ANALYSIS AND DESIGN
OF
FLIGHT VEHICLE STRUCTURES

TRI-STATE OFFSET COMPANY

747 STRUCTURE CUTAWAY

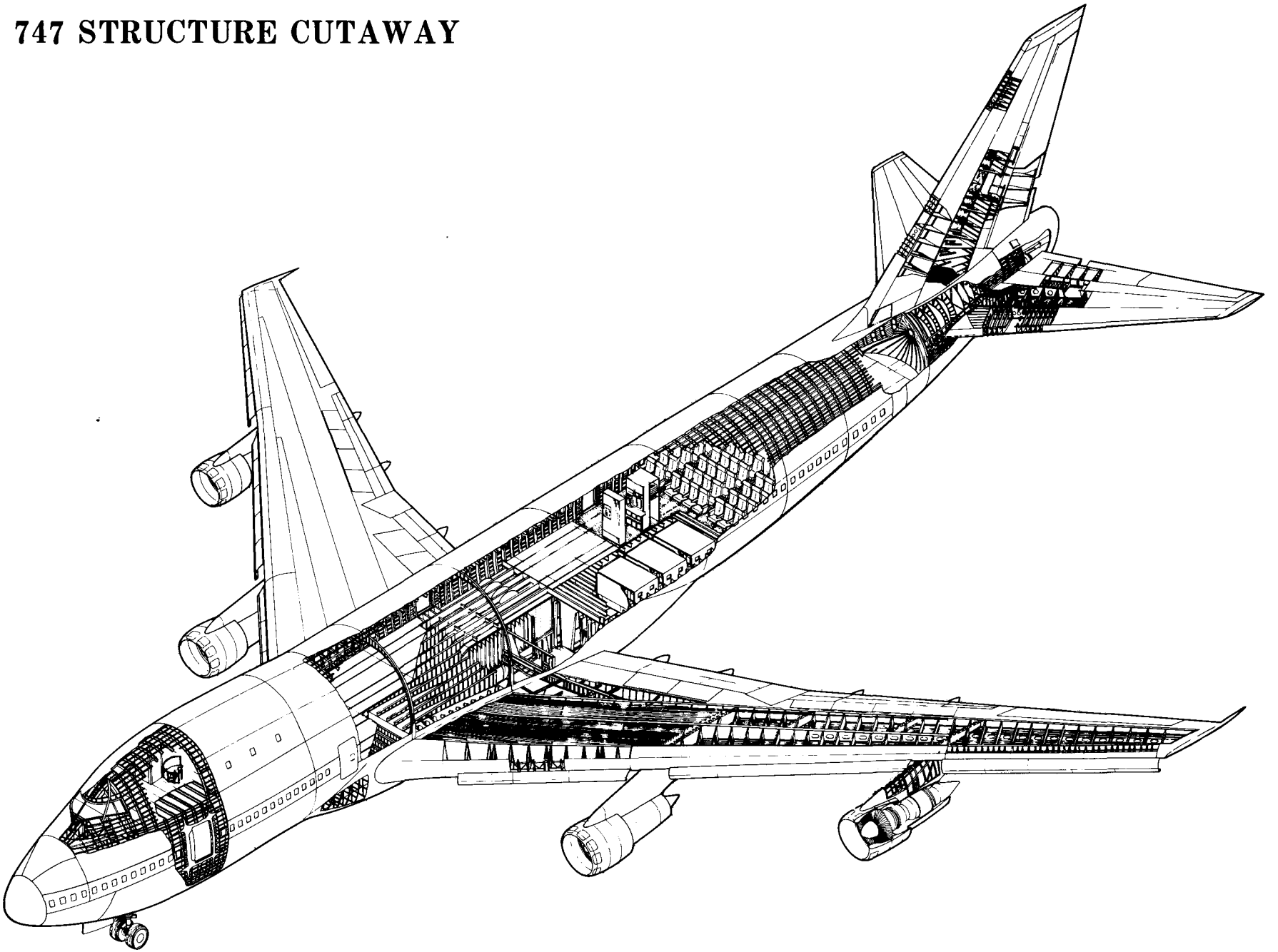

ANALYSIS AND DESIGN
OF
FLIGHT VEHICLE STRUCTURES

By

E. F. Bruhn, B. S., M.S., C.E.

Professor (Emeritus) of Aeronautics and Astronautics

Purdue University

Assisted by the following persons and
the chapters and parts they contributed:

DR. R. J. H. BOLLARD, (Chapters A24, A25, A26)
Head, Department of Aeronautics and Astronautics
University of Washington, Seattle, Washington

LLOYD E. HACKMAN, (Chapters C12)
Consultant on Composite Structures Engineering

DR. GEORGE LIANIS, (Chapter A18)
Professor of Aeronautics and Astronautics
Purdue University

WILLIAM F. McCOMBS, (Chapter CIO-Part 2, Chapter Cll-Part 2, Chapter D3)

DR. A. F. SCHMITT, (Chapters A7, A8, A16, A17, A22)
Litton Systems, Inc.

CLARENCE R. SMITH, (Chapter C13)
Engineering Consultant on Fatigue of Metals and Structures

DR. JOSEPH A. WOLF, JR., (Chapter A23)
Senior Research Engineer
General Motors Research Laboratories

Copyright 1973 by E. F. Bruhn

All rights reserved. including the right of
reproduction in whole or in part in any form.

Portions previously published
under the following titles
"Analysis and Design of Aircraft Structures"
by E. F. Bruhn
"Analysis and Design of Flight Vehicle Structures"
by E. F. Bruhn

Published and Distributed by
Tri-State Offset Company

Printed in U.S.A.

PREFACE

The 1965 edition of the book "Analysis and Design of Flight Vehicle Structures", contained over 950 pages. As time passes it is normal to expect expanded or new material to be added to later editions of a book. Thus it appeared desirable to add some 380 pages of additional material, which meant that a new edition would contain over 1300 pages or too large for a single volume. A decision was made to issue the new edition in two volumes. This two volume edition was practically ready for binding, when a further final decision was made to remain with one volume edition and place the 380 pages of new material referred to above in 3 separate, rather small sized books, Information on these 3 separate books is given on the 3 pages following the Table of Contents. The reader will note that these 3 books deal with special subjects in the structural design field and are available.

This new 1973 one volume edition presents 2 major changes from the 1965 edition. Chapter A23 has been completely revised and expanded by a new co-author, namely, Dr. Joseph A. Wolf, formerly on the faculty of UCLA and now with the General Motors Research Laboratories. Dr. Wolf had the cooperation of Dr. A. F. Schmitt, the author of the A23 Chapter in the 1965 edition. The other major change is the replacement of Chapter C13 on the subject of fatigue in the 1965 edition by a new chapter on fatigue. The Author of this new Chapter C13 is C. R. Smith, a widely known authority in the broad field of fatigue of materials and structures.

This author expresses his thanks to the several co-authors for checking over their material. Only minor corrections have resulted from this check.

A considerable amount of material in various chapters by the author made use of reports, manuals, drawings and photographs supplied to the author by many aerospace companies, in particular, Boeing of Seattle; Douglas Co.; General Dynamics, Fort Worth and San Diego Divisions; Martin in Denver; North American Aviation, Columbus and Tulsa Divisions; and the Vought Division of LTV Corp. The author is deeply grateful for this assistance and cooperation.

As a final note, if any reference in the Chapters of this book refers to Volume 2 it should be discarded by the reader.

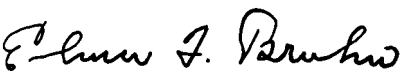

June 1973

DC-10
STRUCTURAL CUTAWAY

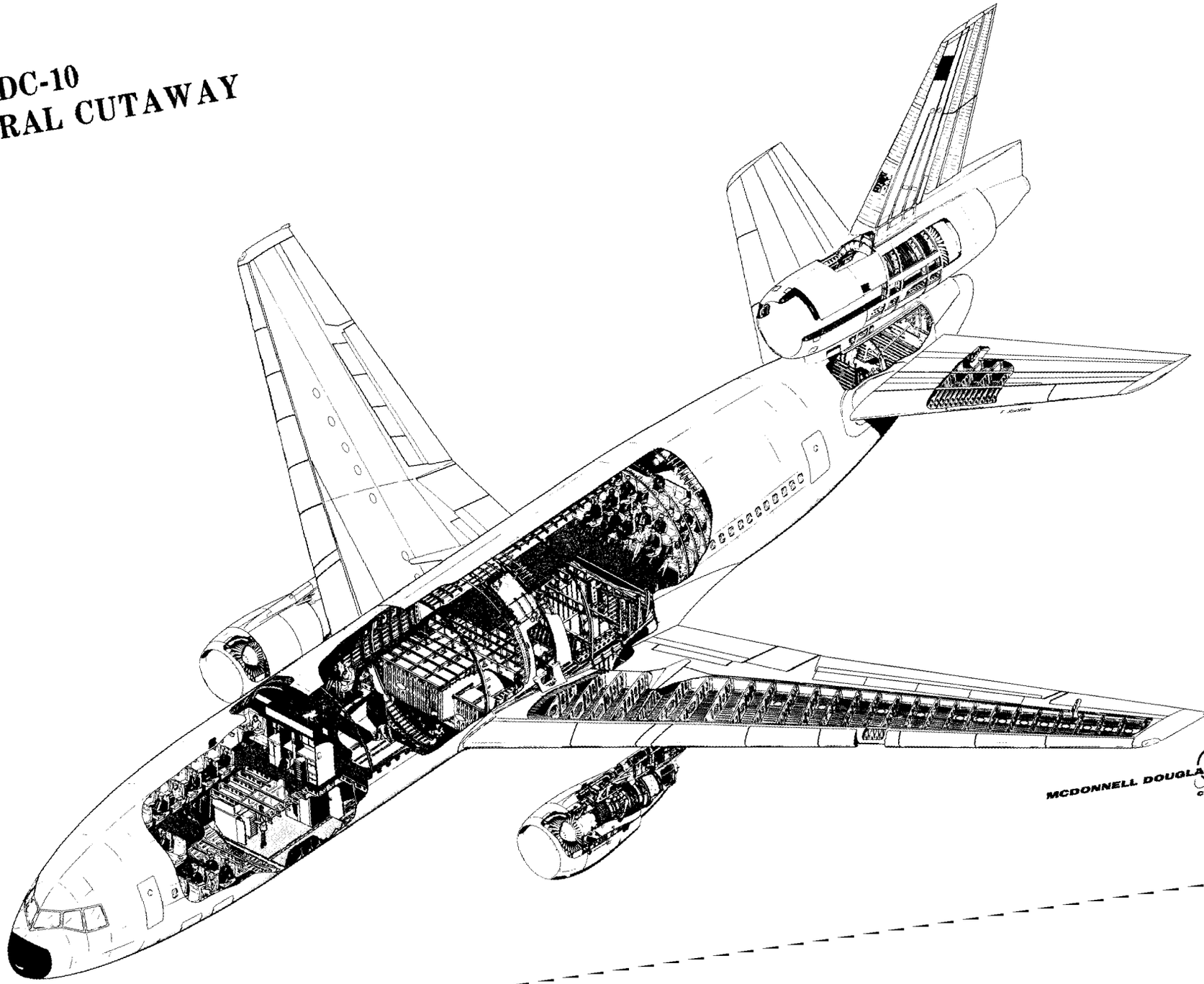

MCDONNELL DOUGLAS CORPORATION

TABLE OF CONTENTS

Chapter No.

A1 The Work of the Aerospace Structures Engineer.

STATICALLY DETERMINATE STRUCTURES

(Loads, Reactions, Stresses, Shears, Bending Moments, Deflections)

A2 Equilibrium of Force Systems. Truss Structures. Externally Braced Wings. Landing Gear.
A3 Properties of Sections - Centroids, Moments of Inertia, etc.
A4 General Loads on Aircraft.
A5 Beams - Shear and Moments. Beam - Column Moments.
A6 Torsion - Stresses and Deflections.
A7 Deflections of Structures. Castigliano's Theorem. Virtual Work. Matrix Methods.

THEORY AND METHODS FOR SOLVING STATICALLY INDETERMINATE STRUCTURES

A8 Statically Indeterminate Structures. Theorem of Least Work. Virtual Work. Matrix Methods.
A9 Bending Moments in Frames and Rings by Elastic Center Method.
A10 Column Analogy Method.
A11 Continuous Structures - Moment Distribution Method.
A12 Slope Deflection Method.

BEAM BENDING AND SHEAR STRESSES. MEMBRANE STRESSES. COLUMN AND PLATE INSTABILITY.

A13 Bending Stresses.
A14 Bending Shear Stresses - Solid and Open Sections - Shear Center.
A15 Shear Flow in Closed Thin-Walled Sections.
A16 Membrane Stresses in Pressure Vessels.
A17 Bending of Plates.
A18 Theory of the Instability of Columns and Thin Sheets.

INTRODUCTION TO PRACTICAL AIRCRAFT STRESS ANALYSIS

A19 Introduction to Wing Stress Analysis by Modified Beam Theory.
A20 Introduction to Fuselage Stress Analysis by Modified Beam Theory.
A21 Loads and Stresses on Ribs and Frames.
A22 Analysis of Special Wing Problems. Cutouts. Shear lag. Swept Wing.
A23 Analysis by the "Method of Displacements".

THEORY OF ELASTICITY AND THERMOELASTICITY

A24 The 3-Dimensional Equations of Thermoelasticity.
A25 The 2-Dimensional Equations of Elasticity and Thermoelasticity.
A26 Selected Problems in Elasticity and Thermoelasticity.

TABLE OF CONTENTS Continued

Chapter No.

FLIGHT VEHICLE MATERIALS AND THEIR PROPERTIES

B1 Basic Principles and Definitions.
B2 Mechanical and Physical Properties of Metallic Materials for Flight Vehicle Structures.

STRENGTH OF STRUCTURAL ELEMENTS AND COMPOSITE STRUCTURES

C1 Combined Stresses. Theory of Yield and Ultimate Failure.
C2 Strength of Columns with Stable Cross-Sections.
C3 Yield and Ultimate Strength in Bending.
C4 Strength and Design of Round, Streamline, Oval and Square Tubing in Tension, Compression, Bending, Torsion and Combined Loadings.
C5 Buckling Strength of Flat Sheet in Compression, Shear, Bending and Under Combined Stress Systems.
C6 Local Buckling Stress for Composite Shapes.
C7 Crippling Strength of Composite Shapes and Sheet-Stiffener Panels in Compression. Column Strength.
C8 Buckling Strength of Monocoque Cylinders.
C9 Buckling Strength of Curved Sheet Panels and Spherical Plates. Ultimate Strength of Stiffened Curved Sheet Structures.
C10 Design of Metal Beams. Web Shear Resistant (Non-Buckling) Type.
Part 1. Flat Sheet Web with Vertical Stiffeners. Part 2. Other Types of Non-Buckling Webs.
C11 Diagonal Semi-Tension Field Design.
Part 1. Beams with Flat Webs. Part 2. Curved Web Systems.
C12 Sandwich Construction and Design.
C13 Fatigue.

CONNECTIONS AND DESIGN DETAILS

D1 Fittings and Connections. Bolted and Riveted.
D2 Welded Connections.
D3 Some Important Details in Structural Design.

Appendix A Elementary Arithmetical Rules of Matrices.

SPECIAL BOOKS NOW AVAILABLE

As explained in the preface, instead of changing to a 2 volume edition in order to include 380 pages of new material, it was decided at the last minute so-to-speak, to remain with one volume and issue this new material on three different subjects as separate books. A description of these 3 books follows:

ENGINEERING COLUMN ANALYSIS

By

WILLIAM F. McCOMBS

Senior Structures Design Specialist

Vought Aeronautics Div. of LTV Corp., Dallas, Texas

"Engineering Column Analysis" has been written to provide the engineer with practical methods for analyzing nearly all types of columns and beam-columns, including those on elastic supports and these loaded into the plastic range of the material. The book has been written in such a manner that no prior study of elastic stability theory is necessary. The only prerequisite is an understanding of elementary strength of materials as given in undergraduate engineering courses.

The numerous methods and techniques of analysis are presented for "hand solutions" by the engineer, but these can, of course, be arranged for analysis by computer if desired. The broad scope of the book is indicated by the following list of Part titles. References are also provided for further reading on specific subjects. Much of the material has been used by the author in classes for practicing engineers in the aircraft industry. It is often surprising to one how easily many seemingly complicated columns or beam-columns can be analyzed for engineering purposes.

Part	Title
A	A Survey of Various Column Problems.
B	Stability and Critical Loads.
C	Columns of Constant Section and Single Span.
D	Columns of Variable Section and Single Span.
E	Beam-Columns of Constant Section and Single Span.
F	Multiple Beam-Columns of Constant Between Supports.
G	Multispan Columns of Constant Section Between Supports.
H	Analysis of Truss Structures for Stability and Strength.
I	Elastic Weight Numerical for Calculations Beam Distortions.
J	Columns of Varying Section and Single Span.
K	Beam-Columns of Varying Section and Single Span.
L	Multispan Columns and Beam-Columns of Varying Section.
M	Beam-Columns on Elastic Supports.
N	Columns on E"lastic Supports.
O	Torsional Buckling of Free Columns (Struts).
P	Torsional Buckling of Restrained Columns.
Q	Special Topics.

DESIGN AND ANALYSIS OF FILAMENTARY COMPOSITE STRUCTURES

By

Lloyd E. Hackman

Consultant on composite structures engineering.

The Author has presented a basic review of a new structural technology. He has also presented an insight into the development of the technology as well as the application of the technology in practical structural elements.

The Author presents the application of the design and analysis methodology from the micro-mechanics of fiber matrix interaction to the use of composite lamination in various types of structural elements and methods of joining. The application analysis also includes the description of failure modes, a statement of failure criteria, and test methods for the experimental evaluation of composite materials.

The Author demonstrates the use of all analysis methodology and failure criteria with example problems taken from ten years of experience in the design with composite materials in the aerospace industry.

TABLE OF CONTENTS

C13.l Introduction

- C13.Ll The Development of a Technology
- C13.L2 The Material Concept
- C13.L3 The Design Approach to Composite Structures
- C14.L4 Nomenclature

C13.2 General Relations for Orthotropic Laminates

- C13.2.l Elastic Relations
- C13.2.2 Strength Relations of Fabric Laminates
- C13-2-3 Properties of Various Constructions
- C13.2.4 Elastic Properties of Oriented Laminates
- C13.2.5 Elastic Properties of Cross Laminates or Parallel Laminates
- C13.2.6 Isotropic Laminates Made with Orthotropic Laminations

C13.3 Relationships of Unidirectional Laminate Materials

- C13.3.l Elastic Relationships for laminae
- C13.3.2 Strength Relationships for a lamina of a Rectangular Array
- C13.3.3 Strength Relationships for a lamina of a Hexagonal Array
- C13.3.4 Multi Laminate Properties and Stresses
- C13.3.5 Compressive Strength of Unidirectional Laminates
- C13.3.6 Effect of voids on Compression Strength

C13.4

- C13.4.l Laminate Failure Criterian
- C13.4.2 Failure modes and Test Methods
- C13.4.3 Nonlinear characteristics of Laminate and Failure Modes

C13.5 Stability of Filamentary Composite Structural Elements

- C13.5.l Flat Rectangular Panels
- C13.5.2 Honeycomb Sandwich

C13.6 Joining of Composite Materials

- C13.6.l Bonded Lap Joints
- C13.6.2 Mechanical Fastened Joints

ANALYSIS AND DESIGN

OF

MISSILE STRUCTURES

By

J. I. ORLANDO, *Branch Chief*
Missile and Space Division
Douglas Aircraft Company

And

J. F. MEYERS, *Section Chief*
Missile and Space Division
Douglas Aircraft Company

This section represents an elaboration for Prof. E. F. Bruhn's book, "Analysis and Design of Flight Vehicle Structures." It has been designed to introduce the student and beginning engineer to the general field of missile structures and to give a limited presentation of the preliminary load, stress analysis, and structural design practices of typical boost missiles.

The first portion is both analytical and descriptive in nature and serves to acquaint the reader with current practices in configuration, material usage, structural techniques, and design factors. The main body, or Parts E1.7 and E1.8, takes a hypothetical multistage vehicle, derives the critical flight load conditions, and indicates analysis for these loads. The analysis techniques derive directly from the body of Professor Bruhn's book, "Analysis and Design of Flight Vehicle Structures"; hence giving the reader examples of practical usage of that data for missile design.

TABLE OF CONTENTS

Part E1.1 HISTORY, TERMINOLOGY, WEIGHT DISTRIBUTION

Part E1.2 PROPULSION SYSTEM FUNDAMENTALS

Part E1.3 MISSILE AND SPACE VEHICLE SPECIFICATIONS

Part E1.4 MISSILE AND SPACE VEHICLE TYPICAL STRUCTURES

Part E1.5 MATERIALS FOR MISSILES

Part E1.6 STRUCTURAL DESIGN FACTORS

Part E1.7 MISSILE LOADS ANALYSIS

Part E1.8 MISSILE STRESS ANALYSIS

Part E1.9 CONCLUSIONS

APPENDIX: Reference Design Charts and Material Taken from "Analysis and Design of Flight Vehicle Structures" by Bruhn.

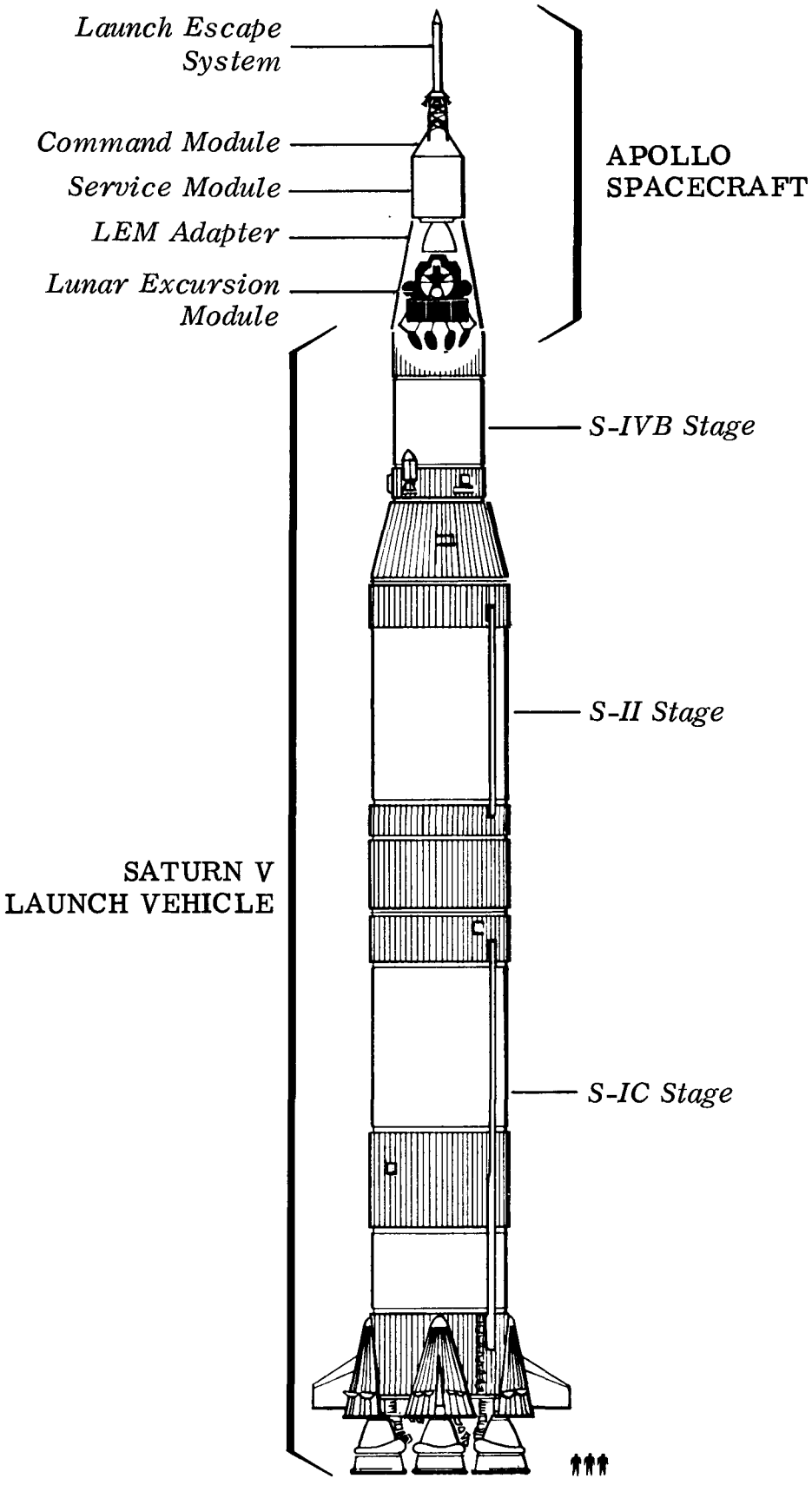

APOLLO/SATURN VEHICLE

Space exploration requires a tremendous launch vehicle, as illustrated, by the Appollo/Saturn vehicle. Note size of vehicle when compared to size of a man.

Such large vehicles present many challenging problems to the structures engineer. (Drawing - Courtesy of N. American Aviation Co.)

1959 - 60 BEGINNING OF THE "JET" AGE OF AIR TRANSPORTATION - 550-650 MPH



BOEING 707 STRATOLINER

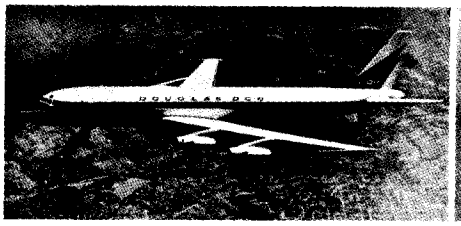

FIRST FLIGHT OF DOUGLAS DC - 8
MAY 30, 1958

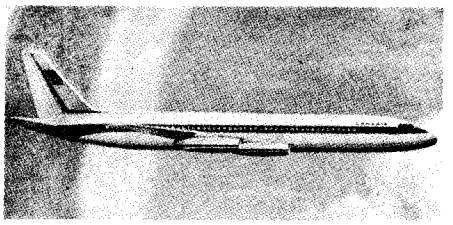

CONVAIR 880 AIRLINER

MODERN TRANSPORTS PRODUCED DURING PERIOD - 1940 - 1956 - 250 -400 MPH

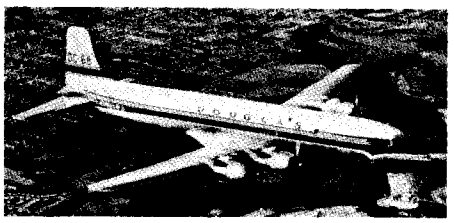

DOUGLAS DC-6B

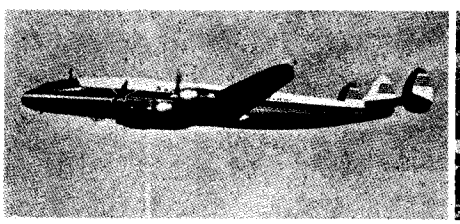

LOCKHEED SUPER CONSTELLATION

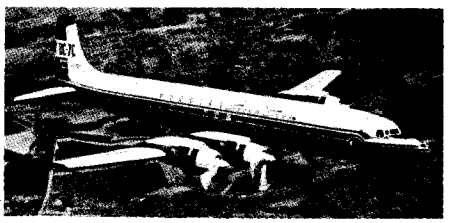

DOUGLAS DC-7C

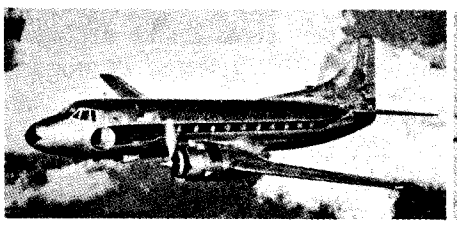

MARTIN "404" TRANSPORT

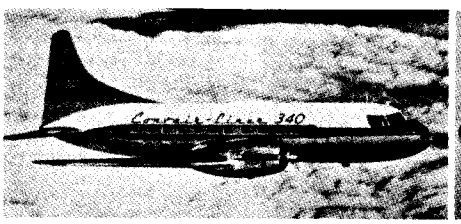

CONVAIR "340" TRANSPORT

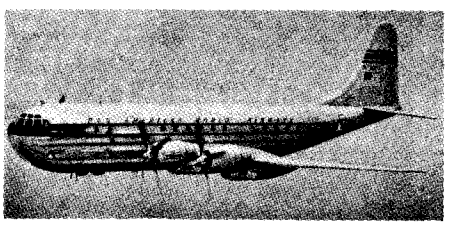

BOEING "STATOCRUISER"

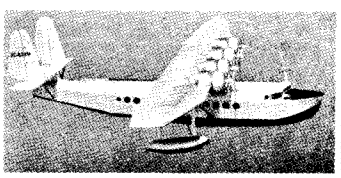

1933 SIKORSKY S-42

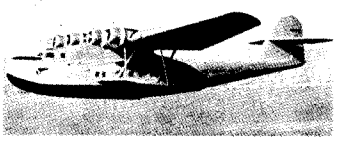

1934 MARTIN BOAT

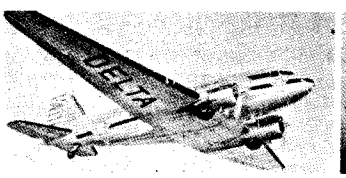

1935 DOUGLAS DC-3

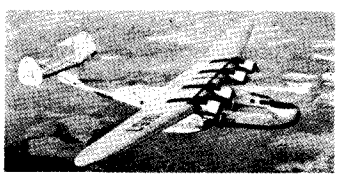

1937 MARTIN "CLIPPER"

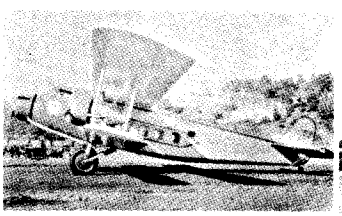

1928 BOEING MODEL 80-A

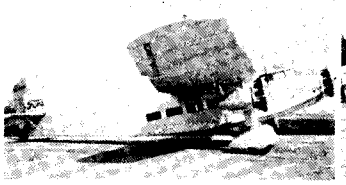

1930 FORD TRI-MOTOR

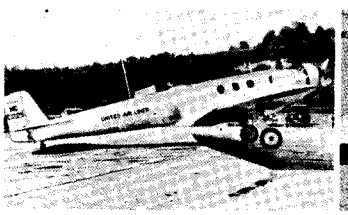

1931 BOEING "MONOMAIL"

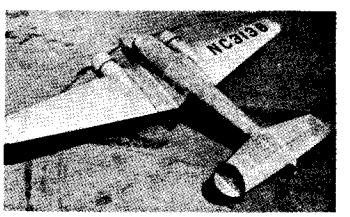

1933 LOCKHEED "ELECTRA"

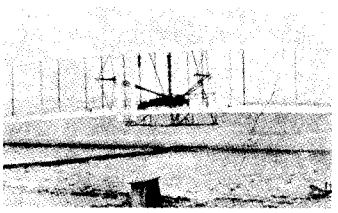

1903 FIRST FLIGHT BY
WRIGHT BROTHERS

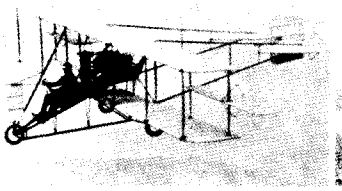

1912 GLEN. L. MARTIN
IN HIS BIPLANE

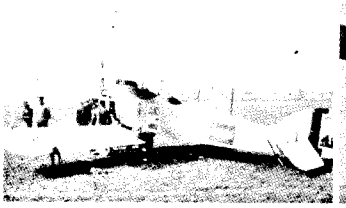

1918 STANDARD AIRCRAFT
CORP BIPLANE



1926 FOKKER TRANSPORT

PHOTOGRAPHS ILLUSTRATING PROGRESS OF AIRCRAFT DESIGN FOR AIR TRANSPORTATION - 40 TO 175 MPH

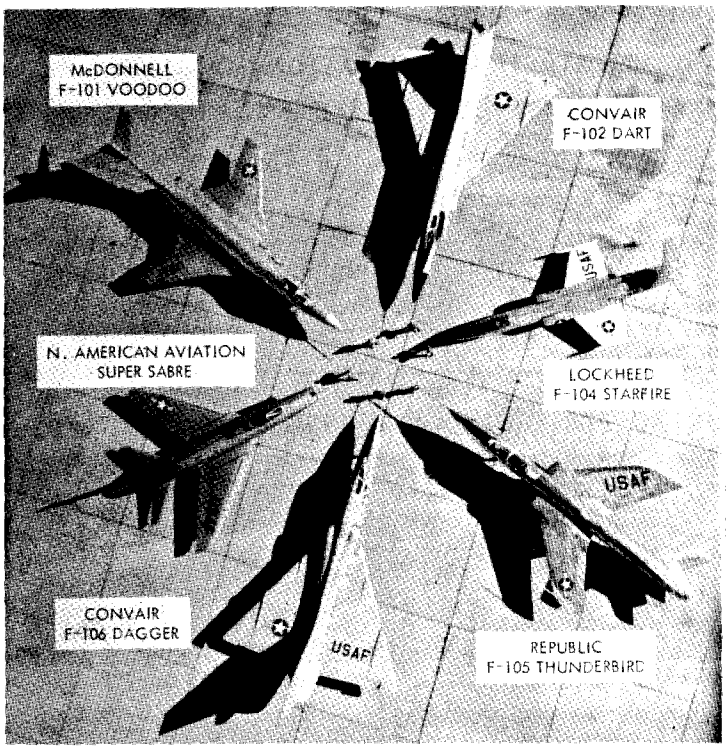

SIX AIR FORCE SUPERSONIC FIGHTERS
SHOWING VARIOUS WING SHAPES
(Picture from United Aircraft Publication "BEEHIVE" Spring 1958)

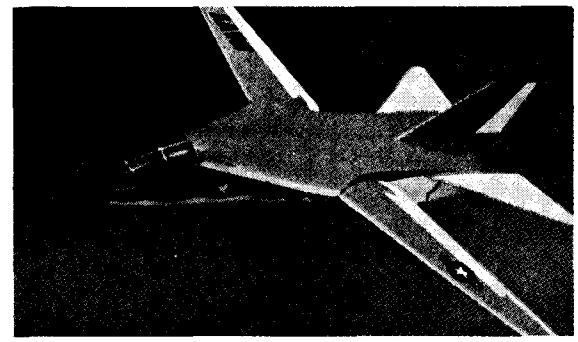

GENERAL DYNAMICS F-111 AIR FORCE/NAVY
TACTICAL FIGHTER. SPEED 2000 M. P. H.
VARIABLE POSITION WING (1965)

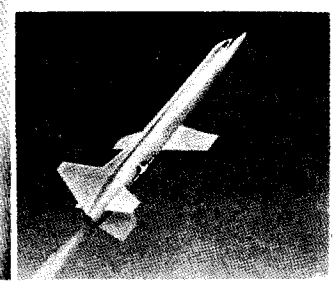

1959 N. AMERICAN
AVIATION
X-15 HYPERSONIC
RESEARCH AIRPLANE

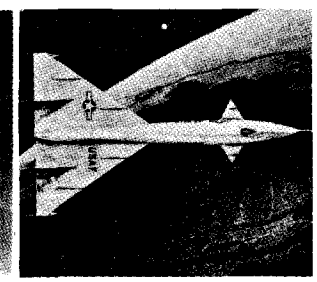

(1964) N. AMERICAN
AVIATION
B-70. SPEED
2000 M. P.H. (PLUS)

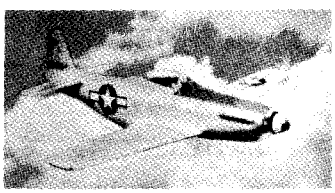

NORTH AMERICAN AVIATION
"MUSTANG"



CONSOLIDATED B-24
"LIBERATOR"

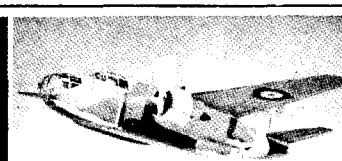

DOUGLAS "BOSTON"
BOMBER

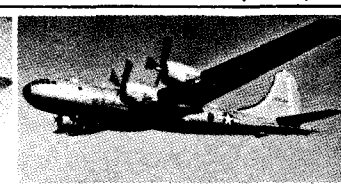

BOEING B-29
"SUPERFORTRESS"



CURTIS P-40 "WAR HAWK"

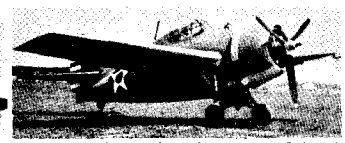

GRUMMAN F4F-4 "WILDCAT"

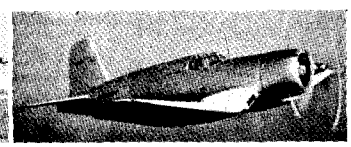

VOUGHT "CORSAIR"



REP. P-47 "THUNDERBOLT"

SOME OUTSTANDING WORLD WAR II AIRCRAFT



1930 MARTIN P3M-1 NAVY

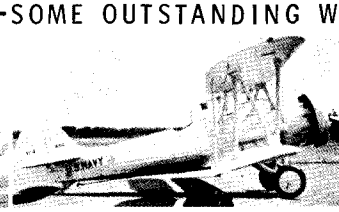

1933 VOUGHT-NAVY SU-4

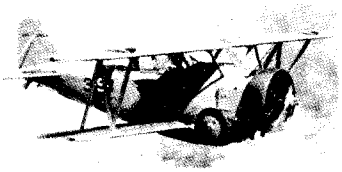

1936 GRUMMAN-NAVY SF-1

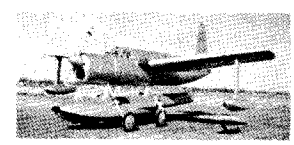

1939 VOUGHT-SIKORSKY SO2U



1908 "WRIGHT" AIRPLANE
FIRST ARMY AIRPLANE

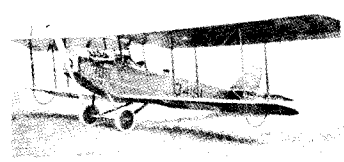

1918 CURTIS "JENNY"



1921 BOEING-ARMY
ARMORED ATTACK AIRPLANE

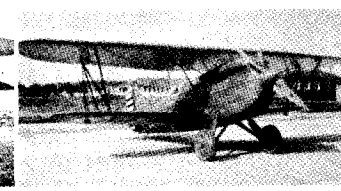

1929 CURTIS P-6 "HAWK"

SOME PRE-WORLD WAR II AIRCRAFT

PHOTOGRAPHS ILLUSTRATING TREMENDOUS PROGRESS OF MILITARY AVIATION

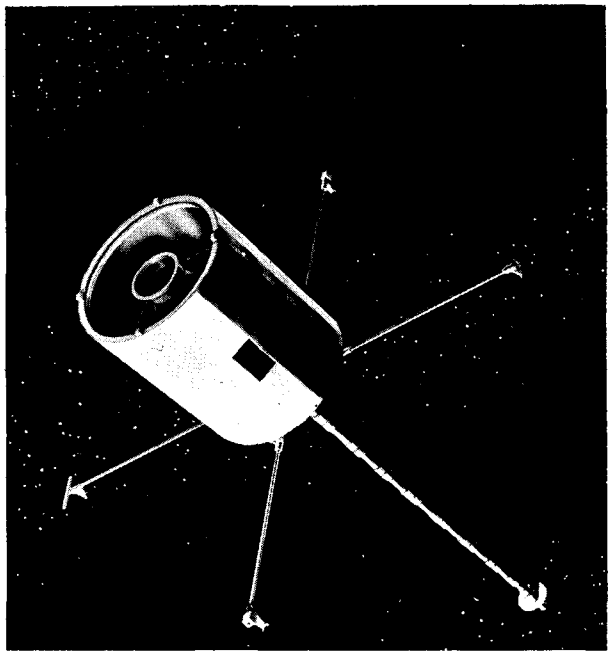

PIONEER. Interplanetary Probing
up to 90 million miles (1965)

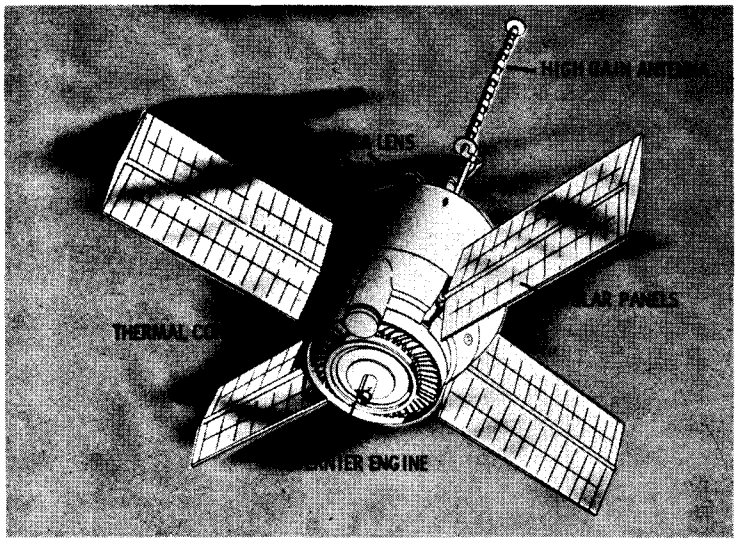

LUNAR ORBITER. Will orbit the moon taking
pictures (1966)

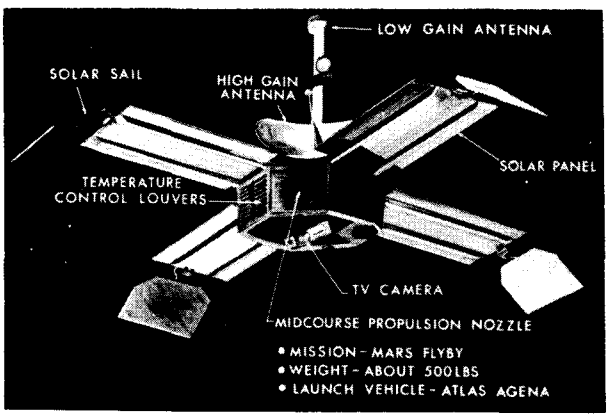

MARINER. To obtain scientific information
on Mars and Venus (1964-65)

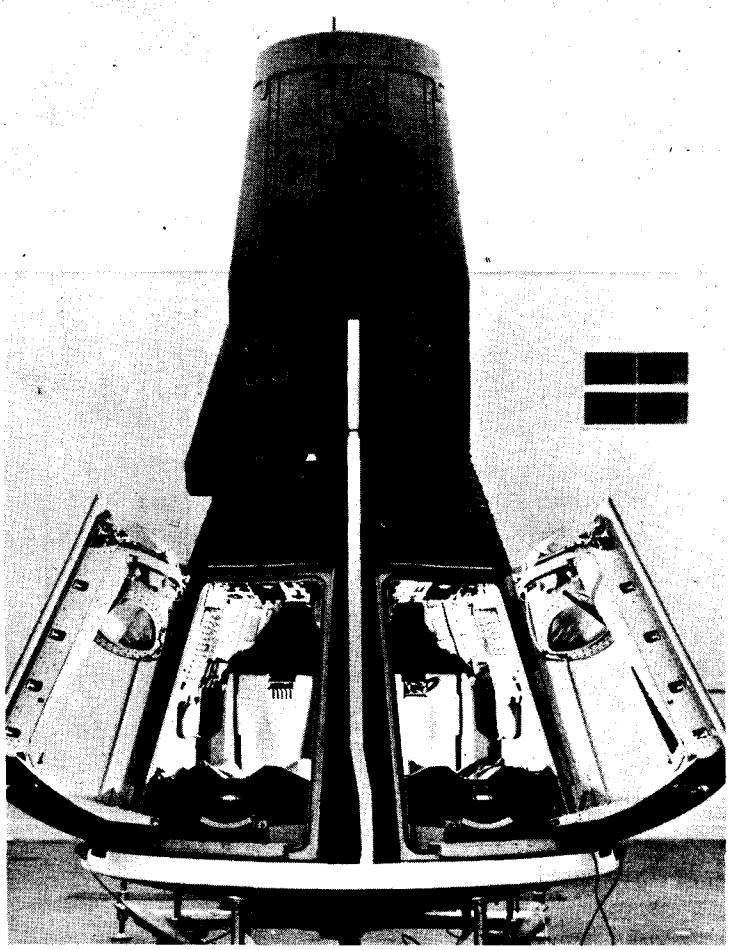

PROJECT GEMINI. Two-man Spacecraft.
(1965)

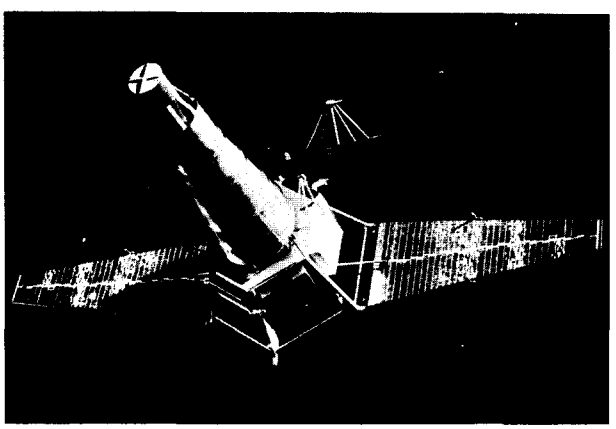

RANGER. Photographed the Lunar Surface.
(1964)

The Age for Spacecraft is just dawning. Regardless of the type of Spacecraft,
its creation will involve the work of the structural designer.

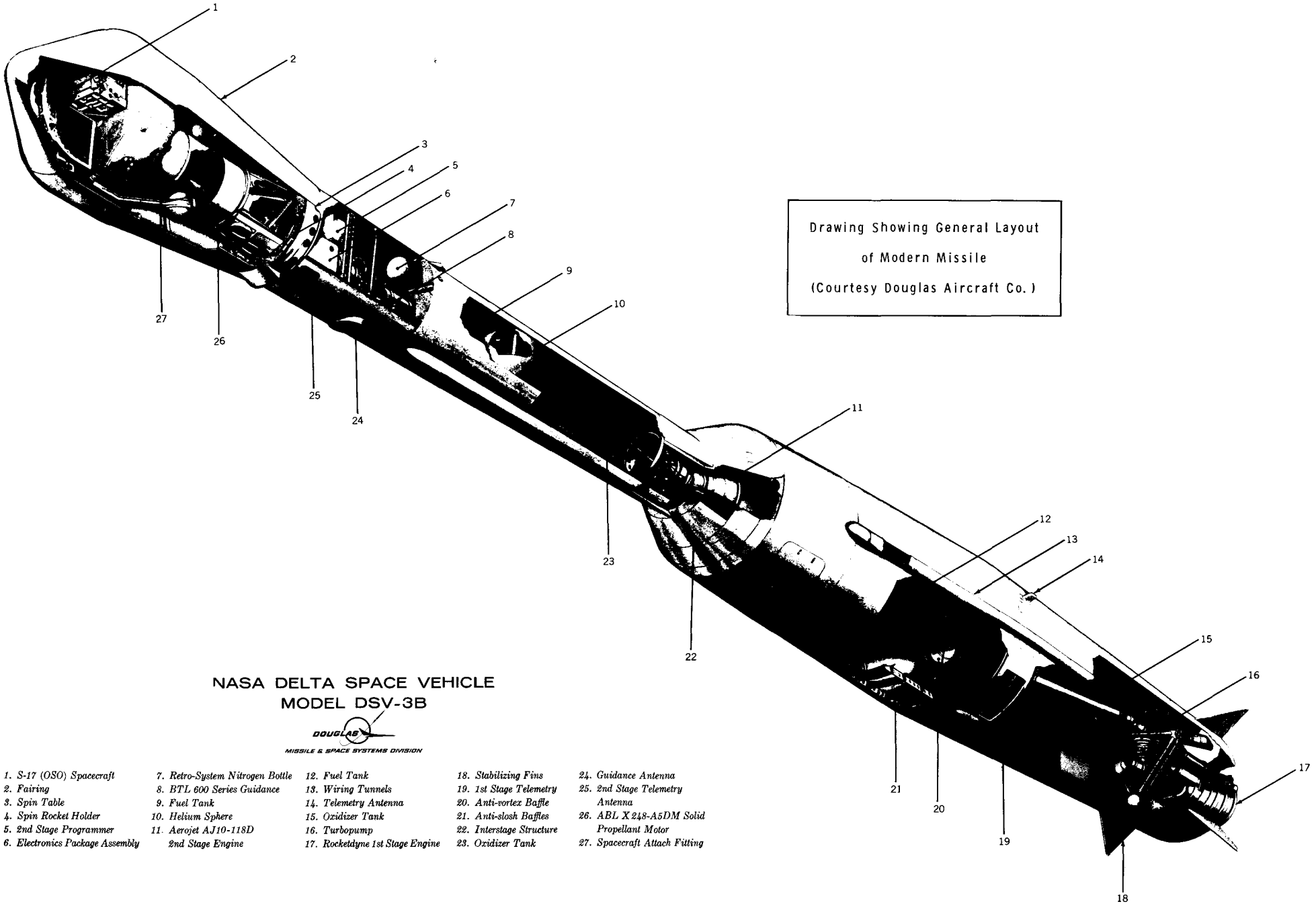

Drawing Showing General Layout
of Modern Missile
(Courtesy Douglas Aircraft Co.)

NASA DELTA SPACE VEHICLE
MODEL DSV-3B

DOUGLAS
MISSILE & SPACE SYSTEMS DIVISION

1. *S-17 (OSO) Spacecraft*
2. *Fairing*
3. *Spin Table*
4. *Spin Rocket Holder*
5. *2nd Stage Programmer*
6. *Electronics Package Assembly*
7. *Retro-System Nitrogen Bottle*
8. *BTL 600 Series Guidance*
9. *Fuel Tank*
10. *Helium Sphere*
11. *Aerojet AJ10-118D 2nd Stage Engine*
12. *Fuel Tank*
13. *Wiring Tunnels*
14. *Telemetry Antenna*
15. *Oxidizer Tank*
16. *Turbopump*
17. *Rocketdyne 1st Stage Engine*
18. *Stabilizing Fins*
19. *1st Stage Telemetry*
20. *Anti-vortex Baffle*
21. *Anti-slosh Baffles*
22. *Interstage Structure*
23. *Oxidizer Tank*
24. *Guidance Antenna*
25. *2nd Stage Telemetry Antenna*
26. *ABL X 248-A5DM Solid Propellant Motor*
27. *Spacecraft Attach Fitting*

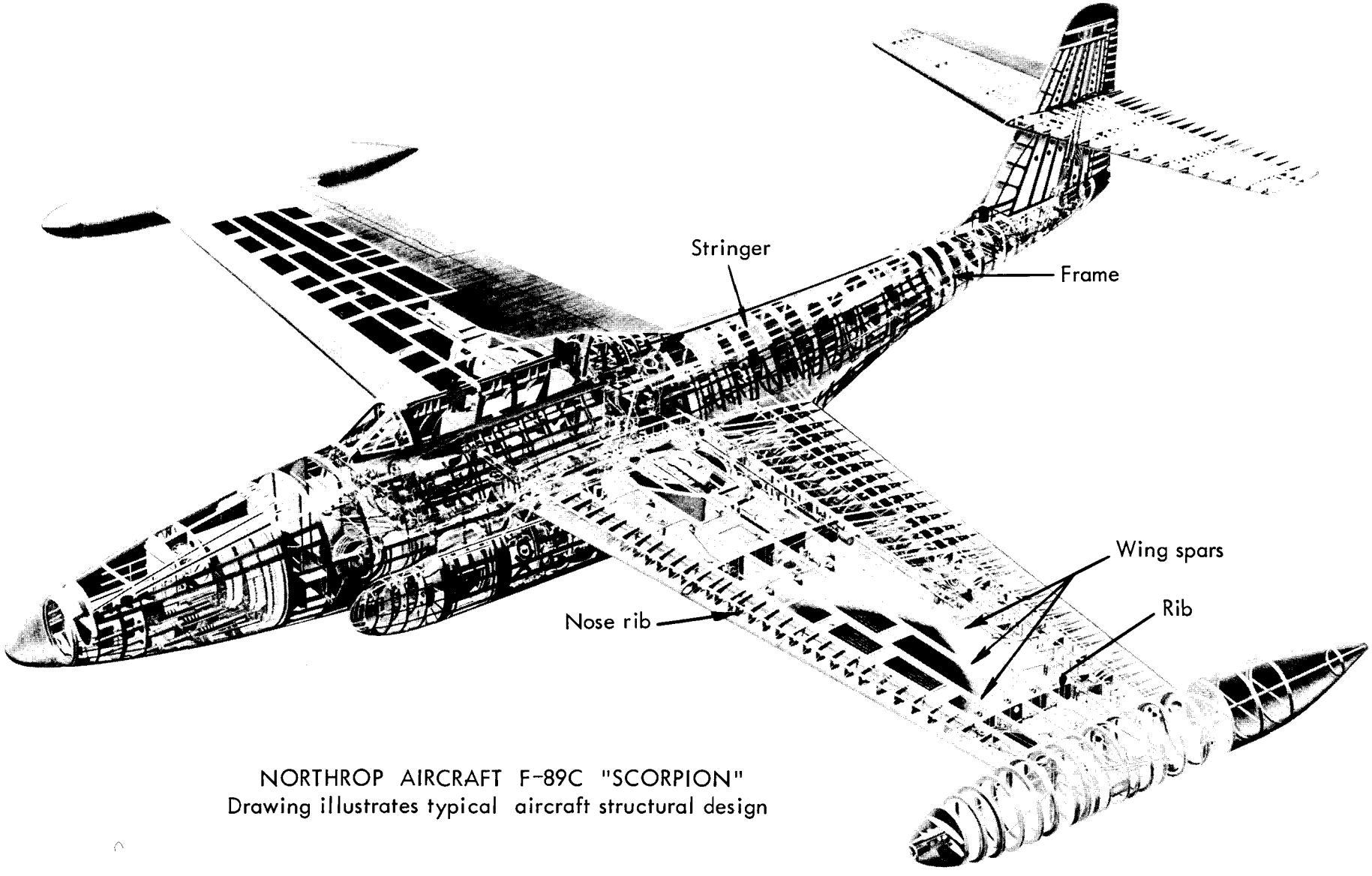

NORTHROP AIRCRAFT F-89C "SCORPION"
Drawing illustrates typical aircraft structural design

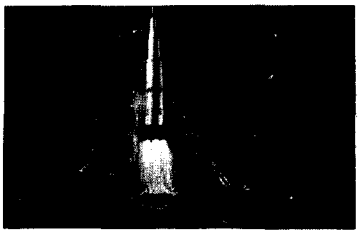

LIFTOFF AT THE CAPE — the huge Saturn V in a 7½-million-pound thrust toward the stars.

1

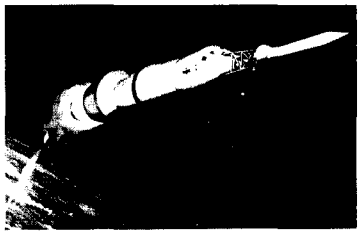

S-IC SEPARATION — first stage drops away, and the Saturn S-II second stage is now ignited.

2

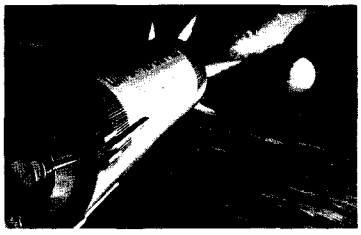

S-IVB IGNITES — S-II stage is jettisoned; S-IVB hurls Apollo spacecraft into earth orbit.

3



TRANSLUNAR INJECTION — S-IVB stage pushes Apollo spacecraft out of earth's gravity pull.

4

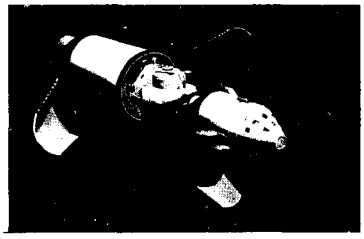

APOLLO — S-IVB SEPARATION — the adapter panels are blown free; Apollo craft separates.

5

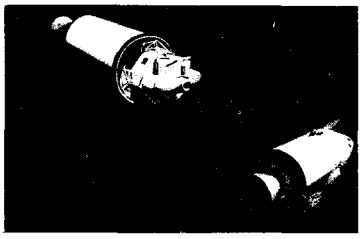

FREE FLY-AROUND — Apollo craft turns around in space to dock with the waiting LEM.

6

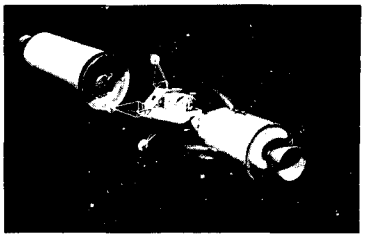

LEM EXPOSED — two crewmen enter LEM for an equipment checkout; S-IVB is left behind.

7



LUNAR ORBIT — Service Module engine retro-fires to put craft in 80-mile lunar orbit.

8

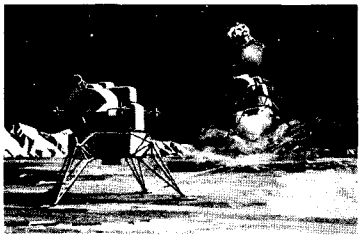

THE DESCENT — Apollo craft remains in orbit while two astronauts guide LEM to the moon.

9



LUNAR EXPLORATION — during moon stay two astronauts undertake scientific observations.

10

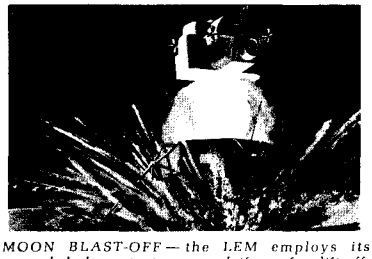

MOON BLAST-OFF — the LEM employs its expended descent stage as platform for lift-off.

11

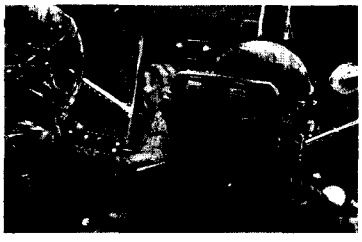

LUNAR RENDEZVOUS — the LEM astronauts line up craft for critical dock/mate maneuver.

12

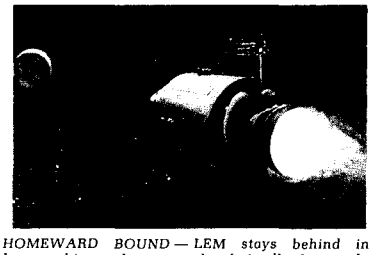

HOMEWARD BOUND — LEM stays behind in lunar orbit as three men head Apollo for earth.

13

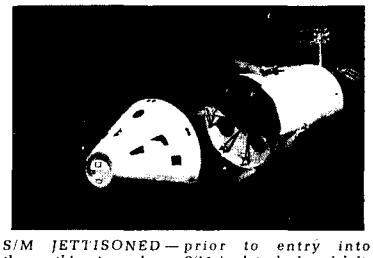

S/M JETTISONED — prior to entry into the earth's atmosphere, S/M is detached and left.

14



REENTRY — pilot now orients Command Module so base heat shield takes friction heat.

15

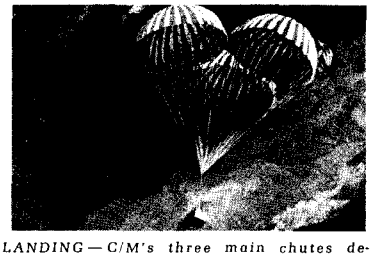

LANDING — C/M's three main chutes deploy to bring the craft back down safely to earth.

16

In the tremendous task of landing on and returning man from the moon, the structures engineer is faced with many new and challenging design requirements.

Appollo II with Astronauts Armstrong, Aldrin and Collins landed on the moon on July 20, 1969.

(Photos - Courtesy of N. American Aviation Co.)

CHAPTER Al
THE WORK OF THE AEROSPACE STRUCTURES ENGINEER

AI. I Introduction.

The first controllable human flight in a heavier than air machine was made by Orville Wright on December 17, 1903, at Kitty Hawk, North Carolina. It covered a distance of 120 feet and the duration of flight was twenty seconds. Today, this initial flight appears very unimpressive, but it comes into its true perspective of importance when we realize that mankind for centuries has dreamed about doing or tried to do what the Wright Brothers accomplished in 1903.

The tremendous progress accomplished in the first 50 years of aviation history, with most of it occurring in the last 25 years, is almost unbelievable, but without doubt, the progress in the second 50 year period will still be more unbelievable and fantastic. As this is written in 1964, jet airline transDortation at 600 MPH is well established and several types of military aircraft have speeds in the 1200 to 2000 MPH range. Preliminary designs of a supersonic airliner with Mach 3 speed have been completed and the government is on the verge of sponsoring the development of such a flight vehicle, thus supersonic air transportation should become common in the early 1970's. The rapid progress in missile design has ushered in the Space Age. Already many space vehicles have been flown in search of new knowledge which is needed before successful exploration of space such as landings on several planets can take place. Unfortunately, the rapid development of the missile and rocket power has given mankind a flight vehicle which, when combined with the nuclear bomb, has the awesome potential to quickly destroy vast regions of the earth. While no person at present knows where or what space exploration will lead to, relative to benefits to mankind, we do know that the next great aviation expansion besides supersonic airline transportation will be the full development and use of vertical take-off and landing aircraft. Thus persons who will be living through the second half century of aviation progress will no doubt witness even more fantastic progress than occurred in the first 50 years of aviation history.

AI. 2 General Organization of an Aircraft Company Engineering Division.

The modern commercial airliner, military airplane, missile and space vehicle is a highly scientific machine and the combined knowledge and experience of hundreds of engineers and scientists working in close cooperation is necessary to insure a successful product. Thus the engineering division of an aerospace company consists of many groups of specialists whose specialized training covers all fields of engineering education such as Physics, Chemical and Metallurgical, Mechanical, Electrical and, of course, Aeronautical Engineering.

It so happens that practically all the aerospace companies publish extenSive pamphlets or brochures explaining the organization of the engineering division and the duties and responsibilities of the many sections and groups and illustrating the tremendous laboratory and test facilities which the aerospace industry possesses. It is highly recommended that the student read and stUdy these free publications in order to obtain an early general uncier-standing of how the modern flight vehicle is conceived, designed and then produced.

In general, the engineering department of an aerospace company can be broken down into six large rather distinct sections, which in turn are further divided into specialized groups, which in turn are further divided into smaller working groups of engineers. To illustrate, the six sections will be listed together with some of the various groups. This is not a complete list, but it should give an idea of the broad engineering set-up that is necessary.

I. Preliminary Design Section.

II. Technical Analysis Section.

- (1) Aerodynamics Group
- (2) Structures Group
- (3) Weight and Balance Control Group
- (4) Power Plant Analysis Group
- (5) Materials and Processes Group
- (6) Controls Analysis Group

III. Component Design Section.

- (1) Structural Design Group (Wing, Body and Control Surfaces)
- (2) Systems Design Group (All mechanical, hydraulic, electrical and thermal installations)

IV. Laboratory Tests Section.

(1) Wind Tunnel and Fluid Mechanics Test Labs.
(2) Structural Test Labs.
(3) Propulsion Test Labs.
(4) Electronics Test Labs.
(5) Electro-Mechanical Test Labs.
(6) Weapons and Controls Test Labs.
(7) Analog and Digital Computer Labs.

V. Flight Test Section.

VI. Engineering Field Service Section.

Since this textbook deals with the subject of structures, it seems appropriate to discuss in some detail the work of the Structures Group. For the detailed discussion of the other groups, the student should refer to the various aircraft company publications.

A1.3 The Work of the Structures Group

The structures group, relative to number of engineers, is one of the largest of the many groups of engineers that make up Section II, the technical analysis section. The structures group is primarily responsible for the structural integrity (safety) of the airplane. Safety may depend on sufficient strength or sufficient rigidity. This structural integrity must be accompanied with lightest possible weight, because any excess weight has detrimental effect upon the performance of aircraft. For example, in a large, long range missile, one pound of unnecessary structural weight may add more than 200 lbs. to the overall weight of the missile.

The structures group is usually divided into sub-groups as follows:-

(1) Applied Loads Calculation Group
(2) Stress Analysis and Strength Group
(3) Dynamics Analysis Group
(4) Special Projects and Research Group

THE WORK OF THE APPLIED LOADS GROUP

Before any part of the structure can be finally proportioned relative to strength or rigidity, the true external loads on the aircraft must be determined. Since critical loads come from many sources, the Loads Group must analyze loads from aerodynamic forces, as well as those forces from power plants, aircraft inertia; control system actuators; launching, landing and recovery gear; armament, etc. The effects of the aerodynamic forces are initially calculated on the assumption that the airplane structure is a rigid body. After the aircraft structure is obtained, its true rigidity can be used to obtain dynamic effects. Results of wind tunnel model tests are usually necessary in the application of aerodynamic principles to load and pressure analysis.

The final results of the work of this group are formal reports giving complete applied load design criteria, with many graphs and summary tables. The final results may give complete shear, moment and normal forces referred to a convenient set of XYZ axes for major aircraft units such as the wing, fuselage, etc.

THE WORK OF STRESS ANALYSIS AND STRENGTH GROUP

Essentially the primary job of the stress group is to help specify or determine the kind of material to use and the thickness, size and cross-sectional shape of every structural member or unit on the airplane or missile, and also to assist in the design of all joints and connections for such members. Safety with light weight are the paramount structural design requirements. The stress group must constantly work closely with the Structural Design Section in order to evolve the best structural over-all arrangement. Such factors as power plants, built-in fuel tanks, landing gear retracting wells, and other large cut-outs can dictate the type of wing structure, as for example, a two spar single cell wing, or a multiple spar multiple cell wing.

To expedite the initial structural design studies, the stress group must supply initial structural sizes based on approximate loads. The final results of the work by the stress group are recorded in elaborate reports which show how the stresses were calculated and how the required member sizes were obtained to carry these stresses efficiently. The final size of a member may be dictated by one or more factors such as elastic action, inelastic action, elevated temperatures, fatigue, etc. To insure the accuracy of theoretical calculations, the stress group must have the assistance of the structures test laboratory in order to obtain information on which to base allowable design stresses.

THE WORK OF THE DYNAMICS ANALYSIS GROUP

The Dynamics Analysis Group has rapidly expanded in recent years relative to number of engineers required because supersonic airplanes, missiles and vertical rising aircraft have presented many new and complex problems in the general field of dynamics. In some aircraft companies the dynamics group is set up as a separate group outside the Structures Group.

The engineers in the dynamics group are responsible for the investigation of vibration and shock, aircraft flutter and the establishment of design requirements or changes for its control or correction. Aircraft contain dozens of mechanical installations. Vibration of any part of these installations or systems may be of such character as to cause faulty operation or danger of failure and therefore the dynamic

characteristics must be changed or modified in order to insure reliable and safe operation.

The major structural units of aircraft such as the wing and fuselage are not rigid bodies. Thus when a sharp air gust strikes a flexible wing in high speed flight, we have a dynamic load situation and the wing will vibrate. The dynamicist must determine whether this vibration is serious relative to induced stresses on the wing structure. The dynamics group is also responsible for the determination of the stability and performance of missile and flight vehicle guidance and control systems. The dynamics group must work constantly with the various test laboratories in order to obtain reliable values of certain factors that are necessary in many theoretical calculations.

THE WORK OF THE SPECIAL PROJECTS GROUP

In general, all the various technical groups have a special sub-group which is working on design problems that will be encountered in the near or distant future as aviation progresses. For example, in the Structures Group, this sub-group might be studying such problems as: (1) how to calculate the thermal stresses in the wing structure at supersonic speeds; (2) how to stress-analyze a new type of wing structure; (3) what type of body structure is best for future space travel and what kind of materials will be needed, etc.

Chart 1 illustrates in general a typical make-up of the Structures Section of a large aerospace company. Chart 2 lists the many items which the structures engineer must be concerned with in insuring the structural integrity of the flight vehicle. Both Charts 1 and 2 are from Chance-Vought Structures Design Manual and are reproduced with their permission.

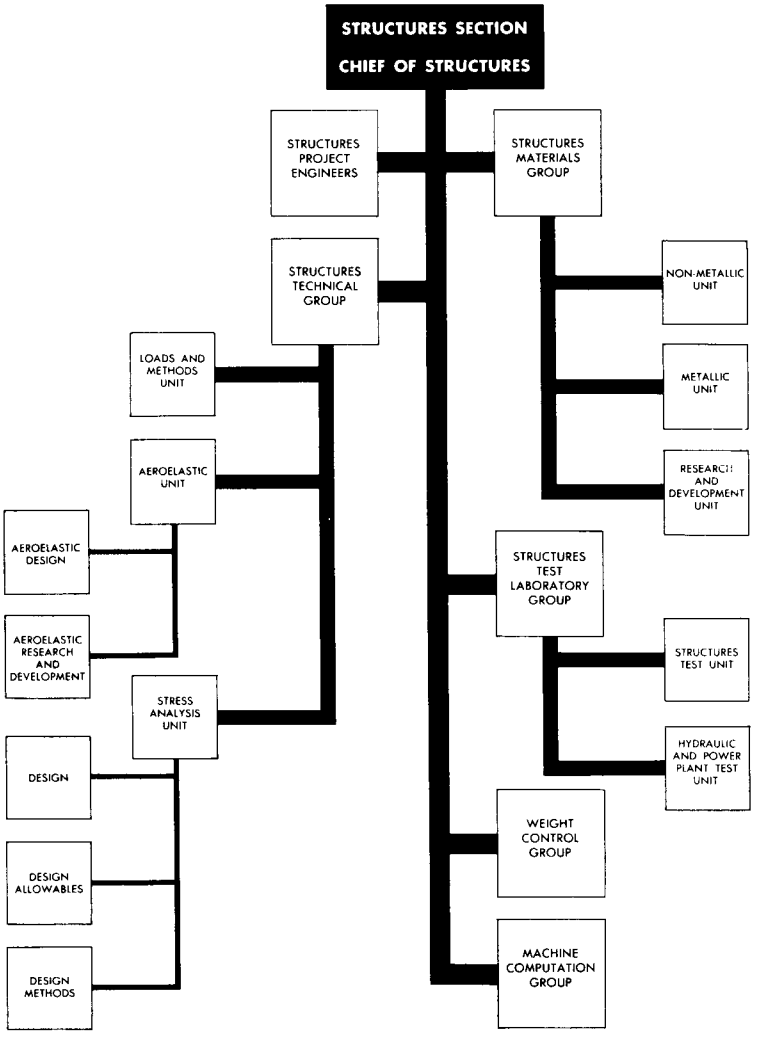

Chart 1. Structures Section Organization Chance-Vought Corp.

THE 7 LINKS TO STRUCTURAL INTEGRITY

. . . . . ARE NO BETTER THAN THE WEAKEST LINK

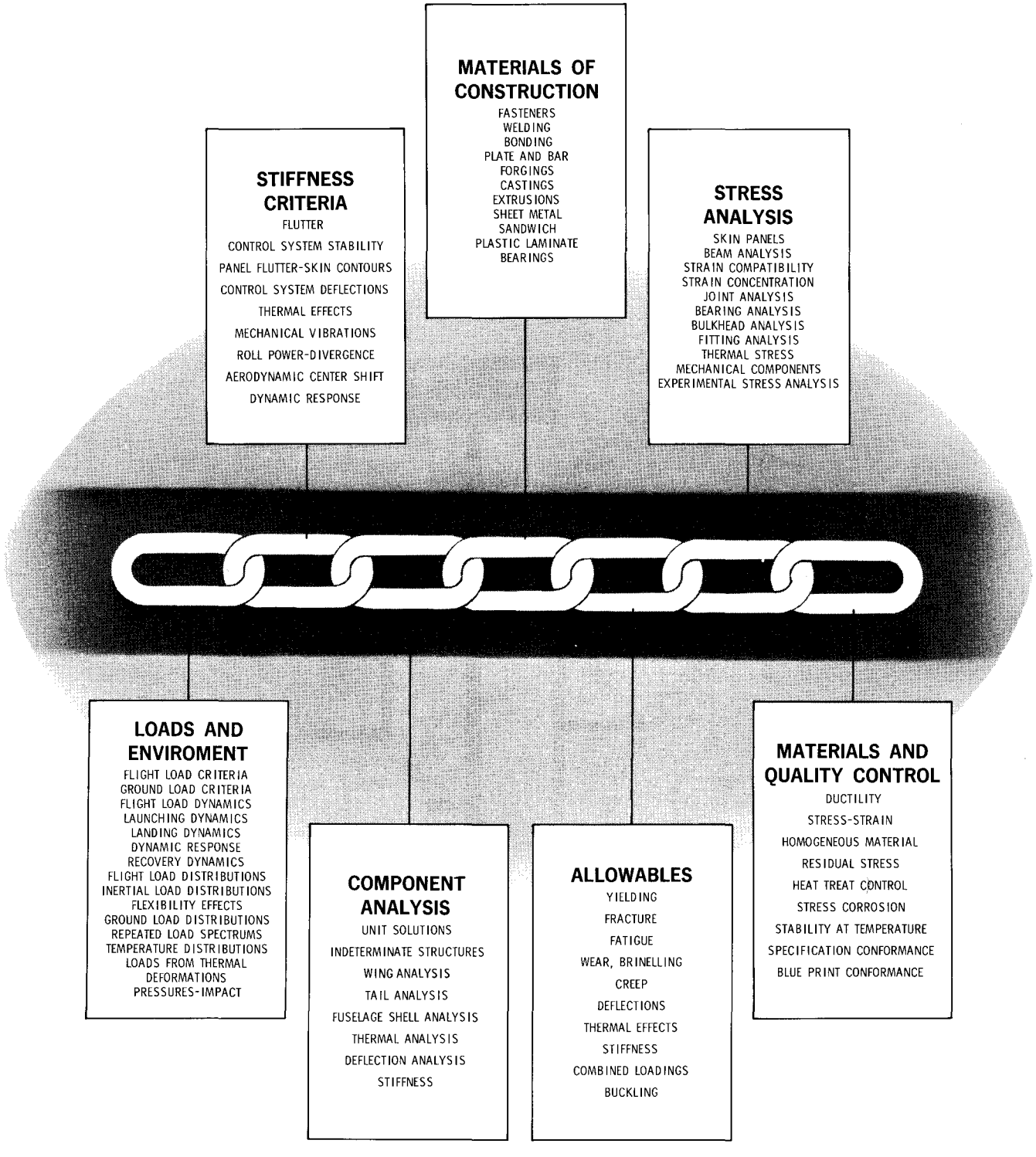

Chart 2
From Chance-Vought Structures Design Manual

CHAPTER A2
EQUILIBRIUM OF FORCE SYSTEMS. TRUSS STRUCTURES

A2.1 Introduction. The equations of static equilibrium must constantly be used by the stress analyst and structural designer in obtaining unknown forces and reactions or unknown internal stresses. They are necessary whether the structure or machine be simple or complex. The ability to apply these equations is no doubt best developed by solving many problems. This chapter initiates the application of these important physical laws to the force and stress analysis of structures. It is assumed that a student has completed the usual college course in engineering mechanics called statics.

A2.2 Equations of Static Equilibrium.

To completely define a force, we must know its magnitude, direction, and point of application. These facts regarding the force are generally referred to as the characteristics of the force. Sometimes the more general term of line of action or location is used as a force characteristic in place of point of application designation.

A force acting in space is completely defined if we know its components in three directions and its moments about 3 axes, for example F_X, F_Y, F_Z and M_X, M_y and M_Z. For equilibrium of a force system there can be no resultant force and thus the equations of equilibrium are obtained by equating the force and moment components to zero. The equations of static equilibrium for the various types of force systems will now be summarized.

EQUILIBRIUM EQUATIONS FOR GENERAL SPACE (NON-COPLANAR) FORCE SYSTEM

$$\left.\begin{array}{ll} \Sigma F_X = 0 & \Sigma M_1 = 0 \\ \Sigma F_y = 0 & \Sigma M_2 = 0 \\ \Sigma F_Z = 0 & \Sigma M_3 = 0 \end{array}\right\} \text{- - - - -(2.1)}$$

Thus for a general space force system, there are 6 equations of static equilibrium available. Three of these and no more can be force equations. It is often more convenient to take the moment axes, 1, 2 and 3, as any set of x, y and z axes. All 6 equations could be moment equations about 6 different axes. The force equations are written for 3 mutually perpendicular axes and need not be the x, y and z axes.

EQUILIBRIUM OF SPACE CONCURRENT-FORCE SYSTEM

Concurrent means that all forces of the force system pass through a common point. The resultant, if any, must therefore be a force and not a moment and thus only 3 equations are necessary to completely define the condition that the resultant must be zero. The equations of equilibrium available are therefore:-

$$\left.\begin{array}{lll} \Sigma F_X = 0 & & \Sigma M_1 = 0 \\ \Sigma F_y = 0 & \text{or} & \Sigma M_2 = 0 \\ \Sigma F_Z = 0 & & \Sigma M_3 = 0 \end{array}\right\} \text{- - - - -(2.2)}$$

A combination of force and moment equations to make a total of not more than 3 can be used. For the moment equations, axes through the point of concurrency cannot be used since all forces of the system pass through this point. The moment axes need not be the same direction as the directions used in the force equations but of course, they could be.

EQUILIBRIUM OF SPACE PARALLEL-FORCE SYSTEM

In a parallel force system the direction of all forces is known, but the magnitude and location of each is unknown. Thus to determine magnitude, one equation is required and for location two equations are necessary since the force is not confined to one plane. In general the 3 equations commonly used to make the resultant zero for this type of force system are one force equation and two moment equations. For example, for a space parallel-force system acting in the y direction, the equations of equilibrium would be:

$$\Sigma F_y = 0, \quad \Sigma M_X = 0, \quad \Sigma M_Z = 0 \quad \text{- - - - -(2.3)}$$

EQUILIBRIUM OF GENERAL CO-PLANAR FORCE SYSTEM

In this type of force system all forces lie in one plane and it takes only 3 equations to determine the magnitude, direction and location of the resultant of such a force system. Either force or moment equations can be used, except that a maximum of 2 force equations can be used. For example, for a force system acting in the xy plane, the following combination of equilibrium equations could be used.

$$\begin{array}{llll} \Sigma F_X = 0 & \Sigma F_X = 0 & \Sigma F_y = 0 & \Sigma M_{Z1} = 0 \\ \Sigma F_y = 0 \text{ or } & \Sigma M_{Z1} = 0 \text{ or } & \Sigma M_{Z1} = 0 \text{ or } & \Sigma M_{Z2} = 0 \quad 2.4 \\ \Sigma M_Z = 0 & \Sigma M_{Z2} = 0 & \Sigma M_{Z2} = 0 & \Sigma M_{Z3} = 0 \end{array}$$

(The subscripts 1, 2 and 3 refer to different locations for z axes or moment centers.)

EQUILIBRIUM OF COPLANAR-CONCURRENT-FORCE SYSTEM

Since all forces lie in the same plane and also pass through a common point, the magnitude and direction of the resultant of this type of force system is unknown but the location is known since the point of concurrency is on the line of action of the resultant. Thus only two equations of equilibrium are necessary to define the resultant and make it zero. The combinations available are,

$$\left.\begin{array}{llll} \Sigma F_X = 0 & \Sigma F_X = 0 & \Sigma F_y = 0 & \Sigma M_{Z_1} = 0 \\ \Sigma F_y = 0 & \Sigma M_Z = 0 & \Sigma M_Z = 0 & \Sigma M_{Z_2} = 0 \end{array}\right\} \quad 2.5$$

(The z axis or moment center locations must be other than through the point of concurrency)

EQUILIBRIUM OF CO-PLANAR PARALLEL FORCE SYSTEM

Since the direction of all forces in this type of force system is known and since the forces all lie in the same plane, it only takes 2 equations to define the magnitude and location of the resultant of such a force system. Hence, there are only 2 equations of equilibrium available for this type of force system, namely, a force and moment equation or two moment equations. For example, for forces parallel to the y axis and located in the xy plane the equilibrium equations available would be: -

$$\left.\begin{array}{ll} \Sigma F_y = 0 & \Sigma M_{Z_1} = 0 \\ \text{or} & \\ \Sigma M_Z = 0 & \Sigma M_{Z_2} = 0 \end{array}\right\} \quad ------ \; 2.6$$

(The moment centers 1 and 2 cannot be on the same y axis)

EQUILIBRIUM OF COLINEAR FORCE SYSTEM

A colinear force system is one where all forces act along the same line or, in other words, the direction and location of the forces are known but their magnitudes are unknown; thus only magnitude needs to be found to define the resultant of a colinear force system. Thus only one equation of equilibrium is available, namely

$$\Sigma F = 0 \quad \text{or} \quad \Sigma M_1 = 0 \quad ---------- \; 2.7$$

where moment center 1 is not on the line of action of the force system

A2.3 Structural Fitting Units for Establishing the Force Characteristics of Direction and Point of Application.

To completely define a force in space requires 6 equations, or 3 equations if the force is limited to one plane. In general a structure is loaded by known forces and these forces are transferred through the structure in some manner of internal stress distribution and then reacted by other external forces, commonly referred to as reactions which hold the known forces on the structure in equilibrium. Since the static equations of equilibrium available for the various types of force systems are limited, the structural engineer resorts to the use of fitting units which establish the direction of an unknown force or its point of application or both, thus decreasing the number of unknowns to be determined. The figures which follow illustrate the type of fitting units employed or other general methods for establishing the force characteristics of direction and point of application.

Ball and Socket Fitting

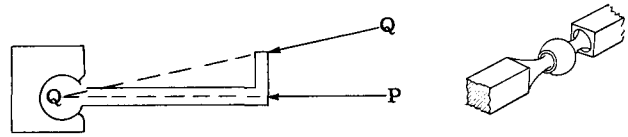

For any space or coplanar force such as P and Q acting on the bar, the line of action of such forces must act through the center of the ball if rotation of the bar is prevented. Thus a ball and socket joint can be used to establish or control the direction and line action of a force applied to a structure through this type of fitting. Since the joint has no rotational resistance, no couples in any plane can be applied to it.

Single Pin Fitting

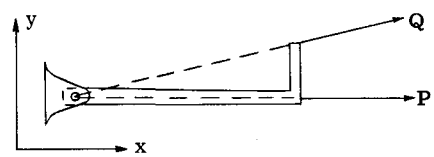

For any force such as P and Q acting in the xy plane, the line of action of such a force must pass through the pin center since the fitting unit cannot resist a moment about a z axis through the pin center. Therefore, for forces acting in the xy plane, the direction and line of action are established by the pin joint as illustrated in the figure. Since a single pin fitting can resist moments about axes perpendicular to the pin axis, the direction and line of action of out-of-plane forces is therefore not established by single pin fitting units.

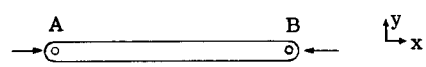

If a bar AB has single pin fittings at each end, then any force P lying in the xy plane and applied to end B must have a direction and line of action coinciding with a line joining the pin centers at end fittings A and B, since the fittings cannot resist a moment about the z axis.

Double Pin - Universal Joint Fittings

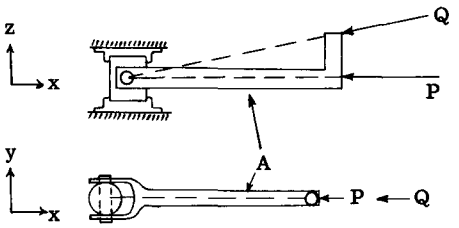

Since single pin fitting units can resist applied moments about axes normal to the pin axis, a double pin joint as illustrated above is often used. This fitting unit cannot resist moments about y or z axes and thus applied forces such as P and Q must have a line of action and direction such as to pass through the center of the fitting unit as illustrated in the figure. The fitting unit can, however, resist a moment about the x axis or in other words, a universal type of fitting unit can resist a torsional moment.

Rollers

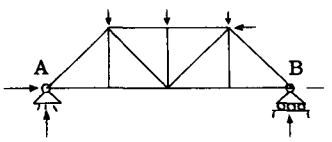

In order to permit structures to move at support points, a fitting unit involving the idea of rollers is often used. For example, the truss in the figure above is supported by a pin fitting at (A) which is further attached to a fitting portion that prevents any horizontal movement of the truss at end (A); however, the other end (B) is supported by a nest of rollers which provide no horizontal resistance to a horizontal movement of the truss at end (B). The rollers fix the direction of the reaction at (B) as perpendicular to the roller bed. Since the fitting unit is joined to the truss joint by a pin, the point of application of the reaction is also known, hence only one force characteristic, namely magnitude, is unknown for a roller-pin type of fitting. For the fitting unit at (A), point of application of the reaction to the truss is known because of the pin, but direction and magnitude are unknown.

Lubricated Slot or Double Roller Type of Fitting Unit.

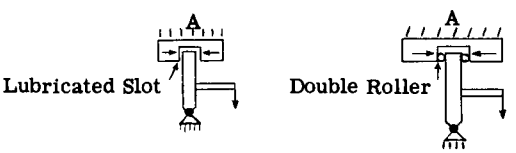

Another general fitting type that is used to establish the direction of a force or reaction is illustrated in the figure at the bottom of the first column. Any reacting force at joint (A) must be horizontal since the support at (A) is so designed to provide no vertical resistance.

Cables - Tie Rods

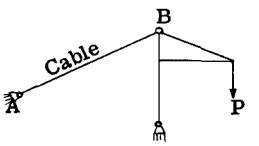

Since a cable or tie rod has negligible bending resistance, the reaction at joint B on the crane structure from the cable must be colinear with the cable axis, hence the cable establishes the force characteristics of direction and point of application of the reaction on the truss at point B.

A2.4 Symbols for Reacting Fitting Units as Used in Problem Solution.

In solving a structure for reactions, member stresses, etc., one must know what force characteristics are unknown and it is common practice to use simple symbols to indicate what fitting support or attachment units are to be used or are assumed to be used in the final design. The following sketch symbols are commonly used for coplanar force systems.

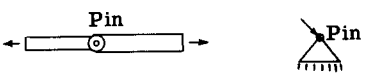

A small circle at the end of a member or on a triangle represents a single pin connection and fixes the point of application of forces acting between this unit and a connecting member or structure.

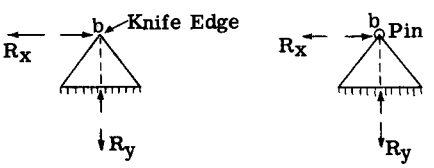

The above graphical symbols represent a reaction in which translation of the attachment point (b) is prevented but rotation of the attached structure about (b) can take place. Thus the reaction is unknown in direction and magnitude but the point of application is known, namely through point (b). Instead of using direction as an unknown, it is more convenient to replace the resultant reaction by two components at right angles to each other as indicated in the sketches.

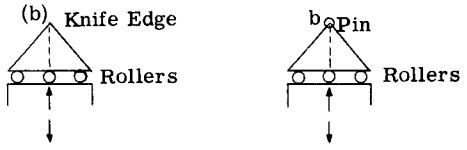

The above fitting units using rollers fix the direction of the reaction as normal to the roller bed since the fitting unit cannot resist a horizontal force through point (b). Hence the direction and point of application of the reaction are established and only magnitude is unknown.

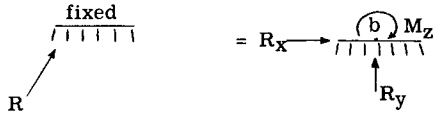

The graphical symbol above is used to represent a rigid support which is attached rigidly to a connecting structure. The reaction is completely unknown since all 3 force characteristics are unknown, namely, magnitude, direction and point of application. It is convenient to replace the reaction R by two force components referred to some point (b) plus the unknown moment M which the resultant reaction R caused about point (b) as indicated in the above sketch. This discussion applies to a coplanar structure with all forces in the same plane. For a space structure the reaction would have 3 further unknowns, namely, R_Z, M_X and M_y.

A2.5 Statically Determinate and Statically Indeterminate Structures.

A statically determinate structure is one in which all external reactions and internal stresses for a given load system can be found by use of the equations of static equilibrium, and a statically indeterminate structure is one in which all reactions and internal stresses cannot be found by using only the equations of equilibrium.

A statically determinate structure is one that has just enough external reactions, or just enough internal members, to make the structure stable under a load system, and if one reaction or member is removed, the structure is reduced to a linkage or a mechanism and is therefore not further capable of resisting the load system. If the structure has more external reactions or internal members than is necessary for stability of the structure under a given load system it is statically indeterminate, and the degree of redundancy depends on the number of unknowns beyond that number which can be found by the equations of static equilibrium. A structure can be statically indeterminate with respect to external reactions alone or to internal stresses alone or to both.

The additional equations that are needed to solve a statically indeterminate structure are obtained by considering the distortion of the structure. This means that the size of all members and the material from which members are made must be known since distortions must be calculated. In a statically determinate structure this information on sizes and material is not required but only the configuration of the structure as a whole. Thus design analysis for statically determinate structures is straightforward, whereas a general trial and error procedure is required for design analysis of statically indeterminate structures.

A2.6 Examples of Statically Determinate and Statically Indeterminate Structures.

The first step in analyzing a structure is to determine whether the structure as presented is statically determinate. If so, the reactions and internal stresses can be found without knowing sizes of members or kind of material. If not statically determinate, the elastic theory must be applied to obtain additional equations. The elastic theory is treated in considerable detail in Chapters A7 to A12 inclusive.

To help the student become familiar with the problem of determining whether a structure is statically determinate, several example problems will be presented.

Example Problem 1.

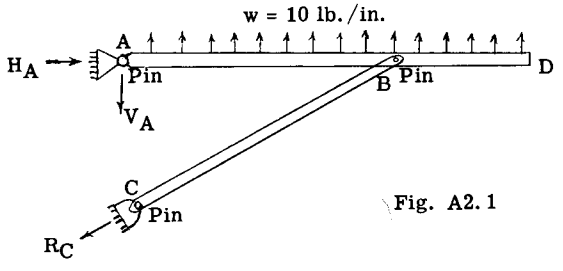

Fig. A2.1

In the structure shown in Fig. 2.1, the known forces or loads are the distributed loads of 10 lb. per inch on member ABD. The reactions at points A and C are unknown. The reaction at C has only one unknown characteristic, namely, magnitude, because the point of application of R_C is through the pin center at C and the direction of R_C must be parallel to line CB because there is a pin at the B end of member CB. At point A the reaction is unknown in direction and magnitude but the point of application must be through the pin center at A. Thus there are 2 unknowns at A and one unknown at C or a total

of 3. With 3 equations of equilibrium available for a coplanar force system the structure is statically determinate. Instead of using an angle as an unknown at A to find the direction of the reaction, it is usually more convenient to replace the reaction by components at right angles to each other as H_A and V_A in the figure, and thus the 3 unknowns for the structure are 3 magnitudes.

Example Problem 2.

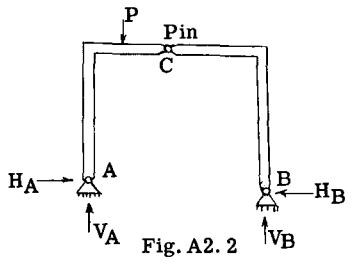

Fig. A2.2

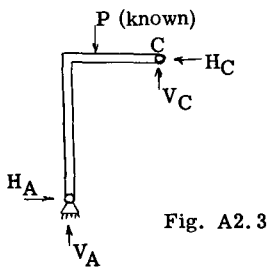

Fig. A2.3

Fig. 2.2 shows a structural frame carrying a known load system P. Due to the pins at reaction points A and B the point of application is known for each reaction; however, the magnitude and direction of each is unknown, making a total of 4 unknowns with only 3 equations of equilibrium available for a coplanar force system. At first we might conclude that the structure is statically indeterminate but we must realize this structure has an internal pin at C which means the bending moment at this point is zero since the pin has no resistance to rotation. If the entire structure is in equilibrium, then each part must likewise be in equilibrium and we can cut out any portion as a free body and apply the equilibrium equations. Fig. 2.3 shows a free body of the frame to left of pin at C. Taking moments about C and equating to zero gives us a fourth equation to use in determining the 4 unknowns, H_A, V_A, V_B and H_B. The moment equation about C does not include the unknowns V_C and H_C since they have no moment about C because of zero arms. As in example problem 1, the reactions at A and B have been replaced by H and V components instead of using an angle (direction) as an unknown characteristic. The structure is statically determinate.

Example Problem 3.

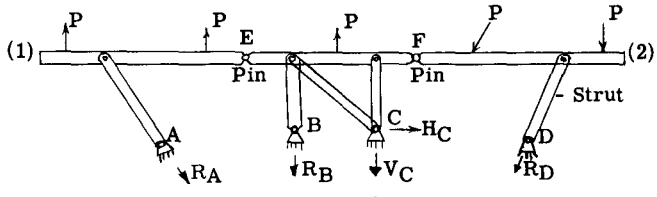

Fig. A2.4

Fig. 2.4 shows a straight member 1-2 carrying a known load system P and supported by 5 struts attached to reaction points ABCD.

At reaction points A, B and D, the reaction is known in direction and point of application but the magnitude is unknown as indicated by the vector at each support. At point C, the reaction is unknown in direction because 2 struts enter joint C. Magnitude is also unknown but point of application is known since the reaction must pass through C. Thus we have 5 unknowns, namely, R_A, R_B, R_D, V_C and H_C. For a coplanar force system we have 3 equilibrium equations available and thus the first conclusion might be that we have a statically indeterminate structure to (5-3) = 2 degrees redundant. However, observation of the structure shows two internal pins at points E and F which means that the bending moment at these two points is zero, thus giving us 2 more equations to use with the 3 equations of equilibrium. Thus drawing free bodies of the structure to left of pin E and to right of pin F and equating moments about each pin to zero, we obtain 2 equations which do not include unknowns other than the 5 unknowns listed above. The structure is therefore statically determinate.

Example Problem 4.

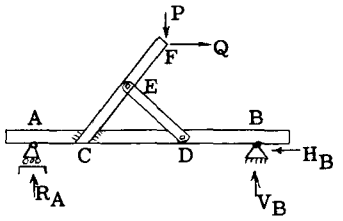

Fig. A2.5

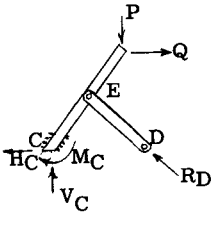

Fig. A2.6

Fig. 2.5 shows a beam AB which carries a super-structure CED which in turn is subjected to the known loads P and Q. The question is whether the structure is statically determinate. The external unknown reactions for the entire structure are at points A and B. At A due to the roller type of action, magnitude is the only unknown characteristic of the reaction since direction and point of application are known. At B, magnitude and direction are unknown but point of application is known, hence we have 3 unknowns, namely, R_A, V_B and H_B, and with 3 equations of equilibrium available we can find these reactions and therefore the structure is statically determinate with respect to external reactions. We now investigate to see if the internal stresses can be found by statics after having found the external reactions. Obviously, the internal stresses will be affected by the internal reactions at C and D, so we draw a free body of the super-structure as illustrated in Fig. 2.6 and consider the internal forces that existed at C and D as external reactions. In the actual structure the members are rigidly attached together at point C such as a welded or

multiple bolt connection. This means that all three force or reaction characteristics, namely, magnitude, direction, and point of application, are unknown; or in other words, 3 unknowns exist at C. For convenience we will represent these unknowns by three components as shown in Fig. 2.6, namely, H_C, V_C and M_C. At joint D in Fig. 2.6, the only unknown regarding the reaction is R_D, a magnitude, since the pin at each end of the member DE establishes the direction and point of application of the reaction R_D. Hence we have 4 unknowns and only 3 equations of equilibrium for the structure in Fig. 2.6, thus the structure is statically indeterminate with respect to all of the internal stresses. The student should observe that internal stresses between points AC, BD and FE are statically determinate, and thus the statically indeterminate portion is the structural triangle CEDC.

Example Problem 5

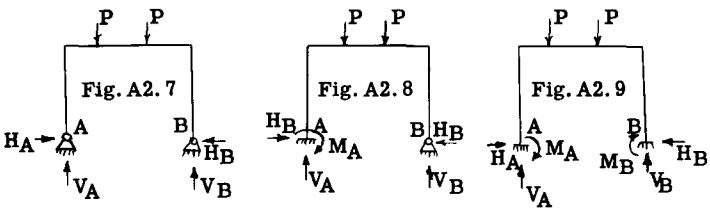

Fig. A2.7 Fig. A2.8 Fig. A2.9

Figs. 2.7, 2.8 and 2.9 show the same structure carrying the same known load system P but with different support conditions at points A and B. The question is whether each structure is statically indeterminate and if so, to what degree, that is, what number of unknowns beyond the equations of statics available. Since we have a coplanar force system, only 3 equations of statics are available for equilibrium of the structure as a whole.

In the structure in Fig. 2.7, the reaction at A and also at B is unknown in magnitude and direction, although their points of application are known. Hence, 4 unknowns (with only 3 equations of statics available) make the structure statically indeterminate to the first degree. In Fig. 2.8, the reaction at A is a rigid one, thus all 3 characteristics of magnitude, direction, and point of application of the reaction, are unknown. At point B, due to pin only 2 unknowns, namely, magnitude and direction, thus making a total of 5 unknowns with only 3 equations of statics available or the structure is statically indeterminate to the second degree. In the structure of Fig. 2.9, both supports at A and B are rigid. Thus, all 3 force characteristics are unknown at each support or a total of 6 unknowns which makes the structure statically indeterminate to the third degree.

Example Problem 6

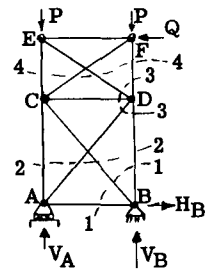

Fig. A2.10

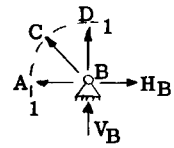

Fig. A2.11

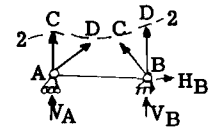

Fig. A2.12

Fig. 2.10 shows a 2 bay truss supported at points A and B and carrying a known load system P, Q. All members of the truss are connected at their ends by a common pin at each joint. The reactions at A and B are applied through fittings as indicated. The question is whether the structure is statically determinate or not. Relative to external reactions at A and B the structure is statically determinate because the type of support produces only one unknown at A and two unknowns at B, namely, V_A, V_B and H_B as shown in Fig. 2.10, and we have 3 equations of static equilibrium available.

We now investigate to see if we can find the internal member stresses after having found the values of the reactions at A and B. Suppose we cut out joint B as indicated by section 1-1 in Fig. 2.10 and draw a free body as shown in Fig. 2.11. Since the members of the truss have pins at each end, the loads in these members must be axial, thus direction and line of action are known and only magnitude is unknown. In Fig. 2.11, H_B and V_B are known but AB, CB, and DB are unknown in magnitude; hence we have 3 unknowns but only 2 equations of equilibrium for a coplanar concurrent force system. If we cut through the truss in Fig. 2.10 by the section 2-2 and draw a free body of the lower portion as shown in Fig. 2.12, we have 4 unknowns, namely, the axial loads in CA, DA, CB, DB but only 3 equations of equilibrium available for a coplanar force system.

Suppose we were able to find the stresses in CA, DA, CB, DB in some manner, and we would now proceed to joint D and treat it as a free body or cut through the upper panel along section 4-4 and use the lower portion as a free body. The same reasoning as used above would show us we have one more unknown than the number of equilibrium equations available and thus we have the truss statically indeterminate to the second degree relative to internal member stresses.

Physically, the structure has two more members than is necessary for the stability of the structure under load, as we could leave out one diagonal member in each truss panel and

the structure would be still stable and all member axial stresses could be found by the equations of static equilibrium without regard to their size of cross-section or the kind of material. Adding the second diagonal member in each panel would necessitate knowing the size of all truss members and the kind of material used before member stresses could be found, as the additional equations needed must come from a consideration involving distortion of the truss. Assume for example, that one diagonal in the upper panel was left out. We would then be able to find the stresses in the members of the upper panel by statics but the lower panel would still be statically indeterminate to 1 degree because of the double diagonal system and thus one additional equation is necessary and would involve a consideration of truss distortion. (The solution of statically indeterminate trusses is covered in Chapter A8.)

A2.7 Example Problem Solutions of Statically Determinate Coplanar Structures and Coplanar Loadings.

Although a student has taken a course in statics before taking a beginning course in aircraft structures, it is felt that a limited review of problems involving the application of the equations of static equilibrium is quite justified, particularly if the problems are possibly somewhat more difficult than most of the problems in the usual beginning course in statics. Since one must use the equations of static equilibrium as part of the necessary equations in solving statically indeterminate structures and since statically indeterminate structures are covered in rather complete detail in other chapters of this book, only limited space will be given to problems involving statics in this chapter.

Example Problem 8.

Fig. A2.14 shows a much simplified wing structure, consisting of a wing spar supported by lift and cabane struts which tie the wing spar to the fuselage structure. The distributed air load on the wing spar is unsymmetrical about the center line of the airframe. The wing spar is made in three units, readily disassembled by using pin fittings at points O and O'. All supporting wing struts have single pin fitting units at each end. The problem is to determine the axial loads in the members and the reactions on the spar.

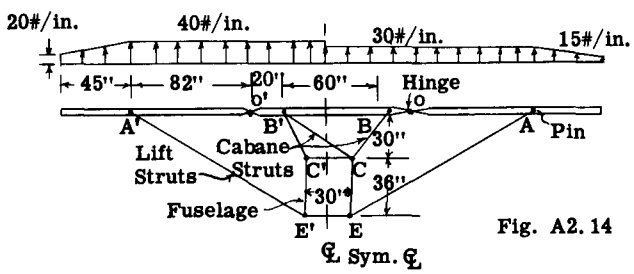

Fig. A2.14

Solution: The first thing to decide is whether the structure is statically determinate. From the figure it is observed that the wing spar is supported by five struts. Due to the pins at each end of all struts, we have five unknowns, namely, the magnitude of the load in each strut. Direction and location of each strut load is known because of the pin at each end of the struts. We have 3 equations of equilibrium for the wing spar as a single unit supported by the 5 struts, thus two more equations are necessary if the 5 unknown strut loads are to be found. It is noticed that the wing spar includes 2 internal single pin connections at points O and O'. This establishes the fact that the moment of all forces located to one side of the pin must be equal to zero since the single pin fitting cannot resist a moment. Thus we obtain two additional equations because of the two internal pin fittings and thus we have 5 equations to find 5 unknowns.

Fig. 2.15 shows a free body of the wing spar to the right of hinge fitting at O.

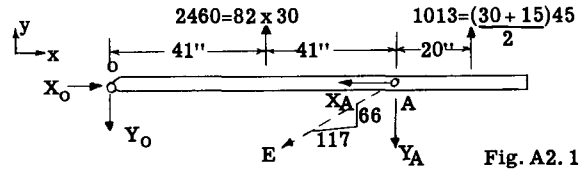

Fig. A2.15

In order to take moments, the distributed load on the spar has been replaced by the resultant load on each spar portion, namely, the total load on the portion acting through the centroid of the distributed load system. The strut reaction EA at A has been shown in phantom as it is more convenient to deal with its components Y_A and X_A. The reaction at O is unknown in magnitude and direction and for convenience we will deal with its components X_O and Y_O. The sense assumed is indicated on the figure.

The sense of a force is represented graphically by an arrow head on the end of a vector. The correct sense is obtained from the solution of the equations of equilibrium since a force or moment must be given a plus or minus sign in writing the equations. Since the sense of a force or moment is unknown, it is assumed, and if the algebraic solution of the equilibrium equations gives a plus value to the magnitude then the true sense is as assumed, and opposite to that assumed if the solution gives a minus sign. If the unknown forces are axial loads in members it is common practice to call tensile stress plus and compressive stress minus, thus if we assume the sense of an unknown axial load as tension, the solution of the equilibrium

equations will give a plus value for the magnitude of the unknown if the true stress is tension and a minus sign will indicate the assumed tension stresses should be reversed or compression, thus giving a consistency of signs.

To find the unknown Y_A we take moments about point O and equate to zero for equilibrium.

$$\Sigma M_O = -2460 \times 41 - 1013 \times 102 + 82Y_A = 0$$

Hence $Y_A = 204000/82 = 2480$ lb. The plus sign means that the sense as assumed in the figure is correct. By geometry $X_A = 2480 \times 117/66 = 4400$ lb. and the load in strut EA equals $\sqrt{4400^2 + 2480^2} = 5050$ lb. tension or as assumed in the figure.

To find X_O we use the equilibrium equation $\Sigma F_X = 0 = X_O - 4400 = 0$, whence $X_O = 4400$ lb.

To find Y_O we use,

$\Sigma F_y = 0 = 2460 + 1013 - 2480 - Y_O = 0$, whence $Y_O = 993$ lb.

To check our results for equilibrium we will take moments of all forces about A to see if they equal zero.

$\Sigma M_A = 2460 \times 41 - 1013 \times 20 - 993 \times 82 = 0$ check

On the spar portion O'A', the reactions are obviously equal to 40/30 times those found for portion OA since the external loading is 40 as compared to 30.

Hence A'E' = 6750, $X_{O'} = 5880$, $Y_{O'} = 1325$

Fig. 2.16 shows a free body of the center spar portion with the reactions at O and O' as found previously. The unknown loads in the struts have been assumed tension as shown by the arrows.

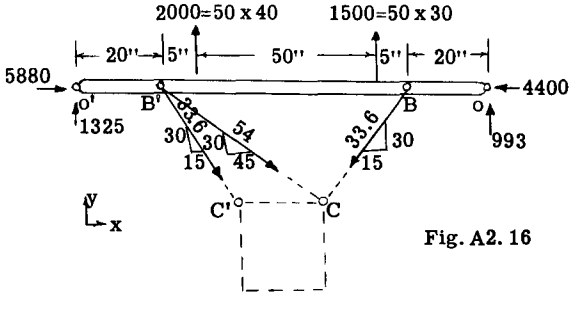

Fig. A2.16

To find the load in strut BC take moments about B'

$$\Sigma M_{B'} = 1325 \times 20 - 2000 \times 5 - 1500 \times 55 - 993 \times 80 + 60\,(BC)\ 30/33.6 = 0$$

Whence, BC = 2720 lb. with sense as assumed.

To find strut load B'C' take moments about point C.

$$\Sigma M_C = 1325 \times 65 + 2000 \times 40 + (5880 - 4400)\ 30 - 1500 \times 10 - 993 \times 35 - 30\,(B'C')\ 30/33.6 = 0$$

whence, B'C' = 6000 lb. with sense as shown.

To find load in member B'C use equation

$$\Sigma F_y = 0 = 1325 + 2000 + 1500 + 993 - 6000\,(30/33.6) - 2720\,(30/33.6) - B'C\,(30/54) = 0$$

whence, B'C = - 3535 lb. The minus sign means it acts opposite to that shown in figure or is compression instead of tension.

The reactions on the spar can now be determined and shears, bending moments and axial loads on the spar could be found. The numerical results should be checked for equilibrium of the spar as a whole by taking moments of all forces about a different moment center to see if the result is zero.

Example Problem 9.

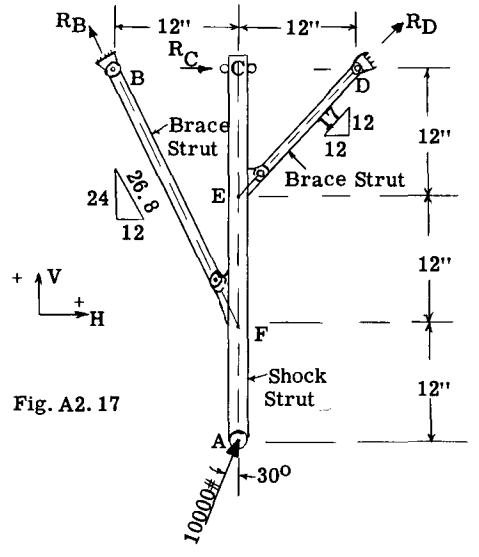

Fig. A2.17

Fig. 2.17 shows a simplified airplane landing gear unit with all members and loads confined to one plane. The brace struts are pinned at each end and the support at C is of the roller type, thus no vertical reaction can be produced by the support fitting at point C. The member at C can rotate on the roller but horizontal movement is prevented. A known load of 10,000 lb. is applied to axle unit at A. The problem is to find the load in the brace struts and the reaction at C.

Solution:

Due to the single pin fitting at each end of the brace struts, the reactions at B and D

are colinear with the strut axis, thus direction and point of application are known for reaction R_B and R_D leaving only the magnitude of each as unknown. The roller type fitting at C fixes the direction and point of application of the reaction R_C, leaving magnitude as the only unknown. Thus there are 3 unknowns R_B, R_C and R_D and with 3 equations of static equilibrium available, the structure is statically determinate with respect to external reactions. The sense of each of the 3 unknown reactions has been assumed as indicated by the vector.

To find R_D take moments about point B:-

$\Sigma M_B = -10000 \sin 30^0 \times 36 - 10000 \cos 30^0 \times 12 - R_D (12/17)\, 24 = 0$

whence, $R_D = -16750$ lb. Since the result comes out with a minus sign, the reaction R_D has a sense opposite to that shown by the vector in Fig. 2.17. Since the reaction R_D is colinear with the line DE because of the pin ends, the load in the brace strut DE is 16750 lb. compression. In the above moment equation about B, the reaction R_D was resolved into vertical and horizontal components at point D, and thus only the vertical component which equals $(12/17)\, R_D$ enters into the equation since the horizontal component has a line of action through point B and therefore no moment. R_C does not enter in equation as it has zero moment about B.

To find R_B take $\Sigma F_V = 0$

$\Sigma F_V = 10000 \times \cos 30^0 + (-16750)(12/17) + R_B (24/26.8) = 0$

whence, $R_B = 3540$ lb. Since sign comes out plus, the sense is the same as assumed in the figure. The strut load BF is therefore 3540 lb. tension, since reaction R_B is colinear with line BF.

To find R_C take $\Sigma H = 0$

$\Sigma H = 10000 \sin 30^0 - 3540\, (12/26.8) + (-16750)\, (12/17) + R_C = 0$

whence, $R_C = 8407$ lb. Result is plus and therefore assumed sense was correct.

To check the numerical results take moments about point A for equilibrium.

$\Sigma M_A = 8407 \times 36 + 3540\, (24/26.8)\, 12 - 3540\, (12/26.8)\, 36 + 16750\, (12/17)\, 12 - 16750\, (12/17)\, 36 = 303000 + 38100 - 57100 + 142000 - 426000 = 0$ (check)

A2.8 Stresses in Coplanar Truss Structures Under Coplanar Loading.

In aircraft construction, the truss type of construction is quite common. The most common is the tubular steel welded trusses that make up the fuselage frame, and less frequently, the aluminum alloy tubular truss. Trussed type beams composed of closed and open type sections are also frequently used in wing beam construction. The stresses or loads in the members of a truss are commonly referred to as "primary" and "secondary" stresses. The stresses which are found under the following assumptions are referred to as primary stresses.

(1) The members of the truss are straight, weightless and lie in one plane.

(2) The members of a truss meeting at a point are considered as joined together by a common frictionless pin and all member axes intersect at the pin center.

(3) All external loads are applied to the truss only at the joints and in the plane of the truss. Thus all loads or stresses produced in members are either axial tension or compression without bending or torsion.

Those stresses produced in the truss members due to the non-fulfillment of the above assumptions are referred to as secondary stresses. Most steel tubular trusses are welded together at their ends and in other truss types, the members are riveted or bolted together. This restraint at the joints may cause secondary stresses in some members greater than the primary stresses. Likewise it is common in actual practical design to apply forces to the truss members between their ends by supporting many equipment installations on these truss members. However, regardless of the magnitude of these so-called secondary loads, it is common practice to first find the primary stresses under the assumption outlined above.

GENERAL CRITERIA FOR DETERMINING WHETHER TRUSS STRUCTURES ARE STATICALLY DETERMINATE WITH RESPECT TO INTERNAL STRESSES.

The simplest truss that can be constructed is the triangle which has three members m and three joints j. A more elaborate truss consists of additional triangular frames, so arranged that each triangle adds one joint and two members. Hence the number of members to insure stability under any loading is:

$$m = 2j - 3 \qquad (2.8)$$

A truss having fewer members than required by Eq. (2.8) is in a state of unstable equilibrium and will collapse except under certain conditions of loading. The loads in the members of a truss with the number of members shown in equation (2.8) can be found with the available equations of statics, since the forces in the members acting at a point intersect at a common point or form a concurrent force system. For this type of force system there are two static equilibrium equations available.

Thus for j number of joints there are 2j

equations available. However three independent equations are necessary to determine the external reactions, thus the number of equations necessary to solve for all the loads in the members is 2j - 3. Hence if the number of truss members is that given by equation (2.8) the truss is statically determinate relative to the primary loads in the truss members and the truss is also stable.

If the truss has more members than indicated by equation (2.8) the truss is considered redundant and statically indeterminate since the member loads cannot be found in all the members by the laws of statics. Such redundant structures if the members are properly placed are stable and will support loads of any arrangement.

ANALYTICAL METHODS FOR DETERMINING PRIMARY STRESSES IN TRUSS STRUCTURES

In general there are three rather distinct methods or procedures in applying the equations of static equilibrium to finding the primary stresses in truss type structures. They are often referred to as the method of joints, moments, and shears.

A2.9 Method of Joints.

If the truss as a whole is in equilibrium then each member or joint in the truss must likewise be in equilibrium. The forces in the members at a truss joint intersect in a common point, thus the forces on each joint form a concurrent-coplanar force system. The method of joints consists in cutting out or isolating a joint as a free body and applying the laws of equilibrium for a concurrent force system. Since only two independent equations are available for this type of system only two unknowns can exist at any joint. Thus the procedure is to start at the joint where only two unknowns exist and continue progressively throughout the truss joint by joint. To illustrate the method consider the cantilever truss of Fig. A2.18. From observation there are only two members with internal stresses unknown at joint L_3. Fig. A2.19 shows a free body of joint L_3. The stresses in the members $L_3 L_2$ and $L_3 U_2$ have been assumed as tension, as indicated by the arrows pulling away from the joint L_3.

The static equations of equilibrium for the forces acting on joint L_3 are ΣH and $\Sigma V = 0$.

$\Sigma V = -1000 - L_3U_2\ (40/50) = 0 \quad -------(a)$

whence, $L_3U_2 = -1250$ lb. Since the sign came out minus the stress is opposite to that assumed in Fig. A2.19 or compression.

$\Sigma H = -500 - (-1250)(30/50) - L_2L_3 = 0 \quad --(b)$

whence, $L_2L_3 = 250$ lb. Since the sign comes out plus, sense is same as assumed in figure

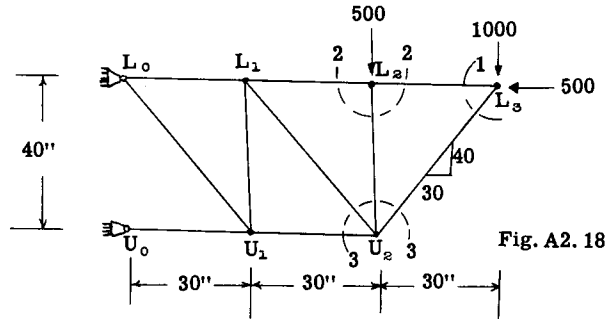

Fig. A2.18

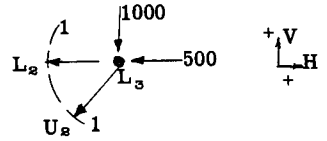

Fig. A2.19

or tension. In equation (b) the load of 1250 in L_3L_2 was substituted as a minus value since it was found to act opposite to that shown in Fig. A2.19. Possibly a better procedure would be to change the sense of the arrow in the free body diagram for any solved members before writing further equilibrium equations. We must proceed to joint L_2 instead of joint U_2, as three unknown members still exist at joint U_2 whereas only two at joint L_2. Fig. A2.20 shows free body of joint L_2 cut out by section 2-2 (see Fig. A2.18). The sense of the unknown member stress L_2U_2 has been assumed as compression (pushing toward joint) as it is obviously acting this way to balance the 500 lb. load.

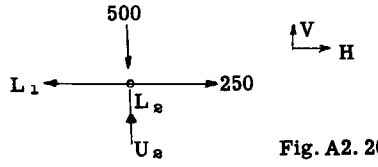

Fig. A2.20

For equilibrium of joint L_2, ΣH and $\Sigma V = 0$
$\Sigma V = -500 + L_2U_2 = 0$, whence, $L_2U_2 = 500$ lb. Since the sign came out plus, the assumed sense in Fig. A2.20 was correct or compression.

$\Sigma H = 250 - L_2L_1 = 0$, whence $L_2L_1 = 250$ lb.

Next consider joint U_2 as a free body cut out by section 3-3 in Fig. A2.18 and drawn as Fig. A2.21. The known member stresses are shown with their true sense as previously found. The two unknown member stresses U_2L_1 and U_2U_1 have been assumed as tension.

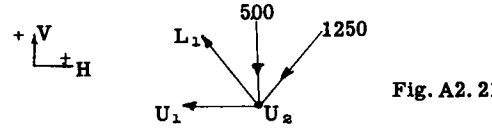

Fig. A2.21

$\Sigma V = -500 - 1250\ (40/50) + U_2L_1\ (40/50) = 0$

whence, $U_2L_1 = 1875$ lb. (tension as assumed.)

$\Sigma H = (-1250)(30/50) - 1875\ (30/50) - U_1U_2 = 0$

whence, $U_1U_2 = -1875$ lb. or opposite in sense to that assumed and therefore compression.

Note: The student should continue with succeeding joints. In this example involving a cantilever truss it was not necessary to find the reactions, as it was possible to select joint L_3 as a joint involving only two unknowns. In trusses such as illustrated in Fig. A2.22 it is necessary to first find reactions R_1 or R_2 which then provides a joint at the reaction point involving only two unknown forces.

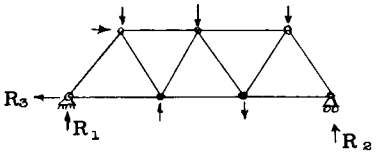

Fig. A2.22

A2.10 Method of Moments.

For a coplanar-non-concurrent force system there are three equations of statics available. These three equations may be taken as moment equations about three different points. Fig. A2.22 shows a typical truss. Let it be required to find the loads in the members F_1, F_2, F_3, F_4, F_5 and F_6.

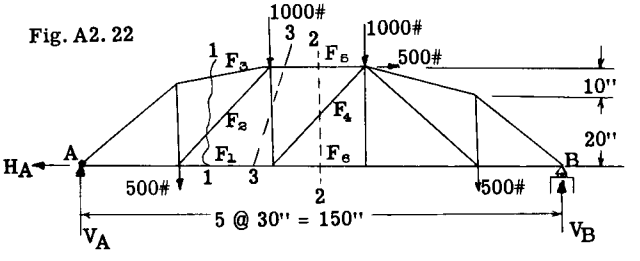

Fig. A2.22

The first step in the solution is to find the reactions at points A and B. Due to the roller type of support at B the only unknown element of the reaction force at B is magnitude. At point A, magnitude and direction of the reaction are unknown giving a total of three unknowns with three equations of statics available. For convenience the unknown reaction at A has been replaced by its unknown H and V components.

Taking moments about point A,

$\Sigma M_A = 500 \times 30 + 1000 \times 60 + 1000 \times 90 + 500 \times 30 + 500 \times 120 - 150\ V_B = 0$

Hence $V_B = 1600$ lb.

Take $\Sigma V = 0$

$\Sigma V = V_A - 1000 - 1000 - 500 - 500 + 1600 = 0$ therefore $V_A = 1400$ lb.

Take $\Sigma H = 0$

$\Sigma H = 500 - H_A = 0$, therefore $H_A = 500$ lb.

The algebraic sign of all unknowns came out positive, thus the assumed direction as shown on Fig. A2.22 was correct.

Check results by taking $\Sigma M_B = 0$

$\Sigma M_B = 1400 \times 150 + 500 \times 30 - 500 \times 120 - 500 \times 30 - 1000 \times 90 - 1000 \times 60 = 0$ (Check)

To determine the stress in member F_1, F_2 and F_3 we cut the section 1-1 thru the truss (Fig. A2.22. Fig. A2.23 shows a free body diagram of the portion of the truss to the left of this section.

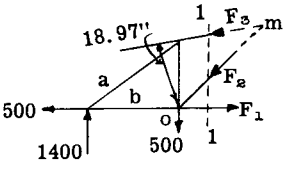

Fig. A2.23

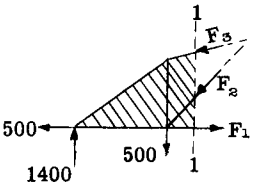

Fig. A2.24

The truss as a whole is in equilibrium. Therefore any portion must be in equilibrium. In Fig. A2.23 the internal stresses in the members F_1, F_2 and F_3 which existed in the truss as a whole now are considered external forces in holding the portion of the truss to the left of section 1-1 in equilibrium in combination with the other loads and reactions. Since the members a and b in Fig. A2.23 have not been cut the loads in these members remain as internal stresses and have no influence on the equilibrium of the portion of the truss shown. Thus the portion of the truss to left of section 1-1 could be considered as a solid block as shown in Fig. A2.24 without affecting the values of F_1, F_2 and F_3. The method of moments, as the name implies, involves the operation of taking moments about a point to find the load in a particular member. Since there are three unknowns a moment center must be selected such that the moment of each of the two unknown stresses will have zero moment about the selected moment center, thus leaving only one unknown force or stress to enter into the equation for moments. For example, to determine load F_3 in Fig. A2.24 we take moments about the intersection of forces F_1 and F_2 or point O.

Thus $\Sigma M_O = 1400 \times 30 - 18.97\ F_3 = 0$

Hence $F_3 = \dfrac{42000}{18.97} = 2215$ lb. compression (or acting as assumed)

To find the arm of the force F_3 from the moment center O involves a small amount of calculation, thus in general it is simpler to resolve the unknown force into H and V components at a point on its line of action such that one of these components passes thru the moment center and the arm of the other component can usually be determined by inspection. Thus in

Fig. A2.25 the force F_3 is resolved into its component F_{3V} and F_{3H} at point O'. Then taking

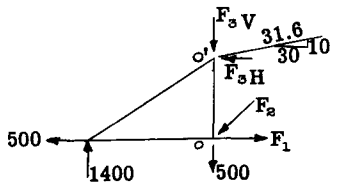

Fig. A2.25

Fig. A2.26

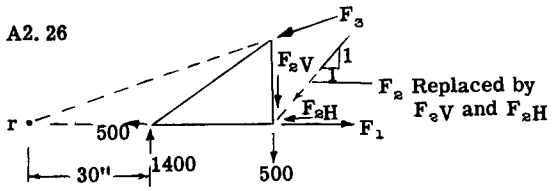

moments about point O as before:-

$$\Sigma M_O = 1400 \times 30 - 20F_{3H} = 0$$

whence, $F_{3H} = 2100$ lb. and therefore

$F_3 = 2100\ (31.6/30) = 2215$ lb. as previously obtained.

The load F_1 can be found by taking moments about point m, the intersection of forces F_2 and F_3 (See Fig. A2.23).

$$\Sigma M_m = 1400 \times 60 + 500 \times 30 - 500 \times 30 - 30F_1 = 0$$

whence, $F_1 = 2800$ lb. (Tension as assumed)

To find force F_2 by using a moment equation, we take moments about point (r) the intersection of forces F_1 and F_3 (See Fig. A2.26). To eliminate solving for the perpendicular distance from point (r) to line of action of F_2, we resolve F_2 into its H and V components at point O on its line of action as shown in Fig. A2.26.

$$\Sigma M_r = -1400 \times 30 + 500 \times 60 + 60\,F_{2V} = 0$$

whence, $F_{2V} = 12000/60 = 200$ lb.

Therefore $F_2 = 200 \times \sqrt{2} = 282$ lb. compression

A2.11 Method of Shears

In Fig. A2.22 to find the stress in member F_4 we cut the section 2-2 giving the free body for the left portion as shown in Fig. A2.27.

The method of moments is not sufficient to solve for member F_4 because the intersection of the other two unknowns F_5 and F_6 lies at infinity. Thus for conditions where two of the 3 cut members are parallel we have a method of solving for the web member of the truss commonly referred to as the method of shears, or the summation of all the forces normal to the two parallel unknown chord members must equal zero. Since the parallel chord members have no component in a direction normal to their line of action, they do not enter the above equation of equilibrium.

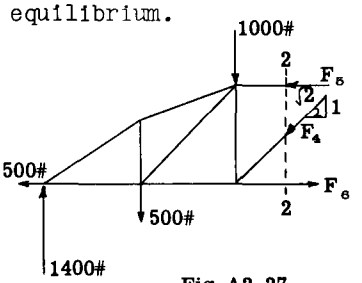

Fig. A2.27

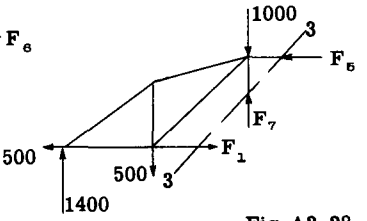

Fig. A2.28

Referring to Fig. A2.27

$$\Sigma V = 1400 - 500 - 1000 - F_4(1/\sqrt{2}) = 0$$

whence $F_4 = -141$ lb. (tension or opposite to that assumed in the figure.

To find the stress in member F_7. we cut section 3-3 in Fig. A2.22 and draw a free body diagram of the left portion in Fig. A2.28. Since F_1 and F_5 are horizontal, the member F_7 must carry the shear on the truss on this section 3-3, hence the name method of shears.

$$\Sigma V = 1400 - 500 - 1000 + F_7 = 0$$

Whence $F_7 = 100$ lb. (compression as assumed)

Note: The student should solve this example illustrating the methods of moments and shears using as a free body the portion of the truss to the right of the cut sections instead of the left portion as used in these illustrative examples. In order to solve for the stresses in the members of a truss most advantageously, one usually makes use of more than one of the above three methods, as each has its advantages for certain cases or members. It is important to realize that each is a method of sections and in a great many cases, such as trusses with parallel chords, the stresses can practically be found mentally without writing down equations of equilibrium. The following statements in general are true for parallel chord trusses:

(1) The vertical component of the stress in the panel diagonal members equals the vertical shear (algebraic sum of external forces to one side of the panel) on the panel, since the chord

members are horizontal and thus have zero vertical component.

(2) The truss verticals in general resist the vertical component of the diagonals plus any external loads applied to the end joints of the vertical.

(3) The load in the chord members is due to the horizontal components of the diagonal members and in general equals the summation of these horizontal components.

To illustrate the simplicity of determining stresses in the members of a parallel chord truss, consider the cantilever truss of Fig. A2.29 with supporting reactions at points A and J.

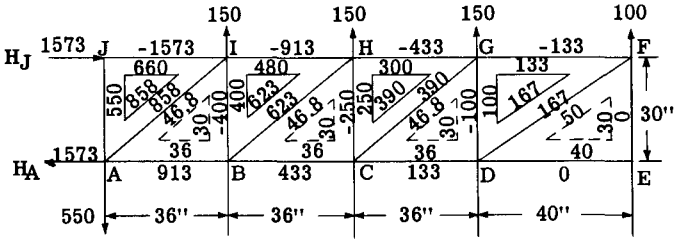

Fig. A2.29

First, compute the length triangles in each panel of the truss as shown by the dashed triangles in each panel. The other triangles in each panel are referred to as load or index triangles and their sides are directly proportional to the length triangles.

The shear load in each panel is first written on the vertical side of each index triangle. Thus, in panel EFGD, considering forces to the right of a vertical section cut thru the panel, the shear is 100 lb., which is recorded on the vertical side of the index triangle.

For the second panel from the free end, the shear is 100 + 150 = 250 and for the third panel 100 + 150 + 150 = 400 lb., and in like manner 550 for fourth panel.

The loads in the diagonals as well as their horizontal components are directly proportional to the lengths of the diagonal and horizontal side of the length triangles. Thus the load in diagonal member DF = 100 (50/30) = 167 and for member CG = 250 (46.8/30) = 390. The horizontal component of the load in DF = 100 (40/30) = 133 and for CG = 250 (36/30) = 300. These values are shown on the index triangles for each truss panel as shown in Fig. A2.29. We start our analysis for the loads in the members of the truss by considering joint E first.

Using $\Sigma V = 0$ gives EF = 0 by observation, since no external vertical load exists at joint E. Similarly, by the same reasoning for $\Sigma H = 0$, load in DE = 0. The load in the diagonal FD equals the value on the diagonal of the panel index triangle or 167 lb. It is tension by observation since the shear in the panel to the right is up and the vertical component of the diagonal FD must pull down for equilibrium.

Considering Joint F. $\Sigma H = - FG - FD_H = 0$, which means that the horizontal component of the load in the diagonal DF equals the load in FG, or is equal to the value of the horizontal side in the index triangle or - 133 lb. It is negative because the horizontal component of DF pulls on Joint F and therefore FG must push against the joint for equilibrium.

Considering Joint D:-

$\Sigma V = DF_V + DG = 0$. But $DF_V = 100$ (vertical side of index triangle)
$\therefore DG = - 100$
$\Sigma H = DE + DF_H - DC = 0$, but DE = 0 and DF_H = 133 (from index triangle)
$\therefore DC = 133$

Considering Joint G:-

$\Sigma H = - GH + GF - GC_H = 0$. But GF = - 133, and GC_H = 300 from index triangle in the second panel. Hence GH = - 433 lb. Proceeding in this manner, we obtain the stress in all the members as shown in Fig. A2.29. All the equilibrium equations can be solved mentally and with the calculations being done on the slide rule, all member loads can be written directly on the truss diagram.

Observation of the results of Fig. A2.29 show that the loads in the truss verticals equal the values of the vertical sides of the index load triangle, and the loads in the truss diagonals equal the values of the index triangle diagonal side and in general the loads in the top and bottom horizontal truss members equal the summation of the values of the horizontal sides of the index triangles.

The reactions at A and J are found when the above general procedure reaches joints A and J. As a check on the work the reactions should be determined treating the truss as a whole.

Fig. A2.30 shows the solution for the stresses in the members of a simply supported Pratt Truss, symmetrically loaded. Since all panels have the same width and height, only one length triangle is drawn as shown. Due to symmetry, the index triangles are drawn for panels to only one side of the truss center line. First, the vertical shear in each panel is written on the vertical side of each index triangle. Due to the symmetry of the truss and

loading, we know that one half of the external loads at joints U_3 and L_3 is supported at reaction R_1 and 1/2 at reaction R_2, or shear in

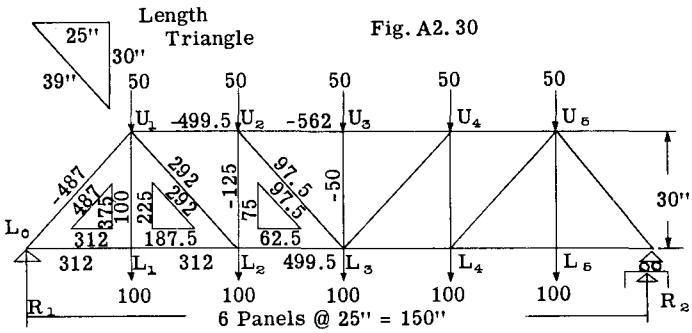

center panel = (100 + 50) 1/2 = 75. The vertical shear in panel $U_1U_2L_1L_2$ equals 75 plus the external loads at U_2 and L_2 or a total of 225 and similarly for the end panel shear = 225 + 50 + 100 = 375. With these values known, the other two sides of the index triangles are directly proportional to the sides of the length triangles for each panel, and the results are as shown in Fig. A2.30.

The general procedure from this point is to find the loads in the diagonals, then in the verticals, and finally in the horizontal chord members.

The loads in the diagonals are equal to the values on the hypotenuse of the index triangles. The sense, whether tension or compression, is determined by inspection by cutting mental sections thru the truss and noting the direction of the external shear load which must be balanced by the vertical component of the diagonals.

The loads in the verticals are determined by the method of joints and the sequence of joints is so selected that the stress in the vertical member is the only unknown in the equation $\Sigma V = 0$ for the joint in question.

Thus for joint U_3, $\Sigma V = -50 - U_3L_3 = 0$ or $U_3L_3 = -50$.

For joint U_2, $\Sigma V = -50 - U_2L_{3V} - U_2L_2 = 0$, but $U_2L_{3V} = 75$, the vertical component of U_2L_3 from index triangle. $\therefore U_2L_2 = -50 - 75 = -125$. For joint L_1, $\Sigma V = -100 + L_1U_1 = 0$, hence $L_1U_1 = 100$.

Since the horizontal chord members receive their loads at the joints due to horizontal components of the diagonal members of the truss, we can start at L_0 and add up these horizontal components to obtain the chord stresses. Thus, $L_0L_1 = 312$ (from index triangle). $L_1L_2 = 312$ from $\Sigma H = 0$ for joint L_1. At joint U_1, the horizontal components of diagonal members = 312 + 187.5 = 499.5. Therefore, load in U_1U_2 = - 499.5. Similarly at joint L_2, L_2L_3 = 312 + 187.5 = 499.5. At joint U_2, the horizontal components of U_1U_2 and U_2U_3 = 499.5 + 62.5 = 562 which must be balanced by - 562 in member U_2U_3.

The reaction R_2 equals the value on the vertical side of our index triangle in the end panel, or 375. This should be checked using the truss as a whole and taking moments about R_2.

If a truss is loaded unsymmetrically, the reactions should be determined first, after which the index triangles can be drawn, starting with the end panels, since the panel shear is then readily calculated.

A2.12 Aircraft Wing Structure. Truss Type with Fabric or Plastic Cover

The metal covered cantilever wing with its better overall aerodynamic efficiency and sufficient torsional rigidity has practically replaced the externally braced wing except for low speed commercial or private pilot aircraft as illustrated by the aircraft in Figs. A2.31 and 32. The wing covering is usually fabric and therefore a drag truss inside the wing is necessary to resist loads in the drag truss direction. Figs. A2.33 and 34 shows the general structural layout of such wings. The two spars or beams are metal or wood. Instead of using double wires in each drag truss bay, a single diagonal strut capable of taking either tension or compressive loads could be used. The external brace struts are stream line tubes.



Fig. A2.31 Piper Tri-Pacer



Fig. A2.32 Champion Traveler

Fig. A2. 33

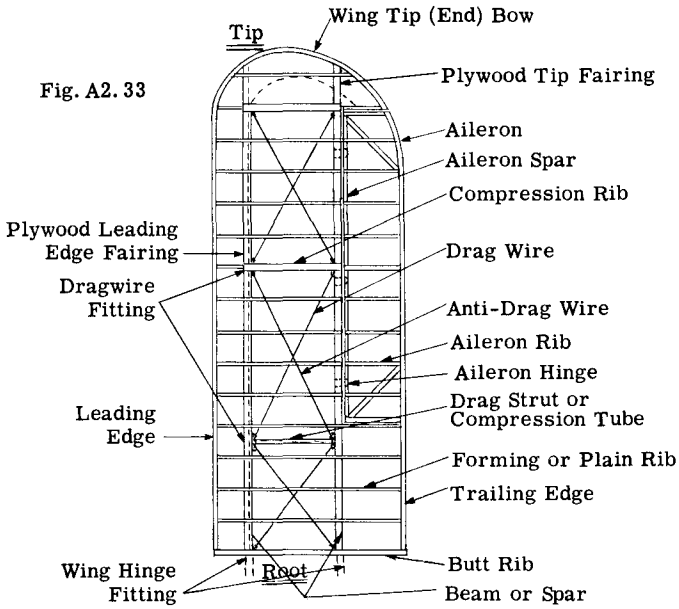

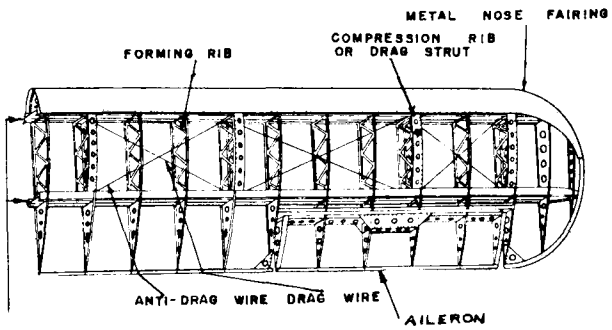

Fig. A2. 34

Example Problem 10. Externally Braced Monoplane Wing Structure

Fig. A2.35 shows the structural dimensional diagram of an externally braced monoplane wing. The wing is fabric covered between wing beams, and thus a drag truss composed of struts and tie rods is necessary to provide strength and rigidity in the drag direction. The axial loads in all members of the lift and drag trusses will be determined. A simplified air loading will be assumed, as the purpose of this problem is to give the student practice in solving statically determinate space truss structures.

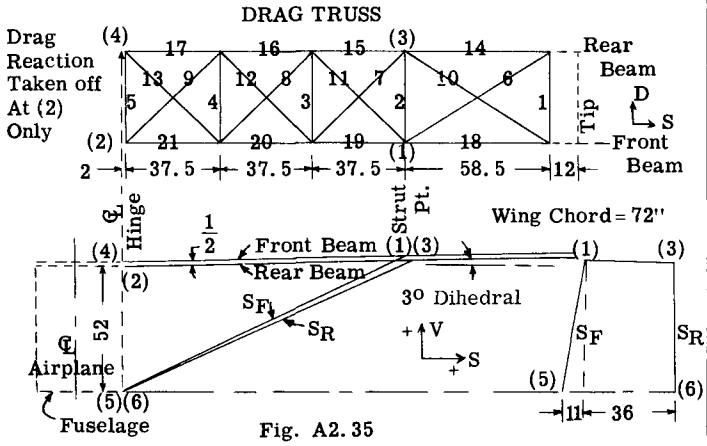

Fig. A2. 35

ASSUMED AIR LOADING:-

(1) A constant spanwise lift load of 45 lb/in from hinge to strut point and then tapering to 22.5 lb/in at the wing tip.

(2) A forward uniform distributed drag load of 6 lb/in.

The above airloads represent a high angle of attack condition. In this condition a forward load can be placed on the drag truss as illustrated in Fig. A2.36. Projecting the air

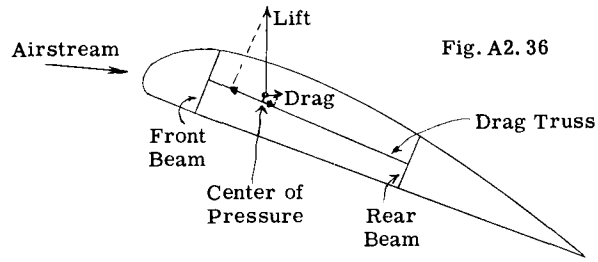

Fig. A2. 36

lift and drag forces on the drag truss direction, the forward projection due to the lift is greater than the rearward projection due to the air drag, which difference in our example problem has been assumed as 6 lb/in. In a low angle of attack the load in the drag truss direction would act rearward.

SOLUTION:

The running loads on the front and rear beams will be calculated as the first step in the solution. For our flight condition, the center of pressure of the airforces will be assumed as shown in Fig. A2.37.

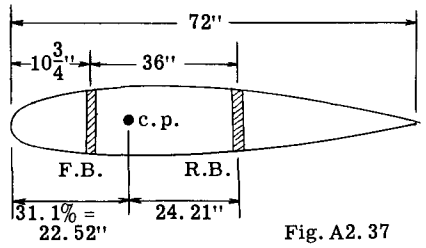

Fig. A2. 37

The running load on the front beam will be 45 x 24.2/36 = 30.26 lb/in., and the remainder or 45 - 30.26 = 14.74 lb/in gives the load on the rear beam.

To solve for loads in a truss system by a method of joints, all loads must be transferred to the truss joints. The wing beams are supported at one end by the fuselage and outboard by the two lift struts. Thus we calculate the reactions on each beam at the strut and hinge points due to the running lift load on each beam.

Front Beam

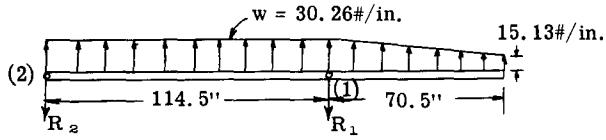

Taking moments about point (2)

$$114.5R_1 - 114.5 \times 30.26 \times 114.5/2 - 15.13 \times 70.5 \times 149.75 - 15.13 \times 35.25 \times 138 = 0.$$

hence

$$R_1 = 3770 \text{ lb.}$$

Take $\Sigma V = 0$ where V direction is taken normal to beam

$$\Sigma V = -R_2 - 3770 + 30.26 \times 114.5 + \frac{(30.26 + 15.13)}{2} 70.5 = 0$$

hence $R_2 = 1295$ lb.

(The student should always check results by taking moments about point (1) to see if $\Sigma M_1 = 0$)

Rear Beam

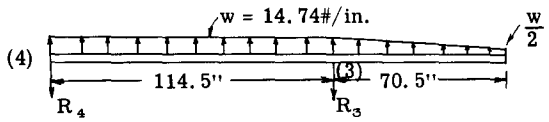

The rear beam has the same span dimensions but the loading is 14.74 lb/in. Hence beam reactions R_4 and R_3 will be 14.74/30.26 = .4875 times those for front beam.

hence $R_3 = .4875 \times 3770 = 1838$ lb.
$R_4 = .4875 \times 1295 = 631$ lb.

The next step in the solution is the solving for the axial loads in all the members. We will use the method of joints and consider the structure made up of three truss systems as illustrated at the top of the next column, namely, a front lift truss, a rear lift truss and a drag truss. The beams are common to both lift and drag trusses.

Table A2.1 gives the V, D and S projections of the lift truss members as determined from information given in Fig. A2.35. The true

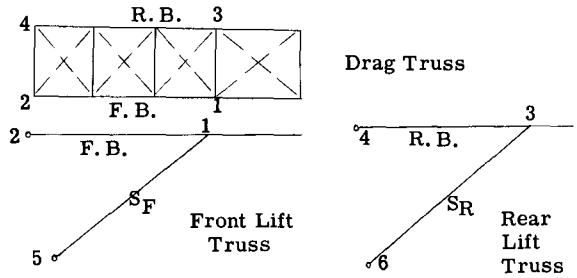

member lengths L and the component ratios then follow by simple calculation.

Table A2.1

Member	Sym.	V	D	S	L	V/L	D/L	S/L
Front Beam	FB	5.99	0	114.34	114.50	.0523	0	.9986
Rear Beam	RB	5.99	0	114.34	114.50	.0523	0	.9986
Front Strut	S_F	57.99	11	114.34	128.79	.4501	.0854	.8878
Rear Strut	S_R	57.49	0	114.34	128.00	.4486	0	.8930

V = vertical direction,
D = drag direction,
S = side direction,
$L = \sqrt{V^2 + D^2 + S^2}$

We start the solution of joints by starting with joint (1). Free body sketches of joint (1) are sketched below. All members are considered two-force members or having pins at each end, thus magnitude is the only unknown characteristic of each member load. The drag truss members coming in to joint (1) are replaced by a single reaction called D_1. After D_1 is found, its influence in causing loads in drag truss members can then be found when the drag truss as a whole is treated. In the joint solution, the drag truss has been assumed parallel to drag direction which is not quite true from Fig. A2.35, but the error on member loads is negligible.

JOINT 1 (Equations of Equilibrium)

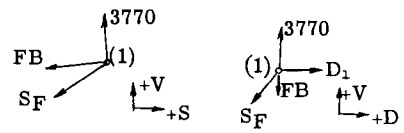

$\Sigma V = 3770 \times .9986 - .0523\ FB - .4501\ S_F = 0$ - (1)
$\Sigma S = -3770 \times .0523 - .9986\ FB - .8878\ S_F = 0$ - (2)
$\Sigma D = -.0854\ S_F + D_1 = 0$ - - - - - - - - - - - (3)

Solving equations 1, 2 and 3, we obtain

FB = - 8513 lb. (compression)
S_F = 9333 lb. (tension)
D_1 = 798 lb. (aft)

Joint (3) (Equations of equilibrium)

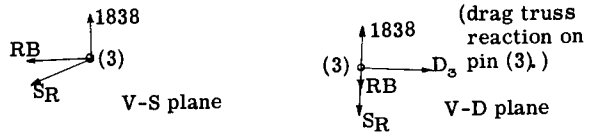

$\Sigma V = 1838 \times .9986 - .0523\ RB - .4486\ S_R = 0$ -(4)
$\Sigma S = -1838 \times .0523 - .9986\ RB - .8930\ S_R = 0$ -(5)
$\Sigma D = D_3 + 0 = 0$ - - - - - - - - - - - - - - - - -(6)

Solving equations 4, 5 and 6, we obtain
RB = - 4189 lb. (compression)
S_R = 4579 lb. (tension)
D_3 = 0

Fig. A2.38 shows the reactions of the lift struts on the drag truss at joints (1) and (3) as found above.

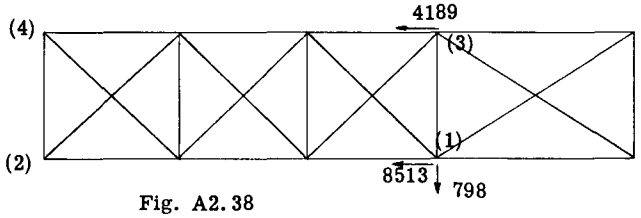

Fig. A2.38

Drag Truss Panel Point Loads Due to Air Drag Load.

It was assumed that the air load components in the drag direction were 6 lb./in. of wing acting forward.

The distributed load of 6 lb./in. is replaced by concentrated loads at the panel points as shown in Fig. A2.39. Each panel point takes one half the distributed load to the adjacent panel point, except for the two outboard panel points which are affected by the overhang tip portion.

Thus the outboard panel point concentration of 254 lb. is determined by taking moments about (3) of the drag load outboard of (3) as follows:

P = 70.5 x 6 x 35.25/58.5 = 254 lb.

To simplify the drag truss solution, the drag strut and drag wires in the inboard drag truss panel have been modified to intersect at hinge points (2) and (4). In the design of the beam and fittings at this point, the effect of the actual conditions of eccentricity should of course be considered.

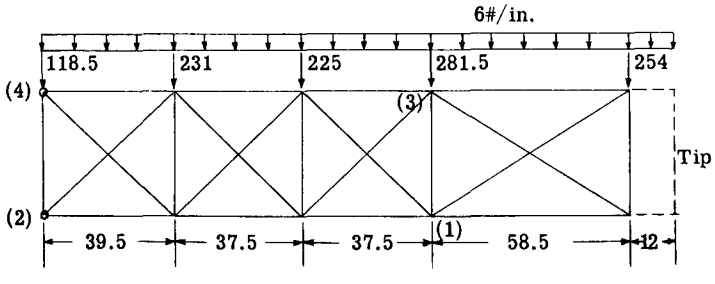

Fig. A2.39

Combined Loads on Drag Truss

Adding the two load systems of Figs. A2.38 and A2.39, the total drag truss loading is obtained as shown in Fig. A2.40. The resulting member axial stresses are then solved for by the method of index stresses (Art. A2.9). The values are indicated on the truss diagram. It is customary to make one of the fittings attaching wing to fuselage incapable of transferring drag reaction to fuselage, so that the entire drag reaction from wing panel on fuselage is definitely confined to one point. In this example point (2) has been assumed as point where drag is resisted. Those drag wires which would be in compression are assumed out of action.

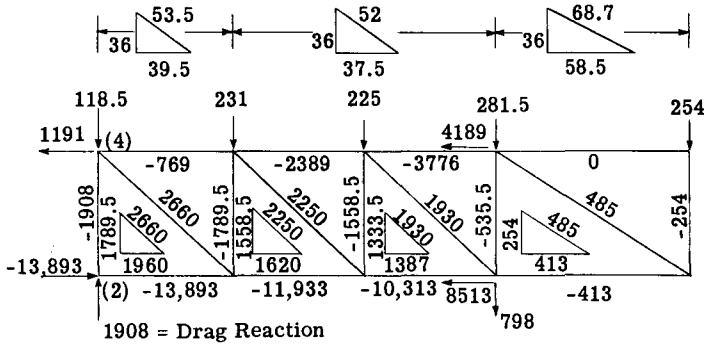

Fig. A2.40

Fuselage Reactions

As a check on the work as well as to obtain reference loads on fuselage from wing structure, the fuselage reactions will be checked against the externally applied air loads. Table A2.2 gives the calculations in table form.

Table A2.2

Point	Member	Load	V	D	S
2	FB	-13893	- 726	0	-13870
	Drag	- 1908	0	-1908	0
	Reaction R_2(Reaction)	- 1295	1294	0	- 67
4	RB	1191	62	0	1190
	R_4(Reaction)	- 631	630	0	- 33
5	F_S	9333	4205	798	8290
6	R_S	4579	2055	0	4090
Totals			7520	-1110	- 400

Applied Air Loads:

V component = (3770 + 1295 + 1838 + 631) .9986 = 7523 lb. (error 3 lb.)
D component = -185 x 6 = 1110 lb. (error = 0)
S component = -(3770 + 1295 + 1838 + 631) .0523 = 394 lb. (error 6 lb.)

The wing beams due to the distributed lift air loads acting upon them, are also subjected to bending loads in addition to the axial loads. The wing beams thus act as beam-columns. The subject of beam-column action is treated in another chapter of this book.

If the wing is covered with metal skin instead of fabric, the drag truss can be omitted since the top and bottom skin act as webs of a beam which has the front and rear beams as its flange members. The wing is then considered as a box beam subjected to combined bending and axial loading.

Example Problem 11. 3-Section Externally Braced Wing.

Fig. A2.41 shows a high wing externally braced wing structure. The wing outer panel has been made identical to the wing panel of example problem 1. This outer panel attached to the center panel by single pin fittings at points (2) and (4). Placing pins at these points make the structure statically determinate, whereas if the beams were made continuous through all 3 panels, the reactions of the lift and cabane struts on the wing beams would be statically indeterminate since we would have a 3-span continuous beam resting on settling supports due to strut deformation. The fitting pin at points (2) and (4) can be made eccentric with the neutral axis of the beams, hence very little is gained by making beams continuous for the purpose of decreasing the lateral beam bending moments. For assembly, stowage and shipping it is convenient to build such a wing in 3 portions. If a multiple bolt fitting is used as points (2) and (4) to obtain a continuous beam, not much is gained because the design requirements of the various governmental agencies specify that the wing beams must also be analyzed on the assumption that a multiple bolt fitting provides only 50 percent of the full continuity.

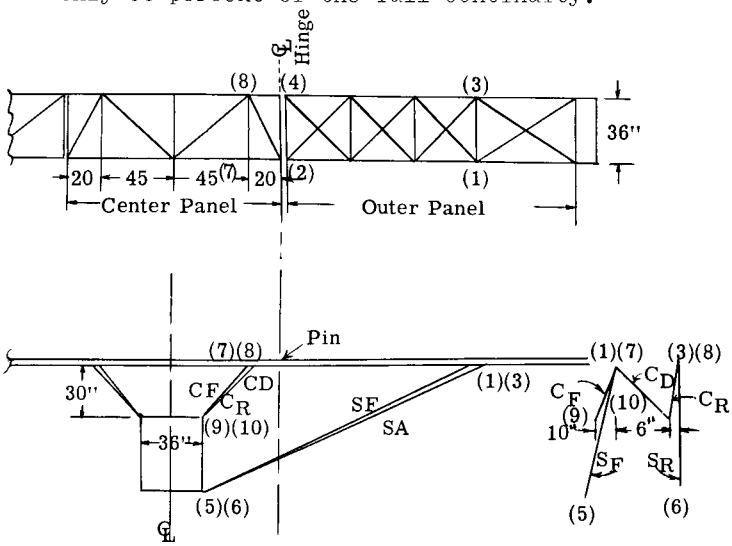

Fig. A2.41

Lengths & Directional Components of Cabane Struts

Member	Sym.	V	D	S	L	V/L	D/L	S/L
Front Cabane	C_F	30	10	27	41.59	.721	.240	.648
Diagonal Cabane Strut	C_D	30	30	27	50.17	.597	.597	.538
Rear Cabane Strut	C_R	29.5	6	27	40.42	.731	.1485	.668

$$L = \sqrt{V^2 + D^2 + S^2}$$

The air loads on the outer panel are taken identical to those in example problem 1. Likewise the dihedral and direction of the lift struts S_F and S_R have been made the same as in example problem 1. Therefore the analysis for the loads in the outer panel drag and lift trus trusses is identical to that in problem 1. The solution will be continued assuming the running lift load on center panel of 45 lb./in. and a forward drag load of 6 lb./in.

Solution of Center Panel

Center Rear Beam

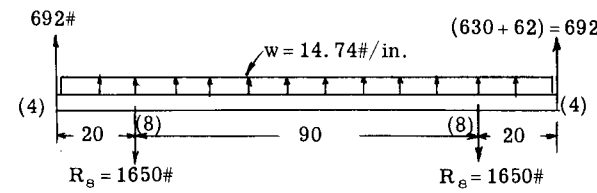

Fig. A2.42

Fig. A2.42 shows the lateral loads on the center rear beam. The loads consist of the distributed air load and the vertical component of the forces exerted by outer panel on center panel at pin point (4). From Table A2.2 of example problem 1, this resultant V reaction equals 630 + 62 = 692 lb.

The vertical component of the cabane reaction at joint (8) equals one half the total beam load due to symmetry of loading or 65 x 14.74 + 692 = 1650 lb.

Solution of force system at Joint 8

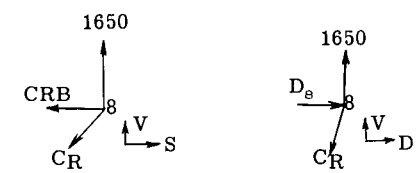

$$\Sigma V = 1650 - .731\, C_R = 0$$

whence

$$C_R = 1650/.731 = 2260 \text{ lb. (tension)}$$

$$\Sigma S = - CRB - 2260 \times .668 = 0$$

whence

$$CRB = -1510 \text{ lb. (compression)}$$

$$\Sigma D = D_s - 2260 \times .1485 = 0$$

whence

$$D_s = 336 \text{ lb. drag truss reaction}$$

Center Front Beam

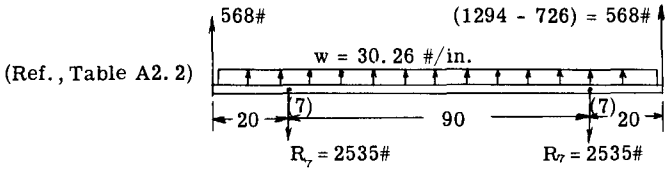

Fig. A2.43

Fig. A2.43 shows the V loads on the center front beam and the resulting V component of the cabane reaction at joint (7).

Solution of force system at Joint 7

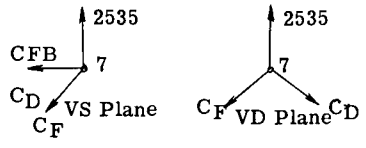

$$\Sigma V = 2535 - .721\ C_F - .597\ C_D = 0$$

$$\Sigma S = - CFB - .648\ C_F - .538\ C_D = 0$$

$$\Sigma D = - .240\ C_F + .597\ C_D = 0$$

Solving the three equations, we obtain

$$CFB = -2281 \text{ (compression)}$$

$$C_F = 2635$$

$$C_D = 1058$$

Solution for Loads in Drag Truss Members

Fig. A2.44 shows all the loads applied to the center panel drag truss. The S and D reactions from the outer panel at joints (2) and (4) are taken from Table A2.2 of problem 1. The drag load of 336 lb. at (8) is due to the rear cabane strut, as is likewise the beam axial load of - 1510 at (8). The axial beam load of - 2281 lb. at (7) is due to reaction of front cabane truss. The panel point loads are due to the given running drag load of 6 lb./in. acting forward.

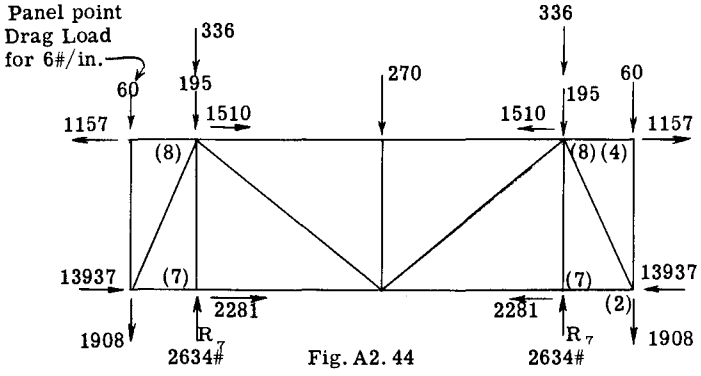

Fig. A2.44

The reaction which holds all these drag truss loads in equilibrium is supplied by the cabane truss at point (7) since the front and diagonal cabane struts intersect to form a rigid triangle. Thus the drag reaction R equals one half the total drag loads or 2634 lb.

Solving the truss for the loading of Fig. A2.44 we obtain the member axial loads of Fig. A2.45.

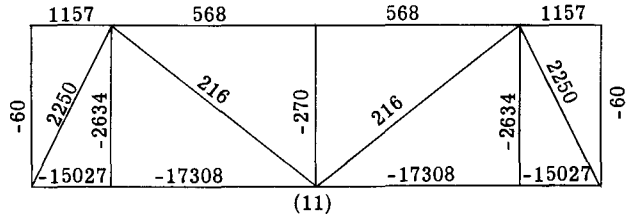

Fig. A2.45

Loads in Cabane Struts Due to Drag Reaction at Point 7

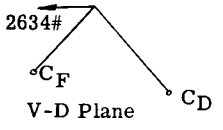

$$\Sigma D = - 2634 - .240\ C_F + .597\ C_D = 0$$

$$\Sigma V = - .721\ C_F - .597\ C_D = 0$$

Solving for C_F and C_D, we obtain

$$C_F = -2740 \text{ lb. (compression)}$$

$$C_D = 3310 \text{ (tension)}$$

adding these loads to those previously calculated for lift loads:

$$C_F = - 2740 + 2635 = - 105$$

$$C_D = 1058 + 3310 = 4368 \text{ lb.}$$

$$C_R = 2260 \text{ lb.}$$

Fuselage Reactions

As a check on the work the fuselage reactions will be checked against the applied loads. Table A2.3 gives the V, D and S components of the fuselage reactions.

Table A2.3

Point	Member	Load	V	D	S
9	Front Strut C_F	-105	-76	-25	-68
10	Rear Strut C_R Dia. Strut C_D	2260 4368	1650 2610	335 -2610	1510 2356
5	Front Lift Strut S_F	9333	4205	798	8290
6	Rear Lift Strut S_R	4579	2055	0	4090
Totals			10444	-1502	16178

Applied Air Loads

V component = 7523 (outer panel) + 65 x 45 = 10448 (check)

D component = - 1110 (outer panel) - 65 x 6 = - 1500 (error 2 lb.)

The total side load on a vertical plane thru centerline of airplane should equal the S component of the applied loads. The applied side loads = - 394 lb. (see problem 1). The air load on center panel is vertical and thus has zero S component.

From Table A2.3 for fuselage reactions have $\Sigma S = 16178$. From Fig. A2.45 the load in the front beam at ℄ of airplane equals - 17308 and 568 for rear beam. The horizontal component of the diagonal drag strut at joints 11 equals 216 x 45/57.6 = 169 lb.

Then total S components = 16178 - 17308 + 568 + 169 = - 393 lb. which checks the side component of the applied air loads.

Example Problem 12. Single Spar Truss Plus Torsional Truss System.

In small wings or control surfaces, fabric is often used as the surface covering. Since the fabric cannot provide reliable torsional resistance, internal structure must be of such design as to provide torsional strength. A single spar plus a special type of truss system is often used to give a satisfactory structure. Fig. A2.46 illustrates such a type of structure, namely, a trussed single spar AEFN plus a triangular truss system between the spar and the trailing edge OS. Fig. A2.46 (a, b, c) shows the three projections and dimensions. The air load on the surface covering of the structure is assumed to be 0.5 lb./in.^{2} intensity at spar line and then varying linearly to zero at the trailing edge (See Fig. d).

The problem will be to determine the axial loads in all the members of the structure. It will be assumed that all members are 2 force members as is usually done in finding the primary loads in trussed structures.

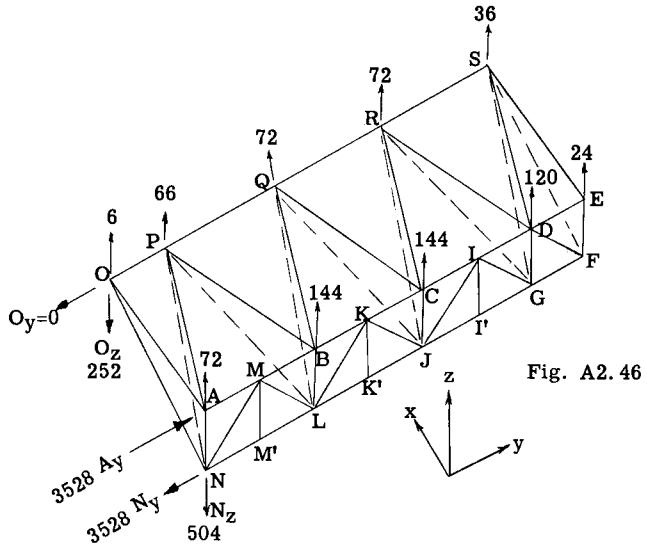

Fig. A2.46

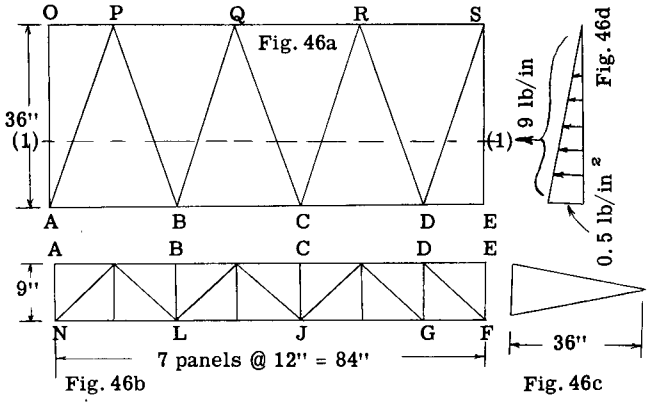

Fig. 46b Fig. 46c

SOLUTION:

The total air load on the structure equals the average intensity per square inch times the surface area or (0.5)(.5)(36 x 84) = 756 lb. In order to solve a truss system by a method of joints the distributed load must be replaced by an equivalent load system acting at the joints of the structure. Referring to Fig. (d), the total air load on a strip 1 inch wide and 36 inches long is 36(0.5)/2 = 9 lb. and its c.g. or resultant location is 12 inches from line AE. In Fig. 46a this resultant load of 9 lb./in. is imagined as acting on an imaginary beam located along the line 1-1. This running load applied along this line is now replaced by an equivalent force system acting at joints OPQRSEDBCA. The results of this joint distribution are shown by the joint loads in Fig. A2.46. To illustrate how these joint loads were obtained, the calculations for loads at joints ESDR will be given.

Fig. A2.48 shows a portion of the structure to be considered. For a running load of 9 lb./in., along line 1-1, reactions will be for

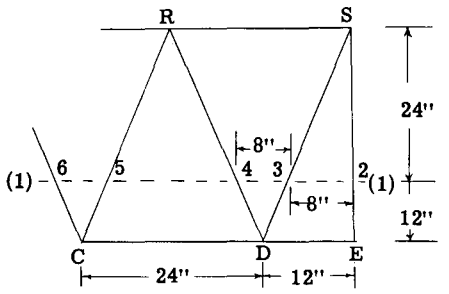

Fig. A2.48

simple beams resting at points 2, 3, 4, 5, etc. The distance between 2-3 is 8 inches. The total load on this distance is 8 x 9 = 72 lb. One half or 36 lb. goes to point (2) and the other half to point (3). The 36 lb. at (2) is then replaced by an equivalent force system at E and S or (36)/3 = 12 lb. to S and (36)(2/3) = 24 to E. The distance between points (3) and (4) is 8 inches and the load is 8 x 9 = 72 lb. One half of this or 36 goes to point (3) and this added to the previous 36 gives 72 lb. at (3). The load of 72 is then replaced by an equivalent force system at S and D, or (72)/3 = 24 lb. to S and (72)(2/3) = 48 to D. The final load at S is therefore 24 + 12 = 36 lb. as shown in Fig. A 2.46. Due to symmetry of the triangle CRD, one half of the total load on the distance CD goes to points (4) and (5) or (24 x 9)/2 = 108 lb. The distribution to D is therefore (108) (2/3) = 72 and (108)/3 = 36 to R. Adding 72 to the previous load of 48 at D gives a total load at D = 120 lb. as shown in Fig. A2.46. The 108 lb. at point (5) also gives (108)/3 = 36 to R or a total of 72 lb. at R. The student should check the distribution to other joints as shown in Fig. A2.46.

To check the equivalence of the derived joint load system with the original air load system, the magnitude and moments of each system must be the same. Adding up the total joint loads as shown in Fig. A2.46 gives a total of 756 lb. which checks the original air load. The moment of the total air load about an x axis at left end of structure equals 756 x 42 = 31752 in. lb. The moment of the joint load system in Fig. A2.46 equals (66 x 12) + (72 x 36) + (72 x 60) + (56 x 84) + 144 (24 + 48) + (120 x 72) + (24 x 84) = 31752 in.lb. or a check. The moment of the total air load about line AE equals 756 x 12 = 9072 in.lb. The moment of the distributed joint loads equals (6 + 66 + 72 + 72 + 36)36 = 9072 or a check.

Calculation of Reactions

The structure is supported by single pin fittings at points A, N and O, with pin axes parallel to x axis. It will be assumed that the fitting at N takes off the spar load in Z direction. Fig. A2.46 shows the reactions O_y, O_z, A_y, N_y, N_z. To find O_z take moments about y axis along spar AEFN.

$$\Sigma M_y = (6 + 66 + 72 + 72 + 36)36 - 36\ O_z = 0$$

whence O_z = 252 lb. acting down as assumed.

To find O_y take moments about z axis through point (A).

$$\Sigma M_z = 0 + 36\ O_y = 0, \quad O_y = 0$$

To find A_y take moments about x axis through point N. The moment of the air loads was previously calculated as - 31752, hence,

$$\Sigma M_x = -31752 + 9\ A_y = 0, \text{ whence, } A_y = 3528 \text{ lb.}$$

To find N_y take $\Sigma F_y = 0$

$$\Sigma F_y = 3528 - N_y = 0, \text{ hence } N_y = 3528 \text{ lb.}$$

To find N_z take $\Sigma F_z = 0$

$$\Sigma F_z = -252 + 756 - N_z = 0, \text{ hence } N_z = 504 \text{ lb.}$$

The reactions are all recorded on Fig. A2.46.

Solution of Truss Member Loads

For simplicity, the load system on the structure will be considered separately as two load systems. One system will include only those loads acting along the line AE and the second load system will be remaining loads which act along line OS. Since no bending moment can be resisted at joint O, the external load along spar AE will be reacted at A and N entirely or in other words, the spare alone resists the loads on line AE.

Fig. A2.49 shows a diagram of this spar with its joint external loading. The axial loads produced by this loading are written on the truss members. (The student should check these member loads.)

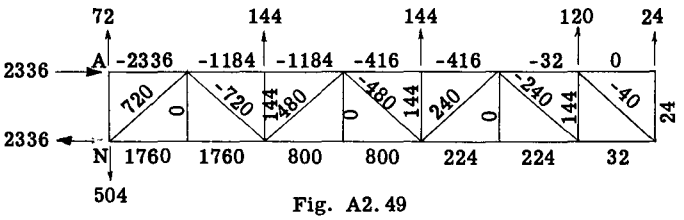

Fig. A2.49

TRIANGULAR TRUSS SYSTEM

The load system along the trailing edge OS causes stresses in both the spar truss and the diagonal truss system. The support fitting at point O provides a reaction in the Z direction but no reacting moment about the x axis. Since the loads on the trailing edge lie on a y axis through O, it is obvious that all these loads flow to point O. Since the bending strength of the trailing edge member is negligible, the

load of 36 lb. at Joint S in order to be transferred to point O through the diagonal truss system must follow the path SDRCQBPAO. In like manner the load of 72 at R to reach O must take the path RCQBPAO, etc.

Calculation of Loads in Diagonal Truss Members:-

Member	z	y	x	L	z/L	y/L	x/L
All Diagonal Truss Members	4.5	12	36	38.2	.118	.314	.943
AO, NO	4.5	0	36	37.5	.120	0	.960

Consider Joint S

The triangular truss SEF cannot assist in transferring any portion of the 36 lb. load at S because the reaction of this truss at EF would put torsion on the spar and the spar has no appreciable torsional resistance.

Considering Joint S as a free body and writing the equilibrium equations:

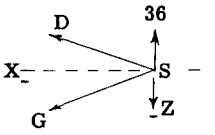

$\Sigma F_X = -.943\ DS - .943\ GS = 0$

whence, $DS = -GS$

$\Sigma F_Z = 36 + .118\ DS - .118\ GS = 0$

Subt. $DS = -GS$ and solving for GS, gives GS = 159 lb.(tension), DS = -159 (compression)

Consider Joint D

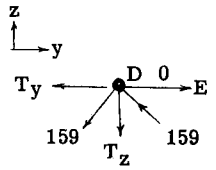

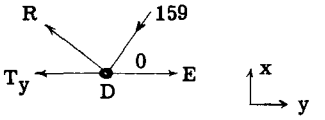

Let T_y and T_Z be reactions of diagonal truss system on spar truss at Joint D.

$\Sigma F_X = -159 \times .943 + .943\ DR = 0$, hence DR = 159 lb.

$\Sigma F_Z = -159 \times .118 + 159 \times .118 - T_Z = 0$

whence $T_Z = 0$, which means the diagonal truss produces no Z reaction or shear load on spar truss at D.

$\Sigma F_y = -.314 \times 159 - .314 \times 159 - T_y = 0$

whence $T_y = -100$ lb.

If joint G is investigated in the same manner, the results will show that $T_Z = 0$ and $T_y = 100$.

The results at joint D shows that the rear diagonal truss system produces no shear load reaction on the spar but does produce a couple force on the spar in the Y direction which produces compression in the top chord of the spar truss and tension in the bottom chord.

Consider Joint R

The load to be transferred to truss RCJR is equal to the 72 lb. at R plus the 36 lb. at S which comes to joint R from truss DRG.

Hence load in RC = (72 + 36)0.5 x (1/.118) = - 457 lb.

Whence RJ = 457, CQ = 457 and JQ = - 457

Joint Q

Load to be transferred to truss QBL = 72 + 72 + 36 = 180 lb.

Hence load in QB = (180 x 0.5)(1/.118) = - 762.

Whence QL = 762, BP = 762, LP = - 762

Joint P

Load = 180 + 66 = 246

Load in PA = (246 x 0.5)(1/.118) = - 1040

Whence PN = 1040

Consider Joint (A) as a free body.

$\Sigma F_X = -1040 \times .943 + .960\ AO = 0$, AO = 1022 lb.

In like manner, considering Joint N, gives NO = - 2022 lb.

Couple Force Reactions on Spar

As pointed out previously, the diagonal torsion truss produces a couple reaction on the spar in the y direction. The magnitude of the force of this couple equals the y component of the load in the diagonal truss members meeting at a spar joint. Let T_y equal this reaction load on the spar.

At Joint C:-

$T_y = -(457 + 457).314 = -287$ lb.

Likewise at Joint J, $T_y = 287$

At Joint B:-

$T_y = -(762 + 762).314 = -479$

Likewise at Joint L, $T_y = 479$

At Joint A:-

$T_y = -(1040 \times .314) = -326$

Likewise at Joint N, $T_y = 326$

These reactions of the torsion truss upon the spar truss are shown in Fig. A2.50. The loads in the spar truss members due to this loading are written adjacent to each truss member. Adding these member loads to the loads in Fig. A2.49, we obtain the final spar truss member loads as shown in Fig. A2.51.

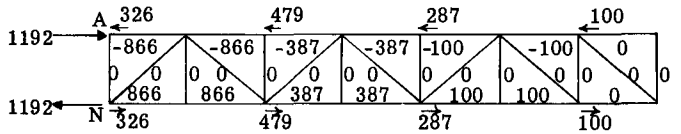

Fig. A2. 50

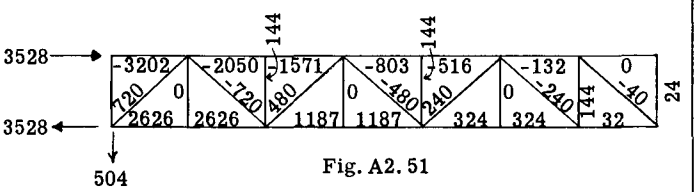

Fig. A2. 51

If we add the reactions in Figs. A2.50 and A2.49, we obtain 3528 and 504 which check the reactions obtained in Fig. A2.46.

A2. 13 Landing Gear Structure

The airplane is both a landborne and airborne vehicle, and thus a means of operating the airplane on the ground must be provided which means wheels and brakes. Furthermore, provision must be made to control the impact forces involved in landing or in taxiing over rough ground. This requirement requires a special energy absorption unit in the landing gear beyond that energy absorption provided by the tires. The landing gear thus includes a so-called shock strut commonly referred to as an oleo strut, which is a member composed of two telescoping cylinders. When the strut is compressed, oil inside the air tight cylinders is forced through an orifice from one cylinder to the other and the energy due to the landing impact is absorbed by the work done in forcing this oil through the orifice. The orifice can be so designed as to provide practically a uniform resistance over the displacement or travel of the oleo strut.

An airplane can land safely with the airplane in various attitudes at the instant of ground contact. Fig. A2.52 illustrates the three altitudes of the airplane that are specified by the government aviation agencies for design of landing gear. In addition to these symmetrical unbraked loadings, special loadings, such as a braked condition, landing on one wheel condition, side load on wheel, etc., are required. In other words, a landing gear can be subjected to a considerable number of different loadings under the various landing conditions that are encountered in the normal operation of an airplane.

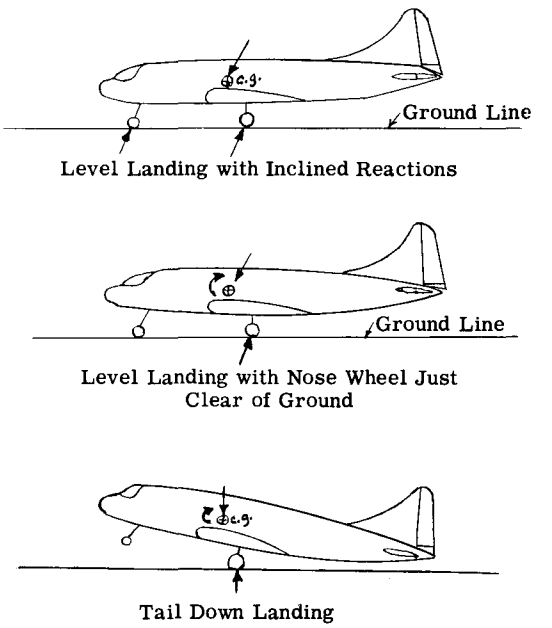

Fig. A2. 52

Fig. A2.53 shows photographs of typical main gear units and Fig. A2.54 for nose wheel gear units.

The successful design of landing gear for present day aircraft is no doubt one of the most difficult problems which is encountered in the structural layout and strength design of aircraft. In general, the gear for aerodynamic efficiency must be retracted into the interior of the wing, nacelle or fuselage, thus a reliable, safe retracting and lowering mechanism system is necessary. The wheels must be braked and the nose wheel made steerable. The landing gear is subjected to relatively large loads, whose magnitudes are several times the gross weight of the airplane and these large loads must be carried into the supporting wing or fuselage structure. Since the weight of landing gear may amount to around 6 percent of the weight of the airplane it is evident that high strength/weight ratio is a paramount design requirement of landing gear, as inefficient structural arrangement and conservative stress analysis can add many unnecessary pounds of weight to the airplane and thus decrease the pay or useful load.

A2. 14 Example Problems of Calculating Reactions and Loads on Members of Landing Gear Units

In its simplest form, a landing gear could consist of a single oleo strut acting as a cantilever beam with its fixed end being the upper end which would be rigidly fastened to the supporting structure. The lower cylinder of the oleo strut carries an axle at its lower

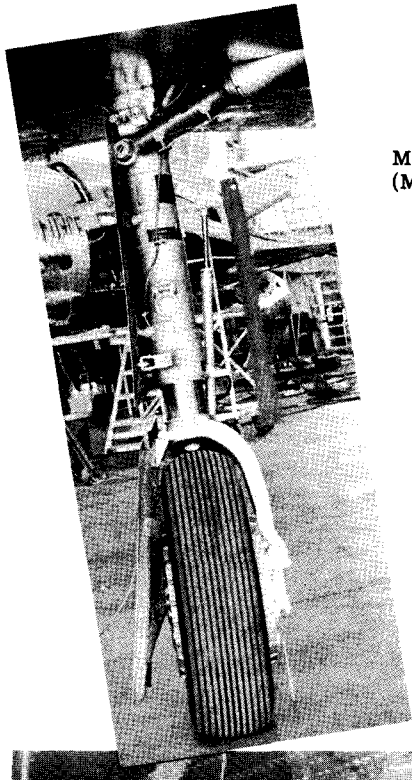

McDonnell Aircraft
(Military Airplane)

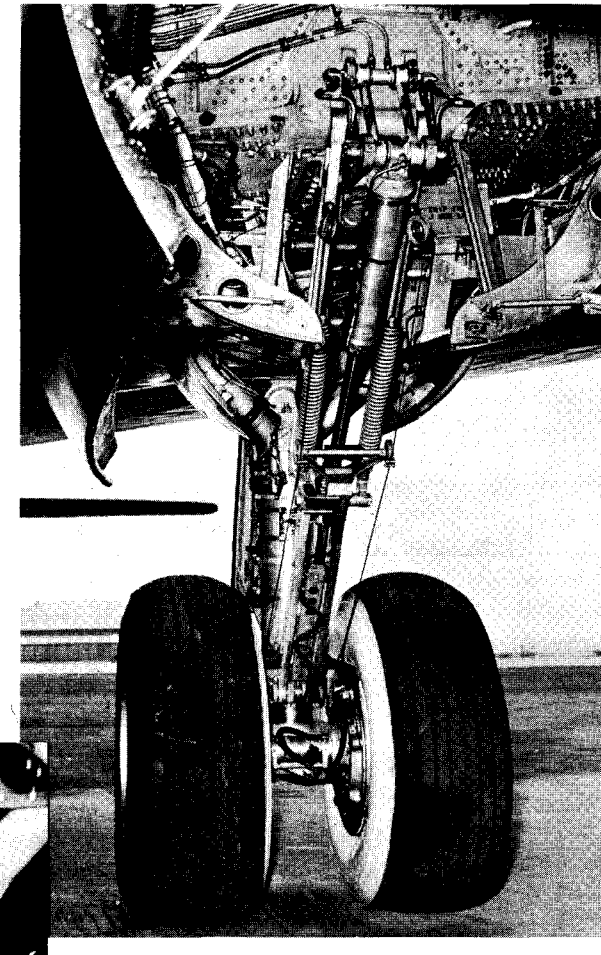

Douglas DC-7 Air Transport

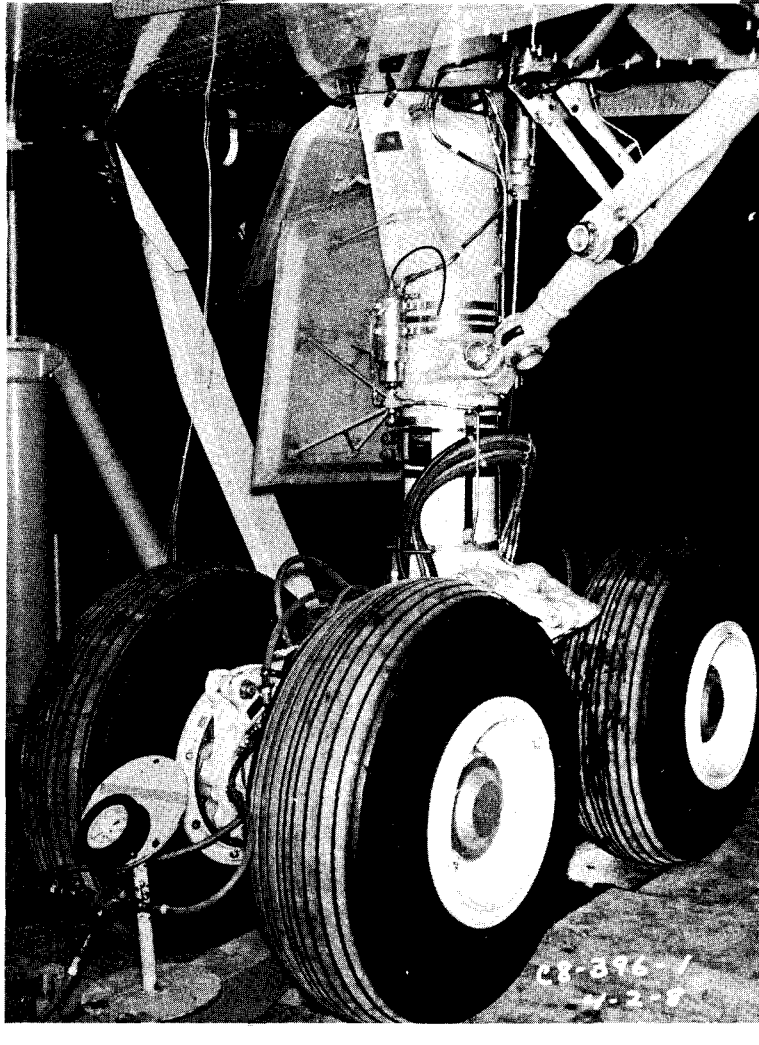

Douglas DC-8
Jet Airliner

Fig. A2.53 Main Landing Gear Illustrations (One Side)

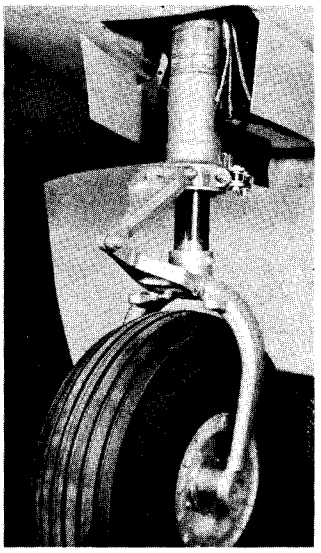

Piper-Apache

Beechcraft Twin Bonanza

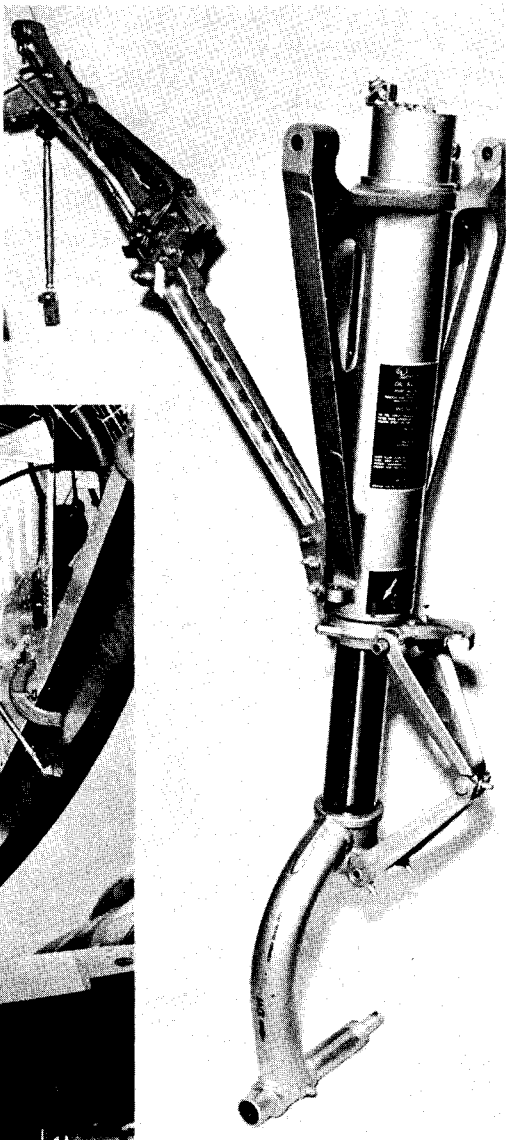



Piper Tri-Pacer

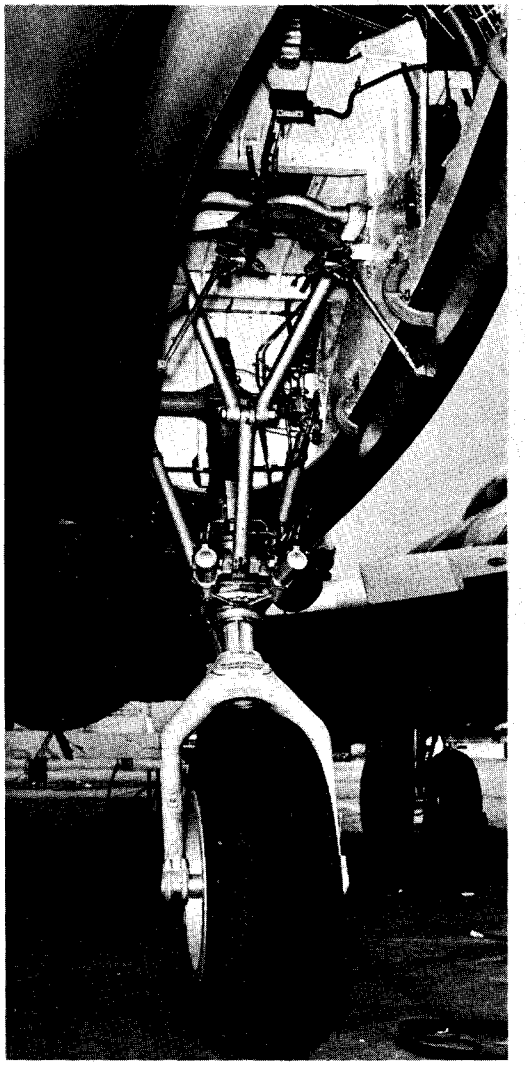

Douglas DC-7 Air Transport

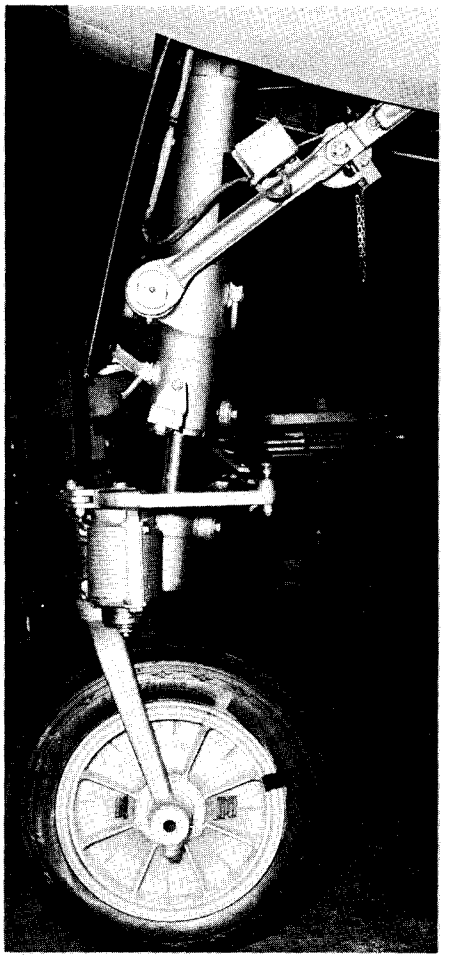

Navy F4-J
North American Aviation Co.

Fig. A2. 54 Nose Wheel Gear Installations

end for attaching the wheel and tire. This cantilever beam is subjected to bending in two directions, torsion and also axial loads. Since the gear is usually made retractable, it is difficult to design a single fitting unit at the upper end of the oleo strut that will resist this combination of forces and still permit movement for a simple retracting mechanism. Furthermore, it would be difficult to provide carry-through supporting wing or fuselage structure for such large concentrated load systems.

Thus to decrease the magnitude of the bending moments and also the bending flexibility of the cantilever strut and also to simplify the retracting problem and the carry-through structural problem, it is customary to add one or two braces to the oleo strut. In general, effort is made to make the landing gear structure statically determinate by using specially designed fittings at member ends or at support points in order to establish the force characteristics of direction and point of application.

Two example problem solutions will be presented, one dealing with a gear with a single wheel and the other with a gear involving two wheels.

Example Problem 13

Fig. A2.55 shows the projections of the landing gear configuration on the VS and VD planes. Fig. A2.56 is a space dimensional diagram. In landing gear analysis it is common to use V, D and S as reference axes instead of the symbols Z, X and Y. This gear unit is assumed as representing one side of the main gear on a tricycle type of landing gear system. The loading assumed corresponds to a condition of nose wheel up or tail down. (See lower sketch of Fig. A2.52). The design load on the wheel is vertical and its magnitude for this problem is 15000 lb.

The gear unit is attached to the supporting structure at points F, H and G. Retraction of the gear is obtained by rotating gear rearward and upward about axis through F and H. The fittings at F and H are designed to resist no bending moment. Hence, reactions at F and H are unknown in magnitude and direction. Instead of using the reaction and an angle as unknowns, the resultant reaction is replaced by its V and D components as shown in Fig. A2.56. The reaction at G is unknown in magnitude only since the pin fitting at each end of member GC fixes the direction and line of action of the reaction at G. For convenience in calculations, the reaction G is replaced by its components G_V and G_D. For a side load on the landing gear, the reaction in the S direction is taken off at point F by a specially designed unit.

SOLUTION

The supporting reactions upon the gear at points F, H, and G will be calculated as a beginning step. There are six unknowns, namely F_S, F_V, F_D, H_V, H_D and G (See Fig. A2.56). With 6 equations of static equilibrium available for a space force system, the reactions can be found by statics. Referring to Fig. A2.56:-

To find F_S take $\Sigma S = 0$

$F_S + 0 = 0$, hence $F_S = 0$

To find reaction G_V take moments about an S axis through points F, H.

$\Sigma M_S = 3119 \times 50 - 24\, G_V = 0$

Whence, $G_V = 6500$ lb. with sense as assumed. (The wheel load of 15000 lb. has been resolved into V and D components as indicated in Fig. A2.55).

With G_V known, the reaction G equals (6500)(31.8/24) = 8610 lb. and similarly the component G_D = (6500)(21/24) = 5690 lb.

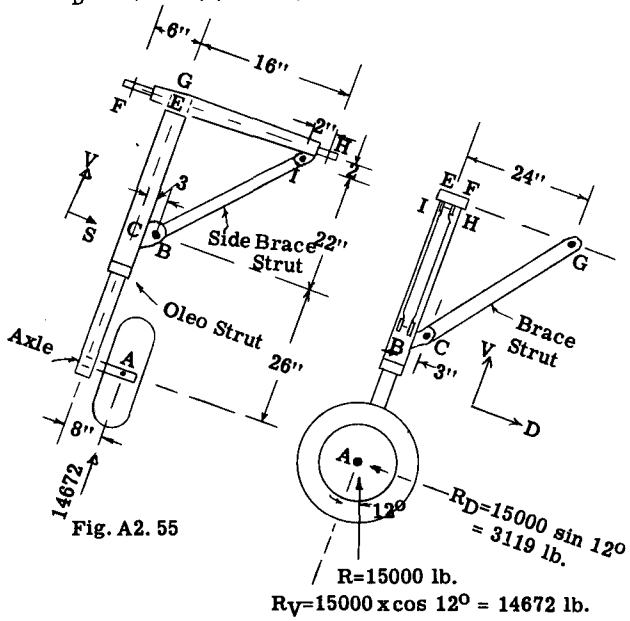

Fig. A2.55

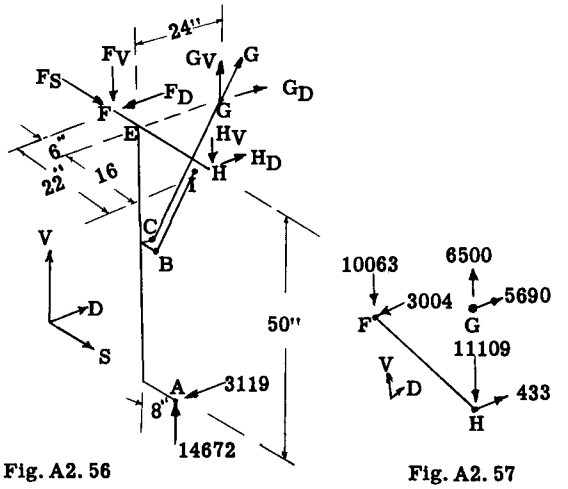

Fig. A2.56

Fig. A2.57

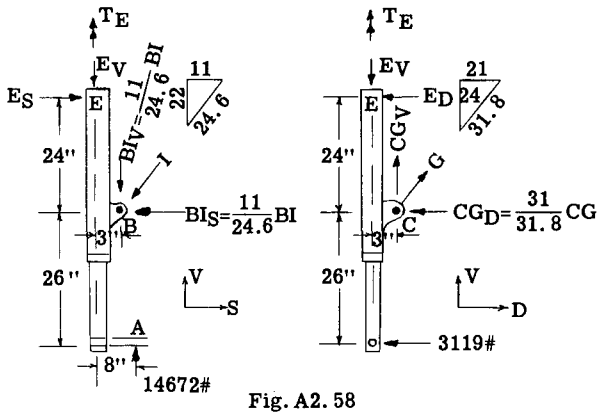

Fig. A2.58

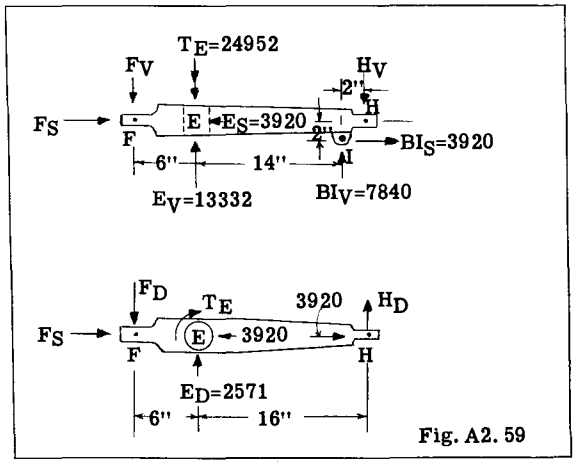

Fig. A2.59

To find F_V, take moments about a D axis through point H.

$$\Sigma M_{H(D)} = 16\ G_V + 14672 \times 8 - 22\ F_V = 0$$
$$= 16 \times 6500 + 14672 \times 8 - 22\ F_V = 0$$

Whence F_V = 10063 lb. with sense as assumed.

To find H_D, take moments about V axis through F.

$$\Sigma M_{F(V)} = -6\ G_D - 22\ H_D + 3119 \times 14 = 0$$
$$= -6 \times 5690 - 22\ H_D + 3119 \times 14$$
$$= 0$$

Whence, H_D = 433 lb.

To find F_D, take $\Sigma D = 0$

$$\Sigma D = -F_D + H_D + G_D - 3119 = 0$$
$$= -F_D + 433 + 5690 - 3119 = 0$$

Whence, F_D = 3004 lb.

To find H_V take $\Sigma V = 0$

$$\Sigma V = -F_V + G_V - H_V + 14672 = 0$$
$$= -10063 + 6500 - H_V + 14672 = 0$$

Whence, H_V = 11109 lb.

Fig. A2.57 summarizes the reactions as found. The results will be checked for equilibrium of the structure as a whole by taking moments about D and V axes through point A.

$$\Sigma M_{A(D)} = -10063 \times 14 + 6500 \times 8 + 11109 \times 8$$
$$= -140882 + 52000 + 88882 = 0 \text{(check)}$$

$$\Sigma M_{A(V)} = 5690 \times 8 - 433 \times 8 - 3004 \times 14$$
$$= 45520 - 3464 - 42056 = 0 \text{ (check)}$$

The next step in the solution will be the calculation of the forces on the oleo strut unit. Fig. A2.58 shows a free body of the oleo-strut-axle unit. The brace members BI and CG are two force members due to the pin at each end, and thus magnitude is the only unknown reaction characteristic at points B and C. The fitting at point E between the oleo strut and the top cross member FH is designed in such a manner as to resist torsional moments about the oleo strut axis and to provide D, V and S force reactions but no moment reactions about D and S axes. The unknowns are therefore BI, CG, E_S, E_V, E_D and T_E or a total of 6 and therefore statically determinate. The torsional moment T_E is represented in Fig. A2.58 by a vector with a double arrow. The vector direction represents the moment axis and the sense of rotation of the moment is given by the right hand rule, namely, with the thumb of the right hand pointing in the same direction as the arrows, the curled fingers give the sense of rotation.

To find the resisting torsional moment T_E take moments about V axis through E.

$$\Sigma M_{E(V)} = -3119 \times 8 + T_E = 0, \text{ hence } T_E$$
$$= 24952 \text{ in.lb.}$$

To find CG take moments about S axis through E.

$$\Sigma M_{E(S)} = 3119 \times 50 - (24/31.8)\ CG \times 3 - 24\ (21/31.8)\ CG = 0$$

Whence, CG = 8610 lb.

This checks the value previously obtained when the reaction at G was found to be 8610. The D and V components of CG thus equal,

$$CG_D = 8610\ (21/31.8) = 5690 \text{ lb.}$$

$$CG_V = 8610\ (24/31.8) = 6500 \text{ lb.}$$

To find load in brace strut BI, take moments about D axis through point E.

$$\Sigma M_{E(D)} = -14672 \times 8 + 3\ (BI)\ 22/24.6 + 24\ (BI)\ 11/24.6 = 0$$

Whence, BI = 8775 lb.

and thus, $BI_V = (8775)(22/24.6) = 7840$ lb.
$BI_S = (8775)(11/24.6) = 3920$ lb.

To find E_S take $\Sigma S = 0$

$\Sigma S = E_S - 3920 = 0$, hence E_S = 3920

To find E_D take $\Sigma D = 0$

$\Sigma D = 5690 - 3119 - E_D = 0$, hence $E_D = 2571$

To find E_V take $\Sigma V = 0$

$\Sigma V = - E_V + 14672 - 7840 + 6500 = 0$, hence $E_V = 13332$ lb.

Fig. A2.59 shows a free body of the top member FH. The unknowns are F_V, F_D, F_S, H_V and H_D. The loads or reactions as found from the analysis of the oleo strut unit are also recorded on the figure. The equations of equilibrium for this free body are:-

$$\Sigma S = 0 = - 3920 + 3920 + F_S = 0, \text{ or } F_S = 0$$

$$\Sigma M_{F(D)} = 22\, H_V - 3920 \times 2 - 7840 \times 20 - 13332 \times 6 = 0$$

Whence, $H_V = 11110$ lb. This check value was obtained previously, and therefore is a check on our work.

$$\Sigma M_{F(V)} = 24952 - 2571 \times 6 - 22\, H_D = 0$$

whence, $H_D = 433$ lb.

$$\Sigma V = - F_V + 13332 + 7840 - 11110 = 0$$

whence, $F_V = 10063$

$$\Sigma D = - F_D + 2571 + 433 = 0$$

whence, $F_D = 3004$ lb.

Thus working through the free bodies of the oleo strut and the top member FH, we come out with same reactions at F and H as obtained when finding these reactions by equilibrium equation for the entire landing gear.

The strength design of the oleo strut unit and the top member FH could now be carried out because with all loads and reactions on each member known, axial, bending and torsional stresses could now be found.

The loads on the brace struts CG and BI are axial, namely, 8610 lb. tension and 8775 lb. compression respectively, and thus need no further calculation to obtain design stresses.

TORQUE LINK

The oleo strut consists of two telescoping tubes and some means must be provided to transmit torsional moment between the two tubes and still permit the lower cylinder to move upward into the upper cylinder. The most common way of providing this torque transfer is to use a double-cantilever-nut cracker type of structure. Fig. A2.60 illustrates how such a torque length could be applied to the oleo strut in our problem.

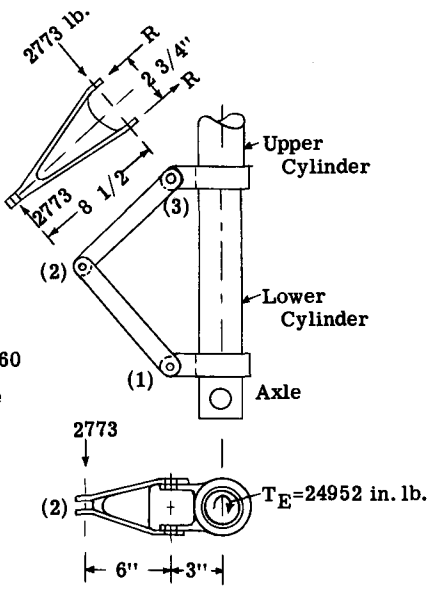

Fig. A2.60
Torque Link

The torque to be transferred in our problem is 24952 in.lb.

The reaction R_2 between the two units of the torque link at point (2), see Fig. A2.60, thus equals 24952/9 = 2773 lb.

The reactions R_3 at the base of the link at point (3) = 2773 x 8.5/2.75 = 8560 lb. With these reactions known, the strength design of the link units and the connections could be made.

Example Problem 14

The landing gear as illustrated in Fig. A2.61 is representative of a main landing gear which could be attached to the under side of a wing and retract forward and upward about line AB into a space provided by the lower portion of the power plant nacelle structure. The oleo strut OE has a sliding attachment at E, which prevents any vertical load to be taken by member AB at E. However, the fitting at E does transfer shear and torque reactions between the oleo strut and member AB. The brace struts GD, FD and CD are pinned at each end and will be assumed as 2 force members.

An airplane level landing condition with unsymmetrical wheel loading has been assumed as shown in Fig. A2.61.

SOLUTION

The gear is attached to supporting structure at points A, B and C. The reactions at these points will be calculated first, treating the entire gear as a free body. Fig. A2.62

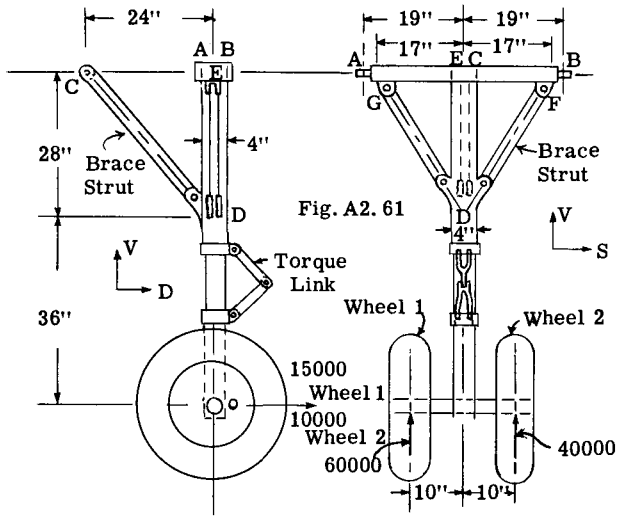

Fig. A2.61

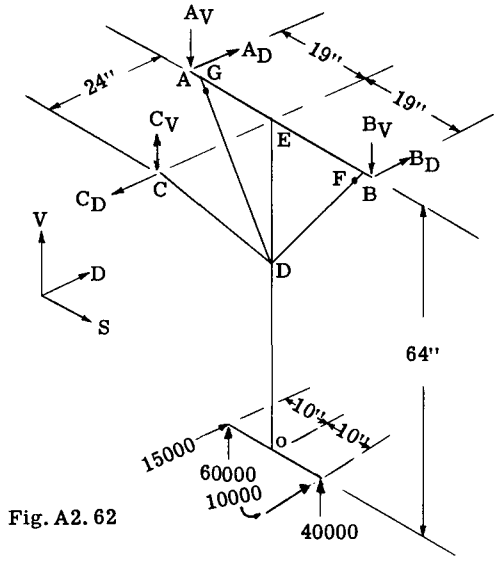

Fig. A2.62

shows a space diagram with loads and reactions. The reactions at A, B and C have been replaced by their V and D components.

To find reaction C_V take moments about an S axis through points AB.

$$\Sigma M_{AB} = -(15000 + 10000)\ 64 + 24\ C_V = 0$$

Whence C_V = 66666 lb. With sense as assumed in Fig. A2.62.

The reaction at C must have a line of action along the line CD since member CD is pinned at each end, thus the drag component and the load in the strut CD follow as a matter of geometry. Hence,

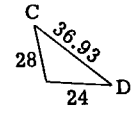

C_D = 66666 (24/28) = 57142 lb.
C_D = 66666 (36.93/28) = 87900 lb. tension

To find B_V take moments about a drag axis through point (A).

$$\Sigma M_{A(D)} = -60000 \times 9 - 40000 \times 29 - 66666 \times 19 + 38\ B_V = 0$$
whence, B_V = 78070 lb.

To find A_V, take $\Sigma V = 0$

$$\Sigma V = -78070 + 60000 + 40000 + 66666 - V_A = 0$$
whence, A_V = 88596 lb.

To find B_D take moments about V axis through point (A).

$$\Sigma M_{A(V)} = 57142 \times 19 - 15000 \times 9 - 10000 \times 29 - 38\ B_D = 0$$
whence, B_D = 17386 lb.

To find A_D take $\Sigma D = 0$

$$\Sigma D = -57142 + 15000 + 10000 + 17386 + A_D = 0$$
whence A_D = 14756 lb.

To check the results take moments about V and D axes through point O.

$$\Sigma M_{O(V)} = 5 \times 10000 + 14756 \times 19 - 17386 \times 19 = 0 \text{ (check)}$$

$$\Sigma M_{O(D)} = 20000 \times 10 - 88596 \times 19 + 78070 \times 19 = 0 \text{ (check)}$$

REACTIONS ON OLEO STRUT OE

Fig. A2.63 shows a free body of the oleostrut OE. The loads applied to the wheels at

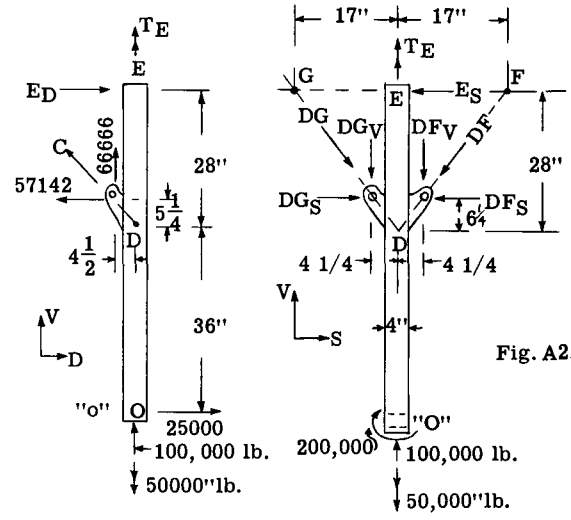

Fig. A2.63

the axle centerlines have been transferred to point (O). Thus the total V load at (O) equals 60000 + 40000 = 100000 and the total D load equals 15000 + 10000 = 25000. The moment of these forces about V and D axes through (O) are $M_{O(V)}$ = (15000 - 10000) 10 = 50000 in.lb. and $M_{O(D)}$ = (60000 - 40000) 10 = 200000 in.lb. These moments are indicated in Fig. A2.63 by the vectors with double arrows. The sense of the moment is determined by the right hand thumb

and finger rule.

The fitting at point E is designed to resist a moment about V axis or a torsional moment on the oleo strut. It also can provide shear reactions E_S and E_D but no bending resistance about S or D axes.

The unknowns are the forces E_S, E_D, DF, DG and the moment T_E.

To find T_E take moments about axis OE.

$\Sigma M_{OE} = -50000 + T_E = 0$, whence $T_E =$ 50000 in.lb.

To find E_S take moments about D axis through point D.

$\Sigma M_{D(D)} = 200000 - 28\ E_S = 0$, whence $E_S = 7143$ lb.

To find force DF_V take moments about D axis through point G.

$\Sigma M_{G(D)} = 200000 - 100000 \times 17 - 66666 \times 17 + 34\ DF_V = 0$

whence, $DF_V = 77451$ lb.

Then $DF_S = 77451\ (17/28) = 47023$ lb.

and $DF = 77451\ (32.72/28) = 90503$ lb.

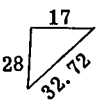

To find DG_V take $\Sigma V = 0$

$\Sigma V = 100000 - 77451 + 66666 - DG_V = 0$, or $DG_V = 89215$

Then, $DG_S = 89215\ (17/28) = 54164$ lb.

$DG = 89215\ (32.73/28) = 104190$ lb.

To find E_D take moments about S axis through point D.

$\Sigma M_{D(S)} = -25000 \times 35 + 28\ E_D = 0$, $E_D = 32143$ lb.

The results will be checked for static equilibrium of strut. Take moments about D axis through point (O).

$\Sigma M_{O(D)} = 200000 + 54164 \times 36 - 47023 \times 36 - 7143 \times 64 = 200000 + 1949904 - 1692828 - 457150 = 0$ (check)

$\Sigma M_{O(S)} = 32143 \times 64 - 57142 \times 36 = 0$ (check)

REACTIONS ON TOP MEMBER AB

Fig. A2.64 shows a free body of member AB with the known applied forces as found from the previous reactions on the oleo strut.

The unknowns are A_D, B_D, A_V and B_V. To find B_V take moments about D axis through A.

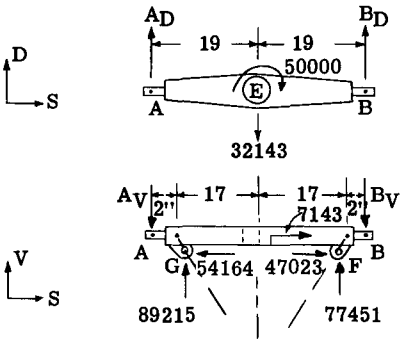

Fig. A2.64

$\Sigma M_{A(D)} = -89215 \times 2 - 77451 \times 36 - 38\ B_V = 0$

whence, $B_V = 78070$ lb.

To find A_V take $\Sigma V = 0$

$\Sigma V = 89215 + 77451 - 78070 - A_V = 0$

whence, $A_V = 88596$ lb.

To find B_D take moments V axis througb A.

$\Sigma M_{V(D)} = 50000 + 32143 \times 19 - 38\ B_D = 0$

whence, $B_D = 17386$ lb.

To find A_D take $\Sigma D = 0$

$\Sigma D = 17386 - 32143 + A_D = 0$, or $A_D =$ 14757 lb.

These four reactions check the reactions obtained originally when gear was treated as a free body, thus giving a numerical check on the calculations.

With the forces on each part of the gear known, the parts could be designed for strength and rigidity. The oleo strut would need a torsion link as discussed in example problem 13 and Fig. A2.60.

A2.15 Problems

(1) For the structures numbered 1 to 10 determine whether structure is statically determinate with respect to external reactions and internal stresses.

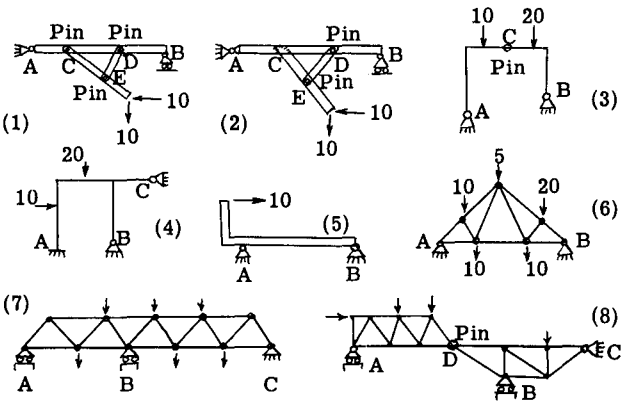

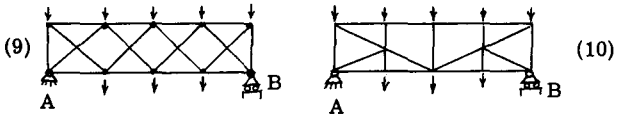

(2) Find the horizontal and vertical components of the reactions on the structures illustrated in Figs. 11 to 15.

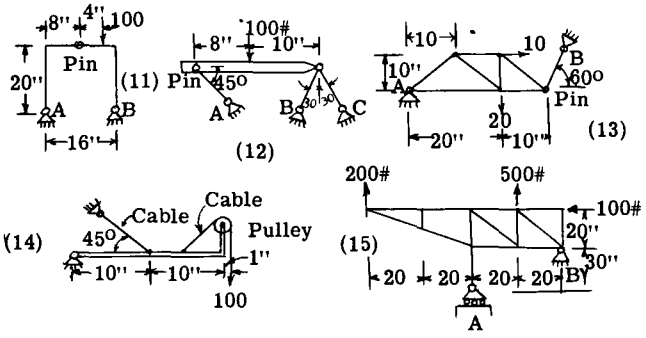

(3) Find the axial loads in the members of the trussed structures shown in Figs. 16 to 18.

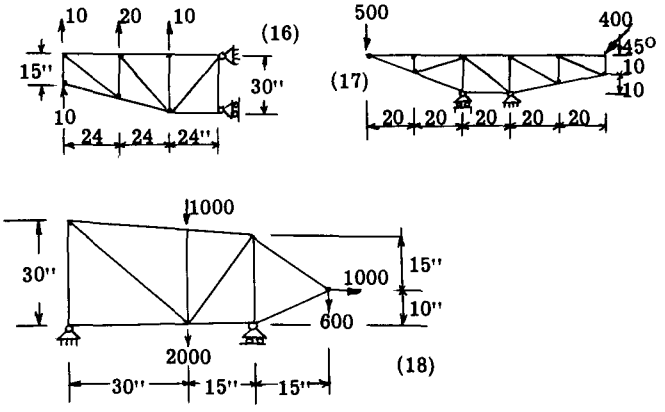

(4) Determine the axial loads in the members of the structure in Fig. 19. The members are pinned to supports at A, B and C.

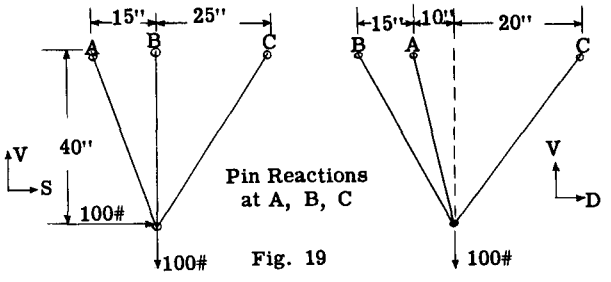

Fig. 19

(5) Fig. 20 shows a tri-pod frame for hoisting a propeller for assembly on engine. Find the loads in the frame for a load of 1000 lb. on hoist.

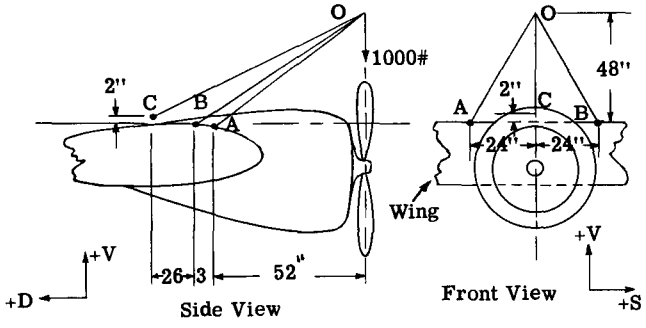

Fig. 20

(6) Fig. 21 shows the wing structure of an externally braced monoplane. Determine the axial loads in all members of the lift and drag trusses for the following loads.

Front beam lift load = 30 lb./in. (upward)
Rear beam lift load = 24 lb./in. (upward)
Wing drag load = 8 lb./in. acting aft

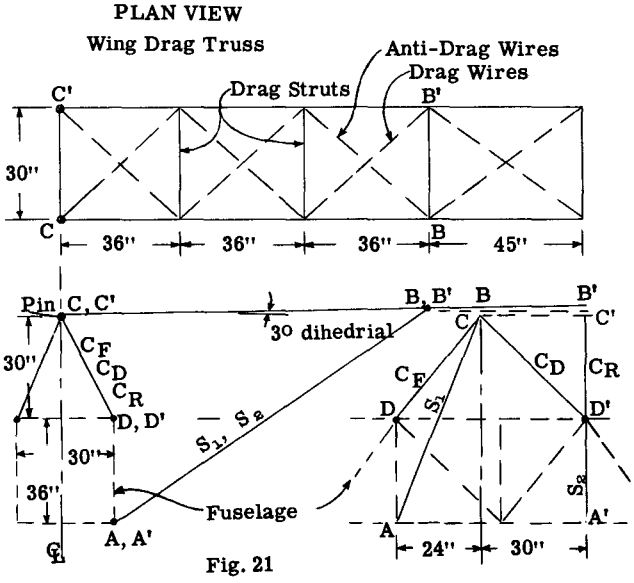

Fig. 21

(7)

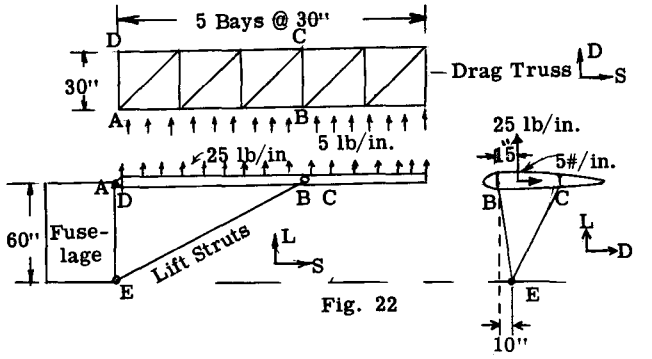

Fig. 22

Fig. 22 shows a braced monoplane wing. For the given air loading, find axial loads in lift and drag truss members. The drag reaction on drag truss is taken off at point A.

(8)

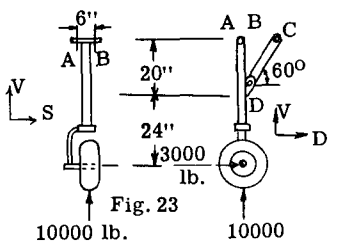

Fig. 23

The fitting at points A and B for the landing gear structure in Fig. 23 provides resistance to V, D and S reactions and moments about D and V axes. Find the reactions at A and B and the load in member CD for given wheel loading.

(9)

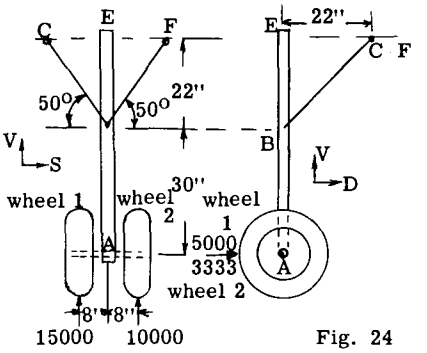

Fig. 24

In the landing gear of Fig. 24, the brace members BC and BF are two force members. The fitting at E provides resistance to V, D and S reactions but only moment resistance about V axis. Find reactions at E and loads in members BF and BC under given wheel loading.

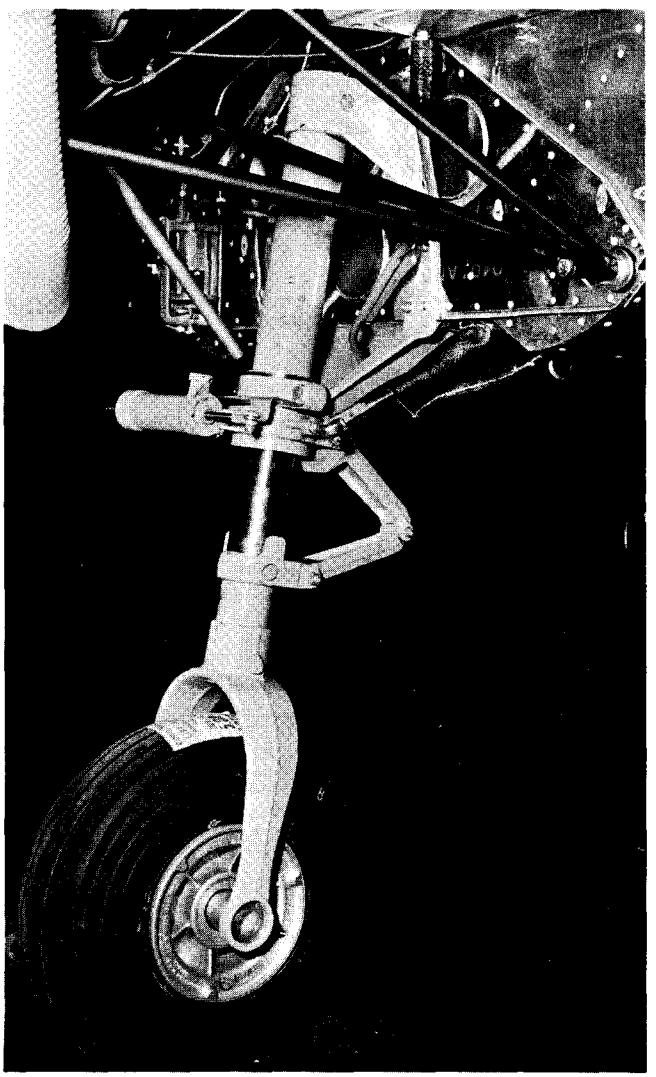

Cessna Aircraft
Nose Wheel Installation (Model 182)

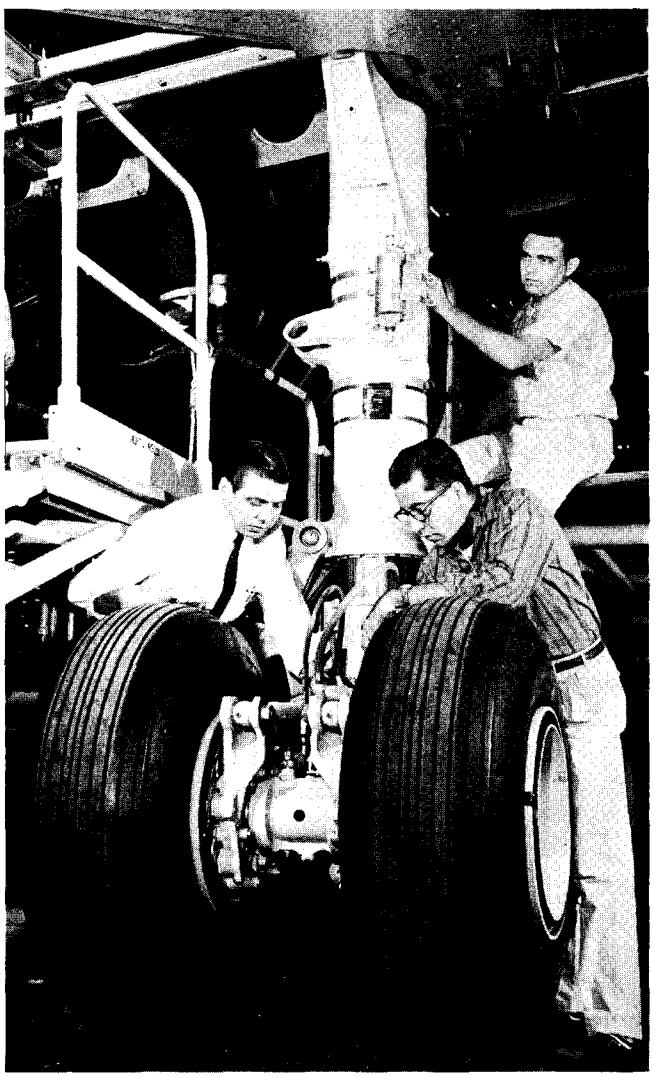

Douglas DC-8 Jet Airliner
Main Landing Gear Unit

CHAPTER A3

PROPERTIES OF SECTIONS - CENTROIDS MOMENTS OF INERTIA ETC.

A3.1 Introduction . In engineering calculations, two terms, center of gravity and moment of inertia, are constantly being used. Thus, a brief review of these terms is in order.

A3.2 Centroids, Center of Gravity. . The centroid of a line, area, volume, or mass is that point at which the whole line, area, volume, or mass may be conceived to be concentrated and have the same moment with respect to an axis as when distributed in its true or natural way. This general relationship can be expressed by the principle of moments, as follows:

Lines:- $\bar{x}L = \Sigma Lx$, hence $\bar{x} = \frac{\Sigma Lx}{L} = \frac{\int x dL}{L}$

Areas:- $\bar{x}A = \Sigma ax$, hence $\bar{x} = \frac{\Sigma ax}{A} = \frac{\int x dA}{A}$

Volumes:- $\bar{x}V = \Sigma Vx$, hence $\bar{x} = \frac{\Sigma Vx}{V} = \frac{\int x dV}{V}$

Masses:- $\bar{x}M = \Sigma xm$, hence $\bar{x} = \frac{\Sigma mx}{M} = \frac{\int x dM}{M}$

If a geometrical figure is symmetrical with respect to a line or plane, the centroid of the figure lies in the given line or plane. This is obvious from the fact that the moments of the parts of the figure on the opposite sides of the line or plane are numerically equal but of opposite sign. If a figure is symmetrical to two lines or planes, the centroid of the figure lies at the intersection of the two lines or the two planes, and likewise, if the figure has 3 planes of symmetry, the centroid lies at the intersection of the 3 planes.

A3.3 Moment of Inertia . The term moment of inertia is applied in mechanics to a number of mathematical expressions which represents second moments of areas, volumes and masses, such as

$\int y^2 dA$, $\int r^2 dV$, $\int r^2 dM$ etc.

A3.4 Moment of Inertia of an Area . As applied to an area, the term moment of inertia has no physical significance, but represents a quantity entering into a large number of engineering problems or calculations. However, it may be considered as a factor which indicates the influence of the area itself in determining the total rotating moment of uniformly varying forces applied over an area.

Let Fig. A3.1 be any plane area referred to three coordinate axes, ox, oy and oz; ox and oy being the plane of area.

Let dA represent an elementary area, with coordinates x, y, and r as shown.

Then

$$I_X = \int y^2 dA,\ I_Y = \int x^2 dA,\ I_Z = \int r^2 dA$$

where I_X, I_Y and I_Z are moments of inertia of the area about the axes xx, yy and zz respectively.

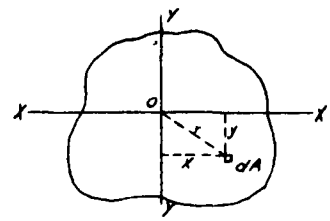

Fig. A3.1

A3.5 Polar Moment of Inertia . In Fig. A3.1, the moment of inertia $I_Z = \int r^2 dA$ about the Z axis is referred to as the polar moment of inertia and can be defined as the moment of inertia of an area with respect to a point in its surface.
Since $r^2 = x^2 + y^2$ (Fig. A3.1)
$I_Z = \int (y^2 + x^2)\, dA = I_X + I_Y$ or; the polar moment of inertia is equal to the sum of the moments of inertia with respect to any two axes in the plane of the area, at right angles to each other and passing thru the point of intersection of the polar axis with the plane.

A3.6 Radius of Gyration . The radius of gyration of a solid is the distance from the inertia axis to that point in the solid at which, if its entire mass could be concentrated, its moment of inertia would remain the same.

Thus, $\int r^2 dM = \rho^2 M$, where ρ is the radius of gyration

Since, $\int r^2 dM = I$, then $I = \rho^2 M$ or $\rho = \sqrt{\frac{I}{M}}$

By analogy, in the case of an area,

$I = \rho^2 A$ or $\rho = \sqrt{\frac{I}{A}}$

A3.7 Parallel Axis Theorem . In Fig. A3.2 let I_y be the moment of inertia of the area referred to the centroidal axis y-y, and let the moment of inertia about axis y_1y_1 be required. y_1y_1 is parallel to yy. Consider the elementary area dA with distance x + d from y_1y_1.

Then, $I_{y_1} = \int (d + x)^2 dA$

$= \int x^2 dA + 2d \int x dA + d^2 \int dA$

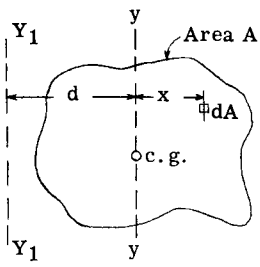

Fig. A3.2

The first term, $\int x^2 dA$, represents the moment of inertia of the body about its centroidal axis y-y and will be given the symbol $\bar{I}$. The second term is zero because $\int x dA$ is zero since yy is the centroidal axis of the body. The last term, $d^2 \int dA = Ad^2$ or, area of body times the square of the distance between axes yy and y_1y_1.

Thus in general,

$I = \bar{I} + Ad^2$

This expression states that the amount of inertia of an area with respect to any axis in the plane of the area is equal to the moment of inertia of the area with respect to a parallel centroidal axis plus the product of the area and the square of the distance between the two axes.

Parallel Axis Theorem For Masses. If instead of area the mass of the body is considered, the parallel axis can be written:

$I = \bar{I} + Md^2$, where M refers to the mass of the body.

A3.7a Mass Moments of Inertia The product of the mass of a particle and the square of its distance from a line or plane is referred to as the moment of inertia of the mass of the particle with respect to the line or plane. Hence,

$I = \Sigma Mr^2$. If the summation can be expressed by a definite integral, the expression may be written $I = \int r^2 dM$

Moments of Inertia of Airplanes. In both flying and landing conditions the airplane may be subjected to angular accelerations. To determine the magnitude of the accelerations as well as the distribution and magnitude of the mass inertia resisting forces, the moment of inertia of the airplane about the three coordinate axes is generally required in making a stress analysis of a particular airplane.

The mass moments of inertia of the airplane about the coordinate X, Y and Z axes through the center of gravity of the airplane can be expressed as follows:

$$I_X = \Sigma wy^2 + \Sigma wz^2 + \Sigma \Delta I_X$$

$$I_Y = \Sigma wx^2 + \Sigma wz^2 + \Sigma \Delta I_Y$$

$$I_Z = \Sigma wx^2 + \Sigma wy^2 + \Sigma \Delta I_Z$$

TABLE 1

Section Properties of Areas

Rectangle 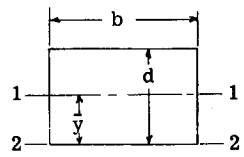	Area = bd $\bar{y} = \frac{d}{2}$ $I_{1-1} = bd^3/12$ $I_{2-2} = \frac{bd^3}{3}$ $\rho_{1-1} = .289\ d$
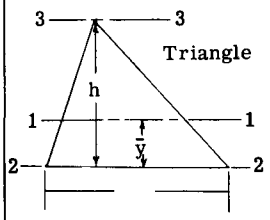	Area = $\frac{bh}{2}$ $\bar{y} = h/3$ $I_{1-1} = \frac{bh^3}{36}$ $I_{2-2} = \frac{bh^3}{12}$ $I_{3-3} = \frac{bh^3}{4}$ $\rho_{1-1} = .236\ h$
Triangle 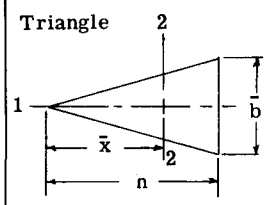	Area = $\frac{bh}{2}$ $\bar{x} = 2/3\ h$ $I_{1-1} = \frac{hb^3}{48}$ $\rho_{1-1} = .204\ h$
Trapezoid 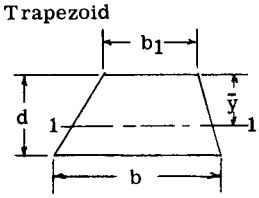	Area = $\frac{d(b + b_1)}{2}$ $\bar{y} = \frac{d(2b + b_1)}{3(b + b_1)}$ $I_{1-1} = d^3 \frac{(b^2 + 4bb_1 + b_1^2)}{36\ (b + b_1)}$
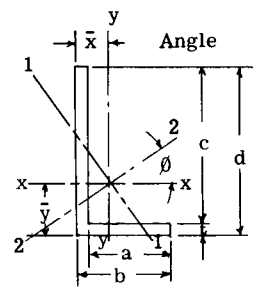	Area = t(b + c) $\bar{x} = \frac{b^2 + ct}{2(b + c)}$ $\bar{y} = \frac{d^2 + at}{2(b + c)}$ $I_X = \frac{1}{3}\left[t(d-y)^3 + by^3 - a(y - t)^3\right]$ $I_Y = \frac{1}{3}\left[t(b - x)^3 + dx^3 - c(x-t)^3\right]$ $\tan 2\emptyset = \frac{2\ I_{XY}}{I_Y - I_X}$, where $I_{XY} = \frac{abcdt}{4(b+c)}$ $I_{1-1} = I_X \sin^2\emptyset + I_Y \cos^2\emptyset + I_{XY} \sin 2\emptyset$ $I_{2-2} = I_X \cos^2\emptyset + I_Y \sin^2\emptyset - I_{XY} \sin 2\emptyset$

TABLE 1 - Continued

Zee

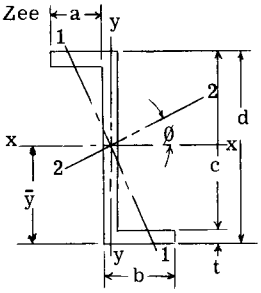

$$\text{Area} = t(d + 2a)$$

$$\bar{y} = d/2$$

$$I_X = \frac{bd^3 - a(d - 2t)^3}{12}$$

$$I_y = d(b + a)^3 - 2a^3c - 6ab^2c$$

$$\tan 2\emptyset = \frac{(dt - t^2)(b^2 - bt)}{I_X - I_y}$$

For I_{1-1} and I_{2-2} see equations as given for angle.

U-section

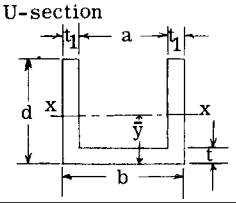

$$\text{Area } A = 2dt_1 + at$$

$$\bar{y} = \frac{d^2t_1 + .5t^2a}{A}$$

$$I_X = \frac{2t_1d^3 + at^3}{3} - A\bar{y}^2$$

Circle

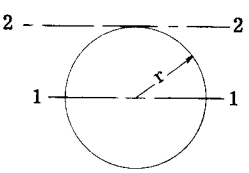

$$\text{Area} = \pi r^2$$

$$I_{1-1} = \frac{\pi r^4}{4}$$

$$I_{2-2} = \frac{5}{4}\pi r^4$$

$$\rho_{1-1} = \frac{r}{2}$$

Ring

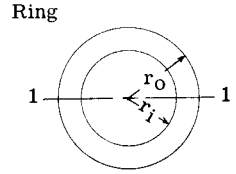

$$\text{Area} = \pi (r_o^2 - r_1^2)$$

$$I_{1-1} = \frac{\pi}{4}(r_o^4 - r_1^4)$$

$$\rho_{1-1} = \sqrt{\frac{r_o^2 + r_1^2}{2}}$$

Semi-circle

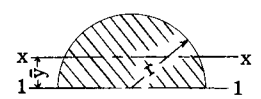

$$\text{Area} = \frac{\pi r^2}{2}$$

$$\bar{y} = .424\ r$$

$$I_X = .1098\ r^4$$

$$\rho_X = .264\ r$$

Semi-circular Ring

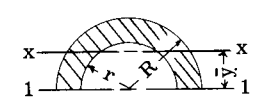

$$\text{Area} = \frac{\pi}{2}(R^2 - r^2)$$

$$y = \frac{4}{3\pi}\frac{(R^2 + Rr + r^2)}{R + r}, \text{approx. } \bar{y} = \frac{2r}{\pi}$$

$$I_X = .1098(R^4 - r^4) - \frac{.283R^2r^2(R - r)}{R + r}$$

$$I_X(\text{approx}) = \frac{.3t(r + R)^3}{2} \text{ when } \frac{t}{r} \text{ is small}$$

Ellipse

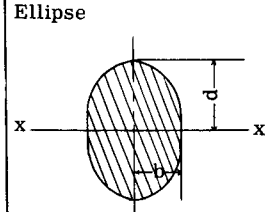

$$\text{Area} = \pi ab$$

$$I_X = \frac{\pi a^3 b}{4}$$

$$\rho_X = \frac{a}{2}$$

Elliptical Ring

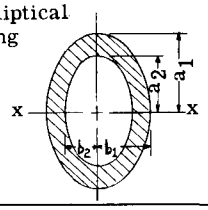

$$\text{Area} = \pi (a_1b_1 - a_2b_2)$$

$$I_X = \frac{\pi}{4}(a_1^3b_1 - a_2^3b_2)$$

$$\rho_X = \sqrt{\frac{I}{\text{Area}}}$$

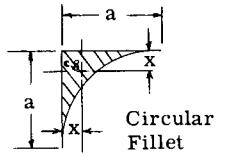

$$\text{Area} = .215\ a^2$$

$$\bar{x} = .223\ a$$

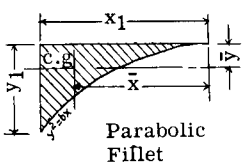

$$\text{Area} = \frac{x_1y_1}{3}$$

$$\bar{x} = \frac{3}{4}x_1$$

$$\bar{y} = .3\ y_1$$

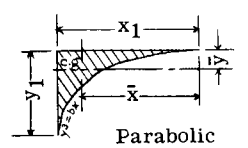

$$\text{Area} = x_1y_1/4$$

$$\bar{x} = \frac{4}{5}x_1$$

$$\bar{y} = \frac{2}{7}y_1$$

TABLE 2

Properties of Solids

Solid Circ. Cyl.

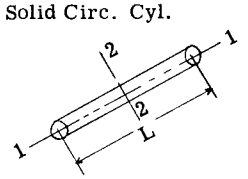

$$\text{Vol.} = \pi r^2L \quad (r = \text{radius})$$

$$M = \frac{W}{g} \quad (\text{Total wt.})$$

$$I_{1-1} = \frac{Mr^2}{2}$$

$$I_{2-2} = M\left[r^2 + (L^2/3)\right]1/4$$

Hollow Circ. Cyl.

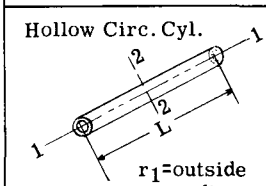

$$\text{Vol.} = \pi L(r_1^2 - r_2^2)$$

$$I_{1-1} = M(r_1^2 + r_2^2)/2$$

$$I_{2-2} = M(r_1^2 + r_2^2 + L^2/3)/4$$

For thin hollow circ. cyl.

$$I_{1-1} = Mr^2$$

Rect. Prism

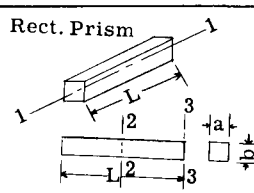

$$\text{Vol.} = abL, \quad M = \frac{W}{g}$$

$$I_{1-1} = M(a^2 + b^2)/12$$

$$I_{2-2} = ML^2/12$$

$$I_{3-3} = ML^2/3$$

Sphere



r_1 = radius of sphere

Solid Sphere

$$\text{Vol.} = (4\pi r^3)/3$$

$$I_{\text{about axis}} = 2Mr^2/5$$

Thin Hollow Sphere

$$\text{Vol.} = \frac{4}{3}\pi(r_1^3 - r_2^3)$$

$$I_{\text{about dia.}} = \frac{2Mr_1^2}{3}$$

TABLE 2 - Continued

Ring with Circular Section

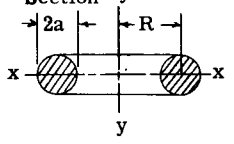

$M = \frac{w}{g}$ = mass per unit volume of body.

$I_{xx} = m\pi^2 Ra^2\left[R^2 + (5a^2/4)\right]$

$I_{yy} = \frac{1}{2} m\pi^2 Ra^2 (4R^2 + 3a^2)$

TABLE 3

Section Properties of Lines
(t is small in comparison to radius)

Circular Arc

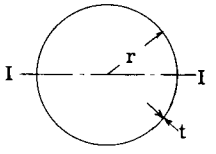

Area = $2\pi rt$

$I_{1-1} = \pi r^3 t$

$I_{polar} = 2\pi r^3 t$

$\rho_x = .707r$

$\rho_{polar} = r$

Semi-circle Arc

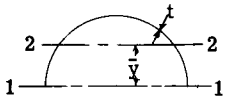

$A = \pi rt$

$\bar{y} = .6366\ r$

$I_{1-1} = \frac{\pi r^3 t}{2}$

$I_{2-2} = .2978\ r^3 t$

Quarter-circular Arc

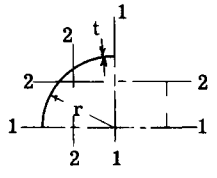

Area = $\frac{\pi rt}{2}$

$\bar{y} = .6366\ r$

$I_{1-1} = \frac{\pi r^3 t}{4}$

$I_{2-2} = .149\ r^3 t$

CIRCULAR ARC

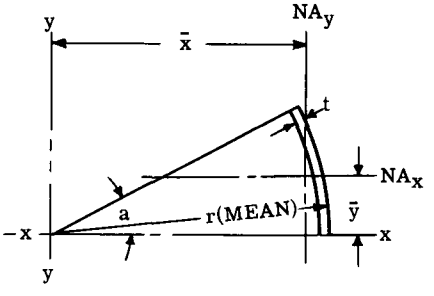

Area = art $\quad$ a in Radians

$\bar{x} = \frac{r \sin a}{a}$, $(M_{yy} = A\bar{x} = r^2 t \sin a)$

$I_{yy} = \frac{r^3 t}{2}\left(a + \frac{\sin 2a}{2}\right)$

$I_{NA_y} = r^3 t\left(\frac{a}{2} + \frac{\sin 2a}{4} - \frac{\sin^2 a}{a}\right)$

$\bar{y} = r\left(\frac{1-\cos a}{a}\right)$, $M_{xx} = A\bar{y} = r^2 t\ (1-\cos a)$

$I_{xx} = \frac{r^3 t}{2}\left(a - \frac{\sin 2a}{2}\right)$

$I_{NA_x} = r^3 t\left(\frac{a}{2} - \frac{\sin 2a}{4} - \frac{(1-\cos a)^2}{a}\right)$

TABLE 4

Centroids of Trapizoidal Areas

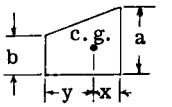

Ratio $\frac{a}{b}$	Distance x	Distance y
1.01	0.4992	0.5008
1.02	0.4984	0.5016
1.03	0.4976	0.5024
1.04	0.4968	0.5032
1.05	0.4960	0.5040
1.06	0.4952	0.5048
1.07	0.4944	0.5056
1.08	0.4936	0.5064
1.09	0.4928	0.5072
1.10	0.4920	0.5080
1.11	0.4912	0.5088
1.12	0.4905	0.5095
1.13	0.4898	0.5102
1.14	0.4890	0.5110
1.15	0.4883	0.5117
1.16	0.4877	0.5123
1.17	0.4870	0.5130
1.18	0.4862	0.5138
1.19	0.4855	0.5145
1.20	0.4849	0.5151
1.22	0.4835	0.5165
1.24	0.4822	0.5178
1.26	0.4809	0.5191
1.28	0.4795	0.5205
1.30	0.4782	0.5218
1.32	0.4770	0.5230
1.34	0.4758	0.5242
1.36	0.4746	0.5254
1.38	0.4733	0.5267
1.40	0.4721	0.5279
1.45	0.4693	0.5307
1.50	0.4667	0.5333
1.55	0.4641	0.5359
1.60	0.4616	0.5384
1.65	0.4592	0.5408
1.70	0.4568	0.5432
1.75	0.4545	0.5455
1.80	0.4523	0.5477
1.85	0.4502	0.5498
1.90	0.4482	0.5518
1.95	0.4462	0.5538
2.00	0.4443	0.5557
2.10	0.4409	0.5591
2.20	0.4375	0.5625
2.30	0.4343	0.5657
2.40	0.4312	0.5688
2.50	0.4284	0.5716
2.60	0.4259	0.5741
2.70	0.4233	0.5767
2.80	0.4209	0.5791
2.90	0.4188	0.5812
3.00	0.4168	0.5832
3.20	0.4128	0.5872
3.40	0.4090	0.5910
3.60	0.4060	0.5940
3.80	0.4030	0.5970
4.00	0.4000	0.6000
4.20	0.3975	0.6025
4.40	0.3950	0.6050
4.60	0.3928	0.6072
4.80	0.3908	0.6092
5.00	0.3889	0.6111
5.50	0.3848	0.6152
6.00	0.3810	0.6190
6.50	0.3778	0.6222
7.00	0.3750	0.6250
7.50	0.3725	0.6275
8.00	0.3702	0.6298
9.00	0.3668	0.6332
10.00	0.3636	0.6364

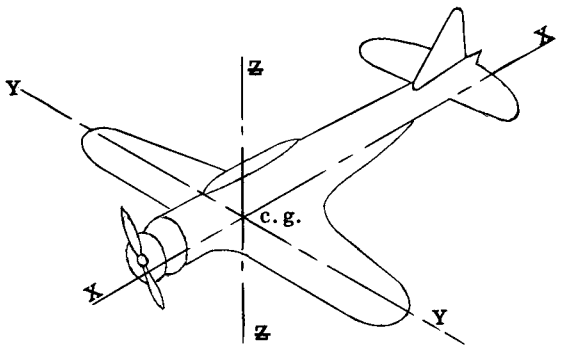

where I_X, I_y, and I_Z are generally referred to as the rolling, pitching and yawing moments of inertia of the airplane.

w = weight of the items in the airplane

x, y and z equal the distances from the axes thru the center of gravity of the airplane and the weights w. The last term in each equation is the summation of the moments of inertia of the various items about their own X, Y and Z centroidal axes.

If w is expressed in pounds and the distances in inches, the moment of inertia is expressed in units of pound-inches squared, which can be converted into slug feet squared by multiplying by 1/32.16 x 144.

Example Problem 1. Determine the gross weight center of gravity of the airplane shown in Fig. A3.3. The airplane weight has been broken down into the 10 items or weight groups, with their individual c.g. locations denoted by the symbol +.

Solution. The airplane center of gravity will be located with respect to two rectangular axes. In this example, a vertical axis thru the centerline of the propeller will be selected as a reference axis for horizontal distances, and the thrust line as a reference axis for vertical distances. The general expressions to be solved are:-

$\bar{x} = \frac{\Sigma wx}{\Sigma w}$ = distance to airplane c.g. from ref. axis Z-Z

$\bar{y} = \frac{\Sigma wy}{\Sigma w}$ = distance to airplane c.g. from ref. axis X-X

Table 4 gives the necessary calculations, whence

$\bar{x} = \frac{417180}{3150} = 133.3$" aft of ℄ propeller

$\bar{y} = \frac{5480}{3150} = -1.74$" (below thrust line)

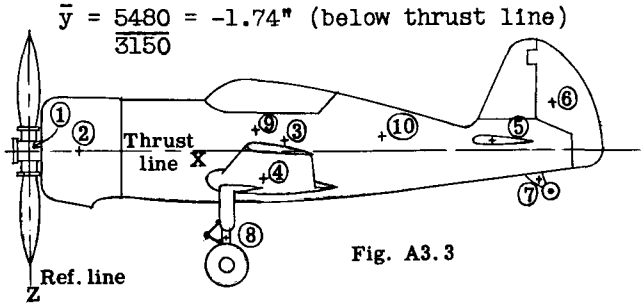

Fig. A3.3

Table 4

Item No.	Name	Weight W#	Horizontal Arm = x	Horizontal Moment = Wx	Vertical Arm = y	Vertical Moment = Wy
1	Propeller	180	0 in.	0	0	0
2	Engine Group	820	46	37720	0	0
3	Fuselage Group	800	182	145600	4	3200
4	Wing Group	600	158	94800	-18	-10800
5	Hori. Tail	60	296	17760	8	480
6	Vert. Tail	40	335	13400	26	1040
7	Tail Wheel	50	328	16400	-20	-1000
8	Front Land. Gear	300	115	34500	-30	- 900
9	Pilot	200	165	33000	10	2000
10	Radio	100	240	24000	5	500
Totals		3150		417180		-5480

Example Problem 2. Determine the moment of inertia about the horizontal centroidal axis for the area shown in Fig. A3.4

Solution. We first find the moment of inertia about a horizontal reference axis. In this solution, this arbitrary axis has been taken as axis x'x' thru the base as shown. Having this moment of inertia, a transfer to the centroidal axis can be made. Table 5 gives the detailed calculations for the moment of inertia about axis x'x'. For simplicity, the cross-section has been divided into the five parts, namely, A, B,C,D, and E.

I_{cx} is moment of inertia about centroidal x axis of the particular part being considered. Distance from axis x'x' to centroidal horizontal axis = $\bar{y} = \frac{\Sigma Av}{\Sigma A} = \frac{17.97}{6.182} = 2.91$"

By parallel axis theorem, we transfer the moment of inertia from axis x'x' to centroidal axis xx.

$I_{xx} = I_{x'x'} - A\bar{y}^2 = 79.47 - 6.18 \times 2.91^2 =$

27.2 in^4

Radius of Gyration, $\rho_{xx} = \sqrt{\frac{I_{xx}}{A}} = \sqrt{\frac{27.2}{6.18}} = 2.1$"

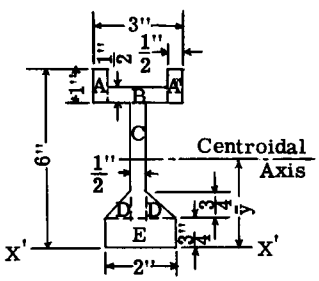

Fig. A3.4

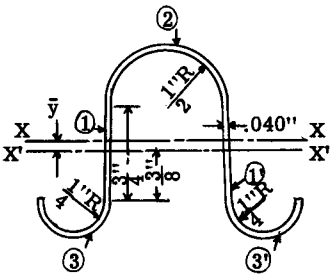

Fig. A3.5

Example Problem #3. Determine the moment of inertia of the stringer cross section shown in Fig. A3.5 about the horizontal centroidal axis.

Solution. A horizontal reference axis x'x' is assumed as shown. The moment of inertia is first calculated about this axis and then transferred to the centroidal axis xx. See Table 6.

Table 5

Portion	Area A	y	Ay	Ay^2	I_{c_x} = moment of inertia of portion about centroidal x axis.	$I_{x'x'} = I_{c_x} + Ay^2$
A	0.50	5.5	2.75	15.13	1/12 x .5 x 1^3 = .04	15.17
A1	0.50	5.5	2.75	15.13	" = .04	15.17
B	1.00	5.25	5.25	27.50	1/12 x 2 x $.5^3$ = .02	27.52
C	2.12	2.875	6.10	17.56	1/12 x .5 x 4.25^3 = 3.19	20.75
D	0.281	1.00	0.28	0.28	bh $^3/36$ = .75 $^4/36$ = 0.01	0.29
D1	0.281	1.00	0.28	0.28	" = 0.01	0.29
E	1.50	0.375	0.56	0.21	1/12 x 2 x $.75^3$ = 0.07	0.28
Sum	6.182		17.97			79.47 in^4

Table 6

Portion	Area	y	Ay	Ay^2	I_{c_x}	$I_{x'x'} = I_{c_x} + Ay^2$
1 + 1'	.06	0	0	0	.00281	.00281
2	.0654	.706	.04617	.0326	.00168	.03428
3 + 3'	.0679	-.547	-.0371	.0203	.000475	.02078
Sum	.1933		.009			.05787

$$\bar{y} = \frac{\Sigma Av}{\Sigma A} = \frac{.009}{.1933} = .0465"$$

$$I_{xx} = I_{x'x'} - A\bar{y}^2 = .05787 - .1933 \times (.0465)^2 = .05745 \text{ in}^4$$

Radius of gyration $\rho_{x-x} = \sqrt{\frac{.05745}{.1933}} = .55"$

Detailed explanation of Table 6:-

Portion 1 + 1'

$$I_{cx} = \frac{1}{12} bd^3 = \left(\frac{.04 \times .\overline{75}^3}{12}\right) \times 2$$

$$= .00281 \text{ in}^4.$$

Portion 2 (ref. table 1)

$$y = .375 + \frac{4}{3\pi} \frac{R^2 + Rr + r^2}{R + r} = .375 + \frac{4}{3\pi} \frac{(.\bar{5}^2 + .5 \times .54 + .54^2)}{(.5 + .54)} = .375 + 331 = .706"$$

By approx. method see Table 1.

$$y = .375 + \frac{2}{\pi} r_1 = .375 + \frac{2}{\pi} \times (.52) = .706"$$

$$I_{cx} = .1098 \times (R^2 + r^2)\, t\, (R + r) - \frac{.283\, R^2 + r^2 t}{R + r}$$

$$= .1098(.2916 + .25) \times .04 \times 1.04 - \frac{.283 \times .2916 \times .25 \times .04}{1.04}$$

$$= .002475 - .000793 = .001682 \text{ in}^4.$$

Approx. $I_{cx} = .3tr_1^3 = .3 \times .04 \times .\overline{52}^3 = .001688 \text{ in}^4.$

Portion 3 + 3' (ref. Table 1)

$$y = .375 + \frac{4}{3\pi} \times \frac{(.0841 + .0725 + .0625)}{.54} = .375 + .172 = .547"$$

approx. $y = .375 + \frac{2}{\pi} r_1 = .375 + .172 = 547"$

$$I_{cx} = \left[.1098(.0841 + .0625) + .04 \times .54 - \frac{.283 \times .0841 \times .0625 \times .04}{.54} \right] = .002375$$

approx. $I_{cx} = .3 \times .04 \times .\overline{27}^3 = .002365 \text{ in}^4$

Problem #4. Determine the moment of inertia of the flywheel in Fig. A3.5a about axis of rotation. The material is aluminum alloy casting (weight = .1 lb. per cu. inch.)

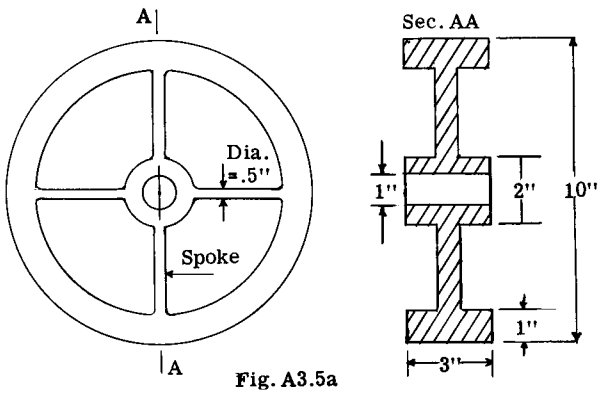

Fig. A3.5a

Solution: The spokes may be treated as slender round rods and the rim and hub as hollow cylinders. (Refer to Table 2)

Rim,

weight $W = \pi(R^2 - r^2) \times 3 \times .1$
$= \pi(5^2 - 4^2) .3 = 8.48$ lb.
$I = .5W(R^2 + r^2) = .5 \times 8.48\ (5^2 + 4^2) = 173.7$ lb. in^2

Hub,

$W = \pi(1^2 - .5^2) \times 3 \times .1 = .707\#$
$I = .5 \times .707\ (1^2 + .5^2) = .44$ lb. in^2

Spokes,

Length of spoke = 3"
Weight of spoke = 3 x $\pi .25^2$ x .1 = .588#
I of one spoke = $WL^2/12 + W\bar{r}^2 = .588 \times 3^2/12 + .588 \times 2.5^2 = 4.10$ lb. in^2
I for 4 spokes = 4 x 4.10 = 16.40

Total I of wheel = 16.40 + .44 + 173.7 = 190.54 lb. in^2

$I = 190.54/32.16 \times 144 = .0411$ slug ft^2

Example Problem #5. Moment of Inertia of an Airplane.

To calculate the moment of inertia of an airplane about the coordinate axes through the gross weight center of gravity, a break down of the airplane weight and its distribution is

necessary, which is available in the weight and balance estimate of the airplane.

Table 6a shows the complete calculation of the moments of inertia of an airplane. This table is reproduced from N.A.O.A. Technical note #575, "Estimation of moments of inertia of airplanes from Design Data."

Explanation of Table

Fig. A3.5b shows the reference of planes and axes which were selected. After the moments of inertia have been determined relative to these axes the values about parallel axes through the center of gravity of the airplane are found by use of the parallel axis theorem.

Column (1) of Table 6a gives breakdown of airplane units or items.
Column (2) gives the weight of each item.
Columns (3), (4) and (5) give the distance of the c.g. of the items from the references planes or axes.
Columns (6) and (7) give the first moments of the item weights about the Y' and X' reference axes.
Columns (8), (9) and (10) give the moment of inertia of the item weights about the reference axes.
Columns (11), (12) and (13) give the moments of inertia of each item about its own centroidal axis parallel to the reference axes. Such items as the fuselage skeleton, wing panels and engine have relatively large values for their centroidal moments of inertia.

The last values in Columns (3) and (5) give the distances from the reference planes to the center of gravity of the airplane.

$$\bar{x}_{c.g.} = \frac{\Sigma wx}{\Sigma w} = \frac{617.024 \text{ (col. 6)}}{5325.3 \text{ (col. 2)}} = 115.9 \text{ in.}$$

$$\bar{z}_{c.g.} = \frac{\Sigma wz}{\Sigma w} = \frac{414.848 \text{ (col. 7)}}{5325.3} = 77.8 \text{ in.}$$

The last values in columns (8), (9) and (10) were obtained by use of the parallel axis theorem, as follows:-

$\Sigma w x^2$ about c.g. of airplane = 97,891,595 - 5325.3 x 115.9^2 = 26,691,595.

$\Sigma wz^2 = 33,252,035 - 5325.3 \times 77.8^2 = 992,035$

The third from the last value in columns (11), (12) and (13) give the moments of inertia of the airplane about the x, y and z axes through the c.g. of airplane. The values are obtained as follows:

$I_y = \Sigma wx^2 + \Sigma wz^2 + \Sigma \Delta I_y = 26,691,595 + 999,035 + 3,120,384 = 30,804,014$ lb. $in.^2$

$I_x = \Sigma wy^2 + \Sigma wz^2 + \Sigma \Delta I_x = 10,287,522 + 992,023 + 2,899,470 = 14,179,027$ lb. $in.^2$

$I_z = \Sigma wy^2 + \Sigma wz^2 + \Sigma \Delta I_z = 10,287,522 + 26,691,595 + 5,157,186 = 42,136,303$ lb. $in.^2$

In order to determine the principal inertia axes, the product of inertia of the weight about the reference axes is necessary. Column (14) gives the values about the reference axes. To transfer the product of inertia to the c.g. axes of the airplane, we make use of the parallel axis theorem. Thus

$\Sigma wxz_{c.g.} = \Sigma wxz_{(Ref.\ axes)} - \Sigma w \bar{x} \bar{z} = 48,857,589 - 5325.3 \times 115.9 \times 77.8 = 839,253$ lb. $in.^2$

To reduce all values to slug $ft.^2$ multiply $\frac{1}{32.17} \times \frac{1}{144}$.

Hence $I_X = 3061$, $I_y = 6680$, $I_Z = 9096$, $I_{XZ} = 181$

Having the inertia properties about the coordinate c.g. axes, the moments of inertia bout the principal axes are determined in a manner as explained for areas. (See A3.13).

The angle $\emptyset$ between the X and Z axes and the principal axes is given by,

$$\tan 2\emptyset = \frac{2I_{XZ}}{I_Z - I_X} = \frac{2 \times 181}{9096-3061} = .05998 \text{ hence } \emptyset = 1^0\ 43''$$

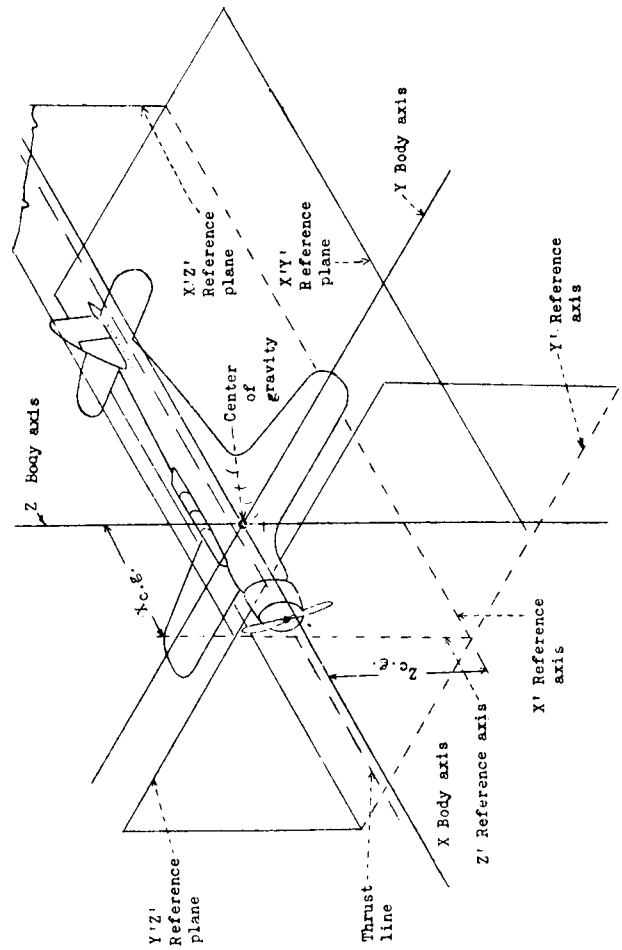

(REF. N.A.C.A. TECH. NOTE No. 575)

Fig. A3.5b

Table 6a

COMPUTATIONS OF MOMENTS OF INERTIA

1.	2.	3.	4.	5.	6.	7.	8.	9.	10.	11.	12.	13.	14.
Item	Weight	x	y	z	wx	wz	wx^2	wy^2	wz^2	ΔI_X	ΔI_Y	ΔI_Z	wxz
Center section nose assembly	108.8	102	-	57	11,098	6,202	1,131,955	-	353,491	261,229	-	261,229	632,563
Center section beam, etc.	204.6	121	-	57	24,757	11,662	2,995,549	-	664,745	491,245	-	491,245	1,411,126
Center section ribs, etc.	84.2	148	-	55	12,462	4,631	1,844,317	-	254,705	202,164	33,680	235,844	685,388
Flap	22.0	180	-	53	3,960	1,166	712,800	-	61,798	48,598	-	48,598	209,880
Outer panel nose	104.6	105	156	65	10,983	6,799	1,153,215	2,545,546	441,935	184,514	-	184,514	713,895
Outer panel beam	155.6	120	156	65	18,672	10,114	2,240,640	3,786,682	657,410	274,478	-	274,478	1,213,680
Outer panel ribs	89.8	139	156	64	12,482	5,747	1,735,026	2,185,373	367,821	158,407	17,601	176,008	798,861
Ailerons	31.4	172	156	62	5,401	1,947	928,938	764,150	120,702	55,390	-	55,390	334,850
Horizontal tail	87.1	367	-	96.7	31,966	8,423	11,731,412	-	814,463	176,378	-	176,378	3,091,083
Vertical tail	31.4	352	-	125	11,053	3,925	3,890,586	-	490,625	110,200	10,174	31	1,381,600
Fuselage skeleton	314.0	176	-	81	55,264	25,434	9,726,464	-	2,060,154	69,394	1,576,594	1,570,000	4,476,384
Engine mount	40.5	60	-	80	2,430	3,240	145,800	-	259,200	5,184	5,184	5,184	194,400
Turtleback (fairing)	48.5	254	-	80	12,319	3,880	3,129,026	-	310,400	15,181	57,861	56,648	985,520
Firewall	11.0	70	-	80	770	880	53,900	-	70,400	2,200	1,100	1,100	61,600
Steps	2.0	170	20	70	340	140	57,800	800	9,800	-	-	-	23,800
N.A.C.A. cowling	70.0	50	-	80	3,500	5,600	175,000	-	448,000	16,940	15,470	15,470	280,000
Cabin and windshield	66.5	146	-	108	9,709	7,182	1,417,514	-	775,656	2,394	106,400	108,794	1,048,572
Foot troughs	2.0	77	5	68	154	136	11,858	50	9,248	-	-	-	10,472
Floor, rear	9.5	210	-	66	1,995	627	418,950	-	41,382	608	1,368	1,976	131,670
Wing fillets	18.5	142	20	58	2,627	1,073	373,034	7,400	62,234	-	18,944	18,944	152,366
Bottom cowling and side frames	27.0	140	11	75	3,780	2,025	529,200	3,267	151,875	-	24,300	24,300	283,500
Arresting door	1.3	284	-	63	369	82	104,853	-	5,160	5	-	5	23,260
Tail-wheel pan, etc.	4.0	365	-	84	1,460	336	532,900	-	28,224	100	-	100	122,640
Side doors	17.0	143	18	82	2,431	1,394	347,633	5,508	114,308	1,088	28,288	27,200	199,342
Baggage door	1.8	165	-	63	297	113	49,005	-	7,144	720	-	720	18,711
Fabric and dope	13.0	254	-	80	3,302	1,040	838,708	-	83,200	4,394	15,509	15,509	264,160
Tail cone	7.5	385	-	91	2,888	683	1,111,688	-	62,108	120	-	120	262,763
Cowling, stations 1-2	12.0	110	-	95	1,320	1,140	145,200	-	108,300	1,200	-	1,200	125,400
Chassis (retracted)	232.4	115	54	51	26,726	11,852	3,073,490	677,678	604,472	-	23,240	23,240	1,363,026
Retracting mechanism	26.6	110	25	67	3,146	1,916	346,060	17,875	128,385	-	-	-	210,782
Wheels, etc.	91.0	141	54	56	12,831	5,096	1,809,171	265,356	285,376	-	-	-	718,536
Tail wheel	26.0	360	-	74	9,360	1,924	3,369,600	-	142,376	26	-	26	692,640
Engine	1049.0	33	-	80	34,617	83,920	1,142,361	-	6,713,600	253,858	253,858	253,858	2,769,360
Engine accessories	90.6	52	-	83	4,711	7,520	244,982	-	624,143	9,060	-	9,060	391,030
Engine controls	11.0	103	10	76	1,133	836	116,699	1,100	63,536	-	-	-	86,108
Propeller	222.0	9.3	-	80	2,065	17,760	19,201	-	1,420,300	177,600	89,300	89,300	165,168
Starting system	37.0	56	-	85	2,072	3,145	116,032	-	267,325	148	333	481	176,120
Lubricating system	26.0	69	-	82	1,794	2,132	123,786	-	174,824	1,274	-	1,274	147,108
Fuel system	82.0	128	-	80	10,496	6,560	1,343,488	-	524,300	22,058	20,008	25,666	839,680
Instruments	38.0	102	-	92	3,876	3,496	395,352	-	321,632	2,432	60,800	63,232	356,592
Surface controls	81.5	160	-	71	13,040	5,787	2,086,400	-	410,842	123,962	130,400	254,362	925,840
Furnishings	160.0	156	-	80	24,960	12,800	3,893,760	-	1,024,000	108,160	400,000	508,160	1,996,800
Electrical equipment	100.7	128	15	81	12,890	8,157	1,649,869	22,658	660,693	-	-	-	1,044,058
Hoist sling	6.0	115	-	102	690	612	79,350	-	62,424	864	-	864	70,380
AIRPLANE EMPTY	3867.4	106.6	0	74.8	412,196	289,138	67,342,573	10,283,443	23,263,736	2,681,572	2,890,404	4,980,508	31,090,714
Pilot	200.0	105	-	90	21,000	18,000	2,205,000	-	1,620,000	33,800	28,800	5,000	1,890,000
Observer	200.0	205	-	89	41,000	17,800	8,405,000	-	1,584,200	33,800	28,800	5,000	3,649,000
Fuel	780.0	132	-	85.5	102,960	66,690	13,590,720	-	5,701,995	141,180	172,380	157,560	8,803,080
Oil	75.0	71	-	85	5,325	6,375	378,075	-	541,875	3,675	-	3,675	452,625
Very Pistol	3.9	195	14	75	761	293	148,298	764	21,938	-	-	-	57,038
Smoke candles	4.0	184	14	96	736	384	135,424	784	36,864	-	-	-	70,656
Float lights	9.0	190	14	72	1,710	648	324,900	1,764	46,656	-	-	-	123,120
Radio	142.7	178	-	85	25,401	12,130	4,521,307	-	1,031,008	5,137	-	5,137	2,159,051
Chart board, etc	3.7	80	3	94	296	348	23,680	33	32,693	-	-	-	27,824
Drift sight	1.6	222	14	84	355	134	78,854	314	11,290	-	-	-	29,837
First aid	4.0	165	10	57	660	228	108,900	400	12,996	-	-	-	37,620
Life raft	34.0	136	-	101	4,624	3,434	628,864	-	346,834	306	-	306	467,024
USEFUL LOAD	1457.9	140.5	0	86.7	204,828	126,464	30,549,022	4,079	10,988,299	217,898	229,980	176,678	17,766,875
TOTALS	5325.3				617,024	414,848	97,891,595	10,287,522	33,252,035	2,899,470	3,120,384	5,157,186	48,857,589
CORRECTION	5325.3	115.9	0	77.8			71,200,000	0	32,260,000				48,018,336
							26,691,595	10,287,522	992,035				839,253
										10,287,522	26,691,595	26,691,595	
										992,035	992,035	10,287,522	
I =										14,179,027	30,804,014	42,136,303	
k^2 =										2,662	5,784	7,912	
k =										51.6	76.1	89	
		$x_{c.g.}$		$z_{c.g.}$			$Wx_{c.g.}{}^2$		$Wz_{c.g.}{}^2$	I_X	I_Y	I_Z	H
													$Wx_{c.g.}z_{c.g.}$

(Table 6a From N.A.C.A. Tech. Note #575)

The principal moments of inertia are given by following equation.

$I_{xp} = I_x \cos^2 \phi + I_z \sin^2 \phi - I_{xz} \sin 2\phi$. (See Art. A3.11)

$I_{yp} = I_y$

$I_z = I_x \sin^2 \phi + I_z \cos^2 \phi + I_{xz} \sin 2\phi$

Substituting

$I_{xp} = 3061 \times (0.9996)^2 + 9096 \times (0.0300)^2 - 181 \times .0599 = 3056$

$I_{zp} = 3061 \times (0.0300)^2 + 9096 \times (0.9996)^2 + 181 \times .0599 = 9102$

$I_{yp} = 6680$

A3.7b Problems

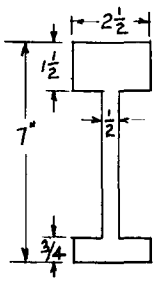

Fig. A3.6

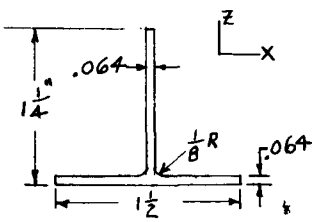

Fig. A3.7

(1) Determine the moment of inertia about the horizontal centroidal axis for the beam section shown in Fig. A3.6.

(2) For the section as shown in Fig. A3.7 calculate the moment of inertia about the centroidal Z and X axes.

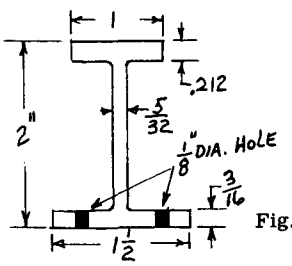

Fig. A3.8

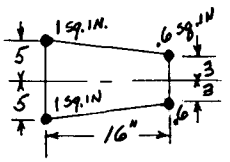

Fig. A3.9

(3) Determine the moment of inertia about the horizontal centroidal axis for the section shown in Fig. A3.8.

(4) In the beam cross-section of Fig. A3.9 assume that the four corner members are the only effective material. Calculate the centroidal moments of inertia about the vertical and horizontal axes.

A3.8 Product of Inertia

In various engineering problems, particularly those involving the calculation of the moments of inertia of unsymmetrical sections, the expression $\int xy\, dA$ is used. This expression is referred to as the product of inertia of the area with respect to the rectangular axes x and y. The term, product of inertia of an area, will be given the symbol I_{xy}, hence

$$I_{xy} = \int xy dA \quad \text{----------(1)}$$

The unit, like that of moment of inertia, is expressed as inches or feet to the 4th power. Since x and y may be either positive or negative, the term I_{xy} may be zero or either positive or negative.

Product of Inertia of a Solid. The product of inertia of a solid is the sum of the products obtained by multiplying the weight of each small portion in which it may be assumed to be divided by the product of its distances from two of the three coordinate planes through a given point.

Thus with respect to planes X and Y

$$I_{xy} = \int xy\, dW$$

$$I_{xz} = \int xz\, dW$$

$$I_{yz} = \int yz\, dW$$

A3.9 Product of Inertia for Axes of Symmetry.

If an area is symmetrical about two rectangular axes, the product of inertia about these axes is zero. This follows from the fact that symmetrical axes are centroidal x and y axes.

If an area is symmetrical about only one of two rectangular axes, the product of inertia, $\int xydA$, is zero because for each product xydA for an element on one side of the axis of symmetry, there is an equal product of opposite sign for the corresponding element dA on the opposite side of the axis, thus making the expression $\int ydA$ equal to zero.

A3.10 Parallel Axis Theorem

The theorem states that, "the product of inertia of an area with respect to any pair of co-planar rectangular axes is equal to the product of inertia of the area with respect to a pair of parallel centroidal axes plus the product of the area and the distances of the centroid of the total area from the given pair of axes". Or, expressed as an equation,

$$I_{xy} = \bar{I}_{xy} + A\bar{x}\bar{y} \quad \text{----------(2)}$$

This equation is readily derivable by referring to Fig. A3.10. $\bar{Y}\bar{Y}$ and $\bar{X}\bar{X}$ are centroidal axes for a given area. YY and XX are parallel axes passing through point O.

The product of inertia about axes YY and XX is $I_{xy} = \int (x + \bar{x})(y + \bar{y})\, dA$

$= \int xydA + \bar{x}\bar{y} \int dA + \bar{x} \int y\, dA + \bar{y} \int xdA$

The last two integrals are each equal to zero, since $\int ydA$ and $\int xdA$ refer to centroidal axes. Hence, $I_{xy} = \int xydA + \bar{x}\bar{y} \int dA$, which can be written in the form of equation (2).

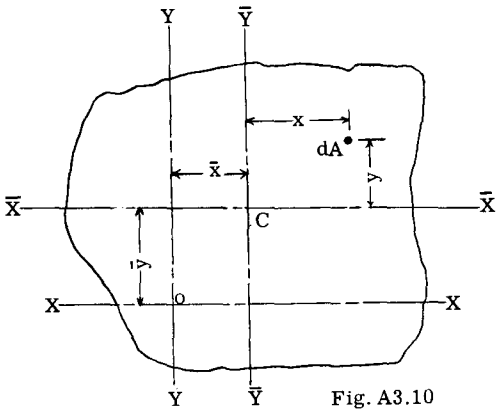

Fig. A3.10

A3.11 Moments of Inertia with Respect of Inclined Axes

Unsymmetrical beam sections are very common in aircraft structure, because the airfoil shape is generally unsymmetrical. Thus, the general procedure with such sections is to first find the moment of inertia about some set of rectangular axes and then transfer to other inclined axes. Thus, in Fig. A3.11 the moment of inertia of the area with respect to axis X_1X_1 is,

$$I_{X_1} = \int y_1^2\, dA = \int (y\cos\phi - x\sin\phi)^2 dA$$

$$= \cos^2\phi \int y^2 dA + \sin^2\phi \int x^2 dA - 2\sin\phi\cos\phi \int xy dA$$

$$= I_X \cos^2\phi + I_y \sin^2\phi - 2 I_{xy} \sin\phi\cos\phi \quad (3)$$

and likewise in a similar manner, the following equation can be derived:

$$I_{y_1} = I_X \sin^2\phi + I_y \cos^2\phi + 2 I_{xy} \sin\phi\cos\phi \quad -(4)$$

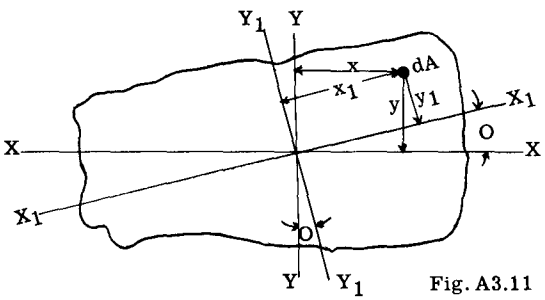

Fig. A3.11

By adding equations (3) and (4), we obtain $I_{X_1} + I_{y_1} = I_X + I_y$ - - - - - - - - - - - - - - - - - - -(5)

or the sum of the moments of inertia of an area with respect to all pairs of rectangular axes, thru a common point of intersection, is constant.

A3.12 Location of Axes for which Product of Inertia is Zero.

In Fig. A3.11

$$I_{X_1 y_1} = \int x_1 y_1\, dA = \int (x\cos\phi + y\sin\phi)(y\cos\phi - x\sin\phi) dA$$

$$= (\cos^2\phi - \sin^2\phi) \int xy dA + \cos\phi\sin\phi \int (y^2 - x^2)\, dA$$

$$= I_{xy} \cos 2\phi + \frac{1}{2} (I_X - I_y) \sin 2\phi$$

Therefore, $I_{X_1 y_1}$ is zero when

$$\tan 2\phi = \frac{2I_{xy}}{I_y - I_X} \quad - - - - - - - - - - - - -(6)$$

A3.13 Principal Axes.

In problems involving unsymmetrical bending, the moment of an area is frequently used with respect to a certain axis called the principal axis. A principal axis of an area is an axis about which the moment of inertia of the area is either greater or less than for any other axis passing thru the centroid of the area.

Axes for which the product of inertia is zero are principal axes.

Since the product of inertia is zero about symmetrical axes, it follows that symmetrical axes are principal axes.

The angle between a set of rectangular centroidal axes and the principal axes is given by equation (6).

Example Problem 4.

Determine the moment of inertia of the angle as shown in Fig. A3.12 about the principal axes passing through the centroid. Solution: Reference axes X and Y are assumed as shown in Fig. A3.12 and the moment of inertia is first calculated about these axes. Table 8 gives the calculations. The angle is divided into the two portions (1) and (2).

Table 8

Part	Area A	x	y	Ay	Ax	Ay^2	Ax^2	Axy	I_{c_x}	I_{c_y}	I_x	I_y
1	.375	.75	.125	.0469	.281	.0058	.211	.0351	$\frac{1}{12} \times 1.5 \left(\frac{1}{4}\right)^3 = .0019$	$\frac{1}{12} \times \frac{1}{4} \times 1.5^3 = .070$	.0077	.281
2	.500	.125	1.25	.625	.0625	.7800	.0078	.0781	$\frac{1}{12} \times \frac{1}{4} \times 2^3 = .167$	$\frac{1}{12} \times 2 \times .25^3 = .0026$	.9470	.010
	.875			.6719	.3435	.7858	.2188	.1132			.9547	.291

*I_{cx} and I_{cy} = moment of inertia of each portion about their own X and Y centroidal axes.

Location of centroidal axes:-

$$\bar{y} = \frac{\Sigma Ay}{\Sigma A} = \frac{.6719}{.875} = .767"$$

$$\bar{x} = \frac{\Sigma Ax}{\Sigma A} = \frac{.3435}{.875} = .392"$$

Transfer moment of inertia and product of inertia from reference X and Y axes to parallel centroidal axes:-

$$\bar{I}_x = I_x - A\bar{y}^2 = .955 - .875 \times .\overline{767}^2 = .440$$

$$\bar{I}_y = I_y - A\bar{x}^2 = .291 - .875 \times .\overline{392}^2 = .157$$

$$\bar{I}_{xy} = \Sigma A_{xy} - A\bar{x}\bar{y} = .1132 - .875 \times .767 \times .392 = -.150$$

Calculate angle between centroidal X and Y axes and principal axes through centroidal as follows:-

$$\tan 2\phi = \frac{2\bar{I}_{xy}}{\bar{I}_y - \bar{I}_x} = \frac{2(-.150}{.157-.440} = \frac{-.30}{-.283} = 1.06$$

$$2\phi = 46^0 - 40' \qquad \phi = 23^0 - 20'$$

Calculate moments of inertia about centroidal principal axes as follows:-

$$\bar{I}_{xp} = \bar{I}_x \cos^2\phi + \bar{I}_y \sin^2\phi - 2\bar{I}_{xy} \sin\phi\cos\phi$$

$$= .44 \times .\overline{918}^2 + .157 \times .\overline{3965}^2 - 2(-.150) \times .3965 \times .918 = .504 \text{ in.}^4$$

$$\bar{I}_{yp} = \bar{I}_x \sin^2\phi + \bar{I}_y \cos^2\phi + 2\bar{I}_{xy} \sin\phi\cos\phi$$

$$= .44 \times .3965 + .157 \times .\overline{918}^2 + 2(-.150) \times .3965 \times .918 = .092 \text{ in.}^4$$

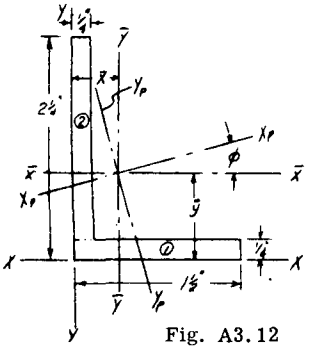

Fig. A3.12

Example Problem 5.

Fig. A3.13 shows a typical distributed flange - 2 cell - wing beam section. The upper and lower surface is stiffened by Z and bulb angle sections. Determine the moment of inertia of the section about the principal axes.

Solution:

The properties of the cross-section depend upon the effective material which can develop resisting axial stresses. The question of effective material is taken up in later chapter. Table 9 shows the calculations for the moment of inertia about the assumed rectangular reference axes XX and YY (see Fig. A3.13). The cross-section has been broken down into 16 stringers as listed in column 1. For the top surface, a width of 30 thicknesses of the .032 skin is assumed to act with the stringers and a width of 25 thicknesses of the .04 skin (see Col. 3). On the lower surface, the skin half way to adjacent stringers is assumed acting with each stringer, or the entire skin is effective. Column 4 gives the combined area of each stringer unit and is considered as concentrated at the centroid of the stringer and effective skin. All distances, x and y, columns 5 and 8, have been scaled from a large drawing.

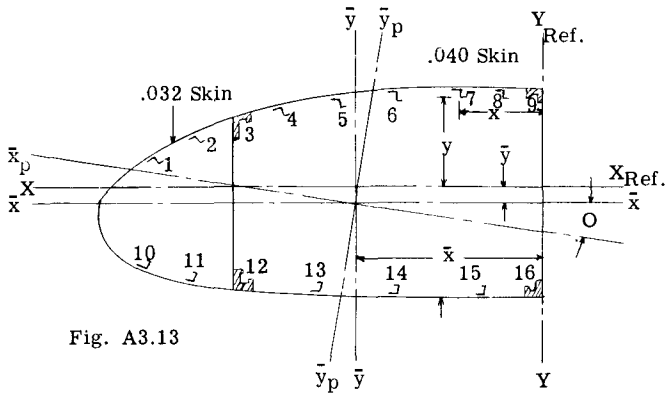

Fig. A3.13

Table 9

1	2	3	4	5	6	7	8	9	10	11
Portion	Stringer Area	Effective Skin	Total Area A	y	Ay	Ay^2	x	Ax	Ax^2	Ixy =Axy
1	.11	.03	.14	4.00	0.560	2.240	-33.15	-4.641	153.85	-18.56
2	.11	.03	.14	6.05	0.847	5.124	-29.28	-4.099	120.02	-24.80
3	.30	.08	.38	7.00	2.660	18.620	-24.85	-9.443	234.66	-66.10
4	.13	.04	.17	7.37	1.253	9.234	-21.18	-3.600	76.25	-26.53
5	.13	.04	.17	7.55	1.288	9.687	-16.60	-2.822	46.84	-21.31
6	.13	.04	.17	7.50	1.275	9.563	-12.60	-2.142	26.99	-16.06
7	.13	.04	.17	7.30	1.241	9.059	- 8.60	-1.462	12.57	-10.67
8	.13	.04	.17	6.90	1.171	8.080	- 4.00	-0.680	2.72	- 4.69
9	.24	.05	.29	6.50	1.885	12.252	- 0.35	-0.100	0.04	-00.65
10	.07	.10	.17	-3.30	-0.561	1.851	-33.25	-5.653	187.96	18.65
11	.07	.10	.17	-4.90	-0.833	4.082	-29.28	-4.978	145.76	24.39
12	.13	.15	.28	-5.95	-1.666	9.913	-24.85	-6.958	172.90	41.40
13	.11	.20	.31	-7.40	-2.294	16.976	-18.70	-5.797	108.40	42.90
14	.11	.20	.31	-8.13	-2.520	20.487	-12.42	-2.850	47.82	31.30
15	.11	.20	.31	-8.62	-2.672	22.432	- 6.10	-1.891	11.54	16.30
16	.24	.11	.35	-8.87	-3.094	27.444	-00.35	-0.122	0.04	1.08
Totals			3.70		-1.465	187.04		-58.238	1348.36	-13.35

Location of centroidal axes with respect to ref. axes, -

$$\bar{y} = \frac{\Sigma Ay}{\Sigma A} = -\frac{1.465}{3.70} = -.396"$$

$$\bar{x} = \frac{\Sigma Ax}{\Sigma A} = -\frac{58.238}{3.70} = -15.74"$$

$$\bar{I}_x = 187.04 - 3.70 \times .\overline{396}^2 = 186.5 \text{ in.}^4$$

$$\bar{I}_y = 1348.36 - 3.70 \times \overline{15.74}^2 = .431.7 \text{ in.}^4$$

$$\bar{I}_{xy} = -13.35 - (3.70 \times .396 \times 15.74) = 36.41 \text{ in.}^4$$

$$\tan 2\phi = \frac{2\bar{I}_{xy}}{\bar{I}_y - \bar{I}_x} = \frac{2(-36.41)}{431.7-186.5} = -.29696$$

$$2\phi = 16^0 - 32.5', \quad \phi = 8^0 - 16.25'$$

$$\bar{I}_{xp} = \bar{I}_x \cos^2\phi + \bar{I}_y \sin^2\phi - 2\bar{I}_{xy} \sin\phi\cos\phi$$

$$= 186.46 \times .9896^2 + 431.7 \times .1438^2 - 2[-36.41 \times .9896 \times (-.1438)] = 181.2 \text{ in.}^4$$

$$\bar{I}_{yp} = \bar{I}_x \sin^2 \phi + \bar{I}_y \cos^2 \phi + 2\ \bar{I}_{xy} \sin \phi \cos \phi = 186.46 \times .14382^2 + 431.7 \times .9896^2 + 2\ -36.41 \times .9896 \times (-.1438) = 437\ \text{in.}^4$$

A3.14 Section Properties of Typical Aircraft Structural Sections.

Table A3.10 through A3.15 and Chart A3.1 give the section properties of a few structural shapes common to aircraft. Use of these tables will be made in later chapters of this book.

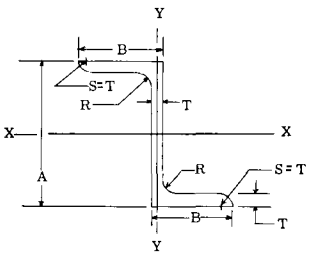

Table A3.10
Properties of
Zee Sections

SECT. NO.	NOMINAL DIMENSIONS A (Inches)	B (Inches)	T (Inches)	R (Inches)	AREA (Square Inches)	SECTION ELEMENTS Ixx ($Inches^4$)	Iyy ($Inches^4$)	ρ_{xx} (Inches)	ρ_{yy} (Inches)
1	.500	.625	.050	.094	.0852	.0035	.0068	.203	.283
2			.063	.125	.1073	.0042	.0082	.197	.277
3		.750	.050	.094	.0977	.0042	.0122	.206	.353
4			.063	.125	.1231	.0049	.0148	.200	.346
5	.625	.625	.050	.094	.0916	.0060	.0069	.255	.274
6			.063	.125	.115	.0071	.0083	.248	.268
7		.750	.050	.094	.104	.0070	.0122	.259	.342
8			.063	.125	.131	.0084	.0148	.253	.336
9		1.000	.063	.125	.163	.0109	.0367	.259	.475
10	.750	.625	.050	.094	.0977	.0090	.0068	.304	.264
11			.063	.125	.123	.0110	.0082	.298	.259
12		.750	.050	.094	.110	.0106	.0122	.310	.333
13			.063	.125	.139	.0128	.0148	.304	.326
14		1.000	.063	.125	.170	.0165	.0367	.312	.464
15	.875	.625	.050	.094	.104	.0130	.0068	.353	.257
16			.063	.125	.131	.0158	.0083	.347	.251
17		.750	.050	.094	.117	.0151	.0122	.360	.323
18			.063	.125	.147	.0184	.0148	.354	.317
19			.078	.125	.177	.0214	.0175	.348	.314
20		.875	.050	.094	.129	.0172	.0197	.365	.391
21			.063	.125	.163	.0210	.0241	.359	.385
22			.078		.197	.0245	.0287	.353	.382
23		1.000	.063		.178	.0236	.0367	.364	.454
24			.078		.216	.0276	.0439	.358	.451
25	1.000	.625	.050	.094	.110	.0176	.0068	.400	.249
26			.063	.125	.139	.0216	.0083	.394	.244
27		.750	.050	.094	.123	.0205	.0121	.408	.315
28			.063		.155	.0251	.0147	.403	.308
29			.078		.187	.0294	.0175	.396	.307
30		.875	.063		.170	.0285	.0242	.409	.377
31			.078	.125	.206	.0335	.0287	.403	.373
32			.094		.244	.0383	.0332	.397	.369
33		1.000	.063		.186	.0320	.0367	.415	.444
34			.078		.226	.0377	.0439	.408	.441
35	1.125	.625	.063	.125	.147	.0285	.0083	.441	.237
36		.875	.050	.094	.142	.0304	.0197	.464	.374
37			.063		.178	.0374	.0241	.458	.368
38			.078		.216	.0441	.0287	.452	.364
39			.094	.125	.256	.0507	.0332	.445	.361
40		1.125	.063		.210	.0467	.0530	.472	.503
41			.078		.255	.0548	.0637	.464	.500
42			.094		.303	.0632	.0744	.457	.496
43	1.250	.750	.063		.170	.0421	.0148	.497	.295
44			.078		.206	.0497	.0175	.491	.291
45		1.000	.063	.125	.202	.0532	.0366	.514	.428
46			.094		.291	.0729	.0511	.501	.419
47		1.250	.078		.294	.0765	.0887	.519	.558
48			.094		.338	.0886	.1039	.512	.555
49	1.375	.750	.063		.178	.0562	.0148	.543	.288
50			.063		.210	.0662	.0367	.562	.418
51		1.000	.078		.255	.0794	.0439	.558	.415
52			.094	.125	.303	.0911	.0511	.549	.411
53		1.250	.078		.294	.0951	.0887	.569	.549
54			.125		.453	.1365	.1308	.549	.537
55	1.500	.750	.078		.226	.0765	.0175	.582	.278
56		1.000	.078	.125	.265	.0961	.0439	.602	.407
57			.094		.314	.1116	.0511	.596	.403
58		1.250	.094		.361	.1349	.1040	.611	.536
59	1.750	.750	.078		.245	.1104	.0175	.671	.267
60		1.000	.078	.125	.284	.1377	.0439	.696	.393
61		1.250	.094		.385	.1925	.1039	.707	.520
62	2.000	.750	.063		.218	.1272	.0148	.765	.261
63		1.000	.094	.125	.361	.2194	.0511	.779	.376
64		1.250	.094		.408	.2621	.1040	.801	.505
65		1.500	.125		.594	.3852	.2346	.806	.629
66	2.500	.750	.063		.249	.2172	.0148	.934	.244
67		.875	.078		.323	.2890	.0288	.945	.298
68			.094	.125	.385	.3383	.0333	.938	.294
69		1.000	.094		.408	.3723	.0512	.955	.354
70			.125		.531	.4707	.0636	.941	.346

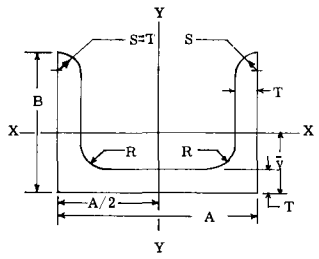

Table A3.11
Properties of
Channel Sections

SECT. NO.	NOMINAL DIMENSIONS A (Inches)	B (Inches)	T (Inches)	R (Inches)	AREA (Square Inches)	SECTION ELEMENTS ȳ (Inch)	Ixx ($Inches^4$)	Iyy ($Inches^4$)	ρ_{xx} (Inches)	ρ_{yy} (Inches)
1	.750	.375	.050	.094	.0727	.106	.0009	.0060	.111	.286
2		.500	.050		.0852	.153	.0020	.0075	.152	.296
3		.625	.050		.0977	.204	.0037	.0090	.195	.304
4			.063		.123	.207	.0045	.0109	.190	.298
5		.875	.063	.125	.155	.315	.0117	.0147	.275	.308
6			.094		.220	.327	.0159	.0193	.269	.296
7	.875	.375	.050		.0790	.0995	.0009	.0087	.106	.332
8		.500	.050	.094	.0916	.146	.0020	.0110	.148	.347
9			.063		.115	.148	.0025	.0132	.144	.339
10		.625	.063	.125	.131	.196	.0047	.0158	.190	.347
11			.078		.158	.201	.0055	.0183	.187	.341
12		.750	.050	.094	.117	.245	.0065	.0151	.237	.360
13			.063		.147	.247	.0079	.0184	.233	.354
14			.078	.125	.177	.253	.0094	.0214	.230	.348
15		1.000	.078		.216	.362	.0213	.0276	.314	.358
16			.125		.328	.379	.0304	.0378	.304	.339
17	1.000	.500	.063		.123	.140	.0026	.0181	.144	.384
18			.078		.148	.145	.0029	.0211	.141	.377
19		.625	.063		.139	.187	.0049	.0216	.187	.394
20			.078		.168	.193	.0058	.0252	.186	.388
21		.750	.063		.155	.229	.0083	.0250	.231	.402
22			.078		.187	.242	.0098	.0294	.229	.393
23			.094	.125	.220	.248	.0113	.0335	.226	.390
24		.875	.063		.170	.289	.0128	.0285	.275	.409
25			.078		.206	.294	.0152	.0335	.271	.403
26			.094		.244	.300	.0176	.0383	.269	.397
27		1.250	.078		.265	.460	.0417	.0460	.397	.417
28			.125		.406	.478	.0607	.0643	.387	.398
29	1.125	.500	.063		.131	.134	.0027	.0241	.143	.429
30			.078		.158	.139	.0031	.0281	.140	.422
31		.625	.063	.125	.147	.178	.0051	.0285	.186	.441
32			.078		.177	.184	.0060	.0334	.184	.434
33		.750	.078		.197	.232	.0102	.0388	.228	.444
34			.094		.232	.237	.0117	.0444	.225	.438
35		.875	.063		.181	.278	.0135	.0379	.274	.458
36			.078		.216	.283	.0158	.0441	.271	.452
37			.094		.256	.289	.0183	.0507	.268	.445
38	1.125		.125	.125	.328	.298	.0225	.0616	.262	.433
39		1.000	.078		.236	.336	.0232	.0495	.314	.458
40			.094		.279	.341	.0269	.0569	.310	.452
41			.125		.359	.352	.0331	.0695	.303	.440
42		1.375	.094		.350	.508	.0661	.0757	.435	.466
43			.125		.453	.519	.0832	.0930	.428	.453
44	1,250	.625	.094		.220	.181	.0071	.0493	.179	.473
45		.875	.094		.267	.278	.0190	.0650	.267	.493
46			.125		.344	.288	.0234	.0796	.261	.481
47		1.125	.078	.125	.265	.377	.0334	.0698	.355	.513
48			.094		.314	.383	.0389	.0807	.352	.507
49			.125		.406	.393	.0484	.0994	.345	.495
50		1.500	.125		.500	.560	.1106	.1292	.470	.508
51	1.375	.625	.078		.197	.169	.0063	.0540	.179	.524
52			.094		.232	.175	.0073	.0621	.177	.517
53		.875	.078		.236	.263	.0169	.0705	.268	.547
54			.094		.279	.268	.0198	.0818	.266	.543
55			.125	.125	.359	.278	.0242	.1002	.259	.528
56		1.125	.094		.326	.371	.0403	.1010	.352	.557
57			.125		.422	.381	.0504	.1246	.346	.544
58			.156		.513	.390	.0591	.1451	.339	.532
59		1.625	.156		.668	.612	.1710	.2035	.506	.552
60	1.500	.625	.094		.244	.168	.0076	.0768	.177	.561
61			.125		.313	.178	.0090	.0939	.170	.548
62		.875	.125	.125	.375	.269	.0249	.1236	.258	.574
63			.156		.455	.278	.0289	.1485	.267	.572
64		1.125	.094		.338	.360	.0414	.1233	.350	.604

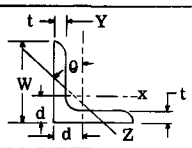

Table A3. 12

Properties of Extruded Aluminum Alloy Equal Leg Angles. (Ref. 1938 Alcoa Handbook)

Dimensions			Area	Axis XX or YY			Axis ZZ		
W	t	R	sq. in.	I	ρ	d	I	ρ	θ
5/8	3/32	1/8	.111	0.004	0.183	0.187	.0015	0.117	45°
3/4	1/16	1/8	.089	0.004	0.220	0.199	.0018	0.142	45°
3/4	3/32	1/8	.132	0.006	0.219	0.214	.0026	0.141	45°
3/4	1/8	1/8	.171	0.008	0.217	0.227	.0034	0.141	45°
1	1/16	1/16	.122	0.012	0.311	0.271	.0048	0.199	45°
1	3/32	1/8	.178	0.016	0.301	0.276	.0066	0.193	45°
1	1/8	1/8	.234	0.021	0.298	0.290	.0085	0.191	45°
1	3/16	1/8	.339	0.029	0.293	0.314	.0124	0.192	45°
1-1/4	3/32	3/32	.230	0.033	0.38	0.34	.014	0.24	45°
1-1/4	1/8	3/16	.30	0.042	0.37	0.35	.017	0.24	45°
1-1/4	3/16	3/16	.43	0.059	0.37	0.37	.025	0.24	45°
1-1/4	1/4	3/16	.56	0.074	0.36	0.40	.032	0.24	45°
1-1/2	3/32	3/16	.28	0.058	0.46	0.40	.024	0.30	45°
1-1/2	1/8	3/16	.36	0.074	0.45	0.41	.031	0.29	45°
1-1/2	3/16	3/16	.53	0.107	0.45	0.44	.044	0.29	45°
1-1/2	1/4	3/16	.69	0.135	0.44	0.46	.057	0.29	45°
1-3/4	3/32	3/32	.32	0.096	0.55	0.47	.039	0.35	45°
1-3/4	1/8	3/16	.42	0.121	0.53	0.47	.050	0.34	45°
1-3/4	3/16	3/16	.62	0.174	0.53	0.50	.072	0.34	45°
1-3/4	1/4	3/16	.81	0.223	0.52	0.52	.093	0.34	45°
2	1/8	1/4	.49	0.18	0.61	0.53	.08	0.40	45°
2	3/16	1/4	.72	0.27	0.61	0.56	.11	0.39	45°
2	1/4	1/4	.94	0.34	0.60	0.58	.14	0.39	45°
2	5/16	1/4	1.16	0.41	0.60	0.61	.17	0.39	45°

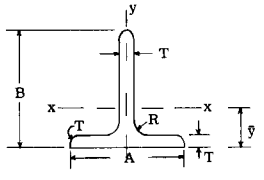

Table A3. 13
Properties of Tee-Sections

SECT. NO.	NOMINAL DIMENSIONS				AREA	SECTION ELEMENTS				
	A	B	T	R		ȳ	Ixx	Iyy	ρ xx	ρ yy
	Inches				Square Inches	Inch	Inches⁴		Inches	
1	1.250	.625	.050	.094	.094	.121	.0028	.0077	.173	.287
2		.750	.063	.125	.127	.160	.0055	.0098	.209	.276
3		.750	.050	.094	.106	.148	.0046	.0103	.209	.312
4	1.375	1.000	.063		.150	.228	.0131	.0129	.296	.293
5		1.000	.078	.125	.183	.235	.0156	.0158	.292	.294
6		1.000	.094		.216	.242	.0182	.0188	.290	.295
7		1.250	.094		.240	.327	.0345	.0188	.379	.280
8	1.500	.750	.063		.141	.141	.0052	.0169	.192	.346
9		.750	.094		.204	.159	.0080	.0244	.198	.346
10		1.000	.078		.193	.225	.0160	.0200	.288	.327
11		1.000	.094	.125	.228	.232	.0186	.0245	.286	.328
12		1.250	.078		.212	.307	.0301	.0206	.377	.312
13		1.250	.094		.252	.314	.0354	.0245	.375	.312
14		1.250	.125		.326	.327	.0449	.0319	.371	.313
15	1.625	.875	.078		.192	.180	.0110	.0263	.240	.370
16		.875	.125		.295	.198	.0161	.0407	.234	.372
17		1.125	.078		.212	.254	.0228	.0263	.328	.352
18		1.125	.125	.125	.326	.274	.0339	.0408	.322	.364
19		1.375	.094		.275	.345	.0475	.0314	.415	.338
20		1.375	.125		.358	.358	.0605	.0408	.411	.338
21		1.375	.156		.437	.370	.0725	.0499	.407	.338
22	1.750	.875	.094		.240	.179	.0131	.0393	.234	.405
23		.875	.125		.311	.191	.0164	.0512	.230	.406
24		1.125	.094		.263	.252	.0273	.0393	.322	.386
25		1.125	.156		.418	.276	.0412	.0628	.314	.387
26		1.375	.094	.125	.287	.333	.0484	.0393	.411	.370
27		1.375	.156		.457	.358	.0741	.0627	.403	.371
28		1.625	.094		.310	.420	.0777	.0394	.500	.356
29		1.625	.125		.405	.434	.0995	.0513	.496	.356
30		1.625	.156		.497	.446	.1200	.0629	.492	.356

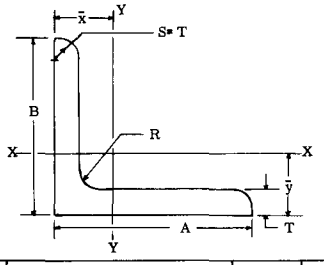

Table A3. 14
Properties of Unequal Angles

SECT. NO.	NOMINAL DIMENSIONS				AREA	SECTION ELEMENTS					
	A	B	T	R		ȳ	x̄	Ixx	Iyy	ρ xx	ρ yy
	Inches				Square Inches	Inch		Inches⁴		Inch	
1	.625	.500	.050	.063	.0535	.126	.187	.0011	.0020	.146	.193
2	.750	.500	.063	.063	.0739	.120	.243	.0014	.0041	.139	.235
3		.625	.063		.0818	.162	.222	.0027	.0044	.181	.232
4	.875	.625	.063	.125	.0922	.150	.269	.0029	.0069	.177	.274
5		.750	.063		.100	.190	.250	.0049	.0073	.221	.270
6			.125		.184	.211	.272	.0082	.0123	.211	.258
7	1.000	.625	.063	.125	.100	.140	.320	.0029	.0100	.170	.316
8			.125		.184	.160	.344	.0050	.0170	.165	.304
9		.750	.063		.108	.178	.299	.0051	.0106	.217	.313
10			.125		.200	.199	.322	.0086	.0182	.208	.302
11		.875	.063		.116	.220	.281	.0079	.0111	.262	.310
12			.094		.167	.231	.292	.0110	.0155	.257	.305
13	1.250	.750	.063	.125	.124	.159	.403	.0054	.0197	.209	.400
14			.094		.179	.170	.416	.0074	.0276	.203	.393
15			.125		.231	.181	.427	.0092	.0346	.200	.387
16		1.000	.063		.139	.239	.361	.0124	.0217	.298	.394
17			.094		.202	.250	.373	.0171	.0306	.291	.389
18			.125		.262	.260	.384	.0215	.0383	.286	.382
19	1.500	.750	.094	.156	.204	.156	.522	.0077	.0463	.194	.476
20			.125		.264	.167	.534	.0096	.0584	.191	.465
21		1.000	.094		.228	.228	.472	.0182	.0512	.282	.474
22			.125		.295	.239	.485	.0226	.0647	.276	.468
23			.156		.361	.249	.495	.0265	.0772	.271	.463
24		1.250	.094		.251	.310	.433	.0347	.0550	.372	.468
25			.125		.327	.321	.444	.0436	.0698	.365	.462
26			.156		.400	.331	.455	.0518	.0834	.360	.457
27	1.750	1.000	.125	.156	.327	.222	.591	.0236	.0998	.269	.553
28		1.250	.125		.358	.300	.545	.0465	.1078	.360	.549
29			.125		.389	.383	.506	.0776	.1144	.447	.542
30		1.500	.156		.478	.393	.517	.0928	.1377	.441	.537

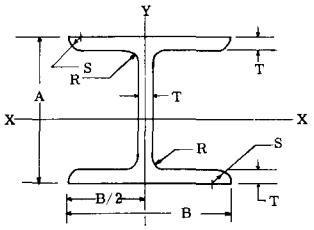

Table A3. 15
Properties of I-Sections

SECT. NO.	NOMINAL DIMENSIONS				AREA	SECTION ELEMENTS			
	A	B	T	R		Ixx	Iyy	ρ xx	ρ yy
	Inches				Square Inches	Inches⁴		Inches	
1	.750	1.250	.063	.125	.207	.0206	.0193	.316	.306
2			.078		.250	.0239	.0235	.310	.307
3		1.500	.078		.289	.0284	.0411	.314	.378
4	.875	1.375	.078	.125	.279	.0373	.0315	.366	.336
5			.094		.329	.0425	.0375	.359	.338
6		1.625	.094		.376	.0497	.0626	.364	.408
7	1.000	1.375	.094	.125	.341	.0580	.0375	.413	.332
8		1.625	.094		.388	.0676	.0626	.418	.402
9		1.750	.094		.411	.0725	.0786	.420	.437
10	1.250	1.375	.094	.125	.364	.0970	.0375	.516	.321
11		1.625	.094		.411	.1128	.0626	.524	.390
12		1.875	.094		.458	.1285	.0971	.530	.460
13		2.125	.094		.505	.1442	.1423	.534	.531
14	1.500	1.500	.094	.125	.411	.1591	.0490	.622	.345
15		1.750	.125		.594	.2268	.1023	.618	.415
16		2.000	.125		.656	.2564	.1543	.625	.485
17		2.500	.125		.781	.3156	.3058	.636	.626
18	2.000	2.000	.094	.125	.552	.3922	.1183	.843	.463
19			.125		.719	.4946	.1544	.830	.464
20	2.500	2.000	.094	.156	.607	.6571	.1184	1.04	.442
21			.125		.789	.8315	.1546	1.03	.443
22	3.000	2.000	.094	.156	.654	.9923	.1184	1.23	.426
23			.125		.851	1.262	.1547	1.22	.426
24	4.000	1.500	.078	.125	.542	1.298	.0413	1.55	.275
25		2.000	.094		.740	1.888	.1184	1.60	.400
26			.125		.969	2.424	.1547	1.58	.400
27		3.000	.156	.188	1.52	4.136	.6586	1.65	.658
28		3.500	.188		2.00	5.521	1.258	1.66	.794
29			.250		2.60	6.968	1.638	1.64	.794
30		4.000	.313	.250	3.53	9.415	3.037	1.63	.928

Table A3.16

SECTION PROPERTIES OF TYPICAL AIRCRAFT EXTRUDED SECTIONS

	Sect. No.	Dimensions							Area in.^{2}	Properties about X-X Axis			Properties about Y-Y Axis		
		A	B	C	t	t_1	t_2	R		I_{xx}	ρ_{xx}	e	I_{yy}	ρ_{yy}	e'
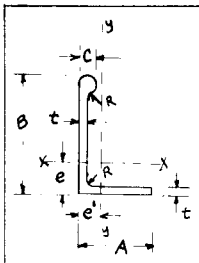	1	17/32	13/16	1/8	.040	.050		1/16	.068	.00686	.317	.319	.00150	.148	.112
	2	1/2	1	7/32	.050	.050		.050	.113	.01515	.3665	.510	.00155	.117	.110
	3	1/2	7/8	3/16	1/16	1/16		3/32	.1025	.0100	.313	.383	.00162	.125	.116
	4	9/16	7/8	3/16	.060	.060		3/32	.1031	.0102	.313	.383	.00215	.114	.130
	5	9/16	7/8	3/16	.050	.078		3/32	.1061	.0120	.329	.345	.00302	.165	.133
	6	3/4	1-1/8	3/16	.075	.075		1/16	.1514	.0239	.397	.435	.00550	.190	.182
	7	3/4	1-5/16	9/32	3/32	3/32		9/64	.230	.0507	.471	.574	.0080	.187	.171
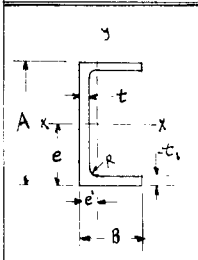	8	7/8	3/8		1/16	1/16		1/16	.095	.0101	.326	.4375	.00111	.108	.108
	9	7/8	3/8		3/32	3/32		3/32	.1375	.0136	.314	.4375	.00148	.104	.118
	10	1	1/2		3/32	3/32		3/32	.1736	.0240	.371	.500	.00376	.147	.158
	11	1-1/4	11/16		3/32	3/32		3/32	.2320	.0536	.480	.625	.00992	.206	.210
	12	1-13/16	1		3/16	3/16		3/32	.644	.2920	.677	.906	.0555	.295	.326
	13	2-1/2	1		1/8	1/8		1/8	.581	.525	.950	1.25	.0662	.338	.323
	14	2-1/4	1-1/8		1/8	3/16		1/8	.666	.524	.888	1.125	.0872	.362	.375
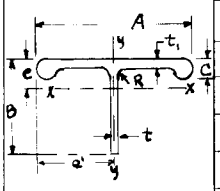	15	1-3/8	11/16	1/8	1/16	1/16		1/16	.137	.00425	.176	.133	.0178	.360	.687
	16	1-5/8	3/4	5/32	1/16	1/16		1/16	.168	.00580	.186	.133	.0335	.446	.812
	17	1-5/8	3/4	5/32	1/16	3/32		5/64	.206	.00589	.170	.121	.0458	.474	.812
	18	2	1-1/16	3/16	3/32	3/32		3/32	.306	.0252	.287	.201	.0791	.509	1.0
	19	2	1-1/4	3/16	1/8	3/32		3/32	.359	.0475	.364	.300	.0827	.479	1.0
	20	2	1-5/32	1/4	3/32	1/8		1/8	.378	.0291	.279	.217	.1095	.541	1.0
	21	2-5/16	1-1/2	5/16	5/32	5/32		5/32	.668	.1075	.401	.338	.2326	.590	1.156
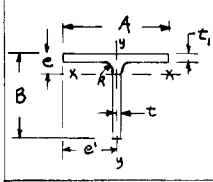	22	1-1/2	1-1/8		1/16	1/16		1/16	.161	.0186	.342	.255	.0171	.326	.750
	23	1-1/2	2		1/8	3/32		1/8	.384	.1562	.641	.658	.0346	.302	.750
	24	1-3/4	2		9/32	1/8		1/8	.760	.315	.643	.757	.0599	.281	.875
	25	1-3/4	2-9/16		1/4	5/32		5/32	.918	.600	.809	.959	.0730	.282	.875
	26	2	2-1/2		5/32	1/8		5/32	.605	.385	.800	.793	.159	.514	1.00
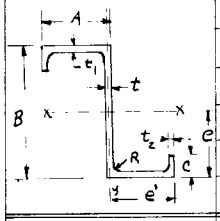	27	11/16	1	1/8	.050	.050	.050	3/32	.135	.0218	.404	.500	.0163	.348	.6625
	28	13/16	1-1/8	3/16	.060	.060	.050	3/32	.180	.0375	.456	.562	.0295	.405	.7825
	29	5/8	1-1/2	3/16	.050	1/16	1/16	3/32	.166	.0603	.595	.75	.0151	.298	.600
	30	3/4	2	1/4	.050	1/16	1/16	3/32	.214	.1382	.793	1.00	.0281	.358	.725
	31	3/4	2	1/4	1/16	1/16	1/16	3/32	.2378	.1449	.773	1.00	.0282	.341	.719
	32	3/4	2	1/4	1/16	3/32	3/32	3/32	.2855	.1820	.795	1.00	.0365	.356	.719
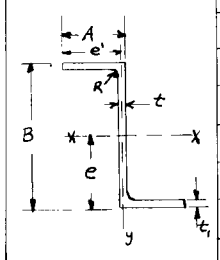	33	9/16	7/8		.050	.050		1/16	.099	.0120	.349	.437	.0056	.238	.537
	34	1/2	7/8		1/16	1/16		1/16	.115	.0135	.341	.437	.00446	.197	.469
	35	9/16	1		1/16	.080		3/32	.151	.0239	.397	.500	.00828	.234	.531
	36	9/16	1 1/4		.075	.075		3/32	.170	.0384	.475	.625	.00876	.227	.525
	37	11/16	1-1/4		1/16	.100		3/32	.213	.0550	.508	.625	.0194	.302	.655
	38	.825	1-1/2		.075	.120		3/32	.302	.110	.604	.750	.0391	.360	.787
	39	3/4	2		.072	.072		1/8	.249	.1446	.757	1.00	.0180	.267	.714
	40	3/4	2		.102	.102		3/32	.330	.1826	.750	1.00	.0228	.265	.700

CHART A3.1 PROPERTIES OF FORMED CHANNEL SECTIONS

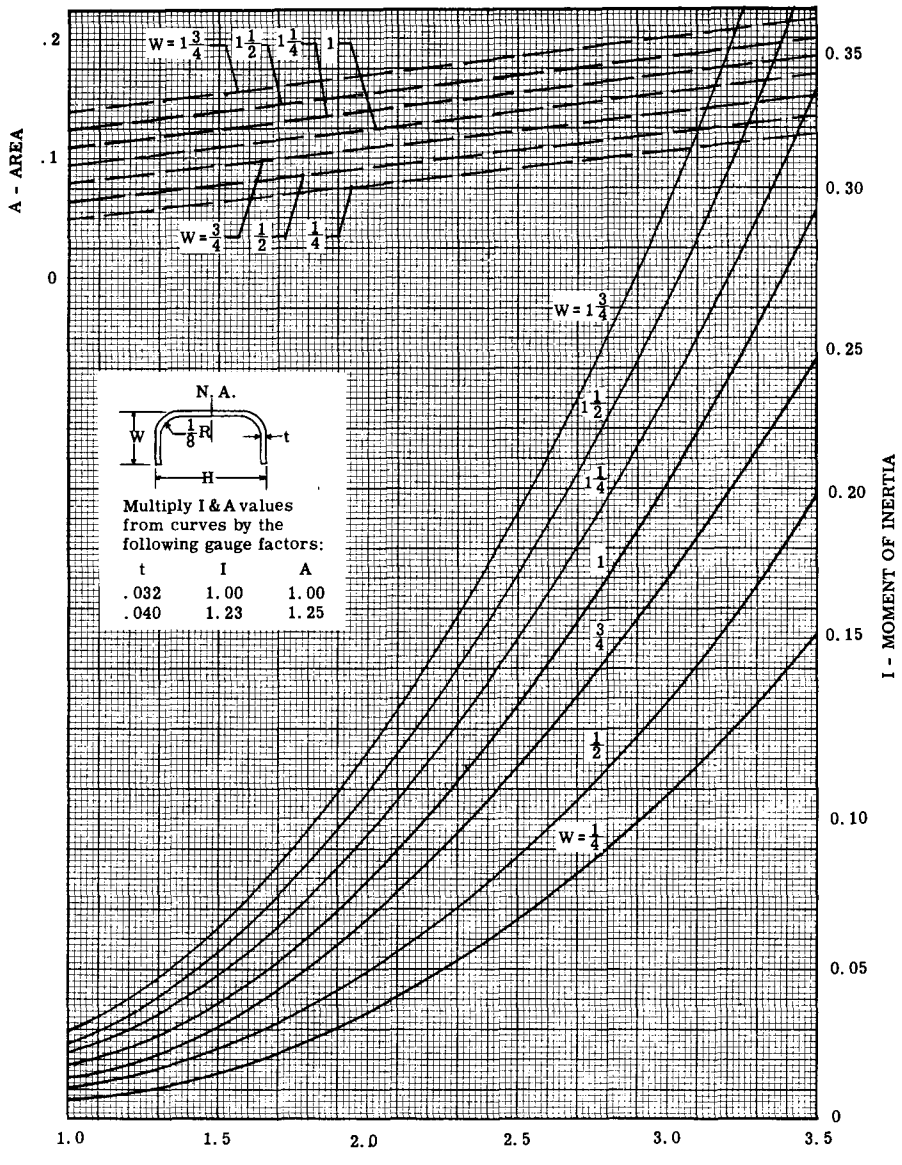

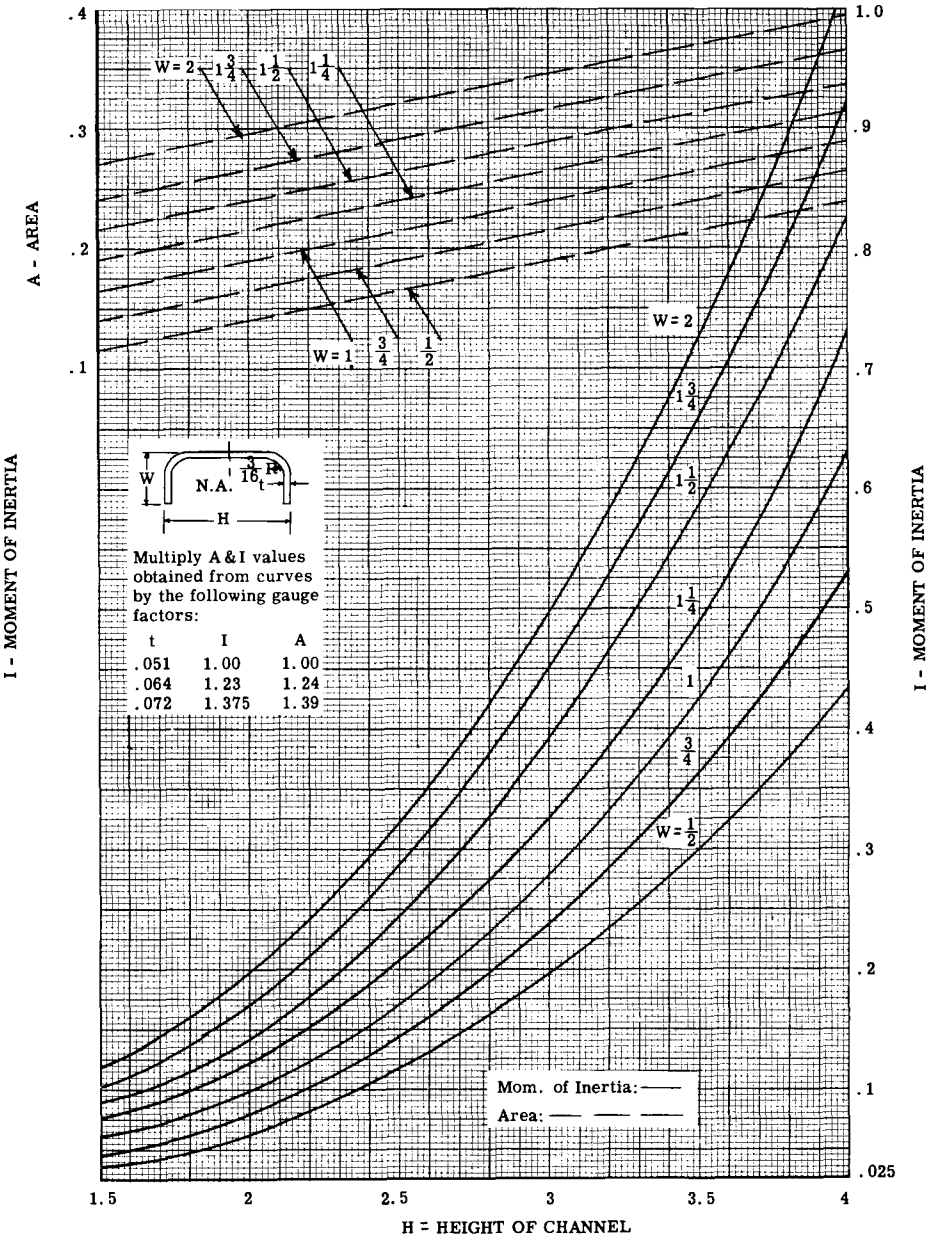

A3.15 Problems

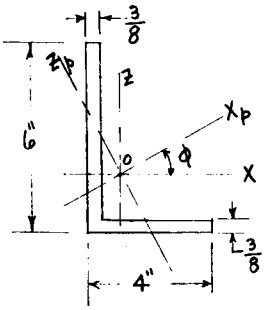

Fig. A3.14

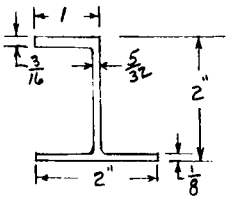

Fig. A3.15

(1) For the section of Fig. A3.14 determine the moment of inertia about each of the principal axes X_p and Z_p.

(2) Calculate the moment of inertia of the section in Fig. A3.15 about the principal axes.

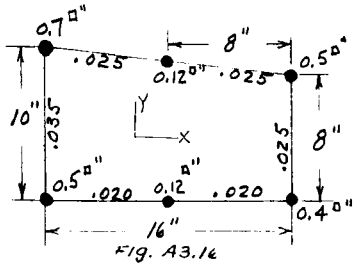

Fig. A3.16

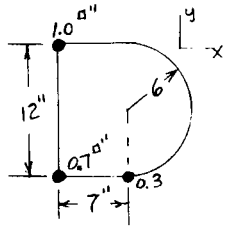

Fig. A3.17

(3) Fig. A3.16 illustrates a box type beam section with six longitudinal stringers. Determine the moment of inertia of the beam section about the principal axes for the following assumptions:-

(a) Assume the beam is bending upward putting the top portion in compression and the lower portion in tension. Therefore, neglect sheet on the top side since it has very little resistance to compressive stresses. The sheet on the bottom side is effective since it is in tension. For simplicity neglect the vertical webs in the calculations.

(b) Reverse the conditions in (a) thus placing top side in tension and lower side in compression.

(4) For the three stringer single cell box beam section in Fig. A3.17, calculate the moments of inertia about the principal axes. Assume all web or wall material ineffective.

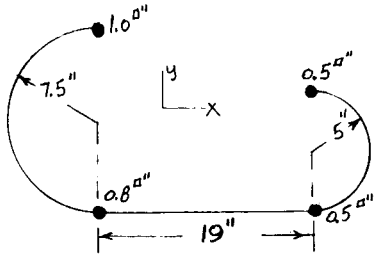

Fig. A3.18

(5) For the beam section in Fig. A3.18, calculate the moment of inertia about the principal axes assuming the four stringers as the only effective material.

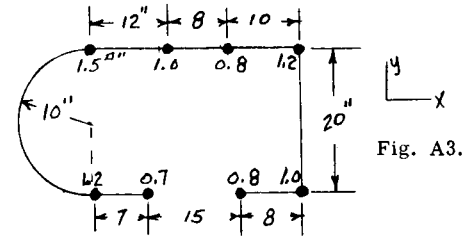

Fig. A3.19

(6) Fig. A3.19 shows a wing beam section with a cut-out on the lower surface. Determine the moments of inertia about the principal axes assuming the eight stringers are the only effective material.

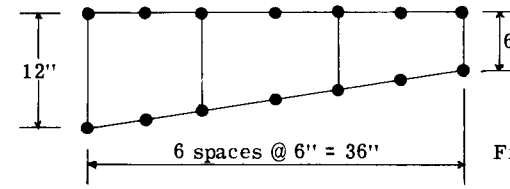

Fig. A3.20

(7) Fig. A3.20 shows a 3 cell multiple flange beam. The 7 flange members on the upper face of beams have an area of .3 sq. in. each and those on the bottom skin 0.2 sq. in. each. The bottom skin is .03 inches in thickness. Compute the moments of inertia about the principle axes assuming that the flange members and the bottom skin comprise the effective material.

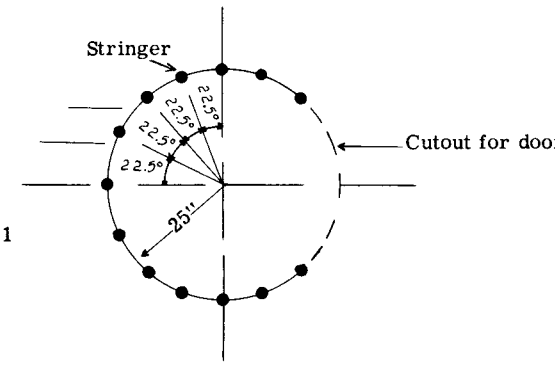

Fig. A3.21

(8) Fig. A3.21 shows the cross-section of a small fuselage. The dashed line represents a cut-out in the structure due to a door. Assume each of the 13 stringers have an area of 0.1 sq. in. Consider fuselage skin ineffective. Calculate the moment of inertia of the effective section about the principal axes.

CHAPTER A4
GENERAL LOADS ON AIRCRAFT

A4.1 Introduction.

Before the structural design of an airplane can be made, the external loads acting on the airplane in flight, landing and take-off conditions must be known. The complete determination of the air loads on an airplane requires a thorough theoretical knowledge of aerodynamics, since modern aircraft fly in sub-sonic, trans-sonic and super-sonic speed ranges. Furthermore, there is a wide range of wing configurations, such as the straight tapered wing, the swept wing and the delta wing, and many of these wings often include leading and trailing edge devices for promoting better lift or control characteristics. The presence of power plant nacelle units, external fuel tanks, etc. are units that affect the airflow around the wing and thus affect the magnitude and distribution of the air forces on the wing. Likewise, the fuselage or airplane body itself influences the airflow over the wing. The theoretical calculation of the airloads on the airplane is too large a subject to be covered in a structures book and it is customary in college aeronautical curricula to provide a separate course for this subject.

In most airplane companies the loads on the airplane are determined by a group of engineers assigned to the Structures Analysis Section and this group is often referred to as the Aircraft Load Calculation group. While the work of this group is primarily based on the use of aerodynamics, it is that phase of aerodynamics which is concerned with determining the magnitude and distribution of the air loads on the airplane so that the airplane structure can be properly designed to support these air forces safely and efficiently. The engineering department of an airplane company has a distinct or separate aerodynamics section, but in general their responsibility is the use of the subject of aerodynamics to insure or guarantee the performance, stability and control of the airplane.

A basic general over-all knowledge of the loads on aircraft is desirable in the study of aircraft structural theory, and hence this chapter attempts to give this information. In a later chapter dealing with wing design, this subject will be further expanded.

A4.2 Limit or Applied Loads. Design Loads.

Because an airplane is designed to carry out a definite job, there result many types of aircraft relative to size, configuration and performance. For example, a commercial transport like the Douglas DC-8 is designed to do a job of transporting a certain number of passengers safely, efficiently and comfortably over various distances between airports. On the other hand the Air Force Fighter type of aircraft has a job of shooting down enemy aircraft or protecting slower friendly aircraft. To do this job efficiently requires a far different configuration as compared to the DC-8 transport. Furthermore the Fighter type airplane must be maneuvered far more sharply to do its required job as compared to the DC-8 in doing its required job.

In general the magnitude of the air forces on an airplane depend on the velocity of the airplane and the rate at which this velocity is changed in magnitude and direction (acceleration). The magnitude of the flight acceleration factor may be governed by the capacity of the human body to withstand these acceleration inertia forces without injury which is the situation in a fighter type of airplane. On the other hand the maneuvering accelerations for the DC-8 are not dictated by what the human body can withstand, but are determined by what is necessary to safely transport passengers from one airport to another.

Designing the airplane structure for loads greater than the airplane suffers in the performance of its required job, obviously will add considerable weight to the airplane and decrease its performance or over-all efficiency relative to the job it is designed to do.

To particularly insure safety in the air-transportation, along with uniformity and efficiency of design, the government aeronautical agencies (civil and military) have definite requirements for the various types of aircraft relative to the magnitude of loads to be used in the structural design of aircraft. In referring in general to these specified aircraft loads two terms are used as follows:-

Limit or Applied Loads.

The terms limit and applied refer to the same loads with the civil agencies (C.A.A.) using the term limit and the military agencies using the term applied.

Limit loads are the maximum loads anticipated on the airplane during its lifetime of service.

The airplane structure shall be capable of supporting the limit loads without suffering detrimental permanent deformations. At all loads up to the limit loads the deformation of the structure shall be such as not to interfere with the safe operation of the airplane.

Ultimate or Design Loads.

These two terms are used in general to mean

the same thing. Ultimate or Design Loads are equal to the limit loads multiplied by a factor of safety (F.S.) or

Design Loads = Limit or Applied Loads times F.S.

In general the over-all factor of safety is 1.5. The government requirements also specify that these design loads be carried by the structure without failure.

Although aircraft are not supposed to undergo greater loads than the specified limit loads, a certain amount of reserve strength against complete structural failure of a unit is necessary in the design of practically any machine or structure. This is due to many factors such as:- (1) The approximations involved in aerodynamic theory and also structural stress analysis theory; (2) Variation in physical properties of materials; (3) Variation in fabrication and inspection standards. Possibly the most important reason for the factors of safety for airplanes is due to the fact that practically every airplane is limited to the maximum velocity it can be flown and the maximum acceleration it can be subjected to in flight or landing. Since these are under the control of the pilot it is possible in emergency conditions that the limit loads may be slightly exceeded but with a reserve factor of safety against failure this exceeding of the limit load should not prove serious from an airplane safety standpoint, although it might cause permanent structural deformations that might require repair or replacements of small units or portions of the structure.

Loads due to airplane gusts, are arbitrary in that the gust velocity is assumed. Although this gust velocity is based on years of experience in measuring and recording gust forces in flight all over the world, it is quite possible that during the lifetime of an airplane, turbulent conditions near storm areas or over mountains or water areas might produce air gust velocities slightly greater than that specified in the load requirements, thus the factor of safety insures safety against failure if this situation would arise.

The broad general category of external loads on conventional aircraft can be broken down into such classifications as follows:-

(1) Air Loads
- Due to Airplane Maneuvers. (under the control of the pilot).
- Due to Air Gusts. (not under control of pilot).

(2) Landing Loads
- Landing on Land. (wheel or ski type).
- Landing on Water.
- Arresting. (Landing on Aircraft Carriers).

(3) Power Plant Loads
- Thrust.
- Torque.

(4) Take off Loads
- Catapulting.
- Assisted take off with auxiliary short period thrust units.

(5) Special Loads
- Hoisting Airplane.
- Towing Airplane.
- Beaching of Hull type Airplane
- Fuselage Pressurizing.

(6) Weight and Inertia Loads.

In resolving external loads for stress analysis purposes, it is convenient to have a set of reference axes. The reference axes XYZ passing through the center of gravity of the airplane as illustrated in Fig. A4.0 are those normally used in stress analysis work as well as for aerodynamic calculations. For convenience the reference axes are often referred to another origin other than the airplane c.g.

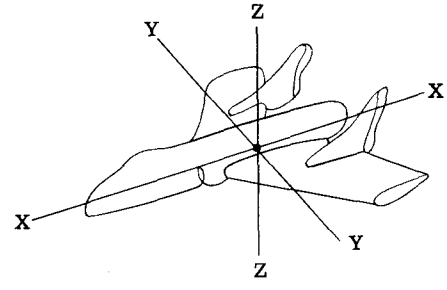

Fig. A4.0

A4.4 Weight and Inertia Forces.

The term weight is that constant force, proportional to its mass, which tends to draw every physical body toward the center of the earth. An airplane in steady flight (uniform velocity) is acted upon by a system of forces in equilibrium, namely, the weight of the airplane, the air forces on the complete airplane, and the power plant forces. The pilot can change this balanced steady flight condition by changing the engine power or by operating the surface controls to change the direction of the airplane velocity. These unbalanced forces thus cause the airplane to accelerate or de-accelerate.

Inertia Forces For Motion of Pure Translation of Rigid Bodies.

If the unbalanced forces acting on a rigid body cause only a change in the magnitude of the velocity of the body, but not its direction, the motion is called translation, and from basic Physics, the accelerating force F = Ma, where M is the mass of the body or W/g. In Fig. A4.1 the unbalanced force system F causes the rigid body to accelerate to the right. Fig. A4.2 shows the effect of this unbalanced force in producing

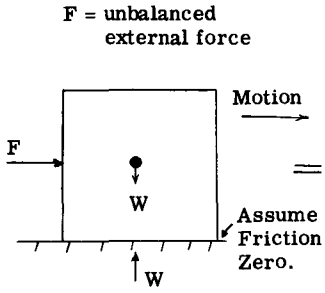

Fig. A4.1

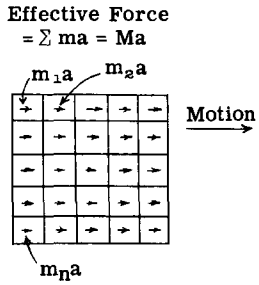

Fig. A4.2

a force on each mass particle of m_1a, m_2a, etc., thus the total effective force is $\Sigma ma = Ma$. If these effective forces are reversed they are referred to as inertia forces. The external forces and the inertia forces therefore form a force system in equilibrium.

From basic Physics, we have the following relationships for a motion of pure translation if the acceleration is constant:-

$$v - v_o = at \quad \text{- - - - - - - - - - - - - - - - - -} \quad (1)$$

$$s = v_o t + \frac{1}{2}at^2 \quad \text{- - - - - - - - - - - - - - - - -} \quad (2)$$

$$v - v_o^2 = 2as \quad \text{- - - - - - - - - - - - - - - - -} \quad (3)$$

where,

s = distance moved in time t.

v_o = initial velocity

v = final velocity after time t.

Inertia Forces on Rotating Rigid Bodies.

A common airplane maneuver is a motion along a curved path in a plane parallel to the XZ plane of the airplane, and generally referred to as the pitching plane. A pull up from steady flight or a pull out from a dive causes an airplane to follow a curved path. Fig. A4.3 shows an airplane following a curved path. If at point A the velocity is increasing along its path, the airplane is being subjected to two accelerations, namely, a_t, tangential to the curve at point A and equal in magnitude to

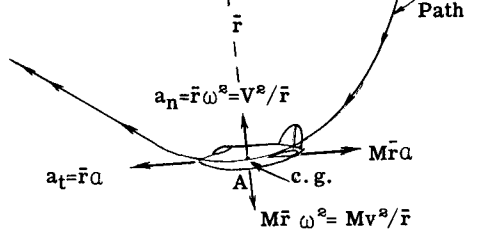

Fig. A4.3

$a_t = \bar{r}\alpha$, and $a_n = \bar{r}\omega^2$ an acceleration normal to the flight path at A and directed toward the center of rotation (o). From Newton's Law the effective forces due to these accelerations are:-

$$F_n = M\bar{r}\omega^2 = Mv^2/r \quad \text{- - - - - - - - - - - - - - -} \quad (4)$$

$$F_t = M\bar{r}\alpha \quad \text{- - - - - - - - - - - - - - - - - - -} \quad (5)$$

where ω = angular velocity at the point A.
α = angular acceleration at point A.
$\bar{r}$ = radius of curvature of flight path at point A.

The inertia forces are equal and opposite to these effective forces as indicated in Fig. A4.3. These inertia forces can then be considered as part of the total force system on the airplane which is in equilibrium.

If the velocity of the airplane along the path is constant, then a_t = zero and thus the inertia force F_t = o, leaving only the normal inertia force F_n.

If the angular acceleration is constant, the following relationships hold.

$$\omega - \omega_o = \alpha t \quad \text{- - - - - - - - - - - - - - - - - -} \quad (6)$$

$$\theta = \omega_o t + \tfrac{1}{2}\alpha t^2 \quad \text{- - - - - - - - - - - - - - - -} \quad (7)$$

$$\omega^2 - \omega_o^2 = 2\alpha\theta \quad \text{- - - - - - - - - - - - - - - -} \quad (8)$$

where θ = angle of rotation in time t.
ω_o = initial angular velocity in rad/sec.
ω = angular velocity after time t.

In Fig. A4.3 the moment T_o of the inertia forces about the center of rotation (o) equals $M\bar{r}\alpha(\bar{r}) = M\bar{r}^2\alpha$. The term $M\bar{r}^2$ is the mass moment of inertia of the airplane about point (o). Since an airplane has considerable pitching moment of inertia about its own center of gravity axis, it should be included. Thus by the parallel axis

$$T_o = I_o\alpha + I_{c.g}\alpha \quad \text{- - - - - - - - - - - - - - - -} \quad (9)$$

where $I_o = M\bar{r}^2$ and $I_{c.g}$ = moment of inertia of airplane about Y axis through c.g. of airplane.

Inertia Forces For Pitching Rotation of Airplane about Y Axis Through c.g. airplane.

In flight, an air gust may strike the horizontal tail producing a tail force which has a moment about the airplane c.g. In some landing conditions the ground or water forces do not pass through the airplane c.g., thus producing a moment about the airplane c.g. These moments cause the airplane to rotate about the Y axis through the c.g.

Therefore for this effect alone the center of rotation in Fig. A4.3 is not at (o) but at

the c.g. of airplane, or $\bar{r} = o$. Thus F_n and F_t equal zero and thus the only inertia force for the pure rotation is $I_{c.g.}\,a$, (a couple) and thus the moment of this inertia couple about the c.g. $= T_{c.g.} = I_{c.g.}\,a$.

As explained before if the inertia forces are included with all other applied forces on the airplane, then the airplane is in static equilibrium and the problem is handled by the static equations for equilibrium.

A4.5 Air Forces on Wing.

The wing of an airplane carries the major portion of the air forces. In level steady flight the vertical upward force of the air on the wing, practically equals the weight of the airplane. The term airfoil is used when referring to the shape of the cross-section of a wing. Figs. A4.4 and A4.5 illustrate the air pressure intensity diagram due to an air-

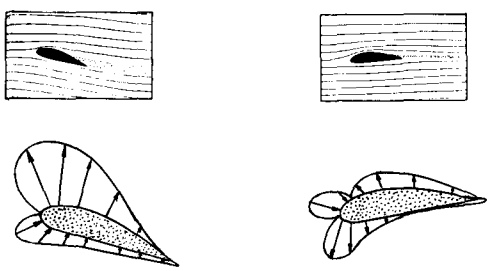

Angle of Attack = 12°

Fig. A4.4

Angle of Attack = - 6°

Fig. A4.5

stream flowing around an airfoil shape for both a positive and negative angle of attack. The shape and intensity of this diagram is influenced by many factors, such as the shape of the airfoil itself, as the thickness to chord ratio, the camber of the top and bottom surfaces etc. A normal wing is attached to a fuselage and it may support external power plants, wing tip tanks etc. Furthermore the normal wing is usually tapered in planform and thickness and may possess leading and trailing slots and flaps to produce high lift or control effects. The airflow around the wing is affected by such factors as listed above and thus wind tunnel tests are usually necessary to obtain a true picture of the air forces on a wing relative to their chordwise spanwise distribution.

Resultant Air Force. Center of Pressure.

It is convenient when dealing with the balancing or equilibrium of the airplane as a whole to deal with the resultant of the total air forces on the wing. For example, consider the two air pressure intensity diagrams in Figs. A4.6 and A4.7. These distributed force systems can be replaced by their resultant (R), which of course must be known in magnitude, direction and location. The location is specified by a term called the center of pressure which is the point where the resultant R intersects the airfoil chord line. As the angle of attack is changed the resultant air force changes in magnitude, direction and center of pressure location.

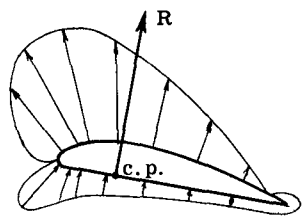

Fig. A4.6

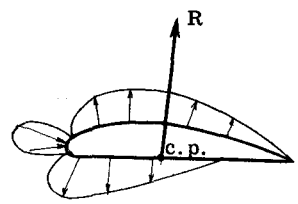

Fig. A4.7

Lift and Drag Components of Resultant Air Force.

Instead of dealing with the resultant force R, it is convenient for both aerodynamic and stress analysis considerations to replace the resultant by its two components perpendicular and parallel to the airstream. Fig. A4.8 illustrates this resolution into lift and drag components.

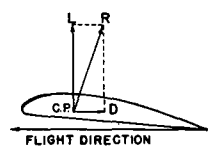

Fig. A4.8

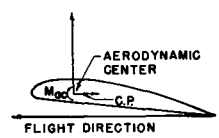

Fig. A4.9

Aerodynamic Center (a.c.). Since an airplane flies at many different angles of attack, it means that the center of pressure changes for the many flight design conditions. It so happens, that there is one point on the airfoil that the moment due to the Lift and Drag forces is constant for any angle of attack. This point is called the aerodynamic center (a.c.) and its approximate location is at the 25 percent of chord measured from the leading edge. Thus the resultant R can be replaced by a lift and drag force at the aerodynamic center plus a wing moment $M_{a.c.}$ as illustrated in Fig. A4.9.

A4.6 Forces on Airplane in Flight.

Fig. A4.10 illustrates in general the main forces on the airplane in an accelerated flight condition.

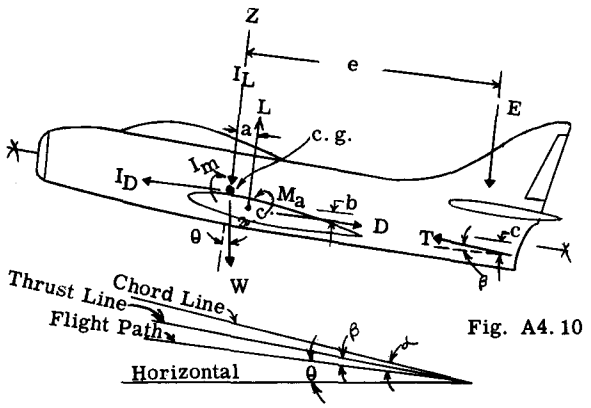

Fig. A4.10

T = engine thrust.
L = total wing lift plus fuselage lift.
D = total airplane drag.
M_a = moment of L and D with reference to wing a.c. (aerodynamic center)
W = weight of airplane.
I_L = inertia force normal to flight path.
I_D = inertia force parallel to flight path.
I_m = rotation inertia moment.
E = tail load normal to flight path.

For a horizontal constant velocity flight condition, the inertia forces I_L, I_D, and I_m would be zero. For an accelerated flight condition involving translation but not angular acceleration about its own c.g. axis, the inertia moment I_m would be zero, but I_L and I_D would have values.

Equations of Equilibrium For Steady Flight.

From Fig. A4.10 we can write:-

$\Sigma F_x = o, \quad D + W \sin \Theta - T \cos \beta = o$

$\Sigma F_{z_*} = o, \quad L - W \cos \Theta + T \sin \beta - E = o$

$\Sigma M_y = o, \quad - M_a - La - Db + Tc \cos \beta + Ee = o$

Equations of Equilibrium in Accelerated Flight.

$\Sigma F_x = o, \quad D + W \sin \Theta - T \cos \beta - I_D = o$

$\Sigma F_z = o, \quad L - W \cos \Theta + T \sin \beta - I_L - E = o$

$\Sigma M_y = o, \quad - M_a - La - Db + Tc \cos \beta + Ee + I_m = o$

Signs used:
- Forces - Plus is up and toward tail.
- Moment - Clockwise is positive.
- Distances from c.g. to force - Plus is up and toward tail.

A4.7 Load Factors.

The term load factor normally given the symbol (n) can be defined as the numerical multiplying factor by which the forces on the airplane in steady flight are multiplied to obtain a static system of forces equivalent to the dynamic force system acting during the acceleration of the airplane. Fig. A4.11 illustrates

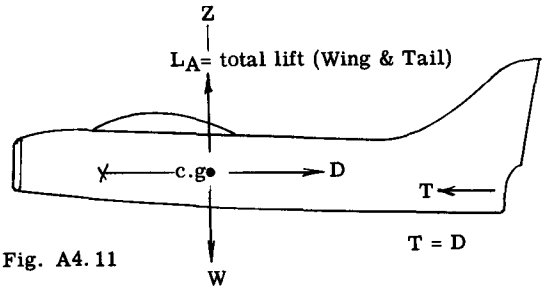

Fig. A4.11

forces in steady horizontal flight. L represents the total airplane lift (wing plus tail). Therefore L = W. Now assume the airplane is accelerated upward along the Z axis. Fig. A4.12 shows the additional inertia force Wa_z/g acting downward, or opposite to the direction of acceleration. The total airplane lift L for the

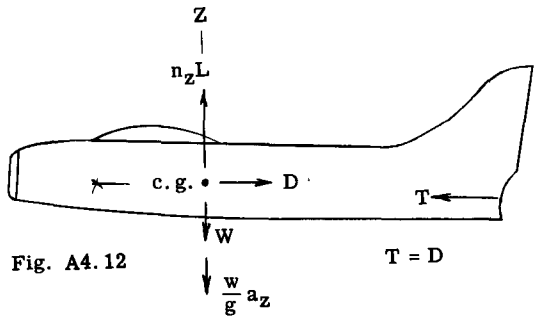

Fig. A4.12

unaccelerated condition in Fig. A4.11 must be multiplied by a load factor n_g to produce static equilibrium in the Z direction.

Thus, $n_g L - W - \frac{W}{g} a_g = o$

Since L = W

Hence $n_g = 1 + \frac{a_g}{g}$

An airplane can of course be accelerated along the X axis as well as the Z axis. Thus in Fig. A4.13 the magnitude of the engine thrust T is greater than the airplane Drag D, which

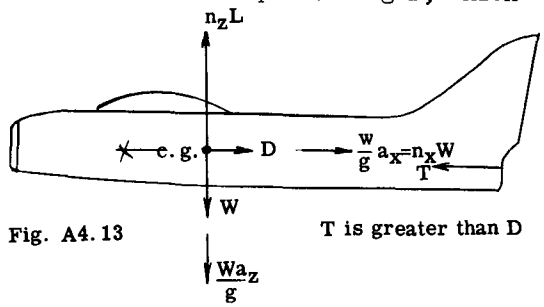

Fig. A4.13

T is greater than D

causes the airplane to accelerate forward. It is convenient to express the inertia force in the X direction in terms of the load factor n_x and the

* The bar through letter Z has no significance. Same meaning without bar.

weight W of the airplane, hence

$n_x W = \frac{W}{g} a_x$ (See Fig. A14.13)

$\Sigma F_x = o$, whence $T-D-n_x W = o$

Hence $n_x = \frac{T-D}{W}$

Therefore the loads on the airplane can be discussed in terms of load factors. The applied or limit load factors are the maximum load factors that might occur during the service of the particular airplane. These loads as discussed in Art. A4.2 must be taken by the airplane structure without appreciable permanent deformation.

The design load factors are equal to the limit load factors multiplied by the factor of safety, and these design loads must be carried by the structure without rupture or collapse, or in other words, complete failure.

A4.8 Design Flight Requirements for Airplane.

The Civil and Military Aeronautics Authorities issue requirements which specify the design conditions for the various classifications of airplanes. Generally speaking, any airplane flight altitude can be defined by stating the existing values of load factors (acceleration) and the airspeed (or more properly the dynamic pressure).

The accelerations on the airplane are produced from two causes, namely, maneuvers and air gusts. The accelerations due to maneuvers are subject to the control of the pilot who can manipulate the controls so as not to exceed a certain acceleration. In highly maneuverable military airplanes, an accelerometer is included in the cockpit instruments as a guide to limit the acceleration factor. For commercial airplanes the maneuver factors are made high enough to safely take care of any maneuvers that would be required in the necessary flight operations of the particular type of airplane. These limiting maneuver factors are based on years of operating experience and have given satisfactory results from a safety standpoint without penalizing the airplane from a weight design consideration.

The accelerations due to the airplane striking an air gust are not under the control of the pilot since it depends on the direction and velocity of the air gust. From much accumulated data obtained by installing accelerometers in commercial and military aircraft and flying them in all types of weather and locations, it has been found that a gust velocity of 30 ft. per second appears sufficient.

The speed or velocity of the airplane likewise affects the loads on the airplane. The higher the velocity the higher the aerodynamic wing moment. Furthermore the gust accelerations increase with airplane velocity. Thus, it is customary to limit the particular airplane to a definite maximum flight velocity. For commercial airplanes the velocity is limited to a reasonable glide speed which is sufficient to take care of reasonable flight operations.

A4.9 Gust Load Factors.

When a sharp edge gust strikes the airplane in a direction normal to the thrust line (X axis), a sudden change takes place in the wing angle of attack with no sudden change in airplane speed. The normal force coefficient (C_{Z_A}) can be assumed to vary linearly with the angle of attack. Thus in Fig. (a), let point (B) represent the normal airplane force coefficient C_{Z_A} necessary to maintain level flight with a velocity V and point (C) the value of C_{Z_A} after a sharp edged gust KU has caused a sudden change $\Delta\alpha$ in the angle of attack without change in V. The total increase in the airplane load in the Z direction can therefore be expressed by the ratio C_{Z_A} at B.

From Fig. (b) for small angles, $\Delta\alpha = KU/V$ and from Fig. (a), $\Delta C_{Z_A} = m\,\Delta\alpha$, where m = the slope of the airplane normal force curve (C_{Z_A} per radian).

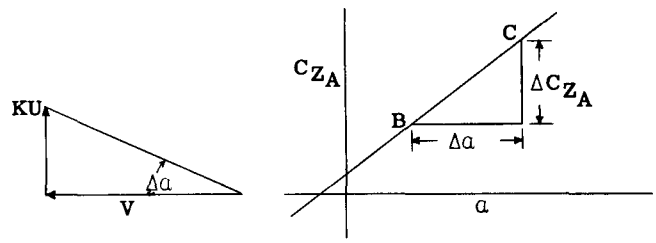

Fig. a

Fig. b

The load factor increment due to the gust KU can then be expressed

$$\Delta n = \frac{\Delta C_{Z_A}}{C_{Z_A}} = \left(\frac{KUm}{V}\right)\left(\frac{\rho V^2 S}{2W}\right) = \frac{KUVS_m}{575\,W} \text{ - - - - - - (A)}$$

where

U = gust velocity in ft./sec.

K* = gust correction factor depending on wing loading (Curves for K are provided by Civil Aeronautics Authorities).

V = indicated air speed in miles per hour.

S = wing area in sq. ft.

W = gross weight of airplane.

* NACA Technical Note 2964 (June 1953), proposes that the alleviation factor K should be replaced by a gust factor, Kg = 0.88 Mg/5.3 + Mg). In this expression Mg is the airplane mass ratio or mass parameter, 2 W/aρcgs, in which c is the mean geometric chord in feet and g the acceleration due to gravity.

If U is taken as 30 ft./sec. and m as the change in C_{Z_A} with respect to angle of attack in absolute units per degree, equation (A) reduced to the following

$$\Delta n = \frac{3KmV}{W/S} \quad \text{- - - - - - - - - - - - - - - - - - -} \quad (B)$$

Therefore the gust load factor n when airplane is flying in horizontal attitude equals

$$n = 1 \pm \frac{3KmV}{W/S} \quad \text{- - - - - - - - - - - - - - - - -} \quad (C)$$

and when airplane is in a vertical attitude

$$n = \pm \frac{3KmV}{W/S} \quad \text{- - - - - - - - - - - - - - - - -} \quad (D)$$

A4.10 Illustration of Main Flight Conditions. Velocity-Load Factor Diagram.

As indicated before the main design flight conditions for an airplane can be given by stating the limiting values of the acceleration and speed and in addition the maximum value of the applied gust velocity. As an illustration, the design loading requirements for a certain airplane could be stated as follows: "The proposed airplane shall be designed for applied positive and negative accelerations of + 6.0g and -3.5g respectively at all speeds from that corresponding to $CL_{max.}$ up to 1.4 times the maximum level flight speed. Furthermore, the airplane shall withstand any applied loads due to a 30 ft./sec. gust acting in any direction up to the restricted speed of 1.4 times the maximum level flight speed. A design factor of safety of 1.5 shall be used on these applied loads".

In graphical form these design requirements can be represented by plotting load factor and velocity to obtain a diagram which is generally referred to as the Velocity-acceleration diagram. The results of the above specification would be similar to that of Fig. A4.14. Thus, the lines AB and CD represent the restricted positive and negative maneuver load factors which are limited to speeds inside line BD which is taken as 1.4 times the maximum level flight speed in this illustration. These restricted maneuver lines are terminated at points A and C by their intersection with the maximum C_L values of the airplane. At speeds between A and B, the pilot must be careful not to exceed the maneuver accelerations, since in general, it would be possible for him to manipulate the controls to exceed these values. At speeds below A and C, there need be no care of the pilot as far as loads on the airplane are concerned since a maneuver producing $C_{L_{max.}}$ would give an acceleration less than the limited values given by lines AB and CD.

The positive and negative gust accelerations due to a 30 ft./sec. gust normal to flight path are shown on Fig. A4.14. In this example diagram, a positive gust is not critical within the restricted velocity of the airplane since the gust lines intersect the line BD below the line AB. For a negative gust, the gust load factor becomes critical at velocities between F and D with a maximum acceleration as given by point E.

For airplanes which have a relatively low required maneuver factor the gust accelerations may be critical for both positive and negative accelerations. Examination of the gust equation indicates that the most lightly loaded condition (smallest gross weight) produces the highest gust load factor, thus involving only partial pay load, fuel, etc.

On the diagram, the points A and B correspond in general to what is referred to as high angle of attack (H,A,A,) and low angle of attack (L.A.A.) respectively, and points C and D the inverted (H.A.A.) and (L.A.A.+ conditions respectively.

Generally speaking, if the airplane is designed for the air loads produced by the velocity and acceleration conditions at points A, B, E, F, and C, it should be safe from a structural strength standpoint if flown within the specified limits regarding velocity and acceleration.

Basically, the flight condition requirements of the Civil Aeronautics Authority, Army, and Navy are based on consideration of specified velocities and accelerations and a consideration of gusts. Thus a student understanding the basic discussion above should have no difficulty understanding the design requirements of these three government agencies.

For stress analysis purposes, all speeds are expressed as indicated air speeds. The "indicated" air speed is defined as the speed which would be indicated by a perfect air-speed indicator, that is, one that would indicate true air speed at sea level under standard atmospheric conditions. The relation between the actual air speed V_a and the indicated air speed V_i is given by the equation

$$V_i = \sqrt{\frac{\rho_a}{\rho_o}}\ V_a$$

where

V_i = indicated airspeed

V_a = actual airspeed

ρ_o = standard air density at sea level

ρ_a = density of air in which V_a is attained

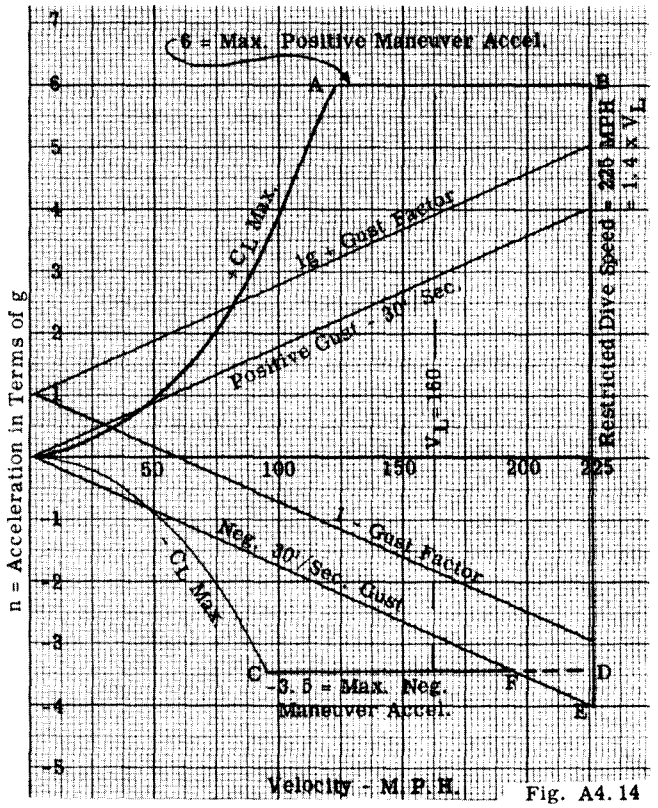

Fig. A4.14

A4.11 Special Flight Design Conditions.

There are many other flight conditions which may be critical for certain portions of the wing or fuselage structure. Most airplanes are equipped with flaps, to decrease the landing speed and such flaps are lowered at speeds at least twice that of the minimum landing speed. Since the flapped airfoil has different values for the magnitude and location of the airfoil characteristics, the wing structure must be checked for all possible flap conditions within the specified requirement relative to maximum speed at which the flaps may be operated. Generally speaking, the flap conditions will effect only the wing portion inboard of the flap and it is usually only critical for the rear beam web or shear wall and for the top and bottom walls of the torsion box. This is due to the fact that the deflection flap moves the center of pressure considerably aft thus producing more shear load on the rear shear wall as well as torsional moment on the conventional cantilever box metal beam.

The airplane must likewise be investigated for aileron conditions. Operation of the ailerons produce a different air load on each side of the airplane wing which produces an angular rolling acceleration of the airplane. Furthermore, the deflected ailerons change the magnitude and location of the airfoil characteristics, thus calculations must be carried out to determine whether the loads in the aileron conditions are more critical than those for the normal flight conditions.

For angular acceleration resulting from pitching moments due to air gusts on the tail, the loads on the wing should be checked for cases where the engines are attached to the wing and are located forward of the leading edge.

In cases where the landing gear is attached to wing or when the fuel and engines are carried in and on the wing, the loads produced on the wing structure in a landing condition may be critical for some portions of the wing structure inboard of landing gear and engine attachment points.

A4.12 Example Problems Involving Accelerated Motion of Rigid Airplane.

As previously explained, it is general practice to place the airplane under accelerated conditions of motion into a condition of static equilibrium by adding the inertia forces to the applied force system acting on the airplane. It is usually assumed that the airplane is a rigid body. Several example problems will be presented to illustrate this general procedure.

Example Problem 1

Fig. A4.15 illustrates an airplane landing on a Navy aircraft carrier and being arrested by a cable pull T on the airplane arresting hook. If the airplane weight is 12,000 lbs. and the airplane is given a constant acceleration of 3.5g (112.7 ft/sec^2), find the hook pull T, the wheel reaction R, and the distance (d) between the line of action of the hook pull and the airplane c.g. If the landing velocity is 60 M.P.H. what is the stopping distance.

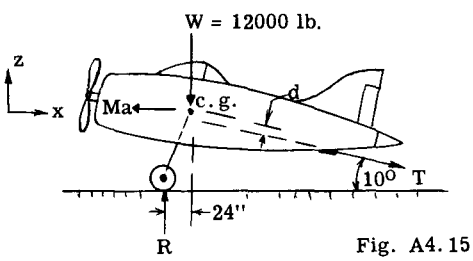

Fig. A4.15

Solution: -

On contact of the airplane with the arresting cable, the airplane is decelerated to the right relative to Fig. A4.15. The motion is pure translation horizontally. The inertia force is

$$Ma = \frac{W}{g} a = \left(\frac{12000}{g}\right) 3.5g = 42000 \text{ lb.}$$

The inertia force acts opposite to the direction of acceleration, hence to the left as shown in Fig. A4.15.

The unknown forces T and R can now be solved for by using the static equations of equilibrium.

$$\Sigma F_x = -42000 + T \cos 10^\circ = 0$$

hence,

$$T = 42700 \text{ lb.}$$

$$\Sigma F_g = -12000 + R - 42700 \times \sin 10^\circ = 0$$

hence,

$$R = 19420 \text{ lb.}$$

To find the distance (d) take moments about c.g. of airplane,

$$\Sigma M_{c.g.} = 19420 \times 24 - 42700\, d = o$$

hence,

$$d = 10.9 \text{ in.}$$

Landing velocity V_o = 6o M.P.H. = 88 ft/sec.

$$V^2 - V_o^2 = 2as$$

Subt: -

$$o^2 - 88^2 = 2(-112.7)\, s$$

hence stopping distance s = 34.4 ft.

Example Problem 2

An airplane equipped with float is catapulted into the air from a Navy Cruiser as illustrated in Fig, A4.16. The catapulting force P gives the airplane a constant horizontal acceleration of 3g(96.6 ft/sec^2). The gross weight of airplane 9000 lb. and the catapult track is 35 ft. long. Find the catapulting force P and the reactions R_1 and R_2 from the catapult car. The engine thrust is 900 lb. What is airplane velocity at end of track run?

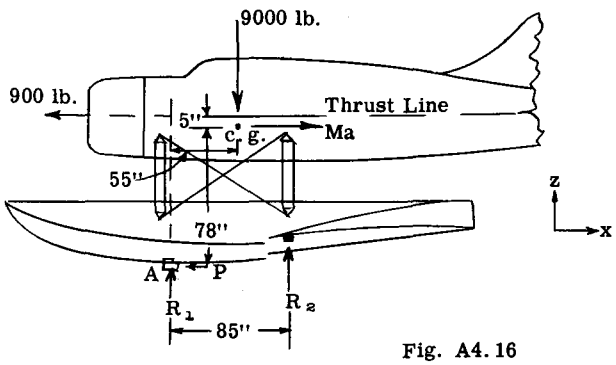

Fig. A4.16

Solution: -

The forces will be determined just after the beginning of the catapult run, where the car velocity is small, and thus the lift on the airplane wing and the airplane drag can be neglected.

Horizontal inertia force acting toward the airplane tail equals,

$$Ma = \left(\frac{9000}{g}\right) 3.0g = 27000 \text{ lb.}$$

From statics: -

$\Sigma F_x = -900 - P + 27000 = o$, hence P = 26100 lb.

To find R_2 take moments about point A,

$$\Sigma M_A = 9000 \times 55 + 27000 \times 78 - 900 \times 83 - 85R_2 = o$$

hence,

$$R_2 = 29800 \text{ lb. (up)}$$

$$\Sigma F_z = 29800 - 9000 + R_1 = o$$

hence,

$$R_1 = -20800 \text{ lb. (acting down)}$$

The velocity at end of catapult track can be found from the following equation

$$V^2 - V_o^2 = 2as$$

$$V^2 - o = 2 \times 96.6 \times 35$$

or

$$V = 82 \text{ ft/sec.} = 56 \text{ M.P.H.}$$

Example Problem 3

Assume that the transport airplane as illustrated in Fig. A4.17 has just touched down in landing and that a braking force of 35000 lb. on the rear wheels is being applied to bring the airplane to rest. The landing horizontal velocity is 85 M.P.H. (125 ft/sec). Neglecting air forces on the airplane and assuming the propeller forces are zero, what are the ground reactions R_1 and R_2. What is the landing run distance with the constant braking force?

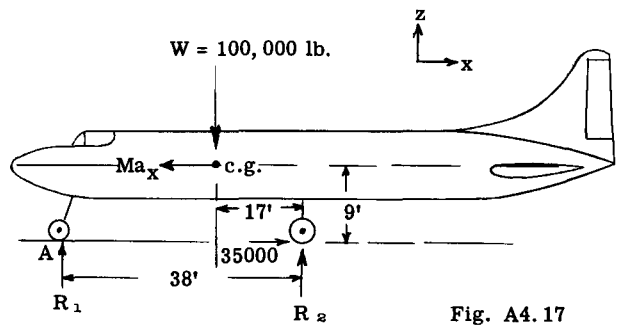

Fig. A4.17

Solution: -

The airplane is being decelerated horizontally hence the inertia force through the airplane c.g. acts toward the front of the airplane. Since the braking force is given we can solve for the deceleration factor by the equilibrium equation,

$$\Sigma F_x = 35000 - Ma_x = 0$$

hence,

$$Ma_x = 35000$$

or

$$\left(\frac{W}{g}\right) a_x = 35000$$

whence

$$a_x = \left(\frac{35000}{100000}\right) 32.2 = 11.27 \text{ ft/sec}^2$$

To find landing run (s),

$$V^2 - V_o^2 = 2\, a_x s$$

$$0 - \overline{125}^2 = 2\,(-11.27)\, s$$

hence,

$$s = 695 \text{ ft.}$$

To find R_2 take moments about point (A)

$$\Sigma M_A = 100{,}000 \times 21 - 35000 \times 9 + 38\, R_2 = 0$$

$$R_2 = 47000 \text{ lb. (2 wheels)}$$

$$\Sigma F_z = 47000 - 100{,}000 + R_1 = 0$$

$$R_1 = 53000 \text{ lb.}$$

Example Problem 4

The airplane in Fig. A4.18 weighs 14,000 lb. It is flying horizontally at a velocity of 500 M.P.H. (733 ft/sec) when the pilot pulls it upward into a curved path with a radius of curvature of 2500 ft. Assume the engine thrust and airplane drag equal, opposite and colinear with each other (not shown on Fig. A4.18).

Find: -

(a) Acceleration of airplane in Z direction
(b) Wing Lift (L) and Tail (T) forces
(c) Airplane Load factor.

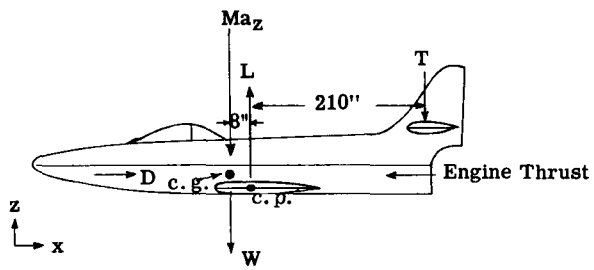

Fig. A4.18

Solution: -

$$\text{Acceleration } a_z = \frac{V^2}{r} = \frac{\overline{733}^2}{2500} = 215 \text{ ft/sec}^2$$

or 214.5/32.2 = 6.68g (upward).

The inertia force normal to the flight path and acting down equals

$$Ma_z = \left(\frac{14000}{g}\right) 6.68g = 93520 \text{ lb.}$$

Placing this force on the airplane through the c.g. promotes static equilibrium, hence to find tail load T take moments about wing aerodynamic center (c.p.)

$$\Sigma M_{c.p.} = -(14000 + 93520)\, 8 + 210\, T = 0$$

hence

$$T = 4100 \text{ lb. (down)}$$

To find Wing Lift (L) use

$$\Sigma F_z = -4100 - 14000 - 93520 + L = 0$$

$$L = 111600 \text{ lb.}$$

$$\text{Airplane Load Factor} = \frac{\text{Airplane Lift}}{W}$$

$$= \frac{111600 - 4100}{14000} = 7.7$$

Example Problem 5

Assume the airplane as used in example problem 4 is in the same attitude as used in that example problem. Now the airplane is further maneuvered by the pilot suddenly pushing the control stick forward so as to give the airplane a pitching acceleration of 4 rad/sec^2.

(a) Find the inertia forces and the tail load T, assuming the lift force on the wing does not change.

(b) Find the forces on the jet engine which weighs 1500 lb. and whose c.g. location is shown in Fig. A4.19.

Assume moment of inertia I_y (pitching) of the airplane equals 300,000 lb. sec^2. in.

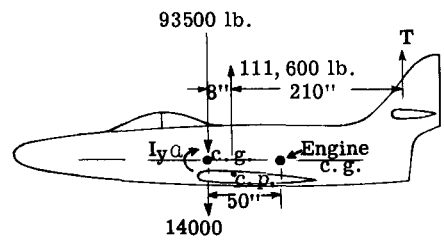

Fig. A4.19

Solution: -

Fig. A4.19 shows a free body of the airplane with the lift and inertia forces as found in Problem 4.

The additional inertia force due to the angular acceleration $\alpha = 4$ rad/sec^2. equals,

$$I_y \alpha = 300000 \times 4 = 1{,}200{,}000 \text{ in. lb.}$$

which acts clockwise or counter to the direction of angular acceleration.

The airplane is now in static equilibrium and to find the tail load T take moments about airplane c.g.

$$\Sigma M_{c.g.} = 1{,}200{,}000 - 111600 \times 8 - 218\, T = 0$$

$$T = 1409 \text{ lb.}$$

To find Ma_g take,

$$\Sigma F_g = 111600 - 14000 + 1409 - Ma_g = 0$$

$$Ma_g = 99009 \text{ lb.}$$

hence, $a_g = \left(\frac{99009}{14000}\right) g = 7.1\ g\ ft/sec^2.$

The c.g. of the engine is 50 inches aft of the airplane c.g. as shown in Fig. A4.19. The force on the engine will be its own weight of 1500 lb., and the inertia forces due to a_g and α.

Inertia force due to a_g equals,

$$Ma_g = \left(\frac{1500}{g}\right) 7.1g = 10630\ lb.$$

Inertia force due to angular acceleration α equals,

$$Mr\alpha = \frac{1500}{32.2 \times 12} \times 50 \times 4 = 776\ lb.\ (down)$$

Then the resultant force on the engine equals

$$1500 + 10630 + 776 = 12906\ lb.\ (down)$$

Note if the engine had been forward of the airplane c.g., the inertia force of 776 lb. would act upward instead of downward.

In calculating the inertia force on a certain airplane item due to angular acceleration, the equation $F = Mr\alpha$ assumes that the particular item had negligible mass moment of inertia about its own centroidal Y axis. In the case of a large item this centroidal mass moment of inertia may be appreciable and should be included in the I_y of airplane.

Then to find the inertia force for such an item the equation $F = Mr\alpha$ should be modified to be

$$F = (I_{c.g.}\ \alpha)/r \qquad \text{where}$$

r = distance or arm from airplane c.g. to c.g. of item.

$I_{c.g.}$ = mass moment of inertia of item about airplane c.g. equals $I_o + Mr^2$, where I_o is mass moment of inertia of item about its own centroidal Y axis.

F = inertia force in lbs. normal to radius r.

Example Problem 6

Fig. A4.20 shows a large transport airplane whose gross weight is 100,000 lb. The airplane pitching mass moment of inertia $I_y = 40{,}000{,}000$ lb. sec². in.

The airplane is making a level landing with nose wheel slightly off ground. The reaction on the rear wheels is 319,000 lb. inclined at such an angle to give a drag component of 100,000 lb. and a vertical component of 300,000 lb.

Find:

(a) The inertia forces on the airplane.

(b) The resultant load on the pilot whose weight is 180 lb. and whose location is shown in Fig. A4.20.

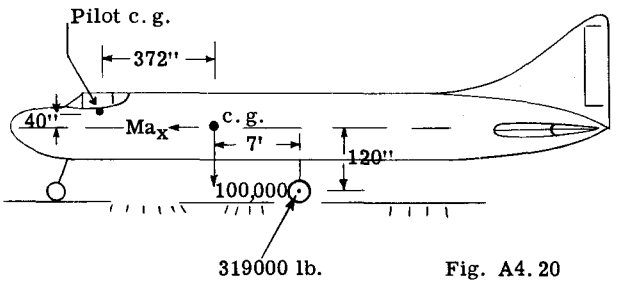

Fig. A4.20

Solution: -

The wing lift will be neglected in this example problem.

The inertia forces on the airplane are forces Ma_x and Ma_g and the couple $I_{c.g.}\alpha$.

To find Ma_x take,

$$\Sigma F_x = 100{,}000 - Ma_x = 0$$

or

$$Ma_x = 100{,}000\ lb.$$

hence,

$$a_x = \frac{100{,}000}{M} = \left(\frac{100{,}000}{100{,}000}\right) g = 1g \rightarrow$$

To find Ma_g take,

$$\Sigma F_g = 300{,}000 - 100{,}000 - Ma_g = 0$$

$$Ma_g = 200{,}000\ lb.$$

hence

$$a_g = \frac{200{,}000}{M} = \left(\frac{200{,}000}{100{,}000}\right) g = 2g \uparrow$$

To find the inertia couple $I_{c.g.}\alpha$, take moments about airplane c.g.,

$$\Sigma M_{c.g.} = -100{,}000 \times 120 - 300{,}000 \times 84 + I_{c.g.}\alpha = 0$$

$$I_{c.g.}\alpha = 37{,}200{,}000\ lb.$$

hence angular acceleration $\alpha = \frac{37{,}200{,}000}{40{,}000{,}000} =$

$$0.93\ rad/sec^2.$$

Calculations of resultant load on pilot: -

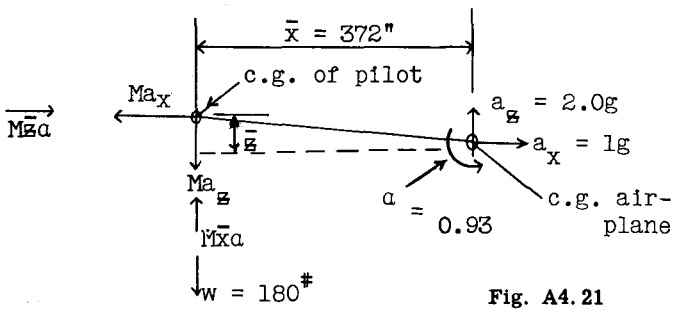

Fig. A4.21

Fig. A4.21 shows the airplane c.g. accelerations.

The forces on the pilot consist of the pilots weight of 180 lb. and the various inertia forces as indicated in the figure.

$$Ma_x = \left(\frac{180}{g}\right) 1g = 180^{\#}$$

$$Ma_z = \left(\frac{180}{g}\right) 2.0g = 360^{\#}$$

The inertia force due to the angular acceleration α acts normal to the radius arm between the airplane c.g. and the pilot. For convenience this normal force will be replaced by its z and x components.

$$F_x = M\bar{z}\alpha = \frac{180}{32.2 \times 12} \times 40 \times 0.93 = 17 \text{ lb.}$$

$$F_z = M\bar{x}\alpha = \frac{180}{32.2 \times 12} \times 372 \times 0.93 = 161 \text{ lb.}$$

Total force in x direction on pilot equals

$$180 - 17 = 163 \text{ lb.}$$

Total force in z direction =

$$360 + 180 - 161 = 379 \text{ lb.}$$

Hence Resultant force R, equals

$$\sqrt{379^2 + 163^2} = 410^{\#}$$

A4.13 Effect of Airplane Not Being a Rigid Body.

The example problems of Art. A4.12 assume that the airplane is a rigid body (suffers no structural deformation). On the basis of this assumption the applied loads on the airplane in either flight or landing conditions are placed in equilibrium with the inertia forces which occur due to the acceleration of the airplane. It is obvious that an airplane structure like any other structure is not a rigid body, particularly a cantilever wing which undergoes rather large bending deflections in both flight and landing conditions. Figure A4.21 shows a composite photograph taken of a test wing for the Boeing B-47 airplane. The maximum upward and downward deflections shown are for design loads, which in general are 1.5 times the applied loads. It would not be correct to say that the wing deflections under the applied loads for these two High Angle of attack conditions would be 2/3 the deflections shown in the photograph since under the design loads a considerable portion of the wing would be stressed beyond the elastic limit of the material or into the plastic range where the stiffness modulus is

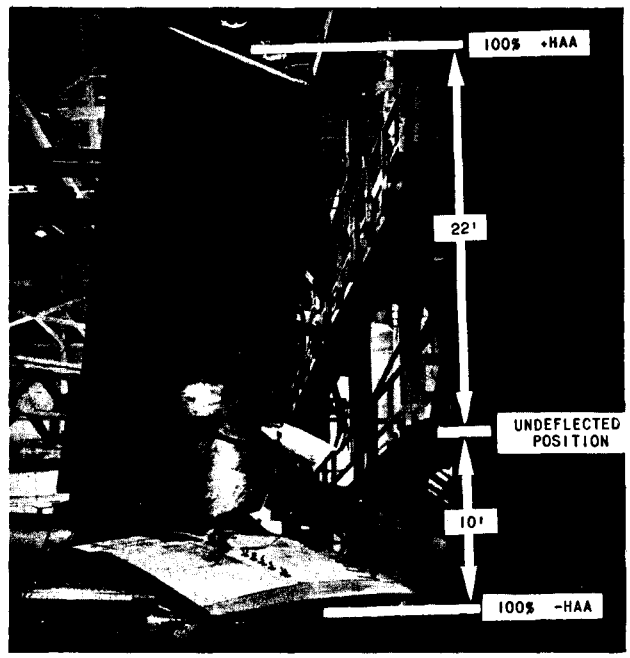

Fig. A4.21

considerably less than the modulus of elasticity, hence the deflections under the applied loads would be somewhat less than 2/3 those shown in the photograph. This photograph thus indicates very strikingly that a wing structure is far from being a rigid body.

Static loads are loads which are gradually applied and cause no appreciable shock or vibration of structure. On high speed aircraft, air gusts, flight maneuvers and landing reactions are applied quite rapidly and thus can be classed as dynamic loads. Therefore when these dynamic loads strike a flexible (non-rigid) airplane cantilever wing, a rather large wing deflection is produced and the wing tends to vibrate. This vibration therefore causes additional accelerations of the mass units of the wing which means additional inertia forces on the wing. Furthermore if the time rate of application of the external applied forces approaches the natural bending frequencies of the wing, the vibration excited can produce large additional wing stresses.

Up until World War II practically all airplanes were assumed as rigid bodies for structural design purposes. During the war failure of aircraft occured under load conditions which the conventional design procedure based on rigid body analysis, indicated satisfactory or safe stresses. The failures were no doubt due to dynamic overstress because the airplane is not a rigid body.

Furthermore, airplane design progress has resulted in thin wings and relatively large wing spans, and in many cases these wings carry concentrated masses, such as, power plants, bombs, wing tip fuel tanks etc,. Thus the flexibility of wings have increased which means the natural bending frequencies have decreased. This fact together with the fact that airplane speeds have greatly increased and thus cause air gust loads to be applied more rapidly, or the loading is becoming more dynamic in character and thus the overall load effect on the wing structure is appreciable and cannot be neglected in the strength design of the wing.

General Dynamic Effect of Air Forces on Wing Loads.

The critical airloads on an airplane are caused by maneuvering the airplane by the pilot or in striking a transverse air gust. A transport airplane does not have to be designed for sharp maneuvers producing high airplane accelerations in its job of transporting passengers, thus the time of applying the maneuver loads is considerably more than a fighter type airplane pulling up sharply from high speeds.

Fig. A4.22 shows the result of a pull-up maneuver on the Douglas D.C.3 airplane at 180 M.P.H. relative to load factor versus time of application of load. As indicated the peak load of load factor 3.25 was obtained at the end of one second of time.

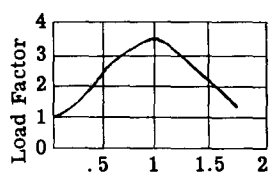

Fig. A4.22

Pull-up of DC-3 Airplane at 180 mph.

The author estimates the natural frequency of the D.C.3 wing to be around 10 to 15 cycles per second, thus a loading time of 1 second against a time of 1/10 or 1/15 for half a wing deflection cycle indicates that dynamic overstress should not be appreciable. In general, it can be said that dynamic over-stress under maneuvering loads on transport airplanes is not as great as from other conditions such as air gusts or landing.

Dynamic Effect of Air Gusts.

The higher the air gust velocity and the higher the airplane velocity, the less the time for applying the load on the wing when striking the air gust.

NACA Technical Note 2424 reports the flight test results on a twin-engine Martin transport airplane. Strain gages were placed at various points on the wing structure, and strains were read for various gust conditions for which the normal airplane accelerations were also recorded. Then slow pull-up maneuvers were run to give similar airplane normal accelerations. The wing had a natural frequency of 3.8 cps and the airplane speed was 250 M.P.H. Two of the conclusions given in this report are: - (1) The bending strains per unit normal acceleration under air gusts were approximately 20 percent higher than those of slow pull-ups for all measuring positions and flight conditions of the tests, and (2) The dynamic component of the wing bending strains appeared to be due primarily to excitation of the fundamental wing bending mode.

These results thus indicate that air gusts apply a air load more rapidly to a wing than a maneuver load giving the same airplane normal acceleration for a commercial transport type of airplane, and thus the dynamic strain effect on the wing is more pronounced for gust conditions.

Figs. A4.23, 24 and 25 show results of dynamic effect of air gusts on a large wing as determined by Bisplinghoff*. The results in these figures show that dynamic effects tend to considerably increase wing forces on some portions of the wing and decrease it on other portions.

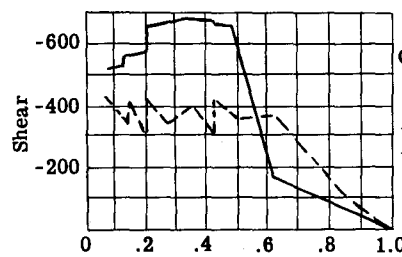

Fig. A4.23

Comparative Shear Distribution

—— **Dynamic Analysis**

– – – **Rigid Airplane Analysis**

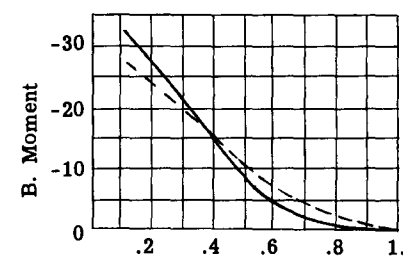

Fig. A4.24

Comparative Bending Moment Distribution

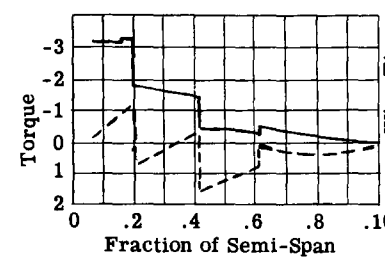

Fig. A4.25
Comparative Distribution of Torque About Elastic Axis.

General Data:-
Wing Span = 189 ft.
Gross Wt. = 184000 lb.
Airlane Vel. =260 mph.

*** Report on an Investigation on Stresses in Aircraft Structures under Dynamic Loading. M.I.T. Publication.**

It has also been found that landing loads applied through the conventional landing gear or by water pressure on a flying boat are applied rapid enough to be classed as dynamic loads and such loads applied to wings of large span produce dynamic stresses which cannot be neglected in the safe design of such structures.

A4.14 General Conclusions on Influence of Dynamic Loading on Structural Design of Airplane.

The advent of the turbo-jet and the rocket type engines has opened up a range of possible airplane airspeeds hardly dreamed of only a few years ago, and already trans-sonic and supersonic speed airplanes are a common development. From an aerodynamic standpoint such speeds have dictated a thin airfoil section which has thus promoted a high density wing. Thus for airplanes with appreciable wing spans like Military bombers and near future jet commercial transports, which usually carry large concentrated masses on the wing such as engines, fuel tanks etc., the assumption that the airplane is a rigid body is not sufficiently accurate enough because the dynamic stresses are appreciable.

The calculation of the dynamic loading on the wing requires that the mass and stiffness distribution of the wing structure be known. Since these factors are not known when the structural design of a wing is started, the general procedure in design would be to first base the design on the assumption that the wing is a rigid body plus correction factors based on past design experience or available research information to approximately take care of the influence of the elastic wing on the airplane aerodynamic characteristics and the build up dynamic inertia forces. With the wing thus initially designed by this procedure, it then can be checked by a complete dynamic analysis and modified as the results dictate and then recalculated for the modified elastic wing. This procedure is now practical because of the availability of high speed computors.

A4.15 PROBLEMS.

(1). The airplane in Fig. A4.26 is being launched from the deck of an aircraft carrier by the cable pull T which gives the airplane a forward acceleration of 3.25g. The gross weight of the airplane is 15,000 lb.

(a) Find the tension load T in the launching cable, and the wheel reactions R_1 and R_2.

(b) If the flying speed is 75 M.P.H., what launching distance is required and the launching time t?

(2). Assume the airplane of Fig. A4.26 is landing at 75 M.P.H. on a runway and brakes are applied to the rear wheels equal to .4 of the vertical rear wheel reaction. What is the horizontal deceleration and the stopping distance for the airplane?

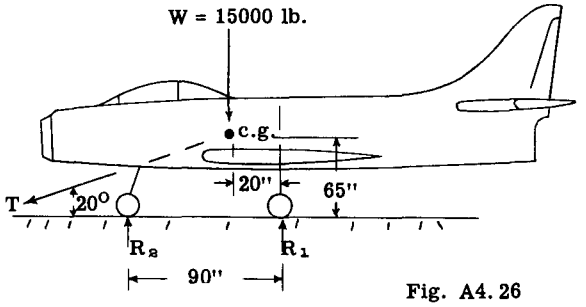

Fig. A4.26

(3). The flying patrol boat in Fig. A4.27 makes a water landing with the resultant bottom water pressure of 250,000 lb. as shown in the figure. Assume lift and tail loads as shown. The pitching moment of inertia of the airplane is 10 million lb. sec.^{2} in. Determine the airplane pitching acceleration. What is the total load on the crew member who weighs 200 lb. and is located in a seat at the rear end of the hull?

Fig. A4.27

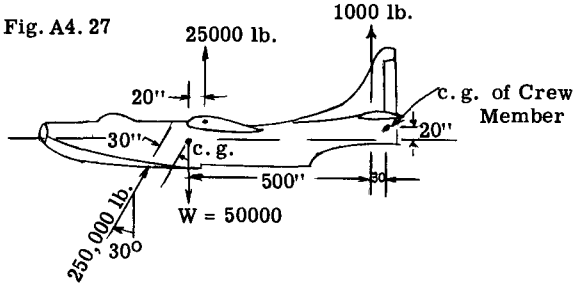

(4). The jet-plane in Fig. A4.28 is diving at a speed of 600 M.P.H. when pilot starts a 8g pull-out. Weight of airplane is 16,000 lb. Assume that engine thrust and total airplane drag are equal, opposite and colinear.

(a) Find radius of flight path at start of pull-out.

(b) Find inertia force in Z direction.

(c) Find lift L and tail load T.

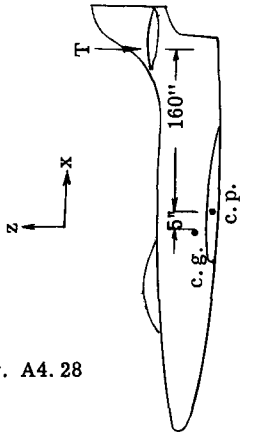

Fig. A4.28

CHAPTER A5
BEAMS - SHEAR AND MOMENTS

A5.1 Introduction.

In general, a structural member that supports loads perpendicular to its longitudinal axis is referred to as a beam. The structure of aircraft provides excellent examples of beam units, such as the wing and fuselage. Very seldom do bending forces act alone on a major aircraft structural unit, but are accompanied by axial and torsional forces. However, the bending forces and the resulting beam stresses due to bending of the beam are usually of primary importance in the design of the beam structure.

A5.2 Statically Determinate and Statically Indeterminate Beams.

A beam can be considered as subjected to known applied loads and unknown supporting reactions. If the distribution of the applied known loads to the supporting reactions can be determined from the conditions of static equilibrium alone, namely, the summation of forces and moments equal zero, then the beam is considered as a statically determinate beam. However, if the distribution of the known applied loads to the supporting beam reactions is influenced by the behavior of the beam material during the loading, then the supporting reactions cannot be found by the statical equilibrium equations alone, and the beam is classified as a statically indeterminate beam. To solve such a beam, other conditions of fact based on the beam deformations must be used in combination with the static equilibrium equations.

A5.3 Shear and Bending Moment.

A given beam is subjected to a certain applied known loading. The beam reactions to hold the beam in static equilibrium are then calculated by the necessary equations of static equilibrium, namely: -

$\Sigma V = 0$, or the algebraic summation of all vertical forces equals zero.

$\Sigma H = 0$, or the algebraic summation of all horizontal forces equals zero.

$\Sigma M = 0$, or the algebraic summation of all the moments equals zero.

With the entire beam in static equilibrium, it follows that every portion of the beam must likewise be in static equilibrium. Now consider the beam in Fig. A5.1. The known applied load of P = 100 lb. is held in equilibrium by the two reactions of 25 and 75 lbs. as shown and are calculated from simple statics. (Beam weight is neglected in this problem). Now consider the beam as cut at section a-a and consider the

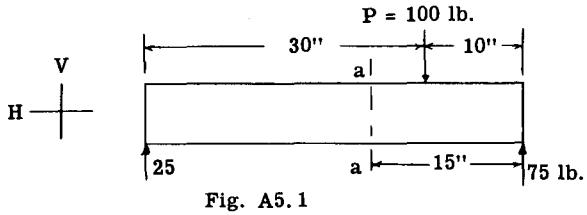

Fig. A5.1

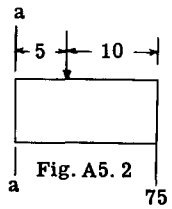

Fig. A5.2

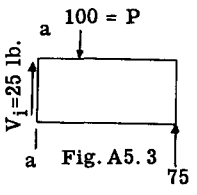

Fig. A5.3

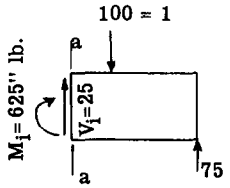

Fig. A5.4

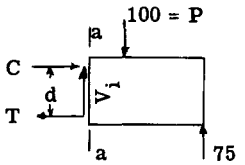

Fig. A5.5

right side portion as a free body in equilibrium as shown in Fig. A5.2. For static equilibrium, ΣV, ΣH and ΣM must equal zero for all forces and moments acting on this beam portion. Considering $\Sigma V = 0$ in Fig. A5.3: -

$$\Sigma V = 75 - 100 = -25 \text{ lb.} \quad \text{-------} \quad (1)$$

thus, under the forces shown, the force system is unbalanced in the V direction, and therefore an internal resisting force V_1 equal to 25 lb. must have existed on section a-a to produce equilibrium of forces in the V direction. Fig. A5.3 shows the resisting shear force, V_1 = 25 lb, which must exist for equilibrium.

Considering $\Sigma M = 0$ in Fig. A5.3, take moments about some point O on section a-a,

$$\Sigma M_o = -75 \times 15 + 100 \times 5 = -625 \text{ in.lb.} \quad (2)$$

or an unbalanced moment of - 625 tends to rotate the portion of the beam about section a-a. A counteracting resisting moment M = 625 must exist on section a-a to provide equilibrium. Fig. A5.4 shows the free body with the V_1 and M_1 acting.

Now ΣH must equal zero. The external forces as well as the internal resisting shear V_1 have no horizontal components. Therefore, the internal forces producing the resisting moment M_1 must be such as to have no horizontal

unbalanced force, which means that the resisting moment M_1 in the form of a couple, as shown in Fig. A5.5, or M_1 = Cd or Td and T must equal C to make $\Sigma H = 0$.

The tendency of the loads and reactions acting on a beam to shear or move one portion of a beam up or down relative to the adjacent portion of the beam is called the External Vertical Shear, or commonly referred to as the beam Vertical Shear and is represented by the term V.

From equation (1), the Vertical Shear at any section of a beam can be defined as the algebraic sum of all the forces and reactions acting to one side of the section at which the shear is desired. If the portion of the beam to the left of the section tends to move up relative to the right portion, the sign of the Vertical Shear is taken as positive shear and negative if the tendency is opposite. Or in other words, if the algebraic sum of the forces is up on the left or down on the right side, then the Vertical Shear is positive, and negative for down on the left and up on the right.

From equation (2), the Bending Moment at any section of a beam can be defined as the algebraic sum of the moments of all the forces acting to either side of the section about the section. If this bending moment tends to produce compression (shortening) of the upper fibers and tension (stretching) of the lower fibers of the beam, the bending moment is classed as a positive bending moment, and negative for the reverse condition.

A5.4 Shear and Moment Diagrams.

In aircraft design, a large proportion of the beams are tapered in depth and section, and also carry a variable distributed load. Thus, to design or check the various sections of such beams, it is necessary to have a complete picture as to the value of the vertical shear and bending moment at all sections along the beam. If these values are plotted as ordinates from a base line, the resulting curves are referred to as Shear and Moment diagrams. A few example Shear and Moment diagrams will be plotted, to refresh the students knowledge regarding these diagrams.

Example Problem 1.

Draw a shear and bending moment diagram for the beam shown in Fig. A5.6. Neglect the weight of the beam.

In general, the first step is to determine the reactions.

To find R_B, take moments about point A.

$\Sigma M_A = -4 \times 500 + 1000 \times 5 + 300 \times 13 - 10R_B = 0$

hence R_B = 690 lb.

$\Sigma V = -500 + R_A - 1000 - 300 + 690 = 0$

hence R_A = 1110 lb.

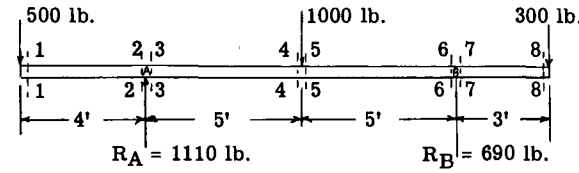

Fig. A5.6

Calculations for Shear Diagram: -

We start at the left end of the beam. Considering a section just to the right of the 500 lb. load, or section 1-1, and considering the portion to the left of the section, the Vertical Shear at 1-1 = $\Sigma V = -500$ (negative, down on left.)

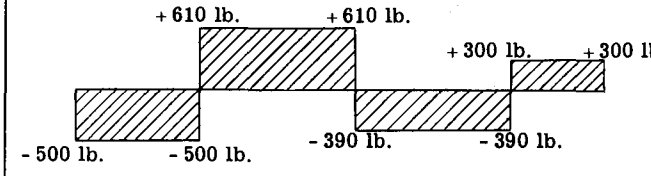

Fig. A5.7 (Shear Diagram)

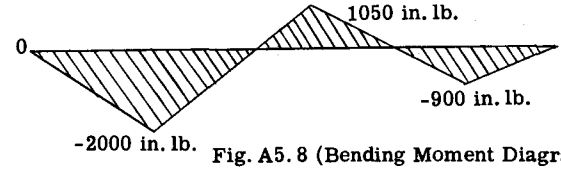

Fig. A5.8 (Bending Moment Diagram)

Next, consider section 2-2, just to left of reaction R_A.

$\Sigma V = -500$, or same as at section 1-1.

Next, consider section 3-3, just to right of R_A.

$\Sigma V = -500 + 1110 = 610$ (positive, up on left side of section).

Next, consider section 4-4, just to left of 1000 load.

$\Sigma V = -500 + 1110 = 610$ (same as at section 3-3).

Section 5-5, to right of 1000 load:

$\Sigma V = -500 + 1110 - 1000 = -390$ (down on left).

Check this shear at section 5-5 by using the portion of the beam to the right of 5-5 as a free body.

$\Sigma V = -300 + 690 = 390$, which checks (sign of shear is minus, because ΣV is up on right). Section 6-6, use the portion to right as a free body:

$\Sigma V = -300 + 690 = 390$ (minus shear).

Section 7-7:

$\Sigma V = -300$ (positive shear, down on right)

Section 8-8:

$\Sigma V = -300$ (positive shear).

Fig. A5.7 shows the plotted values on the shear diagram.

Calculation of the Moment Diagram.

Start at section 1-1, and consider the forces to the left only:

$\Sigma M = -500 \times 0 = 0$

Since sections 2-2 and 3-3 are only a differential distance apart, assume a section just above R_A and consider the forces on the left side only:

$\Sigma M = -500 \times 4 = -2000$ in. lb. (Negative moment, because of tension in the top fibers). Consider the section under the 1000 in. lb. load:

ΣM to left $= -500 \times 9 + 1110 \times 5 = 1050$ in. lb. (positive moment, compressing the top fibers).

Check by considering the forces to the right:

ΣM right $= 300 \times 8 - 690 \times 5 = -1050$ in.lb.

Next, consider a section over R_B:

ΣM right $= 300 \times 3 = 900$ in. lb. (Negative moment, tension in top fibers).

At Section 8-8:

ΣM right $= 300 \times 0 = 0$

Fig. A5.8 shows the plotted values.

From the above results it may be noticed that when the bending moment is obtained from the forces that lie to the left of any section, the bending moment is positive when it is clockwise. If obtained from the forces to the right, it is positive, when counter-clockwise. The student should sketch in the approximate shape of the deflected structure and determine the signs from whether tension or compression exists in the upper and lower fibers.

Example Problem 2

Calculate and draw the shear and moment diagrams for the beam and loading as shown in Fig. A5.9.

First, determine the reactions, R_A and R_B: -

$\Sigma M_A = 36 \times 10 \times 18 + 120 \times 9 - 36R_B = 0.$
hence $R_B = 210$ lb.

$\Sigma V = -120 - 36 \times 10 + 210 + R_A = 0.$
hence $R_A = 270$ lb.

Shear Diagram: -

The vertical shear just to the right of the reaction at A is equal to 270 up, or positive. This is plotted as line AE in Fig. A5.10. The vertical shear at section C just to the left of the load and considering the forces to the left of the section = 270 - 9 x 10 = 180 lb. up, or positive. The vertical shear for any section between A and C at a distance x from A is:

$V_x = 270 - 10x$, and hence, the shear decreases at aconstant rate of 10 lb./in. from 270 at A to 180 at C.

The vertical shear at section D, just to the right of load is,

$V_D = \Sigma V_{left} = 270 - 10 \times 9 - 120 = 60$ up, or positive.

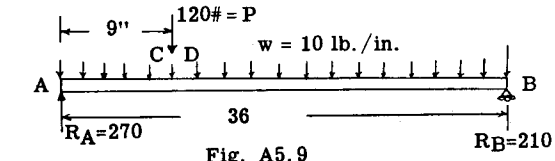

Fig. A5.9

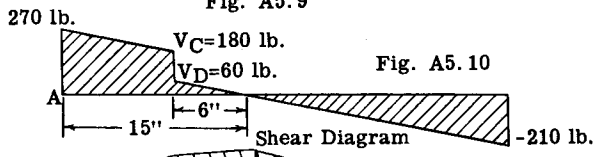

Fig. A5.10

Fig. A5.11

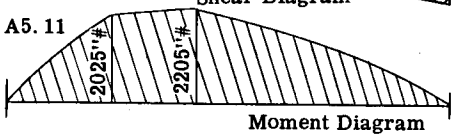

The vertical shear between points D and B, when x is the distance of any section between D and B from A:

$V_{DB} = 270 - 120 - 10x$ - - - - - - - - - - (1)

At point B, x = 36:

hence $V_B = 270 - 120 - 10 \times 36 = -210$ lb., which checks the reaction R_B.

Since the Vertical Shear decreases at a rate of 10 lb/in. from D to B, it will be 6" from D to a point where the shear is zero, since the shear at D is 60 lb.

This point could also be located by equating equation (1) to zero and solving for x as follows:

$0 = 270 - 120 - 10x$, or $x = \frac{150}{10} = 15"$ from A.

If the shear diagram has passed through zero under the concentrated load, then the method of equating the shear equation to zero and solving for x could not be used, thus in general, it is best to draw a shear diagram to find when shear is zero. Fig. A5.10 shows the plotted shear diagram.

Moment Diagram: -

At section A just to the right of reaction R_A the bending moment, considering the forces to the left, is zero, since the arm of R_A is zero.

The bending moment at any section between A and C, at a distance x from the left reaction R_A, is,

$$M_x = R_A x - \frac{wx^2}{2} \quad \text{- - - - - - - - - - - - - - - - (2)}$$

In equation (2), x can not be greater than 9.

The equation for the bending moment between D and B (x greater than 9) is

$$M_x = R_A x - P\,(x-9) - \frac{wx^2}{2} \text{ - - - - - - - - - - } (3)$$

$$= 270\,x - 120\,(x-9) - \frac{10x^2}{2} \text{ - - - - - - -}$$

$$= 1080 + 150\,x - 5x^2 \text{ - - - - - - - - - - } (4)$$

At section C, x = 9", substitute in equation (4)

$M_C = 1080 + 150 \times 9 - 5 \times 9^2 = 2025$ in.lb. (positive, compression in top fibers).

At the point of zero shear, x = 15".

$M = 1080 + 150 \times 15 - 5 \times 15^2 = 2205$

Thus, by substituting in equation (2) and (4) the moment diagram as plotted in Fig. A5.11 is obtained.

A5.5 Section of Maximum Bending Moment.

The general expression for the bending moment on the beam of example problem 2 is from equation (3):

$$M_x = R_A x - P\,(x-9) - \frac{wx^2}{2}$$

Now, the value of x that will make M_x a maximum or minimum is the value that will make the first derivative of M_x with respect to x equal to zero, or

$$\frac{dM_x}{dx} = R_A - P - wx \text{ - - - - - - - - - - - - - - } (5)$$

Therefore, the value of x that will make M_x a maximum or minimum may be found from the equation

$$R_A - P - wx = 0$$

But, observation of this equation indicates that the term Ra - P - wx is the shear for the section at a distance x from the left reaction. Therefore, where the shear is zero, the bending moment is maximum. Thus, the shear diagram which shows where the shear is zero is a convenient medium for locating the points of maximum bending moment.

A5.6 Relation Between Shear and Bending Moment.

Equation (5) can also be written $\frac{dM}{dx} = V$, since the right hand portion of equation (5) is equal to the shear.

Hence, $dM = Vdx$ - - - - - - - - - - - - - - - (6)

Which means that the difference dM between the bending moments at two sections that are a distance dx apart, is equal to the area Vdx under the shear curve between the two sections. Thus, for two sections x_1 and x_2,

$$\int_{M_1}^{M_2} dM = \int_{x_1}^{x_2} V dx$$

Thus, the area of the shear diagram between any two points equals the change in bending moment between these two points.

To illustrate this relationship, consider the shear diagram in example problem 2 (Fig. A5.10). The change in bending moment between the left reaction R_A and the load is equal to the area of the shear diagram between these two points, or

$\frac{270 + 180}{2} \times 9 = 2025$ in.lb. Since the bending moment at the left support is zero, this change therefore equals the true moment at a section under the load P.

Adding to this the area of the small triangle between point D and the point of zero shear, or $\frac{60}{2} \times 6 = 180$, we obtain 2205 in.lb. as the maximum moment. This can be checked by taking the area of the shear diagram between the point of zero shear and point B = $\frac{210}{2} \times 21 = 2205$ in. lb.

Example Problem 3.

Fig. A5.12 illustrates a landing gear oleo strut ADEO braced by struts BD and CE. A landing ground load of 15000 lb. is applied through the wheel axle as shown. Let it be required to find the axial load in all members and the shear and bending moment diagram for the oleo strut.

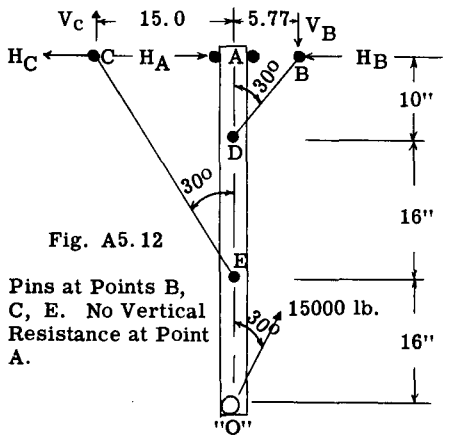

Fig. A5.12

Pins at Points B, C, E. No Vertical Resistance at Point A.

SOLUTION: -

To find V_C take moments about point B, $\Sigma M_B = -15000 \times 0.5 \times 42 + 15000 \times 0.866 \times 5.77 + 20.77\,V_C = 0$.

hence, $V_C = 11550$ lb.

The axial load in member CE therefore equals

11550/cos 30° or 13330 lb. $\therefore H_C = 11550 \times 15/26 = 6660$

To find H_A take moments about point D,

$\Sigma M_D = 11550 \times 15 - 6660 \times 10 - 15000 \times 0.5 \times 32 + 10 H_A = 0.$

hence, $H_A = 13340$ lb.

To find V_B take $\Sigma F_V = 0$,

$\Sigma F_V = 15000 \cos 30° + 11550 - V_B = 0.$

hence, $V_B = 24550$ lb.

The axial load in member BD therefore equals 24550/cos 30° = 28360 lb. (compression). The reaction H_B therefore equals 28360 x sin 30 = 14180 lb.

Fig. A5.13 shows the oleo strut as a free body with the reactions at A, D and E as calculated. Fig. A5.13 also shows the axial load, vertical shear and bending moment diagrams.

The bending moments due to applied loads without regard to bending deformation of the beam are usually referred to as the primary bending moments. If a member carries axial loads additional bending moments will be produced due to the axial loads times the lateral deflection of the beam, and these bending moments are usually referred to as secondary bending moments. (Arts. A23-30 covers the calculation of secondary moments).

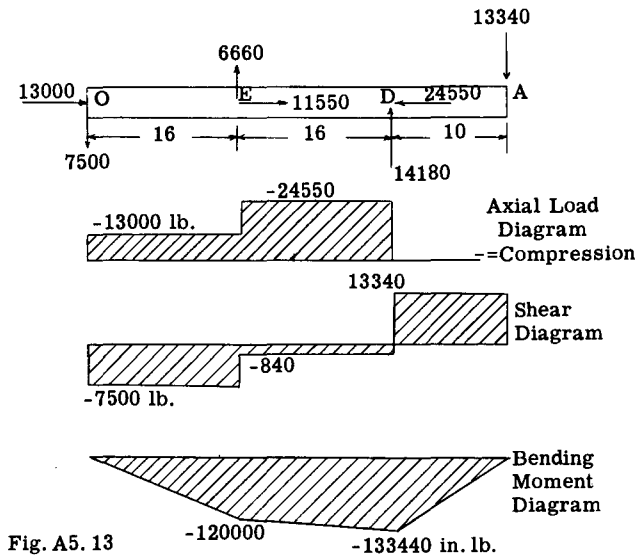

Fig. A5.13

Example Problem 4.

Fig. A5.14 shows a beam loaded with both transverse and longitudional loads. This beam loading is typical of interior beams in the airplane fuselage which support all kinds of fixed equipment. The reactions for the beam are at points A and B. Required: - Shear and bending moment diagrams.

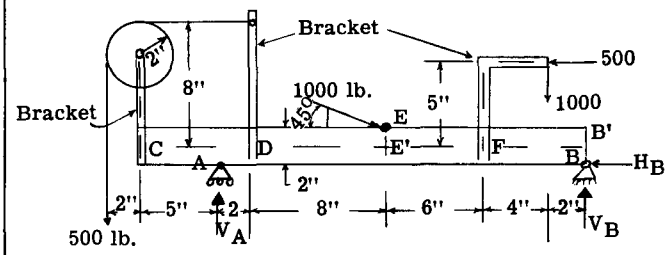

Fig. A5.14

SOLUTION: -

Calculations of reactions at A and B: -

To find V_B take moments about point A,

$\Sigma M_A = - 500 \times 7 - 500 \times 6 + 1000 \times 20 + 1000 \times \sin 45° \times 10 + 1000 \cos 45° \times 2 - 22 V_B = 0.$

hence, $V_B = 999.3$ lb. (up).

To find V_A take $\Sigma V = 0$,

$\Sigma V = 999.3 - 1000 - 1000 \sin 45° - 500 + V_A = 0.$

hence, $V_A = 1207.8$ lb. (up).

To find H_B take $\Sigma H = 0$,

$\Sigma H = - 500 + 1000 \cos 45° - H_B = 0$, hence $H_B = 207.1$.

With the exception of the 1000 lb. load at 45°, all loads are applied to brackets which in turn are fastened to the beam. Therefore the next step is to find the reaction of the loaded brackets at the beam centerline support points. The load at E and the reaction H_B at B will be also referred to beam centerline.

Fig. A5.15 (a,b,c,d) show the cantilever brackets as free bodies. The reactions at the base of these cantilevers will be determined. These reactions reversed will then be the applied loads to the beam at points C, D, F and E.

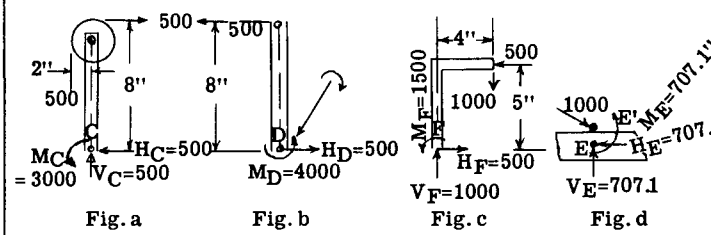

Fig. A5.15

For bracket at C, to find H_C take $\Sigma H = 0$, or obviously $H_C = 500$ lb. In like manner use $\Sigma V = 0$ to find $V_C = 500$ lb. To find M_C take moments about point C. $\Sigma M_C = - 500 \times 2 + 500 \times 8 - M_C = 0$, hence $M_C = 3000$ in. lb. The student should check the reactions at the base of the cantilever brackets at D and F (See Fig. b,c).

The load of 1000 at 45° and applied at point E' will be referred to point E the centerline of beam. Fig. d shows the reaction at E due to the load at E'. The reaction at B should also be referred to the beam centerline. Fig. A5.16 shows the beam with the applied loads at points C D E' F and B'. Figs. A5.17, 18 and 19 show the axial load, vertical shear and bending moment diagrams under the beam loading of Fig. A5.16.

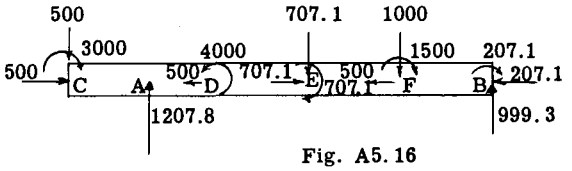

Fig. A5.16

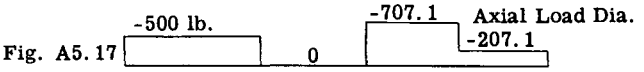

Fig. A5.17

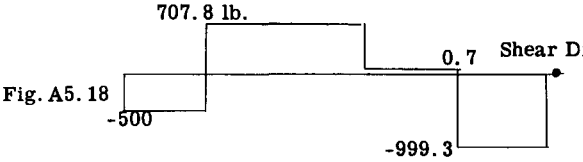

Fig. A5.18

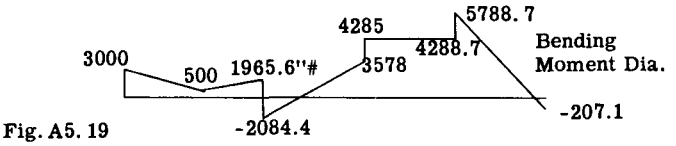

Fig. A5.19

The shear diagram is determined in the same manner as explained before. The applied external couples do not enter into the vertical shear calculations. The bending moment diagram can be calculated by taking the algebraic sum of all couples and moments of all forces lying to the one side of a particular section. If it is desired to use the area of the shear diagram to obtain the bending moments, it is necessary to add the couple moments to the shear areas to obtain the true bending moment. For example, the bending moment just to the left of point E will be equal in magnitude to the area of the shear diagram between C and E plus the sum of all applied couple moments between C and E but not including that at E.

To illustrate the calculations are: -
(- 500 x 5) + (707.8 x 10) = 4578 in. lb. (from area of shear diagram).
(3000 - 4000) = - 1000 in. lb. (from sum of couple moments).
Thus bending moment at E_{left} = 4578 - 1000 = 3578 in. lb.

The bending moment at E_{right} will equal that at E_{left} plus the couple moment at E or 3578 + 707 = 4285 in. lb.

The student should realize that when couple moments are applied to a beam it is possible to have maximum peak moments without the Vertical Shear passing through zero. To illustrate this fact, consider the beam of Fig. A5.20, namely, a simple supported beam with an externally applied couple moment of 10 in. lb. magnitude at point C the center point of the beam. The shear and bending moment diagrams are as indicated and a maximum bending moment occurs at C but the shear diagram does not pass through zero.

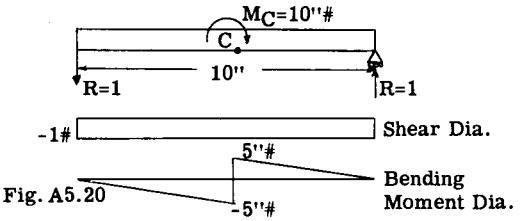

Fig. A5.20

A couple is two equal and opposite forces not in the same straight line. Let it be assumed that the 10 in. lb. couple is made up of forces equal to 100 lb. each and an arm between them of 0.1 inch as illustrated in Fig. A5.21.

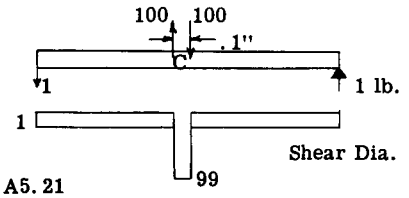

Fig. A5.21

The shear diagram is as shown in Fig. A5.21 and now passes through zero under each of the couple forces. Thus if we assume the couple moment has a dx arm the shear to the right of C is one lb. and then changes to some unknown negative value and then back to one lb. positive as the distance dx is covered in going to the left. Thus the shear goes to zero twice in the region of point C.

A5.7 Moment Diagrams as Made up of Parts.

In calculating the deflection of statically determinate beams (See Chapter A7) and solving statically indeterminate structures (See Chapter A8), the area under the bending moment curve is required, thus it is often convenient to treat each load and reaction as a separate acting force and draw the moment diagram for each force. The true bending moment at a particular point will then equal the algebraic summation of the ordinates of all the various moment curves at this particular point or adding the various separate moment diagrams will give the true bending moment diagram. Figs. A5.22 and A5.23 illustrate the drawing of the bending moment diagram in parts. In these examples, we start from the left end and proceed to the right end and draw the moment curve for each force as though the beam was a cantilever with the fixed

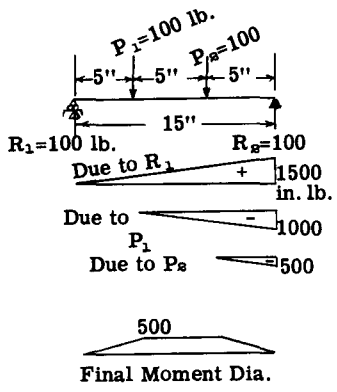

Fig. A5.22

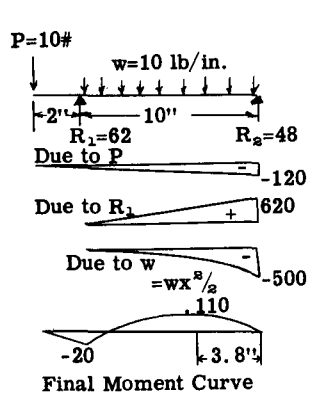

Fig. A5.23

support at the right end. The final bending moment curve for the true given beam then equals the sum of these separate diagrams as illustrated in the figures.

STATIC MOMENT CURVES IN SOLVING STATICALLY INDETERMINATE STRUCTURES

The usual procedure in solving a statically indeterminate structure is to first make the structure statically determinate by removing the necessary redundant or unknown reactions and then calculating the deflection of this assumed statically determinate structure as one step in the overall solution of the problem (See Chapter A8). In the solution of such structures it is likewise convenient to treat the bending moment diagram as made up of parts. To illustrate, Fig. A5.24 shows a loaded rectangular frame fixed at points A and B. The reactions at both

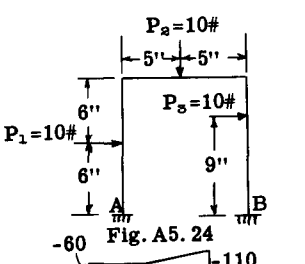

Fig. A5.24

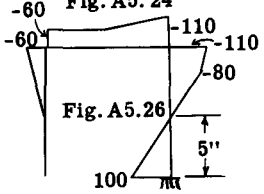

Fig. A5.26

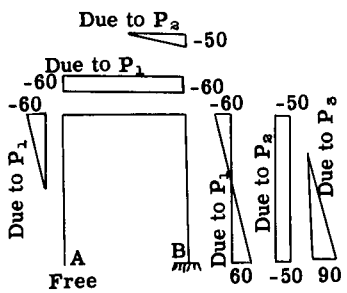

Fig. A5.25

points A and B are unknown in magnitude, direction and location, or each reaction has 3 unknown elements or a total of 6 unknowns for the two reactions. With 3 static equilibrium equations available, the structure is statically indeterminate to the third degree. Fig. A5.25 illustrates one manner in which the structure can be made statically determinate, by freeing the end A to make a bent cantilever beam fixed at B and thus leaving only 3 unknown elements of the reaction at B. Fig. A5.25 shows the bending moment curves for each load acting separately on this cantilever frame. Fig. A5.26 shows the true bending moment as the summation of the various moment curves of Fig. A5.25.

As another solution of this fixed ended frame, one could assume the statically determinate modification as a frame pinned at A and pinned with rollers at B as illustrated in Fig. A5.27. This assumed structure is statically determinate because there are only 3 unknown elements, namely the magnitude and direction of the reaction at A and the magnitude of the reaction at B. For convenience the reaction at A is resolved into two magnitudes as H and V components. The reactions V_A, H_A and V_B can then be found by statics and the results are shown on Fig. A5.27. Fig. A5.28 shows the bending moment diagram on this frame due to each load or reaction acting separately, starting at A and going clockwise to B. Fig. A5.29 shows the true bending moment diagram as the summation of the separate diagrams.

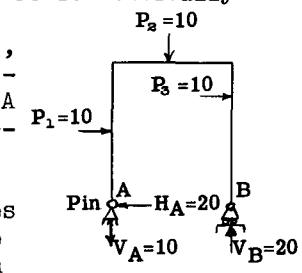

Fig. A5.27

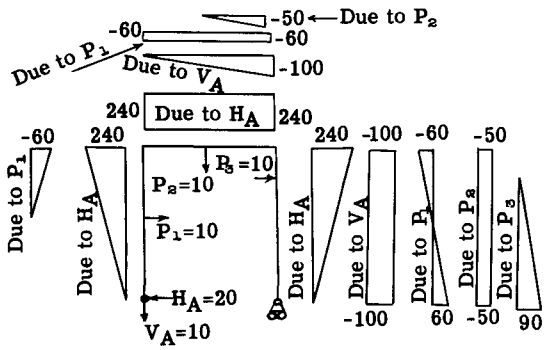

Fig. A5.28

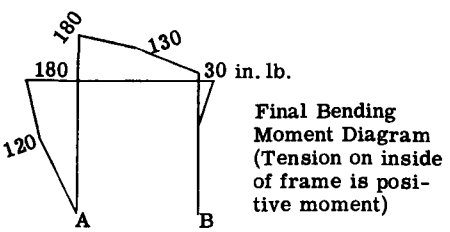

Final Bending Moment Diagram (Tension on inside of frame is positive moment)

Fig. A5.29

A5.8 Forces at a Section in Terms of Forces at a Previous Station.

STRAIGHT BEAMS.

Aircraft structures present many beams which carry a varying distributed load. Minimum structural weight is of paramount importance in aircraft structural design thus it is desirable to have the complete bending moment diagram for the structure so that each portion of the structure can be proportioned efficiently. To decrease the amount of numerical work required in obtaining the complete shear

and bending moment diagrams it usually saves time to express the shear and moment at a given station in terms of the shear and moment at a previous station plus the effect of any loads lying between these two stations. To illustrate, Fig. A5.30 shows a cantilever beam carrying a considerable number of transverse loads F of different magnitudes. Fig. A5.31 shows a free body

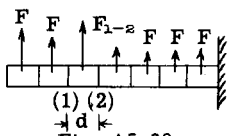

Fig. A5.30

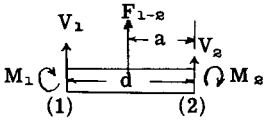

Fig. A5.31

of the beam portion between stations 1 and 2. The Vertical Shear V_1 at station 1 equals the summation of the forces to the left of station 1 and M_1 the bending moment at station 1 equals the algebraic sum of the moments of all forces lying to left of station 1 about station 1.

Now considering station 2: - The Vertical Shear $V_2 = V_1 + F_{1-2}$, or stated in words, the Shear V_2 equals the Shear at the previous station 1 plus the algebraic sum of all forces F lying between stations 1 and 2. Again considering Fig. A5.31, the bending moment M_2 at station 2 can be written, $M_2 = M_1 + V_1 d + F_{1-2} a$, or stated in words, the bending moment M_2 at station 2 is equal to the bending moment M_1 at a previous station 1, plus the Shear V at the previous station 1 times the arm d, the distance between stations 1 and 2 plus the moments of all forces lying between stations 1 and 2 about station 2.

A5.9 Equations for Curved Beams.

Many structural beams carry both longitudional and transverse loads and also the beams may be made of straight elements to form a frame or all beam elements may be curved to form a curved frame or ring. For example the airplane fuselage ring is a curved beam subjected to forces of varying magnitude and direction along its boundary due to the action of the fuselage skin forces on the frame. Since the complete bending moment diagram is usually desirable, it is desirable to minimize the amount of numerical work in obtaining the complete shear and bending moment values. Fig. A5.32 shows a curved beam loaded with a number of different vertical loads F and horizontal loads Q. Fig. A5.33 shows the beam portion 1-2 cut out as a free body. H_1 represents the resultant horizontal force at station 1 and equals the algebraic summation of all the Q forces to the left of station 1. V_1 represents the resultant vertical force at station 1 and equals the sum of all F forces to left of station 1, and M_1 equals the bending moment about point (1) on station 1 due to the moments of all forces lying to the left of point 1.

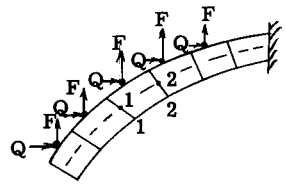

Fig. A5.32

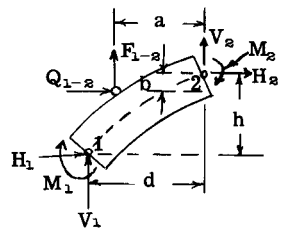

Fig. A5.33

Then from Fig. A5.33 we can write for the resultant forces and moment at point (2) at station 2: -

$$V_2 = V_1 + F_{1-2}$$

$$H_2 = H_1 + Q_{1-2}$$

$$M_2 = M_1 + V_1 d - H_1 h + F_{1-2} a - Q_{1-2} b$$

Having the resultant forces and moments for a given point on a given station, it is usually necessary in finding beam stresses to resolve the forces into components normal and parallel to the beam cross-section and also transfer their location to a point on the neutral axis of the beam cross-section.

For example Fig. A5.34 shows the resultant

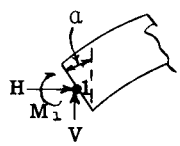

Fig. A5.34

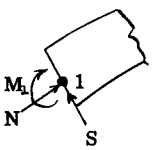

Fig. A5.35

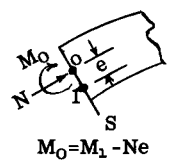

Fig. A5.36

forces and moment at point 1 of a beam cross-section. They can be resolved into a normal force N and a shear force S plus a moment M_1 as shown in Fig. A5.35 where,

$$N = H \cos \alpha + V \sin \alpha$$

$$S = V \cos \alpha - H \sin \alpha$$

Later on when the beam section is being designed it may be found that the neutral axis lies at point O instead of point 1. Fig. A5.36 shows the forces and moments referred to point O, with M_o being equal to $M_1 - Ne$.

A5.10 Torsional Moments.

The loads which cause only bending of a beam are located so that their line of action passes through the flexural axis of the beam. Quite often, the loading on a beam does not act through the flexural axis of the beam and thus the beam undergoes both bending and twisting. The moments which cause the twisting action are usually referred to as torsional moments. The airplane wing is an excellent example of a beam structure that is subjected to combined bending and torsion. Since the center of pressure of the airfoil forces changes with angle of attack, and since there are many flight conditions it is impossible to eliminate torsional moments under all conditions of flight and landing. For the fuselage, the Vertical tail surfaces is normally located above the fuselage and thus a load on this tail unit causes combined bending and twisting of the fuselage.

Fig. A5.34 illustrates a cantilever tube being subjected to a load P acting at point A on a fitting attached to the tube end. The flex-

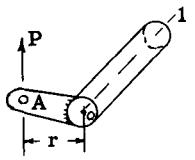

Fig. A5.34

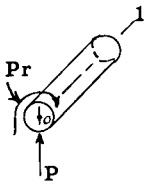

Fig. A5.35

ural axis coincides with the tube centerline, or axis 1-1. Fig. A5.35 shows the load P being moved to the point (0) on the tube axis 1-1, however the original force P had a moment about (0) equal to Pr, thus the moment Pr must be added to the load P acting at (0) if the force system at point (0) is to be equivalent to the original force P at point A. The force P acting through (0) causes bending without twist and the moment Pr causes twisting only.

For the resolution of moments into various resultant planes of action, the student should refer to any textbook on statics.

A5.11 Shears and Moments on Wing.

Arts. A4.5 and A4.6 of Chapter A4 discusses the airloads on the wing and the equilibrium of the airplane as a whole in flight. As explained, it is customary to replace the distributed air forces on an airfoil by two resultant forces, namely, lift and drag forces acting through the aerodynamic center of the airfoil plus a wing moment. The airflow around a wing is not uniform in the spanwise direction, thus the airfoil force coefficients C_L, C_D and C_M vary spanwise along the wing. Fig. A5.36 shows a typical spanwise variation of the C_L and C_D force coefficients in terms of a uniform spanwise variation $\bar{C}_L$ and $\bar{C}_D$.

Any particular type of airplane is designed to carry out a certain job or duty and to do that job requires a certain maximum airplane

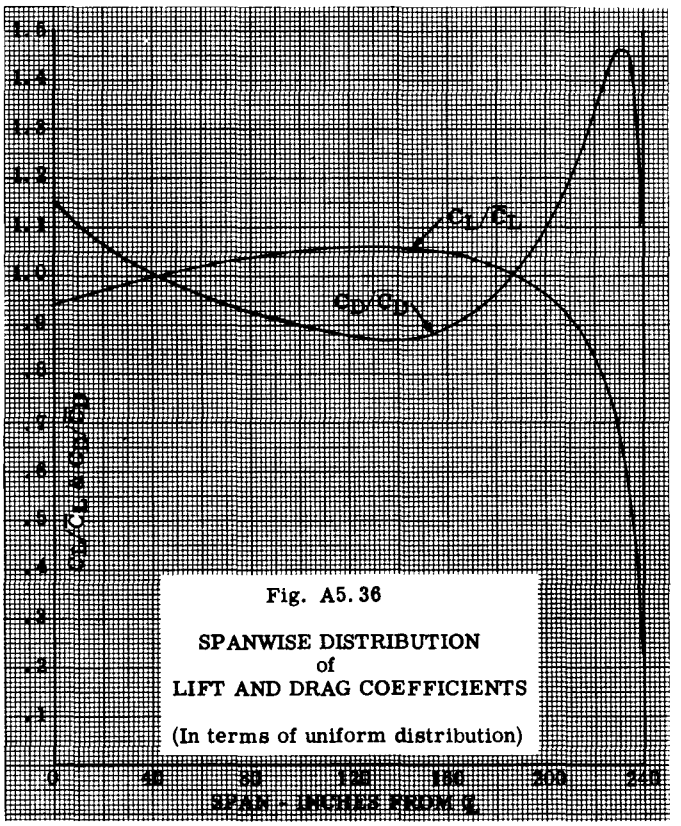

Fig. A5.36

SPANWISE DISTRIBUTION
of
LIFT AND DRAG COEFFICIENTS

(In terms of uniform distribution)

velocity with the maneuvering limited to certain maximum accelerations. These limiting accelerations are usually specified with reference to the X Y Z axes of the airplane. Since the directions of the lift and drag forces change with angle of attack it is simpler and convenient in stress analysis to resolve all forces with reference to the X Y Z axes which remain fixed in direction relative to the airplane.

As a time saving element in wing stress analysis, it is customary to make unit load analysis for wing shears and moments. The wing shears and moments for any design condition then follows as a matter of simple proportion and addition. For example it is customary: -

(1) To assume a total arbitrary unit load acting on the wing in the Z direction through the aerodynamic center of the airfoil section and distributed spanwise according to that of the C_L or lift coefficient.

(2) A similar total load as in (1) but acting in the X direction.

(3) To assume a total unit wing load acting in the Z direction through the aerodynamic center and distributed spanwise according to that of the C_D or drag coefficient.

(4) Same as (3) but acting in the X direction.

(5) To assume a unit total wing moment and distributed spanwise according to that of the $C_{m_{a.c}}$ or moment coefficient.

The above unit load conditions are for conditions of acceleration in translation of the

airplane as a rigid body. Unit load analyses are also made for angular accelerations of the airplane which can also occur in flight and landing maneuvers.

The subject of the calculation of loads on the airplane is far too large to cover in a structures book. This subject is usually covered in a separate course in most aeronautical curricula after a student has had initial courses in aerodynamics and structures. To illustrate the type of problem that is encountered in the calculation of the applied loads on the airplane, simplified problems concerning the wing and fuselage will be given.

A5.12 Example Problem of Calculating Wing Shears and Moments for One Unit Load Condition.

Fig. A5.37 shows the half wing planform of a cantilever wing. Fig. A5.38 shows a wing section at station 0. The reference Y axis has been taken as the 40 percent chord line which happens to be a straight line in this particular wing layout.

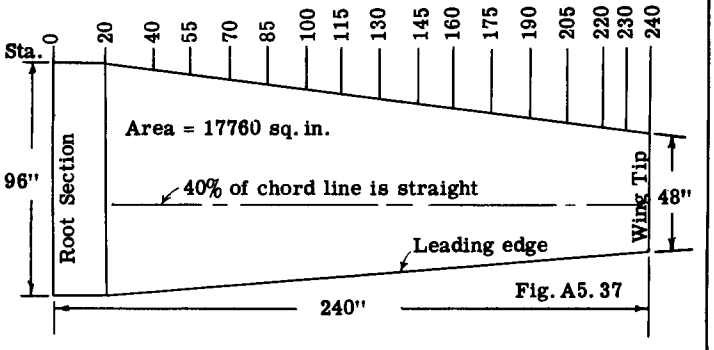

Fig. A5.37

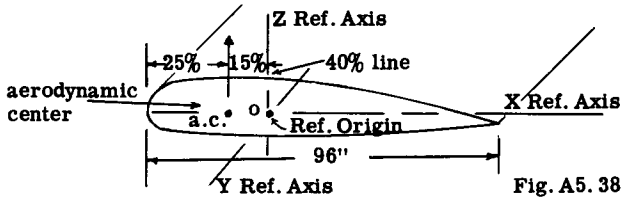

Fig. A5.38

The total wing area is 17760 sq. in. For convenience a total unit distributed load of 17760 lbs. will be assumed acting on the half wing and acting upward in the Z direction and through the airfoil aerodynamic center. The spanwise distribution of this load will be according to the (C_L) lift coefficient spanwise distribution. For simplicity in this example it will be assumed constant.

Table A5.1 shows the calculations in table form for determining the (V_Z) the wing shear in the Z direction, the bending moment M_X or moment about the X axis and M_y the moment about the Y axis for a number of stations between the wing tip station 240 and the centerline station 0.

Column 1 of the table shows the number of stations selected. Column 3 shows the $C_L/\bar{C}_L$ ratio or the spanwise variation of the lift coefficient C_L in terms of a uniform distribution $\bar{C}_L$. In this example we have taken this ratio as unity since we have no wind tunnel or aerodynamic calculations for this wing relative to the spanwise distribution of the lift force coefficient. In an actual problem involving an airplane a curve such as that given in Fig. A5.36 would be available and the values to place in Column 3 of Table A5.1 would be read from such a curve. Column (2) gives the wing chord length at each station. Column (4) gives the wing running load per inch of span at each station point. Since a total unit load of 17760 lb. was assumed acting on the half wing and since the wing area is 17760 sq. in., the running load per inch at any station equals the wing chord length at that station. In order to find shears and moments at the various station points, the distributed load is now broken down into concentrated loads which are equal to the distributed load on a strip and this concentrated strip load is taken as acting through the center of gravity of this distributed strip load. Columns 5, 6, and 7 show the calculations for determining the (ΔP_Z) strip loads. Column 8 shows the location of the ΔP_Z load which is at the centroid of a trapezoidal distributed load whose end values are given in Column (4). In determining these centroid locations it is convenient to use Table A3.4 of Chapter A3.

The values of the shear V_Z and the moment M_X at each station are calculated by the method explained in Art. A5.8. Columns 9, 10, 11 and 12 of Table A5.1 give the calculations. For example, the value of M_X = 9884 in Column (12) for station 220 equals 2436, the M_X moment at the previous station in Column (12) plus 4908 in Column (10) which is the shear at the previous station (230) times the distance 10 inches plus the moment 2540 in Column (9) due to the strip load between stations 230 and 220, which gives a total of 9884 the value in Column (12).

The strip loads ΔP_Z act through the aerodynamic center (a.c.) of each airfoil strip. Column (13) and (14) give the x arms which is the distance from the a.c. to the reference Y axis. (See Fig. A5.38). Column 15 gives the M_y moment for each strip load and Column 16 the M_y moment at the various stations which equals the summation of the strip moments as one progresses from station 240 to zero.

Fig. A5.39 shows the results at station (0) as taken from Table A5.1.

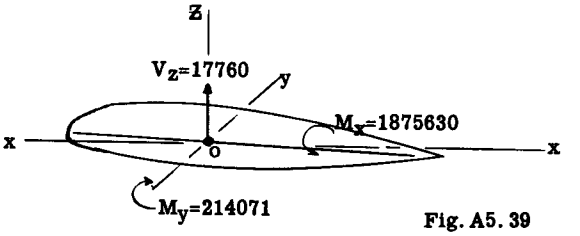

Fig. A5.39

TABLE A5.1

CALCULATION OF WING SHEAR V_z AND WING MOMENTS M_x AND M_y DUE TO TOTAL UNIT DISTRIBUTED HALF WING LOAD OF 17760 LBS., ACTING UPWARD IN Z DIRECTION AND APPLIED AT AERODYNAMIC CENTERS OF WING SECTIONS. (See Figs. A5.37, 38 for Wing Layout)

1	2	3	4	5	6	7	8	9	10	11	12	13	14	15	16
Station = y = Distance From Wing Root Section	Chord Length C Inches	$C_L/\bar{C}_L$ Ratio, Assumed Unity.	Running Load Per Inch of Wing (W). Lbs.	Average Running Load. Wave (lbs.)	Δy = Distance Between Stations	Strip Load ΔP_z = Δy (col. 5)	d = Arm to Centroid of ΔP_z Strip Load	Shear V_z = $\Sigma \Delta P_z$	$V_z \Delta y$ = (Col. 9) (Col. 6)	$\Delta P_z d$ = (Col. 7) (Col. 8)	M_x = Col. 12 previous + Col. 11 + Col. 10.	x = distance from aerodynamic center to Y ref. axis	x_{ave} or strip load distance from Y axis.	$\Delta P_z x_{ave}$ = (Col. 7) (Col. 14)	$My = \Sigma \Delta P_z x_{ave}$ = summation of Col. 15.
240	48	1.0	48					0	0	0	0	7.2			0
				48.54	5.0	242.7	2.49						7.28		
235	49.09	1.0	49.09					242.7	0	605	605	7.36		1767	1767
				49.63	5.0	248.1	2.49						7.44		
230	50.18	1.0	50.18					490.8	1213	618	2436	7.53		1846	3613
				51.27	10.00	512.7	4.97						7.69		
220	52.36	1.0	52.36					1003.5	4908	2540	9884	7.85		3940	7553
				54.00	15.00	810.0	7.43						8.09		
205	55.64	1.0	55.64					1813.5	15052	6020	30956	8.34		6540	14093
				57.27	15.00	859.0	7.43						8.59		
190	58.92	1.0	58.92					2672.5	27020	6490	64466	8.85		7390	21483
				60.56	15.00	908.4	7.43						9.09		
175	62.20	1.0	62.20					3580.9	40087	6760	111313	9.33		8260	29743
				63.84	15.00	957.6	7.43						9.57		
160	65.48	1.0	65.48					4538.5	53713	7100	172126	9.81		9170	38913
				67.13	15.00	1007.0	7.43						10.06		
145	68.78	1.0	68.78					5545.5	68077	7480	247683	10.31		10100	49013
				70.39	15.00	1055.5	7.43						10.55		
130	72.00	1.0	72.00					6601.0	83782	7840	338705	10.80		11100	60113
				73.62	15.00	1104.3	7.43						11.04		
115	75.23	1.0	75.23					7705.3	99015	8200	445920	11.28		11480	71593
				76.89	15.00	1153.4	7.43						11.54		
100	78.55	1.0	78.55					88587	115579	8570	570060	11.80		13270	84863
				80.18	15.00	1202.7	7.43						12.04		
85	81.81	1.0	81.81					10061	132880	8940	702949	12.28		14480	99343
				83.46	15.00	1252.2	7.43						12.52		
70	85.10	1.0	85.10					11313	150915	9310	863174	12.76		15600	114943
				86.73	15.00	1300.9	7.43						13.01		
55	88.35	1.0	88.35					12614	169700	9660	1042534	13.27		16930	131873
				89.98	15.00	1349.7	7.42						13.49		
40	91.62	1.0	91.62					13964	189210	10000	1241744	13.71		18200	150073
				93.81	20.00	1876.3	9.92						14.05		
20	96.00	1.0	96.00					15840	279280	18600	1539624	14.40		26350	176423
				96.00	20.00	1920.0	10.00						14.40		
0	96.00	1.0	96.00					17760	316806	19200	1875630	14.40		27648	214071
								Sum = 17760 Checks Total Limit Load Assumed on Half Wing.							

When the time comes to design the structural make-up of a cross-section to withstand these applied shears and moments, the structural designer may wish to refer the forces to another Y axis as for example one that passes through the shear center of the given section. This transfer of a force system with reference to another set of axes presents no difficulty.

SHEARS AND MOMENTS ON AIRPLANE BODY

A5.13 Introduction.

The body of an airplane acts essentially as a beam and in some conditions of flight or landing as a beam column which may be also subjected to twisting or torsional forces. Thus to design an airplane body requires a complete picture of the shearing, bending, twisting and axial forces which may be encountered in flight or landing. In the load analysis for wings, the direct air forces are the major forces. For the body load analysis the direct air pressures are secondary, the major forces being of a concentrated nature in the form of loads or reactions from units attached to the body, as the power plant, wing, landing gear, tail, etc. In addition, since the body usually serves as the load carrying medium, important forces are produced on the body in resisting the inertia forces of the weight of the interior equipment, installations, pay load etc.

As in the case of the wing, a large part of the load analysis can be made without much consideration as to the structural analysis of the body. The load analysis of an airplane body involves a large amount of calculation, and thus the treatment in this chapter must be of a simplified nature, and is presented chiefly for the purpose of showing the student in general how the problem of load analysis for an airplane body is approached.

A5.14 Design Conditions and Design Weights.

The airplane body must be designed to withstand all loads from specified flight conditions for both maneuver and gust conditions. Since accelerations due to air gusts vary inversely as the airplane weight, it customary to analyze or check the body for a light load condition for flight conditions. In general, the design weights are specified by the government agencies. For landing conditions, however, the normal gross weight is used since it would be more critical than a lightly loaded condition.

The general design conditions which are usually investigated in the design of the body are as follows:

Flight Conditions:

H.A.A.	(High angle of attack)
L.A.A.	(Low angle of attack)
I.L.A.A.	(Inverted low angle of attack)
I.H.A.A.	(Inverted high angle of attack)

The above conditions generally assume only translational acceleration. In addition, it is sometimes specified that the forces due to a certain angular acceleration of the airplane about the airplane c.g. must be considered.

The body is usually required to withstand special tail loads both symmetrical and unsymmetrical which may be produced by air gusts, engine forces, etc. Also, the body should be checked for forces due to unsymmetrical air loads on the wing.

Landing Conditions:

In general, the body is investigated for the following landing conditions. The detailed requirements for each condition are given in the government specifications for both military and commercial airplanes.

Landplanes:
- Level landing.
- Level landing with side load.
- Three point landing.
- Three point landing with ground loop.
- Nose over or turn over condition.
- Arresting. (Usually for only Navy Carrier based airplanes).

Seaplanes or Boats:
- Step landing with and without angular acceleration.
- Bow landing.
- Stern landing.
- Two wave landing.
- Beaching conditions.
- Catapulting conditions (Navy airplanes).

Special Conditions or Forces:
- Towing of airplane.
- Body supercharging.

A5.15 Body Weight and Balance Distribution.

The resisting inertia forces due to the dead weight of the body and its contents plays an important part in the load analysis for the airplane body. When the initial aerodynamic and general layout and arrangement of the airplane is made, it is necessary that a complete weight and balance estimate of the airplane be made. This estimate is usually made by an engineer from the weight control section of the engineering department who has had experience in estimating the weight and distribution of airplane units. This estimate which is presented in report form gives the weights and (c.g.) locations of all major airplane units or installations as well as for many of the minor units which make up these major airplane assemblies or installations. This weight and balance report forms the basis for the dead weight inertia load analysis which forms an important part in the load analysis of the airplane body. The use of this weight and balance estimate will be illustrated in the example problem to follow later.

A5.16 Load Analysis. Unit Analysis.

Due to the many design conditions such as those listed in Art. A5.14, the general procedure in the load analysis of an airplane body is to base it on a series of unit analyses. The loads for any particular design condition then follows as a certain combination of the unit results with the proper multiplying factors. A simplified example problem follows which illustrates this unit method of approach.

A5.17 Example Problem Illustrating the Calculation of Shears and Moments on Fuselage Due to Unit Load Conditions.

Fig. A5.40 and A5.41 shows a layout of the airplane body to be used in this example problem. It happens to be the body of an actual airplane and the wing used in the previous example problem was the wing that went with the airplane.

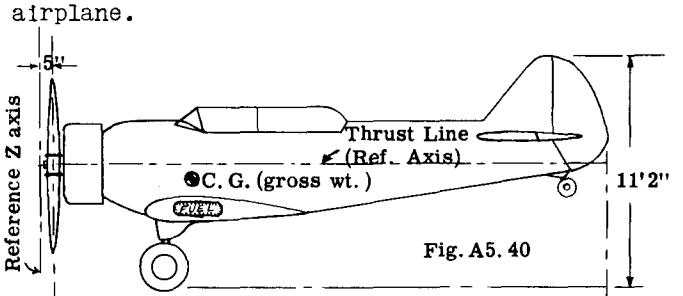

Fig. A5.40

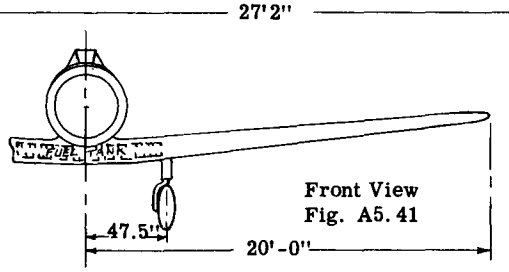

Front View
Fig. A5.41

Table A5.2 gives the Weight and Balance estimate for the total airplane. This table is usually formulated by the Weight and Balance Section of the engineering department and it is necessary to have this information before the airplane load analysis can be made.

TABLE A5.2

AIRPLANE WEIGHT AND BALANCE

Reference Axis { Vert. (Z) arms measured from thrust line (+ is up); Horiz. (X) arms measured from Z axis 5" forward prop. ℄ (+ is aft)

Item No.	Name	W = Wt. #	Horiz. Arm (X) (in.)	Horiz. Moment wx	Vert. Arm (Z)	Vert. Mom. wz
1	Power Plant	1100	19	20900	0	0
2	Fuselage Group	350	113.5	39700	1	350
3	Wing Group	750	97	72750	-18	-13500
4	Tail Group	110	287	31550	24	2640
5	Surface Controls	85	127	10800	-14	- 1190
6	Electrical System	130	61	7930	4	520
7	Chassis Front	235	70	16450	-52	-12200
8	Tail Wheel Group	35	306	10700	-10	- 350
9	Furnishings	220	116	25520	5	1100
10	Radio	125	101	22600	10	1250
	Weight empty =	3150		258900		-21380
11	Pilot	200	151	30200	4	800
12	Student	200	99	19800	4	800
13	Fuel System	760	89	67600	-27	-20500
	Gross weight =	4300		376500		-40280

Calculation of C.G. locations:
Gross wt. x = 376500/4300 = 98.5" aft of Ref. Axis
z = -40280/4300 = 9.4" below thrust line

SOLUTION:

WEIGHT AND BALANCE OF BODY ITEMS.

WEIGHT DISTRIBUTION.

Table A5.3 gives the weight and balance calculations for all items attached to fuselage or carried in the fuselage, except the wing and items attached to the wing as the front landing gear and the fuel.

In order to obtain a close approximation to the true shears and moments on the fuselage due to the dead weight inertia loads, it is necessary to distribute the weights of the various items as given in Table A5.3. Fig. A5.42 shows a side view of the airplane with the center of gravity locations of the weight items of Table A5.3 indicated by the (+) signs. In the various design conditions, the direction of the weight inertia forces changes, thus it is convenient and customary to resolve the inertia forces into X and Z components. Thus, in Fig. A5.43, the weights as given in Table A5.3 are assumed acting in the Z direction through their (c.g.) locations. The loads as shown would not give a true picture as to the shears and moments along the fuselage, thus these loads should be distributed in a manner which should simulate the actual weight distribution. In most weight and balance reports, the weight items are broken down into considerable more detail than that shown in Table A5.3, which makes the weight distribution more evident. The person making the

TABLE A5.3

WEIGHT AND BALANCE OF AIRPLANE LESS WING GROUP AND INSTALLATIONS IN AND ON WING

Ref. Axes: { z equal arm from thrust line. + is up. x is distance from z Ref. Axis 5" forward of propeller. + is aft.

	Item	Name	Weight w	Horiz. Arm x	Horiz. Mom. wx	Vert. Arm z	Vert. Mom. wz
Wt. Empty	1	Powerplant group	1100	19	20900	0	0
	2	Fuselage group	350	113.5	39700	1	350
	4	Tail group	110	287	31550	24	2640
	5	Surface controls	85	127	10800	-14	-1190
	6	Electrical system	130	61	7930	4	520
	8	Tail Wheel group	35	306	10700	-10	- 350
Useful Load	9	Furnishings	220	116	25520	5	1100
	10	Radio	125	181	22600	10	1250
		Weight empty =	2155		169700		4320
	11	Pilot	200	151	30200	4	800
	12	Student	200	99	19800	4	800
		Gross weight = Σ	2555	Σ	219700	Σ	5920

Empty $\bar{x} = \frac{169700}{2155} = 78.7"$ $\bar{z} = \frac{4320}{2155} = 2.00"$

With useful load $\bar{x} = \frac{219700}{2555} = 86.0"$ $\bar{z} = \frac{5920}{2555} = 2.32"$

weight distribution should study the inboard profile drawing of the airplane which shows the general arrangement of all the installations and equipment. Furthermore, he should study the overall structural arrangement as to its possible influence on fuselage weight distribution. The whole process involves considerable common sense if a good approximation to the weight distribution is to be obtained. Fortunately the large dead weight loads, such as the power plant, tail, etc. are definitely located, thus small errors in the distribution of the minor distributed weights does not change the overall shears and moments an appreciable amount.

In order to obtain reasonable accuracy, the fuselage or body is divided into a series of stations or sections. In Fig. A5.42, the sections selected are designed as stations which represent the distance from the Z reference axis. The general problem is to distribute the concentrated loads as shown in Fig. A5.43 into an equivalent system acting at the various fuselage station points.

Obviously, if a weight item from Table A5.3, represents a concentrated load such as a pilot, student, radio, etc., the weight can be distributed to adjacent station points inversely as the distance of the weight (c.g.) from these adjacent stations. However, for a weight item such as the fuselage structure (Item 2 of Table A5.3) whose c.g. location causes it to fall between stations 80 and 120 of Fig. A5.43, it would obviously be wrong to distribute this weight only to the two adjacent stations since the weight of 350# is for the entire fuselage. This weight item of 350# should thus be distributed to all station points. The controlling requirement on this distribution is that the moment of the distributed system about the reference axes must equal the moment of the original weight about the same axes. Fig. A5.44

WEIGHT DISTRIBUTION TO FUSELAGE STATIONS

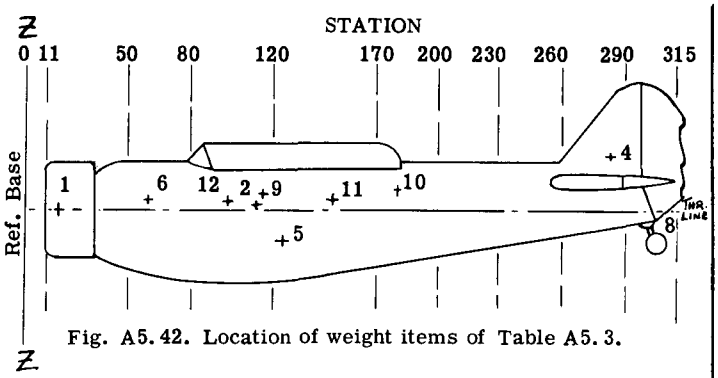

Fig. A5.42. Location of weight items of Table A5.3.

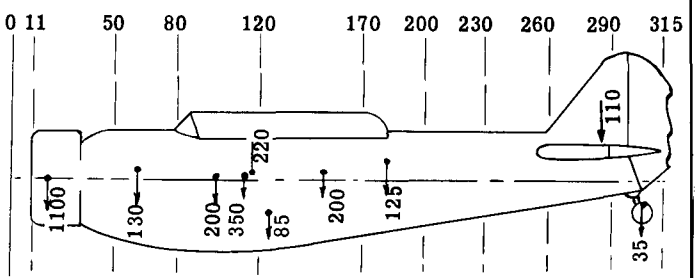

Fig. A5.43. Weight items of Table A5.3 acting in Z direction.

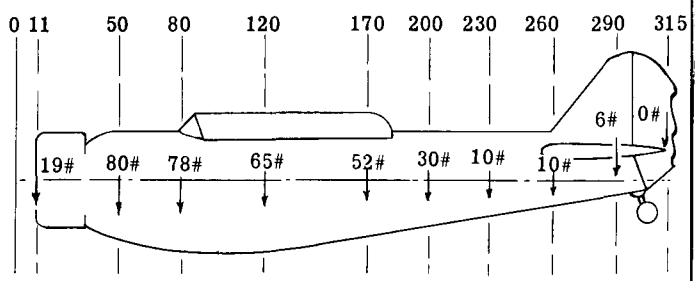

Fig. A5.44. Results of fuselage weight distribution to stations.

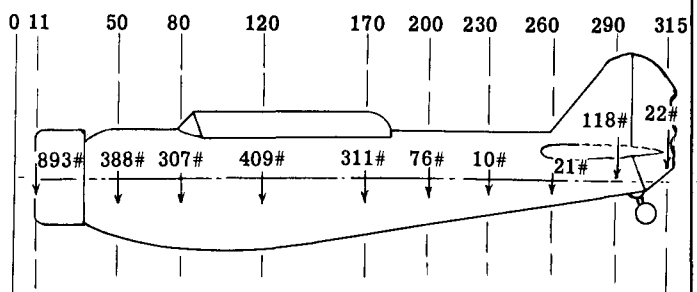

Fig. A5.45. Final weight distribution to station points.

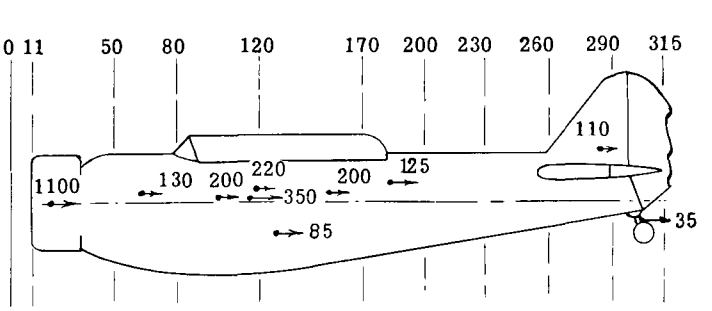

Fig. A5.46. Weight items from Table A5.3 acting in X direction.

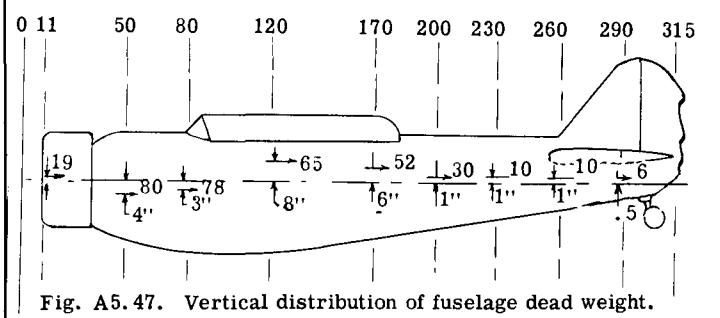

Fig. A5.47. Vertical distribution of fuselage dead weight.

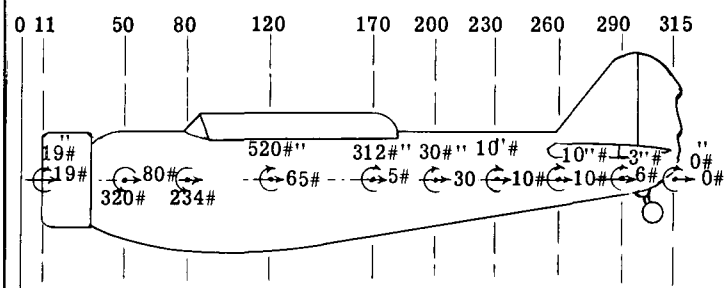

Fig. A5.48. Fuselage weight referred to X axis plus couples.

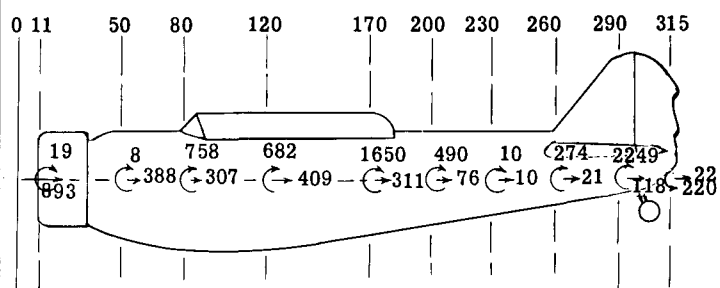

Fig. A5.49. Final weight distribution in X direction referred to X axis plus proper couples.

shows how the dead weight of 350# was distributed to the various station points considering the weights to be acting in the Z direction.

Table A5.4 shows the results of this station point weight distribution for the weight items of Table A5.3. The values in the horizontal rows opposite each weight item shows the distribution to the various fuselage stations. The summation of the weights in each vertical column at each station point as given in the third horizontal row from the bottom of the table gives the final station point weight. These weights are shown in Fig. A5.45 for weights acting in the Z direction. The moment of each total station load about the Z axis is given in the second horizontal row from the bottom of Table A5.4. The summation of the moments in this row must equal the total wx moments of Table A5.3 or 219700"#. This check is shown in the last vertical column of Table A5.4.

The distributed system must also be distributed in the Z or vertical direction in such a manner as to have the same resultant c.g. location as the original weight system which is illustrated in Fig. A5.46. Fig. A5.47 illustrates how the fuselage weight distributed system as shown in Fig. A5.44 is distributed in the vertical direction at the various station points so that the moment of this system about the X axis is equal to that of the original fuselage weight of 350#. For convenience, these distributed fuselage weights can be transferred to the X axis plus a moment as shown in Fig. A5.48.

Table A5.4 shows the vertical distribution of the various items at the various station points. The bottom horizontal row gives the moment about the X axes of the loads at each station point, which equals the individual loads times their Z distances. The summation of the values in this horizontal row must equal the total wz moment of Table A5.3. This check is shown at the bottom of the last vertical column. Fig. A5.49 shows the results as given in Table A5.4 for the weight distribution in the X direction.

TABLE A5.4

PANEL POINT WEIGHT DISTRIBUTION
(Monocoque Type of Fuselage)

Item No.	Name	Wt. W	Station No. = distance x from Ref. z Axis																				
			11		50		80		120		170		200		230		260		290		315		
			w	z	w	z	w	z	w	z	w	z	w	z	w	z	w	z	w	z	w	z	
1	Powerplant group	1100	874	0	226	0																	1100
2	Fuselage group	350	19	1	80	-4	78	-3	65	8	52	6	30	1	10	1	10	1	6	0.5			350
4	Tail group	110															11	24	99	24			110
5	Surface controls	85							73	-14	12	-14											85
6	Electrical system	130			82	4	48	4															130
8	Tail wheel group	35																	13	-10	22	-10	
9	Furnishings	220					76	5	100	5	44	5											220
10	Radio	125									79	10	46	10									125
11	Pilot	200							76	4	124	4											200
12	Student	200					105	4	95	4													200
	Total w	2555	893	.02	388	.02	307	2.47	409	1.67	311	5.3	76	6.45	10	1.0	21	13.06	118	19.1	22	-10	2555
	Horizontal Moment = Σ wx =	9820		19390		24550		49100		52800		15200		2300		5460		34200		6920		219700	
	Vertical Moment = Σ wz =	19		8		758		682		1650		490		10		274		2249		- 220		5920	

x = distance of station from z reference axis which is 5" forward of propeller.
z = distance above or below thrust line or x axis.

A5.18 Unit Analysis for Fuselage Shears and Moments.

Since there are many flight and landing conditions, considerable time can be saved if a unit analysis is made for the fuselage shears, axial and bending forces. The design values in general then follow as a summation of the values in the unit analysis times a proper multiplication factor.

The loads on the fuselage in general consists of tail loads, engine loads, wing reactions, landing gear reactions if attached to fuselage and inertia forces due to the airplane acceleration which may be due to both translational and angular acceleration of the airplane. For simplicity, these loads can be resolved into components parallel to the Z and X axes.

To illustrate the unit analysis procedure, a unit analysis for our example problem will be carried out for the following unit conditions:

(1) Unit acceleration or load factor in Z direction and acting up.

(2) Unit acceleration or load factor in X direction and acting forward.

(3) Unit tail load normal to X axis acting down.

Unit analyses are also usually carried out for engine thrust and engine torque, side load on tail and angular acceleration, but to keep the example calculations from becoming too lengthy only the above 3 unit conditions will be carried out in detail. The others will be discussed in detail in later paragraphs.

Solution for Unit Load Factor in Z Direction.

Fig. A5.50 shows the dead weight loads

acting in the Z direction as taken from Table A5.4 or Fig. A5.45. The wing is attached to the fuselage at stations 73 and 116 as shown on Fig. A5.50. The fittings at these points are assumed as designed to cause all the drag or reaction in the X direction to be taken off entirely at the front fitting on station 73.

To place the fuselage in equilibrium, the wing reaction will be calculated:

$$\Sigma F_X = 0,\ R_H + 0 = 0,\quad \text{hence } R_H = 0$$

$$\Sigma M_{\text{station } 0} = 219700 - 116\,R_R - 73\,R_F = 0 \quad \text{--- (A)}$$

(Note: 219700 from Table A5.3)

$$\Sigma F_Z = -2555 + R_F + R_R = 0 \quad \text{--- (B)}$$

Solving equations (A) and (B) for R_F and R_R:

$$R_F = 1780 \text{ lb.},\ R_R = 775 \text{ lb.}$$

Table A5.5 gives the calculations for the fuselage shears and bending moments at the various station points.

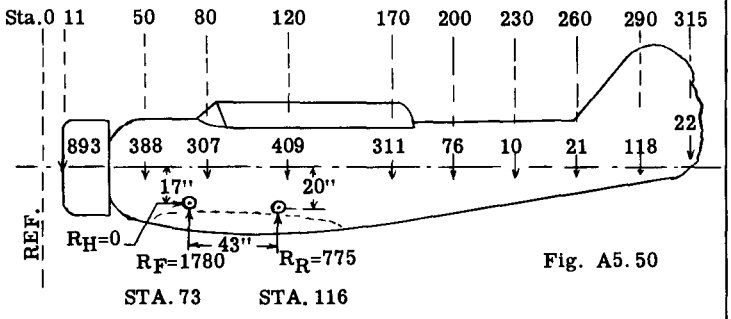

Fig. A5.50

Solution for Unit Load Factor in X Direction.

Fig. A5.51 shows the panel point dead weight distribution for loads acting in the X direction and aft, as taken from Table A5.4 or Fig. A5.40. To place the fuselage in equilibrium the wing reactions at points (A) and (B) will be calculated.

$\Sigma F_X = 2555 - R_H = 0$, hence $R_H = 2555$ lb. (forward)

Take moments about point (A)

$$\Sigma M_A = 2555 \times 17 + 5920 - 43\,R_R = 0,$$
$$\text{hence } R_R = 1147.8 \text{ (up)}$$

(5920 equals the sum of the couples from Table A5.4.

$$\Sigma F_Z = 1147.8 - R_F = 0,$$
$$\text{hence } R_F = 1147.8 \text{ lb. (down)}$$

Table A5.6 gives the calculations for the shears, moments and axial loads for the loading of Fig. A5.51.

TABLE A5.5

FUSELAGE SHEARS AND MOMENTS FOR ONE LOAD FACTOR IN Z DIRECTION
(Dead Weight Acting Down)

1	2	3	4	5	6
Sta. No.	Load or Reaction w	V = shear = Σ w (lbs.)	Δx = Dist. between stations	ΔM = VΔx (in. lbs.)	Moment M* (in. lbs.)
315 +	0	0		0	0
−	− 22	22	25		
290 +	0	22		− 550	− 550
−	− 118	140	30		
260 +	0	140		− 4200	− 4750
−	− 21	161	30		
230 +	0	161		− 4830	− 9580
−	− 10	171	30		
200 +	0	171		− 5130	−14710
−	− 76	247	30		
170 +	0	247		− 7410	−22120
−	− 311	558	50		
120 +	0	558		−27900	−50020
−	− 409	967	4		
116 +	0	967		− 3868	−53888
−	775	192	36		
80 +	0	192		− 6912	−60800
−	− 307	499	7		
73 +	0	499		− 3493	−64290
−	1780	−1281	23		
50 +	0	−1281		+29463	−34827
−	− 388	− 893	39		
11 +	0	− 893		+34827	0
−	− 893	0			

(3) Up on left and down on right side of a section is positive shear.
(6) Tension in upper fuselage portion is negative bending moment.
(1) + refers to aft side of station.
− refers to forward side of station.
* M = M at previous station in col. 6 plus ΔM in col. 5.

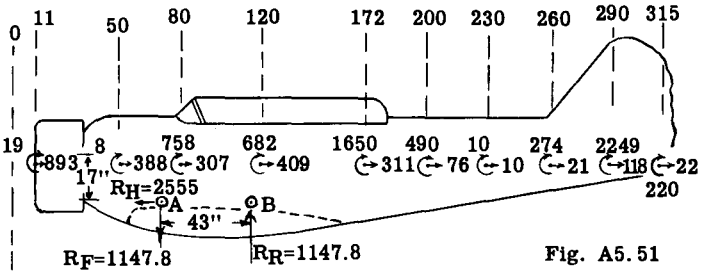

Fig. A5.51

TABLE A5.6

FUSELAGE SHEARS, MOMENTS & AXIAL LOADS FOR ONE LOAD FACTOR IN X DIRECTION

Inertia Loads Acting Aft

1	2	3	4	5	6	7	8	9
Sta. No.	W_X = load in X Dir.	W_Z = load in Z Dir.	$P_X = \Sigma W_X$ = Axial Load	$V = \Sigma W_Z$ = Shear	ΔM_1 = Couple Moment	ΔX = Dist. between Station	$\Delta M_2 = V\Delta x$	M
315 +	0	0	0	0	0		0	0
-	22		22		220	25		220
290 +	0	0	22	0	0		0	220
-	118		140		- 2249	30		- 2029
260 +	0	0	140	0	0		0	- 2029
-	21		161		- 274	30		- 2303
230 +	0	0	161	0	0		0	- 2303
-	10		171		- 10	30		- 2313
200 +	0	0	171	0	0		0	- 2313
-	76		247		- 490	30		- 2803
170 +	0	0	247	0	0		0	- 2803
-	311		558		- 1650	50		- 4453
120 +	0	0	558	0	0		0	- 4453
-	- 409		967		- 682	4		- 5135
116 +	0		967				0	- 5135
-	0	1147.8	967	-1147.8	0	36		- 5135
80 +	0	0	967	-1147.8			41320	36185
-	307	0	1274	-1147.8	- 758	7	0	35427
73 +	0	0	1274	-1147.8	0		8035	43462
-	2555	-1147.8	-1281	0	-43435 *	23	0	27
50 +	388	0	-1281		8		0	27
-	0		- 893	0	0	39		19
11 +	893	0	- 893	0	19		0	19
-	0		0		0			0

* = 17 x (2555) = 43435
\+ refers to aft side of station
Col. 1 - refers to forward side of station
P_X is plus for tension in fuselage.
(Col. 9) M = M at previous station in Col. 9. plus ΔM_1 of col. 6 plus ΔM_2 of col. 8

Solution for Unit Horizontal Tail Load Acting Down.

The fuselage shears and moments will be computed for a unit tail load of 100 lb. on the tail acting in the Z direction, with balancing reactions at the wing attachment points. The center of pressure on the horizontal tail is at station 277.5. Fig. A5.52 shows the fuselage loading. To find wing reactions at (A) and (B):

$$\Sigma M_A = 100 \times (277.5 - 73) - 43\, R_R = 0,$$

hence $R_R = 475.6\#$ (up)

$$\Sigma F_Z = -100 + 475.6 - R_F = 0,$$

hence $R_F = 375.6\#$ (down)

Table A5.7 gives the detailed calculations for the shears and moments at the various station points.

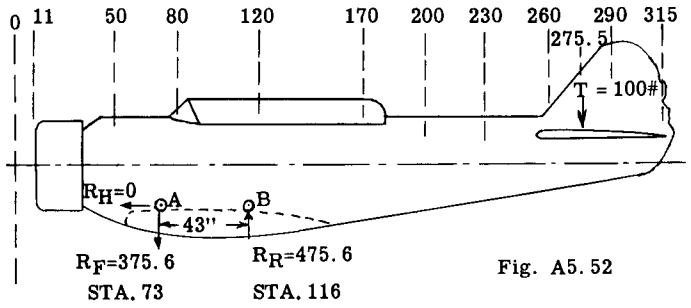

Fig. A5.52

TABLE A5.7

FUSELAGE SHEARS & MOMENTS FOR UNIT HORIZONTAL TAIL LOAD IN Z DIRECTION (Load Acting Down)

1	2	3	4	5	6
Sta.	Load or Reaction w lbs.	V = shear = Σ w lbs.	ΔX = dist. between stations	$\Delta M = V \Delta x$	Moment in. lbs.
315 +	0	0		0	0
-	0	0	25		0
290 +	0	0		0	0
-	0	0	12.5		0
272.5 +	0	0		0	0
-	-100	100	17.5		0
260 +	0	100		- 1750	- 1750
-	0	100	30		- 1750
230 +	0	100		- 3000	- 4750
-	0	100	30		- 4750
200 +	0	100		- 3000	- 7750
-	0	100	30		- 7750
170 +	0	100		- 3000	-10750
-	0	100	50		-10750
120 +	0	100		- 5000	-15750
-	0	100	4		-15750
116 +	0	100		- 400	-16150
-	475.6	-375.6	36		-16150
80 +	0	-375.6		13521	- 2629
-	0	-375.6	7		- 2629
73 +	0	-375.6		2629	0
-	-375.6	0	23		0
50 +	0	0			0
-	0	0	39		0
11 +	0	0			0
-	0	0			0

(Col. 6) = M = M at previous station in Col. 6 plus ΔM in Col. 5.

CALCULATION OF APPLIED FUSELAGE SHEARS, MOMENTS AND AXIAL LOADS FOR A SPECIFIC FLIGHT CONDITION.

Using the results in Tables A5.5, A5.6, and A5.7, the applied shears and moments for a given flight condition follow as a matter of proportion and addition. To illustrate, the applied values for one flight condition will be given.

It will be assumed that the aerodynamic calculations for this airplane for the (H.A.A.) high angle of attack condition gave the following results, which the student will have to accept without knowledge of how they were obtained.

Applied load factor in Z direction = - 6.0 down

Applied load factor in X direction = 1.333 aft.

Applied tail load = 110 lb. up.

Thus with the load factors in the Z and X directions and the tail load known, Table A5.8 can be filled in as illustrated. In a similar manner the values for other flight conditions can be found, the only difference being a new set of multiplying factors since the applied loads would be different.

TABLE A5.8

APPLIED FUSELAGE SHEARS, MOMENTS & AXIAL LOADS FOR FLIGHT CONDITION 1. (H.A.A.)

1	2	3	4	5	6	7	8	9	10
Sta.	V_Z for Z Load Factor (lbs.)	V_Z for X Load Factor (lbs.)	V_Z for Tail Load	App. Shear V_Z	M for Z Load Factor in. lbs.	M for X Load Factor in. lbs.	M for Tail Load in. lbs.	App. Mom. M in. lbs.	Axial Load P_X (lbs.)
315 +	0	0	0	0	0	0	0	0	0
-	132	0	0	132	0	294	0	0	29.3
290 +	132	0	0	132	- 3300	294	0	- 3006	29.3
-	840	0	0	840	- 3300	- 2710	0	- 6010	186.8
260 +	840	0	0	840	- 28500	- 2710	1925	- 29285	186.8
-	966	0	-110	856	- 28500	- 3075	1925	- 29650	215
230 +	966	0	-110	856	- 57480	- 3075	5220	- 55335	215
-	1026	0	-110	916	- 57480	- 3090	5220	- 52030	228
200 +	1026	0	-110	916	- 88260	- 3090	8540	- 82810	228
-	1482	0	-110	1372	- 88260	- 3740	8540	- 83460	330
170 +	1482	0	-110	1372	-132720	- 3740	11820	-124640	330
-	3348	0	-110	3238	-132720	- 6085	11820	-126985	745
120 +	3348	0	-110	3238	-300120	- 6085	17320	-288855	745
-	5802	0	-110	5692	-300120	- 6850	17320	-288650	1290
116 +	5802	0	-110	5692	-323328	- 6850	17770	-312408	1290
-	1152	-1530	413	- 413	-323328	- 6850	17770	-312408	1290
80 +	1152	-1530	413	- 413	-364800	48200	2910	-313690	1290
-	2994	-1530	413	1877	-364800	47250	2910	-314640	1700
73 +	2994	-1530	413	1877	-385740	57900	0	-327840	1700
-	7686	0	0	-7686	-385740	36	0	-385704	-1710
50 +	-7686	0	0	-7686	-208962	36	0	-208926	-1710
-	-5358	0	0	-5358	-208962	25	0	-208937	-1190
11 +	-5358	0	0	-5358	0	25	0	25	-1190
-	0	0	0	0	0	0	0	0	0

NOTES: (Moments & axial loads are referred to the thrust line).

Col. 2 - 6 x values in column 3 of Table A5.5.
Col. 3 - 1.333 x values in column 5 of Table A5.6.
Col. 4 - -1.10 x values in column 3 of Table A5.7.
Col. 5 - column (1) + column (2) + column (3).
Col. 6 - 6 x values in column 6 of Table A5.5.
Col. 7 - 1.333 x values in column 9 of Table A5.6.
Col. 8 - 1.10 x values in column 6 of Table A5.7.
Col. 9 - columns (6) + (7) + (8).
Col.10 - 1.333 x values in column (4) of Table A5.6.

A5.19 Example of Fuselage Shears and Moments for Landing Conditions.

Fig. A5.53 illustrates the airplane in a level landing condition. The ground reaction is assumed to pass the center of landing gear wheel and c.g. of airplane. The fuselage shears, moments and axial loads are required when the vertical ultimate load factor is 7. (Gross weight = 4300#).

SOLUTION:

The vertical or Z component of the ground reaction R is specified as 7 load factors which equals 7 x 4300 = 30100#. One half of this is acting on each wheel.

The horizontal or X component of R is 30100 tan 23° = 425 x 30100 = 12800# and acting aft.

The horizontal load factor on airplane equals 12800/4300 = 2.98.

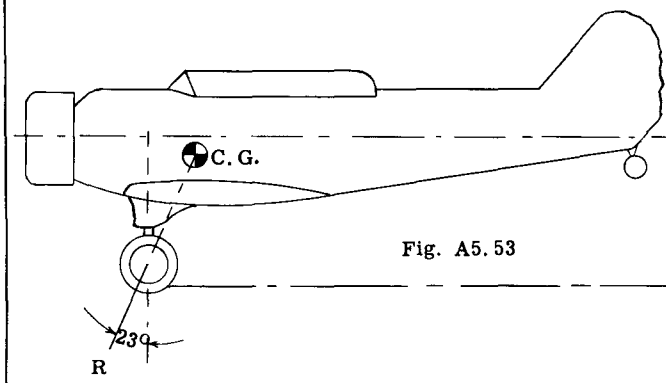

Fig. A5.53

The resistance to these X and Z components of the ground reaction R is provided by the inertia forces of the airplane in the X and Z directions.

Tables A5.5 and A5.6 show the fuselage shears, moments and axial loads for inertia loads due to one load factor in the Z and X directions respectively. Thus to obtain the fuselage forces for this given landing condition, it is only necessary to multiply the values in these two tables by the proper factor and add the results.

Thus fuselage forces due to vertical load factor of 7 would equal 7 times the values in columns (3) of Table A5.5 to obtain shear and 7 times column 6 to obtain bending moment.

Likewise the forces due to the 2.98 load factor in X direction would equal (-2.98) times the values in columns (4), (5) and (9) of Table A5.6 to obtain axial loads, shears and bending moments respectively.

The final or true forces would be the algebraic sum of these results.

Landing with Angular Acceleration

In a level landing condition, it is sometimes specified that the horizontal component of the ground reaction must be a certain proportion of the vertical component, which causes the line of action of the ground reaction R in Fig. A5.53 to not pass through the c.g. of the airplane, which creates an external pitching moment on the airplane. This moment is usually balanced by the inertia forces due to the angular acceleration produced by the unbalanced moment about the c.g. The shears and moments on the fuselage due to this external moment could be found as explained in Art. A5.20.

A5.20 Inertia Loads Due to Angular Acceleration.

In some of the flying conditions, it is sometimes specified that the airplane must be subjected to an angular acceleration as well as translational acceleration. This angular acceleration of the airplane produces inertia forces which must be calculated if the airplane is to be treated as a body in static

equilibrium. In some cases, a tail load due to a gust on the tail is specified which produces a moment about the airplane c.g. which produces angular acceleration of the airplane. In certain landing conditions, the ground forces do not pass through the airplane c.g. thus producing a moment about the c.g. which for stress analysis purposes is balanced by inertia forces.

Moment of Inertia of Airplane

The calculation of the moment of inertia of an airplane about the center of gravity axes was explained on page A3.5 of Chapter A3. A detailed example solution was given in detail in Table 6A of Chapter A3. The general equations for the moments of inertia of the airplane about the reference axes are:

$$I_y = \Sigma\, wx^2 + \Sigma\, wz^2 + \Sigma\, \Delta\, I_y$$

$$I_x = \Sigma\, wy^2 + \Sigma\, wz^2 + \Sigma\, \Delta\, I_x$$

$$I_z = \Sigma\, wy^2 + \Sigma\, wx^2 + \Sigma\, \Delta\, I_z$$

The last term in each of the above equations represents the moment of inertia of each weight item about its own centroidal axes parallel to the reference axes.

A5.21 Solution for Inertia Loads Due to Unit 100,000 In. Lbs. Pitching Moment.

To illustrate the general procedure of determining the balancing inertia loads when the airplane is subjected to an unbalanced moment about the c.g., an analysis will be made for a unit 100,000 in. lb. moment. Table A5.9 gives the necessary calculations.

From kinetics:

Pitching angular acceleration $\alpha = \frac{M_y}{I_y}$ (rad/sec.^{2})

where

M_y = unbalanced external pitching moment about c.g. of airplane.

I_y = pitching moment of inertia of airplane about airplane c.g. = Σwr^2

The tangential inertia force F for a mass w/g due to an angular acceleration α equals,

$$F = \frac{w}{g} r\alpha, \text{ but } \alpha = \frac{M_y}{I_y} g$$

hence

$$F = \frac{M_y}{I_y} w\, r, \text{ where r is the distance from the weight w to the airplane c.g.}$$

It is convenient to treat the inertia force F as resolved into two components F_x and F_z. hence,

$$F_z = \frac{M_y}{I_y} w\, x_c \text{ - - - - - - - - - - - - - - - - - (1)}$$

$$F_x = \frac{M_y}{I_y} w\, z_c \text{ - - - - - - - - - - - - - - - - - (2)}$$

From Table A5.9, I_y = 16097600

M_y was assumed as 100,000

hence

$$F_z = \frac{100000}{16097600} w\, x_c = .00621\, w\, x_c$$

$$F_x = .00621\, w\, z_c$$

where z_c and x_c are the z and x distances of weight w to the airplane c.g.

Columns No. 9 and 10 of Table A5.9 gives the values of these inertia components. Fig. A5.54 shows these inertia loads applied to the fuselage. The reactions at wing attachment points should be computed and then a table of fuselage shears, moments and axial loads should be made up. This unit table could then be used for all conditions involving angular acceleration of the airplane.

It should be realized that the inertia resisting loads in Table A5.9 are only approximately, since the moment of inertia neglects the centroidal moment of inertia of the big items, such as the power plant, wing, etc. The example is only for the purpose of illustrating the general procedure of determining the inertia resisting loads due to angular acceleration. The same general procedure can be followed in considering unbalanced external moments about the Z and X axes, commonly referred to as yawing and rolling moments.

TABLE A5.9

BALANCING INERTIA FORCES FOR UNIT 100,000 IN. LB. MOMENT ABOUT Y AXIS THROUGH AIRPLANE C.G. (PITCHING MOMENT)

1	2	3	4	5	6	7	8	9	10
Fuselage Panel Sta. No.	Sta. Wt. w	Arm Z	Arm X	Arm Z_c	Arm X_c	$X_c^2 + Z_c^2$	$I_y = w(Z_c^2 + X_c^2)$	Inert. Force F_z	Inert. Force F_x
11	893	.02	11	9.42	- 76.5	5949	5300000	-426	-52.1
50	388	.02	50	9.42	- 37.5	1494	580000	- 90.6	-22.6
80	307	2.47	80	11.87	- 7.5	197	60500	- 14.3	-22.6
120	409	1.67	120	11.07	32.5	1182	484000	82.5	-28.2
170	311	5.30	170	14.70	82.5	7016	2180000	159.0	-28.4
200	76	6.45	200	15.85	112.50	12950	985000	53.2	- 7.5
230	10	1.00	230	10.40	142.50	20460	204600	8.9	- 0.6
260	21	13.06	260	22.46	172.50	30270	635000	22.5	- 2.9
290	118	19.10	290	28.50	202.50	31085	3670000	148.3	-20.9
315	22	-10.0	315	- 0.6	227.50	51800	1140000	31.2	- 0.1
Wing	750	-18	97	- 8.6	9.50	164	123000	44.3	40.2
Front Chassis	235	-52	70	-42.6	- 17.50	2120	498000	- 25.6	62.3
Fuel	760	-27	89	-17.6	1.50	312	237500	7.1	83.2
						I_y =	16097600		

Columns (2), (3), & (4) Taken from Table A5.2.
Column (5) $Z_c = Z - 9.4$ } See Table A5.2 for c.g. location
Column (6) $X_c = X - 87.5$
Column (9) $F_z = .00621\, wx_c$
Column (10) $F = .00621\, wz_c$

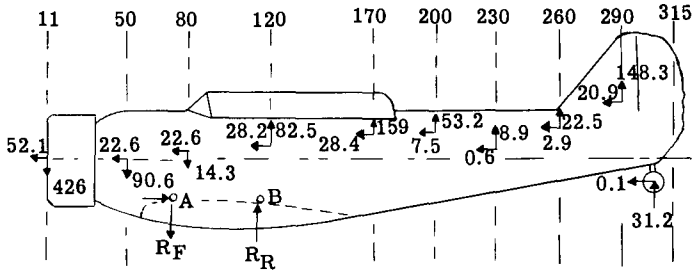

Fig. A5.54

A5.22 Problems

(I) Draw the shear, bending moment and axial load diagrams for loaded structures in Figs. 55 to 60_c.

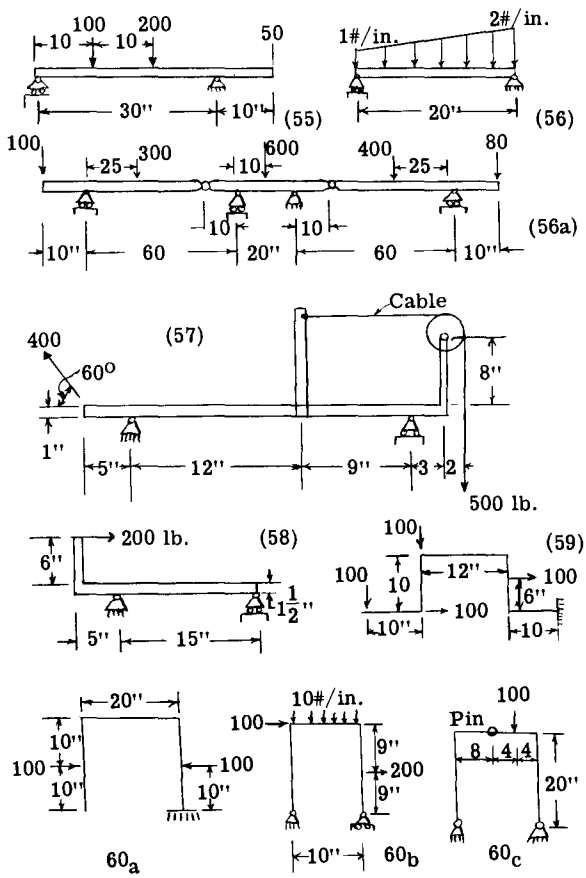

(II) Draw bending moment diagram for structures and loading in Fig. A5.61, abc.

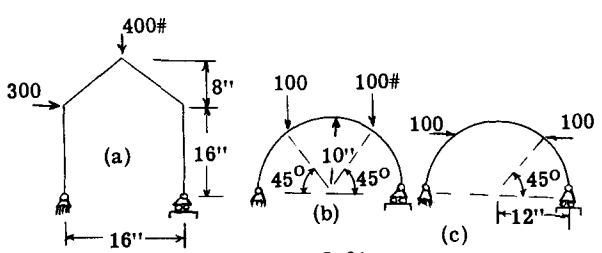

Fig. A5.61

III. Fig. A5.62 shows the plan form of a cantilever wing. Assume a constant normal distributed load on the surface equal to 50 lb./sq.ft. Write expressions for shear and bending moment on wing and find values at 25, 100, 150 and 200 inches from end.

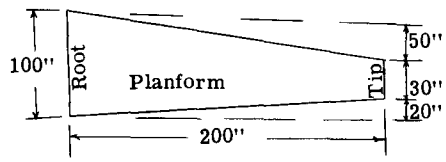

Fig. A5.62

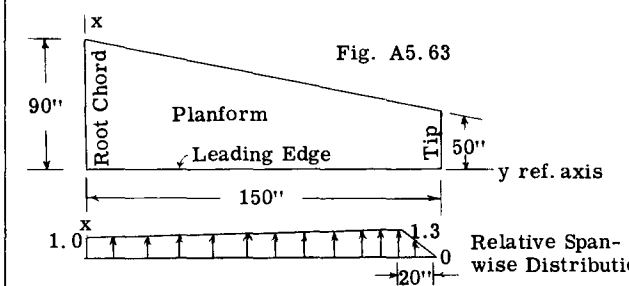

Fig. A5.63

Fig. A5.63 shows plan form of a cantilever wing. The total distributed air load normal to surface is 10000 lb. The relative spanwise distribution is shown. Take center of pressure at 24 percent of chord from leading edge. Divide wing into 10 inch width strips and calculate V_Z, M_X and M_y, and plot curves for same.

IV. Fig. A5,64 shows an externally braced monoplane wing. Take an average wing lift load of 90 lb./sq.ft. normal to wing with center of pressure at 27 percent of the chord from leading edge of wing and calculate and draw the front and rear beam primary shears and bending moment diagrams.

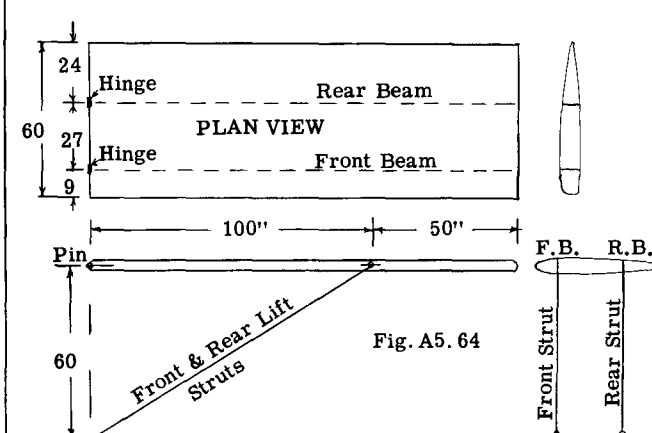

Fig. A5.64

BENDING MOMENTS - BEAM - COLUMN ACTION*

A5.23 Introduction

A beam-column is a member subjected to transverse loads or end moments plus axial loads. The transverse loading, or end moments, produces bending moments which, in turn, produce lateral bending deflection of the member. The axial loads produce secondary bending moments due to the axial load times this lateral deflection. Compressive axial loads tend to increase the primary transverse bending moments, where as tensile axial loads tend to decrease them.

Beam-column members are quite common in airplane structures. For example, the beams of externally braced wing and tail surfaces are typical examples, the air loads producing transverse beam loads and the struts introducing axial beam loads. In landing gears, one member is usually subjected to large bending and axial loads. In tubular fuselage trusses, lateral loads due to installations supported on members between truss joints produce beam-column action.

In general, beam column members in airplane structures are comparatively long and slender compared to those in buildings and bridges; thus, the secondary bending moments due to the axial loads are frequently of considerable proportion and need to be considered in the design of the members.

This chapter deals briefly on the theory of single span beam-column members. A summary of equations and design tables is included together with examples of their use. The information in this chapter is used frequently in other chapters where practical analysis and design of beam-column members is considered. For a completed and comprehensive treatment of beam-column theory and derivation of equations, see Niles and Newell-"Airplane Structures".

A5.24 General Action of a Member Subjected to Combined Axial and Transverse Loads.

Sub-figure a of Fig. A5.65 shows a member subjected to transverse loads W and axial compressive loads P. The transverse loads W produce a primary bending distribution on the member as shown in Fig. b. This bending will produce a transverse deflection curve as illustrated in Fig. c. The end loads P now produce an additional secondary bending moment due to the end load P times the deflection δ , or the bending moment diagram of Fig. d. This first secondary moment distribution produces the additional lateral deflection curve of Fig. e and the end load P will again produce further bending moments due to this deflection. If the axial load is not too large, these successive deflections will gradually converge and the member will reach a state of equilibrium. These secondary bending moments could be found by successive steps by the various deflection principles given in Chapter A7. However, for prismatic beams this convergency can be expressed as a mathematical series and thus save much time over the above successive step method. For members of variable moment of inertia, the secondary moments will usually have to be found by successive steps.

If the end loads P are tension, they will tend to decrease the primary moments; thus, in general, the case of axial compression is more important in practical design, since buckling and instability enter into the problem.

A5.25 Equations for a Compressive Axially Loaded Strut with Uniformly Distributed Side Load.

Fig. A5.66 shows a prismatic beam of length L subjected to a concentric compressive load P and a uniformly transverse distributed load W, with the beam supported laterally at each end, and with end restraining moments M_1 and M_2. It is assumed that the general conditions for the beam theory hold, namely; that plane sections remain plane after bending; that stress is proportional to strain in both tension and compression.

At any point a distance x from the beam end, the moment expression is,

$$M = M_1 + \frac{(M_2 - M_1)}{L} x - \frac{WLx}{2} + \frac{Wx^2}{2} - Py \text{ - - - - - } \quad (A5.1)$$

From applied mechanics, we know that

$M = EI \frac{d^2y}{dx^2}$ therefore, differentiating equation (A5.1) twice with respect to x gives

$$\frac{d^2M}{dx^2} + \frac{P}{EI} M = w \text{ - - - - - - - - - - - - } \quad (A5.2)$$

Fig. A5.65

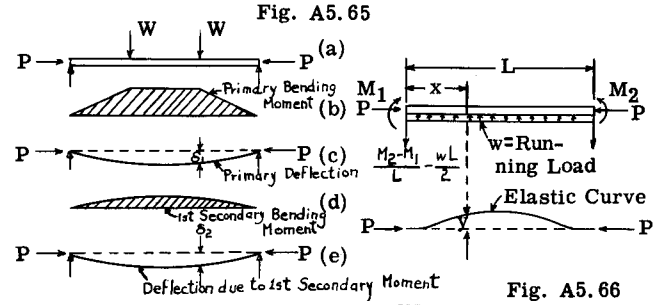

Fig. A5.66

For simplification, let $j = \sqrt{\frac{EI}{P}}$; hence $\frac{P}{EI} = \frac{1}{j^2}$, which, substituted in (A5.2), gives

$$\frac{d^2M}{dx^2} + \frac{1}{j^2} M = w$$

* Also discussed in Chapter C2, Part E.

The solution of this differential equation gives.

$$M = C_1 \sin \frac{x}{j} + C_2 \cos \frac{x}{j} + wj^2 \text{ - - - - (A5.3)}$$

where C_1 and C_2 are constants of integration and $\sin \frac{x}{j}$ and $\cos \frac{x}{j}$ are the limits of an infinite series of variable $\frac{x}{j}$. When x = o, M = M_1 and when x = L, M = M_2, therefore:

$$C_1 = \frac{M_2 - wj^2}{\sin \frac{L}{j}} - \frac{M_1 - wj^2}{\tan \frac{L}{j}}$$

$$= \frac{M_2 - wj^2 - (M_1 - wj^2) \cos \frac{L}{j}}{\sin \frac{L}{j}}$$

and $C_2 = M_1 - wj^2$

Let $D_1 = M_1 - wj^2$ and $D_2 = M_2 - wj^2$. Then, substituting in equation (A5.3),

$$M = \frac{D_2 - D_1 \cos \frac{L}{j}}{\sin \frac{L}{j}} \sin \frac{x}{j} + D_1 \cos \frac{x}{j} + wj^2 \text{ (A5.4)}$$

To find the location of the maximum moment, differentiate equation (A5.3) and equate to zero.

$$\frac{dM}{dx} = o = \frac{C_1}{j} \cos \frac{x}{j} - \frac{C_2}{j} \sin \frac{x}{j}$$

whence

$$\tan \frac{x}{j} = \frac{C_1}{C_2} = \frac{D_2 - D_1 \cos \frac{L}{j}}{D_1 \sin \frac{L}{j}} \text{ - - - - - - - (A5.5)}$$

The value of x must fall within x = 0 to x = L, otherwise M_1 or M_2 is the maximum value.

The value of the maximum span moment can be found by substituting the value from equation (A5.5) in (A5.4), which gives

$$M_{max} = \frac{D_1}{\cos \frac{x}{j}} + wj^2 \text{ - - - - - - - - - (A5.6)}$$

The moment M at any point x along the span can also be written:

$$M = D_1 \left[\left(\tan \frac{x_m}{j} \cdot \sin \frac{x}{j} \right) + \cos \frac{x}{j} \right] + wj^2 \text{ - (A5.7)}$$

where x_m refers to the value of x where the span moment is maximum, or equation (A5.5). Since it is customary to locate the point of maximum span bending moment and its value before investigating other span points, the value of $\tan \frac{x_m}{j}$ is known from equation (A5.5) and thus is available to use in equation (A5.7) for finding moments at other points along the span.

If the equation for the beam deflection is desired, it can be found by substituting the value of M from equation (A5.3) in equation (A5.1), which gives:*

$$y = \frac{1}{P} \left(M_1 + \frac{M_2 - M_1}{L} x - \frac{wLx}{2} + \frac{wx^2}{2} - \frac{D_2 - D_1 \cos \frac{L}{j}}{\sin \frac{L}{j}} \sin \frac{x}{j} - D_1 \cos \frac{x}{j} - wj^2 \right)$$

- - - - - (A5.7a)

The slope of the elastic curve at any point is given by the first derivative of equation (A5.7a)

$$i = \frac{1}{P} \left(\frac{M_2 - M_1}{L} - \frac{wL}{2} + wx - \frac{C_1}{j} \cos \frac{x}{j} + \frac{C_2}{j} \sin \frac{x}{j} \right) \text{ - (A5.8)}$$

A5.26 Formulas for Other Single Span Loadings

In investigating other transverse loadings for a single span carrying axial compression, it is found that the expression for bending moment in the span always takes the form:

$$M = C_1 \sin \frac{x}{j} + C_2 \cos \frac{x}{j} + f(w) \text{ - - - (A5.9)}$$

where f(w) is a term which does not include the axial load P or the end moments M_1 and M_2. The expressions for f(w), C_1 and C_2 depend on the type of the transverse load.

Table A5.I gives the value of these 3 terms for types of transverse loading on a single span which are frequently encountered in airplane structures. The Table also gives equations for the point of maximum bending moment and its magnitude.

Table A5.II is a table of sines, cosines, and tangents for L/j in radians which is more convenient to use than the usual type of trigonometric tables. This table is based on values given in Appendix I of Air Corps Information Circular #493. The Δ difference have been added to facilitate rapid use of the tables.

For single span beams, the critical value of L/j is π; that is, if the axial compressive load is such that the term L/j = π, the center region of the beam will tend to deflect until the combined stresses equal the failing stress of the material.

A5.27 Moments for Combinations of the Various Load Systems as Given in Table A5.I, Margins of Safety. Accuracy of Calculations.

The principle of superposition does not apply to a beam-column, because the sum of the bending moments due to the transverse loads and the axial loads acting separately are not the same as the moments when they act simultaneously. In combining several transverse load systems with their accompanying axial loads, the principle of superposition can be said to apply if each transverse loading is used with the total axial load for the systems which are being combined. Thus, in Table A5.I, to find the moments for several combined loadings, add the values of C_1, C_2 and f(w) for the several loadings and use

* Also see Chapter C2, Part E, Eq. (21).

Table A5.I

Values of Terms C_1, C_2, and f(w) in Equation

$$M = C_1 \sin\frac{x}{j} + C_2 \cos\frac{x}{j} + f(w)$$

Single Span - Axial Compression - Uniform Section

	Loading	C_1	C_2	f(w)	Eq. for Point of Max Bending Moment	Eq. for Max. Span Bending Moment
I	Equal End Moments. No Side Load 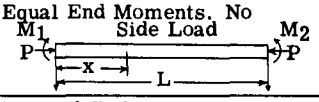	$M_1 \tan\frac{L}{2j}$	M_1	o	$x = \frac{L}{2}$	$M_{max} = \frac{M_1}{\cos\frac{L}{2j}}$
II	Unequal End Moments. No Side Load 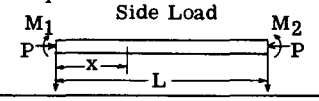	$\frac{M_2 - M_1 \cos\frac{L}{j}}{\sin\frac{L}{j}}$	M_1	o	$\tan\frac{x}{j} = \frac{M_2 - M_1 \cos\frac{L}{j}}{M_1 \sin\frac{L}{j}}$	$M_{max} = \frac{M_1}{\cos\frac{x}{j}}$
III	Uniform Side Load. No End Moments w#/in. 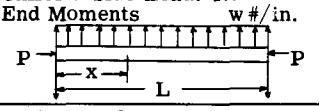	$\frac{wj^2\left[\cos\left(\frac{L}{j}-1\right)\right]}{\sin\frac{L}{j}}$	$-wj^2$	wj^2	$x = .5\,L$	$M_{max} = wj^2(1 - \sec\frac{L}{2j})$
IV	Uniform Side Load Plus End Moments 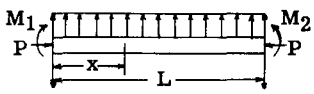 where $D_1 = M_1 - wj^2$ $D_2 = M_2 - wj^2$	$\frac{D_2 - D_1 \cos L/j}{\sin L/j}$	D_1	wj^2	$\tan\frac{x}{j} = \frac{D_2 - D_1 \cos\frac{L}{j}}{D_1 \sin\frac{L}{j}}$	$M_{max} = \frac{D_1}{\cos\frac{x}{j}} + wj^2$
V	Concentrated Side Load. No End Moments 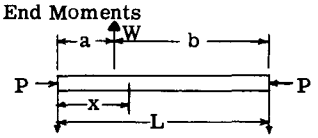	$x < a$, $-\frac{Wj \sin\frac{b}{j}}{\sin\frac{L}{j}}$ $x > a$, $+\frac{Wj \sin\frac{a}{j}}{\tan\frac{L}{j}}$	o $-Wj \sin\frac{a}{j}$	o o	$\tan x/j = \frac{C_1}{C_2}$	$M_{max} = \left(C_1^2 + C_2^2\right)^{\frac{1}{2}}$
VI	Triangular Loading. No End Moments 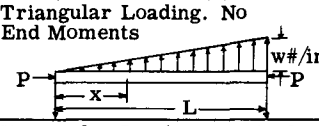	$\frac{-wj^2}{\sin\frac{L}{j}}$	o	$\frac{wj^2 x}{L}$	(NOTE A) To obtain Maximum Moment, compute moment at 3 or 4 points in span. Draw a smooth curve thru plotted results.	
VII	Triangular Loading. No End Moments 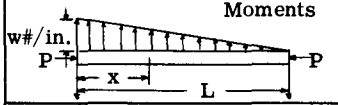	$\frac{wj^2}{\tan\frac{L}{j}}$	$-wj^2$	$wj^2(1-\frac{x}{L})$	(See Note A)	
VIII	Couple Loading (Clockwise) 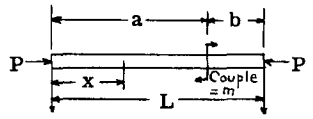	$x < a$, $-\frac{m \cos\frac{b}{j}}{\sin\frac{L}{j}}$ $x > a$, $-\frac{m \cos\frac{a}{j}}{\tan\frac{L}{j}}$	o $m \cos\frac{a}{j}$	o o	(See Note A)	

w or W is positive when upward.
M is positive when it tends to cause compression on the upper fibers of the beam at the section being considered.

Reference: AC1C #493; Niles, Airplane Design; Newell and Niles Airplane Structures

For Table of many other loadings, see NACA T. M. 985.

TABLE A5.II

NATURAL SINES, COSINES, AND TANGENTS OF ANGLES IN RADIANS

L/j in Radians	$\sin {}^{L}/_{j}$	$\Delta \sin {}^{L}/_{j}$	$\cos {}^{L}/_{j}$	$\Delta \cos {}^{L}/_{j}$	$\tan {}^{L}/_{j}$	$\Delta \tan {}^{L}/_{j}$
0.00	0.00000		1.00000		0.00000	
		0.01000		0.00005		0.01000
0.01	0.01000		0.99995		0.01000	
		0.01000		0.00015		0.01000
0.02	0.02000		0.99980		0.02000	
		0.01000		0.00025		0.01000
0.03	0.03000		0.99955		0.03000	
		0.00999		0.00035		0.01002
0.04	0.03999		0.99920		0.04002	
		0.00999		0.00045		0.01002
0.05	0.04998		0.99875		0.05004	
		0.00998		0.00055		0.01003
0.06	0.05996		0.99820		0.06007	
		0.00998		0.00065		0.01005
0.07	0.06994		0.99755		0.07012	
		0.00997		0.00075		0.01005
0.08	0.07991		0.99680		0.08017	
		0.00997		0.00085		0.01007
0.09	0.08988		0.99595		0.09024	
		0.00995		0.00095		0.01010
0.10	0.09983		0.99500		0.10034	
		0.00995		0.00104		0.01011
0.11	0.10978		0.99396		0.11045	
		0.00993		0.00115		0.01012
0.12	0.11971		0.99281		0.12057	
		0.00992		0.00125		0.01016
0.13	0.12963		0.99156		0.13073	
		0.00991		0.00134		0.01019
0.14	0.13954		0.99022		0.14092	
		0.00990		0.00145		0.01022
0.15	0.14944		0.98877		0.15114	
		0.00988		0.00154		0.01024
0.16	0.15932		0.98723		0.16138	
		0.00986		0.00165		0.01027
0.17	0.16918		0.98558		0.17165	
		0.00985		0.00174		0.01032
0.18	0.17903		0.98384		0.18197	
		0.00983		0.00184		0.01036
0.19	0.18886		0.98200		0.19232	
		0.00981		0.00193		0.01039
0.20	0.19867		0.98007		0.20271	
		0.00979		0.00204		0.01043
0.21	0.20846		0.97803		0.21314	
		0.00977		0.00213		0.01048
0.22	0.21823		0.97590		0.22362	
		0.00975		0.00223		0.01052
0.23	0.22798		0.97367		0.23414	
		0.00972		0.00233		0.01058
0.24	0.23770		0.97134		0.24472	
		0.00970		0.00243		0.01062
0.25	0.24740		0.96891		0.25534	
		0.00968		0.00252		0.01068
0.26	0.25706		0.96639		0.26602	
		0.00965		0.00262		0.01074
0.27	0.26672		0.96377		0.27676	
		0.00963		0.00271		0.01080
0.28	0.27636		0.96106		0.28756	
		0.00959		0.00282		0.01085
0.29	0.28595		0.095824		0.29841	
		0.00957		0.00290		0.01093
0.30	0.29552		0.95534		0.30934	
		0.00954		0.00301		0.01098
0.31	0.30506		0.95233		0.32032	
		0.00951		0.00309		0.01107
0.32	0.31457		0.94924		0.33139	
		0.00947		0.00320		0.01114
0.33	0.32404		0.94604		0.34253	
		0.00945		0.00329		0.01121
0.34	0.33349		0.94275		0.35374	
		0.00941		0.00338		0.01129
0.35	0.34290		0.93937		0.36503	
		0.00937		0.00347		0.01137
0.36	0.35227		0.93590		0.37640	
		0.00935		0.00357		0.01146
0.37	0.36162		0.93233		0.38786	
		0.00930		0.00367		0.01155
0.38	0.37092		0.92866		0.39941	
		0.00927		0.00375		0.01164
0.39	0.38019		0.92491		0.41106	
		0.00923		0.00385		0.01174
0.40	0.38942		0.92106		0.42279	
		0.00919		0.00394		0.01184
0.41	0.39861		0.91712		0.43463	
		0.00915		0.00403		0.01194
0.42	0.40776		0.91309		0.44657	
		0.00911		0.00412		0.01205
0.43	0.41687		0.90897		0.45862	
		0.00907		0.00422		0.01216
0.44	0.42694		0.90475		0.47078	
		0.00903		0.00430		0.01228
0.45	0.43497		0.90045		0.48306	
		0.00898		0.00440		0.01239
0.46	0.44395		0.89605		0.49545	
		0.00894		0.00448		0.01251
0.47	0.45289		0.89157		0.50796	
		0.00889		0.00458		0.01265
0.48	0.46178		0.88699		0.52061	
		0.00885		0.00466		0.01278
0.49	0.47063		0.88233		0.53339	
		0.00880		0.00476		0.01301
0.50	0.47943		0.87768		0.54630	

L/j in Radians	$\sin {}^{L}/_{j}$	$\Delta \sin {}^{L}/_{j}$	$\cos {}^{L}/_{j}$	$\Delta \cos {}^{L}/_{j}$	$\tan {}^{L}/_{j}$	$\Delta \tan {}^{L}/_{j}$
0.50	0.47943		0.87758		0.54630	
		0.00875		0.00484		0.01306
0.51	0.48818		0.87274		0.55936	
		0.00870		0.00492		0.01320
0.52	0.49688		0.86782		0.57256	
		0.00865		0.00501		0.01335
0.53	0.50553		0.86281		0.58591	
		0.00861		0.00510		0.01352
0.54	0.51414		0.85771		0.59943	
		0.00855		0.00619		0.01367
0.55	0.52269		0.85252		0.61310	
		0.00850		0.00526		0.01385
0.56	0.53119		0.84726		0.62695	
		0.00844		0.00536		0.01402
0.57	0.53963		0.84190		0.64097	
		0.00839		0.00544		0.01420
0.58	0.54802		0.83646		0.65517	
		0.00834		0.00552		0.01438
0.59	0.55636		0.83094		0.66955	
		0.00828		0.00560		0.01459
0.60	0.56464		0.82534		0.68414	
		0.00823		0.00569		0.01478
0.61	0.57287		0.81965		0.69892	
		0.00817		0.00677		0.01499
0.62	0.58104		0.81388		0.71391	
		0.00810		0.00585		0.01520
0.63	0.58914		0.80603		0.72911	
		0.00806		0.00593		0.01543
0.64	0.59720		0.80210		0.74454	
		0.00799		0.00602		0.01567
0.65	0.60519		0.79608		0.76021	
		0.00793		0.00609		0.01590
0.66	0.61312		0.78999		0.77611	
		0.00787		0.00617		0.01615
0.67	0.62099		0.78382		0.79226	
		0.00780		0.00625		0.01640
0.68	0.62879		0.77757		0.80866	
		0.00775		0.00632		0.01667
0.69	0.63654		0.77125		0.82533	
		0.00768		0.00641		0.01696
0.70	0.64422		0.76484		0.84229	
		0.00761		0.00648		0.01724
0.71	0.65183		0.75836		0.85953	
		0.00755		0.00655		0.01754
0.72	0.65938		0.75181		0.87707	
		0.00749		0.00664		0.01785
0.73	0.66687		0.74517		0.89492	
		0.00742		0.00670		0.01817
0.74	0.67429		0.73847		0.91309	
		0.00735		0.00678		0.01851
0.75	0.68164		0.73169		0.93160	
		0.00728		0.00685		0.01885
0.76	0.68892		0.72484		0.95045	
		0.00722		0.00693		0.01922
0.77	0.69614		0.71791		0.96967	
		0.00714		0.00700		0.01959
0.78	0.70328		0.71091		0.98926	
		0.00707		0.00706		0.01998
0.79	0.71035		0.70385		1.00924	
		0.00701		0.00714		0.02040
0.80	0.71736		0.69671		1.02964	
		0.00693		0.00721		0.02082
0.81	0.72429		0.68950		1.05046	
		0.00686		0.00728		0.02125
0.82	0.73116		0.68222		1.07171	
		0.00678		0.00734		0.02172
0.83	0.73793		0.67488		1.09343	
		0.00671		0.00742		0.02220
0.84	0.74464		0.66746		1.11563	
		0.00664		0.00748		0.02271
0.85	0.75128		0.65998		1.13834	
		0.00656		0.00754		0.02321
0.86	0.75784		0.65244		1.16155	
		0.00649		0.00761		0.02378
0.87	0.76433		0.64483		1.18533	
		0.00641		0.00768		0.02434
0.88	0.77074		0.63715		1.20967	
		0.00633		0.00774		0.02493
0.89	0.77707		0.62941		1.23460	
		0.00626		0.00780		0.02556
0.90	0.78333		0.62161		1.26016	
		0.00617		0.00786		0.02621
0.91	0.78950		0.61375		1.28637	
		0.00610		0.00793		0.02689
0.92	0.79560		0.60582		1.31326	
		0.00602		0.00799		0.02762
0.93	0.80162		0.59783		1.34088	
		0.00594		0.00804		0.02835
0.94	0.80756		0.58979		1.36923	
		0.00586		0.00811		0.02915
0.95	0.81342		0.58168		1.39838	
		0.00577		0.00816		0.02998
0.96	0.81919		0.57352		1.42836	
		0.00570		0.00822		0.03084
0.97	0.82489		0.56530		1.45920	
		0.00561		0.00828		0.03176
0.98	0.83050		0.55702		1.49096	
		0.00553		0.00833		0.03272
0.99	0.83603		0.54869		1.52368	
		0.00544		0.00839		0.03373
1.00	0.84147		0.54030		1.55741	

TABLE A5. II

NATURAL SINES, COSINES, AND TANGENTS OF ANGLES IN RADIANS

L/j in Radians	Sin $^{L}/_{j}$	Δ Sin $^{L}/_{j}$	Cos $^{L}/_{j}$	Δ Cos $^{L}/_{j}$	Tan $^{L}/_{j}$	Δ Tan $^{L}/_{j}$
1.00	0.84147		0.54030		1.55741	
		0.00536		0.00644		0.03480
1.01	0.84683		0.53186		1.59221	
		0.00528		0.00649		0.03592
1.02	0.85211		0.52337		1.62813	
		0.00519		0.00855		0.03712
1.03	0.85730		0.51482		1.66525	
		0.00510		0.00860		0.03836
1.04	0.86240		0.50622		1.70361	
		0.00502		0.00865		0.03971
1.05	0.86742		0.49767		1.74332	
		0.00494		0.00870		0.04110
1.06	0.87236		0.48887		1.78442	
		0.00484		0.00875		0.04261
1.07	0.87720		0.48012		1.82703	
		0.00476		0.00879		0.04419
1.08	0.88196		0.47133		1.87122	
		0.00467		0.00884		0.04588
1.09	0.88665		0.46249		1.91710	
		0.00458		0.00889		0.04766
1.10	0.89121		0.45360		1.96476	
		0.00449		0.00894		0.04958
1.11	0.89570		0.44466		2.01434	
		0.00440		0.00898		0.05161
1.12	0.90010		0.43568		2.06595	
		0.00431		0.00902		0.05380
1.13	0.90441		0.42666		2.11975	
		0.00422		0.00907		0.05613
1.14	0.90863		0.41759		2.17588	
		0.00413		0.00910		0.05861
1.15	0.91276		0.40849		2.23449	
		0.00404		0.00915		0.06131
1.16	0.91680		0.39934		2.29580	
		0.00395		0.00919		0.06418
1.17	0.92075		0.39018		2.35998	
		0.00386		0.00923		0.06728
1.18	0.92461		0.38092		2.42726	
		0.00376		0.00926		0.07064
1.19	0.92837		0.37166		2.49790	
		0.00367		0.00930		0.07425
1.20	0.93204		0.36236		2.57216	
		0.00358		0.00934		0.07818
1.21	0.93562		0.35302		2.65033	
		0.00348		0.00937		0.08243
1.22	0.93910		0.34365		2.73276	
		0.00339		0.00941		0.08706
1.23	0.94249		0.33424		2.81982	
		0.00329		0.00944		0.09212
1.24	0.94578		0.32480		2.91194	
		0.00320		0.00948		0.09763
1.25	0.94898		0.31532		3.00957	
		0.00311		0.00950		0.10371
1.26	0.95209		0.30582		3.11328	
		0.00301		0.00954		0.11035
1.27	0.95510		0.29628		3.22363	
		0.00292		0.00956		0.11772
1.28	0.95802		0.28872		3.34135	
		0.00282		0.00960		0.12586
1.29	0.96084		0.27712		3.46721	
		0.00272		0.00962		0.13489
1.30	0.96356		0.26760		3.60210	
		0.00262		0.00965		0.14498
1.31	0.96618		0.25785		3.74708	
		0.00254		0.00967		0.15627
1.32	0.96872		0.24818		3.90335	
		0.00243		0.00970		0.16896
1.33	0.97115		0.23848		4.07231	
		0.00233		0.00973		0.18331
1.34	0.97348		0.22875		4.25562	
		0.00224		0.00974		0.19961
1.35	0.97572		0.21901		4.45523	
		0.00214		0.00977		0.21821
1.36	0.97786		0.20924		4.67344	
		0.00205		0.00979		0.23962
1.37	0.97991		0.19945		4.91306	
		0.00194		0.00981		0.26438
1.38	0.98185		0.18964		5.17744	
		0.00185		0.00983		0.29326
1.39	0.98370		0.17981		5.47069	
		0.00175		0.00984		0.32719
1.40	0.98545		0.16997		5.79788	
		0.00165		0.00987		0.36749
1.41	0.98710		0.16010		6.16537	
		0.00155		0.00987		0.41573
1.42	0.98865		0.15023		6.58110	
		0.00145		0.00990		0.47436
1.43	0.99010		0.14033		7.05546	
		0.00136		0.00991		0.54636
1.44	0.99146		0.13042		7.60182	
		0.00125		0.00992		0.63628
1.45	0.99271		0.12050		8.23810	
		0.00116		0.00993		0.75052
1.46	0.99387		0.11057		8.98862	
		0.00105		0.00994		0.89878
1.47	0.99492		0.10063		9.88740	
		0.00096		0.00996		1.09698
1.48	0.99588		0.09067		10.98338	
		0.00086		0.00996		1.36653
1.49	0.99674		0.08771		12.34991	
		0.00075		0.00997		1.75151
1.50	0.99749		0.07074		14.10142	

L/j in Radians	Sin $^{L}/_{j}$	Δ Sin $^{L}/_{j}$	Cos $^{L}/_{j}$	Δ Cos $^{L}/_{j}$	Tan $^{L}/_{j}$	Δ Tan $^{L}/_{j}$
1.50	0.99749		0.07074		14.10142	
		0.00066		0.00998		2.32669
1.51	0.99815		0.06076		16.42811	
		0.00056		0.00999		3.2415
1.52	0.99871		0.05077		19.6696	
		0.00046		0.00998		4.8290
1.53	0.99917		0.04079		24.4986	
		0.00036		0.01000		7.9527
1.54	0.99953		0.03079		32.4513	
		0.00025		0.01000		15.6290
1.55	0.99978		0.02079		48.0803	
		0.00018		0.0999		44.5435
1.56	0.99996		0.01080		92.6238	
		0.00004		0.01000		1182.42
1.57	1.00000		0.00080		1275.04	
		0.00004		0.01000		1383.70
1.58	0.99996		-0.00920		-108.661	
		0.00014		0.01000		56.593
1.59	0.99982		-0.01920		-52.0676	
		0.00025		0.01000		17.8347
1.60	0.99957		-0.02920		-34.2329	
		0.00034		0.00999		8.7379
1.61	0.99923		-0.03919		-25.4950	
		0.00044		0.00999		5.1877
1.62	0.99879		-0.04918		-20.3073	
		0.00054		0.00999		3.4361
1.63	0.99825		-0.05917		-16.8712	
		0.00065		0.00998		2.4442
1.64	0.99760		-0.06915		-14.4270	
		0.00073		0.00997		1.8278
1.65	0.99687		-0.07912		-12.59926	
		0.00085		0.00997		1.41867
1.66	0.99602		-0.08909		-11.18059	
		0.00094		0.00995		1.33335
1.67	0.99508		-0.09904		-10.04724	
		0.00104		0.00995		0.92648
1.68	0.99404		-0.10899		- 9.12076	
		0.00114		0.00993		0.77151
1.69	0.99290		-0.11892		- 8.34925	
		0.00123		0.00992		0.65265
1.70	0.99167		-0.12884		- 7.69660	
		0.00134		0.00991		0.55937
1.71	0.99033		-0.13875		- 7.13723	
		0.00144		0.00990		0.48478
1.72	0.98889		-0.14866		- 6.65245	
		0.00153		0.00988		0.42436
1.73	0.98736		-0.15853		- 6.22809	
		0.00164		0.00987		0.37456
1.74	0.98572		-0.16840		- 5.85353	
		0.00173		0.00985		0.33316
1.75	0.98399		-0.17825		- 5.52037	
		0.00184		0.00983		0.29828
1.76	0.98215		-0.18806		- 5.22209	
		0.00192		0.00981		0.26869
1.77	0.98023		-0.19789		- 4.98340	
		0.00204		0.00979		0.24330
1.78	0.97819		-0.20768		- 4.71010	
		0.00212		0.00977		0.22144
1.79	0.97607		-0.21745		- 4.48866	
		0.00222		0.00975		0.20230
1.80	0.97385		-0.22720		- 4.28627	
		0.00233		0.00973		0.18577
1.81	0.97152		-0.23693		- 4.10050	
		0.00241		0.00970		0.17113
1.82	0.96911		-0.24663		- 3.92937	
		0.00252		0.00968		0.15819
1.83	0.96659		-0.25631		- 3.77118	
		0.00261		0.00965		0.14668
1.84	0.96398		-0.26596		- 3.62450	
		0.00271		0.00963		0.13644
1.85	0.96127		-0.27559		- 3.48806	
		0.00280		0.00960		0.12723
1.86	0.95847		-0.28519		- 3.36083	
		0.00290		0.00957		0.11895
1.87	0.95557		-0.29476		- 3.24188	
		0.00300		0.00954		0.11149
1.88	0.95257		-0.30430		- 3.13039	
		0.00308		0.00951		0.10473
1.89	0.94949		-0.31381		- 3.02556	
		0.00319		0.00948		0.09856
1.90	0.94630		-0.32329		- 2.92710	
		0.00328		0.00945		0.09296
1.91	0.94302		-0.33274		- 2.83414	
		0.00338		0.00941		0.08784
1.92	0.93964		-0.34215		- 2.74630	
		0.00346		0.00938		0.08314
1.93	0.93618		-0.35163		- 2.66316	
		0.00356		0.00934		0.07883
1.94	0.93262		-0.36087		- 2.58433	
		0.00366		0.00931		0.07486
1.95	0.92896		-0.37018		- 2.50947	
		0.00375		0.00927		0.07119
1.96	0.92521		-0.37945		- 2.43828	
		0.00384		0.00923		0.06779
1.97	0.92137		-0.38868		- 2.37049	
		0.00393		0.00920		0.06467
1.98	0.91744		-0.39788		- 2.30582	
		0.00403		0.00916		0.06534
1.99	0.91341		-0.40705		- 2.24048	
		0.00411		0.00912		0.05544
2.00	0.90930		-0.41615		- 2.18504	

TABLE A5.II

NATURAL SINES, COSINES, AND TANGENTS OF ANGLES IN RADIANS

L/j in Radians	Sin $L/_j$	Δ Sin $L/_j$	Cos $L/_j$	Δ Cos $L/_j$	Tan $L/_j$	Δ Tan $L/_j$
2.00	0.90930		-0.41615		- 2.18504	
		0.00421		0.00907		0.05651
2.01	0.90509		-0.42522		- 2.12853	
		0.00430		0.00903		0.05416
2.02	0.90079		-0.43425		- 2.07437	
		0.00438		0.00898		0.05195
2.03	0.89641		-0.44323		- 2.02242	
		0.00448		0.00895		0.04990
2.04	0.89193		-0.45218		- 1.97252	
		0.00457		0.00889		0.04766
2.05	0.88736		-0.46107		- 1.92456	
		0.00466		0.00885		0.04615
2.06	0.88270		-0.46992		- 1.87841	
		0.00473		0.00881		0.04445
2.07	0.87797		-0.47873		- 1.83396	
		0.00484		0.00875		0.04284
2.08	0.87313		-0.48748		- 1.79112	
		0.00491		0.00871		0.04135
2.09	0.86822		-0.49619		- 1.74977	
		0.00503		0.00866		0.03993
2.10	0.86319		-0.50485		- 1.70984	
		0.00507		0.00860		0.03857
2.11	0.85812		-0.51345		- 1.67127	
		0.00518		0.00856		0.03732
2.12	0.85294		-0.52201		- 1.63395	
		0.00526		0.00850		0.03610
2.13	0.84768		-0.53051		- 1.59785	
		0.00535		0.00845		0.03498
2.14	0.84233		-0.63896		- 1.56287	
		0.00543		0.00840		0.03389
2.15	0.83690		-0.54736		- 1.52898	
		0.00552		0.00834		0.03288
2.16	0.83138		-0.55570		- 1.49610	
		0.00559		0.00828		0.03191
2.17	0.82579		-0.56398		- 1.46419	
		0.00569		0.00823		0.03098
2.18	0.82010		-0.57221		- 1.43321	
		0.00576		0.00818		0.03011
2.19	0.81434		-0.58039		- 1.40310	
		-0.00585		0.00811		0.02928
2.20	0.80849		-0.58850		- 1.37382	
		0.00591		0.00806		0.02848
2.21	0.80258		-0.59656		- 1.34534	
		0.00601		0.00799		0.02773
2.22	0.79657		-0.60455		- 1.31761	
		0.00609		0.00794		0.02701
2.23	0.79048		-0.61249		- 1.29060	
		0.00616		0.00787		0.02631
2.24	0.78432		-0.62036		- 1.26429	
		0.00625		0.00781		0.02566
2.25	0.77807		-0.62817		- 1.23863	
		0.00632		0.00775		0.02503
2.26	0.77175		-0.63592		- 1.21360	
		0.00639		0.00769		0.02444
2.27	0.76536		-0.64361		- 1.18916	
		0.00648		0.00762		0.02385
2.28	0.75888		-0.65123		- 1.16531	
		0.00655		0.00756		0.02332
2.29	0.75233		-0.65879		- 1.14199	
		0.00662		0.00749		0.02278
2.30	0.74571		-0.66628		- 1.11921	
		0.00669		0.00742		0.02227
2.31	0.73902		-0.67370		- 1.09694	
		0.00678		0.00736		0.02180
2.32	0.73224		-0.68104		- 1.07514	
		0.00685		0.00728		0.02133
2.33	0.72539		-0.68834		- 1.05381	
		0.00692		0.00722		0.02089
2.34	0.71847		-0.69556		- 1.03292	
		0.00699		0.00715		0.02045
2.35	0.71148		-0.70271		- 1.01247	
		0.00707		0.00708		0.02005
2.36	0.70441		-0.70979		- 0.99242	
		0.00713		0.00701		0.01966
2.37	0.69728		-0.71680		- 0.97276	
		0.00721		0.00694		0.01927
2.38	0.69007		-0.72374		- 0.95349	
		0.00726		0.00686		0.01892
2.39	0.68281		-0.73060		- 0.93457	
		0.00733		0.00679		0.01856
2.40	0.67547		-0.73739		- 0.91602	
		0.00741		0.00672		0.01823
2.41	0.66806		-0.74411		- 0.89779	
		0.00748		0.00685		0.01790
2.42	0.66058		-0.75076		- 0.87989	
		0.00754		0.00656		0.01759
2.43	0.65304		-0.75732		- 0.86230	
		0.00760		0.00651		0.01728
2.44	0.64544		-0.76383		- 0.84502	
		0.00767		0.00640		0.01701
2.45	0.63777		-0.77023		- 0.82801	
		0.00774		0.00634		0.01671
2.46	0.63003		-0.77657		- 0.81130	
		0.00779		0.00626		0.01645
2.47	0.62224		-0.78283		- 0.79485	
		0.00786		0.00718		0.01619
2.48	0.61438		-0.78901		- 0.77866	
		0.00792		0.00611		0.01594
2.49	0.60846		-0.79512		- 0.76272	
		0.00799		0.00602		0.01569
2.50	0.59847		-0.80114		- 0.74703	

L/j in Radians	Sin $L/_j$	Δ Sin $L/_j$	Cos $L/_j$	Δ Cos $L/_j$	Tan $L/_j$	Δ Tan $L/_j$
2.50	0.59847		-0.80114		- 0.74703	
		0.00804		0.00596		0.01548
2.51	0.59043		-0.80709		- 0.73165	
		0.00810		0.00586		0.01523
2.52	0.58233		-0.81295		- 0.71632	
		0.00818		0.00578		0.01503
2.53	0.57417		-0.81873		- 0.70129	
		0.00821		0.00571		0.01482
2.54	0.56596		-0.82444		- 0.68647	
		0.00827		0.00561		0.01461
2.55	0.55769		-0.83005		- 0.67186	
		0.00833		0.00554		0.01442
2.56	0.54936		-0.83559		- 0.65744	
		0.00649		0.00545		0.01422
2.57	0.54097		-0.84104		- 0.64322	
		0.00844		0.00537		0.01405
2.58	0.53253		-0.84641		- 0.62917	
		0.00848		0.00528		0.01387
2.59	0.52405		-0.85169		- 0.61530	
		0.00855		0.00520		0.01370
2.60	0.51550		-0.85689		- 0.60160	
		0.00859		0.00511		0.01354
2.61	0.50591		-0.86200		- 0.58806	
		0.00664		0.00503		0.01338
2.62	0.49827		-0.86703		- 0.57468	
		0.00870		0.00494		0.01323
2.63	0.48957		-0.87197		- 0.56145	
		0.00875		0.00485		0.01308
2.64	0.48082		-0.87682		- 0.54837	
		0.00878		0.00476		0.01293
2.65	0.47204		-0.88158		- 0.53544	
		0.00885		0.00468		0.01280
2.66	0.46319		-0.88626		- 0.52264	
		0.00888		0.00459		0.01267
2.67	0.45431		-0.89085		- 0.50997	
		0.00893		0.00449		0.01253
2.68	0.44538		-0.89534		- 0.49744	
		0.00898		0.00441		0.01242
2.69	0.43640		-0.89975		- 0.48502	
		0.00902		0.00432		0.01229
2.70	0.42738		-0.90407		- 0.47273	
		0.00907		0.00423		0.01218
2.71	0.41831		-0.90830		- 0.46055	
		0.00909		0.00414		0.01206
2.72	0.40922		-0.91244		- 0.44849	
		0.00915		0.00404		0.01196
2.73	0.40007		-0.91648		- 0.43653	
		0.00918		0.00396		0.01186
2.74	0.39089		-0.92044		- 0.42467	
		0.00922		0.00386		0.01175
2.75	0.38167		-0.92430		- 0.41292	
		0.00927		0.00377		0.01166
2.76	0.37240		-0.92807		- 0.40126	
		0.00930		0.00358		0.01156
2.77	0.36310		-0.93175		- 0.38970	
		0.00933		0.00368		0.01148
2.78	0.35377		-0.93533		- 0.37822	
		0.00937		0.00350		0.01138
2.79	0.34440		-0.93883		- 0.36684	
		0.00941		0.00339		0.01131
2.80	0.33499		-0.94222		- 0.35553	
		0.00944		0.00331		0.01122
2.81	0.32555		-0.94563		- 0.34431	
		0.00947		0.00320		0.01115
2.82	0.31608		-0.94873		- 0.33316	
		0.00950		0.00312		0.01107
2.83	0.30658		-0.95185		- 0.32209	
		0.00954		0.00302		0.01100
2.84	0.29704		-0.95487		- 0.31109	
		0.00956		0.00292		0.01095
2.85	0.28748		-0.95779		- 0.30014	
		0.00960		0.00282		0.01086
2.86	0.27788		-0.96061		- 0.28928	
		0.00961		0.00274		0.01081
2.87	0.26827		-0.96335		- 0.27847	
		0.00965		0.00263		0.01074
2.88	0.25862		-0.96598		- 0.26773	
		0.00967		0.00254		0.01069
2.89	0.24895		-0.96852		- 0.25704	
		0.00970		0.00244		0.01063
2.90	0.23925		-0.97096		- 0.24641	
		0.00973		0.00234		0.01058
2.91	0.22952		-0.97330		- 0.23583	
		0.00973		0.00225		0.01054
2.92	0.21979		-0.97555		- 0.22529	
		0.00977		0.00215		0.01048
2.93	0.21002		-0.97770		- 0.21481	
		0.00979		0.00205		0.01044
2.94	0.20023		-0.97975		- 0.20437	
		0.00981		0.00195		0.01040
2.95	0.19042		-0.98170		- 0.19397	
		0.00982		0.00186		0.01035
2.96	0.18060		-0.98356		- 0.18362	
		0.00984		0.00175		0.01032
2.97	0.17076		-0.98531		- 0.17330	
		0.00987		0.00166		0.01029
2.98	0.16089		-0.98697		- 0.16301	
		0.00988		0.00156		0.01025
2.99	0.15101		-0.98853		- 0.15276	
		0.00989		0.00146		0.01022
3.00	0.14112		-0.98999		- 0.14254	

TABLE A5.II

NATURAL SINES, COSINES, AND TANGENTS OF ANGLES IN RADIANS

$L/_j$ in Radians	Sin $L/_j$	Δ Sin $L/_j$	Cos $L/_j$	Δ Cos $L/_j$	Tan $L/_j$	Δ Tan $L/_j$
3.00	0.14112		-0.98999		-0.14254	
		0.00991		0.00136		0.01019
3.01	0.13121		-0.99135		-0.13235	
		0.00992		0.00127		0.01016
3.02	0.12129		-0.99262		-0.12219	
		0.00993		0.00116		0.01013
3.03	0.11136		-0.99378		-0.11206	
		0.00994		0.00106		0.01011
3.04	0.10142		-0.99484		-0.10195	
		0.00996		0.00097		0.01010
3.05	0.09146		-0.99581		-0.09185	
		0.00996		0.00086		0.01008
3.06	0.08150		-0.99667		-0.08177	
		0.00997		0.00077		0.01006
3.07	0.07153		-0.99744		-0.07171	
		0.00998		0.00066		0.01004
3.08	0.06155		-0.99810		-0.06167	
		0.00999		0.00057		0.01003
3.09	0.05156		-0.99867		-0.05164	
		0.00997		0.00046		0.01002
3.10	0.04159		-0.99913		-0.04162	
		0.01000		0.00037		0.01001
3.11	0.03159		-0.99950		-0.03161	
		0.00999		0.00027		0.01001
3.12	0.02160		-0.99977		-0.02160	
		0.01000		0.00016		0.01000
3.13	0.01160		-0.99993		-0.01160	
		0.01000		0.00007		0.01000
3.14	0.00160		-1.00000		-0.00160	
		0.01001		0.00003		0.01001
3.15	-0.00841		-0.99997		0.00841	
		0.01000		0.00014		0.01000
3.16	-0.01841		-0.99984		0.01841	
		0.00999		0.00023		0.01000
3.17	-0.02840		-0.99960		0.02841	
		0.01000		0.00034		0.01002
3.18	-0.03840		-0.99926		0.03843	
		0.00999		0.00043		0.01002
3.19	-0.04839		-0.99883		0.04845	
		0.00999		0.00053		0.01003
3.20	-0.05838		-0.99830		0.05848	
		0.00998		0.00064		0.01004
3.21	-0.06836		-0.99766		0.06852	
		0.00997		0.00073		0.01005
3.22	-0.07833		-0.99693		0.07857	
		0.00996		0.00084		0.01007
3.23	-0.08829		-0.99609		0.08864	
		0.00996		0.00093		0.01009
3.24	-0.09825		-0.99516		0.09873	
		0.00995		0.00103		0.01010
3.25	-0.10820		-0.99413		0.10883	

these values in the general expression for M as given at the top of the Table.

In a beam-column member, the bending moments do not vary directly as the load is increased. Thus, the student should realize that margins of safety based on direct proportion of moments to loads are incorrect and lie on the unsafe side.

It is recommended that four significant figures be used in computations, making use of the so-called precise equations, since the results in many cases involve small differences between large numbers.

A5.28 Example Problems*

Example Problem #1

Fig. A5.67 illustrates a typical upper, outer panel wing beam of a biplane. Let it be required to determine the maximum negative bending moment between points (1) and (2), generally referred to as the maximum span moment. To obtain the true bending moments on the beam, the axial beam load as well as the end moments at (1) and (2) are necessary since they influence the deflection of the beam.

Solution:-

To obtain the horizontal component T_h of the lift strut load, we take moments about the

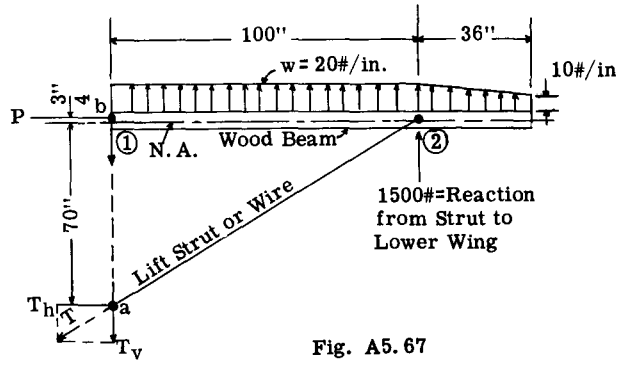

Fig. A5.67

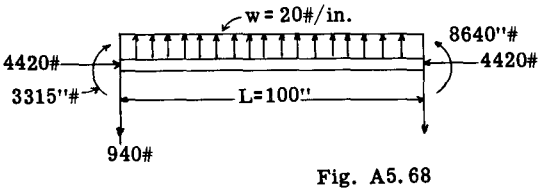

Fig. A5.68

hinge point at the left end.

$$\Sigma M_b = -2000 \times 50 - 540 \times 116 - 1500 \times 100 + 70.75\, T_h = 0$$

hence

$$T_h = 4420\#$$

The axial compressive load induced by the lift strut at point (2) then equals - 4420#.

Taking $\Sigma H = 0$ for the load system of Fig. A5.67 gives $P = -T_h = 4420\#$. The end moment on the beam at (1) equals the end load times the eccentricity of the hinge from the neutral axis of the beam, or 4420 x .75 = 3315"# positive because it produces compression in the top fibers. The moment at (2) due to the cantilever overhang equals $\frac{(20+10)}{2}$ 36 x 16 = 8640"#. Fig. A5.68 shows the beam portion between points (1) and (2) as a free body.

From Art. A5.25, we have the following precise equations for a beam carrying a transverse uniform distributed load with end compressive loads.

$$\tan \frac{x}{j} = \frac{D_2 - D_1 \cos \frac{L}{j}}{D_1 \sin \frac{L}{j}} \qquad \text{----------(A)}$$

and

$$M_{max} = \frac{D_1}{\cos \frac{x}{j}} + wj^2 \qquad \text{----------(B)}$$

Evaluating terms for substitution in these equations, we obtain,

$M_1 = 3315\#$

$M_2 = 8640\#$

$P = 4420\#$ compression

$I = 10$ in^4 given and assumed constant throughout the span.

$$j = \sqrt{\frac{1.3 \times 10^6 \times 10}{4420}} = \sqrt{2941} = 54.23$$

$wj^2 = 20 \times 2941 = 58820$

$D_1 = M_1 - wj^2 = 3315 - 58820 = -55505$

$D_2 = M_2 - wj^2 = 8640 - 58820 = -50180$

$$\frac{L}{j} = \frac{100}{54.23} = 1.844$$

From Table A5.II $\sin \frac{L}{j} = .96290$ and $\cos \frac{L}{j} = -.26981$

Substituting in equation (A)

$$\tan \frac{x}{j} = \frac{D_2 - D_1 \cos \frac{L}{j}}{D_1 \sin \frac{L}{j}}$$

$$= -\frac{50180 - (-55505 \times -.26981)}{-55505 \times .96290} = \frac{-65156}{-53441} = 1.2192$$

$$\frac{x}{j} = \tan^{-1} 1.2192 = .88383$$

Hence, x = .88383 x 54.23 = 48", which equals the distance from the left end of the beam to the point of maximum span moment.

$$M_{max} = \frac{D_1}{\cos \frac{x}{j}} + wj^2, \quad \cos \frac{x}{j} = .63419 \text{ from Table A5.II}$$

Hence

$$M_{max} = -\frac{55505}{.63419} + 58820 = -28{,}700\#$$

To obtain an idea as to the magnitude of the secondary bending moment, that is, the moment due to the axial load times the lateral beam deflection, the primary bending moment at a point 48"

*Additional examples are presented in Chapter C2, Part E, with stress analysis.

from the left end will be computed.

$$M_{as} = 3315 + 48 \times 20 \times 24 - 940 \times 48 = -18765"\#$$

Thus the secondary bending moment equals $-28700 + 18765 = -9935"\#$ which is a large percentage of the primary moment. The transverse deflection of the beam at the point of max. span moment then equals $\frac{-9935}{-4420} = 2.25$ inches upward.

Bending Moment at any Point Along Span

Let the moment at a point 10" from point (2) be required. In this case, $x = 100 - 10 = 90$

$$M = D_1\left[(\tan\frac{Xm}{j} \cdot \sin\frac{x}{j}) + \cos\frac{x}{j}\right] + wj^2 \text{ (Ref. Eq. A5.7)}$$

$$\frac{x}{j} = \frac{90}{54.23} = 1.6596, \sin\frac{x}{j} = .99605$$

$$\cos\frac{x}{j} = -.08867$$

$\tan\frac{X_m}{j} = 1.2192$ = value for x at the point of maximum bending moment

Hence,

$$M = -55505\left[(1.2192 \times .99605) + -.08867\right] + 58820 = -3664"\#$$

Example Problem #2

Fig. A5.69 shows a simplified landing gear structure carrying a vertical load of 12000# on the axle. Member ABC is continuous thru B and pinned at C. Let it be required to determine the bending moment at the midpoint of member BC and its lateral deflection due to the 12000# vertical design load.

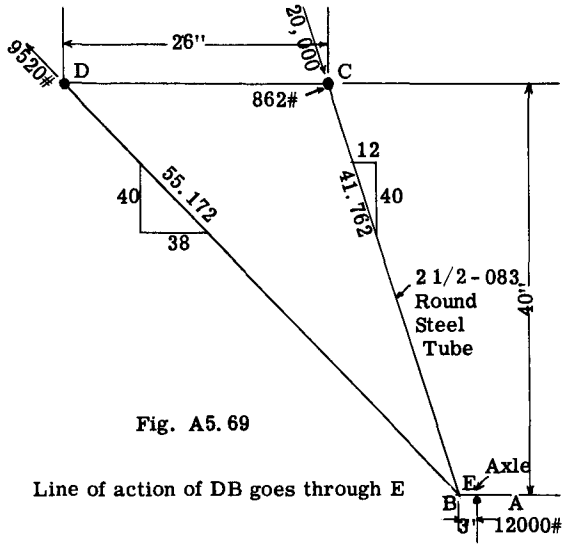

Fig. A5.69

Line of action of DB goes through E

Solution:-

Solving for reactions at C by statics, we obtain the axial load in BC = -20000. The bending moment at B due to 3" eccentricity of the wheel load = 3 x 12000 = 36000"#.

Fig. A5.70 shows a free body of portion BC of member ABC. From Table A5.I

$$M = C_1 \sin\frac{x}{j} + C_2 \cos\frac{x}{j} + f(w)$$

Substituting values of C_1 and C_2 and f(w) from Table A5.I in the above equations:

$$M = \frac{(M_2 - M_1 \cos L/j) \sin x/j}{\sin L/j} + M_1 \cos x/j$$

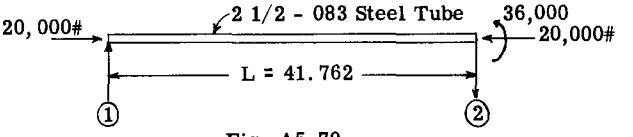

Fig. A5.70

But, $M_1 = 0$ in our problem, hence,

$$M = \frac{M_2 \sin x/j}{\sin L/j}$$

$$j = \sqrt{\frac{EI}{P}} = \sqrt{\frac{29 \times 10^6 \times .46}{20000}} = \sqrt{667} = 25.826$$

$$L/j = \frac{41.762}{25.826} = 1.617 \text{ - - - } \sin L/j = .99892$$

$$x = L/2 = 20.881$$

$$x/j = \frac{20.881}{25.80} = .8085 \text{ - - - } \sin x/j = .72327$$

Substituting in the above equations for M

$$M = \frac{36000 \times .72327}{.99892} = 26066"\#$$

This compares with a primary moment of 36000/2 = 18000"#. The deflection at the midpoint of BC = $\frac{26066 - 18000}{20000} = .403$ in.

The maximum moment is given by the equation:

$M_{max} = \frac{M_2}{\sin\frac{L}{j}}$ and it occurs at $x = \frac{\pi j}{2}$ (See Table A5.I)

A5.29 Stresses Above Proportional Limit Stress of Material.*

The equations as presented in this chapter assume that E is constant or in other words the stresses are within the elastic range. In aircraft structural design the applied or limit loads must be taken without suffering permanent deformation, hence E is constant under such loads. However the aircraft structure must take the design loads which equal the limit loads times a factor of safety (usually 1.5) without failure. In many cases structural failure will occur under stresses in the plastic range where the material stiffness is less and not constant.

A good approximation for an effective modulus E' is obtained as follows:-

(1) Compute $F_C = P/A$ for the given number.

(2) With this value of F_C enter the basic column curve diagram for the given material (for end fixity C = 1) and find value of L'/ρ corresponding to the stress F_C.

* Also see Chapter C2, Part E.

(3) Using these values of L'/ρ and F_c, compute

$$E' = \frac{F_c}{\pi^2}\left(\frac{L'}{\rho}\right)^2$$

(4) Then $j = \left(\frac{E'I}{\rho}\right)^{1/2}$

Basic column curves for various materials are given in another chapter of this book.

A5.30 Problems*

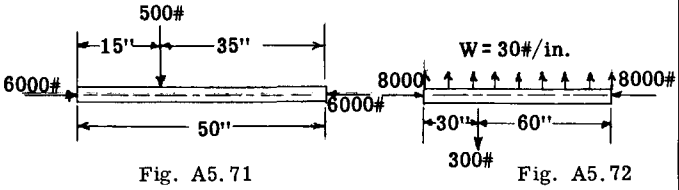

Fig. A5.71

Fig. A5.72

(1) Fig. A5.71 shows a 1-1/2 - .065 steel tube subjected to both end and lateral loads. Determine the maximum bending moment on the tube. Compare the result with the bending moment due to the side load only. E = 29 x 10^6 psi. I of tube = .075 $in.^4$ Compute lateral deflection at point of maximum bending moment. Area tube = 0.293 sq. in.

(2) The beam column member in Fig. A5.72 is made of 24ST aluminum alloy. Calculate and plot a curve of the bending moments on the member. Also plot bending moment due to lateral loads only. E = 10.3 x 10^6 psi. I = 5.0 $in.^4$

(3) Determine the maximum bending moment for the wood wing beam and loading of Fig. A10.9. I of beam section = 17 $in.^4$ E = 1.3 x 10^6.

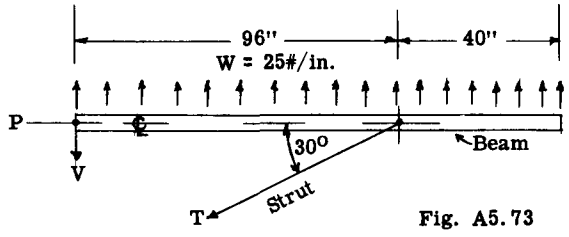

Fig. A5.73

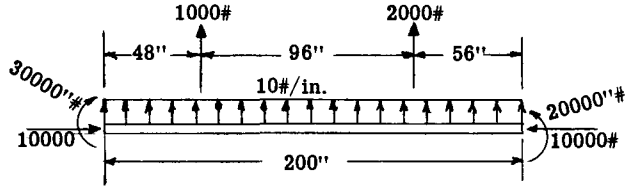

Fig. A5.74

(4) Determine the bending moment at the centerline of the beam-columns shown in Fig. A10.10 Assume EI = 64,000,000 lb. in. sq.

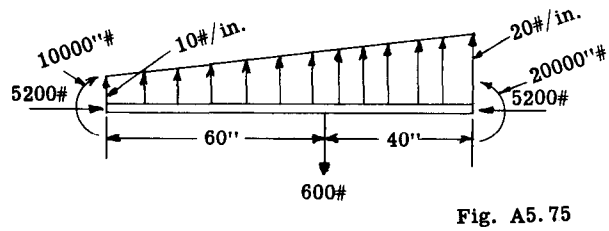

Fig. A5.75

(5) For the beam-column in Fig. A5.75 calculate the bending moment of the centerline of the member. Assume E = 1,300,000 psi. and I = 10 $in.^4$

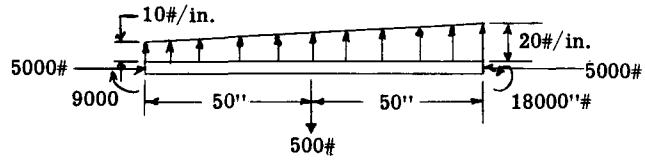

Fig. A5.76

(6) For the beam-column loading in Fig. A5.76, calculate bending moment at center point of beam. Take E = 1,200,000 psi and I = 10 $in.^4$

A5.31 Beam-Columns in Continuous Structures.

The secondary moments in a particular member due to beam-column action also effect or influence the deflections in adjacent members of a continuous structure. This rather involved problem can be handled quite simply and rapidly by the moment distribution method as explained and illustrated in Arts. A11.12 to 15 of Chapter A11 and in Part F of Chapter C2.

A numerical procedure for such beam-columns having a varying EI and/or a varying axial load is presented and illustrated in Part K and L of Chapter C2.

Beam-columns on elastic supports are discussed in Part M of Chapter C2.

CHAPTER A6
TORSION. - STRESSES AND DEFLECTIONS

A6.1 Introduction.

Problems involving torsion are common in aircraft structures. The metal covered airplane wing and fuselage are basically thin-walled tubular structures and are subjected to large torsional moments in certain flight and landing conditions. The various mechanical control systems in an airplane often contain units of various cross-sectional shapes which are subjected to torsional forces under operating conditions, hence a knowledge of torsional stresses and distortions of members is necessary in aircraft structural design.

A6.2. Torsion of Members with Circular Cross Sections.

The following conditions are assumed in the derivation of the equations for torsional stresses and distortions: -

(1) The member is a circular, solid or hollow round cylinder.

(2) Sections remain circular after application of torque.

(3) Diameters remain straight after twisting of section.

(4) Material is homogeneous, isotropic and elastic.

(5) The applied loads lie in a plane or planes perpendicular to the axis of the shaft or cylinder.

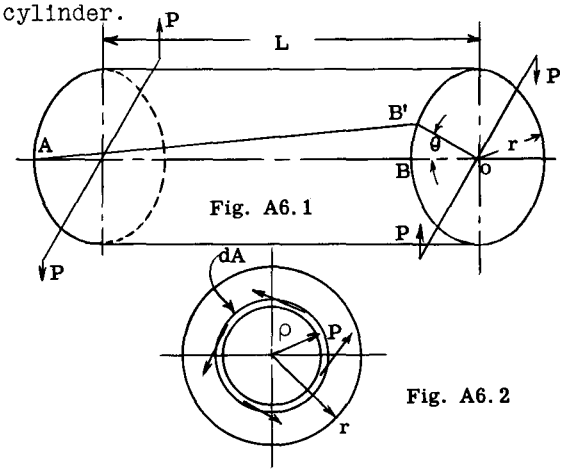

Fig. A6.1

Fig. A6.2

Fig. A6.1 shows a straight cylindrical bar subjected to two equal but opposite torsional couples. The bar twists and each section is subjected to a shearing stress. Assuming the left end as stationary relative to the rest of the bar a line AB on the surface will move to AB' under these shearing stresses and this rotation at any section will be proportional to the distance from the fixed support. It is assumed that any radial line undergoes angular displacement only, or OB remains straight when moving to OB'.

The unit shearing strain in a distance L equals,

$$\varepsilon = \frac{BB'}{AB} = \frac{r\,\theta}{L}$$

Let G equal modulus of rigidity of the material and let τ equal the unit shearing stress at the extreme fiber on the cross-section.

$$\text{Hence, } \tau = \varepsilon G = \frac{r\,\theta\,G}{L} \quad \text{- - - - - - - - - - -} \quad (1)$$

In Fig. A6.2 let τ_ρ equal the unit shearing stress on a circular strip dA at a distance ρ from O. Then

$$\tau_\rho = \frac{\rho}{r}\tau = \frac{\rho\,r\,\theta\,G}{r\,L} = \frac{\rho\,\theta\,G}{L}$$

The moment of the shearing stress on the circular strip dA about O the axis of the bar is equal to,

$dM = \tau_\rho\,\rho dA = \frac{\rho^2\theta G dA}{L}$ and thus the total internal torsional resisting moment is,

$$M_{int.} = \int \frac{G\rho^2\theta dA}{L}$$

For equilibrium, the internal resisting moment equals the external torsional moment T, and since $G\theta/L$ is a constant, we can write,

$$T = M_{int.} = \frac{G\theta}{L}\int_o^r \rho^2 dA = \frac{G\theta J}{L} \quad \text{- - - - - - -} \quad (2)$$

where J = polar moment of inertia of the shaft cross section and equals twice the moment of inertia about a diameter.

From equation (1) $\frac{G\theta}{L} = \frac{\tau}{r}$

$$\text{Hence, } T = \frac{\tau J}{r} \quad \text{- - - - - - - - - - - - - - - -} \quad (3)$$

$$\text{or} \qquad \tau = \frac{T r}{J} \quad \text{- - - - - - - - - - - - - - - -} \quad (4)$$

also from equation (2), solving for the twist θ,

$$\theta = \frac{TL}{GJ} \quad \text{- - - - - - - - - - - - - - - -} \quad (5)$$

(θ is measured in radians).

A6.3 Transmission of Power by a Cylindrical Shaft.

The work done by a twisting couple T in moving through an angular displacement is equal to the product of the magnitude of the couple and the angular displacement in radians. If the angular displacement is one revolution, the work done equals $2\pi T$. If T is expressed in inch-pounds and N is the angular velocity in revolutions per minute, then the horsepower transmitted by a rotating shaft may be written,

$$H.P. = \frac{2\pi N T}{396000} \quad \text{- - - - - - - - - - - - - - - - - (6)}$$

where 396000 represents inch pounds of work of one horsepower for one minute. Equation (6) may be written:

$$T = \frac{H.P. \times 396000}{2\pi N} = \frac{63025\ H.P.}{N} \quad \text{- - - - - - - (7)}$$

EXAMPLE PROBLEMS.

Problem 1.

Fig. A6.3 shows a conventional control stick-torque tube operating unit. For a side load of 150 lbs. on stick grip, determine the shearing stress on aileron torque tube and the angle of twist between points A and B.

SOLUTION:

Torsional moment on tube AB due to side stick force of 150# = 150 x 26 = 3900 in. lb. The resistance to this torque is provided by the

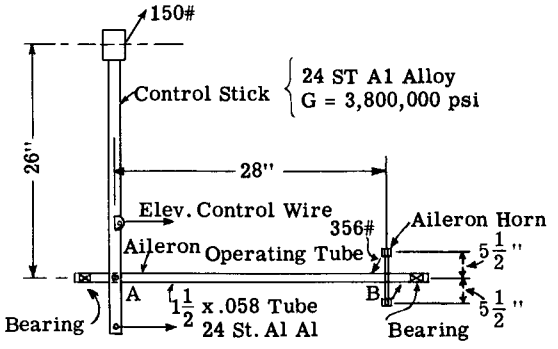

Fig. A6.3

aileron operating system attached to aileron horn and the horn pull equals 3900/11 = 356 lb. The polar moment of inertia of a $1\frac{1}{2}$ - 0.058 round tube equals 0.1368 in^4.

Maximum Shearing stress = $\tau = Tr/J$ = (3900 x 0.75)/0.1368 = 21400 psi.

The angular twist of the tube between points A and B equals

$$\theta = \frac{TL}{GJ} = \frac{3900 \times 28}{3{,}800{,}000 \times 0.1368} = 0.21 \text{ radians}$$

or 12 degrees.

Problem 2.

Fig. A6.4 illustrates an aileron control surface, consisting of a circular torque tube (1-1/4 - .049 in size) supported on three hinge brackets and with the control rod fitting attached to the torque tube above the center support bracket. Find the maximum torsional shearing stress in the tube if the air load on the aileron is as indicated in Fig. A6.4, and also compute the angle of twist of tube between horn section and end of aileron.

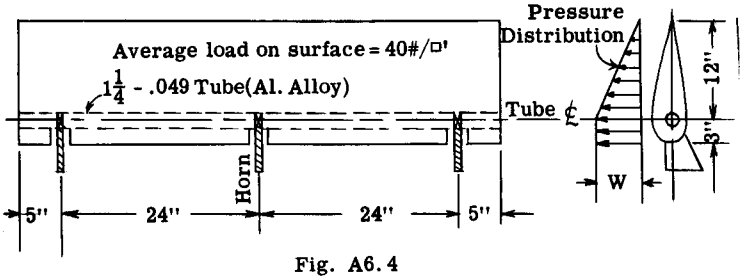

Fig. A6.4

SOLUTION:

The airload on the surface tends to rotate the aileron around the torque tube, but movement is prevented or created by a control rod attached to the torque tube over the center supporting bracket.

The total load on a strip of aileron one inch wide = 40(15 x 1/144) = 4.16 lb.

Let w equal intensity of loading per inch of aileron span at the leading edge point of the aileron surface, (see pressure diagram in Fig. A6.4).

Then 3w + (0.5 w)12 = 4.16

hence w = 0.463 lb./in.

The total load P_1 forward of the centerline of torque tube = 0.463 x 3 = 1.389 lb. and P_2 the load on aileron portion aft of hinge line = 0.463 x 0.5 x 12 = 2.778 lb.

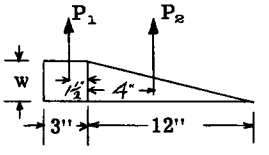

The torsional moment per running inch of torque tube: = - 1.389 x 1.5 + 2.778 x 4 = 9.0 in. lb. Hence, the maximum torque, which occurs at the center of the aileron, equals 9.0 x 29 = 261 in. lb.

$$\tau_{(max.)} = \frac{Tr}{J} = \frac{261 \times 0.625}{0.06678} = 2450 \text{ psi.}$$

$(J = 0.06678\ in^4.)$

Since the tube section is constant and the torque

varies directly as the distance from the end of the ailerons, the angle of twist θ can be computed by using the average torque as acting on entire length of the tube to one side of horn or a distant L = 29", hence

$$\theta = \frac{TL}{GJ} = \frac{261 \times 29}{2 \times 3800000 \times 0.06678} 57.3 = 0.86 \text{ degrees}$$

A6.4 Torsion of Members with Non-Circular Cross-Sections.

The formulas derived in Art. A6.2 cannot be used for non-circular shapes since the assumptions made do not hold. In a circular shaft subjected to pure torsion, the shearing stress distribution is as indicated in Fig. A6.5, namely, the maximum shearing stress is located at the most remote fiber from the centerline axis of the bar and is perpendicular to the radius to the stressed point. At a given distance from the axis of rotation the shear stress



Fig. A6.5

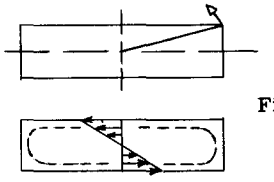

Fig. A6.6

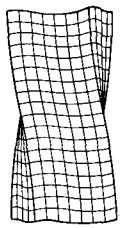

Fig. A6.7

τ max.

is constant in both directions as illustrated in Fig. A6.5, which means that ends of segments of the bar as it twists remain parallel to each other or in other words the bar sections do not warp out of their plane when the bar twists.

If the conditions of Fig. A6.5 are applied to the rectangular bar of Fig. A6.6, the most stressed fibers will be at the corners and the stress will be directed as shown. The stress would then have a component normal to the surface as well as along the surface and this is not true. The theory of elasticity shows that the maximum shear stress occurs at the centerline of the long sides as illustrated in Fig. A6.6 and that the stress at the corners is zero. Thus when a rectangular bar twists, the shear stresses are not constant at the same distances from the axis of rotation and thus the ends of segments cut through the bar would not remain parallel to each other when the bar twists or in other words, warping of the section out of its plane takes place. Fig. A6.7 illustrates this action in a twisted rectangular bar. The ends of the bar are warped or suffer distortion normal to the original unstressed plane of the bar ends.

Further discussion and a summary of equations for determining the shear stresses and twists of non-circular cross-sections is given in Art. A6.6.

A6.5 Elastic Membrane Analogy.

The shape of a warped cross-section of a non-circular cross-section in torsion is needed in the analysis by the theory of elasticity, and as a result only a few shapes such as rectangles, elipses, triangles, etc., have been solved by the theoretical approach. However, a close approximation can be made experimentally for almost any shape of cross-section by the use of the membrane analogy.

It was pointed out by Prandtl that the equation of torsion of a bar and the equation for the deflection of a membrane subjected to uniform pressure have the same form. Thus if an elastic membrane is stretched over an opening which has the same shape as the cross-section of the bar being considered and then if the membrane is deflected by subjecting it to a slight difference of pressure on the two sides, the resulting deflected shape of the membrane provides certain quantities which can be measured experimentally and then used in the theoretical equations. However, possibly the main advantage of the membrane theory is, that it provides a method of visualizing to a considerable degree of accuracy how the stress conditions vary over a complicated cross-section of a bar in torsion.

The membrane analogy provides the following relationships between the deflected membrane and the twisted bar.

(1) Lines of equal deflection on the membrane (contour lines) correspond to shearing stress lines of the twisted bar.

(2) The tangent to a contour line at any point on the membrane surface gives the direction of the resultant shear stress at the corresponding point on the cross-section of the bar being twisted.

(3) The maximum slope of the deflected membrane at any point, with respect to the edge support plane is equal in magnitude to the shear stress at the corresponding point on the cross-section of the twisted bar.

(4) The applied torsion on the twisted bar is proportional to twice the volume included between the deflected membrane and a plane through the supporting edges.

To illustrate, consider a bar with a rectangular cross-section as indicated in Fig. A6.8. Over an opening of the same shape we stretch a thin membrane and deflect it normal to the cross-section by a small uniform pressure. Equal deflection contour lines for this deflected membrane will take the shape as illustrated in Fig. A6.9. These contour lines which correspond to direction of shearing stress in the twisted bar are nearly circular near the center region of the bar, but tend

to take the shape of the bar boundary as the boundary is approached. Fig. A6.9a shows a section through the contour lines or the deflected membrane along the lines 1-1, 2-2 and 3-3 of Fig. A6.9. It is obvious that the slopes of the deflected surface along line 1-1 will be greater than along lines 2-2 or 3-3. From this we can conclude that the shear stress at any point on line 1-1 will be greater than the shear stress for corresponding points on lines 2-2 and 3-3. The maximum slope and therefore the maximum

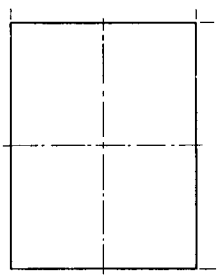

Fig. A6.8

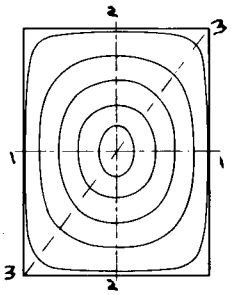

Fig. A6.9

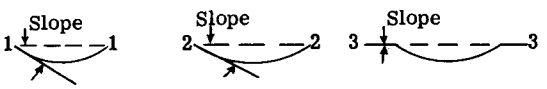

Fig. A6.9a

stress will occur at the ends of line 1-1. The slope of the deflected membrane will be zero at the center of the membrane and at the four corners, and thus the shear stress at these points will be zero.

A6.6 Torsion of Open Sections Composed of Thin Plates.

Members having cross-sections made up of narrow or thin rectangular elements are sometimes used in aircraft structures to carry torsional loads such as the angle, channel, and Tee Shapes.

For a bar of rectangular cross-section of width b and thickness t a mathematical elasticity analysis gives the following equations for maximum shearing stress and the angle of twist per unit length.

$$\tau_{MAX} = \frac{T}{\alpha\, b\, t^2} \quad \text{- - - - - - - - - - - - - - - - - -} \quad (6)$$

$$\theta = \frac{T}{\phi\, b\, t^3\, G} \text{ in radians} \quad \text{- - - - - - - - - - -} \quad (7)$$

Values of α and ϕ are given in Table A6.1.

TABLE A6.1

CONSTANTS α AND ϕ

b/t	1.00	1.50	1.75	2.00	2.50	3.00	4	6	8	10	∞
α	0.208	0.231	0.239	0.246	0.258	0.267	0.282	0.299	0.307	0.313	0.333
ϕ	0.141	0.196	0.214	0.229	0.249	0.263	0.281	0.299	0.307	0.313	0.333

From Table A6.1 it is noticed that for large values of b/t, the values of the constants is 1/3, and thus for such narrow rectangles, equations (6) and (7) reduce to,

$$\tau_{MAX} = \frac{3\,T}{bt^2} \quad \text{- - - - - - - - - - - - - - - - -} \quad (8)$$

$$\theta = \frac{3\,T}{bt^3G} \quad \text{- - - - - - - - - - - - - - - - - -} \quad (9)$$

Although equations (8) and (9) have been derived for a narrow rectangular shape, they can be applied to an approximate analysis of shapes made up of thin rectangular members such as illustrated in Fig. A6.10. The more generous the fillet or corner radius, the smaller the stress concentration at these junctions and therefore the more accuracy of these approximate formulas. Thus for a section made up of a continuous plate such as illustrated in

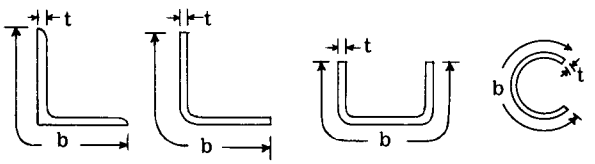

Fig. a

b can be taken as centerline length for above type of sections

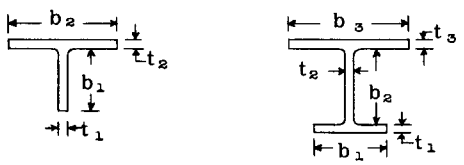

Fig. A6.10

Fig. (a) of Fig. A6.10, the width b can be taken as the total length of the cross-section. For sections such as the tee and H section in Fig. A6.10, the polar moment of inertia J can be taken as $\Sigma\, bt^3/_3$. Thus for the tee section of Fig. A6.10:

$$\theta = \frac{T}{GJ} = \frac{3\,T}{G\,\Sigma\, bt^3}$$

$$= \frac{3\,T}{G\,(b_1t_1^3 + b_2t_2^3)}$$

For the maximum shearing stress on leg b_1

$$\tau_{b_1} = \frac{T\,t_1}{J} = \frac{3\,T\,t_1}{\Sigma\, bt^3} = \frac{3\,T\,t_1}{b_1t_1^3 + b_2t_2^3} \quad \text{- - - -} \quad (10)$$

and for the plate b_2,

$$\tau_{b_2} = \frac{T\,t_2}{J} = \frac{3\,T\,t_2}{b_1t_1^3 + b_2t_2^3} \quad \text{- - - - - - - - -} \quad (11)$$

If $t_1 = t_2 = t$, then

$$\theta = \frac{3\,T}{G\,t^3(b_1 + b_2)} \quad \text{- - - - - - - - - - - - -} \quad (12)$$

$$\tau = \frac{3\,T}{t^3(b_1 + b_2)} \quad \text{- - - - - - - - - - - - - -} \quad (13)$$

EXAMPLE PROBLEM SHOWING TORSIONAL STIFFNESS OF CLOSED THIN WALLED TUBE COMPARED TO OPEN OR SLOTTED TUBE.

Fig. A6.11a shows a 1 inch diameter tube with .035 wall thickness, and Fig. A6.11b shows the same tube but with a cut in the wall making it an open section.

For the round tube $J_1 = 0.02474$ in^4.

For open tube $J_2 = \frac{1}{3} \times 3.14 \times .035^3 = 0.000045$

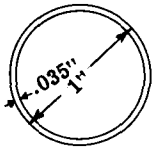

Fig. A6.11a

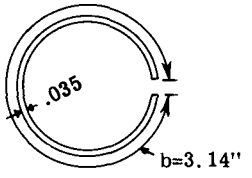

Fig. A6.11b

Let θ_1 equal twist of closed tube and θ_2 equal twist of open tube. The twist, will then be inversely proportional to J since $\theta = \frac{T}{JG}$. Therefore the closed tube is $J_1/J_2 = 0.02474/0.000045 = 550$ times as stiff as the open tube. This result shows why open sections are not efficient torsional members relative to torsional deflection.

TABLE A6.3

FORMULAS FOR TORSIONAL DEFLECTION AND STRESS

$\theta = \frac{T}{KG}$ = twist in radians per inch of length.
T = Torsional Moment (in. lb.).
G = Modulus of Rigidity.
K (in^4) From Table.

SECTION	K	FORMULA FOR SHEAR STRESS
SOLID ELLIPITICAL SECTION. 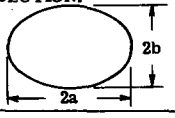	$K = \frac{\pi a^3 b^3}{a^2 + b^2}$	$\tau_{MAX} = \frac{2T}{\pi ab^2}$ (at ends of minor axis).
SOLID SQUARE. 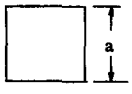	$K = 0.141 a^4$	$\tau_{MAX} = \frac{T}{0.208 a^3}$ (at midpoint of each side).
SOLID RECTANGLE. 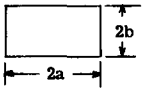	$K = ab^3\left[\frac{16}{3} - 3.36\frac{b}{a}\left(1 - \frac{b^4}{12a^4}\right)\right]$	$\tau_{MAX} = \frac{T(3a - 1.8b)}{8a^2b^2}$ midpoint of longside.
SOLID TRIANGLE. 	$K = \frac{1.73 a^4}{80}$	$\tau_{MAX} = \frac{2OT}{a^3}$ at midpoint of side.

For an extensive list of formulas for many shapes both solid and hollow, refer to book, "Formulas For Stress and Strain" by Roark, 1954 Edition.

A6.7 Torsion of Solid Non-Circular Shapes and Thick-Walled Tubular Shapes.

Table A6.3 summarizes the formulas for torsional deflection and stress for a few shapes. These formulas are based on the assumption that the cross-sections are free to warp (no end restraints). Material is homogeneous and stresses are within the elastic range.

A6.8 Torsion of Thin-Walled Closed Sections.

The structure of aircraft wings, fuselages and control surfaces are essentially thin-walled tubes of one or more cells. Flight and landing loads often produce torsional forces on these major structural units, thus the determination of the torsional stress and deformation of such structures plays an important part in aircraft structural analysis and design.

Fig. A6.12 shows a portion of a thin-walled cylindrical tube which is under a pure torsional moment. There are no end restraints on the tube or in other words the tube ends and tube cross-sections are free to warp out of their plane.

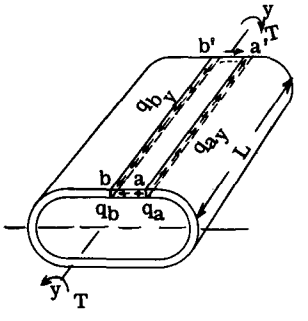

Fig. A6.12

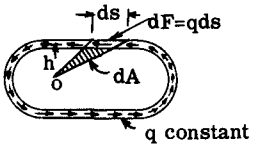

Fig. A6.13

Let q_a be the shear force intensity at point (a) on the cross-section and q_b that at point (b).

Now consider the segment a a' b' b of the tube wall as shown in Fig. A6.12 as a free body. The applied shear force intensity along the segment edges parallel to the y axis will be given the values q_{a_y} and q_{b_y} as shown in Fig. A6.12. For a plate in pure shear the shearing stress at a point in one plane equals the stress in a plane at right angles to the first plane, hence $q_a = q_{a_y}$ and $q_b = q_{b_y}$.

Since the tube sections are free to warp there can be no longitudinal stresses on the tube wall. Considering the equilibrium of the segment in the Y direction,

$\Sigma F_y = 0 = q_{a_y}L - q_{b_y}L = 0$, hence $q_{a_y} = q_{b_y}$ and therefore $q_a = q_b$ or in other words the shear force intensity around the tube wall is constant. The shear stress at any point $\tau = q/t$. If the wall thickness t changes the shear stress

changes but the shear force q does not change, or

$$\tau_a t_a = \tau_b t_b = \text{constant.}$$

The product τt is generally referred to as the shear flow and is given the symbol q. The name shear flow possibly came from the fact that the equation τt = constant, resembles the equation of continuity of fluid flow qS = constant where q is the flow velocity and S the tube cross-sectional area.

We will now take moments of the shear flow q on the tube cross-section about some point (o). In Fig. A6.13 the force dF on the wall element dF = qds. Its arm from the assumed moment center (o) is h. Thus the moment of dF about (o) is q ds h. However, ds times h is twice the area of the shaded triangle in Fig. A6.13.

Hence the torsional moment dT of the force on the element ds equals,

$$dT = qhds = 2qdA$$

and thus for the total torque for the entire shear flow around the tube wall equals,

$$T = \int_A 2qdA \quad \text{and since q is constant}$$

$$T = q\,2A \qquad (14)$$

or

$$q = \frac{T}{2A} \qquad (15)$$

where A is the enclosed area of the mean periphery of the tube wall.

The shear stress τ at any point on the tube wall is equal to q, the shear force per inch of wall divided by the area of this one inch length or 1 x t or

$$\tau = q/t = \frac{T}{2At} \qquad (16)$$

TUBE TWIST

Consider a small element cut from the tube wall and treated as a free body in Fig. A6.14, with ds in the plane of the tube cross-section and a unit length parallel to the tube axis. Under the shearing strains the plate element

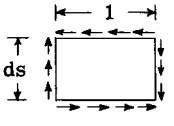

Fig. A6.14

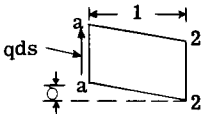

Fig. A6.15

deforms as illustrated in Fig. A6.15, that is, the face a-a moves with respect to face 2-2 a distance δ. The force on edge a-a equals q ds and it moves through a distance δ.

The elastic strain energy dU stored in this element therefore equals,

$$dU = \frac{qds}{2}\,\delta$$

However the shear strain δ can be written,

$$\delta = \frac{\tau}{G} = \frac{q}{Gt}, \text{ but } q = \frac{T}{2A}$$

hence $$dU = \frac{T^2}{8A^2Gt}\,ds$$

or $$U = \oint \frac{T^2}{8A^2Gt}\,ds, \text{ the integral } \oint$$

is the line integral around the periphery of the tube. From Chapter A7 from Castigliano's theorem,

$$\theta = \frac{\partial U}{\partial T} = \oint \frac{T}{4A^2Gt}\,ds \qquad (17)$$

since all values except t are constant, equation (17) can be written,

$$\theta = \frac{T}{4A^2G} \oint \frac{ds}{t} \qquad (18)$$

and since T = 2 qA, then also,

$$\theta = \frac{q}{2AG} \oint \frac{ds}{t} \qquad (19)$$

where θ is angle of twist in radians per unit length of one inch of tube. For a tube length of L

$$\theta = \frac{q\,L}{2AG} \oint \frac{ds}{t} \qquad (20)$$

A6.9 Expression for Torsional Moment in Terms of Internal Shear Flow Systems for Multiple Cell Closed Sections.

Fig. A6.16 shows the internal shear flow pattern for a 2-cell thin-walled tube, when the tube is subjected to an external torque. q_1, q_2 and q_3 represent the shear load per inch on the three different portions of the cell walls.

For equilibrium of shear forces at the junction point of the interior web with the outside wall, we know that

$$q_1 = q_2 + q_3 \qquad (21)$$

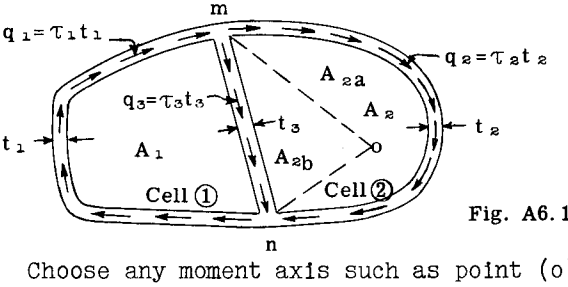

Fig. A6.16

Choose any moment axis such as point (o). Referring back to Fig. A6.13, we found that the moment of a constant shear force q acting along a wall length ds about a point (o) was equal in

magnitude to twice the area of the geometrical shape formed by radii from the moment center to the ends of the wall element ds times the shear flow q.

Let T_o = moment of shear flow about point (o). Then from Fig. A6.16,

$$T_o = 2q_1 (A_1 + A_{2b}) + 2q_2A_{2a} - 2q_3A_{2b}$$

$$= 2q_1A_1 + 2q_1A_{2b} + 2q_2A_{2a} - 2q_3A_{2b} \quad ---- \quad (22)$$

But from equation (21), $q_3 = q_1 - q_2$. Substituting the value of q_3 in (22)

$$T_o = 2q_1A_1 + 2q_1A_{2b} + 2q_2A_{2a} - 2q_1A_{2b} + 2q_2A_{2b}$$

But $A_2 = A_{2a} + A_{2b}$

Hence, $T_o = 2q_1A_1 + 2q_2A_2$ ---------- (23)

where A_1 = area of cell (1) and A_2 = area of cell (2). Therefore, the moment of the internal shear system of a multiple cell tube carrying pure torsional shear stresses is equal to the sum of twice the enclosed area of each cell times the shear load per inch which exists in the outside wall of that cell. (Note: The web mn is referred to as an inside wall of either cell).

A6.10 Distribution of Torsional Shear Stresses in a Multiple-Cell Thin-Walled Closed Section. Angle of Twist.

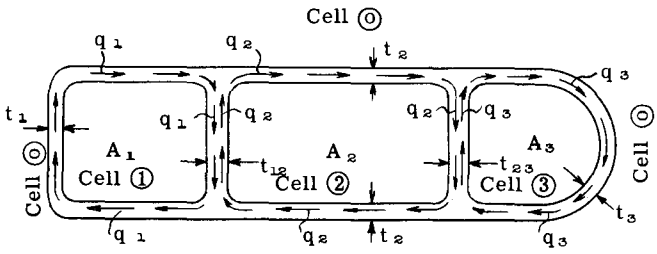

Fig. A6.17

Fig. A6.17 shows in general the internal shear flow pattern on a 3-cell tube produced by a pure torque load on the tube. The cells are numbered (1), (2) and (3), and the area outside the tube is designated as cell (o). Thus, to designate the outside wall of cell (1), we refer to it as lying between cells 1-0; for the outside wall of cell 2, as 2-0; and for the web between cells (1) and (2) as 1-2, etc.

q_1 = shear load per inch = τ_1t_1 in the outside wall of cell (1), where τ_1 equals the unit stress and t_1 = wall thickness. Likewise, $q_2 = \tau_2t_2$ and $q_3 = \tau_3t_3$ = shear load per inch in outside walls of cells (2) and (3) respectively. For equilibrium of shear forces at the junction points of interior webs with the outside walls, we have $(q_1 - q_2)$ equal to the shear load per inch in the web 1-2 and $(q_2 - q_3)$ for web 2-3.

For equilibrium, the torsional moment of the internal shear system must equal the external torque on the tube at this particular section. Thus, from the conclusions of article A6.9, we can write:

$$T = 2q_1A_1 + 2q_2A_2 + 2q_3A_3 \quad -------- \quad (24)$$

For elastic continuity, the twist of each cell must be equal, or $\theta_1 = \theta_2 = \theta_3$.

From equation (19), the angular twist of a cell is

$$\theta = \frac{q}{2AG} \oint \frac{ds}{t} \quad \text{or}$$

$$2G\theta = \frac{q}{A} \oint \frac{ds}{t} \quad ---------- \quad (25)$$

Thus, for each cell of a multiple cell structure an expression $\frac{q}{A} \oint \frac{ds}{t}$ can be written and equated to the constant value $2G\theta$. Let a_{1o}, represent a line integral $\oint \frac{ds}{t}$ for cell wall 1-0, and a_{12}, a_{2o}, a_{23} and a_{3o} the line integrals $\oint \frac{ds}{t}$ for the other outside wall and interior web portions of the 3-cell tube. Let clockwise direction of wall shear stresses in any cell be positive in sign. Now, substituting in Equation (25), we have:

$$\text{cell (1)} \quad \frac{1}{A_1}\left[q_1 a_{1o} + (q_1 - q_2)\, a_{12}\right] = 2G\theta \quad (26)$$

$$\text{cell (2)} \quad \frac{1}{A_2}\left[(q_2 - q_1)a_{12} + q_2a_{2o} + (q_2 - q_3)a_{23}\right]$$

$$= 2G\theta \quad ---------- \quad (27)$$

$$\text{cell (3)} \quad \frac{1}{A_3}\left[(q_3 - q_2)a_{23} + q_3a_{3o}\right] = 2G\theta \quad (28)$$

Equations (24, 26, 27 and 28) are sufficient to determine the true values of q_1, q_2, q_3 and θ.

Thus, to determine the torsional stress distribution in a multiple cell structure, we write equation (25) for each cell and these equations together with the general torque equation, similar to equation (24), provides sufficient conditions for the solution of the shear stresses and the angle of twist.

A6.11 Stress Distribution and Angle of Twist for 2-Cell Thin-Wall Closed Section.

For a two cell tube, the equations can be simplified to give the values of q_1, q_2 and θ directly. For tubes with more than two cells, the equations become too complicated, and thus the equations should be solved simultaneously. Equations for two-cell tube (Fig. A6.18): -

$$q_1 = \frac{1}{2}\left[\frac{(a_{20}A_1 + a_{12}A)}{a_{20}A_1^2 + a_{12}A^2 + a_{01}A_2^2}\right] T \quad ---- (29)$$

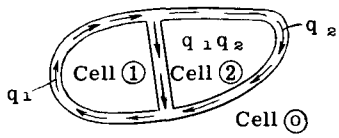

Fig. A6.18

$$q_2 = \frac{1}{2}\left[\frac{a_{01}A_2 + a_{12}A}{a_{20}A_1^2 + a_{12}A^2 + a_{01}A_2^2}\right] T \quad ---- (30)$$

$$J = 4\left[\frac{a_{20}A_1^2 + a_{12}A^2 + a_{01}A_2^2}{a_{01}a_{12} + a_{12}a_{20} + a_{20}a_{01}}\right] ----- (31)$$

$$\theta = \frac{T}{G\,J} \quad ---------- (32)$$

where $A = A_1 + A_2$.

A6.12 Example Problems of Torsional Stresses in Multiple-Cell-Thin-Walled Tubes.

Example 1 - Torsional Stresses in Un-symmetrical Two-Cell-Tube.

Fig. A6.19 shows a typical 2-cell tubular section as formed by a conventional airfoil shape, and having one interior web. An external applied torque T of 83450 in. lb. is assumed acting as shown. The internal shear resisting pattern is required.

Calculation of Cell Constants

Cell areas: - A_1 = 105.8 sq. in.
A_2 = 387.4 sq. in.
A = 493.2 sq. in.

Line integrals $a = \oint \frac{ds}{t}$: -

$$a_{10} = \frac{26.9}{.025} = 1075; \quad a_{12} = \frac{13.4}{.04} = 335$$

$$a_{20} = \frac{25.25}{.04} + \frac{15.7}{.05} + \frac{25.3}{.032} = 1735$$

Solution by equating angular twist of each cell.

General equation $2G\theta = \frac{q}{A}\oint \frac{ds}{t}$. Clockwise flow of q is positive.

Cell 1 Subt. in general equation

$$2G\theta = \frac{1}{105.8}\left[-q_1 \times 1075 + (-q_1 + q_2)\,335\right] =$$

$$-13.33\,q_1 + 3.165\,q_2 \quad ---------- (33)$$

Cell 2

$$2G\theta = \frac{1}{387.4}\left[-(q_2 - q_1)\,335 - 1735\,q_2\right] =$$

$$.865\,q_1 - 5.34\,q_2 \quad ---------- (34)$$

Equating (33) and (34)

$$-14.195\,q_1 + 8.505\,q_2 = 0 \quad ---------- (35)$$

The summation of the external and internal resisting torque must equal zero.

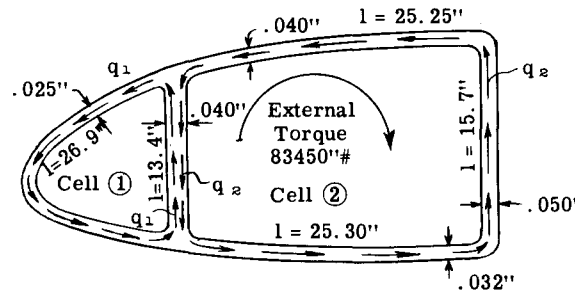

Fig. A6.19

$$83450 - 2 \times 105.8\,q_1 - 2 \times 387.4\,q_2 = 0 \quad (36)$$

Solving equations (35) and (36), q_1 = 55.6#/in. and q_2 = 92.5#/in. Since results come out positive, the assumed direction of counter-clockwise was correct for q_1 and q_2 or true signs are q_1 = - 55.6 and q_2 = - 92.5.

q_{12} = - 55.6 + 92.5 = 36.9#/in. (as viewed from Cell 1).

Fig. A6.20 shows the resulting shear pattern. The angular twist of the complete cell can be found by substituting values of q_1 and q_2 in either equations (33) or (34), since twist of each cell must be the same and equal to twist of tube as a whole.

Fig. A6.20

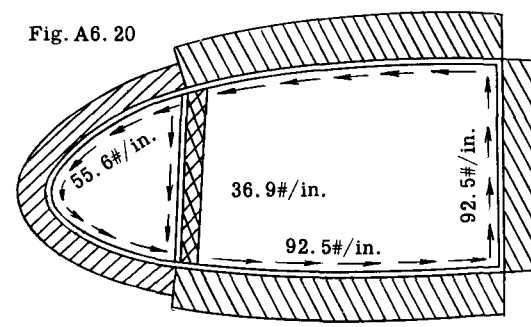

SOLUTION BY SUBSTITUTING IN EQUATIONS (29) & (30)

$$q_1 = \frac{1}{2}\left[\frac{a_{20}A_1 + a_{12}A}{a_{20}A_1^2 + a_{12}A^2 + a_{10}A_2^2}\right] T =$$

$$\left[\frac{1735 \times 105.8 + 335 \times 493.2}{1735 \times 105.8^2 + 335 \times 493.2^2 + 1075 \times 387.4^2}\right]\frac{T}{2}$$

$$= .000665\ T = .000665 \times 83450 = 55.6\#/in.$$

$$q_2 = \frac{1}{2}\left[\frac{a_{10}A_2 + a_{12}A}{a_{20}A_1^2 + a_{12}A^2 + a_{10}A_2^2}\right]T =$$

$$\left[\frac{1075 \times 387.4 + 335 \times 493.2}{1735 \times 105.8^2 + 335 \times 493.2^2 + 1075 \times 387.4^2}\right]\frac{T}{2}$$

$$= .001107\ T = .001107 \times 83450 = 92.5\#/in.$$

Example Problem 2.

Determine the torsional shear stresses in the symmetrical 2 cell section of Fig. A6.21 when subjected to a torque T. Neglect any resistance of stringers in resisting torsional moment.

Fig. A6.21

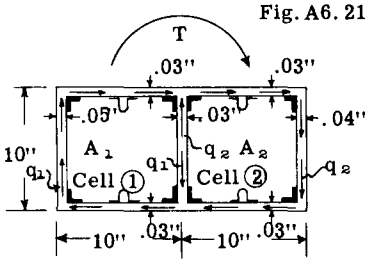

SOLUTION:

Calculation of terms

Area of cells: -

$A_1 = 100$ $A_2 = 100$

$A = A_1 + A_2 = 200$

Line integrals $a = \oint \frac{ds}{t}$: -

$$a_{10} = \frac{10}{.05} + \frac{20}{.03} = 866.7$$

$$a_{12} = \frac{10}{.03} = 333.3$$

$$a_{20} = \frac{20}{.03} + \frac{10}{.04} = 916.7$$

Solution of Equations from Article A6.11: -

$$q_1 = \frac{1}{2}\left[\frac{a_{20}A_1 + a_{12}A}{a_{20}A_1^2 + a_{12}A^2 + a_{10}A_2^2}\right]T$$

$$q_1 = \frac{1}{2}\left[\frac{916.7 \times 100 + 333.3 \times 200}{916.7 \times 100^2 + 333.3 \times 200^2 + 866.7 \times 100^2}\right]T$$

$$= .002540\ T$$

$$q_2 = \frac{1}{2}\left[\frac{a_{10}A_2 + a_{12}A}{a_{20}A_1^2 + a_{12}A^2 + a_{01}A_2^2}\right]T$$

$$= \frac{1}{2}\left[\frac{866.7 \times 100 + 333.3 \times 200}{916.7 \times 100^2 + 333.3 \times 200^2 + 866.7 \times 100^2}\right]T$$

$$= .002456\ T$$

$$J = 4\left[\frac{a_{20}A_1^2 + a_{12}A^2 + a_{10}A_2^2}{a_{10}a_{12} + a_{12}a_{20} + a_{20}a_{10}}\right]$$

$$= 4\left[\frac{916.7 \times 100^2 + 333.3 \times 200^2 + 866.7 \times 100^2}{866.7 \times 333.3 + 333.3 \times 916.7 + 916.7 \times 866.7}\right]$$

$$= 89.76$$

$$\theta = \frac{T}{JG} = \frac{T}{G \times 89.76} = .01116\frac{T}{G}\ \text{(rad.) per unit length of cell.}$$

A6.13 Example 3 - Three-Cell-Tube.

Fig. A6.22 shows a thin-walled tubular section composed of three cells. The internal shear flow pattern will be determined in resisting the external torque of 100,000"# as shown.

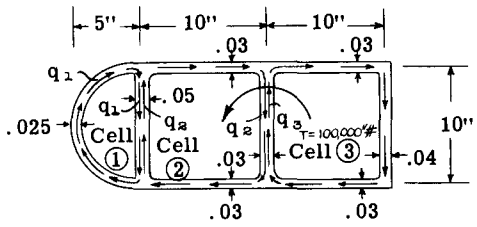

Fig. A6.22

SOLUTION:

Calculation of cell constants

Cell areas: -

$A_1 = 39.3$ $A_2 = 100$ $A_3 = 100$

Line integrals $a = \oint \frac{ds}{t}$. -

$$a_{10} = \frac{\pi \times 10}{2 \times .025} = 629 \qquad a_{12} = \frac{10}{.05} = 200$$

$$a_{20} = \frac{20}{.03} = 667 \qquad a_{23} = \frac{10}{.03} = 333$$

$$a_{30} = \frac{20}{.03} + \frac{10}{.04} = 917$$

Equating the external torque to the internal resisting torque: -

$$2q_1A_1 + 2q_2A_2 + 2q_3A_3 + T = 0$$

Substituting:

$$78.6\ q_1 + 200\ q_2 + 200\ q_3 - 100{,}000 = 0 \quad - (37)$$

Writing the expression for the angular twist of each cell: -

Cell (1)

$$2G\theta = \frac{1}{A_1}\left[q_1a_{10} + (q_1 - q_1)\ a_{12}\right]$$

Substituting:

$$2G\theta = \frac{1}{39.3}\left[629\, q_1 + 200\, q_1 - 200\, q_2\right] - - - \quad (38)$$

Cell (2)

$$2G\theta = \frac{1}{A_2}\left[(q_2 - q_1)\, a_{12} + q_2 a_{20} + (q_2 - q_3)\, a_{23}\right]$$

Substituting:

$$2G\theta = \frac{1}{100}\left[200\, q_2 - 200\, q_1 + 667\, q_2 + 333\, q_2 - 333\, q_3\right] \quad - - - - - - - - - - - - - - - - - - \quad (39)$$

Cell (3)

$$2G\theta = \frac{1}{A_3}\left[(q_3 - q_2)\, a_{23} + q_3 a_{30}\right]$$

Substituting:

$$2G\theta = \frac{1}{100}\left[333\, q_3 - 333\, q_2 + 917\, q_3\right] \quad - - - \quad (40)$$

Solving equations (37) to (40), we obtain,

$q_1 = 143.4\#/\text{in.}$

$q_2 = 234.1\#/\text{in.}$

$q_3 = 208.8\#/\text{in.}$

$q_2 - q_1 = 90.7\#/\text{in.}$

$q_2 - q_3 = 25.3\#/\text{in.}$

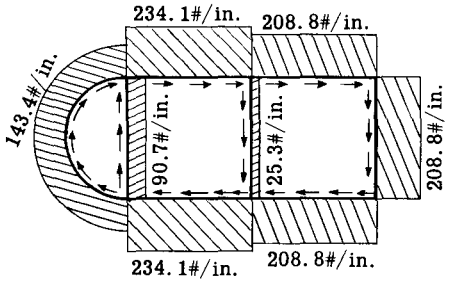

Fig. A6.23

Fig. A6.23 shows the resulting internal shear flow pattern. The angle of twist, if desired, can be found by substituting values of shear flows in any of the equations (38) to (40).

A6.14 Torsional Shear Flow in Multiple Cell Beams by Method of * Successive Corrections.

The trend in airplane wing structural design particularly in high speed airplanes is toward multiple cell arrangement as illustrated in Fig. A6.24, namely a wing cross-section made up of a relatively large number of cells.

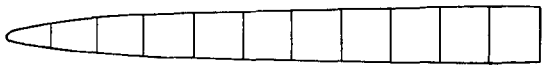

Fig. A6.24

With one unknown shear flow q for each cell, the solution by the previous equations becomes quite laborious.

The method of successive approximations provides a simple, rapid method for finding the shear flow in multiple cells under pure torsion.

EXPLANATION OF SUCCESSIVE CORRECTION METHOD.

Consider a two cell tube as shown in Fig. a. To begin with assume each cell as acting independently, and subject cell (1) to such a shear flow q_1 as to make $G\theta_1 = 1$.

From equation (19) we can write,

$$G\theta = \frac{q}{2A}\oint \frac{ds}{t}$$

Now assume $G\theta = 1$, then

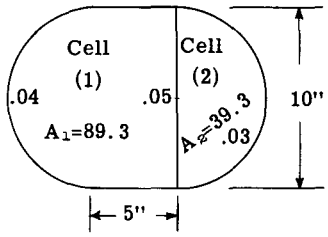

Fig. a

$$q = \frac{2A}{\oint \frac{ds}{t}}$$

Since practically all cellular aircraft beams have wall and web panels of constant thickness for each particular unit, the term $\oint \frac{ds}{t}$ for simplicity will be written $\Sigma \frac{L}{t}$, where L equals the length of a wall or web panel and t its thickness. Thus we can write,

$$q = \frac{2\,A}{\Sigma_{cell}\frac{L}{t}} \quad - - - - - - - - - - - - - - - \quad (41)$$

Therefore assuming $G\theta_1 = 1$ for cell (1) of Fig. a, we can write from equation (41): -

* Based on Paper, "Numerical Transformation Procedures for Shear Flow Calculations" by S. U. Benscoter. Journal, Institute of Aeronautical Sciences, Aug. 1946.

$$q_1 = \frac{2A_1}{\Sigma \frac{L}{T}} \quad \frac{2 \times 89.3}{\frac{25.7}{.04} + \frac{10}{.05}} = \frac{178.6}{842} = 0.212 \text{ lb./in.}$$

Fig. b. shows the results.

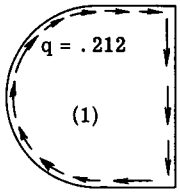

Fig. b

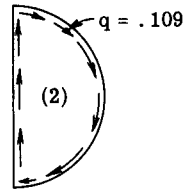

Fig. c

In a similar manner assume cell (2) subjected to a shear flow q_2 to make $G\theta_2 = 1$. Then

$$q_2 = \frac{2A_2}{\Sigma \frac{L}{t}} \quad \frac{2 \times 39.3}{\frac{10}{.05} + \frac{15.7}{.03}} = \frac{78.6}{723} = 0.109\#/\text{in.}$$

Fig. c shows the results.

Now assume the two cells are joined together with the interior web (1-2) as a common part of both cells. See Fig. d. The interior web is now subjected to a resultant shear flow of $q_1 - q_2 = (.212 - .109) = .103\#/\text{in.}$ Obviously this change of shear flow on the interior web will cause the cell twist to be different for each cell instead of the same when the cells were considered acting separately. To verify this conclusion the twist measured by the term $G\theta$ will be computed for each cell.

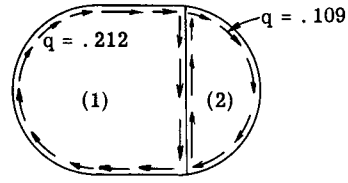

Fig. d

Cell (1), $\quad G\theta_1 = \frac{1}{2A_1} \Sigma q \frac{L}{t} =$

$$= \frac{1}{2 \times 89.3}\left[.212 \times \frac{25.7}{.04} + (.212 - .109)\frac{10}{.05}\right] =$$

$$= 0.875$$

Cell (2), $\quad G\theta_2 = \frac{1}{2A_2} \Sigma q \frac{L}{t} =$

$$= \frac{1}{2 \times 39.3}\left[.109 \times \frac{15.7}{.03} - (.212 - .109)\frac{10}{.05}\right] =$$

$$= 0.466$$

Since θ_1 must equal θ_2 if the cross-section is not to distort from its original shape, it is evident that the above shear flows are not the true ones when the two cells act together as a unit.

Now consider cell (1) in Fig. d. In bringing up and attaching cell (2) the common web (1-2) is subjected to a shear flow $q_2 = - .109\#/\text{in.}$ (counterclockwise with respect to cell (1) and therefore negative), in addition to the shear flow $q_1 = .212$ of cell (1). The negative shear flow $q_2 = - .109$ on web 1-2 decreases the twist of cell (1) as calculated above with the resulting value for $G\theta_1 = 0.875$ instead of 1.0 as started with.

Thus in order to make $G\theta_1 = 1$ again, we will have to add a constant shear flow q_1' to cell (1) which will cancel the negative twist due to q_2 acting on web (1-2). Since we are considering only cell (1) we can compare cell wall strains instead of cell twist since in equation (41), the term 2A is constant.

Thus adding a constant shear flow q_1' to cancel influences of q_2 on web 1-2, we can write:

$$q_1' \left(\Sigma \frac{L}{t}\right) \text{ cell (1)} - q_2 \left(\frac{L}{t}\right)_{\text{web 1-2}} = 0$$

hence

$$q_1' = q_2 \left[\frac{\left(\frac{L}{t}\right) \text{ web 1-2}}{\left(\Sigma \frac{L}{t}\right) \text{ cell (1)}}\right] \quad - - - - - - - - - (42)$$

Substituting values in equation (42)

$$q_1' = q_2 \left[\frac{\frac{10}{.05}}{\frac{25.7}{.04} + \frac{10}{.05}}\right] = \frac{200}{842} q_2 = .237\, q_2$$

Thus to make $G\theta_1$ equal to 1 we must correct the shear flow in cell (1) by adding a constant shear flow equal to .237 times the shear flow q_2 in cell (2) which equals $.237 \times .109 = .0258\#/\text{in.}$ Since this shear flow is in terms of the shear flow q_2 of the adjacent cell it will be referred to as a correction carry over shear flow, and will consist of a carry over correction factor times q_2.

Thus the carry over factor from cell (2) to cell (1) may be written as

$$\text{C.O.F. (2 to 1)} = \frac{\left(\frac{L}{t}\right) \text{ web (1-2)}}{\left(\Sigma \frac{L}{t}\right) \text{ cell (1)}} \text{ which equals}$$

.237 as found above in substitution in equation (42).

Now consider cell (2) in Fig. d. In bringing up and attaching cell (1), the common web (2-1) is subjected to a shear flow of $q_1 = - 0.212\#/\text{in.}$ (counterclockwise as viewed from cell 2 and therefore negative). This additional shear flow changes $G\theta_2$ twist of cell (2) to a relative value of 0.4375 instead of 1.0 (see previous $G\theta_2$ calculations). Therefore to make $G\theta_2$ equal to 1.0 again, a corrective constant shear flow q_2' must be added to cell (2) to

cancel the twist effect of $q_1 = 0.212$ on web (2-1). Therefore we can write,

$$q'_2 \left(\Sigma \frac{L}{t}\right) \text{cell (2)} - q_1 \left(\frac{L}{t}\right) \text{web (2-1)} = 0$$

hence

$$q'_2 = \frac{q_1 \left(\frac{L}{t}\right) \text{web (2-1)}}{\left(\Sigma \frac{L}{t}\right) \text{cell (2)}} \quad \text{- - - - - - - - - - - -} \quad (43)$$

Substituting in equation (43): -

$$q'_2 = q_1 \left(\frac{200}{723}\right) = .277\, q_1 = .277 \times .212 = .0587\#/\text{in.}$$

Thus the carry over factor from cell (1) to cell (2) in terms of q_1 to make $G\theta_2 = 1$ again can be written

$$\text{C.O.F.}_{(1 \text{ to } 2)} = \frac{\left(\frac{L}{T}\right) \text{web (2-1)}}{\left(\Sigma \frac{L}{t}\right) \text{cell (2)}} = \frac{200}{723} = .277$$

Fig. e shows the constant shear flow q'_2 and q'_1 that were added to make $G\theta = 1$ for each cell. However these corrective shear flows were added assuming the cells were again independent of each other or did not have the common web (1-2). Thus in bringing the cells together again the interior web is subjected to be resultant shear flow of $q'_1 - q'_2$. In other words if we were to add the shear flows of Fig. e to those of Fig. d, we would not have $G\theta_1$ and $G\theta_2$ equal to 1. The resulting values would be closer to 1.0 than were found for the shear flow system of Fig. d.

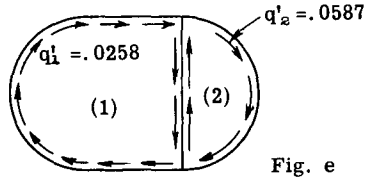

Fig. e

Considering Fig. e, we will now add a second set of corrective shear flows q''_1 and q''_2 to cells (1) and (2) respectively to make $G\theta_1$ and $G\theta_2 = 1$ for cells acting independently.

Considering cell (1), and proceeding with same reasoning as before,

$$q''_1 \left(\Sigma \frac{L}{t}\right) \text{cell (1)} - q'_2 \left(\frac{L}{t}\right) \text{web 1-2} = 0$$

Hence

$$q''_1 = \frac{q'_2 \left(\frac{L}{t}\right) \text{1-2}}{\Sigma \left(\frac{L}{t}\right) \text{cell (1)}} = .0587 \times .237 = .0139\#/\text{in.}$$

or

$$q''_1 = (\text{C.O.F.})_{2 \text{ to } 1} \text{ times } q'_2 = .237 \times .0587 = .0139$$

Considering Cell (2)

$$q''_2 = q'_1 (\text{C.O.F.})_{1 \text{ to } 2} = .0258 \times .277 = .00717\#/\text{in.}$$

Fig. f shows the resulting second set of corrective constant shear flows for each cell. Since our corrective shear flows are rapidly getting smaller, the continuation of the process depends on the degree of accuracy we wish for the final results. Suppose we add one more set of corrective constant shear flows q'''_1 and q'''_2, Using the carry over correction factors previously found we obtain,

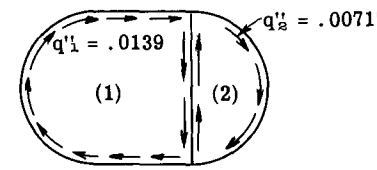

Fig. f

$$q'''_1 = .237 \times .00717 = .0017\#/\text{in.}$$

$$q'''_2 = .277 \times .0139 = .00385\#/\text{in.}$$

Fig. g shows the results.

The final or resulting cell shear flows then equal the original shear flows plus all corrective cell shear flows, or

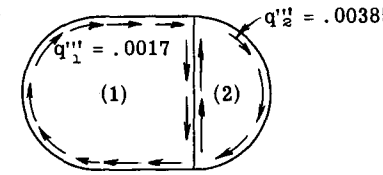

Fig. g

$$q_{1\,(\text{final})} = q_1 + q'_1 + q''_1 + q'''_1$$

$$q_{2\,(\text{final})} = q_2 + q'_2 + q''_2 + q'''_2$$

Fig. h shows the final results.

To check the final twist of each cell the value $G\theta$ will be computed for each cell using the q values in Fig. h.

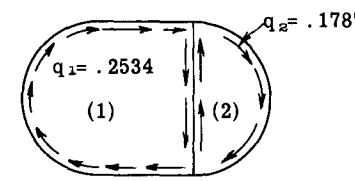

Fig. h

Cell (1)

$$G\theta_1 = \frac{1}{2 \times 89.3}\left[.2534 \times \frac{25.7}{.04} + .0747 \times \frac{10}{.05} \right] = .997$$

$$G\theta_2 = \frac{1}{2 \times 39.3}\left[.1787 \times \frac{15.7}{.03} - .0747 \times \frac{10}{.05} \right] = .997$$

A6.15 Use of Operations Table to Organize Solution by Successive Corrections.

Operations Table 1 arranges the calculations so that the steps dealing with the corrective shear flows can be carried out rapidly and with a minimum of thought.

OPERATIONS TABLE 1

	Cell 1		Cell 2
1	C.O. Factor	.277	.237
2	Assumed q	.212	.109
3	C.O. q	.0258	.0587
4	C.O. q	.0139	.00717
5	C.O. q	.0017	.00385
6	Final q = Σ	.2534	.1787
7	T = 2Aq	45.2"#	14.1"#
8	Total T	59.3"#	

Explanation of Table 1

Line 1 gives the carry over factors for each cell, computed as explained before. Line 2 gives the necessary constant shear flow q in each cell to give unit rate of twist to each cell acting independently. ($G\theta = 1$). Line 3 gives the first set of constant corrective shear flows to add to each cell. The corrective q referred to as the carry over q or C.O.q in the table consists of the q in the adjacent cell times the C.O. factor of that cell.

Thus .237 x .109 = .0258 is carry over from cell (2) to cell (1) and .277 x .212 = .0587 is carry over from cell (1) to cell (2).

Line 4 gives the second set of corrective carry over shear flows, namely .277 x .0258 = .00717 to cell (2) and .237 x .0587 = .0139 to cell (1). Line 5 repeats the corrective carry over process once more. Line 6 gives the final q values which equal the original q plus all carry over q values.

Example Problem 1 (2 cells)

Determine the internal shear flow system for the two cell tube in Fig. A6.25 when subjected to a torque of 20,000 in. lbs.

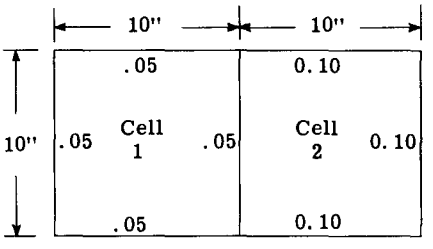

Fig. A6.25

OPERATIONS TABLE 2

	Cell 1		Cell 2
1	C.O. Factor	0.4	0.25
2	Assumed q	25.0	40.0
3	C.O. q	10	10
4	C.O. q	2.5	4
5	C.O. q	1.0	1
6	C.O. q	0.25	0.4
7	C.O. q	0.10	0.1
8	Final q = Σ	38.85	55.5
9	2Aq	7770	11100
10	T (Total)	18870	
11	q for T=20,000	41.2	58.9

Explanation of solution as given in Table (2):

Line 1 gives the values of the carry over factors. The values are calculated as follows:

C.O. factor cell (1) to cell (2):

$$C.O._{(1-2)} = \frac{\left(\frac{L}{t}\right)_{\text{web 1-2}}}{\Sigma\left(\frac{L}{t}\right)_{\text{cell 2}}} = \frac{\frac{10}{.05}}{\frac{10}{.05} + \frac{30}{0.1}} = .40$$

$$C.O._{(2-1)} = \frac{\left(\frac{L}{t}\right)_{\text{web 2-1}}}{\Sigma\left(\frac{L}{t}\right)_{\text{cell 1}}} = \frac{\frac{10}{.05}}{\frac{40}{.05}} = .25$$

Line 2 gives the shear flow q in each cell, when it is assumed each cell is acting separately and is subjected to a unit rate of twist or $G\theta = 1$.

The calculations for the q values are as follows: -

For cell (1)

$$q_1 = \frac{2A_1}{\Sigma\left(\frac{L}{t}\right)_{\text{cell 1}}} = \frac{2 \times 100}{\frac{40}{.05}} = .25$$

For cell (2)

$$q_2 = \frac{2A_2}{\Sigma\left(\frac{L}{t}\right)_{\text{cell 2}}} = \frac{2 \times 100}{\frac{10}{.05} + \frac{30}{0.1}} = .4$$

A_1 and A_2 equal cell area of cells (1) and (2) respectively. L = length of wall element and t its corresponding thickness.

In order not to start out with decimal values of q, the values above will arbitrarily be multiplied by 100 to make $q_1 = 25\#/in.$ and $q_2 = 40\#/in.$ Since we want only relative values of terms this is permissible. These values are shown in line 2 of Table (2). The corrective carry over process proper is started in line 3 of table (2). In cell (1) the amount carried over of $q_1 = 25$ to cell (2) equals the C.O. factor times 25 or 0.4 x 25 = 10 which is written along the vertical line under cell (2). Likewise in cell (2) the amount of $q_2 = 40$ that is carried over to cell (1) equals the C.O. factor times q_2 or .25 x 40 = 10, which is written along the vertical line under cell (1).

The second set of corrective carry over constant shear flows are given in line 4 of Table (2), thus, .4 of the $q_1 = 10 = 4.0$ is carried over to cell (2) and .25 x value of $q_1 = 10 = 2.5$ is carried over to cell (1). Line 5 repeats the process namely 0.4 x 2.5 = 1 to cell (2) and .25 x 4 = 1.0 to cell (1).

This process of carrying over values of q is continued until the values are small or negligible. Line 8 gives the final q values in each cell as the summation of the assumed q value plus all carry over values of q. Thus in cell (1) q = 38.85#/in. and for cell (2) q = 55.5. Line 9 gives the torque that these values of cell shear flow can produce.

$$T = 2Aq$$

For cell (1) T = 2 x 100 x 38.85 = 7770 in. lb.
For cell (2) T = 2 x 100 x 55.5 = 11100 in. lb.

Line 10 gives the sum of the above two values which equals 18870 in. lb.

The original requirement of the problem was the shear flow system for a torque of 20,000"#. Therefore the required q values follow by direct proportion, whence

$$q_1 = \frac{20000}{18870} \times 38.85 = 41.2\#/\text{in.}$$

$$q_2 = \frac{20000}{18870} \times 55.5 = 58.9\#/\text{in.}$$

These values are shown in line 11 of Table 2. Check on twist of cells under final q values.

The relative total strain around each cell boundary is given by the term $\frac{1}{A} \Sigma\, q \frac{L}{t}$ for the cell.

Thus for cell (1)

$$\frac{1}{A_1} \Sigma\, q \frac{L}{t} = \frac{1}{100}\left[41.2 \left(\frac{30}{.05}\right) + (41.2 - 58.9) \frac{10}{.05}\right] =$$

$$= 212$$

For cell (2),

$$\frac{1}{A_2} \Sigma\, q \frac{L}{t} = \frac{1}{100}\left[(58.9 - 41.2) \frac{10}{.05} + 58.9 \times \left(\frac{30}{0.1}\right)\right]$$

$$= 212$$

Thus both cells have the same twist.

In the above calculations q_1 and q_2 act clockwise in each cell, hence the shear flow on the interior common web is the difference of the two q values.

Example Problem 2. Three cells

The three cell structure in Fig. A6.26 is subjected to an external torque of - 100,000 in. lb. Determine the internal resisting shear flow pattern.

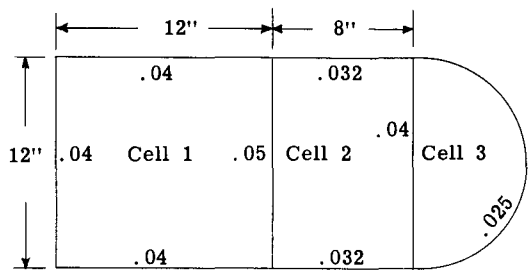

Fig. A6.26

OPERATIONS TABLE 3

		Cell 1	Cell 2	Cell 3
1	C.O. Factor	.23	.21 .284	.288
2	Assumed q	25.30	18.45	10.70
3	C.O. q	3.88	5.82 3.08	5.25
4	C.O. q	1.87	0.894 1.51	2.53
5	C.O. q	0.505	0.430 0.73	0.685
6	C.O. q	0.244	0.116 0.197	0.330
7	C.O. q	0.066	0.056 0.095	0.088
8	Final q = Σ	31.87	31.37	19.58
9	2Aq	9200	6020	2215
10	T (Total) =	9200 + 6020 + 2215 = 17435"#		
11	q - for T = 100,000	183	180	112.5

Explanation of solution as given in Table 3: -

Cell (1)	Cell (2)	Cell (3)
$A_1 = 144$	$A_2 = 96$	$A_3 = 56.5$
$\Sigma \frac{L}{t} = 1140$	$\Sigma \frac{L}{t} = 1040$	$\Sigma \frac{L}{t} = 1055$

Shear flow q for $G\Theta = 1$ for each cell acting independently: -

Cell (1) $$q = \frac{2A_1}{\Sigma \frac{L}{t}} = \frac{288}{1140} = .253$$

Cell (2) $$q = \frac{2A_2}{\Sigma \frac{L}{t}} = \frac{192}{1040} = .1845$$

Cell (3) $$q = \frac{2A_3}{\Sigma \frac{L}{t}} = \frac{113}{1055} = .107$$

To avoid small numbers these values of q are multiplied by 100 and entered on line 2 of the table. Calculation of carry factors as given in line 1 of Table 3.

Cell (1) to (2)

$$C.O._{(1-2)} = \frac{\left(\frac{L}{t}\right) \text{web } 1\text{-}2}{\Sigma \left(\frac{L}{t}\right) \text{cell } 2} = \frac{240}{1040} = .23$$

Cell (2) to (1)

$$C.O._{(2-1)} = \frac{\left(\frac{L}{t}\right) \text{web } 2\text{-}1}{\Sigma \left(\frac{L}{t}\right) \text{cell } 1} = \frac{240}{1140} = .21$$

Cell (2) to (3)

$$C.O._{(2-3)} = \frac{\left(\frac{L}{t}\right) \text{web } 2\text{-}3}{\Sigma \left(\frac{L}{t}\right) \text{cell } 3} = \frac{300}{1055} = .284$$

Cell (3) to (2)

$$C.O._{(3-2)} = \frac{\left(\frac{L}{t}\right)_{\text{web 2-3}}}{\Sigma\left(\frac{L}{t}\right)_{\text{cell 2}}} = \frac{300}{1040} = .288$$

The balance of the solution or procedure in Table 3 is the same as explained for Problem 1 in Table (2). It should be noticed that cell (2) being between two cells receives carry over q values from both adjacent cells and these two values are added together before being distributed or carried over again to adjacent cells. For example consider line 3 in Table (3) and cell (2). The q value 5.82 representing .23 x 25.3 is brought over from cell (1) and the q value 3.08 = .288 x 10.70 from cell (3). These two values are added together or 5.82 + 3.08 = 8.90. The carry over q to cell (1) is then .21 x 8.90 = 1.87 and to cell (3) is .284 x 8.90 = 2.53.

In line 8, the final q in cell (2) equals the original q of 18.45 plus all carry over q values from each adjacent cell.

Line 10 in Table (3) shows the total torque developed by the resultant internal shear flow is 17435"#. Since the problem was to find the shear flow system for a torque of - 100,000 in. lb., the values of q in line 8 must be multiplied by the factor 100,000/17435.

Line 11 shows the final q values.

Example Problem 3. Four cells.

Determine the internal shear flow system for the four cell structure in Fig. A6.27 when subjected to a torsional moment of - 100,000 in. lb.

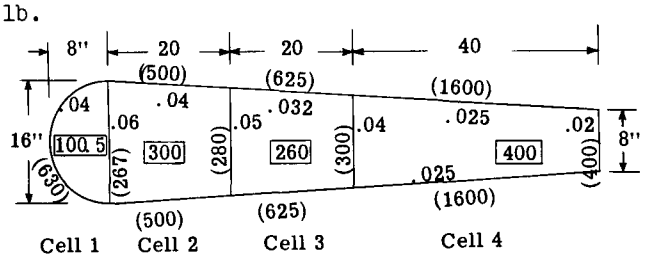

Fig. A6.27

OPERATIONS TABLE 4

		Cell 1	Cell 2	Cell 3	Cell 4
1	C.O.F.	.173	.298 .153	.181 .078	.164
2	q	22.4	38.8	28.4	20.50
3	C.O.	11.6 3.88	5.14 5.94	3.36	2.22
4	C.O.	2.69 2.00	1.68 1.38	0.36	0.73
5	C.O.	1.10	0.47 0.32	0.57 0.12	0.13
6	C.O.	0.15	0.19 0.12	0.08 0.02	0.15
7	Σq	37.95	52.60	40.23	23.63
8	2Aq	7620	31560	22550	18900
9	Total T = 80630				
10	q	47.1	65.3	49.9	29.41

In Fig. A6.27 the values in the rectangles represent the cell areas. The values in ( ) represent the L/t values for the particular wall or web. After studying example problems 1 and 2 one should have no trouble checking the values as given in Table 4. Line 10 shows the correction of q values to develop a resisting torque of 100,000"#. The multiplying factor is 100,000/80630.

A6.16 Torsion of Thin-Walled Cylinder Having Closed Type Stiffeners.

The airplane thin-walled structure usually contains longitudinal stiffeners spaced around the outer walls as illustrated in Figs. A6.28 and A6.29.

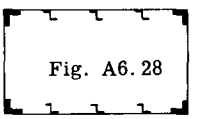

Open Type Stiffener

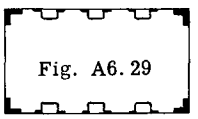

Closed Type Stiffener

For the open type stiffener as illustrated in Fig. A6.28, the torsional rigidity of the individual stiffeners as compared to the torsional rigidity of the thin-walled cell is so small to be negligible. However a closed type stiffener is essentially a small sized tube and its stiffness is much greater than an open section of similar size. Thus a cell with closed type stiffeners attached to its outer walls could be handled as a multiple cell structure, with each stiffener acting as a cell with a common wall with the outside surrounding cell. Since in general the stiffness provided by the stiffeners is comparatively small compared to the over-all cell, the approximate simplified procedure as given in NACA T.N. 542 by Kuhn can be used to usually give sufficient accuracy. In this approximate method, the thin-walled tube and closed stiffeners are converted or transformed into a single thin-walled tube by modifying the closed stiffeners by either one of the following procedures: -

(1) Replace each closed stiffener by a doubler plate having an effective thickness $t_e = t_{ST} s/d$, and calculate $\oint ds/t$ with these doubler plates in place. The enclosed area of the torsion tube still remains (A) or the same. See Fig. A6.30.

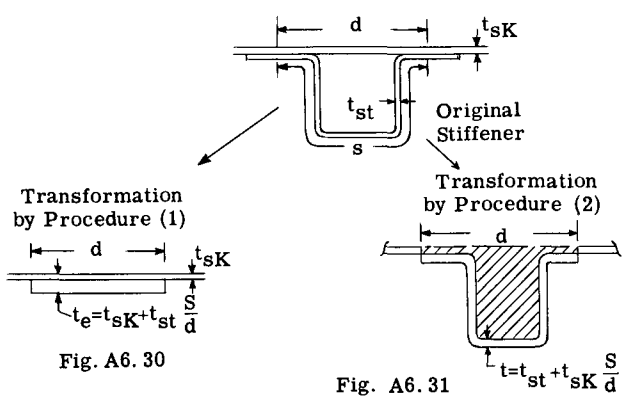

Fig. A6.30

Fig. A6.31

(2) Replace the skin over each stiffener by a "liner" in the stiffener having a thickness $t_e = t_{SK}\, d/s$. (See Fig. A6.31.) The enclosed area (A) of the cell now equals the original area less that area cross-latched in Fig. A6.31.

Procedure (1) slightly overestimates and procedure (2) slightly underestimates the stiffness effect of the stiffeners.

The corner members of a stiffened cell are usually open or solid sections and thus their torsional resistance can be simply added to the torsional stiffness of the thin-walled over-all cell.

A6.17 Effect of End Restraint on Members Carrying Torsion.

The equations derived in the previous part of this chapter assumed that cross-sections throughout the length of the torsion members were free to warp out of their plane and thus there could be no stresses normal to the cross-sections. In actual practical structures restraint against this free warping of sections is however often present. For example, the airplane cantilever wing from its attachment to a rather rigid fuselage structure is restrained against warping at the wing-fuselage attachment point. Another example of restraint is a heavy wing bulkhead such as those carrying a landing gear or power plant reaction. The flanges of these heavy bulkheads often possess considerable lateral bending stiffness, hence they tend to prevent warping of the wing cross-section. Since only torsional forces are being considered here as being applied to the member, the stresses produced normal to the cross-section of the member namely, tension and compression must add up zero for equilibrium. Thus the applied torque is carried by pure torsion action of the member and part by the longitudional stresses normal to the member cross-sections. The percentage of the total torque carried by each action depends on the dimensions and shape of the cross-section and the length of the member.

Fig. A6.32 illustrates the distortion of an open section, namely, a channel section subjected to a pure torsional force T at its free end and fixed at the other or supporting end. Near the fixed end the applied torque is practically all resisted by the lateral bending of the top and bottom legs of the channel acting as short cantilever beams, thus forming the couple with H forces as illustrated in the Figure. Near the free end of the member, these top and bottom legs are now very long cantilever beams and thus their bending rigidity is small and thus the pure torsional rigidity of the section in this region is greater than the bending rigidity of the channel legs.

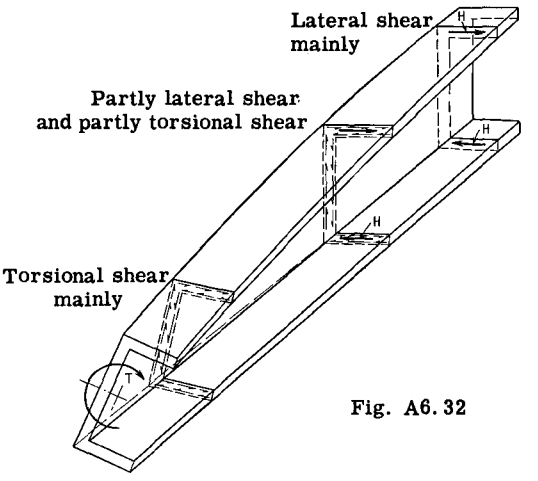

Fig. A6.32

A6.18 Example Problem Illustrating Effect of End Restraint on a Member in Torsion.

Fig. A6.33 shows an I-beam subjected to a torsional moment T at its free end. The problem will be to determine what proportion of the torque T is taken by the flanges in bending and what proportion by pure shear, at two different sections, namely 10 inches and 40 inches from the fixed end of the I-beam.

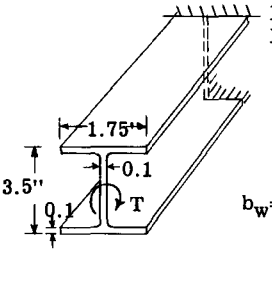

Fig. A6.33

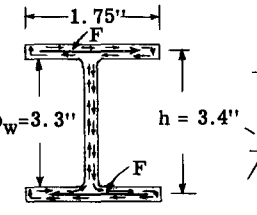

Fig. A6.34

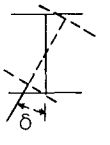

Fig. A6.35

Fig. A6.34 shows the torque dividing into two parts, namely the couple force F-F formed by bending of the flanges of the I-beam and the pure shearing stress system on the cross-section. Fig. A6.35 shows the twisting of the section through a distance δ.

The solution will consist in computing the angle of twist θ under the two stress conditions and equating them.

Let T_B be the proportion of the total torque T carried by the flanges in bending forming the couple F-F in Fig. A6.34. From Fig. A6.35, the angle of twist can be written

$$\theta_B = \frac{\delta}{0.5h} = \frac{\frac{F\,L^3}{3\,EI}}{0.5h} = \frac{2}{3}\,\frac{T_B\,L^3}{h^2\,EI}$$

Note: The deflection of a cantilever beam with a load F at its end equals $FL^3/3EI$, and I the moment of inertia of a rectangle about its center axis = $tb^3/12$.

hence $$\theta_B = \frac{8\,L^3}{E\,b^3 t\,h^2}\,T_B$$

Now let T_t be the portion of the total torque carried by the member in pure torsion. The approximate solution for open sections composed of rectangular elements as given in Art. A6.6, equation (12) will be used.

$$\theta_t = \frac{3\,T_t\,L}{Gt^3(b + b_w)}$$

Equating θ_B to θ_t, we can write

$$\frac{T_B}{T_t} = \frac{3\,E\,h^2\,b^3}{8L^2Gt^2(2b + b_w)}$$

Substituting values when L = 10 inches.

$$\frac{T_B}{T_t} = \frac{3 \times 10.5 \times 10^6 \times 3.4^2 \times 1.75^3}{8 \times 10^2 \times 3.7 \times 10^6 \times 0.1^2(2 \times 1.75 + 3.3)} =$$

$$= 9.65$$

Therefore, percent of total torsional T taken by bending of flanges equals,

$$\frac{T_B}{T_B + T_t}(100) = \frac{T_B}{T_B + \frac{T_B}{9.65}}(100) = 90.5 \text{ percent.}$$

If we consider the section 40 inches from the fixed end, then L = 40 inches. Thus if 40^2 is placed in the above substitution instead of 10^2 the results for T_B/T_t would be 0.602 and the percent of the torque carried by the flanges in bending would be 36 as compared to 90.5 percent at L = 10 inches from support. Thus in general the effect of the end restraint decreases rapidly with increasing value of L.

The effect of end restraint on thin walled tubes with longitudinal stiffeners is a more involved problem and cannot be handled in such a simplified manner. This problem is considered in other Chapters.

A6.19 Problems.

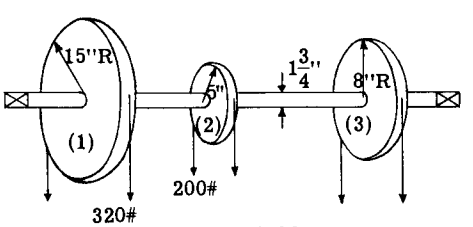

Fig. A6.36

(1) In Fig. A6.36 pulley (1) is the driving pulley and (2) and (3) are the driven pulleys, The shaft rotates at constant speed. The difference in belt pull on two sides of a pulley are shown on the figure. Calculate the maximum torsional shearing stress in the 1-3/4 inch shaft between pulleys (1) and (2) and between (2) and (3).

(2) A 1/2 HP. motor operating at 1000 RPM rotates a 3/4-.035 aluminum alloy torque tube 30 inches long which drives the gear mechanism for operating a wing flap. Determine the maximum torsional stress in the torque shaft under full power and RPM. Find the angular deflection of shaft in the 30 inch length. Polar moment of inertia of tube = .01 in. Modulus of rigidity G = 3800,000 psi.

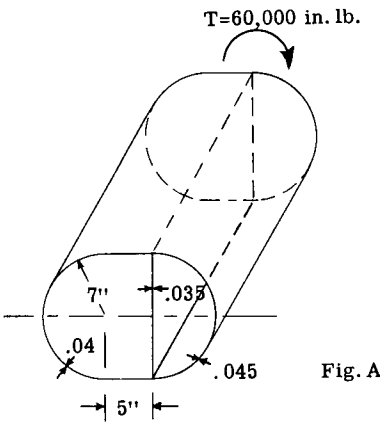

Fig. A6.36

(3) In the cellular section of Fig. A6.36 determine the torsional shear flow in resisting the external torque of 60000 in.lb. Web and wall thickness are given on the figure. Assume the tube is 100 in. long and find the torsional deflection. Material is aluminum alloy. (G = 3800,000 psi.)

(4) In Fig. A6.36 remove the interior .035 web and compute torsional shear flow and deflections.

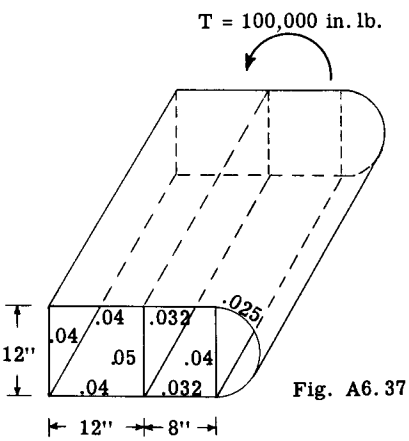

Fig. A6.37

(5) In the 3-cell structure of Fig. A6.37 determine the internal resisting shear flow due to external torque of 100,000 in. lb. For a length of 100 inches calculate twist of cellular structure if G is assumed 3,800,000 psi.

(6) Remove the .05 interior web of Fig. A6.37 and calculate shear flow and twist.

(7) Remove both interior webs of Fig. A6.37 and calculate shear flow and twist.

(8) Each of the cellular structures in Fig. A6.38 is subjected to a torsional moment of 120,000 in.lbs. Using the method of successive approximation calculate resisting shear flow pattern.

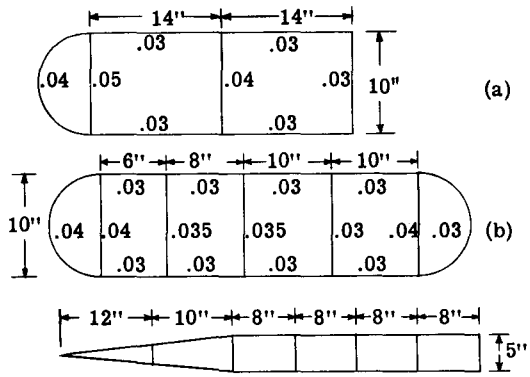

All interior webs = .05 thickness
Top skin .084" thickness
Bottom skin .064" thickness

Fig. A6.38

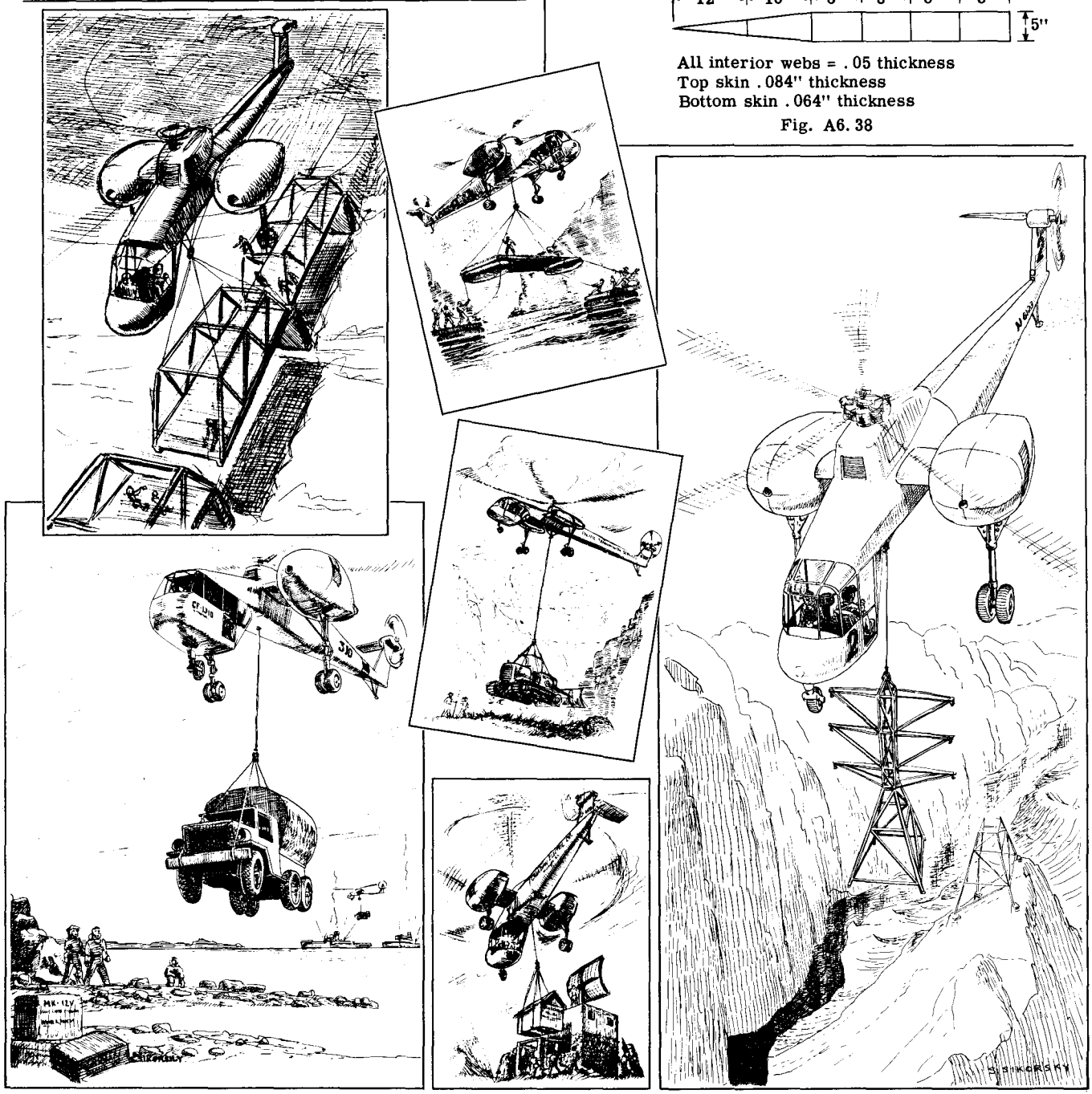

The big helicopters of the future will be used in many important industrial and military operations. The helicopter presents many challenging problems for the structures engineer.

(Sketches from United Aircraft Corp. Publication "BEE-HIVE", Jan. 1958. Sikorsky Helicopters)

CHAPTER A7
DEFLECTIONS OF STRUCTURES

ALFRED F. SCHMITT[1]

A7.1 Introduction.

Calculations of structural deflections are important for two reasons: -

(1) A knowledge of the load-deformation characteristics of the airplane is of primary importance in studies of the influence of structural flexibility upon airplane performance.

(2) Calculations of deflections are necessary in solving for the internal load distributions of complex redundant structures.

The elastic deflection of a structure under load is the cumulative result of the strain deformation of the individual elements composing the structure. As such, one method of solution for the total deflection might involve a vectorial addition of these individual contributions. The involved geometry of most practical structures makes such an approach prohibitively difficult.

For complex structures the more popular techniques are analytical rather than vectorial. They deal directly with quantities which are not themselves deflections but from which deflections may be obtained by suitable operations. The methods employed herein for deflection calculations are analytical in nature.

A7.2 Work and Strain Energy.

Work as defined in mechanics is the product of force times distance. If the force varies over the distance then the work is computed by the integral calculus. Thus the work done by a varying force P in deforming a body an amount δ is

$$\text{Work} = \int_0^{\delta} P\,d\delta$$

and is represented by the area under the load deformation (P-δ) curve as shown in Fig. A7.1.

If the deformed body is perfectly elastic the energy stored in the body may be completely recovered, the body unloading along the same P-δ curve followed for increasing load. This energy is called the elastic strain energy of deformation (hereafter the strain energy, for brevity) and is denoted by the symbol U. Thus $U = \int_0^{\delta} P\,d\delta$. Should the body be linearly elastic (as are most bodies dealt with in structural analysis) then the load-deformation

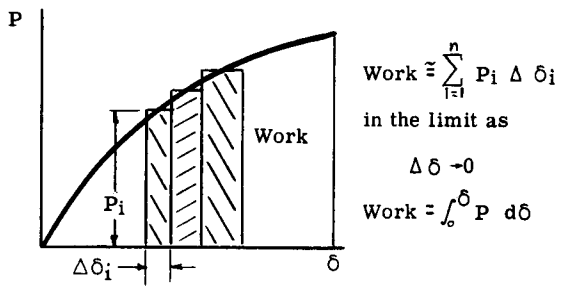

Fig. A7.1

curve is a straight line whose equation is $P = k\delta$ and the strain energy is readily computed to be

$$U = \frac{k\delta^2}{2} \text{ or, equally, } U = \frac{P^2}{2k}.$$

A7.3 Strain Energy Expressions for Various Loadings.

STRAIN ENERGY OF TENSION

A tensile load S acting at the end of a uniform bar of length L, cross sectional area A and elastic modulus E causes a deformation $\delta = SL/AE$. Hence $S = \frac{AE}{L}\delta$ and

$$U = \int_0^{\delta} S\,d\delta = \frac{AE}{L}\frac{\delta^2}{2} \quad \text{- - - - - - - - - - - - - - (1)}$$

Alternately,

$$U = \frac{S^2 L}{2AE} \quad \text{- (2)}$$

Equations (1) and (2) are equivalent expressions for the strain energy in a uniform bar, the former expressing U in terms of the deformation and the latter expressing U in terms of load. The second form of expression is more convenient for general usage and succeeding strain energy formulas will be put in this form.

For a tensile bar having non-uniform properties (varying AE), or for which the axial load S varies, the strain energy is computed by the calculus. Thus the energy in a differential element of length dx is given by eq. (2) as

$$dU = \frac{S^2 dx}{2AE} \text{ where S and AE}$$

are average values over the length of element.

The total energy in the bar is obtained by summing over the length of the bar.

$$U = \int dU = \int \frac{S^2 dx}{2AE} \quad \text{- - - - - - - - - - - - - - -} \quad (3)$$

Example Problem 1

A linearly tapered aluminum bar is under an axial load of 1500 lbs. as shown in Fig. A7.2. Find U.

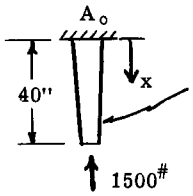

$A(x) = A_o(1 - \frac{x}{80})$

$A_o = 2 \text{ in}^2$

Fig. A7.2

Solution:

From statics, the internal load $S = -1500^{\#}$ at every section.

$$U = \int_0^L \frac{S^2 dx}{2AE} = \int_0^{40} \frac{(-1500)^2 dx}{4(1 - \frac{x}{80})10 \times 10^6}$$

($\tau = x/40$ introduced for convenience)

$$= \frac{2(-1500)^2}{10^6} \int_0^1 \frac{d\tau}{2-\tau} = 4.5 \ln 2 \text{ inch lbs.}$$

Note that although P was a negative (compressive) load the strain energy remained positive.

Example Problem 2

Find U in a uniform bar under a running load

$q = q_o \cos \frac{\pi x}{2L}$ (Fig. A7.3).

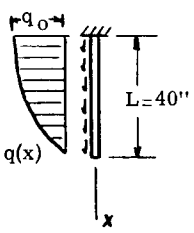

$L = 40"$
$A = 2 \text{ in}^2$
$E = 10 \times 10^6$ psi
$q_o = 25$ lb/in

Fig. A7.3

Solution:

The equation for S (x) was found by statics.

$$S(x) = \int_x^L q dx = \int_x^L q_o \cos \frac{\pi x}{2L} dx$$

$$= q_o \frac{2L}{\pi} \sin \frac{\pi x}{2L} \Big]_x^L = q_o \frac{2L}{\pi} \left(1 - \sin \frac{\pi x}{2L}\right).$$

Substitution into eq. (3) gave

$$U = \frac{2q_o^2 L^2}{\pi^2 AE} \int_0^L \left(1 - \sin \frac{\pi x}{2L}\right)^2 dx =$$

$$\frac{2(25)^2 (40)^2}{9.87(2)(10 \times 10^6)}(.227)(40) = 0.0920 \text{ in lbs.}$$

STRAIN ENERGY OF FLEXURE

A uniform beam of length L under the action of a pure couple undergoes an angular rotation proportional to the couple. Thus, from elementary strength of materials

$$\theta = \frac{L}{EI} M$$

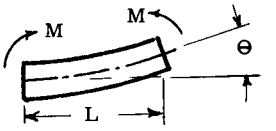

where the constant EI, the product of elastic modulus by section moment of inertia, is called the "bending stiffness".

Since the rotation θ builds up linearly with M the strain energy stored is

$$U = \frac{1}{2} M\theta$$

or

$$U = \frac{1}{2} \frac{M^2 L}{EI} \quad \text{- - - - - - - - - - - - - - - - - -} \quad (4)$$

For a beam having non-uniform properties (varying EI) and/or for which M varies along the beam, the strain energy is computed by the calculus. From eq. (4) the strain energy in a beam element of differential length is

$$dU = \frac{1}{2} \frac{M^2 dx}{EI}$$

Hence summing over the complete beam to get the total strain energy one has

$$U = \int dU = \frac{1}{2} \int \frac{M^2 dx}{EI} \quad \text{- - - - - - - - - - - - -} \quad (5)$$

Example Problem 3

For the beam of Fig. A7.4 derive the strain energy expression as a function of M_o.

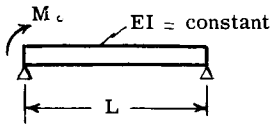

Fig. A7.4

Solution:

The bending moment diagram (Fig. A7-4a) was found and an analytic expression written for M.

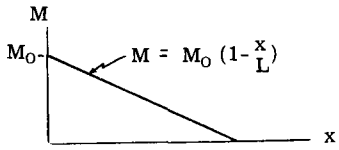

Fig. A7.4a

Then

$$U = \frac{1}{2EI}\int_o^L M_o^2\left(1 - \frac{x}{L}\right)^2 dx$$

$$= \frac{M_o^2 L}{6EI}$$

Example Problem 4

Determine the strain energy of flexure of the beam of Fig. A7.5. Neglect shear strain energy.

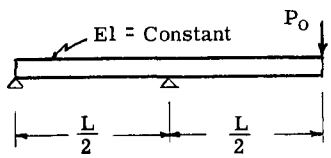

Fig. A7.5

Solution:

The bending moment diagram was drawn first (Fig. A7.5a) and analytic expressions were written for M.

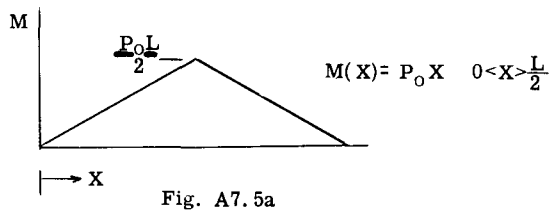

Fig. A7.5a

Inspection of the diagram revealed that the energy of flexure in the right half of the beam must be identical with that of the left half. Hence

$$U = 2 \cdot \frac{1}{2EI} \cdot \int_o^{L/2} (P_o x)^2 dx$$

$$= \frac{P_o^2 L^3}{24\ EI}$$

STRAIN ENERGY OF TORSION

A uniform circular shaft carrying a torque T experiences a total twist in a length L proportional to the torque. Thus from elementary strength of materials

$$\phi = \frac{L}{GJ} T \quad - - - - - - - - - - - - - - - - - - \quad (6)$$

where the constant GJ, the product of the elastic modulus in shear by the cross section polar moment of inertia, is called the "torsional stiffness".

Since the twist ϕ builds up linearly with T the strain energy stored is

$$U = \frac{1}{2} T \phi$$

or

$$U = \frac{1}{2}\frac{T^2 L}{GJ} \quad - - - - - - - - - - - - - - - - - - \quad (7)$$

For a shaft of non-uniform properties and varying loading one has

$$U = \frac{1}{2}\int \frac{T^2 dx}{GJ} \quad - - - - - - - - - - - - - - - - - - \quad (8)$$

In passing it is worth remarking that one often encounters the group symbol "GJ" in use for the torsional stiffness of a non-circular shaft or beam such as an aircraft wing. In such a case the torsional stiffness has not been computed literally as G x J, but rather as defined by eq. (6), viz. the ratio of torque to rate of twist.

Example Problem 5

For a certain flight condition the torque on an airplane wing due to aerodynamic loading is given as shown graphically in Fig. A7.6. The variation of torsional stiffness GJ is given in like manner. Find the strain energy stored.

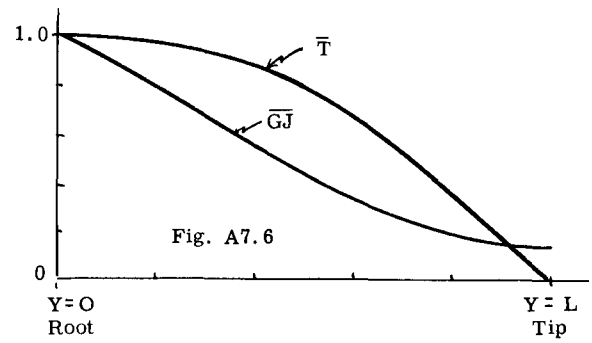

Fig. A7.6

Solution:

A numerical integration of eq. (8) was performed using Simpson's rule. The work is shown in tabular form in table A7.1.

Values of T and GJ for selected wing stations were taken from the graphs provided and were entered in the table. For convenience in handling the numerical work all the variables were treated in non-dimensional form, eq. (8) being changed as follows

$$U = \frac{1}{2}\int_o^{L_R} \frac{T^2}{GJ} dy = \frac{1}{2}\frac{LT_R^2}{GJ_R}\int_o^1 \frac{(\bar{T})^2}{\overline{GJ}} d\tau$$

where

$$\bar{T} \equiv T/T_R \ , \quad \tau = y/L$$

$$\overline{GJ} \equiv GJ/GJ_R$$

The subscript R denotes "root" value (y=o). The coefficients for Simpson's rule appearing in column (6) were taken from the expression for odd n

$$I = \frac{\Delta\tau}{3}\ (f_o + 4f_1 + 2f_2 + 4f_3 + - - - -$$

$$- - - - + \frac{15}{4}f_{n-2} + 3f_{n-1} + \frac{5}{4}f_n)$$

TABLE A7.1

STA. τ	$\bar{T}$	$(\bar{T})^2$	$\overline{GJ}$	$\frac{(\bar{T})^2}{\overline{GJ}}$	Coeff.	$\frac{(\bar{T})^2}{\overline{GJ}}$ x Coeff.
0	1.0	1.0	1.0	1.0	.0667	.0667
.2	.98	.96	.76	1.26	.267	.336
.4	.94	.88	.54	1.63	.133	.216
.6	.67	.45	.37	1.22	.250	.305
.8	.29	.084	.24	.35	.200	.070
1.0	0	0	.14	0	.0833	0.0
						Σ = .994

Therefore the strain energy was

$$2U = \frac{LT_R^2}{GJ_R} \times .994$$

STRAIN ENERGY OF SHEAR

A rectangular element "dx" by "dy" of thickness "t" into the page under the action of uniform shear stress τ (psi) is shown in Fig. A7.6a.

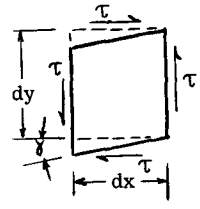

Fig. A7.6a

From elementary strength of materials the angle of shear strain γ is proportional to the shear stress τ as

$\gamma = \frac{\tau}{G}$ where G is the material elastic modulus in shear. For the displacements as shown in the sketch only the down load on the left hand side does any work. (In general all four sides move, but if the motion is referred to axes lying along two adjacent sides of the element, as was done here, the derivation is simplified). This load is equal to τ x dy x t and moves an amount γ x dx. Then

$$dU = \frac{1}{2}\tau\gamma t\ dx\ dy$$

$$= \frac{1}{2}\ \frac{\tau^2}{G}\ tdxdy \ - - - - - - - - - - - - - - - - - \ (9)$$

Eq. (9) may be used to compute the shear strain energy in a beam under the action of a transverse shear loading V(lbs)*. For this purpose V = τ x dy x t and t x dy is called A, the beam cross sectional area. Hence

$$dU = \frac{V^2 dx}{2AG} \ , \text{ and}$$

therefore the elastic strain energy of shear for the entire beam is given by

$$U = \int \frac{V^2 dx}{2AG} \ - - - - - - - - - - - - - - - - - - \ (10)$$

Example Problem 6

Determine the strain energy of shear in the beam of Example Problem 4.

Solution:

The shear load diagram was drawn first from the right end.

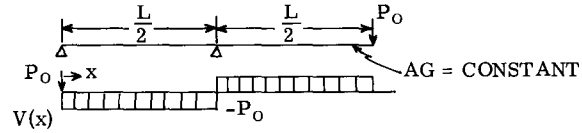

Then

$$U = \frac{1}{2AG} \times 2 \times \int_0^{L/2} P_o^2\, dx$$

$$= \frac{P_o^2 L}{2AG}$$

Eq. (9) may be used to compute the shear strain energy in a thin sheet. The element dx x dy is visualized as but one of many in the sheet and the total energy is obtained by summing. Thus

$$U = \frac{1}{2}\int\int \frac{\tau^2 t\ dx\ dy}{G} \ - - - - - - - - - - - - - \ (11)$$

Here a double integration is required, the summation being carried out in both directions over the sheet. In dealing with thin sheet the use of the shear flow $q \equiv \tau t$ is often convenient so that eq. (11) rewrites

$$U = \frac{1}{2}\int\int \frac{q^2 dx\ dy}{Gt} \ - - - - - - - - - - - - - \ (11a)$$

A very important special case occurs when a homogenous sheet of constant thickness is analyzed assuming q is constant everywhere. In this case one has

$$U = \frac{q^2}{2Gt}\int\int dxdy = \frac{q^2 S}{2Gt} \ - - - - - - - - - - - - - \ (12)$$

where $S = \int\int dxdy$ is the surface area of the sheet.

* The sketch is visualized as a side view of an element of length dx taken from a beam of total height dy.

Example Problem 7

Find the shear strain energy stored in a cantilever box beam of uniform rectangular cross section under the action of torque T. (Fig. A7.8).

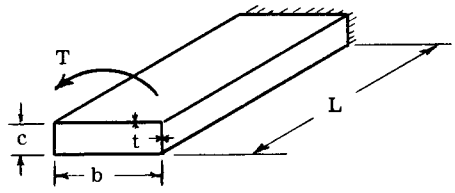

Fig. A7.8

Solution:

The shear flow was assumed given by Bredt's formula (Ref. Chapter A-6)

$$q = \frac{T}{2A} = \frac{T}{2bc} ,$$

constant around the perimeter of any section. Then

$$U = \Sigma \frac{q^2 S}{2Gt} = \frac{T^2}{8Gb^2c^2t} 2L(b+c)$$

$$= \frac{T^2 L(b+c)}{4Gb^2c^2t}$$

THE TOTAL ELASTIC STRAIN ENERGY OF A STRUCTURE

The strain energy by its definition is always a positive quantity. It also is a scalar quantity (one having magnitude but not direction) and hence the total energy of a composite structure, having a variety of elements under various loadings, is readily found as a simple sum.

$$U_{TOT} = \int \frac{S^2 dx}{2AE} + \int \frac{M^2 dx}{2EI} + \int \frac{T^2 dx}{2GJ}$$

$$+ \int \frac{V^2 dx}{2AG} + \iint \frac{q^2 dxdy}{2Gt} \quad - - - - - - - - - - - - - - \quad (13)$$

The integral symbols and common use of "x" an an index of integration should not be taken too literally. It is probably best to read these terms as "the sum of so and so over the structure" rather than "the integral of", for quite often the terms are formed as simple sums without resort to the calculus. The calculus is only used as an aid in some applications.

It is seldom that all the terms of eq. (13) need be employed in a calculation. Many of the loadings, if actually present, may be of a localized or of a secondary nature and their energy contribution may be neglected.

A7.4 The Theorems of Virtual Work and Minimum Potential Energy.

An important relationship between load and deformation stems directly from the definitions of work and strain energy. Consider Fig. A7.9(a).

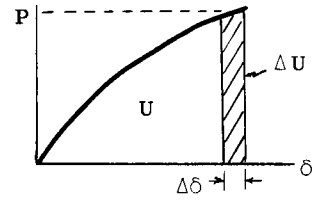

Fig. A7.9a

Thus

$$\frac{dU}{d\delta} = P \quad - \quad (14)$$

In words,

"The rate of change of strain energy with respect to deflection is equal to the associated load".

Eq. (14) and the above quotation are statements of the Theorem of Virtual Work. The reader may find this theorem stated quite differently in the literature on rigid body mechanics but should be able to satisfy himself that the expressions are nevertheless compatible.

A useful restatement of the above theorem is obtained by rewriting eq. (14) as

$$dU - Pd\delta = 0$$

It is next argued that if the change in displacement dδ is sufficiently small the load P remains sensibly constant and hence

$$dU - d(P\delta) = 0$$

$$d(U-P\delta) = 0 \quad - - - - - - - \quad (15)$$

The quantity U - Pδ is called the total potential of the system and eq. (15), resembling as it does the mathematical condition for the minimum value of a function, is said to be a statement of the Theorem of Minimum Potential.

From the foregoing it is clear that the Theorem of Minimum Potential is a restatement of the Theorem of Virtual Work.

In structural analysis the most important uses of these theorems are made in problems concerning buckling instability and other non-linearities. No applications will be made at this point.

A7.5 The Theorem of Complementary Energy and Castigliano's Theorem.

Again in the case of an elastic body, examination of the area above the load-deformation curve shows that increments in this area (called

the complementary energy, U^*), are related to the load and deformation by (see Fig. A7.9(b).

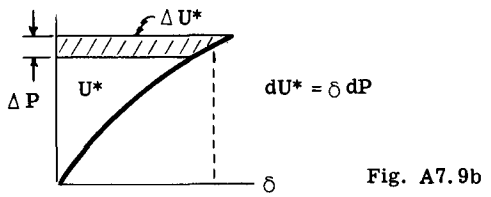

Fig. A7.9b

$$\frac{dU^*}{dP} = \delta \quad \text{- - - -

$$P = \frac{\pi^2 EI}{2L^2} \quad \text{(incorrect)}$$

Moral: Do not use Castigliano's theorem for non-linear problems.

Fortunately the above restriction upon the use of Castigliano's theorem is not a very severe one, the majority of every day structural problems being linear. Castigliano's theorem is quite useful in performing deflection calculations and a variety of applications will be made in the following sections.

A7.6 Calculations of Structural Deflections by Use of Castigliano's Theorem.

As the examples of Art. A7.3 have illustrated, the strain energy of a structure can be expressed as a function of the external loadings provided the internal load or stress distribution is calculable. Having the strain energy so expressed the deflections at points of load application can be determined with the aid of eq. (17), Castigliano's Theorem.

In the examples to follow the deflections of a variety of statically determinate structures are computed. Methods of handling redundant structures are considered in subsequent articles.

Example Problem 8

Find the vertical deflection at the point of load application of the crane of Fig. A7.11.

Cross sectional areas are given on each member. The stranded cables have effective modulii of 13.5 x 10^6 psi. E = 29,000,000 for other members.

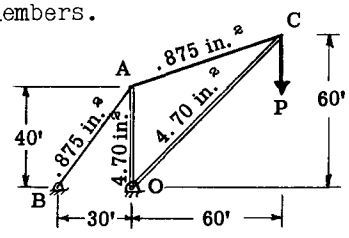

Fig. A7.11

Solution:

The strain energy considered here was that due to axial loading in each of the four members. The load distribution was obtained from statics and the energy calculation was made in tabular form as follows:

TABLE A7.2

MEMBER	S LBS	L FT	AE x 10^6 LBS	$\frac{S^2L}{AE}$ x 10^6
OA	-1.50 P	40.0	136	0.66 P^2
AB	2.50 P	50.0	11.8	26.48 P^2
AC	1.58 P	63.0	11.8	13.33 P^2
OC	-2.12 P	84.5	136	2.79 P^2
				Σ = 43.26 P^2

Then

$$2U = 43.26 \times 10^{-6} P^2 \text{ LB FT}$$

$$\delta_p = \frac{dU}{dp} = \underline{43.26 \times 10^{-6} P} \text{ ft.}$$

Note that in this problem the only use made of the calculus was in the differentiation. A simple sum was used to form U, as per eq. (2).

Example Problem 9

Derive Bredt's formula for the rate of twist of a hollow, closed, thin-walled tube:

$$\Theta = \frac{T}{4A^2G} \oint \frac{ds}{t} \qquad \text{Ref. chap. A6.}$$

The strain energy is stored in shear according to

$$U = \frac{1}{2} \iint \frac{q^2 dxdy}{Gt} .$$

This is the only energy stored, secondary effects neglected. Over a given cross section q is a constant and is given by Bredt's equation $q = \frac{T}{2A}$, where A is the enclosed area of the tube (Ref. Chap. A.5).

Solution:

Since the twist per unit length was desired the strain energy per unit length only was written. Thus, assuming y in the axial direction, no integration was made with respect to y. The integration in the remaining direction was to be carried out around the perimeter of the tube and so the index was changed from "x" to the more appropriate "s". Hence (compare with Example Prob. 7)

$$U = \frac{1}{2G} \oint \frac{q^2 ds}{t} = \frac{T^2}{8A^2G} \oint \frac{ds}{t}$$

The symbol $\oint$ means the integration is carried out around the tube perimeter. Therefore

$$\Theta = \frac{dU}{dT} = \frac{T}{4A^2G} \oint \frac{ds}{t} .$$

USE OF FICTITIOUS LOADS

In the following example the desired deflection is at the free end of the bar where no load is applied. A fictitious load will be added for purposes of the calculation. The rate of change of strain energy with respect to this fictitious load will be found after which the load will be set equal to zero. This technique gives the desired result in as much as the deflection is equal to the rate of change of strain energy with respect to the load and such a rate exists even though the load itself be zero.

Example Problem 10

Compute the axial motion of the free end of the tapered bar of Fig. A7.12.

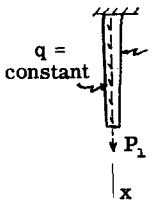

q = 40#/in.
A_0 = 4 in.²
L = 40 in.
E = 10 x 10⁶ psi

Fig. A7.12

Solution:

After addition of the fictitious end load P_1 the axial load from statics was found to be

$$S(x) = P_1 + q\,(L - x)$$

Hence, since loadings other than tensile are of a secondary nature

$$U = \frac{1}{2}\int_0^L \frac{S^2 dx}{AE} \quad \text{- - - - See Eq. 3}$$

$$= \frac{1}{2}\int_0^L \frac{\left[P_1 + q\,(L - x)\right]^2}{A_0 E\left(1 - \frac{x}{2L}\right)}\,dx$$

$$= \frac{P_1^2}{2A_0E}\int_0^L \frac{dx}{\left(1 - \frac{x}{2L}\right)} + \frac{P_1 q}{A_0 E}\int_0^L \frac{(L - x)\,dx}{\left(1 - \frac{x}{2L}\right)}$$

$$+ \frac{q^2}{2A_0E}\int_0^L \frac{(L - x)^2 dx}{\left(1 - \frac{x}{2L}\right)}$$

Before evaluating the integrals it was observed that the steps to follow, in which U was to be differentiated with respect to P_1 and the subsequent setting of $P_1 = 0$ would drop out both the first and last terms. Hence only the second term was evaluated.

$$U = X + \frac{2L^2 P_1 q}{A_0 E}(1 - \ln 2) + X$$

Then

$$\delta = \frac{dU}{dP_1} = \frac{2L^2 q}{A_0 E}\,(1 - \ln 2)$$

DIFFERENTIATION UNDER THE INTEGRAL SIGN

An important labor savings may be had in the calculation of deflections by Castigliano's theorem.

In the strain energy integrals arising in this class of problems, the load P_1, with respect to which the deflection is to be found, acts as an independent parameter in the integral. Provided certain requirements for continuity of the functions are met - and they invariably are in these problems - the differentiation with respect to P may be carried out before the integration is made. The resulting integrals generally are easier to evaluate.

Example Problem 11

Find the deflection at point B of the beam of Fig. A7.13.

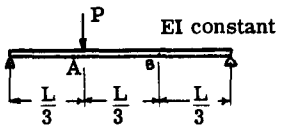

Fig. A7.13

Solution:

A fictitious load P_1 was added at point B and the bending moment diagram was drawn in two parts.

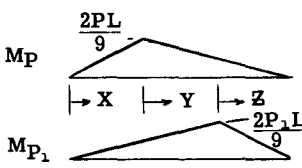

Fig. A7.13a

Then neglecting the energy of shear as being small*

$$U = \frac{1}{2EI}\int_0^{L/3}\left[(2P + P_1)\,\frac{X}{3}\right]^2 dx$$

$$+ \frac{1}{2EI}\int_0^{L/3}\left[\frac{P}{9}(2L - 3Y) + \frac{P_1}{9}\,(L + 3Y)\right]^2 dy$$

$$+ \frac{1}{2EI}\int_0^{L/3}\left[\frac{(P + 2P_1)}{9}\,(L - 3Z)\right]^2 dZ\,.$$

Differentiation under the integral sign with respect to P_1 gave

$$\delta_B = \frac{\partial U}{\partial P_1} = \frac{1}{EI}\int_0^{L/3}\left[(2P + P_1)\frac{X}{3}\right]\frac{X}{3}\,dx$$

$$+ \frac{1}{EI}\int_0^{L/3}\left[\frac{P}{9}(2L - 3y) + \frac{P_1}{9}(L + 3y)\right]\frac{(L + 3y)}{9}\,dy$$

$$+ \frac{1}{EI}\int_0^{L/3}\left[\frac{P + 2P_1}{9}(L - 3Z)\right]\frac{2(L - 3Z)}{9}\,dZ\,.$$

* For beams of usual high length - to - depth ratios the shear strain energy is small compared to the energy of flexure. Neglecting the shear energy is equivalent to neglecting the shear deflection contribution. (see p. A7.14)

The fictitious load P_1, having served its purpose, was set equal to zero before completing the work.

$$\delta_B = \frac{1}{EI} \cdot \frac{2P}{9} \int_0^{L/3} x^2 dx$$

$$+ \frac{1}{EI} \frac{P}{81} \int_0^{L/3} (2L - 3y)(L + 3y)\, dy$$

$$+ \frac{1}{EI} \frac{2P}{81} \int_0^{L/3} (L - 3z)^2\, dz$$

$$\delta_B = \frac{7}{486} \frac{PL^3}{EI}$$

Example Problem 12

Fig. A7.14 shows a cantilever round rod of diameter D formed in a quarter circle and acted upon by a torque T_o. Find the vertical movement of the free end.

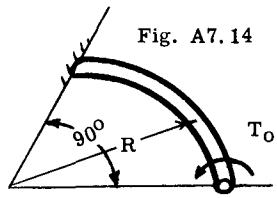

Fig. A7.14

Solution:

Fig. A7.14a shows the vector resolution of the applied torque T_o on beam elements. $T_1(\theta) = T_o \cos\theta$ and the moment $M_1(\theta) = T_o \sin\theta$. Application of a fictitious vertical load P (down) at the point of desired deflection gave the loadings shown in Fig. A7.14b.

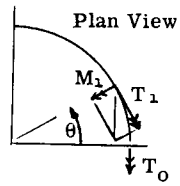

Fig. A7.14a

The total loadings were

$$M = M_1 - M_2 = (T_o - PR)\sin\theta$$

$$T = T_1 + T_2 = T_o \cos\theta + PR(1 - \cos\theta)$$

Thus

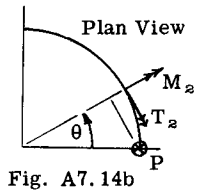

Fig. A7.14b

$$U = \frac{1}{2EI} \int_0^{\pi/2} (T_o - PR)^2 \sin^2\theta\, R\, d\theta$$

$$+ \frac{1}{2GJ} \int_0^{\pi/2} \left[T_o \cos\theta + PR(1 - \cos\theta)\right]^2 R\, d\theta$$

(Note use of "Rdθ" for the length of a differential beam element instead of "dx"). Differentiating under the integral sign

$$\frac{\partial U}{\partial P} = -\frac{(T_o - PR)R^2}{EI} \int_0^{\pi/2} \sin^2\theta\, d\theta$$

$$+ \frac{R^2}{GJ} \int_0^{\pi/2} \left[T_o \cos\theta + PR(1 - \cos\theta)\right](1 - \cos\theta)\, d\theta.$$

Putting P, the fictitious load equal to zero and integrating gave

$$\delta_{VERT} = \frac{\partial U}{\partial P} = \frac{T_o R^2}{4} \left(\frac{4 - \pi}{GJ} - \frac{\pi}{EI}\right)$$

Since $J = 2I$ and $G \approx E/2.6$ the deflection was negative (UP).

A7.7 Calculation of Structural Deflections by the Method of Dummy-Unit Loads (Method of Virtual Loads).

The strict application of the calculus to Castigliano's theorem as in Art. A7.6, leads to a number of cumbersome techniques ill-suited to the solution of large complex structures. A more flexible approach, readily adapted to improved "book keeping" techniques is the Method of Dummy-Unit Loads developed independently by J. C. Maxwell (1864) and O. Z. Mohr (1874).

That the equations for the Method of Dummy-Unit Loads may be derived in a number of ways is attested to by the great variety of names applied to this method in the literature ⓪ . Presented below are two derivations of the equations stemming from different viewpoints. One derivation obtains the equations by a reinterpretation of the symbols of Castigliano's theorem - essentially an appeal to the concepts of strain energy. The other derivation uses the principles of rigid body mechanics. Based as they are upon a common set of consistent assumptions, all the methods must, of course, yield the same result.

Derivation of Equations for the Method of Dummy-Unit Loads (Virtual Loads)

I - From Castigliano's Theorem

Beginning with the general expression for strain energy, eq. (13)

II - From the Principle of Virtual Work

When a system of forces whose resultant is zero (a system in equilibrium) is displaced a

⓪ Variously called the Maxwell-Mohr Method, Method of Virtual Velocities, Method of Virtual Work, Method of Auxilliary Loads, Dummy Loads, Method of Work, etc.

I Cont'd.

$$U = \frac{1}{2}\int \frac{S^2dx}{AE} + \frac{1}{2}\int \frac{M^2dx}{EI} + \frac{1}{2}\int \frac{T^2dx}{GJ} + \text{- - - etc.}$$

differentiate under the integral sign with respect to P_i to obtain

$$\delta_i = \int \frac{S\frac{\partial S}{\partial P_i}dx}{AE} + \int \frac{M\frac{\partial M}{\partial P_i}dx}{EI} + \text{- - - - - - - - etc.}$$

Consider the symbols

$$\frac{\partial S}{\partial P_i}, \frac{\partial M}{\partial P_i}, \frac{\partial T}{\partial P_i}, \text{- - - - - - - - - - - - - - - etc.}$$

Each of these is the "rate of change of so-and-so with respect to P_i" or "how much so-and-so changes when P_i changes a unit amount" OR EQUALLY, "the so-and-so loading for a unit load P_i".

Thus, to compute these partial derivative terms one need only compute the internal loadings due to a unit load (the virtual load) applied at the point of desired deflection. For example, the term $\partial M/\partial P_i$ could be computed in either of the two ways shown in Fig. A7.15a.

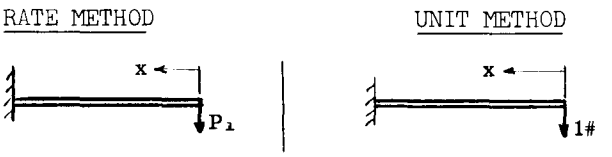

Fig. A7.15a

$M = P_1 x$ | m = dummy loading

$\frac{\partial M}{\partial P_1} = x$ | $= x \left(= \frac{\partial M}{\partial P_1}\right)$

Likewise, $\partial S/\partial P_C$, where P_C is a load (real or fictitious) applied at joint c of Fig. A7.15b, is given by the loadings for the unit load applied as shown.

In practice the use of the unit load is most convenient. Using the notation

$$u \equiv \frac{\partial S}{\partial P_i}, \; m \equiv \frac{\partial M}{\partial P_i}, \; t \equiv \frac{\partial T}{\partial P_i}$$

$$v \equiv \frac{\partial V}{\partial P_i}, \; \bar{q} \equiv \frac{\partial q}{\partial P_i}$$

for the unit loadings, the deflection equation becomes

$$\delta_i = \int \frac{Sudx}{AE} + \int \frac{Mmdx}{EI} + \int \frac{Ttdx}{GJ} + \int \frac{Vvdx}{AG} + \iint \frac{q\,\bar{q}\,dxdy}{Gt} \quad \text{- - - - - - - - - -} \quad (18)$$

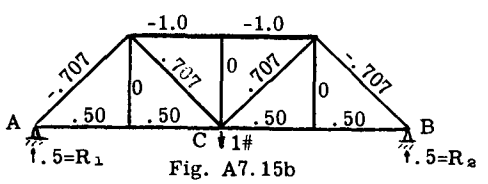

Fig. A7.15b

"u" loads due to a unit (virtual) load.

II Cont'd.

small amount without disturbing the equilibrium balance, the work done is zero - obviously, since zero resultant force moving through a distance does zero work.

Consider now the set of equilibrium forces applied to the truss of Fig. A7.15(b). The set may be divided into two parts: the "external system", consisting of the unit load applied at the point whose deflection is desired and the two reactions fixing the line of reference, and the "internal system" consisting of the axial loads acting on the truss members to produce equilibrium. These latter are denoted by the symbol "u". This set of forces is considered small enough so as not to affect the actual behavior of the structure during subsequent application of a real set of major loads. This unit load set is present solely for mathematical reasons and is called a "virtual loading" or "dummy loading".

Assume now that the structure undergoes a deformation due to application of a set of real loads, the virtual loads "going along for the ride". Each member of the structure suffers a deformation denoted by Δ ①. The virtual loading system, being in equilibrium (zero resultant) by hypothesis, does work ("virtual work") equal to zero. Or, considering the subdivision of the virtual loading system, the work done by the external virtual load must equal that absorbed by the internal virtual loads. The work done by the external virtual forces is equal to one pound times the deflection at joint C, the reactions R_1 and R_2 not moving. That is

$$\text{External Virtual Work} = 1^{\#} \times \delta_C .$$

The internal virtual work is the sum over the structure of the products of the member virtual loads u by the member distortions Δ. That is,

$$\text{Internal Virtual Work} = \Sigma\, u \cdot \Delta .$$

Then equating these works,

$$1 \times \delta_C = \Sigma\, u \cdot \Delta .$$

If the deformations Δ are the result of elastic strains due to real member loads S then $\Delta = SL/AE$ for each member and one has

$$\delta_C = \Sigma\, u \frac{SL}{AE}$$

The argument given above may be extended quickly to include the internal virtual work of virtual bending moments (m), torsion loads (t), shear loads (v), and shear flows ($\bar{q}$) doing work during deformations due to real moments (M), torques (T), shear loads (V), and shear flows (q). The general expression becomes

$$\delta_i = \int \frac{Sudx}{AE} + \int \frac{Mmdx}{EI} + \int \frac{Ttdx}{GJ} + \int \frac{Vvdx}{AG} + \iint \frac{q\,\bar{q}\,dxdy}{Gt} \quad \text{- - - - -} \quad (18)$$

① Note that the deformations are not restricted to those due to elastic strains only. They may be the result of elastic or inelastic strains, temperature strains or misalignment corrections.

In applying eq. (18) the labor of a deflection calculation divides conveniently into several steps:

i. Calculation of the real (actual) load distribution (S,M,T, etc.)

ii. Calculation of the unit (virtual) load distribution (u,m,t, etc.) due to a unit (virtual) load applied at the point of desired deflection and reacted at the reference point(s).

iii. Calculation of flexibilities,

$\frac{1}{AE}$, $\frac{1}{EI}$, etc.

iv. Summation and/or Integration.

Here again note the general nature of the terms "load" and "deflection". (See p. A7.6)

The following examples apply the method of dummy-unit loads to the determination of absolute and relative deflections, both rotation and translation.

Example Problem 13

The pin-jointed truss of Fig. A7.16 is acted upon by the external loading system shown. The member loads are given on the figure. Member properties are given in Table A7.3. Find the vertical movement of joint G and the horizontal movement of joint H.

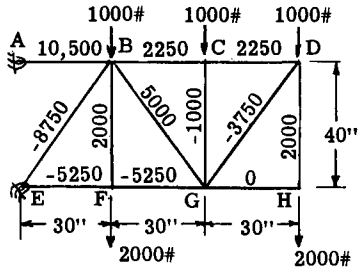

Fig. A7.16

Solution:

Only the energy of axial loadings in the members was considered. Unit (virtual) loads were applied successively at joints G and H as shown in Figs. A7.16a and A7.16b. All S and u loadings were entered in Table A7.3 and the calculation for $\delta = \int \frac{Sudx}{AE}$ was carried out by forming the sum of SuL/AE terms for the members of the truss, i.e. $\delta = \Sigma \frac{SuL}{AE}$

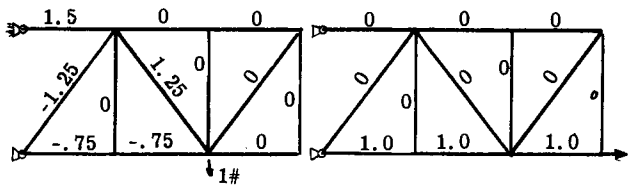

"u_1" loads

Fig. A7.16a

"u_2" loads

Fig. A7.16b

TABLE A7.3

MEM.	L_{in}	AE x 10^{-6} lbs	$\frac{L}{AE}$ x 10^6 in/lb	S	u_1	u_2	$\frac{Su_1L}{AE_{inch}}$ x 10^3	$\frac{Su_2L}{AE_{inch}}$ x 10^3
AB	30	4.785	6.270	10,500	1.5	0	98.75	0
BC	30	3.074	9.759	2,250	0	0	0	0
CD	30	3.074	9.759	2,250	0	0	0	0
EF	30	5.365	5.591	-5,250	-0.75	1	22.01	-29.36
FG	30	5.365	5.591	-5,250	-0.75	1	22.01	-29.36
GH	30	3.48	8.621	0	0	1	0	0
BE	50	10.15	4.926	-8,750	-1.25	0	53.88	0
BG	50	3.48	14.368	5,000	1.25	0	89.80	0
DG	50	5.365	9.320	-3,750	0	0	0	0
BF	40	3.074	13.012	2,000	0	0	0	0
CG	40	3.074	13.012	-1,000	0	0	0	0
DH	40	3.074	13.012	2,000	0	0	0	0
							Σ = 286.4	Σ = -58.72

Answers: $\delta_{G_{VER}}$ = 0.286"

$\delta_{H_{HOR}}$ = -.0587" (the negative sign means the joint moves to the LEFT since the unit load was drawn to the RIGHT in Fig. A7.16b).

Example Problem 14

For the truss of Fig. A7.16 find the following relative displacements of joints:

c) the movement of joint C in the direction of a diagonal line joining C and F.

d) the movement of joint G relative to a line joining points F and H.

Relative deflections are determined by applying unit (virtual) loads at the points where the deflections are desired and by supporting such unit load systems at the reference points of the motion. Thus, for solution to part (c) a unit load system was applied as shown in Fig. A7.16c and for the solution of

part (d) the system of unit loads of Fig. A7.16d was used. Table A7.4 completes the solution, the real loads and member flexibilities $\left(\frac{L}{AE}\right)$ being the same as for example problem 13.

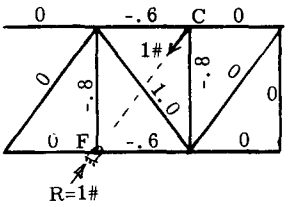

"u_3" loads

Fig. A7.16c

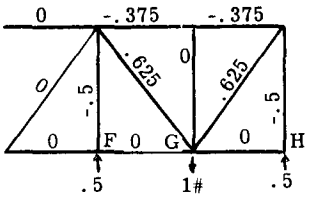

"u_4" loads

Fig. A7.16 d

TABLE A7.4						
MEM.	$\frac{L}{AE}$ x 10^6 in/lb (See Table A7.3)	$S_{lb.}$	u_3	u_4	$\frac{Su_3L}{AE}$ x 10^3 inch	$\frac{Su_4L}{AE}$ x 10^3 inch
AB	6.270	10,500	0	- 0	0	0
BC	9.759	2,250	-.6	-.375	-13.17	-8.23
CD	9.759	2,250	0	-.375	0	-8.23
EF	5.591	-5,250	0	0	0	0
FG	5.591	-5,250	-.6	0	17.61	0
GH	8.621	0	0	0	0	0
BE	4.926	-8,750	0	0	0	0
BG	14.368	5,000	1.0	.625	71.84	44.9
DG	9.320	-3,750	0	.625	0	-21.8
BF	13.012	2,000	-.8	-.50	-20.82	-13.0
CG	13.012	-1,000	-.8	0	+10.41	0
DH	13.012	2,000	0	-.50	0	-13.0
					Σ = 65.87	Σ =-19.36

Therefore the movement of joint c towards joint F was δ = .06587 inches and the motion of joint G relative to a line between F and H was δ = -.0194 inches, the negative sign indicating an upward movement.

Example Problem 15

For the truss of Fig. A7.16 determine

e) the absolute rotation of member DG

f) the rotation of member BG relative to member CG.

Rotations, both absolute and relative are determined by applying unit (virtual) couples to the member or portion of structure whose rotation is desired. The unit couple is resisted by reactions placed on the line of reference for the rotation. Thus Figs. A7.16e and A7.16f show the unit (virtual) loadings for parts (e) and (f) respectively. Table A7.5 completes the calculation, the real loads and member flexibilities $\left(L/_{AE}\right)$ being the same as for example problem 13.

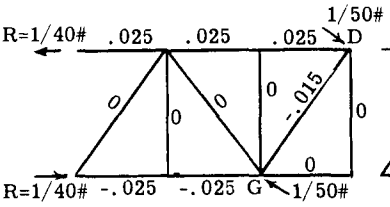

"u_5" loads

Fig. A7.16e

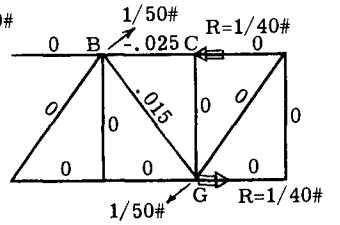

"u_6" loads

Fig. A7.16f

TABLE A7.5						
MEM.	$\frac{L}{AE}$ x 10^6 in/lb (See Table A7.3)	S_{lb}	$u_5$inch^{-1}	$u_6$inch^{-1}	$\frac{Su_5L}{AE}$ x 10^3	$\frac{Su_6L}{AE}$ x 10^3
AE	6.270	10,500	.025	0	1.65	0
BC	9.759	2,250	.025	-.025	.55	-0.55
CD	9.759	2,250	.025	0	.55	0
EF	5.591	-5,250	-.025	0	+.73	0
FG	5.591	-5,250	-.025	0	+.73	0
GH	8.621	0	0	0	0	0
BE	4.926	-8,750	0	0	0	0
BG	14.368	5,000	0	.015	0	1.08
DG	9.320	-3,750	-.015	0	.52	0
BF	13.012	2,000	0	0	0	0
CG	13.012	-1,000	0	0	0	0
DH	13.012	2,000	0	0	0	0
					Σ = 4.73	Σ = 0.53

Therefore the absolute rotation of member DG was Θ_{DG} = .00473 radians and the rotation of BG relative to CG was $\Theta_{BG - CG}$ = .00053 radians.

Example Problem 16

Find the vertical deflection of point C for the cantilever beam of Fig. A7.17 carrying a concentrated load P at its end. Also find slope of elastic curve at C.

Solution:

$$\delta_C = \int \frac{Mmdx}{EI}$$

With origin at B

$$M = -Px \quad \text{(Fig. A7.17)}$$

For virtual loading (Fig. A7.17a)

$$m = 0, \text{ for } x<b$$
$$m = -1\,(x - b), \text{ for } x>b$$

Hence $Mmdx = -Px(-x + b)dx = (Px^2 - Pbx)dx$

Whence $\delta_C = \frac{P}{EI}\int_b^L (x^2 - bx)dx = \frac{P}{EI}\left[\frac{x^3}{3} - \frac{bx^2}{2}\right]_b^L$

$$= \frac{P}{3EI}\left[L^3 - \frac{3L^2b}{2} + \frac{b^3}{2}\right]$$

If b = zero, then $\delta_B = PL^3/3EI$

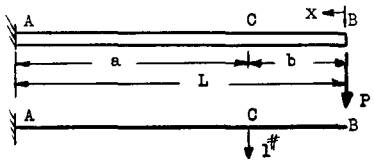

Fig. A7.17

Fig. A7.17a

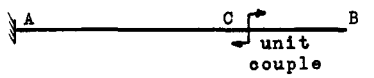

Fig. A7.17b

$$\theta_c = \int \frac{Mmdx}{EI}$$

For virtual loading see Fig. A7.17b

$$m = 0, \; x<b, \quad m = -1, \; x>b$$

Hence $Mmdx = (-Px)(-1)\,dx = Px\,dx$

$$\therefore \theta_c = \int \frac{Mmdx}{EI} = \frac{P}{EI}\int_b^L x\,dx = \frac{P}{2EI}(L^2 - b^2)$$

If b = 0, $\theta_B = \frac{PL^2}{2EI}$

Example Problem 17

For the uniformly loaded cantilever beam of Fig. A7.18, find the deflection of point D relative to the line joining points C and E on the elastic curve of the beam. This is representative of a practical problem in aeronautics, in that AB might represent a rear wing beam and points C, D, E, the attachment points of an aileron or a flap. The wing beam deflection bends the aileron or flap structure by applying a load at D thru aileron supporting bracket. To know this force the deflection of the wing beam at D relative to line CE must be known.

Solution:

Origin at B: -

$$M = 30\,x \cdot \frac{x}{2} = 15\,x^2$$

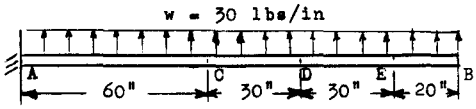

Fig. A7.18

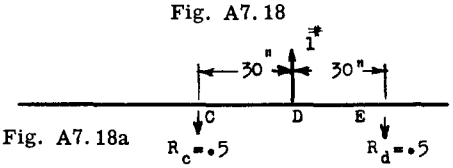

Fig. A7.18a

$m = 0, \; x < 20$

$m = -.5\,(x - 20) = -.5x + 10$, when x = 20 to 50

$m = -.5\,(x - 20) + 1\,(x - 50) = .5x - 40$, when x = 50 to 80

$$\delta_{D(CE)} = \int \frac{Mmdx}{EI}$$

$$= \frac{1}{EI}\int_{20}^{50} 15\,x^2\,(-.5x + 10)dx + \frac{1}{EI}\int_{50}^{80} 15\,x^2\,(.5x - 40)\,dx$$

$$= \frac{1}{EI}\left[\frac{-7.5\,x^4}{4} + \frac{150\,x^3}{3}\right]_{20}^{50} + \frac{1}{EI}\left[\frac{7.5\,x^4}{4} - \frac{600\,x^3}{3}\right]_{50}^{80}$$

$$= \frac{10^6}{EI}\left[-11.72 + 6.25 + .300 - .400 + 76.8 - 102.4 - 11.72 + 25.0\right]$$

$$= -\frac{17.9 \times 10^6}{EI}$$

Therefore deflection of point D relative to line joining CE is down because result comes out negative and therefore opposite to direction of virtual load.

Example Problem 18

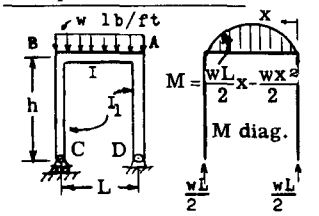

Fig. A7.19

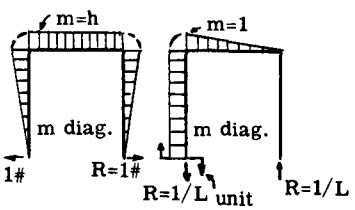

Fig. A7.20

Find the horizontal deflection of point C for the frame and loading of Fig. A7.19. Also angular deflection of C with respect to line CD.

Solution:

Fig. b shows the static moment curve for the given loading and Fig. c the moment diagram for the virtual loading of a unit horizontal load applied at C and resisted at D.

$$\delta_{C(H)} = \int \frac{Mmdx}{EI} \; ; \quad M = \frac{wLx}{2} - \frac{wx^2}{2} \; ; \quad m = h$$

hence

$$\delta_C = \int_0^L \frac{\left(\frac{wLx}{2} - \frac{wx^2}{2}\right)}{EI} h dx = \left[\left(\frac{wLx^2}{4} - \frac{wx^3}{6}\right)\frac{h}{EI}\right]_0^L =$$

$$= \frac{1}{12} \frac{whL^3}{EI}$$

To find angular deflection at C apply a unit imaginary couple at C with reactions at C and D. Fig. A7.20 shows the virtual m diagram.

$$\theta_c = \int_0^L \frac{Mmdx}{EI} = \frac{1}{EI} \int_0^L \left(\frac{wLx}{2} - \frac{wx^2}{2}\right) \frac{x}{L} dx = \frac{1}{EI} \int_0^L$$

$$\left(\frac{wLx^2}{2L} - \frac{wx^3}{2L}\right) dx = \frac{1}{EI}\left[\frac{wx^3}{6} - \frac{wx^4}{8L}\right]_0^L =$$

$$= \frac{1}{24} \frac{wL^3}{EI}$$

Linear Deflection of Beams Due to Shear by Virtual Work.

Generally speaking, shear deflections in beams are small compared to those due to bending except for comparatively short beams and therefore are usually neglected in deflection calculations. A close approximation is sometimes made by using a modulus of elasticity slightly less than that for bending and using the bending deflection equations.

The expression for shear deflection of a beam is derived from the same reasoning as in previous derivations. The virtual work equation for the hypothetical unit load system for a shear detrusion dy (Fig. A7.21) considering only dx elastic is 1 x δ=vdy where v is shear on section due to unit hypothetical load at point O, and dy is the shear detrusion of the element dx due to any given load system or any other cause.

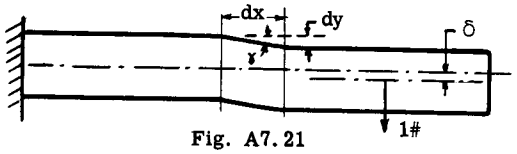

Fig. A7.21

dy = γ dx and $\gamma = \frac{V}{AE_S}$, where A = cross sectional area of beam at section and E_S = modulus of rigidity*, and assuming that the shearing stress $\frac{V}{A}$ is uniform over the cross-section.

Therefore 1 x $\delta = \frac{Vvdx}{AE_S}$. Then the total deflection for the shear slips of all elements of the beam equals

$$\delta \text{ total} = \int_0^L \frac{Vvdx}{AE_S} \qquad \text{--------(a)}$$

where V is the shear at any section due to given loads. v = shear at any section due to unit hypothetical load at the point where the deflection is wanted and acting in the desired direction of the deflection. The reactions to the hypothetical unit load fix the line of reference for the deflection.

A is the cross-sectional area and E_S the modulus of rigidity. Equation (a) is slightly in error as the shearing stress is not uniform over the cross-section, e.g. being parabolic for a rectangular section. However, the average shearing stress gives close results.

For a uniform load of w per unit length, the center deflection on a simply supported beam is: -

$$\delta_{center} = 2\int_0^{\frac{L}{2}} \frac{Vvdx}{AE_S} = 2\int_0^{\frac{L}{2}} \frac{\left(\frac{wL}{2} - wx\right)}{AE_S} \cdot \frac{1}{2} dx =$$

$$= \frac{wL^2}{8AE_S}$$

For bending deflection for a simply supported beam uniformly loaded the center deflection is

$$\frac{5\ wL^4}{384\ EI}$$

Hence

$$\frac{\frac{wL^2}{8AE_S}}{\frac{5wL^4}{384EI.}} = 24\left(\frac{r}{L}\right)^2, \text{ using } E_S = .4E,$$

r = radius of gyration.

For I beams and channels r is approximately $\frac{1}{2}$ d

and for rectangular sections $r = \frac{d}{\sqrt{12}}$. (d = depth)

In aircraft structures a ratio of $\frac{d}{L}$ is seldom greater than $\frac{1}{12}$.

Thus the shearing deflection in percent of the bending deflection equals 4.1% for a $\frac{d}{L}$ ratio of $\frac{1}{12}$ for I-beam sections and 1.4 percent for rectangular sections.

* Sometimes "G", instead. See p. A7.4

Example Problem 19

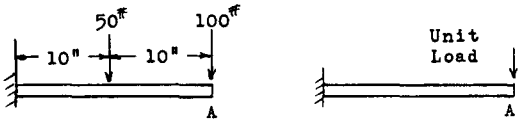

Fig. A7.22

Find the vertical deflection of free end A due to shear deformation for beam of Fig. A7.22 assuming shearing stress uniform over cross-section, and AE_S constant.

$$\delta_A = \int \frac{Vvdx}{AE_S}$$

V = 100# for x = 0 to 10

V = 150 for x = 10 to 20

v = 1 for x = 0 to 20

hence

$$\delta_A = \frac{1}{AE_S}\int_0^{10} 100 \cdot 1\, dx + \frac{1}{AE_S}\int_{10}^{20} 150 \cdot 1\, dx$$

$$= \frac{1}{AE_S}\left[100x\right]_0^{10} + \frac{1}{AE_S}\left[150x\right]_{10}^{20} = \frac{2500}{AE_S}$$

Method of Virtual Work Applied to Torsion of Cylindrical Bars.

The angle of twist of a circular shaft due to a torsional moment may be found by similar reasoning as used in previous articles for finding deflection due to bending or shear forces. The resulting expressions are: -

$$\delta = \int \frac{Ttdx}{E_S J} \quad \text{- - - - - - - - - - - - - - - (A)}$$

$$\theta = \int \frac{Ttdx}{E_S J} \quad \text{- - - - - - - - - - - - - - - (B)}$$

In equation (A), for translation deflections,

T = twisting moment at any section due to applied twisting forces.

t = torsional moment at any section due to a virtual unit 1 lb. force applied at the point where deflection is wanted and applied in the direction of the desired displacement. (in lbs/lb)

E_S = shearing modulus of elasticity for the material. (also "G")

J = polar moment of inertia of the circular cross-section.

In equation (B), for rotational deflections,

θ = angle in twist at any section due to the applied twisting moments in planes perpendicular to the shaft axis. Angle in radians.

t = torsional moment at any section due to a unit virtual couple acting at section where angle of twist is desired and acting in the plane of the desired deflection. (inch lbs/inch lb)

Example Problem

Example Problem 20

Fig. A7.23 shows a cantilever landing gear strut-axle unit ABC lying in XY plane. A load of 1000# is applied to axle at point A normal to XY plane. Find the deflection of point A normal to XY plane. Assume strut and axle are tubular and of constant section.

Solution:

The loading shown causes both bending and twisting of the strut axle unit. First find bending and torsional moments on axle and strut due to 1000# load.

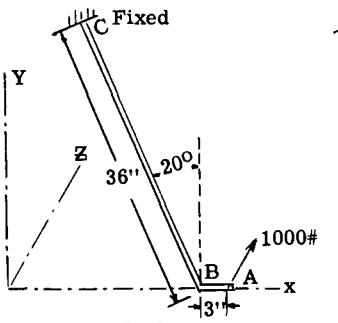

Fig. A7.23

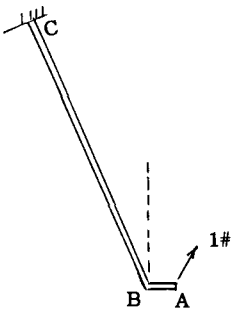

Fig. A7.24

$$\delta = \int \frac{Mmdx}{EI} + \frac{Ttdx}{E_S J}$$

Member AB M = 1000 x, (for x = 0 to 3)
T = 0

Member BC M_{BC} = 3000 sin 20° + 1000 x, (for x = 0 to 36)

T_{BC} = 3000 cos 20° constant between B and C.

Now apply a unit 1# force at A normal to xy plane as shown in Fig. A7.24 and find bending and torsional moments due to this 1# force.

Member AB

m = 1. x = x, (for x = 0 to 3)

t = 0

Member BC

m = 3 sin 20° + 1. x (for x = 0 to 36)

t = 3 cos 20° constant between B and C.

Subt.

$$\delta = \int \frac{Mmdx}{EI} + \int \frac{Ttdx}{E_S J}$$

$$= \frac{1}{EI}\int_0^3 1000\,x \cdot x\,dx + \frac{1}{EI}\int_0^{36} [(1000\,x + 1026)$$

$$(x + 1.026)]\,dx + \frac{1}{E_S J}\int_0^{36} (2820)\,(2.82)\,dx$$

$$= \frac{1}{EI}\left(\left[333\,x^3\right]_0^3 + \left[333\,x^3 + 1026\,x^2 + 1050\right.\right.$$

$$\left.\left. x\right]_0^{36}\right) + \frac{1}{E_S J}\left[7952\right]_0^{36} = \frac{1}{EI}\,(16{,}92500) +$$

$$\frac{1}{E_S J}\,(286200)$$

Note: A practical landing gear strut would involve a tapered or reinforced section involving a variable I and J and the integration would have to be done graphically or numerically.

Example Problem 21

For the thin-web aluminum beam of Fig. A7.25 determine the deflection at point G under the loading shown. Stringer section areas are given on the figure.

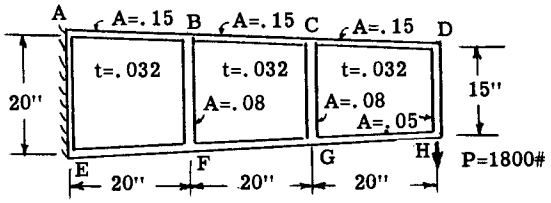

Fig. A7.25

Solution:

It was assumed that the webs did not buckle and carried shear only. Fig. A7.26 is an exploded view of the beam showing the internal real loads carried as determined by statics.*

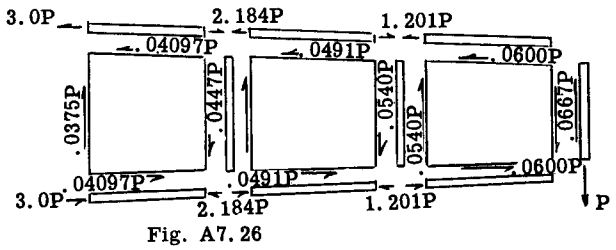

Fig. A7.26

* The equations of statics for tapered beam webs are derived in Art. A15.18, Ch. A-15.

The shear flows shown on the (nearly) horizontal edges of the web panels are average values. Fig. A7.27 is an exploded view of the beam showing the unit (virtual) loads.

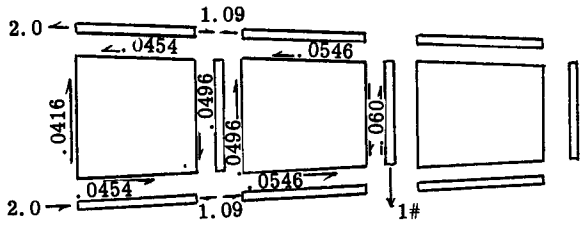

Virtual loading. Fig. A7.27

Since both axial loads and shear flows were considered, the form of deflection equation used was

$$\delta_G = \int \frac{Sudx}{AE} + \iint \frac{\bar{q}\,q\,dxdy}{Gt}$$

Integrations in the flanges were made assuming linear load variations. Such an integration carried out over a uniform flange of length L whose real load varies from S_i to S_j and whose virtual load varies from u_i to u_j yields

$$\int_0^L \frac{Sudx}{AE} = \frac{L}{AE}\left(\frac{S_i\,u_i}{3} + \frac{S_i\,u_j}{6} + \frac{S_j\,u_i}{6} + \frac{S_j\,u_j}{3}\right).$$

The integrations in the trapezoidal sheet panels were made using the shear flows on the (nearly) horizontal sides as average values, assumed constant over the panel. With this simplification $\iint \frac{q_{AV}\,\bar{q}_{AV}\,dxdy}{Gt} = q_{AV}\,\bar{q}_{AV}\,\frac{S}{Gt}$

where S is the panel area.

The calculation was completed in Table A7.6.

TABLE A7.6

(1) Flange Member	(2) S_i	(3) S_j	(4) u_i	(5) u_j	(6) $\frac{2u_i + u_j}{3}$	(7) $\frac{2u_j + u_i}{3}$	(8) $\frac{L}{AE} \times 10^{6*}$	(9) (2) x (6) + (3) x (7)	(10) (8) x (9) ÷ 2 $\int \frac{Sudx}{AE} \times 10^6$
AB	3.00 P	2.184 P	2.00	1.09	1.697	1.393	13.34	8.133 P	108.5 P
BC	2.184 P	1.201 P	1.09	0	.727	.363	13.34	2.024 P	27.0 P
CD	1.201 P	0	0	0	0	0	13.34	0	0
EF	-3.00 P	-2.184 P	-2.00	-1.09	-1.697	-1.393	13.34	8.133 P	108.5 P
FG	-2.184 P	-1.201 P	-1.09	0	- .727	- .363	13.34	2.024 P	27.0 P
GH	-1.201 P	0	0	0	0	0	-	0	0
DH	P	0	0	0	0	0	-	0	0
CG	0	0	1	0	.67	.33	-	0	0
BF	0	0	0	0	0	0	-	0	0
									Σ = 271.0 P/2

Web Member	$q_{(AVG)}$	$\bar{q}_{(AVG)}$	S	$\frac{1}{Gt} \times 10^6$	$q_{AV}\bar{q}_{AV}\frac{S}{Gt} \times 10^6$
A-B-E-F	.04097 P	.0454	383	8.14	5.80
B-C-F-G	.0491 P	.0546	350	8.14	7.64
C-D-G-H	.0600 P	0	-	-	0
					Σ = 13.44 P

E = 10,000,000
G = 3,800,000

NOTE:
The denominator of terms in cols. 6 & 7 should be 6 instead of 3. To correct this error, total sum of col. 10 is divided by 2.

$$\therefore \delta_G = \left(\frac{271.0}{2} + 13.4\right) P \times 10^{-6} =$$

$$.147\ (1800)\ 10^{-3}\ \text{in} = .265\ \text{in.}$$

A7.8 Deflections Due to Thermal Strains.

As noted in the "virtual work derivation" of the dummy-unit load deflection equations, the real internal strains of the structure may be due to any cause including thermal effects. Hence, provided the temperature distribution and thermal properties of a structure are known, the dummy-unit load method provides a ready means for computing thermal deflections.

Example Problem 22

Find the axial movement at the free end of a uniform bar due to heat application to the fixed end, resulting in the steady state temperature distribution shown in Fig. A7.28. Assume material properties are not functions of temperature.

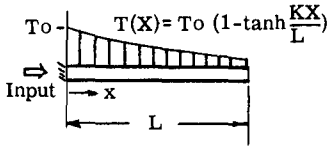

Fig. A7.28

T = temperature above ambient temperature

K = an empirical constant depending upon thermal properties and rate of heat addition.

Solution:

The thermal coefficient of expansion of the rod material was α. Hence a rod element of length dx experienced a thermal deformation $\Delta = \alpha \cdot T \cdot dx$. Application of a unit load at the bar end gave u = 1. Therefore

$$\delta = \int u \cdot \alpha \cdot T \cdot dx = \alpha T_o \int_o^L \left(1 - \tanh \frac{Kx}{L}\right) dx$$

$$= \alpha T_o L \left[1 - \frac{1}{K} (\ln \cosh K)\right]$$

Example Problem 23

The idealized two-flange cantilever beam of Fig. A7.29a undergoes rapid heating of the upper flange to a temperature T, uniform spanwise, above that of the lower flange. Determine the resulting displacement of the free end.

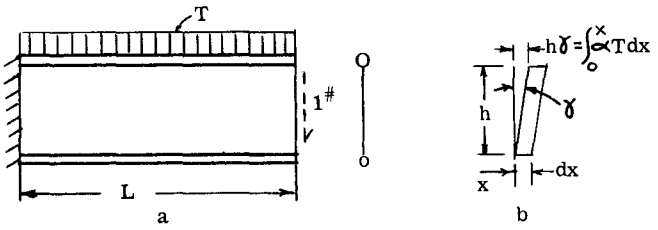

Fig. A7.29

Solution:

The axial deformation of a differential element of the upper flange (subscript U) was assumed given by $\Delta_U = \alpha T\, dx$ where α was the material thermal coefficient of expansion. The lower flange, having received no heating underwent no expansion.

Inasmuch as a thermal expansion is uniform in all directions no shear strain can occur on a material element. Hence no shear strain occurs in the web. The apparent anomaly here - that web elements appear to undergo shear deformations $\gamma = \frac{\alpha T x}{h}$ (Fig. A7.29b) - is explained as follows: The temperature varies linearly over the beam depth. The various horizontal beam "fibers" thus undergo axial deformations which vary linearly also in the manner of Fig. A7.29b giving the apparent shear deformation. No virtual work is done during this web deformation since no axial virtual stresses are carried in the web.

With the addition of a unit (virtual) load to the free end, the virtual loadings obtained in the flanges were:

$$u_U = \frac{L - x}{h} \quad (= -u_L)$$

Then the deflection equation was

$$\delta = \int u_U \Delta_U + \int u_L \Delta_L = \int_o^L \frac{L - x}{h} \cdot \alpha T\, dx + \int o$$

$$\delta = \frac{\alpha T L^2}{2h}$$

Example Problem 24

The first step in computing the thermal stresses in a closed ring (3 times indeterminate) involves cutting the ring to make it statically determinate and finding the relative movement of the two cut faces.

Fig. A7.30a shows a uniform circular ring whose inside surface is heated to a temperature T above the outside surface. The temperature is constant around the circumference and is assumed

to vary linearly over the depth of the cross section. Find the relative movement of the cut surfaces shown in Fig. A7.30b.

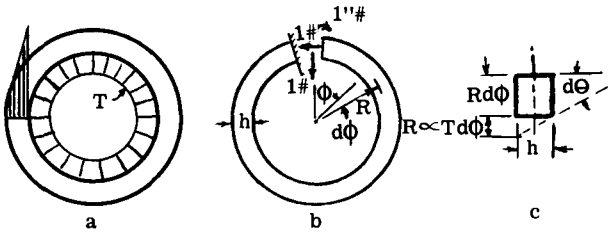

Fig. A7.30

Solution:

An element of the beam of length $Rd\phi$ is shown in Fig. A7.30c. Due to the linear temperature variation an angular change $d\theta = \frac{R\alpha T}{h} d\phi$ occurred in the element. The change in length of the midline (centroid) of the section was $\Delta = \frac{R\alpha T}{2} d\phi$. Unit redundant loads were applied at the cut surface as shown in Fig. A7.30b giving the following unit loadings around the ring.

From unit redundant couple (X)

$$m_x = 1 \quad \text{(m positive if it tends to open the ring).}$$

$$u_x \text{ (= axial load)} = o \text{ (positive of tensile)}$$

From unit redundant axial (horizontal) load (Y)

$$m_y = -R\,(1 - \cos\phi)$$

$$u_y = \cos\phi$$

From unit redundant shear (vertical) load (Z)

$$m_z = -R \sin\phi$$

$$u_z = -\sin\phi$$

The deflection equation by the dummy-unit load method is

$$\delta = \int u \cdot \Delta + \int m \cdot d\theta$$

Then

$$\delta_X = \int o \cdot \Delta + \int_o^{2\pi} 1 \cdot \frac{R\alpha T}{h} d\phi = 2\pi \frac{R\alpha T}{h}$$

$$\delta_Y = \int_o^{2\pi} \cos\phi \frac{R\alpha T}{2} d\phi + \int_o^{2\pi} (-) R(1-\cos\phi) \frac{R\alpha T}{h} d\phi$$

$$= -\frac{2\pi R^2 \alpha T}{h} \quad \text{(negative indicating movement to the right)}$$

$$\delta_Z = \int_o^{2\pi} (-\sin\phi) \frac{R\alpha T}{2} d\phi + \int_o^{2\pi} (-R \sin\phi) \frac{R\alpha T}{h} d\phi = o$$

Remarks:

In the three elementary examples given above no stresses were developed inasmuch as the idealizations yielded statically determinate structures which, with no loads applied, can have no stresses. Indeterminate structures are treated in Chapter A.8.

A7.9 Matrix Methods in Deflection Calculations.

Introduction. There is much to recommend the use of matrix methods[9] for the handling of the quantity of data arising in the solutions of stress and deflection calculations of complex structures: The data is presented in a form suitable for use in the routine calculatory procedures of high speed digital computers; a flexibility of operation is present which permits the solution of additional related problems by a simple expansion of the program; The notation itself suggests new and improved methods both of theoretical approach and work division.

The methods and notations employed here and later are essentially those presented by Wehle and Lansing[8] in adapting the Method of Dummy-Unit Loads to matrix notation. Other appropriate references are listed in the bibliography.

BASIS OF METHOD

Assume the structure to be analyzed has been idealized into a truss-like assembly of rods, bars, tubes and panels (sheets) upon which are acting the external loads applied as concentrated loads P_m or P_n, each with a different numerical

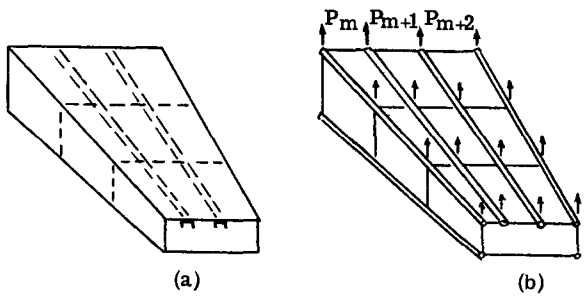

Fig. A7.31. Idealization into an assembly of bars and panels.

[9] For the reader not familiar with the elementary arithmetic rules of matrix operations employed here, a short appendix has been included in the present edition.

[8] L. B. Wehle Jr. and Warner Lansing, A Method for Reducing the Analysis of Complex Redundant Structures to a Routine Procedure, Journ. of Aero. Sciences, 19, October 1952.

subscript. Thus the system of Fig. A7.31a is idealized into that of Fig. A7.31b.

With the above idealization an improved scheme may be employed to systematize the computation of deflection calculations. The following steps summarize the procedure which is discussed in detail in succeeding sections.

I. A set of internal generalized forces, denoted by q_i or q_j (i, j are different numerical subscripts), is used to describe the internal stress distribution. The q's may represent axial loads, moments, shears, etc. In conjunction with a set of member flexibility coefficients, a_{ij}, the q's are employed to express the strain energy U. a_{ij} gives the displacement of point i per unit force at point j.*

II. Equilibrium conditions are used to relate the internal generalized forces q_i, q_j to the external applied loads, P_m or P_n. With this relationship the strain energy expression obtained in I, above is then transformed to give U as a function of the P's.

III. Castigliano's Theorem is used to compute deflections.

CHOICE OF GENERALIZED FORCES

Consider for example the problem of writing the strain energy (of flexure) of the stepped cantilever beam of Fig. A7.32a, assuming external loads are to be applied as transverse point loads at A and B. The set of internal generalized forces of Fig. A7.32b will completely determine the bending moment distribution in the beam elements and hence the strain energy. Set (b) then is a satisfactory choice of generalized forces.

It should be pointed out that set (b) is not a unique set. Other satisfactory choices (not an exhaustive display) are shown in Figs. A7.32c, d and e. The final selection may be made for convenience or personal taste.

Note that only as many generalized forces are used per element as are required to determine the significant loadings in that element.

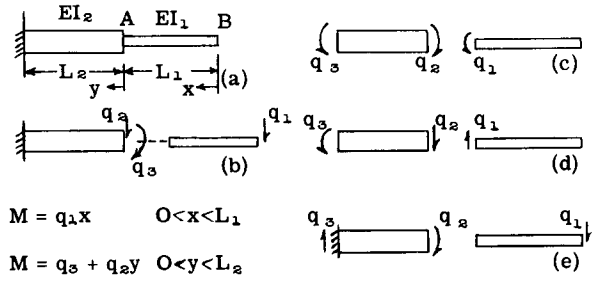

Fig. A7.32. Some possible choices of generalized forces.

*("Relative displacements in the individual member")

THE STRAIN ENERGY

It is next desired to write the strain energy as a function of the q's. Continuing the illustrative example, write

$$U = \frac{1}{2}\int_0^{L_1}\frac{M^2dx}{EI_1} + \frac{1}{2}\int_0^{L_2}\frac{M^2dy}{EI_2}$$

$$= \frac{1}{2}q_1^2\int_0^{L_1}\frac{x^2dx}{EI_1} + \frac{1}{2}q_2^2\int_0^{L_2}\frac{y^2dy}{EI_2}$$

$$+ 2 \times \frac{1}{2}q_2 q_3\int_0^{L_2}\frac{ydy}{EI_2} + \frac{1}{2}q_3^2\int_0^{L_2}\frac{dy}{EI_2}$$

Observe that each of the integral terms in the above expression is a property of the structural element (variation of EI) and of the nature of the associated generalized force (exponent on variable). Introducing the notation

$$a_{11} \equiv \int_0^{L_1}\frac{x^2dx}{EI_1} \qquad a_{22} \equiv \int_0^{L_2}\frac{y^2dy}{EI_2}$$

$$a_{23} = \int_0^{L_2}\frac{ydy}{EI_2} \qquad a_{33} = \int_0^{L_2}\frac{dy}{EI_2}$$

the strain energy becomes

$$U = \frac{1}{2}q_1^2 a_{11} + \frac{1}{2}q_2^2 a_{22} + 2 \times \frac{1}{2}q_2 q_3 a_{23}$$

$$+ \frac{1}{2}q_3^2 a_{33} \quad \text{- - - - - - - - - - - - - - - - - - (19)}$$

Equation (19) is an expression for U which could have been written immediately from physical considerations. Each coefficient a_{ij} is the displacement at point i per unit change in force at point j. This identity is easily seen by applying Castigliano's Theorem to eq. (19). With this interpretation the first term in eq. (19), representing the strain energy in the outer beam portion, is written by analogy to eq. (2) of Art. A7.3 $\left(U = \frac{1}{2}\frac{S^2L}{AE}\right)$. The remaining three terms, representing the energy stored in the inner beam segment by q_2 and q_3, are likewise readily written, with proper account taken for the cross influence of one force upon another (the "$a_{23}\ q_2\ q_3$" term).

Note that

$$a_{ij} = \frac{\partial^2 U}{\partial q_i \partial q_j} = \frac{\partial^2 U}{\partial q_j \partial q_i} = a_{ji} \quad \text{- - - - - - - - - (20)}$$

Hence

$$a_{ij} = a_{ji} \text{ (Maxwell's Reciprocal Theorem)}$$

The general form of strain energy expression is (expanding eq. (19) by induction)

$$2U = q_1q_1\,a_{11} + q_1q_2\,a_{12} + \cdots + q_1\,q_N\,a_{1N}$$
$$+ q_2q_1\,a_{21} + q_2q_2\,a_{22} + \cdots$$
$$+ q_3q_1\,a_{31} + q_3q_2\,a_{32} + \cdots$$
$$+ q_4q_1\,a_{41} + \cdots$$
$$\vdots$$
$$+ q_Nq_1\,a_{N1} + \cdots + q_N\,q_N\,a_{NN}$$

In matrix notation this equation is written (see appendix)

$$2U = \lfloor q_1q_2 \cdots q_N \rfloor \begin{bmatrix} a_{11} & a_{12} & \cdots & a_{1N} \\ a_{21} & a_{22} & \cdots & \\ \vdots & & & \\ a_{N1} & \cdots & & a_{NN} \end{bmatrix} \begin{Bmatrix} q_1 \\ q_2 \\ \vdots \\ q_N \end{Bmatrix} \quad (21)$$

or, more concisely,

$$2U = \lfloor q_i \rfloor \left[a_{ij}\right] \{q_j\} \ .$$

In the matrix $[a_{ij}]$ many (if not most) of the elements are zero. In the specific example, eq. (21) would be written

$$2U = \lfloor q_1q_2q_3 \rfloor \begin{bmatrix} a_{11} & 0 & 0 \\ 0 & a_{22} & a_{23} \\ 0 & a_{32} & a_{33} \end{bmatrix} \begin{Bmatrix} q_1 \\ q_2 \\ q_3 \end{Bmatrix}$$

The problem of computing and tabulating various a_{ij}'s is considered in detail later.

RELATING THE INTERNAL GENERALIZED FORCES TO THE EXTERNAL APPLIED LOADS

For the statically determinate structures considered in this chapter the internal forces are related to the external loads by use of the equations of static equilibrium. A set of linear equations results. Thus, in the specific example considered, if P_1 and P_2 are the external loads applied as in Fig. A7.32f, then by statics (refer to Fig. A7.32b)

$$q_1 = P_1$$
$$q_2 = P_1 + P_2$$
$$q_3 = P_1 L_1$$

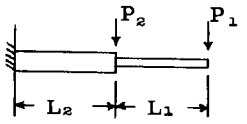

Fig. A7.32f

In matrix notation

$$\begin{Bmatrix} q_1 \\ q_2 \\ q_3 \end{Bmatrix} = \begin{bmatrix} 1 & 0 \\ 1 & 1 \\ L_1 & 0 \end{bmatrix} \begin{Bmatrix} P_1 \\ P_2 \end{Bmatrix}$$

Symbolically these relationships are written

$$\{q_i\} = \left[G_{im}\right] \{P_m\} \quad \cdots\cdots\cdots\cdots\cdots (22)$$

The matrix $[G_{im}]$ is called the "unit load distribution" inasmuch as any one column of $[G_{im}]$, say the mth column, gives the values of the generalized forces (the q's) for a unit value of load P_m, all other external loads zero.

THE STRAIN ENERGY IN TERMS OF APPLIED LOADS

If eq. (22) and its transpose are used to substitute for the q_i's in eq. (21) one gets

$$2U = \lfloor P_m \rfloor \left[G_{mi}\right] \left[a_{ij}\right] \left[G_{jn}\right] \{P_n\} \quad \cdots\cdots\cdots (23)$$

In the notation here i and j are used interchangeably as are m and n. Also $[G_{mi}]$ is the transpose of $[G_{im}]$, i.e. interchange of subscripts denotes transposition (see appendix).

If the matrix triple product in eq. (23) is formed and defined as

$$\left[A_{mn}\right] \equiv \left[G_{mi}\right] \left[a_{ij}\right] \left[G_{jn}\right] \quad \cdots\cdots\cdots (24)$$

then

$$2U = \left[P_m\right] \left[A_{mn}\right] \left\{P_n\right\} \quad \text{- - - - - - - - - -} \quad (25)$$

Eq. (25) expresses the strain energy as a function of the external applied loads.

In the specific example being used

$$\left[A_{mn}\right] \equiv \begin{bmatrix} 1 & 1 & L_1 \\ 0 & 1 & 0 \end{bmatrix} \begin{bmatrix} a_{11} & 0 & 0 \\ 0 & a_{22} & a_{23} \\ 0 & a_{32} & a_{33} \end{bmatrix} \begin{bmatrix} 1 & 0 \\ 1 & 1 \\ L_1 & 0 \end{bmatrix}$$

DEFLECTIONS BY CASTIGLIANO'S THEOREM

Application of Castigliano's theorem to eq. (25),

$$2U = \left[P_m\right] \left[A_{mn}\right] \left\{P_n\right\} \quad \text{- - - - - - - - - -} \quad (25)$$

yields

$$\left\{\frac{\partial U}{\partial P_m}\right\} = \left\{\delta_m\right\} = \left[A_{mn}\right] \left\{P_n\right\} \text{ - - - - - - -} \quad (26)$$

The steps in passing to eq. (26) may be demonstrated readily by writing out eq. (25) for, say, a set of three loads (m, n = 1,2,3), differentiating successively with respect to P_1, P_2 and P_3 and then re-collecting in matrix form.

The matrix $\left[A_{mn}\right]$ gives the deflection at the external points "m" for unit values of the loads P_n and is therefore, by definition, the matrix of influence coefficients.

COMPARISON WITH DUMMY-UNIT LOADS EQUATIONS

It is instructive to write eq. (26) out as

$$\left\{\delta_m\right\} = \left[G_{mi}\right] \left[a_{ij}\right] \left[G_{jn}\right] \left\{P_n\right\} \text{ - - - -} \quad (26a)$$

and compare the expression with a typical term from the dummy-unit load method equations, say $\delta = \Sigma\, u \frac{SL}{AE}$. In the matrix equation (26a) the $\left[G_{mi}\right]$ is the unit (virtual) matrix corresponding to the symbol "u" in the simple sum. The $\left[a_{ij}\right]$ are the member flexibilities corresponding to $\frac{L}{AE}$. The matrix product $\left[G_{jn}\right] \left\{P_n\right\}$ gives the member load distributions due to the real applied loads, hence these are the "S" loads. Finally the operation of matrix multiplication itself yields a summation to complete the calculation.

From this last discussion it is clear that eq. (26a) also may be derived by formulating the Dummy-Unit Load equations (Art. A7.7) in matrix notation.

To illustrate the application of the matrix methods presented thus far, a brief and elementary example is worked with those tools already developed.

Example Problem 25

Determine the influence coefficient matrix for transverse forces to be applied to the uniform cantilever of Fig. A7.33 at the three points indicated.

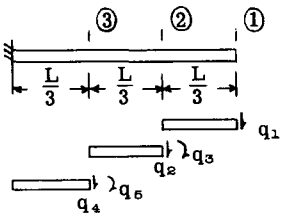

Fig. A7.33

Solution:

The choice and numbering of generalized forces are shown on the figure. These forces were placed so that previously derived expressions for the a's could be used. The following member flexibility coefficients were computed. Note that the only non-zero coefficients of mixed subscripts (i not equal to j) are those for loads common to an element.

$$a_{11} = \int_0^{L/3} \frac{x^2 dx}{EI} = \frac{L^3}{81EI} = a_{22} = a_{44}$$

This expression was adopted from that developed for a transverse shear force on a cantilever beam segment in the preceding illustrative example.

$$a_{33} = a_{55} = \int_0^{L/3} \frac{dy}{EI} = \frac{L}{3EI}$$

This expression is for a couple on the end of a cantilever segment (of length L/3).

$$a_{23} = a_{45} = \int_0^{L/3} \frac{y dy}{EI} = \frac{L^2}{18EI}$$

This expression is for the cross influence of a couple and a shear load on a cantilever segment. Collecting in matrix form,

$$\left[a_{ij}\right] = \frac{L^3}{3EI}\begin{bmatrix} \frac{1}{27} & 0 & 0 & 0 & 0 \\ 0 & \frac{1}{27} & \frac{1}{6L} & 0 & 0 \\ 0 & \frac{1}{6L} & \frac{1}{L^2} & 0 & 0 \\ 0 & 0 & 0 & \frac{1}{27} & \frac{1}{6L} \\ 0 & 0 & 0 & \frac{1}{6L} & \frac{1}{L^2} \end{bmatrix}$$

The unit load matrix $\left[G_{im}\right]$ was computed by successively applying unit loads at points 1, 2 and 3 and computing the values of the q's by statics.

$$\left[G_{im}\right] = \begin{bmatrix} 1 & 0 & 0 \\ 1 & 1 & 0 \\ L/3 & 0 & 0 \\ 1 & 1 & 1 \\ 2L/3 & L/3 & 0 \end{bmatrix}$$

Note that the first column of $\left[G_{im}\right]$ gives the values of the q's obtained for a unit load at point "1" with no other loads applied. The second column gives the q's for a unit load at point "2" only, and so forth.

Finally,

$$\left[A_{mn}\right] = \frac{L^3}{3EI}\begin{bmatrix} 1 & 1 & L/3 & 1 & 2L/3 \\ 0 & 1 & 0 & 1 & L/3 \\ 0 & 0 & 0 & 1 & 0 \end{bmatrix}\begin{bmatrix} \frac{1}{27} & 0 & 0 & 0 & 0 \\ 0 & \frac{1}{27} & \frac{1}{6L} & 0 & 0 \\ 0 & \frac{1}{6L} & \frac{1}{L^2} & 0 & 0 \\ 0 & 0 & 0 & \frac{1}{27} & \frac{1}{6L} \\ 0 & 0 & 0 & \frac{1}{6L} & \frac{1}{L^2} \end{bmatrix}\begin{bmatrix} 1 & 0 & 0 \\ 1 & 1 & 0 \\ L/3 & 0 & 0 \\ 1 & 1 & 1 \\ \frac{2L}{3} & L/3 & 0 \end{bmatrix}$$

Multiplying (see appendix),

$$\left[A_{mn}\right] = \frac{L^3}{162EI}\begin{bmatrix} 54 & 28 & 8 \\ 28 & 16 & 5 \\ 8 & 5 & 2 \end{bmatrix}$$

Should the deflections be desired at the three points one forms

$$\begin{Bmatrix} \delta_1 \\ \delta_2 \\ \delta_3 \end{Bmatrix} = \frac{L^3}{162EI}\begin{bmatrix} 54 & 28 & 8 \\ 28 & 16 & 5 \\ 8 & 5 & 2 \end{bmatrix}\begin{Bmatrix} P_1 \\ P_2 \\ P_3 \end{Bmatrix}$$

as per eq. (26).

The matrix $\left[A_{mn}\right]$ is seen to be symmetric about the main diagonal as it must be: from Maxwell's reciprocal theorem $A_{mn} = A_{nm}$ (see eq. (20)).

A7.10 Member Flexibility Coefficients: Compilation of a Library.

Several member flexibility coefficients are derived below for various members and loadings. A more comprehensive listing is available in the paper by Wehle and Lansing referenced earlier.

BARS

The energy in a uniform bar under varying axial force (Fig. A7.34) is

$$U = \frac{1}{2AE}\int_0^L \left[q_1 + \frac{q_j - q_i}{L}\,x\right]^2 dx$$



Fig. A7.34

Then referring to eq. (20),

$$a_{11} = \frac{\partial^2 U}{\partial q_1^2} = \frac{1}{AE}\int_0^L \left(1-\frac{x}{L}\right)^2 dx$$

$$= \frac{L}{3AE}\quad \left(= a_{jj}\right).$$

and,

$$a_{ij} = \frac{\partial^2 U}{\partial q_i \partial q_j} = \frac{1}{AE}\int_0^L \frac{x}{L}\left(1-\frac{x}{L}\right) dx$$

$$= \frac{L}{6AE}\quad \left(= a_{ji}\right)$$

An equally likely choice of generalized forces for the above case is shown in Fig. A7.34a. The strain energy is (x measured from free end)

$$U = \frac{1}{2AE}\int_0^L \left[q_1 + q_j\,x\right]^2 dx$$

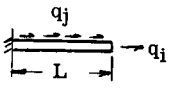

Fig. A7.34a

$$a_{11} = \frac{\partial^2 U}{\partial q_1^2} = \frac{1}{AE}\int_0^L dx = \frac{L}{AE}.$$

$$a_{jj} = \frac{\partial^2 U}{\partial q_j^2} = \frac{1}{AE}\int_0^L x^2 dx = \frac{L^3}{3AE}$$

$$a_{ij} = \frac{\partial^2 U}{\partial q_i \partial qj} = \frac{1}{AE}\int_0^L x\,dx = \frac{L^2}{2AE}$$

In the case of tapered members the coefficients are determined by evaluating integrals of the form

$$a_{ij} = \frac{1}{E}\int_0^L \frac{f(x)dx}{A(x)}$$

Such a quadrature can always be made in these problems. For the linearly tapered bar the results may be obtained as functions of the end area ratios. Thus, Wehle and Lansing give

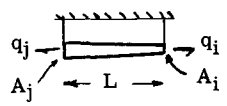

Fig. A7.34b

$$a_{ii} = \frac{L}{3A_iE}\cdot\phi_{ii}$$

$$a_{ij} = \frac{L}{6A_iE}\cdot\phi_{ij}$$

$$a_{jj} = \frac{L}{3A_jE}\cdot\phi_{jj}$$

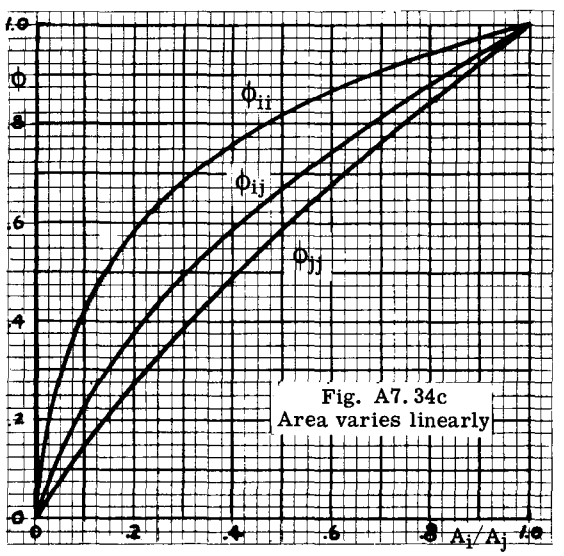

Fig. A7.34c
Area varies linearly

BEAMS

The energy in the uniform beam of Fig. A7.34d is given by

$$U = \frac{1}{2EI}\int_0^L \left[q_1 + \left(\frac{q_j - q_i}{L}\right)x\right]^2 dx$$



Fig. A7.34d

Then

$$a_{ii} = \frac{\partial^2 U}{\partial q_i^2} = \frac{L}{3EI} \quad (= a_{jj})$$

$$a_{ij} = \frac{\partial^2 U}{\partial q_i \partial q_j} = \frac{L}{6EI} \quad (= a_{ji})$$

An alternate choice of generalized forces for the beam of Fig. A7.34d is shown in Fig. A7.34e.

$$U = \frac{1}{2EI}\int_0^L \left[q_1 + q_j x\right]^2 dx$$

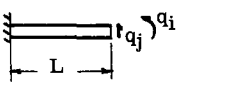

Fig. A7.34e

and from which

$$a_{ii} = \frac{L}{EI}$$

$$a_{ij} = a_{ji} = \frac{L^2}{2EI}$$

$$a_{jj} = \frac{L^3}{3EI}$$

NOTE: The coefficients for bars and beams are directly analogous (compare several cases) so that for tapered beams one uses the results for tapered bars with EI in place of AE.

SHEAR PANELS

For the rectangular shear panel with a uniform shear flow q_1 on all edges (Fig. A7.34f)

$$U = \frac{q_1^2}{2Gt}S$$

S = surface area

$$a_{ii} = \frac{S}{Gt}$$

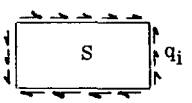

Fig. A7.34f

The trapezoidal shear panel (Fig. A7.34g) is treated approximately by using the average shear flow on the non-parallel sides as though it were constant throughout the sheet. Thus

$$U = \frac{q_1^2}{2Gt}S$$

S = surface area

$$a_{ii} = \frac{S}{Gt}$$

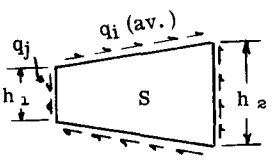

Fig. A7.34g

Since by statics $q_j = q_1\frac{h_2}{h_1}$, one could use q_j as an alternate choice of generalized force and $a_{jj} = \left(\frac{h_1}{h_2}\right)^2\frac{S}{Gt}$.

TORSION BAR

A uniform shaft under torque q_1 has strain energy

$$U = \frac{q_1^2 L}{2GJ}. \quad \text{Then } a_{11} = \frac{L}{GJ}.$$

A7.11 Application of Matrix Methods to Various Structures.

Example Problem 26

The tubular steel truss of Fig. A7.35 is to be analyzed for vertical deflections at points E and F under several load conditions in which vertical loads are to be applied to all joints excepting A and D. The cross sectional areas of tube members are given on the figure.

Set up the matrix form of expression for the

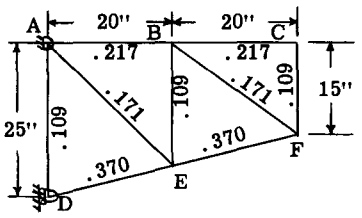

Fig. A7.35

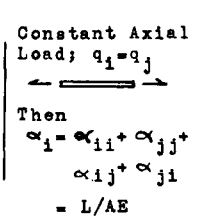

Fig. A7.35a

deflections at points E and F.

Solution:

The member flexibility coefficient for a uniform bar under constant axial load is L/AE. Fig. A7.36a gives the numbering scheme applied to the members and the q's (these being one and the same, since q is constant in a given member). Fig. A7.36b shows the numbering scheme adopted for the external loading points.

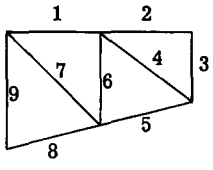

Fig. A7.36a

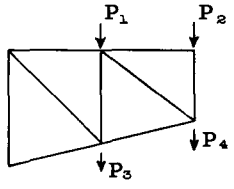

Fig. A7.36b

Member flexibility coefficients were collected in matrix form as

$$\left[\alpha_{ij}\right] = \frac{1}{E}$$

i \ j	1	2	3	4	5	6	7	8	9
1	92.2	0	0	0	0	0	0	0	0
2	0	92.2	0	0	0	0	0	0	0
3	0	0	138	0	0	0	0	0	0
4	0	0	0	146	0	0	0	0	0
5	0	0	0	0	55.7	0	0	0	0
6	0	0	0	0	0	183	0	0	0
7	0	0	0	0	0	0	165	0	0
8	0	0	0	0	0	0	0	55.7	0
9	0	0	0	0	0	0	0	0	229

In the case of a pin jointed truss, where only a single generalized force is required to describe the strain energy per member, the matrix of member flexibility coefficients is a diagonal matrix as above.

Unit load distributions were obtained by placing unit loads successively at external loading points 1, 2, 3 and 4 (Fig. A7.36b). The results were collected in matrix form as

$$\left[G_{im}\right] =$$

i \ m	1	2	3	4
1	0	1.0	0	1.0
2	0	0	0	0
3	0	-1.0	0	0
4	0	1.25	0	1.25
5	0	-1.03	0	-1.03
6	-1.0	- .75	0	- .75
7	1.13	.848	1.13	.848
8	-.825	-1.65	-.825	-1.65
9	.20	0.40	.20	0.40

Then the matrix triple product

$$\left[A_{mn}\right] = \left[G_{mi}\right]\left[a_{ij}\right]\left[G_{jn}\right]$$

was formed giving, per eq. (26),

$$\begin{Bmatrix}\delta_1\\ \delta_2\\ \delta_3\\ \delta_4\end{Bmatrix} = \frac{1}{E}\begin{bmatrix}440 & 389 & 257 & 389\\ 389 & 927 & 252 & 789\\ 257 & 252 & 257 & 252\\ 389 & 789 & 252 & 789\end{bmatrix}\begin{Bmatrix}P_1\\ P_2\\ P_3\\ P_4\end{Bmatrix}$$ inches

The results here give the deflections of all four points. Since only the deflections of points 3 and 4 were desired the first two rows of $\left[A_{mn}\right]$ may be dropped out. The same result could have been achieved by leaving out the first two rows of $\left[G_{mi}\right]$ (the transpose of $\left[G_{im}\right]$).

The matrix form of equation above is useful in organizing the computation of deflections for a number of different loading conditions. Thus, should there be several different sets of external loads P_n, corresponding to various loading conditions, each set is placed in column form giving the loads as the rectangular matrix $\left[P_{nk}\right]$, k different numerical subscripts for the load conditions. The matrix product

$$\left[\delta_{mk}\right] = \left[A_{mn}\right]\left[P_{nk}\right] \quad \text{- - - - - - - - - -} \quad (26b)$$

now gives the deflections at each point (m) for the various load conditions (k).

Example Problem 27

Deflections at points 1, 2, 3 and 4 of the truss of Fig. A7.35 are desired for the following loading conditions:

Condition No.	P_1	P_2	P_3	P_4 (see Fig. A7.36b)
1	2500	2000	800	450
2	-1200	-800	-2100	-1750
3	1800	1470	-1200	-1100

Solution:

The matrix product formed per eq. (26b) was set up as

$$\left[\delta_{mk}\right] = \frac{1}{E}\begin{bmatrix} 440 & 389 & 257 & 389 \\ 389 & 927 & 252 & 789 \\ 257 & 252 & 257 & 252 \\ 389 & 789 & 252 & 789 \end{bmatrix}\begin{bmatrix} 2500 & -1200 & 1800 \\ 2000 & -800 & 1470 \\ 800 & -2100 & -1200 \\ 450 & -1750 & -1100 \end{bmatrix}$$

Example Problem 28

For the landing gear unit of Example Problem 20, Fig. A7.23 find the matrix of influence coefficients relating deflections due to lift and drag loads acting at point A and torque about the axle A-B.

Solution:

The structure was divided into elements and the set of internal generalized forces applied as shown in Fig. A7.37a. (Torques and moments are shown vectorially by R.H. rules). Axial stresses were neglected in C-B.

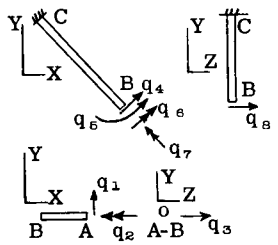

Fig. A7.37a

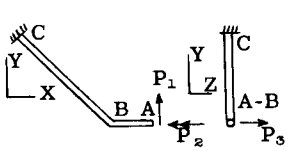

Fig. A7.37b

The following member flexibility coefficients were determined

$$a_{11} = a_{33} = \frac{L^3}{AB/3EI}, \quad a_{22} = \frac{L}{AB/GJ}$$

$$a_{44} = a_{88} = \frac{L^3}{BC/3EI}, \quad a_{77} = \frac{L}{BC/GJ}$$

$$a_{45} = a_{68} = \frac{L^2}{BC/2EI}, \quad a_{55} = a_{66} = \frac{L}{BC/EI}$$

Collected in matrix form $\left(\text{noting that } GJ = \frac{EI}{1.3}\right)$

$$\left[a_{ij}\right] = \frac{1}{EI}$$

	1	2	3	4	5	6	7	8
1	9.0	0	0	0	0	0	0	0
2	0	3.9	0	0	0	0	0	0
3	0	0	9.0	0	0	0	0	0
4	0	0	0	15,600	648	0	0	0
5	0	0	0	648	36.0	0	0	0
6	0	0	0	0	0	36.0	0	648
7	0	0	0	0	0	0	46.8	0
8	0	0	0	0	0	648	0	15,600

The unit load distributions $\left[G_{im}\right]$ were obtained by applying unit external applied loads, numbered and directed as in Fig. A7.37b.

$$\left[G_{im}\right] =$$

i \ m	1	2	3
1	1.0	0	0
2	0	1.0	0
3	0	0	1.0
4	.342	0	0
5	3	0	0
6	0	-.937	1.026
7	0	.342	2.811
8	0	0	1.0

At this point the engineer may consider the problem as solved, for the remaining computation is a routine operation:

$$\left[A_{mn}\right] = \left[G_{mi}\right]\left[a_{ij}\right]\left[G_{jm}\right]$$

Example Problem 29

The beam of example problem 21 is to be resolved by the matrix methods presented herein.

Influence coefficients for points F, G and H are to be found.

Solution:

Fig. A7.38 shows the choice and numbering of generalized forces.

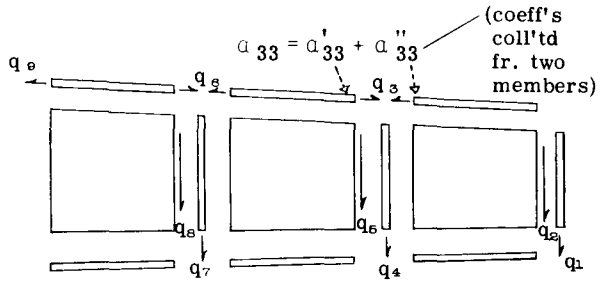

Fig. A7.38

No forces were shown applied to the lower flange elements as these were known to be equal to those of the upper flange due to symmetry. Entries were made for a_{ij} in matrix form as below. Entries for a_{33} and a_{66} were quadrupled as these occur in two identical members each on top and bottom. Entries for a_{36}, a_{69} and a_{99} were doubled. (See Art. A7.10 for coefficient formulae.)

$[a_{ij}] = 10^{-4}$ ×

i \ j	1	2	3	4	5	6	7	8	9
1	10								
2		2085							
3			17.8			4.45			
4				6.95					
5					2350				
6			4.45			17.8			4.45
7							7.64		
8								2600	
9						4.45			8.89

Unit load values were obtained as in Fig. A7.27, considered to be external loading number "two". Similar diagrams were drawn for unit loads at points "one" (H) and "three" (F). (cf. Fig. A 7-25)

$[G_{im}] =$

i \ m	1	2	3
1	1.0	0	0
2	.0667	0	0
3	1.201	0	0
4	0	1.0	0
5	.0540	.0600	0
6	2.184	1.09	0
7	0	0	1.0
8	.0447	.0496	.0545
9	3.00	2.00	1.00

The matrix triple product

$$[A_{mn}] = [G_{mi}] [a_{ij}] [G_{jn}]$$

completes the calculation.

Example Problem 30

Deflections of statically indeterminate structures often may be computed successfully by the methods of this chapter provided that some auxiliary means is employed to obtain an approximation to the true internal force distribution. The exact internal force distribution is not necessarily required in making deflection calculations inasmuch as such a calculation amounts to an integration over the structure - an operation which tends to average out any errors. Thus one may use the engineering theory of bending (E.T.B.), experimental data, previous experience, etc. to obtain reasonable estimates of the internal force distribution for unit loadings.

In the following problem the matrix of influence coefficients is determined for a single cell, three-bay box beam (3 times indeterminate) by using the E.T.B.

Fig. A7.39a shows an idealized doubly symmetric single cell cantilever box beam having three bays. Determine the matrix of influence coefficients for the six point net indicated.

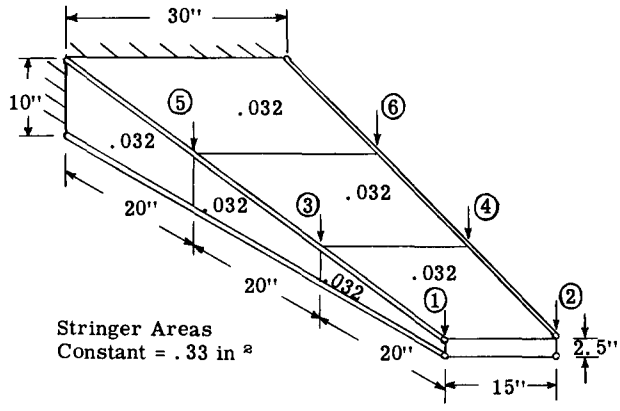

Fig. A7.39a

Solution:

Fig. A7.39b is an exploded view of the beam showing the placement and numbering of the internal generalized forces. Note that only the upper side of the beam was numbered, the lower side being identical by symmetry.

Member flexibility coefficients were computed by the formulas of Art. A7.10 and entered in matrix form as below. Note that all entries for which there were corresponding loads on the lower surface of the beam were doubled. By this means the total strain energy of the beam

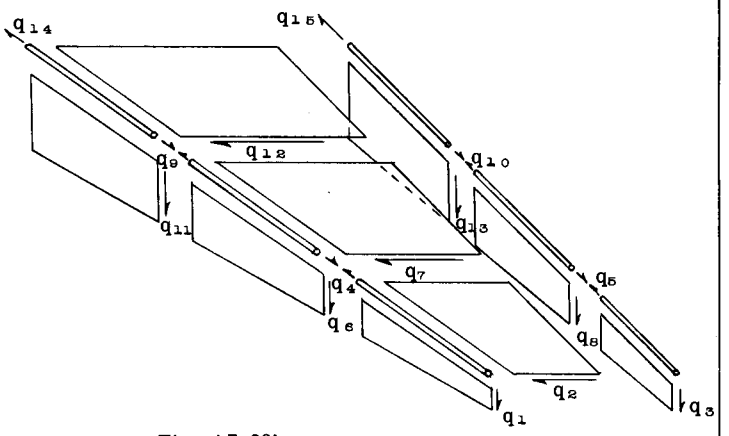

Fig. A7.39b

was accounted for. Note also that entries for a_{44}, a_{55}, a_{99} and $a_{10,10}$ were re-doubled as each of these q's act on two (identical) members.

$$[a_{ij}] = \frac{1}{E}$$

i \ j	1	2	3	4	5	6	7	8	9	10	11	12	13	14	15
1	1520														
2		32,000													
3			1520												
4				80.96					20.24						
5					80.96					20.24					
6						4510									
7							46,800								
8								4510							
9				20.24					80.96					20.24	
10					20.24					80.96					20.24
11											8000				
12												62,000			
13													8000		
14									20.24					40.48	
15										20.24					40.48

Note: VOID SPACES INDICATE ZEROS.

Unit load distributions were obtained for successive applications of unit loads to points one through six (Fig. A7.39a). The internal forces predicted by the E.T.B, for a load through the shear center (center of beam, due to symmetry) were superposed on the uniform shear flow $\left(q = \frac{T}{2A}\right)$ due to the torque developed in transferring the load to one side.

$$[G_{im}] =$$

i \ m	1	2	3	4	5	6
1	0.3	0.1				
2	0.1	-0.1				
3	0.1	0.3				
4	2	2				
5	2	2				
6	.0875	.0125	0.15	0.05		
7	.0375	-.0375	0.05	-0.05		
8	.0125	.0875	0.05	0.15		
9	2.67	2.67	1.33	1.33		
10	2.67	2.67	1.33	1.33		
11	.0423	.0023	.0713	.0179	0.100	.0333
12	.020	-.020	.0267	-.0267	.0333	-.0333
13	.0023	.0423	.0179	.0713	.0333	.100
14	3	3	2	2	1	1
15	3	3	2	2	1	1

The matrix triple product

$$[A_{mn}] = [G_{mi}] [a_{ij}] [G_{jn}]$$

completes the solution.

A7.12 Deflections and Angular Change of the Elastic Curve of Simple Beams by the "Method of Elastic Weights" (Mohr's Method).

In the calculation of structural deflections there occur many steps involving simple integral properties of elementary functions. The Method of Elastic Weights (and the Area Moment Method to follow in Art. A7.14) owes its popularity in large measure to the fact that it enables the analyst to write down many of these integral properties almost by inspection, relying as it does upon the analyst's familiarity with the properties of simple geometric figures.

For finding the deflection of a point on a simply supported beam relative to a line joining the supports, the Method of Elastic Weights states:

The deflection at point A on the elastic curve of a simple beam is equal to the bending moment at A due to the $\frac{M}{EI}$ diagram acting as a distributed beam load.

Spelled out in steps:

i - The $\frac{M}{EI}$ diagram is drawn just as it occurs due to the applied beam load

ii - This diagram is visualized as being the loading on a second beam (the conjugate beam) supported at the points of reference for the deflection desired

iii - The bending moment in this conjugate beam is found at the station where the deflection of the original beam was desired. This bending moment is equal to the desired deflection.

To prove the theorem, consider the dummy-unit load (virtual work) equation

$$1^{\#} \cdot \delta = m \cdot d\theta = m \cdot \frac{Mdx}{EI} .$$

This expression equates the external virtual work done by a unit load, applied at a point deflecting an amount δ, to the internal virtual work on a beam element experiencing an angular change $d\theta = \frac{Mdx}{EI}$. The sum (integral) of such expressions throughout a beam gives the total

deflection at the point (cf. eq. 18). We now show that the deflection expression, using the above equation, is the same as the bending moment expression for a simple beam loaded by an "elastic weight" $\frac{Mdx}{EI}$.

In Fig. A7-40, the loading of (a) produces the real moments of (b). Consider the deflections of points B and C due to the angular change $\frac{Mdx}{EI}$ in a beam element at A* (Fig. A7-40c).

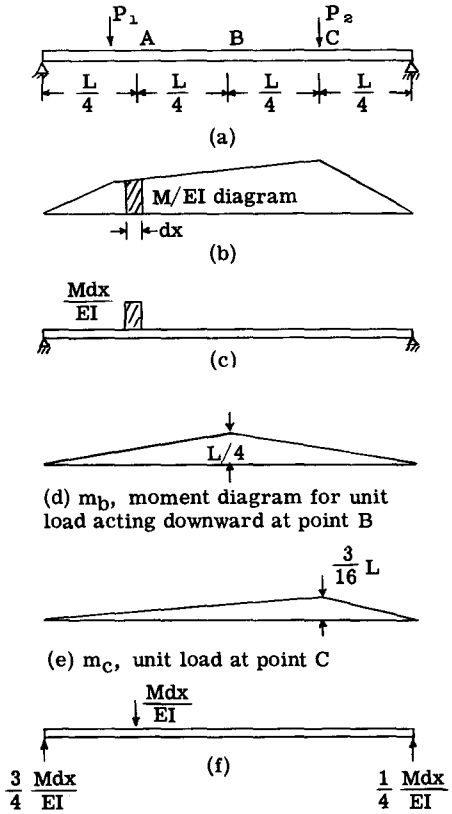

Fig. A7.40

For a unit load at point b, Fig. d shows the m diagram. The value of m at the midpoint of dx (point A) = L/8. Hence

$$\delta_b = \frac{Mdx}{EI} \cdot \frac{L}{8} = \frac{MLdx}{8EI}$$

For deflection of point c, draw m diagram for a unit load at C (see Fig. e). Value of m on element dx = $\frac{L}{16}$

Hence

$$\delta_c = \frac{Mdx}{EI} \cdot \frac{L}{16} = \frac{MLdx}{16EI}$$

* For simplicity the points A, B and C were placed at the one-quarter span points. The reader may satisfy himself with the general character of the proof by substituting x_A, x_B and x_C for the point locations and then following through the argument once again.

In Fig. f consider $\frac{Mdx}{EI}$ as a load on a simply supported beam and determine the bending moment at points b and c due to $\frac{Mdx}{EI}$ acting at point a.

$$M_b = \frac{Mdx}{4EI} \cdot \frac{L}{2} = \frac{MLdx}{8EI}$$

$$M_c = \frac{Mdx}{4EI} \cdot \frac{L}{4} = \frac{MLdx}{16EI}$$

These values of the beam bending moments at points b and c are identical to the deflections at b and c by the virtual work equations. The moment diagram m for a unit load at b and c (Figs. d and e) is numerically precisely the same as the influence line for moment at points b and c.

Therefore deflections of a simple beam can be determined by considering the $\frac{M}{EI}$ curve as an imaginary beam loading. The bending moment at any point due to this $\frac{M}{EI}$ loading equals the deflection of the beam under the given loads.

Likewise it is easily proved that the angular change at any section of a simply supported beam is equal to the shear at that section due to the $\frac{M}{EI}$ diagram acting as a beam load.

A7.13 Example Problems

Example Problem 31. Find the vertical deflection and slope of points a and b for beam and loading shown in Fig. A7.41. The lower Fig. shows the moment diagram for load P acting at center of a simple beam.

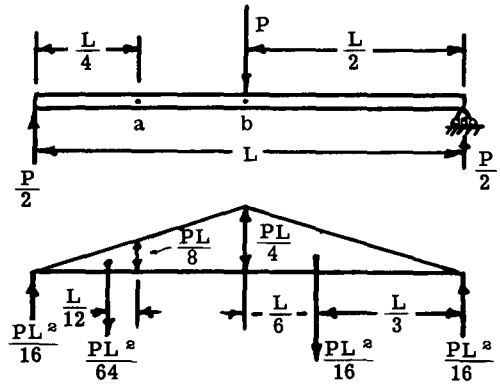

Fig. A7.41

Deflection at point a equals bending moment due to M diagram as a load divided by EI. (See lower Fig. of Fig. A7.41)

$$\delta_a = \left(\frac{PL^2}{16} \cdot \frac{L}{4} - \frac{PL^2}{64} \cdot \frac{L}{12}\right)\frac{1}{EI} = \frac{11}{768}\frac{PL^3}{EI}$$

$$\delta_b = \left(\frac{PL^2}{16} \cdot \frac{L}{2} - \frac{PL^2}{16} \cdot \frac{L}{6}\right)\frac{1}{EI} = \frac{1}{48}\frac{PL^3}{EI}$$

The angular change of any point equals the shear due to M/EI diagram as a load.

$$\alpha_a = \left(\frac{PL^2}{16} - \frac{PL^2}{64}\right)\frac{1}{EI} = \frac{3}{64}\frac{PL^2}{EI}$$

$$\alpha_b = \left(\frac{PL^2}{16} - \frac{PL^2}{16}\right)\frac{1}{EI} = 0$$ (Slope is horizontal or no change from original direction of beam axis.)

Example Problem 32. Determine the deflection of a simple beam loaded uniformly as shown in Fig. A7.42. The bending moment expression for a uniform load $M = \frac{wlx}{2} - \frac{wx^2}{2}$ or parabolic as shown in Fig. A7.42a. The deflection at midpoint equals the bending moment due to M diagram as a load.

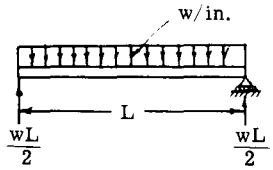

Fig. A7.42

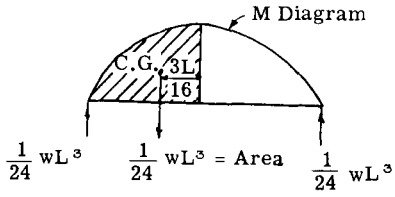

Fig. A7.42a

$$\delta_{center} = \left(\frac{1}{24}wL^3 \cdot \frac{L}{2} - \frac{1}{24}wL^3 \cdot \frac{3}{8}\frac{L}{2}\right)\frac{1}{EI} = \frac{5}{384}\frac{wL^4}{EI}$$

$$\alpha_{center} = \left(\frac{1}{24}wL^3 - \frac{1}{24}wL^3\right)\frac{1}{EI} = 0$$

Slope at supports = the reaction = $\frac{1}{24}\frac{wL^3}{EI}$.

Example Problem 33.

Fig. A7.43 shows the plan view of one-half of a cantilever wing. The aileron is supported on brackets at points D, E and F with self-aligning bearings. The brackets are attached to the wing rear beam at points A, B,and C. When the wing bends under the air load the aileron must likewise bend since it is connected to wing at three points. In the design of the aileron beam and similarly for cases of wing flaps this deflection produces critical bending moments. Assuming that the running load distributed to the rear beam as the wing bends as a unit is as shown in the Fig., find the deflection of point B with respect to straight line joining points A and C, which will be the deflection of E with respect to line joining D and F if bracket deflection is neglected. The moment of inertia of the rear beam between A and C varies as indicated in the Table A7.6

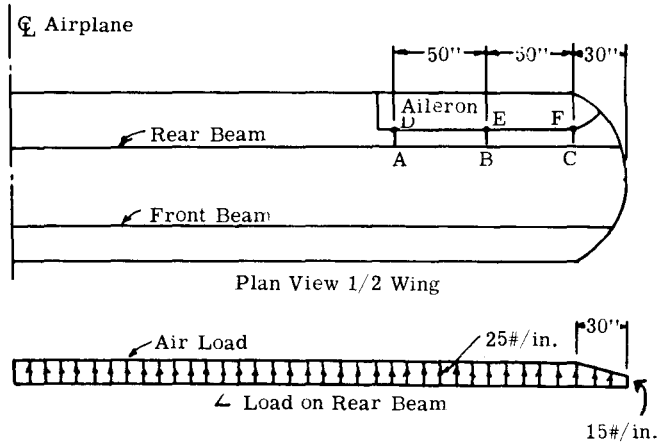

Fig. A7.43

Solution:- Due to the beam variable moment of inertia the beam length between A and C will be divided into 10 equal strips of 10 inches each. The bending moment M at the midpoint of each will be calculated. The elastic weight for each strip will equal $\frac{Mds}{I}$, where ds = 10" and I the moment of inertia at midpoint of the strip. These elastic loads are then considered as loads on an imaginary beam of length AC and simply supported at A and C. The bending moment on this imaginary beam at point B will equal the deflection of B with respect to line joining AC.

The bending moment at C = 15 x 30 x 15 + 10 x 15 x 10 = 8250"#

The shear load at C = $\frac{(15+25)}{2} \times 30 = 600\#$

Bending moment expression between points C and A equals, $M = 8250 + 600x + 12.5x^2$, where x = 0 to 100.

Table A7.6 gives the detailed calculations for the strip elastic loads. The I values assumed are typical values for a aluminum alloy beam carrying the given load. The modulus of elasticity E = 10 x 10^6 is constant and thus can be omitted until the final calculations. The figure below the table shows the elastic loads on the imaginary beam.

Table A7.6

Strip No.	ds in.	M = moment at mid-point	I at mid-point	Elastic load $\frac{Mds}{I}$
1	10	11563	5.5	21000
2	10	20063	6.5	30900
3	10	31063	7.5	41450
4	10	44580	8.5	52300
5	10	60580	9.5	63850
6	10	79050	12.0	65940
7	10	100050	16.0	62530
8	10	123550	20.0	61770
9	10	149550	24.0	62320
10	10	178150	28.0	63600

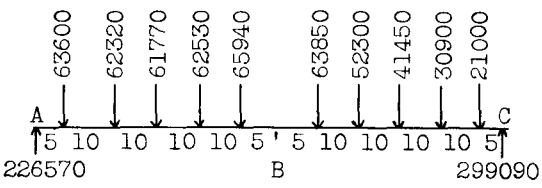

Bending moment at point B due to above elastic loading = 7,100,000 .˙. deflection at B relative to line AC = $\frac{7,100,000}{E=10,000,000}$ = .71 inch

Example Problem 34

Fig. A7.43a shows a section of a cantilever wing sea plane. The wing beams are attached to the hull at points A and B. Due to wing loads the wing will deflect vertically relative to attachment points AB. Thus installations such as piping, controls, etc., must be so located as not to interfere with the wing deflections between A and B. For illustrative purposes a simplified loading has been assumed as shown in the figure. EI has been assumed as constant whereas the practical case would involve variable I. For the given loading determine the deflection of point C with respect to the support points A and B. Also determine the vertical deflection of the tip points D and E.

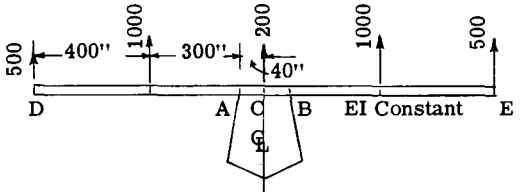

Fig. A7.43a

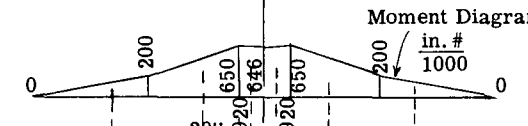

Fig. A7.43b

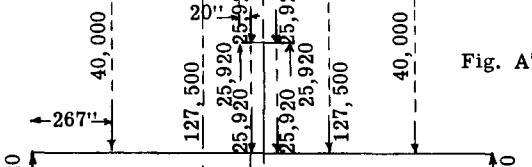

Fig. A7.43c



Fig. A7.43d

Solution:- Fig. A7.43b shows the bending moment diagram for the given wing loading. To find the deflection of C normal to line joining AB we treat the moment diagram as a load on a imaginary beam of length AB and simply supported at A and B (See Fig. A7.43c.) The deflection of C is equal numerically to the bending moment on this fictitious beam.

Hence $EI\delta_C = 25920 \times 40 - 25920 \times 20$

$$\text{or } \delta_C = \frac{518000}{EI}$$

To find the tip deflection, we place the elastic loads (area of moment diagram) on an imaginary beam simply supported at the tip D and E (See Fig. A7.43d). The bending moment on this imaginary beam at points A or B will equal numerically the deflection of these points with respect to the tip points D and E and since points A and B actually do not move this deflection will be the movement of the tip points with respect to the beam support points.

Bending moment at A = 193420 x 700 - 40000 x 433 - 127500 x 124 = 102200000. .˙. $\delta_{tip} = \frac{102,200,000}{EI}$.

A7.14 Deflections of Beams by Moment Area Method*

For certain types of beam problems the method of moment areas has advantages and this method is frequently used in routine analysis.

Angular Change Principle. Fig. A7.44 shows a cantilever beam. Let it be required to determine the angular change of the elastic line between the points A and B due to any given loading. From the equation of virtual work, we have

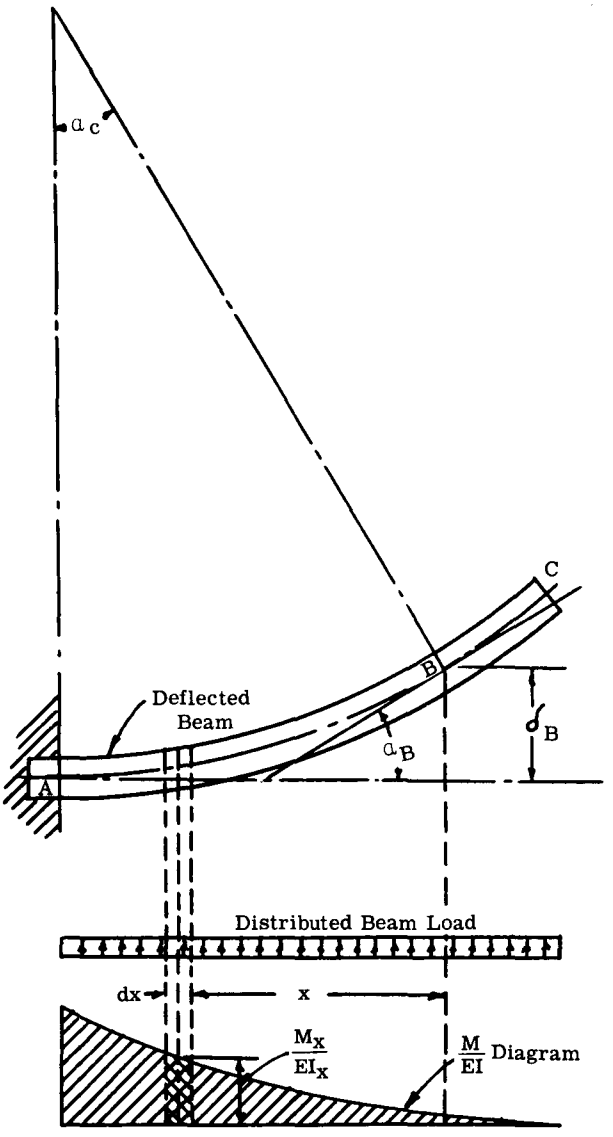

Fig. A7.44

$\alpha_b = \int_B^A \frac{Mdx}{EI} m$, where m is the moment at any section, distant x from B due to unit hypothetical couple applied at B. But m = unity at all points between B and A.

Therefore $\alpha_B = \int_B^A \frac{Mdx}{EI}$

(*Moment area first developed by Prof. C. E. Greene and published in 1874.)

Referring to Fig. A7.44, this expression represents the area of the $\frac{M}{EI}$ diagram between points B and A. Thus the first principle:- "The change in slope of the elastic line of a beam between any two points A and B is numerically equal to the area of the $\frac{M}{EI}$ diagram between these two points."

Deflection Principle

In Fig. A7.44 determine the deflection of point B normal to tangent of elastic curve at A. In Fig. A7.44 this deflection would be vertical since tangent to elastic line at A is horizontal.

From virtual work expression $\delta_B = \int_B^A \frac{Mdx}{EI} m$,

where m is the moment at any section A distance x from B due to a unit hypothetical vertical load acting at B. Hence m = 1.x = x for any point between B and A.

Hence

$$\delta_B = \int_B^A \frac{Mdx}{EI} \cdot x$$

This expression represents the 1st moment of the $\frac{M}{EI}$ diagram about a vertical thru B. Thus the deflection principle of the moment area method can be stated as follows:- "The deflection of a point A on the elastic line of a beam in bending normal to the tangent of the elastic line at a point B is equal numerically to the statical moment of the $\frac{M}{EI}$ area between points "A" and "B" about point A".

Illustrative Problems

Example Problem 35. Determine the slope and vertical deflection at the free end B of the cantilever beam shown in Fig. A7.45. EI is constant.

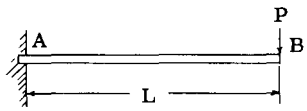

Fig. A7.45

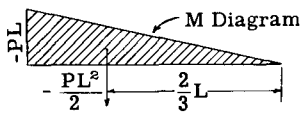

Solution:- The moment diagram for given load is triangular as shown in Fig. A7.45. Since the beam is fixed at A, the elastic line at A is horizontal or slope is zero. Therefore true slope at B equals angular change between A and B which equals area of moment diagram between A and B divided by EI.

Hence

$$\alpha_B = (-PL.\ L/2)\ \frac{1}{EI} = -\frac{PL^2}{2EI}$$

The vertical deflection at B is equal to the 1st moment of the moment diagram about point B divided by EI, since tangent to elastic curve at A is horizontal due to fixed support.

Hence

$$\delta_B = \left(-\frac{PL^2}{2} \cdot \frac{2}{3} L\right) \frac{1}{EI} = -\frac{PL^3}{3EI}$$

Example Problem 36

Fig. A7.46 illustrates the same simplified wing and loading as used in example problem 34. Find the deflection of point C normal to line joining the support points A and B. Also find the deflection of the tip points D and E relative to support points A and B.

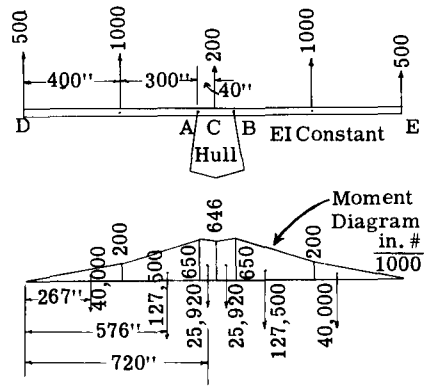

Fig. A7.46

Solution:-

Due to symmetry of loading, the tangent to the deflected elastic line at the center line of airplane is horizontal. Therefore, we will find the deflection of points A or B away from the horizontal tangent of the deflected beam at point C which is equivalent to vertical deflection of C with respect to line AB.

Thus to find vertical deflection of A with respect to horizontal tangent at C take moments of the $\frac{M}{EI}$ diagram as a load between points A and C about point A.

Whence

$$\frac{\delta_A}{1000}\ (\text{tangent at C}) = \frac{1}{EI}\left(\frac{650+646}{2}\right)40 \times 20 =$$

$$\frac{1}{EI}\ (518400) = \text{deflection of C normal to AB.}$$

To find the vertical deflection of the tip point D with respect to line AB, first find deflection of D with respect to horizontal tangent at C and subtract deflection of a with respect to tangent at C.

$$\frac{\delta_D}{1000}\ (\text{respect to tangent at C}) = \frac{1}{EI}\ (40000 \times 267 + 127500 \times 576 + 25920 \times 720) = \frac{1}{EI}\ (102700,000)$$

(See Fig. A7.46 for areas and arms of M/EI diagram). Subtracting the deflection of A with respect to C as found above we obtain

$$\frac{\delta_D}{1000}\ (\text{respect to line AB}) = \frac{1}{EI}\ (102,700,000 - 518400) = \frac{1}{EI}\ (102,180,000)$$

A7.15 Beam Fixed End Moments by Method of Area Moments

From the two principles of area moments as given in Art. A7.14, it is evident that the deflection and slope of the elastic curve depend on the amount of bending moment area and its location or its center of gravity.

Fig. A7.47 shows a beam fixed at the ends and carrying a single load P as shown. The bending moment shown in (c) can be considered as made up of two parts, namely that for a load P acting on a simply supported beam which gives the triangular diagram with value Pa (L-a)/L for the moment at the load point, and secondly a trapezoidal moment diagram of negative sign with values of M_A and M_B and of such magnitude as to make the slope of the beam elastic curve zero or horizontal at the support points A and B, since the beam is considered fixed at A and B.

The end moments M_A and M_B are statically indeterminate, however, with the use of the two moment area principles they are easily determined. In Fig. b the slope of elastic curve at A and B is zero or horizontal, thus the change in slope between A and B is zero. By the 1st

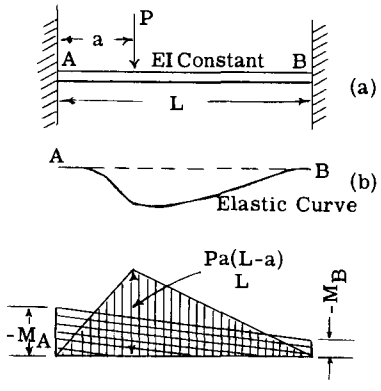

Fig. A7.47

principle of area moments, this means that the algebraic sum of the moment areas between A and B equal zero. Hence in Fig. c

$$\frac{(-M_A - M_b)}{2} L + \frac{(Pa\ (L-a)}{L} \cdot \frac{L}{2} = 0 \text{ - - - - - - - -(A)}$$

In Fig. b the deflection of B away from a tangent to elastic curve at A is zero, and also deflection of A away from tangent to elastic curve at B is zero.

Thus by moment area principle, the moment of the moment diagrams of Fig. C about points A, or B is zero.

Taking moments about point A:-

$$\Sigma M_A = \frac{Pa^2(L-a)}{2L} \cdot \frac{2a}{3} + \frac{Pa(L-a)^2}{2L} \times \left(a + \frac{L-a}{3}\right) + \frac{M_A L}{2} \times \frac{L}{3} +$$

$$\frac{M_B L}{2} \times \frac{2}{3} L = 0 \text{ - - - - - - - - - - - - - - - - -(B)}$$

Solving equations A and B for M_A and M_B

$$M_A = -\frac{Pab^2}{L^2} \text{ and } M_B = -Pba^2/L^2 \text{ where } b = (L-a)$$

To find the fixed end moments for a beam with variable moment of inertia use the M/I diagrams in place of the moment diagrams.

Example Problem 37

Fig. A7.48 shows a fix-ended beam carrying two concentrated loads. Find the fixed-end moments M_A and M_B.

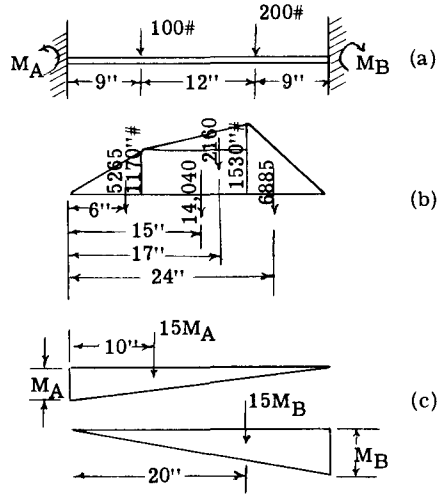

Fig. A7.48

Solution:- Fig. b shows the static moment diagram assuming the beam simply supported at A and B. For simplicity in finding areas and taking moments of the moment areas the moment diagram has been divided into the 4 simple shapes as shown. The centroid of each portion is shown together with the area which is shown as a concentrated load at the centroids.

Fig. C shows the moment diagrams due to unknown moments M_A and M_B. The area of these triangles is shown as a concentrated load at the centroids.

Since the change in slope of the elastic curve between A and B is zero, the area of these moment diagrams must equal zero, hence

$$5265 + 14040 + 2160 + 6885 + 15M_A + 15M_B = 0$$

or

$$15M_A + 15M_B + 28350 = 0 \text{ - - - - - - - - - - -(1)}$$

The deflection of point A away from tangent to elastic curve at B is zero, therefore the first moment of the moment diagrams about point A equals zero. Hence,

$5265 \times 6 + 15 \times 14040 + 17 \times 2160 + 24 \times 6885 + 150M_A + 300\ M_B = 0$ or $150\ M_A + 300\ M_B + 444600 = 0$- - - -(2)

Solving equations (1) and (2), we obtain

$M_A = -816$ in. lb.

$M_B = -1074$ in. lbs.

With the end moments known, the deflection or slope of any point on the elastic curve between A and B can be found by use of the 2 principles of area moments.

A7.16 Truss Deflection by Method of Elastic Weights

If the deflection of several or all the joints of a trussed structure are required, the method of elastic weights may save considerable time over the method of virtual work used in previous articles of this chapter. The method in general consists of finding the magnitude and location of the elastic weight for each member of a truss due to a strain from a given truss loading or condition and applying these elastic weights as concentrated loads on an imaginary beam. The bending moment on this imaginary beam due to this elastic loading equals numerically the deflection of the given truss structure.

Consider the truss of diagram (1) of Fig. A7.49. Diagram (2) shows the deflection curve for the truss for a ΔL shortening of member bc, all other members considered rigid. This deflection diagram can be determined by the virtual work ex pression $\delta = u\Delta L$. Thus for deflection of joint O, apply a uhit vertical load acting down at joint O. The stress m in bar bc due to this unit load $= \frac{2}{3} \cdot \frac{2P}{r} = \frac{4P}{3r}$. Therefore

$\delta_O = \Delta L_{bc} \cdot \frac{4P}{3r}$. The deflection at other lower chord joints could be found in a similar manner by placing a unit load at these joints. Diagram (2) shows the resulting deflection curve. This diagram is plainly the influence line for stress in bar bc multiplied by ΔL_{bc}.

Diagram (3) shows an imaginary beam loaded with an elastic load $\frac{\Delta L_{bc}}{r}$ acting along a vertical line thru joint O, the moment center for obtaining the stress in bar bc. The beam reactions for this elastic loading are also given. Diagram (4) shows the beam bending moment diagram due to the elastic load at point O. It is noticed that this moment diagram is identical to the deflection diagram for the truss as shown in diagram (2).

The elastic weight of a member is therefore equal to the member deformation divided by the arm r to its moment center. If this elastic load is applied to an imaginary beam corresponding to the truss lower chord, the bending moment on this imaginary beam will equal to the true truss deflection.

Diagram 5, 6 and 7 of Fig. A7.49 gives a similar study and the results for a ΔL lengthening of member CK. The stress moment center for this diagonal member lies at point O', which lies outside the truss. The elastic weight $\frac{\Delta L}{r_1}$ at point O' can be replaced by an equivalent system at points O and k on the imaginary beam as shown in Diagram (6). These elastic loads produce a bending moment diagram (Diagram 7) identical to the deflection diagram of diagram (5).

Table A7.7 gives a summary of the equations for the elastic weights of truss chord and web members together with their location and sign.

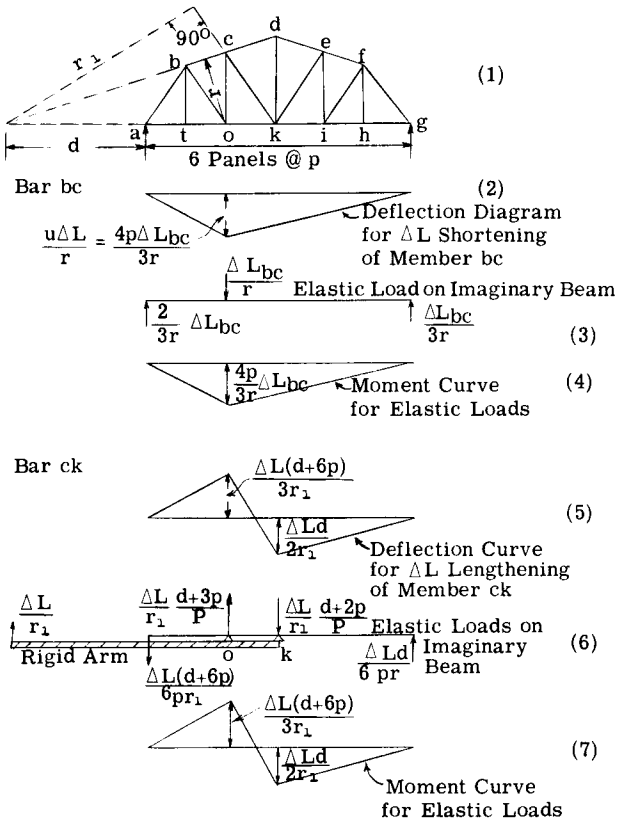

Fig. A7.49

Table A7.7 Equations for Elastic Weights
Elastic-Weight for Chord Members
(See Member ab)

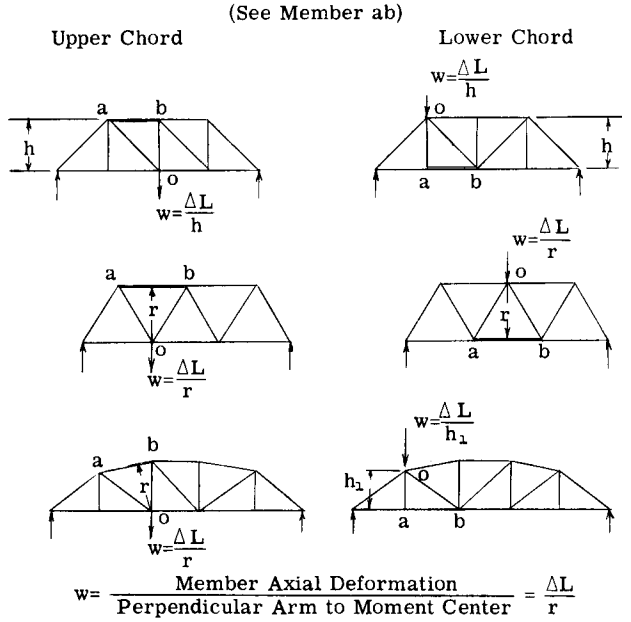

$$w = \frac{\text{Member Axial Deformation}}{\text{Perpendicular Arm to Moment Center}} = \frac{\Delta L}{r}$$

The moment center O of a chord member is the intersection of the other two members cut by the section used in determining the load in that member by the method of moments

The sign of the elastic weight w for a chord member is plus if it tends to produce downward deflection of its point of application. Thus for a simple truss compression in top chord or tension in botton chord produces downward or positive elastic weight

Table A7.7 (continued)

WEB DIAGONAL MEMBERS (See Member ab)

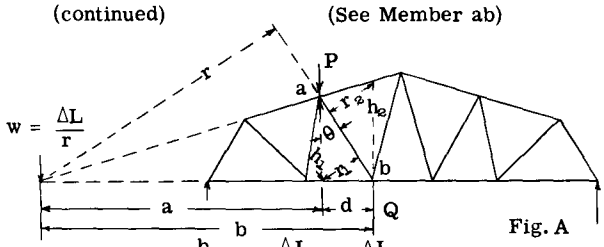

Fig. A

$P = \frac{b}{d}w = \frac{\Delta L}{h_1 \sin\theta} = \frac{\Delta L}{r_1}$

$Q = \frac{a}{d}w = \frac{\Delta L}{h_2 \sin\theta} = \frac{\Delta L}{r_2}$

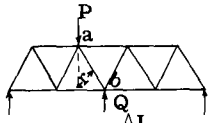

$P = Q = \frac{\Delta L}{r}$

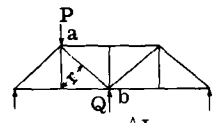

$P = Q = \frac{\Delta L}{r}$

For a truss diagonal member the elastic weights P & Q have opposite signs and are assumed to be directed toward each other or away according as the member is in compression or tension. In fig. a, P is greater than Q and P is located at the end of the diagonal nearest the moment center O. Downward elastic weights are plus.

TABLE A7.7 (CONTINUED)

Truss Verticals (See Member ab)

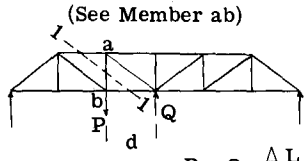

$P = Q = \frac{\Delta L}{d}$

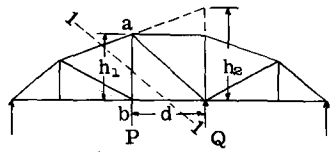

$P = \frac{h_1}{h_2}\frac{\Delta L}{d}$ $\quad Q = \frac{\Delta L}{d}$

The elastic weight P acts at foot of vertical and downward if vertical is in tension. Q acts opposite to P at far end of chord member cut by index section 1-1 used in finding stress in ab by method of sections.

A7.17 Solution of Example Problems.

The method of elastic weights as applied to truss deflection can be best explained by the solution of several simple typical trusses.

Example Problem 38

Fig. A7.50 shows a simply supported truss symmetrically loaded. Since the axial deformations in all the members must be found, the first step is to find the loads in all the members due to the given loading. The results of

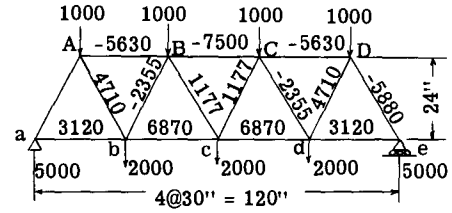

Fig. A7.50

this step are given in the figure, the stresses being written adjacent to each member. The next step or steps is to compute the member elastic weights, their location and their sense or direction. Tables A7.8 and A7.9 gives these calculations.

Table A7:8

Member	Length L	Chord Member Elastic Weights: Area A	Load P	$\frac{PL}{AE} = \frac{\Delta L}{E=29\times10^6}$	Arm r	Elastic wt. $w = \frac{\Delta L}{r}$	Point of application joint
AB	30	.2172	-5630	-.0268	24	.Q01117	b
BC	30	.2172	-7500	-.0357	24	.001487	c
CD	30	.2172	-5630	-.0268	24	.001117	d
ab	30	.1198	3120	.0269	24	.001117	A
bc	30	.1198	6870	.0592	24	.002465	B
cd	30	.1198	6870	..0592	24	.002465	C
de	30	.1198	3120	.0269	24	.001117	D

Table A7.9 Web Member Elastic Weights.

Member	Length L	Area A	Load P	$\Delta L = \frac{PL}{AE}$	r_1	$P = \frac{\Delta L}{r_1}$	Apply at	r_2	$Q = \frac{\Delta L}{r_2}$	Apply at
aA	28.25	.242	-5880	-.0236	12.75	-.00185	a	12.75	.00185	A
Ab	"	.146	4710	.0314	""	-.00246	A	"	.00246	b
bB	"	.146	-2355	-.0157	"	-.00123	b	"	.00123	B
Bc	"	.093	1177	.0123	"	-.000965	B	"	.000965	c
cC	"	.093	1177	.0123	"	-.000965	C	"	.000965	c
Cd	"	.146	-2355	-.0157	"	-.00123	d	"	.00123	C
Dd	"	.146	4710	.0314	"	-.00246	D	"	.00246	d
De	"	.242	-5580	-.0236	"	-.00185	e	"	.00185	D

Fig. A7.51 shows the elastic weights obtained from Tables 8 and 9 applied to an imaginary beam whose span equals that of the given truss. These elastic weights are the algebraic sum of the elastic weights acting at each truss joint.

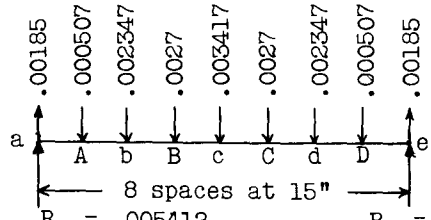

Fig. A7.51

The deflection at any joint equals the bending moment on the imaginary beam of Fig. A7.51.

Defl. at A = (.005412 + .00185)15 = .007262 x 15 = .109"

Defl. at b = .109 + (.007262 - .000507)15 = .109 + .006755 x 15 = .209"

Defl. at B = .209 + (.006755 - .002347)15 = .209 + .004408 x 15 = .275"

Defl. at c = .275 + (.004408 - .0027)15 = .301"
The slope of the elastic curve at the truss joint points equals the vertical shear at these points for the beam of Fig. A7.51.

Example Problem 39

Find the vertical deflection of the joints of the Pratt truss as shown in Fig. A7.52. The member deformations ΔL for each member due to the given loading are written adjacent to each member. Table A7.10 gives the calculation of member elastic weights. Fig. A7.53 shows the imaginary beam loaded with the elastic weights from Table A7.10. The deflections are equal numerically to the bending moments on this beam.

δ_b = .01855 x 25 = .465"
δ_B = .465 + .053 (ΔL in Bar Bb) = .518"
δ_c = .01855 x 50 - .00387 x 25 - .833"
δ_c = .833 + .031 (ΔL of Cc) = .864
δ_D = .01855 x 75 - .00387 x 50 - .00623 x 25 = 1.03"

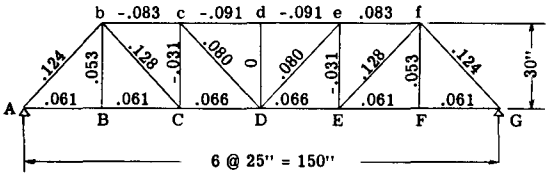

Fig. A7.52

Table A7.10

Elastic Weight Chord Members				
Member	Δ L	r	$w = \frac{\Delta L}{r}$	Joint
AB	.061	30	.00203	b
BC	.061	30	.00203	b
CD	.066	30	.0022	c
bc	-.083	30	.00277	C
Cd	-.091	30	.00304	D

Elastic Weight of Web Members							
		P			Q		
Member	Δ L	r_1	$P = \frac{\Delta L}{r_1}$	Joint	r_2	$Q = \frac{\Delta L}{r_2}$	Joint
Ab	.124	19.2	-.00648	A	19.2	.00648	b
Bb	.053	∞			∞		
bC	.128	19.2	-.00667	b	19.2	.00667	C
cC	-.031	25	-.00124	C	25	.00124	D
CD	.080	19.2	-.00417	c	19.2	.00417	D
Dd	0						

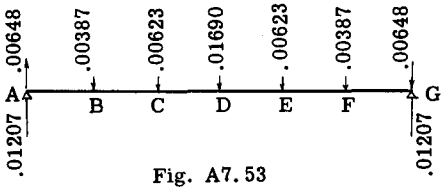

Fig. A7.53

Example Problem 40

Find the vertical joint deflections for the unsymmetrically loaded truss of Fig. A7.54. The ΔL deformations for all members are given on the Figure. Table A7.11 gives the calculation of the elastic weights, their signs and points of application. Fig. A7.55 shows the imaginary beam loaded with the elastic weights from Table A7.11. Table A7.12 gives the calculation for the joint deflections.

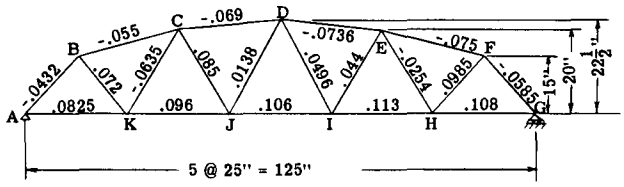

Fig. A7.54

Table A7.11

Elastic Weight of Chord Members				
Member	Δ L	r	$w = -\frac{\Delta L}{r}$	Joint
AK	.0825	15.0	.00550	B
BC	-.055	17.17	.00320	K
KJ	.096	20.0	.00480	C
CD	-.069	21.14	.00322	J
JI	.106	22.50	.00471	D
DE	-.0736	21.14	.00348	I
IH	.113	20.0	.00565	E
EE	-.075	17.17	.00437	H
HG	.108	15.00	.00720	F

Elastic Weight of Web Members

Member	Δ L	r_1	$P = -\frac{\Delta L}{r_1}$	Joint	r_2	$Q = \frac{\Delta L}{r_2}$	Joint
AB	-.0432	9.60	-.00450	A	9.60	.00450	B
BK	.072	9.60	-.00748	B	11.20	.00643	K
KC	-.0635	9.27	-.00685	K	10.60	.00600	C
CJ	.085	10.60	-.00802	C	11.26	.00755	J
JD	.0138	10.33	.00134	J	10.93	-.00126	D
ID	.0496	10.33	.00480	I	10.93	-.00454	D
EI	.044	10.60	-.00415	E	11.26	.00891	I
HE	-.0254	9.27	-.00274	H	10.60	.00240	E
FH	.0985	9.60	-.01028	F	11.20	.00878	H
GF	-.0585	9.60	-.00610	G	9.60	.00610	F

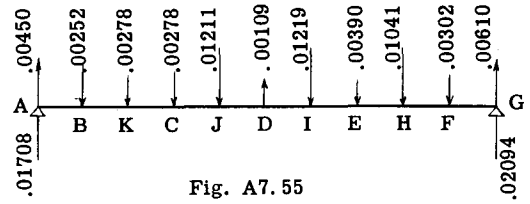

Fig. A7.55

Table A7.12

Panel	Panel Shear	Σ Shear	Moment = 12.5 x Shear = deflection	Point
		0	0	A
AB	.02158	.02158	.27	B
BK	.01906	.04064	.508	K
KC	.01628	.05692	.710	C
CJ	.01350	.07042	.881	J
JD	.00139	.07181	.900	D
DI	.00248	.07429	.930	I
IB	-.00971	.06458	.810	E
EH	-.01361	.05097	.638	H
HF	-.02402	.02695	.336	F
FG	-.02704	.00009*	0	G

*error

Example Problem 41

Fig. A7.56 shows a simply supported truss with cantilever overhang on each end. This simplified truss is representative of a cantilever wing beam the fuselage attachment points being

at e and e". The ΔL deformation in each truss member due to the given external loading is given on the figure. The complete truss elastic loading will be determined. With the elastic loading known the truss deflections from various reference lines are readily determined.

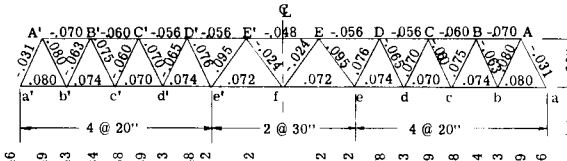

Fig. A7.56

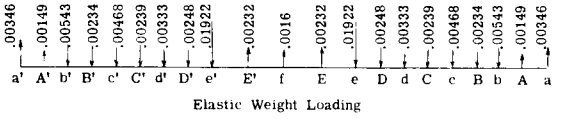

Fig. A7.57

Table A7.13

Elastic Weights of Chord Members

Member	ΔL	r	$w = \frac{\Delta L}{r}$	Apply at Joint
ab	.080	20	.0040	A
AB	-.070	20	.0035	b
bc	.074	20	.0037	B
BC	-.060	k0	.0030	c
cd	.070	20	.0035	C
CD	-.056	20	.0028	d
de	.074	20	.0037	D
DE	-.056	20	.0028	e
ef	.072	20	.0036	E
EE	-.048	20	.0024	f

Elastic Weights of Web Members

Member	ΔL	r_1	$P = \frac{\Delta L}{r_1}$	apply at joint	r_2	$Q = \frac{\Delta L}{r_2}$	apply at joint
aA	-.031	8.95	-.00346	a	8.95	.00346	A
Ab	.080	8.95	-.00895	A	8.95	.00895	b
bB	-.063	8.95	-.00702	b	8.95	.00702	B
Bc	.075	8.95	-.00838	B	8.95	.00838	c
cC	-.060	8.95	-.00670	c	8.95	.00670	C
Cd	.070	8.95	-.00781	C	8.95	.00781	d
dD	-.065	8.95	-.00728	d	8.95	.00728	D
De	.076	8.95	-.00850	D	8.95	.00850	e
eE	.095	12.0	.00792	e	12.0	-.00792	E
Ef	.024	12.0	.0020	E	12.0	-.0020	f

Table A7.13 gives the calculations for the magnitude of the member elastic weights. The signs and also the joint locations for locating the elastic loads are also given. Combining algebraically the elastic weights for each joint from Table A7.13 the beam elastic loading as shown in Fig. A7.57 is obtained.

Let it first be required to determine the vertical deflection of Joint f relative to the truss support points at e and e'.

To determine the deflections of the truss between the supports e a d e' it is only necessary to consider the elastic weight loading between these points. Fig. A7.58 shows the portion of the imaginary beam of Fig. A7.57 between these points. The deflection at f relative to line ee' is equal to the bending moment at f for the portion of the imaginary beam between joints e and e' and simply supported at these points.

Hence deflection at f = - .00312 x 30 + .00232 x 15 = .0586" (upward since minus is up).

Find the vertical deflection of the cantilever over-hang portion of the truss relative to support points e and e'.

Since the cantilever portion is not fixed at e since the restraint is determined by the truss between e' and e, this fact must be taken into account in loading the cantilever portion. The reactions on the beam of Fig. A7.58 represent the slope at e due to the elastic loading between e and e'. This elastic reaction in acting in the reverse direction is therefore applied as a load to the imaginary beam between e and a as shown in Fig. A7.59.

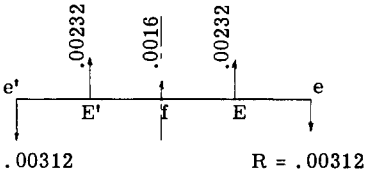

Fig. A7.58

In finding deflections this overhang elastically loaded portion is considered as fixed at a and free at e. The bending moment at any point on this beam equals the magnitude of the vertical deflection at that point.

Thus to find the deflection of the truss end (Joint a) we find the bending moment at point a of the imaginary beam of Fig. A7.59.

Hence

deflection at a = ΣM_a (calling counterclockwise positive). = (.01922 - .00312) 80 + .00248 x 70 + .00333 x 60 + .00239 x 50 + .00468 x 40 + .00234 x 30 + .00543 x 20 - .00149 x 10 = 2.13" upward. Due to symmetry of truss and loading of the truss we know the slope of the elastic curve at the center line of the truss is horizontal or zero. Thus to find the deflection of any point with reference to Joint f we can make use of the deflection principle of the moment area method. Thus in Fig. A7.60 the vertical deflection of any point for example joint a, relative to Joint f equals the moment of all elastic loads between a and f about a.

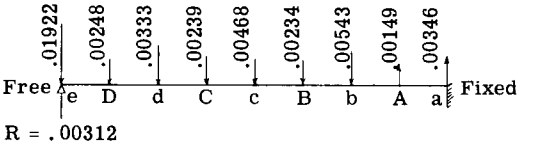

Fig. A7.59

ΣM_a = 2.077" (student should make calculations). Previously the deflection of f with respect to e was found to be -.0586". Thus deflection of a with respect to point e = 2.077 + .0586 = 2.135" which checks value found above. Let it be required to find the deflection of joint c relative to a line connecting joints b and d.

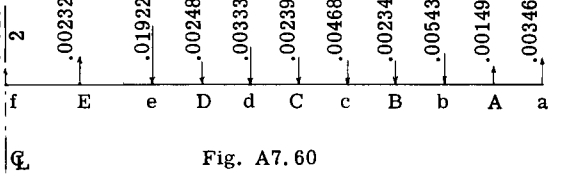

Fig. A7.60

For this problem we need only to consider the elastic loads between points b and d as loads on a simple beam supported at b and d (See Fig. A7.61) The deflection at C with respect to a line bd of the deflected truss equals the bending moment at point c for the loaded beam of Fig. A7.61.
hence

δ_C = .004743 x 20 - .00239 x 10 = .07 inches

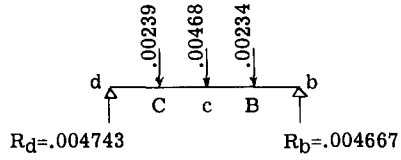

Fig. A7.61

A7.18 Problems

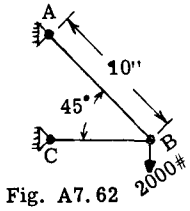

Fig. A7.62

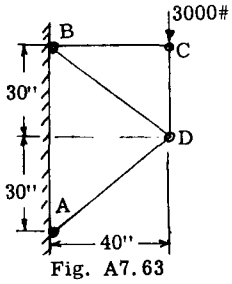

Fig. A7.63

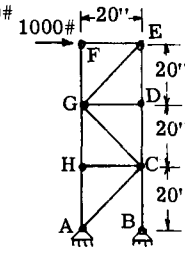

Fig. A7.64

(1) Find vertical and horizontal deflection of joint B for the structure in Fig. A7.62. Area of AB = 0.2 sq. in. and BC = 0.3. E = 10,000,000 psi.

(2) For the truss in Fig. A7.63, calculate the vertical deflection of joint C. Use AE for each member equal to 2 x 10^7.

(3) For the truss of Fig. A7.64 determine the horizontal deflection of joint E. Area of each truss member = 1 sq. in., E = 10,000,000 psi.

(4) Determine the vertical deflection of joint E of the truss in Fig. A7.64

(5) Determine the deflection of joint D normal to a line joining joint CE of the truss in Fig. A7.64.

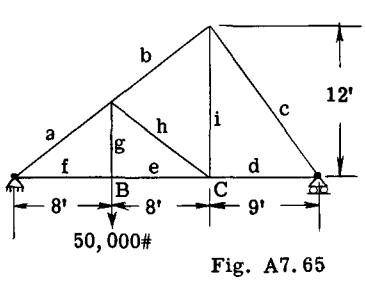

Fig. A7.65

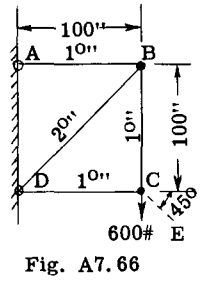

Fig. A7.66

(6) Calculate the vertical displacement of joint C for the truss in Fig. A7.65 due to the load at joint B. Members a, b, c and h have areas of 20 sq. in. each. Members d, e, f, g and i have areas of 2 sq. in. each. E = 30,000,000 psi.

(7) For the truss in Fig. A7.66 calculate the deflection of joint C along the direction CE. E = 30,000,000 psi.

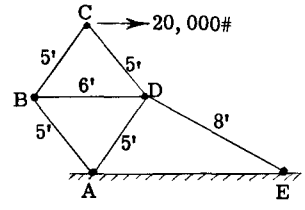

Fig. A7.67

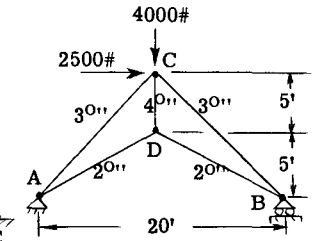

Fig. A7.68

(8) For the truss in Fig. A7.67, find the vertical and horizontal displacement of joints C and D. Take area of all members carrying tension as 2 sq. in. each and those carrying compression as 5 sq. in. each. E = 30,000,000 psi.

(9) For the truss in Fig. A7.68, determine the horizontal displacement of points C and B. E = 28,000,000 psi.

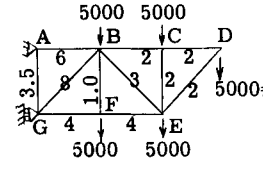

Fig. A7.69

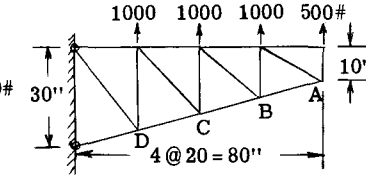

Fig. A7.70

(10) For the truss in Fig. A7.69, find the vertical deflection of joint D. Depth of truss = 180". Width of each panel is 180". The area of each truss member is indicated by the number on each bar in the figure. E = 30,000,000 psi. Also calculate the angular rotation of bar DE.

(11) For the truss in Fig. A7.70, calculate the vertical and horizontal displacement of joints A and B. Assume the cross-sectional area for members in tension as 1 sq. in. each and those in compression as 2 sq. in. E = 10,300,000 psi.

(12) For the truss in Fig. A7.70 calculate the angular rotation of member AB under the given truss loading.

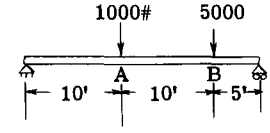

Fig. A7.71

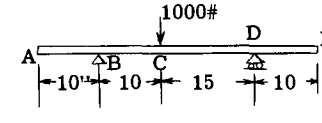

Fig. A7.72

(13) For the beam in Fig. A7.71 determine the deflection at points A and B using method of elastic weights. Also determine the slopes of the elastic curve at these points. Take E = 1,000,000 psi and I = 1296 $in.^4$

(14) For the beam in Fig. A7.72 find the deflection at points A and E. Also the slope of the elastic curve at point C. Assume EI equals to 5,000,000 lb in. sq.

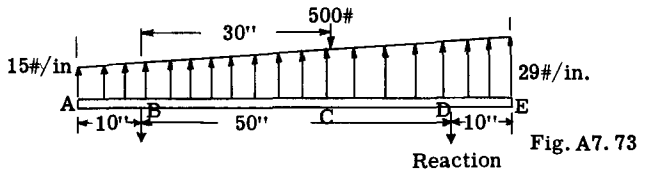

Fig. A7.73

(15) Fig. A7.73 illustrates the airloads on a flap beams ABCDE. The flap beams is supported at B and D and a horn load of 500# is applied at C. The beam is made from a 1"-.049 aluminum alloy round tube. I = .01659 in^4; E = 10,300,000 psi. Compute the deflection at points C and E and the slope of the elastic curve at point B.

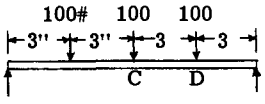

Fig. A7.74

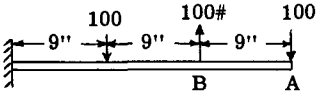

Fig. A7.75

(16) For the beam of Fig. A7.74 determine the deflections at points C and D in terms of EI which is constant. Also determine slopes of the elastic curve at these same points.

(17) For the cantilever beam of Fig. A7.75 determine the deflections and slopes of the elastic curve at points A and B. Take EI as constant. Express results in terms of EI.

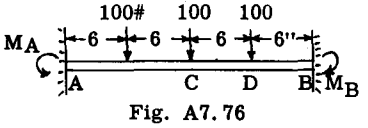

Fig. A7.76

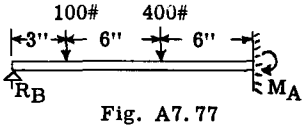

Fig. A7.77

(18) For the loaded beam in Fig. A7.76 determine the value of the fixed end moments M_A and M_B. EI is constant. Also find the deflection at points C and D in terms of EI.

(19) In Fig. A7.77 determine the magnitude of the fixed end moment M_A and the simple support R_B.

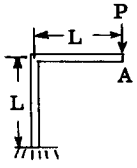

Fig. A7.78

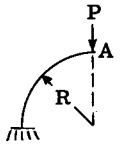

Fig. A7.79

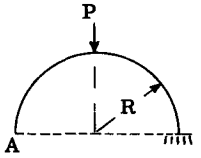

Fig. A7.80

(20) In Fig. A7.78 EI is constant throughout. Calculate the vertical deflection and the angular rotation of point A.

(21) For the curved beam in Fig. A7.79 find the vertical deflection and the angular rotation of point A. Take EI as constant.

(22) For the loaded curved beam of Fig. A7.80, determine the vertical deflection and the angular rotation of the point A. Take EI as constant.

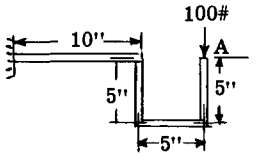

Fig. A7.81

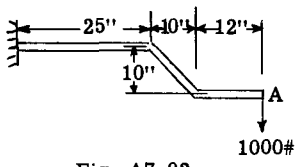

Fig. A7.82

(23) In Fig. A7.81 find the vertical movement and the angular rotation of point A. Take EI = 12,000,000.

(24) Determine the vertical deflection of point A for the structure in Fig. A7.82. EI = 14,000,000.

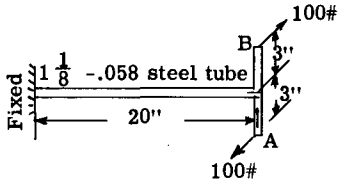

Fig. A7.83

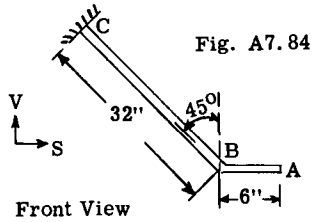

Front View

Fig. A7.84

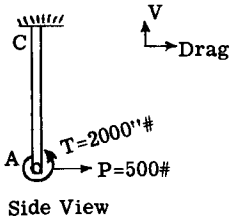

Side View

(25) The cantilever beam of Fig. A7.83 is loaded normal to the plane of the paper by the two loads of 100# each as shown. Find the deflection of point A normal to the plane of the paper by the method of virtual work. The rectangular moment of inertia for the tube is 0.0277 in^4. E = 29,000,000.

(26) The cantilever landing gear strut in Fig. A7.84 is subjected to the load of 500# in the drag direction at point A and also a torsional moment of 2000 in. lb. at A as shown. Determine the displacement of point A in the drag direction. The tube size for portion CB is 2"-.083 and for portion BA, 2"-.065 round tube. Material is steel with E = 29,000,000 psi.

(27) Using the matrix equation $2U = \{q_i\}[a_{ij}]\{q_j\}$ compute the strain energy in the truss of Fig. A7.63 (Problem 2). The member flexibility coefficient for a member under uniform axial load is L/AE (see Fig. A7.35a). Ans. U = 22.4 lb.in.

(28) Using matrix equation (23) compute the strain energy in the beam of Fig. A7.71. Note: the choice of generalized forces should be made so as to permit computation of the member flexibility coefficients by the equations of p. A7.19. Ans. U = 3533 lb. in.

(29) Re-solve the problem of example problem 25 for a stepped cantilever beam whose I doubles at point "2" and doubles again at "3". (Heaviest section at built-in end.)

(30) For the truss of Fig. A7 85 determine the influence coefficient matrix relating vertical deflections due to loads P_1, P_2, P_3 and P_4 applied as shown. Member areas are shown on the figure.

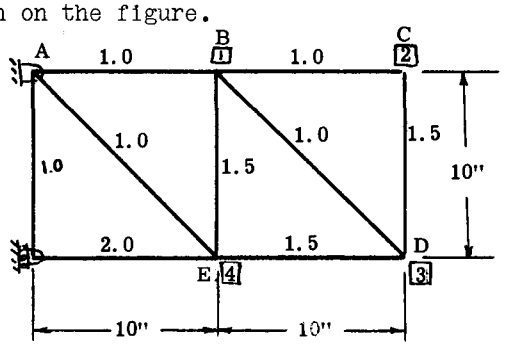

Fig. A7.85

Answer.

$$[A_{mn}] = \frac{1}{E}\begin{bmatrix} 39.67 & 44.95 & 44.95 & 33.28 \\ 44.95 & 106.56 & 99.9 & 38.28 \\ 44.95 & 99.9 & 99.9 & 38.28 \\ 33.28 & 38.28 & 38.28 & 33.28 \end{bmatrix}$$

(31) For the truss of problem (30) determine which of the following two loading conditions produces the greatest deflection of point 4, (All loads in pounds).

Condition No.	P_1	P_2	P_3	P_4
1	1000	500	800	400
2	300	700	400	600

(32) Determine the matrix of influence coefficients relating drag load (positive aft), braking torque (positive nose up) and moment in the V-S plane (positive right wing down) as applied to the free end of the gear strut assembly of Problem 26.

Answer.

$$[A_{mn}] = 10^{-6}\begin{bmatrix} 2500 & -50.7 & 0 \\ -50.7 & 6.97 & 0 \\ 0 & 0 & 6.00 \end{bmatrix}$$

(33) Find the deflection of the load applied to the cantilever panel of Fig. A7.86. (Assume the web does not buckle). Use matrix notation. Ans. $\delta = 7.94 \times 10^{-3}$ inches.

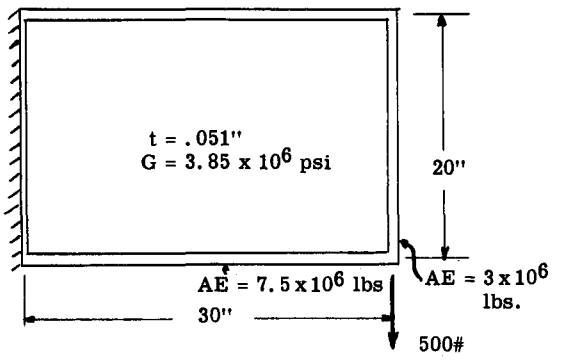

Fig. A7.86

(34) Find the influence coefficients relating deflections at points 1 and 2 of the simply supported beam of Fig. A7 87. Use matrix methods.

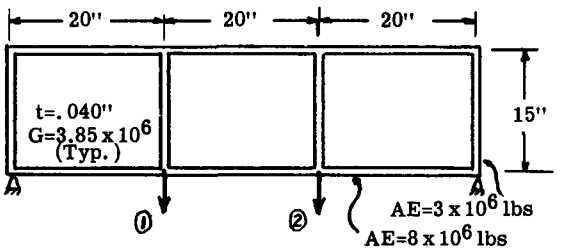

Fig. A7.87

Ans.

$$[A_{mn}] = 10^{-6}\begin{bmatrix} 12.34 & 7.102 \\ 7.102 & 12.34 \end{bmatrix}$$

Note to student: It will be highly instructive to re-work problems 33 and 34 using the alternate choice of generalized forces in the stringers from those used in your first solution. See p. A7.22 for alternate generalized forces on a stringer.

References for Chapters A7, A8.

TEXT BOOKS ON STRUCTURAL THEORY

"Advanced Mechanics of Materials", F. Seely and J. O. Smith, 2nd Ed., John Wiley, New York.

"Advanced Strength of Materials", J. P. Den Hartog, McGraw-Hill, N. Y.

"Theory of Elasticity", S. Timoshenko, McGraw-Hill, N. Y.

TEXT BOOKS WITH MATRIX APPLICATIONS

"Elementary Matrices", R. A. Frazer, W. J. Duncan and A. R. Collar, Cambridge University Press.

"Introduction to the Study of Aircraft Vibration and Flutter", R. Scanlan and R. Rosenbaum, Mac Millan, New York.

TECHNICAL PAPERS

Benscoter, S. U., "The Partitioning of Matrices in Structural Analysis", Journ. of Appl. Mechs. Vol. 15, 1948.

Wehle, L. and Lansing, W., A Method for Reducing the Analysis of Complex Redundant Structures to a Routine Procedure, Journ. of Aero. Sci. Vol. 19, 1952.

Langefors, B., Analysis of Elastic Structures by Matrix Transformation with Special Regard to Semi Monocoque Structures, Journ. of Aero. Sci. 19, 1952.

Langefors, B., Matrix Methods for Redundant Structures, Journ. of Aero. Sci. Vol. 20, 1953.

Falkenheiner, H. Systematic Analysis of Redundant Elastic Structures by Means of Matrix Calculus, Journ. of Aero. Sci., 20, 1953.

Argyris, J. and Kelsey, S., Energy Theorems in Structural Analysis, Aircraft Engineering, Oct. 1954, et. seq.

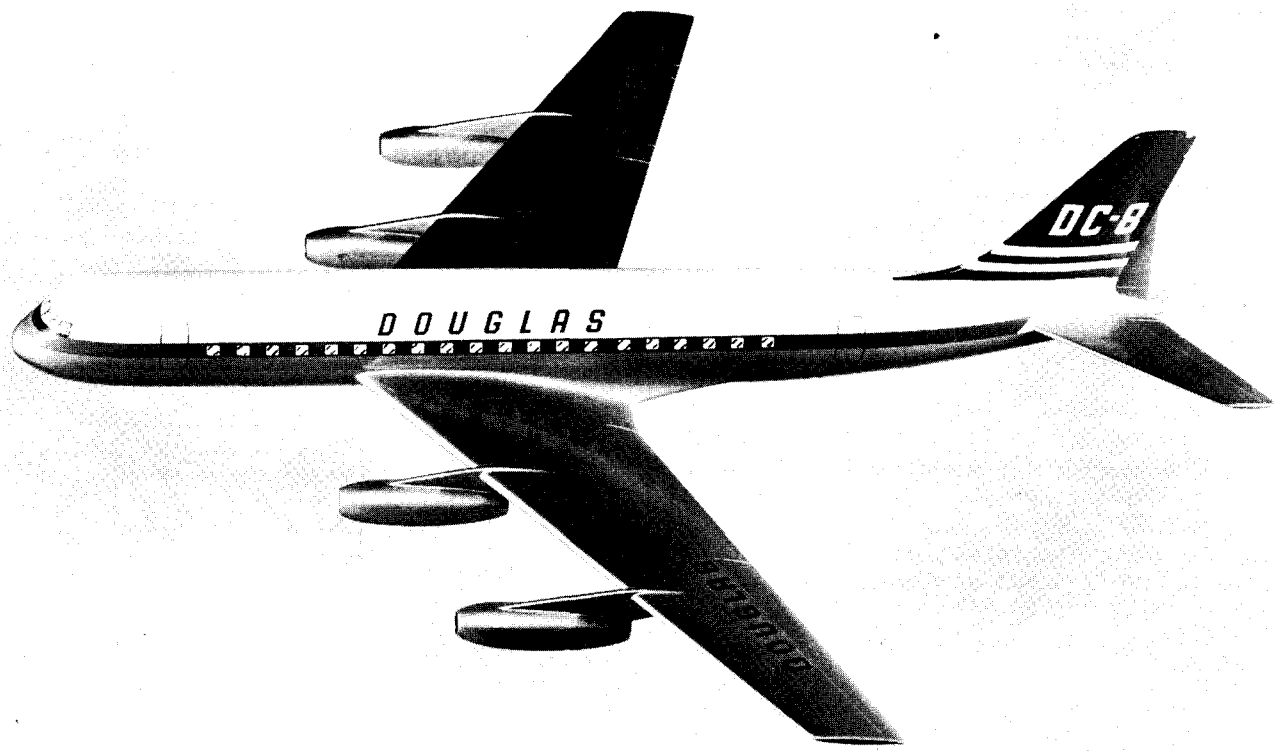

Many problems involving calculation of deflections are encountered in the structural design of a large modern airplane such as the Douglas DC-8.

CHAPTER A8
STATICALLY INDETERMINATE STRUCTURES

ALFRED F. SCHMITT

A8.00 Introduction.

A statically indeterminate (redundant) problem is one in which the equations of static equilibrium are not sufficient to determine the internal stress distribution. Additional relationships between displacements must be written to permit a solution.

The "Theory of Elasticity" shows that all structures are statically indeterminate when analyzed in minute detail. The engineer however, is often able to make a number of assumptions and coarse approximations which render the problem determinate. In addition, auxiliary aids are available such as the Engineering Theory of Bending $\left(\frac{MY}{I}\right)$ and the constant-shear-flow rules of thumb ($q = T/2A$) (see Chaps. A-5, A-6 and A-13 through A-15). While these latter are certainly not laws of "statics", the engineer employs them often enough so that problems in which they are used to obtain stress distributions are often thought of as being "determinate".

It is frequently the case in aircraft structural analysis that, in view of the requirements for efficient design, one cannot obtain a determinate problem without sacrificing necessary accuracy. The Theory of Elasticity assures the existence of a sufficient number of auxiliary conditions to permit a solution in such cases.

This chapter employs extensions of the methods of Chapter A-7 to effect the solution of typical redundant problems. Special methods of handling particular structural configurations are shown in later chapters.

A8.0 The Principle of Superposition.

The general principle of superposition states that the resultant effect of a group of loadings or causes acting simultaneously is equal to the algebraic sum of the effects acting separately. The principle is restricted to the condition that the resultant effect of the several loadings or causes varies as a linear function. Thus, the principle does not apply when the member material is stressed above the proportional limit or when the member stresses are dependent upon member deflections or deformations, as, for example, the beam-column, a member carrying bending and axial loads at the same time.

A8.1 The Statically Indeterminate Problem.

Several characteristics (and interpretations thereof) of the statically indeterminate problem may be pointed out. These characteristics are individually useful in forming the bases for methods of solution.

A. There are more members in the structure than are required to support the applied loads. If n members may be removed (cut) while leaving a stable structure the original structure is said to be "n-times redundant".

-COROLLARY-

In an n-times redundant structure the magnitude of the forces in n members may be assigned arbitrarily while establishing stresses in equilibrium with the applied loads. Thus, in Fig. A8.1 (a singly redundant structure), the internal force distribution of (a) is in equilibrium with the external loads for any and all values of X, the force in member BD.

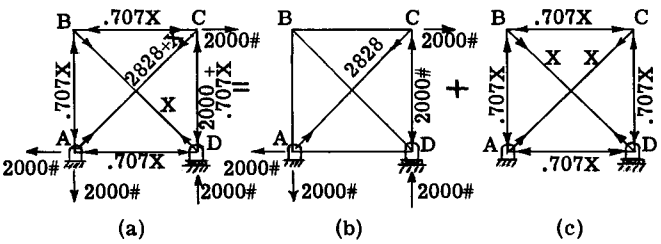

Fig. A8.1

Singly redundant stress distribution, (a) consisting of a stress in static equilibrium with the applied loads, (b), with one zero-resultant stress distribution, (c), superposed.

Only the system (b) is actually required to equilibrate the external loads (corresponding to $X = 0$). Note that the system (c) has zero external resultant.

B. Of all the possible stress (force) distributions satisfying static equilibrium the one correct solution is that one which results in kinematically possible strains (displacements), i.e. retains continuity of the structure.

Thus, for example, there are an infinite number of bending moment distributions satisfying static equilibrium in Fig. A8.1 (d) since M_o can assume any value. Of these, only one will result in the zero deflection of the right hand beam tip necessary to maintain structural continuity with the support at that point.

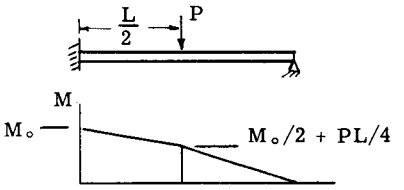

Fig. A8.1d

Singly redundant beam with root bending moment M_0 undetermined by statics.

-COROLLARY-

If n member loads have been assigned arbitrarily while establishing equilibrium with the external loads, relative movements of the elements will result, violating continuity at n points. n zero-resultant stress (force) distributions may then be superposed to reduce the relative motions to zero. The resulting stress distribution is the correct one.

A8.2 The Theorem of Least Work.

A theorem extremely useful in the solution of redundant problems may be obtained from Castigliano's Theorem. Consider first the problem of redundant reactions such as in a beam over three supports (Fig. A8.2). One of the reactions cannot be obtained by statics.

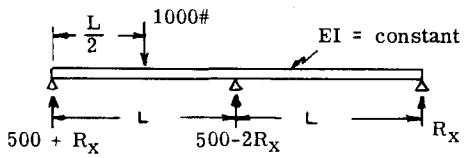

Fig. A8.2

A singly redundant beam with one reaction given an arbitrary value (R_X).

If the unknown reaction (say that on the far right) is given a symbol, R_X, then the remaining reactions and the bending moments may be determined from statics. The strain energy U may then be written as a function of R_X, i.e., $U = f(R_X)$. Next form

$$\frac{\partial U}{\partial R_X} = \delta_{R_X}$$

This is the deflection at R_X due to R_X. But this must also be zero, since the support is rigid. Hence

$$\frac{\partial U}{\partial R_X} = 0 \qquad \text{- - - - - - - - - - - - - - - - - - - (1)}$$

Eq. (1) is true for all redundant reactions occuring at fixed supports. Because it corresponds to the mathematical condition for the minimum of a function, eq. (1) is said to state the Theorem of Least Work. In words; "the rate of change of strain energy with respect to a fixed redundant reaction is zero".

A8.2.1 Determination of Redundant Reactions by Least Work.

Example Problem A

By way of illustration, the problem posed by Fig. A8.2 was carried to completion. The bending moment was given by (x, y, z measured from the left ends of the three beam divisions)

$$M = (500 + R_X)\,x \qquad 0<x<L/2$$

$$M = \frac{(500 + R_X)\,L}{2} + (R_X - 500)\,y \qquad 0<y<L/2$$

$$M = R_X\,(L - z) \qquad 0<z<L$$

Then

$$U = \frac{1}{2}\int\frac{M^2 dx}{EI} = \frac{1}{2EI}\int_0^{L/2}(500+R_X)^2 x^2 dx$$

$$+ \frac{1}{2EI}\int_0^{L/2}\left[\frac{(500+R_X)L}{2} + (R_X - 500)y\right]^2 dy$$

$$+ \frac{1}{2EI}\int_0^{L} R_X^2 (L - z)^2 dz$$

Differentiating under the integral sign, (see p. A7.8)

$$\frac{\partial U}{\partial R_X} = \frac{1}{EI}\int_0^{L/2}(500 + R_X)\,x^2 dx$$

$$+ \frac{1}{EI}\int_0^{L/2}\left[\frac{(500 + R_X)L}{2} + (R_X - 500)y\right]\left(\frac{L}{2} + y\right) dy$$

$$+ \frac{1}{EI}\int_0^{L} R_X\,(L - z)^2\,dz$$

$$\frac{\partial U}{\partial R_X} = 0 = (500 + R_X)\int_0^{L/2} x^2\,dx$$

$$+ \frac{(500 + R_X)L}{2}\int_0^{L/2}\left(\frac{L}{2} + y\right) dy +$$

$$(R_X - 500)\int_0^{L/2} y\left(\frac{L}{2} + y\right) dy + R_X\int_0^{L}(L - z)^2 dz$$

Completion of the computation gave

$$R_X = -\frac{1500}{16}\ \text{lbs.} = -\ 93.8\ \text{lbs.},$$

the negative sign indicating that R_X was down.

Example Problem B

Determine the redundant fixed end moments for the beam of Fig. A8.2(a).

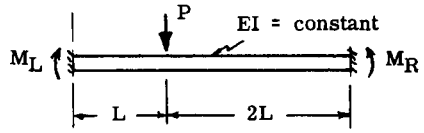

Fig. A8.2a

A doubly redundant beam with two reactions given two arbitrary values.

Solution:

The redundant end moments were designated as M_L and M_R for the left and right beam ends respectively and were taken positive as shown. The moment equations for the two beam portions (x from left end, y from right) were

$$M = M_L + \frac{M_R + 2PL - M_L}{3L}\,x \qquad 0<x<L$$

$$M = M_R + \frac{M_L + PL - M_r}{3L}\,y \qquad 0<y<2L$$

Then

$$U = \frac{1}{2EI}\int_0^L \left[M_L + \frac{M_R + 2PL - M_L}{3L}\,X\right]^2 dx + \frac{1}{2EI}\int_0^{2L}\left[M_R + \frac{M_L + P_L - M_R}{3L}\,y\right]^2 dy$$

Differentiating under the integral sign (see remarks on p. A7-8)

$$\frac{\partial U}{\partial M_L} = 0 = \int_0^L \left[M_L + \frac{M_R + 2P_L - M_L}{3L}\,X\right]\left(1 - \frac{X}{3L}\right) dx + \int_0^{2L}\left[M_R + \frac{M_L + P_L - M_R}{3L}\,y\right]\frac{y}{3L}\,dy\ .$$

$$\frac{\partial U}{\partial M_R} = 0 = \int_0^L \left[M_L + \frac{M_R + 2PL - M_L}{3L}\,X\right]\frac{X}{3L}\,dx + \int_0^{2L}\left[M_R + \frac{M_L + PL - M_R}{3L}\,y\right]\left(1 - \frac{y}{3L}\right) dy\ .$$

$$0 = M_L\int_0^L\left(1 - \frac{x}{3L}\right)dx + \frac{M_R + 2PL - M_L}{3L}\int_0^L X\left(1 - \frac{X}{3L}\right)dx + M_R\int_0^{2L}\frac{y}{3L}\,dy + \frac{M_L + PL - M_R}{3L}\int_0^{2L}\frac{y^2}{3L}\,dy\ .$$

$$0 = M_L\int_0^L\frac{X}{3L}\,dx + \frac{M_R + 2PL - M_L}{3L}\int_0^L\frac{X^2}{3L}\,dx + M_R\int_0^{2L}\left(1 - \frac{y}{3L}\right)dy + \frac{M_L + PL - M_R}{3L}\int_0^{2L} y\left(1 - \frac{y}{3L}\right)dy\ .$$

Evaluating the integrals and solving simultaneously gave

$$M_L = -\frac{4}{9}\,PL$$

$$M_R = -\frac{2}{9}\,PL$$

A8.2.2 Redundant Stresses by Least Work.

The Theorem of Least Work may be applied to the problem of determining redundant member forces within a statically indeterminate structure. Thus, in an n-times redundant structure if the redundant member forces are assigned symbols X, Y, Z, - - - etc., the values which these forces must assume for continuity of the structure are such that the displacements associated with these forces (the discontinuities) must be zero. Hence, by an argument parallel to that used for redundant reactions, one writes,

$$\left.\begin{array}{l} \dfrac{\partial U}{\partial X} = 0 \\ \dfrac{\partial U}{\partial Y} = 0 \\ \vdots \\ \text{etc.} \end{array}\right\} \text{- - - - - - - - - (2)}$$

In words, "the rate of change of strain energy with respect to the redundant forces is zero".

Eqs. (2), like eq. (1), are statements of the Theorem of Least Work. They provide n equations for the n-times redundant structure. The simultaneous solution of these equations yields the desired solution of the problem.

Example Problem C

The cantilever beam and cable system of Fig. A8.3(a) is singly redundant. Find the member loadings by use of the Least Work Theorem.

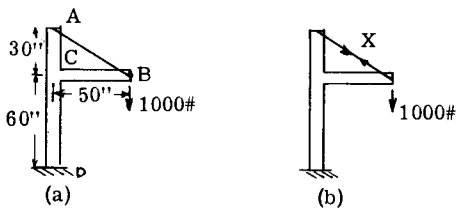

Fig. A8.3

A singly redundant structure with one member force given an arbitrary value (X).

Solution:

The tensile load in the cable was treated as the redundant load and was given the symbol X (Fig. A8.3(b)). The strain energies considered were those of flexure in portions AC, CD and BC and that of tension in the cable AB. Energies due to axial forces in the beam portions were considered negligible.

The bending moment in BC (origin at B) was

$$M_{BC} = \left(1000 - \frac{30}{58.3}X\right)x$$

In AC, (origin at A):

$$M_{AC} = \frac{50}{58.3}X \cdot y$$

In CD:

$$M_{CD} = 50{,}000$$

The strain energy was therefore

$$U = \frac{X^2}{2}\left(\frac{L}{AE}\right)_{AB} + \frac{1}{2EI_{BC}}\int_0^{50}\left(1000 - \frac{30}{58.3}X\right)^2 x^2 dx + \frac{1}{2EI_{AC}}\int_0^{30}\left(\frac{50}{58.3}X\right)^2 y^2 dy + \frac{1}{2EI_{CD}}\int_0^{60}(50{,}000)^2 ds$$

Obviously there was no need to consider the energy in CD as its loading did not depend upon X and hence could not enter the problem. Differentiating under the integral sign

$$\frac{\partial U}{\partial X} = \frac{58.3\,X}{EA_{AB}} - \frac{30}{58.3}\frac{\left(1000 - \frac{30}{58.3}X\right)}{EI_{BC}}\int_0^{50} x^2\,dx + \left(\frac{50}{58.3}\right)^2\frac{X}{EI_{AC}}\int_0^{30} y^2\,dy = 0$$

$$\frac{58.3\,X}{EA_{AB}} + \frac{11{,}032\,X}{EI_{BC}} + \frac{6620\,X}{EI_{AC}} = \frac{21.44 \times 10^6}{EI_{BC}}$$

Putting

$$A_{AB} = 0.025\ \text{in}^2$$

$$I_{BC} = 8.0\ \text{in}^4$$

$$I_{AC} = 10.0\ \text{in}^4$$

gave

$$X = 613\ \text{lbs.}$$

Then

$$M_{BC} = \left[1000 - \frac{30}{58.3}(613)\right]x = 685x$$

$$M_{AC} = \frac{50}{58.3}\,613 \cdot y = 526\,y$$

Example Problem D

A semicircular pin-ended, uniform ring is supported and loaded as shown in Fig. A8.3(c). As a first approximation the horizontal floor tie is to be assumed rigid axially. Find the bending moment distribution in the ring.

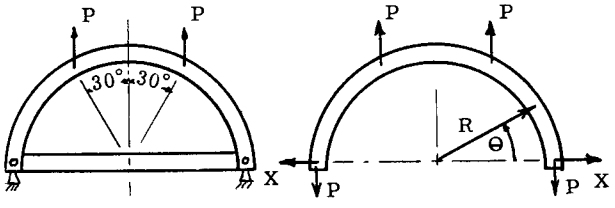

(c) Fig. A8.3 (d)

Solution:

The axial load in the floor was taken to be the redundant (since the floor was assumed rigid, this could have been thought of as a redundant floor reaction from fixed supports). The loading is shown in Fig. A8.3(d).

The bending moment distribution was

$$M = X\,R\,\sin\theta - PR\,(1 - \cos\theta) \qquad 0<\theta<60°$$

$$M = X\,R\,\sin\theta - PR/2 \qquad 60°<\theta<90°$$

The axial loadings were

$$S = P\cos\theta + X\sin\theta \qquad 0<\theta<60°$$

$$S = X\sin\theta \qquad 60°<\theta<90°$$

The strain energy (for only half the structure) was *

$$U = \frac{1}{2EI}\int_0^{60°}\left[X\,R\,\sin\theta - PR\,(1-\cos\theta)\right]^2 Rd\theta$$

$$+\frac{1}{2EI}\int_{60°}^{90°}\left[X\,R\,\sin\theta - PR/2\right]^2 Rd\theta$$

$$+\frac{1}{2AE}\int_0^{60°}\left[P\cos\theta + X\sin\theta\right]^2 Rd\theta$$

$$+\frac{1}{2AE}\int_{60°}^{90°}\left[X\sin\theta\right]^2 Rd\theta$$

* Zero strain energy in the rigid floor ($AE \to \infty$).

Differentiating under the integral sign

$$\frac{\partial U}{\partial X} = \frac{R^3}{EI}X\int_0^{60°}\sin^2\theta\,d\theta$$

$$-\frac{R^3P}{EI}\int_0^{60°}(1-\cos\theta)\sin\theta\,d\theta$$

$$+\frac{R^3X}{EI}\int_{60°}^{90°}\sin^2\theta\,d\theta$$

$$-\frac{R^3P}{2EI}\int_{60°}^{90°}\sin\theta\,d\theta$$

$$+\frac{PR}{AE}\int_0^{60°}\cos\theta\sin\theta\,d\theta$$

$$+\frac{XR}{AE}\int_0^{60°}\sin^2\theta\,d\theta + \frac{XR}{AE}\int_{60°}^{90°}\sin^2\theta\,d\theta$$

Evaluating,

$$\frac{\partial U}{\partial X} = 0 = \frac{\pi}{4}X\left(\frac{R^3}{EI}+\frac{R}{AE}\right)$$

$$+\frac{3}{8}P\left(\frac{R}{AE}-\frac{R^3}{EI}\right)$$

Therefore

$$X = \frac{3P}{2\pi}\,\frac{\left(\frac{R^3}{EI}-\frac{R}{AE}\right)}{\left(\frac{R^3}{EI}+\frac{R}{AE}\right)}$$

Example Problem E

The portal frame of Fig. A8.3(e) is three times redundant. Set up the simultaneous equations in the redundant forces. The relative bending stiffnesses of the segments are given on the figure.

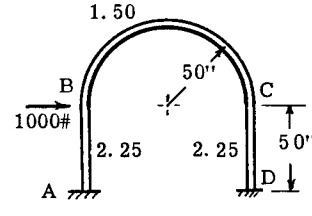

Fig. A8.3e

Solution:

The redundant forces selected were the bending moment, the transverse shear force and the axial force, all at point A. The four figures A8.3(f) through A8.3(i) show the bending moment diagrams of the structure due to applied loads and due to redundant forces

acting individually (it being easier to compute the loadings in this fashion). The complete loading was obtained by superposition.

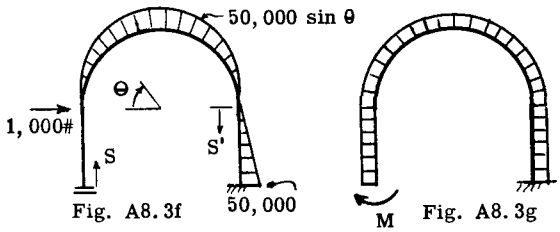

Fig. A8.3f

Fig. A8.3g

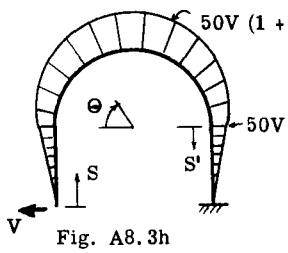

Fig. A8.3h

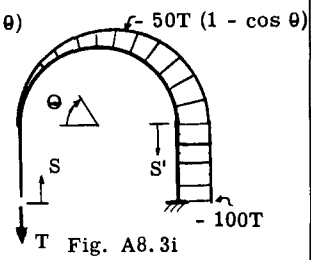

Fig. A8.3i

The composite bending moments as functions of s, θ and s' were

$$M_{AB} = M + Vs$$

$$M_{BC} = -50{,}000 \sin\theta + M + 50V + 50V \sin\theta - 50T(1 - \cos\theta)$$

$$M_{CD} = 1000s' + M - Vs' + 50V - 100T$$

Then since

$$U = \frac{1}{2}\int \frac{M^2 ds}{EI} \quad \text{and} \quad \frac{\partial U}{\partial M} = \frac{\partial U}{\partial V} = \frac{\partial U}{\partial T} = 0,$$

one has,

$$\frac{\partial U}{\partial M} = 0 = \int_0^{50} \frac{(M + Vs)}{2.50}\, ds$$

$$+ \int_0^{\pi} \left[\frac{-50{,}000 \sin\theta + M + 50V(1 + \sin\theta) - 50T(1 - \cos\theta)}{1.50}\right] 50 d\theta$$

$$+ \int_0^{50} \frac{(1000s' + M - Vs' + 50V - 100T)}{2.25}\, ds'$$

$$\frac{\partial U}{\partial V} = 0 = \int_0^{50} \frac{(M + Vs)\, sds}{2.25}$$

$$+ \int_0^{\pi} \left[\frac{-50{,}000 \sin\theta + M + 50V(1 + \sin\theta) - 50T(1 - \cos\theta)}{1.50}\right] (1 + \sin\theta)\, \overline{50} d\theta$$

$$+ \int_0^{50} \frac{(1000s' + M - Vs' + 50V - 100T)(50 - s')}{2.25}\, ds'$$

$$\frac{\partial U}{\partial T} = 0 = + \int_0^{50} \left[\frac{1000s' + M - Vs' + 50V - 100T}{2.25}\right] (-100)\, ds'$$

$$+ \int_0^{\pi} \left[\frac{-50{,}000 \sin\theta + M + 50V(1 + \sin\theta) - 50T(1 - \cos\theta)}{1.50}\right] (\cos\theta - 1)\overline{50}^2 d\theta$$

After evaluation of the integrals the equations obtained were

$$\begin{cases} .1492M + 9.682V - 7.459T = 2.778 \times 10^3 \\ 9.682M + 763.1V - 484.0T = 288.3 \times 10^3 \\ -7.459M - 484.0V + 614.9T = -111.15 \times 10^3 \end{cases}$$

A8.3 Redundant Problems by The Methods of Dummy-Unit Loads.

While the Theorem of Least Work may be made the basis of redundant problem analysis, its direct application by the calculus, as in Art. A8-2.1 and A8-2.2, is often impractical. For the majority of problems the work is facilitated if carried out by the techniques of the Method of Dummy-Unit Loads.

The following derivation is for a doubly redundant truss structure. The extension to a more general n-times redundant structure, in which other loadings in addition to axial (flexure, torsion and shear) are present, is indicated later.

Consider the doubly redundant truss of Fig. A8.4(a). It may be made statically determinate by "cutting" two members such as the diagonals indicated. Application of the external loads to this determinate ("cut") structure gives a load distribution, "S", computed by satisfying static equilibrium. At this time discontinuities appear at the cuts "x" and "y" due to the strains developed.

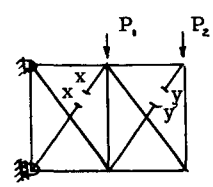

S loads

Fig. A8.4a

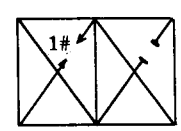

u_x loads

Fig. A8.4b

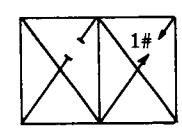

u_y loads

Fig. A8.4c

To compute these and subsequent displacements the Method of Dummy-Unit Loads may be used (Art. A7-7). For this purpose virtual loads are placed alternately at the x and y cuts as in Figs. A8.4(b) and (c). From the dummy-unit load equations

$$\left.\begin{aligned}\delta_{xo} &= \Sigma \frac{Su_xL}{AE}\\ \delta_{yo} &= \Sigma \frac{Su_yL}{AE}\end{aligned}\right\} \text{- - - - - - - - - - - - - - - (3)}$$

u_x and u_y are the unit-redundant stress distributions as indicated in Figs. A8-4b, c. The subscript "o" indicates these relative displacements occur in the determinate ("cut") structure with the "original" stress distribution.

It is now desired to close up the discontinuities by application of redundant loads X and Y to the x and y cuts, respectively, as in Fig. A8-4(d). Load X causes a stress distribution Xu_x and, likewise, Y causes a distribution Yu_y. The relative displacement at cut x due to redundant load X is given by (δ_{xx} is read "displacement at x due to X").

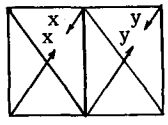

Fig. A8.4d

$$\delta_{xx} = \Sigma \frac{Xu_x \cdot u_xL}{AE} = X \Sigma \frac{u_x^2L}{AE}$$

and at cut y by (read δ_{yx} as "displacement at y due to X").

$$\delta_{yx} = \Sigma \frac{Xu_x \cdot u_yL}{AE} = X \Sigma \frac{u_xu_yL}{AE}$$

Similarly the load Y causes displacements at the cuts y and x given respectively by

$$\delta_{yy} = \Sigma \frac{Yu_y \cdot u_yL}{AE} = Y \Sigma \frac{u_y^2L}{AE}$$

and

$$\delta_{xy} = \Sigma \frac{Yu_y \cdot u_xL}{AE} = Y \Sigma \frac{u_yu_xL}{AE}$$

Now the net relative displacement at each cut under the simultaneous action of the three stress systems S, $X \cdot u_x$ and $Y \cdot u_y$ is

$$\delta_{xo} + \delta_{xx} + \delta_{xy} = \Sigma \frac{Su_xL}{AE} + X \Sigma \frac{u_xu_xL}{AE} + Y \Sigma \frac{u_y u_xL}{AE}$$

and

$$\delta_{yo} + \delta_{yx} + \delta_{yy} = \Sigma \frac{Su_yL}{AE} + X \Sigma \frac{u_xu_yL}{AE} + Y \Sigma \frac{u_yu_yL}{AE}$$

For continuity these net relative displacements must be zero. Equating the above expressions each to zero, and rearranging, gives the simultaneous equations

$$\left.\begin{aligned}X \Sigma \frac{u_x^2L}{AE} + Y \Sigma \frac{u_xu_yL}{AE} &= -\Sigma \frac{Su_xL}{AE}\\ X \Sigma \frac{u_yu_xL}{AE} + Y \Sigma \frac{u_y^2L}{AE} &= -\Sigma \frac{Su_yL}{AE}\end{aligned}\right\} \text{- - - - - - (4)}$$

Eqs. (4) are two simultaneous equations in the two unknowns X and Y. Upon solution for X and Y the true stress distribution may be computed as

$$S_{TRUE} = S + Xu_x + Yu_y \text{ - - - - - - - - - - - - (5)}$$

For a structure which is only <u>singly</u> redundant, eqs. (4) and (5) are applied by setting Y = o giving

$$X \Sigma \frac{u_x^2L}{AE} = -\Sigma \frac{Su_xL}{AE}$$

or, simply,

$$X = -\frac{\Sigma \frac{Su_xL}{AE}}{\Sigma \frac{u_x^2L}{AE}} \text{ - - - - - - - - - - - - - - - (4a)}$$

and,

$$S_{TRUE} = S + X u_x \text{ - - - - - - - - - - - - - - (5a)}$$

A8.4 Example Problems - Trusses With Single Redundancy.

<u>Example Problem #1</u>

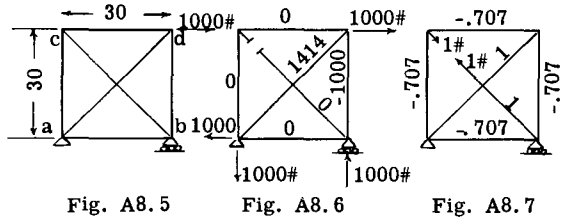

Fig. A8.5 Fig. A8.6 Fig. A8.7

Fig. A8.5 shows a single bay pin connected truss. The truss is statically determinate with respect to external reactions, but statically indeterminate with respect to internal member loads, since at any joint there are 3 unknowns with only two equations of statics available for a concurrent force system. The truss is therefore redundant to the first degree. The general procedure for solution is to make the truss statically determinate by cutting one of the members; on Fig. A8.6, member bc has been selected as the redundant member, and it is cut as shown. The member stresses S for the truss of

Fig. A8.6 are then determined, the results being recorded on the members and also entered in Table A8.1. In Fig. A8.7, a unit 1# tensile dummy load has been applied at the cut section of the redundant member bc, and the loads in all the members due to this unit load are calculated. The results are recorded on the figure and also in Table A8.1 under the head of u stresses. The solution for the redundant load X in the redundant member bc is given at the bottom of Table A8.1. The true load in any member equals the S stress plus X times its u stress.

Table A8.1

Member	L	A	S	u	$\frac{SuL}{A}$	$\frac{u^2L}{A}$	True Stress = S + Xu
ab	30	1	0	-.707	0	15	395
bd	30	1	-1000	-.707	21210	15	-605
dc	30	1	0	-.707	0	15	395
ca	30	1	0	-.707	0	15	395
cb	42.4	2	0	1.0	0	21.2	-559
ad	42.4	1.5	1414	1.0	40000	28.3	855
					Σ 61210	109.5	

X = true load in redundant member bc

$$X = -\frac{\Sigma \frac{SuL}{A}}{\Sigma \frac{u^2L}{A}} = \frac{-61210}{109.5} = -559\#$$

Example Problem #2

Fig. A8.8 shows a singly redundant 3-member frame. Find the member loadings. Member areas are shown on the figure.

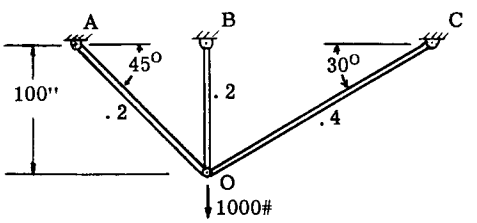

Fig. A8.8

Solution: Member OC was selected as the redundant and was cut in figuring the S-loads, as in Fig. A8.9. Fig. A8.10 shows the u-load calculation. The table completes the calculation.

Mem.	L	A	S	u	$\frac{SuL}{A}$	$\frac{u^2L}{A}$	True Load = S + X u
AO	141.4	0.2	0	1.224	0	1059	335.5
BO	100.0	0.2	1000	-1.366	-6.83×10^5	933	625.6
CO	200.0	0.4	0	1.000	0	500	274.1
				Σ	-6.83×10^5	2492	

$$X = -\frac{\Sigma \frac{SuL}{A}}{\Sigma \frac{u^2L}{A}} = 274.1 \text{ lb.}$$

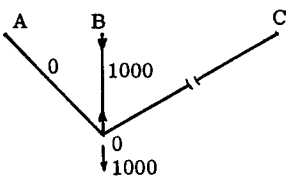

Fig. A8.9
S loads

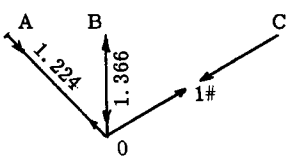

Fig. A8.10
u loads

Example Problem # 1-A; Deflection Calculation in a Redundant Truss

Calculations of the deflections under load of a redundant structure are made by application of the methods of Chapter A-7. Since, however, there are certain pitfalls as regards symbols and also some important special techniques, the following examples are given at this time. The extension of the method to more complex structures is immediate and no further work on deflections of redundant structures is given in this chapter (excepting in the case of the matrix methods of Arts. A8.10 et. seq.).

Find the horizontal movement of point "d" of Example Problem # 1 under the action of the load applied there.

Solution: The equation used to find the deflection is Eq. (18) of Chapter A-7. Written for application to truss deflections it is (see Example Problem 13, p. A7.11)

$$\delta = \Sigma \frac{SuL}{AE} \text{ - - - - - - - - - - - - - - - - (A)}$$

Now for a deflection calculation the symbols "S" and "u" must be carefully reinterpreted from their meanings in the redundant stress calculation. For a deflection calculation the symbols of eq. (A), above, mean: "S-loads" are the true loads of the redundant structure due to application of the real external loading; "u-loads" are the loads due to a dummy-unit (virtual) load applied at the external point where the deflection is desired and in the direction of the desired deflection.

Thus, the "S loads" for use in Eq. (A) are the true stresses (the solution) of Example Problem # 1.

The "u-loads" represent additional information which would, in general, appear to necessitate another redundant stress calculation. As will be seen, such is fortunately not the case. In the present problem the dummy-unit load is applied identically as is the 1000# real load and hence the u-loads are simply equal to the "S-loads" properly scaled down. The following table completes the calculation.

Mem.	L	A	S*	u**	SuL/A
ab	30	1	395	.395	4,680
bd	30	1	-605	-.605	10,980
dc	30	1	395	.395	4,680
ca	30	1	395	.395	4,680
cb	42.4	2	-559	-.559	6,620
ad	42.4	1.5	855	.855	20,660
				Σ	52,300

$$\therefore \delta = \frac{52,300}{E}$$

* identical with the "true stress" of Table A8.1.

** simply 1/1000th of the "S-loads" since the dummy-unit load is applied exactly as is the 1000# real load.

Example Problem #2-A.

Find the horizontal deflection of point O of Example Problem #2 under application of the vertical 1000# load shown in Fig. A8.8.

Solution: To compute the deflection use

$$\delta = \Sigma \frac{SuL}{AE}$$

Again the symbols "S" and "u" are to be re-interpreted for a deflection calculation as explained above in Example Problem #1-A. The "S-loads" are now the "true loads" computed in Example Problem #2, above. The "u-loads" are loads due to placing a dummy-unit load acting horizontally on the structure at point O. Since this load acts on a redundant structure it would appear that another redundant stress calculation is required. However, this is not necessary.

Theorem: For the u-loads in a deflection calculation any set of stresses (loads) in static equilibrium with the dummy-unit load may be used, even from the simplest of "cut" structures.

This theorem says that to get the "u-loads" for this deflection calculation we may "cut" any one of the three members and get a satisfactory set of u-loads by simple statics! Before proving the theorem we complete the calculation in tabular form as shown. The "u-loads" were obtained by cutting member OC and applying a unit load horizontally at O.

Mem.	L	A	S*	u	$\frac{SuL}{A}$
AO	141.4	.2	335.5	$\sqrt{2}$	3.355×10^5
BO	100	.2	625.6	-1	-3.128×10^5
CO	200	.4	274.1	0	0
					0.227×10^5

$$\therefore \delta = \frac{22,700}{E}$$

* true loads from Example Problem #2.

By way of demonstration another set of u-loads, called u', were found for this same problem, this time by cutting member OA. The corresponding calculations follow:

S	u'	$\frac{Su'L}{A}$
335.5	0	0
625.6	.578	1.808×10^5
274.1	-1.155	-1.583×10^5
	Σ	0.225×10^5

The results are identical (allowing for round-off errors).

Proof of Theorem

To prove the theorem above we return to the virtual work principle and the argument from which the dummy-unit loads deflection equation, Eq. (18) of Chapter A-7, was derived (refer to p. A7.10). It will be remembered that the deflection was shown to be equal to the work done by the internal virtual loads (u-loads) moving through the distortions (Δ) due to the real loads, i.e., $\delta = \Sigma u \Delta$. The internal virtual loads are those loads due to a unit load acting at the point of desired deflection.

Now for the statically indeterminate structure these internal virtual loads (u-loads) are, in general, indeterminate since the dummy-unit load is applied at an external point of the structure. However, we recall that,

1 - any stress distribution in static equilibrium with the "applied load" (for the moment now we are thinking of the dummy-unit load as the "applied load") differs from the correct (true) distribution only by a stress distribution having zero external resultant (p. A8.1).

11 - a zero-resultant stress distribution moving through a set of displacements does zero work.

Mathematically expressed these points are;

$$\text{i} \;.\; u_{TRUE} = u_{STATIC} + u_{R=0}$$

where u_{STATIC} is a u-load distribution obtained from statics in a simple "cut" structure under the action of the externally applied dummy-unit load and $u_{R=0}$ is the zero-resultant u-load system which must be superposed to give the true u-load distribution

$$\text{ii} \;.\; \Sigma \Delta \cdot u_{R=0} = 0$$

It follows, therefore, that any set of u-loads in static equilibrium with the externally applied dummy-unit load will do the same amount of virtual work when the structure undergoes its distortion as would a "true" set of u-loads computed by an indeterminate stress calculation. That is,

$$\delta = \Sigma \Delta \cdot u_{TRUE} =$$

$$\Sigma \Delta \cdot (u_{STATIC} + u_{R=0}) =$$

$$\Sigma \Delta \cdot u_{STATIC} + \Sigma \Delta \cdot u_{R=0} =$$

$$\Sigma \Delta \cdot u_{STATIC}$$

Q.E.D.

A8.5 Trusses With Double Redundancy

Trusses with double redundancy are handled directly by Eqs. (4). By way of illustration, the structure of Fig. A8.4, from which Eqs. (4) were derived, will be solved for a loading $P_1 = 2000\#$ and $P_2 = 1000\#$. Choices of redundants were made identical with those of Fig. A8.4a. Figs. A8.11, A8.12 and A8.13 show the S, u_x and u_y load calculations respectively.

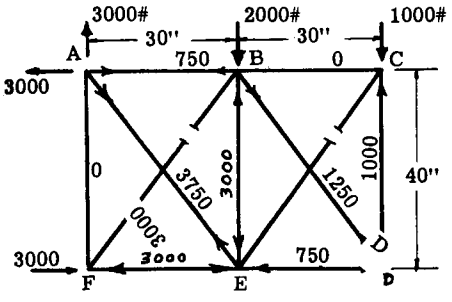

Fig. A8.11
S loads

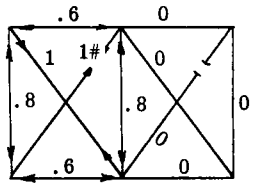

Fig. A8.12
u_x loads

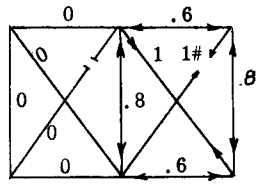

Fig. A8.13
u_y loads

We note here the rule by which the degree of redundancy of a planar pinjointed truss can be determined. For a truss of m members with p joints, the truss is n times redundant where n = m - (2p - 3). For a spatial truss (3 dimensional truss) n = m - (3p - 6).

In the present problem n = 11 - (12 - 3) = 2.

The calculation is carried out in tabular form in Table A8.2. The member dimensions are given in the table.

Table A8.2

Member	L	A	S	u_x	u_y	$\frac{Su_xL}{A}$	$\frac{Su_yL}{A}$	$\frac{u_x^2L}{A}$	$\frac{u_y^2L}{A}$	$\frac{u_xu_yL}{A}$	True Load = $S + X u_x + Y u_y$
AB	30	.5	750	-.6	0	-27,000	0	21.6	0	0	1680
BC	30	.25	0	0	-.6	0	0	0	43.2	0	560
CD	40	.5	-1000	0	-.8	0	64,000	0	51.2	0	-255
BD	50	.25	1250	0	1	0	250,000	0	200	0	318
CE	50	.5	0	0	1	0	0	0	100	0	-932
BE	40	.7	-3000	-.8	-.8	137,000	137,000	36.6	36.6	36.6	-1015
ED	30	.5	-750	0	-.6	0	27,000	0	21.6	0	-190
BF	50	.8	0	1	0	0	0	62.5	0	0	-1550
AE	50	.5	3750	1	0	375,000	0	100	0	0	2200
EF	30	.7	-3000	-.6	0	77,200	0	15.4	0	0	-2070
AF	40	.25	0	-.8	0	0	0	105.0	0	0	1240
					Σ	562,200	478,000	341.1	452.6	36.6	

Substituting from the table into Eqs. (4) gives (common factor of E divided out)

$$\begin{cases} X \Sigma \frac{u_x^2L}{A} + Y \Sigma \frac{u_xu_yL}{A} = - \Sigma \frac{Su_xL}{A} \\ X \Sigma \frac{u_xu_yL}{A} + Y \Sigma \frac{u_y^2L}{A} = - \Sigma \frac{Su_yL}{A} \end{cases}$$

$$\begin{cases} 341.1\, X + 36.6\, Y = - 562{,}000 \\ 36.6\, X + 452.6\, Y = - 478{,}000 \end{cases}$$

Solving,

$X = - 1550\#$

$Y = - 932\#\#$

Finally (see Table A8.2)

True Load = $S + Xu_x + Yu_y$.

A8.5 Trusses With Double Redundancy, cont'd.

Example Problem 3

Fig. A8.14 shows a structure composed of four co-planar members supporting a 2000# load. With only two equations of statics available for the concurrent force system the structure, relative to loads in the members, is redundant to the second degree.

Solution:

Fig. A8.15 shows the assumed statically determinate structure; the two members CE and DE were taken as the redundants and were cut at points x and y as shown. The member stresses for this structure and loading are recorded on the members. Figs. A8.16 and A8.17 give the u_x and u_y member stresses due to unit (1#) tensile loads applied at the cut faces x and y. Table A8.3 gives the complete calculations for eqs. (4) and (5). The load in the redundant member CE was designated X and that in DE as Y.

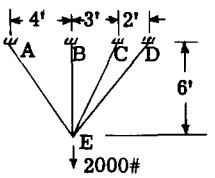

Fig. A8.14

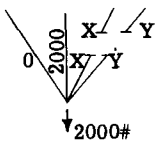

Fig. A8.15

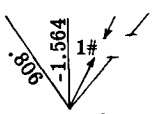

u_x loads

Fig. A8.16

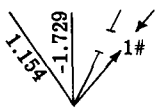

u_y loads

Fig. A8.17

$$X \Sigma \frac{u_x^2 L}{A} + Y \Sigma \frac{u_x u_y L}{A} = - \Sigma \frac{S u_x L}{A}$$

Substituting values from table

$$2446\ X + 2350\ Y = 2{,}253{,}000.$$

$$X \Sigma \frac{u_x u_y L}{A} + Y \Sigma \frac{u_y^2 L}{A} = - \Sigma \frac{S u_y L}{A}$$

Substituting:

$$2350\ X + 3039\ Y = 2{,}488{,}000.$$

TABLE A8.3

Member	Area	L	S	u_x	u_y	$\frac{Su_xL}{A} \times 10^{-6}$	$\frac{Su_yL}{A} \times 10^{-6}$	$\frac{u_x^2L}{A}$	$\frac{u_y^2L}{A}$	$\frac{u_xu_yL}{A}$	True Load = $S + X_{ux} + Y_{uy}$
AE	.2	86.5	0	.806	1.154	0	0	280.5	576.5	402	900
BE	.1	72	2000	-1.564	-1.729	-2.253	-2.488	1763	2150	1948	465
CE	.2	80.5	0	1.00	0	0	0	402.5	0	0	521
DE	.3	93.7	0	0	1.00	0	0	0	312.5	0	416
Total Σ						-2.253	-2.488	2446	3039	2350	

Solving the two equations for X and Y, one obtains X = 521# and Y = 416#. The true load in any member = $S + Xu_x + Yu_y$ which gave the values in the last column of the table.

A8.6 Trusses With Multiple Redundancy.

By induction, eqs. (4) may be extended for application to trusses which are three or more times redundant. Thus for a triple redundancy,

$$\left.\begin{aligned} X \Sigma \frac{u_x^2 L}{AE} + Y \Sigma \frac{u_x u_y L}{AE} + Z \Sigma \frac{u_x u_z L}{AE} &= - \Sigma \frac{S u_x L}{AE} \\ X \Sigma \frac{u_x u_y L}{AE} + Y \Sigma \frac{u_y^2 L}{AE} + Z \Sigma \frac{u_y u_z L}{AE} &= - \Sigma \frac{S u_y L}{AE} \\ X \Sigma \frac{u_x u_z L}{AE} + Y \Sigma \frac{u_y u_z L}{AE} + Z \Sigma \frac{u_z^2 L}{AE} &= - \Sigma \frac{S u_z L}{AE} \end{aligned}\right\} \text{-(6)}$$

and after solving for X, Y, Z,

$$\text{True Stresses} = S + Xu_x + Yu_y + Zu_z \quad \text{-----(7)}$$

A8.7 Redundant Structures With Members Subjected to Loadings in Addition to Axial Forces.

Eqs. (6) are extended readily to cover problems in which flexural, torsional, and shear loadings occur. Thus, for a three times redundant structure

$$\left.\begin{aligned} Xa_{xx} + Ya_{xy} + Za_{xz} &= - \delta_{xo} \\ Xa_{yx} + Ya_{yy} + Za_{yz} &= - \delta_{yo} \\ Xa_{zx} + Ya_{zy} + Za_{zz} &= - \delta_{zo} \end{aligned}\right\} \text{---------(8)}$$

where

$$a_{xx} = \Sigma \frac{u_x^2 L}{AE} + \int \frac{m_x^2 dx}{EI} + \int \frac{t_x^2 dx}{GJ} + \iint \frac{\bar{q}_x^2\, dx\, dy}{Gt}$$

$$a_{xy} = a_{yx} = \Sigma \frac{u_x u_y L}{AE} + \int \frac{m_x m_y dx}{EI} + \int \frac{t_x t_y dx}{GJ} + \iint \frac{\bar{q}_x \bar{q}_y\, dx dy}{Gt}$$

$$a_{yy} = \Sigma \frac{u_y^2 L}{AE} + \int \frac{m_y^2 dx}{EI} + \text{----- etc.}$$

,
,
,
,
,

and

$$\delta_{xo} = \left\{ \frac{Su_x L}{AE} + \int \frac{Mm_x dx}{EI} + \int \frac{Tt_x dx}{GJ} \right.$$

$$\left. + \iint \frac{q\bar{q}_x dxdy}{Gt} \right.$$

$$\delta_{yo} = \left\{ \frac{Su_y L}{AE} + \int \frac{Mm_y dx}{EI} + \int \frac{Tt_y dx}{GJ} \right.$$

$$\left. + \iint \frac{q\bar{q}_y \, dx \, dy}{Gt} \right.$$

,
,
,
,

etc.

and where

S, M, T, q are the real loads in the determinate structure;

u_x, m_x, t_x, $\bar{q}_x$ are the unit (virtual) loadings due to a unit load at cut x;

u_y, m_y, t_y, $\bar{q}_y$ are for a unit load at cut y; etc.

The redundant force(s) need not be an axial force but may be a moment, torque etc.

After solution for the redundants, True Axial Forces =

$$\left.\begin{array}{l} S + X\,u_x + Y\,u_y + Z\,u_z \\ \text{True Bending Moments} = \\ M + X\,m_x + Y\,m_y + Z\,m_z \end{array}\right\} \text{- - - - - - - - (9)}$$

,
,
,

etc.

Example Problem 4

The symmetric sheet stringer panel of Fig. A8.18 is to be analyzed for distribution of load P between stringers. As a first approximation, assume constant shear flow in the sheet panels. All stringers have the same area.

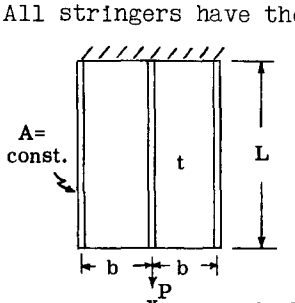

Fig. A8.18

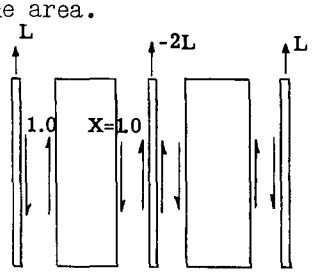

u_x, $\bar{q}_x$ loadings

Fig. A8.19

Solution:

The shear flow in the sheet panels was chosen as redundant. Because of symmetry the problem was only singly redundant. Fig. A8.19 shows the u_x and $\bar{q}_x$ loadings due to the redundant shear flow X = 1. The real loading in the determinate structure consisted of a constant load P in the central stringer alone. The equation solved was (ref. eqs. (8)).

$$X\left(\int \frac{u_x^2 \, dx}{AE} + \iint \frac{\bar{q}_x^2 \, dxdy}{Gt} \right) =$$

$$= -\left(\int \frac{Su_x \, dx}{AE} + \iint \frac{q\,\bar{q}_x \, dxdy}{Gt} \right)$$

where

$$\text{REAL LOADS} \begin{cases} S = P = \text{constant, in central stringer} \\ S = o \text{ in side stringers} \\ q = o \end{cases}$$

$$\text{VIRTUAL LOADS} \begin{cases} u_x = L - x \text{ in side stringers} \\ \quad = 2(x-L) \text{ in central stringers} \\ \bar{q}_x = 1.0 \end{cases}$$

When evaluated, (note that the double integrals simply reduce to a constant times the panel area)

$$X\left(2\,\frac{L^3}{AE} + \frac{2bL}{Gt} \right) = -\left(\frac{-PL^2}{AE} \right)$$

$$X = \frac{P}{2L}\left(\frac{1}{1 + \frac{bAE}{GtL^2}} \right)$$

Therefore the true stresses were

$$P_{ROOT} = P - 2LX = P\,\frac{1}{1 + \frac{L^2Gt}{AEb}} \text{ in central stringer}$$

$$P_{ROOT} = LX = \frac{P}{2}\,\frac{1}{1 + \frac{AEb}{L^2Gt}} \text{ in side stringers}$$

Example Problem 5

The problem of Fig. A8.19 is doubly redundant as shown. Determine the bending moment distribution. Both members have equal sectional properties.

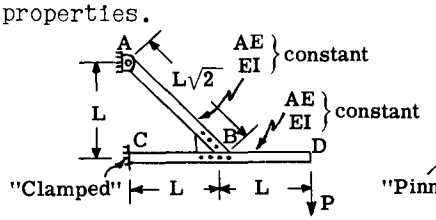

Fig. A8.19

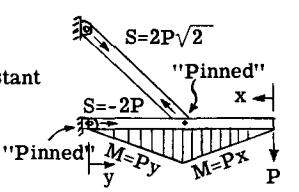

Fig. A8.20
S, M loadings

Solution:

The bending moments at point C in member CBD and at point B in member AB were selected as redundants yielding (when cut) the pin-jointed determinate structure of Fig. A8.20. The virtual loadings were as shown in Figs. A8.21 and A8.22.

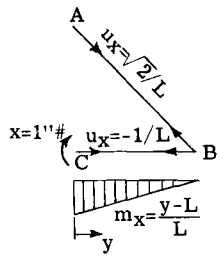

u_x, m_x loadings
Fig. A8.21

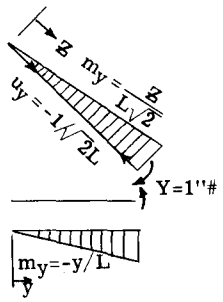

u_y, m_y loadings
Fig. A8.22

Note that in Fig. A8.22 the unit redundant loading was applied as a self-equilibrating set of unit couples. The real and virtual loadings were as follows: (member portion BD, having no virtual loadings, was omitted. It could not enter the calculation.)

Member	S	M	u_x	m_x	u_y	m_y
AB	$2P\sqrt{2}$	0	$\sqrt{2}/L$	0	$-1/L\sqrt{2}$	$z/L\sqrt{2}$
BC	-2P	Py	$-1/L$	$\frac{y-L}{L}$	0	$-y/L$

The equations which were solved were (Ref. eq. (8)).

$$X\left(\int\frac{u_x^2L}{AE}+\int\frac{m_x^2dx}{EI}\right)+Y\left(\int\frac{u_xu_yL}{AE}+\int\frac{m_xm_ydx}{EI}\right)=-\left(\int\frac{Su_xL}{AE}+\int\frac{Mm_xdx}{EI}\right)$$

$$X\left(\int\frac{u_xu_yL}{AE}+\int\frac{m_xm_ydx}{EI}\right)+Y\left(\int\frac{u_y^2L}{AE}+\int\frac{m_y^2dx}{EI}\right)=-\left(\int\frac{Su_yL}{AE}+\int\frac{Mm_ydx}{EI}\right)$$

After evaluation of the integrals and multiplying through by L^2 these become

$$X\left((1+2\sqrt{2})\frac{L}{AE}+\frac{L^3}{3EI}\right)+Y\left(-\frac{L\sqrt{2}}{AE}+\frac{L^3}{6EI}\right)=-PL\left(\frac{(2+4\sqrt{2})L}{AE}-\frac{L^3}{6EI}\right)$$

$$X\left(-\frac{L\sqrt{2}}{AE}+\frac{L^3}{6EI}\right)+Y\left(\frac{L}{\sqrt{2}AE}+\frac{(1+\sqrt{2})L^3}{3EI}\right)=-PL\left(\frac{2L\sqrt{2}}{AE}-\frac{L^3}{3EI}\right)$$

For a specific case it was assumed that

$$\frac{AE}{L}=100\,\frac{EI}{L^3}\qquad\text{giving}$$

$$\begin{cases}.3716\,X+.1526\,Y=.09011\,PL\\ .1526\,X+.8121\,Y=.3616\,PL\end{cases}$$

$$\begin{cases}X=.0645\,PL\\ Y=.456\,PL\end{cases}$$

Then as usual

$$\text{True Stresses}=S+X\,u_x+Y\,u_y$$

$$\text{True Moments}=M+Xm_x+Ym_y$$

A8.8 Initial Stresses.

In a redundant structure initial stresses are developed if, upon assembly, certain members must be forced into place because of lack of fit. In some situations intentional misfits are employed to obtain more favorable stress distributions under load ("prestressing").

If, in Fig. A8.4(a), the redundant member with the "x cut" was initially oversize (too long) an amount δ_{Xi} (an oversize, corresponding to a distortion in the positive X direction, is a positive δ_{xi}), the modified condition for continuity at the x cut would be (compare with the equations just preceding eqs. (4)).

$$\delta_{x0}+\delta_{xi}+\delta_{xx}+\delta_{xy}=0$$

Similarly if the Y redundant member were too long

$$\delta_{y0}+\delta_{yi}+\delta_{yx}+\delta_{yy}=0$$

Then using the previous notations, the appropriate equations for the redundant forces are

$$\left.\begin{aligned}X\left\{\frac{u_x^2L}{AE}+Y\left\{\frac{u_xu_yL}{AE}\right.\right.&=-\left\{\frac{Su_xL}{AE}-\delta_{xi}\right.\\ X\left\{\frac{u_xu_yL}{AE}+Y\left\{\frac{u_y^2L}{AE}\right.\right.&=-\left\{\frac{Su_yL}{AE}-\delta_{yi}\right.\end{aligned}\right\}\quad\text{---(10)}$$

The "S loads" of eq. (10) are present because of applied external loads. These may or may not be zero depending upon the problem.

Example Problem 6

If in example problem 3 member CE was 0.01 inches too short before assembly, determine the stress distribution after assembly and load application.

Solution:

Data obtained from the previous problem was substituted into eqs. (10) along with

$\delta_{xi} = -.01"$ (negative because "too short")

$\delta_{yi} = 0$

to give

$$\begin{cases} 2446\ X + 2350\ Y = 2.253 \times 10^6 + .01E \\ 2350\ X + 3039\ Y = 2.488 \times 10^6 \end{cases}$$

with $E = 29 \times 10^6$ the redundant forces were

$$X = 985 \text{ lbs.}$$
$$Y = 57 \text{ lbs.}$$

Then, as usual,

$$\text{True stresses} = S + Xu_x + Yu_y.$$

Example Problem 7

Assume that in the structure of example problem 5 an angular misalignment occurred between members AB and CBD at joint B such that the end of member AB had to be rotated 2.7° clockwise to fit upon assembly. Determine the moments developed without external loads applied.

Solution:

The initial imperfection was $\delta_{yi} = -\,{}^{2.7}/_{57.3} = -\,.0471$ radians

The sign was determined by noting that the original misalignment was in the negative direction of the redundant couple Y.

The equations used from the previous problem were (noting the equations there had been multiplied by $L^2 \times EI/L^3 = EI/L$).

$$\begin{cases} .3716\ X + .1526\ Y = 0 \\ .1526\ X + .8121\ Y = .0471\ \dfrac{EI}{L} \end{cases}$$

Solving,

$$X = -\,.0258\ EI/L$$
$$Y = .0630\ EI/L$$

True initial stresses and moments were determined as usual.

If, as is sometimes the case, the number of misalignments exceeds the number of redundancies, or if the misalignment does not coincide with the redundant cut chosen but occurs elsewhere, one may use the virtual work principle to compute the effect of these misalignments on the redundant cuts proper. Thus, referring to the "virtual work" derivation of the Dummy-Unit load equations, (Chap. A7) one has

$$\delta_{xi} = \Sigma\ u_x\ \Delta_i \quad - - - - - - - - - - - - - - - - (11)$$

where δ_{xi} is the initial misalignment in the determinate structure at the X redundancy-cut due to initial imperfections (equivalent to initial strains) Δ_i throughout the structure. u_x as before, is the unit loading due to a virtual load at cut x. Eq. (11) and similar expressions for the Y, Z, etc. cuts may be inserted in eqs. (10).

Example Problem 8

Referring back to example problems numbers 3 and 6, assume that member BE is .025" too long. Determine the initial stresses if the other members are of proper length and no external load is applied.

Solution:

To employ the same equations as those of example problem 3, the initial imperfections occurring at the same x and y cuts used there were computed, in this case due to the initial elongation of BE. Thus

$$\delta_{xi} = \Sigma\ u_x \Delta_i = (-1.564)(.025") = -.0391"$$
$$\delta_{yi} = \Sigma\ u_y \Delta_i = (-1.729)(.025) = -.0432"$$

Then, use of those previously computed coefficients in eqs. (10) gave,

$$2446\ X + 2350\ Y = .0391\ E$$
$$2350\ X + 3039\ Y = .0432\ E$$

With $E = 29 \times 10^6$ psi

$$X = 263 \text{ lbs.}$$
$$Y = 209 \text{ lbs.}$$

Finally,

$$\text{True Initial Stresses} = S + Xu_x + Yu_y$$

A8.9 Thermal Stresses.

Stresses induced in redundant structures by thermal strains may be computed by application of methods presented above. The problem may be approached from the point of view of computing the

relative motions at the cuts of the determinate structure caused by the thermal strains and then restoring continuity by applying redundant member forces to the cuts.

Specifically, consider a doubly redundant truss such as that of Fig. A8.4(a). After making cuts "x" and "y" to render the structure determinate, the application of the temperature distribution is visualized. Relative displacements occur at the cuts, denoted by δ_{xT} and δ_{yT}. These displacements may be computed by the Dummy-Unit Load method as shown in Art. A7.8 of Chap. A7. After this calculation is accomplished, the problem proceeds as for initial strains, Art. A8.8. Thus, the continuity condition at the cut gives (compare with the equations immediately preceding eqs. (4) and assume for simplicity that the external loads are absent, making $\delta_{xo} = \delta_{yo} = 0$)

$$\left.\begin{aligned} \delta_{xT} + \delta_{xx} + \delta_{xy} &= 0 \\ \delta_{yT} + \delta_{yx} + \delta_{yy} &= 0 \end{aligned}\right\}$$

In a truss, the thermal strains produce relative displacements at the cuts given by the "virtual work" derivation of the Dummy-Unit Load equations (ref. Chap. A7, Arts. A7.7 and A7.8) as

$$\left.\begin{aligned} \delta_{xT} &= \int u_x\, \alpha\, T\, dx \\ \delta_{yT} &= \int u_y\, \alpha\, T dx \end{aligned}\right\} \quad - - - - - - - - - - - - (12)$$

where α is the material thermal coefficient of expansion, T is the temperature above the ambient temperature and u_x and u_y are the unit load distributions due to virtual loads at the x and y cuts, respectively. The sums in eqs. (12) are written as integrals rather than finite sums to allow for possible variation in α and T, along the members as well as from member to member. Then the final equations for thermal stresses in a doubly redundant truss become

$$\left.\begin{aligned} X\left\{\frac{u_x^2 L}{AE}\right. + Y\left\{\frac{u_x u_y L}{AE}\right. &= -\int u_x\, \alpha\, T\, dx \\ X\left\{\frac{u_x u_y L}{AE}\right. + Y\left\{\frac{u_y^2 L}{AE}\right. &= -\int u_y\, \alpha\, T\, dx \end{aligned}\right\} \quad - - (13)$$

Equations (13) may, of course, be extended for application to structures other than trusses. The expressions appropriate to other loadings have been developed previously (eqs. (8) et seq. in this chapter and other equations in Art. A7.8).

Example Problem 9

The end upright of the truss of Fig. A8.23 is heated to the temperature distribution shown. Determine the stresses and reactions developed.

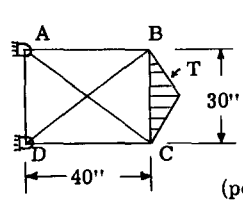

Fig. A8.23

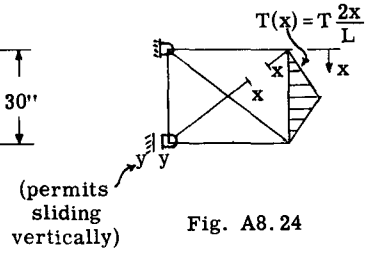

Fig. A8.24

Solution:

The structure was made determinate by cuts x and y as in Fig. A8.24. The unit loadings are shown in Fig. A8.25.

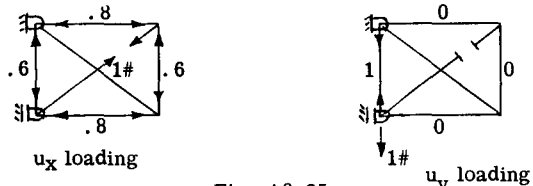

Fig. A8.25

The thermal coefficient α was assumed constant. The calculation was set up in tabular form.

TABLE A8.4

Mem.	L	AE x 10^{-6}	u_x	u_y	$\frac{u_x^2 L}{AE}$ x 10^6	$\frac{u_y^2 L}{AE}$ x 10^6	$\frac{u_x u_y L}{AE}$ x 10^6	T(x)	$\int u_x \alpha T\, dx$	$\int u_y \alpha T\, dx$	Stresses = $Xu_x + Yu_y$
AB	40	30	- .8	0	.853	0	0	0	0	0	-1.61αTx10^6
BC	30	20	- .6	0	.540	0	0	$\frac{2x}{L}$T	- 9 α T	0	-1.21 "
CD	40	30	- .8	0	.853	0	0	0	0	0	-1.61 "
DA	30	20	- .6	1.0	.540	1.50	- .90	0	0	0	0.0 "
AC	50	45	1.0	0	1.111	0	0	0	0	0	2.01 "
DB	50	45	1.0	0	1.111	0	0	0	0	0	2.01 "
					5.008 x 10^{-6}	1.50 x 10^{-6}	- .90 x 10^{-6}		- 9 α T		

Substituting into eqs. (13)

$$\left\{\begin{aligned} 5.008\, X - .90\, Y &= 9\, \alpha\, T \times 10^6 \\ -\ .90\, X + 1.50\, Y &= 0 \end{aligned}\right.$$

Solving,

$$X = 2.01\, \alpha\, T \times 10^6$$

$$Y = 1.21\, \alpha\, T \times 10^6$$

True stresses are given in Table A8.4.

Example Problem 10

The upper surface of the built-in beam of Fig. A8.26 is heated to a uniform temperature T.

Through the depth of the beam the temperature varies linearly to normal (T = 0) at the lower surface. Determine the end moments developed, neglecting axial constraint and influence of axial forces.

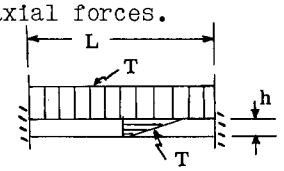

EI constant
Fig. A8.26a

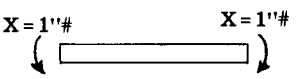

Virtual Loading
Fig. A8.26b

Solution:

The problem was only singly redundant because of symmetry and was made determinate by cutting the end bending restraints. Application of unit couples (Fig. A8.26b) gave m = 1 = const. Then (see Example Problem 24, Art. A7.8) the thermal deflection at the "cut" was

$$\delta_{xT} = \int_0^L m d\theta = \int_0^L 1 \cdot \frac{T\alpha dx}{h} = \frac{T\alpha L}{h}$$

The redundant moment equation was (by analogy to eq. 13)

$$X \int \frac{m_x^2 dx}{EI} = - \delta_{xT}$$

Therefore

$$X \frac{L}{EI} = - T\alpha L/h$$

$$X = - \frac{T\alpha EI}{h}$$

The redundant moment compresses the upper fibers as was to be expected.

Example Problem 11

Complete the problem begun in Example Problem 24 Art. A7.8, viz, that of computing the thermal stresses in a closed ring whose inner surface is uniformly heated to a temperature T above the outside.

Solution:

The ring was made determinate by cutting at the top as in Fig. A7.30(b). The unit loadings and thermal deflections were determined in the referenced example. The results of deflection calculations made previously were

$$\delta_{xT} = 2\pi \frac{R\alpha T}{h}$$

$$\delta_{yT} = -2\pi \frac{R^2 \alpha T}{h}$$

$$\delta_{zT} = 0$$

Then the equations corresponding to eqs. (13) were written (see also eqs. (8)).

$$X\left(\int \frac{u_x^2 ds}{AE} + \int \frac{m_x^2 ds}{EI}\right) + Y\left(\int \frac{u_x u_y ds}{AE} + \int \frac{m_x m_y ds}{EI}\right)$$

$$+ Z\left(\int \frac{u_x u_z ds}{AE} + \int \frac{m_x m_z ds}{EI}\right) = - \delta_{xT}$$

$$X\left(\int \frac{u_x u_y ds}{AE} + \int \frac{m_x m_y ds}{EI}\right) + Y\left(\int \frac{u_y^2 ds}{EI} + \int \frac{m_y^2 ds}{EI}\right)$$

$$+ Z\left(\int \frac{u_y u_z ds}{AE} + \int \frac{m_y m_z ds}{EI}\right) = - \delta_{yT}$$

$$X\left(\int \frac{u_x u_z ds}{AE} + \int \frac{m_x m_z ds}{EI}\right) + Y\left(\int \frac{u_y u_z ds}{AE} + \int \frac{m_y m_z ds}{EI}\right)$$

$$+ Z\left(\int \frac{u_z^2 ds}{AE} + \int \frac{m_z^2 ds}{EI}\right) = - \delta_{zT}$$

Evaluated, the equations were

$$\begin{cases} \frac{1}{EI} X - \frac{R}{EI} Y + 0 \cdot Z = + \frac{\alpha T}{h} \\ \frac{-R}{EI} X + \frac{1}{2}\left(\frac{1}{AE} + \frac{R^2}{EI}\right) Y + 0 \cdot Z = - \frac{\alpha R T}{h} \\ 0 \cdot X + 0 \cdot Y + \left(\frac{1}{AE} + \frac{R^2}{EI}\right) Z = 0 \end{cases}$$

Note that from the last of these equations Z = 0, as it must because of the symmetry of the ring. Solving the first two equations

$$X = \frac{\alpha T EI}{h}$$

$$Y = 0$$

A non-zero value of Y would produce a varying bending moment which cannot be because of symmetry. Hence this result too, is rational.

A8.10 Redundant Problem Stress Calculations by Matrix Methods.

In the following section the indeterminate structural problem is formulated in matrix notation. The reader is assumed to be familiar with the matrix applications of Art. A7.9 and the elements of matrix notation and arithmetic (see Appendix).

The stress distribution of the structure is specified by a set of internal generalized forces, q_i, q_j.* (ref. Art. A7.9). Unlike the case of the determinate structure, these q_i, q_j cannot be

* In the case of indeterminate structures, wherein some of the support reactions may also be redundant, these reactions also are denoted by q's. (see Example Problem 13a).

related immediately to the external loads by the equations of statics. Thus a certain subset of the q_i, q_j are redundants and are denoted by q_r, q_s, (r, s different numerical subscripts). When, finally, the redundant forces, q_r, q_s, are computed (by satisfying continuity) the true values of all the q_i, q_j may be found by statics.

SYMBOLS

q_i, q_j - internal generalized forces acting on structural elements and reactions at support points.

q_r, q_s - redundant generalized forces and redundant reactions

P_m, P_n - applied external loads

g_{im} $(=g_{jn})$ - the value of q_i, (q_j) in the determinate structure under application of a unit external load $P_m = 1$ $(P_n = 1)$

g_{ir} $(=g_{js})$ - the value of q_i (q_j) in the determinate structure due to application of a unit redundant force $q_r = 1$ $(q_s = 1)$

G_{im} $(=G_{jn})$ - the true value of q_i (q_j) in the redundant structure due to application of load $P_m = 1$ $(P_n = 1)$

G_{rm} $(=G_{sn})$ - the true value of q_r (q_s) for a unit value of applied load $P_m = 1$ $(P_n = 1)$.

a_{ij} - member flexibility coefficient: deflection at point i for a unit force, $q_j = 1$ (see Arts. A7.9, 10)

a_{mn} - influence coefficient for the determinate structure: displacement at external loading point m for a unit applied load, $P_n = 1$. $(a_{mn} = a_{nm})$

a_{rn} $(=a_{sm})$ - influence coefficient for the determinate structure: displacement at redundant cut r (s) for a unit applied load, $P_n = 1$ $(P_m = 1)$. $(a_{rn} = a_{nr})$

a_{rs} - influence coefficient for the determinate ("cut") structure: displacement at redundant cut r for a unit redundant force $q_s = 1$. $(a_{rs} = a_{sr})$

A_{mn} - influence coefficient for complete redundant structure: deflection at external loading point m for a unit applied load, $P_n = 1$. $(A_{mn} = A_{nm})$

SYMBOLS - continued

T_i, T_j - the temperature (above normal) at points i, j.

Δ_{iT}, Δ_{jT} - the member thermal distortions associated with q_i, q_j.

In the notation of Arts. A8.3 et seq, the final true values of the stresses were expressed as (eq. (5) Art. A8.3)

$$S_{TRUE} = S + Xu_x + Yu_y \quad - - - - - - - - - - - - (5)$$

In the notation to be employed here, this equation is restated as

$$\left\{q_i\right\} = \left[g_{im}\right]\left\{P_m\right\} + \left[g_{ir}\right]\left\{q_r\right\} - - - - - - \quad (14)$$

Here:

$\left[g_{im}\right]\left(=\left[g_{jn}\right]\right)^*$ is the matrix of unit-load stress distributions in the determinate ("cut") structure found by the application of unit (virtual) loads at the external loading points. The product $\left[g_{im}\right]\left\{P_m\right\}$ then gives the real loads in the determinate structure, corresponding to the "S" loads of eq. (5).

$\left[g_{ir}\right]\left(=\left[g_{js}\right]\right)$ is the matrix of unit-load stress distributions found by application of unit (virtual) forces at the redundant cuts in the determinate ("cut") structure. Hence this is the matrix of u_x, u_y, etc. loads.

The $\left\{q_r\right\}$, of course, correspond to X, Y, etc.

Note that the $\left[g_{im}\right]$ and $\left[g_{ir}\right]$ matrices are load distributions computed and arranged in much the same fashion as was $\left[G_{im}\right]$ of Art. A7.9. The small letter "g" is used to indicate load distribution in the "cut" structure.

By way of illustration, the final result for Example Problem 3, Art. A8.5 is expressed below. FIRST, in the form of eq. (5):

True Stresses = S + X (u_x) + Y (u_y)

AE = 0 + 521 (.806) + 416 (1.154)

BE = 2000 + 521 (-1.564) + 416 (-1.729)

CE = 0 + 521 (1.00) + 416 (0)

DE = 0 + 521 (0) + 416 (1.00)

* Note that within each of the sets of subscript symbols (i, j), (r, s), (m, n) the symbols may be used interchangeably.

SECOND, in the form of eq. (14):

$$\begin{Bmatrix} q_1 \\ q_2 \\ q_3 \\ q_4 \end{Bmatrix} = \begin{Bmatrix} 0 \\ 1 \\ 0 \\ 0 \end{Bmatrix} \cdot 2000 + \begin{bmatrix} .806 & 1.154 \\ -1.564 & -1.729 \\ 1.00 & 0 \\ 0 & 1.00 \end{bmatrix} \begin{Bmatrix} 521 \\ \\ 416 \\ \\ \end{Bmatrix}$$

Note that in this case $[g_{im}]$ consisted of only one column, inasmuch as there was only a single external load.

In Art. A7.9 the strain energy was written

$$2U = \lfloor q_i \rfloor [a_{ij}] \{q_j\} \quad \text{- - - - - - - - - - (15)}$$

where $[a_{ij}]$ is the matrix of member flexibility coefficients (Art. A7.10). If now eq. (14) and its transpose are used to substitute into (15) the expression becomes (note the use of (i,j), (r,s), and (m,n) interchangeably)

$$2U = \left(\lfloor P_m \rfloor [g_{mi}] + \lfloor q_r \rfloor [g_{ri}] \right) x$$

$$[a_{ij}] \, x \left([g_{js}] \{q_s\} + [g_{jn}] \{P_n\} \right).$$

Multiplying out

$$2U = \lfloor P_m \rfloor [g_{mi}] [a_{ij}] [g_{jn}] \{P_n\} +$$

$$2 \lfloor q_r \rfloor [g_{ri}] [a_{ij}] [g_{jn}] \{P_n\} +$$

$$\lfloor q_r \rfloor [g_{ri}] [a_{ij}] [g_{js}] \{q_s\}$$

The reader may satisfy himself that the "cross product" term in the middle of the above result is correct by observing that, because of the symmetry of $[a_{ij}]$,

$$\lfloor q_r \rfloor [g_{ri}] [a_{ij}] [g_{jn}] \{P_n\} =$$

$$\lfloor P_m \rfloor [g_{mi}] [a_{ij}] [g_{js}] \{q_s\}$$

The various matrix triple products occurring above are assigned the following symbols, each having the interpretation given (compare with eq. (24) of Art. A7.9)

$$[a_{mn}] \equiv [g_{mi}] [a_{ij}] [g_{jn}] \quad \text{- - - - - - - - - -(16)}$$

- the matrix of external-point influence coefficients in the "cut" structure: deflection at point m per unit load at point n.

$$[a_{rn}] \equiv [g_{ri}] [a_{ij}] [g_{jn}] \quad \text{- - - - - - - - - (17)}$$

- the matrix of influence coefficients relating relative displacements at the "cuts" to external loads: displacement at cut r per unit load at point n.

$$[a_{rs}] \equiv [g_{ri}] [a_{ij}] [g_{js}] \quad \text{- - - - - - - - - (18)}$$

- the matrix of influence coefficients relating relative displacements at the "cuts" to redundant loads at the "cuts": displacement at cut r per unit redundant force at cut s.

With the above notation one may write

$$2U = \lfloor P_m \rfloor [a_{mn}] \{P_n\} + 2 \lfloor q_r \rfloor [a_{rn}] \{P_n\}$$

$$+ \lfloor q_r \rfloor [a_{rs}] \{q_s\} \quad \text{- - - - - - - - - - - - (19)}$$

Now according to the Theorem of Least Work $\partial U / \partial q_r = 0$ for continuity. Then, differentiating eq. (19):

$$\frac{\partial U}{\partial q_r} = 0 = [a_{rn}] \{P_n\} + [a_{rs}] \{q_s\} \quad \text{- - - - (20)}$$

This last result may be verified by writing eq. (19) out in expanded form, differentiating and then recombining in matrix form. Rearranged, eq. (20) gives

$$[a_{rs}] \{q_s\} = - [a_{rn}] \{P_n\} \quad \text{- - - - - - - - (21)}$$

Eq. (21) is a set of simultaneous equations for the redundant internal forces q_r, q_s. It may be compared with eq. (6) of Art. A8.6, to which it corresponds. Eq. (21) may be solved directly from the form there displayed or its solution may be obtained by computing $[a_{rs}^{-1}]$, the inverse of the matrix of coefficients, giving

$$\{q_s\} = - [a_{rs}^{-1}] [a_{rn}] \{P_n\} \quad \text{- - - - - - - (22)}$$

The matrix product $- [a_{rs}^{-1}] [a_{rn}]$ gives the values of the redundant forces for unit values of the external loads. This may be given the symbol $[G_{sn}]$ so that

$$\{q_s\} = [G_{sn}] \{P_n\} \quad \text{- - - - - - - - - - - - (22a)}$$

If now eq. (22) is substituted into eq. (14) one gets (with exchange of r for s and m for n)

$$\{q_i\} = [g_{im}]\{P_m\} - [g_{ir}][a_{sr}^{-1}][a_{sm}]\{P_m\}$$

$$= \left([g_{im}] - [g_{ir}][a_{sr}^{-1}][a_{sm}]\right)\{P_m\}$$

$$= \left([g_{im}] + [g_{ir}][G_{rm}]\right)\{P_m\}$$

The matrix set off in parentheses above, gives the internal force distribution per unit value of the external loads. It is given the symbol

$$[G_{im}] \equiv [g_{im}] - [g_{ir}][a_{sr}^{-1}][a_{sm}] \quad \text{- - -} \quad (23)$$

$$\equiv [g_{im}] + [g_{ir}][G_{rm}]$$

so that

$$\{q_i\} = [G_{im}]\{P_m\} \quad \text{- - - - - - - - - - - - - -} \quad (24)$$

Eqs. (23), (24) constitute the major result, inasmuch as they present the means for computing the internal force distribution in a redundant structure.

Example Problem 13

The doubly redundant beam of Fig. A8.27 (a) is to be analyzed for the bending moment distribution. The beam is loaded by couples over the supports as shown.

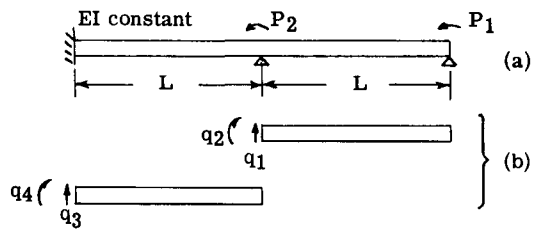

Fig. A8.27

Solution:

The choice of internal generalized forces is shown in Fig. A8.27 (b). The appropriate member flexibility coefficients were arranged in matrix form as (ref. Art. A7.10 for coefficient expressions).

$$[a_{ij}] = \frac{L}{EI}\begin{bmatrix} L^2/3 & L/2 & 0 & 0 \\ L/2 & 1 & 0 & 0 \\ 0 & 0 & L^2/3 & L/2 \\ 0 & 0 & L/2 & 1 \end{bmatrix}$$

The moments q_2 and q_4 were taken as the redundants. With these set equal to zero, the internal force distributions due to application of unit values of P_1 and P_2 were determined, giving

$$[g_{im}] = \begin{bmatrix} 1/L & 0 \\ 0 & 0 \\ 0 & 1/L \\ 0 & 0 \end{bmatrix}$$

With the applied loads set equal to zero, unit values of the redundants were applied yielding

$$(r =) \qquad (2) \qquad (4)$$

$$[g_{ir}] = \begin{bmatrix} -1/L & 0 \\ 1 & 0 \\ 1/L & -1/L \\ 0 & 1 \end{bmatrix}$$

Note that redundant load q_2 was applied as a self-equilibrating internal couple, acting on both beam halfs.

The following matrix products were formed:

$$[a_{rs}] = [g_{ri}][a_{ij}][g_{js}]$$

$$= \frac{L}{EI}\begin{bmatrix} -1/L & 1 & 1/L & 0 \\ 0 & 0 & -1/L & 1 \end{bmatrix}\begin{bmatrix} L^2/3 & L/2 & 0 & 0 \\ L/2 & 1 & 0 & 0 \\ 0 & 0 & L^2/3 & L/2 \\ 0 & 0 & L/2 & 1 \end{bmatrix}\begin{bmatrix} -1/L & 0 \\ 1 & 0 \\ 1/L & -1/L \\ 0 & 1 \end{bmatrix}$$

$$= \frac{L}{6EI}\begin{bmatrix} 4 & 1 \\ 1 & 2 \end{bmatrix}$$

$$[a_{rn}] = [g_{ri}][a_{ij}][g_{jn}]$$

$$= \frac{L}{EI}\begin{bmatrix} -1/L & 1 & 1/L & 0 \\ 0 & 0 & -1/L & 1 \end{bmatrix}\begin{bmatrix} L^2/3 & L/2 & 0 & 0 \\ L/2 & 1 & 0 & 0 \\ 0 & 0 & L^2/3 & L/2 \\ 0 & 0 & L/2 & 1 \end{bmatrix}\begin{bmatrix} 1/L & 0 \\ 0 & 0 \\ 0 & 1/L \\ 0 & 0 \end{bmatrix}$$

$$= \frac{L}{6EI}\begin{bmatrix} 1 & 2 \\ 0 & 1 \end{bmatrix}$$

The inverse of $[a_{rs}]$ was found (ref. appendix)

$$[a_{rs}^{-1}] = \frac{6EI}{7L}\begin{bmatrix} 2 & -1 \\ -1 & 4 \end{bmatrix}$$

Next, the unit redundant load distribution was found (eq. 22).

$$[G_{sn}] = -[a_{rs}^{-1}][a_{rn}] = -\frac{1}{7}\begin{bmatrix} 2 & 3 \\ -1 & 2 \end{bmatrix}$$

$$= \begin{bmatrix} -.286 & -.428 \\ .143 & -.286 \end{bmatrix}$$

Finally, the true unit stress distribution was computed.

$$[G_{im}] = [g_{im}] + [g_{ir}][G_{rm}]$$

$$= \frac{1}{L}\begin{bmatrix} 1 & 0 \\ 0 & 0 \\ 0 & 1 \\ 0 & 0 \end{bmatrix} + \begin{bmatrix} -1/L & 0 \\ 1 & 0 \\ 1/L & -1/L \\ 0 & 1 \end{bmatrix}\begin{bmatrix} -.286 & -.428 \\ .143 & -.286 \end{bmatrix}$$

$$= \frac{1}{L}$$

i \ m	1	2
1	1.286	.428
2	- .286L	-.428L
3	- .429	.858
4	.143L	-.286L

(The tabular form of presentation of the matrix G_{im}, above, is used here only to indicate clearly the functioning of the subscript notational scheme. In general, it should be unnecessary to call out the subscripts in this fashion excepting for the larger matrices, for the handling of which, the tabular form may prove helpful.)

Example Problem 13a

The redundant beam problem of Fig. A8.27 is to be re-solved using the redundant reactions as the unknowns.

Solution:

The support reactions under the loads P_1 and P_2 were given the symbols q_5 and q_6, respectively, positive up. These forces did not enter into the strain energy expression so that, although the matrix of member flexibility coefficients was expanded to a 6 x 6, the coefficients for q_5 and q_6 were zero. Thus,

$$[a_{ij}] = \frac{L}{EI}\begin{bmatrix} L^2/3 & L/2 & 0 & 0 & 0 & 0 \\ L/2 & 1 & 0 & 0 & 0 & 0 \\ 0 & 0 & L^2/3 & L/2 & 0 & 0 \\ 0 & 0 & L/2 & 1 & 0 & 0 \\ 0 & 0 & 0 & 0 & 0 & 0 \\ 0 & 0 & 0 & 0 & 0 & 0 \end{bmatrix}$$

With the redundants q_5 and q_6 set equal to zero, successive applications of unit external couples P_1 and P_2 gave the stress distribution

$$[g_{im}] = \begin{bmatrix} 0 & 0 \\ 1 & 0 \\ 0 & 0 \\ 1 & 1 \\ 0 & 0 \\ 0 & 0 \end{bmatrix}$$

and, with P_1 and P_2 zero, successive applications of unit redundant forces q_5 and q_6 gave

$$[g_{ir}] = \begin{bmatrix} -1 & 0 \\ L & 0 \\ -1 & -1 \\ 2L & L \\ 1 & 0 \\ 0 & 1 \end{bmatrix}$$

Then, multiplying out per eqs. (17) and (18)

$$[a_{rn}] = \frac{L^2}{2EI}\begin{bmatrix} 4 & 3 \\ 1 & 1 \end{bmatrix}$$

$$[a_{rs}] = \frac{L^3}{6EI}\begin{bmatrix} 16 & 5 \\ 5 & 2 \end{bmatrix}$$

The inverse was found:

$$[a_{rs}^{-1}] = \frac{6EI}{7L^3}\begin{bmatrix} 2 & -5 \\ -5 & 16 \end{bmatrix}$$

Finally,

$$[G_{im}] = [g_{im}] - [g_{ir}][a_{sr}^{-1}][a_{sm}]$$

$$= \frac{1}{L} \begin{bmatrix} 1.286 & .428 \\ -.286L & -.428L \\ -.428 & .857 \\ .143L & -.286L \\ -1.286 & -.428 \\ 1.714 & -.428 \end{bmatrix}$$

(Compare with solution to Example Problem 13).

Example Problem 14

The continuous truss of Fig. A8.28 is twice redundant. It is desired to analyze it for stress distributions under a variety of loading conditions consisting of concentrated vertical loads applied at the four external points indicated.

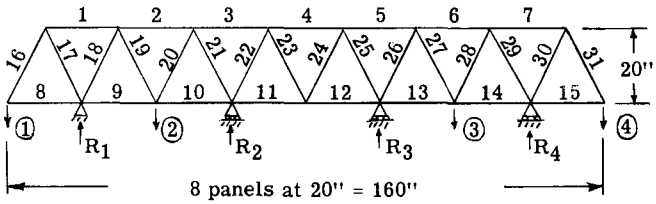

Fig. A8.28

Solution:

The internal generalized forces (q_i, q_j) employed were the axial loads in the various members. These were numbered from one to thirty-one as shown on the figure. The member flexibility coefficients in this case were of the form $a_i = {}^{L}/_{AE}$ (Ref. Fig. A7.35a). The coefficients are written as a column matrix below. (They were employed as the diagonal elements of a square matrix in the matrix multiplications, but are written here as a column to conserve space.)

Member loads q_3 and q_6 were selected as redundants. With q_3 and q_6 set equal to zero ("cut"), unit loads were applied successively at external loading points one through four, the four stress distributions thus found being arranged in four columns giving the matrix $[g_{im}]$ (below). By way of illustration, the loading figure used to obtain the second column of $[g_{im}]$ is shown in Fig. A8.29.

Next, unit forces were applied successively at the redundant cuts "three" and "five" as shown in Figs. A8.30a and A8.30b. These loads were arranged in two columns to give the matrix $[g_{ir}]$

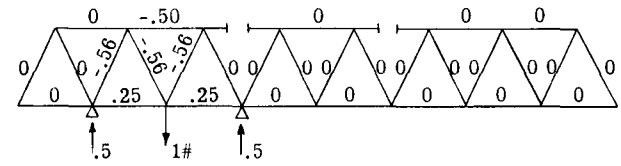

Loading for column $\{g_{i2}\}$ of the matrix $[g_{im}]$

Fig. A8.29

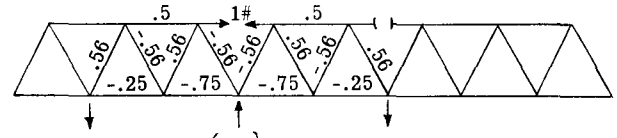

Fig. A8.30a $\{g_{i3}\}$ loading

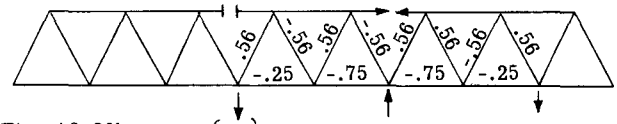

Fig. A8.30b $\{g_{i5}\}$ loading

$$a_i = \frac{1}{E} \begin{Bmatrix} 20 \\ 20 \\ 20 \\ 20 \\ 20 \\ 20 \\ 20 \\ 40 \\ 40 \\ 40 \\ 40 \\ 40 \\ 40 \\ 40 \\ 40 \\ 22.4 \\ 22.4 \\ 22.4 \\ 22.4 \\ 22.4 \\ 22.4 \\ 22.4 \\ 22.4 \\ 22.4 \\ 22.4 \\ 22.4 \\ 22.4 \\ 22.4 \\ 22.4 \\ 22.4 \end{Bmatrix}$$

$[g_{ir}] =$

i \ r	3	5
1	0	0
2	.5	0
3	1.0	0
4	.5	.5
5	0	1.0
6	0	.5
7	0	0
8	0	0
9	-.25	0
10	-.75	0
11	-.75	-.25
12	-.25	-.75
13	0	-.75
14	0	-.25
15	0	0
16	0	0
17	0	0
18	.56	0
19	-.56	0
20	.56	0
21	-.56	0
22	-.56	.56
23	.56	-.56
24	-.56	.56
25	.56	-.56
26	0	-.56
27	0	.56
28	0	-.56
29	0	.56
30	0	0
31	0	0

$[g_{im}]$ =

i \ m	1	2	3	4
1	1.0			
2	.50	-.50		
3				
4				
5				
6			-.50	.50
7				1.0
8	- .50			
9	- .75	.25		
10	- .25	.25		
11				
12				
13			.25	- .25
14			.25	- .75
15				- .50
16	1.12			
17	-1.12			
18	- .56	-.56		
19	.56	.56		
20	- .56	.56		
21	.56	-.56		
22				
23				
24				
25				
26			-.56	.56
27			.56	- .56
28			.56	.56
29			-.56	- .56
30				-1.12
31				1.12

NOTE: VOIDS INDICATE ZEROES

Multiplying out gave

$$[a_{rs}] = [g_{ri}]\,[a_{ij}]\,[g_{js}] = \frac{1}{E}\begin{bmatrix} 136 & -8.0 \\ -8.0 & 136 \end{bmatrix}$$

$$[a_{rn}] = [g_{ri}]\,[a_{ij}]\,[g_{jn}]$$

$$= \frac{1}{E}\begin{bmatrix} -8.0 & -15.0 & 0 & 0 \\ 0 & 0 & -15.0 & -8.0 \end{bmatrix}$$

The inverse of $[a_{rs}]$ was found (ref. appendix)

$$[a_{rs}^{-1}] = \frac{E}{18{,}432}\begin{bmatrix} 136 & 8.0 \\ 8.0 & 136 \end{bmatrix}$$

Next, the values of the redundant forces, for unit values of the applied loads, were found per eq. (22).

$$[G_{sn}] = -[a_{rs}^{-1}]\,[a_{rn}]$$

$$= \begin{bmatrix} .059 & .111 & .0065 & .0035 \\ .0035 & .0065 & .111 & .059 \end{bmatrix}$$

The calculation was completed as per eq. (23) to give $[G_{im}]$, the values of the member forces for unit applied external loads.

$[G_{im}]$ =

i \ m	1	2	3	4
1	1.0	0	0	0
2	.529	-.445	.003	.001
3	.059	.111	.006	.003
4	.031	.059	.059	.031
5	.003	.006	.111	.059
6	.001	.003	-.445	.529
7	0	0	0	1.0
8	- .50	0	0	0
9	- .764	.222	-.001	0
10	- .294	.167	-.003	- .002
11	- .045	-.085	-.032	- .017
12	- .017	-.032	-.085	- .045
13	- .002	-.003	.167	- .294
14	0	-.001	.222	- .764
15	0	0	0	- .50
16	1.12	0	0	0
17	-1.12	0	0	0
18	- .527	-.498	.003	.001
19	.527	.498	-.003	- .001
20	- .527	-.622	.003	.001
21	.527	.622	-.003	- .001
22	- .031	-.058	.058	.031
23	- .031	.058	-.058	- .031
24	.031	-.058	.058	.031
25	- .031	.058	-.058	- .031
26	- .001	-.003	-.622	.527
27	.001	.003	.622	- .527
28	- .001	-.003	-.498	.527
29	.001	.003	.498	- .527
30	0	0	0	-1.12
31	0	0	0	1.12

Example Problem 14a

Fig. A8.31 shows the two bays of a steel tubular tail fuselage truss which is loaded by tail air loads to be resolved into three concentrated loads applied as shown. The fuselage bulkhead at the attach-points station (A-E-F-K) is heavy enough so that it may be assumed to be rigid in its own plane. Hence, the truss may be analyzed as if cantilevered from A-E-F-K as shown. All members are steel tubes, their lengths and areas being tabulated below.

Solution:

The generalized forces were taken to be the member axial loads, these being numbered as in the table below. Member flexibility coefficients, L/A, (E set equal to unity for convenience) were also tabulated.

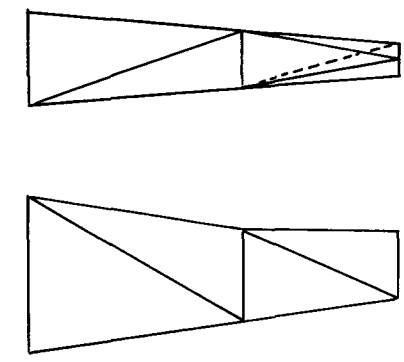

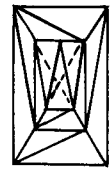

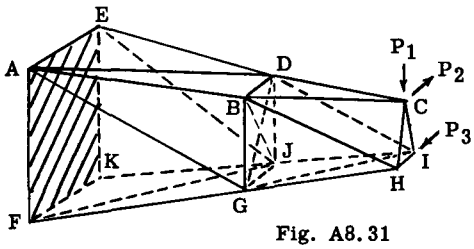

Fig. A8.31

MEMBER	NUMBER	LENGTH	AREA	L/A
AB	1	35.47	.565	62.8
BC	2	25.43	.499	51.0
BD	3	9.20	.165	55.8
CD	4	25.43	.499	51.0
DE	5	35.47	.565	62.8
FG	6	35.47	.565	62.8
GH	7	25.34	.565	44.85
HI	8	5.00	.165	30.3
IJ	9	25.34	.565	44.85
GJ	10	9.20	.165	55.8
JK	11	35.47	.565	62.8
AG	12	40.4	.630	64.1
BG	13	15.0	.165	90.9
BH	14	27.57	.500	55.14
HC	15	11.70	.395	29.62
IC	16	11.70	.395	29.62
DI	17	27.57	.500	55.14
DJ	18	15.0	.165	90.9
EJ	19	40.4	.630	64.1
AD	20	37.36	.565	66.1
FJ	21	37.36	.565	66.1
GI	22	26.23	.500	52.46
DG	23	17.60	.165	106.6
BJ	24	17.60	.165	106.6

The structure was three times redundant. In a space framework of p joints, 3p-6 independent equations of statics may be written (p. A8.10). Here, however, stress details in the plane AEKF are to be sacrificed; six equations are lost thereby since only net forces in two directions in this plane can be summed. 3 x 11 - 6 - 6 = 21 equations; 24 member unknowns. Members 22, 23 and 24 were cut.

The next step was to compute the unit stress distributions $[g_{im}]$ and $[g_{ir}]$. Rather than apply successive unit loads and forces at points m = 1, 2, 3 and r = 22, 23, 24 and then carry each loading through the structure, another procedure, often better adapted to large complex structures, was employed.

In the method used, the equations of static equilibrium were written for each of the seven joints.* Summation of forces in three directions on each joint gave 21 equations in 24 q's (the unknowns) and the three applied loads P_1, P_2 and P_3. Some typical equations obtained were:

From Σ F on Joint C.

$$\begin{cases} .21368\,q_{16} - .21368\,q_{18} + .18334\,q_4 - .18334\,q_2 = -P_2 \\ q_4 + q_2 = 0 \\ q_{16} + q_{18} = -1.0236\,P_1 \end{cases}$$

From Σ F on Joint B.

$$\begin{cases} .081759\,q_1 - .18334\,q_2 - q_3 - .07617\,q_{16} = .5227\,q_{24} \\ q_1 - q_2 - .91593\,q_{14} = 0 \\ -.1410\,q_1 + q_{13} + .4146\,q_{14} = -.8523\,q_{23} \end{cases}$$

And so forth, for the other joints.

Note that in each case the equations were arranged with the applied loads (P_n) and the redundant q's (q_{22}, q_{23}, q_{24}) grouped on the right hand side of the equal sign. This arrangement was observed for all 21 equations, after which the equations were placed in matrix form as

$$\left[C_{ij}\right]\left\{q_j\right\} = \left[D_{in} \vdots D_{is}\right]\left\{\begin{matrix} P_n \\ \cdots \\ q_s \end{matrix}\right\}$$

$$i,j = 1,2, \ldots\ldots 24$$
$$n = 1,2,3$$
$$s = 22,23,24$$

(Note that there were 24 equations here, the additional three equations being the identities

$$q_{22} = q_{22}$$
$$q_{23} = q_{23}$$
$$q_{24} = q_{24} \quad)$$

On the right hand side of the above matrix equation the matrices are shown "partitioned". The first three columns of [D] are the coefficients of P_n and the last three are the

* For structures other than trusses the equilibrium equations are written for the various structural elements, equilibrium of joints alone being inappropriate.

coefficients of the q_s.

The matrix equation was solved for the q_j by finding the inverse of $[C_{ij}]$ (see appendix). Thus,

$$\left\{q_j\right\} = \left[g_{jn} \vdots g_{js}\right]\left\{\begin{matrix} P_n \\ \cdots \\ q_s \end{matrix}\right\}$$

where

$$\left[g_{jn} \vdots g_{js}\right] = \left[C_{ij}^{-1}\right]\left[D_{in} \vdots D_{is}\right].$$

Thus, the unit stress distributions in the determinate structure were found by a procedure having as its main advantage the reduction of the work to a routine mathematical operation. In the conduct of this work appropriate standardized techniques may be employed.*

The result in this case was

$\left[g_{im} \vdots g_{ir}\right] =$

m, r / i	1	2	3	22	23	24
1	.8416	2.727	6.574	-2.3059	0	0
2	0	2.727	2.727	- .9565	0	0
3	- .00117	- .2771	- .2824	.0991	0	- .5227
4	0	-2.727	-2.727	.9560	0	0
5	.8440	-4.059	-7.943	2.786	1.236	-1.236
6	-1.217	.5456	-5.016	2.725	1.209	-1.209
7	- .8445	0	-3.8607	1.354	0	0
8	.1094	0	.5000	- .1754	0	0
9	- .8446	0	3.862	-2.3205	0	0
10	0	.00013	- .0007	- .1914	- .5224	0
11	-1.4234	- .5800	5.926	-3.734	-2.417	2.417
12	.4415	- .6473	1.371	- .4809	-1.435	1.435
13	- .2623	.3845	- .8145	.2856	0	- .8523
14	.9186	0	4.200	-1.473	0	0
15	- .5118	0	-2.340	.8208	0	0
16	- .5118	0	2.340	- .8208	0	0
17	.9190	0	-4.202	1.4737	0	0
18	- .2619	- .4090	.7882	- .2764	- .8327	- .01962
19	.3605	.6884	- .9593	.2445	1.401	-1.401
20	.00058	1.3745	1.399	- .4906	-1.302	1.302
21	- .06621	- .0003	.3044	.2941	1.302	-1.302
22	0	0	0	1.0	0	0
23	0	0	0	0	1.0	0
24	0	0	0	0	0	1.0

The member flexibility coefficients L/A were arranged as the diagonal elements of the matrix $[a_{ij}]$. Then, multiplying out according to eqs. (17) and (18),

$$[a_{rn}] = \begin{bmatrix} 177.9 & -1137.0 & -6430.3 \\ 195.0 & -151.7 & -2263.0 \\ -154.4 & 161.6 & 2273.3 \end{bmatrix}$$

$$[a_{rs}] = \begin{bmatrix} 2970 & 1150 & -1148 \\ 1150 & 1221 & -1035 \\ -1148 & -1035 & 1224 \end{bmatrix}$$

* See references in appendix.

The inverse was found (see appendix)

$$[a_{rs}^{-1}] = 10^{-3}\begin{bmatrix} .5555 & - .2880 & .2775 \\ -.2880 & 3.0412 & 2.3015 \\ .2775 & 2.3015 & 3.023 \end{bmatrix}$$

Then (referring to eqs. (22) and (22a))

$$[G_{sn}] \equiv -[a_{rs}^{-1}][a_{rn}] = 10^{-3}\begin{bmatrix} .18 & 543 & 2289 \\ -186.4 & -238 & -201.0 \\ - 31.4 & 176 & 121.3 \end{bmatrix}$$

Finally, the complete unit stress distribution was obtained as

$$[G_{im}] = [g_{im}] + [g_{ir}][G_{rm}]$$

$=$

m / i	1	2	3
1	.8412	1.475	1.296
2	- .00017	2.208	.538
3	.01523	- .3153	- .1190
4	.00017	-2.208	- .539
5	.6529	-3.058	-1.957
6	-1.404	1.5247	.832
7	- .8443	.7352	- .761
8	.1094	- .0952	.0985
9	- .8450	-1.260	-1.450
10	.0973	.0205	- .3338
11	-1.0494	-1.607	-1.842
12	.6638	- .3143	.733
13	- .2355	.3896	- .2641
14	.9185	- .7998	.8283
15	- .5116	.4457	- .461
16	- .5120	- .4457	.461
17	.9193	.8002	- .829
18	- .1061	- .3638	.3205
19	.1434	.2411	- .8512
20	.2023	1.6471	.6956
21	- .2680	- .3796	.5580
22	.0002	.543	2.289
23	- .1864	- .238	- .2010
24	- .0314	.176	.1213

Example Problem 15

The doubly symmetric four flange idealized box beam of Fig. A8.32 is to be analyzed for stresses due to load application at the six points indicated. Flange areas* taper linearly from root to tip while sheet thicknesses are constant in each panel. The beam is mounted rigidly at the root, providing full restraint

* These are the "effective areas", being the flange area plus adjacent effective cover sheet area plus one-sixth of the web area. (The factor of one-sixth provides the same moment of inertia as the distributed web area).

against warping of the root cross section due to any torsion loadings.

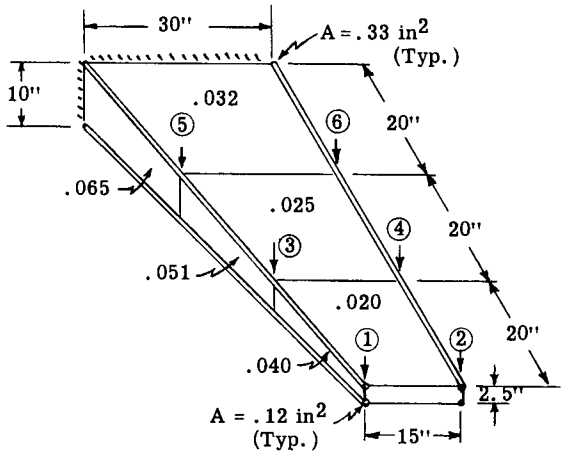

Fig. A8.32

Solution:

The generalized forces employed are shown on the exploded view, Fig. A8.33. No forces were shown for the lower surface, its members and forces being equal to those of the upper surface because of symmetry. In the $[a_{ij}]$ matrix this fact was accounted for by doubling the member flexibility coefficients for the members of the upper surface.

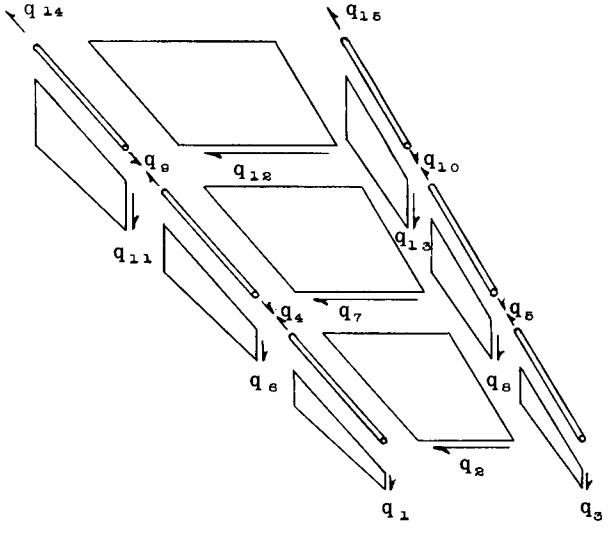

Fig. A8.33

The member flexibility coefficients were collected in matrix form as shown below. Note that entries for a_{44}, a_{55}, a_{99} and $a_{10,10}$ were collected from two stringers each (as well as being doubled as discussed above). Coefficients for these tapered stringers were computed from the formulas of Art. A7.10.

j / i	1	2	3	4	5	6	7	8	9	10	11	12	13	14	15
1	1220														
2		51,200													
3			1220												
4				134.4					25.2						
5					134.4					25.2					
6						2830									
7							60,000								
8								2830							
9				25.2					80.8					15.28	
10					25.2					80.8					15.28
11											3940				
12												62,000			
13													3940		
14									15.28					27.6	
15										15.28					27.6

NOTE: VOIDS INDICATE ZEROES. E = 1, G = .385

Cover sheet shear flows q_2, q_7 and q_{12} were selected as redundants. With these set equal to zero, and with unit loads placed successively at loading points "one" through "six", the $[g_{im}]$ matrix was obtained. When the cover sheets are "cut" the two webs act independently as plane-web beams. The details of the stress calculation for such beams are similar to those of Example Problem 21, Art. A7.7 and are not shown here.

$[g_{im}]$ =

m / i	1	2	3	4	5	6
1	.400					
2						
3		.400				
4	4.006					
5		4.006				
6	.100		.200			
7						
8		.100		.200		
9	5.341		2.671			
10		5.341		2.671		
11	.04445		.08887		.1333	
12						
13		.04445		.08887		.1333
14	6.231		4.006		2.003	
15		6.231		4.006		2.003

NOTE: VOIDS INDICATE ZEROES.

Calculations for $[g_{ir}]$ were made by successively assigning unit values to the redundants q_2, q_7 and q_{12}. The calculations are illustrated by the exploded view of the end bay in Fig. A8.34 showing the calculation in that part of the structure for $q_2 = 1$. Note that $q_2 = 1$ was applied as a self-equilibrating pair of shear flows acting one on each side of the "cut". The ribs were considered rigid in their own planes.

Put $q_2 = 1$

From equilibrium of end rib: (Σ M, Σ F)

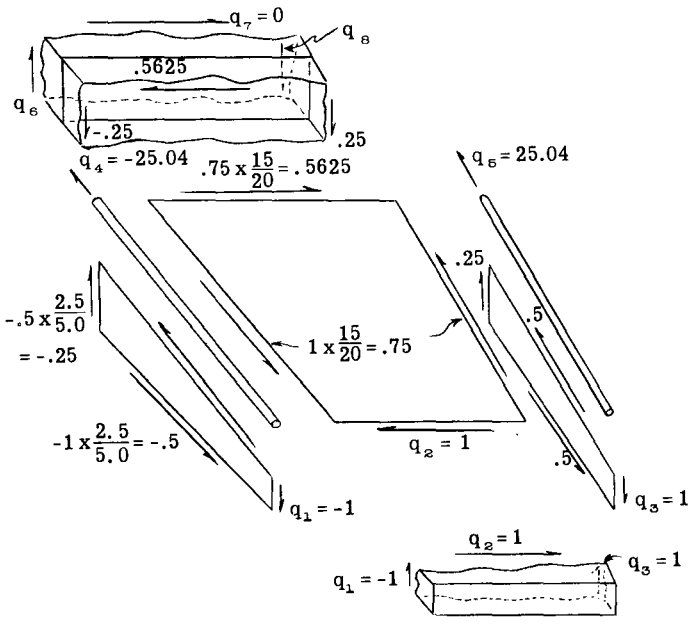

Fig. A8.34

$q_1 = -1.0$

$q_3 = 1.0$

From equilibrium of 2nd rib:

$q_8 = -(.5625 - .25) = -.3125$

$q_6 = .3125$

$q_7 = 0$, by hypothesis

So on, into the next bay. In the idealization used here, the ribs have zero stiffness normal to their own plane so that the axial flange loads are transmitted directly to the flange ends of the adjacent bay (see q_4, q_7, q_8, q_{10} of Fig. A8.33).

$[g_{ir}] =$

i \ r	2	7	12
1	- 1.00		
2	1.00		
3	1.00		
4	-25.04		
5	25.04		
6	.3125	- 1.00	
7		1.00	
8	- .3125	1.00	
9	-20.87	-29.38	
10	20.87	29.38	
11	.1387	.1955	- 1.00
12			1.00
13	- .1387	- .1955	1.00
14	-18.79	-26.44	-31.71
15	18.79	26.44	31.71

NOTE: VOIDS INDICATE ZEROES.

The following matrix products were formed:

Per eq. (18):

$$[a_{rs}] = \frac{10^6}{E} \begin{bmatrix} .3774 & .1789 & .0520 \\ .1789 & .2678 & .07322 \\ .0520 & .07322 & .1254 \end{bmatrix}$$

Per eq. (17):

$$[a_{rn}] = \frac{10^6}{E} \begin{bmatrix} -.03356 & .03356 & -.009318 & .009318 & -.001605 & .001605 \\ -.02324 & .02324 & -.01156 & .01156 & -.002259 & .002259 \\ -.008216 & .008216 & -.005150 & .005150 & -.002278 & .002278 \end{bmatrix}$$

The inverse of $[a_{rs}]$ was found (ref. appendix).

$$[a_{rs}^{-1}] = \frac{E}{10^6} \begin{bmatrix} 3.882 & -2.562 & -.1137 \\ -2.562 & 6.137 & -2.521 \\ -.1137 & -2.521 & 9.499 \end{bmatrix}$$

Then

$$[G_{sn}] = -[a_{rs}^{-1}][a_{rn}]$$

$$= \begin{bmatrix} .0699 & -.0699 & .00598 & -.00598 & .00016 & -.00016 \\ .03593 & -.03593 & .03409 & -.03409 & .00403 & -.00403 \\ .01568 & -.01568 & .01872 & -.01872 & .01578 & -.01578 \end{bmatrix}$$

Finally, the true stresses were (per eq. 23)

$$[G_{im}] = [g_{im}] - [g_{ir}][G_{rm}]$$

$=$

i \ m	1	2	3	4	5	6
1	.330	.0699	- .0060	.0060	-.0002	.0002
2	.0699	- .0699	.0060	- .0060	.0002	-.0002
3	.0699	.330	.0060	- .0060	.0002	-.0002
4	2.26	1.75	- .150	.150	-.0040	.0040
5	1.75	2.26	.150	- .150	.0040	-.0040
6	.0859	.0141	.168	.0322	-.0040	.0040
7	.0359	- .0359	.0341	- .0341	.0040	-.0040
8	.0141	.0359	.0322	.168	.0040	-.0040
9	2.83	2.51	1.545	1.126	-.122	.122
10	2.51	2.83	1.126	1.545	.122	-.122
11	.0454	- .0010	.0776	.0112	-.0150	.0150
12	.0157	- .0157	.0187	- .0187	.0158	-.0158
13	- .0010	.0454	.0112	.0776	.0150	-.0150
14	3.47	2.76	2.40	1.61	.610	-.610
15	2.76	3.47	1.61	2.40	-.610	.610

The reader will observe that the result displays the "bending stresses due to torsion"; that is, the buildup of axial flange stresses near the root of a beam under torsion when the root is restrained against warping. The solution for application of a torque is readily

found by superposing stresses for $P_1 = 1$ and $P_2 = -1$. Thus, one finds that under this condition there is a root flange load of

$$q_{14} = 3.47 - 2.76 = 0.71 \text{ lbs.}$$

for a torque of 15 inch lbs.

A8.11 Redundant Problem Deflection Calculations by Matrix Methods.

Deflections (and in particular, the matrix of influence coefficients) are readily computed from the results of Art. A8.10.

Assume that the redundant forces $\{q_s\}$ have been determined from eq. (22). The total deflection of external loading points is then easily computed as the sum of, ONE, the deflection due to external loads acting on the "cut" structure, $[a_{mn}]\{P_n\}$ (ref. eq. 16) and, TWO, the deflections due to the redundant forces acting on this same cut structure, $[a_{ms}]\{q_s\}$ (ref. eq. 17). Thus,

$$\{\delta_m\} = [a_{mn}]\{P_n\} + [a_{ms}]\{q_s\}.$$

Substituting from eq. (22)

$$\{\delta_m\} = [a_{mn}]\{P_n\} - [a_{ms}][a_{rs}^{-1}][a_{rn}]\{P_n\}$$

$$= \left([a_{mn}] - [a_{ms}][a_{rs}^{-1}][a_{rn}]\right)\{P_n\}$$

The matrix expression set off in parentheses above, giving as it does the deflections for unit values of the applied loads, is the matrix of influence coefficients. Let

$$[A_{mn}] \equiv [a_{mn}] - [a_{ms}][a_{rs}^{-1}][a_{rn}] \quad ---- \quad (25)$$

so that

$$\{\delta_m\} = [A_{mn}]\{P_n\} \quad ---------- \quad (26)$$

Example Problem 16

Determine the matrix of influence coefficients for the redundant truss of example problem 14.

Solution:

From the previous work the following matrix products were formed

$$[a_{mn}] = [g_{mi}][a_{ij}][g_{jn}] = \frac{1}{E}\begin{bmatrix} 144 & -15.0 & 0 & 0 \\ -15.0 & 38.0 & 0 & 0 \\ 0 & 0 & 38.0 & -15.0 \\ 0 & 0 & -15.0 & 144 \end{bmatrix}$$

$$-[a_{ms}][a_{rs}^{-1}][a_{rn}] = -\frac{1}{E}\begin{bmatrix} .472 & .888 & .0525 & .028 \\ .888 & 1.665 & .0975 & .0525 \\ .0525 & .0975 & 1.665 & .888 \\ .028 & .0525 & .888 & .472 \end{bmatrix}$$

Finally, the sum of the above two matrices gave

$$[A_{mn}] = \frac{1}{E}\begin{bmatrix} 144 & -15.9 & -.052 & -.028 \\ -15.9 & 36.3 & -.098 & -.052 \\ -.052 & -.098 & 36.3 & -15.9 \\ -.028 & -.052 & -15.9 & 144 \end{bmatrix}$$

Example Problem 17

Determine the matrix of influence coefficients for the box beam of example problem 15.

Solution:

An alternate procedure to that shown by eq. (25) was followed. The influence coefficient matrix was formed as in Chapter A-7, Art. A7.9, by the product.

$$[A_{mn}] = [G_{mi}][a_{ij}][G_{jn}]$$

This product was formed readily, inasmuch as $[G_{im}]$ was available from example problem 15. The result was

$$[A_{mn}] = \frac{1}{E}\begin{bmatrix} 4363 & 3500 & 1522 & 1243 & 29.7 & -29.7 \\ 3500 & 4363 & 1243 & 1522 & -29.7 & 29.7 \\ 1522 & 1243 & 897.8 & 594.2 & 33.7 & -33.7 \\ 1243 & 1522 & 594.2 & 897.8 & -33.7 & 33.7 \\ 29.7 & -29.7 & 33.7 & -33.7 & 36.8 & -36.8 \\ -29.7 & 29.7 & -33.7 & 33.7 & -36.8 & 36.8 \end{bmatrix}$$

A8.12 Precision and Accuracy in Redundant Stress Calculations.

Matters of precision are dependent upon the number of significant figures obtained and retained in dealing with the geometry of the structure and in the care with which arithmetic operations are performed. In the discussion to follow it is assumed that all due caution is exercised with regard to the precision of the work.

Matters of accuracy have to do with the number of significant figures finally obtained in the answer as influenced by the manner of formu-

lation of the problem. The accuracy of the result may be affected by a number of factors, two of the most important of which are discussed here.

Two factors influencing accuracy often are considered together under the heading "choice of redundants". They are:

● - the number of significant figures which may be retained in the solution for the inverse of the redundant force coefficient matrix, $[a_{rs}]$. (eq. 21).

●● - the magnitude of the redundant forces relative to the size of the determinate forces.

These two factors are concerned respectively with the left hand side and the right hand side of eq. 21, viz.

$$[a_{rs}]\{q_s\} = -[a_{rn}]\{P_n\};$$

they are discussed in detail below.

● - ACCURACY OF INVERSION OF $[a_{rs}]$;

THE CONDITION OF THE MATRIX.

The characteristic of the matrix $[a_{rs}]$ which determines the accuracy with which its inverse can be computed is its condition. The condition of the matrix is an indication of the magnitude of elements off the main diagonal (upper left to lower right) relative to those on. The smaller are the relative sizes of elements off the main diagonal, the better is the condition of the matrix. A well conditioned matrix is more accurately inverted than a poorly conditioned one. Two extreme cases are now given for illustration:

a) the diagonal matrix. Its off-diagonal elements are zero, so that it is ideally conditioned. Thus, the inverse of

$$\begin{bmatrix} 2 & 0 & 0 \\ 0 & 7 & 0 \\ 0 & 0 & -3 \end{bmatrix}$$

is easily and accurately obtained as

$$\begin{bmatrix} 1/2 & 0 & 0 \\ 0 & 1/7 & 0 \\ 0 & 0 & -1/3 \end{bmatrix}$$

b) a matrix all of whose elements are equal in each row. All the elements off the main diagonal are equal to those on. The determinant of such a matrix is zero and hence its inverse cannot be found (ref. appendix). Its condition is terrible. Example:

$$\begin{bmatrix} 2 & 2 & 2 \\ 7 & 7 & 7 \\ -3 & -3 & -3 \end{bmatrix}$$

In the matrix $[a_{rs}]$ the off-diagonal elements are measures of the structural cross-coupling of one redundant force with another. The strength of this cross-coupling is dependent upon the choice of redundants made in "cutting" the structure to make it statically determinate.

FOR EXAMPLE, the doubly redundant beam of Fig. A8.35(a) may be made statically determinate by "cutting" any two constraints.

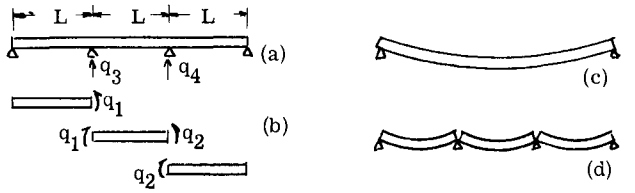

Fig. A8.35

Fig. A8.35(b) shows the choice of generalized forces. Only two (q_1 and q_2) are required to describe the strain energy, but the central support reactions were also given symbols as it was desired to consider them in the discussion. Then

$$[a_{ij}] = \frac{L}{EI}\begin{bmatrix} 2/3 & 1/6 & 0 & 0 \\ 1/6 & 2/3 & 0 & 0 \\ 0 & 0 & 0 & 0 \\ 0 & 0 & 0 & 0 \end{bmatrix}$$

FIRST, suppose the beam was made determinate by selecting the support reactions q_3 and q_4 as redundants. The "cut structure" in this case may be visualized as the beam of Fig. A8.35(c) whose central supports have been removed. Application of unit redundant forces $q_3 = 1$ and $q_4 = 1$ gave

$[g_{ir}] =$

i \ r	3	4
1	$-\frac{2}{3}L$	$-\frac{1}{3}L$
2	$-\frac{1}{3}L$	$-\frac{2}{3}L$
3	1	0
4	0	1

Multiplying out,

$$[a_{rs}] = [g_{ri}]\,[a_{ij}]\,[g_{js}] = \frac{L^3}{18EI}\begin{bmatrix} 8 & 7 \\ 7 & 8 \end{bmatrix}$$

$$r, s = 3, 4$$

The condition of this matrix is poor. Physically, a unit load at point "3" causes almost as much deflection at point "4" as at "3" itself. The cross-coupling is large.

SECOND, suppose the moments q_1 and q_2 had been chosen as redundants. The "cut structure" in this case being visualized as in Fig. A8.35(d). Application of unit redundant forces $q_1 = 1$ and $q_2 = 1$ gave

$[g_{ir}] =$

i \ r	1	2
1	1	0
2	0	1
3	$-\frac{2}{L}$	$\frac{1}{L}$
4	$\frac{1}{L}$	$-\frac{2}{L}$

Multiplying out,

$$[a_{rs}] = [g_{ri}]\,[a_{ij}]\,[g_{js}] = \frac{L}{6EI}\begin{bmatrix} 4 & 1 \\ 1 & 4 \end{bmatrix}$$

$$r, s = 1, 2$$

The condition of this redundant matrix is obviously better than that obtained with the first choice of redundants. There is less cross-coupling between the redundant forces.

Thus the analyst, by choice of redundants, determines the condition of the matrix. The choice may be critical in the case of a highly redundant structure, for it may prove impossible to invert a large, ill-conditioned matrix with the limited number of significant figures available from the initial data. The following statements and rules-of-thumb may be useful in the treatment of highly redundant problems.

(1) It is always possible to find a set of redundants for which the cross-coupling is at a minimum-zero, in fact. Theoretically then, by proper choice of redundants, the matrix $[a_{rs}]$ may be reduced to a diagonal matrix (ideally conditioned).

(1a) The choice of redundants which gives zero cross-coupling ("orthogonal functions") is not readily found in general. In some special structures, such as rings and frames, orthogonal redundants may be chosen simply. In most structures, however, the additional labor involved in seeking an orthogonal set of redundants is not warranted.

(2) In choosing a set of redundants which will yield a well-conditioned redundant matrix, it is best to make such "cuts" as will leave a statically determinate structure retaining as many of the characteristics of the original structure as possible. Thus, one may consider that the structure of Fig. A8.35(d) retains more of the features of the original continuous-beam structure than does that of Fig. A8.35(c).

(3) The degree to which one redundant influences another (extent of cross-coupling) can be visualized by observing how much their individual unit-load diagrams "overlap".

To elaborate on this last point, refer once again to the above illustrative example. The cross-coupling of q_3 with q_4 may be expected to be large if their unit-load diagrams are drawn as below in Fig. A8.36(a). This deduction follows easily if it is recalled that the dummy-unit load equation for such a cross-coupling term is of the form $\int \frac{m_3 m_4\, dx}{EI}$*, obviously large for m_3, m_4. Strictly, the comparison is with the terms $\int \frac{m_3^2\, dx}{EI}$, $\int \frac{m_4^2\, dx}{EI}$ which form the on-diagonal elements of the matrix $[a_{rs}]$

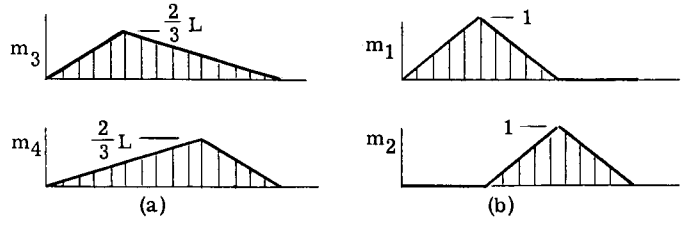

Fig. A8.36

Study of the unit-load diagrams for the redundant choice q_1, q_2 (Fig. A8.36b) reveals that the cross-coupling should be small here since an integral of the form $\int \frac{m_1 m_2\, dx}{EI}$ can have a contribution from the center span only. Hence, the $\int \frac{m_1 m_2\, dx}{EI}$ is obviously considerably smaller than $\int \frac{m_1^2\, dx}{EI}$ or $\int \frac{m_2^2\, dx}{EI}$. Thus, a visual inspection of Fig. A.36 reveals that q_1, q_2 is a better choice of redundants than is q_3, q_4.

---

* see eq. (8) Art. A8.7.

(4) Combinations of redundants may be employed to yield new unit-redundant stress distributions which do not "overlap" as extensively as do those of the individual redundants originally chosen.

For example, suppose that in the previous illustrative problem, the choice q_3, q_4 for redundants had been made originally, leading to the unit-load diagrams of Fig. A8.37(a). Inspection of the diagrams leads one to anticipate a strong degree of cross-coupling and hence a new set of redundants is sought. Rather than return to the structure to choose new "cuts", combinations of the m_3 and m_4 diagrams are looked for which will have less "overlap" and hence less cross-coupling.

It is observed by inspection that two new stress distributions which have the desired property may be formed from the m_3, m_4 diagrams by proper combination. Thus, if one half the m_4 diagram is subtracted from the m_3 diagram to form one new stress distribution and one half the m_3 diagram is subtracted from the m_4 diagram to form the other new stress distribution, the results are as shown in Fig. A.37b. There is obviously less "overlap" of the diagrams for these new combinations.

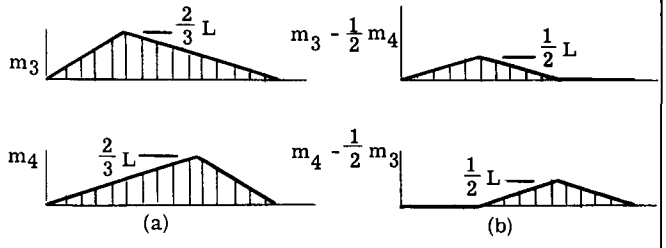

Fig. A8.37

New unit-redundant-force stress distributions (b) obtained by combining previous distributions (a).

In this way two new unknowns are introduced by linear combination. In matrix notation, the old stress distributions $\left[g_{ir}\right]$ are transformed to a new set $\left[g_{i\rho}\right]$ by forming

$$\left[g_{i\rho}\right] = \left[g_{ir}\right]\left[B_{r\rho}\right]$$

$$= \begin{bmatrix} -\frac{2}{3}L & -\frac{1}{3}L \\ -\frac{1}{3}L & -\frac{2}{3}L \\ 1 & 0 \\ 0 & 1 \end{bmatrix} \begin{bmatrix} 1 & -1/2 \\ -1/2 & 1 \end{bmatrix}$$

The transformation matrix $\left[B_{r\rho}\right]$ is written in such a way that the product $\left[g_{ir}\right]\left[B_{r\rho}\right]$ does exactly what is desired, viz., "take one times the q_3 column minus one half the q_4 column to give the first column of the new distribution $\left[g_{i\rho}\right]$". Then "take minus one half of the q_3 column plus one times the q_4 column to give the second column of the new distribution $\left[g_{i\rho}\right]$".

Multiplying out in the above example

$$\left[g_{i\rho}\right] = \begin{bmatrix} -\frac{1}{2}L & 0 \\ 0 & -\frac{1}{2}L \\ 1 & -\frac{1}{2} \\ -\frac{1}{2} & 1 \end{bmatrix}$$

Now form the matrix of redundant coefficients for the new unknowns (subscripts ρ, σ; $\left[g_{i\rho}\right] = \left[g_{j\sigma}\right]$)

$$\left[a_{\rho\sigma}\right] \equiv \left[g_{\rho i}\right]\left[a_{ij}\right]\left[g_{j\sigma}\right]$$

$$= \frac{L^3}{24EI} \begin{bmatrix} 4 & 1 \\ 1 & 4 \end{bmatrix}$$

The condition of this matrix is greatly improved over that obtained for q_3, q_4 alone (previously computed), viz.,

$$\left[a_{rs}\right] = L^3/18EI \begin{bmatrix} 8 & 7 \\ 7 & 8 \end{bmatrix} \quad (r, s = 3, 4)$$

(That the $\left[a_{\rho\sigma}\right]$ matrix obtained here happens to be similar to that obtained for q_1, q_2 in a previous example, is coincidental.)

Once a transformation has been performed, leading to a new unit redundant matrix $\left[g_{i\rho}\right]$, the problem may be completed in the "ρ, σ system". The appropriate equations are obtained from eqs. (14), (21), (23) and (25) simply by replacing all "r, s," by "ρ, σ". Thus

$$\left\{q_i\right\} = \left[g_{im}\right]\left\{P_m\right\} + \left[g_{i\rho}\right]\left\{q_\rho\right\} - - - - - - \quad (29)$$

where the redundants q_ρ ($= q_\sigma$) are the solutions of

$$\left[a_{\rho\sigma}\right]\left\{q_{\sigma}\right\} = -\left[a_{\rho n}\right]\left\{P_{n}\right\} \quad \text{- - - - - - - - -} \quad (30)$$

and where

$$\left[a_{\rho\sigma}\right] \equiv \left[g_{\rho i}\right]\left[a_{ij}\right]\left[g_{j\sigma}\right] \quad \text{- - - - - - - - -} \quad (30a)$$

$$\left[a_{\rho n}\right] \equiv \left[g_{\rho i}\right]\left[a_{ij}\right]\left[g_{jn}\right] \quad \text{- - - - - - - - -} \quad (30b)$$

The final unit load distribution is

$$\left[G_{im}\right] = \left[g_{im}\right] - \left[g_{i\rho}\right]\left[a_{\sigma\rho}^{-1}\right]\left[a_{\sigma m}\right] \quad \text{- - - -} \quad (31)$$

and the matrix of influence coefficients is given by

$$\left[A_{mn}\right] = \left[a_{mn}\right] - \left[a_{m\sigma}\right]\left[a_{\rho\sigma}^{-1}\right]\left[a_{\rho n}\right] \quad \text{- - - -} \quad (32)$$

● ● - THE MAGNITUDE OF THE REDUNDANT FORCES; SIZE OF ELEMENTS IN $\left[a_{rn}\right]$

Inspection of eqs. (14) or (29) reveals that the redundant forces act in the nature of corrections to the determinate stress distributions originally assumed (the $\left[g_{im}\right]$). It is apparent that if these corrections are large, then any inaccuracies in the redundants (arising from the difficulties inherent in accurately inverting $\left[a_{rs}\right]$ or $\left[a_{\rho\sigma}\right]$) will have an important effect on the accuracy of the final stress distribution. Thus, as a matter of general practice, it is desirable to keep the magnitudes of the redundant forces as small as possible.

It follows immediately that one should use for the determinate stress distribution one requiring a minimum of correction, i.e., Select as the determinate stress distribution one which approximates the true stress distribution as closely as possible.

The rule given in connection with the "choice of redundants" (rule 2, above) is an aid in making a good selection for the determinate stress distribution. If, as suggested, a determinate structure is obtained by making "cuts" which leave a system having properties similar to the original, the stress distribution obtained therein by statics should be a fair approximation to the final true stress distribution.

However, it is even more important to realize that the determinate stress distribution only need be in static equilibrium with the external applied loads and that it may be determined with the aid of any appropriate auxiliary rules, test information, or even intuitive guess-work which leads to a distribution close to the final true distribution. There is no need to set the redundant (cut) member forces equal to zero in establishing the determinate distribution. Instead, reasonable approximate values may be employed for them. (The corrections to these values become the unknown redundants!)

Mathematically, the magnitudes of the redundant forces are directly dependent upon the magnitudes of the elements in the matrices $\left[a_{rn}\right]$ or $\left[a_{\rho n}\right]$ on the right-hand side of eqs. (21) or (30). (The right-hand side of such a set of simultaneous equations is called the non-homogeneous part.) Thus, the relative merits of several possible determinate stress distributions may be judged by forming the matrix product $\left[a_{rn}\right]$ with each and comparing results.

FOR EXAMPLE, if the doubly redundant structure of Example Problem 3, Art. A8.5 were formulated in matrix form the $\left[g_{ir}\right]$ and $\left[a_{ij}\right]$ matrices would be (see Fig. A8.38 for numbering scheme)

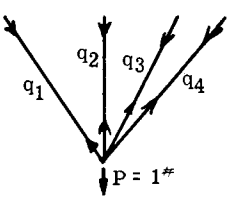

Fig. A8.38

Generalized force numbering scheme in illustrative problem. q_3 and q_4 selected as redundants.

$$\left[a_{ij}\right] = \frac{1}{E}\begin{bmatrix} 432 & 0 & 0 & 0 \\ 0 & 720 & 0 & 0 \\ 0 & 0 & 402 & 0 \\ 0 & 0 & 0 & 312 \end{bmatrix}$$

$$\left[g_{ir}\right] = \begin{bmatrix} .806 & 1.154 \\ -1.564 & -1.729 \\ 1.0 & 0 \\ 0 & 1.0 \end{bmatrix}$$

Several possible determinate stress distributions $\left[g_{im}\right]$ will now be tried. FIRST, the stress distribution obtained by statics alone in the "cut" structure ($q_3 = q_4 = 0$)

$$\left\{g_{im}\right\}_{CUT} = \begin{Bmatrix} 0 \\ 1 \\ 0 \\ 0 \end{Bmatrix}$$

(This is certainly a poor approximation to the final stress distribution). Multiplying out

$$\left[a_{rn}\right]_{CUT} = \left[g_{ri}\right]\left[a_{ij}\right]\left\{g_{jn}\right\}_{CUT} = \begin{Bmatrix} -1126 \\ -1245 \end{Bmatrix} \frac{1}{EI}$$

SECOND, a stress distribution in which loads of 0.40 lbs were guessed at for q_1 and q_3. (In a two times redundant structure any two forces may be assigned values arbitrarily while satisfying static equilibrium.) q_2, q_4 were found by statics. Thus,

$$\left\{g_{im}\right\}_{GUESS} = \begin{Bmatrix} 0.40 \\ 0.258 \\ 0.40 \\ 0.0672 \end{Bmatrix}.$$

Multiplying out one finds

$$\left[a_{rn}\right]_{GUESS} = \begin{Bmatrix} 9.49 \\ -101 \end{Bmatrix}.$$

Note that a reasonable guess at a stress distribution resulted in non-homogenous terms only one-tenth as great as those obtained by use of the "cut" distribution. The magnitudes of redundants are correspondingly reduced.

THIRD, as a matter of interest, the true stress distribution, obtained in Example Problem 3, was used. The result:

$$\left\{g_{im}\right\}_{TRUE} = \begin{Bmatrix} .450 \\ .232 \\ .260 \\ .280 \end{Bmatrix}; \quad \left[a_{rn}\right]_{TRUE} = \begin{Bmatrix} .16 \\ -.16 \end{Bmatrix} \frac{1}{E}$$

The non-homogeneous terms are practically zero, as they should be*. The redundant forces would be zero also.

---

* The demonstration here suggests a useful check upon the final result of a redundant stress calculation. After obtaining the final true stresses $\left[G_{im}\right]$ (= $\left[G_{jn}\right]$), one forms

$$\left[a_{rn}\right]_{TRUE} \equiv \left[g_{ri}\right]\left[a_{ij}\right]\left[G_{jn}\right]$$

and compares the result element-by-element with the matrix previously computed,

$$\left[a_{rn}\right] \equiv \left[g_{ri}\right]\left[a_{ij}\right]\left[g_{jn}\right].$$

The "true-matrix" elements ought to be zero, or nearly so, if $\left[G_{im}\right]$ is error-free.

Example Problem 18

It is desired to increase the accuracy of the calculation in the case of the box beam, Example Problem 15. It will be assumed for this purpose that the initial data of that problem were sufficiently precise to warrant an increase of accuracy.

Solution:

The first step taken was an examination of the unit-redundant stress distributions obtained with the choice previously made of q_2, q_7 and q_{12} as redundants. The three unit-redundant stress distributions were represented graphically as in Fig. A8.39.

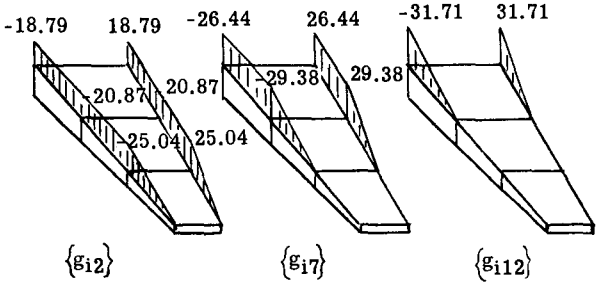

Fig. A8.39

Unit-redundant-force stress distributions - axial flange forces.

Inspection of the figures showed that the following combinations of distributions should give new distributions likely to have considerably less "overlap".

$$(1)\text{----} \quad 1 \times \left\{g_{i_2}\right\} - \frac{20.87}{29.38}\left\{g_{i_7}\right\} + 0 \times \left\{g_{i,12}\right\}$$

$$(2)\text{----} \quad 0 \times \left\{g_{i_2}\right\} + 1 \times \left\{g_{i_7}\right\} - \frac{26.44}{31.71}\left\{g_{i,12}\right\}$$

$$(3)\text{----} \quad 0 \times \left\{g_{i_2}\right\} + 0 \times \left\{g_{i_7}\right\} + 1 \times \left\{g_{i,12}\right\}$$

In matrix form the transformation was

$$\left[g_{ip}\right] = \left[g_{ir}\right]\begin{bmatrix} 1 & 0 & 0 \\ -.7103 & 1 & 0 \\ 0 & -.8330 & 1 \end{bmatrix}$$

Using $\left[g_{ir}\right]$ as previously computed, the multiplication gave

$[g_{i\rho}]$ =

i \ p	1	2	3
1	- 1.00		
2	1.00		
3	1.00		
4	-25.04		
5	25.04		
6	1.023	- 1.00	
7	- .7103	1.00	
8	- 1.023	1.00	
9		-29.38	
10		29.38	
11		1.0285	- 1.00
12		- .8330	1.00
13		- 1.0285	1.00
14	- .010	- .026	-31.71
15	.010	.026	31.71

NOTE: VOIDS DENOTE ZEROES.

Fig. A8.39a shows plots of the new distributions, these having greatly reduced "overlap" (compare with Fig. A8.39).

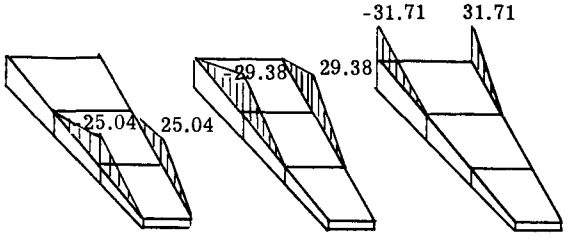

Fig. A8.39a
New unit redundant stress distributions, $[g_{i\rho}]$

The new redundant coefficient matrix $[a_{\rho\sigma}]$ was obtained by multiplying out per eq. (30a).

$$[a_{\rho\sigma}] = \frac{10^6}{E} \begin{bmatrix} .2584 & -.01132 & .0000175 \\ -.01132 & .2566 & -.03124 \\ .0000175 & -.03124 & .1254 \end{bmatrix}$$

This matrix is very well conditioned, being a considerable improvement over that of $[a_{rs}]$ found originally in Example Problem 15, viz.,

$$[a_{rs}] = \frac{10^6}{E} \begin{bmatrix} .3774 & .1789 & .0520 \\ .1789 & .2678 & .07322 \\ .0520 & .07322 & .1254 \end{bmatrix}$$

It remained to select a determinate stress distribution which would reduce the magnitude of the redundants. For this purpose, the engineering theory of bending was employed to compute stress distributions satisfying equilibrium for each application of a unit external load. The result was (refer to Example Problem 30, Art. A7.11).

$[g_{im}]$ =

i \ m	1	2	3	4	5	6
1	.30	.10				
2	.10	- .10				
3	.10	.30				
4	2.0	2.0				
5	2.0	2.0				
6	.0875	.0125	0.15	.05		
7	.0375	- .0375	.05	- .05		
8	.0125	.0875	.05	.15		
9	2.67	2.67	1.33	1.33		
10	2.67	2.67	1.33	1.33		
11	.0423	.0023	.0713	.0179	.100	.0333
12	.020	- .020	.0267	- .0267	.0333	-.0333
13	.0023	.0423	.0179	.0713	.0333	.100
14	3.00	3.00	2.00	2.00	1.0	1.0
15	3.00	3.00	2.00	2.00	1.0	1.0

NOTE: VOIDS DENOTE ZEROES.

Next the matrix $[a_{\rho n}]$ was obtained by multiplying out per eq. (30b)

$$[a_{\rho n}] = \frac{1}{E} \begin{bmatrix} 3495 & -3495 & -1841 & 1841 & 0 & 0 \\ 1167 & -1167 & 1554 & -1554 & -1450 & 1450 \\ 1082 & -1082 & 1445 & -1445 & 1802 & -1802 \end{bmatrix}$$

This result compared very favorably with $[a_{rn}]$ previously obtained, the elements being from one-half to one-tenth as large.

The solution may be carried to completion in the "ρ,σ system" using the matrices $[g_{i\rho}]$, $[a_{\rho\sigma}]$, $[g_{im}]$ and $[a_{\rho n}]$ in eqs. (31) and (32).

A8.13 Thermal Stress Calculations by Matrix Methods.

The thermal stress problem is conveniently formulated in matrix notation by an extension of the techniques presented above.

First, consider eq. (21), written in the form

$$\left[a_{rs}\right]\left\{q_s\right\} + \left[a_{rn}\right]\left\{P_n\right\} = 0.$$

In light of the physical interpretations given to $\left[a_{rs}\right]$ and $\left[a_{rn}\right]$, the equation is seen to be a matrix-form statement of the condition for continuity at the redundant cuts, viz., the displacement at each cut caused by the redundant forces plus the displacement at each cut caused by the external loads, must be equal to zero. To modify this equation for thermal stresses, the appropriate expressions for thermal displacements at the cuts must be added. Following the argument used in Art. A8.9 one writes

$$\left\{\delta_{rT}\right\} + \left[a_{rs}\right]\left\{q_s\right\} + \left[a_{rn}\right]\left\{P_n\right\} = 0$$

where δ_{rT} is the displacement at the rth cut due to thermal straining in the determinate structure. The explicit form for this term will be derived below. Rewritten,

$$\left[a_{rs}\right]\left\{q_s\right\} = -\left[a_{rn}\right]\left\{P_n\right\} - \left\{\delta_{rT}\right\} \quad ---- \quad (33)$$

Eq. (33) is a modified form of eq. (21), giving as its solution the redundant forces in an indeterminate structure under the application of both external loads and a temperature distribution.

To derive an explicit expression for δ_{rT}, the virtual work concept may be employed to advantage. Thus, following the argument of the "virtual work" derivation for deflections (Arts. A7.7, A7.8), the thermal deflection at the rth redundant cut must be equal to the total internal virtual work done by the rth-redundant force virtual stresses (due to a unit r^{th}-redundant force) moving through distortions caused by thermal strains.

Since the internal stress distribution is expressed in terms of the internal generalized forces q_i, q_j, it is convenient to employ these q's in writing the virtual work of straining. If one lets Δ_{iT} be the displacement of internal generalized force q_i due to thermal straining, then the virtual work done by a single generalized force is $q_i\,\Delta_{iT}$. The quantity Δ_{iT} will be called the member thermal distortion. The total virtual work throughout the structure is obtained by summing, giving the deflection at the rth cut as the matrix product

$$\delta_{rT} = \left\lfloor g_{ri} \right\rfloor \left\{\Delta_{iT}\right\} \quad ---------- \quad (34)$$

where g_{ri} is the value of the q_i due to a unit (virtual) load at cut r. Note that the term Δ_{iT} may consist of the sum of several contributions should q_i act on more than one member.

Because δ_{rT} is desired at each of the redundant cuts, eq. (34) is expanded by writing

$$\left\{\delta_{rT}\right\} = \left[g_{ri}\right]\left\{\Delta_{iT}\right\} \quad ---------- \quad (35)$$

$\left[g_{ri}\right]$ is, of course, the transpose of $\left[g_{ir}\right]$, the unit redundant force stress distribution in the determinate structure. Substitution of eq. (35) into eq. (33) gives

$$\left[a_{rs}\right]\left\{q_s\right\} = -\left[a_{rn}\right]\left\{P_n\right\} - \left[g_{ri}\right]\left\{\Delta_{iT}\right\} \quad (36)$$

Solution of eq. (36) gives the values of the redundants q_s, after which the problem may be completed in the usual fashion, viz,

$$\left\{q_i\right\} = \left[g_{ir}\right]\left\{q_r\right\}^{*}.$$

It is obvious that the use of combinations of redundants (the "ρ,σ" system of Art. A8.12) is possible. One makes a direct substitution of $\left[g_{i\rho}\right]$ for $\left[g_{ir}\right]$, $\left[a_{\rho n}\right]$ for $\left[a_{rn}\right]$, etc. into eq. (36).

MEMBER THERMAL DISTORTIONS

It remains to establish the forms for Δ_{iT}.

Thermal strains on an infinitestinal element of homogeneous material can cause uniform normal extensions only, so that no shear strains develop. Hence only normal (as opposed to shear) virtual stresses need be considered in computing the internal virtual work. Note that normal stresses associated with flexure must be included. It follows that only virtual work in axially loaded bars and in beams in flexure need be considered. Hence Δ_{iT} is zero for all q_i which are shear flows on panels or torques on shafts.

BARS

The general expression for the virtual work done by virtual axial loads u in a bar under varying temperature T is

$$W = \int u \cdot \alpha\, T\, dx$$

where α is the material thermal coefficient of expansion.

---

* It will be convenient later to designate by q_{sT} the solution to eq. (36) when the mechanical loads P_n are zero, the stresses in such a case being purely "thermal".

Several specific cases are now treated.

A bar under linearly varying load with linearly varying temperature is shown in Fig. A8.40.

In this case

$$u = q_j + \frac{q_i - q_j}{L} x$$

$$T = T_j + \frac{T_i - T_j}{L} x$$

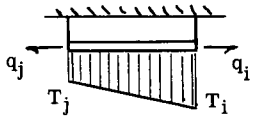

Fig. A8.40

Then, assuming α constant

$$W = \alpha \int_0^L \left(q_j + \frac{q_i - q_j}{L} \right) \left(T_j + \frac{T_i - T_j}{L} x \right) dx$$

$$= \alpha L \frac{2T_i + T_j}{6} q_i + \alpha L \frac{T_i + 2T_j}{6} q_j$$

This expression may be put in the form

$$W = q_i \Delta_{iT} + q_j \Delta_{jT}$$

where

$$\Delta_{iT} \equiv \alpha L \frac{2T_i + T_j}{6}$$

$$\Delta_{jT} \equiv \alpha L \frac{T_i + 2T_j}{6}$$

Note that variation in the cross sectional area of the bar does not affect the distortions Δ_{iT}, Δ_{jT}.

The alternate choice of generalized forces for the bar under varying axial load is shown in Fig. A8.41. By a derivation similar to that above one finds

$$W = q_i \Delta_{iT} + q_j \Delta_{jT}$$

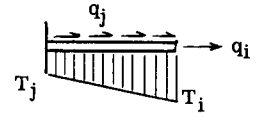

Fig. A8.41

where

$$\Delta_{iT} = \alpha L \frac{T_i + T_j}{2}$$

$$\Delta_{jT} = \alpha L^2 \frac{T_i + 2T_j}{6}$$

The simpler cases of uniform load ($q_i = u$ = constant) and uniform T ($T_i = T_j$) follow immediately by specialization of the above forms. For example, for a bar under constant load $q_i = q_j$, and constant temperature, $T_i = T_j = T$, one has $\Delta_{iT} = \alpha LT$.

BEAMS

For a beam the general form of expression for the virtual work done during thermal straining by a top-to-bottom-surface temperature difference δT, varying linearly over the beam depth, is (see Art. A7.8, Ex. Prob. 24).

$$W = \alpha \int m \cdot \frac{\delta T \, dx}{h}$$

where

m = virtual moment (positive for compression on top fiber)

$\delta T = T_{BOTTOM} - T_{TOP}$

h = beam depth.

Applied to the case of Fig. A8.42 one gets

$$W = \frac{\alpha}{h} \int_0^L \left(q_j + \frac{q_i - q_j}{L} x \right) \left(\delta T_j + \frac{\delta T_i - \delta T_j}{L} x \right) dx$$

$$= \frac{\alpha L}{h} \left(\frac{2\delta T_i + \delta T_j}{6} \right) q_i + \frac{\alpha L}{h} \left(\frac{\delta T_i + 2\delta T_j}{6} \right) q_j$$

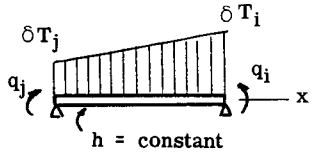

Fig. A8.42

or

$$W = q_i \Delta_{iT} + q_j \Delta_{jT}$$

where

$$\Delta_{iT} \equiv \frac{\alpha L}{h} \left(\frac{2\delta T_i + \delta T_j}{6} \right)$$

$$\Delta_{jT} \equiv \frac{\alpha L}{h} \left(\frac{\delta T_i + 2\delta T_j}{6} \right)$$

Special forms of the thermal distortion expressions for beams of varying depth may be derived readily as required.

Example Problem 19

The upper surface of the beam of Fig. A8.43 is subjected to a temperature δT above that of the lower surface, varying linearly as shown (i.e.,

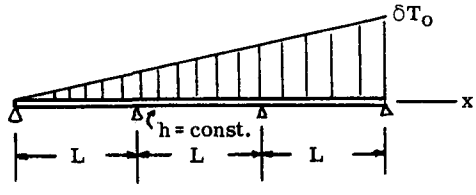

Fig. A8.43

the temperatures are equal at the left end and differ by δT_o at the right end). Determine the center reactions assuming α is constant.

Solution:

In the illustrative example of Art. A8.12 this structure was analyzed by employing as generalized internal forces the bending moments q_1 and q_2 over the central supports (see Fig. A8.35). The two central reactions were denoted by q_3 and q_4. The matrix of redundant coefficients, considering q_1 and q_2 as redundants (the better choice, it will be recalled) was (ref. Art. A8.12)

$$\left[a_{rs}\right] = \frac{L}{6EI}\begin{bmatrix} 4 & 1 \\ 1 & 4 \end{bmatrix}$$

The unit redundant load distribution for $q_1 = 1$ and $q_2 = 1$ was

$$\left[g_{ir}\right] = \begin{array}{|c|c|c|} \hline i \backslash r & 1 & 2 \\ \hline 1 & 1 & 0 \\ \hline 2 & 0 & 1 \\ \hline 3 & -\frac{2}{L} & \frac{1}{L} \\ \hline 4 & \frac{1}{L} & -\frac{2}{L} \\ \hline \end{array}$$

Member thermal distortions were computed. (Note that δT was negative according to the convention adopted earlier).

$$\Delta_{1T} = \frac{\alpha L}{h}(-)\frac{2 \times \frac{1}{3}\delta T_o}{6} + \frac{\alpha L}{h}(-)\left(\frac{\frac{2}{3}\delta T_o + 2 \times \frac{1}{3}\delta T_o}{6}\right)$$

$$= -\frac{\alpha L}{3H}\delta T_o$$

$$\Delta_{2T} = \frac{\alpha L}{h}(-)\left(\frac{2 \times \frac{2}{3}\delta T_o + \frac{1}{3}\delta T_o}{6}\right) + \frac{\alpha L}{h}(-)\left(\frac{\delta T_o + 2 \times \frac{2}{3}\delta T_o}{6}\right)$$

$$= -\frac{2}{3}\frac{\alpha L}{h}\delta T_o$$

Then from eq. (36)

$$\frac{L}{6EI}\begin{bmatrix} 4 & 1 \\ 1 & 4 \end{bmatrix}\begin{Bmatrix} q_1 \\ q_2 \end{Bmatrix} = (-)\begin{bmatrix} 1 & 0 & -\frac{2}{L} & \frac{1}{L} \\ 0 & 1 & \frac{1}{L} & -\frac{2}{L} \end{bmatrix}\begin{Bmatrix} -\frac{\alpha L \delta T_o}{3h} \\ -\frac{2\alpha L}{3h}\delta T_o \\ 0 \\ 0 \end{Bmatrix}$$

$$\begin{bmatrix} 4 & 1 \\ 1 & 4 \end{bmatrix}\begin{Bmatrix} q_1 \\ q_2 \end{Bmatrix} = \frac{2EI\ \alpha\ \delta T_o}{h}\begin{Bmatrix} 1 \\ 2 \end{Bmatrix}$$

Solving

$$\begin{Bmatrix} q_1 \\ q_2 \end{Bmatrix} = \frac{EI\ \alpha\ \delta T_o}{h}\begin{Bmatrix} .267 \\ .933 \end{Bmatrix}$$

The final stress distribution was

$$\left\{q_i\right\} = \left[g_{im}\right]\left\{P_m\right\} + \left[g_{ir}\right]\left\{q_r\right\}$$

$$= 0 + \frac{EI\ \alpha\ \delta T_o}{h}\begin{bmatrix} 1 & 0 \\ 0 & 1 \\ -\frac{2}{L} & \frac{1}{L} \\ \frac{1}{L} & -\frac{2}{L} \end{bmatrix}\begin{Bmatrix} .267 \\ .933 \end{Bmatrix}$$

$$\left\{q_i\right\} = \frac{EI\ \alpha\ \delta T_o}{h}\begin{Bmatrix} .267 \\ .933 \\ .399/L \\ -1.60/L \end{Bmatrix}$$

Thus the reactions were

$$q_3 = .399\ \frac{EI\ \alpha\ \delta T_o}{Lh}$$

$$q_4 = -1.60\ \frac{EI\ \alpha\ \delta T_o}{Lh}$$ (negative indicates DOWN)

Example Problem 20

The symmetric sheet-stringer panel of Fig. A8.44(a) is to be analyzed for thermal stresses developed by heating the two outside stringers to a uniform temperature T above the center stringer. Assume G = 0.385E.

Solution:

The panel was divided for convenience into three bays. The numbering and placing of generalized forces is shown in Fig. A8.44(b). Transverse members (ribs, not shown on Figure) were considered rigid in their own planes - a satisfactory assumption for symmetric panels. Because of symmetry only one half the panel was handled. All member flexibility coefficients and thermal distortions were doubled where appropriate.

The matrix of flexibility coefficients was set up as (VOIDS DENOTE ZEROES)

$$[a_{ij}] = \frac{1}{E}$$

177.6	44.4							
44.4	177.6	44.4						
	44.4	88.8						
			88.8	22.2				
			22.2	88.8	22.2			
				22.2	44.4			
						62,400		
							62,400	
								62,400

The matrix of member thermal distortions was

$$\{\Delta_{1T}\} = \alpha T \begin{Bmatrix} 40 \\ 40 \\ 20 \\ 0 \\ 0 \\ 0 \\ 0 \\ 0 \\ 0 \end{Bmatrix}$$

Here, for example $\Delta_{1T} = 2 \times 2 \times 10 = 40$ (doubled once because q_1 acts on two stringer ends and doubled again to account for the other half of the panel).

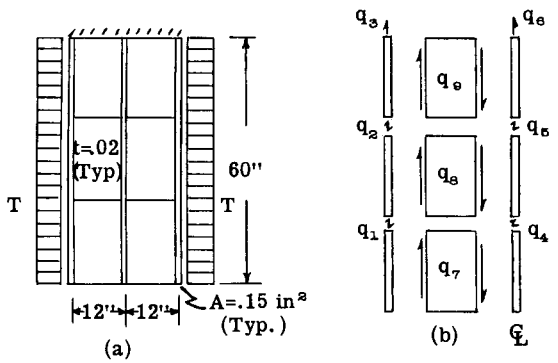

Fig. A8.44

The structure was three times redundant. Stringer loads q_4, q_5 and q_6 were selected as redundants. Fig. A8.45 shows the unit redundant load sketches for $q_4 = 1$, $q_5 = 1$ and $q_6 = 1$.

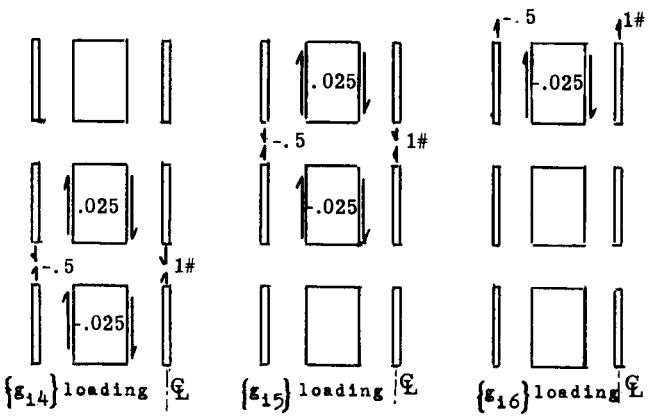

Fig. A8.45

Then

$$[g_{1r}] = \begin{bmatrix} -.5 & 0 & 0 \\ 0 & -.5 & 0 \\ 0 & 0 & -.5 \\ 1.0 & 0 & 0 \\ 0 & 1.0 & 0 \\ 0 & 0 & 1.0 \\ -.025 & 0 & 0 \\ .025 & -.025 & 0 \\ 0 & .025 & -.025 \end{bmatrix}$$

Multiplying out per eq. 18,

$$[a_{rs}] = \frac{1}{E} \begin{bmatrix} 211.2 & -5.7 & 0 \\ -5.7 & 211.2 & -5.7 \\ 0 & -5.7 & 105.6 \end{bmatrix}$$

and

$$[g_{r1}]\{\Delta_{1T}\} = \alpha T \begin{bmatrix} -.5 & 0 & 0 & 1.0 & 0 & 0 & -.025 & -.025 & 0 \\ 0 & -.5 & 0 & 0 & 1.0 & 0 & 0 & -.025 & .025 \\ 0 & 0 & -.5 & 0 & 0 & 1.0 & 0 & 0 & -.025 \end{bmatrix} \begin{Bmatrix} 40 \\ 40 \\ 20 \\ 0 \\ 0 \\ 0 \\ 0 \\ 0 \\ 0 \end{Bmatrix}$$

$$= \alpha T \begin{Bmatrix} -20 \\ -20 \\ -10 \end{Bmatrix}$$

Then the redundant equations, per eq. (36), were

$$\frac{1}{E} \begin{bmatrix} 211.2 & -5.7 & 0 \\ -5.7 & 211.2 & -5.7 \\ 0 & -5.7 & 105.6 \end{bmatrix} \{q_s\} = 10\,\alpha T \begin{Bmatrix} 2 \\ 2 \\ 1 \end{Bmatrix}.$$

Solving,

$$\{q_{rT}\} = \alpha T E \begin{Bmatrix} 0.0974 \\ 0.100 \\ 0.100 \end{Bmatrix}$$

Finally, the complete thermal stress distribution was

$$\{q_{1T}\} = [g_{1r}]\{q_{rT}\} = \alpha T E \times 10^{-3} \begin{Bmatrix} -48.7 \\ -50.0 \\ -50.0 \\ 97.4 \\ 100.0 \\ 100.0 \\ -2.44 \\ -0.065 \\ 0 \end{Bmatrix}$$

The result compares favorably with "exact" solutions made under the same assumptions (ref. NACA TN 2240) as far as the stringer loads are concerned. The shear flow result is not very satisfactory, primarily due to the use of too few "bays" in this analysis.

Example Problem 21

The uniform four-flange box beam of Fig. A8.46a is to be analyzed for the thermal stresses developed upon heating one flange to a temperature T, uniform spanwise, above the other three flanges.

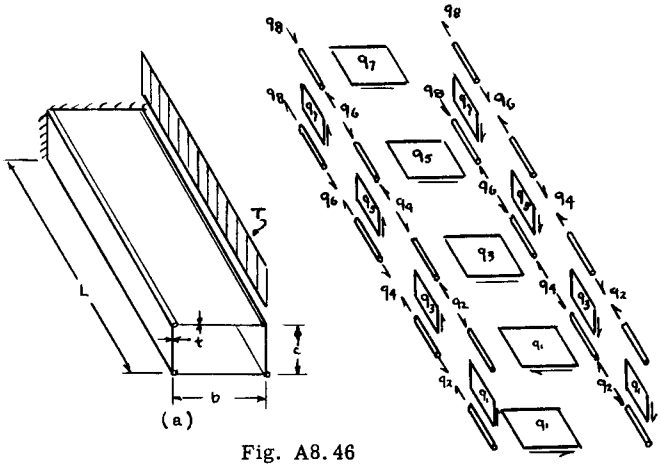

Fig. A8.46

Solution:

The beam was divided into four equal bays giving a four times redundant problem. Four self-equilibrating (zero-resultant) independent stress distributions were taken as the unknowns, these being shown in Fig. A8.46(b). Such zero-resultant stress distributions are the only ones possible in a structure having no applied loads*.

The matrix of member flexibility coefficients was formed by collecting coefficients from the several members. Unit redundant stress distributions were prepared, taking q_1, q_3, q_5 and q_7 as the redundants and setting these equal to unity successively.

$$[a_{ij}] = \frac{L\,(b+c)}{Gt}$$

.500							
	.667k²		.1667k²				
		.500					
	.1667k²		.667k²		.1667k²		
				.500			
			.1667k²		.667k²		.1667k²
						.500	
					.1667k²		.333k²

where $k^2 = Gt / AE\,(b + c)$

* Since external loads are not to be applied it follows from statics that the generalized forces for adjacent webs and cover sheets are equal, as are the loads in front and rear spar caps at any given station. Hence an economy of numbering in the generalized force scheme is possible. Much labor is saved in the handling of data when the same symbol can be employed on several members whose loads are known to be equal.

$$[g_{ir}] =$$

1			
$L/2$			
	1		
$L/2$	$L/2$		
		1	
$L/2$	$L/2$	$L/2$	
			1
$L/2$	$L/2$	$L/2$	$L/2$

Multiplying out per eq. (18),

$$[a_{rs}] = \frac{L^3k^2\,(b+c)}{Gt}$$

$\frac{.500}{L^2k^2} + .833$	.625	.375	.125
.625	$\frac{.500}{L^2k^2} + .583$	.375	.125
.375	.375	$\frac{.500}{L^2k^2} + .333$	.125
.125	.125	.125	$\frac{.500}{L^2k^2} + .0833$

For a specific case let $k^2L^2 = 1$. The inverse was computed to be

$$[a_{rs}^{-1}] = \frac{Gt}{L\,(b+c)}$$

1.070	- .5291	- .2337	- .06587
- .5291	1.366	- .3613	- .1018
- .2337	- .3613	1.497	- .1934
- .06587	- .1018	- .1934	1.792

Member thermal distortions (Δ_{iT}) were computed for loads q_2, q_4, q_6 and q_8 and were collected from the one heated flange only.

$$\left\{\Delta_{iT}\right\} = \frac{a\,L\,T}{8}\begin{Bmatrix}0\\2\\0\\2\\0\\2\\0\\1\end{Bmatrix}$$

(Note that if two adjacent flanges are heated equally, one must set the corresponding Δ_{iT} equal to zero; this because the virtual loads being of opposite sign in adjacent flanges, the virtual work must cancel).

Multiplying out:

$$[g_{ri}]\left\{\Delta_{iT}\right\} = \frac{a\,T\,L^2}{16}\begin{Bmatrix}7\\5\\3\\1\end{Bmatrix}$$

Then the solution to eq. (36) was written as

$$\left\{q_{s_T}\right\} = -\left[a_{rs}^{-1}\right]\left[g_{ri}\right]\left\{\Delta_{iT}\right\}$$

which, when multiplied out gave

$$\left\{q_{s_T}\right\} = -\frac{G t a L T}{16\,(b+c)}\begin{Bmatrix} 4.079 \\ 1.938 \\ .8562 \\ .2413 \end{Bmatrix}.$$

Finally the complete set of thermal stresses were (still for the case $L^2k^2 = 1$)

$$\left\{q_{jT}\right\} = \left[g_{js}\right]\left\{q_{s_T}\right\} = -\frac{G t a L T}{16(b+c)}\begin{Bmatrix} 4.079 \\ 2.039\ L \\ 1.938 \\ 3.008\ L \\ .8562 \\ 3.437\ L \\ .2413 \\ 3.558\ L \end{Bmatrix}$$

The result compares favorably with an exact solution (NACA TN 2240) insofar as flange stresses are concerned, an error of less than 1 percent being present at the root. Shear flow values in the sheet are less satisfactory due to the (relatively) crude assumption of constant shear in each beam quarter.

A8.14 Thermal Deflections by Matrix Methods.

A. STATICALLY DETERMINATE STRUCTURES

The problem of the thermal deflections of a statically determinate structure was considered earlier in Art. A7.8 in non-matrix form. It should be apparent from the derivation, that the matrix method presented for the calculation of redundant-cut thermal deflections may be applied equally well to the problem of computing the thermal deflections of external points of a determinate structure. Thus

$$\left\{\delta_{m_T}\right\} = \left[G_{mi}\right]\left\{\Delta_{iT}\right\} \quad - - - - - - - - - - - \quad (37)$$

where δ_{m_T} is the thermal deflection of external point m, and $\left[G_{mi}\right]$ is the transpose of $\left[G_{im}\right]$, the unit-applied load stress distribution (compare with eq. 35).

B. REDUNDANT STRUCTURES

In the case of the redundant structure, additional strains are present due to the thermal stresses set up; the effect of these strains upon the deflection of external points must be included in the calculation.

The appropriate equation is most easily derived by visualizing the action in two stages. FIRST, the redundant structure is "cut" making it determinate, after which the temperature distribution is applied producing thermal deflections

$$\left\{\delta_{m_{T_1}}\right\} = \left[g_{mi}\right]\left\{\Delta_{iT}\right\}$$

at the external points (compare with eqs. (35) and (37)). Simultaneously the redundant cuts will experience relative displacements.

SECOND, the redundant cuts are restored to zero displacement by the application of redundant forces (this problem was solved in Art. A8.13). The q_s are given by eq. (36); they produce additional deflections at points m

$$\left\{\delta_{m_{T_2}}\right\} = \left[a_{ms}\right]\left\{q_{s_T}\right\}.$$

The total deflection of point m is then

$$\left\{\delta_{m_T}\right\} = \left[g_{mi}\right]\left\{\Delta_{iT}\right\} + \left[a_{ms}\right]\left\{q_{s_T}\right\}.$$

But

$$\left[a_{ms}\right] = \left[g_{mi}\right]\left[a_{ij}\right]\left[g_{js}\right].$$

Therefore

$$\left\{\delta_{mT}\right\} = \left[g_{mi}\right]\left\{\Delta_{iT}\right\} + \left[g_{mi}\right]\left[a_{ij}\right]\left[g_{js}\right]\left\{q_{sT}\right\}$$

or,

$$\left\{\delta_{mT}\right\} = \left[g_{mi}\right]\left(\left\{\Delta_{iT}\right\} + \left[a_{ij}\right]\left\{q_{jT}\right\}\right) \quad - - - \quad (38)$$

The matrix quantity in parentheses is the total strain (thermal plus "mechanical").

For definite reasons the equation for thermal deflections has been left in the form of eq. (38) rather than the more polished forms which might be obtained by substitution from eq. (36), FIRST, the q_{jT}, the thermal stresses, will probably have been solved for previously and will be readily available in explicit form. SECOND, and far more important from a labor saving standpoint, the unit load distribution $\left[g_{im}\right]$ (whose transpose is used in eq. 38) may be any convenient stress distribution satisfying statics in the simplest of "cut" structures. One need not even use the same $\left[g_{im}\right]$ distribution (and same choice of "cuts") as employed in the redundant thermal stress calculation; a more convenient choice of cuts may be employed. In principle, any stress distribution statically equivalent to the unit applied load(s) may be used for $\left[g_{im}\right]$ in eq. (38). (See p. A8.9).

Example Problem 22

Compute the rotation occurring at the right hand end of the beam of Fig. A8.43.

Solution:

To compute the rotation a unit couple was applied (positive counterclockwise) at the right hand end. An additional generalized force, called q_5, also was added at that point. Then,

$$\Delta_{5T} = \frac{aL}{h}(-)\left(\frac{\frac{2}{3}\delta T_o \cdot + 2\delta T_o}{6}\right) = \frac{-4\,a\,L\,\delta T_o}{9h}$$

and, using some results from Example Prob. 19,

$$\left\{\Delta_{iT}\right\} = -\frac{a\,L\,\delta T_o}{9h}\begin{Bmatrix}3\\6\\4\end{Bmatrix} \quad i = 1, 2, 5$$

Note that q_3 and q_4, the intermediate support reactions, were omitted from consideration. They do not enter into any expression for the internal virtual work of the structure; or, equally, they are not used to describe the strain energy of the structure. Hence they are not included in writing the total strain. (Their Δ_{iT} are zero.)

The member flexibility coefficient matrix was

$$\left[a_{ij}\right] = \frac{L}{6EI}\begin{bmatrix}4 & 1 & 0\\1 & 4 & 1\\0 & 1 & 2\end{bmatrix} \quad i = 1, 2, 5$$

From Example Problem 19, the true thermal stress distribution was

$$\left\{q_i\right\} = \frac{EI\,a\,\delta T_o}{h}\begin{Bmatrix}.267\\.933\\0\end{Bmatrix} \quad i = 1, 2, 5$$

(q_5 was zero by inspection)

To determine $\left[g_{im}\right]$, a unit couple $q_5 = 1$ was applied. Taking as the "cut" structure one where $q_1 = q_2 = 0$ one has simply

$$\left\{g_{im}\right\} = \begin{Bmatrix}0\\0\\1\end{Bmatrix}; \quad \left\lfloor g_{mi}\right\rfloor = \begin{bmatrix}0 & 0 & 1\end{bmatrix}$$

Then substituting into eq. (38),

$$\left\{\delta_{m_T}\right\} = \begin{bmatrix}0 & 0 & 1\end{bmatrix}\left(-\frac{aL\delta T_o}{9h}\begin{Bmatrix}3\\6\\4\end{Bmatrix} + \frac{L}{6EI}\begin{bmatrix}4 & 1 & 0\\1 & 4 & 1\\0 & 1 & 2\end{bmatrix}\frac{EI\,a\,\delta T_o}{h}\begin{Bmatrix}.267\\.933\\0\end{Bmatrix}\right)$$

$$= \frac{a\,L\,\delta T_o}{h}\begin{bmatrix}0 & 0 & 1\end{bmatrix}\begin{Bmatrix}0\\0\\-.289\end{Bmatrix}$$

$$\delta_T = -.289\,\frac{a\,L\,\delta T_o}{h}$$

It is apparent that the values of the redundant moments q_1, q_2 could have been chosen arbitrarily in $\left\{g_{im}\right\}$, above, without affecting the result. Here, clearly, $\left\{g_{im}\right\}$ for any "cut" structure visualized will lead to the same result, q_5 being equal to unity in all cases.

Example Problem 23

Compute the axial movement of the free end of the central stringer of the panel of Fig. A8.44.

Solution:

An additional generalized force, q_{10}, was added axially to the free end of the central stringer (ref. Fig. A8.44b). Then

$$\left[a_{ij}\right] = \frac{1}{E}\begin{bmatrix}
177.6 & 44.4 & & & & & & & & \\
44.4 & 177.6 & 44.4 & & & & & & & \\
 & 44.4 & 88.8 & & & & & & & \\
 & & & 88.8 & 22.2 & & & & & 22.2 \\
 & & & 22.2 & 88.8 & 22.2 & & & & \\
 & & & & 22.2 & 44.4 & & & & \\
 & & & & & & 62,400 & & & \\
 & & & & & & & 62,400 & & \\
 & & & & & & & & 62,400 & \\
 & & & 22.2 & & & & & & 44.4
\end{bmatrix}$$

$$\left\{\Delta_{iT}\right\} = \begin{Bmatrix}40\\40\\20\\0\\0\\0\\0\\0\\0\\0\end{Bmatrix}$$

Using the q_{j_T} as obtained in Example Problem 20 (with $q_{10} = 0$), the following product was formed:

$$\left[a_{ij}\right]\left\{q_{j_T}\right\} = \begin{Bmatrix}-10.87\\-13.26\\-6.660\\10.87\\13.26\\6.66\\-152.2\\-4.06\\0.00\\2.162\end{Bmatrix} \times a\,T$$

Then, substituting into eq. (38),

$$\delta_{m_T} = \alpha T \left\lfloor g_{mi} \right\rfloor \begin{Bmatrix} 29.13 \\ 26.74 \\ 13.34 \\ 10.87 \\ 13.26 \\ 6.66 \\ -152.2 \\ - 4.06 \\ 0.00 \\ 2.162 \end{Bmatrix}$$

It remained to find the determinate stress distribution for $q_{i_0} = 1$. .

As the determinate distribution $\left\{ g_{im} \right\}$, the stresses due to a unit load $q_{i_0} = 1$ were computed in the "cut" structure obtained when $q_1 = q_2 = q_3 = 0$. (Note that this is a different choice of redundant cuts from that employed in computing the thermal stresses in Example Problem 20.) Thus

$$\left\{ g_{im} \right\} = \begin{Bmatrix} 0 \\ 0 \\ 0 \\ 1 \\ 1 \\ 1 \\ 0 \\ 0 \\ 0 \\ 1 \end{Bmatrix}$$

and finally,

$$\delta_{m_T} = \alpha T \left\lfloor 0\ 0\ 0\ 1\ 1\ 1\ 0\ 0\ 0\ 1 \right\rfloor \begin{Bmatrix} 29.13 \\ 26,74 \\ 13.34 \\ 10.87 \\ 13.26 \\ 6.66 \\ -152.2 \\ - 4.06 \\ 0.00 \\ 2.162 \end{Bmatrix}$$

$= 33.0\, \alpha\, T$ (ANSWER)

As a matter of interest, a different unit stress distribution was employed with a different choice of "cuts". If the forces q_4, q_5 and q_6 are set equal to zero ("cut"), application of a unit load $q_{i_0} = 1$ gives (writing the transpose of $\left\{ g_{im} \right\}$)

$$\left\lfloor g_{mi} \right\rfloor = \left\lfloor .50\ .50\ .50\ 0\ 0\ 0\ .025\ 0\ 0\ 1 \right\rfloor$$

Then multiplying out for the thermal deflection: $\delta_{m_T} = 33.0\, \alpha\, T$ (same answer).

It is apparent from the above result that the simplest determinate ("cut") structure should be used to compute $\left[g_{im} \right]$; it is completely adequate.

CLOSURE

The general thermal stress problem is complicated by the fact that the material properties E, G and α vary with temperature. The problem created thereby is primarily one of bookkeeping - computing the member flexibility coefficients (a_{ij}) and the member thermal distortions (Δ_{iT}) for a structure whose properties vary from point to point with the temperature. The variations of E, G and α with T will, of course, have to be known from test data.

Two additional complications, not considered here, are the lowering of the yield point with heating (and the attendant increased likelihood of developing inelastic strains) and the phenomenon of "creep" (the time-dependent development of inelastic strains under steady loading).

Should it prove necessary to analyze for thermal stresses under more than one temperature distribution, the member thermal distortion matrix $\left\{ \Delta_{iT} \right\}$ may be generalized easily into a rectangular form such as

$$\left[\Delta_{iR} \right] = \left[C_{ij} \right] \left[T_{jR} \right]$$

where Δ_{iR} is the member thermal distortion associated with force q_i from thermal loading condition R. The matrix $\left[C_{ij} \right]$ of member thermal coefficients consists of the constant coefficients in the Δ_{iT} expressions previously presented, while T_{jR} would be the temperature associated with q_j for condition R. (compare with eq. (26b), Art. A7.11).

A8.15 Problems.

Note: Problems (1) through (9) below may be worked by either the Least Work or Dummy Unit Load Methods. The student will be well advised to try some problems both ways for comparison.

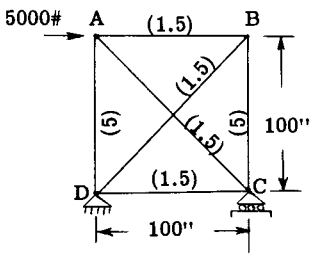

Fig. a

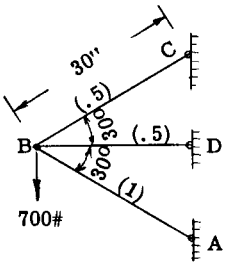

Fig. b

(1) Determine the load in all the members of the loaded truss shown in Fig. (a). Values in ( ) on members represent the cross-sectional area in sq. in. for that member. All members of same material.

(2) For the structure in Fig. (b), determine the load in each member for a 700# load at joint B. Areas of members are given by the values in ( ) on each member. All members made of same material.

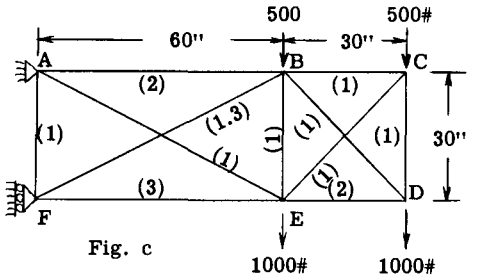

Fig. c

(3) For the loaded truss in Fig. c, determine the axial load in all members, Values in parenthesis adjacent to members represent relative areas. E is constant for all members.

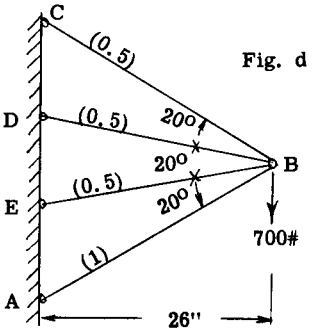

Fig. d

(4) For structure in Fig. d, calculate the axial loads in all the members. Values in parenthesis adjacent to each member represent relative areas. E is constant or same for all members.

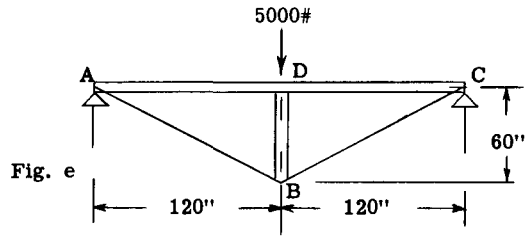

Fig. e

(5) For the "King post" truss in Fig. e, calculate the load in member BD. Members AB, BC and BD have area of 2 sq. in. each. The continuous member ADC has an area of 9.25 sq. in. and moment of inertia of 216 in^4. E is same for all members.

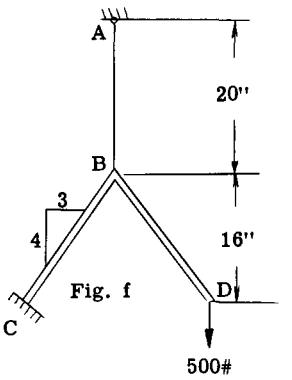

Fig. f

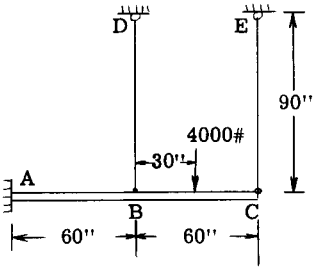

Fig. g

(6) In Fig. f, AB is a steel wire 0.50 sq. in. area. The steel angle frame CBD has a 4 in. sq, cross section. Determine the load in member AB. E = 30,000,000 psi.

(7) In Fig. g find the loads in the two tie rods BD and CE. I_{ac} = 72 in.^{4}; A_{bd} = 0.05 sq. in. A_{ce} = 0.15 sq. in. E is same for all members.

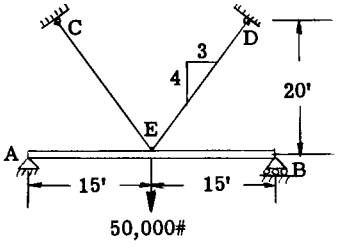

Fig. h

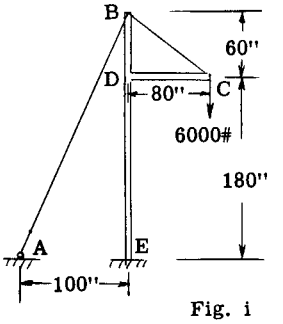

Fig. i

(8) For the structure in Fig. h, determine the reactions at points A, B. Members CE and ED are steel tie rods with areas of 1 sq. in. each. Member AB is a wood beam with 12" x 12" cross section. E_{steel} = 30,000,000 psi. E_{wood} = 1,300,000 psi.

(9) For the structure in Fig. i, determine the axial loads, bending moments and shears in the various members. The structure is continuous at joint D. Members AB, BC are wires. The member areas are AB = 1.2, BC = 0.6; CD = 6.0; BDE = 10.0. The moment of inertia for members CD = 60.0 in.^{4}; for BDE = 140 in.^{4}

(10) Re-solve Example Problem 10, p. A8.15 using as redundants the two restraints at one end (couple and transverse force). Solved in this way the problem is doubly redundant as no advantage is made of the symmetry of the structure.

(11) Add two additional members, diagonals FB and EC (each with areas 1.0 in^2) to the truss of Fig. A7.85, chapter A-7. Find the matrix of

influence coefficients.

Ans.

$$\left[A_{mn}\right] = \frac{1}{E}\begin{bmatrix} 21.8 & 27.2 & 27.5 & 18.3 \\ 27.2 & 68.5 & 65.4 & 26.4 \\ 27.5 & 65.4 & 68.4 & 26.2 \\ 18.3 & 26.4 & 26.2 & 20.6 \end{bmatrix}$$

(12) Re-solve the doubly redundant beam of Example Problem B, page A8.3 by matrix methods. The redundant reactions should be given "q" symbols. (See Example Problem 13a, page A8.20).

(13) Re-solve Example Problem 5, page A8.12 by matrix methods. For simplicity, make your choice of generalized forces including those designated as X and Y in the example so that Figs. A8.21 and A8.22 can be used to give the g_{1r} loadings.

(14) By matrix methods re-solve Example Problem 4, p. A8.12 using 3 equal bay divisions along the panel (3 times redundant). Use the same structural dimensions as in Example Problem 20, p. A8.36. Compare the results with those obtained from the formulas developed in Example Problem 4.

(15) Show that the matrix equation eq. (21) is modified to cover the initial stress problems of Art. A8.8 by writing

$$\left[a_{rs}\right]\left\{q_s\right\} = -\left[a_{rn}\right]\left\{P_n\right\} - \left[g_{ri}\right]\left\{\Delta_i\right\}$$

where Δ_i is the initial imperfection associated with force q_i. Refer to the argument leading to eq. (11) of Art. A8.8.

(16) Using the equation of problem (15), above, re-solve Example Problem 6, p. A8.14.

(17) Using the equation of problem (15) above, re-solve Example Problem 7, p. A8.14.

(18) Using the matrix methods of Art. A8.13, re-solve Example Problem 9, p. A8.15.

(19) For the doubly symmetric four flange box beam of Example Problem 15, p. A8.24, determine the redundant stresses q_8, q_7 and q_{12} if one flange is heated to a temperature T, uniform spanwise, above the remainder of the structure.

Ans.

$$\begin{Bmatrix} q_8 \\ q_7 \\ q_{12} \end{Bmatrix} = \frac{-E\,a\,T}{10^6}\begin{Bmatrix} 2081 \\ 1599 \\ 741 \end{Bmatrix}$$

REFERENCES.

See references at the end of Chapter A-7.



Douglas DC-8 airplane. Photograph showing simulated aerodynamic load being applied to main entrance door of fuselage test section.

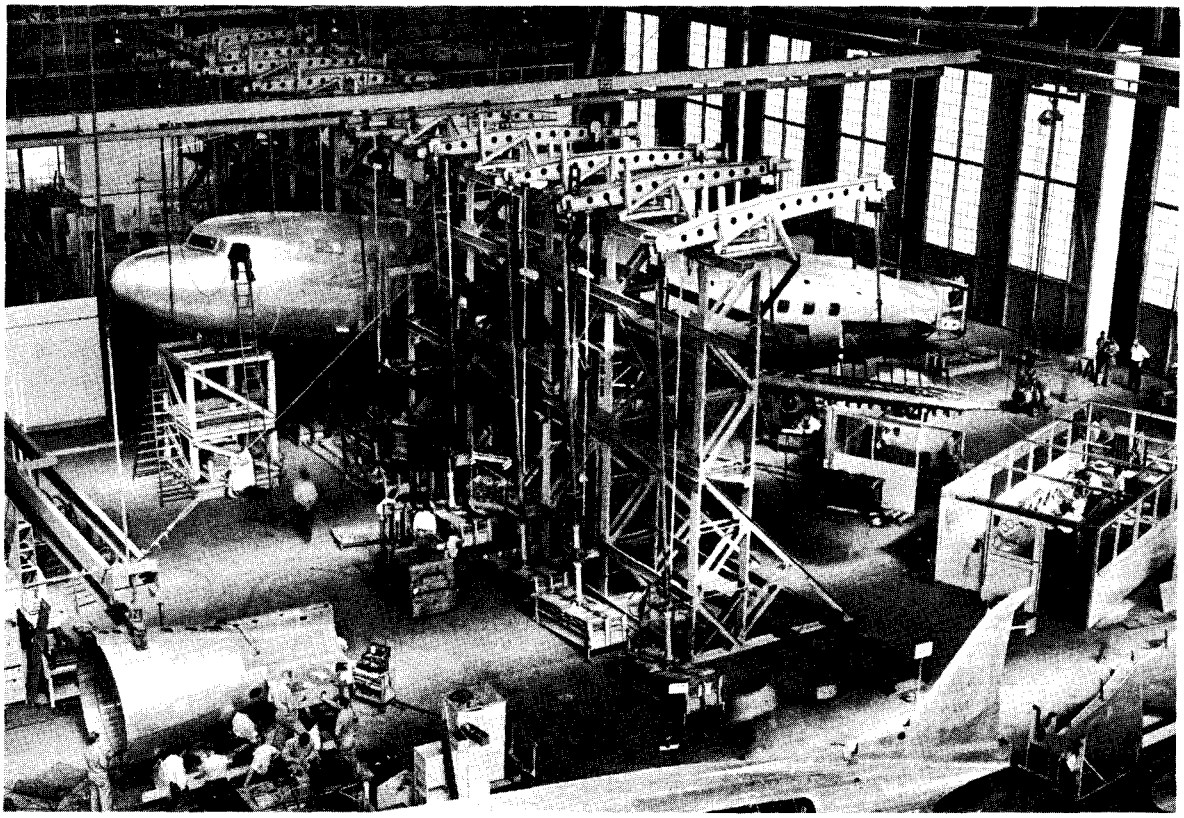

PROOF TEST OF DOUGLAS AIRCRAFT MODEL DC-6

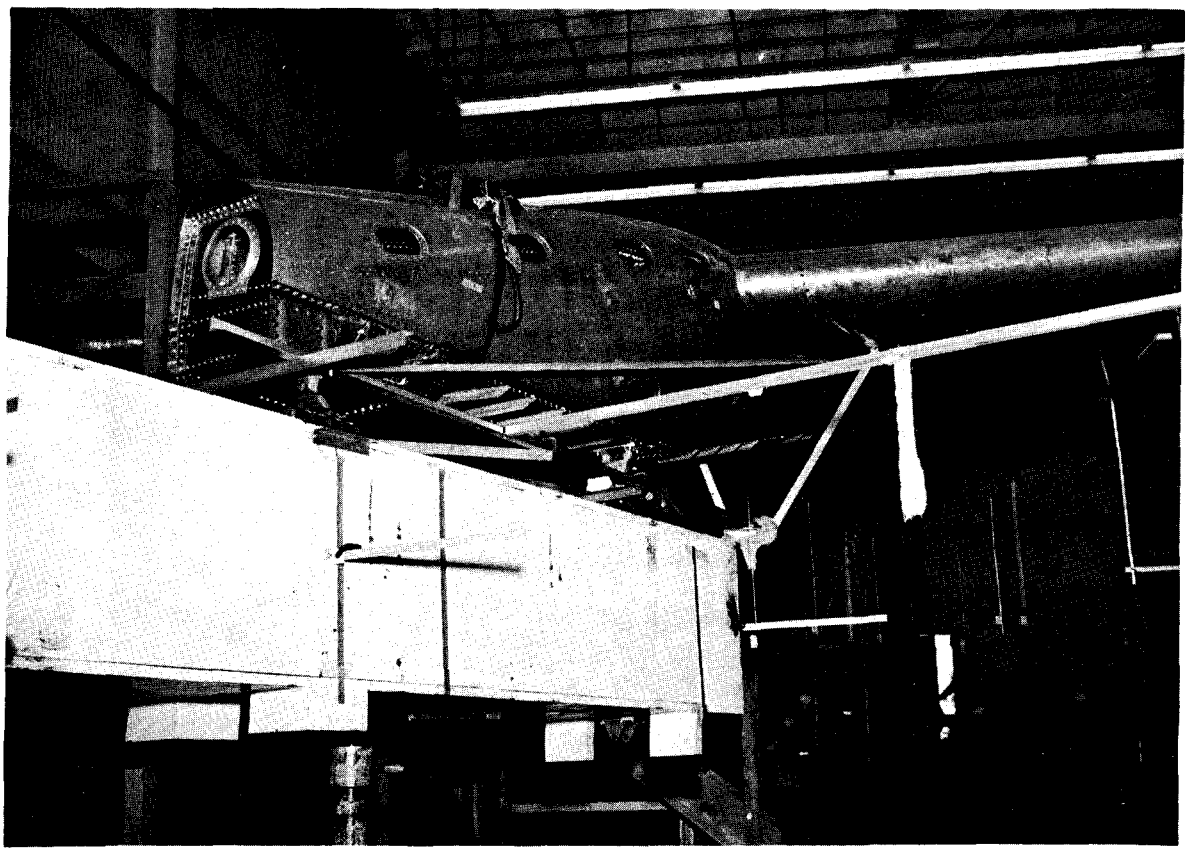

DOUGLAS DC-8 AIRPLANE. An outboard engine pylon mounted on a section of wing for static and flutter tests. The steel box represents the weight and moment of inertia of the engine.

CHAPTER A9
BENDING MOMENTS IN FRAMES AND RINGS
BY
ELASTIC CENTER METHOD

A9.1 Introduction

In observing the inside of an airplane fuselage or seaplane hull one sees a large number of structural rings or closed frames. Some appear quite light and are essentially used to maintain the shape of the body metal shell and to provide stabilizing supports for the longitudinal shell stringers. At points where large load concentrations are transferred between body and tail, wing power plant, landing gear, etc., relatively heavy frames will be observed. In hull construction, the bottom structural framing transfers the water pressure in landing to the bottom portion of the hull frames which in turn transfers the load to the hull shell.

In general the frames are of such shape and the load distribution of such character that these frames or rings undergo bending forces in transferring the applied loads to the other resisting portions of the airplane body. These bending forces produce frame stresses in general which are of major importance in the strength proportioning of the frame, and thus a reasonable close approximation of such bending forces is necessary.

Such frames are statically indeterminate relative to internal resisting stress and thus consideration must be given to section and physical properties to obtain a solution of the distribution of the internal resisting forces.

General Methods of Analysis:

There are many methods of applying the principles of continuity to obtain the solution for the redundant forces in closed rings or frames and bents. The author prefers the one which is generally referred to as the "Elastic Center" method and has used it for many years in routine airplane design. The method was originated by Muller-Breslau[1]. The main difference in this method as compared to most other methods of solution is that the redundant forces are assumed acting at a special point called the elastic center of the frame which gives resulting equations for the redundants which are independent of each other.

[1] Muller-Breslau, H., Die Neueren Hethden der Festigkeitslehre und der Statik der Baukonstruktionen. Leipzig, 1886.

Assumptions

In the derivations which follow the distortions due to axial and shear forces are neglected. In general these distortions are small compared to frame bending distortions and thus the error is small.

In computing distortions plane sections are assumed to remain plane after bending. This is not strictly true because the curvature of the frame changes this linear distribution of bending stresses on a frame cross-section. (Corrections for curvature influence are given in Chapter A13.

Furthermore it is assumed that stress is proportional to strain. Since the airplane stress analyst must calculate the ultimate strength of a frame, this assumption obviously does not hold with heavy frames where the rupturing stresses for the frame are above the proportional limit of the frame material.

This chapter will deal only with the theoretical analysis for bending moments in frames and rings by the elastic center method. Practical questions of body frame design are covered in a later chapter.

The following photographs of a portion of the structural framing of the hull of a seaplane illustrate both light and heavy frames.

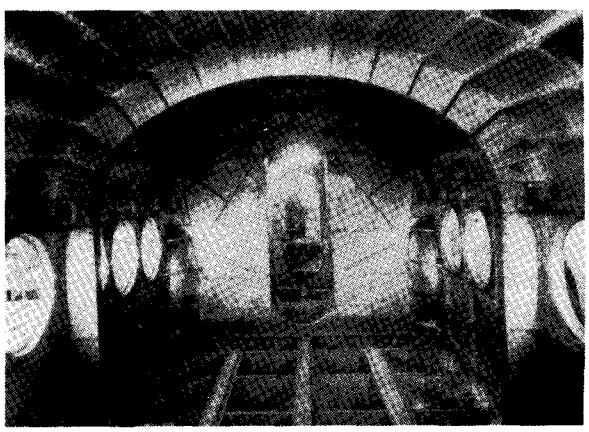

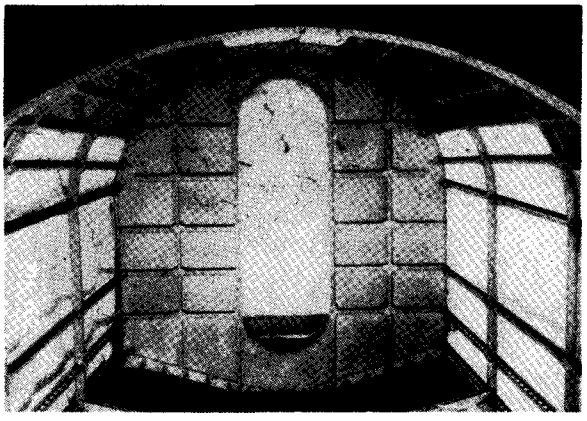

A9.2 Derivation of Equations. Unsymmetrical Frame.

Fig. A9.1 shows an unsymmetrical curved beam fixed at ends (A) and (B) and carrying some external loading P_1, P_2, etc. This structure is statically indeterminate to the third degree because the reactions at (A) and (B) have three unknown elements, namely, magnitude, direction and line of action, making a total of six unknowns with only three equations of static equilibrium available.

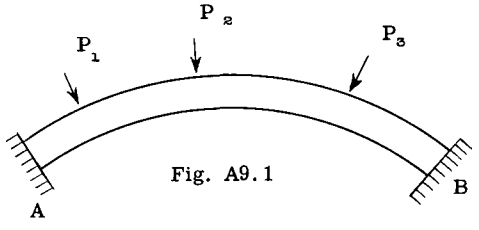

Fig. A9.1

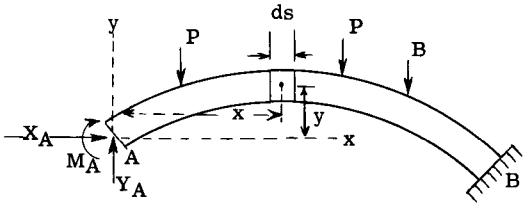

Fig. A9.2

In Fig. A9.2 the reaction at (A) has been replaced by its 3 components, namely, the forces X_A and Y_A and the moment M_A and the structure is now treated as a cantilever beam fixed at end (B) and carrying the redundant loads at (A) and the known external loading P_1, P_2, etc. Because joint (A) is actually fixed it does not suffer translation or rotation when structure is loaded, thus the movement of end (A) under the loading system of Fig. A9.2 must be zero. Therefore, three equations of fact can be written stating that the horizontal, vertical and angular deflection of point (A) must equal zero.

Consider a small element ds of the curved beam as shown in Fig. A9.2. Let M_S equal the bending moment on this small element due to the given external load system. The total bending moment on the element ds thus equals,

$$M = M_S + M_A - X_A y + Y_A x \quad \text{--------(1)}$$

(Moments which cause tension on the inside fibers of the frame are regarded as positive moments.)

The following deflection equations for point (A) must equal zero:-

$\theta = o$. (angular rotation of (A) = zero)
$\Delta_X = o$. (movement of (A) in x direction = o)
$\Delta_y = o$. (movement of (A) in y direction = o)

From Chapter A7, which dealt with deflection theory, we have the following equations for the movement of point (A):-

$$\theta = \Sigma \frac{Mmds}{EI} \quad \text{----------(2)}$$

$$\Delta_X = \Sigma \frac{Mmds}{EI} \quad \text{----------(3)}$$

$$\Delta_y = \Sigma \frac{Mmds}{EI} \quad \text{----------(4)}$$

In equation (2) the term m is the bending moment on a element ds due to a unit moment applied at point (A) (See Fig. A9.3). The bending moment is thus equal one or unity for all ds elements of frame.

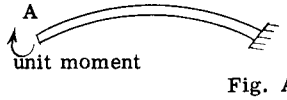

Fig. A9.3

Then substituting in equation (2) and using value of M from equation (1) we obtain -

$$\theta = \Sigma\frac{M_S ds}{EI} + M_A\Sigma\frac{1.ds}{EI} - X_A\Sigma\frac{1.yds}{EI} + Y_A\Sigma\frac{1.xds}{EI} = o$$

whence,

$$\theta = \Sigma\frac{M_S ds}{EI} + M_A\Sigma\frac{ds}{EI} - X_A\Sigma\frac{yds}{EI} + Y_A\Sigma\frac{xds}{EI} = o \quad (5)$$

In equation (3) the term m represents the bending moment on a element ds due to a unit load applied at point (A) and acting in the x direction, as illustrated in Fig. A9.4.

The applied unit load has a positive sign as it has been assumed acting toward the right. The distance y to the ds element is a plus distance as it is

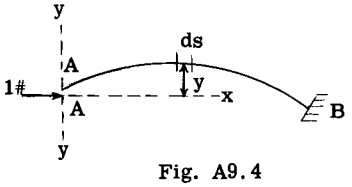

Fig. A9.4

measured upward from axis x-x through (A). However the bending moment on the ds element shown is negative (tension in top fibers), thus the value of m = - (1) y = -y. The minus sign is necessary to give the correct bending moment sign.

Substituting in Equation (3) and using M from Equation (1):-

$$\Delta_X = -\Sigma\frac{M_S y ds}{EI} - M_A\Sigma\frac{yds}{EI} + X_A\Sigma\frac{y^2ds}{EI} - Y_A\Sigma\frac{xyds}{EI} = o \text{--(6)}$$

In equation (4) the term m represents the bending moment on a element ds due to a unit load at point (A) acting in Y direction as illustrated in Fig. A9.5. Hence, m = 1(x) = x Substituting in equation (4) and using M from equation (1), we obtain,

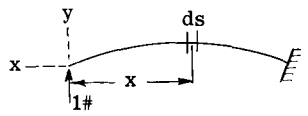

Fig. A9.5

$$\Delta_y = \Sigma\frac{M_S x ds}{EI} + M_A\Sigma\frac{xds}{EI} - X_A\Sigma\frac{xyds}{EI} + Y_A\Sigma\frac{x^2ds}{EI} = o \text{ - - - - - - - - - - - - - - - -(7)}$$

Equations 5, 6, 7 can now be used to solve for the redundant forces M_A, X_A and Y_A. With these values known the true bending moment at any point on structure follows from equation (1).

REFERRING REDUNDANTS TO ELASTIC CENTER

For the purpose of simplifying equations 5, 6, 7, let it be assumed that end A is attached to a inelastic arm terminating at a point (o) as illustrated in Fig. A9.6. The point (o) coincides with the centroid of the ds/EI values for the structure. Reference axes x and y will now be taken with point (o) as the origin. The redundant reactions will now be placed at point (o) the end of the

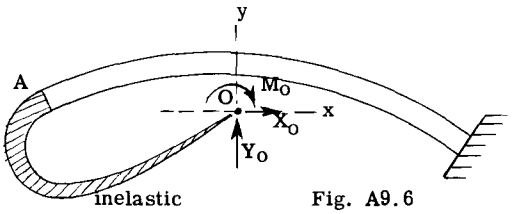

Fig. A9.6

inelastic bracket, as shown in Fig. A9.6. Since point A suffers no movement in the actual structure, then we can say that point (o) must undergo no movement since (o) is connected to point (A) by a rigid arm.

Thus equations 5, 6, and 7 can be re-written using the redundants X_O, Y_O, and M_O in place of X_A, Y_A and M_A respectively.

The axes x and y through the point (o) are centroidal axes for the values ds/EI of the structure. This fact means that the summations-

$$\Sigma\frac{yds}{EI} = o \quad \text{and} \quad \Sigma\frac{xds}{EI} = o$$

The expressions $\Sigma x^2ds/EI$, $\Sigma y^2ds/EI$ and $\Sigma xyds/EI$ also appear in equations 6 and 7. These terms will be referred to as elastic moments of inertia and product of inertia of the frame about y and x axes through the elastic center of the frame, and for simplicity will be given the following symbols.

$$\Sigma\frac{x^2ds}{EI} = I_y \ , \ \Sigma\frac{y^2ds}{EI} = I_x \ , \ \Sigma\frac{xyds}{EI} = I_{xy}$$

Equations 5, 6 and 7 will now be rewritten using the redundant forces at point (o).

$$\theta = \Sigma\frac{M_S ds}{EI} + M_O\Sigma\frac{ds}{EI} = o$$

hence,

$$M_O = \frac{-\Sigma\frac{M_S ds}{EI}}{\Sigma\frac{ds}{EI}} \text{ - - - - - - - - - - - - - (8)}$$

$$\Delta_X = -\Sigma\frac{M_S dsy}{EI} + X_O I_X - Y_O I_{xy} = o \text{ - - - (9)}$$

The term $M_O\Sigma$ yds/EI is zero since Σ yds/EI is zero, thus M_O drops out when substituting in Equation (6).

$$\Delta_y = \frac{M_S dsx}{EI} - X_O I_{xy} + Y_O I_y = o \text{ - - - -(10)}$$

The term $M_S ds/EI$ represents the angle change between the end faces of the ds element when acted upon by a constant static moment M_S. This angle change which actually is equal in value to the area of the M_S/EI diagram on the element ds will be given the symbol ϕ_S, that is, $\phi_S = M_S ds/EI$. With this symbol substitution, equations 8, 9, 10 can now be rewritten as follows:-

$$M_O = -\frac{\Sigma\,\phi_S}{\Sigma\,ds/EI} \text{ - - - - - - - - - - - - -(11)}$$

$$-\Sigma\,\phi_S y + X_O I_X - Y_O I_{xy} = o \text{ - - - - - -(12)}$$

$$\Sigma\,\phi_S x - X_O I_{xy} + Y_O I_y = o \text{ - - - - - - -(13)}$$

Solving equations (12) and (13) for the redundant forces X_O and Y_O we obtain,

$$X_o = \frac{\Sigma \phi_s y - \Sigma \phi_s x \left(\frac{I_{xy}}{I_y}\right)}{I_x \left(1 - \frac{I^2_{xy}}{I_x I_y}\right)} \quad \text{--------(14)}$$

$$Y_o = \frac{-\left[\Sigma \phi_s x - \Sigma \phi_s y \left(\frac{I_{xy}}{I_x}\right)\right]}{I_y \left(1 - \frac{I^2_{xy}}{I_x I_y}\right)} \quad \text{------(15)}$$

A9.3 Equations for Structure with Symmetry About One Axis through Elastic Center.

If the structure is such that either the x or y axis through the elastic center is a axis of symmetry than the product of inertia $\Sigma xyds/EI = I_{xy} =$ zero. Thus making the term $I_{xy} = o$ in equations 11, 14 and 15 we obtain,

$$M_o = \frac{-\Sigma \phi_s}{\Sigma ds/EI} \quad \text{----------(16)}$$

$$X_o = \frac{\Sigma \phi_s y}{I_x} \quad \text{----------(17)}$$

$$Y_o = \frac{-\Sigma \phi_s x}{I_y} \quad \text{----------(18)}$$

A9.4 Example Problem Solutions. Structures with at least One Axis of Symmetry.

Example Problem 1

Fig. A9.7 shows a rectangular frame with fixed supports at points A and D, and carrying a single load as shown. The problem is to determine the bending moment diagram under this loading.

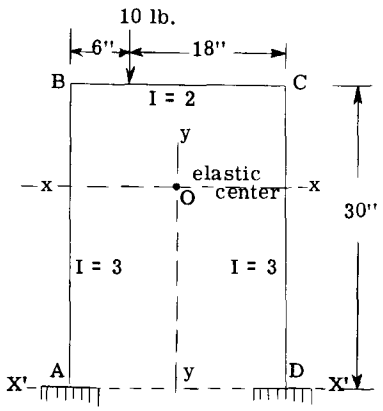

Fig. A9.7

The first step in the solution is to find the location of the elastic center of the frame and the elastic moments of inertia I_x and I_y.

Due to symmetry of the structure about the Y axis the centroidal Y axis is located midway between the sides of the frame, and thus the elastic center (o) lies on this axis.

Table A9.1 shows some of the necessary calculations to determine the location of the elastic center and the elastic moments of inertia. The reference axes used are x^1-x^1 and y-y.

Table A9.1

Portion	$w=\frac{ds}{I}$	y= dist. from x^1-x^1	x= dist. from y-y	wx	wy	$I_x = wy^2 + i_x$	$I_y = wx^2 + i_y$
AB	$\frac{30}{3}=10$	15	-12	-120	+150	$wy^2 = 2250$ $i_x = \frac{30^3}{12x3} = 750$	$wx^2 = 1440$ $i_y = \frac{30}{12x3^3} = 0$
BC	$\frac{24}{2}=12$	30	0	0	360	$wy^2 = 10800$ $i_x = \frac{24}{12x2^3} = 0$	$wx^2 = 0$ $i_y = \frac{24^3}{12x2} = 576$
CD	$\frac{30}{3}=10$	15	12	120	150	$wy^2 = 2250$ $i_x = 750$	$wx^2 = 1440$ $i_y = \frac{30}{12x3^3} = 0$
Sum	32			0	660	16800	3456

The terms i_x and i_y are the elastic moment of inertia of each portion of the frame about its centroidal x and y axes. Since I is constant over each portion the centroidal moment of inertia of each portion is identical to that of a rectangle about its centroidal axis.

To explain for member AB:-

Referring to Fig. a,

$$i_x = \frac{1}{12}bh^3 = \frac{1}{12} \times \frac{1}{3} \times 30^3 = 750$$

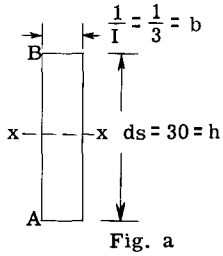

Fig. a

Referring to Fig. b,

$$i_y = \frac{1}{12}bh^3 = \frac{1}{12} \times 30 \times \frac{1}{3^3} = .09 \text{ (negligible)}$$

The distance from the two reference axes to the elastic center can now be calculated:-

$$\bar{y} = \frac{\Sigma wy}{\Sigma w} = \frac{660}{32} = 20.625 \text{ in.}$$

$$\bar{x} = \frac{\Sigma wx}{\Sigma w} = \frac{0}{32} = o$$

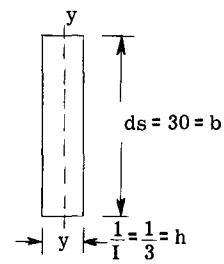

Fig. b

Having the moment of inertia about axis x^1x^1 we can now find its value about the centroidal axis xx of the frame, by use of the parallel axis theorem.

$$I_x = I_x - \Sigma w(\bar{y}^2) = 16800 - 32 \times 20.625^2 = 3188$$

$$I_y = I_y - \Sigma w(\bar{x}^2) = 3456 - 32(o) = 3456$$

The problem now consists in solving equations (16), (17) and (18) for the redundants at the elastic center, namely

$$M_o = \frac{-\Sigma \phi_s}{\Sigma ds/I} = \frac{\text{Area of static M/I diagram}}{\text{Total elastic weight of structure}}$$

$$X_o = \frac{\Sigma \phi_s y}{I_x} = \frac{\text{Moment of static M/I diagram about x axis}}{\text{Elastic moment of inertia about x axis}}$$

$$Y_o = \frac{-\Sigma \phi_s x}{I_y} = \frac{\text{Moment of static M/I diagram about y axis}}{\text{Elastic moment of inertia about y axis}}$$

Thus to solve these three equations we must assume a static frame condition consistent with the given frame and loading. In general there are a number of static conditions that can be chosen. For example in this problem we might select one of the statically determinate conditions illustrated in Fig. A9.8 cases 1 to 5.

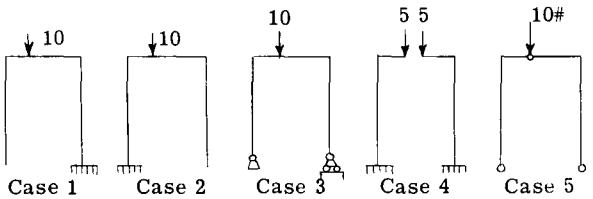

Fig. A9.8

To illustrate the use of different static conditions, three solutions will be presented with each using a different static condition.

Solution No. 1

In this solution we will use Case 3 as the static frame condition. The bending moment on the frame for this static frame condition is given in Fig. A9.9. The equations

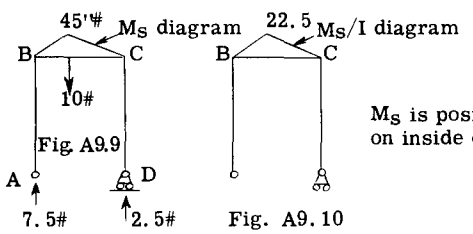

Fig. A9.10

M_S is positive, tension on inside of frame.

for the redundants require ϕ_S the area of the M_S/I diagram. Fig. A9.10 shows the M_S/I curve which is obtained by dividing the values in Fig. A9.9 by the term 2 which is the moment of inertia of member BC as given in the problem. Since the equations for X_o and Y_o require the moment of the M_S/I diagram as a load about axes through the elastic center of frame, the area of the M_S/I diagram will be concentrated at the centroid of the diagram and along the centerline of the frame, or more accurately along the neutral axis of the frame members.

In Fig. A9.10 the area of the M_S/I diagram equals $\phi_S = 22.5 \times 24/2 = 270$. The centroid by simple calculations of this triangle would fall 10 inches from B. Fig. A9.11 now shows the frame with its M_S/I or its ϕ_S load. ϕ_S is positive since M_S is positive. The next step is to solve the equations for the redundant at the elastic center. The signs of the distances x and y from the axes x and y are conventional.

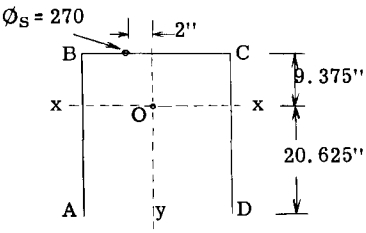

Fig. A9.11

Thus,

$$M_o = \frac{-\Sigma \phi_S}{\Sigma ds/I} = \frac{-(270)}{32 \text{ (from Table A9.1}} = -8.437 \text{ in.lb.}$$

$$X_o = \frac{\Sigma \phi_S y}{I_x} = \frac{270(9.375)}{3188} = 0.7939 \text{ lb.}$$

$$Y_o = \frac{-\Sigma \phi_S x}{I_y} = \frac{-(270)(-2)}{3456} = 0.1562 \text{ lb.}$$

Fig. A9.12 shows these values of the redundants acting at the elastic center.

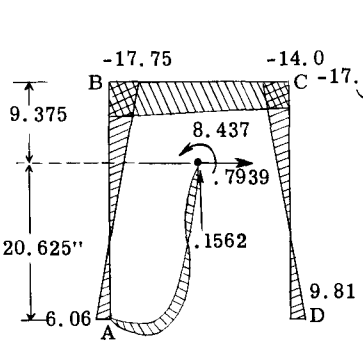

Fig. A9.12

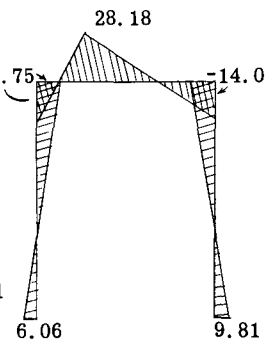

Fig. A9.13

The bending moments due to these redundant forces will now be calculated.

$$M_A = -8.437 - .1562 \times 12 + .7939 \times 20.625 = 6.06 \text{ in.lb.}$$

$$M_B = -8.437 - .7939 \times 9.375 - .1562 \times 12 = -17.75 \text{ in.lb.}$$

$$M_C = -8.437 - .7939 \times 9.375 + .1562 \times 12 = -14.00 \text{ in.lb.}$$

$$M_D = -8.437 + .7939 \times 20.625 + .1562 \times 12 = 9.81 \text{ in.lb.}$$

These resulting values are plotted on Fig. A9.12 to give the bending moment diagram due to the redundant forces at the elastic center.

Adding this bending moment diagram to the static bending diagram of Fig. A9.9 we obtain the final bending moment diagram of Fig. A9.13.

The final bending moments could also be obtained by substituting directly in equation (1) using subscript (o) instead of (A). Thus,

$$M = M_S + M_O - X_O y + Y_O x \quad -------(19)$$

For example, determine bending moment at point B.

For point B, x = -12 and y = 9.375, M_S = 0 substituting in (19)

$$M_B = 0 + (-8.437) - .7939 \times 9.375 + .1562\ (-12) = -17.75$$ as previously found

AT POINT D. x = 12, y = -20.625, M_S = 0.

$$M_D = 0 + (-8.437) - .7939\ (-20.625) + .1562 \times 12 = 9.81$$ in.lb.

Solution No. 2

In this solution we will use Case 4 (See Fig. A9.8) as the assumed static condition, that is two cantilever beams with half the external load or 5 lb. acting on each cantilever. Fig. A9.14 shows the static bending moment diagram and Fig. A9.15 the M_S/I diagram.

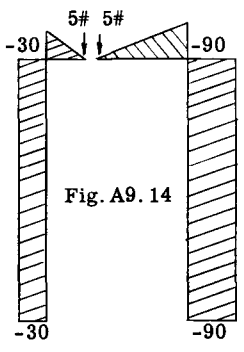

Fig. A9.14

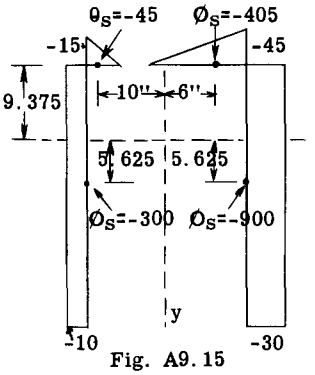

Fig. A9.15

Fig. A9.15 also shows the results of calculating the $\emptyset_S$ value for each portion of the M_S/I diagram and its centroid location. Substituting in the equations for the redundants we obtain,

$$M_O = \frac{-\Sigma\emptyset_S}{\Sigma ds/I} = \frac{-(-45-405-300-900)}{32} = 51.56 \text{ in.lb.}$$

$$X_O = \frac{\Sigma\emptyset_S y}{I_x} = \frac{(-45-405)9.375+(-900-300)(-5.625)}{3188}$$

$$= 0.7939 \text{ lb.}$$

$$Y_O = \frac{-\Sigma\emptyset_S x}{Iy} = \frac{-[-45(-10)-405x6-300(-12)-900x12]}{3456}$$

$$= \frac{-(-9180)}{3456} = 2.656 \text{ lb.}$$

The final moments at any point can now be found by equation (19).

Consider point B:-

M_S = -30 from Fig. A9.14
x = -12, y = 9.375

Subt. in (19)

M_B = -30+51.56-.7939x9.375+2.656(-12)
= -17.75 in.lb. which checks first solution.

Consider point D:-

M_S = -90, x = 12, y = -20.625

Subt. in (19)

M_D = -90+51.56 - 7939(-20.625) + 2.656 x 12
= 9.80 in.lb.

Solution No. 3

In this solution we will use Case 5 (Fig. A9.8) as the assumed static condition, namely a frame with 3 hinges at points A, D and E, as illustrated in Fig. A9.16.

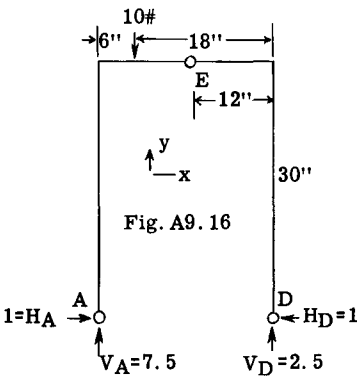

Fig. A9.16

Before the bending moment diagram can be calculated the reactions at A and D are necessary.

To find V_D take moments about point A.

ΣM_A = 10x6 - 24V_D
= o

hence, V_D = 2.5

To find V_A take ΣF_y = o = -10 + 2.5 + V_A = o hence V_A = 7.5.

To find H_D take moments about hinge at E of all forces on frame to right side of E and equate to zero.

ΣM_E = -2.5 x 12 + 30H_D = o, hence H_D = 1.

Then using ΣF_X = o for entire frame, we obtain ΣF_X = -1 + H_A = o, hence H_A = 1.

The frame static bending moment diagram can now be calculated and drawn as shown in Fig. A9.17.

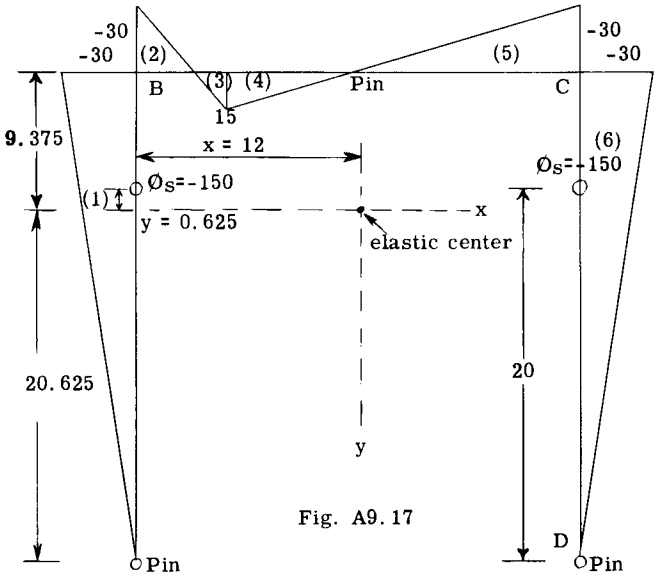

Fig. A9.17

The moment diagram is labeled in 6 parts 1 to 6 as indicated by the values in the small circles on each portion. Most of the calculations from this point onward can be done conveniently in table form as illustrated in Table A9.2.

Table A9.2

1	2	3	4	5	6	7	8
Mom. Diagram Portion	A = Area of Mom. Dia.	I for Beam Section	$\emptyset_S = \frac{A}{I}$	x = dist. from Y axis to C.g. of $\emptyset_S$	y = dist. from X axis to C.g. of $\emptyset_S$	$\emptyset_S x$	$\emptyset_S y$
1	-450	3	-150	-12.00	-0.625	1800	93
2	- 60	2	- 30	-10.67	9.375	320	-281
3	15	2	7.5	- 6.67	9.375	- 50	70
4	45	2	22.5	- 4.00	9.375	- 90	211
5	-180	2	- 90	8.00	9.375	- 720	-844
6	-450	3	-150	12.00	-0.625	-1800	93
Sum			-390			- 540	-658

In order to take moments of the $\emptyset_S$ values in column (4) of the table, the centroid of each portion of the diagram must be determined. For example, the centroid of the two triangular bending moment portions marked 1 and 6 is .667 x 30 from the lower end or 20 inches as shown in Fig. A9.17. Thus the distances x and y from this $\emptyset_S$ location to the y and x axes through the frame elastic center are then calculated as -12 and -0.625 inches respectively.

$$M_o = \frac{-\Sigma\emptyset_S}{\Sigma ds/I} = \frac{-(-390)}{32} = 12.19 \text{ in. lb.}$$

$$X_o = \frac{\Sigma\emptyset_S y}{I_x} = \frac{-648}{3188} = -0.203 \text{ lb.}$$

$$Y_o = \frac{-\Sigma\emptyset_S x}{I_y} = \frac{-(-540)}{3456} = 0.1562 \text{ lb.}$$

The final moments at any point can now be found by use of equation (19), namely

$$M = M_S + M_o - X_o y + Y_o x \quad \text{-------(19)}$$

Consider point B:-

$$x = -12, \quad y = 9.375, \quad M_S = -30$$

Substituting -

$$M_B = -30+12.19-(-0.203)9.375+0.1562(-12)$$
$$= -17.76 \text{ in.lb.(checks previous solutions)}$$

Consider point D:-

$$x = 12, \quad y = -20.625, \quad M_S = o$$

Subt. in (19)

$$M_D = 0+12.19-(-0.203)(-20.625)+0.1562x12$$
$$= 9.82 \text{ in.lb. (checks previous solutions)}$$

The final complete bending moment diagram would of course be the same as drawn in Fig. A9.13 for the results of Solution No. 1.

Example Problem 2.

Fig. A9.18 shows a rectangular closed frame supported at points A and B and carrying the external loads as shown. The reaction at D due to rollers is vertical. The frame at point A is continuous through the joint but the reaction is applied through a pin at the center of the joint. The problem is to determine the bending moment diagram.

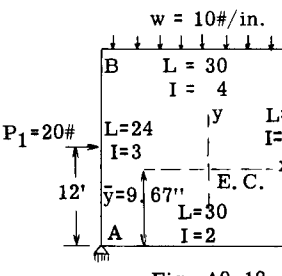

Fig. A9.18

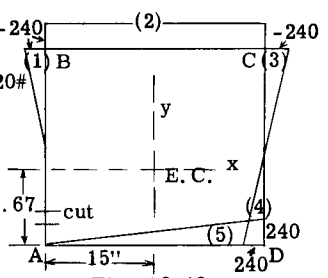

Fig. A9.18
M_S diagram for load P_1

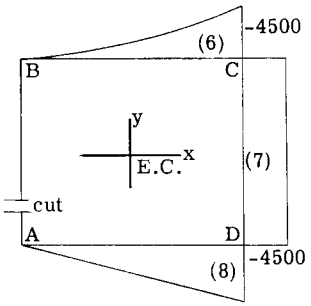

Fig. A9.19
M_S diagram for w loading

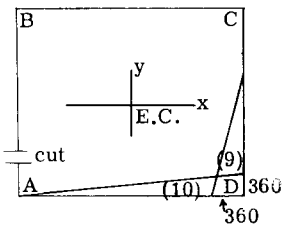

Fig. A9.20
M_S diagram for P_2 load.

Solution:

The first step is to find the location of the elastic center of the frame. Due to symmetry of frame about the y axis, the elastic center will be on a y axis through the middle of the frame. The vertical distance $\bar{y}$ measured from a axis through AD equals,

$$\bar{y} = \frac{\Sigma\left(\frac{ds}{I}\right)y}{\Sigma\frac{ds}{I}} = \frac{\frac{30}{4}x24+\frac{24}{3}x12x2}{\frac{30}{4}+\left(\frac{24}{3}\right)2+\frac{30}{2}} = \frac{372}{38.5} = 9.67"$$

The next step is to determine the elastic moment of inertia of the frame about x and y axes through the elastic center of the frame.

Moment of inertia about x axis = I_X :-

Members AB and DC,

$$I_X = \left(\frac{1}{3} \times \frac{1}{3} \times 14.33^3\right) 2 = 653.9$$
$$\left(\frac{1}{3} \times \frac{1}{3} \times 9.67^3\right) 2 = 200.9$$

Member BC and AD

$$I_X = (30/4)(14.33^2) = 1540.0$$
$$(30/2)(9.67^2) = 1402.7$$
$$I_X = 3797.5$$

Moment of inertia about y axis = I_y :-

Members AD and BC,

$$I_y = \frac{1}{12} \times \frac{1}{4} \times 30^3 = 563$$
$$\frac{1}{12} \times \frac{1}{2} \times 30^3 = 1126$$

Members AB, CD,

$$I_y = \left(\frac{24}{3} \times 15^2\right)2 = 3600$$
$$I_y = 5289$$

The next step is to choose a static frame condition and determine the static (M_S) bending moment diagram. In this solution the frame is assumed cut on member AB just above point A as illustrated in Figs. A9.18, 19 and 20. For simplicity the static moment curve has been drawn in three parts, with each part considering only one of the three external given loads on the structure. Figs. A9.18, 19, 20 show these resulting bending moment curves. The portions of these bending moment diagrams numbered 1 to 10 are shown in the parenthesis on each portion.

The next step in the solution consists of finding the area of the M_S/I diagrams and the first moment of these diagrams about the x and y axes through the elastic center. These simple calculations can best be done in table form as illustrated in Table A9.3.

Table A9.3

Portion of M_S Diagram ( )	Area of M_S Portion = A	I	$\emptyset_S = \frac{A}{I}$	x = dist. to Y Axis	y = dist. to X Axis	$\emptyset_S x$	$\emptyset_S y$
1	- 1440	3	- 480	-15	10.33	7200	- 4958
2	- 7200	4	- 1800	0	14.33	0	- 25794
3	- 1440	3	- 480	15	10.33	- 7200	- 4958
4	1440	3	480	15	- 5.67	7206	- 2726
5	3600	2	1800	5	- 9.67	9000	- 17406
6	- 45000	4	-11250	7.5	14.33	- 84375	-161212
7	-108000	3	-36000	15	2.33	-540000	- 83880
8	- 67500	2	-33750	5	- 9.67	-168750	326362
9	3240	3	1080	15	- 3.67	16200	- 3964
10	5400	2	2700	5	- 9.67	13500	- 26109
Sum			-77700			-747225	- 4645

Solving for the redundants at the elastic center,

$$M_O = \frac{-\Sigma\emptyset_S}{\Sigma ds/I} = \frac{-(-77700)}{38.5} = 2018 \text{ in.lb.}$$

$$X_O = \frac{\Sigma\emptyset_S y}{I_x} = \frac{-4645}{3797} = -1.22 \text{ lb.}$$

$$Y_O = \frac{-\Sigma\emptyset_S x}{I_y} = \frac{-(-747225)}{5289} = 141.28 \text{ lb.}$$

Fig. A9.21 shows these redundant forces acting at the elastic center. Fig. A9.22 shows the bending moment diagram due to these redundant forces. The calculations with reference to Fig. A9.21 are -

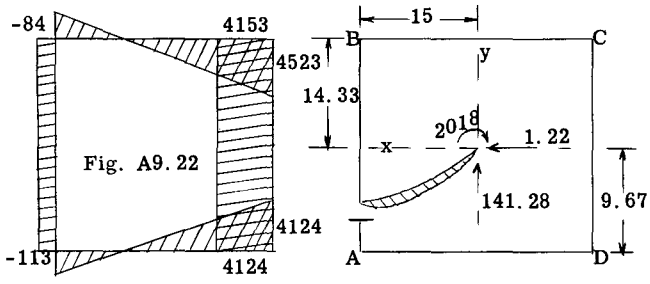

Fig. A9.21

M_A = 2018 - 141.28 x 15 - 1.22 x 9.67 = -113

M_B = 2018 - 141.28 x 15 + 1.22 x 14.33 = -84

M_C = 2018 + 141.28 x 15 + 1.22 x 14.33 = 4153

M_D = 2018 + 141.28 x 15 - 1.22 x 9.67 = 4124

Combining the bending moment diagrams of Figs. A9, 18, 19, 20 with Fig. A9.22 would give the true or final bending moment diagram.

Example Problem 3. Circular Ring.

Fig. A9.23 shows a circular ring of constant cross-section subjected to a symmetrical loading as shown. The problem is to determine the bending moment diagram.

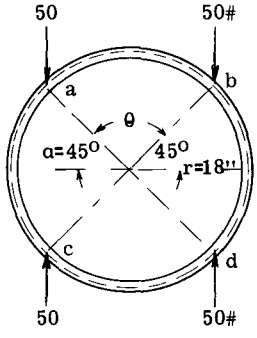

Fig. A9.23

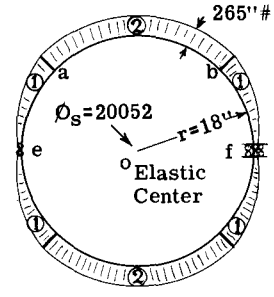

Fig. A9.24

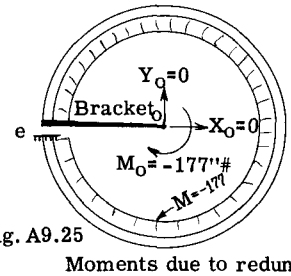

Fig. A9.25

Moments due to redundant forces.

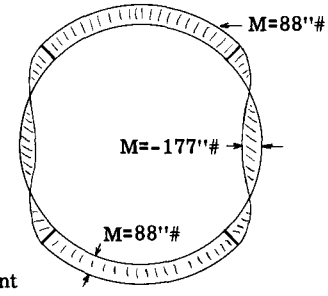

Fig. A9.26

Solution. Due to symmetry of the ring structure the elastic center falls at the center of the ring. Since the ring has been assumed with constant cross-section, a relative value of one will be used for I.

Total elastic weight of ring =

$$\Sigma \frac{ds}{I} = \frac{\pi (36)}{1} = 113.1$$

The elastic moment of inertia about x and y axes through center point of ring are the same for each axis and equal

$$I_x = I_y = \pi r^3 = \pi \times 18^3 = 18300$$

The next step in the solution is to assume a static ring condition and determine the static (M_S) diagram. In general it is good practice to try and assume a static condition such that the M_S diagram is symmetrical about one or if possible about both x and y axes through the elastic center, thus making one or both of the redundants X_o and Y_o zero and thus reducing considerably the amount of numerical calculation for the solution of the problem.

In order to obtain symmetry of the M_S diagram and also the M_S/I diagram since I is constant, the static condition as shown in Fig. A9.24 is assumed, namely, a pin at (e) and rollers at (f). The static bending moment at points (a), (b), (c) and (d) are the same magnitude and equal,

$$M_S = 50(18 - 18 \cos 45^\circ) = 265 \text{ in.lb.}$$

The sign is positive because the bending moment produces tension on the inside of the ring.

The next step is to determine the $\emptyset_S$, $\emptyset_S x$ and $\emptyset_S y$ values.

$\emptyset_S$ is the area of the M_S/I diagram, however since I is unity it is the area of the M_S diagram. The static M_S diagram of Fig. A9.24 is divided into similar portions labeled (1) and (2). Hence

$\emptyset_{S(1)}$ = area of portion (1) = $Pr^2(\alpha - \sin \alpha)$, where P = 50 lb. and $\alpha = 45^\circ$.

Substituting and multiplying by 4 since there are four portions labeled (1).,

$$\emptyset_{S(1)} = 4\left[50 \times 18^2 (0.785 - 0.707)\right] = 5052$$

The area of portion labeled (2) equals,

$$Pr^2\theta(1 - \cos \alpha).$$

Since there are two areas (2) we obtain,

$$\emptyset_{S(2)} = 2\left[50 \times 18^2 \times \frac{\pi}{2} (1-0.707)\right] = 15000$$

Hence, total $\emptyset_S$ = 15000 + 5052 = 20052

Since the centroid of the M_S diagram due to symmetry about both x and y axes coincides

with the center or elastic center of the frame, the terms $\Sigma\phi_S x$ and $\Sigma\phi_S y$ will be zero.

Substituting to determine the value of the redundants at the elastic center we obtain,

$$M_O = \frac{-\Sigma\phi_S}{\Sigma ds/I} = \frac{-(20052)}{113.1} = -177 \text{ in.lb.}$$

$$X_O = \frac{\Sigma\phi_S y}{I_X} = \frac{20052(0)}{18300} = 0$$

$$Y_O = \frac{-\Sigma\phi_S x}{Iy} = \frac{-(20052)(0)}{18300} = 0$$

Fig. A9.25 shows the values acting at the elastic center and the bending moment diagram produced by these forces. Adding the bending moment diagram of Fig. A9.25 which is a constant value over entire frame of -177 to the static moment diagram of Fig. A9.24 gives the final bending moment diagram as shown in Fig. A9.26.

Example Problem 4. Hull Frame

Fig. A9.27 shows a closed frame subjected to the loads as shown. The problem is to determine the bending moment diagram.

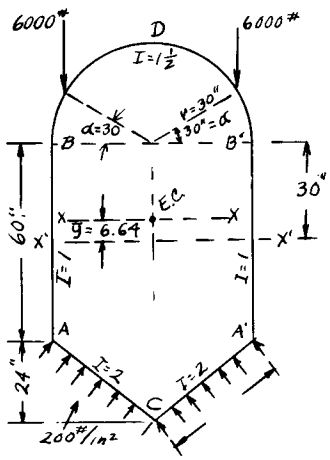

Fig. A9.27

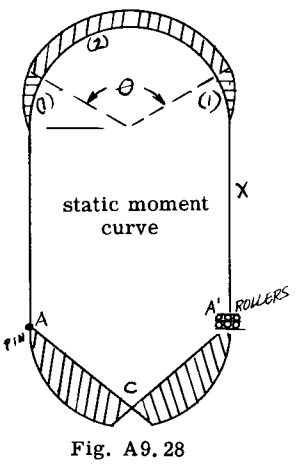

Fig. A9.28

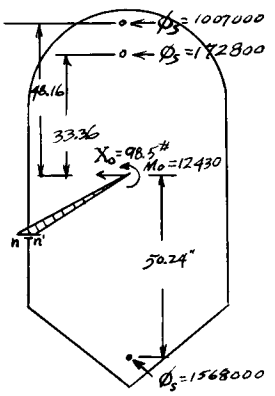

Fig. A9.29

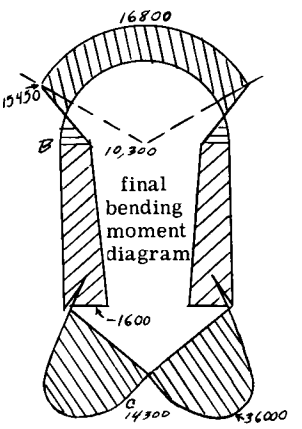

Fig. A9.30

Solution:

The first step is to determine the elastic center of the frame and the elastic moments of inertia. Table A9.4 shows the calculations. A reference axis x'-x' has been selected at the midpoint of the side AB. Since a static frame condition has been selected to make the M_S diagram symmetrical about y axes through the elastic center (see Fig. A9.28), it is not necessary to determine I_y since the redundant Y_O will be zero due to this symmetry.

Table A9.4

Member	Length ds	I	$w = \frac{ds}{I}$	y	wy	$I_{X'X'} = i_x + wy^2$
BDB'	94.25	1.5	62.8	$\frac{2r}{\pi} + 30 = 49.1$	3080	5400+151200 = 156600
AB	60.0	1.0	60.0	0	0	18000 + 0 = 18000
A'B'	60.0	1.0	60.0	0	0	18000 + 0 = 18000
AC	38.4	2.0	19.2	-42	-806	922 + 33850 = 34772
CA'	38.4	2.0	19.2	-42	-806	922 + 33850 = 34772
Totals			221.2		1468	262140

In the last column of Table A9.4 the term i_X is the moment of inertia of a particular member about its own centroidal x axis. Thus for member BDB;

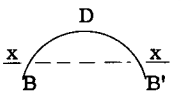

$$i_X = \frac{.3r^3}{I} = .3 \times 30^3/1.5 = 5400$$

For members AC and CA ,

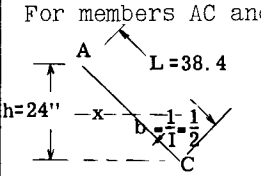

$$i_X = \frac{1}{12} b L h^2$$

$$= \frac{1}{12} \times \frac{1}{2} \times 38.4 \times 24^2 = 922$$

Let $\bar{y}$ = distance from X'X' ref. axis to centroidal elastic axis X-X.

$$\bar{y} = \frac{\Sigma wy}{\Sigma w} = \frac{1468}{221.2} = 6.64 \text{ in.}$$

By parallel axis theorem,

$$I_X = I_{X'} - 6.64^2(\Sigma w)$$

$$= 262140 - 6.64^2(221.2) = 252400$$

The next step in the solution is to compute the static moment elastic weights ϕ_S and their centroid locations. In Fig. A9.28, the static frame condition assumed is a pin at point A and rollers at point A', which gives the

general shape of static moment curve as shown in the figure.

Consider member BDB',

The bending moment curve will be considered in two parts, namely (1) and (2). The term $\emptyset_S$ represents the area of the M_S/I diagram.

Thus for portion (1) and (1')

$$\emptyset_{S(1)} + \emptyset_{S(1')} = 2\left[\frac{Pr^2}{I}(a - \sin a)\right]$$
$$= 2\left[\frac{6000 \times 30^2}{1.5}(0.524 - 0.5)\right] = 172800$$

The vertical distance from the line BB' to centroid of M_S curve for portion (1) and (1') is,

$$y = \frac{r(1 - \cos a - \frac{\sin^2 a}{2})}{a - \sin a} = \frac{30(1 - 0.867 - \frac{0.5^2}{2})}{0.524 - 0.5}$$

$$= 10 \text{ in.}$$

For portion (2) of the M_S diagram the area of the M_S/I diagram which equals $\emptyset_S$ is

$$\emptyset_{S(2)} = \frac{Pr^2\theta}{I}(1 - \cos a) = \frac{6000 \times 30^2 \times 2.1}{1.5}(1-0.867)$$

$$= 1{,}007{,}000$$

Consider member AC,

From free body diagram of bottom portion of frame (Fig. A9.31a) the equation for bending moment

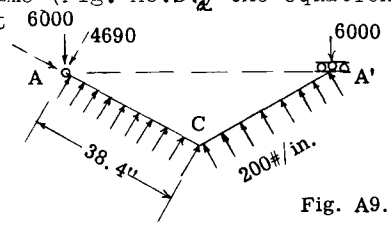

Fig. A9.31a

on member AC equals:

$$M_X = 4690 \times -100 x^2$$

Area of M/I curve between A and C when I = 2 equals,

$$1/2\int_0^{38.4} (4690 \times - 100 x^2)dx$$

$$= 1/2\left[\frac{4690 x^3}{2} - \frac{100 x^3}{3}\right]_0^{38.4} = 784000$$

Distance to centroid of M/I curve along line AC from A.

$$\bar{X} = \frac{1/2\int_0^{38.4} (4690 \times 100 x^2)xdx}{78400}$$

$$= \frac{1/2\left[\frac{4690 x^3}{3} - \frac{100 x^4}{4}\right]_0^{38.4}}{78400} = 21.77"$$

Vertical distance from line AA' to centroid = 21.77 x 24/38.4 = 13.6". The static moment weight for A'C' is same as for AC, thus

$$\emptyset_{AC} + \emptyset_{A'C'} = 2 \times 784000 = 1568000$$

Fig. A9.29 shows the frame with the moment weights $\emptyset_S$ located at the centroids, together with the redundant forces M_o and X_o at the elastic center. It makes no difference where the frame is cut to form our residual cantilever, if one of the cut faces is attached to elastic center and the other is considered fixed. With the elastic properties and moment weights known the redundants can be solved for:

$$M_o = -\frac{\Sigma\emptyset_S}{\Sigma w} = -\frac{(1007000 + 172800 + 156800)}{221.2} =$$

$$12430"\#$$

$$X_o = \frac{\Sigma\emptyset_S y}{I_{xx}} =$$

$$= \frac{1007000 \times 48.16 + 172800 \times 33.36 + 156800 \times -5.24}{252400}$$

$$= -98.5\#$$

Y_o is zero because of the symmetrical frame and loading. The final or true bending moment at any point equals

$$M = M_S + M_o - X_o y$$

Thus for point B

$$M_B = 0 + (-12430) - (-98.5 \times 23.36) =$$
$$-10130"\#$$

For point C

$$M_S \text{ at point C} = 4690 \times 38.4 - 200x(38.4)^2/2$$
$$= 32700$$

Hence $M_C = 32700 - 12430 - (-98.5 \times -60.64) =$
$$14300"\#$$

Fig. A9.30 shows the general shape of the true frame bending moment diagram.

Example Problem 5

Fig. A9.31 shows the general details of one

half of a symmetrical hull frame that was used in an actual seaplane. The main external load on such frames is the water pressure on the hull bottom plating. The hull bottom stringers transfer the bottom pressure as concentrations on the frame bottom as shown. The resistance to this bottom upward load on the frame is provided by the hull metal covering which exerts tangential loads on the frame contour. The question as to the distribution of these resisting forces is discussed in later chapters. In this problem the resisting shear flow in the hull sheet has been assumed constant between the chine point and the upper heavy longeron. For analysis purposes the frame has been divided into 20 strips. The centroid of these strips located on the neutral axis of the frame sections are numbered 1 to 20 in Fig. A9.21. The tangential skin resisting forces are shown as concentrations on frame strips #6 to #16. On the figure these tangential loads have been replaced by their horizontal and vertical components. The sum of the vertical components should equal the vertical component of the bottom water pressure.

Table A9.5 shows the complete calculations for determining the bending moment on the frame. Columns 1 to 7 give the calculations for the elastic properties of the frame, namely the elastic weight of the frame; the elastic center location, and the elastic centroidal moment of inertia about the horizontal centroidal elastic axis. A reference horizontal axis X'X' has been selected as shown. All distance recorded in the table have been obtained by scaling from a large drawing of the frame.

The static condition assumed for computing the M_S moments is a double symmetrical cantilever beam as illustrated in Fig. A9.32. The frame is cut at the top to form the free end of the cantilever beams, and the fixed end has been taken at the centerline bottom frame section. The static bending moment diagram will be symmetrical about the y axis through the elastic center of the frame and thus the redundant Y_0 at the elastic center will be zero since the term $\Sigma \phi_S x$ will be zero. The calculations for determining the static moments M_S in Column 8 of Table A9.5 are not shown. The student should refer to Art. A5.9 of Chapter A5 to refresh his thinking relative to bending moment calculations on curved beams.

Columns 9 and 10 give the calculations of the ϕ_S values (area of M_S/I diagram) and the first moment ($\phi_S x$ values). The summations of columns 3, 9, 10 permits the solution for the redundants M_0 and X_0 as shown below the table. The final bending moment M at any point on the frame is by simple statics equals,

$$M = M_S + M_0 - X_0 y.$$

The moment of inertia of the frame cross sections are given in column 2 of Table A9.6 which have been determined from a consideration of the actual dimensions of the frame members.

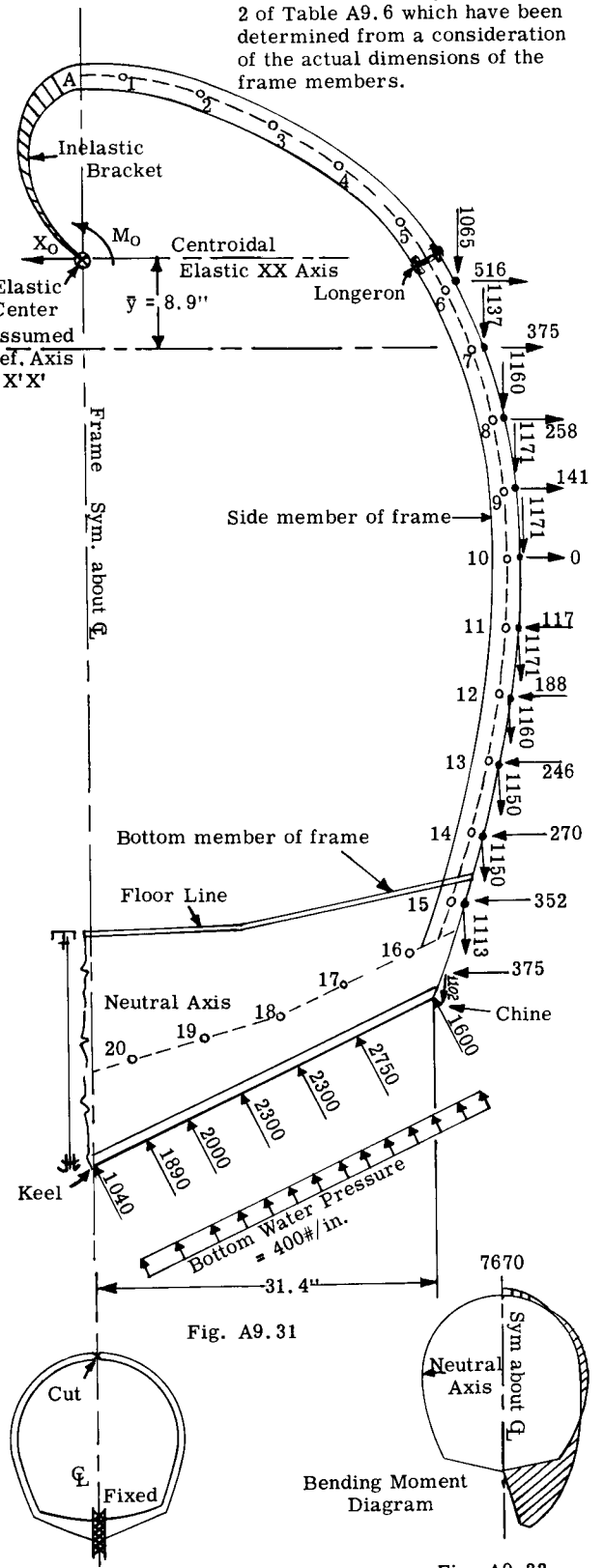

Fig. A9.31

Fig. A9.32

Fig. A9.33

Table A9.5

Calculation of Frame Elastic Properties							Calculation of Moment Weights and Solution of Redundants						
Col.	1	2	3	4	5	6	7	8	9	10	11	12	13
Station	Strip Length ds	Moment of Inertia I	Elastic Weight w = ds / I	Arm to Ref. Axis X'X' = y'	w y'	w y'^{2}	Arm to Axis XX = y	Static Moment M_S	Moment Weight $\phi_S = \frac{M_S w}{1000}$	ϕ_S y	M_O	$-X_O y$	*Total Moment M
1	7.6	.065	117.00	26.1	3050	79700	17.2	0	0	0	-9020	16650	7630
2	7.6	.065	117.00	24.4	2850	69500	15.5	0	0	0	"	15020	6000
3	7.6	.065	117.00	21.4	2497	53300	12.5	0	0	0	"	12100	3080
4	7.6	.065	117.00	17.3	2025	35020	8.4	0	0	0	"	8130	- 890
5	7.6	.065	117.00	12.0	1403	16820	3.1	0	0	0	"	3000	-6020
6	6.4	.25	25.60	5.9	151	892	- 3.0	1220	31.2	- 93.7	"	- 2910	-10710
7	6.4	.25	25.60	0	0	0	- 8.9	2880	71.6	- 637	"	- 8610	-14840
8	6.4	.25	25.60	- 6.3	-161	1017	-15.2	6230	159.3	- 2420	"	-14720	-17510
9	6.4	.25	25.60	-12.6	-323	4060	-21.5	11260	286.5	- 6160	"	-20830	-18590
10	6.4	.25	25.60	-19.1	-488	9320	-28.0	18470	473.0	- 13220	"	-27100	-17650
11	6.4	.30	21.30	-25.5	-543	13850	-34.4	29020	618.0	- 21250	"	-33300	-13300
12	6.4	.34	18.82	-32.0	-602	19250	-40.9	43180	814.0	- 33100	"	-39700	- 5540
13	6.4	.34	18.82	-38.3	-720	27600	-47.2	58980	1110.0	- 52400	"	-45600	4360
14	6.4	.34	18.82	-44.6	-840	57500	-53.5	77330	1455.0	- 77800	"	-51700	16610
15	6.4	.34	18.82	-50.8	-959	48750	-59.9	99030	1865.0	-111300	"	-57900	32110
Chine							-63.0	111700				-61100	41600
16	7.0	12.0	0.58	-55.4	- 32	1780	-64.3	149700	86.7	- 5570	"	-62200	78500
17	7.0	12.0	0.58	-58.4	- 34	1980	-67.3	221400	128.3	- 8650	"	-65100	147300
18	7.0	18.0	0.39	-61.4	- 24	1470	-70.3	271200	105.8	- 7440	"	-68100	194100
19	7.0	34.0	0.21	-63.2	- 13	840	-72.1	308600	64.9	- 4680	"	-70000	229600
20	7.0	50.0	0.14	-64.8	- 9	588	-73.7	327900	45.9	- 3385	"	-71400	247500
Keel							-75.0	332900			-9020	-72600	251280
Totals			811.48		7228	423237			7315.0	-348106			

$\bar{y} = 7228/811.48 = 8.9''$

$I_{XX} = 423237 - 811.48 \times 8.9^2 = 358940$

$M_O = \frac{-\Sigma\phi_S}{\Sigma w} = -\frac{(7315.7 \times 1000)}{811.5} = -9020''\#$

$X_O = \frac{\Sigma\phi_S y}{I_{XX}} = \left[-\frac{348106 \times 1000}{35894}\right] = -968\#$

*Total Moment M at any station = $M_S + M_O - X_O y$

Columns 11 and 12 record the values of M_O and $-X_O y$ for each station point. For example, the value of $-X_O y$ for station (1) equals - (-968 x 17.2) = 16650 and for station (20) = - [-968(-73.7)] = -71400.

Fig. A9.44 shows the shape of the final moment curve as the result of the values in column 13.

A9.5 Unsymmetrical Structures. Example Problem Solutions.

Example Problem 1

Fig. A9.34 shows an unsymmetrical frame carrying the loads as shown. Determine the bending moments at points A, B, C and D.

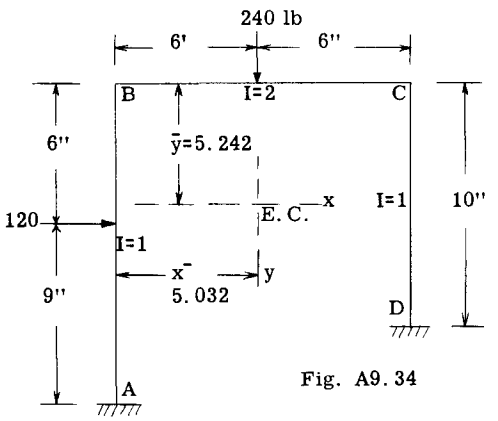

Fig. A9.34

Solution:-

The elastic weight of frame = $\Sigma ds/I$ = (15/1) + (12/2) + 10/1 = 31

The distance $\bar{x}$ from the line AB to the elastic center is,

$$\bar{x} = \frac{(15)0 + 6 \times 6 + 10 \times 12}{31} = 5.032 \text{ in.}$$

The distance $\bar{y}$ from line BC to elastic center equals,

$$\bar{y} = \frac{15 \times 7.5 + 6 \times 0 + 10 \times 5}{31} = 5.242 \text{ in.}$$

The elastic moments of inertia I_x and I_y and the product of inertia I_{xy} are required.

$$I_x = \frac{(15)^3}{12} + (15)(2.258)^2 + \frac{(12)}{2}(5.242)^2 + \frac{(10)^3}{12}$$

$$+ (10)(0.242)^2 = 606.51$$

$$I_y = (15)(5.032)^2 + \frac{(12)^3}{2 \times 12} + (\frac{12}{2})(0.968)^2 +$$

$$(10)(6.968)^2 = 942.96$$

$$I_{xy} = (15)(-5.032)(-2.258) + (\frac{12}{2})(0.968)(5.242)$$

$$+ (10)(6.968)(0.242) = 217.74$$

The next step is to assume some static frame condition and draw the static bending moment diagram. Fig. A9.35 shows that the frame has been assumed cut near point C which gives two cantilever beams. The bending moment diagram in three parts for this static condition is also shown on Fig. A9.35.

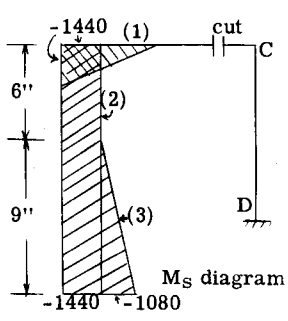

Fig. A9.35

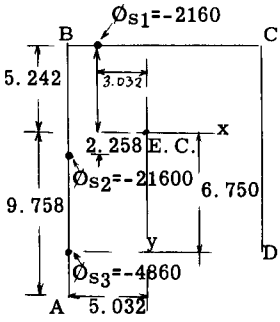

Fig. A9.36

The $\emptyset_S$ values which equal the area of the M_S diagram divided by the I values of the particular portion will be calculated.

$$\emptyset_{S_1} = 3(-1440)/2 = -2160$$

$$\emptyset_{S_2} = -1440 \times 15 = -21600$$

$$\emptyset_{S_3} = 4.5(-1080) = -4860$$

$$\Sigma\emptyset_S = -2160 - 21600 - 4860 = -28620$$

Fig. A9.36 shows the centroid locations of the $\emptyset_S$ values along the center line of the frame. The moment of these $\emptyset_S$ values about the x and y axes will now be calculated.

$$\Sigma\emptyset_S x = (-2160)(-3.032) + (-21600)(-5.032) + (-4860)(-5.032) = 139700$$

$$\Sigma\emptyset_S y = (-2160)(5.242) + (-21600)(-2.258) + (-4860)(-6.758) = 70290$$

The values of the redundants at the elastic center can now be calculated using equations (11), (14), (15), namely

$$M_o = \frac{-\Sigma\emptyset_S}{\Sigma ds/I} = \frac{-(-28620)}{31} = 923 \text{ in. lb.}$$

$$X_o = \frac{\Sigma\emptyset_S y - \Sigma\emptyset_S x \frac{I_{xy}}{I_y}}{I_x (1 - \frac{I^2_{xy}}{I_x I_y})}$$

$$= \frac{70290 - 139700 (\frac{217.74}{942.96})}{606.51 (1 - \frac{217.74^2}{(606.51)(942.96)})} = 68.46 \text{ lb.}$$

$$Y_o = \frac{-\left[\Sigma\emptyset_S x - \Sigma\emptyset_S y (\frac{I_{xy}}{I_x})\right]}{I_y (1 - \frac{I_{xy}^2}{I_x I_y})}$$

$$= \frac{-\left[139700 - 70290 (\frac{217.74}{606.51})\right]}{942.96 (1 - \frac{217.74^2}{(606.51)(942.96)})} = -132.36 \text{ lb.}$$

The bending moment at any point from eq. (19) equals,

$$M = M_S + M_o - X_o y + Y_o x, \text{ for example,}$$

Consider point A.

$$x = -5.032, \; y = -9.758, \; M_S = -2520$$

$$M_A = -2520 + 923 - 68.46 (-9.758) + (-132.36)(-5.032) = -263 \text{ in. lb.}$$

Point B. $x = -5.032, \; y = 5.242, \; M_S = -1440$

$$M_B = -1440 + 923 - 68.46 \times 5.242 + (-132.36)(-5.032) = -209 \text{ in. lb.}$$

Point C. $x = 6.968, \; y = 5.242, \; M_S = 0$

$$M_C = 0 + 923 - 68.46 \times 5.242 + (-132.36)(6.968) = -357 \text{ in. lb.}$$

Thus, the complete bending moment diagram could be determined by computing several more values such as point D and the external load points.

Example Problem 2. Fig. A9.37 shows an unsymmetrical closed frame. The bending moment diagram will be determined under the given frame loading.

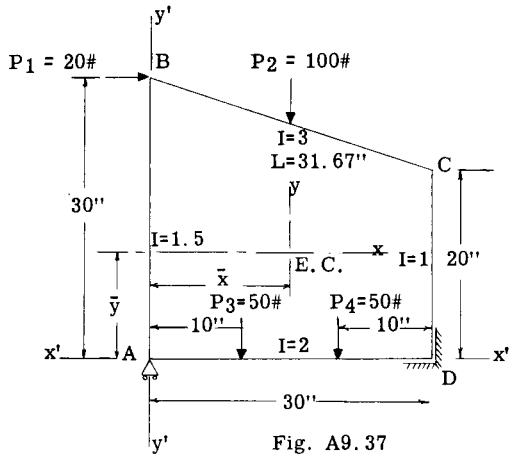

Fig. A9.37

Solution: -

The elastic weight of frame equals

$$\Sigma \frac{ds}{I} = \frac{30}{1.5} + \frac{31.67}{3} + \frac{20}{1} + \frac{30}{2} = 65.58$$

The location of the elastic axes will be determined with reference to assumed axes x'x' and y'y' as shown on Fig. A9.37.

$$\bar{x} = \frac{(\frac{30}{1.5})(0)+(\frac{31.67}{3})(15)+(\frac{20}{1})(30)+(\frac{30}{2})(15)}{65.58} = 15"$$

$$\bar{y} = \frac{(\frac{30}{1.5})(15)+(\frac{31.67}{3})(25)+(\frac{20}{1})(10)+(\frac{30}{2})(0)}{65.58} =$$

$$11.657"$$

These distances $\bar{x}$ and $\bar{y}$ locate the x and y elastic axes as shown in Fig. A9.37.

The elastic moments of inertia and the elastic product of inertia will now be calculated.

Calculation of I_x -

Member AB, $I_x = \frac{1}{3} \times \frac{1}{1.5}(\overline{18.343}^3 + \overline{11.657}^3) = 1723.51$

Member CD, $I_x = \frac{1}{3} \times \frac{1}{1}(8.343^3 + 11.657^3) = 721.58$

Member BC, $I_x = (\frac{31.67}{3})(13.343^2) + \frac{1}{12}(\frac{31.67}{3})(10^2) = 1967.48$

Member AD, $I_x = (\frac{30}{2})(11.657^2) + \frac{1}{12} \times 30 \times (0.5)^3 = 2038.50$

Total $I_x = 6451.07$

Calculation of I_y -

Member AB, $I_y = \frac{30}{1.5} \times 15^2 + \frac{1}{12} \times 30(0.667)^3 = 4500.7$

Member BC, $I_y = \frac{1}{12} \times \frac{31.67}{3} \times 30^3 = 791.7$

Member CD, $I_y = \frac{20}{1} \times 15^2 + \frac{1}{12} \times 20(1)^3 = 4501.7$

Member AD, $I_y = \frac{1}{12} \times \frac{1}{2} \times 30^3 = 1125.0$

Total $I_y = 10919$

Calculation of I_{xy} -

Member AB, $I_{xy} = \frac{30}{1.5}(-15)(3.343) = -1002.9$

Member BC, $I_{xy} = \frac{31.67}{3}(13.343)(0) - \frac{1}{12} \times \frac{31.67}{3}(30)(10) = -263.92$

Member CD, $I_{xy} = \frac{20}{1}(15)(-1.657) = -497.1$

Member AD, $I_{xy} = 0$

Total $I_{xy} = -1763.9$

The next step in the solution is to assume a static frame condition and draw the M_S diagram. Fig. A9.38 shows the assumed static condition, namely pinned at point A and supported as rollers at point D. The bending moment diagram is drawn in parts as shown.

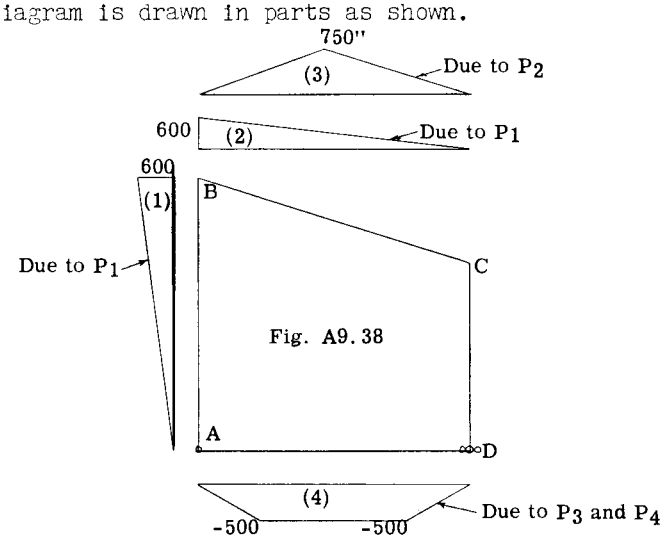

Fig. A9.38

The next step is to compute the value of ϕ_S for each portion of the moment diagram. ϕ_S is the area of the M_S/I diagram. For reference the portions of the M_S diagram have been labeled 1 to 4.

Portion (1). $\phi_S = \frac{600}{2} \times \frac{30}{1.5} = 6000$

Portion (2). $\phi_S = \frac{600}{2} \times \frac{31.67}{3} = 3167$

Portion (3). $\phi_S = \frac{31.67}{2} \times \frac{750}{3} = 3958$

Portion (4). $\phi_S = -500(\frac{10}{2}) - 500(\frac{10}{2}) = -5000$

$\Sigma\phi_S = 13125 - 5000 = 8125$

The individual ϕ_S values are now concentrated at the c.g. of each of the M_S diagrams. Fig. A9.39 shows the location of the ϕ_S values with respect to the x and y axes through the elastic center.

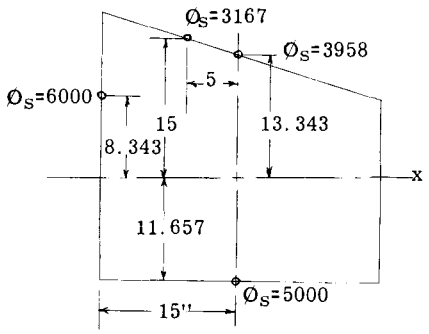

Fig. A9.39

$\Sigma\phi_S x = 6000(-15) + 3167(-5) = -105835$

$\Sigma\phi_S y = 6000(8.343) + 3167(15) +$
$3958(13.343) - 5000(-11.657) = 208659$

The values of the redundants at the elastic center can now be calculated.

$$M_O = \frac{-\Sigma\phi_S}{\Sigma ds/I} = \frac{-(8125)}{65.58} = -124.8 \text{ in.lb.}$$

$$X_O = \frac{\Sigma\phi_S\, y - \Sigma\phi_S x\, (\frac{I_{xy}}{I_y})}{I_x\,(1 - \frac{I_{xy}^2}{I_x I_y})}$$

$$= \frac{208659 - (-105835)(\frac{-1763.9}{10919})}{6451\left[1 - \frac{(-1763.9^2)}{10919 \times 6451}\right]} = 31.07 \text{ lb.}$$

$$Y_O = \frac{-\left[\Sigma\phi_S x - \Sigma\phi_S y\, (\frac{I_{xy}}{I_x})\right]}{I_y\,(1 - \frac{I_{xy}^2}{I_x I_y})}$$

$$= \frac{-\left[-105835 - 208659(\frac{-1763.9}{6451})\right]}{10919\left[1 - \frac{(-1763.9^2)}{10919 \times 6451}\right]} = 4.674 \text{ lb.}$$

The bending moment at any point equals the original static M_S plus the moment due to the redundant forces as shown in Fig. A9.40.

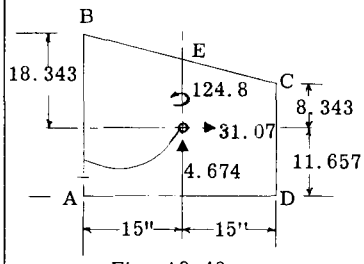

Fig. A9.40

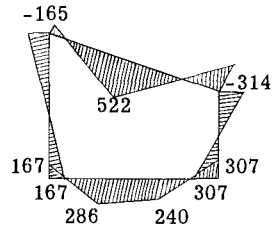

Fig. A9.41

Consider point A: - $M_S = 0$

$M_A = 0 - 124.8 - 4.674 \times 15 + 31.07 \times 11.657$
$= 167$ in. lb.

Point B. $M_S = 600$

$M_B = 600 - 124.8 - 4.674 \times 15 - 31.07 \times 18.343$
$= -165$ in.lb.

Point C. $M_S = 0$

$M_C = 0 - 124.8 - 31.07 \times 8.343 + 4.674 \times 15$
$= -314$ in.lb.

Point D. $M_S = 0$

$M_D = 0 - 124.8 + 4.674 \times 15 + 31.07 \times 11.657$
$= 307$ in.lb.

Fig. A9.41 shows the true bending moment diagram.

A9.6 Analysis of Frame with Pinned Supports.

Fig. A9.42 shows a rectangular frame and loading. This frame is identical to example problem 1 of Art. A9.3, except it is pinned at points A and D instead of fixed.

The first step will be to determine the elastic weight of the frame, the elastic center location and the elastic moments of inertia about axes through the elastic center.

The term ds/EI of a beam element of length ds represents the angle change between its two end faces when the element is acted upon by a unit moment. In this chapter this term has been called the elastic weight of the element. Physically, the elastic weight is the ability of the element to cause rotation when acted upon by a unit moment. When a unit moment is applied to a rigid support, the support suffers no rotation since the support is rigid, therefore a rigid support has zero elastic weight and therefore does not figure in the frame elastic properties.

If a support is pinned or hinged it has no resistance to rotation and thus a unit moment acting on a hinge would have infinite angle change or rotation and therefore a hinge or pin possesses infinite elastic weight.

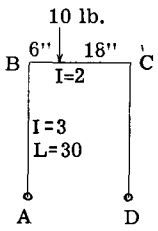

Fig. A9.42

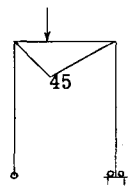

Fig. A9.44

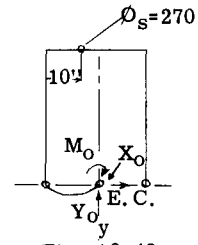

Fig. A9.43

Due to symmetry of structure about the centerline y axis the elastic center will lie on this axis. Since the two hinges at A and B have infinite elastic weight, the centroid or elastic center of the frame will obviously lie midway between A and B. Fig. A9.43 shows the elastic center O connected to the point A by a rigid bracket.

$\Sigma ds/EI$ for frame is infinite because of the hinges at A and B.

The elastic moment of inertia about a y axis through elastic center is infinite since the hinge supports have infinite elastic weight.

I_X is calculated as follows: -

For Portion AB $= \frac{1}{3} \times \frac{1}{3} \times 30^3 = 3000$

For Portion CD $= \frac{1}{3} \times \frac{1}{3} \times 30^3 = 3000$

For Portion BC $= 24 \times \frac{1}{2} \times 30^2 = 10800$

$I_X = 16800$

Fig. A9.44 shows the static frame condition assumed to obtain the M_S values.

The value of $\emptyset_S$ for member BC equals the area of the M_S curve divided by I for BC, hence $\emptyset_S = 45 \times \frac{24}{2} \times \frac{1}{2} = 270$. The centroid of this $\emptyset_S$ value is 10 inches from point B. The redundant forces at the elastic center can now be solved for

$$M_O = \frac{-\Sigma \emptyset_S}{\Sigma \frac{ds}{EI}} = \frac{-270}{\text{infinity}} = 0$$

$$Y_O = \frac{-\Sigma \emptyset_S x}{Iy} = \frac{-(270)10}{\text{infinity}} = 0$$

$$X_O = \frac{\Sigma \emptyset_S y}{I_X} = \frac{270 \times 30}{16800} = 0.482 \text{ lb.}$$

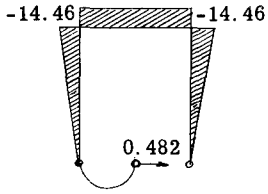

Fig. A9.45

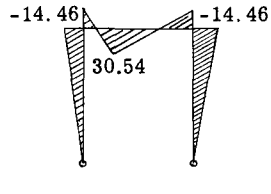

Fig. A9.46

Fig. A9.45 shows the bending moment diagram due to the redundant X_O. Adding this diagram to the original static diagram gives the final bending moment curve in Fig. A9.46.

A9.7 Analysis of Frame with One Pinned and One Fixed Support.

Fig. A9.47 shows the same frame and loading as in the previous example but point D is fixed instead of hinged.

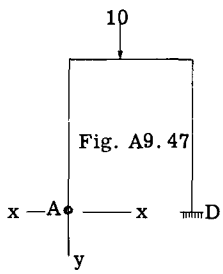

Fig. A9.47

The support D has zero elastic weight and the pin at A has infinite elastic weight, therefore the elastic center of the frame lies at point A. The total elastic weight of frame is infinite because of pin at A.

The elastic moments of inertia will be calculated about x and y axes through A.

$I_X = 16800$ (Same as previous example)

$I_y = (\frac{30}{3} \times 24^2) + (\frac{1}{3} \times \frac{1}{2} \times 24^3) = 8064$

$I_{xy} = (\frac{30}{3} \times 15 \times 24) + (\frac{24}{2} \times 30 \times 12) = 7920$

The static frame condition will be assumed the same as in the previous example problem, hence $\emptyset_S = 270$ and acts 10" from B (Fig. A9.48).

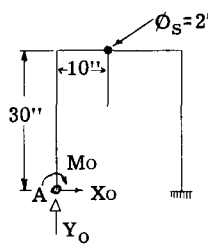

Fig. A9.48

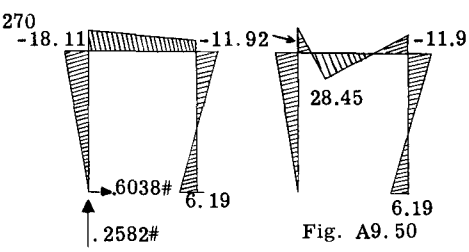

Fig. A9.49

Fig. A9.50

Since the frame is unsymmetrical, the x and y axes through the elastic center at A are not principal axes, hence

$$X_o = \frac{\Sigma\phi_s y - \Sigma\phi_s x\ (\frac{I_{xy}}{I_y})}{I_x\ (1 - \frac{I_{xy}^2}{I_x I_y})}$$

$$= \frac{270 \times 30 - 270 \times 10\ (\frac{7920}{8064})}{16800\ (1 - \frac{7920^2}{16800 \times 8064})} = 0.6038 \text{ lb.}$$

$$Y_o = \frac{-\left[\Sigma\phi_s x - \Sigma\phi_s y\ (\frac{I_{xy}}{I_x})\right]}{I_y\ (1 - \frac{I_{xy}^2}{I_x I_y})}$$

$$= \frac{-\left[270 \times 10 - 270 \times 30(\frac{7920}{16800})\right]}{8064\ (1 - \frac{7920^2}{16800 \times 8064})} = .2582 \text{ lb.}$$

$$M_o = \frac{-\Sigma\phi_s}{\Sigma ds/EI} = \frac{-270}{\text{infinity}} = 0$$

Fig. A9.49 shows the redundant values at point A. The bending moments at the points B, C and D are,

$M_B = -.6038 \times 30 = -18.11$ in.lb.

$M_C = -18.11 + .2582 \times 24 = -11.92$

$M_D = .2582 \times 24 = 6.19$

Adding the static moment curve to that of Fig. A9. gives the final moment curve of Fig. A9.50.

A9.8 Solution of Unsymmetrical Frames Using Principal Axes.

For the frame of A9.51 the axes x and y through the elastic center are not principal axes because the elastic product of inertia

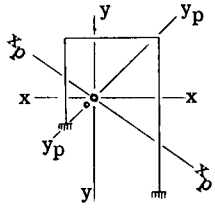

Fig. A9.51

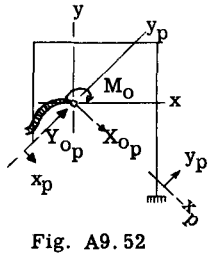

Fig. A9.52

I_{xy} is not zero. However, for the principal axes x_p and y_p as shown, the product of inertia is zero. Thus if the redundant forces at the elastic center are referred to the principal axes as illustrated in Fig. A9.52, then the same form of equations for the redundants result as for symmetrical structure, namely

$$M_o = \frac{-\Sigma\phi_s}{\Sigma ds/I} \text{ (Same)} - - - - - - - - - - - (19)$$

$$X_{o_p} = \frac{\Sigma\phi_s y_p}{I_{x_p}} - - - - - - - - - - - - - (20)$$

$$Y_{o_p} = \frac{-\Sigma\phi_s x_p}{I_{y_p}} - - - - - - - - - - - - - (21)$$

Where I_{x_p} and I_{y_p} are the elastic moments of inertia about the principal axes and y_p and x_p the perpendicular distance from the ϕ_s loads to the principal axes.

The author prefers to use the longer equations (14) and (15) which avoid finding the principal axes location, the properties about these axes and the perpendicular distances with respect to these axes, thus decreasing the numerical work required.

The student should use equations (19), (20) and (21) to solve example problem 1 of Art. A9.5 in order to compare the two methods of solution.

A9.9 Problems.

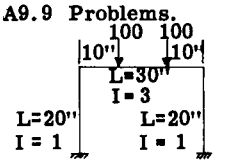

Fig. A9.52

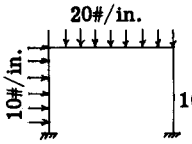

Fig. A9.53

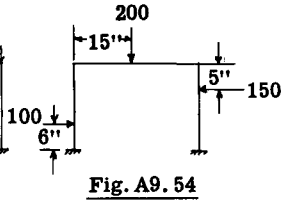

Fig. A9.54

(1) Figs. A9.52, 53 and 54 show the same frame with three different loadings. Determine bending moment diagram for each loading.

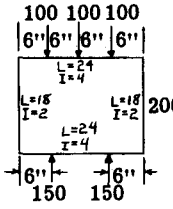

Fig. A9.55

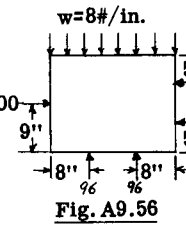

Fig. A9.56

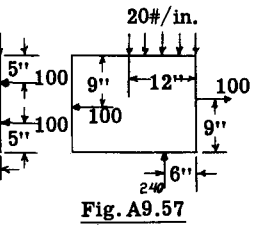

Fig. A9.57

(2) Figs. A9.55, 56 and 57 show same frame with 3 different loadings. Determine bending moment diagram for each loading.

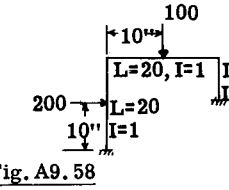

Fig. A9.58

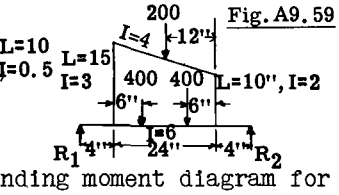

Fig. A9.59

(3) Determine the bending moment diagram for the frame and loading in Figs. A9.57 and A9.58.

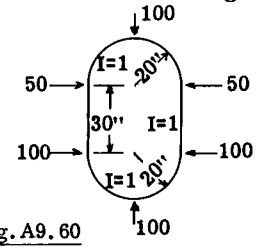

Fig. A9.60

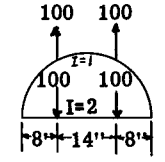

Fig. A9.61

(4) Determine the bending moment diagram for the frames and loadings as shown in Figs. A9.59 and A9.60.

CHAPTER A10

STATICALLY INDETERMINATE STRUCTURES
SPECIAL METHOD - THE COLUMN ANALOGY METHOD

A10.1 General. The Column Analogy* method is a method that is widely used by engineers in determining the bending moments in a bent or ring type structure. The method considers only distortions due to bending of the structure.

The numerical work in using the column analogy method is practically identical to that carried out in applying the elastic center method of Chapter A9.

A10.2 General Explanation of Column Analogy Method.

Fig. A10.1 shows a short column loaded in compression by a load P located at distances (a) and (b) from the principal axes x and y of the column cross-section.

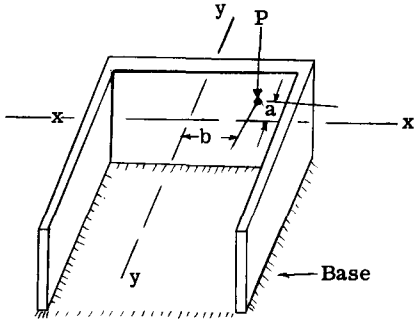

Fig. A10.1

To find the bearing stress between the supporting base and the lower end of the column, it is convenient to transfer the load P to the column centroid plus moments about the principal axes. Then if we let σ equal the bearing stress intensity at some point a distance x and y from the yy and xx axes, we can write

$$\sigma = \frac{P}{A} \pm \frac{(Pa)y}{I_x} \pm \frac{(Pb)x}{I_y}$$

Where A is the area of the column cross-section and Pa and Pb the moment of the load P about the xx and yy axes respectively. If we let $Pa = M_x$ and $Pb = M_y$, the above equation can be written,

$$\sigma = \frac{P}{A} \pm \frac{M_x y}{I_x} \pm \frac{M_y x}{I_y} \quad - - - - - - - - - - - - \quad (1)$$

*Method of Analysis due to Prof. Hardy Cross. See "The Column Analogy" Univ. Ill. Eng. Expt. Sta. Bull. 215.

Now assume we have a frame whose centerline length and shape is identical to that of the column section in Fig. A10.1. The width of each portion of this frame will be proportional to 1/EI of the member. Fig. A10.2 shows this assumed frame. Furthermore, assume that end B of the frame is fixed and that a rigid bracket is attached to the end A and terminating at point (0) the elastic center of the frame. The frame is subjected to an external loading, w_1, w_2, etc.

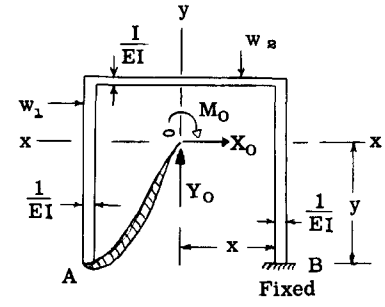

Fig. A10.2

This cantilever structure will suffer bending distortion under the external load system w_1, w_2, etc., and point (0) will be displaced. Point (0) can be brought back to its original undeflected position by applying a couple and two forces at (0), namely, M_0, X_0 and Y_0 as shown in Fig. A10.2. Since point (0) is attached to frame end A by the rigid bracket these three forces at the elastic center (0) will cause point A to remain stationary or in other words to be fixed. Therefore, for the frame in Fig. A10.2 fixed at A and B, the moment and two forces acting at the elastic center cause the statically indeterminate moments M_1 when resisting a given external loading causing static moments M_S. The final true bending moment M at a point on the frame than equals

$$M = M_S + M_1.$$

From Fig. A10.2 we can write for a point on the frame such as B that the indeterminate bending moment M_1 equals,

$$M_1 = M_0 + X_0 y + Y_0 x \quad - - - - - - - - - - - \quad (2)$$

In Chapter A9, Art. A9.3, the equations for M_0, X_0 and Y_0 were derived. They are,

$$M_o = \frac{-\Sigma \phi_S}{\Sigma ds/I}, \quad Y_o = \frac{-\Sigma \phi_S x}{I_y}, \quad X_o = \frac{\Sigma \phi_S y}{I_x}$$

The term $\Sigma\phi_S$ represents the area of the static M_S/I curve. (E has been assumed constant and therefore omitted). Let the term $\Sigma\phi_S$ be called the elastic load and give it a new symbol P. The term $\Sigma ds/I$ equals the elastic weight of the frame and equals the sum of the length of each member times its width which equals 1/I. Let this total frame elastic weight be given a new symbol A.

In the expressions for Y_o and X_o the terms $\Sigma\phi_S x$ and $\Sigma\phi_S y$ represent the moment of the static M/I curve acting as a load about the y and x axes respectively passing through the frame elastic center. Therefore let $\Sigma\phi_S x$ be given a new symbol M_y and $\Sigma\phi_S y$ a new symbol M_x. With these new symbols, equation (2) can now be rewritten as follows: -

$$M_1 = \frac{P}{A} + \frac{M_x y}{I_x} + \frac{M_y x}{I_y} \quad \text{- - - - - - - - - - - - (3)}$$

Comparing equations (1) and (3) we see they are similar. In other words, the indeterminate bending moments M_1 in a frame are analogous to the column bearing pressures σ, hence the name "Column Analogy" for the method using equation (1). With this general explanation, the method can now be clearly explained by giving several example problem solutions.

A10.3 Frames with One Axis of Symmetry.

From the previous discussion we can write,

(1) The cross-section of the analogous column consists of an area, the shape of which is the same as that of the given frame and the thickness of any part equals 1/EI of that part.

(2) The loading applied to the top of the analogous column is equal to the M_S/EI diagram, where M_S is the statical moment in any basic determinate structure derived from the given frame. If M_S causes bending compression on the inside face of the frame it is a positive bending moment and the analogous load P on the column acts downward.

(3) The indeterminate bending moment M_1 at a given frame point equals the base pressure at this same point on the analogous column. Thus the indeterminate moment at any point on the frame equals (from eq. 3),

$$M_1 = \frac{P}{A} + \frac{M_x y}{I_x} + \frac{M_y x}{I_y} \quad \text{- - - - - - - - - - - - (4)}$$

(4) The final or true bending moment M at any point then equals,

$$M = M_S - M_1 \quad \text{- - - - - - - - - - - - - - (5)}$$

Example Problem 1.

Fig. A10.3 shows a rectangular frame with fixed supports at points A and D. The bending moments at points A, B, C and D will be determined by the column analogy method. This frame and loading is identical to example problem 1 of Art. A9.4 of Chapter A9 where the solution was made by the elastic center method.

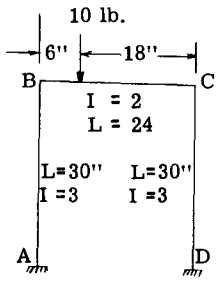

Fig. A10.3

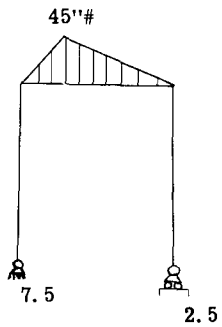

Fig. A10.4

SOLUTION NO. 1

We first consider the frame centerline shape as shown in Fig. A10.3 as the cross-section of a short column (see Fig. A10.5). The width of each portion of the column section is equal to 1/EI of the member cross-section. Since E is constant, it will be made unity and the widths will then equal 1/I.

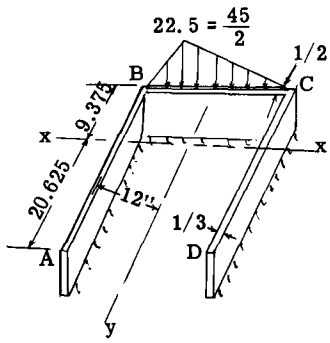

Fig. A10.5

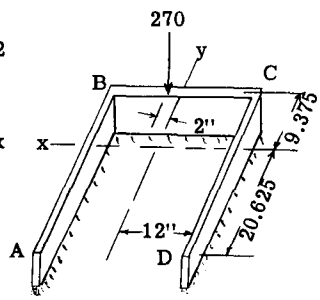

Fig. A10.6

The first step in the calculations is to compute the area (A) of the column cross-section in Fig. A10.5 and the moments of inertia of the column cross-section about x and y centroidal axes.

$$\text{Area } A = \Sigma \frac{ds}{I} = \frac{30}{3} + \frac{30}{3} + \frac{24}{2} = 32$$

The calculation of the location of the centroidal axes and the moments of inertia I_x

and I_y would be identical to the complete calculations given in Art. A9.4, and Table A9.1 where this same problem is solved by the elastic center method. These calculations will not be repeated here. The results were, $I_x = 3188$ and $I_y = 3456$.

Since the frame is statically indeterminate the next step is to assume a static frame condition consistent with the given frame and loading. Fig. A10.4 shows the condition assumed for this solution, namely, pinned at point A and a pin with rollers at point D. The static M_S diagram is therefore as shown in Fig. A10.4. We now load the column cross-section with the M_S/I diagram as a load as shown in Fig. A10.5. The static moment sign is positive because the static condition causes tension on the inside face of the frame. In the column analogy method a positive M_S/I loading is a downward or compressive load on top of column, and therefore a negative M_S/I value would be an upward or tension load on the column.

Equation (3) requires the values of the M_x and M_y the moment of the M_S/I diagram as a load about the x and y axes. Equation (3) also requires the total column load P which equals the area of the M_S/I diagram.

For this problem the value of P from Fig. A10.5 equals,

$$P = 22.5 \times 24/2 = 270$$

The centroid of this triangular loading is 2 inches to left of y axis. Fig. A10.6 shows the column section with this resultant load P.

We now use equation (3) to find the indeterminate moments M_1 which are equal to the base pressures on the column. Equation (3) involves bending moments M_x and M_y and distances x and y, all of which must have signs. The signs will be determined as follows:

When moment M_x produces compression on base on that portion above x axis, then M_x is positive.

When moment M_y produces compression on base on that portion to right of y axis, then M_y is positive.

A distance y measured upward from x axis is positive; measured downward is negative.

A distance x measured to right from y axis is positive, to left negative.

From Fig. A10.6: -

$P = 270$

$M_x = 270 \times 9.375 = 2530$ (positive because base pressure is compressive on column portion above x axis).

$M_y = -(270 \times 2) = -540$ (negative because base pressure is tension on column portion to right of y axis).

Substitution in equation (3).

Frame Point A. $x = -12"$, $y = -20.625"$

$$M_1 = \frac{P}{A} + \frac{M_x y}{I_x} + \frac{M_y x}{I_y}$$

$$M_1 = \frac{270}{32} + \frac{2530\ (-20.625)}{3188} + \frac{(-540)(-12)}{3456}$$

$$= 8.44 - 16.38 + 1.88 = -6.06 \text{ in.lb.}$$

The true bending moment from equation (5),

$$M = M_S - M_1$$

$M_S = 0$, see Fig. A10.5

whence, $M_A = 0 - (-6.06) = 6.06$ in.lb.

Frame Point B. $x = -12"$, $y = 9.325"$

$$M_1 = \frac{270}{32} + \frac{2530 \times 9.375}{3188} + \frac{(-540)(-12)}{3456}$$

$$= 8.44 + 7.44 + 1.88 = 17.77$$

$$M_B = M_S - M_1 = 0 - (17.77) = -17.77 \text{ in.lb.}$$

Frame Point C. $x = 12$, $y = 9.325$

$$M_1 = \frac{270}{32} + \frac{2530 \times 9.325}{3188} + \frac{(-540)12}{3456}$$

$$= 8.44 + 7.44 - 1.88 = 14.0$$

$$M_C = M_S - M_1 = 0 - (14.0) = -14.0 \text{ in.lb.}$$

Frame Point D. $x = 12$, $y = -20.625$

$$M_1 = \frac{270}{32} + \frac{2530(-20.625)}{3188} + \frac{(-540)12}{3456}$$

$$= 8.44 - 16.38 - 1.88 = -9.82$$

$$M_D = M_S - M_1 = 0 - (-9.82) = 9.82 \text{ in.lb.}$$

Fig. A10.7 shows the final bending moment diagram, which of course checks the solution by the elastic center method in Art. A9.4. The student should note that the numerical work in the column analogy method is practically the same as in the elastic center method.

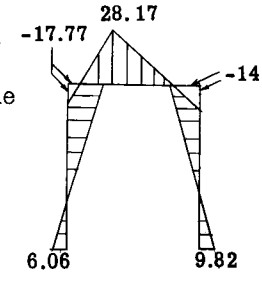

Fig. A10.7

Solution No. 2

In this solution a different static frame condition will be assumed as shown in Fig. A10.8, namely the frame is cut under the load and one-half the 10 lb. load will be assumed as going to each cantilever part. Fig. A10.9 shows the static moment diagram and Fig. A10.10 the static M_S/I diagram with centroid locations of each portion of diagram which

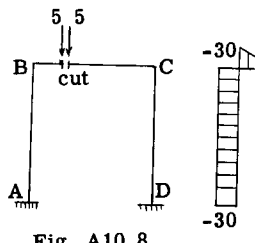

Fig. A10.8

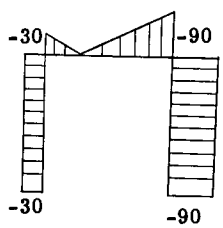

Fig. A10.9

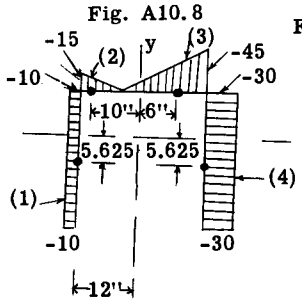

Fig. A10.10

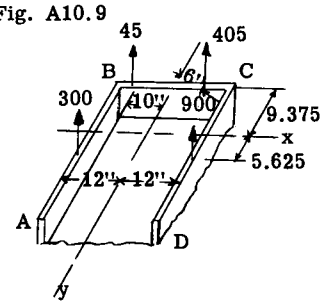

Fig. A10.11

are numbered (1), (2), (3) and (4). The area of each of these portions will represent a load P_1, P_2, etc. on the column in Fig. A10.11. Since the static moment is negative on each portion the load on the column section will be upward.

$$P_1 = -10(30) = -300, \quad P_3 = -45 \times 9 = -405$$

$$P_2 = -15(6)/2 = -45, \quad P_4 = -30 \times 30 = -900$$

$$P = \Sigma P = -300 - 45 - 405 - 900 = -1650$$

From Fig. A10.11

$$M_X = -(45 + 405)\ 9.375 + (300 + 900)\ 5.635$$
$$= 2531$$

$$M_Y = 300 \times 12 + 45 \times 10 - 405 \times 6 - 900 \times 12$$
$$= -9180$$

$$M_1 = \frac{P}{A} + \frac{M_X y}{I_X} + \frac{M_Y x}{I_Y}$$

POINT A. $x = -12, \quad y = -20.625$

$$M_1 = \frac{-1650}{32} + \frac{2531(-20.625)}{3188} + \frac{(-9180)(-12)}{3456}$$
$$= -36.06$$

$$M_A = M_S - M_1 = -30 - (-36.06) = 6.06 \text{ in.lb.}$$

which checks solution 1.

Frame Point B. $x = -12, \quad y = 9.375$

$$M_1 = \frac{-1650}{32} + \frac{2531 \times 9.325}{3188} + \frac{(-9180)(-12)}{3456}$$
$$= -12.23$$

$$M_B = M_S - M_1 = -30 - (-12.33) = -17.77 \text{ in.lb.}$$

Frame Point C. $x = 12, \quad y = 9.375$

$$M_1 = \frac{-1650}{32} + \frac{2531 \times 9.375}{3188} + \frac{(-9180)12}{3456}$$
$$= -76.0$$

$$M_C = M_S - M_1 = -90 - (-76.0) = -14.0 \text{ in.lb.}$$

Frame Point D. $x = 12, \quad y = -20.625$

$$M_1 = \frac{-1650}{32} + \frac{2531(-20.625)}{3188} + \frac{(-9180)12}{3456}$$
$$= -99.82$$

$$M_D = M_S - M_1 = -90 - (-99.82) = 9.82 \text{ in.lb.}$$

Thus solution 2 checks solution 1. The student should solve this problem using other static conditions.

A10.4 Unsymmetrical Frames or Rings.

In applying the column analogy method to unsymmetrical frames and rings, the moment of the M/EI diagram must be taken about principal axes and the moments of inertia with respect to principal axes.

However, as explained for the elastic center method in Chapter A9, the moments and section properties with regard to centroidal axes can be used if M_X, M_Y, I_X and I_Y are modified to take care of the dis-symmetry of the structure. In Art. A9.2 it was shown that the redundant forces at the elastic center to unsymmetrical frame sections was, (see equations 11, 14, 15 of Art. A9.2).

$$M_O = \frac{\Sigma \phi_S}{\Sigma ds/EI} = \frac{P}{A} \text{ (same as for symmetrical frame)}$$

$$X_O = \frac{\Sigma \phi_S y - \Sigma \phi_S x \left(\frac{I_{XY}}{I_Y}\right)}{I_X \left(1 - \frac{I_{XY}^2}{I_X I_Y}\right)} \quad \text{- - - - - - - - (a)}$$

$$Y_O = \frac{\Sigma \phi_S x - \Sigma \phi_S y \left(\frac{I_{XY}}{I_X}\right)}{I_Y \left(1 - \frac{I_{XY}^2}{I_X I_Y}\right)} \quad \text{- - - - - - - - (b)}$$

As previously done in Art. A10.2 let,

$$M_y = \Sigma \emptyset_S x \quad \text{and} \quad M_x = \Sigma \emptyset_S y$$

Furthermore, let,

$$M'_y = M_y \left(\frac{I_{xy}}{I_y}\right) \text{ and } M'_x = M_x \left(\frac{I_{xy}}{I_x}\right)$$

$$\text{and } k = \left(1 - \frac{I_{xy}^2}{I_x I_y}\right)$$

Then substituting in equations (a) and (b) we obtain,

$$X_o = \frac{M_x - M'_y}{k\, I_x}, \quad Y_o = \frac{M_y - M'_x}{k\, I_y}$$

From equation (2) we have,

$$M_1 = M_o + X_o y + Y_o x$$

Substituting values of X_o and Y_o into this equation, we obtain as the equation for M_1 the indeterminate moment in the column analogy method, the following -

$$M_1 = \frac{P}{A} + \frac{(M_x - M'_y)y}{kI_x} + \frac{(M_y - M'_x)x}{kI_y} \quad - - - \quad (6)$$

The true moment is the same as for the symmetrical section, namely,

$$M = M_S - M_1$$

Thus the solution of an unsymmetrical frame by the column analogy method follows the same procedure as for a symmetrical section except that equation (6) is used instead of equation (3).

A10.5 Example Problem - Unsymmetrical Section.

Fig. A10.12 shows a loaded unsymmetrical frame fixed at points A and D. Required, the true bending moments at points A, B, C and D. This problem is identical to example problem 1 of Art. A9.5 where a solution was given by the elastic center method.

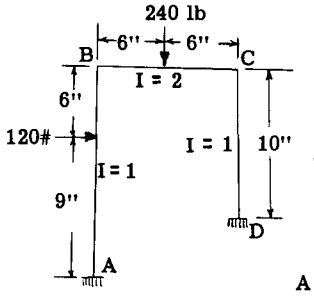

Fig. A10.12

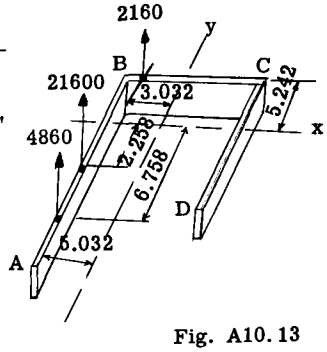

Fig. A10.13

SOLUTION:

Fig. A10.13 shows the cross-section of the analogous column. The length of each member of the column section being the same as in Fig. A10.12, and the width of each portion being 1/I. The first step in the solution is to find the column section properties.

The total area (A) of column section equals (15/1) + (10/1) + (12/2) = 31.

The other properties required are: - I_x, I_y and I_{xy}.

The calculations to determine the location of the centroidal x and y axes and the above properties about these axes would be identical to that given in example problem 1 of Art. A9.5 of Chapter A9, where this same problem was solved by elastic center method. The results were I_x = 606.51, I_y = 942.96 and I_{xy} = 217.74. The location of the axes were as shown in Fig. A10.13.

The next step in the solution is to choose a static frame condition and determine the static (M_S) diagram. Fig. A10.14 shows the assumed static condition, namely, two cantilevers because of the frame cut as shown. The figure also shows the static bending moment diagram made up of three portions labeled (1), (2) and (3). The area of each portion of the moment diagram divided by the (I) for that frame portion will give the loads P on the column.

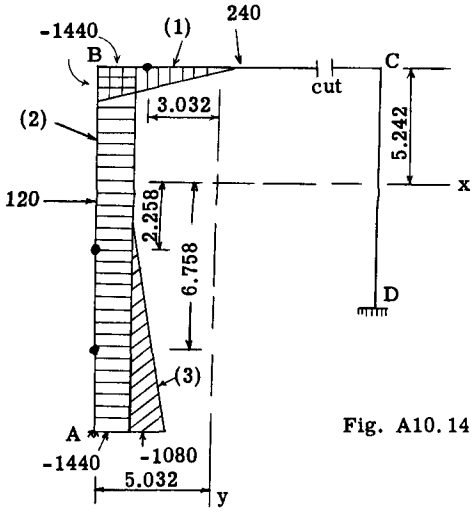

Fig. A10.14

$$P_1 = -1440 \times 3/2 = -2160$$

$$P_2 = -1440 \times 15/1 = -21600$$

$$P_3 = -1080 \times 4.5/1 = -4860$$

$$\Sigma P = -28620$$

These loads act on the centerline of the frame members and through the centroid of the geometrical moment diagram shapes. These centroid locations are indicated by the heavy dots in Fig. A10.14 and their locations are given with respect to the centroidal x and y axes. The loads P_1, P_2 and P_3 are now placed on the column in A10.13, acting upward because they are negative.

We now find the moments M_x and M_y which equal the moments of the loads P about the centroidal axes.

$$M_x = -2160 \times 5.242 + 21600 \times 2.258 + 4860 \times 6.758 = 70290$$

$$M_y = 2160 \times 3.032 + 21600 \times 5.032 + 4860 \times 5.032 = 139700$$

To solve equation (6) we must have the terms M'_x, M'_y and k.

$$M'_x = M_x \left(\frac{I_{xy}}{I_x}\right) = 70290 \times 217.74/606.51 = 25234$$

$$M'_y = M_y \left(\frac{I_{xy}}{I_y}\right) = 139700 \times 217.74/942.96 = 32258$$

$$k = \left(1 - \frac{I_{xy}^2}{I_x I_y}\right) = \left(1 - \frac{217.74^2}{606.51 \times 942.96}\right) = .9171$$

Substituting values in equation (6) we obtain,

$$M_1 = \frac{-28620}{31} + \frac{(70290 - 32258)y}{0.9171 \times 606.51} + \frac{(139700 - 25234)x}{0.9171 \times 942.96}$$

whence,

$$M_1 = -923 + 68.37y + 132.36x \quad - - - - - (7)$$

For Frame Point A. $x = -5.032$, $y = -9.758$

$$M_1 = -923 + 68.37(-9.758) + 132.36(-5.032) = -923 - 667.15 - 666.0 = -2256$$

$$M_A = M_S - M_1 = -1440 - 1080 - (-2256) = -264 \text{ in.lb.}$$

For Frame Point B. $x = -5.032$, $y = 5.242$

$$M_1 = -923 + 68.37 \times 5.242 + 132.36(-5.032) = -923 + 358.39 - 666.0 = -1230.6$$

$$M_B = M_S - M''_C = -1440 - (-1230.6) = -209.4 \text{ in.lb.}$$

Frame Point C. $x = 6.968$, $y = 5.242$

$$M_1 = -923 + 68.37 \times 5.242 + 132.36 \times 6.968 = 357.7$$

$$M_C = M_S - M_1 = 0 - (357.7) = -357.7 \text{ in.lb.}$$

Frame Point D. $x = 6.968$, $y = -4.758$

$$M_1 = -923 + 68.37(-4.758) + 132.36 \times 6.968 = -326$$

$$M_D = M_S - M_1 = 0 - (-326) = 326 \text{ in.lb.}$$

The above results check the solution of this same problem by the elastic center method in Art. A9.5 of Chapter A9. The student should solve this problem by choosing other static frame conditions.

A10.6 Problems

(1) Determine the bending moment diagram for the loaded structures of Figs. A10.15 to A10.20.

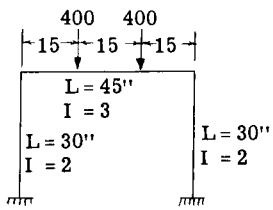

Fig. A10.15

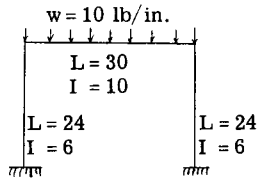

Fig. A10.16

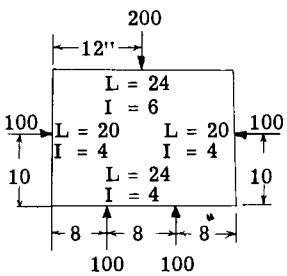

Fig. A10.17

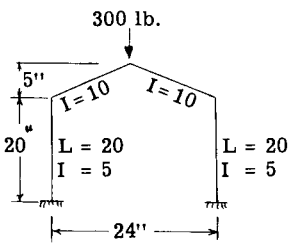

Fig. A10.18

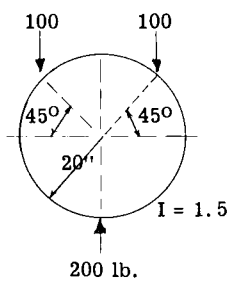

Fig. A10.19

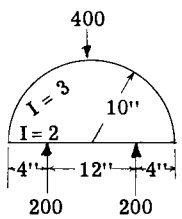

Fig. A10.20

(2) Solve problems (2) and (3) at the end of Chapter A9, Art. A9.9.

CHAPTER A11
CONTINUOUS STRUCTURES - MOMENT DISTRIBUTION METHOD*

A11.1 Introduction. The moment distribution method was originated by Professor Hardy Cross.** The method is simple, rapid and particularly adapted to the solution of continuous structures of a high degree of redundancy, where it avoids the usual tedious algebraic manipulations of numerous equations. Furthermore, it possesses the merit of giving one a better conception of the true physical action of the structure in carrying its loads, a fact which is usually quite obscure in some methods of solution.

The method of procedure in the Cross method is in general the reverse of that used in the usual methods where the continuous structure is first made statically determinate by removing the continuous feature and the value of the redundant then solved for which will provide the original continuity. In the Cross method each member of the structure is assumed in a definite restrained state. Continuity of the structure is thus maintained but the statics of the structure are unbalanced. The structure is then gradually released from its arbitrary assumed restrained state according to definite laws of continuity and statics until every part of the structure rests in its true state of equilibrium.

The general principles of the Cross method can best be explained by reference to a specific structure.

Fig. A11.1 shows a continuous 2 span beam. Let it be required to determine the bending moment diagram. We first arbitrarily assume that each span is completely restrained against rotation at its ends. In the example selected ends A and C are already fixed so no restraint must be added to these points. Joint B is not fixed so this joint is imagained as locked so it cannot rotate. The bending moments which exist at the ends of each member under the assumed condition are then determined. Fig. A11.2 shows the moment curves for this condition. (For calculation and formulas for fixed end moments see following articles). Fig. A11.3 shows the general shape of the elastic curve under this assumed condition. It is noticed that continuity of the structure at B is maintained, however from the moment curves of Fig. A11.2 it is found that the internal bending moments in the beams over support B are not statically balanced, or specifically there is an unbalance of 270. The next step is to statically balance this joint, so it is unlocked from its imaginary locked state and obviously joint B will rotate (See Fig. A11.4) until equilibrium is established, that is, until resisting moments equal to 270 have been set up in the two beams at B. The question is how much of this moment is developed by each beam. The physical condition which establishes the ratio of this distribution to the two beams at B is the fact that the B end of both beams must rotate through the same angle and thus the unbalanced moment of 270 will be distributed between the two beams in proportion to their ability of resisting the rotation of their B end thru a common angle. This physical characteristic of a beam is referred to as its stiffness. Thus let it be considered that the stiffness factors of the beam BA and BC are such that 162 is distributed to BC and - 108 to BA as shown in Fig. A11.4. (The question of stiffness factors is discussed in a following article).

Referring to Fig. A11.4 again it is evident that when the elastic curve rotates over joint B that it tends to rotate the far ends of the beams at A and C, but since these joints are fixed, this rotation at A and C is prevented or moments at A and C are produced. These moments produced at A and C due to rotation at B are referred to as carry-over moments. As shown by the obvious curvature of the elastic curves (Fig. A11.4), the carry-over moment is of opposite sign to the distributed moment at the rotating end. The ratio of the carry-over moment to the distributed moment, referred to as the carry-over factor, depends on the physical properties of the beam and the degree of restraint of its far end. (Carry-over factors are discussed in a following article. For a beam of constant section and fixed at the far end, the carry-over factor is -1/2). In figure A11.4 a factor of -1/2 has been assumed which gives carry-over moments of 54 and -81 to A and C respectively. To obtain the final end moments we add the original fixed end moments, the distributed balancing moments and the carry-over moments as shown in Fig. A11.4. With the indeterminate moments thus determined, the question of shear, reactions and span moments follow as a matter of statics.

A11.2 Definitions and Derivations of Terms

1. Fixed-end moments:

By "fixed end moment" is meant the moment which would exist at the ends of a member if these ends were fixed against rotation.

2. Stiffness Factor:

The stiffness factor of a member is a value proportional to the magnitude of a couple that must be applied at one end of a member to cause unit rotation of that end, both ends of the member being assumed to have no movement of

* Also see Chapter C2, Parts F, L and M.

** Paper - A.S.C.E. Proceedings, May 1930).

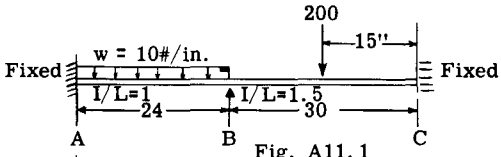

Fig. A11.1

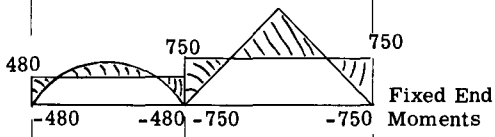

Fig. A11.2

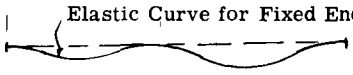

Fig. A11.3

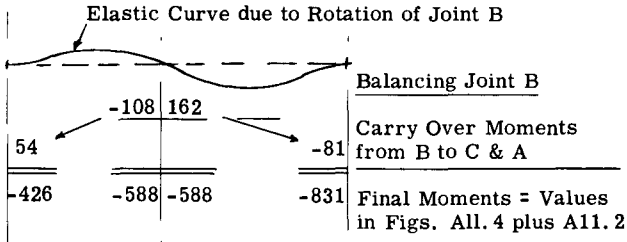

Fig. A11.4

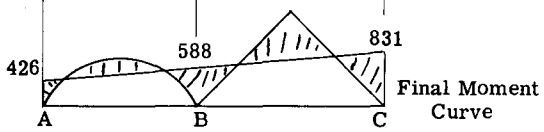

translation. The value of the stiffness factor will depend in part on the restraint or degree of fixity of the opposite end of the member from which the couple is applied. The letter K is used as a symbol for stiffness factor.

3. Carry-over Factor:

If a beam is simply supported at one end and restrained to some degree at the other, and a moment is applied at the simply supported end, a moment is developed at the restrained end. The carry-over factor is the ratio of the moment at the restrained end to that at the simply supported end. For a prismatic beam without axial load the carry-over factor is 0.5 when far end is fixed. The letter C will be used to designate carry-over factor.

4. Distribution Factor:

If a moment is applied at a joint where two or more members are rigidly connected the distribution factor for each member is the proportional part of the applied moment that is resisted by that member. The distribution factor for any member which will be given the symbol D equals $K/\Sigma K$, where K equals stiffness factor of a particular member and ΣK equals the sum of K values for all the Joint members. The sum of the D values for any joint must equal unity.

5. Sign Convention:

Due to the fact that in many problems where members come into a joint from all directions as is commonly found in airplane structure, the customary sign convention for moments may produce confusion in applying the moment distribution method. The following sign convention is used in this book: a clockwise moment acting on the end of a member is positive, a counterclockwise one is negative. It follows that a moment tending to rotate a joint clockwise is negative. It should be understood that when indeterminate continuity moments are determined by the moment distribution method using the above adopted sign convention, that they should be transferred into the convential signs before proceeding with the design of the member proper.

The following sketches illustrate the adapted sign convention.

Illustrations of Sign Conventions for End Moments.

Example 1

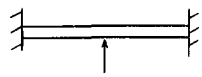

Fixed end beam with lateral loads.

Conventional moment signs + +

+ tension in bottom fibers is positive bending moment.

Adopted sign convention



moments which tend to rotate end of member clockwise are positive.

Example 2



Translation of supports of fixed ended beam.

Conventional moment signs − +

Adopted sign convention



Example 3

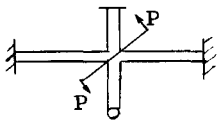

External applied moment at joint in structure

adopted sign

joint

moment

Moments which tend to rotate joint counter-clockwise are positive.

A11.3 Calculation of Fixed End Moments

Since the fixed end moments are statically indeterminate, additional facts must be obtained from the laws of continuity in order to solve for them. In this book the theorem of area moments will be used to illustrate the calculation of the fixed end moments as well as the other terms which are used in the moment distribution method. (Ref. Chapter A7)

The following well known principles or theorem of area moments will be used:-

(1) The deflection of any point "A" on the elastic curve of a beam away from a tangent to the elastic curve at another point "B" is equal to the moment of the area of the $\frac{M}{EI}$ diagram between the points A and B about point "A".

(2) The change in slope between two points "A" and "B" on the elastic curve of a beam is equal to the area of the $\frac{M}{EI}$ diagram between the two points "A" and "B".

The "area moment" theorems will be illustrated by the applications to the solution of a simple problem. Fig. A11.5 shows a simply supported beam of constant moment of inertia and modulus of elasticity carrying a single concentrated load. Figs. A11.6 and A11.7 show the static moment curve and the shape of the beam elastic curve. Now assume that the ends are fixed as shown in Fig. A11.8 and let the value of the fixed end moments be required. Fig. A11.9 shows the shape of the final moment curves made up of the static moment curve and the unknown trapizoidal moment curve formed by the unknown end moments. Fig. A11.10 shows the shape of the elastic curve, the slope at the two supports being made zero by fixity at these points.

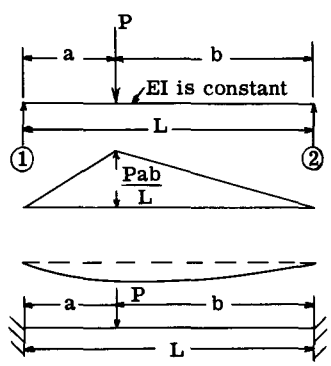

Fig. A11.5

Fig. A11.6

Fig. A11.7

Fig. A11.8

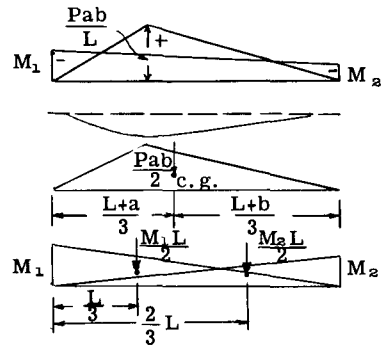

Fig. A11.9

Fig. A11.10

Fig. A11.11

Fig. A11.12

Since the change in slope of the elastic curve between ends (1) and (2) is zero, theorem (2) as applying to fixed end beams can be restated as follows.

The sum of the areas of the moment diagram must equal zero. And from theorem (1) the static moment of the areas of the moment diagram about any point must equal zero or in equation form:

$\Sigma M = 0$ - - - - - - - - - - - - - - - - - - -(1)

$\Sigma Mx = 0$ - - - - - - - - - - - - - - - - - - -(2)

For a beam with variable moment of inertia the conditions for fixity are:-

$\int Mdx/EI = 0$

$\int Mxdx/EI = 0$

Figs. A11.11 and A11.12 show the static and continuity moment areas, the total area of each portion and its c.g. location.

Substituting in Equation (1)

$$M = \frac{Pab}{2} + \frac{M_1L}{2} + \frac{M_2L}{2} = 0 \quad - - - - - - - - -(3)$$

and from equation (2)

$$M_X \text{ about left end} = \frac{Pab}{2} \cdot \frac{L+a}{3} + \frac{M_1L}{2} \cdot \frac{L}{3} + \frac{M_2L}{2} \cdot \frac{2L}{3} = 0 \quad - - - - - -(4)$$

The values of M_1 and M_2 for any value of a or b can now be found by solving equations (3) and (4)

Table A11.1 gives a summary of beam fixed end moments for most of the loadings encountered in routine design and analysis.

TABLE A11.1

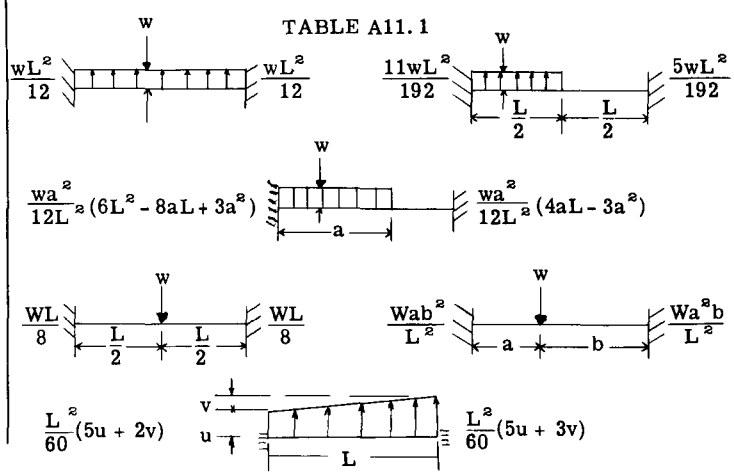

Table A11.1 - Continued

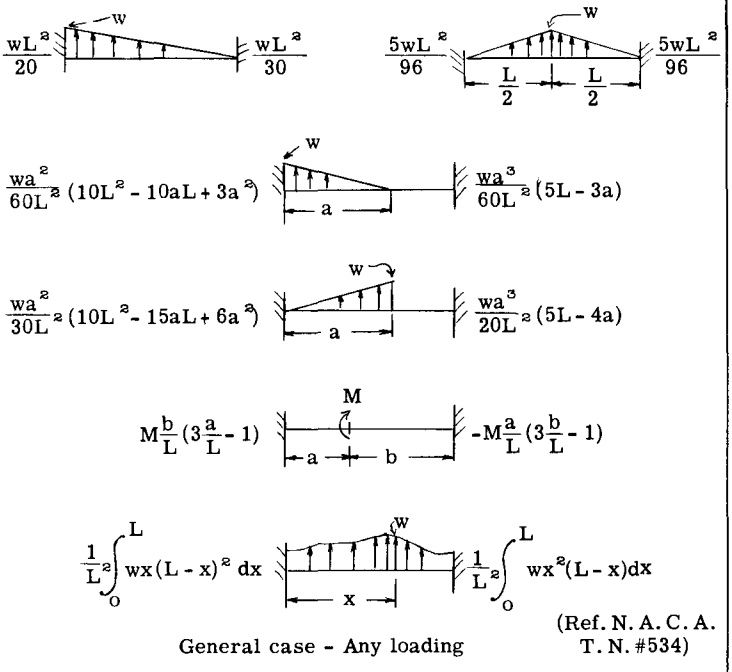

(Ref. N. A. C. A. T. N. #534)

General case - Any loading

A11.4 Stiffness Factor; Carry over Factor: - Derivation of:

(For definitions of these terms see page A11.2)

Consider the beam of Figure A11.13. By Mohr's theorem (see Art. A7.12), the slope of a tangent to the elastic curve at point A relative to a line AB is equal to the shear at A on a simply supported beam AB due to the $\frac{M}{EI}$ curve between A and B acting as a load.

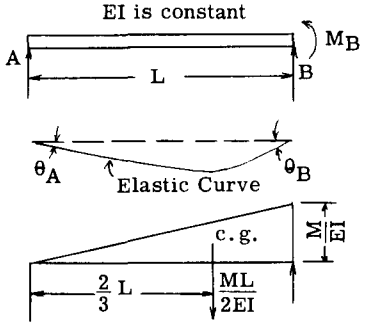

Fig. A11.13

Thus

$$\theta_A = -\frac{(\frac{ML}{2EI} \times 1/3)}{} = -\frac{ML}{6EI}$$ (Positive Shear = Neg. Slope)

$$\theta_B = \frac{ML}{2EI} \times 2/3 = \frac{ML}{3EI}$$

Let θ_B = unity

Then $1 = \frac{ML}{3EI}$ or $M_B = \frac{3EI}{L}$ = stiffness Factor of Beam BA of Fig. A11.13. A moment applied at B produces no moment at A since end A is freely supported. Thus the carry-over factor for a beam freely supported at its far end is obviously zero. Consider the beam of Fig. A11.14. Due to complete fixity at end A, the slope of the elastic curve at A is zero.

$$O_A = \frac{M_B L}{2EI} \cdot 1/3 + \frac{M_A L}{2EI} \cdot 2/3 = 0$$

or

$$M_A = -\frac{M_B}{2}$$

Thus the carry over factor for a beam fixed at its far end is 1/2. Using the conventional moment signs, the carry over moment is of the opposite sign as shown by the above equation, However, for our adopted sign convention inspection of the shape of the elastic curve as shown in Fig. A11.14 tells us that the sign of the carry-over moment is of the same sign as the rotating moment at the near end. That is, the moment acting on each end of the member is in the same direction, and therefore of the same sign.

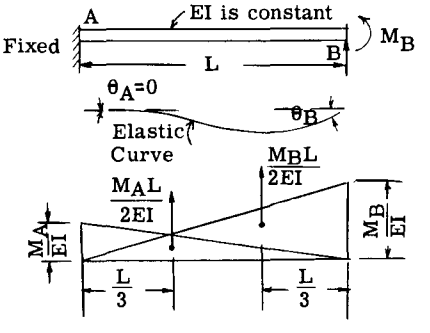

Fig. A11.14

$$\theta_B = \frac{M_B L}{2EI} \cdot 2/3 + \frac{M_A L}{2EI} \cdot 1/3 = \frac{M_B L}{3EI} + \frac{M_A L}{6EI}, \text{ but } M_A = -\frac{M_B}{2}$$

Then $\theta_B = \frac{M_B L}{3EI} - \frac{M_B L}{12EI} = \frac{M_B L}{4EI}$

Let θ_B = unity, then $M_B = \frac{4EI}{L}$ = stiffness factor of beam BA of Fig. A11.14.

A comparison of the stiffness factor of this beam to that of Fig. A11.13 shows that the stiff-

ness factor of a beam freely supported at its far end is 3/4 as great as one fixed at its far end. Furthermore in one case the carry-over factor is zero and in the other case it is 1/2. It is therefore obvious that the values of these two terms depends in part upon the restraint or degree of fixation of the far end of the beam.

A11.5 General Expressions for Stiffness and Carry-over Factor in Terms of Fixation Factor (F) at Far End of a Beam

In the beam of Fig. A11.14 (F) fixation factor at A was unity since beam had been taken as completely fixed at A. It was found that:-

$$M_B = \frac{4EI\theta_B}{L} \quad \text{and} \quad M_A = -\frac{2\,EI\,\theta_B}{L}$$

Then θ_B = unity and let $\frac{EI}{L} = K$ for simplicity.

Then $M_B = 4K$

$M_A = -2K$

Likewise the results for the beam of Fig. A11.13 give

$M_B = 3K$

$M_A = 0$

Figs. A11.15 and A11.16 show these results. Fig. A11.17 shows the general case, the fixation factor at A being F. The difference between Figs. A11.15 and A11.17 is that the slope at end A has changed but θ_B the slope at end B remains the same.

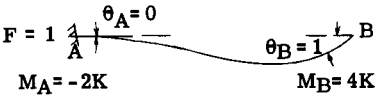

Fig. A11.15

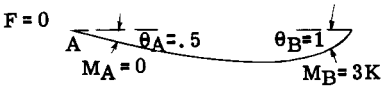

Fig. A11.16

The change in moment at end A when changing beam A11.15 to that of A11.17 = 2K - 2KF = 2K(1-F). Since θ_B is kept the same value, one-half of the moment change at end A appears at end B but of opposite sign, or

$$M_B = 4K - 1/2 \quad 2K(1-F) = 3K + KF = K\,(3+F) = \frac{EI}{L}\,(3+F)$$

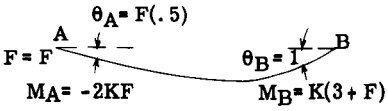

Fig. A11.17

Thus the general expression for the stiffness factor of a beam of constant section equals $\frac{EI}{L}$ (3+F). The carry-over factor from B to A = $\frac{M_A}{M_B} = -\frac{2KF}{K(3+F)} = -\frac{2F}{3+F}$ which is the general expression for carry-over factor for a degree of fixation F.

A11.5a Example Problems

To obtain a definite conception of the true mechanics of the "Cross" method, the reader is advised to follow thru the detailed solution of the following simple problems. In these problems, the moment of inertia in any span has been taken as constant and all joints have been assumed to undergo no translation. Problems involving variable I and joint translation will be considered later.

Example Problem #1

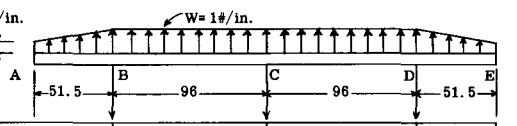

Stiffness Factor $\frac{EI}{L} = K$	0	1	1	1	0
Distribution Factor K/ΣK	0	1	.5	.5	1	0
Carry Over Factor	0	.5	.5	.5	.5	0
Fixed End Moments	*-883	768=.0833wL²=-768	768=.0833wL²=-768	883
1st Balancing	0	115	0	0	-115	0
Carry Over 1/2		0	57.5	-57.5	0	
2nd Balancing	0	0	0	0	0	0
Final Moments	-883	883	-710.5	710.5	-883	883
Conventional Moment Signs	+	+	+	+	+	+

*Overhang Moment = .5 x 51.5 x 25.75 + .25 x 51.5 x 17.17 = 883

Example Problem 1 shows a two-span continuous beam with over-hanging ends. We first assume all the joints B, C and D to be locked against rotation or the beams BC and CD are arbitrarily assumed in a fixed-end condition.

The first line in the solution gives the stiffness factor of each beam. From Art. A11.5 the general expression for stiffness factor is EI(3+F)/L, where F = fixation factor of far end, which equals 1, since all joints have been considered fixed. Thus, stiffness factor K = EI (3+1)/L = 4 EI/L. Since EI/L is the same for each span BC and CD, the stiffness factor has been written as one since it is only the relative values that are necessary. The cantilever BA has zero stiffness.

The second row gives the member distribution factor D at each joint or D = K/ΣK. For example at joint B, the distribution factor to BA = 0/(1 + 0) = 0 and to BC = 1/(1 + 0) = 1. At joint C, the distribution factor to CB = 1/(1 + 1) = .5 and likewise to CD.

The third row gives the carry-over factors. From Art. A11.5, the carry-over factor C = 2F/(3 + F) = 2 x 1/(3 + 1) = .5 assuming the far end fixed or F = 1 for each member.

The next step as shown by the 4th horizontal row is the calculation of the fixed end moments. The signs of the moments are according to our adopted sign convention, that is an internal resisting moment which tends to rotate the

end of a member clockwise is positive.

We now begin the solution proper by first unlocking joint B from its assumed fixed state. We find a moment of -883 on one side and 768 on the other side of joint or a static unbalance of -115. Joint B therefore will rotate until a resisting moment of 115 is set up in the members BA and BC.

The resistance of these members to a rotation of Joint B is proportional to their stiffness. The distribution factor based on the stiffness factors is 0 for BA and 1 for BC. Thus 1 x 115 = 115 is distributed to BC at B and 0 x 115 = 0 to BA. Joint B is now imagined as again locked against rotation and we proceed to Joint C, which is now released from its assumed locked state. Since the joint is already statically balanced, no rotation takes place and the distributing balancing moment to each span is zero. Next proceed to joint D, and release it. The unbalanced moment is, 115 so the joint is balanced by distributing -115 between DE and DC as explained above for joint B.

As pointed out in Art. A11.5, when we rotate one end of a beam it tends to rotate the far fixed end of the beam by exerting a moment equal to some proportion of the moment causing rotation at the near end. For beams of constant section and fixed at their far ends, the carry over factor is 1/2 as explained before. Thus the distributing balancing moments in line 4 produce the carry-over moments as shown in line 5 of the table. This completes one cycle of the moment distribution method, which is repeated until there is nothing to balance or carry-over, or in other words until all artificial restraints have been removed and the structure rests in its true state of equilibrium.

To continue with the second cycle, go back to joint B and release it again from its assumed locked state. There is no unbalance since the carry over moment from point C was zero, thus there is nothing to distribute or carry-over. Proceed to point C, releasing the joint, we find it balanced under the carry-over moments of 57.5 and -57.5. Thus the distributing balancing moments are zero. Joint D is likewise in balance since the carry-over moment from C is zero. All joints can now be released without any rotation since all joints are in equilibrium. To obtain the final moments we add the original fixed end moments plus all distributed balancing and carry over moments.

A11.6 General Summary of Proceedure

1. All computations should be written on, or adjacent to the diagram of the structure.
2. Determine the stiffness factor K for each end of each member. $K = (3 + F)\,EI/L$, where F is the degree of fixity at far end of member. If all members are assumed fixed at far end then K is proportional to I/L assuming E as constant.
3. Determine the distribution factor D for each member at each joint of structure. $D = K/\Sigma K$.
4. Calculate the carry-over factor C for each end of all members $C = 2F/(3+F)$. Thus for beams fixed at far end F = 1 and thus C = 1/2. For pinned at far end F = 0, hence C = 0.
5. Calculate the fixed end moments (f) for given transverse member loadings or support deflections, using equations in summary Table A11.1. End moments which tend to rotate end of beam clockwise are positive moments. (See Art. A11.2)
6. Considering one joint at a time, unlock it from its assumed fixed state, all other joints remaining locked. If an unbalanced moment exists balance it statically by distributing a counter acting moment of opposite sign among the connecting members according to their D or distribution factors.
7. These distributed balancing moments produce, carry over moments at far-end of members equal to the distributed moment times the carry-over factor C and of the same sign as the distributed moment. Record these carry-over moments at far ends for all distributed moments.
8. Repeat the proceedure of unlocking each joint, distributing, and carrying over moments until the desired precision is obtained, stopping the solution after a distribution. The final moment at the end of any member equals the algebraic sum of the original fixed end moments and all distributed and carry over moments.

Example Problem #2

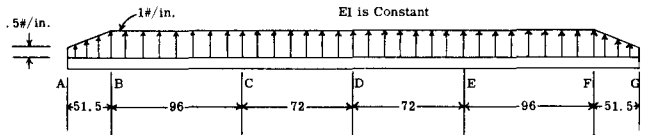

Stiffness Factor $\frac{EI}{L}=K$		0	.0104 = $\frac{1}{96}$ = .0104		.0139=$\frac{1}{72}$=.0139		.0139=$\frac{1}{72}$=.0139		.0104 = $\frac{1}{96}$ = .0104				
Distribution Factor $D=\frac{K}{\Sigma K}$		0	1	.428	.572	.5	.5	.572	.428	1			0
Carry-Over Factor C		0	.5	.5	.5	.5	.5	.5	.5	.5			0
Fixed End Moments		-883	768 = $\frac{1}{12}wL^2$ = -768		432=$\frac{1}{12}wL^2$=-432		432=$\frac{1}{12}wL^2$=-432		768 = $\frac{1}{12}wL^2$ = -768				883
1st Balancing		0	115	144	192	0	0	-192	-144	-115			0
Carry-Over			72	57.5	0	96	-96	0	-57.5	-72			
2nd Balancing		0	-72	-24.6	-32.9	0	0	32.9	24.6	72			0
Carry-Over			-12.3	-36	0	-16.5	16.5	0	36	12.3			
3rd Balancing		0	12.3	15.4	20.6	0	0	-20.6	-15.4	-12.3			0
Carry-Over			7.7	6.1	0	10.3	-10.3	0	-6.1	-7.7			
4th Balancing		0	-7.7	-2.6	-3.5	0	0	3.5	2.6	7.7			0
Carry-Over			-1.3	-3.9	0	-1.8	1.8	0	3.9	1.3			
5th Balancing		0	1.3	1.7	2.2	0	0	-2.2	-1.7	-1.3			0
Final Moments		-883	883	-610.4	610.4	-344	344	-610.4	610.4	-883			883
Conventional Signs		+	+	+	+	+	+	+	+	+			+

Example Problem 2 is similar to problem 1 but two spans have been added. We first assume all joints locked against rotation. The stiffness factor of each span is proportional to EI/L or 1/L since EI is constant. The carry-over factor is 1/2 as in previous example. Fixed end moments are calculated as shown. Unlock joint B, the unbalanced moment is -115. Balance the joint by distributing 1 x 115 to BC and zero to BA. Proceed to joint C,

and unlock, all other joints remaining fixed against rotation. The unbalanced moment is (-768 + 432) = - 336. Balance by distributing .428 x 336 = 144 to CB and .572 x 336 = 192 to CD. Proceed to joint D, and release. The unbalanced moment is zero which means that joint D is in equilibrium, thus no distribution is necessary. Proceed to joint E and F and balance in a similar manner. The distributed moments will be the same as the values for joints B and C due to symmetry of structure and loading, however, the signs will be opposite under our adopted sign conventions. The next step is the carry-over moments which are equal to 1/2 the distributed balancing moments. This operation is shown clearly in the table. Values of all moments are given only to first decimal place. The first cycle has now been completed. Cycle two is started by again releasing joint B. We find the joint has been unbalanced by the carry-over moment of 72. Balance the joint by distributing - 72 x 1 = - 72 to BC and zero to BA. Proceed to joint C. The unbalanced moment is 57.5. Balance by distributing - 57.5 x .428 = - 24.6 to CB and the remainder - 32.9 to CD. Proceed to joint D. There is no unbalance at this joint since the carry-over moments are in balance, thus no distribution is necessary. Proceed to joints E and F in a similar manner.

The carry over moments equal to 1/2 of the 2nd set of balancing distributed moments are now carried over as shown in the table. The second cycle has now been completed. This operation has been repeated five times in the solution shown, or until the values of the balancing and carry over moments are quite small or negligible. The final moments equal the algebraic summation of the original fixed end moments plus all distributed and carry over moments. One requirement of the final end moments at any joint is that the algebraic sum must equal zero. The other requirement consistant with the common slope to all members at any joint is given by equation (5) of Art. A11.8. The results at joint C will be checked using this equation.

$$\frac{\Delta M_{cd} - .5\,\Delta M_{dc}}{\Delta M_{cb} - .5\,\Delta M_{bc}} = \frac{K_{cd}}{K_{cb}}$$

Subt. values

$$\frac{(610.4 - 432) - .5\,[344 - (-432)]}{[-610.4 - (-768)] - .5\,(883 - 768)} = \frac{178.6 - 44}{157.6 - 57.3} =$$

1.343

Ratio of stiffness factors = $\frac{K_{cd}}{K_{cb}} = \frac{.0139}{.0104} = 1.34$.

Thus the distribution is according to the K ratios of the adjacent members.

Simplifying Modifications - Example Problem #3

The solution as given in Problem #2 represents the "Cross" method in its fundamental and most elementary detailed form. Many modifications of the general method have been presented, in the most part for the purpose of eliminating part of the arithmetic or the number of cycles necessary. These modifications usually involve rather long expressions for expressing the stiffness and carry over factors of a member in terms of the fixation given by adjacent members. It is felt that it is best to keep the method in its simplest form which means that very little is to be remembered and then the method can be used infrequently without refreshing ones mind as to many required formulas or equations.

There are however several quite simple modifications which are easily understood and remembered and which reduce the amount of arithmetic required considerably.

For example in Problem #2, joints B and F are in reality freely supported, thus it is needless arithmetic to continue locking and unlocking a joint which is definitely free to rotate. Likewise due to symmetry of structure and loading it is only necessary to solve one half of the structure. Due to symmetry joint D does not rotate and thus can be considered fixed, which eliminates the repeated locking and unlocking of this joint.

A second solution of Problem #2 is given in Example Problem #3. As before we assume each joint locked and calculate the fixed end moments. Now release or unlock joint B and balance as explained in previous example #2. Before proceeding to joint C, carry over to C from B the carry over moment equal to 115 x 1/2 = 57.5. Joint B is now left free to rotate or in its natural condition. Proceed to joint C and unlock. The unbalanced moment = (-768 + 432 + 57.5) = - 278.5 or 278.5 is necessary for equilibrium. This moment is distributed between two beams, CD which is fixed at its far end D and CB which is freely supported at the far end B. The stiffness factor is equal to (3 + F) EI/L (See Art. A11.5).

Hence for CD stiffness factor = (3 + 1) EI/L = 4 EI/L. For CB stiffness factor = (3 + 0) EI/L = 3 EI/L or in other words the stiffness of a beam freely supported at its far end is 3/4 as great as when fixed at its far end. Thus the stiffness factor of CB at C is .75 x .0104 = .0078. The carry-over factor C to B is zero since B is left free to rotate. (See Art. A11.5)

Example Problem #3. Simplified Solution of Problem #2

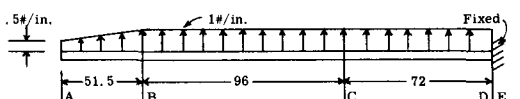

Stiffness Factor (k)	0	.0104=1/96	.75x.0104=.0078	.0139 = 1/72 = .0139		∞
Distribution Factor D = K/ΣK	0	1	.36	.64	0	1
Carry-over factor (C)	0	.5	0	.5	.5	
Fixed end moments	-883	768	-768	432	-432	
Balance joint B	0	115				
Carry-over 1/2 to C			57.5			
Balance joint C			-100.1	178.4		
Carry-over to B, D		0			89.2	
Balance joint D					0	342.8
Carry-over to C				0		
Final moments	-883	883	-610.4	610.4	-342.8	342.8
Conventional signs	+	+	+	+	+	+

The stiffness factor of the fixed support is infinity, that is a rigid support has infinite resistance to rotation.

Joint C is now balanced by distributing 278.5 x .36 = 100.1 to CB and 278.5 x .64 = 178.4 to CD. Now carry over to joint B, 0 x 100.1 = 0 and 0.5 x 178.4 = 89.2 to D. Proceed to joint D and release it from its assumed locked state. The unbalanced moment is -432 + 89.2 = - 342.8, we balance by distributing 342.8 between DC which has a stiffness of 0.139 and the support E which has an infinite stiffness or zero goes to DC and 342.8 goes to rigid support. The carry over moment to C from D is zero since 0.5 x 0 = 0. The final moments thus equals the summations as shown which of course are equal to the results shown in Problem #2.

Example Problem #4

Problem 4 is similar to Problem #2 and #3, except that the support at D is assumed as having 50 percent fixity. Thus 50 percent of any moment at this point produces rotation of the member DC at D.

In continuous wing beams, which fasten together by fittings on a support, it is commonly required that the beam be considered as being fully continuous and also that the degree of continuity be taken as 50 percent. Solution 1 of Problem 4 is a detailed solution. The only change that has been made is in the stiffness factor of the support E, which has been taken as equal to the beam DC, thus any unbalanced moment at this point is equally divided between the beam and the support.

Solution 2 is a modified solution which eliminates considerable arithmetic. Thus it is unnecessary to lock and unlock joint B and D since we know definitely that one is freely supported and the other 50 percent fixed. Therefore, once we have released these joints from their assumed fixed end state, we leave them in their natural state. The stiffness and carry-over factors for beams CB and CD must then be determined for these beams with their modified end conditions.

By reference to the fundamental equations for stiffness and carry over factors in Art. A11.5, it is readily seen that the stiffness factor for CB is 3/4 as much as when fixed at its far end B and the carry over moment is zero. For beam CD the stiffness is 7/8 as much as when fixed at end D, and the carry over factor is 2F/3 + F = (2 x .5)/3 + .5 = .286. With these modifications the solution is carried thru with a relatively small number of steps. Thus in solution #2, joint B is unlocked. The unbalanced moment of -115 is balanced statically by distributing 115 to BC. The carry-over moment of .5 x 115 = 57.5 is carried over to C as shown. Joint B is now left unlocked or free to rotate. Joint D is unlocked next. The unbalanced moment is -432. It is balanced by distributing 216 to DC and 216 to E since support at E is considered to give 50% fixity. The carry-over moment of

Solution #1
Example Problem #4

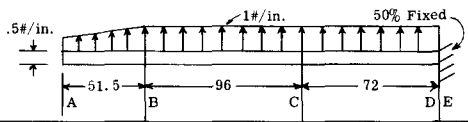

Stiffness Factor k		0	.0104 = 1/96 = .0104	.0139=1/72=.0139	.0139	
Distribution Factor D=$\frac{K}{\Sigma K}$		0	1	.428	.572	.5	.5
Carry-Over Factor		0	.5	.5	.5	.5	
Fixed End Moments	-883	768	-768	432	-432		
1st Balancing	0	115	144	192	216	216	
Carry-Over		72	57.5	108	96		
2nd Balancing	0	-72	-70.7	-94.8	-48	-48	
Carry-Over		-35.3	-36.0	-24.0	-47.4		
3rd Balancing	0	35.3	25.7	34.3	23.7	23.7	
Carry-Over		12.9	17.6	11.8	17.2		
4th Balancing	0	-12.9	-12.6	-16.8	-8.6	-8.6	
Carry-Over		-6.3	-6.4	-4.3	-8.4		
5th Balancing	0	6.3	4.6	6.1	4.2	4.2	
Final Moments	-883	883	-644.3	644.3	-187.3	187.3	
Conventional Signs		+	+	+	+	+	

.5 x 216 = 108 is carried over to C. Joint D is left unlocked or in its true state of restraint. Joint C is now unlocked. The unbalanced moment

Solution #2
Example Problem #4

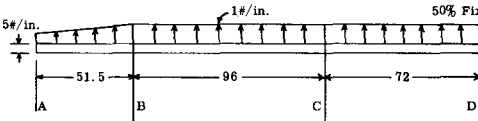

Stiffness Factor K	-883	.0104=$\frac{1}{96}$	.75x.0104=.0078	.0121=$\frac{7}{8}$x$\frac{1}{72}$	$\frac{1}{72}$=.0139	.0139
Distribution Factor=$\frac{K}{\Sigma K}$		0	1	.392	.608	.50	.50
Carry-over Factor		1/2	0	.286	1/2		
Fixed End Moments	-883	768	-768	432	-432		
Balance Joint B	0	115					
Carry-over to C			57.5				
Balance Joint D						216	216
Carry-over to C				108			
Balance Joint C			66.8	103.7			
Carry-over to D					29.6		
Balance D							29.6
Final Moments	-883	883	-643.7	643.7	-186.4	186.4	

equals (-768 + 432 + 57.5 + 108) = - 170.5, or 170.5 is necessary for equilibrium. Joint C is balanced by distributing .392 x 170.5 = 66.8 to CB and the remainder of 103.7 to CD. The carry-over moment to B is zero and to D it equals 103.7 x .286 = 29.6. The final moments in solution #2 are slightly different than solution #1. If another cycle had been added in solution #1 the discrepancy would be considerably smaller.

A11.7 Continuous Beams with Yielding or Deflected Supports*

In wing, elevator and rudder beams the support points usually deflect due to the deformation of the supporting struts or wires in the case of a wing, or to the deflection of the stabilizer or fin in the case of elevator and rudder beams. If these beams are continuous this deflection of their support points causes additional bending moments in the beams. The moment distribution method can of course be used to find the additional moments due to this deflection. Thus Example Problem #5, shows a solution illustrating a problem which involves the deflecting of the supports of a continuous beam. Due to symmetry of structure and loading, the slope at D is zero or the beam may be considered fixed at

* Also see Chapter C2, Parts F, M and Q.

Joint D. Since the moment of inertia is constant and the spans are constant, the relative stiffness factor of the beam is 1. In the solution shown since beam is freely supported at B this joint is left free to rotate after releasing and thus the stiffness factor of beam CB is 3/4 x 1 = 3/4, when compared to one having full fixity at B.

Since the first step in the solution proper is to assume the joints fixed against rotation, it is evident that deflecting one support relative to an adjacent support will produce moments at the ends which are assumed fixed against rotation.

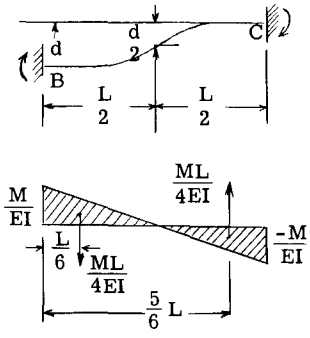

Fig. A11.18

A11.8 Fixed End Moments Due to Support Deflections

Fig. A11.18 shows a fixed end beam. The support B is deflected a distance d relative to the support point C. If the member is of constant cross-section the point of inflection will fall at the beam midpoint and $M_B = -M_C$.

By moment area principal deflection

$$-d = \frac{ML}{4EI} \cdot \frac{L}{6} - \frac{ML}{4EI} \cdot \frac{5}{6} L$$

or $$d = \frac{ML^2}{6EI}$$

hence

$$M = \frac{6EId}{L^2}$$ the magnitude for the fixed end moment due to a transverse support settlement of d.

Example Problem #5. Continuous beam with deflected supports.

General data:

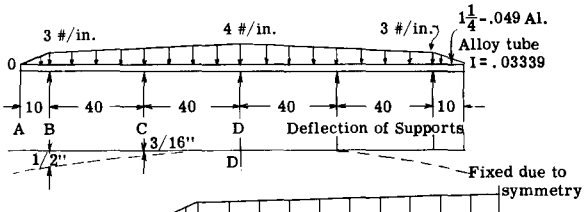

Solution:

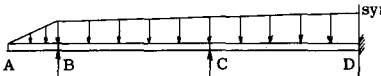

Stiffness Factor K	0	1	3/4x1=.75	1	1	∞
Distribution Factor = K/ΣK	0	1	.429	.571	0	1
Carry-over Factor		1/2	0	1/2	1/2	
Fixed End Moments: Due to Lateral Load	50	-426	440	-494	507	
Fixed End Moments: Due to support deflection	0	390	390	234	234	
Balance joint B	0	-14				
Carry-over to C			-7			
Balance joint C			-241	-322		
Carry-over to B, D		0			-161	
Balance joint D					0	-580
Final Moments	50	-50	582	-582	580	-580
Conventional Signs	-	-	-	-	-	

Since the fixed end moments are due to both lateral loads and support deflection, the values as listed in the solution table will be explained in detail.

Fixed End Moment For Lateral Beam Loading

The distributed airload is trapezoidal in shape. The fixed-end moments for a trapezoidal loading from Table A11.4 are:

$$M_{1-2} = \frac{L^2}{60}(5u + 2v) \quad \text{(See Fig. (a))}$$

$$M_{2-1} = \frac{L^2}{60}(5u + 3v) \quad \text{(See Fig. (a))}$$

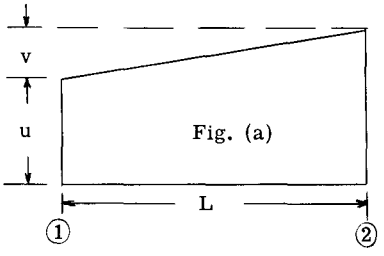

For Span BC:

$$M_{bc} = \frac{40^2}{60}(5 \times 3 + 1) = 426 \text{ in. lb.}$$

$$M_{cb} = \frac{40^2}{60}(5 \times 3 + 1.5) = 440 \text{ in. lb.}$$

For Span CD:

$$M_{cd} = \frac{40^2}{60}(5 \times 3.5 + 1) = 494 \text{ in. lb.}$$

$$M_{dc} = \frac{40^2}{60}(5 \times 3.5 + 1.5) = 507 \text{ in. lb.}$$

Fixed End Moments Due to Support Movement

From Art. A11.8 $M = 6EId/L^2$

For Span BC:

Deflection of B relative to C = 5/16 inch. Hence,

$M_{bc} = M_{cb} = 6 \times 10{,}000{,}000 \times .03339 \times .3125/40^2 = 390$ in. lb.

For Span CD:

$M_{cd} = M_{dc} = 6 \times 10{,}000{,}000 \times .03339 \times .1875/40^2 = 234$ in. lb.

For signs of the moments due to these deflections see Art A11.2. Having determined the fixed end moments the general distributing and carrying over process follows as indicated in the solution table. Thus at joint B, the unbalanced moment = (50-426 + 390) = 14. Balance by distributing - 14 x 1 = - 14 to BC and zero to BA. Carry over .5 x -14 = - 7 to C. Considering joint C, the unbalanced moment = (440 + 390 + 234 - 494 - 7) = 563. Balance bydistributing - 563 x .571 = - 322 to CD and -563 x .429 = - 241 to CB. Carry over .5 x -322 = - 161 to D. At joint D the unbalanced moment = (507 + 234 - 161) = 580. This is balanced by distributing zero to DC and -580 to the fixed support.

A11.8 Check on Final Moments

To satisfy statics, the algebraic sum of the moments in all the members at a joint must equal zero. This requirement alone will not prove that the final moments are correct, as errors could have been made in the various distributing and carry over moments. Continuity tells us that the final slope of the elastic curve at any joint is common to all members meeting at that joint, thus for a complete check it is necessary to prove that the final moments are consistent with equal slopes for the various members. The rotation of the joints from their original assumed fixed or locked condition is due entirely to the distributed and carry over moments. The actual rotation will therefore equal the rotation of the end of a simply supported beam when subjected to end moments equal to those produced by the algebraic sum of the distributed and carry over moments. These end moments equal the final moments minus the original fixed end moments and will be referred to as ΔM moments.

From Chapter A7, the slope at any point on a simply supported beam equals the shear due to the M/EI diagrams as a loading.

The slope θ_A from Fig.a' equals the beam shear at A or equals the reaction at A.

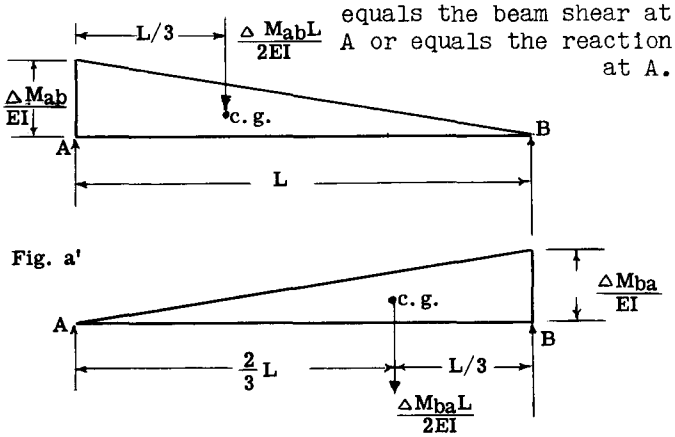

Fig. a'

$$\theta_A = -\frac{\Delta M_{ab} L}{2EI} \cdot 2/3 - \frac{\Delta M_{ba} L}{2EI} \cdot \frac{1}{3}$$

$$= -\frac{(\Delta M_{ab} + .5\,\Delta M_{ba})}{3EK_{ab}}$$

where

$$K_{ab} = \frac{I}{L} \text{ of AB}$$

Since the angle θ_A must be the same for members meeting at A, the general relation between the moment increments of any two members such as AB and AC must be,

$$\frac{\Delta M_{ab} + .5\,\Delta M_{ba}}{\Delta M_{ac} + .5\,\Delta M_{ca}} = \frac{K_{ab}}{K_{ac}}$$

To make this equation consistent with the assumed sign convention, that is, the carry over moment has the same sign as the balancing distributed moment, the above equation must be modified as follows:-

$$\frac{\Delta M_{ab} - .5\Delta M_{ba}}{\Delta M_{ac} - .5\Delta M_{ca}} = \frac{K_{ab}}{K_{ac}} \quad \text{----------(5)}$$

If equation (5) is satisfied the accuracy of the moment distributions is established.

A11.9 End Moments for Continuous Frameworks Whose Members are not in a Straight Line. Joint Rotation Only*

Continuous truss frame works are quite common in aircraft construction. Welded steel tubular fuselages are composed of members which maintain continuity thru the joints due to the welding. Landing gears frequently have two members which are made continuous at their points of connection. The members of such structures usually carry high axial stresses which cause joint translation which in turn produces bending of the members since the joints are rigid. These moments produce lateral deflection of the members which introduces additional secondary moments due to member axial loads times the lateral member deflections. These influences are treated in later articles. In this article to further familiarize the student with the moment distribution procedure, the effect of joint translation and secondary moments will be neglected.

Example Problem #6

Fig. A11.19 illustrates a simplified landing gear chassis problem. Let it be required to determine the bending moments in the two members due to the vertical load on the axle. The problem has been solved using three different degrees of restraint at ends A and B. Joint O is a welded joint and full continuity is assumed thru this joint. The solutions as given in Fig. A11.20 give only the moments due to joint rotation under primary bending moments. The effect of axial deformation and secondary moments due to member deflections is omitted in these solutions. These factors are treated in later articles.

In a practical problem the degree of restraint at points A and B would be determined by the type of fitting used and also on the rigidity of the adjacent fuselage or wing structure. As illustrated in later examples, the moment distribution method permits the consideration of the rigidity of the adjacent structure without adding any difficulty, while such methods as least work

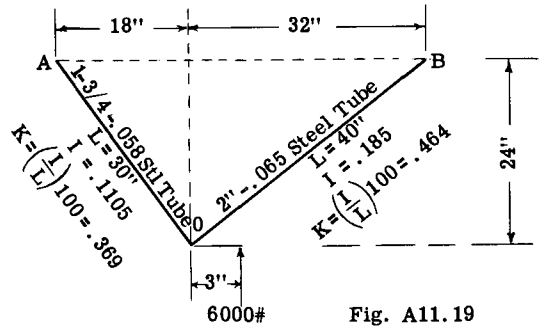

Fig. A11.19

* Also see Chapter C2, Part H.

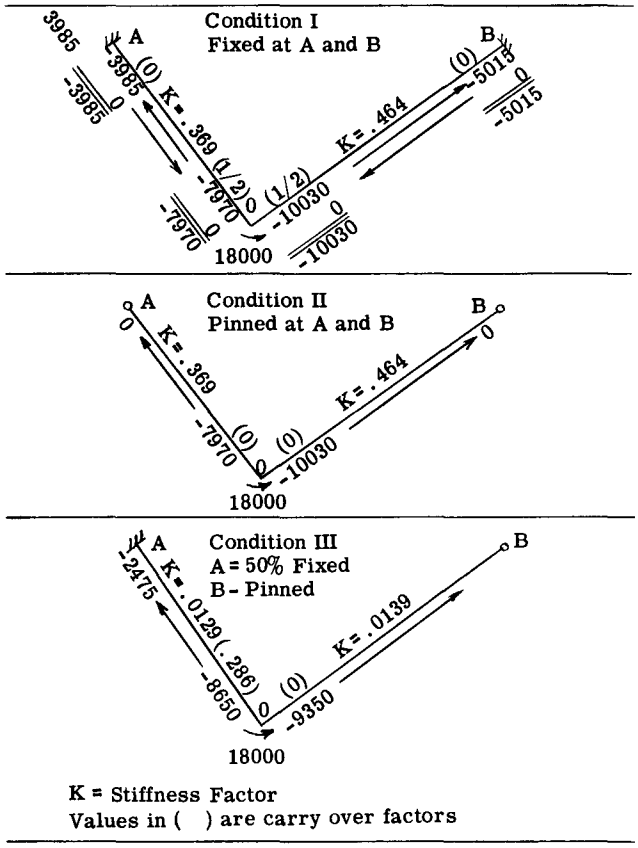

Fig. A11.20

are not practicable because of the large number of equations that must be solved to obtain values for the many unknowns.

Solution for Condition I, Fixed at Ends A and B

Referring to Fig. A11.20, all joints are assumed locked against rotation or fixed. The vertical axle load of 6000# produces a counter-clockwise moment of 3 x 6000 = 18000 in. lb. about joint 0. The sign is positive (See Art. A11.2). Release or unlock joint 0, the unbalanced moment is 18000 or - 18000 is required for static equilibrium of joint 0. Joint 0 is balanced by distributing - 18000(.464/.464 + .369) =-10030 to member OB and the remainder or or -18000(.369/.464 + .369) = -7970 to OA. These distributed balancing moments at 0 produce carry over moments at A and B.

Thus carry over to B, .5 x - 10030 = - 5015
and carry over to A, .5 x - 7970 = - 3985

Proceeding to joint A which is a fixed joint, the unbalanced moment of -3985 is balanced entirely by the rigid support, or no rotation takes place when joint is released from its imaginary fixed state. Similar action takes place at joint B. The final end moments are as shown in the Figure.

Solution for Condition II. End A and B Pinned

For this condition the ends A and B are freely supported. Instead of locking and unlocking these joints which are definitely known to be free to be freely supported, they will be left in their true state. Thus the carry over moments from end 0 will be zero. Since A and B are both pinned, the relation between the relative stiffness factors of members OA and OB remain the same as in condition I, thus the same K or stiffness factors that were used in condition I can be used in distributing moments at joint 0. Joint 0 is balanced in same manner as condition I but with zero carry over moments to A and B.

Solution for Condition III. A is 50% Fixed and B is Pinned.

Since each member has a different degree of fixity at its upper end, the stiffness and carry over factors will be considered in detail. In condition I since both members were fixed at their upper ends the relative stiffness factor of each member was proportional to I/L for the member and this ratio was used. The general expression for stiffness factor is K = EI (3 + F)/L carry over factor = $\frac{2F}{3+F}$. For member OA, F equals .5 since A is 50% fixed, and for member OB, F is zero since B is freely supported. Hence for member OA

$$K = \frac{EI}{L}(3 + .5) = \frac{3.5\ EI}{L} = \frac{3.5 \times .1105\ E}{30} = .0129\ E$$

$$\text{C.O. Factor from 0 to A} = \frac{2 \times .5}{3 + .5} = .286$$

For member OB

$$K = \frac{EI}{L}(3 + 0) = \frac{3 \times .185 \times E}{40} = .0139E$$

$$\text{C.O. Factor From 0 to B} = \frac{2 \times 0}{3 + 0} = 0$$

Considering joint 0 in Fig. A11.20 the external moment of 18000 in.lb. is balanced by distributing - 18000 between the two members in proportion to their stiffness factors. Hence - 18000 (.0129/.0129 + .0139) = -8650 in lbs. is resisted by OA and the remainder of -18000 (.0139/.0129 + .0139)= -9350 to OB. The carry over moment from 0 to A = .286 x -8650 = -2475 and zero from 0 to B. (See Fig. A11.20)

Example Problem #7

Fig. A11.21 shows a structure composed of 3 members. Member AO is subjected to a transverse load of 120# at its midpoint. Joint A is fixed, B is freely supported, C is 25 percent fixed and joint 0 is considered to maintain continuity between all members at 0. The end moments on the three members due to the transverse loading on member AO will be determined.

Solution #1. Fig. A11.21 gives a solution using the "Cross" method in its fundamental unmodified state. The solution is started by assuming all three members as fix-ended. The relative stiffness factor K of each member is therefore proportional to I/L of each member. These K values are listed in Fig. A11.21. The distribution

factor D for each member at each joint which equal K/ΣK is recorded in □ on each member around each joint. Thus any balancing moment is distributed between the joint members as per these distribution factors. The carry over factors for all members is 1/2. The fixed end moments due to external loading are computed for the three members. For member AO, the fixed end moments equal PL/8 = 120 x 20/8 = 300 in. lb. The other two members having no transverse loading, the fixed end moments are zero.

In this solution the order of joint consideration has been AOBC and repeat. Starting with joint A the joint is released but since the member AO is actually held by a fixed support, no rotation takes place and the balancing moment of 300 is provided entirely by the support and zero by the member AO. The carry over moment C, to O is zero. Releasing joint O, the unbalanced moment of 300 is balanced by distributing - 300 between the three members according to their D values, thus - 300 x .416 = - 125 to OA; - 300 x .168 = - 50 to OC and - 125 to OB. To prevent confusion it is recommended that a line be drawn under all distributed balancing moments, thus any values above these lines need not be given further consideration and only values below the lines need be considered in later balancing of the joints. Immediately after distributing the moments at joint O the proper carry over moments should be taken over to the far end of each member, thus - 62.5 to A, - 62.5 to B and - 25 to C. Joint B is next considered. The unbalanced moment is -62.5 and it is balanced by distributing 62.5 to BO since the pin support has zero stiffness, or no resistance to rotation. A line is drawn under the 62.5 and the carry over moment of 31.25 is placed at O. Joint C is considered next. The unbalanced moment of -25 is balanced

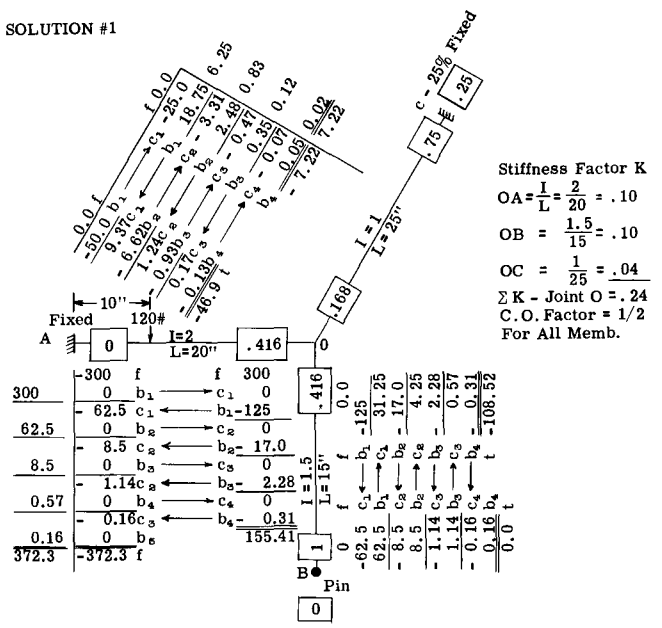

Fig. A11.21

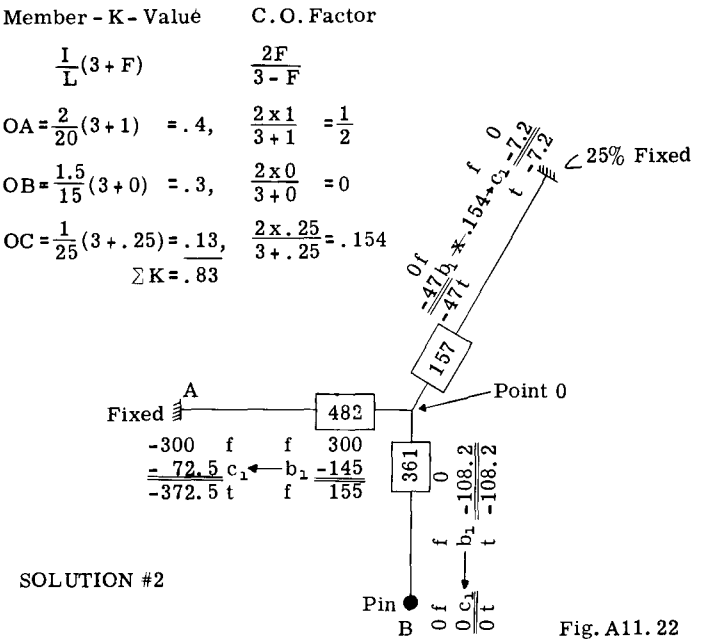

Fig. A11.22

by distributing .75 x 25 = 18.75 to CO and the remainder of 6.25 to the support, since the fixity of the support at C has been assumed as 25 percent. A line is drawn under the 18.75 and the carry over moment of 9.37 is taken over to O. One cycle has now been completed. Returning to joint A, we find -62.5 below the line. This is balanced by distributing zero to OA and 62.5 to the fixed support. A line is drawn under the zero distributed moment to AO and the carry over moment of zero is placed at O. Considering joint O for the second time the unbalanced moment is 9.37 + 31.25 + 0 = 40.62 or the sum of all values below the column horizontal lines. The joint is balanced by distributing - 17 to OA and OB and -6.62 to OC. Lines are drawn under these balancing moments as shown in Fig. A11.21 and the carry over moments are taken over to the far ends before proceeding to joint B.

This general process is repeated until joint A has been balanced 5 times and the other joints 4 times each, as indicated in the figure the distributing values have become quite small and it is evident that a high degree of accuracy has been obtained. The final end moments at each joint equal the algebraic sum of the values in each column. A double line is placed above the final moments as a distinguishing symbol. In the figure the letters b and c refer to balancing and carry over moments, the subscripts referring to the member of the balancing or carry over operation. Any order of joint consideration can be used in reaching the same result.

Solution #2 of Problem 7

Fig. A11.22 gives a second solution. With the end conditions known at A, B and C, the modified stiffness factors of the members can be found together with the modified carry over factors, thus making it necessary to balance joint O only once and carry over this final far end

moments of each member. The figure gives the calculation of the modified or actual stiffness and carry over factors. With these known the solution is started as before by computing the fixed end moments due to transverse loading on member AO. Joints B and C are released and since no fixed end moments exist, no balancing is required and the joints are left in their true state of restraint instead of locking and unlocking as in solution #1. Releasing joint O from its imaginary fixed state the unbalanced moment is 300 which is balanced by distributing - 300 between the 3 connecting members according to the new distribution factors at joint O. Thus - 300 x .482 = - 145 to OA; - 300 x .361 = - 108.2 to OB and - 300 x .157 = - 47 to OC. The carry over moment to A = - 145 x .5 = - 72.5 to B = - 108.2 x 0 = 0 and -47 x .154 = - 7.2 to C.

Example Problem #8

Figure A11.23 shows the forward portion of a fuselage side truss. Due to eccentricity of engine mount and landing gear members, external moments are produced on joints A, B and D as shown. Furthermore lateral loads due to equipment installation are shown acting on members BE and CD. Assuming the fuselage welded joints produce rigid continuity of members thru the joint, the problem is to find the end moments in all the members due to the eccentric joint moments and two lateral loads. The effect of joint translation and secondary moments due to deflections and axial loads is to be neglected in this example.

Solution:

Table A11.2 gives the calculation of the stiffness factor for each truss member. The fuselage truss aft of joints I and H have been assumed to give 50% fixity to these joints. In Table A11.2 a modified stiffness factor is calculated for members GI, FI, and FH using a 50 percent fixity at their far ends. The last column of Table A11.2 gives the summation of the member stiffness factors for members intersecting at each joint.

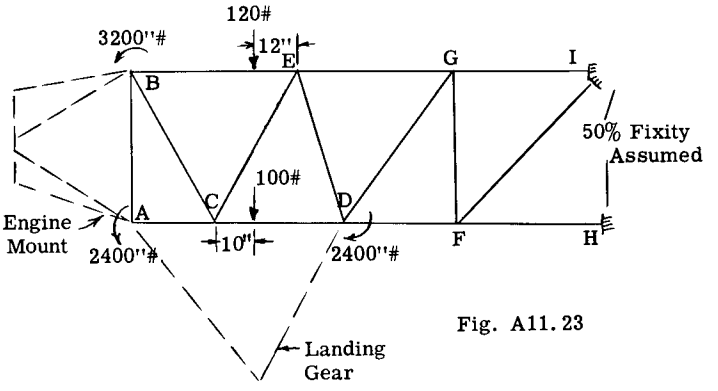

Fig. A11.23

TABLE A11.2

Member	Size Tube	Length L	I	I x 1000 / L Stiffness K Factor	Σ I/L for each joint: Joint	Σ I/L for each joint: Stiffness
BE	1-1/8 - .049	41.25"	.0240	0.582	A	5.80
EG	1-1/8 - .049	38.75	.0240	0.619	B	4.81
GI	1-1/8 - .049	34.0	.0240	.618*	C	6.95
AC	1-1/2 - .049	19.25	.0588	3.06	D	6.14
CD	1-1/2 - .049	30.0	.0588	1.96	E	2.58
DF	1-1/2 - .049	30.0	.0588	1.96	F	4.42
FH	1-3/8 - .049	34.0	.0449	1.16*	G	3.21
AB	1-3/4 - .049	34.5	.0947	2.74		
ED	1-1/4 - .049	35.4	.03339	0.944		
FG	1-1/8 - .049	34.5	.0240	0.695		
BC	1-1/2 - .049	39.5	.0588	1.49	(E is constant for all members)	
CD	1-1/8 - .035	41.0	.0178	0.434		
DG	1-1/2 - .049	46.0	.0588	1.28		
FI	1-1/4 - .049	48.5	.03339	0.602*		

(*stiffness factor - 7/8 I/L because of 50% fixity)

Fig. A11.24

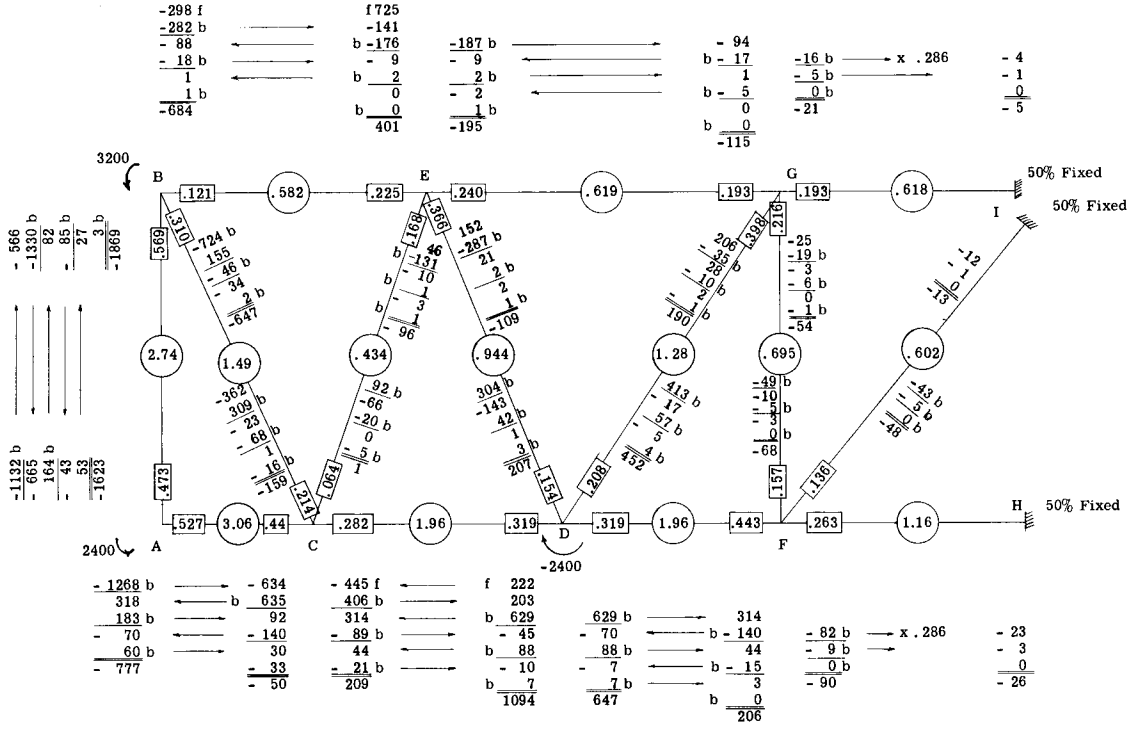

Fig. A11.24 gives the solution of the problem. The procedure in this solution was as follows:

The stiffness factor K for each member as computed in Table A11.2 is recorded in the circles adjacent to each truss member. The carry over factors for all members is 1/2 except for modified members GI, FI and FH for which the carry over factor to the 50% fixed ends is .286. The distribution factor for each member at each joint is recorded at the end of each member, and equals K/ΣK.

The next step in the solution is to compute the fixed end moments due to the transverse loads on members.

For member BE

$M_{BE} = Pab^2/L^2 = 120 \times 29.25 \times 12^2/41.25^2 = -298$"#

$M_{EB} = 120 \times 29.25^2 \times 12/41.25^2 = 725$"#

$M_{CD} = 100 \times 20^2 \times 10/30^2 = -445$

$M_{DC} = 100 \times 10^2 \times 20/30^2 = 222$

These moments are placed at the ends of the members on Fig. A11.23 together with the eccentric joint moments. The process of unlocking the joints, distributing and carrying over moments can now be started. In the solution as given the order of joint consideration is ABCDEFG and repeat, and each joint has been balanced three times.

Consider joint A:-

Unbalanced moment = 2400. Balance by distributing - 2400 as follows:-

To AC = - 2400 x .527 = -1268. Carry over to C = -634

To AB = - 2400 x .473 = -1132. Carry over to B = -566

Proceed to Joint B:-

Unbalanced moment = (-566 + 3200 - 298) = 2336. Joint is balanced by distributing - 2336 to connecting members as follows:-

To BA = - 2336 x .569 = - 1330. Carry over to A = - 665

To BC = - 2336 x .310 = - 724. Carry over to C = - 362

To BE = - 2336 x .121 = - 282. Carry over to E = - 141

The convenient device of drawing a line under all balancing moments is used to prevent confusion in later balances of the joint.

Proceed to Joint C:-

Unbalanced moment = (-634 - 362 - 445) = -1441. The joint is balanced by distributing 1441 as follows:-

To CA = 1441 x .44 = 635. Carry over to A = 318

CB = 1441 x .214 = 309. Carry over to B = 155

CE = 1441 x .064 = 92. Carry over to E = 46

CD = 1441 x .282 = 406. Carry over to D = 203

This process is continued for the remainder of the truss joints. After all joints has been balanced once, on returning to joint A we find below the lines an unbalanced moment of (318 - 665) = -347. The joint is balanced a second time by distributing 183 to AC and 164 to AB with carry over moments of half these values to ends C and B respectively.

The student should now be able to check the rest of the solution as given on Fig. A11.24.

The solution could be made with any order of joint consideration. If any particular joint appears to be nearly balanced, it is best to skip it for the time being and consider those joints which are considerably unbalanced.

The final moments at the end of each member are given below the double lines.

Example Problem #9

Fig. A11.25 represents a cross section of a welded tubular steel fuselage. The top and bottom members which are web members in the top and bottom fuselage trusses are subjected to the equipment installation transverse loads as shown. Let it be required to determine the end bending moments in the rectangular frame due to these transverse loads assuming full continuity thru joints.

Solution:

Fig. A11.26 shows the solution. The distribution factors based on the member stiffness factors are shown in □ at ends of each member. The first step is to compute the fixed end moments due to transverse loads, on members AB and CD using equations from Table A11.1. The magnitudes are 1890"# for AB and 2025"# for CD.

Joint B is now released from its assumed fixed state. The unbalanced moment of 1890 is balanced by distributing - 1890 x .247 = - 467 to BA and the remainder of -1423 to BD. The carry over moment to A = - 465 x .5 = - 233. Due to symmetry of structure and loading only one half of frame need be considered and hence these carry over moments to A are not recorded. However, in balancing joint A it will throw over to B the same magnitude of carry over moments as thrown over to A from B but of opposite sign since the original fixed end moment at B is minus. Thus 233 comes to B from first balance of A as shown in the figure. The distributing moment to B of -1423 produces a carry over moment of -1423 x .5= -712 at D.

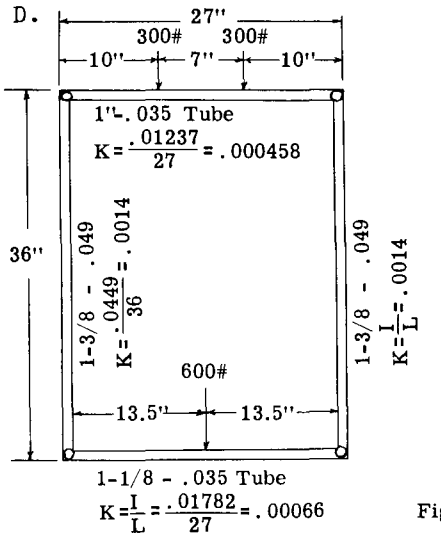

Fig. A11.25

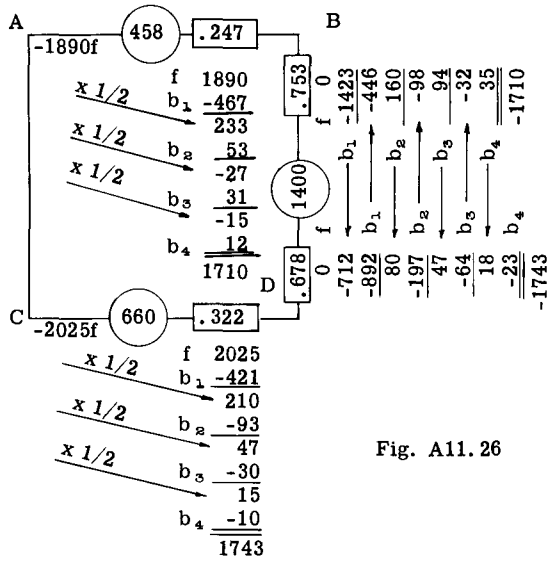

Fig. A11.26

Joint D is considered next: The unbalanced moment of (2025 - 712) = 1313 is balanced by distributing - 1313 to the connecting members.

To member DB = - 1313 x .678 = - 892 and the remainder of -421 to DC. The carry-over moment to B is - 446. The carry-over from C to D is one-half the balancing moment B = - 421 but of opposite sign or 210, due to symmetry as explained before for member AB.

Returning to joint B, the unbalanced as recorded below the single lines is (233 - 446) = - 213. To balance 160 is distributed to BD and 53 to BA. Carry-over 80 to D and bring over from A to B .5 x -53 = - 27. Continue this process until joints A and D have been balanced 4 times or 4 cycles have been completed. The final moments are shown below the double lines. Fig.A11.26a shows the resulting moment diagram on frame.

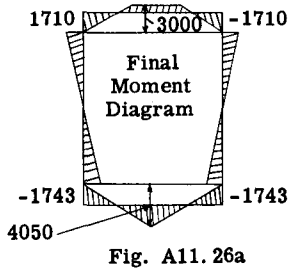

Fig. A11.26a

A11.10 Continuous Structures with Members of Variable Moment of Inertia*

In Arts.A11.3, 4 and 5 consideration was given to the derivation of expressions for fixed end moments, stiffness and carry-over factors for beams of uniform cross-section. Many cases occur in routine design where members have a variable cross section. This article will illustrate the calculation of the fixed end moments, stiffness and carry-over factor for a beam with variable moment of inertia. The effect of axial load on these factors will not be considered here but will be treated in a later article.

*Also see Chapter C2, Part L.

(A) Calculation of Fixed End Moments for a Given Beam Load

Fig.A11.27 shows a fixed end beam with a variable moment of inertia and carrying a single concentrated load of 100#. The beam moment diagram for this load is considered in three parts. Fig.A11.28 shows the static moment curve assuming the beam simply supported at A and B and carrying the load of 100#. Fig.A11.29 shows the other two parts, namely the triangular moment diagram due to the unknown moments M_A and M_B which produce fixity at the two ends. In this figure M_A and M_B have arbitrarily been taken as 100, instead of unity.

Fig.A11.30 shows the M/I diagram for the 3 moment diagrams of Fig.A11.29. The beam is divided into ten equal strips, and the M/I curves are obtained by dividing the moment values at the end of each strip or portion by the corresponding I value from Fig. A11.27.

From the conditions of fixity at the beam ends, we know that the slope of the beam elastic curve is zero at each end. Likewise the deflection of one end of the beam away from a tangent at the other end is zero. Stating these facts in terms of the moment area principles, we obtain

$$\int_0^L \frac{M dx}{I} = 0 \quad -(5)$$ (Area of M/I diagrams equal zero)

$$\int_0^L \frac{M x dx}{I} = 0 \quad -(6)$$ (Moment of the M/I diagram as a load about either end equals zero)

(Note: Since E is usually considered constant it has been omitted from denominator of the above equations.)

TABLE A11.3

Beam Portion	Static M/I curve			Trial $\frac{M_A}{I}$ curve			Trial $\frac{M_B}{I}$ curve		
	Av. Ord. = y	Mom. arm left end = x	Mom. about left end = yx	Av. Ord. (y)	Mom. arm left end x	yx	Av. Ord. = y	Arm x	Mom. yx
1	107	2.67	286	110	2.06	227	6.7	2.67	18
2	397	6.31	2510	133	6.07	807	24.9	6.27	156
3	770	10.16	7800	143	10.0	1430	48.2	10.16	488
4	1120	14.10	15800	130	13.94	1810	70.0	14.10	990
5	1440	18.07	26000	110	17.96	1976	90.0	18.06	1630
6	1760	22.06	38900	90	21.92	1970	110.0	22.05	2430
7	1615	25.88	41600	67.3	25.88	1740	123.5	26.04	3480
8	975	29.77	29000	40.7	29.76	1215	117.0	29.94	3490
9	420	33.65	14180	17.5	33.68	590	91.0	33.88	3080
10	100	37.33	3733	4.2	37.33	157	62.5	37.86	2360
*Σy	8504			845.7			743.8		
Σyx			179809			11922			18122

$\bar{x} = \frac{\Sigma yx}{\Sigma} = \frac{179809}{8504} = 21.15"$ $\quad \bar{x} = \frac{11922}{845.7} = 14.1"$ $\quad \bar{x} = \frac{18122}{743.8} = 24.4"$

* Actual area is 4 times the results shown. For calculation of fixed end moments $S\Sigma$c.o. factors only relative values are necessary.

Fig. A11.27

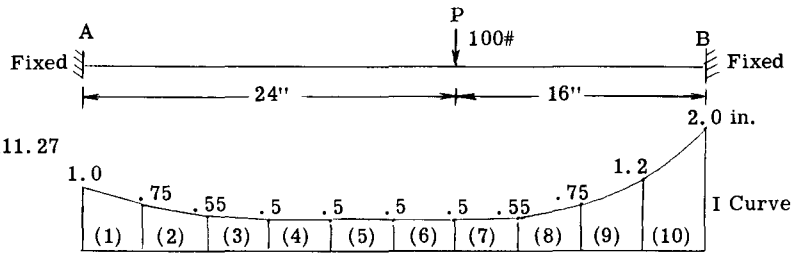

Fig. A11.28

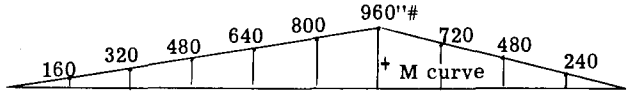

Fig. A11.29

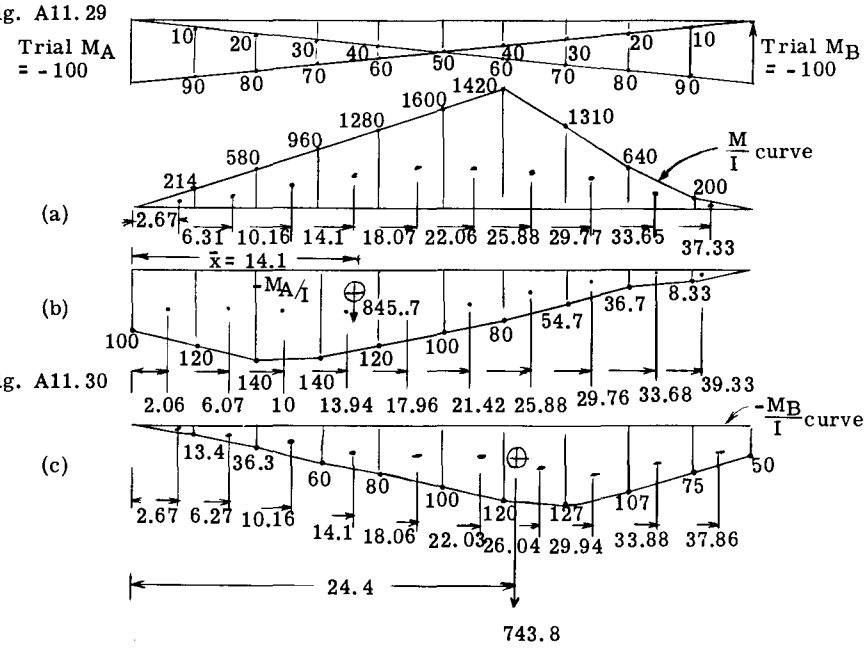

Table A11.3 shows the calculations for computing the areas and the centroids of the three M/I diagrams of Fig. A11.30. Substituting values from Table in equations (5) and (6).

$$\frac{845.7}{100} M_A + \frac{743.8}{100} M_B + 8504 = 0 \text{ - - - - - -(7)}$$

$$\frac{11922}{100} M_A + \frac{18122}{100} M_B + 179809 = 0 \text{ - - - - - -(8)}$$

The value 100 in the denominators is due to the fact that trial values of 100 were assumed for M_A and M_B. Solving equations (7) and (8) we obtain;

M_A = - 315"# and M_B = - 785"#.

(B) Calculation of Carry Over Factors

To determine the carry over factor from A to B consider end A as freely supported and B as fixed. A moment M_A = 100 is applied at A which produces the M/I curve of Fig. A11.30b. Due to the deflection of the beam under this loading a restraining moment at B to cause tangent of elastic curve to remain horizontal will exist. This unknown fixed moment at B has arbitrarily been taken as 100, thus producing a M/I curve identical to Fig. A11.30c. For the conditions of support assumed, the deflection of A away from a tangent to the elastic curve at B is zero. Thus by the deflection principle of area moments, the moment of the M/I diagrams of Figs. A11.30 (a and b) about end A equals zero. Thus,

$$845.7 \times 14.1 + \frac{743.8}{100} M_B \times 24.4 = 0$$

or

M_B = - 66"#

Since M_A was assumed 100, then carry over factor from A to B = $\frac{-66}{100}$ = - .66.

To find carry over factor from B to A, take moments about B and equate to zero.

Hence

$$743.8 \times 15.6 + \frac{845.7}{100} M_A \times 25.9 = 0$$

whence

M_A = - 53.2"#

Therefore carry over factor B to A = $-\frac{53.2}{100}$ = - .532

(Note: For the moment sign convention used in this book carry over factor would be plus.)

(C) Calculation of Beam Stiffness Factors

When a beam is freely supported at one end A and fixed at the far end B, the stiffness factor at the A end is measured by the moment necessary at A to produce unit rotation of the elastic curve at A.

In Art. A11.4 it was proved for beams of uniform section that $E\Theta_A = M_A L/4I$ or $M_A = 4EI\Theta_A/L$. In a continuous structure at any joint all members have the same Θ, thus $4E\Theta$ is constant and the stiffness K of any prismatic beam is proportional to I/L. For beams of variable section the stiffness factor K may be written:-

$$K = cI_o/L \text{ - - - - - - - - - - - - - - - - -(9)}$$

where I_o is the moment of inertia at a particular reference section and c is a constant to be found for each non-uniform member. Thus for non-uniform members

$$E\Theta_A = M_A L/4cI_o \text{ - - - - - - - - - - - - - (10)}$$

By the moment area slope principle, the slope at A when B is fixed equals the area of the M/I diagram between A and B.

Taking M_A = 100, M_B was found to equal -66"#. Thus $E\Theta_A = 4(845.7 - .66 \times 743.8) = 1419$. The value 4 is due to the strip width since true area is wanted and only average ordinate was used in Table A11.3.

Equating this result to Equation (10)

$$1419 = \frac{100 \times 40}{4c \times 1}, \text{ whence } c = .707$$

I_0 was taken as the value at the A end or 1. (See Fig. All.27).
Therefore $K_{AB} = .707\ I_A/L$

Similarly for end B:-

$$E\theta_B = 4(743.8 - .532 \times 845.7) = \frac{100 \times 40}{4c \times 1}$$

whence

$$c = .85 \text{ and } K_{BA} = .85\ I_A/L$$

A11.11 Frames with Unknown Joint Deflections Due to Sidesway *

In the example problems so far treated the joints of the particular structure were assumed to rotate without translation or with a definite amount of translatory movement. Translation of the joints may however, be produced by shortening and lengthening of the members due to axial loads and by lateral sway due to lack of diagonal shear members. The problem relative to the effect of joint translation due to axial stresses is treated in a later article. In this article only the effect of sidesway of rectangular frames on the frame bending moments will be considered.

Fig. All.31 illustrates cases of frames where only rotation of joints takes place (neglecting axial deformation) whereas Fig.All.32 illustrates conditions in which sidesway takes place and the joints suffer translation as well as rotation.

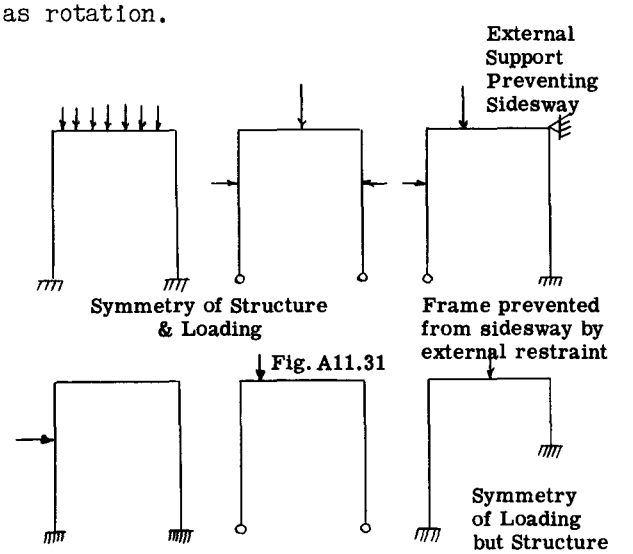

Fig. A11.32

There are several methods of determining the bending moments due to sidesway. Only one method will be presented here and it can best be explained by the solution of example problems.

Example Problem 1.

Fig. All.33 shows a single bay rectangular bent carrying a distributed side load on one leg as shown. The K or I/L values for each member are given on the figure.

Under the given loading it is obvious that the frame will sway to the right or in other words, joints B and C will undergo considerable horizontal movement. The moment distribution method assumes that only joint rotation takes place. To make this assumption true for this structure we will add an imaginary support at joint C which will prevent sidesway of the frame as illustrated in Fig.All.34. The end moments in the frame will then be found by the moment distribution process. Fig. All.34 shows the results of this process. To explain, the solution begins with computing the fixed end moment on member AB = $WL^2/12 = (300 \times 25^2)/12 = 15.63$ thousands of foot lbs. This value with the proper sign is written at the head of a column of figures on member AB as shown in Fig.All.34.

Now considering Joint B, the unbalanced joint moment of 15.63 is distributed as follows:-
To Member BA = - 15.63 (40/190) = - 3.27. Carry over to Joint A = - 3.27/2 = - 1.63

To Member BC = - 15.63 (150/190) = - 12.36. Carry over to Joint C = - 12.36/2 = - 6.18

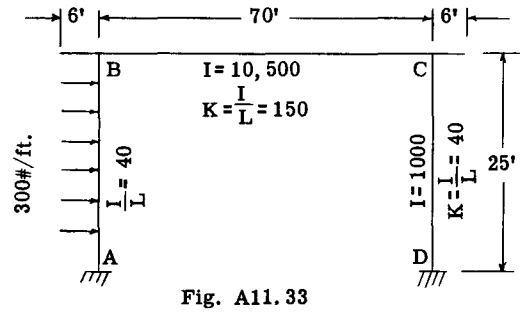

Fig. A11.33

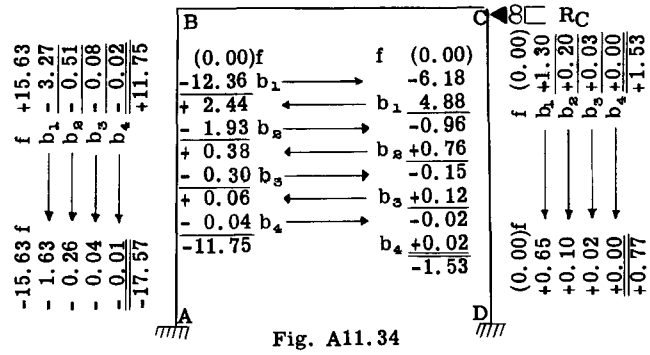

Fig. A11.34

* Also see Chapter C2, Part M.

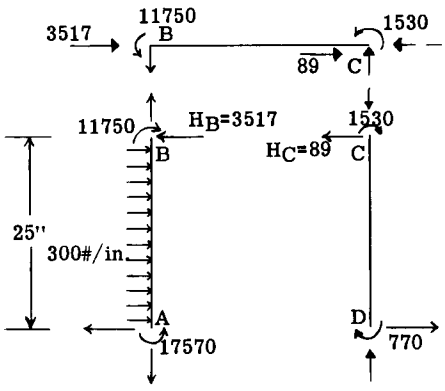

Fig. A11.35

Now consider Joint C:-

The unbalanced moment is -6.18. To balance we distribute to CB = 6.18 x 150/190 = 4.88. Carry over to B = 2.44; to CD = 6.18 x 40/190 = 1.30. Carry over to D = 0.65

The balancing and carry over procedure is now repeated for joints B and C, until the unbalanced moments become of negligible magnitude. Fig.A11.34 shows that 4 cycles have been carried through. By keeping the ratio 150/190 set on the slide rule the unbalanced moments at joints B and C are distributed and chased back and forth as rapidly as one can write them down. Since joints A and D are assumed fixed, they absorb moments but do not give out any.

Fig. A11.35 shows a free body diagram of each portion of the frame. The end moments are taken from the results in Fig. A11.34. Consider member AB as a free body. To find the horizontal reaction H_B we take moments about point A.

$$\Sigma M_A = 300 \times 25 \times 12.5 + 11750 - 17570 - 25H_B = 0$$

hence $H_B = 87930/25 = 3517$ lb.

Now consider member CD as a free body. To find H_C take moments about D.

$$\Sigma M_D = 1530 + 770 - 25H_C = 0, \text{ hence } H_C = 89 \text{ lb.}$$

We now place these horizontal forces on the top member BC as a free body as shown in the upper portion of Fig. A11.35. The unknown imaginary reaction R_C at point C that was added in Fig. A11.34 to prevent sidesway is also shown. To find R_C take $\Sigma F_h = 0$

$$\Sigma F_h = 3517 + 89 - R_C = 0, \text{ hence } R_C = 3606 \text{ lb.}$$

Since the external reaction of 3606 does not exist, we must eliminate it and find the bending moments due to the sidesway of the frame. In other words, the frame will sway sideways until bending of the frame develops a horizontal shear reaction at the upper end of the vertical legs of the frame equal to 3606 lb.

Bending Moments Due to Sidesway.

Assume the structure sways sideways as illustrated in Fig. A11.36, but with no rotation of the upper joints. It was proven in Art. A11.8 that the end moments produced by the lateral movement of one end of a beam whose ends are fixed against rotation are equal to $6EId/L^2$ where d is the lateral movement. In Fig. A11.36 the load P causes both vertical members to suffer the same horizontal displacement at their upper ends, hence their end moments due to this displacement are proportional to EI/L^2.

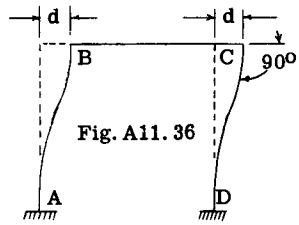

Fig. A11.36

Sidesway Without Rotation of Joints

Since EI and L are the same for each vertical member in our structure, the fixed end moments will be the same magnitude for each member. Therefore, for convenience we will assume fixed end moments of 10,000 ft.lbs. are produced by the sidesway. We now use the moment distribution process in permitting the upper joints to rotate as illustrated in Fig. A11.37. The procedure is similar to that in Fig. A11.34. For example the solution is started by considering joint B. The unbalanced moment is -10. This is balanced by distributing 10 x 150/190 = 7.89 to BC and the remainder of 2.11 to BA. The carry over moments are 7.89/2 = 3.95 to C and 2.11/2 = 1.06 to A. Due to symmetry of loading and structure, the distributing and carry over moments at joint C will be same as at joint B, hence it is needless work to show calculations at these joints. The carry over moments from C to B will be identical to those from B to C. Fig. A11.37 shows the 5 cycles have been carried out to obtain the final end moments as shown below the double lines.

+ 7.89 b		
+ 3.95	← 1/2	Due to symmetry of loading and structure it is not necessary to consider right hand portion as calculations will be identical as shown for left side.
- 3.12 b		
- 1.56	← 1/2	
+ 1.23 b		
+ 0.62	←	
- 0.49 b		
- 0.25	←	
+ 0.20 b		
+ 8.47		

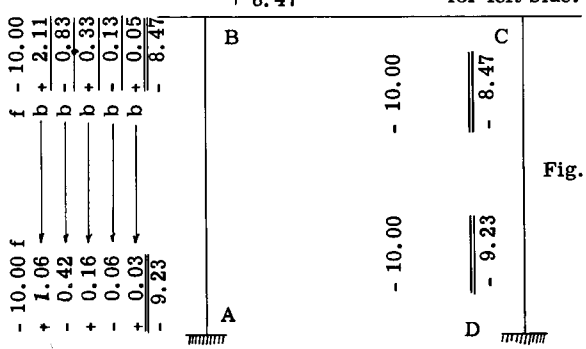

Fig. A11.37

Fig. All.38 shows a free body diagram of the frame vertical members with the end moments as found in Fig. All.37. The shear reactions H_B and H_C are each equal to (8470 + 9230)/25 = 708 lb. These shear reactions are then placed on the free body of member BC in Fig. All.38. For equilibrium the summation of the horizontal forces must equal zero. Thus P = 708 + 708 = 1416 lb. and acting to the right as shown in Fig. All.38. Since the reaction R_C = -3606 in Fig. All.35 must be liquidated and since the liquidating force P produced by the moments in Fig. All.37 is 1416 lb. it is obvious the values in Fig. All.37 must be multiplied by a factor equal to 3606/1416 = 2.545. Therefore, the final bending moment values equal those of Fig. All.34 plus 2.545 times those in Fig. All.37. Fig. All.39 shows the results and Fig. All.40 the final moment diagram.

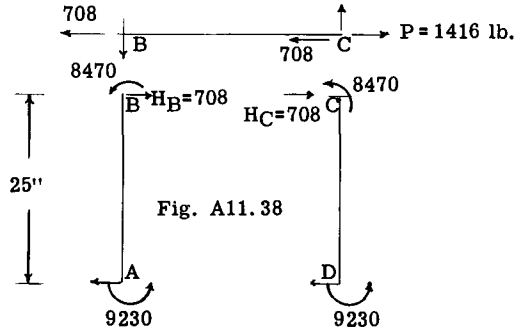

Fig. All.38

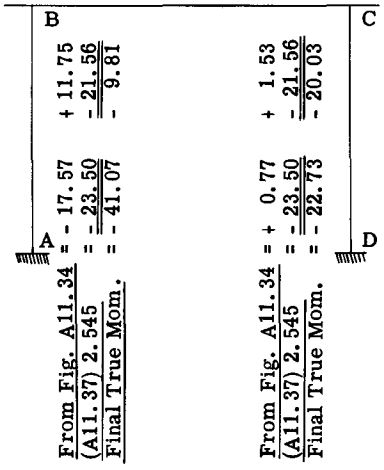

- 11.75 + 21.56 + 9.81
- 1.53 + 21.56 + 20.03

Fig. All.39

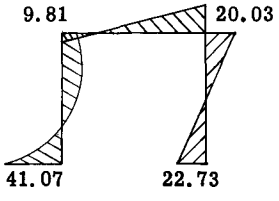

Fig. All.40

Example Problem 2. Bent with Unequal Length Legs and Pinned Ends.

Fig. All.41 shows a loaded unsymmetrical frame. The final bending moments at B and C will be determined.

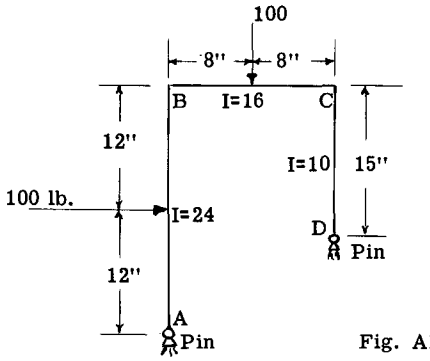

Fig. All.41

SOLUTION:

Relative Stiffness Factors: -

$K_{BA} = \frac{3I}{L} = \frac{3 \times 24}{24} = 3$, $K_{BC} = \frac{4I}{L} = \frac{4 \times 16}{16} = 4$

$K_{CD} = \frac{3I}{L} = \frac{3 \times 10}{15} = 2$

The distribution factors for each member at joints B and C, which equal K/ΣK are recorded in the small ☐ on Fig. All.41a.

Fixed End Moments: -

For Member AB = PL/8 = 100 x 24/8 = 300 in.lb.
For Member BC = PL/8 = 100 x 16/8 = 200

As explained in example problem 1, the moment distribution is carried out in two steps, one for joint rotation only and the other for effect of sidesway or horizontal translation of joints B and C. Fig. All.41a shows the moment distribution for no sidesway by placing an imaginary reaction R_C at joint C. The process is started at joint A and the order of joint balancing is ABCBC. As soon as a joint is balanced the carry over moments are immediately carried over before proceeding to the next joint. When a joint is balanced a horizontal line is drawn.

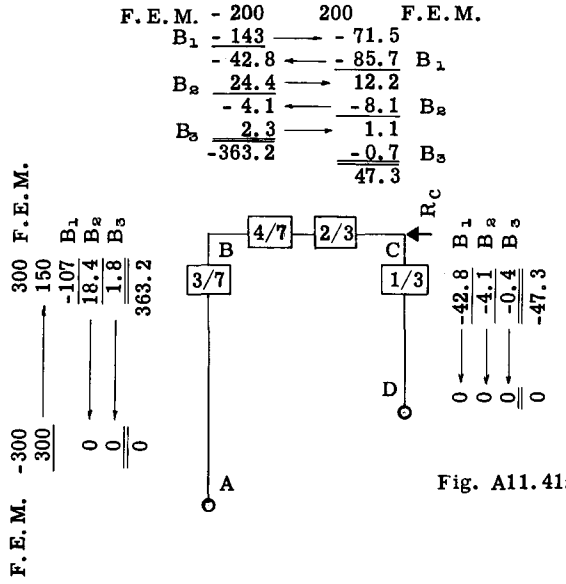

Fig. All.41a

With the end moments known the reaction R_C can be calculated by a consideration of the free body of each member as shown in Fig. A11.41b.

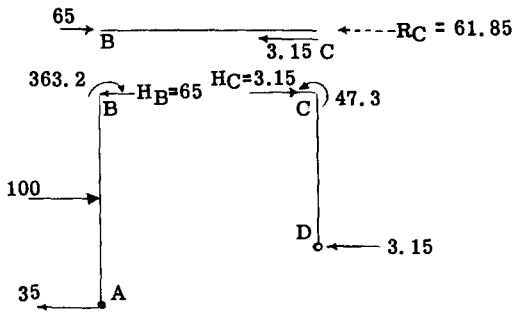

Fig. A11.41b

To find H_B take moments about A,

$$100 \times 12 + 362.3 - 24H_B = 0, \quad H_B = 65 \text{ lb.}$$

To find H_C take moments about D,

$$-47.3 + 15H_C = 0, \quad H_C = 3.15$$

Placing these shear reactions on member BC and writing equilibrium of horizontal forces we find that $R_C = 65 - 3.15 = 61.85$ lb. We now must liquidate this reaction R_C and permit frame to sidesway.

We will assume that the frame is fixed ended and that an unknown horizontal force P at C will deflect the frame sideways. The fixed end moments for equal horizontal deflection of B and C will be proportional to EI/L^2 of the vertical member.

For member AB, $\frac{I}{L^2} = \frac{24}{24^2} = .0417$

For member DC, $\frac{I}{L^2} = \frac{10}{15^2} = .0445$

For convenience we will assume 417 in.lb. as the fixed end moments on AB and 445 on DC. The assumed fixed ends will now be eliminated by the moment distribution process as shown in Fig. A11.41c. The order of joint balance was ABDCBCBC.

Fig. A11.41d shows the shear reaction on the vertical members at B and C. These forces reversed on the top member show an unbalanced force of 6.02 + 10.85 = 16.87 lb. Therefore a force P = 16.87 was necessary to produce the bending moments that resulted on the frame due to sidesway.

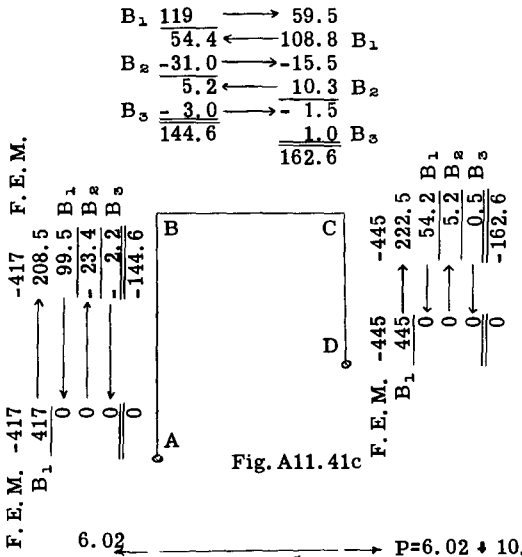

Fig. A11.41c

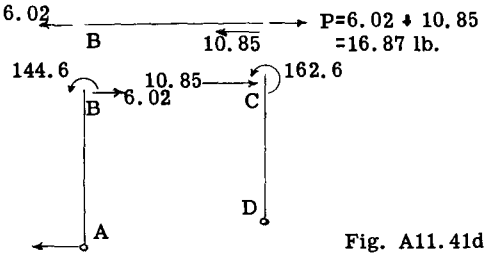

Fig. A11.41d

To liquidate the reaction $R_C = 61.85$ it will therefore require 61.85/16.87 = 3.67 times the moments in Fig. A11.41c. Therefore the final bending moments equal those in Fig. A11.41a plus 3.67 times those in Fig. A11.41c. Fig. A11.41e shows the results. The bending moment and shear diagram and the axial loads now follow as a simple matter of statics.

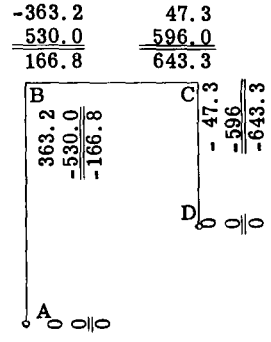

Fig. A11.41e

Example Problem 3. Bending Moments in Truss Involving One Panel Without Diagonal Shear Member.

Frequently, in aircraft structures a truss is used in which a diagonal member must be left out of one or more truss bays. The external shear load on such bays must be carried by the truss chord members in bending. Fig. A11.42 shows a 3 bay truss with no diagonal member in the center bay. The bending moments on the truss members will be determined for the truss

loading as shown in the figure.

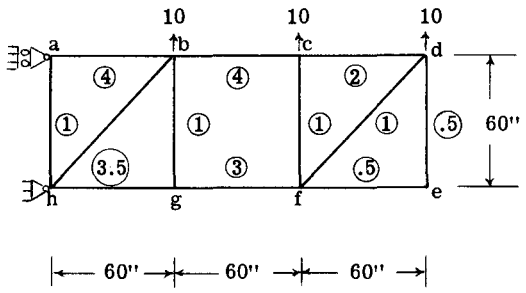

Fig. A11.42

SOLUTION:

The relative moment of inertia values for each member are given in the circles on the truss in Fig. A11.42.

The distribution factor to each member at each joint is then computed and equals K/ΣK. The values are recorded in the □ on each member in Fig. A11.43. The stiffness factor K is proportional to I/L for the member. For example for joint c: -

$$\Sigma K = \Sigma \frac{I}{L} = \frac{4}{60} + \frac{2}{60} + \frac{1}{60} = \frac{7}{60}$$

Then the distribution factors are: -

To Member cb = 4/7 = .57

To Member cf = 1/7 = .14

To Member cd = 2/7 = .29

In this problem there are no loads applied to the members between joints. The external shear load on the truss to the right of the center truss panel which equals 10 + 10 = 20 must be carried through the center panel by the truss chord members in bending. This bending causes the center truss to sway or deflect until a resisting shear force equal to 20 is developed.

We will assume the truss center panel is fixed at joints b, c, f, and g. The right end of this assumed fixed ended truss will be given an upward deflection. This deflection will cause fixed end moments in members bc and gf which are proportional to I/L^2 for each member. Since L is the same for each member, the fixed end moments will be proportional to I of the member.

$$I_{bc} = 4, \quad I_{gf} = 3.$$

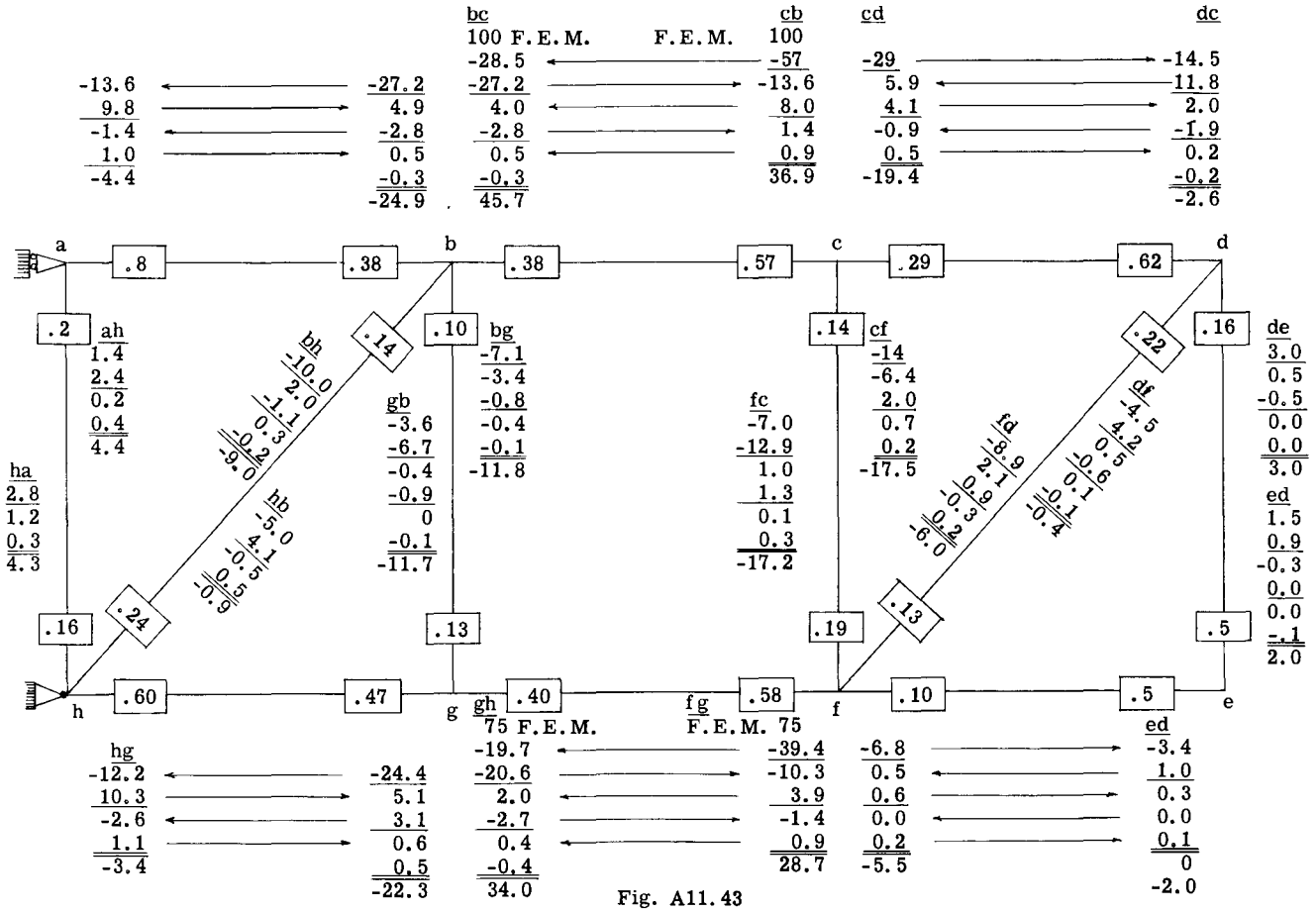

Fig. A11.43

Therefore the fixed end moments on member gf will be 75 percent of those on member bc.

Assume 100 as the fixed end moments on bc. Then a 75 x 10 = 75 is the accompanying fixed end moment on gf.

We now remove the imaginary fixed supports on the center truss and let them rotate to equilibrium by the moment distribution process as shown in detail in Fig. A11.43.

The first step is to record the assumed fixed end moments of 100 at each end of member bc and 75 at each end of member gf with due regard for sign. The moment distribution process will be started at joint C. The unbalanced moment is 100 or -100 is necessary for static balance. Using the distribution factors on joint C, we find -57 goes to cb, -29 to cd and -14 to cf. Short lines are drawn below each of these numbers. Fifty percent of these balancing moments are carried over to the far end of each of these members. This process is repeated at each joint until the remaining balancing moments are negligible. In Fig. A11.43 the order of joint balance was cfdebghacfdebghacfdebg. If the student will follow this order he should be able to check the figures in Fig. A11.43.

Fig. A11.44 shows free bodies of the truss members bc and gf with end moments from Fig. A11.43. The shear reaction at ends c and f by statics equals

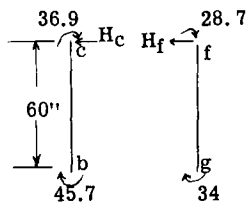

Fig. A11.44

$$H_c + H_f = \frac{36.9 + 45.1}{60} + \frac{28.7 + 34}{60} =$$

$$1.377 + 1.045 = 2.422 \text{ lb.}$$

The external truss shear at line cf = 20 lb. Therefore it will take 20/2.422 = 8.25 times the final bending moments as found in Fig. A11.43 to develop a bending shear reaction of 20 lb. Thus the final moments are 8.25 times those in Fig. A11.43.

The solution as given neglects the effect of axial loads upon the value of the stiffness and carry over factors. Art. A11.12 explains how to include these effects.

A11.12 Effect of Axial Load on Moment Distribution

In the previous articles the effect of axial loads upon the member end moments of a continuous structure was neglected. The axial loads produce bending in the members of a continuous structure in two ways. (1) The shortening or lengthening of the various members due to axial loads produces translation of the joints of the structure. Since the angles between the members at a joint remain the same due to continuity, this translation of joints bends the members between joints. (2) The bending moments on the members due to external joint or lateral loads or those due to joint rotation produce lateral deflection of the members between joints. The member axial loads times these lateral deflections produce secondary moments. These secondary moments can be handled by the general method of moment distribution however the stiffness and carry over factors and the fixed end moments are not constant but become functions of the axial loads.

Fig. A11.45 shows a prismatic beam simply supported at A and fixed at B, with a moment M_A applied at A and carrying an axial compressive load P. Sub. Figure a, b and c show the 3 parts which make up the moment diagram on the beam. Without the axial load P the portion (c) would be omitted.

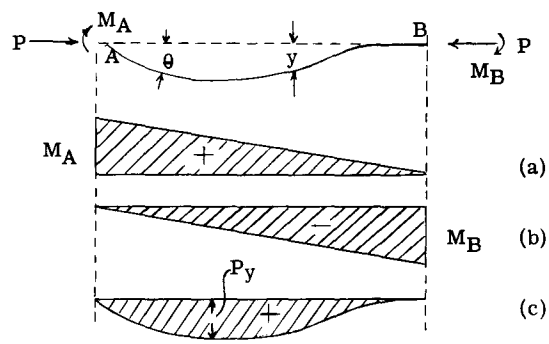

MOMENT DIAGRAMS

Fig. A11.45

By definition the stiffness factor of beam AB is measured by the necessary moment M_A to produce unit rotation ($\theta = 1$) for elastic line at point A. By the moment area principles, the slope at A equals the shear at A due to the moment diagrams acting as a load on a simply supported beam at A and B. For a given unit slope at A it is obvious that the required M_A is less when the load P is acting as it produces a moment load in (Fig. c) of the same sign as the moment load due to M_A. Thus the stiffness of AB is less when carrying an axial compressive load compared to that without it. For a tension axial load diagram C becomes a negative moment diagram and thus M_A must become larger to give unit slope at A. Or in other words a member carrying a tensile axial load has a greater stiffness than one without axial loads. It is evident that the moment diagram due to P will also effect the magnitude of any

fixed end moments and also the carry over factor.

A11.13 Fixed End Moments, Stiffness and Carry over Factors for Beam Columns of Constant Section *

In deriving expressions for fixed end moments, stiffness and carry over factors the beam columns formulas of Chapter A5, must be used in finding slopes, deflection and moments.

Mr. B. W. James in an excellent thesis at Stanford University and later published by N.A.C.A. as Technical Note #534 has derived expressions for these factors and has provided graphs of these factors for use in routine design. Figures A11.46 to A11.56 inclusive are taken from this thesis. The use of these Figures can best be illustrated by the solution of several problems.

A11.14 Illustrative Problems**

Example Problem #12

Fig. A11.57 shows the same continuous beam as used in Example Problem #4 (and solution #2). For this example it has been assumed that such axial compression loads exist in spans BC and CD as to make the term L/j = 2.5 and 2.0 for these spans respectively, where $j = \sqrt{EI/P}$. Due to the axial loads, new values of stiffness and carry over moments as well as fixed end moments must determined as follows.

Span BC

$$K = \frac{I}{L} = \frac{1}{96} = .0104$$

From Fig. A11.47 when L/j = 2.5, correction factor for stiffness factor = .775 when far end is fixed and .36 when far end is pinned. Hence,

K_{BC} = .0104 x .775 = .00806

K_{CB} = .0104 x .36 = .00374

From Fig. A11.46, when L/j = 2.5 the carry over factors are C_{BC} = .73 and C_{CB} = 0 if B is considered freely supported.

From Fig. A11.48 when L/j = 2.5 fixed end moments for uniform load = $wL^2/10.67 = 1 \times 96^2/10.67$ = 865 in. lb.

Span CD

K = I/L = 1/72 = .0139, L/j = 2.0

From Fig. A11.47 correction factor = .86, hence $K_{CD} = K_{DC}$ = .86 x .0139 = .01198. Carry over factor from Fig. A11.46 = .62. Fixed end moments from Fig. A11.48 = $wL^2/11.2 = 1 \times 72^2/11.2$ = 462

The distribution factor at joint C equals (.00374/.00374 + .01198) = .238 to CB and the remainder .762 to CD.

The balancing and carry over process is similar to that in Example Problem #4.

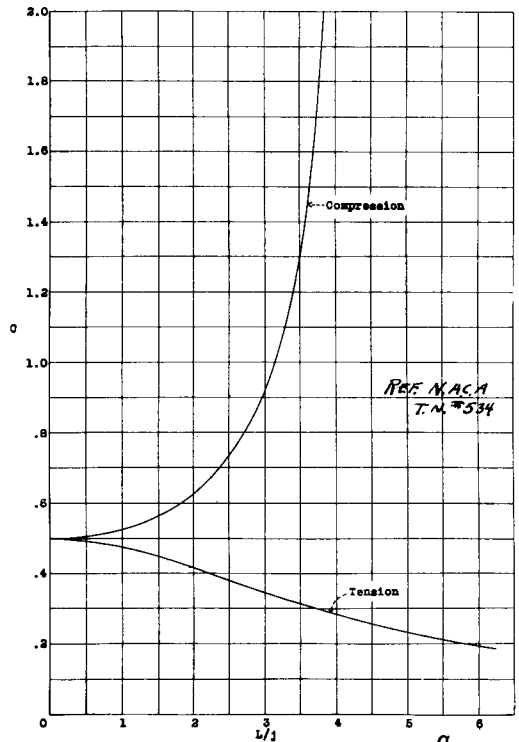

Carry-over factor. $C = \frac{\alpha}{2\beta}$

Fig. A11.46

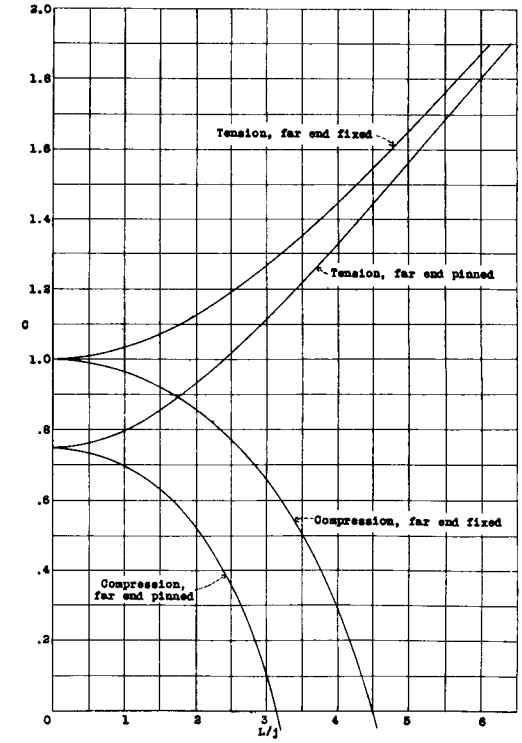

Stiffness factor coefficient. $K = C\frac{I}{L}$

Fig. A11.47

* See Chapter C2, Part L for members having a varying EI.

** Additional examples in Chapter C2, Parts G, L and M.

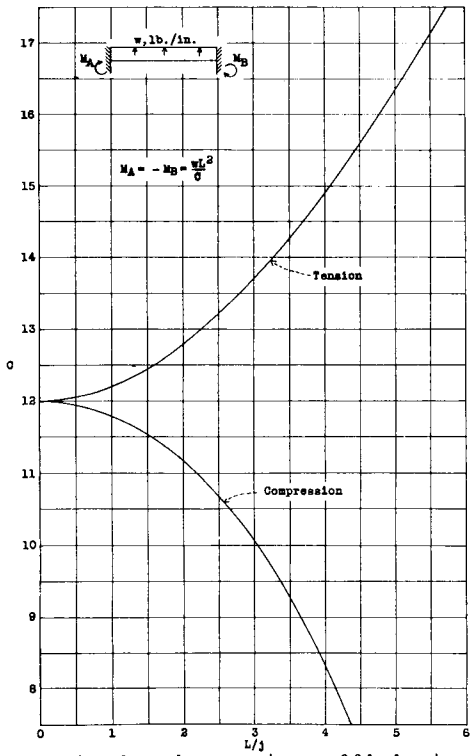

Fixed-end moment coefficient.
Uniform Load.

Fig. A11.48

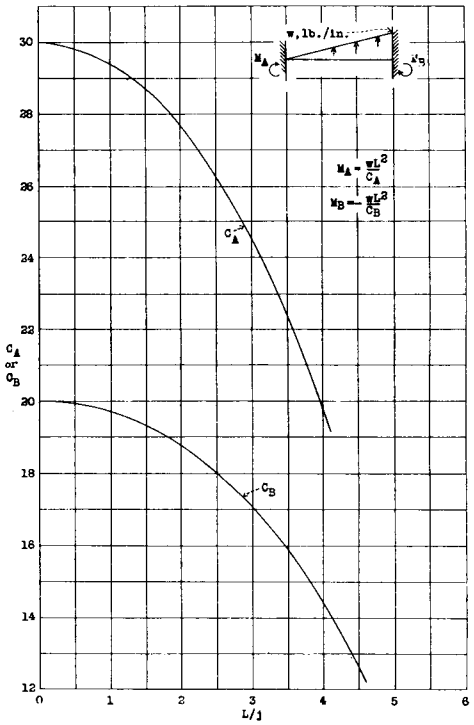

Fixed-end moment coefficient.
Uniformly varying load.
Axial compression.

Fig. A11.49

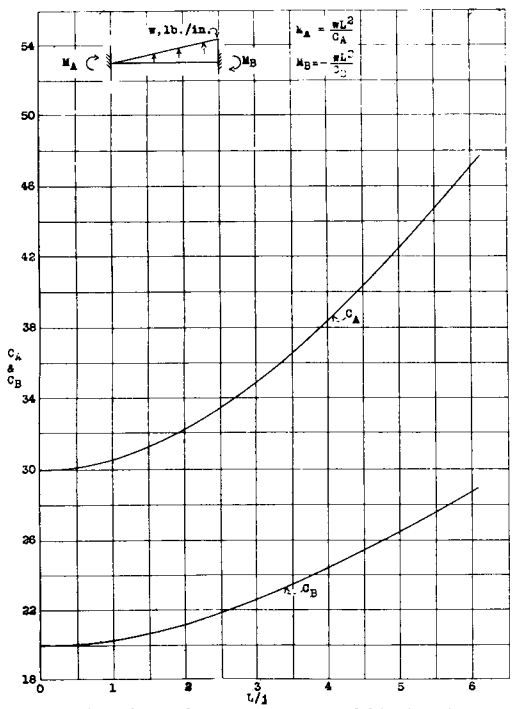

Fixed-end moment coefficient.
Uniformly varying load.
Axial tension.

Fig. A11.50

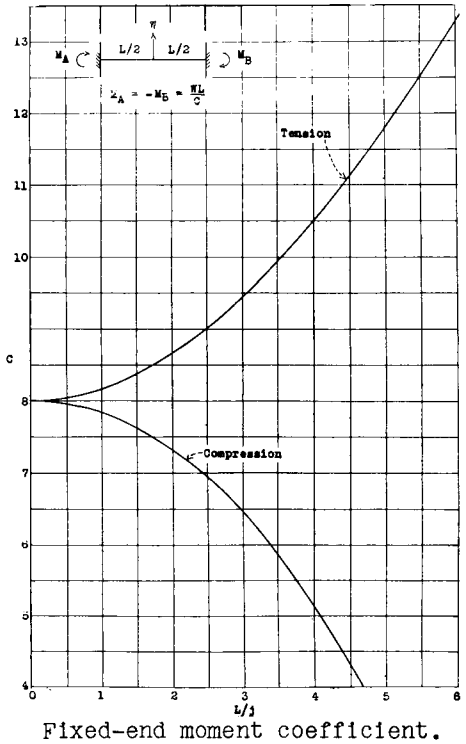

Fixed-end moment coefficient.
Concentrated load at mid-span.

Fig. A11.51

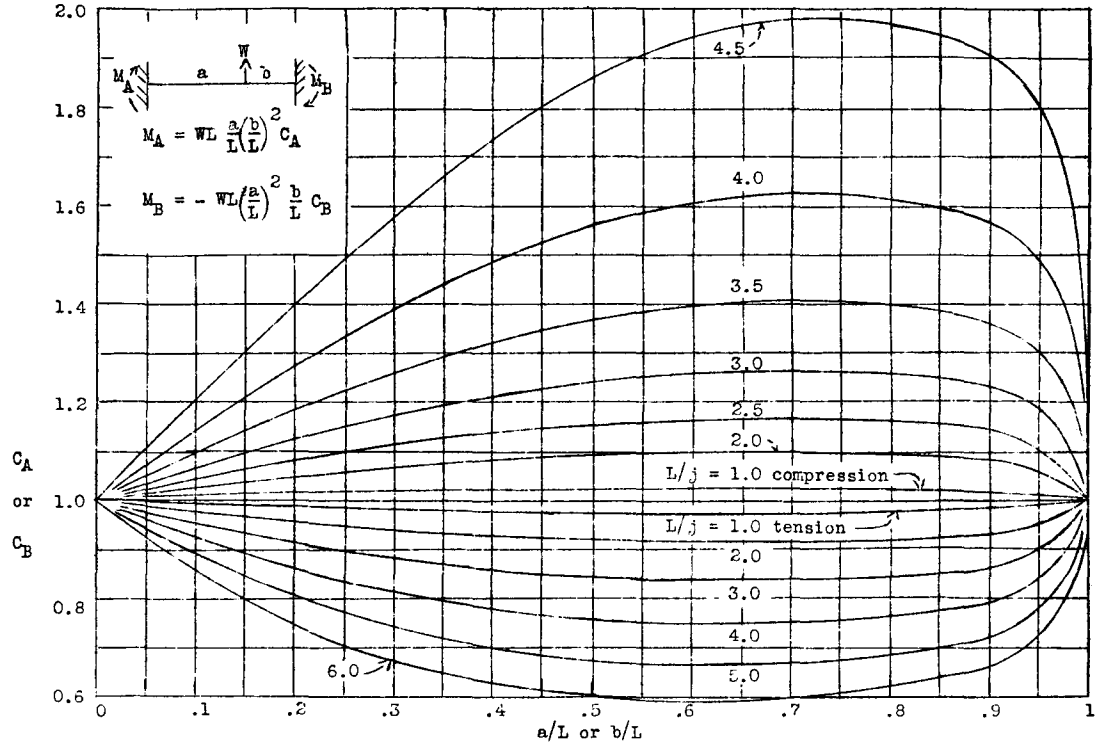

Fig. A11.52 Fixed-end moment coefficient. Concentrated load. REF. NACA T.N. 534

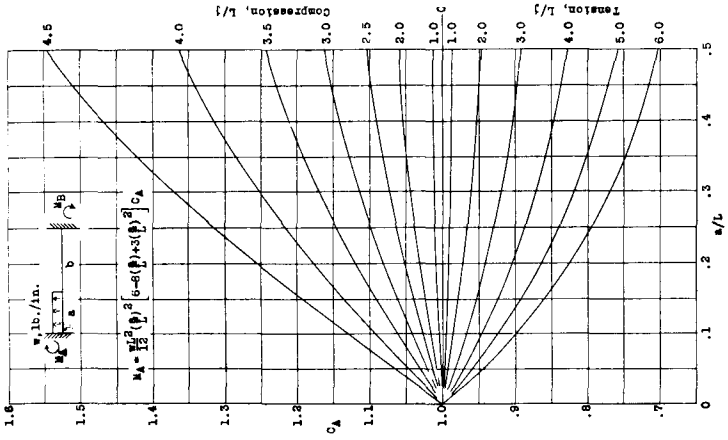

Fig. A11.54 Fixed-end moment coefficient for M_A. Uniform load over part of the span.

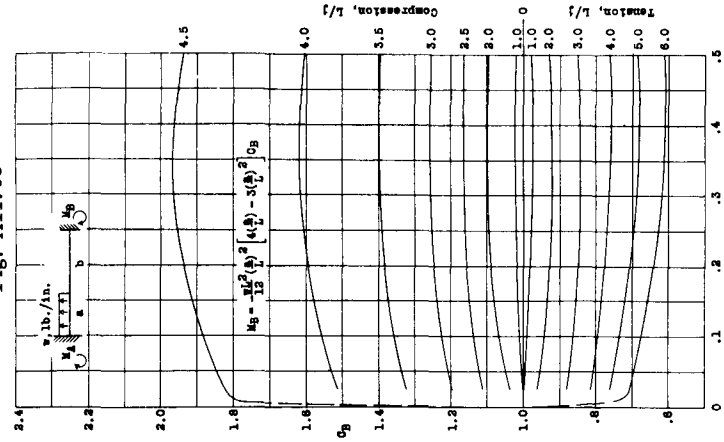

Fig. A11.55 Fixed-end moment coefficient for M_B. Uniform load over part of the span.

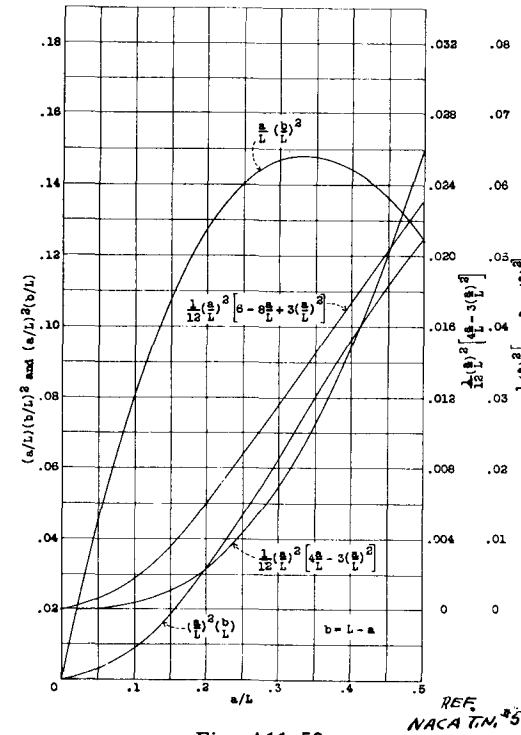

REF. NACA T.N. 534

Fig. A11.53

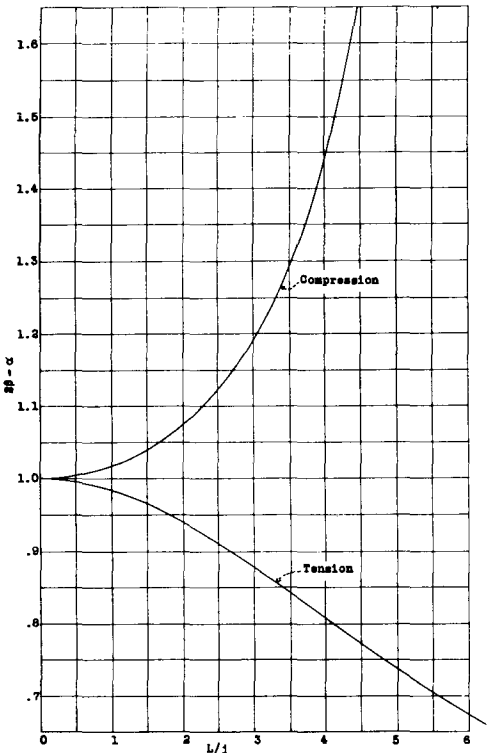

Column distribution factor. $2\beta - \alpha$.

Fig. A11.56

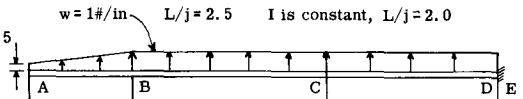

Fig. A11.57

Stiff. Fact. K	0	.00806	.00374	.01198	.01198	∞
Distribution Fac.	0	1	.238	.762	0	1
C.O. Factor	0	.73	0	.62	.62	
Fixed End Mom.	-883	865	-865	462	-462	
Balance Joint B	0	18				
C.O. to C			13.2			
Bal. Joint C			146.0	243.8		
Carry-over		0			148	
Balance D					0	314
Carry-over				0		
Final Mom.	-883	883	-705.8	705.8	-314	314

Comparing these results with those of Problem #3 we find moment at C is increased 15.7 percent and that at D is decreased 8.5 percent. For larger values of L/j the difference would be greater.

Example Problem #13

Fig. A11.58 shows the upper wing of a biplane. The wing beams are continuous over 3 spans. The distributed air loads on the front beam are shown in the figure, also the axial loads on front beam induced by the lift and drag truss. The bay sections of the spruce are shown in Fig. A11.58. The moment of inertia in each span will be assumed constant, neglecting the influence of tapered filler blocks at strut points.

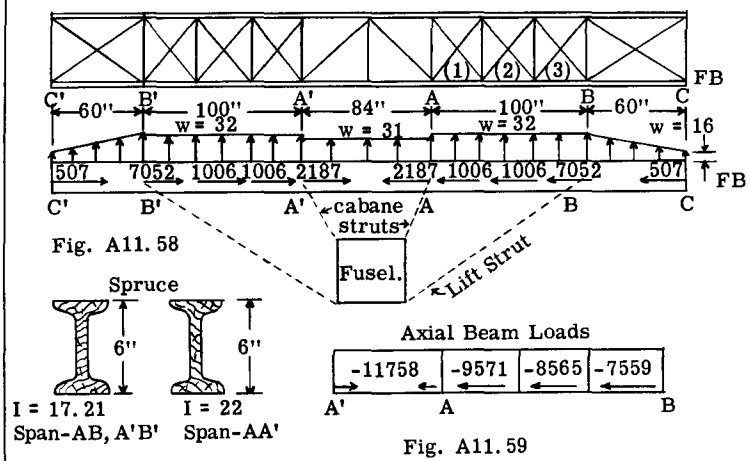

Fig. A11.58

Fig. A11.59

Fig. A11.59 shows the total beam axial loads in the various portions of the beam by adding the values shown in Fig. A11.58. The outer span AB due to the axial loads induced by drag wires of drag truss is subjected to a varying load. As is customary in design of such wing beams the axial load in span AB will be taken as equal to the average load or (-9571-8565-7559)/3=-8565#.

The beam bending moments at the support points will be determined by the moment distribution method.

Calculation of Factors:-

Span AB

I = 17.21, L = 100, I/L = .172

E = 1300,000, P = 8565

$$j = \sqrt{\frac{EI}{P}} = \sqrt{\frac{1300{,}000 \times 17.21}{8565}} = 51.1$$

L/j = 100/51.1 = 1.96

From Fig. A11.47 when L/j = 1.96, correction factor = .86 for fixed far end and .52 for pinned far end. Therefore

K_{AB} = .52 x .172 = .0895

K_{BA} = .86 x .172 = .148

From Fig. A11.46, when L/j = 1.96, the carry over factors are:-

$C.O._{BA}$ = .62, and zero from A to B since B is considered in its true state or freely supported. From Fig. A11.48 when L/j = 1.96 equation for fixed end moment for uniform load = $wL^2/11.25 = 32 \times \overline{100}^2/11.25 = 28420$"#.

The overhand moment M_{BC} = 60 x 26.6 x (32 + 16)/2 = 38300"#.

Center Span AA':-

I = 22, I/L = 22/84 = .262, P = - 11758

$$j = \sqrt{\frac{1{,}300{,}000 \times 22}{11758}} = 49.4$$

L/j = 84/49.4 = 1.70

$K_{AA'} = K_{A'A}$ = .262 x .895 = .234

C.O. Factor = .585

Fixed end moment = $wL^2/11.35$ = 31 x $\overline{84}^2/11.35$ = 19300"#

The moment distribution process is given in Fig. A11.60. If the axial loads were neglected, the bending moment, at support A and A' would be 19480, thus the axial influence increases the moment at A approximately 7.5 percent.

Fig. A11.60

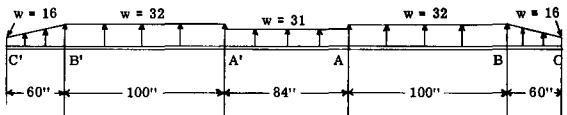

K Value	0	.148	.0895	.234	.234	.0895	.148	0
Distri. Factor	0	1	.276	.724				
C.O. Factor	0	.62	0	.585	.585	0	.62	0
F.E.Mom.	-38300	28420	-28420	19300	-19300	28420	-28420	38300
Bal. B' & B	0	9880					-9880	0
C.O.			6125			-6125		
Bal. A' & A			828	2167	-2167	-828		
C.O.		0		-1265	1265		0	
Bal. A' & A			347	918	-918	-347		
C.O.		0		-538	538		0	
Bal. A' & A			148	390	-390	-148		
C.O.		0		-228	228		0	
Bal.			63	165	-165			
Final Mom.	-38300	38300	-20909	20909	-20909	20909	-38300	38300

Example Problem #14

Fig. A11.61 shows a triangular truss composed of two members fixed at A and B and rigidly joined at C to the axle bar. Let it be required to determine the end moments on the two members considering the effect of axial loads on joint rotation and translation.

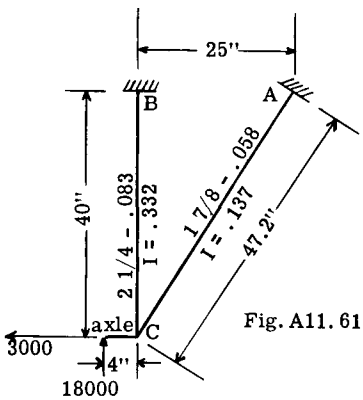

Fig. A11.61

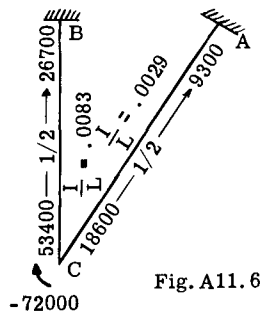

Fig. A11.62

Solution:-

The magnitude of the axial loads in the members is influenced by the unknown restraining moments at A and B. To obtain a close approximation of the axial loads, the end moments in the two members will be determined without consideration of axial loads. Thus the external joint moment of 4 x 18000 = 72000 in. lb. at C is distributed between the two members as shown in Fig. A11.62. With the member end moments known the axial loads and shear reactions at A and B can be found by statics. The resulting axial loads are

P_{AC} = 7360# and P_{BC} = - 24240# and the shear reactions, S_A = 198# and S_B = 2332#.

With the axial loads known the modified beam factors can be determined.

For member BC

P = - 27150, I/L = .0083, I = .332

$$j = \left(\frac{29{,}000{,}000 \times .332}{27150}\right)^{1/2} = 18.82, \quad L/j = \frac{40}{18.82} = 2.12$$

From Fig. A11.47, stiffness factor = .82 x .0083 = .00681

From Fig. A11.46 C.O. Factor = .66

For Member AC

P = 10400#, I/L = .0029, I = .137

$$j = \sqrt{\frac{29{,}000{,}000 \times .137}{10400}} = 19.58, \quad \frac{L}{j} = \frac{47.20}{19.58} = 2.42$$

Stiffness factor = .0029 x 1.18 = .00342

C.O. factor = .39

Fig. A11.63 shows the moment distribution solution which includes the effect of axial loads on joint rotation. Comparing the results in Figs. A11.62 and 63, the moment M_{CA} of 24050 is 29 percent larger than that in Fig. 62, and the moment at B is 18 percent larger. The effect on the axial loads of these new final moments will be quite small, and thus further revision is unnecessary.

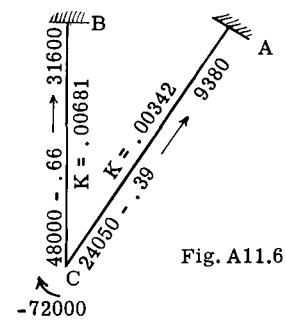

Fig. A11.63

Effect on End Moments Due to Translation of Joint C Due to Axial Loads.

The movement of joint C normal to each member will be calculated by virtual work. (Reference Chapter A7). Fig. A11.64 shows the virtual loading of 1# normal to each member at C. The Table shows the calculation of the normal deflections at C.

Table

Mem.	L/AE	S	U_a	$\frac{S_{u_a}L}{AE}$	U_b	$\frac{S_{u_b}L}{AE}$
AC	.0000049	10400	1.89	.0962	1.6	.0816
BC	.00000244	-27150	-1.60	.1060	-1.89	.1250
				.202		.207

Thus the deflection of joint C normal to BC equals .202" in the direction assumed for the unit load, and the deflection of C normal to AC = .207".

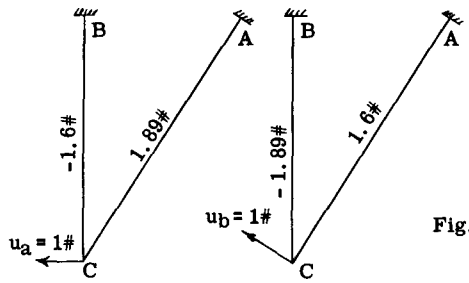

Fig. A11.64

The fixed end moments due to support deflection equals $M = 6EId/L^2$ as derived in Art. A11.7. However, the secondary moments due to axial loads times lateral deflection modify this equation. "James" has shown that the modified equation is,

$$M_{\text{fixed end}} = \frac{6EId}{L^2(2\beta-\alpha)}, \text{ if } K = \frac{I}{L} \text{ and } R = \frac{d}{L}, \text{ than}$$

$$M = \frac{6KER}{2\beta-\alpha},$$

Fig. A11.56 shows a plot of $2\beta-\alpha$ against L/j. For Member BC:-

$R = .202/40 = .00505 \quad K = I/L = .0083,$

$2\beta-\alpha = 1.08$ for $L/j = 2.12.$

Hence, fixed end moments due to translation of joint C equals-

$$M_{BC} = M_{CB} = \frac{6 \times .0083 \times .00505 \times 29{,}000{,}000}{1.08} = -6750\text{"#}$$

For Member AC

$R = .207/47.2 = .00438 \quad K = .0029, \quad 2\beta-\alpha = .92$

when $L/j = 2.42$ and member is in tension.

hence

$$M_{AC} = M_{CA} = \frac{6 \times .00438 \times .0029 \times 29{,}000{,}000}{.92} =$$

$$-2400\text{"#}$$

The signs are minus because inspection shows that the moments tend to rotate ends of members counter clockwise. (Ref. Art. A11.2)

Fig. A11.65 shows the moment distribution for these moments. The magnitude of the moment at B is 6.7 percent of that in Fig. A11.63 and 10.4 percent at Joint C, however, it is relieving in this example.

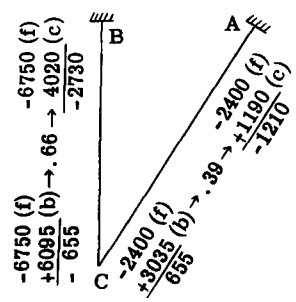

Fig. A11.65

A11.15 Secondary Bending Moments in Trusses with Rigid Joints. *

Often in airplane structural design trusses with rigid joints are used. Rigid joints are produced because of welding the members together at the truss joints or by the use of gusset plates bolted or riveted to each member at a truss joint. When a truss bends under loading the truss joints undergo different amounts of movement or deflection. Since the truss members are held rigidly at the joints, any joint displacement will tend to bend the truss members. The bending moments produced in the truss members due to the truss joint deflections are generally referred to as secondary moments and the stresses produced by these moments as secondary stresses.

Since fatigue strength is becoming more important in aircraft structural design, the question of secondary stresses becomes of more importance than in the past. The moment distribution method provides a simple and rapid method for determining these secondary moments in truss members due to truss deflection. The general procedure would be as follows: -

(1) Find the horizontal and vertical displacements of each truss joint due to the critical design condition. (See Chapter A7 for methods of finding truss deflections).

(2) From these displacements, the transverse deflection of one end of a member with respect to the other can be found for each truss member.

(3) Compute the fixed end moments on each member due to these transverse displacements.

(4) Calculate stiffness and carry-over factors for each truss member.

(5) Calculate distribution factors for each truss joint.

(6) Carry out the moment distribution process to find the secondary moments at the ends of each member.

(7) Calculate the stresses due to these secondary moments and combine with the primary axial stresses in the truss members due to truss action with pinned truss joints.

A11.16 Structures with Curved Members.

The moment distribution method can be applied to continuous structures which include curved as well as straight members. The equations for finding the stiffness factors, carry over factors and fixed end moments for straight members cannot be used for curved members. The elastic center method as presented

* Also see Chapter C2, Part H.

in Chapter A9 provides a rapid and simple method for determining these values for curved members. The use of the elastic center method in determining the value of stiffness and carry over factors will now be explained.

A11.17 Structures with Curved Members.

Before considering a curved member a straight member of constant EI will be considered. Fig. A11.66 shows a beam freely

Fig. A11.66

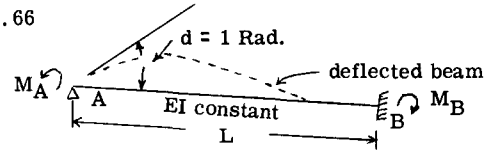

Fig. A11.67

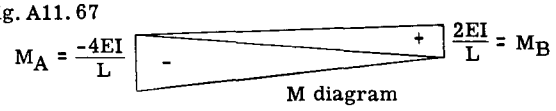

Fig. A11.68

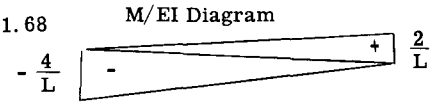

supported at end A and fixed at end B. A moment M_A is applied at end A of such magnitude as to turn end A through a unit angle of one radian as illustrated in Fig. A11.66. By definition, the necessary moment M_A to cause this unit rotation at A is referred to as the stiffness of the beam AB. In Art. A11.4 it was shown that this required moment was equal in magnitude to -4EI/L. It was also proved that this moment at A produced a moment at the fixed end B of 2EI/L or a moment of one half the magnitude and of opposite sign to that at A. Fig. A11.67 shows the bending moment diagram which causes one radian rotation of end A. Fig. A11.68 shows the M/EI diagram, which equals the moment diagram divided by EI which has been assumed constant.

The total moment weight $\emptyset$ as explained in Chapter A9 equals the area of the M/EI diagram. Thus $\emptyset$ for the M/EI diagram in Fig. A11.68 equals,

$$-\frac{4}{L}\left(\frac{L}{2}\right)+\frac{2}{L}\left(\frac{L}{2}\right) = -2 + 1 = -1$$

In other words the total elastic moment weight $\emptyset$ equals one or unity.

The location of this total moment weight $\emptyset$ will coincide with the centroid of the M/EI diagram. Thus to find the distance $\bar{x}$ from B to this centroid we take moments of the M/EI diagram about B and divide by $\emptyset$ the total area of the M/EI diagram. Thus

$$\bar{x} = \frac{-2(.667L) + 1(.333L)}{-2 + 1} = \frac{-L}{-1} = L$$

Thus the centroid of the total moment weight $\emptyset$ which equals one lies at point A or a distance L to left of B.

In using the elastic center method to determine the stiffness and carry-over factor for a straight beam, we assume that the bending moment curve due to a moment applied at A is of such magnitude as to turn the end A through an angle of 1 radian. As shown above, the moment weight $\emptyset$ for this loading is unity or 1 and its centroid location is at A. Then by the elastic center method we find the moment required to turn end A back to zero rotation. The value of this moment at A will then equal the stiffness factor of the beam AB. In order to simplify the equations for the redundant forces the elastic center method refers them to the elastic center. From Chapter A9 the equations for the redundant forces at the elastic center for a structure symmetrical about one axis are: -

$$M_O = \frac{-\Sigma\, \emptyset_S}{\Sigma\, ds/EI} \quad \text{- - - - - - - - - - - - - - - (1)}$$

$$Y_O = \frac{-\Sigma\, \emptyset_S\, X}{I_y} \quad \text{- - - - - - - - - - - - - - - (2)}$$

$$X_O = \frac{\Sigma\, \emptyset_S\, y}{I_x} \quad \text{- - - - - - - - - - - - - - - (3)}$$

Fig. A11.69 shows beam of Fig. A11.66 replaced by a beam with the reaction at end A replaced by a rigid bracket terminating at point (O) the elastic center of the beam, which due to symmetry of the beam lies at the midpoint of the beam. The elastic moment loading is $\emptyset_S = 1$ and its location is at A as shown in Fig. A11.69.

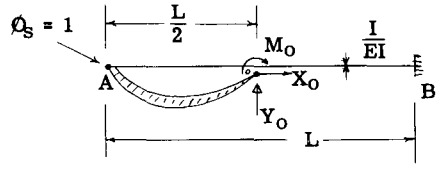

Fig. A11.69

Solving for redundants at (O) by equations (1), (2) and (3).

$$M_O = \frac{-\emptyset_S}{\Sigma\, ds/EI} = \frac{-1}{L/EI} = -EI/L$$

$$Y_o = \frac{-\Sigma \phi_S x}{I_y} = \frac{-1(-\frac{L}{2})}{\frac{1}{12}\frac{1}{EI} L^3} = \frac{6EI}{L^2}$$

$X_o = \frac{\Sigma \phi_S y}{I_x} = 0$, because y the vertical distance of ϕ_S load to x axis through elastic center (0) is zero.

Fig. A11.70 shows these forces acting at the elastic center.

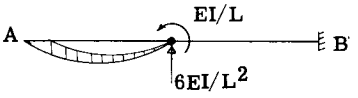

Fig. A11.70

The bending moment at end A equals

$$-\frac{EI}{L} - \frac{6EI}{L^2}\left(\frac{L}{2}\right) = -\frac{4EI}{L}$$

By definition the stiffness factor is the moment at A which is required to turn end A through an angle of 1 radian. Thus 4EI/L is the stiffness factor and this result checks the value as previously derived in Art. A11.4.

The bending moment at B in Fig. A11.70 equals,

$$= -\frac{EI}{L} + \frac{6EI}{L^2}\left(\frac{L}{2}\right) = \frac{2EI}{L}$$

Hence the carry-over factor from A to B is .5 and the carry-over moment is of opposite sign to that of the moment at A.

A11.18 Stiffness and Carry-Over Factors For Curved Members.

Fig. A11.71 shows a curved member, namely, a half circular arc of constant EI cross-section. The end B is fixed and the end A is freely supported. A moment M_A is applied at A of such magnitude as to cause a rotation at A of 1 radian as illustrated in the Fig. Fig. A11.72 shows the general shape of the bending moment curve which is statically indeterminate. In Fig. A11.73 the support at A is removed and end A is connected by a rigid bracket terminating at the elastic center of the structure. We will now find the required forces at (0) to cancel the unit rotation at A which was assumed in Fig. A11.71.

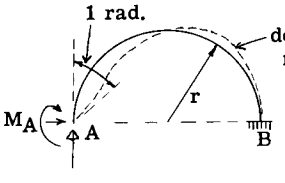

Fig. A11.71

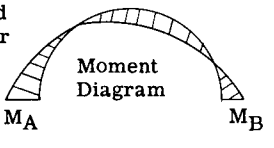

Fig. A11.72

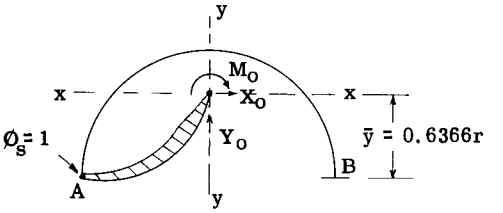

Fig. A11.73

The total area of the M/EI curve for the curve in Fig. A11.72 if calculated would equal one or unity as explained in detail for a straight member. The centroid of this M/EI diagram would if calculated fall at point A. Thus in Fig. A11.73 we apply a unit ϕ_S load at A and find the redundant force at O. Due to symmetry of structure about a vertical or y axis the elastic center lies on this symmetrical axis. The vertical distance from base line AB to elastic center equals $\bar{y} = .6366r$. (See page A3.4 of Chapter A3).

The elastic moments of inertia I_X and I_y can be calculated or taken from reference sources such as the table on page A3.4.

Whence,

$$I_X = .2978r^3t, \text{ but } t = \frac{1}{EI}$$

Hence $I_X = \frac{.2978r^3}{EI}$

$$I_y = \frac{\pi r^3 t}{2} = \frac{\pi r^3}{2EI}$$

Solving the equations for the redundants at (0), remembering $\phi_S = 1$ and located at point A.

$$M_o = -\frac{\Sigma \phi_S}{\Sigma\, ds/EI} = \frac{-(1)}{\frac{\pi r}{EI}} = \frac{-EI}{\pi r}$$

$$Y_o = -\frac{\Sigma \phi_S x}{I_y} = \frac{-(1)(-r)}{\frac{\pi r^3}{2EI}} = \frac{2EI}{\pi r^2}$$

$$X_o = \frac{\Sigma \phi_S y}{I_X} = \frac{(1)(-.6366r)}{\frac{0.2978r^3}{EI}} = -2.14\frac{EI}{r^2}$$

Fig. A11.74 shows these forces acting at the elastic center. The bending moment at A equals the stiffness factor for the curved beam fixed at far end B and freely supported at near

end A. The ratio of the bending moment at point B to that at point A will give the carry-over factor.

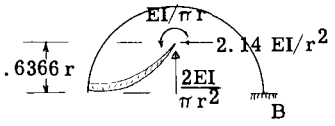

Fig. A11.74

Bending moment at A,

$$M_A = \frac{-EI}{\pi r} - 2.14\frac{EI}{r^2}(0.6366r) - (\frac{2EI}{\pi r^2})r$$

$$= \frac{-0.318EI}{r} - \frac{1.36EI}{r} - 0.636\frac{EI}{r} = -2.314\frac{EI}{r}$$

Bending moment at B,

$$M_B = \frac{-0.318EI}{r} - \frac{1.36EI}{r} + \frac{0.636EI}{r} = -1.042\frac{EI}{r}$$

Therefore the stiffness factor for a half-circular arch of constant EI is 2.314 EI/r.

The carry-over factor equals the ratio of M_B to M_A or $(-1.042\ EI/r)/(-2.314\ EI/r) = 0.452$. It should be noticed that the carry-over moment has the same sign as the applied moment at A as compared to the opposite sign for straight members. In other words, there are two points of inflection in the elastic curve for the curved arch as compared to one for the straight member.

FIXED END MOMENTS

The fixed end moments on a curved member for any external loading can be determined quite rapidly by the elastic center method as illustrated in Chapter A9 and thus the explanation will not be repeated here.

The student should realize or understand that when the end moments on a straight member in a continuous structure are found from the moment distribution process, the remaining end forces are statically determinate, whereas for a curved member in a continuous structure, knowing the end moments does not make the curved member statically determinate, since we have six unknowns at the two supports as illustrated in Fig. A11.75 and only 3 equations of static equilibrium. Even when the end moments are determined from the moment distribution process there still remains one unknown, namely the horizontal reaction at one of the beam ends.

Fig. A11.75

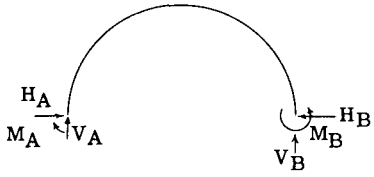

The method of how to handle this remaining redundant force can best be explained by presenting some example problem solutions.

A11.19 Example Problems. Continuous Structures Involving Curved Members.

Example Problem 1

Fig. A11.76 shows a frame consisting of both straight and curved members. Although simplified relative to shape, this frame is somewhat representative of a fuselage frame with two cross members, one between A and C to support installations above cabin ceiling and the other between F and D to support the cabin floor loads. The frame supporting forces are assumed provided by the fuselage skin as shown by the arrows on the side members. Eccentricity of these skin supporting forces relative to neutral axis of frame member is neglected in this simplified example problem, since the main purpose of this example problem is to illustrate the application of the moment distribution method to solving continuous structures involving curved members.

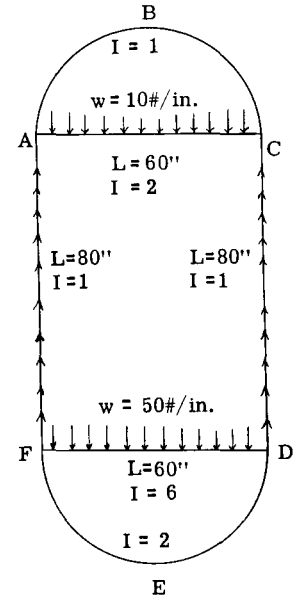

Fig. A11.76

SOLUTION

Due to symmetry of structure and loading, no translation of the frame joints takes place due to frame sidesway.

The frame cross members AC and FD prevent horizontal movement of joints A, C, F, and D due to bending of the two arches. Any horizontal movement of these joints due to axial deformation is usually of minor importance relative to causing bending of frame members. Therefore it can be assumed that the frame joints suffer rotation only and therefore the moment distribution method is directly applicable.

Calculation of stiffness (K) values for each member of frame: -

Upper curved member ABC: -

$K_{ABC} = K_{CBA} = 2.314\frac{EI}{r}$. This value was derived in the previous Art. A11.18.

Substituting: -

$$K_{ABC} = K_{CBA} = \frac{2.314 \times 1}{30} = .0770$$ (E is constant and therefore omitted since only relative values are needed for the K values.)

The relative moment of inertia of the cross-section of each frame member is given on Fig. A11.76.

$$K_{FED} = K_{DEF} = \frac{2.314 \times 2}{30} = .1540$$

For all straight members, the stiffness factor equals 4EI/L. Hence,

$$K_{AC} = K_{CA} = 4 \times 2/60 = 0.1333$$

$$K_{FD} = K_{DF} = 4 \times 6/60 = 0.4000$$

$$K_{AF} = K_{FA} = 4 \times 1/80 = 0.0500$$

$$K_{CD} = K_{DC} = 4 \times 1/80 = 0.0500$$

DISTRIBUTION FACTORS AT EACH JOINT: -

JOINT A.

$$\Sigma K = 0.1333 + .0770 + .0500 = 0.2603$$

Let D equal symbol for distribution factor.

$$D_{ABC} = .0770/0.2603 = 0.296$$

$$D_{AC} = .1333/0.2603 = 0.512$$

$$D_{AF} = .0500/0.2603 = 0.192$$

JOINT F.

$$\Sigma K = .0500 + 0.400 + 0.1540 = 0.6040$$

$$D_{FA} = .0500/.6040 = .082$$

$$D_{FD} = .4000/.6040 = .663$$

$$D_{FED} = .1540/.6040 = .255$$

Carry-Over Factors: -

For the straight members the carry-over factor is 0.5 and the moment sign is the same as the distributed moment when the sign convention adopted in this chapter is used.

For a half circular arch of constant I, the carry-over factor was derived in the previous article and was found to be 0.452. The sign of this carry-over moment was the same sign as the distributed moment at the other end of the beam. However, using the sign convention as adopted for the moment distribution in this book, the carry-over factor would be minus or of opposite sign to the distributed moment.

Calculation of Fixed End Moments.

The curved members of the frame have no applied external loadings hence the fixed end moments on the curved members is zero.

For member AC, fixed end moment equals $WL^2/12 = 10 \times 60^2/12 = 3000$ in. lb. and for member FD = $50 \times 60^2/12 = 15000$ in.lb.

Since the supporting skin forces on the side members have been assumed acting along centerline of frame members, the fixed end moments on members AF and CD are zero.

Moment Distribution Process: -

Fig. A11.77 shows the calculations in carrying out the successive cycles of the moment distribution process. Due to symmetry

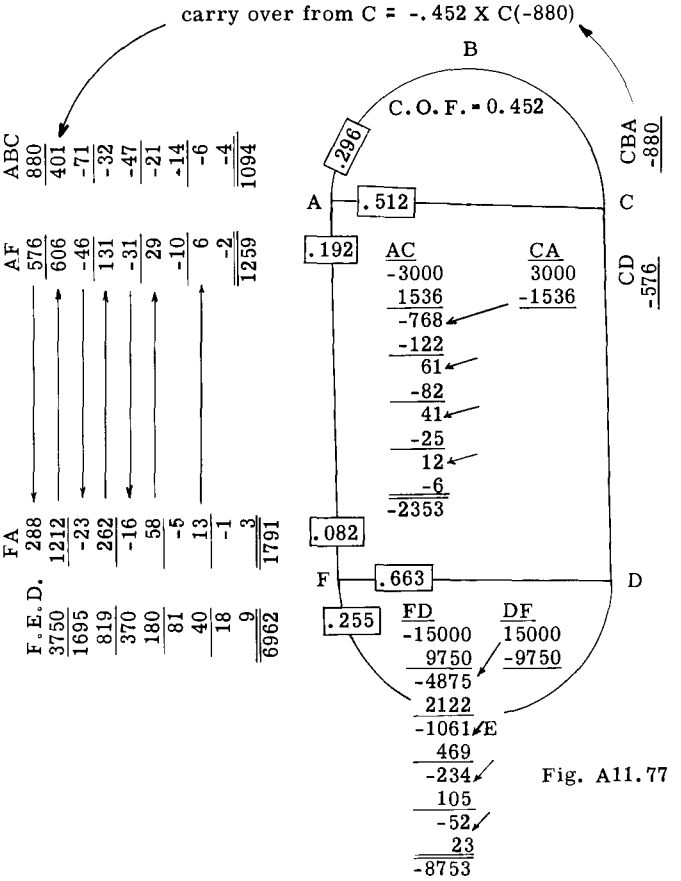

Fig. A11.77

of frame and loading, the process need only be carried out for one-half of frame, thus in Figure A11.77, only joints A and F are considered since the numerical results at D and C would be the same as at A and F respectively. In the figure the distribution factors are shown in

the □ at each joint. The process is started by placing the fixed end moments with due regard to sign at the ends of members AC and FD, namely, -3000 at AC, 3000 at CA, -15000 at FD and 15000 at DF. We now unlock joint A and find an unbalanced moment of -3000 which means a plus 3000 is needed for static balance. Joint A is therefore balanced by distributing .512 x 3000 = 1536 to AC, .296 x 3000 = 880 to ABC, and .192 x 3000 = 576 to AF. Short horizontal lines are then drawn under each of these distributed values to indicate that these are balancing moments. Carry-over moments are immediately taken care of by carrying over to joint F, .5 x 576 = 288. From A to C the carry-over moment would be .5 x 1536 = 768 and therefore the carry-over from C to A would be .5(-1536) = -768 which is recorded at A as shown. For the arch member ABC, the carry-over moment from A to C would be -0.452 x 880 = -401 (not shown) and therefore from C to A = -0.452 x (-880) = 401 as shown at joint A in the figure for arch member CBA. Joint C in the figure has been balanced once for the purpose of helping the student understand the sign of the carry-over moments which flow to the left side from the right side of the frame.

After balancing joint A and taking care of the carry-over moments, we imagine A as fixed again and proceed to joint F where we find an unbalanced moment of -15000 + 288 = -14712, thus plus 14712 is necessary for balancing. The balancing distribution is .255 x 14712 = 3750 to FED, .663 x 14712 = 9750 to FD and .082 x 14712 = 1212 to FA. The carry-over moments are .5 x 1212 = 606 to A, .452 x 3750 = 1695 from D to F by way of the arch member and -.5 x 9750 = -4875 from D on member FD. We now go back to joint A which has been unbalanced by the carry-over moments and repeat the balancing and carrying-over cycle. In the complete solution as given in Figure A11.77 each joint A and F was balanced five times. The final bending moments at the ends of the members at each joint are shown below the double short lines.

The arch member ABC has 3 unknown forces at each end A and C or a total of 6 unknowns. With 3 equations of static equilibrium available plus the known values of the end moments at A and C as found from the moment distribution process, the arch member is still statically indeterminate to one degree. Thus the horizontal reaction at A or C as provided by the axial load in member AC must be found before the bending moments on arch ABC can be calculated.

The first step in this problem is to find the elastic center of the frame portion composed of members ABC and AC, as shown in Fig. A11.78, and then find the elastic moments of inertia about x and y axes through the elastic center.

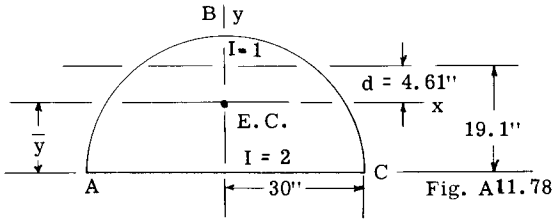

Fig. A11.78

$$\bar{y} = \frac{19.1 \times \pi\ (30/1)}{\frac{\pi \times 30}{1} + \frac{60}{2}} = 14.49"$$

(NOTE:- 19.1 equals distance from line AC to centroid of arch member ABC.)

Calculation of moment of inertia I_x: -

Member ABC

$$I_x = \frac{.3r^3}{I} + \frac{\pi r d^2}{I}$$

$$= \frac{.3 \times 30^3}{1} + \frac{\pi \times 30}{1} \times 4.61^2 = 10100$$

Member AC $= \frac{60}{2} \times 14.49^2 = 6310$

I_x total $= 16410$

Total elastic weight of structure equals $\Sigma\ ds/I = (\pi \times 30/1) + 60/2 = 124.24$.

The next step in the solution is to draw the bending moment curves on this frame portion due to the given load on member AC and the end moments as found by the moment distribution process in Fig. A11.77. It is composed of three parts labeled (1) to (3) in Fig. A11.79. Portions (1) and (2) are due to the end moments and portion (3) due to the distributed lateral load on member AC.

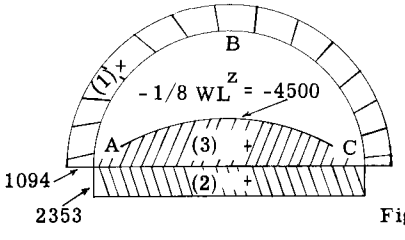

Fig. A11.79

The next step is to find the ϕ_s (area of M/I curve) for each portion and its centroid location.

ϕ_{S_1} = 1094 x π x 30/1 = 103000

ϕ_{S_2} = 60 x 2353/2 = 70590

ϕ_{S_3} = (-.667 x 60 x 4500)/2 = -90000

$\Sigma\phi_S$ = 83590

Fig. All.80 shows the ϕ_S values concentrated at their centroid locations and referred to the x and y axes through the elastic center.

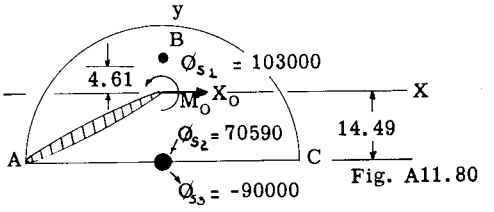

Fig. All.80

The frame has been imagined cut at A and the arch end at A has been connected by a rigid bracket to the elastic center. The redundants at the elastic center which will cancel any relative movement of the cut faces at A can now be computed.

$$M_O = \frac{-\Sigma\phi_S}{\Sigma\, ds/I} = \frac{-83590}{124.24} = -673 \text{ in.lb.}$$

$$X_O = \frac{\Sigma\phi_S y}{I_X} = \frac{[103000\,(4.61) + 70590\,(-14.49) - 90000\,(-14.49)]}{16410} = 46 \text{ lb.}$$

$$Y_O = \frac{-\Sigma\phi_S x}{I_y} = 0 \text{ because } x = \text{zero.}$$

The bending moment at any point on ABC or AC equals that due to M_O and X_O plus the moments in Fig. All.79.

For example,

At point A on member ABC,

M_A = 1094 - 670 + 46 x 14.49 = 1091 (should be 1094 since moment as found in Fig. All.77 is correct one. Small error due to slide rule accuracy.

At point B on member ABC: -

M_B = 1094 - 670 - 46 x 15.51 = -289 in. lb.

The horizontal reaction at A will not produce any bending on member AC, thus the values in Fig. All.79 are the true moments.

The axial load in member AC by statics from Fig. All.80 equals X_O or a tension load of 46 lb. The member AC also suffers an axial load due to the shear reactions at the top of members FA and DC. Fig. All.81 shows free bodies of the side member FA and DC with the end moments as found in Fig.All.77.

The shear reaction at A and C can be found by taking moments about lower ends. Thus for FD, R_A = (1259 + 1791)/80 = 38.1 lb. Likewise R_C = 38.1 lb. These reactions react on cross member AC in the opposite directions thus giving a compression load of 38.1 lb. in member AC, which must be added to the tension load of 46 lb. from the arch reaction to obtain the final load in the cross-member.

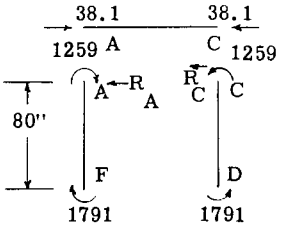

Fig. A11.81

Bending Moment in Lower Arch Member FED

The horizontal reaction on arch FED must be found before the true bending moments on the arch can be found. The procedure is the same as for the upper arch. Figs. All.81, 82, 83 show the results for the lower frame portion.

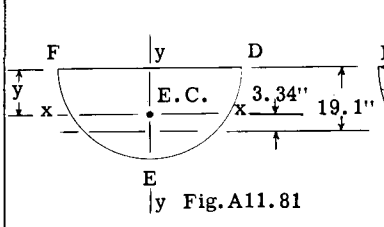

Fig.A11.81

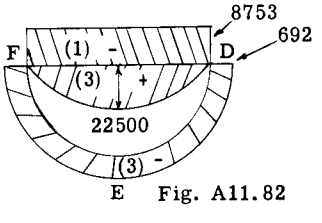

Fig. A11.82

$$\bar{y} = \frac{19.1 \times \pi(30/2)}{\pi \times \frac{30}{2} + \frac{60}{6}} = \frac{900}{57.1} = 15.76" \qquad \Sigma\frac{ds}{I} = 57.1$$

$$I_X = \frac{.3 \times 30^3}{2} + 15\pi \times 3.34^2 = 4578$$
$$(60/6)(15.76)^2 = 2478$$
$$I_X = 7056$$

From Fig. All.82,

ϕ_{S_1} = -8753 x 60/6 = - 87530

ϕ_{S_2} = .667 x 22500 x 60/6 = 150000

ϕ_{S_3} = - 6962π x (30/2) = -328000

$\Sigma\phi_S$ = -265500

Solving for Redundant forces M_O and X_O (See Fig. All.83)

$$M_O = \frac{-\Sigma\phi_S}{\Sigma\, ds/I} = \frac{-(-265500)}{57.1} = 4650 \text{ in. lb.}$$

$$X_o = \frac{\Sigma \emptyset_S y}{I_x} = \frac{-87530 \times 15.76 + 150000 \times 15.76 - 328000(-3.34)}{7056}$$

X_o = 294 lb.

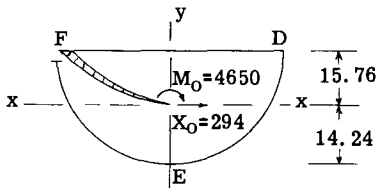

Fig. A11.83

Bending moment at F on member FED,

M_F = -6962 + 4650 - 294 x 15.76 = -6962 in.lb.

M_E = -6962 + 4650 + 294 x 15.76 = 2340 in.lb.

The axial load in member FD = 294 lb. compression plus 38.1 lbs. tension due to shear reaction from side members at points F and D or a resultant load of 255.9 lb. compression. Fig. A11.84 shows the final bending moment diagram on each member of the frame.

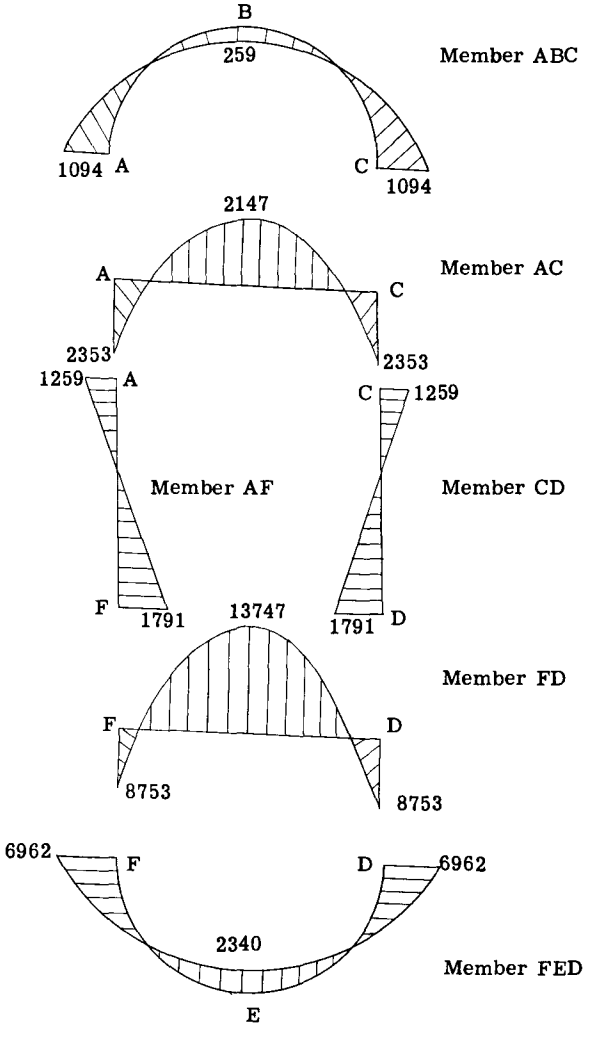

Figs. A11.84. Final Bending Moment Curves on Each Member of Frame.

Example Problem 2. External Loads on Curved Members.

Fig. A11.85 shows a frame which has external loads applied to the curved member as well as to the straight members. The frame supporting forces have been assumed as acting uniformly along the side members AD and CE. The problem will be to determine the bending moments at frame points ABCDE.

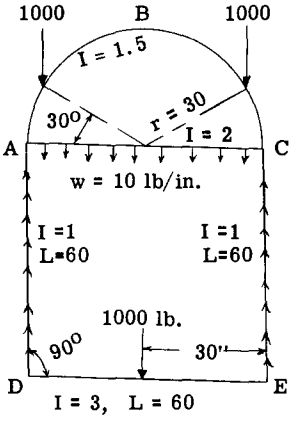

Fig. A11.85

SOLUTION:-

Calculation of stiffness factors K.

Member ABC. K_{ABC} = 2.314 I/r = 2.314 x 1.5/30 = .1158

K_{AC} = 4I/L = 4 x 2/60 = .1333

K_{AD} = 4I/L = 4 x 1/60 = .0667

K_{DE} = 4I/L = 4 x 3/60 = .2000

Calculation of Distribution Factors D.

JOINT A. ΣK = .1158 + .1333 + .0667 = .3158

D_{ABC} = .1158/.3158 = .366

D_{AC} = .1333/.3158 = .422

D_{AD} = .0667/.3158 = .212

JOINT D. ΣK = .0667 + .2000 = .2667

D_{DA} = .0667/.2667 = .25

D_{DE} = 2000/.2667 = .75

The carry-over factor for ABC is -0.452 as previously derived for a half circle arc, and 0.5 for the straight members.

Calculation of Fixed End Moments

For member AC, $M_A = M_B = \frac{1}{12} wL^2 = \frac{1}{12} \times 10 \times \overline{60}^2 =$

3000

For DE, $M_B = M_E$ = PL/8 = 1000 x 60/8 = 7500

Curved member ABC.

The fixed end moments on this curved member due to the external loads will be determined by the elastic center method. The assumed static frame condition will be an arch pinned at A and supported on rollers at B. (See Fig. A11.86)

Fig. A11.87 shows the general shape of the static moment.curve. For the frame portion between the reactions and the load points, the bending moment equation is $M=P(r-r\cos\alpha)$.

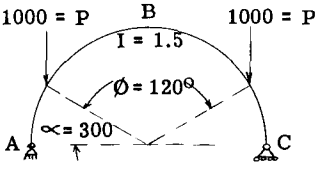

Fig. A11.86

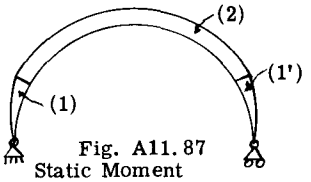

Fig. A11.87 Static Moment Curve.

For the beam portion between the two 1000 lb. loads, the bending moment is constant and equals, $M=P(r-r\cos 30^0)$

Calculation of $\emptyset_S$ Values.

The $\emptyset_S$ values equal the area of the M/I curves. The moment curve in Fig. A11.87 has been broken down into three parts labeled (1) (1') and (2).

$$\emptyset_{S_1}+\emptyset_{S_2}=2\left[\frac{Pr^2}{I}(\alpha-\sin\alpha)\right]$$

$$=2\left[\frac{1000\times 30^2}{1.5}(.524-.5)\right]=28800$$

The vertical distance $\bar{y}$ from line AC to centroid of $\emptyset_{S_1}$ and $\emptyset_{S_2}$ values is,

$$\bar{y}=\frac{r(1-\cos\alpha-\frac{\sin^2\alpha}{2})}{\alpha-\sin\alpha}=\frac{30(1-.867-0.5/2)}{.524-.50}=$$

10 in.

$$\emptyset_{S_2}=\frac{Pr^2\theta}{I}(1-\cos\alpha).\quad \theta=120^0,\ \alpha=30^0.$$

$$\emptyset_{S_2}=\frac{1000\times 30^2\times 2.1}{1.5}(1-.867)=167300$$

Vertical distance $\bar{y}$ from line AC to centroid of $\emptyset_{S_2}$ equals,

$$\bar{y}=\frac{2r\sin\theta/2}{\theta}=\frac{2\times 30\times 0.867}{2.1}=24.8\text{ in.}$$

Fig. A11.88 shows the $\emptyset_S$ values and their location with respect to x and y axes through the arch elastic center.

The elastic center method requires the total elastic weight of member and its elastic moments of inertia about axes through the elastic center.

$$\text{TOTAL ELASTIC WEIGHT}=\Sigma\, ds/I=\frac{\pi r}{1.5}=\frac{\pi\times 30}{1.5}$$

$$=62.83$$

Distance $\bar{y}$ from line AC to elastic center of arch ABC equals $0.6366r = .6366\times 30 = 19.1$ in.
$I_X = 0.2978r^3/I = 2978\times 30^3/1.5 = 5350$

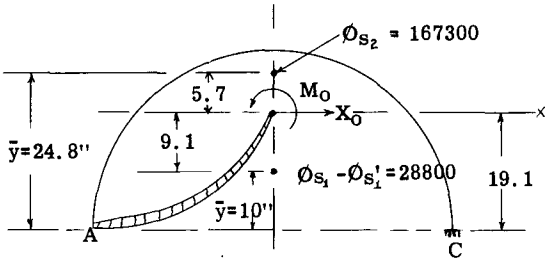

Fig. A11.88

Calculation of redundant forces at elastic center.

$$M_O=-\frac{\Sigma\,\emptyset_S}{\Sigma\, ds/I}=\frac{-(28800+167300)}{62.83}=-3122\text{ in.lb.}$$

$$X_O=\frac{\Sigma\,\emptyset_S y}{I_X}=\frac{167300\times 5.7+28800(-9.1)}{5350}=129.3\text{ lb.}$$

$$Y_O=\frac{-\Sigma\,\emptyset_S x}{I_y}=0\ \text{(because x = 0)}$$

The fixed end moments at ends A and C will equal the moment due to the redundant forces M_O and Y_O since the static moment assumed was zero at A and C.

$$M_A=M_C=M_O+X_O y=-3122+129.3\,(-19.1)$$
$$=-652\text{ in.lb.}$$

Moment Distribution Process

Having determined the fixed end moments, distribution and carry-over factors, the moment distribution can now be carried out. Fig. A11.89 shows the solution. The first cycle will be explained. Starting at joint (A) the unbalanced moment is -3000 - 652 = - 3652. The joint is balanced by distributing .432 x 3652 = 1543 to AC; .364 x 1543 = 1333 to ABC and .212 x 3652 = 776 to AD. The carry-over moment from C to A = .5(-1543) = -772; from C on member CBA to A = - .452(-1332) = 601; and from A to D = .5 x 776 = 388. Now proceeding to joint D the unbalanced moment is -7500 + 388 = -7112. The joint is balanced by distributing .75 x 7112 = 5340 to DE and the remainder 25 per cent = 1772 to DA.

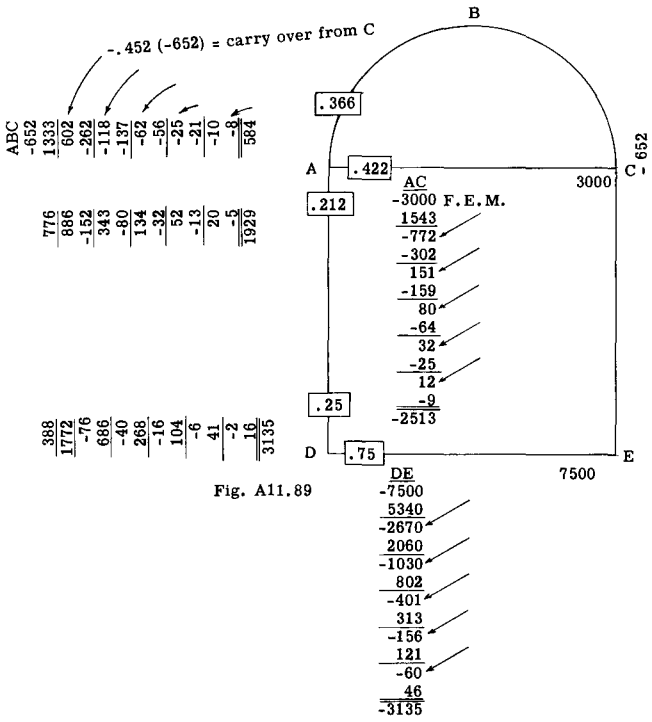

Fig. A11.89

The carry-over moments are: -

From E to D = .5 x (-5340) = -2670

To A from D = .5 (1772) = 886

The first cycle is now completed. Five more cycles are carried out in Fig. A11.89 in order to obtain reasonable accuracy of results. The final end moments are listed below the double short lines.

On arch member ABC the end moments of 584 are correct. However before the end moments at any other point on the arch can be found the horizontal reaction on the arch at A must be determined. This reaction will be determined by the elastic center method.

Fig. A11.90 shows the bending moment curves for members ABC and AC as made up of 5 parts labeled 1 to 5.

Calculation of ϕ_S values which equal area of each moment curve divided by I of member.

$2\phi_{S_1}$ = 28800

ϕ_{S_2} = 167300

ϕ_{S_3} = 584 x π x 30/1.5 = 36800

ϕ_{S_4} = - (.667 x 4500 x 60/2) = -90000

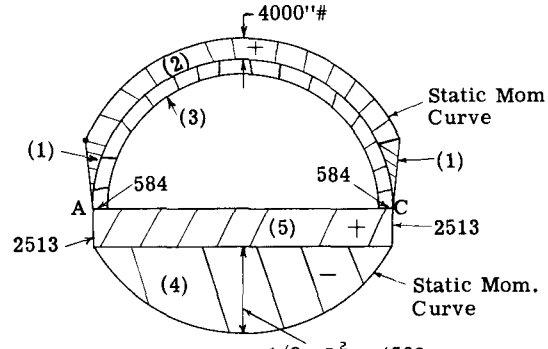

Fig. A11.90

ϕ_{S_5} = 2513 x 60/2 = 75390

$\Sigma\phi_S$ = 218290

Calculation of elastic center location and I_X.

Distance $\bar{y}$ from line AC to elastic center =

$$\frac{19.1 \times \pi \times 30/1.5}{\frac{\pi \times 30}{1.5} + \frac{60}{2}} = \frac{1202}{92.83} = 12.97"$$

TOTAL ELASTIC WEIGHT = 92.83.

$$I_X = \frac{.2978 \times 30^3}{1.5} + \frac{\pi \times 30}{1.5}(6.13)^2 + \frac{60}{2} \times 12.97^2$$

$$= 12713$$

Fig. A11.91 shows the elastic center location and the ϕ_S values together with their centroid locations.

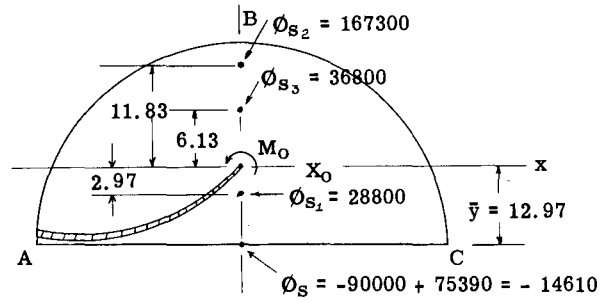

Fig. A11.91

Solving for redundant forces at elastic center.

$$M_O = \frac{\Sigma\,\phi_S}{\Sigma\,ds/I} = \frac{-218290}{92.83} = -2356$$

$$X_O = \frac{\Sigma\,\phi_S y}{I_X} = \frac{167300 \times 11.83 + 36800 \times 6.13}{12713} +$$

$$\frac{28800\,(-2.97) - 14610\,(-12.97)}{12713} = 181 \text{ lb.}$$

The bending moment at any point on member AC or ABC equals the values in Fig. A11.90 plus those due to M_o and X_o in Fig. A11.91.

Thus at point A on member ABC,
$M_{ABC} = 584 - 2356 + 181 \times 12.97 = 584$ in. lb.
which is the same as found by the moment distribution process.

At point B on arch: -

M_B from Fig. A11.90 = $584 + 4000 = 4584$

M_B from Fig. A11.91 = $-2356 - 181 \times (30 - 12.97)$

$= -5476$

Hence $M_B = 4584 - 5476 = -892$ in.lb.

STRUCTURES WITH JOINT DISPLACEMENTS

For unsymmetrical frames or for frames loaded unsymmetrically, the assumption that only joint rotation occurs may give resulting moments considerably in error. Joint displacement can be handled in a manner as previously explained and illustrated for frames composed of straight members.

The distribution of the skin supporting forces on the frame boundary are usually taken as following the shear flow distribution for the shell in bending as explained in a later chapter.

A11.20 Problems.*

(1) Determine the bending moment diagram for the loaded structures shown in Figs. 1 to 6.

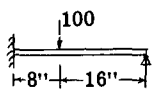

Fig. 1

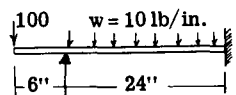

Fig. 2

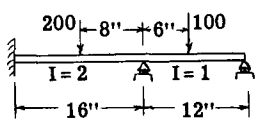

Fig. 3

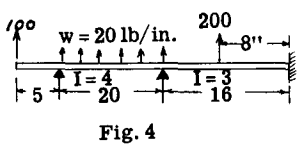

Fig. 4

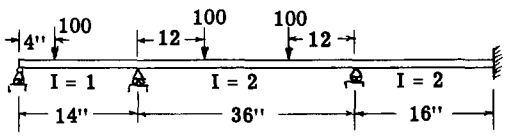

Fig. 5

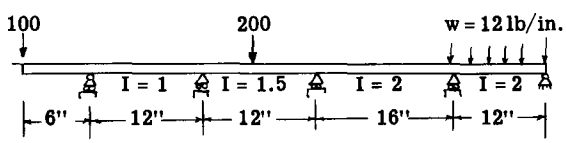

Fig. 6

* Also see Chapter C2, Parts F, L, M and Q.

(2) Find the bending moments at all joints and support points of the loaded structures in Figs. 7 to 10.

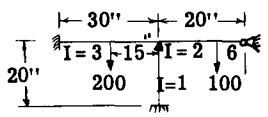

Fig. 7

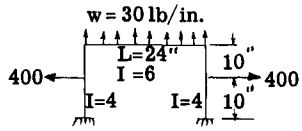

Fig. 8

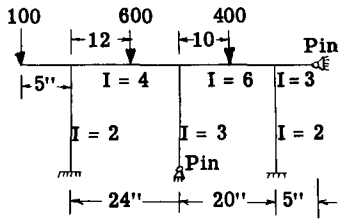

Fig. 9

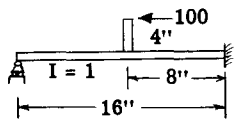

Fig. 10

(3)

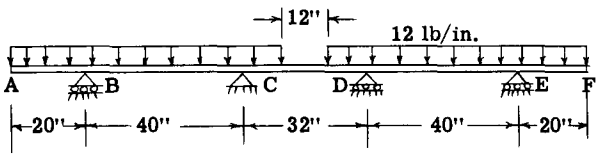

Fig. 11

In the loaded beam of Fig. 11, the supports B and E of the elevator beam deflect 0.1 inch more than supports C and D. Compute the resultant bending moments at the supports and find reactions. EI = 320,000 lb.in.sq.

(4) Fig. 12 illustrates a continuous 3 span wing beam, carrying a uniform air load of 20 lb./in. Determine the beam bending moments at strut points A and B. Take

$I_{AB} = 17$ in., $I_{AA'} = 20$ in., and $E = 1.3 \times 10^6$ in.^{2}

Neglect effect of support deflection due to strut axial deformation.

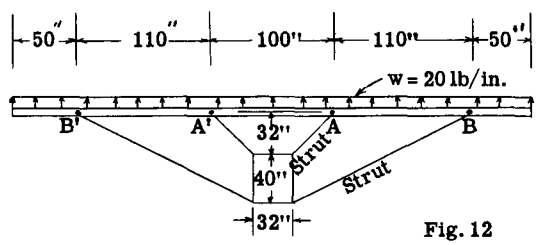

Fig. 12

(5) Figs. 13 to 15 are loaded structures that suffer joint translation. Determine bending moment diagram.

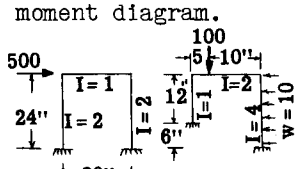

Fig. 13

Fig. 14

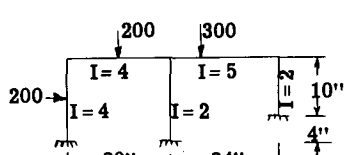

Fig. 15

CHAPTER A12

SPECIAL METHODS - SLOPE DEFLECTION METHOD

A12.1 General. The slope-deflection method is another widely used special method for analyzing all types of statically indeterminate beams and rigid frames. In this method as in the moment distribution method all joints are considered rigid from the standpoint that all angles between members meeting at a joint are assumed not to change in magnitude as loads are applied to the structure. In the slope deflection method the rotations of the joints are treated as the unknowns. For a member bounded by two end joints, the end moments can be expressed in terms of the end rotations. Furthermore for static equilibrium the sum of the end moments on the members meeting at a joint must be equal to zero. These equations of static equilibrium provide the necessary conditions to handle the unknown joint rotations and when these unknown joint rotations are found, the end moments can be computed from the slope-deflection equations. The advantages of the slope deflections method will be discussed at the end of the chapter after the method has been explained and applied to problem solution.

A12.2 Derivation of Slope Deflection Equation.

The problem is to determine the relationships between the displacements of the end supports of a beam and the resulting end moments on the beam.

Fig. A12.1a shows a beam restrained at ends 1 and 2. It is assumed unloaded and of constant cross-section or moment of inertia. This beam is now displaced as shown in Fig. b, namely, that the ends are rotated through the angles θ_1 and θ_2 plus a vertical displacement d_1 and d_2 of its ends from its original position, which produces a relative deflection Δ of its two ends. The angle ϕ representing the swing of the member equals Δ/L.

The problem is to derive equations for M_1 and M_2 in terms of the end slopes θ_1 and θ_2, the length of the beam and EI. Figs. c, d and e illustrate how the total beam deflection in Fig. b is broken down into three separate deflections. In Fig. c, the end (2) is considered fixed and a moment M'_1 is applied to rotate end (1) through an angle θ_1. In Fig.d, end (1) is considered fixed and a moment M''_2 is applied at (2) to rotate end (2) through an angle θ_2. In Fig. e, both ends are considered fixed and end (2) is displaced downward a distance Δ which causes end moments M'''_1 and M'''_2. In deriving the slope deflection equations each of the three beam deflections will be considered separately and the results are then added to give the final equations. Fig. A12.2 shows Fig. c repeated.

Fig. A12.1a

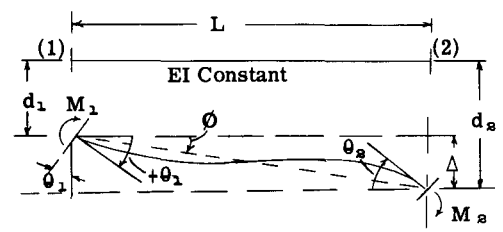

Fig. b

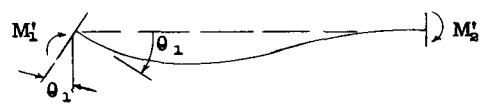

Fig. c

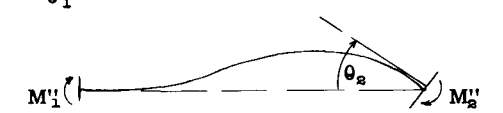

Fig. d

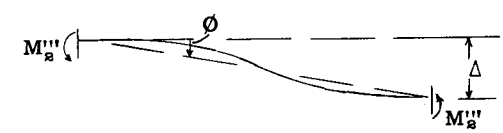

Fig. e

Figs. A12.1

Fig. A12.2

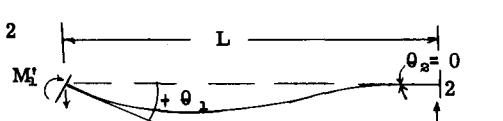

Fig. A12.3

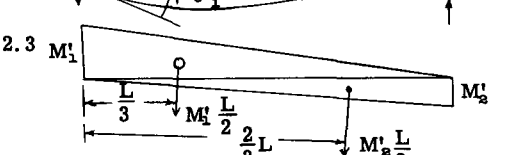

Fig. A12.4

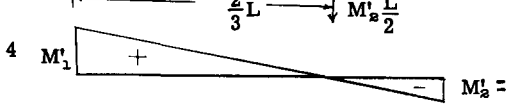

The applied moment M'_1, is positive (tension in bottom fibers). Since end (2) is assumed fixed an unknown moment M'_2 is produced at (2). Fig. A12.3 shows the bending moment diagram made up of two triangles. M'_2 being unknown will be

assumed also positive, as the algebraic solution will determine the true sign of M''_2.

Two moment area theorems will be used in deriving the slope-deflection equations, namely (I) that the change in slope of the beam elastic curve between two points on the beam is equal in magnitude to the area of the M/EI diagram between the two points, and (II) the deflection of a point (A) on the elastic curve away from a tangent to the elastic curve at (B) is equal in magnitude to the first moment about A of the M/EI diagram between (A) and (B) acting as a load.

In Fig. A12.2 since $\theta_2 = 0$, then θ_1 will equal the area of the M curves divided by EI.

$$\theta_1 = \frac{(M'_1 L/2)}{EI} + \frac{(M'_2 L/2)}{EI} = \frac{(M'_1 + M'_2)L}{2EI} \quad \text{- - - (1)}$$

The deflection of end (1) away from a tangent at (2) equals zero, thus we take moments of the moment diagram about (1) and equate to zero.

$$\left(\frac{M'_1 L}{2EI}\right)\frac{L}{3} + \left(\frac{M'_2 L}{2EI}\right)\frac{2L}{3} = \frac{M'_1 L^2}{6EI} + \frac{M'_2 L^2}{3EI} = 0$$

whence $-M'_2 = M'_1/2$ - - - - - - - - - - - - - - (2)

Fig. A12.4 shows the true shape of moment diagram.

Substituting results in equation (2) in equation (1) we obtain,

$$\theta_1 = \frac{M'_1 L}{4EI} \quad \text{or} \quad M'_1 = \frac{4EI\theta_1}{L} \quad \text{- - - - - - - (3)}$$

Then from equation (2)

$$M'_2 = -\frac{2EI\theta_1}{L} \quad \text{- - - - - - - - - - - - - - (4)}$$

Fig. A12.5

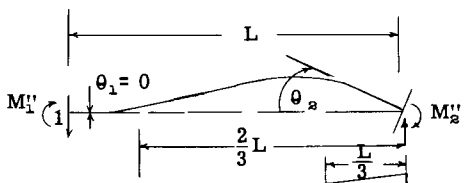

Fig. A12.6

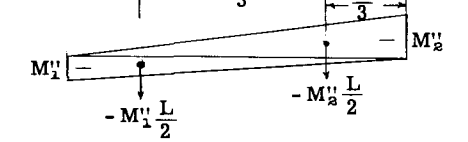

Fig. A12.7



Fig. A12.6 shows the moment diagram for an applied bending moment $-M''_2$ which rotates end (2) through an angle θ_2 when other end (1) is fixed (See Fig. A12.5). In a similar manner as described before,

$$\theta_2 = \frac{(-M''_1 L/2)}{EI} + \frac{(-M''_2 L/2)}{EI} = \frac{-(M''_1 + M''_2)L}{2EI} \quad \text{- (5)}$$

Taking moments of M/EI diagram about (2),

$$\left(\frac{M''_2 L}{2EI}\right)\frac{L}{3} + \left(\frac{M''_1 L}{2EI}\right)\frac{2L}{3} = 0$$

or, $-M''_2 = 2M''_1$ - - - - - - - - - - - - (6)

whence,

$$\theta_2 = \frac{M''_1 L}{2EI} \text{ and } M''_1 = \frac{2EI\theta_2}{L} \quad \text{- - - - - - - (7)}$$

Then from equation (6)

$$M''_2 = -\frac{4EI\theta_2}{L} \quad \text{- - - - - - - - - - - - - (8)}$$

Fig. A12.8 shows the third part of the beam deflection, namely, support (2) is deflected downward a distance Δ assuming both ends fixed.

Fig. A12.8

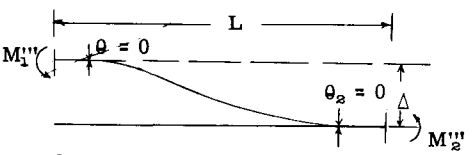

Fig. A12.9

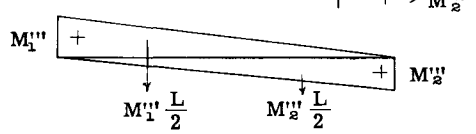

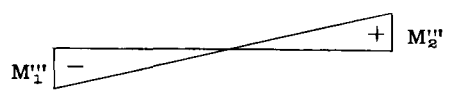

Fig. A12.10

The change in slope of the elastic curve between the ends equal zero, thus by the moment area theorem the area of M/EI diagram equals zero.

Hence, $\frac{(M'''_1 + M'''_2)L}{2EI} = 0$

whence $M'''_1 = -M'''_2$ - - - - - - - - - - - - - - (9)

From the deflection theorem,

$$\frac{M'''_1 L}{2EI}\left(\frac{2}{3}L\right) + \frac{M'''_2 L}{2EI}\left(\frac{L}{3}\right) = -\Delta \quad \text{- - - - - - (10)}$$

Subt. (9) in (10)

$$M'''_1 = -\frac{6EI\Delta}{L^2} \quad \text{- - - - - - - - - - - - (11)}$$

$$M_2''' = \frac{+ 6EI\Delta}{L^2} - - - - - - - - - - - - - \quad (12)$$

The combined effect of deflection O_1, O_2 and Δ can now be obtained by adding the separate results.

$$M_{1-2} = M_1' + M_1'' + M_1''' = \frac{2EI}{L}(2\theta_1 + \theta_2 - 3\Delta/L)$$

Let $K = \frac{EI}{L}$ and $\emptyset = \Delta/L$

Then, $M_{1-2} = 2K\ (2\theta_1 + \theta_2 - 3\emptyset)$ - - - - - - (13)

and $M_{2-1} = -2K\ (2\theta_2 + \theta_1 - 3\emptyset)$ - - - - - (14)

These end moments due to the distortion of the supports must be added to the moments due to any applied loads on the beam when considered as fixed ended. Let these fixed end moments be labeled M_{F_1} and M_{F_2}. Then equations (13) and (14) can be written including these moments.

$$M_{1-2} = 2K\ (2\theta_1 + \theta_2 - 3\emptyset) - M_{F_1} \quad - - - \quad (15)$$

$$M_{2-1} = -2K\ (2\theta_2 + \theta_1 - 3\emptyset) - M_{F_2} \quad - - - \quad (16)$$

MODIFIED SIGN CONVENTION

Equations (15) and (16) have been developed using the conventional signs for bending moments. In general there are advantages of using a statical sign convention as was used in the moment distribution method in Chapter A11. Therefore, the following sign convention will be used in this chapter: -

(1) The rotation of a joint or member is positive if it turns in a clockwise direction.

(2) An end moment is considered positive if it tends to rotate the end of the member clockwise or the joint counterclockwise.

This adopted sign convention is the same as adopted for the moment distribution method (See Art. A11.2).

When equations (15) and (16) are revised for this new sign convention they become: -

$$M_{1-2} = 2K\ (2\theta_1 + \theta_2 - 3\emptyset) + M_{F_1} \quad - - - - \quad (17)$$

$$M_{2-1} = 2K\ (2\theta_2 + \theta_1 - 3\emptyset) + M_{F_2} \quad - - - - \quad (18)$$

Equations (17) and (18) are referred to as the slope-deflection equations where $K = EI/L$ and $\emptyset = \Delta/L$.

For no yielding or transverse movement of supports, $\Delta = 0$ and equations (17) and (18) become

$$M_{1-2} = 2K\ (2\theta_1 + \theta_2) + M_{F_1} \quad - - - - - - \quad (18a)$$

$$M_{2-1} = 2K\ (2\theta_2 + \theta_1) + M_{F_2} \quad - - - - - - \quad (18b)$$

A12.3 Hinged End. Slope Deflection Equation.

Consider that end (2) of beam 1-2 is freely supported or in other words hinged. This means that M_{2-1} is zero. Thus equation (18) can be equated to zero.

$$M_{2-1} = 2K\ (2\theta_2 + \theta_1 - 3\emptyset) + M_{F_2} = 0$$

whence

$$2K\theta_2 = -K\theta_1 + 3K\emptyset - .5M_{F_2}$$

Substituting this value in equation (17)

$$M_{1-2} = 3K(\theta_1 - \emptyset) + M_{F_{1-2}} - 0.5M_{F_{2-1}} - - - (19)$$

A12.4 Example Problems.

Problem 1

Fig. A12.11 shows a two span continuous beam fixed at ends (1) and (3) and carrying lateral loads as shown. The bending moments at points 1, 2 and 3 will be determined. Relative values of I are shown for each member.

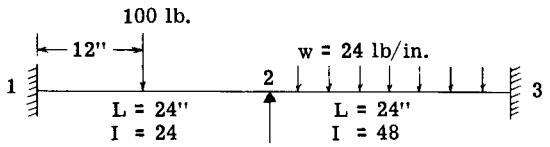

Fig. A12.11

SOLUTION:

Calculation of fixed end moments due to applied loads -

$$M_{F_{1-2}} = -PL/8 = 100 \times 24/8 = -300 \text{ in. lb.}$$

$$M_{F_{2-1}} = PL/8 = 300$$

The signs as shown are determined from the fact that the end moment at (1) tends to rotate the end of the member counterclockwise which is a positive moment according to our adopted sign convention. By similar reasoning the fixed in moment at (2) is positive because the moment tends to rotate end of member clockwise. For span 2-3: -

$$M_{F_{2-3}} = wL^2/12 = 24 \times 24^2/12 = -1152 \text{ in.lb.}$$

$$M_{F_{3-2}} = 1152$$

K Values K = EI/L. Since E is constant it will be considered unity.

FOR BEAM 1-2, K = I/L = 24/24 = 1
FOR BEAM 2-3, K = 48/24 = 2

Substituting in slope-deflection equations 18a and 18b. (ϕ = 0 since supports do not translate.)

Beam 1-2. $\theta_1 = 0$ because of fixity at (1).

$$M_{1-2} = 2K(2\theta_1 + \theta_2) + M_{F_1}$$

$$M_{1-2} = 2 \times 1 (0 + \theta_2) - 300$$

$$M_{1-2} = 2\theta_2 - 300 \quad - - - - - - - - - - - - \quad (a)$$

$$M_{2-1} = 2K(2\theta_2 + \theta_1) + M_{F_2}$$

$$M_{2-1} = 2 \times 1 (2\theta_2 + 0) + 300$$

$$M_{2-1} = 4\theta_2 + 300 \quad - - - - - - - - - - - - \quad (b)$$

Beam 2-3. $\theta_3 = 0$, because of fixity at (3).

$$M_{2-3} = 2K(2\theta_2 + \theta_3) + M_{F_2}$$

$$M_{2-3} = 2 \times 2 (2\theta_2 + 0) - 1152$$

$$M_{2-3} = 8\theta_2 - 1152 \quad - - - - - - - - - - - - \quad (c)$$

$$M_{3-2} = 2K(2\theta_3 + \theta_2) + M_{F_3}$$

$$M_{3-2} = 2 \times 2 (0 + \theta_2) + 1152$$

$$M_{3-2} = 4\theta_2 + 1152 \quad - - - - - - - - - - - - \quad (d)$$

At joint (2) $\Sigma M = 0$ for static equilibrium.

Hence

$$M_{2-1} + M_{2-3} = 0$$

Substituting from (b) and (c)

$$4\theta_2 + 300 + 8\theta_2 - 1152 = 0$$

whence $\theta_2 = 71$

With θ_2 known the final end moments can be found by substituting in equations (a), (b), (c) and (d) as follows: -

$$M_{1-2} = 2 \times 71 - 300 = -158 \text{ in.lb.}$$

$$M_{2-1} = 4 \times 71 + 300 = 584$$

$$M_{2-3} = 8 \times 71 - 1152 = -584$$

$$M_{3-2} = 4 \times 71 + 1152 = 1436$$

Changing the resulting moment signs to the conventional sign practice, gives

$$M_{1-2} = -158, \; M_{2-1} = M_{2-3} = -584,$$

$$M_{3-2} = -1436$$

Example Problem 2

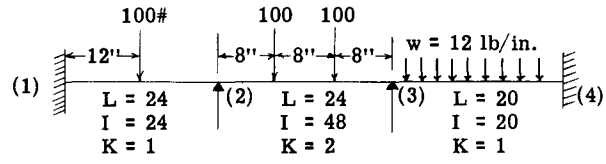

Fig. A12.12

Fig. A12.12 shows a loaded 3 span beam fixed at points (1) and (4). This fixity at (1) and (4) causes θ_1 and θ_4 to be zero.

Fixed end moments: -

$$M_{F_{1-2}} = -PL/8 = 100 \times 24/8 = -300,$$

$$M_{F_{2-1}} = 300$$

$$M_{F_{2-3}} = (100 \times 8 \times 16^2/24) + (100 \times 16 \times 8^2/24^2)$$
$$= -534$$

$$M_{F_{3-2}} = 534$$

$$M_{F_{3-4}} = wL^2/12 = 12 \times 20^2/12 = -400,$$

$$M_{F_{4-3}} = 400$$

SLOPE DEFLECTION EQUATIONS (ϕ = 0)

$$M_{1-2} = 2 \times 1(0 + \theta_2) - 300 = 2\theta_2 - 300 \quad - - \quad (a)$$

$$M_{2-1} = 2 \times 1(2\theta_2 + 0) + 300 = 4\theta_2 + 300 \quad - \quad (b)$$

$$M_{2-3} = 2 \times 2(2\theta_2 + \theta_3) - 534 = 8\theta_2 + 4\theta_3 - 534 \quad - - - - - - - - - - - - - - - \quad (c)$$

$$M_{3-2} = 2 \times 2(2\theta_3 + \theta_2) + 534 = 8\theta_3 + 4\theta_2 + 534 \quad - - - - - - - - - - - - - - - \quad (d)$$

$$M_{3-4} = 2 \times 1(2\theta_3 + 0) - 400 = 4\theta_3 - 400 - \quad - \quad (e)$$

$$M_{4-3} = 2 \times 1(0 + \theta_3) + 400 = 2\theta_3 + 400 \quad - - \quad (f)$$

Joint-Moment equilibrium equations: -

JOINT (2) $M_{2-1} + M_{2-3} = 0$

whence

$$4\theta_2 + 300 + 8\theta_2 + 4\theta_3 - 534 = 0 \quad \text{or}$$

$$12\theta_2 + 4\theta_3 - 234 = 0 \quad - - - - - - - - - - - \quad (g)$$

JOINT (3) $M_{3-2} + M_{3-4} = 0$

$$8\theta_3 + 4\theta_2 + 534 + 4\theta_3 - 400 = 0 \quad \text{or}$$

$$12\theta_3 + 4\theta_2 + 134 = 0 \quad - - - - - - - - - - - \quad (h)$$

Solving equations (g) and (h) for θ_2 and θ_3 gives,

$$\theta_2 = 26.15, \quad \theta_3 = -19.9$$

Substituting in equations (a) to (f) inclusive to find final end moments.

$$M_{1-2} = 2\theta_2 - 300 = 2 \times 26.15 - 300 = -247.7 \text{ in.lb.}$$

$$M_{2-1} = 4\theta_2 + 300 = 4 \times 26.15 + 300 = 404.6$$

$$M_{2-3} = 8\theta_2 + 4\theta_3 - 534 = 8 \times 26.15 + 4\,(-19.9) - 534 = -404.6$$

$$M_{3-2} = 8\theta_3 + 4\theta_2 + 534 = 8\,(-19.9) + 4 \times 26.15 + 534 = 479.4$$

$$M_{3-4} = 4\theta - 400 = 4\,(-19.9) - 400 = -479.4$$

$$M_{4-3} = 2\theta_3 + 400 = 2\,(-19.9) + 400 = 360.2$$

(Note: - Student should convert to conventional moment signs and draw complete bending moment diagram).

Example Problem 3. Beam with Simple Supports.

Fig. A12.13 shows a loaded 3 span continuous beam with hinged supports at points (1) and (4), which means that M_{1-2} and $M_{4-3} = 0$. The moments at supports (2) and (3) will be determined.

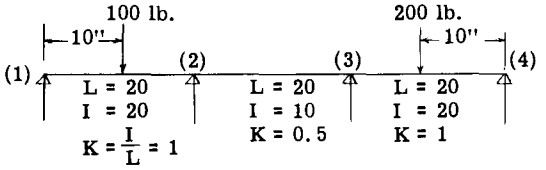

Fig. A12.13

SOLUTION:

Fixed end moments: -

$$M_{F_{1-2}} = -PL/8 = 100 \times 20/8 = -250, \quad M_{F_{2-1}} = 250$$

$$M_{F_{2-3}} = M_{F_{3-2}} = 0 \text{ (No load on span 2-3)}$$

$$M_{F_{3-4}} = PL/8 = 200 \times 20/8 = -500, \quad M_{4-3} = 500$$

Slope-deflection equations: -

Since supports at (1) and (4) are hinged or free to rotate we use equation (19) in writing equations for M_{2-1} and M_{3-4}.

$$M_{2-1} = 3K\theta_2 + M_{F_{2-1}} - 0.5\, M_{F_{1-2}}. \quad (\emptyset \text{ is zero})$$

$$M_{2-1} = 3 \times 1 \times \theta_2 + 250 - 0.5\,(-250) = 3\theta_2 + 375 \text{ - - - - - - - - - - - - (a)}$$

$$M_{3-4} = 3K\theta_3 + M_{F_{3-4}} - 0.5\, M_{F_{4-3}}$$

$$M_{3-4} = 3 \times 1 \times \theta_3 - 500 - 0.5\,(500) = 3\theta_3 - 750 \text{ - - - - - - - - - - - - - - (b)}$$

Using equations 18a and 18b and substituting,

$$M_{2-3} = 2K(2\theta_2 + \theta_3) + M_{F_{2\ 3}}$$

$$M_{2-3} = 2 \times 0.5(2\theta_2 + \theta_3) + 0 = 2\theta_2 + \theta_3 \text{ - - (c)}$$

$$M_{3-2} = 2K(2\theta_3 + \theta_2) + M_{F_{3-2}}$$

$$M_{3-2} = 2 \times 0.5(2\theta_3 + \theta_2) + 0 = 2\theta_3 + \theta_2 \text{ - - (d)}$$

For statical equilibrium of joints: -

JOINT (2) $M_{2-1} + M_{2-3} = 0$

Subt. $3\theta_2 + 325 + 2\theta_2 + \theta_3 = 0$

or $5\theta_2 + \theta_3 + 375 = 0$ - - - - - - - - - - - - (e)

JOINT (3) $M_{3-2} + M_{3-4} = 0$

$$2\theta_3 + \theta_2 + 3\theta_3 - 750 = 0$$

or $5\theta_3 + \theta_2 - 750 = 0$ - - - - - - - - - - - - - (f)

Solving (e) and (f) for θ_2 and θ_3 gives,

$$\theta_2 = -109.4, \quad \theta_3 = 172$$

The end moments at (2) and (3) can now be found from equation (a) to (d) inclusive.

$$M_{2-1} = 3\theta_2 + 375 = 3\,(-109.4) + 375 = 46.8 \text{ in.lb.}$$

$$M_{2-3} = 2\theta_2 + \theta_3 = 2\,(-109.4) + 172 = -46.8$$

$$M_{3-2} = 2\theta_3 + \theta_2 = 2 \times 172 + (-109.4) = 234$$

$$M_{3-4} = 3\theta_3 - 750 = 3 \times 172 - 750 = -234$$

A12.5 Loaded Continuous Beam with Yielding Supports.

The movable control surfaces of an airplane, namely the elevator, rudder and aileron are attached at several points to the stabilizer, fin and wing respectively. These supporting surfaces are usually cantilever structures and thus the supporting points for the movable control surfaces suffer a displacement thus promoting a continuous beam on yielding or deflected

supports. The slope deflection equations can take care of this support displacement as illustrated in the following example problem.

Example Problem.

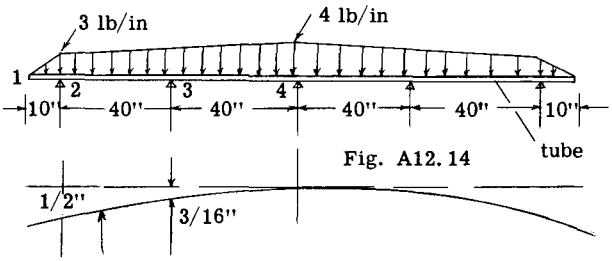

Fig. A12.14

Fig. A12.15

Fig. A12.14 is representative of an elevator beam attached to deflecting stabilizer structure at the five reaction points as indicated in the figure. The elevator beam is a round aluminum tube 1-1/4 - .049 in size. The moment of inertia (I) of this tube equals 0.03339 and the modulus of elasticity (E) of the material equals 10 million psi. The air load on the elevator beam is variable as indicated in Fig. A12.14.

Fig. A12.15 shows the shape of the deflecting supporting structure, which means that supports (2) and (3) move downward through the distances indicated on the figure. The problem will be to determine the bending moment at the supports under the combined action of transverse loading and settling of supports.

SOLUTION: -

Calculation of fixed end moments: -

For a trapeqoidal loading as shown in Fig. a, the fixed end moments are,

$$M_{1-2} = \frac{L^2}{60}(5u + 2v)$$

$$M_{2-1} = \frac{L^2}{60}(5u + 3v)$$

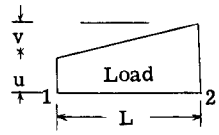

Fig. a

Substituting in these equations for the loading values as shown in Fig. A12.4,

$$M_{F_{2-3}} = \frac{40^2}{60}(5 \times 3 + 1) = -426 \text{ in.lb.}$$

$$M_{F_{3-2}} = \frac{40^2}{60}(5 \times 3 + 1.5) = 440$$

$$M_{F_{3-4}} = \frac{40^2}{60}(5 \times 3.5 + 1) = -494$$

$$M_{F_{4-3}} = \frac{40^2}{60}(5 \times 3.5 + 1.5) = 507$$

The beam has a constant section, hence, K for all spans equals,

$$K = EI/L = (10{,}000{,}000 \times 0.03339)\ 40 = 8347$$

Calculation of ϕ values.

Span 2-3. The settlement of support (2) with respect to support (3) = (0.5 - .1875) = .3125 inches = Δ

$$\phi = -\Delta/L = -.3125/40 = -0.007812 \text{ rad.}$$

(Since (2) moves counterclockwise with respect to (3) the sign of ϕ is negative.

Span 3-4. Δ = .1875 inches

$$\phi = -\Delta/L = -.1875/40 = -.004688 \text{ rad.}$$

Since the beam, external loading and support settlement is symmetrical about support (4), the slope of the beam elastic curve at (4) is horizontal or zero and therefore $\theta_4 = 0$. Thus only one-half of the structure need be considered in the solution. Due to the fact that (2) is a simple support with a cantilever overhang, the moment M_{2-1} is statically determinate and equals 5 x 3 x 3.33 = 50 in.lb. Then for static equilibrium of joint (2), M_{2-3} must equal - 50.

Substitution in slope deflection equations (17) and (18): -

$$M_{2-3} = 2K(2\theta_2 + \theta_3 - 3\phi) + M_{F_{2-3}}$$

$$-50 = 2 \times 8347\left[2\theta_2 + \theta_3 - 3(.007812)\right] - 426$$

or $= 33388\theta_2 + 16694\theta_3 + 15 = 0$ - - - - - - - (1)

$$M_{3-2} = 2K(2\theta_3 + \theta_2 - 3\phi) + M_{F_{3-2}} = 2 \times 8347$$
$$\left[2\theta_3 + \theta_2 - 3(-.007812)\right] + 440$$

whence $M_{3-2} = 33388\theta_3 + 16694\theta_2 + 831$ - - - - (2)

$$M_{3-4} = 2K(2\theta_3 + \theta_4 - 3\phi) + M_{F_{3-4}} \qquad (\theta_4 = 0)$$

$$M_{3-4} = 2 \times 8347\left[2\theta_3 + 0 - 3(-.004688)\right] - 494$$

whence $M_{3-4} = 33388\theta_3 - 259$ - - - - - - - - (3)

$$M_{4-3} = 2K(2\theta_4 - \theta_3 - 3\phi) + M_{F_{4-3}}$$

$$M_{4-3} = 2 \times 8347\left[0 + \theta_3 - 3(-.004688)\right] + 507$$

whence $M_{4-3} = 16694\theta_3 + 742$ - - - - - - - - (4)

For static equilibrium of joint (3),

$M_{3-2} + M_{3-4} = 0$, hence

$$33388\theta_3 + 16694\theta_2 + 831 + 33388\theta_3 - 259 = 0$$

whence, $66776\theta_3 + 16694\theta_2 + 572 = 0$ - - - - - (5)

Solving equations (1) and (5) for θ_2 and θ_3 we obtain $\theta_2 = 0.00439$ and $\theta_3 = -0.00967$.

Substituting in equations (2), (3) and (4) gives the moments at these points.

$M_{3-2} = 33388\ (-.00967) + 16694 \times .00439 + 831 = 582$ in.lb.

$M_{3-4} = 33883\ (-.00967) - 259 = -582$

$M_{4-3} = 16694\ (-.00967) + 742 = 580$

Converting these signs to the conventional signs would give $M_2 = -50$, $M_3 = -582$ and $M_4 = -580$.

A12.6 Statically Indeterminate Frames. Joint Rotation Only.

The slope deflection equations can be used in solving all types of framed structures. In frames as compared to straight continuous beams, the axial loads in the members are usually more important, however the influence on joint displacement due to axial deformation of members is relatively small and is therefore usually neglected in most simple framed structures. To illustrate the slope-deflection method as applied to frames, the structure shown in Fig. A12.16 will be solved.

Example Problem 1.

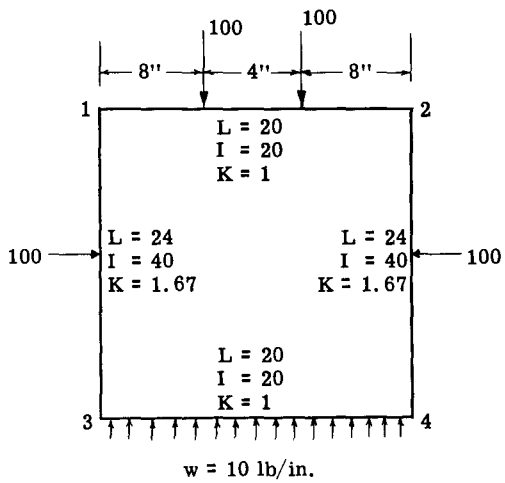

Fig. A12.16

Fig. A12.16 shows a closed rectangular frame subjected to loadings on its four sides which hold the frame in equilibrium. The bending moments at the frame joints will be determined.

SOLUTION: -

FIXED END MOMENTS: -

$M_{F_{1-2}} = (100 \times 8 \times 12^2)/20^2 + (100 \times 12 \times 8^2)/20^2 = -480$

$M_{F_{2-1}} = 480$

$M_{F_{1-3}} = 100 \times 24/8 = 300.$ $\quad M_{F_{3-1}} = -300$

$M_{F_{3-4}} = 10 \times 20^2/12 = 334.$ $\quad M_{F_{4-3}} = -334$

Due to symmetry of loading we know that $\theta_1 = -\theta_2$ and $\theta_3 = -\theta_4$, which fact will shorten the solution.

Slope deflection equations: -

$M_{1-2} = 2K\ (2\theta_1 + \theta_2) + M_{F_{1-2}}$

$M_{1-2} = 2 \times 1\ (2\theta_1 - \theta_1) - 480$

$M_{1-2} = 2\theta_1 - 480$ - - - - - - - - - - - - (a)

$M_{1-3} = 2K\ (2\theta_1 + \theta_3) + M_{F_{1-3}}$

$M_{1-3} = 2 \times 1.67\ (2\theta_1 + \theta_3) + 300$

$M_{1-3} = 6.67\theta_1 + 3.33\theta_3 + 300$ - - - - - - (b)

$M_{3-1} = 2K\ (2\theta_3 + \theta_1) + M_{F_{3-1}}$

$M_{3-1} = 2 \times 1.67\ (2\theta_3 + \theta_1) - 300$

$M_{3-1} = 6.67\theta_3 + 3.33\theta_1 - 300$ - - - - - - (c)

$M_{3-4} = 2K\ (2\theta_3 + \theta_4) + M_{F_{3-4}}$

$M_{3-4} = 2 \times 1\ (2\theta_3 - \theta_3) + 334$

$M_{3-4} = 2\theta_3 + 334$ - - - - - - - - - - - - (d)

Static Joint Equations: -

JOINT (1).

$M_{1-2} + M_{1-3} = 0$ which gives,

$2\theta_1 - 480 + 6.67\theta_1 + 3.33\theta_3 + 300 = 0$

whence $8.67\theta_1 + 3.33\theta_3 - 180 = 0$ - - - - - - (e)

JOINT (3).

$M_{3-1} + M_{3-4} = 0$ which gives,

$6.67\theta_3 + 3.33\theta_1 - 300 + 2\theta_3 + 334 = 0$

whence $8.67\theta_3 + 3.33\theta_1 + 34 = 0$ - - - - - - - (f)

Solving equations (e) and (f) for θ_3 and θ_1 gives,

$\theta_1 = 26.3, \quad \theta_3 = -13.94$

Subt. in equation (a)

$$M_{1-2} = 2 \times 26.3 - 480 = -428 \text{ in.lb.}$$

Subt. in equation (d)

$$M_{3-4} = 2(-13.94) + 334 = 306 \text{ in.lb.}$$

Fig. A12.17 shows the resulting bending moment diagram.

Fig. A12.17

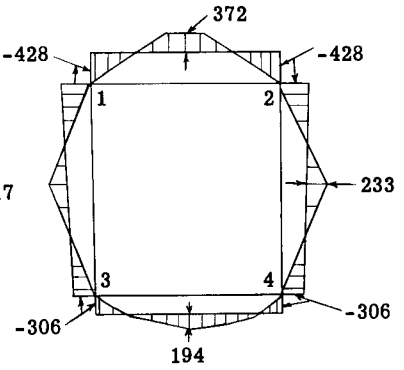

A12.7 Frames with Joint Displacements.

In the previous example problems, the conditions were such that only joint rotations took place, or if any transverse joint displacement took place as in the example problem of Art. A12.5, these displacements were known, or in other words the value of $\emptyset$ in the slope-deflection was known.

In many practical frames however, the joints suffer unknown displacements as for example in the frame of Fig. A12.18. The term $\emptyset = \Delta/L$ in the slope-deflection equation was derived on the basis of transverse displacement of the member ends when both ends were fixed. Thus in Fig. A12.18 under the action of the external loads, will sway to the right as magnified by the dashed lines. Neglecting any joint displacement due to axial deformation, the upper end of each member will move through the same displacement Δ. Then we can write,

$$\emptyset_{2-1} = \Delta/L_{1-2}, \quad \emptyset_{4-3} = \Delta/L_{3-4}, \quad \emptyset_{6-5} = \Delta/L_{5-6}$$

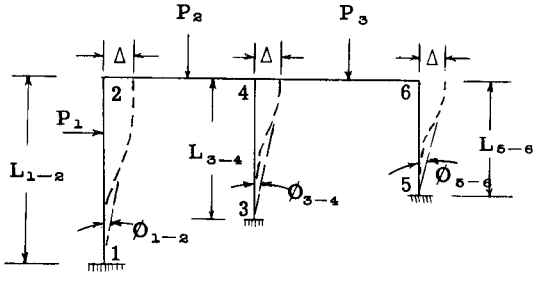

Fig. A12.18

Due to the fixity at joints (1), (3) and (5), $\theta_{1-2} = \theta_{3-4} = \theta_{5-6} = 0$. Therefore, the unknowns are θ_{2-1}, θ_{4-3}, θ_{6-5} and Δ.

There are three statical joint equations of equilibrium available, namely,

$$M_{2-1} + M_{2-4} = 0, \quad M_{4-2} + M_{4-6} = 0, \text{ and}$$
$$M_{6-4} + M_{6-5} = 0$$

Another equation is necessary because there are four unknowns. This additional equation is obtained by applying the equations of statics to the free bodies of the vertical members. Fig. A12.19 shows the free bodies.

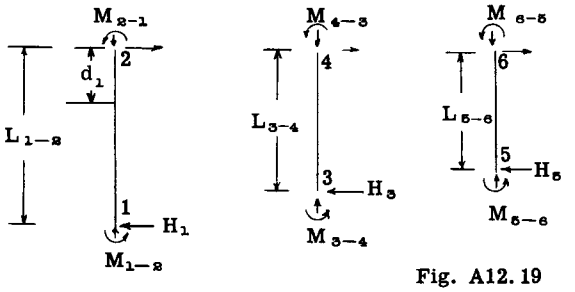

Fig. A12.19

Treating each member separately, we take moments about the upper end and equate to zero and then solve for the horizontal reaction at the bottom end. The results are,

$$H_1 = \frac{P_1 d_1}{L_{1-2}} + \frac{M_{2-1} + M_{1-2}}{L_{1-2}}$$

$$H_3 = \frac{M_{4-3} + M_{3-4}}{L_{3-4}}$$

$$H_5 = \frac{M_{6-5} + M_{5-6}}{L_{5-6}}$$

With these horizontal reactions known the static equation $\Sigma H = 0$ can now be applied to the frame as a whole, which gives,

$$P_1 - H_1 - H_3 - H_5 = 0 \text{ - - - - - - - - - - } (20)$$

Equation (20) is generally referred to as the bent or shear equation and is an equation that supplies the necessary extra condition to take care of the additional unknown Δ.

A12.8 Example Problems of Frames with Unknown Joint Displacement.

Example Problem 1

Fig. A12.20 shows an unsymmetrical frame with unsymmetrical loading. The bending moment curve will be determined.

SOLUTION: -

The relative moment of inertia of each

member is given on the figure. The relative K = I/L values are also indicated adjacent to each member.

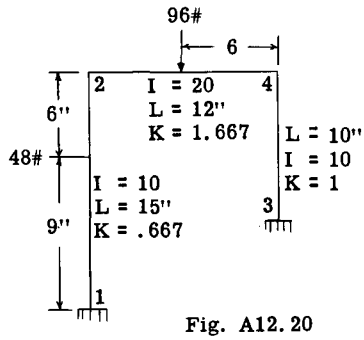

Fig. A12.20

Relative values of Ø due to sidesway of frame: -

The angles Ø are proportional to the Δ/L for each member where Δ is same for members (1-2) and (3-4) and zero for member (2-4). (See Fig. A12.10).

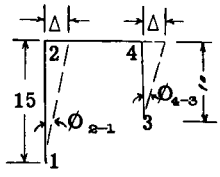

Fig. A12.10

Hence,

$$\emptyset_{2-1} = \frac{1}{15} = .0667\emptyset$$

$$\emptyset_{3-4} = \frac{1}{10} = 0.10\emptyset$$

$$\emptyset_{2-4} = \frac{0}{12} = 0$$

FIXED END MOMENTS: -

Member 1-2.

$$M_{F_{1-2}} = -(48 \times 6^2 \times 9)/15^2 = -69.12 \text{ in.lb.}$$

$$M_{F_{2-1}} = (48 \times 9^2 \times 6)/15^2 = 103.68$$

Member 2-4.

$$M_{F_{2-4}} = -(96 \times 12)/8 = -144$$

$$M_{F_{4-2}} = 144$$

Member 3-4 has no lateral loads and thus fixed end moments are zero.

The slope-deflection equations are: -

$$M_{1-2} = 2K(2\theta_1 + \theta_2 - 3\emptyset) + M_{F_1} \quad - - - - \quad (17)$$

$$M_{2-1} = 2K(2\theta_2 + \theta_1 - 3\emptyset) + M_{F_2} \quad - - - - \quad (18)$$

Writing above equations for each member and noting that θ_1 and θ_3 are zero because frame is fixed at support points, gives,

$$M_{1-2} = 2 \times 0.667(0 + \theta_2 - 3 \times .0667\emptyset) - 69.12$$

$$M_{1-2} = 1.333\theta_2 - 0.2667\emptyset - 69.12 - - - - \quad (a)$$

$$M_{2-1} = 2 \times 0.667(2\theta_2 + 0 - 3 \times .0667\emptyset) + 103.68$$

$$M_{2-1} = 2.667\theta_2 - 0.2667\emptyset + 103.68 - - - \quad (b)$$

$$M_{2-4} = 2 \times 1.667(2\theta_2 + \theta_4 - 0) - 144$$

$$M_{2-4} = 6.667\theta_2 + 3.333\theta_4 - 144 - - - - - \quad (c)$$

$$M_{4-2} = 2 \times 1.667(2\theta_4 + \theta_2 - 0) + 144$$

$$M_{4-2} = 6.667\theta_4 + 3.333\theta_2 + 144 - - - - - \quad (d)$$

$$M_{3-4} = 2 \times 1(0 + \theta_4 - 3 \times 0.1\emptyset) + 0$$

$$M_{3-4} = 2\theta_4 - 0.6\emptyset - - - - - - - - - - - - \quad (e)$$

$$M_{4-3} = 2 \times 1(2\theta_4 + 0 - 3 \times 0.1\emptyset) + 0$$

$$M_{4-3} = 4\theta_4 - 0.6\emptyset - - - - - - - - - - - - \quad (f)$$

Equilibrium equations: -

JOINT (2). $M_{2-1} + M_{2-4} = 0$

Substituting: -

$$2.667\theta_2 - 0.2667\emptyset + 103.68 + 6.667\theta_2 + 3.333\theta_4 - 144 = 0$$

whence, $9.333\theta_2 - 0.2667\emptyset + 3.333\theta_4 - 40.32 = 0 - - - - - - - - - - - - - - - - - \quad (g)$

JOINT (4). $M_{4-2} + M_{4-3} = 0$

$$6.667\theta_4 + 3.333\theta_2 + 144 + 4\theta_4 - 0.6\emptyset = 0$$

whence, $10.667\theta_4 + 3.333\theta_2 - 0.6\emptyset + 144 = 0 \quad - (h)$

Writing the bent equation (See Eq. 20).

$$H_1 + H_3 - 48 = 0 - - - - - - - - - - - - - - \quad (i)$$

In order to get H_1 and H_3 in terms of end moments see Fig. A12.21.

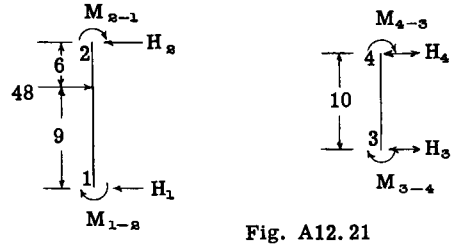

Fig. A12.21

For free body of member 1-2 take moments about (2) and equate to zero.

$$M_{2-1} + M_{1-2} - 6 \times 48 + 15H_1 = 0$$

hence, $H_1 = \dfrac{288 - (M_{2-1} + M_{1-2})}{15}$

Subt. values of M_{2-1} and M_{1-2} in the equation,

$$H_1 = -0.2667\theta_2 + .03555\emptyset + 16.88 - - - - \quad (j)$$

For free body of member 3-4 take moments about (4) and equate to zero.

$$M_{3-4} + M_{4-3} + 10H_3 = 0$$

whence, $H_3 = -\frac{(M_{3-4} + M_{4-3})}{10}$

Substituting values of M_{3-4} and M_{4-3} in above equations, gives,

$$H_3 = -0.6\theta_4 + 0.12\phi \text{ - - - - - - - - - - (k)}$$

Substituting values of H_1 and H_3 in equation (i), gives,

$$-0.2667\theta_2 - .6\theta_4 + .1555\phi - 31.12 = 0 \text{ - - (l)}$$

Solving equations (g), (h), (l) for the unknowns θ_2, θ_4 and ϕ gives,

$$\phi = 196.9,\ \theta_2 = 12.17,\ \theta_4 = -6.22$$

The final end moments can now be found by substituting these values in equations (a) to (f) inclusive.

$$M_{1-2} = 1.333 \times 12.17 - .2667 \times 196.9 - 69.12 = -105.4 \text{ in.lb.}$$

$$M_{2-1} = 2.667 \times 12.17 - .2667 \times 196.9 + 103.68 = -83.6$$

$$M_{2-4} = 6.667 \times 12.17 + 3.333\ (-6.22) - 144 = 83.6$$

$$M_{4-2} = 6.667\ (-6.22) + 3.333 \times 12.17 + 144 = 142.9$$

$$M_{4-3} = 4\ (-6.22) - 0.6 \times 196.9 = -142.9$$

$$M_{3-4} = 2\ (-6.22) - 0.6 \times 196.9 = -130.45$$

Fig. A12.22 shows the bending moment diagram. The student should also draw the shear diagram, find axial load in members since all these loads are needed when the

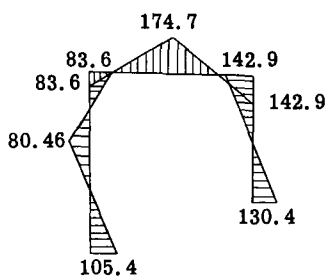

Fig. A12.22

strength of the frame members are computed and compared against the stresses caused by the frame loading.

Example Problem 2.

Fig. A12.23 shows a gable frame, carrying the symmetrical distributed load as shown.

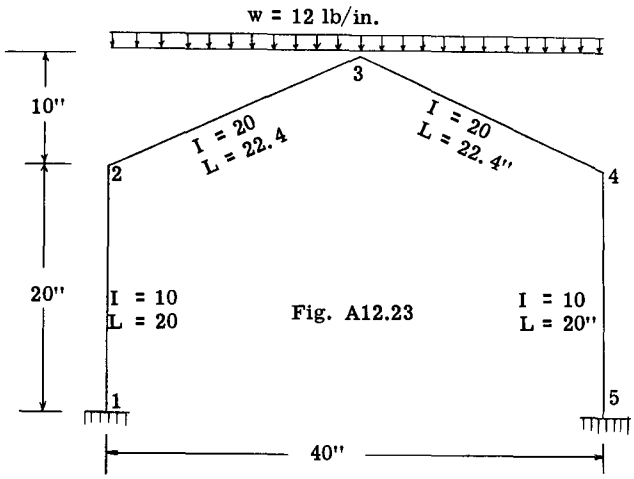

Fig. A12.23

The bending moment diagram under the given loading will be determined.

SOLUTION: -

Relative Stiffness (K values)

Members 1-2 and 4-5, K = 10/20 = 0.5

Members 2-3 and 4-3, K = 20/22.4 = 0.892

Fixed end moments:

$$M_{F_{2-3}} = wL_h^2/12 = (12 \times 20^2)/12 = -400 \text{ in.lb.}$$

$$M_{F_{3-2}} = 400,\ M_{F_{4-3}} = 400,\ M_{F_{3-4}} = -400$$

Relative values of ϕ: -

Due to the sloping members, the relative transverse deflections of each member are not as obvious as when the vertical members are connected to horizontal members as in the previous example. In this example, joints (1) and (5) are fixed. Because of symmetry of frame and loading, joints (2) and (4) will move outward the same distance Δ as indicated in Fig. A12.24. Furthermore, due to symmetry, joint (3) will undergo vertical movement only.

In Fig. A12.24, draw a line from point (2') parallel to 2-3 and equal in length to 2-3 to locate the point (3"). Erect a perpendicular to 2'-3" at 3" and where it intersects a vertical through (3) locates the point (3') the final location of joint (3). The length of 2'-3' equals 2-3. In the triangle 3-3'-3", the side 3'-3" = $\sqrt{5}\Delta$. The relative values of ϕ which are measured by Δ/L for each member can now be calculated.

$$\phi_{1-2} = -\frac{1}{20} = -.05\phi \qquad \phi_{2-3} = \frac{\sqrt{5}}{22.4} = 0.1\phi$$

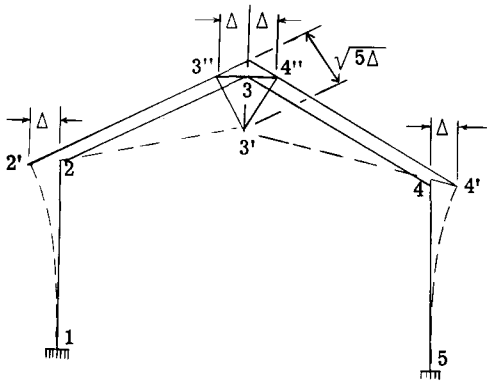

Fig. A12.24

$\phi_{3-4} = -0.1\phi$ $\qquad$ $\phi_{4-5} = .05\phi$

Substitution in Slope Deflection Equations: -

We know that $\theta_1 = \theta_5 = 0$, due to fixity at joints (1) and (5). Also $\theta_3 = 0$ due to symmetry or only vertical movement of joint (3). Furthermore due to symmetry $\theta_4 = -\theta_2$

$$M_{1-2} = 2K(2\theta_1 + \theta_2 - 3\phi) + M_{F_{1-2}}$$

$$M_{1-2} = 2 \times 0.5(0 + \theta_2 + .05 \times 3\phi) + 0$$

$$M_{1-2} = \theta_2 + 0.15\phi \text{ - - - - - - - - - - - - (a)}$$

$$M_{2-1} = 2K(2\theta_2 + \theta_1 - 3\phi) + M_{F_{2-1}}$$

$$M_{2-1} = 2 \times 0.5(2\theta_2 + .05 \times 3\phi) + 0$$

$$M_{2-1} = 2\theta_2 + 0.15\phi \text{ - - - - - - - - - - - - (b)}$$

$$M_{2-3} = 2K(2\theta_2 + \theta_3 - 3\phi) + M_{F_{2-3}}$$

$$M_{2-3} = 2 \times 0.892(2\theta_2 + 0 - .3 \times 0.1\phi) - 400$$

$$M_{2-3} = 3.568\theta_2 - 0.5352\phi - 400 \text{ - - - - (c)}$$

$$M_{3-2} = 2K(2\theta_3 + \theta_2 - 3\phi) + M_{F_{3-2}}$$

$$M_{3-2} = 2 \times .892(0 + \theta_2 - 3 \times 0.1\phi + 400$$

$$M_{3-2} = 1.784\theta_2 - 0.5352\phi + 400 \text{ - - - - (d)}$$

$$M_{3-4} = 2K(2\theta_3 + \theta_4 - 3\phi) + M_{F_{3-4}}$$

$$M_{3-4} = 2 \times .892(0 - \theta_2 + 3 \times 0.1\phi) - 400$$

$$M_{3-4} = -1.784\theta_2 + 0.5352\phi - 400 \text{ - - - (e)}$$

$$M_{4-3} = 2K(2\theta_4 + \theta_3 - 3\phi) + M_{F_{4-3}}$$

$$M_{4-3} = 2 \times .892(-2\theta_2 + 0 + 3 \times 0.1\phi) + 400$$

$$M_{4-3} = -3.568\theta_2 + 0.5352\phi + 400 \text{ - - - (f)}$$

$$M_{4-5} = 2K(2\theta_4 + \theta_5 - 3\phi) + M_{F_{4-5}}$$

$$M_{4-5} = 2 \times 0.5(-2\theta_2 + 0 - 3 \times .05\phi) + 0$$

$$M_{4-5} = -2\theta_2 - 0.15\phi \text{ - - - - - - - - - - (g)}$$

$$M_{5-4} = 2K(2\theta_5 + \theta_4 - 3\phi) + M_{F_{5-4}}$$

$$M_{5-4} = 2 \times 0.5(0 - \theta_2 - 3 \times .05\phi) + 0$$

$$M_{5-4} = -\theta_2 - 0.15\phi \text{ - - - - - - - - - - (h)}$$

JOINT (2). Equilibrium equation.

$M_{2-1} + M_{2-3} = 0$, substituting -

$$2\theta_2 + 0.15\phi + 3.568\theta_2 - 0.5352\phi - 400 = 0$$

whence, $5.568\theta_2 - 0.3852\phi - 400 = 0$ - - - - (i)

The joint equilibrium equations at (3) and (4) will not provide independent equations because in the previous substitutions in the slope-deflection equations θ_3 was made equal to zero and θ_4 was equal to $-\theta_2$.

Shear Equations: -

Due to symmetry the horizontal reactions at points (1) and (5) are equal and opposite and therefore in static balance. Since we have two unknowns θ_2 and ϕ, we need another equation to use with equation (i). This equation can be obtained by stating that the horizontal reaction H_{2-1} on member 2-1 at end (2) must be equal and opposite to H_{2-3}, the horizontal reaction at end (2) of member 2-3.

Fig. A12.25 and 26 show free body sketches of members 1-2 and 2-3.

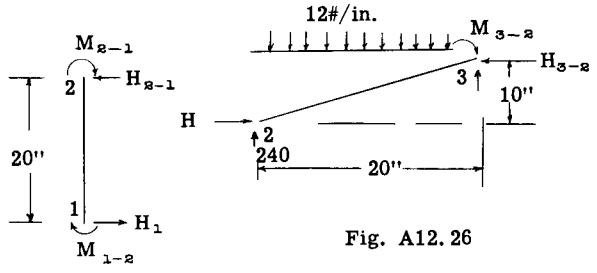

Fig. A12.26

Fig. A12.25

In Fig. A12.25 take moments about (1) and equate to zero.

$$M_{1-2} + M_{2-1} - 20H_{2-1} = 0$$

whence, $H_{2-1} = \dfrac{M_{1-2} + M_{2-1}}{20}$

and in Fig. A12.26, taking moments about (3),

$$M_{2-3} + M_{3-2} + 240 \times 20 - 20 \times 12 \times 10 - 10H_{2-3} = 0$$

whence, $H_{2-3} = \dfrac{M_{2-3} + M_{3-2} + 2400}{10}$

Shear equation, $H_{2-1} = H_{2-3}$

whence,

$$\frac{M_{1-2}+M_{2-1}}{20} = \frac{M_{2-3}+M_{3-2}+2400}{10}$$

Substituting values for the end moments: -

$$\frac{\theta_2 + 0.15\phi + 2\theta_2 + 0.15\phi}{20} = \frac{3.568\theta_2 - 0.5352\phi}{10}$$

$$\frac{-400 + 1.784\theta_2 - 0.5352\phi + 400 + 2400}{10}$$

whence,

$$0.3852\theta_2 - 0.122\phi + 240 = 0 \text{ - - - - - - (j)}$$

Solving equations i and j for θ_2 and ϕ, gives

$$\phi = 2805, \quad \theta_2 = 265.8$$

Substituting these values in equations (a) to (h), the end moments are obtained as follows: -

$M_{1-2} = \theta_2 + 0.15\phi = 265.8 + 0.15 \times 2805$
$= 686.5$ in.lb.

$M_{2-1} = 2\theta_2 + 0.15\phi = 531.6 + 420.7 = 952$

$M_{2-3} = 3.568\theta_2 - 0.5352\phi - 400$
$= 3.568 \times 265.8 - 0.5352 \times 2805 - 400$
$= -952$

$M_{3-2} = 1.784\theta_2 - 0.5352\phi + 400$
$= 1.784 \times 265.8 - 0.5352 \times 2805 + 400$
$= 628$

$M_{3-4} = -1.784\theta_2 + 0.5352\phi - 400 = -628$

$M_{4-3} = 952$

$M_{4-5} = -952$

$M_{5-4} = -686.5$

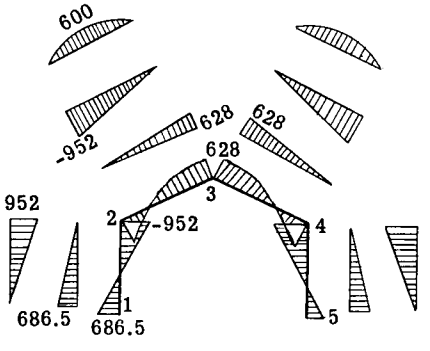

Fig. A12.27

Fig. A12.27 shows the resulting bending moment diagram, first drawn in parts for each member of the frame and then added to form the composite diagram plotted directly on the frame. The shears and axial loads follow as a matter of statics. With the moment diagram known the frame deflected shape is readily calculated.

A12.9 Comments on Slope-Deflection Method.

The example problems solutions indicate that the method of slope-deflection has two advantages, namely, (1) it reduces the number of equations to be solved simultaneously and (2) it presents equations that are easily and rapidly formulated.

Thus for structures with a high degree of redundancy, the slope-deflection method should be considered as possibly the best method of solution. The solving of the equations in this method are readily programmed for solution by high speed computing machinery.

A12.10 Problems.

(1) Determine the bending moments at support points A, B, C, D, for the continuous beam shown in Fig. A12.28.

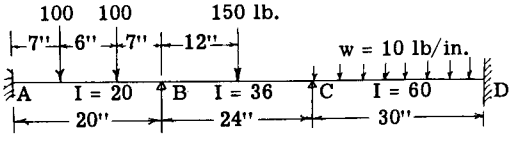

Fig. A12.28

(2) Same as problem (1) but consider support A as freely supported instead of fixed.

(3) Determine the bending moment diagram for the various loaded structures in Fig.A12.29.

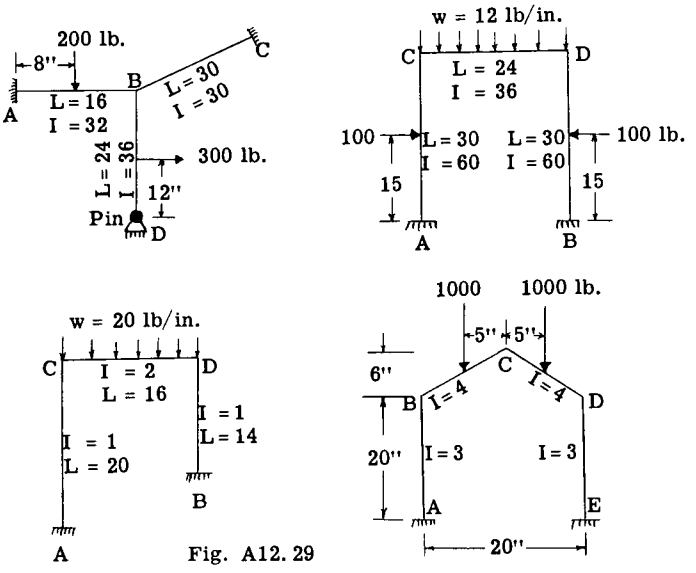

Fig. A12.29

CHAPTER A13
BENDING STRESSES

A13.0 Introduction.

The bar AB in Fig. a is subjected to an axial compressive load P. If the compressive stresses are such that no buckling of the bar takes place, then bar sections such as 1-1 and 2-2 move parallel to each other as the bar shortens under the compressive stress.

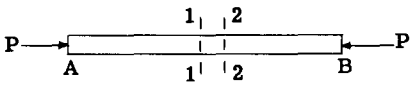

Fig. a

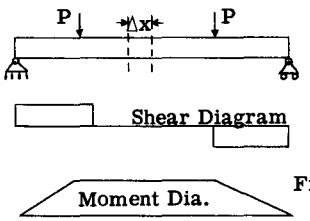

Fig. b

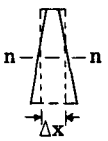

Fig. c

In Fig. b the same bar is used as a simply supported beam with two applied loads P as shown. The shear and bending moment diagrams for the given beam loading are also shown. The portion of the beam between sections 1-1 and 2-2 under the given loading are subjected to pure bending since the shear is zero in this region.

Experimental evidence for a beam segment Δx taken in this beam region under pure bending shows that plane sections remain plane after bending but that the plane sections rotate with respect to each other as illustrated in Fig. c, where the dashed line represents the unstressed beam segment and the heavy section the shape after pure bending takes place. Thus the top fibers are shortened and subjected to compressive stresses and the lower fibers are elongated and subjected to tensile stresses. Therefore at some plane n-n on the cross-section, the fibers suffer no deformation and thus have zero stress. This location of zero stress under pure bending is referred to as the neutral axis.

A13.1 Location of Neutral Axis.

Fig. d shows a cantilever beam subjected to a pure moment at its free end, and under this applied moment the beam takes the exaggerated deflected shape as shown.

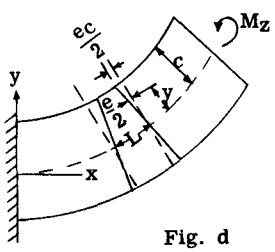

Fig. d

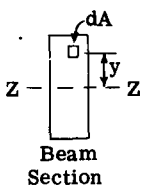

The applied bending moment vector acts parallel to the Z axis, or in other words the applied bending moment acts in a plane perpendicular to the Z axis. Consider a beam segment of length L. Fig. d shows the distortion of this segment when plane sections remain plane after bending of the beam.

It will be assumed that the beam section is homogeneous, that is, made of the same material, and that the beam stresses are below the proportional limit stress of the material or in other words that Hooke's Law holds.

From the geometry of similar triangles,

$$\frac{e}{y} = \frac{e_c}{c} \text{ or } e = \frac{y}{c} e_c \quad \text{- - - - - - - - - - - - - (A)}$$

We have from Youngs Modulus E, that

$$E = \frac{\text{unit stress}}{\text{unit strain}} = \frac{-\sigma_y}{e/L}$$

where σ_y is the bending stress under a deformation e and since it is compression it will be given a minus sign.

Solving for σ_y,

$$\sigma_y = - E \frac{e_c}{c} \frac{y}{L}$$

The most remote fiber is at a distance y = c. Hence

$$\sigma_y = - E \frac{e_c}{L}$$

whence

$$\sigma_y = - \frac{\sigma_c}{c} y \quad \text{- - - - - - - - - - - - - - - - - (B)}$$

For equilibrium of the bending stress perpendicular to the beam cross-section or in the X direction, we can write $\Sigma F_X = 0$, or

$$\Sigma F_X = - \frac{\sigma_c}{c} \int y da = 0.$$

however in this expression, the term $\frac{\sigma_c}{c}$ is not zero, hence the term $\int y da$ must equal zero and this can only be true if the neutral axis coincides with the centroidal axis of the beam cross-section.

The neutral axis does not pass through the beam section centroid when the beam is nonhomogeneous that is, the modulus of elasticity is not constant over the beam section and also when Hooke's Law does not apply or where the stress-strain relationship is non-linear. These beam conditions are described later in this Chapter.

A13.2 Equations for Bending Stress, Homogeneous Beams, Stresses Below Proportional Limit Stress.

In the following derivations, it will be assumed that the plane of the external loads contain the flexural axis of the beam and hence, the beam is not subjected to torsional forces which, if present, would produce bending stresses if free warping of the beam sections was restrained, as occurs at points of support. The questions of flexural axes and torsional effects are taken up in later chapters.

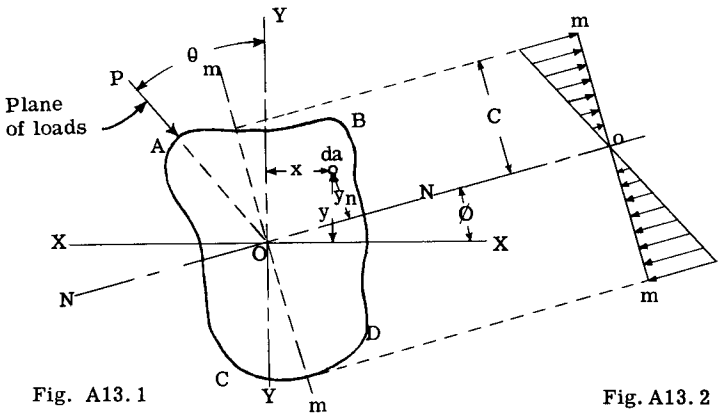

Fig. A13.1 Fig. A13.2

Fig. A13.1 represents a cross-section of a straight cantilever beam with a constant cross-section, subjected to external loads which lie in a plane making an angle θ with axis Y-Y through the centroid O. To simplify the figure, the flexural axis has been assumed to coincide with the centroidal axis, which in general is not true.

Let NN represent the neutral axis under the given loading, and let Ø be the angle between the neutral axis and the axis X-X. The problem is to find the direction of the neutral axis and the bending stress σ at any point on the section.

In the fundamental beam theory, it is assumed that the unit stress varies directly as the distance from the neutral axis, within the proportional limit of the material. Thus, Fig. A13.2 illustrates how the stress varies along a line such as mm perpendicular to the neutral axis N-N.

Let σ represent unit bending stress at any point a distance y_n from the neutral axis. Then the stress σ on da is

$$\sigma = k y_n \quad \text{- - - - - - - - - - - - - - - - - - - -} \quad (1)$$

where k is a constant. Since the position of the neutral axis is unknown, y_n will be expressed for convenience in terms of rectangular coordinates with respect to the axes X-X and Y-Y.

Thus, $y_n = (y - x \tan \phi) \cos \phi$ - - - - - -

$= y \cos \phi - x \sin \phi$ - - - - - - - - - - - - - - (2)

Then Eq. (1) becomes

$$\sigma = k (y \cos \phi - x \sin \phi) \quad \text{- - - - - - - - - -} \quad (3)$$

This equation contains three unknowns, σ, k, and Ø. For solution, two additional equations are furnished by conditions of equilibrium namely, that the sum of the moments of the external forces that lie on one side of the section ABCD about each of the rectangular axes X-X and Y-Y must be equal and opposite, respectively, to the sum of the moments of the internal stresses on the section about the same axes.

Let M represent the bending moment in the plane of the loads; then the moment about axis X-X and Y-Y is $M_x = M \cos \theta$ and $M_y = M \sin \theta$. The moment of the stresses on the beam section about axis X-X is $\int \sigma \, da \, y$. Hence, taking moments about axis X-X, we obtain for equilibrium,

$$M \cos \theta = \int \sigma \, da \, y$$

$$= \int k (\cos \phi \, y^2 da - \sin \phi \, xyda)$$

$$= k \cos \phi \int y^2 da - k \sin \phi \int xyda \quad \text{- - - -} \quad (4)$$

In similar manner, taking moments about the Y-Y axis

$$M \sin \theta = \int \sigma \, da \, x$$

whence

$$M \sin \theta = - k \sin \phi \int x^2 da + k \cos \phi \int xyda \quad (4a)$$

A13.3 Method 1. Stresses for Moments About the Principal Axes.

In equation (4), the term $\int y^2 da$ is the moment of inertia of the cross-sectional area about axis X-X, which we will denote by I_x, and the term $\int xyda$ represents the product of inertia about axes X-X and Y-Y. We know, however, that the product of inertia with respect to the principal axes is zero. Therefore, if we select XX and YY in such a way as to make them coincide with the principal axes, we can write equation (4):

$$M \cos \theta = k \cos \phi \, I_{x_p} \quad \text{- - - - - - - - - - -} \quad (5)$$

In like manner, from equation (4a)

$$M \sin \theta = - k \sin \phi \, I_{y_p} \quad \text{- - - - - - - - - -} \quad (6)$$

To find the unit stress σ at any point on the cross-section, we solve equation (5) for cos Ø and equation (6) for sin Ø, and then substituting these values in (3), we obtain the following expressing, giving σ the subscript b to represent bending stress: -

$$\sigma_b = \frac{M \cos \theta \, y_p}{I_{x_p}} + \frac{M \sin \theta \, x_p}{I_{y_p}}$$

Let the resolved bending moment M cos θ and M sin θ about the principal axes be given the symbols M_{x_p} and M_{y_b}. Then we can write

$$\sigma_b = - \frac{M_{x_p} y_p}{I_{x_p}} - \frac{M_{y_p} x_p}{I_{y_p}} \quad - - - - - - - - - - - - \quad (7)$$

The minus signs have been placed before each term in order to give a negative value for σ_b when we have a positive bending moment, or M_{xp} is the moment of a couple acting about X_p-X_p, positive when it produces compression in the upper right hand quadrant. M_{y_p} is the moment about the Y_p-Y_p axis, and is also positive when it produces compression in the upper right hand quadrant.

BENDING STRESS EQUATION FOR SYMMETRICAL BEAM SECTIONS

Since symmetrical axes are principal axes (term $\int$ xyda = 0), the bending stress equation for bending about the symmetrical XX and YY axes is obviously,

$$\sigma_b = - \frac{M_x y}{I_x} - \frac{M_y x}{I_y} \quad - - - - - - - - - - - - - \quad (7a)$$

A13.4 Method 2. Stresses by use of Neutral Axis for Given Plane of Loading.

The direction of the neutral axis NN, measured from the XX_p principal axis is given by dividing equation (6) by (5).

$$\text{Tan } \alpha = - \frac{I_{x_p}}{I_{y_p}} \tan \theta \quad - - - - - - - - - - - - - \quad (8)$$

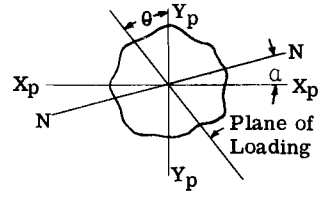

The negative sign arises from the fact that θ is measured from one principal axis and Ø is measured in the same direction from the other principal axis.

Since equation (8) gives us the location of the neutral axis for a particular plane of loading, the stress at any point can be found by resolving the external moment into a plane perpendicular to the neutral axis N-N and using the moment of inertia about the neutral axis, hence

$$\sigma_b = \frac{[M \cos (\theta - \alpha)] \, y_n}{I_n} = \frac{M_n y_n}{I_n} \quad - - - - - - \quad (9)$$

I_n can be determined from the relationship expressed in Chapter A3, namely,

$$I_n = I_{x_p} \cos^2 \alpha + I_{y_p} \sin^2 \alpha \quad - - - - - - - - - \quad (10)$$

A13.5 Method 3. Stresses from Moments, Section Properties and Distances Referred to any Pair of Rectangular Axes through the Centroid of the Section.

The fiber stresses can be found without resort to principal axes or to the neutral axis.

Equation (4) can be written:

$$M_x = k \cos \phi \, I_x - k \sin \phi \, I_{xy} \quad - - - - - - \quad (11)$$

where $I_x = \int y^2 da$ and $I_{xy} = \int xyda$, and M_x = M cos θ.

In like manner,

$$M_y = - k \sin \phi \, I_y + k \cos \phi \, I_{xy} \quad - - - - - \quad (12)$$

Solving equations (11) and (12) for sin Ø and cos Ø and substituting their values in equation (3), we obtain the following expression for the fiber stress σ_b: -

$$\sigma_b = - \frac{(M_y I_x - M_x I_{xy})}{I_x I_y - I_{xy}^2} x - \frac{(M_x I_y - M_y I_{xy}) y}{I_x I_y - I_{xy}^2} \quad (13)$$

For simplification, let

$$K_1 = I_{xy}/(I_x I_y - I^2_{xy})$$

$$K_2 = I_y/(I_x I_y - I^2_{xy})$$

$$K_3 = I_x/(I_x I_y - I^2_{xy})$$

Substituting these values in Equation (13): -

$$\sigma_b = - (K_3 M_y - K_1 M_x) x - (K_2 M_x - K_1 M_y) y \quad (14)$$

In Method 2, equation (8) was used to find the position of the neutral axis for a given plane of loading. The location of the neutral axis can also be found relative to any pair of rectangular centroidal axes X and Y as follows: - Since the stress at any point on the neutral axis must be zero, we can write from equation (14) that: -

$(K_3 M_y - K_1 M_x)x = - (K_2 M_x - K_2 M_y)y$ for all points located on the neutral axis. From Fig. A13.1 $\tan \phi = \frac{y}{x}$,

Thus $$\tan \phi = - \frac{(K_3 M_y - K_1 M_x)}{(K_2 M_x - K_1 M_y)} \quad - - - - - - - \quad (15)$$

It frequently happens that the plane of the bending moment coincides with either the X-X or the Y-Y axis, thus making either M_X or M_y equal to zero. In this case, equation (15) can be simplified. For example, if $M_y = 0$

$$\tan \phi = \frac{I_{xy}}{I_y} \quad \text{- - - - - - - - - - - - - - - - - - (16)}$$

and if $M_X = 0$

$$\tan \phi = \frac{I_x}{I_{xy}} \quad \text{- - - - - - - - - - - - - - - - - - (17)}$$

A13.6 Advantages and Disadvantages of the Three Methods.

Method 2 (bending about the neutral axis for a given plane of loading) no doubt gives a better picture of the true action of the beam relative to its bending as a whole. The point of maximum fiber stress is easily determined by placing a scale perpendicular to the neutral axis and moving it along the neutral axis to find the point on the beam section farthese away from the neutral axis. In airplane design, there are many design conditions, which change the direction of the plane of loading, thus, several neutral axes must be computed for each beam section, which is a disadvantage as compared to the other two methods.

In determining the shears and moments on airplane structures, it is common practice to resolve air and landing forces parallel to the airplane XYZ axes and these results can be used directly in method 3, whereas method 1 requires a further resolution with respect to the principal axes. Methods 1 and 3 are more widely used than method 2.

Since bending moments about one principal axis produces no bending about the other principal axis, the principal axes are convenient axes to use when calculating internal shear flow distribution.

A13.7 Deflections.

The deflection can be found by using the beam section properties about the neutral axis for the given plane of loading and the bending moment resolved in a plane normal to the neutral axis. The deflection can also be found by resolving the bending moment into the two principal planes and then using the properties about the principal axes. The resultant deflection is the vector sum of the deflections in the direction of the principal planes.

A13.8 Illustrative Problems. Example Problem 1.

Fig. A13.3 shows a unsymmetrical one cell box beam with four corner flange members a, b, c and d. Let it be required to determine the bending axial stress in the four corner members due to the loads P_X and P_y acting 50" from the section abcd.

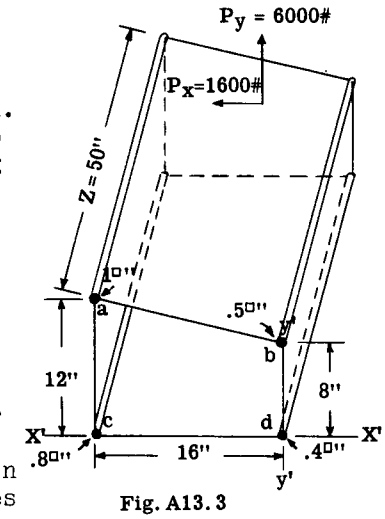

Fig. A13.3

In this example solution the sheet connecting the corner members will be considered ineffective in bending. The stresses will be determined by each of the three methods as presented in this chapter.

SOLUTION

The first step common to all three methods is the calculation of the moments of inertia about the centroidal X and Y axes. Table A13.1 gives the detailed calculations. The properties are first calculated about the reference axes x'x' and y'y' and then transferred to the parallel centroidal axes.

TABLE A13.1

Mem.	Area "A"	y'	x'	Ay'	Ax'	Ay'^{2}	Ax'^{2}	Ax'y'
a	1.0	12	-16	12	-16	144.0	256.0	-192
b	0.5	8	0	4	00	32.0	0	0
c	0.8	0	-16	0	-12.8	0	204.8	0
d	0.4	0	0	0	0	0	0	0
Totals	2.7			16	-28.8	176.0	460.8	-192

Calculation of Centroid of Section: -

$$\bar{x} = \frac{\Sigma Ax'}{\Sigma A} = \frac{-28.8}{2.7} = -10.667"$$

$$\bar{y} = \frac{\Sigma Ay'}{\Sigma A} = \frac{16}{2.7} = 5.926"$$

$$I_x = 176 - 2.7 \times \overline{5.926^2} = 81.18$$

$$I_y = 460.8 - 2.7 \times \overline{10.667^2} = 153.58$$

$$I_{xy} = -192 - (2.7 \times -10.667 \times 5.926) = -21.33$$

Solution by Method 1 (bending about principal axes)

The angle ϕ between the x axis and the principal axes is given by the equation,

$$\tan 2\phi = \frac{2 I_{xy}}{I_y - I_x} = \frac{2 (-21.33)}{153.58 - 81.18} = \frac{-42.66}{72.40} =$$

$$= -.589$$

$$2\phi = 30^\circ - 30', \quad \phi - 15^\circ = 15'$$

$$I_{x_p} = I_x \cos^2 \phi + I_y \sin^2 \phi - 2 I_{xy} \sin \phi \cos \phi$$

$$= 81.18 \times \overline{.9648}^2 + 153.58 \times \overline{.2636}^2 - (-21.33 \times$$

$$- .2636 \times .9648)2$$

$$= 75.56 + 10.67 - 10.85 = 75.38 \text{ in.}^4$$

$$I_{y_p} = I_x \sin^2 \phi + I_y \cos^2 \phi + 2 I_{xy} \sin \phi \cos \phi$$

$$= 81.18 \times \overline{.2636}^2 + 153.58 \times \overline{.9647}^2 + 10.85 =$$

$$159.34 \text{ in.}^4$$

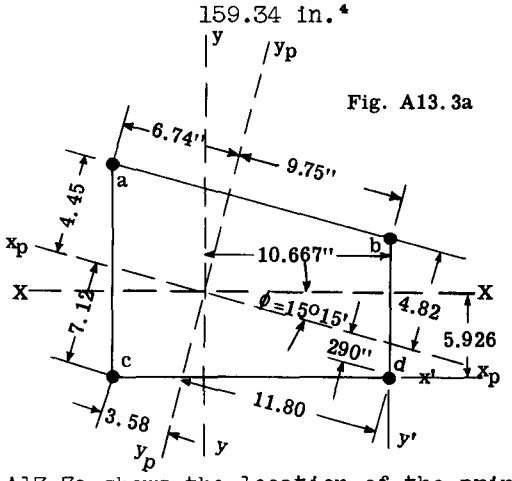

Fig. A13.3a

Fig. A13.3a shows the location of the principal axes, as well as the perpendiuclar distances from each corner member to each of the principal axes. These distances are readily determined from elementary trigonometry.

The external bending moment about the X and Y axes equal,

$$M_x = 6000 \times 50 = 300{,}000 \text{"\#}$$

$$M_y = -1600 \times 50 = -80{,}000 \text{"\#}$$

These moments will be resolved into bending moments about the x_p and y_p principal axes.

$$M_{x_p} = 300{,}000 \times \cos 15^\circ - 15' - 80000 \times$$

$$\sin 15^\circ - 15' = 289700 - 21000 = 268700 \text{"\#}$$

$$M_{y_p} = -300000 \times \sin 15^\circ - 15' - 80000 \times$$

$$\cos 15^\circ - 15' = -79000 - 77200 = -156200 \text{"\#}$$

(Positive moments produce compression in upper right hand quadrant).

Calculation of Stresses

$$\sigma_b = -\frac{M_{xp}\, y_p}{I_{xp}} - \frac{M_{yp}\, x_p}{I_{yp}}$$

Stringer a

$$x_p = -6.74, \quad y_p = 4.45$$

hence

$$\sigma_b = -\frac{268700 \times 4.45}{75.38} - \frac{-156200 (-6.74)}{159.34}$$

$$= -15900 - 6600 = -22500 \#/\text{in.}^2$$

Stringer b

$$x_p = 9.75", \quad y_p = 4.82$$

$$\sigma_b = -\frac{268700 \times 4.82}{75.38} - \frac{-156200 \times 9.75}{159.34}$$

$$= -17180 + 9570 = -7610 \#/\text{in.}^2$$

Stringer c

$$x_p = -3.58, \quad y_p = -7.12$$

$$\sigma_b = \frac{-268700 \times -7.12}{75.38} - \frac{-156200 (-3.58)}{159.34}$$

$$= 25400 - 3520 = 21880$$

and similarly for stringer d, $\sigma_b = 21900$.

Solution by Method 2 (Neutral Axis Method)

Let θ' = angle between yy axis and plane of loading.

$$\tan \theta' = \frac{-80000}{300000} = -.2667$$

hence

$$\theta' = 14^\circ - 56' \text{ and } \theta = 14^\circ - 56' + 15^\circ - 15' =$$

$$= 30^\circ - 11$$

Let α = angle between neutral axis NN and the X_p axis,

$$\tan \alpha = -\frac{I_{xp} \tan \theta}{I_{yp}} = \frac{-75.38 (-0.5816)}{159.34} = .275$$

hence $\alpha = 15^\circ - 24'$ (see Fig. A13.3b).

Since the angle between the X axis and the neutral axis is only 9', we can say $I_N = I_x = 81.18$.

Resolving the external bending moments normal to neutral axis, we obtain

M_N = 300000 x .9999 + 80000 x sin 0° - 9' = 300200"#. The bending stress at any point is given by,

$$\sigma_b = \frac{M_n\, y_n}{I_n}$$

Stringer a

$$y_n = 6.074 + 5.33 \times .0025 = 6.087"$$

$$\sigma_b = \frac{-\ 300\ 200 \times 6.087}{81.18} = -\ 22500\#/in.^2$$

Stringer b

$$y_n = 2.055"$$

$$\sigma_b = \frac{-\ 300\ 200 \times 2.05}{81.18} = -\ 7570$$

Stringer c

$$y_n = -\ 5.92$$

$$\sigma_b = \frac{-\ 300\ 200\ (-\ 5.92)}{81.18} = 21850$$

Stringer d

$$y = -\ 5.95$$

$$\sigma_b = \frac{-\ 300\ 200\ (-\ 5.95)}{81.18} = 22000$$

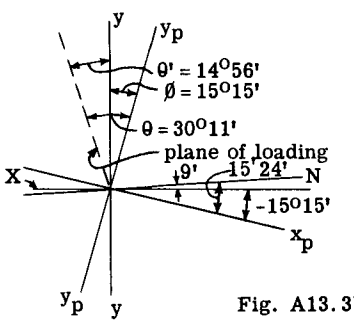

Fig. A13.3b

Solution by Method 3 (Method Using Properties About X and Y Axes)

M_x = 300000, M_y = - 80000

I_x = 81.18, I_y = 153.58,

I_{xy} = - 21.33

$$K_1 = I_{xy}/(I_x I_y - I_{xy}^2) = \frac{-\ 21.33}{81.18 \times 153.58 - 21.33^2} =$$

$$\frac{-\ 21.33}{12016} = -\ .00177$$

$$K_2 = I_y/(I_x I_y - I_{xy}^2) = 153.58/12016 = .012794$$

$$K_3 = I_x/(I_x I_y - I_{xy}^2) = 81.18/12016 = .00674$$

$$\sigma_b = -\ (K_3 M_y - K_1 M_x)\ x - (K_2 M_x - K_1 M_y)\ y$$

Stringer a

$$x = -\ 5.333", \quad y = 6.074"$$

$$\sigma_b = -\ \Big[.00674\ (-\ 80000) + .00177 \times 300000\Big]\ x -$$

$$\Big[.012794 \times 300000 - .00177\ (-\ 80000)\Big]\ y$$

$$\text{hence } \sigma_b = (8)\ x - (3697) y;$$

$$\text{hence } \sigma_b = 8 \times -\ 5.33 - 3697 \times 6.074 = -\ 22450$$

Stringer b

$$x = 10.667, \quad y = 2.074$$

$$\sigma_b = 8 \times 10.667 - (3697)\, 2.074 = 85 - 7660 = -\ 7575$$

Stringer c

$$x = -\ 5.333, \quad y = -\ 5.926$$

$$\sigma_b = 8 \times -\ 5.333 - (3697 \times -\ 5.926) = -$$

$$42 + 21900 = 21862$$

Stringer d

$$x = 10.667, \quad y = -\ 5.926$$

$$\sigma_b = 8 \times 10.667 - (3697 \times -\ 5.926) =$$

$$= 85 + 21900 = 21985$$

NOTE: The stresses σ_b by the three methods were calculated by 10" slide rule, hence the small discrepancy between the results for the three methods.

Error in Stresses Due to Assumption that Section Bends About X and Y Centroidal Axes Due to M_x and M_y.

$$\sigma_b = -\ \frac{M_x\, y}{I_x} - \frac{M_y\, x}{I_y} \qquad \text{(Equation 7a)}$$

Stringer a

$$y = 6.074, \quad x = -\ 5.33$$

$$\sigma_b = -\ \frac{300000 \times 6.074}{81.18} - \frac{-\ 80000 \times -\ 5.33}{153.58} = -\ 25190$$

Stringer b

$$y = 2.07, \quad x = 10.667$$

Stringer b - cont'd.

$$\sigma_b = - \frac{300000 \times 2.07}{81.18} - \frac{- 80000 \times 10.667}{153.58} = - 2110$$

In like manner for stringers c and d

$$\sigma_{b_c} = 19130 \quad \text{and} \quad \sigma_{b_c} = 27440$$

Comparing these results with the previous results it is noticed that considerable error exists. Under these eroneous stresses the internal resisting moment does not equal the external bending moments about the X and Y axis.

Example Problem 2.

Fig. A13.4 shows a portion of a cantilever 2-cell stressed skin wing box beam. In this example, the beam section is considered constant, and the section is identical to that used in

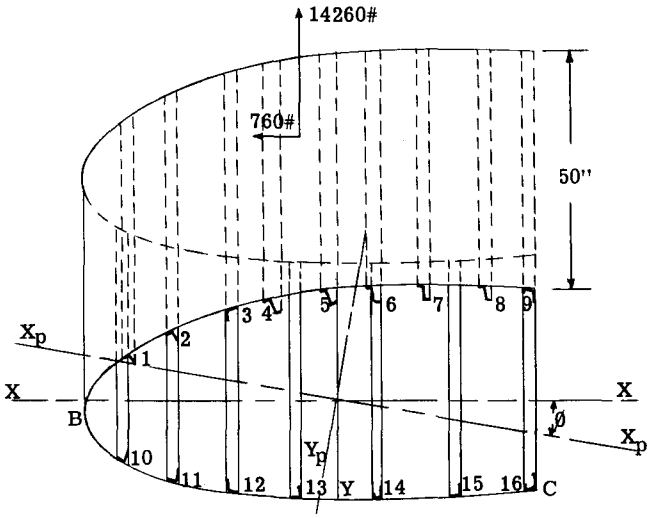

Fig. A13.4

Fig. A3.13 of Chapter A3 for which the section properties were computed and are as follows: -

I_X = 186.5 in.^{4} I_y = 431.7 in.^{4} I_{xy} = 36.41 in.^{4}
Ø = 8° - 16.25" I_{x_p} = 181.2 I_{y_p} = 437

The resultant air load on the wing outboard of section ABC is 14260# acting up in the Y direction and 760# acting forward in the X direction, and the location of these resultant loads is 50 from section ABC (Fig. A13.4).

The bending stress intensity at the centroids of stringers number (1), (9) and (12) will be calculated using all three methods.

Solution by Method 1 (Bending about Principal Axes)

The bending moment at section ABC about the X and Y axes is,

$$M_x = 14260 \times 50 = 713{,}000"\#$$

$$M_y = - 760 \times 50 = - 38000"\#$$

These moments are resolved into bending moments about the principal axes, as follows: -

$$M_{x_p} = 713000 \times \cos Ø - 38000 \times \sin Ø = 700{,}000"\#$$

$$M_{y_p} = - 71300 \times \sin Ø - 38000 \times \cos Ø = -140000"\#$$

From equation (7), the general formula for σ_b is:

$$\sigma_b = - \frac{M_{x_p}\, y_p}{I_{x_p}} - \frac{M_{y_p}\, x_p}{I_{y_p}}$$

Stress on Stringer 1:

y_p = 1.85" and x_p = - 17.86" (scaled from full size drawing).

$$\sigma_b = - \frac{(700000 \times 1.85)}{181.17} - \frac{- 140000 \times (- 17.86)}{437}$$

$$= - 7150 - 5700 = - 12850\#/\text{sq. in.}$$

Stress on Stringer 9:

$$y_p = 9.04", \quad x_p = 14.24"$$

$$\sigma_b = - \frac{(700000 \times 9.04)}{181.17} - \frac{- 140000 \times 14.24}{437}$$

$$= - 34{,}900 + 4560 = - 30340\#/\text{sq. in.}$$

Stress on Stringer 12:

$$y_p = - 6.80", \quad x_p = - 8.22"$$

$$\sigma_b = - \frac{700000 \times (- 6.80)}{181.17} - \frac{- 140000 \times (- 8.22)}{437} =$$

$$= 26200 + 2630 = + 23570\#/\text{sq. in.}$$

Solution by Method 2 (Neutral Axis Method)

In Fig. A13.5 let Θ' be the angle between the Y-Y axis and the plane of the resultant bending moment. Resultant bending moment,

$$M = \sqrt{713000^2 + 38000^2} = 714600" \text{ lb.}$$

$$\tan Θ' = \frac{- 38000}{713000} = - .0533, \text{ hence } Θ' = - 3° - 3'$$

Let Θ equal the angle between the plane of the resultant moment and the Y_p axis.

Then Θ = Θ' + Ø = 3° - 3' + 8° - 16' = 11° - 19'

From equation (8), the angle between the X_p axis and the neutral axis = α, and

$$\tan α = - \frac{I_{xp} \tan Θ}{I_{yp}} = - \frac{181.17 \times (- .200)}{437} =$$

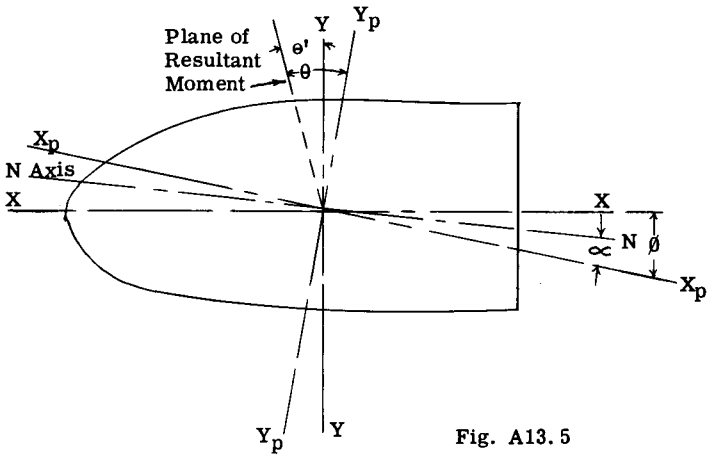

Fig. A13.5

= .083. Hence, α = 4° - 45'

Fig. A13.5 shows the relative positions of the neutral axis, principal axes, and plane of loading.

The component of the external resultant moment about the neutral axis N equals: -

$$M_N = 714060 \times \sin 83° - 26' = 709350 \text{ in. lb.}$$

$$I_N = I_{xp} \cos^2 \alpha + I_{yp} \sin^2 \alpha$$

$$= 181.17 \times \overline{.9966}^2 + 437 \times \overline{.0878}^2 = 183.37 \text{ in.}^4$$

Stress on Stringer 1:

$$y_{n_1} = (y_p + x_p \tan \alpha) \cos \alpha = (1.85 + 17.86 \times .083)\ .9966 = 3.32"$$

$$\sigma_{b_1} = -\frac{M_n\, y_n}{I_n} = \frac{-\ 709350 \times 3.32}{183.37} = -\ 12850\#/\text{sq. in.}$$

Stress on Stringer 9:

$$y_{n_9} = (9.04 - 14.24 \times .083)\ .9966 = 7.84"$$

$$\sigma_{b_9} = \frac{-\ 709350 \times 7.84}{183.37} = -\ 30300\#/\text{sq. in.}$$

Stress on Stringer 12:

$$y_{n_{12}} = (6.80 + 8.22 \times .083)\ .9966 = 6.10$$

$$\sigma_{b_{12}} = \frac{-\ 709350 \times -\ 610}{183.37} = 23600\#/\text{sq. in.}$$

Solution by Method 3

$$M_X = 713000"\#, \quad M_y = -\ 38000"\#$$

$I_X = 186.46$ $I_y = 431.7$ $I_{xy} = -\ 36.41$

The constants K_1, K_2, and K_3 are first determined -

$$K_1 = I_{xy}/(I_X I_y - I^2_{xy}) = \frac{-\ 36.41}{186.46 \times 431.7 - 36.41^2}$$

$$= -\ .00046$$

$$K_2 = I_y/(I_X I_y - I^2_{xy}) = \frac{431.7}{186.46 \times 431.7 - 36.41^2}$$

$$= \frac{431.7}{793000} = .00545$$

$$K_3 = I_X/(I_X I_y - I^2_{xy}) = \frac{186.46}{793000} - = .002355$$

Stress on Stringer 1:

$$y_1 = 4.39", \quad x_1 = -\ 17.41"$$

$$\sigma_b = -\ (K_3 M_y - K_1 M_X)x - (K_2 M_X - K_1 M_y)y$$

$$\sigma_{b_1} = \left[.002355 \times (-\ 38000) - (-\ .00046 \times 713000)\right]$$

$$(-\ 17.41\ )$$

$$-\ \left[.00545 \times 713000 - (-\ .00046 \times -\ 38000)\right] 4.39$$

$$= -\ (238.5)(-\ 17.41) - (3868)\ 4.39$$

$$= 4150 - 17000 = -\ 12850\#/\text{in.}^2$$

Stress on Stringer 9:

$$y_9 = 6.89", \quad x_9 = 15.39"$$

$$\sigma_{b_9} = -\ \left[238.5\right] 15.39 = \left[3868\right] 6.89 = -\ 30320\#/\text{in.}^2$$

Stress on Stringer 12:

$$y_{12} = -\ 5.55", \quad x_{12} = -\ 9.11"$$

$$\sigma_{b_{12}} = -\ \left[238.5\right] (-\ 9.11) - \left[3868\right] (-\ 5.55) =$$

$$= 23620\#/\text{in.}^2$$

NOTE: In the three solutions, the distance from the axis in question to the stringers 1, 9, and 12 have been taken to the centroid of each stringer unit. Thus, the stresses obtained are average axial stresses on the stringers. If the maximum stress is desired, the arm should refer to the most remote part of the stringer or the skin surface.

Approximate Method.

It is sometimes erroneously assumed that the external bending moments M_X and M_y produce bending about the X and Y axes as though they were neutral axes. To show the error of this assumption, the stresses will be computed for stringers 1 and 9.

Stringer 1:

$$y_1 = 4 + .39 = 4.39$$

$$x_1 = -33.15 + 15.74 = -17.41$$

$$\sigma_b = \frac{-M_x y}{I_x} - \frac{M_y x_1}{I_y}$$

$$\sigma_b = \frac{-713000 \times 4.39}{186.46} - \frac{(-38000 \times -17.41)}{431.7} =$$

$$-18330\#/in^2.$$

Stringer 9:

$$y_9 = 6.89, \quad x_9 = 15.39$$

$$\sigma_b = \frac{-713000 \times 6.89}{186.46} - \frac{(-38000 \times 15.39)}{431.7} -$$

$$-25000\#/in^2.$$

Example Problem 3.

The previous example problems were solved by substituting in the bending stress equations. The student should solve bending stress problems by equating the internal resisting moment at a beam section to the external bending moment at the same section. To illustrate Fig. A13.6 shows a simply supported loaded beam. The shear and bending moment diagram for the given beam loading is also shown. Fig. A13.7 shows the beam section which is constant along the span.

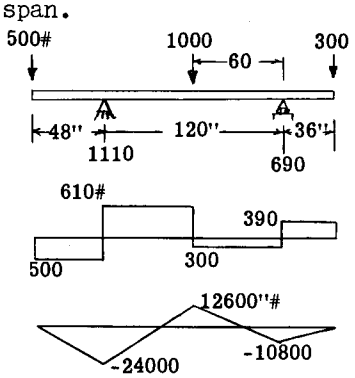

Fig. A13.6

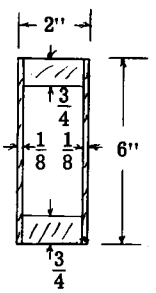

Fig. A13.7

The maximum bending moment occurs over the left support and equals - 24000 in. lbs. Due to symmetry of the beam cross-section the centroidal horizontal axis is the center line of the beam and thus the neutral axis is at the midpoint of the beam.

Fig. A13.8 shows a free body of that portion of the beam from the left end to a section over the left support where the bending moment is maximum. The triangular bending stress intensity diagram is shown acting on the cut section, with a value of σ_b at the most remote fiber. The forces T_A, T_B etc. represent the total load on the beam cross-sectional areas labeled A and B respectively in Fig. A13.9. The

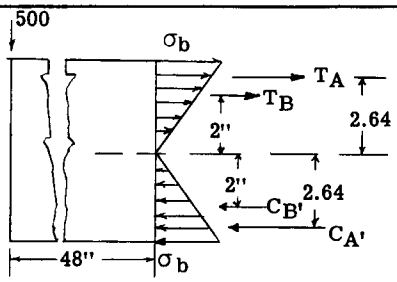

Fig. A13.8

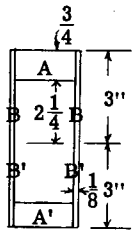

Fig. A13.9

stress intensity at bottom edge of portion A is σ_b $(2.25/3) = 0.75\ \sigma_b$.

$T_A = C_A'$ = Average stress times area

$$= \left(\frac{\sigma_b + 0.75\sigma_b}{2}\right)(1.75 \times 0.75) = 1.15\sigma_b$$

The distance from the neutral axis to the centroid of the trapizoidal stress loading on portion A is 2.64 inches. In like manner,

$$T_B = C_B' = \left(\frac{0 + \sigma_b}{2}\right) 3 \times 0.25 = 0.375\sigma_b$$

The arm to T_B is $0.667 \times 3 = 2$ inches.

For equilibrium of the beam free body, take moments about point (0) and equate to zero.

$$\Sigma M_0 = -500 \times 48 + 2.64 \times T_A + 2.64\ C_A' + 2\ T_B +$$

$$2\ C_B' = 0$$

Substituting values as found for T_A, T_B etc,

$$-500 \times 48 + 2.64 \times 1.15\ \sigma_b + 2.64 \times 1.15\ \sigma_b$$

$$+ 2 \times 0.375\ \sigma_b + 2 \times 0.375\ \sigma_b = 0$$

hence $$\sigma_b = \frac{24000}{7.58} = 3170 \text{ psi.}$$

Solution using Bending Stress Formula.

$\sigma_b = \frac{M\,c}{I}$ where M = - 24000
c = 3"
I = Moment of inertia about Neutral axis.

Calculation of I.

For Portions A and A'

$$I = \frac{1}{12} \times 1.75\ (6^3 - \overline{4.5}^3) = 18.26\ in^4.$$

For Web Portions b, b",

$$I = \frac{1}{12} \times 0.25 \times 6^3 = \underline{4.50\ in^4.}$$

$$I_{Total} = 22.76\ in^4.$$

hence

$$\sigma_b = \frac{-\ 24000 \times 3}{22.76} = -\ 3170 \text{ psi.},$$

which checks first solution.

Example Problem 4.

Fig. A13.10 shows a loaded beam and Fig. A13.11 shows the cross-section of the beam at section a-a'. Determine the magnitude of the maximum bending stress at section a-a' under the given beam loading. The beam section is unsymmetrical about the horizontal centroidal axis. Simple calculations locate the neutral axis as shown in Fig. A13.11.

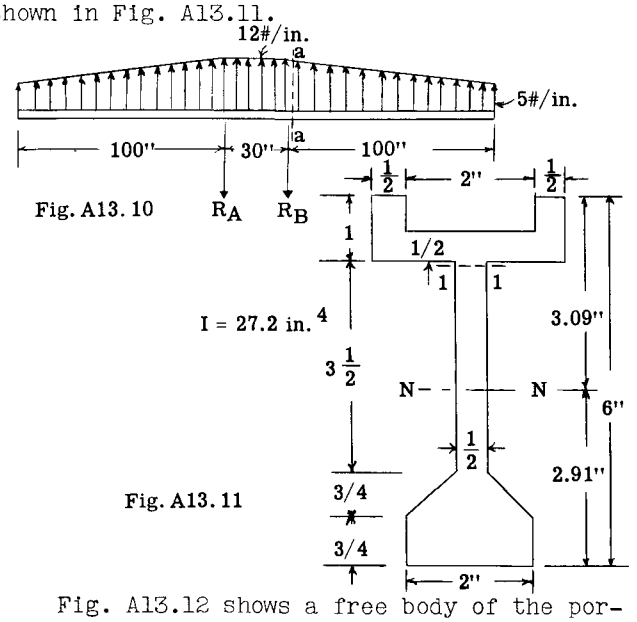

Fig. A13.11

Fig. A13.12 shows a free body of the portion of the beam to the right of section a-a. The bending stress intensity diagram is shown by the horizontal arrows acting on the beam face at section a-a. Fig. A13.13 shows the cross-section of the beam at section a-a.

The general procedure will be to determine the total bending stress load on each portion, 1 to 6, of the cross-section and then the moment of each of these loads about the neutral axis, the summation of which must equal the external bending moment.

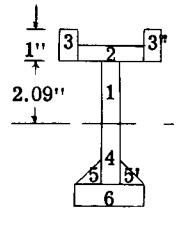

Fig. A13.13

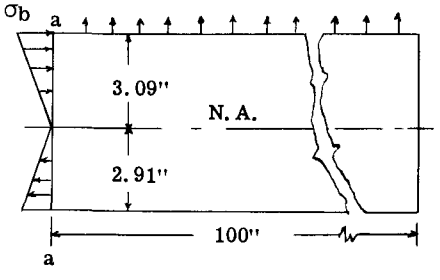

Fig. A13.12

This method of solution involves more calculations than that required in substituting in the bending stress formula, however, the student should obtain a better understanding of the internal force action from this method of solution. In solving nonhomogeneous beams and beams stressed above the elastic limit stress, this method of solution often proves necessary or advantageous because no simple beam bending stress formula can be derived.

In Fig. A13.12, let σ_b be the intensity on the most remote fiber, or 3.09" above the neutral axis. Table A shows the calculations of the total stress on each of the portions of the cross-section and their moment about the neutral axis, all in terms of the unknown stress, σ_b.

TABLE A

1	2	3	4	5	6
Portion See Fig. A13.13	Area A	Average Stress in terms of σ_b	Total Load = (2) x (3)	y = arm to N.A.	Resisting moment (4) x (5)
1	1.045	$-.337\sigma_b$	$-.353\sigma_b$	1.39	$-.490\ \sigma_b$
2	1.00	-.757	-.757	2.35	-1.780
3 - 3'	1.00	-.837	-.837	2.62	-2.190
4	1.09	.350	.387	-1.44	-0.557
5 - 5'	0.56	.578	.323	-1.93	-0.622
6	1.50	$.821\sigma_b$	$1.237\sigma_b$	-2.57	$-3.180\ \sigma_b$
Totals	6.19		$0.000\sigma_b$		$-8.82\ \sigma_b$

Explanation of Table A.

Column 3 gives the average stress on each of the 6 portions. For example, the stress on portion (1) varies from zero at the neutral axis to $\frac{2.09}{3.09}\sigma_b = .674\ \sigma_b$ at the upper edge of (1). Thus, the average stress $= \frac{.674\ \sigma_b + 0}{2} = .337\ \sigma_b$. On part 3 or 3', the stress on the lower edge $= .674\ \sigma_b$ and σ_b on the upper edge. Then, the average stress $= \frac{(1 + .674)}{2}\sigma_b = .837\ \sigma_b$. Column 5 is the distance from the neutral axis to the centroid of the load on each of the blocks. For portion (1) the stress pattern is triangular, and y = 2/3 x 2.09 = 1.39". On portions (2), (3), (5) and (6) the bending stress distribution is trapezoidal, and the arm is to the centroid of this trapezoid.

The total internal resisting moment of $-\ 8.82\ \sigma_b$ from Table A equals the external bending moment of 36670"#.
Thus,

$$\sigma_b = \frac{-\ 36670}{8.82} = -\ 4160\#/\text{in.}^2.$$

For equilibrium, the total compressive stresses on the cross-section of the beam must be equal to the total tensile stresses, or ΣH must equal zero. Column 4 of Table A gives the

total load on each portion of the cross-section and the total of this column is zero.

The bending stress on the lower fiber of the cross-section is directly proportional to the distance from the neutral axis or, $\sigma_{b_{lower}} = \frac{2.91}{3.09} \times 4160 = 3930\#/in.^2$

SOLUTION USING BENDING STRESS FORMULA.

$\sigma_b = \frac{M\,y}{I_{N.A.}}$ $\qquad I_{N.A.} = 27.2\ in.^4$

hence

σ_b (upper fiber) $= \frac{-\ 36670 \times 3.09}{27.2} = -\ 4160$ psi.

which checks the above solution.

A13.9 Bending Stresses in Beams with Non-Homogeneous Sections, Stresses within the Elastic Ranges.

In general, beams are usually made of one material, but special cases often arise where two different materials are used to form a beam section. For example, a commerical airplane in its lifetime often undergoes a number of changes or modifications such as the addition of additional installations, fixed equipment, larger engines, etc. This increase in airplane weight increases the structural stresses and it often becomes necessary to strengthen various structural members at the critical stress points. Since space limitations are usually critical, it often necessitates that the reinforcing material be stiffer than the original material. Years ago, when spruce wood was a common material for wing beams, it was normal practice to use reinforcements at critical stress points of stiffer wood material such as maple in order to cut down the size of the reinforcements. In aluminum alloy beams, the use of heat-treated alloy steel reinforcements are often used because steel is 29000,000/10500,000 or 2.76 times stiffer than aluminum alloy.

SOLUTION BY MEANS OF TRANSFORMED BEAM SECTION.

To illustrate how the stresses in a composite beam can be determined, two example problems will be presented.

Example Problem 5.

Fig. A13.14 shows the original beam section which is entirely spruce wood. Fig. A13.15 shows the reinforced or modified beam section. Two ears of maple wood have been added to the upper part as shown and a steel strap has been added to the bottom face of the beam. The problem is to find the stress at the top and bottom points on the beam section when the beam section is subjected to an external bending moment of 60000 in. lbs. about a horizontal axis which causes compression in the upper beam portion. The modulus of elasticity (E) for the 3 different materials is: -

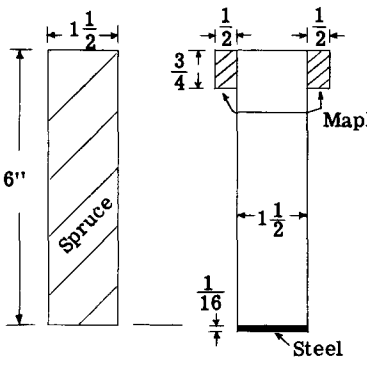

Fig. A13.14 Fig. A13.15

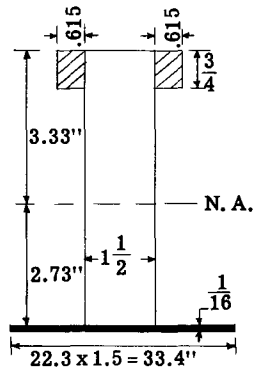

Fig. A13.16 Transformed Section into Equivalent Spruce

$E_{spruce} = 1{,}300{,}000$ psi.

$E_{maple} = 1{,}600{,}000$ psi.

$E_{steel} = 29{,}000{,}000$ psi.

SOLUTION:

The first step in the solution is to transform the reinforced beam section of Fig. A13.15 into an equivalent beam section composed of the same material throughout. This is possible, because the modulus of elasticity of each material gives us the measure of stiffness for that material. In this solution the reinforced beam will be transformed into a spruce beam section as illustrated in Fig. A13.16.

$$\frac{E_{maple}}{E_{spruce}} = \frac{1{,}600{,}000}{1{,}300{,}000} = 1.23$$

$$\frac{E_{steel}}{E_{spruce}} = \frac{29{,}000{,}000}{1{,}300{,}000} = 22.3$$

Thus to transform the maple reinforcing strips in Fig. A13.15 into spruce we increase the width of each strip to 1.23 x 0.5 = 0.615 inches as shown in Fig. A13.16. Likewise, to transform the steel reinforcing strip into spruce, we make the width equal to 22.3 x 1.5 = 33.4 inches as shown in Fig. A13.16.

This transformed equivalent section is now handled like any homogeneous beam section which is stressed within the elastic limit of the materials. The usual calculation would locate the neutral axis as shown and the moment of inertia of the transformed section about the neutral axis would give a value of 51.30 in. .

Bending stress at upper edge of beam section: -

$$\sigma_{b_c} = \frac{-\ M_x\ y}{I_x} \qquad \frac{-\ 60000 \times 3.33}{51.30} = -\ 3900 \text{ psi.}$$

Referring to Fig. A13.15, this stress would be

the stress in the spruce section. Since the reinforcing strips are maple, the stress at the top edge of these maple strips would be 1.23 times (- 3900) = - 4880 psi.

The bending stress at the lower edge of the transformed beam section of Fig. A13.16 would be:

$$\sigma_{b_t} = - \frac{60000 \times (- 2.73)}{51.30} = 3200 \text{ psi.}$$

The stress in the steel reinforcing strap thus equals 22.3 times 3200 = 71500 psi.

Since all these stresses are below the elastic limit stress for the 3 materials the beam bending stress formula as used is applicable.

Example Problem 6.

Fig. A13.17 shows an unsymmetrical beam section composed of four stringers, a,b,c and d of equal area each and connected by a thin web. The web will be neglected in this example problem. Each of the stringers is made from different material as indicated on Fig. A13.17. The beam section is subjected to the bending moment M_x and M_y as indicated. Let it be required to determine the stress and total load on each stringer in resisting these applied external bending moments.

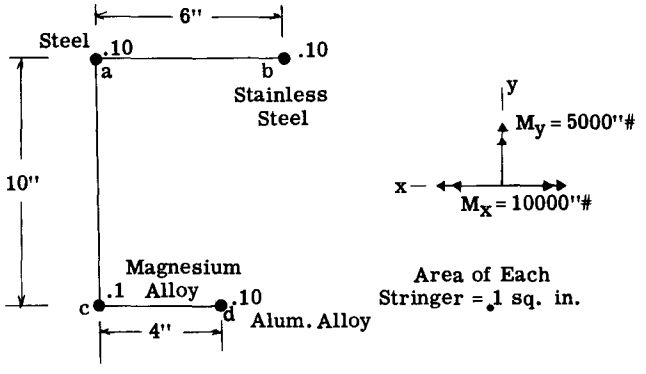

Fig. A13.17

SOLUTION:

Since the 4 stringers are made of different materials we will transform all the materials into an equivalent beam section with all 4 stringers being magnesium alloy.

$E_{mag.}$	= 6,500,000	$\frac{E_{steel}}{E_{mag.}} = \frac{29}{6.5}$	= 4.46
E_{steel}	= 29,000,000		
$E_{stain.steel}$	= 28,000,000	$\frac{E_{S.S.}}{E_{mag.}} = \frac{28}{6.5}$	= 4.31
$E_{alum.alloy}$	= 10,500,000	$\frac{E_{alum.}}{E_{mag.}} = \frac{10.5}{6.5}$	= 1.615

Using the ratio of stiffness values as indicated above gives the transformed beam section of Fig. A13.18 where all material is now magnesium alloy. The original area of 0.1 sq. in. each have been multiplied by these stiffness ratio values.

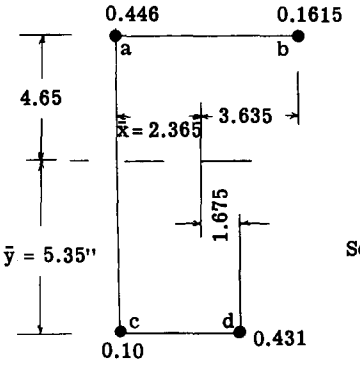

Fig. A13.18 Transformed Beam Section into Magnesium Alloy.

The solution for the beam section of Fig. A13.18 is the same as for any other unsymmetrical homogeneous beam section.

The first step is to locate the centroid of this section and determine the moments of inertia of this section about centroidal X and Y axes.

$$\bar{y} = \frac{\Sigma Ay}{\Sigma A} = \frac{.446 \times 10 + 0.1615 \times 10}{1.1385} = 5.35"$$

$$\bar{x} = \frac{\Sigma AX}{\Sigma A} = \frac{0.1615 \times 6 + .431 \times 4}{1.1385} = 2.365"$$

$$I_x = 0.6075 \times \overline{4.65}^2 + 0.531 \times \overline{5.35}^2 = 28.27 \text{ in.}^4$$

$$I_y = 0.546 \times \overline{2.365}^2 + 0.165 \times \overline{3.635}^2 + 0.431 \times \overline{1.635}^2 = 6.34 \text{ in.}^4.$$

$$\begin{aligned} I_{xy} = {} & 0.446\ (- 2.365)(4.65) = - 4.90 \\ & 0.1615 \times 3.635 \times 4.65 = 2.73 \\ & 0.10\ (- 2.365)(- 5.35) = 1.27 \\ & 0.431 \times 1.635\ (- 5.35) = - 3.77 \\ & \text{TOTAL} = - 4.67 \text{ in.}^4 = I_{xy} \end{aligned}$$

The bending stresses will be calculated by using method 3 of Art. A13.5.

From Equation (14) Art. A13.5 --

$$\sigma = - (K_3 M_y - K_1 M_x)x - (K_2 M_x - K_1 M_y)y$$

$$K_1 = \frac{I_{xy}}{I_x I_y - I_{xy}^2} = \frac{- 4.67}{28.27 \times 6.34 - 4.67^2} =$$

$$\frac{- 4.67}{157.4} = - 0.0296$$

$$K_2 = \frac{I_y}{I_x I_y - I_{xy}^2} = \frac{6.34}{157.4} = 0.0403$$

$$K_3 = \frac{I_x}{I_x I_y - I_{xy}^2} = \frac{28.27}{157.4} = 0.1797$$

M_x = - 10,000 in. lb. M_y = 5000 in. lb.

Consider Stringer (c): -

$$x = -2.365, \quad y = -5.35$$

Substituting in σ_b equation

$$\sigma_c = -\left[0.1797 \times 5000 - (-0.0296)(-10000)\right]x$$

$$-\left[(0.0403)(-10000) - (-.0296 \times 5000)\right] y$$

$$= -(898 - 296)\, x - \left[(-403) + 148\right] y$$

$$\sigma_c = -602\, x + 255\, y \quad \text{---------- (18)}$$

For stringer (c) $x = -2.365$, $y = -5.35$ hence

$$\sigma_c = -602\ (-2.365) + 255\ (-5.35)$$

$$= 1423 - 1360 = 63 \text{ psi.}$$

The total load P_c in stringer (c) thus equals σ_c (Area) = 63 x 0.1 = 6 lbs. tension.

Stringer (a):

$$x = -2.365, \quad y = 4.65$$

from equation (18)

$$\sigma_a = -602\ (-2.365) + 255 \times 4.65 = 2613 \text{ psi.}$$

$$P_a = 2613 \times 0.446 = 1167. \text{ lb. tension.}$$

Since the true area of this stringer is 0.1 square the stress in this steel stringer equals 1167 /0.1 = 11670 psi. tension.

Stringer (b):

$$x = 3.635, \quad y = 4.65$$

$$\sigma_b = -602 \times 3.635 + 255 \times 4.65 = -1006 \text{ psi.}$$

$$P_b = -1006 \times 0.1615 = -162 \text{ lbs.}$$

True stress in stainless steel stringer = - 162 /0.1 = - 1628 psi.

Stringer (d):

$$x = 1.635, \quad y = -5.35$$

$$\sigma_d = -602 \times 1.635 + 255\ (-5.35) = -2345 \text{ psi.}$$

$$P_d = -2345 \times 0.431 = -1010 \text{ lbs.}$$

$$\text{True stress} = \frac{-1010}{0.1} = -10100 \text{ psi.}$$

To check the results, check total stringer loads to see if they equal zero.

$$\Sigma P = 6 + 1167 - 162 - 1010 = 1 \text{ check.}$$

Forthermore the moments of the stringer loads about the X and Y axes must equal the applied external bending moments.

Take moments about a Y axis through stringers (a) and (c).

$$\Sigma M_y = -6 \times 162 - 4 \times 1010 + 5000$$

$$= -12 \text{ in. lb.}$$

Take moments about X axis through stringers (c) and (d),

$$\Sigma M_x = 1162 \times 10 - 162 \times 10 - 10000$$

$$= 0 \text{ in. lb.}$$

(The calculations in this example being done on a slide rule can not provide exact checks).

A13.10 Bending Stresses of Homogeneous Beams Stressed above the Elastic Limit Stress Range.

In structural airplane design, the applied loads on the airplane must be taken by the structure without suffering permanent strain which means the stresses should fall within the elastic range. The airplane structural design loads which in general equal the applied loads times a factor of safety of 1.5 must be taken by the structure without collapse or rupture with no restriction on permanent strain. Many airplane structural beams will not fail until the stresses are considerably above the elastic stress range for the beam material.

Since the stress-strain relationship in the inelastic range is not linear and also since the stress-strain curve for a material in the inelastic range is not the same under tensile and compressive stresses (See Fig. A13.19), the beam bending stress formulas as previously derived do not apply since they were based on a linear variation of stress to strain. Experimental tests however, have shown that even when stressed in the inelastic range, that plane sections before bending remain plane after after bending, thus strain deformation is still linear which fact simplifies the problem since the stress corresponding to a given strain can be found from a stress-strain curve for the beam material.

A general method of approach to solving beams that are stressed above the elastic range can best be explained by the solution of a problem.

Example Problem 7.

Portion (a) of Fig. A13.20 shows a solid round bar made from 24ST aluminum alloy material. Fig. A13.19 shows a stress-strain curve for this material. Let it be assumed

that the maximum failing compressive stress occurs at a strain of 0.01 in. per inch. The problem is to determine the ultimate resisting moment developed by this round bar and then compare the result with that obtained by using the beam bending stress formula based on linear variation of stress to strain.

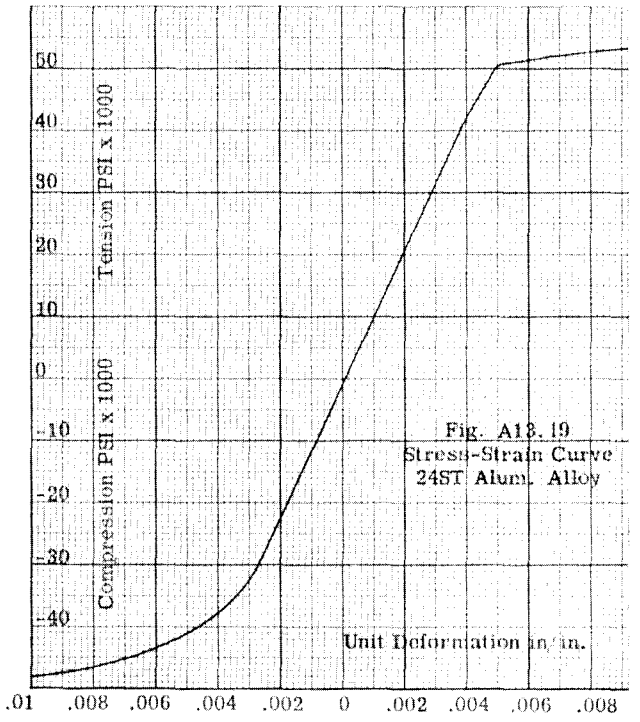

Fig. A13.19
Stress-Strain Curve
24ST Alum. Alloy

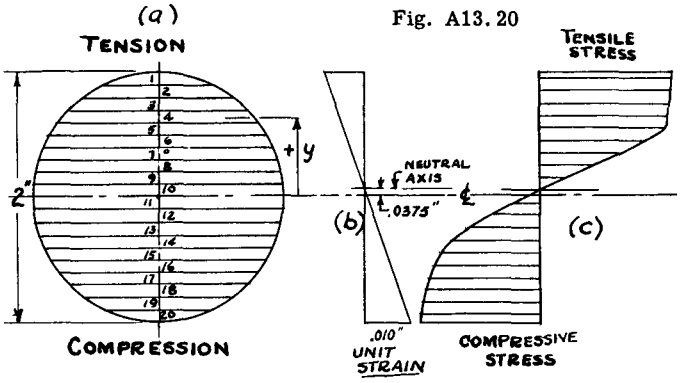

Fig. A13.20

SOLUTION:

Since the stress-strain diagram in tension is different from that in compression (See Fig. A13.19) the neutral axis will not coincide with the centroidal axis of the round bar regardless of the fact that it is a symmetrical shape. Thus the method of solution is a trial and error one since the location of the neutral axis can not be solved for directly. In Fig. b of Fig. A13.20 the neutral axis has been assumed 0.0375 inches above the centerline axis of the bar. It was assumed toward the tension side because observation of the stress-strain curve of Fig. A13.19 shows that for a given strain in the inelastic range the resulting tensile stress is higher than the resulting compressive stress, and furthermore from internal equilibrium the total tensile stress on the cross-section must equal the total compressive stress.

The problem as stated assumed that a compressive unit strain of 0.01 caused failure. Fig. b thus shows the strain picture on the beam just before failure since plane sections remain plane after bending in the inelastic range. Table A13.2 gives the detailed calculations for determining the internal resisting moment developed under the given strain condition.

TABLE A13.2

1	2	3	4	5	6	7
Strip No.	Strip Area "A"	y	ε	Unit Stress σ	F = σA	Res. Moment M = Fr
1	.058	0.935	.00867	53000	3075	2760
2	.102	0.840	.00773	52500	5350	4300
3	.135	0.75	.00685	52100	7025	5040
4	.153	0.65	.00591	51500	7870	4820
5	.165	0.55	.00494	51000	8410	4310
6	.180	0.45	.00398	43000	7740	3200
7	.185	0.35	.00302	33200	6140	1920
8	.195	0.25	.00205	22800	4450	945
9	.197	0.15	.00108	12500	2460	280
10	.200	0.05	.00012	3200	640	10
11	.200	-0.05	-.00084	- 7250	-1450	130
12	.197	-0.15	-.00181	-17800	-3510	660
13	.195	-0.25	-.00276	-29500	-5750	1650
14	.185	-0.35	-.00374	-35500	-6560	2540
15	.180	-0.45	-.00470	-40000	-7200	3510
16	.165	-0.55	-.00566	-43000	-7100	4170
17	.153	-0.65	-.00663	-44800	-6850	4710
18	.135	-0.75	-.00759	-46000	-6210	4880
19	.102	-0.84	-.00846	-47200	-4810	4210
20	.058	-0.935	-.00937	-48000	-2780	2690
Total	3.140				740	56735

Col. 1 Rod divided into 20 strips .1" thick.
Col. 3 y = distance from centerline to strip c.g.
Col. 4 ε = strain at midpoint = (y - .0375)/103.75
Col. 5 Unit stress for ε strain from Fig. A13.19
Col. 6 Total stress on strip.
Col. 7 Moment about neutral axis. M = (y - .0375)F.

The summation of column (6) should be zero. Since the discrepancy is 740 lbs., it means that the assumed position for the neutral axis is a little too high, however the discrepancy is negligible. The total internal resisting moment is 56735 in. lbs. (Col. 7).

If we take a maximum unit compressive strain of 0.01 we find the corresponding stress from Fig.A13.19 to be 48500 psi. If this stress is used as the failing stress in the beam formula $M = \frac{\sigma I}{c}$ we obtain,

$$M = 48500 \times 0.785 = 38000 \text{ in. lbs.}$$

$$(0.785 = \frac{I}{c} \text{ of round bar} = \pi r^3/4)$$

Thus using the same failing stress at the far extreme fiber the beam formula based on linear stress-strain relationship gives an ultimate bending strength of 38000 as compared to a true strength of 56735 or only 67 percent as much.

Fig. c of Fig. A13.10 shows the true stress distribution on the cross-section, which explains why the resisting moment is higher than when a triangular distribution is used.

The problem of the ultimate bending strength of structural shapes is discussed in detail in Volume II.

A13.11 Curved Beams. Stresses Within the Elastic Range.

The equations derived in the previous articles of this chapter were for beams that were straight. Thus in Fig. A13.21, the element of length (L) used in the derivation was constant over the depth of the beam. The strain ($\Delta L/L$) was therefore directly proportional to ΔL which had a linear variation.

In a curved beam, the assumption that plane sections remain plane after bending still applies, however the beam segment of a curved beam cannot have equal width over the depth of the beam because of the curvature as illustrated in Fig. A13.22, or in other words the length of the segment is greater on the outside edge (L) than on the inside edge (L_i). Thus in calculating the strain distribution over the beam depth the change in length ΔL at a point must be divided by the segment width at that point. Thus even though plane sections remain plane the strain distribution over the section will not be linear. The width of the segment at any point is directly proportional to the radius of curvature of the segment and thus the strain at a point on the segment is inversely to the radius of curvature. This gives a hyperbolic type of strain distribution as illustrated in Fig. A13.22, and if the strains are within the elastic limit the stress distribution will be similar. The development of a beam formula based on a hyperbolic stress distribution is given in most books on advanced engineering mechanics and will not be repeated here.

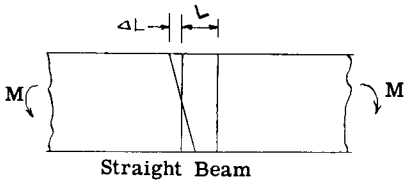

Straight Beam

Fig. A13.21

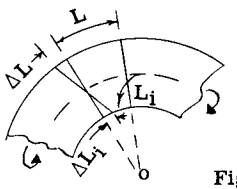

Curved Beam

Fig. A13.22

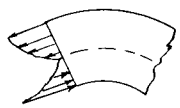
Stress Distribution

It is convenient however to express the influence of the beam curvature in the form of a correction factor K by which the stresses obtained by the beam formula for straight beams can be multiplied to obtain the true stresses for the curved beams. Thus for a curved beam the maximum stress can be calculated from the equation

$$\sigma = K \frac{M c}{I} \qquad \text{- - - - - - - - - - - - - - - - - (19)}$$

Table A13.3 gives the value of K for various beam section shapes and beam radius of curvatures. The table shows that for only rather sharp curvatures is the correction appreciable. In general for airplane fuselage rings on frames the curvature influence can be neglected. However there are often fittings and mechanical structural units in airplane construction whose parts involve enough curvature to make the influence on the stress of primary importance. The concentration of stress on the inside edge of a curved unit in bending may influence the fatigue strength of unit considerably, thus a consideration of the possible influence of curvature should be a regular part of design procedure.

In the inelastic or plastic stress range, the influence of beam curvature should be considerably less since the stiffness of a material in the inelastic range is much less than in the elastic stress range and changes rather slowly as the stress increases.

A13.12 Problems.

(1) Fig. A13.23 shows the cross-section of a single cell beam with 12 stringers. Assume the walls and webs are ineffective in bending. Calculate load in each stringer by use of beam formula. Also calculate stringer loads by equating internal resisting moment to external bending moment. Each stringer area is same and equals 0.1 sq. in. applied bending moment M_x = - 100,000 in.lb.

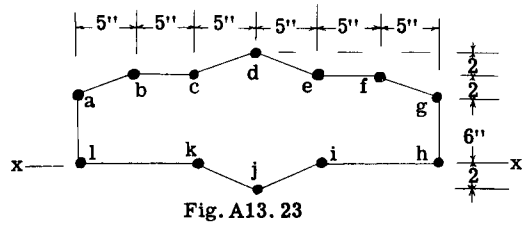

Fig. A13.23

(2) Same as problem (1) but change external bending moment to M_y = 200,000 in.lb.

(3) Fig. A13.24 shows a beam section with 4 stringers. Assume web and walls ineffective in bending. Stringer areas

TABLE A13.3

VALUES OF K FOR USE IN THE BEAM FORMULA $\sigma = K\frac{Mc}{I}$

SECTION	$\frac{R}{c}$	FACTOR K		$\frac{e^*}{R}$
		INSIDE FIBER	OUTSIDE FIBER	
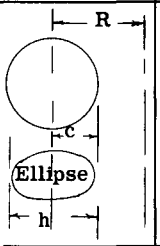	1.2	3.41	0.54	0.224
	1.4	2.40	0.60	0.151
	1.6	1.96	0.65	0.108
	1.8	1.75	0.68	0.084
	2.0	1.62	0.71	0.069
	3.0	1.33	0.79	0.030
	4.0	1.23	0.84	0.016
	6.0	1.14	0.89	0.0070
	8.0	1.10	0.91	0.0039
	10.0	1.08	0.93	0.0025
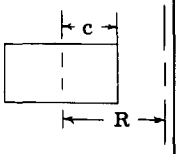	1.2	2.89	0.57	0.305
	1.4	2.13	0.63	0.204
	1.6	1.79	0.67	0.149
	1.8	1.63	0.70	0.112
	2.0	1.52	0.73	0.090
	3.0	1.30	0.81	0.041
	4.0	1.20	0.85	0.021
	6.0	1.12	0.90	0.0093
	8.0	1.09	0.92	0.0052
	10.0	1.07	0.94	0.0033
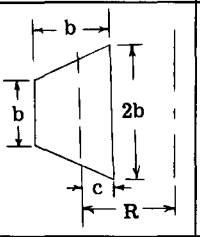	1.2	3.01	0.54	0.336
	1.4	2.18	0.60	0.229
	1.6	1.87	0.65	0.168
	1.8	1.69	0.68	0.128
	2.0	1.58	0.71	0.102
	3.0	1.33	0.80	0.046
	4.0	1.23	0.84	0.024
	6.0	1.13	0.88	0.011
	8.0	1.10	0.91	0.0060
	10.0	1.08	0.93	0.0039
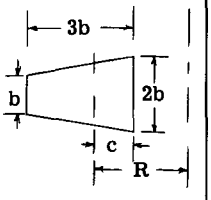	1.2	3.09	0.56	0.336
	1.4	2.25	0.62	0.229
	1.6	1.91	0.66	0.168
	1.8	1.73	0.70	0.128
	2.0	1.61	0.73	0.102
	3.0	1.37	0.81	0.046
	4.0	1.26	0.86	0.024
	6.0	1.17	0.91	0.001
	8.0	1.13	0.94	0.0060
	10.0	1.11	0.95	0.0039
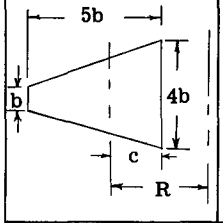	1.2	3.14	0.52	0.352
	1.4	2.29	0.54	0.243
	1.6	1.93	0.62	0.179
	1.8	1.74	0.65	0.138
	2.0	1.61	0.68	0.110
	3.0	1.34	0.76	0.050
	4.0	1.24	0.82	0.028
	6.0	1.15	0.87	0.012
	8.0	1.12	0.91	0.0060
	10.0	1.12	0.93	0.0039
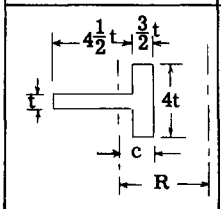	1.2	3.63	0.58	0.418
	1.4	2.54	0.63	0.299
	1.6	2.14	0.67	0.229
	1.8	1.89	0.70	0.183
	2.0	1.73	0.72	0.149
	3.0	1.41	0.79	0.069
	4.0	1.29	0.83	0.040
	6.0	1.18	0.88	0.018
	8.0	1.13	0.91	0.010
	10.0	1.10	0.92	0.0065

TABLE A13.3 (continued)

VALUES OF K FOR USE IN THE BEAM FORMULA $\sigma = K\frac{Mc}{I}$

SECTION	$\frac{R}{c}$	FACTOR K		$\frac{e^*}{R}$
		INSIDE FIBER	OUTSIDE FIBER	
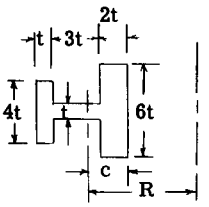	1.2	3.55	0.67	0.409
	1.4	2.48	0.72	0.292
	1.6	2.07	0.76	0.224
	1.8	1.83	0.78	0.178
	2.0	1.69	0.80	0.144
	3.0	1.38	0.86	0.867
	4.0	1.26	0.89	0.038
	6.0	1.15	0.92	0.018
	8.0	1.10	0.94	0.010
	10.0	1.08	0.95	0.0065
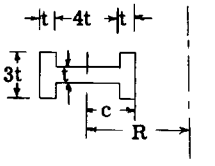	1.2	2.52	0.67	0.408
	1.4	1.90	0.71	0.285
	1.6	1.63	0.75	0.208
	1.8	1.50	0.77	0.160
	2.0	1.41	0.79	0.127
	3.0	1.23	0.86	0.058
	4.0	1.16	0.89	0.030
	6.0	1.10	0.92	0.013
	8.0	1.07	0.94	0.0076
	10.0	1.05	0.95	0.0048
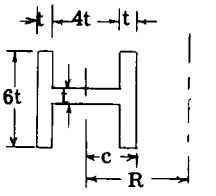	1.2	2.37	0.73	0.453
	1.4	1.79	0.77	0.319
	1.6	1.56	0.79	0.236
	1.8	1.44	0.81	0.183
	2.0	1.36	0.83	0.147
	3.0	1.19	0.88	0.067
	4.0	1.13	0.91	0.036
	6.0	1.08	0.94	0.016
	8.0	1.06	0.95	0.0089
	10.0	1.05	0.96	0.0057
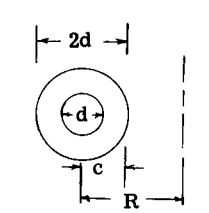	1.2	3.28	0.58	0.269
	1.4	2.31	0.64	0.182
	1.6	1.89	0.68	0.134
	1.8	1.70	0.71	0.104
	2.0	1.57	0.73	0.083
	3.0	1.31	0.81	0.038
	4.0	1.21	0.85	0.020
	6.0	1.13	0.90	0.0087
	8.0	1.10	0.92	0.0049
	10.0	1.07	0.93	0.0031
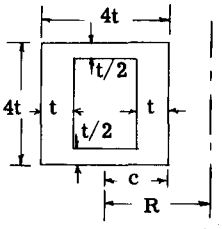	1.2	3.55	0.67	0.409
	1.4	2.48	0.72	0.292
	1.6	2.07	0.76	0.224
	1.8	1.83	0.78	0.178
	2.0	1.69	0.80	0.144
	3.0	1.38	0.86	0.067
	4.0	1.26	0.89	0.038
	6.0	1.15	0.92	0.018
	8.0	1.10	0.94	0.010
	10.0	1.08	0.95	0.0065

*e equals distance from centroidal axis to neutral axis.

References: Wilson and Quereau. "A Simple Method of Determining Stresses in Curved Flexural Members,"
"Advanced Strength of Materials", by Seely.

shown in () on figure. External applied bending moments are;

M_x= -500,000 in.lb. and M_y = 200,000 in.lb.

Find stress on all four stringers by all three methods which were explained in this chapter.

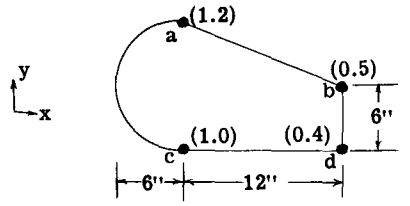

Fig. A13.24

(4) The Zee section shown in Fig. A13.25 is subjected to bending moments of M_x = 500 in.lb. and M_y = 2000 in.lb. Find bending stresses at points a,b,c,d.

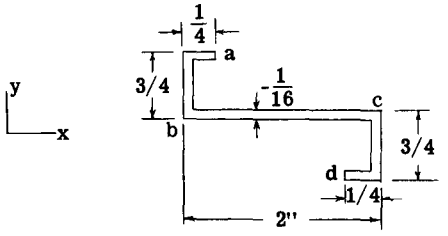

Fig. A13.25

(5) Fig. A13.26 shows a beam section composed of three different materials. Find the stress at top and bottom points on beam due to a bending moment M_x= 80,000 in.lb.

$E_{Mag.}$= 6.5 x 10^6

E_{Steel}= 29 x 10^6

$E_{Alum.}$= 10.5 x 10^6

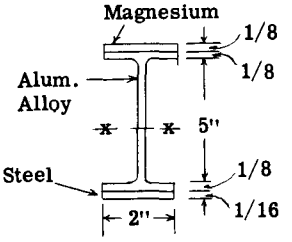

Fig. A13.26

(6) Fig. A13.26 shows a cross-section of a wood beam composed of 3 kinds of wood labeled A, B and C, glued together to form a composite beam. If the beam is subjected to a bending moment M_x = 75000 in.lb., find intensity of bending stress at top edge of beam. Also find total end load on portions B and C.

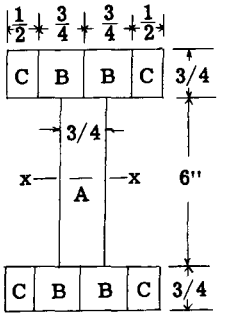

Fig. A13.26

A = Spruce. E = 1,300,000 psi
B = Maple. E = 1,500,000 psi
C = Fir. E = 1,600,000 psi

(7) Fig. A13.27 shows 3 different beam sections. They are made of aluminum alloy whose stress-strain diagram is the same as that plotted in Fig. A13.19. Determine the ultimate internal resisting moment if the maximum compressive strain is limited to 0.01 in./in. Consider that upper portion is in compression. Compare the results obtained with formula $M = \sigma_b I/c$, where σ_b = compressive stress when unit strain is 0.01.

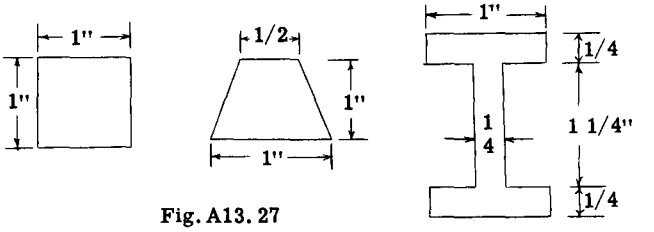

Fig. A13.27

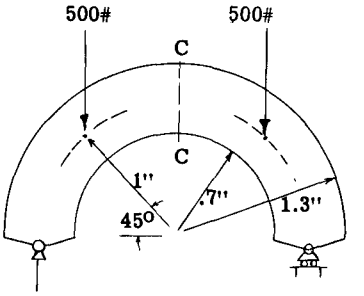

Fig. A13..28

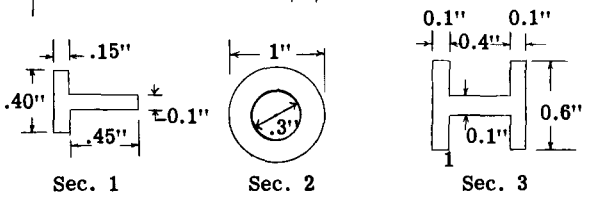

(8) Fig. A13.28 shows a curved beam, carrying two 500 lb. loads. Find bending stresses at points C and C", when beam cross-section is made 3 different ways is indicated by sections 1, 2 and 3. Use Table A13.3.

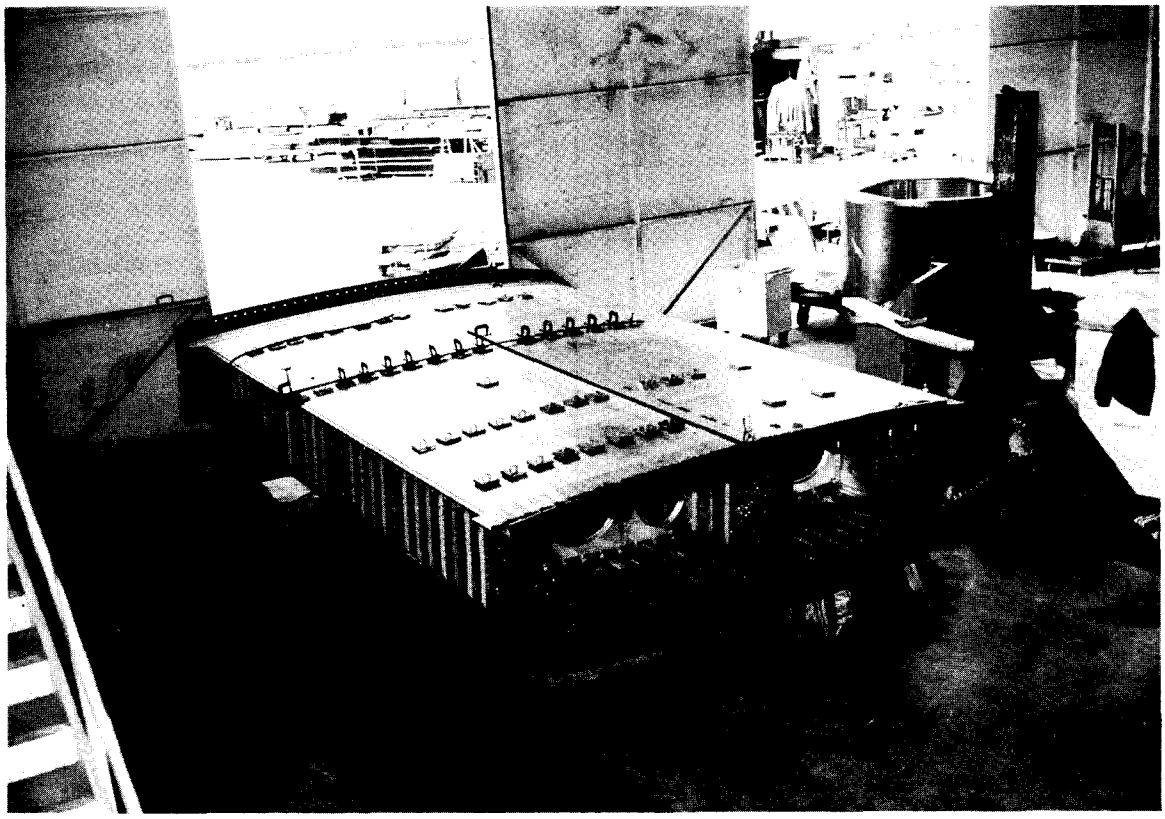

DOUGLAS DC-8 AIRPLANE. Over-all view of the test wing section representing center wing section of DC-8.

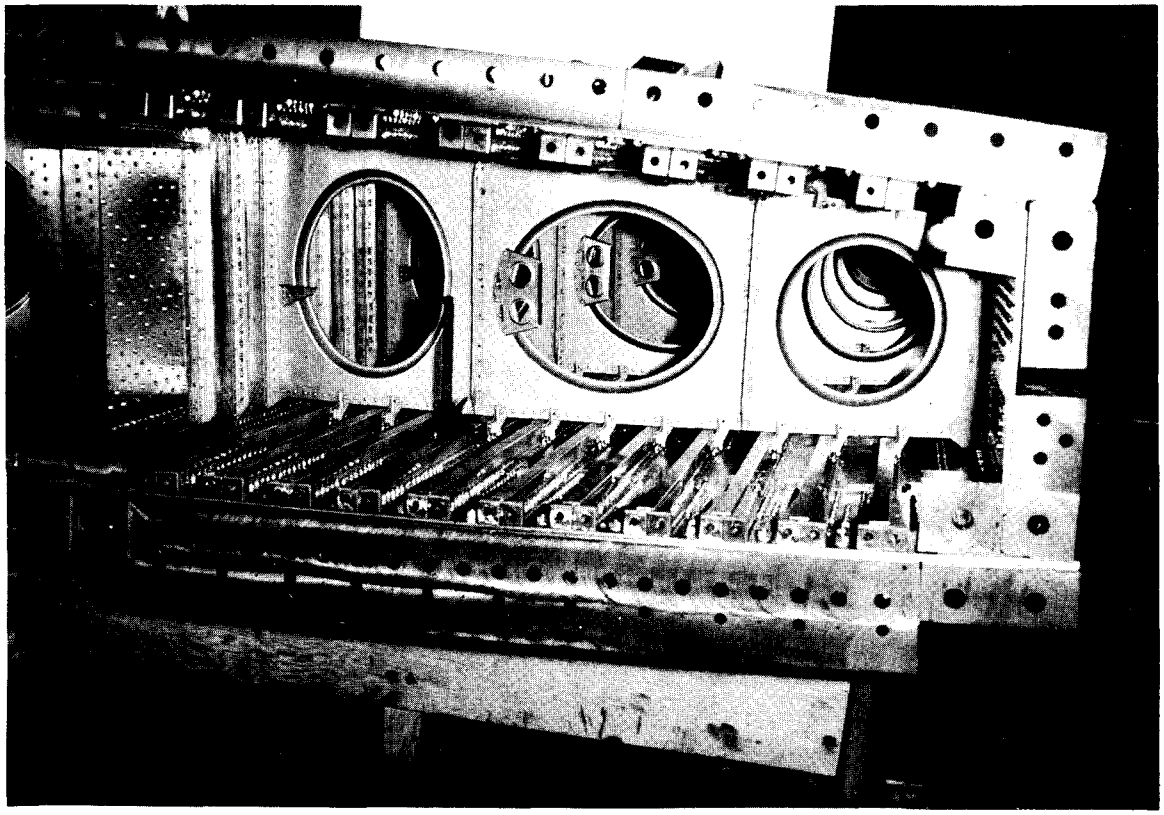

A close-up view of wing test section showing details of wing ribs, stringers, etc.

CHAPTER A 14
BENDING SHEAR STRESSES - SOLID AND OPEN SECTIONS SHEAR CENTER

A14.1 Introduction.

In Chapter A6, the shear stresses in a member subjected to pure torsional forces were considered in detail. In Chapter A13, the subject of bending stresses in a beam subjected to pure bending was considered in considerable detail. In practical structures however, it seldom happens that pure bending forces (couples) are the loading forces on the beam. The usual case is that bending moments on a beam are due to a transfer of external shear forces. Thus bending of a beam usually involves both bending (longitudinal tension and compression stresses) and shear stresses.

The same assumptions that were made in Chapter A13 in deriving the bending stress equations are likewise used in deriving the equations for flexural shear stresses. With flexural shear stresses existing, the assumption that plane sections remain plane after bending is not completely true, since the shearing strains cause the beam sections to slightly warp out of their plane when the beam bends. This warping action is usually referred to by the term "shear lag". However, except in cases of beams with wide thin flanges, the error introduced by neglecting shearing strains is quite small and therefore neglected in deriving the basic flexural shear stress formula. The problem of shear lag influence is considered in other chapters.

A14.2 Shear Center.

When a beam bends without twisting, due to some external load system, shearing stresses are set up on the cross sections of the beam. The centroid of this internal shear force system is often referred to as the shear center for the particular section. The resultant external shear load at this section must pass through the shear center of the section if twist of the section is to be prevented. Thus, if the shear center is known, it is possible to represent the external load influences by two systems, one that causes flexure and the other which causes only twist.

A14.3 Derivation of Formula for Flexural Shear Stress.

Fig. A14.1 shows a loaded simply supported beam. When the beam bends downward due to the given loading, the beam portion above the neutral axis is placed in compression and that below the neutral axis in tension. Consider a short portion dx of the beam at points DF on the beam and treat it as a free body as shown in Fig. A14.3. The variation of tensile and compressive stress on each face of the beam portion

Fig. A14.2

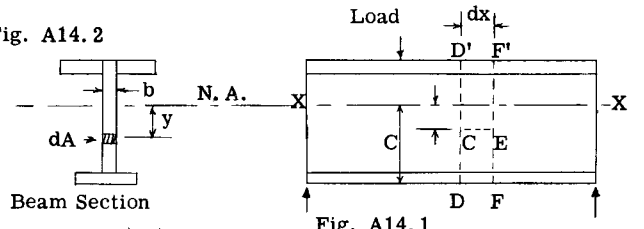

Fig. A14.1

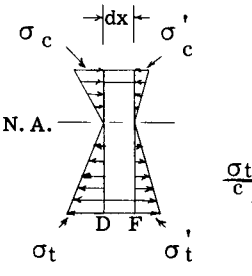

Fig. A14.3

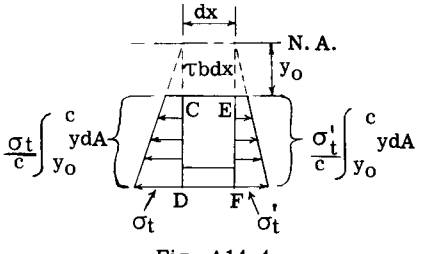

Fig. A14.4

is as indicated. The stress σ_t is greater than σ_t' because the bending moment due to the given beam loading is greater at beam section DD' than at FF'. Now consider that this beam portion dx is further cut as indicated by the notch DCEF in Fig. A14.1, and this segment is shown in Fig. A14.4 as a free body with the forces as indicated.

Let σ_t = maximum tensile stress at a distance c from the neutral axis,

Then the stress at a distance y from neutral axis is $\sigma_y = \sigma_t\, y/c$.

The total load on an element of area dA of the beam cross-section (see Fig. A14.2) thus equals $\frac{\sigma_t}{c} \int y\, dA$.

Now, referring to Fig. A14.4, the total tensile load on each face of this segment will be calculated.

$$\text{Total load on face CD} = \frac{\sigma_t}{c}\int_{y_o}^{c} y\, dA \quad ----- \quad (1)$$

$$\text{Total load on face FE} = \frac{\sigma_t'}{c}\int_{y_o}^{c} y\, dA \quad ---- \quad (2)$$

From Chapter A13, the equation for flexural stress σ was derived, namely $\sigma_t = Mc/I$. Let M equal the bending moment at beam section DD' and M' that at beam section FF' and let I and I' the moment of the inertia of the cross-sectional area about the neutral axis at these same beam sections respectively. Then substituting value of σ_t in equations (1) and (2) we can write,

$$\text{Total load on face CD} = \frac{M}{I}\int_{y_o}^{c} y\, dA \quad ----- \quad (3)$$

Total load on face FE = $\frac{M'}{I'}\int_{y_o}^{c} y\,dA$ - - - - (4)

Now let τ b dx equal the shearing force on face CE of the segment in Fig. A14.4 where τ equals the shearing stress and b dx the shearing area. For equilibrium of the segment, the total forces parallel to x-x axis must be zero. If the beam is of uniform cross-section, which is the case in our problem, then I = I' and c and y_o are the same in both equations (3) and (4).

Then the resultant horizontal force on the sides of the segment equals the difference of the values in (3) and (4), or

$$\text{Resultant horizontal load} = \frac{M - M'}{I}\int_{y_o}^{c} y\,dA.$$

For equilibrium of segment in x-x direction,

$$\Sigma F_X = -\frac{M - M'}{I}\int_{y_o}^{c} y\,dA + \tau\, b\, dx = 0$$

$$\text{hence } \tau = \frac{M - M'}{I\, b\, dx}\int_{y_o}^{c} dA \quad - - - - - - - - - - - - \quad (5)$$

However $\frac{M - M'}{dx} = \frac{dM}{dx} = V$ = the external shear on the beam section.

$$\text{hence } \tau = \frac{V}{I\, b}\int_{y_o}^{c} y\,dA \quad - - - - - - - - - - - - \quad (6)$$

It is important to note that equation (6) applies only to beams of uniform section (constant moment of inertia). In airplane wing structures the common case is for beams to vary in cross-section or moment of inertia, and if this variation is considerable, equation (6) should not be used and resort should be made to equations (3) and (4). This fact is illustrated in example problem 2. This matter of variable cross-sections is discussed later in this chapter.

A14.4 Example Problems. Symmetrical Sections. External Shear Loads Act Thru Shear Center.

Example Problem 1.

Fig. A14.5 shows the cross section of a beam symmetrical about the Y-Y axis. Assume that a beam with this cross-section is subjected to a loading which produces a shear load in the Y direction = to V_y = 850 lb. Its location is through the shear center of the section which lies on the centroidal y axis of the beam section due to the symmetry of the section about this axis. Let it be required to determine the shearing stress at the neutral axis x-x and at points 1-1 and 2-2 of the cross-section as shown in Fig. A14.5. The neutral axis location and moment of inertia of the section about the neutral axis are given on the figure.

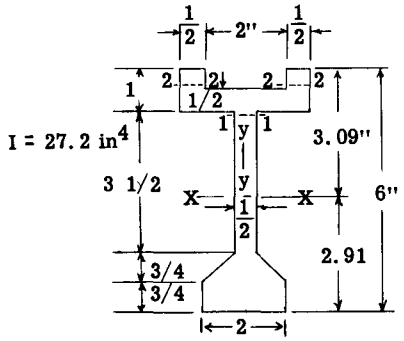

Fig. A14.5

SOLUTION: -

Shear stress at neutral axis x-x

$$\tau_{x-x} = \frac{V_y}{I_x\, b}\int_{o}^{3.09} y\,dA$$

Table A shows the calculation of the term $\int_{o}^{3.09} y\,dA$.

TABLE A. REFER TO FIG. a.

PORTION	Area d A	y	y dA
1	2.09 x 0.5 = 1.045	1.045	1.096
2	3 x 0.5 = 1.50	2.34	3.510
3	0.5 x 0.5 = 0.25	2.84	0.710
3'	0.5 x 0.5 = 0.25	2.84	0.710
		SUM	6.026

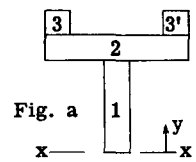

Fig. a

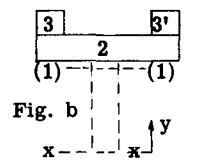

Fig. b

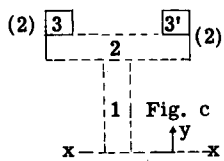

Fig. c

hence $\tau = \frac{850 \times 6.026}{27.2 \times 0.5} = 377$ psi.

Calculation of shear stress at point 1-1, : -

$$\tau_{1-1} = \frac{V_y}{I_x\, b}\int_{2.09}^{3.09} y\,dA\ .$$

Fig. b shows the effective areas in this intregration, thus in Table A, we leave out portion 1, hence $\int y\,dA = 4.93$.

Substituting, $\tau_{1-1} = \frac{850 \times 4.93}{27.2 \times 0.5} = 308$ psi.

This shearing stress is at a section just adjacent to portion (2). If it was taken just adjacent to portion (1), then the width b in the equation would be 3 inches instead of 0.5 inch and the shearing stress would be 0.5/3 times that shown above, or in other words the shearing stress changes abruptly when the shear area changes abruptly.

Shearing stress at point 2-2 on cross-section: -

Fig. c shows effective area, thus in Table A, the portions (1) and (2) are omitted and

$$\int_{2.59}^{3.09} y\,dA \text{ equals } 1.42.$$

Substituting, $\tau_{2-2} = \dfrac{850 \times 1.42}{27.2 \times 1.0} = 44.4$ psi.

(The width b = 0.5 + 0.5 for the two portions 3, 3').

The shearing stresses as calculated act in the plane of the beam cross-section in the Y direction and also with the same intensity parallel to the Z axis which is normal to the beam section.

Example Problem 2. VARIABLE MOMENT OF INERTIA.

Fig. A14.6 shows a cantilever beam loaded with a single load of 600 lb. at the end and acting through the centroid of the beam cross-section. The beam section is constant between stations 0 and 132, then it tapers uniformly to the sections shown for stations 175 and 218. The shear stress distribution on the beam cross-section at stations 175 and 218 will be determined.

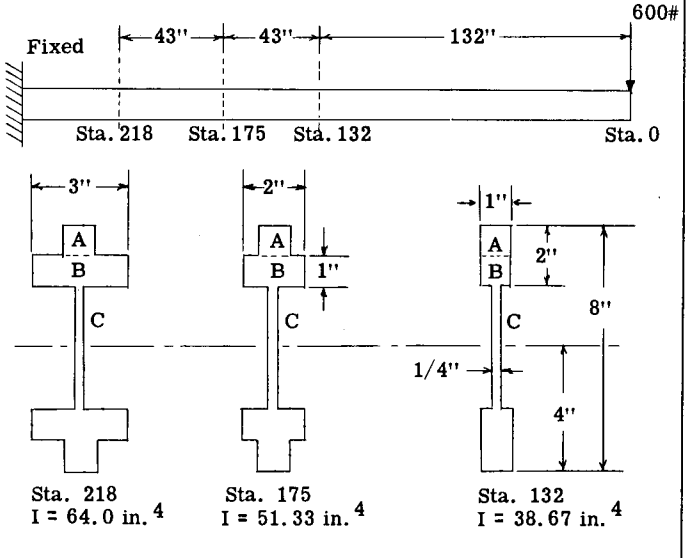

Fig. A14-6

SOLUTION: -

Bending Moments: -

$M_{132} = -600 \times 132 = -79{,}200$"#

$M_{175} = -600 \times 175 = -105{,}000$"#

$M_{218} = -600 \times 218 = -130{,}800$"#

Table A14.1 shows the results of calculating the bending stresses at 3 points on each side of the neutral axis for the 3 stations. For example for station 132

$$\sigma_{MAX.} = \pm\left(\frac{M\,c}{I}\right) = \pm\left(\frac{79200 \times 4}{38.67}\right) = \pm\ 8180 \text{ psi.}$$

(tension at top edge and compression at lower edges).

For a point 1 inch from either edge of the beam

$$\sigma = \pm\left(\frac{79200 \times 3}{38.67}\right) = \pm\ 6135 \text{ psi.}$$

TABLE A14.1

1	2	3	4	5	6	7	8
Beam Station	Bending Moment M	Bend. Stress σ_b = My/I			Total Bending Stress Load on: -		
		On Top or Bottom Fiber y = 4"	Point 1" From Top or Bottom y = 3"	Point 2" From Top or Bottom y = 2"	Portion "A"	Portion "B"	Portion "C"
132	79,200"#	±8180	±6135	±4090	7157#	5112#	1023#
175	105,000"#	±8180	±6135	±4090	7157	10224	1023
218	130,800"#	±8180	±6135	±4090	7157	15336	1023

From the results in Table A14.1, it should be noticed that the change in moment of inertia between the three stations is directly porportional to the change in bending moment, hence the same value for the bending stresses for all three stations. Columns 6, 7 and 8 give the total bending stress load on portions A, B and C of the three cross-sections (see Fig. A14.6). These values equal the average stress on the portions times the area of the portion; for example, for station 132, the load on portion A:

$$\text{load} = \frac{8180 + 6135}{2} \times 1 \times 1 = 7157\#, \text{ and for}$$

portion C:

$$\text{load} = \frac{4090 + 0}{2} \times 2 \times .25 - 1023\#$$

Fig. A14.7 shows the tension and compressive stresses acting on a portion of the beam between

stations 175 and 218. Fig. A14.8 shows the resulting horizontal shear stress pattern resulting from the loads in Fig. A14.7. For example, if we take a section along the beam 1" from the top or bottom edge of the beam and treat this portion as a free body as shown in Fig. A14.12 applying $\Sigma H = 0$,

$$\Sigma H = -7157 + 7157 + \tau \times 43 \times 1.0 = 0, \text{ hence } \tau = 0$$

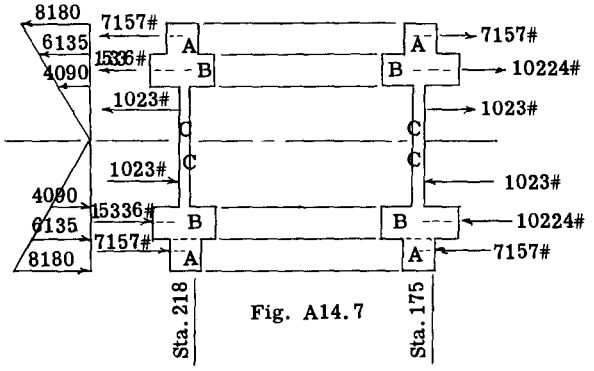

Fig. A14.7

Fig. A14.8 Fig. A14.10 Fig. A14.9

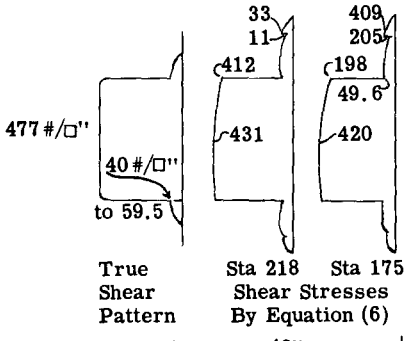

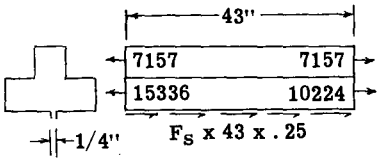

Fig. A14.13

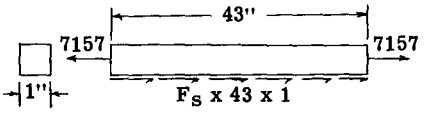

Fig. A14.12

Similarly, treating the portion between the edge of the beam and a point 2" from the edge as a free body diagram as shown in Fig. A14.13,

$$\Sigma H = -7157 + 7157 - 15336 + 10224 + \tau \times 43 \times .25 = 0, \text{ therefore } \tau = 477 \text{ psi.}$$

Obviously, the shear stress on portion C is constant, since the end load on this portion at both stations is the same, or 1023#.

Fig. A14.8 shows the general shape of the shear stress distribution on the beam section at any point between stations 175 and 218. The shear stresses between stations 132 and 175 would be the same, since the change in bending moment and moment of inertia have been made the same as between stations 175 and 218.

Figs. A14.9 and A14.10 show the shear stress patterns if the formula $\tau = \frac{V \int y\, dA}{I\, b}$ be used for each station. The discrepancy is considerable as the equation does not apply to beams of varying section.

To illustrate the calculation by the shear stress formula, the shear stress will be calculated at the neutral axis for the beam section at station 175.

$$\tau = \frac{V}{I\, b} \int_0^4 y\, dA$$

where $\int_0^4 y\, dA = 1 \times 1 \times 3.5 + 2 \times 1 \times 2.5 + 2 \times 0.25 \times 1 = 9.0$

hence, $\tau = \frac{600 \times 9.0}{51.33 \times 0.25} = 420$ psi. as compared to the true shear stress of 477 in Fig. A14.8.

TABLE A14.2

MAXIMUM SHEAR STRESS FOR SIMPLE SECTIONS

Cross Section	Max. Shear Stress	Location of Max. Shear Stress
N—□—N	$\tau = \frac{3V}{2A}$	e = 0
N—○—N	$\tau = \frac{4V}{3A}$	e = 0
N—(d, D)—N	$\tau = \frac{4V}{3A}\left(1 + \frac{Dd}{D^2 + d^2}\right)$	e = 0
d, N—△—e, N	$\tau = \frac{3V}{2A}$	$e = \frac{d}{6}$
e, e, x—◇—N, d	$\tau = \frac{9V}{8A}$	$e = \frac{d}{8}$
Ellipse N—⬭—N	$\tau = \frac{4V}{3A}$	e = 0

A14.5 Maximum Shear Stresses for Simple Cross-Sections.

Table A14.2 gives the value of the maximum shear stress on a few simple sections and where it occurs on the cross section, (e is distance from neutral axis to point of maximum shear stress). V equals the shear load normal to the neutral axis and it acts along the centerline axis, thus no twisting on the section. A is the total cross-sectional area. The maximum shear stress is given in terms of the average shear stress which equals V/A.

A14.6 Derivation of Flexural Shear Flow Equation. Symmetrical Beam Section.

To emphasize further the fundamental relationships, a second derivation of the equation for shear stress distribution will be presented. Fig. A14.14 shows a portion of a cantilever beam carrying a load P at the free end as shown. This load is so located as to cause the beam to bend in the YZ plane without twist about a Y axis. The problem is to derive relationships which will give the magnitude and sense of the shear flow distribution on the cross-section of the beam.

Fig. A14.15 shows a free body of a small portion of the beam cut out from the upper flange of the beam at points (a b) in Fig. A14.14. Under the given external load P it is obvious that the upper half of the beam is subjected to compressive stresses. In Fig. A14.15, C_y' is larger than C_y since the cantilever bending moment is greater at station Y'.

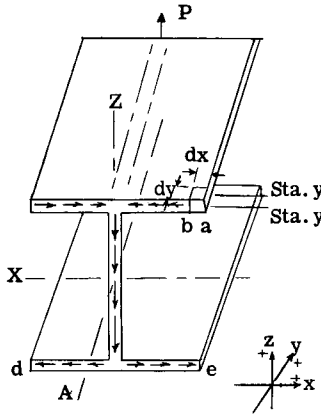

Fig. A14.14

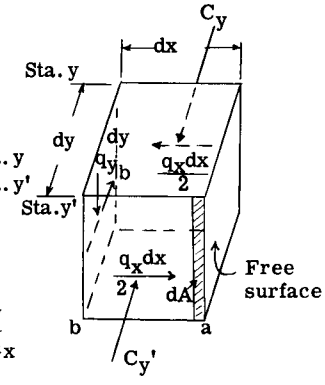

Fig. A14.15

Fig. A14.16

The free edge of beam flange forms the right side face of the element in Fig. A14.15 and thus the shear flow force on this face is zero as indicated. The shear flow forces on the internal or cut faces in lbs. per inch are q_y and q_x as indicated. Since the sense of these shear forces is unknown, they will be assumed as acting in the positive direction. (See Fig. A14.16 for positive sense of forces acting parallel to each of the coordinate axes XYZ.

Now consider the equilibrium of forces in the Y direction for the element in Fig. A14.15 $\Sigma F_y = 0$, or

$$q_{y_b}\, dy + \left(C_y' - C_y\right) = 0 \text{ , hence}$$

$$q_{y_b} = -\frac{\left(C_y' - C_y\right)}{dy}$$

But $\left(C_y' - C_y\right) = \dfrac{M_X' - M_X}{I_X} \displaystyle\int_a^b z\, dA$ (See Art. A14.3)

hence $$q_{y_b} = -\frac{dM}{dy}\frac{1}{I_X}\int_a^b z\, dA$$

however $\dfrac{dM}{dy} = V_Z$, the external shear in the Z direction.

hence $$q_{y_b} = -\frac{V_Z}{I_X}\int_a^b z\, dA \quad \text{- - - - - - - - - - - (7)}$$

Equation (7) gives the change in shear flow force q_y between points (a) and (b) and since in figure A14.15 the value of q_y at (a) is zero because of a free surface, the value of q_{y_b} in equation (7) is the true shear flow force in lbs. per inch at point (b). The student should realize that equation (7) gives the shear flow q in the Y direction. The minus sign in equation (7) means that the positive sense as assumed by the arrowhead on q_{y_b} in Fig. A14.15 is incorrect or should be reversed.

The initial problem was to determine the shear flow force system in the plane of the beam cross-section or the ZX plane. From elementary engineering mechanics, we know that if a shearing stress occurs on one plane at a point in a body, a shearing stress of the same intensity exists on planes at right angles to the first plane, or in general at a point,

$$q_y = q_X = q_Z \quad \text{- - - - - - - - - - - - - - - - - - (8)}$$

Before the shear flow in other planes is completely defined its sense (positive or negative) must be known. Equation (7) gives the magnitude and sense for q_y at any desired point on the cross-section. The question of the sense of the associated q_X and q_Z is easily determined from an observation involving equilibrium of moments. This fact will be explained by referring to a number of free body diagrams.

Fig. A14.17 shows a free body of a small element cut from the beam in Fig. A14.14 at point (a) on the cross-section. The forces on this free body are the compressive forces C" and C on the front and rear faces and the shear forces on the various faces as indicated. The right side face of the element is a free surface and thus q on this face is zero.

The shear flow q_y on the left side face is calculated from equation (7) namely

$$q_y = -\frac{V_Z}{I_X}\,\Sigma\, Z\, A \text{ .}$$

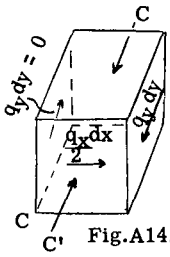

Fig.A14.18

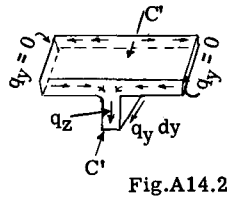

Fig.A14.21

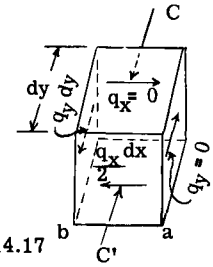

Fig.A14.17

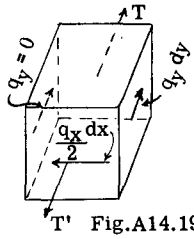

Fig.A14.19

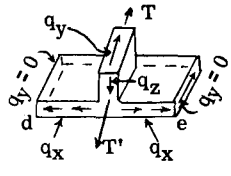

Fig.A14.22

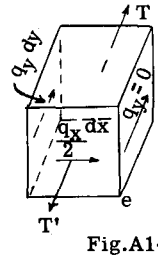

Fig.A14.20

For the given beam loading in Fig. A14.14 the load P is up, therefore V_z has a positive sign. For any portion of area (A) of the cross-section the distance z in the above equation is therefore positive. Therefore in substituting in the above equation q_y comes out negative for any point above neutral axis, and likewise for any point on beam section below the neutral axis the distance z would have a negative sign and q_y would come out positive. Therefore the sense of the calculated shear flow q_y on the left side of the element in Fig. A14.17 is negative or as indicated by the arrow on the force vector. Now to find the sense of the shear flow q_x on the front face take moments about a Z axis acting in the plane of the rear face and through point (O) which is on the line of action of the forces C' and C. Only two forces have moments, namely the side shear force q_y dy and the front face shear force $(q_x/2)dx$. It is obvious by observation that q_x on front face must act to the left as shown if the moment is to equal zero. The total shear force on front face is $(q_x/2)dx$ because shear flow at right edge is zero and it varies linearly to q_x at left edge of front face.

Figs. A14.18, 19 and 20 show free bodies of elements taken at the other three corners of the beam section which are labeled c, d, e in Fig. A14.14. For all free surfaces q is zero. The sense of q_y as before is given by the equation as explained before, hence q_y is negative in Fig. A14.18 and positive in figures 19 and 20. A simple consideration of moment equilibrium as explained for Fig. A14.17 gives the sense of the shear flow q_x as shown in the 3 figures.

Fig. A14.21 shows a free body of the entire upper beam flange and a short portion of the beam web. q_y from the equation is negative and this acts as shown in the figure. Now if we take moments about a X axis in the plane of the back side and through a point on the line of action of C' and C, the shear flow q_z on the front face must act downward in order to balance the moment due to q_y.

Fig. A14.22 shows the results for a free body of the lower flange plus a small web portion. q_y is positive from equation and thus q_z must be downward for moment equilibrium.

From the results obtained for these 6 different locations, a simple rule can be stated relative to sense of shear flows in the plane of the cross-section, namely: -

If the calculated shear flow is directed toward the boundary line between the two intersecting planes of the particular free body, then the shear flow on the other plane is also directed toward the common boundary line, and conversely directed away if the calculated shear flow is directed away.

Fig. A14.14 shows the sense of the shear flow pattern on the beam section as determined for the given external loading.

A14.7 Shear Stresses and Shear Center for Beam Sections with One Axis of Symmetry.

Example Problem. CHANNEL SECTION.

Fig. A14.23 shows a cantilever beam with channel shaped cross-section carrying a 100 lb. downward load as shown. The problem is to determine the lateral position of this load so that the beam will bend without twist. This position will coincide with the lateral position of the centroid of the shear flow system on the beam cross-section which holds the external load in equilibrium without twisting of the beam section. The cantilever beam has been cut at a section a b c d (Fig. A14.23) which is far enough from the fixed end of the beam (not shown) so that the effects of beam end restraint against section warping can be neglected. In Fig. A14.23, the internal forces holding the beam in equilibrium are sketched in. They consist of a longitudinal stress system of tension and compression and variable shear flow system in the plane of the cross-section. In this problem we are only considered with the internal resisting shear flow system.

For solution of this problem the moment of inertia I_x must be known. If calculated it would be $I_x = 0.2667$ in^4.

SOLUTION: - From equation (7)

$$q_y = - \frac{V_z}{I_x} \Sigma\, z\, A \text{ - - - - - - - - - - - - - - - - - (8)}$$

we know that the shear stress is zero at a free edge, thus the solution of equation (8) is started at either points (a) or (d).

The shear V_z is - 100 lb. Thus equation (8) for our problem reduces to,

$$q_y = - \frac{-100}{0.2667} \Sigma\, z\, A = 375 \Sigma\, z\, A \text{ - - - - - - - - (9)}$$

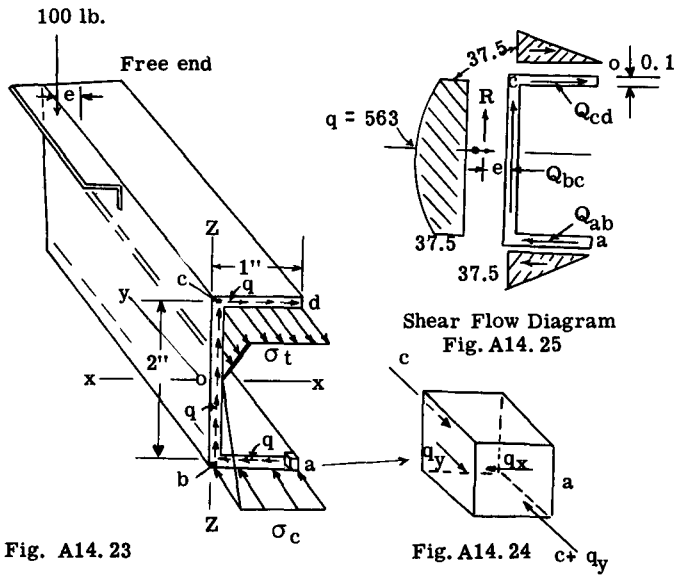

Fig. A14.23 Fig. A14.24

We will start at point (a) in solving equation (9) and proceed around the section.

Point (a) $q_{y_a} = 0$ (free surface)

Point (b) $z = -1$, A = area between (a) and (b).

$$q_{y_b} = q_{y_a} + 375 \, \Sigma_a^b z \, A$$

$$q_{y_b} = 0 + 375 \, (-1)(1 \times 0.1) = -37.5 \text{ lb/in.}$$

Point (0) on X axis.

$$q_{y_o} = -37.5 + 375 \, \Sigma_b^o z \, A$$

$$= -37.5 + 375 \, (-0.5)(1 \times 0.1) = -56.3 \text{ lb./in.}$$

Point (c).

$$q_{y_c} = -56.3 + 375 \, (0.5)(1 \times 0.1) = -37.5 \text{ lb./in.}$$

Point (d).

$$q_{y_d} = -37.5 + 375 \, (1)(1 \times 0.1) = 0 \text{ (free surface)}$$

We know that the intensity of shear flow in the ZX plane at any point equals that in the Y direction at the same point. Thus q_X or q_Z equal the q_y values above. The sense of the q_X and q_Z shear flows must be known before they are completely defined or known. Fig. A14.24 shows a free body of a small element at point (a) on the end of the lower beam flange. For any point below the X centroidal axis equation (9) will give a minus sign for q_y. Thus in Fig. A14.24 q_y acts as shown, or directed toward the boundary line between the side face and the front face. Then by the simple rule as given in the previous article q_X is also directed toward this common boundary line as shown in Fig. A14.24.

Common sense tells us that the resisting shear flow q_Z on the channel web must be directed upward because it is the only force system that can balance the 100 lb. load as far as $\Sigma F_Z = 0$ is concerned.

In general the shear flow is continuous around the section and only reverses when it passes through zero which only happens in closed tubular sections. In general, it is possible in most cases by observation only, to determine the sense of the shear flow at some one point on the beam cross-section. The shear flow being like a flow of liquid will continue in the same general direction along the center line of the parts that make up the beam section.

The small arrows on the beam section of Fig. A14.23 show the sense of the shear flow pattern over the beam section. In Fig. A14.25, the shear flow values as calculated at the various points are plotted to form a shear flow diagram for the beam section. Between points a and b or d and c, the arm z in equation (9) is constant and thus q varies linearly as plotted. Between b and 0 or 0 and c the arm z changes and the area is also a function of z, thus q varies as z^2 or parabolic as plotted.

The initial problem was to locate the centroid of this final shear flow system which is generally referred to as the shear center. In Fig. A14.25, Q_{ab}, Q_{bc} and Q_{cd} represent the resultant of the shear flow force system on these three portions of the beam cross-section. Each force is equal in magnitude to the area of the shear flow diagram for the particular beam section portion. Hence,

$$Q_{ab} = 1 \times 37.5/2 = 18.75 \text{ lb.}$$

$$Q_{bc} = 2 \times 37.5 + (56.3 - 37.5) \times 2 \times {}^2/_3 = 100 \text{ lb.}$$

$$Q_{cd} = 1 \times 37.5/2 = 18.75 \text{ lb.}$$

The resultant R of these three shear forces will now be determined.

$\Sigma F_Z = 100$ lb., $\Sigma F_X = 18.75 - 18.75 = 0$

Hence

$$R = \left(\Sigma F_Z^2 + \Sigma F_X^2\right)^{1/2} = \left(100^2 + 0\right)^{1/2} = 100 \text{ lb.}$$

The moment of the resultant about any point such as (b) in Fig. A14.17 must equal the moment of the shear flow force system about point (b). Let e be distance from point b to line of action of the resultant R.

Hence $R\,e = \Sigma M_b$ (of shear flow system) or

$$100 \, e = 18.75 \times 2, \quad \text{or } e = 0.375 \text{ inches.}$$

Thus the centroid of the internal shear resisting force system lies on a vertical line

0.375 inches to left of point b as shown in Fig. A14.23. For bending about the centroidal Z axis without twist the resultant of the internal shear flow system would obviously, due to symmetry of section about X centroidal axis, lie on the X axis, hence shear center for the given channel section is at point O in Fig. A14.23. The external load of 100 lb. would have to be located 0.375 inches to the left of the centerline of the channel web if bending of the channel without twist is to occur.

A14.8 Shear Stresses for Unsymmetrical Beam Sections.

In chapter A13, which dealt with bending stresses in beams, three methods were presented for determining the bending stresses in beams with unsymmetrical beam sections. The bending stress equations for these three methods will be repeated here: -

Method 1. The Principal Axis Method.

$$\sigma = - \frac{M_{x_p} z_p}{I_{x_p}} - \frac{M_{z_b} x_p}{I_{z_p}} \quad \text{- - - - - - - - - - - -} \quad (9)$$

Method 2. The Neutral Axis Method.

$$\sigma = - \frac{M_n z_n}{I_n} \quad \text{- - - - - - - - - - - - - - - - -} \quad (10)$$

Method 3. The Method using section properties about centroidal Z and X axes. For brevity this method will be called the k method.

$$\sigma = - (k_3 M_Z - k_1 M_X) x - (k_2 M_X - k_1 M_Z) z \quad (11)$$

where,

$$k_1 = \frac{I_{XZ}}{I_X I_Z - I_{XZ}^2}, \quad k_3 = \frac{I_X}{I_X I_Z - I_{XZ}^2}$$

$$k_2 = \frac{I_Z}{I_X I_Z - I_{XZ}^2}$$

In referring back to the derivations of equations (5), (6) and (7) the above equations (9), (10) and (11) can be written in terms of beam external shears instead of external bending moments as follows: -

Method 1. The Principal Axis Method.

$$q_y = - \frac{V_{z_p}}{I_{x_p}} \Sigma z_p A - \frac{V_{x_p}}{I_{z_p}} \Sigma x_p A \quad \text{- - - - - - -} \quad (12)$$

Method 2. The Neutral Axis Method.

$$q_y = - \frac{V_n}{I_n} \Sigma z_n A \quad \text{- - - - - - - - - - - - - - -} \quad (13)$$

Method 3. The k Method.

$$q_y = - (k_3 V_X - k_1 V_Z) \Sigma x A - (k_2 V_Z - k_1 V_X) \Sigma z A \quad \text{- - - - - - - -} \quad (14)$$

EXAMPLE PROBLEM USING THE THREE DIFFERENT METHODS.

Fig. A14.26 shows a Zee Section subjected to a 10,000 lb. shear load acting through the shear center of the section and in the direction as shown. The problem will be to calculate the shear flow q_y at two points on the beam section, namely points b and c as indicated on the figure. The shear flow at these two places will be calculated by all 3 methods.

Since all 3 methods require the use of beam section properties and since the direction of either the principal axes or the neutral axis are unknown the first step in the solution regardless of which method is used is to calculate the section properties about centroidal X and Z axes. Table A14.3 gives the calculations. The section has been divided into 4 portions labeled 1, 2, 3 and 4.

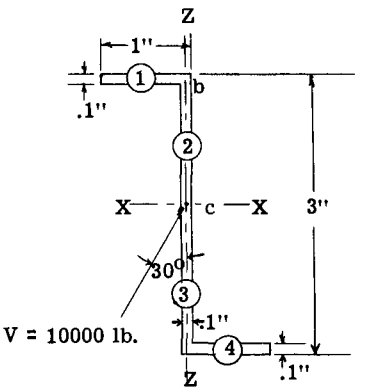

Fig. A14.26

TABLE A14.3

Portion	Area (A)	Arm z	Arm x	Axz	Az^2	Ax^2	i_z	i_x
1	0.10	1.45	-0.45	-.06525	.21025	.02025	.00838	.000017
2	0.14	0.70	0	0	.06860	0	.000117	.02287
3	0.14	-0.70	0	0	.06860	0	.000117	.02287
4	0.10	-1.45	0.45	-.06525	.21025	.02025	.00838	.000017
			Σ	-.1305	.55770	.04050	.01690	.04577

$$I_X = \Sigma A z^2 + \Sigma i_X = .6035 \text{ in}^4.$$

$$I_Z = \Sigma A x^2 + \Sigma i_Z = .0574$$

$$I_{XZ} = \Sigma A xz = - .1305$$

(Note: In Table A14.3 i_X and i_Z are the moments of inertia of each portion about its own centroidal axis).

SOLUTION BY PRINCIPAL AXES METHOD. (Method 1)

Let ϕ be angle between Principal axes and the X and Z axes. From chapter A13,

$$\tan 2\phi = \frac{2 I_{XZ}}{I_Z - I_X}$$

$$= \frac{2 (- 0.1305)}{0.0574 - 0.6035} = 0.4778$$

hence $2\phi = 25° - 32.2'$ or $\phi = 12° - 46.1'$.

$\sin \phi = 0.2210$ and $\cos \phi = 0.97527$.

The moments of inertia about the principal axes can now be calculated.

$$I_{x_p} = I_x \cos^2 \phi + I_z \sin^2 \phi - 2 I_{xz} \sin \phi \cos \phi$$

$$= 0.6035 \times \overline{.97527}^2 + .0574 \times \overline{.2210}^2 - 2 (-0.1305) \times .97527 \times .2210 = .63316 \text{ in}^4.$$

$$I_{z_p} = I_x \sin^2 \phi + I_z \cos^2 \phi + 2 I_{xz} \sin \phi \cos \phi$$

$$= 0.6035 \times \overline{0.2210}^2 + .0574 \times \overline{.97527}^2 + 2 (-0.1305) \times .97527 \times 0.2210 = 0.02782 \text{ in}^4.$$

The equation for shear flow q is,

$$q = - \frac{V_{z_p}}{I_{x_p}} \Sigma z_p - \frac{V_{x_p}}{I_{z_p}} \Sigma x_p \qquad \text{- - - - - - - - (15)}$$

In Fig. A14.26 the external shear load is 10000 lbs. acting in a direction as shown. Resolving this shear load into z and x components, we obtain,

$$V_z = 10000 \times \cos 30° = 8667 \text{ lb.}$$

$$V_x = 10000 \times \sin 30° = 5000 \text{ lb.}$$

Resolving these z and x components further into components along the principal axes we obtain,

$$V_{z_p} = 8667 \times .97527 - 5000 \times .2210 = 7348 \text{ lb.}$$

$$V_{x_p} = 8667 \times .2210 + 5000 \times .97527 = 6792 \text{ lb.}$$

Calculation of shear flow at point (b). (See Fig. A14.26).

Fig. A14.27 shows the position of the principal axes as calculated. The shear flow at the free edge of the upper portion (1) is zero. For the shear flow at point (b), the area to be used in the summations $\Sigma z_p A$ and $\Sigma x_p A$ is the area of element (1). The arms z_p and x_p can be calculated by simple trigonometry. Fig. A14.27 shows the value of these distances, namely $x_p = - 0.1184$ and $z_p = 1.5136$.

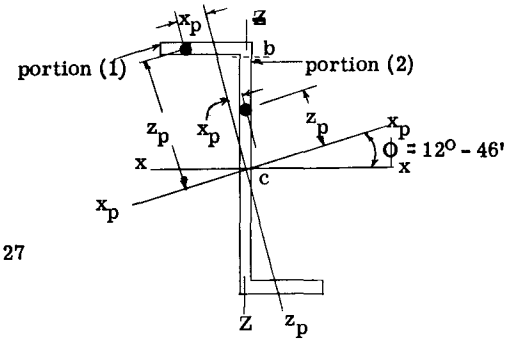

Fig. A14.27

Now substituting in equation (15)

$$q_b = - \frac{7348}{0.63316} (1 \times 0.1 \times 1.5136)$$

$$- \frac{6792}{0.02782} (1 \times 0.1) (- 0.1184) = - 1756 + 2890$$

$$= 1134 \text{ lb/in.}$$

Calculation of shear flow at point (c).

For portion (2) area $A = 1.4 \times 0.1 = 0.14$

$z_p = .70 \times .97527 = 0.6825$ in.

$x_p = .70 \times .2210 = 0.1547$

The shear flow at point (c) equals the shear flow at point (b) plus the effect of the portion (2) between points (b) and (c)., hence

$$q_c = 1134 - \frac{7348}{0.63316} (0.14 \times 0.6825) -$$

$$\frac{6792}{0.02782} (0.14 \times 0.1547) = 1134 - 1109 - 5285 =$$

$$- 5260 \text{ lb./in.}$$

The shear stresses at these two points (b) and (c) would equal $q/t = 1134/0.1$ and $- 5260/0.1$ or 11340 psi and - 52600 psi respectively,

SOLUTION BY NEUTRAL AXIS METHOD. (Method 2)

In this solution it is necessary to find the neutral axis for the given external loading. In Fig. A14.28, the angle θ is the angle between the plane of loading and the z_p principal axis, and this angle θ equals $30° + 12° - 46' = 42° - 46'$.

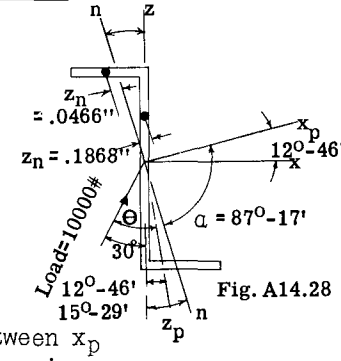

Fig. A14.28

Let α equal angle between x_p principal axis and neutral axis n-n.

From chapter A13, we find,

$$\tan \alpha = - \frac{I_{x_p} \tan \theta}{I_{z_p}}$$

$$= - \frac{0.63316 \times 0.9245}{0.02782} = - 21.052$$

whence, $\alpha = - 87° - 17'$ (See Fig. A14.28 for location of neutral axis.

$\sin \alpha = 0.9989$, $\cos \alpha = 0.04742$

$I_n = I_{x_p} \cos^2 \alpha + I_{z_p} \sin^2 \alpha$, substituting,

$I_n = 0.63316 \times \overline{.04742}^2 + .02782 \times \overline{.9989}^2 = .02919$

The component of the given external shear load normal to the neutral axis n-n equals

$$V_n = 10000 \times \sin 45° - 29' = 7130 \text{ lb.}$$

From equation (13)

$$q = - \frac{V_n}{I_n} \Sigma z_n A$$

Shear flow at point (b): -

The distance from the neutral axis to the centroid of portion (1) equal $z_n = - 0.0466$ in. hence

$$q_b = - \frac{7130}{.02919} (1 \times 0.1) (- 0.0466) = 1135 \text{ lb/in.}$$

Shear flow at point (c): - $z_n = 0.1868$ in.

$$q_c = 1135 - \frac{7130}{.02919} (1.4 \times 0.1) .1868$$

$$= 1135 - 6390 = - 5255 \text{ lb./in.}$$

SOLUTION BY METHOD 3 - (The k Method).

In this method, only the section properties about the centroidal X and Z axes are needed. These properties as previously calculated in Table A14.3 are,

$$I_X = 0.6035, \quad I_Z = 0.0574, \quad I_{XZ} = - 0.1305$$

The shear flow equation from eq. (14) is,

$$q = - (k_3 V_X - k_1 V_Z) \Sigma xA - (k_2 V_Z - k_1 V_X) \Sigma z A \quad \text{- - - - - - - - - - - - - - - - - - (16)}$$

$$k_1 = \frac{I_{XZ}}{I_X I_Z - I_{XZ}^2} = \frac{- 0.1305}{0.6035 \times .0574 - (- 0.1305)^2} =$$

$$= \frac{- 0.1305}{.01762} = - 7.406$$

$$k_2 = \frac{I_Z}{I_X I_Z - I_{XZ}^2} = \frac{0.0574}{.01762} = 3.257$$

$$k_3 = \frac{I_X}{I_X I_Z - I_{XZ}^2} = \frac{0.6035}{0.01762} = 34.25$$

Resolving the external shear load of 10,000 into x and z components, we obtain,

$$V_X = 10000 \sin 30° = 5000 \text{ lb.}$$

$$V_Z = 10000 \cos 30° = 8667 \text{ lb.}$$

Substituting values of V_X, V_Z and k values in equation (16) we obtain -

$$q = - \left[34.25 \times 5000 - (- 7.406 \times 8667)\right] \Sigma xA - \left[3.257 \times 8667 - (- 7.406 \times 5000)\right] \Sigma z A, \text{ whence}$$

$$q = - 235438 \Sigma x A - 65258 \Sigma z A$$

Shear flow at point (b)

For portion (1), $x = - 0.45$ in., $z = 1.45$ in.

$$A = 1 \times 0.1 = .1$$

Substituting,

$$q_b = - 235438 (- 0.45) 0.1 - 65258 \times 1.45 \times 0.1$$

$$= 10597 - 9462 = 1135 \text{ lb./in.}$$

Point (c)

For portion (2), $x = 0$, $z = 0.7$, $A = 1.4 \times .1 = .14$

$$q_c = 1135 - 235438 (0) .14 - 65258 \times 0.7 \times 0.1$$

$$= 1135 - 0 - 6395 = - 5260 \text{ lb./in.}$$

General Comments.

The author prefers solution method number 3 since it avoids the calculation of additional angles and section properties as required in methods 1 and 2. Furthermore, in calculating the shears and moments on the airplane wing, fuselage and other major sturctural units it is convenient to refer these shears and moments to the conventional X Y Z axes, and thus these values can be used in method 3 without further resolution. From an investigation of many airplane stress analysis reports, it appears that the engineers of most airplane companies prefer to use method 3.

A14.9 Beams with Constant Shear Flow Webs.

Fig. A14.29 shows a beam composed of heavy flange members and a curved thin web. For bending about the X-X axis, the web on the compressive, side of the beam absorbs very little compressive stress, since buckling of the web will take place under low stresses, particularly when the curvature of the web is small. On the tension side, the web will be more effective, but if the flange areas are relatively large, the proportion of the total bending tensile stress carried by the web is small as compared to that carried by the tension flange. Thus for beams composed of individual flange members connected by thin webs it is often assumed that the flanges develop the entire longitudinal bending resistance which therefore means that the shear flow is constant

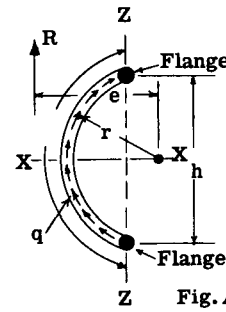

Fig. A14.29

over a particular web. In other words in the shear flow equation $q = \frac{V_Z}{I_X} \int z\, d\, A$, if the area of the web is neglected then q is constant between flange members.

RESULTANT OF CONSTANT SHEAR FLOW FORCE SYSTEMS

Fig. A14.29 shows a beam assumed to be carrying a downward shear load (not shown) and to cause bending about axis x-x without twist. Assuming the two flanges develop the entire bending resistance, the shear flow q is constant on the web and acts upward along the web to balance the assumed external downward load. The resultant of this resisting shear flow force system will give the lateral position of the shear center for this beam section. The problem then is to find the resultant of the shear flow system.

Let q = load per inch along web (constant).

Let R = resultant of the q force system.

From elementary mechancis,

$R = \sqrt{\Sigma\, q_x^2 + \Sigma\, q_z^2}$, where q_x and q_y are the x and y components of the q forces along the web. Since q is constant, $\Sigma\, q_x$ is zero, hence,

$$R = \Sigma\, q_z = q\, h \quad - - - - - - - - - - - - - - - \quad (17)$$

Equation (17) states that the magnitude of the resultant of a constant flow force system is equal to the shear flow q times the straight line distance between the two ends of the shear flow system.

Since $\Sigma\, q_x$ is zero, the direction of the resultant is parallel to the straight line joining the ends of the web.

The location of the resultant force is found by using the principle of moments, namely, that the moment of the resultant about any point must equal the moment of the original force system about the same point. In Fig. A14.29 assume point (0) as a moment center.

Then $R\, e = q\, L\, r$

but $R = q\, h$

$$\text{hence } e = \frac{q\, L\, r}{q\, h} = \frac{L\, r}{h} \quad - - - - - - - - - - \quad (18)$$

In equation (18) the term L r is equal to twice the area (A), where area (A) is the enclosed area formed by drawing straight lines from moment center (0) to the ends of the shear flow force system. Thus

$$e = \frac{2\, A}{h} \quad - - - - - - - - - - - - - - - \quad (19)$$

The shear center thus lies at a distance e to the left of point (0), and the external shear load would have to act through this point if twisting were to be eliminated.

EXAMPLE PROBLEM - RESULTANT OF A CONSTANT FLOW FORCE SYSTEM.

Fig. A14.30 shows a constant flow force system thru points A B C D E with q = 10 lb. per inch. The resultant of this force system is required.

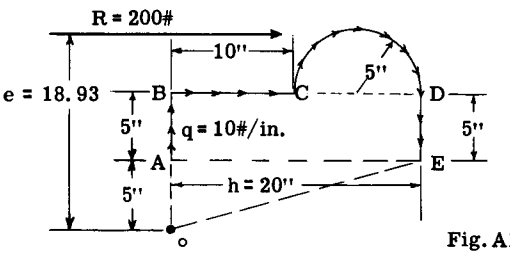

Fig. A14.30

SOLUTION: -

Draw closing line between the beginning and end points of force system. (line AE). The length h of this closing line is 20 inches.

From eq. (17) $R = q\, h = 10 \times 20 = 200$ lb.

The direction of the resultant is parallel to line AE or horizontal in this problem. To find the location of R take moments about any point such as (0). Draw lines from point (0) to points A and E. The enclosed area (A) equals

$5 \times 10 + 5 \times 10 + .5\pi \times 5^2 + 10 \times 5 = 189.3$ sq. in.

From eq. (19)

$$e = \frac{2\, A}{h} = \frac{2 \times 189.3}{20} = 18.93 \text{ in.}$$

Fig. A14.30 shows the resultant of 200 lb. acting at a distance e from (0) and parallel to line AE.

A14.10 Example Problems for Beams with Constant Shear Flows Between Flange Members.

EXAMPLE PROBLEM 1. Beam Section Symmetrical About One Axis.

Fig. A14.31 shows an open beam section composed of 8 flange members connected by thin

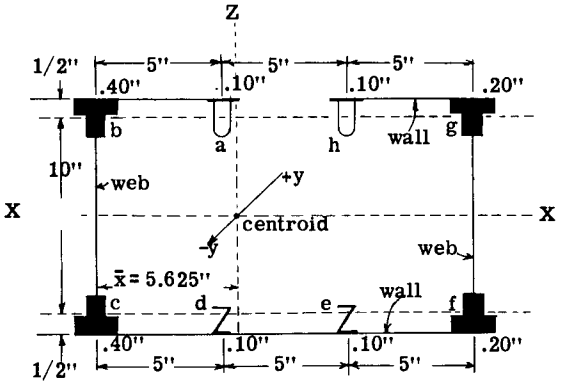

Fig. A14.31

sheet to form the webs and walls. The flange members are numbered a to h and the areas of each are given on the figure. It will be assumed that the webs and walls develop no bending resistance and thus the shear flow between adjacent flange members will be constant. The problem is to determine the shear center for the beam section.

SOLUTION: -

Since the beam section is symmetrical about the X axis, the centroidal X and Z axes are also principal axes, since the product of inertia I_{xz} is zero.

The vertical position of the beam section centroid due to symmetry is midway between the upper and lower flanges.

To find the horizontal position of the centroid, take moments of the flange areas about the left end or line bc:

$$\bar{x} = \frac{\Sigma A x}{\Sigma A} = \frac{0.4 \times 15 + 0.2 \times 10 + 0.2 \times 5}{1.6}$$

$$= 5.625 \text{ in.}$$

The moments of inertia for the section about the centroidal x and y axes are: -

$$I_x = \Sigma A z^2 = (0.8 \times 5^2)\, 2 = 40 \text{ in}^4.$$

$$I_z = 0.8 \times 5.625^2 + 0.2 \times 0.625^2 + 0.2 \times 4.375^2 + 0.4 \times 9.375^2 = 64.4 \text{ in}^4.$$

HORIZONTAL POSITION OF SHEAR CENTER: -

The horizontal position of the shear center will coincide with the centroid of the shear flow system due to bending about axis xx without twist. For simplicity, to eliminate large decimal values for shear flow values an external upward shear load V_z = 100 lb. will be assumed and the internal resisting shear flow system will be calculated for this external loading.

From equation (8)

$q_y = -\frac{V_z}{I_x} \Sigma z A$, substituting values of V_z and I_x

$$q_y = -\frac{100}{40} \Sigma z A = -2.5 \Sigma z A$$

We could start the solution at either of two points (a) or h since these points are free edges and thus q_y is zero. In this solution, we will start at the free edge at point (a) and go counterclockwise around the beam section. The area of each flange member has been concentrated at a point coinciding with the centroid of each flange area. In solving for the q values the subscript y will be omitted, and subscripts using the flange letters will be used in order to indicate at what point the shear flow q is being calculated.

$$q_{ab} = -2.5 \Sigma_a z A = -2.5 \times 5 \times 0.1 =$$

$$= 1.25 \text{ lb./in.}$$

The first letter of the subscript refers to the flange member where the shear flow q is being calculated and the second letter indicates on which adjacent side of the particular flange member. Hence q_{ab} means the shear flow at flange (a) but on the side toward (b).

$q_{ab} = q_{ba} = -1.25$ (Since no additional flange area is added, and thus shear flow is constant on sheet ab.

$q_{bc} = q_{ba} - 2.5 \Sigma_b z A$

$= -1.25 - 2.5 \times 5 \times 0.4 = -6.25$ lb./in.

$q_{cb} = -6.25$

$q_{cd} = q_{cb} - 2.5 \Sigma_c z A$

$= -6.25 - 2.5 \times (-5 \times 0.4) = -1.25$

$q_{dc} = q_{cd} = -1.25$

$q_{de} = q_{dc} - 2.5 \Sigma_d z A = -1.25 - 2.5 (-5 \times 0.1) = 0$

$q_{ed} = q_{de} = 0$

$q_{ef} = 0 - 2.5 \Sigma_e z A = 0 - 2.5 (-5 \times 0.1) = 1.25$

$q_{fe} = q_{ef} = 1.25$

$q_{fg} = 1.25 - 2.5 \Sigma_f z A = 1.25 - 2.5 (-5 \times 0.2) = 3.75$

$q_{gf} = q_{fg} = 3.75$

$q_{gh} = 3.75 - 2.5 \Sigma_g z A = 3.75 - 2.5 \times 5 \times 0.2 = 1.25$

$q_{hg} = q_{gh} = 1.25$

$q_{ha} = 1.25 - 2.5 \Sigma_h z A = 1.25 - 2.5 \times 5 \times 0.1 =$ 0 (checks free edge at h).

The sign or sense of each shear flow is for the shear flow in the y direction as explained in the derivations of the shear flow equations. The procedure now is to determine the sense of the shear flow in the plane of the cross-section or in the xz plane. It is only necessary to determine this sense at the beginning point, that is in sheet panel ab. The surest way to determine this sense is to draw a simple free body sketch of flange member (a) as illustrated in Fig. A14.31. The shear flow on the cut face is $q_{y(ab)} = -1.25$ and this value is shown on the free body. By simple rule given at the end of Art. A14.6, the shear flow in the plane of the cross-

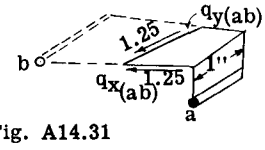

Fig. A14.31

section is also directed toward the common boundary line and thus $q_{x(ab)}$ has a sense as shown in Fig. A14.31. The sense of the shear flow on the cross-section will now continue in this direction until the sign changes in the origional calculation, which means therefore the shear flow sense will reverse. Fig. A14.32 shows a plot of the shear flow pattern with the sense indicated by the arrow heads.

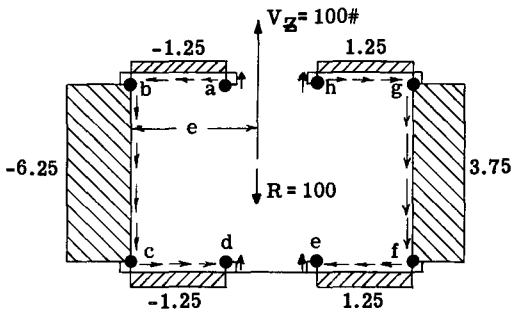

Fig. A14.32

The results will be checked to see if static equilibrium exists relative to ΣF_x and $\Sigma F_z = 0$.

ΣF_z = 100 (ext. load) - 10 x 6.25 - 10 x 3.75 + 1.25 x 0.5 x 4 - 1.25 x 0.5 x 4 = 0 (check).

ΣF_x = - 5 x 1.25 + 5 x 1.25 - 5 x 1.25 + 5 x 1.25 = 0 (check).

The shear flow force system in Fig. A14.32 causes the section to bend about axis xx without twist. The resultant of this system is 100 lb. acting down in the z direction. The position of this resultant will thus locate the lateral position of the shear center.

Equating the moments of the shear flow system about some point such as (c) to the moment of the resultant about the same point we obtain: -

$$100\ e = 10 \times 3.75 \times 15 - 1.25 \times 0.5 \times 2 \times 5 - 1.25 \times 0.5 \times 2 \times 10 + 1.25 \times 0.5 \times 2 \times 15$$

$$\text{hence } e = 562.5/100 = 5.625 \text{ inches.}$$

Thus the shear center lies on a vertical line 5.625 inches to right of line bc.

CALCULATION OF VERTICAL POSITION OF SHEAR CENTER.

For convenience as before, we will assume a shear load V_x = 100 lb. and compute the resisting shear flow system to resist this load in bending about axis zz without twist. The resultant of this shear flow system will give the vertical location of the shear center. The shear flow equation is,

$$q_y = -\frac{V_x}{I_z} \Sigma\ x\ A = -\frac{100}{64.4} \Sigma\ x\ A = -\ 1.55\ \Sigma\ x\ A$$

We will again start at the free edge adjacent to flange (a) where q_y = 0.

q_{ab} = - 1.55 Σ_a x A = - 1.55 (- 0.625 x 0.1) = 0.0971 lb./in.

$q_{ba} = q_{ab}$ = 0.0971

q_{bc} = 0.0971 - 1.55 Σ_b x A = 0.0971 - 1.55 (- 5.625 x 0.4) = 3.592

$q_{cb} = q_{bc}$ = 3.592

q_{cd} = 3.592 - 1.55 Σ_c x A = 3.592 - 1.55 x 5.625 x 0.4) = 7.087

q_{dc} = 7.087

q_{de} = 7.087 - 1.55 (- 0.625 x 0.1) = 7.184

q_{ed} = 7.184

q_{ef} = 7.184 - 1.55 x 4.375 x 0.1 = 6.504

q_{fe} = 6.504

q_{fg} = 6.504 - 1.55 x 9.375 x 0.2 = 3.589

q_{gf} = 3.589

q_{gh} = 3.589 - 1.55 x 9.375 x 0.2 = 0.674

Fig. A14.33 shows the plotted shear flow results. The signs of the calculated shear flows are for shear flows in the y direction. Simple consideration of a free body of flange member (a) will give the sign or sense of the shear flow in the plane of the beam section. Thus in Fig. A14.34 q_x must act as shown when q_y is positive.

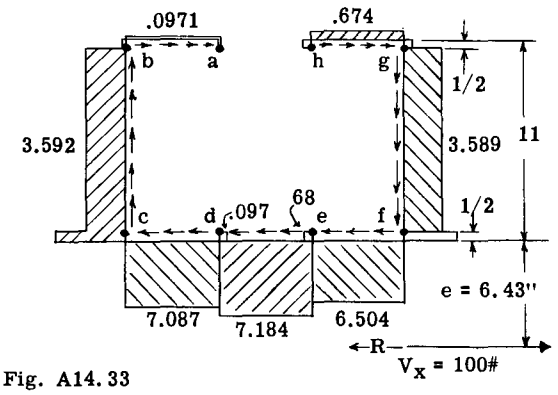

Fig. A14.33

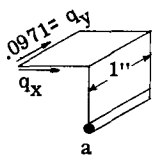

Fig. A14.34

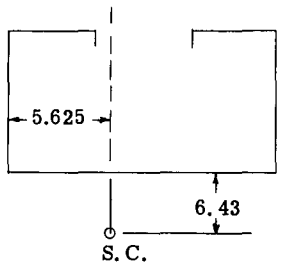

Fig. A14.35

Checking to see if $\Sigma F_Z = 0$ and $\Sigma F_X = 0$: -

$\Sigma F_Z = 3.592 \times 10 - 3.589 \times 10 + .5 \times .0971 - .5 \times .0971 + 5 \times .674 - .5 \times .674 + .5 \times .0971 - .5 \times .674 - .5 \times 6.504 + .5 \times 7.087 = 0$ (check)

$\Sigma F_X = 100 + 5 \times .0971 + 5 \times .674 - 5\ (7.087 + 7.184 + 6.504) = 0$ (check)

The resultant R of the internal shear flow system is a horizontal force of 100 lb. acting toward the left. To find the location of the resultant take moments about a point 0.5 inch below point (c).

$$Re = \Sigma M$$

$100\ e = 5\ (.0971 + .674)\ 11 + 10 \times 3.589 \times 15 + .5 \times .0971 \times 5 - (.5 \times .674 \times 10) + .5 \times .674 \times 15 + .5 \times 6.504 \times 15 + .5 \times .674 \times 10 - (.5 \times .0971 \times 5)$

$$100\ e = 643$$

$$e = 643/100 = 6.43 \text{ inches}$$

Fig. A14.35 shows the resulting shear center location for the given beam section.

EXAMPLE PROBLEM 2. Unsymmetrical Beam Section.

Fig. A14.36 shows a four flange beam section. The areas of each flange are shown adjacent to flange. The external shear load V equals 141.14 lb. and acts in a direction as shown. The problem is to find the line of action of V so that section will bend without twisting.

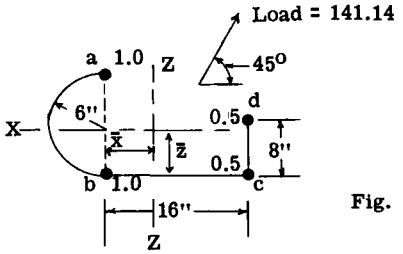

Fig. A14.36

SOLUTION: -

To solve this problem, method (3) will be used.

To locate centroidal x and z axes: -

$$\bar{z} = \frac{\Sigma A x}{\Sigma A} = \frac{1 \times 12 + 0.5 \times 8}{3} = 5.333 \text{ in.}$$

$$\bar{x} = \frac{\Sigma A z}{\Sigma A} = \frac{(0.5 + 0.5)\ 16}{3} = 5.333 \text{ in.}$$

Calculation of I_X, I_Z and I_{XZ} —

$$I_X = \Sigma A z^2 = .5\ (5.333^2 + 2.667^2) + 1\ (5.333^2 + 6.667^2) = 90.667$$

$I_Z = \Sigma A x^2 = 1\ (10.667^2) + 2\ (5.333^2) = 170.667$

$I_{XZ} = \Sigma A xz = 1 \times 6.667\ (- 5.333) + 1\ (- 5.333)\ (- 5.333) + 0.5 \times 10.667 \times 2.667 + 0.5 \times 10.667\ (- 5.333) = - 21.333$

The constants k_1, k_2 and k_3 are now determined —

$$k_1 = \frac{I_{XZ}}{I_X I_Z - I_{XZ}^2} = \frac{- 21.333}{90.667 \times 170.667 - 21.333^2} = \frac{- 21.333}{15019} = - .00142$$

$$k_2 = \frac{I_Z}{I_X I_Z - I_{XZ}^2} = \frac{170.667}{15019} = 0.01136$$

$$k_3 = \frac{I_X}{I_X I_Z - I_{XZ}^2} = \frac{90.667}{15019} = 0.006037$$

Resolving the given shear load of 141.14 into z and x components, we obtain,

$$V_Z = 141.14 \times \sin 45° = 100 \text{ lb.}$$

$$V_X = 141.14 \times \cos 45° = 100 \text{ lb.}$$

From equation (14) -

$$q_y = - (k_3 V_X - k_1 V_Z) \Sigma x A - (k_2 V_Z - k_1 V_X) \Sigma z A$$

Substituting —

$$q_y = - \left[.006037 \times 100) - (- .00142 \times 100\right] \Sigma x A - \left[.01136 \times 100 - (- .00142 \times 100)\right] \Sigma z A$$

whence

$$q_y = - 0.7457 \Sigma x A - 1.278 \Sigma z A$$

We will start at flange member (a) where q_y is zero on the free edge side of the member.

$q_{ab} = - 0.7457 \times 1\ (- 5.333) - 1.278 \times 1 \times 6.667 = - 4.544$

$q_{ba} = q_{ab} = - 4.544$

$q_{bc} = - 4.544 - 0.7457 \times 1\ (- 5.333) - 1.278 \times 1\ (- 5.333) = 6.249$ lb./in.

$q_{cb} = q_{bc} = 6.249$

$q_{cd} = 6.249 - 0.7457 \times 0.5 \times 10.667 - 1.278 \times 0.5\ (-5.333) = 5.680$

$q_{dc} = q_{cd} = 5.680$

$q_{da} = 5.680 - 0.7457 \times .5 \times 10.667 - 1.278 \times 0.5 \times 2.667 = 5.680 - 3.977 - 1.704 =$ 0 (checks free edge at d where q_y must be zero.)

Fig. A14.37 shows the resulting shear flow resisting pattern. The sense of the shear flow in

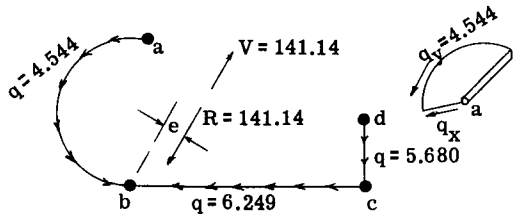

Fig. A14.37a

Fig. A14.37

the plane of the cross-section is determined in web at flange member (a) by the simple free body diagram of stringer (a) in Fig. A14.37a

Check ΣF_X and ΣF_Z to see if each equals 100.

$\Sigma F_X = -6.249 \times 16 = -99.99$ (checks $V_X = 100$)

$\Sigma F_Z = -12 \times 4.544 - 8 \times 5.68 = -99.94$ (checks $V_Z = 100$).

The resultant of the internal resisting shear flow system equals $\sqrt{100^2 + 100^2} = 141.14$ lb.

To locate this resultant we use the principle of moments. Taking point (b) as a moment center,

$$141.14\ e = 8 \times 5.68 \times 16 - 4.544 \times 36\ \pi$$

$$\text{hence } e = \frac{212}{141.14} = 1.50 \text{ inch.}$$

Therefore external load must act at a distance e = 1.50" from (b) as shown in Fig. A14.37. The load so located will pass thru shear center of section. To obtain the shear center location, another loading on the beam can be assumed, and where the line of action of the resultant of the resisting shear flow system intersects the resultant as found above would locate the shear center as a single point. If the shear center location is desired it is convenient to assume a unit V_Z and V_X acting separately and find the horizontal and vertical locations of the shear center from the 2 separate shear flow force systems.

A14.11 Shear Center Location By Using Neutral Axis Method.

In a beam subjected to bending there is a definite neutral axis position for each different external plane of loading on the beam. The shear flow equation with respect to the neutral axis is,

$$q_y = -\frac{V_n}{I_n} \Sigma Z_n A \text{ - - - - - - - - - - - - (20)}$$

where, V_n = Shear resolved normal to neutral axis

I_n = Moment of inertia about neutral axis

Z_n = Distance to neutral axis

In finding the shear center location of an unsymmetrical section, it is convenient to assume that the Z and X axes are neutral axis and find the shear flow system for bending about each axis by equation (20). The resultant of each of these shear flow force systems will pass through the shear center, thus the intersection of these two resultant forces will locate the shear center.

Example Problem

The same beam section as used in the previous article (see Fig. A14.36) will be used to illustrate the neutral axis method.

Fig. A14.38 shows the section with the centroidal axis drawn in. The X axis will now

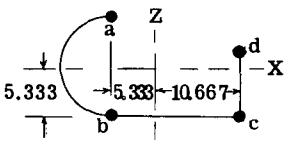

Fig. A14.38

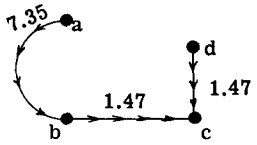

Fig. A14.39

be assumed as the neutral axis for an external plane of loading as yet unknown. We will further assume that when this unknown external loading is resolved normal to the X neutral axis, that it will give a value of 100 lb., or $V_Z = 100$. From the previous article $I_X = 90.667$.

Since the X axis has been assumed as the neutral axis, equation (20) can be written

$$q_y = -\frac{V_Z}{I_X} \Sigma ZA, \text{ hence,}$$

$$q_{ab} = -\frac{100}{90.667} \times 6.667 \times 1.0 = -7.35 \text{ lb./in.}$$

$$q_{bc} = -7.35 - \frac{100}{90.667} \times (-5.333)1 = -1.47$$

$$q_{cd} = -1.47 - \frac{100}{90.667}\ (-5.333)\ 0.5 = 1.47$$

Fig. A14.39 shows the resulting shear flow values.

$\Sigma F_x = 1.47 \times 16 = 23.52$ lb.

$\Sigma F_z = 7.35 \times 12 + 8 \times 1.47 = 99.96$ lb. (check)

$R = \sqrt{100^2 + 23.52^2} = 103$ lb.

$\tan \theta = 23.52/100 = .2352$

hence $\theta = 13^0 - 16'$

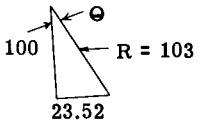

Let e = distance from resultant R to point b.

Equating moments of resultant about (b) to that of shear flow system about (b),

$$103e = -7.35 \times 6\pi^2 + 1.47 \times 8 \times 16$$

$$e = -\frac{644}{103} = -6.25 \text{ in.}$$

Fig. A14.40 shows the location of the resultant. We know the shear center lies on the line of action of this resultant. Thus we

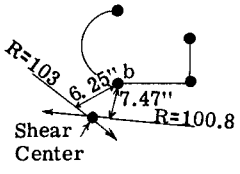

Fig. A14.40

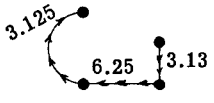

Fig. A14.41

must obtain another resultant force which passes through the shear center before we can definitely locate the shear center. Therefore we will now assume that the Z centroidal axis is a neutral axis and that a resolution of the external load system gives a shear $V_x = 100$ lb.

$$q_y = -\frac{V_x}{I_z} \Sigma XA, \quad I_z = 170.667$$

$$q_{ab} = -\frac{100}{170.667} \times (-5.333)1 = 3.125 \text{ lb./in.}$$

$$q_{bc} = 3.125 - \frac{100}{170.66} (-5.333)1 = 6.25 \text{ lb./in}$$

$$q_{cd} = 6.25 - \frac{100}{170.66} (0.5)(10.667) = 3.13$$

Fig. A14.41 shows the shear flow results.

$\Sigma F_x = -6.25 \times 16 = -100$ lb.

$\Sigma F_z = -8 \times 3.13 + 12 \times 3.125 = 12.5$ lb.

$R = \sqrt{100^2 + 12.5^2} = 100.8$

$\tan \theta = \frac{12.5}{100} = .125$

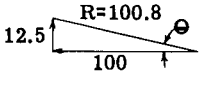

Take moments about (b) and let (e) equal distance to resultant R.

$$100.8e = 3.125 \times \pi \times 6^2 + 3.13 \times 8 \times 16$$

$$e = 753/100.8 = 7.47 \text{ in.}$$

Fig. A14.40 shows the position of this resultant force. Where it intersects the previous resultant force gives the shear center location.

A14.12 Problems

(1) Fig. A14.42 shows the cross-section of a wood beam glued together on lines a-a and a-b. The beam is subjected to a vertical shear V = 2400 lb. Determine shearing stress on sections a-a and a-b. Find maximum shearing stress on beam section.

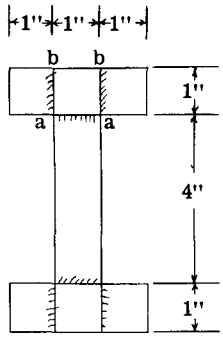

Fig. A14.42

(2) Fig. A14.43 shows a Zee section loaded by a 1000 lb. load acting through the shear center as shown. Find the shear stress at sections a-a and b-b by three different methods.

Fig. A14.43

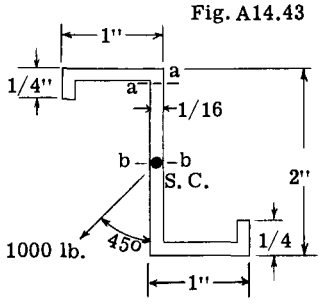

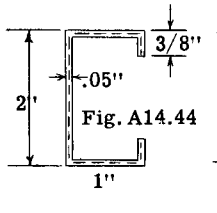

Fig. A14.44

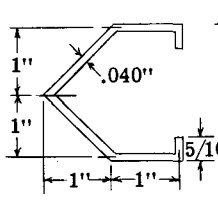

Fig. A14.45

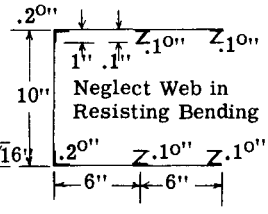

Fig. A14.46

(3) Determine the shear flow diagram and the shear center location for bending about horizontal centroidal axis for the beam sections as given in Figs. A14.44 to A14.46.

Fig. A14.47

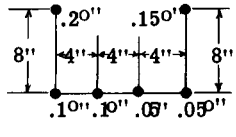

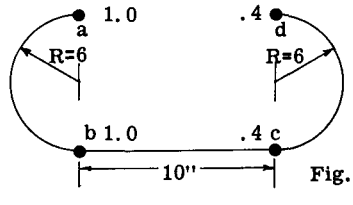

Fig. A14.48

(4) Determine the shear center location for the beam sections in Figs. A14.47 and A14.48. As-

sume flange members develop entire bending stress resistance.

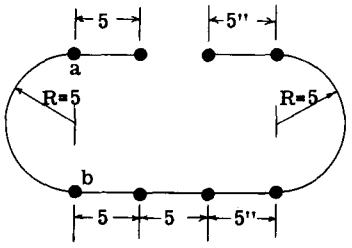

Fig. A14.49

(5) Determine the shear center for the beam section of Fig. A14.49. Assume only the 8 stringers as being effective in bending. Area of stringers (a) and (b) = 2 sq. in. each. All other stringers 1 sq. in. each.

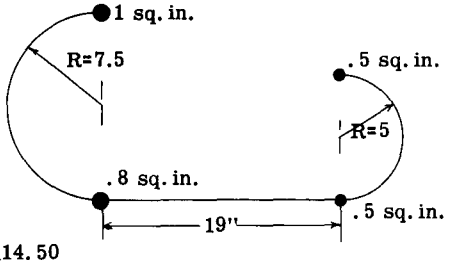

Fig. A14.50

(6) Determine the shear center for the unsymmetrical beam section of Fig. A14.50. Assume sheet connecting the four stringers as ineffective. Areas of stringers shown on Fig.

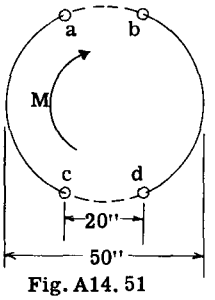

Fig. A14.51

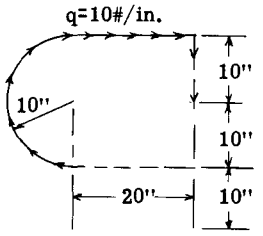

Fig. A14.52

(7) In Fig. A14.51, the shell structure is subjected to a torsional moment M = 50,000 in. lb. The shell skin shown dashed is cut out, thus the torsional moment is resisted by the constant shear flow on the two curved sheet elements ac, and bd. Determine the value of the shear flow.

(8) Determine the moment of the constant flow force system in Fig. A14.52 about point (O). Also find the resultant of this force system.

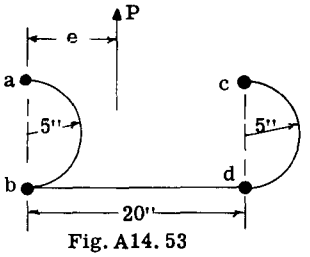

Fig. A14.53

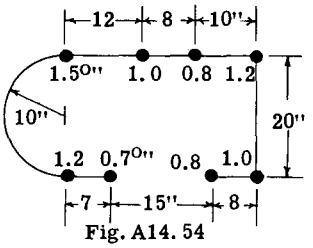

Fig. A14.54

(9) In Fig. A14.53, the four stringers a, b, c and d have the same area. Assume the webs ineffective in resisting bending stresses. Determine the distance (e) to product bending about the horizontal axis without twist.

(10) For the wing cell beam section in Fig. A14.54, determine the location of the shear center. Assume webs and walls ineffective in bending.

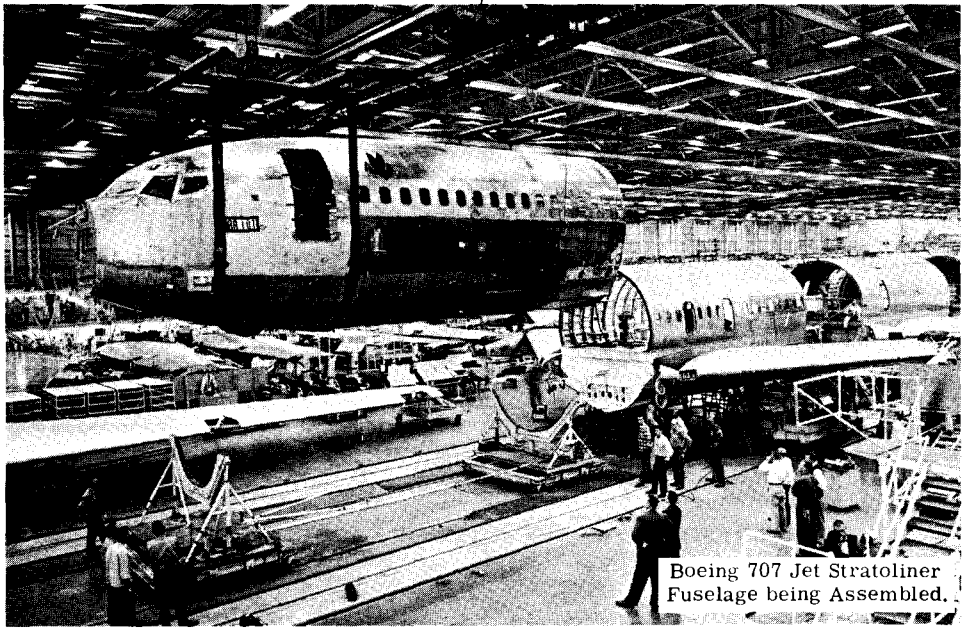

Boeing 707 Jet Stratoliner Fuselage being Assembled.

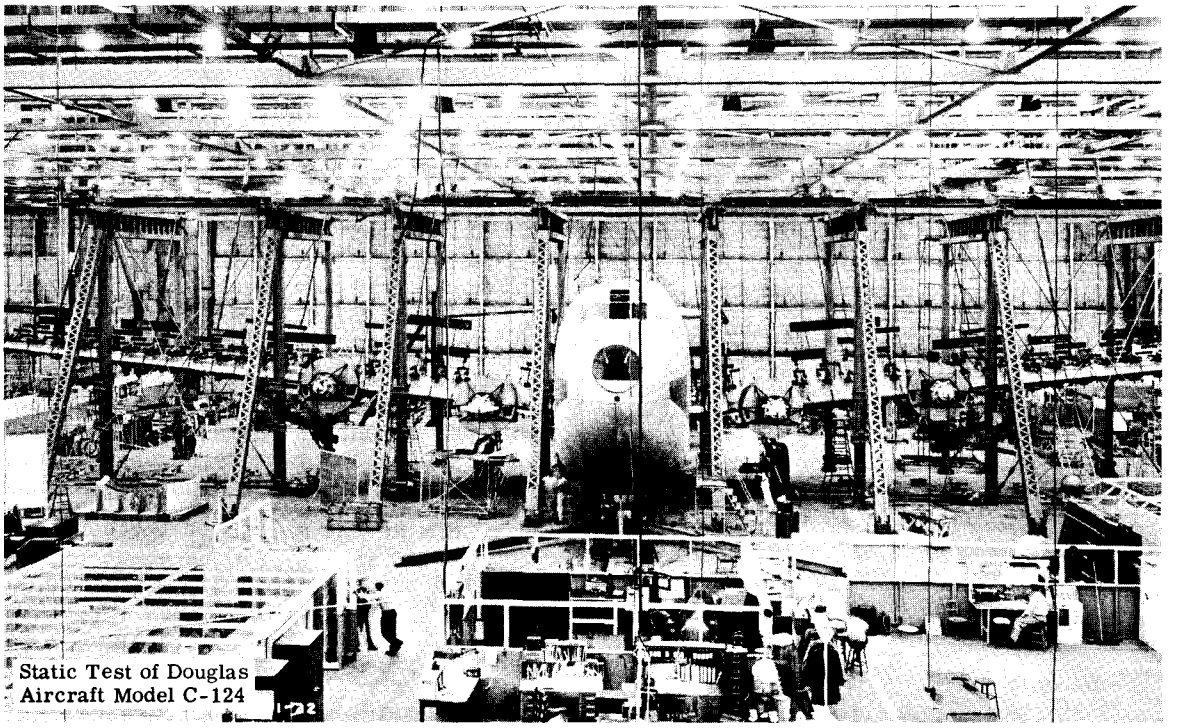

Static Test of Douglas Aircraft Model C-124

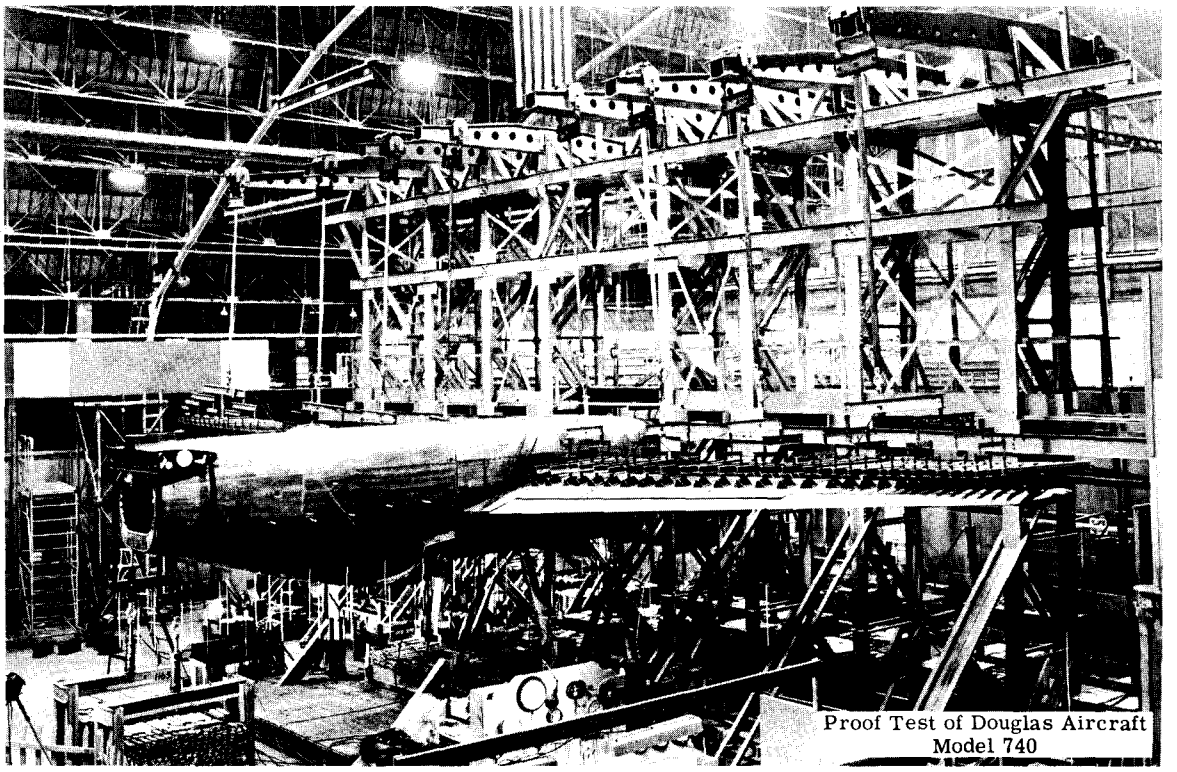

Proof Test of Douglas Aircraft Model 740

STRUCTURAL TESTING IS AN IMPORTANT PHASE OF STRUCTURAL DESIGN.

CHAPTER A 15
SHEAR FLOW IN CLOSED THIN - WALLED SECTIONS

A15.1 Introduction. The wing, fuselage and empennage structure of modern aircraft is essentially a single or multiple cellular beam with thin webs and walls. The design of such structures involves the consideration of the distribution of the internal resisting shear stresses. This chapter introduces the student to the general problems of shear flow distribution. Chapter A14 should be covered before taking up this chapter.

A15.2 Single Cell Beam. Symmetrical About One Axis. All Material Effective in Resisting Bending Stresses.

Fig. A15.1 shows a single cell rectangular beam carrying the load of 100 lb. as shown. The problem is to find the internal resisting shear flow pattern at section abcd.

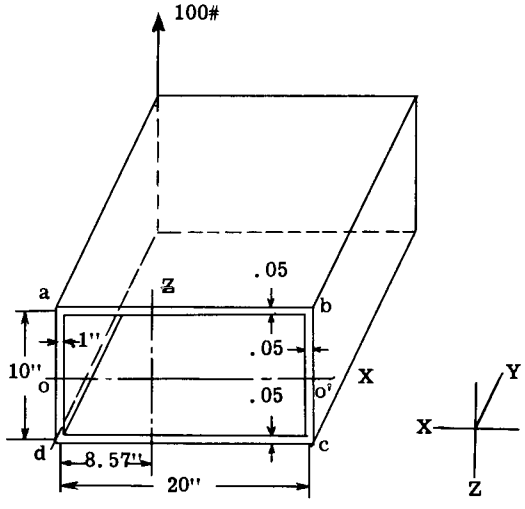

Fig. A15-1

Solution 1

Due to symmetry of material the X centroidal axis lies at the mid-height of the beam. The shear flow equation requires the value of I_X, the moment of inertia of the section about the X axis.

$$I_X = \frac{1}{12} x .15 \times 10^3 + 2\left[20 \times .05 \times 5^2\right] = 62.5 \text{ in.}^4$$

From Chapter A14, the equation for shear flow is,

$$q_y = -\frac{V_Z}{I_X} \Sigma\, zA \quad - - - - - - - - - - - - - - - \quad (1)$$

This equation gives the change in shear flow between the limits of the summation. In open sections we could start the summation at a free surface where q would be zero, thus the summation to any other point would give the true shear flow q_y. In a closed cell there is no free end, therefore the value of q_y is unknown for any point.

Equation (1) gives the shear distribution for bending about the X axis without twist. The general procedure is to assume a value of the shear flow q_y at some point and then find the shear flow pattern for bending without twist under the given external load. The centroid of this internal shear flow system will be the location where the external shear load should act for bending without twist. Since the given external shear would have a moment about this centroid, this unbalanced moment must be made zero by adding a constant shear flow system to the cell.

To illustrate we will assume q_y to be zero at point O on the web ad.

$q_o = 0$. The term $\frac{V_Z}{I_X} = 100/62.5 = 1.6$

$$q_{ao} = -1.6\, \Sigma_o^a zA = -1.6 \times 2.5 \times 5 \times 0.1 = -2 \text{ lb/in.}$$

$$q_{ba} = -2 - 1.6\, \Sigma_a^b zA = -2 - 1.6 \times 5 \times 20 \times .05 = -10$$

$$q_{o'b} = -10 - 1.6\, \Sigma_b^{o'} zA = -10 - 1.6 \times 2.5 \times 5 \times .05 = -11$$

$$q_{co'} = -11 - 1.6\, \Sigma_{o'}^c zA = -11 - 1.6 \times (-2.5) 5 \times .05 = -10$$

$$q_{cd} = -10 - 1.6\, \Sigma_c^d zA = -10 - 1.6(-5)20 \times .05 = -2$$

$$q_{od} = -z - 1.6\, \Sigma_d^o zA = -2 - 1.6(-2.5)5 \times 0.1 = 0$$

Fig. A15.2 shows a plot of the shear flow results. On the vertical web the increase in shear is parabolic since the area varies directly with distance z.

The intensity of q_X and q_Z in the plane of the cross-section is equal to the values of q found above which are in the y direction. The sense of q_X and q_Z is determined as explained in detail in Art. A14.6 of Chapter A14.

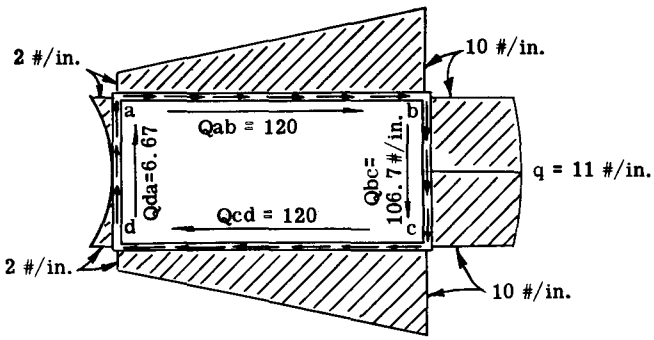

Fig. A15-2

Fig. A15.2 also shows the resultant shear flow force on each of the four walls of the cell. The resultant shear force on each equals the area of the shear flow diagram on each position.

For example,

$$Q_{ab} = \left(\frac{2 + 10}{2}\right)20 = 120 \text{ lb.}$$

$$Q_{da} = \frac{1}{3} \times 2 \times 10 = 6.67 \text{ lb.}$$

$$Q_{bc} = 10 \times 10 + 0.667 \times 1 \times 10 = 106.7$$

The internal shear flow force system as given in Fig. A15.2 will now be checked forω equilibrium with given external shear loading of 100 lb. as shown in Fig. A15.1.

$$\Sigma F_Z = 100 \text{ (external)} + 6.67 - 106.67$$
$$= 0 \text{ (check)}$$

$$\Sigma F_X = 120 - 120 = 0 \text{ (check)}$$

Equilibrium of moments must also be satisfied. Take moments of all forces about point d. The external load has no moment about d.

$$\Sigma M_d = 120 \times 10 + 106.67 \times 20$$
$$= 3344 \text{ in. lb. clockwise}$$

Thus we have an unbalanced moment which must be made zero if we are to have equilibrium.

The unbalanced moment of 3334 in. lb. can be balanced by adding a constant shear in a counter-clockwise direction around the cell. The value of this balancing shear flow would equal,

$$q = -\frac{M}{2A} = \frac{-3334}{2 \times 200} = -8.34 \text{ lb/in.}$$

(A equals area of cell = 10 x 20)

Adding this constant shear flow to that of Fig. A15.2 we obtain the final shear flow pattern of A15.3.

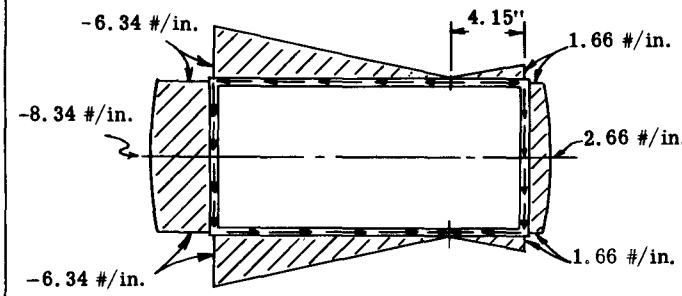

Fig. A15-3

If this constant shear flow of -8.34 was not added then the external load of 100 lb. would have to be re-located so that it passed through the centroid of the shear flow pattern in A15.2. To find this centroid location, we can equate the moment of the internal shear flow pattern about some point to the moment of the resultant of the system about the same point.

$$\text{Resultant } R = \sqrt{\Sigma F_X{}^2 + \Sigma F_Z{}^2} = \sqrt{100^2 + 0}$$
$$= 100 \text{ acting down.}$$

Take moments about point d. Let $\bar{x}$ equal distance to resultant.

$$R\bar{x} = \Sigma M_d \text{ (internal system)}$$

$$100\ \bar{x} = 120 \times 10 + 106.67 \times 20$$

hence $\bar{x} = 33.33$ in. Thus the external load would have to be moved 33.33 inches to right if the pattern of A15.2 would hold it in equilibrium. Since we assume q = zero at point 0, this means an open cell with the free end at 0 would bend without twist if the external load was moved the distance $\bar{x}$.

The student should work this same problem by assuming q_y at some other point is zero instead of point 0 as assumed in the above solution.

Solution No. 2. Shear Center Method.

In this solution, we determine the centroid of the internal shear flow system for bending of the closed section about axis X without twist. This point is called the shear center. The external shear load can then be resolved into a shear force acting through the shear center plus a torsional moment about the shear center.

We start the solution, exactly as in solution 1, by assuming the shear flow q = o at point 0. In a sense we are cutting the cell at 0 and making it an open section. The resulting shear flow is as given in A15.2. This open

section will bend without twist if the external shear load acts through the shear center of the open section.

The closed section will be assumed to bend without twist, and the resulting shear flow pattern will be determined.

The equation for angular twist θ (See Chapter A6) per inch length of beam is,

$$\theta = \frac{1}{2AG} \Sigma \frac{qL}{t}$$, where L equals the length of a web or wall.

or $2A\theta = \frac{1}{G} \Sigma \frac{qL}{t}$. The right hand side of this equation represents the total shearing strain around the cell which must be zero for no twist of cell. Since G is constant, we can assume it as unity as only relative values of strain are needed in the solution. Thus the total shearing strain δ around cell is proportional to,

$$\delta = \Sigma \frac{qL}{t} \text{ - - - - - - - - - - - - - - - - (2)}$$

Using the values of q from Fig. A15.2 and substituting in (2),

$$\delta = \Sigma \frac{qL}{t} = \left[\frac{2 \times 5}{3 \times .1} + \frac{(10 + 2)}{2} \frac{20}{.05} + \frac{10 \times 5}{.05} + \frac{(11 - 10)(.667 \times 5)}{.05} \right] 2 = 7000$$

Since the section and shear flow pattern is symmetrical about the X axis, the substitution above is written for one-half of the cell and the results multiplied by 2. When the shear flow q varies over a portion the average shear flow is used in the above substitution.

If the cell is not to twist the relative twist of 7000 must be cancelled by adding a constant shear flow q around the cell to give a total shear strain of -7000.

The shearing strain for a constant q equals,

$$\delta = \Sigma \frac{qL}{t} = q \left[\frac{5}{0.1} + \frac{20}{.05} + \frac{5}{.05} \right] 2 = -7000$$

hence $q = -\frac{7000}{1106} = -6.36$ lb/in.

Fig. A15.4 shows the resultant shear flow pattern if the constant shear flow of -6.36 is added to the shear flow pattern of A15.2.

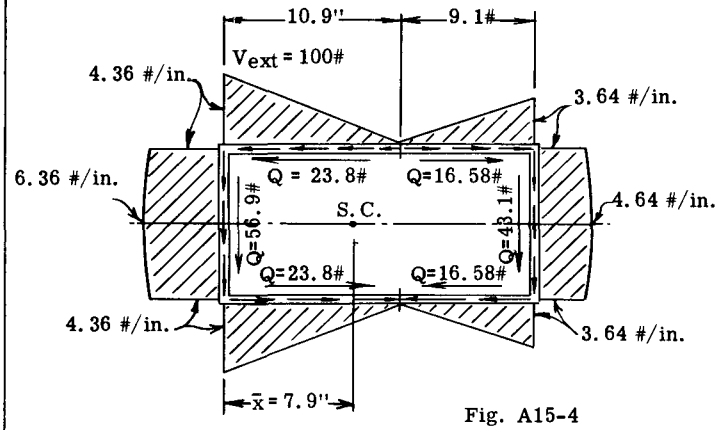

Fig. A15-4

The location of the resultant of the shear flow force system of Fig. A15.4 will locate the horizontal position of the shear center. Due to symmetry of the section about the X axis, the vertical position of the shear center will be on the X axis, because for bending about the Z axis, the shear flow would be symmetrical and thus, the resultant would coincide with the X axis.

Fig. A15.4 also shows the resultant shear load Q on each portion of the cell wall which equals the area of the shear flow diagram for various portions as shown.

$\Sigma F_Z = -56.9 - 43.1 = -100$, which balances the external load of 100 lb.

$\Sigma F_X = 0$ by observation. Take moments about point O, the intersection of axis XX and side ad.

$$\bar{x} = \frac{\Sigma M_O}{\Sigma F_Z} = \frac{43.1 \times 20 + (-23.8 + 16.58)10}{100} = 7.90 \text{ in.}$$

Hence the shear center lies on the X axis, 7.9" from side ad.

The moment of the external load of 100 lb. about shear center equals 100 x 7.9 = 790 in. lb. clockwise. The moment of the internal shear flow of Fig. A15.4 is zero thus we have an unbalanced moment of 790. Therefore for equilibrium of moments we must add a constant shear flow q around cell to develop -790 in.lb. or

$$q = \frac{M}{2A} = \frac{-790}{2 \times 200} = -1.98 \text{ lb/in.}$$

Adding this constant shear flow to that of Fig. A15.4, we obtain the final shear flow pattern which will be identical to that in Fig. A15.3 or the results of solution 1.

A15.3 Single Cell - 2 Flange Beam. Constant Shear Flow Webs.

As discussed in Art. A14.9, the common aircraft cellular beam is made up of thin sheet

walls and webs which are stiffened by members usually referred to as flange members. A simplifying common assumption is to assume that the flange members alone develop the resistance to the bending moment. This assumption therefore means that the shear flow is constant between flange members.

Fig. A15.5 shows a single cell beam with two flanges at A and B. Find the internal shear flow force system when the beam carries the external load of 100 lb. as shown.

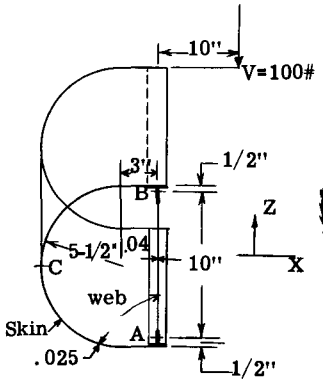

Fig. A15-5

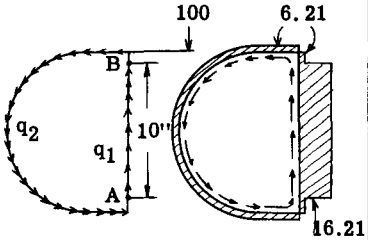

Fig. A15-6

Fig. A15-7

It is assumed that the two flanges develop the entire bending stress resistance. This means that shear flow is constant on each web. Let q_1 and q_2 be the constant shear flow as shown in Fig. A15.6. The sense or direction of these shear flows will be assumed as indicated by the arrow heads in the figure.

The force system in the plane of the cross-section has 2 unknowns, namely q_1 and q_2 and thus we can solve for q_1 and q_2 by simple statics.

To find q_2 take moments about point A.

$$\Sigma M_A = 100 \times 10 - q_2 (2 \times 80.52) = 0$$

hence $q_2 = 1000/lb\ 161.04 = 6.21$ lb/in.

The sign of q_2 comes out plus, thus the assumed sense of q_2 as shown in Fig. A15.6 is correct.

In the above equation of moments about point A, the moment of the constant flow system q_2 about A, equals q_2 times double the enclosed area formed by lines running from A to the ends of the web which carries the shear flow q_2. In this case the area is the area of the cell, or 80.52 sq. in.

To find the remaining unknown q_1 we use the equilibrium equation,

$$\Sigma F_Z = 0 = -100 - 10 \times 6.21 + 10q_1 = 0$$

hence $q_1 = 16.21$ lb/in. (sign comes out positive, hence assumed sense of q_1 is correct).

Fig. A15.7 shows a plot of the internal shear flow resisting system.

A single cell beam having only two flanges can resist only external loads which are parallel to the line AB, and thus a two flange box beam is not used very often in aircraft structure. When the bending moment in a plane at right angles to line AB is small, the resistance of the curved panel to compressive bending stresses may be sufficient to resist such external bending moments and thus be satisfactory.

A15.4 Shear Center of Single Cell - Two Flange Beam.

Let it be required to find the shear center of the beam as given in Fig. A15.5. In other words where would the external load have to be placed so that the beam would bend without twist.

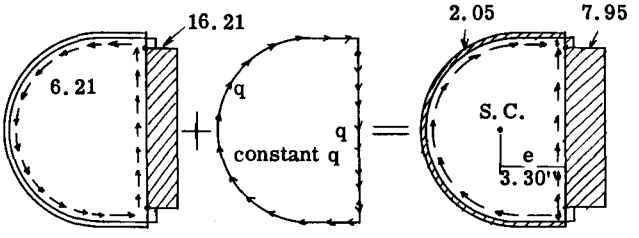

Fig. A15-8 Fig. A15-9 Fig. A15-10

Fig. A15.8 shows the resulting shear flow system in resisting the 100 lb. external load acting as shown in Fig. A15.5. This shear flow system will cause the cell to twist. Therefore we add a constant shear flow q to the cell to produce zero twist (Fig. A15.9). The centroid of the combined shear flow system will then locate the lateral location of the shear center.

To find q we must write an expression which measures the twist when subjected to the shear flows of Figs. A15.8 and 9 and equate the result to zero, and then solve for the one unknown q.

$$\delta = \Sigma \frac{qL}{t} = 0. \quad \text{(Clockwise q is positive)}$$

Substituting, using the shear flows of Figs. A15.8 and A15.9,

$$\delta = -\frac{16.21 \times 10}{.04} - \frac{6.21 \times 24.28}{.025} + \frac{10q}{.04}$$

$$+ \frac{24.28q}{.025} = 0$$

hence q = 8.26 lb.in.

Adding this constant shear flow to that of Fig. A15.8, we obtain the shear flow of Fig. A15.10.

The lateral position of the shear center is given by the location of the resultant of the shear flow system of Fig. A15.10.

The resultant $R = \sqrt{\Sigma F_X^2 + \Sigma F_Z^2}$

$\Sigma F_X = 0$

$\Sigma F_Z = 10 \times 7.95 + 2.05 \times 10 = 100$ lb.

Therefore R = 100 lb.

Equate moments of R about point A to moment of shear flow system about A.

$Re = \Sigma M_A$

$100e = 2.05\ (2 \times 80.52)$

$e = 3.30$ in.

Thus shear center lies 3.30 inches to left of line AB. (See Fig. A15.10).

Thus if the given external load of 100 lb. acts through the shear center, it will produce the shear flow system of Fig. A15.10. However it acts 13.3 to right of shear center, hence it produces a clockwise moment of 100 x 13.3 = 1330 in.lb. on the cell. For equilibrium, this moment must be balanced by a constant resisting shear flow around cell which will produce a moment of -1330.

The required $q = \frac{-1330}{2 \times 80.52} = -8.26$ lb.in., which if added to the shear flow system of A15.10 will give the true shear flow system of A15.8.

Thus having the shear center location, the external load system can be broken down into a load through the shear center plus a moment about the shear center. The shear flow due to each is then added to give the true resisting shear flow.

It should be noticed that the web or skin thickness does not influence the magnitude of the shear flow system in a single cell beam. A change in thickness, however, effects the unit shearing stress and therefore the shearing strain and thus in computing angular twist of the cell, the web and wall thickness do influence the amount of twist for a given torsional load. In the shear center solution, it is known what portion of the shear flow is due to torque or pure twist, and also that due to bending without twist, which fact is sometimes of importance.

TORSIONAL DEFLECTION OF CELL

The angular twist as given by the final shear flow pattern of Fig. A15.8 equals $2\Theta AG = \Sigma qL/t$, whence

$$2\Theta AG = \frac{-6.21 \times 24.28}{.025} - \frac{16.21 \times 10}{.04} = -10082 \quad -- \quad (3)$$

After finding the shear center location, we found that the external load had a moment of 1330 in. lb. about shear center, which was resisted by a constant shear flow of - 8.26 lb/in. The angular twist under this pure torque shear flow should therefore give the same result as equation (3) above.

$$2\Theta AG = \frac{-8.26 \times 24.28}{.025} - \frac{8.26 \times 10}{.04} = -10082$$

which checks the result of equation (3).

A15.5 Single Cell-Three Flange Beam. Constant Shear Flow Webs.

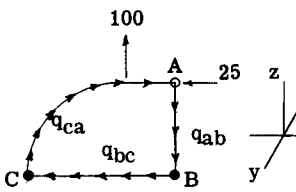

Fig. A15-12

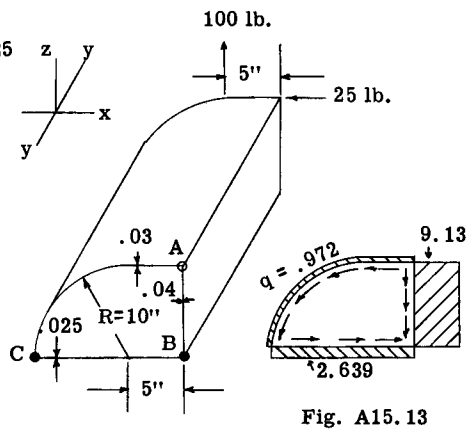

Area Cell = 128.54 sq. in.

Fig. A15.13

Fig. A15.11

Fig. A15.11 shows a single cell beam with three flange members, A, B and C, carrying the external load as shown. A three flange box if the flanges are not located in a straight line can take bending in any direction and therefore is often used in design because of its simplicity.

For such a structure, there are six unknowns, namely, the axial load in each stringer and the shear flow q in each of the three sheet panels that make up the cell. For a space structure, we have six static equations of equilibrium, thus a three flange single cell

beam can be solved by statics if we assume that the three flange members develop all the bending stress resistance, thus producing constant shear flow webs.

Fig. A15.12 shows the cross section ABC. The three unknown resisting shear flows have been assumed with a positive sign. (Clockwise flow is positive shear flow). These three unknown shear flows can be determined by statics.

To find q_{ca} take moments about point B and equate to zero.

$$\Sigma M_B = 100 \times 5 - 25 \times 10 + q_{ca}(128.54 \times 2) = 0$$

hence $q_{ca} = -\frac{250}{257.08} = -0.972$ lb/in.

To find q_{ab} take $\Sigma F_z = 0$

$$\Sigma F_z = 100 - 10 \times 0.972 - 10q_{ab} = 0$$

$$q_{ab} = 9.13 \text{ lb/in.}$$

To find q_{bc} take $\Sigma F_x = 0$

$$\Sigma F_x = -15 \times 0.972 - 25 - 15q_{bc} = 0$$

hence $q_{bc} = -2.639$ lb/in.

The signs of q_{ca} and q_{bc} came out negative, hence the sense of the shear flow on these cell wall portions is opposite to that assumed in Fig. A15.12. The resulting shear flow pattern is plotted in Fig. A15.13.

The student should realize the thickness of the wall elements does not influence the shear flow distribution if we assume the three flanges develop the entire resistance to the bending moment.

A15.6 Shear Center of Single Cell-Three Flange Beam. Constant Shear Flow Webs.

Let it be required to determine the shear center location for the beam in Fig. A15.11. The shear center is a point on the beam cross-section through which the resultant external shear must act if the cell is to bend without twist.

The shear center location will be determined in two steps, first its horizontal location and then its vertical location.

Calculation of horizontal location:-

We will assume any vertical shear load, as the example, the same vertical shear as used in the problem of Art. A15.4, namely, a 100 lb. load acting five inches from A, as illustrated in the following Fig. A15.14.

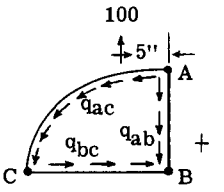

Fig. A15-14

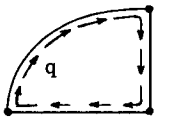

Fig. A15-15

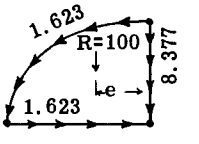

Fig. A15-16

The three unknown resisting shear flows will be assumed with the sense as indicated by the arrow heads.

To find q_{ac} take moments about B

$$\Sigma M_B = 100 \times 5 - q_{ac}(128.54 \times 2) = 0$$

$$q_{ac} = 1.945 \text{ lb/in.}$$

$$\Sigma F_x = -15 \times 1.945 + 15q_{bc} = 0$$

$$q_{bc} = 1.945$$

$$\Sigma F_z = 100 - 10 \times 1.945 - 10q_{ab} = 0$$

$$q_{ab} = 8.055 \text{ lb/in.}$$

The algebraic signs of the unknown q value all come out positive, thus the assumed direction of shear flows in Fig. A15.14 is correct.

To make the cell twist zero, we must add a constant shear flow q to the cell (see Fig. A15.15). The relative twist under the shear flow of Figs. 14 and 15 will be equated to zero.

$$\Sigma \frac{qL}{t} = -\frac{1.945 \times 20.71}{.03} - \frac{1.945 \times 15}{.025} + \frac{8.055 \times 10}{.04} + \frac{20.71q}{.03} + \frac{10q}{.04} + \frac{15q}{.025} = 0$$

Whence, q = 0.322 lb/in. with sense as assumed in Fig. A15.15. Adding this constant shear flow to that of Fig. A15.14 we obtain the shear flow system of Fig. A15.16. The resultant R of this shear flow system is obviously - 100 lb., since the external load was 100 lb. The location of this resultant R will therefore locate the horizontal position of the shear center. Equate moment of resultant R about point B to the moment of the shear flow system about B, whence,

$$100e = 1.623 (128.54 \times 2)$$

or e = 417/100 = 4.17 in. from line AB. (Fig. A15.16)

Calculation of Vertical Position of Shear Center

A convenient horizontal shear load will be

assumed acting on the cell. Since we used a 25 lb. load in the example problem of Art. 15.5, we will assume the same load in this solution. Fig. A15.17 shows the loading and the assumed directions of the three unknown shear flows.

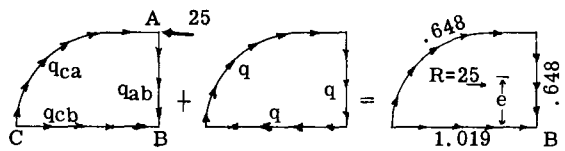

Fig. A15-17 Fig. A15-18 Fig. A15-19

Solving for the three unknown shear flows in Fig. A15.17.

$$\Sigma M_B = -25 \times 10 + q_{ca}\,(128.54 \times 2) = 0$$

$$q_{ca} = 0.972 \text{ lb/in.}$$

$$\Sigma F_X = -25 + .972 \times 15 + 15q_{cb} = 0$$

$$q_{cb} = 0.695$$

$$\Sigma F_Z = 10 \times 0.972 - 10q_{ab} = 0$$

$$q_{ab} = 0.972$$

A constant shear flow q is now added to cell to make twist zero (Fig. A15.18).

Writing $\Sigma qL/t$ for both loadings and equating to zero:-

$$\Sigma qL/t = \frac{0.972 \times 20.71}{.03} - \frac{0.695 \times 15}{.025} + \frac{0.972 \times 10}{.04} + \frac{20.71q}{.03} + \frac{10q}{.04} + \frac{15q}{.025} = 0$$

whence, q = - 0.324 lb/in.

Adding this constant shear flow to that of Fig. A15.17 we obtain the values in Fig. A15.19.

R (the resultant) = 25 lb.

Equating moment of resultant about B to moment of shear flow system about B,

$$Re = \Sigma M_B$$

$$25e = 0.648\,(128.54 \times 2)$$

Therefore e = 6.65 inches.

Thus shear center lies 6.65 inches above B, and 4.17 inches to left of B as previously found.

A15.7 Single Cell-Multiple Flange-One Axis of Symmetry.

Fig. A15.20 shows a single cell beam with 8 flange members, carrying a 100 lb. shear load. The resisting shear flow system will be calculated.

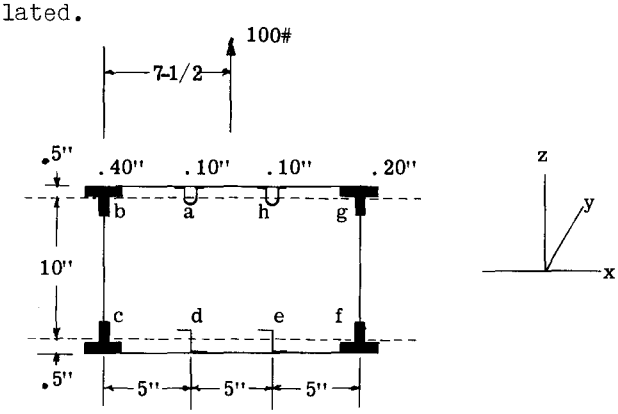

Fig. A15-20

The beam section which is symmetrical about the X axis is identical to the beam section relative to flange material which was used in example problem 1 of Art. A14.10.

SOLUTION:-

Assuming the 8 flanges develop all the bending stress resistance, the shear flow will therefore be constant between flanges. Since the beam section is a closed one the value of the shear flow q at any point is unknown. Thus we will imagine the top cover cut between flange members a and h, thus making q zero in this panel due to the free end at the cut. We now find the internal resisting shear flow system for bending of this open section about axis x-x under a external shear load V_Z = 100 lb.

The calculations would be exactly like those in example problem 1 of Art. A14.10 and will not be repeated here. Fig. A15.21 shows the plotted results as recopied from Fig. A14.32.

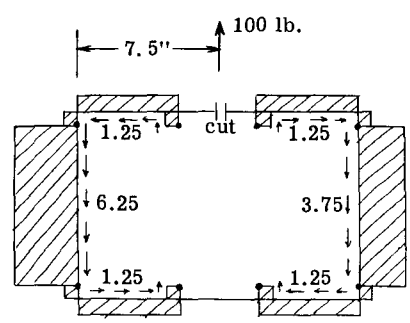

Fig. A15-21

If ΣF_X and ΣF_Z are considered for equilibrium of external and internal loads, they will be found to equal zero.

To check ΣM_y = zero take moments about some point such as C.

$$\Sigma M_C = -100 \times 7.5 + 10 \times 3.75 \times 15 - 1.25 \times 5 - 1.25 \times 10 + 1.25 \times 15 = -187.5 \text{ in.lb.}$$

Therefore to make $\Sigma M_C = 0$, a constant shear flow q equal to $M/2A = (187.5/2 \times 11 \times 15) = 0.57$ lb./in. is required. Adding this constant shear flow to that in Fig. A15.21, we obtain the final shear flow pattern of Fig. A15.22. This final pattern is not much different from that of Fig. A15.21, the reason being that the location of the imaginary cut to make q equal zero, was not far from the true fact, since the final q in this panel was only 0.57. If we had started the solution by assuming the web bc cut or $q_{bc} = 0$, then the correction constant flow that would be needed to satisfy $\Sigma M_y = 0$ would have come out q = -5.88, since this is the final q in web bc. Since the shear flow which is a load on the cell wall influences the required thickness of sheet required, it is good practice to try to place the imaginary cut at a point where the shear is near zero, so that preliminary estimates in routine design relative to shell thickness required will be based on shear flow values that are near the final values.

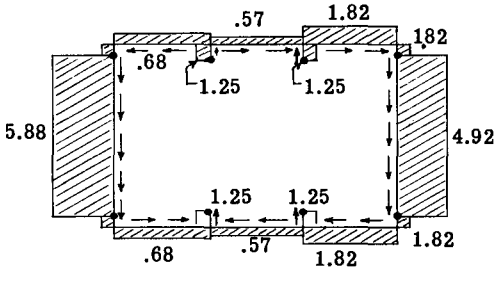

Fig. A15-22

A15.8 Single Cell - Unsymmetrical - Multiple Flange.

Example Problem 1

Fig. A15.23 shows a 4 flange unsymmetrical single cell beam carrying two external loads as shown. This beam is identical to the one used in example problem 1 of Art. A13.8 which dealt with bending stresses.

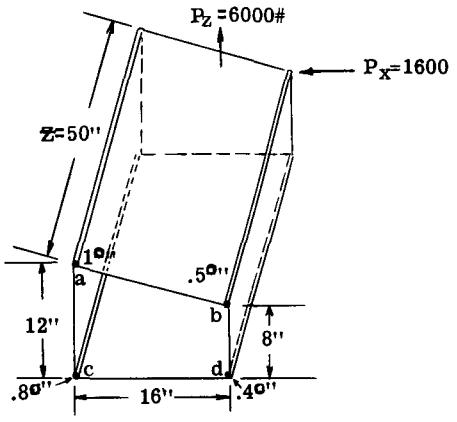

Fig. A15-23

Solution 1. Using Section Properties and External Shears with Reference to Centroidal Axes (The K Method).

In Art. A13.8 the calculations for this beam section gave -

$$I_X = 81.18, \quad I_Z = 153.58, \quad I_{XZ} = -21.33$$

Fig. A15.23a shows the location of x and z centroidal axes.

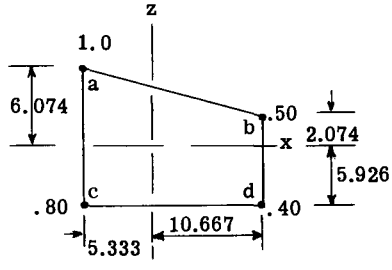

Fig. A15-23a

In Art. A14.8 of Chapter A14, the method of solution was referred to as the K method. The shear flow equation (see Eq. 14 of Art. A14.8) is,

$$q_y = -(k_3 V_X - k_1 V_Z)\,\Sigma xA - (k_2 V_Z - k_1 V_X)\,\Sigma zA$$

$$k_1 = I_{XZ}/I_X I_Z - I_{XZ}^2 = \frac{-21.33}{81.18 \times 153.58 - 21.33^2} = \frac{-21.33}{12016} = -.001775$$

$$k_2 = I_Z/I_X I_Z - I_{XZ}^2 = 153.58/12016 = .01279$$

$$k_3 = I_X/I_X I_Z - I_{XZ}^2 = 81.18/12016 = .00674$$

For the given beam loading the external shear loads at section abcd are,

$$V_Z = 6000 \text{ lb.}, \quad V_X = -1600 \text{ lb.}$$

Substituting in the equation for q_y as given above,

$$q_y = -\left[.00674\ (-1600) - (-.00177 \times 6000)\right]\Sigma xA - \left[.01279 \times 6000 - (-.00177)(-1600)\right]\Sigma zA$$

whence

$$q_y = 0.16\ \Sigma xA - 73.91\ \Sigma zA \text{ - - - - - -} \quad (4)$$

In using equation (4) to compute the shear flow pattern we will imagine top panel ab cut, thus making the shear flow q_y = zero in this panel. Subt. in (4) - - - -

$$q_{ac} = 0 + .16 \times 1\ (-5.333) - 73.91 \times 1 \times 6.074 = -449.78 \text{ lb/in.}$$

$$q_{cd} = -449.78 + .16 \times .8\ (-5.333) - 73.91 \times .8 \times (-5.926) = -100.05$$

$$q_{db} = -100.05 + .16 \times .4 \times 10.667 - 73.91 \times .4\ (-5.926) = 75.80$$

$$q_{ba} = 75.80 + .16 \times .5 \times 10.667 - 73.91 \times .5 \times 2.074 = 0$$

Fig. A15.24 shows the plotted shear flow results. This pattern satisfies $\Sigma F_z = 0$ and $\Sigma F_x = 0$. To check equilibrium of moments

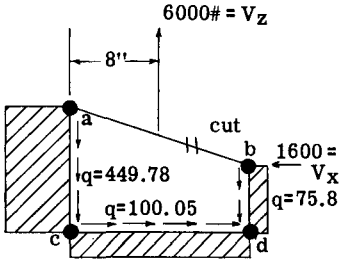

Fig. A15-24

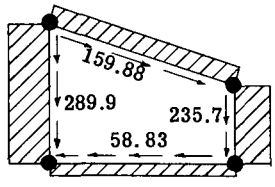

Fig. A15-25

about a y axis. Assume a y axis going through point d.

$$\Sigma M_d = 6000 \times 8 - 1600 \times 8 - 449.78 \times 12 \times 16 = -51160 \text{ in.lb.}$$

Thus for equilibrium a moment of plus 51160 in.lb. is required. This is produced by adding a constant shear flow q around the cell walls, where

$$q = \frac{M}{2A} = \frac{51160}{2 \times 160} = 159.88 \text{ lb.in.}$$

(A = area of cell = 160)

Adding this value of q to those in Fig. A15.24 we obtain the final shear flow resisting pattern in Fig. A15.25.

Solution 2. Principal Axes Method

The shear flow system can of course be found by referring section properties and external shear loads to the principal axes of the beam section. The equation for shear flow is (see Eq. 15 of Chapter A14),

$$q_y = -\frac{V_{zp}}{I_{xp}}\Sigma\ z_p A - \frac{V_{xp}}{I_{zp}}\Sigma\ x_p A \text{ - - - - -} \quad (5)$$

(The subscript p refers to principal axes.)

The section properties about the principal axes were computed for this same beam section on page A13.5 of Chapter A13. The values are:-

$$I_{xp} = 75.38, \quad I_{zp} = 159.34$$

Fig. A15.26 which was also taken from page A13.5 shows the location of the principal axes and the distances from the four flange members to the principal axes.

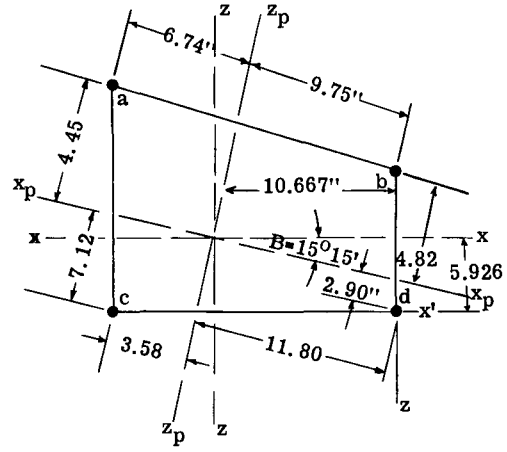

Fig. A15-26

Before substitution in equation (5) can be made, the given shear loads $V_z = 6000$, and $V_x = -1600$ must be resolved normal to the principal axes.

$$V_{z_p} = 6000 \cos 15^\circ\text{-}15' - 1600 \sin 15^\circ\text{-}15' = 5367.9 \text{ lb.}$$

$$V_{x_p} = -6000 \sin 15^\circ\text{-}15' - 1600 \cos 15^\circ\text{-}15' = -3121.8 \text{ lb.}$$

Hence $\frac{V_{z_p}}{I_{x_p}} = 71.21$ and $\frac{V_{x_p}}{I_{z_p}} = -19.59$

Subt. in equation (5),

$$q_y = -71.21\ \Sigma\ z_p A + 19.59\ \Sigma\ x_p A \text{ - - - -} \quad (6)$$

Assume $q_y = 0$ in top panel ab.

$q_{ac} = -71.21 \times 4.45 \times 1 + 19.59 \times (-6.74) \times 1 = -448.92$

$q_{cd} = -448.92 - 71.21\ (-7.12).8 + 19.59\ (-3.58).8 = -\ 99.41$

$q_{db} = -\ 99.41 - 71.21\ (-2.90).4 + 19.59 \times 11.80 \times .4 = 75.65$ lb/in.

$q_{ba} = 75.65 - 71.21\ (4.82).5 + 19.59 \times 9.75 \times .5 = 0$ (check)

These shear flows are practically the same as obtained in solution no. 1 as recorded in Fig. A15.24. Discrepancies are due to slide rule accuracy.

For equilibrium of moments, take moments about (b).

$\Sigma M_b = 6000 \times 8 - 1600 \times 8 - 448.92 \times 12 \times 16 = -50993$ in.lb.

A constant shear flow q around cell must be added to produce 50993 in.lb. for equilibrium. This balancing shear flow is,

$$q = \frac{M}{2A} = \frac{50993}{2 \times 160} = 159.35 \text{ lb/in.}$$

which is the same as in solution no. 1.

Example Problem 2

Fig. A15.27 illustrates a typical single cell wing beam with multiple flange members. The external shear load on this beam section is $V_Z = 1000$ and $V_X = 400$ located as shown. The internal shear flow resisting pattern will be calculated.

This beam section is the same as that used in example problem 5 of Chapter A3, where the calculations of the section properties were made.

The results were:

$I_X = 186.5$, $I_Z = 431.7$, $I_{XZ} = 36.41$

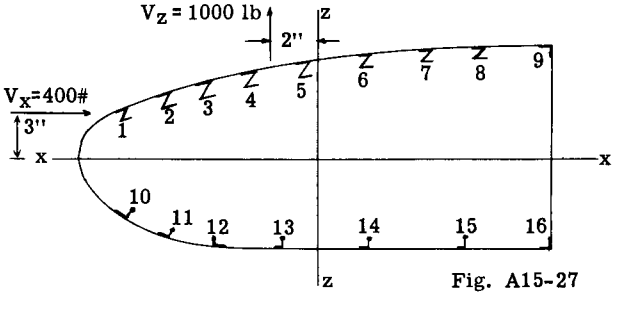

Fig. A15-27

Solution. The K method of solution will be used.

$$k_1 = \frac{I_{XZ}}{I_X I_Z - I_{XZ}^2} = \frac{36.41}{186.5 \times 431.7 - 36.41^2} = \frac{36.41}{79185} = .0004598$$

$$k_2 = \frac{I_Z}{I_X I_Z - I_{XZ}^2} = \frac{431.7}{79185} = .005452$$

$$k_3 = -\frac{I_X}{I_X I_Z - I_{XZ}^2} = \frac{186.5}{79185} = .002355$$

$$q_y = (k_3 V_X - k_1 V_Z)\Sigma xA - (k_2 V_Z - k_1 V_X)\Sigma zA$$

Substituting in above equation,

$$q_y = -(.002355 \times 400 - .0004598 \times 1000)\Sigma xA - (.005452 \times 1000 - .0004598 \times 400)\Sigma zA$$

$$q_y = -0.4822\ \Sigma xA - 5.268\ \Sigma zA \quad - - - - - \quad (7)$$

Since the value of the shear flow is unknown at any point on the cell walls, it will be assumed that the cell wall is cut between flange members 1 and 10, thus making q zero on the sheet panel numbered (1-10). Then using equation (7) the shear flow is calculated in going clockwise around the panel. Columns 1 to 10 of Table A15.1 show the calculations in solving equation (7). For explanation on how to determine sense of shear flows q_y in Columns 9, 10, and 11, review Art. A14.6 of Chapter A14.

The shear flow values in column 11 would be the results if the external loads as given were so located as to act through the centroid of this shear flow force system. Since they do not we will solve for the unbalanced moment on the beam section about point (0) the centroid of the beam cross-section. The moment of the shear flow force on a sheet panel between any two adjacent flange members is equal in magnitude to q times double the enclosed area formed by drawing lines from the moment center (0) and the ends of the particular sheet panel. Fig. A15.28 illustrates this explanation. The value m in column 12 of the table lists the double areas of these various triangular areas.

Taking moments of all forces both external and internal about point (0),

$\Sigma M_0 = 1000 \times 2 + 400 \times 3 + 17123 = 20323$ in.lb.

(17123 equals summation of column 13)

Thus for equilibrium a negative moment of -20323 is needed. This moment is provided by adding a

Table A15.1

1	2	3	4	5	6	7	8	9	10	11	12	13	14
Member	Area A	Arm Z	ZA	Arm X	XA	ΣZA	ΣXA	$q_y = -0.4822$ (Σ xA)	$q_y = -5.268$ (Σ zA)	q_{xz} = (col 9 + col 10)	m sq. in.	$q_{xz}m$	Final q = q_{xz} -20.6
						0	0	0	0	0		0	-20.6
1	0.14	4.396	0.615	-17.41	-2.437	0.615	-2.437	1.175	- 3.240	2.065	55.2	114	-18.53
2	0.14	6.446	0.902	-13.54	-1.896	1.517	-4.333	2.089	- 7.991	5.902	44.2	261	-14.70
3	0.38	7.396	2.810	- 9.11	-3.462	4.327	-7.795	3.758	-22.794	19.036	32.0	609	- 1.56
4	0.17	7.766	1.320	- 5.44	-0.925	5.647	-8.720	4.205	-29.748	25.543	38.2	976	4.94
5	0.17	7.946	1.351	- 0.86	-0.146	6.988	-8.866	4.275	-36.865	32.590	33.0	1075	11.99
6	0.17	7.896	1.342	3.14	0.534	8.340	-8.332	4.017	-43.935	39.908	33.2	1325	19.31
7	0.17	7.696	1.308	7.14	1.214	9.648	-7.118	3.432	-50.825	47.393	40.2	1905	26.79
8	0.17	7.296	1.240	11.74	1.996	10.888	-5.722	2.470	-57.358	54.888	32.6	1789	34.29
9	0.29	6.896	2.000	15.39	4.463	12.888	-0.659	0.318	-67.894	67.576	251.8	1702	46.98
16	0.35	-8.411	-2.964	15.39	5.386	9.924	4.727	-2.279	-52.280	54.559	46	2509	33.16
15	0.31	-8.224	-2.587	9.64	2.988	7.327	7.715	-3.720	-38.862	42.582	48.2	2052	21.98
14	0.31	-7.734	-2.395	3.32	1.629	4.982	8.744	-4.216	-26.245	30.44	46.4	1413	9.84
13	0.31	-7.004	-2.171	- 2.96	-0.917	2.813	7.827	-3.774	-14.819	18.59	47.6	885	- 2.01
12	0.28	-5.554	-1.554	- 9.11	-2.551	1.259	5.276	-2.544	- 6.632	9.176	36.6	336	-11.43
11	0.17	-4.504	-0.766	-13.54	-2.302	0.493	2.974	-1.434	- 2.597	4.031	42.6	172	-16.57
10	0.17	-2.904	-0.493	-17.51	-2.976	0	0	0		0		0	-20.6
1												Σ 17123	

constant negative shear flow around cell where magnitude equals

$$q = \frac{M}{2A} = \frac{20323}{2 \times 493} = -20.6 \text{ lb./in.}$$

(493 = area of cell)

Adding this constant shear flow to that in column 11, we obtain the final shear flow in column 14. Fig. A15.29 shows true shear flow pattern.

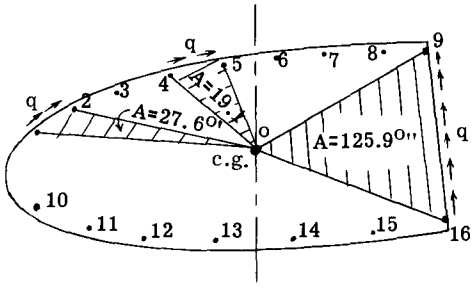

Fig. A15-28

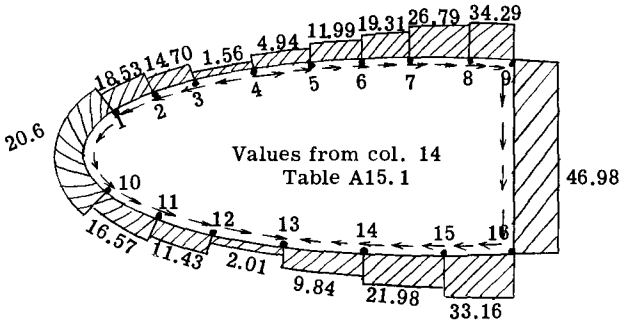

Fig. A15-29

A15.9 Two Cell-Multiple Flange Beam. Symmetrical About One Axis.

Fig. A15.30 shows a two cell cantilever beam with 10 flange stringers. The cross-section is constant. Let it be required to determine the internal shear flow in resisting the 1000 lb. load acting as shown. For simplification, the top and bottom sheet covering and the three vertical webs will be considered ineffective in taking bending flexural loads. Since the beam section is symmetrical about the X axis, the beam will bend about this axis in resisting the given external load. The moment of inertia of the section about the X axis equals 250 in.^{4}

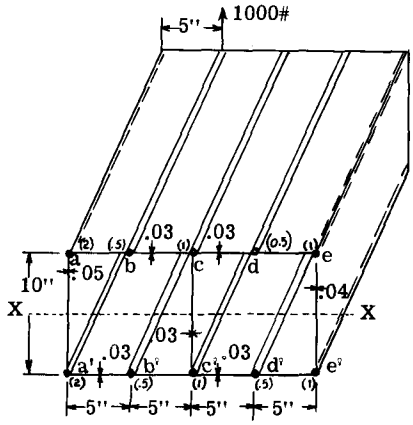

Fig. A15-30

Solution 1 (Without use of shear center)

The internal shear flow is statically indeterminate to the second degree, since the

shear flow at any point in each cell is unknown. Therefore, to make the flexural shear flow statically determinate, a value for the shear flow q in each cell will be assumed at some point, and the flexural shear flow for each cell will then be calculated, consistent with the assumed conditions. These resulting static shear flow systems will, in general, produce a different total shearing strain around the perimeter of each cell, or in other words, produce a different cell twist. Since full continuity exists between cells, this condition cannot exist, and therefore an unknown constant shear flow of q_1 in cell (1) and q_2 in cell (2) must be added to make the twist of both cells identical. This fact gives us the basis for one equation and the other equation necessary for the solution of the two unknowns q_1 and q_2 is given by the requirement of equilibrium, namely, that the moment of the external and the internal shear forces about any point in the plane of the cross section must equal zero. In Fig. A15.31 the flexural shear flow has been assumed as zero just to the left of stringer c in cell (1) and just right of stringer c in cell (2). The balance of the flexural shear system consistent with this assumption is calculated as follows:

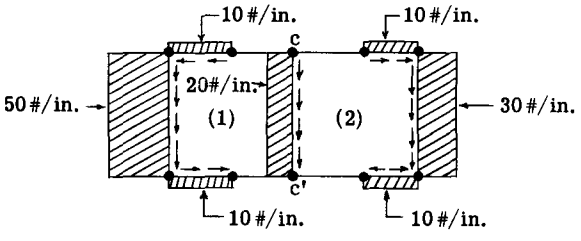

Fig. A15-31

The general shear flow equation is,

$$q_y = -\frac{V_z}{I_x}\Sigma zA = -\frac{1000}{250}\Sigma zA = -4\Sigma zA$$

Cell (1). Starting in panel cb where the shear has been assumed zero and proceding counter-clockwise around cell

q_{cb} = zero (assumed)

$q_{ba} = -4\Sigma zA = 0 - 4 \times 5 \times 0.5 = -10$ lb./in.

$q_{aa'} = -10 - 4 \times 5 \times 2 = -50$ lb./in.

$q_{a'b'} = -50 - 4 \times (-5) \times 2 = -10$ lb./in.

$q_{b'c'} = -10 - 4 \times (-5) \times 0.5 = 0$ lb./in.

We cannot proceed beyond stringer c' because there are two connecting webs with unknown shear flows. We can get around this difficulty by going back to stringer c, where the shear flow on each side of c was assumed zero. Thus the shear flow in the vertical web cc' is determined by the stringer c alone, namely

$$q_{cc'} = -4\Sigma_c^{c'} zA = -4 \times 1 \times 5 = -20 \text{ lb./in.}$$

We can now continue around cell (2) starting with stringer c' where we were previously stopped.

$$q_{c'd'} = q_{b'c'} + q_{cc'} - 4\Sigma_{c'}^{d'} zA$$
$$= 0 - 20 - 4 \times (-5)\ 1 = 0$$

$q_{d'e'} = 0 - 4 \times (-5)\ 0.5 = 10$ lb./in.

$q_{e'e} = 10 - 4 \times (-5)\ 1 = 30$ lb./in.

$q_{ed} = 30 - 4 \times 5 \times 1 = 10$ lb./in.

$q_{dc} = 10 - 4 \times 5 \times 0.5 = 0$, which checks the assumed value of q = 0 in panel cd.

The shear flows in cell (2) could of course been found by starting in panel cd where the shear has been assumed zero and proceeding clockwise around cell as for example

$q_{de} = 0 - 4 \times 5 \times .5 = -10$ lb./in.

$q_{ee'} = -10 - 4 \times 5 \times 1 = -30$ lb./in.

$q_{e'd'} = -30 - 4 \times (-5)\ 1 = -10$ lb./in.

$q_{d'c'} = -10 - 4 \times (-5)\ 0.5 = 0$ lb./in.

The magnitude of the results are the same as previously calculated but the signs are opposite. As emphasized previously the shear flow calculated together with its sign is in the y direction or q_y. The direction of the shear flow along the cell walls in the xz plane can be determined by the simple rule as given in Art. A14.6 of Chapter A14. To illustrate, refer to the free bodies in Figs. A, B, and C. The shear flow q_y in panel ba was calculated to be -10. This value is shown in Fig. A with its calculated sense and acts toward the intersection point (0). Then by the rule of Art. A14.6, q_{ba_x} must also act toward point (0), thus giving the sense as shown in Fig. A.

To obtain the shear flow in web panel cc', the calculations started at point c and went toward point c'. q_y on this panel was calculated to be -20. The free body in Fig. B shows this value of $q_y = -20$, acting with its true sense or acting toward point (0'). Then q_{cc_z} must also act toward point (0'), as shown in Fig. B. The free body in Fig. C shows how the sense of q_{de_x} was obtained.

Fig. (A)

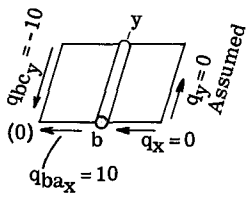

Fig. (B)

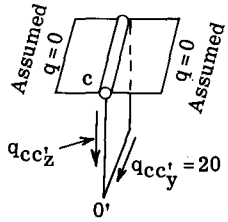

Fig. (C)

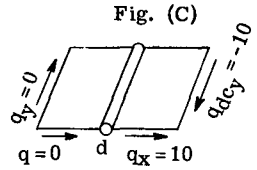

Fig. A15.32 illustrates the unknown constant shear flow systems q_1 and q_2 which must act on cells (1) and (2) respectively to produce the same cell twist when added to the shear flow system of Fig. A15.31. The sense of q_1 and q_2 has been assumed clockwise or positive in each cell.

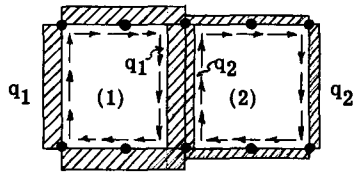

Fig. A15-32

The equation for the angular twist θ per unit length of beam is,

$$2AG\theta = \Sigma q \frac{L}{t}$$

using the shear flow values in Figs. A15.31 and 32, the angular twist of each cell will be calculated by substituting in the above equation.

For cell (1)

$$2A_1G\theta_1 = -\frac{10 \times 5}{.03} - \frac{50 \times 10}{.05} - \frac{10 \times 5}{.03} + \frac{20 \times 10}{.03} + \frac{10q_1}{.05} + \frac{3 \times 10q_1}{.03} - \frac{10q_2}{.03}.$$ Hence, $2A_1G\theta_1 = 1200q_1 - 333q_2 - 6670$ - (1)

For cell (2)

$$2A_2G\theta_2 = \frac{10 \times 5 \times 2}{.03} + \frac{30 \times 10}{.04} - \frac{20 \times 10}{.03} + \frac{3 \times 10q_2}{.03} + \frac{10q_2}{.04} - \frac{10q_1}{.03}.$$ Hence, $2A_2G\theta_2 = -333q_1 + 1250q_2 + 4170$ - (2)

Since there is continuity between cells, $\theta_1 = \theta_2$. Also since area of each cell is the same, $A_1 = A_2$. Equating (1) and (2),

$1533q_1 - 1583q_2 - 10840 = 0$ - - - - - - - - - (3)

One other equation is necessary to solve for unknowns q_1 and q_2, and it is given by the moments of the external and internal shear forces about any point in the plane of the cross section, which must equal zero for equilibrium.

Take moments about point (b) of the shear flow system of Figs. A15.31 and A15.32 and also the external shear load of 1000 lb., which in this case has no moment about our assumed moment center.

$\Sigma M_b = -50 \times 10 \times 5 + 20 \times 10 \times 5 + 10 \times 30 \times 15 + 200q_1 + 200q_2 = 0$

hence, $200q_1 + 200q_2 + 3000 = 0$ - - - - - - - - (4)

Solving equations (3) and (4) for q_1 and q_2, we obtain

$q_1 = -4.07$ lb./in. $\qquad q_2 = -10.80$ lb./in.

The final or true internal shear flow system then equals that of Fig. A15.31 plus that of Fig. A15.32 when $q_1 = -4.07$ and $q_2 = -10.80$ lb./in., which gives the shear flow diagram of Fig. A15.33.

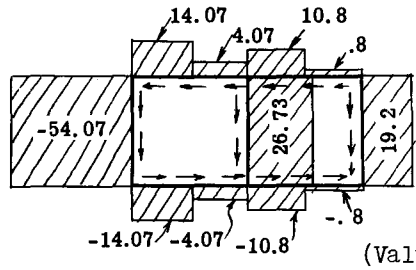

(Values in lb./in.)

Fig. A15-33

Solution 2 (By use of shear center)

In this solution, we find the flexural shear flow for bending about axis X-X without twist. The centroid of this internal shear system locates the shear center. The moment of the external shear load about the shear center produces pure torsion on the 2 cell beam. Thus, adding the shear due to this pure torsion to that of pure bending, we obtain the final resisting internal shear flow.

In bending about axis X-X without twist, the shearing strain for each cell as given by equations (1) and (2) must equal zero. Hence:

$1200q_1 - 333q_2 - 6670 = 0$ - - - - - - - - (5)

$-333q_1 + 1250q_2 + 4170 = 0$ - - - - - - - - (6)

Solving equations (5) and (6) for q_1 and q_2, we obtain $q_2 = -2.0$ lb./in. $q_1 = 5.00$ lb./in. Therefore, taking these values of q_1 and q_2 in Fig. A15.32 and adding the results to that of Fig. A15.31, we obtain the shear flow pattern of Fig. A15.34 which is the shear flow system for bending without twist about X axis. The centroid of this shear system locates the shear center.

In Fig. A15.34,

$\Sigma V = 0 = -10 \times 45 - 10 \times 28 - 10 \times 27 = -1000$ lb., which checks the external shear of 1000 lb. $\Sigma H = 0$ by observation of Fig. A15.34.

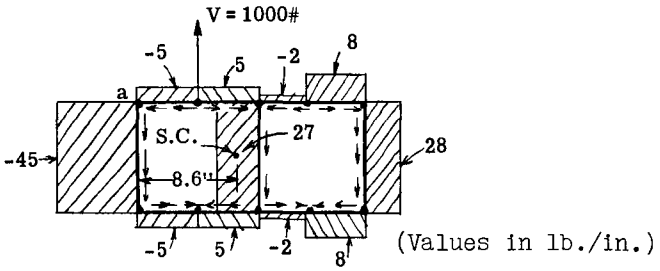

Fig. A15-34

To find the horizontal position of the centroid of the shear flow in Fig. A15.34 take moments about point a:

$$\Sigma M_a = 10 \times 27 \times 10 + 10 \times 28 \times 20 + 5 \times 8 \times 10 - 5 \times 2 \times 10 = 8600 \text{ in.lb.}$$

hence, $\bar{x} = \frac{8600}{1000} = 8.6$" to the right of web aa'.

The external shear load of 1000 lb. acts 5" to the right of aa', and therefore causes a moment about the shear center equal to $(8.6 - 5.0)\ 1000 = 3600$ in.lb. To resist this torsional moment, a constant torsional shear flow $q_{t(1)}$ and $q_{t(2)}$ must act on cells (1) and (2) respectively.

The values of $q_{t(1)}$ and $q_{t(2)}$ can be found by using equations (29) and (30) of Art. A6.11 of Chapter A5. Thus

$$q_{t(1)} = -\frac{1}{2}\left[\frac{a_{20}A_1 + a_{12}A}{a_{20}A_1^2 + a_{12}A^2 + a_{01}A_2^2}\right] T$$

$$q_{t(1)} = -\frac{1}{2}\left[\frac{\left(\frac{10}{.03}+\frac{10}{.04}+\frac{10}{.03}\right)100 + \frac{10}{.03}\times 200}{\left(\frac{10}{.03}+\frac{10}{.04}+\frac{10}{.03}\right)100^2 + \frac{10}{.03}\times 200^2 + \left(\frac{10}{.03}+\frac{10}{.05}+\frac{10}{.03}\right)100^2}\right] T = \frac{1}{2}\left[\frac{158200}{31190000}\right] T = .00254T$$

Since the external torque equals 3600 in.lb., the resisting internal torque must therefore equal -3600. Therefore,

$$q_{t(1)} = .00254(-3600) = -9.17 \text{ lb./in.}$$

Solving for $q_{t(2)}$

$$q_{t(2)} = \frac{1}{2}\left[\frac{a_{01}A_2 + a_{12}A}{31190000}\right] T$$

$$= \frac{1}{2}\left[\frac{\left(\frac{10}{.03}+\frac{10}{.03}+\frac{10}{.05}\right)100 + \frac{10}{.03}\times 200}{31190000}\right] T = .00245T$$

hence: $q_{t(2)} = .00245 \times -3600 = -8.85$ lb/in.

Therefore, if we add to the shear flow system of Fig. A15.34, a constant shear flow of -9.17 lb./in. to cell (1) and -8.85 lb./in. to cell (2), we will obtain the true internal resisting shear flow of Fig. A15.35, which checks solution 1, any discrepancy being due to slide rule accuracy.

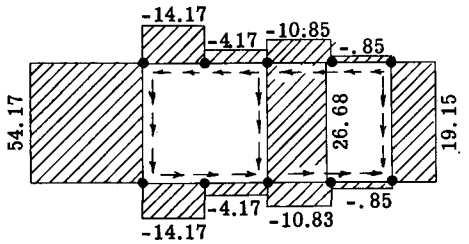

Fig. A15-35

Torsional Deflections

The angular twist of each cell is the same. The value of the angular twist θ per unit length of the beam can be found using the shear flow pattern of Fig. A15.35 which is the true resultant shear flow, or the pure torsional shear flows of $q_{t(1)} = -9.17$ lb./in. and $q_{t(2)} = -8.85$ lb./in. may be used if desired.

The results will, of course, be the same. For example:

For cell (1) due to $q_{t(1)} = -9.17$ lb./in. and $q_{t(2)} = -8.85$ lb./in.

$$2\theta GA_1 = \frac{\Sigma qL}{t} = \frac{(9.17 \times 10)}{(.03)}3 + \frac{9.17 \times 10}{.05} - \frac{8.85 \times 10}{.03} = 8000$$

Cell (2)

$$2\theta GA_2 = \frac{\Sigma qL}{t} = \frac{(8.85 \times 10)}{(.03)}3 + \frac{8.85 \times 10}{.04} - \frac{9.17 \times 10}{.03} = 8000$$

Cell (1) Final stresses - Fig. A15.35

$$2\theta GA_1 = \frac{\Sigma qL}{t} = \frac{(14.17 \times 5)2}{(.03)} + \frac{(4.17 \times 5)2}{(.03)} + \frac{54.17 \times 10}{.05}$$

$$- \frac{26.68 \times 10}{.03} = 8000$$

Cell (2) Final stresses

$$2\theta GA_2 = \frac{\Sigma qL}{t} = \frac{(10.85 \times 5)2}{(.03)} + \frac{(0.85 \times 5)2}{(.03)} + \frac{26.68 \times 10}{.03}$$

$$\frac{-19.15 \times 10}{.04} = 8000$$

A15.10 Three Cell - Multiple Flange Beam. Symmetrical About One Axis.

Fig. A15.36 shows a 3-cell box beam subjected to an external shear load of 1000 lbs. as shown. The section is symmetrical about axis XX. The area of each stringer is shown in parenthesis at each stringer point. The internal shear flow system which resists the external load of 1000 lbs. will be calculated assuming that the webs and walls take no bending loads, or, the stringers are the only effective material in bending. The moment of inertia about the XX axis of effective material equals 250 in ^{4}. (Note: this beam section is identical to the two cell beam of Fig. A15.30 plus the leading edge cell (3).

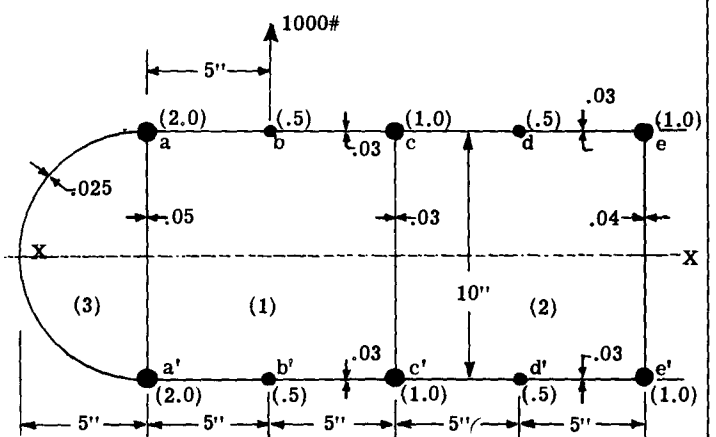

Fig. A15-36

Solution No. 1 (Without use of shear center)

The system is statically indeterminate, to the third degree, since the value of the shear flow q at any point in each cell is unknown.

The value of the shear flow will be assumed at a point in each cell and the flexural shear flow for bending about the XX axis will be determined consistent with this assumption. A constant unknown shear flow q_1, q_2, and q_3 for cells (1) and (2) and (3) respectively will be added to the static flexural shear flow so as to make the angular twist θ of each cell the same, since if any twisting takes place, all cells must suffer the same amount. Furthermore, for equilibrium, the moment of the internal shear flow system plus the moment of the external shear load must equal zero.

For bending about axis XX, the flexural shear flow will be assumed as zero at a point just to the left of stringer a in cell (3) and just to the left and right of stringer c in cells (1) and (2) respectively. One might consider the cells as cut at these three points. Fig. A15.37 shows the flexural shear flow under these assumptions. Since the leading edge cell (3) has no stringers and the covering is considered ineffective in bending, the shear flow will be zero on the leading edge portion since the shear flow was assumed zero just to the left of stringer a. The resulting flexural shear flow for the 3 cell section will therefore be identical to Fig. A15.31 and the calculations for the flexural shear flow will be identical to those in Art. A15.7.

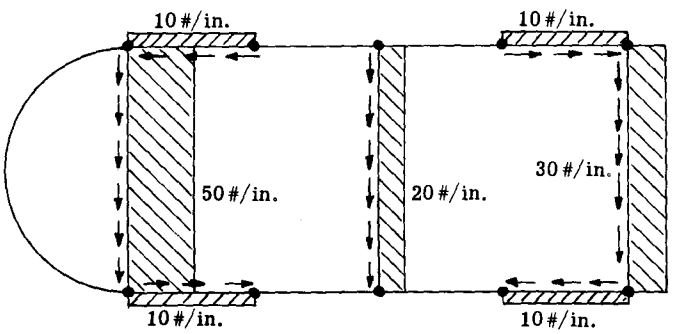

Fig. A15-37

Fig. A15.38 shows the unknown constant shear flows q_1, q_2, and q_3 which must be added to the flexural shear flow of Fig. A15.37 to make the twist θ of each cell the same. The sense of each has been assumed positive in each cell.

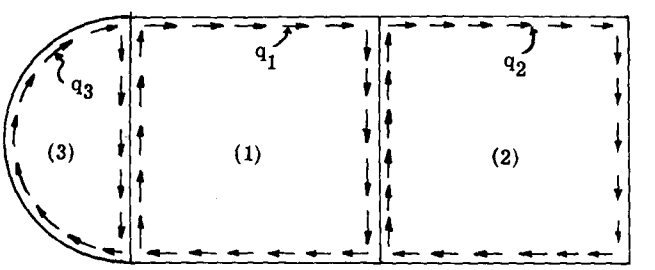

Fig. A15-38

The angular twist θ for each cell equals $\theta = \frac{1}{2AG} \Sigma\, q\, L/t$

Using the values of q in Figs. A15.37 and A15.38, the value θG will be computed for each cell.

Cell (3)

$$2\Theta A_3 G = \frac{\Sigma qL}{t}$$

$$2\Theta \times 39.4G = \frac{10 \times 50}{.05} + \frac{15.71}{.025} q_3 + \frac{10q_3}{.05} - \frac{10q_1}{.05}$$

$$\text{or } \Theta G = 10.5q_3 - 2.55q_1 + 127 \text{ - - - - - - - - - (1)}$$

Cell (1)

$$2\Theta A_1 G = \frac{\Sigma qL}{t}$$

$$2\Theta \times 100G = \frac{-50 \times 10}{.05} - \frac{2(10 \times 5)}{.03} + \frac{10 \times 20}{.03} + \frac{3(10q_1)}{.03}$$

$$+ \frac{10q_1}{.05} - \frac{10q_3}{.05} - \frac{10q_2}{.03} \text{ hence } \Theta G = 6q_1 - q_3 - 1.67q_2$$

$$- 33.34 \text{ - (2)}$$

Cell (2)

$$2\Theta A_2 G = \frac{\Sigma qL}{t}$$

$$2\Theta \times 100 \times G = -\frac{20 \times 10}{.03} + \frac{2(10 \times 5)}{.03} + \frac{10 \times 30}{.040} +$$

$$\frac{3 \times 10 \times q_2}{.03} + \frac{10q_2}{.04} - \frac{10q_1}{.03} \text{ hence } \Theta G = 6.25q_2 -$$

$$1.67q_1 + 20.83 \text{ - - - - - - - - - - - - - - - - (3)}$$

Taking moments of the internal shear flow systems of Fig. A15.37 and A15.38 and the external load of 1000 lbs. about stringer a and equating to zero:-

$$\Sigma M_a = 10 \times 20 \times 10 + 10 \times 30 \times 20 - 5 \times 1000$$
$$+ 78.6q_3 + 200q_1 + 200q_2 = 0$$
$$= 3000 + 78.6q_3 + 200q_1 + 200q_2 = 0 \text{ - - (4)}$$

Solving equations (1) (2) (3) and (4) for the unknown q_1, q_2, q_3 and ΘG we obtain:

$q_1 = -2.12$ lb./in.

$q_2 = -7.09$ lb./in.

$q_3 = -14.5$ lb./in.

$\Theta G = -19.9$

Adding these constant shear flows to the flexural shear flow of Fig. A15.37, we obtain the true internal resisting shear flow as shown in Fig. A15.39.

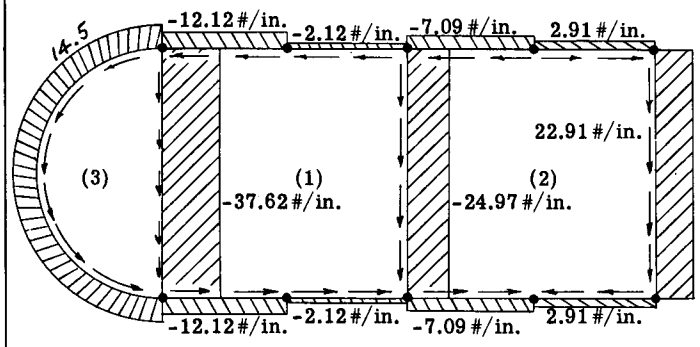

Fig. A15-39

A15.11 Shear Flow in Beam with Multiple Cells. Method of Successive Approximations.

The general trend in airplane structural design appears to be to the use of a relatively large number of cells. There are various reasons for this trend some of which are: (1) using multiple interior webs, the detrimental effect of shear deformation on bending stress distribution is decreased; (2) the fail safe characteristic of the wing is increased because the wing is made statically indeterminate to a high degree and thus failure of individual units due to fatigue or shell fire can take place without greatly decreasing the over-all ultimate strength of the wing; (3) the ultimate compressive strength of wing flange units is usually increased because column action is prevented by the multiple webs which attach to flange members.

In Chapter A6, Art. A6.13, the method of successive approximation was presented by determining the resisting shear flow system when a multiple cell beam was subjected to a pure torsional moment. This method of approach has now been extended to determine the resisting shear flow when the beam is subject to flexural bending without twist*. Using these two methods the shear flow in a beam with a relatively large number of cells can be determined rather rapidly as compared to the usual method of solving a number of equations.

PHYSICAL EXPLANATION OF THE METHOD

Fig. A15.40 shows a 3-cell beam carrying and external shear load V acting through the shear center of the beam section but as yet unknown in location. In other words, the beam bends about the symmetrical axis X-X without twist. The problem is to determine the internal resisting shear flow system for bending without

* "The Analysis of Shear Distribution for Multi-Cell Beams in Flexure by Means of Successive Numerical Approximations." By D. R. SAMSON. Journal of the Royal Aeronautical Society, Feb. 1954.

twist. In this example, it is assumed that the bending moment is resisted entirely by the flange members as represented by the small circles on the figure, which means that the shear flow will be constant between the flange members.

The first step in the solution is to make the structure statically determinate relative to shear flow stresses for bending without twist. In Fig. A15.41 imagine each cell cut at points a, b and c as shown. For the given shear load V, the static shear flow q_S can be calculated, assuming the modified section bends about axis X with no twist. Fig. A15.41 shows the general shape of this static shear flow pattern.

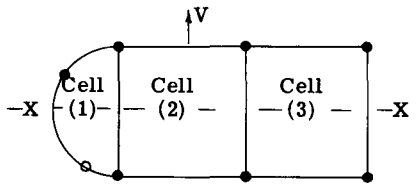

Fig. A15-40

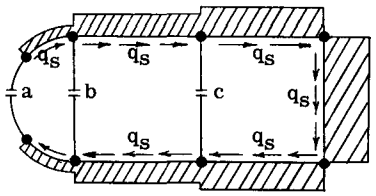

Fig. A15-41

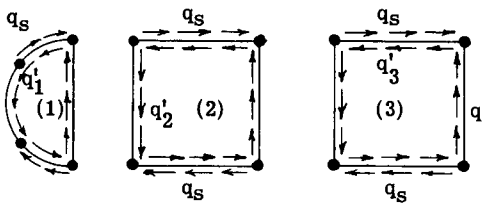

Fig. A15-42

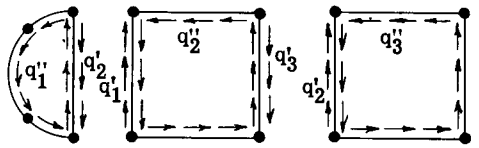

Fig. A15-43

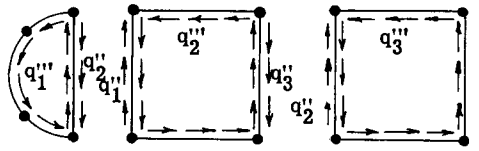

Fig. A15-44

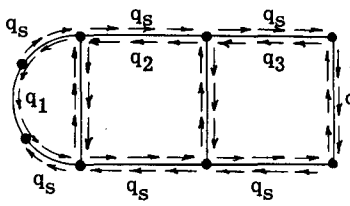

Fig. A15-45

Now consider each cell as a separate cell. The static shear flow q_S acting on each cell will cause each cell to twist. Since zero twist is necessary a constant shear flow q_1' to cell (1), q_2' to cell (2), and q_3' to cell (3) must be added as shown in Fig. A15.42, and the magnitudes of such value as to make the twist of each cell zero. However, the cells are actually not separate but have a common web between adjacent cells, thus the shear flow q_2' acts on web 2-1 which is part of cell (1), and thus causes cell (1) to twist. Likewise cell (3) is twisted by q_2' and cell (2) by both q_1' and q_3'. Therefore to cancel this additional cell twist, we must add additional constant shear flows q_1'', q_2'' and q_3'' as shown in Fig. A15.43, and considering each cell separate again. However, since the cells are not separate these additional shear flows effect the twist of adjacent cells through the common web. As before this disturbance in cell twist is again cancelled or made zero by adding further closing shear flows q_1''', q_2''', q_3''' as shown in Fig. A15.44. This procedure is repeated until the closing shear flows become negligible. In general the converging of this system is quite rapid and only a few cycles are necessary to give the desired accuracy of results.

The total closing shear flows q_1, q_2 and q_3 are then equal to -

$$q_1 = q_1' + q_1'' + q_1''' + - - - -$$
$$q_2 = q_2' + q_2'' + q_2''' + - - - -$$
$$q_3 = q_3' + q_3'' + q_3''' + - - - -$$

The final shear flow on any panel then equals, (See Fig. A15.45)

$$q = q_S + q_1 + q_2 + q_3 \; - - - - - - - - - - (1)$$

The centroid of this final shear flow system locates the shear center of the section, relative to bending about the X axis.

DERIVATION OF EQUATIONS FOR USE IN SUCCESSIVE APPROXIMATION METHOD

Fig. A15.46 shows cell (2) of the 3-cell beam shown in Fig. A15.45. q_S is the static shear flow and q_1, q_2 and q_3 are the redundant or unknown shear flows. Since cell (2) does not twist under these shear flows we can write in general,

$$\Sigma q \frac{L}{t} = 0 \; - - - - - - \quad (1)$$

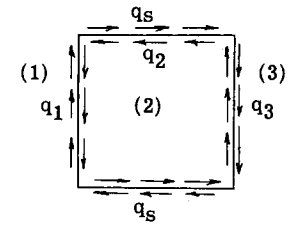

Fig. A15-46

Substituting the various shear flows on cell (2) in Fig. A15.46 into eq. (1),

$$\sum_{s} q_S \frac{L}{t} - q_2 \sum_{2} \frac{L}{t} + q_1 \sum_{1-2} \frac{L}{t} + q_3 \sum_{3-2} \frac{L}{t} = 0 \text{ - - - - (2)}$$

The subscript (s) on the summation symbol implies summation completely around cell (2) whereas the subscripts $1-2$ and $3-2$ implies summation only along webs 1-2 or 3-2 respectively. L is the length of a sheet panel and t its thickness.

Solving equation (2) for q

$$q_2 = \frac{\sum_{2} q_S \frac{L}{t}}{\sum_{2} \frac{L}{t}} + \left(\frac{\sum_{1-2} \frac{L}{t}}{\sum_{2} \frac{L}{t}} \right) q_1 + \left(\frac{\sum_{3-2} \frac{L}{t}}{\sum_{2} \frac{L}{t}} \right) q_3 \text{ - - - (3)}$$

The first term in equation (3) represents the proportion of the static shear flow q_S which must act as a constant shear flow around cell (2) to cancel the twist due to q_S. The resulting value of this first term will be given the term q'_2.

The second and third terms in (3) represent the constant closing shear flows required in cell (2) to cancel the twist of cell (2) due to the influence of q_1 and q_3 in the adjacent cells acting on the common webs between the cells. The ratio in equation (3) before q_1 will be referred to as the carry over influence factor from cell (1) on cell (2) and will be given the symbol C_{1-2}, and the ratio before q_3 in equation (3), the carry over influence factor from cell (3) to cell (2) and it will be given the symbol C_{3-2}. Thus equation (3) can now be written as,

$$q_2 = q'_2 + C_{1-2} q_1 + C_{3-2} q_3 \text{ - - - - - - - - - - (4)}$$

As explained above, q'_2 is the value of the necessary closing shear flow for zero twist when the adjacent cell shear flows are zero. Hence first approximations to the final shear flows in each cell can be taken as neglecting the effect of adjacent cells, or in other words each cell is considered separate. Hence the first approximations are,

$$\left.\begin{aligned} q_1 &\simeq q'_1 \\ q_2 &\simeq q'_2 \\ q_3 &\simeq q'_3 \end{aligned}\right\} \quad (5)$$

By substituting (5) in (4) a second approximation for q_2 is obtained, namely,

$$q_2 \simeq q'_2 + C_{1-2} q'_1 + C_{3-2} q'_3 \text{ - - - - - - (6)}$$

$$\text{or, } q_2 \simeq q'_2 + q''_2 \text{ - - - - - - - - - - (7)}$$

where q''_2 is the correction added to the first approximation. In a similar manner corrections q''_1 and q''_3 are made to the approximations for q_1 and q_3. Therefore as a third estimate for q_2, these further corrections should be added and thus equation (7) becomes,

$$q_2 \simeq q'_2 + C_{1-2}(q'_1 + q''_1) + C_{3-2}(q'_3 + q''_3) \text{ - - - (8)}$$

Thus by repeating the above procedure, a power series of the carry over influence factor is obtained. In general the convergency is rapid and only a relatively few cycles or operations are needed for sufficient accuracy for final shear flows. A solution of a problem will now be given to show how the necessary operations form a very simple routine.

A15.12 Example Problem Solution. Problem No. 1.

Fig. A15.47 shows a cellular beam with five cells. The flange areas and the web and wall thicknesses are labeled on the figure. The problem will be to determine the internal shear flow pattern when resisting an external shear load of V_Z = 1000 lbs. without twist of the beam. Having determined this shear flow system the shear center location follows as a simple matter.

Fig. A15.48 shows the assumed static condition for determining the shear flow system in carrying a V_Z load of 1000 lb. without twist. The static condition is that all webs except the right end web have been imagined cut as indicated thus making the shear flow q_S at these points zero.

In this example problem it will be assumed that the flange members develop all the bending stress resistance, which assumption makes the shear flow constant between adjacent flange members.

The total top flange area equals 5.5 in.^{2}, and also the total bottom flange area. Due to symmetry the centroidal X axis lies at the mid-depth point.

$$\text{Hence, } I_X = (5.5 \times 5^2)2 = 275 \text{ in.}^4$$

$$q_S = -\frac{V_Z}{I_X} \Sigma zA = -\frac{1000}{275} \Sigma zA = -3.636 \, \Sigma zA$$

Starting at the lower left hand corner, the static shear flow q_S will be computed going counter-clockwise around beam.

$$q_{ab} = -3.636(-5)2 = 36.36 \text{ lb./in.}$$

$$q_{bc} = 36.36 - 3.636(-5)1 = 54.55 \text{ lb./in.}$$

$$q_{cd} = 54.55 - 3.636(-5)0.5 = 63.64$$

Continuing in like manner around the beam, the values of q_S as shown in Fig. A15.48 would be obtained.

The solution from this point onward is made in table form as shown in Table A15.2 which should be located below a drawing of the

cellular beam as illustrated, and the numbers in the Table should be lined up with respect to the cells as indicated.

The solution as presented in Table A15.2 is carried out in 17 simple steps. The first step as given in row 1 of the Table is to compute for each cell the value for $\Sigma\, q_s \frac{L}{t}$, where q_s is the static shear flow on each sheet panel of a cell; L the length of the panel and t its thickness. Values for q_s are taken from Fig. A15.48.

For example, for Cell 1

$$\Sigma\, q_s \frac{L}{t} = 2(36.36 \times 10)\frac{1}{.04} = 18180$$

The sign is positive because q_s is positive. (Clockwise shear flow on a cell is positive.) Row 1 in the Table shows the values as calculated for the 5 cells.

The second step as indicated in row 2 of the Table is to calculate the value of the expression Σ L/t for each cell.

For example, for Cell 1,

$$\Sigma_1 \frac{L}{t} = \frac{10}{.064} + \frac{(10)2}{.04} + \frac{10}{.05} = 856$$

For cell 2,

$$\Sigma_2 \frac{L}{t} = \frac{10}{.05} + \frac{2(10)}{.04} + \frac{10}{.04} = 950$$

The third step as indicated in row 3 is to calculate the value for the L/t of the common web between two adjacent cells.

For example, for web bb' between cells (1) and (2),

$$\left(\frac{L}{t}\right)_{1-2} = \frac{10}{.05} = 200$$

The fourth step is to determine the carry over factor from one cell to the adjacent cell. The results are recorded in row 4 of the Table.

Referring to equation (3) for general explanation, the carry over factor from cell (1) to cell (2) is,

$$C_{1-2} = \frac{\left(\frac{L}{t}\right)_{1-2}}{\Sigma_2 \frac{L}{t}} = \frac{200}{950} = .2105$$

and the carry over factor from cell (2) to cell (1) equals,

$$C_{2-1} = \frac{\left(\frac{L}{t}\right)_{2-1}}{\Sigma_1 \frac{L}{t}} = \frac{200}{856} = .2336$$

We are now ready to start the solution proper by successive approximations. In row 5 of the Table, the first approximation is to assume a value q' added to each cell which will cancel the twist due to the static shear flow when the cell webs are not cut, but each cell is considered separate or independent of the other. This constant closing shear flow q' equals,

$$q' = -\frac{\Sigma q_s \frac{L}{t}}{\Sigma \frac{L}{t}}.$$ The minus sign is necessary because the twist under the static shear flow must be canceled. The values for q' are recorded in row 5 of the Table.

For example for cell (1),

$$q' = -\frac{18180}{856} = -21.238$$

For cell (2),

$$q' = -\frac{27275}{950} = -28.71$$

Steps 6 to 13 as recorded in rows 6 to 13 of the Table are identical in operation, namely, the carry over influence from one cell to the adjacent cell because of the common web between the cells. As a closing shear flow is added to each cell to make the cell twist zero when they are considered separate, this result is continually disturbed because of the common web. Gradually these corrective shear flows become smaller and smaller until the cells reach their true state and possess zero twist. In the Table, arrows have been used for two cycles to help clarify the operations.

For example in row 6, the carry over shear flow from cell (1) to cell (2) is,

$$-6.700 \times .2105 = -1.414$$

From cell (2) to cell (1), the carry over value is

$$(-4.480 - 8.330)\ 0.2336 = -3.000$$

From cell (2) to cell (3),

$$(-4.480 - 8.330)\ 0.250 = -3.216$$

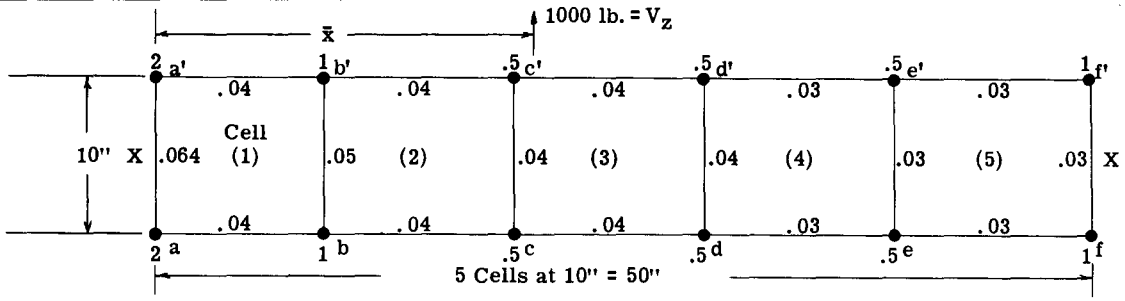

Fig. A15-47 Flange and Web Data

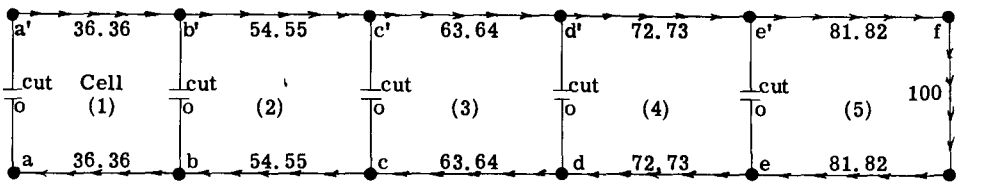

Fig. A15-48 Assumed Static Condition for Shear Flow q_s

Table A15.2

Row	OPERATION									
1.	Σq_s L/t for each cell	18180		27275		31820		48487		87880
2.	Σ L/t for each cell	856		950		1000		1250		1333
3.	L/t of cell web	200		250		250		333		
4.	Carry Over Factor (C)	.2105	.2336	.250	.2633	.200	.250	.250	.266	
5.	1st Approx. $q' = -\Sigma q_s$ L/t/Σ L/t	-21.238		-28.71		-31.82		-38.79		-65.910
6.	q" = Cq' (Carry over)	- 6.700	-4.480	-8.380	-7.170	-9.700	-6.364	-17.560	- 9.700	
7.	q'" = Cq" (Carry over)	- 3.000	-1.414	-4.430	-3.216	-5.975	-3.372	-2.580	- 5.975	
8.	ETC (Carry over)	- 1.362	-0.631	-2.518	-1.460	-1.489	-1.837	-1.592	- 1.489	
9.	Carry over	- 0.736	-0.287	-0.777	-0.787	-0.872	-0.590	-0.396	- 0.872	
10.	Carry over	- 0.248	-0.155	-0.436	-0.266	-0.246	-0.332	-0.232	- 0.246	
11.	Carry over	- 0.138	-0.052	-0.135	-0.148	-0.141	-0.102	-0.065	- 0.141	
12.	Carry over	- 0.044	-0.029	-0.076	-0.047	-0.042	-0.058	-0.037	- 0.045	
13.	Carry over	- 0.003	-0.009	-0.003	-0.003	-0.003	-0.002	-0.012	- 0.003	
14.	q = q' + q" + q'" + - - -)	-33.47		-52.52		-63.39		-73.92		-84.38
15.	1st Reiteration	-12.27	-7.05	-16.69	-13.13	-18.48	-12.68	-22.44	-18.48	
16.	q' from row 5	-21.238		-28.71		-31.82		-38.79		-65.91
17.	q	-33.51		-52.45		-63.43		-73.91		-84.39
18.	2nd Reiteration	12.23	-7.05	-16.70	-13.10	-18.48	-12.69	-22.44	-18.48	
19.	q' from row 5	-21.238		-28.71		-31.82		-38.79		-65.91
20.	q	-33.47		-52.46		-63.40		-73.92		-84.39

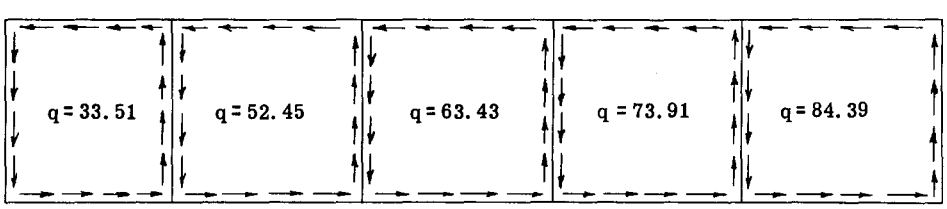

Fig. A15-49 Closing Shear Flows to Make Twist of Each Cell Equal Zero

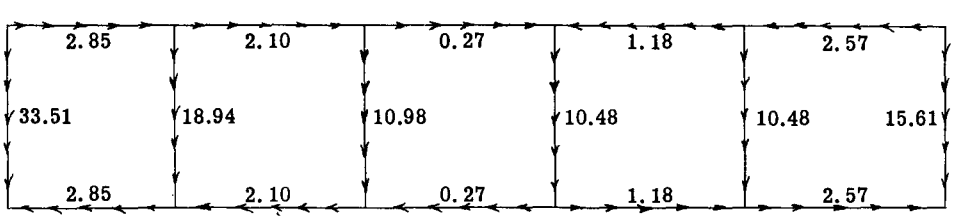

Fig. A15-50 Final Shear Flows. (Fig. A15.48 plus Fig. A15.49)

CALCULATION OF SHEAR CENTER LOCATION

In Fig. A15.47 let $\bar{x}$ = distance from left end of beam to shear center. Taking moments about upper left corner of the shear flow forces in Figs. A15.48 and A15.49 and equating to 1000 $\bar{x}$.

$1000\bar{x} = 10(36.36+54.55+63.64+72.73+81.82)10 + 100 \times 10 \times 50 - 2 \times 100(33.51 + 52.45 + 63.43 + 73.91 + 84.39)$, hence $1000\bar{x} = 19472$ or $\bar{x} = 19.47$ inches.

In row 13 of the Table, the carry over values are so small that the process is terminated. The final constant shear flow that must be added to each cell to cancel the twist due to the static shear flow equals the algebraic sum of the values from the beginning row 5 to row 14. The results are shown in row 14 of the Table.

The results in row 14 are obtained after a considerable number of multiplications and additions of numbers, thus it is easy to make a numerical mistake. To check whether any appreciable mistakes have been made, we take the values in row 14 and consider these values of constant shear flow in each cell as that causing zero twist if cells are separate. Then bringing the cells together, through the common webs causes a disturbance in twist and this is made zero by the carry over values. This step in the Table is referred to as a reiteration and is indicated in row 15. Then adding the values in row 15 to the initial approximation q' in row 5, which value is repeated in row 16, we obtain the final value of q in row 17. The values in row 17 are practically the same magnitude as in row 14, thus no appreciable mistakes have been made. If the difference was appreciable, then a second, and if needed, even a greater number of reiterations should be carried out. In the Table a second reiteration is shown in rows 18, 19, 20 and the results in row 20 are practically the same as in row 17.

It will be assumed that the solution was stopped after first iteration, and thus the values in row 17 are the constant shear flows that must be added to the static shear flows to produce bending without twist. Fig. A15.49 shows these final closing constant shear flows. Adding these values to those in Fig. A15.48 we obtain the final shear flows in Fig. A15.49.

The lateral location of the shear center for this given 5 cell beam coincides with the centroid of the shear flow force system in Fig. A15.50. The calculations for locating the shear center are given below Fig. A15.50.

Solution 2 of Problem 1

In solution 1, the assumed static condition involved cutting all vertical webs except the right end web. Thus the static beam section became an open channel section and the resulting static shear flows must obviously be far different than the final true shear flow values, since the webs always carry the greater shear flows in bending without twist. This fact is indicated by the relatively large number of steps required in Table A15.2 to reach a state where successive corrections were small enough to give a desired accuracy of final result. Thus it is logical to assume a static condition where the static shear flows in the webs should be much closer to the final values and thus hasten the convergency in the successive approximation procedure.

Thus in Fig. A15.51, we have assumed the top panel in each cell as cut to give the static condition. The static shear flow is now confined to the vertical webs and zero values for top and bottom sheet. Table A15.3 shows the calculations for carrying out the successive approximations and needs no further explanation. It should be noticed that after the first approximation was made in row 5, only three carry over cycles were needed in rows 6, 7 and 8 to obtain the same degree of accuracy as required in 8 cycles in Table A15.2 for solution 1. Fig. A15.52 shows the final shear flows which equal the constant shear flows in each cell from row 9 of Table added to the static shear flows in Fig. A15.51. These values check the results of solution 1 as given in Fig. A15.50, within slide rule accuracy. In Table A15.3 no reiteration steps were given. The student should make it a practice to use such checks.

A15.13 Example Problem 2.
All Material Effective in Bending Resistance.

The general trend in supersonic wing structural design is toward a large number of cells and relatively thick skins, thus in general, all cross-sectional material of the wing is effective in resisting bending stresses and thus the shear flow varies in intensity along the walls and webs of the beam cells. Fig. A15.53 shows a ten cell beam with web and wall thicknesses as shown. It will be assumed that all beam material is effective in bending. The shear flow resisting system for bending about the horizontal axis without twist will be determined. The centroid of this system will then locate the shear center.

Fig. A15.54 shows the static condition that has been assumed, namely, that the upper sheet panel in each cell has been imagined cut at its midpoint, thus making the static shear flow zero at these points. The static shear flow values q_s are shown on Fig. A15.54. To explain how they were calculated, a sample calculation will be given.

The moment of inertia of the entire cross-section about the horizontal centroidal axis is,

I_X for top and bottom skins,
$= (50 \times 0.125 \times 2.5^2)2 = 78.0$
I_X of all webs $= (0.912 \times 5^3)/12 = 9.5$
Total $I_X = 87.5$ in^4

For convenience an external shear load $V_Z = 8750$ lb. will be assumed acting on this beam section.

Hence, $q = -\frac{V_Z}{I_X}\Sigma zA = -\frac{8750}{87.5}\Sigma zA = -100\,\Sigma zA$

Now consider Fig. A15.55 which shows a sketch of cell (1) plus half of cell (2). As previously explained the upper cell panels were assumed cut at their midpoints (a) and (m).

Starting at point (a) in cell (1) where the shear flow is zero and going counter-clockwise around the cell, the static shear flows are as follows: -

(Cont. on pg. A15.23 ⟶)

Solution II

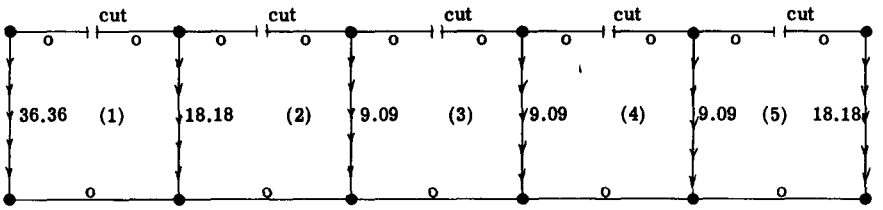

Fig. A15-51 Assumed Static Condition for Shear Flow q_s and Resulting q_s Values.

Table A15.3

Row OPERATION										
1. $\Sigma q_s L/t$ for each cell	-2045		-1362		0		758		3031	
2. $\Sigma L/t$ for each cell	856		950		1000		1250		1333	
3. L/t of cell web	200		250		250		333			
4. Carry over factor C	.2105	.2336	.250	.2633	.200	.250	.250	.266		
5. 1st approx. $q' = -\Sigma q_s L/t / \Sigma L/t$	2.389		1.434		0		-0.606		-2.274	
6. $q'' = Cq'$ (carry over)	0.334	0.503	0	0.358	-.152	0	-.605		-0.152	
7. $q''' = Cq''$ (carry over)	0.118	0.071	.055	0.126	-.152	0.041	-.041		-0.152	
8. ETC (carry over)	0.029	0.025	-.007	0.031	0	-0.005	-.040		0	
9. $q = q' + q'' + q''' + - - -$)	2.870		2.081		0.211		-1.256		-2.578	

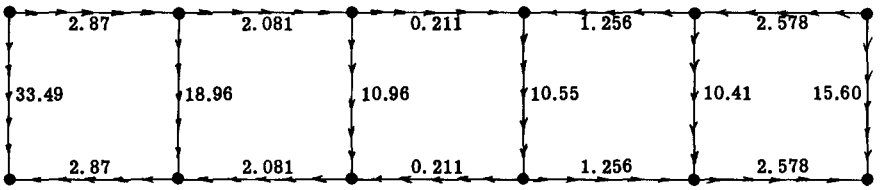

Fig. A15-52 Final Shear Flows (Row 9 Plus Fig. A15-51) Compare Results with Solution I (See Fig. A15-50)

Example Problem 2 Ten Cell Beam - All Material Effective in Bending.

Top Skin = .125 Inches Thick

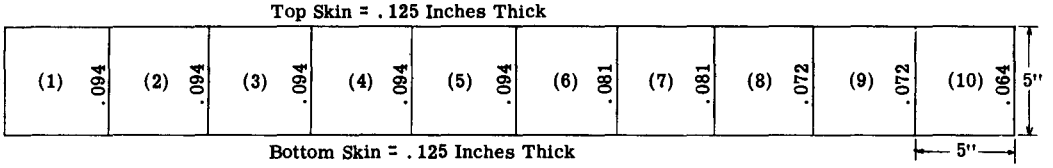

Bottom Skin = .125 Inches Thick

Fig. A15-53

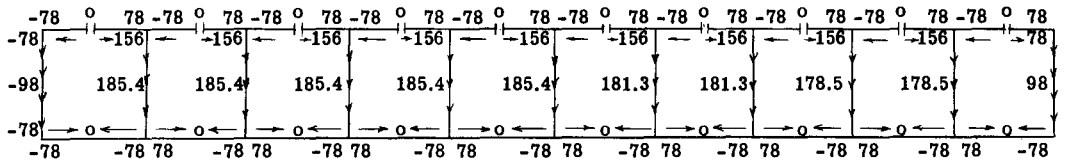

Fig. A15-54

Table A15.4

$\Sigma q_s L/t$	2200	0	0	0	0	1350	0	1190	0	-4760
$\Sigma L/t$ cell	211.4	186.4	186.4	186.4	186.4	195	203.6	211.3	219	227.7
L/t web	53.2	53.2	53.2	53.2	53.2	61.8	61.8	69.5	69.5	
C	.285	.252 .285	.285	.285	.285	.285	.285	.304	.316 .292	.304 .317 .329 .306 .317
$q' = -\Sigma q_s L/t / \Sigma L/t$	-10.42	0	0	0	0	-6.92	0	-5.63	0	20.91
C.O.	0	-2.98 0	0	0 0	0	0 -1.97	0 0	-2.10 -1.71	0 0	-1.78 6.63 0
C.O.	-0.75	0 0	-0.86	0 0	-0.57	0 0	-0.56 -1.20	0 0	-1.11 1.60	0 0 1.48
C.O.	0	-0.21 -0.25	0	-0.16 -0.25	0	-0.16 -0.50	0 0	-0.53 0.15	0 0	0.15 0.47 0
C.O.	-0.11	0 -0.00	-0.13	-0.07 -0.05	-0.19	-0.07 0	-0.19 0.11	0 0	-0.11 0.20	0 0 0.19
C.O.	-0.00	-0.03 -0.06	-0.00	-0.07 -0.06	-0.02	-0.07 -0.08	-0.02 0	-0.09 0.03	0 0	0.03 0.06 0
q	-11.28	-3.53	-1.29	-1.14	-2.85	-9.00	-4.25	-5.05	5.56	22.58
Reiterate	-0.89	-3.21 -0.36	-1.01	-0.32 -0.36	-0.81	-0.32 -2.56	-0.81 -1.34	-2.74 -1.53	-1.24 1.83	-1.60 7.15 1.70
q'	-10.42	0	0	0	0	-6.92	0	-5.63	0	20.91
q	-11.31	-3.57	-1.33	-1.17	-2.88	-9.07	-4.27	-5.04	5.55	22.61

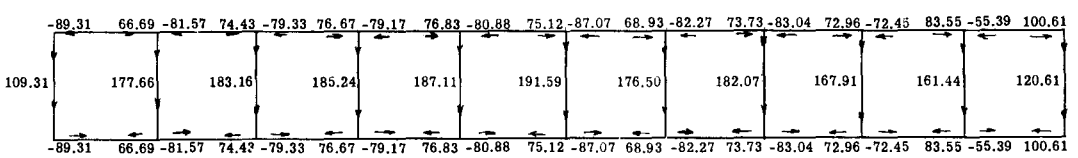

Fig. A15-57. Final Shear Flow Values.
(Note: Shear Flow at Ends of Webs Equal Sum of Shear Flows in Adjacent Skin Panels.)

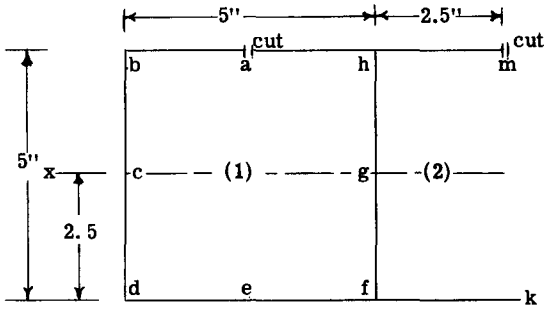

Fig. A15-55

$q_a = 0$

$q_b = -100\sum_a^b ZA = -100 \times 2.5 \times 2.5 \times 0.125$

$= -78$ lb./in.

$q_c = q_b - 100\sum_b^c ZA = -78 - 100\ (1.25 \times 2.5 \times 0.064) = -78 - 20 = -98$ lb./in.

$q_d = -98 - \sum_c^d ZA = -98 - 100\ (-1.25)(2.5 \times 0.064) = -98 + 20 = -78$

$q_e = -78 - \sum_d^e ZA = -78 - 100\ (-2.5)(2.5 \times 0.125) = -78 + 78 = 0$

$q_{fe} = 0 - \sum_e^f ZA = 0 - 100\ (-2.5)(2.5 \times 0.125)$

$= 78$

At point (f) there are two other connecting sheet panels so we cannot proceed past this joint in calculating the shear flow in the two connecting sheets at (f).

Thus we go back to point (a) and go clockwise,

$q_a = 0$

$q_{ha} = 0 + 100\sum_a^h ZA = 0 + 100\ (2.5 \times 2.5 \times 0.125)$

$= 78$ lb./in.

With two other webs intersecting at joint (f) the shear flow summation cannot continue past (f), hence we go to point (m) in cell (2) where shear flow is zero due to the assumed cut at point (m).

$q_m = 0$

$q_{hm} = 0 - 100\sum_m^h ZA = -100(2.5 \times 2.5 \times 0.125)$

$= -78$

Now at joint (h) we have the shear flow of 78 magnitude on each top panel, thus the shear flow in the vertical web at (h) equals the sum of these two shear flows or 156.

Proceeding to (g)

$q_g = q_{hg} + 100\sum_h^g ZA = 156 + 100\ (1.25 \times 2.5 \times .094) = 156 + 29.4 = 185.4$ lb./in.

$q_{fg} = 185.4 + 100\sum_g^f ZA = 185.4 + 100\ (-1.25)(2.5 \times .094) = 156$ lb./in.

$q_{fk} = q_{fg} - q_{fe} = -156 + 78 = -78$

$q_{kf} = -78 - 100\sum_f^k ZA = -78 - 100\ (-2.5)(2.5 \times 0.125) = -78 + 78 = 0$

Fig. A15.56 shows a plot of these calculated values. The arrows give the sense of the shear flows.

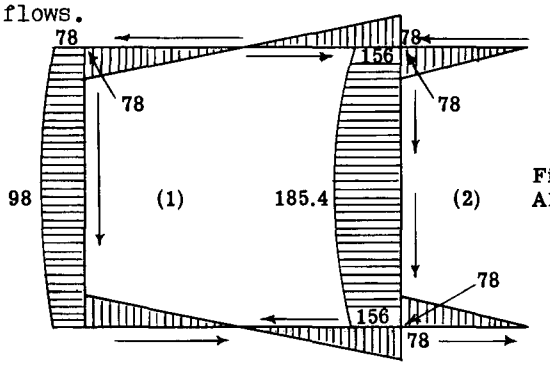

Fig. A15-56

Fig. A15.54 shows the calculated static shear flow values for the entire 10 cells. The values are recorded at the ends of each sheet panel and at the midpoints of each sheet panel. Clockwise shear flow in a cell is positive shear flow. Since an interior web is part of two adjacent cells, the sign of the shear flow on vertical webs is referred to the left hand cell in order to determine whether sense is positive or negative.

Having determined the static shear flows which will be referred to as q_s, we can now start the operations Table A15.4. The first horizontal row gives the calculations of the twist of each cell under the static shear flows, which is relatively measured by the term $\Sigma q_s \frac{L}{t}$ for each cell.

With all material effective in bending the shear flow varies along each sheet. Fig. A15.56 shows this variation on the sheet panels of cell (1). The term $\Sigma q_s\ L/t$ is nothing more than the area of the shear flow diagram on each sheet divided by the sheet thickness. To illustrate, consider cell (1) in Fig. A15.56.

Upper sheet panel: -

$$\Sigma q_s \frac{L}{t} = \frac{-(0+78)}{2}\frac{2.5}{0.125} + \frac{(0+78)}{2}\frac{2.5}{0.125} = 0$$

For lower sheet panel: -

$\Sigma q_s \frac{L}{t} = 0$ (Same figure as for upper sheet)

For left hand vertical web: -

Treating the shear flow diagram as a rectangle with height 78 and a parabola with height 98 - 78 = 20,

$$\Sigma q_s \frac{L}{t} = \frac{-78 \times 5}{0.064} - \frac{(20 \times 5 \times 0.667)}{0.064} = -7142$$

For right hand web of cell (1),

The shear flow diagram is likewise made up of a rectangle and a parabola.

$$\Sigma q_s \frac{L}{t} = \frac{156 \times 5}{0.094} + (186.5 - 156)5 \times \frac{0.667}{0.094} = 9342$$

Therefore for entire cell (1)

$\Sigma q_s \frac{L}{t} = -7142 + 9342 = 2200$, which is the value in row (1) of Table A15.4 under cell (1). The results for the other nine cells as calculated in a similar manner are recorded in row 1 of the Table. The procedure as followed in the remaining rows of Table 4 is the same as explained in detail for example problem 1. In Table A15.4 only one reiteration is carried through as the values in the bottom or last row are practically the same as arrived at after the fifth carry over cycle. Adding the constant shear flow values in the last row in the Table to the static shear flow values in Fig. A15.54 we obtain the final shear flow values of Fig. A15.57. The resultant of this shear flow pattern is a force of 8750 acting down in the Z direction. Its location would be through the centroid of the shear flow force system. Let $\bar{x}$ equal distance from upper left hand corner of beam to line of action of shear flow resultant force.

Taking moments of shear flow force system of Fig. A15.54 plus the constant shear closing values in each cell as given in the last row of Table A15.4 and equating to 8750 $\bar{x}$, we obtain;

Due to uniform static shear flow on each web: -

$$M = (156 \times 5)(5 + 10 + 15 + 20 + 25 + 30 + 35 + 40 + 45) + 78 \times 5 \times 50 = 175000$$

Due to parabolic static shear flow in each web:-

$$M = (29.4 \times 5 \times 0.667)(5 + 10 + 15 + 20 + 25) + 25.3 \times 5 \times 0.667(30 + 35) + 22.5 \times 5 \times 0.667 (40 + 45) + 20 \times 5 \times 0.667 \times 50 = 22520$$

Due to constant closing shear flows as listed in last row in Table A15.4: -

$$M = +(-11.31 - 3.57 - 1.33 - 1.17 - 2.88 - 9.07 - 4.27 - 5.04 + 5.55 + 22.61)\ 2 \times 25 = -520$$

Total Moment = 175000 + 22520 - 520 = 197000 hence $\bar{x}$ = 197000/8750 = 22.5 in., which equals the distance from left end of beam to shear center location.

Referring to the final shear flow values in Table A15.57, it will be noticed that the final results are not much different from the assumed static shear flows with the possible exception of the two end webs. If we had assumed all the webs cut except one to form the static condition, then Table A15.4 would have required several times as many carry over cycles to obtain the same accuracy of final results.

A15.14 Use of Successive Approximation Method for Multiple Cell Beams when Subjected to Combined Bending and Torsional Loads.

The internal shear flow resisting force system for a beam subjected to bending and twisting loads at the same time is carried out in two distinct steps and the results are added to given the true final shear flow system. First, the shear flow resisting system is found for being without twist as was explained in this chapter. The results of this first step locates the shear center. The external load system is then transferred to the sheat center, which normally would produce a torsional moment about the shear center. The internal resisting shear flow system to balance this torsional moment is then handled by the successive approximation method as explained and illustrated in detail in Art. A6.13 of Chapter A6.

A15.15 Shear Flow in Cellular Beams with Variable Moment of Inertia.

The previous part of this chapter dealt entirely with beams of constant moment of inertia along the flange direction. In airplane wing and fuselage structures, the common case is a beam of non-uniform section in the flange direction. In cases where the change of the cross-sectional areas is fairly well distributed between the various flange members which make up the beam cross section, the shear flow results as given by the solution for beams of constant moment of inertia are not much in error. For beams where this is not the case, the shear flow results may be considerably different from the actual shear flows. This fact will be illustrated later by the solution of a few example problems.

A15.16 The Determination of the Flexural Shear Flow Distribution by Considering the Changes in Flange Loads. (The ΔP Method.)

Fig. A15.58 shows a single cell distributed

flange beam. Consider the beam acts as a cantilever beam with the bending moment existing at section (A) being greater than that existing at section (B) and that the bending moment produces compression on the upper surface. By the use of the flexural stress equations, the bending stress on each stringer can be found, which if multiplied by the stringer area gives the stringer axial load. Thus at beam section (B), let P_1, P_2, P_3, etc. represent the axial loads due to a bending moment M. The external bending

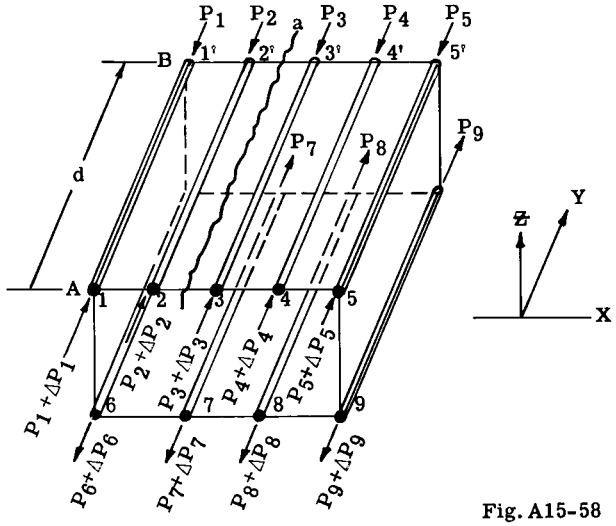

Fig. A15-58

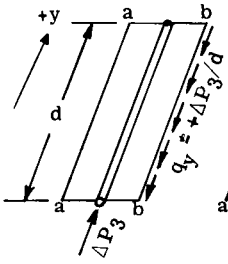

Fig. A15-59

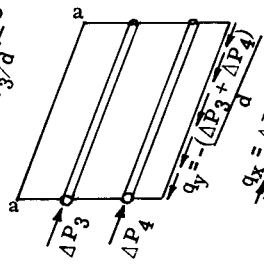

Fig. A15-60

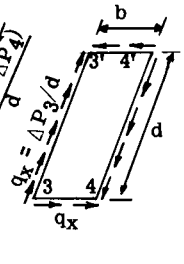

Fig. A15-61

moment at section (A) is M + ΔM, hence the stringer axial loads at section (A) will equal $P_1 + \Delta P_1$, $P_2 + \Delta P_2$, $P_3 + \Delta P_3$, etc. These stringer axial loads are shown on Fig. A15.58.

Imagine the upper sheet panel 2, 2', 3, 3' is cut along line (a-a). Furthermore consider stringer number (3) cut out and shown as a free body in Fig. A15.59. Let q_y be the average shear flow per inch over the distance d on the sheet edge bb. It has been assumed positive relative to sense along y axis.

For equilibrium of this free body,

$\Sigma F_y = 0$, hence $\Delta P_3 + q_y d = 0$

whence $q_y = -\Delta P_3/d$

For a free body including two stringers or flange members, see Fig. A15.60. Again $\Sigma F_y = 0$,

whence $\Delta P_3 + \Delta P_4 + q_y d = 0$

or $q_y = -\dfrac{(\Delta P_3 + \Delta P_4)}{d}$

Therefore starting at any place where the value of q_y is known, the change in the average shear flow to some other section equals

$$q_y = -\Sigma \frac{\Delta P}{d} \text{ - - - - - - - - - - - - - - - -(1)}$$

If the summation is started where q_y is zero then equation (1) will give the true average shear flow q_y.

Fig. A15.61 shows sheet panel (3,3',4,4') isolated as a free body. Taking moments about corner 4' and equating to zero for equilibrium,

$$\Sigma M_{4'} = \frac{d(\Delta P_3)b}{d} - q_x bd = 0$$

whence, $q_x = \Delta P_3/d$ - - - - - - - - - - -(2)

Thus for rectangular sheet panels between flange members the shear flow q_x or q_z equals the average shear q_y.

The same rules as previously presented to determine the sense of q_x or q_z after having q_y can be used and will not be repeated here.

To show that equation (1) reduces to the shear flow equation previously derived and used, consider a beam with constant cross-section and take a beam length d = 1 inch. Then,

$\Delta M = V_z d = V_z(1) = V_z$

$\Delta P = \dfrac{\Delta M}{I_x} ZA = \dfrac{V_z}{I_x} ZA$ (where A = area of stringer)

From equation (1) $q_y = -\Sigma \Delta P$

Substituting value of ΔP found above,

$q_y = -\dfrac{V_z}{I_x} \Sigma ZA$ - - - - - (3) which is the shear flow equation previously derived for beams with constant moment of inertia.

A15.17 Example Problem to Compare Results in Using Equations (1) and (3).

Fig. A15.62 shows a square single cell beam with six flange stringers. Between points B and C, the beam has a constant flange section which is shown in Section B-B. The numerals beside each stringer represent the area of the stringer. Between points B and D, the flange material tapers uniformly with the flange material at point A as indicated in Section A-A. It should be noticed that the increase in flange area is

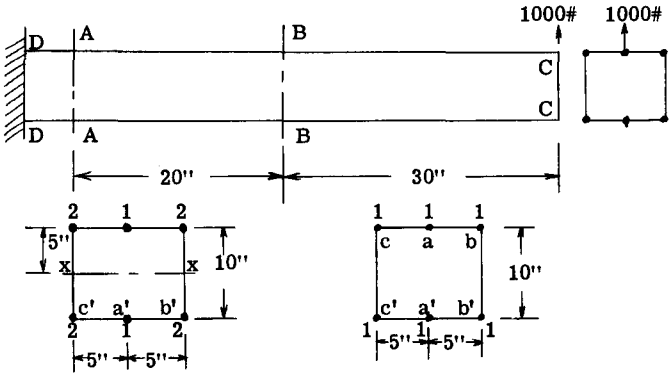

Fig. A15-62

obtained by increasing only corner stringers b and c. The shear flow on section A-A will be computed using equation (3) which applies only to beams with constant section and also by equation (1) which applies to beams with varying moment of inertia.

Solution 1. Using Shear Flow Equation for Beams of Constant Cross-Section. (Equation 3)

Since q_y at any point on the cell is unknown, it will be assumed that the upper surface on Section A-A is cut through the midpoint of flange stringer (a), thus making the shear flow q_y equal to zero on this free surface. One-half of stringer (a) thus acts with each side of the top surface. In this solution the webs and walls will be assumed ineffective in resisting bending stresses, thus the shear flow is constant between adjacent stringers.

Starting at midpoint of stringer (a) and going counter-clockwise around cell,

$$q_a = 0 \text{ (assumed cut)}$$

$$q_{ac} = -\frac{V_Z}{I_X} \Sigma ZA = -\frac{1000}{250} \times 5 \times 0.5 = -10 \text{ lb/in}$$

$$q_{CA} = -10$$

$$q_{cc'} = -10 - \frac{1000}{250} \times 5 \times 2 = -50 \text{ lb/in.}$$

Proceeding around the cell the balance of the shear flow could be calculated, but due to symmetry enough values have been found for the shear flow to draw the complete shear flow picture for bending about the X axis when it is assumed that one-half of the area of stringer (a) acts with each adjacent web. Fig. A15.63 shows the resulting shear flow diagram. The resultant of this shear flow pattern is a 1000 lb. force in the Z direction and its location through the midpoint of the box since the flow is symmetrical. The external load of 1000 lb. also acts through the midpoint of the cell hence the external load is in equilibrium with the shear flow system of Fig. A15.63, which therefore is the final shear flow system for this method of solution.

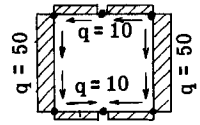

Fig. A15-63

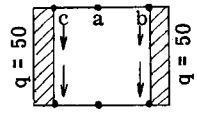

Fig. A15-64

Solution No. 2. Considering ΔP Loads in Flange Stringers. (Equation 1)

Bending moment at section AA = 1000 x 50 = 50000 in.lb.

Bending moment at section BB = 1000 x 30 = 30000 in.lb.

Considering Section B-B:

Bending stress intensity at midpoint of stringers by the flexural formula:

$$\sigma_b = \frac{M_Z}{I_X} = \frac{30000 \times 5}{150} = 1000 \text{ psi.}$$

Axial load in each of the stringers a, b, and c = 1000 x 1 = 1000 lb.

Considering Section A-A:

$$\sigma_b = \frac{M_Z}{I_X} = \frac{50000 \times 5}{250} = 1000 \text{ psi.}$$

Axial load in stringer (a) = 1000 x 1 = 1000 lb.

Axial load in stringer (b) or (c) = 1000 x 2 = 2000 lb.

These resulting axial loads are shown acting on the portion between points A and B in Fig. A15.65, which equals the results as shown in Fig. A15.66.

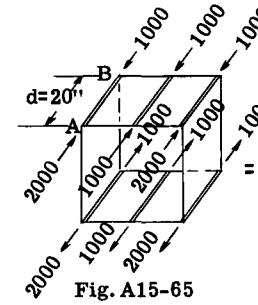

Fig. A15-65 Fig. A15-66

Having found the ΔP flange loads over a length (d) of 20", the shear flow can be computed by equation (1).

It will be assumed that one-half of the ΔP load in stringer (a) will flow to each adjacent wet. However, there is no ΔP load in stringer (a) hence $q_{ab} = q_{ac} = 0$. Then from equation (1),

$$q_{bb'} = 0 - \Sigma \frac{\Delta P_b}{d} = 0 - \frac{1000}{20} = -50 \text{ lb./in.}$$

$$q_{b'a'} = -50 + \Sigma\frac{\Delta P_{b'}}{d} = -50 - \frac{-1000}{20} = 0$$

Due to symmetry the left side of cell would give the same results. The results are plotted in Fig. A15.64. Since the increase in section moment of inertia between beam points B and A is increasing at the same rate as the external bending moment, the average shear of 50 lb./in. is constant between the two beam section A and B. Comparing Figs. 63 and 64, we find the first method gives a shear flow of 10 lb./in. in the top and bottom webs, whereas actually it is zero. This seems reasonable since the entire increase of flange area was placed in stringers b and c.

Example Problem No. 2

The same beam as in Problem 1 will be used except that the cross-sections at beam points B and A are as shown in Fig. A15.67. The increase in flange area between beam points B and A has been placed entirely in stringer (a) which changes from 1 sq. in. at B to 3 sq. in. at A.

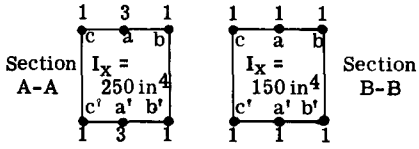

Fig. A15-67

The results of using equations (3) and (1) relative to the shear flow pattern are given in Figs. A15.68 and A15.69 respectively. (The student should check these results.) It should be noticed that the true shear flow is greater in the top and bottom skin than that given by equation (1) which applies only for beams of constant cross-section.

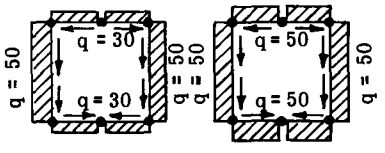

Fig. A15-68

Fig. A15-69

A15.18 Shear Flow in Tapered Sheet Panel.

Major aircraft structural units such as the wing, fuselage, etc., are tapered in both plan form and depth and therefore the sheet panels between flange members usually are tapered in width. Fig. A15.70 shows a cantilever beam tapered in depth and carrying a load V at its end. The flange reactions at the left end have been found by statics. A free body diagram of the web is shown in Fig. A15.71. Take moments about point (0) and equate to zero.

$$\Sigma M_0 = \left(\frac{Vd}{b_1}\right) b_2 - q_1 b_1 d = 0$$

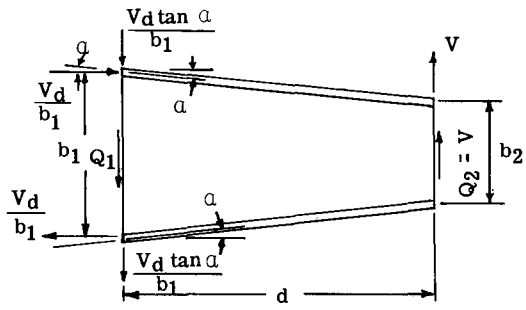

Fig. A15-70

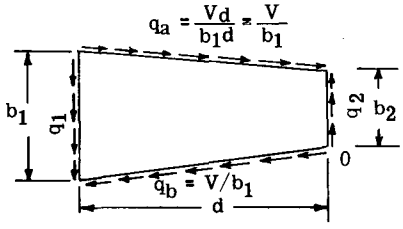

Fig. A15-71

whence $q_1 = \frac{Vb_2}{b_1^2}$

But $V = q_2 b_2$, whence

$$q_1 = \left(\frac{b_2}{b_1}\right)^2 q_2 \quad \text{- - - - - - - - - - - - - - - - (4)}$$

From Fig. A15.71

$$q_a = \frac{V}{b_1} = \frac{q_2 b_2}{b_1}, \text{ hence } q_2 = \frac{b_1 q_a}{b_2}$$

Substituting value of q in (4)

$$q_1 = \left(\frac{b_2}{b_1}\right) q_a \quad \text{- - - - - - - - - - - - - - - - (5)}$$

Thus having the shear flow on the stringer edge of the sheet panel, the shear flow on the large end of the tapered panel can be found by equation (5).

A15.19 Example Problem of Shear Flow in Tapered Multiple Flange Single Cell Beam.

Fig. A15.72 shows a tapered single cell beam with 6 spanwise stringers or flange members. The beam is loaded by a 1000 lb. load located as shown. Assuming the webs ineffective in bending the internal resisting shear flow pattern will be determined.

In this solution the shear flow at Station 120 will be determined by considering the ΔP flange loads over a length of 30" or between Stations 90 and 120.

Consider section at Station 120:-

Bending stress $\sigma_b = \frac{Mc}{I} = \frac{1000 \times 120 \times 5}{450} = 1333.33$ psi.

The horizontal component of the axial load in a stringer equals $\sigma_b A$ (where A = area of the stringer).

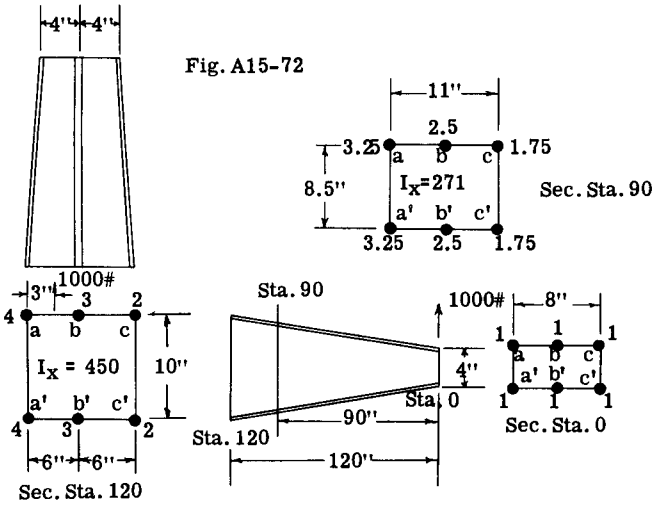

hence, the horizontal components, of stringer loads are,

$$P_a = 4 \times 1333.33 = 5333.33 \text{ lb.}$$

$$P_b = 3 \times 1333.33 = 4000 \text{ lb.}$$

$$P_c = 2 \times 1333.33 = 2666.7 \text{ lb.}$$

Consider beam section at Station 90:-

$$\sigma_b = \frac{1000 \times 90 \times 4.25}{271} = 1411.5 \text{ psi.}$$

hence stringer loads are,

$$P_a = 3.25 \times 1411.5 = 4587.4$$

$$P_b = 2.50 \times 1411.5 = 3528.7$$

$$P_c = 1.75 \times 1411.5 = 2470.1$$

The change in axial load ΔP in the stringers between stations 90 and 120 equals the difference between the above loads, whence

$$\Delta P_a = 746, \quad \Delta P_b = 471, \quad \Delta P_c = 196.6$$

Fig. A15.73 shows these ΔP loads acting on wing portion. Since shear flow is unknown at any point, assume q equals zero in web aa'. The average shear flow in each sheet panel over a length d = 30 inches.can now be calculated by using equation (1).

$$q_y = q_{a'a} - \frac{\Sigma \Delta P}{d}, \quad q_{a'a} = 0 \text{ (assumed)}$$

$$q_{y(ab)} = 0 - \frac{746}{30} = - 24.87 \text{ lb./in.}$$

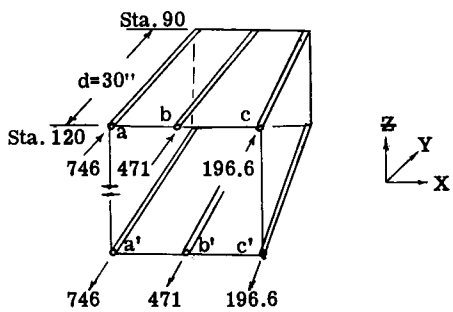

Fig. A15-73

Since panel ab is tapered in width from 6" at station 120 to 5.5" at station 90, the shear flow $q_{x(ab)}$ at station 120 can be found from equation (5).

$$q_{x(ab)} = - 24.87 \times 5.5/6 = - 23.2 \text{ lb./in.}$$

$$q_{y(bc)} = - 24.87 - 471/30 = - 40.57$$

$$q_{x(bc)} = - 40.57 \times 5.5/6 = - 37.2$$

$$q_{y(cc')} = - 40.57 - 196.6/30 = - 47.12$$

$$q_{z(cc')} = - 47.12 \times 8.5/10 = - 40.0 \text{ lb./in.}$$

Since the ΔP loads are the same on the lower stringers but tension the shear flow calculations if continued would give the same values as found on the top surface. Fig. A15.74 shows the shear flow pattern on station 120.

IN PLANE FORCES PRODUCED BY INCLINATION OF FLANGE MEMBERS

Since the box tapers in depth and width, the flange stringers are not normal to section 120, thus X and Z force components are produced on section by the stringer loads.

These in plane force components are:-

For stringers a and a',

$$P_x = 5333.33 \times 2/120 = 88.9 \text{ lb.}$$

$$P_z = 5333.33 \times 3/120 = 133.3 \text{ lb.}$$

For stringers b and b',

$$P_x = 4000 \times 0/120 = 0$$

$$P_z = 4000 \times 3/120 = 100 \text{ lb.}$$

For stringers c and c',

$$P_x = 2666.7 \times 2/120 = 44.4 \text{ lb.}$$

$$P_z = 2666.7 \times 3/120 = 66.7 \text{ lb.}$$

Fig. A15.74 shows these in plane force components due to the flange axial loads.

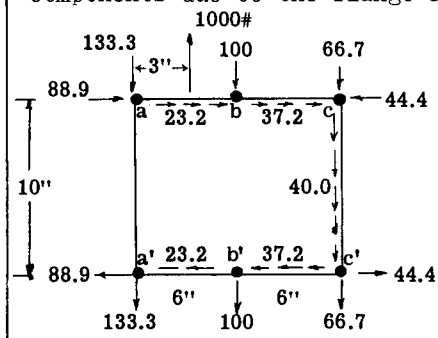

Fig. A15-74

The forces in Fig. A15.74 will be checked for equilibrium.

$$\Sigma F_z = 1000 - 266.6 - 200 - 133.4 - 10 \times 40 = 0$$

$\Sigma F_x = 0$ by observation.

Take moments about stringer (a),

$$\Sigma M_a = -3 \times 1000 + 200 \times 6 + 133.4 \times 12 + 10 \times 40 \times 12 + (+88.9 - 44.4)10 + 23.2 \times 6 \times 10 + 37.2 \times 6 \times 10 = 8670 \text{ in.lb.}$$

For equilibrium a moment of -8670 is needed, which is provided by a constant shear flow q = M/2A = -8670/240 = -36.1 lb./in. Adding this constant shear flow to that of Fig. A15.74 gives the final shear flow as shown in Fig. A15.75.

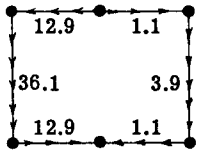

Fig. A15-75

Solution No. 2

This same beam and loading will now be solved using the shear flow equation derived for beams of constant cross-section.

Since the stringers are not perpendicular to the beam cross-section they have a z force component which thus assists in carrying the external shear load in the z direction. These P_z components at station 120 have been calculated in the other solution.

$$\Sigma P_z = -(2 \times 133.3 + 2 \times 100 + 2 \times 66.7) = -600 \text{ lb}$$

Total V_z (external) = 1000 lb.

Let $V_{z(net)}$ be shear load to be taken by cell walls,

$$V_{z(net)} = V_z - \Sigma P_z = 1000 - 600 = 400 \text{ lb.}$$

Calculation of static shear flow assuming q in sheet panel aa" is zero.

$$q_{y(ab)} = \frac{V_{z(net)}}{I_x} \Sigma ZA = \frac{400}{450} \times 5 \times 4 = 17.8 \text{ lb.in.}$$

This corresponds to value of 23.2 in previous solution (see Fig. A15.74).

$$q_{y(bc)} = 17.8 + \frac{400}{450} \times 5 \times 3 = 31.1 \text{ lb./in.}$$

As compared to 37.2 in Fig. A15.74.

$$q_{y(cc')} = 31.1 + \frac{400}{450} \times 5 \times 2 = 40.0 \text{ lb.in.}$$

which is the same as in Fig. A15.74.

Taking moments about point a of the forces in Fig. A15.74 but replacing the shear flows in the top and bottom panels by the values found above, we would obtain an unbalanced moment of 7970 in.lb. instead of 8670 previously found. The correcting shear flow would then be q = -7970/240 = -33.2 instead of -36.1 as previously found. The final shear flow pattern would be as shown in Fig. A15.76, which values should be compared to those in Fig. A15.75.

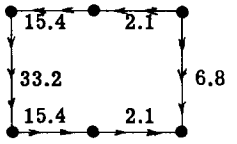

Fig. A15-76

A15.20 Problems

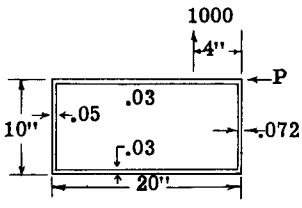

Fig. A15-77

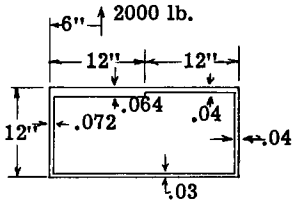

Fig. A15-78

(1) Determine the resisting shear flow pattern for the loaded single cell beam as shown in Fig. A15.77. Assume load P = zero in this problem. Assume all material effective in bending. Make two solutions, one of them involving the use of the shear center.

(2) Same as problem (1) but add load P = 1000 lb.

(3) Fig. A15.78 shows an unsymmetrical single cell beam loaded as shown. Assume all material effective in bending. Determine resisting shear flow diagram.

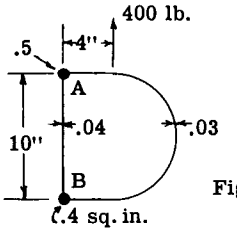

Fig. A15-79

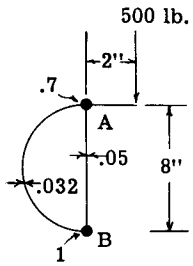

Fig. A15-80

(4) Figs. A15.79 and A15.80 show two loaded single cell - 2 flange beams. Assume the flanges develop all the bending resistance. Determine the shear flow resisting pattern by two solutions, namely, without and with use of shear center.

(5) Fig. A15.81 shows a single cell - 3 flange beam subjected to loads as shown. Assume the 3

flanges develop the entire bending resistance. Determine the internal shear flow resisting system.

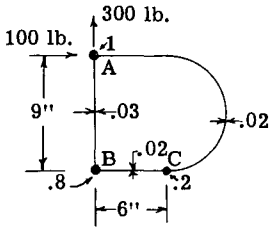

Fig. A15-81

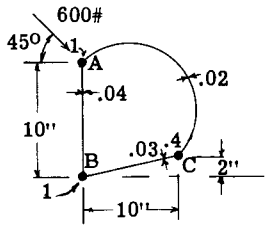

Fig. A15-82

(6) Find shear center location for beam in Fig. A15.81 if the 3 flanges provide the entire bending resistance.

(7) Find the internal resisting shear flow pattern for the 3 flange-single cell beam of Fig. A15.82. Assume webs or walls ineffective in bending.

(8) Determine shear center location for beam of Fig. A15.82. Webs and walls are ineffective in bending.

Fig. A15-83

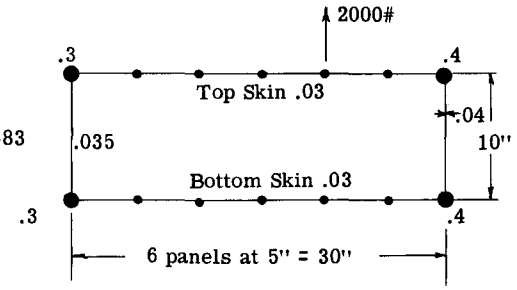

(9) Fig. A15.83 shows a multiple flange-single cell beam section. Find resisting shear flow system if webs and skin are ineffective in resisting bending stresses. All skin flange members have area of 0.1 sq. in. each.

(10) Find shear center location for beam section in Fig. A15.83, if webs and skin are ineffective in bending.

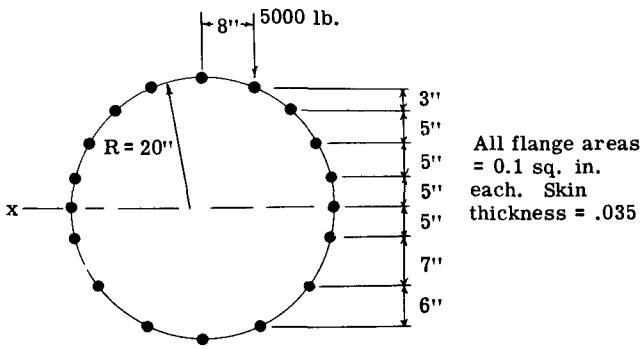

Fig. A15-84

(11) Fig. A15.84 shows a multiple flange-circular beam section. Find the resisting shear flow pattern when carrying the external shear load of 5000 lb. as located in figure. Assume cell skin ineffective in resisting beam bending stresses.

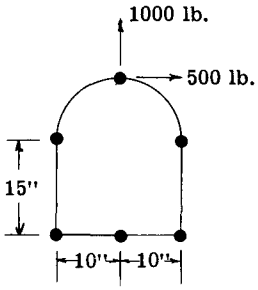

Fig. A15-85

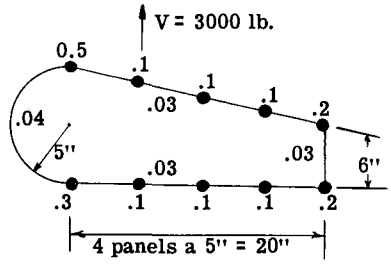

Fig. A15-86

(12) Determine the shear flow resisting system for the beam section of Fig. A15.85. The 6 flanges have areas of 0.2 sq. in. each. Skin is .032 thickness. Assume skin ineffective in bending.

(13) Find the shear flow resisting system for the unsymmetrical beam section in Fig. A15.86. Flange areas and skin thicknesses are given on figure. Assume skin ineffective in bending.

(14) Determine shear center location for beam section in Fig. A15.86.

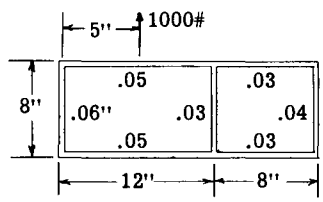

Fig. A15-87

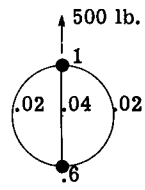

Fig. A15-88

(15) Fig. A15.87 shows a 2 cell beam section. Consider all material effective in resisting bending stresses. For the given beam loading determine the internal resisting shear flow system.

(16) Find shear center location for beam section in Fig. A15.87. All material effective in bending.

(17) For the 2 flange-2 cell beam in Fig. A15.88, determine the resisting shear flow pattern when beam section is loaded as shown. Webs are ineffective in bending.

(18) Fig. A15.89 shows a 4 cell beam section with 6 flange members. Assume walls and webs ineffective in bending.

(a) As a first problem assume that the left and right curved sheet panels are removed,

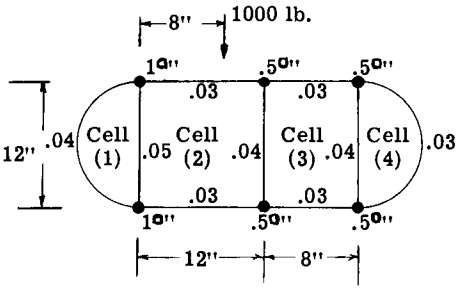

Fig. A15-89

leaving a 2 cell beam section. Find the resisting shear flow system under the given loading.

(b) Now add the left curved sheet to form cell (1) thus giving a 3 cell beam. Find shear flow system.

(c) Now add the right curved sheet to form cell (4), thus giving a 4 cell beam section. Find the shear flow system.

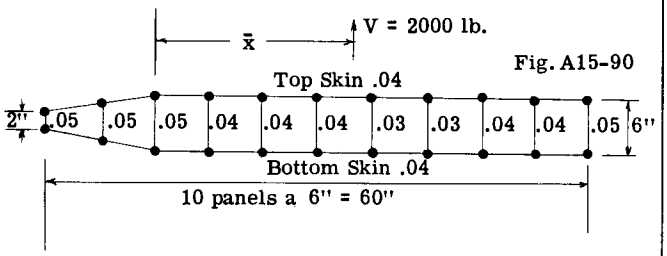

Fig. A15-90

(19) Fig. A15.90 shows a 10 cell multiple flange beam section. Area of each of the 22 flange members equal 0.3 sq. in. Assume webs and skin ineffective in resisting bending stresses. Find internal resisting shear flow system for 2000 lb. shear load acting through shear center of beam section. Find location of shear center. For solution use method of successive approximation.

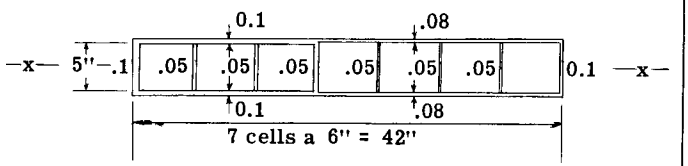

Fig. A15-91

(20) Find the shear center for the 7 cell beam section of Fig. A15.91 for bending about xx axis without twist. All beam material effective in bending. For solution use method of successive approximation.

(21) Fig. A15.92 shows a single cell-6 flange tapered beam carrying a 1000 lb. load as shown. Calculate resisting shear flow pattern at section A-A by two methods. (1) By ΔP method over a distance of 20 inches between sections A-A and B-B, and (2) By using general shear flow equation for beams of constant section. Compare the results. All six flange members have 0.2 sq. in. area each at section A-A and tapers uniformly to 0.1 sq. in. at end C-C.

Fig. A15-92

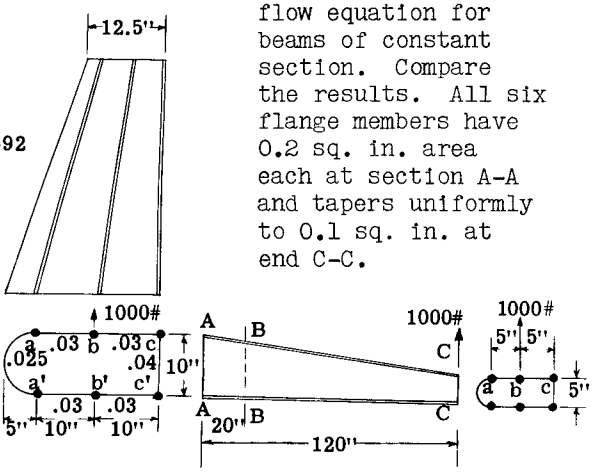

(22) Add two interior webs to the beam of Fig. A15.92, connecting flange members a-a" and b-b", thus making it a 3 cell beam. Find the shear flow resisting pattern at section A-A by the ΔP method.

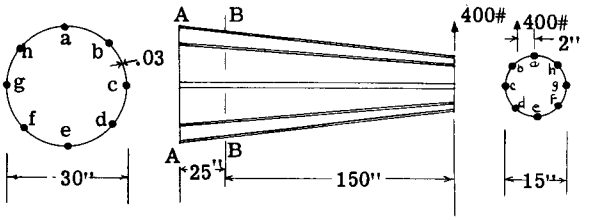

Fig. A15-93

(23) Fig. A15.93 shows a circular single cell beam with 8 flange members. The area of each flange member is 0.1 sq. in. throughout the beam length. For the given 400 lb. external loading determine the resisting shear flow pattern at section A-A using the ΔP method over a distance of 25 inches between sections A-A and B-B. Assume cell wall ineffective in resisting bending stresses.

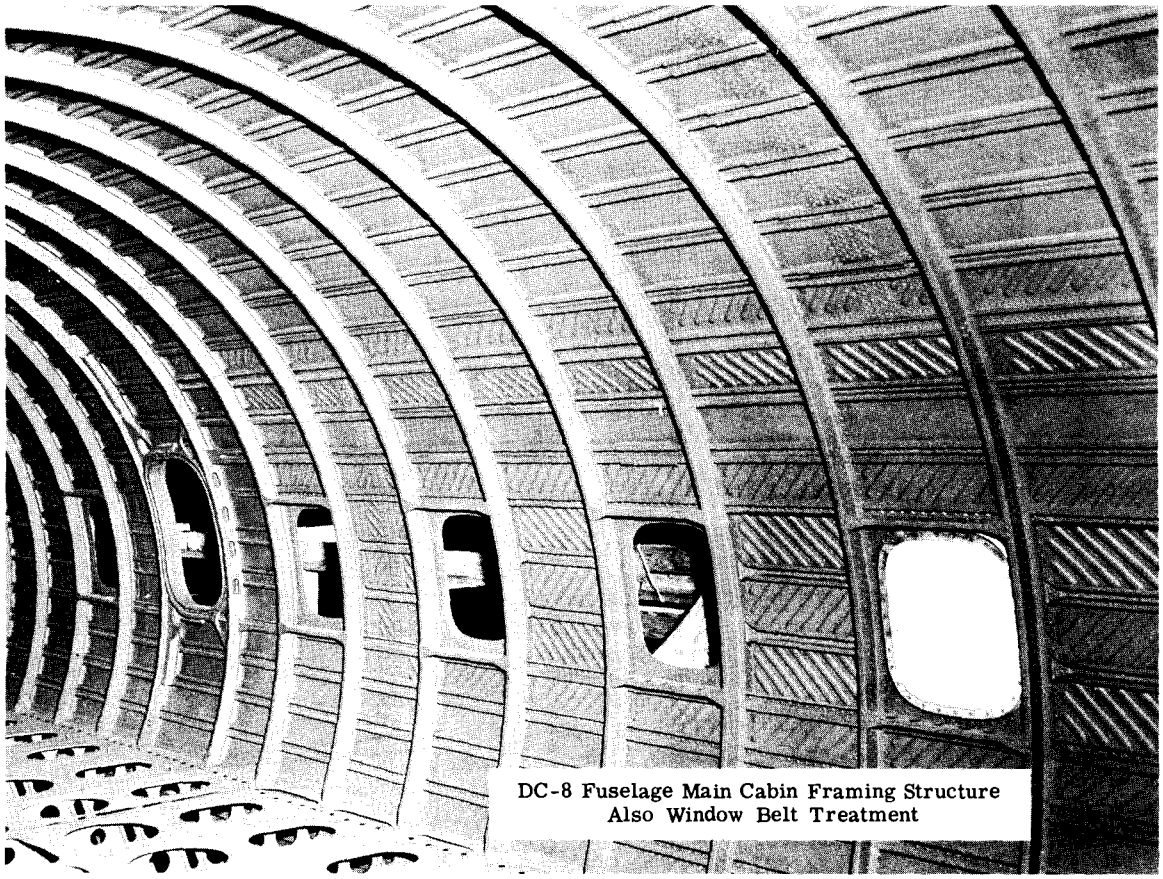

DC-8 Fuselage Main Cabin Framing Structure
Also Window Belt Treatment

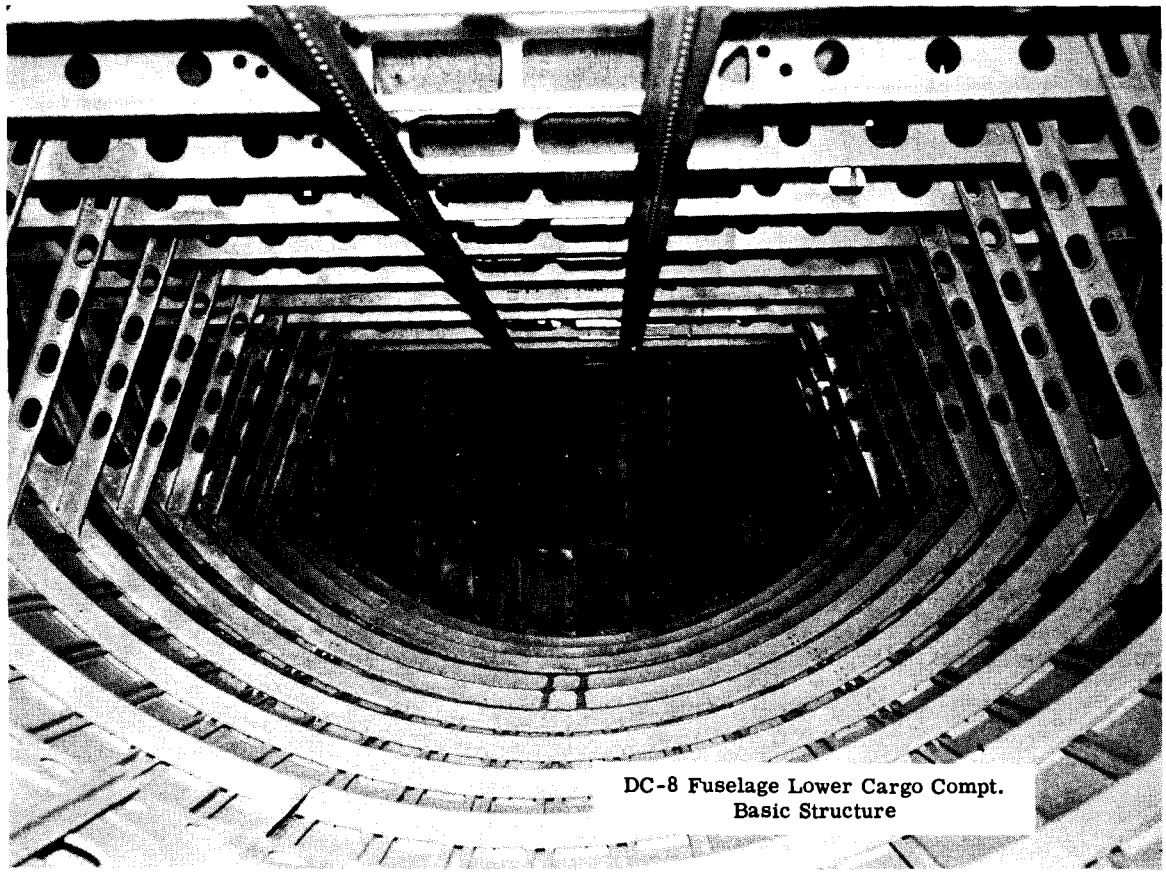

DC-8 Fuselage Lower Cargo Compt.
Basic Structure

DOUGLAS DC-8 JET AIRLINER. BASIC FUSELAGE CONSTRUCTION

CHAPTER A-16

MEMBRANE STRESSES IN PRESSURE VESSELS

ALFRED F. SCHMITT

A16.1 Introduction.

The structural designer is often called upon to develop a vessel which is to contain a fluid under pressure. Occasionally the design of such a vessel is not critical from either a weight or shape standpoint and almost any suitably strong sealed vessel will suffice. More often, the strength, weight and form of such a unit are closely prescribed and rigidly controlled. Thus, the pressurized cabin of a modern aircraft is a sealed pressure vessel containing an atmosphere at near sea level pressures and whose functional requirements include:

i - the transmittal of heavy loads from the tail surfaces and from internal dead loads,

ii - the necessity for nonstructural cutouts for doors and windows,

iii - an efficient shape from both the aerodynamic and space utilization points of view,

iv - a minimum of weight.

Structurally, the most efficient form of pressure vessel is one in which the lateral pressures are supported by tensile stresses alone in the curved walls of the vessel. Examples of such shapes are those assumed by pressurized rubber balloons and canvas fire hoses and by the free surface of a drop of water (in which the surface tension forces provide the support). The walls of these vessels have zero bending stiffnesses and hence have the properties of a membrane. The stresses developed, lying wholly in tangential directions at each point, are called membrane stresses.

In shells of technical importance, the walls do, of course, have some bending stiffness and hence may carry some transverse loadings by flexural stresses. Indeed, the boundary conditions imposed on the shell may be such as to necessitate some localized bending near edges and seams. An efficient pressure vessel design is one in which the configuration minimizes these departures from a true membrane stress system, i.e., minimizes the degree of local bending stresses induced.

A16.2 Membrane Equations of Equilibrium: Shells of Revolution Under Rotationally Symmetric Pressure Loadings.

Consider the equilibrium of a differential element cut from the shell of revolution of Fig. A16-1. (The figure is drawn to resemble a familiar folding paper Christmas bell, since such an object may aid in visualization.) The element is cut out by the intersection of a pair of adjacent meridian curves and a pair of adjacent parallels.

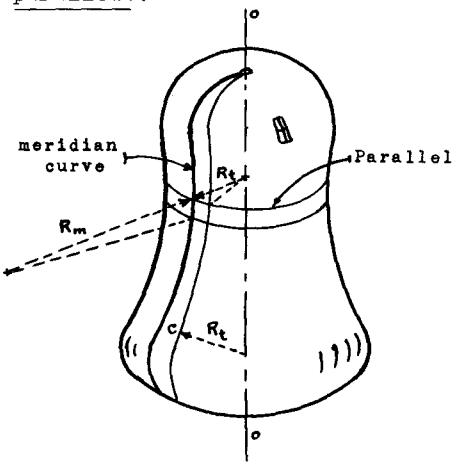

Fig. A16.1

The radii R_m and R_t shown on the figure are found by erecting local normals to the surface of the element at its corners. R_m is the radius of curvature of the meridian curve: it may be either positive (inward pointing), negative (outward pointing as in Fig. A16-1), or infinite (at inflection points or straight-line meridian segments). R_t is the radius of curvature of the section normal to the meridian curve. For simple forms of pressure vessel R_t is always positive; all radii R_t point inward and intersect the axis O-O, although not generally normal to O-O (see radius R_t erected from point C of Fig. A16-1).

Fig. A16-2 is a detail of the surface element. The forces per unit length* in the meridional and tangential directions are denoted by N_m and N_t, respectively. Shear stresses are

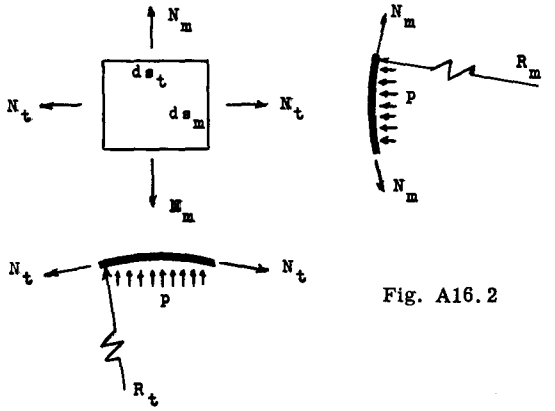

Fig. A16.2

* Hereafter referred to as "stresses" although their units are pounds per inch rather than psi.

absent due to the symmetry of the problem. The included angles between the pairs of meridional and tangential forces are ds_m/R_m and ds_t/R_t, respectively.

Summing forces normal to the differential element, one has

$$ds_t\, N_m \frac{ds_m}{R_m} + ds_m\, N_t \frac{ds_t}{R_t} = p\, ds_m\, ds_t$$

or,

$$\frac{N_m}{R_m} + \frac{N_t}{R_t} = p \quad \text{- - - - - - - - - - - - - - - - - -} \quad (1)$$

Here p is the internal pressure, positive outward. Note that the shell wall thickness does not enter eq. (1). The pressure p may vary in the meridional direction but is constant in the tangential direction by hypothesis (rotational symmetry assumed).

Eq. (1) is one equation containing two unknowns. Another equation may be obtained by the condition of equilibrium of a portion of the shell above or below a parallel circle. Thus in Fig. A16-3, the pressures acting downward on the lower portion of the shell are equilibrated by the upward vertical components of the meridional stresses, N_m.

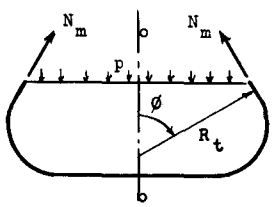

Fig. A16.3

Summing forces vertically

$$p\,\pi\,(R_t \sin\phi)^2 = 2\,\pi\,(R_t \sin\phi)\, N_m \sin\phi$$

Solving,

$$N_m = p\,\frac{R_t}{2} \quad \text{- - - - - - - - - - - - - - - - - -} \quad (2)$$

Eqs. (1) and (2) determine completely the membrane stress state in the rotationally symmetric shell problem: the problem is thus seen to be statically determinate.

We note that eq. (2) should not be used in cases of hydrostatic pressure loadings. The basic concept is that of shell equilibrium, and consequently for this class of problems the manner of shell support must be considered. Thus, in the tank of Fig. A16-4a, the upper cylindrical portion requires no meridional stresses since the load is reacted at the supporting ring 0-0. (In these analyses the structural weight, which always requires some stresses for its support, is neglected.) In the lower hemispherical portion meridional stresses are required as shown in Fig. A16-4b. Hence, in this class of problems it is best to derive the necessary second equilibrium equation (corresponding to eq. 2) by considering the individual characteristics of the structure.

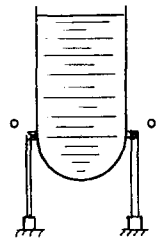

Fig. A16.4a

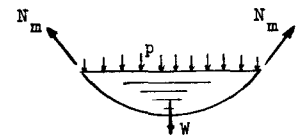

Fig. A16.4b

A16.3 Applications to Simple Pressure Vessels.

Example Problem 1

Determine the membrane stresses in a cylindrical pressure vessel of circular cross section (radius R_o), having hemispherical ends, if the internal gas pressure is p. Also find the greatest combined normal stress.

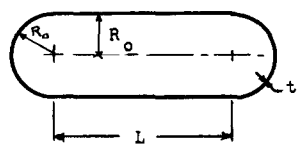

Fig. A16.5

SOLUTION:

In the hemispherical ends $N_m = N_t$ by symmetry and, of course, $R_m = R_t = R_o$. Hence eq. (1) is sufficient to determine the stresses in this portion of the structure. One has

$$2\,\frac{N_m}{R_o} = 2\,\frac{N_t}{R_o} = p$$

$$N_m = N_t = \frac{p\,R_o}{2}$$

$$\text{Stress} = \frac{N_m}{t} = \frac{N_t}{t} = \frac{p\,R_o}{2t}$$

In the cylindrical portion the radii are

$R_m = \infty$ (the curve of Fig. A16-5 is the meridian curve and this is a straight line for the cylindrical portion).

$$R_t = R_o$$

Eq. (1) becomes

$$\frac{N_m}{\infty} + \frac{N_t}{R_o} = p$$

$$N_t = p\,R_o$$

$$\text{Stress} = \frac{N_t}{t} = \frac{p\,R_o}{t}$$

The meridional stress in the cylindrical portion is found from eq. (2):

$$N_m = \frac{p\,R_o}{2}$$

$$\text{Stress} = \frac{p\,R_o}{2t}$$

Since shear stresses are absent everywhere in the meridional and tangential directions, these are the directions of principal stresses. Hence the greatest combined normal stress is identically equal to the greatest meridional or tangential stress as just computed. It is seen to be

$$s_{max} = p\,R_o/t\ .$$

Example Problem 2.

An important problem in pressurized cabin design concerns the shape of the end bulkheads. While hemispherical bulkheads (such as used in Example Problem 1) are highly desirable from a stress standpoint, such forms are uneconomical as regards space utilization. On the other extreme, a flat bulkhead, while providing far more useful volume, cannot resist the pressure loading by membrane stresses and hence is structurally inefficient. A compromise configuration is that shown in Fig. A16-6, in which the bulkhead is a spherical surface of low curvature, ("dished head") supporting the pressure loading by membrane stresses. A reinforcing ring, placed at the seam, resists the radial component of these stresses. Problem: find the compressive load acting in the reinforcing ring.

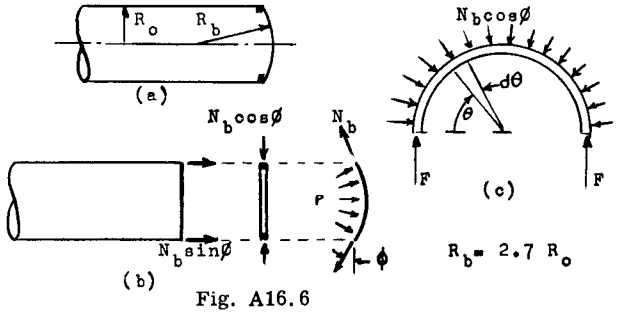

Fig. A16.6

Solution: as shown in the exploded view, Fig. A16-6b, the radial components of the bulkhead stresses are resisted by the reinforcing ring, the cylinder wall being presumed to offer no resistance to concentrated transverse forces.

For this case $\phi = \text{arc sin}\ \frac{1}{2.7} = 21.7°$.

From eq. (1), with $N_m = N_t = N_b$,

$$N_b = \frac{2.7\,R_o\,p}{2}$$

Therefore

$$N_b \cos\phi = \frac{2.7\,R_o\,p}{2}\ (.929)$$

$$= 1.25\,R_o\,p$$

Finally, the compressive ring load, F, is (ref. Fig. A16-6c)

$$2F = \int_o^{\pi} 1.25\,R_o\,p \sin\theta\,R_o\,d\theta = 2.5\,R_o^2\,p$$

In computing reinforcing ring stresses from this result it is necessary to include some effective skin from the adjacent shell walls when the ring cross sectional area is figured.

Example Problem 3.

Another form of bulkhead used to close a circular pressure cylinder is elliptical in section as shown in Fig. A16-7. Such a bulkhead shape provides tangential meridional forces at the seam (requiring no reinforcing ring as in the last example) and yet is reasonably efficient as regards space utilization. Problem: determine the membrane stresses in such a bulkhead.

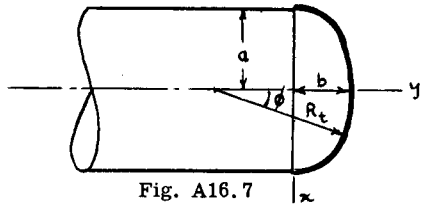

Fig. A16.7

Solution: In cartesian coordinates the equation of the bulkhead meridian is

$$\frac{x^2}{a^2} + \frac{y^2}{b^2} = 1$$

From the calculus, the radius of curvature of this meridian curve is

$$R_m = \frac{\left[1 + \left(\frac{dy}{dx}\right)^2\right]^{3/2}}{\frac{d^2y}{dx^2}} = \frac{(a^4y^2 + b^4a^2)^{3/2}}{a^4b^4}$$

The radius R_t is found most readily by observing that it is normal to a tangent to the meridian curve (see figure). After finding the

slope of the tangent (angle ϕ), one computes $R_t = x/\sin\phi$. The results are

$$\sin\phi = \frac{b^2 x}{(a^4y^2 + b^4x^2)^{1/2}}$$

$$R_t = \frac{(a^4y^2 + b^4x^2)^{1/2}}{b^2}$$

The meridional stress is found from eq. (2). Thus,

$$N_m = \frac{p\,R_t}{2} = \frac{p}{2}\,\frac{(a^4y^2 + b^4x^2)^{1/2}}{b^2}$$

Substituting the expressions for R_m, R_t and N_m into eq. (1) one finds

$$N_t = p\,\frac{(a^4y^2 + b^4x^2)^{1/2}}{b^2}\left[1 - \frac{a^4b^2}{2\,(a^4y^2 + b^4x^2)}\right]$$

Of particular interest are the stresses at the seam. Here $y = 0$ and $x = a$. One finds

$$N_m = \frac{pa}{2}$$

$$N_t = pa\left(1 - \frac{a^2}{2b^2}\right)$$

This last result is important since it indicates that compressive tangential stresses are possible if $a > b\sqrt{2}$. As will be seen below, such a situation is undersirable because of the large resultant difference in radial expansions between the cylinder and bulkhead (the bulkhead actually contracts radially if N_t is negative) producing high secondary bending stresses in the vessel walls.

Example Problem 4.

Determine the weight per unit length of the double-cylinder fuselage cross section as a function of the internal pressure, allowable stress and the geometric parameters of Fig. A16-8. For structural efficiency it is desired to maintain equal membrane stresses in the skin and floor.

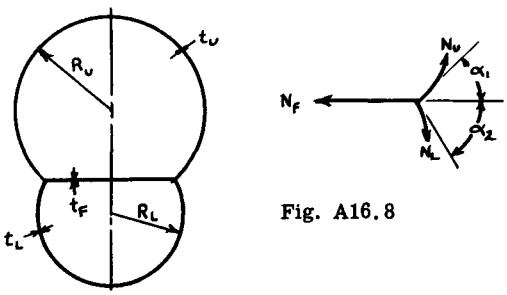

Fig. A16.8

SOLUTION:

From eq. (1) the "hoop" loadings in the upper and lower cylindrical lobes are

$$N_U = p\,R_U$$

$$N_L = p\,R_L \quad .$$

Summing forces horizontally at the floor joint:

$$N_f = p\,(R_U \cos\alpha_1 + R_L \cos\alpha_2) \quad .$$

Assume all stresses are equal and are given by s.

$$s_U = s = p\,R_U/t_U$$

$$s_L = s = p\,R_L/t_L$$

$$s_f = s = \frac{p}{t_f}\,(R_U \cos\alpha_1 + R_L \cos\alpha_2)$$

Letting the weight density of the material be w, the weight per unit length (axially) along the cabin is (w times the developed length of walls and floor).

$$W = w\left\{2\,t_U R_U\,(\pi - \alpha_1) + 2\,t_L R_L\,(\pi - \alpha_2) + 2\,t_f\,R_U \sin\alpha_1\right\} .$$

Solving for the various thicknesses from above and substituting, one finds (to obtain a result symmetric in appearance use was made of the fact that $R_U \sin\alpha_1 = R_L \sin\alpha_2$)

$$W = \frac{2wp}{s}\left\{R_U^2\left(\pi - \alpha_1 + \frac{1}{2}\sin 2\alpha_1\right) + R_L^2\left(\pi - \alpha_2 + \frac{1}{2}\sin 2\alpha_2\right)\right\}$$

Since one may show that the cross sectional area of this fuselage is

$$\mathbf{A = R_U^2\left(\pi - \alpha_1 + \frac{1}{2}\sin 2\alpha_1\right) + R_L^2\left(\pi - \alpha_2 + \frac{1}{2}\sin 2\alpha_2\right),}$$

an important consequence of this calculation is that the ratio of shell weight to shell volume is

$$\frac{W}{A} = \frac{2wp}{s}$$

and is therefore independent of the combinations of R_U, R_L, α_1 and α_2 used. The designer is thus free to choose these shape parameters so as to satisfy other requirements.

Example Problem 5.

Determine the membrane stresses in a conical vessel of height h and half apex angle α. The cone forms the bottom of a large vessel filled with a liquid of specific weight w and having a head of liquid H above the cone. The complete unit is supported from above.

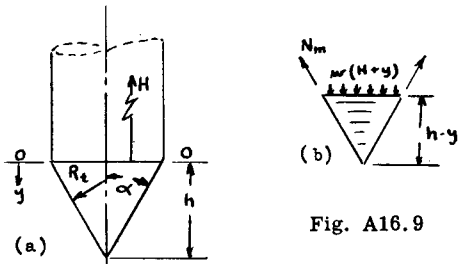

Fig. A16.9

SOLUTION:

The meridian curve of the cone has a radius of curvature $R_m = \infty$ and, at any point a distance y down from the top of the cone, the radius R_t is

$$R_t = \frac{(h - y) \tan \alpha}{\cos \alpha}$$

Then from eq. 1, at any level y

$$N_t = p\, R_t = \frac{w\,(H + y)\,(h - y) \tan \alpha}{\cos \alpha}$$

To find the meridional stresses N_m in the cone, the equilibrium of a segment of height h - y is considered (Fig. A16-9b). Summing forces vertically,

$$N_m \cdot 2\pi\,(h - y) \tan \alpha \cos \alpha =$$

$$\pi\,(h - y)^2 \tan^2 \alpha \cdot w\,(H + y) +$$

$$+ w \frac{\pi}{3} (h - y)^2 \tan^2 \alpha \cdot (h - y)$$

Solving

$$N_m = \frac{w}{2} \frac{\tan \alpha}{\cos \alpha} (h - y) \left[H + y + \frac{1}{3} (h - y) \right]$$

A16.4 Displacements, Boundary Conditions and Local Bending in Thin Walled Shells.

It is appropriate at this point to examine some of the foregoing illustrative cases to determine whether or not the membrane stresses computed gave satisfactorily accurate measures of the shell stresses. Anticipating the answer, we state that, while the membrane analysis will give the primary stress system in a shell-like pressure vessel, a careful (and often lengthy) analysis of induced bending caused by boundary effects will reveal localized secondary stress peaks. In static strength analyses of properly designed* vessels it is the practice to neglect these secondary stress peaks, arguing that local yielding of the material will level them out. However, such stress peaks may prove to be of great importance in cases of repeated loadings wherein fatigue failure is considered likely.

To point up the major weakness in the membrane analysis one need only compute the radial displacements in the two different elements that make up the pressure vessel of Fig. A16-5, viz., the cylinder and the hemispherical bulkhead. By Hooke's law, the tangential strain in the cylinder is

$$\varepsilon_{t_{CYL}} = \frac{1}{E} (s_t - \mu\, s_m) \qquad (\mu = \text{Poisson's ratio, } = .3 \text{ for aluminum})$$

$$= \frac{p\, R_o}{Et} \left(1 - \frac{\mu}{2}\right) = .85 \frac{p\, R_o}{Et}$$

By integration the radial displacement of any point on the cylinder is seen to be (ref. Fig. A16-10).

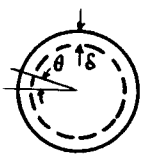

Fig. A16.10

$$\delta_{CYL} = \int_0^{\pi/2} \varepsilon_{t_{CYL}} \cos\theta\, R_o d\theta =$$

$$.85 \frac{p\, R_o}{E\, t}$$

Adjacent to the seam, the tangential strain in the hemispherical bulkhead is

$$\varepsilon_{t_{BLKHD}} = \frac{p\, R_o}{2Et} (1 - \mu) = .35 \frac{p\, R_o}{Et} .$$

Hence, by integration

$$\delta_{BLKHD} = .35 \frac{p\, R_o^2}{Et}$$

Thus the cylinder tends to expand more than the bulkhead - a situation prevented by the seam between these elements. It follows then that the seam experiences a transverse shearing action as indicated in Fig. A16-11. These shear forces in turn produce bending moments in the shell wall as shown on the figure.

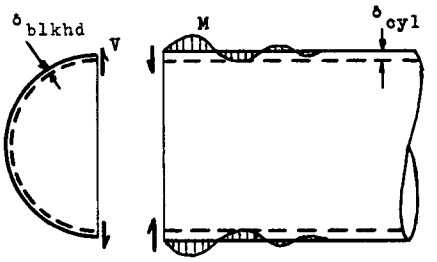

Fig. A16.11

* various codes and standards give proportions of common vessels which will correctly limit secondary stresses. See for example reference (1).

While it is not our purpose here to take up shell bending in detail, some indication of the character and magnitude of these bending stresses should be available to place them in proper perspective. The most striking thing about these wall moments is that they are quickly damped out, becoming negligibly small (down to 1% of their maximum value) at a distance of about $4\sqrt{R_o t}$ from the seam. Thus, for an instance, in a circular cylindrical shell of 40" radius and .065" wall thickness, these moments are so damped at 6.5" from the seam.

The next important consideration is an appreciation of the magnitude of these secondary bending stresses. For the case of the pressure vessel of Fig. A16-5, the meridional stresses are increased about 30% at the point of maximum moment, while the tangential stresses are increased only about 3%. Fortunately, in this class of vessel, the tangential stresses are the ones designed by (they are twice as great as the meridional stresses) and hence the secondary stresses have little importance for this case (see Chap. 11, pp. 389-422 of reference 2). In other configurations one is not always so fortunate, and detailed analysis may be required. (see references 3, 4, 5 and 6).

The situation at the seam of the above vessel is typical of many seams or boundaries where elements are joined which would experience different expansions if loaded separately. Among such seams and boundaries are those:

i - where the meridional curvature changes abruptly. It changes from $R_m = R_o$ to $R_m = \infty$ at the seam in Fig. A16-5.

ii - where a sudden change in direction of the meridian curve occurs. In Example Problem 5, above, considerable shell wall bending would be induced near the seam. In fact, a reinforcing ring would probably have to be added at the seam as was done in Example Problem 2, above.*

iii - at which structural members of different stiffnesses and different loadings join. In Example Problem 2, the cylinder tends to expand the most, the bulkhead quite a bit less and the reinforcing ring, being loaded in compression, tends to contract. Other seams and/or boundaries of this type are those where an abrupt change in shell wall thickness occurs (addition of a doubler) or where a shell is fastened into a foundation.

Good design tends to minimize the magnitude of the secondary bending stresses by avoiding combinations of elements which would have highly incompatible distortions. Thus, the analysis of Example Problem 3 shows that if one closes a circular pressure cylinder with an elliptical bulkhead in which a = 2 b, compressive tangential stresses would develop in the bulkhead. In such a case the bulkhead would tend to contract radially while the main cylinder would tend to expand as always. Thus, the shear and induced moment at the seam would be aggravated, producing (as it happens) a tangential maximum stress 13% above the membrane stress (as against only 3% above for the hemispherical bulkhead) (reference 2, p. 410). For this type of bulkhead, boiler codes sometimes permit a ratio of a/b as high as 2.6, however.

*certain details of the design of such reinforcing rings are given in the codes and standards.

A16.4 Special Problems in Pressurized Cabin Stress Analysis.

Because of functional requirements over and above those of a simple pressure vessel, the pressurized cabin shell of an airplane has a number of stress analysis problems peculiar to its configuration. Several of the more general of these will be considered here.

DISTRIBUTION OF STRESSES BETWEEN SHELL AND STRINGERS.

To stabilize the shell wall in transmitting heavy tail loads through the fuselage, longitudinal stringers are added. These same stringers will also help to carry the meridional pressure loads. The skin and stringers must, of course, have equal strains in the longitudinal directions but, because the skin is in a two-dimensional state of stress, they cannot have equal longitudinal stresses: hence the following analysis.

Let the meridional (longitudinal) stresses in the skin and stringers be s_m and s_L, respectively. s_t will be the tangential (hoop) stress in the skin. From eq. (1) we again have

$$s_t = \frac{p R_o}{t}$$

If N is the total number of stringers, each of cross sectional area A_L, then equilibrium longitudinally requires

$$p \pi R_o^2 = 2 \pi R_o t s_m + N A_L s_L.$$

The condition of equal longitudinal strain in the skin and stringers yields

$$E \varepsilon = s_L = s_m - \mu s_t$$

where μ is Poisson's ratio (= .3 for aluminum).

Solving these three equations one finds

$$s_t = \frac{p R_o}{t}$$

$$s_m = \frac{p R_o}{2t} \frac{(1 + 2 \mu \alpha)}{(1 + \alpha)} = \frac{p R_o}{2t} \frac{(1 + .6 \alpha)}{(1 + \alpha)}$$

$$s_L = \frac{p R_o}{2t} \frac{(1 - 2 \mu)}{(1 + \alpha)} = \frac{p R_o}{2t} \frac{.4}{(1 + \alpha)}$$

where $\alpha = N A_L / 2\pi R_o t$ is the ratio of total stringer area to skin area. A little study will show that $t(1 + \alpha)$ is a sort of "effective shell wall thickness": it is the result of taking all the cross sectional area (skin plus stringers)

and distributing it uniformly around the perimeter. On this basis, the results are a little disappointing: the stringers are carrying only 40% of the stress one might expect if the net longitudinal load ($p \pi R_o^2$) were distributed evenly over the entire cross sectional area ($2 \pi R_o t (1 + \alpha)$).

The meridional skin stresses are reduced by the factor $(1 + .6\alpha)/(1 + \alpha)$ from what they would be without the stringers. For structures of usual proportions this decrease may amount to 20 to 30% but clearly can never exceed 40%. Inasmuch as the bending stresses due to tail loads will be superposed on these pressure membrane stresses, the reduction is certainly beneficial*.

INTERACTION BETWEEN RINGS AND SHELL.

Because of the necessity for transmitting various concentrated loads from within the cabin and from the wings and tail to the main shell and because it is also necessary to provide some lateral restraint which will stabilize the stringers and skin against an overall instability failure, the pressurized fuselage of an airplane contains a considerable number of rings and frames distributed along the length of the shell. These rings are seldom, if ever, spaced closely enough such that they can be considered effective in carrying a part of the hoop stresses (in the way the stringers were effective in carrying part of the meridional stress). Rather, they act more like widely spaced restraining bands having the effect shown exaggerated in Fig. A16-12.

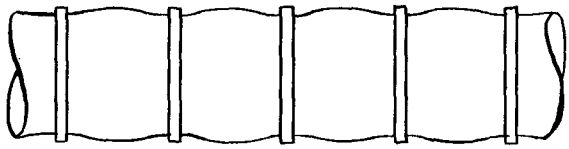

Fig. A16.12 Restraining rings along a pressurized tank. The action is representative of a fuselage with widely spaced rings inside.

It is obvious that the rings in this case will produce secondary bending stresses in the skin and hence may have a detrimental effect on the simple membrane stress system. Equally harmful are the tensile loadings developed in the rivets joining the skin and rings. Detailed analyses which will permit quantitative evaluations of these effects in a specific case are to be found in references 2 (pp. 395-406), 6 and 8.

One proposed solution to the ring-shell interaction problem is the floating skin. Basically, the idea is to reduce the radial stiffness of the connection between the shell and the rings so as to allow the shell to expand freely under the pressure loading. The connection between ring and skin must still retain its shear stiffness so that ring loads may be transferred to the shell wall by tangential shear flows. Fig. A16-13 shows the basic idea of the radially flexible connection. Many



Fig. A16.13 Ring skin cross section showing the action of a radially flexible connection.

variations of this type of "mount" suggests themselves, some of which may have merit for other reasons. For instance, the transmittal of wind and other vibration noise into the cabin of a high speed transport is a problem which might be treated simultaneously by the proper choice of connection between the ring and the shell.

DOORS AND WINDOWS.

The various cutouts in the shell of a pressurized cabin require special consideration if an excessive weight penalty is to be avoided.

Consider the panel removed from the pressurized cylinder of Fig. A16-14a. Following a

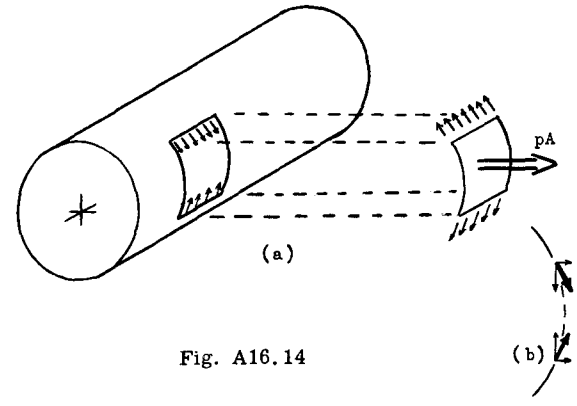

Fig. A16.14

common practice in dealing with cutouts, we determine what forces the panel-to-be-removed applies to the main structure around the border of the cutout, and then superpose a set of equal but opposite, self-equilibrating stresses to cancel these. The cutout border is then unstressed and the panel may be removed without disturbing the new stress system in the main structure.

* If one looks at the problem from the point of view of a stiffened shell, loaded primarily by bending and shear loads from the tail, on which the pressure membrane loadings are to be superposed, an interesting effect appears. Because the internal pressure tends to stabilize the curved skin panels on the compression side, the effective width of skin acting with the stringers is increased. The section properties of the cross section may then change in such a way as to produce little or no variation in the maximum fiber stresses. Indeed, the maximum tensile stresses may actually be reduced by the addition of the internal pressure loading! (see reference 7).

In examining the figure to determine what sort of canceling stress system must be supplied, we see that the tangential hoop stresses bordering the cutout cannot be canceled by a self-equilibrating set since they have a radial component. However, the radial component of these stresses will actually be supplied by the door or window pressing outward against its frame. Hence, it is only the component of the hoop stresses along a chord which need to be canceled (Fig. A16-14b)*.

The immediate problem becomes one of designing a structure to effectively support a set of uniformly distributed self-equilibrating stresses acting in the plane of the chord connecting the upper and lower edges of the opening (Fig. A16-15a).

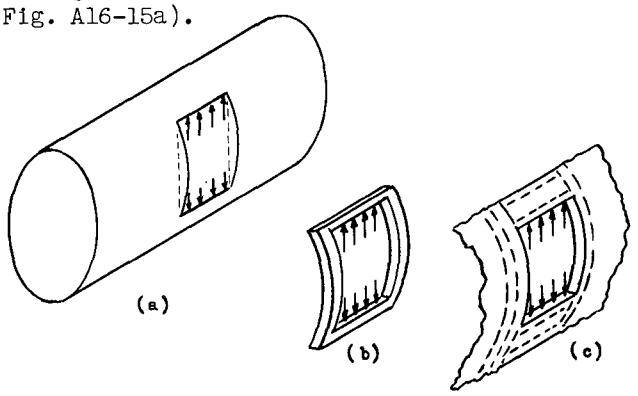

Fig. A16.15

All that appears necessary to support the stress system is to provide horizontal headers at the top and bottom of the cutout, which, as beams, will carry the loads across to the sides of the frames where the loads cancel (Fig. A16-15b). For cutouts of usual sizes in pressurized fuselages, the stress system to be supported in this manner is quite large and it proves uneconomical to design a single horizontal frame member of sufficient bending stiffness to resist them. Instead, the shell wall itself is employed to help carry these loads across. The skin is used to form a beam of considerable depth, the skin being the web of this beam, with the horizontal frame member and one or more longitudinals forming the beam flanges (Fig. A16-15c).

Because of the heavy shear flows and direct stresses developed, the skin is usually doubled in this region. Additional stringers may also be added to relieve the stresses. The rings bordering the cutout (and forming part of the frame) are extended some distance above and below the cutout proper (unless they coincide with a regular ring location, in which case they carry all the way around).

***Clearly one of the design requirements will be to make the frame sufficiently stiff in bending against radial forces so that the door or window can bear up evenly against the frame.**

Fig. A16-16 shows the typical cutout structural arrangement. While analytical approaches have been tried, it is probably safe to say that the true elastic stress distribution in such a configuration cannot be computed. The necessity for avoiding high intensity stress concentrations (with their attendant fatigue likelihood) makes empirical information most useful in such cases. On the other hand, a simple rational analysis, based on principles outlined above, will very likely suffice for a static strength check and for most design purposes.

The above discussion has concentrated attention on the problems of carrying the hoop stresses around a cutout. The longitudinal pressure stresses, while being smaller themselves, are intensified by bending stresses from the tail loads. Hence, the longitudinal stresses across the cutout may make this condition (or the combination) most severe.

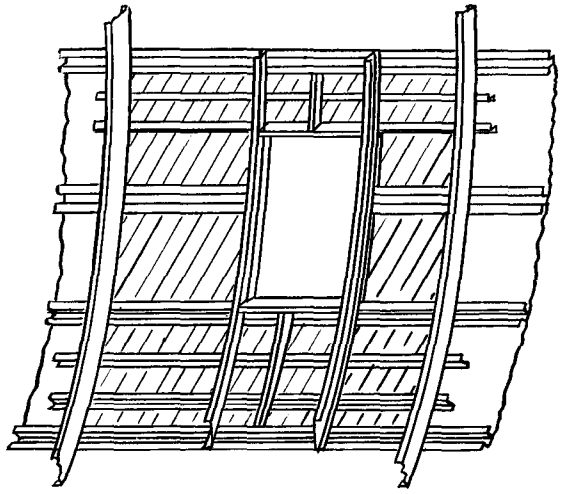

Fig. A16.16 Structural arrangement around a cutout. Most or all of the shaded skin area would probably be doubled.

LARGE DEFLECTIONS OF PLANE PANELS; "QUILTING".

The use of flat skin panels in a pressurized fuselage cannot always be avoided. Since the thin skin has little bending stiffness, it cannot support the lateral pressure as a beam ("plate", more correctly) and hence must deflect to develop some tensile membrane stresses which will then carry the loading. The resultant bulges of the rectangular skin panels between their bordering stiffeners give a "quilted" appearance to the surface.

Even in the case of curved skin panels quilting will occur: if the internal stiffening framework (transverse rings and frames and longitudinal stringers) is relatively rigid and is everywhere tightly fastened to the skin, then each skin panel is restrained along its

four sides (borders) against the radial expansion normally associated with the shell membrane stresses. The result is a sort of three-dimensional-case of the behavior depicted in Fig. A16-12*.

From a structural viewpoint, the unfortunate aspects of quilting lie in the high concentration of stresses occurring near the panel edges and in the tensile loadings on the rivets which join shell to stiffeners. The aerodynamic characteristics of a quilted surface are highly undesirable in a high performance airplane; hence again quilting is to be avoided.

Computations of stresses in quilted panels, inasmuch as they involve large, nonlinear deflections, are difficult. An additional (and quite necessary) complication is that of having to introduce the stiffness properties of the bordering members. The reader is referred to Chapter A.17 for a further discussion of the problem. A simplified approach, indicative of trends, is given there along with further references to the literature.

A16.5 Shells of Revolution Under Unsymmetrical Loadings.

Problems in which the shell of revolution experiences unsymmetrical loadings are not uncommon in aircraft structural analysis. The nose of a fuselage, the external fuel tank and the protruding radome are shells of revolution which may be loaded unsymmetrically by external aerodynamic pressures. Again, the same external fuel tank shell receives an unsymmetric internal hydrostatic pressure load from the weight of fuel directed normal to the shell axis.

Because of the unsymmetry of the problem, membrane shear stresses are now present and so the analyst must solve not two, but three equations in three unknowns (N_m, N_t and N_s). Moreover, these become differential rather than algebraic equations.

Because the derivation of the differential equations of equilibrium is rather lengthy, and because their general solution cannot be written (rather, only specific solutions for certain cases may be be found), no details are reproduced here. The reader is referred to pp. 373-379 of reference 2 for the derivation of the equations and for an example problem.

REFERENCES

(1) API-ASME* Unified Pressure Vessel Code 1951 Edition, et. seq.

(2) Timoshenko, S. "Theory of Plates and Shells" McGraw-Hill, N.Y., 1940

(3) Watts, G. and Lang, H., Stresses in a Pressure Vessel With a Conical Head, Trans. ASME, vol. 74, 1952, pp. 315-324.

(4) ———————, Stresses in a Pressure Vessel With a Flat Head Closure, Trans. ASME, vol. 74, 1952, pp. 1083-1090.

(5) ———————, Stresses in a Pressure Vessel With a Hemispherical Head, Trans. ASME, vol. 75, 1953, pp. 83-89.

(6) Roark, R. J. "Formulas for Stress and Strain", McGraw-Hill, N. Y. 3rd Edition, 1954.

(7) Howland W. and Beed, C. Tests of Pressurized Cabin Structures, Journ. Aero. Sci. vol. 8, Nov. 1940.

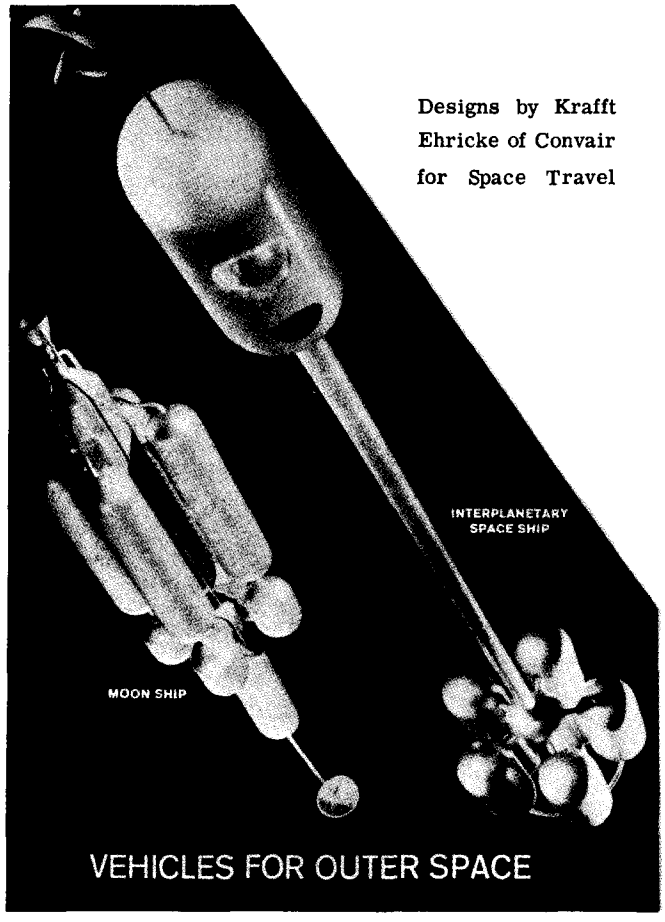

Outer Space Vehicles will Present Many New Problems to the Aeronautical Structures Engineer.

* One design which reduces quilting in the curved skin, fastens rings and frames to the inner surface of "hat" section stringers only. Thus the ring is not directly fastened to the skin which is therefore not continuously restrained around each ring circumference. The result is a modified floating skin.

* American Petroleum Institute - American Society of Mechanical Engineers.

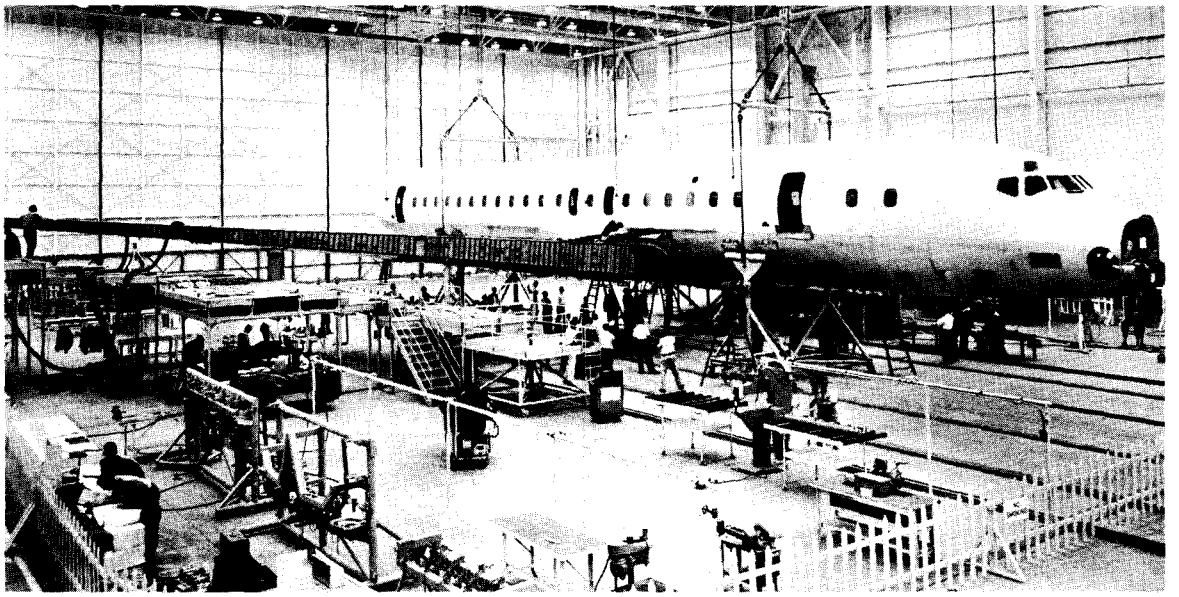

Douglas DC-8 Under Construction and Assembly. Fuselage is Pressurized to Permit High Altitude Flight.

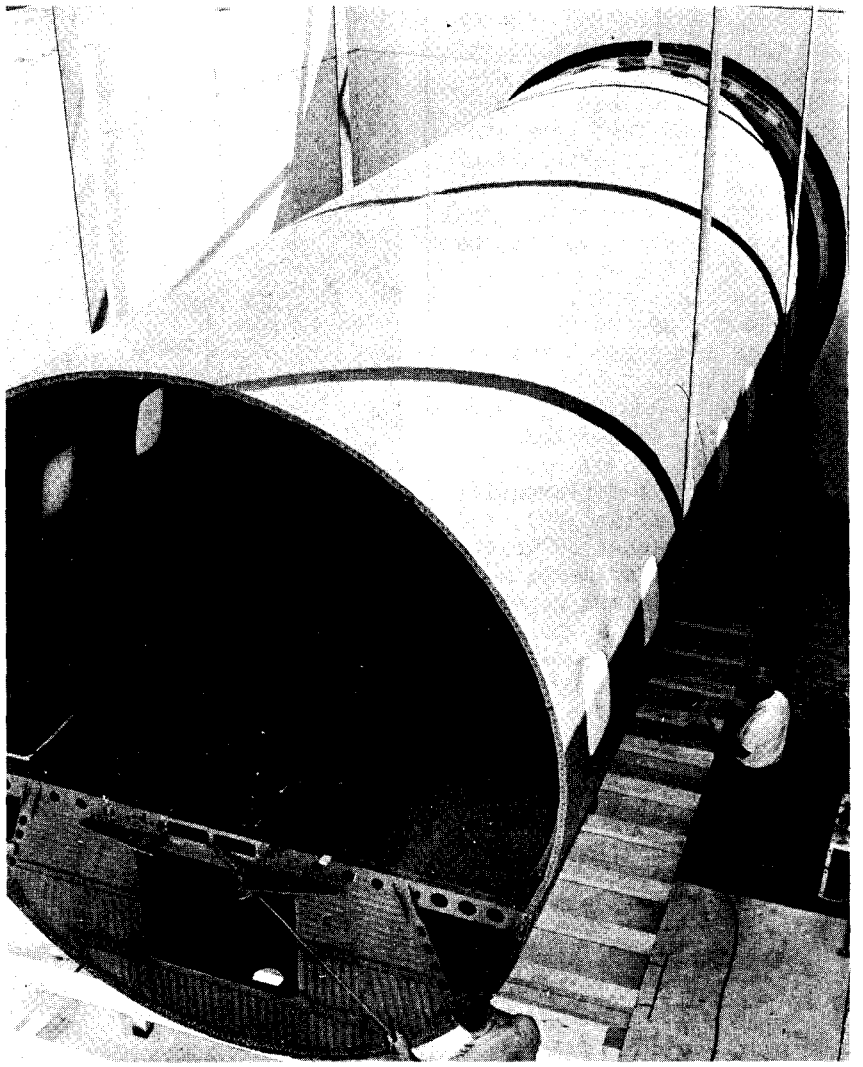

Section of DC-8 Fuselage being Lowered into Hydrostatic Test Tank.

CHAPTER A-17
BENDING OF PLATES

ALFRED F. SCHMITT

A17.1 Introduction.

It was seen in the last chapter that thin curved shells can resist lateral loadings by means of tensile-compressive membrane stresses. As will be seen later, thin flat sheets, by deflecting enough to provide both the necessary curvature and stretch, may also develop membrane stresses to support lateral loads. In the analysis of these situations no bending strength is presumed in the sheet (membrane theory).

In contrast to the membrane, the plate is a two-dimensional counterpart of the beam, in which transverse loads are resisted by flexural and shear stresses, with no direct stresses in its middle plane (neutral surface).

The skin may also be classified as either a plate or a membrane depending upon the magnitude of transverse deflections under loads. Transverse deflections of plates are small in comparison with the plates' thicknesses - on the order of a tenth of the thickness. On the other hand, the transverse deflections of a membrane will be on the order of ten times its thickness.*

Unfortunately for the engineers' attempt at an orderly cataloging of problems, most aircraft skins fall between the above two extremes and hence behave as plates having some membrane stresses.

Plate bending investigations have for a longtime been important in aircraft structural analyses in their relation to sheet buckling problems. Recently they have assumed new importance with the introduction of thick skinned construction and still more recently with the use of very thin low aspect ratio wings and control surfaces which behave much like large plates, or even are plates in some cases.

It is the purpose of this chapter to present briefly the classic plate formulas and some applications. Appropriate references are cited in lieu of an exhaustive treatise, which could hardly be presented in one chapter (or even one volume) as witness the voluminous literature on the subject.

A17.2 Plate Bending Equations**.

Technical literature in this field abounds with many excellent and elegant derivations of the plate bending equations (references 1 and 2, for instance). Rather than labor the subject with another such, we write the equations down by a direct appeal to past experience and intuition.

Fig. A17-1 shows the differential element of a thin, initially flat plate, acted upon by bending moments (per unit length) M_x and M_y about axes parallel to the y and x directions respectively. Sets of twisting couples M_{xy} (= $- M_{yx}$) also act on the element.

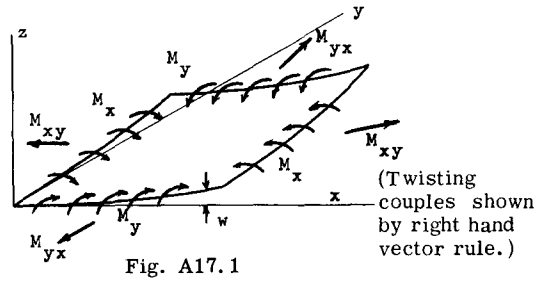

Fig. A17.1

As in the case of a beam, the curvature in the x, z plane, $\partial^2 w/\partial x^2$, is proportional to the moment M_x applied. The constant of proportionality is 1/EI, the reciprocal of the bending stiffness. For a unit width of beam $I = t^3/12$. In the case of a plate, due to the Poisson effect, the moment M_y also produces a (negative) curvature in the x, z plane. Thus, altogether, with both moments acting, one has

$$\frac{\partial^2 w}{\partial x^2} = \frac{12}{Et^3}(M_x - \mu M_y)$$

where μ is Poisson's ratio (about .3 for aluminum). Likewise, the curvature in the y, z plane is

$$\frac{\partial^2 w}{\partial y^2} = \frac{12}{Et^3}(M_y - \mu M_x) .$$

These two equations are usually rearranged to give the moments in terms of the curvature. They are written

$$M_x = D\left(\frac{\partial^2 w}{\partial x^2} + \mu \frac{\partial^2 w}{\partial y^2}\right) - - - - - - - - - - - \quad (1)$$

$$M_y = D\left(\frac{\partial^2 w}{\partial y^2} + \mu \frac{\partial^2 w}{\partial x^2}\right) - - - - - - - - - - - \quad (2)$$

where $D = Et^3/12(1 - \mu^2)$

The twist of the element, $\partial^2 w/\partial x \partial y$ (= $\partial^2 w/\partial y \partial x$) is the change in x-direction-slope per unit distance in the y-direction (and

---

* As will be seen later, the presence or absence of membrane stresses is not wholly dependent upon the magnitude of deflections, but is also determined by the form of deflection surface assumed by the sheet (in turn dependent upon the shape of boundary and loading).

** the assumptions implicit in the following analysis are spelled out in detail in Art. A17.5, below.

(and visa versa)***. It is proportional to the twisting couple M_{xy}. A careful analysis (see references 1 and 2) gives the relation as

$$M_{xy} = D\,(1-\mu)\,\frac{\partial^2 w}{\partial x \partial y} \qquad \text{- - - - - - - - - - - - -} \qquad (3)$$

Equations (1), (2) and (3) relate the applied bending and twisting couples to the distortion of the plate in much the same way as does $M = EI\ d^2y/dx^2$ for a beam.

While a few highly instructive problems may be solved with these equations (see reference 1, pp. 45-49 and reference 2, pp. 111-113), they are of little technical importance. Hence we move on to consider bending due to lateral loads.

Fig. A17-2 shows the same plate element as in Fig. A17-1, but with the addition of internal shear forces Q_x and Q_y (corresponding to the "V" of beam theory) and a distributed transverse pressure load q (psi). With the presence of these shears, the bending and twisting moments now vary along the plate as indicated in Fig. A17-2a. (For clarity, the several systems of forces on the plate element were separated into the two figures of Fig. A17-2. They do, of course, all act simultaneously on the single element).

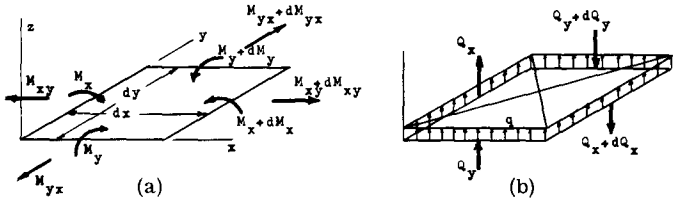

Fig. A17.2. The differentials are increments which should be written more precisely as, for instance, $dQ_y = (\partial Q_y/\partial y)\,dy$.

The next relations are obtained by summing moments in turn about the x and y axes. For example, we visualize the two loading sets of Fig. A17-2 acting simultaneously on the single element, and sum moments about the y axis.

$$M_x\,dy + (M_{yx} + d\,M_{yx})\,dx + (Q_x + d\,Q_x)\,dx\,dy =$$

$$(M_x + d\,M_x)\,dy + M_{yx}\,dx$$

Dividing by dx dy and discarding the term of higher order gives

$$Q_x = \frac{\partial M_x}{\partial x} - \frac{\partial M_{yx}}{\partial y}$$

or,

$$Q_x = \frac{\partial M_x}{\partial x} + \frac{\partial M_{xy}}{\partial y} \qquad \text{- - - - - - - - - - - - - -} \qquad (4)$$

*** If w, the deflection function, is a continuous function of x and y (as it must be, of course, in any technically important plate problem) then at each point $\partial^2 w/\partial x \partial y = \partial^2 w/\partial y \partial x$, as is proven in the calculus.

In a similar manner, a moment summation about the x axis yields

$$Q_y = \frac{\partial M_y}{\partial y} + \frac{\partial M_{xy}}{\partial x} \qquad \text{- - - - - - - - - - - - -} \qquad (5)$$

(Equations (4) and (5) correspond to V = dM/dx in beam theory).

One final equation is obtained by summing forces in the z direction on the element:

$$q = \frac{\partial Q_x}{\partial x} + \frac{\partial Q_y}{\partial y} \qquad \text{- - - - - - - - - - - - - -} \qquad (6)$$

Equations (4), (5) and (6) provide three additional equations in the three additional quantities Q_x, Q_y and q. The plate problem is thus completely defined.

To summarize, we tabulate below the quantities and equations obtained above. For comparison, the corresponding items from the engineering theory of beams are also listed.

CLASS	ITEM	PLATE THEORY	BEAM THEORY
Geometry	Coordinates	x y	x
	Deflections	w	y
	Distortions	$\frac{\partial^2 w}{\partial x^2}$, $\frac{\partial^2 w}{\partial y^2}$, $\frac{\partial^2 w}{\partial x \partial y}$	$\frac{d^2y}{dx^2}$
Structural Characteristic	Bending Stiffness	$D = \frac{Et^3}{12\,(1-\mu^2)}$	EI
Loadings	Couples	M_x, M_y, M_{xy}	M
	Shears	Q_x, Q_y	V
	Lateral	q	q or w
"Hooke's Law"	Moment-Distortion Relation	$M_x = D\left(\frac{\partial^2 w}{\partial x^2} + \mu \frac{\partial^2 w}{\partial y^2}\right)$ $M_y = D\left(\frac{\partial^2 w}{\partial y^2} + \mu \frac{\partial^2 w}{\partial x^2}\right)$ $M_{xy} = D\,(1-\mu)\,\frac{\partial^2 w}{\partial x \partial y}$	$M = EI\,\frac{d^2y}{dx^2}$
Equilibrium	Moments	$Q_x = \frac{\partial M_x}{\partial x} + \frac{\partial M_{xy}}{\partial y}$ $Q_y = \frac{\partial M_y}{\partial y} + \frac{\partial M_{xy}}{\partial x}$	$V = \frac{d\,M}{d\,x}$
	Forces	$q = \frac{\partial Q_x}{\partial x} + \frac{\partial Q_y}{\partial y}$	$q = \frac{d\,V}{d\,x}$

Finally, one very important equation is obtained by eliminating all internal forces (M_x, M_y, M_{xy}, Q_x, Q_y) between the above six equations. The result (which the student should obtain by himself as an exercise) is a relation between the lateral loading q and the deflections w*:

$$\frac{\partial^4 w}{\partial x^4} + 2\,\frac{\partial^4 w}{\partial x^2\,\partial y^2} + \frac{\partial^4 w}{\partial y^4} = \frac{q}{D} \qquad \text{- - - - - -} \qquad (7)$$

* the corresponding equation for a simple beam is $q/EI = d^4y/dx^4$.

The plate bending problem is thus reduced to an integration of eq. (7). For a given lateral loading q (x, y), a deflection function w (x, y) is sought which satisfies both eq. (7) and the specified boundary conditions. Once found, w (x, y) can be entered into eqs. (1) to (5) to determine the internal forces and stresses.

A17.3 An Illustrative Plate Bending Analysis.

Assume a lateral loading applied to a rectangular plate having all edges simply supported (hinged). The coordinates are chosen as in Fig. A17-3. With foreknowledge of the general usefulness of the result, we assume a sinusoidal loading of the form

$$q = q_{mn} \sin \frac{m \pi x}{a} \sin \frac{n \pi y}{b} \quad \text{- - - - - - - - -} \quad (8)$$

$$m, n = 1, 2, 3, \text{ - - - - -}$$

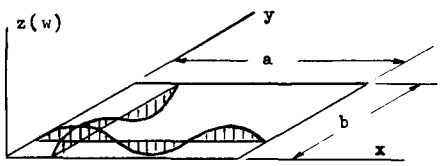

Fig. A17.3 Sinusoidal loading on a rectangular plate. Sections through the loading shown for m=3, n=2.

To find the resulting deflected shape of the plate we try a solution of the form

$$w = A_{mn} \sin \frac{m \pi x}{a} \sin \frac{n \pi y}{b} \quad \text{- - - - - - - -} \quad (9)$$

where A_{mn} is the unknown deflection amplitude. This trial deflection function is known to satisfy the boundary conditions on the plate since at x = 0, a and at y = 0, b we have

$w = 0$ (zero deflection at the supported edges)

$\frac{\partial^2 w}{\partial x^2} = \frac{\partial^2 w}{\partial y^2} = 0$ (zero moment at the hinged edges: see eqs. 1 and 2)

It remains only to find the value of A_{mn} which will satisfy eq. (7). Substituting (8) and (9) into (7) one obtains

$$A_{mn} \frac{m^4 \pi^4}{a^4} + 2 A_{mn} \frac{m^2 \pi^2}{a^2} \frac{n^2 \pi^2}{b^2} + A_{mn} \frac{n^4 \pi^4}{b^4} =$$

$$= q_{mn}/D \quad *$$

or

$$A_{mn} = \frac{q_{mn}}{D \pi^4} \frac{1}{\left(\frac{m^2}{a^2} + \frac{n^2}{b^2} \right)^2} .$$

Hence the required deflection surface (and the solution to the problem**) has the equation

$$w = \frac{q_{mn}}{D \pi^4} \frac{1}{\left(\frac{m^2}{a^2} + \frac{n^2}{b^2} \right)^2} \sin \frac{m \pi x}{a} \sin \frac{n \pi y}{b} \quad \text{- (10)}$$

The maximum deflection is seen to occur where the trigonometric functions have values of unity and q is also a maximum.

If eq. (10) is substituted into eqs. (1), (2) and (3) one obtains

$$M_x = - \frac{q_{mn}}{\pi^2 \left(\frac{m^2}{a^2} + \frac{n^2}{b^2} \right)^2} \left(\frac{m^2}{a^2} + \frac{\mu n^2}{b^2} \right) \sin \frac{m \pi x}{a} \sin \frac{n \pi y}{b}$$

$$M_y = - \frac{q_{mn}}{\pi^2 \left(\frac{m^2}{a^2} + \frac{n^2}{b^2} \right)^2} \left(\frac{\mu m^2}{a^2} + \frac{n^2}{b^2} \right) \sin \frac{m \pi x}{a} \sin \frac{n \pi y}{b}$$

$$M_{xy} = \frac{q_{mn} (1 - \mu)}{\pi^2 \left(\frac{m^2}{a^2} + \frac{n^2}{b^2} \right)^2} \frac{mn}{ab} \cos \frac{m \pi x}{a} \cos \frac{n \pi y}{b}$$

In a similar manner the transverse shears may be found from eqs. (4) and (5).

With such results as these the plates' stresses may be determined as desired. For example, the maximum direct bending stresses are seen to occur where the shear stresses (due to M_{xy}) are zero. Thus

$$s_x \left(= \frac{Mc}{I} \right) = \frac{M_x t}{2I} = \frac{6 M_x}{t^2}$$

and hence

$$s_{x_{MAX}} = \frac{6 q_{mn} \left(\frac{m^2}{a^2} + \frac{\mu n^2}{b^2} \right)}{t^2 \pi^2 \left(\frac{m^2}{a^2} + \frac{n^2}{b^2} \right)} \quad \text{- - - - - - - - - - (11)}$$

The reader having a familiarity with Fourier series methods will recognize immediately that the above analysis provides the key to the solution of the problem of any general loading q (x, y) on the same plate. Such an application is made by determining the proper combination of sinusoidal pressure terms (each of the form of eq. 8) such that their sum will closely represent the desired loading. The sum of the corresponding deflection functions (each of the form of eq. 10) gives the desired solution. Details of this type of analysis are to be found in reference 1 on pp. 113-176 and 199-256.

In common with all problems which are formulated in terms of a partial differential

---

* the common factor $\sin \frac{m \pi x}{a} \sin \frac{n \pi y}{b}$ has been divided out.

** the uniqueness of solutions to the differential equation of the form of eq. (7) is a classical proof appearing in numerous advanced texts on mathematics and mathematical physics. Since the equation is known to have a unique solution, then any solution found for it is the one and only correct solution.

equation, the solution of the plate bending problem depends strongly upon the boundary conditions (both the shape of the boundary and the types of support provided there). The above example may be said to have been deceptively easy because of both the simple shape of the boundary and the type of support. Plate problems wherein the plate planform is not a simple geometric figure must be solved by numerical means. As to the type of support, a full discussion of boundary conditions for plates is to be found in reference 1, pp. 89-95.

A17.4 Compilations of Results for Plate Bending Problems.

Fortunately for the practicing engineer, it is not necessary to perform analytic computations as discussed above for the great majority of practical plate problems. Problems of the type illustrated above, plus the myriad variations possible, became very fashionable exercises amongst mathematicians following the discovery by LaGrange of eq. (7) in the year 1811. The results of many researchers' labors have been compiled in various forms for handy reference.

A common and important case is that of a uniformly loaded rectangular plate (Fig. A17-4). The major engineering results are the values of the maximum deflections and the maximum stresses developed. These may be put in the form (a is the length of the short side):

$$w_{MAX} = \alpha \frac{q\,a^4}{E\,t^3} \qquad (12)$$

$$s_{MAX} = \beta \frac{q\,a^2}{t^2} \qquad (13)$$

where the coefficients α and β are given in Table A17.1 for the four most common edge conditions.

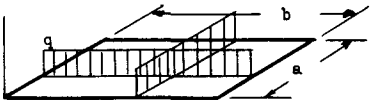

Fig. A17.4

Similar presentations may be made for many dozens of other cases. With the ready availability of comprehensive catalogings of these problems in references devoted to the purpose, there appears to be little virtue in duplication here. Hence the following list of selected references is presented. Additional references are to be found in turn within these works. We note that, because of the linearity of the plate bending problem, superposition of solutions is possible to extend even further the usefulness of these extensive listings.

TABLE A17.1

Stress and Deflection Coefficients for a Uniformly Loaded Rectangular Plate Having Various Edge Conditions

	All Sides Pinned		Long Sides Pinned, Short Sides Clamped		Short Sides Pinned, Long Sides Clamped		All Sides Clamped	
b/a	α	β	α	β	α	β	α	β
1.0	.0443	.2874	.0209	.420	.0209	.420	.0138	.3078
1.2	.0616	.3756	.0340	.522	.0243	.462	.0188	.3834
1.4	.0770	.4518	.0502	.600	.0262	.486	.0226	.4356
1.6	.0906	.5172	.0658	.654	.0273	.500	.0251	.4680
1.8	.1017	.5688	.0799	.690	.0279	.502	.0267	.4872
2.0	.1106	.6102	.0987	.714	.0284	.504	.0277	.4974
3.0	.1336	.7134	.128	.750	-	-	-	-
4.0	.1400	.7410	-	-	-	-	-	-
5.0	.1416	.7476	-	-	-	-	-	-
∞	.1422	.7500	.1422	.750	.0284	.498	.0284	.498

Rectangular Plates Under Various Loadings

- S. Timoshenko, "Theory of Plates and Shells", pp. 113-176, 199-256.
- J. P. Den Hartog, "Advanced Strength of Materials", pp. 132-134.
- R. J. Roark, "Formulas for Stress and Strain", pp. 202-207.

Circular Plates Under Various Loadings

(same three references, in order)

- pp. 55-84, 257-287.
- pp. 128-132.
- pp. 194-201, 209-211.

A17.5 Deflection Limitations in Plate Analyses.

In the introductory remarks of this chapter it was stated that a plate may be distinguished from a membrane by the small order of its deflections (on the order of a few tenths of its thickness). We will re-examine this statement here to show that this is not so much a definition as it is an accuracy limitation imposed by one of the assumptions made in the plate analysis.

There are several familiar assumptions from beam theory which, of course, carry over here, inasmuch as the plate analysis resembles the beam analysis rather closely. These "beam theory assumptions" are:

i - elastic stresses only are presumed,

ii - small slopes (so that $\partial^2 w/\partial x^2$ and $\partial^2 w/\partial y^2$ are good approximations to the curvatures),

iii - at least one transverse dimension (length or width) be large compared to the thickness so that shear deflections may be neglected.

However, the beam theory assumptions do not place a very severe restriction on the magnitude of deflections permitted. Deflections of several times the plate thickness would be permissible if these were the only restricting assumptions.

In deriving the plate bending equations it was assumed that no stresses acted in the middle (neutral) plane of the plate (no membrane stresses). Thus, in summing forces to derive eq. (6), no membrane stresses were present to help support the lateral load. Now in the solutions to the great majority of all plate bending problems (solved as in Art. A17.3), the deflection surface solution found is a non-developable surface, i.e., a surface which cannot be formed from a flat sheet without some streching of the sheets' middle surface*. But, if appreciable middle surface strains must occur, then large middle surface stresses will result, invalidating the assumption upon which eq. (6) was derived.

Thus, practically all loaded plates deform into surfaces which induce some middle surface stresses. It is the necessity for holding down the magnitude of these very powerful middle surface stretching forces that results in the more severe rule-of-thumb restriction that plate bending formulae apply accurately only to problems in which deflections are a few tenths of the plates' thickness.

A17.6 Membrane Action in Very Thin Plates.

There is still another source of middle surface strains in plates: this is the restraint against in-plane movements offered by the edge supports. While not important in problems wherein deflections are limited in accordance with the restriction of the last article, such restraint does assume great importance in the case of large deflections of very thin plates which support a major share of the load by membrane action. It is, in fact, useful to consider the limiting case of the flat membrane which cannot support any of the lateral load by bending stresses and hence has to deflect and stretch to develop both the necessary curvatures and membrane stresses.

The two-dimensional membrane problem is a nonlinear one whose solution has proven to be very difficult. Rather than attempt to treat the complete problem, we can study a simplified version whose solution retains the desired general features. The one-dimensional analysis of a narrow (unit width) strip will be treated. This strip is cut from an originally flat membrane whose extent in the y-direction is very great (Fig. A17-5a).

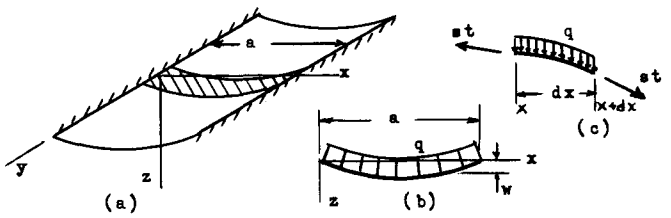

Fig. A17.5

Fig. A17-5b shows the desired one-dimensional problem which now resembles a loaded cable. The differential equation of equilibrium is obtained by summing vertical forces on the element of Fig. A17-5c (draw with all quantities; loads, deflections, slopes and curvatures shown positive). One obtains

$$s\,t\left[\left.\frac{dw}{dx}\right|_{x+dx} - \left.\frac{dw}{dx}\right|_{x}\right] + q\,dx = 0$$

or

$$\frac{d^2w}{dx^2} = -\frac{q}{s\,t} \qquad \text{- - - - - - - - - - - - - - - - - (14)}$$

where s is the membrane stress in psi.

Eq. (14) is the differential equation of a parabola. Its solution is

$$w = \frac{q\,x}{2\,s\,t}(a - x) \qquad \text{- - - - - - - - - - - - - - - (15)}$$

The (as yet) unknown stress in eq. (15) can be found by computing the change in length of the strip as it deflects. This "stretch" is given by the difference between the curved arc length and the original straight length (a). Thus:

$$\delta = \int_0^a ds - a \quad *$$

$$= \int_0^a \sqrt{dw^2 + dx^2} - a$$

$$= \int_0^a \sqrt{1 + \left(\frac{dw}{dx}\right)^2}\,dx - a$$

Since the slope dw/dx is small compared with unity, we use the binomial theorem to write

$$\left(1 + \left(\frac{dw}{dx}\right)^2\right)^{1/2} \simeq 1 + \frac{1}{2}\left(\frac{dw}{dx}\right)^2$$

* The cone and cylinder are examples of developable surfaces, the sphere is a nondevelopable one. It is a familiar experience that the skin of an orange cannot be developed into a flat sheet without tearing.

* here "ds" is the differential arc length of the calculus and has no kinship with the s which denotes the membrane stress throughout the remainder of the analysis.

Hence

$$\delta = \int_0^a \left[1 + \frac{1}{2}\left(\frac{dw}{dx}\right)^2\right] dx - a$$

$$= \frac{1}{2}\int_0^a \left(\frac{dw}{dx}\right)^2 dx \ .$$

Substituting through the use of eq. (15) and integrating we find

$$\delta = \frac{q^2 a^3}{24\, s^2 t^2}$$

Now by elementary considerations

$$\delta = \frac{s\, a}{E}$$

Equating these last and solving we find

$$s = .347 \left[E\left(\frac{q\, a}{t}\right)^2\right]^{1/3} \text{- - - - - - - - - - - - - (16)}$$

If eq. (16) is substituted into eq. (15) one gets for the maximum deflection $\left(x = \frac{a}{2}\right)$

$$w_{MAX} = .360\, a \left(\frac{q\, a}{E\, t}\right)^{1/3} \text{- - - - - - - - - - - (17)}$$

Equations (16) and (17) display the essential nonlinearity of the problem, the stress and the deflection both varying as fractional exponents of the lateral pressure q.

Solutions of the complete two-dimensional nonlinear membrane problem have been carried out*, the results being expressed in forms identical with those obtained above for the one-dimensional problem, viz.,

$$w_{MAX} = n_1\, a \left(\frac{q\, a}{E\, t}\right)^{1/3} \text{- - - - - - - - - - - - (18)}$$

$$s_{MAX} = n_2 \left[E\left(\frac{q\, a}{t}\right)^2\right]^{1/3} \text{- - - - - - - - - - - (19)}$$

Here "a" is the length of the long side of the rectangular membrane and n_1 and n_2 are given in Table A17.2 as functions of the panel aspect ratio a/b.

The maximum membrane stress (s_{MAX}) occurs at the middle of the long side of the panel. We note that the limiting case, a/b = 0, corresponds to the one-dimensional case analyzed earlier. Unfortunately, an extrapolation of these two-dimensional results to that limit does not show agreement with the one-dimensional result. Presumably the discrepancy may be traced to the excessive influence of inaccuracies in the assumed deflection shape of the membrane as used in the approximate two-dimensional solutions.

Experimental results reported in reference 4 show good agreement with the theory for square panels in the elastic range.

TABLE A17.2

Membrane Stress and Deflection Coefficients

a/b	1.0	1.5	2.0	2.5	3.0	4.0	5.0
n_1	.318	.228	.16	.125	.10	.068	.052
n_2	.356	.37	.336	.304	.272	.23	.205

A17.7 Large Deflections in Plates**.

In the previous articles of this chapter the results of analyses were outlined for the two extreme cases of sheet panels under lateral loads. At one extreme, sheets whose bending stiffness is great relative to the loads applied (and which therefore deflect only slightly) may be analyzed satisfactorily by the plate bending solutions. At the other extreme, very thin sheets, under lateral loads great enough to cause large deflections, may be treated as membranes whose bending stiffness is ignored.

As it happens, the most efficient plating designs generally fall between these two extremes. On the one hand, if the designer is to take advantage of the presence of the interior stiffening structure (rings, bulkheads, stringers, etc.), which is usually present for other reasons anyway, then it is not necessary to make the skin so heavy as to behave like a "pure" plate. On the other hand, if the skin is made so thin as to necessitate supporting all pressure loads by stretching and developing membrane stresses, then permanent deformation results, producing "quilting" or "washboarding".

The exact analysis of the two-dimensional plate which undergoes large deflections and thereby supports the lateral loading partly by its bending resistance and partly by membrane action is very involved. A one-dimensional

* The work of Henky and Foppl is summarized in reference 3, pp. 258-290 and in reference 4. The partial differential equation solved is given in reference 1 on p. 344 (eq. 202) and the approximate method of solution usually employed is sketched out on pp. 345, 346 of this same reference. The reader who would compare presentations amongst these references should note the differences in the definitions of the plate dimensioning symbols "a" and "b".

** The discussion to follow will be concerned primarily with problems dealing with the support of a uniform pressure load on a flat skin panel. It may, therefore, help the reader to fix his ideas if he visualizes the discussion as applied to the problems of analysis of a single rectangular skin panel taken between the stringers and bulkheads of a seaplane hull bottom. Equally useful is the picture of the very nearly flat panel between rings and stringers in the slightly curved side of a large pressurized fuselage.

analysis, parallel to that of Art. A17.6, is to be found in reference 1, pp. 4-10. A more elaborate two-dimensional analysis is shown on pp. 347-350 of this same reference.

An approximate solution of the large deflection plate problem can be obtained by adding together the flat plate and membrane solutions in the following way:

Solve eq. (12), the plate bending relation, for q; call it q',

$$q' = \frac{w_{MAX}\, E\, t^3}{\alpha\, a^4}$$

Now solve eq. (18), the membrane relation, for q; call it q",

$$q'' = \frac{w_{MAX}^3\, E\, t}{n_1^3\, a^4}$$

The sum of these two pressures gives the total lateral pressure, called simply, q.

$$q = q' + q''$$

$$q = \frac{1}{\alpha}\,\frac{Et^3}{a^4\,\left(\frac{b}{a}\right)^4}\,w_{MAX} + \frac{1}{n_1^3}\,\frac{Et}{a^4}\,w_{MAX}^3 \qquad \text{- - - - - - (20)}$$

Eq. (20), we see, is based upon summing the individual stiffnesses of the two extreme behavior mechanisms by which a flat sheet can support a lateral load. No interaction between stress systems is assumed and, since the system is nonlinear, the result can be an approximation only.

Eq. (20) is best rewritten as

$$\frac{q\,a^4}{E\,t^4} = \frac{1}{\alpha}\left(\frac{w_{MAX}}{t}\right)\left(\frac{a}{b}\right)^4 + \frac{1}{n_1^3}\left(\frac{w_{MAX}}{t}\right)^3 \qquad \text{- - - - - (21)}$$

Fig. A17-6 shows eq. (21) plotted for a square plate using values of α and n_1 as taken from Tables A17.1 and A17.2. Also plotted are the results of an exact analysis (reference 5). As may be seen, eq. (21) is somewhat conservative inasmuch as it gives a deflection which is too large for a given pressure.

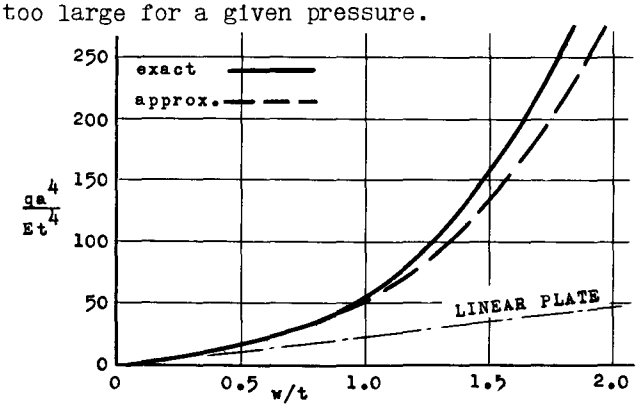

Fig. A17.6 Deflections at the midpoint of a simply supported square panel by two large-deflection theories.

The approximate large-deflection method outlined above has serious shortcomings insofar as the prediction of stresses is concerned. For simply supported edges the maximum combined stresses are known to occur at the panel midpoint. Fig. A17-7 shows plots of these stresses for a square panel as predicted by the approximate method (substituting q' and q" into eqs. (13) and (14) respectively and cross plotting with the aid of Fig. A17-6*). Also shown are the maximum stresses computed by the exact large-deflection theory (reference 5).

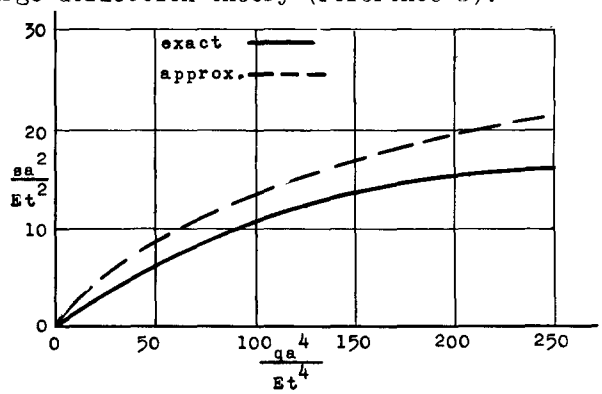

Fig. A17.7 Large-deflection theories' midpanel stresses; simply supported square panel.

Because of the obvious desirability of using the results of the more exact theory, some of these are presented in Table A17.3. The treatment of additional cases (other types of edge support) may be found in reference 6, pp. 221, 222.

TABLE A17.3

Large Deflection Rectangular Plate Coefficients
(Uniform Pressure Load, q. Simply Supported Edges)

a/b	Deflection or Stress Coefficient	Pressure Coefficient, qa^4/Et^4							
		12.5	25	50	75	100	150	200	250
1	w/t	0.4055	0.6083	0.846	1.0031	1.1240	1.3104	1.4557	1.5770
	sb^2/Et^2	3.191	5.158	7.770	9.720	11.339	14.055	16.364	18.424
	s_Mb^2/Et^2	0.609	1.377	2.683	3.792	4.785	6.542	8.103	9.533
2 to ∞	w/t	0.6958	0.9463	1.241	1.440	1.596	1.840	2.033	2.196
	sb^2/Et^2	4.871	7.164	10.26	12.62	14.61	18.01	20.93	23.55
	s_Mb^2/Et^2	1.293	2.403	4.155	5.612	6.911	9.220	11.28	13.16

Notes: 1. s = total stress = $s_B + s_M$
2. s_B = "bending stress" component of stress
3. s_M = "membrane stress" component of stress

A17.8 Considerations in the Applications of Large-Deflection Plate and Membrane Analyses.

Before concluding this chapter it is pertinent to note several serious omissions in the developments outlined above with regard to their application to flat pressure-panel analyses within a ship hull or fuselage. The

---

*but using n_2 = .260 in eq. (19), This value gives the stresses at the center of a square panel whereas n_2 = .356 in Table A17.2 is for stresses at the panel edge.

large-deflection plate and the membrane analyses were developed for applications where the plate bending analysis appeared inadequate. However, these analyses themselves presumed conditions seldom encountered in practice.

FIRST, the analyses assume unyielding supports on the boundaries of the sheet panel. In practice, the skin is stretched across an elastic framework of stringers and bulkheads. It follows, therefore, that the heavy membrane tensile forces developed during large deflections will cause the supports to deflect towards each other thereby increasing the plate deflection and relieving some of the stresses.

A simple one-dimensional analysis for a membrane strip having elastic edge supports (parallel to the analysis of Art. A17.6), shows errors on the order of 25 per cent are likely if the framework elasticity is neglected (reference 7). At this writing no two-dimensional treatment of this problem is known to the writer.

SECOND, it is seldom that the analyst has to check a panel for lateral pressure loads alone. Most often, the entire "field" of panels on the framework of stringers and bulkheads must simultaneously transmit in-plane loadings from the tail load bending stresses and the cabin pressurization stresses.

Inasmuch as the large-deflection plate and membrane analyses are nonlinear, it follows that correct stresses cannot be found by a straight superposition. The magnitude of the error introduced by such a procedure is difficult to estimate in the absence of an exact analysis. A one-dimensional analysis, parallel to that of Art. A17.6, but with elastic supports and axial load, is given in reference 7. These results, which indicate the effect of the axial load to be quite important, may be used as a guide in lieu of more complete two-dimensional studies. The interested reader is referred to the original work for details.

REFERENCES

1. Timoshenko, S. "Theory of Plates and Shells", McGraw-Hill, N. Y., 1940.
2. Den Hartog, J. P. "Advanced Strength of Materials", McGraw-Hill, N. Y., 1952.
3. Sechler, E. and Dunn, L. "Airplane Structural Analysis and Design", John Wiley, N. Y., 1942.
4. Heubert, M. and Sommer, A., Rectangular Shell Plating Under Uniformly Distributed Hydrostatic Pressure, NACA TM 965.
5. (selected large-deflection plate references).
   a) Moness, E. Flat Plates Under Pressure, Journ. Aero. Sci., 5, Sept. 1938.
   b) Ramberg, W., McPherson, A. and Levy, S., Normal Pressure Tests of Rectangular Plates, NACA TR 748, 1942.
   c) Levy, S. Square Plate With Clamped Edges Under Normal Pressure Producing Large Deflections, NACA TR 740, 1942.
   d) Levy, S. Bending of Rectangular Plates With Large Deflections, NACA TR 737, 1942.
   e) Chi-Teh Wang, Nonlinear Large Deflection Boundary-value Problems of Rectangular Plates, NACA TN 1425, 1948.
   f) Chi-Teh Wang, Bending of Rectangular Plates With Large Deflections, NACA TN 1462, 1948.
6. Roark, R. J. "Formulas for Stress and Strain", McGraw-Hill, N. Y. 3rd Edition, 1954.
7. Flugge, W. Stress Problems in Pressurized Cabins, NACA TN 2612, 1952.
8. Engineering Research Bulletins of Oklahoma State University.
   a) No. 15. Influence Coefficients for Circular Plates.
   b) No. 17. Analysis of Thin Plates Supported on their Corners.
   c) No. 118. Analysis of Flat Plates by Algebraic Carryover Method.

CHAPTER A18

THEORY OF THE INSTABILITY OF COLUMNS AND THIN SHEETS

(BY DR. GEORGE LIANIS)

PART 1

ELASTIC AND INELASTIC INSTABILITY OF COLUMNS

A18.1 Introduction.

Part 1 of this chapter will be confined to the theoretical treatment of the instability of a perfect elastic column and an imperfect elastic column. The column is the simplest of the various types of structural elements that are subject to the phenomenon of instability. The theory as developed for columns forms the basis for the study of the instability of thin plates, which subject is treated in Part 2.

A18.2 Combined Bending and Compression of Columns.

Consider a column with one end simply supported and the other end hinged (Fig. A18.1) under the simultaneous action of a compressive load P and a transverse load Q. Without the load P the bending moment due to Q would be:-

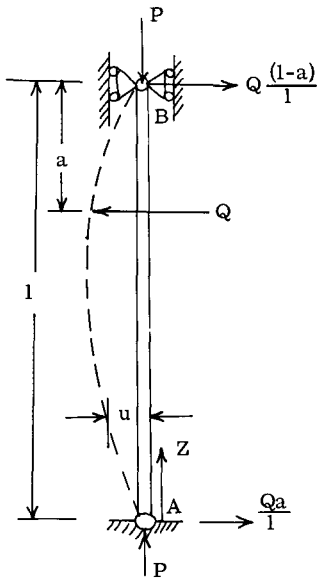

Fig. A18.1

On the lower portion of the column

$$M_1 = \frac{Qaz}{l} \quad - - - - - - - - - - - - - - - \text{(a)}$$

On the upper portion

$$M_1^1 = \frac{Q(1-a)(1-z)}{l} \quad - - - - - - - - - - \text{(b)}$$

Due to the deflection u(z), the axial load P contributes to the bending moment by the amount:-

$$M_2 = Pu \quad - - - - - - - - - - - - - - - - \text{(c)}$$

Thus the total bending moment at section z will be:-

$$M = Pu + \frac{Qaz}{l} \text{ on upper portion} \quad - - - - \text{(d)}$$

$$M = Pu + Q\frac{(1-a)(1-z)}{l} \text{ on lower portion} \quad \text{(e)}$$

From mechanics of simple bending, we have the deflection equation,

$$\frac{d^2u}{dz^2} = -\frac{M}{EI_y} \quad - - - - - - - - - - - - - - \text{(1)}$$

Thus the deflection u(Z) of the column is,

$$EI\frac{d^2u}{dz^2} = -Pu - \frac{Qaz}{l}, \quad (0 \leq z \leq 1-a)$$

$$EI\frac{d^2u}{dz^2} = -Pu - Q\frac{(1-a)(1-z)}{l},$$

$$(1-a \leq z \leq 1) \quad - - - - - \text{(2)}$$

If we introduce the notation,

$$\frac{P}{EI} = K^2 \quad - - - - - - - - - - - - - - - - - \text{(3)}$$

The general solution of eq. (2) is:

$$u = C_1 \cos Kz + C_2 \sin Kz - \frac{Qaz}{Pl},$$

$$(0 \leq z\ 1-a) \quad - - - - - - - - - - \text{(4a)}$$

$$u = C_3 \cos Kz + C_4 \sin Kz - Q\frac{(1-a)(1-z)}{l},$$

$$(1-a \leq z \leq 1) \quad - - - - - - - - - \text{(4b)}$$

where C_1, C_2, C_3, and C_4 are constants of integration to be determined from boundary conditions.

For eqs. (4), since u = 0 for z = 0 and z = l, it follows that:

$$C_1 = 0 \text{ and } C_3 = -C_4 \tan Kl \quad - - - - - \text{(f)}$$

At z = (l - a) the two portions of the deflection curve given by (4a) and (4b) respectively must have the same deflection and slope. From these two conditions we determine C_2 and C_4.

$$C_3 = \frac{Q \sin Ka}{PK \sin Kl}\ ,\quad C_4 = -\frac{Q \sin K(1-a)}{PK \tan Kl} \quad ----\ (g)$$

Substituting (f) and (g) into eq. (2), we obtain:

$$u = \frac{Q \sin Ka}{PK \sin Kl} \sin Kz - \frac{Qa}{Pl} z\ ,$$

$$(0 \le z \le 1 - a) \quad ----------(5a)$$

$$u = \frac{Q \sin K(1-a)}{PK \sin Kl} \sin K(1-z) - \frac{Q(1-a)(1-z)}{Pl}\ ,$$

$$(1 - a \le z \le 1) \quad ----------(5b)$$

If load Q is applied at the middle of the column the maximum deflection is:-

$$u_{max} = \frac{Q \tan \frac{Kl}{2}}{2\,PK} - \frac{Ql}{4P} \quad --------\ (6)$$

It is obvious that for $\frac{Kl}{2} = \frac{\pi}{2}$,

$\tan \frac{KI}{2} \longrightarrow \infty$. Thus the maximum deflection of column becomes infinite for $KI = \pi$ and from eq. (3).

$$P_{cr} = \frac{\pi^2 EI}{l^2} \quad ----------\ (7)$$

Equation (7) is an important equation derived first by Euler. It gives the critical compressive load which causes infinite deflection in a column and it specifies the ultimate strength of a column in compression.

It is obvious from eq. (7) that Euler's critical load is independent of the magnitude of the transverse load Q. It seems, therefore, that even in the absence of the transverse load Q, the maximum deflection becomes infinite under the action of only a compressive load as given by eq. (7).

A18.3 Elastic Stability of a Column.

The above conclusion as to the critical load was based on purely mathematical reasoning. We have found a critical value of a compressive load which causes infinite deflection.

Far more important, however, is an investigation of the stability of a column which should be based on physical arguments. The question arises as to what happens before the load P reaches its critical value as given by eq. (7) and also how the column behaves if this critical value is exceeded.

An elastic system is called stable under given loads when infinitesimal loads added to the body would cause only infinitesimal changes in the displacements and the body recovers if the added loads are removed. When the displacements are continuously increased with little or no further increment of loads, the system is unstable. If the body will remain in the displaced position after the removal of the disturbance, the body is said to be in neutral equilibrium. Having these definitions, we will not investigate the behavior of the column before and after the critical load is reached.

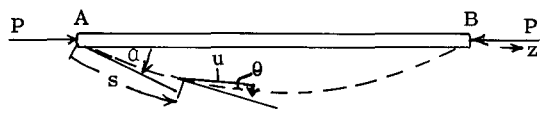

Fig. A18.2

Assume, as shown in Fig. A18.2, that a simply supported column loaded by an axial load P is bent by a small disturbance. If the deflection at a distance s along the deflected axis is u, the bending moment due to P is Pu.

From engineering theory of bending, we know that,

$$\frac{EI}{R} = -M\ ,\ \text{whence}$$

$$\frac{EI}{R} = -Pu \quad ----------(8a)$$

The exact expression for the curvatuve of the neutral axis is:-

$\frac{1}{R} = \frac{d\theta}{ds}$, where s is the arc length of the deformed axis, and θ the angle between the tangent to the curve and the z axis. Thus,

$$EI \frac{d\theta}{ds} + Pu = 0 \quad ----------(8b)$$

Differentiating (8b) with respect to s and since $\frac{du}{ds} = \sin \theta$, we obtain:

$$EI \frac{d^2\theta}{ds^2} + P \sin \theta = 0 \quad --------(8c)$$

Multiplying (8c) by $d\theta$ and noting that:-

$$\frac{d^2\theta}{ds^2} d\theta = \frac{d\theta}{ds} d \left(\frac{d\theta}{ds}\right)\ ,\ \text{and integrating}$$

$$EI \int \frac{d\theta}{ds} d \left(\frac{d\theta}{ds}\right) + P \int \sin \theta d\theta = C,\ \text{or}$$

$$\frac{EI}{2} \left(\frac{d\theta}{ds}\right)^2 - P \cos \theta = C \quad -------(8d)$$

Since at end A, $\theta = -a$ and $M = EI \frac{d\theta}{ds} = 0$, we find that $C = - P \cos a$.

Now let $k = \sqrt{\frac{P}{EI}}$ - - - - - - - - - - (8e)

Then eq. (8d) becomes,

$$\frac{1}{\sqrt{2}} \frac{d\theta}{ds} = k \sqrt{\cos\theta - \cos\alpha}, \text{ or}$$

$$ds = \frac{d\theta}{\sqrt{2k^2(\cos\theta - \cos\alpha)}} \text{ - - - - - - (8f)}$$

The total length of the column in the deflected shape is given by:-

$$l = \int_A^B ds = \int_{-\alpha}^{\alpha} \frac{d\theta}{\sqrt{2}\, k \sqrt{\cos\theta - \cos\alpha}} \text{ - - - (8h)}$$

$$\text{or } l = \int_{-\alpha}^{\alpha} \frac{d\theta}{2k\sqrt{\sin^2\frac{\alpha}{2} - \sin^2\theta/2}} \text{ - - - - (8i)}$$

Denoting $\sin\frac{\alpha}{2}$ by p and introducing a new variable ϕ :-

$$\sin\frac{\theta}{2} = p \sin\phi$$

Equation (8i) then becomes,

$$l = \frac{2}{k} \int_0^{\frac{\pi}{2}} \frac{d\phi}{\sqrt{1-p^2\sin^2\phi}} = \frac{2K}{k} \text{ - - - - - - (8j)}$$

where $K = \int_0^{\frac{\pi}{2}} \frac{d\theta}{\sqrt{1-p^2\sin^2\phi}}$ is called the complete elliptic integral of the first kind, and it can be found in tables. If α and therefore p is very small, then $p^2\sin^2\phi$ can be neglected in equation (8j) and then

$$l = \frac{2}{k} \int_0^{\frac{\pi}{2}} d\phi = \frac{\pi}{k} = \pi\sqrt{\frac{EI}{P}}$$

whence $P = \frac{\pi^2 EI}{l^2}$ - - - - - - - - - - - - (8k)

The deflection at the midpoint of column is:- $\theta = 0$, $du = ds \sin\theta$, and from Eq. (8f)

$$u\left(z=\frac{l}{2}\right) = \delta = \frac{l}{2k} \int_0^{\alpha} \frac{\sin\theta d\theta}{\sqrt{\sin^2\frac{\alpha}{2} - \sin^2\frac{\theta}{2}}} \text{ - - - (8l)}$$

or in terms of ϕ:-

$$\delta = \frac{2P}{k} \int_0^{\frac{\pi}{2}} \sin\phi d\phi = \frac{2P}{k} \text{ - - - - - - - - - (8m)}$$

From equation (8j) and equation (8k), we obtain

$$\frac{P}{P_{cr}} = \frac{Pl^2}{\pi^2 EI} = \frac{4K^2}{\pi^2} \text{ - - - - - - - - - - - - - (8n)}$$

$$\frac{\delta}{l} = \frac{2P}{\pi\sqrt{\frac{P}{P_{cr}}}} \text{ - - - - - - - - - - - - - - - (8o)}$$

Let us now write the bending moment $M = P\delta$ at the middle point in non-dimensional form:

$$m = \frac{P}{P_{cr}} \cdot \frac{\delta}{l} = \frac{4KP}{\pi^2} \text{ - - - - - - - - - - (8p)}$$

Since $p = \sin\frac{\alpha}{2}$ is a function of α so is the elliptic integral K and the ratios $\frac{P}{P_{cr}}$ and $\frac{\delta}{l}$ calculated from equations (8a) and (8o).

Thus $\frac{P}{P_{cr}}$ is a function of $\frac{\delta}{l}$ calculated by means of tables giving elliptic integrals. Thus m can be plotted against δ/l as shown in Fig. A18.3.

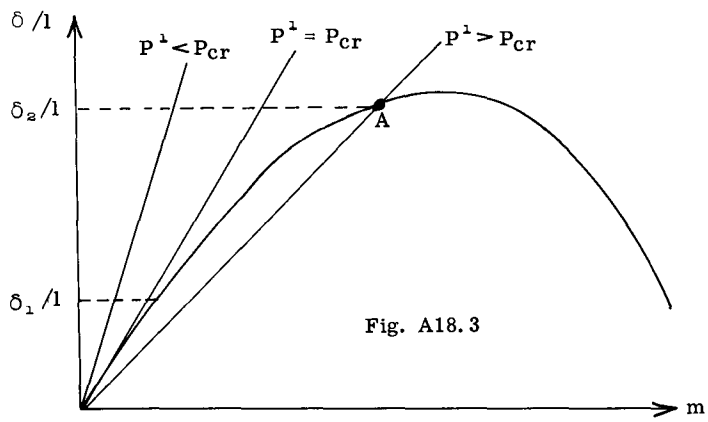

Fig. A18.3

Let us now examine the stability of various equilibrium configurations. Assume that a load P^1 is acting on the column and the column has a certain maximum deflection δ where P^1 does not correspond to δ.

The non-dimensional maximum bending moment is:-

$$m^1 = \frac{P^1}{P_{cr}}\left(\frac{\delta}{l}\right) \text{ - - - - - - - - - - - (8g)}$$

The m^1 versus δ/l curves are straight lines. The column is in equilibrium if $m = m^1$, or in other words, if the $m^1(\delta/l)$ curve intersects the $m(\delta/l)$ curve.

We see from Fig. A18.3 that these curves intersect at the origin only if $P^1 < P_{cr}$. The column, therefore, has only one possible equilibrium form, for example, that for which $\delta/l = 0$, which is the straight form. When $P^1 > P_{cr}$, there are two points of intersection,

one when $\delta/l = 0$ and the other (point A) for which $\delta/l \neq 0$. The column thus has two possible equilibrium forms, one straight and one bent.

Let us now assume that at $\delta = 0$, the column is displaced by a small disturbance and acquires a deflection δ_1. For $P' < P_{cr}$, we see from Fig. 3 that $m > m'$. Thus P' is not sufficient to maintain the column in equilibrium in the bent form and it will spring back to its straight form. Thus for $P' < P_{cr}$, the straight form is stable.

If $P' > P_{cr}$, then $m' > m$. Thus m' will bend the column still further. This means that if $P' > P_{cr}$, the straight form of equilibrium is unstable. The column will continue to bend until m' becomes equal to m (point A in Fig. 3). If the column is displaced further from A, the deflection becomes larger than δ_2 and $m > m'$ at the new position. The column will spring back to point A. Point A is therefore stable.

At $P = P_{cr}$, the m' versus δ/l line is tangent to the m curve at the origin. Therefore, for an infinitesimal disturbance, the column will remain in equilibrium at the displaced position since for such small disturbances m' remains equal to m. The column is therefore in neutral equilibrium.

A18.4 The Failure of Columns by Compression.

In discussing the stability of a column in the previous section, it was shown that below the critical Euler load (Eq. 7), the straight form is stable, above the P_{cr} the bent form is stable and at P_{cr} the equilibrium is neutral. By plotting the curve P/P_{cr} versus δ/l as shown in Fig. A18.4, we observe the following behavior.

(a) Below $P/P_{cr} = 1$, there is only one equilibrium position, $\delta/l = 0$.

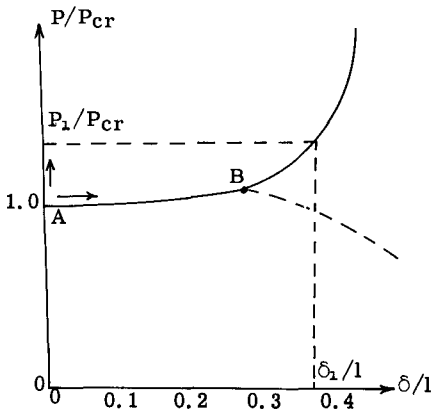

Fig. A18.4

(b) At $P/P_{cr} = 1$, or at point (A), a bifurcation of equilibrium occurs and the column starts to acquire two possible neighbor positions of equilibrium, the straight and the bent.

(c) Above $P/P_{cr} = 1$, the column has two possible equilibrium positions $\delta/l = 0$ and $\delta_1/l \neq 0$.

Thus as far as initiation of instability is concerned, the Euler load as given by Eq. 7 can be considered as the critical load. The question arises whether this load has a practical use for design purposes. A logical design criterion is obviously the maximum load which a column can sustain. We observe from Fig. A18.4 that the load P increases for increasing displacement δ. This behavior is due to the development of large deflections due to bending. However, over a considerable range of deflections δ, the $P \rightarrow \delta$ curve is practically horizontal (for instance, between points A and B the ratio δ/l varies from zero to ≈ 0.4). For such large deflections for which the column load does not change practically, it is obvious that the column ceases to function properly. Therefore, from this point of view, the Euler load can be considered that which characterizes the maximum strength of the column.

The rising part of the curve BD holds as long as the material behaves elastically. At some point B, however, inside the almost flat portion of the curve, the inner fibers of the column acquire maximum stress equal to the yield stress. If we carry out an elastic-plastic analysis of the subsequent behavior, we observe that the curve drops almost immediately. Again this maximum load P_B is very near the Euler load. For design purposes, therefore, the Euler load, which is a buckling load, is a very good approximation to the ultimate load which the column can sustain.

Another argument will confirm the above conclusion. In discussing the buckling of columns in the previous paragraphs, we have assumed that the column is initially straight, centrally loaded and made of homogeneous material. Actual columns, however, are imperfect due to initial crookedness (for instance, due to unavoidable tolerances in their manufacture), due to slight load eccentricities and due to lack of complete homogenity. Therefore, a certain amount of bending is always present even for small loads.

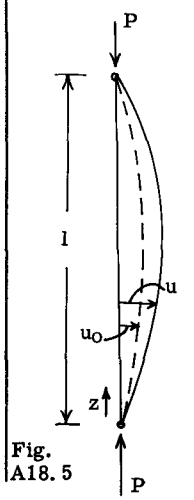

Fig. A18.5

Let us now examine the behavior of such initially imperfect columns by assuming a certain initial deflection u_0 of the column axis (see Fig. A18.5). For small deflections,

the change of curvature due to subsequent bending (after loading) is:-

$$\delta\left(\frac{1}{R}\right) = \frac{d^2u}{dz^2} - \frac{d^2u_0}{dz^2}$$

In the differential equation of deflection one can prove that 1/R is the change of curvature which for an initial straight column coincides with the curvature itself. Thus in the present case, where the bending moment is Pu, the equation of deflection becomes:-

$$\frac{d^2u}{dz^2} - \frac{d^2u_0}{dz^2} = -k^2u \quad \text{- - - - - - - - - (9)}$$

Let us express u_0 in Fournier series:-

$$u_0 = \sum_1^\infty \bar{\delta}_n \sin\frac{\pi u z}{l} \quad \text{- - - - - - - - -(10)}$$

Substituting (10) in (9), we find the solution which satisfies the boundary conditions (u = 0 for z = 0, z = 1) is:-

$$u = \sum_{n=1}^{\infty} \delta_n \sin\frac{\pi z}{l} \quad \text{- - - - - - - - (11a)}$$

where $\delta_n = \dfrac{\bar{\delta}_n}{1 - P/P_n}$ - - - - - - - - - - (11b)

$$P_n = \frac{n^2\pi^2 EI}{l^2}$$

The deflection of the column at the center is:-

$$\delta_{max} = \delta_1 - \delta_3 + \delta_5 \quad \text{- - - - - - - - -(12)}$$

If we plot the deflection versus the load we obtain the curve (Fig. A18.6), which

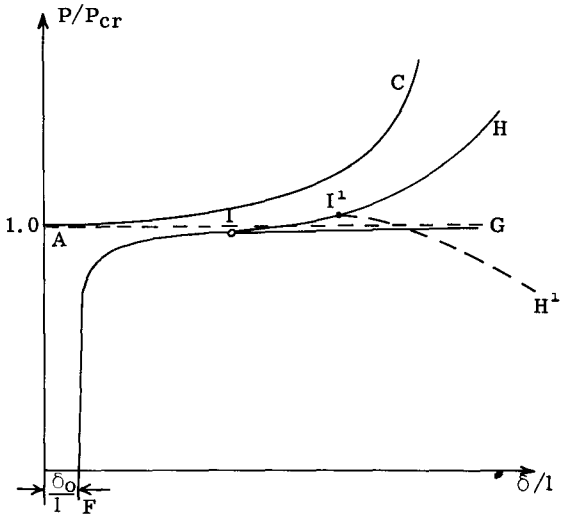

Fig. A18.6

approaches the horizontal line $P/P_{cr} = 1$ asymptotically. This curve, however, is valid for small deflections for which the approximation:-

$$\delta\left(\frac{1}{R}\right) \cong \frac{d^2u}{dz^2} - \frac{d^2u_0}{dz^2} \quad \text{is valid.}$$

By a treatment similar to that in the previous paragraph, we will find that for large deflections the load deflection curve raises after the point I (curve FIH). Due to the onset of plasticity, the actual curve drops at the point I^1 (curve FII^1H^1). The failing load at I^1 can be either greater or smaller than P_{cr}, but it is usually very near to it.

In the above discussions we have shown that for all practical purposes the Euler buckling load can be considered as the ultimate load which a real or practical column can sustain. Besides its closeness to the actual ultimate load, the critical load can be easily calculated from equation (7) without the necessity of carrying out a lengthy calculation which will include the initial imperfections and plastic effects.

It should be noted, however, that the buckling load given by equation (7) is valid when the uniform stress due to a compressive load ($\sigma = P/A$, where A is cross-sectional area) is below yield stress. If σ is above the yield stress, the theory of plasticity predicts another value for the buckling load. Referring now to equations (11) we find:-

$$P_n = n^2 P_{cr} \quad (P_{cr} \text{ from equation 7})$$

$$\delta_n = \frac{\bar{\delta}_n}{1 - \dfrac{P}{n^2 P_{cr}}}$$

Thus as P approaches P_{cr}, we see that

$$\frac{\delta_1}{\bar{\delta}_1} \to \infty \quad \frac{\delta_2}{\bar{\delta}_2} \to \frac{4}{3}, \quad \frac{\delta_3}{\bar{\delta}_3} \to 9/8 \quad \text{etc.}$$

Thus $\delta_1 >> \delta_2 >> \delta_3$ and:-

$$\delta_{max} \cong \delta_1 = \frac{\bar{\delta}_1}{1 - P/P_{cr}}$$

In a buckling test we measure $\delta = \delta_{max} - \bar{\delta}$, where $\bar{\delta}$ is the initial deflection at the middle point. Thus:-

$$\delta \cong \delta_{max} - \bar{\delta}_1 = \frac{\bar{\delta}_1}{\dfrac{P_{cr}}{P} - 1} \quad \text{and,}$$

$$P_{cr}\frac{\delta}{P} - \delta = \bar{\delta}_1 \quad \text{- - - - - - - - - - - (13)}$$

If in a buckling test we plot δ/P versus δ, we can obtain the critical load experimentally without knowing the initial deflection $\bar{\delta}_1$. It is simply the inverse of the slope of this curve.

A18.5 Buckling Loads of Columns with Various End Conditions.

From the conclusions reached in the previous discussion, we can consider the buckling problem as an instability problem of an initially straight column. Thus we assume a certain deflected position near the straight configuration as another possible equilibrium form and seek the loads under which the non-straight form is possible. Furthermore, only a small deflection analysis is necessary.

The general differential equation of bending-buckling is:-

$$\frac{d^4u}{dz^2} + k^2 \frac{d^2u}{dz^2} = 0 \quad \text{- - - - - - - - - - (14)}$$

and the general solution is:-

$$u = C_1 \sin kz + C_2 \cos kz + C_3 z + C_4 \quad \text{- - (15)}$$

The coefficients C_1, C_2, C_3 and C_4 depend on the conditions of the end supports. The various end conditions are:-

Free end:- $\frac{d^2u}{dz^2} = 0$, $\frac{d^3u}{dz^3} = 0$

Pin end: - $u = 0$, $\frac{d^2u}{dz^2} = 0$

Fixed end:- $u = 0$, $\frac{du}{dz} = 0$

Thus we have 4 end conditions. These give systems of four linear homogenous equations. A trivial solution of these is the zero solution. For the buckling state, however, C_1, C_2, C_3, C_4 are not all zero. The condition of non-zero solution of the above system is that the determinant of the coefficients of C_1, C_2, C_3 and C_4 is equal to zero. From this equation, we calculate the buckling load.

For example, in a simply supported beam, ($u = 0$, $\frac{d^2u}{dz^2} = 0$, at both ends), the end conditions furnish give

$$C_2 + C_4 = 0 \quad , \quad C_2 = 0$$

$$C_1 \sin kl + C_2 \cos kl + C_3 l + C_4 = 0$$

For buckling we must have:-

$$\begin{vmatrix} 0 & 1 & 0 & 1 \\ 0 & 1 & 0 & 0 \\ \sin kl & \cos kl & 1 & 1 \\ -\sin kl & -\cos kl & 0 & 0 \end{vmatrix} = 0$$

or $\sin kl = 0$ or $kl = n\pi$ $(n = 1, 2, 3 - - -)$

whence $P_n = \frac{n^2\pi^2 EI}{l^2}$ - - - - - - - - - - - (16a)

Thus for P_n equal to the right hand side of equation (16a), we have a possible form of equilibrium of the bent form. The smallest value of P_n occurs at $n = 1$, and this is the buckling load:

$$P_{cr} = \frac{\pi^2 EI}{l^2} \quad \text{- - - - - - - - - - - - - (16b)}$$

The buckling load for other end conditions can be derived in similar manner.

INELASTIC COLUMN STRENGTH

A18.6 Inelastic Buckling. Introduction.

Euler's theory of buckling is valid as long as the stress in the column nowhere exceeds the elastic limit of the column material. We have seen that the analysis for perfect and imperfect elastic columns leads to the same result, namely, equation (7).

The case of the inelastic buckling, that is, instability under axial load exceeding the elastic limit stress, presents some difficulties. As we will see, the perfect column analysis leads to a different expression for the critical load than for the perfect column. This is due to the fact that in the plastic stress range, the material behaves differently under loading and unloading, as illustrated in Fig. A18.7. Let us now examine the two cases:

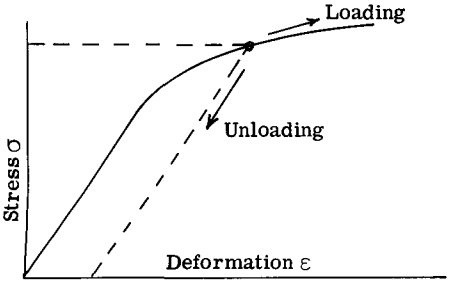

Fig. A18.7

A18.7 Perfect Column. Reduced Modulus Theory.

Let us assume that the perfect column is first compressed uniformly up to the stress σ. To study the critical value, σ_{cr}, of σ for which

the column becomes unstable we assume:-

(1) That the displacements are small so that the relation between the radius of curvature R and the deflection u of the elastic axis is,

$$\frac{1}{R} = \frac{d^2u}{dz^2} \quad \text{- - - - - - - - - - - - - - - (17a)}$$

(2) Plane sections remain plane, therefore the change of strain due to bending at a distance h on the plane of bending is,

$$\delta\varepsilon = \frac{h}{R} = h\frac{d^2u}{dz^2} \quad \text{- - - - - - - - - - - - (17b)}$$

(3) The stress-strain relation follows the simple tension curve for the material.

(4) The plane of bending is a plane of symmetry of the cross-section.

Assume now a column with the cross-section as shown in Fig. A18.8a be compressed in the

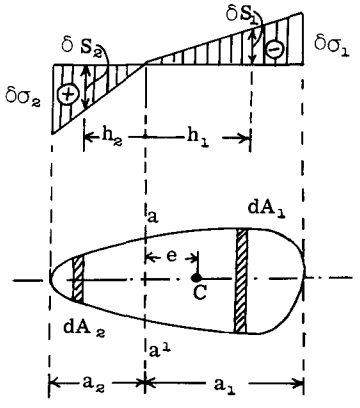

Fig. A18.8a

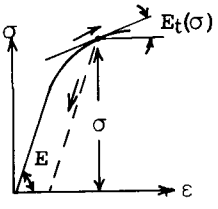

Fig. A18.8b

plastic stress range and that the compressive stress prior to instability be σ. To consider the condition of buckling, let the column be slightly deflected transversely. The stress on one side of the column will then increase due to the bending following the stress-strain curve, while on the other side the stress will decrease and will therefore follow the unloading elastic line shown in Fig. A18.8b.

For small changes of the stress, on the first side, the variation of stress is related to the variation of strain by:-

$$\delta S_1 = E_t(\sigma)\,\delta\varepsilon_1 \quad \text{- - - - - - - - - - (18)}$$

where $E_t(\sigma)$ is the slope of the stress-strain curve at stress σ. On the second side the changes will follow the elastic relation, that is,

$$\delta S_2 = E\,\delta\varepsilon_2 \quad \text{- - - - - - - - - - - - (19)}$$

The distribution of the compressive (-) stress and the tensile (+) stress due to bending is shown in Fig. A18.8a. The stress becomes zero on line (a a¹), which is at a distance e from the centroid c. For equilibrium of stresses on the cross-section we have,

$$-\int_0^{a_1}\delta S_1 dA + \int_0^{a_2}\delta S_2 dA = 0 \quad \text{- - - - (20)}$$

and for equilibrium for moments,

$$-\int_0^{a_1}\delta S_1(h_1+e)dA + \int_0^{a_2}\delta S_2(h_2-e)dA = Pu \quad \text{- - (21)}$$

Due to the linear distribution of stress, we have:-

$$\delta S_1 = \frac{\delta\sigma_1}{a_1}h_1, \qquad \delta S_2 = \frac{\delta\sigma_2}{a_2}h_2 \quad \text{- - - - - - - - - - - - (22)}$$

Introducing now (17b), (18), (19) and (22) in equation (20), we obtain,

$$-E_t Q_1 + EQ_2 = 0 \quad \text{- - - - - - - - - - (23)}$$

where,

$$Q_1 = \int_0^{a_1} h_1 dA\,, \quad Q_2 = \int_0^{a_2} h_2 dA \quad \text{- - - (24)}$$

are the moments of the cross-sectional areas to the right and left of line a a¹.

From eq. (21) we obtain,

$$\bar{E}I\frac{d^2u}{dz^2} = Pu \quad \text{- - - - - - - - - - - - - (25)}$$

where,

$$\bar{E} = \frac{EI_1 + E_t I_2}{I} \quad \text{- - - - - - - - - - (26)}$$

$\bar{E}$ is the so-called reduced modulus, and I_1 and I_2 being the moment of inertia of the two sides.

We observe that the position of the neutral axis in terms of the axial stress is given by eq. (24), while the buckling eq. (25) is similar to the elastic buckling eq. (14). However, the value of K here is not given by eq. (3), but by,

$$K = \sqrt{\frac{A\sigma}{\bar{E}I}} \quad \text{- - - - - - - - - - - - - (27)}$$

Therefore all the results of the previous analysis will be valid for the case of inelastic buckling. For instance, for a simply

supported column according to eq. (7), we will have,

$$\sigma_{cr} = \frac{\pi^2 \bar{E} I}{Al^2} \quad - - - - - - - - - - - - - - (28)$$

Since $\bar{E}$ is a function of σ_{cr} given by eq. (28) and the value of E_t at the unknown σ_{cr}, the calculation of the critical stress requires a trial and error simultaneous solution of equations (23), (26) and (28).

A18.8 Imperfect Column. Tangent-Modulus Theory.

The tangent-modulus theory, originally proposed by Engesser (Ref. 1), is based on the assumption that at the critical state, no stress reversal takes place, and the critical stress, therefore, is determined only by the tangent modulus E_t. This theory was abandoned early since according to the previous discussion with the classical definition of instability (perfect column, bifurcation of equilibrium) strain reversal does take place. In recent years, however, this tangent modulus theory has been proved useful.

Under the assumption of no strain reversal both sides of the cross-section in Fig. A18.8a, will be characterized by the same linear stress distribution, corresponding to the tangent-modulus E_t. Thus the buckling equation will be,

$$E_t I \frac{d^2u}{dz^2} + Pu = 0 \quad - - - - - - - - - - - - (29)$$

and the critical stress for simply supported end conditions becomes,

$$\sigma_t = \frac{\pi^2 E_t I}{Al^2} \quad - - - - - - - - - - - - - - (30)$$

Since $I_1 + I_2 > I$ and $E > E_t$, it follows from (26)

$$\bar{E} > E_t \text{ and } \sigma_r > \sigma_t \quad - - - - - - - - - - (31)$$

The critical stress σ_t, therefore predicted by the tangent-modulus theory is smaller than σ_r from the reduced modulus theory. Although for perfect columns, the assumption of no strain reversal is in contradiction to the material behavior in the plastic range, most experiments have given results more closely to the results by the tangent-modulus theory.

To resolve this controversy, Shanley (Ref. 2), proposed the following explanation. For simplicity, let a two-flange buckled column be formed by two rigid legs (see Fig. A18.9) joined in the middle by a plastic hinge. Assume that this column starts to buckle as soon as σ_t is reached. By considering the effect of a load P above the critical load P_t corresponding to tangent-modulus, Shanley proves the relation,

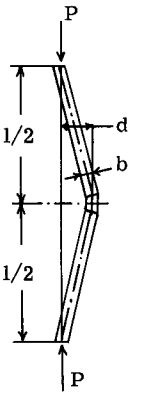

Fig. A18.9

$$P = P_t \left(1 + \frac{1}{\frac{b}{2d} + \frac{1+\tau}{1-\tau}}\right) \quad - - - - - - - (32)$$

where

$$\tau = E_t/E$$

It must be emphasized that the buckled configuration is a stable one similar to that considered in the refined Euler's theory. Shanley has recognized the fact that such a stable configuration may exist after exceeding the tangent modulus load.

If $R = P/P_t$, Shanley found that the relation between the variation of stress due to bending and the compressive strain e_t corresponding to σ_t is:-

$$\text{Concave side: } \frac{\delta\varepsilon_1}{\varepsilon_t} = \frac{2\left(\frac{1}{\tau} - R\right)}{\frac{1-\tau}{R-1} - (1+\tau)}$$

$$\text{Convex side: } \frac{\delta\varepsilon_2}{\varepsilon_t} = \frac{2\,(R-1)}{\frac{1-\tau}{R-1} - (1+\tau)} \quad - - - - (33)$$

In Fig. A18.10, $\delta\varepsilon_1/\varepsilon_t$ and $\delta\varepsilon_2/\varepsilon_t$ are plotted against R for $\tau = 0.75$. We observe that while the strain on the concave side increases very rapidly and reaches an infinite value at the reduced-modulus load, the strain on the convex side decreases initially very slowly. Due to this picture we can conceive that in a real column, which has initial imperfections, the compressive strain will increase more rapidly. Furthermore, the rapid increase of $\delta\varepsilon_1$ will cause a fast reduction of E_t. The column, therefore, loses its usefulness after the tangent-modulus has been slightly increased. Thus the tangent-

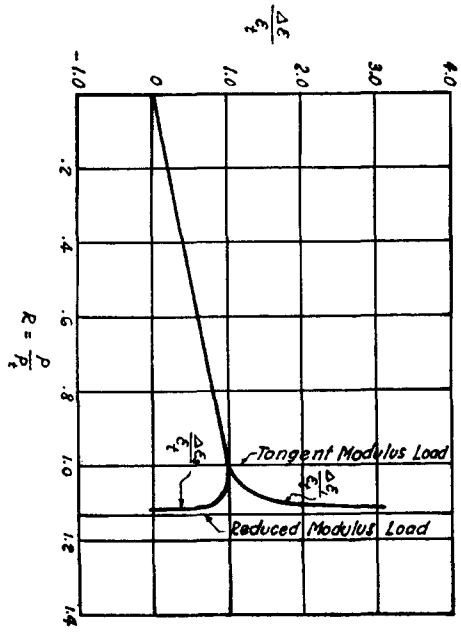

Fig. A18.10

modulus, even though it does not actually define an unstable configuration, it represents the lower limit of a spectrum of possible buckled configurations, the upper limit of which is the reduced modulus load which corresponds to infinite deflections.

Thus to summarize, sufficient experimental results are available to show that the failing stress of a column in the inelastic range can be found by replacing E by the tangent modulus E_t in Euler's equation, or,

$$\sigma_{cr} = \frac{\pi^2 E_t}{(L/r)^2}, \quad r = \sqrt{\frac{I}{A}} \qquad \text{- - - - - - - - (34)}$$

Figs. A18.11 and 12 show how experimental results check the strength as given by the Euler equation using the tangent-modulus E_t.

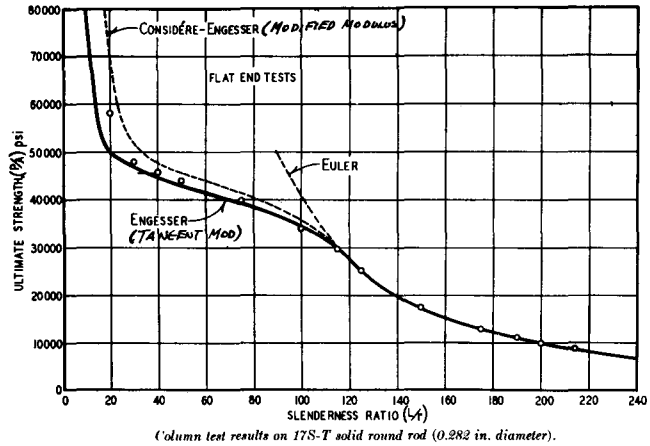

Column test results on 17S-T solid round rod (0.282 in. diameter).

Fig. A18.11

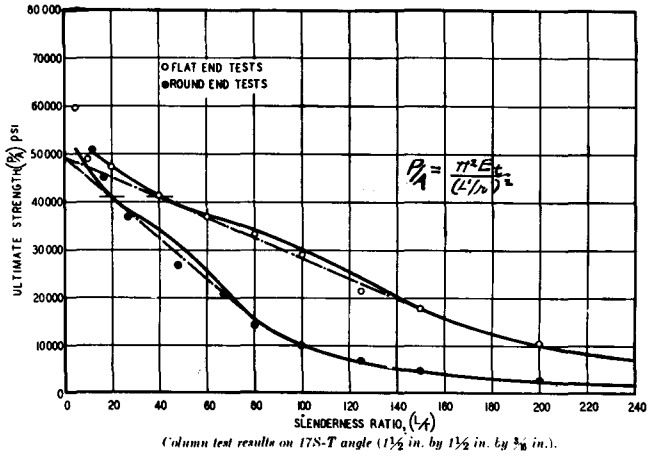

Column test results on 17S-T angle (1½ in. by 1½ in. by 5/16 in.).

Fig. A18.12

References:

Ref. 1. Engesser F., Schweezeriche Bauer Zeitung. Vol. 26, p. 24, 1895.

Ref. 2. Shanley, F.R., Inelastic Column Theory, Jour. Aeronautical Sciences, 1947, p. 261.

PART 2

THEORY OF THE ELASTIC INSTABILITY OF THIN SHEETS

A18.9 Introduction.

Thin sheets represent a very common and important structural element in aerospace structures since the major units of such structures are covered with thin sheet panels. Since compressive stresses cannot be eliminated in aerospace structures, it is important to know what stress intensities will cause thin sheet panels to buckle. Equations for the buckling of thin sheet panels under various load systems and boundary conditions have been derived many years ago and are readily available to design engineers. Part C of this book takes up the use of the many buckling equations in the practical design of thin sheet structural elements. The purpose of this chapter is to introduce the student to the theory of thin plate instability or how these buckling equations so widely in use by design engineers were derived. For a broad comprehensive treatment of the subject of instability of structural elements, the student should refer to some of the references as listed at the end of this chapter.

A18.10 Pure Bending of Thin Plates.

To derive the theory of instability of thin plates, we must first derive the theory of the pure bending of thin plates.

In the following the analysis will be confined to small deformations. Let x, y be the middle plane of the plate before bending occurs and z be the axis normal to that plane. Points of the x, y plane undergo small displacements, w in the z-direction, which will be referred as the deflection of the plate. The slope of the middle-surface in the x- and y-directions after bending are

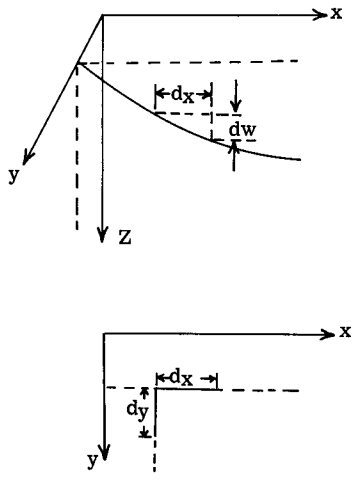

Fig. 1

$$i_x = \frac{\partial w}{\partial x} \ , \quad i_y = \frac{\partial w}{\partial y}$$

For small deflections, the curvature of the middle surface can be found approximately by omitting powers of $\frac{\partial w}{\partial x}$, $\frac{\partial w}{\partial y}$, as compared to unity, as it has been done for the curvature of beams. Thus the curvature of the deflected middle surface in planes parallel to xz and yz planes respectively are:

$$\frac{1}{R_x} = -\frac{\partial^2 w}{\partial x^2} \ , \quad \frac{1}{R_y} = -\frac{\partial^2 w}{\partial y^2} \qquad \text{- - - - - - - - (1a)}$$

Another quantity used in the problem of plates is the so-called twist of the middle surface given by:

$$\frac{1}{R_{xy}} = \frac{\partial^2 w}{\partial x \partial y} \qquad \text{- - - - - - - - - - - - - - - - - (1b)}$$

The strains can now be expressed by means of curvatures and twist of the middle surface. In the case of pure bending of prismatic bar a rigorous solution was obtained by assuming that cross-sections of the bars remain plane after bending and rotate so as to remain perpendicular to the deflected neutral axis. Combination of such bending in two perpendicular directions brings us to pure bending of plates.

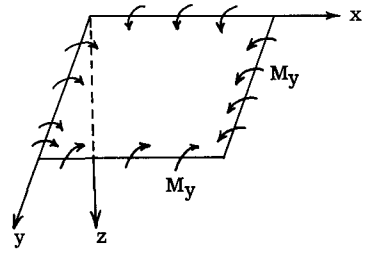

Fig. 2a

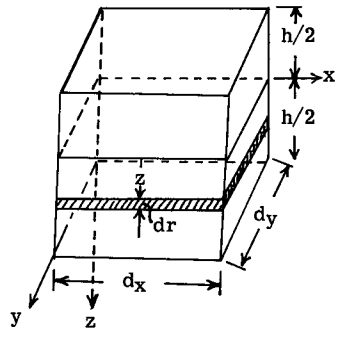

Fig. 2b

Let Fig. (2a) represent a thin rectangular plate loaded by uniformly distributed bending

M_x, M_y per unit length at its edges. These moments are considered positive when they are directed as shown in the figure, i.e. when they produce compression in the upper surface of the plate and tension in the lower. Let also (Fig. 2b) be a rectangular element cut out of the plate with sides dx, dy, t. The thickness t is considered very small compared with the other dimensions. Obviously the stress conditions at the edges of all such elements will be identical to that of Fig. 2a. Assume now that the lateral sides of the element remain plane during bending and rotate about the axes so as to remain normal to the deflected middle surface. Due to symmetry the middle surface does not undergo any extension and it is therefore the neutral surface.

From the geometry of the above described form of deformation the displacements in the x, y, z directions can be found as follows:

A point B on the middle surface has been displaced to B^1 by W in the z-direction. An element of surface dzdy has rotated by an angle equal to the slope of the deflected middle surface in the direction so as to remain normal to the middle surface. See Fig. 3.

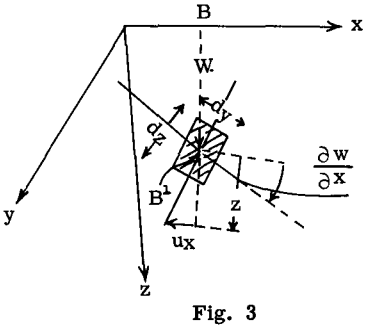

Fig. 3

This angle for small displacements is obviously equal to $\frac{\partial w}{\partial x}$. Thus the horizontal displacement u_x in the x-direction of a point at distance z from the middle surface is:

$$u_x = - z \frac{\partial w}{\partial x}$$ (The sign - indicates negative displacement for positive z).

In a similar manner we find the displacement in the y-direction. The complete displacement system is:

$$u_x = - z\frac{\partial w}{\partial x}\ ,\ u_y = - z\frac{\partial w}{\partial y}\ ,\ u_z = w(x,y) \quad - - (2)$$

The corresponding strains are:

$$\varepsilon_x = - z \frac{\partial^2 w}{\partial x^2} = \frac{z}{R_x}\ ,\quad \varepsilon_y = - z \frac{\partial^2 w}{\partial y^2} = \frac{z}{R_y}\ ,$$

$$\varepsilon_{xy} = 2z \frac{\partial^2 w}{\partial x \partial y} = \frac{2z}{R_{xy}} \quad - - - - - - - - - - - - (3)$$

Since we treat the problem of plates as a plane stress problem, we find by means of Hook's law

$$\sigma_x = \frac{Ez}{(1-\nu^2)} \left(\frac{1}{R_x} + \frac{\nu}{R_y}\right) =$$

$$- \frac{Ez}{(1-\nu^2)} \left(\frac{\partial^2 w}{\partial x^2} + \nu \frac{\partial^2 w}{\partial y^2}\right) \quad - - - - - - - - (4a)$$

$$\sigma_z = \frac{Ez}{(1-\nu^2)} \left(\frac{1}{R_y} + \frac{\nu}{R_x}\right) =$$

$$- \frac{Ez}{(1-\nu^2)} \left(\frac{\partial^2 w}{\partial y^2} + \nu \frac{\partial^2 w}{\partial x^2}\right) \quad - - - - - - - - (4b)$$

These normal stresses are linearly distributed over the plate thickness. Their resultants must be equal to M_x and M_y respectively:

$$\int_{-h/2}^{h/2} \sigma_x\, z\ dydz = M_x dy$$

$$\int_{-h/2}^{h/2} \sigma_y\, z\ dxdz = M_y dx$$

Substituting from (4) we find:

$$M_x = -D \left(\frac{\partial^2 w}{\partial x^2} + \nu \frac{\partial^2 w}{\partial y^2}\right) \quad - - - - - - - (5a)$$

$$M_y = -D \left(\frac{\partial^2 w}{\partial y^2} + \nu \frac{\partial^2 w}{\partial x^2}\right) \quad - - - - - - - (5b)$$

where $D = \frac{Eh^3}{12(1-\nu^2)}$ = the <u>flexural rigidity</u> of the plate. If besides the flexural moments M_x, M_y, there are uniformly distributed twisting moments M_{xy} and M_{yx} along the sides of the plate of Fig. 2a, these must be equal to the resultant of distributed shear forces σ_{xy}, σ_{xz} along the sides of the element of Fig. 2b.

From eq. (3) we obtain:

$$\sigma_{xy} = \sigma_{yx} = \frac{2Gz}{R_{xy}} = 2Gz \frac{\partial^2 w}{\partial x \partial y} \quad - - - - - (4c)$$

$$M_{xy}dx = \int_{-h/2}^{h/2} \sigma_{xy} z\ dxdz\ ,\ M_{yz}dy =$$

$$\int_{-h/2}^{h/2} \sigma_{yx} z\ dydz\ ,\ M_{xy} = M_{yx} =$$

$$D(1-\nu) \frac{\partial^2 w}{\sigma x \sigma y} \quad - - - - - - - - - - - - (5c)$$

Equations (5) give the moments per unit length for pure bending and twisting of a plate.

A18.11 The Differential Equation of the Deflection Surface.

To develop the theory of small deflections of thin plates we make one more assumption. At the boundary of the plate we assume that its edges are free to move in the plane of the plate.

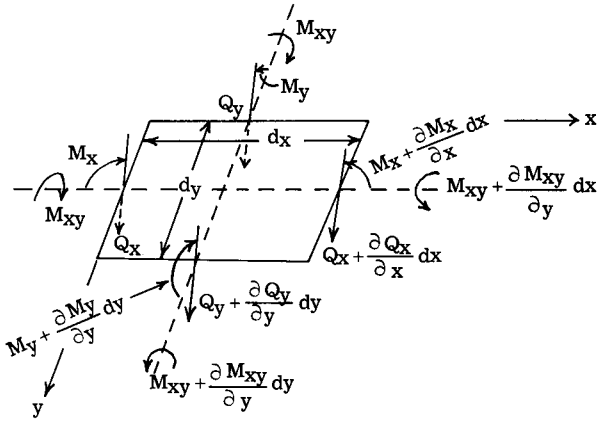

Fig. 4

Thus the reactive forces at the edges due to the supports are normal to the plate. With these assumptions we can neglect any strain in the middle plane during bending.

Let us consider, Fig.4, an element dxdy of the middle plane. Along its edge the moments M_x, M_y, M_{xy} are distributed. These are the resultants of the bending and twisting stresses distributed linearly along the thickness of the plate (see eqs. 4 and 5). If the plate is loaded by external forces normal to the middle plane in addition to the above moments there are vertical shearing forces Q_x, Q_y, acting on the sides of the element of Fig. 4.

$$Q_x = \int_{-h/2}^{h/2} \sigma_{xz} dr, \quad Q_y = \int_{-h/2}^{h/2} \sigma_{yz} dz \quad -- \quad (6)$$

Let q be the transverse load per unit area acting normally to the upper face of the plate. Considering the force equilibrium in the z-direction of the element of Fig. 4 we find:

$$\frac{\partial Q_x}{\partial x} dxdy + \frac{\partial Q_y}{\partial y} dydx + q dxdy = 0 \quad \text{or} \quad =$$

$$\frac{\partial Q_x}{\partial x} + \frac{\partial Q_y}{\partial y} + q = 0 \quad - - - - - \quad (6a)$$

Taking the equilibrium of the moments acting in the x-direction we obtain:

$$\frac{\partial M_{xy}}{\partial x} dxdy - \frac{\partial M_y}{\partial y} dxdy + Q_y dxdy = 0 \quad \text{or}$$

$$\frac{\partial M_{xy}}{\partial x} - \frac{\partial M_y}{\partial y} + Q_y = 0 \quad - - - \quad (6b)$$

From the moment equilibrium in the y-direction we find:

$$\frac{\partial M_{xy}}{\partial y} + \frac{\partial M_x}{\partial x} - Q_x = 0 \quad - - - - - - - - - \quad (6c)$$

By eliminating Q_x, Q_y from 6 a,b,c, we find the equilibrium relation between the moments:

$$\frac{\partial^2 M_x}{\partial x^2} + \frac{\partial^2 M_y}{\partial y^2} - 2 \frac{\partial^2 M_{xy}}{\partial x \partial y} = - q \quad - - - - \quad (7)$$

To represent this equation in terms of the deflections w of the plate, we make the assumption that the expression (5) derived for pure bending holds approximately also in the case of laterally loaded plates. This assumption is equivalent to neglecting the effect on bending of the shearing forces and the compressive stress σ_z. This is an extension of the engineering theory of bending of beams. As in the case of beams it gives good approximation for bending of plates under transverse loads.

Introducing equation (4) into (7) we find:

$$\frac{\partial^4 w}{\partial x^4} + \frac{\partial^4 w}{\partial y^4} + 2 \frac{\partial^4 w}{\partial x^2 \partial y^2} = \frac{q}{D} \quad - - - - - - \quad (8)$$

The problem of bending of plates is thus reduced to integrating eq. (8) for w. The corresponding shearing forces in terms of the displacements are found from eqs. 4 and 6b and c:

$$Q_x = \frac{\partial M_{xy}}{\partial y} + \frac{\partial M_x}{\partial x} = - D \frac{\partial}{\partial x} \left(\frac{\partial^2 w}{\partial x^2} + \frac{\partial^2 w}{\partial y^2} \right) \quad - - - \quad (9a)$$

$$Q_y = \frac{\partial M_y}{\partial y} - \frac{\partial M_{xy}}{\partial x} = - D \frac{\partial}{\partial y} \left(\frac{\partial^2 w}{\partial x^2} + \frac{\partial^2 w}{\partial y^2} \right) \quad - - - \quad (9b)$$

The above analysis is sufficient to seek solutions of specific problems. The general procedure is to find approximate solution of the fourth order differential equation (8) which satisfies the given boundary displacement and force conditions.

A18.12 Strain Energy in Pure Bending of Plates.

In evaluating the strain energy of a thin plate we shall ignore the contribution of the shear strains which are generally small for small deflections.

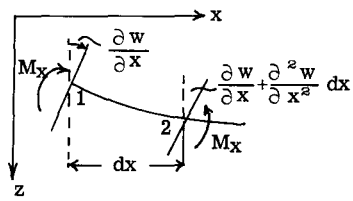

Fig. 5a

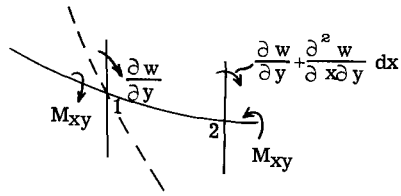

Fig. 5b

The strain energy stored in a plate element is obtained by calculating the work done by the moments $M_x dy$, and $M_y dx$ on the element during bending. Since the sides of the element remain plane during bending the work done by $M_x dy$ is obtained by taking half the product of $M_x dy$ and the relative angle of rotation of the two sides of the element. Since the curvature in the x-direction is $-\frac{\partial^2 w}{\partial x^2}$, the relative angle of rotation of the sides 1 and 2 of distance dx will be $-\frac{\partial^2 w}{\partial x^2}dx$. Thus the work due to $M_x dy$ is:

$$dV_x = -\frac{1}{2} M_x \frac{\partial^2 w}{\partial x^2} dxdy \quad - - - - - - - - \text{(a)}$$

Similarly the work due to $M_y dx$ is:

$$dV_y = -\frac{1}{2} M_y \frac{\partial^2 w}{\partial x^2} dxdy \quad - - - - - - - - \text{(b)}$$

The twisting moment $M_{xy}dy$ also does work against rotation of the element about the x-axis. The relative angle of rotation of the two sections 1, 2 is obviously $\frac{\partial^2 w}{\partial x \partial y}dx$. Thus the work done by $M_{xy}dy$ is:

$$dV_{xy} = \frac{1}{2} M_{xy} \frac{\partial^2 w}{\partial x \partial y} dxdy \quad - - - - - - - - \text{(c)}$$

and the work due to $M_{yx}dx = M_{xy}dx$ is:

$$dV_{yx} = \frac{1}{2} M_{xy} \frac{\partial^2 w}{\partial x \partial y} dxdy \quad - - - - - - - - \text{(d)}$$

(It is noted that the twist does not affect the work produced by the bending moments, neither the bending affect the work produced by the torsional moments).

Thus the total strain energy per unit volume of the plate is:

$$V_o = \frac{dV_x + dV_y + dV_{xy} + dV_{yx}}{dxdy} =$$

$$\frac{1}{2}\left[- M_x \frac{\partial^2 w}{\partial x^2} - M_y \frac{\partial^2 w}{\partial y^2} + 2M_{xy} \frac{\partial^2 w}{\partial x \partial y} \right] \quad - - - - \text{(10)}$$

Substituting M_x, M_y, M_{xy} in terms of the displacement from eqs. (5) we find:

$$V_o = \frac{1}{2} D \left(\frac{\partial^2 w}{\partial x^2} + \frac{\partial^2 w}{\partial y^2}\right)^2 -$$

$$2(1-\nu)\left[\frac{\partial^2 w}{\partial x^2} \cdot \frac{\partial^2 w}{\partial y^2} - \left(\frac{\partial^2 w}{\partial x \partial y}\right)^2\right] \quad - - - - - - - \text{(11)}$$

This expression will be modified later when we will consider the superposition of compressive loads in the plane of the plate which are related to the problem of plate buckling.

A18. 13 Bending of Rectangular Plates.

The general differential equation for bending plates was given in section C2.3 (eq. 8). Two very useful methods of solution have been widely used, namely, the Fourier Series Method and the Energy Method. Both methods will be developed in the following for rectangular plates and various edge-supporting conditions. The edge support conditions are classified as follows:

a) Built-in edge or Fixed: The deflection along the built-in side is zero and the tangent plane to the deflected middle surface is horizontal. Thus if for instance the x-axis coincides with the built-in edge these conditions are:

$$(w)_{y=o} = 0 \quad \left(\frac{\partial w}{\partial y}\right)_{y=o} = 0 \quad - - - - \text{(12a)}$$

b) Simply supported edge: The deflection along the simply-supported side is zero and the bending moment parallel to this side is also zero. Thus if the plate is simply supported along the x-axis we have:

$$(w)_{y=o}=0 \quad (M_y)_{y=o}=\left(\frac{\partial^2 w}{\partial y^2}+\frac{\partial^2 w}{\partial x^2}\right)_{y=o} = 0 \quad - - - \text{(12b)}$$

c) Free edge: The bending moment, twisting moment and shear force along the free side is zero. Thus if the free side coincides with the straight line x = aL we have:

$$(M_x)_{x=a} = 0 \qquad (M_{xy})_{x=a} = 0 \qquad (Q_x)_{x=a} = 0$$

However, as was proved by Kirchoff two boundary conditions are only necessary to find a unique solution of the bending problem. He has shown that the two last equations of the above conditions can be replaced by one condition.

$$\left(\frac{\partial^3 w}{\partial x^3} + (2-\nu)\frac{\partial^3 w}{\partial x \partial y^2}\right)_{x=a} = 0$$

Expressing the condition $(M_x)_{x=a} = 0$ in terms of w we find the final form of the boundary conditions along the free edge:

$$\left(\frac{\partial^2 w}{\partial x^2} + \frac{\partial^2 w}{\partial y^2}\right)_{x=a} = 0 \quad , \quad \left[\frac{\partial^3 w}{\partial x^3} + (2-\nu)\frac{\partial^3 w}{\partial x \partial y^2}\right]_{x=a} = 0$$

- - - - - - - - - (12c)

In the following solutions for various edge conditions will be developed.

1. Simply supported rectangular plates

Let a plate with sides a and b and axes x, y, as shown in Fig. 6, be simply supported around the whole periphery and loaded by a distributed load q = f (x,y).

Two methods of solutions will be developed:

a) Navier solution by means of double Fourier Series:

We can always express f (x,y) in the form of a double trigonometric (Fourier) series:

$$q = f(x,y) = \sum_{m=1}^{\infty}\sum_{m=1}^{\infty} a_{mn} \sin\frac{m\pi x}{a} \sin\frac{n\pi y}{b} \quad -(13a)$$

where: $$a_{mn} = \frac{4}{ab}\int_0^a \int_0^b f(x,y) \sin\frac{m\pi x}{a}\sin\frac{n\pi y}{b}\,dx\,dy$$

- - - - - - - - - -(13b)

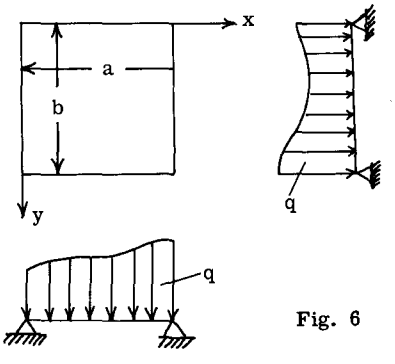

Fig. 6

The boundary conditions are:

W = 0 , M_x = 0 at x = 0, x = a

W = 0 , M_y = 0 at y = 0, y = b , or:

(1) W = 0 (2) $\frac{\partial^2 w}{\partial x^2} = 0$ at x = 0, x = a

(3) W = 0 (4) $\frac{\partial^2 w}{\partial y^2} = 0$ at y = 0, y = b

These boundary conditions are satisfied if we take:

$$W = \sum_{m=1}^{\infty}\sum_{n=1}^{\infty} C_{mn} \sin\frac{m\pi x}{a}\sin\frac{n\pi y}{b} \quad - - - (14a)$$

By substituting in eq. (18) with q given by eq. (13) we find:

$$\sum_{m=1}^{\infty}\sum_{n=1}^{\infty} C_{mn} \pi^4 \left(\frac{m^2}{a^2}+\frac{n^2}{b^2}\right)^2 \sin\frac{m\pi x}{a}\sin\frac{n\pi y}{b} =$$

$$\frac{1}{D}\sum_{m=1}^{\infty}\sum_{n=1}^{\infty} a_{mn} \sin\frac{m\pi x}{a}\sin\frac{n\pi y}{b} \quad - - - - - (14b)$$

This relation is identity if:

$$C_{mn} = \frac{a_{mn}}{\pi^4 D \left(\frac{m^2}{a^2}+\frac{n^2}{b^2}\right)^2}$$

and thus:

$$W = \frac{1}{\pi^4 D}\sum_{m=1}^{\infty}\sum_{n=1}^{\infty} \frac{a_{mn}}{\left(\frac{m^2}{a^2}+\frac{n^2}{b^2}\right)^2} \sin\frac{m\pi x}{a}\sin\frac{n\pi y}{b}$$

- - - - - (14c)

In the case of a load q_o uniformly distributed over the whole surface we have:

$$f(x,y) = q_o = \text{const.}$$

$$a_{mn} = \frac{4q_o}{ab}\int_0^a \int_0^b \sin\frac{m\pi x}{a} \cdot \sin\frac{n\pi y}{b}\,dx\,dy =$$

$$\frac{16 q_o}{\pi^2 mn} \quad - - - - - (15a)$$

where m, n are both odd integers. If either or both are even a_{mn} = 0 and substituting in (14c):

$$W = \frac{16 q_o}{\pi^6 D}\sum_{m=1,3,5}^{\infty}\sum_{n=1,3,5}^{\infty} \frac{\sin\frac{m\pi x}{a}\sin\frac{n\pi y}{b}}{mn\left(\frac{m^2}{a^2}+\frac{n^2}{b^2}\right)^2}$$

- - - - - (15b)

with maximum deflection at the center,

$$W_{mkx} = \frac{16 q_o}{\pi^6 D}\sum_{m=1,3,5}^{\infty}\sum_{n=1,3,5}^{\infty} \frac{(-1)^{\frac{m+n}{2}-1}}{mn\left(\frac{m^2}{a^2}+\frac{n^2}{b^2}\right)^2}$$

- - - - - (15c)

This is a rapidly converging series and a satisfactory approximation is obtained by taking only the first term. For a square

plate this approximation becomes:

$$W_{max} \simeq \frac{4q_o a^4}{\pi^6 D} = 0.0454 \frac{q_o a^4}{Eh^3} \quad (\text{for } \nu = 0.3)$$

which is by 2-1/2% is error with the exact solution.

The expressions for bending and twisting moments are not so quickly convergent. To improve the solution another series solution can be developed as follows:

b) Levy alternate single series solution:

The method will be developed for uniform load q_o = const. Levy suggested a solution in the form:

$$W = \sum_{m=1}^{\infty} Y_m (y) \sin \frac{m\pi x}{a} \quad - - - - - - - - (16)$$

where Y_m is a function of y only. Each term of the series satisfies the boundary conditions $w = 0, \frac{\partial^2 w}{\partial x^2} = 0$ at $x = a$. It remains to determine Y_m so as to satisfy the remaining two boundary conditions $w = 0, \frac{\partial^2 w}{\partial y^2} = 0$ at $y = b$.

A further simplification can be made if we take the solution in the form

$$w = w_1 + w_2 \quad - - - - - - - - - - - - - - - (17a)$$

where

$$w = \frac{q_o}{24D} (x^4 - 2ax^3 + a^3 x) \quad - - - - - (17b)$$

is the deflection of a very long strip with the long side in the x-direction loaded by a uniform load q_o supported at the short sides $x = o$, $x = a$, and free at the two long sides. Since (17b) satisfies the differential equation and the boundary conditions at $x = o$, $x = a$, the problem is solved if we find the solution of:

$$\frac{\partial^4 w_2}{\partial x^4} + 2 \frac{\partial^4 w_2}{\partial x^2 \partial y^2} + \frac{\partial^4 w_2}{\partial y^4} = 0 \quad - - - - (18)$$

with w_2 in the form of (16) and satisfying together with w_1 of eq. (17b) the boundary conditions $w = o, \frac{\partial^2 w}{\partial y^2} = 0$ at $y = \pm \frac{b}{2}$ (see Fig. 7).

Substituting (16) into (18) we obtain:

$$\sum_{m=1}^{\infty} \left(Y_m^{IV} - \frac{2m^2\pi^2}{a^2} Y_m'' + \frac{m^4\pi^4}{a^4} Y_m\right) \sin \frac{m\pi x}{a} = 0$$

$$- - - - (19a)$$

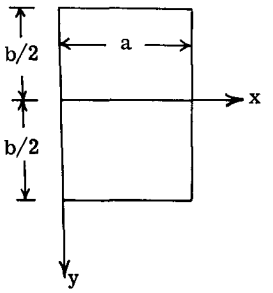

Fig. 7

where for symmetry m = 1,3,5 . . .

This equation can be satisfied for all values of x if:

$$Y_m^{IV} - \frac{2m^2\pi^2}{a^2} Y_m'' + \frac{m^4\pi^4}{a^4} Y_m = 0 \quad - - - - - - (19b)$$

The general solution of (19b) is:

$$Y_m (y) = \frac{qa^4}{D} \left[A_m \cos h \frac{m\pi y}{a} + B_m \frac{m\pi y}{a} \sin h \frac{m\pi y}{a} + C_m \sin h \frac{m\pi y}{a} + D_m \frac{m\pi y}{a} \cos h \frac{m\pi y}{a}\right]$$

$$- - - - - - (20)$$

Since the deflection is symmetric with respect to the x-axis it follows that $C_m = D_m = 0$. Thus:

$$w = \frac{q}{24D} (x^4 - 2ax^3 + a^3 x) + \frac{qa^4}{D} \sum_{m=1,3,5}^{\infty} \left(A_m \cos h \frac{m\pi y}{a} + B_m \frac{m\pi y}{a} \sin h \frac{m\pi y}{a}\right) \sin \frac{m\pi x}{a}$$

or

$$W = \frac{qa^4}{D} \sum_m \left(\frac{4}{\pi^5 m^5} + A_m \cos h \frac{m\pi y}{a} + B_m \frac{m\pi y}{a} \sin h \frac{n\pi y}{a}\right) \sin \frac{m\pi x}{a}$$

where m = 1,3,5 . . . . Substituting this expression into the boundary conditions:

$$w = 0, \quad \frac{\partial^2 w}{\partial y^2} = 0 \quad \text{for } g = \pm \frac{b}{2} \quad \text{we find:}$$

$$A_m \cos h\, \alpha_m + \alpha_m B_m \sin h\, \alpha_m + \frac{4}{\pi^5 m^5} = 0$$

$$- - (21a)$$

$$(A_m + 2B_m) \cos h\, \alpha_m + \alpha_m B_m \sin h\, \alpha_m = 0$$

where $\alpha_m = m\pi b/2a$

From these equations we find:

$$A_m = \frac{2(a_m \tanh a_m + 2)}{\pi^5 m^5 \cosh a_m},$$

$$B_m = \frac{2}{\pi^5 m^5 \cosh a_m} \quad \text{- - - - - - - - - (21b)}$$

Thus:

$$W = \frac{4qa^4}{\pi^6 D} \sum_{m=1,3,5}^{\infty} \frac{1}{m^5} \left[1 - \frac{(a_m \tanh a_m + 2)}{2 \cosh a_m} \cosh \frac{2a_m y}{b} + \frac{a_m}{2 \cosh a_m} \cdot \frac{2y}{b} \sinh \frac{2a_m y}{b} \right] \sin \frac{m\pi x}{a} \quad \text{- - - - - - - - - - - - - - - (21c)}$$

The maximum deflection occurs at the middle $x = \frac{a}{2}$. $y = 0$:

$$W_{max} = \frac{4qa^4}{\pi^5 D} \sum_{m=1,3,5}^{\infty} \frac{(-1)^{\frac{m-1}{2}}}{m^5} \left(1 - \frac{a_m \tanh a_m + 2}{2 \cosh a_m} \right) \quad \text{- - - - - - - - - (21d)}$$

The summation of the first series of terms corresponds to the solution of the middle of a uniformly loaded strip, eq. (17b). Thus:

$$W_{max} = \frac{5}{384} \frac{qa^4}{D} - \frac{4qa^4}{\pi^5 D} \sum_{m=1,3,5}^{\infty} \frac{(-1)^{\frac{m-1}{2}}}{m^5} \cdot \frac{a_m \tanh a_m + 2}{2 \cosh a_m} \quad \text{- - - - - - - - - (21e)}$$

This series converges very rapidly. Taking a square plate, a/b = 1, we find from (21a):

$$a_1 = \frac{\pi}{2}, \quad a_3 = \frac{3\pi}{2} \quad \text{e.t.c.}$$

$$W_{max} = \frac{5}{384} \frac{qa^4}{D} - \frac{4qa^4}{\pi^6 D} (0.68562 - 0.00025 + \ldots.)$$

$$\cong 0.00406 \frac{qa^4}{D}$$

We observe that only the first term of the series in (21e) need to be taken into consideration.

The bending moments are found by substituting (21c) into eqs. (5). The maximum bending moments at $x = \frac{a}{2}$, $y = 0$ are:

$$(M_x)_{max} = \frac{qa^2}{8} + (1-\nu) qa^2 \pi^2 \sum_{m=1,3,5}^{\infty} (-1)^{\frac{m-1}{2}} m^2 \left(A_m - \frac{2\nu}{1-\nu} B_m \right)$$

$$(M_y)_{max} = \nu \frac{qa^2}{8} - (1-\nu) qa^2 \pi^2 \sum_{m=1,3,5}^{\infty} (-1)^{\frac{m-1}{2}} m^2 \left(A_m + \frac{2}{1-\nu} B_m \right) \quad \text{- - - - - - - - (21f)}$$

c) Solution by means of the principle of virtual work

From the discussion of the method (a) we can represent w in double Fourier Series:

$$W = \sum_{m=1}^{\infty} \sum_{n=1}^{\infty} C_{mn} \sin \frac{m\pi x}{a} \sin \frac{n\pi y}{b} \quad \text{- - - (22a)}$$

The coefficients C_{mn} may be considered as the co-ordinate defining the deflection surface. A virtual displacement will have the form:

$$\delta w = \delta C_{mn} \cdot \sin \frac{m\pi x}{a} \cdot \sin \frac{n\pi y}{b} \quad \text{- - - - - (22b)}$$

The strain energy V_1 can be found by substituting (22a) into eq. (6). After a few algebraic manipulations we find:

$$V_1 = \int_0^a \int_0^b V_0 dx dy = \frac{\pi^4 ab}{8} D \sum_{m=1}^{\infty} \sum_{n=1}^{\infty} C_{mn}^2 \left(\frac{m^2}{a^2} + \frac{n^2}{b^2} \right)^2 \quad \text{- - - - - (23)}$$

Let us now examine the deflection of the plate of Fig. 6 with a concentrated load P at the point with co-ordinates $x = \xi$, $y = n$. The increment of strain energy due to the increment of the deflection by:

$$\delta w = \delta C_{mn} \sin \frac{m\pi x}{a} \sin \frac{n\pi y}{b} \quad \text{- - - - - - (24a)}$$

is found from (23)

$$\delta V_1 = \frac{\pi^4 ab}{4} C_{mn} \left(\frac{m^2}{a^2} + \frac{n^2}{b^2} \right)^2 \delta C_{mn} \quad \text{- - - - (24b)}$$

The increment of the work of the load P is:

$$\delta W = P \delta C_{mn} \sin \frac{m\xi}{a} \sin \frac{n\eta}{b} \quad \text{- - - - - - (24c)}$$

From $\delta V_1 - \delta W = 0$ we obtain:

$$\left[\frac{\pi^4 ab}{4} C_{mn} \left(\frac{m^2}{a^2} + \frac{n^2}{b^2}\right)^2 - P \sin\frac{m\pi\xi}{a} \cdot \sin\frac{n\pi\eta}{b}\right]$$

$$\delta C_{mn} = 0$$

Since δC_{mn} is arbitrary its coefficient must be zero. Thus:

$$C_{mn} = \frac{4P \sin\frac{m\pi\xi}{a} \cdot \sin\frac{n\pi\eta}{b}}{\pi^4 abD \left(\frac{m^2}{a^2} + \frac{n^2}{b^2}\right)^2}$$

$$W = \frac{4P}{\pi^4 abD} \sum_{m=1}^{\infty} \sum_{n=1}^{\infty} \frac{\sin\frac{m\pi\xi}{a} \cdot \sin\frac{n\pi\eta}{b}}{\left(\frac{m^2}{a^2} + \frac{n^2}{b^2}\right)^2} \cdot \sin\frac{m\pi x}{a} \cdot \sin\frac{n\pi y}{b} \quad \text{- - - - - - - - -(24d)}$$

This series converges rapidly. For a square plate (a/b = 1):

$$W_{max} = \frac{4Pa^2}{\pi^4 D} \sum_{m=1}^{\infty} \sum_{n=1}^{\infty} \frac{1}{(m^2 + n^2)^2} \quad \text{- - - -(24e)}$$

By taking only the first four terms we find

$$W_{max} \cong 0.01121 \frac{Pa^2}{D}$$

which is 3-1/2% less than the correct value.

(2) Rectangular plate with two opposite edges simply supported, the third edge free and the fourth edge built-in or simply supported.

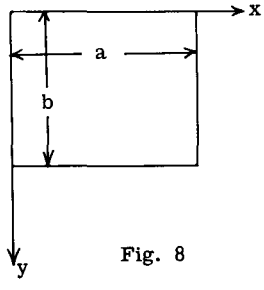

Fig. 8

Assume that the edges x = 0 and x = a are simply supported, the edge y = b free and the edge y = 0 built-in (Fig. 8). In such a case the boundary conditions are:

$$w = 0, \frac{\partial^2 w}{\partial x^2} = 0, \text{ for } x = 0, x = a \quad (a)$$

$$w = 0, \frac{\partial w}{\partial y} = 0, \text{ for } y = 0 \quad (b)$$

$$\left(\frac{\partial^2 w}{\partial x^2} + \frac{\partial^2 w}{\partial y^2}\right) = 0, \quad \text{- - (25)}$$

$$\left[\frac{\partial^3 w}{\partial y^3} + 2(1-\nu)\frac{\partial^3 w}{\partial x^2 \partial y}\right] = 0 \text{ for } y = b \quad (c)$$

Let us consider the case of a uniform load q. we write the deflection in the form:

$$W = w_1 + w_2 \quad \text{- - - - - - - - - - - -(26a)}$$

where w_1 is the deflection of a simply supported strip of length, a, which for the system of axes of Fig. 8 can be written (see Levy's method in previous section):

$$w_1 = \frac{4qa^4}{\pi^5 D} \sum_{m=1,3,5}^{\infty} \frac{1}{m^5} \sin\frac{m\pi x}{a},$$

and w_2 is represented by the series:

$$w_2 = \sum_{m=1,3,5}^{\infty} Y_m(y) \sin\frac{m\pi x}{a} \quad \text{- - - -(26c)}$$

where w_2 being a solution of

$$\frac{\partial^4 w_2}{\partial x^4} + \frac{\partial^4 w_2}{\partial y^4} + 2\frac{\partial^4 w_2}{\partial x^2 \partial y^2} = 0$$

is found as in the previous section:

$$Y_m = \frac{qa^4}{D}\left(A_m \cosh\frac{m\pi y}{a} + B_m \frac{m\pi y}{a} \sinh\frac{m\pi y}{a} + C_m \sinh\frac{m\pi y}{a} + D_m \frac{m\pi y}{a} \cosh\frac{m\pi y}{a}\right) \quad \text{- -(26d)}$$

It is obvious that the two first boundary conditions are identically satisfied by $w = w_1 + w_2$. The coefficients A_m, B_m, C_m, D_m must be determined so as to satisfy the last four boundary conditions. Using the conditions (25b) we obtain:

$$A_m = -\frac{4}{\pi^5 m^5}, \quad C_m = -D_m$$

By the conditions (25c) we find:

$$B_m = \frac{4}{\pi^5 m^5} \cdot \frac{(3+\nu)(1-\nu)\cosh^2 B_m + 2\nu\cosh B_m - \nu(1-\nu)B_m \sinh B_m - (1-\nu^2)}{(3+\nu)(1-\nu)\cosh^2 B_m + (1-\nu)^2 B_m^2 + (1+\nu)^2}$$

$$C_m = \frac{4}{\pi^5 m^5} \cdot \frac{(3+\nu)(1-\nu)\sinh B_m \cosh B_m + \nu(1+\nu)\sinh B_m - \nu(1-\nu)B_m \cosh B_m - (1-\nu)^2 B_m}{(3+\nu)(1-\nu)\cosh^2 B_m + (1-\nu)^2 B_m^2 + (1+\nu)^2} \quad \text{- - - -(26e)}$$

Substituting A_m, B_m, C_m and D_m in eq. (26d) we find the deflection. The maximum deflection occurs at the middle of the free edge.

A18. 14 Combined Bending and Tension or Compression of Thin Plates.

In developing the differential equations of equilibrium in previous pages, it was assumed that the plate is bent by transverse loads normal to the plate and the deflections were so small that the stretching of the middle plane can be neglected. If we consider now the case where only edge loads are active coplanar

with the middle surface (Fig. 9) we have a plane stress problem. If we assume that the stresses are uniformly distributed over the thickness and denote by N_x, N_y, N_{xy}, N_{yx} the resultant force of these stresses per unit length of linear element in the x and y-directions (Fig. 9) it is obvious that:

$$N_x = h\sigma_x \ , \ N_y = h\sigma_y$$
$$N_{xy} = N_{yx} = h\sigma_{xy} = h\sigma_{yx} \qquad \text{- - - - - - - - (27)}$$

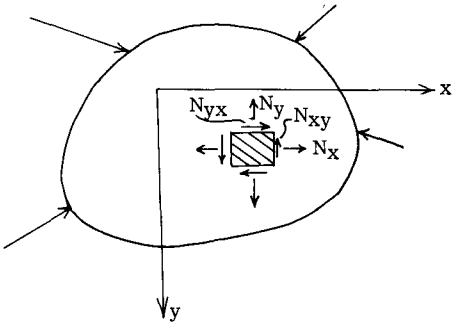

Fig. 9

The equations of equilibrium in the absence of body forces can be written now in terms of these generalized stresses N_x, N_y, N_{xy} by substituting from eq. (27) to the equations of equilibrium

$$\frac{\partial N_x}{\partial x} + \frac{\partial N_{xy}}{\partial y} = 0 \ , \ \frac{\partial N_y}{\partial y} + \frac{\partial N_{xy}}{\partial x} = 0 \qquad \text{- - - - - (28)}$$

On the other hand if the plate is loaded by transverse loads the stresses give rise to pure bending and twisting moments only. The equations of equilibrium for the latter have been given in before (see eqs. 6, 7, 8). If both transverse loads and coplanar edge loads are acting simultaneously, then for small vertical deflections the state of stress is the superposition of the stresses due to N_x, N_y, N_{xy} and M_x, M_y, M_{xy}. For large vertical deflection of the plate, however, there is interaction of the coplanar stresses and the deflections. These stresses give rise to additional bending moments due to the non-zero lever arm of the edge loads from the deflected middle surface, as in the case of beams. When the edge loads are compressive this additional moments might cause instability and failure of the plate due to excessive vertical deflections.

In this chapter the problem of instability of plates will be examined.

When the edge loads are compressive and give rise to additional bending moments eq. (8) must be modified.

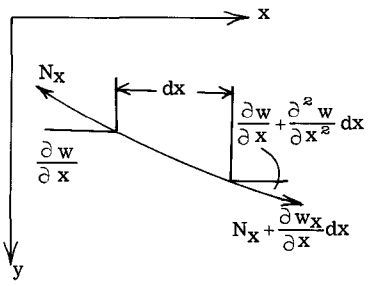

Fig. 10a

Consider an element of the middle surface dx, dy (Fig. 10a). The conditions of force equilibrium in the x, y-directions are given by eq. (28). Consider now the projection of the stresses N_x, N_y, N_{xy} in the z-direction:

(a) Projection of N_x: From Fig. 10a it follows that the resultant projection is:

$$- N_x \, \partial y \, \frac{\partial w}{\partial x} + (N_x + \frac{\partial w_x}{\partial x} dx)(\frac{\partial w}{\partial x} + \frac{\partial^2 w}{\partial x^2} dx)$$

and neglecting terms of higher order:

$$(N_x \frac{\partial^2 w}{\partial x^2} + \frac{\partial N_x}{\partial x} \cdot \frac{\partial w}{\partial x}) \qquad \text{- - - - - - - - - - - - (a)}$$

(b) Projection of N_y: By similar argument we find that this projection is equal to:

$$(N_y \frac{\partial^2 w}{\partial y^2} + \frac{\partial N_y}{\partial y} \frac{\partial w}{\partial y}) \qquad \text{- - - - - - - - - - - - (b)}$$

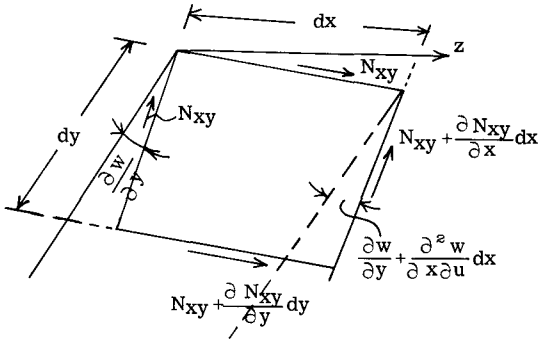

Fig. 10b

(c) Projection of N_{xy} and N_{yx}: From Fig. 10b we find:

$$- N_{xy} \frac{\partial w}{\partial y} + (N_{xy} + \frac{\partial N_{xy}}{\partial x} dx) \ (\frac{\partial w}{\partial y} + \frac{\partial^2 w}{\partial x \partial y} dx)$$

and neglecting terms of higher order:

$$(N_{xy} \frac{\partial^2 w}{\partial x \partial y} + \frac{\partial N_{xy}}{\partial x} \cdot \frac{\partial w}{\partial y}) \, dxdy \qquad \text{- - - - - - - - (c)}$$

Similarly we find the projection of $N_{yx} = N_{xy}$:

$$\left(N_{xy}\frac{\partial^2 w}{\partial x\partial y}+\frac{\partial N_{xy}}{\partial y}\cdot\frac{\partial w}{\partial x}\right)dxdy \quad -------- (d)$$

Thus in eq. (6a) the terms given by (a), (b), (c) and (d) should be added (divided of course by dxdy):

$$\frac{\partial Q_x}{\partial x}+\frac{\partial Q_y}{\partial y}+q+N_x\frac{\partial^2 w}{\partial x^2}+N_y\frac{\partial^2 w}{\partial y^2}+2N_{xy}\frac{\partial^2 w}{\partial x\partial y}+$$

$$\left(\frac{\partial N_x}{\partial x}+\frac{\partial N_{xy}}{\partial y}\right)\frac{\partial w}{\partial x}+\left(\frac{\partial N_y}{\partial y}+\frac{\partial N_{xy}}{\partial x}\right)\frac{\partial w}{\partial y}=0 \quad -- (e)$$

But due to the equation of equilibrium (28) the two terms inside the parentheses in (e) are zero. Thus:

$$\frac{\partial Q_x}{\partial x}+\frac{\partial Q_y}{\partial y}+q+N_x\frac{\partial^2 w}{\partial x^2}+$$

$$N_y\frac{\partial^2 w}{\partial y^2}+2N_{xy}\frac{\partial^2 w}{\partial x\partial y}=0 \quad --------(29)$$

Eq. (29) replaces eq. (6a) when edge loads are present. Eqs. (6b) and (6c) are, however, still valid since they express moment equilibrium of the element dxdy in which the contribution of N_x, N_y, N_{xy} is zero. Thus eliminating Q_x, Q_y between (6b), (6c) and (29) we find:

$$\nabla^4 w=\frac{\partial^4 w}{\partial x^4}+\frac{\partial^4 w}{\partial y^4}+2\frac{\partial^4 w}{\partial x^2\partial y^2}=$$

$$\frac{1}{D}\left(q+N_x\frac{\partial^2 w}{\partial x^2}+N_y\frac{\partial^2 w}{\partial y^2}+2N_{xy}\frac{\partial^2 w}{\partial x\partial y}\right) \quad ----(30)$$

Eq. (30) replaces eq. (128) when edge loads are present and the deflections are large so that instability might occur.

The distribution of the coplanar stresses N_x, N_y, N_{xy} can be found from eqs. (28) by solving the plane stress problem. In the following the above theory will be applied to rectangular plates.

A18.15 Strain Energy of Plates Due to Edge Compression and Bending.

The energy expression for pure bending, eq. (11), must be complemented to include the contribution of the edge coplanar loads. Assume that first the edge loads are applied. Obviously the strains due to the stresses N_x, N_y, N_{xy} are:

$$\varepsilon_x^\circ=\frac{1}{hE}(N_x-\nu N_y),\quad \varepsilon_y^\circ=\frac{1}{hE}(N_y-\nu N_x),$$

$$\gamma^\circ_{xy}=\frac{N_{xy}}{hG} \quad ----------(31)$$

The strain energy is:

$$V_{1N}=\frac{1}{2}\iint(N_x\varepsilon_x^\circ+N_y\varepsilon_y^\circ+N_{xy}\gamma^\circ_{xy})\,dxdy=$$

$$\frac{1}{2hE}\iint(N_x^2+N_y^2-2\nu N_xN_y+2(1+\nu)N_{xy}^2) \quad -- (a)$$

During bending due to transverse loads or/and due to buckling we assume that the edge loads and consequently N_x, N_y, N_{xy}, remain constant. Its variation is thus zero and we do not consider it in the following. Let us apply now the transverse load that produces bending. (We can also consider bending due to other transverse disturbance, which is the case of buckling). If u, v, are the displacements of the middle surface due to the coplanar loads (which are assumed constant across the thickness) and w the bending deflection of the plate it can be shown that the strains are:

$$\varepsilon_x=\frac{\partial u}{\partial x}+\frac{1}{2}\left(\frac{\partial w}{\partial x}\right)^2$$

$$\varepsilon_y=\frac{\partial v}{\partial y}+\frac{1}{2}\left(\frac{\partial w}{\partial y}\right)^2$$

$$\gamma_{xy}=\frac{\partial u}{\partial y}+\frac{\partial v}{\partial x}+\frac{\partial w}{\partial x}\cdot\frac{\partial w}{\partial y} \quad ------- (b)$$

Let us apply now bending with constant coplanar stresses. Due to stretching of the middle surface the energy is:

$$\iint(N_x\varepsilon_x+N_y\varepsilon_y+N_{xy}\gamma_{xy})\,dxdy \quad ---- (c)$$

Introducing (b) into (c) and adding the strain energy due to bending, eq. (11), we find the total change of strain energy due to bending which is:

$$V_1=\iint\left[N_x\frac{\partial u}{\partial x}+N_y\frac{\partial v}{\partial y}+N_{xy}\left(\frac{\partial u}{\partial y}+\frac{\partial v}{\partial x}\right)\right]dxdy+$$

$$\frac{1}{2}\iint\left[N_x\left(\frac{\partial w}{\partial x}\right)^2+N_y\left(\frac{\partial w}{\partial y}\right)^2+2N_{xy}\frac{\partial w}{\partial x}\cdot\frac{\partial w}{\partial y}\right]dxdy+$$

$$\frac{1}{2}D\iint\left(\frac{\partial^2 w}{\partial x^2}+\frac{\partial^2 w}{\partial y^2}\right)^2-$$

$$2(1-\nu)\left[\frac{\partial^2 w}{\partial x^2}\cdot\frac{\partial^2 w}{\partial y^2}-\left(\frac{\partial^2 w}{\partial x\partial y}\right)^2\right]dxdy \quad -- (d)$$

Here u, v are the additional coplanar displacements after bending has started. It can be shown by integrating by parts that the first integral is the work done during bending by the edge loads. For instance taking a rectangular plate this integral becomes:

$$\int_0^a\int_0^b\left[N_x\frac{\partial u}{\partial x}+N_y\frac{\partial v}{\partial y}+N_{xy}\left(\frac{\partial u}{\partial y}+\frac{\partial v}{\partial x}\right)\right]dxdy=$$

$$\int_0^b\left(\left|N_xu\right|_0^a+\left|N_{xy}v\right|_0^a\right)dy+\int_0^a\left(\left|N_yv\right|_0^b+\left|N_{xy}u\right|_0^b\right)dx-$$

$$\int_0^a\int_0^b\left\{u\left(\frac{\partial N_x}{\partial x}+\frac{\partial N_{xy}}{\partial y}\right)+v\left(\frac{\partial N_y}{\partial y}+\frac{\partial N_{xy}}{\partial x}\right)\right\}dxdy \quad -- (e)$$

Obviously the first two integrals represent the work done by the edge loads while the second integral is zero due to the equilibrium equations (28). Thus the work of the edge loads is:

$$W_N = \iint \left[N_x \frac{\partial u}{\partial x} + N_y \frac{\partial v}{\partial y} + N_{xy} \left(\frac{\partial u}{\partial y} + \frac{\partial v}{\partial x}\right)\right] dxdy \quad - - \quad (f)$$

We assume now that for small deflections the stretching of the middle surface of the plate is negligible. (This is the so-called inextensional theory of plates). In this case by zeroing the strains in eq. (b) and substituting in (f) we find:

$$W_N = -\frac{1}{2} \iint \left[N_x \left(\frac{\partial w}{\partial x}\right)^2 + N_y \left(\frac{\partial w}{\partial y}\right)^2 + 2N_{xy} \frac{\partial w}{\partial x} \cdot \frac{\partial w}{\partial y}\right] dxdy$$

- - - - - - - - - (32a)

In the strain energy expression, eq. (a) the first two terms cancel each other and the strain energy is due only to bending:

$$V_1 = \frac{1}{2} D \iint \left\{ \left(\frac{\partial^2 w}{\partial x^2} + \frac{\partial^2 w}{\partial y^2}\right)^2 - 2(1-\nu) \left[\frac{\partial^2 w}{\partial x^2} \cdot \frac{\partial^2 w}{\partial y^2} - \left(\frac{\partial^2 w}{\partial x \partial y}\right)^2 \right] \right\} dxdy \quad - - \quad (32b)$$

In the absence of transverse loads the work of external forces is simply due to the edge loads:

$$W = W_N \quad - - - - - - - - - - - - - - - - \quad (32c)$$

Expressions (32b) and (c) will be used in solving the buckling problem by means of the principle of virtual work.

A18.16 Buckling of Rectangular Plates with Various Edge Loads and Support Conditions.

General discussion

In calculating critical values of edge loads for which the flat form of equilibrium becomes unstable and the plate begins to buckle, the same methods and corresponding reasonings as for compressed bars will be employed.

The critical values can be obtained by assuming that the plate has a slight initial curvature or a small transverse load. These values of the edge loads for which the lateral deflection w becomes infinite are the critical values (see Part 1 for similar treatment in columns).

Another way of investigating such instability is to assume that the plate buckles due to a certain external disturbance and then to calculate the edge loads for which such a buckled configuration (deflections different from zero) is possible. It was found in the case of column that this latter solution (Euler's solution) approaches asymptotically the first at the limit where the deflections become extremely large but for even small deflections the edge load acquires a value very near the Euler's critical value. The latter technique is mathematically more convenient and it gives for plates also a very good estimate of their compressive strength. In the following we shall use this latter approach by assuming a plate with edge loads and no transverse load. Eq. (30) becomes in this case:

$$\frac{\partial^4 w}{\partial x^4} + 2 \frac{\partial^4 w}{\partial x^2 \partial y^2} + \frac{\partial^4 w}{\partial y^4} = \frac{1}{D} \left(N_x \frac{\partial^2 w}{\partial x^2} + N_y \frac{\partial^2 w}{\partial y^2} + 2N_{xy} \frac{\partial^2 w}{\partial x \partial y}\right)$$

- - - - - - - - - (33)

By solving eq. (33) we will find that the assumed buckling made is possible ($w \neq 0$) for certain definite values of the edge loads, the smallest of which determines the critical load. The energy method can also be used in investigating buckling problems. In this method we assume that the plate is initially under the plane stress conditions due to the edge loads and the stress distribution is assumed as known. We then consider the buckled state as a possible configuration of equilibrium. The change of the work is given by eq. (32a). We interpret here w as a virtual displacement though we do not use the variation symbol δ. Thus the increment of work δW is given by (32a) and the increment of strain energy δV_1 is given by eq. (32b). If $\delta W < \delta V_1$ for every possible shape of buckling the flat equilibrium is stable. If $\delta W > \delta V_1$ for a certain shape of buckling then the flat configuration is unstable and the plate will buckle under any load above the critical load. If $\delta W = \delta V_1$, the equilibrium is neutral and from this equation we find the critical load. The critical load therefore is found from the equation:

$$-\frac{1}{2} \iint \left[N_x \left(\frac{\partial w}{\partial x}\right)^2 + N_y \left(\frac{\partial w}{\partial y}\right)^2 + 2N_{xy} \frac{\partial w}{\partial x} \cdot \frac{\partial w}{\partial y} \right] dxdy =$$

$$\frac{D}{2} \iint \left\{ \left(\frac{\partial^2 w}{\partial x^2} + \frac{\partial^2 w}{\partial y^2}\right)^2 - 2(1-\nu) \left[\frac{\partial^2 w}{\partial x^2} \cdot \frac{\partial^2 w}{\partial y^2} - \left(\frac{\partial^2 w}{\partial x \partial y}\right)^2 \right] \right\} dxdy$$

- - - - - - - - - (34)

Here w is a certain assumed deflection which satisfies the boundary conditions (virtual deflection).

A18.17 Buckling of Simply Supported Rectangular Plates Uniformly Compressed in One Direction.

Let a plate of sides a and b (Fig. 11) simply supported around its periphery be compressed by load N_x uniformly distributed along the sides x = o and x = a. From the

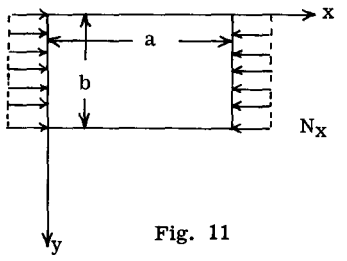

Fig. 11

obvious solution of the corresponding plane stress problem we find that the state of stress is everywhere a simple compression equal to N_x (the load at the periphery).

The deflection surface of a simply supported plate when bending takes place have been found previously (see eq. 14a). Its general expression can be written in a double series form:

$$W = \sum_{m=1}^{\infty} \sum_{n=1}^{\infty} C_{mn} \sin \frac{m\pi x}{a} \cdot \sin \frac{n\pi y}{b} \quad - - - \quad (35a)$$

The increment of strain energy found by substituting (35a) in the right-hand side of (34) is:

$$\delta V_1 = \frac{\pi^4 ab}{8} D \sum_{m=1}^{\infty} \sum_{n=1}^{\infty} C_{mn}^2 \left(\frac{m^2}{a^2} + \frac{n^2}{b^2}\right)^2 - - - \quad (35b)$$

The increment of work done by the external forces is found by substituting (35a) into the left-hand side of eq. (34) and N_x = const, $N_x = N_{xy} = 0$. Thus:

$$\delta W = \frac{1}{2} N_x \int_0^a \int_0^b \left(\frac{\partial w}{\partial x}\right)^2 dxdy =$$

$$\frac{\pi^2 b}{8a} N_x \sum_{m=1}^{\infty} \sum_{n=1}^{\infty} m^2 C_{mn}^2 \quad - - - - - - - \quad (35c)$$

From the equality $\delta W = \delta V_1$, solving for N_x, we obtain:

$$N_x = \frac{\pi^2 a^2 D \sum_{m=1}^{\infty} \sum_{n=1}^{\infty} C_{mn}^2 \left(\frac{m^2}{a^2} + \frac{n^2}{b^2}\right)^2}{\sum_{m=1}^{\infty} \sum_{n=1}^{\infty} m^2 C_{mn}^2} \quad - - - \quad (35d)$$

Here C_{mn} is arbitrary. We are interested, however, to find that values of C_{mn} which make N_x minimum. To that effect we use the following mathematical reasoning:

Imagine a series of fractions:

$$\frac{a}{b}, \frac{c}{d}, \frac{e}{f}, \ldots\ldots\ldots \quad - - - - - - - \quad (a)$$

If we add the numerators and the denominators we obtain the fraction:

$$\frac{a + c + e + \ldots\ldots\ldots}{b + d + f + \ldots\ldots\ldots} \quad - - - - - - - \quad (b)$$

This fraction has some intermediate value between the maximum and the minimum of the fractions (a). It follows that if we wish to make the fraction (b), which is similar to the fraction of eq. 35d, a minimum, we must take only one term in the numerator and the corresponding term in the denominator. Thus to make the fraction of eq. (35d) minimum, we must put all the parameters C_{11}, C_{12}, C_{21} .... except one, zero. This is equivalent to assuming that the buckling configuration is of simple sinusoidal form in both directions, i.e. $W_{mn} = C_{mn} \sin \frac{m\pi x}{a} \cdot \sin \frac{n\pi y}{b}$. The minimum expression for C_{mn} obtained by dropping all the terms except C_{mn} becomes:

$$N_x = \frac{\pi^2 a^2 D}{m^2} \left(\frac{m^2}{a^2} + \frac{n^2}{b^2}\right)^2 \quad - - - - - - - \quad (35e)$$

It is obvious that the smallest value of N_x is obtained by taking n = 1. This means that the plate buckles always in such a way that there can be several half-waves in the direction of compression but only are half-wave in the perpendicular direction. Thus for n = 1, eq. (35e) becomes:

$$(N_x)_{cr} = \frac{\pi^2 D}{a^2} \left(m + \frac{1}{m} \frac{a^2}{b^2}\right)^2 \quad - - - - - - \quad (36a)$$

The value of m (in other words the number of half-waves) which makes this critical value the smallest possible depends on the ratio a/b and can be found as follows:

Let us express (36a) in the form:

$$(N_x)_{cr} = k \frac{\pi^2 D}{b^2} \quad - - - - - - - - - - \quad (36b)$$

where k is a numerical factor depending on $\left(\frac{a}{b}\right)$. From (36a) and (36b) we have:

$$k = \frac{b^2}{a^2} \left(m + \frac{1}{m} \frac{a^2}{b^2}\right)^2 \quad - - - - - - - - - \quad (36c)$$

If we plot k against $\frac{a}{b}$ for various values of the integer m = 1, 2, 3, ... we obtain the curves of Fig. (12). From these curves the critical load factor k and the corresponding number of half-waves can readily be determined. It is only necessary to take the corresponding point $\left(\frac{a}{b}\right)$ as the axis of abcissas and to choose that curve which gives the smallest k. In Fig. 12 the portion of the various curves which give the critical values of k are shown by full lines. The transition from m to (m + 1) half-waves occurs at the intersection of the two corresponding lines. From eq. (36c) we find:

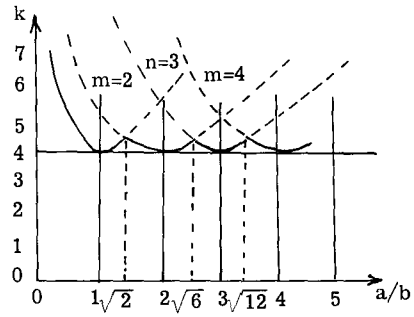

Fig. 12

$$\frac{mb}{a} + \frac{a}{mb} = \frac{(m+1)b}{a} + \frac{a}{(m+1)b} \qquad \text{or:}$$

$$\frac{a}{b} = \sqrt{m\,(m+1)} \qquad \text{- - - - - - - - - - - - (36d)}$$

Thus the transition from one to two half-waves occur for:

$$\frac{a}{b} = \sqrt{1\,(1+1)} = \sqrt{2}$$

from two to three for

$$\frac{a}{b} = \sqrt{2\,(2+1)} = \sqrt{6}$$

..... and so on.

The number of half-waves increases with the ratio a/b and for very long plates m is very large.

$$\frac{a}{b} \approx m$$

This means that a very long plate buckles in half-waves the lengths of which approach the width of the plate. The buckled plate is subdivided into squares.

The critical value of the compression stress is:

$$\sigma_{xv} = \frac{(N_x)_{cr}}{h} = \frac{k\pi^2 E}{12(1-\nu^2)} \cdot \frac{t^2}{b^2} \text{- - - - (36e)}$$

(t = thickness)

A18.18 Buckling of Simply Supported Rectangular Plate Compressed in Two Perpendicular Directions.

Let (Fig. 13) N_x, N_y the uniformly distributed edge compressions. Using the same as before expression for the deflections (eq. 35a) and applying the energy equation (33) with N_x, N_y = constants (which is the solution of the corresponding plane stress problem) we find:

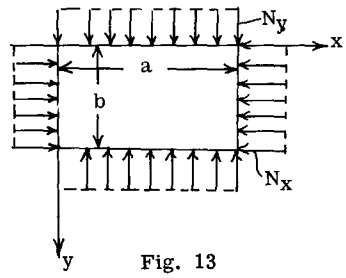

Fig. 13

$$N_x \frac{m^2\pi^2}{a^2} + N_y \frac{n^2\pi^2}{b^2} = D\left(\frac{m^2\pi^2}{a^2} + \frac{n^2\pi^2}{b^2}\right)^2 \text{ - (37a)}$$

and by introducing the parameter:

$$\sigma_e = \frac{\pi^2 D}{a^2 h} \qquad \text{- - - - - - - - - - - - - (37b)}$$

We obtain:

$$\sigma_x m^2 + \sigma_y n^2 \frac{a^2}{b^2} = \sigma_e \left(m^2 + n^2 \frac{a^2}{b^2}\right)^2 \text{ - - (37c)}$$

Taking any integer m and n the corresponding deflection surface of the buckled plate is given by:

$$W_{mn} = C_{mn} \sin\frac{m\pi x}{a} \cdot \sin\frac{n\pi y}{b} \text{ - - - - (38)}$$

and the corresponding σ_x, σ_y are given by (37c) which is a straight line in the diagram σ_y, σ_x (Fig. 14). By plotting such lines for various pairs of m and n we find the region of stability and the critical combination of σ_x, σ_y which is on the periphery of the polygon formed by the full lines of Fig. 14.

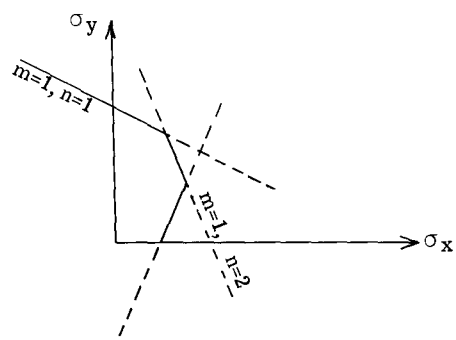

Fig. 14

A18.19 Buckling of Simply Supported Rectangular Plate Under Combined Bending and Compression.

Let us consider a simply supported rectangular plate (Fig. 15). Along the sides x = o, x = a there are linearly distributed edge loads given by the equation:

$$N_x = N_o\left(1 - \lambda\frac{y}{b}\right) \qquad \text{- - - - - - - - - - (39a)}$$

which is a combination of pure bending and pure compression. Let us take the deflection again in the form:

$$w = \sum_{m=1}^{\infty} \sum_{n=1}^{\infty} C_{mn} \sin \frac{m\pi x}{a} . \sin \frac{n\pi y}{b} \quad - - - \quad (39b)$$

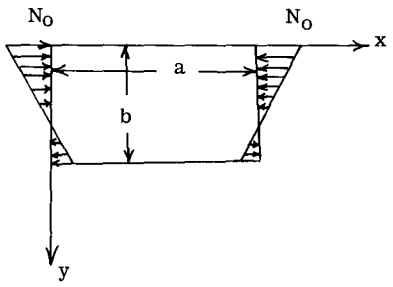

Fig. 15

Substituting in the right-hand side of eq. (34) we find the variation of strain energy:

$$\Delta V_i = D \frac{ab\pi^4}{8} \sum \sum C_{mn}^2 \left(\frac{m^2}{a^2}+\frac{n^2}{b^2}\right)^2 \quad - - - - - \quad (39c)$$

while the increment of work is:

$$\Delta W = \frac{1}{2} \int_0^a \int_0^b N_o \left(1-\lambda \frac{y}{b}\right) \left(\frac{\partial w}{\partial x}\right)^2 dxdy =$$

$$\frac{N_o}{4} \left\{ \frac{ab}{2} \sum \sum C_{mn}^2 \frac{m^2\pi^2}{a^2} - \frac{\lambda a}{b} \sum_{m=1}^{\infty} \frac{m^2\pi^2}{a^2} \right.$$

$$\left. \left[\frac{b}{4} \sum_{n=1}^{\infty} C_{mn}^2 - \frac{8b^2}{\pi^2} \sum_{n=1}^{\infty} \sum_{i=1}^{\infty} \frac{C_{mn}\, C_{mi}\, ni}{(n^2-i^2)^2} \right] \right\} \quad - - \quad (39d)$$

Equating (39c) and (39d) and solving for N_o we find:

$$(N_o)_{cr} = \frac{\pi^4 D \sum_{1}^{\infty} \sum_{1}^{\infty} C_{mn}^2 \left(\frac{m^2}{a^2}+\frac{n^2}{b^2}\right)^2}{\sum\sum_{1\,1}^{\infty\infty} C_{mn}^2 \frac{m^2\pi^2}{a^2} - \frac{\lambda}{2} \sum_{m=1}^{\infty} \frac{m^2\pi^2}{a^2} \left[\sum_{n=1}^{\infty} C_{mn}^2 - \frac{32}{\pi^2} \Sigma\Sigma \frac{C_{mn} \cdot C_{mi} ni}{(n^2-i^2)^2} \right]}$$

$$- - - - \quad (39e)$$

The coefficients now C_{mn} are so adjusted that $(N_o)_{cr}$ becomes minimum. By taking the derivative of expression (38e) with respect to each coefficient C_{mn} and equating these to zero we find:

$$DC_{mn}\pi^4 \left(\frac{m^2}{a^2}+\frac{n^2}{b^2}\right)^2 = (N_o)_{cr} \left\{ C_{mn} \frac{m^2\pi^2}{a^2} - \frac{\lambda}{2} \frac{m^2\pi^2}{a^2} \right.$$

$$\left. \left[C_{mn} - \frac{16}{\pi^2} \sum_{i}^{\infty} \frac{C_{mi}\, ni}{(n^2-i^2)^2} \right] \right\} \quad - - - - - - - \quad (39f)$$

We examine for each value of m the solutions of the system (38f). Starting from m = 1 and denoting:

$$\sigma_{cr} = \frac{(N_o)_{cr}}{h} \quad - - - - - - - - - - \quad (39g)$$

we obtain from (39f):

$$C_{ln} \left[\left(1 + n^2 \frac{a^2}{b^2}\right) - \sigma_{cr} \frac{a^2 h}{\pi^2 b} \left(1-\frac{\lambda}{2}\right) \right] -$$

$$8\lambda\sigma_{cr} \frac{a^2 h}{\pi^4 D} \sum_{i}^{\infty} \frac{C_{li}\, ni}{(n^2-j^2)^2} - - - - - - - - \quad (39h)$$

These are homogeneous equations in a_{11}, a_{12} ... etc. The system possesses a non-zero solution (which indicates the possibility of buckling of the plate) if the determinant of eq. (39h) is zero. From this condition an equation is obtained for σ_{cr}. Obviously the system (39h) is of infinite number of equations (n = 1, 2, 3 ...). A sufficient approximation is obtained by taking a large but finite number of terms and find the solution of the finite determinant (using for example digital computers). Thus a curve of σ_{cr} versus a/b is obtained for m = 1 like that of Fig. 12. Repeating the same calculation for m = 2, 3 ... etc., we find similar curves of two, three, etc. half-wave lengths. The regions of the curves with minimum ordinates define the region of stability as in Fig. (12).

A18. 20 Inelastic Buckling of Thin Sheets

The problem of the inelastic buckling of thin sheets has been extensively studied by various authors. The main difficulty in such studies is in reference to the stress-strain relations of plasticity under complex states of stress. Many controversial discussions have appeared in literature without resolving the theoretical difficulties. For this reason we will not develop the theory of inelastic buckling in this chapter. Some of the better references on this subject are listed below.

Chapter C4 presents the plasticity correction factors to use in calculating the inelastic buckling strength of thin sheets.

A18. 21 References.

(1) Bleich, F: Buckling Strength of Metal Structures. Book by McGraw-Hill.
(2) Stowell, E.Z., A Unified Theory of Plastic Buckling of Columns and Plates. NACA Report 898, 1948.
(3) Gerard and Becker: Handbook of Structural Stability. NACA T.N. 3781, 1957.
(4) Gerard: Introduction to Structural Stability Theory. Book by McGraw-Hill Co., 1962.

BOEING
747

PART 3
STRENGTH OF COLUMNS WITH STABLE CROSS-SECTIONS

(BY PROFESSOR E. F. BRUHN)

A18.22 Methods of Column Failure. Column Equations.

In Part 1, the theory of the elastic and inelastic instability of the column was presented. The equations from Part 1 for a pin end support condition are:-

For elastic primary failure,

$$F_c = \frac{\pi^2 E}{(L/\rho)^2} \quad \text{- - - - - - - - - - - - - (1)}$$

For inelastic primary failure,

$$F_c = \frac{\pi^2 E_t}{(L/\rho)^2} \quad \text{- - - - - - - - - - - - - (2)}$$

Where F_c = compressive unit stress at failure = P/A stress.

E = Young's modulus

E_t = tangent modulus

L = column length

ρ = radius of gyration of cross-section

Fig. 16 shows a typical plot of F_c versus L/ρ. If the column dimensions are such as to cause it to fail in range CD in Fig. 16, the primary failure is due to elastic instability and equation (1) holds. This range of L/ρ values is often referred to by engineers as the long column range.

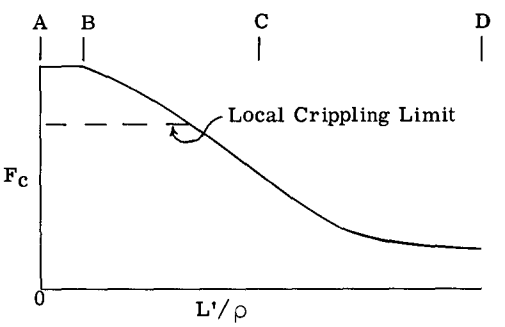

Fig. 16

The range BC represents the range of L/ρ values where failure is due to inelastic instability of the column as a whole and equation (2) applies. This range BC is often referred to as the short column range.

The range AB in Fig. 16 is for a range of L/ρ values of below 20 to 25, and represents a range where failure is due to plastic crushing of the column. In other words, the column is too short to buckle or bow under end load but crushes under the high stresses. This column range of stresses is usually referred to as the block compression strength.

A column, however, may fail by local buckling or crippling due to distortion of the column cross-section in its own plane. The horizontal dashed line in Fig. 16 represents the condition where the primary column strength is limited by the local weakness. This line moves up or down according to the value of the local weakness. The determination of the column strength when failure is due to local weakness is covered in volume 2.

A18.23 Column End Restraint. Fixity Coefficients. Column Effective Length.

The column strength is influenced by the end support restraint against rotation and by any lateral supports between the column ends. The letter c is commonly used to indicate the end fixity coefficient, and C = 1.0 for zero end restraint against rotation, which can be produced mechanically by a pin or ball and socket end support fitting. Thus including the end restraint effect equations (1) and (2) can be written,

$$F_c = \frac{c\pi^2 E}{(L/\rho)^2}, \quad F_c = \frac{c\pi^2 E_t}{(L/\rho)^2} \quad \text{- - - - - (3)}$$

Let L' = effective length of the column which equals the length between inflection points of the deflected column under load.

Then $L' = L/\sqrt{c}$ - - - - - - - - - - - (4)

Thus equation (3) can be written as,

$$F_c = \frac{\pi^2 E}{(L'/\rho)^2}, \quad F_c = \frac{\pi^2 E_t}{(L'/\rho)^2} \quad \text{- - - (5)}$$

If we let P = failing or critical load, equation (5) can be written as equation (6) by realizing that $P = F_c A$ and $\rho = \sqrt{I/A}$.

$$P = \frac{\pi^2 E I}{(L')^2}, \quad P = \frac{\pi^2 E_t I}{(L')^2} \quad \text{- - - - - - (6)}$$

Fig. 17 shows the deflected column curve under the load P for various end and lateral support conditions. The effective lengths L' and the end fixity coefficients are also listed.

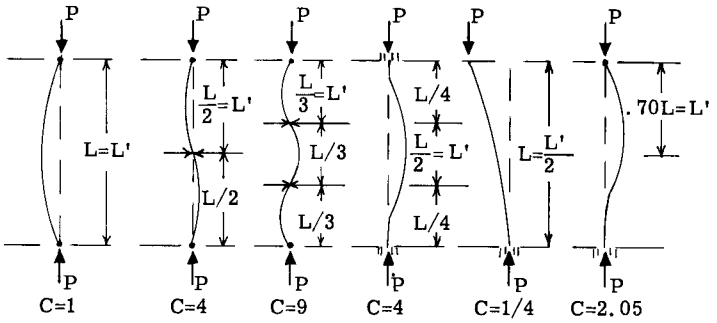

Fig. 17

A18.24 Design Column Curves for Various Materials.

For routine design purposes it is convenient to have column curves of allowable failing column stress F_c versus the effective slenderness ratio L'/ρ. In equation (5) we will assume values of F_c, then find the tangent modulus E_t corresponding to this stress and then solve for the term L'/ρ. Table A18.1 shows the calculations for 17.7 PH (TH1050) stainless steel sheet at room temperature. The results are then plotted in Fig. 18 to give the column strength curve. Similar data was calculated for the material under certain exposure time to different elevated temperatures and the results are also plotted in Fig. 18. Figs. 19 to 22 give column curves for other materials under various temperature conditions.

A18.25 Selection of Materials for Elevated Temperature Conditions.

Light weight is an important requirement in aerospace structural design. For columns that fail in the inelastic range of stresses, a comparison of the F_{cy}/w ratio of materials gives a fairly good picture of the efficiency of compression members when subjected to elevated temperature conditions. In this ratio F_{cy} is the yield stress at the particular temperature and w is the weight per cu. inch of the material. Fig. 23 shows a plot of F_{cy}/w for temperature ranges up to 600° F. with 1/2 hour time exposure for several important aerospace materials.

A18.26 Example Problem.

PROBLEM

Fig. 24 shows a forged (I) section member 30 inches long, which is to be used as

TABLE A18.1

17-7 PH(TH1050) Stainless Steel Sheet
F_{tu} = 180,000
F_{cy} = 162,000
E = 29 x 10^6

F_c	E_t*	$L'/\rho = \pi\sqrt{E_t/F_c}$
20,000	29 x 10^6	119.56
30,000	29 x 10^6	97.62
40,000	29 x 10^6	84.54
50,000	29 x 10^6	75.62
60,000	29 x 10^6	69.03
70,000	29 x 10^6	63.91
80,000	29 x 10^6	59.78
89,600	29 x 10^6	56.49
96,000	27.55 x 10^6	53.19
102,000	26.10 x 10^6	50.22
107,400	24.65 x 10^6	47.57
112,200	23.20 x 10^6	45.15
117,000	21.75 x 10^6	42.81
121,500	20.30 x 10^6	40.58
125,800	18.85 x 10^6	38.43
130,000	17.40 x 10^6	36.32
134,000	15.95 x 10^6	34.25
137,700	14.50 x 10^6	32.22
147,000	11.60 x 10^6	27.89
158,100	8.70 x 10^6	23.29
167,600	5.80 x 10^6	18.47
173,800	2.90 x 10^6	12.82

*Values of E_t calculated from stress-strain diagram for this material.

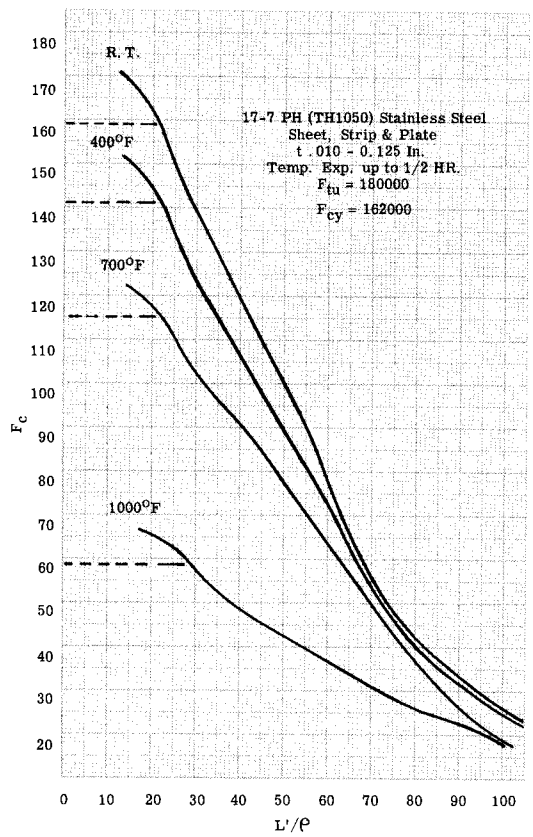

Fig. 18

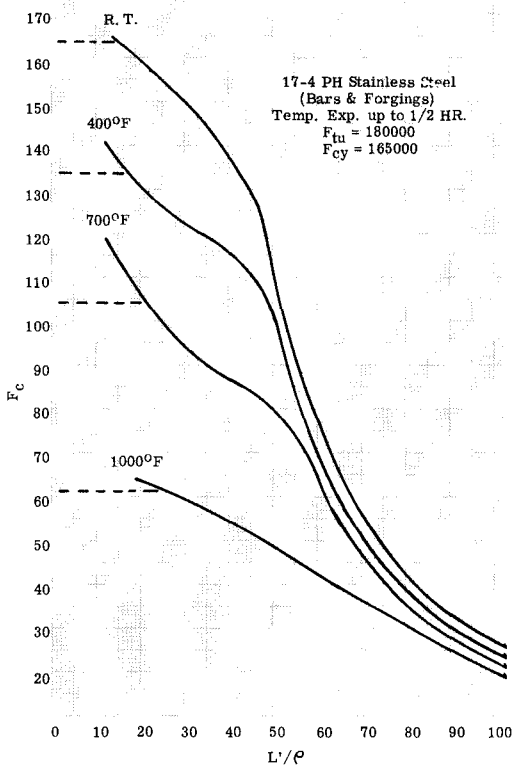

Fig. 19

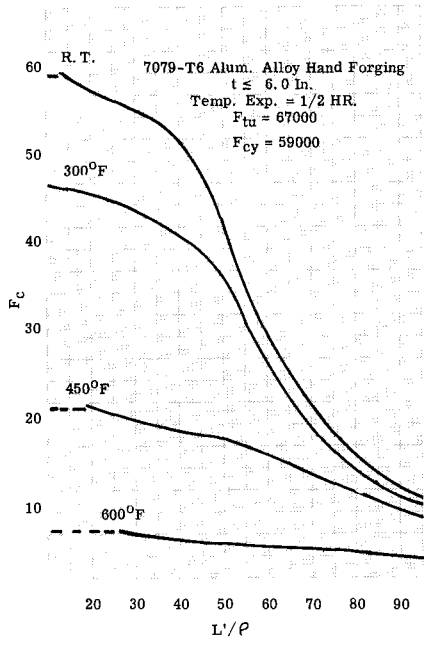

Fig. 20

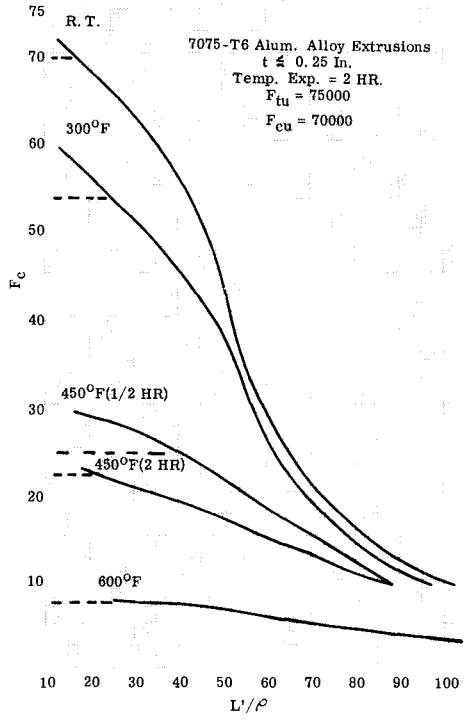

Fig. 21

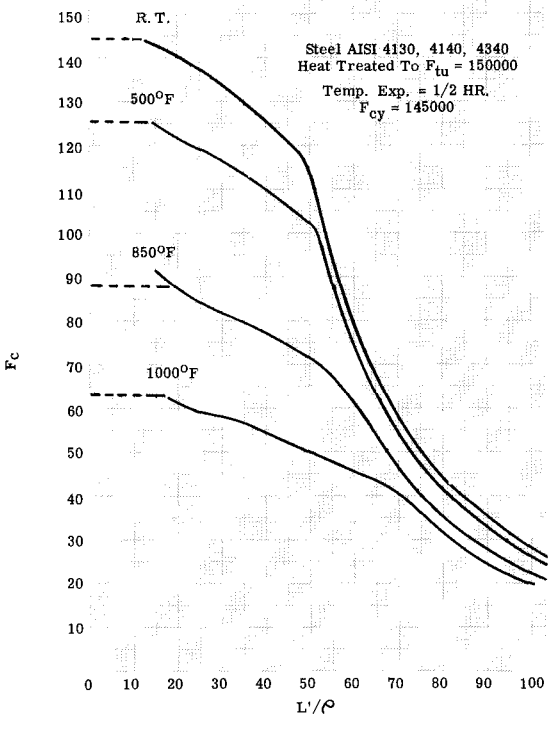

Fig. 22

Values of F_c in KSI. The horizontal dashed line is the compressive yield stress. Values above these cut-off lines should be substantiated by tests.

Fig. 23

(1) AISI Steel, $F_{tu} = 180,000$

(2) 17-7PH. Stainless Steel, $F_{tu} = 210,000$

(3) 7075-76 Alum. Alloy

(4) AZ31B Magnesium Alloy

(5) 6AL-4V Titanium Alloy

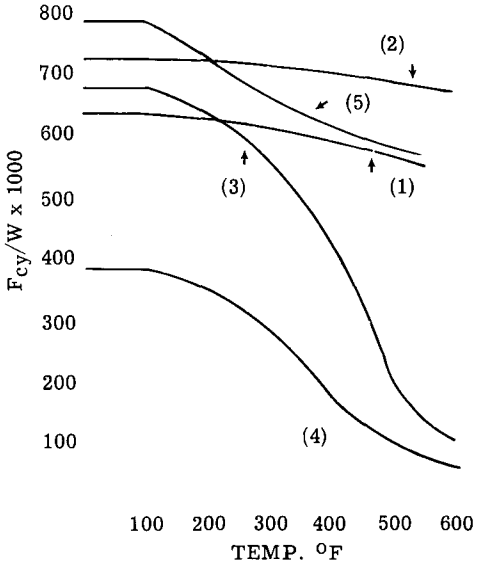

a compression member. Find the ultimate strength of the member if made from the following materials and subjected to the given temperature and time conditions.

Case 1. Material 7079-T6 Alum. Alloy hand forging and room temperature.

Case 2. Same as Case 1, but subjected 1/2 hour to a temperature of 300°F.

Case 3. Same as Case 2, but for 600°F.

Case 4. Material 17-4 PH stainless steel, hand forging at room temperature.

Fig. 24

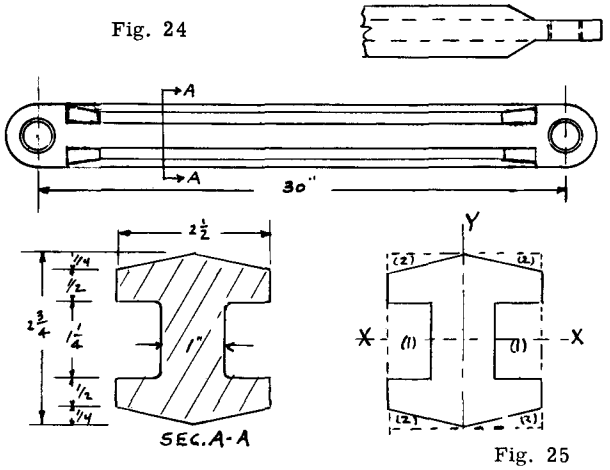

Fig. 25

Solution:

Since the column may fail by bending about either the X or Y axes, the column strength for bending about each of these axes will be calculated. Since the column strength is a function of the radius of gyration of the cross-section, the first step in the solution will be the calculation of I_x and I_y, from which ρ_x and ρ_y can be found.

Calculating I_x: In Fig. 25 the section will be first considered a solid rectangle 2.5 x 2.75 and then the properties of portions (1) and (2) will be subtracted.

$$I_x \text{ (rectangle)} = \frac{1}{12} \times 2.5 \times 2.75^3 = 4.32$$

Portions (1) and (2)

$$I_x = -\frac{1}{12} \times 1.5 \times 1.25^3 - 4(.625 \times .25 \times 1.292^2) = -1.29$$

(I_o of (2) about its x centroidal axis is negligible)

$$I_x = 4.32 - 1.29 = 3.03 \text{ in.}^4$$

$$\rho_x = \sqrt{\frac{I_x}{A}}, \text{ Area } A = 2.5 \times 2.75 - 2 \times .75 \times 1.25 - 4 \times .25 \times .625) = 4.375 \text{ sq. in.}$$

$$\rho_x = \sqrt{3.03/4.375} = .83 \text{ in.}$$

Calculation of I_y:

$$I_y \text{ (solid)} = \frac{1}{12} \times 2.75 \times 2.5^3 = 3.58$$

$$\text{Portion (1)} = -(1.25 \times .75 \times .875^2)2 - (1.25 \times .75^3/12)2 = -1.52$$

$$\text{Portion (2)} = -(.25 \times .625 \times .833^2)4 - 4(.25 \times 1.25^3/36) = -.488$$

$$I_y = 3.58 - 1.52 - .488 = 1.58 \text{ in.}^4$$

$$\rho_y = \sqrt{1.58/4.375} = .60"$$

Column strength is considerably influenced by the end restraint conditions. For failure by bending about the x-x axis, the end restraint against rotation is zero as the single fitting bolt has an axis parallel to the x-x axis and thus c the fixity coefficient is 1. For failure by bending about the y-y axis we have end restraint which will depend on the rigidity of the bolt and the adjacent fitting and structure. For this example problem, this restraint will be such as to make the end fixity coefficient c = 1.5.

For failure about x-x axis,

$$L' = L/\sqrt{c} = 30/\sqrt{1} = 30, \quad L'/\rho_x = 30/.83 = 36$$

For failure about y-y axis,

$$L' = 30/\sqrt{1.5} = 24.6, \quad L'/\rho_y = 24.6/.60 = 41$$

Therefore failure is critical for bending about y-y axis, with $L'/\rho = 41$.

Case 1. The material is 7079-T6 Alum. Alloy hand forging. Fig. 20 gives the failing stress F_c for this material plotted against the L'/ρ ratio. Thus using $L'/\rho = 41$ and the room temperature curve, we read $F_c = 50500$ psi. Thus the failing load if $P = F_cA = 50500 \times 4.375 = 220{,}000$ lbs.

Case 2. Using the 300°F curve in Fig. 20 for the same L'/ρ value, we read $F_c = 40{,}400$, and thus $P = 40{,}400 \times 4.375 = 177{,}000$.

Case 3. Using the 600°F curve, F_c reads 6100 and thus $P = 6100 \times 4.375 = 26700$ lbs. Thus subjecting this member to a temperature of 600°F for 1/2 hour reduces its strength from 220,000 to 26,700 lbs., which means that Alum. Alloy is a poor material for carrying loads under such temperatures since the reduction in strength is quite large.

Case 4. Material 17-4 PH stainless steel forging. Fig. 19 gives the column curves for this material. For $L'/\rho = 41$ and using the room temperature curve we read $F_c = 135{,}200$ and thus $P = 135{,}200 \times 4.375 = 591{,}000$ lbs.

A18.27 Comprehensive Treatment of Column Strength.

Columns with stable cross-sections fail as described in Art. A18.22. However, compression members having open sections such as angle, channel and zee shapes, often fail by twisting or by local buckling or crippling of one or more of the elements that make up the shape of the cross-section. Furthermore, the end fixity condition influences the column strength and these end conditions depend on the type of end fitting or connection to the adjacent structure. Furthermore, to save weight columns are often tapered in cross-section, that is, a variable moment of inertia along the column length, these equations (1) and (2) which assure constant moment of inertia do not apply. Since elevated temperature conditions effect the strength of a material, the column strength of a structural member is likewise influenced. (See Figs. 26, 27, 28).

Since this Volume 1 is concerned primarily with stress and strain analysis of structure, the subject of column strength is only slightly considered or presented. However, Volume 2, which deals primarily with materials and strength analysis and design of structure, presents a very complete and broad coverage of column design, involving over 180 pages of theory, design charts and many sample design problems.

A18.28 Some Mechanical and Physical Properties of a Few Typical Aircraft Materials.

In order to determine the true deflections or distortions of structures under a given load system, the values of the stiffness properties of the material used in the structure must be known. Chapters A7 and A8 involve the deflections of structures, thus the value of (E), modulus of elasticity and (G), modulus of rigidity must be known if true deflections are to be wanted. Table A18.2 gives these stiffness values for a few common aircraft structural materials and also several other strength properties.

When a material is subjected to elevated temperatures for various periods of time, the strength and stiffness properties are considerably influenced as illustrated in Figs. 26 to 28, which have been taken from Volume 2.

For a comprehensive treatment of the behavior of aircraft materials and their mechanical and physical properties, the reader is referred to Chapter B1 and B2 of Volume 2, where over 50 pages are devoted to this important subject.

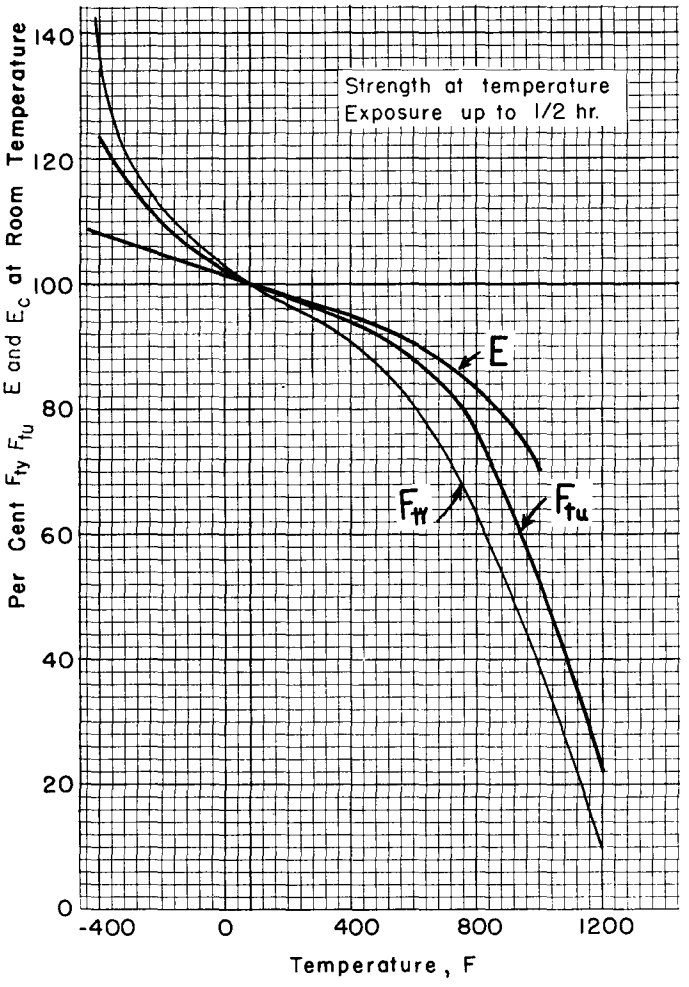

Fig. 26. Effect of Temperature on F_{tu}, F_{ty} and E of AISI alloy steel

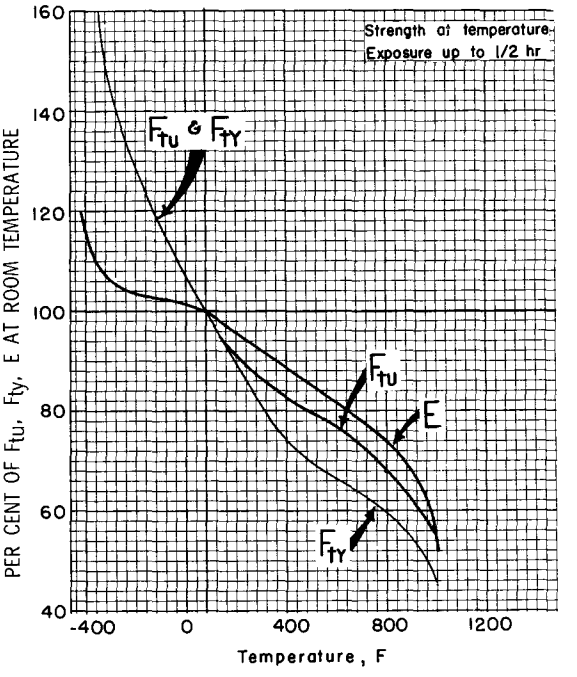

Fig. 27. Effect of temperature on F_{tu}, F_{ty} and E of 6Al-4V annealed titanium alloy (sheet and bar)

TABLE A18.2

Material	Symbol	Form	F_{tu} KSI	F_{ty} KSI	E psi/10^6	E_c psi/10^6	G psi/10^6	W lbs./ Cu. in.
AISI Alloy Steel	4140	Sheet-Tube	95	75	29.0	29.0	11.0	0.283
AISI Steel - Heat Tr.	4130	Sheet-Tube	180	163	29.0	29.0	11.0	0.283
Stainless Steel	17-7PH	Sheet	180	150	29.0	30.0	11.0	0.276
Aluminum Alloy	2024	Sheet-Tube	62	40	10.9	10.7	4.0	0.100
Aluminum Alloy	7075	Extrusion	78	70	10.3	10.5	4.9	0.101
Magnesium Alloy	AZ31B	Sheet	32	15	6.5	6.5	2.4	0.064
Titanium Alloy	6A1-4V	Sheet	130	120	16.0	16.4	6.2	0.160
Inconel Steel	X	Sheet	155	100	31.0	31.0	--	0.304

F_{tu} = Ultimate Tensil Str. F_{ty} = Yield Tensile Str.
E = Modulus of Elasticity. G = Modulus of Rigidity.

EFFECT OF TEMPERATURE ON 7075 ALUMINUM ALLOYS

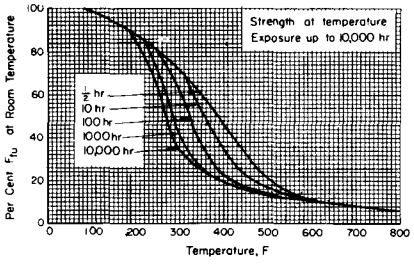

*Effect of temperature on the ultimate tensile strength (F_{tu}) of 7075-T6 aluminum alloy (all products).

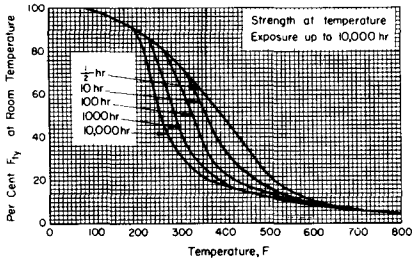

Effect of temperature on the tensile yield strength (F_{ty}) of 7075-T6 aluminum alloy (all products).

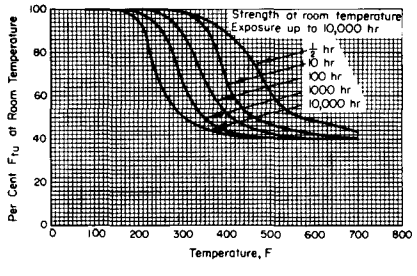

Effect of exposure at elevated temperatures on the room-temperature ultimate tensile strength (F_{tu}) of 7075-T6 aluminum alloy (all products).

Fig. 28

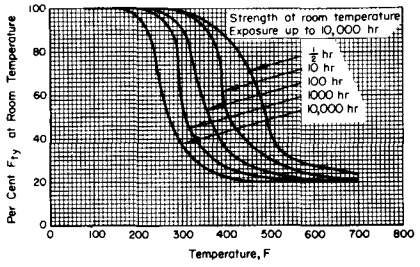

Effect of exposure at elevated temperatures on the room-temperature tensile yield strength (F_{ty}) of 7075-T6 aluminum alloy (all products).

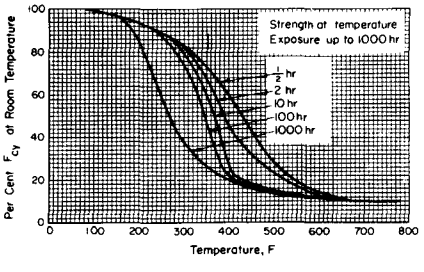

Effect of temperature on the compressive yield strength (F_{cy}) of 7075-T6 aluminum alloy (all products).

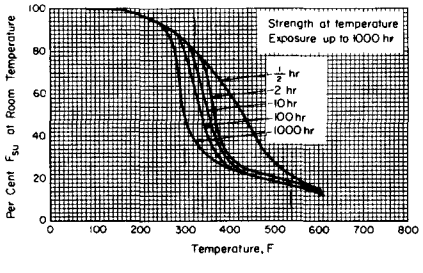

Effect of temperature on the ultimate shear strength (F_{su}) of 7075-T6 aluminum alloy (all products).

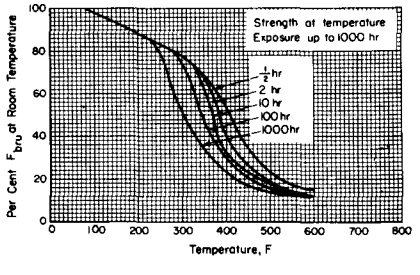

Effect of temperature on the ultimate bearing strength (F_{bru}) of 7075-T6 aluminum alloy (all products).

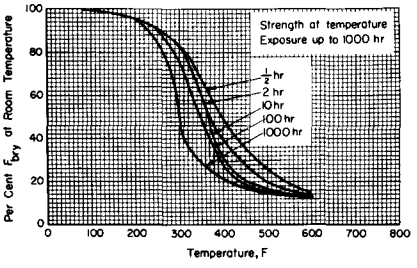

Effect of temperature on the bearing yield strength (F_{bry}) of 7075-T6 aluminum alloy (all products).

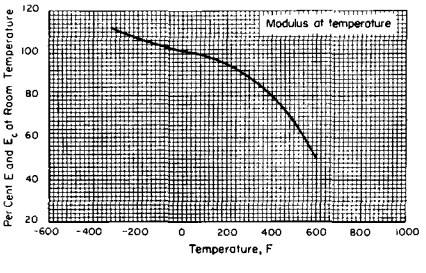

Effect of temperature on the tensile and compressive modulus (E and E_c) of 7075-T6 aluminum alloy.

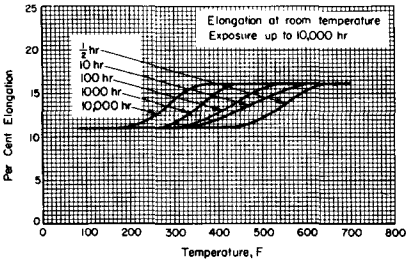

Effect of exposure at elevated temperatures on the elongation of 7075-T6 aluminum alloy (all products except thick extrusions).

CHAPTER A19
INTRODUCTION TO WING STRESS ANALYSIS

A19.1 Typical Wing Structural Arrangement

For aerodynamic reasons, the wing cross-section must have a streamlined shape commonly referred to as an airfoil section. The aerodynamic forces in flight change in magnitude, direction and location. Likewise in the various landing operations the loads change in magnitude, direction and location, thus the required structure must be one that can efficiently resist loads causing combined tension, compression, bending and torsion. To provide torsional resistance, a portion of the airfoil surface can be covered with a metal skin and then adding one or more internal metal webs to produce a single closed cell or a multiple cell wing cross-section. The external skin surface which is relatively thin for subsonic aircraft is efficient for resisting torsional shear stresses and tension, but quite inefficient in resisting compressive stresses due to bending of wing. To provide strength efficiency, spanwise stiffening units commonly referred to as flange stringers are attached to the inside of the surface skin. To hold the skin surface to airfoil shape and to provide a medium for transferring surface air pressures to the cellular beam structure, chordwise formers and ribs are added. To transfer large concentrated loads into the cellular beam structure, heavy ribs, commonly referred to as bulkheads, are used.

Figs. A19.1 and A19.2 illustrate typical structural arrangements of wing cross-sections for subsonic aircraft. The surface skin is relatively thin. In general the wing structural flange arrangement can be classified into two types; (1) the concentrated flange type where flange material is connected directly to internal webs and (2) the distributed flange type where stringers are attached to skin between internal webs.

Fig. A9.3 shows several structural arrangements for wing cross-sections for supersonic aircraft. Supersonic airfoil shapes are relatively thin compared to subsonic aircraft.

Fig. a

Fig. b

Fig. c

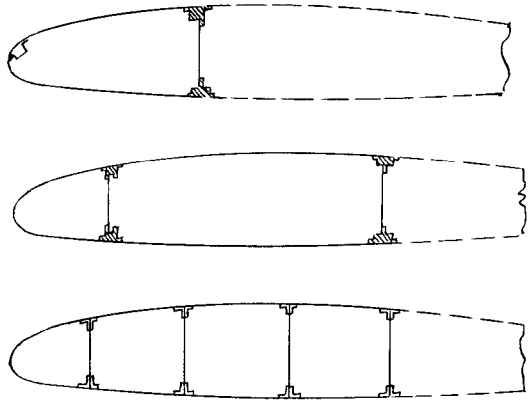

Fig. A19.1

Concentrated Flange Type of Wing Beam.

Dashed line represents secondary structure. In many cases this portion is fabric covered.

Distributed Flange Type of Wing Beam.

Fig. d

Fig. e

Fig. f

Fig. g

Fig. h

Fig. i

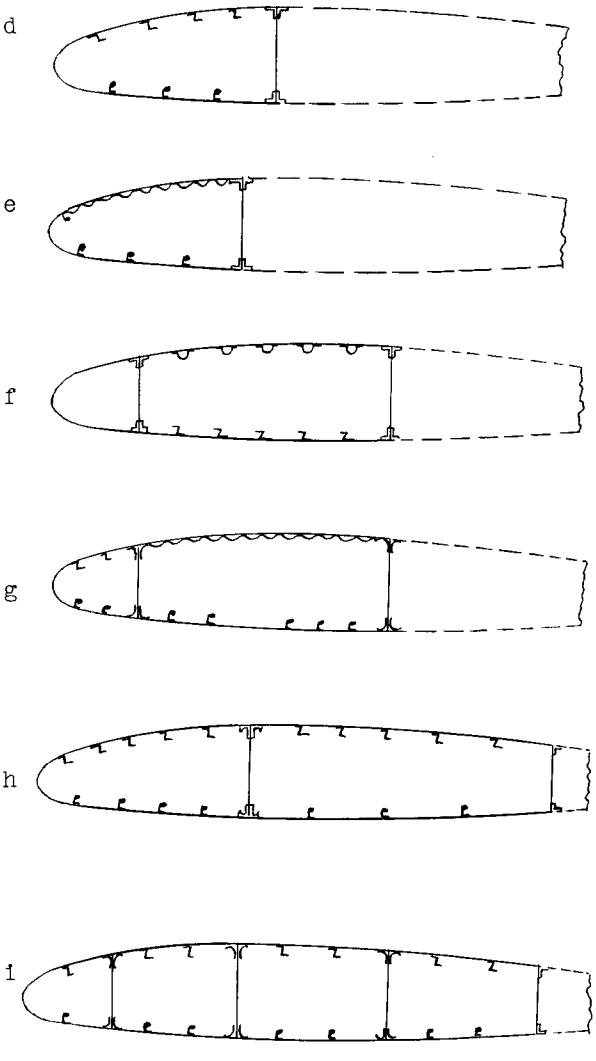

Fig. A19.2 Common Types of Wing Beam Flange Arrangement.

To withstand the high surface pressures and to obtain sufficient strength much thicker wing skins are usually necessary. Modern milling machines permit tapering of skin thicknesses. To obtain more flange material integral flange units are machined on the thick skin as illustrated in Fig. k.

Fig. j

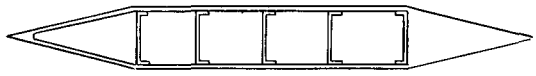

Fig. k

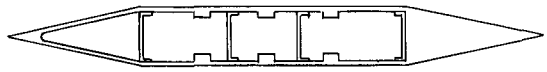

Fig. l

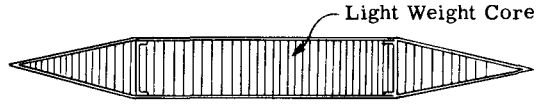

Fig. A19.3 Wing Sections - Supersonic Aircraft

In a cantilever wing, the wing bending moments decrease rapidly spanwise from the maximum values at the fuselage support points. Thus thick skin construction must be rapidly tapered to thin skin for weight efficiency, but thinner skin decreases allowable compressive stresses. To promote better efficiency sandwich construction can be used in outer portion of wing (Fig. l). A light weight sandwich core is glued to thin skin and thus the thin skin is capable of resisting high compressive stresses since the core prevents sheet from buckling.

A19.2 Some Factors Which Influence Wing Structural Arrangements

(1) Light Weight:

The structural designer always strives for the minimum weight which is practical from a production and cost standpoint. The higher the ultimate allowable stresses, the lighter the structures. The concentrated flange type of wing structures as illustrated Fig. (a, b and c) of Fig. A19.1 permits high allowable compressive flange stresses since the flange members are stabilized by both web and covering sheet, thus eliminating column action, which permits design stresses approaching the crippling stress of the flange members. Since the flange members are few in number, the size or thickness required is relatively large, thus giving a high crippling stress. On the other hand, this type of design does not develop the effectiveness of the metal covering on the compressive side, which must be balanced against the saving in the weight of the flange members.

In the distributed type of flange arrangement (Fig. A19.2), a portion of the covering on the compression side is made effective since it is attached to closely spaced stringers or corrugations. However, the flange stringers between cell webs are supported only at rib or bulkhead points and thus suffer column action normal to the cell covering. This factor reduces the flange allowable compressive stresses since it is not practical to space wing ribs less than 12 to 18 times the flange stringer depth. Thus, if there were no other controlling factors, one could easily make calculations to determine which of the above would prove lightest. In general, if the torsional forces on the wing are small, thus requiring only a thin covering, the concentrated flange type of wing structure should prove the lightest.

In general, the flange material should be placed to give the largest moment of inertia in the Z direction, which means in general that the flange material should be placed between the 15 and 50 per cent of wing chord from the leading edge.

The secondary or distributing structure aft of the structural box beam should be made as light as possible and thus in general the farther forward the rear closing web of the box beam, the lighter the wing structure as a whole.

In the layout of the main spanwise flange members bends or changes in direction should be avoided as added weight is required in splicing or in transverse stiffeners which are necessary to change the direction of the load in the flange members. If flange members must be spliced, care should be taken not to splice them in the region of a maximum cross-section. Furthermore, in general, the smaller the number of fittings, the lighter the structure.

(2) Wing-Fuselage Attachment:

If the airplane is of the low wing or the high wing type, the entire wing structure can continue in the way of the airplane body. However, in the mid-wing type or semi-low wing type, limitations may prevent extending the entire wing through the fuselage, and some of the shear webs as well as the wing covering must be terminated at the side of the fuselage. If a distributed flange type of cell structure were used, the axial load in the flange stringers would have to be transferred to the members extending through the fuselage. To provide for this transfer of large loads requires structural weight and thus a concentrated flange type of box structure might prove the best type of structure.

(3) Cut-outs in Wing Surface:

The ideal arrangement where continuity of structure is maintained over the entire surface

of the structural box is seldom obtained in actual airplane design due to cut-outs in the wing surface for such items as retractable landing gears, mail compartments and bomb and gun bays. If the distributed flange type of box beam is used, they are interrupted at each cut-out, which requires that means must be provided for drifting the flange loads around the opening, an arrangement which adds weight because conservative overlapping assumptions are usually made in the stress analysis. The additional structure and riveting to provide for the transfer of flange load around large openings adds considerably to the production cost.

For landing gears as well as many other installations, the wing cut-outs are confined to the lower surface, thus a structural arrangement as illustrated in Fig. A19.4 is quite common. The upper surface is of the distributed flange type whereas the lower flange material is concentrated at the two lower corners of the box. In the normal flying conditions, the lower surface is in tension and thus cell sheet covering between the cut-outs is equally effective in bending if shear lag influence is discounted. For negative accelerated flying conditions, the lower surface is in compression thus sheet covering between corner flanges would be ineffective in bending. However, since the load factors in these flight conditions are approximately one half the normal flight load factors, this ineffectiveness of the lower sheet in bending is usually not critical.

Cut-outs likewise destroy the continuity of intermediate interior shear webs of such sections as illustrated in Figs. (c and i), and the shear load in these interrupted webs must be transferred around the opening by special bulkheads on each side of the cut-out, which means extra weight.

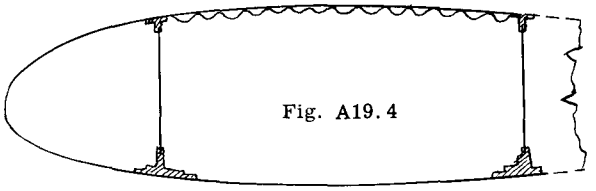

Fig. A19.4

In many cases, cut-outs in the leading edge are necessary due to power plant installations, landing gear wells, etc. Furthermore, in many airplanes, it is desirable to make the leading edge portion removable for inspection of the many installations which occupy this space in the portion of the wing near the fuselage. If such is the case, then an interior web should be located near the front of the wing section.

Inspection doors for the central portion of the box beam structure are usually located on the lower side of the wing. They are usually fastened to two spanwise stringers with screws and the removable panels are effective in resisting bending and shear load. (See Fig.A19.5)

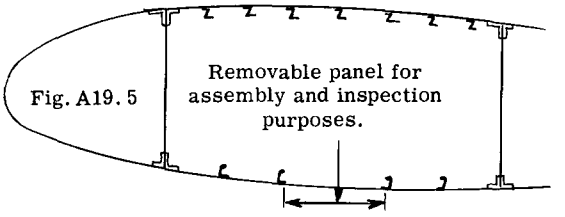

Fig. A19.5

Cutouts in the wing structural box destroys the continuity of the torsional resistance of the cell and thus special consideration must be given to carrying torsional forces around the cut-out. This special problem is discussed later.

(4) Folding-Wings:

For certain airplanes, particularly Carrier based Naval airplanes, it is necessary that provision be made to fold the outer wing panels upward. This dictates definite hinge points between the outer and center wing panels. If a distributed flange type of structure is used, the flange forces must be gathered and transferred to the fitting points, thus a compromise solution consisting of a small number of spanwise members is common practice.

(5) Wing Flutter Prevention:

With the high speeds now obtained by modern airplanes, careful attention to wing flutter prevention must be given in the structural layout and design of the wing. In general, the critical flutter speed depends to a great extent on the torsional rigidity of the wing. When the mass center of gravity moves aft of the 25 per cent of chord point, the critical flutter speed decreases, thus it is important to keep weight of the wing forward. At high speeds where "compressibility" effects become important, the torsional forces on the wing are increased, which necessitates extra skin thickness or a larger cell. Designing for flutter prevention is a highly specialized problem.

(6) Ease and Cost of Production:

The airplane industry is a mass production industry and therefore the structural layout of the wing must take into account production methods. The general tendency at this time is to design the wing and body structure, so that sub-assemblies of the various parts can be made, which are finally brought together to form the final assembly of the wing panel. To make this process efficient requires careful consideration in the details and layout of the wing structure. Photograph A19.6 illustrates the sub-assembly

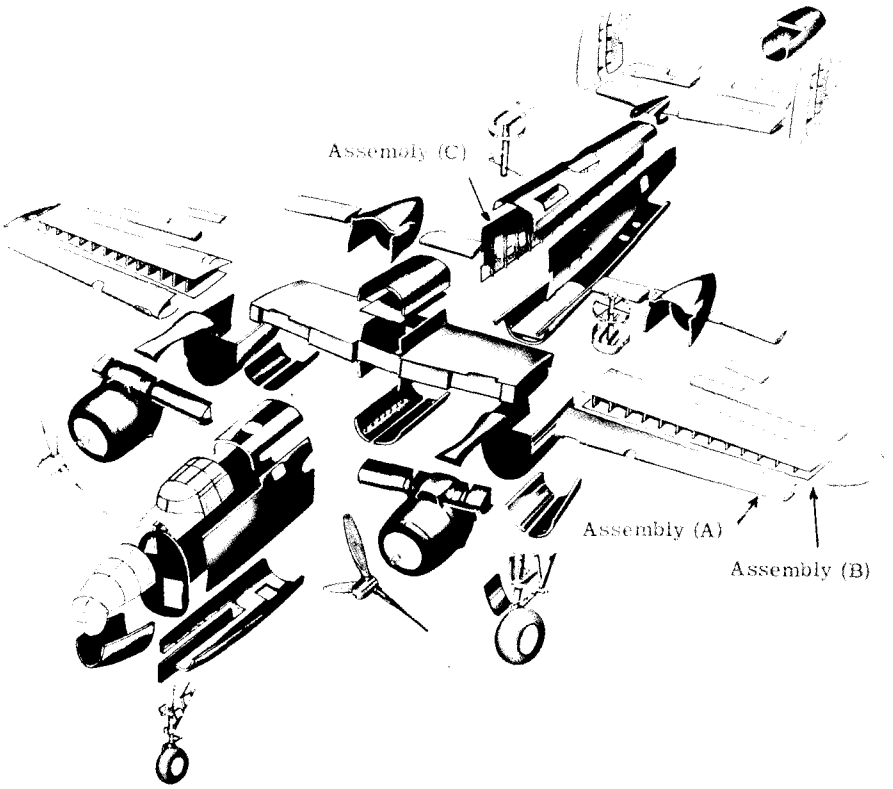

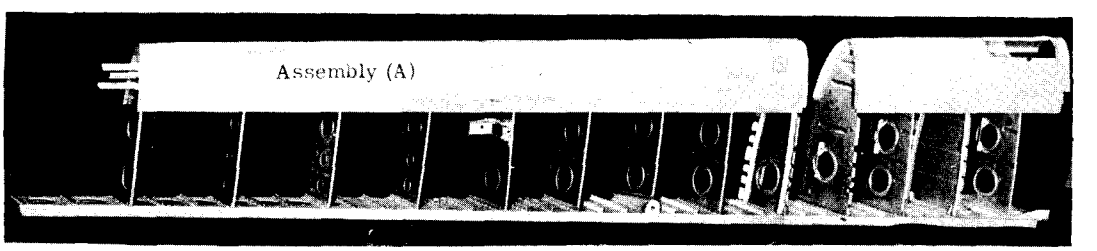

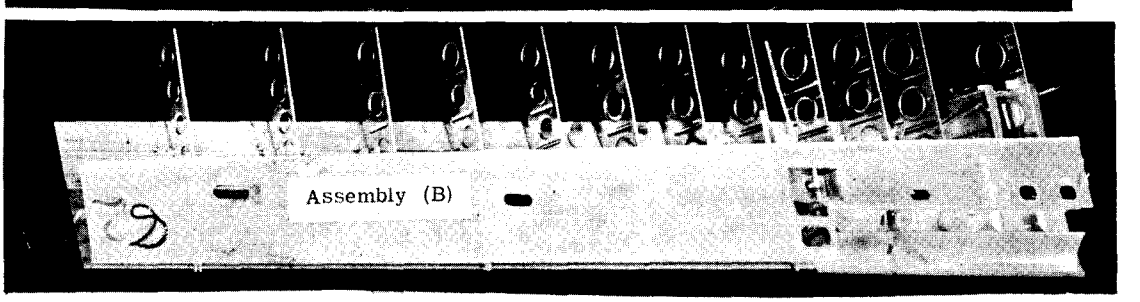

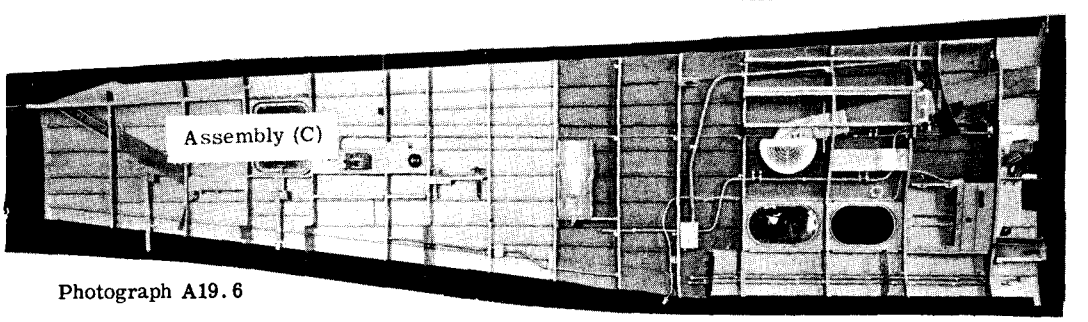

Photograph A19.6

Designing To Facilitate Production.

Photographs by courtesy of North American Aviation Co.

break-down of the structural parts of an airplane of a leading airplane company. Fabrication and assembly of these units permits the installation of much equipment before assembly of the units to the final assembly.

A19.3 Wing Strength Requirements

Two major strength requirements must be satisfied in the structural design of a wing. They are: - (1) Under the applied or limit loads, no part of the structure must be stressed beyond the yield stress of the material. In general, the yield stress is that stress which causes a permanent strain of 0.002 inches per inch. The terms applied or limit refer to the same loads, which are the maximum loads that the airplane should encounter during its lifetime of operations. (2) The structure shall also carry Design Loads without rupture or collapse or in other words failure. The magnitude of the Design Loads equals the Applied Loads times a factor of safety (F.S.). In general, the factor of safety for aircraft is 1.5, thus the structure must withstand 1.5 times the applied loads without failure. In missiles, since no human passengers are involved, the factor of safety is less and appears at this time to range between 1.15 to 1.25.

Aircraft factors of safety are rather low compared to other fields of structural design, chiefly because weight saving is so important in obtaining a useful transportation vehicle relative to useful load and performance. Since safety is the paramount design requirement, the correctness of the theoretical design must be checked by extensive static and dynamic tests to verify whether the structure will carry the design loads without failure.

A19.4 Wing Stress Analysis Methods

In many of the previous chapters of this book, internal forces were calculated for both statically determinate and statically indeterminate structures. The internal loads in a statically determinate structure can be found by the use of the static equilibrium equations alone. The over-all structural arrangement of members is necessary, but the size or shape of no individual member is required. In other words, design consists of finding internal loads and then supplying a member to carry this load safely and efficiently. In a statically indeterminate structure, additional equations beyond the static equilibrium equations are necessary to find all the internal stresses. The additional equations are supplied from a consideration of structural distortions, which means that the size and shape and kind of material for members of the structure must be known before internal stresses can be determined. This fact means a trial and error method is necessary. Another important distinction is that a statically determinate wing structure has just enough members to produce stability and if one member is removed or fails, the entire structure will usually fail, whereas a statically indeterminate structure has one or more additional members than are necessary for static stability and thus some members could fail without causing the entire structure to collapse. In other words, the structure has a fail safe characteristic in that a redistribution of internal stress can take place if some members are over loaded. In general, statically indeterminate structures can be designed lighter and with smaller overall deflections.

METHODS OF STRESS ANALYSIS FOR STATICALLY INDETERMINATE WING STRUCTURES

Two general methods are commonly used, namely,

(1) Flexural beam theory with simplifying assumptions.

(2) Solving for redundant forces and stresses by applying the principles of the elastic theory by various methods such as virtual work, strain energy, etc.

The second method is no doubt more accurate since less assumptions are necessary. A wing structure composed of several cells and many spanwise stringers is a many degree redundant structure. Before the development of high speed computing machinery, so-called rigorous methods were not usable because the computing requirements were impossible or entirely impractical. However, present day computer facilities have changed the situation and rigorous methods are now being more and more used in aircraft structural analysis. Art. A7.9 and A8.10 in Chapters A7 and A8 present matrix methods for finding deflections and stresses to be used with computer facilities.

A19.5 Example Problem I. 3-Flange ~ Single Cell Wing.

Fig. A19.7 shows a portion of a cantilever wing. To provide torsional strength a single closed cell (1) is formed by the interior web AB and the metal skin cover forward of this web. Thin sheet is relatively weak in resisting compressive stresses thus 3 flange stringers A, B and C are added to develop efficient bending resistance. The structure to the rear of spar AB is referred to as secondary structure and consists of thin metal or fabric covering attached to chordwise wing ribs. The air load on this portion is therefore carried forward by the ribs to the single cell beam.

A wing is subjected to many flight condi-

tions. The engineers who calculate the applied loads on the wing usually refer the resulting shears and moments to a set of convenient x, y and z axes. Fig. A19.7 shows the location of these reference axes. The job of the stress engineer is to provide structure to resist these loads safely and efficiently. The general procedure is to find the stresses or loads in all parts of the cell cross-section at several stations along the spanwise direction and from these loads or stresses proportion the required areas, thicknesses and shapes.

In this example, the internal loads will be calculated for only one section, namely, that at Station 240. It will be assumed that the design critical loads from the critical flight condition are as follows.

M_X = 1,100,000 in.lb. V_Z = 11,500 lb.

M_Z = 80,000 in.lb. V_X = 700 lb.

M_y = 460,500 in.lb.

Fig. A19.8 shows these shears and moments referred to the reference axes with origin at point (O). Moments are represented by vectors with double arrow head. The sense of the moment follows the right hand rule.

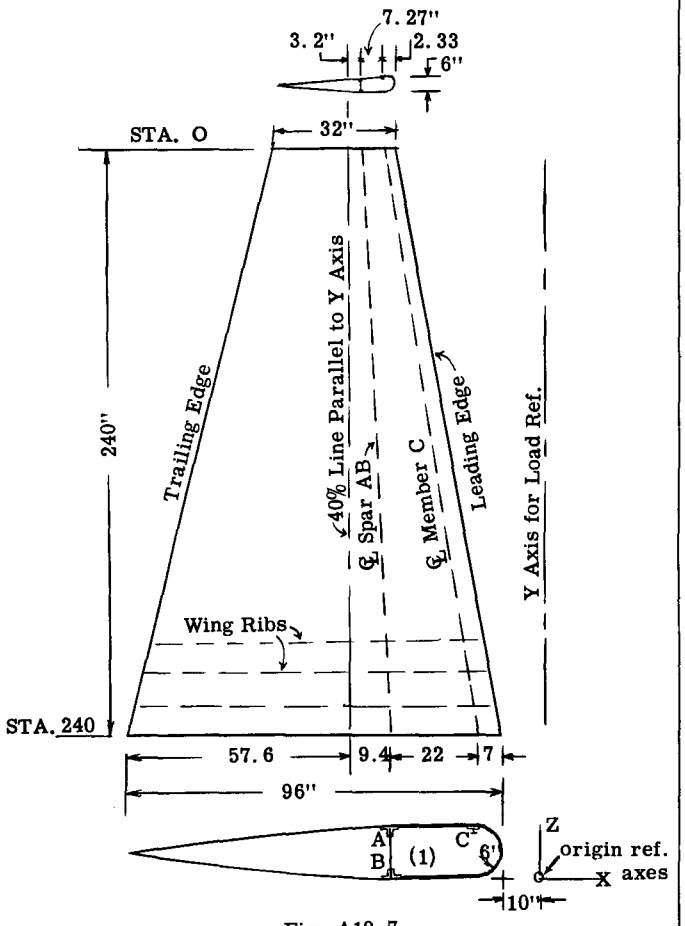

Fig. A19.7

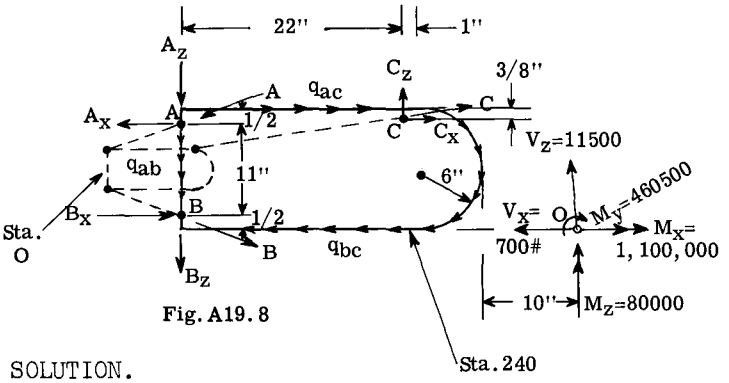

Fig. A19.8

SOLUTION.

ASSUMPTIONS: - It will be assumed that the 3 flange stringers A, B and C develop the entire resistance to the bending moments about the Z and X axes. For skin under compression this assumption is nearly correct since the skin will buckle under relatively low stress. Since sheet can take tensile stresses, this assumption is conservative. However, since the thin sheet cover must resist the shear stresses we will make this conservative assumption. The main advantage of this approximate assumption is that it makes the structure statically determinate.

Fig. A19.8 shows the wing cut at Station 240. The unknown forces are the three axial loads in the stringers A, B and C and the three shear flows q_{ab}, q_{ac} and q_{bc} on the three sheet panels, making a total of 6 unknowns and since there are 6 static equilibrium equations available for a space structure, the structure is statically determinate.

Since the size and shape of flange members A, B and C are unknown, we guess their centroid locations as indicated by the dots in Fig.A19.8. The axial load in each of the 3 stringers has been replaced by its x, y and z components as shown on the figure. The external applied loads are given at the reference origin (O) as shown in Fig.A19.8. Y axis is normal to cross section.

We now apply the equations of equilibrium to find the 6 unknowns.

To find C_y take moments about Z axis through points A and B. C_y is normal to cross section.

$$\Sigma M_{Z(ab)} = -22\,C_y + 80000 = 0, \text{ whence}$$
$$C_y = 3636 \text{ lb.}$$

The result comes out with a plus sign thus indicating that the assumed sense of tension was correct.

To find B_y take moments about an X axis thru (A). B_y is normal to section.

$$\Sigma M_{X(A)} = -11\,B_y + 1{,}100{,}000 + 3636 \times$$
$$0.125 = 0$$

whence, B_y = 100,043 lb. tension as assumed.

To find A_y take $\Sigma F_y = 0$

$\Sigma F_y = -100{,}043 - 3636 + A_y = 0$,

whence, A_y = 103679 lb. and compression as assumed.

Since the direction of the 3 stringers is known, we can find the X and Z components of the stringer loads by simple geometry.

The y, x, and z length components of the three stringers from the dimensions given in Fig. A19.7 are found to be,

Member	y	x	z
A	240	6.2	3
B	240	6.2	3
C	240	20.93	3

The force components are therefore: -

$A_Z = 103679 \times 3/240 = 1296$ lb.

$A_X = 103679 \times 6.2/240 = 2679$ lb.

$B_Z = 100043 \times 3/240 = 1250$ lb.

$B_X = 100043 \times 6.2/240 = 2584$ lb.

$C_Z = 3636 \times 3/240 = 45$ lb.

$C_X = 3636 \times 20.93/240 = 316$ lb.

Fig. A19.9 shows these forces applied in the plane of the cross-section at Station 240, together with the unknown shear flows and the external forces acting in the plane of the cross-section.

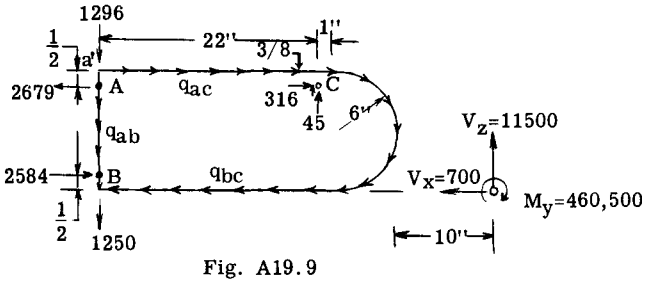

Fig. A19.9

To find q_{bc} take moments about point (a')

$\Sigma M_{a'} = +2679 \times .5 - 2584 \times 11.5 - 316 \times 0.375 - 45 \times 22 + 700 \times 12 - 11500 \times 39 + 460{,}500 - q_{bc}(665) = 0$

whence $q_{bc} = \frac{+9065}{665} = +13.66$ lb./in. and having the sense as assumed.

In the above moment equation the moment of the shear flow q_{bc} about point (a') equals q_{bc} times twice the area of the cell or 665.

To find q_{ac} take $\Sigma F_X = 0$

$\Sigma F_X = -2679 + 2584 + 316 + 22\, q_{ac} - 22 \times 13.66 - 700 = 0$

whence q_{ac} = 35.45 lb./in. with sense as assumed.

To find q_{ab} take $\Sigma F_Z = 0$

$\Sigma F_Z = -1296 - 1250 + 45 + 35.45 \times 0.5 - 11.5 \times 13.66 + 11500 - 11\, q_{ab} = 0$

whence, q_{ab} = 805 lb./in.

The loads on the stringers and sheet panels have now been determined. The axial load in the stringers is practically equal to their y component since axial load equals their y force component divided by the cosine of a small angle. The stress engineer would find similar stresses at a number of stations along the span. These 6 stresses are generally referred to as primary stresses. Usually in most structures there are secondary stress effects which must be considered before final member sizes can be determined. For example, internal webs of a box type beam are designed usually as semi-tension field beams. Tension field beam theory shows that the flange members are subjected to additional stresses besides the primary stresses as found above. The subject of secondary stresses and the strength design of members and their connections to carry given stress loads is taken up in detail in later chapters.

A19.6 Example Problem 2. Metal Covered Wing With Single External Brace Strut.

In Chapter A2, the stress analysis of an externally braced fabric covered monoplane wing was considered. To provide sufficient torsional strength and rigidity, two external brace struts were necessary. However, if a wing is metal covered, a single external brace strut can be used, since the closed cell or cells formed by the metal sheet covering and the internal webs provide the torsional resistance and the wing can be designed as a simply supported beam with cantilever overhang. An excellent example of this type of wing structure is the Cessna aircraft Model 180 as shown in the photograph. An excellent airplane relative to performance, ease of manufacture and maintenance.

To introduce the student to the general approach of stress analyzing such a wing struc-

ture, a limited discussion with a few calculations will be presented.



Cessna Aircraft Model 180
Metal Covered Wing with
One External Strut

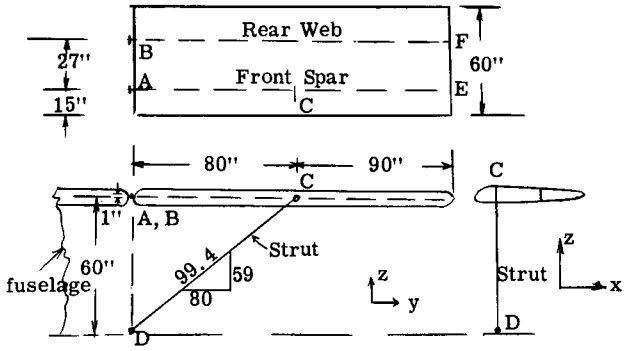

Fig. A19.10

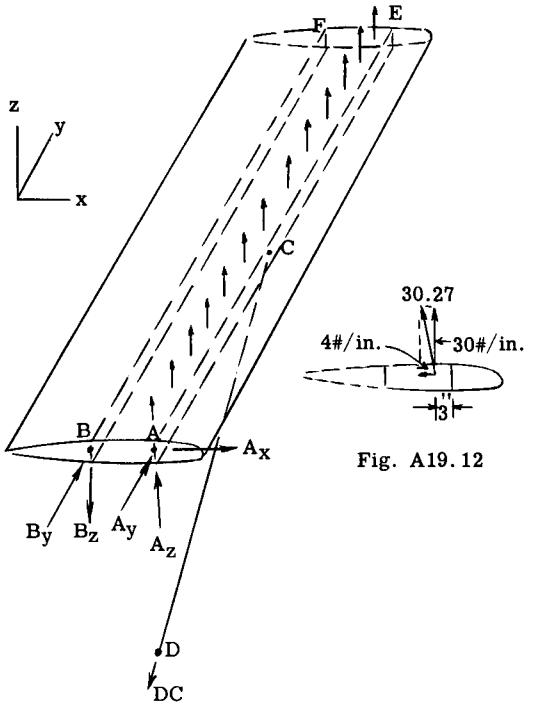

Fig. A19.11

Fig. A19.12

Fig. A19.10 and A19.11 shows the wing dimensions and general structural layout of a monoplane wing with one external brace strut. The wing panel is attached to fuselage by single pin fittings at points A and B with pin axes parallel to x axis. The mating lugs of the fittings at point A are made snug fit but those at B with some gap, thus drag reaction of wing loads on fuselage is resisted entirely at fitting A. Since the fittings at A and B cannot resist moments about x axis, it is necessary to add an external brace strut DC to make structure stable. The panel structure consists of a main spar ACE and a rear spar BF. The entire panel is covered with metal skin forward of the rear spar.

A simplified air load has been assumed as shown in Fig. A19.12, namely, a uniform load w = 30.27 lb./in. of span acting at the 30 per cent of chord point. When this resultant load is resolved into z and x components the results are w_z = 30 lb./in. and w_x = 4 lb./in. as shown in Fig. A19.12.

The general physical action of the wing structure in carrying these air loads can be considered as 3 rather distinct actions, namely, (1) The front spar ACE resists the bending moments and shears due to load w_z., (2) The skin and webs of the two-cell tube resists all moments about y axis or broadly speaking torsional moments, (3) the entire panel cross-section resists the bending moment and flexural shear due to drag load w_x, with the top and bottom skin acting as webs and the two spars as the flanges of this box beam.

General Calculations: -

The unknown external reactions (see Fig. A19.11) are A_y, A_z, A_x, B_y, B_z and DC., or a total of 6. Since 6 static equations of equilibrium are available, the reactions are statically determinate. Reaction DC is also the load in brace strut DC.

To find reaction DC take moments about x axis through points A, B

$$\Sigma M_{X(AB)} = (-\ 170 \times 30 \times 170/2) + DC(80/99.4)60 = 0$$

whence, DC = 8979 lb. (The sign comes out plus so the sense assumed in Fig. A19.11 was correct.) The load in the strut is therefore 8979 lb. tension.

To find B_y, take moments about a z axis through point (A).

$$\Sigma M_{Z(A)} = -\ (4 \times 170 \times 170/2) + 27\ B_y = 0$$

whence, B_y = 2141 lb. acting with sense assumed.

To find A_y take $\Sigma F_y = 0$

$\Sigma F_y = 2141 - 8979\ (80/99.4) + A_y = 0$

whence $A_y = 5085$ lb.

To find B_Z take moments about y axis through (A).

$\Sigma M_{y(A)} = + (30 \times 170 \times 3) - 27\ B_Z = 0$

whence $B_Z = 567$ lb. acting as assumed.

To find A_Z take $\Sigma F_Z = 0$

$\Sigma F_Z = 170 \times 30 - 567 - (8979 \times 59/99.4) + A_Z = 0$

whence $A_Z = 796$ lb. acting as assumed.

The fittings at A and B should be designed to take the reactions at these points as found above. The external strut DC and its end fittings must carry the tension load of 8979 lb.

The next step is to find the stresses and loads on the structural parts of the wing panel.

Since the spar ACE must resist the bending moments about x axis the airloads in Fig. A19.12 are moved to the spar centerline as shown in Fig. A19.13.

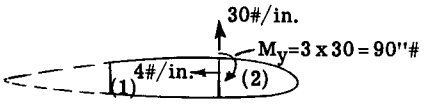

Fig. A19.13

The torsional moment of 90 in. lb. per inch of span is resisted by the cellular tube made up of two cells (1) and (2). In many designs the leading edge cell is neglected in resisting the torsional moments due to many cutouts, etc., thus cell one could be assumed to provide the entire torsional shear resistance and the shear flow for this case would be $q = M_y/2A$ where M_y equals the torsional moment at a given panel section and A the enclosed area of cell (1). If both cells were considered effective then the sheet thickness is necessary before solution for shear flow can be computed. Refer to Chapter A6 for computing torsional shear flow in multiple cell tubes.

The maximum torsional moment would be at the fuselage end of the wing panel and its magnitude would be 170 x 90 = 15300 in. lb. Since the top and bottom skin is not attached to fuselage, this torsional moment must be thrown off on a rib at the end of the panel and this rib in turn transfers this moment in terms of a couple reaction on the spars at points A and B. This couple force equals the moment divided by distance between spars or 15300/27 = 566.7 lb.

Front spar (ACE) loads due to $w_Z = 30$ lb/in:

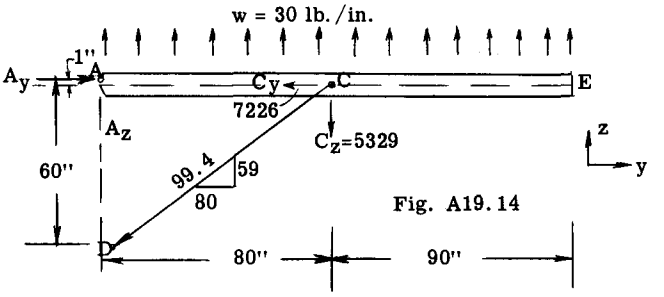

Fig. A19.14

Fig. A19.14 shows free body of front spar ACE. To find strut load DC take moments about (A).

$\Sigma M_A = (- 30 \times 170 \times 170/2) + 60\ (DC \times 80/99.4) = 0$

whence DC = 8979 lb. Tension which checks value previously found.

The y and z components of the strut reaction at C will then be,

$C_y = 8979\ (80/99.4) = 7226$ lb.

$C_Z = 8979\ (59/99.4) = 5329$ lb.

These values are indicated on Fig. A19.14.

To find A_y take $\Sigma F_y = 0$

$\Sigma F_y = - 7226 + A_y = 0$, hence $A_y = 7226$ lb.

In finding the reaction A_y previously, the value was 5085 lb. The difference is due to the drag bending moment which tends to put a tension load on front spar and compression on the rear spar.

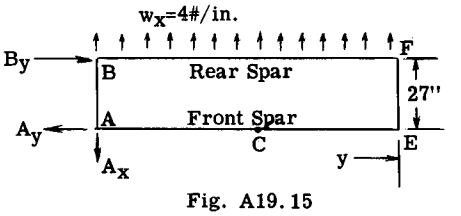

Fig. A19.15

Fig. A19.15 shows the air drag load of 4 lb./in. The bending moment on panel at a distance y from the wing tip equals $w_x\ (y)(y/2) = 4y^2/2 = 2y^2$. The axial load P_y in either spar at any distance y from tip thus equals bending moment divided by arm of 27" or $P_y = 2y^2/27 = .074y^2$. The axial load at points A and B thus equal $.074 \times 170^2 = 2141$ lb. (tension in front spar and compression in rear spar). Thus each spar is subjected to an axial load

increasing from zero at tip to 2141 lb. at fuselage attachment points and varying as y^2. At point C on from spar the axial tension load would be .074 (90^2) = 600 lb.

The design of the front spar between points C and E would be nothing more than a cantilever beam subjected to a bending forces plus an axial tensile load plus a torsional shear flow. The design of the spar between points C and A is far more complicated since we have appreciable secondary bending moments to determine, which must be added to the primary bending moments. Fig. A19.15a shows a free body of spar portion AC.

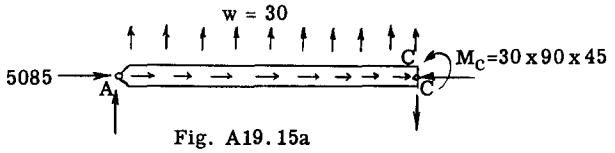

Fig. A19.15a

The lateral load of 30 lb./in. bends the beam upward, thus the axial loads at A and C will have a moment arm due to beam deflection which moments are referred to as secondary moments. To find deflections the beam moment of inertia must be known, thus the design of this beam portion would fall in the trial and error procedure. Articles A5.23 to 28 of Chapter A5 explain and illustrate solution of problems involving beam-column action and such a procedure would have to be used in actually designing this beam portion.

The rear spar BF receives two load systems, namely a varying axial load of zero at F to 2141 lb. at B and the web of this spar receives a shear load from the torsional moment. The rear spar is not subjected to bending moments.

In Fig. A9.10 the secondary structure consisting of chordwise ribs and spanwise light stringers riveted to skin are not shown. This secondary structure is necessary to hold wing contour shape and transfer air pressures to the box structure. This secondary structure is discussed in Chapter A21. The broad subject of designing a member or structure to withstand stresses safely and efficiently is considered in detail in later chapters.

A19.7 Single Spar - Cantilever Wing - Metal Covered

A single spar cantilever wing with metal covering is often used particularly in light commercial or private pilot aircraft.

Suppose in the single spar externally braced wing of Fig. A19.11, that the external brace strut DC was removed. Obviously the wing would be unstable as it would rotate about hinge fittings at points A and B. To make the structure stable the single pin fitting at (A) would have to be replaced by two fittings, one on the upper flange and the other on the lower flange in order to be able to resist a M_X moment. Fig. A19.16 shows this modification. The fitting at B could remain as before, a single pin fitting.

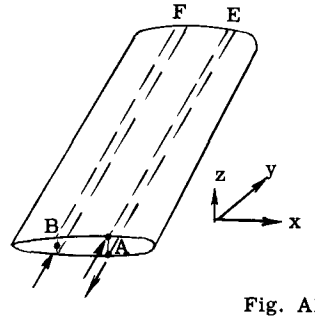

Fig. A19.16

The stress analysis of this wing would consist of the spar AE resisting all the M_X moments and the V_Z shears and acting as a cantilever beam. The torsional moment about a y axis coinciding with spar AE would be resisted by shear stresses in the cellular tubes formed by the skin and the spar webs. The drag bending and shear forces would be resisted by the beam whose flanges are the front and rear spars and the web being the top and bottom skin.

A19.8 Stress Analysis of Thin Skin - Multiple Stringer Cantilever Wing. Introduction and Assumptions.

The most common type of wing construction is the multiple stringer type as illustrated by the six illustrative cross-sections in Fig. A19.2. A structure with many stringers and sheet panels is statically indeterminate to many degrees with respect to internal stresses. Fortunately, structural tests of complete wing structures show that the simple beam theory gives stresses which check fairly well with measured stresses if the wing span is several times the wing chord, that sweep back is minor and wing is free of major cutouts and discontinuities. Thus it is common procedure to analyze and design a wing overall by the beam theory and then investigate those portions of the wing where the beam theory may be in error by using more rigorous analysis methods such as those explained and illustrated in Art. A8.10 of Chapter A8.

ASSUMPTIONS - BEAM THEORY

In this chapter the wing bending and shear stresses will be calculated using the unsymmetrical beam theory. The two main assumptions in this theory are: -

(1) Transverse sections of the beam originally plane before bending remain plane after bending of beam. This assumption means that longitudinal strain varies directly as the distance from

the neutral axis or strain variation is linear.

(2) The longitudinal stress distribution is directly proportional to strain and therefore from assumption (1) is also linear. This assumption actually means that each longitudinal element acts as if it were separate from every other element and that Hook's law holds, namely, that the stress-strain curve is linear.

Assumption (1) neglects strain due to shear stresses in skin, which influence is commonly referred to as shear lag effect. Shear lag effects are usually not important except near major cut-outs or other major discontinuities and also locations where large concentrated external forces are applied.

Assumption (2) is usually not correct if elastic and inelastic buckling of skin and stringers occur before failure of wing. In applying the beam theory to practical wings, the error of this assumption is corrected by use of a so-called effective section which is discussed later.

A19.9 Physical Action of Wing Section in Resisting External Bending Forces from Zero to Failing Load.

Fig. A19.17 shows a common type of wing cross-section structural arrangement generally referred to as the distributed flange type.

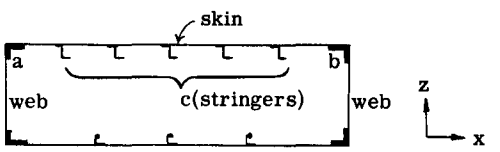

Fig. A19.17

The corner members (a) and (b) are considerably larger in area than the stringers (c). The skin is relatively thin. Now assume the wing is subjected to gradually increasing bending forces which place the upper portion of this wing section in compression and the bottom portion in tension. Under small loading the compressive stresses in the top surface will be small and the stress will be directly proportional to strain and the beam formula $\sigma_c = M_X z/I_X$ will apply and the moment of inertia I_X will include all of the cross-section material. As the external load is increased the compressive stresses on the thin sheets starts to buckle the sheet panels and further resistance decreases rapidly as further strain continues, or in other words, stress is not directly proportional to strain when sheet buckles. Buckling of the skin panels however does not cause the beam to fail as the stringers and corner members are lowly stressed compared to their failing stress. The stringers (c) are only supported transversely at wing rib points and thus the stringers act as columus and fail by elastic or inelastic bending. The corner flange members (a) and (b) are stabilized in two directions by the skin and webs and usually fail by local crippling.

Now continuing the loading of the wing after the skin has buckled, the stringers and corner members will continue to take additional compressive stress. Since the ultimate strength of the stringers is less than that of the corner members, the stringers (c) will start to bend elastically or inelastically and will take practically no further stress as additional strain takes place. The corner members still have considerable additional strength and thus additional external loading can be applied until finally the ultimate strength of the corner members is reached and then complete failure of the top portion of the beam section takes place. Therefore, the true stress - strain relationship does not follow Hook's Law when such a structure is loaded to failure.

In the above discussion the stringers (c) were considered to hold their ultimate buckling load during considerable additional axial strain. This can be verified experimentally by testing practical columns. Practical columns are not perfect relative to straightness, uniformity of material, etc. Fig. A19.18 shows the load versus lateral deflection of column midpoint as a column is loaded to failure and fails by elastic bending. Fig. A19.19 shows similar results when the failure is inelastic bending.

Fig. A19.18

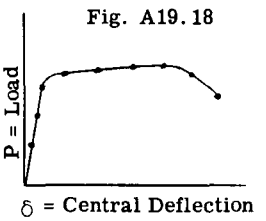

Fig. A19.19

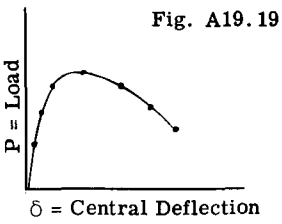

The test results show that a compression member which fails in bending, normally continues to carry approximately the maximum load under considerable additional axial deformation. Thus in the beam section of Fig. A19.17 when the stringers (c) reach their ultimate load, failure of the beam does not follow since corner members (a) and (b) still have remaining strength.

A19.10 Ultimate Strength Design Requirement

The strength design requirements are: -

(1) Under the applied or limit loads, no structural member shall be stressed above the material yield point, or in other words, there must be no permanent deformation or deflection of any part of the structure.

(2) Under the design loads which equal the applied loads times a factor of safety, no failure of the structure shall occur. The usual factor of safety for conventional aircraft is 1.5, or the structure must carry loads 50 percent greater than the applied loads without failure. The higher the stress at failure of a member the less material required and therefore the less structural weight. The stress engineer thus tries to design members which fail in the inelastic zone.

The bending stress beam formula $\sigma_c = Mc/I$ does not take care of this non-linear stress-strain action and thus some modification of the moment of inertia of the beam cross-section is necessary if the ultimate strength of a wing section is to be computed fairly accurately. The stress engineer usually solves this problem by using a modified cross-section, usually referred to as the effective cross-section.

A19.11 Effective Section at Failing Load.

In order to use the beam formula which assumes linear stress-strain relation, corrections to take care of skin buckling and stringer buckling must be formulated. The effectiveness of the skin panels will be considered first.

When a compressive load is applied to a sheet stringer combination, the thin sheet buckles at rather low stress. For further loading the compressive stress various over the panel width as illustrated in Fig. A19.20. The stress in the sheet at the stringer attachment line is the same as in the stringer since it cannot buckle and therefore suffers the same strain as the stringer. Between the stringers the sheet stress decreases as shown by the dashed line in Fig. A19.20. This variable stress condition is difficult to handle so the stress engineer makes a convenient substitution by replacing the actual sheet with its variable stress by a width of sheet carrying a uniform

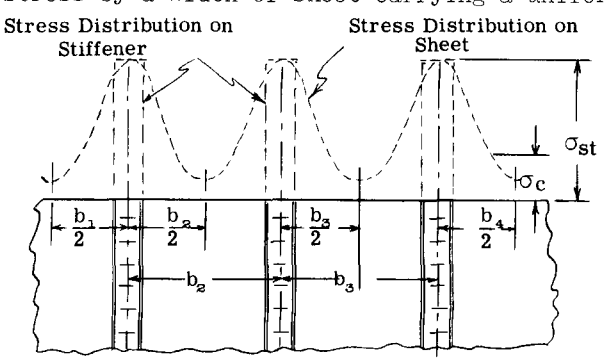

Fig. A19.20

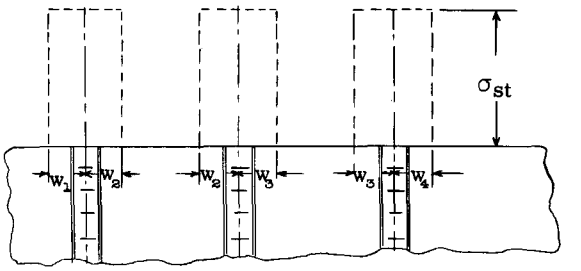

Fig. A19.21

stress equal to the stringer stress. In Fig. A19.21 2w is the effective sheet width to go with each stringer. The total stress on the effective widths carrying a uniform stress equal to the stringer stress equals the total load on the sheet panels carrying the actual varying stress distribution. The equation for effective width is usually written in the form,

$$* \quad 2w = kt\,(E/\sigma_{st})^{\frac{1}{2}}$$

a widely used value for K = 1.9, whence

$$2w = 1.90\,t\,(E/\sigma_{st})^{\frac{1}{2}} \text{ - - - - - - - - - - (1)}$$

σ_{st} = stress in stringer

Therefore if we know the stress in the stringer we can find the width of sheet to use with the stringer to obtain an effective section to take care of the sheet buckling influence.

Effective Factor for Buckled Stringers.

Consider the beam section in Fig. A19.17. If we take a stringer (c) and attach a piece of sheet to it equal to 2w, the effective width and test it in compression and brace it in a plane parallel to the sheet, the resulting test stress versus strain shortening curve (c) of Fig. A19.22 will result. The length of the test specimen would equal the rib spacing in the wing. The corner members (a) or (b) in Fig. A19.17 being stabilized in two directions will fail by local crippling, thus if a short piece of this member is tested to failure in compression the test curve (A) in Fig. A19.22 is obtained. Curve (C) shows that the stringer holds approximately its maximum load for a considerable strain period. Curve (A) shows that for the same unit strain member (a) can take considerable higher stress. If we take a unit strain of .006, the point at which the maximum stress of 47000 is obtained in member (a) (see point (3) on Curve A) then the stress at the same strain for member (C) will be 38000 (see point (2) on Curve C).

* The buckling of sheets is taken up in detail in Chapter C5.

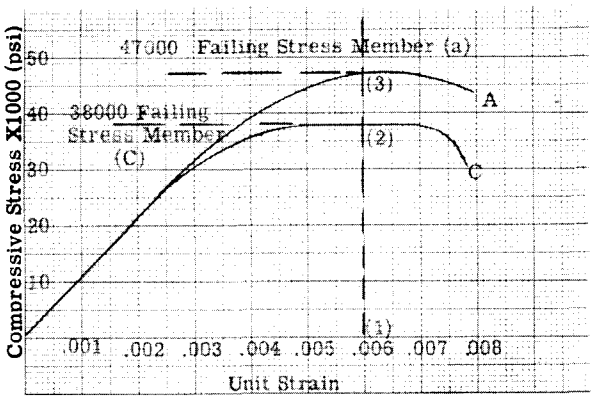

Fig. A19.22

For stress analysis procedure using the beam formula, we assume a linear stress variation from zero to 47000 psi. Since stringers (c) can only take 38000 psi at the same strain, or in other words, stringer (c) is less effective than members (a) and (b). The effectiveness factor for stringer (c) equals its ultimate strength divided by the ultimate strength of member (a) or 38000/47000 = .808.

A19.12 Example Problem

The wing section in Fig. A19.23 is subjected to a design bending moment about the x axis of 500,000 in.lb., acting in a direction to put the upper portion in compression. The problem is to determine the margin of safety for this design bending moment. The material is 2024 aluminum alloy.

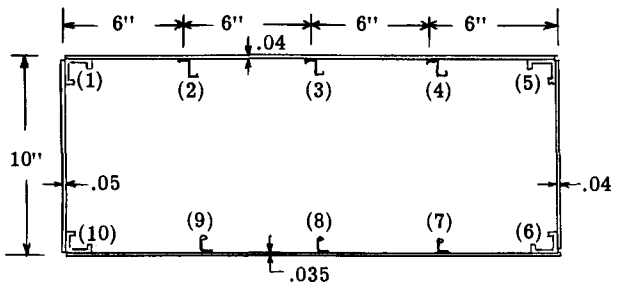

Fig. A19.23

SOLUTION

The beam formula for bending stress at any point is $\sigma_b = M_x z/I_x$. To solve this equation we must have the effective moment of inertia of the beam cross-section. The bottom surface being in tension under the given design bending moment is entirely effective, however the top surface has a variable effectiveness since the skin, stringers and corner flange members have different ultimate failing stresses.

From equation (1) the effective width of sheet to use with each rivet line depends on the stress in the stringer to which it is attached. The failing stress for the stringer will be used, which means that the failing stress of the stringers and corner flanges must be known before the effective width can be found. For this example the zee stringers have been selected of such a size as to give an ultimate column failing stress of 38000 psi, and the corner flange members have been made of such size and shape as to give a failing stress of 47000 psi. These failing stresses can be computed by theory and methods as given in Chapter C7. The sizes have purposely been selected to given strengths represented by the test curves of Fig. A19.22.

The effective width with each rivet line from equation (1) would be,

For zee stringer $2w = 1.90 \times .04 (10.5 \times 10^6/38000)^{\frac{1}{2}} = 1.25$ inches

Thus the area of effective skin = 1.25 x .04 = .05 in.^{2}. The area of the zee stringer is 0.135 sq. in. which added to the effective skin area gives 0.185 sq. in. which value is entered in Column (2) of Table I opposite zee stringers numbered 2, 3 and 4 in Fig. A19.23. The same procedure is done for the corner members 1 and 5 with the resulting effective areas as given in Table I. On the bottom side which is in tension all material is effective. The skin width equal to one-half the distance to adjacent stringers is assumed to act with each stringer. Taking the area of the angle section as 0.11 and adding skin area equal to 6 x .035 = .21 or a total of 0.32 sq. in. which value is shown in Column 2 of Table I opposite stringers 7, 8 and 9. The areas of the lower corner members plus bottom skin and web skin would come out as recorded in the Table.

The next step is to correct for stringer effectiveness in compression. The failing stress for the zee stringer was given as 38000 and for the corner members 47000 psi. The effectiveness factor for the zee stringer thus equals 38000/47000 = .808. This factor is recorded in Column 3 of Table I. For the corner members 1 and 5 and all the tension members the factor is of course unity. The balance of Table I gives the calculation of the effective moment of inertia ΣAz^2 about the x neutral axis.

The compressive stress intensity at the centroid of the zee stringers thus equals,

$\sigma_b = M_x z/I_x = 500{,}000 \times 5.57/59.80 = 46600$ psi.

The true stress equals the effectiveness factor times this stress = .808 x 46600 = 37400 psi. The failing stress equals 38000 hence margin of safety = (38000/37400) - 1 = .01 or one percent.

TABLE A19.1

1	2	3	4	5	6	7	8
Stringer Number	Stringer Area Plus Effective Skin	Stringer Effectiveness Factor	Effective Area (A)	z'	Az'	z=z'-$\bar{z}$	Az^2
1	0.37	1.0	0.370	4.50	1.664	5.47	11.05
2	0.185	0.808	0.149	4.60	0.685	5.57	4.62
3	0.185	0.808	0.149	4.60	0.685	5.57	4.62
4	0.185	0.808	0.149	4.60	0.685	5.57	4.62
5	0.370	1.0	0.370	4.50	1.664	5.47	11.05
6	0.417	1.0	0.417	-4.60	-1.920	-3.63	5.50
7	0.320	1.0	0.320	-4.63	-1.480	-3.66	4.28
8	0.320	1.0	0.320	-4.63	-1.480	-3.66	4.28
9	0.320	1.0	0.320	-4.63	-1.480	-3.66	4.28
10	0.417	1.0	0.417	-4.63	-1.920	-3.63	5.50
		Σ	2.981		-2.897	I_X=	59.80

z' = distance from ℄ x axis to centroid of stringer area

$\bar{z} = \Sigma Az'/\Sigma A = -2.897/2.981 = -.97$ in.

On corner members (1) and (5) the compressive stress = 500,000 x 5.47/59.80 = 45000 psi. With the failing stress being 47000 the margin of safety is 2 percent.

Now suppose we would have omitted consideration of the stringer effectiveness factor and omitted column (3) of Table I. Carrying through the calculations of Table I, the value of $\bar{Z}$ would be -0.76" and I_X would be 63.08. The stress intensity on the zee stringers would then be 500000 x 5.36/63.08 = 42500 psi. Since the failing stress for stringer is 38000 the margin of safety would be (38000/42500) - 1 = a negative 10.5 percent. The previous result was a plus 1 percent, thus a difference of 11.5 percent in the results.

The purpose of this simple example problem was to emphasize to the student that failure of real aircraft stiffened skin structures occurs under non-linear stress-strain conditions and the elastic theory must be modified if fairly accurate estimates of the failing strength of a composite structure is to be obtained.

A19.13 Bending and Shear Stress Analysis of Tapered - Multiple Stringer Cantilever Wing. Unsymmetrical Beam Method.

In general cantilever wings are tapered in both depth and planform. Fig. A19.24 illustrates a typical structural layout of the outer wing panel for a small airplane. The structure consists of a front and rear beam (spar) with spanwise stringers between the two beams. Tapering in cross-sectional material is obtained by decreasing size of members by cutting off portions of the spanwise stringers and corner flanges and decreasing the skin and web thickness.

The stress analysis of this wing would show the resulting bending and shear stresses for a number of spanwise stations for the critical design load conditions. In this example solution the bending longitudinal stresses will be determined on cross-sections at two stations, namely, stations 20 and 47.5, and the shear stresses will be determined for station 20. In this example problem, the leading edge cell will be considered ineffective as well as any structure to rear of rear beam, hence structure is a one cell beam with multiple stringers. A second solution including the leading edge cell to form a two cell beam will also be presented.

ANALYSIS FOR BENDING LONGITUDINAL STRESSES

Longitudinal stresses (tension or compression) are produced by external forces normal to the cross-section and by bending moments about x and z axes. The stress equations are:

$$\sigma_n = P/A \quad - - - - - - - - - - - - - - - - - (2)$$

where σ_n = longitudinal stress

P = external load acting through centroid of effective wing cross-section

A = effective area of cross-section.

For any given flange member with area (a) the load P_n on the member would be,

$$P_n = \sigma_n a \quad - - - - - - - - - - - - - - - - - (3)$$

The stresses due to bending moments are from Chapter A13, Art. A13.5: -

$$\sigma_b = -(K_3 M_Z - K_1 M_X)x - (K_2 M_X - K_1 M_Z)z - \quad (4)$$

where σ_b = bending stress with plus being tension

$$K_1 = I_{XZ}/(I_X I_Z - I_{XZ}^2)$$

$$K_2 = I_Z/(I_X I_Z - I_{XZ}^2)$$

$$K_3 = I_X/(I_X I_Z - I_{XZ}^2)$$

The normal component of the axial load in a flange member equals σ_b a) where (a) is the area of the flange member. Since the angle between the normal to the beam section and the centroidal axis of a stringer is generally quite small, the difference between the cosine of a small angle and unity is negligible and thus the normal component can be considered as the axial load in the stringer.

Before equations 2, 3 and 4 can be solved, the effective cross-section area must be known as well as the moments of inertia and product of inertia about x and z centroidal axes.

WING BODY SECTION PLAN VIEW LOOKING INBOARD FROM TIP

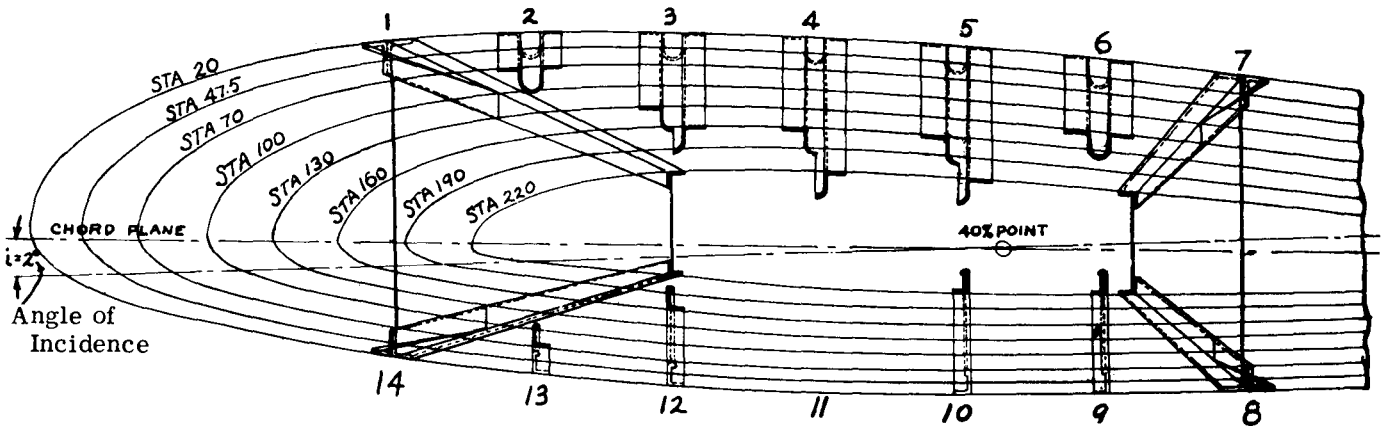

UPPER SURFACE STRINGER AND SKIN ARRANGEMENT

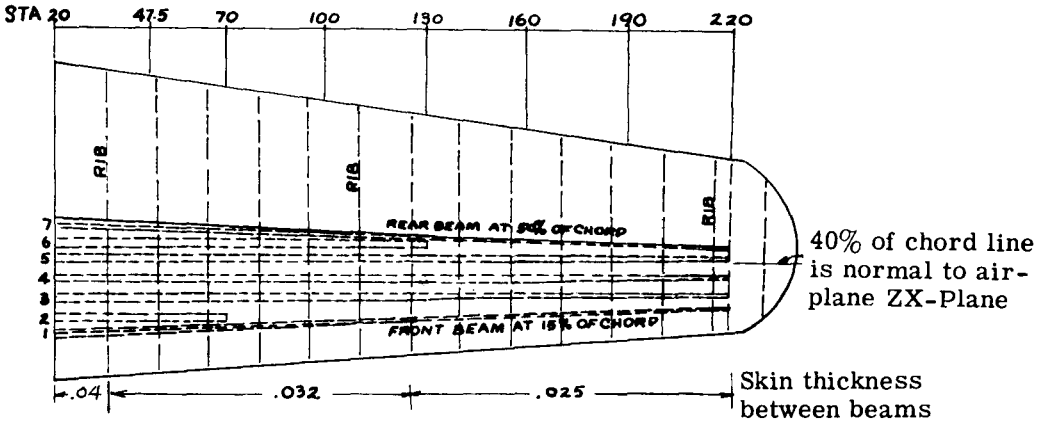

LOWER SURFACE STRINGER AND SKIN ARRANGEMENT

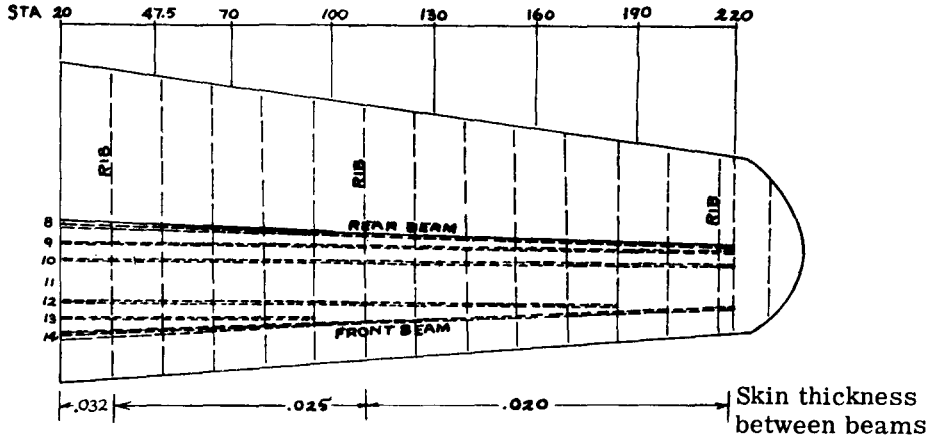

Fig. A19. 24 Structural Layout of Tapered Cantilever Wing

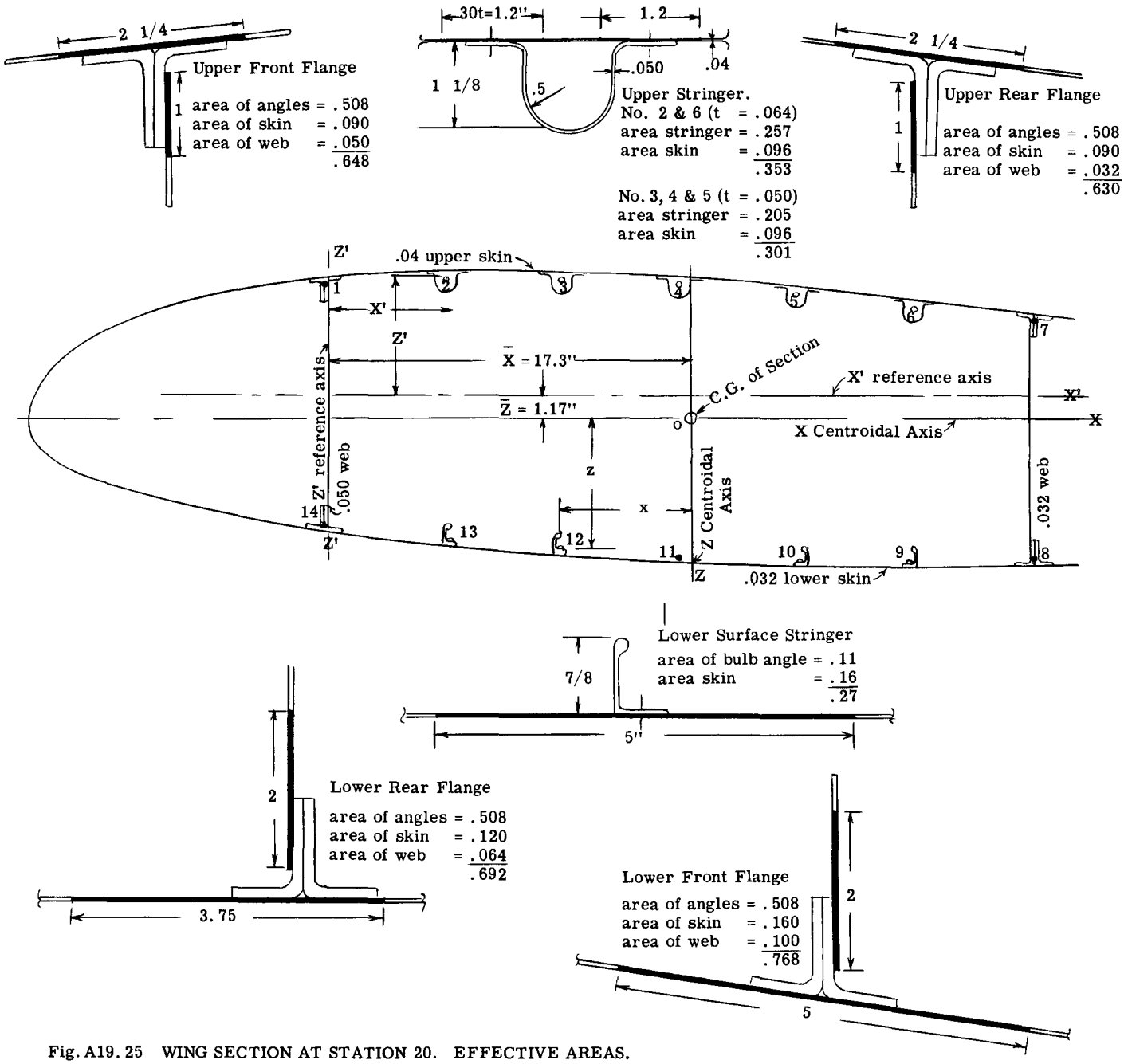

Fig. A19.25 WING SECTION AT STATION 20. EFFECTIVE AREAS.

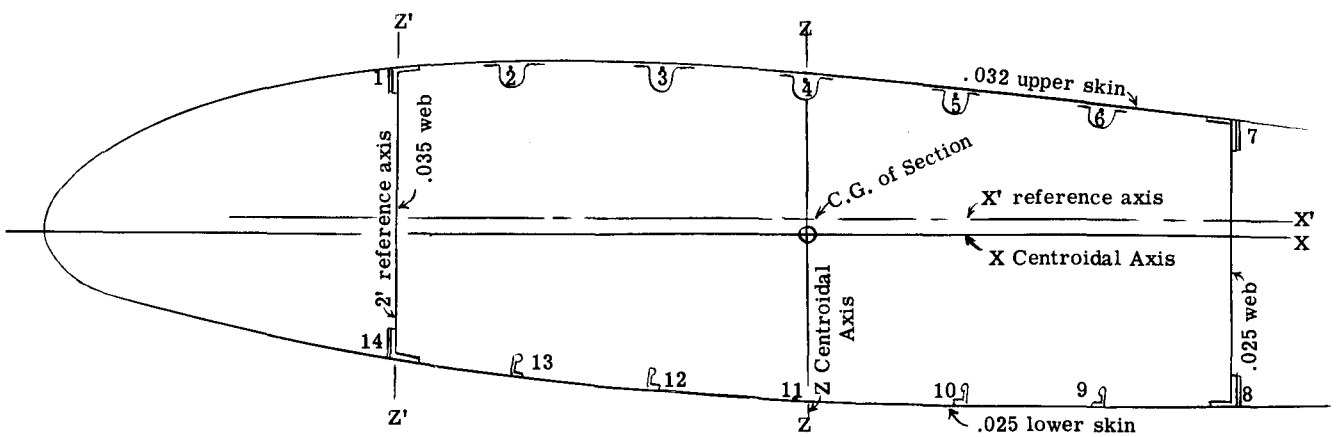

Fig. A19.26 WING SECTION STATION 47.5

Fig. A19.25 shows the cross section at Station 20 divided into 14 longitudinal units numbered 1 to 14. Since the external load condition to be used places the top surface in compression, the skin will buckle and thus we use the effective width procedure to obtain the skin portion to act with each stringer. Fig. A19.25 shows the effective skin which is used with each flange member to give the total area of numbers (1) to (7). The skin on the bottom surface being in tension is all effective and Fig. A19.25 shows the skin area used with each bottom flange member.

The next factor to decide is the stringer effectiveness as discussed and explained in the previous example problem. For the structure of Fig. A19.25 we will assume that the compressive failing stress of the stringers is the same as that for the corner members, thus we will have no correction factor to take care of the situation of flange members having different ultimate strengths.

Table A19.2, columns 1 to 11, and the calculations below the table give the calculations for determining the section properties at Station 20, namely A, I_X, I_Z and I_{XZ}. Table A19.3 gives the same for wing section at Station 47.5. The areas in column (2) are less since sizes have changed between Stations 20 and 47.5.

Calculation of longitudinal stress due to M_X and M_Y bending moments: -

The design bending moments will be assumed and are as follows: -

Station 20 M_X = 1,300,000 in.lb.
M_Z = - 285,000 in.lb.

Station 47.5 M_X = 1,000,000 in.lb.
M_Z = - 215,000 in.lb.

The moments about the y axes are not needed in the bending stress analysis but are needed in the shear analysis which will be made later.

To solve equation (4) the constants K_1, K_2 and K_3 must be known.

For Station 20 from Table A19.2, I_X = 230.3, I_Z = 1030 and I_{XZ} = - 50, whence -

$$K_1 = I_{XZ}/(I_X I_Z - I_{XZ}^2) = -50/(230.3 \times 10.30 - 50^2) = -50/235500 = -.0002125$$

$$K_2 = I_Z/235500 = 1030/235500 = .004378$$

$$K_3 = I_X/235500 = 230.3/235500 = .00098$$

Substituting in equation (4)

$$\sigma_b = -\left[.00098 \times - 285000 - (-.0002125 \times 1300000)\right] x - \left[.004378 \times 1{,}300{,}000 - (-.0002125 \times - 285000)\right] z$$

whence, $\sigma_b = 3.3\ x - 5639\ z$ - - - - - - - - (5)

Column 12 of Table A19.2 gives the results of this equation for values of x and z in columns 10 and 11. Multiplying these bending stresses by the stringer areas, the stringer loads are given in column 13. The sum of the loads in this column should be zero since total tension must equal total compression on a section in bending.

Stresses at station 47.5:

I_X = 157.4, I_Z = 700, I_{XZ} = -35.4 (Table A19.3)

$K_1 = 35.4/(157.4 \times 700 - 35.4^2) = -35.4/108950 = -.000324$

$K_2 = 700/108950 = .00643$

$K_3 = 157.4/108750 = .001447$

$$\sigma_b = -\left[.001447 \times -215000 - (-.000324 \times 1{,}000{,}000)\right] x - \left[(.00643 \times 1{,}000{,}000 - (-.00324 \times -215000)\right] z$$

whence

$$\sigma_b = -14.5 \times -6360\ z$$

Column 12 of Table A19.3 gives the results of this equation and column 13, the total stringer loads at station 47.5.

The stresses in column 12 of each table would be compared to the failing stress of the flange members to obtain the margin of safety.

ANALYSIS FOR SHEAR STRESSES IN WEBS AND SKIN

The shear flow distribution will be calculated by using the change in axial load in the stringers between stations 20 and 47.5, a method commonly referred to as the ΔP method. For explanation of this method, refer to Art. A15.16 of Chapter A15.

The shear flow in the y direction at a point n of the cell wall equals,

$$q_{y_n} = q_o - \sum_{o}^{n} \frac{\Delta P}{d} \quad \text{- - - - - - - - - - - - (6)}$$

where q_o is a known value of shear flow at some point o and the second term is the change in shear flow between points o and n.

TABLE A19.2

SECTION PROPERTIES ABOUT CENTROIDAL X AND Z AXES

Wing Section at Station 20 (Compression on upper surface)

1	2	3	4	5	6	7	8	9	10	11	12	13
Flange No.	Area A	Z'	AZ'	AZ'^{2}	X'	AX'	AX'^{2}	AX'Z'	$Z = Z' - \bar{Z}$	$X = x' - \bar{x}$	σ_b	$P = \sigma_b A$
1	.648	5.50	3.56	19.61	-0.10	-0.06	0	-0.36	6.68	-17.4	-37660	-24390
2	.353	5.90	2.08	12.30	5.65	1.99	11.30	11.78	7.08	-11.65	-39940	-14070
3	.300	5.85	1.76	10.28	11.20	3.36	37.60	19.67	7.03	- 6.10	-39620	-11890
4	.300	5.55	1.66	9.25	16.85	5.05	85.00	28.10	6.73	- 0.45	-37950	-11370
5	.300	5.05	1.52	7.65	22.40	6.72	150.50	34.00	6.23	5.10	-35115	-10510
6	.353	4.40	1.55	6.83	28.00	9.89	277.00	43.50	5.58	10.70	-31450	-11090
7	.630	3.55	2.24	7.95	35.72	23.15	826.00	80.00	4.73	18.42	-26560	-16700
8	.692	-8.40	-5.81	48.90	35.72	24.70	881.00	-208.00	-7.22	18.42	40750	28230
9	.270	-8.50	-2.30	19.55	27.80	7.50	208.00	- 64.00	-7.32	10.50	41280	11180
10	.270	-8.50	-2.30	19.55	22.60	6.10	138.00	- 52.00	-7.32	5.30	41250	11170
11	.160	-8.30	-1.33	11.05	16.70	2.67	44.60	- 22.20	-7.12	- 0.60	40100	6430
12	.27	-8.00	-2.16	17.30	10.90	2.94	32.00	- 23.50	-6.82	- 6.40	38400	10390
13	.27	-7.50	-2.02	15.20	5.60	1.51	8.45	- 11.35	-6.32	-11.7	35570	9600
14	.768	-6.50	-5.00	32.50	- 0.10	.08	0	0.50	-5.32	-17.40	29950	23020
Σ	5.584		-6.56	238.0		96.44	2700	-163.8				0.00

$\bar{z} = \frac{-6.56}{5.584} = -1.176$

$\bar{X} = \frac{96.44}{5.584} = 17.3$

$I_x = 238 - 5.584 \times 1.176^2 = 230.3$ in.^{4}

$I_z = 2700 - 5.584 \times 17.3^2 = 1030$ in.^{4}

$I_{xz} = -163.8 - 5.584 \times -1.176 \times 17.3 = -50$

General Notes:

See Fig. A19.25 for Section at Station 20.

Reference axes X'X' and Z'Z' are assumed as shown.

Properties are calculated with respect to these axes and transferred to the centroidal X and Z axes.

$\sigma_b = 3.3 X - 5639 Z$

TABLE A19.3

SECTION PROPERTIES ABOUT CENTROIDAL X AND Z AXES

Wing Section at Station 47.5 (Compression on upper Surface)

1	2	3	4	5	6	7	8	9	10	11	12	13
Flange No.	Area A	Z'	AZ'	AZ'^{2}	X'	AX'	AX'^{2}	AX'Z'	$Z = Z' - \bar{Z}$	$X = X' - \bar{X}$	σ_b	$P = \sigma_b A$
1	.476	5.60	2.66	14.95	- 0.10	- 0.05	0	- 0.27	6.21	-15.60	-39275	-18700
2	.318	5.83	1.86	10.80	4.40	1.40	6.16	8.16	6.44	-11.10	-40790	-12990
3	.266	5.75	1.53	8.80	10.00	2.66	26.60	15.30	6.36	- 5.50	-4025	-10710
4	.266	5.42	1.44	7.81	15.60	4.15	64.75	22.40	6.03	0.10	-38400	-10200
5	.266	4.90	1.30	6.40	21.20	5.64	120.00	27.60	5.51	5.70	-35075	- 9320
6	.318	4.30	1.37	5.88	26.70	8.50	226.50	36.60	4.91	11.20	-31360	-10000
7	.476	3.60	1.71	6.17	31.70	15.10	478.00	54.40	4.21	16.20	-27030	-12880
8	.553	-7.10	-3.93	27.90	31.70	17.51	555.00	-124.50	-6.49	16.20	41050	22770
9	.235	-7.40	-1.74	12.90	26.50	6.23	165.00	- 46.10	-6.79	11.00	43090	10140
10	.235	-7.40	1.74	12.90	21.30	5.00	107.00	- 37.18	-6.79	5.80	43180	10160
11	.135	-7.20	-0.90	6.48	15.10	1.89	28.50	- 13.60	-6.59	- 0.40	41900	5240
12	.235	-6.90	-1.62	11.20	9.60	2.26	21.70	- 15.60	-6.29	-55.90	40085	9410
13	.235	-6.25	-1.47	9.20	4.50	1.06	4.75	- 6.61	-5.84	-11.00	36060	8470
14	.605	-5.40	-3.27	17.70	- 0.10	- 0.06	0	0.33	-4.79	-15.60	30725	18600
Σ	4.61		-2.80	159.1		71.3	1804	- 79.0				0

$\bar{Z} = -2.80/4.61 = -0.61"$

$\bar{X} = 71.3/4.61 = 15.50"$

$I_x = 159.1 - 4.61 \times .61^2 = 157.4$

$I_z = 1804 - 4.61 \times 15.5^2 = 700$

$I_{xz} = -79 - 4.61 \times -.61 \times 15.5 - 35.4$

General Notes:

See Fig. A19.26 for section at Station 47.5.

Reference axes X'X' and Z'Z' are assumed as shown.

$\sigma_b = -14.5 X - 6360 Z$

ΔP equals the change in stringer axial load over a distance d in the y direction.

Since the cell in our problem is closed the value q_0 at any point is unknown. We assume it zero on web 1-14 by imagining that the web is cut as shown in Fig. A19.27. Equation (6) thus reduces to,

$$q_y = - \Sigma \frac{\Delta P}{27.5} \quad - - - - - - - - - - - - - - (7)$$

Columns 1 to 5 of Table A19.4 show the solution of equation (7). The shear flow values of q_y in column 5 are plotted on the cell wall in Fig. A19.27, remembering that $q_y = q_x = q_z$. For rules giving direction of q_x and q_z refer to Chapter A14, Art. A14.6.

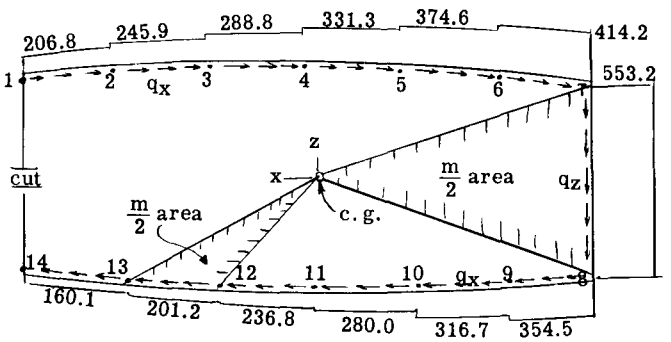

Fig. A19.27

TABLE A19.4

Calculation of Flexural Shear Flow Assuming q - zero in Web Between Flange Members (1) and (14).

(Shear values are average between stations 20 and 47.5)

1	2	3	4	5	6	7	8	9
Flange No.	P at Station 20	P at Station 47.5	$-\frac{\Delta P}{27.5}$	$q = \Sigma \frac{\Delta P}{27.5}$	m sq. in.	mq	q_1	$q_r = q + q_1$
1	-24390#	-18700	206.8	206.8	48.4	10000	-328	-121.2
2	-14070	-12990	39.1	245.9	43.8	10780	-328	- 82.1
3	-11890	-10710	42.9	288.8	42.0	12120	-328	- 39.2
4	-11370	-10200	42.5	331.3	42.6	14100	-328	3.3
5	-10510	- 9320	43.3	374.6	43.6	16340	-328	46.6
6	-11090	-10000	39.6	414.2	42.0	17500	-328	86.2
7	-16700	-12880	139.0	553.2	197.0	108900	-328	225.2
8	28230	22770	-198.7	354.5	47.4	16800	-328	26.5
9	11180	10140	- 37.8	316.7	37.2	11800	-328	- 11.3
10	11170	10160	- 36.7	280.0	40.8	11420	-328	- 48.0
11	6430	5240	- 43.2	236.8	42.2	10000	-328	- 91.2
12	10390	9410	- 35.6	201.2	38.0	7650	-328	-126.8
13	9600	8470	- 41.1	160.1	54.0	8650	-328	-167.9
14	23020	18600	-160.3	0	204.0	0	-328	-328
1								
Total mq =						256060		

For equilibrium of all the forces in the plane of the cross-section ΣM_y must equal zero. For convenience we will select a moment y axis through the c.g. of the cross-section. The moment of the shear flow q on any sheet element equal q times double the area of the triangle formed by joining the c.g. with lines going to each end of the sheet element. These double areas are referred as m values (See Fig. A19.27). Column 6 of Table A19.4 records these double areas which were obtained by use of a planimeter. Column (7) gives the moment of each shear flow about the c.g. and the total of this column gives the moment about the c.g. of the complete shear flow system of Fig. A19.27 or a value of 256060 in.lb.

The double areas (m) can be found approximately as follows:

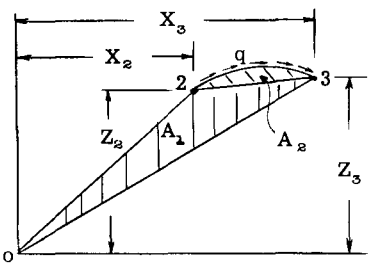

The moment of the shear flow q on the web (2-3) about point O equals q times twice the area $(A_1 + A_2)$. In most cases, the area A_2 can be neglected.

By simple geometry, the area $A_1 = 1/2 (X_3 Z_2 - X_2 Z_3)$. The moment of the shear flow q on web (2-3) thus equals $q (X_3 Z_2 - X_2 Z_3)$. Since values of X and Z for all flange points with reference to section (c.g.) are given in the Table A19.2, it is unnecessary to use the planimeter except for regions of sharp curvature.

MOMENT OF EXTERNAL LOADS ABOUT c.g. OF STATION 20

As stated before the engineers in the applied loads calculation group supply the shears and moments at various spanwise stations. We will assume that these loads are: $V_Z = 12000$ lb., $V_X = +2700$ lb., $M_y = - 390{,}000$ in.lb. The location of the reference y axis used by the loads group will be assumed as located at point O in Fig. A19.28 relative to cross-section at Station 20.

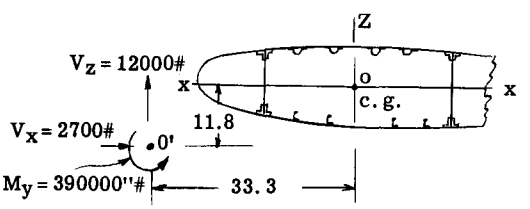

Fig. A19.28

Therefore moment of external loads about c.g. is,

$$\Sigma M_{c.g.} = 12000 \times 33.3 - 2700 \times 11.8 - 390000$$
$$= 41800 \text{ in.lb.}$$

Moments Produced by Inclination of Flange Loads With Beam Section.

Since the flange members in general are not normal to the beam sections, the flange loads

have components in the Z and X directions. Columns (4) and (7) of the Table A19.5 give the values of these in plane components. The slopes dx/dy between stations 20 and 47.5 are found by scaling from Fig. A19.24. Fig. A19.29 shows these induced in plane forces as found in Table A19.5.

TABLE A19.5

In Plane Moments About Section c.g. Produced by in Plane Components of Flange Loads

Station 20

1	2	3	4	5	6	7	8
Flange No.	p	$\frac{dx}{dy}$	$P_x = p\frac{dx}{dy}$	$M_{c.g.} = P_x Z$	$\frac{dz}{dy}$	$P_z = p\frac{dz}{dy}$	$M_{c.g.} = -(P_z X)$
1	-24390	-.046	1120	7480	.025	-610	-10600
2	-14070	0	0	0	.022	-310	- 3610
3	-11890	0	0	0	.022	-262	- 1600
4	-11370	0	0	0	.022	-250	- 112
5	-10510	0	0	0	.022	-231	1180
6	-11090	0	0	0	.025	-278	2970
7	-16700	.021	- 350	-1660	.025	-417	7770
8	28230	.021	594	-4300	.018	-508	9350
9	11180	0	0	0	.017	-190	2000
10	11170	0	0	0	.015	-167	885
11	6430	0	0	0	.015	- 96	- 57
12	10390	0	0	0	.017	-177	- 1130
13	9600	0	0	0	.018	-173	- 2020
14	23020	-.046	-1060	5640	.018	-416	- 7250
			Σ	7160			- 2224

NOTES:
Column (2); P from Table A19.2
Column (5) and (8): Values of Z and X are found in Columns 10, 11 of Table A19.2

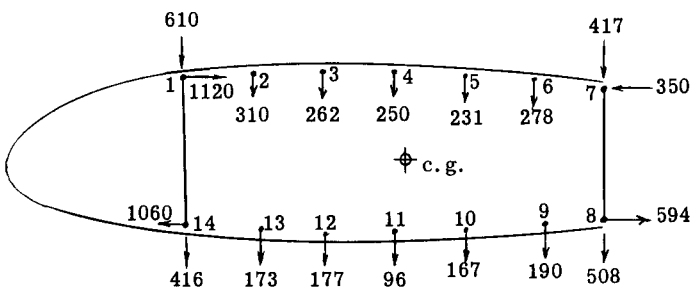

Fig. A19.29 In plane forces produced by flange axial loads.

The moments of these in plane components about the section c.g. are given in Columns (5) and (8) of Table A19.5. In general, these moments are not large.

Total Moments of All Forces About Section c.g. at Station 20:

Due to flanges = 7160 - 2224 = 4936 in.lb. (Ref. Table A19.5)

Due to assumed static shear flow = 256060 in.lb. (Ref. Table A19.4)

Due to external loads = 41800 in.lb.

Then the total unbalanced moment = 4936 + 256060 + 41800 = 302796 in.lb.

For equilibrium, this must be balanced by a constant shear flow q_1.

hence

$$q_1 = \frac{M}{2A} = -\frac{302796}{2 \times 461.5} = -328 \text{ lb./in.}$$

(Note: 461.5 = total area of cell)

The shear stresses q_1 are listed in Column (8) of Table A19.4.

The final or resultant shear flow q_r at any point therefore equals

$$q_r = q + q_1$$

The resulting values are given in Column 9 of Table A19.4. Fig. A19.30 illustrates the results graphically.

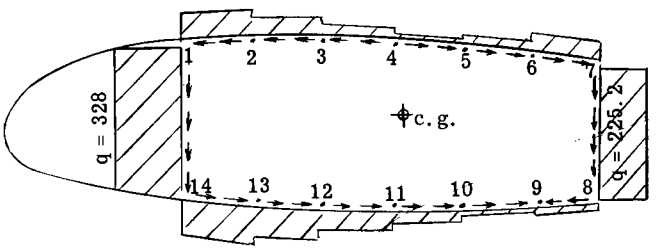

Fig. A19.30 Final shear flow diagram. For values see Column 9 of Table A19.4.

Having determined the shear flows, the shear stress on any panel would be q/t. In checking the sheet for strength in shear and combined shear and tension, interaction relationships are necessary. The strength design of sheet panels under combined stresses is covered in considerable detail in Chapter C5.

A19.14 Bending and Shear Stress Analysis of 2-Cell Multiple Stringer Tapered Cantilever Wing.

A two-cell beam is also quite common in wing structural design. A two-cell structure in bending and torsion is statically indeterminate to the second degree since the shear flow at any one point in each cell is unknown. However, due to continuity between cells the angular twist of each cell must be the same, which gives the additional equation necessary for solving a two-cell beam as compared to the single cell analysis.

Example Problem

To avoid repetition of similar type calcu-

lations as was used in the previous single cell problem, the bending and shear stresses will be determined for the same structure as in the previous example except that the leading edge cell is considered effective, thus making a 2-cell structure. Since there are no spanwise stringers in the leading edge, very little skin on the compressive side will be effective. On the tension side, the leading edge skin would be effective in resisting bending axial loads and thus the moment of inertia would be slightly different from that found in example problem 1. Since this problem is only for the purpose of illustrating the use of the equations, the leading edge skin will be neglected in computing the bending flexural stresses. With this assumption, the bending stresses and flange loads at stations 20 and 47.5 are the same as for the previous problem. (See values in column 12 and 13 of Tables A19.2 and A19.3.)

Shear Flow Calculations: -

To compute the static shear flow, each cell is assumed cut at one point as shown in Fig. A19.31, and thus the shear flow is zero at points (a) and (b).

Fig. A19.31

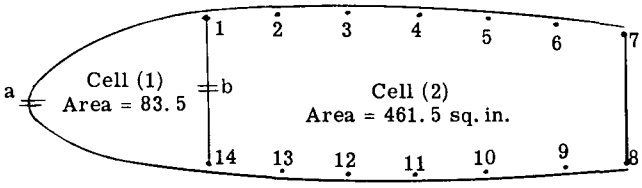

Table A19.6 (Column 5) gives the value of the static shear flow under these assumptions.

The first 7 columns of this table are the same as in Table A19.4, since no stringers have been added to cell (1), and the shear q is assumed zero in cell (1).

To make the twist of each cell the same and also to make the summation of all torsional forces zero will require two unknown constant shear flows, q_1 in cell (1) and q_2 in cell (2). Thus two equations will be written, namely:

$$\theta_1 = \theta_2 \quad \text{- - - - - - - - - - - - - - - - - (8)}$$

$$\Sigma M_{c.g.} = 0 \quad \text{- - - - - - - - - - - - - - - - - (9)}$$

The twist θ per unit length of a cell equals

$$\theta = \frac{1}{2AG} \Sigma qL/t \quad \text{- - - - - - - - - - - - - (10)}$$

The modulus of rigidity G will be assumed constant and thus will be omitted.

Consider cell (1): (Refer to Table A19.6, Columns 10 and 11)

Area of cell (1) = 83.5 sq. in.

$$\theta_1 = \frac{1}{2A_1}\left[\Sigma\, q\, L/t + \Sigma\, q_1\, L/t + \Sigma\, q_2\, L/t\right]$$

$$\theta_1 = \frac{1}{2 \times 83.5}\left[0 + 1278\, q_1 - 230\, q_2\right], \text{ whence}$$

$$\theta_1 = 7.65\, q_1 - 1.378\, q_2 \text{ - - - - - - - - (a)}$$

For cell (2):

Area of cell (2) = 461.5 sq. in.

TABLE A19.6

SHEAR FLOW - 2 CELL - MULTIPLE FLANGE TAPERED BEAM
(Average Shear Flow Between Stations 20 and 47.5)

1	2	3	4	5	6	7	8	9	10		11		12	13	14
Flange No.	P at Sta. 20	P at Sta. 47.5	$-\frac{\Delta P}{27.5}$	$q = \frac{\Sigma \Delta P}{27.5}$	m	mq	L (in.)	t	L/t Cell (1)	L/t Cell (2)	q(L/t) Cell (1)	q(L/t) Cell (2)	q_1	q_2	$q_r = q+q_1+q_2$
1	-24390	-18700	206.8	206.8	48.4	10000	5.75	.04		144		29800	0	-317	-110.2
2	-14070	-12990	39.1	245.9	43.8	10780	5.50	.04		137		33700	0	-317	- 71.1
3	-11890	-10710	42.9	288.8	42.8	12120	5.50	.04		137		39600	0	-317	- 28.2
4	-11370	-10200	42.5	331.3	42.6	14100	5.50	.04		137		45400	0	-317	14.3
5	-10510	- 9320	43.3	374.6	43.6	16340	5.50	.04		137		51400	0	-317	57.6
6	-11090	-10000	39.6	414.2	42.0	17500	5.50	.04		137		56700	0	-317	97.2
7	-16700	-12880	139.0	553.2	197.0	108900	12.25	.032		382		211500	0	-317	236.2
8	28230	22770	-198.7	354.5	47.4	16800	5.5	.032		172		61000	0	-317	37.5
9	11180	10140	- 37.8	316.7	37.2	11800	5.0	.032		156		49400	0	-317	0
10	11170	10160	- 36.7	280.0	40.8	11420	5.8	.032		181		50650	0	-317	- 37
11	6430	5240	- 43.2	236.8	42.2	10000	5.8	.032		181		42900	0	-317	- 80.2
12	10390	9410	- 35.6	201.2	38.0	7650	5.3	.032		166		33400	0	-317	-115.8
13	9600	8470	- 41.1	160.1	54.0	8650	5.5	.032		172		27600	0	-317	-156.9
14	23020	18600	160.3	0	204	0	11.75	.051	230	230	0	0	-62.8	-317	-254.2
1															
Lead edge web				0	371		33.5	.032	1048		0		-62.8		-62.8
Sum						256060			1278	2469	0	733050			

NOTES: L = length of web sheet between flange members. Col. 4 = (Col. 2 + Col. 3)/27.5
t = web thickness.

$$\theta_2 = \frac{1}{2 \times 461.5}\left[733050 - 230\, q_1 + 2469\, q_2\right]$$

$$\theta_2 = 794 - .2495\, q_1 + 2.678\, q_2 \quad - - - - \text{(b)}$$

For continuity θ_1 must equal θ_2, hence equating (a) and (b):

$$7.899\, q_1 - 4.056\, q_2 - 794 = 0 \quad - - - - \text{(c)}$$

For equilibrium the summation of all moments in the plane of the cross-section about the section (c.g.) must be equal to zero, or

$$\Sigma M_{c.g.} = 0$$

The moment of the external loads about the section c.g. is the same as in previous problem.

$$M_{\text{external forces}} = 41800 \text{ in.lb.}$$

The induced moment due to the in plane components of the flange axial loads is likewise the same as in previous problem (see Table A19.5).

$$M_{\text{due to flange loads}} = 4936 \text{ in.lb.}$$

The torsional moment due to the static shear flow from Column (7) of Table A19.6 equals 256060 in.lb. The torque due to the unknown constant shear flows of q_1 and q_2 is equal to twice the enclosed area of each cell times the shear flow in that cell, whence

$$M_{(\text{due to } q_1 \text{ and } q_2)} = 2 \times 83.5\, q_1 + 2 \times 461.6\, q_2$$
$$= 167\, q_1 + 923\, q_2$$

$$\text{Therefore } \Sigma M_{c.g.} = 167\, q_1 + 923\, q_2 + 302796 = 0 \quad - - - - - \text{(d)}$$

Solving equations (c) and (d), we obtain,

$$q_1 = -62.8 \text{ lb./in.}, \quad q_2 = -317 \text{ lb./in.}$$

These values are listed in columns (12) and (13) of Table A19.6. The final or resultant shear flow q_r on any sheet panel equals the sum of $q + q_1 + q_2$. The results are shown in column (14) of Table A19.6. Fig. A19.32 shows the potted shear flow pattern. Comparing this figure with Fig. A19.30 shows the effect of adding the leading edge cell to the single cell of the previous problem.

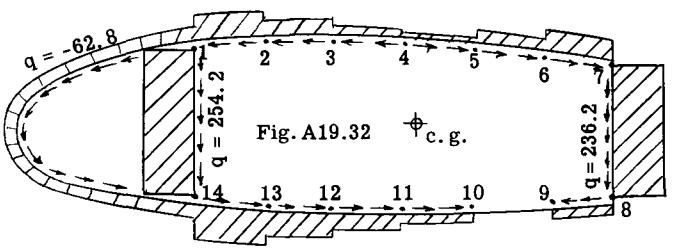

A19.15 Bending Strength of Thick Skin - Wing Section

Figs. i and k of Fig. A19.3 illustrate approximate shapes for airfoils of supersonic aircraft. Such airfoils have relatively low thickness ratios and since supersonic military aircraft have comparatively high wing loadings, it is necessary to go to thick skin in order to resist the wing bending moments efficiently. The ultimate compressive stress of such structures can be made rather uniform and occurring at stresses considerably above the yield point of the material. Since structures must carry the design loads without failure, it is necessary to be able to calculate the ultimate bending resistance of such a wing section if the margin of safety is to be given for various load conditions.

The question of the ultimate bending resistance of beam sections that fail at stresses beyond the elastic stress range is treated in Article A13.10 and example problem 7 of Chapter A13 and should be studied again before proceeding with the following example problem.

A19.16 Example Problem

To illustrate the procedure of Art. A13.10, a portion of a thick skin wing section as illustrated in Fig. A19.34 will be considered.

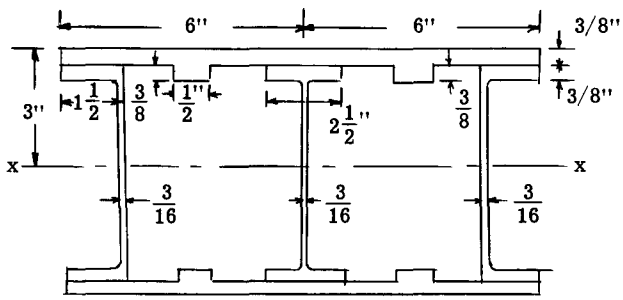

Fig. A19.34

For simplicity the section has been drawn symmetrical about the x-x axis. The material is aluminum alloy. In this problem the material stress-strain curves will be assumed the same in both tension and compression. The problem is to determine the margin of safety for this beam section when subjected to a design bending moment M_X = 1,850,000 in.lb.

SOLUTION:

Since it is desirable to use the beam formula $\sigma_b = M_X z / I_X$, it is necessary to obtain a modified beam section to correct for the non-linear stress-strain relationship since the give structure will fail under stresses in the inelastic zone. The maximum compressive stress at surface of beam will be assumed at 50000 psi. This value could be calculated from a consider-

ation of crippling and column strength of the stiffened skin, a subject treated later.

Curve (A) of Fig. A19.35a is a portion of the compressive stress-strain diagram of the aluminum alloy material from zero to 50,000 psi.

Due to symmetry about the x-x axis, we need only to consider one half of the beam section. We divide the upper half of the beam section into horizontal strips, each 3/8 inch thick. Each beam portion along these horizontal strips can be placed together to form the areas labeled (1) to (8) in Fig. b of Fig. A19.35. Since plane sections remain plane after bending in both elastic and inelastic stress zones, Fig. c shows the beam section strain picture.

Fig. A19.35

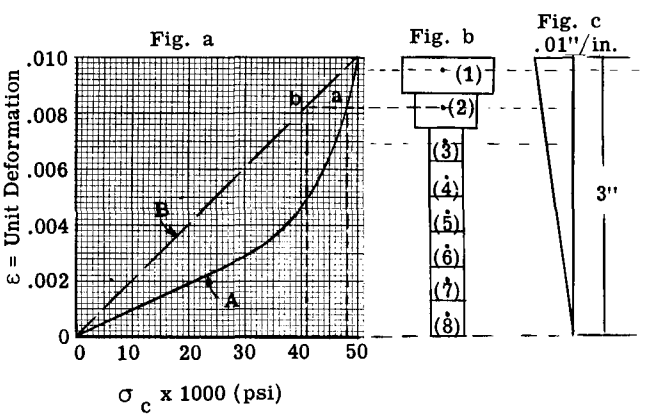

Table A19.7 shows the calculations for obtaining the modified moment of inertia of the cross-section to use with the linear beam formula.

TABLE A19.7

1	2	3	4	5	6	7	8
Portion	Area A	σ_c	σ_c'	K = σ_c/σ_c'	A_e = KA	Arm Z	A_eZ^2
1	4.500	49200	46900	1.049	4.71	2.8125	37.30
2	2.437	48000	40600	1.182	2.88	2.4375	17.14
3	0.211	46000	34400	1.340	0.282	2.0625	1.20
4	0.211	43200	28100	1.539	0.324	1.6875	0.92
5	0.211	39200	21840	1.790	0.378	1.3125	0.65
6	0.211	33200	15620	2.121	0.449	0.9375	0.38
7	0.211	20500	9360	2.190	0.461	0.5625	0.15
8	0.211	7000	3120	2.240	0.473	0.1875	0.02
						Σ	57.76
							2
						I_x =	115.52

Col. (2) = Area of Strip
Col. (3) Stress at midpoint of strip as read from Curve (A)
Col. (4) Stress at midpoint of strip as read from Curve (B)
Col. (5) Nonlinear Correction Factor K = σ_c/σ_c'
Col. (6) Modified Area = A_e = KA
Col. (7) Arm from Neutral Axis to Midpoint of Strip
Col. (8) Modified section moment of inertia

The values in column (3) of Table A19.7 represents the true compressive stress at the midpoint of a strip area when the beam is resisting its maximum or failing bending moment. The values in column (4) represent the compressive stress at the midpoint of the strip areas if the bending stress is linear and varying from zero at neutral axis to 50000 psi at edge of beam section (Curve B of Fig. A19.35a).

To illustrate, consider strip area number (2) in Fig. b of A19.35. Project a horizontal dashed line from midpoint of this strip until it intersects curves A and B at points (a) and (b) respectively. From these intersection points project downward to read values of 48000 and 40600 psi respectively.

In using the linear beam formula, the stress intensity on strip (2) would be 40600 but actually it is 48000. The ratio between the two is given the symbol K. Thus to modify the linear stress to make it equal to the nonlinear stress we increase the true strip areas by the factor K, giving the results of column (6).

The modified moment of inertia (column 8) equals I_x = 115.52.

The design bending moment was 1,850,000 in.lb.

Consider point at midpoint of strip (1)

Z = 2.8125 inches

$\sigma_b = M_x Z/I_x$ = (1,850,000 x 2.8125)/115.52
= 45100 psi.

This stress is based on the modified strip areas. The true stress $\sigma_{b(t)}$ on strip 1 thus equals $K\sigma_b$ = 1.049 x 45100 = 47400. The allowable stress at failure equals 49200 from column (3) of Table A19.7. Hence margin of safety = (49200/47400) - 1 = .04 or 4 percent.

The margin of safety for other points on the beam section will likewise be 4 percent. For example at midpoint of strip (3), Z = 2.0625. K=1.34

whence $\sigma_{c_t} = \left[(1{,}850{,}000 \times 2.0625)/115.52\right]1.34$
= 44400.

whence margin of safety = (46000/44400)
- 1 = .04

The moment of inertia without modifying the strip areas would come out to be I_x = 104.42 hence the stress at midpoint of strip (1) would calculate to be σ_b = (1,850,000 x 2.8125)/104.42 = 49900. The allowable stress for linear stress variation would be 46900 from column (4) of Table. Hence margin of safety would be

(46900/49900) - 1 = -.06. The elastic theory thus gives a margin of safety 10 percent less than the strength given when true stress-strain or non-linear relationship is used.

If the same comparison was made for bending about Z axis of this same beam section the difference would be considerably more than 10 percent as more beam area is acting in the region of greater discrepancy between curves A and B.

A19.17 Application to Practical Wing Section

A practical wing section involves these facts: - (1) The section is unsymmetrical; (2) external load planes change their direction under different flight conditions; (3) the material stress-strain curves are different in tension and compression in the inelastic range.

Since the stress analyst must determine critical margins of safety for many conditions, it would be convenient to have an interaction curve involving M_X and M_Z bending moments which would cause failure of the wing section. This interaction curve could be obtained as follows:-

(1) Choose a neutral axis direction and its location.

(2) Assuming that plane sections remain plane, and taking the maximum strain as that causing failure of the compressive flange, use the stress-strain curve to determine the longitudinal stress and then the internal load on each element of the cross-section. A check on the location of the assumed neutral axis is that the total compression on cross-section must equal total tension. Since the location was assumed or guessed, the neutral axis must be moved parallel to itself to another location and repeated until the above check is obtained.

(3) Find the internal resisting moment about the neutral axis and an axis normal to the neutral axes. Resolve these moments into moments about x and z axes or M_X and M_Z. These resulting values of M_X and M_Z are bending moments which acting together will cause failure of the wing in bending.

(4) Repeat steps 1, 2 and 3 for several other directions for a neutral axis which results will give additional combinations of M_X and M_Z moments to cause wing failure. Thus an interaction curve involving values of M_X and M_Z which cause failure of wing in bending is obtained and thus the margin of safety for any design condition is readily obtainable.

A19.18 Shear Lag Influences

In the beam theory, the assumption is made that plane sections remain plane after bending. In a beam involving sheet and stringer panels, this assumption means that the sheet panels have infinite shearing rigidity, which of course is not true as shearing stresses produce shearing strains. The effect of sheet panel shear strains is to cause some stringers to resist less axial load than those calculated by beam theory. This decreased effectiveness of stringers is referred to as "shear lag" effect, since some stringers tend to lag back from the position they would take if plane sections remain plane after bending.

In general, the shear lag effect in sheet-stringer structures is not appreciable except for the following situations: -

(1) Cutouts which cause one or more stringers to be discontinued.

(2) Large abrupt changes in external load applications.

(3) Abrupt changes in stringer areas.

In Chapters A7 and A8, strains due to shearing stresses were considered in solving for distortions and stresses in structures involving sheet-stringer construction. Even in these so-called rigorous methods, simplifying assumptions must be made as for example, shear stress is constant over a particular sheet panel and estimates of the modulus of rigidity for sheet panels under a varying state of buckling must be made. The number of stringers and sheet panels in a normal wing is large, thus the structure is statically indeterminate to many degrees and solutions necessitate the use of high speed computors. Before such analyses can be made, the size and thickness of each structural part must be known, thus rapid approximate methods of stress analysis are desirable in obtaining accurate preliminary sizes to use in the more rigorous elastic analysis.

To illustrate the shear lag problem in its simplest state, consider the three stringer-sheet panel unit of Fig. A19.36. The three stringers are supported rigidly at B and equal loads P are applied to the two edge stringers labeled (1) at point (A). The center stringer (2) has zero axial load at (A), but as end B is approached, the sheet panels transfer some of the load P to the center stringer by shear stresses in the sheet. At the support points B the transfer of load from side stringers to center stringer is such as to make the load in all three stringers approximately equal or equal to 2P/3.

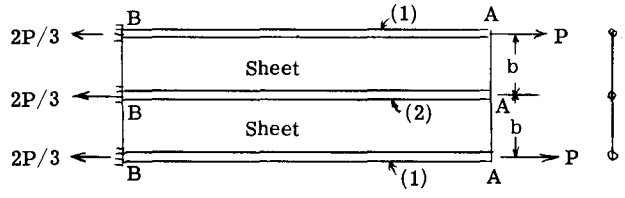

Fig. A19.36

The theoretical load in center stringer can be calculated by methods of Chapter A7 and A8, and the results would give the solid curve of Fig. A19.37. To simplify the solution, it is common practice to assume the load distribution in the center stringer to vary according to the dashed curve in Fig. A19.37 which indicates that in a distance 3b, the load 2P is equalized between the three stringers.

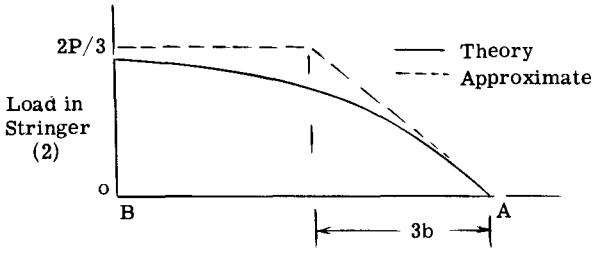

Fig. A19.37

A19.19 Application of Shear Lag Approximation to Wing with Cut-Out.

Fig. A19.38 shows the top of a multiple stringer wing which includes a cut-out in the surface. The stringers (5), (6) and (7) must be discontinued through the cut-out region.

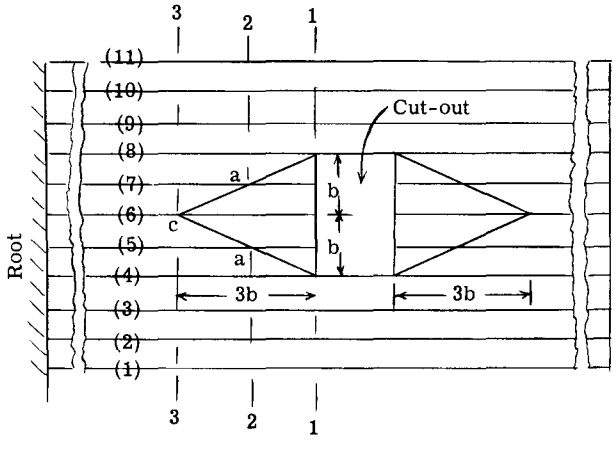

Fig. A19.38

It is assumed that the effectiveness of these 3 interrupted stringers is given by the triangles in the figure. At beam section 1-1 these stringers have zero end load. The stringer load is then assumed to increase linearly to full effectiveness when it intersects the sides of this triangle whose height equals 3b. At beam section 2-2 stringers (5) and (7) have become effective since they intersect triangle at points (a) on section 2-2. At section 3-3 point c, stringer (6) becomes fully effective.

To handle shear lag effect in a practical wing problem another column would be inserted in Table A19.1 between columns (3) and (4) to take care of the shear lag effect. The shear lag effectiveness factor which we will call R would equal the effectiveness obtained from a triangle such as illustrated in Fig. A19.38.

For example, the shear lag factor R at beam section 1-1 in Fig. A19.38 would be zero for stringers (5), (6) and (7) and one for all other stringers. At beam section 2-2 stringers (5) and (7) have a factor R = 1.0 since they are fully effective at points (a). Stringer (6) is only 50 percent effective since section 2-2 is halfway from section 1-1 to point (c), thus R = 0.5 for stringer (6). At beam section 3-3, stringer (6) becomes fully effective and thus R = 1.0 for all stringers. The final modified stringer area (A) in column (4) of Table A19.1 would then equal the true stringer area plus its effective skin times the factors KR. The procedure from this point would be the same as discussed before. Thus shear lag approximations can be handled quite easily by modifying the stringer areas. Using these modified stringer areas, the true total loads in the stringers are obtained. The true stresses equal these loads divided by the true stringer area, not the modified area.

A19.20 Approximate Shear Lag Effect in Beam Regions where Large Concentrated Loads are Applied.

Wing and fuselage structures are often required to resist large concentrated forces as for example power plant reactions, landing gear reactions, etc. To illustrate, Fig. A19.39 represents a landing condition, with vertical load. The wing is a box beam with 7 stringers

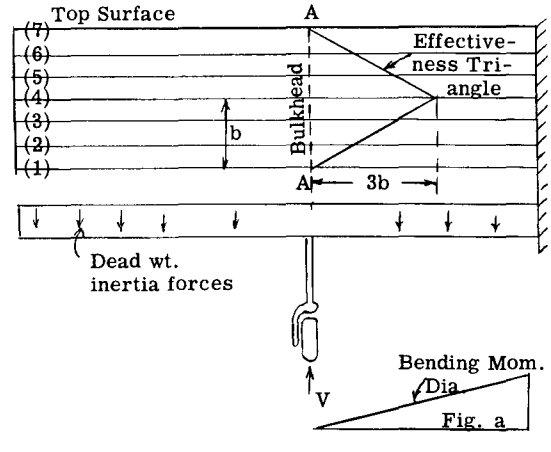

Fig. A19.39

and flange members. Fig. (a) shows the bending moment diagram due to the landing gear reaction alone. The internal resistance to this bending moment cannot be uniform on a beam section adjacent to section A-A because of the shear strain in the sheet panels or what is called shear lag effect. To approximate this stringer effectiveness, a shear lag triangle of length 3b is assumed, and the same procedure as discussed in the previous article on cut-outs is used in finding the longitudinal stresses. It should be understood that the bending moments due to the distributed forces on the wing such as air loads and dead weight inertia loads are not included in the shear lag considerations, only the forces that are applied at concentrated points on the structure and must be distributed into the beam. A side load on the gear or power plant would produce a localized couple plus an axial force besides a shear force as in Fig. A19.39. The resistance to this couple and axial force would likewise be based on the effectiveness triangle in Fig. A19.39.

A19.21 Approximation of Shear Lag Effect for Sudden Change in Stringer Area

Stringers of one size are often spliced to stringers of smaller size thus creating a discontinuity because of the sudden change in stringer area.

Fig. A19.40 shows the stringer arrangement in a typical sheet-stringer wing. Stringer B is spliced at point indicated. The stringer area A_2 is decreased suddenly by splicing into a stringer with less area A_1.

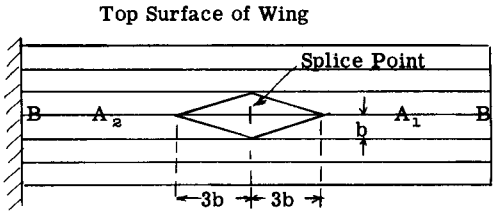

Fig. A19.40

To approximate the shear lag effect, assume the area of stringer B at splice point to be the average area of the two sides or $(A_1 + A_2)/2$. This average area is then assumed to taper to A_2 and A_1 at a distance 3b from the splice point. The shear lag effectiveness factor R will therefore be greater than 1.0 on the side toward the smaller stringer A, and less than one on the side toward the stringer with the greater area A_2, since the average area was used for the splice point.

A19.22 Problems

(1) Fig. A19.41 shows a cantilever, 3 stringer, single cell wing. It is subjected to a distributed airload of 2 lb./in.^{2} average intensity acting upward in the z direction and 0.25 lb./in.^{2} average intensity acting rearward in the x direction. The center of pressure for z forces is on the 25 percent of chord line measured from the leading edge edge and at mid-height of spar AB for the x air forces. Assume the 3 stringers A, B, C develop the entire resistance to external bending moments. Find axial loads in stringers A, B, C and the shear flow in the 3 sheet panels of cell (1) at wing stations located 50", 100" and 150" from wing tip. Consider structure to rear of cell (1) as only carrying airloads forward to cell (1) and not resisting wing torsion or bending.

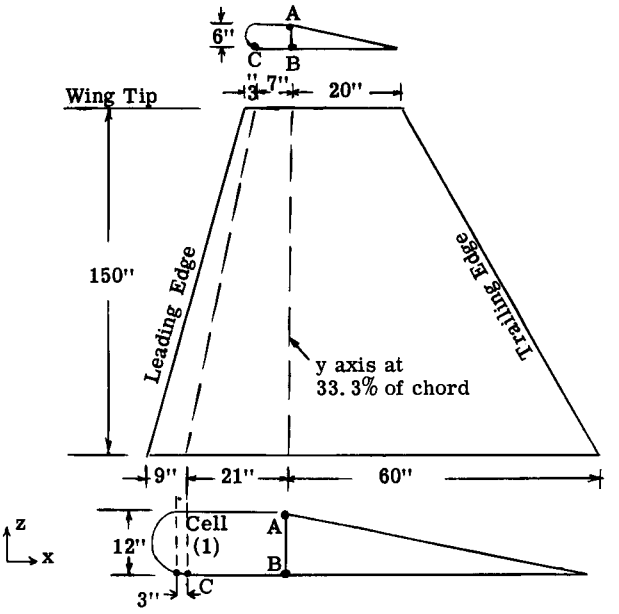

Fig. A19.41

Fig. A19.42

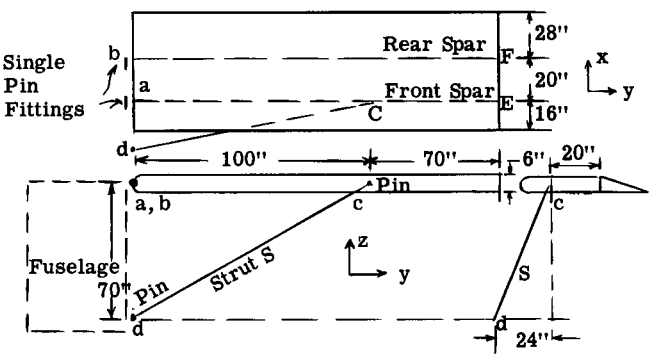

(2) Fig. A19.42 shows a monoplane wing with one external brace strut. The wing is fastened to fuselage by single pins at points (a) and (b). The fitting at (b) is designed to take off drag reaction. The airloads are w_Z = 40 lb./in. of wing span, with center of pressure at 30 percent of chord from leading edge and acting upward,

and w_x = 5 lb./in., acting to rear and located at mid-depth of wing. Find reactions at points (a), (b) and (d). Find axial loads on front and rear spars. Find primary bending moments on front spar. Find shear flow on webs and walls. Neglect structure forward of front spar and rearward of rear spar.

(3) Fig. A19.43 shows a portion of a single cell - multiple stringer cantilever wing. The external air loads are:

w_z = 100 lb./in. acting upward and whose center of pressure is along a y axis coinciding with stringer (8).

w_x = 6 lb./in. acting to rear and located at mid-depth of wing.

Table A gives the stringer areas at stations 0 and 150. Assume stringers have linear variation in area between these two stations. Use 30t as effective skin with compression stringers.

Find axial loads in stringers at stations 150 and 130 and determine shear flow system at station 150.

(4) Same as problem (3) but add an internal web of .04 thickness connecting stringers (3) and (8).

(5) Same as problem (4) but add a leading edge cell with radius equal to one-half the front spar depth. Take skin thickness as .04 inches.

TABLE A

Flange No.	Area	
	Sta. 150	Sta. 0
1	1.0	.20
2	.25	.10
3	.25	.10
4	.25	.10
5	.80	.10
6	.70	.10
7	.25	.10
8	.25	.10
9	.25	.10
10	.85	.20

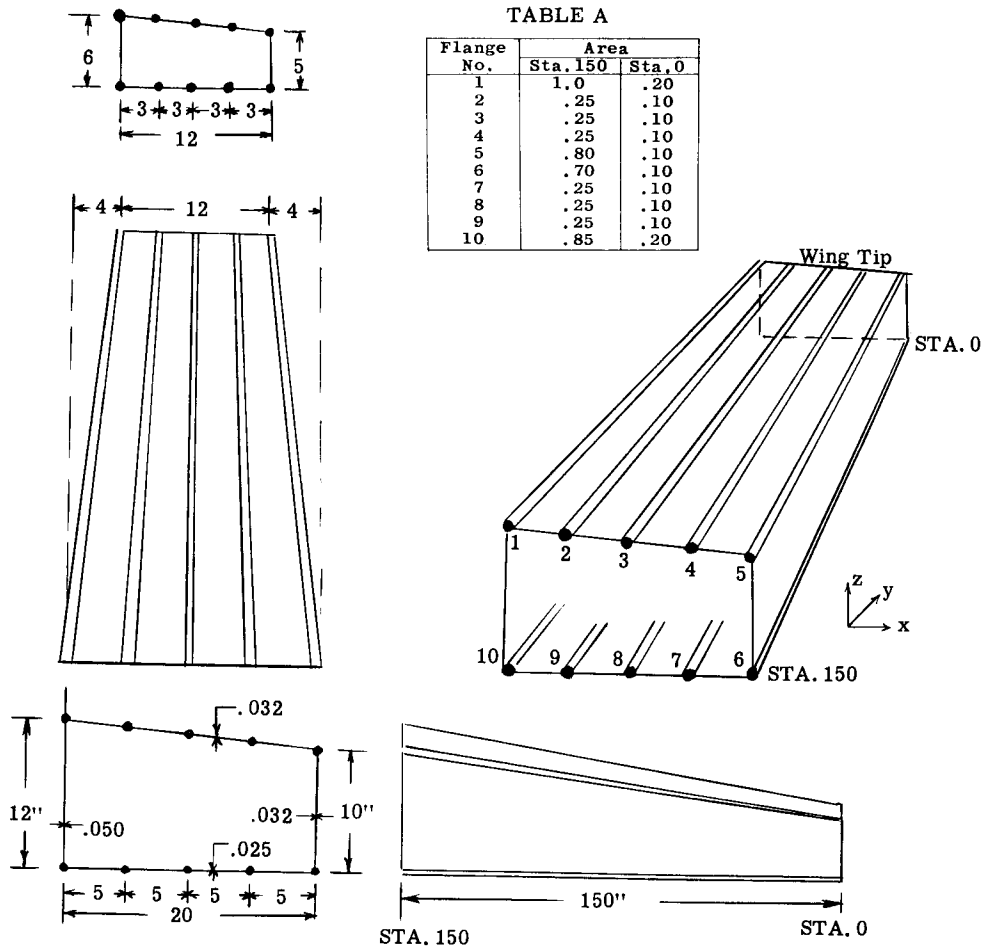

Fig. A19.43

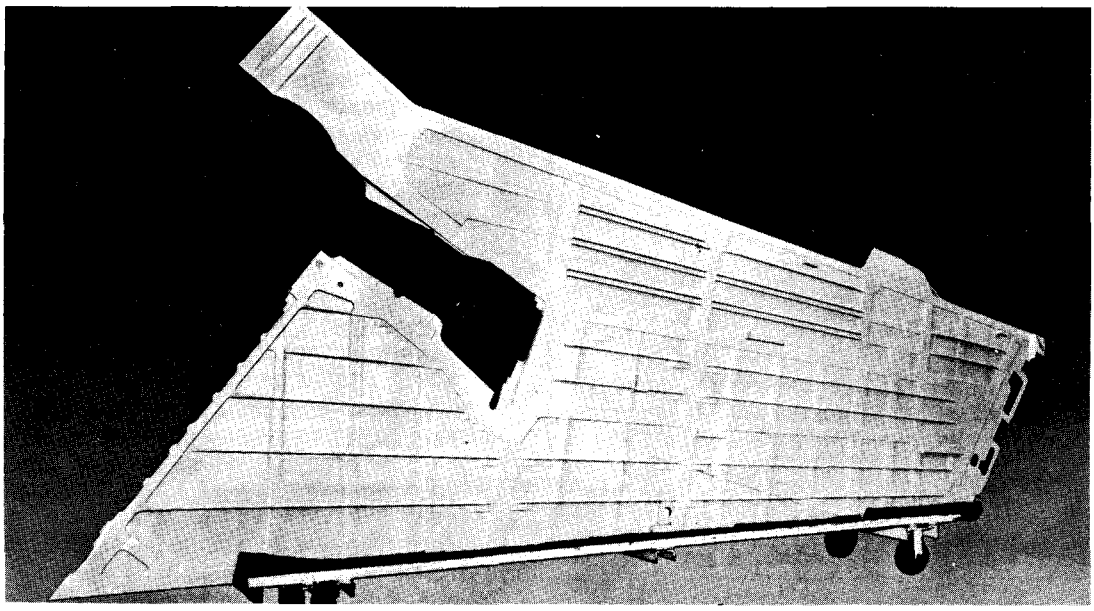

North American Aviation FJ3 "Fury Jet". View Shows Bottom Wing Skin. Note Integral Construction of Skin and Stringers.

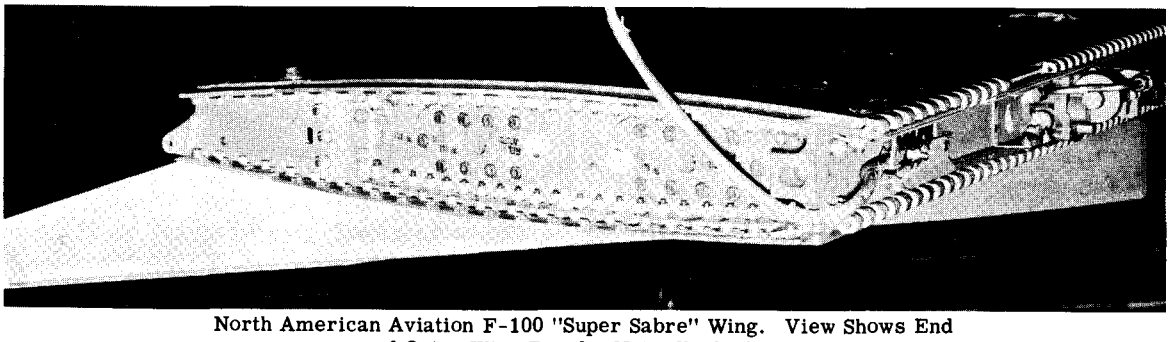

North American Aviation F-100 "Super Sabre" Wing. View Shows End of Outer Wing Panel. Note Thick Skin.

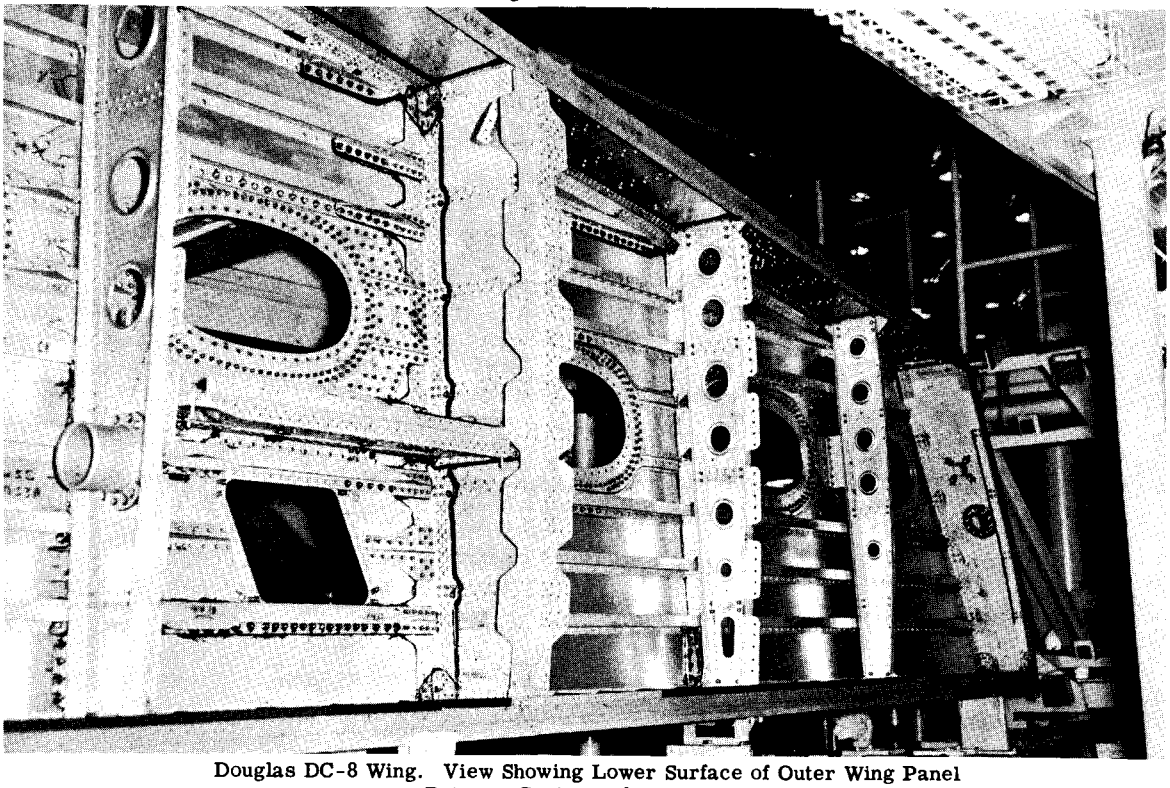

Douglas DC-8 Wing. View Showing Lower Surface of Outer Wing Panel Between Center and Rear Spar.

CHAPTER A20
INTRODUCTION TO FUSELAGE STRESS ANALYSIS

A20.1 General. In general the purpose of an airplane is to transport a commercial payload or a military useful load. The commercial payload of a modern airliner may be 100 or more passengers and their baggage. These passengers must be transported safely and comfortably. For example, an airliner flies at high altitudes where temperatures may be far below zero and where the air density is such as not to sustain human life. These facts mean that the body which carries the passengers must be heated, ventilated and pressurized to provide the necessary safety. Air travel must be acceptable to the passengers, thus the airplane body must shield the passengers from excessive noise and vibration, and furthermore efficient, restful and attractive furnishings must be provided to make travel enroute comfortable and enjoyable. The portion of the airplane which houses the passengers on payload is referred to as the fuselage. Fuselages vary greatly in size and configuration. For example, the fuselage of a supersonic military airplane may house only one passenger, the pilot, the remainder of the fuselage interior space being used to house the power plant, to provide retracting space for landing gear, and to house the many mechanical and electronic installations which are necessary to fly the airplane and carry out the various operations for which the airplane was designed to accomplish. Many groups of engineers with various backgrounds of training and experience are therefore concerned with the design of the fuselage. The structures engineer plays a very important part because he is responsible for the strength, rigidity and light weight of the fuselage structure.

A20.2 Loads. Basic Structure.

The wing, being the lifting body is subjected to large distributed surface air forces, whereas the fuselage is subjected to relatively small surface air forces. The fuselage is subjected to large concentrated forces such as the wing reactions, landing gear reactions, empennage reactions, etc. In addition the fuselage houses many items of various sizes and weights which therefore subject the fuselage to large inertia forces. In addition, because of high altitude flight, the fuselage must withstand internal pressures, and to handle these internal pressures efficiently requires a circular cross-section or a combination of circular elements.

The student should refer to Chapter A4 for further discussion of loads on aircraft and also to Chapter A5, where example calculations of fuselage shears and moments are presented.

The basic fuselage structure is essentially a single cell thin walled tube with many transverse frames or rings and longitudinal stringers to provide a combined structure which can absorb and transmit the many concentrated and distributed applied forces safely and efficiently. The fuselage is essentially a beam structure subjected to bending, torsional and axial forces. The ideal fuselage structure would be one free of cut-outs or discontinuities, however a practical fuselage must have many cut-outs. Fig. (a) shows the basic interior fuselage structure of a small airplane with skin removed. It consists of transverse frames and longitudinal stringers. Photographs 1, 2 and 3 illustrate fuselage construction of late model large aircraft.

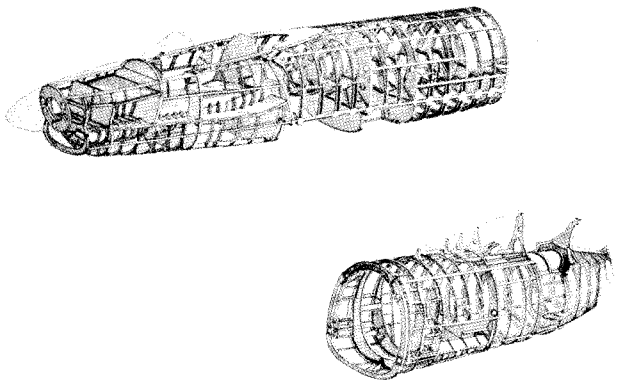

Fig. (a)

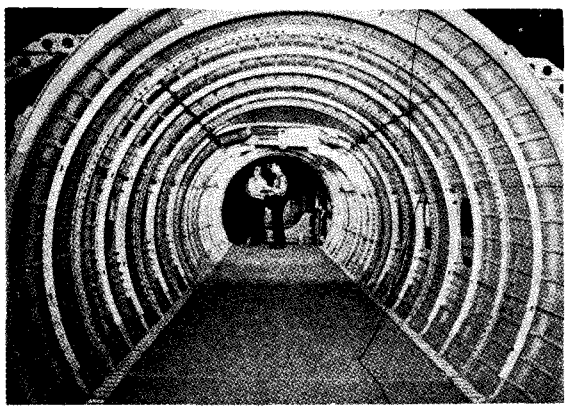

PHOTO. NO. 1
Fuselage Construction of Fairchild F-27 Transport

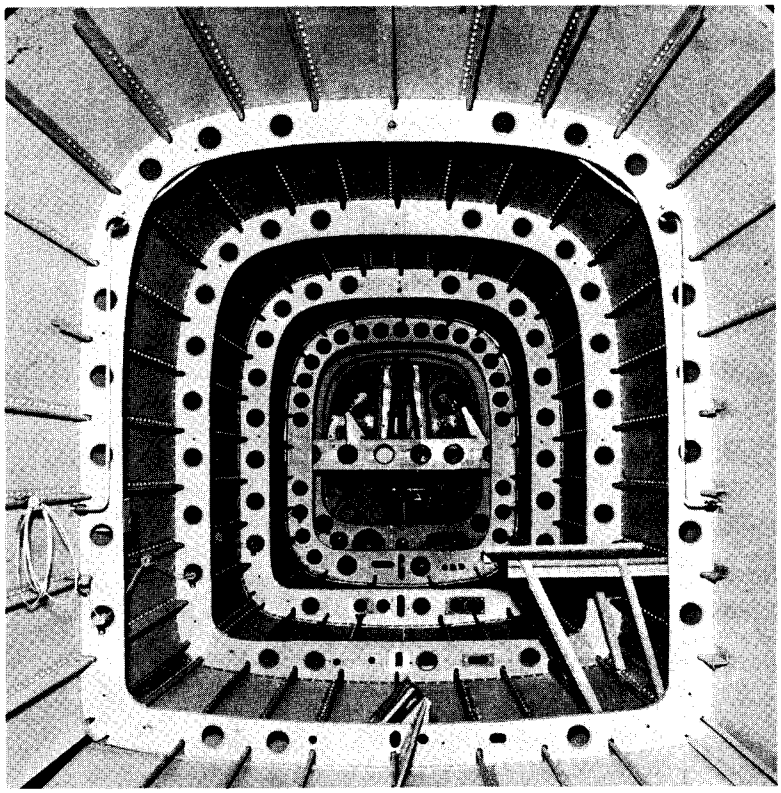

PHOTO. NO. 2
View Looking Inside of Rear Portion of Fuselage of Beechcraft Twin-Bonanza Airplane.

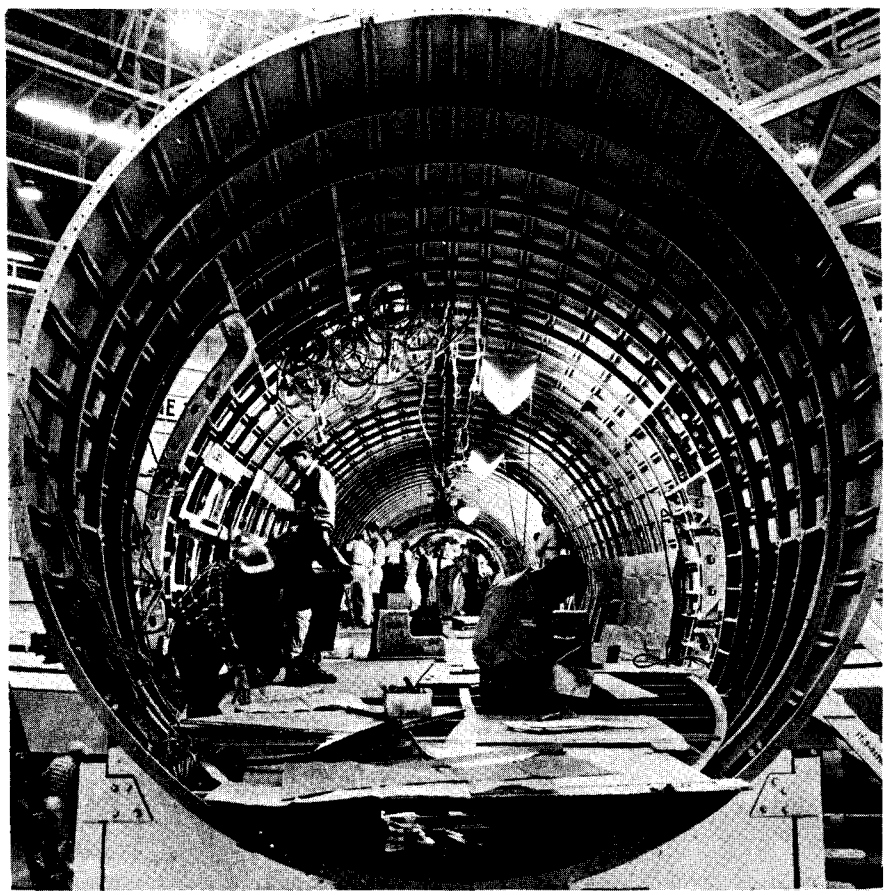

PHOTO. NO. 3
Fuselage Construction of Boeing 707 Jet Airliner.

(FOR GENERAL DETAILS OF DOUGLAS DC-8 FUSELAGE CONSTRUCTION SEE PAGE A15. 32)

A20.3 Stress Analysis Methods. Effective Cross-Section.

It is common practice to use the simplified beam theory in calculating the stresses in the skin and stringers of a fuselage structure. If the fuselage is pressurized, the stresses in the skin due to this internal pressure must be added to the stresses which resist the flight loads. In wings the skin in the middle region of the airfoil is relatively flat and thus the skin is usually considered as made up of flat sheet panels. In fuselages, however, the skin is curved and curved sheet panels have a higher critical compressive buckling stress than flat panels of the same size and thickness. In small airplanes, the radius of curvature of the fuselage skin is relatively small and thus the additional buckling strength due to this curvature may be appreciable. A simple procedure of approximately including the effect of sheet curvature will now be explained.

Fig. A20.1 illustrates a distributed stringer type of fuselage section. Assume that external loads are applied which produce bending of the beam about the Y axis with compression on the upper portion of the cell.

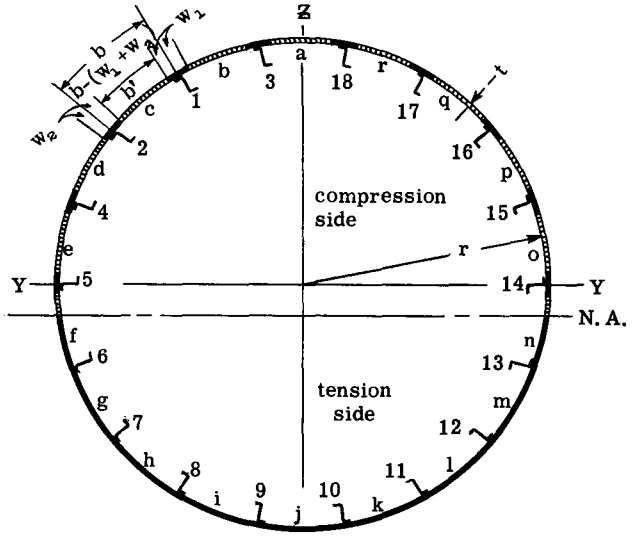

Fig. A20.1

Up to the point of buckling of the curved sheet between the skin stringers, all the material in the beam section can be considered fully effective and the bending stresses can be computed by the general flexure formula $\sigma_b = Mz/I_y$, where I_y is the centroidal moment of inertia of the entire section. When a bending compression stress is reached which causes the curved sheet between stringers to buckle, a re-arrangement takes place in the stress distribution on the section as a whole. Theory as well as experimental results indicate that the ultimate compressive strength of a curved sheet with edge stringers can be approximated by the following two assumptions.

(1) A small width of sheet w_1 on each side of the attachment line of skin to stringer is considered as carrying the same compressive stress as the stringer, as was discussed in Chapter A19. These effective sheet widths w_1 are shown as the blackened elements adjacent to the stringers on the compressive side in Fig. A20.1.

(2) The remainder of the curved sheet between stringers, namely, $b-(w_1 + w_2)$ carries a maximum compressive stress $\sigma_{cr} = .3\ E\ t/r$. This value for σ_{cr} is conservative. E is the modulus of elasticity of the skin material, t the skin thickness, and r the radius of curvature of the skin. These curved sheet elements are shown by the hatched skin lengths in Fig. A20.1.

Since the thin curved skin between the stringers normally buckles under a compressive stress far below the buckling strength of the stringers, the curved sheet is treated as an element with varying effective thickness which depends on the ratio of the curved sheet buckling stress σ_{cr} to the bending stress σ_b existing at that point for bending of the fuselage section. Hence the effective sheet thickness for the curved sheet panels can be written,

$$t_e = t\ (\sigma_{cr}/\sigma_b) \quad \text{- - - - - - - - - - - - (1)}$$

or an effective area can be written

$$A_e = b't\ (\sigma_{cr}/\sigma_b) \quad \text{- - - - - - - - - - - - (2)}$$

where b' is the width of curved sheet between the effective sheet widths w_1, w_2, etc. (See Fig. A20.1).

To illustrate this approach in obtaining the effective cross-section of a fuselage section, an example problem will be presented. The example problem will be broadened to some extent for the purpose of introducing the student to design procedure.

A20.4 Example Problem.

Let it be required to determine the stringer arrangement for the approximate elliptical shaped fuselage section shown in Fig. A20.2.

The following data will be assumed: -

Design bending moment about y axis = 1,600,000 in. lb. (producing compression on upper portion).
Zee stringers, one inch deep and with an area equal to 0.12 sq. in. shall be used.
The ultimate compressive strength of the zee stringer plus its effective skin and a length equal to fuselage frame spacing is assumed to be 32000 psi. The skin thickness is .032 and all material is (2024) aluminum alloy with E = 10,300,000 psi. The fuselage stringers are to be symmetrical about section center lines.

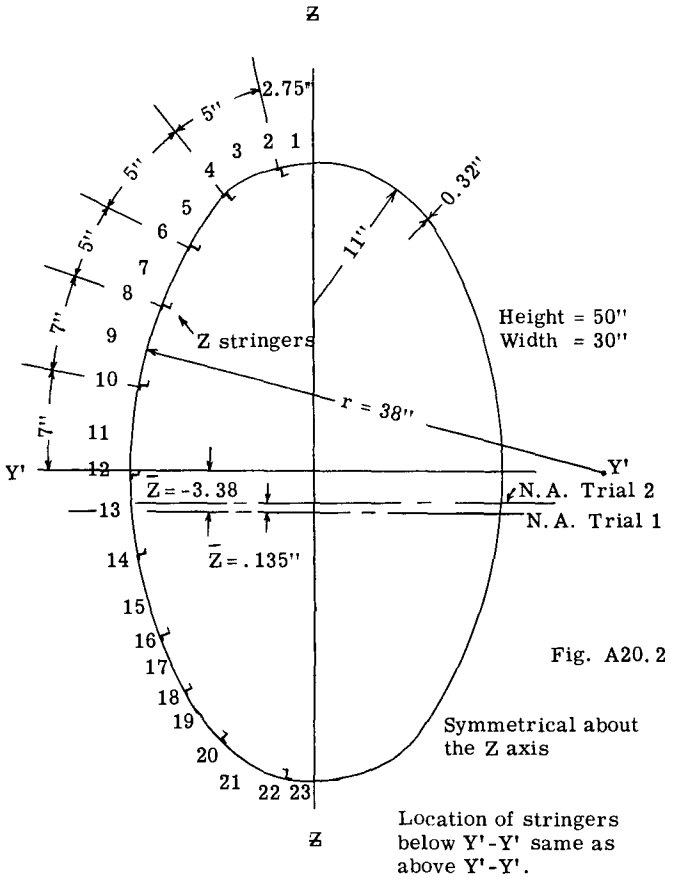

Fig. A20.2

Solution:

The first thing to do is to determine approximately how many Z stringers will be required so that a section can be obtained to work with. Since the internal resisting moment must equal the external bending moment, one can guess at the internal resisting couple in terms of total compressive flange stress and an effective internal couple arm.

For elliptical and circular sections with distributed flange material, the approximate effective resisting arm of the internal couple can be taken as 0.75 times the height h, and the average tension or compressive stress as 2/3 the maximum stress. Thus equating the external bending moment to the internal resisting moment an approximate total area A_c for the compressive side of the fuselage section can be obtained.

$$M_y = A_c\ (.67\ \sigma_b)(.75\ h), \text{ whence,}$$

$$A_c = \frac{1{,}600{,}000}{.75 \times 50 \times .67 \times 32000} = 2.0 \text{ sq. in.}$$

Part of this total area is provided by the effective skin area. The effective width to use with each rivet line equals $w = Ct\sqrt{E/\sigma_{st}}$. We will take C = 1.7 which is a commonly used value.

$$w = 1.7 \times .032\sqrt{10{,}300{,}000/32000} = .975 \text{ in.}$$

which equals a width of .975/.032 = 30.5 sheet thicknesses. Since the bending stress decreases to zero as the neutral axis is approached, and since the curved sheet between the Z stringers can carry loads up to its buckling strength, a preliminary value of effective width w = 40t will be assumed acting with each stringer. Thus total area of stringer plus effective skin equals 0.12 + 40 x .032² = 0.16 sq. in. The number of stringers required is therefore 2.00/0.16 = 12.

Fig. A20.2 shows how the stringers were placed to give 12 stringers on the top half. Since the skin on the lower half is in tension and therefore fully effective, the neutral axis will fall below the center line and thus the two stringers on the center line will be considered as part of the required 12 stringers. A fuselage cross-section has now been obtained. The desired final result is that the maximum compressive stress will be near but not over 32000 psi. The procedure from this point is still a trial and error process since the effective sheet on the compressive side depends on the magnitude of the compressive bending stress which in turn is influenced by the amount of effective sheet and the buckling load carried by the curved sheet.

Using the preliminary stringer arrangement of Fig. A20.2, Tables A20.1 and A20.2 give the calculation of the effective moment of inertia of the section about the horizontal neutral axis, Table A20.1 deals with the stringers and the effective sheet elements and Table A20.2 deals with the curved buckled sheet elements.

In the trial No. 1, the following assumptions are made:

(1) A width of 30 thicknesses of skin act with each stringer on the upper or compressive side.

(2) The area of the curved sheet between the effective sheet widths as found in (1) is modified to give an effective area by multiplying by a K factor of σ_{cr}/σ_b, where σ_{cr} is the buckling compressive stress and σ_b is the bending stress at the center of the curved sheet element assuming 32000 at the extreme upper fiber of the beam section and zero at the horizontal center line, with linear variation in between these points.

NOTE: Since the entire skin on the lower half is effective, a more logical assumption would be to guess at the location of the neutral axis and use a variation of σ_b between the neutral axis and the extreme fiber. This approach will not be used in this example.

TABLE A20.1

	TRIAL NO. 1				TRIAL NO. 2						
1	2	3	4	5	6	7	8	9	10	11	12
Flange Element No.	Area a sq.in.	Arm z'	az'	az'^{2}	$z = z' - \bar{z}$	$\sigma_b = Mz/I = -1090z$	Eff.skin w-1.7t$\sqrt{E/\sigma_b}$	Eff.skin area = wt.	Revised Eff.area a	az	az^2
2	.15	24.2	3.63	87.8	27.58	-30020	1.0	.032	.152	4.19	115.4
4	.15	22.0	3.30	72.6	25.38	-27700	1.03	.033	.153	3.88	98.5
6	.15	18.2	2.73	49.7	21.58	-23550	1.12	.036	.156	3.36	72.4
8	.15	13.3	1.99	26.4	16.68	-18200	1.28	.041	.161	2.69	44.7
10	.15	6.9	1.04	7.2	10.28	-11200	1.66	.053	.173	1.78	18.3
12	.12	0	0	0	3.38	- 3680	2.88	.092	.212	0.72	2.4
13	.224	-3.2	-0.72	2.3	-0.18				.224	- .04	0.7
14	.120	-6.9	-0.83	5.7	-3.52				.120	-0.42	1.5
15	.224	-10.1	-2.28	23.0	-6.72				.224	-1.52	10.2
16	.12	-13.3	-1.60	21.3	-9.92				.12	-1.19	11.8
17	.160	-15.8	-2.53	40.0	-12.42				.160	-1.99	24.7
18	.12	-18.2	-2.19	39.8	-14.82				.12	-1.78	26.4
19	.16	-20.3	-3.24	65.8	-16.92				.16	-2.70	45.6
20	.12	-22.0	-2.64	58.0	-18.62				.12	-2.24	41.6
21	.16	-23.7	-3.80	90.0	-20.32				.16	-3.25	66.0
22	.12	-24.2	-2.90	70.2	-20.82				.12	-2.50	52.1
23	.088	24.9	-2.19	54.5	-21.52				.088	-1.89	40.7
Stringers & Effective Skin						Sheet in Tension	Skin in Tension				
SUM = 2.49			-12.23	714.3					2.627	-2.86	673

Explanatory Notes for Table A20.1

TRIAL NO. 1

Col. 1 For numbering of stiffeners and sheet elements, see Fig. A20.2.

Col. 2 Stiffener area = .12 + 30 x .032 x .032 = .15 sq. in. For stiffeners 2, 4, 6, 8, 10. Below the centerline each stiffener is considered acting separately. The entire skin between stiffeners is considered as a unit.

Col. 3 All arms z' are measured to horizontal centerline axis.

4.5

TRIAL NO. 2

Col. 6 z = distance to neutral axis as found from results of Trial No. 1.

Col. 7 σ_b = 1600000 z/1470

Col. 8 = effective width based on stress in Col. 7

TABLE A20.2

	TRIAL NO. 1											TRIAL NO. 2						
	1	2	3	4	5	6	7	8	9	10	11	12	13	14	15	16	17	18
Buckled sheet	Sheet Element No.	b'	t	r	$\sigma_{cr} = .3Et/r$ psi	Assumed σ_b	Eff. Fact. $K = \sigma_{cr}/\sigma_b$	Eff. Area a = K t b'	z'	az'	az'^{2}	$z = z' - \bar{z}$	$\sigma_b = \frac{Mz}{I_{NA}} = -1090z$	Rev. Eff. Fact. $K = \sigma_{cr}/\sigma_b$	Revised Width b'	Revised Eff. Area a = K t b'	az	az^2
	1	2.27	.032	11	-9000	-31900	.282	.020	24.9	0.50	12.4	28.28	-30800	.292	2.25	.021	.59	16.7
	3	4.04	.032	11	-9000	-30300	.296	.038	23.7	0.90	21.3	27.08	-29500	.305	3.99	.039	1.06	28.7
	5	4.04	.032	24	-4510	-26000	.173	.022	20.3	0.45	9.1	23.68	-25800	.174	3.93	.022	0.52	12.3
	7	4.04	.032	38	-2600	-20200	.128	.016	15.8	0.25	3.9	19.18	-20900	.124	3.80	.015	0.29	5.5
	9	6.04	.032	38	-2600	-12900	.201	.039	10.1	0.40	4.0	13.48	-14700	.177	5.53	.031	0.42	5.7
	11	6.52	.032	38	-2600	- 4100	.63	.131	3.2	0.42	1.3	6.58	- 7200	.362	4.73	.055	0.36	2.4
TOTALS								.266		2.92	52.0	TOTALS				.183	3.24	71.3

Explanatory Notes for Table A20.2

Trial No. 1

Col. 1, 2, 3, 4 (see Fig. A20.1 for meaning of terms)

Col. 5 E = 10,300,000 for aluminum alloys

Col. 6 σ_b varies as a straight line from 32000 at top of cell to zero at centerline

Col. 9 z' = distance from centroid of element to centerline axis of cell

Explanatory Notes for Table A20.2

Trial No. 2

Col. 12 z - distance to neutral axis as found in results of Trial No. 1

Col. 13 σ_b = 1600000 z/1470

Col. 14 based on stress σ_b of Col. 13

Results of Trial No. 1

Considering results of both Tables and multiplying by 2 since only one half of cell was considered:

$\sum a$ = total effective area = (2.49 + .266)2

= 5.51 sq. in.

$\sum az'$ = (-12.23 + 2.92)2 = -18.62

$\bar{z} = \sum az'/\sum a$ = -18.62/5.51 = -3.38"

$I_{NA} = 2(714.3 + 52) - 5.51 \times \overline{3.38}^2 = 1470$ in.^{4}

Results of Trial No. 2

Total effective area = (2.627 + .183)2 = 5.62

$\sum az$ = (-2.86 + 3.24)2 = 0.76

$\bar{z}$ = .76/5.62 = .135" above N.A. of trial 1.

$I_{NA} = 2(673 + 71.3) - 5.62 \times .135^2 = 1489$

Due to the symmetry of the section, Tables A20.1 and A20.2 give calculations for only one-half of the material, thus the results are multiplied by two. General explanatory notes are given below each table.

The results of trial No. 1 give a neutral axis 3.38" below the center line and a moment of inertia of 1470 in.^{4}. In Trial No. 2, the effective sheet widths are based on the moment of inertia of 1470. The results of trial No. 2 give a moment of inertia of 1489 in.^{4} with a neutral axis .135" above the first location. If a third trial were used, making use of the 1489 moment of inertia, the change would be quite small since the effect of a small change in stress on the effective sheet width is negligible.

The compressive stress on stringer No. 2 using the resulting moment of inertia and neutral axis location, therefore becomes

$$\sigma_b = M_y Z/I_y = 1{,}600{,}000 \times 27.45/1489 = 29{,}500 \text{ psi}$$

The allowable stress was 32000, hence the margin of safety is (32000/29500) - 1 = .08 or eight percent. If a smaller margin of safety was desired some material would be eliminated and the calculations of Tables A20.1 and A20.2 would be repeated.

Calculation of Shear Stress in Skin at Neutral Axis

The equation for the shear flow q at some point on the skin is,

$$q = q_o - \frac{V_Z}{I_y} \Sigma az \qquad (3)$$

Due to symmetry of cross-section about the Z axis the shear flow q_o is zero at a point on the center line Z axis. The summation of the term az between a point on the Z axis and the neutral axis is given in Table A20.3. The values of areas (a) and arms (z) are taken from Tables A20.1 and A20.2.

TABLE A20.3

Element No.	az
(1)	.021(28.28 - .13) = 0.59
(2)	.152(27.58 - .13) = 4.17
(3)	.039(27.08 - .13) = 1.05
(4)	.153(25.38 - .13) = 3.86
(5)	.022(23.68 - .13) = 0.52
(6)	.156(21.58 - .13) = 3.34
(7)	.015(19.18 - .13) = 0.28
(8)	.161(16.68 - .13) = 2.66
(9)	.031(13.48 - .13) = 0.41
(10)	.173(10.28 - .13) = 1.75
(11)	.055(6.58 - .13) = 0.35
(12)	.212(3.38 - .13) = 0.69
	Total az 19.67

Substituting in equation (3)

$$q_{N.A.} = q_o + \frac{V_Z}{I_y} \Sigma az$$

$$= 0 + \frac{(V_Z)}{1489} 19.67 = .0132\ V_Z \text{ lb./in.}$$

The shear stress $\tau = q/t = .0132\ V_Z/.032 = .413\ V_Z$

The average shear stress on the section would be $\tau_{av.} = V_Z/2ht = V_Z/2 \times 50 \times .032 = .312\ V_Z$.

Thus for this shape of cross-section and stringer arrangement the maximum shear stress is .413/.312 times the average shear stress or approximately 4/3 times as large.

The procedure as given above is quite conservative relative to the true or actual margin of safety, because a linear variation of stress with strain has been assumed and failure of the section is assumed to occur when the most remote stringer reaches its ultimate compressive stress. Actually in a static test of a fuselage to destruction, the fuselage section as a whole will not collapse when one stringer buckles, but will continue to take increasing load until other stringers have reached their ultimate strength. Furthermore, in a typical fuselage structure, stringers of various sizes, shapes and therefore different compressive strengths are used, and thus to obtain a better measure of the ultimate strength of a fuselage section, modifications in stress procedures are made to measure stringer effectiveness. This subject was discussed in some detail in Arts. 11 and 12 of Chapter A19. To illustrate stringer effectiveness in fuselage bending stress analysis, a simple example problem will be presented.

A20.5 Ultimate Bending Strength of Fuselage Section. Example Calculation.

Fig. A20.3 shows the cross-section of a circular fuselage. The Z stringers are arranged symmetrically with respect to the center line Z and X axes.

Three sizes of Z stringers are used as illustrated in Fig. A20.4 and are labeled S_1, S_2 and S_3. These symbols are used on Fig. A20.3 to indicate where each type of stringer is used. The stringers on each side of the section are numbered 1 to 13 as shown on Fig. A20.3. Fig. A20.5 shows a plot of the stress-strain curve for the three stringer types loaded in compression and with a column length equal to the fuselage frame spacing. Fig. A20.5 also shows a tension stress-strain diagram for the material which is aluminum alloy (2024). The ultimate bending strength will be calculated for bending which places the upper portion in compression.

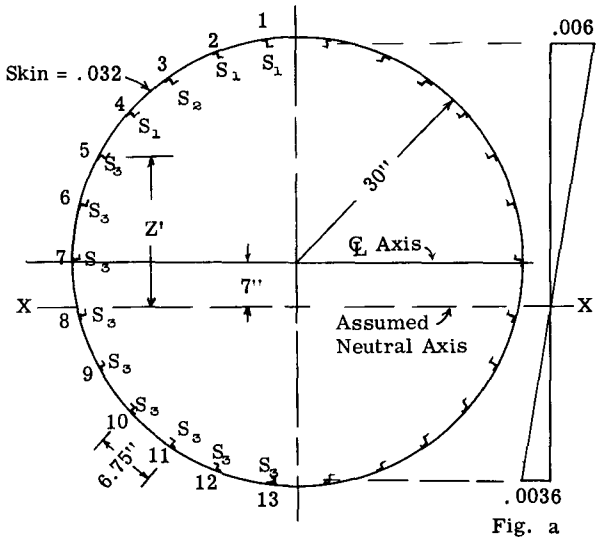

Fig. A20.3

Fig. a Strain Diagram

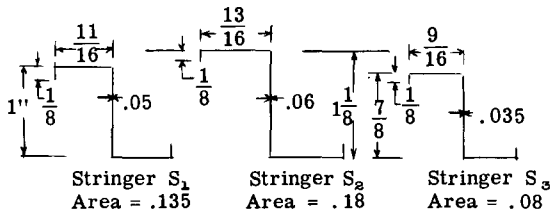

Fig. A20.4

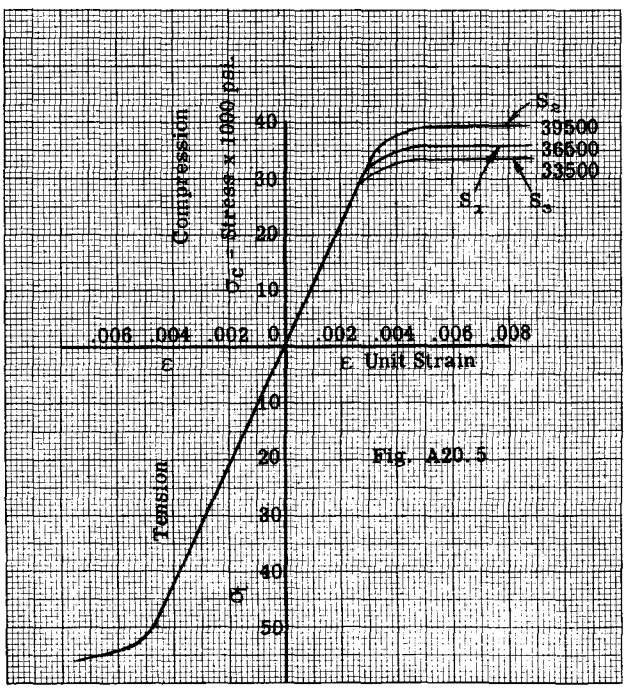

Fig. A20.5

Since the location of the neutral axis is unknown, a location will be assumed, namely, 7 inches below the center line axis as shown in Fig. A20.3. The entire calculations for determining the effective moment of inertia can best be done in Table form, as shown in Table A20.4. Due to symmetry about the Z axis only one-half of the structure need be considered since the results can be multiplied by two.

Column (1) lists the stringer numbers relative to location and Column (2) according to types S_1, S_2 and S_3. Column (3) gives the stringer area. On the tension or lower side of the section, the skin is all effective and that area of skin halfway to each adjacent stringer is assumed to act with stringers numbered 9 to 13 and this skin area is recorded in Column (5). On the compressive side the skin is only partially effective. The effective width w for each stringer rivet line depends on the stringer stress. We will take the effective width $w = 1.9t\sqrt{E/\sigma_{ST}}$. The effective area A_e will then equal wt. These effective skin areas are recorded in Column (5). In solving this equation the stringer stress σ_{ST} has been taken as -36500 psi on stringer number (1), and then varying linearly to zero at the neutral axis as indicated in Column (4). This assumption is not true but accurate enough to obtain effective skin areas. To illustrate, consider stringer number (1). The effective area A_e equals $wt^2 = 1.9 \times .032^2(10{,}300{,}000/36500)^{\frac{1}{2}} = .032$ sq. in. Column (6) gives the sum of the stringer and effective skin areas or $A_S + A_e$.

In this example problem, the effectiveness of the curved sheet panels between the sheet effective widths will be neglected since its influence is small. It could be included as illustrated in the previous example problem. Column (7) lists the distances from the assumed neutral axis to the centroid of each stringer-skin unit. We now assume that plane sections remain plane or a linear strain variation. Referring to Fig. A20.5, it is noticed that when a unit strain of .006 is obtained in stringer S_1 type the compressive stress is 36500, which represents its ultimate stress. Stringer (1) is of S_1 type and is located farthest from the neutral axis. Sub. Fig. (a) of Fig. A20.3 shows the strain diagram with .006 at stringer (1) and varying as a straight line to zero at the neutral axis. Column (8) of Table A20.4 records the unit strain at each stringer centroid. The true stress at each stringer point due to these strain values is read from the curves on Fig. A20.5 and recorded in column (9) of the Table. It should be noted that stringer (3) although closer to the neutral axis than stringer (1) carries a higher stress than stringer (1). This is possible because when stringer (1) reaches its maximum-stress, it bends but continues to hold the same stress with

TABLE A20.4

1	2	3	4	5	6	7	8	9	10	11	12	13
Stringer		Stringer Area A_S	Linear Stress σ_b^1	Effect-ive Skin Area A_e	Total Stringer Area A	Arm Z^1 (in)	Unit Strain ε	Stress $AT\varepsilon.$ σ	$K = \sigma/\sigma^1$	KA	KAZ^1	KAZ^2 $(Z = Z^1)$
No.	Type											
1	S_1	0.135	-36500	.032	.167	35.7	-.00600	-36500	1.00	.167	5.96	213
2	S_1	0.135	-34700	.034	.169	33.8	-.0057	-36500	1.05	.178	6.00	203
3	S_2	0.180	-31000	.036	.216	30.3	-.0051	-39100	1.26	.272	8.25	250
4	S_1	0.135	-26600	.039	.174	26.0	-.0048	-36000	1.35	.235	6.10	159
5	S_3	0.080	-20500	.044	.124	20.1	-.0034	-31500	1.54	.191	3.85	77
6	S_3	0.080	-13400	.054	.134	13.7	-.0023	-24000	1.79	.240	3.30	45
7	S_3	0.080	-7150	.074	.154	7.0	-.0012	-12500	1.75	.270	1.89	13
8	S_3	0.080	0	0	.080	10.0	0	0	1.0	.080	0	0
9	S_3	0.080	6130	.216	.296	- 6.0	.0010	10000	1.63	.483	-2.88	17
10	S_3	0.080	12280	.216	.296	-12.0	.0020	20500	1.67	.494	-5.91	71
11	S_3	0.080	16800	.216	.296	-16.5	.0028	30000	1.78	.526	-8.69	144
12	S_3	0.080	20400	.216	.296	-20.0	.0034	35000	1.71	.506	-10.10	202
13	S_3	0.080	21700	.216	.296	-21.2	.0036	38000	1.75	.517	-10.93	232
									Σ	4.159	-3.16	1626

increasing strain, but stringer (3) which has not reached its maximum strength of 39000 continues to take increasing load.

Since we wish to use the beam formula $\sigma_b = M_y Z/I_X$ in computing stresses, we must modify the stringer areas to give a linear stress variation since the formula is based on a linear stress variation. The stringer modification factor K equals the ratio of the true stress in column (9) of Table to linear stress value in column (4) or $K = \sigma/\sigma^1$. The results are recorded in column (10). The modified stringer areas are then equal to KA and are recorded in column (11). Column (12) gives the first moment of the modified areas about the assumed neutral axis, giving a total value of -3.16.

The distance $\bar{Z}$ from the assumed neutral axis to the true neutral axis is thus,

$$\bar{Z} = \Sigma KAZ^1/\Sigma KA$$

$$= \frac{-3.16}{4.159} = -0.76"$$

The true N.A. would fall about .70 inches below assumed position. The effect on total sum of Column (13) would be negligible, thus Table A20.4 will not be revised.

Column (13) gives the calculation of the effective moment of inertia with Z^1 being equal to Z. The effective moment of inertia is therefore twice the sum of Column (13) or 3252.

Calculation of Ultimate Resisting Moment.

The maximum stress at the most remote stringer which is number (1) is 36500. From the beam formula,

$$M_X = \sigma_b I_X/Z$$

$$= (36500 \times 3252)/35.7 + 0.7$$

$$= 3{,}260{,}000 \text{ in.lb.}$$

This bending strength when compared to any design bending moment about the X axis would give the margin of safety relative to bending strength.

If the moment of inertia had been computed without regard to non-linear stress variation, or in other words, using K equal 1 for all stringers the neutral axis would have come out 4.9 inches below the centerline axis and the moment of inertia would have calculated to be 2382 $in.^4$. The resisting moment developed would then be $(36500 \times 2382)/33.6 = 2{,}600{,}000$ in.lbs. Thus the true strength is 25 percent greater than the strength for linear stress variation. This result explains why such structures test overstrength if designed on linear stress variation basis.

After stringer stresses are obtained

using the modified areas of Table A20.4, the true stringer areas must be used to find the true stringer loads, which must be used in the shear flow analysis.

A20.6 Shear Flow Analysis for Fuselage Structures

The shear flow analysis can be made once the effective cross-sections of the fuselage are obtained. The procedure is the same as was illustrated for wing structures in Chapter A19. To illustrate, two example problems will be presented.

Example Problem 1. Symmetrical Tapered Section.

Fig. A20.6 shows a portion of a tapered circular shaped fuselage structure that might be representative of the rear portion of a fuselage for a small airplane. Since this example is only for the purpose of illustrating shear flow analysis, it will be assumed that the 16 stringers are the only effective material. In an actual stress analysis, the effective cross-section would have to be used as illustrated in previous articles A20.3 to A20.5.

The problem will be to determine the stringer stresses and the skin shear flow stress system at Station (0) under a given load system at Station (150) as shown in Fig. A20.6.

Solution No. 1 - Solution by Considering Beam Properties at Only One Section.

If the change in longitudinal stringer or flange material is fairly uniform this method can be used with little error in the resulting shear flow stresses.

Moment of inertia of section at station (0) about centroidal Y axis:

$$I_y = (15^2 \times .1 \times 2) + (13.86^2 + 10.61^2 + 5.74^2).1 \times 4 = 180 \text{ in.}^4$$

Table A20.5 gives the necessary calculations for determining the flange bending stresses and the net total shear load to be taken by the cell skin. Since the cell is tapered, the stringers have a z component, thus the stringer axial loads help resist the external shear load. The summation of column (8) of Table A20.5 gives -333.4 lb. for a summation for half the fuselage section.

Hence, net web shear at station 0 equals:

$$V_{web} = V_{ext.} + V_{flange} = 2000 + (2 \times -333.4) = 1333.2 \text{ lb.}$$

The results in this particular problem show that at station 0 the flange stringer system resists one third of the external shear load. At station 150 the web system will resist the entire external shear load of 2000 lb. since the load in the stringers is zero.

In actual design the net web shear should be used since in many cases it will decrease the sheet thickness required one or more gauges.

Calculation of Flexural Shear Flow.

$$q = q_o - \frac{V_{z(web)} \Sigma a z}{I_y} = q_o - \frac{1333.2}{180} \Sigma az$$

$$= q_o - 7.40 \Sigma az \text{ - - - - - - - - - - - (A)}$$

Due to symmetry of the section about the Z axis, the flexural shear flow in the web at the center line is zero. Therefore, q_o will be taken as zero and the summation in equation (A) will

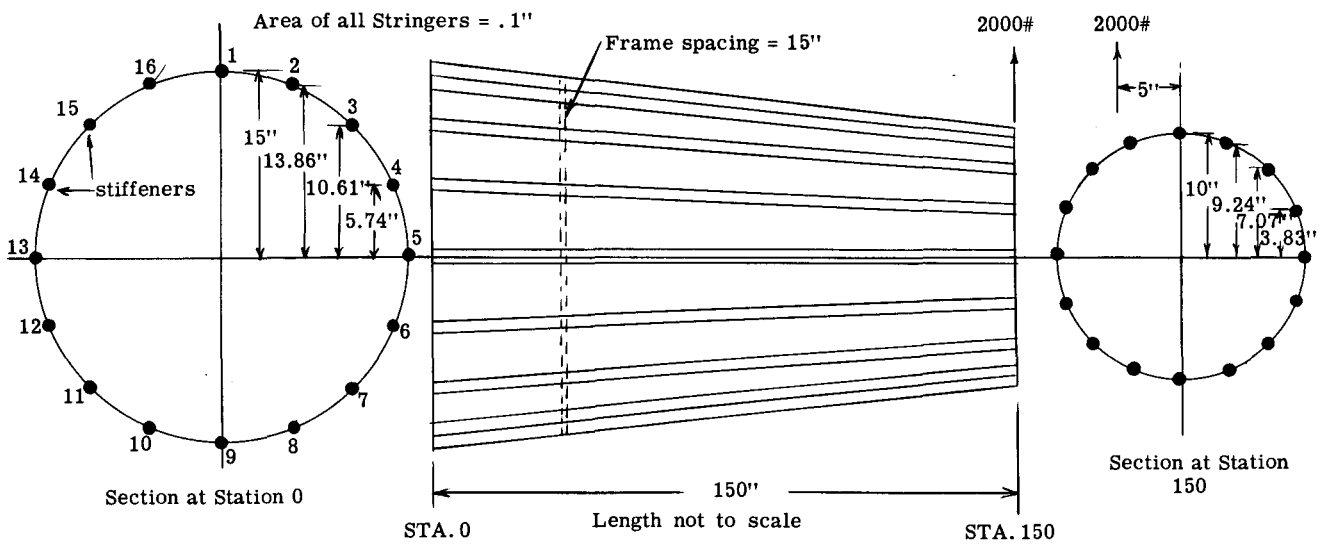

Fig. A20.6

TABLE A20.5

1	2	3	4	5	6	7	8	9
Stiffener No.	Arm z	Area a	σ_b = -1667z (psi)	$P_x=\sigma_b a$ (3)(4) lbs.	$\frac{dz}{dx}$	$\frac{dy}{dx}$	P_z = -P x $\frac{dz}{dx}$	P_y = -P x $\frac{dy}{dx}$
1	15	*.05	-25000	-1250	-.0333	0	-41.6	0
2	13.86	.10	-23100	-2310	-.0308	-.0127	-71.3	-29.4
3	10.61	.10	-17700	-1770	-.0236	-.0236	-41.7	-41.7
4	5.74	.10	- 9550	- 955	-.0127	-.0308	-12.1	-29.5
5	0	.10	0	0	0	-.0333	0	0
6	- 5.74	.10	9550	955	.0127	-.0308	-12.1	29.5
7	-10.61	.10	17700	1770	.0236	-.0236	-41.7	41.7
8	-13.86	.10	23100	2310	.0308	-.0127	-71.3	29.4
9	-15	*.05	25000	1250	.0333	0	-41.6	0
				Shear taken by stringers =			-333.4	0

*1/2 of stringer one is assumed acting with each half of cell.

NOTES:

Col. 4 $\sigma_b = -Mz/I_y = -2000 \times 150 \times z/180 = -1667z$

Col. 5 Total x component of load in stringer member. For practical purposes, it equals axial load in stringers since cosine of a small angle is practically one.

Col. 6 The slope of the stringers in the z and y directions can be calculated from the dimensions of the two end sections and the length of the cell. (see Fig. A20.6)

Col. 8 & 9 The in plane components of the stringer axial loads at station 0.

start with stringer (1)

$q_{12} = 0 - 7.40 \times .05 \times 15 = -5.55$ lb./in.

$q_{23} = -5.55 - 7.40 \times .1 \times 13.86 = -15.80$

$q_{34} = -15.80 - 7.40 \times .1 \times 10.61 = -23.66$

$q_{45} = -23.66 - 7.40 \times .1 \times 5.74 = -27.91$

The torsional moment T about the centroid of the section at station (0) equals 5 x 2000 = 10000 in. lb. (clockwise when looking toward station 150). Due to the symmetry of the section at station 0, the in-plane components of the stringer loads produce zero moment about the section centroid.

For equilibrium a constant internal shear flow q_1 is necessary to make $\Sigma M_X = 0$

$$q_1 = \frac{T}{2A} = \frac{-10000}{2 \times \pi \times 15^2} = -7.06 \text{ lb./in.}$$

Adding the torsional shear flow q_1 to the flexural shear flow q, the following results are obtained:

$q_{12} = -7.06 + 5.55 = -1.51$ lb./in.

$q_{23} = -7.06 + 15.80 = 8.74$

$q_{34} = -7.06 + 23.66 = 16.60$

$q_{45} = -7.06 + 27.91 = 20.85$ etc.

Fig. A20.7 shows the results in graphical form, on the left side of the section the shears are of the same sign and therefore add together.

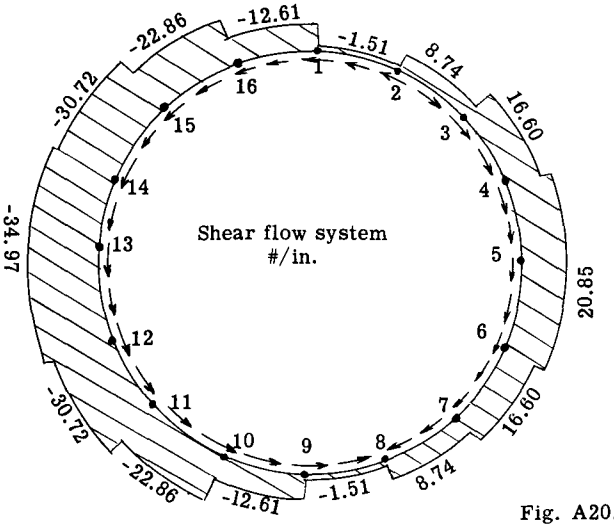

Fig. A20.7

Solution No. 2. Shear Flow by Change in Stringer Loads Between Adjacent Stations. ΔP Method.

The shear flow will be calculated by considering the change in the axial load in the longitudinal stringers between fuselage sections at stations (0) and (30).

Fig. A20.8 shows the beam section at station 30, the stringer areas being the same as at station 0, but the section as a whole is smaller due to the taper of the cell.

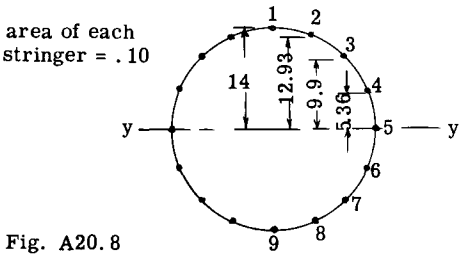

Fig. A20.8

Table A20.6 gives the calculations for the flexural shear system. The procedure is the same as illustrated for wing structures in Chapter A19.

Comparing the results of column 13 with the flexural shear flow as found by solution No. 1, we find the second solution gives a maximum shear flow of 28.95 lb./in. against a value of 27.91 for the first solution. The first method deals with the properties at only one section and this cannot include the effects of change in moment of inertia on the shear flow. The

TABLE A20.6

1	2	3	4	5	6	7	8	9	10	11	12	13
Stringer No.	Sta. 0 Area a sq. in.	Sta. 30 Area a sq. in.	Sta. 0 Arm z	Sta. 30 Arm z	Sta. 0 σ_b = -1667Z (psi.)	Sta. 30 σ_b = -1522Z (psi.)	Stringer Load Sta. 0 $P_x = \sigma_b a$	Stringer Load Sta. 30 $P_x = \sigma_b a$	$\frac{\Delta P}{30}$ - $\frac{\text{(Col. 8 - Col. 9)}}{30}$	Panel Taper Corr. Factor K	$\frac{\Delta PK}{30}$	Flexural Shear Flow $q = \Sigma \frac{\Delta PK}{30}$ lb./in.
1	.05	.05	15.00	14.00	-25000	-21300	-1250	-1065	6.17	.935	5.76	5.76
2	.10	.10	13.86	12.93	-23100	-19700	-2310	-1970	11.33	.935	10.60	16.36
3	.10	.10	10.61	9.90	-17700	-15050	-1770	-1505	8.83	.935	8.25	24.61
4	.10	.10	5.74	5.36	- 9550	- 8155	- 955	- 815	4.65	.935	4.34	28.95
5	.10	.10	0	0	0	0	0	0	0	0	0	28.95
6	.10	.10	- 5.74	- 5.36	9550	8155	955	815	- 4.65	.935	- 4.34	24.61
7	.10	.10	-10.61	- 9.90	17700	15050	1770	1505	- 8.83	.935	- 8.25	16.36
8	.10	.10	-13.86	-12.93	23100	19700	2310	1970	-11.33	.935	-10.60	5.76
9	.05	.05	-15.00	-14.0	25000	21300	1250	1065	- 6.17	.935	- 5.76	

NOTES:

Col. 6 $\sigma_b = -2000 \times 150\ z/180 = -1667\ z$

Col. 7 $\sigma_b = -2000 \times 120\ z/157.2 = -1522\ z$

Col. 10 Change in axial load in each stringer between stations 0 and 30 divided by distance between Stations. This result represents the average shear flow induced by the loading up of each stringer between stations 0 and 30.

Col. 11 The width of a skin panel at Station 0 is 5.88 inches and 5.5 inches at Station 30. The shear flow on the edge of the panels at Station 0 equals (5.5/5.88) $\Delta P/30$. (See Art. A15.18 of Chapter A15 for explanation). This refinement is usually neglected and the average values as given in Col. 10 are used which are conservative.

Col. 13 Due to symmetry of structure, the shear flow is zero on z axis. Thus shear flow at any station equals the progressive summation of the shear flow values in Col. 12.

second method is recommended for practical analysis procedure.

Since the section is symmetrical, there are no moments induced by the in-plane components of the stringer forces at station 0.

The torsional shear flow forces are the same as in solution method No. 1 and these are added to the values of column 13 of Table A20.6 and give a pattern similar to Fig. A20.7.

A20.7 Example Problem. Tapered Circular Fuselage with Unsymmetrical Stringer Areas.

Fuselage cross-sections are seldom all symmetrical relative to stringer and skin areas because the practical fuselage has cut-outs such as doors, etc. To illustrate the unsymmetrical case a simplified case will be presented.

Fig. A20.9 shows a portion of a tapered fuselage. The stringer areas are such as to make the cross-sections unsymmetrical relative to bending material. Again for simplicity, we will assume the stringers are the only effective material. In actual design practice the effectiveness of the skin and each stringer would have to be considered as explained in Articles A20.4 and 5.

The problem will be to determine the stringer stresses and the skin shear flow values at station (0) due to the given external loads of P_Z = 4000 lb., P_Y = 1000 lb. and P_X = 1500 acting at station (150) as shown in Fig. A20.9.

SOLUTION:

Since we choose to use the ΔP method in finding the shear flow system at station (0), we will find the stringer loads at two stations, namely, station (0) and station (30). The first step is to find the moment of inertia of each fuselage section about centroidal z and y axes and the product of inertia about these axes. Table A20.7 (Columns 1 to 11) gives the calculations of the section properties for station

Fig. A20.9

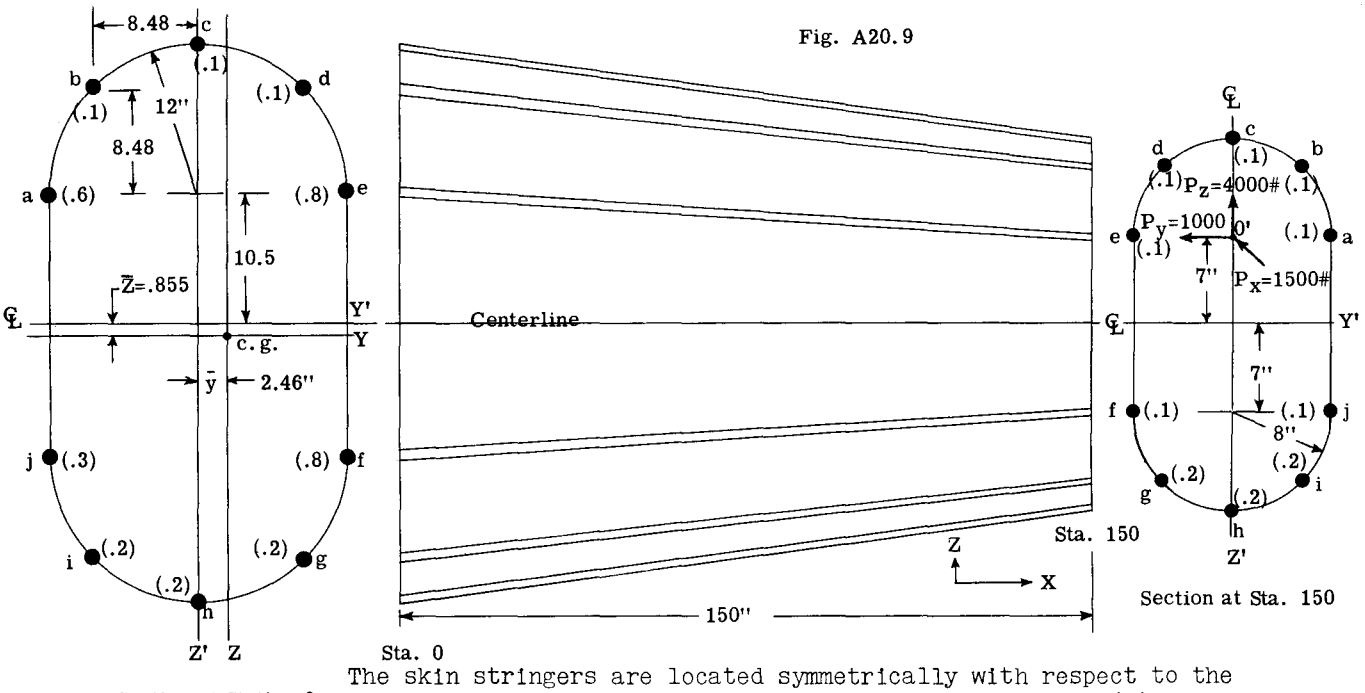

The skin stringers are located symmetrically with respect to the centerline axes, however the stringer areas as given in( ) on the figure are not symmetrical with these axes. It is assumed in this problem that the stringers taper uniformly between the values as given for station 0 and 150. The cell would of course have interior transverse frames which are not shown on the figure.

TABLE A20.7

Section Properties at Sta. 0											Total Stringer Loads at Sta. 0		
1	2	3	4	5	6	7	8	9	10	11	12	13	14
Stringer No.	Area a	Arm z'	Arm y'	az'	az'^{2}	ay'	ay'^{2}	az'y'	z = z' - $\bar{z}$	y = y' - $\bar{y}$	σ_b	σ_c = F/Σa = -1500/3.40	P_s = a(σ_b + σ_c) = (2) (12 + 13)
a	.60	10.5	-12.00	6.30	66.20	-7.20	86.50	- 75.50	11.36	-14.46	-15080	-441	-9312
b	.10	18.98	- 8.48	1.90	36.00	-0.85	7.20	- 16.10	19.84	-10.94	-21960	-441	-2239
c	.10	22.50	0	2.25	50.80	-0	0	0	23.36	- 2.46	-22600	-441	-2304
d	.10	18.98	8.48	1.90	36.00	0.85	7.20	16.10	19.84	6.02	-16742	-441	-1719
e	.80	10.5	12.00	8.40	88.10	9.60	115.10	100.80	11.36	9.54	- 7692	-441	-6506
f	.80	-10.5	12.00	-8.40	88.10	9.60	115.10	-100.80	- 9.65	9.54	11958	-441	9216
g	.20	-18.98	8.48	-3.80	72.00	1.70	14.40	- 32.30	-18.13	6.02	18798	-441	3673
h	.20	-22.50	0	-4.50	101.60	0	0	0	-21.65	- 2.46	19485	-441	3809
i	.20	-18.98	- 8.48	-3.80	72.00	-1.70	14.40	32.30	-18.13	-10.94	13610	-441	2634
j	.30	-10.50	-12.00	-3.15	33.10	-3.60	43.25	37.80	- 9.65	-14.46	4592	-441	1246
Sum	3.40			-2.90	643.9	8.40	403.2	- 37.70					-1500

Reference Axes Z' and Y' are taken as the centerline axes. (see Fig. A20.9)

Location of centroid and transfer of properties to centroidal axes.

$\bar{z}$ = -2.90/3.40 = -.855"

$\bar{y}$ = 8.40/3.40 = 2.46"

I_y = 643.9 - 3.40 x 855^2 = 641.4

I_z = 403.2 - 3.40 x 2.46^2 = 382.6

I_{zy} = -37.7 - 3.40 x 2.46 x -.855 = -30.55

General Notes:

Col. 12 σ_b = 307.0y - 936.1z

Col. 14 Since the total tensile stresses equal to total compressive stresses in bending, the sum of Col. 14 should equal the external applied normal load.

TABLE A20.8

Section Properties at Sta. 30											Total Stringer Loads at Sta. 30		
1	2	3	4	5	6	7	8	9	10	11	12	13	14
Stringer No.	Area a	Arm z'	Arm y'	az'	az'^{2}	ay'	ay'^{2}	az'y'	z = z' - $\bar{z}$	y = y' - $\bar{y}$	σ_b	$\sigma_c = F/\Sigma a$ = -1500/2.98	$P_s = a(\sigma_b + \sigma_c)$
a	.50	9.80	-11.2	4.90	48.1	-5.60	62.8	-54.9	10.90	-13.31	-14800	-503	-7651
b	.10	17.72	- 7.92	1.77	31.4	-0.79	6.3	-14.0	18.82	-10.03	-21090	-503	-2159
c	.10	21.00	0	2.10	44.1	0	0	0	22.10	- 2.11	-21447	-503	-2195
d	.10	17.72	7.92	1.77	31.4	0.79	6.3	14.0	18.82	5.81	-15647	-503	-1615
e	.66	9.8	11.20	6.47	63.2	7.40	83.0	72.5	10.90	9.09	- 7088	-503	-5011
f	.66	- 9.8	11.20	-6.47	63.2	7.40	83.0	-72.5	- 8.7	9.09	-11282	-503	7100
g	.20	-17.72	7.92	-3.54	62.8	1.58	12.6	-28.0	-16.60	5.81	-17583	-503	3416
h	.20	-21.00	0	-4.20	88.2	0	0	0	-19.90	- 2.11	17943	-503	3489
i	.20	-17.72	- 7.92	-3.54	62.8	-1.58	12.6	28.0	-16.60	-10.02	12135	-503	2327
j	.26	- 9.8	-11.20	-2.55	25.0	-2.92	32.6	28.6	- 8.70	-13.31	3570	-503	797
Sum	2.98			-3.29	520.2	6.28	299.2	-26.3					-1500

NOTES:

Reference Z' and Y' axes are taken as the centerline axes.

$\bar{z} = -3.29/2.98 = -1.10''$

$\bar{y} = 6.28/2.98 = 2.11$

$I_y = 520.2 - 2.98 \times 1.10^2 = 516.6$

$I_z = 299.2 - 2.98 \times 2.11^2 = 286.0$

$I_{zy} = -26.3 - 2.98 \times 2.11 \times -1.10 = -19.4$

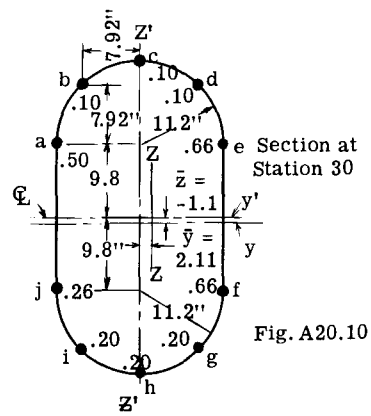

Fig. A20.10

(0) and the similar columns of Table A20.8 gives the calculations for station (30).

Before the bending and shear stresses can be calculated, the external bending moments, shears and normal forces at stations (0) and (30) must be known.

At station (0): -

The bending moment about y neutral axis at station (0) equals,

$M_y = P_Z\ (150) + P_X\ (7.85)$

$= 4000 \times 150 + 1500 \times 7.85 = 611800$ in.lb.

$M_Z = P_y\ (150) - P_X\ (2.46)$

$= -1000 \times 150 + 1500 \times 2.46 = -146310$ in.lb.

The shears at station (0) are $V_Z = P_Z = 4000$ lb. and $V_y = P_y = -1000$ lb.

The normal load P_n at station (0) referred to centroid of section equals $\Sigma P_X = -1500$ lb.

In a similar manner, the values at station (30) are, (see Fig. A20.10)

$M_y = 4000 \times 120 + 1500 \times 8.10 = 492150$ in.lb.

$M_Z = -1000 \times 120 + 1500 \times 2.11 = 116820$ in.lb.

$P_n = -1500$ lb., $V_Z = 4000$ lb., $V_y = -1000$ lb.

Calculation of Bending Stresses.

Station (0):

$$\sigma_b = -(K_3 M_Z - K_1 M_y)y - (K_2 M_y - K_1 M_Z)\ z$$

where

$K_1 = I_{yz}/(I_y I_Z - I_{yz}^2)$

$K_2 = I_Z/(I_y I_Z - I_{yz}^2)$

$K_3 = I_y/(I_y I_Z - I_{yz}^2)$

Substituting values from Tables A20.7 and A20.8:

$K_1 = -30.55/(641.4 \times 382.6 - 30.55^2) =$

$= -30.55/244670 = -.0001248$

$K_2 = 382.6/244670 = .00156$

$K_3 = 641.4/244670 = .00262$

Substituting K values in equation for σ_b:

$$\sigma_b = -\left[.00262 \times -146310 - (-.0001248 \times 611800)\right] y - \left[.00156 \times 611800 - (-.0001248 \times -146310)\right] z$$

whence

$$\sigma_b = 307.0\, y - 936.1\, z \text{ (plus } \sigma_b \text{ is tension)}$$

Station (30):

$$K_1 = -19.4/(516.6 \times 286 - 19.4^2) = -19.4/147620 = -.0001315$$

$$K_2 = 286/147620 = .001936$$

$$K_3 = 516.6/147620 = .0035$$

$$\sigma_b = -\left[.0035\, c - 116800 - (-.0001315 \times 492150)\right] y - \left[.001936 \times 492150 - (-.0001315 \times 116820)\right] z$$

whence

$$\sigma_b = 344.3\, y - 937.7\, z$$

Column (12) in Tables A20.7 and A20.8 gives the results of solving the equations for σ_b.

Since an external load of 1500 lb. is acting normal to the sections and through the section centroids, an axial compressive stress σ_c is produced on the sections. (See Columns 13). The total load P_s in each stringer equals the area of the stringer times the combined bending and axial stresses. (See column 14 of each table).

Calculation of Flexural Shear Flow q.

Table A20.9 gives the necessary calculations to determine the shear flow at station (0) based on the change in stringer loads between stations (0) and (30). The correction of the average shear due to the taper in the skin panels as was done in example problem (1), Table A20.6, column (11), is omitted in this solution since it tends toward the conservative side. Since the effective cross section is unsymmetrical, the value of the flexural shear flow q at any point is unknown thus a value for q at some point is assumed. In Table A20.9 the shear flow q in the web aj is assumed zero. Column (5) gives the results at other points under this assumption.

Moment of Shear Flow about Intersection of Centerline Axes

For equilibrium in the plane of the cross section at station (0), the summation of the moments in the plane, of all internal and external forces must be zero. Column (7) of Table A20.9 gives the moment of the flexural shear about this point. (See notes and Fig. below Table for explanation.)

TABLE A20.9

SHEAR FLOW CALCULATIONS

1	2	3	4	5	6	7	8	9
Stringer No.	P_x at Sta. 0	P_x at Sta. 30	$\frac{\Delta P_x}{30}$	$q = \sum \frac{\Delta P_x}{30}$	m sq. in.	mq	q_1	$q_r = q + q_1$
a	-9312	-7651	55.37					
				55.37	150.04	8300	-52	3.37
b	-2239	-2159	2.67					
				58.04	202.46	11820	-52	6.04
c	-2304	-2195	3.63					
				61.67	202.46	12500	-52	9.67
d	-1719	-1615	3.47					
				65.14	150.04	9780	-52	13.14
e	-6506	-5011	49.83					
				114.97	252.0	29000	-52	62.97
f	9216	+7100	-70.53					
				44.44	150.04	6660	-52	- 7.56
g	3673	3416	- 8.57					
				35.87	202.46	7270	-52	-16.13
h	3809	3489	-10.67					
				25.20	202.46	5100	-52	-26.8
i	2634	2327	-10.23					
				14.97	150.04	2240	-52	-37.03
j	1246	797	-14.97					
				0	252.0	0	-52	-52.0
a								
					Sum	92670		

NOTES:

Col. (2) and (3) from tables A20.7 and A20.8

Col. (4) $\Delta P_x = -\left[P_{x_{Sta.0}} - P_{x_{Sta.30}}\right]$

Col. (6) m = double areas (see Fig. a).

Col. (7) mq = moment of shear flow q on each web element about 0' (Fig. a)

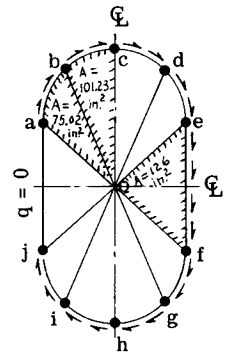

Fig. a

Moments Due to In Plane Components of Stringer Loads.

Since the stringers are not normal to the section at station (0), the stringers have in-plane components which may produce a moment about the intersection of the symmetrical axes which has been selected as a moment center. Table A20.10 gives the calculations for the in-plane components and their moments about point 0'.

Moment of External Load System About Point (0').

The 1000 lb. load at station (150) acting in the Y direction has a moment arm of 7" about the point 0' of station (0).

Hence external moment = 1000 x 7 = 7000 in.lb.

Therefore the total moment about the assumed moment center 0' =

TABLE A20.10

MOMENTS DUE TO IN PLANE COMPONENTS OF STRINGER LOADS

1	2	3	4	5	6	7	8
Stringer No.	P_x (lbs.)	$\frac{dy}{dx}$	$P_y = P_x \frac{dy}{dx}$	$M_o = P_y z'$	$\frac{dz}{dx}$	$P_z = P_x \frac{dy}{dx}$	$M_o = P_z y'$
a	-9312	.0026	248	2600	-.0233	217	-2600
b	-2239	.0188	42	798	-.0421	94	- 796
c	-2304	0	0	0	-.050	115	0
d	-1719	-.0188	32	- 608	-.0421	72	610
e	-6506	-.0266	173	-1820	-.0233	152	1820
f	9216	-.0266	245	-2570	.0233	214	2560
g	3673	-.0188	69	-1310	.0421	154	1307
h	3809	0	0	0	.050	190	0
i	2634	.0188	49	930	.0421	111	- 941
j	1246	.0266	33	346	.0233	29	- 348
			Sum	-1634			1612

NOTES:

Col. (2) from Table A20.7
Col. (3) equals the slope of stringers in y and z directions. (see Fig. A20.9)
Col. (5) Values of z' and (8) and y' from Table A20.7. Fig. b shows the P_y and P_z components from Cols. (4) and (7).

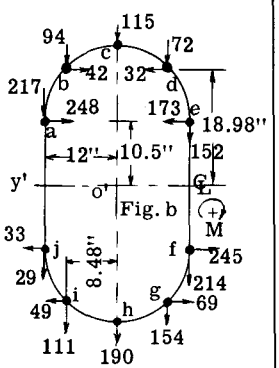

Looking Toward Sta. 150

Total moment about 0' = -1634 + 1612 = -22"#

92670 due to shear flow q
-22 due to in plane components of stringers.
7000 due to the external loads.

Total= 99648 in. lb.

Therefore for equilibrium a moment of -99646 is required which can be provided by a constant shear flow q_1 around the cell, hence

$$q_1 = \frac{T}{2A} = \frac{-99648}{2 \times 957} = -52 \text{ lb./in.}$$ (957 = enclosed area of cell)

This value of q is entered in column 8 of Table A20.9. The resulting shear flow in any web portion q_r equals the algebraic sum of q and q_1. (See Col. 9, Table A20.9). Fig. A20.11 shows the results in graphical form.

A20.8 Discontinuities - Shear Lag - Pressurization Stresses - Combined Stresses.

A practical fuselage has many cut-outs. The approximate effect of these discontinuities as well as the shear lag effect at sections

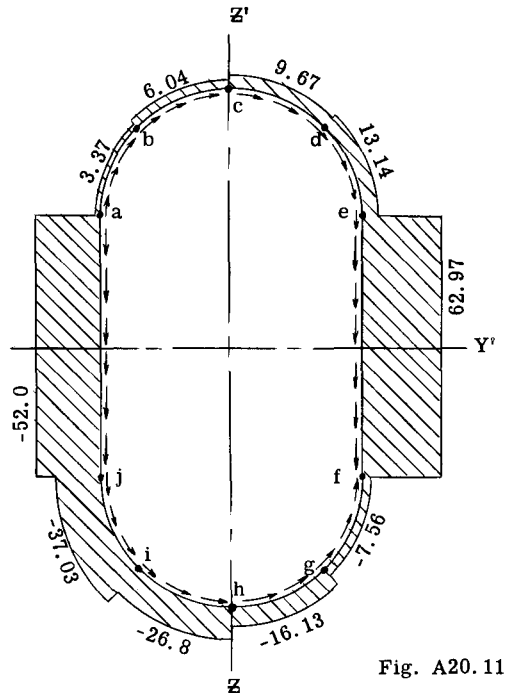

Fig. A20.11

Shear flow distribution.

where large concentrated loads are applied can be determined by the procedure given in Articles 18 to 20 of Chapter A19. A more rigorous analysis can be made by the application of the basic theory as given in Chapter A8.

The problem of shell stresses due to internal pressures is presented in Chapter A16. The strength design of the fuselage skin involves a question of combined stresses. The broad problem of the strength design of structural elements and their connections under all types of stress conditions is covered in Volume II.

A20.9 Problems.

(1)

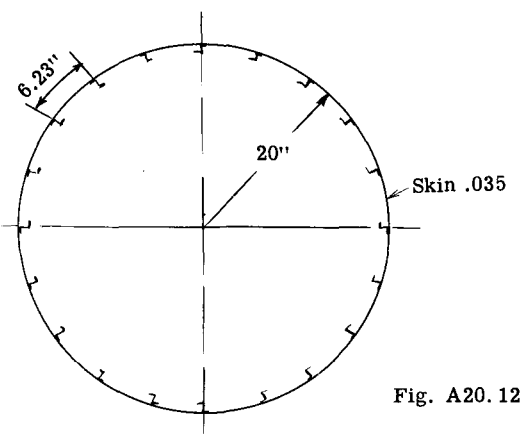

Fig. A20.12

Fig. A20.12 shows the cross-section of a circular fuselage. All stringers have same area, namely 0.12 sq. in. Skin thickness is .035 inches. Stringers are 1 inch in depth.

All material is aluminum alloy. E = 10,500,000 psi. The ultimate compressive strength of stringer plus its effective skin is 35000 psi. For effective sheet width use $w = 1.9t\,(E/\sigma_{ST})^{\frac{1}{2}}$. For buckling strength of curved panels use $\sigma_{cr} = .3\,Et/r$. Determine the ultimate bending moment that the fuselage section will develop for bending about horizontal neutral axis. Use linear stress distribution. Follow procedure as given in example problem in Art. A20.4.

(2)

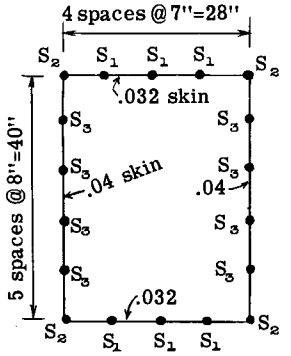

Fig. A20.13

Fig. A20.13 shows the cross-section of a rectangular fuselage. The dots represent stringer locations. Three types of stringers are used, namely, S_1, S_2 and S_3. Fig. A20.14 shows the ultimate compressive stress-strain curve for each of the three stringer types and also the tension stress-strain curve of the material.

Determine the ultimate bending resistance of the fuselage section about the horizontal neutral axis if the maximum unit compressive strain is limited to .008. Refer to Art. A20.5 for method of solution.

ADDITIONAL DATA. Area stringer S_1 = .12 sq.in.; S_2 = .25 sq.in.; S_3 = .08 sq.in. E = 10,500,000 psi..

(3) Fig. A20.15 shows a tapered circular fuselage with 8 stringers. The area of each stringer is 0.1 sq.in. Assume stringers develop entire bending resistance. Find the axial load in stringers at station (110) due to P_Z and P_X loads at station (0). Also find shear flow system at station 110 using ΔP method. Use properties at station (90) IN OBTAINING AVERAGE SHEAR FLOWS.

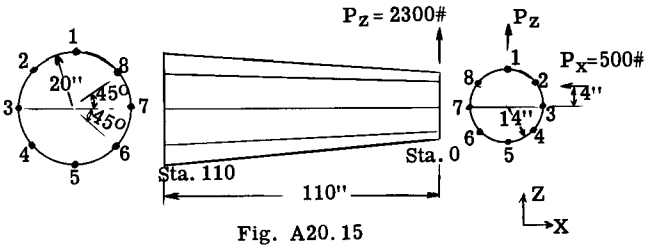

Fig. A20.15

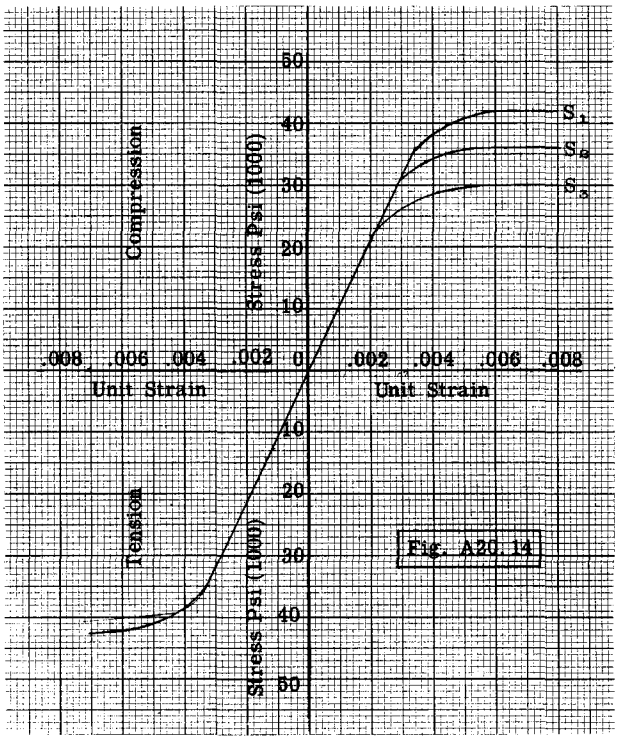

(4) Same as Problem (3) but change area of stringer no. (2) to 0.3 sq. in., thus making an unsymmetrical section.

A20.10 Secondary Stresses in Fuselage Stringers and Rings.

The stresses that are found in the stringers or longerons of a typical fuselage by use of the modified beam theory or by the more rigorous theory of Chapter A8, are referred to as primary stresses. Because of the necessity of weight saving, most fuselage structures are designed to permit skin buckling, which means that shear loads in the skin are carried by diagonal semi-tension field action. This diagonal tension in the skin panels produces additional stresses in the stringers and also in the fuselage rings. These resulting stresses are referred to as secondary stresses and must be properly added to the primary stresses in the strength design of the individual stringer or ring. Chapter C11 covers the subject of these secondary stresses due to diagonal semi-tension field action in skin panels. It is suggested to the student that after studying Chapters A19 and A20, that Chapters C10 and C11 be referred to in order to obtain a complete stress picture for skin covered structures.

CHAPTER A21
LOADS AND STRESSES ON RIBS AND FRAMES

A21.1 Introduction. For aerodynamic reasons the wing contour in the chord direction must be maintained without appreciable distortion. Unless the wing skin is quite thick, spanwise stringers must be attached to the skin in order to increase the bending efficiency of the wing. Therefore to hold the skin-stringer wing surface to contour shape and also to limit the length of stringers to an efficient column compressive strength, internal support or brace units are required. These structural units are referred to as wing ribs. The ribs also have another major purpose, namely, to act as a transfer or distribution unit. All the loads applied to the wing are reacted at the wing supporting points, thus these applied loads must be transferred into the wing cellular structure composed of skin, stringers, spars, etc., and then reacted at the wing support points. The applied loads may be only the distributed surface airloads which require relatively light internal ribs to provide this carry through or transfer requirement, to rather rugged or heavy ribs which must absorb and transmit large concentrated applied loads such as those from landing gear reactions, power plant reactions and fuselage reactions. In between these two extremes of applied load magnitudes are such loads as reactions at supporting points for ailerons, flaps, leading edge high lift units and the many internal dead weight loads such as fuel and military armament and other installations. Thus ribs can vary from a very light structure which serves primarily as a former to a heavy structure which must receive and transfer loads involving thousands of pounds.

Since the airplane control surfaces (vertical and horizontal stabilizer, etc.) are nothing more than small size wings, internal ribs are likewise needed in these structures.

The skin-stringer construction which forms the shell of the fuselage likewise needs internal forming units to hold the fuselage cross-section to contour shape, to limit the column length of the stringers and to act as transfer agents of internal and externally applied loads. Since a fuselage must usually have clear internal space to house the payload such as passengers in a commercial transport, these internal fuselage units which are usually referred to as frames are of the open or ring type. Fuselage frames vary in size and strength from very light former type to rugged heavy types which must transfer large concentrated loads into the fuselage shell such as those from landing gear reactions, wing reactions, tail reactions, power plant reactions, etc. The dead weight of all the payload and fixed equipment inside the fuselage must be carried to frames by other structure such as the fuselage floor system and then transmitted to the fuselage shell structure. Since the dead weight must be multiplied by the design acceleration factors, these internal loads become quite large in magnitude.

Another important purpose or action of ribs and frames is to redistribute the shear at discontinuities and practical wings and fuselages contain many cut-outs and openings and thus discontinuities in the basic structural layout.

A21.2 Types of Wing Rib Construction.

Figs. A21.1 to 6 illustrate the common types of wing construction. Fig. 1 illustrates a sheet metal channel for a leading edge 3

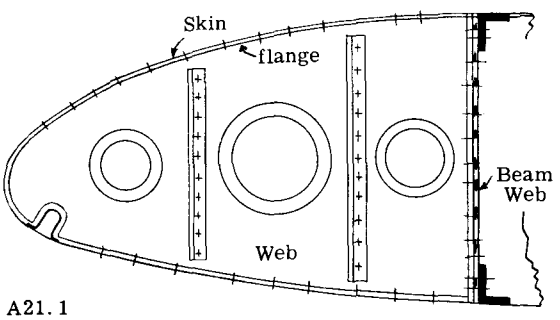

Fig. A21.1

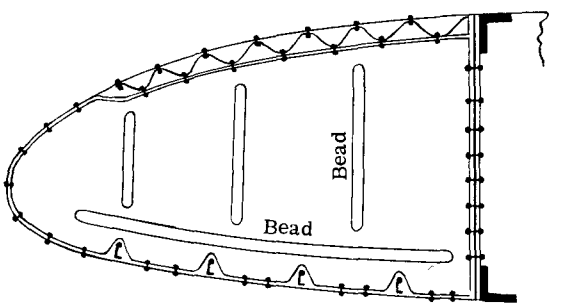

Fig. A21.2

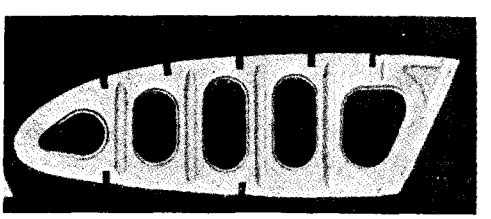

Fig. A21.3

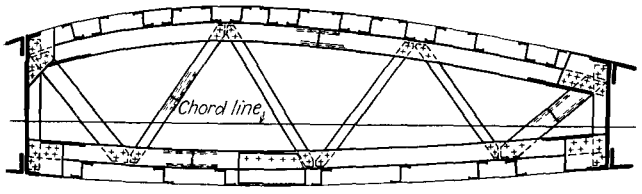

Fig. A21.4

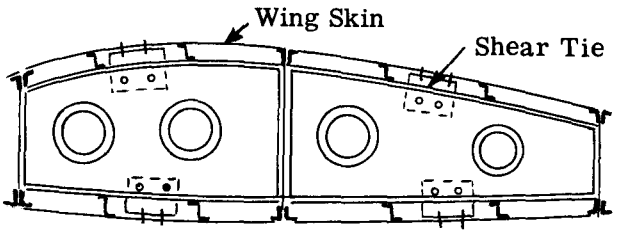

Ribs in 3 Spar Wing.

Fig. A21.5

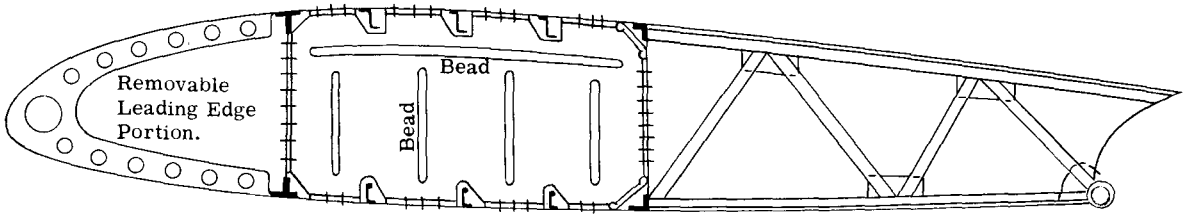

Fig. A21.6

stringer, single spar, single cell wing structure. The rib is riveted, or spot-welded, or glued to the skin along it boundary. Fig. 2 shows the same leading edge cell but with spanwise corrugations on the top skin and stringers on the bottom. On the top the rib flange rests below the corrugations, whereas the stringers on the bottom pass through cut-outs in the rib. Fig. 3 illustrates the general type of sheet metal rib that can be quickly made by use of large presses and rubber dies. Figs. 4 and 5 illustrate rib types for middle portion of wing section. The rib flanges may rest below stringers or be notched for allowing stringers to pass through. Ribs that are subjected to considerable torsional forces in the plane of the rib should have some shear ties to the skin. For ribs that rest below stringers this shear tie can be made by a few sheet metal angle clips as illustrated in Fig. 5. Fig. A21.7 shows an artist's drawing of the wing structure of the Beechcraft Bonanza commercial airplane. It should be noticed that various types and shapes of ribs and formers are required in airplane design. Photographs A21.1 to 3 illustrate typical rib construction in various type aircraft, both large and small. Since ribs compose an appreciable part of the wing structural weight, it is important that they be made as light as safety permits and also be efficient relative to cost of fabrication and assembly. Rib development and design involves considerable static testing to verify and assist the theoretical analysis and design.

A21.3 Distribution of Concentrated Loads to Thin Sheet Panels.

In Art. A21.1 it was brought out that ribs were used to transmit external loads into the wing cellular beam structure. Concentrated external loads must be distributed to the rib before the rib can transfer the load to the wing beam structure. In other words, a concentrated load applied directly to the edge of a thin sheet would cause sheet to buckle or cripple under the localized stress. Thus a structural element usually called a web stiffener or a web flange is fastened to the web and the concentrated load goes into the stiffener which in turn transfers the load to the web. To get the load into the stiffener usually requires an end fitting. In general the distributed air loads on the wing surface are usually of such magnitude that the loads can be distributed to rib web by direct bearing of flange normal to edge of rib web without causing local buckling, thus stiffeners are usually not needed to transfer air pressures to wing ribs.

EXAMPLE PROBLEM ILLUSTRATING TRANSFER OF CONCENTRATED LOAD TO SHEET PANEL.

Fig. A21.8 shows a cantilever beam composed of 2 flanges and a web. A concentrated load of 1000 lb. is applied at point (A) in the direction shown. Another concentrated load of 1000 lb. is applied at point (E) as shown.

To distribute the load of 1000 lb. at (A), a horizontal stiffener (AB) and a vertical stiffener (CAD) are added as shown. A fitting would be required at (A) which would be attached to both stiffeners. The horizontal component of the 1000 lb. load which equals 800 lb. is taken by the stiffener (AB) and the vertical component which equals 600 lb. is taken by the

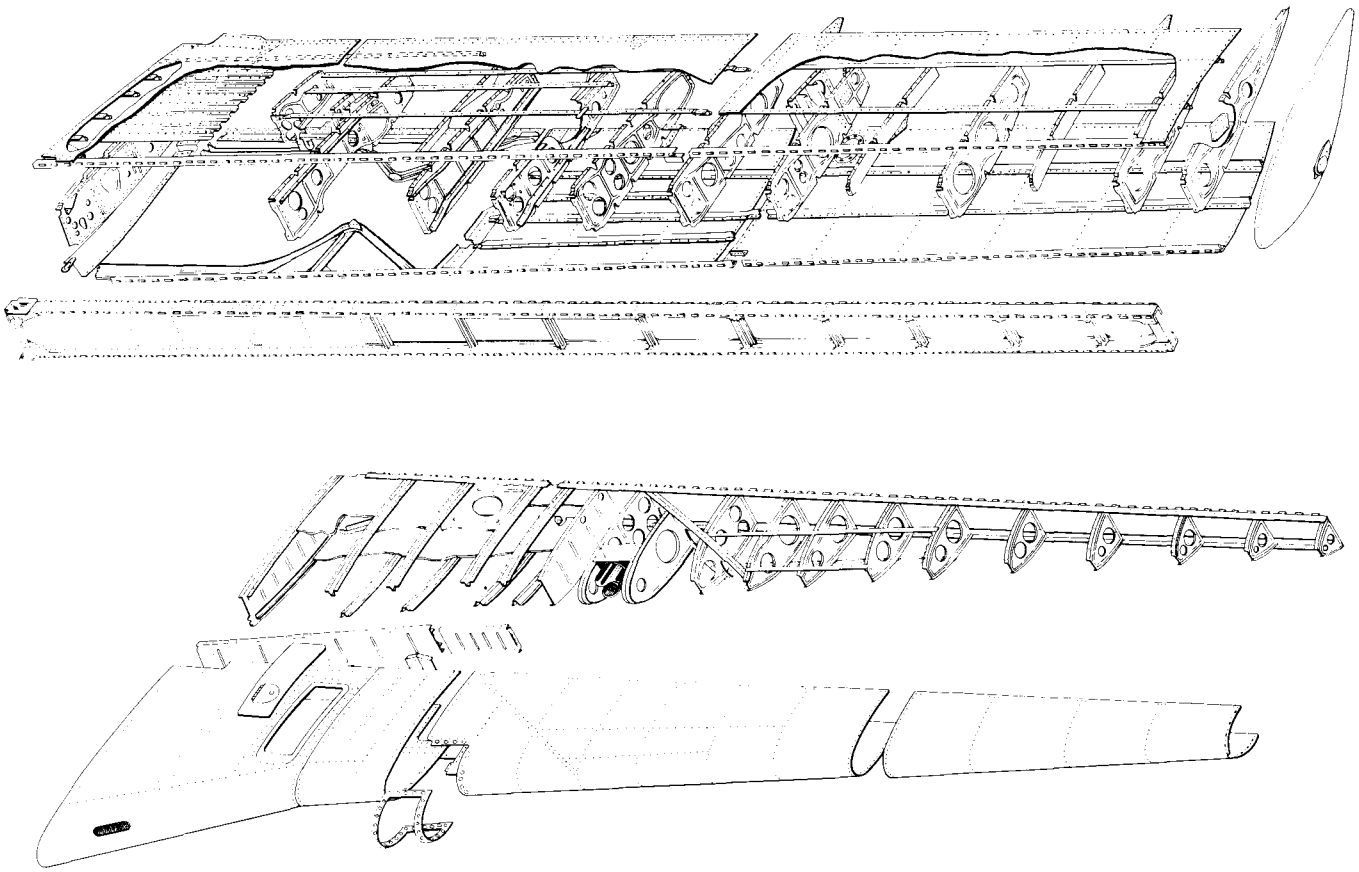

Fig. A21.7 General Structural Details of Wing for Beechcraft "Bonanza" Commercial Airplane.

vertical stiffener CD. The vertical load at E would be transferred to stiffener EF through fitting at E. The problem is to find the shear flows in the web panels, the stiffener loads and the beam flange loads.

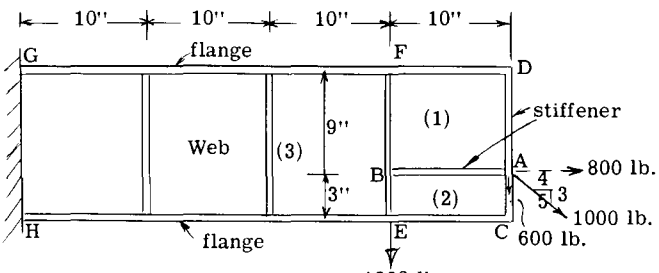

Fig. A21.8

Figs. A21.9 and A21.10 show free bodies of that portion including web panels (1) and (2) and stiffeners CAD and AB and the external load at (A). In Fig. A21.9 the shear flows q_1 and q_2

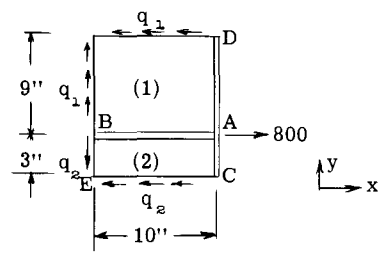

Fig. A21.9

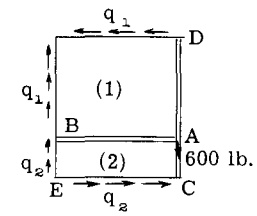

Fig. A21.10

SOLUTION: It will be assumed that the beam flanges develop the entire resistance to beam bending moments, thus shear flow is constant on a web panel.

The shear flows on web panels (1) and (2) will be computed treating each component of the 1000 lb. load as acting separately and the results added to give the final shear flow.

on the top and bottom edges respectively have been assumed with the sense as shown. Taking moments about point E,

$$\Sigma M_E = 800 \times 3 - 12 \times 10 q_1 = 0, \text{ whence } q_1 = 20 \text{ lb./in.}$$

$$\Sigma F_X = 800 - 20 \times 10 - 10 q_2 = 0, \text{ whence } q_2 = 60 \text{ lb./in.}$$

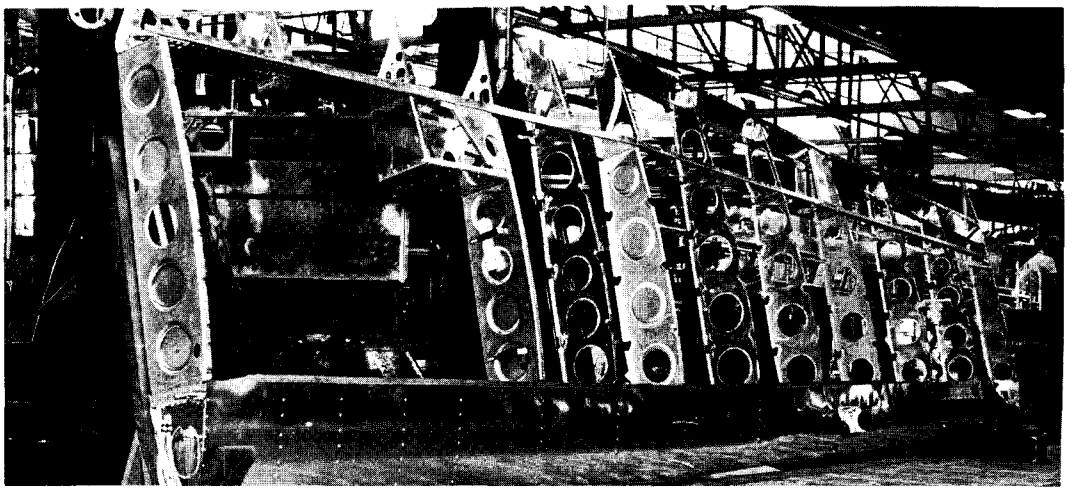

PHOTO. A21.1 Type of Wing Ribs Used in Cessna 180 Model Airplane, a 4 Place Commercial Airplane.

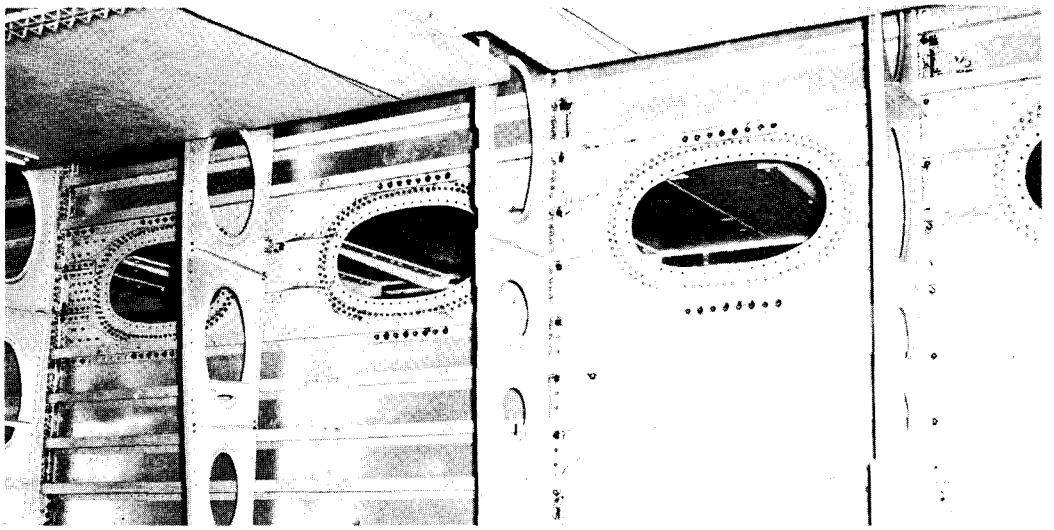

PHOTO. A21.2 Rib Type Used in Outer Panel-Fuel Tank Section- of Douglas DC-8 Commercial Jet Airliner.

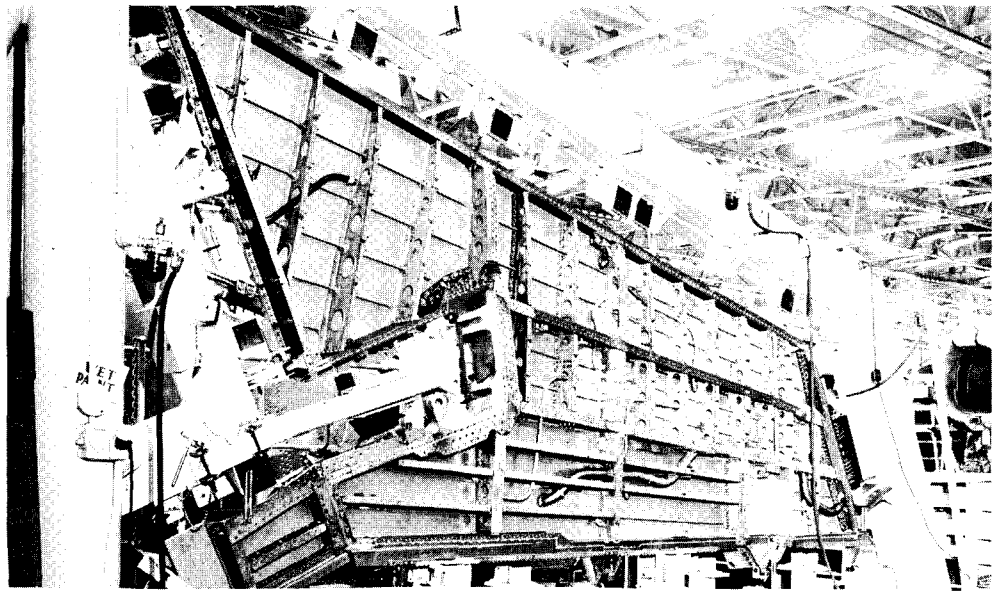

PHOTO. A21.3 Rib Construction and Arrangement in High Speed, Swept Wing, Fighter Type of Aircraft. North American Aviation - Navy Fury - Jet Airplane.

Referring to Fig. A21.10,

$\Sigma M_E = 600 \times 10 - 12 \times 10q_1 = 0$, whence $q_1 =$ 50 lb. in.

$\Sigma F_X = -50 \times 10 + 10q_2 = 0$, whence $q_2 =$ 50 lb./in.

Combining the two shear flows for the two loads,

$q_1 = 20 + 50 = 70$ lb./in.

$q_2 = 60 - 50 = 10$ lb./in.

Fig. A21.11 shows the results. Fig. A21.12 shows stiffener AB as a free body, and Fig. A21.13 the axial load diagram on stiffener AB, which comes directly from Fig. A21.11 by starting at one end and adding the shear flows.

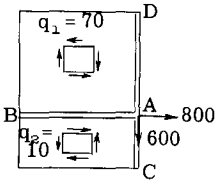

Fig. A21.11

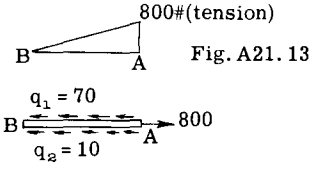

Fig. A21.13

Fig. A21.12

Fig. A21.14 shows a free body of the vertical stiffener CAD, and Fig. A21.15 the axial load diagram for the stiffener.

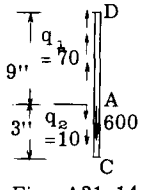

Fig. A21.14

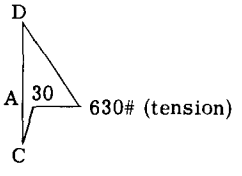

Fig. A21.15

The shear flows q_1 and q_2 could of course be determined using both components of forces at (A) acting simultaneously. For example, consider free body in Fig. A21.15a.

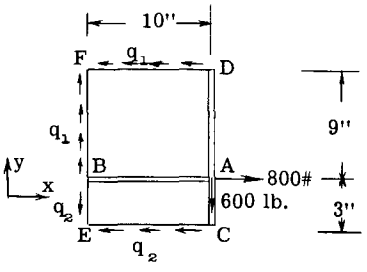

Fig. A21.15a

$\Sigma F_X = 800 - 10q_1 - 10q_2 = 0$ - - - - - (1)

$\Sigma F_y = -600 + 9q_1 - 3q_2 = 0$ - - - - - - (2)

Solving equations (1) and (2) gives,

$q_1 = 70$ lb./in., $q_2 = 10$ lb./in., which checks first solution.

The shear flow q_3 in web panel (3) is obtained by considering stiffener EBF as a free body, see Fig. A21.16.

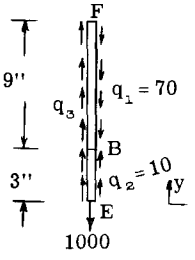

Fig. A21.16

$\Sigma F_y = 12q_3 + 10 \times 3 - 9 \times 70 - 1000 = 0$

whence, $q_3 = 133.33$ lb./in.

The shear flow q_3 could also be found by treating entire beam to right of section through panel (3). For this free body,

$\Sigma F_y = -600 - 1000 + 12q_3 = 0$

whence, $q_3 = 133.33$

Fig. A21.17 shows diagram of axial load in stiffener EF as determined from Fig. A21.16 by starting at one end and adding up the forces to any section.

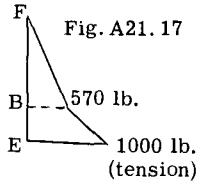

Fig. A21.17

After the web shear flows have been determined the axial loads in the beam flanges follow as the algebraic sum of the shear flows. Fig. A21.18 shows the shear flows along each beam flange as previously found. The upper and lower beam flange loads are indicated by the diagrams adjacent to each flange.

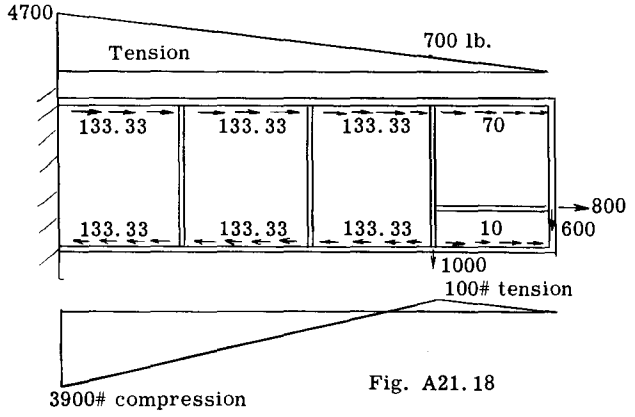

Fig. A21.18

In this example problem the applied external load at point (A) was acting in the plane of the beam web, thus two stiffeners were sufficient to take care of its two components. Often

loads are applied which have three rectangular components. In this case, the structure should be arranged so that line of action of applied force acts at intersection of two webs as illustrated in Fig. A21.19 where a load P is applied at point (0) and its components P_Z, P_y

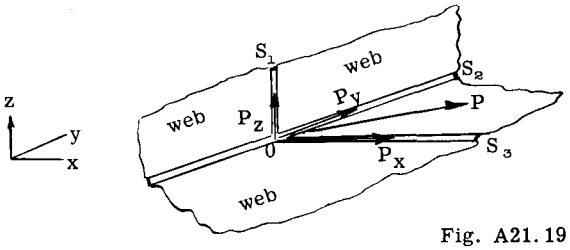

Fig. A21.19

and P_X are distributed to the web panels by using three stiffeners S_1, S_2 and S_3 intersecting at (0).

In cases where a load must be applied normal to the web panel, the stiffener must be designed strong enough or transfer the load in bending to adjacent webs.

In this chapter, the webs are assumed to resist pure shear along their boundaries. In most practical thin web structures, the webs will buckle under the compressive stresses due to shear stresses and thus produce tensile field stresses in addition to the shear stresses. The subject of tension field beams is discussed in detail in Volume II. In general the additional stresses due to tension field action can be superimposed on those found for the non-buckling case as explained in this chapter.

STRESSES IN WING RIBS

A21.4 Rib for Single Cell 2 Flange Beam.

Fig. A21.20 illustrates a rib in a 2-flange single cell leading edge type of beam. Assume that the air-load on the trailing edge portion (not shown in the figure) produces a couple reaction P and a shear reaction R as shown. These loads are distributed to the cell walls by the rib which is fastened continuously to the cell walls. Let q = shear flow per inch on rib perimeter which is necessary to hold rib in equilibrium under the given loads P and R.

Taking moments about some point such as (1) of all forces in the plane of the rib:

$$\Sigma M_1 = -Ph + 2Aq = 0$$

hence

$$q = Ph/2A. \quad (A = \text{enclosed area of cell})$$

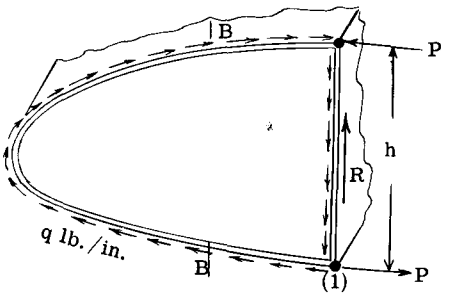

Fig. A21.20

With q known the shear and bending moment at various sections along the rib can be determined. For example, consider the section at B-B in Fig. A21.20. Fig. A21.21 shows a free body of the portion forward of this section.

The bending moment at section B-B equals:

$M_B = 2qA_1$ where A_1 is the area of the shaded portion.

Let F_X equal the horizontal component of the flange load at this section.

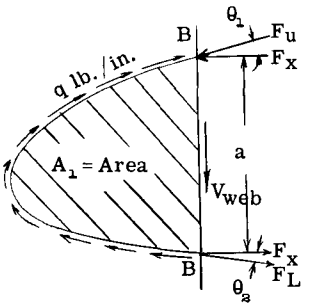

Fig. A21.21

$$F_X = M_B/a = 2qA_1/a$$

The true upper flange load $F_U = F_X/\cos\theta_1$ and the lower flange load equals $F_L = F_X/\cos\theta_2$.

The vertical shear on the rib web at B-B equals the vertical component of the shear flow q minus the vertical components of the flange loads. Hence

$$V_{web} = q\,a - F_X \tan\theta_1 - F_X \tan\theta_2$$

$$= q\,a - \frac{2\,q\,A_1}{a}(\tan\theta_1 + \tan\theta_2)$$

Illustrative Problem

The rib in the leading edge portion of the wing as illustrated in Fig. A21.22 will be analyzed.

A distributed external load as shown will be assumed.

Solution:

The total air load aft of beam = 8 x 40/2 = 160 lb. The arm to its c.g. location from the beam equals 40/3 = 13.33". Hence the reactions at the beam flange points due to the loads on the trailing edge portion equals:

$P = 160 \times 13.33/10 = 213.2$ lb. (See Fig. A21.23)

Shear reaction $V_r = 160$ lb.

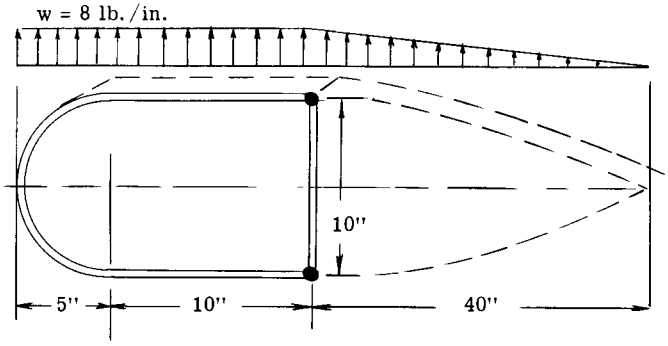

Fig. A21.22

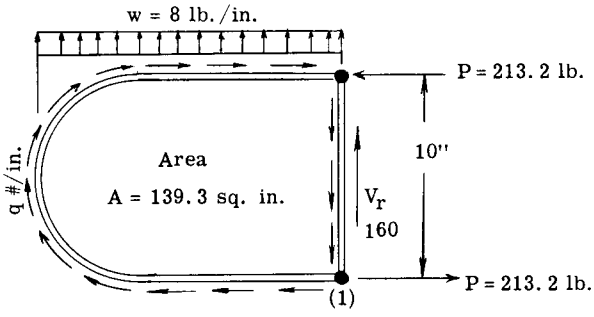

Fig. A21.23

Let q be the constant flow reaction of the cell skin on the rib perimeter which is necessary to hold the rib in equilibrium under the applied air loads.

Take moments about some point such as the lower flange (1).

$\Sigma M = -213.2 \times 10 + 8 \times 15 \times 7.5 + 2 \times 139.3\ q = 0$

whence, $q = 1232/278.6 = 4.42$ lb./in.

With the applied forces on the rib known, the shears and bending moments at various sections as desired can be calculated. For example, consider a section B-B, 2.5" from the leading edge. Fig. A21.24.

Bending moment at section B-B =

$8 \times 2.5 \times 1.25 + 4.42 \times 2 \times 15.4 = 161$ in.lb.

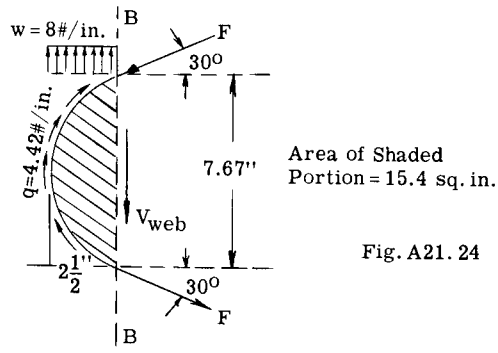

Area of Shaded Portion = 15.4 sq. in.

Fig. A21.24

A21.5 Stresses in Rib for 3 Stringer Single Cell Beam.

Fig. A21.25 shows a rib that fits into a single cell beam with 3 stringers labeled (a), (b) and (c). An external load is applied at point (a) whose components are 5000 and 3000 lbs. as shown. Additional reactions from a trailing edge rib are shown at points (b) and (c). A vertical stiffener ad is necessary to distribute the load of 5000 lb. at (a). The following values will be determined: -

(1) Rib web shear loads on each side of stiffener ad.

(2) Rib flange load at section ad.

(3) Rib flange and web load at section just to left of line bc.

Fig. A21.25

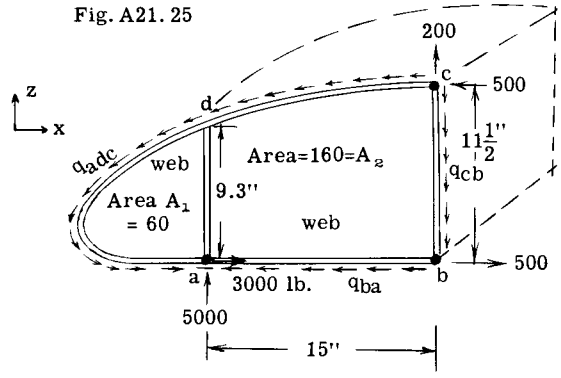

SOLUTION. It will be assumed that the 3 stringers develop the entire wing beam bending resistance, thus the wing shear flow is constant between the stringers. The wing rib is riveted to the wing skin and thus the edge forces on the rib boundary will be assumed to be the same as the shear flow distribution. In other words, the three shear flows q_{adc}, q_{ba} and q_{cb} hold the external loads in equilibrium. The sense of these 3 unknown shear flows will be assumed as shown in Fig. A21.25.

To find q_{adc}, take moments about point (b)

$$\Sigma M_b = -2(A_1 + A_2)\, q_{adc} + 5000 \times 15 - 500 \times 11.5 = 0$$

$$= -2(60 + 160)\, q_{adc} + 75000 - 5750 = 0$$

whence, q_{adc} = 157.3 lb./in. with sense as assumed.

To find q_{cb} take $\Sigma F_Z = 0$

$$\Sigma F_Z = 5000 + 200 - 157.3 \times 11.5 - 11.5\, q_{cb} = 0$$

whence, q_{cb} = 295 lb./in.

To find q_{ba} take $\Sigma F_X = 0$

$$\Sigma F_X = -500 + 3000 + 500 - 157.3 \times 15 - 15\, q_{ba} = 0$$

whence, q_{ba} = 42.7 lb./in.

With these supporting skin forces on the rib boundary, the rib is now in equilibrium and thus the web shears and flange loads can be determined. Consider as a free body that portion of the rib just to the left of the stiffener ad centerline as shown in Fig. A21.26.

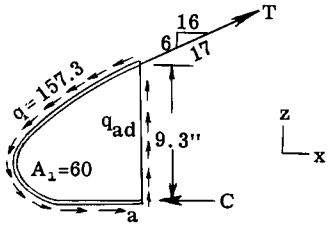

Fig. A21.26

To find flange load T take moments about point (a),

$$\Sigma M_a = (16/17)T \times 9.3 - 157.3 \times 60 \times 2 = 0$$

whence, T = 2158 lb.

To find flange load C take $\Sigma F_X = 0$

$\Sigma F_X = 2158\ (16/17) - C = 0$, whence C = 2034 lb.

To find web shear q_{ad} take $\Sigma F_Z = 0$

$\Sigma F_Z = 2158\ (6/17) - 157.3 \times 9.3 + 9.3\, q_{ad} = 0$

whence, q_{ad} = 74.6 lb./in.

To find the shear in the web just to right of stiffener ad, consider the free body formed by cutting through the rib on each side of the stiffener attachment line as shown in Fig. A21.27. The forces as found above are shown on this free body.

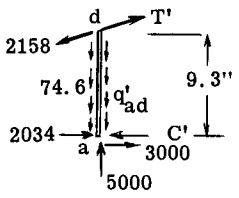

Fig. A21.27

To find web shear q'_{ad} take $\Sigma F_Z = 0$

$$\Sigma F_Z = 5000 - 9.3 \times 74.6 - 9.3\, q'_{ad} = 0$$

whence, q'_{ad} = 463 lb./in.

To find flange load C' take $\Sigma F_X = 0$, considering joint (a) as a free body,

$\Sigma F_X = 2034 + 3000 - C' = 0$, whence, C' = 5034 lb.

At joint (d) T' obviously equals 2158 lb. The stiffener ad carries a compressive load of 5000 lb. at its (a) end and decreases uniformly by the amount equal to the two shear flows or 463 + 74.6 = 537.6 lb./in.

The results obtained by considering Fig. A21.27 could also be obtained by treating the entire rib portion to the left of a section just to right of stiffener ad, as shown in Fig. A21.28.

To find rib flange load T' take moments about point (a).

$$\Sigma M_a = (16/17)\, T' \times 9.3 - 157.3 \times 60 \times 2 = 0$$

whence, T' = 2158 lb.

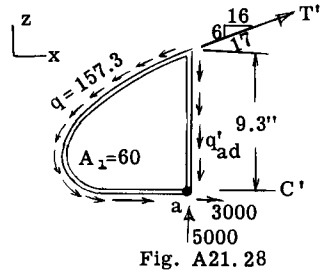

Fig. A21.28

To find flange load C' take $\Sigma F_X = 0$

$$\Sigma F_X = -C' + 3000 + 2158(16/17) = 0$$

whence, C' = 5034 lb.

To find q'_{ad} take $\Sigma F_Z = 0$

$$\Sigma F_Z = 2158(6/17) - 157.3 \times 9.3 + 5000 - 9.3\, q'_{ad} = 0$$

whence, q'_{ad} = 463 lb./in.

The above values are the same as previously obtained.

The rib flange loads and web shear will be calculated for a section just to left of line

cb. Fig. A21.29 shows the free body for the rib to left of this section.

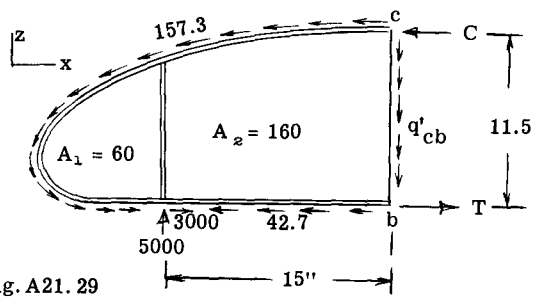

Fig. A21.29

To find flange load C take moments about point (b).

$$\Sigma M_b = -157.3 \times 2\ (160 + 60) + 5000 \times 15$$
$$-11.5\ C = 0$$

whence, C = 500 lb.

To find flange load T take $\Sigma F_X = 0$

$$\Sigma F_X = 3000 - 157.3 \times 15 - 15 \times 42.7 - 500 + T = 0$$

whence, T = 500 lb.

To find q'_{cb} take $\Sigma F_Z = 0$

$$\Sigma F_Z = 5000 - 157.3 \times 11.5 - 11.5\ q'_{cb} = 0$$

whence, q'_{cb} = 278 lb./in.

The above results could have been obtained with less numerical work by considering the forces to right of section cb in Fig. A21.29.

A21.6 Stress Analysis of Rib for Single Cell Multiple Stringer Wing.

When there are more than three spanwise stringers in a wing, there are four or more panels in the cell walls, thus the reactions of the cell walls upon the rib boundary cannot be found by statics as was possible in the 3 stringer case of the previous example problem.

Fig. A21.30 illustrates a wing section consisting of four spanwise flange members. The concentrated loads acting at the four corners of the box might be representative of reactions from the engine mount or nacelle structure and the reactions from a rib which supports the wing flap. These loads must be distributed into the walls of the wing box beam which necessitates a rib. Before the rib can be designed, the bending and shear forces on the rib must be determined. The calculations which follow illustrate a method of procedure.

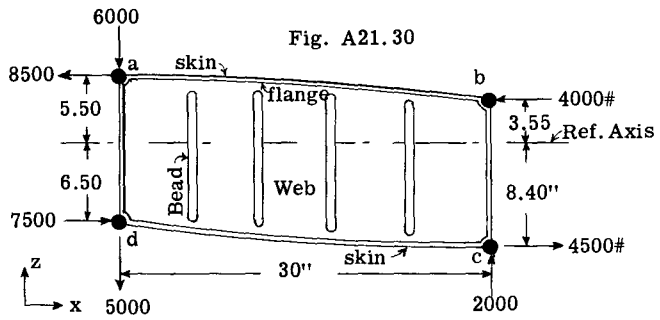

Fig. A21.30

SOLUTION:

The total shear load on the wing in the Z direction equals $V_Z = -6000 - 5000 + 2000 = -9000$ lb. and $V_X = -8500 + 7500 - 4000 + 4500 = -500$ lb.

The boundary forces on the rib will be equal to the shear flow force system on the cell walls due to the given external force system.

From Chapter A14, page A14.8, equation (14), the expression for shear flow is,

$$q_y = -(K_3 V_X - K_1 V_Z)\ \Sigma xA - (K_2 V_Z - K_1 V_X)\ \Sigma zA \quad \text{- - - - - - - - - - - - - - - - (1)}$$

The constants K depend on the section properties of the wing cross-section. Table A21.1 gives the calculation of the moment of inertia and product of inertia about centroidal Z and X axes. In this example the 4 stringers a, b, c and d have been considered as the entire effective material in resisting wing bending stresses.

TABLE A21.1

1	2	3	4	5	6	7	8	9	10	11
Flange No.	Area A	Z'	X'	AZ'	AZ'^2	AX'	AX'^2	AX' z'	$Z=Z'-\bar{Z}$	$X=X'-\bar{X}$
a	2.00	5.50	0	11.00	60.5	0	0	0	6.36	-11.8
b	1.25	3.55	30	4.43	15.72	37.50	1125	132.9	4.41	18.2
c	1.15	-8.40	30	- 9.66	82.20	34.50	1035	-289.8	-7.54	18.2
d	1.70	-6.50	0	-11.04	71.90	0	0	0	-5.64	-11.8
Σ	6.10			- 5.27	230.3	72.00	2160	-156.9		

$$\bar{z} = \Sigma AZ'/\Sigma A = -5.27/6.10 = -.865"$$
$$\bar{x} = \Sigma AX'/\Sigma A = 72.0/6.10 = 11.8"$$

Centroidal x and z moments of inertia:

$$I_X = 230.3 - 6.10 \times .865^2 = 225.8$$
$$I_Z = 2160 - 6.10 \times 11.8^2 = 1310$$
$$I_{XZ} = -156.9 - 610 \times -.865 \times 11.8 = -94.7$$

With the wing section properties known, the constants K can be calculated.

$$K_1 = I_{XZ}/(I_X I_Z - I_{XZ}^2)$$
$$= -94.7/(225.8 \times 1310 - 94.7^2) =$$
$$-94.7/286700 = -.00033$$

$$K_2 = I_Z/286700 = 1310/286700 = .00456$$

$$K_3 = I_X/286700 = 225.8/286700 = .000786$$

Substituting in equation (1),

$$q_y = -\left[.000786\ (-500) - (-.00033)(-9000)\right] \Sigma xA - \left[.00456\ (-9000) - (-.00033)(-500)\right] \Sigma zA$$

whence,

$$q_y = 3.363\ \Sigma xA + 41.205\ \Sigma zA \quad - - - - - \quad (2)$$

Since the shear flow at any point on the cell walls is unknown, it will be assumed zero on web ad, or imagine the web is cut as shown in Fig. A21.31. The static shear flows can now be found.

$$q_{ab} = 3.363\ (-11.8)(2.0) + 41.205 \times 6.36 \times 2 = 444 \text{ lb./in.}$$

$$q_{bc} = 444 + 3.363 \times 18.2 \times 1.25 + 41.205 \times 4.41 \times 1.25 = 748 \text{ lb./in.}$$

$$q_{cd} = 748 + 3.363 \times 18.2 \times 1.15 + 41.205\ (-7.54)(1.15) = 461 \text{ lb./in.}$$

These shear flows are plotted on Fig. A21.31. Refer to Chapter A14 regarding sense of shear flows.

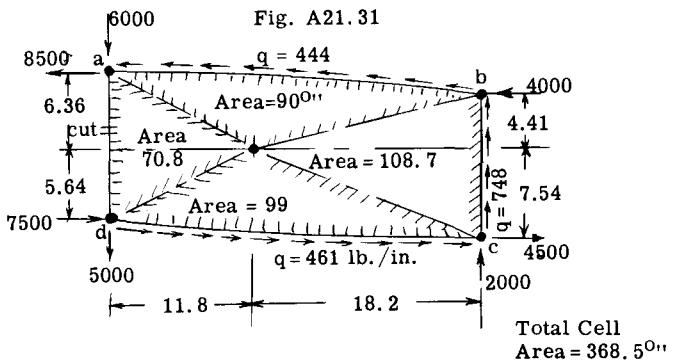

Fig. A21.31

The moments of the forces in the plane of the rib will now be calculated:

Taking moments about the c.g. of the beam cross section (See Fig. A21.31):

$$\Sigma M_{c.g.} = -11000 \times 11.8 - 8500 \times 6.36 - 7500 \times 5.65 - 4000 \times 4.41 - 4500 \times 7.54 - 2000 \times 18.2 - 444 \times 2 \times 90 - 748 \times 2 \times 108.7 - 461 \times 2 \times 99 = -648400 \text{ in.lb.}$$

For equilibrium $\Sigma M_{c.g.}$ must equal zero, therefore a constant flow shear q_1 acting around the rib perimeter is necessary which will produce a moment of 648400 in.lb.

$$q_1 = \frac{M}{2A} = \frac{648400}{2 \times 368.5} = 880 \text{ lb./in.}$$

(Note: 368.5 = total area of cell)

Adding this shear flow to that of Fig. A21.31, the resulting force system of Fig. A21.32 is obtained. The reactions of the beam cell walls on the rib have now been determined and the bending moments and shears on the rib can now be calculated.

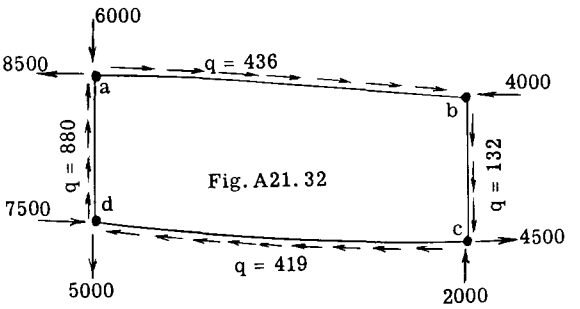

Fig. A21.32

To illustrate, consider the rib section B-B which passes through the c.g. of the beam section. Fig. A21.33 shows a free body of the bulkhead portion to the left of section B-B.

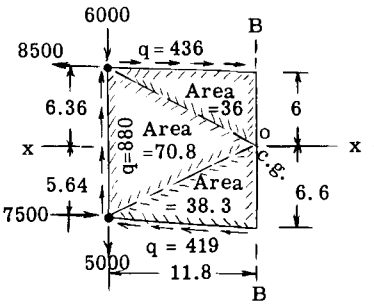

Fig. A21.33

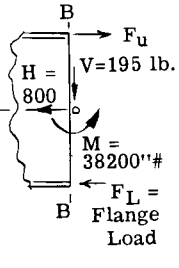

Fig. A21.34

Moments at section B-B will be referred to the point (O):

$$\Sigma M_O = -11000 \times 11.8 - 8500 \times 6.36 - 7500 \times 5.64 + 436 \times 2 \times 36 + 880 \times 2 \times 70.8 + 419 \times 2 \times 38.3 = -38200 \text{ in.lb.}$$

The resultant external shear force along the section B-B equals the summation of the z components of all the forces.

$$V = \Sigma F_Z = -11000 + 12 \times 880 - 436 \times 0.36 + 419 \times 0.96 = -195 \text{ lb.}$$

The resultant load normal to the section B-B equals the summation of the force components in the x direction.

$$H = \Sigma F_X = -8500 + 7500 + (436 - 419)\ 11.8 = -800 \text{ lb.}$$

Fig. A21.34 shows these resultant forces referred to point (O) of the cross-section. If we assume that the rib flanges develop the entire resistance to normal stresses, we can find flange loads by simple statics.

To find upper flange load F_u take moments about lower flange point.

$$\Sigma M = 12.6\ F_u - 38200 - 800 \times 6.6 = 0$$

whence, F_u = 3443 lb. tension

To find F_L use $\Sigma F_X = 0$

$\Sigma F_X = 3443 - 800 - F_L = 0$, whence F_L = 2643 lb. compression.

The shear flow on web equals V/12.6 = 195/12.6 = 15.5 lb./in. This result neglects effect of flanges not being normal to section B-B, which inclination is negligible in this case.

If the entire cross-section of rib is effective in bending, then the web thickness and flange sizes of the rib would be needed to obtain the section moment of inertia which is necessary in the beam equation for bending stresses. The forces at (O) would then be referred to neutral axis of section before bending and shear stresses on the rib section could be calculated.

To obtain a complete picture of the web and flange forces, several sections along the rib span should be analyzed as illustrated for section B-B.

A21.7 Rib Loads Due to Discontinuities in Wing Skin Covering.

As referred to before, ribs in addition to transmitting external loads to wing cell structure are also a means of re-distributing the shear forces at a discontinuity, the most common discontinuity being a cut-out in one or more of the webs or walls of the wing beam cross section. The usual procedure in finding the boundary forces on a rib located adjacent to a cut-out is to find the applied shear flows in the wing on two sections, one on each side of the rib. Then the algebraic sum of these two shear flows will give the rib boundary forces. With the boundary forces known the rib web and flange stresses can be found as previously illustrated. The procedure can best be illustrated by example problems.

A21.8 Example Problem. Wing with Cut-Out Subjected to Torsion.

Fig. A21.35 shows a rectangular single cell wing beam with four stringers or flanges located at the four corners. The upper surface skin is discontinued in the center bay (2). The wing is subjected to a torsional moment of

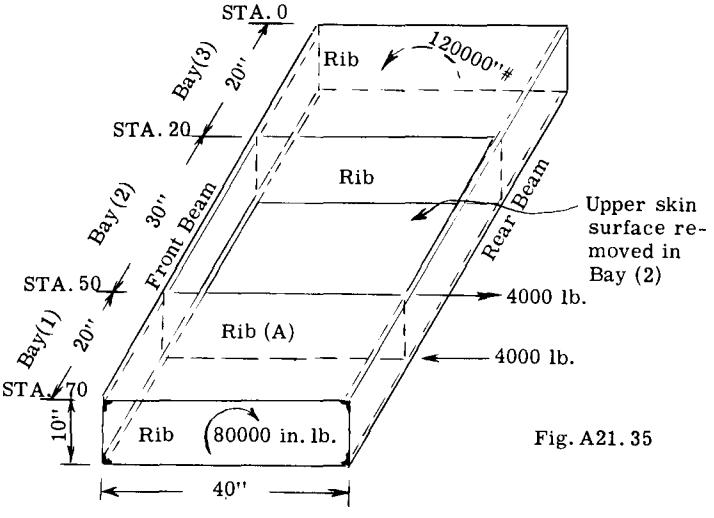

Fig. A21.35

80000 in.lb. at Station (70) and a couple force at Station (50) as shown in Fig. A21.35. The problem will be to determine the applied forces on rib (A).

SOLUTION:

The applied shear flow on the cell walls will be found for two cross-sections of the wing, one on each side of rib (A).

In bay (1) the torsional moment M is 80000 in.lb. The applied shear flow on a cross-section of the wing in bay (1) thus equals,

$$q = \frac{M}{2A} = \frac{80000}{2 \times 10 \times 40} = 100 \text{ lb./in.}$$

This shear flow system is shown on Fig. A21.36 which is a free body of rib (A). In bay (2), since the top skin is removed, the torsional moment must be taken by the front and rear vertical webs, since any shear flow in the bottom skin could not be balanced.

The torsional moment in bay (2) is,

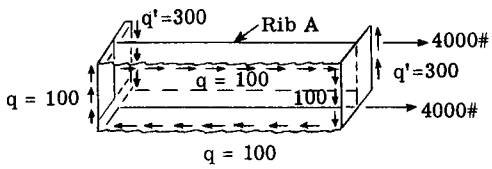

Fig. A21.36

$M = 80000 + 4000 \times 10 = 120000$ in.lb.

The total shear load on each vertical web thus equals 120000/40 = 3000 lb., which gives a shear flow q' = 3000/10 = 300 lb./in. on each web. This applied shear is shown on the free body of rib (A) in Fig. A21.36. On the left end of the rib a shear flow of 100 is acting

Fig. A21.37

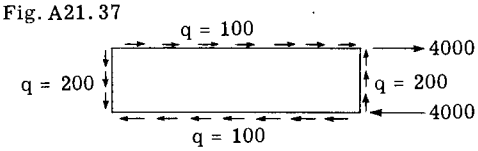

up and on the other side a shear flow of 300 is acting down, thus the rib web must take the difference or 200 acting down. On the right end of the rib the load on the rib web is 200 lb./in. up. The loads on the top and bottom flanges of the rib is obviously 100 lb./in. Fig. A21.37 shows the loads applied to the rib boundary when the torsion in bay (1) and the external couple force is transferred to the cross-section of bay (2).

ADDITIONAL EFFECTS DUE TO DIFFERENTIAL BENDING OF BEAMS IN BAY (2).

The torsion in bay (1) and the external couple force are thrown off as couple force on the front and rear beams of middle bay (2), with the total shear load on each beam being 3000 lb. as previously calculated. These beam shear loads must be transmitted to bay (3) and thus cause bending of the beams in bay (2). Since each beam is attached to relative rigid box structures at each end, namely bays (1) and (3), the beams tend to bend with no rotation of their ends. If we neglect the deflections of these end box structures, we can assume that the beams bend with no rotation of their ends or each beam is fixed ended. Fig. A21.38a illustrates the deflection of the front beam in bay (2) under the assumption of no end rotation. The beam elastic curve has a point of inflection at the span midpoint. Figs. 38b, c show the beams bending moment and shear diagrams.

The end moments are $M = VL/2 = 3000 \times 30/2 = 45000$ in.lb. Assuming the beam flanges develop the entire bending resistance the beam

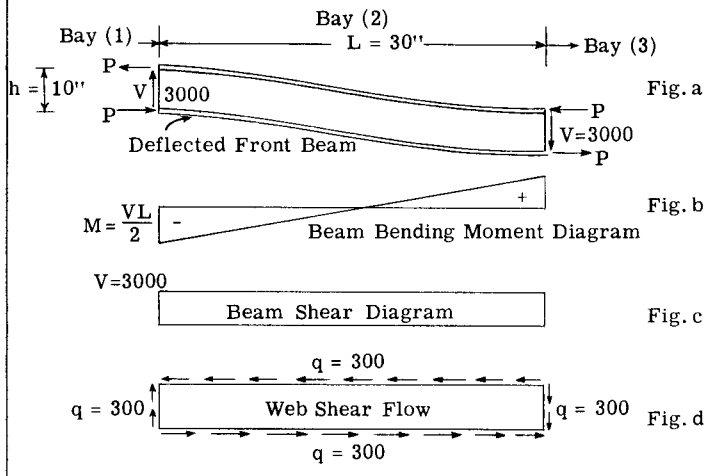

Fig. A21.38

flange loads at the beam ends are P = 45000/10 = 4500 lb. (See Fig. a).

The deflection of the rear beam would be the reverse of Fig. a, and thus all forces would also be reversed.

Fig. A21.39 shows bay (1) of the wing as a free body acted upon by the flange loads due to bending of the beams in bay (2). These internal flange forces from bay (2) must be held in equilibrium by the internal stresses in the adjacent wing structure of bay (1).

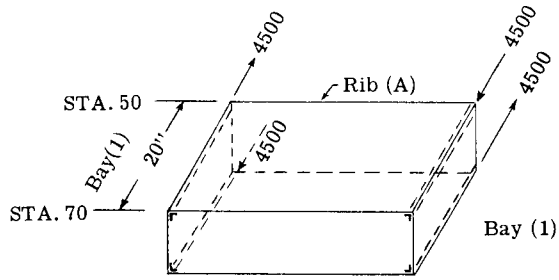

Fig. A21.39

According to the well known principle of mechanics formulated by Saint Vennat, the stresses resulting from such an internal force system will be negligible at a distance from the forces. This distance in case of a cut-out is usually assumed as approximately equal to the width of the cut-out, or in general to the width of the adjacent wing bay. Thus in Fig. A21.39 the flange loads of 4500 lbs. each are assumed to be dissipated at a uniform rate for a distance of 20 inches. Thus the shear flow created by each stringer load which equals the change in axial load per inch in the stringer in bay (1) equals 4500/20 = 225 lb.

Fig. A21.40 shows a segment 1 inch wide cut from wing bay (1) with the ΔP load in each

flange member. To find the shear flow on the cross-section the front web is first assumed cut, and thus the static shear flow $q_S = \Sigma\Delta P$ from cut face where q_S is zero. Fig. A21.40 shows this static shear flow.

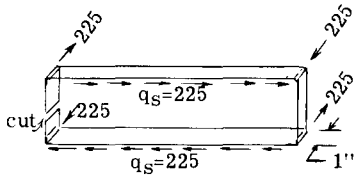

Fig. A21.40

For equilibrium of the cross-section, the moment of the forces in the plane of the cross-section must equal zero. Taking moments about lower left hand corner of the q_S force system,

M = 225 x 40 x 10 = 90000 in.lb. For equilibrium a moment of -90000 is necessary. Therefore a constant shear flow system q must be added to develop a moment of -90000. Thus q = M/2A = (-90000/2 x 10 x 40) = -112.5 lb./in. Adding this shear flow to that for q_S in Fig. A21.40 gives the final values in Fig. A21.41. This shear flow system represents the stress

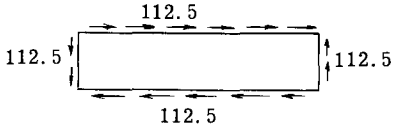

Fig. A21.41

system caused on cross-section of bay (1) due to the differential bending of the beams in bay (2). This shear flow system must therefore be resisted by rib (A) as it must terminate at end of bay (1). Therefore the shear flows in Fig. A21.41 are applied boundary loads to rib (A) and these must be added to the rib loads in Fig. A21.37 to give the final rib loads of Fig. A21.42. With the final rib loads

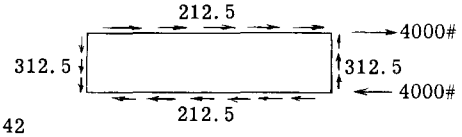

Fig. A21.42

known, the rib flange and web stresses can be found as previously explained.

A21.9 Example Problem. Wing with Cut-Out Subjected to Bending and Torsional Loads.

Fig. A21.43 shows a portion of a 4 stringer single cell cantilever beam composed of 3 bays formed by the four ribs. The loads on the structure consist of loads applied to end of bay (1) as shown. The areas of corner stringers a, b, c and d are shown in ( ) adjacent to each stringer.

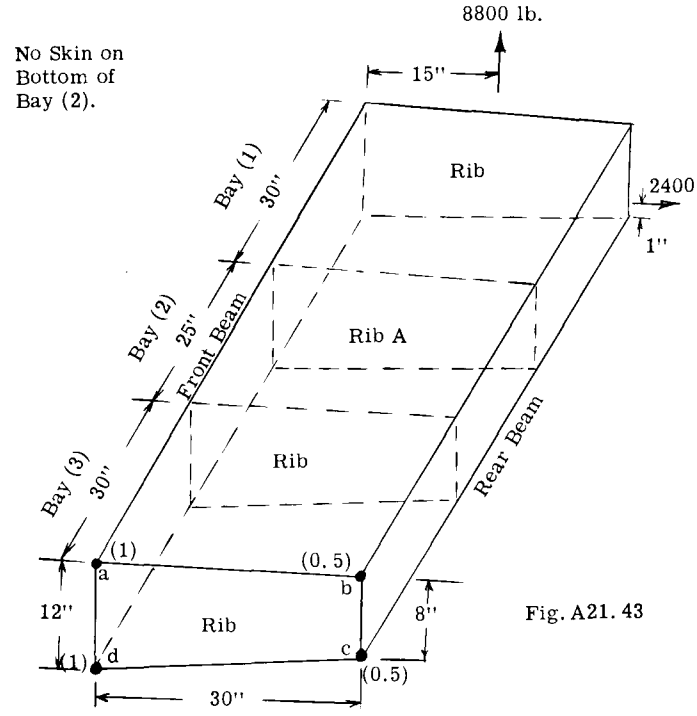

Fig. A21.43

The middle bay (2) has no skin on the bottom surface, or in other words, the middle bay has a channel cross-section, which fact often happens in practical wing design as for example a space or well for a retractable landing gear. The problem will be to find the shear flow in bays (1) and (2) and the boundary loads on rib (A) between bays (1) and (2).

Solution No. 1

This method of solution will make use of the shear center location for bay (2) in order to obtain the true torsional moment on bay (2). With this torsional moment known, the procedure is similar to the previous example involving wing torsion only.

We will first calculate the shear flow in wing bay (1). Fig. A21.44 shows the cross-section.

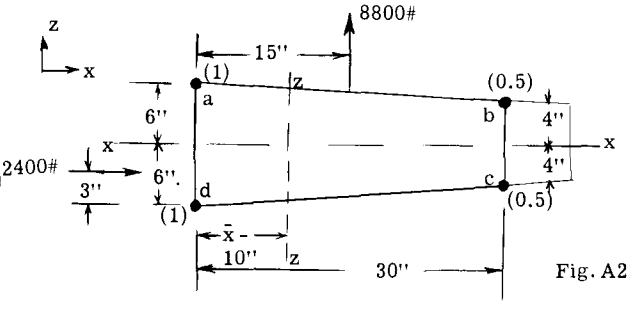

Fig. A21.44

The section moments of inertia are needed in calculating shear flows.

$$I_x = (1 \times 6^2 \times 2) + (0.5 \times 4^2 \times 2) = 88 \text{ in.}^4$$

$$\bar{X} = \Sigma Ax/\Sigma A = (1 \times 30)/3 = 10 \text{ in.}$$

$$I_z = (2 \times 10^2) + (1 \times 20^2) = 600 \text{ in.}^4$$

$$V_z = 8800 \text{ lb.}, \quad V_x = 2400 \text{ lb.}$$

$$q_y = -\frac{V_z}{I_x} \Sigma zA - \frac{V_x}{I_z} \Sigma xA, \text{ substituting}$$

$$q_y = -100\ \Sigma zA - 4\ \Sigma xA \quad - - - - - - - - - - - \quad (a)$$

Since the shear flow is unknown at any point on cell, we will assume front web (ad) as cut or carrying zero shear.

$$q_{dc} = -100\ (-6)(1) - 4\ (-10)(1) = 640 \text{ lb./in}$$

$$q_{cb} = 640 - 100\ (-4)(0.5) - 4\ (20)\ 0.5 = 800$$

$$q_{ba} = 800 - 100\ (4)(0.5) - 4\ (20)\ 0.5 = 560$$

Fig. A21.45 shows these static shear flows.

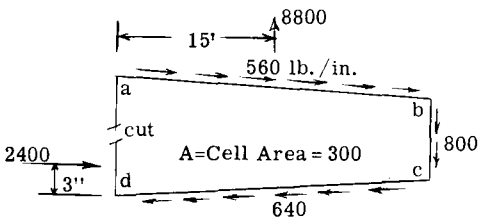

Fig. A21.45

To this shear flow, a constant shear flow must be added to make $\Sigma M = 0$. Take moments about point (d).

$$\Sigma M_d = -8800 \times 15 + 2400 \times 3 + 560 \times 30 \times 12 + 800 \times 8 \times 30 = 268800 \text{ in. lb., or } -266800$$

is required for equilibrium, hence the required constant shear flow $q = -M/2A = -268800/2 \times 300 = -448$. Adding this shear flow to that of Fig. A21.45, we obtain the shear flow of Fig. A21.46.

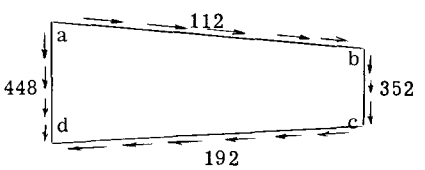

Fig. A21.46

This shear flow system would be the shear flow system for all 3 bays if the bottom skin in bay (2) was not removed. Removing the bottom skin in bay (2) will modify these shear flows of Fig. A21.46.

Therefore we consider bay (2) in its true condition with bottom skin removed. Fig. A21.47 shows the cross-section of bay (2).

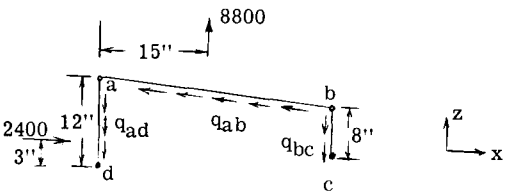

Fig. A21.47

The three shear flows can be determined by statics.

$$\Sigma F_x = 2400 - 30\ q_{ab} = 0, \text{ whence } q_{ab} = 80$$

$$\Sigma M_d = 2400 \times 3 - 8800 \times 15 - 80 \times 30 \times 12 + q_{bc}\ (8 \times 30) = 0, \text{ whence } q_{bc} = 640$$

$$\Sigma F_z = 8800 - 8 \times 640 + 2 \times 80 - 12\ q_{ad} = 0$$

whence $q_{ad} = 320$

Fig. A21.48 shows the results. This shear flow system is the final or true shear on bay (2).

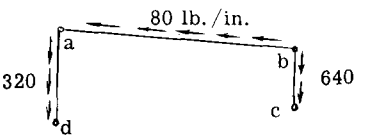

Fig. A21.48

Since we have a channel or open wing cross-section in bay (2), any torsional moment on this bay must be transmitted by differential bending of the front and rear beams. To obtain the torsional moment on bay (2), the shear center location must be known.

Horizontal location of shear center: - Assume the section bends about centroidal X axis without twist under a V_z load of 8800 lb.

$$q = -\frac{V_z}{I_x} \Sigma zA, \text{ or } q = -100\ \Sigma zA$$

$$q_{cb} = -100\ (-4)(0.5) = 200$$

$$q_{ba} = 200 - 100\ (4)(0.5) = 0$$

$$q_{ad} = 0 - 100\ (6)(1) = -600$$

Fig. A21.49 shows the shear flow results for bending about x-x without twist. The line of action of the resultant of this shear flow force system locates the horizontal position of the shear center.

$$\bar{X} = (200 \times 8 \times 30)/8800 = 5.45 \text{ in.}$$

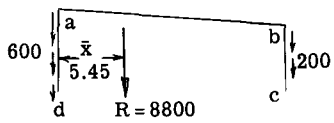

Fig. A21.49

Vertical position of shear center: -

Assume section bends about centroidal z axis without twist under a load of V_x = 2400 lb.

$$q = -\frac{V_x}{I_z}\Sigma xA = -4\,\Sigma xA$$

$$q_{cb} = -4 \times 20 \times 0.5 = -40 \text{ lb./in.}$$

$$q_{ba} = -40 - 4 \times 20 \times 0.5 = -80$$

$$q_{ad} = -80 - 4\,(-10)\,1 = -40$$

Fig. A21.50 shows the shear flow results.

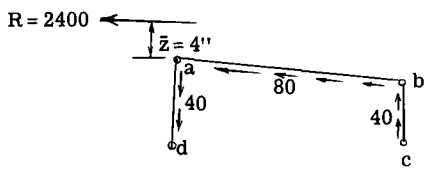

Fig. A21.50

The vertical distance $\bar{Z}$ from point (a) to the line of action of the resultant which locates the vertical location of shear center is,

$$\bar{Z} = \Sigma M_a/2400 = (40 \times 8 \times 30)/2400 = 4 \text{ in.}$$

Fig. A21.51 shows the shear center location and the external loads. The moment about the shear center which equals the torsion on the wing bay (2) equals,

$$M_{s.c.} = -8800 \times 9.55 - 2400 \times 13 = -115240 \text{ in.lb.}$$

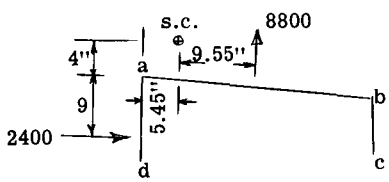

Fig. A21.51

This torsional moment must be resisted by front and rear beams. Hence shear load on each beam = 115240/30 = 3841 lb.

As in the previous example problem involving torsion, the beams in bay (2) will be assumed to bend without rotation of their ends, or in other words the bending moment at midpoint of bay is zero. The flange loads at points a, b, c and d on bay (1) from the differential bending of beams in bay (2), thus equal the beam shear times half the span of bay (2) divided by the beam depth.

For front beam P = 3841 x 12.5/12 = 4000 lb.

For rear beam P = 3841 x 12.5/8 = 6000 lb.

Fig. A21.52 shows these flange loads applied to bay (1). These loads are dissipated

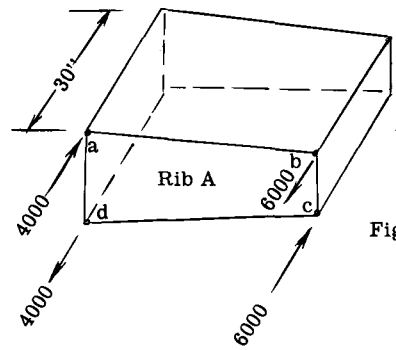

Fig. A21.52

uniformly in bay (1) over a distance of 30 inches, or the shear flow per inch produced by these flange loads equals ΔP = P/30, whence

$$\Delta P_a = \Delta P_d = 4000/30 = 133.3 \text{ and } \Delta P_b = \Delta P_c = 6000/30 = 200 \text{ lb.}$$

Fig. A21.53 shows an element of bay (1) one inch wide with these ΔP loads. The shear flow q assuming the front web cut equals ΣΔP. The resulting static shear flows which equals ΣΔP is shown in Fig. A21.53.

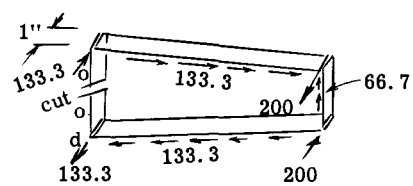

Fig. A21.53

The moment of this shear flow system about point (d) = 133.33 x 30 x 12 - 66.7 x 8 x 30 = 31980. For ΣM = 0, we need a constant shear flow q = - 31980/2 x 300 = -53.3 lb./in. Adding this constant shear flow to that of Fig. A21.53 gives the shear flow system of Fig. A21.54. These results represent the effect on bay (1)

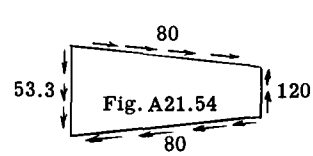

Fig. A21.54

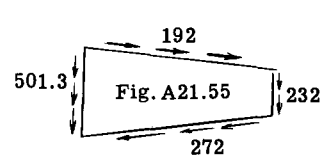

Fig. A21.55

of removing the bottom skin in bay (2). Adding the shear flows of Fig. A21.54 to those of Fig. A21.46, we obtain the final shear flows in bay (1) as shown in Fig. A21.55.

BOUNDARY LOADS ON RIB (A)

The boundary loads on rib (A) will equal the difference between the shear flows in bays (1) and (2). Fig. A21.56 shows a free body of rib (A) with the shears flows obtained from Figs. A21.55 and A21.48.

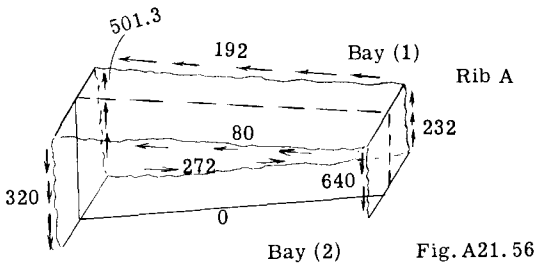

Fig. A21.56

The resulting applied boundary forces to the rib equal the algebraic sum of the shear flows on each side of the rib which gives the values in Fig. A21.57.

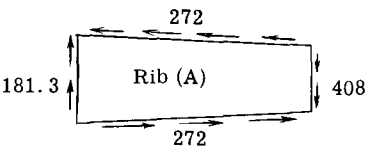

Fig. A21.57

With the rib boundary loads known, the stresses in the rib can be found as previously illustrated in this chapter.

Solution No. 2

This method of solution first finds the shear flow in all bays assuming bottom skin is not removed in center bay (2). This gives a shear flow in the bottom skin. However, the skin in bay (2) is actually removed so a corrective set of shear flows on bay (2) along the boundary lines of the bottom skin must be applied to eliminate the shear flows found in the bottom skin. The problem then consists of finding the influence of these corrective shear flows upon the shear flows as found for bays (1) and (2) when bottom skin in bay (2) was not removed.

The first step is to find the shear flows in all bays assuming bottom skin in bay (2) is not removed. The calculations would be exactly like those in solution (1) and the shear flow in all bays would be those in Fig. A21.46. The bottom skin in Fig. A21.46 has a shear flow of 192 with sense as shown. Since this skin is missing we reverse this shear flow and find the resisting shear flows on the other three sides of the bay cross-section. Fig. A21.58 shows the section, with the 3 unknown shear flows q_{ab}, q_{bc} and q_{ad}.

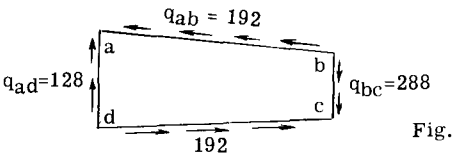

Fig. A21.58

To find q_{ab} use $\Sigma F_x = 0$, $192 \times 30 - 30\ q_{ab} = 0$

whence, $q_{ab} = 192$

$\Sigma M_d = -30 \times 192 \times 12 + 8\ q_{bc} \times 30 = 0$

whence, $q_{bc} = 288$

$\Sigma F_z = 4 \times 192 - 8 \times 288 + 12\ q_{ad} = 0$

whence, $q_{ad} = 128$

Adding the shear flows of Fig. A21.58 to those of Fig. A21.46 gives the final shear flows in bay (2) as shown in Fig. A21.59. These results check the results in Fig. A21.48 obtained in solution method (1).

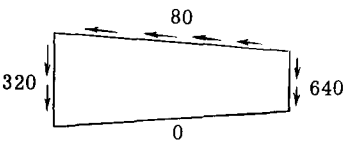

Fig. A21.59

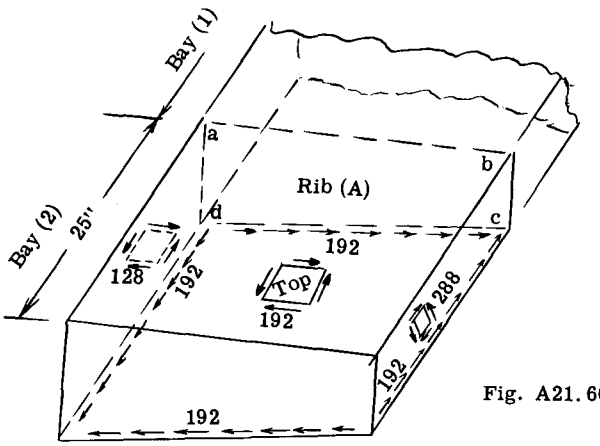

Fig. A21.60

Fig. A21.60 shows the corrective shear flows of Fig. A21.58 applied to bay (2). On the bottom skin the corrective shear flow is shown on the boundary of the cut-out. These shear

flows cause differential bending of the front and rear beams in bay (2). If we make the assumption that the beam end suffer no rotation, the bending moment is zero at midpoint of the bay and thus the flange loads at points a, b, c and d of bay (1) equal the algebraic sum of the shear flows on each side of a flange times half the span of bay (2) or 12.5 inches. Thus from Fig. A21.60,

$P_a = (192 + 128)12.5 = 4000$ lb. compression

$P_b = (288 + 192)12.5 = 6000$ lb. tension

$P_c = (288 + 192)12.5 = 6000$ compression

$P_d = (128 + 192)12.5 = 4000$ tension

Referring to Fig. A21.52, we find that the P values above are the same as the P values obtained by solution (1). Thus the remainder of solution (2) would be identical to that in solution (1), and therefore the calculations will not be repeated here.

A21.10 Fuselage Frames

Frames in a fuselage serve the same purpose as ribs in wing structures. Ribs are usually of beam or truss construction and can be stress analyzed fairly accurately by statics. Fuselage frames however, are of the closed ring type of structure and are therefore statically indeterminate relative to internal stresses. Once the applied loads on a frame are known the internal stresses can be found by the application of the elastic theory as covered in Chapters A8, A9, A10 and A11. The loads on fuselage frames due to discontinuities in the fuselage structure, such as those due to windows and doors, can be approximately determined by the procedures previously presented for wing ribs.

The photographs on page 32 of Chapter A15 show some of the frame construction of the Douglas DC-8 airliner. Other pictures of fuselage construction are given in Chapter A20. Photographs A21.4 and 5 illustrate typical frame construction and arrangement.

A21.11 Supporting Boundary Forces on Fuselage Frames.

When external concentrated loads are applied to a fuselage frame through a suitable fitting or connection, the frame is held in equilibrium by reacting fuselage skin forces which are usually transferred to the frame boundary by rivets which fasten fuselage skin to frame. Since the fuselage shell is usually stress analyzed by the beam theory, it is therefore consistent to determine the distribution of the supporting skin forces by the same theory.

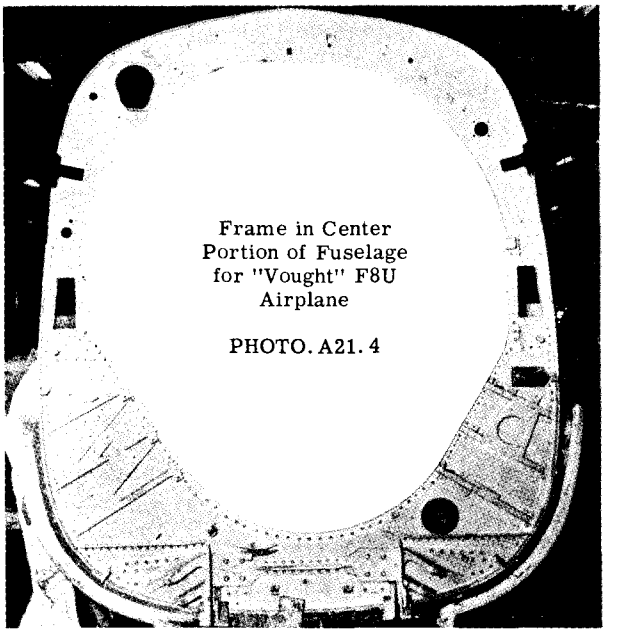

Frame in Center Portion of Fuselage for "Vought" F8U Airplane

PHOTO. A21.4

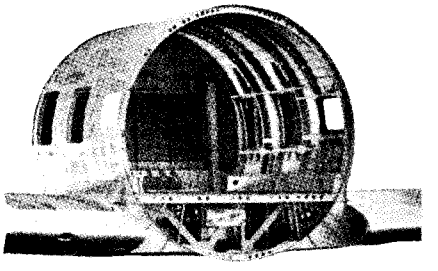

PHOTO. A21.5
Fuselage-Wing Portion of "Martin" 404 Transport

A21.12 Calculation of Frame Boundary Supporting Forces.

Example Problem 1

Fig. A21.61 illustrates a cross-section of a circular fuselage. Two concentrated loads of 2000 lb. each are applied to the fuselage frame at the points indicated. The problem is to determine the reacting shear flow forces in the fuselage skin which will balance the two externally applied loads. This fuselage section might be considered as the aft portion of a medium size fuselage and the loads are due to air loads on the horizontal tail surfaces. To make the numerical calculations short the fuselage stringer arrangement has been assumed symmetrical.

Solution:

In this solution the fuselage skin resisting forces will be assumed to vary according to the general beam theory. The general flexural shear flow equation for bending about the Y axis is,

$$q = -\frac{V_Z}{I_y} \Sigma zA \ , \quad \text{where } V_Z = 4000 \text{ lb.}$$

The moment of inertia I_y of the fuselage cross-section is required. In this simplified illustration, the area of each stringer plus its effective skin will be taken as .15 sq.in. The student should of course realize after studying Chapters A19 and A20 that the true effective area should be used on the compressive side and that the skin on the tension side of the fuselage is entirely effective. These facts would tend to make the effective cross-section unsymmetrical about the Y axis. Since the only purpose of this illustrative solution is to show how the frame loads are balanced, the section being assumed as symmetrical which will greatly decrease the amount of calculations required.

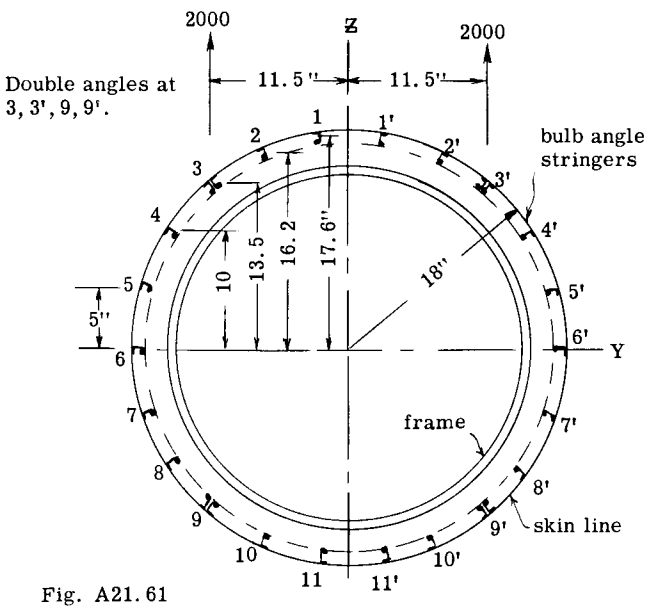

Fig. A21.61

Moment of inertia of fuselage section about Y axis which is the neutral axis under our simplified assumptions.

$$I_y = .15\ (17.6^2 + 16.2^2 + 13.5^2 + 13.5^2 + 10^2 + 5^2)4 = 637 \text{ in.}^4$$

Due to symmetry of effective section and external loading, the shear flow in the fuselage skin on the z axis or between stringers 1 and 1 and 11 or 11 will be zero. Thus starting with stringer (1) the shear flow in the skin resisting the external loads of 4000 lb. can be written around the circumference of the section.

$$q = -\frac{V_Z}{I_y} \Sigma zA = -\frac{4000}{637} \Sigma zA = -6.275\ \Sigma zA$$

$$q_{1-2} = -6.275 \times .15 \times 17.6 = -16.57 \text{ lb./in.}$$

$$q_{2-3} = -16.57 - 6.275 \times .15 \times 16.2 = -31.82$$

$$q_{3-4} = -31.82 - 6.275 \times .30 \times 13.5 = -57.22$$

$$q_{4-5} = -57.22 - 6.275 \times .15 \times 10 = -66.62$$

$$q_{5-6} = -66.62 - 6.275 \times .15 \times 5 = -71.32$$

Due to symmetry of effective cross-section, the shear flow is symmetrical about the Y axis.

As a check on the above work, the summation of the z components of the shear flow on each skin panel between the stringers should equal the external load of 4000 lb.

ΣF_Z of skin shear flow equals the vertical projected length of each panel times the shear flow q on that panel, or

$$\Sigma F_Z = [1.4 \times 16.57 + 2.7 \times 31.82 + 3.5 \times 57.22 + 5 \times 66.62 + 5 \times 71.32]\ 4 = 4000 \text{ lb.}$$ (check)

Fig. A21.62 shows the frame with its balanced load system. The internal stresses can now be found by the methods of Chapters A8 to A11.

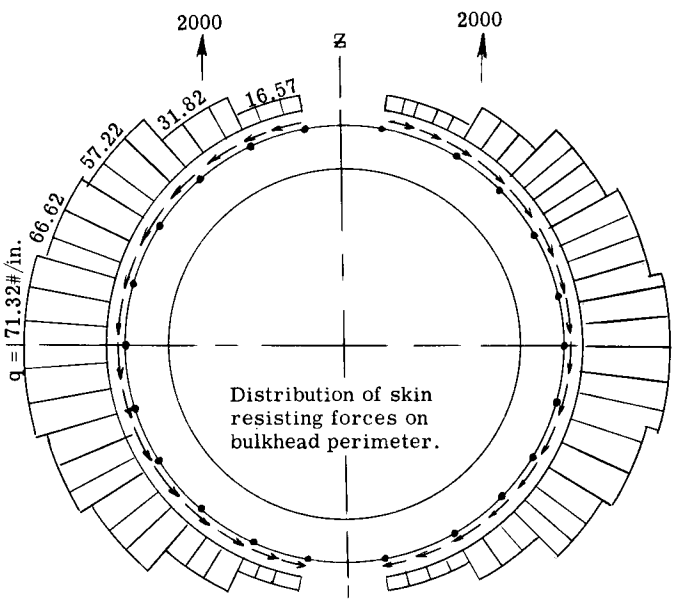

Fig. A21.62

Example Problem 2. Unsymmetrical Vertical Loading

In certain conditions in flying and landing, unsymmetrical concentrated loads are applied to the fuselage or hull structure. For example, Fig. A21.63 shows the same section and frame as was used in Problem 1. Due to an unsymmetrical load on the horizontal tail, the reactions from the tail on the fuselage are as illustrated in the figure. The total load in the z direction is still 4000 lb. but the loads are not symmetrical about the z axis. For analysis purposes, consider the loads as transferred to the

c.g. of the section as indicated in Fig. A21.64. The moment of the two loads about the c.g. = 1500 x 11.5 - 2500 x 11.5 = -11500 in.lb. The shear load V_Z = 4000 produces the same shear flow pattern as Fig. A21.62. To balance the moment of -11500, a constant shear flow q_1 around the frame is necessary.

$$q = \frac{M}{2A} = \frac{11500}{2 \times \pi \times 18^2} = 5.65 \text{ lb./in.}$$

(A = area of fuselage cross-section)

Adding this constant force system to that of Fig. A21.62, gives the final boundary supporting forces on the frame as illustrated in Fig. A21.65. The elastic stress analysis of the frame can now proceed.

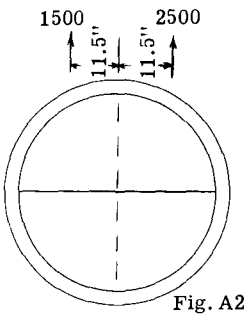

Fig. A21.63

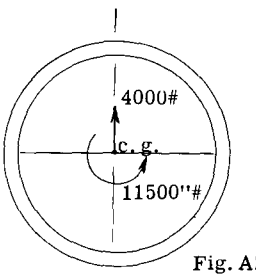

Fig. A21.64

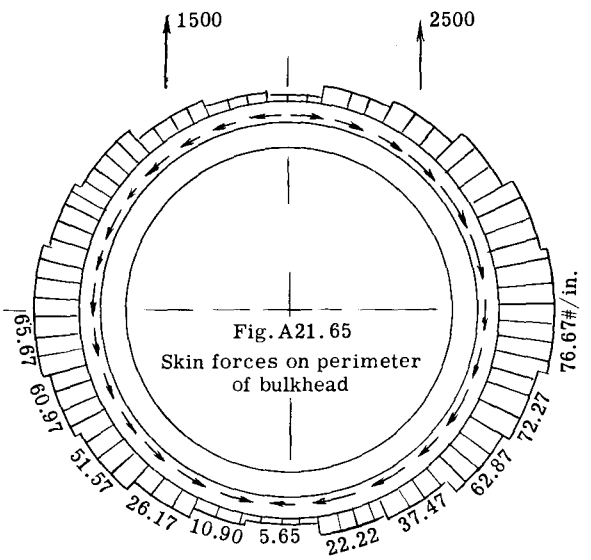

Fig. A21.65
Skin forces on perimeter of bulkhead

A21.13 Problems.

(1) Fig. A21.66 shows a cantilever beam loaded as shown. Find the shear flow in each of the 4 web panels. Draw axial load diagram for each of the vertical web stiffeners and also the horizontal stiffener be. Plot axial load diagram for beam flange members as obtained from web shear flows.

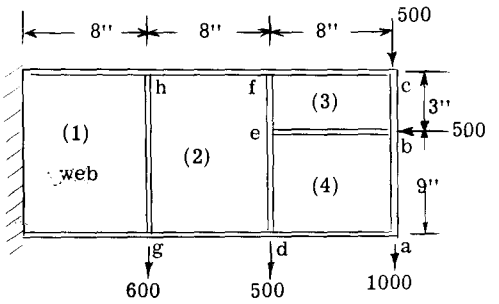

Fig. A21.66

(2)

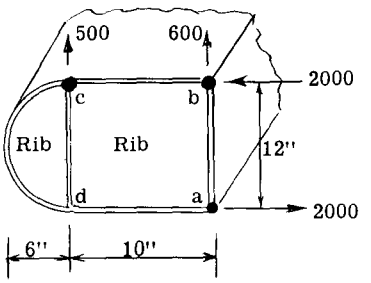

Fig. A21.67

Fig. A21.67 shows a wing rib inserted in a 3 flange single cell wing beam, which is subjected to the external loads as shown.

(1) Find rib flange loads at (c) and (d).

(2) Find rib web shear flow on each side of stiffener cd.

(3) Find rib flange and web loads at section 5" to left of line ab.

(3)

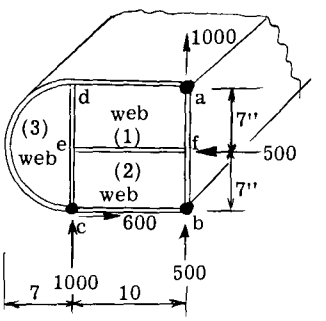

Fig. A21.68

Fig. A21.68 shows a 3 stringer single cell wing beam. A rib is inserted to distribute the concentrated loads as shown.

(1) Find shear flows in rib web panel (1) (2) and (3).

(2) Find rib flange loads at sections dc and ab.

(4)

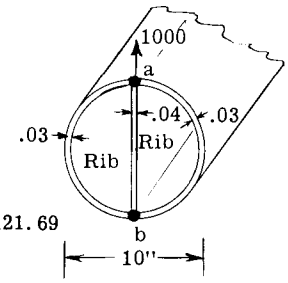

Fig. A21.69

Fig. A21.69 shows a 2 stringer, 2 cell wing beam. A rib is inserted to transfer 1000 lb. load to beam structure.

Find shear flow in rib web in each cell adjacent to line ab. Also rib flange loads adjacent to points (a) and (b).

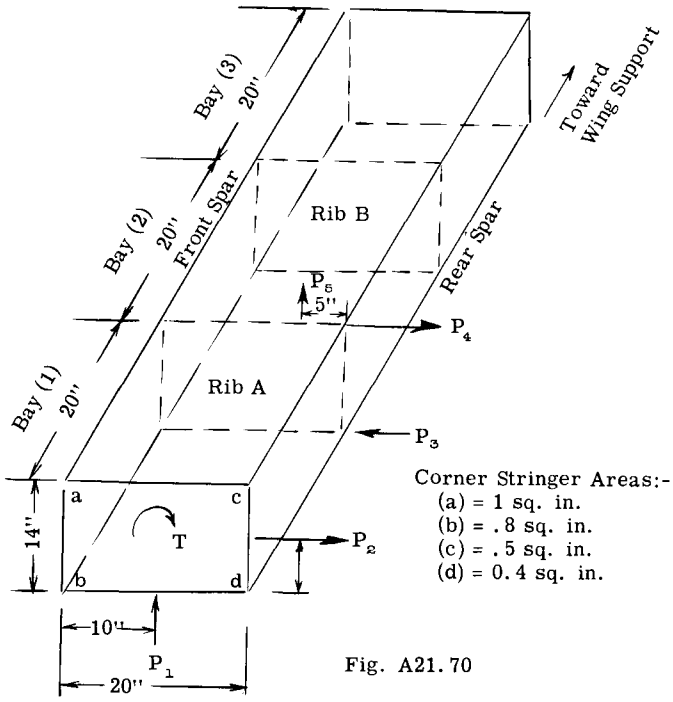

Fig. A21.70

(5) Fig. A21.70 shows 3 bays of a cantilever single cell, 4 stringer wing beam. The bottom skin in bay (2) is removed. Find the shear flows in all bays and boundary loads on ribs (A) and (B) when the external wing loads are as follows: T = 56000 in.lb., P_1 = 0, P_2 = 0, P_3 = 2000 lb., P_4 = 2000 lb., P_5 = 0.

(6) Same as problem (5) but upper skin in bay (2) is removed instead of the lower skin.

(7) Same as problem (5) but with the following external loads.

T = 56000 in.lb., P_1 = 5000 lb.,

P_2 = 2000 lb., P_3 = P_4 = 0 and P_5 = 1000 lb.

(8) Same as problem (7) but with top skin removed instead of lower skin.

(9) Same as (5) but with read spar web removed instead of bottom skin.

(10) Same as problem (7) but with rear spar web removed instead of bottom skin.

(11) In Fig. A21.71 the external bulkhead loads P_1 and P_2 equal 4000 lb. each and P_3 equals zero. The fuselage stringer material consists of four omega sections with an area of .25 sq. in. each. Determine the skin resisting forces on the bulkhead in balancing the above loads. Neglect any effective skin in this problem.

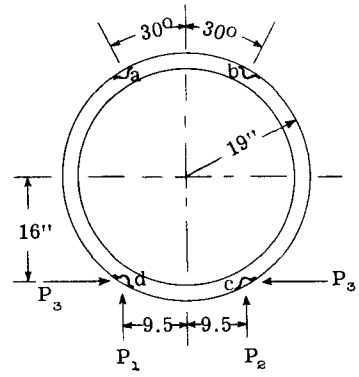

Fig. A21.71

(12) Same as problem (11) but make P_1 = 4000 and P_2 = 6000.

(13) Same as problem (12) but add P_3 = 3000 lb.

(14) In a water landing condition the hull frame of Fig. A21.72 is subjected to a normal bottom pressure of 200 lb. per in. The area of the bulb angle stringers is .11 sq. in. each and they are 7/8 in. deep. The area of the Z stringers is .18 sq. in. each and the depth 1.5 in. The area of the stringers a, b, c, d and e is .20 sq. in. each. Neglecting any effective skin determine the skin resisting forces on the frame in balancing the bottom water pressures.

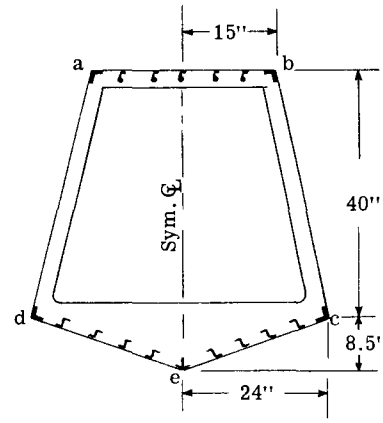

Fig. A21.72

(15) Same as problem (14) but consider that the water pressure is only acting on one side of the bottom of the frame.

CHAPTER A22
ANALYSIS OF SPECIAL WING PROBLEMS

ALFRED F. SCHMITT

A22.1 Introduction.

In a previous chapter (A19) analyses of wing beams were carried out using the engineering theory of bending and rational modifications thereof. As discussed there, wing configurations which depart radically from the usual conception of a "beam" present the engineer with the choice of making approximate and/or empirical corrections to beam theory, or of following a complete analytic treatment of the structure.

This chapter illustrates the latter approach to several special problems associated with aircraft wing structures, viz.,*

Art. A22.2 - stresses around a panel cutout
Art. A22.3 - shear lag problem
Art. A22.4 - cutout in a box beam
Art. A22.5 - swept wing box beam

Aside from presenting one analytic treatment of these problems, a discussion is given of the physical nature of each phenomenon. An understanding of the nature of the problem is of prime importance, since no one analytic technique can be all-powerful in the solution of stress problems. The analyst must exercise judgment and ingenuity in approaching each new situation.

In this chapter all analyses are made using the matrix formulation of the Method of Dummy Unit Loads (Chapters A7, A8), a familiarity with which is assumed.

Such problems as those listed above are too unwieldy to be studied here in great detail; hence no attempt at exhaustive analyses has been made. To bring into relief the main features of each problem, the structure selected for analysis is one which is simple in construction and so loaded as to exhibit clearly the phenomenon under study. Many practical details, such as the effects of sheet wrinkling, rivet and fitting "give", stress concentrations, etc., have been side-stepped so as not to becloud the objective. Further, the problems of idealization of the original structure, into the one finally analyzed, are treated only lightly; additional references are cited where appropriate.

The analyses shown are strictly applicable to (reasonably) thin-skinned wings only, wherein the "constant shear flow" assumptions are valid, viz.

i - the sheet carries shear stresses only
ii - normal (direct) stresses are carried in the flanges (spar caps and stringers) with effective areas of skin lumped in. In all cases handled here the skin was assumed fully effective (stresses below skin buckling stress - see Art. A19.11, Chapter A19).

To enhance the usefulness of these problems, all the structures chosen for analysis were taken from referenced NACA (National Advisory Committee for Aeronautics) publications wherein the reader may find detailed discussions of the problems, other methods of analysis and data obtained from tests upon the specimens. Where available, these data have been used herein for comparison.

A22.2 Stresses Around a Panel Cutout

"Cutouts in wings and fuselages constitute one of the most troublesome problems confronting the aircraft designer. Because the stress concentrations caused by cutouts are localized, a number of valuable partial solutions of the problem can be obtained by analyzing the behavior, under load, of simple skin-stringer panels" (1)**

Thus, in the case of a wing beam with a panel cutout of the upper surface (Fig. A22.1), it would be feasible to analyze the section immediately around the cutout as a flat sheet-stringer panel under the action of axial stringer loads and edge shears (coming from the spar webs). The axial stringer forces could be computed with sufficient accuracy by the engineering theory of bending (E.T.B.) since these are removed sufficiently far from the cutout proper. The edge shear flows are readily computed by those elementary considerations which give the spar-web shear flows.

* One other important special problem - the so-called "bending stresses due to torsion" - is not treated here specifically. As indicated in Chapter A8, the general box beam analysis presented there encompasses this problem (Example Prob. 15, p.p. A8.24 through A8.27).

** Numbers in parentheses refer to the bibliography at the end of the chapter.

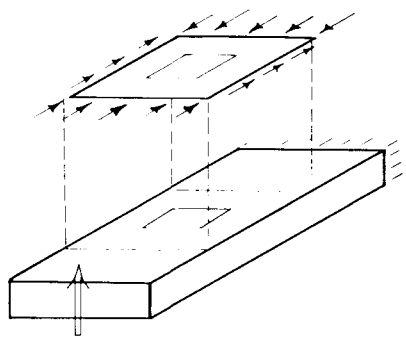

Fig. A22.1

The sheet-stringer panel may, in general, contain a large number of longitudinal elements (stringers). The labor involved in treating this multi-element structure in detail is prohibitive, and thus an appropriate idealization must be made. First, it is likely that the panel may be considered to be symmetric about a longitudinal axis, so that only the half-panel need be handled. Second, the complex, multi-stringer structure is replaced by one having but three stringers. As indicated in Fig. A22.2, these stringers are:

#1, a substitute stringer having for its area all the effective area of the fully continuous members to one side of the "combing stringer" (the stringer bordering the cutout) and placed at the centroid of the area of material for which it substitutes. The stress which this stringer develops is then the average stress for the material it replaces.

#2, the combing stringer, being simply the main continuous stringer bordering the cutout.

#3, another substitute stringer, this one replacing all of the effective material made discontinuous by the cutout. It is located at the centroid of the material it replaces, and its stress is the average stress for this same material.*

The sheet thicknesses used are the same as those of the actual structure.**

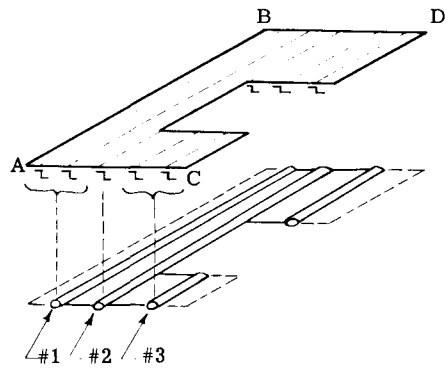

Fig. A22.2 Idealization of the half panel by use of substitute stringers

Fig. A22.3 gives the geometry of the idealized panel.

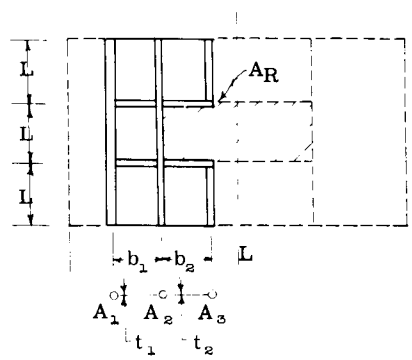

Fig. A22.3

$A_1 = .703$ in^2
$A_2 = .212$ in^2
$A_3 = 1.045$ in^2
$A_R = 0.25$ in^2
$t_1 = 0.0331$ in
$t_2 = 0.0331$ in
$b_1 = 5.96$ in
$b_2 = 7.56$ in
$L = 15.0$ in

SOLUTION:

Fig. A22.4 is an exploded view of the half-panel showing the placement and numbering of the internal generalized forces (Art. A7.9, Chapter A7) and the external loading. Note that the applied axial stresses were assumed to be constant chordwise, giving stringer loads proportional to the stringer areas; their sum is P_2, one of external loads.

The applied edge shear flows, coming from the spar web, were assumed constant spanwise, as from a constant shear load. Other load distributions may be handled by allowing these applied shears to vary from panel to panel. For very extreme load variations additional transverse members could be inserted to create more spanwise panels allowing a better fit to the spar shear variation. The applied shear flows were considered as the other external load and designated P_1.

Panels on the centerline have zero shear due to symmetry (Fig. A22.3).

---

* An alternate idealization, in which stringers #1 and #3 are located along the lines AB and CD, respectively (Fig. A22.2), was used in Reference (2) for a box beam loaded in torsion.

** When the longitudinal members themselves contribute to the shear stiffness of the cover (as is the case for "hat" section stringers riveted to the skin so as to form small closed cross sections), an effective thickness must be used. This point is discussed in Reference (3). In this source, however, the increase in shear stiffness is accounted for, not by increasing skin thickness, but by decreasing the panel width - an equivalent procedure.

q_{17}=.359 (P_2+3P_1L)
q_{18}=.108 (P_2+3P_1L)
q_{19}=.533 (P_2+3P_1L)

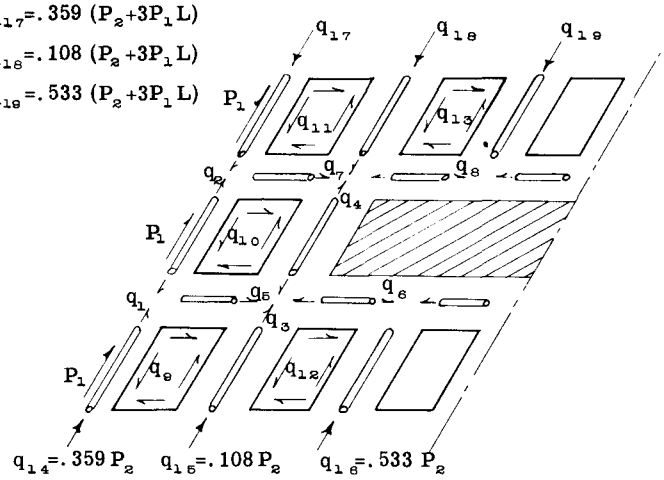

Fig. A22.4

Experience has shown that for symmetric panels symmetrically loaded it is satisfactory to consider transverse members to be rigid in their own planes (4). Thus, in this problem, member flexibilities for forces q_5, q_6, q_7 and q_8 may be taken to be zero. In the actual NACA test specimen with which results are to be compared, those transverse members bordering the cutout appeared to have been heavily reinforced (to an extent unknown to the writer). Hence it is logical to take their stiffnesses as great.

Member flexibility coefficients were collected in matrix form as below using the formulas of Chapter A7. Note that the coefficients for subscripts 5, 6, 7 and 8 were set equal to zero (rigid transverse members).

The half panel was twice indeterminate. Member loads q_6 and q_8 were selected as redundants. With these set equal to zero, successive applications of loads P_1 and P_2 were made. Also, successive applications of unit values of q_6 and q_8 were made. The results:

$[g_{im} \vdots g_{ir}]$ =

i \ m,r	1	2	6	8
1	4.755	.316	-1.68	- .840
2	9.510	.316	- .840	-1.68
3	-19.76	-1.316	1.68	.840
4	-39.51	-1.316	.840	1.68
5	0	- .268	1.00	0
6	0	0	1.00	0
7	-12.09	- .268	0	1.00
8	0	0	0	1.00
9	- 1.317	- .0450	.112	.056
10	- 1.317	0	- .056	.056
11	.711	.0450	- .056	- .112
12	0	.0355	0	0
13	- 1.599	- .0355	0	0
14	0	.359	0	0
15	0	.108	0	0
16	0	.533	0	0
17	16.16	.359	0	0
18	4.86	.108	0	0
19	23.98	.359	0	0

α_{ij}, MEMBER FLEXIBILITY COEFFICIENTS (E = 1) (Voids denote zeros)

i \ j	1	2	3	4	5	6	7	8	9	10	11	12	13	14	15	16	17	18	19
1	14.22	3.56												-3.56					
2	3.56	14.22															-3.56		
3			47.17	11.79											-11.79				
4			11.79	47.17														-11.79	
5																			
6																			
7																			
8																			
9									7,024										
10										7,024									
11											7,024								
12												8,909							
13													8,909						
14	-3.56													7.11					
15			-11.79												23.58				
16																4.785			
17		-3.56															7.11		
18				-11.79														23.58	
19																			4.785

The "off diagonal" values have negative sign because the sense of those internal generalized forces having subscripts (14), (15), (17) and (18) was taken opposite to that used in the derivation in Art. A7.10. A change in sense requires a change in sign in off-diagonal coefficients only.

The following matrices were formed:

Per eq. (17) of Chapter A8:

$$\left[\alpha_{rn}\right] = \begin{bmatrix} -5206 & -262.8 \\ -6633 & -262.8 \end{bmatrix}$$

Per eq. (18) of Chapter A8:

$$\left[\alpha_{rs}\right] = \begin{bmatrix} 392.1 & 293.5 \\ 293.5 & 392.1 \end{bmatrix}$$

The inverse of this last was found;

$$\left[\alpha_{rs}^{-1}\right] = 10^{-3} \begin{bmatrix} 5.802 & -4.343 \\ -4.343 & 5.802 \end{bmatrix}$$

Finally, per eq. (23) of Chapter A8, the unit load stress distribution was,

$\left[G_{im}\right]$ =

i \ m	1	2
1	-10.93	-.65
2	-18.34	-.65
3	- 4.08	-.351
4	-11.66	-.351
5	1.40	.115
6	1.40	.383
7	3.79	.115
8	15.88	.383
9	- .270	.019
10	- .510	0
11	- 1.15	-.019
12	0	.0355
13	- 1.60	-.0355
14	0	.359
15	0	.108
16	0	.533
17	16.16	.359
18	4.86	.108
19	23.98	.359

The above analytical results are compared with NACA test data (1) in Fig. A22.5 for the loading $P_2 = 1$, $P_1 = 0$. Agreement is seen to be good.

EFFECT OF RIB FLEXIBILITY:

To investigate the influence of rib flexibility, the problem was reworked assuming aluminum rib caps, of constant area A = .25 in.^{2}, as the transverse members bordering the cutout. The appropriate member flexibility coefficients

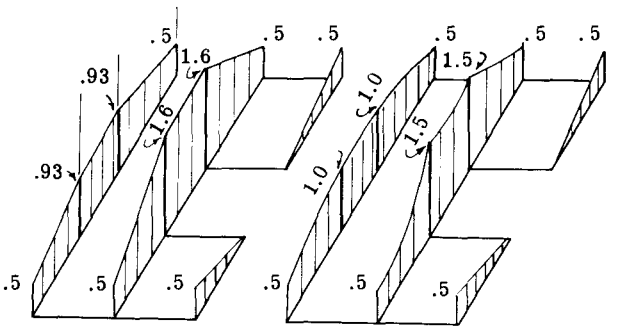

CALCULATED MEASURED

Fig. A22.5 Comparison between calculated and measured stresses (psi) on the half-panel.

inserted in the α_{ij} matrix (in place of the zeroes used above) were

$\left[\alpha_{ij}\right]$ =

i \ j	5	6	7	8
5	18.03	5.04		
6	5.04	10.08		
7			18.03	5.04
8			5.04	10.08

The problem was solved retracing the same steps as before, but using the modified $\left[\alpha_{ij}\right]$ matrix, to yield the stresses:

$\left[G_{im}\right]_{\text{FLEXIBLE RIBS}}$ =

i \ m	1	2
1	-11.11	-.621
2	-16.83	-.621
3	- 3.90	-.379
4	-13.17	-.379
5	2.14	.104
6	2.14	.372
7	2.52	.104
8	14.61	.372
9	- .26	.017
10	- .62	0
11	- 1.05	-.017
12	0	.036
13	- 1.60	-.036
14	0	.359
15	0	.108
16	0	.533
17	16.11	.359
18	4.86	.108
19	23.98	.359

Comparison of this result with the previous one for the rigid ribs reveals that the most important effect of rib flexibility was to increase the concentration of stresses in the combing stringer bordering the cutout. It should be noted, however, that for this symmetric panel, the use of a very flexible rib as compared with a rigid rib led to stress increases of the order of only 10% in the combing stringer. Thus, the "rule of thumb" that transverse flexibilities may be neglected in symmetric panels is re-affirmed.

A22.3 Shear Lag Analysis of Box Beams

"The bending stresses in box beams do not always conform very closely to the predictions of the engineering theory of bending. The deviations from the theory are caused chiefly by the shear deformations in the cover of the box that constitutes the flange of the beam. The problem of analyzing these deviations from the engineering theory of bending has become known as the shear lag problem, a term that is convenient though not very descriptive." (3)

Fig. A22.6 illustrates the basic problem. The beam cover sheet is loaded along the edges by shear flows from the spar webs. These shear flows are resisted by axial forces developed in the longitudinal members (spar caps and stringers). According to elementary considerations, the stringer stresses should be uniform chordwise at any given beam station ("elementary theory" in the figure). Actually, the central stringers tend to "lag behind" the others in picking up the load because the

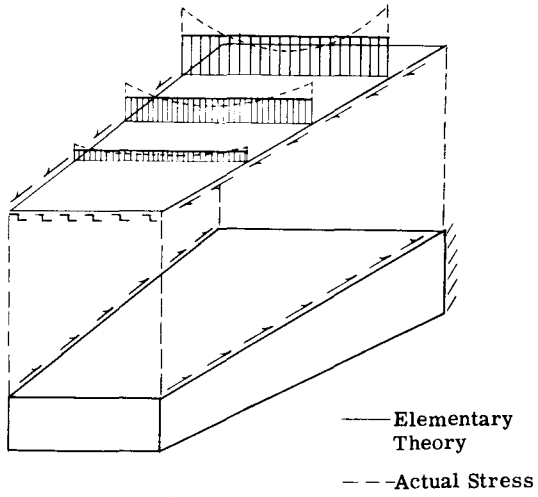

Fig. A22.6

intermediate sheet, which transfers the loads in from the edges, is not perfectly rigid in shear. The action may be comprehended readily by visualizing an extreme case: a large degree of "lag" would occur if the load transferring skin were made of a highly flexible material such as a plastic sheet or even rubber. In such a case the inside stringers would be out of action almost entirely! With the inside stringer stresses lagging, the outside stringers and spar caps must carry an over-stress to maintain equilibrium ("actual" in the figure).

Fig. A22.7 shows the beam analyzed herein.

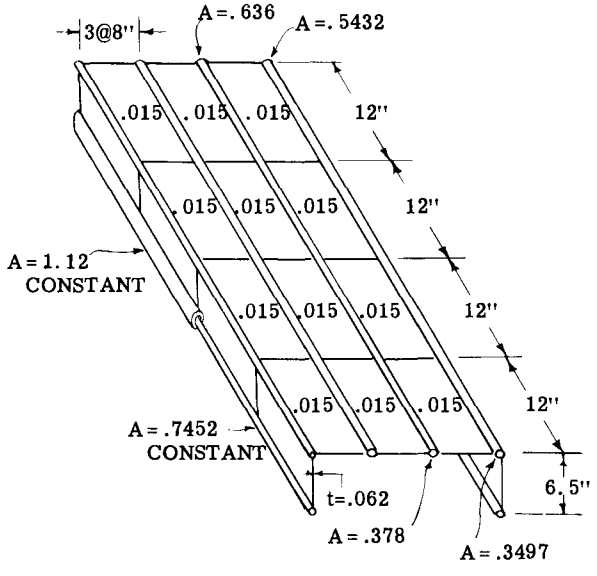

Fig. A22.7

The beam is an idealization of one tested by the NACA and reported in reference (3). Note that the beam has no lower cover sheet and that it is symmetric about a vertical axis. Transverse bulkheads are located at stations 12", 24", 36" and 48" from the root.

The actual beam specimen had three more stringers than shown in the idealized structure, these being located one each midway between the pairs of longitudinals shown on the beam cover of Fig. A22.7. In the idealizing process, these extra stringer areas were divided equally between adjacent longitudinals. The stringer areas shown are the effective areas, with those in the top cover tapering linearly from root to tip. All skin was considered effective in carrying direct stresses.

Some detailed discussions of the techniques of idealization of practical beams are given in references (5) and (5a).

SOLUTION:

To permit the handling of the calculation in a limited space, it was elected to analyze

the structure for a single transverse (vertical) tip load symmetrically placed. In that case, because of symmetry, it was necessary to treat only one-half of the structure. In addition, no shear flows could appear in the middle panels. Further, it is known that the influence of rib flexibility on shear lag is slight for symmetric systems, so that the ribs were considered rigid in their own planes; hence no generalized forces were needed on the ribs to describe their strain energies.

Fig. A22.8 shows the placement and numbering of the generalized forces on the half-beam.

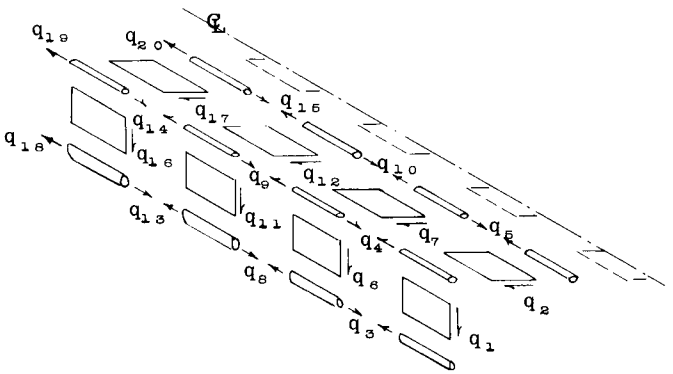

Fig. A22.8 Choice of generalized forces for shear lag problem.

Member flexibility coefficients were computed with the formulas of Chapter A7 and arranged in a matrix.

The shear flows q_2, q_7, q_{12} and q_{17} were selected as redundants. Setting these equal to zero, the stress distribution due to a one-half pound load at the tip (a unit load divided equally between beam halves) was readily computed.

$$[g_{im}] = \begin{Bmatrix} .07692 \\ 0 \\ -.9230 \\ .9230 \\ 0 \\ .07692 \\ 0 \\ -1.8461 \\ 1.8461 \\ 0 \\ .07692 \\ 0 \\ -2.769 \\ 2.769 \\ 0 \\ .07692 \\ 0 \\ -3.692 \\ 3.692 \\ 0 \end{Bmatrix}$$

Next, the unit redundant stress distribution was computed. Fig. A22.9 illustrates a typical calculation, showing the stresses in the tip bay for $q_2 = 1$, $q_7 = q_{12} = q_{17} = 0$.

α_{ij}, MEMBER FLEXIBILITY COEFFICIENTS (E = 1)

i \ j	1	2	3	4	5	6	7	8	9	10	11	12	13	14	15	16	17	18	19	20
1	3271																			
2		16,640																		
3			10.74					2.684												
4				20.05					4.724											
5					17.99					4.202										
6						3271														
7							16,640													
8			2.684					8.939					1.785							
9				4.724					17.84					4.255						
10					4.202					15.78					3.708					
11											3271									
12												16,640								
13								1.785					7.142					1.785		
14									4.255					16.084					3.840	
15										3.708					13.89					3.324
16																3271				
17																	16,640			
18													1.785					3.571		
19														3.840					7.518	
20															3.324					6.439

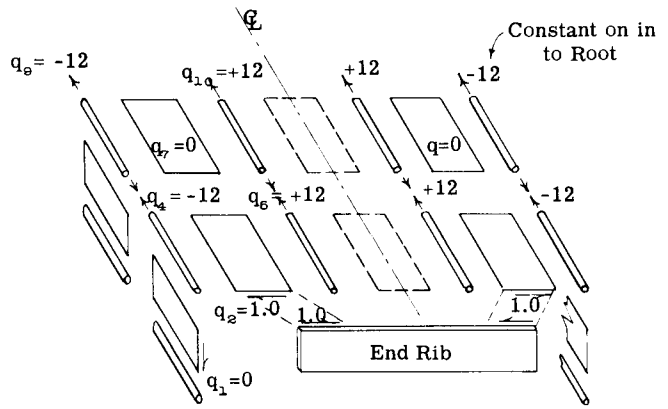

Fig. A22.9 Application of a self-equilibrating unit redundant stress q_8.

The complete redundant stresses were:*

$$\left[g_{1r} \right] =$$

1 \ r	2	7	12	17
1	0	0	0	0
2	1	0	0	0
3	0	0	0	0
4	-12	0	0	0
5	12	0	0	0
6	0	0	0	0
7	0	1	0	0
8	0	0	0	0
9	-12	-12	0	0
10	12	12	0	0
11	0	0	0	0
12	0	0	1	0
13	0	0	0	0
14	-12	-12	-12	0
15	12	12	12	0
16	0	0	0	0
17	0	0	0	1
18	0	0	0	0
19	-12	-12	-12	-12
20	12	12	12	12

The following matrix products were formed (per eqs. (17), (18) of Chapter A8):

$$\left[\alpha_{rn} \right] = \begin{Bmatrix} -2175 \\ -1848 \\ -1260 \\ -460.7 \end{Bmatrix}$$

$$\left[\alpha_{rs} \right] = \begin{bmatrix} 40,210 & 16,810 & 9,536 & 3,041 \\ 16,810 & 32,160 & 9,536 & 3,041 \\ 9,536 & 9,536 & 25,030 & 3,041 \\ 3,041 & 3,041 & 3,041 & 18,650 \end{bmatrix}$$

The inverse of the latter was formed:

$$\left[\alpha_{rs}^{-1} \right] = 10^{-6} \begin{bmatrix} 3.285 & -1.505 & -.656 & -.183 \\ -1.505 & 4.219 & -1.000 & -.279 \\ -.656 & -1.000 & 4.687 & -.495 \\ -.183 & -.279 & -.495 & 5.519 \end{bmatrix}$$

and, finally, per eq. (23) of Chapter A8,

$$\left[G_{1m} \right] = \begin{Bmatrix} .07692 \\ .03453 \\ -.9230 \\ .5086 \\ .4144 \\ .07692 \\ .03136 \\ -1.846 \\ 1.055 \\ .7907 \\ .07692 \\ .02401 \\ -2.7691 \\ 1.690 \\ 1.079 \\ .07692 \\ .01005 \\ -3.692 \\ 2.493 \\ 1.199 \end{Bmatrix}$$

Fig. A22.10 shows the above computed stresses and those reported by the NACA as obtained by test. Agreement is seen to be quite good.

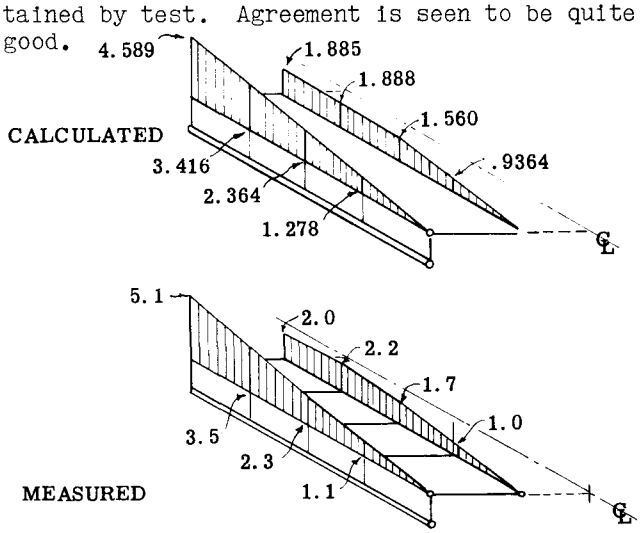

Fig. A22.10 Comparison between calculated and measured stresses (psi) in a box beam

* This is an obvious place in which to use combinations of redundants to decrease the structural coupling (reference Chapter A8, pp. A8.29, 30). (Recommended as an exercise for the student.)

A22.4 Stress Analysis of a Box Beam With a Cutout.

In Article A22.2, one technique was employed for computing the stresses around a cutout. In that analysis the effect of the cutout was presumed to have been localized about the cutout region; consequently, the problem was treated by isolating the affected panel. Quite often, when the cutout is placed well inboard on the wing, its influence on the root stresses is appreciable. Therefore, it is desirable to be able to consider the overall problem of the box beam with a cutout for such cases.

"The most convenient and the most rapid method of analyzing structures with cutouts is the indirect, or inverse, method. The analysis by the indirect method is made in two steps. First, the structure is analyzed for the basic condition that exists before the cutout is made. The results of this basic analysis are used to calculate the internal forces that exist along the boundary of the proposed cutout. External forces equal and opposite to these internal forces are then introduced; these external forces reduce the stresses to zero along the boundary of the proposed cutout, and consequently the cutout can now be made without disturbing the stresses." (3)*

It is desired to modify the calculation of the previous article (A22.3, "Shear Lag Analysis") to allow for the presence of two cutouts symmetrically placed. Panel "q_{12}" was removed while the single tip load remained. Since the unit remained symmetric, the data from the previous analysis, in which the transverse rib stiffnesses were taken to be infinitely great, should still yield satisfactory results.

SOLUTION:

The calculation was accomplished in three steps:

1) The stress distribution was found in the "basic structure" (no cutout). This work was carried out in Article A22.3 where it was found that $q_{12} = .02401$ lbs./inch.

2) A stress distribution was found for an "applied load" of $q_{12} = 1$. Such a loading has zero external resultant.

3) .02401 times this last stress distribution was subtracted from the first.

The calculation for step (2) above, will now be carried out by considering a unit shear flow, $q_{12} = 1$, applied while all other loads are zero. Under this loading condition the relative displacements at redundant cuts 2, 7 and 17 are equal to $\alpha_{2,12}$, $\alpha_{7,12}$ and $\alpha_{17,12}$ respectively, where these coefficients have been computed previously in Article A22.3.

To restore continuity (reduce the relative displacements to zero) three redundant forces are applied, one each, at the cuts 2, 7 and 17. The appropriate equations specifying continuity are

$$\begin{bmatrix} \alpha_{2,2} & \alpha_{2,7} & \alpha_{2,17} \\ \alpha_{7,2} & \alpha_{7,7} & \alpha_{7,17} \\ \alpha_{17,2} & \alpha_{17,7} & \alpha_{17,17} \end{bmatrix} \begin{Bmatrix} q_2 \\ q_7 \\ q_{17} \end{Bmatrix} = - \begin{Bmatrix} \alpha_{2,12} \\ \alpha_{7,12} \\ \alpha_{17,12} \end{Bmatrix}$$

Note that these equations say simply that the deflections at the redundant cuts due to the (unknown) redundant forces must be equal and opposite to the deflections due to $q_{12} = 1$.

All coefficients in the above equation were computed in Art. A22.3. Specifically,

$$\begin{bmatrix} 40{,}210 & 16{,}810 & 3{,}041 \\ 16{,}810 & 32{,}160 & 3{,}041 \\ 3{,}041 & 3{,}041 & 18{,}650 \end{bmatrix} \begin{Bmatrix} q_2 \\ q_7 \\ q_{17} \end{Bmatrix} = - \begin{Bmatrix} 9{,}536 \\ 9{,}536 \\ 3{,}041 \end{Bmatrix}$$

The above matrix is the $[\alpha_{rs}]$ of Art. A22.3, with the "q_{12} row" and "q_{12} column" removed.

The equations were solved** to give the values of the redundants for a unit applied load, $q_{12} = 1$, as

$$\{G_{s,12}\} = \begin{Bmatrix} q_2 \\ q_7 \\ q_{12} \\ q_{17} \end{Bmatrix} = \begin{Bmatrix} -.1399 \\ -.2134 \\ 1.00 \\ -.1055 \end{Bmatrix} \quad q_{12} = 1$$

The q_{12} force is included in the above for later convenience. Then the complete stress distribution, due to applying a unit shear flow $q_{12} = 1$, was

---

* The procedure described here is quite generally useful for studies of the effect of removing one or more members; such might be required for an analysis of the effects of structural damage.

** See Appendix for a method of "extracting" the inverse of this matrix from that previously found for the complete $[\alpha_{rs}]$ matrix.

$$\left\{G_{1,12}\right\} = \left[g_{1r}\right] \left\{G_{r,12}\right\}$$

$$= \begin{Bmatrix} 0 \\ -.1399 \\ 0 \\ 1.679 \\ -1.679 \\ 0 \\ -.2134 \\ 0 \\ 4.240 \\ -4.240 \\ 0 \\ 1.00 \\ 0 \\ -7.760 \\ 7.760 \\ 0 \\ -.1055 \\ 0 \\ -6.494 \\ 6.494 \end{Bmatrix}$$

($\left[g_{1r}\right]$ taken from Art. A22.3)

To obtain the stresses in the loaded beam with the cutout, 0.02401 times the above stresses were subtracted from the "basic" stress distribution of Art. A22.3, as previously explained.

$$\left\{G_{1m}\right\}_{CUTOUT} = \left\{G_{1m}\right\}_{BASIC} - .02401\left\{G_{1,12}\right\} = \begin{Bmatrix} .07692 \\ .03789 \\ -.9230 \\ .4683 \\ .4547 \\ .07692 \\ .03648 \\ -1.8461 \\ .9536 \\ .8925 \\ .07692 \\ 0 \\ -2.7691 \\ 1.8763 \\ .8927 \\ .07692 \\ .01258 \\ -3.692 \\ 2.649 \\ 1.037 \end{Bmatrix}$$

Note that q_{12} is now zero and the cutout panel may be "lifted out".

In the case of a structure under a variety of external loadings (m = 1, 2, 3 ---), the more general equation, corresponding to the above, is

$$\left[G_{1m}\right]_{CUTOUT} = \left[G_{1m}\right]_{BASIC} - \left\{G_{1,12}\right\} \left\lfloor G_{12,m} \right\rfloor$$

where the row matrix $\left\lfloor G_{12,m} \right\rfloor$ is simply the "12 row" of $\left[G_{1m}\right]_{BASIC}$

COMPARISON WITH TEST DATA:

Reference 3 reports test data for the case analyzed, the stringer stresses being plotted below in Fig. A22.11.

In the actual test specimen a stringer passing through the cutout was severed, it having zero stress at stations 12 and 24, therefore. However, during the idealization process discussed in Art. A22.3 (for the beam without cutout) the area for this stringer was placed partly with the combing stringer and partly with the spar cap. In the same way, some effective sheet from the midportion of the panel, now made discontinuous by the cutout, was added also to the spar cap and combing stringer.

It follows then that the full idealized areas of the combing stringer and spar cap should not be used in figuring the stresses at stations 12 and 24 (produced by forces q_9, q_{10}, q_{14}, q_{15}). With these areas reduced by the appropriate subtractions, the stresses were computed and are plotted in Fig. A22.11. Agreement with test data is seen to be quite satisfactory.

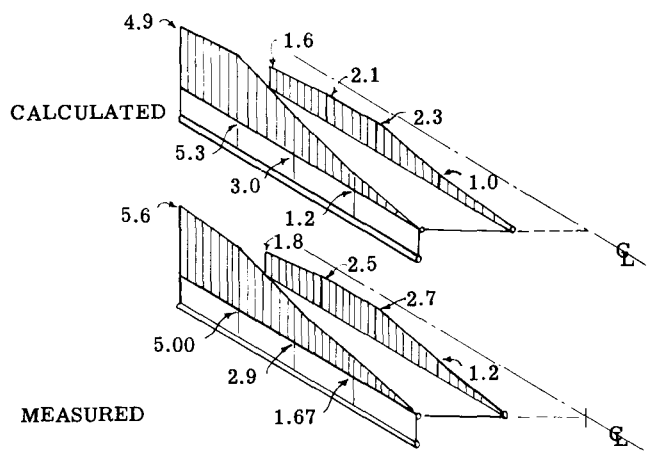

Fig. A22.11 Comparison between calculated and measured stresses (psi) in a box beam with cutouts.

A22.5 Analysis of a Swept Box Beam.

"Experimental investigations of swept box beams have shown that the stresses and distortions in a swept wing can be appreciably different in character from those that would exist if the root were normal to the wing axis. The principle effect of sweepback on the stresses occurs under bending loads and consists in a concentration of bending stress and vertical

shear in the rear spar near the fuselage. With regard to distortions, the effect of sweep is to produce some twist under loads that would produce only bending of an unswept wing and some bending under loads that would produce only twist of an unswept wing." (6)

In the following example a swept box beam is analyzed by the matrix methods of Chapter A8 and, in particular, by the specific techniques of reference (7). The method accounts for the interaction between the swept cover panels and the longitudinal members. It is this action that is responsible for the distinctive structural characteristics of the swept box beam.

Again, we emphasize that the method used here is strictly applicable to thin-skinned wings of beam-like proportions only. Considering the wide variety of structural layouts which may be employed in swept wing configurations, a comprehensive treatment cannot be given here. An excellent review of methods better adapted to thick-skinned construction and to "plate-like" (very thin, wide) wings, may be found in reference (8). One method of analyzing such wings is given in Chapter A23.

THE STRUCTURE:

The structure shown is Fig. A22.12 is an idealization of the NACA test beam of references (6) and (9), in which a single substitute stringer has been employed along the cover sheet to allow for the antitipated shear lag effect. The figure shows only one-half of the complete unit, which was built symmetrically about the axis corresponding to the longitudinal axis of the airplane.

Only tip loads were to be applied (at points A and B). The outer section of the beam was assumed to carry stresses which could be calculated reasonably well by the engineering theory of bending (E.T.B.). For this purpose it was judged satisfactory to consider the outer 66" of the beam as a single bay (A-B-D-C). If loads were to have been applied inboard of the tip, it would have been necessary to consider additional bay divisions between A-B and C-D (that is, insert additional ribs at stations

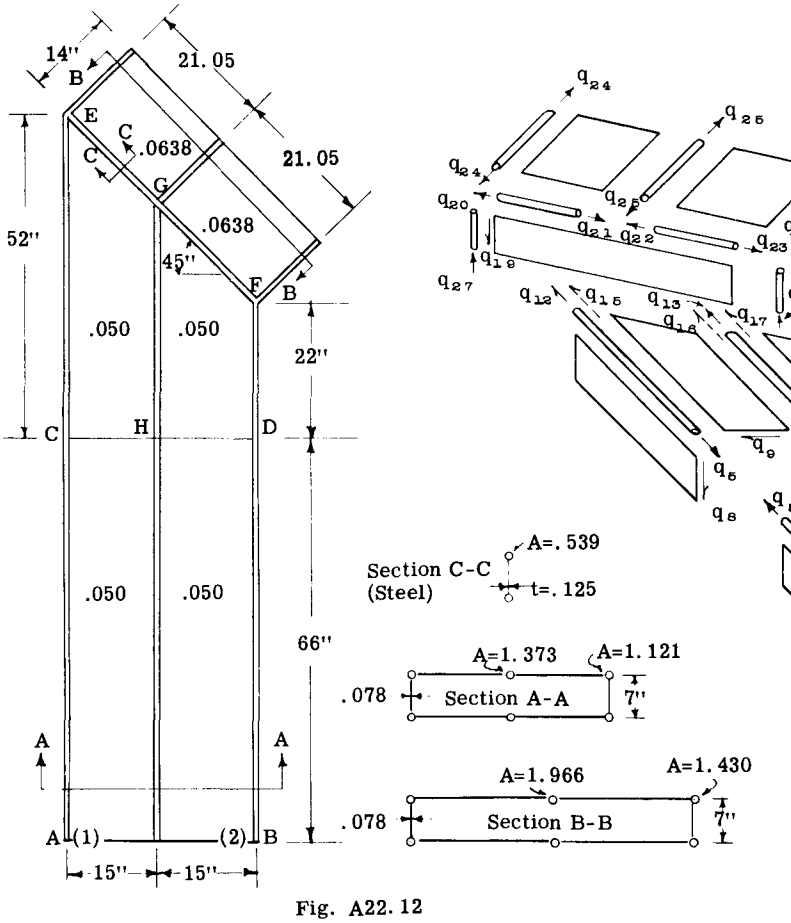

Fig. A22.12

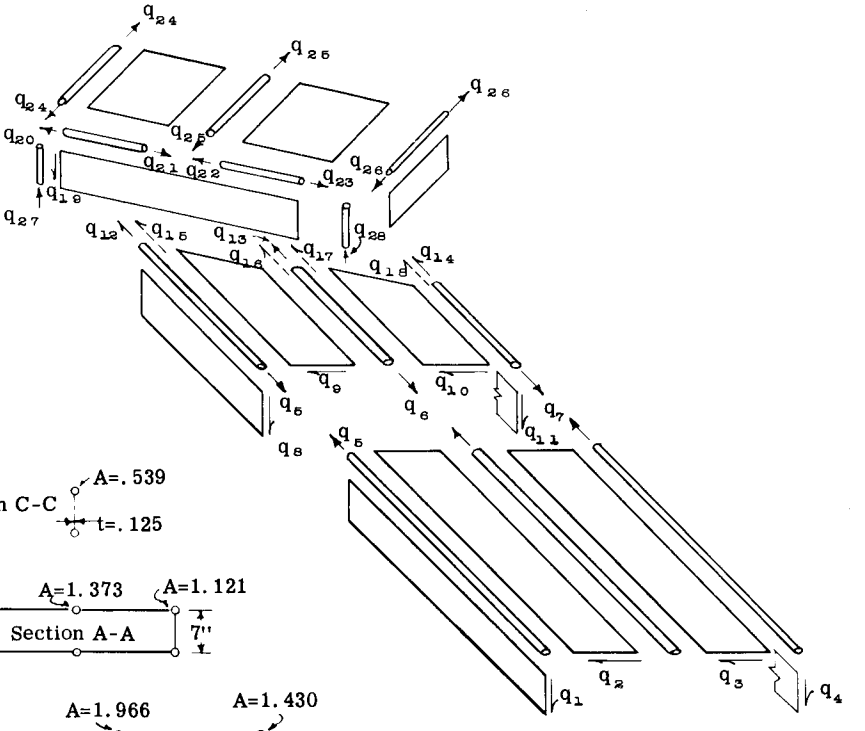

Fig. A22.13

of load application). Rib C-D was located at one of the actual rib locations in the NACA test specimen and was assumed rigid in its own plane.

The choice of bay C-D-F-E as a single bay was somewhat arbitrary. For improved accuracy, additional ribs inboard of C-D could have been used. Note that any ribs placed inboard of point F will produce triangular skin panels in the cover sheets. Examples of treatments for such panels may be found in references (9), (10) and (11).

Rib E-F was considered flexible in its own plane, it being known that the flexibility of a rib is important at a location where a structure changes direction.* Note that this rib was made of steel in the test specimen.

Effective areas of longitudinals as shown in Fig. A22.12 were computed by considering all of the skin to be effective. The spar cap areas are equal to the sum of the areas of the angle member at the cap location, plus one-half of the effective area of material between the cap and the substitute stringer (this area includes several stringers as well as skin) plus one-sixth of the attached spar web area.** The substitute stringer area was collected in like manner from the half-panels to either side.

The method used in calculating the effective areas of the rib caps (E-F) is given in detail in reference (9), from which the value used here was taken. The "carry-through bay" cover sheet thickness is equal to that used on the specimen (.050") plus a weighted increase to allow for the presence of splice plates along the plane of symmetry (see reference 9).

INTERNAL GENERALIZED FORCES:

Fig. A22.13 shows the choice and numbering of the generalized forces.

The beam was rigidly supported at points E, F and at the two corresponding points on the other beam half. These might correspond to the fuselage ring attach points in an airplane. The vertical end caps on rib E-F were considered rigid axially, so that no flexibility coefficients were associated with the reactions q_{25} and q_{26}. Flexibility of these members affects total deflections only and can be omitted in a stress analyses where deflections are not sought.

Since only symmetric loadings were considered in this analysis no shear was transmitted by the carry-through bay and hence no shear flows were shown in that portion.

Sets of additional axial forces (q_{15} through q_{18}) were applied to the ends of the flanges and stringers adjacent to the obliquely cut ends of the cover sheet panels in bay C-D-F-E. These forces are necessary to account for the interaction between the swept covers and the longitudinals. As shown in Fig. A22.14, the pure shear flow on the oblique edge is obtained by superposing onto the panel a zero-resultant system consisting of a uniform tensile stress of intensity 2q plus a pair of concentrated balancing loads. The balancing loads must be contributed by the bordering longitudinals and hence react on these as tensile loads (Fig. A22.14c). The balancing loads applied to the stringers are shown dashed since they are internal forces within the bay and are not to be entered into the equilibrium equations for the structure.

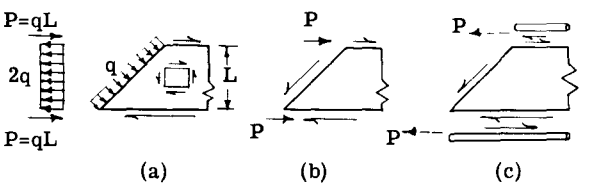

Fig. A22.14 Showing how the uniform shear stress on an oblique panel end (b) is created by superposition of a uniform tensile stress plus two balancing forces (a). The balancing forces react as tensile loads on the bordering longitudinals (c).

From an energy viewpoint, these dashed forces account for the additional strain energy stored by the axial components of shear flows in the non-rectangular panels. This energy is stored in the cover panels themselves (and is accounted for in this manner since the longitudinals contain the effective area from the cover sheet***) and in the longitudinals which react against these components.

"Dashed loads" are applied to the longitudinals adjacent to any obliquely cut panel end. Similar dashed loads would be applied to

* The effect of neglecting this rib's flexibility is demonstrated later in this example.

** The factor of 1/6 is used so that the effective area contribution of the web results in a structure having the same moment of inertia about a horizontal axis as the original. Some of the problems of idealization are discussed in reference (2), p. 16.

*** This much of the energy could be accounted for in another fashion by modifying the member flexibility coefficient for the sheet panel. See Reference 12, where this was done. However, that reference incorrectly neglects the additional energy stored in the longitudinals, as was demonstrated in Reference 13.

the outboard ends of the panels in bay C-D-F-E if they too were cut obliquely. Such panel configurations arise often in swept wing construction having ribs parallel to the airstream. Formulae for more general quadrilateral panels are given in Reference 7.

THE STRESS DISTRIBUTIONS

For the symmetric loadings considered here the structure was indeterminate only two times since the outer bay was assumed to be determinate by the E.T.B.

Stresses in outer bay by E.T.B.:

Flange stresses at rib C-D (for both $P_1 = 1$ and $P_2 = 1$)

$M = 66"\#$

$I = 88.57$ in.^{4}; $C = 3.5"$

$f_b = \frac{MC}{I} = 2.608$ psi

Therefore,

$q_5 = q_7 = 2.608 \times 1.121 = 2.924$ lbs.

$q_6 = 2.608 \times 1.373 = 3.581$ lbs.

For a unit transverse load at the shear center (midpoint, because of symmetry)

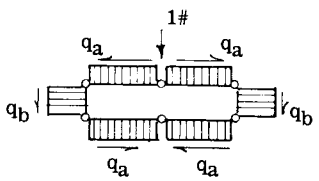

$$q_a = \frac{3.581}{2 \times 66} = .02713 \ \frac{\text{lbs}}{\text{in}}$$

$$q_b = .02713 + \frac{2.924}{66}$$

$$= .07143 \ \frac{\text{lbs}}{\text{in}}$$

The unit load was shifted 15" to either side by application of a torque, T = 15 in.lbs. The uniform shear flow superposed was

$$q = \frac{T}{2A} = \frac{15}{2 \times 210} = .03571 \ \frac{\text{lbs}}{\text{in}}$$

Finally, superposition gave the stresses for the outer bay as

$$\left[g_{im} \right] =$$

i \ m	1	2
1	.1071	.03572
2	.06284	- .00858
3	.00858	- .06284
4	.03572	.1071
5	2.924	2.924
6	3.581	3.581
7	2.924	2.924

Stresses in inner bays:

According to the discussion of Art. A8.12, Chapter A8, the determinate stress distribution, $\left[g_{im} \right]$, may be any stress distribution in equilibrium with the applied loads, and preferably one close to the final true stress distribution. The magnitude of the redundant forces is reduced by use of a satisfactory estimate of the true stresses.

The stresses in the two inner bays were determined for both g_{im} and g_{ir} simultaneously. Since this inner portion of the structure is two times indeterminate we can estimate two loads. For this purpose the two flange loads q_{12} and q_{14} were written as

$$q_{12} = q'_{12} + q''_{12}$$

$$q_{14} = q'_{14} + q''_{14}$$

where the (single) primed values are approximate values determined by the E.T.B. and the double primed values are the unknown corrections (the redundants). Using My/I at stations 66" and 118" from the tip gave*

$$q'_{12} = 5.228 \ P_1 + 5.228 \ P_2$$

$$q'_{14} = 3.899 \ P_1 + 3.899 \ P_2$$

The equilibrium equations for the elements of the structure were written next by summing forces and moments.

Joint F

$$q_{23} + q_{26} = 0$$

$$q_{23} + q_{26} = 1.414 \ q_{14}$$
$$= 5.513 \ P_1 + 5.513 \ P_2 + 1.414 \ q''_{14}$$

Joint E

$$q_{24} + q_{20} = 0$$

$$q_{24} - q_{20} = 1.414 \ q_{12}$$
$$= 7.392 \ P_1 + 7.392 \ P_2 + 1.414 \ q''_{12}$$

ΣM about E-F

$$q_{24} + q_{25} + q_{26} = 11.918 \ P_1 + 8.888 \ P_2$$

* This is a rather crude way to estimate these loads and is used here only for simplicity. The analyst is generally better advised to exercise a little more ingenuity in making these estimates, even to the extent of being guided by other swept wing solutions.

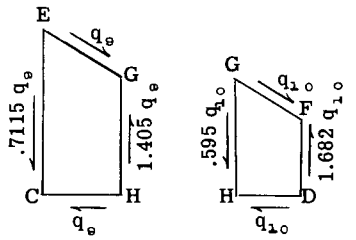

Shear Flows around the non-rectangular panels. (Check by summing moments about E, G and F.)

Cap EC

$$q_8 - .7115\, q_9 = .04431\, P_1 + .04431\, P_2 + .01923\, q''_{12}$$

Rib Vertical at E

$$q_8 - q_{19} = -.1403\, P_1 - .211\, P_2$$

Cap EG

$$-21.2\, q_9 - 21.2\, q_{19} - q_{20} + q_{21} = 0$$

Joint G

$$.707\, q_{13} - q_{25} = 0$$
$$.707\, q_{13} - q_{21} + q_{22} = 0$$

Cap GF

$$q_{10} + q_{19} + .04717\,(q_{22} - q_{23}) = 0$$

Rib Vertical at F

$$q_{11} + q_{19} = .2831\, P_1 + .3540\, P_2$$

Cap DF

$$q_{11} + 1.682\, q_{10} = .04432\,(P_1 + P_2) + .04545\, q''_{14}$$

The first five of the above equations were readily solved by substitution, yielding:

$$q_{23} = q_{26} = 2.756\, P_1 + 2.756\, P_2 + .707\, q''_{14}$$
$$-q_{20} = q_{24} = 3.696\, P_1 + 3.696\, P_2 + .707\, q''_{12}$$
$$q_{25} = 5.466\, P_1 + 2.436\, P_2 - .707\, q''_{12} - .707\, q''_{14}$$

Also, from equilibrium of joint G:

$$q_{13} = 7.729\, P_1 + 3.444\, P_2 - q''_{12} - q''_{14}$$

The remaining seven equations were arranged for solution thus:

$$\begin{bmatrix} 1 & 0 & 0 & 0 & -1 & 0 & 0 \\ 1 & -.7115 & 0 & 0 & 0 & 0 & 0 \\ 0 & 0 & 21.2 & 0 & 21.2 & 0 & 1 \\ 0 & 0 & 1.682 & 1 & 0 & 0 & 0 \\ 0 & 0 & 0 & 1 & 1 & 0 & 0 \\ 0 & -21.2 & 0 & 0 & -21.2 & 1 & 0 \\ 0 & 0 & 0 & 0 & 0 & -1 & 1 \end{bmatrix} \begin{Bmatrix} q_8 \\ q_9 \\ q_{10} \\ q_{11} \\ q_{19} \\ q_{21} \\ q_{22} \end{Bmatrix} =$$

$$= \begin{bmatrix} -.1403 & -.2111 & 0 & 0 \\ .04431 & .04431 & .01923 & 0 \\ 2.756 & 2.756 & 0 & .707 \\ .04432 & .04432 & 0 & .04545 \\ .2831 & .3540 & 0 & 0 \\ -3.696 & -3.696 & -.707 & 0 \\ -5.466 & -2.436 & .707 & .707 \end{bmatrix} \begin{Bmatrix} P_1 \\ P_2 \\ q''_{12} \\ q''_{14} \end{Bmatrix}$$

After inverting the matrix of coefficients on the left hand side of this last equation, and multiplying through thereby, the stresses were obtained as

$$\begin{Bmatrix} q_8 \\ q_9 \\ q_{10} \\ q_{11} \\ q_{19} \\ q_{21} \\ q_{22} \end{Bmatrix} = \begin{bmatrix} .1006 & .0295 & .00676 & -.00676 \\ .0791 & -.0208 & -.01753 & -.00950 \\ .0013 & -.0411 & .00401 & .0230 \\ .0422 & .1135 & -.00675 & .00675 \\ .2409 & .2409 & .00676 & -.00676 \\ 3.087 & .964 & -.9355 & -.3444 \\ -2.379 & -1.473 & -.2284 & .3625 \end{bmatrix} \begin{Bmatrix} P_1 \\ P_2 \\ q''_{12} \\ q''_{14} \end{Bmatrix}$$

The complete determinate and unit-redundant stress distributions, using the results up to this point, were therefore:

$[g_{im} : g_{ir}] =$

i \ m,r	1	2	12"	14"
1	.1071	.03572	0	0
2	.06284	- .00858	0	0
3	.00858	- .06284	0	0
4	.03572	.1071	0	0
5	2.924	2.924	0	0
6	3.581	3.581	0	0
7	2.924	2.924	0	0
8	.1006	.0295	.00676	- .00676
9	.0791	- .0208	- .01753	- .00950
10	.0013	- .0411	.00401	.0230
11	.0422	.1135	- .00675	.00675
12	5.228	5.228	1.0	0
13	7.729	3.444	-1.0	-1.0
14	3.899	3.899	0	1.0
15	- .989	.260	.2191	.1188
16	-1.384	.360	.3068	.1662
17	- .0146	.460	- .0449	- .2576
18	- .0244	.773	- .0754	- .4324
19	.2409	.2409	.00676	- .00676
20	-3.696	-3.696	- .707	0
21	3.087	.964	- .9355	- .3444
22	-2.379	-1.473	- .2284	.3625
23	2.756	2.756	0	.707
24	3.696	3.696	.707	0
25	5.466	2.436	- .707	- .707
26	2.756	2.756	0	.707

DASHED LOAD CALCULATIONS:

In the above matrix, loads q_{15}, q_{16}, q_{17} and q_{18} were obtained from q_9 and q_{10} following formulas given in reference 7 for general quadrilateral panels. The equations applicable to a parallel-sided panel are:

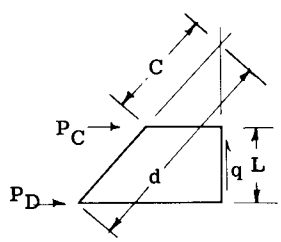

$P_C = \frac{d}{c+d}\, qL \times 2$

$P_D = \frac{c}{c+d}\, qL \times 2$

Balancing Load (= Dashed Load) Formulae from Ref. 7

For the panel CEGH; c = 52.3", d = 73.5", c + d = 125.8", L = 15". Hence

$$q_{16} = "P_D" = 2 \times \frac{52.3}{125.8} \times 15 \times (-)\, q_9 = -12.5\, q_9$$

$$= -.989\, P_1 + .260\, P_2 + .2191\, q''_{12} + .1188\, q''_{14}$$

$$q_{16} = "P_C" = 2 \times \frac{73.5}{125.8} \times 15 \times (-)\, q_9 = -17.5\, q_9$$

$$= -1.384\, P_1 + .360\, P_2 + .3068\, q''_{12} + .1662\, q''_{14}$$

Similarly, for the panel HGFD;

$$q_{17} = -.0146\, P_1 + .460\, P_2 - .0449\, q''_{12} - .2576\, q''_{14}$$
$$q_{18} = -.0244\, P_1 + .773\, P_2 - .0754\, q''_{12} - .4324\, q''_{14}$$

The following matrix products were formed: (cf. eqs. 17, 18, 23 of Chapter A8)

$$[\alpha_{rn}] = \begin{bmatrix} 17.70 & 250.2 \\ -173.7 & -50.43 \end{bmatrix}$$

$$[\alpha_{rs}] = \begin{bmatrix} 114.5 & 42.96 \\ 42.96 & 83.54 \end{bmatrix}$$

$$[\alpha_{rs}^{-1}] = \begin{bmatrix} 0.01082 & -.005563 \\ -.005563 & 0.01483 \end{bmatrix}$$

Finally, the true stress distribution was found as,

$[G_{im}] =$

i \ m	1	2
1	.1071	.03572
2	.06284	- .00858
3	.00858	- .06284
4	.03572	.1071
5	2.924	2.924
6	3.581	3.581
7	2.924	2.924
8	.0747	- .0051
9	.0740	.0112
10	.0581	- .0039
11	.0681	.1481
12	4.070	2.241
13	6.213	4.292
14	6.573	6.038
15	- .925	- .140
16	-1.295	- .201
17	- .6514	.0431
18	-1.093	.073
19	.2150	.2060
20	-2.877	-1.584
21	3.249	3.022
22	-1.145	- .015
23	4.646	4.268
24	2.877	1.584
25	4.394	3.036
26	4.652	4.268

MATRIX OF MEMBER FLEXIBILITY COEFFICIENT α_{ij} (E = 1) (Formulas from Chapter A7 and Reference 7)

1	2	3	4	5	6	7	8	9	10	11	12	13	14	15	16	17	18	19	20	21	22	23	24	25	26
15,400																									
	102,960																								
		102,960																							
			15,400																						
				70.170							15.46			15.46											
					50.01							8.984			8.984	8.984									
						52.33							6.542				6.542								
							12,130																		
								69,400																	
									46,000																
										5,130															
				15.46							30.92			30.92											
					8.984							17.97			17.97	17.97									
						6.542							13.08				13.08								
				15.46							30.92			30.92											
					8.984							17.97			17.97	17.97									
					8.984							17.97			17.97	17.97									
						6.542							13.08				13.08								
																		2130							
																			9.046	4.523					
																			4.523	9.046					
																					9.046	4.523			
																					4.523	9.046			
																							19.58		
																								14.24	
																									19.58

COMPARISON WITH TEST DATA:

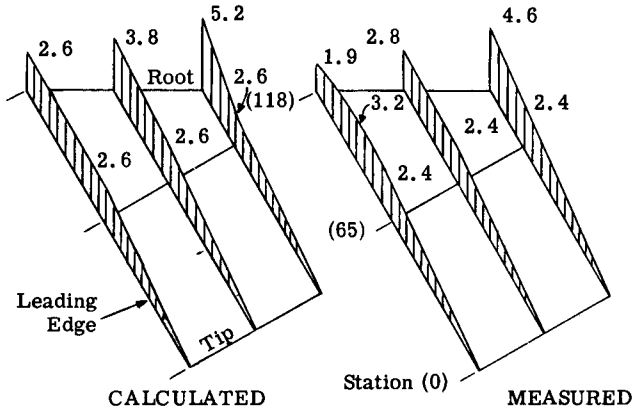

Fig. A22.15 Comparison Between Calculated and Measured Stresses (psi) in a Swept Box Beam.

Fig. A22.15 shows a comparison between the calculated stringer stresses and those measured by the NACA as reported in Reference 6. The stresses shown are for a unit tip load, centrally placed ($P_1 = P_2 = 1/2$ lb.).

Considering the limitations on the analysis the agreement is generally satisfactory. Thus, the discrepancy in the My/I stresses at station 65 may be attributed to a lack of precise knowledge of the test parameters. The calculated stresses in the leading edge spar between stations 65 and 118 cannot duplicate the experimental variation since only a single bay was employed in this region in the idealization. The fact that the calculated root stresses run consistently above the test values is difficult to explain. Inasmuch as the calculated stresses satisfy equilibrium, the test values, all being lower, would seem to defy this fundamental requirement. More details concerning the testing techniques and method of data presentation would probably resolve this conflict. Both test and calculated values clearly exhibit the characteristic build-up of stresses in the rear spar of a swept wing.

RIB E-G-F RIGID:

As a matter of interest, it was decided to investigate the effect upon stresses when rib E-G-F is taken to be rigid. Such a calculation is readily achieved by putting the member flexibility coefficients for the rib equal to zero.

Thus, in the matrix $[\alpha_{ij}]$, those coefficients with subscripts 19, 20, 21, 22 and 23 were set equal to zero and the complete calculation was repeated.

The results, for spar cap loads at the wing root (a most sensitive point), were:

$[G_{im}]_{\text{RIGID RIB}}$ =

i \ m	1	2
12	3.824	1.792
14	6.993	6.610

A comparison with the flexible rib calculations follows:

LOADING	SPAR CAP FORCE	FLEX. RIB	RIGID RIB	% DIFF.
Simple Bending; $P_1=P_2=1$	q_{12}	6.311	5.616	11
	q_{14}	12.61	13.60	8
Torsion; $P_1=-P_2=1$	q_{12}	1.829	2.032	11
	q_{14}	0.535	0.383	28

Considering that rib EGF was relatively rigid to begin with - being made of heavy gage steel - it may be seen that neglect of the flexibility of a corresponding all-aluminum rib could lead to serious errors.

REFERENCES

(1) Kuhn, P., Duberg, J. E., and Diskin, J. H., Stresses Around Rectangular Cut-Outs in Skin-Stringer Panels Under Axial Load - II, NACA WR L368 (ARR 3J02), Oct. 1943

(2) Rosecrans, R., A Method for Calculating Stresses in Torsion-Box Covers with Cut-outs, NACA TN 2290, Feb. 1951

(3) Kuhn, P., and Chiarito, P. T., Shear Lag in Box Beams: Methods of Analysis and Experimental Investigations, NACA TR 739, 1942

(4) Hoff, N. J., and Libby, P. A., Recommendations for Numerical Solutions of Reinforced Panel and Fuselage-Ring Problems, NACA TR 934, 1949

(5) Kuhn, P., Approximate Stress Analysis of Multi-Stringer Beams with Shear Deformation of the Flanges, NACA TR 636, 1938

(5a) Kuhn, P., Deformation Analysis of Wing Structures, NACA TN 1361, July 1947

(6) Zender, G., and Libove, C., Stress and Distortion Measurements in a 45° Swept Box Beam Subjected to Bending and Torsion, NACA TN 1525

(7) Wehle, L. B., and Lansing, W., A Method for Reducing the Analysis of Complex Redundant Structures to a Routine Procedure, Journal of Aero. Sci., 19, Oct. 1952

(8) Williams, M. L., A Review of Certain Analysis Methods for Swept Wing Structures, Journ. of Aero. Sci., 19, p. 615, 1952

(9) Heldenfels, R., Zender, G., and Libove, C., Stress and Distortion Analysis of a Swept Box Beam Having Bulkheads Perpendicular to the Spars, NACA TN 2232.

(10) Bisplinghoff, R., and Lang, A., An Investigation of Deformations and Stresses in Sweptback and Tapered Wings with Discontinuities, Mass. Inst. of Tech. Rept., July, 1949
(See also, Journ. of Aero. Sci. 18, p. 705, 1951)

(11) Denke, P., The Matric Solution of Certain Non-Linear Problems in Structural Analysis, Journ. of Aero. Sci., 23, 1956

(12) Levy, S., Computation of Influence Coefficients for Aircraft Structures with Discontinuities and Sweepback, Journ. of Aero. Sci., 14, Oct. 1947

(13) Islinger, J. S., Stress Analysis and Stress Measurements for a Swept Back Wing Having Ribs Parallel to the Airstream, McDonnell Aircraft Corp. Report 1127, April 1949.

CHAPTER A23

ANALYSIS BY THE METHOD OF DISPLACEMENTS

JOSEPH A. WOLF, Jr.

A23.1 Introduction

The displacement or stiffness method (1-4)* is a structural analysis procedure using displacements as the independent variables (and unknown quantities) rather than the forces. As applied here, the displacement method will be used in conjunction with a structural modeling using finite elements. Typical elements used are rod and beam segments, thin sheet and plate sections, and conical shell frusta. The number of unknown displacements is determined by the number of elements chosen and the level of sophistication or detail used in modeling. It is assumed that the description given by displacements of selected nodal points is adequate to represent the deformation of the structure. If a better representation is needed, the structure may be modeled by more nodes and hence more elements. The actual loading is replaced by a set of nodal forces calculated using the method of virtual work.

The displacement method has the following advantages:

1. The coordinate transformation matrix is easy to visualize and easy to generate, being determined solely by the geometry of the system,

2. There is no difficulty in deciding how to choose redundant reactions to yield a well-conditioned problem,

3. Matrices tend to be banded ones when using the displacement method, resulting in economies during computer storage and matrix manipulations,

4. The treatment of structural dynamics and structural stability are simplified because the inertial and geometric properties of elements and systems transform from coordinate system to coordinate system using the same matrices as are used in transforming the element and system stiffness properties,

5. The number of unknowns is based on the number of coordinates chosen, while in the force method redundant forces are the unknowns. Thus the displacement method is favored for analyzing highly-redundant structures such as frames.

* Numbers in parentheses designate References at end of Chapter.

Of course both methods can be used to describe structural behavior. For example, some of the disadvantages of the force method can be overcome by means of programmed automatic redundant selectors or "structure cutters." The engineer must be familiar with both methods in order to perform the analysis function efficiently.

The formulation of the displacement method has been perfected within the last 15 years, prompted by the availability of large electronic digital computers. In 1950, the solution of a system involving ten or twelve independent coordinates represented a massive effort for an analyst working by hand with a desk calculator. Present computer programs routinely handle structures represented by thousands of coordinates. Structural analysis can now be used in the design process for preliminary or parametric calculations because of this increase in capability and speed. With on-line graphics equipment, the design engineer can even manipulate his design by supplying and receiving information directly during computer calculations.

We note here, as an aside, that the Moment Distribution Method of Chapter A11, the Slope Deflection Method of Chapter A12 and the Method of Successive Corrections of Chapters A6 and A15 are all examples of the Displacement Method of structural analysis. In each of these methods the displacements are taken as the independent variables, and these are adjusted to achieve equilibrium of the loaded structure. The adjustment may appear as a systematic relaxation of artificial constraints (Moment Distribution and Successive Corrections) or it may be done mathematically in one stroke by the solution of a set of simultaneous equations (Slope Deflection Method). The latter approach-solution of a set of simultaneous equations-is essentially that followed herein, the solution usually being effected by matrix inversion or Gaussian elimination.

A23.2 Structural Coordinates

It would be impossible to consider the deflections of each particle of a structure. Instead, we characterize the system by a finite number of quantities which describe in a gross way (but a sufficiently useful way) the deformed shape of the system. These quantities are called

coordinates, and are of two kinds, discrete and distributed. Both kinds involve a simplified modeling of reality.

Discrete coordinates are used if the principal modes of deformation can be identified in terms of displacements of a finite number of points.

For example, with a beam element, we assume that the deformed shape can be adequately described in terms of the motion of the ends of the element. For each end there are six components of motion, three for linear displacement and three for rotation (Fig. A23.1). The deformation of the element therefore is described only to the degree possible by defining the deflection and rotation of ends. This description is obviously completely adequate if no external loads are applied along the element. If loads are applied along the element and greater detail is desired, nodal points can be defined at interior locations, effectively breaking each member into two or more elements.

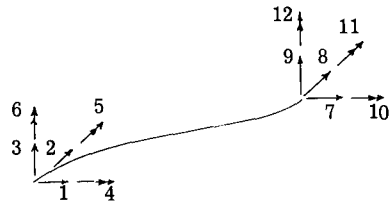

Fig. A23.1

Distributed coordinates are space functions which simultaneously approximate the displacements of all points of an elastic member. For example, if we have a simply supported beam, we might describe it using the ϕ functions shown in Fig. A23.2.

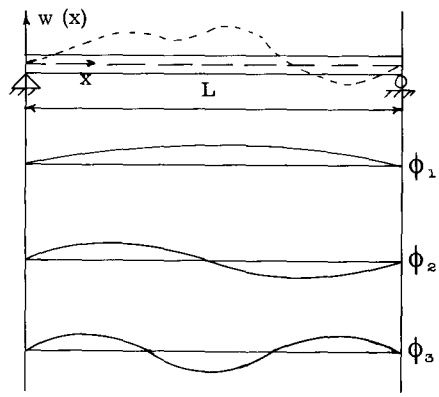

Fig. A23.2

Thus

$$w(x) = u_1\phi_1(x) + u_2\phi_2(x) + u_3\phi_3(x) + \ldots \quad - - - - \quad (1)$$

Here again, an exact representation cannot be given because, for practical reasons, the series used is of finite extent.

When a collection of elements are joined into a system, there are certain connectivity or constraint conditions and boundary conditions which characterize the system, and which distinguish it from a mere pile of elements.

To fix these concepts, we consider the example of a simple portal frame whose deformation is assumed to be restricted to the plane of the figure (Fig. A23.3).

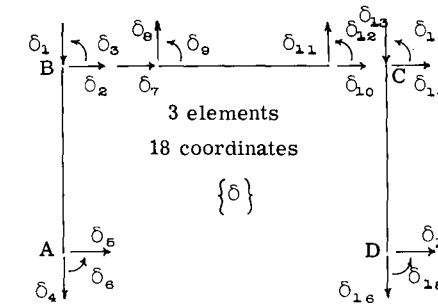

Fig. A23.3

The constraints and boundary conditions are

1. Fixed end conditions (no deflection) at points A and D.

2. Kinematic constraints at points B and C, such that deflections and rotations of elements 1 and 2 are the same at point B, and of elements 2 and 3 are the same at point C.

After eliminating duplicate coordinates, we are left with six system coordinates as shown in Fig. A23.4. Element coordinates are denoted by δ and structural system coordinates by u, respectively. (The symbols used generally follow those of Rubinstein, Refs. 1 and 2. Thus the reader interested in studying the theory in greater detail will not need to learn a new glossary).

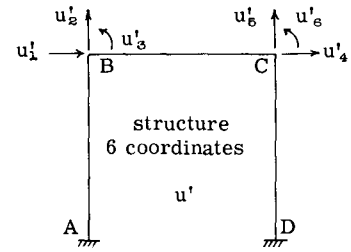

Fig. A23.4

As a practical matter, the kinematic constraints are taken into account when compiling the system stiffness matrix. The boundary conditions may be treated in the same way or, if

desired, may be applied all at once in a subsequent step. A further simplification is common in many structural problems. The stresses and strains due to axial loads within an element are often much smaller than those produced by bending loads. For such cases one may assume that the frame members are inextensible. Thus, in Fig. A23.4, we may take $u'_2 = u'_5 = 0$, and $u'_4 = u'_1$, and are left with three generalized coordinates for this level of modeling abstraction. Fig. A23.5 shows the structural deformation patterns corresponding to these generalized coordinates.

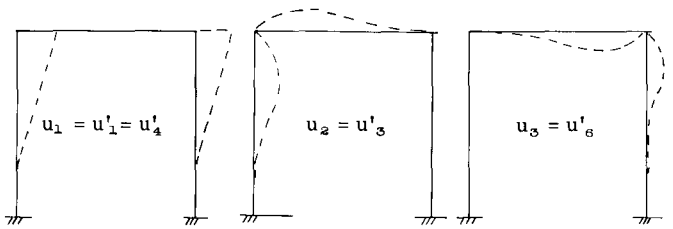

Fig. A23.5

Three Generalized System Coordinates for Portal Frame

A23.3 Theoretical Basis of the Method of Displacements

To perform a static analysis of a given structure, we must derive relationships between external, applied forces $\{F\}$ and the nodal points' generalized deflections $\{u\}$. In particular, since the deflections are to be treated as independent quantities, we seek to derive an equation

$$\{F\} = [K]\{u\} \quad - - - - - - - - - - - - - - - (2)$$

where the matrix $[K]$ is the system stiffness matrix. (Throughout this chapter, matrix notation has been employed. The symbols used are defined in Appendix A, except where noted).

To give the elements of the stiffness matrix physical meaning, we may consider an experiment in which one of the u's, say u_s, is given a unit deflection. The elements of the sth column of $[K]$ are equal to the forces necessary to give the structure this deflected configuration, or equally, the elements of the sth column are the forces developed at each of the nodal points when coordinate s is deflected a unit amount with all other coordinates held fixed. Within this sth column, the element K_{rs} is the force developed at coordinate r in that deformed configuration. The system stiffness matrix is compiled by adding together the individual element stiffness matrices, as will be demonstrated later.

Stiffness properties of structural elements are defined by applying the theory of elasticity to the particular configuration of interest. Various methods have been used; we will illustrate the procedure by employing the theorem of virtual work in the case of an elastic rod, and the differential equation of flexure in the case of a beam. The forces and displacements of elements will be denoted by P and δ, respectively, as distinguished from forces and displacements at nodal points of a structural system, denoted by F and u, respectively.

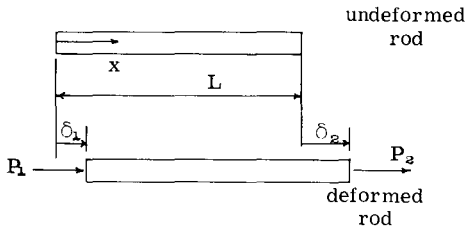

Fig. A23.6

For a uniform elastic rod subject to axial displacements δ_1 and δ_2 at the ends, the displacement at any section x is given by

$$\delta = \delta_1 + (\delta_2 - \delta_1)\frac{x}{L} \quad - - - - - - - - - (3)$$

The total axial strain is uniform, and given by

$$e_x = \frac{1}{L}(\delta_2 - \delta_1) \quad - - - - - - - - - - - (4)$$

If the rod is subjected to an increase in temperature of T degrees as well as an axial stress (load), the total strain e_x is equal to the elastic strain ε_x, plus the thermal strain αT. The elastic strain is the quantity needed to calculate the strain energy, that is,

$$\varepsilon_x = \frac{1}{L}(\delta_2 - \delta_1) - \alpha T \quad - - - - - - - - - - (5)$$

Rewriting Eq. 2, page A7.1, in terms of strain, using the substitutions $\sigma_x A = S$ and $\varepsilon_x E = \sigma_x$ for the elastic rod, we find

$$U = \frac{AEL}{2}\varepsilon_x^2 = \frac{AE}{2L}\left[(\delta_2 - \delta_1) - \alpha TL\right]^2 - - - (6)$$

Using the theorem of virtual work (Eq. 14, page A7.5)

$$P_r = \frac{\partial U}{\partial \delta_r} \quad - - - - - - - - - - - - - - - - - (7)$$

so

$$P_1 = \frac{\partial U}{\partial \delta_1} = -\frac{AE}{L}\left[(\delta_2 - \delta_1) - \alpha TL\right] - - - (8a)$$

and

$$P_2 = \frac{\partial U}{\partial \delta_2} = \frac{AE}{L}\left[(\delta_2 - \delta_1) - \alpha TL\right] \quad - - - (8b)$$

where the forces have the same positive directional sense as δ_1 and δ_2. This information can be exhibited in matrix form as

$$\begin{Bmatrix} P_1 \\ P_2 \end{Bmatrix} = \frac{AE}{L} \begin{bmatrix} 1 & -1 \\ -1 & 1 \end{bmatrix} \begin{Bmatrix} \delta_1 \\ \delta_2 \end{Bmatrix} + AE\alpha T \begin{Bmatrix} 1 \\ -1 \end{Bmatrix} \quad - - (9)$$

and we recognize the square matrix as $[k]$, the element stiffness matrix for axial deflection of an elastic rod. The elements of $[k]$ may also be calculated directly by rewriting the Theorem of Virtual Work. Recalling the definition of k_{rs}, it is the force P_r per unit deflection in coordinate δ_s. Thus

$$k_{rs} = \frac{\partial P_r}{\partial \delta_s} = \frac{\partial^2 U}{\partial \delta_r \partial \delta_s} \quad - - - - - - - - - - - - (10)$$

This result is of interest also because it demonstrates the symmetry of the stiffness matrix, $k_{rs} = k_{sr}$.

As a second illustration, we will use the solution of the differential equation of flexure to derive the stiffness matrix of a beam. Consider a unit end deflection, $\delta_3 = 1$, in Fig. A23.7.

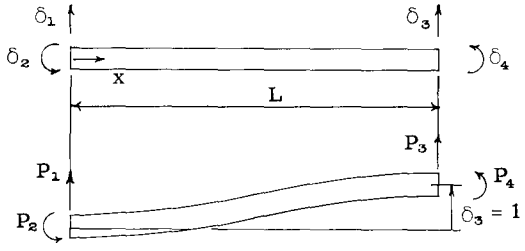

Fig. A23.7

The differential equation for a beam is (page A17.2)

$$EI \frac{d^2w}{dx^2} = M(x) = P_1 x - P_2 \quad - - - - - - - - (11)$$

subject here to the boundary conditions

$$\left.\begin{aligned} w &= \delta_1 = 0 \\ \frac{dw}{dx} &= \delta_2 = 0 \end{aligned}\right\} \text{ at } x = 0 \quad - - - - - - - - - (12a)$$

$$\left.\begin{aligned} w &= \delta_3 = 1 \\ \frac{dw}{dx} &= \delta_4 = 0 \end{aligned}\right\} \text{ at } x = L \quad - - - - - - - - - (12b)$$

After integrating twice with respect to x, the result is

$$EIw = \frac{P_1 x^3}{6} - \frac{P_2 x^2}{2} + C_1 x + C_2 \quad - - - - - - (13)$$

Using the boundary conditions at $x = 0$, we find that $C_1 = C_2 = 0$. The conditions at $x = L$ provide two equations in the unknowns P_1 and P_2,

$$\frac{P_1 L^3}{6} - \frac{P_2 L^2}{2} = EI \quad - - - - - - - - - - - - (14a)$$

$$\frac{P_1 L^2}{2} - P_2 L = 0 \quad - - - - - - - - - - - - (14b)$$

which have the solution $P_1 = -\frac{12EI}{L^3}$ and $P_2 = -\frac{6EI}{L^2}$. The values of P_3 and P_4, found from the equations of static equilibrium, are $P_3 = \frac{12EI}{L^3}$ and $P_4 = -\frac{6EI}{L^2}$. These results establish the third column of the stiffness matrix. The remaining terms are found by a similar procedure, with the result

$$\begin{Bmatrix} P_1 \\ P_2 \\ P_3 \\ P_4 \end{Bmatrix} = \frac{EI}{L^3} \begin{bmatrix} 12 & 6L & -12 & 6L \\ 6L & 4L^2 & -6L & 2L^2 \\ -12 & -6L & 12 & -6L \\ 6L & 2L^2 & -6L & 4L^2 \end{bmatrix} \begin{Bmatrix} \delta_1 \\ \delta_2 \\ \delta_3 \\ \delta_4 \end{Bmatrix} \quad - - (15)$$

The method of superposition provides an alternate derivation of the stiffness coefficients (ref. Fig. A23.8)

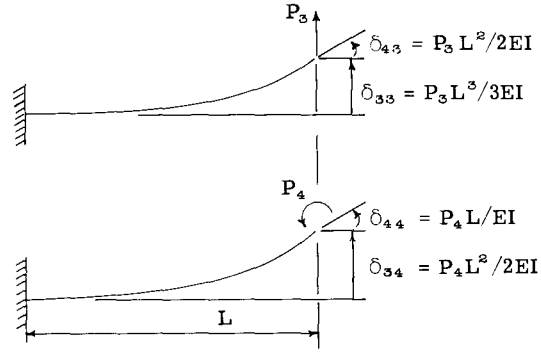

Fig. A23.8

Using the boundary conditions

$$\delta_3 = \delta_{33} + \delta_{34} = \frac{P_3 L^3}{3EI} + \frac{P_4 L^2}{2EI} = 1 \quad - - (16a)$$

$$\delta_4 = \delta_{43} + \delta_{44} = \frac{P_3 L^2}{2EI} + \frac{P_4 L}{EI} = 0 \quad - - (16b)$$

we find, as before, $P_3 = \frac{12EI}{L^3}$ and $P_4 = -\frac{6EI}{L^2}$. In this case, P_1 and P_2 are determined from static equilibrium. The remaining coefficients are determined in the same way. Note also that the reciprocity manifest in the symmetry of the stiffness matrix is demonstrated by the result $\delta_{43}/P_3 = \delta_{34}/P_4 = \frac{L^2}{2EI}$, a restatement of Maxwell's reciprocity theorem.

A23.4 Tabulation of Element Properties

In each case, the generalized force is taken to have the same positive sense as the

associated generalized displacement coordinate shown.

A. Bar with Axial Forces



$$\begin{Bmatrix} P_1 \\ P_2 \end{Bmatrix} = \frac{AE}{L} \begin{bmatrix} 1 & -1 \\ -1 & 1 \end{bmatrix} \begin{Bmatrix} \delta_1 \\ \delta_2 \end{Bmatrix}$$

B. Bar with Torsion



$$\begin{Bmatrix} P_1 \\ P_2 \end{Bmatrix} = \frac{GJ}{L} \begin{bmatrix} 1 & -1 \\ -1 & 1 \end{bmatrix} \begin{Bmatrix} \delta_1 \\ \delta_2 \end{Bmatrix}$$

C. Beam



$$\begin{Bmatrix} P_1 \\ P_2 \\ P_3 \\ P_4 \end{Bmatrix} = \frac{EI}{L^3} \begin{bmatrix} 12 & 6L & -12 & 6L \\ 6L & 4L^2 & -6L & 2L^2 \\ -12 & -6L & 12 & -6L \\ 6L & 2L^2 & -6L & 4L^2 \end{bmatrix} \begin{Bmatrix} \delta_1 \\ \delta_2 \\ \delta_3 \\ \delta_4 \end{Bmatrix}$$

Note that the stiffness matrix of a beam element subject to a general (three-dimensional) case of loading at the ends (a 12 x 12 matrix) may be compiled from the above information. Referring to Fig. A23.1, we associate coordinates 2 and 8 with coordinates δ_1 and δ_2 of case A, above, and coordinates 5 and 11 with coordinates δ_1 and δ_2 of case B. Further, assuming that the transverse coordinate axes are chosen to coincide with the principal axes of the beam cross section, the results of case C provide the remaining information for the general case. Specifically, we associate coordinates 3 and 4 (or 1 and 6) with coordinates δ_1 and δ_2, and coordinates 9 and 10 (or 7 and 12) with coordinates δ_3 and δ_4 of case C. The parentheses indicate the coordinate correspondence for the other transverse direction.

D. Tapered Beam

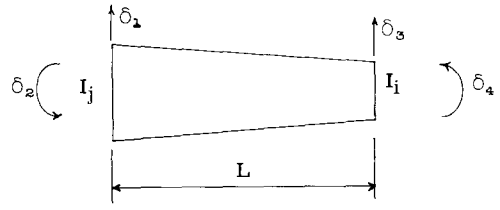

$$\begin{Bmatrix} P_1 \\ P_2 \\ P_3 \\ P_4 \end{Bmatrix} = \frac{3EI_j}{2DL^3} \begin{bmatrix} A & BL & -A & CL \\ BL & 2L^2\phi_{ii} & -BL & L^2\phi_{ij} \\ -A & -BL & A & -CL \\ CL & L^2\phi_{ij} & -CL & 2L^2\phi_{jj} \end{bmatrix} \begin{Bmatrix} \delta_1 \\ \delta_2 \\ \delta_3 \\ \delta_4 \end{Bmatrix}$$

where

$$A = 2\,(\phi_{ii} + \phi_{jj} + \phi_{ij})$$

$$B = 2\phi_{ii} + \phi_{ij}$$

$$C = \phi_{ij} + 2\phi_{jj}$$

$$D = \phi_{ii}\,\phi_{jj} - \frac{1}{4}\,\phi_{ij}^2$$

and ϕ_{ii}, ϕ_{ij} and ϕ_{jj} are given in Fig. A7.34c as functions of the ratio I_i/I_j, rather than A_i/A_j. Note that these functions have been derived for the case of a beam whose moment of inertia varies linearly.

E. Bar with Linearly Varying Axial Force

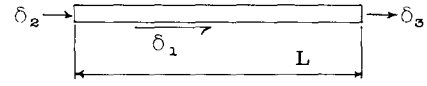

$$\begin{Bmatrix} P_1 \\ P_2 \\ P_3 \end{Bmatrix} \frac{2AE}{L^3} \begin{bmatrix} 6 & -3L & -3L \\ -3L & 2L^2 & L^2 \\ -3L & L^2 & 2L^2 \end{bmatrix} \begin{Bmatrix} \delta_1 \\ \delta_2 \\ \delta_3 \end{Bmatrix}$$

note that the shear flow P_1 and the associated deflection δ_1 have the units of pounds per inch and square inches, respectively (Ref. section A7.5). It is difficult to give a physical interpretation to δ_1, but we note that the product of P_1 and δ_1 has the units of strain energy, as expected. As an exercise, the reader may show that the flexibility matrix for this case (Sec. A7.10) is the inverse of the stiffness matrix.

F. Shear Panel

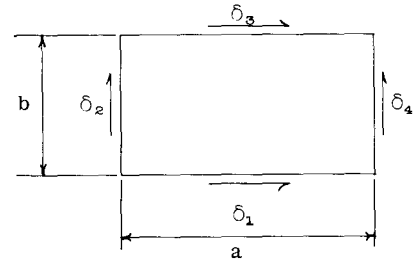

$$\begin{Bmatrix} P_1 \\ P_2 \\ P_3 \\ P_4 \end{Bmatrix} = \frac{Gt}{ab} \begin{bmatrix} 1 & 1 & -1 & -1 \\ 1 & 1 & -1 & -1 \\ -1 & -1 & 1 & 1 \\ -1 & -1 & 1 & 1 \end{bmatrix} \begin{Bmatrix} \delta_1 \\ \delta_2 \\ \delta_3 \\ \delta_4 \end{Bmatrix}$$

In this case, also, the units are pounds per inch and square inches for the "forces" and "displacements," respectively. Note that there is only one independent coordinate here, which is represented physically by the change in angle at one of the corners due to the shearing action of the applied forces.

G. Other Elements

Only the simplest elements have been shown in this section. Fortunately, many practical problems can be worked using this information, since a comprehensive catalog of elements could easily fill a separate chapter. Other elements having widespread application are two-dimensional elements with membrane forces (including triangular, square, and trapezoidal elements), two-dimensional plate bending elements (including triangular, square and trapezoidal elements), thin shell elements (including conical frusta and doubly curved elements), axisymmetric thick shell elements (including ring elements having various cross-section configurations), and general three-dimensional elements (including tetrahedron and hexahedron elements). These and other elements are being developed and perfected by structural analysts. It is worth noting that lack of interelement compatibility is an important shortcoming with the more complex finite elements, and provides the motivation for much continuing work. For details, the reader is referred to the abundant literature in this field.

A23.5 Transformation of Coordinates

We will often need to transform displacements between original coordinates (or coordinates in which it was convenient to define element properties) and generalized or independent coordinates. For this purpose, we use geometry to define a transformation matrix $[\beta]$ given by

$$\{\delta\} = [\beta]\{u\} \quad \text{- - - - - - - - - - - - - - (17)}$$

For the portal frame of Figs. A23.3 and A23.5, by inspection, we have

$$\begin{Bmatrix} \delta_1 \\ \delta_2 \\ \delta_3 \\ \delta_4 \\ \delta_5 \\ \delta_6 \\ \hline \delta_7 \\ \delta_8 \\ \delta_9 \\ \delta_{10} \\ \delta_{11} \\ \delta_{12} \\ \hline \delta_{13} \\ \delta_{14} \\ \delta_{15} \\ \delta_{16} \\ \delta_{17} \\ \delta_{18} \end{Bmatrix} = \begin{bmatrix} 0 & 0 & 0 \\ 1 & 0 & 0 \\ 0 & 1 & 0 \\ 0 & 0 & 0 \\ 0 & 0 & 0 \\ 0 & 0 & 0 \\ -- & -- & -- \\ 1 & 0 & 0 \\ 0 & 0 & 0 \\ 0 & 1 & 0 \\ 1 & 0 & 0 \\ 0 & 0 & 0 \\ 0 & 0 & 1 \\ -- & -- & -- \\ 0 & 0 & 0 \\ 1 & 0 & 0 \\ 0 & 0 & 1 \\ 0 & 0 & 0 \\ 0 & 0 & 0 \\ 0 & 0 & 0 \end{bmatrix} \begin{Bmatrix} u_1 \\ u_2 \\ u_3 \end{Bmatrix} \quad \text{- - (18)}$$

For convenience, the system $[\beta]$ matrix may be partitioned into element $[\beta_e]$ matrices, as shown. These smaller matrices may be used one at a time to transform element properties, as will be shown subsequently.

Similarly, we will want to transform forces from system to system. The method for doing this is derived from the expression for virtual work.

Consider forces F, associated with the u coordinate system. For a set of virtual displacements $\{\Delta u\}$, the virtual work is*

$$\Delta W = \{F\}^T \{\Delta u\} \quad \text{- - - - - - - - - - - - (19)}$$

For the δ system,

$$\Delta W = \{P\}^T \{\Delta\delta\} \quad \text{- - - - - - - - - - - - (20)}$$

We also have the compatibility relationship

$$\{\Delta\delta\} = [\beta]\{\Delta u\} \quad \text{- - - - - - - - - - - - (21)}$$

derived from the coordinate transformation. Now, since virtual work is a scalar, and since the P's and F's are in equilibrium, and the δ's and u's are compatible, the virtual work is the same in either system.

Thus

$$\{F\}^T \{\Delta u\} = \{P\}^T \{\Delta\delta\} = \{P\}^T [\beta]\{\Delta u\} \quad \text{- (22)}$$

* $\{\ \}^T$ and $[\ ]^T$ denote transpose of column and rectangular matrices respectively.

and since the Δu's are independent

$$\{F\}^T = \{P\}^T [\beta] \text{ or } \{F\} = [\beta]^T \{P\} \text{ - - - (23)}$$

which is the desired relationship.

We next ask how the stiffness and flexibility matrices are transformed from one set of coordinates to another. The appropriate formula can be derived from the expression for the strain energy in an element.

$$U = \frac{1}{2} \{\delta\}^T [k] \{\delta\} = \frac{1}{2} \{u\}^T [K] \{u\} \text{ - - - - (24)}$$

with $\{\delta\} = [\beta] \{u\}$, so the first expression may be rewritten

$$U = \frac{1}{2} \{u\}^T [\beta]^T [k] [\beta] \{u\} \text{ - - - - - - - - - (25)}$$

and, since the u's are independent,

$$[K] = [\beta]^T [k] [\beta] \text{ - - - - - - - - - - - (26)}$$

For transforming the flexibility matrices (denoted by $[a]$ and $[a]$ for element and system, respectively) a further result is needed. From equilibrium, we can find a relationship between element forces $\{P\}$ and external nodal point forces $\{F\}$

$$\{P\} = [b] \{F\} \text{ - - - - - - - - - - - - - - (27)}$$

which defines $[b]$ (for an indeterminant structure, see below). Writing the strain energy of an element

$$U = \frac{1}{2} \{P\}^T [a] \{P\} = \frac{1}{2} \{F\}^T [a] \{F\} \text{ - - - - (28)}$$

we can then substitute for $\{P\}$ using Eq. 27 and derive the final expression

$$[a] = [b]^T [a] [b] \text{ - - - - - - - - - - - (29)}$$

where we have used the fact that the $\{F\}$ forces are independent.

Often there will be displacements in $\{u\}$ which are associated with zero applied forces in those coordinates. Let

$$\{u\} = \left\{\begin{array}{c} u^* \\ \hline u^0 \end{array}\right\} \text{ - - - - - - - - - - - - - - - (30)}$$

where the $\{u^*\}$ are displacements on coordinates with applied forces $\{F^*\}$, and the $\{u^0\}$ are displacements on coordinates with zero valued applied forces.

Then $$\left\{\begin{array}{c} F^* \\ \hline 0 \end{array}\right\} = \left[\begin{array}{c|c} K_{11} & K_{12} \\ \hline K_{21} & K_{22} \end{array}\right] \left\{\begin{array}{c} u^* \\ \hline u^0 \end{array}\right\} \text{ - - - - - - - - (31)}$$

so $$\{F^*\} = [K_{11}] \{u^*\} + [K_{12}] \{u^0\} \text{ - - - - (32a)}$$

and $$\{0\} = [K_{21}] \{u^*\} + [K_{22}] \{u^0\} \text{ - - - - (32b)}$$

or $$\{u^0\} = - [K_{22}]^{-1} [K_{21}] \{u^*\} \text{ - - - - - (33)}$$

Substituting back into Eq. 32a,

$$\{F^*\} = \left([K_{11}] - [K_{12}] [K_{22}]^{-1} [K_{21}]\right) \{u^*\} \text{ - (34)}$$

Therefore we may define a reduced stiffness matrix

$$[K^*] = [K_{11}] - [K_{12}] [K_{22}]^{-1} [K_{21}] \text{ - (35)}$$

and, once the $\{u^*\}$ are known in any given problem, the $\{u^0\}$ may be found immediately from Eq. 33.

Similarly, the flexibility method is useful in statically indeterminate structures where the opposite situation pertains - that is, where forces are associated with (redundant) zero displacements.

We extend $\{F\}$ to include a set of self-equilibrating forces corresponding to the number of redundants in the structure. For the portal frame, there are three redundants, as shown in Fig. A23.9. The displacements at the redundants are actually zero.

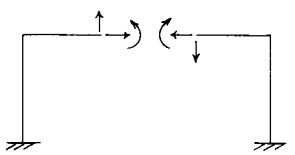

Fig. A23.9

Thus we have

$$\left\{\begin{array}{c} u^* \\ \hline 0 \end{array}\right\} = \left[\begin{array}{c|c} a_{11} & a_{12} \\ \hline a_{21} & a_{22} \end{array}\right] \left\{\begin{array}{c} F^* \\ \hline F^0 \end{array}\right\} \text{ - - - - - - - (36)}$$

and by analogy with the case of zero forces

$$\{u^*\} = [a^*] \{F^*\} \text{ - - - - - - - - - - - (37)}$$

where

$$[a^*] = [a_{11}] - [a_{12}] [a_{22}]^{-1} [a_{21}] \text{ - (38)}$$

The flexibility method is useful also in deriving a relationship between system forces and element forces for a statically indeterminate structure.

For the extended set of forces, including redundants, we may write

$$\{P\} = \left[\begin{array}{c|c} b^* & b^o \end{array}\right] \left\{\begin{array}{c} F^* \\ \hline F^o \end{array}\right\} \quad - - - - - - - - - (39)$$

based upon static equilibrium. At this point the $\{F^o\}$ are not known.

However, from Eq. 36, we found

$$[a_{21}]\{F^*\} + [a_{22}]\{F^o\} = \{0\}$$

or

$$\{F^o\} = -[a_{22}]^{-1}[a_{21}]\{F^*\} - - - - - - (40)$$

so

$$\{P\} = \left([b^*] - [b^o][a_{22}]^{-1}[a_{21}]\right)\{F^*\} \quad - (41)$$

which is the desired transformation. We have seen how to transform information about forces, displacements, stiffnesses and/or flexibilities from one coordinate system to another. Our next task is to apply these methods to transform from element properties to system properties. Rather than repeat the several derivations, the results are tabulated below.

Table A23.1

	Stiffness Method	Flexibility Method
Element Properties	$\{P\} = [k]\{\delta\}$	$\{\delta\} = [a]\{P\}$
System Properties	$\{F\} = [K]\{u\}$	$\{u\} = [a]\{F\}$
Transformation of Displacements and Forces	$\{\delta\} = [\beta]\{u\}$ $\{F\} = [\beta]^T\{P\}$	$\{P\} = [b]\{F\}$ $\{u\} = [b]^T\{\delta\}$
Transformation of Structural Properties	$[K] = [\beta]^T[k][\beta]$ or $[K] = \sum_{e=1}^{m} [\beta_e]^T[k_e][\beta_e]$	$[a] = [b]^T[a][b]$ or $[a] = \sum_{e=1}^{m} [b_e][a_e][b_e]$
where m = number of elements in structural system		

In the case of zero force coordinates

$$\{F^*\} = \left([K_{11}] - [K_{12}][K_{22}]^{-1}[K_{21}]\right)\{u^*\}$$

$$= [K^*]\{u^*\}$$

In the case of zero displacement (redundant) coordinates

$$\{u^*\} = \left([a_{11}] - [a_{12}][a_{22}]^{-1}[a_{21}]\right)\{F^*\}$$

$$= [a^*]\{F^*\}$$

Example Problem 1

Fig. A23.10 shows the singly redundant three member frame previously analyzed in section A8.4

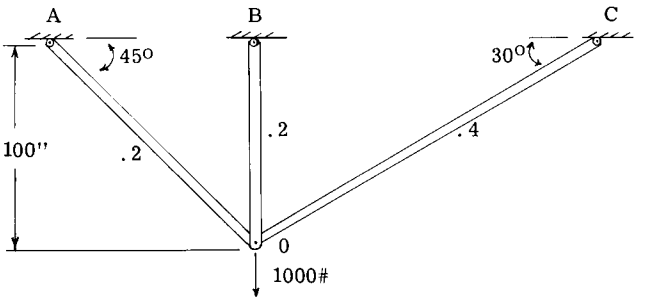

Fig. A23.10

The coordinates chosen are shown in Fig. A23.11.

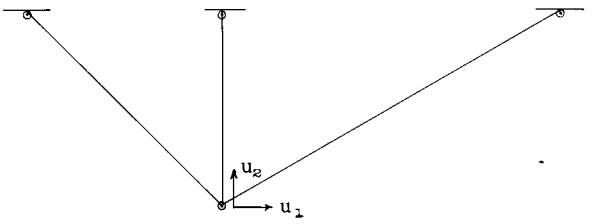

Fig. A23.11a

System Coordinates

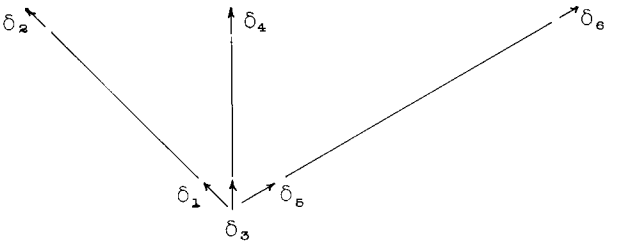

Fig. A23.11b

Element Coordinates

Note that system coordinates at the boundary points A, B and C could have been included, but would have dropped out when the boundary conditions were applied. For simplicity, these coordinates have been deleted at the beginning of the analysis. To compile the system stiffness matrix, the contribution from each element must be found. For example, for element OC, the element stiffness is given by

$$[k_{oc}] = \frac{A_{oc}E}{L_{oc}}\begin{bmatrix} 1 & -1 \\ -1 & 1 \end{bmatrix} = \frac{E}{10^3}\begin{bmatrix} 2 & -2 \\ -2 & 2 \end{bmatrix} \quad - - (42)$$

and the transformation from element to system coordinates is given by $\{\delta_{oc}\} = [\beta_{oc}]\{u\}$

or, from Figs. A23.10 and A23.11,

$$\begin{Bmatrix} \delta_5 \\ \delta_6 \end{Bmatrix} = \begin{bmatrix} 0.866 & 0.500 \\ 0 & 0 \end{bmatrix} \begin{Bmatrix} u_1 \\ u_2 \end{Bmatrix} \quad \text{- - - - - (43)}$$

Thus element OC contributes the term,

$$[K_{oc}] = [\beta_{oc}]^T [k_{oc}] [\beta_{oc}] = \frac{E}{10^3} \begin{bmatrix} 1.5 & 0.866 \\ 0.866 & 0.5 \end{bmatrix}$$

- (44)

to the system stiffness matrix. Similarly, the following information may be compiled for elements OA and OB.

Table A23.2

Quantity	Element	
	OA	OB
Element Stiffness in Local Coordinates $[k_e]$	$\frac{E}{10^3}\begin{bmatrix} 1.414 & -1.414 \\ -1.414 & 1.414 \end{bmatrix}$	$\frac{E}{10^3}\begin{bmatrix} 2 & -2 \\ -2 & 2 \end{bmatrix}$
Coordinate Transformation $[\beta_e]$	$\begin{bmatrix} -0.707 & 0.707 \\ 0 & 0 \end{bmatrix}$	$\begin{bmatrix} 0 & 1 \\ 0 & 0 \end{bmatrix}$
Element Stiffness in System Coordinates $[K_e]$	$\frac{E}{10^3}\begin{bmatrix} 0.707 & -0.707 \\ -0.707 & 0.707 \end{bmatrix}$	$\frac{E}{10^3}\begin{bmatrix} 0 & 0 \\ 0 & 2 \end{bmatrix}$

The system stiffness matrix is given by

$$[K] = \sum_{e=1}^{3} [K_e] = \sum_{e=1}^{3} [\beta_e]^T [k_e] [\beta_e] \quad \text{- - - - - (45)}$$

or

$$[K] = \frac{E}{10^3} \begin{bmatrix} 2.207 & 0.159 \\ 0.159 & 3.207 \end{bmatrix} \quad \text{- - - - - (46)}$$

which provides the relationship between system forces and deflections.

Example Problem 2

Assemble the system stiffness matrix for the portal frame of Fig. A23.12a, assuming uniform element properties and neglecting axial deformation. The element coordinates are shown in Fig. A23.12b, and the element stiffness matrix is given by case C of section A23.4.

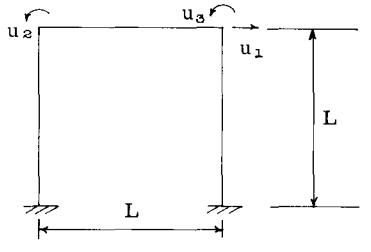

Fig. A23.12a
System Coordinates

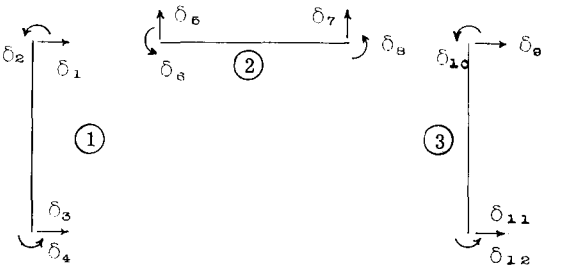

Fig. A23.12b
Element Coordinates

In general, $[K] = [\beta]^T [k] [\beta]$, where

$$[\beta] = \begin{bmatrix} \beta_1 \\ \beta_2 \\ \beta_3 \end{bmatrix} = \left[\begin{array}{ccc} 1 & 0 & 0 \\ 0 & 1 & 0 \\ 0 & 0 & 0 \\ 0 & 0 & 0 \\ \hline 0 & 0 & 0 \\ 0 & 1 & 0 \\ 0 & 0 & 0 \\ 0 & 0 & 1 \\ \hline 1 & 0 & 0 \\ 0 & 0 & 1 \\ 0 & 0 & 0 \\ 0 & 0 & 0 \end{array}\right] \quad \text{- - - - (47)}$$

and

$$[k] = \left[\begin{array}{c|c|c} k_1 & 0 & 0 \\ \hline 0 & k_2 & 0 \\ \hline 0 & 0 & k_3 \end{array}\right] \quad \text{- - - - - - - (48)}$$

with each $[k_e]$ equal to the result given in case C, section A23.4.

The final result, after carrying out the indicated operations (using either the complete matrices of Eqs. 47 and 48, or the partitioned form of Eq. 45) is

$$[K] = \frac{EI}{L^3} \begin{bmatrix} 24 & 6L & -6L \\ 6L & 8L^2 & 2L^2 \\ -6L & 2L^2 & 8L^2 \end{bmatrix} \quad \text{- - - - - - (49)}$$

A23.6 Calculation of Displacements and Stresses

There are several methods for solving for the deflections resulting from the application of given forces. The most straightforward is

to invert the stiffness matrix (for details, see Appendix A)

so that

$$\{u\} = [K]^{-1}\{F\} \quad - - - - - - - - - - - - \quad (50)$$

or for the three member frame of example problem 1, section A23.5,

$$\begin{Bmatrix} u_1 \\ u_2 \end{Bmatrix} = \frac{10^3}{E}\begin{bmatrix} 4.547 & -0.225 \\ -0.225 & 3.129 \end{bmatrix}\begin{Bmatrix} F_1 \\ F_2 \end{Bmatrix} \quad - - - \quad (51)$$

Given that $F_1 = 0$ and $F_2 = -1000$ lb., we find that the horizontal deflection $u_1 = 22500/E$ inches and the vertical deflection $u_2 = -312900/E$ inches. The final step is to compute element forces. To do this, the element deflections must be found using the transformation matrix $[\beta]$ or $[\beta_e]$. For member OC, using Eq. 43,

$$\begin{Bmatrix} \delta_1 \\ \delta_2 \end{Bmatrix} = \begin{bmatrix} 0.866 & 0.500 \\ 0 & 0 \end{bmatrix}\begin{Bmatrix} \frac{22500}{E} \\ \frac{-312900}{E} \end{Bmatrix} = \begin{Bmatrix} \frac{-137000}{E} \\ 0 \end{Bmatrix} \quad - \quad (52)$$

and $\{P\} = [k]\ \{\delta\}$

or

$$\begin{Bmatrix} P_5 \\ P_6 \end{Bmatrix} = \frac{E}{10^3}\begin{bmatrix} 2 & -2 \\ -2 & 2 \end{bmatrix}\begin{Bmatrix} \frac{-137000}{E} \\ 0 \end{Bmatrix} = \begin{Bmatrix} -274 \\ 274 \end{Bmatrix} \quad - - \quad (53)$$

Thus the force in member OC is 274 lb. tension which checks with the result found previously in section 8.4. Similarly, the forces in members OA and OB are 335 lb. and 626 lb. respectively.

A23.7 Method of Gaussian Elimination

For large systems, involving solution for tens, hundreds, or, often, thousands of unknowns, the matrix inversion method is more time-consuming than other techniques. Basically, the alternate solution methods are divided into two categories, elimination methods, and iteration methods (5,6).

The method of Gaussian elimination or variants such as Cholesky decomposition are widely used as practical solution methods for large systems of equations. The basic Gaussian elimination will be described and used here. Consider a system of linear equations,

$$\begin{aligned}
C_{11}X_1 + C_{12}X_2 + C_{13}X_3 + \ldots + C_{1n}X_n &= C_{1n+1} \\
C_{21}X_1 + C_{22}X_2 + C_{23}X_3 + \ldots + C_{2n}X_n &= C_{2n+1} \\
C_{31}X_1 + C_{32}X_2 + C_{33}X_3 + \ldots + C_{3n}X_n &= C_{3n+1} \\
\ldots & \qquad \ldots \\
C_{n1}X_1 + C_{n2}X_2 + C_{n3}X_3 + \ldots + C_{nn}X_n &= C_{nn+1}
\end{aligned} \quad - - \quad (54)$$

We wish to systematize the solution by first triangularizing the left-hand side of the equations, resulting in fewer unknowns in each successive equation, and culminating in a final equation in the single unknown x_n. The solution is completed by solving first for the last unknown, x_n, then using this information to solve for x_{n-1}, and so on. In the triangularized form, each unknown, x_r say, depends only on the x_m, with $n \geq m > r$.

The first step in the triangularization consists of calculating new coefficients for the second equation and all subsequent equations using

$$C_{ij}^{(1)} = C_{ij} - \frac{C_{i1}}{C_{11}}C_{1j} \qquad \begin{matrix} i = 2,\ldots, n \\ j = 2,\ldots, n+1 \end{matrix} \quad - - \quad (55)$$

which brings the equations to the form

$$\begin{aligned}
C_{11}X_1 + C_{12}X_2 + C_{13}X_3 + \ldots + C_{1n}X_n &= C_{1n+1} \\
C_{22}^{(1)}X_2 + C_{23}^{(1)}X_3 + \ldots + C_{2n}^{(1)}X_n &= C_{2n+1}^{(1)} \\
C_{32}^{(1)}X_2 + C_{33}^{(1)}X_3 + \ldots + C_{3n}^{(1)}X_n &= C_{3n+1}^{(1)} \\
\ldots & \qquad \ldots \\
C_{n2}^{(1)}X_2 + C_{n3}^{(1)}X_3 + \ldots + C_{nn}^{(1)}X_n &= C_{nn+1}^{(1)}
\end{aligned} \quad - - \quad (56)$$

The final form is

$$\begin{aligned}
C_{11}X_1 + C_{12}X_2 + C_{13}X_3 + \ldots + C_{1n}X_n &= C_{1n+1} \\
C_{22}^{(1)}X_2 + C_{23}^{(1)}X_3 + \ldots + C_{2n}^{(1)}X_n &= C_{2n+1}^{(1)} \\
C_{33}^{(2)}X_3 + \ldots + C_{3n}^{(2)}X_n &= C_{3n+1}^{(2)} \\
\ldots & \qquad \ldots \\
C_{nn}^{(n-1)}X_n &= C_{nn+1}^{(n-1)}
\end{aligned} \quad - - \quad (57)$$

where at any step, the coefficients are given by

$$C_{ij}^{(k)} = C_{ij}^{(k-1)} - \frac{C_{ik}^{(k-1)}}{C_{kk}^{(k-1)}}C_{Kj}^{(K-1)}; \quad \begin{matrix} k = 1,2,\ldots,n-1 \\ j = k+1,\ldots,n+1 \\ i = k+1,\ldots,n \end{matrix} \quad (58)$$

and $C_{ij}^{(0)} = C_{ij}$

The back substitution then takes the symbolic form

$$X_i = \frac{1}{C_{ii}^{(i-1)}}\left[C_{i,n+1}^{(i-1)} - \sum_{j=i+1}^{n} C_{ij}^{(i-1)}X_j\right], \quad i=n,\ldots,1$$

$$- - - - - - - - - - - - \quad (59)$$

Example Problem 3

Fig. A23.13 shows the single bay pin connected truss which was discussed on page A8.7.

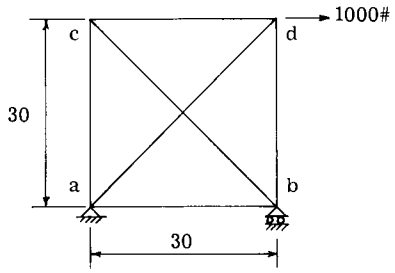

Fig. A23.13

This truss will now be solved by the displacement method, using Gaussian elimination. The initial step of the solution is to compile the system stiffness matrix. The required element information is tabulated below.

Table A23.3

Member	$\frac{AE}{L}$	$\cos\theta_e$	$\sin\theta_e$
ab	1.0×10^6	1.0	0.0
bd	1.0×10^6	0.0	1.0
dc	1.0×10^6	1.0	0.0
ca	1.0×10^6	0.0	1.0
cb	1.4142×10^6	0.7071	-0.7071
ad	1.607×10^6	0.7071	0.7071

Note that θ is the angle between the global (system) x axis and the structural axis of a member.

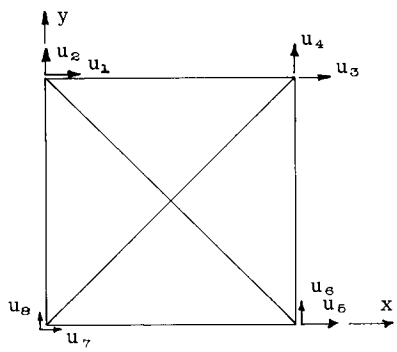

Fig. A23.14
System Coordinates

The transformation matrix for an element is then given by

$$[\beta_e] = \begin{bmatrix} \text{Cos } \theta_e & \text{Sin } \theta_e \\ -\text{Sin } \theta_e & \text{Cos } \theta_e \end{bmatrix} \quad \text{- - - - - - (60)}$$

and the total system stiffness matrix is

$$[K] = 10^6 \begin{bmatrix} 1.7071 & -0.7071 & -1 & 0 & -0.7071 & 0.7071 & 0 & 0 \\ & 1.7071 & 0 & 0 & 0.7071 & -0.7071 & 0 & -1 \\ & & 1.5303 & 0.5303 & 0 & 0 & -0.5303 & -0.5303 \\ & & & 1.5303 & 0 & -1 & -0.5303 & -0.5303 \\ & & & & 1.7071 & -0.7071 & -1 & 0 \\ & & & & & 1.7071 & 0 & 0 \\ & \text{Symmetrical} & & & & & 1.5303 & 0.5303 \\ & & & & & & & 1.5303 \end{bmatrix} \quad (61)$$

Equation 2 may be rewritten as

$$\left\{\begin{matrix} F \\ \hline R \end{matrix}\right\} = \left[\begin{matrix} K_{11} \\ \hline K_{21} \end{matrix} \vdots \begin{matrix} K_{12} \\ \hline K_{22} \end{matrix}\right] \left\{\begin{matrix} u^c \\ \hline 0 \end{matrix}\right\} \quad \text{- - - - - - - (62)}$$

where R denotes the forces at the constraints (boundaries), and u^c represents system coordinates remaining after applying the boundary conditions. The constrained statics problem is thus obtained simply by deleting rows and columns corresponding to the fixed coordinates. For this example, the boundary conditions are $u_6 = u_7 = u_8 = 0$ for all loading conditions. The problem formulation may be simplified by eliminating the constrained coordinates, leaving

$$\{F\} = [K_{11}]\{u^c\} \quad \text{- - - - - - - - - - - (63)}$$

where

$$[K_{11}] = 10^6 \begin{bmatrix} 1.7071 & -0.7071 & -1 & 0 & -0.7071 \\ -0.7071 & 1.7071 & 0 & 0 & 0.7071 \\ -1 & 0 & 1.5303 & 0.5303 & 0 \\ 0 & 0 & 0.5303 & 1.5303 & 0 \\ -0.7071 & 0.7071 & 0 & 0 & 1.7071 \end{bmatrix} \quad (64)$$

If desired, the reaction forces may be found from

$$\{R\} = [K_{21}]\{u^c\} = [K_{21}][K_{11}]^{-1}\{F\} \quad (65)$$

The solution procedure outlined above can be modified to account for yielding supports, etc. if desired.

To solve for the displacements, the method of Gaussian elimination will be used. The result of the triangularization step, corresponding to Eq. 57, is the matrix equation

$$10^6 \begin{bmatrix} 1.7071 & -0.7071 & -1 & 0 & -0.7071 \\ 0 & 1.4142 & -0.4142 & 0 & 0.4142 \\ 0 & 0 & 0.8232 & 0.5303 & -0.2929 \\ 0 & 0 & 0 & 1.1887 & 0.1887 \\ 0 & 0 & 0 & 0 & 1.1588 \end{bmatrix} \begin{Bmatrix} u_1 \\ u_2 \\ u_3 \\ u_4 \\ u_5 \end{Bmatrix}$$

$$= \begin{Bmatrix} F_1 \\ F_2 + 0.4142\,F_1 \\ F_3 + 0.2929\,F_2 + 0.7071\,F_1 \\ F_4 - 0.6442\,F_3 - 0.1887\,F_2 - 0.4555\,F_1 \\ F_5 - 0.1587\,F_4 + 0.4580\,F_3 - 0.1588\,F_2 + 0.6168\,F_1 \end{Bmatrix} \quad (66)$$

For the problem to be analyzed, F_3 is the only force to be considered. Thus the right-hand side for the back substitution process is

$$F_3 \begin{Bmatrix} 0 \\ 0 \\ 1 \\ -0.6442 \\ 0.4580 \end{Bmatrix}$$

Each row of the matrix equation represents an algebraic equation in the unknown u values. These are solved in inverse order, with the following results

$$u_5 = 0.3952 \times 10^{-6}\, F_3$$
$$u_4 = -0.6047 \times 10^{-6}\, F_3$$
$$u_3 = 1.7450 \times 10^{-6}\, F_3$$
$$u_2 = 0.3953 \times 10^{-6}\, F_3$$
$$u_1 = 1.3497 \times 10^{-6}\, F_3$$

The static deflections are found by substituting the given value of $F_3 = 1000$.

Member forces are determined in the usual way, by means of the appropriate $[\beta_e]$ and $[k_e]$ matrices as before. The results are shown in Fig. A23.15.

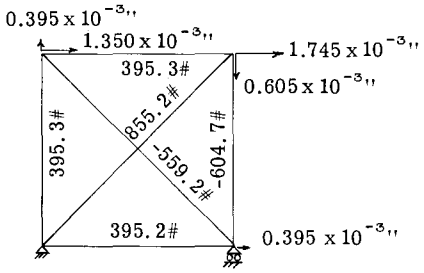

Fig. A23.15

A23.8 Gauss-Seidel Iteration

A second class of solution methods involves the use of iteration. Iterative methods of solution are particularly appealing for structures whose description results in sparse matrices, that is, matrices containing relatively few nonzero elements. Large space frames and two- and three-dimensional solid bodies modeled with finite elements are examples of such structures. One widely used iteration technique is the Gauss-Seidel method. In this method, an initial solution vector is generated, often by guessing plausible values. This trial solution is then systematically improved, by solving the linear equations in sequence, using the current values for all unknowns other than the one being evaluated. As soon as an unknown has been determined, it is incorporated in the values used for subsequent steps within a given iteration cycle, rather than waiting until the cycle has been completed. As an illustration, consider the portal frame of Example Problem 2, with an applied force $F_1 = 24000$ lb. Assume values of $EI = 10^9$ lb. in.^{2} and $L = 100$ inches, and calculate the deflections using Gauss-Seidel iteration. After making the indicated substitutions, and dividing through by the common factor of 8000, the problem may be brought to the form

$$\begin{bmatrix} 3 & 75 & -75 \\ 75 & 10000 & 2500 \\ -75 & 2500 & 10000 \end{bmatrix} \begin{Bmatrix} u_1 \\ u_2 \\ u_3 \end{Bmatrix} = \begin{Bmatrix} 3 \\ 0 \\ 0 \end{Bmatrix} \quad ---- \quad (67)$$

For the iteration, a further reduction is worthwhile, wherein only one unknown appears on the left-hand side of each scalar equation. Following this manipulation, the equations to be solved are

$$u_1 = 1 - 25u_2 + 25u_3 \quad ---------(68a)$$

$$u_2 = -0.0075u_1 - 0.25u_3 \quad ---------(68b)$$

$$u_3 = 0.0075u_1 - 0.25u_2 \quad ---------(68c)$$

As a trial solution, we take $u_1 = 1$, $u_2 = u_3 = 0$, inasmuch as we expect sidesway to be the dominant deflection. The results at selected steps of the procedure are given in Table A23.4. The convergence does not appear to be rapid, but methods exist for accelerating the solution. For further details, the reader is referred to a text on numerical analysis.

Table A23.4

Step of Solution	u_1	u_2	u_3
Initial Trial	1	0	0
Initial Result of Eq. 68a	1	0	0
Initial Result of Eq. 68b	1	-0.0075	0
Initial Result of Eq. 68c (End of First Iteration)	1	-0.0075	0.0094
Second Result of Eq. 68a	1.4225	-0.0075	0.0094
Second Result of Eq. 68b	1.4225	-0.0130	0.0094
Second Result of Eq. 68c (End of Second Iteration)	1.4225	-0.0130	0.0139
End of Fifth Iteration	1.8925	-0.0187	0.0189
End of Tenth Iteration	1.995	-0.0199	0.0199
Exact Solution	2.0	-0.02	0.02

A23.9 Calculation of Nodal Forces for Loads Acting Between Nodal Points

In many practical situations, the structure is loaded at locations other than the nodal points. Of course, in the case of concentrated loads, this complication may be resolved by introducing nodes at the loading sites. However, for distributed loads, such as pressure, there is no way of avoiding the problem. Therefore, we wish to derive a method for calculating equivalent nodal forces which are consistent with the finite element formulation of the problem. To do this, we employ the method of virtual work. As an example, consider the case of an elastic beam element. Associated with each nodal coordinate, there is a deflected shape or distributed coordinate for the entire finite element, found from the solution of the differential equation of beam bending. These shapes are shown in Fig. A23.16.

Thus, from Eq. 1, the connection between nodal coordinates and the deformed shape of the element is

$$w(X) = u_1\phi_1(X) + u_2\phi_2(X) + u_3\phi_3(X) + u_4\phi_4(X) \quad - (69)$$

Let the applied load be given by f(x) as shown in Fig. A23.16e. Then the total virtual work produced by the applied load acting through a virtual displacement Δw is

$$\Delta W = \int_0^L f(X)\ \Delta w(X)\ dx \quad - - - - - - - - - (70)$$

or substituting from Eq. 69,

$$\Delta W = \sum_{i=1}^{4} \int_0^L f(X)\phi_i(X)\, dx\, \Delta u_i \quad - - - - - (71)$$

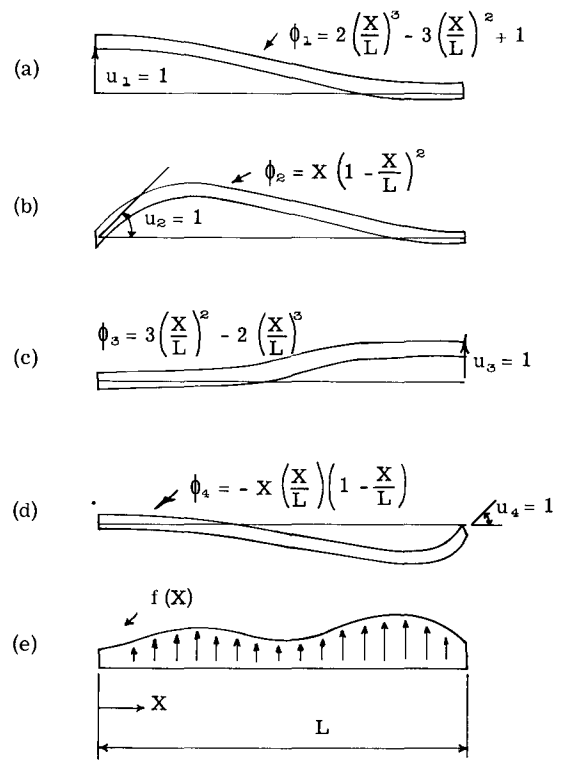

Fig. A23.16

By analogy, the total virtual work is also given by calculating the work done by the nodal forces, P_i, acting through the compatible nodal virtual displacements, Δu_i. The result is

$$\Delta W = \sum_{i=1}^{4} P_i \Delta u_i \quad - - - - - - - - - - - - (72)$$

and since the Δu_i are independent, the right-hand sides of Eqs. 71 and 72 may be equated term by term, giving the desired equation,

$$P_i = \int_0^L f(X)\phi_i(X)dx,\ i = 1, \ldots, 4 \quad - (73)$$

In the case of moments acting between nodal points, a parallel development gives the result

$$P_i = \int_0^L m(X)\phi_i'(X)dx,\ i = 1, \ldots, 4 \quad - (74)$$

where m(X) is the applied moment and $\phi_i' \equiv d\phi/dx$.

Several loading cases occur often enough to justify tabulating the associated nodal forces. Table A23.5 contains the nodal forces appropriate to the loads shown in Fig. A23.17.

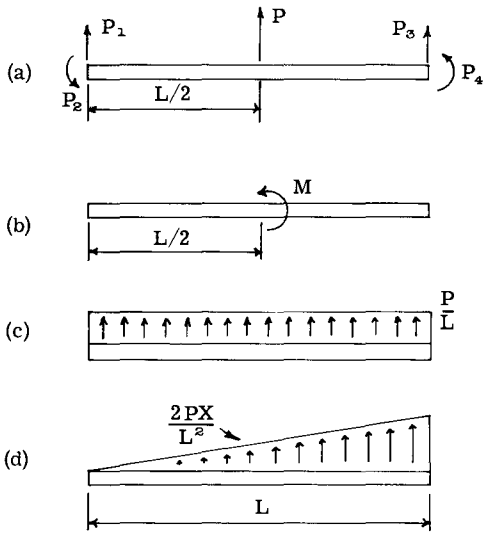

Fig. A23.17

Table A23.5

Case	P_1	P_2	P_3	P_4
(a) Concentrated Force at Midspan	P/2	PL/8	P/2	-PL/8
(b) Concentrated Moment at Midspan	$-\frac{3M}{2L}$	$-\frac{M}{4}$	$\frac{3M}{2L}$	$-\frac{M}{4}$
(c) Uniform Load	P/2	PL/12	P/2	-PL/12
(d) Triangular Load	3P/10	PL/15	7P/10	-PL/10

Note that these nodal forces are related to the fixed end moments used in the moment distribution method of Chapter All. The moments P_2 and P_4 are fixed end moments, while the reactions P_1 and P_3 may be obtained by statics. For other cases of interest, the reader is referred to the information displayed in Chapter All, Table All.1, herein, from which the appropriate nodal forces can be derived. Loadings not appearing in the table can often be obtained by superimposing the given cases.

A23.10 Structural Modeling Using Finite Elements

The process of structural modeling occurs at several levels of abstraction during the course of any design. Typically, one first has a conceptual model, selecting the type of structure necessary to transmit the applied loads from among many possibilities, including trusses, cables, frames, arches, and shells. A more detailed model is necessary when making the design drawings. One must detail connections and brackets, size members based on available sheet metal gages, and rolled or extruded sections, actual material properties, etc. An analytical model is required as well, relating to both the conceptual and detail models, and reducing the structure to a properly formulated mathematical problem. The numbers produced by the solution of the mathematical problem are then used to verify the design concept and to provide a rational basis for redesign, where necessary. Finite element modeling is one method for producing a mathematical description of the structure. The next two sections comprise several representative example problems, intended to provide the reader with an appreciation for the nature of typical finite element models and the kinds of results which can be obtained with them.

Example Problem 4

Reconsider the truss of Fig. A7.16, reproduced in Fig. A23.18. A truss is defined as a pinned structure wherein moments are not transmitted between members at the joints. This idealization is seldom met, and the truss is, in reality, a frame composed of relatively slender members. The structure shown will be reanalyzed as a frame, and the results compared with the truss analysis presented in section A7.7. The previous problem statement does not include data on section properties for the members of the structure. Calculated values have been supplied, based on a plausible design philosophy. Assuming that the material is aluminum, having a modulus of elasticity $E = 10^7$ psi, member areas can be found from Table A7.3. A typical aircraft I section is shown in Fig. A23.19, along with dimensions given in terms of the material thickness. For this section, we have

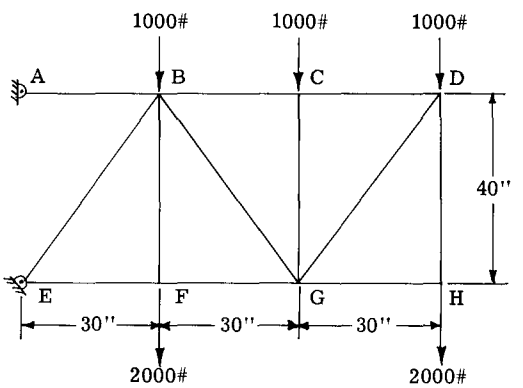

Fig. A23.18

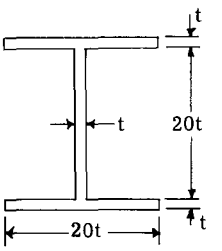

Fig. A23.19

the relationships

$$A = 60\,t_2 \quad \text{- - - - - - - - - - - - - - - -} \quad (75)$$

and $$I = 5080\,t^4 \quad \text{- - - - - - - - - - - - - - -} \quad (76a)$$

or $$I = 1.439\,A^2 \quad \text{- - - - - - - - - - - - - -} \quad (76b)$$

which have been used to calculate the moments of inertia given in Table A23.6.

Table A23.6

Member	L in.	A in.^{2}	I in.^{4}	S_{truss} lb.	S_{frame} lb.	M_{frame} in.-lb.
AB	30	0.4785	0.323	10500	10500	208
BC	30	0.3074	0.130	2250	2262	692
CD	30	0.3074	0.130	2250	2244	95
EF	30	0.5365	0.406	-5250	-5239	732
FG	30	0.5365	0.406	-5250	-5225	204
GH	30	0.348	0.171	0	10	355
BE	50	1.015	1.45	-8750	-8728	805
BG	50	0.348	0.171	5000	4939	120
DG	50	0.5365	0.406	-3750	-3723	86
BF	40	0.3074	0.130	2000	1981	348
CG	40	0.3074	0.130	-1000	- 965	387
DH	40	0.3074	0.130	2000	1980	252

A finite element model of the structure has been used, with each member represented by a six by six stiffness matrix. This stiffness matrix is found by combining results of cases A and C of section A23.4 to provide the relation between forces and displacements in one rotational and two translational coordinates at each end of the member. There are 12 elements in the structure, connected at eight nodal points. Thus the connectivity conditions at the joints produce a reduction from 72 element coordinates to 24 system coordinates. Finally, applying two boundary conditions each at nodes A and E, one finds there are 20 generalized coordinates for this analysis. The system description and loads were read into a digital computer, programmed to solve the problem using the method of Gaussian elimination.

The results of the analysis are shown in Table A23.6. The effect of neglecting end fixity is slight for the axial forces. However, the inclusion of induced bending moments in the calculation of outer fiber stresses produces large differences for several members. For example, the maximum stress in member BC is given by (S/A) = 7320 psi for the truss analysis and by (S/A) + (Mc/I) = 11540 psi for the frame analysis, a difference of 58 per cent. The structural designer must be aware of the possibility of this effect, and examine its significance for the particular structure being analyzed.

Example Problem 5

The redundant portal frame of Fig. A23.20 is to be analyzed by the method of displacements.

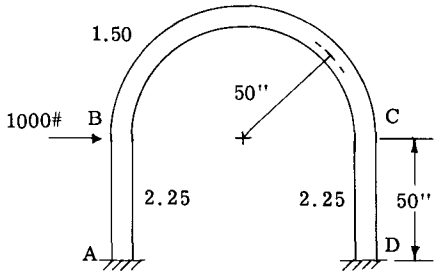

Fig. A23.20

The relative bending stiffnesses of the segments are given on the figure. The frame is modeled using beam elements, whose stiffness properties are given by case C of section A23.4. The curved portion of the frame is approximated by 30 straight beam elements (chords), connecting equally spaced nodal points located on the elastic axis of the curved portion. Here the model contains 32 elements, and, after accounting for connectivity and boundary conditions, there are 93 generalized coordinates in the system. A computer solution was performed, again using the Gaussian elimination method. As a check, the computed values of reactions at point A have been compared with results of an analysis given in section A8.2.2. The equations obtained in Chapter A8 are satisfied by the values M = -27650 in.-lb., V = 801.3 lb., and T = 114.6 lb., with the sign conventions given in Fig. A8.3g,h, i. The comparison is given in Table A23.7, along with results for three other models, involving 15, eight, and four beam elements to approximate the curved portion of the portal frame, and one element for each column.

Table A23.7

Model	M_A in.-lb.	V_A lb.	T_A lb.
Analytical (Sec. A8.2.2)	-27650	801.3	114.6
32 elements	-27627	801.13	114.92
17 elements	-27589	800.68	115.34
10 elements	-27461	799.19	116.78
6 elements	-26955	793.29	122.78

The bending moment is plotted as a function of position on the frame in Fig. A23.21. This gives a good approximation for the spatial variation of outer fiber stresses, since bending is the predominant type of deformation in this problem.

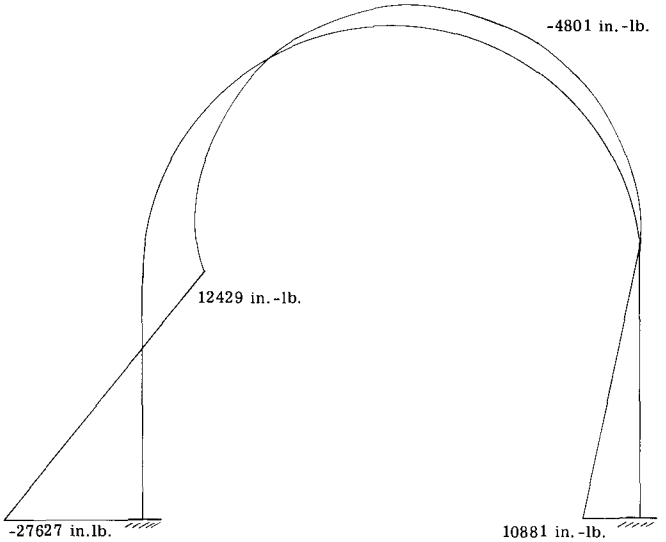

Fig. A23.21

Example Problem 6

The thick walled pipe of Fig. A23.22 is to be modeled using finite elements. The dimensions of the pipe are ℓ = 24 in., r_i = 4 in., and r_o = 10 in.

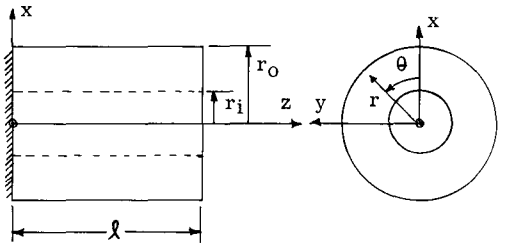

Fig. A23.22

An applied shear load acts at the free end of the pipe with the resultant force parallel to the x axis. The model consists of annular elements having a square cross section. A typical element and its associated coordinates are shown in Fig. A23.23. The stress components are also defined in Fig. A23.23. (For a more detailed discussion, see Chapter A24). Two grid sizes are used in the analysis, as shown in Fig. A23.24.

The loading is applied by means of equivalent shear stresses (τ_{zr} and $\tau_{z\theta}$) acting in the

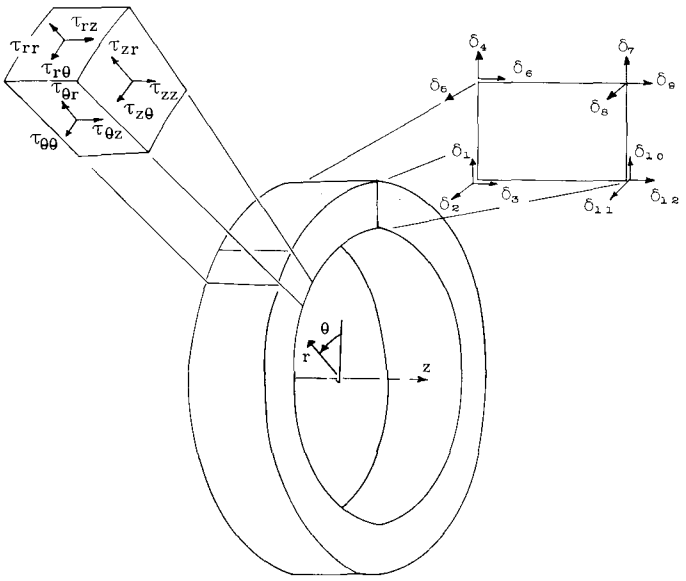

Fig. A23.23

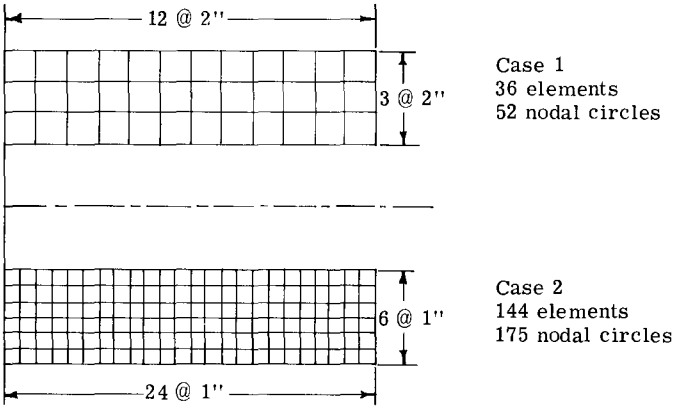

Fig. A23.24

plane of the free end. These end stresses were set equal to the theoretical values at the centers of the element faces for a resultant shear load of 4200π lb., equivalent to an uniform vertical shear stress of 50 psi. The interior stress distributions have been derived from the theory of elasticity (7) and are plotted along with computed values in Fig. A23.25 and A23.26. Reported values for each station represent averages of values for the adjacent elements, referred to the midpoint of the bounding face. In the derivation of these theoretical values, the nature of the end condition at the wall is neglected. Thus, the two results should show good agreement at intermediate stations, but not near the wall. These features are observed in Figs. A23.25 and A23.26. Near the wall, the finite element model gives more realistic stress values, based on the actual boundary conditions. This is often true, especially in cases where the

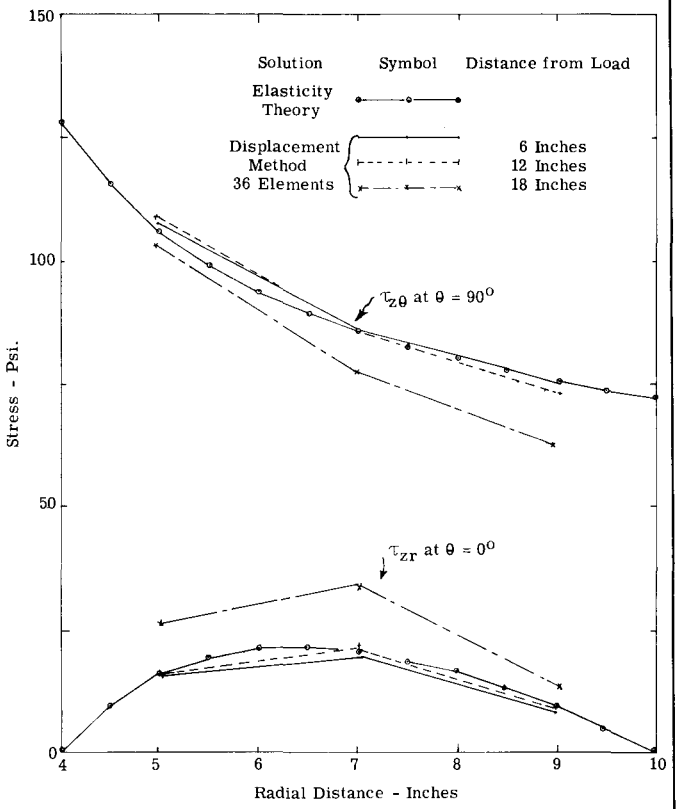

Fig. A23.25

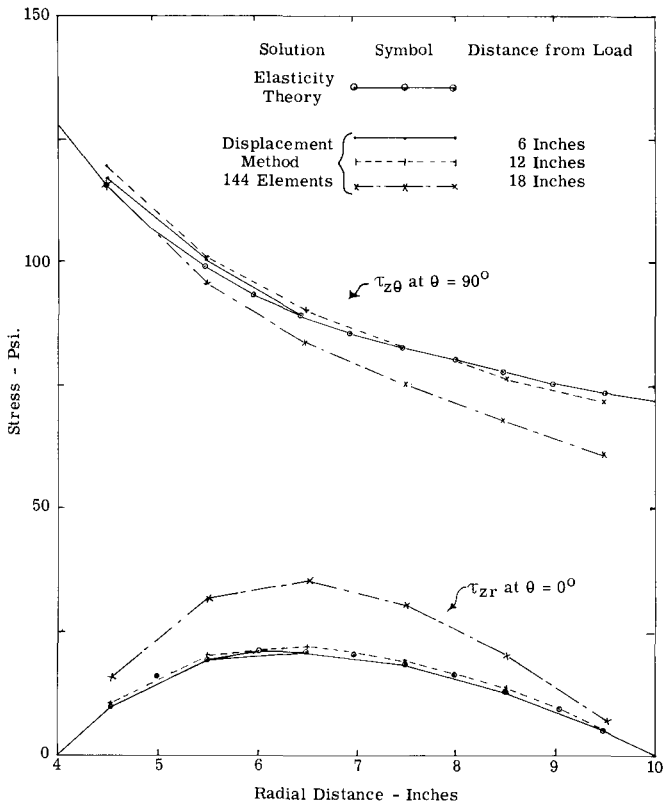

Fig. A23.26

system is sufficiently complex to preclude an analytical solution in closed form. Note that the coarser nodal grid gives results comparable in accuracy to those achieved with the refined division using 144 elements. The decision regarding how many elements to use must be based on experience with comparative studies of this sort.

A23.11 A Delta Wing Example Problem*

The idealized delta wing structure of Fig. A23.27 will be analyzed to determine the influence coefficients and the internal stresses as functions of the applied loads. This problem will also illustrate the use of substructures in analysis.

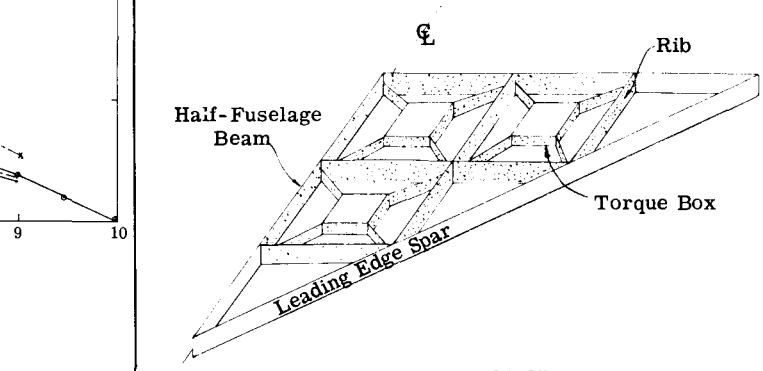

Fig. A23.27
Idealized Delta Wing Structure

IDEALIZATION

The delta wing has been idealized into a grid-like structure having grid points numbered as in Fig. A23.28. Grid numbers increase to the rear and outward.

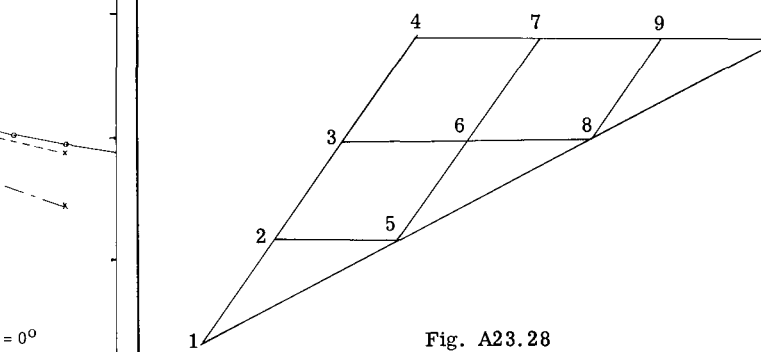

Fig. A23.28
Grid Numbering Scheme

The torsional stiffness of the wing's shear-carrying cover sheet is accounted for by the presence of quadrilateral "torque boxes" connecting points of intersection of the spars and ribs. The resistance of a torque box having a corner at, say, point 6 of the grid (e.g., box

* By Alfred F. Schmitt

6-7-8-9) is a result of the tendency for the box to keep all four corners in the same plane. Obviously, three-cornered "boxes" have no such resistance; hence none are shown in Fig. A23.27.

In the structure under consideration member 1-2-3-4 lies on the airplane centerline. The bending stiffness of this member includes that of the half-fuselage plus one-half of the "carry-through structure." More detailed representations of the structure in this region are generally desirable, the oversimplified model used here being employed to limit the amount of data to be handled. Some techniques which may be applied in idealizing the structure in this region are given in Reference (11)

Idealization, particularly with regard to effective skin areas, has been discussed in some detail by Levy (8). The complexities of this phase of the problem are too great to permit an expansive treatment here.* Briefly, Levy's recommendations are:

(a) all skin may be considered effective between spanwise spars when computing the cap areas of such spars. This assumption is subject to modification, of course, if spanwise stresses are anticipated which will buckle the skin.

(b) for streamwise ribs an effective width of 0.362L, where L is the rib length, may be taken as acting with each rib cap (Fig. A23.29a).

(c) for the leading edge spar an effective width of skin of .181 of the span between spanwise spars is taken as acting with the cap of each such spar segment (Fig. A23.29b).

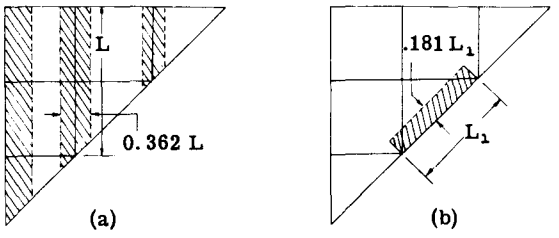

Fig. A23.29

Effective Widths of Cover Sheet for Rib and Oblique Spar Caps (After Levy, Ref. 8)

* A rational, systematic means of treating cover sheet panels is given in Reference 10).

STRUCTURAL PROPERTIES SUMMARIZED

The properties of the structure (Fig. A23.27) after idealization, are summarized as follows:

Net Point (see Fig. A23.28)	Beam Depth (inches)
1	5.56
2	9.12
3	7.80
4	3.16
5	4.88
6	7.26
7	3.06
8	4.02
9	2.74
10	0.72

All cover skin t = .051"

BEAM ELEMENT PROPERTIES

(Moments of inertia, in (inches^4), are assumed to vary linearly between numbered points)

1/2 Fuselage Beam (1-2-3-4)

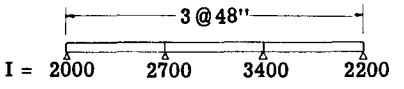

Spar 2-5

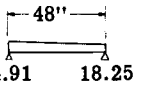

Rib 5-6-7

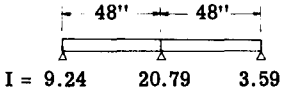

Spar 3-6-8

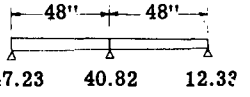

Rib 8-9

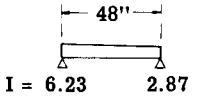

Spar 4-7-9-10

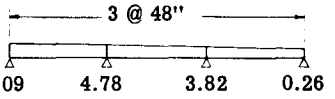

Leading Edge Spar (1-5-8-10)

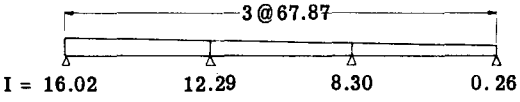

SIGN CONVENTION

The sign convention adopted in conjunction with the grid numbering scheme of Fig. A23.28 is as follows:

Element Forces, P_m

Transverse Force at a joint,

+ UP

or, Pitching Moment at a joint,

+ NOSE DOWN

or, Rolling Moment at a joint,

+ RIGHT WING DOWN

or, Moment on an Oblique Member,

acting in the plane of that member,

+ COUNTER CLOCKWISE WHEN THE MEMBER IS VIEWED WITH ITS JOINT NUMBERS INCREASING LEFT TO RIGHT.

Element Displacements, δ_m

Follow same numbering and sign convention as do corresponding forces.

With the above sign convention any beam element (spar or rib) which is viewed so that its joint numbers increase left to right will have forces and displacements taken in a sense compatible with the beam element tabulations of Sec. A23.4.

CALCULATION OF ELEMENT STIFFNESSES

The element stiffness matrices are computed next for the beam segments and torque boses. For the beam segments the equations of Case D, Sec. A23.4 are used. The torque boxes are treated expressly, below.

Beam Segment Stiffness Matrices

For the beam segments the spar between grid points 2 and 5 typifies the calculation. From the beam element properties given earlier, and Fig. A7.34C

$$I_i/I_j = 0.281$$
$$\phi_{ii} = 0.670$$
$$\phi_{ij} = 0.480 \qquad \phi_{ij}/2 = 0.240$$
$$\phi_{jj} = 0.370$$

Then $D_{2-5} = (0.670)\,(0.370) - (0.240)^2 = 0.1903$

and $$\left[k_{2-5}\right] = \begin{bmatrix} 0.003954 & 0.1136 & -0.003954 & 0.07616 \\ 0.1136 & 4.015 & -0.1136 & 1.438 \\ 0.003954 & -0.1136 & 0.003954 & -0.07616 \\ 0.07616 & 1.438 & -0.07616 & 2.217 \end{bmatrix}$$

where we have taken E = 1 for convenience. It is understood that forces and displacements of the beam element (spar 2-5) are applied in positive sense and arrayed in numeric order as in Case D, Sec. A23.4, when the beam element is viewed with grid numbers increasing left to right.

In like manner, the element stiffnesses for the remaining fourteen (14) beam segments (spar, rib and leading edge spar segments) are computed. They are not tabulated here for reasons of space conservation.

Torque Box Stiffness Matrices

In the case of the torque boxes, the stiffness matrices may be computed directly (they are determinate). The following approximate analysis is suggested as being satisfactory for most torque boxes. A more detailed analysis may be in order for boxes with extreme geometries. An alternate method is presented in Reference (8) and an appropriate discussion may be found in Reference (12). A completely different treatment of the cover skin is given in Reference (10).

Consider the quadrilateral box of Fig. A23.30.

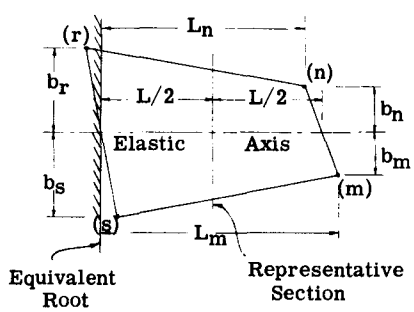

Fig. A23.30

For purposes of this immediate analysis, the box is considered cantilevered from one end, such as r-s. An elastic axis (e.a.) is assumed to exist midway between the long sides and an "effective root" is employed. The torque on the box is

$$T = P_m\, b_m - P_n\, b_n$$

An (assumed) average rate of twist, θ, is computed approximately by using the GJ at a representative section half way along the box.*

$$\theta = \frac{T}{GJ} = \frac{P_m b_m - P_n b_n}{GJ}$$

Then the deflection δ_n and δ_m are given by

$$\delta_n = \theta L_n b_n = \frac{P_m b_m - P_n b_n}{GJ} L_n b_n$$

$$\delta_m = \theta L_m b_m = \frac{P_m b_m - P_n b_n}{GJ} L_m b_m$$

By summing moments about the effective root, P_n is found in terms of P_m and then eliminated from the above equations to give

$$\delta_n = \frac{P_m L_n b_n}{GJ} \quad \frac{L_n b_m + L_m b_n}{L_n}$$

$$\delta_m = \frac{P_m L_m b_m}{GJ} \frac{L_n b_m + L_m b_n}{L_n}$$

Since it is only the deflection of one corner (say, point m) which is to be related to the corner reactions, the box is now rotated about the effective root axis to reduce δ_n to zero. The resulting total deflection of point m is

$$\delta_{m_{TOTAL}} = \delta_m + \frac{L_m}{L_n}\delta_n$$

$$= \frac{P_m L_m}{GJ}\left(\frac{L_n b_m + L_m b_n}{L_n}\right)(b_n + b_m)$$

Re-solving this, we write

$$P_m = \frac{GJ}{L_m(b_n + b_m)} \quad \frac{L_n}{(L_n b_m + L_m b_n)}$$

This last expression relates the load at point m to the deflection at that point, with the other three corners undeflected. Thus the deflection of point m as defined was relative to the plane m n r s. This relative displacement may be related by geometry to the case where all four corners are displaced (in effect, removing the rigid body displacements).

$$\delta_{m_{relative}} = \begin{bmatrix} 1 & -L_m/L_n & A_1 & A_2 \end{bmatrix} \begin{Bmatrix} \delta_m \\ \delta_n \\ \delta_r \\ \delta_s \end{Bmatrix}$$

where

$$A \equiv \frac{L_n b_m + L_m b_n + b_s (L_m - L_n)}{L_n (b_r + b_s)}$$

$$A \equiv \frac{-(L_n b_m + L_m b_n) + b_r (L_m - L_n)}{L_n (b_r + b_s)}$$

This last relation corresponds to Equation 17 of this chapter. Then using equation 26 we obtain the square stiffness matrix

$$\begin{matrix} & mnrs \\ m \\ n \\ r \\ s \end{matrix} \begin{bmatrix} K \end{bmatrix} = \frac{GJ\ L_n/L_m}{(L_n b_m + L_m b_n)(b_n + b_m)} \begin{Bmatrix} 1 \\ -L_m/L_n \\ A_1 \\ A_2 \end{Bmatrix} \begin{bmatrix} 1 & -\frac{L_m}{L_n} & A_1 & A_2 \end{bmatrix}$$

In the above derivation the torsional stiffness GJ at a representative section is used. The stiffness is obtained from Bredt's equation for the twist of a single cell thin-walled tube (Eq. 18, Chapter A6)

$$\theta = \frac{T}{4A^2 G} \oint \frac{ds}{T}$$

from which, by definition

$$GJ = \frac{4A^2 G}{\oint \frac{ds}{T}}$$

Here A is the area enclosed within the tube cross section by the median line of the tube wall and the integration is carried out around the tube perimeter (index s gives distance along the perimeter). For the torque boxes encountered in delta wings it is probably satisfactory to neglect the ds/t contribution from the vertical webs, it being small compared with the corresponding contribution from the cover sheets.

In the example wing three boxes (2-3-5-6, 3-4-6-7 and 6-7-8-9) are to be used. These boxes are each 48 inches square in plan and have average depths (assumed here to be the uniform depths of the representative sections) of 7.26", 5.32" and 4.27", respectively. Fig. A23.31 shows the assumed representative cross section of box 2-3-5-6 and its GJ calculation.

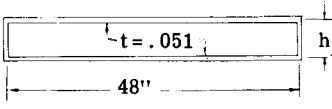

$A = 7.26 \times 48 = 348 \text{ in}^2$

$$\oint \frac{ds}{t} = 2 \times \frac{48}{.051} = 1.88 \times 10^3$$

Note: $G = \frac{E}{2.6}$

$$GJ_{E=1} = \frac{4(348)^2 \cdot 1}{1.88 \times 10^3 \times 2.6} = 99.3 \text{ lb. in.}^2$$

(ds/t contribution of vertical webs neglected)

Fig. A23.31

Calculation of GJ for the Representative Section of Box 2-3-5-6

In similar fashion one finds:

For box 3-4-6-7

$GJ_{E=1} = 53.3$

* Calculation of this GJ is discussed later.

For box 6-7-8-9

$$GJ_{E=1} = 34.3$$

Finally, the stiffness matrices for the three boxes of the example become:

For box 2-3-5-6

$$[K] = 0.000898 \begin{bmatrix} 1 & -1 & -1 & 1 \\ -1 & 1 & 1 & -1 \\ -1 & 1 & 1 & -1 \\ 1 & -1 & -1 & 1 \end{bmatrix}$$

For box 3-4-6-7

$$[K] = 0.000482 \begin{bmatrix} 1 & -1 & -1 & 1 \\ -1 & 1 & 1 & -1 \\ -1 & 1 & 1 & -1 \\ 1 & -1 & -1 & 1 \end{bmatrix}$$

For box 6-7-8-9

$$[K] = 0.000310 \begin{bmatrix} 1 & -1 & -1 & 1 \\ -1 & 1 & 1 & -1 \\ -1 & 1 & 1 & -1 \\ 1 & -1 & -1 & 1 \end{bmatrix}$$

SYSTEM DISPLACEMENTS/TRANSFORMATION OF COORDINATES

The element displacements of the foregoing element stiffness matrices may now be related to (transformed to) the system displacements chosen for the overall wing structure. Fig. A23.32 shows the system displacements which may be chosen.

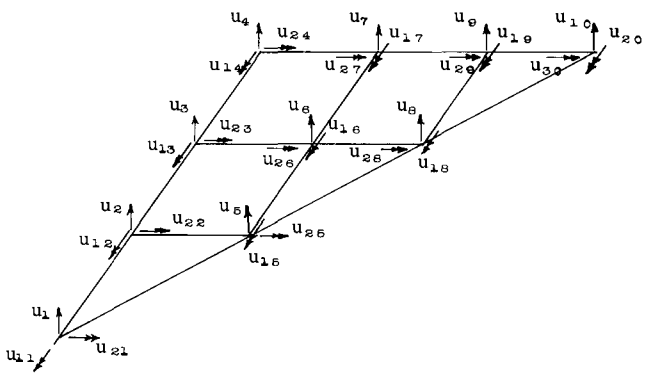

Fig. A23.32

Delta Wing System Displacements.
All rotations positive by right-hand rule.

One now writes the relations which transform the displacements. As an example, one writes

$\beta_{2-5} =$

δ \ u	1	2	3	4	5	6	-----	11	12	13	14	15	16	-----	--29	30
1	0	1	0	0	0	0	-----	0	0	0	0	0	0	----	0	0
2	0	0	0	0	0	0	-----	0	1	0	0	0	0		0	0
3	0	0	0	0	1	0	-----	0	0	0	0	0	0		0	0
4	0	0	0	0	0	0	-----	0	0	0	0	1	0		0	0

Then

$$[K_{2-5}] = \beta'_{2-5}\, k_{2-5}\, \beta_{2-5}$$

$=$

	2	5	12	15
2	.003850	-.003850	.1108	.07404
5	-.003850	.003850	-.1108	-.07404
12	.1108	-.1108	3.929	1.387
15	.07404	-.07404	1.387	2.167

Here for economy we have written only the non-zero terms of the transformed element stiffness matrix. These simple transformations, involving no coordinate rotations may be written by inspection since obviously, for element 2-5

$$\delta_1 \longrightarrow u_2$$
$$\delta_2 \longrightarrow u_{12}$$
$$\delta_3 \longrightarrow u_5$$
$$\delta_4 \longrightarrow u_{15}$$

For the leading edge spar there are geometric transformations. Thus, for element 1-5,

$\beta_{1-5} =$

δ \ u	1	5	11	15	21	25
1	1	0	0	0	0	0
2	0	0	.707	0	.707	0
3	0	1	0	0	0	0
4	0	0	0	.707	0	.707

where, again, only displacements having non-zero entries are shown explicitly.

Then

$$K_{1-5} = \beta'_{1-5}\quad k_{1-5}\quad \beta_{1-5}$$

$=$

	1	5	11	15	21	25
1	.0005295	-.0005295	.01326	.01214	.01326	.01214
5	-.0005295	.0005295	-.01326	-.01214	-.01326	-.01214
11	.01326	-.01326	.4361	.2004	.4361	.2004
15	.01214	-.01214	.2004	.3821	.2004	.3821
21	.01326	-.01326	.4361	.2004	.4361	.2004
25	.01214	-.01214	.2004	.3821	.2004	.3821

Proceeding in the above manner, stiffness matrices for all 15 beam elements are transformed. The torque boxes are already in "system" coordinates since each was designated by the grid numbers of its four corners.

ANALYSIS BY SUBSTRUCTURES

From this point on the analysis proceeds in a very direct manner as previously illustrated. However, as is also apparent, any large structure having many nodal points is going to yield a very high order matric equation when analyzed in such a completely elemental fashion.

It is possible, however, to reduce the order of the problem by some preliminary recombining of the elements into substructures in the course of which one can

(a) use certain a priori information to eliminate some loads (and corresponding displacements)

(b) extract some portions of the problem out of the main calculation, putting them into subproblems solved on the substructures.

These devices will be employed in the following section.

Certain of the external loads associated with the displacements of Fig. A23.32 are known to be zero by nature of the load modeling used in this problem. Thus, only transverse forces, F_6 through F_{10}, are to be applied as loads at the wing grid points, reacted by transverse loads F_1 through F_4 and rolling moments F_{11} through F_{14} along the airplane centerline.

For this structure and this loading it is then known a priori that many element loads are zero. For example, there can be no couples on the beam elements at grid point 10*. It is, in effect, as if this joint was a pin joint and only its translation was considered.

Many element loads are not zero but need not be solved for explicitly in the main problem if they can be computed subsequently by analysis of a substructure within which they are subsumed. For example, the bending moments on the beam elements 7-9 and 9-10 meeting at grid point 9 are equal and may be found easily once the transverse element load at point 10 is found on span 9-10. This situation suggests that a single beam, continuous across grid point 9, be used instead of the separate elements.

The substructures selected for this problem, along with their element deflections, are shown in Fig. A23.33. They are the rather natural choices of the continuous wing beams (spars and ribs) with only the minimum necessary deflections considered. While the foregoing reasoning had dealt largely with forces, it is the corresponding element displacements which are used as the variables and are so-shown in the figure.

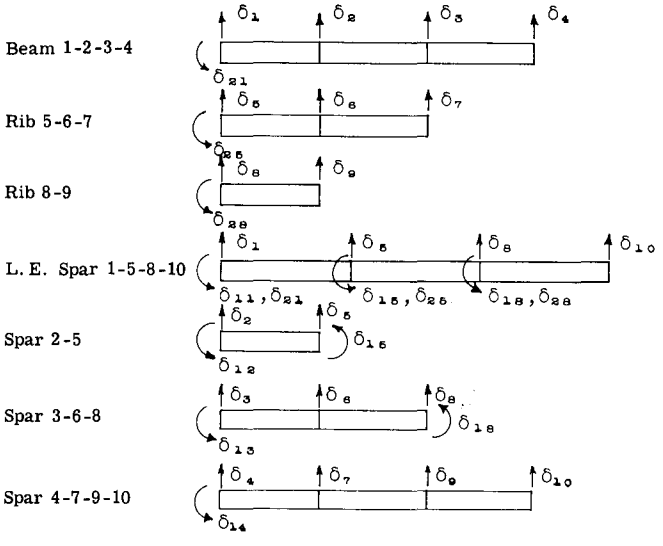

Fig. A23.33

Substructures and Their Element Displacements. Note numbering of displacements has been kept consistent with system numbering of Fig. A23.32.

The substructure of spar 4-7-9-10 illustrates the motivation in the substructure variable choices. It was modeled as shown since it was known there were no applied couples at grid points 7, 9 and 10 and hence the rotational displacements at those points need not be considered. Elimination of variables at no-load points can, of course be done on the final complete system stiffness matrix (obtaining a reduced stiffness matrix per Equation 35). Such a reduction may involve manipulation of very large matrices. Using substructures this reduction process is divided into several smaller, more tractable problems while simultaneously reducing the order of the main problem. The rotational displacements thus eliminated can be easily obtained via a subcalculation, if desired, (ref. Equation 33).

Couples must be considered to act wherever three or more nonorthogonal beam elements

* The implication here is that beam torsional stiffnesses are not considered in such interactions. This assumption is probably quite satisfactory in general, bending stiffnesses being much greater than torsional stiffnesses for most beam elements. On occasion, a beam will have considerable torsional stiffness and it will then be necessary to account for it. The leading edge spar might be such a beam if it replaces the "D" nose section of the wing in the idealization.

intersect to account for their interaction; hence the rotational displacements at grid points 5 and 8 on all ribs and spars intersecting there and at grid point 1. (The other wing half provides the third structure at that point.)

Looking ahead we see a complete system stiffness matrix of 19th order (u_1 through u_{15} plus u_{18}, u_{21}, u_{25} and u_{28}) instead of 30th order. This matrix can be subsequently reduced in order because of five known zero external loads (there are no externally applied moments at the points where the nonorthogonal beams intersect). This reduction will require inversion of a 5th order matrix rather than the 16th order matrix otherwise required to reduce the 30th order problem to an equivalent system of equations.

SUBSTRUCTURE STIFFNESS MATRICES

Calculation of the substructure stiffness matrices follows the procedure established for any structure built up of elements. For example, consider beam 3-6-8 which comprises elements 3-6 and 6-8. The substructure is shown below with all displacements indicated, including δ_{18}, even though it is to be eliminated because the applied load P_{18} is known to be zero.

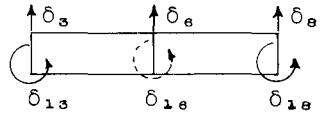

The stiffness matrix is collected from that of each of the elements 3-6 and 6-8.

K_{3-6} =

	3	6	13	16
3	.004746	-.004746	.1166	.1112
6	-.004746	.004746	-.1166	-.1112
13	.1166	-.1166	3.775	1.819
16	.1112	-.1112	1.819	3.521

K_{6-8} =

	6	8	16	18
6	.002558	-.002558	.07305	.04974
8	-.002558	.002558	-.07305	-.04974
16	.07305	-.07305	2.574	.9325
18	.04974	-.04974	.9325	1.455

Adding these together gives

K_{3-6-8}

	3	6	8	13	16	18
3	.004746	-.004746		.1166	.1112	
6	-.004746	.007304	-.002558	-.1166	-.0382	.04974
8		-.002558	.002558		-.07305	-.04974
13	.1166	-.1166		3.775	1.819	
16	.1112	-.0382	-.07305	1.819	6.095	.9325
18		.04974	-.04974		.9325	1.455

(Voids denote zeroes)

The constraint of generalized force u being zero is now applied using Equation 35. The inverse "K_{22}^{-1}" in this instance is merely 1/6.095 and the matrix "K_{21}" is the row (.1112, -.0382, -.07305, 1.819, 0.9325). Applying the equation leads to

K^*_{3-6-8} =

	3	6	8	13	18
3	.002718	-.004049	.001332	.0834	-.0170
6	-.004049	.007065	-.003016	-.1052	.05558
8	.001332	-.003016	.001683	.02179	-.03857
13	.0834	-.1052	.02179	3.232	-.2782
18	-.0170	.05558	-.03857	-.2782	1.312

The foregoing procedure is followed to obtain reduced stiffness matrices for each of the remaining substructures.

COMPLETE WING STIFFNESS MATRIX

The stiffness matrix for the composite wing now may be obtained by forming the sum of the complete stiffness matrices for the beam substructures and the torque boxes. For this purpose a large matric table is laid out and entries from the individual stiffness matrices are transferred into the appropriate locations. Wherever multiple entries occur in a box these are summed.

Before the large wing matrix is laid out it is necessary to observe first that the matrix which would be obtained as just indicated would be singular, i.e., its determinant would be zero, and hence it could not be inverted to yield the flexibility influence coefficients (see Appendix A). This condition arises due to the fact that the equations represented (19 in number in the example problem) are not independent; three of these equations can be obtained as linear combinations of the others.

That there are three such interdependencies may be seen from the existence of the three equations of statics which may be applied to the wing (summation of normal forces and summation of moments in two vertical planes):

hence three of the reactions expressed by the structural equations in the matrix may be found from the others by the equations of statics. To remove the "singularity" from the stiffness matrix it is only necessary to drop out three equations - achieved by removing three rows and corresponding columns (so as to retain a symmetric stiffness matrix).

The act of removing the three equations selected is also equivalent to assuming the corresponding deflections to be zero. In this way a reference base for the deflections is also established. The choice of reference base is somewhat arbitrary, but, following a suggestion of Williams (13), a triangular base will be employed as shown in Fig. A23.34.

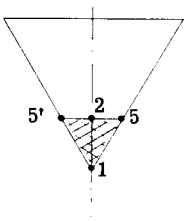

Fig. A23.34

Deflection Reference Base

Here the deflections at points 1 and 5 are zero, fixing the reference triangle, since the point corresponding to 5 in the other half of the wing (say, 5'), will have zero deflection also due to symmetry. The third condition is applied to point 2: point 2 will be assumed to have zero rolling rotation ($u_{12} = 0$) for symmetric wing loadings and to have zero transverse deflection ($u_2 = 0$) for antisymmetric loadings.*

Hence the following equations (rows and columns) are to be omitted from the wing stiffness matrix:

F_1, u_1
F_5, u_5
F_{12}, u_{12}
} for symmetric loadings

F_1, u_1
F_5, u_5
F_2, u_2
} for antisymmetric loadings

The 16 x 16 wing stiffness matrices thus obtained can now be inverted as they are nonsingular. However, if this step is carried out one finds that the resultant influence coefficients are those for only the half-wing acting alone and supported by constraints as assumed above. To account for the presence of the other half of the wing, it is necessary to specify additional geometric conditions along the airplane centerline. This step is accomplished by assuming the following deflections zero (eliminating their corresponding rows and columns from the matrix):

u_{11}
u_{13}
u_{14}
} for symmetric loadings (zero lateral slope or rolling rotation along the airplane centerline)

u_3
u_4
u_{21}
u_{22}
u_{23}
u_{24}
} for antisymmetric loadings (zero transverse deflections and pitching rotations along the airplane centerline

It will be seen that in both cases additional equations are eliminated from the 16 x 16 matrices further reducing them. In general there is no reason why the matrices for the symmetric and antisymmetric cases have to be the same size since the modeling of applied loads is not the same in these cases (for example, no forces F_1, F_2, F_3 or F_4 are applied in an antisymmetric loading).

Written below is the 13 x 13 wing stiffness matrix for the symmetric case ($u_1 = u_5 = u_{11} = u_{12} = u_{13} = u_{14} = 0$). As explained earlier, each entry therein is the sum of all corresponding stiffnesses for all elements meeting at the point. A typical multiple entry occurs for joint 6 - (row F_6, column u_6). These comprise:

0.007065	from spar 3-6-8
0.001730	from rib 5-6-7
0.000310	from box 6-7-8-9
0.000898	from box 2-3-5-6
0.000482	from box 3-4-6-7
0.010485	TOTAL

* The antisymmetric loading pattern is one wherein the wing is loaded equally, but in opposite sense, on corresponding points of the two wing halves. Any general loading may be resolved into the sum of one symmetric and one antisymmetric loading.

$K_{Wing\ Symm.}$ =

	u_2	u_3	u_4	u_6	u_7	u_8	u_9	u_{10}	u_{15}	u_{18}	u_{21}	u_{25}	u_{28}
F_2	0.4299	-.2670	.07314	.000898					.07616		-5.393		
F_3	-.2670	.2753	-.1027	-.005429	.000482	.001332				-.01700	1.449		
F_4	.07314	-.1027	.04629	.000482	-.0009328		.0001586	-.00002122			-.2450		
F_6	.000898	-.005429	.000482	.010485	-.001380	-.003326	.000310			.05558		-.02658	
F_7		.000482	-.0009328	-.001380	.001776	.000310	-.0006789	.00008089				.004706	
F_8		.001332		-.003326	.000310	.002564	-.0004515	-.0000499	-.009686	-.04470		-.009686	.000664
F_9			.0001586	.000310	-.0006789	-.0004515	.0007662	-.0001045					-.006796
F_{10}			-.00002122		-.00008089	-.0000499	-.0001045	.0000947		-.002394			-.002394
F_{15}	.07616					-.009686			2.9213	.1425	.2004	.7043	.1425
F_{18}		-.0170		.05558		-.04470		-.002394	.1425	1.6937		.1425	.3817
F_{21}	-5.393	1.449	-.2450						.2004		155.44	.2004	
F_{25}				-.02658	.004706	-.009686			.7043	.1425	.2004	1.5285	.1425
F_{28}						.000664	-.006796	-.002394	.1425	.3817		.1425	.7078

REDUCED WING STIFFNESS MATRIX

The wing stiffness matrix as derived above contains all the necessary geometric constraints to represent correctly the wing behavior under a symmetric loading. It may, however, be further reduced by the application of certain zero-loading constraints which exist purely because of the external load modeling used. Specifically, the load modeling sets the couples F_{15}, F_{18}, F_{21}, F_{25} and F_{28} equal to zero. Hence Equation 35 may be used to derive a reduced matrix. This reduced matrix offers the advantages of simpler handling if the further computing tasks of deriving wing influence coefficients (by inverting the wing stiffness matrix) and internal wing stresses (i.e., specific element loads) are undertaken.

A23.12 Accuracy, Convergence and Error Bounds

We have to deal with two kinds of accuracy; first, the accuracy associated with the finite element model; and second, the accuracy associated with the numerical solution, once a model has been chosen. It is worth pointing out that the results although given by the computer to many decimal places may be useless, due to a conceptual defect in the model, or a computational defect in the solution.

Of the two processes, that of choosing a finite element model is more dependent on experience and judgment. For some types of elements, convergence to an exact (theory of elasticity or continuous) solution is assured by taking a sequence of models with more and more (smaller) elements. Example problems 5 and 6 illustrate this situation. It may be worthwhile to bound the desired result by considering limiting, simpler problems with similar boundary conditions. In regions of high stress and strain gradients, extreme care must be taken in modeling and interpretation of results, to assure obtaining useful values of stress and deflection.

Concerning the numerical solution, the stiffness matrix derived from the displacement method is a positive definite symmetric matrix, for which nontrivial, unique solutions can be guaranteed a priori. The real difficulty lies in finding a computationally efficient algorithm for determining these solutions.

Several methods have been illustrated in the example problems of this chapter, including direct solution by inverting the stiffness matrix (example problem 1) or by Gaussian elimination (example problem 3), and solution by iteration with a Gauss-Seidel algorithm (example problem 2). As a rule of thumb, direct solution is best for small, fully populated matrices, while both types of solution are used for large, sparsely populated matrices. The preferred method of solution, and the demarcation between large and small problems varies from authority to authority, and in fact, the choice of method may be overriden at a given facility by a reliable, debugged procedure of either type. Problem bookkeeping should be optimized as well. For example, where possible, modes should be numbered to produce a banded stiffness matrix to minimize storage requirements.

Certain practical measures may be employed to facilitate numerical calculation. In the case of one or more extremely stiff elements, associated coordinates can be eliminated (as in example problem 2) to yield better conditioning of the problem.

Computational errors arise from two sources, termed roundoff error and truncation error. Roundoff error occurs because a finite number of digits are carried in the calculations; double precision arithmetic is often necessary to avoid loss of significant figures. In some algorithms, the order of operations is altered by interchanging pairs of rows and columns, again to avoid loss of significant figures in subtraction and achieve better accuracy. Truncation error is typically associated with iteration methods, whose

accuracy is assured only by completing an infinite number of steps. By terminating the calculations after a finite number of iterations, we produce a truncation error. Further error may be produced if the matrix coefficients are obtained empirically. Placing bounds on the errors is a difficult but important part of the calculation procedure. For details, the reader is referred to texts on the subject of numerical analysis (5,6).

A23.13 Management of Problem for the Computer

A discussion of the management of a structural problem for solution on an electronic digital computer could easily occupy a separate book. We will be content here to give the reader a checklist of topics which can be considered as a guide to the questions he should consider and discuss with a computer consultant. It is assumed that the desirability and feasibility of performing a computer analysis have already been determined, and the analytical approach has been selected.

At this point the key factor is the cost of the calculation for a given degree of accuracy. The method employed, and thus the cost will be intimately related to the rate structure at the local computer facility. Often costs not central to the computation are the controlling ones. A typical charge rate includes central processor unit time, number of input-output requests, and required storage region size. Other factors, such as cost of cards and printed output, tape and disk storage charges, graphic plotter usage, etc., may be prorated or charged directly. For a given computer, one of the elements of the rate structure generally dominates the programming strategy. Earlier in the evolution of computers, processing time and storage were the limiting factors. With improvements in these areas, current computer technology is often bound by input-output limitations. In addition to cost considerations, the possibility of committing a blunder in data inputting has led to use of special data generation routines and checking programs. Graphical output is especially useful in detecting errors in nodal point location and in checking element definitions. Because of input-output costs, it is desirable to keep as much of the program in core storage as possible. The cost of storing and fetching information may exceed the cost of regenerating data by a factor of ten, twenty, or more. When moving data in and out of the central processing unit, the format used can have a critical influence on cost. It is often advantageous to transfer many record lines at a time using the simplest format definition available.

Every program contains errors or bugs which must be discovered and corrected before reliable production runs can be performed. Use of on-line terminals operating on a time-sharing system is an efficient way to debug, as it eliminates most of the waiting time between runs. This is especially useful during the initial runs to discover spelling and syntax errors. Often a machine failure will terminate a run before completion. It is desirable to output intermediate results so that something is learned from every run. The amount of running time for each portion of the program can be checked easily, and can pinpoint those parts of the calculations where reprogramming would be most productive.

Once a program is ready for production, it should be compiled and stored on tape or disk in machine language rather than FORTRAN or PL/I. This will save considerable time per run. Where possible, established, widely used programs should be used; with a new program debugging represents a significant proportion of the work required to produce results. However, one must beware of poorly documented programs; the cost of the learning cycle could easily exceed the cost of writing and debugging a new program.

REFERENCES

(1) Rubinstein, M. F., Structural Systems - Statics, Dynamics and Stability, Prentice-Hall, Englewood Cliffs, N. J., 1970.

(2) Rubinstein, M. F., Matrix Computer Analysis of Structures, Prentice-Hall, Englewood Cliffs, N. J., 1966.

(3) Przemieniecki, J. S., Theory of Matrix Structural Analysis, McGraw-Hill, New York, 1968.

(4) Zienkiewicz, The Finite Element Method in Structural and Continuum Mechanics, McGraw-Hill, Ltd., London, 1967.

(5) Crandall, S. H., Engineering Analysis, McGraw-Hill, New York, 1956.

(6) Ralston, A., A First Course in Numerical Analysis, McGraw-Hill, New York, 1965.

(7) Sokolnikoff, I. S., Mathematical Theory of Elasticity, McGraw-Hill, New York, 1956.

(8) Levy, S., Structural Analysis and Influence Coefficients for Delta Wings, Journal of the Aeronautical Sciences, 20, 1953.

(9) Schuerch, H., Delta Wing Design Analysis, Society of Automotive Engineers National Aeronautic Meeting Preprint No. 141, September, 1953.

(10) Turner, M. J., Clough, R. W., Martin, H. C., and Topp, L. J., Stiffness and Deflection Analysis of Complex Structures, Journal of the Aeronautical Sciences, 23, September, 1956.

(11) Kroll, W., Effect of Rib Flexibility on the Vibration Modes of a Delta Wing Aircraft, Institute of Aeronautical Sciences, Preprint No. 585, 1956.

(12) Wooley, Ruth, Check of Method for Computing Influence Coefficients of Delta and Other Wings, National Bureau of Standards Report 3655, 1954. (Available as ASTIA No. AD46866).

(13) Williams, D., Recent Developments in the Structural Approach to Aeroelastic Problems, Journal of the Royal Aeronautical Society, 58, 1954 (see also, Aircraft Engineering, 25, 1954).

INTRODUCTION TO
THE THEORY OF ELASTICITY AND THERMOELASTICITY

BY

R. J. BOLLARD, Ph.D.

CHAPTER A24
THE 3-DIMENSIONAL EQUATIONS OF THERMOELASTICITY

A24.1 Assumptions: There are two most important assumptions in the classical theory of elasticity concerning the state of an elastic body throughout its volume.

(i) The material is homogeneous.

(ii) The material is isotropic.

The first requires that the elastic body possess the same material properties at all points throughout its volume and on the surface. When homogeneity does not exist, such as in the case of an inclusion of foreign material or of a laminated structure of different material in each lamination, the mechanical and elastic constants become functions of position in the body. This is also the case where the material properties become functions of temperature in a non-uniformly heated body.

The second requires that the elastic properties are the same in all directions at any point in the elastic body. If a material is non-isotropic, such as in extruded graphite or laminated plastics, the relationships between stress and strain are no longer the simple equations containing two independent elastic constants. In the most general non-isotropic material it requires 21 elastic constants to define the stress-strain relationship. The existence of planes of elastic symmetry reduces this number.(4)

A third important assumption is that the displacements are so small that the position of a point in the body does not require redefinition after deformation and that the higher order terms of displacement derivatives are negligible. If these assumptions are not made the relationship between strains and displacements become non-linear and the much more difficult theory of large deformations must be employed.

The final assumption is that the material behaves elastically. This assumption requires that a deformed body returns to its original shape upon removal of the deformation source, be it external loads or temperature. If one considers the simple tension stress strain curve, this assumption requires that at no point in the body can the stress level be above the yield point. If this stress level is exceeded the problem again becomes non-linear since the stress-strain relations no longer follow Hooke's Law. This non-linear response is idealized in the theory of plasticity. It is usual, also, in the application of the classical theory of elasticity to ignore the visco-elastic behavior of materials but the extension to this case where the stress-strain relations contain only linear time derivatives of stress and strain is quite straightforward. Since this type of behavior, the best known of which is creep, becomes more pronounced as the temperature increases, this possible extension in the linear case will be mentioned in Chapter A27.

The violation of these last two assumptions, small deformations and linear stress-strain relations, leading to the non-linear problem where, of course, the rules of superposition no longer apply, is mentioned not to cause confusion but to serve as a warning of the limitations of the theory presented herein.

A24.2 Formulation of the 3-Dimensional Equations of Thermoelasticity.

The problem of thermoelasticity is to determine at any point within and on the boundary of a heated elastic body subject to external loads and constraints the stresses, strains and displacements. The stress condition at any chosen point within or on the boundary of the body must be such that equilibrium of forces and moments exists at that point. Consequently, the expression of the equilibrium state of the stress components will be independent of the material properties, the deformations, the temperature and temperature distribution, the stress-strain law, etc. The relationship between stress components must be only such as to satisfy the equations of equilibrium. It is well known that the stress at a point, being the force intensity in a chosen direction, can be represented by a single vector, having magnitude and direction, which is related to a chosen cut

(4) **Numbers in parentheses refer to the bibliography at the end of the chapter.**

plane surface of infinitesimal area at that point. Thus the definitions of the stress at the point requires more than the statement of the stress vector. It requires in addition the definition of the cutting plane through the point of interest to which the stress vector is referred. The stress at a point can be fully defined by choosing a sufficient number of cutting planes and determining the stress vectors, usually defined by its components, associated with each. In 3-dimensional bodies a minimum of 3 cutting planes which are mutually at right angles to each other (orthogonal) is required. Thus, when each stress vector associated with one of these cutting planes is defined by its 3 components, there will exist 9 stress components to be determined. These 9 components of the stress at a point make-up the stress tensor[4] which is the most convenient representation for the more difficult problems in theoretical analysis. The three cutting planes are usually chosen parallel to a chosen space fixed cartesian coordinate system, the choice usually clearly indicated for the physical system under analysis, and thus, the stress components will all be parallel to this axis system. Other axis systems such as cylindrical axes, can be chosen so long as there is provided the 3 mutually perpendicular planes at the point of interest. These 9 stress components are related by the equilibrium equations as shown in the next section. There will be 6 equations of equilibrium and thus there exists more unknowns (9) than there are equations which fact prevents any possible general solution.

Under the influence of this stress field the elastic body will deform in a manner dependent upon the stress strain relations. The stress strain relations for the isothermal problem (the same temperature throughout) are well known from the linear Hook's Law.[2,3,4] The introduction of temperature modifies these relations by the addition of another strain component due to the thermal expansion properties of the material being studied. These stress-strain relations provide 6 more equations but at the same time 6 additional unknown strain components are introduced. The system of equations is still incomplete.

The strains give rise to displacements. The relationship between strains and displacements which are independent of temperature and temperature distribution requires 6 equations for definition and at the same time introduces only 3 unknowns which are the displacement components.

The number of unknowns is now 18 and there exists 18 equations so that the equation set is complete and a general solution is possible. This general solution will be the unique solution when all 18 equations are simultaneously satisfied. The development of the solution to a specific problem requires a set of boundary condition equations for evaluation of the unknown coefficients existing in the general solution.

As in the theory of elasticity, the solution to a chosen physical problem in thermoelasticity must satisfy the defined 18 equation set and, as well, the boundary conditions. The equations of thermoelasticity are derived in the following sections in the following sequence.

(A) Equilibrium Equations

(B) Strain - Displacement Relations

(C) Stress-Strain Relations

(D) Boundary Conditions

It should be noted at this time that the only change that is necessary in the equations of the linear theory of elasticity to the linear theory of thermoelasticity is in the stress-strain relations.

A24.3 The Equilibrium Equations.

Consider the point O in an elastic body which is subject to external loading and internal, or body, forces. It is desired to determine the state of stress at O. This could be done completely by defining the resultant stress tensor with respect to some spatial reference but is most commonly done in the following manner. Take the point of interest O as the origin of three mutually perpendicular axes oriented parallel to a chosen spatial cartesian axis system. The choice of this reference axis system is usually clearly indicated by the geometry of the system under study.

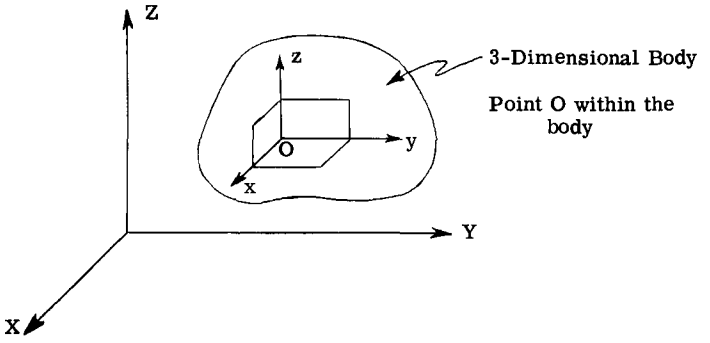

Assume that the body is cut by the planes xy, xz, yz, having the common point of intersection O. Associated with each of these cutting planes there will be a resultant stress vector at O requiring three components for definition. It is logical to choose the di-

rections of these components as those of the axis system.

For example, consider the cutting plane yz. The resultant stress vector at O associated with this cutting plane can be defined by the three components σ_x; τ_{xy}; τ_{xz} where

σ_x = component normal to the zy plane and therefore parallel to the x - axis, hence the subscript x

τ_{xy} = one of the stress components in the yz plane which is identified by the normal direction x, hence the first subscript, and in the y direction as indicated by the second subscript. This component could be written as $\tau_{(yz)y}$ but since the axes are mutually perpendicular the yz plane is more economically identified by the subscript x as shown.

τ_{xz} = the other in-plane component at right angles to τ_{xy} where again the first subscript identifies the cutting plane yz and the second the direction.

With the adoption of a sign convention these vector components can be considered scalar quantities. Associated with the cutting plane xz will be the components σ_y, τ_{yx}, τ_{yz} and with the cutting plane xy the components σ_z, τ_{zx}, τ_{zy}. Any other of the infinitely many possible cutting planes passing through O can be defined in terms of coordinates associated with the three mutually perpendicular planes xy, xz, yz. Thus, definition of the 9 stress components σ_x, σ_y, σ_z, τ_{xy}, τ_{xz}, τ_{yx}, τ_{yz}, τ_{zx}, τ_{zy} will completely define the stress condition at the point O in the body. The magnitudes of these vector components will be obtained from the solutions of the differential equations of equilibrium, stress-strain and strain-displacement relations and the boundary conditions, wherein the components are treated as scalar quantities since the sign convention illustrated in the next section is always implied and the direction is that of the chosen cartesian coordinate system.

To establish the equations of equilibrium the fundamental laws of statics are employed, viz;

$$\Sigma F_X = \Sigma F_Y = \Sigma F_Z = \Sigma M_O = 0$$

where F_X indicates a force in the direction x, etc., and M_O a moment about O.

Since it is forces which satisfy this equation, surface areas over which the stresses (being force intensities) are acting must be provided. This is most conveniently done by considering the stress components acting over the faces of a small parallelepiped constructed with faces in or parallel to the cutting planes contained in the cartesian coordinate system with the point of interest O as the origin. This parallelepiped is considered arbitrarily small and in the limit as the edge dimensions approach zero the equations resulting from equilibrium of the element will describe the stress conditions at the point O. Consider then such a parallelepiped which is already considered infinitesimally small with edge dimensions then correctly specified as dx, dy and dz. The stress components on those faces

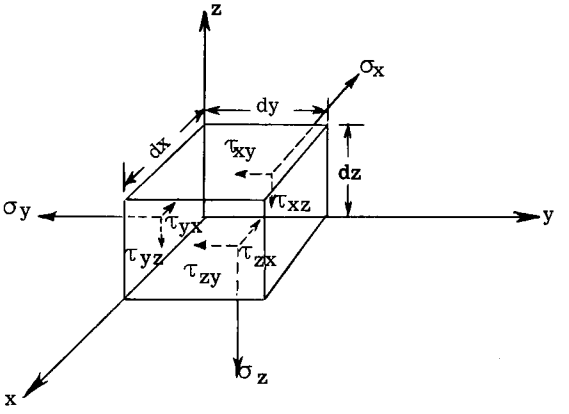

contained in the cutting planes xz, xy and yz are shown according to the positive sign convention. According to this same sign convention the stress components on those faces parallel to the cutting planes are shown in the next figure. It is these components which are of interest from the physical interpretation of the stress condition at O since, because of the limiting process mentioned above, it is these directions which are indicated by positive values in the solution to the differential equations of equilibrium. It is observed that positive values of σ_X, σ_y and σ_Z indicate tension of the elastic material at the point O.

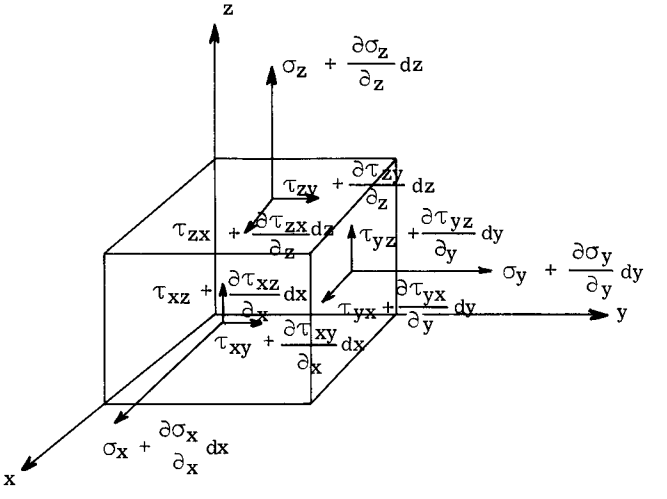

When in doubt during the physical interpretation of solutions to the equations of elasticity one should return to these two figures which define the positive sense of the stress components.

The stress components have all been increased an amount equal to the rate change of magnitude in the direction of movement times the distance moved. This increase is, of course, the change in magnitude between the components on the planes passing through O and those displaced an infinitesimal distance away in the positive direction. In this volume element, dxdydz, it will also be possible to have body forces X, Y, Z defined as the force per unit volume and which can arise as gravitational forces, magnetic forces, etc., acting in the direction x, y and z respectively and through the centroid of the volume element. It should be borne in mind that these are internal forces within the element considered and are distinct from the external forces which will appear in the equations defining the boundary conditions.

The equations of equilibrium are obtained directly from the static equilibrium conditions:

$$\left.\begin{aligned}\Sigma F_X &= 0\\ \Sigma F_y &= 0\\ \Sigma F_Z &= 0\end{aligned}\right\} \quad - - - - - - - - - - - - - - - \quad (1)$$

To illustrate the procedure the forces in the x direction are summed and equated to zero.

$$(\sigma_x + \frac{\partial \sigma_x}{\partial x} dx)dy\ dz - \sigma_x dydz + (\tau_{yx} + \frac{\partial \tau_{yx}}{\partial y} dy)dzdx$$

$$- \tau_{yx}\ dz\ dx + (\tau_{zx} + \frac{\partial \tau_{zx}}{\partial z} dz)\ dy\ dx - \tau_{zx}\ dy\ dx +$$

$$X\ dx\ dy\ dz = 0$$

which, on simplification, gives

$$\frac{\partial \sigma_x}{\partial x} + \frac{\partial \tau_{yx}}{\partial y} + \frac{\partial \tau_{zx}}{\partial z} + X = 0 \quad - - - - - - - \quad (2)$$

Similarly

$$\frac{\partial \tau_{xy}}{\partial x} + \frac{\partial \sigma_y}{\partial y} + \frac{\partial \tau_{zy}}{\partial z} + Y = 0 \quad - - - - - - - \quad (3)$$

$$\frac{\partial \tau_{xz}}{\partial x} + \frac{\partial \tau_{yz}}{\partial y} + \frac{\partial \sigma_z}{\partial z} + Z = 0 \quad - - - - - - - \quad (4)$$

It can be readily shown, by taking moments about the volume center and satisfying the equation of static equilibrium, $\Sigma M_O = 0$ that the complementary components of the shear stress are equal, ie.

$$\tau_{xy} = \tau_{yx}\ ;\ \tau_{xz} = \tau_{zx}\ ;\ \tau_{yz} = \tau_{zy} \quad - - - \quad (5)$$

The equations 2, 3, 4 and the three equations of 5 make up the 6 equilibrium equations. In the following discussions equations 5 will be accepted and thus the preceding discussion on the equation set of 18 must be modified to the set of 15 with a similar reduction of 3 in the number of unknowns.

It should be noted that these equations 2, 3 and 4 define the equilibrium state of the volume element and their derivation requires no limiting assumptions as to the elastic nature of the material. The equations are thus quite general and will be the same for non-linear systems and those in which displacements are created by temperature differences. For convenience, these equilibrium equations are written in cylindrical coordinates r, θ and z.

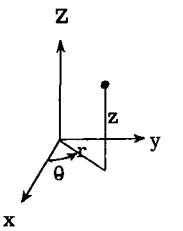

$$\frac{\partial \sigma_r}{\partial r} + \frac{1}{r}\frac{\partial \tau_{r\theta}}{\partial \theta} + \frac{\partial \tau_{rz}}{\partial z} + \frac{\sigma_r - \sigma_\theta}{r} + R = 0$$

$$\frac{\partial \tau_{rz}}{\partial r} + \frac{1}{r}\frac{\partial \tau_{\theta r}}{\partial \theta} + \frac{\partial \sigma_z}{\partial z} + \frac{\tau_{rz}}{r} + Z = 0$$

$$\frac{\partial \tau_{r\theta}}{\partial r} + \frac{1}{r}\frac{\partial \sigma_\theta}{\partial \theta} + \frac{\partial \tau_{\theta z}}{\partial z} + \frac{2\tau_{r\theta}}{r} + \Theta = 0$$

where the body force components in the r, z and θ directions are identified as R, Z and Θ respectively, and in spherical coordinates r, θ and Ø

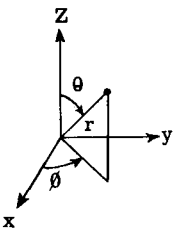

$$\frac{\partial \sigma_r}{\partial r} + \frac{1}{r}\frac{\partial \tau_{r\theta}}{\partial \theta} + \frac{1}{r\ \sin\theta}\frac{\partial \tau_{r\phi}}{\partial \phi} + \frac{1}{r}(2\sigma_r - \sigma_\theta - \sigma_\phi + \tau_{r\theta}\ \cot\theta) + R = 0$$

$$\frac{\partial \tau_{r\theta}}{\partial r} + \frac{1}{r}\frac{\partial \sigma_\theta}{\partial \theta} + \frac{1}{r\ \sin\theta}\frac{\partial \tau_{\theta\phi}}{\partial \phi} + \frac{1}{r}\left[(\sigma_\theta - \tau_{\phi\theta})\ \cot\theta + 3\tau_{r\theta}\right] + \Theta = 0$$

$$\frac{\partial \tau_{r\phi}}{\partial r} + \frac{1}{r}\frac{\partial \tau_{\theta\phi}}{\partial \theta} + \frac{1}{r\ \sin\theta}\frac{\partial \sigma_\phi}{\partial \phi} + \frac{1}{r}\left[3\tau_{r\phi} + 2\tau_{\theta\phi}\ \cot\theta\right] + \Phi = 0$$

where the body forces in the r, θ and Ø directions are given by R, Θ and Φ respectively.

A24.4 Strain - Displacement Relations.

Equations 2, 3, and 4 being three equations with six unknowns are insufficient to establish solutions for these unknowns σ_x, σ_y, σ_z, τ_{xy}, τ_{xz}, τ_{yz}. One looks therefore to equations relating the stresses to the deformations of the deformable elastic body for the further equations necessary to provide a complete set. Consider first the strain displacement relations. The discussion of the relation between these strains and the stresses will follow.

If a fictitious fiber of unit length lies in the positive x - direction before deformation, one has only to determine the increase in length of this fiber after deformation to obtain the strain at the point of origin of the fiber. With the assumption that this change in length is sufficiently small that second order terms of this change can be neglected and further, that rotation of this fiber away from the x - direction is small, it is easy to show by simple trigonometry that the strain ε_x is given by

$$\varepsilon_x = \frac{\partial u}{\partial x} \qquad \text{- - - - - - - - - - - - - - - - - (6)}$$

By considering fibers originally in the y and z directions the same development, given in all texts in elasticity, gives

$$\varepsilon_y = \frac{\partial v}{\partial y} \qquad \text{- - - - - - - - - - - - - - - - - (7)}$$

$$\varepsilon_z = \frac{\partial w}{\partial z} \qquad \text{- - - - - - - - - - - - - - - - - (8)}$$

where u, v and w are the displacements of the point of interest, the origin of the three fibers considered, from the undeformed body position. The shear strains are readily obtained, when the same restrictions on the magnitude of length change and rotation of the fiber are enforced, by consideration of the two fibers lying in the same plane. Consider those two projections in the x-y plane starting from the point of interest O in the body.

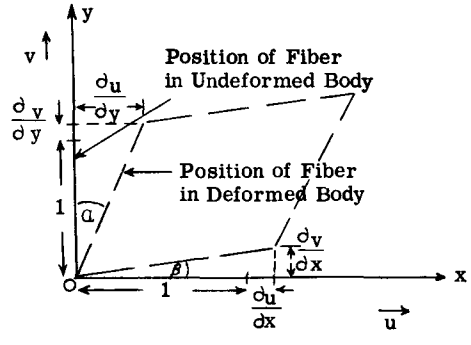

The shear strain $\gamma_{xy} = \alpha + \beta$

$$= \frac{\partial u}{\partial y} + \frac{\partial v}{\partial x}$$

within the assumptions stated above. In similar fashion the remaining two components of shear strain can be obtained to give the complete set

$$\gamma_{xy} = \frac{\partial u}{\partial y} + \frac{\partial v}{\partial x} \qquad \text{- - - - - - - - - - - - - (9)}$$

$$\gamma_{xz} = \frac{\partial w}{\partial x} + \frac{\partial u}{\partial z} \qquad \text{- - - - - - - - - - - - - (10)}$$

$$\gamma_{yz} = \frac{\partial v}{\partial z} + \frac{\partial w}{\partial y} \qquad \text{- - - - - - - - - - - - - (11)}$$

Again, for future convenience, these strain displacement relations are written in cylindrical and spherical coordinates below.

In cylindrical coordinates,

$$\varepsilon_r = \frac{\partial u}{\partial r} \; ; \; \varepsilon_z = \frac{\partial w}{\partial z} \; ; \; \varepsilon_\theta = \frac{u}{r} + \frac{1}{r}\frac{\partial v}{\partial \theta}$$

$$\gamma_{r\theta} = \frac{1}{r}\frac{\partial u}{\partial \theta} + \frac{\partial v}{\partial r} - \frac{v}{r} \; ; \; \gamma_{rz} = \frac{\partial u}{\partial z} + \frac{\partial w}{\partial r} \; ;$$

$$\gamma_{z\theta} = \frac{\partial v}{\partial z} + \frac{1}{r}\frac{\partial w}{\partial \theta}$$

where u, v and w represent displacements in the r, θ and z directions respectively. And in spherical coordinates,

$$\varepsilon_r = \frac{\partial u}{\partial r} \; ; \; \varepsilon_\theta = \frac{u}{r} + \frac{1}{r}\frac{\partial v}{\partial \theta} \; ;$$

$$\varepsilon_\phi = \frac{u}{r} + \frac{v}{r}\cot\theta + \frac{1}{r \sin\theta}\frac{\partial w}{\partial \phi}$$

$$\gamma_{r\theta} = \frac{1}{r}\frac{\partial u}{\partial \theta} + \frac{\partial v}{\partial r} - \frac{v}{r}$$

$$\gamma_{r\phi} = \frac{1}{r \sin\theta}\frac{\partial u}{\partial \phi} + \frac{\partial w}{\partial r} - \frac{w}{r}$$

$$\gamma_{\theta\phi} = \frac{1}{r}\left(\frac{\partial w}{\partial \theta} - w\cot\theta\right) + \frac{1}{r \sin\theta}\frac{\partial v}{\partial \phi}$$

where u, v, w represent the displacements in the r, θ and ϕ directions respectively.

It must be noted that these equations apply only under the restrictive assumptions on the order of magnitude of displacements. These are the linear strain-displacement relations of the classical theory of elasticity. An obvious extension to the classical theory immediately presents itself as the theory of large deformations wherein the higher order terms of the displacement derivative are considered. This difficult non-linear theory is being actively

developed since many structural problems, such as the buckling and post-buckling behavior of structures, involve large deformations.

We now possess a set of 9 equations, the 3 equations of equilibrium and the 6 strain-displacement relations, with the 15 unknowns σ_x, σ_y, σ_z, τ_{xy}, τ_{yz}, τ_{xz}, ε_x, ε_y, ε_z, γ_{xy}, γ_{yz}, γ_{xz}, u, v, w so the equation set is even more incomplete than before. However, by means of the stress-strain relations, Hooke's Law, the equation set will be completed to 15.

A24.5 Stress-Strain Relations.

In accord with the limiting assumptions of the linear theory of elasticity the general statement of Hooke's Law requires 36 constants in the isothermal problem. For isotropic materials, wherein the elastic properties at any chosen point throughout the body are the same for all possible directions of observation, these 36 constants are readily shown to be dependent[1, 2, 3, 4] and can be reduced to the two most commonly used, E, Young's modulus and ν, Poisson's ratio, or the Lamé constants λ and μ. For the isothermal problem the stress-strain relations can be written as;

$$\varepsilon_x = \frac{1}{E}\left[\sigma_x - \nu(\sigma_y + \sigma_z)\right]$$

$$\varepsilon_y = \frac{1}{E}\left[\sigma_y - \nu(\sigma_z + \sigma_x)\right]$$

$$\varepsilon_z = \frac{1}{E}\left[\sigma_z - \nu(\sigma_y + \sigma_x)\right]$$

$$\gamma_{xy} = \frac{1}{G}\tau_{xy}$$

$$\gamma_{yz} = \frac{1}{G}\tau_{yz}$$

$$\gamma_{xz} = \frac{1}{G}\tau_{xz}$$

where E = Young's modulus = slope of the uni-axial stress strain curve

$$G = \text{shear modulus} = \frac{E}{2(1+\nu)}$$

ν = Poisson's ratio = 0.3 for steel

= 0.25 → 0.50 for all elastic materials at room temperature.

It is often more convenient to express the stress strain relations with the Lamé constants of linearity. In three-dimensional elasticity these relations become

$$\sigma_x = \lambda e + 2\mu\varepsilon_x$$

$$\sigma_y = \lambda e + 2\mu\varepsilon_y$$

$$\sigma_z = \lambda e + 2\mu\varepsilon_z$$

$$\tau_{xy} = \mu\gamma_{xy}$$

$$\tau_{yz} = \mu\gamma_{yz}$$

$$\tau_{zx} = \mu\gamma_{zx}$$

where the Lamé constants

$$\lambda = \frac{\nu E}{(1+\nu)(1-2\nu)}$$

$$\mu = \frac{E}{2(1+\nu)} = G$$

and

$$e = \varepsilon_x + \varepsilon_y + \varepsilon_z = \text{the dilatation of the volume element.}$$

It should be further noted that

$$3\lambda + 2\mu = 3k$$

where

$$k = \frac{E}{3(1-2\nu)}$$

In the case of the heated elastic body these strain expressions must be modified by the addition of a component arising from the thermal expansion property of all structural materials. This component will be proportional to the temperature level, T, above or below some reference temperature (usually room temperature). The constant of proportionality is the familiar linear coefficient of thermal expansion, which, for isotropic materials is the same in all directions of observation at the point O. It is obvious that the direct strain components, ε_x, ε_y, ε_z, being the change in length per unit length of a fictitious fiber oriented in the x, y, z directions respectively, are directly affected by the thermal expansion. The shear stress components will not, however, be affected for isotropic materials since the angular deformation of a small volume element located at O will not be changed during the uniform expansion of this volume element. The stress-strain relations for thermoelasticity thus become:

$$\varepsilon_x = \frac{1}{E}\left[\sigma_x - \nu(\sigma_y + \sigma_z)\right] + \alpha T \quad - - - - \quad (12)$$

$$\varepsilon_y = \frac{1}{E}\left[\sigma_y - \nu(\sigma_x + \sigma_z)\right] + \alpha T \quad - - - - \quad (13)$$

$$\varepsilon_z = \frac{1}{E}\left[\sigma_z - \nu(\sigma_x + \sigma_y)\right] + \alpha T \quad - - - - \quad (14)$$

$$\gamma_{xy} = \frac{1}{G}\tau_{xy} \quad - - - - - - - - - - - - - \quad (15)$$

$$\gamma_{xy} = \frac{1}{G}\tau_{xz} \quad - - - - - - - - - - - - - \quad (16)$$

$$\gamma_{yz} = \frac{1}{G}\tau_{yz} \quad - - - - - - - - - - - - - \quad (17)$$

These equations can be inverted to express the stresses as functions of strains. This is left as an exercise for the student but these relations containing the Lamé constants are given here for completeness of treatment.

$$\sigma_x = \lambda e + 2\mu\varepsilon_x - (3\lambda + 2\mu)\alpha T$$

$$\sigma_y = \lambda e + 2\mu\varepsilon_y - (3\lambda + 2\mu)\alpha T$$

$$\sigma_z = \lambda e + 2\mu\varepsilon_z - (3\lambda + 2\mu)\alpha T$$

$$\tau_{xy} = \mu\gamma_{xy}$$

$$\tau_{yz} = \mu\gamma_{yz}$$

$$\tau_{zx} = \mu\gamma_{zx}$$

where the definitions of λ, μ and e remain unchanged from those previously given in the isothermal equations relating stress and strain.

A24.6 The General Equations of 3-Dimensional Thermoelasticity.

The unknowns are:

6 stress components $\sigma_x, \sigma_y, \sigma_z, \tau_{xy}, \tau_{xz}, \tau_{yz}$
6 strain components $\varepsilon_x, \varepsilon_y, \varepsilon_z, \gamma_{xy}, \gamma_{xz}, \gamma_{yz}$
3 displacement components u, v, w
15

The necessary 15 equations are given by

3 equations of equilibrium

$$\frac{\partial\sigma_x}{\partial x} + \frac{\partial\tau_{xy}}{\partial y} + \frac{\partial\tau_{xz}}{\partial z} + X = 0$$

$$\frac{\partial\sigma_y}{\partial y} + \frac{\partial\tau_{xy}}{\partial x} + \frac{\partial\tau_{yz}}{\partial z} + Y = 0$$

$$\frac{\partial\sigma_z}{\partial z} + \frac{\partial\tau_{xz}}{\partial x} + \frac{\partial\tau_{yz}}{\partial y} + Z = 0$$

6 strain - displacement relations

$$\varepsilon_x = \frac{\partial u}{\partial x} \qquad \gamma_{xy} = \frac{\partial u}{\partial y} + \frac{\partial v}{\partial x}$$

$$\varepsilon_y = \frac{\partial v}{\partial y} \qquad \gamma_{yz} = \frac{\partial v}{\partial z} + \frac{\partial w}{\partial y}$$

$$\varepsilon_z = \frac{\partial w}{\partial z} \qquad \gamma_{xz} = \frac{\partial u}{\partial z} + \frac{\partial w}{\partial x}$$

6 strain-stress relations

$$\varepsilon_x = \frac{1}{E}\left[\sigma_x - \nu(\sigma_y + \sigma_z)\right] + \alpha T$$

$$\varepsilon_y = \frac{1}{E}\left[\sigma_y - \nu(\sigma_x + \sigma_z)\right] + \alpha T$$

$$\varepsilon_z = \frac{1}{E}\left[\sigma_z - \nu(\sigma_x + \sigma_y)\right] + \alpha T$$

$$\gamma_{xy} = \frac{1}{G}\tau_{xy}$$

$$\gamma_{xz} = \frac{1}{G}\tau_{xz}$$

$$\gamma_{yz} = \frac{1}{G}\tau_{yz}$$

The equation set is now complete since the number of independent equations is equal to the number of unknowns.

A24.7 The Compatability Equations.

It will be noted in the strain displacement equations that 6 strain components are necessary to define the 3 displacement components. Thus, if one were to choose at random a set of 6 strain components this does not mean that there exists a possible set of 3 displacement components which will allow satisfaction of the strain-displacement equations.

Consequently the choice of these 6 strain components cannot be arbitrary and, in fact, must be such that the compatability equations, which are equations relating the derivatives of the strain components, are satisfied. These compatability equations thus ensure the existence of continuous single-valued displacement functions. This, of course, ensures the uniqueness of the solution when, as is possible, the analysis is formulated in terms of stresses and strains only. These equations are automatically satisfied if the complete 15 equation set is satisfied.

These equations are derived in the following manner.

From equation 9

$$\gamma_{xy} = \frac{\partial u}{\partial y} + \frac{\partial v}{\partial x}$$

therefore

$$\frac{\partial^2\gamma_{xy}}{\partial x\,\partial y} = \frac{\partial^3 u}{\partial x\partial y^2} + \frac{\partial^3 v}{\partial x^2\partial y}$$

$$= \frac{\partial^2}{\partial y^2}\left(\frac{\partial u}{\partial x}\right) + \frac{\partial^2}{\partial x^2}\left(\frac{\partial v}{\partial y}\right)$$

or from equations 6 and 7

$$\frac{\partial^2 \gamma_{xy}}{\partial x \partial y} = \frac{\partial^2 \varepsilon_x}{\partial y^2} + \frac{\partial^2 \varepsilon_y}{\partial x^2}$$

The remaining 5 compatability equations are derived in similar manner and the complete set appears as follows

$$\frac{\partial^2 \gamma_{yz}}{\partial x \partial y} = \frac{\partial^2 \varepsilon_y}{\partial y^2} + \frac{\partial^2 \varepsilon_z}{\partial x^2} \quad - - - - - - - - - (18)$$

$$\frac{\partial^2 \gamma_{xz}}{\partial x \partial z} = \frac{\partial^2 \varepsilon_x}{\partial z^2} + \frac{\partial^2 \varepsilon_z}{\partial x^2} \quad - - - - - - - - - (19)$$

$$\frac{\partial^2 \gamma_{yz}}{\partial y \partial z} = \frac{\partial^2 \varepsilon_y}{\partial z^2} + \frac{\partial^2 \varepsilon_z}{\partial y^2} \quad - - - - - - - - - (20)$$

$$\frac{\partial^2 \gamma_{xy}}{\partial x \partial z} + \frac{\partial^2 \gamma_{xz}}{\partial x \partial y} - \frac{\partial^2 \gamma_{yz}}{\partial x^2} = 2\frac{\partial^2 \varepsilon_x}{\partial y \partial z} \quad - - - (21)$$

$$\frac{\partial^2 \gamma_{xy}}{\partial y \partial z} - \frac{\partial^2 \gamma_{xz}}{\partial y^2} + \frac{\partial^2 \gamma_{yz}}{\partial x \partial y} = 2\frac{\partial^2 \varepsilon_y}{\partial x \partial z} \quad - - - (22)$$

$$- \frac{\partial^2 \gamma_{xy}}{\partial z^2} + \frac{\partial^2 \gamma_{xz}}{\partial y \partial z} + \frac{\partial^2 \gamma_{yz}}{\partial x \partial z} = 2\frac{\partial^2 \varepsilon_z}{\partial x \partial y} \quad - - - (23)$$

As will be noted later, these compatability equations are automatically satisfied if the problem is formulated in terms of displacements and then the general solution must satisfy only the equilibrium equations with these equations written in terms of displacements. In comparison, if the problem is formulated completely in terms of stresses then both the equilibrium and the compatability equations must be satisfied. The 3 equilibrium and the 6 stress-strain relations together with the 6 compatability equations again provide a complete set of equations for the general solution to a problem formulated in terms of stresses and strains only.

It now remains only to obtain the specific solution to this complete set of equations for the chosen physical problem. This requires the use of the equations which state the boundary conditions into which the general solution is substituted to obtain a set of algebraic equations from which the unknown constants of the general solution can be evaluated.

A24.8 Boundary Conditions

It is obvious that the boundary conditions can be prescribed in three different possible ways. Consider each case in turn.

Case 1. All external boundary conditions are prescribed in terms of external surface loads with no geometrical restraints imposed. Since the derived equations are in terms of stresses, these loads are converted to load intensities (lb. force/unit area) and are then termed surface tractions. Simple examples of a system having these boundary conditions would be a general 3-dimensional elastic body subjected to hydrostatic pressure or the same body non-uniformly heated. In the first example the surface tractions are the pressure levels acting normal to the surface and in the latter the surfaces are traction free (the boundary tractions all zero). If the surface tractions at any point on the surface are represented by the vector components $\bar{X}$, $\bar{Y}$, $\bar{Z}$ parallel to the x, y, z axes respectively, the equations of equilibrium at the boundary give the boundary condition equations:

$$\left.\begin{aligned} \bar{X} &= \sigma_x l + \tau_{xy} m + \tau_{xz} n \\ \bar{Y} &= \sigma_y m + \tau_{yz} n + \tau_{xy} l \\ \bar{Z} &= \sigma_z n + \tau_{xz} l + \tau_{yz} m \end{aligned}\right\} \quad - - - (24)$$

where l, m, n are the direction cosines of the surface normal drawn outward from the surface.

Case 2. All external boundaries are constrained by geometrical restraints and thus, all boundary displacements are specified. This case is relatively rare in engineering structures. A simple example would be that of a heated insert fully contained within a rigid body. If the boundary displacements are specified over the whole boundary, the boundary conditions can be written as:

$$\left.\begin{aligned} u &= f(s) \\ v &= g(s) \\ w &= h(s) \end{aligned}\right\} \quad - - - - - - - - - (25)$$

where s is the surface point and f, g, and h are known functions prescribed by the specified displacements.

Case 3. The boundary conditions are specified by stresses over part of the surface and by displacements over the remainder. A simple example is that of a heated cantilever wing where the assumption of a rigid root fixity prescribes zero displacements at the root while over the remainder of the structure surface the surface tractions are zero, for the unloaded wing, or

prescribed by the external loading. This problem is discussed in some detail later in the text of Chapter A25. Both sets of equations stated in the above two cases must then be used where appropriate.

A24.9 General Notes.

Only the linear theory of thermoelasticity is being considered herein and consequently the rules of superposition apply. This means, of course, that one can determine the stresses, strains and displacements of an elastic structure due to one of several causes and add the results of each cause treated independently to determine the stresses, strains and displacements due to all the causes acting simultaneously. In the thermoelastic analysis of heated loaded structures it is frequently most convenient to determine the stress, strain and displacement distribution due to temperature alone and to then add to this result the isothermal analysis of the loaded structure according to the well documented theory of elasticity to obtain the final distribution. In determining the stress, strain and displacement due to temperature one can rightly consider all surfaces to be traction free so long as, in the isothermal analysis, deformations at geometrical restraints due to the temperature are restored to the prescribed values by such boundary condition equations as:

$$u = f(s) - u_T(s)$$

$$v = g(s) - v_T(s) \qquad \text{- - - - - - - - - - (26)}$$

$$w = h(s) - w_T(s)$$

The functions u_T, v_T, w_T will be the boundary displacements calculated from the thermoelastic analysis considering all surfaces free of tractions.

This technique has the distinct advantage that the thermoelastic problem can then always be formulated in terms of stresses only, leaving the mixed boundary condition problem to the isothermal analysis. It will be seen later, however, that this is not always advantageous and it is often desirable to retain the prescribed boundary displacement conditions in both the thermal and isothermal analyses. Unfortunately no rules of choice can be given and the decision must be made by the analyst based on his own experience. The examples to be considered in the next chapter will assist in this choice however.

Mention is made in the above of a stress formulation. This point deserves clarification. The fifteen equations of the 3-dimensional theory of elasticity and thermoelasticity contain the 15 unknown stress, strain and displacement components. If the boundary conditions are, as in Case 1 of the preceding section, given by surface tractions only, the boundary condition equations contain 6 stress components. It is then desirable to formulate the 15 equations in terms of 6 stress equations. These will be the 3 equilibrium equations and the first 3 compatability equations written in terms of stresses by use of the stress-strain and strain-displacement relations. The remaining 3 compatability equations must also be satisfied to ensure a unique solution. The specific solution is obtained in terms of stresses only from the set of 9 equations and the 3 boundary condition relations. This formulation is the one employed in the thermal stress analysis where all surfaces are considered traction free. It is important to remember that in this stress formulation the equations of equilibrium and compatability (written in terms of stresses) must be satisfied simultaneously by the general solution.

If, on the other hand, the boundary conditions are those of Case 2 then the boundary condition equations contain only 3 known displacements. The problem is then formulated in terms of displacements. Since, by the choice of displacements over the boundary, the equations of compatability are automatically satisfied it remains only to obtain a solution of the 3 equations of equilibrium which have been rewritten in terms of displacements, again by the use of the stress-strain and strain-displacement relations. Unfortunately, as stated before, this most desirable case rarely exists in engineering analysis.

If the boundary conditions are of the mixed type of Case 3 then no one formulation is the more desirable.

References:

1. "Theory of Elasticity" by S. Timoshenko, McGraw-Hill Book Co., Inc., New York, N. Y.

2. "Mathematical Theory of Elasticity" by A.E.H. Love; Dover Publications, New York, 1944.

3. "Analysis of Stress and Strain" by A. J. Durelli, E. A. Phillips and C. H. Tsao, McGraw-Hill Book Co., Inc., New York, N.Y.

4. "Mathematical Theory of Elasticity" by I.S.Sokolnikoff, McGraw-Hill Book Co., Inc., New York, N.Y.

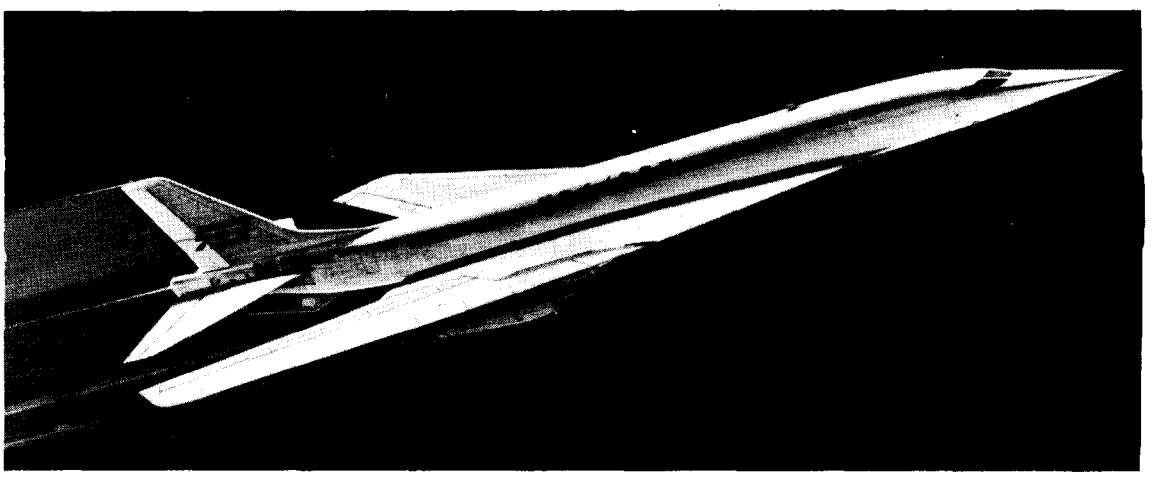

BOEING

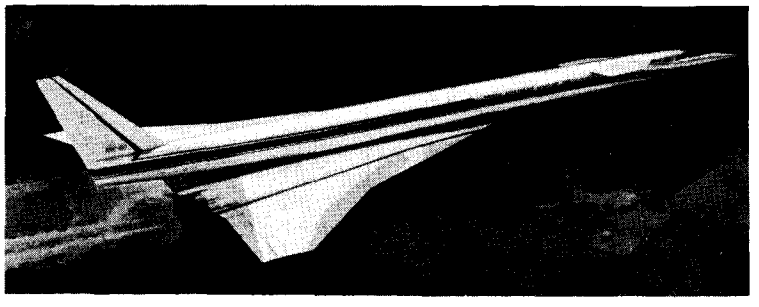

NORTH AMERICAN

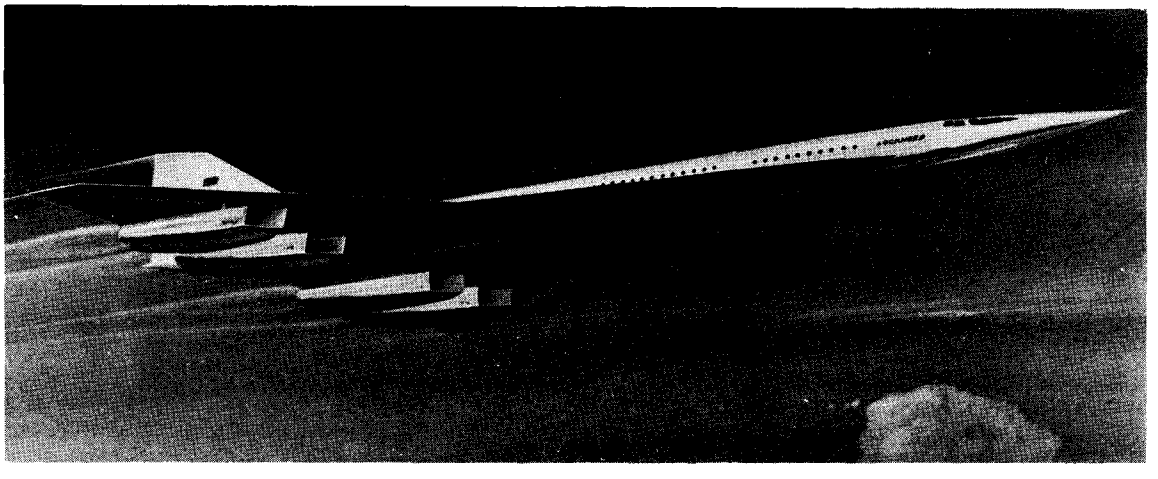

LOCKHEED

Proposed Designs For Supersonic Airliners. Boeing won the competition but later changed design to fixed wing type. Later Congress killed the SST project, a bad decision in this author's opinion.

CHAPTER A25
THE 2-DIMENSIONAL EQUATIONS OF ELASTICITY AND THERMOELASTICITY

A25.1 Introduction: In any elastic body wherein the stress components at a point of interest all lie in the one plane and, due to symmetry in the body itself or in the external loading, the stresses throughout the body all lie in this one plane, the stress analysis becomes 2-dimensional. All stresses normal to this plane are zero. The analysis is then referred to as one of plane stress.

In the same manner, if all strains lie in one plane (all strain components normal to the plane being zero) the problem is again two dimensional and the analysis is referred to as one of plane strain.

The restriction to a planar surface is, of course, not necessary and the statement of the 2-dimensional problem of stress or strain should be generalized to that wherein the general 3-dimensional equations can be reduced to a 2-dimensional form by the possible neglect of the stress or strain components parallel to one of the axes of reference.

The equations for plane stress are different from those of plane strain and, consequently, each in turn is treated in the following development.

In the following development the equations of thermoelasticity are derived and discussed. The equations of elasticity follow directly by deletion of all terms containing the temperature, T.

A25.2 Plane Stress.

For illustrative purposes only, the discussion is limited to a physical problem of such geometry that the system is best defined by a cartesian coordinate system. The extension to a system defined by cylindrical or spherical coordinates follows directly.

With the above limitation, the plane stress problem requires that all stress components parallel to one of the axes are zero. Let this axis be the z - axis. Then

$$\sigma_z = \tau_{xz} = \tau_{yz} = 0 \qquad 25.1$$

is the equation which defines completely the state of plane stress. One simple example to which this equation applies is that of a thin slice where the faces are unloaded and not

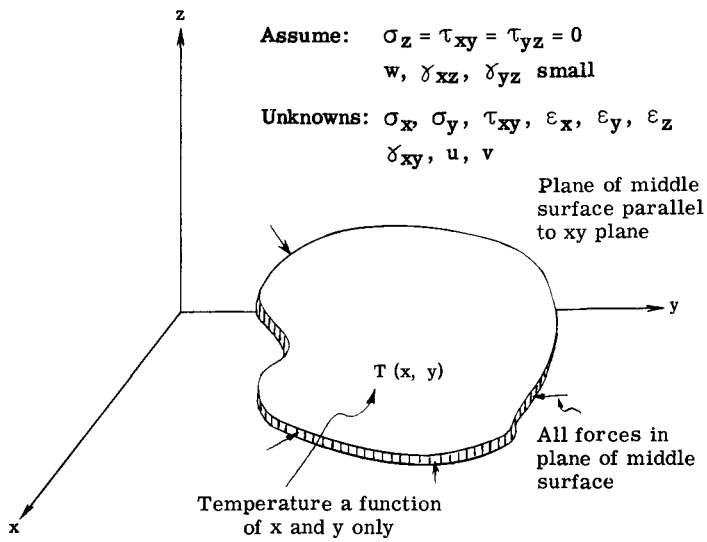

Figure A25.1 Plane Stress

restrained and where the temperature does not vary through the thickness as illustrated in Fig. A25.1. The problem of the thin cantilever wing with no temperature variation through the thickness is a physical system satisfying this statement as is the isothermal problem of a simple cantilever beam. Both of these examples will be discussed in some detail in Chapter A26.

In equation 25.1 the unknowns are reduced to the following:

σ_x	ε_x	u	(w is assumed negligibly small and the results must therefore be approximate if w does exist at all.)
σ_y	ε_y	v	
τ_{xy}	γ_{xy}		

Where the statement of there being only the two displacement components u and v is an assumption consistent with that of the thin slice where the edge loadings are symmetric about the middle surface so that no bending displacements out of the plane occur. This required symmetry of loading for the plane stress formulation must be carefully considered in those systems defined by cylindrical or spherical coordinates such as in the problems of thin cylindrical and spherical shells.

The 8 equations, necessary for a general solution, can be derived directly from the pre-

ceding chapter by substitution of equation 25.1 into the equation set of A24.7.

The two equations of equilibrium

$$\frac{\partial \sigma_x}{\partial x} + \frac{\partial \tau_{xy}}{\partial y} + X = 0 \qquad 25.2$$

$$\frac{\partial \sigma_y}{\partial y} + \frac{\partial \tau_{xy}}{\partial x} + Y = 0 \qquad 25.3$$

The three stress-strain relations are: -

$$\varepsilon_x = \frac{1}{E}(\sigma_x - \nu\sigma_y) + \alpha T \qquad 25.4$$

$$\varepsilon_y = \frac{1}{E}(\sigma_y - \nu\sigma_x) + \alpha T \qquad 25.5$$

$$\gamma_{xy} = \frac{1}{G}\tau_{xy}, \qquad 25.6$$

where T = 0 for the elasticity problem and the three strain-displacement relations are,

$$\varepsilon_x = \frac{\partial u}{\partial x} \qquad 25.7$$

$$\varepsilon_y = \frac{\partial v}{\partial y} \qquad 25.8$$

$$\gamma_{xy} = \frac{\partial u}{\partial y} + \frac{\partial v}{\partial x} \qquad 25.9$$

The equation set is complete for the general solution. There is still required an equation for the strain components ε_z and the compatability equation required for uniqueness of solution from a stress formulation. The expression for ε_z is not usually included in the completed set since it results directly from the solution of this set and is given by,

$$\varepsilon_z = -\frac{\nu}{E}(\sigma_x + \sigma_y) + \alpha T \qquad 25.10$$

The compatability equation is given by

$$\frac{\partial^2 \gamma_{xy}}{\partial x \partial y} = \frac{\partial^2 \varepsilon_x}{\partial y^2} + \frac{\partial^2 \varepsilon_y}{\partial x^2} \qquad 25.11$$

in terms of strains, or by

$$\nabla^2(\sigma_x + \sigma_y) + E\alpha\nabla^2 T = 0 \qquad 25.12$$

in terms of stresses where

$$\nabla^2 = \frac{\partial^2}{\partial x^2} + \frac{\partial^2}{\partial y^2}, \qquad 25.13$$

$X = Y = 0$,

and E and α are constants (independent of temperature and position in the body). See note in section A25.4 for case where X = 0, Y = 0.

Boundary Conditions:

The boundary condition equations from Chapter A24 reduce to the following in each case.

Case 1, traction boundary conditions at the slice edges,

$$\bar{X} = \sigma_x l + \tau_{xy} m$$

$$\bar{Y} = \sigma_y m + \tau_{xy} l \qquad 25.14$$

$$\bar{Z} = 0$$

where $\bar{X}$, $\bar{Y}$ are the components of the external surface forces per unit area in the directions x and y respectively.

Case 2, displacement boundary conditions and where in the thermal stress analysis it is usual to assume $\bar{X} = \bar{Y} = 0$.

$$u = f(s)$$

$$v = g(s) \qquad 25.15$$

$$w = 0$$

The discussion of Chapter A24 applies to these boundary conditions and should be studied again if necessary. This discussion outlines the usual procedure of treating the thermal stress problem in stress formulation with all surfaces traction free and then determining the effect of external loads and removal of thermal displacements where prescribed by means of an isothermal analysis.

A25.3 Derivation of Equations.

For those to whom this subject is new it will be well to derive, in this section, the complete equation set in some more detail. These derivations can be found in any text in the theory of elasticity and are repeated here merely for the convenience of the reader. In many two-dimensional stress problems it is necessary to develop the strain-displacement relations from fundamental consideration of possible deformation in space of a chosen fiber so that special attention should be paid to the development of the most simple case presented here.

The equations of equilibrium.

Consider the figure shown in Chapter A24 on which the positive stress components are shown for an element extracted from a three-dimensional body. If one were to view this figure from the z-axis in a positive z-direction the following figure would be observed.

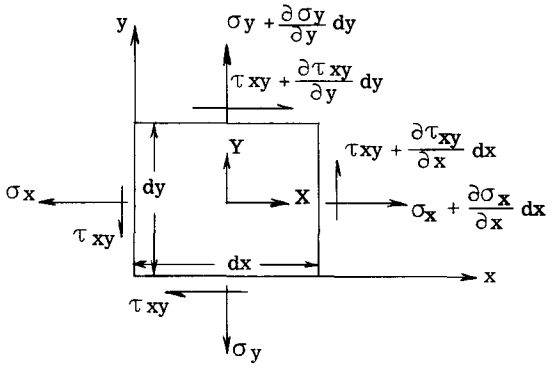

For the plane stress problem the stress components shown are all that will be acting since, by definition, the stress components out of the x-y plane are zero. The equations of equilibrium are then readily derived by summing the forces in the x and y direction, remembering that the figure actually represents a plan view of a three-dimensional element of depth dz, and equating this algebraic sum to zero.

Consider $\Sigma Fy = 0$.

$$(\sigma_y + \frac{\partial \sigma_y}{\partial y} dy) dxdz - \sigma_y \, dxdz +$$

$$(\tau_{xy} + \frac{\partial \tau_{xy}}{\partial x} dx) \, dydz - \tau_{xy} \, dydz + Y \, dxdydz = 0.$$

Thus, upon dividing through by the element volume, dxdydz, and cancelling,

$$\frac{\partial \sigma_y}{\partial y} + \frac{\partial \tau_{xy}}{\partial x} + Y = 0$$

From the equation $\Sigma Fx = 0$,

$$\frac{\partial \sigma_x}{\partial x} + \frac{\partial \tau_{xy}}{\partial y} + X = 0.$$

If the elastic material is to be in equilibrium the variation of stress components and the body forces must satisfy these equations.

The stress-strain relations.

Consider the elastic isothermal problem. The generalized statement of Hooke's Law provides that each of the independent components of stress (σ_x, σ_y, τ_{xy}) may be expressed as a linear function of the strain components (ε_x, ε_y, γ'_{xy}) and visa versa. Thus follows the mathematical expressions,

$$\sigma_x = a_{11} \varepsilon_x + a_{12} \varepsilon_y + a_{13} \gamma'_{xy}$$

$$\sigma_y = a_{21} \varepsilon_x + a_{22} \varepsilon_y + a_{23} \gamma'_{xy}$$

$$\tau_{xy} = a_{31} \varepsilon_x + a_{32} \varepsilon_y + a_{33} \gamma'_{xy}.$$

Now, if the material is isotropic it follows that the directions of principal stress are also the directions of principal strains. The relationship between principal stresses and strains can then be written as

$$\sigma_1 = a_{11} \varepsilon_1 + a_{12} \varepsilon_2$$

$$\sigma_2 = a_{21} \varepsilon_1 + a_{22} \varepsilon_2 .$$

In matrix form, these equations can be written as

$$\begin{Bmatrix} \sigma_1 \\ \sigma_2 \end{Bmatrix} = \begin{bmatrix} a_{11} & a_{12} \\ a_{21} & a_{22} \end{bmatrix} \begin{Bmatrix} \varepsilon_1 \\ \varepsilon_2 \end{Bmatrix}$$

and from Cramer's Rule it therefore follows that

$$\varepsilon_1 = \frac{\sigma_1 \, a_{22}}{a_{11} a_{22} - a_{21} a_{12}} - \frac{\sigma_2 \, a_{12}}{a_{11} a_{22} - a_{21} a_{12}}$$

and that

$$\varepsilon_2 = - \frac{\sigma_1 \, a_{21}}{a_{11} a_{22} - a_{21} a_{12}} + \frac{\sigma_2 \, a_{11}}{a_{11} a_{22} - a_{21} a_{12}}$$

Again, from the assumption of isotropy, which states that the elastic properties are the same in all directions at a point in the elastic body, it follows that since the principal direction subscripts can be arbitrarily prescribed a complete interchange of subscripts can be made. Thus it follows that

$$a_{12} = a_{21}$$

$$a_{11} = a_{22} .$$

The constant $\frac{a_{11}}{a_{11} a_{22} - a_{21} a_{12}} = \frac{1}{E}$

and the constant $\frac{a_{12}}{a_{11} a_{22} - a_{21} a_{12}} = \frac{\nu}{E}$

Thus the direct extensions are related by the simple formulae, wherein the 9 general constants have been reduced to two,

$$\varepsilon_1 = \frac{1}{E} (\sigma_1 - \nu \sigma_2)$$

$$\varepsilon_2 = \frac{1}{E} (\sigma_2 - \nu \sigma_1) .$$

If, however, as is generally the case, the coordinate directions are not the principal directions then shear stresses and strains will exist simultaneously with the direct extensions. The shear strain is independent of the direct extensions and is related to the shear stress by the relation

$$\gamma'_{xy} = \frac{1}{G} \tau_{xy}$$

where, it can be shown

$$G = \frac{E}{2(1+\nu)}$$

Thus, in the general case where the coordinate axes are not the principal axes the two-dimensional equations relating stress and strain can be written

$$\varepsilon_x = \frac{1}{E}(\sigma_x - \nu\sigma_y)$$

$$\varepsilon_y = \frac{1}{E}(\sigma_y - \nu\sigma_x)$$

$$\gamma_{xy} = \frac{1}{G}\tau_{xy}$$

If the elastic body is heated it should be obvious that the small element under consideration will expand uniformly and the resulting deformation due to temperature T will be equal direct extensions αT, where α is the linear coefficient of thermal expansion, in both the x and y directions. The shear strain component will be unaffected. Thus the thermoelastic stress strain relations in the plane stress problem can be written as,

$$\varepsilon_x = \frac{1}{E}(\sigma_x - \nu\sigma_y) + \alpha T$$

$$\varepsilon_y = \frac{1}{E}(\sigma_y - \nu\sigma_x) + \alpha T$$

$$\gamma_{xy} = \frac{1}{G}\tau_{xy}$$

Strain - Displacement Relations.

Consider a point, O, in an elastic two-dimensional body. Under the influence of external loads and temperature differences this point will be displaced to a new position O_1 through the displacement components u and v. As discussed in Chapter A24, it is a necessary assumption of the linear theory of elasticity that these displacements be sufficiently small that no redefinition of the point O is required after deformation or that the squares and products of their derivatives may be neglected. The strain-displacement relations are derived by consideration of the deformation of a fiber oriented originally in the direction of the chosen component direction.

Consider the figure below,

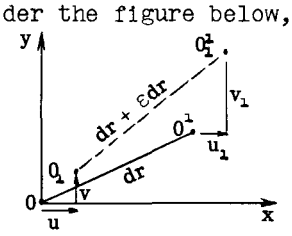

The figure shows an unstrained fiber $O\text{-}O^1$ located in the elastic body at the point O and at known orientation with respect to the axes x and y. Upon deformation of the body the fiber takes up the new position $O_1\text{-}O_1^1$. The original length of the straight fiber is dr and the length in the displaced position becomes $dr + \varepsilon dr$. The quantity ε is known as the strain of the fiber. The end displacements of the fiber are u, v and u_1, v_1 as shown. These end displacements are related by the equations

$$u_1 = u + \frac{\partial u}{\partial x} l\,dr + \frac{\partial u}{\partial y} m\,dr$$

$$v_1 = v + \frac{\partial v}{\partial x} l\,dr + \frac{\partial v}{\partial y} m\,dr$$

where l and m are the direction cosines of the fiber. The coordinates of O_1 are u and v. The coordinates of O^1 are l dr and m dr. The coordinates of O_1^1 are

$$l\,dr + u_1$$
$$\text{and } m\,dr + v_1$$

Thus the projection of the strained fiber on the x-axis is given by

$$l dr + u_1 - u = l dr + \frac{\partial u}{\partial x} l dr + \frac{\partial u}{\partial y} m dr$$

and along the y-axis by

$$m dr + (v_1 - v) = m dr + \frac{\partial v}{\partial x} l dr + \frac{\partial v}{\partial y} m dr \ .$$

From the right angle triangle it follows that

$$(dr + \varepsilon dr)^2 = (l dr + \frac{\partial u}{\partial x} l dr + \frac{\partial u}{\partial y} m dr)^2 + (m dr + \frac{\partial v}{\partial x} l dr + \frac{\partial v}{\partial y} m dr)^2$$

which leads to

$$\varepsilon = l^2 \frac{\partial u}{\partial x} + m^2 \frac{\partial v}{\partial y} + lm\left(\frac{\partial u}{\partial y} + \frac{\partial v}{\partial x}\right)$$

since $l^2 + m^2 = 1$.

Thus the strain of any fiber of a given orientation can be found if the derivatives of displacements are known. Consider the strain in the x-direction. This is obtained by considering a fiber originally aligned with the x-axis. In this case l = 1, m = 0 and

$$\varepsilon_x = \frac{\partial u}{\partial x}$$

Similarly the strain in the y-direction is given by

$$\varepsilon_y = \frac{\partial v}{\partial y}$$

The term $\frac{\partial u}{\partial y} + \frac{\partial v}{\partial x}$ is known as the shear strain. The physical meaning can be seen by consideration of a fiber oriented at an angle of 45^0 to the x-y axis system and therefore subtending an angle of 90^0 at the origin. It is left as an exercise to prove then that $\frac{\partial u}{\partial y} + \frac{\partial v}{\partial x}$ is the reduction in this subtended angle when the fiber is strained. This physical picture is, perhaps, better understood by reference to the figure below.

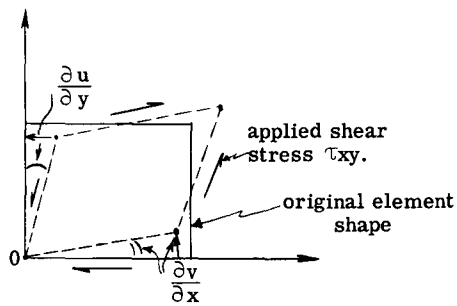

γ_{xy} = reduction in original 90° angle.

$$= \frac{\partial u}{\partial y} + \frac{\partial v}{\partial x}$$

It should be noted that the general expression for strain, ε, can now be rewritten in terms of ε_x, ε_y and γ_{xy} as follows,

$$\varepsilon = l^2\varepsilon_x + m^2\varepsilon_y + lm\,\gamma_{xy}$$

which is exactly analogous to the direct stress expression on a cutting plane oriented at an angle to the x-y axis system, viz:

$$\sigma = l^2\sigma_x + m^2\sigma_y + lm\,\tau_{xy}\,.$$

It is readily verified, therefore, that the directions of principle stress coincide with the direction of principal strains.

A25.4 Formulation of Plane Stress Problem.

(a) Stress Formulation - All boundary conditions given in terms of surface tractions.

The 2 equilibrium equations are already written in terms of the 3 stress components σ_x, σ_y, τ_{xy}. The compatability equation is given by 25.12. The equations which must therefore be satisfied by the three unknowns σ_x, σ_y, τ_{xy} are:

$$\left.\begin{aligned}\frac{\partial \sigma_x}{\partial x} + \frac{\partial \tau_{xy}}{\partial y} &= 0\\ \frac{\partial \sigma_y}{\partial y} + \frac{\partial \tau_{xy}}{\partial x} &= 0\end{aligned}\right\} \quad \text{when the body forces } X = Y = 0 \qquad 25.16$$

and

$$\frac{\partial^2\sigma_x}{\partial x^2} + \frac{\partial^2\sigma_x}{\partial y^2} + \frac{\partial^2\sigma_y}{\partial x^2} + \frac{\partial^2\sigma_y}{\partial y^2} + E\alpha\left(\frac{\partial^2 T}{\partial x^2} + \frac{\partial^2 T}{\partial y^2}\right) = 0 \qquad 25.17$$

when both E and α are independent of the temperature, T, and position in the body. The derivation of this compatability equation in terms of stresses is left as an exercise for the student.

The specific solution to a problem in this formulation requires those values of σ_x, σ_y and τ_{xy} which satisfy the above 3 equations and the boundary condition equations of 25.14.

When X = Y = 0 (body forces not present) or when these body forces can be represented by a potential function, V, in the following manner

$$X = -\frac{\partial v}{\partial x}\,, \quad Y = -\frac{\partial v}{\partial y} \qquad 25.18$$

the inverse solution technique usually proves the most profitable. Since, in the linear problems of elasticity and thermoelasticity, the stress formulation occurs most frequently this inverse approach is illustrated here in some detail. This approach is not restricted to the plane stress problem now under discussion and can be applied equally as well to plane strain or any two-dimensional stress formulations.

In general, one can choose a stress function ϕ defined by the relations

$$\sigma_x = \frac{\partial^2\phi}{\partial y^2}$$

$$\sigma_y = \frac{\partial^2\phi}{\partial x^2} \qquad 25.19$$

$$\tau_{xy} = -\frac{\partial^2\phi}{\partial x \partial y}$$

This function ϕ is commonly referred to as the Airy stress function since Airy first applied this well known mathematical technique to problems in elasticity.

It is obvious that the equilibrium equations are automatically satisfied by ϕ when chosen according to 25.19. To obtain a general solution for the stresses it remains, therefore, to solve only the compatability equation, 25.17, which, when written in terms of ϕ, becomes

$$\nabla^4 \phi = - E\alpha \nabla^2 T \qquad 25.20$$

when X = Y = 0

and

$$\nabla^4 \phi + (1-\nu)\nabla^2 v = -E\alpha \nabla^2 T \qquad 25.21$$

when the body forces X & Y are defined by 25.18.

In both 25.20 and 25.21

$$\nabla^4 \phi = \nabla^2(\nabla^2 \phi) = \frac{\partial^4 \phi}{\partial x^4} + \frac{\partial^4 \phi}{\partial y^4} + 2\frac{\partial^4 \phi}{\partial^2 x \partial^2 y}$$

and E and α are not functions of temperature. The general solution for ϕ is obtained by solving 25.20 or 25.21 for a given temperature distribution. The general solution for stresses follows directly from 25.19. The specific solution is obtained by substitution into 25.14, the boundary conditions.

In this case, where the boundary conditions are those of traction free boundary conditions, the equation 25.14 can be written in terms of ϕ as

$$\phi = 0$$

and $$\frac{\partial \phi}{\partial n} = 0 \qquad 25.22$$

where n is the outward drawn surface normal at all points on the boundary. Thus, the specific solution can be obtained in terms of ϕ directly and the specific solutions for σx, σy, and τxy by direct substitution into 25.19.

It should be noted that in this case of traction free boundary conditions there will exist no thermal stresses at all if the temperature distribution is such as to satisfy the equation

$$\nabla^2 T = 0 \qquad 25.23$$

and body forces do not exist. Thus, if T is constant or a linear function of x and y, no thermal stresses will result.

It is wise to repeat at this time that if there is any displacement restraint placed on the boundaries, stresses due to the restraint of thermal strains will result even though T is such as to satisfy the equation $\nabla^2 T = 0$. (See discussion in Chapter A24).

It is convenient, at this point, to present the definition of the stress function for cylindrical coordinates (equivalent to equation 25.19 and obtained therefrom by the simple transformation from the x-y plane to r-θ plane with z the axial direction.

$$r^2 = x^2 + y^2$$

$$\theta = \tan^{-1}\frac{y}{x}),$$

and the compatability equation from which the general solution is obtained (equivalent to equation 25.20 when the body forces are considered zero).

The stress function, ϕ, is defined by the equations

$$\sigma_r = \frac{1}{r}\frac{\partial \phi}{\partial r} + \frac{1}{r^2}\frac{\partial^2 \phi}{\partial \theta^2}$$

$$\sigma_\theta = \frac{\partial^2 \phi}{\partial r^2}$$

$$\tau r_\theta = \frac{1}{r^2}\frac{\partial \phi}{\partial \theta} - \frac{1}{r}\frac{\partial^2 \phi}{\partial r \partial \theta}$$

$$= -\frac{\partial}{\partial r}\left(\frac{1}{r}\frac{\partial \phi}{\partial \theta}\right)$$

and the compatability equation becomes

$$\left(\frac{\partial^2}{\partial r^2} + \frac{1}{r}\frac{\partial}{\partial r} + \frac{1}{r^2}\frac{\partial^2}{\partial \theta^2}\right)\left(\frac{\partial^2 \phi}{\partial r^2} + \frac{1}{r}\frac{\partial \phi}{\partial r} + \frac{1}{r^2}\frac{\partial^2 \phi}{\partial \theta^2}\right) =$$

$$-\Sigma\alpha\left(\frac{\partial^2 T}{\partial r^2} + \frac{1}{r}\frac{\partial T}{\partial r} + \frac{1}{r^2}\frac{\partial^2 \phi}{\partial \theta^2}\right)$$

This reduction of the 3-dimensional case to the 2-dimensional plane stress problem can be generalized to an equivalent problem which includes the case where the temperature varies through the plate or slice thickness, t, by employing the equations

$$\sigma_z = 0$$

$$\tau_{xz} = \tau_{yz} = 0 \qquad 25.24$$

at the upper and lower surfaces. The equations are analogous to 25.1. This equation requires that the stress components, the temperature, the displacements and the edge loadings be taken as average values across the thickness. For example, the temperature would be written as

$$T = \int_{-t/2}^{+t/2} T dz$$

The quantities τ_{xz}, τ_{yz}, γ_{xz}, γ_{yz} and w must be sufficiently small across the thickness that they can be neglected. This is not the exact plane stress problem and some care must be taken in its application as will be demonstrated in Chapter A26. The results will be average values of σ_x, σ_y, γ_{xy}, ε_x, ε_y, u, v across the thickness.

(b) Displacement Formulation - The bound-

ary conditions given in terms of boundary displacements. By choosing the displacement formulation the compatability equation is automatically satisfied. The general solution for the two displacements u and v are obtained from the two equilibrium equation written in terms of displacements as follows:

$$\frac{E}{2(1-\nu)}\frac{\partial}{\partial x}\left(\frac{\partial u}{\partial x}+\frac{\partial v}{\partial y}\right)+\frac{E}{2(1+\nu)}\nabla^2 u - \frac{\alpha E}{(1-\nu)}\frac{\partial T}{\partial x}+X=0$$

$$\frac{E}{2(1-\nu)}\frac{\partial}{\partial y}\left(\frac{\partial u}{\partial x}+\frac{\partial v}{\partial y}\right)+\frac{E}{2(1+\nu)}\nabla^2 v - \frac{\alpha E}{(1-\nu)}\frac{\partial T}{\partial y}+Y=0 \qquad 25.25$$

where, again, E, α and ν are constants. These equations are derived directly by the substitution of equations 25.4, .5, .6, .7, .8 and .9 into equations 25.2 and .3.

The specific solution is obtained by substituting the general solution into the boundary condition equations, 25.15, and solving for the unknown constants.

A25.5 Plane Strain.

The plane strain problem requires that no displacement exists in one of the coordinate axes directions, say the z-direction. Thus w = 0 and u and v are functions of x and y only. This is equivalent to requiring that the following strain components are zero,

$$\varepsilon_z = \gamma_{xz} = \gamma_{yz} = 0 \qquad 25.26$$

It follows that the 8 unknowns will be σ_x, σ_y, τ_{xy}, γ_{xy}, ε_x, ε_y, u and v. In this case of plane strain σ_z will be a function of σx and σy and is, therefore, not considered as an unknown. The substitution of 25.26 into the 15 equations of A24, reduces the number of independent equations to 8, the two equilibrium equations, the 3 stress-strain relations and the 3 strain-displacement relations. Thus the equation set is complete.

The condition that w = 0, displacements normal to the x-y plane do not exist, requires that any cut surface originally lying in the x-y plane remains parallel to this plane after deformation. One such physical system in which this situation will exist is that of a long cylindrical body subjected to external loads and temperature which are independent of the z, or axial, component and all loads and body forces act normal to the axial direction (i.e. all loading lies in the x-y plane and is independent of axial position in the body.) Such systems are common in missiles and rockets (the cylindrical shell body, the solid fuel grain, the rocket nozzle) atomic reactors (cylindrical fuel rods, heat exchanger tubes) etc.

The question of whether a system under analysis can be considered one of plane stress or one of plane strain is frequently raised and should be answered at this point. One must consider the system carefully and check as to whether all the requirements pertinent to one or the other states has been satisfied. If any have not then the problem is essentially a 3-dimensional one and the 15-equation set must be employed. However, in some cases, this decision is not a clear cut one. Consider, for example, the case of a cylindrical shell of finite length h, of diameter b, and which is loaded normal to its axis, body forces are zero and temperature is independent of the axial coordinate. If one considers the ratio of length to diameter, h/b, the problem can be classified as follows

$\frac{h}{b} \gg 1$ plane strain

$\frac{h}{b} \ll 1$ plane stress

$\frac{h}{b} \doteq 1$ 3-dimensional

It should be noted, that in actual fact, the plane stress problem is a three-dimensional strain problem and the plane strain problem one of three-dimensions in stress due to the possible presence of ε_z in the first and σ_z in the second.

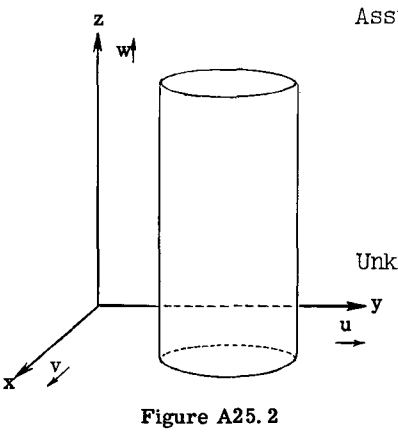

Assume: w=0; u=u(x,y); v=v(x,y)

Unknowns: $\gamma_{xz}=\gamma_{yz}=\varepsilon_z=0$; $\tau_{xz}=\tau_{yz}=0$; $\varepsilon_x=\varepsilon_x(x,y)$; $\varepsilon_y=\varepsilon_y(x,y)$; $\gamma_{xy}=\gamma_{xy}(x,y)$; $\sigma_x=\sigma_x(x,y)$; $\sigma_y=\sigma_y(x,y)$; $\tau_{xy}=\tau_{xy}(x,y)$

Figure A25.2

$\sigma_z = f(\sigma_x,\sigma_y)$ Known.

The distinction between plane stress and plane strain problems is clearly portrayed by comparison between figures 25.1 and 25.2.

By direct substitution of 25.26 into the general equations of Chapter A24 the following

8 equations of the plane strain problem result:

2 equations of equilibrium

$$\frac{\partial \sigma_x}{\partial x} + \frac{\partial \tau_{xy}}{\partial y} + X = 0 \qquad 25.27$$

$$\frac{\partial \tau_{xy}}{\partial x} + \frac{\partial \sigma_y}{\partial y} + Y = 0 \qquad 25.28$$

3 stress-strain relations (where $\varepsilon_z = 0$

$$\therefore \sigma_z = \underset{-E\alpha T}{\nu(\sigma_x+\sigma_y)}.$$

$$\varepsilon_x = \frac{1-\nu^2}{E}\left(\sigma_x - \frac{\nu}{1-\nu}\sigma_y\right) + (1+\nu)\alpha T \qquad 25.29$$

$$\varepsilon_y = \frac{1-\nu^2}{E}\left(\sigma_y - \frac{\nu}{1-\nu}\sigma_y\right) + (1+\nu)\alpha T \qquad 25.30$$

$$\gamma_{xy} = \frac{2(1+\nu)}{E}\tau_{xy} \qquad 25.31$$

3 strain-displacement relations

$$\varepsilon_x = \frac{\partial u}{\partial x} \qquad 25.32$$

$$\varepsilon_y = \frac{\partial v}{\partial y} \qquad 25.33$$

$$\gamma_{xy} = \frac{\partial u}{\partial y} + \frac{\partial v}{\partial x} \qquad 25.34$$

Boundary Conditions

The boundary condition equations from Chapter A24 reduce to the following in each case;

Case 1. Traction boundary conditions.

$$\bar{X} = \sigma_x l + \tau_{xy} m$$

$$\bar{Y} = \sigma_y m + \tau_{xy} l \qquad 25.35$$

In this plane strain problem there will result from the solution an apparent surface traction at the free ends given by

$$\bar{Z} = \sigma_z = \nu(\sigma_x + \sigma_y) - E\alpha_1 T$$

This is, of course, non-zero and therefore this boundary condition is not satisfied under the assumption of traction-free surfaces and only by the most rare chance would this coincide with a prescribed applied surface traction. This apparent surface traction must be removed by the application of an equal and opposite traction the results of which, as derived from an isothermal analysis, must be superimposed on the thermal stress analysis. If a surface traction is prescribed over this and the other surfaces a further isothermal analysis of the resulting stress, strain and displacement components would then be carried out and superimposed on the preceding solutions to obtain the actual solution.

This problem arises from the fact that σ_z is prescribed by the solution of the complete equation set. A similar problem would arise in the plane stress problem if surface strains were prescribed as boundary conditions which, of course, is never done.

Case 2. Displacement boundary conditions.

The boundary condition equations become

$$u = f(s)$$

$$v = g(s) \qquad 25.36$$

and the third displacement w must be zero since this was the governing equation of the plane strain problem.

Case 3. Mixed boundary conditions.

If the surface tractions are prescribed over part of the surface and displacements over the remainder then the equations of Case 1 and Case 2 must be applied where appropriate.

However, it is repeated here for emphasis that the linear thermoelastic analysis is usually broken down into a thermal stress analysis assuming all surfaces unrestrained and traction free, and upon the results of this part is superimposed an isothermal analysis in which the effect of external loading and satisfaction of prescribed boundary displacements is taken into account.

A25.6 Mathematical Equality of the Plane Stress and Plane Strain Problems.

It will be noted that if one makes the following substitutions,

$$E_1 = \frac{E}{1-\nu^2}$$

$$\nu_1 = \frac{\nu}{1-\nu} \qquad 25.37$$

$$\alpha_1 = \alpha(1+\nu)$$

the strain-stress equations, 25.29, 25.30 and 25.31, can be written

$$\varepsilon x = \frac{1}{E_1}(\sigma_x - \nu\sigma_y) + \alpha_1 T$$

$$\varepsilon y = \frac{1}{E_1}(\sigma_y - \nu_1\sigma_x) + \alpha_1 T \qquad 25.38$$

$$\gamma_{xy} = \frac{1}{G}\tau_{xy}$$

These equations are exactly of the same form as the same relations 25.4, 25.5, 25.6 in the plane stress problem. In fact the two equation sets are now identical except for the change in the elastic constants as given above. Thus the mathematical problem is identically the same and consequently the discussion of section A25.4 pertaining to the mathematical formulation is directly applicable to this plane strain problem so long as the reader changes the elastic constants E, ν and α to E_1, ν_1 and α_1. To avoid any confusion these discussions are briefly repeated here and the pertinent equations rewritten.

A25.7 Formulation of Plane Strain Problem.

As in the preceding case, the plane-strain problem can be formulated in terms of stresses or displacements.

(a) Stress Formulation:

The equations which must be satisfied by the three stress components σ_x, σ_y and τ_{xy} are

$$\left.\begin{aligned} \frac{\partial \sigma_x}{\partial x} + \frac{\partial \tau_{xy}}{\partial y} + X = 0 \\ \frac{\partial \sigma_y}{\partial y} + \frac{\partial \tau_{xy}}{\partial x} + Y = 0 \end{aligned}\right\} \text{ equilibrium} \qquad 25.39$$

$$\nabla^2(\sigma_x+\sigma_y) + E_1\alpha_1\nabla^2 T = 0 \quad \text{compatability}$$

$$= \nabla^2(\sigma_x+\sigma_y) + \frac{E\alpha}{1-\nu}\nabla^2 T, \qquad 25.40$$

where E, ν and α are constants, for the general solution, and for the specific solution, the boundary conditions just discussed.

If X = Y = 0 (body forces zero) the inverse formulation using the stress function ϕ, as defined in 25.19, is the most profitable approach requiring only the solution to the equation

$$\nabla^4 \phi = -E_1\alpha_1\nabla^2 T = -\frac{E\alpha}{1-\nu}\nabla^2 T \qquad 25.41$$

for the general solution.

If X and Y are non-zero and derivable from the relations $X = -\frac{\partial V}{\partial x}$, $Y = -\frac{\partial V}{\partial y}$ as discussed in A25.4a, the equation becomes

$$\nabla^4 \phi + (1-\nu_1)\nabla^2 V = -E_1\alpha_1\nabla^2 T.$$

$$\text{or} \quad \nabla^4 \phi + \frac{1-2\nu}{1-\nu}\nabla^2 V = -\frac{E\alpha}{1-\nu}\nabla^2 T. \qquad 25.42$$

(b) Displacement Formulation

In this case again only the equilibrium equations expressed in terms of displacements must be satisfied for the general solution. These two equilibrium equations are:

$$\frac{E_1}{2(1-\nu_1)}\frac{\partial}{\partial x}\left(\frac{\partial u}{\partial x}+\frac{\partial v}{\partial y}\right) + \frac{E_1}{2(1+\nu_1)}\nabla^2 u - \frac{\alpha_1 E_1}{(1-\nu_1)}\frac{\partial T}{\partial x} + X = 0$$

$$\frac{E_1}{2(1-\nu_1)}\frac{\partial}{\partial y}\left(\frac{\partial u}{\partial x}+\frac{\partial v}{\partial y}\right) + \frac{E_1}{2(1+\nu_1)}\nabla^2 v - \frac{\alpha_1 E_1}{(1-\nu_1)}\frac{\partial T}{\partial y} + Y = 0 \qquad 25.43$$

or, using E and ν, are:

$$\frac{E}{2(1+\nu)(1-2\nu)}\frac{\partial}{\partial x}\left(\frac{\partial u}{\partial x}+\frac{\partial v}{\partial y}\right) + \frac{E}{2(1-\nu^2)}\nabla^2 u - \frac{\alpha E}{1-2\nu}\frac{\partial T}{\partial x} + X = 0$$

$$\frac{E}{2(1+\nu)(1-2\nu)}\frac{\partial}{\partial y}\left(\frac{\partial u}{\partial x}+\frac{\partial v}{\partial y}\right) + \frac{E}{2(1-\nu^2)}\nabla^2 v - \frac{\alpha E}{(1-2\nu)}\frac{\partial T}{\partial y} + Y = 0 \qquad 25.44$$

The specific solution is obtained by use of the boundary condition equations just discussed.

A25.8 Concluding Discussion.

The 2-dimensional formulation of plane stress and plane strain just presented applies to the majority of structural systems with which the engineering stress analyst will have to deal. There will, however, arise heated structural shapes in which the stress, strain, and displacement components will not obviously be such as to comply with the restrictions imposed by the plane stress and plane strain idealization. In such cases the general equations of 3-dimensional thermoelasticity must be employed. These equations should be simplified as much as possible by assuming appropriate stress, strain, and displacement components either zero or negligible. In all such problems it is advisable to investigate the thermal stress analysis under the assumption of unrestrained and traction free boundary conditions leaving the evaluation of effects of external loading and boundary displacement restraint to an isothermal analysis. This approach will be illustrated in the later chapters where the thermoelastic analysis of shells of revolution is discussed.

A25.9 Problems.

(1) By direct substitution and use of the equilibrium equations 25.2 and 25.3 prove that the compatability equation 25.12

$$\nabla^2(\sigma_x + \sigma_y) + E\alpha\nabla^2 T = 0$$

follows from the equation

$$\frac{\partial^2 \gamma_{xy}}{\partial x \partial y} = \frac{\partial^2 \varepsilon_x}{\partial y^2} + \frac{\partial^2 \varepsilon_y}{\partial x^2}$$

(2) From the stress diagram in section A25.3 derive the equilibrium equations

$$\frac{\partial \sigma_x}{\partial x} + \frac{\partial \tau_{xy}}{\partial y} + X = 0$$

$$\frac{\partial \sigma_y}{\partial y} + \frac{\partial \tau_{xy}}{\partial x} + Y = 0$$

(3) For the inverse solution technique establish that the condition of zero surface traction can be written in terms of the stress function ϕ as

$$\phi = 0$$

$$\frac{\partial \phi}{\partial n} = 0$$

where n is the outward drawn normal.

(4) Prove that the equilibrium equations in cylindrical coordinates are given by

$$\frac{\partial \sigma_r}{\partial r} + \frac{1}{r}\frac{\partial \tau_{r\theta}}{\partial \theta} + \frac{\sigma_r - \sigma_\theta}{r} = 0$$

$$\frac{1}{r}\frac{\partial \sigma_\theta}{\partial \theta} + \frac{\partial \tau_{r\theta}}{\partial r} + \frac{2\tau_{r\theta}}{r} = 0$$

(5) Prove that the definition of the stress function in cylindrical coordinates is given by the equations

$$\sigma_r = \frac{1}{r}\frac{\partial \phi}{\partial r} + \frac{1}{r^2}\frac{\partial^2 \phi}{\partial \theta^2}$$

$$\sigma_\theta = \frac{\partial^2 \phi}{\partial r^2}$$

$$\tau_{r\theta} = -\frac{\partial}{\partial r}\left(\frac{1}{r}\frac{\partial \phi}{\partial \theta}\right)$$

when the r - θ plane corresponds to the x-y plane and body forces are absent.

(6) Establish the plane stress compatability equation as given in the text and, by direct substitution for the elastic constants, write the compatability equation for the plane strain thermoelastic problem. Modify both these equations to include the existence of body forces X and Y derivable from the function V as defined in 25.18.

(7) If a body force, R, acting only in the radial direction and independent of θ is defined as

$$R = \sqrt{X^2 + Y^2}$$

where X and Y are body forces in the x and y directions respectively and defined by

$$X = -\frac{\partial v}{\partial x}$$

$$Y = -\frac{\partial v}{\partial y}$$

prove, from the simple transformation from cartesian to cylindrical coordinates, that

$$R = \frac{\partial v}{\partial r}$$

and thus, for this special case, the equilibrium equations become

$$\frac{\partial \sigma_r}{\partial r} + \frac{1}{r}\frac{\partial \tau_{r\theta}}{\partial \theta} + \frac{\sigma_r - \sigma_\theta}{r} + \frac{\partial v}{\partial r} = 0$$

$$\frac{1}{r}\frac{\partial \sigma_\theta}{\partial \theta} + \frac{\partial \tau_{r\theta}}{\partial r} + 2\frac{\tau_{r\theta}}{r} = 0$$

REFERENCES

(1) "Elasticity in Engineering" E. E. Sechler, Galcit Aeronautical Series, John Wiley & Sons, Inc., 1952.

(2) "Applied Elasticity" Chi-Teh Wang, McGraw-Hill Book Co., Inc., 1953.

(3) All references of Chapter A24.

CHAPTER A26
SELECTED PROBLEMS IN ELASTICITY AND THERMOELASTICITY

A26.1 Introduction. The preceding chapter presented the general formulation of the two-dimensional equations of elasticity and thermoelasticity. This chapter is devoted to the development of solutions of simple problems in elasticity and thermoelasticity employing these equations rather than the Strength of Materials approach which will be discussed in the chapter on beams. These problems have been selected to illustrate clearly the formulation of the governing equations for the chosen mathematical model, the solution of these equations and the interpretation of the results. A large store of such problems exist in the literature, especially in the case of the isothermal analysis, which is referenced at the close of this chapter. Consequently the problems chosen for this chapter are to illustrate the technique only and, while they may appear trivial to some readers, they are intended to provide a reasonably sound knowledge of the techniques so that the literature can be read easily and with confidence. In all of the problems of this chapter the basic assumptions of Chapter A24 are observed and consequently the discussion is restricted to elastic materials whose properties are not affected by temperature.

The chapter opens with a selection of simple one-dimensional problems which are interjected at this point merely to provide the student with an understanding of the behaviour of metals when they are heated and the elastic constants are not affected by the temperature rise. This section is then followed by a selection of problems in which the formulations of the preceding chapter are employed.

A26.2 One-Dimensional Problems.

Example 1.

Consider a cylindrical bar of metal mounted between two rigid walls as shown in Figure A26.1.

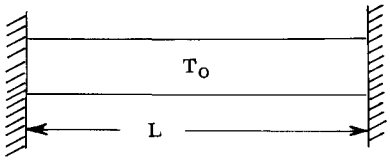

Fig. A26.1

The geometrical properties of the bar at the initial temperature, T_0, are completely prescribed by the cross-sectional area A and the length L. The only restraint is that imposed on the length L by the rigid walls. The problem is to determine the stress distribution throughout the bar and the change in shape when temperature is increased to T.

Assume the bar is unrestrained during the heating. The change in length will be

$$\Delta L = \alpha(T - T_0)L$$

or, the new heated total length will be

$$L_1 = L\left[1 + \alpha(T - T_0)\right]$$

$T - T_0$ = Temperature change

where α = Coefficient of linear thermal expansion

= Change in length per unit length (at a chosen reference temperature level) per degree change in temperature.

In engineering it is common practice to measure temperature change in $^{\circ}F$ and to use the reference temperature as $32^{\circ}F$. So long as α is a constant the reference temperature could be as well chosen as the original temperature since, by the definition above, the value of α would be the same. However, for most materials, α is a coefficient of the temperature and therefore the values given in the following table are applicable only over the stated temperature

TABLE A26.1
REPRESENTATIVE VALUES OF α
(Original length measured at $32^{\circ}F$)

Material	Temp. $^{\circ}F$	α
Aluminum (99.95%)	68 - 212	13.22×10^{-6}
Commercial	68 - 212	13.33×10^{-6}
Beryllium (98.9%)	68 - 212	6.83×10^{-6}
Brass (66 Cu, 34 Zn)	32 - 212	10.42×10^{-6}
Bronze (93.5 Cu, 6.5 Sn)	68 - 212	9.72×10^{-6}
Graphite	100	4.37×10^{-6}
Copper	70 - 212	9.33×10^{-6}
Glass	32 - 212	4.63×10^{-6}
Steel	32 - 212	5.88×10^{-6}
Molybdenum	70 - 212	2.72×10^{-6}
Invar (Nickel Steel)	100	0.46×10^{-6}
Stainless Steel	70 - 212	5.33×10^{-6}
Tungsten (99.978%)	- 212	2.33×10^{-6}
	32 - 950	2.56×10^{-6}
(powder metallurgy)	4000	5.65×10^{-6}
Magnesium Oxide	75 - 212	5.6×10^{-6}

range. Furthermore, every alloy of the materials shown possess a characteristic α. The table can, therefore, be used only as a guide to the appropriate values of α and the exact value obtained from a more extensive source.

Now, for the example under discussion, it can be seen that the bar will have to be compressed an amount ΔL to fit between the rigid walls. This will give rise to a compressive strain of $\Delta L/L$, or

$\varepsilon = -\alpha(T - T_0)$ in the axial direction, and a compressive stress of

$$\sigma = -E\alpha(T - T_0)$$

Thermal expansion in the radial direction as well as an elastic strain due to Poisson's effect will also occur. However there will be no stresses in the radial direction since there are no restraints or expansion in this direction and no surface tractions are applied. Thus there will exist the compressive stress uniformly distributed over the cross-section throughout the length of the bar, if, and only if, no restraints on the radial deformations exist at the ends against the walls. The total load reacting against the wall will be

$$P = -E\alpha(T - T_0)\, A_1$$

where A_1 is the area of the final cross-section shape and thus the change in this cross-section could be significant in the calculation of P if the material possessed a large value for α and the temperature rise was large. The Poisson effect is usually negligible. It is left as an exercise for the student to determine A_1 in Problem 26.1.

Example 2.

Consider the system of two cylindrical bars supported between rigid, frictionless walls and heated to temperature T above the ambient temperature T_0 when the bars were a perfect fit between the walls. The system is shown below in Figure A26.2.

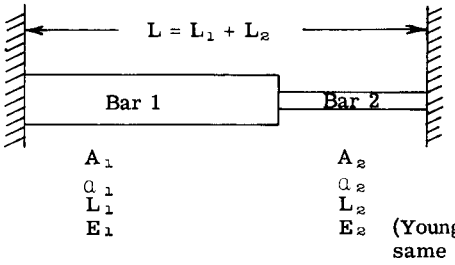

Fig. A26.2

The geometrical properties and the linear coefficient of thermal expansion are different for each bar. The problem is to determine the axial stress in each bar and the displacement of the interface under the assumption of no restraints in the radial direction and no surface tractions.

Again we remove the restraint from one end. The total expansion will be

$$\Delta L = \alpha_1 L_1 (T - T_0) + \alpha_2 L_2 (T - T_0)$$

and the bars must be compressed by a common force P so that this total displacement is removed.

The stress in bar 1 will be $\sigma_1 = \dfrac{-P}{A_1}$

and the stress in bar 2 will be $\sigma_2 = \dfrac{-P}{A_2}$

The corresponding strains will be

$$\varepsilon_1 = -\frac{P}{A_1 E}$$

and $$\varepsilon_2 = -\frac{P}{A_2 E}$$

The corresponding displacement, or change in length, of each bar will be

$$u_1 = -\frac{P}{A_1 E} L_1$$

and $$u_2 = -\frac{P}{A_2 E} L_2$$

Now $u_1 + u_2 = \Delta L$

$$\therefore -P\left[\frac{L_1}{A_1 E} + \frac{L_2}{A_2 E}\right] = (\alpha_1 L_1 + \alpha_2 L_2)(T - T_0)$$

or $$P = -\frac{(\alpha_1 L_1 + \alpha_2 L_2)\,(T - T_0)}{\left(\frac{L_1}{A_1 E} + \frac{L_2}{A_2 E}\right)}$$

It then follows that

$$\sigma_1 = -\frac{(\alpha_1 L_1 + \alpha_2 L_2)\,(T - T_0)}{\left(\frac{L_1}{E} + \frac{A_1 L_2}{A_2 E}\right)}$$

and $$\sigma_2 = -\frac{(\alpha_1 L_1 + \alpha_2 L_2)\,(T - T_0)}{\left(\frac{A_2 L_1}{A_1 E} + \frac{L_2}{E}\right)}$$

The final position of the interface will be located at a distance x from the left hand wall given by the original length of bar 1 plus its thermal elongation plus u_1, or

$$x = L_1 + \alpha_1 L_1 (T - T_0) - \frac{L_1}{E}\,\frac{(\alpha_1 L_1 + \alpha_2 L_2)(T - T_0)}{\left(\frac{L_1}{E} + \frac{A_1 L_2}{A_2 E}\right)}$$

It is interesting to note that this problem is essentially not this simple. The analysis re-

quires the assumption that the interface stress distribution is uniform across the section of each bar. In the case of bar 1 this will certainly not be the case. The extension to the problem where this two-dimensional stress field is taken into account is beyond the scope of this chapter. It is sufficient to note that this effect will be negligible in all cases except where the ratio of A_1 / A_2 is large and, again, where the value of P is large.

Besides this obvious extension of the problem the following meaningful studies are apparent.

(a) The investigation of the stability of the simple column system and
(b) The investigation of the flow behavior at very high temperatures for both or one of the materials.

These significant and difficult aspects of this seemingly simple problem will be returned to in later chapters.

Example 3.

The same problem will be analyzed in a more direct manner which does not require the technique of considering the system completely unrestrained to begin with and then determining the loads necessary to restore the original, or defined, shape. While this stated technique has been discussed in Chapters A24.4 and A24.5 as being the most desirable, the direct approach is sometimes the more rational and, therefore, must not be overlooked. This problem serves as a good comparative example at this stage in the development of the theory of thermoelasticity.

Consider the Figure A26.3 which is the same as Figure A26.2 but shows the positive coordinate system, the boundary conditions with a possible deformed position illustrated.

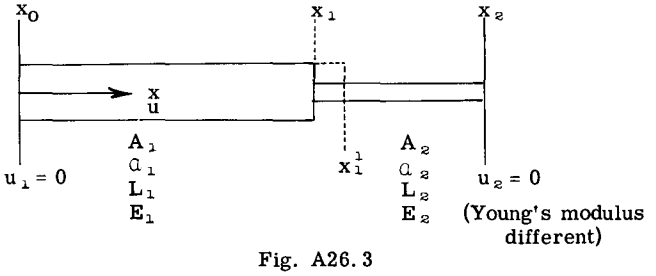

Fig. A26.3

The total strain in the system will be

$$\varepsilon_X = \varepsilon_{X_1} + \varepsilon_{X_2}$$

where

$$\varepsilon_{X_1} = \frac{\sigma_{X_1}}{E_1} + \alpha_1(T - T_0)$$

and

$$\varepsilon_{X_2} = \frac{\sigma_{X_2}}{E_2} + \alpha_2(T - T_0)$$

From the strain-displacement relations where, in this case, u is a function of x only

$$\varepsilon_{X_1} = \frac{du_1}{dx}$$

$$\varepsilon_{X_2} = \frac{du_2}{dx}$$

It then follows that

$$u_1 = \int_0^{X_1} \left[\frac{\sigma_{X_1}}{E_1} + \alpha_1(T - T_0)\right] dx$$

and

$$u_2 = \int_{X_1}^{X_2} \left[\frac{\sigma_{X_2}}{E_2} + \alpha_2(T - T_0)\right] dx$$

But $u_1 + u_2 = 0$ if the interface is to remain, as such and no total elongation is allowed. Furthermore, since the same force is transmitted through each bar,

$$\sigma_{X_1} A_1 = \sigma_{X_2} A_2$$

Consequently

$$\int_0^{X_1} \left[\frac{\sigma_{X_1}}{E_1} + \alpha_1(T-T_0)\right] dx + \int_{X_1}^{X_2} \left[\frac{\sigma_{X_1}}{E_2}\frac{A_1}{A_2} + \alpha_2(T-T_0)\right] dx = 0$$

Since σ_X, E, E_2, A_1, A_2, α_1 and α_2 are constants throughout the system the integration in this case is straight forward and since $0 \rightarrow x_1 = L_1$ and $x_1 \rightarrow x_2 = L_2$.

$$\frac{\sigma_{X_1}}{E_1} L_1 + \alpha_1(T-T_0)L_1 + \frac{\sigma_{X_1}}{E_2}\frac{A_1}{A_2} L_2 + \alpha_2(T-T_0)L_2 = 0$$

It then follows directly that

$$\sigma_{X_1} = -\frac{(\alpha_1 L_1 + \alpha_2 L_2)(T - T_0)}{\left(\frac{L_1}{E_1} + \frac{L_2}{E_2}\frac{A_1}{A_2}\right)}$$

$$\sigma_{X_2} = -\frac{(\alpha_1 L_1 + \alpha_2 L_2)(T - T_0)}{\left(\frac{L_1}{E_1} + \frac{L_2}{E_2}\frac{A_1}{A_2}\right)}\frac{A_1}{A_2}$$

and

$$u_1 = -u_2 = \alpha_1 L_1(T-T_0) - \frac{L_1}{E_1}\frac{(\alpha_1 L_1 + \alpha_2 L_2)(T-T_0)}{\left(\frac{L_1}{L_1} + \frac{A_1 L_2}{A_2 E_2}\right)}$$

which is the same as before. The inherent advantage in this direct approach is the generalization of the problem to take into account possible variations in cross-section shape and

variation of the physical properties in the axial direction.

Example 4.

A direct application of the preceding examples is the determination of shear and tensile stresses developed in bolts of a bolted connection. Consider the bolted connection between two dissimilar metals which are heated to different temperatures T_1 and T_2 above ambient temperature T_0. Initial bolt clearances are normally allowed in bolted connections to relieve thermal stresses and such clearances are shown in Figure A26.4 as C_1 and C_2.

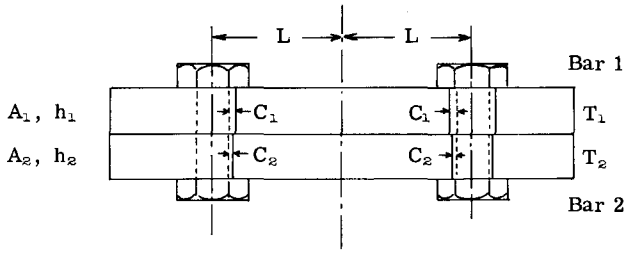

Fig. A26.4

Associated with bar 1 and bar 2 are the material constants E_1, α_1 and E_2, α_2 respectively.

Determination of shear load transmitted: -

Due to symmetry we need consider only one side of the above system. Assume $T_1 > T_2$ and $\alpha_1 > \alpha_2$ (the generalization to other combinations is straight forward and will follow the same development).

Assume the bolt removed.

Bar 1 expands an amount $\alpha_1(T_1 - T_0)L$ = displacement of hole center line.

Bar 2 expands an amount $\alpha_2(T_2 - T_0)L$

Thus the relative displacement of the hole center line will be

$$\alpha_1(T_1 - T_0)L - \alpha_2(T_2 - T_0)L$$

The allowable clearance will be $C_1 + C_2$ so that the relative displacement between the two bars necessary to realign the holes so that the bolt will just fit will be given by

$$-\alpha_1(T_1 - T_0)L + \alpha_2(T_2 - T_0)L + (C_1 + C_2)$$

If all of this motion is obtained by compressing bar 1, inserting the bolt and then releasing the system the two bars will expand together to an equilibrium position wherein the same force, P, exists in each. The total motion of the precompressed bar 1 after the insertion of the pin will be

$$\left[\alpha_1(T_1 - T_0)L - \alpha_2(T_2 - T_0)L - (C_1 + C_2)\right] - \frac{PL}{E_1A}$$

and the motion of bar 2 will be $\frac{PL}{E_2A_2}$. Since these motions must be the same it follows directly that

$$P = \frac{\alpha_1(T_1 - T_0) - \alpha_2(T_2 - T_0) - \left(\frac{C_1 + C_2}{L}\right)}{\left(\frac{1}{A_1E_1} + \frac{1}{A_2E_2}\right)}$$

In this chosen case, P will produce compression in the bar 1 and tension in bar 2 since the expansion of bar 1 was initially greater than that of bar 2 and it was assumed that this relative expansion was greater than the total clearance, which, of course, is necessary for the creation of thermal stresses at all. The solution should be generalized to

$$P = \frac{\pm\ \alpha_1(T_1 - T_0) \mp \alpha_2(T_2 - T_0) - \left(\frac{C_1 + C_2}{L}\right)}{\left(\frac{1}{A_1E_1} + \frac{1}{A_2E_2}\right)}$$

and the appropriate signs chosen from an initial estimate of the relative displacements. It is an interesting extension of this problem to take into account the elastic deformation of the bolt in an array of bolts.

The tension load on the bolt, additive to any bolt prestress, can be deduced in the following way. The total expansion in the bars in the bolt axis direction will be (due to thermal expansion) in each sheet.

$$\alpha_1(T_1 - T_0)h_1 \quad \text{and} \quad \alpha_2(T_2 - T_0)h_2$$

There will be an elastic contraction however, due to the bolt increased tension force P which will be

$$P\left(\frac{h_1}{E_1A_1}\right) \quad \text{and} \quad P\left(\frac{h_2}{E_2A_2}\right) \quad \text{respectively.}$$

where A_1 and A_2 are assumed bar areas affected by the bolt tension. A commonly used estimate of this area is that contained in the circle of two bolt diameters about the bolt centerline. Consequently the total bar deformation in the bolt axis direction will be

$$\alpha_1(T_1 - T_0)h_1 + \alpha_2(T_2 - T_0)h_2 - \frac{Ph_1}{E_1A_1} - \frac{Ph_2}{E_2A_2}$$

Now, the total extension in the bolt, assuming it to be at a temperature T_3, will be

$$\alpha_B\ (T_3 - T_0)(h_1 + h_2) + \frac{P}{E_B}\ \frac{(h_1 + h_2)}{A_B}$$

where the subscript B refers to the bolt.

These extensions must, of course, be the same and therefore

$$P = \frac{\alpha_1(T_1-T_0)h_1+\alpha_2(T_2-T_0)h_2-\alpha_B(T_3-T_0)(h_1+h_2)}{\frac{h_1+h_2}{E_B A_B} + \frac{h_1}{E_1 A_1} + \frac{h_2}{E_2 A_2}}$$

The extension of this last formula to multiple layers, bolts of varying diameters wherein the temperature varies along the length, etc., is obvious from the above development and the discussion in example 3 as it applies to varying temperature along the bolt axis.

Example 5.

It is becoming relatively common practice to design primary structures to avoid thermal stresses. One obvious way of doing so is to replace the usual flanged wing beam with a statically determinant truss for no thermal stresses can exist in such structures so long as no restraints are imposed on the thermal expansion of the whole truss system.

The use of corrugated webs is one example of a structural technique designed to relieve thermal stresses. In such structures, however, the thermal strains and hence, deflections, become large and must be considered.

Redundant structures will contain thermal stresses whenever non-uniform heating is present even though there are no geometrical restraints imposed. In the case of statically indeterminant trusses or space frames wherein individual members are at different temperatures the analysis is the same as for the isothermal problem wherein the readily computed thermal strains and deflections are introduced as initial deformations. This problem is discussed in detail in article A8.9 of Chapter A8 and consequently is not treated here.

Attention will be now directed to continuous structures such as plates and beams, wherein the two-dimensional formulations of Chapter A25 will be required.

A26.3 Two-dimensional Problems.

Example 1.

As the first example let us consider the problem of the simple beam subjected to an externally applied moment and with the whole system at room temperature. The physical system is as shown below in Figure A26.5.

The problem is to determine the stress, strain and displacement distribution throughout the beam under the influence of the positive end moments shown. The mathematical model is

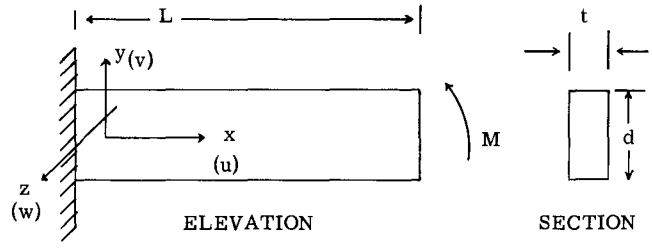

Fig. A26.5

the same geometrically as that shown in the Figure A26.5 but with the following assumptions:

(1) There are no displacements out of the x-y plane, i.e., w = 0.

(2) All deformations are small so that the equations of the basic formulation apply.

(3) Since the beam is thin (t is small), the applied moment lies in the plane x-y, and there are no surface forces on the sides of the beam, thus there exists no stress components in the z-direction.

(4) There are no body forces present, i.e. X = Y = Z = 0.

From assumption (3) it is obvious that all stresses lie in the plane x-y and the problem is therefore one of plane stress. (It so happens that under assumption (2), which is applied merely as a convenience at this time, the problem is also one of plane strain.)

The question now is to determine stress functions for σ_x, σ_y and τ_{xy} which will satisfy the equation of equilibrium, compatability and the boundary conditions. The basic equations are: -

$$\left.\begin{aligned} \frac{\partial\sigma_x}{\partial x} + \frac{\partial\tau_{xy}}{\partial y} &= 0 \\ \frac{\partial\sigma_y}{\partial y} + \frac{\partial\tau_{xy}}{\partial x} &= 0 \end{aligned}\right\} \quad \text{equilibrium}$$

$$\frac{\partial^2\gamma_{xy}}{\partial x\partial y} = \frac{\partial^2\varepsilon_x}{\partial y^2} + \frac{\partial^2\varepsilon_y}{\partial x^2} \qquad \text{compatability}$$

and the boundary conditions

$$\int_{-\frac{d}{2}}^{+\frac{d}{2}} t\sigma_x \, dy = 0 \quad \text{(applied end thrust is zero)}$$

$$\int_{-\frac{d}{2}}^{+\frac{d}{2}} t\sigma_x y \, dy + M = 0 \quad \text{(summation of moments = 0)}$$

From assumption (3)

$$\sigma_z = \tau_{xz} = \tau_{yz} = 0$$

and thus

$$\varepsilon_z = \gamma_{xz} = \gamma_{yz} = 0$$

Since the external loading is bending only and there is no variation of same in the x-direction, it is reasonable to assume the strain distribution to be of the following form:

$$\varepsilon_x = C_0 + C_1 y \quad \text{(plane sections remain plane)}$$
$$\varepsilon_y = f(y)$$

and thus

$$\sigma_x = E(C_0 + C_1 y)$$

$$\sigma_y = E f(y)$$

From the first equilibrium equation it then follows that τ_{xy} must be a constant or a function of x only. Then, from the second equilibrium equation

$$\frac{\partial \sigma_y}{\partial y} = -\frac{\partial \tau_{xy}}{\partial x}$$

or $E\frac{df(y)}{dy} = 0$, a constant or a function of x.

Due to the symmetry of loading the last possibility does not exist, the second possibility allows f(y) to be linear function of y and the third allows f(y) to be a constant. Neither of these are possible since there are no normal forces along the top and bottom edges to balance a σ_y component. The only solution for f(y), and therefore for σ_y, which will satisfy the equilibrium equations is therefore

$$f(y) = \frac{\sigma_y}{E} = 0$$

Thus we have two possible stress components

$$\sigma_x = (C_0 + C_1 y)E$$

$$\tau_{xy} = f(x)$$

The first equation of equilibrium is satisfied but, from the second and the discussion on f(y) it is obvious that

$$\tau_{xy} = 0$$

(This could have been assumed directly, of course, since there is no externally applied shear present, but the matter of zero internal shear has been belabored since many students appear to have some difficulty in grasping this simple fact.)

Thus the only stress component present is σ_x and the equations of equilibrium are satisfied. It is obvious also that since

$$\varepsilon_x = C_0 + C_1 y$$

$$\varepsilon_y = -\frac{\nu}{E}\sigma_x$$

$$\gamma_{xy} = 0 ,$$

the equation of compatability is also satisfied. Thus we have the unique general solution to the mathematical model chosen.

$$\sigma_x = E(C_0 + C_1 y)$$

$$\sigma_y = \tau_{xy} = \tau_{xz} = \tau_{yz} = \sigma_z = 0.$$

It now remains to obtain the specific solution which satisfies the boundary conditions. By direct substitution into the boundary condition equations, the constants C_0 and C_1 are readily evaluated as

$$C_0 = 0$$

$$C_1 = -\frac{M}{E\int_{-\frac{d}{2}}^{+\frac{d}{2}} t y^2 \, dy} = -\frac{M}{EI}$$

and thus $\sigma_x = -\frac{M}{I} y$, the well known simple beam formula where the negative sign indicates compression. Now the strain distribution throughout the beam will be given by

$$\varepsilon_x = -\frac{My}{EI} \quad , \quad \varepsilon_y = \frac{\nu My}{IE}$$

$$\varepsilon_z = \gamma_{xy} = \gamma_{xz} = \gamma_{yz} = 0.$$

and the displacement distribution, from the strain-displacement relations

$$\left.\begin{aligned} \varepsilon_x &= \frac{\partial u}{\partial x} \\ \varepsilon_y &= \frac{\partial v}{\partial y} \\ \gamma_{xy} &= \frac{\partial u}{\partial y} + \frac{\partial v}{\partial x} \end{aligned}\right\} \quad \begin{aligned} u &= -\frac{My}{EI}.x + f_1(y) \\ v &= g_1(x) + \frac{\nu My^2}{2IE} \end{aligned}$$

Since u = 0 at x = 0, it follows that $f_1(y) = 0$. Then, from the third strain-displacement relation it follows that

$$\frac{dg_1(x)}{dx} = \frac{Mx}{EI}$$

and therefore

$$g_1(x) = \frac{Mx^2}{EI2} + h$$

Since, at x = 0, v = 0 then it follows that h = 0 at y = 0. Thus the displacement distribution will be

$$u = \frac{Myx}{EI}$$

$$v = \frac{Mx^2}{2EI} + \nu\frac{My^2}{2EI}$$

$$w = 0.$$

Example 2.

Consider now the same problem but with the external load a transverse force, P, applied at the end.

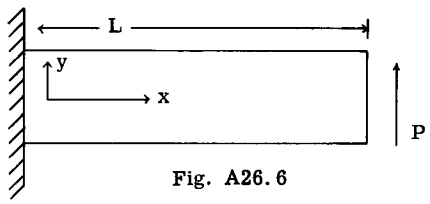

Fig. A26.6

The same basic assumptions are made as in the previous example and the basic equations are the same. The boundary condition equations are the same when the applied moment, M, is given by

$$M = P(L - x)$$

We will again assume that the strain distribution is of the following form

$$\varepsilon_x = (C_0 + C_1 y)g(x)$$

$$\varepsilon_y = f(y)$$

$$\varepsilon_z = 0$$

The assumption for ε_x is more meaningful in this case for it limits the discussion to beams such that the bending action is predominant. This means that the solution developed under this assumption applies only to beams where $L \gg d$. Let us consider one station, i.e., one value of x, along the beam and consider first the boundary condition equations. From the first, viz;

$$\int_{-\frac{d}{2}}^{+\frac{d}{2}} \sigma_x t\,dy = 0$$

it follows, as before, that $C_0 = 0$.

From the second and letting $C_1 g(x) = C_2(x)$

$$EC_2 \int_{-\frac{d}{2}}^{\frac{d}{2}} ty^2\,dy + P(L - x) = 0$$

and therefore

$$C_2 = -\frac{P(L - x)}{EI}$$

so that

$$\sigma_x = -\frac{P(L - x)}{I}\,y$$

From the first equation of equilibrium it follows that

$$\frac{\partial \tau_{xy}}{\partial y} = -\frac{Py}{I}$$

By integration

$$\tau_{xy} = -\frac{Py^2}{2I} + f(x)$$

Now, since there must be zero shear on the top and bottom faces of the beam, i.e., at $x = \pm\frac{d}{2}$ it follows directly that f(x) is a constant given by

$$C_3 = \frac{Pd^2}{8I}$$

and therefore $\tau_{xy} = \frac{P}{2I}\left(\frac{d^2}{4} - y^2\right)$

From the second equation of equilibrium it follows that

$$\frac{\partial \sigma_y}{\partial y} = 0$$

and thus, from the same argument as in the previous example, it follows that

$$\sigma_y = 0$$

The strain distribution follows directly

from Hooke's law and the assumptions to give

$$\varepsilon_z = \gamma_{xz} = \gamma_{yz} = 0$$

$$\varepsilon_x = -\frac{P}{EI}(L - x)y$$

$$\varepsilon_y = +\frac{\nu}{EI}P(L - x)y$$

$$\gamma_{xy} = \frac{P}{2IG}\left(\frac{d^2}{4} - y^2\right)$$

These strain components obviously satisfy the compatability equations.

The displacement distribution can be obtained from the strain-displacement relations as follows:

$$\text{Since } \varepsilon_x = \frac{\partial u}{\partial x} = -\frac{P}{EI}(L - x)y$$

$$\text{it follows that } u = -\frac{PLyx}{EI} + \frac{Px^2y}{2EI} + f(y)$$

$$\text{and since } \varepsilon_y = \frac{\partial v}{\partial y} = \frac{\nu}{EI}P(L - x)y$$

$$\text{it follows that } v = k(x) + \frac{\nu}{EI}P(L - x)\frac{y^2}{2}$$

Since $u = 0$ at $x = 0$ it follows directly that $f(y) = 0$. From the third strain-displacement relation, viz:

$$\gamma_{xy} = \frac{\partial u}{\partial y} + \frac{\partial v}{\partial x}$$

it follows, by direct substitution, that

$$\frac{P}{2IG}\left(\frac{d^2}{4} - y^2\right) = \frac{PLx}{EI} + \frac{Px^2}{2EI} + \frac{\partial v}{\partial x}$$

We are interested in the deflection of the neutral axis only, that is the plot of $\bar{v}\ (x, y = 0)$ and therefore we can rewrite this equation as

$$\frac{d\bar{v}}{dx} = \frac{Pd^2}{8IG} + \frac{PLx}{EI} - \frac{Px^2}{2EI}$$

Consequently we are imposing the boundary condition that at $x = 0$, $\frac{d\bar{v}}{dx} = 0$.

Upon integration and satisfaction of the boundary condition $\bar{v} = 0$ at $x = 0$, the general expression for the deformation of the neutral axis will be obtained as:

$$\bar{v} = \frac{Pxd^2}{8IG} - \frac{Px^3}{6EI} + \frac{PLx^2}{2EI}$$

and the deflection at the tip will be

$$\bar{v}_{x=L} = \frac{PL^3}{3EI} + \frac{PLd^2}{8IG}$$

It is interesting to note that this solution differs from that developed from the Strength of Materials approach. The term $\frac{PLd^2}{8IG}$ arises from the shearing force and is effectively a rotation at the end $x = 0$ given by

$$\left.\frac{\partial v}{\partial x}\right|_{\substack{x=0\\y=0}} = \frac{Pd^2}{8IG}$$

If this rotation is prevented, as it is in this case, then the tip deflection should be:

$$v_{\substack{y=0\\x=L}} = \frac{PL^3}{3EI}$$

which would have been the solution had we imposed the boundary condition at the station $x = 0$

$$\left.\frac{\partial v}{\partial x}\right|_{\substack{x=0\\y=0}} = 0$$

The fixed end is not free to distort and thus allow the displacement distribution obtained above and therefore the stress and strain distribution will not be that obtained in the vicinity of this fixed end. The solution will be valid throughout the beam for all points $x > d$ (Saint-Venant's Principle). It should be mentioned also that for the solution to be valid in the neighborhood of the free end the shear load P must be applied according to the shear distribution

$$\frac{P}{2I}\left(\frac{d^2}{4} - y^2\right)$$

If this is not done then the solution will not apply in the region of the free end.

This matter of the fixed end boundary conditions deserves more study and is therefore discussed in the next example. For an even more exhaustive discussion the reader is referred to Reference 1.

Example 3.

In the previous example the stress distribution was obtained as

$$\sigma_x = -\frac{P(L - x)y}{I}$$

$$\sigma_y = 0$$

$$\tau_{xy} = \frac{P}{2I}\left(\frac{d^2}{4} - y^2\right)$$

Therefore, from Hooke's Law and assuming $\nu \neq 0$, the strain distribution will be

$$\varepsilon_x = -\frac{P}{EI}(L - x)y$$

$$\varepsilon_y = \frac{\nu P}{EI}(L - x)y$$

$$\gamma_{xy} = \frac{P}{2IG}\left(\frac{d^2}{4} - y^2\right)$$

and then, from the strain-displacement relations

$$u = -\frac{Pxy}{EI}\left(L - \frac{x}{2}\right) + f(y)$$

$$v = \frac{\nu P}{2EI}(L - x)y^2 + g(x)$$

where $f(y)$ and $g(x)$ are functions respectively of y and x alone. It is the aim in this example to evaluate these functions in a more general sense than was done in Example 2. Substitution of the expressions for u and v in the third strain-displacement relation, viz:

$$\gamma_{xy} = \frac{\partial u}{\partial y} + \frac{\partial v}{\partial x}$$

gives

$$\frac{P}{2IG}\left(\frac{d^2}{4} - y^2\right) = -\frac{Px}{EI}\left(L - \frac{x}{2}\right) + f'(y) - \frac{\nu Py^2}{2EI} + g'(x)$$

where $f'(y) = \frac{df}{dy}$ and $g'(x) = \frac{dg}{dx}$

This equation must hold for all values of x and y and we can therefore investigate the nature of the functions $f'(y)$ and $g'(x)$ by alternately letting x and y be zero. For $y = 0$,

$$\frac{Pd^2}{8IG} = -\frac{Px}{EI}\left(L - \frac{x}{2}\right) + f'(o) + g'(x)$$

For $x = 0$ $\quad \frac{P}{2IG}\left(\frac{d^2}{4} - y^2\right) = f'(y) - \frac{\nu Py^2}{2EI} + g'(o)$

For $x = 0$, $y = 0$

$$\frac{Pd^2}{8IG} = f'(o) + g'(o)$$

Now $f'(o)$ and $g'(o)$ are constants C_1 and C_2 respectively. Therefore

$$g'(x) = \frac{Pd^2}{8IG} + \frac{Px}{EI}\left(L - \frac{x}{2}\right) - C_1$$

$$f'(y) = \frac{P}{2IG}\left(\frac{d^2}{4} - y^2\right) + \frac{\nu Py^2}{2EI} - C_2$$

By direct integration it then follows that

$$g(x) = \frac{Pd^2x}{8IG} + \frac{Px^2L}{2EI} - \frac{Px^3}{6EI} - C_1x + C_3$$

$$f(y) = \frac{P}{2IG}\left(\frac{d^2y}{4} - \frac{y^3}{3}\right) + \frac{\nu Py^3}{6EI} - C_2y + C_4$$

Thus, the complete expressions for u and v will be

$$u = -\frac{Pxy}{EI}\left(L - \frac{x}{2}\right) + \frac{P}{2IG}\left(\frac{d^2y}{4} - \frac{y^3}{3}\right) + \frac{\nu Py^3}{6EI} - C_2Y + C_4$$

$$v = \frac{\nu P}{2EI}(L - x)y^2 + \frac{Pd^2x}{8IG} + \frac{Px^2L}{2EI} - \frac{Px^3}{6EI} - C_1x + C_3$$

Now to fix the beam at the end $x = 0$ it is necessary to prevent a translation in the u and v directions and to prevent rotation at this end. Thus the end conditions can be written as

$$u_{(o,o)} = v_{(o,o)} = 0$$

and $\left.\frac{\partial u}{\partial y}\right|_{x=0,\ y=0} = 0$

on $\left.\frac{\partial v}{\partial x}\right|_{x=0,\ y=0} = 0$

There is a choice on these last two since we need only 3 boundary conditions in addition to the equation

$$\frac{Pd^2}{8IG} = C_1 + C_2$$

to evaluate C_1, C_2, C_3 and C_4. Thus the boundary conditions are over prescribed and different solutions for the displacement distribution can be obtained by choosing different sets of three. The choice is only two, however, since no translation is allowed. The solution for the set containing the condition

$$\left.\frac{\partial u}{\partial y}\right|_{x=0,\ y=0} = 0$$

is that of example 2. Therefore, let us consider the set containing the condition

$$\left.\frac{\partial v}{\partial x}\right|_{x=0,\ y=0} = 0$$

Applying these conditions and using the other available equation in C_1 and C_2 provides

the following solution for the displacements.

$$u = -\frac{Pxy}{EI}\left(L - \frac{x}{2}\right) + \frac{P}{2IG}\left(\frac{d^2y}{4} - \frac{y^3}{3}\right) + \frac{\nu P y^3}{6EI}$$

$$v = \frac{\nu P}{2EI}(L - x)y^2 + \frac{Px^2L}{2EI} - \frac{Px^3}{6EI}$$

and we note now that the tip deflection at $y = 0$, $x = L$ becomes

$$v = \frac{PL^3}{3EI}$$

Example 4.

Let us now consider the same beam with an externally applied distributed load as shown in Figure 26.7.

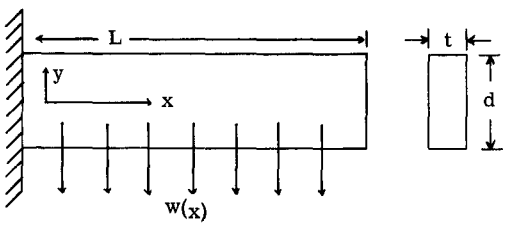

Fig. A26.7

It is common engineering practice to ignore the local effects in the stress field due to the applied load and to thus retain the argument that $\sigma y = 0$ for all values of y. The only non-zero stress components are thus σ_x and τ_{xy}. The solution technique is therefore the same as in the preceding example but where now the moment M is given in the form, for the coordinate system shown,

$$M(x) = \int_0^{L-x} w(x)\alpha\, d\alpha$$

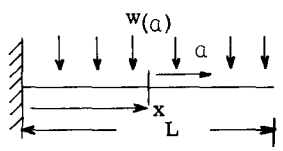

The solution follows directly the steps of the preceding example. In the majority of problems the variation of w along the beam is linear, lumped into a sequence of discrete loads, or w is a constant. In any of these cases this integral is readily evaluated in the initial steps of the problem solution. For example, if w = constant,

$$M(x) = \frac{w}{2}(L - x)^2$$

and the stress field is given by

$$\sigma_x = -\frac{w(L - x)^2}{2EI}y$$

$$\sigma_y = 0$$

$$\tau_{xy} = \frac{w(L - x)}{2EI}\left[\frac{d^2}{4} - y^2\right]$$

and the displacements are determined as before.

The actual problem is not as simple however as for the above solution where the upper and lower edges of the beam are considered stress free. The applied load as shown will require that σ_y be now-zero on one, or both, of these faces. In fact, all three stress components σ_x, σ_y and τ_{xy} will be now-zero throughout the beam. The solution is not simple but the reader has now the techniques to attack it. The solution follows the same steps as before with careful observation of the boundary conditions along the top and bottom edges where σ_y is now-zero on the loaded edge. The most simple example of this problem is where w is constant along the beam. It is left as an exercise for the reader to show that for this case and where the constant load is hung on the bottom surface giving rise to the boundary condition

$$\sigma_y = w, \text{ at } y = -\frac{d}{2}$$

that the stress components are:

$$\sigma_x = \frac{wt}{I}y(L-x)^2 - \frac{wt}{I}\frac{y^3}{3} + \frac{wt}{I}\frac{d^2}{20}y$$

$$\sigma_y = \frac{wt}{I}\frac{y^3}{6} - \frac{wt}{8I}d^2y + \frac{wtd^3}{124}$$

$$\tau_{xy} = \frac{wt}{I}(L-x)\frac{y^2}{2} - \frac{wt}{I}(L-x)\frac{d^2}{8}$$

and the deflection of the neutral axis is given by

$$\bar{v} = -\frac{wt}{GI}\left\{Lx - \frac{x^2}{2}\right\}\frac{d^2}{8} - \frac{wt}{EI}\left\{\frac{L^2x^2}{4} - \frac{Lx^3}{6} + \frac{x^4}{24}\right\}$$

$$- \frac{wt}{EI}\frac{d^2}{40}x^2 - \frac{\nu}{E}\frac{wt}{I}\frac{d^2}{16}x^2 + \frac{1}{G}\frac{wt}{I}\frac{d^2}{8}Lx$$

General Note: Since we are dealing with linear problems, it is possible to break down any loading given into components matching those of the problems given above and by direct superposition of the separate solutions corresponding to these component loadings obtain the final solution for the complex combined loading states. This general technique will be employed to obtain solutions to general thermoelastic problems in beams.

Example 5.

Consider the cantilever beam shown subjected to a non-linear temperature distribution in the depth direction but constant in the spanwise direction, $T = T(y)$. This general distribution is an approximation to the

temperature distribution in high speed aircraft wings.

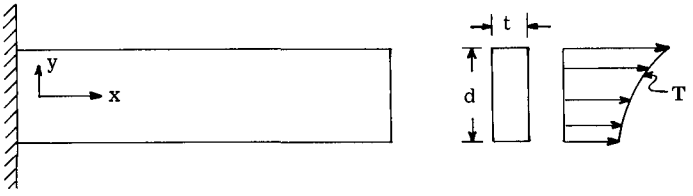

Assumptions: (i) The assumptions governing the basic theory as discussed in Chapter A25.
(ii) $\sigma_y = \tau_{xy} = \sigma_y = 0$.
(iii) The restraint to deformation v at the root (x = 0) is negligible. This assumption is questionable when the root fixing is considered. The effect of the inclusion of root restraint on v can be evaluated by superposing a self-equilibrating isothermal stress pattern to restrain v. The effect will only be appreciable in an area local to the root of a beam ($L >> d$) and therefore will be neglected.
(iv) Material properties are independent of temperature.

Basic equations: (Refer again to Chapter A25.) Since there are no boundary tractions along the edges and it is assumed that there is no resistance to expansion at the root station, it follows that $\tau_{xy} = 0$. It is also now apparent that σ_x will be a function of y only (σ_x constant in the spanwise direction) for this case of thermal loading only.

The compatibility equation (See eq. 25.12), thus reduces to

$$\nabla^2 (\sigma_x + E\alpha T) = 0$$

Since σ_x and T are functions of y only, this equation further reduces to the ordinary differential equation

$$\frac{d^2}{dy^2} (\sigma_x + E\alpha T) = 0$$

Boundary Conditions.
The cantilever beam is replaced by a beam of length 2L to satisfy the condition imposed by symmetry of zero deformation in the x-direction at the root. On this beam all surfaces must be zero. Hence the boundary conditions on σ_x can be written as;

(i) The resultant force over the end face at $x = \pm L$ is zero or

$$\int_{-\frac{d}{2}}^{\frac{d}{2}} \sigma_x t dy = 0 \qquad \text{and}$$

(ii) The resultant moment on these faces must be zero or

$$\int_{-\frac{d}{2}}^{\frac{d}{2}} \sigma_x t y dy = 0$$

Solution:

The general solution is obtained by direct integration as

$$\sigma_x = - \alpha E T + C_1 y + C_2$$

Use of the boundary conditions allows the evaluation of C_1 and C_2 as

$$C_1 = \frac{12\alpha E}{d^3} \int_{-\frac{d}{2}}^{\frac{d}{2}} T y dy$$

$$C_2 = \frac{\alpha E}{d} \int_{-\frac{d}{2}}^{\frac{d}{2}} T dy$$

Hence, the stress distribution at any station is given by:

$$\sigma_x = \alpha E \left[-T + \frac{1}{d} \int_{-\frac{d}{2}}^{\frac{d}{2}} T dy + \frac{12}{d^3} y \int_{-\frac{d}{2}}^{\frac{d}{2}} T y dy \right] \qquad \text{- - - Eq. (A)}$$

and it follows directly from the general stress-strain relations with $\sigma_y = 0$;

$$\varepsilon_x = \alpha \left[\frac{1}{d} \int_{-\frac{d}{2}}^{\frac{d}{2}} T dy + \frac{12}{d^3} y \int_{-\frac{d}{2}}^{\frac{d}{2}} T y dy \right]$$

and

$$\varepsilon_y = -\nu\alpha\left[\frac{1}{d}\int_{-\frac{d}{2}}^{\frac{d}{2}} T\,dy + \frac{12}{d^3}\,y\int_{-\frac{d}{2}}^{\frac{d}{2}} T\,y\,dy\right]$$

$$+ \alpha T\,(1+\nu)$$

$$\gamma_{xy} = 0.$$

and the displacements obtained by direct integration of the strain-displacement relations with satisfaction of the boundary conditions $u = 0$ at $x = 0$.

$$u = \alpha x\left[\frac{1}{d}\int_{-\frac{d}{2}}^{\frac{d}{2}} T\,dy + \frac{12}{d^3}\,y\int_{-\frac{d}{2}}^{\frac{d}{2}} T\,y\,dy\right]$$

Again we are interested in the deformation of the "neutral" axis or, in this case, any line at y = constant. Since $\gamma_{xy} = 0$ it follows from the strain displacement relations that

$$\frac{\partial v}{\partial x} = -\frac{\partial u}{\partial y}$$

and $$\frac{\partial^2 v}{\partial x^2} = -\frac{\partial^2 u}{\partial x \partial y}$$

$$= -\alpha\,\frac{12}{d^3}\int_{-\frac{d}{2}}^{\frac{d}{2}} T\,y\,dy$$

$$= \text{constant}.$$

Thus the curvature is constant along the length of the beam and v can be considered due to an effective end moment of value

$$\alpha E\,\frac{12}{d^3}\,y\int_{-\frac{d}{2}}^{\frac{d}{2}} T\,y\,dy$$

Thus the solution is complete.

Example 6.

The preceding problem can, of course, be solved employing the inverse formulation in terms of the stress function ϕ as outlined in Chapter A25.

The thermal gradient has been chosen as a function of y only, and since $\sigma_y = 0$, it follows that ϕ will be a function of y only. The general equation

$$\nabla^4\phi = -E\alpha\nabla^2 T$$

reduces to

$$\frac{d^4\phi}{dy^4} = -E\alpha\,\frac{d^2T}{dy^2}$$

Integrating both sides, with respect to y, will give

$$\phi = -\alpha E\int_{-\frac{d}{2}}^{y}\int_{-\frac{d}{2}}^{y} T\,dy\,dy + C_1 y^3 + C_2 y^2$$

$$+ C_3 y + C_4$$

and the boundary conditions on ϕ, necessary for the evaluation of C_1, C_2, C_3 and C_4 will follow from Chapter A25 as $\phi = \frac{d\phi}{dy} = 0$ at the boundaries $y = \pm\frac{d}{2}$. The stresses can then be obtained directly from

$$\sigma_x = \frac{d^2\phi}{dy^2}$$

and the strains and displacements obtained as in the preceding example.

Note that if T is linear, or satisfies $\nabla^2 T = 0$, then $\phi = 0$ everywhere and consequently no stresses will result. Strains, however, will exist and therefore deformations will result.

Example 7. Numerical example.

Consider a cantilever beam with the following dimensions and material properties.

$L = 10$ ins. $\quad \alpha = 7 \times 10^{-6}$

$d = 2$ ins. $\quad E = 30 \times 10^6$ (assumed constant)

$t = \frac{1}{8}$ ins. $\quad \nu = 0.3$

and subject to the following chordwise thermal gradient

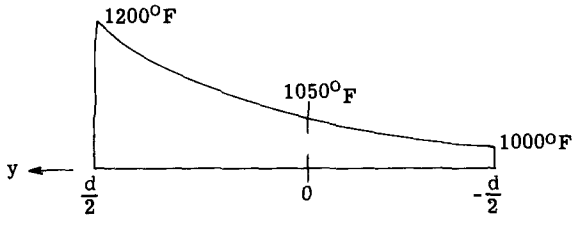

Assuming a parabolic temperature distribution it follows that

$$T(y) = 50y^2 + 100y + 1050$$

Then $\int_{-1}^{1} T\,dy = 2133$; $\int_{-1}^{1} Ty\,dy = 66.$

Then $\sigma_x = 210\,(-50y^2 + 16)$ From Eq. A

Thus $\sigma_x \Big/_{y = \pm \frac{d}{2}} = -6{,}740$ lb./ins.^{2} compression

$\sigma_x \Big/_{y = 0} = 3360$ lb./ins.^{2} tension.

The two symmetric nodes will be at

$$y = \pm \left(\frac{16}{50}\right)^{1/2}$$

$$= \pm\ 0.57 \text{ ins.}$$

The stress profile is therefore approximately (numbers in solution are approximate) symmetric as shown in the plot

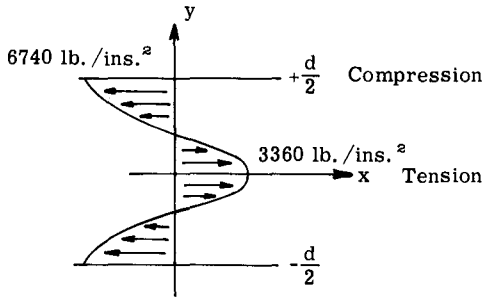

Station x.

It should be noted that the boundary condition of zero normal stresses at the boundary $x = \pm L$ is not satisfied. The solution obtained is valid only over the range $x = \pm (L - d)$ according to St. Venant's principle. If the solution is to be extended over the range $-L < x < L$ then a self-equilibrating stress-distribution must be applied at the ends to balance the normal stresses. This is a difficult problem and beyond the scope of this discussion.

Example 8.

In accordance with the discussion of Chapter A25 it is possible now to obtain the solutions to the simple beam problem when the beam is subjected to external loadings and chordwise varying temperature distributions by employing direct superposition of separate solutions. For example, consider the case of the simple cantilever beam where the external loading is an end moment M and the temperature distribution is linear across the depth and given by $T(g) = A + By$. The stress components will then be given by

$$\sigma_x = \sigma_{x_1} \text{ (due to moment M)} + \sigma_{x_2} \text{ (due to temperature)}$$

$$\sigma_y = 0$$

$$\nu_{xy} = 0$$

and the displacements by

$$u = u_1 \text{ (due to moment M)} + u_2 \text{ (due to temperature)}$$

$$v = v_1 \text{ (due to moment M)} + v_2 \text{ (due to temperature)}$$

It is left as an exercise for the reader to show that

$$\sigma_{x_1} = -\frac{My}{I}$$

$$\sigma_{x_2} = 0$$

$$u_1 = -\frac{Myx}{EI}$$

$$u_2 = \alpha\,(A + By)\,x\ .$$

$$v_1 = \frac{M}{2EI}\,(x^2 + \nu y^2)$$

$$v_2 = \alpha y\,(A + \tfrac{1}{2}\,By) - \tfrac{1}{2}\,\alpha B x^2\ .$$

Concluding Remarks.

The examples given above illustrate how problems in two-dimensional elasticity are attacked and how problems involving complex loading states can be simplified by consideration of separate more simple components of the loading state and obtaining the final solution by employing superposition. This technique is further illustrated in those problems dealing with thermal stresses.

It should be borne in mind that the simplification of the general three-dimensional elasticity problem to the two-dimensional plane-stress or plane-strain problem must be done with care and the consequences of this idealization, as it is in the majority of problems, not overlooked.

All of the illustrative problems presented in this chapter are almost mathematically

trivial problems in the theory of elasticity and thermoelasticity. We have restricted our attention to simple beam problems where the beam depth is small compared to the length and where the temperature varies across the depth only. However, the basic equations and solution techniques are basic to the solution of more complex problems where the temperature is a function of two spatial coordinates, $T = T(x,y)$, and the geometry is that of a general two dimentional plate. In these problems all the stress components will exist and displacements in the z-direction may occur in the general two-dimensional plate problem. Generalization of the techniques illustrated here in this class of problems is beyond the scope of this discussion and the reader who wishes to pursue this subject is referred to references listed in next column which can now be read with ease.

An important assumption basic to all of the preceding discussion on thermoelasticity and inherent in the references cited is that there exists no "thermo-mechanical coupling". This allows the calculation of the temperature field as a separate problem with no cross-coupling with the mechanical response (without the inclusion of the kinematical variables) and that the elasticity problem due to this temperature distribution can be considered separately. This assumption is valid only if the rate processes involved are slow.

REFERENCES

1. Boley, Bruno A. and Weiner, Jerome H., "Theory of Thermal Stresses". John Wiley & Sons, New York, 1960.

2. Gatewood, B. E., "Thermal Stresses" with Application to Airplanes, Missiles, Turbines and Nuclear Reactors. McGraw Hill, New York, 1957.

3. Timoshenko, S. H. and Goodier, J. N., "Theory of Elasticity", 2nd Ed., Chapter 14, McGraw Hill, New York, 1951.

4. Sokolinkoff, I. S., "Mathematical Theory of Elasticity", 2nd Ed., Section 101, McGraw Hill, New York, 1956.

PART B
FLIGHT VEHICLE MATERIALS AND THEIR PROPERTIES

CHAPTER B1
BASIC PRINCIPLES AND DEFINITIONS

B1.1 Introduction.

The flight vehicle structures engineer faces a major design requirement of a high degree of structural integrity against failure, but with as light structural weight as possible. Structural failure in flight vehicles can often prove serious relative to loss of life and the vehicle. However, experience has shown that if a flight vehicle, whether military or commercial in type, is to be satisfactory from a payload and performance standpoint, major effort must be made to save structural weight, that is, to eliminate all structural weight not required to insure against failure.

Since a flight vehicle is subjected to various types of loading such as static, dynamic and repeated, which may act under a wide range of temperature conditions, it is necessary that the structures engineer have a broad knowledge of the behavior of materials under loading if safe and efficient structures are to be obtained. This Part B provides information for the structures design engineer relative to the behavior of the most common flight vehicle materials under load and the various other conditions encountered in flight environment, such as elevated temperatures.

B1.2 Failure of Structures.

A flight vehicle like any other machine, is designed to do a certain job satisfactorily. If any structural unit of the vehicle suffers effects which in turn effects in some manner the satisfactory performance of the vehicle, the unit can be considered as having failed. Failure of a structural unit is therefore a rather broad term. For example, failure of a structural unit may be due to too high a stress or load causing a complete fracture of the unit while the vehicle is in flight. If this unit should happen to be one such as a wing beam or a major wing fitting, the failure is a serious one as it usually involves loss of the airplane and loss of life. Likewise the collapse of a strut in landing gear structure during a landing operation of the airplane can be a very serious failure. Failure of a structural unit may be due to fatigue and since fatigue failure is of the fracture type without warning indications of impending failure, it can also prove to be a very serious type of failure.

Failure in a different manner can result from a structural unit being too flexible, and this flexibility might influence aerodynamic forces sufficiently as to produce unsatisfactory vehicle flying characteristics. In some cases this flexibility may not be serious relative to the loss of the vehicle, but it is still a degree of failure because changes must be made in the structure to provide a satisfactory operating vehicle. In some cases, excessive distortion such as the torsional twist of the wing can be very serious as this excessive deflection can lead to a build-up of aerodynamic-dynamic forces to cause flutter or violent vibration which can cause failure involving the loss of the airplane.

To illustrate another degree of failure of a structural unit, consider a wing built in fuel tank. The stiffened sheet units which make up the tank are also a part of the wing structure. In general these sheet units are designed not to wrinkle or buckle under airplane operating conditions in order to insure against leakage of fuel around riveted connections. Therefore if portions of the tank walls do wrinkle in operation resulting in fuel leakage, which in turn require repair or modification of the structure, we can say failure has occurred since the tank failed to do its job satisfactory, and involves the item of extra expense to make satisfactory. To illustrate further, the flight vehicle is equipped with many installations, such as the control systems for the control surfaces, the power plant control system etc., which involves many structural units. In many cases excessive elastic or inelastic deformation of a unit can cause unsatisfactory operation of the system, hence the unit can be considered as having failed although it may not be a serious failure relative to causing the loss of the vehicle. Thus the aero-astro structures engineer is concerned with and responsible for preventing many degrees of failure of structural units which make up the flight vehicle and its installations and obviously the greater his knowledge regarding the behavior of materials, the greater his chances of avoiding troubles from the many degrees of structural failure.

B1.3 General Types of Loading.

Failure of a structural member is influenced by the manner in which the load is

applied. Relative to the length of time in applying the load to a member, two broad classifications appear logical, namely, (1) Static loading and (2) Dynamic loading. For purposes of explanation and general discussion, these two broad classifications will be further broken down as follows:-

- Static Loading
  - Continuous Loading.
  - Gradually or slowly applied loading.
  - Repeated gradually applied loading.
- Dynamic Loading
  - Impact or rapidly applied loading.
  - Repeated impact loading.

Static Continuous Loading. A continuous load is a load that remains on the member for a long period of time. The most common example is the dead weight of the member or the structure itself. When an airplane becomes airborne, the weight of the wing and its contents is a continuous load on the wing. A tank subjected to an internal pressure for a considerable period of time is a continuous load. Since a continuous load is applied for a long time, it is a type of loading that provides favorable conditions for creep, a term to be explained later. For airplanes, continuous loadings are usually associated with other loads acting simultaneously.

Static Gradually or Slowly Applied Loads. A static gradually applied load is one that slowly builds up or increases to its maximum value without causing appreciable shock or vibration. The time of loading may be a matter of seconds or even hours. The stresses in the member increases as the load is increased and remains constant when the load becomes constant. As an example, an airplane which is climbing with a pressurized fuselage, the internal pressure loading on the fuselage structure is gradually increasing as the difference in air pressure between the inside and outside of the fuselage gradually increases as the airplane climbs to higher altitudes.

Static Repeated Gradually Applied Loads. If a gradually applied load is applied a large number of times to a member it is referred to as a repeated load. The load may be of such nature as to repeat a cycle causing the stress in the member to go to a maximum value and then back to zero stress, or from a maximum tensile stress to a maximum compressive stress, etc. The situation envolving repeated loading is important because it can cause failure under a stress in a member which would be perfectly safe, if the load was applied only once or a small number of times. Repeated loads usually cause failure by fracturing without warning, thus repeated loads are important in design of structures.

Dynamic or Impact Loading. A dynamic or impact loading when applied to a member produces appreciable shock or vibration. To produce such action, the load must be applied far more rapid than in a static loading. This rapid application of the load causes the stresses in the member to be momentarily greater than if the same magnitude of load was applied statically, that is slowly applied. For example, if a weight of magnitude W is gradually placed on the end of a cantilever beam, the beam will bend and gradually reach a maximum end deflection. However if this same weight of magnitude W is dropped on the end of the beam from even such a small height as one foot, the maximum end deflection will be several times that under the same static load W. The beam will vibrate and finally come to rest with the same end deflection as under the static load W. In bringing the dynamic load to rest, the beam must absorb energy equal to the change in potential energy of the falling load W, and thus dynamic loads are often referred to as energy loads.

From the basic laws of Physics, force equals mass times acceleration ($F = Ma$) and acceleration equals time rate of change of velocity. Thus if the velocity of a body such as an airplane or missile is changed in magnitude, or the direction of the velocity of the vehicle is changed, the vehicle is accelerated which means forces are applied to the vehicle. In severe flight airplane maneuvers like pulling out of a dive from high speeds or in striking a severe transverse air gust when flying at high speed, or in landing the airplane on ground or water, the forces acting externally on the airplane are applied rather rapidly and are classed as dynamic loads. Chapter A4 discusses the subject of airplane loads relative to whether they can be classed as static or dynamic and how they are treated relative to design of aircraft structures.

B1.4 The Static Tension Stress-Strain Diagram.

The information for plotting a tension stress-strain diagram of a material is obtained by loading a test specimen in axial tension and measuring the load with corresponding elongation over a given length, as the specimen is loaded statically (gradually applied) from zero to the failing load. To standardize results standard size test specimens are specified by the (ASTM) American Society For Testing Materials. The speed of the testing machine cross-head should not exceed 1/16 inch per inch of gage length per minute up to the yield point of the material

and it should not exceed 1/2 inch per inch of gage length per minute from the yield point to the rupturing point of the material. The instrument for measuring the elongation must be calibrated to read 0.0002 inches or less. The information given by the tension stress-strain diagram is needed by the engineer since it is needed in strength design, rigidity design, energy absorption, quality control and many other uses.

Fig. B1.1 shows typical tensile stress-strain diagrams of materials that fall in three broad classifications. In the study of such diagrams various facts and relationships have been noted relative to behavior of materials and standard terms and symbols have been provided for this basic important information. These terms will be explained briefly.

Modulus of Elasticity (E). The mechanical property that defines resistance of a material in the elastic range is called stiffness and for ductile materials is measured by the value termed Modulus of Elasticity, and, designated by the capital letter E. Referring to Fig. B1.1, it is noticed that the first part of all three diagrams is a straight line, which indicates a constant ratio between stress and strain over this range. The numerical value of this ratio is referred to as the modulus of Elasticity (E). E is therefore the slope of the initial straight portion of the stress-strain diagram and its numerical value is obtained by dividing stress in pounds per square inch by a strain which is non-dimensional or $E = f/\varepsilon$, and thus E has the same units as stress, namely pounds per square inch.

The clad aluminum alloys have two E values as indicated in the lower diagram of Fig. B1.1. The initial modulus is the same as for other aluminum alloys, but holds only up to the proportional limit stress of the soft pure aluminum coating material. Immediately above this point there is a short transition stage and the material then exhibits a secondary modulus of Elasticity up to the proportional limit stress of the stronger core material. This second modulus is the slope of the second straight line in the diagram. Both modulus values are based on a stress using the gross area which includes both core and covering material.

Tensile Proportional Limit Stress. (F_{tb}). The proportional limit stress is that stress which exists when the stress strain curve departs from the initial straight line portion by a unit strain of 0.0001. In general the proportional limit stress gives a practical dividing line between the elastic and inelastic range of the material. The modulus of elasticity is considered constant up to the proportional limit stress.

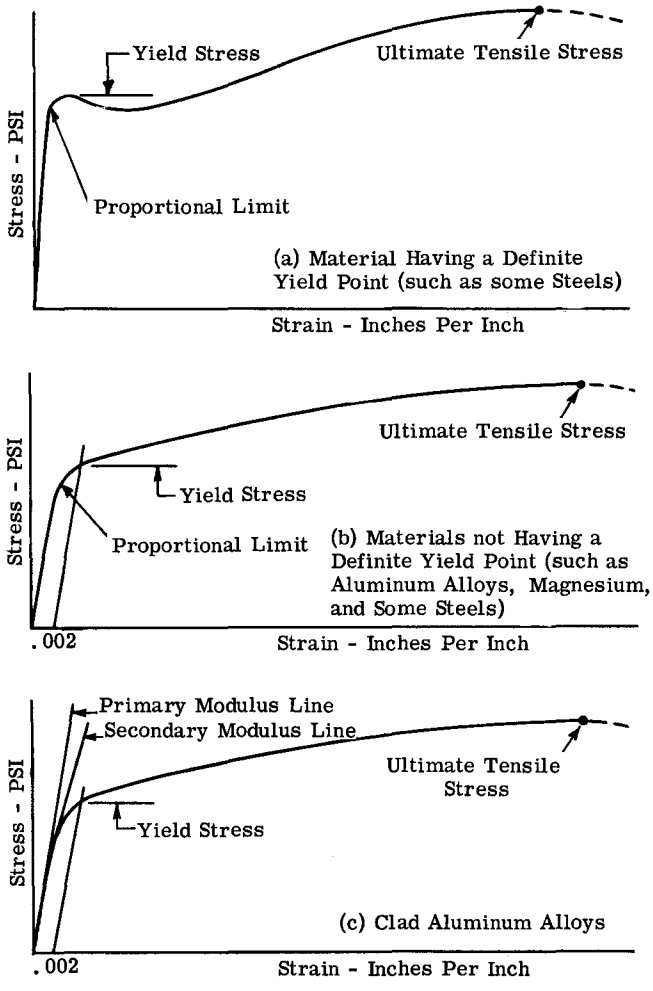

Fig. B1.1

Tensile Yield Stress (F_{ty}). In referring to the upper diagram in Fig. B1.1, we find that some materials show a sharp break at a stress considerably below the ultimate stress and that the material elongates considerably with little or no increase in load. The stress at which this takes place is called the yield point or yield stress. However many materials and most flight vehicle materials do not show this sharp break, but yield more gradually as illustrated in the middle diagram of Fig. B1.1, and thus there is no definite yield point as described above. Since permanent deformations of any appreciable amount are undesirable in most structures or machines, it is normal practice to adopt an arbitrary amount of permanent strain that is considered admissible for design purposes. Test authorities have established this value of permanent strain or set as 0.002 and the stress which existed to cause this permanent strain when released from the material is called the yield stress. Fig. B1.1 shows how

it is determined graphically by drawing a line from the 0.002 point parallel to the straight portion of the stress-strain curve, and where this line intersects the stress-strain curve represents the yield strength or yield stress.

Ultimate Tensile Stress (F_{tu}). The ultimate tensile stress is that stress under the maximum load carried by the test specimen. It should be realized that the stresses are based on the original cross-sectional area of the test specimen without regard to the lateral contraction of the specimen during the test, thus the actual or true stresses are greater than those plotted in the conventional stress-strain curve. Fig. B1.2 shows the general relationship between actual and the apparent stress as plotted in stress-strain curves. The difference is not appreciable until the higher regions of the plastic range are reached.

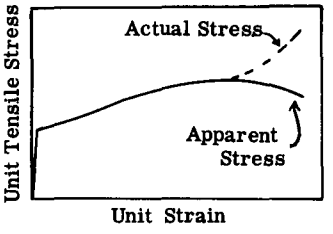

Fig. B1.2

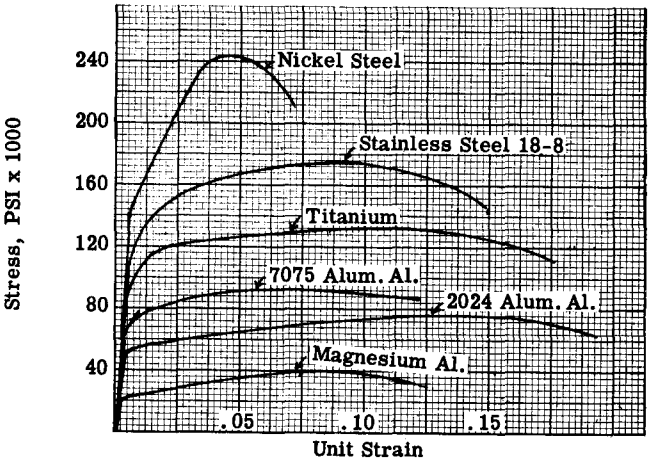

Fig. B1.3 Stress-Strain Curves. Entire Range.

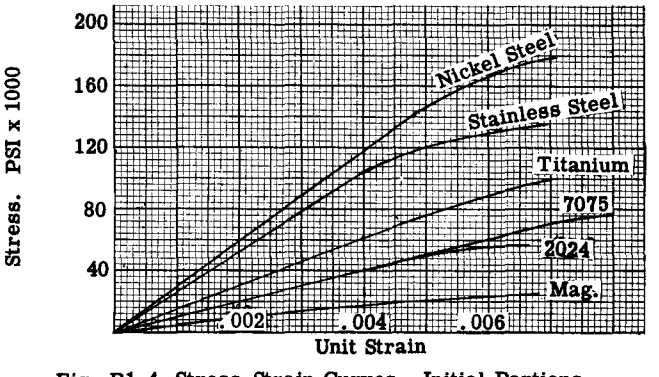

Fig. B1.4 Stress-Strain Curves. Initial Portions.

Figs. B1.3 and B1.4 compare the shapes of the tension stress-strain curves for some common aircraft materials.

B1.5 The Static Compression Stress-Strain Diagram.

Because safety and light structural weight are so important in flight vehicle structural design, the engineer must consider the entire stress-strain picture through both the tension and compressive stress range. This is due to the fact that buckling, both primary and local, is a common type of failure in flight vehicle structures and failure may occur under stresses in either the elastic or plastic range. In general the shape of the stress-strain curve as it departs away from the initial straight line portion, is different under compressive stresses than when under tensile stresses. Furthermore, the various flight vehicle materials have different shapes for the region of the stress-strain curve adjacent to the straight portion. Since light structural weight is so important, considerable effort is made in design to develop high allowable compressive stresses, and in many flight vehicle structural units, these allowable ultimate design compressive stresses fall in the inelastic or plastic zone.

Fig. B1.5 shows a comparison of the stress-strain curves in tension and compression for four widely used aluminum alloys. Below the proportional limit stress the modulus of elasticity is the same under both tension and compressive stresses. The yield stress in compression is determined in the same manner as explained for tension.

Compressive Ultimate Stress (F_{cu}). Under a static tension stress, the ultimate tensile stress of a member made from a given material is not influenced appreciably by the shape of the cross-section or the length of the member, however under a compressive stress the ultimate compressive strength of a member is greatly influenced by both cross-sectional shape and length of the member. Any member, unless very short and compact, tends to buckle laterally as a whole or to buckle laterally or cripple locally when under compressive stress. If a member is quite short or restrained against lateral buckling, then failure for some materials such as stone, wood and a few metals will be by definite fracture, thus giving a definite value for the ultimate compressive stress. Most aircraft materials are so ductile that no fracture is encountered in compression, but the material yields and swells out so that the increasing cross-sectional area tends to carry increasing load. It is therefore practically impossible to select a value of the ultimate compressive stress of ductile materials without having

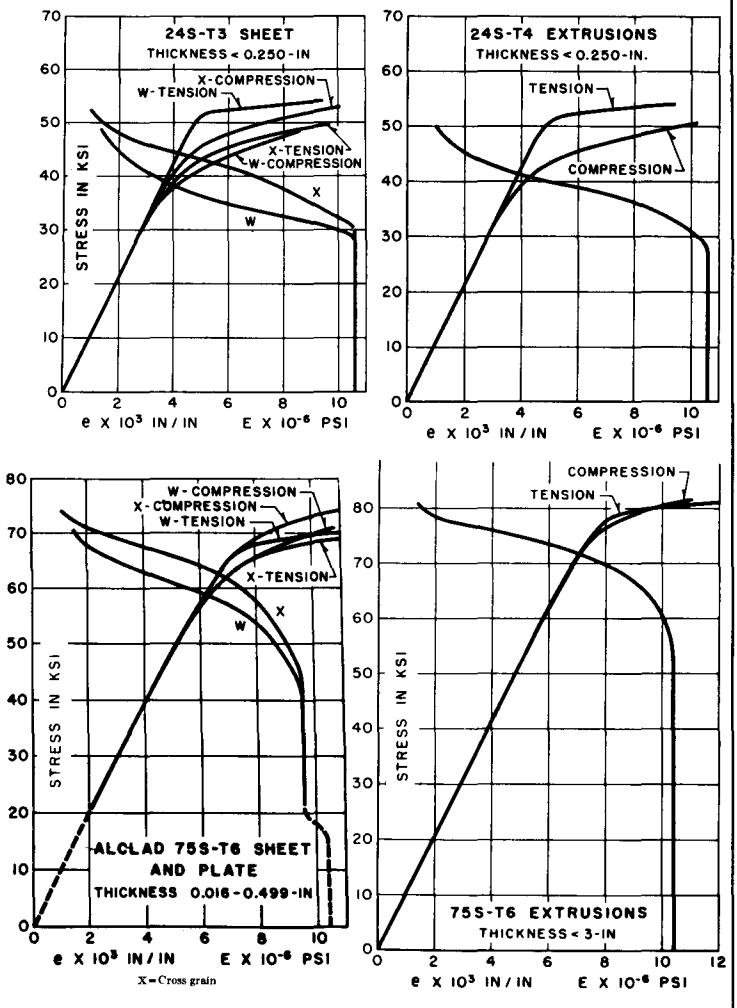

Fig. B1.5

some arbitrary measure or criteron. For wrought materials it is normally assumed that F_{cu} equals F_{tu}. For brittle materials, that are relatively weak in tension, an F_{cu} higher than F_{tu} can be obtained by compressive tests of short compact specimens and this ultimate compressive stress is generally referred to as the block compressive stress.

B1.6 Tangent Modulus. Secant Modulus.

Modern structural theory for calculating the compressive strength of structural members as covered in detail in other chapters of this book, makes use of two additional terms or values which measure the stiffness of a member when the compressive stresses in the member fall in the inelastic range. These terms are tangent modulus of elasticity (E_t) and secant modulus of elasticity (E_s). These two modifications of the modulus of elasticity (E) apply in the plastic range and are illustrated in Fig. B1.6. The tangent modulus E_t is determined by drawing a tangent to the stress-strain diagram at the point under consideration.

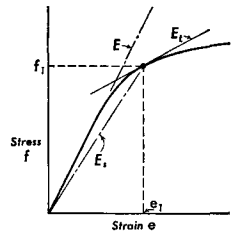

Fig. B1.6

The slope of this tangent gives the local rate of change of stress with strain. The secant modulus E_s is determined by drawing a secant (straight line) from the origin to the point in question. This modulus measures the ratio between stress and actual strain. Curves which show how the tangent modulus varies with stress are referred to as tangent modulus curves. Fig. B1.5 illustrates such curves for four different aluminum alloys. It should be noted that the tangent modulus is the same as the modulus of elasticity in the elastic range and gets smaller in magnitude as the stress gets higher in the plastic range.

B1.7 Elastic - Inelastic Action.

If a member is subjected to a certain stress, the member undergoes a certain strain. If this strain vanishes upon the removal of the stress, the action is called elastic. Generally speaking, for practical purposes, a material is considered elastic under stresses up to the proportional limit stress as previously defined. Fig. B1.7 illustrates elastic action. However, if when the stress is removed, a residual strain remains, the action is generally referred to as inelastic or plastic. Fig. B1.8 illustrates inelastic action.

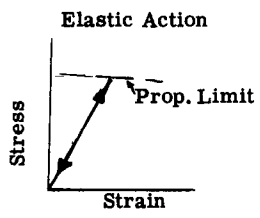

Fig. B1.7

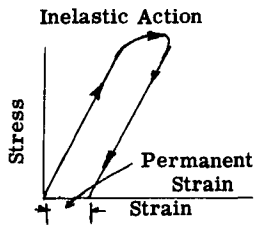

Fig. B1.8

B1.8 Ductility.

The term ductility from an engineering standpoint indicates a large capacity of a material for inelastic (plastic) deformation in tension or shear without rupture, as contrasted with the term brittleness which indicates little capacity for plastic deformation without failure. From a physical standpoint, ductility is a term which measures

the ability of a material to be drawn into a wire or tube or to be forged or die cast. Ductility is usually measured by the percentage elongation of a tensile test specimen after failure, for a specified gage length, and is usually an accurate enough value to compare materials.

$$\text{Percent elongation} = \left(\frac{L_a - L_o}{L_o}\right) 100 = \text{measure of ductility.}$$

where L_o = original gage length and L_a = gage length after fracture. In referring to ductility in terms of percent alongation, it is important that the gage length be stated, since the percent elongation will vary with gage length, because a large part of the total strain occurs in the necked down portion of the gage length just before fracture.

B1.9 Capacity to Absorb Energy. Resilience. Toughness.

Resilience. The capacity of a material to absorb energy in the elastic range is referred to as its resilience. For measure of resilience we have the term modulus of resilience, which is defined as the maximum amount of energy per unit volume which can be stored in the material by stressing it and then completely recovered when the stress is removed. The maximum stress for elastic action for computing the modulus of resilience is usually taken as the proportional limit stress. Therefore for a unit volume of material (1 cu. in.) the work done in stressing a material up to its proportional limit stress would equal the average stress $f_p/2$ times the elongation (ε_p) in one inch. If we let U represent modulus of resilience, then

$$U = \left(\frac{f_p}{2}\right) \varepsilon_p \quad \text{- - - - - - - - - - - - - - - - - (1)}$$

But $\varepsilon_p = f_p/E$, hence

$$U = \left(\frac{f_p}{2}\right)\left(\frac{f_p}{E}\right) = f_p^2/2E \quad \text{- - - - - - - - - - - (2)}$$

Under a condition of axial loading, the modulus of resilience can be found as the area under the stress-strain curve up to the proportional limit stress. Thus in Fig. B1.9, the area OAB represents the energy absorbed in stressing the material from zero to the proportional limit stress.

High resilience is desired in members subjected to shock, such as springs. From equation (1), a high value of resilience is obtained when the proportional limit stress is high and the strain at this stress is high, or from equation (2), when the proportional limit stress is high and modulus of elasticity is low.

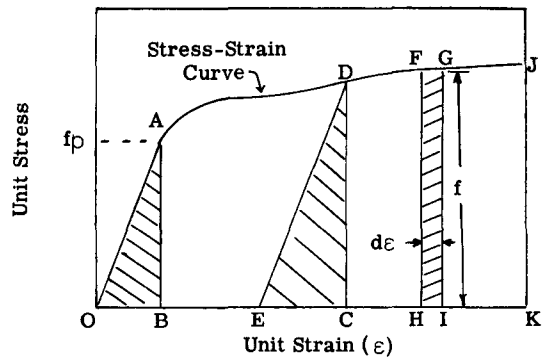

Fig. B1.9

In Fig. B1.9 if the stress is released from point D in the plastic range, the recovery diagram will be approximately a straight line DE parallel to AO, and the area CDE represents the energy released, and often referred to as hyper-elastic resilience.

Toughness. Toughness of a material can be defined as its ability to absorb energy when stressed in the plastic range. Since the term energy is involved, another definition would be the capacity of a material for resisting fracture under a dynamic load. Toughness is usually measured by the term modulus of Toughness which is the amount of strain energy absorbed per unit volume when stressed to the ultimate strength value.

In Fig. B1.9, let f equal the average stress over the unit strain distance dε from F to G. Then work done per unit volume in stressing F to G is fdε which is represented by the area FGHI. The total work done in stressing to the ultimate stress f_u would then equal $\int^{\varepsilon k} f d\varepsilon$, which is the area under the entire stress-strain curve up to the ultimate stress point, or the area O A J K O in Fig. B1.9 and the units are in. lb. per cu. inch. Strictly speaking it should not include the elastic resilience or the energy absorbed in the elastic range, but since this area is small compared to the area under the curve in the plastic range it is usually included in toughness measurements.

It should be noted that the capacity of a member for resisting an axially applied dynamic load is increased by increasing the length of a member, because the volume is increased directly with length. However, the ultimate strength remains the same since it is a function of cross-sectional area and not of volume of the material.

Toughness is a desirable characteristic when designing to resist impact or dynamic loads as it gives a reserve strength or factor of safety against failure by fracture when over-loading in actual use should happen to cause the member to be stressed fairly high into the plastic zone.

The property of ductility helps to produce toughness, but does not alone control toughness as illustrated in Fig. B1.10, which shows the

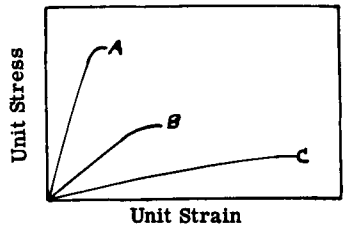

Fig. B1.10

stress-strain curves for three different materials. Material (A) is strong but brittle, whereas material (C) is weak and ductile, and material (B) represents average strength and ductility. However, all three materials have the same modulus of toughness since the areas under all three curves is the same.

B1.10 Poisson's Ratio.

When a material is stressed, it will deform in the direction of the stress and also at right angles to it. For axial loading and for stress below the proportional limit stress, the ratio of the unit strains at right angles to the stress, to the unit strain in the direction of the stress is called Poisson's ratio. It is determined by direct measurement in a tensile or compressive test of a specimen, and is approximately equal to 0.3 for steel and 0.33 for non-ferrous materials. In many structures there are members which are subjected to stresses in more than one direction, say along all three coordinate axes. Poisson's ratio is used to determine the resultant stress and deformation in the various directions.

Poisson's Ratio in Plastic Range. Information is somewhat limited as to Poisson's ratio in the plastic range and particularly during the transition range from elastic to plastic action. For the assumption of a plastically incompressible isotropic solid, Poisson's ratio assumes a value of 0.5. Gerard and Weldform found from their research, that the transition of Poisson's ratio from the elastic value of around 1/3 to 1/2 in the plastic range is gradual and is most pronounced in the yield point region of the stress-strain curve.

B1.11 Construction of a Stress-Strain Curve Through a Given Yield Stress by Using a Known Test Stress-Strain Curve.

Materials in general are produced to satisfy certain guaranteed minimum strength properties such as yield stress, ultimate tensile stress, etc. Thus in the design of important members in a composite structure, the minimum guaranteed properties must be used to provide the required degree of safety. In general, most materials will give properties slightly above the guaranteed values, thus the test stress-strain curve of purchased material cannot be used for design purposes. The stress-strain curve passing through a given yield point stress can be readily obtained for a test stress-strain curve as follows:

In Fig. B1.11, the heavy curve O B C represents a known typical stress-strain curve for the given material. Let the minimum guaranteed yield stress be the value as shown at point A, using the 0.2 percent method. Then proceed as follows:

(1) Draw a straight line through point O and point A which will intersect the typical curve at point B. Point B may be above or below the typical curve.

(2) Locate any other point on the typical curve such as point C, and draw line from O through C.

(3) Locate point D on line O C by the following ratio:-

$$OD = \frac{OA}{OB} \times OC$$

(4) Repeat step 3 to obtain a number of points as shown by dots on Fig. B1.11, and draw smooth curve through these points to obtain desired stress-strain curve.

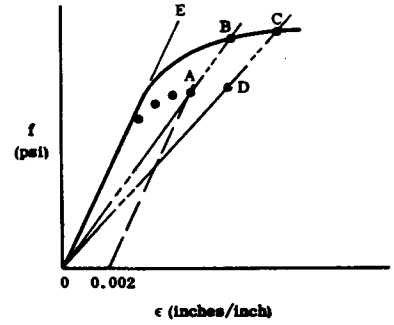

Fig. B1.11

B1.12 Non-Dimensional Stress-Strain Curves.

The structural designer is constantly confronted with the design of structural units which fail by inelastic instability. The

solution of such problems requires information given by the compressive stress-strain curve. Since flight vehicles make use of many different materials, and each material usually has many different states of manufacture which give different mechanical properties, the question of time required to obtain certain design information from stress-strain curves becomes important. For example, in the aluminum alloys alone there are about 100 different alloys, and when elevated temperatures at various time exposures are added, the number of stress-strain curves required is further greatly increased.

Fortunately, this time consuming work was greatly lessened when Ramsberg and Osgood (Ref. 1) proposed an equation to describe the stress-strain curve in the yield range. Their proposed equation specifies the stress-strain curve by the use of three parameters, the modulus of elasticity E, the secant yield stress $F_{0.7}$, which is taken as the line of slope 0.7E drawn from origin (see Fig. B1.12), and a parameter n which describes the shape of the stress-strain curve in the yield region. In order to evaluate the term n, another stress $F_{0.85}$ is needed, which is the intersection of the curve by a line of slope of 0.85E through the origin (see Fig. B1.12).

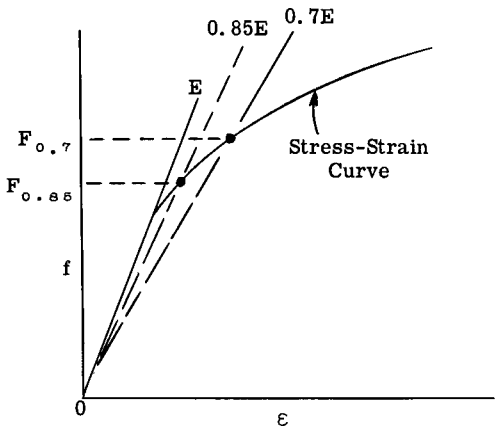

Fig. B1.12

The Ramsberg and Osgood proposed three parameter representation of stress-strain relations in the inelastic range is:-

$$\frac{E\varepsilon}{F_{0.7}} = \frac{f}{F_{0.7}} + \left(\frac{f}{F_{0.7}}\right)^n \quad - - - - - - - - - - - (3)$$

The equation for n is,

$$n = 1 + \log_e (17/7)/\log_e(F_{0.7}/F_{0.85}) \quad - - - (4)$$

Fig. B1.13 is a plot of equation (4). The quantities $E\varepsilon/F_{0.7}$ are non-dimensional and may be used in determining the non-dimensional curves of Fig. B1.14. E, n, and $F_{0.7}$ must be known to use these curves in obtaining values on the stress-strain curve. Table B1.1 gives the values of $F_{0.7}$, $F_{0.85}$, n, etc., for many flight vehicle materials. Notice that the shape parameter varies widely for materials, being as low as 4 and as high as 90.

B1.13 Influence of Temperature on Material Properties.

Before the advent of the supersonic airplane or the long range missile, the aeronautical structures engineer could design the airframe of aircraft using the normal static mechanical properties of materials, since the temperature rise encountered by such aircraft had practically no effect on the material strength properties. The development of the turbine jet and rocket jet power plants provided the means of opening up the whole new field of supersonic and space flight. The flight environmental conditions were now greatly expanded, the major change being that aerodynamic heating caused by high speeds in the atmosphere caused surface temperatures on the airframe which would greatly effect the normal static material strength properties and thus temperature and time became important in the structural design of certain types of flight vehicles.

B1.14 Creep of Materials.

It is obvious that temperature can weaken a material because if the temperature is high enough the material will melt or flow and thus have no load carrying capacity as a structural member. When a stressed member is subjected to temperature, it undergoes a change of shape in addition to that of the well known thermal expansion. The term creep is used to describe this general influence of temperature and time on a stressed material. Creep is defined in general as the progressive, relatively slow change in shape under stress when subjected to an elevated temperature. A simple illustration of creep is a person standing on a bituminous road surface on a very hot summer day. The longer he stands on the same spot the deeper the shoe soles settle into the road surface, whereas on a cold winter day the same time of standing on one spot would produce no noticeable penetration of the road surface.

High temperature, when used in reference to creep, has different temperature values for different materials for the same amount of creep. For example, mercury, which melts at -38°F, may creep a certain amount at -75°F, whereas tungsten, which melts at 6170°F, may not creep as much at 2000°F as the mercury under -75°F. All materials creep under conditions of temperature, stress and time of stress application. The simplest manner in which to obtain the effects of creep is to study its effect on the static stress-strain diagram for the material.

Fig. B1.13

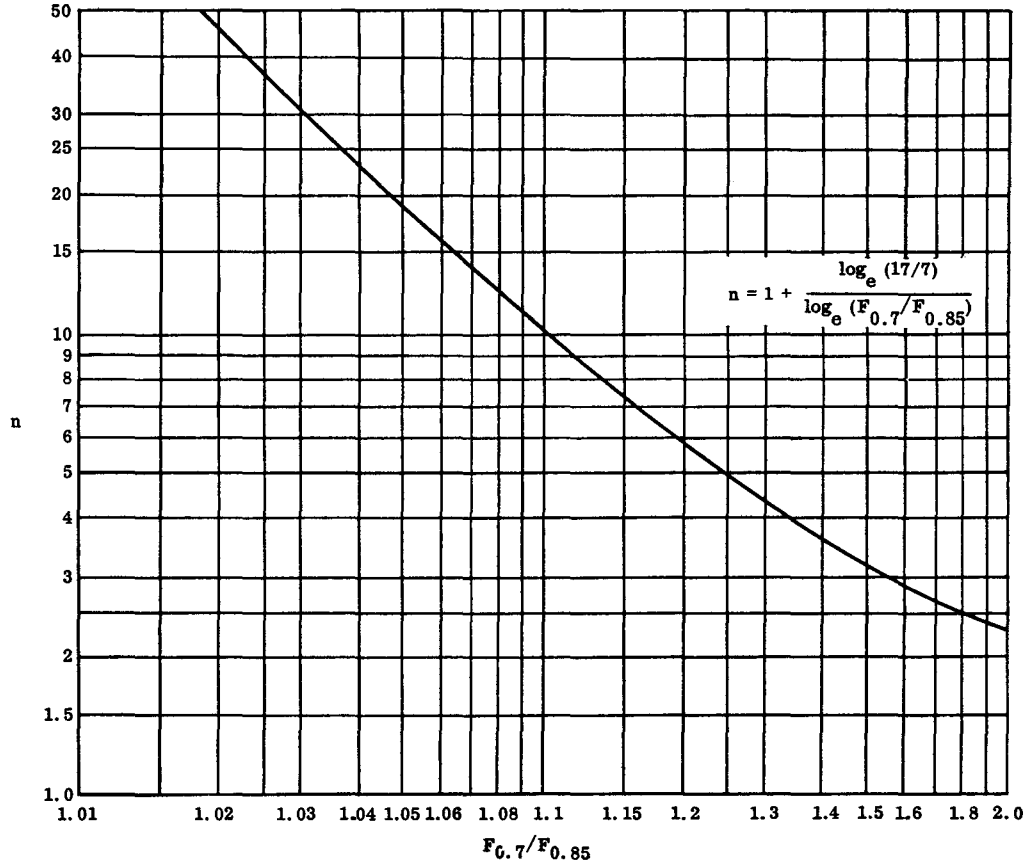

Fig. B1.14

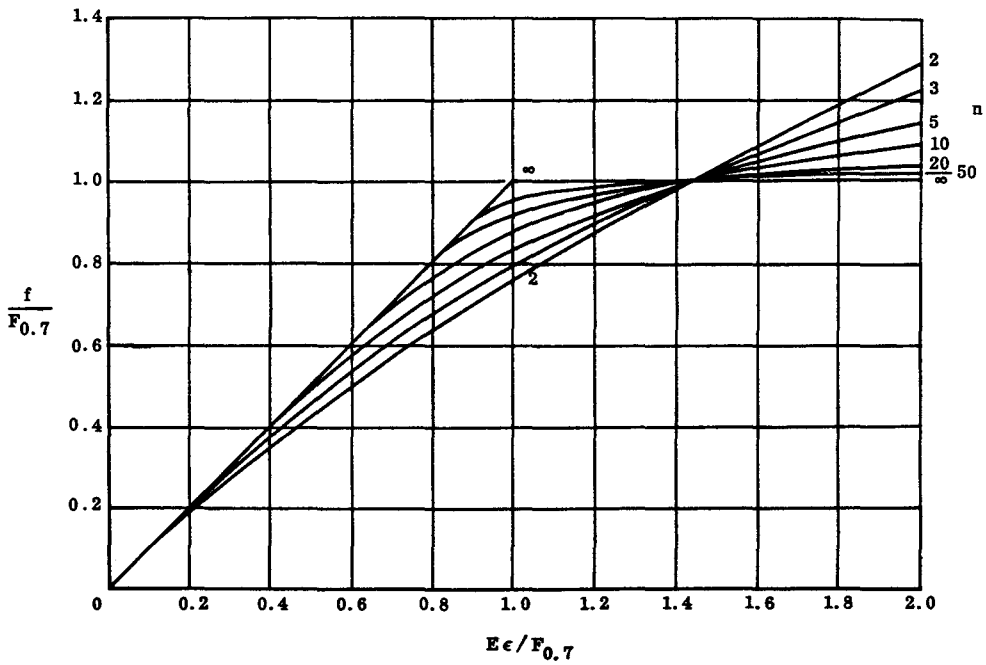

Table B1.1 Values of F_{tu}, F_{cy}, E_c, $F_{0.7}$, $F_{0.85}$, n, for Various Materials Under Room & Elevated Temperatures (From Ref. 6)

MATERIAL	Temp. Exp. Hr.	Temp. °F	e, %	F_{tu}, ksi	F_{cy}, ksi	E_c 10^6psi	$F_{0.7}$ ksi	$F_{0.85}$ ksi	n
STAINLESS STEEL									
AISI 301 1/4 Hard Sheet	1/2	RT	25	125	80	27.0	73	63	6.9
Transverse Compression									
Longitudinal Compression	1/2	RT	25	125	43	26.0	28.2	23	5.2
AISI 301 1/2 Hard Sheet	1/2	RT	15	150	118	27.0	116.5	105	9.2
Transverse Compression	1/2	400		118	108.5	23.2	108.5	97	8.6
	1/2	600		110	107.5	20.9	108.5	96.5	8.2
	1/2	1000		86	86	16.2	94.5	83.5	8.0
Longitudinal Compression	1/2	RT	15	150	58	26.0	48	37	4.4
	1/2	400		118	53.3	22.4	45.5	36	4.7
	1/2	600		110	52.8	20.1	44	31	3.5
	1/2	1000		86	45.2	15.6	40	30.5	4.3
AISI 301 3/4 Hard Sheet	1/2	RT	12	175	160	27.0	163.5	151.5	13.2
Transverse Compression	1/2	400		148	148	24.1	153	142.5	13.2
	1/2	600		138	138	22.4	152	140	11.2
	1/2	1000		112	112	18.9	127	121	19.2
Longitudinal Compression	1/2	RT	12	175	76	26.0	70	61.5	7.6
	1/2	400		148	71	23.3	65	56	6.8
	1/2	600		138	70.3	21.6	65.5	56.5	6.8
	1/2	1000		112	59.3	18.2	55	46	5.9
AISI 301 Full Hard Sheet	1/2	RT	8	185	179	27.0	183	172	16
Transverse Compression	1/2	400		168	168	25.1	174	164	16
	1/2	600		159	159	23.8	172	162	16
	1/2	1000		131	130	21.6	141.5	135.5	21.5
Longitudinal Compression	1/2	RT	8	185	85	26.0	77.5	63	5.2
	1/2	400		168	80.8	24.2	74	59.5	5
	1/2	600		159	79.9	22.9	74	58	4.6
	1/2	1000		131	66.3	20.8	58	42.5	3.9
17-4 PH Bar & Forgings	1/2	RT	6	180	165	27.5	166	160	24
	1/2	400		162	135	25.3	137	129	16
	1/2	700		146	105.5	23.1	106	97	11
	1/2	1000		88	62.6	21.2	60	52	7.1
17-7 PH (TH1050) Sheet, Strip & Plate,	1/2	RT		180	162	29.0	166	145	7.4
t = .010 to .125 in.	1/2	400		169	144	27.8	146	126	6.8
	1/2	700		144	118	24.9	117	104	8.4
	1/2	1000		88	61.5	20.3	56	47	6
17-7 PH (RH950) Sheet, Strip & Plate,	1/2	RT		210	205	29.0	208	196	16.4
t = .010 to .125 in.									
19-9DL (AMS 5526) & 19-9DX	1/2	RT	30	95	45	29.0	36.5	32	7.6
(AMS 5538), Sheet, Strip & Plate									
19-9DL (AMS 5527) & 19-9DX	1/2	RT	12	125	90	29.0	85	74	7.2
(AMS 5539) Sheet, Strip & Plate									
PH15-7Mo (TH1050) Sheet & Strip,	1/2	RT	5	190	170	28.0	171	164	22.5
t = .020 to .187 in.									
PH15-7Mo (RH950) Sheet & Strip,	1/2	RT	4	225	200	28.0	218	189	7.3
t = .020 to .187 in.									
LOW CARBON & ALLOY STEELS									
AISI 1023 & 1025 Tube, Sheet & Bar,									
Cold Finished		RT	22	55	36	29.0	32.7	31.5	24
AISI 4130 Normalized, t > .188 in.	1/2	RT	23	90	70	29.0	61.5	53	6.8
	1/2	500		81	61.5	27.3	55	48	7.3
	1/2	800		68	46.2	23.8	40	32.5	5.2
	1/2	1000		46	30.8	20.6	28	22	4.7
AISI 4130, 4140, 4340 Heat Treated	1/2	RT	23	125	113	29.0	111	102	10.9
	1/2	500		113	98.3	27.3	96	88	10.9
	1/2	850		88	68.9	23.2	66.5	61.5	12
	1/2	1000		64	49.7	20.6	45.5	41	9.2
AISI 4130, 4140, 4340 Heat Treated	1/2	RT	18.5	150	145	29.0	145	140	25
	1/2	500		135	126	27.3	126	122	29
	1/2	850		105	88.5	23.2	88	83.5	18.5
	1/2	1000		76	63.8	20.6	62	57	10.9
AISI 4130, 4140, 4340 Heat Treated	1/2	RT	15	180	179	29.0	179	176	50
	1/2	500		162	156	27.3	156	153	46
	1/2	850		126	109.3	23.2	109.4	105	22
	1/2	1000		92	77	20.6	75	68	9.8
AISI 4130, 4140, 4340 Heat Treated	1/2	RT	13.5	200	198	29.0	198	196	90
	1/2	500		180	170	27.3	172.5	169	46
	1/2	850		140	121	23.2	121.5	117	25
	1/2	1000		104	87.1	20.6	87	83	19
HEAT RESISTANT ALLOYS									
A-286 (AMS 5725A) Sheet, Plate	1/2	RT	15	140	95	29.0	93	87	14
& Strip	1/2	600		129	88.4	24.4	87	81	13.5
	1/2	1000		115	81.7	19.8	81	75	12.5
	1/2	1400		52	50.3	14.2	50	47	15.3
K-MONEL Sheet, Age Hardened	1/2	RT	15	125	90	26.0	88	82	13.5
MONEL Sheet, Cold Rolled & Annealed	1/2	RT	35	70	28	26.0	20	17	6.4
INCONEL-X	1/2	RT	20	155	105	31.0	104	100	23.5
	1/2	400		152	95.6	28.9	94	89	17
	1/2	800		141	90.2	26.4	88.6	84	18.5
	1/2	1200		104	83	23.2	82	78.6	21

Table B1.1 Values of F_{tu}, F_{cy}, E_c, $F_{0.7}$, $F_{0.85}$, n, for Various Materials Under Room & Elevated Temperatures (From Ref. 6) (Continued)

MATERIAL	Temp. Exp. Hr.	Temp. °F	e, %	F_{tu}, ksi	F_{cy}, ksi	E_c 10^6psi	$F_{0.7}$ ksi	$F_{0.85}$ ksi	n
ALUMINUM ALLOYS									
2014-T6 Extrusions	2	RT	7	60	53	10.7	53	50.3	18.5
$t \leq 0.499$ in.	2	300		51	42.5	10.2	41.5	40	24
	2	450		28	21	9.2	20.5	19.5	25
	2	600		10	8.0	7.4	5.5	4.5	5.4
	1/2	300		51	43.5	10.2	44.0	42.5	25
	1/2	450		31	26	9.2	26	25.2	29
2014-T6 Forgings	2	RT	7	62	52	10.7	52.3	50	20
$t \leq 4$ in.	2	300		53	41	10.2	40.5	38.5	19
	2	450		29	22	9.2	21.5	20	12.6
	2	600		10	7.5	7.4	4.5	3.0	3.2
	1/2	300		53	43	10.2	42.5	40	15.8
	1/2	450		32	25.5	9.2	25.0	23.5	15.6
2024-T3 Sheet & Plate,	2	RT	12	65	40	10.7	39	36	11.5
Heat Treated, $t \leq .250$ in.	2	300			37	10.3	35.7	33.5	15
	2	500			26	8.4	24.8	22.8	10.9
	2	700			7.5	6.4	6.2	5.5	8.2
2024-T4 Sheet & Plate,	2	RT	12	65	38	10.7	36.7	34.5	15.6
Heat Treated, $t \leq 0.50$ in.	2	300			34	10.3	32.5	30.5	14.6
	2	500			24	8.4	23	21	10.2
	2	700			7	6.4	60	5.7	18.5
2024-T3 Clad Sheet & Plate,	2	RT	12	60	37	10.7	35.7	33	12
Heat Treated, t = .020 to .062 in.	2	300			34	10.3	33	30.3	11
	2	500			24.5	8.4	22.7	20	7.9
	2	700			6.5	6.4	5.8	5.5	18.5
2024-T6 Clad Sheet & Plate,	2	RT	8	62	49	10.7	49	45	11
Heat Treated, $t \geq 0.063$ in.	2	300			45	10.3	44.3	40.7	11
	2	500			22	8.4	31.5	28	8.3
	2	700			6	6.4	7.0	6.0	6.6
2024-T6 Clad Sheet & Plate,	2	RT	8	60	47	10.7	47	43	10.6
Heat Treated, $t < 0.063$ in.	2	300			43.2	10.3	42.3	38.7	10.8
	2	500			21	8.4	29.5	26	7.8
	2	700			6	6.4	5.00	4.0	4.9
2024-T81 Clad Sheet, Heat Treated,	2	RT	5	62	55	10.7	56	51.6	11.2
$t < 0.064$ in.	2	300			50.5	10.3	51.2	46.5	10
	2								
	2								
6061-T6 Sheet, Heat Treated & Aged,	1/2	RT	10	42	35	10.1	35	34	31
$t < 0.25$ in.	1/2	300			29.5	9.5	29	28	26
	1/2	450			20.5	8.5	19.3	17.7	10.9
	1/2	600			7.5	7.0	6.6	6.2	15.2
7075-T6 Bare Sheet & Plate,	2	RT	7	76	67	10.5	70	63	9.2
$t \leq 0.50$ in.	2	300			54	9.4	55.8	52.5	15.6
	2	425			25.5	8.1	25.4	23.5	12.1
	2	600			8	5.3	7.2	5.2	3.7
	1/2	425			30	8.1	34.5	32.5	16
7075-T6 Extrusions,	2	RT	7	75	70	10.5	72	68	16.6
$t \leq 0.25$ in.	2	300			54	9.4	58.5	54.5	13.4
	2	450			22.5	7.8	21.3	18.5	7.2
	2	600			8	5.3	6.5	4.3	3.2
	1/2	450			25	7.8	29	26	8.8
7075-T6 Die Forgings,	2	RT	7	71	58	10.5	58.5	55.1	15.2
$t \leq 2$ in.	2	300			47.6	9.4	47.8	45	15.6
	2	450			18.5	7.8	17.3	16	12
	2	600			7.0	5.3	5.0	3.7	3.9
	1/2	450			23	7.8	24	22	10.9
7075-T6 Hand Forgings,	2	RT	4	72	63	10.5	63.8	61.5	25
Area ≤ 16 sq. in.	2	300			51.6	9.4	52.2	50	21.5
	2	450			20.2	7.8	20.3	19	13.7
	2	600			7.6	5.3	6.0	5.0	5.8
	1/2	450			24	7.8	26.5	25.3	19.5
7075-T6 Clad Sheet & Plate,	2	RT	8	70	64	10.5	64.5	61.6	19.5
$t \leq 0.50$ in.	2	300			50	9.4	54	51.7	20
	2	450			20.5	7.8	19.7	17.5	4.6
	2	600			7.7	5.3	7.7	5.5	3.6
	1/2	450			23	7.8	27.2	25.3	12.4
7079-T6 Hand Forgings,	1/2	RT	4	67	59	10.5	59.5	57.5	26
$t \leq 6.0$ in.	1/2	300			47	9.4	46.5	45	29
	1/2	450			21	7.8	20	18.5	12
	1/2	600			7.0	5.3	5.5	3.5	3.0
MAGNESIUM ALLOYS									
AZ61A Extrusions,		RT	8	38	14	6.3	12.9	12.3	19
$t \leq 0.249$ in.									
HK31A-0 Sheet	1/2	RT	12	30	12	6.5	10	8.4	6
t = 0.016 to 0.250 in.	1/2	300		20	11.1	6.16	8.9	6.9	4.5
	1/2	500		15	9.3	4.94	7.5	5.6	4.2
	1/2	600		10	4.9	3.77	3.3	1.6	2.2
HK31A-H24 Sheet,	1/2	RT	4	34	19	6.5	17.3	14.6	6.2
$t < 0.250$ in.	1/2	300		22	17.7	6.2	15.6	12.6	5.1
	1/2	500		17	14.8	4.9	13.1	10.5	4.9
	1/2	600		11	7.8	3.8	6.7	5.2	4.5
TITANIUM ALLOYS									
Ti-8Mn Annealed Sheet,	1000	RT	10	120	110	15.5	119.5	102	13.7
Plate & Strip									
Ti-6A1-4V Annealed Bar	1/2	RT	10	130	126	16.0	127	124.5	43
& Sheet, $t \leq .187$ in.	1/2	400		105	96	14.1	97	93	22
	1/2	600		99	84.5	13.0	85.5	82	22
	1/2	800		87	79.4	11.8	80.5	77	21.5
	1/2	1000		70	60.6	7.7	61	59.5	36

Fig. B1.15 (curves A and B) show the stress-strain curve for a material. Curve (A) is for a low elevated temperature condition and curve (B) that of a high elevated temperature condition. The results were obtained by a normal testing machine procedure requiring a short time test period, hence the results can be considered as independent of time.

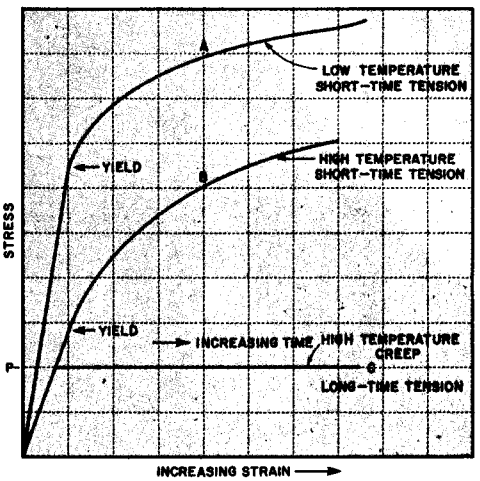

Fig. B1.15 (Ref. 2) - Effect of temperature and time on the strength characteristics of metals.

The figure shows that the higher temperature (curve B) reduces the ultimate strength, yield strength and modulus of elasticity of the material as compared to curve (A) which is a test at a lower temperature.

EFFECT OF TIME

If temperature and stress are of such combination as to produce appreciable creep, then time becomes an important effect. For example, in Fig. B1.15, if the material at low temperature (curve A) is stressed to a value P within the elastic limit of the material, and this stress is maintained for a considerable time period, very little creep, if any, will be detected, and when the stress is removed, the material will practically resume its original dimensions. However, if the material is stressed to the same value P but under a high temperature condition, creep will occur just as long as the stress P remains applied and the stress-strain curve will take a shape like curve (C) in Fig. B1.15. This time dependent strain will follow a characteristic pattern. The material will never return to its original shape after creep has taken place regardless if the stress is removed. If both stress and high temperature continue, rupture produced by creep will finally occur.

B1.15. The General Creep Pattern.

A typical manner of plotting creep-rupture test data is illustrated in Fig. B1.16. For metals tested at high value of stress or temperature, three stages in the creep-time relation can be observed as shown in Fig. B1.16. The initial stage, often called the stage of primary creep, includes the elastic deformation and that region where the rate of creep deformation decreases rather rapidly with time, which no doubt indicates an influence of strain hardening. The second stage, often referred to as the secondary creep stage, represents a stage where the rate of strain has decreased to a constant value (except for high stress) for a considerable time period, and this stage represents the period of minimum creep rate. The third stage, often called the tertiary creep stage, represents the period where the reduction in cross-sectional area leads to a higher stress, a greater creep rate and finally rupture.

Transition Point. The inflection point between the constant creep rate of the second stage and the increasing rate of the third stage is referred to as the transition point. Failure generally occurs in a relatively short time after the transition point. Transition points may not occur at very low stresses and may also not be definable at very high stresses. Minimum creep rate is that indicated in the second stage, where the creep rate is practically constant.

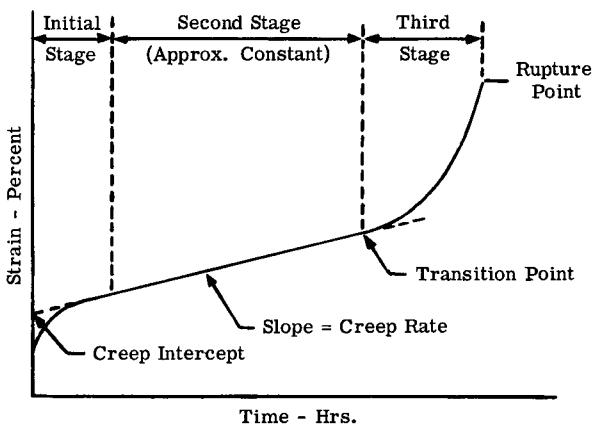

Fig. B1.16 Typical creep-rupture curve.

Fig. B1.17 shows a plot of creep-time curves for a material at constant temperature and several stress levels. It is noticed that increasing stress changes the creep-time relationship considerably.

B1.16 Stress-Time Design Charts.

In many structural design problems involving elevated temperatures such as power

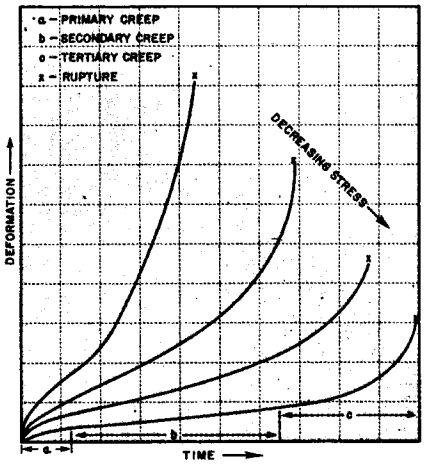

Fig. B1.17 (Ref. 2) Creep curves for a material at constant temperature and various stress levels showing the characteristic stages of creep behavior.

plants, the critical design factor is not strength but the permissible amount of creep that can be allowed to still permit the structure or machine to function or operate satisfactorily. Extensive tests are usually necessary to provide reliable creep design information and such test information is often recorded in the form as illustrated in Fig. B1.18.

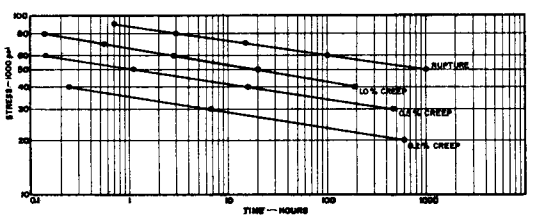

Fig. B1.18 (Ref. 2) - Stress-time design chart at a single constant temperature for selecting limiting stress values.

B1.17 Effect of Time of Exposure.

In general materials can be roughly classified into those which time of exposure to elevated temperatures has great influence on the mechanical properties and those where such exposure produces relatively small effect.

This general fact is illustrated in Figs. B1.19 and B1.20. The yield strength of the aluminum alloy in Fig. B1.19 is far more influenced by time of exposure to elevated temperature than the steel alloy as shown in Fig. B1.20.

B1.18 Effect of Rapid Rate of Heating

Supersonic aircraft and missiles are subjected to rapid aerodynamic heating. The results of tests indicate that in general metals can withstand substantially higher

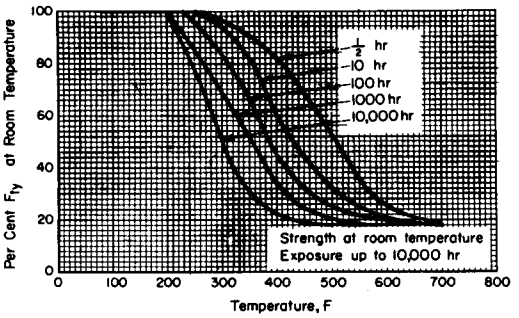

Fig. B1.19 (Ref. 3) - Effect of exposure at elevated temperatures on the room-temperature tensile yield strength (F_{ty}) of 7079-T6 aluminum alloy (hand forgings).

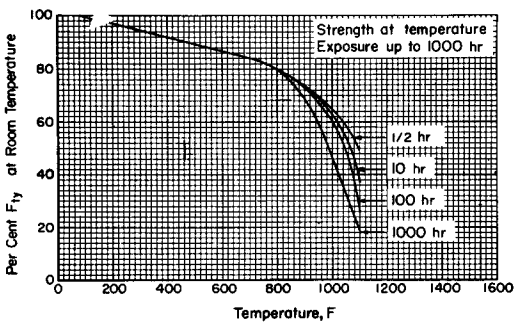

Fig. B1.20 (Ref. 3) - Effect of temperature on the tensile yield strength (F_{ty}) of 5 Cr-Mo-V aircraft steels.

stresses at a given temperature when heated from zero up to 200°F per second under constant load conditions than when loaded after the material has been 1/2 hour or longer at constant temperature. Increasing the temperature rate from 200°F to 2000°F per second or more results in only a small increase in strength. Figs. B1.21 and B1.22 (Ref. 4) show the effect of temperature rates up to 100°F per second upon the yield and ultimate

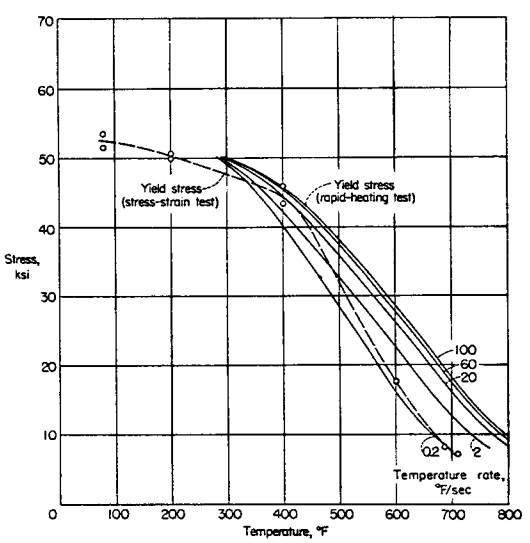

Fig. B1.21 - Tensile yield stress of 2024-T3 aluminum alloy for temperature rates from 0.2°F to 100°F per second and of stress-strain tests for 1/2-hour exposure.

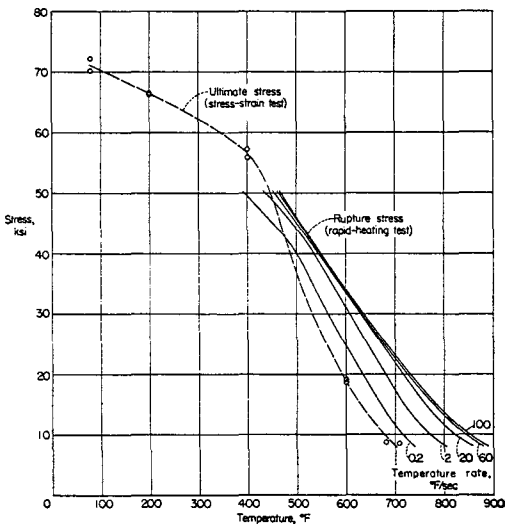

Fig. B1.22 - Tensile rupture stress of 2024-T3 aluminum alloy for temperature rates from 0.2°F to 100°F per second and ultimate tensile stress of stress-strain tests for 1/2-hour exposure.

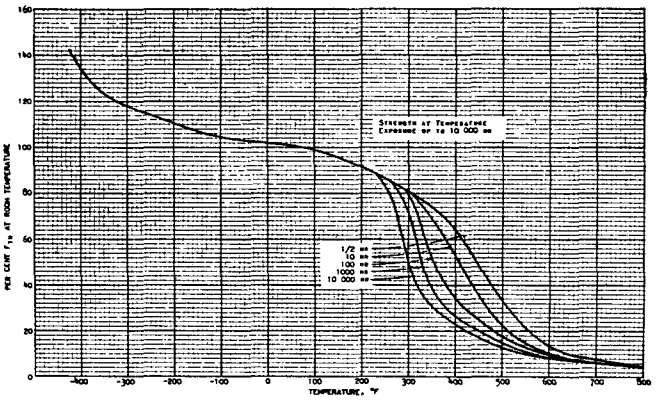

Fig. 1.23 (Ref. 3) - Effect of Temperature on Ultimate Strength (F_{tu}) of 2014-T 6 Aluminum Alloy.

strength respectively of aluminum alloy as compared to values when loaded after the material has been exposed 1/2 hour at constant temperature.

B1.19 General Effect of Low Temperatures Upon Material Properties.

The development of the missile and the space vehicle brought another factor into the ever increasing number of environmental conditions that effect structural design, namely, extremely low temperatures. For example, in space the shady side of the flight vehicle is subjected to very low temperatures. Missiles carry fuels and oxidizers such as liquid hydrogen and oxygen which boil at -423 and -297°F respectively. In general, low temperatures increase the strength and stiffness of materials. This effect tends to decrease the ductility of the material or, in other words, produce brittleness, a property that is not desirable in structures because of the possibility of a catastrophic failure. In general, the hexagonal closely packed crystalline structures are best suited for giving the best service under low temperatures. The most important of such materials are aluminum, titanium, and nickel-base alloys. Fig. B1.23 shows the effect of both elevated and low temperatures on the ultimate tensile strength of 2014-T6 aluminum alloy under various exposure times.

B1.20 Fatigue of Materials.

Designing structures to provide safety against what is called fatigue failure is one of the most important and difficult problems facing the structural designer of flight vehicles. Fatigue failure is failure due to being stressed a number of times. For example, a beam may be designed to safely and efficiently carry a design static load and it will carry this static load indefinitely without failure. However, if this load is repeated a large enough number of times, it will fail under this static design load. The higher the beam stress under the static design load, the less the number of repeated loadings to cause failure.

To date no adequate theory has been developed to clearly explain the fatigue failure of materials. Fatigue failure appears to begin with a crack starting at a point of weakness in the material and progressing along crystal boundaries. A microscopic examination of metals indicates there are many small cracks scattered throughout a material. Under the action of repeated stress these small cracks open and close during the stress cycle. The cracks cause higher stress to exist at the base of the crack as compared to the stress if there were no crack. Under this repeated concentration of stress, the cracks will gradually extend across the section of the member and finally causing complete failure of the member.

Fatigue testing consists of 3 types:- (1) the testing of material crystals, (2) the testing of small structural test specimens, and (3) the testing of complete composite structures. A tremendous amount of test information is available for the second type of testing. More and more attention is being given to the third type of testing. For example, a complete airplane wing or fuselage is often subjected to elaborate fatigue testing in order to insure the safe design life of the airplane.

The presence of cracks initially is not necessary to start a fatigue or progressive failure as irregularities such as slag inclusions, surface scratches, pitting, etc., can cause corrosive action to start, thus supplying the condition for the promotion of cracks and the resultant progressive failure.

The strength of ferrous metals under repeated stresses is often referred to as the endurance or fatigue limit. The endurance limit stress is the stress that can be repeated an infinite number of times without causing fracture of the material. Non-ferrous materials, such as the aluminum alloys do not have an endurance limit as defined above but continue to weaken as the stress cycles are increased. Due to this fact and also since the required service life of structures and machines vary greatly, it is customary to refer to the strength under repeated stresses as endurance or fatigue strength instead of endurance limit. Thus the fatigue strength is the maximum stress that can be repeated for a specified number of cycles without producing failure of the structural unit.

The results of testing a specimen under repeated stresses such as tension, compression, bending, etc., is often plotted in a form which is referred to as the S-N (stress versus cycles) diagram, as illustrated in Fig. B1.24.

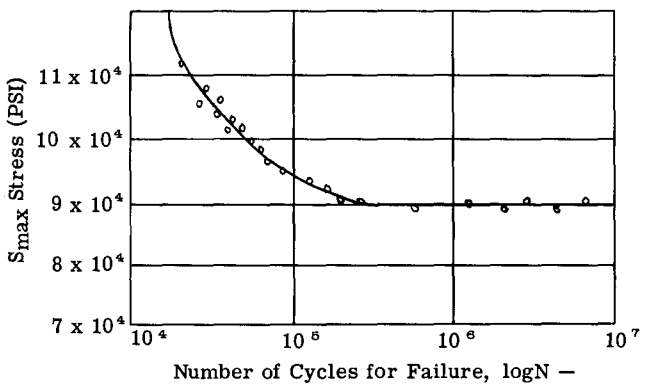

Fig. B1.24

The problem of fatigue design of aircraft airframes is covered in Chapter C13 of this book.

B1.21 Effect of Impact Loading on Material Properties.

An impact load when applied to a structure produces appreciable shock or vibration. To produce such action, the load must be applied rapidly, that is, in a short interval of time. The effect of impact loads differs from that of static loads in that impact loads appreciably effect the magnitude of the stresses produced in a member and also the resistance properties or behavior of the material under load. The importance and effect of dynamic loads on the magnitude of stresses in aircraft structures is discussed briefly in Chapter A4. The limited discussion which follows will deal only with the effect of impact loads on the behavior of materials.

IMPACT TESTING METHODS

There are in general two types of tests to determine the behavior of materials under impact loads. The usual impact test which has been conducted for many years is referred to as the notched bar test and consists of subjecting notched specimens to axial, bending and torsional loads by the well known Charpy or Izod impact testing machines. In both of these machines an impact load is applied to the specimen by swinging a weight W from a certain vertical height (h) to strike and rupture the notched specimen and then stopping at a vertical height (h'). The energy expended in rupturing the specimen is then equal approximately to (Wh-Wh'). This type of test is primarily used for studying the influence of metallurgical variables.

The other type of impact testing is made on unnotched specimens and the general purpose is to obtain the stress-strain diagram of materials under impact load or the load-distortion diagram of a structural member or composite structure as the unit is completely fractured under an impact load.

B1.22 Examples of Some Results of Impact Testing of Materials.

Figs. B1.25, 26 and 27 show the results of impact tests upon the stress-strain curve as compared to the static stress-strain diagram (Ref. 5).

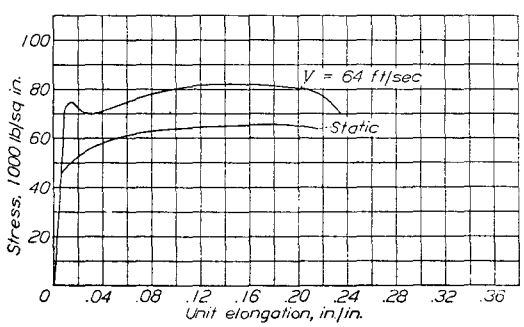

Fig. B1.25 - Stress-Strain curves, 24ST aluminum alloy.

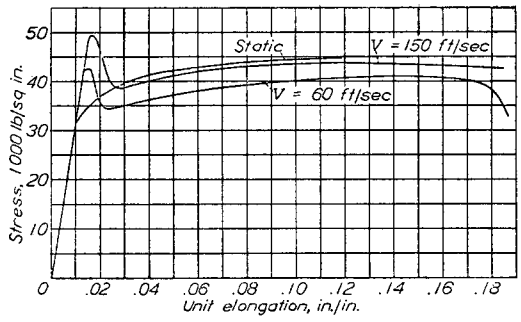

Fig. B1.26 - Stress-strain curves, Dow metal X.

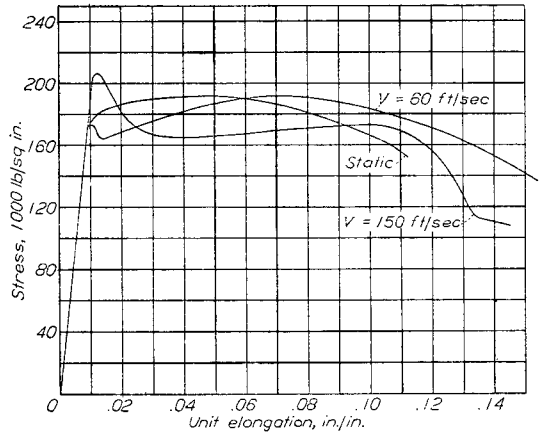

Fig. B1.27 - Stress-strain curves, SAE 6140, drawn 1020°F.

Table B1.2 shows additional impact testing results as compared to the static test results.

Table B1.2

Comparison of Strengths, Ductility and Energy Absorption Under Impact and Static Loads.[xxx]

Material	Ratio of Impact to Static Value For,			
	Yield Point	Maximum Load	Elong-ation	Energy
SAE No. 6140[x]		1.020	2.205	2.865
SAE No. 1015[xx]	1.328	1.285	1.418	1.376
SAE No. 1018	1.995	1.397	0.992	0.946
18-8 Alloy	1.224	1.212	0.682	0.600
17ST Alum. Al.	1.294	1.094	1.000	0.885
Brass[xx]	1.387	1.142	1.163	1.203
Aluminum	1.522	1.323	1.628	1.627
Copper	1.433	1.390	1.527	1.597

[x] Oil quenched from 1620°F.
[xx] Cold-rolled.
[xxx] From "Stress-Strain Relations Under Tension and Impact Loading" by D. S. Clark & G. Datwyler, Proc. A.S.T.M. 1938, Vol. 38.

REFERENCES

Ref. 1. Ramberg & Osgood. Description of Stress-Strain Curves of 3 Parameters. NACA, Tech. Note 902.
Ref. 2. Time and Temperature Gremlins of Destruction. By L. A. Yerkorvich, Cornell Aero. Lab. Research Trends. Sept. 1956.
Ref. 3. Military Handbook (MIL-HDBK-5) Aug. 1962.
Ref. 4. NACA Technical Note 3462.
Ref. 5. NACA Technical Note 868.
Ref. 6. From Structures Manual, Convair Astronautics.

CHAPTER B2

MECHANICAL AND PHYSICAL PROPERTIES OF METALLIC MATERIALS FOR FLIGHT VEHICLE STRUCTURES

General Explanation. It would require several hundred pages to list the properties of the many materials used in flight vehicle structural design. The metallic materials presented in this chapter are those most widely used and should be sufficient for the use of the student in his structural analysis and design problems. All Tables and Charts in this chapter are taken from the government publication "Military Handbook, MIL-HDBK-5, August, 1962. Metallic Materials and Elements for Flight Vehicle Structures". This publication is for sale by the Supt. of Public Documents, Washington 25, D.C. The properties given in the various tables are for a static loading condition under room temperature. The effect of temperature upon the mechanical properties is given in the various graphs.

AISI ALLOY STEELS

Table B2. 1 (AISI) Alloy Steels

Alloy	AISI 4130, 8630, and 8735		AISI 4130, 4140, 4340, 8630, 8735, and 8740			4140 4340 8740	AISI 4340
Form	Sheet, strip, plate, tubing		All wrought forms				
Condition	N		Heat treated (quenched and tempered) to obtain F_{tu} indicated				
Thickness or diameter, in.	≤0.187	>0.187					
Basis	.....	.....	.....	.....	.....	.....	[a]
Mechanical properties:							
F_{tu}, ksi	95	90	125	150	180	200	260
F_{ty}, ksi	75	70	103	132	163	176	217
F_{cy}, ksi	75	70	113	145	179	198	242
F_{su}, ksi	55	55	82	95	109	119	149
F_{bru}, ksi:							
$(e/D=1.5)$	.....	.....	194	219	250	272	347
$(e/D=2.0)$	140	140	251	287	326	355	440
F_{bry}, ksi							
$(e/D=1.5)$	.....	.....	151	189	230	255	312
$(e/D=2.0)$	.....	.....	180	218	256	280	346
e, percent	See table 2.3.1.1(b)		See table 2.3.1.1(c)				[b] L 10 [b] T 3
E, 10^6 psi	29.0						
E_c, 10^6 psi	29.0						
G, 10^6 psi	11.0						
Physical properties:							
ω, lb/in.^{3}	0.283.						
C, Btu/(lb)(F)	0.114 (at 32° F).						
K, Btu/[(hr)(ft^2)(F)/ft]	22.0 (at 32° F).						
α, 10^{-6} in./in./F	6.3 (0° to 200° F).						

AISI ALLOY STEELS (Cont.)

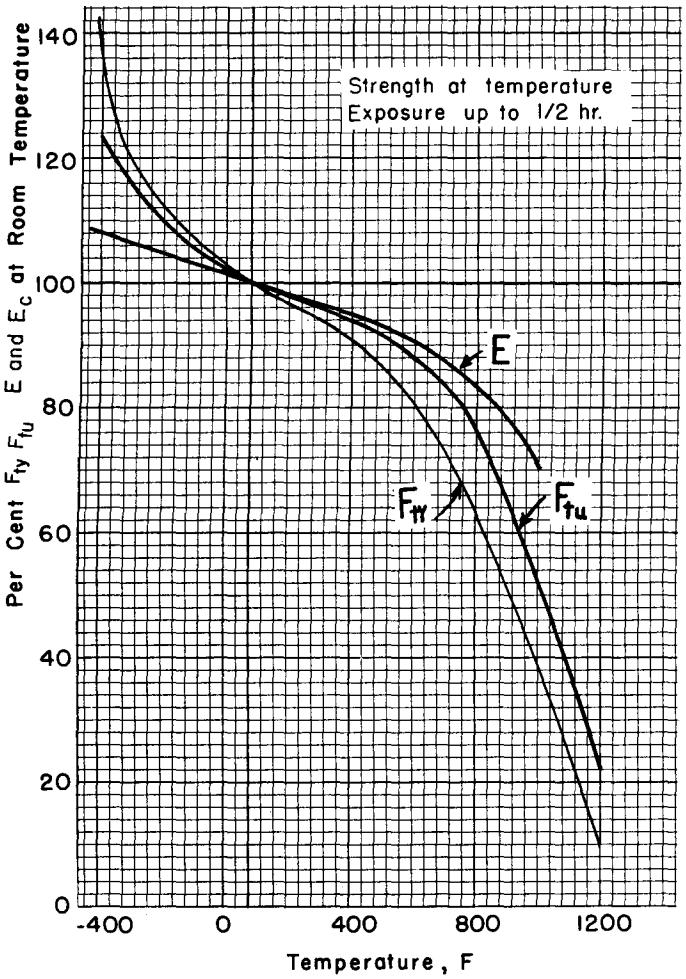

Fig. B2.1. Effect of temperature on F_{tu}, F_{ty}, and E of AISI alloy steel

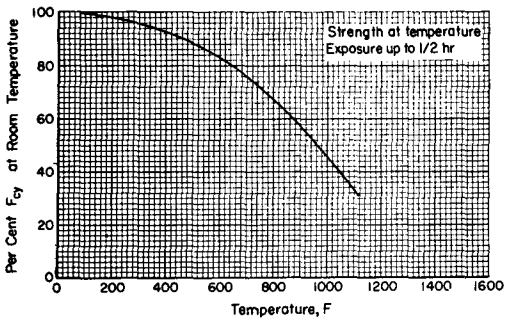

Fig. B2.2. Effect of temperature on the compressive yield strength (F_{cy}) of heat-treated AISI alloy steels.

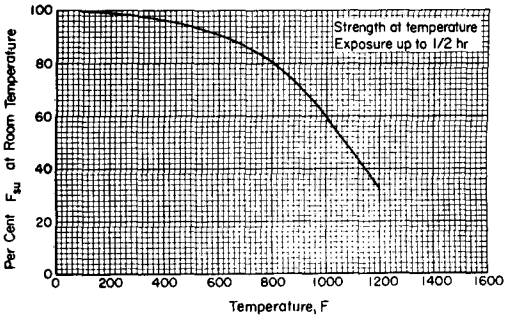

Fig. B2.3. Effect of temperature on the ultimate shear strength (F_{su}) of heat-treated AISI alloy steels.

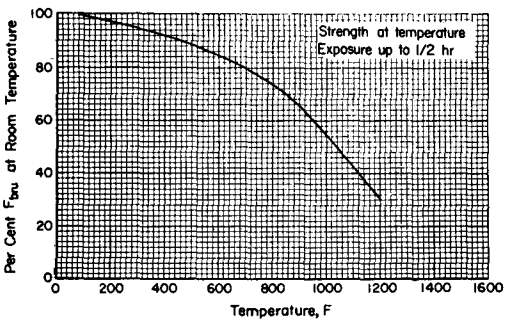

Fig. B2.4. Effect of temperature on the ultimate bearing strength (F_{bru}) of heat-treated AISI alloy steels.

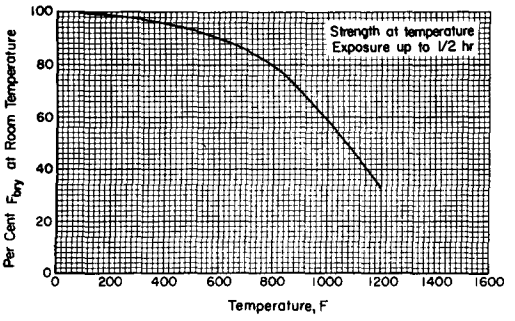

Fig. B2.5. Effect of temperature on the bearing yield strength (F_{bry}) of heat-treated AISI alloy steels.

5 Cr-Mo-V AIRCRAFT STEEL

Table B2.2 Design Mechanical and Physical Properties of 5Cr-Mo-V Aircraft Steel

Alloy	5Cr-Mo-V aircraft steel.		
Form	All wrought forms.		
Condition	Heat treated to obtain the F_{tu} indicated.		
Section size	Up to 12 in. diam. or equivalent.		
Basis	(a)	(a)	(a)
Mechanical properties:			
F_{tu}, ksi	240	260	280
F_{ty}, ksi	200	220	240
F_{cy}, ksi	220	240	260
F_{su}, ksi	145	155	170
F_{bru}, ksi:			
$(e/D=1.5)$	.....	.....	.....
$(e/D=2.0)$	400	435	465
F_{bry}, ksi:			
$(e/D=1.5)$	.....	.....	.....
$(e/D=2.0)$	315	340	365
e, percent:			
Bar, in 4D	9	8	7
Sheet, in 2 in. (b)	6	5	4
Sheet, in 1 in	8	7	6
E, 10^6 psi	30.0		
E_c, 10^6 psi	30.0		
G, 10^6 psi	11.0		
Physical properties:			
ω, lb/in.^{3}	0.281.		
C, Btu/(lb)(F)	0.11(c) (32° F).		
K, Btu/[(hr)(ft^2)(F)/ft]	16.6 (400° to 1,100° F).		
α, 10^{-6} in./in./F	7.1 (80° to 800° F); 7.4 (80°–1,200° F).		

(a) Minimum properties expected when heat treated as recommended in section 2.5.1.0.

(b) For sheet thickness greater than 0.050 inch.

(c) Calculated value.

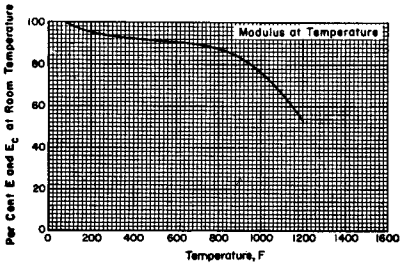

Fig. B2.8 Effect of temperature on the tensile and compressive modulus (E and E_c) of 5 Cr-Mo-V aircraft steels.

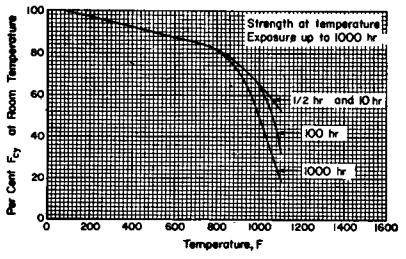

Fig. B2.9 Effect of temperature on the compressive yield strength (F_{cy}) of 5 Cr-Mo-V aircraft steels.

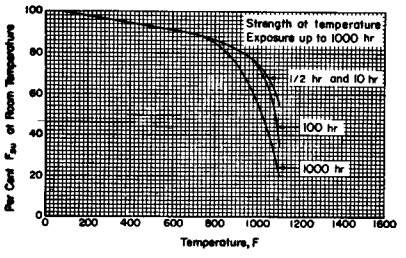

Fig. B2.10 Effect of temperature on the ultimate shear strength (F_{su}) of 5 Cr-Mo-V aircraft steels.

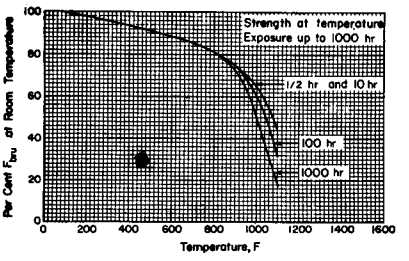

Fig. B2.11 Effect of temperature on the ultimate bearing strength (F_{bru}) of 5 Cr-Mo-V aircraft steels.

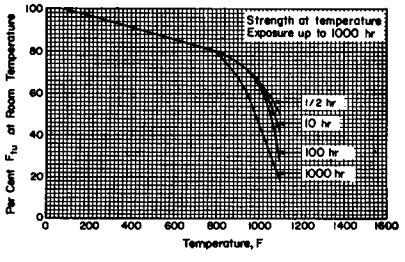

Fig. B2.6 Effect of temperature on the ultimate tensile strength (F_{tu}) of Cr-Mo-V aircraft steels.

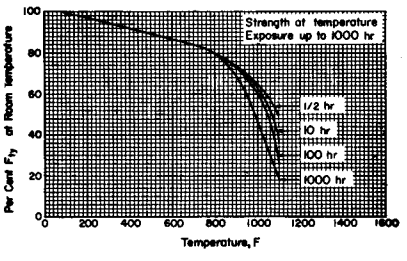

Fig. B2.7 Effect of temperature on the tensile yield strength (F_{ty}) of 5 Cr-Mo-V aircraft steels.

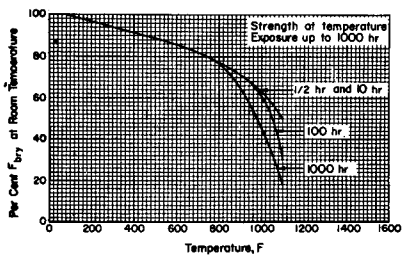

Fig. B2.12 Effect of temperature on the bearing yield strength (F_{bry}) of 5 Cr-Mo-V aircraft steels.

17-7 PH STAINLESS STEEL

Table B2.3 Design Mechanical and Physical Properties of 17-7 PH Stainless Steel

Alloy	17-7 PH				
Form	Sheet, strip, and plate[a]			Bars and Forgings[b]	
Condition	TH 1050	RH 950		TH 1050	RH 950
Thickness or diameter, in.	0.005 to 0.500	0.005 to 0.1874	0.1875 to 0.500	6 and under	
Basis	S			S[c]	
Mechanical properties:					
F_{tu}, ksi	180	210	200	170	185
F_{ty}, ksi	150	190	180	140	150
F_{cy}, ksi	158	200	189	147	158
F_{su}, ksi	117	136	130	111	120
F_{bru}, ksi:					
$(e/D=1.5)$	297	346	330	280	305
$(e/D=2.0)$	360	420	400	340	370
F_{bry}, ksi:					
$(e/D=1.5)$	225	285	270	210	225
$(e/D=2.0)$	247	313	297	231	247
e, percent	See table 2.7.2.1(b)			6	6
E, 10^6 psi	29.0				
E_c, 10^6 psi	30.0				
G, 10^6 psi	11.0				
Physical properties:					
ω, lb/in.^{3}	0.276.				
C, Btu/(lb)(F)	0.11.[d]				
K, Btu/[(hr)(ft^2)(F)/ft]	9.75 (at 300° F).				
α, 10^{-6} in./in./F	6.3 (70° to 600° F) for TH 1050. 6.8 (70° to 600° F) for RH 950.				

[a] Test direction longitudinal for widths less than 9 in.; transverse for widths 9 in. and over.

[b] Test direction longitudinal; these properties not applicable to the short transverse (thickness) direction.

[c] Vendors guaranteed minimums for F_{tu}, F_{ty}, and e.

[d] Calculated value.

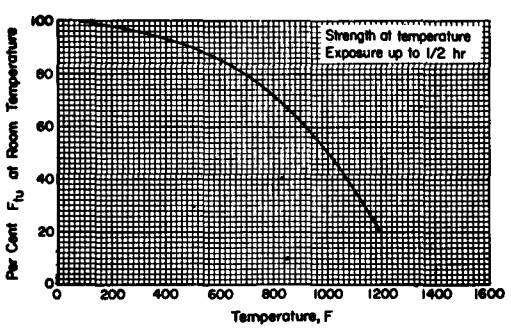

Fig. B2.13. Effect of temperature on the ultimate tensile strength (F_{tu}) of 17-7 PH (TH1050) stainless steel.

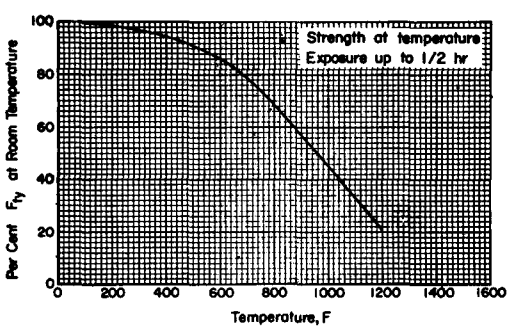

Fig. B2.14. Effect of temperature on the tensile yield strength (F_{ty}) of 17-7 PH (TH1050) stainless steel.

17-7 PH STAINLESS STEEL (Cont.)

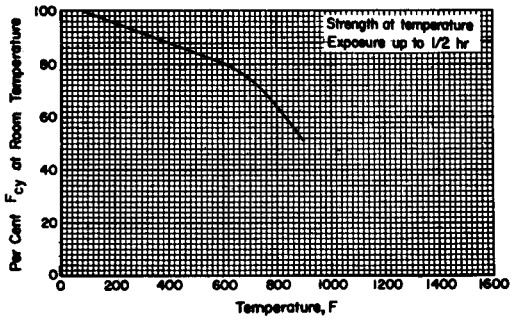

Fig. B2.15. Effect of temperature on the compressive yield strength (F_{cy}) of 17-7 PH (TH1050) stainless steel.

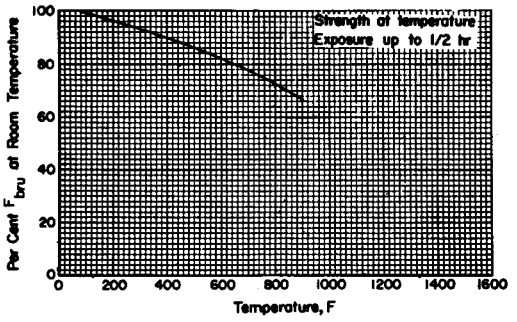

Fig. B2.18. Effect of temperature on the ultimate bearing strength (F_{bru}) of 17-7 PH (TH1050) stainless steel.

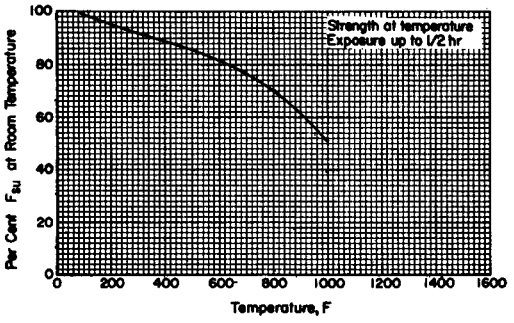

Fig. B2.16. Effect of temperature on the ultimate shear strength (F_{su}) of 17-7 PH (TH1050) stainless steel.

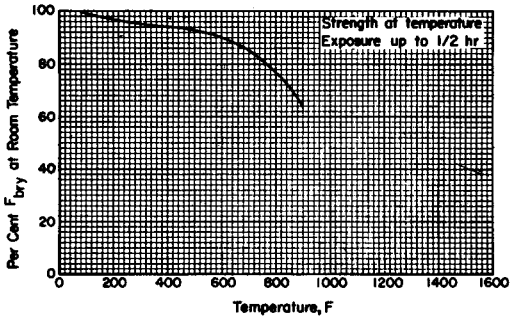

Fig. B2.19. Effect of temperature on the bearing yield strength (F_{bry}) of 17-7 PH (TH1050) stainless steel.

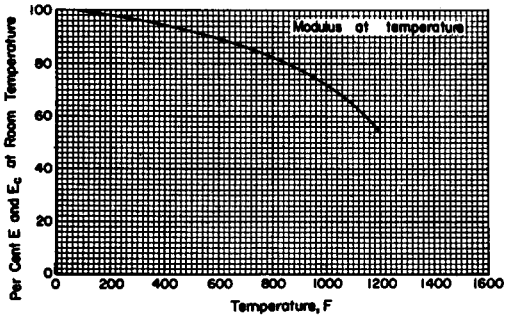

Fig. B2.20. Effect of temperature on the tensile and compressive modulus (E and E_C) of 17-7 PH (TH1050) stainless steel.

17-4 PH STAINLESS STEEL

Table B2.4 Design Mechanical and Physical Properties of 17-4 PH Stainless Steel

Alloy	17-4 PH	
Form	Plate	Bars and forgings[b]
Condition	H 900	H 900
Thickness or diameter, in.		8 and under
Basis	S[a]	S
Mechanical properties:		
F_{tu}, ksi	190	190
F_{ty}, ksi	170	170
F_{cy}, ksi	178	178
F_{su}, ksi	123	123
F_{bru}, ksi:		
$(e/D=1.5)$	313	313
$(e/D=2.0)$	380	380
F_{bry}, ksi:		
$(e/D=1.5)$	255	255
$(e/D=2.0)$	280	280
e, percent:		
In 2 in.	10	...
In 4 D	...	10
E, 10^6 psi	29.0	
E_c, 10^6 psi	30.0	
G, 10^6 psi	11.0	
Physical properties:		
ω, lb/in.^{3}	0.282.	
C, Btu/(lb)(F)	0.11 (32° to 212° F).	
K, Btu/[(hr)(ft^2)(F)/ft]	10.3 (at 300° F); 11.2 (at 500° F); 13.1 (at 900° F).	
α, 10^{-6} in./in./F	6.0 (70° to 200° F); 6.1 (70° to 400° F); 6.5 (70° to 900° F).	

[a] Vendors guaranteed minimums for F_{tu}, F_{ty}, and e.

[b] Test direction longitudinal; these properties not applicable to the short transverse (thickness) direction.

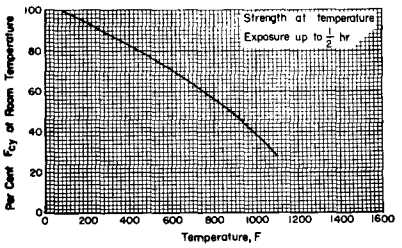

Fig. B2.23 Effect of temperature on the compressive yield strength (F_{cy}) of 17-4 PH (H900) stainless steel.

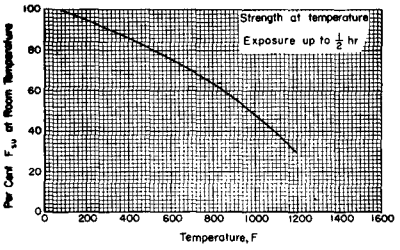

Fig. B2.24 Effect of temperature on the ultimate shear strength (F_{su}) of 17-4 PH (H900) stainless steel.

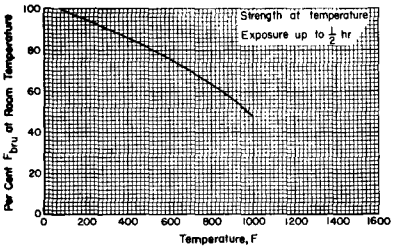

Fig. B2.25 Effect of temperature on the ultimate bearing strength (F_{bru}) of 17-4 PH (H900) stainless steel.

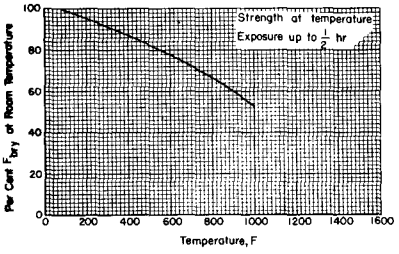

Fig. B2.26 Effect of temperature on the bearing yield strength (F_{bry}) of 17-4 PH (H900) stainless steel.

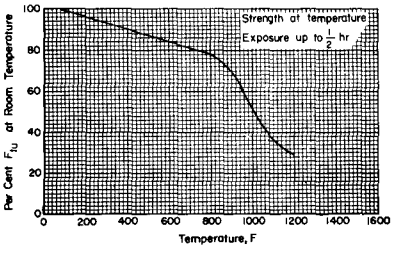

Fig. B2.21 Effect of temperature on the ultimate tensile strength (F_{tu}) of 17-4 PH (H900) stainless steel.

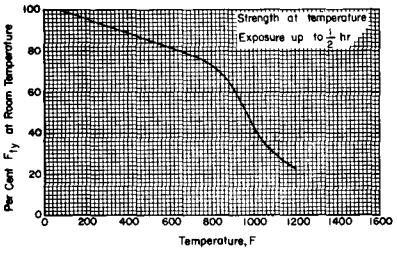

Fig. B2.22 Effect of temperature on the tensile yield strength (F_{ty}) of 17-4 PH (H900) stainless steel.

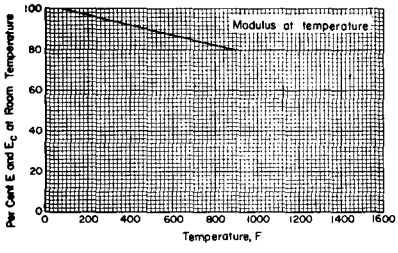

Fig. B2.27 Effect of temperature on the tensile and compressive modulus (E and E_c) of 17-4 PH (H900) stainless steel.

AM-350 STAINLESS STEEL

Table B2.5 Design Mechanical and Physical Properties of AM-350 Stainless Steel

Alloy	AM-350	
Form	Sheet and strip[a]	Sheet and strip[a]
Condition	DA	SCT
Thickness, in.	0.187 and under	0.187 and under
Basis	S	S
Mechanical properties:		
F_{tu}, ksi	165	185
F_{ty}, ksi	135	150
F_{cy}, ksi	142	158
F_{su}, ksi	107	120
F_{bru}, ksi:		
$(e/D=1.5)$	272	305
$(e/D=2.0)$	330	370
F_{bry}, ksi:		
$(e/D=1.5)$	202	225
$(e/D=2.0)$	223	247
e, percent	10	10
E, 10^6 psi	29.0	
E_c, 10^6 psi	30.0	
G, 10^6 psi	11.0	
Physical properties:		
ω, lb/in.^{3}	0.282.	
C, Btu/(lb)(F)	0.12 (32° to 212° F).	
K, Btu/[(hr)(ft^2)(F)/ft]	8.4 (at 100° F); 11.7 (at 800° F).	
α, 10^{-6} in./in./F	6.3 (70° to 212° F); 7.2 (70° to 932° F).	

[a] Test direction longitudinal for widths less than 9 in.; transverse for widths 9 in. and over.

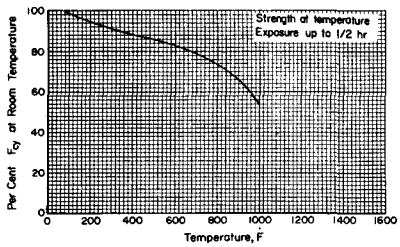

Fig. B2.30 Effect of temperature on the compressive yield strength (F_{cy}) of AM-350 stainless steel (double-aged).

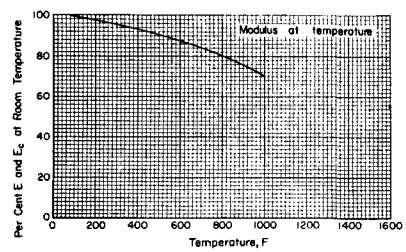

Fig. B2.31 Effect of temperature on the tensile and compressive modulus (E and E_C) of AM-350 stainless steel (double-aged).

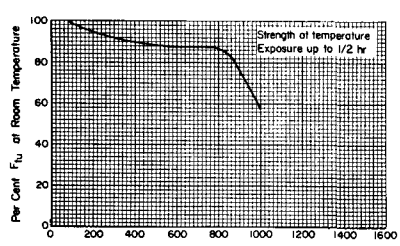

Fig. B2.32 Effect of temperature on the ultimate tensile strength (F_{tu}) of AM-350 stainless steel (SCT).

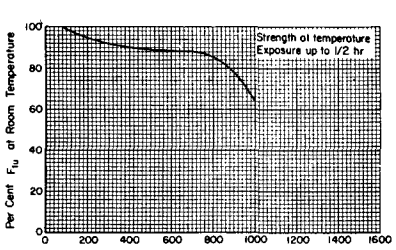

Fig. B2.28 Effect of temperature on the ultimate tensile strength (F_{tu}) of AM-350 stainless steel (double-aged).

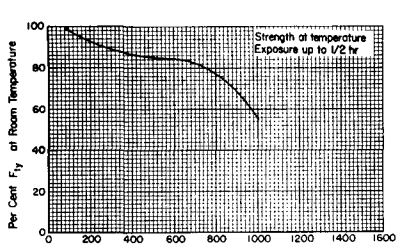

Fig. B2.29 Effect of temperature on the tensile yield strength (F_{ty}) of AM-350 stainless steel (double-aged).

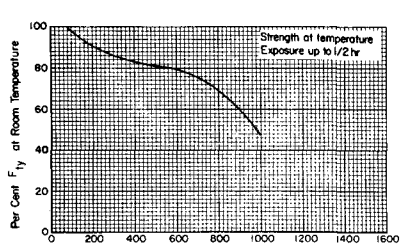

Fig. B2.33 Effect of temperature on the tensile yield strength (F_{ty}) of AM-350 stainless steel (SCT).

AM-350 STAINLESS STEEL (Cont.)

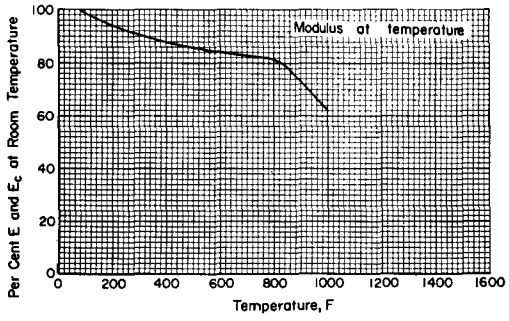

Fig. B2.34 Effect of temperature on the tensile and compressive modulus (E and E_c) of AM-350 stainless steel (SCT).

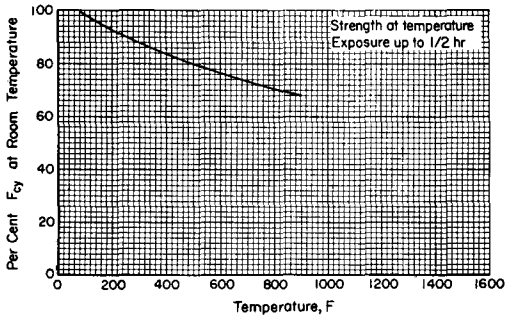

Fig. B2.36 Effect of temperature on the compressive yield strength (F_{cy}) of AM-350 stainless steel (SCT).

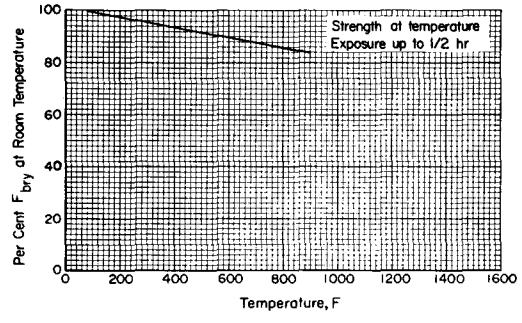

Fig. B2.35 Effect of temperature on the bearing yield strength (F_{bry}) of AM-350 stainless steel (SCT).

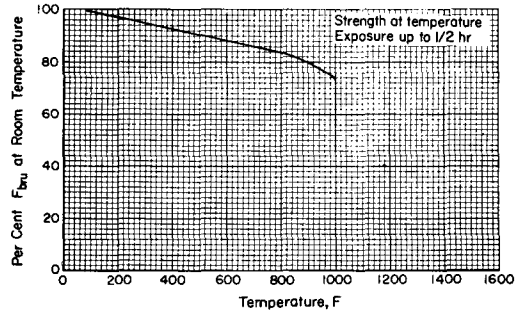

Fig. B2.37 Effect of temperature on the ultimate bearing strength (F_{bru}) of AM-350 stainless steel (SCT).

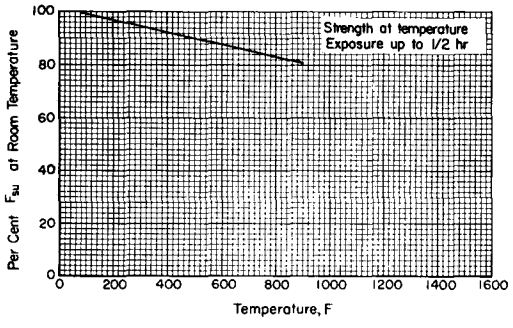

Fig. B2.38 Effect of temperature on the ultimate shear strength (F_{su}) of AM-350 stainless steel (SCT).

AISI 301 STAINLESS STEEL

Table B2.6 Design Mechanical and Physical Properties of AISI 301 Stainless Steel

Alloy	AISI 301 [a]				
Form	Plate [b], sheet, and strip				
Condition	Annealed	¼ hard	½ hard	¾ hard	Full hard
Basis	S	S	S	S	S
Mechanical properties:					
F_{tu}, ksi:					
L	75	125	150	175	185
T	75	125	150	175	185
F_{ty}, ksi:					
L	30	75	110	135	140
T	30	75	110	135	140
F_{cy}, ksi:					
L	35	43	58	76	85
T	35	80	118	160	179
F_{su}, ksi	40	67.5	80	95	100
F_{bru}, ksi:					
$(e/D=1.5)$	.....	.....	.....	.....	.....
$(e/D=2.0)$	150	250	300	350	370
F_{bry}, ksi:					
$(e/D=1.5)$	.....	.....	.....	.....	.....
$(e/D=2.0)$	50	140	200	240	270
e, percent	[c]	[c]	[c]	[c]	[c]
E, 10^6 psi:					
L	29.0	27.0	26.0	26.0	26.0
T	29.0	28.0	28.0	28.0	28.0
E_c, 10^6 psi:					
L	28.0	26.0	26.0	26.0	26.0
T	28.0	27.0	27.0	27.0	27.0
G, 10^6 psi	12.5	12.0	11.5	11.0	11.0
Physical properties:					
ω, lb/in.^{3}	0.286.				
C, Btu/(lb)(F)	0.108 (at 32° F).				
K, Btu/[(hr)(ft^2)(F)/ft]	7.74 (at 32° F).				
α, 10^{-6} in./in./F	9.2 (70° to 200° F).				

[a] Properties for annealed condition also applicable to annealed AISI 302, 303, 304, 321, and 347.

[b] Only annealed condition applicable to plate.

[c] See table 2.8.1.1(b).

NOTE.—Yield strength, particularly in compression, and modulus of elasticity in the longitudinal direction may be raised appreciably by thermal stress-relieving treatment in the range 500° to 800° F.

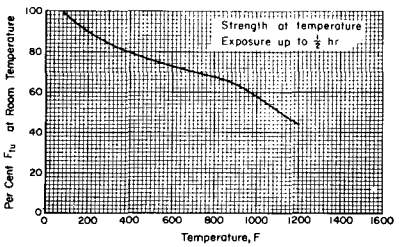

Fig. B2.39 Effect of temperature on the ultimate tensile strength (F_{tu}) of AISI 301 (half-hard) stainless steel.

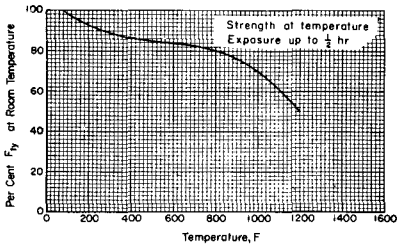

Fig. B2.40 Effect of temperature on the tensile yield strength (F_{ty}) of AISI 301 (half-hard) stainless steel.

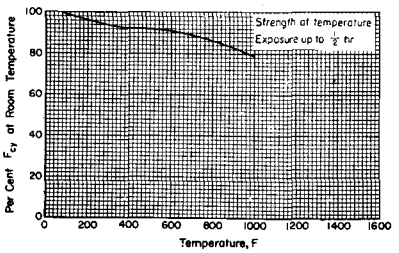

Fig. B2.41 Effect of temperature on the compressive yield strength (F_{cy}) of AISI 301 (half-hard) stainless steel.

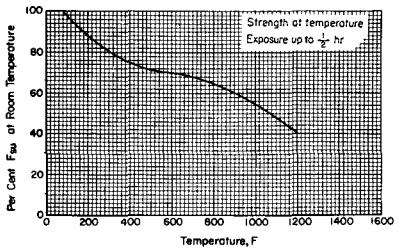

Fig. B2.42 Effect of temperature on the ultimate shear strength (F_{su}) of AISI 301 (half-hard) stainless steel.

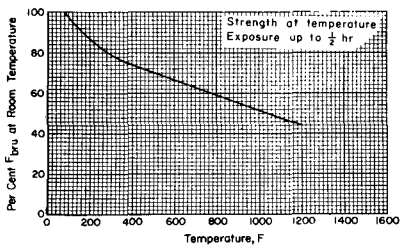

Fig. B2.43 Effect of temperature on the ultimate bearing strength (F_{bru}) of AISI 301 (half-hard) stainless steel.

AISI 301 STAINLESS STEEL (Cont.)

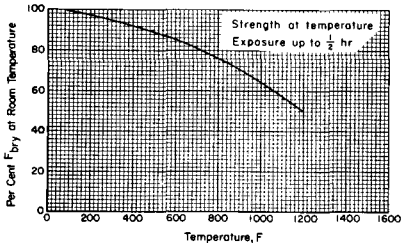

Fig. B2.44 Effect of temperature on the bearing yield strength (F_{bry}) of AISI 301 (half-hard) stainless steel.

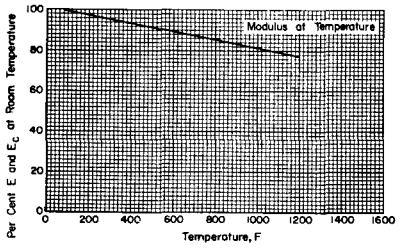

Fig. B2.45 Effect of temperature on the tensile and compressive modulus (E and E_c) of AISI 301 (half-hard) stainless steel.

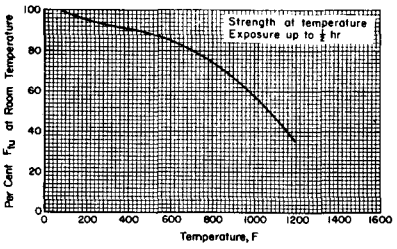

Fig. B2.46 Effect of temperature on the ultimate tensile strength (F_{tu}) of AISI 301 (full-hard) stainless steel.

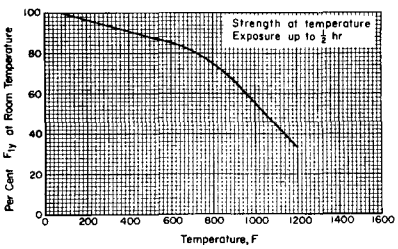

Fig. B2.47 Effect of temperature on the tensile yield strength (F_{ty}) of AISI 301 (full-hard) stainless steel.

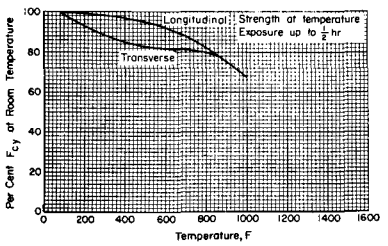

Fig. B2.48 Effect of temperature on the compressive yield strength (F_{cy}) of AISI 301 (full-hard) stainless steel.

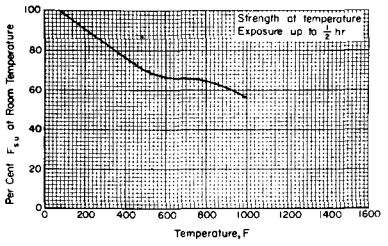

Fig. B2.49 Effect of temperature on the ultimate shear strength (F_{su}) of AISI 301 (full-hard) stainless steel.

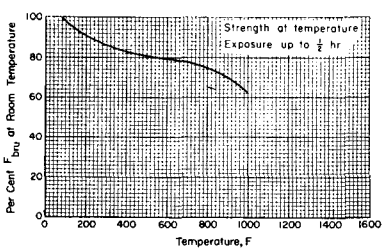

Fig. B2.50 Effect of temperature on the ultimate bearing strength (F_{bru}) of AISI 301 (full-hard) stainless steel.

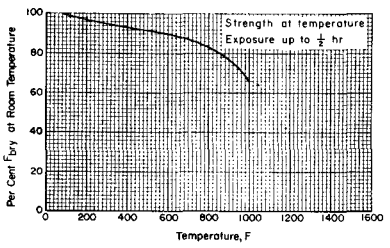

Fig. B2.51 Effect of temperature on the bearing yield strength (F_{bry}) of AISI 301 (full-hard) stainless steel.

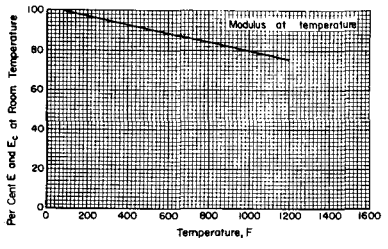

Fig. B2.52 Effect of temperature on the tensile and compressive modulus (E and E_c) of AISI 301 (full-hard) stainless steel.

2014 ALUMINUM ALLOYS (SHEET & PLATE, EXTRUSIONS, FORGINGS)

NOTE: Values in (A) columns are minimum guaranteed values. Values in (B) column will be met or exceeded by 90 percent of material supplied.

Table B2.7 Design Mechanical and Physical Properties of 2014 Aluminum Alloy (Sheet and Plate)

Alloy	2014										
Form	Sheet and plate										
Condition	-T6[a]										
Thickness, in.	0.020–0.039		0.040–0.499		0.500–1.000		1.001–1.500		1.501–2.000	2.001–3.000	3.001–[b] 4.000
Basis	A	B	A	B	A	B	A	B	A	A	A
Mechanical properties:											
F_{tu}, ksi											
L	65	67	68	70	68	70	67	68	65	63	59
T	64	66	67	69	67	69	67	68	65	63	59
ST	..	..	..	..	..	..	..	..	..	58	54
F_{ty}, ksi											
L	58	60	60	62	60	62	59	62	59	57	55
T	57	59	59	61	59	61	59	62	59	57	55
ST	..	..	..	..	..	..	..	..	..	53	51
F_{cy}, ksi											
L	..	..	60	62	60	62	61	64	61	59	57
T	..	..	61	63	61	63	61	64	61	59	57
ST	..	..	..	..	..	..	..	..	..	59	57
F_{su}, ksi	..	..	41	42	41	42	41	41	40	39	37
F_{bru}, ksi[c]											
$(e/D=1.5)$	..	..	102	105	102	105	101	102	98	89	88
$(e/D=2.0)$	..	..	129	133	129	133	127	129	124	129	112
F_{bry}, ksi[c]											
$(e/D=1.5)$	..	..	84	87	84	87	83	87	83	80	77
$(e/D=2.0)$	..	..	96	99	96	99	94	99	94	91	88
e, percent											
L	..	..	8	..	6	..	6	..	6	4	3
T	6	..	8	..	6	..	4	..	3	2	1.5
ST	..	..	..	..	..	..	..	..	..	1	..
E, 10^6 psi	10.5										
E_c, 10^6 psi	10.7										
G, 10^6 psi	4.0										
Physical properties:											
ω, lb/in.^{3}	0.101										
C, Btu/(lb)(F)	0.23 (at 212°F)										
K, Btu/[(hr)(ft^2)(F)/ft]	90 (at 77°F)										
α, 10^{-6} in./in./F	12.5 (68° to 212°F)										

2014 ALUMINUM ALLOYS (SHEET & PLATE, EXTRUSIONS, FORGINGS) (Cont.)

Table B2.8 Design Mechanical and Physical Properties of Clad 2014 Aluminum Alloy (Clad Sheet and Plate)

Alloy	Clad 2014							
Form	Sheet and plate							
Condition	-T6[a]							
Thickness, in	≤0.039		0.040–0.499		0.500–1.000		1.001–1.500	
Basis	A	B	A	B	A	B	A	B
Mechanical properties:								
F_{tu}, ksi								
L	64	64	65	67	65	67	64	65
T	63	63	64	66	64	66	64	65
ST	..	..	..	..	..	..	..	..
F_{ty}, ksi								
L	56	56	58	60	58	60	57	60
T	55	55	57	59	57	59	57	60
ST	..	..	..	..	..	..	..	..
F_{cy}, ksi								
L	56	56	58	60	58	60	59	62
T	57	57	59	61	59	61	59	62
ST	..	..	..	..	..	..	..	..
F_{su}, ksi	39	39	39	40	39	40	39	40
F_{bru}, ksi[b]								
$(e/D=1.5)$	96	96	98	101	98	101	96	98
$(e/D=2.0)$	122	122	124	127	124	127	122	124
F_{bry}, ksi[b]								
$(e/D=1.5)$	78	78	81	84	81	84	80	84
$(e/D=2.0)$	90	90	93	96	93	96	91	96
e, percent								
L	7	..	8	..	6	..	6	..
T	7	..	8	..	6	..	4	..
E, 10^6 psi	10.5							
E_c, 10^6 psi	10.7							
G, 10^6 psi	4.0							

Table B2.9 Design Mechanical and Physical Properties of 2014 Aluminum Alloy (Extrusions)

Alloy	2014											
Form	Extruded rod, bar, and shapes											
Condition	-T6[c]										>25, ≤32	Heat treated and aged by user[a] -T62
Cross-sectional area, in.[2]	≤25										>25, ≤32	Up to 32
Thickness, in.[b]	0.125–0.499		0.500–0.749		0.750–1.499		1.500–2.999		3.000–4.499		≥0.750	0.125–4.499
Basis	A	B	A	B	A	B	A	B	A	B	A	A
Mechanical properties:												
F_{tu}, ksi												
L	60	61	64	68	68	73	68	73	68	73	68	60
T	60	61	64	67	63	66	61	63	58	61	56	56
F_{ty}, ksi												
L	53	57	58	62	60	65	60	65	60	65	58	53
T	53	57	55	59	54	58	52	55	49	53	47	47
F_{cy}, ksi												
L	55	59	60	64	62	67	62	67	62	67	..	53
T	53	56	58	62	57	61	57	61	57	61	..	48
F_{su}, ksi	35	35	37	39	39	42	39	42	39	42	39	35
F_{bru}, ksi												
$(e/D=1.5)$	90	92	96	102	88	95	88	95	88	95	..	..
$(e/D=2.0)$	114	116	122	129	109	117	109	117	109	117	..	..
F_{bry}, ksi												
$(e/D=1.5)$	74	80	81	87	78	85	78	85	78	85	..	..
$(e/D=2.0)$	85	91	93	99	84	91	84	91	84	91	..	..
e, percent												
L	7	..	7	..	7	..	7	..	7	..	6	7
T[d]	5	..	5	..	2	..	2	..	1	..	1	..
E, 10^6 psi	10.5											
E_c, 10^6 psi	10.7											
G, 10^6 psi	4.0											

2014 ALUMINUM ALLOYS (SHEET & PLATE, EXTRUSIONS, FORGINGS) (Cont.)

Table B2.10 Design Mechanical and Physical Properties of 2014 Aluminum Alloy (Forgings)

Alloy	2014									
Form	Die forgings		Hand forgings Length ≤3 times width				Hand forgings Length >3 times width			
Condition	-T4		-T6							
Thickness, in.	≤4 inches		≤6 inches							
Cross-sectional area, in.²			≤16	>16, ≤36	>36, ≤144	>144, ≤256	≤16	>16, ≤36	>36, ≤144	>144, ≤256
Basis	A	A	A	A	A	A	A	A	A	A
Mechanical properties:										
F_{tu}, ksi										
L	55	65	65	65	62	60	65	65	62	60
T	52	62	63	63	59	58	63	63	59	58
ST	..	..	60	60	56	55	60	60	56	55
F_{ty}, ksi										
L	30	55	55	53	53	52	55	53	53	52
T	28	52	55	53	52	50	55	53	52	50
ST	..	..	55	53	52	50	55	53	52	50
F_{cy}, ksi										
L	30	55	55	53	53	52	55	53	53	52
T_e	28	52	55	53	52	50	55	53	..	..
ST	..	..	..	..	..	..	..	..	..	..
F_{su}, ksi	34	39	40	40	38	37	40	40	..	..
F_{bru}, ksi										
$(e/D=1.5)$	..	..	91	91	87	84	91	91	87	84
$(e/D=2.0)$	..	..	117	117	112	108	117	117	112	108
F_{bry}, ksi										
$(e/D=1.5)$	..	..	77	74	74	73	77	74	74	73
$(e/D=2.0)$	..	..	88	85	85	83	88	85	85	83
e, percent										
L	11	7	10	9	7	5	10	9	7	5
T	..	3	6	5	3	2	4	3	2.5	2
ST	..	..	3	2	1	1	2	2	1	1
E, 10^6 psi	10.5									
E_c, 10^6 psi	10.7									
G, 10^6 psi	4.0									

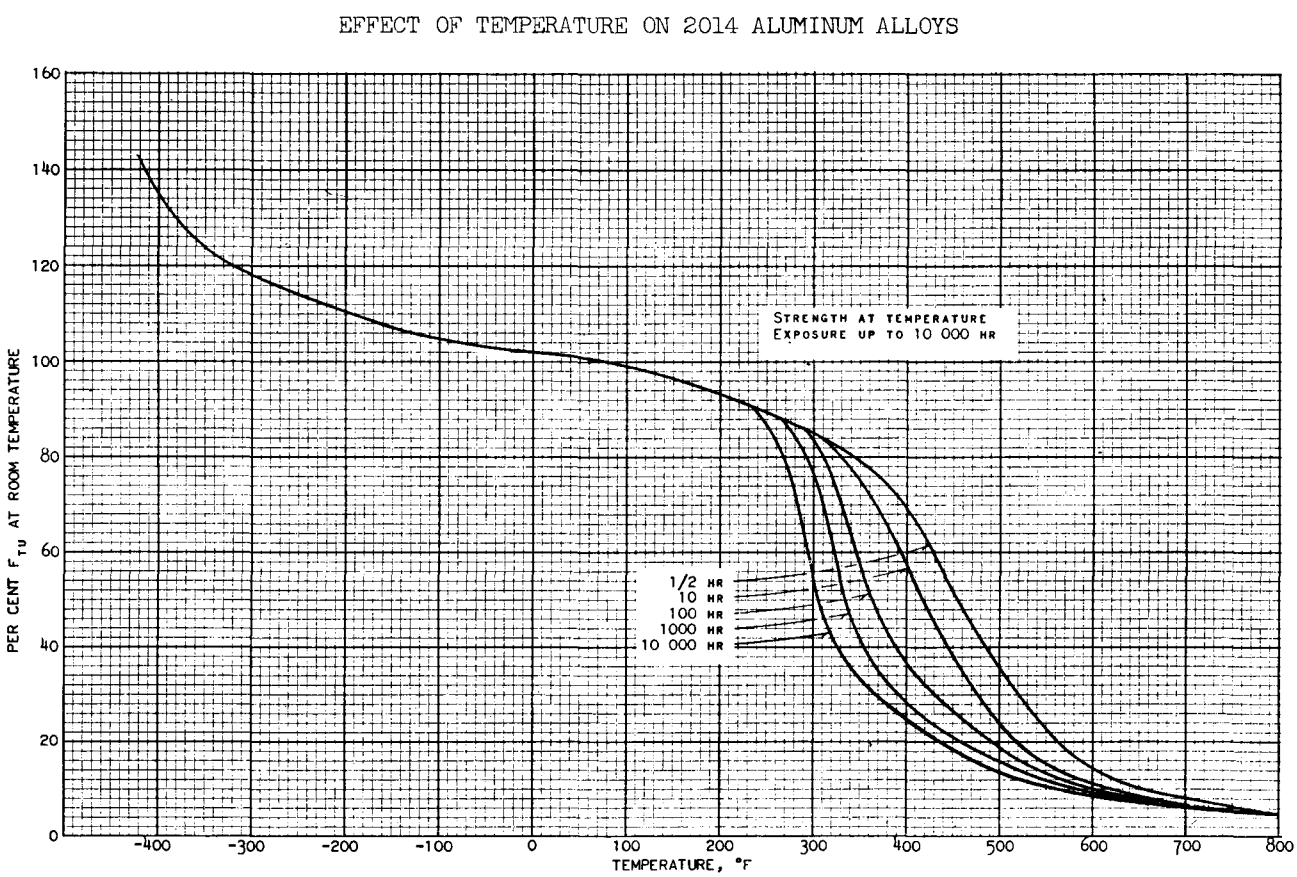

Fig. B2.53 Effect of temperature on the ultimate strength (F_{tu}) of 2014-T6 aluminum alloy (bare and clad sheet 0.020-0.039 in. thick; bare and clad plate 1.501-4.000 in. thick; rolled bar, rod and shapes; hand and die forgings; extruded bar, rod and shapes 0.125-0.749 in. thick with cross-sectional area $\leq$ 25 sq. in.).

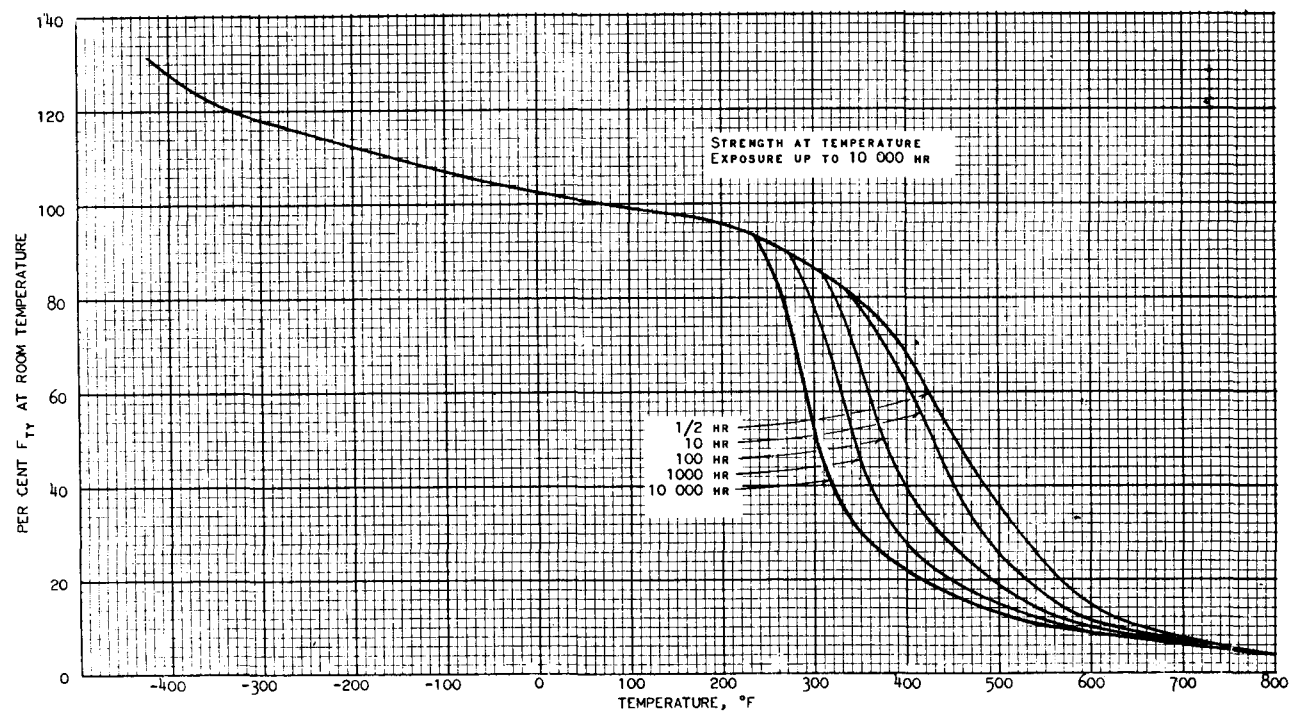

Fig. B2.54 Effect of temperature on the tensile yield strength (F_{ty}) of 2014-T6 aluminum alloy (bare and clad plate 3.001-4.000 in. thick; rolled bar, rod and shapes; hand and die forgings; extruded bar, rod and shapes 0.125-0.499 in. thick with cross-sectional area $\leq$ 25 sq. in.).

EFFECT OF TEMPERATURE ON 2014 ALUMINUM ALLOYS (Cont.)

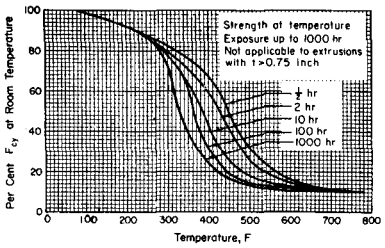

Fig. B2.55 Effect of temperature on the compressive yield strength (F_{cy}) of 2014-T6 aluminum alloy (all products except thick extrusions).

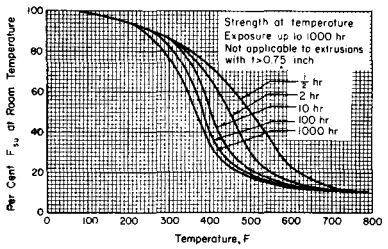

Fig. B2.56 Effect of temperature on the ultimate shear strength (F_{su}) of 2014-T6 aluminum alloy (all products except thick extrusions.

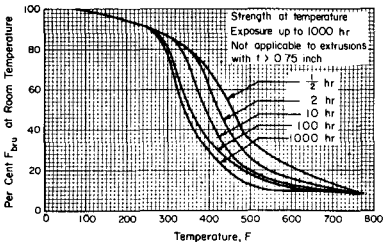

Fig. B2.57 Effect of temperature on the ultimate bearing strength (F_{bru}) of 2014-T6 aluminum alloy (all products except thick extrusions).

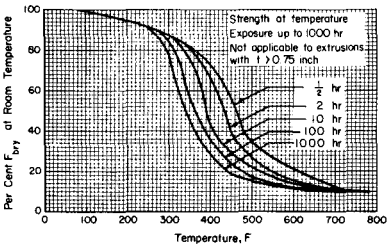

Fig. B2.58 Effect of temperature on the bearing yield strength (F_{bry}) of 2014-T6 aluminum alloy (all products except thick extrusions).

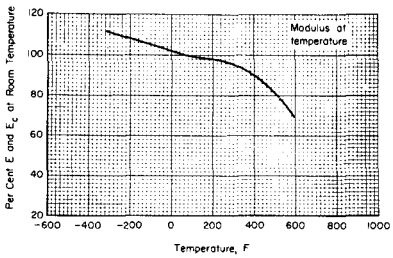

Fig. B2.59 Effect of temperature on the tensile and compressive modulus (E and E_c) of 2014 and 2017 aluminum alloys.

2024 ALUMINUM ALLOY (BARE SHEET & PLATE, EXTRUSIONS, BAR, ROD & WIRE)

Table B2.11 Design Mechanical and Physical Properties of 2024 Aluminum Alloy (Sheet and Plate)

Alloy	2024																	
Form	Sheet and plate																Coiled sheet	
Condition	Heat treated by user[a]					Heat treated[b]									Heat treated and rolled		Heat treated	
	-T42					-T3		-T4							-T36		-T4	
Thickness (in.)	<0.250	0.250–0.500	0.501–1.000	1.001–2.000	2.001–3.000	0.010–0.249		0.250–0.500		0.501–1.000		1.001–2.000		2.001–3.000		0.020–0.500		0.012–0.128	
Basis	A	A	A	A	A	A	B	A	B	A	B	A	B	A	B	A	B	A	B
Mechanical properties:																			
F_{tu}, ksi																			
L	62	64	62	60	56	65	68	65	67	63	68	61	64	..	..	70	72	62	66
T	62	64	62	60	56	64	67	64	66	62	67	60	63	56	59	69	71	62	66
F_{ty}, ksi																			
L	40	38	38	38	38	48	51	46	49	44	48	42	46	..	..	60	62	40	41
T	40	38	38	38	38	42	44	40	43	40	44	40	44	40	44	52	54	40	41
F_{cy}, ksi																			
L	40	38	38	38	38	40	42	38	41	38	42	38	42	..	..	49	51	40	41
T	40	38	38	38	38	45	47	43	46	43	47	42	46	..	..	56	58	40	41
F_{su}, ksi	37	38	37	36	34	40	42	40	41	38	41	36	38	..	..	43	44	37	40
F_{bru}, ksi[c]																			
(e/D = 1.5)	93	96	93	90	84	98	102	98	101	95	102	92	96	..	..	105	108	93	99
(e/D = 2.0)	118	122	118	114	106	124	129	124	127	120	129	116	122	..	..	133	137	118	126
F_{bry}, ksi[c]																			
(e/D = 1.5)	56	53	53	53	53	69	71	64	69	62	67	60	66	..	..	84	88	56	57
(e/D = 2.0)	64	61	61	61	61	79	82	74	78	70	77	68	75	..	..	96	100	64	66
e, percent																			
T	(d)	12	8	(d)	4	(d)	..	12	..	8	..	(d)	..	4	..	(d)	..	(d)	..
E, 10^6 psi	10.5																		
E_c, 10^6 psi	10.7																		
G, 10^6 psi	4.0																		

Table B2.12 Design Mechanical and Physical Properties of 2024 Aluminum Alloy (Extrusions)

Alloy	2024													
Form	Extruded bars, rods, and shapes													
	Heat treated												Heat treated by user[b]	Heat treated cold worked and aged
Condition	-T4[c]												-T42	-T81
Thickness, in	0.050–0.249		0.250–0.499		0.500–0.749		0.750–1.499		1.500–2.999		3.000≥		All thickness	≤0.250
Cross-sectional area, in.^{2}	≤25								≥25, ≤32				≤32	
Basis	A	B	A	B	A	B	A	B	A	B	A	B	A	A
Mechanical properties:														
F_{tu}, ksi														
L	57	61	60	62	60	62	65	70	70	74	70	74	57	64
T	57	61	60	62	60	62	58	61	54	57	50	53	50	.....
F_{ty}, ksi														
L	42	47	44	47	44	47	46	54	52	54	52	54	38	56
T	42	46	43	46	42	45	41	44	38	41	36	39	36	.....
F_{cy}, ksi														
L	38	41	39	42	39	42	44	52	50	52	50	52	38	.....
T	38	41	39	42	39	42	42	48	42	44	42	44	38	.....
F_{su}, ksi	30	32	32	33	32	33	34	38	38	40	38	40	30	.....
F_{bru}, ksi														
$(e/D=1.5)$	85	91	85	91	85	91	85	91	85	91	85	91	85	.....
$(e/D=2.0)$	108	114	108	114	108	114	108	114	108	114	108	114	108	.....
F_{bry}, ksi														
$(e/D=1.5)$	59	66	60	66	60	66	61	66	62	66	62	66	53	.....
$(e/D=2.0)$	67	75	69	75	69	75	71	75	73	75	73	75	61	.....
e, percent														
L	12	....	12	....	12	....	10	....	10	....	10	....	12	.....
T[a]	....	....	6	....	6	....	5	....	2	....	2	....	.....	.....
E, 10^6 psi	10.5													
E_c, 10^6 psi	10.7													
G, 10^6 psi	4.0													

2024 ALUMINUM ALLOY (BARE SHEET & PLATE, EXTRUSIONS, BAR, ROD & WIRE)(Cont.)

Table B2.13 Design Mechanical and Physical Properties of 2024 Aluminum Alloy (Bar, Rod, and Wire); Rolled, Drawn or Cold Finished; Rolled Tubing

Alloy	2024										
Form	Bar, rod and wire; rolled, drawn or cold-finished							Tubing			
Condition	–T4 or –T351							Heat treated		Heat treated by user [c]	Heat treated cold worked and aged
Cross-sectional area, in	⩽36							–T3		–T42	–T81
Thickness, in	Up to 1.000	1.001–2.000	2.001–3.000	3.001–4.000	4.001–5.000 [a]	5.001–6.000 [a]	6.001–6.500 [a]	0.018 to 0.500		0.018–0.500	
Basis	A	A	A	A	A	A	A	A	B	A	A
Mechanical properties:											
F_{tu}, ksi											
L	62	62	62	62	62	62	62	64	70	62	68
T	61	59	57	55	54	52	.....	.....	.....	.....	.....
F_{ty}, ksi											
L	40	40	40	40	40	40	40	42	46	40	60
T	40	39	38	37	37	36	.....	.....	.....	.....	.....
F_{cy}, ksi											
L	32	32	32	32	32	32	.....	42	46	40	.....
T	.....	.....	.....	.....	.....	.....	.....	.....	.....	.....	.....
F_{su}, ksi	37	37	37	37	37	37	37	39	42	39	.....
F_{bru}, ksi											
$(e/D=1.5)$	93	93	93	93	93	93	.....	93	105	96	.....
$(e/D=2.0)$	118	118	118	118	118	118	.....	118	133	122	.....
F_{bry}, ksi											
$(e/D=1.5)$	56	56	56	56	56	56	.....	59	64	56	.....
$(e/D=2.0)$	64	64	64	64	64	64	.....	67	74	64	.....
e, percent											
L	10 [b]	10	10	10	10	10	10	10 [d]	.....	.....	.....
T	10	8	6	4	2	2	.....	.....	.....	.....	.....
E, 10^6 psi	10.5										
E_c, 10^6 psi	10.7										
G, 10^6 psi	4.0										
Physical properties:											
ω, lb/in.^{3}	0.100										
C, Btu/(lb)(F)	0.23 (at 212° F)										
K, Btu/[(hr)(ft^2)(F)/ft]	70 (at 77° F) [e]										
α, 10^{-6} in./in./F	12.6 (68° to 212° F)										

Table B2.14 Design Mechanical and Physical Properties of Clad 2024 Aluminum Alloy (Sheet, Plate, and Coiled Sheet)

Alloy	Clad 2024																																			
Form	Sheet and plate																						Coiled sheet				Sheet and plate									
					Heat treated and rolled						Heat treated [a]								Heat treated by user [b]								Heat treated		Heat treated and aged		Heat treated, cold worked, and aged					
Condition	-T3				-T36						-T4								-T42								-T4		-T6		-T81	-T86				
Thickness, in.	0.010–0.062		0.063–0.249		0.020–0.062		0.063–0.499		0.500[c]		0.250–0.499		0.500–1.000[c]		1.001–2.000[c]		2.001–3.000[c]		0.008–0.062		0.063–0.249		0.250–0.499		0.500–1.000[c]		1.001–2.000[c]		2.001–3.000[c]		0.010–0.062		0.063–0.128		0.010–0.062	0.063–0.249	≤0.063 ≥0.063		0.020–0.062		0.063–0.249		0.250–0.499		0.500[c]	
Width, in.					≷48																																	
Basis	A	B	A	B	A	B	A	B	A	B	A	B	A	B	A	B	A	B	A	B	A	B	A	B	A	B	A	B	A		A		A		A	B	A	B	A	B	A	B	A	B
Mechanical properties:																																											
F_{tu}, ksi																																											
L	60	62	63	65	63	66	67	69	67	69	63	65	61	65	59	62	...	...	56	58	59	61	62	60	58	54	58	61	61	63	60	62	64	67	67	69	71	73	70	71	69	70
T	59	61	62	64	62	65	66	68	66	68	62	64	60	64	58	61	54	57	56	58	59	61	62	60	58	54	58	61	61	63	60	62	62	65	66	68	70	72	70	71	69	70
F_{ty}, ksi																																											
L	45	47	46	48	55	58	58	60	58	60	46	48	42	46	40	44	...	...	34	35	36	38	38	36	36	36	37	38	38	40	47	49	57	59	63	65	67	69	65	66	64	65
T	39	41	40	42	48	50	50	52	50	52	40	42	38	42	38	42	38	42	34	35	36	38	38	36	36	36	37	38	38	40	47	49	51	56	62	64	66	68	65	66	64	65
F_{cy}, ksi																																											
L	37	39	38	40	46	48	48	48	49	49	38	40	36	40	36	40	...	...	34	35	36	38	38	36	36	36	37	38	38	40	47	49	55	57	63	65	67	69	65	66	64	65
T	42	44	43	45	51	54	54	56	54	56	43	45	41	45	40	44	...	...	34	35	36	38	38	36	36	36	37	38	38	40	47	49	55	57	65	67	69	71	68	69	67	68
F_{su}, ksi	38	39	40	41	39	41	41	42	41	42	40	41	37	39	...	...	...	...	34	35	35	37	37	36	...	...	35	37	37	38	36	37	38	39	39	40	41	42	41	42	41	41
F_{bru}, ksi[d]																																											
$(e/D)=1.5$	90	93	95	98	95	99	101	104	101	104	95	98	92	98	89	93	...	...	84	87	89	92	93	90	87	81	87	92	92	95	90	93	96	100	100	103	106	109	105	106	103	105
$(e/D)=2.0$	114	118	120	124	120	125	127	131	127	131	120	124	116	124	112	118	...	...	106	110	112	116	118	114	110	103	110	116	116	120	114	118	122	127	127	131	135	139	133	135	131	133
F_{bry}, ksi[d]																																											
$(e/D)=1.5$	64	67	64	67	77	81	81	84	81	84	61	69	59	64	56	62	...	...	48	49	50	53	53	50	50	50	52	53	53	56	66	69	78	83	88	91	94	97	91	92	90	91
$(e/D)=2.0$	73	76	74	78	88	93	93	96	93	96	74	78	67	74	61	70	...	...	54	56	58	61	61	58	58	58	59	61	61	64	75	78	90	94	101	104	107	110	104	106	102	104
e, percent																																											
T	(e)	...	(e)	...	8	...	9	...	10	...	11	...	8	...	(e)	...	4	...	(e)	...	15	...	11	8	(e)	4	(e)	...	15	...	8	8	5	5	3	...	4	...	4	...	4	...
E, 10^6 psi																																											
Pri	10.5																																										
Sec	9.5		10		9.5		10.0												9.5		10.0								9.5		10.0		9.5	10.0	9.5	10.0	9.5		10.0					
E_c, 10^6 psi																																											
Pri	10.7																																										
Sec	9.7		10.2		9.7		10.2												9.7		10.2								9.7		10.2		9.7	10.2	9.7	10.2	9.7		10.2					
G, 10^6 psi																																											
Physical properties:																																											
ω, lb/in^3	0.100																																										
C, Btu/(16)(F)	0.23 (at 212° F)																																										
K, Btu/[(hr)(ft^2)(F)]	70 (at 77° F)																																										
α 10^{-6} in./in./F	12.6 (68° to 212° F)																																										

[a] For the stress relieved temper–T351 (plate only), all values for the –T4 temper apply with the exception of F_{cy} which may be somewhat lower.

[b] "Heat treated by user" refers to all material solution heat treated by the user regardless of the prior temper of the material.

[c] Specification minimums for clad material 0.500 inch thick and heavier are for the core material, inasmuch as a round test specimen is required for testing. The values given here for thickness 0.500 inch and greater have been adjusted to represent the average properties across the whole section, including the cladding.

[d] See Table 3.1.1.1.1.

[e] The elongation values for these columns are found in Table 3.2.3.0 (e).

EFFECT OF TEMPERATURE ON 2024 ALUMINUM ALLOYS

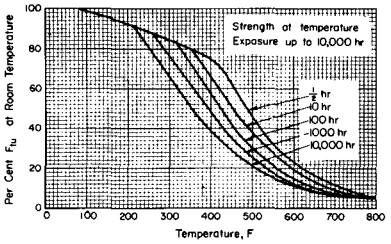

Fig. B2.60 Effect of temperature on the ultimate tensile strength (F_{tu}) of 2024-T3 and 2024-T4 aluminum alloy (all products except extrusions).

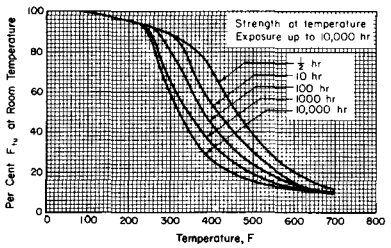

Fig. B2.61 Effect of temperature on the ultimate tensile strength (F_{tu}) of 2024-T3 and 2024-T4 aluminum alloy (extrusions).

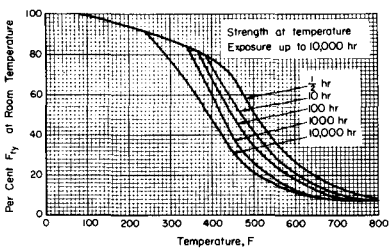

Fig. B2.62 Effect of temperature on the tensile yield strength (F_{ty}) of 2024-T3 and 2024-T4 aluminum alloy (all products except extrusions).

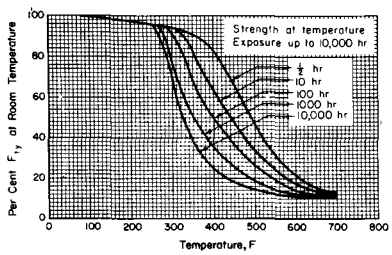

Fig. B2.63 Effect of temperature on the tensile yield strength (F_{ty}) of 2024-T3 and 2024-T4 aluminum alloy (extrusions).

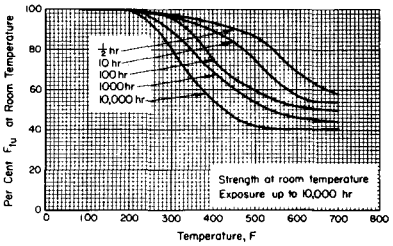

Fig. B2.64 Effect of exposure at elevated temperatures on the room-temperature ultimate tensile strength (F_{tu}) of 2024-T3 and 2024-T4 aluminum alloy (all products except thick extrusions).

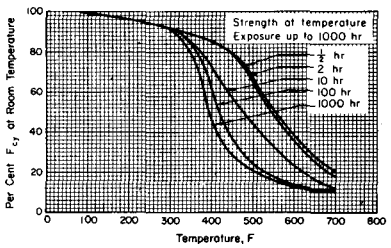

Fig. B2.65 Effect of temperature on the compressive yield strength (F_{cy}) of clad 2024-T3 and clad 2024-T4 aluminum alloy (sheet).

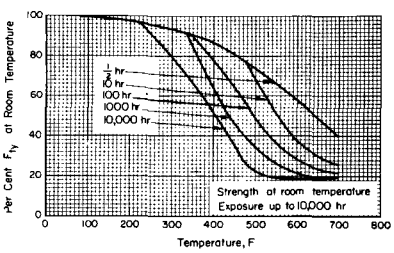

Fig. B2.66 Effect of exposure at elevated temperatures on the room-temperature tensile yield strength (F_{ty}) of 2024-T3 and 2024-T4 aluminum alloy (all products except thick extrusions).

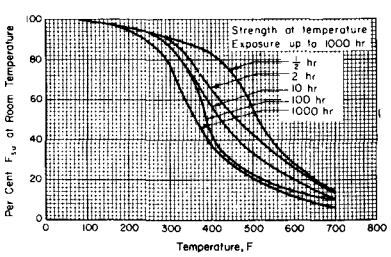

Fig. B2.67 Effect of temperature on the ultimate shear strength (F_{su}) of clad 2024-T3 and clad 2024-T4 aluminum alloy (sheet).

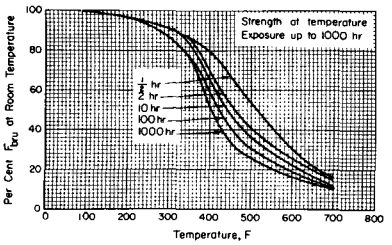

Fig. B2.68 Effect of temperature on the ultimate bearing strength (F_{bru}) of clad 2024-T3 and clad 2024-T4 aluminum alloy (sheet).

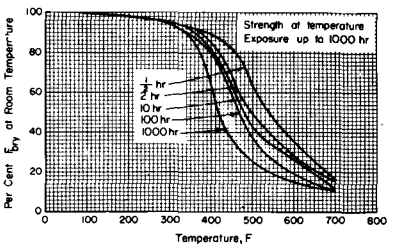

Fig. B2.69 Effect of temperature on the bearing yield strength (F_{bry}) of clad 2024-T3 and clas 2024-T4 aluminum alloy (sheet).

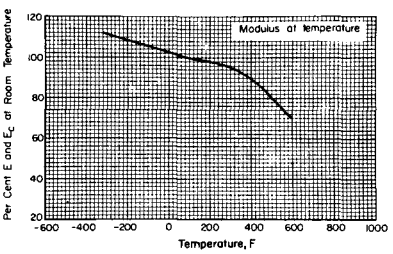

Fig. B2.70 Effect of temperature on the tensile and compressive modulus (E and E_c) of 2024 aluminum alloy.

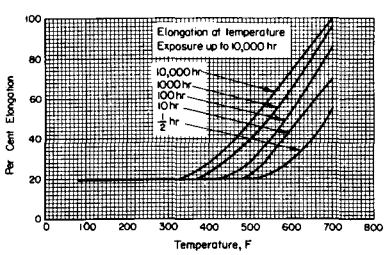

Fig. B2.71 Effect of temperature on the elongation of 2024-T3 and 2024-T4 aluminum alloy (all products except thick extrusions).

Table B2. 15 Design Mechanical and Physical Properties of 7075 Aluminum Alloy (Sheet and Plate)

Alloy	7075															
Form	Sheet and plate															
Condition	-T6[a]															
Thickness, in.	0.015–0.039		0.040–0.249		0.250–0.500		0.501–1.000		1.001–2.000		2.001–2.500		2.501–3.000		3.001–3.500	3.501–4.000
Basis	A	B	A	B	A	B	A	B	A	B	A	B	A	B	A	A
Mechanical properties:																
F_{tu}, ksi																
L	76	78	77	79	77	79	79	82	78	80	73	75	70	72	68	66
T	76	78	77	79	77	79	77	80	77	79	73	75	70	72	68	66
ST	..	..	..	..	..	..	..	..	..	..	67	69	64	66	64	62
F_{ty}, ksi																
L	66	69	67	70	67	69	69	72	68	71	62	65	60	62	58	56
T	65	68	66	69	66	68	66	69	66	69	62	65	60	62	58	56
ST	..	..	..	..	..	..	..	..	..	..	61	63	59	60	56	54
F_{cy}, ksi																
L	67	70	68	71	69	71	69	72	68	71	65	67	63	65	62	60
T	70	73	71	74	69	71	69	72	68	71	65	67	63	65	62	60
ST	..	..	..	..	..	..	..	..	..	..	64	66	62	63	62	60
F_{su}, ksi	46	47	46	47	46	47	47	49	46	47	43	45	41	43	40	39
F_{bru}, ksi[b]																
$(e/D=1.5)$	114	117	116	119	108	110	110	115	109	112	102	105	98	101	95	94
$(e/D=2.0)$	144	148	146	150	139	142	142	147	140	144	131	135	126	130	122	119
F_{bry}, ksi[b]																
$(e/D=1.5)$	92	97	94	98	87	90	90	94	88	92	81	84	78	81	75	73
$(e/D=2.0)$	106	110	107	112	100	104	104	108	102	106	93	97	90	93	87	84
e, percent																
L	7	..	8	..	8	..	6	..	5	..	5	..	5	..	5	..
T	7	..	8	..	8	..	6	..	4	..	3	..	3	..	3	2
ST	..	..	..	..	..	..	..	..	..	..	1	..	1	..	1	..
E, 10^6 psi	10.3															
E_c, 10^6 psi	10.5															
G, 10^6 psi	3.9															
Physical properties:																
ω, lb/in.^{3}	0.101															
C, Btu/(lb)(F)	0.23 (at 212°F)															
K, Btu/[(hr)(ft^2)(F)/ft]	76 (at 77°F)															
α, 10^{-6} in./in./F	12.9 (68° to 212°F)															

a For the stress relieved temper -T651, all values for the -T6 temper apply with the exception of F_{cy}. Applicable F_{cy} values are as follows:

Thickness (in.)	Direction of test	Fcy (A values)
0.250–2.000	L	66
2.001–2.500	L	62
2.501–3.000	L	60

b See Table 3.1.1.1.1.

Table B2.16 Design Mechanical and Physical Properties of Clad 7075 Aluminum Alloy (Sheet and Plate)

Alloy	Clad 7075																			
Form	Sheet and plate																			
Condition	–T6[a]																			
Thickness, in.	0.015–0.039		0.040–0.062		0.063–0.187		0.188–0.249		0.250–0.499		0.500–1.000[b]		1.001–2.000[b]		2.001–2.500[b]		2.501–3.000[b]		3.001–3.500[b]	3.501–4.000[b]
Basis	A	B	A	B	A	B	A	B	A	B	A	B	A	B	A	B	A	B	A	A
Mechanical properties:																				
F_{tu}, ksi—L	70	73	72	74	73	75	75	77	75	77	77	79	76	78	71	73	68	70	66	64
T	70	73	72	74	73	75	75	77	75	77	75	77	75	77	71	73	68	70	66	64
ST	..	..	..	..	..	..	..	..	..	..	..	..	..	..	67	69	64	66	64	62
F_{ty}, ksi—L	61	64	63	65	64	66	65	67	65	67	66	68	66	69	60	62	58	60	56	54
T	60	63	62	64	63	65	64	66	64	66	64	66	64	67	60	62	58	60	56	54
ST	..	..	..	..	..	..	..	..	..	..	..	..	..	..	61	63	59	60	56	54
F_{cy}, ksi—L	62	65	64	66	65	67	66	68	66	69	66	69	66	69	62	64	61	62	60	58
T	64	67	66	68	67	69	68	70	66	69	66	69	66	69	62	64	61	62	60	58
ST	..	..	..	..	..	..	..	..	..	..	..	..	..	..	64	66	62	63	62	60
F_{su}, ksi[c]	42	44	43	44	44	45	45	46	45	46	46	47	45	46	42	43	40	41	39	38
F_{bru}, ksi—(e/D = 1.5)	105	110	108	111	110	112	112	116	105	108	108	111	106	109	99	102	95	98	92	90
(e/D = 2.0)	133	139	137	141	139	142	142	146	135	139	139	142	137	140	128	131	122	126	119	115
F_{bry}, ksi[c]—(e/D = 1.5)	85	90	88	91	90	92	91	94	84	87	86	88	86	90	78	81	75	78	73	70
(e/D = 2.0)	98	102	101	104	102	106	104	107	98	100	99	102	99	104	90	93	87	90	84	81
e, percent—L	7	..	8	..	8	..	8	..	8	..	6	..	5	..	5	..	5	..	5	..
T	7	..	8	..	8	..	8	..	8	..	6	..	4	..	3	..	3	..	3	2
ST	..	..	..	..	..	..	..	..	..	..	..	..	..	..	1	..	1	..	1	..
E, 10^6 psi—Pri.	10.3				10.3		10.3													
Sec.	9.5				9.8		10.0													
E_c, 10^6 psi—Pri.	10.5				10.5		10.5													
Sec.	9.7				10.0		10.2													
G, 10^6 psi																				
Physical properties:																				
ω, lb/in.³	0.101																			
C, Btu/(lb)(F)	0.23 (at 212°F)																			
K, Btu/[(hr)(ft²)(F)/ft]	76 (at 77°F)																			
α, 10^{-6} in./in./F	12.9 (68° to 212°F)																			

[a] For the stress relieved temper –T651, all values for the –T6 temper apply with the exception of F_{cy}. Applicable F_{cy} values are as follows:

Thickness (in.)	Direction of test	Fcy (A values)
0.250–0.499	L	62
0.500–2.000	L	64
2.001–2.500	L	60
2.501–3.000	L	58

[b] These values except in the ST direction have been adjusted to include the influence of the 1 1/2% per side nominal cladding thickness.

[c] See Table 3.1.1.1.1.

Table B2. 17 Design Mechanical and Physical Properties of 7075 Aluminum Alloy (Extrusions)

Alloy	7075															
Form	Extrusions (rod, bars, and shapes)															
Condltion	−T6[a]															
Cross-sectional area, in.^{2}	≤20										≤20		>20, ≤32		≤32	
Thickness [b], in.	Up to 0.249		0.250–0.499		0.500–0.749		0.750–1.499		1.500–2.999		3.000–4.499				4.500–5.0	
Basis	A	B	A	B	A	B	A	B	A	B	A	B	A	B	A	B
Mechanical properties:																
F_{tu}, *ksi*																
L	78	82	81	85	81	85	81	85	81	85	81	84	78	81	78	81
T	76	78	77	79	73	75	72	74	66	68	62	64	62	64	60	62
F_{ty}, *ksi*																
L	70	74	73	77	72	76	72	76	72	76	71	74	70	73	68	71
T	64	67	66	68	63	66	62	64	56	58	54	56	54	56	53	55
F_{cy}, *ksi*																
L	71	75	74	78	73	77	72	76	72	75	72	75	68	72	.....	.....
T	71	75	74	78	73	77	72	75	69	72	65	68	.....	.....	.....	.....
F_{su}, *ksi*	43	45	45	47	45	47	45	47	45	47	45	46	43	44	43	44
F_{bru}, *ksi*																
(e/D=1.5)	101	107	97	102	97	102	97	102	97	102	97	101	94	97	94	97
(e/D=2.0)	125	131	130	136	130	136	130	136	130	136	122	126	117	125	117	125
F_{bry}, *ksi*																
(e/D=1.5)	91	96	80	85	79	84	79	84	79	84	78	81	77	80	75	78
(e/D=2.0)	98	104	102	108	101	106	101	106	101	106	92	96	91	95	88	92
e, percent																
L	7	8	7	8	7	8	7	8	7	8	7	8	6	.....	6	.....
T	5	.....	5	.....	4	.....	3	.....	1	.....	1	.....	1	.....	1	.....
E, 10^6 *psi*	10.3															
E_c, 10^6 *psi*	10.5															
G, 10^6 *psi*	3.9															
Physical properties:																
ω, lb/in.^{3}	0.101															
C, Btu/(lb)(F)	0.23 (at 212°F)															
K, Btu/[(hr)(ft^2)(F)/ft]	76 (at 77° F)															
α, 10^{-6} in./in./F	12.9 (68° to 212°F)															

[a] For the stress relieved tempers -T6510 and -T6511, all values for the -T6 temper apply, with the exception of F_{cy}-L. Applicable F_{cy} values are listed below:

Thickness (in.)	*Area (sq. in.)*	*Direction of test*	F_{cy} *(A values)*
≤0.249	≤20	L	70
0.250–0.749	≤20	L	72
0.750–1.499	≤20	L	71
1.500–2.999	≤20	L	70
3.000–4.499	≤32	L	66
4.500–5.000	≤32	L	65

[b] For extrusions with outstanding legs, the load carrying ability of such legs shall be determined on the basis of the properties of the appropriate column corresponding to the leg thickness.

7075 ALUMINUM ALLOY (EXTRUSIONS, FORGINGS, BAR, ROD, WIRE) (Cont.)

Table B2.18 Design Mechanical and Physical Properties of 7075 Aluminum Alloy
(Hand Forgings and Die Forgings)

Alloy	7075						
Form	Hand-forged stock, length ≤3 times width			Hand-forged stock, length >3 times width			Die forgings
Condition	-T6[a]						-T6
Thickness, in.							≤3
Cross-sectional area, in.²	≤16	>16, ≤36	>36, ≤144	≤16	>16, ≤36	>36, ≤144	
Basis	A	A	A	A	A	A	A
Mechanical properties:							
F_{tu}, ksi							
L	75	73	71	75	73	71	75
T	75	71	69	73	71	69	71
ST	72	68	66	70	68	66	..
F_{ty}, ksi							
L	64	61	60	63	60	59	65
T	63	60	58	61	59	57	62
ST	63	60	58	61	59	57	..
F_{cy}, ksi							
L	64	61	60	63	60	59	65
T	63	60	58	61	59	57	58
ST	..	..	..	..	..	..	..
F_{su}, ksi	45	44	43	45	44	43	45
F_{bru}, ksi							
$(e/D=1.5)$	97	95	85	97	95	85	..
$(e/D=2.0)$	135	124	114	135	124	114	..
F_{bry}, ksi							
$(e/D=1.5)$	90	79	78	88	78	77	..
$(e/D=2.0)$	96	91	90	94	90	88	..
e, percent							
L	9	7	4	9	7	4	7
T	4	3	2	4	3	2	3
ST	2	2	1	2	2	1	..
E, 10^6 psi	10.3						
E_c, 10^6 psi	10.5						
G, 10^6 psi	3.9						

7075 ALUMINUM ALLOY (EXTRUSIONS, FORGINGS, BAR, ROD, WIRE) (Cont.)

Table B2.19 Design Mechanical and Physical Properties of 7075 Aluminum Alloy
(Bar, Rod, Wire and Shapes; Rolled, Drawn or Cold-Finished)

Alloy	7075			
Form	Bar, rod, wire and shapes, rolled, drawn or cold-finished			
Condition	—T6 or —T651			
Thickness, in	Up to 1.000 [a]	1.001 2.000 [a]	2.001 3.000 [a]	3.001 4.000 [a]
Basis	A	A	A	A
Mechanical properties:				
F_{tu}, ksi:				
L	77	77	77	77
LT	77	75	72	69
F_{ty}, ksi:				
L	66	66	66	66
LT	66	66	63	60
F_{cy}, ksi:				
L	64	64	64	64
LT				
F_{su}, ksi	46	46	46	46
F_{bru}, ksi:				
$(e/D=1.5)$	100	100	100	100
$(e/D=2.0)$	123	123	123	123
F_{bry}, ksi:				
$(e/D=1.5)$	86	86	86	86
$(e/D=2.0)$	92	92	92	92
e, percent:				
L	[b] 7	7	7	7
LT	4	3	2	1
E, 10^6 psi	10.3			
E_c, 10^6 psi	10.5			
G, 10^6 psi	3.9			

EFFECT OF TEMPERATURE ON 7075 ALUMINUM ALLOYS

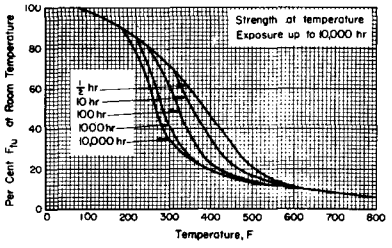

Fig. B2.72 Effect of temperature on the ultimate tensile strength (F_{tu}) of 7075-T6 aluminum alloy (all products).

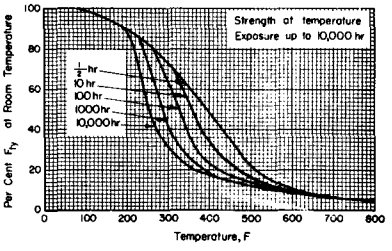

Fig. B2.73 Effect of temperature on the tensile yield strength (F_{ty}) of 7075-T6 aluminum alloy (all products).

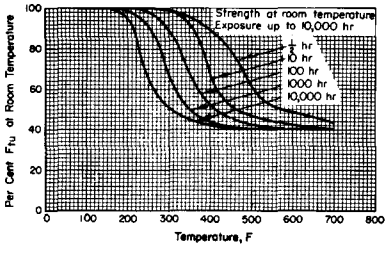

Fig. B2.74 Effect of exposure at elevated temperatures on the room-temperature ultimate tensile strength (F_{tu}) of 7075-T6 aluminum alloy (all products).

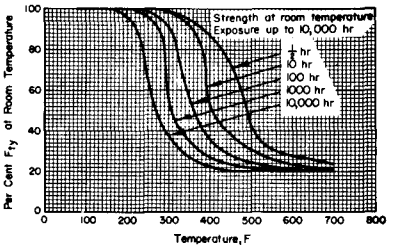

Fig. B2.75 Effect of exposure at elevated temperatures on the room-temperature tensile yield strength (F_{ty}) of 7075-T6 aluminum alloy (all products).

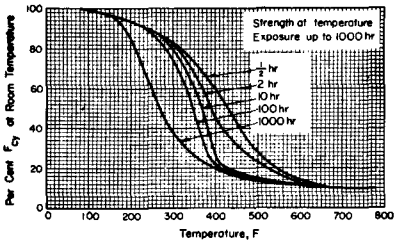

Fig. B2.76 Effect of temperature on the compressive yield strength (F_{cy}) of 7075-T6 aluminum alloy (all products).

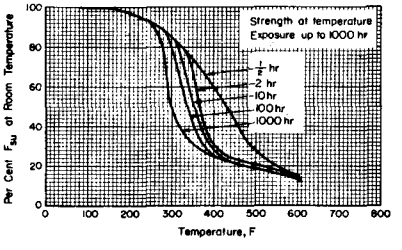

Fig. B2.77 Effect of temperature on the ultimate shear strength (F_{su}) of 7075-T6 aluminum alloy (all products).

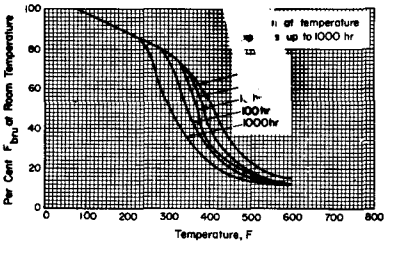

Fig. B2.78 Effect of temperature on the ultimate bearing strength (F_{bru}) of 7075-T6 aluminum alloy (all products).

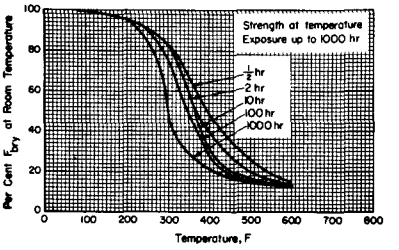

Fig. B2.79 Effect of temperature on the bearing yield strength (F_{bry}) of 7075-T6 aluminum alloy (all products).

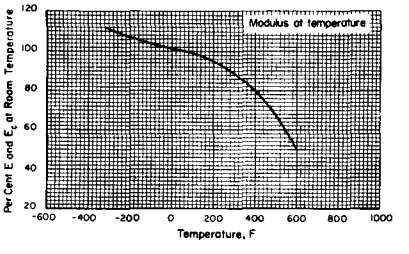

Fig. B2.80 Effect of temperature on the tensile and compressive modulus (E and E_c) of 7075-T6 aluminum alloy.

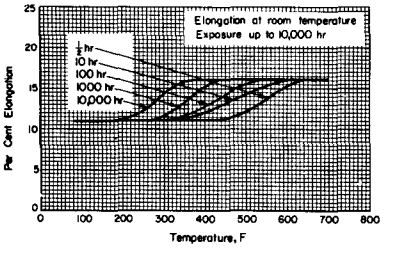

Fig. B2.81 Effect of exposure at elevated temperatures on the elongation of 7075-T6 aluminum alloy (all products except thick extrusions).

Table B2.20 Design Mechanical and Physical Properties of AZ31B Magnesium Alloy (Sheet and Plate)

Alloy	AZ31B																		
Form	Sheet and plate																		
Condition	-O						-H24						-H26						
Thickness (in.)	0.016–0.060		0.061–0.249		0.250–0.500	0.501–2.000	0.016–0.249		0.250–0.374	0.375–0.500	0.501–1.000	1.001–2.000	0.250–0.374	0.375–0.438	0.439–0.500	0.501–0.750	0.751–1.000	1.001–1.500	1.501–2.000
Basis	A	B	A	B			A	B											
Mechanical properties:																			
F_{tu}, *ksi.*																			
L	32	36	32	36	32	30	39	40	38	37	36	34	39	38	38	37	37	35	35
T	....	....	....	....	.....	.....	40	....	39	38	37	35	40	39	39	38	38	36	36
F_{ty}, *ksi.*																			
L	18	19	15	19	15	15	29	30	26	24	22	20	27	26	26	25	23	22	21
T	....	....	....	....	.....	.....	32	....	29	27	25	23	30	29	29	28	26	25	24
F_{cy}, *ksi.*																			
L	12	13	12	14	10	10	24	25	20	16	13	10	22	21	18	17	16	15	14
T[b]	....	....	....	....	.....	.....	.....	.....	.....	.....	.....	.....	.....	.....	.....	.....	.....	.....	.....
F_{su}, *ksi*	17	23	17	23	17	.....	18	26	18	18	.....	.....	18	18	18	.....	.....	.....	.....
F_{bru}, *ksi.*																			
$(e/D=1.5)$	50	52	50	52	50	.....	58	60	56	54	.....	.....	58	56	56	.....	.....	.....	.....
$(e/D=2.0)$	60	61	60	61	60	.....	68	70	65	63	.....	.....	68	65	65	.....	.....	.....	.....
F_{bry}, *ksi.*																			
$(e/D=1.5)$	29	30	29	31	27	.....	43	44	38	34	.....	.....	40	39	36	.....	.....	.....	.....
$(e/D=2.0)$	29	30	29	31	27	.....	43	44	38	34	.....	.....	40	39	36	.....	.....	.....	.....
e, percent																			
L	12	18	12	19	12	10	6	8	8	8	8	8	6	6	6	6	6	6	6
T	....	....	....	....	.....	.....	8	....	10	10	10	10	8	8	8	8	8	8	8
E, 10^6 *psi*	6.5																		
E_c, 10^6 *psi*	6.5																		
G, 10^6 *psi*	2.4																		
Physical properties:																			
ω, lb/in.^{3}	0.0639																		
C, BTU/(lb)(F)	0.25 (at 78° F)[a]																		
K, BTU/(hr)(ft^2)(F)/ft	56 (212 to 572° F)																		
α, $10^{*}t$ in./in./F	14 (65 to 212° F)																		

[a] Estimated. [b] Transverse F_{sy} allowables are equal to or greater than the longitudinal F_{sy} allowables.

AZ31B MAGNESIUM ALLOY (SHEET & PLATE) (Cont.)

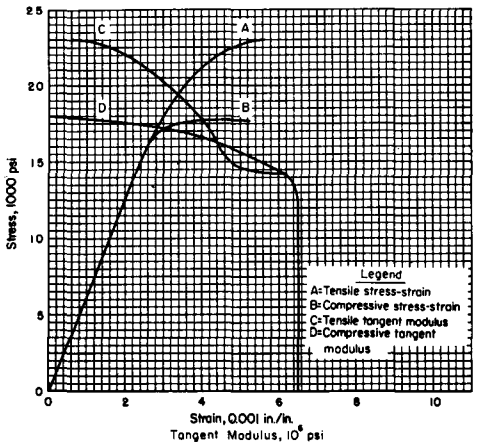

Fig. B2.82 Typical stress-strain and tangent-modulus curves for AZ31B-O magnesium alloy at room temperature (longitudinal).

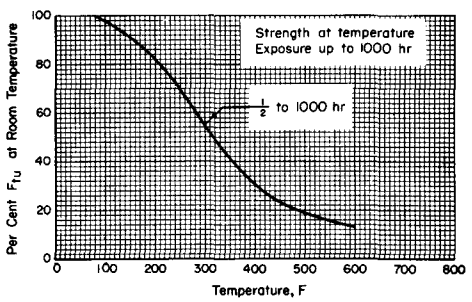

Fig. B2.83 Effect of temperature on the ultimate tensile strength (F_{tu}) of AZ31B-H24 magnesium alloy.

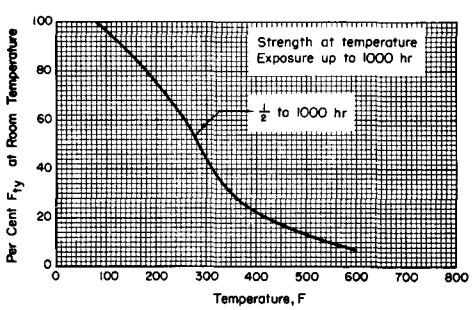

Fig. B2.84 Effect of temperature on the tensile yield strength (F_{ty}) of AZ31B-H24 magnesium alloy.

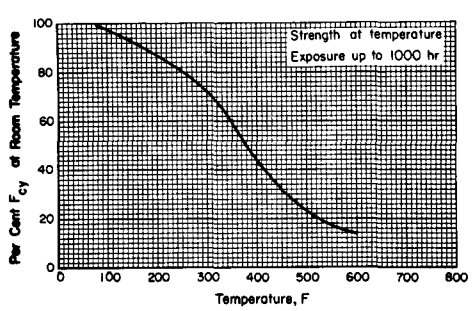

Fig. B2.85 Effect of temperature on the compressive yield strength (F_{cy}) of AZ31B-H24 magnesium alloy.

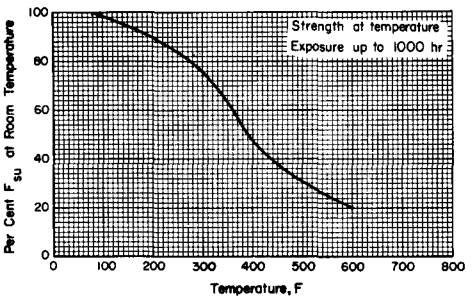

Fig. B2.86 Effect of temperature on the ultimate shear strength (F_{su}) of AZ31B-H24 magnesium alloy.

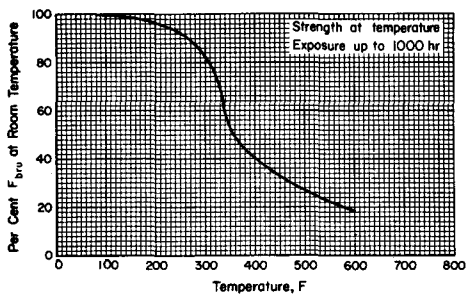

Fig. B2.87 Effect of temperature on the ultimate bearing strength (F_{bru}) of AZ31B-H24 magnesium alloy.

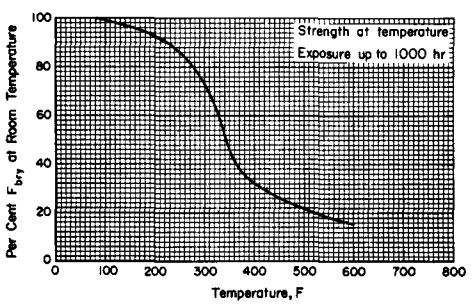

Fig. B2.88 Effect of temperature on the bearing yield strength (F_{bry}) of AZ31B-H24 magnesium alloy.

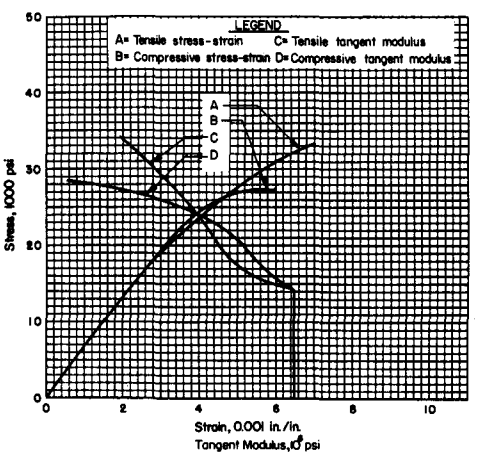

Fig. B2.89 Typical stress-strain and tangent-modulus curves for AZ31B-H24 magnesium alloy at room temperature.

Table B2.21 Design Mechanical and Physical Properties of HK31A Magnesium Alloy (Sheet, Plate and Sand Castings)

Alloy	HK31A													
Form	Sheet [a] and plate [a]													Sand castings [b]
Condition	-O					-H24								-T6
Thickness, in.	0.016–0.250		0.251–0.500	0.501–1.000	1.001–3.000	0.016–0.125		0.126–0.250		0.251–0.500	0.501–1.000	1.001–2.000	2.001–3.000	.....
Basis	A	B				A	B	A	B					(c)
Mechanical properties:														
F_{tu}, *ksi*	30	32	30	30	29	34	36	34	35	34	34	33	33	27
F_{ty}, *ksi*	18	19	16	15	14	26	28	23	24	21	18	15	15	13
F_{cu}, *ksi*	12	13	10	10	10	20	21	19	22	18	13	11	11	13
F_{su}, *ksi*	22	22	22	22	.....	23	23	23	23	23	23	.....	.....	.....
F_{bru}, *ksi*														
(e/D=1.5)	43	46	43	.....	.....	49	52	49	51	49	.....	.....	.....	.....
(e/D=2.0)	51	54	51	.....	.....	57	60	57	58	57	.....	.....	.....	.....
F_{bry}, *ksi*														
(e/D=1.5)	24	25	21	.....	.....	34	35	33	36	31	.....	.....	.....	.....
(e/D=2.0)	24	25	21	.....	.....	34	35	33	36	31	.....	.....	.....	.....
e, percent	12	20	12	12	12	4	6	4	8	4	10	10	8	4
E, 10^6 *psi*	6.5													
E^c, 10^6 *psi*	6.5													
G, 10^6 *psi*	2.4													
Physical properties:														
ω, lb./in.^{3}	0.0647													
C, BTU/(lb.)(F)	0.25 (32° to 212° F)													
K, BTU/(hr.)(ft.^{2})(F) ft	60.0 (at 68° F)													
α, 10^{-6} in./in./F	15 (68° to 392° F)													

[a] Properties for sheet and plate are taken parallel to the direction of rolling. Transverse properties are equal to or greater than the longitudinal properties.

[b] Reference should be made to the specific requirements of the procuring or certificating agency with regard to the use of the above values in the design of castings.

[c] Mechanical properties are based upon the guaranteed tensile properties from separately-cast test bars. The mechanical properties of bars cut from castings may be as low as 75 percent of the tabulated values.

HK31A MAGNESIUM ALLOY (SHEET, PLATE & SAND CASTINGS) (Cont.)

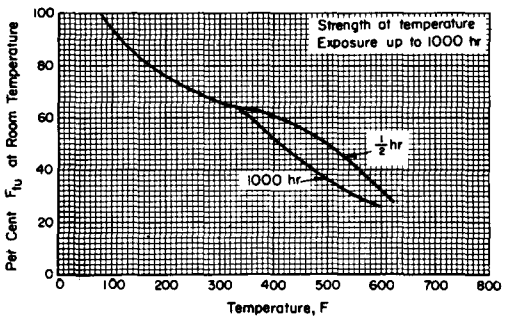

Fig. B2.90 Effect of temperature on the ultimate tensile strength (F_{tu}) of HK31A-H24 magnesium alloy.

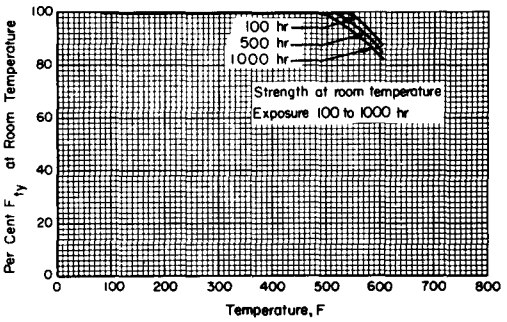

Fig. B2.93 Effect of exposure at elevated temperatures on the room-temperature tensile yield strength (F_{ty}) of HK31A-H24 magnesium alloy.

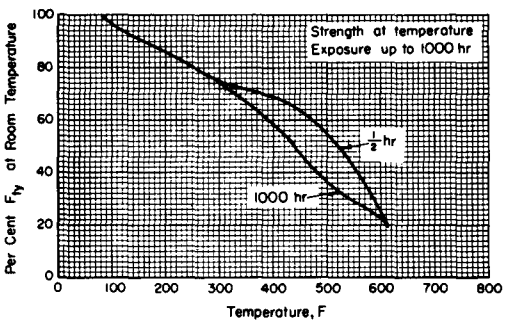

Fig. B2.91 Effect of temperature on the tensile yield strength (F_{ty}) of HK31A-H24 magnesium alloy.

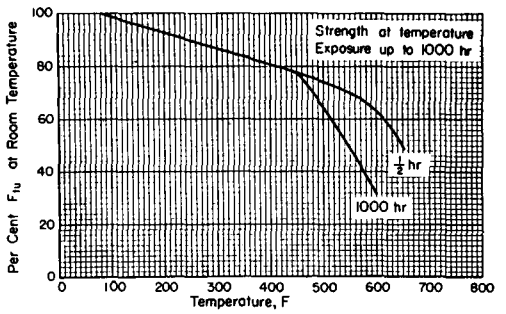

Fig. B2.94 Effect of temperature on the ultimate tensile strength (F_{tu}) of HK31A-T6 magnesium alloy (sand casting).

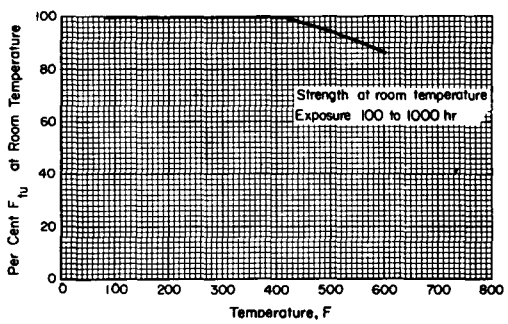

Fig. B2.92 Effect of exposure at elevated temperatures on the room-temperature ultimate tensile strength (F_{tu}) of HK31A-H24 magnesium alloy.

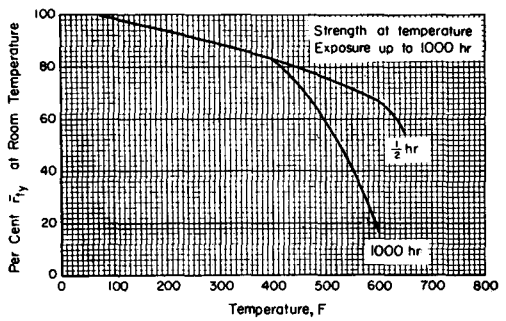

Fig. B2.95 Effect of temperature on the tensile yield strength (F_{ty}) of HK31A-T6 magnesium alloy (sand casting).

AZ61A, AZ63A, AZ80A MAGNESIUM (EXTRUSIONS, FORGINGS, CASTINGS)

Table B2.22 Design Mechanical and Physical Properties of AZ61A[a] Magnesium Alloy (Extrusions and Forgings)

Alloy	AZ61A				
Form	Extruded bar, rod, and solid shapes		Extruded Hollow shapes	Extruded Tubes	Forging
Condition	-F				
Thickness, in	≷0.249	0.250–2.499		0.028–0.750	
Basis					
Mechanical properties:					
F_{tu}, ksi					
L	38	39	36	36	38
T	..	..	..	..	..
F_{ty}, ksi					
L	21	24	16	16	22
T	..	..	..	..	..
F_{cy}, ksi					
L	14	14	11	11	14
T	..	..	..	..	..
F_{su}, ksi	19	19	..	..	19
F_{bru}, ksi					
$(e/D=1.5)$	45	45	..	..	50
$(e/D=2.0)$	55	55	..	..	60
F_{bry}, ksi					
$(e/D=1.5)$	28	28	..	..	28
$(e/D=2.0)$	32	32	..	..	32
e, percent	8	9	7	7	6
E, 10^6 psi	6.3				
E_c, 10^6 psi	6.3				
G, 10^6 psi	2.4				
Physical properties:					
ω, lb/in.^{3}	0.0647				
C, Btu/(lb)(F)	0.25 (at 78°F)[b]				
K, Btu/[(hr)(ft^2)(F)/ft]	46 (212° to 572°F)				
α, 10^{-6} in./in./F	14 (65° to 212°F)				

a Properties for extruded bars, rods, shapes, tubes, and forgings are taken parallel to the direction of extrusion or maximum metal flow during fabrication.

b Estimated.

AZ61A, AZ63A, AZ80A MAGNESIUM (EXTRUSIONS, FORGINGS, CASTINGS) (Cont.)

Table B2.23 Design Mechanical and Physical Properties of AZ80A[a] Magnesium Alloy (Extrusions and Forgings)

Alloy	AZ80A							
Form	Extruded bars, rods, and solid shapes						Forgings	
Condition	-F			-T5			-F	-T5
Thickness, in.	≤0.249	0.250–1.499	1.500–2.499	≤0.249	0.250–1.499	1.500–2.499	..	..
Basis								
Mechanical properties:								
F_{tu}, ksi								
L	43	43	43	47	48	48	42	42
T	..	..	..	..	..	..	..	..
F_{ty}, ksi								
L	28	28	28	30	33	33	26	28
T	..	..	..	..	..	..	..	..
F_{cy}, ksi								
L	..	17	17	..	28	27	18	25
T	..	..	..	..	..	..	..	..
F_{su}, ksi	19	19	19	20	20	20	20	20
F_{bru}, ksi								
$(e/D=1.5)$	48	48	48	..	..	..	..	50
$(e/D=2.0)$	56	56	56	..	..	..	..	70
F_{bry}, ksi								
$(e/D=1.5)$	36	36	36	..	..	..	..	42
$(e/D=2.0)$	40	40	40	..	..	..	..	..
e, percent	9	8	6	4	4	4	5	2
E, 10^6 psi	6.5							
E_c, 10^6 psi	6.5							
G, 10^6 psi	2.4							

Table B2.24 Material Specifications for AZ63A Magnesium Alloy

Specification	Type of product
QQ-M-56	Sand castings
QQ-M-55	Permanent-mold castings

TABLE 4.2.3.0(*b*). *Design Mechanical and Physical Properties of AZ63A Magnesium[a] Alloy (Castings)*

Alloy	AZ63A			
Form	Sand and permanent-mold castings			
Condition	-F	-T4	-T5	-T6
Thickness (in.)				
Basis[b]				
Mechanical properties:				
F_{tu}, ksi	24	34	24	34
F_{ty}, ksi	10	10	11	16
F_{cy}, ksi	10	10	11	16
F_{su}, ksi	16	17	..	19
F_{bru}, ksi				
$(e/D=1.5)$	36	36	..	50
$(e/D=2.0)$	50	50	..	65
F_{bry}, ksi				
$(e/D=1.5)$	28	32	..	36
$(e/D=2.0)$	30	36	..	45
e, percent	4	7	2	3
E, 10^6 psi	6.5			
E_c, 10^6 psi	6.5			
G, 10^6 psi	2.4			

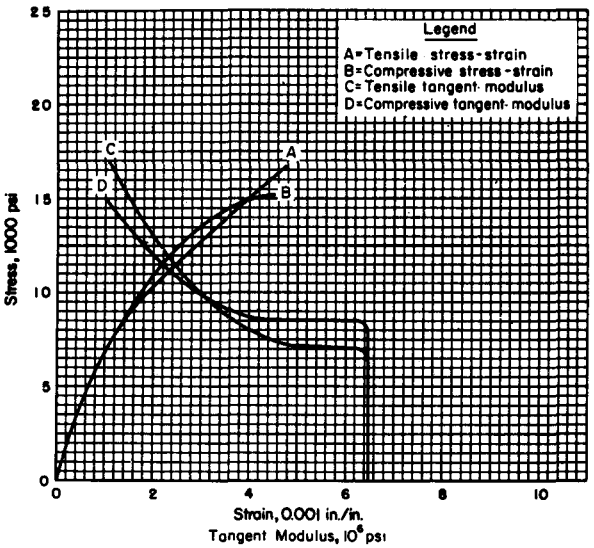

Fig. B2.96 Typical stress-strain and tangent-modulus curves for AZ63A-T4 magnesium alloy (sand casting) at room temperature.

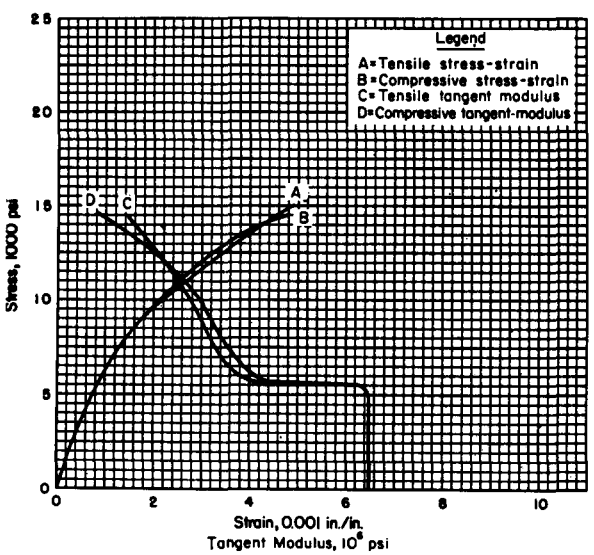

Fig. B2.97 Typical stress-strain and tangent-modulus curves for AZ63A-F magnesium alloy (sand casting) at room temperature.

Table B2.25 Design Mechanical and Physical Properties of 8Mn Titanium Alloy

Alloy	8Mn
Form	Sheet, plate, and strip
Condition	Annealed
Thickness, in	..
Basis	A
Mechanical properties:	
F_{tu}, *ksi*	
L	120
T	120
F_{ty}, *ksi*	
L	110
T	110
F_{cy}, *ksi*	
L	110
T	110
F_{su}, *ksi*	84
F_{bru}, *ksi*	
$(e/D=1.5)$	170
$(e/D=2.0)$	..
F_{bry}, *ksi*	
$(e/D=1.5)$	130
$(e/D=2.0)$	..
e, percent	10
E, 10^6 *psi*	15.5
E_c, 10^6 *psi*	16.0
G, 10^6 *psi*	..
Physical properties:	
ω, lb/in.^{3}	0.171
C, Btu/(lb)(F)	0.118 (at 68°F)
K, Btu/[(hr)(ft^2)(F)/ft]	6.3
α, 10^{-6} in./in./F	4.8 (at 200°F)

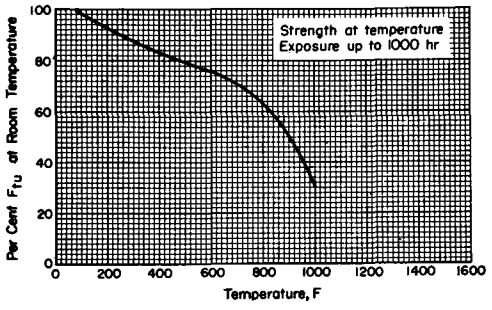

Fig. B2.98 Effect of temperature on the ultimate tensile strength (F_{tu}) of 8Mn annealed titanium alloy.

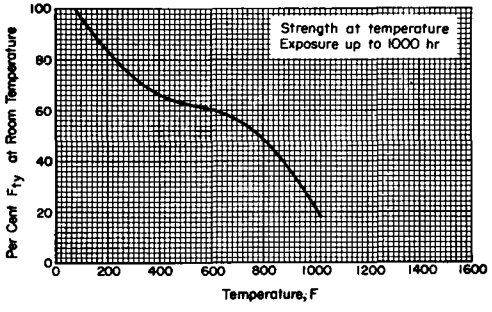

Fig. B2.99 Effect of temperature on the tensile yield strength (F_{ty}) of 8 Mn annealed titanium alloy.

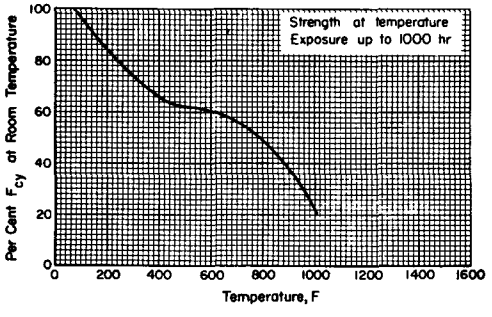

Fig. B2.100 Effect of temperature on the compressive yield strength (F_{cy}) of 8 Mn annealed titanium alloy.

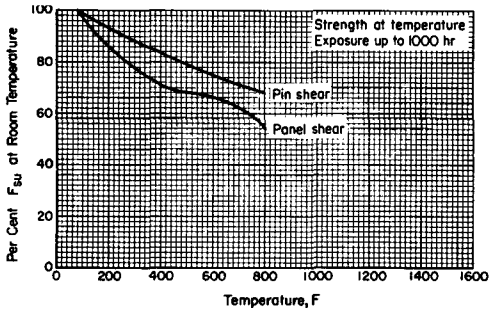

Fig. B2.101 Effect of temperature on the ultimate shear strength (F_{su}) of 8 Mn annealed titanium alloy.

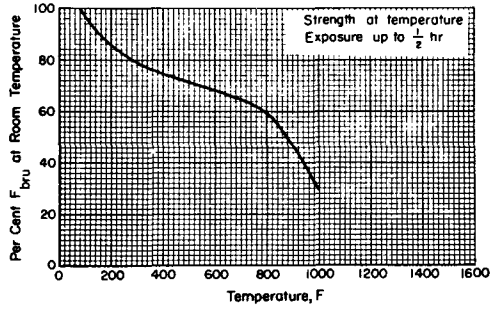

Fig. 2.102 Effect of temperature on the ultimate bearing strength (F_{bru}) of 8 Mn annealed titanium alloy.

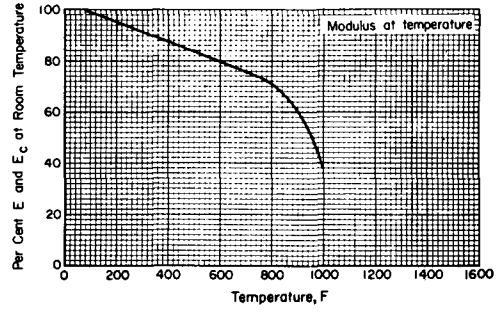

Fig. 2.103 Effect of temperature on the tensile and compressive modulus (E and E_c) of 8Mn titanium alloy.

6Al-4V TITANIUM ALLOY (BAR & SHEET)

Table B2. 26 Design Mechanical and Physical Properties of 6Al-4V Titanium Alloy

Alloy	6Al-4V	
Form	Bar	Sheet
Condition	Annealed	
Thickness, in.	≷1.5	≷0.187
Basis	A	A
Mechanical properties:		
F_{tu}, ksi		
L	130	130
T	..	130
F_{ty}, ksi		
L	120	120
T	..	120
F_{cy}, ksi		
L	126	126
T	..	126
F_{su}, ksi	80	76
F_{bru}, ksi		
(e/D=1.5)	196	191
(e/D=2.0)	248	244
F_{bry}, ksi		
(e/D=1.5)	174	163
(e/D=2.0)	205	198
e, percent	10	10
E, 10^6 psi		
L	16.0	15.4
T	..	16.4
E_c, 10^6 psi		
L	16.4	16.0
T	..	16.9
G, 10^6 psi	6.2	..
Physical properties:		
ω, lb/in.³	0.160	
C, Btu/(lb)(F)	0.135 (at 68°F)	
K, Btu/[(hr)(ft²)(F)/ft]	3.8 (at 63°F)	
α, 10^{-6} in./in./F	4.6 (at 200°F)	

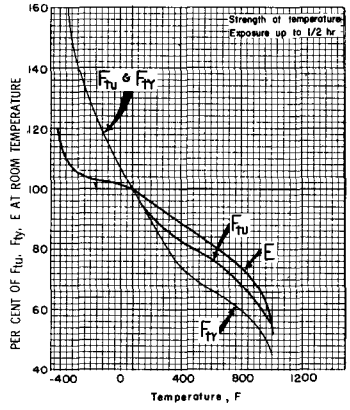

Fig. B2. 104 Effect of temperature on F_{tu}, F_{ty} and E of 6Al-4V annealed titanium alloy (sheet and bar)

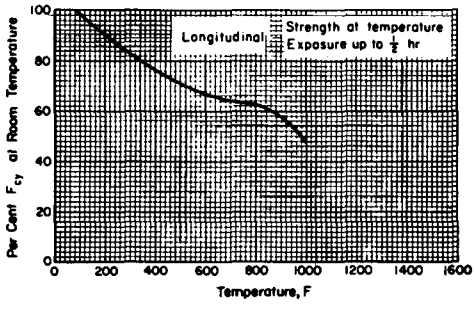

Fig. B2. 105 Effect of temperature on the compressive yield strength (F_{cy}) of 6Al-4V annealed titanium alloy (sheet and bar).

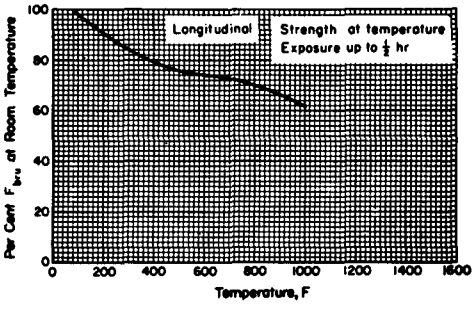

Fig. B2. 106 Effect of temperature on the ultimate bearing strength (F_{bru}) of 6Al-4V annealed titanium alloy (sheet and bar).

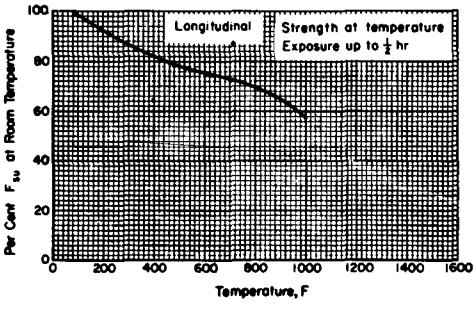

Fig. B2. 107 Effect of temperature on the ultimate shear strength (F_{su}) of 6Al-4V annealed titanium alloy (sheet and bar).

INCONEL X NICKEL ALLOY (SHEET)

Table B2.27 Design Mechanical and Physical Properties of Inconel X Nickel Alloy

Alloy	Inconel X
Form	Sheet
Condition	Precipitation heat-treated
Thickness, in.	
Basis	
Mechanical properties:	
F_{tu}, ksi	
L	155
T	155
F_{ty}, ksi	
L	100
T	100
F_{cy}, ksi	
L	105
T	105
F_{su}, ksi	108
F_{bru}, ksi	
$(e/D=1.5)$	..
$(e/D=2.0)$	286
F_{bry}, ksi	
$(e/D=1.5)$	..
$(e/D=2.0)$	186
e, percent	20
E, 10^6 psi	31.0
E_c, 10^6 psi	31.0
G, 10^6 psi	
Physical properties:	
ω, lb/in.^{3}	0.304
C, Btu/(lb)(F)	0.109
K, Btu/[(hr)(ft^2)(F)/ft]	8.7 (80° to 212°F)
α, 10-^{6} in./in./F	6.4 (100° to 200°F)

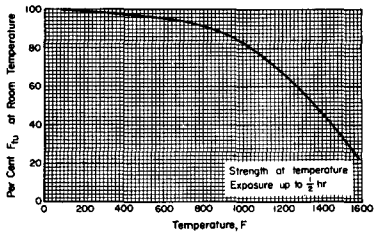

Fig. B2.108 Effect of temperature on the ultimate tensile strength (F_{tu}) of precipitation heat treated Inconel X nickel alloy.

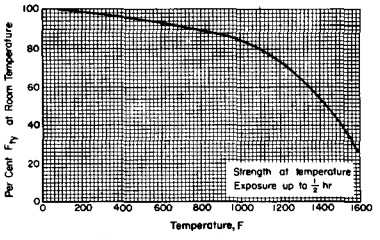

Fig. B2.109 Effect of temperature on the tensile yield strength (F_{ty}) of precipitation heat treated Inconel X nickel alloy.

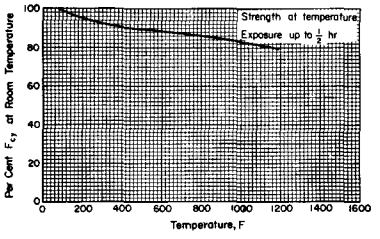

Fig. B2.110 Effect of temperature on the compressive yield strength (F_{cy}) of precipitation heat treated Inconel X nickel alloy.

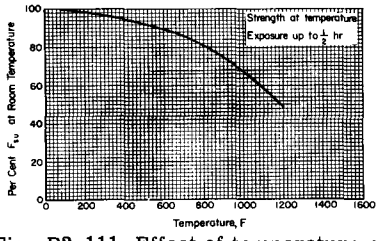

Fig. B2.111 Effect of temperature on the ultimate shear strength (F_{su}) of precipitation heat treated Inconel X nickel alloy.

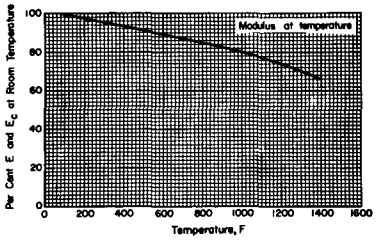

Fig. B2.112 Effect of temperature on the tensile modulus (E) of Inconel X nickel alloy.

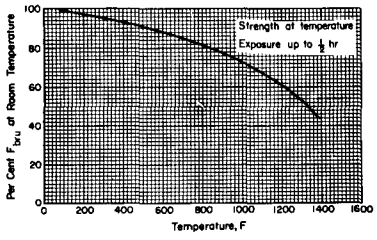

Fig. B2.113 Effect of temperature on the ultimate bearing strength (F_{bru}) of precipitation heat treated Inconel X nickel alloy.

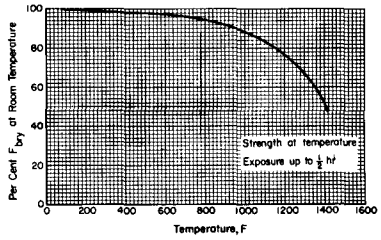

Fig. B2.114 Effect of temperature on the bearing yield strength (F_{bry}) of precipitation heat treated Inconel X nickel alloy.

PART C
PRACTICAL STRENGTH ANALYSIS & DESIGN OF STRUCTURAL COMPONENTS

CHAPTER C1
COMBINED STRESSES. THEORY OF YIELD AND ULTIMATE FAILURE.

C1.1 Uniform Stress Condition

Aircraft structures are subjected to many types of external loadings. These loads often cause axial, bending and shearing stresses acting simultaneously. If structures are to be designed satisfactorily, combined stress relationships must be known. Although in practical structures uniform stress distribution is not common, still sufficient accuracy for design practice is provided by using the stress relationships based on uniform stress assumptions. In deriving these stress relationships, the Greek letter sigma (σ) will represent a stress intensity normal to the surface and thus a tensile or compressive stress and the Greek letter tau (τ) will represent a stress intensity parallel to the surface and thus a shearing stress.

C1.2 Shearing Stresses on Planes at Right Angles.

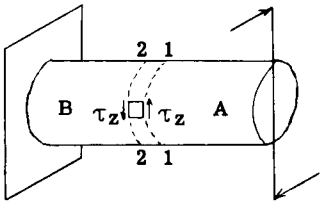

Fig. C1.1

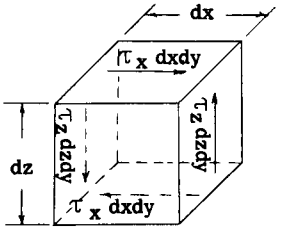

Fig. C1.2

Fig. C1.1 shows a circular solid shaft subjected to a torsional moment. The portion (A) of the shaft exerts a shearing stress τ_z on section (1-1) and portion (B) exerts a resisting shearing stress τ_z on section (2-2). Fig. C1.2 illustrates a differential cube cut from shaft between sections (1-1) and (2-2). For equilibrium a resisting couple must exist on top and bottom face of cube. Taking moments about lower left edge of cube:

$$\tau_x \, dxdy \, (dz) - \tau_z \, dzdy \, (dx) = 0$$

$$\text{hence, } \tau_x = \tau_z \quad - - - - - - - - - - - - - - - - \quad (1)$$

Thus if a shearing unit stress occurs on one plane at a point in a body, a shearing unit stress of same intensity exists on planes at right angles to the first plane.

C1.3 Simple Shear Produces Tensile and Compressive Stresses.

Fig. C1.3 shows an elementary block of unit dimensions subjected to pure shearing stresses.

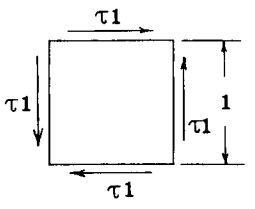

Fig. C1.3

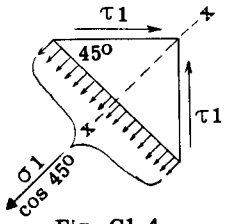

Fig. C1.4

Fig. C1.4 shows a free body after the block has been cut along a diagonal section.

For equilibrium the sum of the forces along the x-x axis equals zero.

$$\Sigma F_x = - \frac{\sigma(1)}{\cos 45} + 2 \, (\tau 1 \cos 45^\circ) = 0$$

$$\text{hence, } \sigma = \frac{2 \, (\tau \, 1 \cos 45^\circ) \cos 45^\circ}{1} = \tau \quad - - \quad (2)$$

Therefore when a point in a body is subjected to pure shear stresses of intensity τ, normal stresses of the same intensity as the shear stresses are produced on a plane at 45° with the shearing planes.

C1.4 Principal Stresses

For a body subjected to any combination of stresses 3 mutually perpendicular planes can be found on which the shear stresses are zero. The normal stresses on these planes of zero shear stress are referred to as principal stresses.

C1.5 Shearing Stresses Resulting From Principal Stresses.

In Fig. C1.5 the differential block is subjected to tensile principal stresses σ_x and σ_z and zero principal stress σ_y. The block is cut along a diagonal section giving the free body of Fig. C1.6. The stresses on the diagonal section have been resolved into stress components parallel and normal to the section as shown. For equilibrium the summation of the stresses along the axes (1-1) and (2-2) must equal zero.

$$\Sigma F_{1-1} = 0$$

$$\sigma_n \, dudy - \sigma_x \, dzdy \cos\theta - \sigma_z \, dydx \sin\theta = 0,$$

$$\text{whence } \sigma_n = \frac{\sigma_x \, dzdy \cos\theta}{dudy} + \frac{\sigma_z \, dydx \sin\theta}{dudy}$$

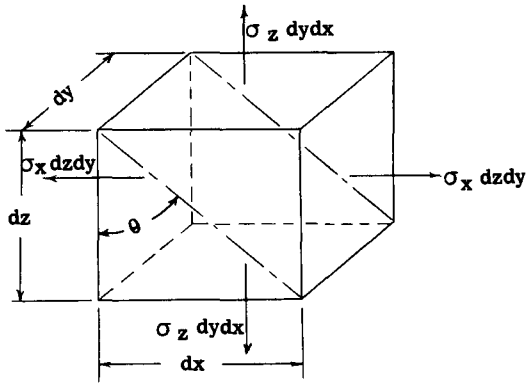

Fig. C1.5

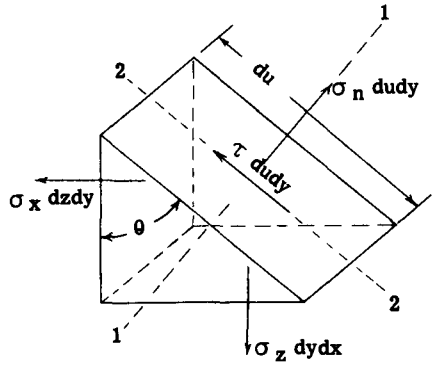

Fig. C1.6

But $\frac{dzdy}{dudy} = \cos\theta$ and $\frac{dydx}{dudy} = \sin\theta$, whence

$$\sigma_n = \sigma_X \cos^2\theta + \sigma_Z \sin^2\theta \text{ - - - - - - - - - - (2a)}$$

The normal stress σ_n at a point is always less than the maximum principal stress σ_X or σ_Z at the point.

$$\Sigma F_{s-s} = 0$$

$$-\tau\, dudy - \sigma_X\, dzdy \sin\theta + \sigma_Z\, dydx \cos\theta = 0$$

But $\frac{dzdy}{dudy} = \cos\theta$ and $\frac{dydx}{dudy} = \sin\theta$

hence, $\tau = \sigma_Z \sin\theta \cos\theta - \sigma_X \cos\theta \sin\theta$

or, $\tau = (\sigma_Z - \sigma_X) \sin\theta \cos\theta$

or, $\tau = (1/2)(\sigma_Z - \sigma_X) \sin 2\theta$, where σ_Z is maximum principal stress and σ_X is minimum principal stress.

Since $\sin 2\theta$ is maximum when $\theta = 45^\circ$,

$$\tau = (\sigma_{max} - \sigma_{min})/2 \text{ - - - - - - - - - - (3)}$$

Stated in words, the maximum value of the shearing unit stress at a point in a stressed body is one-half the algebraic differences of the maximum and minimum principal unit stresses.

C1.6 Combined Stress Equations

Fig. C1.7 shows a differential block subjected to normal stresses on two planes at right angles to each other and with shearing forces on the same planes. The maximum normal and shearing unit stresses will be determined.

Fig. C1.8 shows a free body diagram of a portion cut by a diagonal plane at angle θ as shown.

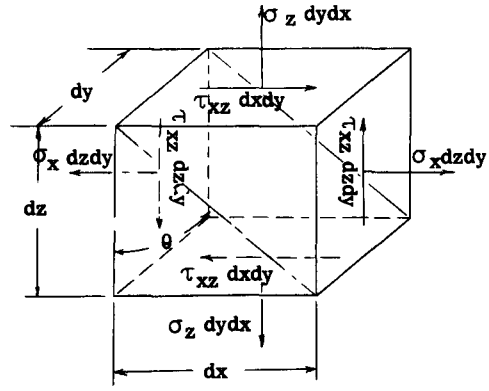

Fig. C1.7

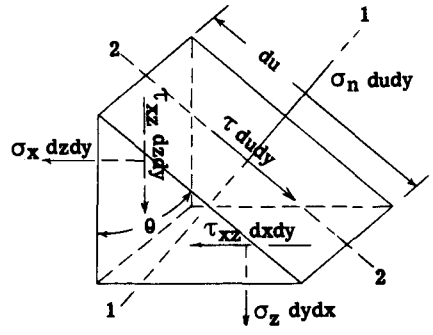

Fig. C1.8

For equilibrium the sum of the forces in the z and x directions must equal zero.

$$\Sigma F_X = 0$$

$$\sigma_n\, dudy \cos\theta + \tau\, dudy \sin\theta - \sigma_X\, dzdy - \tau_{XZ} dxdy = 0 \text{ - (4)}$$

$$\Sigma F_Z = 0$$

$$\sigma_n\, dudy \sin\theta - \tau\, dudy \cos\theta - \sigma_Z\, dydx - \tau_{XZ} dzdy = 0 \text{ - (5)}$$

By dividing each equation by du and noting that $\frac{dzdy}{dudy} = \cos\theta$ and $\frac{dydx}{dudy} = \sin\theta$, we obtain:

$$(\sigma_n - \sigma_X) \cos\theta + (\tau - \tau_{XZ}) \sin\theta = 0 \text{ - - - - (6)}$$

$$(\sigma_n - \sigma_z) \sin\theta - (\tau - \tau_{xz}) \cos\theta = 0 \quad ---(7)$$

The maximum normal stress σ_n will be maximum when θ equals such angle θ' as to make τ = zero. Thus if $\tau = 0$ and $\theta = \theta'$ in equations (6) and (7), we obtain,

$$(\sigma_n - \sigma_x) \cos\theta' - \tau_{xz} \sin\theta' = 0 \quad -----(8)$$

$$(\sigma_n - \sigma_z) \sin\theta' - \tau_{xz} \cos\theta' = 0 \quad -----(9)$$

In equations (8) and (9) σ_n represents the principal stress. Dividing one equation by another to eliminate θ',

$$\frac{\sigma_n - \sigma_x}{\tau_{xz}} = \frac{\tau_{xz}}{\sigma_n - \sigma_z} \quad \text{whence,}$$

$$\sigma_n^2 - (\sigma_x - \sigma_z)\sigma_n + \sigma_x\sigma_z = \tau_{xz}^2, \quad \text{or}$$

$$\sigma_n = \frac{\sigma_x + \sigma_z}{2} \pm \sqrt{\left(\frac{\sigma_x - \sigma_z}{2}\right)^2 + \tau_{xz}^2} \quad --(10)$$

In equation (10), tensile normal stress is plus and compression minus. For maximum σ_n use plus sign before radical and minus sign for minimum σ_n.

To find the plane of the principal stresses, the value of θ' may be solved for from equations (8) and (9), which gives:

$$\tan 2\theta' = \frac{2\tau_{xz}}{\sigma_x - \sigma_z} \quad ---------- (11)$$

θ' is measured from the plane of the largest normal stress σ_x or σ_z. The direction of rotation of θ' from this plane is best determined by inspection. Thus if only the shearing stresses τ_{xz} were acting, the maximum principal stress would be one of the 45° planes, the particular 45° plane being easily determined by inspection of the sense of the shear stresses. Furthermore if only the largest normal stress were acting it would be the maximum principal stress and θ' would equal zero. Thus if both σ and τ act, the plane of the principal stress will be between the plane on which σ acts and the 45° plane. As stated before σ refers to either σ_x or σ_z whichever is the largest.

Maximum Value of Shearing Stress. ($\tau_{max.}$)

The maximum value of τ from equation (3) equals,

$$\tau_{max.} = (\sigma_{n(max.)} - \sigma_{n(min.)})/2 \quad ----- (12)$$

Substituting the maximum and minimum values of σ_n from (10) in (12), we obtain maximum shearing stress as follows:

$$\tau_{max.} = \pm \sqrt{\left(\frac{\sigma_x - \sigma_z}{2}\right)^2 + \tau_{xz}^2} \quad --(13)$$

C1.7 Mohr's Circle for Determination of Principal Stresses.

It is sometimes convenient to solve graphically for the principal stresses and the maximum shear stress. Mohr's circle furnishes a graphical solution. (Fig. C1.9a). In the Mohr method, two rectangular axes x and z are chosen to represent the normal and shearing stresses respectively. Taking point O as the origin lay off to scale the normal stresses σ_x and σ_z equal to OB and OA respectively. If tension, they are laid off to right of point O and to the left if compression. From B the shear stress τ_{xz} is laid off parallel to O_z and with the sense of the shear stress on the face DC of Fig. C1.9b, thus locating point C. With point E the midpoint of AB as the center and with radius EC describe a circle cutting OB at F and G. AD will equal BC and will represent the shear on face AB of Fib. b. It can be proven that OF and OG are the principal stresses $\sigma_{max.}$ and $\sigma_{min.}$ respectively and EC is the maximum shear stress $\tau_{max.}$. The principal stresses occur on planes that are parallel to CF and CG. (See Figs. c and d). The maximum shear stress occurs on two sections parallel to CH and CI where HEI is perpendicular to OB. If σ_x should equal zero then O would coincide with A.

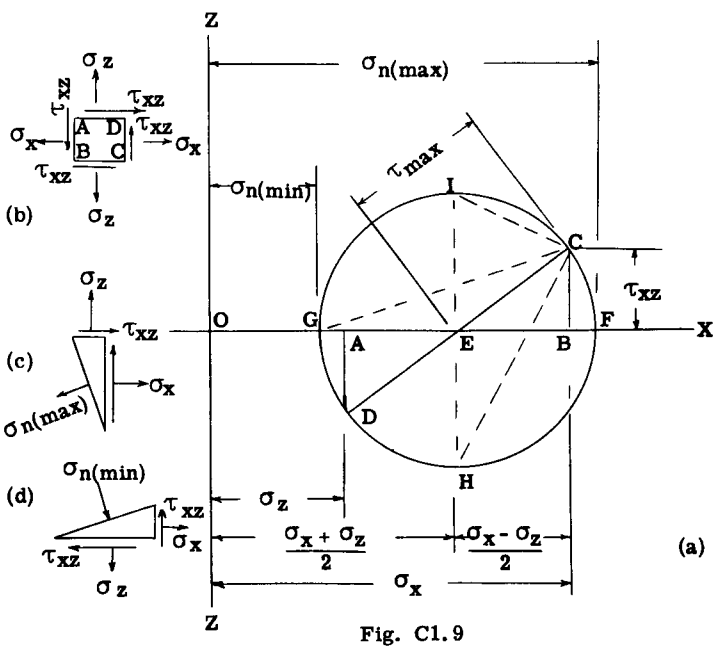

Fig. C1.9

C1.8 Components of Stress From Principal Stresses by Mohr's Circle.

In certain problems the principal stresses may be known as in Fig. C1.9 and it is desired to find the stress components on other planes designated by angle θ. In Fig. C1.11 the axes x and z represent the normal and shear stresses respectively. The principal stresses are laid off to scale on ox giving points D and E respectively. Construct a circle with A the midpoint of DE and with diameter ED. Draw angle CAB equal

to 2θ. It can be proven that OB represents the normal stress on the plane defc of Fig. C1.10, and CB represents the shear stress τ on this plane.

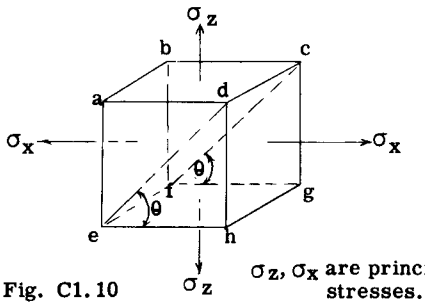

Fig. C1.10 σ_z, σ_x are principal stresses.

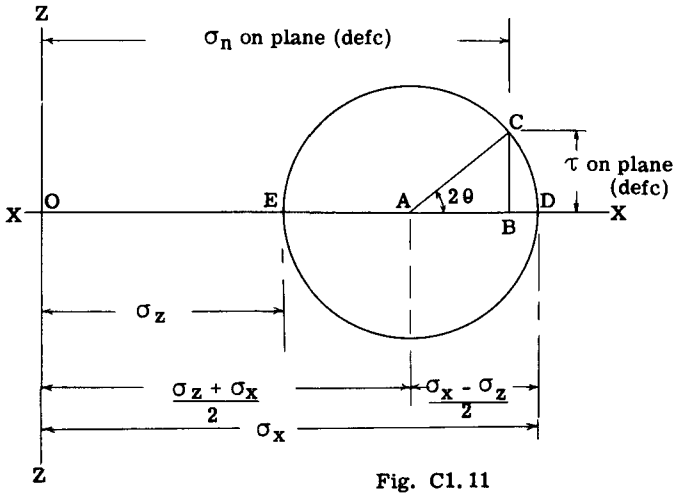

Fig. C1.11

C1.9 Example Problems.

Example Problem 1.

The maximum normal and shear stresses will be determined for the block loaded as shown in Fig. C1.12.

The graphical solution making use of Mohr's circle is shown in Fig. C1.13. From reference axes x and z thru point O, the given normal stresses σ_x = 10000 is laid off to scale on ox and toward the right giving point B. From B the shear stress τ_{xz} = 5000 is laid off parallel to oz to locate point C. With E the midpoint of OB as the center of the circle and with radius EC a circle is drawn which cuts the Ox axis at F and G. The maximum and minimum principal stresses are then equal to oF and oG which equals 12070 and -2070 respectively. The maximum shear stress equals EC or 7070.

Algebraic Solution: From eq. (10),

$$\sigma_n = \frac{\sigma_x + \sigma_z}{2} \pm \sqrt{\left(\frac{\sigma_x - \sigma_z}{2}\right)^2 + \tau_{xz}^2}$$

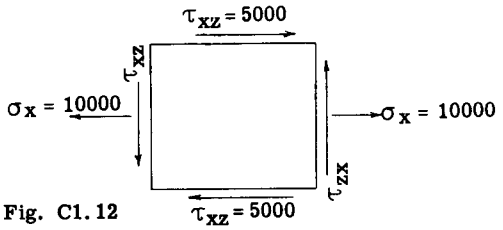

Fig. C1.12

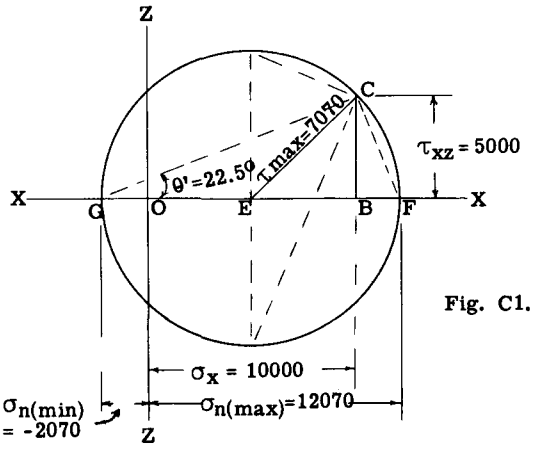

Fig. C1.13

Substituting values,

$$\sigma_n = \frac{10000 + 0}{2} \pm \sqrt{\left(\frac{10000 + 0}{2}\right)^2 + 5000^2} = 5000 + 7070$$

hence, $\sigma_{n(max.)} = 5000 + 7070 = 12070$ psi

$\sigma_{n(min.)} = 5000 - 7070 = -2070$ psi

$\tau_{max.} = (1/2)(\sigma_{n(max.)} - \sigma_{n(min.)})$ (Ref.Eq.12)

$= (1/2)(12070 - (-2070)) = 7070$ psi

$\tau_{max.}$ can also be computed by equation (13),

whence,

$$\tau_{max.} = \pm \sqrt{\left(\frac{10000 + 0}{2}\right)^2 + 5000^2} = \pm 7070 \text{ psi}$$

$$\tan 2\theta^n = \frac{2\,\tau_{xz}}{\sigma_x - \sigma_z} = \frac{2 \times 5000}{10000 - 0} = 1$$

hence, $\theta^n = 22.5^\circ$.

Example Problem 2.

The maximum normal and shear stresses will be determined for the block loaded as shown in Fig. C1.14.

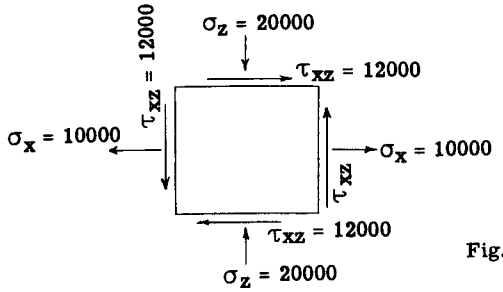

Fig. C1.14

Fig. C1.15 shows the graphical solution using Mohr's circle. From point O, σ_X = 10000 and σ_Z = -20000 are laid off equal to OB and OA respectively. τ_{XZ} equal to 12000 is laid off parallel to OZ at B locating C. With E the midpoint of AB as the center of a circle of radius EC a circle is drawn which cuts the ox axis at F and D. The maximum normal and shear stresses are indicated on the figure.

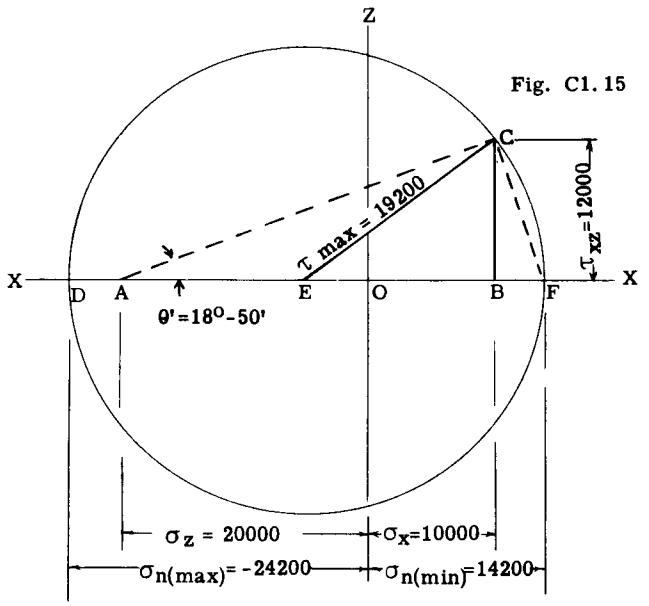

Fig. C1.15

Algebraic Solution

$$\sigma_n = \frac{\sigma_X + \sigma_Z}{2} \pm \sqrt{\left(\frac{\sigma_X - \sigma_Z}{2}\right)^2 + \tau_{XZ}^2}$$

$$= \frac{10000 - 20000}{2} \pm \sqrt{\left(\frac{10000-(-20000)}{2}\right)^2 + 12000^2}$$

$$= -5000 \pm 19200$$

hence, $\sigma_{n(max.)} = -5000 - 19200 = -24200$ psi

$\sigma_{n(min.)} = -5000 + 19200 = 14200$

$\tau_{max.} = \pm 19200$, $\tan 2\theta' \dfrac{2 \times 12000}{1000 - (-20000)} = .8$

$\theta' = 18^\circ - 50'$

C1.10 Triaxial or Three Dimensional Stresses

For bodies which are stressed in three directions, the state of stress can be defined completely by the six stress components as illustrated in Fig. C1.16. Using the same procedure as was carried out for a two-dimensional stress system, it can be shown that there are three principal stresses σ_1, σ_2 and σ_3, whose values are the three roots of σ in the following cubic equation.

$$\sigma^3 - (\sigma_X + \sigma_Y + \sigma_Z)\sigma^2 + (\sigma_X\sigma_Y + \sigma_Y\sigma_Z + \sigma_X\sigma_Z - \gamma_{YZ}^2 - \gamma_{XY}^2)\sigma - (\sigma_X\sigma_Y\sigma_Z + 2\gamma_{YZ}\gamma_{XZ}\gamma_{XY} - \sigma_X\gamma_{YZ}^2 - \sigma_Y\gamma_{XZ}^2 - \sigma_Z\gamma_{XY}^2 = 0 \quad \text{----------(14)}$$

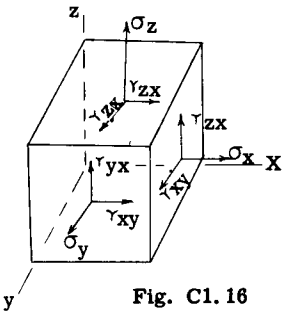

Fig. C1.16

Fig. C1.17 shows the principal stress system which replaces the system of Fig. C1.16. It can be shown that the maximum shear stress max. is one of the following values.

$$\left.\begin{aligned} \gamma_{max.} &= \pm \frac{1}{2}(\sigma_1 - \sigma_2) \\ \text{or } \gamma_{max.} &= \pm \frac{1}{2}(\sigma_2 - \sigma_3) \\ \text{or } \gamma_{max.} &= \pm \frac{1}{2}(\sigma_3 - \sigma_1) \end{aligned}\right\} \quad \text{------(15)}$$

The planes on which these shear stresses act are indicated by the dashed lines in Fig. C1.18, namely, adhe, bdge and dcef. The largest of the shear stresses in equations (15) depends on the magnitude and signs of the principal stresses, remembering that tension is plus and compression is minus when making the substitution in equations (15).

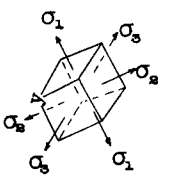

Fig. C1.17

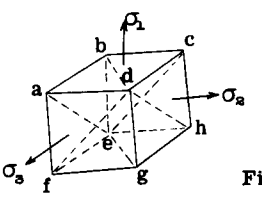

Fig. C1.18

C1.11 Principal Strains

The strains under combined stresses are usually expressed as strains in the direction of the principal stresses. Consider a case of simple tension as illustrated in Fig. C1.19. The stress σ_1 causes a lengthening unit strain ε in the direction of the stress σ_1, and a shortening unit strain ε' in a direction at right angles to the stress σ_1.

The ratio of ε' to ε is called Poisson's ratio and is usually given the symbol μ. Thus, $\mu = \varepsilon'/\varepsilon$

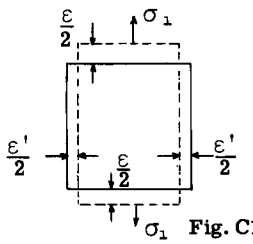

Fig. C1.19

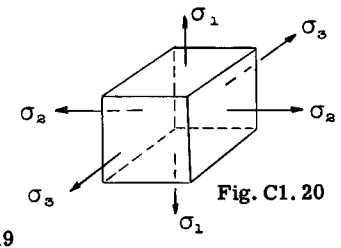

Fig. C1.20

Since $\varepsilon = \sigma_1/E$, we obtain,

$$\varepsilon' = \mu\,\sigma_1/E \quad \text{----------(16)}$$

Now consider the cubical element in Fig. C1.20 subjected to the three principal stresses σ_1, σ_2 and σ_3, all being tension. The total unit strain ε_1 in the direction of stress σ_1 will be expressed. Obviously, σ_1 tends to stretch the element in the direction of σ_1 whereas stresses σ_2 and σ_3 tend to shorten the element in the direction of σ_1, hence,

$$\varepsilon_1 = \frac{\sigma_1}{E} - \frac{\mu\sigma_2}{E} - \frac{\mu\sigma_3}{E}\text{, whence}$$

$$\left.\begin{aligned} \varepsilon_1 &= \frac{\sigma_1}{E} - \frac{\mu}{E}(\sigma_2 + \sigma_3) \\ \text{and similarly for } \varepsilon_2 \text{ and } \varepsilon_3, & \\ \varepsilon_2 &= \frac{\sigma_2}{E} - \frac{\mu}{E}(\sigma_3 + \sigma_1) \\ \varepsilon_3 &= \frac{\sigma_3}{E} - \frac{\mu}{E}(\sigma_1 + \sigma_2) \end{aligned}\right\} \quad \text{-----(17)}$$

For a two-dimensional stress system, that is, stresses acting in one plane, $\sigma_3 = 0$ and the principal strains become,

$$\left.\begin{aligned} \varepsilon_1 &= \frac{1}{E}(\sigma_1 - \mu\sigma_2) \\ \varepsilon_2 &= \frac{1}{E}(\sigma_2 - \mu\sigma_1) \\ \varepsilon_3 &= \frac{1}{E}(\sigma_1 + \sigma_2) \end{aligned}\right\} \quad \text{-----(18)}$$

Equations 17 and 18 give the strains when all the principal stresses are tensile stresses. For compressive principal stresses use a minus sign when substituting the principal stresses in the equations.

C1.12 Elastic Strain Energy

The strain energy in the elastic range for the unit cube in Fig. C1.20 when subjected to combined stresses is equal to the work done by the three gradually applied principal stresses σ_1, σ_2 and σ_3. These stresses produce strains equal to ε_1, ε_2 and ε_3 and thus the work done per unit volume equals the strain energy. Thus if U equals the strain energy, we obtain,

$$U = \frac{\sigma_1\varepsilon_1}{2} + \frac{\sigma_2\varepsilon_2}{2} + \frac{\sigma_3\varepsilon_3}{2} \quad \text{-------(19)}$$

The strain energy can be expressed in terms of stress by substituting values of ε in terms of σ from equations (17) into equation (19), which gives,

$$U = \frac{1}{2E}\left(\sigma_1^2 + \sigma_2^2 + \sigma_3^2 - 2\mu(\sigma_1\sigma_2 + \sigma_2\sigma_3 + \sigma_3\sigma_1)\right)$$
$$\text{----------(20)}$$

For a two dimensional stress system, $\sigma_3 = 0$ and equation (20) becomes

$$U = \frac{1}{2E}\left(\sigma_1^2 - 2\mu\,\sigma_1\sigma_2 + \sigma_2^2\right) \quad \text{-----(21)}$$

C1.13 Structural Design Philosophy. Limit and Ultimate Loads. Factors of Safety. Margin of Safety.

The basic philosophy governing the structural design of a flight vehicle is to develop an adequate light weight structure that will permit the vehicle to accomplish the operations or missions that were established as design requirements. The job of a commercial airliner is to carry passengers and cargo from place to place at the lowest cost. To carry out this job a certain amount of flight and ground maneuvering is required and the loads due to these maneuvers must be carried safely and efficiently by the structure. A military fighter airplane must be maneuvered in flight far more severely to accomplish its desired job as compared to the commercial airliner, thus the flight acceleration factors for the military fighter airplane will be considerably higher than that of the airliner. In other words, every type of flight vehicle will undergo a different load environment, which may be repeated frequently or infrequently during the life of the vehicle. The load environment may involve many factors such as flight maneuvering loads, air gust loads, take off and landing loads, repeated loads, high and low temperature conditions, etc.

Limit Loads. Limit loads are the calculated maximum loads which may be subjected to the flight vehicle in carrying out the job it is designed to accomplish during its life time of use. The term limit was no doubt chosen because every flight vehicle is limited relative to the extent of its operations. A flight vehicle could easily be designed for loads greater than the limit loads, but such extra strength which is not necessary for safety would only increase the weight of the structure and decrease the commercial or military payload or in general be detrimental to the design.

Factor of Safety. Factor of safety can be defined as the ratio considered in structural design of the strength of the structure to the maximum calculated operational loads, that is, the limit loads.

Yield Factor of Safety. This term is defined as the ratio of the yield strength of the structure to the limit load.

Ultimate Factor of Safety. This term is defined as the ratio of the ultimate strength of the structure to the limit load.

Yield Load. This term is defined as the limit load multiplied by the yield factor of safety.

Ultimate Load. This term can be defined as the limit load multiplied by the ultimate factor of safety. This resulting load is often referred to by engineers as the design load, which is misleading because the flight vehicle structure must be designed to satisfy both yield and ultimate failure and either one may be critical.

Yield Margin of Safety. This term usually expressed in percent represents the additional yield strength of the structure over that strength required to carry the limit loads.

$$\text{Yield Margin of Safety} = \frac{\text{Yield Strength}}{\text{Limit Load}} - 1$$

Ultimate Margin of Safety. This term usually expressed in percent represents the additional ultimate strength of the structure over that strength required to carry the ultimate loads.

$$\text{Ultimate Margin of Safety} = \frac{\text{Ultimate Strength}}{\text{Ultimate Load}} - 1$$

C1.14 Required Strength of Flight Structures.

Under Limit Loads:-

The flight vehicle structure shall be designed to have sufficient strength to carry simultaneously the limit loads and other accompanying environmental phenomena for each design condition without undergoing excessive elastic or plastic deformation. Since most materials have no definite yield stress, it is common practice to use the unit stress where a .002 inches per inch permanent set exists as the yield strength of the material, and in general this yield strength stress can be used as the maximum stress under the limit loads unless definitely otherwise specified.

Under Ultimate Loads:-

The flight vehicle structure shall be designed to withstand simultaneously the ultimate loads and other accompanying environmental phenomena without failure. In general no factor of safety is applied to the environmental phenomena but only to the limit loads.

Failure of a Structure:-

This term in general refers to a state or condition of the structure which renders it incapable of performing its required function. Failure may be due to rupture or collapse or due to excessive deflection or distortion.

C1.15 Determination of the Ultimate Strength of a Structural Member Under a Combined Load System. Stress Ratio-Interaction Curve Method.

Since the structural designer of flight vehicles must insure that the ultimate loads can be carried by the structure without failure, it is necessary that reliable methods be used to determine the ultimate strength of a structure. Structural theory as developed to date is in general sufficiently developed to accurately determine the ultimate strength of a structural member under a single type of loading, such as axial tension or compression, pure bending or pure torsion. However, many of the members which compose the structure of a flight vehicle are subjected simultaneously to various combinations of axial, bending and torsional load systems and thus a method must be available to determine the ultimate strength of a structure under combined load systems. A strictly theoretical approach appears too difficult for solution since failure may be due to overall elastic or inelastic buckling, or the local elastic or inelastic instability.

The most satisfactory method developed to date is the so-called stress ratio, interaction curve method, originally developed and presented by Shanley. In this method the stress conditions on the structure are represented by stress ratios, which can be considered as non-dimentional coefficients denoting the fraction of the allowable stress or strength for the member which can be developed under the given conditions of combined loading.

For a single simple stress, the stress ratio can be expressed as,

$$R = \text{stress ratio} = \frac{f}{F} \qquad \text{-------(22)}$$

where f is the applied stress and F the allowable stress. The margin of safety in terms of the stress ratio R can be written,

$$\text{M.S.} = \frac{1}{R} - 1.0 \qquad \text{----------(23)}$$

Load ratios can be used instead of stress ratios and is often more convenient.

For example for axial loading,

$R = P/P_a$, where P = applied axial load and P_a the allowable load.

For pure bending,

$R = M/M_a$, where M = applied bending moment and M_a the allowable bending moment.

For pure torsion,

$R = T/T_a$, where T is applied torsional moment and T_a the allowable torsional moment.

For combined loadings the general conditions for failure are expressed by Shanley as follows:-

$$R_1^x + R_2^y + R_3^z + \text{------} = 1.0 \quad ----(24)$$

In this above expression, R_1, R_2 and R_3 could refer to compression, bending and shear and the exponents x, y, and z give the relationship for combined stresses. The equation states that the failure of a structural member under a combined loading will result only when the sum of the stress ratios is equal to or greater than 1.0.

For some of the simpler combined load systems, the exponents of the stress ratios in equation (24) can be determined by the various well known theories of yield and failure that have been developed. However, in many cases of combined loading and for particular types of structures the exponents in equation (24) must be determined by making actual failure tests of combined load systems.

Since the stress ratio method was presented by Shanley many years ago, much testing has been done and as a result reliable interaction equations with known exponents have been obtained for many types of structural members under the various combined load systems. In a number of the following chapters, the interaction equations which apply will be used in determining the ultimate strength design of structural members.

C1.16 Determination of Yield Strength of a Structural Member Under a Combined Load System.

As explained in Art. C1.14, the flight vehicle structure must carry the limit loads without yielding, which in general means the yield strength of the material cannot be exceeded when the structure is subjected to the limit loads. In some parts of a flight vehicle structure involving compact unit or pressure vessels, biaxial or triaxial stress conditions are often produced and it is necessary to determine whether any yielding will occur under such combined stress action when carrying the limit loads. For cases where no elastic instability occurs, the following well known theories of failure have been developed.

1. Maximum Principal Stress Theory
2. Maximum Shearing Stress Theory
3. Maximum Strain Theory
4. Total Strain Energy Theory
5. Strain Energy of Distortion Theory
6. Octahedral Shear Stress Theory

The reader may review the explanation and derivation of these 6 theories by referring to such books as listed at the end of this chapter.

Test results indicate that the yield strength at a point in a stressed structure is more accurately defined by theories 5 and 6 followed in turn by theory 2. Since theories 5 and 6 give the same result, they might be considered as the same general theory. In this chapter we will only give the resulting equations as derived by theory 6, since theories 5 and 6 appear to be the theories used in flight vehicle structural design.

C1.17 The Octahedral Shear Stress Theory.

Since this theory gives the same results as the well known energy of distortion method it is often referred to as the Equivalent Stress Theory. The octahedral shear stress theory may be stated as follows:- In elastic action at any point in a body under combined stress action begins only when the octahedral shearing stress becomes equal to 0.47 f_e, where f_e is the tensile elastic strength of the material as determined from a standard tension test. Since the elastic tensile strength is somewhat indefinite, it is common practice to use the engineering yield strength F_{ty}. In this theory it is assumed that the tensile and compressive yield strengths are the same.

Figs. C1.21 and C1.22 illustrate the conditions of equilibrium involving the octahedral shear stress. In Fig. C1.21, the cube is subjected to the 3 principal stresses as shown. A tetrahedron is cut from the cube and shown in Fig. C1.22. Three of the sides of this tetrahedron are parallel to the

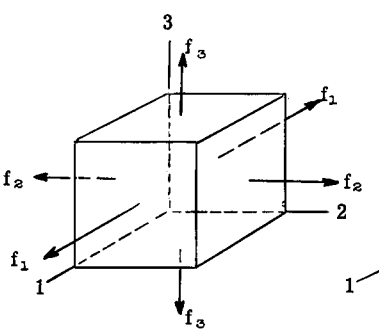

Fig. C1.21

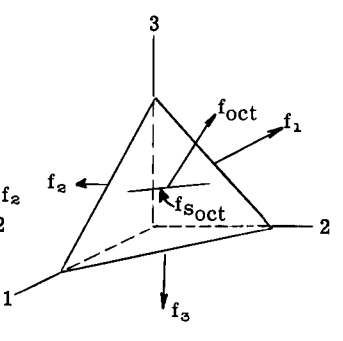

Fig. C1.22

principal axes, while the normal to the fourth side makes equal angles with the principal axes. The octahedral shear and normal stresses are the resulting stresses on the fourth side.

The equation for the value of the normal octahedral stress is,

$$f_{oct} = \frac{1}{3}(f_1 + f_2 + f_3) \quad ------(25)$$

The equation for the octahedral shear stress is,

$$f_{s_{oct}} = \frac{1}{3}\sqrt{(f_1-f_2)^2+(f_2-f_3)^2+(f_3-f_1)^2} \quad --(26)$$

Now the octahedral shear stress is 0.47 of the normal stress.

Let $\bar{f}$ be the effective axial stress in uniaxial tension or compression which results in the given octahedral shear stress.

$$\bar{f} = f_{s_{oct}}/0.47 = \frac{3}{\sqrt{2}} f_{s_{oct}} \quad -----(27)$$

Therefore multiplying Eq. (26) by $3/\sqrt{2}$ we obtain for a condition of principal triaxial stresses,

$$\bar{f} = \frac{1}{\sqrt{2}}\sqrt{(f_1-f_2)^2+(f_2-f_3)^2+(f_3-f_1)^2} \quad ----(28)$$

Let F equal the allowable tensile or compressive stress. If the yield strength is being determined then

$$\text{Margin of Safety M.S.} = \frac{F}{\bar{f}} - 1 \quad ---(29)$$

For a biaxial stress system taking $f_3 = 0$, we obtain,

$$\bar{f} = \sqrt{f_1^2 + f_2^2 - f_1 f_2} \quad -------(30)$$

It is often more convenient to use the x, y and z component of stresses instead of the principal stresses. Fig. C1.23 illustrates the various component stresses.

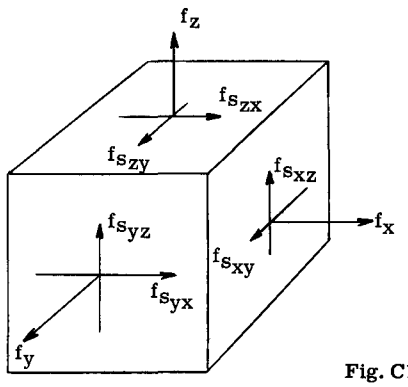

Fig. C1.23

For a triaxial stress system,

$$\bar{f} = \frac{1}{\sqrt{2}}\sqrt{(f_x-f_z)^2+(f_z-f_y)^2+(f_y-f_x)^2+6(f_{s_{xz}}+f_{s_{zy}}+f_{s_{yx}})^2} \quad ----------(31)$$

For a biaxial stress system, f_y, $f_{s_{yz}}$, $f_{s_{yx}} = 0$

$$\bar{f} = \sqrt{f_x^2 + f_z^2 - f_x f_z + 3f_{s_{xz}}^2} \quad ---(32)$$

C1.18 Example Problem 1.

A cylindrical stiffened thin sheet fuselage is fabricated from 2024 aluminum alloy sheet which has a tensile yield stress $F_{ty} = 40000$. Find the yield margin of safety under the following limit load conditions.

(1) A limit bending moment produces a bending stress of 37000 psi (tension) at top point of fuselage section. The flexural shear stress is zero at this point.

(2) Same as condition (1) but pressurization of fuselage produces a circumferential tension stress of 8600 psi and a longitudinal tension stress of 4300 psi.

(3) Same as condition (2) but a yawing maneuver of airplane produces a limit torsional shearing stress of 8000 psi in fuselage skin.

SOLUTION: Condition (1)

This is a uniaxial stress condition for point being considered.

$$\text{Yield M.S.} = \frac{F_{ty}}{f_t} - 1 = \frac{40000}{37000} - 1 = .08$$

SOLUTION: Condition (2)

There are no flexural shear stresses at the fuselage point being considered. Since no torsion is being applied to fuselage no torsional shear stresses exist. The stress system at the point being considered is thus a biaxial stress system and f_1 and f_2 are principal stresses.

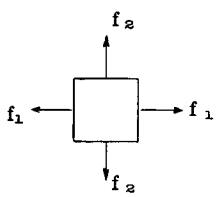

$f_1 = 37000 + 4300 = 41300$ psi

$f_2 = 8600$ psi

From equation (30),

$$\bar{f} = \sqrt{f_1^2 + f_2^2 - f_1 f_2}$$

$$= \sqrt{41300^2 + 8600^2 - 41300 \times 8600}$$

whence $\bar{f}$ = 37700 psi

$$M.S. = \frac{F}{\bar{f}} - 1 = \frac{40000}{37700} - 1 = .06$$

SOLUTION: Condition (3)

Since a torsional shear stress has now been added, the new stress is still two dimentional, however the given tension stresses are not principal stresses due to the addition of the torsional shear stress.

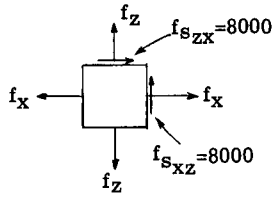

f_x = 41300 psi. f_z = 8600 psi. f_s = 8000 psi.

Instead of finding the principal stresses and using Eq. (30), we will use the f_x and f_z stresses and use Eq. (32)

$$\bar{f} = \sqrt{f_x^2 + f_z^2 - f_x f_z + 3f_s^2}$$

$$= \sqrt{41300^2 + 8600^2 - 41300 \times 8600 + 3 \times 8000^2}$$

$\bar{f}$ = 40200 psi. $M.S. = \frac{40000}{40200} - 1 = -.01$

Thus yield is indicated since M.S. is negative.

Example Problem 2.

A cylindrical pressure vessel is 100 inches in diameter and 1 inch thick. The vessel is made of steel with F_{ty} = 42000 psi. Determine the internal pressure that will produce yielding.

SOLUTION: This applied stress system is biaxial with no flexural or torsional shear.

Let: p equal internal pressure
t = wall thickness = 1 in.
d = diameter = 100"

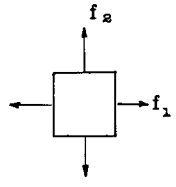

f_2 = circumferential stress due to pressure p

$f_2 = \frac{pd}{2t}$ and $f_1 = \frac{pd}{4t}$

From Eq. 30

$$\bar{f} = \sqrt{f_1^2 + f_2^2 - f_1 f_2}$$

The vessel wall is to be stressed to the yield stress of 42000, thus $\bar{f}$ = 42000.

Whence

$$(42000)^2 = \left(\frac{pd}{4t}\right)^2 + \left(\frac{pd}{2t}\right)^2 - \left(\frac{pd}{4t}\right)\left(\frac{pd}{2t}\right)$$

Solving, p = 970 psi.

PROBLEMS

(1) The combined stress loading at a point in a structure is as follows:- f_z = -1000, f_x = -2500, f_s = 2000. Determine the magnitude and direction of the principal stresses. Determine the maximum shearing stress. Solve both analytically and graphically.

(2) Same as Problem 1, but change f_z to 4000 and f_x to -3000 and f_s to 2500.

(3) A solid circular shaft is subjected to a limit bending moment of 122000 inch pounds and a torsional moment of 250,000 inch pounds. If diameter is 4 inches and the yield tensile stress is 42,000, what is yield Margin of Safety.

(4) A thin walled cylinder of diameter 6 inches is subjected to an axial tensile load of 15,000 pounds, and a torsional moment of 12,000 inch pounds. What should be the wall thickness if the permissible yield stress is 30,000 psi.

(5) A closed end cylindrical vessel is 15 inches in diameter and a wall thickness of 0.25 inches. The vessel is subjected to an internal pressure of 10,000 psi, and a tensile load of 22,000 pounds. If the yield tensile stress of the material is 75,000 p i, what torsional moment can be added without causing yield.

REFERENCES: -

Nadai, Theory of Flow and Fracture of Solids.

Timoshenko, Strength of Materials.

Freudenthal, The Inelastic Behavior of Engineering Materials and Structures.

Marin, J., Engineering Materials.

Seely & Smith, Advanced Mechanics of Materials.

CHAPTER C2
STRENGTH OF COLUMNS WITH STABLE CROSS-SECTIONS

C2.1 Methods of Column Failure. Column Equations.

In Chapter A18, the theory of the elastic and inelastic instability of the column was presented. The equations from Chapter A18 for a pin end support condition are:-

For elastic primary failure,

$$F_c = \frac{\pi^2 E}{(L/\rho)^2} \quad \text{- - - - - - - - - - - - - - (1)}$$

For inelastic primary failure,

$$F_c = \frac{\pi^2 E_t}{(L/\rho)^2} \quad \text{- - - - - - - - - - - - - - (2)}$$

Where F_c = compressive unit stress at failure = P/A stress.

E = Young's modulus

E_t = tangent modulus

L = column length

ρ = radius of gyration of cross-section

Fig. C2.1 shows a typical plot of F_c versus L/ρ. If the column dimensions are such as to cause it to fail in range CD in Fig. C2.1, the primary failure is due to elastic instability and equation (1) holds. This range of L/ρ values is often referred to by engineers as the long column range.

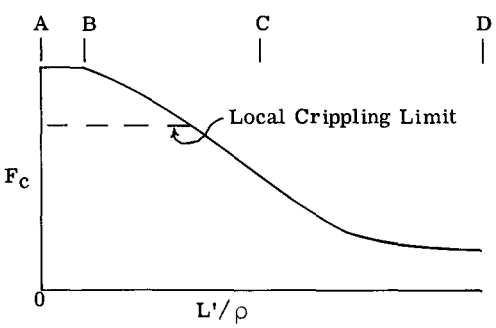

Fig. C2.1

The range BC represents the range of L/ρ values where failure is due to inelastic instability of the column as a whole and equation (2) applies. This range BC is often referred to as the short column range.

The range AB in Fig. C2.1 is for a range of L/ρ values of below 20 to 25, and represents a range where failure is due to plastic crushing of the column. In other words, the column is too short to buckle or bow under end load but crushes under the high stresses. This column range of stresses is usually referred to as the block compression strength.

A column, however, may fail by local buckling or crippling due to distortion of the column cross-section in its own plane. The horizontal dashed line in Fig. C2.1 represents the condition where the primary column strength is limited by the local weakness. This line moves up or down according to the value of the local weakness. The determination of the column strength when failure is due to local weakness is covered in another chapter.

C2.2 Column End Restraint. Fixity Coefficients. Column Effective Length.

The column strength is influenced by the end support restraint against rotation and by any lateral supports between the column ends. The letter c is commonly used to indicate the end fixity coefficient, and c = 1.0 for zero end restraint against rotation, which can be produced mechanically by a pin or ball and socket end support fitting. Thus including the end restraint effect equations (1) and (2) can be written,

$$F_c = \frac{c\pi^2 E}{(L/\rho)^2} \quad , \quad F_c = \frac{c\pi^2 E_t}{(L/\rho)^2} \quad \text{- - - - - (3)}$$

Let L' = effective length of the column which equals the length between inflection points of the deflected column under load.

Then $L' = L/\sqrt{c}$ - - - - - - - - - - - (4)

Thus equation (3) can be written as,

$$F_c = \frac{\pi^2 E}{(L'/\rho)^2} \quad , \quad F_c = \frac{\pi^2 E_t}{(L'/\rho)^2} \quad \text{- - - (5)}$$

If we let P = failing or critical load, equation (5) can be written as equation (6) by realizing that $P = F_c A$ and $\rho = \sqrt{I/A}$.

$$P = \frac{\pi^2 EI}{(L')^2} \quad , \quad P = \frac{\pi^2 E_t I}{(L')^2} \quad \text{- - - - - - (6)}$$

Fig. C2.2 shows the deflected column curve under the load P for various end and lateral support conditions. The effective lengths L' and the end fixity coefficients are also listed.

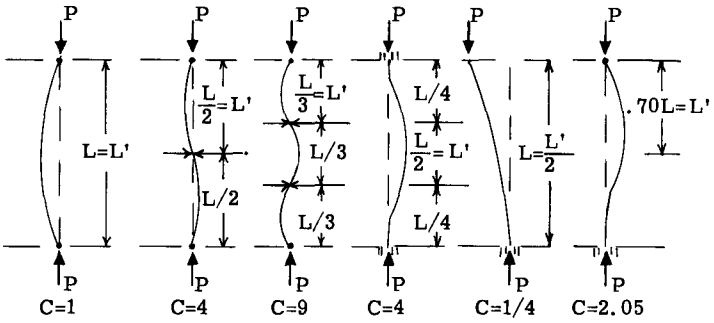

Fig. C2.2

C2.3 Design Column Curves for Various Materials.

For routine design purposes it is convenient to have column curves of allowable failing column stress F_c versus the effective slenderness ratio l'/ρ. In equation (5) we will assume values of F_c, then find the tangent modulus E_t corresponding to this stress and then solve for the term L'/ρ. Table C2.1 shows the calculations for 17.7 PH (TH1050) stainless steel sheet at room temperature. The results are then plotted in Fig. C2.7 to give the column strength curve. Similar data was calculated for the material under certain exposure time to different elevated temperatures and the results are also plotted in Fig. C2.7. Figs. C2.3 to C2.15 give column curves for other materials under various temperature conditions. Use of these curves will be made in example problems later in this chapter. The horizontal dashed line is the compressive yield stress. Values above these cut-off lines should be substantiated by tests.

C2.4 Tangent Modulus E_t from Ramberg-Osgood Equation.

The basic Ramberg-Osgood relationship for E_t is given as follows: (See Ref. 1)

$$\frac{E_t}{E} = \frac{1}{1 + \frac{3}{7} n \left(\frac{F}{F_{0.7}}\right)^{n-1}} \qquad \text{(7)}$$

E_t = tangent modulus of elasticity

E = modulus of elasticity

For definition of other terms see Article B1.12 of Chapter B1.

TABLE C2.1

17-7 PH(TH1050) Stainless Steel Sheet
F_{tu} = 180,000
F_{cy} = 160,000
$E = 29 \times 10^6$

F_c	E_t	$L'/\rho = \pi\sqrt{E_t/F_c}$
20,000	29×10^6	119.56
30,000	29×10^6	97.62
40,000	29×10^6	84.54
50,000	29×10^6	75.62
60,000	29×10^6	69.03
70,000	29×10^6	63.91
80,000	29×10^6	59.78
89,600	29×10^6	56.49
96,000	27.55×10^6	53.19
102,000	26.10×10^6	50.22
107,400	24.65×10^6	47.57
112,200	23.20×10^6	45.15
117,000	21.75×10^6	42.81
121,500	20.30×10^6	40.58
125,800	18.85×10^6	38.43
130,000	17.40×10^6	36.32
134,000	15.95×10^6	34.25
137,700	14.50×10^6	32.22
147,000	11.60×10^6	27.89
158,100	8.70×10^6	23.29
167,600	5.80×10^6	18.47
173,800	2.90×10^6	12.82

This equation is plotted in Fig. C2.16. For a given material, n, $F_{0.7}$ and E must be known. Then assuming values of F, we can find corresponding values of E_t/E from Fig. C2.16. For values of E, $F_{0.7}$ and n refer to Table B1.1 in Chapter B1.

C2.5 Non-Dimensional Column Curves.

Quite useful non-dimentional column curves have been derived by Cozzone and Melcon (See Ref. 3).

The Euler column equation is $F = \pi^2 E_t/(L'/\rho)^2$, which can be written,

$$\frac{E_t}{F} = \frac{(L'/\rho)^2}{\pi^2}$$

The problem therefore resolves itself into obtaining and expression for E_t/F from the non-dimensional relationship. To do this multiply both sides of equation (7) by $F_{0.7}/F$ and equate to B^2.

$$\left(\frac{E_t}{E}\right)\left(\frac{F_{0.7}}{F}\right) = \frac{1}{\frac{F}{F_{0.7}} + \frac{3}{7} n \left(\frac{F}{F_{0.7}}\right)^n} = B^2 \qquad \text{(8)}$$

Fig. C2.17 shows a plot of this equation as taken from Ref. 3, and shows $F/F_{0.7}$ versus B for various values of n.

The shape of the knee of the stress-strain curve is given by the shape parameter n and the abscissa B incorporates the

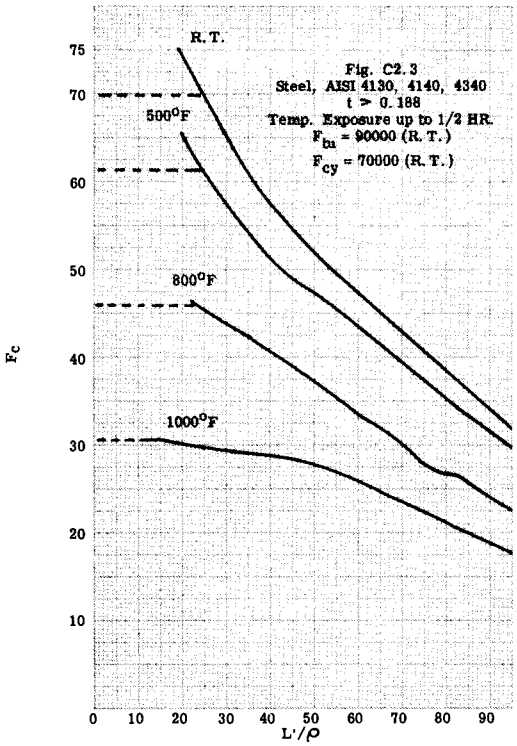

Figure C2.3

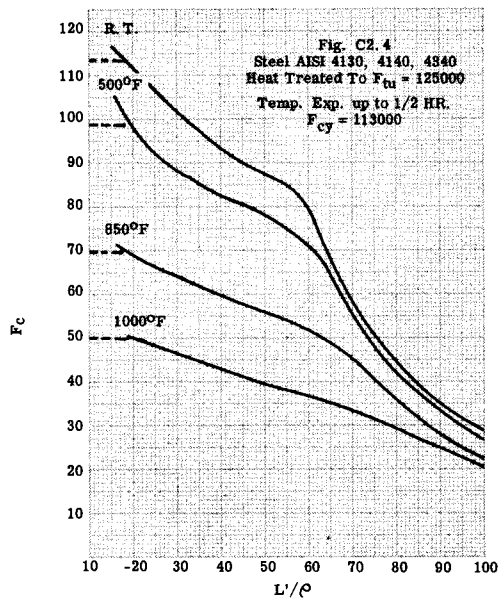

Figure C2.4

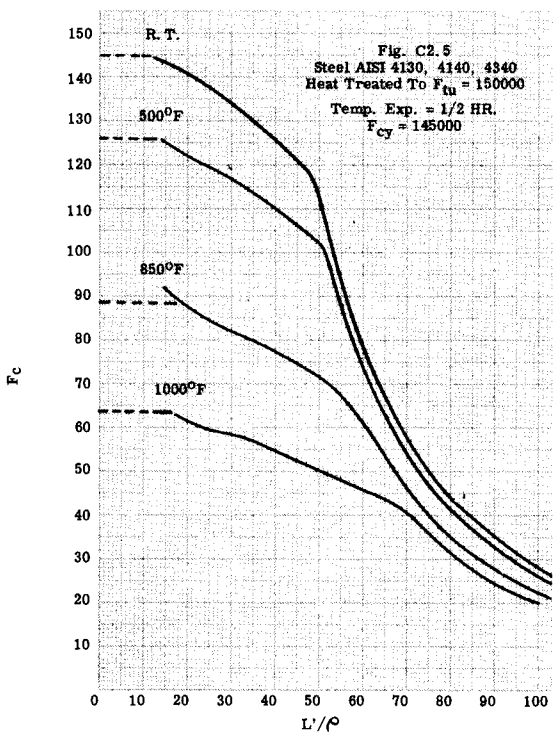

Figure C2.5

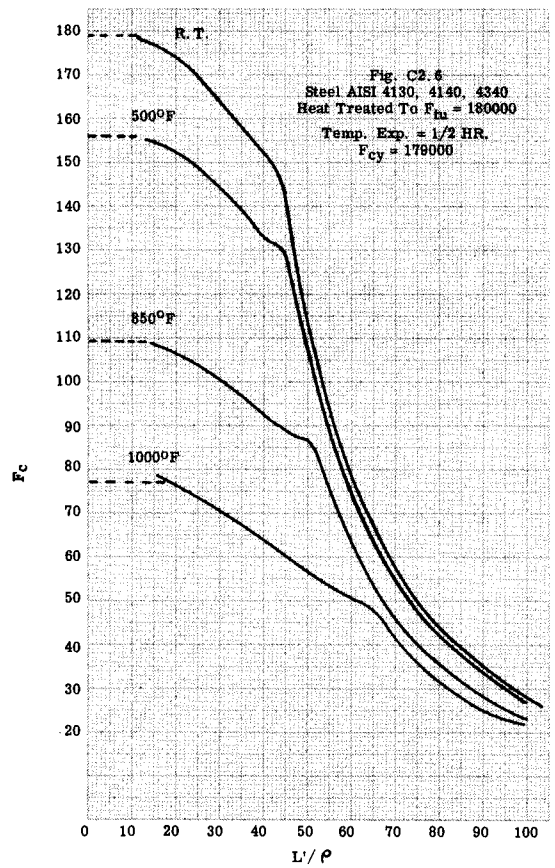

Figure C2.6

F_c is in ksi

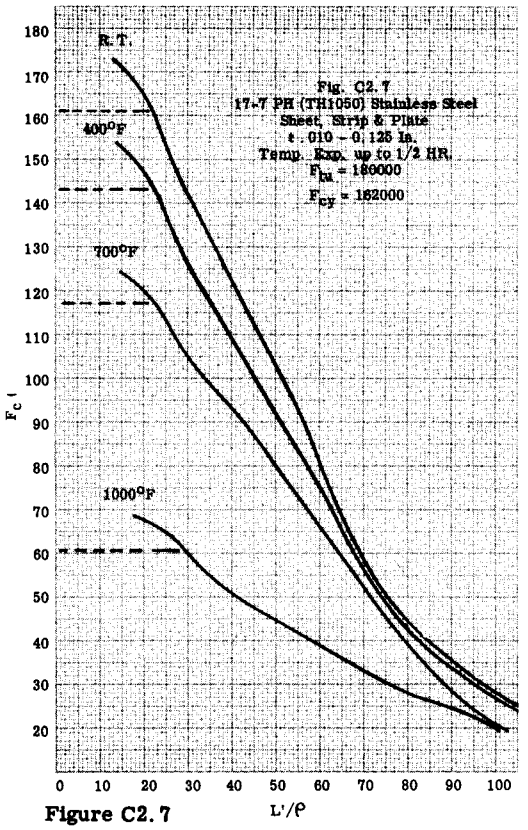

Figure C2.7

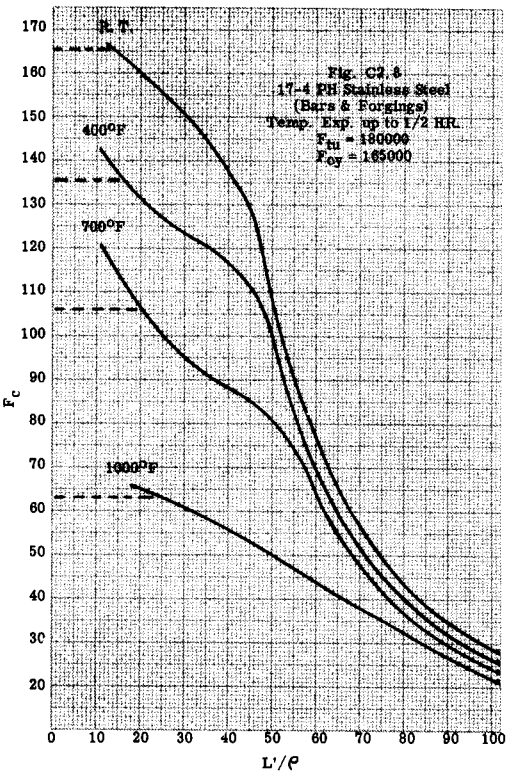

Figure C2.8

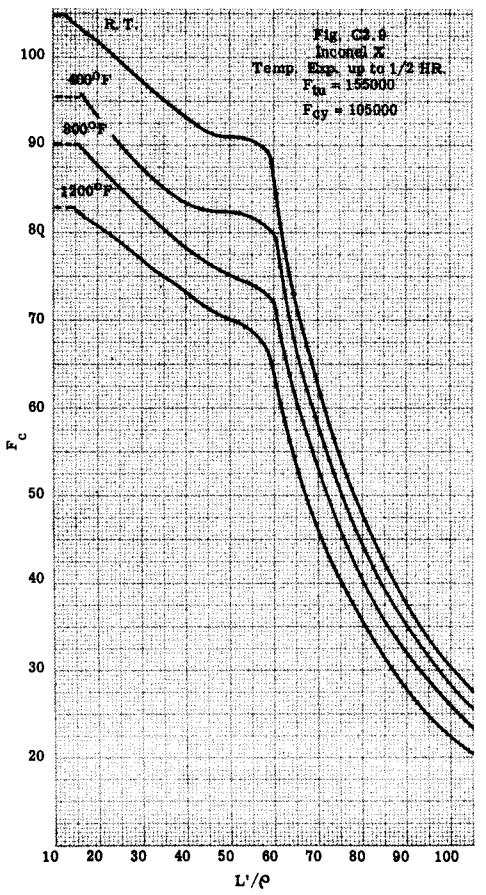

Figure C2.9

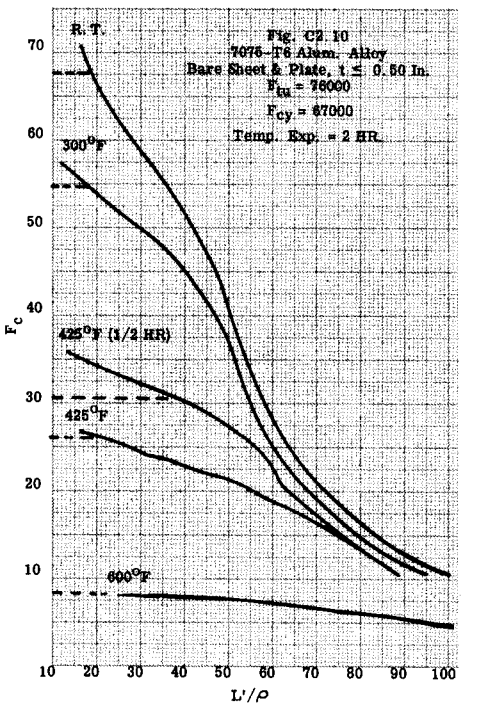

Figure C2.10

F_c is in ksi

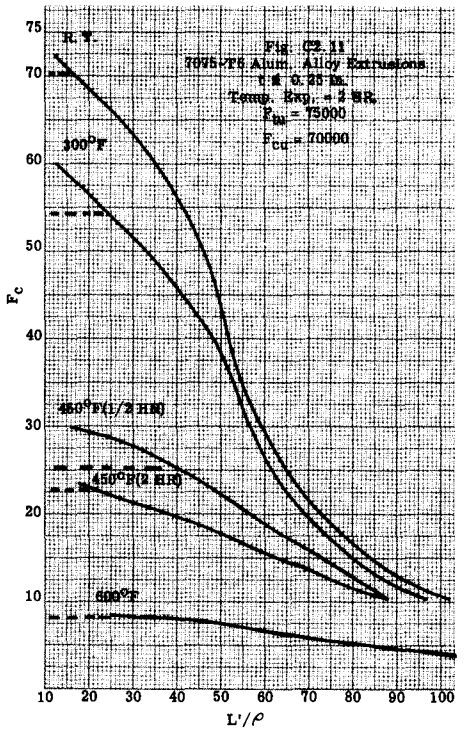

Figure C2.11

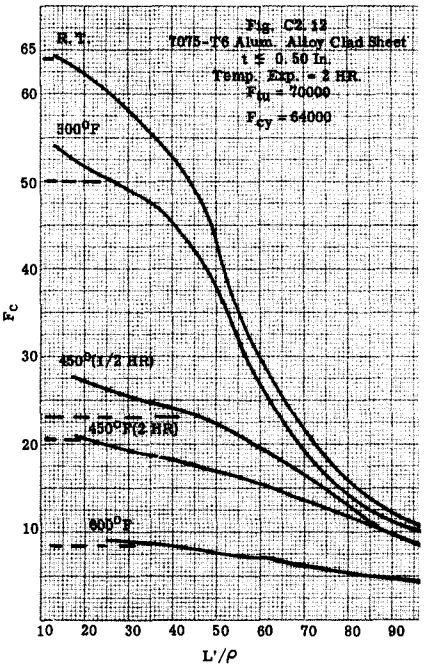

Figure C2.12

F_c is in ksi

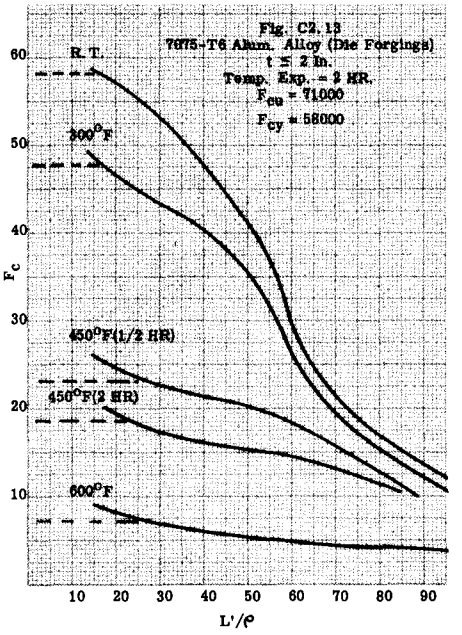

Figure C2.13

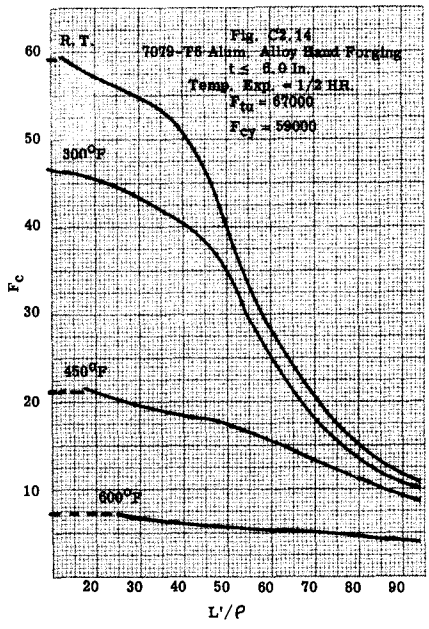

Figure C2.14

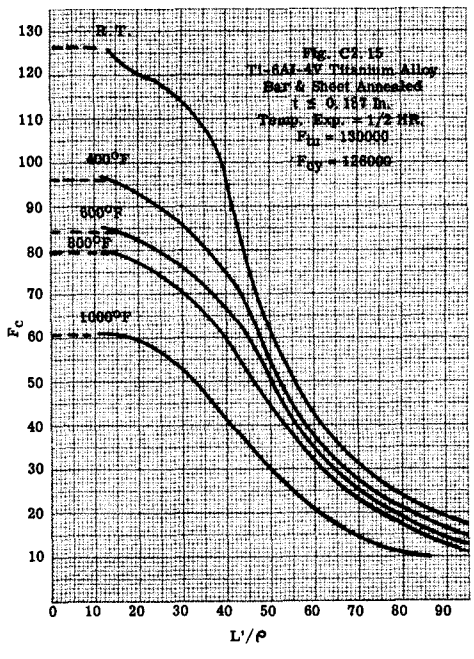

Figure C2.15

F_c is in ksi

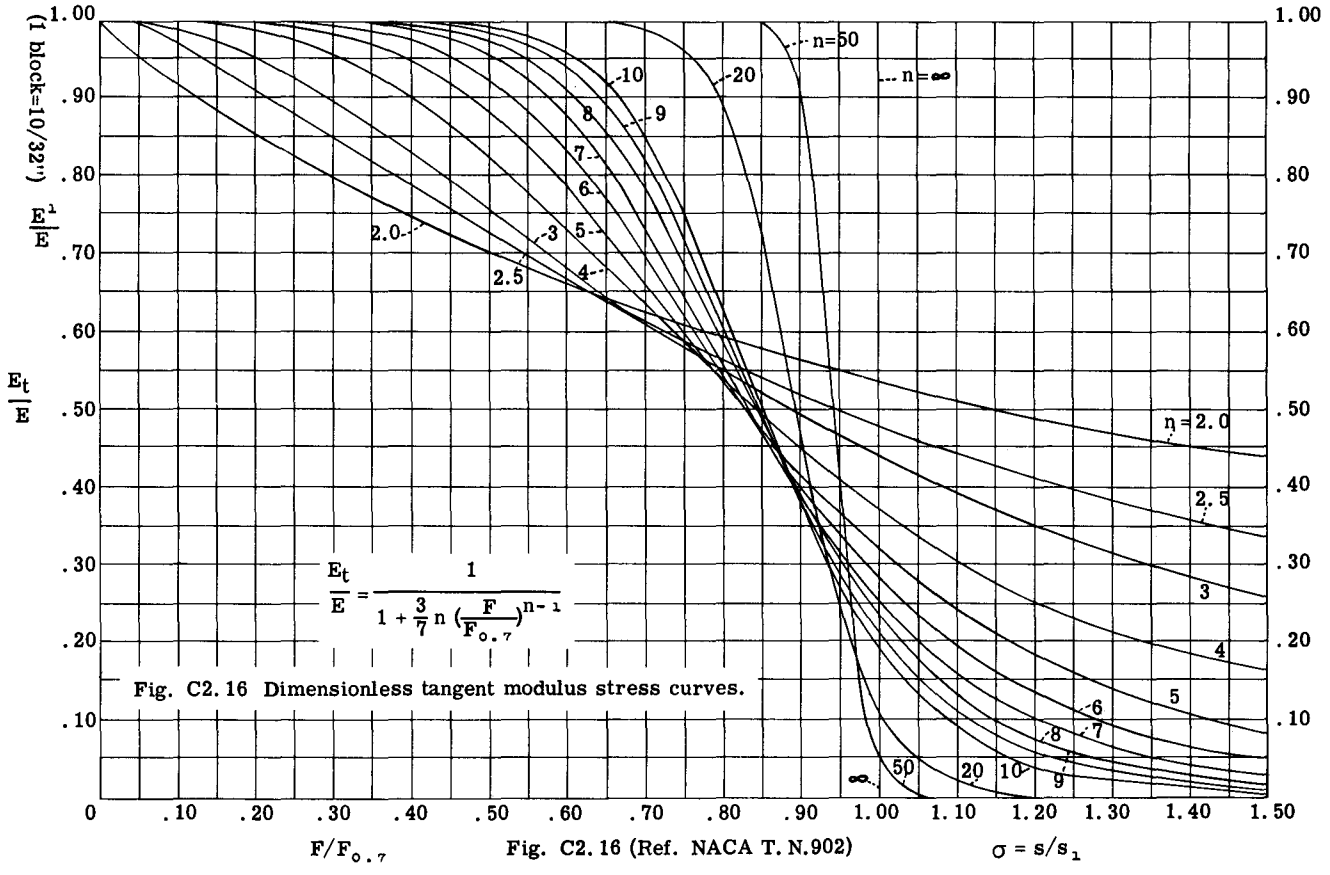

Fig. C2.16 Dimensionless tangent modulus stress curves.

Fig. C2.16 (Ref. NACA T. N.902)

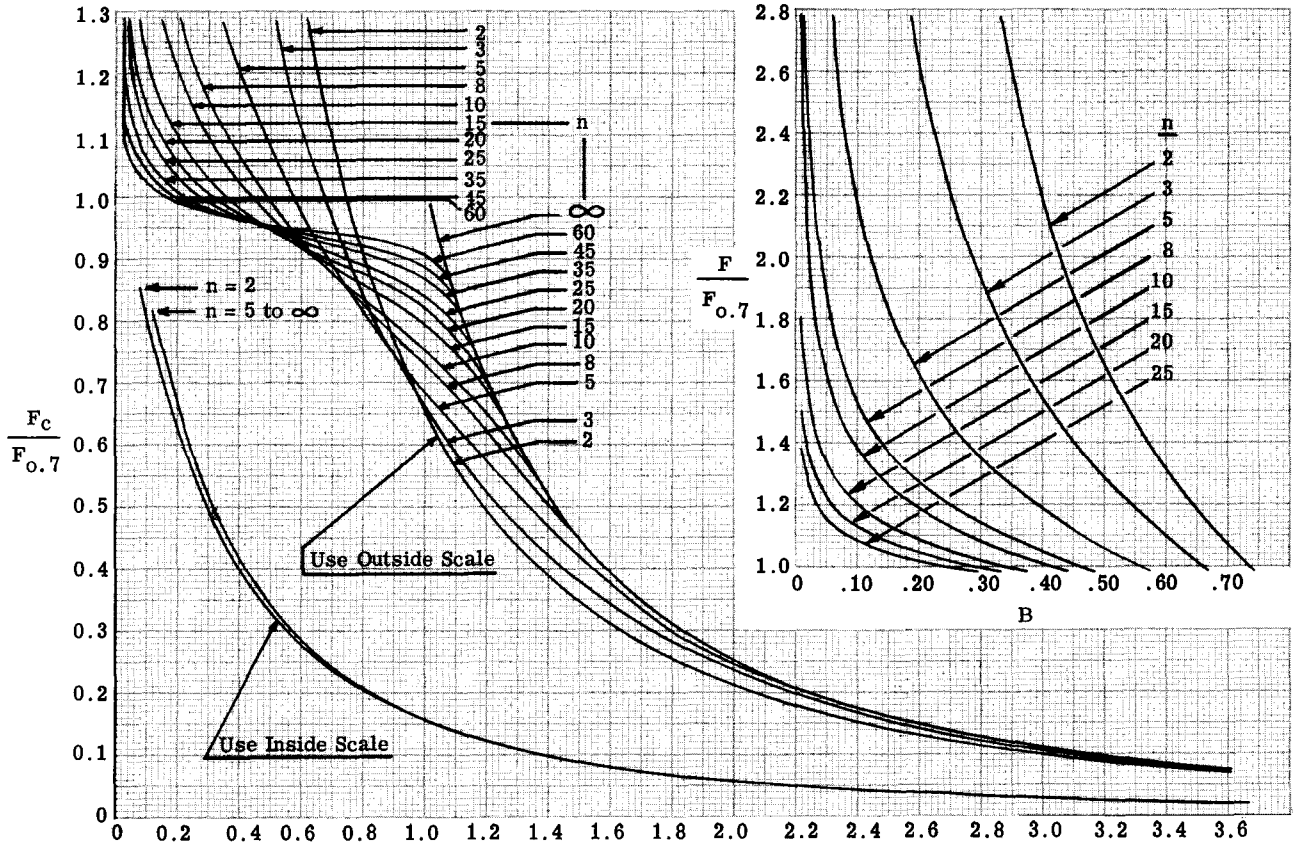
$\frac{F_C}{F_{0.7}}$
n = 2
n = 5 to ∞
Use Outside Scale
Use Inside Scale
n
2
3
5
8
10
15
20
25
35
45
60
∞
$\frac{F}{F_{0.7}}$
B
$B = \frac{1}{\pi}\sqrt{\frac{F_{0.7}}{E}}(L'/\rho)$

Fig. C2.17

particular properties of the material $E_{o.7}/F$.

Inserting value of $F = \pi^2 E_t/(L'/\rho)^2$ in equation (8),

$$\left(\frac{E_t}{\pi^2 E_t/(L'/\rho)^2}\right)\left(\frac{F_{o.7}}{E}\right) = B^2$$

$$\text{or } B = \frac{1}{\pi}\sqrt{\frac{F_{o.7}}{E}}\left(\frac{L'}{\rho}\right) \quad ------- (9)$$

The use of the curves in Fig. C2.17 will be illustrated later in the example problem solutions.

C2.6 Strength of Columns with Variable Cross-Section or Moment of Inertia.

To save weight in a built up column or forged column, the member is tapered or is made with a non-uniform cross-section. To find the ultimate strength of such columns, it is usually necessary to use a trial and error method. The general method of solution involving a consideration of column deflection will be illustrated for a case of a long column with uniform cross-section.

Fig. C2.18 shows a pin ended column in a deflected neutral equilibrium position when carrying the ultimate or critical load P. Assume that the shape of the deflected column follows a sine curve relationship with the deflection at midpoint equal to unity (see Fig. C2.18).

The equation of the deflected column curve is $y = \frac{\sin \pi x}{L}$. If P is the end load, the bending moment at any point = $M = Py = P \sin \frac{\pi x}{L}$.

By the well known "moment area" principle (see Chapter A7; Art. A7.14), the deflection of a point (A) on the elastic curve away from a tangent to elastic curve (B) equals the first moment of the M/EI diagram between (A) and (B) about (A).

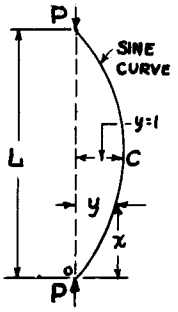

Fig. C2.18

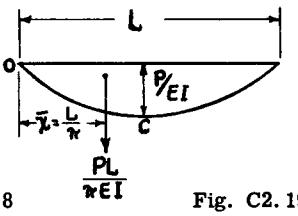

Fig. C2.19

Thus in Fig. C2.18, the deflection of point (O) away from tangent at midpoint c equals unity in our assumed conditions and it also equals the first moment of the area of the M/EI diagram between (O) and (C) about (O). (Fig. C2.19).

The value of the ordinate for M/EI diagram at any point x from O is $\frac{P}{EI}\sin\frac{\pi x}{L}$.
The total area under the curve is,

$$\text{area} = \frac{P}{EI}\int_0^L \sin\frac{\pi}{L}x\,dx = \frac{P}{EI}\left[-\frac{L}{\pi}\cos\frac{\pi}{L}x\right]_0^L$$

$$= \frac{P}{EI} - \left\{\left[\frac{L}{\pi}(-1)\right]\left[-\frac{L}{\pi}(1)\right]\right\} = \frac{P}{EI}\left(\frac{L}{\pi}+\frac{L}{\pi}\right)$$

$$\text{hence area} = \frac{2PL}{\pi EI} \text{ and half area} = \frac{PL}{\pi EI}$$

The center of gravity of the half area is

$$A\bar{x} = \int x\,da$$

$$\left(\frac{PL}{\pi EI}\right)\bar{x} = \frac{P}{EI}\int_0^{L/2} x \sin\frac{\pi}{L}x\,dx,$$

$$\frac{L}{\pi}\bar{x} = \int_0^{L/2} x \sin\frac{\pi}{L}x\,dx$$

Integrating this simple expression and solving for x we obtain:

$$\bar{x} = L/\pi$$

Taking moments about point (O) of the M/EI diagram between O and C about O:

$$y_o = 1 = \frac{PL}{\pi EI}\cdot\frac{L}{\pi} = \frac{PL^2}{\pi^2 EI} \quad \text{hence, } P = \frac{\pi^2 EI}{L^2}$$

which is the Euler equation, and thus the assumed sine curve was the proper one for the deflected elastic curve of the column.

Suppose that the elastic curve of deflected column had been assumed as a parabola with unit deflection at midpoint. Fig. C2.20 shows the M/EI diagram.

The area of one-half the diagram = $\frac{1}{2}\left(\frac{2}{3}L\times\frac{P}{EI}\right) = \frac{PL}{3EI}$

Taking moments about O of the area between O and C;

$$y_o = 1 = \frac{PL}{3EI}\cdot\frac{5}{16}L = \frac{5PL^2}{48EI} \quad \text{hence,}$$

$P = \frac{48EI}{5L^2} = \frac{9.6\ EI}{L^2}$, which compares with $P = 9.9EI/L^2$ of the Euler equation or an error of 3 percent.

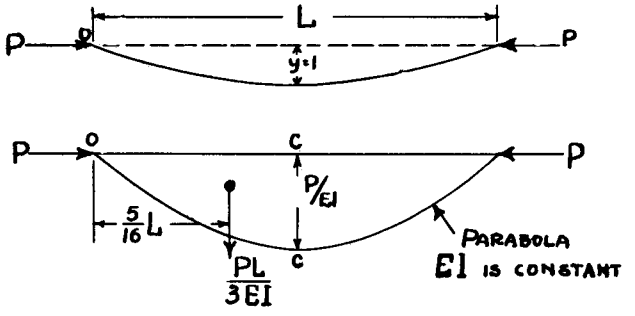

Fig. C2.20

We can now apply the same procedure to a column with non-uniform cross-section. The steps in this procedure for a column symmetrical about the center point are as follows:-

(1) Assume a sine curve for the deflected column with unit deflection at center point.

(2) Plot a moment of inertia (I) curve for column cross-section.

(3) Find the bending moment curve due to end load P times the lateral deflection.

(4) Divide these moment values by the EI values to obtain M/EI curve. The modulus of elasticity E is considered constant.

(5) Find the deflected column curve due to this M/EI loading.

(6) Compare the shape of the derived column deflection curve with that originally assumed as a sine curve. This can be done by multiplying the computed deflections by a factor that makes the center deflection equal to unity. Since the assumed sine curve is not the true column deflection curve, the computed deflection will differ somewhat from the sine curve.

(7) With the computed deflection curve, modified to give unity at center point, repeat steps 3, 4, 5 and 6. The results this time will show derived deflection curve still closer to the assumed deflection curve.

(8) To obtain the desired accuracy, the procedure in step (7) will usually have to be repeated again.

(9) Solve for load P by writing an expression for the deflection at the center point which equals unity. This is done by using the moment area principle as was done in the previous example problem involving a column with uniform section.

In the above outlined procedure, E has been assumed constant or, in other words, the column failure is elastic or failing stresses are below the proportional limit stress of the material. The practical problem usually involves a slenderness ratio where failure is due to inelastic bending and thus E is not constant. For this case, a trial and error method of solution in necessary using the tangent modulus of elasticity which varies with stress in the inelastic stress range.

C2.7 Design Column Curves for Columns with Non-Uniform Cross-Section.

Figs. C2.21 and C2.22 give curves for rapid solution of two types of stepped columns. Figs. C2.23 and C2.24 gives curves for the rapid solution of two forms of tapered columns. Use of these curves will be illustrated later in this chapter.

C2.8 Column Fixity Coefficients c for Use with Columns with Elastic Side Restraints and Known End Bending Restraint.

Figs. C2.25 and C2.26 give curves for finding fixity coefficient c for columns with one and two elastic lateral restraints and Fig. C2.27 gives curves for finding c when restraining moments at column ends are known. Use of these various curves will be illustrated later.

C2.9 Selection of Materials for Elevated Temperature Conditions.

Light weight is an important requirement in aerospace structural design. For columns that fail in the inelastic range of stresses, a comparison of the F_{cy}/w ratio of materials gives a fairly good picture of the efficiency of compression members when subjected to elevated temperature conditions. In this ratio F_{cy} is the yield stress at the particular temperature and w is the weight per cu. inch of the material. Fig. C2.28 shows a plot of F_{cy}/w for temperature ranges up to 600° F. with 1/2 hour time exposure for several important aerospace materials.

C2.10 Example Problems.

PROBLEM 1.

Fig. C2.29 shows a forged (I) section member 30 inches long, which is to be used as

CRITICAL LOADS-NON-UNIFORM COLUMNS

Single Stepped - Pin Ended

Fig. C2.21

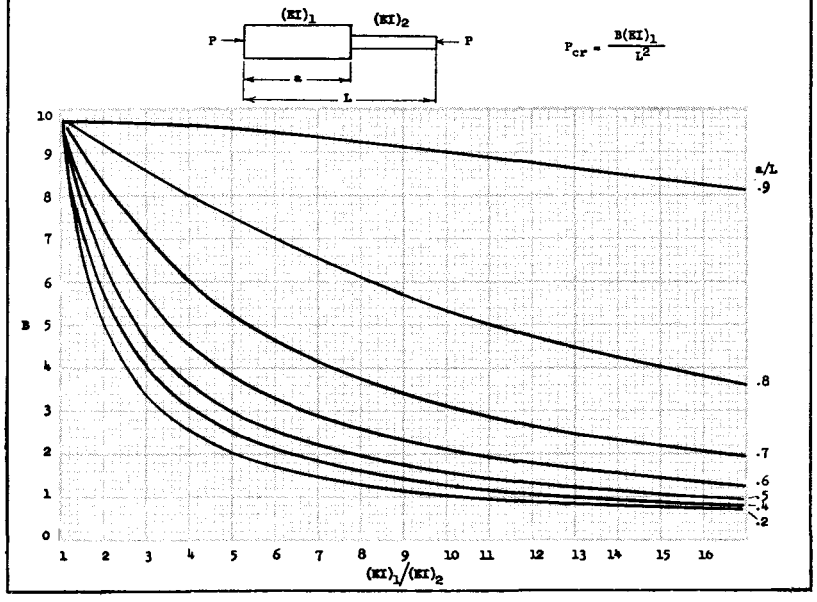

CRITICAL LOADS-NON-UNIFORM COLUMNS

Double Stepped - Pin Ended

Fig. C2.22

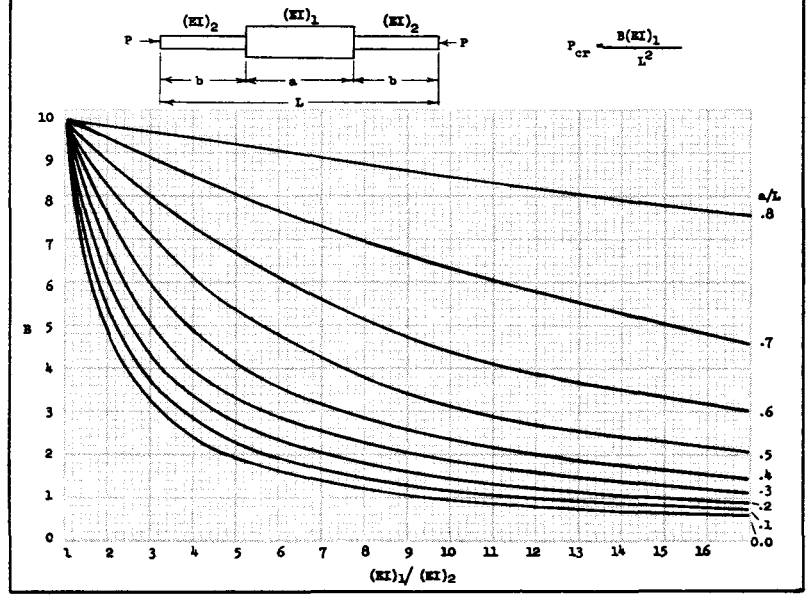

CRITICAL LOADS-NON-UNIFORM COLUMNS

Constant Thickness - Taper in Plan-Form

$P_{cr} = \frac{B(EI)_1}{L^2}$

Fig. C2.23

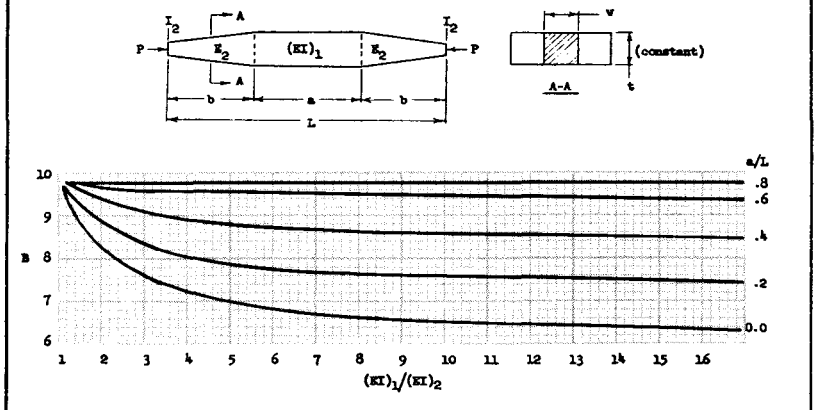

CRITICAL LOADS-NON-UNIFORM COLUMNS

Solid Prisms Tapering in Width and Thickness
Solid Cylinders Tapering to Cones

$P_{cr} = \frac{B(EI)_1}{L^2}$

Fig. C2.24

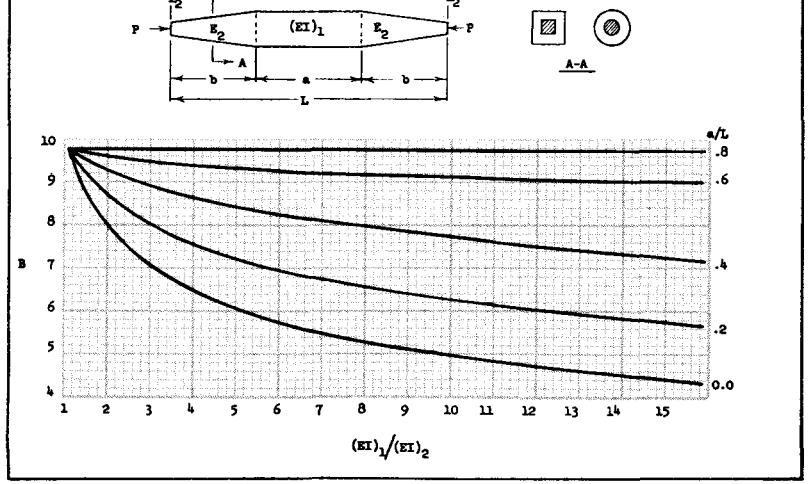

Reference - N. American Avaiation Structures Manual

SIMPLY SUPPORTED COLUMNS WITH ONE ELASTIC RESTRAINT

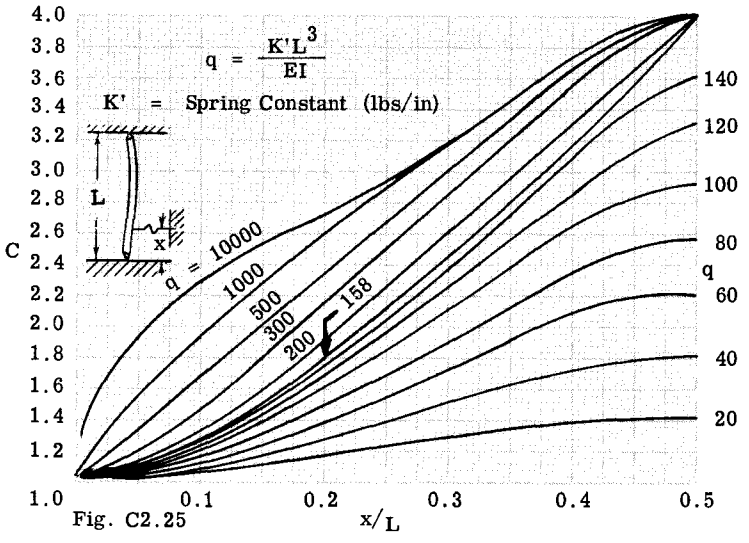

Fig. C2.25

SIMPLY SUPPORTED COLUMNS WITH TWO ELASTIC RESTRAINTS

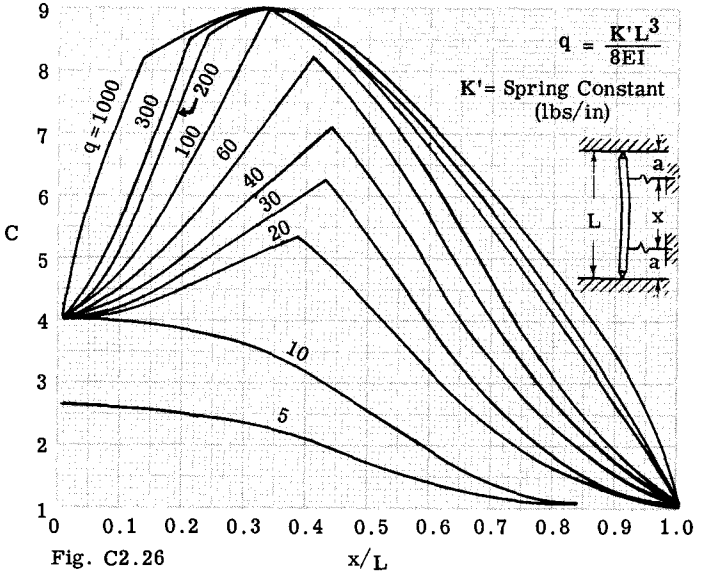

Fig. C2.26

FIXITY CONSTANT FOR COLUMN WITH END SUPPORT HAVING A KNOWN BENDING RESTRAINT

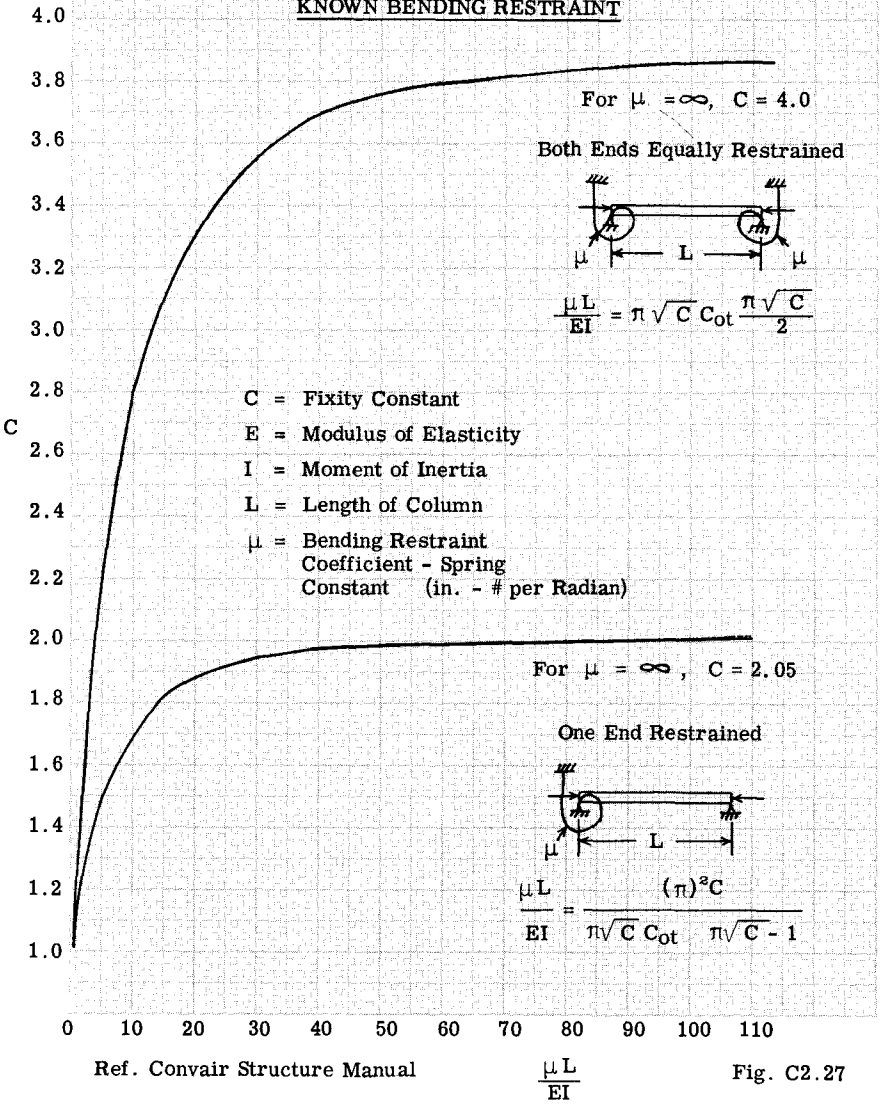

Ref. Convair Structure Manual

Fig. C2.27

Fig. C2.28

(1) AISI Steel, $F_{tu} = 180,000$

(2) 17-7PH. Stainless Steel, $F_{tu} = 210,000$

(3) 7075-76 Alum. Alloy

(4) AZ31B Magnesium Alloy

(5) 6AL-4V Titanium Alloy

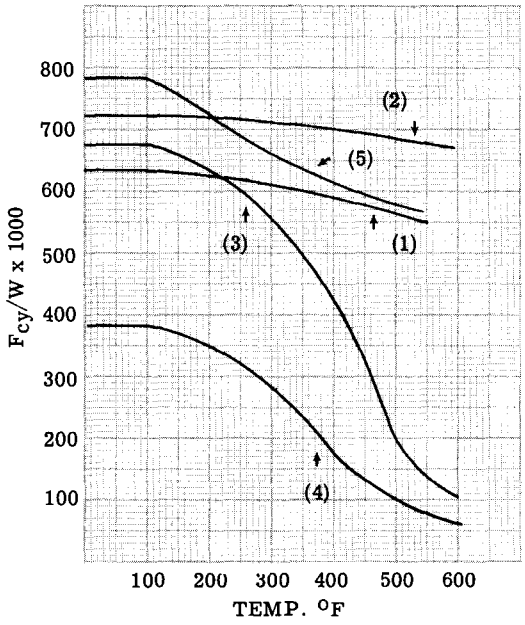

a compression member. Find the ultimate strength of the member if made from the following materials and subjected to the given temperature and time conditions.

Case 1. Material 7079-T6 Alum. Alloy hand forging and room temperature.

Case 2. Same as Case 1, but subjected 1/2 hour to a temperature of 300°F.

Case 3. Same as Case 2, but for 600°F.

Case 4. Material 17-4 PH stainless steel, hand forging at room temperature.

Fig. C2.29

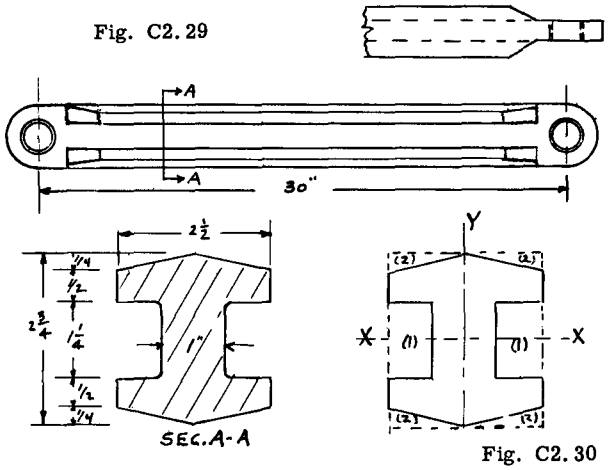

Fig. C2.30

Solution:

Since the column may fail by bending about either the X or Y axes, the column strength for bending about each of these axes will be calculated. Since the column strength is a function of the radius of gyration of the cross-section, the first step in the solution will be the calculation of I_x and I_y, from which ρ_x and ρ_y can be found.

Calculating I_x: In Fig. C2.30 the section will be first considered a solid rectangle 2.5 x 2.75 and then the properties of portions (1) and (2) will be subtracted.

$$I_x \text{ (rectangle)} = \frac{1}{12} \times 2.5 \times 2.75^3 = 4.32$$

Portions (1) and (2)

$$I_x = -\frac{1}{12} \times 1.5 \times 1.25^3 - 4(.625 \times .25 \times 1.292^2) = -1.29$$

(I_o of (2) about its x centroidal axis is negligible)

$$I_x = 4.32 - 1.29 = 3.03 \text{ in.}^4$$

$$\rho_x = \sqrt{\frac{I_x}{A}}, \text{ Area } A = 2.5 \times 2.75 - 2 \times .75 \times 1.25 - 4 \times .25 \times .625) = 4.375 \text{ sq. in.}$$

$$\rho_x = \sqrt{3.03/4.375} = .83 \text{ in.}$$

Calculation of I_y:

$$I_y \text{ (solid)} = \frac{1}{12} \times 2.75 \times 2.5^3 = 3.58$$

$$\text{Portion (1)} = -(1.25 \times .75 \times .875^2)2 - (1.25 \times .75^3/12)2 = -1.52$$

$$\text{Portion (2)} = -(.25 \times .625 \times .833^2)4 - 4(.25 \times 1.25^3/36) = -.488$$

$$I_y = 3.58 - 1.52 - .488 = 1.58 \text{ in.}^4$$

$$\rho_y = \sqrt{1.58/4.375} = .60"$$

Column strength is considerably influenced by the end restraint conditions. For failure by bending about the x-x axis, the end restraint against rotation is zero as the single fitting bolt has an axis parallel to the x-x axis and thus c the fixity coefficient is 1. For failure by bending about the y-y axis we have end restraint which will depend on the rigidity of the bolt and the adjacent fitting and structure. For this example problem, this restraint will be such as to make the end fixity coefficient c = 1.5.

For failure about x-x axis,

$$L' = L/\sqrt{c} = 30/\sqrt{1} = 30, \quad L'/\rho_x = 30/.83 = 36$$

For failure about y-y axis,

$$L' = 30/\sqrt{1.5} = 24.6, \quad L'/\rho_y = 24.6/.60 = 41$$

Therefore failure is critical for bending about y-y axis, with $L'/\rho = 41$.

Case 1. The material is 7079-T6 Alum. Alloy hand forging. Fig. C2.14 gives the failing stress F_c for this material plotted against the L'/ρ ratio. Thus using $L'/\rho = 41$ and the room temperature curve, we read $F_c = 50500$ psi. Thus the failing load if $P = F_cA = 50500 \times 4.375 = 220{,}000$ lbs.

Case 2. Using the 300°F curve in Fig. C2.14 for the same L'/ρ value, we read $F_c = 40{,}400$, and thus $P = 40{,}400 \times 4.375 = 177{,}000$.

Case 3. Using the 600°F curve, F_c reads 6100 and thus $P = 6100 \times 4.375 = 26700$ lbs. Thus subjecting this member to a temperature of 600°F for 1/2 hour reduces its strength from 220,000 to 26,700 lbs., which means that Alum. Alloy is a poor material for carrying loads under such temperatures since the reduction in strength is quite large.

Case 4. Material 17-4 PH stainless steel forging. Fig. C2.8 gives the column curves for this material. For $L'/\rho = 41$ and using the room temperature curve we read $F_c = 135{,}200$ and thus $P = 135{,}200 \times 4.375 = 591{,}000$ lbs.

C2.10 Solution Without Using Column Curves.

When primary bending failure occurs at stresses above the proportional limit stress, the failing stress is given by equation (5) which is,

$$F_c = \pi^2 E_t/(L'/\rho)^2$$

Since E_t is the tangent modulus of elasticity, it varies with F_c, and thus the relation of E_t to F_c must be known before the equation can be solved. To plot column curves for all materials in their many manufactured forms plus the various temperature conditions would require several hundred individual column charts. The use of such curves can be avoided if we know several values or parameters regarding the material as presented by Ramsburg and Osgood and expanded by Cozzone and Melcon (see Arts. C2.4 and C2.5) for use in column design.

Thus we make use of the curves in Fig. C2.17.

Case 1. Material 7079-T6 Alum. Alloy forging. Table B1.1 of Chapter B1 summarizes certain material properties. The properties needed to use Fig. C2.17 are the shape factor n, the moduls E_c and the stress $F_{o.7}$. Referring to Table B1.1, we find that $n = 26$, $E_c = 10{,}500{,}000$ and $F_{o.7} = 59{,}500$.

The horizontal scale in Fig. C2.17 involves the parameter,

$$B = \frac{1}{\pi}\sqrt{\frac{F_{o.7}}{E_c}}\,(L'/\rho)$$

Substituting:-

$$B = \frac{1}{\pi}\sqrt{\frac{59{,}500}{10{,}500{,}000}}\,(41) = 1.01$$

Using Fig. C2.17 with 1.01 on bottom scale and projecting vertically upward to n = 26 curve and then horizontal to scale at left side of chart we read $F_c/F_{o.7} = .842$.

Then $F_c = 59{,}500 \times .842 = 50{,}100$, as compared to 50,500 in the previous solution using Fig. C2.14.

Case 2. From Table B1.1 for this material subjected to a temperature of 600°F for 1/2 hour, we find $n = 29$, $F_c = 9{,}400{,}000$ and $F_{o.7} = 46{,}500$.

Then $B = \frac{1}{\pi}\sqrt{\frac{46{,}500}{9{,}400{,}000}}\,(41) = .917$

From Fig. C2.17 for $B = .917$ and $n = 29$, we read $F_c/F_{o.7} = .88$, thus $F_c = 46{,}500 \times .88 = 40{,}900$ as compared to 40,400 in the previous solution.

EXAMPLE PROBLEM 2.

Fig. C2.31 shows an extruded (I) section. A member composed of this section is 32 inches long. The member is braced laterally in the x direction, thus failure will occur by bending about x-x axis. The member is pin ended and thus c = 1. The material is 7075-T6 Extrusion. The problem is to find the failing stress F_c under room temperature conditions.

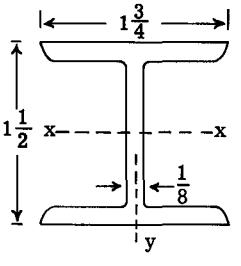

Fig. C2.31

This (I) section corresponds to Section 15 in Table A3.15 in Chapter A3. Reference

to this table gives,

$A = .594$ sq. in. $P_x = .618$

$L' = L$, sin c = 1, $L'/\rho_x = 32/.618 = 51.7$

Fig. C2.11 gives the column curves for this material. For $L'/\rho = 51.7$ and room temperature we read $F_c = \underline{38,500}$ psi.

Solution by using Fig. C2.17,

From Table B1.1, n = 8.8, $E_c = 7,800,000$ and $F_{o.7} = 29,000$.

$$B = \frac{1}{\pi}\sqrt{\frac{29,000}{7,800,000}}\,(51.7) = 1.00$$

From Fig. C2.17 we find $F_c/F_{o.7} = .74$

Then $F_c = .74 \times 29,000 = \underline{21,450}$ psi

Consider the member is subjected to a temperature of 450°F for 1/2 hour.

From Fig. C2.11, $F_c = \underline{21400}$ psi

Using Fig. C2.17:-

From Table B1.1, n = 8.8, $E_c = 7,800,000$ and $F_{o.7} = 29,000$.

$$B = \frac{1}{\pi}\sqrt{\frac{29,000}{7,800,000}}\,(51.7) = 1.00$$

From Fig. C2.17 we find $F_c/F_{o.7} = .74$

Then $F_c = .74 \times 29,000 = \underline{21,450}$ psi

A very common aluminum alloy in aircraft construction is 2014-T6 extrusions. Let it be required to determine the allowable stress F_c for our member when made of this material.

Since we have not presented column curves for this material, we will use Fig. C2.17.

From Table B1.1, for our material, we find n = 18.5, $E_c = 10,700,000$ and $F_{o.7} = 53,000$

$$\text{Then } B = \frac{1}{\pi}\sqrt{\frac{53,000}{10,700,000}}\,(51.7) = 1.16$$

From Fig. C1.17 for B = 1.16 and n = 18.5, we read $F_c/F_{o.7} = .71$, hence $F_c = .71 \times 53,000 = \underline{37,600}$.

The result shows that the 2014-T6 material gave a failing stress of 37,600 as compared to 38,900 for the 7075-T6 material which has a F_{cy} of 70,000 as compared to $F_{cy} = 53,000$ for the 2014-T6 material. The reason for the 7075 material not showing much higher column failing stress F_c over that for the 2014 alloy is due to the fact that the stress existing under a L'/ρ value of 51.7 is near the proportional limit stress or E_t is not much different than E_c, the elastic modulus.

To illustrate a situation where the 7075 material becomes more efficient in comparison to the 2014 alloy, let us assume that our member has a rigid connection at its end which will develop an end restraint equivalent to a fixity coefficient c = 2.

Then $L' = 32/\sqrt{2} = 22.6$ and $L'/\rho = 22.6/.618 = 36.7$.

For the 7075 material from Fig. C2.11, $F_c = \underline{58,300}$

For the 2014 material, we use Fig. C2.17

$$B = \frac{1}{\pi}\sqrt{\frac{53,000}{10,700,000}}\,(36.7) = .823.$$

From Fig. C2.17 for B = .823 and n = 18.5, we read $F_c/F_{o.7} = .87$, when $F_c = .87 \times 53,000 = \underline{46,100}$ as compared to 58,300 for the 7075 material, thus 7075 material would permit lighter weight of required structural material.

The student should realize that if the stress range is such as to make $E_t = E_c$, then the bending failure is elastic instead of inelastic and equation (5), using Young's modulus of elasticity E_c, can be solved directly without resort to column curves or a consideration of E_t, since E_t is equal to E_c.

The student should realize that equation (5) is for strength under primary column failure due to bending as a whole and not due to local buckling or crippling of the member or by twisting failure. The subject of column design when local failure is involved is covered in a later chapter.

In example problem 2, we have assumed that local crippling is not critical, which calculation will show is true as explained and covered in a later chapter.

C2.12 Strength of Stepped Column.

The use of curves in Fig. C2.22 will be illustrated by the solution for the strength of two stepped columns in order to illustrate both elastic and inelastic failure of such columns.

Case 1. Elastic failure.

Fig. C2.32 shows a double stepped pin ended column. The member is machined from a 1 inch diameter extruded rod made from

7075-T6 material. The problem is to find the maximum compressive load this member will carry.

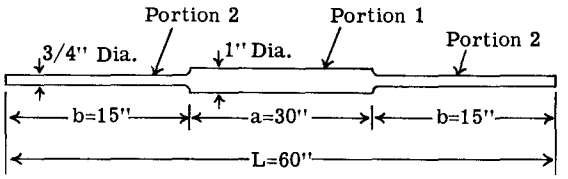

Fig. C2.32

PORTION 1	PORTION 2
$A_1 = .7854$ in.^{2}	$A_2 = .4418$
$I_1 = .0491$ in.^{4}	$I_2 = .0155$
$E_C = 10{,}500{,}000$	$E_C = 10{,}500{,}000$

From Fig. C2.22, $P_{cr} = \dfrac{B(EI_1)}{L^2}$. This is the Euler equation for failure under elastic bending. If the ratio a/L equals 1 or a uniform section, B becomes π^2 or 10 as shown in Fig. C2.22. The curves in Fig. C2.22 apply only to elastic failure. Since the member in Fig. C2.32 is rather slender we will assume the failure is elastic and then check this assumption.

$$\frac{EI_1}{EI_2} = \frac{10{,}500{,}000 \times .0491}{10{,}500{,}000 \times .0155} = 3.17, \quad a/L = 30/60 = 0.5$$

From Fig. C2.22 for a/L = 0.5 and $EI_1/EI_2 = 3.17$ we read B = 7.0

$$\text{Whence, } P_{cr} = \frac{B\ EI_1}{L^2} = \frac{7 \times 10{,}500{,}000 \times .0491}{60^2} = 1000 \text{ lb.}$$

The stresses in each portion are,

$f_1 = 1000/0.7854 = 1280$ psi

$f_2 = 1000/.4418 = 2270$ psi

These compressive stresses are below the proportional limit stress of the material so E_C is constant and our solution is correct.

Case 2. Inelastic Failure.

The column has been shortened to the dimensions as shown in Fig. C2.33. The diameters and material remain the same as in Case 1.

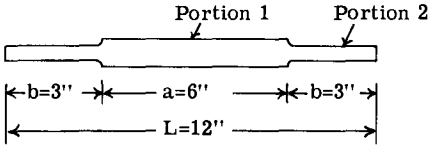

Fig. C2.33

This is a relatively short column so the failing stress should fall in the inelastic range where E is not constant, therefore the solution is a trial and error procedure. We will base our first guess or trial on an average L/ρ value.

ρ for portion 1 is 0.25 inches

ρ for portion 2 is 0.1875

Average ρ = (6 x .25 + 6 x 0.1875)/12 = 0.22

Then L/ρ = 12/0.22 = 54.5, use 55.

Fig. C2.11 is a column curve for 7075-T6 Alum. Alloy extruded material. With L/ρ = 55, we read allowable stress F_C = 33,500 psi. Therefore

$$P = F_C\ A = 33{,}500 \times 0.7854 = 26{,}300 \text{ lb.}$$

$f_1 = 33{,}500$ and $f_2 = 26{,}300/.4418 = 59{,}500.$

The stress f in portion 2 is above the proportional limit stress so a plasticity correction must be made in using the curves in Fig. C2.22.

Referring to Table B1.1 in Chapter B1, we find the following values for 7075-T6 extrusions:- n = 16.6, $F_{0.7}$ = 72,000, E_C = 10,500,000.

The tangent modulus E_t will be found for the stresses f_1 and f_2.

For Portion 1, $f_1/F_{0.7} = 33{,}500/72{,}000 = .465$

Referring to Fig. C2.16 and using 0.465 and n = 16.6, we read $E_t/E = 1.0$, thus $E_t = E$ and thus no plasticity correction for Portion 1.

For Portion 2, $f_2/F_{0.7} = 59{,}500/72{,}000 = .826$

From Fig. C2.16, we obtain $E_t/E = .675$ whence, $E_t = .675 \times 10{,}500{,}000 = 7{,}090{,}000$.

$$\frac{EI_1}{EI_2} = \frac{10{,}500{,}000 \times .0491}{7{,}090{,}000 \times .0155} = 4.7$$

From Fig. C2.22 for a/L = .5, we obtain B = 5.6.

$$\text{Then } P_{cr} = \frac{B\ EI_1}{L^2} = \frac{5.6 \times 10{,}500{,}000 \times .0491}{144} = 20{,}000 \text{ lb.}$$

Our guessed strength was 26,300 lb. Our guessed strength and calculated strength must be the same so we must try again.

Trial 2. Assume a critical load P = 23500 lb.

$f_1 = 23500/.7854 = 29900$

$f_2 = 23500/.4418 = 53100$

Portion 1. $f_1/F_{0.7} = 29900/72000 = .415$

From Fig. C2.16 for n = 16.6, we read $E_t/E = 1.0$.

Portion 2. $f_2/F_{0.7} = 53100/72000 = .738$

From Fig. C2.16, $E_t/E = .90$, whence $E_t = .90 \times 10{,}500{,}000 = 9{,}450{,}000$.

$$\frac{EI_1}{EI_2} = \frac{10{,}500{,}000 \times .0491}{9{,}450{,}000 \times .0155} = 3.52.$$

From Fig. C2.22 for a/L = .5, we read B = 6.62.

$$\text{The } P_{cr} = \frac{B\,EI_1}{L^2} = \frac{6.62 \times 10{,}500{,}000 \times .0491}{144} =$$

23,650 lb.

This practically checks the assumed value, thus the answer is between 23,500 and 23,650 and if further accuracy is desired another trial should be carried through.

The other types of columns with non-uniform cross-sections as shown in Figs. C2.21, C2.23 and C2.24 are solved in a similar manner. These charts are to be used only with pin ended columns. The end fixity coefficient c for tapered columns is not the same as for uniform section columns.

C2.13 Column Strength With Known End Restraining Moment.

Fig. C2.27 shows curves for finding the end fixity coefficient c for two conditions of known end bending restraint.

To illustrate the use of these curves, a simple problem will be solved.

Fig. C2.34 shows a 3-bay welded steel tubular truss. The problem is to determine the allowable compressive stress for member AB. This strength is influenced by the fixity existing at ends A and B. The diameter and wall thickness of each tube in the truss is shown on the figure. The material is AISI steel, $F_{tu} = 90{,}000$, $F_{ty} = 70{,}000$, $E = 29{,}000{,}000$.

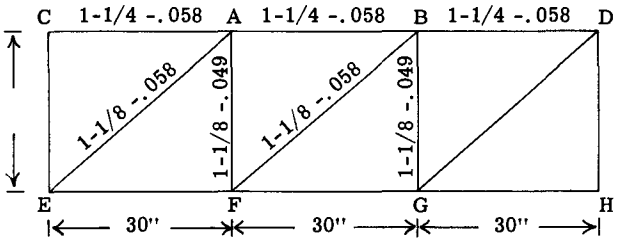

Fig. C2.34

The member AB is welded to three adjacent tubes at joints (A) and (B). Since these tubes are the same at joints (A) and (B), the fixity at the ends (A) and (B) of member AB is the same.

Referring to Fig. C2.27, the term μ is defined as the bending restraint coefficient-spring constant expressed as inch pounds per radian. In Fig. A, the moment M required to rotate end (A) through 1 radian when far end is fixed is 4EI/L. For derivation of this value refer to Art. A11.4 of Chapter A11. If the far end (B) is pinned in (Fig. A), a moment M = 3EI/L will rotate end (A) through one radian. To be slightly conservative, we will assume the far ends of members coming into joints (A) and (B) as pinned. Thus μ = 3EI/L. The sum of μ = 3EI/L will be computed for the 3 members which form the support of member AB at end (A).

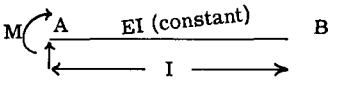

Fig. A

Member AC:- I = .03867, I/L = .001289
Member AE:- I = .02775, I/L = .00071
Member AF:- I = .02402, I/L = .000962

$\mu = \Sigma\, 3EI/L$

$= 3(.001289 + .00071 + .000962)\ 29{,}000{,}000$

$\mu = 258{,}000$

In Fig. C2.27 we need term μ L/EI. The L/EI refers to member AB. Thus μ L/EI = $(258{,}000 \times 30)/29{,}000{,}000 \times .0367 = 7.28$.

We use the upper curve in Fig. C2.27 since restraint at both ends of member AB is the same. Thus for μ L/EI = 7.28, we read end fixity coefficient c = 2.58.

Then $L' = L/\sqrt{c} = 30/\sqrt{2.58} = 18.6$.

ρ for member = .422 inches.

$L'/\rho = 18.6/.422 = 44.0$

From column curve in Fig. C2.3, we read

allowable failing stress to be F_c = 55,200 psi.

If the far ends of the connecting members were assumed fixed instead of pinned, then $\mu = 4EI/L$, or we can multiply previous value of 7.28 by 4/3, which gives 9.7 which, used in Fig. C2.27, gives c = 2.80.

$L'/\rho = 30/\sqrt{2.8} \times .422 = 42.5$. Then from Fig. C2.3, F_c = 56,600 psi. Since the far ends are less than fixed, the assumption that far ends are pinned gives fairly accurate results.

In a truss structure all members are carrying axial loads and axial loads affect the ability of members to resist rotation of their ends. Art. A11.12 of Chapter A11 explains how to take account of the effect of axial load upon the stiffness of a member as required in calculating the end restraint coefficient μ.

C2.14 Columns With Elastic Lateral Supports.

Figs. C2.25 and C2.26 provide curves for finding the end fixity coefficient c to take care of elastic lateral supports at points midway between the column ends.

To illustrate the use of these charts, a round bar 0.5 inches in diameter and 24 inches long is braced laterally as shown in Fig. C2.35. The bar is made of AISI Steel, heat treated to F_{tu} = 125,000. The spring constant for the lateral support is 775 lbs. per inch.

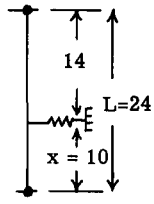

Moment of Inertia of 1/2" rod = .003068,

Radius of Gyration = .125 inches.

Fig. C2.35

$$q = \frac{K'L^3}{EI} = \frac{775 \times 24^3}{29{,}000{,}000 \times .003068} = 120$$

From Fig. C2.25 for x/L = 10/24 = .416 and q = 120, we find c = 2.92.

Then $L' = L/\sqrt{c} = 24/\sqrt{2.92} = 14.08$

$L'/\rho = 14.08/0.125 = 113$

$$F_c = \frac{\pi^2 E}{(L'/\rho)^2} = \frac{\pi^2 \times 29{,}000{,}000}{(113)^2} = 22{,}500 \text{ psi}$$

If the stress is above the proportional limit stress for the material, then the trial and error approach must be used as illustrated in the problem dealing with a tapered column.

C2.15 Problems.

(1) 6061-T6 Aluminum Alloy sheet, heat-treated and aged has the following properties:

(a) Under room temperature:- $F_{0.7}$ = 35,000 psi, E_c = 10,100,000 psi, and n = 31

(b) For 1/2 hr.exposure at 300°F:- $F_{0.7}$ = 29,000, E_c = 9,500,000 and n = 26.

For the above two cases (a) and (b), determine E_t (tangent modulus values) from Fig. C2.16 and then calculate and plot column curves for these 2 material conditions.

(2) Fig. C2.36 shows the cross-section of a compression member. Calculate the failing compressive load under the following cases:-

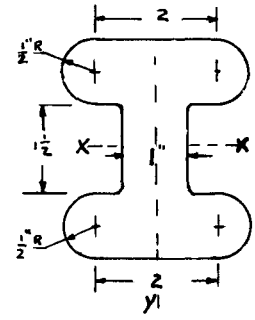

Fig. C2.36

Case 1. L = 25 inches. Material AISI Steel 4140, F_{tu} = 180,000. Take end fixity coefficient c = 1 for bending about x-x axis and 1.5 about axis y-y.

(3) Same as Problem (2) but member is subjected to a temperature of 850°F for 1/2 hour.

(4) Two extruded channel sections identical to Section No. 50 in Table A3.11 in Chapter A3, are riveted back to back and used as a column member. If member is 26 inches long and end fixity is C = 1 and material is 7075-T6 extrusion, what is the failing compressive load.

If member is fastened rigidly to adjacent structure which provides a fixity c = 2, what will be the failing load.

(5) Consider the column in problem (4) is made from 2014-T6 Aluminum Alloy extrusion. Find failing load.

(6) The pin ended single stepped column as shown in Fig. C2.37 is made of AISI-4130 normalized steel, F_{tu} = 90,000, F_{cy} = 70,000. Determine the maximum compressive load member will carry.

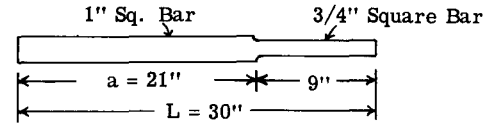

Fig. C2.37

(7) Same as Problem (5) but member is exposed 1/2 hour to a temperature of 500°F.

(8) Same as Problem (5) but change dimension (a) to 10 inches, and L to 14.28 inches.

(9) Find the failing compressive load for the doubly stepped column in Fig. C2.38 if member is made from 7079-T6 hand forging.

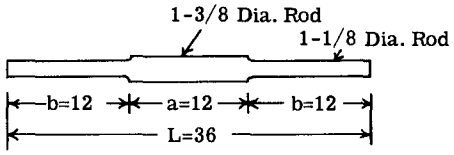

Fig. C2.38

(10) Same as Problem (7) but change dimensions a = 6", b = 4", L = 14".

(11) The cylindrical tapered member in Fig. C2.39 is used as a compression member. If member is made from AISI Steel 4140, F_{tu} = 125,000, what is the failing load.

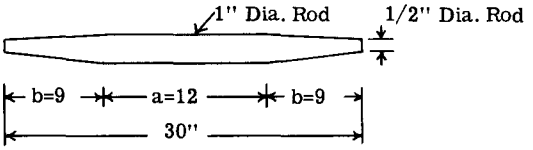

Fig. C2.39

(12) Same as Problem (7) but change dimensions to a = 6", b = 4.0", L = 14 inches.

References:

(1) NACA Technical Note 902.
(2) Non-dimensional Buckling Curves, by Cozzone Σ Melcon, Jr. of Aero. Sciences, October, 1946.
(3) Chart from Lockheed Aircraft Structures Manual.

CHAPTER C3
YIELD AND ULTIMATE STRENGTH IN BENDING

C3.1 Introduction.

Members subjected to bending alone or in combination with axial and torsional loads are quite common in flight vehicle structures. The limit design loads on a structural member must be carried without permanent distortion and the ultimate design loads must be carried without rupture or failure. The well known bending stress equation $f_b = Mc/I$, assumes a linear variation of stress with strain or, in other words, the equation holds for stresses below the proportional limit stress or, in general, the elastic range. Failure of a member in bending, unless there is local weakness, does not occur at stresses in the elastic range but occurs at stresses in the inelastic range. Since the ultimate strength of a member is needed to compare against the ultimate design load to be carried, a theory or procedure is necessary which will accurately determine the ultimate and yield strength of a member in bending.

C3.2 Basic Approach to Finding the Bending Strength of Members.

The problem is to determine the internal resisting moment of a beam section when subjected to stresses which fall in the inelastic range of stresses. This stress can be taken as the ultimate tensile or compressive stress of the material or limited to some stress or deformation in the inelastic range. To obtain the true internal resisting moment, we must know how the normal tension and compressive stress varies over the cross-section. The stress-strain curve for the material provides the source for obtaining the true stress picture. If a material has a different shape in the tensile and compressive inelastic zones, the neutral axes does not coincide with the centroidal axis, thus adding some difficulty to an analysis method. The analysis procedure for determining the true internal resisting moment is best explained by an example solution.

C3.3 Bending Strength of a Solid Round Bar.

Fig. C3.1a shows the cross-section of a round solid bar made of aluminum alloy. The stress-strain curve up to a unit strain of .010 in. per inch is given in Fig. C3.2. Note that the shape of the curve in the inelastic zone is not the same for both tension and compression. In this example solution, we will find the internal resisting moment when we limit the unit strain at the extreme edge on the compressive side of the beam section to 0.010. Now plane sections remain plane after bending in both elastic and inelastic stress conditions when member is in pure bending. We will guess the neutral axis as located 0.0375 inches above the centroidal axis as shown in Fig. C3.1b. Having assumed the maximum unit strain as .010, we can draw the strain diagram of Fig. C3.1b. We now divide the cross-section in Fig. C3.1a into 20 narrow horizontal strips. Having the strain curve in Fig. C3.1b, we can find the unit

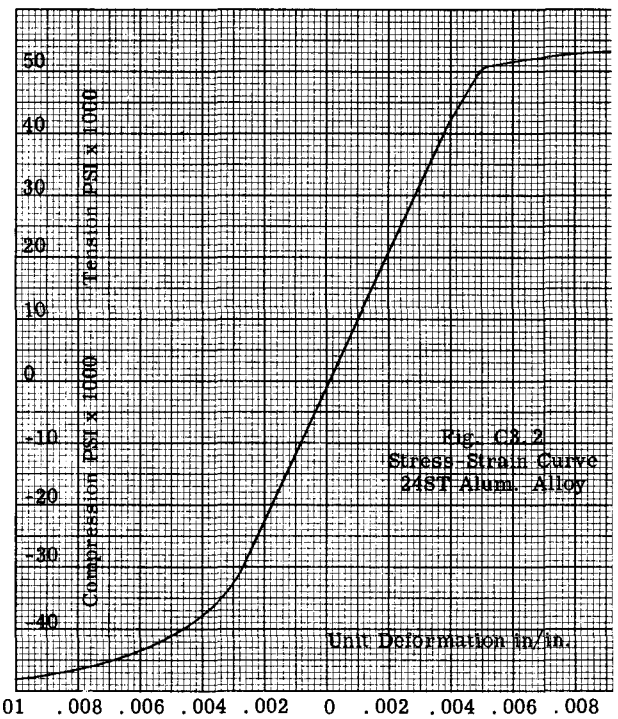

Fig. C3.2
Stress-Strain Curve
24ST Alum. Alloy

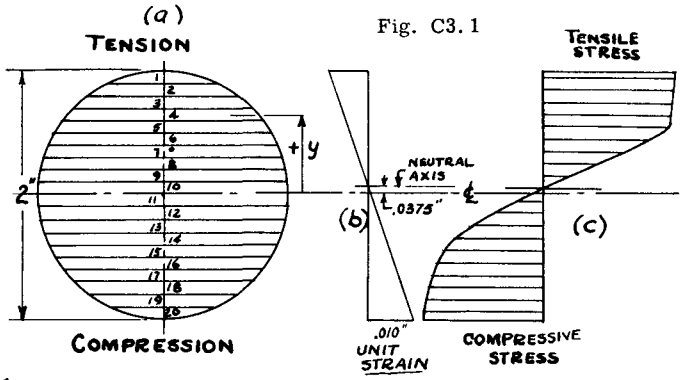

Fig. C3.1

strain at the midpoint of each strip. With the strain known on each strip, the stress existing can be found by use of the stress-strain curve in Fig. C3.2. The total load on each strip then equals the stress times the area of the strip. The internal resisting moment then equals the summation of the load on each strip times the distance from the strip to the neutral axis.

Table C3.1 shows the detail calculations. If the neutral axis has been selected in the correct position, the values in column (6) of the table should add up to zero since total tension must equal the total compression on the beam cross-section. The small discrepancy of 740 pounds in the summation of column (6) is not enough to change the location of the neutral axis or the total internal resisting moment appreciably. Column (7) gives the total internal resisting moment as 56735 in. lbs. when the strain is limited to the .010 strain as previously discussed. The stress at this strain from Fig. C3.2 is 49000 psi. Using this stress in the well known beam formula M = fI/c, we obtain M = 49000 x 0.785 = 38450, which is much less than the true value of 56735.

TABLE C3.1

1	2	3	4	5	6	7
Strip No.	Strip Area "A"	y	ε	Unit Stress σ	$F = \sigma A$	Res. Moment M = Fr
1	.058	0.935	.00867	53000	3075	2760
2	.102	0.840	.00773	52500	5350	4300
3	.135	0.75	.00685	52100	7025	5040
4	.153	0.65	.00591	51500	7870	4820
5	.165	0.55	.00494	51000	8410	4310
6	.180	0.45	.00398	43000	7740	3200
7	.185	0.35	.00302	33200	6140	1920
8	.195	0.25	.00205	22800	4450	945
9	.197	0.15	.00108	12500	2460	280
10	.200	0.05	.00012	3200	640	10
11	.200	-0.05	-.00084	- 7250	-1450	130
12	.197	-0.15	-.00181	-17800	-3510	660
13	.195	-0.25	-.00276	-29500	-5750	1650
14	.185	-0.35	-.00374	-35500	-6560	2540
15	.180	-0.45	-.00470	-40000	-7200	3510
16	.165	-0.55	-.00566	-43000	-7100	4170
17	.153	-0.65	-.00663	-44800	-6850	4710
18	.135	-0.75	-.00759	-46000	-6210	4880
19	.102	-0.84	-.00846	-47200	-4810	4210
20	.058	-0.935	-.00937	-48000	-2780	2690
Total	3.140				740	56735

Col. 1 Rod divided into 20 strips . 1" thick.
Col. 3 y = distance from centerline to strip c. g.
Col. 4 ε = strain at midpoint = (y - .0375)/103.75.
Col. 5 Unit stress for ε strain from Fig. C3.2.
Col. 6 Total stress on strip.
Col. 7 Moment about neutral axis. r = (y - .0375).

Since it is desirable to use the beam formula in finding bending stresses due to a given bending moment, and also for determining the true internal resisting moment of a beam section, structural design engineers make use of a fictitious failing bending stress F_b, which is referred to as a modulus of rupture stress in pure bending. Then the ultimate bending moment that can be developed by a given beam cross-section and a given material is $M = F_b I/C$. Design curves for finding F_b, the modulus of rupture, are given later in this chapter.

Since there are many flight vehicle materials and all kinds of shapes used in structural members, the basic approach for solution as illustrated in Table C3.1 becomes very time consuming. Design engineers always search for simplified methods which give sufficient accuracy. Thus Cozzone (Ref. 1) has developed a simplified procedure for finding the modulus of yield or rupturing bending stress F_b. The method is widely used in the aerospace industry in structural design.

C3.4 The Cozzone Simplified Procedure.

The Cozzone method in its simplest form assumes a symmetrical rectangular beam section and the same shape of the stress-strain curve in both tension and compression. Fig. C3.3 represents the true bending stress variation over the beam cross-section when failure occurs. Cozzone now replaces this true curve by a trapizoidal stress variation as shown in Fig. C3.4. The stress f_o is a fictitious stress which is assumed to exist at the neutral axis or at zero strain.

Fig. C3.3

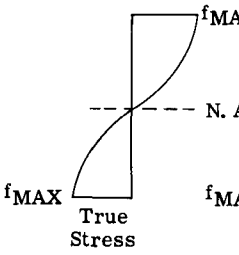

Fig. C3.4

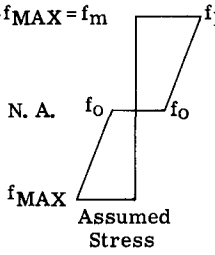

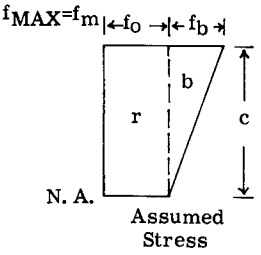

Fig. C3.6

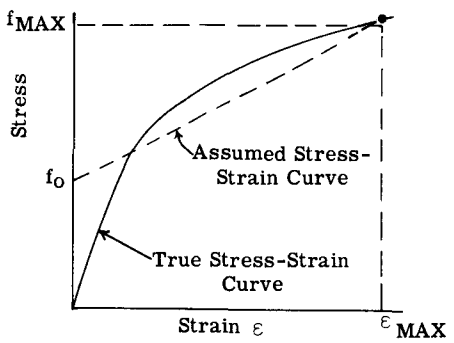

Fig. C3.5

The value of f_o is determined by making the requirement that the internal moment of the true stress system must equal the moment of the assumed trapezoidal stress system which results from the assumed stress-strain curve as shown in Fig. C3.5. Fig. C3.6 shows the trapezoidal stress pattern drawn to a larger scale and showing only one half of the symmetrial beam section. The trapezoidal stress pattern has been divided into a rectangle (r) and a triangle (b) as shown in the figure.

Let, M_b = total internal resisting moment.
m_r = internal moment developed by portion (r).
m_b = internal moment developed by portion (b).

Then $M_b = m_r + m_b$

Since f_b varies linearly from zero to f_b, the stress is elastic and thus the beam equation holds, or

$m_b = f_b I/c$ for entire beam section. The stress variation on portion (r) is constant or rectangular, thus

$$m_r = f_o \int_o^c y dA, \text{ let } \int_o^c y dA = Q$$

Then $m_r = f_o 2Q$ for entire beam section

But $f_b = f_m - f_o$ (from Fig. C3.6)

Thus, $M_b = (f_m - f_o)\frac{I}{c} + 2f_oQ$, or

$$\frac{M_b c}{I} = f_m + f_o\left(\frac{2Q}{I/c} - 1\right) \text{ - - - - - - - - (1)}$$

$$\text{Let } k = \frac{2Q}{I/c} \text{ - - - - - - - - - - - - - (2)}$$

k is a beam section shape factor.

Let $F_b = M_b c/I$, then from equation (1)

$$F_b = f_m + f_o(k - 1) \text{ - - - - - - - - - (3)}$$

F_b is a fictitious Mc/I stress or the modulus of rupture for a particular cross-section at a given maximum stress level.

The values of k vary between 1 and 2.0. If calculated value of k is greater than 2 use 2.0. Fig. C3.7 shows the value of the shape factor k for several typical shapes. Fig. C3.8 shows curves for the rapid determination of the k factor for 3 common beam sections.

Fig. C3.7 k Factor for Some Typical Shapes

Shape	K	Shape	K
	1		1.25 to 1.7
	4/3		1.7
	1 to 1.5		2
	1.5		

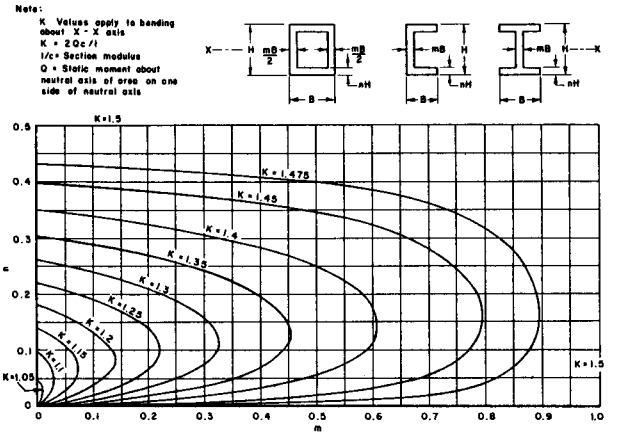

Fig. C3.8 Section Factor K for I, □, and C Sections (Ref. 2)

C3.5 Design Curves for Finding Modulus of Rupture (F_b).

The modulus of rupture F_b may be a yield modulus, that is, in equation (3) the value of f_m is equal to the yield stress of the material. It may also be the ultimate modulus of rupture, in which case the value of f_m in equation (3) equals the ultimate strength of the material. The modulus of rupture may be limited to a stress between the yield and ultimate stress of the material because of local crippling or by excessive distortion. Regardless of what value is used for f_m in equation (3), the corresponding value of f_o must be known before the value of F_b can be determined. Figs. C3.9 to C3.23 give strain curves for various material and the corresponding f_o curve. The use of these two curves permit the determination of F_b if the k shape factor for the particular beam section being considered is known. In deriving the values of f_o, the following assumptions are made.

(1) The stress-strain curve is assumed the same in tension and compression.

(2) The neutral axis is assumed to coincide with the centroidal axis.

(3) During bending plane sections remain plane.

(4) The cross-section is not subject to local or torsional instability.

(5) Beam-column, curvature and shear lag effects are considered negligible.

C3.6 General Accuracy of Method.

(1) It is exact for a rectangular section under pure bending with moment vector parallel to a principal axis.

(2) For double symmetric sections under pure bending and moment vector parallel to a principal axis, the accuracy should be within 5 percent.

(3) Single symmetric sections will vary from practically exact to definitely unconservative (moment vector normal to axis of symmetry).

(4) For sections subject to combined bending and axial load, the results will vary from practically exact to conservative.

(5) For unsymmetrical bending, with and without axial load, the results will vary from practically exact to conservative.

C3.7 Example Problems in Finding Bending Strength.

EXAMPLE PROBLEM 1.

A rectangular beam section is 0.25 inches wide and 1.5 inches deep. What yield and ultimate bending moment will the section develop when made from 7075-T6 extruded aluminum alloy.

Solution: The modulus of bending stress is given by equation (3),

$$F_b = f_m + f_o\,(k - 1) \quad - - - - - - - - - (3)$$

$$k = \frac{2Q}{I/c} = \frac{2 \times 0.75 \times .25 \times .375 \times}{(\frac{1}{12})\ .25 \times 1.5^3 (1/.75)} = \frac{.1408}{.0938}$$

$$k = 1.50$$

The value of k could also be found in Fig. C3.7.

Material is 7075-T6 aluminum alloy. From Fig. C3.17, F_{tu} = 75000, F_{ty} = 65000.

To find the yield bending strength, the value of f_m in equation (3), the maximum stress permitted on the most remote fiber is 65000, the yield stress of the material. To find f_o, we go to Fig. C3.17 and find the point on the stress-strain curve that corresponds to a stress of 65000. This point is projected vertically downward to intersect the curve f_o. This point is then projected to the stress scale at the edge of the chart to give the value of f_o. The value of f_o from this chart operation gives f_o = 29000. Then from equation (3)

$F_{b_{yield}}$ = 65000 + 29000 (1.5 - 1) = 79500 psi.

Then yield bending moment = $M_{yp} = F_b I/c$

Thus M_{yp} = 79500 x .0938 = 7460 in. lb.

For finding the ultimate resisting bending, we use F_{tu} which is 75000 as the value of f_m in equation (3). Again going to Fig. C3.17 to stress of 75000 on stress-strain curve and the vertically down to f_o curve, we obtain f_o = 70500.

Then $F_{b(ult)}$ = 75000 + 70500(1.5-1)= 110250 psi

Then $M_{ult} = F_b I/c$ = 110250x.0938 = 10370 in.lb.

Let us assume that is is desired to limit the strain in the extreme fiber to .03 inches per inch. What would be the bending moment developed under this limitation.

From Fig. C3.17 for a unit strain of .03 the corresponding stress from the stress strain curve is 74700 and the f_o stress is 61200.

Then F_b = 74700 + 61200 (1.5-1) = 105300

Then $M = F_b I/c$ = 105300 x .0938 = 9900 in. lb.

EXAMPLE PROBLEM 2.

The symmetrical I beam section in Fig. (a) is subjected to an ultimate design pure bending moment M = 14000 in. lb. What is the margin of safety if the beam is made of magnesium forging AZ61A which has F_{tu} = 38000 and F_{ty} = 22000.

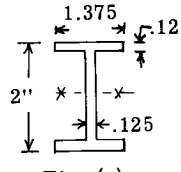

Fig. (a)

$$I_x = \frac{1}{12} \times 1.375 \times 2^3 - \frac{1}{12} \times 1.25 \times 1.75^3$$

$$= .916 - .558 = .358.$$

$$I_{x/c} = .358/1 = 0.358$$

$$Q = 1.375 \times .125 \times .9375 + .875 \times .125 \times .4375 = 0.209$$

$$k = \frac{2Q}{I_{x/c}} = \frac{2 \times .209}{0.358} = 1.17$$

k could have been from Fig. C3.8 when using m = .125/1.375 = .091, and n = .125/2.00 = .062.

From Fig. C3.19, for $f_m = F_{tu} = 38000$ we find in projecting vertically downward to f_o curve gives $f_o = 23700$. Then subt. in equation (3)

$F_b = 38000 + 23700\ (1.17 - 1) = 40770$

$M_{ult} = F_b I/c = 40770 \times .358 = \underline{15000}$ in. lb.

Margin of Safety $= \frac{M_{ult}}{M} - 1 = \frac{15000}{14000} - 1 = \underline{.07}$

Assume we desire the stress intensity at a point 0.5 inches from neutral axis if full bending strength was developed. From Fig. C3.19, the unit strain when stress is 38000 is .035. Then since plane sections remain plane after bending, the unit strain at point .50 inch from neutral axis is (.5/1) (.035) = .0175. From Fig. C3.19, the stress existing at this strain is f = 31000 psi. A linear variation of stress as used in the flexural equation would give half the maximum stress or 38000/2 = 19000 psi as against the true stress of 31000.

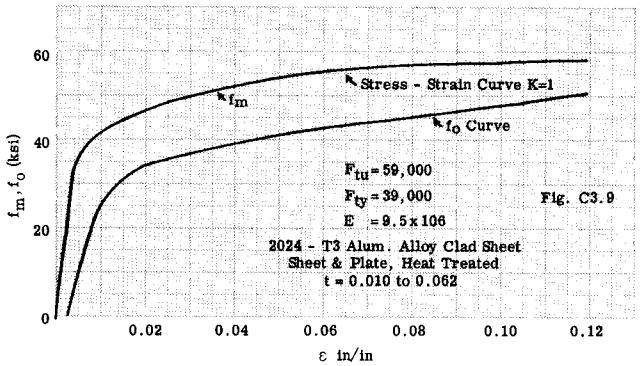

Fig. C3.9

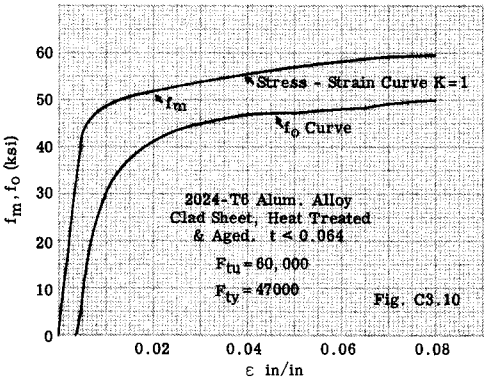

Fig. C3.10

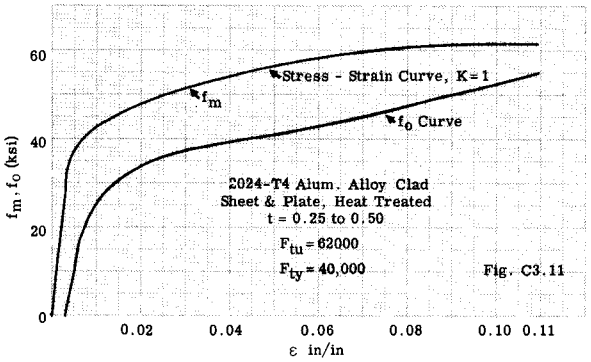

Fig. C3.11

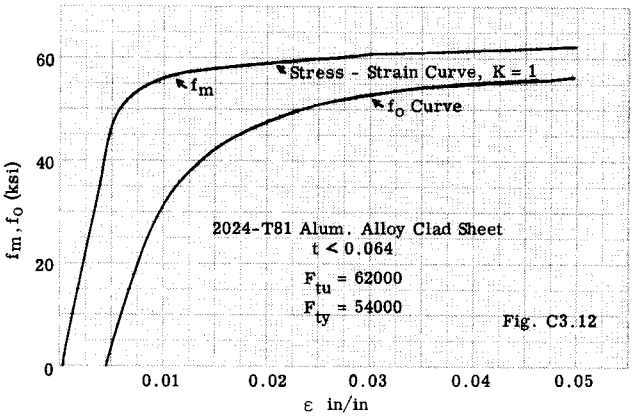

Fig. C3.12

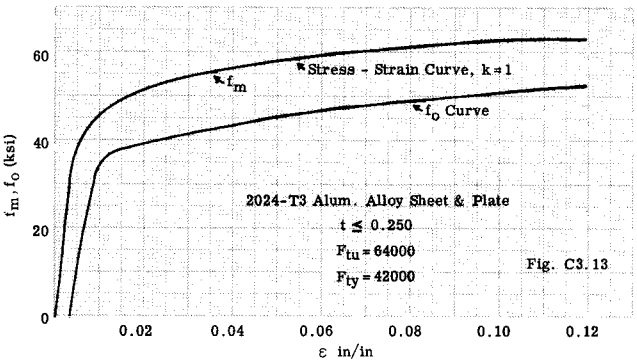

Fig. C3.13

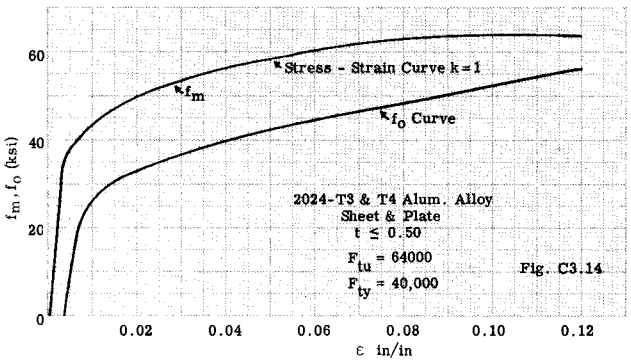

Fig. C3.14

Curves for finding F_b. $F_b = f_m + f_o\ (k - 1)$.

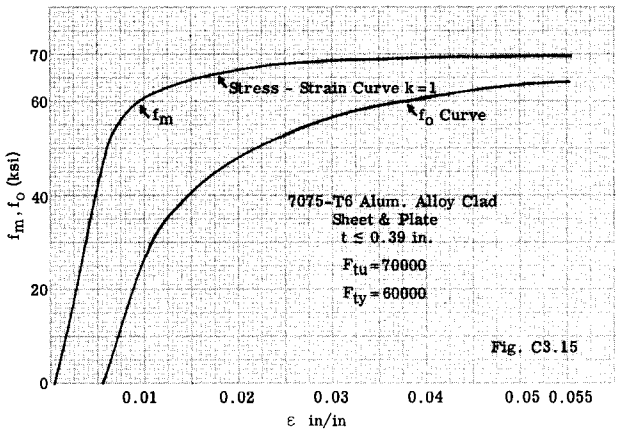

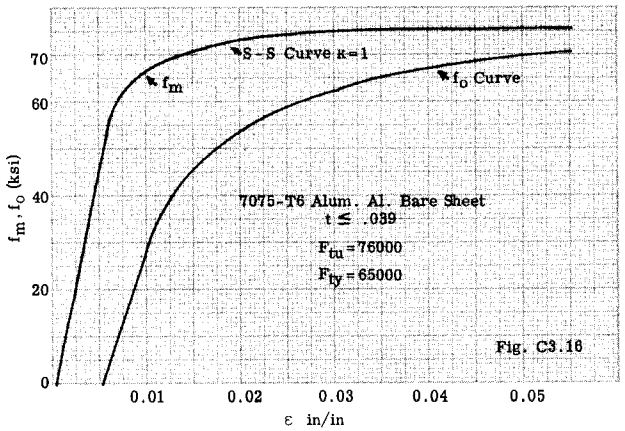

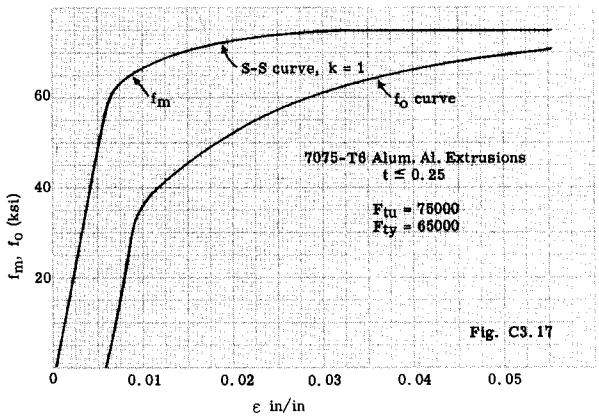

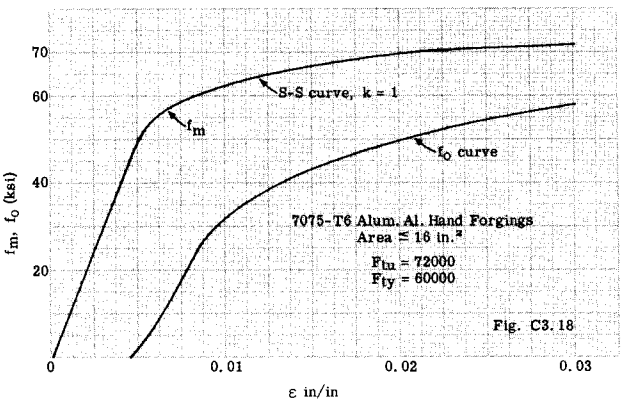

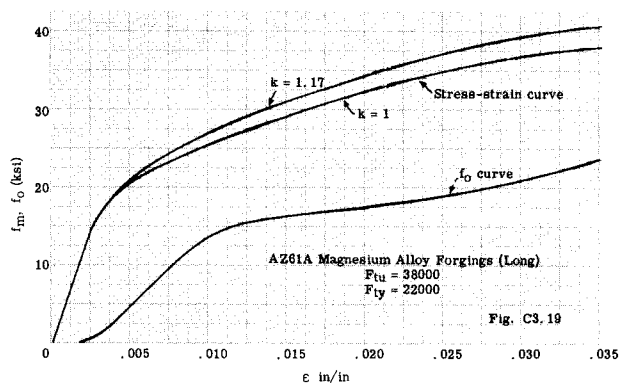

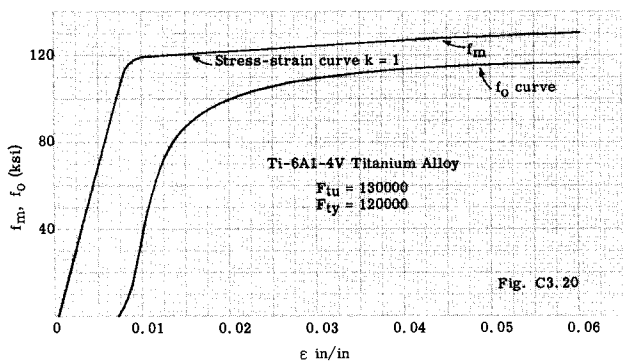

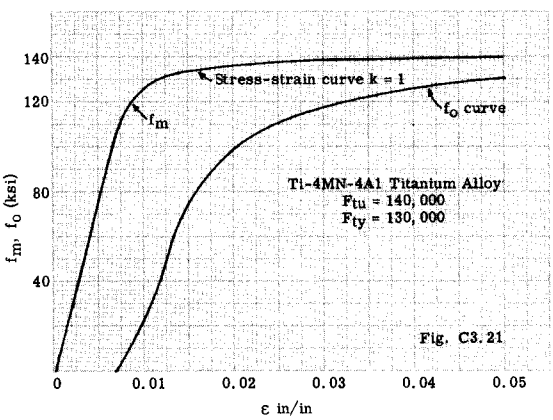

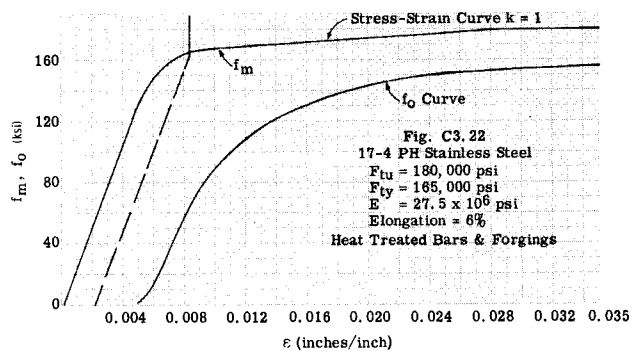

Curves for finding F_b. $F_b = f_m + f_o (k - 1)$.

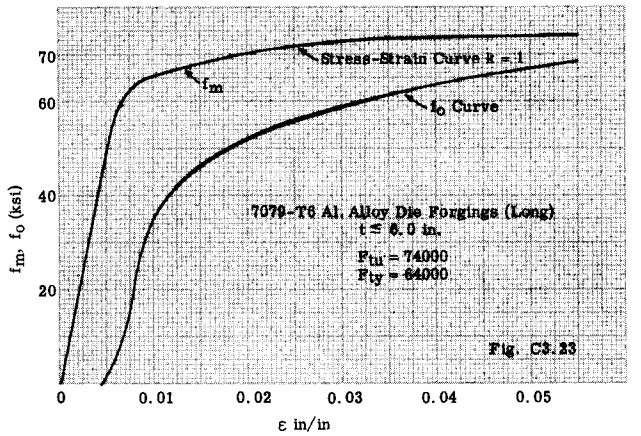

EXAMPLE PROBLEM 3. Unsymmetrical Section.

Fig. (b) shows a tee beam section, symmetrical about the vertical axis. If the material is 17-4 PH stainless steel, what ultimate bending moment will be developed if bottom portion is the tension flange.

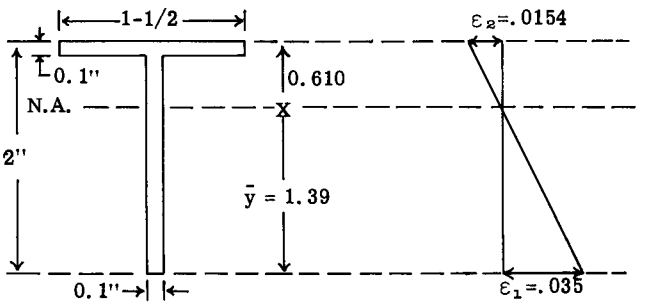

The neutral axis will first be determined.

$$\bar{y} = \frac{\Sigma Ay}{\Sigma A} = \frac{2 \times .1 \times 1 + 1.4 \times .1 \times 1.95}{2 \times .1 + 1.4 \times .1} = 1.39$$

Fig. (c) shows the unit strain picture. The lower edge of the beam section is strained to the maximum value of .035 as shown on the stress-strain curve in Fig. C3.22. Since plane sections remain plane the unit strain ε_2 at the upper edge of section is ε_2 = .035 x .61/1.39 = .0154.

Solution 1

Equation (3) was derived for a symmetrical section about the neutral axis. The equation involves finding the resisting moment developed by one half the beam section and multiplying by 2. This is permissible since the unit strain at both top and bottom edges is the same. In this solution we will continue to use equation (3). To do this it is necessary to make symmetrical sections for the portion on each side of the neutral axis of the entire section.

Label the beam portion below the neutral axis as (1) and that above by (2).

Portion 1. Fig. (d) shows how the lower portion (1) is made a symmetrical section about neutral axes by adding the dashed portion. The internal bending resistance will be found for this entire section in Fig. (d). One half of this amount will then be the true moment developed by portion (1).

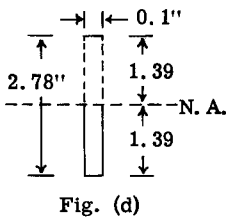

Fig. (d)

$$I = \frac{1}{12} bh^3 = \frac{1}{12} \times 0.1 \times 2.78^3 = 0.178$$

$$I_1/c_1 = 0.178/1.39 = .128$$

$$Q_1 = 1.39 \times 0.1 \times .695 = .0965$$

$$2Q_1 = .193$$

$$k_1 = 2Q_1/I_1/c_1 = \frac{0.193}{0.128} = 1.5$$

From Fig. C3.22, F_{tu} = 180000 which equals f_m.

f_o from curve = 156000

Then $F_{b_1} = f_m + f_o (k - 1)$

$= 180000 + 156000 (1.5 - 1) = 258000$

$$M = (F_{b_1} I_1/c_1)\frac{1}{2} = 258000 \times .128 \times 0.5 = 16550 \text{ in. lb.}$$

The factor 1/2 is due to the fact that portion (1) is only one half the beam section in Fig. (d).

Portion 2. Fig. (e) shows the developed symmetrical section for the upper portion (2) of the beam section.

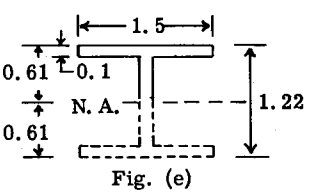

Fig. (e)

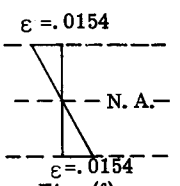

Fig. (f)

The unit strain picture is shown in Fig.(f)

$$I_2 = \frac{1}{12} \times 1.5 \times 1.22^3 - \frac{1}{12} \times 1.4 \times 1.02^3 = .104$$

$I_2/c_2 = .104/.61 = .1704$

$Q_2 = .61 \times .1 \times .305 + 1.4 \times 0.1 \times 0.56 = .097$

$2Q_2 = 0.194$

$k_2 = 0.194/.1704 = 1.14$

The stress for a unit strain of .0154 from the stress strain curve in Fig. C3.22 is 172000, and $f_0 = 129400$.

Then $F_{b_2} = 172000 + 129400\ (1.14-1) = 190100$

$$M_2 = \frac{1}{2}(F_{b_2} I_2/c_2) = 190100 \times .1704 = 16200$$

Total resisting moment = $M_1 + M_2 = 16550 + 16200 = \underline{32750}$ in. lbs.

Solution 2.

Instead of making each portion a symmetrical section as was done in solution (1) and dividing the results by two, we will find the internal bending resistance of each portion as is when bending about the neutral axis of the entire section. Equation (3) now becomes for each portion of beam section,

$$F_b = f_m + f_0\ (k - 1) \text{ - - - } 3'$$

where $k_1 = \frac{Q_1}{I_1/c_1}$, $k_2 = \frac{Q_2}{I_2/c_2}$

The section modulus of each portion refers to neutral axis of entire beam section. Fig. (g) shows lower portion (1).

$I_1 = \frac{1}{3}bc_1^3 = \frac{1}{3} \times .1 \times 1.39^3$

$= .0895$

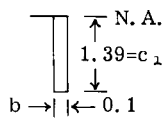

Fig. (g)

$I_1/c_1 = .0895/1.39 = .0645$

$Q_1 = 1.39 \times .1 \times .695$

$= .0965$

$k_1 = Q_1/I_1/c_1 = .0965/.0645 = 1.50$

From equation (3'), $F_b = 180000 + 156000\ (1.50 - 1) = 258000$

$M_1 = F_{b_1} \times I_1/c_1 = 258000 \times .0645 = 16620$

Fig. (h) shows upper portion (2)

$I_2 = \frac{1}{3} \times 1.5 \times .61^3 -$

$\frac{1}{3} \times 1.4 \times .51^3$

$= .0514$

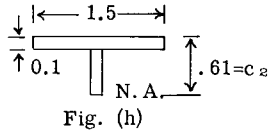

Fig. (h)

$I_2/c_2 = .0514/.61 = .0842$,

$Q_2 = 0.61 \times 0.1 \times .305 + 1.4 \times .1 \times .561$

$= .0971$

$k_2 = .0971/.0842 = 1.15$

As explained in solution (1), for $\varepsilon = .0154$, $f_m = 172000$ and $f_0 = 129400$.

$F_{b_2} = 172000 + 129400\ (1.15-1) = 191400$

$M_2 = 191400 \times .0842 = 16100$

$M_{total} = M_1 + M_2 = 16620 + 16100 =$

$\underline{32720}$ in. lb.

EXAMPLE PROBLEM 4. Fig. C3.24 shows an unsymmetrical I beam section. The material is 7079-T6 aluminum alloy die forging. The upper portion is in bending compression. It will be assumed that the compressive crippling stress for the outstanding upper legs of the section is 65000 psi. (The theory and method of calculating crippling compressive strength is given in another chapter.) The ultimate design bending moment is 16500 in. lb. Find M.S.

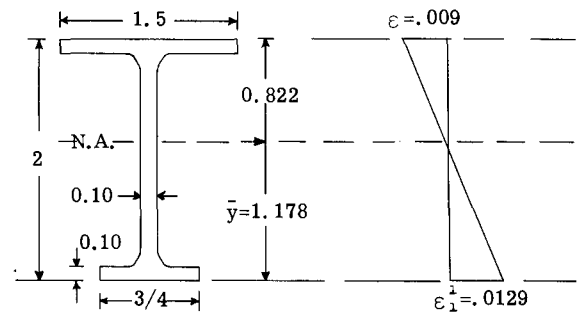

Fig. C3.24

Fig. C3.25

Solution:

$$\bar{y} = \frac{2x0.1x1+1.4x.1x1.85+.65x0.1x.05}{2x0.1+1.4x0.1+0.65x0.1} = 1.178$$

The maximum compressive stress permitted is 65000 psi. From Fig. C3.23, using the stress-strain curve, we obtain a unit strain of .009 for this stress. The unit strain at the bottom edge of section is .009 (1.178/0.822) = .0129 as shown in Fig. C3.25. From Fig. C3.23 this strain causes a stress of 67500 psi.

Upper portion: (See Fig. 1)

$I_{NA} = \frac{1}{3} \times 1.5 \times .822^3 - \frac{1}{3}$

$\times 1.4 \times 0.722^3 = .102$

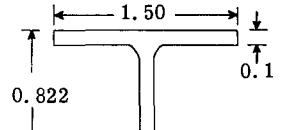

Fig. (i)

$I/c = .102/.822 = .124$

$Q = 0.822 \times 0.1 \times 0.411 + 1.4 \times 0.1 \times 0.772$
$= .1418$

$k = .1418/.124 = 1.142$

$f_{max} = 65000$. From Fig. C3.23, $f_o = 30000$

Then $f_b = 65000 + 30000\ (1.142-1) = 69260$

$m_1 = f_b I/c = 69260 \times .124 = \underline{8580}$ in. lb.

Lower Portion.

$I_{NA} = \frac{1}{3} \times 0.75 \times 1.178^3$
$- \frac{1}{3} \times 0.65 \times 1.078^3$

$I_{NA} = .137$, $I/c = .137/1.178 = .1164$

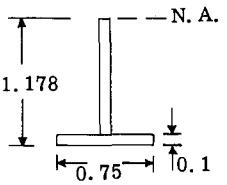

Fig. (j)

$k = .1425/.1164 = 1.222$

$f_{max} = 67500$

From Fig. C3.23, $f_o = 44500$

$f_b = 67500 + 44500\ (1.222-1) = 77370$ psi

$m_2 = .1164 \times 77370 = \underline{9000}$ in. lb.

Total internal allowable resisting moment $= m_1 + m_2$

or $M_a = 8580 + 9000 = \underline{17580}$ in. lb.

$$R_b = \frac{M}{M_a} = \frac{16500}{17580} = 0.94 \text{ (Load ratio)}$$

$$M.S. = \frac{1}{R_b} - 1 = \frac{1}{0.94} - 1 = .06$$

C3.8 Complex Bending. Symmetrical Section. Moment Vector Not Parallel to Principal Axis.

Fig. C3.26 shows a double symmetric section. The x and y axes are therefore principal axes.

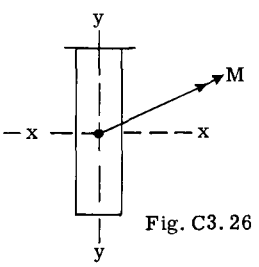

Fig. C3.26

The following procedure can be followed which is quite conservative.

(1) Resolve the given moment into components about x and y axes, or M_x and M_y.

(2) Using M_x follow the procedure as given in the example problems and find $R_{b_x} = M_x/M_{ax}$, where M_{ax} is the internal moment section will develop in bending about x axes and M_x the design bending.

(2) Using M_y, carry out the same procedure for bending about y axes and find,

$R_{b_y} = M_y/M_{ay}$

Then the moment ratio R_b for combined bending is,

$R_b = R_{b_x} + R_{b_y}$

Then margin of safety $M.S. = \frac{1}{R_b} - 1.$

C3.9 Section with One Axis of Symmetry.with Moment Vector not Parallel to Either Axis.

Since the symmetrical axis is a principal axis, the procedure in this case is the same as for the double symmetric case.

$R_b = R_{b_x} + R_{b_y}$

$M.S. = \frac{1}{R_b} - 1$

C3.10 Unsymmetrical Section with No Axis of Symmetry.

Fig. C3.27 shows an unsymmetrical section subjected to the applied moment vector M.

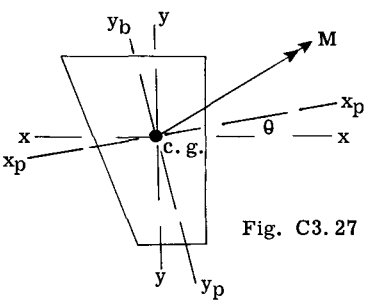

Fig. C3.27

For this case the procedure is as follows:

(1) Determine principal axes location by equation,

$$\tan 2\theta = \frac{2I_{xy}}{I_y - I_x}$$

where x and y are centroidal axes, I_x and I_y are moments of inertia about these axes and I_{xy} the product of inertia.

(2) Resolve the given moment M into components M_{x_p} and M_{y_p}.

(3) Follow the same procedure as before.

(4) The stress ratio $R_b = R_{b_{x_p}} + R_{b_{y_p}}$

$M.S. = \frac{1}{R_b} - 1$

C3.11 Alternate More Exact Method for Complex Bending.

A beam section when resisting a pure external bending moment bends about an axis that is called the neutral axis. No matter what the shape of the beam cross-section for any given external moment, there is an axis about which bending takes place. The general case involves an unsymmetrical beam cross-section and material which has different stress-strain curves in compression and tension in the inelastic range. The neutral axis therefore does not pass through the centroid of the cross-section and thus the method of solution is a trial and error approach. The solution procedure is outlined in Chapter A19, Article A19.17, and therefore will not be repeated here. Also the chapter dealing with the design of beams with non-buckling webs explains and illustrates how the ultimate bending resistance of an entire beam section is determined.

C3.12 Strength Under Combined Bending and Flexural Shear.

The previous part of this chapter has dealt with the determination of the strength of a beam section in pure bending. The usual beam design problem involves flexural shear with bending. In finding the true internal resisting moment, the Cozzone simplified method derives a trapezoidal bending stress distribution which will produce the same internal resisting moment as the true internal bending stress system. A triangular stress system is then derived which will also give the true bending moment.

Now the equation for flexural shear stress for a triangular bending stress distribution is

$$f_s = \frac{VQ}{It} \quad - - - - - - - - - - - - - - - (A)$$

Thus to use equation (A) for a trapizoidal bending stress, a correction factor (C) must be applied or equation (A) becomes

$$f_s = \frac{CVQ}{It} \quad - - - - - - - - - - - - - - - (B)$$

To illustrate how the correction factor (C) can be determined, the I beam section used in example problem (2) will be used.

We will assume the ultimate design moment of 14000 in. lbs. is produced by a load of 600 lbs. acting on a cantilever beam at a point 23.30 inches from the fixed end of the beam. Thus the beam section at the support is subjected to bending moment of 14000 and a shear V = 600 lbs. The problem is to find the margin of safety under this combined loading.

For pure bending only the stress ratio is $R_b = \frac{M}{M_a} = \frac{14000}{15000} = .933$ (the value of 15000 is obtained from example problem 2).

The stress ratio in shear is $R_s = f_s/F_{su}$, where f_s is the flexural shear stress and F_{su} the ultimate shear stress of the material. The problem therefore is to find the value of f_s.

The equivalent trapezoidal and triangular bending stress distribution will be determined for the design bending moment of 14000 in. lbs.

For a triangular stress variation, $F_b = Mc/I = 14000/0.358 = 39150$ psi.

From example problem (2) the shape factor k was 1.17. On Fig. C3.19, the curve for k = 1.17 has been plotted. Starting with the F_b stress of 39150 at the left scale, run horizontal to an intersection with the k = 1.17 curve, the projecting vertically downward to intersections with the stress- strain curve and the f_o curve to give 35800 for f_m and 19700 for f_o. The stress results are shown graphically in Fig. C3.28a and Fig. C3.28b.

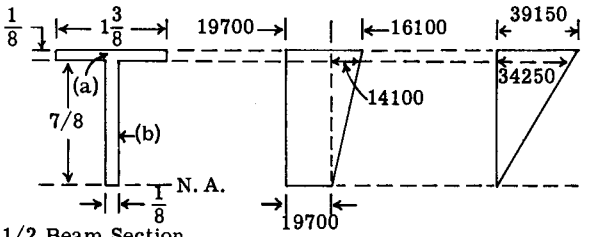

1/2 Beam Section

Fig. C3.28a Case 1

Fig. C3.28b Case 2

The flexural shear stress is a function of the rate of change of the bending stress. Thus we can obtain a shear correction factor C by comparing the bending stresses in the two stress distribution diagram.

The shear stress is maximum at the neutral axis in this particular problem. The total normal force on the cross-section of beam above the neutral axis equals the stress times the area.

For simplification, the beam section will be divided into the two portions labeled (a) and (b).

For Case 1:-

Load on portion (a) is,

$19700 \times 1.375 \times 0.125 = 3380$ lb.

$\frac{16100 + 14100}{2} \times 1.375 \times 0.125 = 2600$ lb.

Portion (b)

$19700 \times 0.875 \times 0.125 = 2155$

$14100 \times 0.5 \times 0.875 \times 0.125 = 771$

Total Force 8906 lbs.

For Case 2:-

Portion (a)

$\frac{39150 + 34250}{2} \times 1.375 \times 0.125 = 6300$

Portion (b)

$34250 \times 0.5 \times 0.875 \times 0.125 = \frac{1874}{8174}$ lbs.

Thus the correction factor is,

$C = 8906/8174 = 1.09$

Then f_s at neutral axis is,

$$f_s = \frac{CVQ}{It} = \frac{1.09 \times 600 \times 0.209}{0.358 \times 0.125} = 3060 \text{ psi.}$$

The ultimate shear stress for this particular magnesium material is 19000 psi. (See chapter on material properties.)

$$\text{Stress Ratio } R_S = \frac{f_s}{F_{sw}} = \frac{3060}{19000} = 0.161$$

The interaction equation for combined bending and flexural shear is

$$R_b^2 + R_s^2 = 1$$

whence, Margin of Safety $= \frac{1}{\sqrt{R_b^2 + R_s^2}} - 1$

or, M.S. $= \frac{1}{\sqrt{.933^2 + .161^2}} - 1 = .05$

Thus the effect of the flexural shear stress was to reduce the margin of safety of .07 in pure bending to .05 in the combined stress action.

As further calculation of the shear correction factor C, its value for the shear stress at the upper edge of portion (b) of the cross-section will be determined. The correction factor for this point is found by comparing the loads on portion (a) for Case 1 and Case 2 stress patterns.

Case 1. Load on (a) = 3380 + 2600 = 5980

Case 2. Load on (a) = 6300.

Hence, C = 5980/6300 = .95

C3.13 Strength Under Combined Bending Flexural Shear and Axial Compression.

The subject of the ultimate strength design under combined loads is treated in detail in a later chapter.

A conservative interaction equation for combined bending, shear and axial load is,

$$(R_a + R_b)^2 + R_s^2 = 1$$

$$\text{or M.S.} = \frac{1}{\sqrt{(R_a + R_b)^2 + R_s^2}} - 1$$

R_b includes effect of secondary bending moment due to axial load times deflection.

C3.14 Further Values of f_m and f_o.

Table C3.2 gives the yield and ultimate values of f_m and f_o for a number of other materials common to the aerospace field of structures. The yield and ultimate modulus in bending F_b is found by substituting in the equation.

$$F_b = f_m + f_o (k - 1)$$

TABLE C3.2 Values of f_m and f_o for Finding F_b

$F_b = f_m + f_o (k - 1)$		Yield		Ultimate	
Material	Size	$f_m = F_{ty}$	f_o	$f_m = F_{tu}$	f_o
2014-T6 Alum. Al. Die Forgings	$t \leq 4$ in.	52	18.8	62	57.5
6061-T6 Alum. Al. Sheet	$t \geq 0.02$	35	17.5	42	40.5
7075-T6 Alum. Al. Die Forgings	$t \leq 2.0$	65	25.5	75	70.0
7079-T6 Alum. Al. Hand Forgings(L)	$t \leq 6.0$	62	33.5	71	67.0
A-Z61A Magnesium Al. Extru. (Long)	$t \leq 0.25$	21	7.6	38	15.7
HK31A-0 Magnesium Al. Sheet	.016-0.25	18	4.0	30	22.6
ZK60A Magnesium Al. Forgings (Long)		26	7.5	42	30.8
AISI Alloy Steel (Normalized)	> 0.188	70	43.2	90	83.1
AISI Alloy Steel (Normalized)	$t \leq 0.188$	75	47.1	95	86.0
AISI Alloy Steel (Heat Treated)		103	51.6	125	118.0
AISI Alloy Steel (Heat Treated)		132	66.0	150	146.0
AISI Alloy Steel (Heat Treated)		163	53.0	180	172.0
AISI Alloy Steel (Heat Treated)		176	65.0	200	192.0
17-7PH Stainless Steel		150	62.0	180	161.0
PH15-7 MO (RH950) Stainless Steel		200	55.0	225	160.0
Ti-8MN Titanium Alloy		110	36.0	120	116.0

PROBLEMS

(1) A round tube 1-1/2 inches in diameter has a wall thickness of .095 inches. It is made of aluminum alloy whose stress-strain curve is shown in Fig. C3.2. If the maximum unit strain in

compression is limited to .008, what bending resisting moment will the section develop. (Note, since stress-strain curve has different shape in tension and compression, neutral axis does not coincide with center line axis, thus use trial and error method.

(2) Same as Problem (1) but use a square tube with 1-1/4 inch outside dimension and .081 inch wall thickness.

Use the Cozzone method for solving the following problems.

(3) Find the ultimate bending moment that each of the following beam sections will develop when bending about the principal axis and made from each of the following materials.

(a) 7075-T6 Aluminum Alloy Extrusion. F_{tu} = 75000, F_{ty} = 65000.

(b) Ti-6Al-4V Titanium Alloy. F_{tu} = 130,000, F_{ty} = 120,000.

Fig. 1

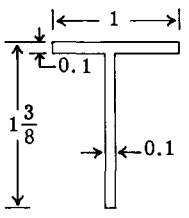

Fig. 2

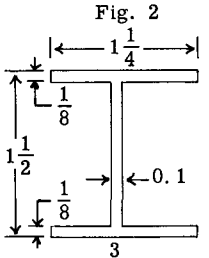

Fig. 3

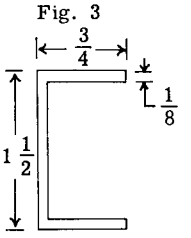

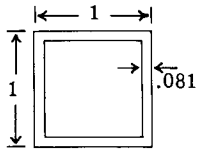

Fig. 4

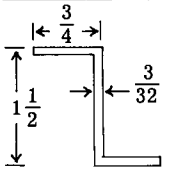

Fig. 5

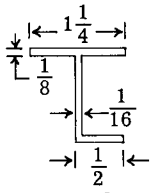

Fig. 6

(4) A simply supported beam has a span of 24 inches. Depth of beam limited to 2 inches. It must carry an ultimate load of 4000 lbs. located at midpoint of beam. Material is 7075-T6 aluminum alloy extrusion. Design an I shaped section to carry this load. Neglect areas of corner fillets that would be used in extruded shapes.

REFERENCES.

Ref. 1. Bending Strength in Plastic Range. By F. P. Cozzone, J. Aeronautical Sci., May, 1943.

Ref. 2. Vought Structures Manual.

CHAPTER C4

STRENGTH AND DESIGN OF ROUND, STREAMLINE, OVAL AND SQUARE TUBING IN TENSION, COMPRESSION, BENDING, TORSION AND COMBINED LOADINGS.

C4.1 Introduction.

Before the advent of the stressed-skin structure for aircraft, or during the period when fuselage and wing were fabric covered, round, oval and square tubing were used in designing the major structure of the fuselage and wing. If the wing and tail were externally braced, streamline tubing was used. The development of the metal covered structure eliminated the use of tubing in fuselage and wing design, however, tubing continued to be used for landing gear structure, engine mounts, control systems, fixed equipment such as passenger seats, etc.

With the opening of the space age, tubing as a structural unit in space vehicles is again being widely used because drag in space is not an important factor. Round tubing is the best shape for transmitting torsional forces and thus is widely used in control systems. Round and square tubing permit simple connection or end fitting design. The metals industry has made available a large number of diameter and wall thicknesses and thus the structural designer has a large number of sizes to select from.

C4.2 Design for Tension.

In general the strength design requirements are that the limit loads must be carried without exceeding the tensile yield stress (F_{ty}) of the material and the ultimate design load which is equal to the limit load times a factor of safety must be carried without failure, which means the tensile stress cannot exceed the (F_{tu}) of the material. In general for aircraft, the factor of safety is 1.5. For unmanned missiles and space vehicles the factor of safety may be as low as 1.2. Since the ratio of F_{tu} to F_{ty} for materials varies widely, sometimes the yield under limit loads is more critical than failure under the ultimate design loads, thus the student should always be sure he has the critical situation.

Since elevated temperature and time of exposure effect the yield and ultimate strength of materials, the problem of material selection relative to light weight becomes an important design factor. Fig. C4.1 shows a plot of the F_{tu}/w ratio versus elevated temperatures up to 800 degrees, where w is the density of the material. The tube materials are AISI alloy steel and 2024 aluminum alloy. Observation of Fig. C4.1 shows that for temperatures below 350°F, aluminum alloy is lighter unless the steel is heat-treated to F_{tu} = 180,000 or above. Above 350°F, the ultimate strength of aluminum alloy falls off rapidly, but steel continues its rather uniform decrease in tensile strength.

The graph explains why aluminum alloy cannot be used entirely for the surface of supersonic airplanes flying at speeds around 2000 miles per hour, as aerodynamic heating would produce surface temperatures in the region where the strength of aluminum alloy decreases rapidly.

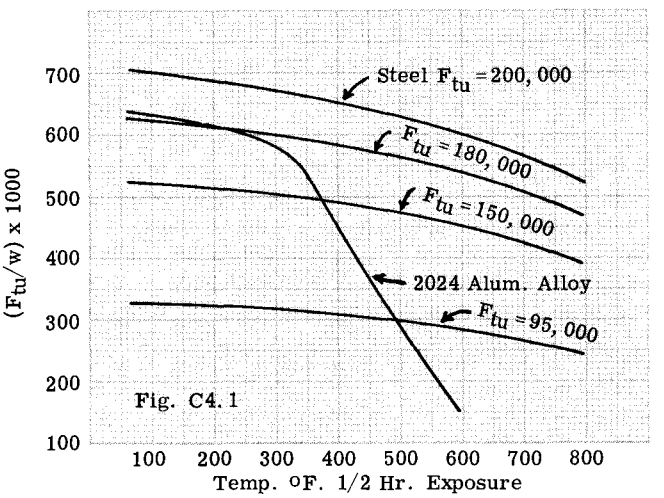

Fig. C4.1

Practically every structural tubular member in a flight vehicle structure must be fastened or attached to another adjacent member. The connection can be made by using some sort of end fitting which is fastened to the tube by rivets or bolts or by welding. If rivets or bolts are used, holes are cut in the tube walls which means the tube is weakened since tube area is cut away, thus net area on any tube cross-section must be used in calculating the tube tensile strength. If welding is used in the connection, the welding heat causes grain growth in the tube material adjacent to the weld area, which decreases the tube strength, thus a welding correction factor must be used in calculating the ultimate tensile strength. Designing for tension will be illustrated later in this chapter.

C4.3 Design for Compression.

The strength of members with stable cross-sections when acting as columns can be calculated by Euler's equation if the bending failure is elastic, or E is constant (eq. C4.1) and for inelastic bending failure, Euler's equation with the tangent modulus E_t replacing E (eq. C4.2) checks test results. (The student should refer to Chapters A18 and C2 for theory on column strength.)

$$F_c = \frac{\pi^2 E}{(L'/\rho)^2} \quad \text{- - - - - - - - - - - - (C4.1)}$$

$$F_c = \frac{\pi^2 E_t}{(L'/\rho)^2} \quad \text{- - - - - - - - - - - - (C4.2)}$$

L' is the effective length and equals $L/\sqrt{c}$, where c is the column end fixity coefficient.

Long and Short Columns

For many years the problem or subject of inelastic column strength or failure was treated almost entirely from a consideration of test results. That is, sufficient tests were made to establish the shape of the failing stress curve in the region where the failure was at stresses above the proportional limit stress of the material. Mathematical curves were then derived to fit the test results. Engineers referred to the columns which failed by inelastic bending as short columns, and thus referred to the equations that fit the test data as short column equations. The columns that failed by elastic bending were then referred to as long columns. The test curve for long columns would follow the Euler column equation (C4.1) and thus tests were not necessary to establish allowable failing stresses in the so-called long column range. Thus over the years short column equations based on test results have been presented by official government agencies for use in structural design. The official publication for the aerospace field is the Military Handbook MIL-HDBK (Ref. 1).

C4.4 Column Formulas for Round Steel Tubes.

From (Ref. 1) the basic short column equations are:-

$$F_c = F_{co}\left[1 - F_{co}\,(L'/\rho)^2/4\pi^2 E\right] \text{- - - - - (C4.3)}$$

$$F_c = F_{co}\left\{1 - 0.3027\left[(L'/\rho)/\pi\sqrt{E/F_{co}}\right]^{1.6}\right\} \text{- - - - - - - - (C4.4)}$$

Where F_{co} is the column yield stress (upper limit of column stress for primary failure). It can be determined from test results by extending the short column curve to a point corresponding to zero length, ignoring any tendency of the test curve to rise rapidly for very short lengths where failure is by block compression. Table C4.1 shows the resulting short and long column equations after values of F_{co} and E have been substituted in equations C4.3 and C4.4 and E in the Euler equation. The column headed transitional L'/ρ, represents the value of L'/ρ where failure change from inelastic to elastic failure or, in other words, it is the dividing point between the so-called long and short column range. Thus if the equations are used, the L'/ρ value must be known in order to select the proper equation.

C4.5 Column Formulas for Aluminum Alloy Tubes.

From (Ref. 1), the basic short column equations for aluminum alloys are:-

$$F_c = F_{co}\left[1 - 0.385\,(L'/\rho)/\pi\sqrt{E/F_{co}}\right] \text{- - (C4.5)}$$

$$F_c = F_{co}\left[1 - 0.333\,(L'/\rho)/\pi\sqrt{E/F_{co}}\right] \text{- - (C4.6)}$$

$$F_c = F_{co}\left[1 - 0.272\,(L'/\rho)/\pi\sqrt{E/F_{co}}\right] \text{- - (C4.7)}$$

For long columns:-

$$F_c = \pi^2 E/(L'/\rho)^2 \quad \text{- - - - - - - - - - - - (C4.8)}$$

The equations for determining F_{co} are given in Table C4.2 (from Ref. 1). The table also indicates which of the three short column equations to use for the various aluminum alloy materials.

To illustrate the use of Table C4.2, the column formula for 2024-T3 aluminum alloy tubing will be derived:-

From Chapter B2, we find the following strength properties for 2024-T3 tubing,

$$F_{tu} = 64000\,, \quad F_{cy} = 42000$$

From Table C4.2, the equation for F_{co} is,

$$F_{co} = F_{cy}\left(1 + \sqrt{F_{cy}/1000}\right), \text{ substituting,}$$

$$F_{co} = 42000\left(1 + \sqrt{42/1000}\right) = 42000\,(1 + .205) = 50600$$

From Table C4.2, we note that short column equation C4.5 applies.

Substituting in this equation,

$$F_c = 50600\left[1 - 0.385(L'/\rho/\pi\sqrt{10{,}500{,}000/50600}\right]$$

$$\text{or } F_c = 50600 - 431\,L'/\rho \text{ - - - - - - - - (C4.9)}$$

C4.6 Column Formulas for Magnesium Alloys.

From (Ref. 1) the following short column equations for various magnesium alloy materials

Table C4.1 Column Formulas for Round Steel Tubes

Material	F_{tu}, ksi	F_{ty}, ksi	F_{co}, ksi	Short columns [a]		Transitional [c] L'/ρ	Long columns [b]	Local failure
				Column formula [b]	Basic equation			
1025	55	36	36	$36,000-1.172(L'/\rho)^2$ ...	C4.3	122	$286 \times 10^6/(L'/\rho)^2$	[d]
4130	95	75[e]	79.5	$79,500-51.9(L'/\rho)^{1.5}$..	C4.4	91	$286 \times 10^6/(L'/\rho)^2$	[d]
Heat-treated [e] alloy steel	125	103	113	$113,000-11.15(L'/\rho)^2$..	C4.3	73	$286 \times 10^6/(L'/\rho)^2$	[d]
Heat-treated alloy steel	150	132	145	$145,000-18.36(L'/\rho)^2$..	C4.3	63	$286 \times 10^6/(L'/\rho)^2$	[d]
Heat-treated alloy steel	180	163	179	$179,000-27.95(L'/\rho)^2$..	C4.3	56	$286 \times 10^6/(L'/\rho)^2$	[d]

[a] Equation C4.1 may be used in the short column range if E is replaced by E_t obtained from the combined stress-strain curves for the material.

[b] $L'/\rho = L/\rho\sqrt{c}$: L'/ρ shall not exceed 150 without specific authority from the procuring or certificating agency.

[c] Transitional L/ρ is that above which columns are "long" and below which they are "short." These are approximate values.

[d] Not necessary to investigate for local instability when $D/t < 50$.

[e] This value is applicable when the material is furnished in condition N (MIL-T-6736) but the yield strength is reduced when normalized subsequent to welding to 60 ksi.

are given in Tables C4.4 and C4.4a.

Table C4.4 Column Formulas for Magnesium-Alloy Extruded Open Shapes[a]

GENERAL FORMULA

$$F_c = \frac{K(F_{cy})^n}{(L'/\rho)^m}$$

(Stress values are in ksi)

Alloy	K	n	m	Max. F_c
M1A	180	1/2	1.0	0.90 F_{cy}
AZ31B, AZ61A, AZ80A. .	2,900	1/4	1.5	F_{cy}
AZ80A-T6, ZK60A-T5 . .	3,300	1/4	1.5	0.96 F_{cy}

[a] Formulas given above are for members that do not fail by local buckling.

Table C4.4a Column Formula for AZ31B-H24 Magnesium-Alloy Sheet

$$F_c = 1.05\,F_{cy} - \frac{(1.05\,F_{cy})^2(L'/\rho)^2}{4\pi^2 E}$$

Max. $F_c = F_{cy}$

C4.7 Short Column Equations for Other Materials.

For other metals for which short column equations are not available, the use of Euler's equation, using the tangent modulus E_t can be used (eq. C4.2). Refer to Chapter C2 for information on how to construct column strength curves using this equation.

C4.8 Column Failure Due to Local Failure.

The equations as presented give the allowable stress due to failure by bending of the column as a whole and the action is elastic or inelastic instability of the column as a whole. As the slenderness ratio L'/ρ gets smaller, the F_c stress increases. Now if the diameter of the tube is relatively large and the wall thickness relatively small or, in other words, if the diameter/thickness (D/t) ratio is large, failure will result by local crippling or crushing of the tube wall and this local failing stress is usually represented by the symbol F_{cc}. The values of F_{cc} in general have been determined by tests (see design charts for F_{cc} versus D/t ratio).

C4.9 Design Column Charts.

In design, column strength charts are a great time-saver as compared to substituting in the various column equations, thus a number of column charts are presented in this chapter to facilitate the strength check of columns and the strength design of columns. Fig. C4.2 is a chart of L'/ρ versus F_c for heat treated round alloy steel tubing. Fig. C4.3 is a similar type of chart for aluminum alloy round tubing. Fig. C4.4 gives column charts for magnesium alloy materials. All three charts are taken from (Ref. 1). Figs. C4.5 and C4.6 represent a further simplication for the design of steel and aluminum round tubing.

C4.10 Section Properties of Round Tubing.

Table C4.3 gives the section properties of round tubing. A tube is designated by giving its outside wall diameter (D) and its wall thickness (t). Thus a 2-1/4 - .058 means a tube with 2-1/4 inch outside diameter and a wall thickness in inches of .058. Since a tube is symmetrical about any axis, the polar moment of inertia, which is needed in torsion problems, equals twice the rectangular moment of inertia as given in Table C4.3. For weight comparison, the weight of steel and aluminum tubing is

Table C4.2 Column Formulas for Aluminum Alloys

Alloy and Temper	Product	F_{co}	Short Columns	Transitional L'/ρ	Long Columns
2014–T3, T4, T451 2024–T3, T351, T36, T4, T42	Sheet and Plate*; Rolled Rod, Bar and Shapes; Drawn Tube	$F_{cy}(1+\sqrt{F_{cy}/1000})$	Equation C4.5	$1.732\pi\sqrt{E/F_{co}}$	Equation C4.8
5052—All Tempers 5083—All Tempers 5086—All Tempers 5454—All Tempers 5456—All Tempers 6061–T4, T451, T4510, T4511	All Products				
All Cast Alloys and Tempers	Sand and Permanent Mold Castings				
2024–T3510, T3511, T4, T42	Extrusions	$F_{cy}(1+\sqrt{F_{cy}/1333})$	Equation C4.6	$1.346\pi\sqrt{E/F_{co}}$	Equation C4.8
2014–T6, T651 2024–T6, T81, T86, T851 7075–T6, T651 7178–T6, T651	Sheet and Plate*; Rolled Rod, Bar and Shapes; Drawn Tube				
6061–T6, T651	Sheet and Plate*				
2014–T6, T651, T6510, T6511, T652 2024–T6, T81, T8510, 2024–T6, T81, T8510, T8511, T852 7075-T6, T6510, T6511, T652 7079–T6, T6510, T6511, T652 7178–T6, T6510, T6511	Extrusions, Forgings	$F_{cy}(1+\sqrt{F_{cy}/2000})$	Equation C4.7	$1.224\pi\sqrt{E/F_{co}}$	Equation C4.8
6061–T6, T651, T6510, T6511	Rolled Rod, Bar and Shapes; Drawn Tube; Extrusions				
X2020–T6, T651	Sheet and Plate*				

*Includes clad as well as bare sheet and plate.

Transitional L'/ρ is that above which the columns are "long" and below which they are "short".

Equation C4.8 may be used in the short column range if E' is replaced by E_t obtained from the compressive stress-strain curve for the material.

given in the last two columns of the table.

C4.11 Some General Facts in Tubing Design.

1. For a given area, the larger the tube diameter, the greater the column strength if failure due to local crippling is not critical.

2. The higher the D/t ratio of tube the lower the crippling or local failure strength.

3. If columns fall within the long column category, the use of higher strength alloy steel or aluminum alloy will not increase strength of column since E is practically constant for all chrome-moly steel alloys and likewise for all aluminum alloys. Failure is due to elastic buckling of the column as a whole and is therefore a function only of I, L' and E.

4. The column end restraint affects the necessary tube size. Consult the design requirements of the Army, Navy, and C.A.A. in this matter. In general with welded steel tubular trusses a coefficient of C = 2 is permissible except for engine mount and Nacelle structures. For trusses with riveted joints a value of not over 1.5 is generally permissible.

5. The student should realize that practical limitations such as clearance requirements may determine the diameter of the tube instead of strength-weight considerations. Thus design can consist of checking the tubes available under the given restrictions.

C4.12 Effect of Welding of Steel Tubes Upon the Tension and Column Strength.

Since welding affects the grain structure of the tube material adjacent to the weld, tests show the strength of the material adjacent to the weld is decreased as compared to the unwelded material. If a tapered weld is used, the effect of the weld is decreased. Table C4.5 shows the allowable stresses in tension to use when tension loads are carried.

In short columns, the primary column failing stress may be greater than the local crippling strength of the tube adjacent to the weld at the end of the tube. This local failing stress due to welding is referred to as the weld cut-off stress and the column compressive stress F_c should not exceed this value. This cut-off weld stress is shown by the horizontal lines in Fig. C4.2 and C4.5.

Table C4.5

Tension Allowables Near Welds in Steel Tubing (X-4130)

Type of Weld	Normalized Tube Welded	Welded after HT or Norm. after Weld	HT after Welding
*Tapered Welds of 30° or Less	.947 F_{tu}	90,000 psi	.90 F_{tu}
All others	.841 F_{tu}	80,000 psi	.80 F_{tu}

*Note: Gussets or plate inserts considered 0° "taper" with ℄.

** For (X-4130) Special, comparable, values to the F_{tu}, equal to 90,000 and 80,000, are stresses 94,500 and 84,100 psi, respectively.

Ref. Anc-5

C4.13 Illustrative Problems in Strength Checking and Design of Round Steel Tubes as Columns and Tension Members.

PROBLEM 1

Tube size = 1-1/2 - .058, Length L = 30 in. End fixity coefficient C = 1. Material:- Alloy steel, F_{tu} = 95000. The tube is welded at ends. Ultimate design loads are:- P = -14,500 lbs. compression, and P = 18500 lbs. tension. Required the Margin of Safety (M.S.)

Solution: The compressive (M.S.) will be determined first. As the simplest solution, we can use the column curves in Fig. C4.5. For a length of 30 and C = 1, from the upper right chart we project upward to the intersection with the 1-1/2 diameter tube and then horizontally to the left hand scale to read the column strength of 14800 lbs. which we will call the allowable failing P_a.

$$M.S. = \frac{P_a}{P} - 1 = \frac{14800}{14500} - 1 = .02$$

The tube strength could also be found by using Fig. C4.2 as follows:

$$L' = L/\sqrt{c} = 30/\sqrt{1} = 30$$

$L'/\rho = 30/.5102 = 58.7$. ρ is found from Table C4.3 as well as the tube area 0.2628 sq. in. Using 58.7 for L'/ρ on lower scale and projecting upward to the F_{tu} = 95000 curve, which is the lower curve, and then horizontally to left hand scale we read F_c = 56500 psi.

Whence, $P_a = F_c A$ = 56500 x .2628 = 14850 lb.

The solution obviously could be made by substituting in the short column equation for steel having F_{tu} = 95000, or

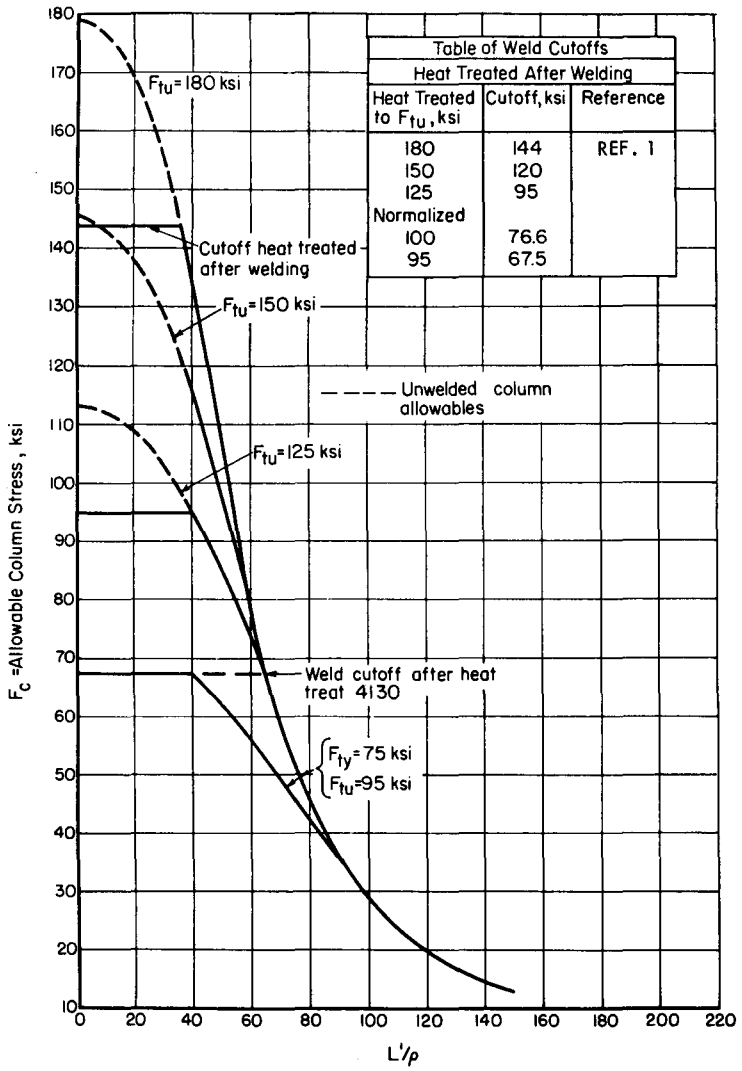

Fig. C4.2 Allowable column stress for heat-treated alloy-steel round tubing.

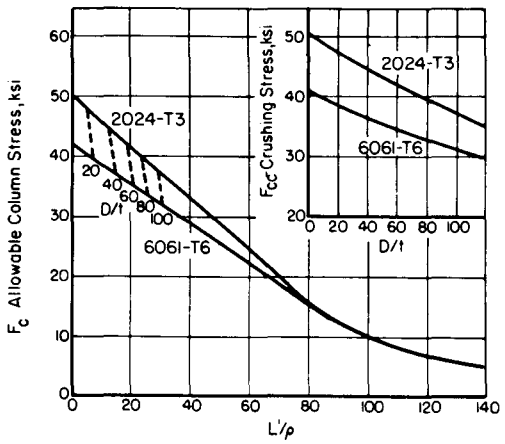

Fig. C4.3 2024-T3 and 6061-T6 round aluminum alloy tubing.

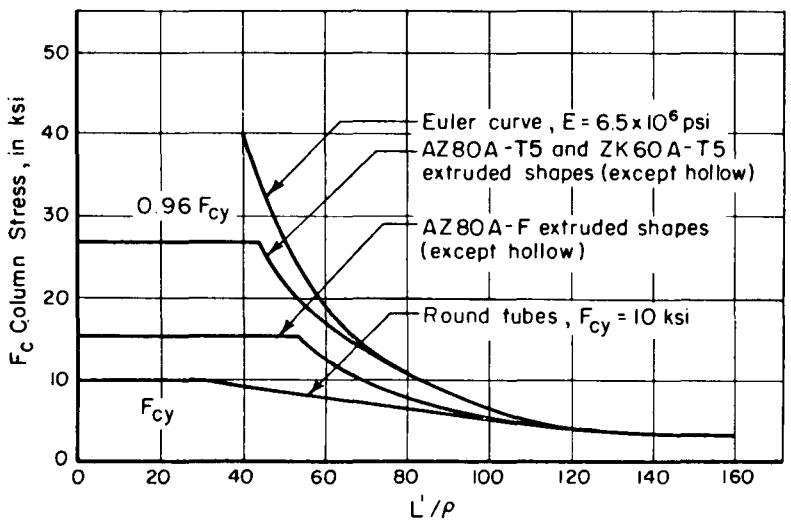

Fig. C4.4 Allowable column stresses for magnesium-alloy columns.

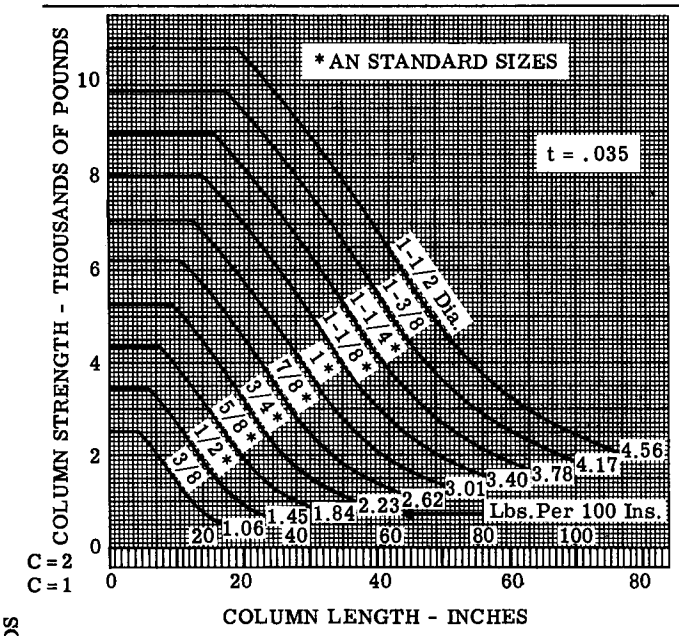

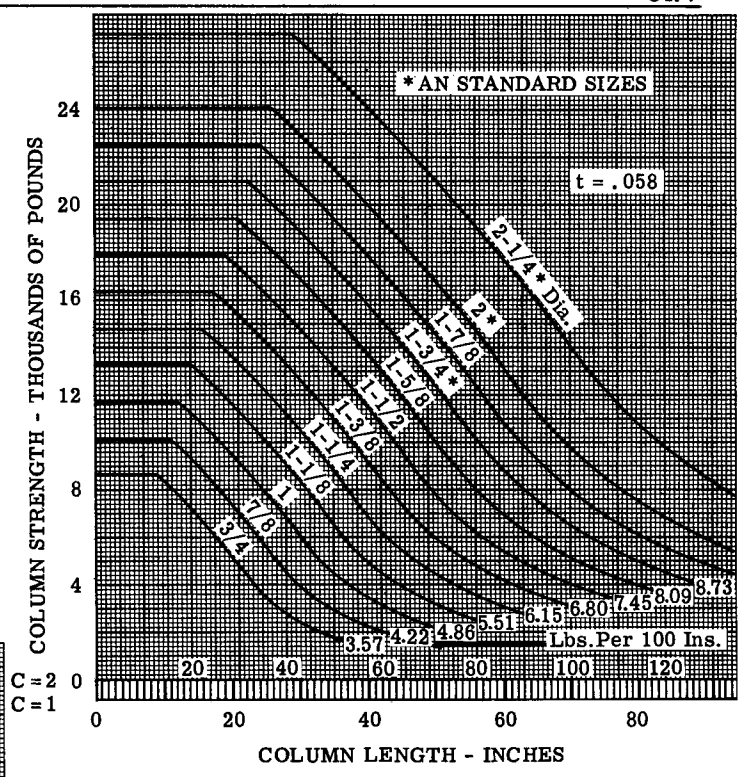

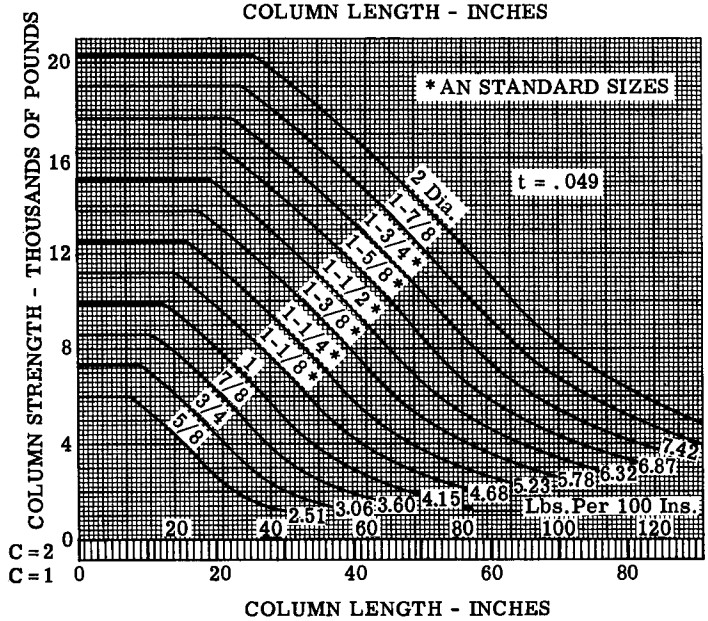

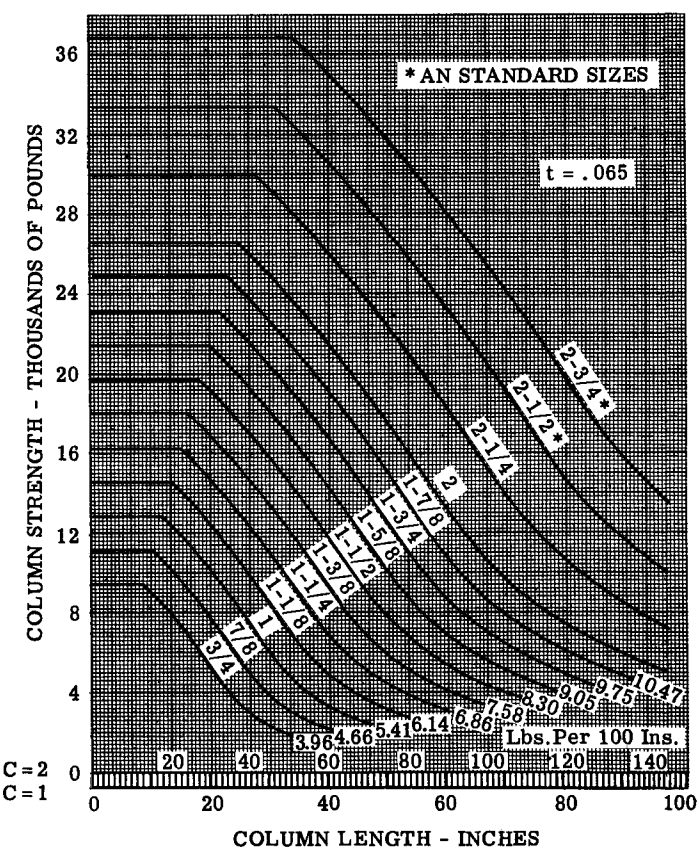

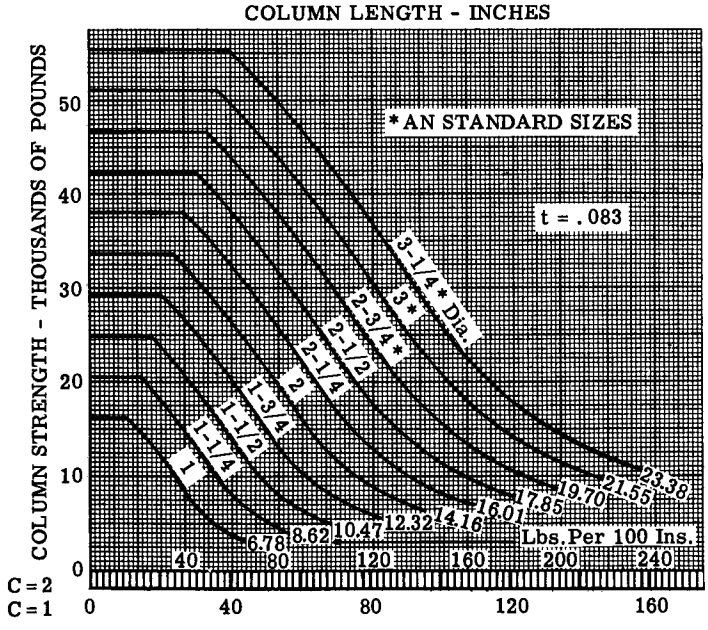

Fig. C4.5

STRENGTH OF CHROME MOLY ROUND STEEL TUBES

F_{TY} = 75,000 PSI F_{TU} = 95,000 PSI

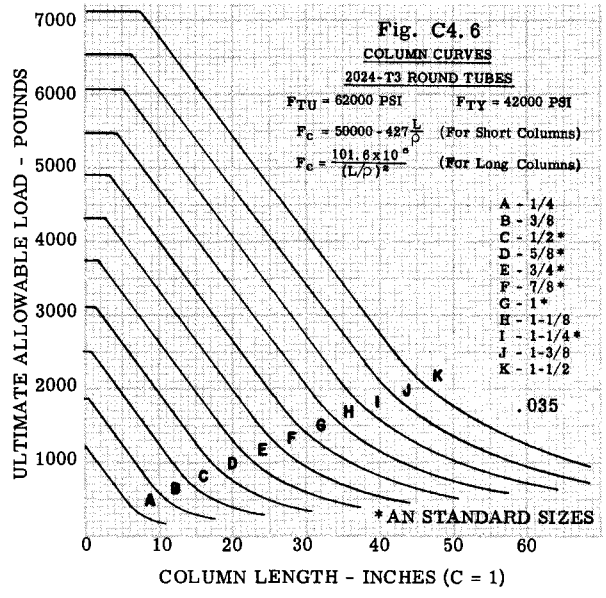
Fig. C4. 6
COLUMN CURVES
2024-T3 ROUND TUBES
F_{TU} = 62000 PSI
F_{TY} = 42000 PSI
$F_c = 50000 - 427\frac{L}{\rho}$ (For Short Columns)
$F_c = \frac{101.6 \times 10^6}{(L/\rho)^2}$ (For Long Columns)
A - 1/4
B - 3/8
C - 1/2*
D - 5/8*
E - 3/4*
F - 7/8*
G - 1*
H - 1-1/8
I - 1-1/4*
J - 1-3/8
K - 1-1/2
.035
*AN STANDARD SIZES
ULTIMATE ALLOWABLE LOAD - POUNDS
COLUMN LENGTH - INCHES (C = 1)

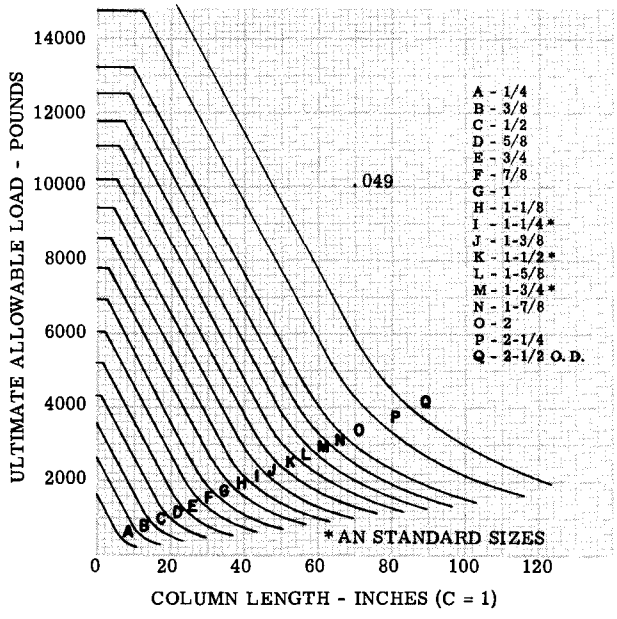
A - 1/4
B - 3/8
C - 1/2
D - 5/8
E - 3/4
F - 7/8
G - 1
H - 1-1/8
I - 1-1/4*
J - 1-3/8
K - 1-1/2*
L - 1-5/8
M - 1-3/4*
N - 1-7/8
O - 2
P - 2-1/4
Q - 2-1/2 O.D.
.049
*AN STANDARD SIZES
ULTIMATE ALLOWABLE LOAD - POUNDS
COLUMN LENGTH - INCHES (C = 1)

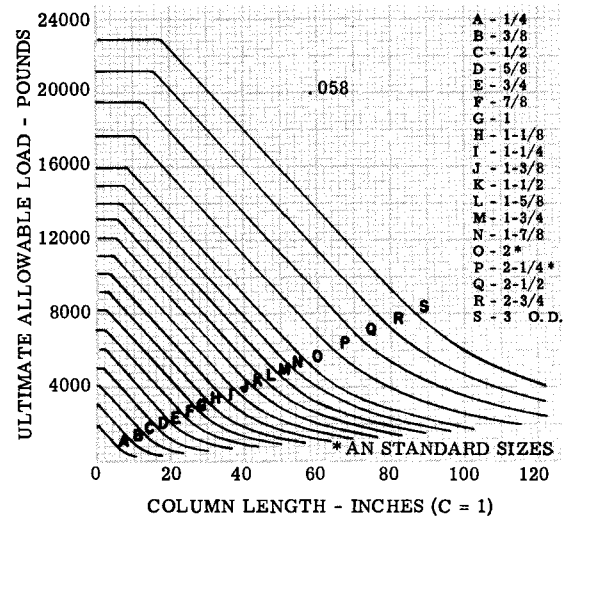
A - 1/4
B - 3/8
C - 1/2
D - 5/8
E - 3/4
F - 7/8
G - 1
H - 1-1/8
I - 1-1/4
J - 1-3/8
K - 1-1/2
L - 1-5/8
M - 1-3/4
N - 1-7/8
O - 2*
P - 2-1/4*
Q - 2-1/2
R - 2-3/4
S - 3 O.D.
.058
*AN STANDARD SIZES
ULTIMATE ALLOWABLE LOAD - POUNDS
COLUMN LENGTH - INCHES (C = 1)

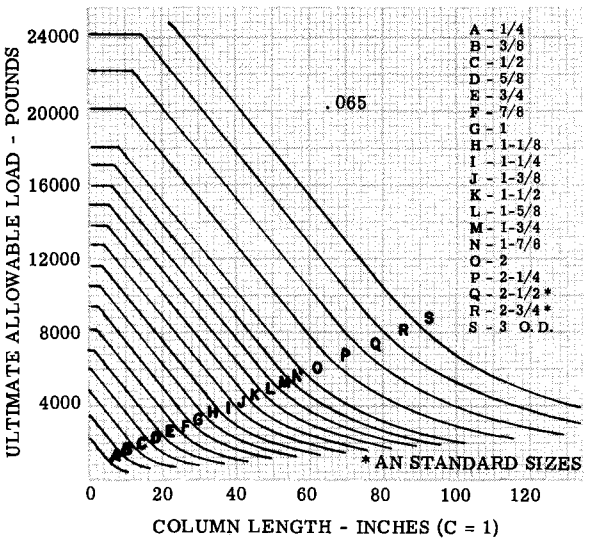
A - 1/4
B - 3/8
C - 1/2
D - 5/8
E - 3/4
F - 7/8
G - 1
H - 1-1/8
I - 1-1/4
J - 1-3/8
K - 1-1/2
L - 1-5/8
M - 1-3/4
N - 1-7/8
O - 2
P - 2-1/4
Q - 2-1/2*
R - 2-3/4*
S - 3 O.D.
.065
*AN STANDARD SIZES
ULTIMATE ALLOWABLE LOAD - POUNDS
COLUMN LENGTH - INCHES (C = 1)

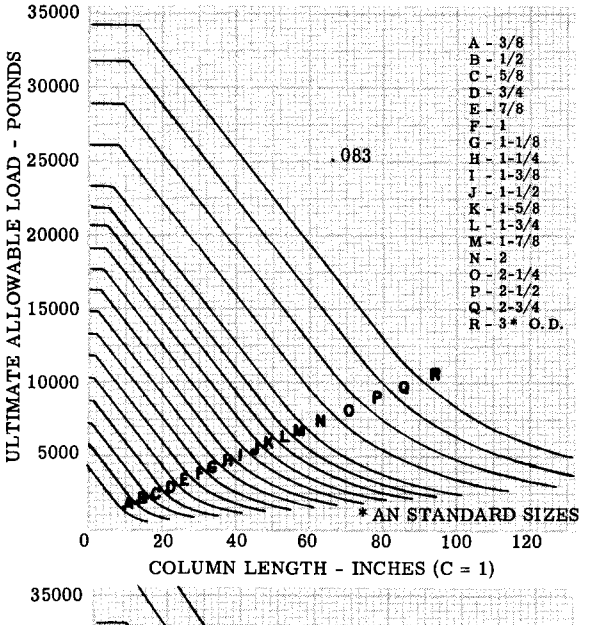
A - 3/8
B - 1/2
C - 5/8
D - 3/4
E - 7/8
F - 1
G - 1-1/8
H - 1-1/4
I - 1-3/8
J - 1-1/2
K - 1-5/8
L - 1-3/4
M - 1-7/8
N - 2
O - 2-1/4
P - 2-1/2
Q - 2-3/4
R - 3* O.D.
.083
*AN STANDARD SIZES
ULTIMATE ALLOWABLE LOAD - POUNDS
COLUMN LENGTH - INCHES (C = 1)

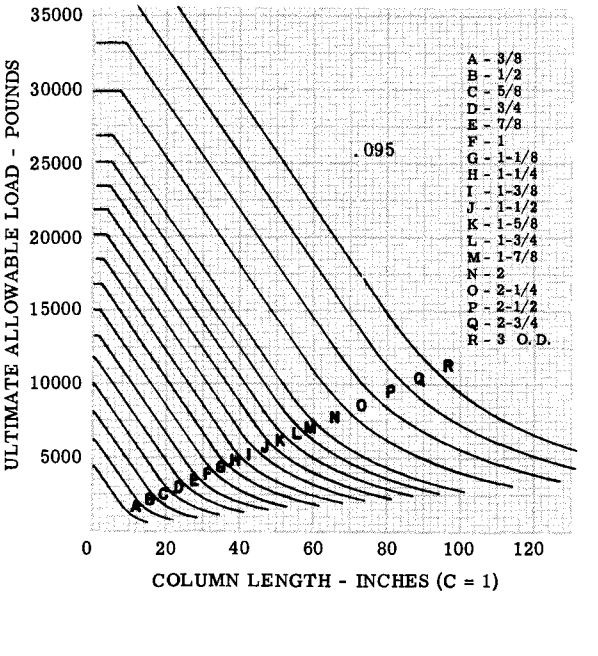
A - 3/8
B - 1/2
C - 5/8
D - 3/4
E - 7/8
F - 1
G - 1-1/8
H - 1-1/4
I - 1-3/8
J - 1-1/2
K - 1-5/8
L - 1-3/4
M - 1-7/8
N - 2
O - 2-1/4
P - 2-1/2
Q - 2-3/4
R - 3 O.D.
.095
ULTIMATE ALLOWABLE LOAD - POUNDS
COLUMN LENGTH - INCHES (C = 1)

Table C4.3 PROPERTIES OF ROUND TUBING

Dia.	Gage	A	ρ	I	I/Y	D/t	Weight Lb/100 ins. Steel	Weight Lb/100 ins. Dural
1/4	.022	.01576	.0810	.000103	.000825	11.38	.45	.16
	.028	.01953	.0791	.000122	.000978	8.23	.55	.20
3/8	.028	.03063	.1231	.000462	.002466	13.39	.86*	.31
	.035	.03739	.1208	.000546	.002912	10.72	1.06	.38
	.049	.06018	.1166	.000682	.003636	7.65	1.43	.51
1/2	.~~028~~	.04152	.1672	.001160	.004641	17.85	1.17	.42
	.035	.05113	.1649	.001390	.005559	14.28	1.45*	.52*
	.040	.06943	.1576	.001786	.007144	10.20	1.96	.70
5/8	.028	.05252	.2113	.002345	.007503	22.30	1.49	.54
	.035	.06487	.2090	.002833	.009065	17.85	1.84*	.66*
	.049	.08867	.2044	.003704	.011852	12.77	2.51	.90
	.058	.10331	.2016	.004195	.013425	10.79	2.93	1.05
3/4	.028	.06351	.2555	.004145	.011052	26.80	1.80	.65
	.035	.07862	.2531	.005036	.013429	21.42	2.23*	.80*
	.049	.10791	.2485	.006661	.017762	15.30	3.06	1.09
	.058	.12609	.2455	.007601	.02027	12.94	3.57	1.28
	.065	.13988	.2433	.008278	.02208	11.53	3.96	1.42
7/8	.028	.07451	.2996	.006689	.015289	31.23	2.11	.76
	.035	.09236	.2973	.008161	.018653	25.00	2.62*	.94*
	.049	.12715	.2925	.010882	.02487	17.85	3.60	1.29
	.058	.14887	.2896	.012484	.02853	15.10	4.22	1.51
	.065	.16541	.2865	.013653	.03121	13.47	4.66	1.68
1	.035	.10611	.3414	.012368	.02474	28.56	3.01*	1.07*
	.049	.14640	.3367	.016594	.03319	20.40	4.15	1.48
	.058	.17164	.3337	.019111	.03822	17.25	4.86	1.74
	.065	.19093	.3314	.020970	.04193	15.38	5.41	1.93
1 1/8	.035	.11985	.3856	.01782	.03168	32.10	3.40*	1.21
	.049	.16564	.3808	.02402	.04270	22.95	4.68*	1.68
	.058	.19442	.3780	.02775	.04933	19.40	5.51	1.97
	.065	.21650	.3755	.03052	.05425	17.30	6.14	2.20
1 1/4	.035	.13360	.4297	.02467	.03948	35.70	3.78*	1.35*
	.049	.18488	.4250	.03339	.05342	25.50	5.23*	1.87*
	.058	.2172	.4219	.03867	.06187	21.55	6.15	2.20
	.065	.2420	.4196	.04260	.06816	19.22	6.86	2.45
1 3/8	.035	.1473	.4739	.03309	.04814	39.25	4.17	1.49
	.049	.2041	.4691	.04492	.06534	28.05	5.78*	2.07
	.058	.2400	.4661	.05213	.07583	23.70	6.80	2.43
	.065	.2675	.4638	.05753	.08367	21.15	7.58	2.70
1 1/2	.035	.1611	.5181	.04324	.05765	42.80	4.56	1.63
	.049	.2234	.5132	.05885	.07847	30.60	6.32*	2.26*
	.058	.2628	.5102	.06841	.09121	25.85	7.45	2.66
	.065	.2930	.5079	.07558	.10079	23.05	8.30	2.97
	.083	.3695	.5018	.09305	.12407	18.08	10.47	3.74
1 5/8	.035	.1748	.5622	.05528	.06803	46.40	4.95	1.77
	.049	.2426	.5575	.07540	.09279	33.15	6.87*	2.46
	.058	.2855	.5544	.08776	.10801	28.00	8.09	2.89
	.065	.3186	.5520	.09707	.11948	25.00	9.05	3.23
	.083	.4021	.5459	.11985	.14751	19.58	11.40	4.06
1 3/4	.035	.1885	.6065	.06936	.07927	50.00	5.32	1.91
	.049	.2618	.6017	.09478	.10832	35.70	7.42*	2.65*
	.058	.3083	.5986	.11046	.12624	30.20	8.73*	3.12
	.065	.3441	.5962	.12230	.13977	26.90	9.75	3.48
	.083	.4347	.5901	.~~16136~~	.17299	21.10	12.32	4.40
1 7/8	.035	.2023	.6507	.08565	.09136	53.60	5.73	2.04
	.049	.2811	.6458	.11720	.12500	38.25	7.95	2.84
	.058	.3311	.6427	.13677	.14589	32.30	9.38	3.35
	.065	.3696	.6404	.15156	.16166	28.80	10.47	3.74
	.083	.4673	.6342	.18797	.20050	22.60	13.25	4.73
2	.049	.3003	.6900	.14299	.14299	40.80	.50	3.04
	.058	.3539	.6869	.16696	.16696	34.45	10.03*	3.58*
	.065	.3951	.6845	.18514	.18514	30.75	11.19	4.00
	.083	.4999	.8783	.2300	.2301	24.10	14.16	5.06
	.095	.5885	.6744	.2586	.2586	21.05	16.11	5.76
2 1/4	.049	.3388	.7783	.2052	.1824	45.90	9.59	3.43
	.058	.3994	.7753	.2401	.2134	38.80	11.30*	4.05*
	.065	.4462	.7728	.2665	.2369	34.60	12.64	4.52
	.083	.5651	.7667	.3322	.2953	27.15	16.01	5.72
	.095	.6432	.7626	.3741	.3325	23.70	18.22	6.51
2 1/2	.049	.3773	.8667	.2834	.2267	51.00	10.68	3.82
	.058	.4450	.8635	.3318	.2655	43.10	12.60	4.50
	.065	.4972	.8613	.3688	.2950	38.45	14.09*	5.03*
	.083	.6302	.8550	.4607	.3686	30.10	17.85	6.38
	.095	.7178	.8509	.5197	.4158	26.30	20.34	7.27
2 3/4	.049	.4158	.9551	.3793	.2759	56.10	11.78	4.20
	.058	.4905	.0521	.4446	.3233	47.40	13.90	4.96
	.065	.5483	.9496	.4944	.3596	42.30	15.50*	5.55*
	.083	.6954	.9434	.6189	.4501	33.15	19.70*	7.04
	.095	.7924	.9393	.6991	.5084	28.95	22.48	8.03
3	.058	.5361	1.0403	.5802	.3868	51.70	16.18	5.42
	.065	.5993	1.0380	.6457	.4305	46.20	16.95	6.06
	.083	.7606	1.0318	.8097	.5398	36.15	21.55*	7.70*
	.095	.8670	1.0276	.9156	.6104	31.58	24.56	8.78
	.120	1.0857	1.0191	1.1276	.7518	25.00	30.76	11.00
3 1/4	.058	.5816	1.1287	.7410	.4560	56.10	16.47	5.89
	.065	.6504	1.1263	.8251	.5077	50.00	18.40	6.58
	.083	.8258	1.1201	1.0361	.6376	39.15	23.38*	8.35*
	.095	.9416	1.1160	1.1727	.7217	34.20	26.66	9.52
	.120	1.1800	1.1074	1.4472	.8906	27.10	33.43	11.95
3 1/2	.065	.7014	1.2147	1.0349	.5914	53.80	19.85	7.09
	.083	.8910	1.2085	1.3012	.7435	42.20	25.20	9.01
	.095	1.0162	1.2043	1.4739	.8422	36.85	28.70*	10.25*
	.120	1.2742	1.1958	1.8220	1.0411	29.15	36.00	12.89
3 3/4	.065	.7525	1.3031	1.2777	.6814	57.60	21.30	7.60
	.083	.9562	1.2968	1.6080	.8576	45.20	27.06	9.67
	.095	1.0908	1.2927	1.8228	.9722	39.50	30.84*	11.04*
	.120	1.3685	1.2841	2.2565	1.2035	31.25	38.70	13.82
4	.065	.8035	1.3915	1.5557	.7779	61.50	22.75	8.12
	.083	1.0214	1.3852	1.9597	.9799	42.20	28.95	10.32
	.095	1.1655	1.3810	2.2228	1.1114	42.10	32.95	11.78
	.120	1.4627	1.3725	2.7552	1.3776	33.33	41.40*	14.80*
4 1/4	.134	1.7327	1.4557	3.6732	1.7408	31.75	49.10*	17.55*
4 1/2	.156	2.1289	1.5369	5.0282	2.2347	28.80	60.40*	21.55*
4 3/4	.188	2.6944	1.6143	7.0213	2.9563	25.25	76.25*	27.20*

* AN STANDARD TUBING

$F_c = 79500 - 51.9\ (L'/\rho)^{1.5}$

$= 79500 - 51.9\ (58.7)^{1.5} = 56500$ psi

The short column equation applies since, as shown in Table C4.1, the transitional L'/ρ is 91 and the value for our tube is 58.7.

Tensile Strength

Since the tube is welded, the tube material adjacent to the weld is weakened. The weld correction values are given in Table C4.5. We will assume a weld other than tapered. Let P_a = allowable or failing tensile strength of tube.

$P_a = F_{tu}$ (weld factor) (area of tube)

$= 95000 \times .841 \times .2628 = 21000$ lbs.

M.S. = $(P_a/\rho)-1 = (21000/18500) - 1 =$ 0.13, thus compression is critical.

PROBLEM 2

Case 1. Tube size 1-1/4 - .049, L = 40 in. c = 1
Material: Alloy steel, $F_{tu} = 95000$
Find ultimate compressive load it will carry.

Solution: From Fig. C4.5, $P_a =$ 6000 lbs.

Case 2. If tube was heat treated to $F_{tu} =$ 150,000, what compressive load would it carry.

Solution: Fig. C4.5 cannot be used since $F_{tu} = 150{,}000$, thus we will use Fig. C4.2.

$L' = L/\sqrt{c} = 40/\sqrt{1} = 4$. From Table C4.3, $\rho = .425$ and area (A) = .1849.

$L'/\rho = 40/.425 = 94$. From Fig. C4.2, using the 150,000 curve, we find $F_c = 32500$. Then $P_a = F_cA = 32500 \times .1849 =$ 6000 lb. Thus heat treating the tube from 95000 to 150,000 for F_{tu} did not increase the column strength. For a $L'/\rho = 94$, it is a long column and failure is elastic and E is constant.

The strength could also be calculated by Euler's equation from Table C4.1.

$F_c = 286{,}000{,}000/(L'/\rho)^2$

$= 286{,}000{,}000/(94)^2 =$ 32500 psi, the same as previously calculated.

Case 3. Same as Case 1, but assume tube is welded to several other tubes at its end and that the end fixity developed is c = 2.

$L' = L/\sqrt{c} = 40/\sqrt{2} = 28.4$

In Fig. C4.5 we can use L = 40 and c = 2 scale at bottom of chart or use c = 1 scale and L' = 28.4. Reading the chart we obtain $P_a =$ 9200 lbs. Thus the c = 2 fixity increased the strength of the tube from 6000 to 9200.

Case 4. Same as Case 3 but heat treated to $F_{tu} = 150{,}000$ after welding.

$L'/\rho = 28.4/.425 = 66.8$

From Fig. C4.2 using 150,000 curve, we read $F_c = 63000$, whence

$P_a = F_cA = 63000 \times .1849 =$ 11650 lb.

In this case heat treating produced additional strength, whereas in Case 2 it did not. The reason for this is that failure occurs in the inelastic stress range and heat treating raises the material properties in the inelastic range. The end fixity changed the column from a so-called long column to a short column.

The strength could be found also by substituting in the short column equal for 150,000 steel as given in Table C4.1,

$F_c = 145000 - 18.36\ (L'/\rho)^2$

$= 145000 - 18.36\ (66.8)^2 =$ 63000 psi.

PROBLEM 3

Case 1. Tube size 2 - .065, L = 24, c = 1.5
Material $F_{tu} = 95000$. Welded at ends.
Ultimate design load = 25000 lbs.
What is M.S.

Solution: $L' = L/\sqrt{c} = 24/\sqrt{1.5} = 19.7$

From Fig. C4.5 for L = 19.7 on c = 1 scale, we project upward to the 2 inch tube and note that it intersects the horizontal weld cut-off line which gives an allowable column load at left scale of $P_a = 26700$ lb. Failure in this case is local crippling adjacent to welds at the tube ends.

M.S. = $P_a/p = 26700/25000 - 1 = .07$

Case 2. Assume tube is heat treated to F_{tu} = 125000 after welding. What is tube strength.

$L'/\rho = 19.7/.6845 = 28.8$

Using Fig. C4.2 with $L'/\rho = 28.8$ and projecting up to 125000 curve, we again note that horizontal weld cut-off line is intersected

giving F_c = 95000, whence P_a = 95000 x .3951 = 37500 lbs.

If the tube had not been welded at ends the dashed part of the column curve could have been used, thus giving additional strength.

PROBLEM 4

Fig. C4.7 shows a steel tubular engine mount structure for a 1050 H.P. radial engine. The ultimate design tension and compressive load in each member as determined from a stress analysis for the various flying and landing conditions are shown in ( ) adjacent to each member. The true length L of each member is also shown. Using chrome-moly steel tubes, F_{tu} = 95000, select tube sizes for the given loads. It is common practice to assume the column end fixity c = 1 for engine mount members, since the mount is subjected to considerable vibration and the true rigidity given by the engine mount ring is difficult to accurately determine.

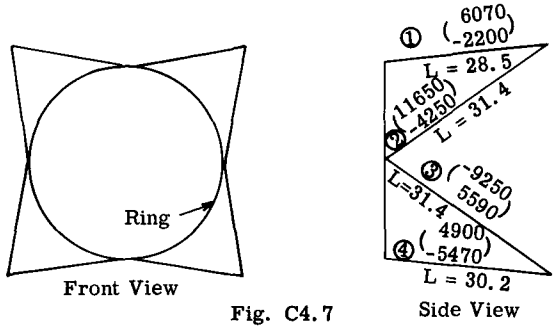

Fig. C4.7

Consider member (3). Ultimate design load = - 9250. Referring to the column charts of Fig. C4.5, we find for C = 1 and L = 31.4 the following tube sizes for a strength near - 9250 lbs.

1-1/2 - .035, P_a = 8850 (weak). (Note - P_a = allowable load).

1-3/8 - .049, P_a = - 10350, weight=5.78 lb./100", M.S. = (10350/9250) - 1 = .12

1-1/4 - .058, P_a = -10000, weight = 6.15, M.S. = 10000/9250) - 1 = .08

Thus use 1-3/8 - .049 since it is the lightest as well as the strongest.

Consider member (4), Load = - 5470, L = 30, c = 1

From Fig. C4.5:

1-1/8 - .049, P_a = -7100, wt.= 4.68, M.S.= .30

1-1/4 - .035, P_a = -6500, wt.= 3.78, M.S.= .19

1" - .058, P_a = -6000, wt.= 4.86, M.S.= .10

The results show that 1-1/4 - .035 is the lightest. Since there is danger in welding .035 thickness to the other heavier tube gauges particularly the engine mount ring which is usually relatively heavy for this size engine, a minimum tube thickness of .049 will be used, hence the 1-1/8 - .049 tube will be selected.

Consider Member (2)

Design loads 11650 tension and 4250 compression. Since the tension load appears critical, the tube will be designed for the tension load and then checked for the compressive load. The F_{tu} of the material equals 95000 psi. Since the engine mount in a welded structure, the strength of the tube adjacent to the end welds must be reduced to .841 x 95000 = 80000 psi (see Table C4.5).

Hence tube area required = 11650/80000 = 0.146 sq, in. From Table C4.3, which gives the section properties of round tubes, we select the following sizes:

1 - .049, Area = .146, M.S. = (.146/.146) - 1 = 0

1 - .058, Area = .172, M.S. = (.172/.146) - 1 = .19

1-1/8 - .049, Area = .166, M.S. = .14

1-3/8 - .035, Area = .147, M.S. = 0

To obtain a reasonable margin of safety, the 1-1/8 - .049 will be selected.

Many structural designers prefer to have large margins of safety on engine mount members as considerable trouble has been encountered in the failure or cracking of engine mount members.

The strength of the 1-1/8 - .049 tube as a column for length = 31.4 and c = 1 equals -6700 lbs. from Fig. C4.5 which gives a margin of safety of (6700/4250) - 1 = .58 on the maximum compressive load. The student should select a tube size for member (1).

C4.14 Illustrative Problems Using Aluminum Alloy and Magnesium Round Tubes as Columns and Tension Members.

In general alloy steel round tubes must be heat treated to around 180,000 to 200,000 ultimate tension strength before they can compare favorably with aluminum round tubes on a material weight basis. However, aluminum alloy as used for tubes cannot be welded satisfactorily and thus in a truss structure the end connections involving riveted and bolted connections add weight and design difficulties as compared to welded connections in steel trusses.

PROBLEM 1

Case 1. Tube size 1 - .049 round.
L = 24, c = 1, Material 2024-T3
Find failing compressive load.

Solution: The column curves in Fig. C4.6 are slightly conservative because the equation used was slightly different from the equation now specified in (Ref. 1).

Use L = 24, we read for 1-049 tube a failing load of 2800 lb.

As a second solution, we will use Fig. C4.3. $L' = L/\sqrt{c} = 24/\sqrt{1} = 24$. $L'/P = 24/.3367 = 71.3$. From Fig. C4.3, we read $F_c = 20000$. Then $P_a = F_cA = 20000 \times .1464 =$ 2930 lb.

The answer could be obtained by substituting in equation C4.9,

$$F_c = 50600 - 431\ L'/\rho$$
$$= 50600 - 431\ (71.3) = 19900$$
$$P_a = 19900 \times .1464 = 2920 \text{ lb.}$$

A column may also fail by local crushing or crippling of the tube wall, thus the crushing stress F_{cc} should be determined to see if it is less than the primary bending failing stress for the column.

For our tube the diameter over thickness ratio D/t = 1.0/.049 = 20.40. Values of D/t are given in Table C4.3.

Referring to the small chart in the upper right hand corner of Fig. C4.3, we find for a D/t of 20.4 that $F_{cc} = 47500$ psi. Since this stress is greater than the bending failing column stress of 20,000, it is not critical.

Case 2. Same as Case 1 but use c = 1.5 and change material to 6061-T6 aluminum alloy.

$L' = L/\sqrt{c} = 24/\sqrt{1.5} = 19.7$, $L'/\rho = 19.7/.3367 = 58.5$

From Fig. C4.3, $F_c = 22500$

Whence $P_a = 22500 \times .1464 =$ 3300 lb.

F_{cc} for D/t = 20.4 from Fig. C4.3 = 38500 (not critical).

Case 3. Same as Case 2 but change material to magnesium alloy, $F_{cy} = 10{,}000$.

For $L'/\rho = 58.5$ and using lower curve on Fig. C4.4, we read $F_c = 7600$. Then $P_a = F_cA =$ $7600 \times .1464 =$ 1110 lb.

C4. 15 Strength of Streamline Tubing.

If a round tube is exposed to the airstream, the air drag is about 15 times greater than if it were given a streamlined shape, thus streamline tubes are used when the member is exposed to the airstream.

Streamline tubes are drawn from round tubes. In designating a streamline tube, the round tube from which it was made is used and then the fineness ratio is also given. The fineness ratio is the ratio L/D, which dimensions are shown in Fig. C4.8. The most common fineness ratio used is 2.5 to 1. Table C4.6 shows the section properties of streamline tubing having a fineness ratio of 2.5 to 1. Figs. C4.9 and C4.10 give curves for finding the column failing stress F_c and the local crushing stress F_{cc}.

Fig. C4. 8

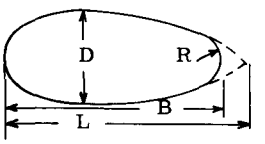

B = .944L R = .19D
D = .5714d L = 2.5D
d = Equiv. Round Dia.

PROBLEM 1. Case 1.

A streamline tube made from a basic round tube of 2-1/2 - .065 size has a fineness ratio of 2.5 to 1. The length L is 30 in. Take c = 1. Material is alloy steel $F_{ty} = 75000$. Find the ultimate compressive load the member will carry.

Solution: From Table C4.6 for 2-1/2 - .065 size we find the following section properties:- Area (A) = .4972, ρ (major axis) = .5137 in. Then $L' = L/\sqrt{c} = 30/\sqrt{1} = 30$, and $L'/\rho = 30/.5137 = 58.5$
D/t value for tube = 2.5/.065 = 38.5

From Fig. C4.9 for $L'/\rho = 58.5$ and D/t = 38.5, we read $F_c = 46500$ psi. For D/t = 38.5 and reading from small chart in upper right hand corner of Fig. C4.9, we read $F_{cc} = 66500$. Thus F_c is critical and $P_a = 46500 \times .4972 =$ 23000 lb.

Case 2. Same as Case 1 but change material to 2024-T6 aluminum alloy.

For this material we use Fig. C4.10. For $L'/\rho = 58.5$, we read $F_c = 26000$ psi. For D/t = 38.5, we read $F_{cc} = 37500$ (not critical). Thus $P_a = 26000 \times .4972 =$ 12900 lb.

C4. 16 Strength of Oval and Square Shaped Tubes in Compression.

Tables C4.8 and C4.7 give the section properties for square and oval shaped tubes respectively. For the design of these shaped

Streamline TABLE C4. 6 SECTION PROPERTIES OF STREAMLINE TUBING (Fineness Ratio 2. 5 to 1)

Equiv. Round O.D.	Wall Dec'l	Wall Gage	Axes Major	Axes Minor	Area	Wt. per ft.	I Major	Z Major	ρ Major	I Minor	Z Minor	ρ Minor
¾	.035	20	1.0114	.4286	.0786	.2673	.0017	.0079	.1486	.0073	.0140	.3046
	.049	18	"	"	.1079	.3668	.0022	.0103	.1435	.0097	.0187	.2998
⅞	.035	20	1.1800	.5000	.0924	.3140	.0028	.0112	.1753	.0118	.0195	.3572
	.049	18	"	"	.1272	.4323	.0037	.0148	.1703	.0158	.0261	.3525
	.058	17	"	"	.1489	.5061	.0042	.0168	.1671	.0182	.0301	.3495
1	.035	20	1.3485	.5714	.1061	.3607	.0043	.0151	.2020	.0178	.0257	.4100
	.049	18	"	"	.1464	.4977	.0057	.0200	.1972	.0239	.0345	.4044
	.058	17	"	"	.1716	.5835	.0065	.0228	.1939	.0278	.0402	.4023
1⅛	.035	20	1.5170	.6428	.1199	.4074	.0063	.0196	.2292	.0257	.0329	.4626
	.049	18	"	"	.1656	.5631	.0083	.0258	.2240	.0347	.0445	.4573
	.058	17	"	"	.1944	.6609	.0094	.0292	.2205	.0402	.0516	.4549
	.065	16	"	"	.2165	.7359	.0103	.0320	.2182	.0443	.0569	.4525
1¼	.035	20	1.6857	.7143	.1336	.4542	.0088	.0246	.2559	.0355	.0409	.5154
	.049	18	"	"	.1849	.6285	.0116	.0325	.2509	.0482	.0557	.5107
	.058	17	"	"	.2172	.7384	.0133	.0372	.2477	.0560	.0647	.5077
	.065	16	"	"	.2420	.8226	.0145	.0406	.2451	.0618	.0714	.5053
1⅜	.035	20	1.8543	.7857	.1473	.5009	.0118	.0300	.2828	.0476	.0549	.5683
	.049	18	"	"	.2041	.6939	.0157	.0400	.2777	.0648	.0680	.5635
	.058	17	"	"	.2400	.8158	.0181	.0461	.2745	.0754	.0791	.5604
	.065	16	"	"	.2675	.9094	.0198	.0504	.2719	.0833	.0875	.5581
1½	.035	20	2.0228	.8571	.1611	.5476	.0154	.0359	.3096	.0621	.0597	.6209
	.049	18	"	"	.2234	.7593	.0207	.0483	.3045	.0848	.0815	.6162
	.058	17	"	"	.2627	.8932	.0239	.0555	.3014	.0988	.0951	.6131
	.065	16	"	"	.2934	.9962	.0262	.0611	.2989	.1093	.1052	.6108
	.083	14	"	"	.3695	1.256	.0316	.0737	.2923	.1351	.1302	.6047
1⅝	.035	20	2.1913	.9285	.1748	.5943	.0198	.0426	.3365	.0793	.0704	.6736
	.049	18	"	"	.2426	.8248	.0266	.0573	.3314	.1085	.0964	.6689
	.058	17	"	"	.2855	.9707	.0308	.0448	.3282	.1266	.1124	.6659
	.065	16	"	"	.3186	1.083	.0338	.0728	.3256	.1402	.1245	.6634
	.083	14	"	"	.4021	1.367	.0410	.0883	.3192	.1738	.1545	.6574
	.095	13	"	"	.4566	1.552	.0453	.0976	.3149	.1949	.1732	.6541
1¾	.035	20	2.3600	1.0000	.1886	.6411	.0249	.0498	.3633	.0995	.0820	.7263
	.049	18	"	"	.2618	.8902	.0336	.0672	.3583	.1363	.1123	.7216
	.058	17	"	"	.3083	1.048	.0389	.0778	.3551	.1592	.1312	.7186
	.065	16	"	"	.3441	1.170	.0428	.0856	.3525	.1765	.1455	.7163
	.083	14	"	"	.4347	1.478	.0521	.1042	.3461	.2192	.1809	.7101
	.095	13	"	"	.4939	1.679	.0577	.1154	.3418	.2463	.2034	.7061
1⅞	.035	20	2.5285	1.0714	.2023	.6878	.0308	.0575	.3902	.1227	.0943	.7789
	.049	18	"	"	.2811	.9556	.0417	.0779	.3851	.1685	.1296	.7743
	.058	17	"	"	.3311	1.126	.0482	.0900	.3815	.1969	.1515	.7712
	.065	16	"	"	.3696	1.257	.0532	.0993	.3794	.2186	.1683	.7690
	.083	14	"	"	.4673	1.589	.0650	.1214	.3729	.2719	.2093	.7624
	.095	13	"	"	.5312	1.806	.0722	.1348	.3687	.3598	.2770	.7523
2	.035	20	2.6970	1.1428	.2161	.7345	.0376	.0658	.4170	.1494	.1076	.8313
	.049	18	"	"	.3003	1.021	.0510	.0893	.4120	.2053	.1480	.8269
	.058	17	"	"	.3539	1.203	.0591	.1034	.4088	.2402	.1732	.8238
	.065	16	"	"	.3951	1.343	.0652	.1141	.4062	.2668	.1925	.8217
	.083	14	"	"	.4999	1.699	.0799	.1398	.3998	.3325	.2399	.8156
	.095	13	"	"	.5685	1.933	.0889	.1556	.3954	.3744	.2703	.8115
2¼	.049	18	3.0343	1.2857	.3388	1.152	.0735	.1144	.4657	.2946	.1887	.9325
	.058	17	"	"	.3994	1.358	.0854	.1329	.4625	.3450	.2212	.9294
	.065	16	"	"	.4462	1.517	.0944	.1469	.4600	.3835	.2458	.9271
	.083	14	"	"	.5650	1.921	.1161	.1807	.4533	.4794	.3075	.9223
	.095	13	"	"	.6432	2.186	.1298	.2020	.4492	.5409	.3470	.9170
	.120	11	"	"	.8030	2.730	.1556	.2421	.4402	.6629	.4255	.9086
2½	.049	18	3.3713	1.4285	.3773	1.283	.1018	.1425	.5194	.4063	.2343	1.0377
	.058	17	"	"	.4450	1.513	.1186	.1660	.5163	.4764	.2747	1.0346
	.065	16	"	"	.4972	1.690	.1312	.1837	.5137	.5300	.3057	1.0325
	.083	14	"	"	.6302	2.143	.1621	.2269	.5071	.6640	.3832	1.0265
	.095	13	"	"	.7178	2.440	.1815	.2541	.5028	.7504	.4333	1.0224
	.120	11	"	"	.8972	3.050	.2188	.3063	.4938	.9226	.5329	1.0141
2¾	.049	18	3.7085	1.5714	.4158	1.414	.1366	.1739	.5732	.5434	.2848	1.1432
	.058	17	"	"	.4905	1.668	.1593	.2028	.5699	.6372	.3340	1.1398
	.065	16	"	"	.5483	1.864	.1765	.2247	.5674	.7099	.3723	1.1379
	.083	14	"	"	.6954	2.364	.2188	.2785	.5609	.8907	.4673	1.1318
	.095	13	"	"	.7924	2.694	.2455	.3125	.5566	1.0081	.5289	1.1279
	.120	11	"	"	.9915	3.371	.2973	.3785	.5476	1.2427	.6523	1.1196
3	.058	17	4.0455	1.7142	.5361	1.822	.2085	.2433	.6236	.8318	.3997	1.2456
	.065	16	"	"	.5993	2.037	.2312	.2698	.6211	.9265	.4452	1.2434
	.083	14	"	"	.7606	2.586	.2872	.3352	.6145	1.1645	.5599	1.2373
	.095	13	"	"	.8670	2.947	.3229	.3768	.6103	1.3184	.6338	1.2332
	.120	11	"	"	1.0857	3.691	.3925	.4580	.6013	1.6289	.7839	1.2249
	.156	9/32	"	"	1.3959	4.746	.4824	.5630	.5879	2.0497	.9869	1.2118
3¼	.058	17	4.3828	1.8571	.5816	1.977	.2668	.2873	.6773	1.0617	.4708	1.3511
	.065	16	"	"	.6504	2.211	.2961	.3189	.6747	1.1830	.5248	1.3487
	.083	14	"	"	.8258	2.807	.3689	.3973	.6684	1.4886	.6604	1.3426
	.095	13	"	"	.9416	3.201	.4150	.4470	.6639	1.6873	.7489	1.3386
	.120	11	"	"	1.1800	4.011	.5062	.5452	.6549	2.0887	.9275	1.3304
	.156	5/32	"	"	1.5186	5.163	.6251	.6732	.6416	2.6353	1.1707	1.3173
3½	.065	16	4.7200	2.0000	.7014	2.385	.3723	.3723	.7286	1.4831	.6108	1.4541
	.083	14	"	"	.8910	3.029	.4645	.4645	.7220	1.8686	.7699	1.4481
	.095	13	"	"	1.0162	3.455	.5234	.5234	.7177	2.1194	.8733	1.4442
	.120	11	"	"	1.2742	4.332	.6400	.6400	.7087	2.6269	1.0828	1.4358
	.156	5/32	"	"	1.6414	5.580	.7934	.7934	.6952	3.3221	1.3705	1.4227
3¾	.065	16	5.0570	2.1428	.7525	2.558	.4604	.4297	.7822	1.8299	.7033	1.5594
	.083	14	"	"	.9562	3.251	.5754	.5371	.7757	2.3073	.8871	1.5534
	.095	13	"	"	1.0908	3.708	.6490	.5777	.7713	2.6195	1.0075	1.5497
	.120	11	"	"	1.3685	4.652	.7955	.7425	.7624	3.2505	1.2502	1.5412
	.156	5/32	"	"	1.7641	5.997	.9894	.9235	.7489	4.1192	1.5855	1.5281
4	.065	16	5.3940	2.2856	.8035	2.732	.5614	.4912	.8359	2.2270	.8025	1.6648
	.083	14	"	"	1.0214	3.472	.7024	.6146	.8293	2.8161	1.0148	1.6604
	.095	13	"	"	1.1655	3.962	.7933	.6941	.8250	3.1917	1.1506	1.6549
	.120	11	"	"	1.4627	4.973	.9739	.8522	.8160	3.9661	1.4303	1.6467
	.156	5/32	"	"	1.8867	6.414	1.2153	1.0634	.8026	5.0332	1.8164	1.6333
	.188	3/16	"	"	2.2457	7.635	1.4109	1.2345	.7926	5.9364	2.1431	1.6259
4¼	.065	16	5.7313	2.4285	.8546	2.905	.6761	.5568	.8895	2.6784	.9082	1.7704
	.083	14	"	"	1.0866	3.694	.8473	.6978	.8830	3.3817	1.1471	1.7641
	.095	13	"	"	1.2400	4.216	.9574	.7885	.8787	3.8426	1.3035	1.7604
	.120	11	"	"	1.5570	5.293	1.1779	.9701	.8698	4.7789	1.6216	1.7519
	.156	5/32	"	"	2.0095	6.832	1.4729	1.2131	.8573	6.0748	2.0628	1.7387
	.188	3/16	"	"	2.3930	8.135	1.7144	1.4120	.8464	7.1732	2.4365	1.7314
4½	.083	14	6.0683	2.5713	1.1517	3.915	1.0105	.7860	.9367	4.0256	1.2894	1.8696
	.095	13	"	"	1.3147	4.469	1.1429	.8889	.9324	4.5759	1.4662	1.8656
	.120	11	"	"	1.6512	5.613	1.4082	1.0953	.9235	5.6952	1.8254	1.8572
	.156	5/32	"	"	2.1322	7.249	1.7650	1.3728	.9098	7.2508	2.3247	1.8441
	.188	3/16	"	"	2.5403	8.636	2.0580	1.6007	.9001	8.5740	2.7498	1.8372
	.219	7/32	"	"	2.9421	10.01	2.3221	1.8061	.8884	9.8001	3.1451	1.8251

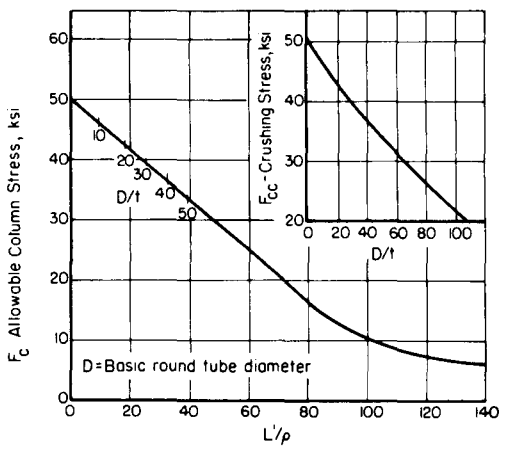

Fig. C4. 10 Streamline 2024-T3 Tubing

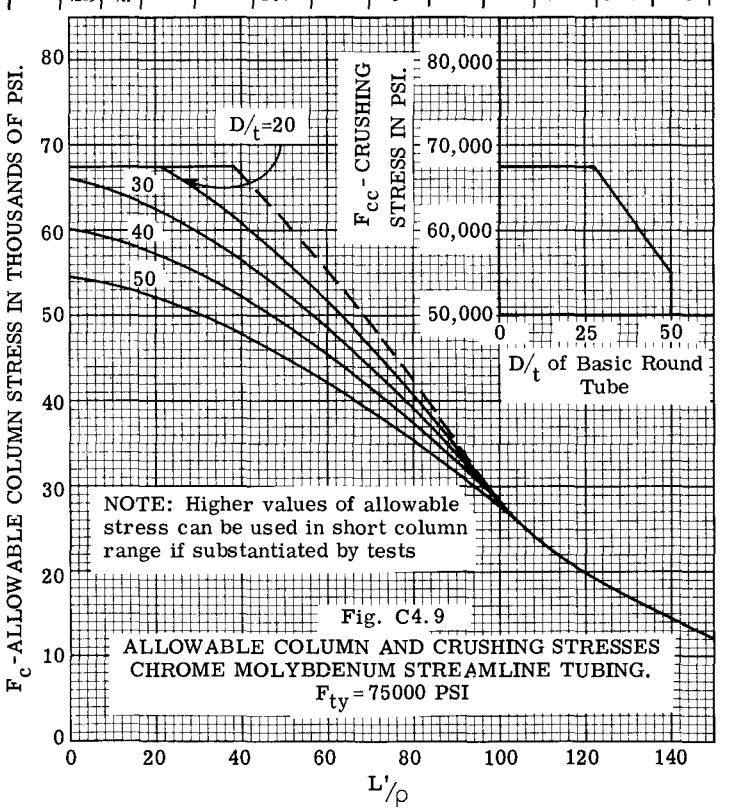

Fig. C4.9
ALLOWABLE COLUMN AND CRUSHING STRESSES CHROME MOLYBDENUM STREAMLINE TUBING.
F_{ty} = 75000 PSI

Squares TABLE C4.8 SECTION PROPERTIES OF STREAMLINE TUBING

Size	Wall		Area	Wt. per ft.	I	Z	ρ
Dist. Across Flats	Dec'l	Gage					
⅜	.022	24	.0294	.0998	.0006	.0031	.1415
	.028	22	.0368	.1252	.0007	.0038	.1396
	.035	20	.0453	.1589	.0009	.0045	.1372
	.049	18	.0612	.2081	.0011	.0057	.1318
½	.022	24	.0396	.1348	.0016	.0065	.2023
	.028	22	.0499	.1697	.0020	.0079	.1991
	.035	20	.0616	.2096	.0024	.0094	.1956
	.049	18	.0841	.2861	.0030	.0120	.1892
	.058	17	.0980	.3330	.0033	.0134	.1853
	.065	16	.1084	.3684	.0035	.0141	.1804
⅝	.022	24	.0483	.1641	.0033	.0104	.2600
	.028	22	.0630	.2143	.0040	.0129	.2526
	.035	20	.0780	.2652	.0048	.0155	.2489
	.049	18	.1071	.3640	.0063	.0201	.2420
	.058	17	.1251	.4253	.0071	.0227	.2379
	.065	16	.1388	.4717	.0077	.0245	.2348
¾	.028	22	.0761	.2588	.0064	.0168	.2890
	.035	20	.0944	.3209	.0078	.0206	.2866
	.049	18	.1300	.4419	.0103	.0274	.2816
	.058	17	.1522	.5175	.0118	.0313	.2784
	.065	16	.1692	.5751	.0129	.0342	.2760
	.083	14	.2113	.7184	.0154	.0408	.2700
⅞	.028	22	.0892	.3033	.0103	.0236	.3390
	.035	20	.1108	.3766	.0125	.0288	.3364
	.049	18	.1528	.5193	.0168	.0386	.3320
	.058	17	.1794	.6098	.0193	.0445	.3283
	.065	16	.1996	.6785	.0212	.0487	.3528
	.083	14	.2502	.8504	.0255	.0588	.3194
1	.028	22	.1023	.3479	.0154	.0309	.3883
	.035	20	.1271	.4322	.0190	.0380	.3867
	.049	18	.1758	.5978	.0256	.0511	.3813
	.058	17	.2065	.7020	.0295	.0591	.3782
	.065	16	.2300	.7819	.0324	.0649	.3756
	.083	14	.2890	.9824	.0394	.0788	.3693
	.095	13	.3272	1.112	.0436	.0873	.3652
1⅛	.035	20	.1435	.4878	.0275	.0489	.4340
	.049	18	.1988	.6757	.0369	.0657	.4311
	.058	17	.2336	.7942	.0427	.0759	.4265
	.065	16	.2604	.8852	.0471	.0838	.4241
	.083	14	.3278	1.114	.0576	.1024	.4191
	.095	13	.3716	1.263	.0640	.1138	.4151
	.120	11	.4600	1.564	.0760	.1351	.4064
1¼	.035	20	.1599	.5435	.0378	.0604	.4891
	.049	18	.2217	.7536	.0513	.0821	.4831
	.058	17	.2608	.8865	.0595	.0952	.4778
	.065	16	.2908	.9886	.0657	.1051	.4753
	.083	14	.3666	1.246	.0806	.1290	.4960
	.095	13	.4161	1.414	.0899	.1438	.4647
	.120	11	.5161	1.755	.1074	.1718	.4561
1⅜	.035	20	.1763	.5992	.0506	.0736	.5360
	.049	18	.2446	.8316	.0689	.1003	.5309
	.058	17	.2879	.9787	.0801	.1166	.5276
	.065	16	.3212	1.092	.0886	.1288	.5251
	.083	14	.4055	1.378	.1091	.1587	.5187
	.095	13	.4605	1.566	.1219	.1773	.5145
	.120	11	.5723	1.946	.1464	.2130	.5058

Side	Wall		Area	Wt. per ft.	I	Z	ρ
	Dec'l	Gage					
1½	.035	20	.1926	.6549	.0661	.0881	.5859
	.049	18	.2675	.9095	.0902	.1203	.5807
	.058	17	.3150	1.071	.1051	.1401	.5776
	.065	16	.3516	1.195	.1162	.1550	.5750
	.083	14	.4443	1.510	.1436	.1915	.5686
	.095	13	.5050	1.717	.1608	.2144	.5643
	.120	11	.6284	2.136	.1940	.2586	.5556
1¾	.049	18	.3134	1.065	.1451	.1658	.6804
	.058	17	.3693	1.255	.1691	.1932	.6766
	.065	16	.4124	1.402	.1877	.2146	.6747
	.083	14	.5220	1.774	.2331	.2663	.6682
	.095	13	.5938	2.019	.2618	.2992	.6640
	.120	11	.7307	2.484	.3175	.3628	.6592
2	.049	18	.3592	1.221	.2180	.2180	.7790
	.058	17	.4236	1.440	.2557	.2557	.7769
	.065	16	.4732	1.609	.2838	.2838	.7744
	.083	14	.5996	2.038	.3536	.3536	.7679
	.095	13	.6827	2.321	.3981	.3981	.7636
	.120	11	.8530	2.900	.4859	.4856	.7548
	.156	9/16	1.0912	3.710	.6010	.6010	.7422
2¼	.049	18	.4051	1.377	.3080	.2738	.8721
	.058	17	.4778	1.624	.3607	.3207	.8689
	.065	16	.5341	1.816	.4000	.3556	.8654
	.083	14	.6773	2.302	.5007	.4451	.8598
	.095	13	.7716	2.623	.5640	.5013	.8549
	.120	11	.9652	3.281	.6918	.6149	.8466
	.156	9/16	1.2372	4.206	.8765	.7791	.8418
2½	.058	17	.5321	1.809	.5074	.4035	.9757
	.065	16	.5949	2.022	.5643	.4488	.9739
	.083	14	.7549	2.566	.7071	.5625	.9678
	.095	13	.8605	2.925	.7981	.6530	.9631
	.120	11	1.0775	3.663	.9809	.7806	.9541
	.156	5/16	1.3831	4.702	1.2256	.9760	.9413
	.188	3/16	1.6479	5.602	1.4257	1.3183	.9301
2¾	.058	17	.5864	1.993	.6792	.4940	1.0763
	.065	16	.6557	2.229	.7559	.5497	1.0737
	.083	14	.8326	2.830	.9481	.6896	1.0671
	.095	13	.9494	3.227	1.0724	.7799	1.0628
	.120	11	1.1898	4.045	1.3213	.8653	1.0541
	.156	5/16	1.5291	5.198	1.6569	1.1121	1.0410
	.188	3/16	1.8238	6.200	1.9334	1.3264	1.0296
3	.065	16	.7166	2.436	.9860	.6573	1.1730
	.083	14	.9102	3.094	1.2394	.8263	1.1669
	.095	13	1.0383	3.530	1.4032	.9355	1.1625
	.120	11	1.3021	4.426	1.7325	1.1550	1.1544
	.156	5/16	1.6750	5.694	2.1793	1.4529	1.1406
	.188	3/16	1.9997	6.798	2.5503	1.7002	1.1381
	.219	7/32	2.3081	7.847	2.8873	1.9249	1.1184

Ovals TABLE C4.7 SECTION PROPERTIES OF OVAL TUBING

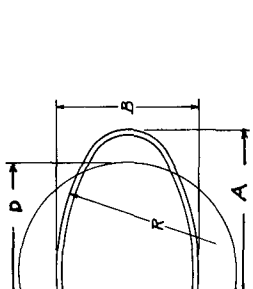

A = 2
B = 1.50 D
A = 1.90 D
B = .65 D
R = 1.100 D (Approx.)
r = .206 D (Approx.)
D = Equiv. Round Dia.

Equiv. Round O.D.	Wall		Axes		Area	Wt. per ft.	I		Z		ρ
	Dec'l	Gage	Major	Minor			Major	Minor	Major	Minor	
¾	.035	20	.9728	.4864	.0786	.2673	.0023	.0069	.0094	.0145	.2971
⅞	.035	20	1.1348	.5674	.0924	.3140	.0037	.0112	.0132	.0198	.3485
	.049	18	"	"	.1272	.4323	.0049	.0150	.0265	.0487	.3437
1	.035	20	1.2972	.6486	.1061	.3607	.0057	.0176	.0176	.0262	.4003
	.049	18	"	"	.1464	.4977	.0075	.0229	.0233	.0353	.3954
1⅛	.035	20	1.4592	.7296	.1199	.4074	.0083	.0254	.0226	.0335	.4518
	.049	18	"	"	.1656	.5631	.0110	.0331	.0301	.0453	.4469
1¼	.035	20	1.6212	.8106	.1336	.4542	.0115	.0287	.0287	.0418	.5034
	.049	18	"	"	.1849	.6285	.0153	.0459	.0378	.0567	.4986
	.058	17	"	"	.2172	.7384	.0176	.0533	.0435	.0657	.4952
1⅜	.035	20	1.7824	.8912	.1473	.5009	.0154	.0453	.0345	.0508	.5546
	.049	18	"	"	.2041	.6939	.0207	.0616	.0464	.0692	.5496
	.058	17	"	"	.2400	.8158	.0238	.0716	.0535	.0804	.5463
1½	.035	20	1.9456	.9728	.1611	.5476	.0202	.0587	.0415	.0604	.6038
	.049	18	"	"	.2234	.7593	.0272	.0809	.0539	.0831	.6016
	.058	17	"	"	.2627	.8932	.0314	.0941	.0646	.0967	.5983
	.065	16	"	"	.2930	.9962	.0346	.1070	.0711	.1070	.5960
1⅝	.049	18	2.1076	1.0538	.2426	.8248	.0349	.1035	.0663	.0982	.6531
	.058	17	"	"	.2855	.9707	.0404	.1206	.0767	.1145	.6492
	.065	16	"	"	.3186	1.083	.0445	.1336	.0845	.1267	.6467
1¾	.049	18	2.2700	1.1350	.2618	.8902	.0440	.1301	.0776	.1146	.7050
	.058	17	"	"	.3083	1.048	.0510	.1518	.0900	.1338	.7017
	.065	16	"	"	.3441	1.170	.0563	.1682	.0992	.1482	.6992
1⅞	.049	18	2.4320	1.2160	.2811	.9556	.0546	.1608	.0897	.1323	.7564
	.058	17	"	"	.3311	1.126	.0653	.1878	.1042	.1545	.7532
	.065	16	"	"	.3696	1.257	.0699	.2083	.1150	.1713	.7507
	.083	14	"	"	.4673	1.589	.0859	.2589	.1413	.2129	.7443
2	.049	18	2.5940	1.2970	.3003	1.021	.0666	.1961	.1027	.1512	.8080
	.058	17	"	"	.3539	1.203	.0775	.2292	.1194	.1767	.8047
	.065	16	"	"	.3951	1.343	.0856	.2543	.1320	.1961	.8023
	.083	14	"	"	.4999	1.699	.1054	.3166	.1625	.2441	.7958
	.095	13	"	"	.5685	1.933	.1177	.3563	.2747	.2747	.7917
2¼	.058	17	2.9184	1.4592	.3994	1.358	.1117	.3293	.1531	.2257	.9080
	.065	16	"	"	.4462	1.517	.1237	.3658	.1695	.2507	.9055
	.083	14	"	"	.5650	1.921	.1529	.4568	.2095	.3130	.8991
	.095	13	"	"	.6432	2.186	.1713	.5150	.2348	.3529	.8948
2½	.058	17	3.2428	1.6214	.4450	1.513	.1549	.4550	.1911	.2806	1.0112
	.065	16	"	"	.4972	1.690	.1716	.5060	.2117	.3121	1.0088
	.083	14	"	"	.6302	2.143	.2129	.6332	.2626	.3905	1.0024
	.095	13	"	"	.7178	2.440	.2390	.7150	.2948	.4410	.9981
	.120	11	"	"	.8972	3.050	.2900	.8781	.3577	.5416	.9893
2¾	.065	16	3.5668	1.7834	.5483	1.864	.2306	.6778	.2586	.3800	1.1118
	.083	14	"	"	.6954	2.364	.2868	.8498	.3216	.4765	1.1054
	.095	13	"	"	.7924	2.694	.3225	.9607	.3617	.5387	1.1001
	.120	11	"	"	.9915	3.371	.3927	1.1829	.4404	.6633	1.0923
	.156	5/16	"	"	1.2732	4.328	.4841	1.4820	.5430	.8310	1.0789
3	.065	16	3.8912	1.9456	.5993	2.037	.3019	.8848	.3103	.4548	1.2151
	.083	14	"	"	.7606	2.586	.3763	1.1111	.3868	.5711	1.2086
	.095	13	"	"	.8670	2.947	.4238	1.2576	.4357	.6464	1.2044
	.120	11	"	"	1.0857	3.691	.5176	1.5517	.5321	.7976	1.1955
	.156	5/16	"	"	1.3959	4.746	.6409	1.9501	.6776	1.0024	1.1820
	.188	3/16	"	"	1.6967	5.632	.7396	2.2803	.8589	1.1721	1.1732
3¼	.065	16	4.2152	2.1076	.6504	2.211	.3862	1.1301	.3664	.5362	1.3180
	.083	14	"	"	.8258	2.807	.4823	1.4208	.4576	.6742	1.3117
	.095	13	"	"	.9416	3.201	.5438	1.6095	.5161	.7657	1.3074
	.120	11	"	"	1.1800	4.011	.6660	1.9896	.6320	.9441	1.2985
	.156	5/16	"	"	1.5186	5.163	.8279	2.5071	.7856	1.1896	1.2849
	.188	3/16	"	"	1.8040	6.133	.9586	2.9096	.9343	1.3943	1.2763
3½	.065	16	4.5396	2.2698	.7014	2.385	.4851	1.4172	.4274	.8316	1.4215
	.083	14	"	"	.8910	3.029	.6068	1.7839	.5347	.8253	1.4150
	.095	13	"	"	1.0162	3.455	.6850	2.0223	.6036	.8217	1.4107
	.120	11	"	"	1.2742	4.332	.8408	2.5037	.8123	1.1031	1.4017
	.156	5/16	"	"	1.6414	5.580	1.0486	3.1620	1.0239	1.3931	1.3880
	.188	3/16	"	"	1.9512	6.663	1.2177	3.7136	1.0729	1.7900	1.3796

tubes the primary column strength can be found by using the curves in Figs. C4.9 and C4.10. The crushing stress F_{cc} for oval shaped tubes can conservatively be taken as that for streamline tubes as given in Figs. C4.9 and C4.10. For square tubes the local crushing stress F_{cc} can be taken as the crippling stress of a flat plate. For this stress refer to the chapter which covers the buckling and crippling stress of flat plates with various widths, thickness and boundary edge conditions.

ULTIMATE BENDING STRENGTH OF ROUND TUBES

C4.17 Charts for Finding Modulus of Rupture Stress.

Chapter C3 was concerned with the theory and methods of determining the ultimate yield and failing stress of a section in pure bending. It was concerned with finding a fictitious stress F_b which, when substituted in the well known beam formula $M = F_bI/c$, would give the value of the bending moment which would cause failure.

The same procedure as was used in Chapter C3 can be used to find the modulus of rupture stress (F_b) for round tubes. However, since round tubes have been a standard and available structural member for many years, much testing has been done on tubes and as a result rather complete design curves are available for finding the modulus of rupture in bending (F_b) for round tubes. Figs. C4.11 to C4.14 inclusive give curves for finding modulus of rupture F_b round tubes when fabricated from alloy steels, aluminum alloys, magnesium alloys and titanium alloy.

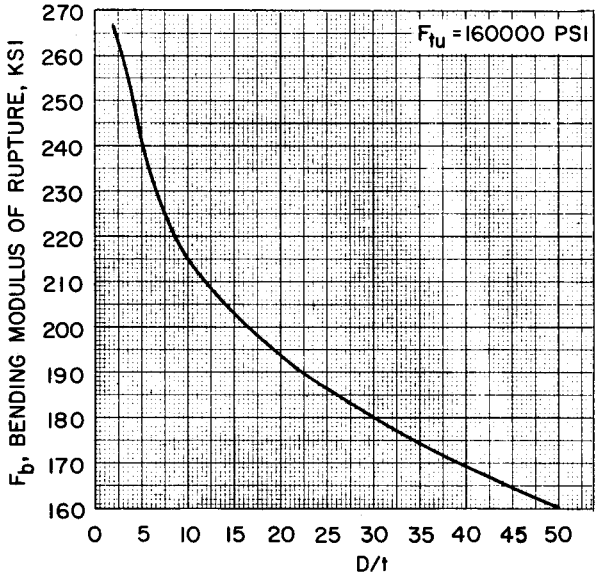

Fig. C4.14 Bending modulus of rupture for round 6Al-4V tubing. (Titanium)

C4.18 Problems Involving Bending Strength of Tubes.

PROBLEM 1

A 1-1/4 - .058 round tube is used as a simply supported beam with the supports at the ends. The span or length of the beam is 24 inches. It carries a uniform distributed load w in pounds per inch. Find the value of w to cause the tube to fail in bending if the tube is made from the following materials:- alloy steel F_{tu} = 95000, 6061-T6 aluminum alloy, and 6AL-4V titanium.

Solution: The maximum bending moment occurs at the midpoint of the span and equals $wL^2/8 = w \times 24^2/8 = 72w$ in. lb.

The section properties for the tube are D/t = 21.55, and I/y = .06187 obtained from Table C4.3.

The beam equation involving the modulus of rupture F_b is $M = F_bI/y$. Substituting 72w for M, we obtain:

$$w = \frac{F_bI}{72y}$$

Consider the alloy steel, F_{tu} = 95000. From Fig. C4.11 for D/t = 21.55, we read F_b = 117000. Then w = (117000 x .06187)/72 = 100.2 lb. per inch. Consider tube material as 6061-T6 which has a F_{tu} = 42000 psi.

From Fig. C4.12 for D/t = 21.55, we read that F_b/F_{tu} = 1.06. Thus F_b = 42000 x 1.06 = 44500.

Then w = (44500 x .06187)/72 = 38.1. Tube material 6AL-4V titanium.

From Fig. C4.14 for D/t = 21.55, we read F_b = 191600. Then w = (191600 x .06187)/72 = 118.7 lbs. per in.

PROBLEM 2

A beam simply supported at its ends has a span of 30 inches. The ultimate design load consists of two equal loads of 2000 lbs. each. The beam is symmetrically loaded with each load located 12 inches from the ends.

Select the lightest round tube when made from the following material: (1) alloy steel F_{tu} = 220000, (2) 7075-T6 aluminum alloy. Compare the resulting tube weights.

Solution: The maximum bending moment is constant and occurs between the load points.

M = 2000 x 12 = 24000 in. lb.

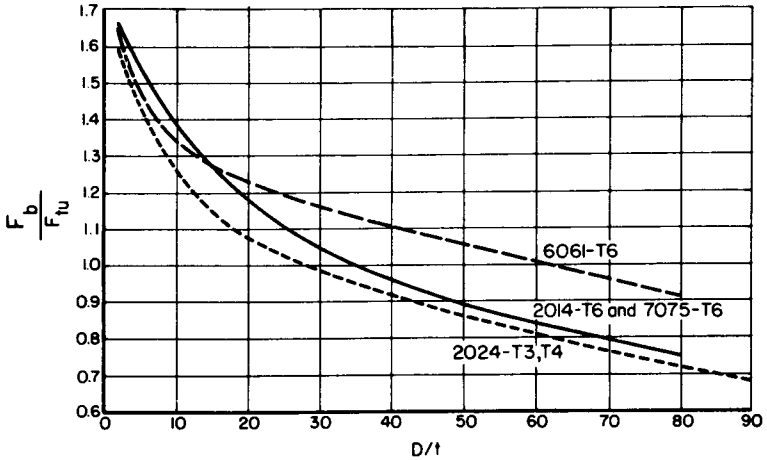

Fig. C4.12 Bending modulus of rupture for aluminum-alloy round tubing.

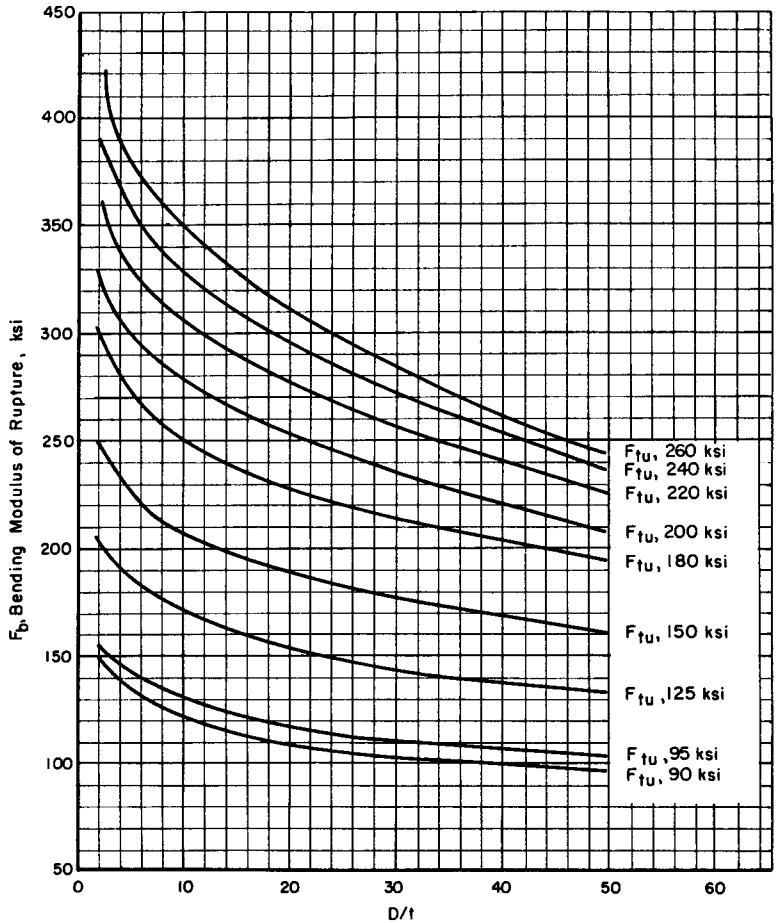

Fig. C4.11 Bending modulus of rupture for round alloy-steel tubing.

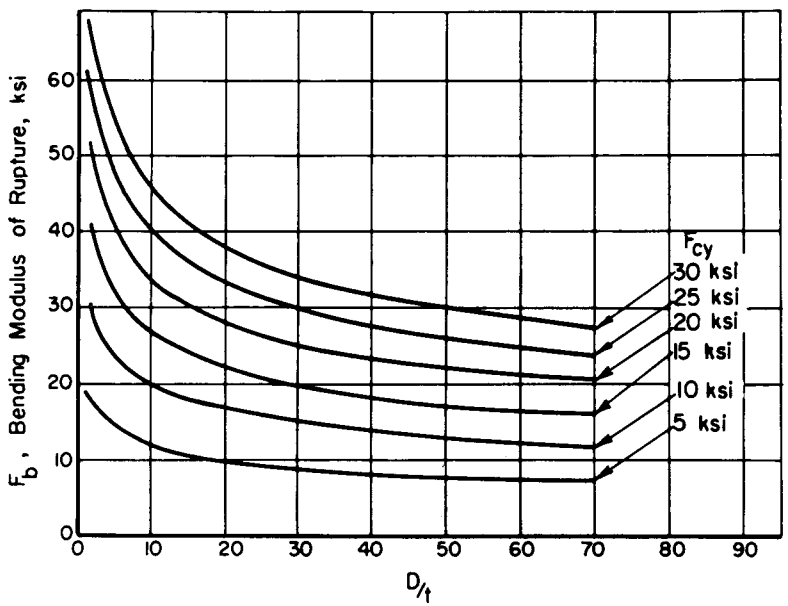

Fig. C4.13 Bending modulus of rupture of magnesium-alloy round tubing.

Since the allowable or failing bending stress is a function of D/t, and since we do not have a tube size, the design or solution procedure is by trial and error.

Observation of the modulus of rupture curves show that as D/t increases F_b decreases. This is due to the fact that failure in bending is a local failure and the thinner the wall and larger the diameter, the lower the buckling or crushing stress. However, the larger the D/t value the greater the section modulus I/y of the tube, which means increasing bending resistance. Thus we have two influences which act oppositely relative to effecting the bending strength.

There are many ways of guessing a tube size for checking purposes. In this example problem we will assume two values for D/t and see what I/y would calculate to be. The two values of D/t will be 45 and 25.

Consider the material alloy steel F_{tu}=220000:-

For D/t = 45 from Fig.C4.11, F_b=232000

Then $I/y = M/F_b = 24000/232000 = .103$

For D/t = 25, $F_b = 266000$

Then $I/y = 24000/266000 = .089$

Therefore we will refer to Table C4.3 and select tubes that have an I/y value near the .089 to .103 range and then find their true bending strength. Table (A) shows the selection and the necessary calculations, using Fig. C4.11.

Table A

Tube Size	I/y	Area	D/t	F_b	$M=F_bI/y$	M. S. = (Ma/M)-1
1-7/8 -.035	.09136	.2023	53.6	227000	20800	-0.13
1-3/4 -.049	.1083	.2618	35.7	248000	26400	+0.10
1-5/8 -.049	.0928	.2426	33.15	250000	23200	-0.04

The lightest available tube with a positive margin of safety is 1-3/4 - .049 and its weight for a 30 inch length is 30 x .2618 x 0.283 = 2.22 lbs.

Consider the tube made from 7075-T6 aluminum alloy material which has a F_{tu} = 77000.

From Fig. C4.12:-

For D/t = 60, F_b/F_{tu} = .84, thus F_b = .84 x 77000 = 64700

$I/y = M/F_b = 24000/64700 = .37$

For D/t = 30, F_b/F_{tu} = 1.045, thus F_b = 1.045 x 77000 = 80500

$I/y = 24000/80500 = .30$

Therefore we will select a tube from Table C4.3 that has a I/y value in the region of .30 to .37.

Try 2-3/4 - 058. I/y = .3233, D/t = 47.4. From Fig. C4.12, F_b/F_{tu} = 0.90. Then F_b = .90 x 77000 = 69300 psi. Then $M_a = F_b\ I/y$ = 69300 x .3233 = 22400. This is less than the design bending moment of 24000 so this tube is weak.

Try 3-058. I/y = .3868, D/t = 51.7
F_b/F_{tu} = .885 , F_b = .885 x 77000 = 68000
$M_a = F_b\ I/y$ = 68000 x .3868 = 26300
M.S. = (26300/24000)-1 = .09.

A study of other tubes in Table C4.3 shows that no other tube would be lighter in weight.

Tube weight = 30 x .5361 x .101 = 1.70 lbs., as against 2.22 lbs. for the alloy steel heat treated to 220,000. Thus aluminum alloy tubes from a weight standpoint usually yield results better than most materials. This conclusion applies to only low temperatures, below 250°F, as aluminum alloys lose strength rapidly for temperatures above 250° to 300°F.

The student should calculate the lightest titanium tube and the lightest magnesium tube using Figs. C4.14 and C4.13 respectively and compare the weight results with the steel and aluminum as found above.

ULTIMATE TORSIONAL STRENGTH OF ROUND TUBES

C4.19 Torsional Modulus of Rupture.

In Article A6.2 of Chapter A6, the torsion formula for circular sections, $f_s = Tr/J$, was derived. This equation assumes the maximum shear stress on the cross-section of a round bar or tube does not exceed the proportional limit of the material, or the stress variation is linear as shown in Fig. C4.15 and this situation exists under the flight vehicle limit loads. Before a round bar made of ductile

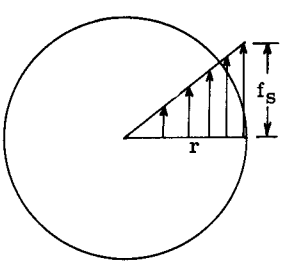

Fig. C4.15

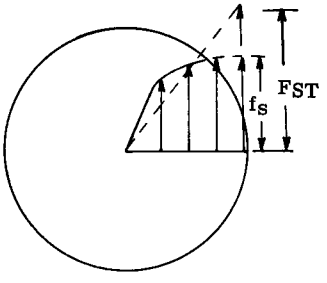

Fig. C4.16

material fails in torsion, the shear stresses fall in the inelastic or plastic range and

thus the internal shear stress distribution is similar to that indicated in Fig. C4.16. The shear stress-strain curve is similar in shape to the tension stress-strain curve.and is equal to approximately 0.6 of the ordinates. Thus to find the ultimate internal torsional resisting moment, we can divide the cross-section into a number of circular elements. From the stress curve in Fig. C4.16, the stress at the midpoints of the circular elements can be found. Multiplying the area of the element by this stress times the distance of the element from the center axis gives the moment developed, and adding up the moment of the shear force on all the circular elements gives the total allowable or ultimate internal resisting moment T_a.

If this moment T_a is to be used in the torsion equation, we must replace the true stress curve in Fig. C4.16 by a triangular stress curve with maximum value F_{st} which will produce the same internal resisting moment as the true stress curve. Thus

$T_a = F_{st}\, J/r$, or $F_{st} = T_a\, r/J$ - - - - (C4.10)

F_{st} is called the torsional modulus of rupture stress. It is a fictitious stress, being higher than the ultimate shear stress of the material. Tubes subjected to torsion usually fail by inelastic or plastic instability or by elastic instability if the D/t ratio is large. To obtain reliable values of F_{st}, resort is usually made to tests, and since the round tube or rod is the most efficient and most available shape, much testing has been done over the years thus design curves are readily available for round tubes of the most common flight vehicle materials.

C4.20 Torsional Modulus of Rupture Curves.

Figs. C4.17 to C4.24 inclusive present curves for finding the modulus of rupture stress F_{st} for steel alloys from F_{tu} = 95000 to 260,000 psi. It should be noted that the torsional strength is influenced by the D/t and the L/D values of the tube. Figs. C4.25 to C4.30 inclusive give curves for the various aluminum alloys and Fig. C4.31 gives information for one magnesium alloy. All of these curves were taken from (Ref. 1).

The curves are based on a theoretical investigation by Lee and Ades (see Ref. 2), and have been found to be in good agreement with experimental results.

C4.21 Problems Illustrating Use of Torsional Modulus of Rupture Curves.

Problem 1. A 1-5/8 - .065 round tube is 16.25 inches long. What ultimate torsional moment

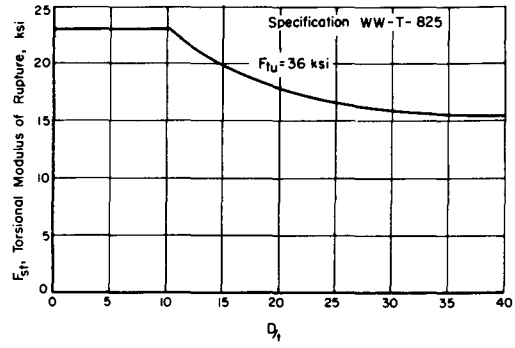

Fig. C4.31 Torsional modulus of rupture for magnesium-alloy round tubing.

will it develop if made of the following materials: (1) alloy steel F_{tu} = 95000, (2) aluminum alloy 2024-T3.

Solution: D/t = 25. J/r = 2(I/y) = 2 x 0.11948 = 0.2390. L/D = 16.25/1.625 = 10. For alloy steel, F_{tu} = 95000, we use Fig. C4.17 where for D/t = 25 and L/D = 10, we read $F_{st}/1000$ = 47.3. Thus F_{st} = 47300.

$T_a = F_{st}\, J/r$ = 47300 x 0.2390 = 11300 in.lb.

For 2024-T3 aluminum alloy, we refer to Fig. C4.26 where we read F_{st} = 29000.

Then $T_a = F_{st}\, J/r$ = 29000 x 0.2390 = 6930 in. lb.

Problem 2.

A round tube 10 inches long is to carry an ultimate torsional moment of 7000 in. lb. Select the lightest tube if made from aluminum alloy 2024-T4 and alloy steel F_{tu} = 200,000 and compare the resulting weight of each.

Solution: Since the modulus of rupture depends on D/t and L/D and since the tube size is unknown, we will use the trial and check approach. The design calculations can conveniently be made in table form as follows:

Trial Tube Size	Area	D/t	J/r	L/D	F_{st}	$T_a = F_{st}J/r$	M.S. = $\frac{T_a}{T}$ -1
Alum. Alloy 2024-T4 (Fig. C4.27)							
1-1/2 -.065	.2930	23.05	.2016	6.7	30000	6050	-.14
1-3/4 -.058	.3083	30.20	.2525	5.7	28000	7060	.01
1-7/8 -.049	.2811	38.25	.2500	5.3	26000	6500	-.07
2.0 -.049	.3003	40.30	.2860	5.0	26000	7440	.06
Alloy Steel F_{tu} = 200,000 (Fig. C4.21)							
1 - .035	.1061	28.56	.0495	10	98000	4850	-.31
1 - .049	.1461	20.40	.0664	10	106000	7050	.01
1-1/4 -.035	.1336	35.70	.0790	8	94000	7430	.06

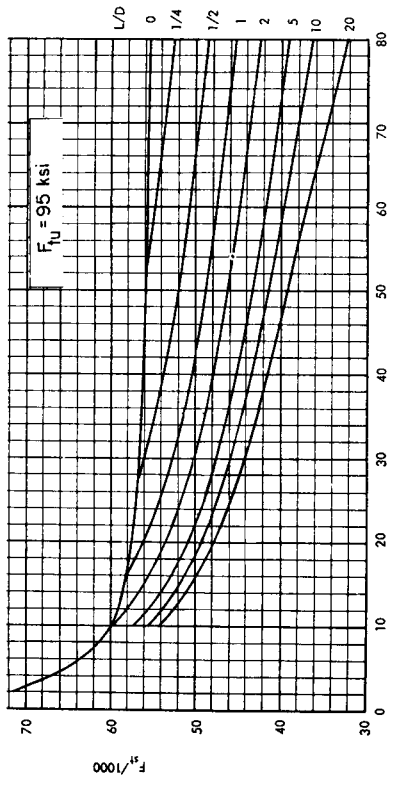

Fig. C4.17 Torsional modulus of rupture - alloy steels heat treated to F_{tu} = 95 ksi.

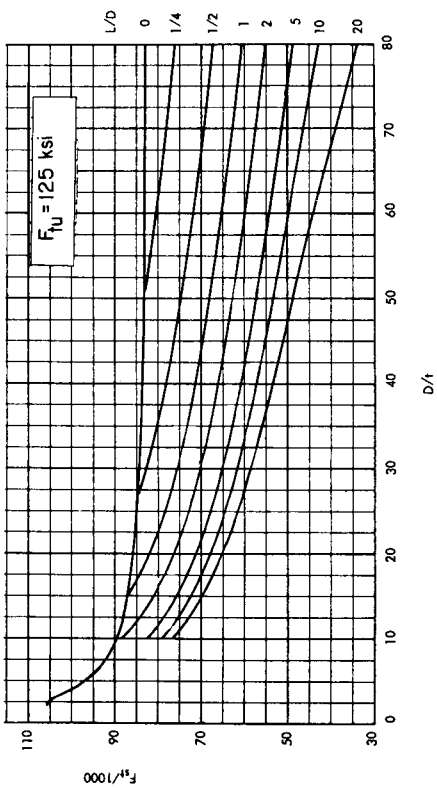

Fig. C4.18 Torsional modulus of rupture - alloy steels heat treated to F_{tu} = 125 ksi.

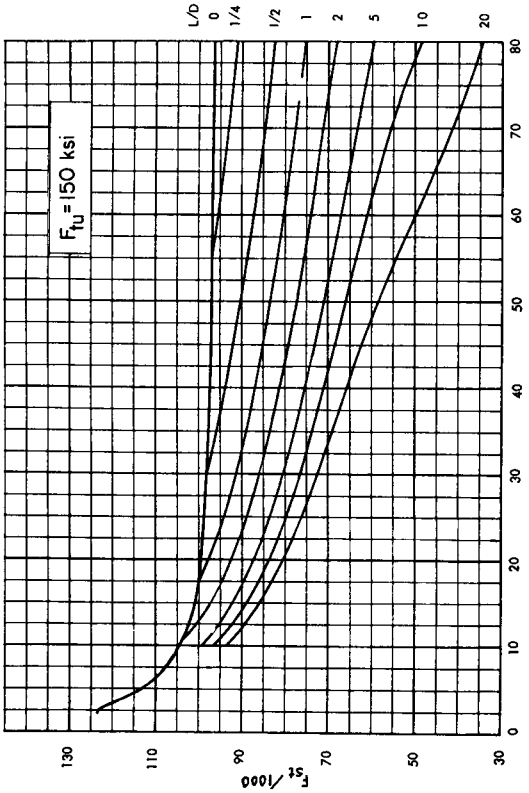

Fig. C4.19 Torsional modulus of rupture - alloy steels heat treated to F_{tu} = 150 ksi.

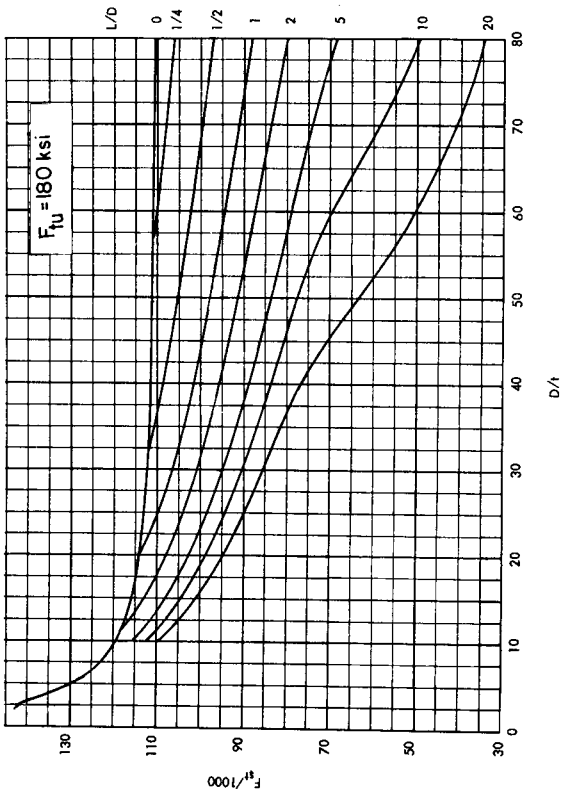

Fig. C4.20 Torsional modulus of rupture - alloy steels heat treated to F_{tu} = 180 ksi.

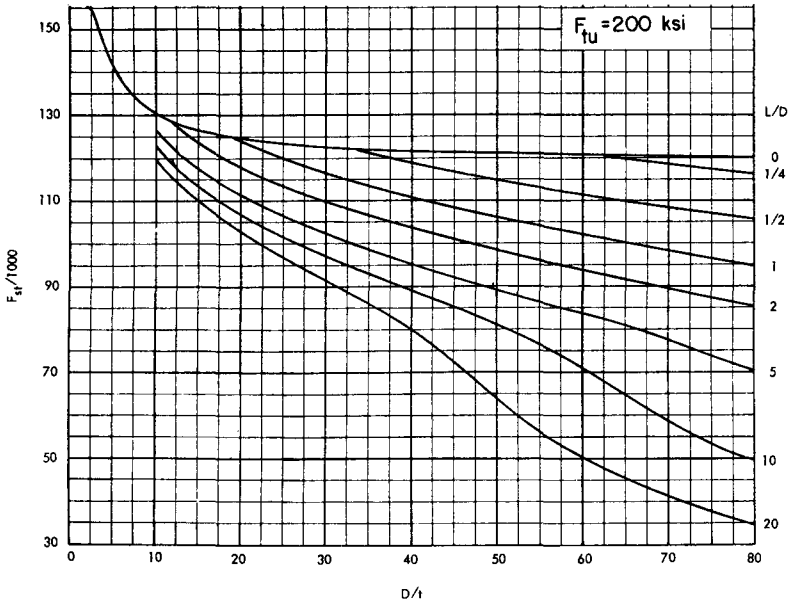

Fig. C4.21 Torsional modulus of rupture - alloy steels heat treated to F_{tu} = 200 ksi.

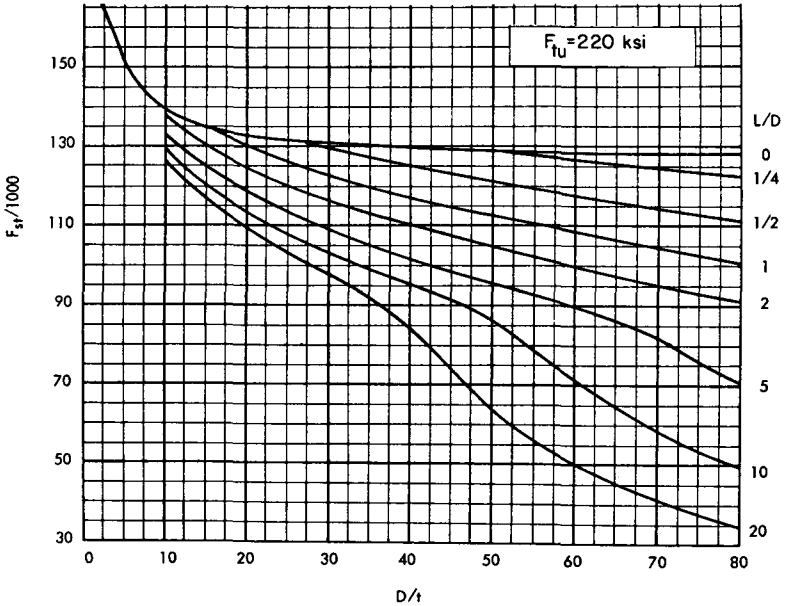

Fig. C4.22 Torsional modulus of rupture - alloy steels heat treated to F_{tu} = 220 ksi.

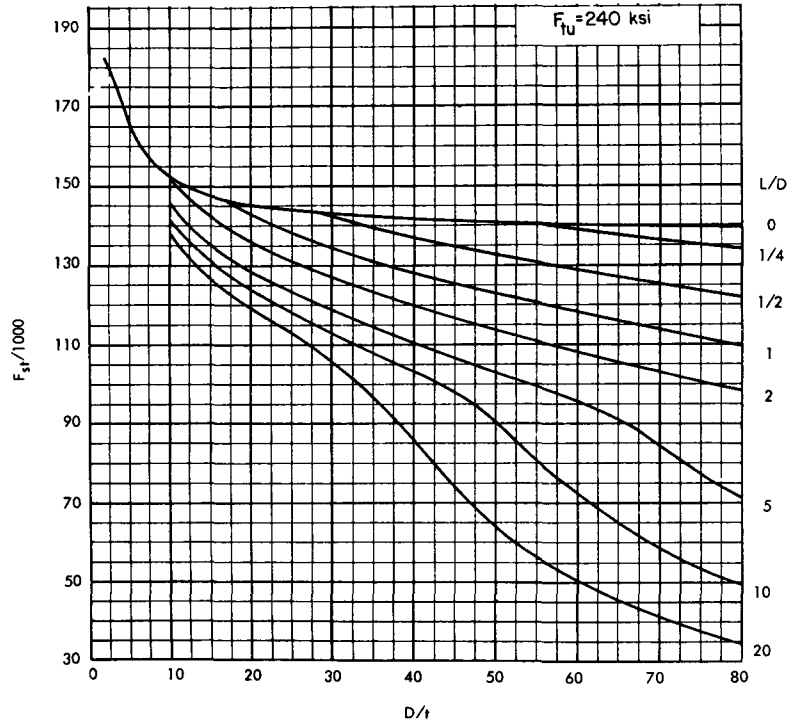

Fig. C4.23 Torsional modulus of rupture - alloy steels heat treated to F_{tu} = 240 ksi.

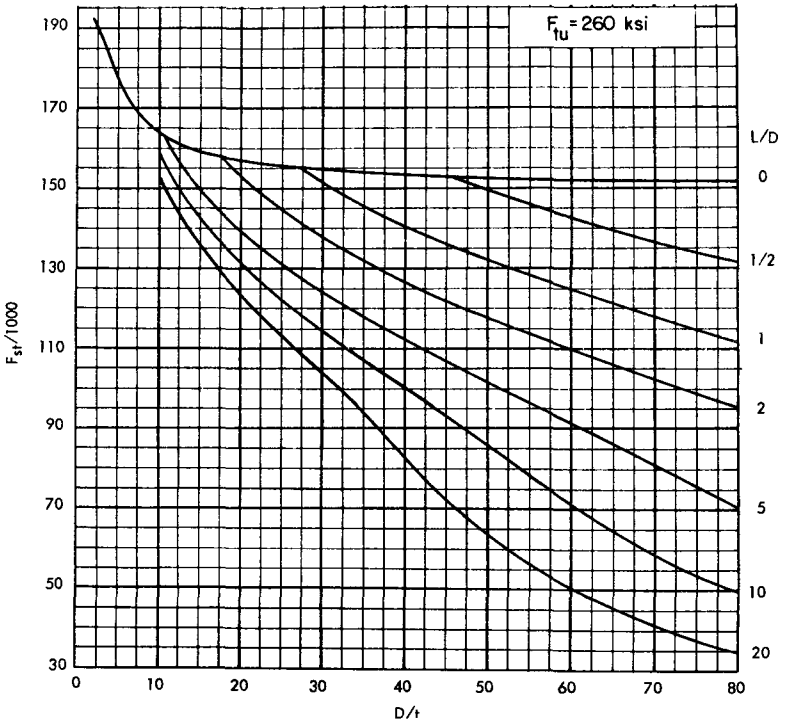

Fig. C4.24 Torsional modulus of rupture - alloy steels heat treated to F_{tu} = 260 ksi.

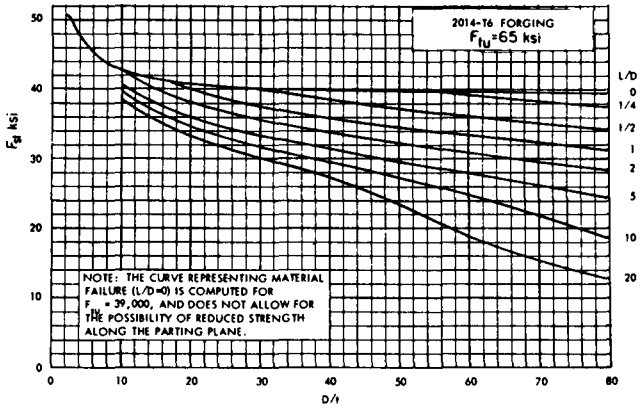

Fig. C4.25 Torsional modulus of rupture - 2014-T6 aluminum alloy forging.

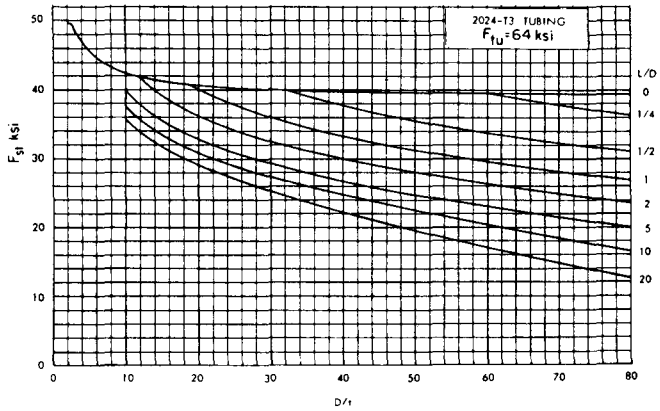

Fig. C4.26 Torsional modulus of rupture - 2024-T3 aluminum alloy tubing.

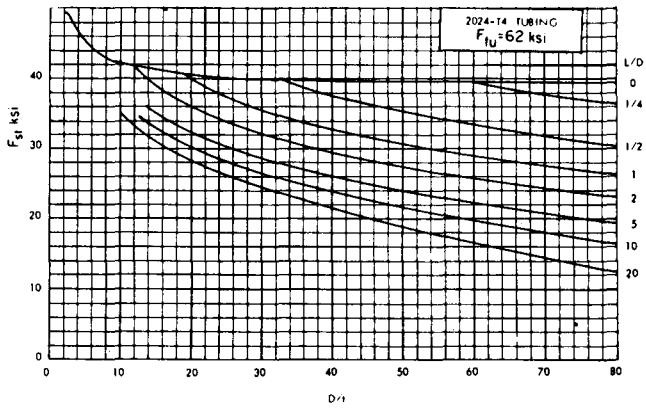

Fig. C4.27 Torsional modulus of rupture - 2024-T4 aluminum alloy tubing.

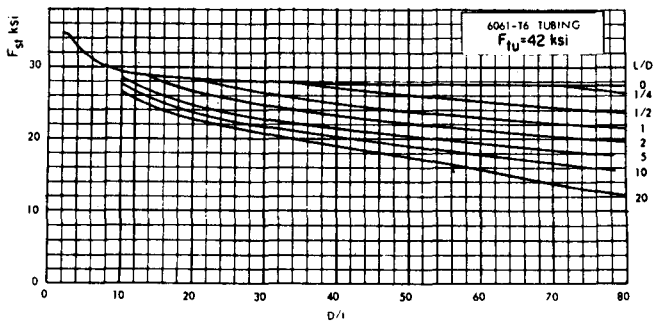

Fig. C4.28 Torsional modulus of rupture - 6061-T6 aluminum alloy tubing.

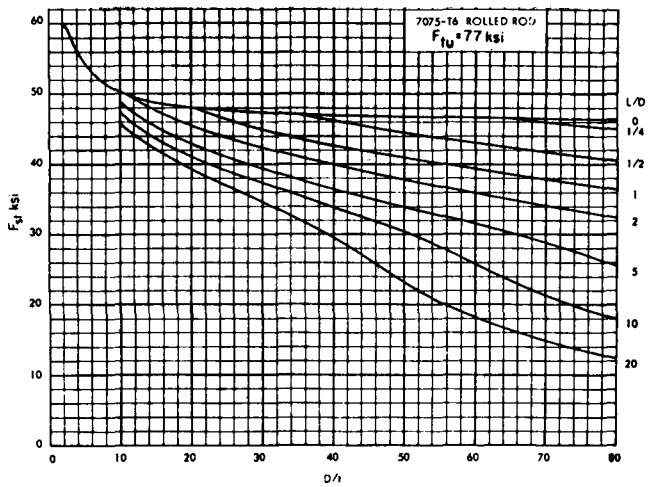

Fig. C4.29 Torsional modulus of rupture - 7075-T6 aluminum alloy rolled rod.

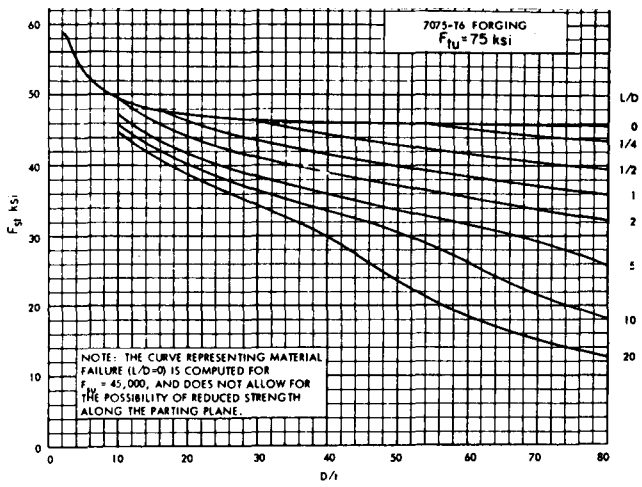

Fig. C4.30 Torsional modulus of rupture - 7075-T6 aluminum alloy forging.

The lightest aluminum tube with a positive margin of safety is 2 - .049. The weight of a 10 in. length = .3003 x .101 x 10 = .303 lbs. The lightest steel tube is 1-1/4 - .035 and its weight is 0.1336 x .283 x 10 = .378 lbs. Although the steel is heat treated to F_{tu} = 200,000, it still is heavier than the aluminum alloy tube.

STRENGTH OF ROUND TUBES UNDER COMBINED LOADINGS

Reference should be made to Artiale C1.15 of Chapter C1 for general explanation of stress-ratios and interaction equations as used in determining the ultimate strength of structural members under combined loadings.

C4.22 Combined Bending & Compression.

In tubes subjected to combined bending and compression, the stress due to compression is uniform over the cross-section whereas the bending stress is not uniform over the cross-section. The following stress ratio equation is possibly somewhat conservative but is recommended by (Ref. 1).

$$R_c + R_b' = 1 \quad \text{- - - - - - - - - - - - - (C4.11)}$$

which can be written

$$\frac{f_c}{F_c} + \frac{f_b'}{F_b} = 1.0 \quad \text{- - - - - - - - - - - - - (C4.12)}$$

Where f_b' equals the maximum bending stress including the secondary moments due to axial load times beam deflection

F_b = Bending modulus of rupture stress

f_c = Compressive column axial stress

F_c = Allowable column stress

Equation C4.12 could also be written,

$$\frac{P}{P_a} + \frac{M}{M_a} = 1.0 \quad \text{- - - - - - - - - - - - - (C4.13)}$$

Where P = column load

P_a = allowable column load at failure

M = bending moment

M_a = allowable ultimate bending moment

Fig. C4.32 shows a plot of equation C4.11.

The margin of safety equation is,

$$M.S. = \frac{1}{R_c + R_b'} - 1 \quad \text{- - - - - - - - - - (C4.14)}$$

Fig. C4.32 shows margin of safety curves for estimating closely the M.S. values if equation C4.14 is not used.

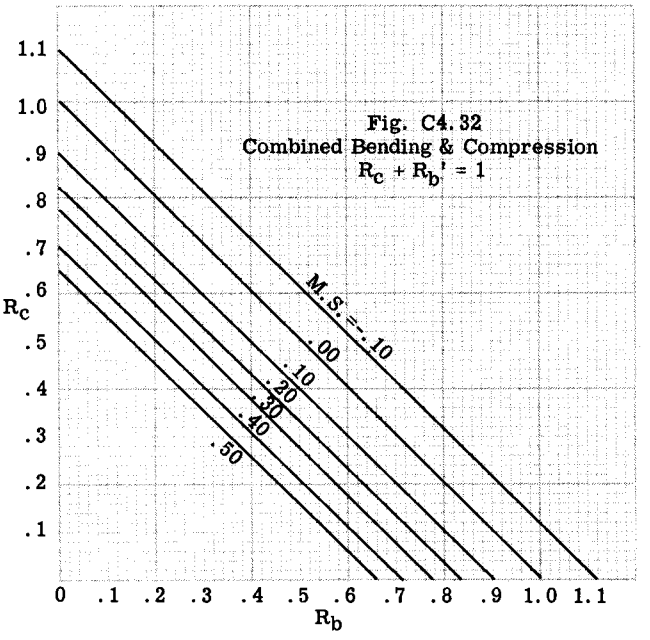

Fig. C4.32
Combined Bending & Compression
$R_c + R_b' = 1$

C4.23 Illustrative Problem Involving Combined Bending and Compression.

Fig. C4.33 shows a round 2024-T3 tube acting as a beam-column. It is supported at pin A and by the inclined strut BC at point C. Let it be required to determine the margin of safety when carrying a uniform lateral load of 10 lb./in.

To find the axial load in tube AC, take moments about point (B).

$$\Sigma M_B = -40 \times 10 \times 20 + 20\, R_{A_H} = 0, \text{ hence}$$

$$R_{A_H} = 400 \text{ lb.}$$

Thus axial load in tube is 400 lb. compression.

The column strength of a 2024-T3 1-1/4 - .049 round tube 40 inches long with end fixity C = 1 is obtained from Fig. C4.6 and equals - 2100 lb., hence stress ratio

$$R_c = \frac{\text{Column load}}{\text{Column strength}} = \frac{-400}{-2100} = .191$$

The bending moment will be maximum at the center of span because of symmetry of loading and the value of the moment is obtained from the following equation which includes the secondary moments due to deflection. (Reference table A5.1 of Chapter A5.)

$$M_{max} = wj^2 \left(1 - \sec \frac{L}{2j}\right) \quad \text{- - - - - - - - - - (A)}$$

$$j = \sqrt{\frac{EI}{P}} = \sqrt{\frac{10{,}700{,}000 \times .0334}{400}} = \sqrt{860} = 29.3$$

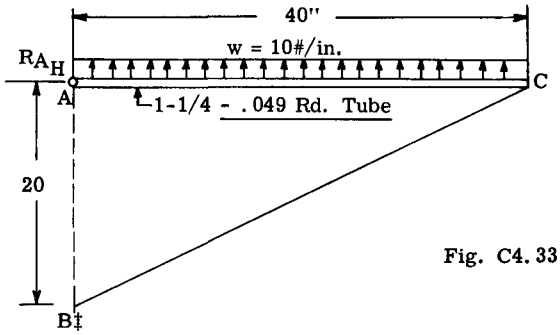

Fig. C4.33

$wj^2 = 10 \times 860 = 8600$

$\frac{L}{2j} = \frac{40}{58.6} = .683 \qquad \sec \frac{L}{2j} = \frac{1}{\cos \frac{L}{2j}}$

From Table A5.2 of Chapter A5 cos of .683 = .7757.

hence $\frac{1}{\cos L/2j} = 1/.7757 = 1.29$

Substituting in equation (A)

$M_{max.} = 8600\ (1 - 1.29) = -2490$ in. lb.

From Fig. C4.12 for D/t = 25.5, we read $F_b/F_{tu} = 1.03$. Hence $F_b = 1.03 \times 62000 = 64000$ psi. Then $M = F_b I/y = 64000 \times .0534 = 3420$ in. lbs.

Stress ratio in bending $R_b = \frac{2490}{3420} = .728$

$R_c + R_b = .191 + .728 = .917$ which shows that member is not weak.

Margin of safety $M.S. = (\frac{1}{R_c + R_b}) - 1 = (\frac{1}{.191 + .728}) - 1 = .09$

The margin of safety could be read directly from curves in Fig. C4.32.

The student should notice that the maximum bending moment of 2490 in. lb. is 24 percent greater than the primary moment which equals $wL^2/8 = 10 \times 40^2/8 = 2000$. The lateral deflection at the midpoint of the tube thus equals 490/400 = 1.22 inch.

The secondary moments due to lateral deflection do not vary linearly, so if design loads were increased the calculation of the maximum bending should be repeated instead of assuming that the moment would increase directly as the applied load to the beam.

C4.23a Combined Bending and Tension

The interaction equation for combined bending and tension on round tubes, which is widely used, is

$R_b + R_t^{1.5} = 1 \qquad$ - - - - - - - - - (C4.15)(Ref.2)

This equation is plotted in Fig. C4.34. The stress ratio $R_t = f_t/F_{tu}$. The figure is based on D/t = 10 and in general is conservative for other D/t ratios.

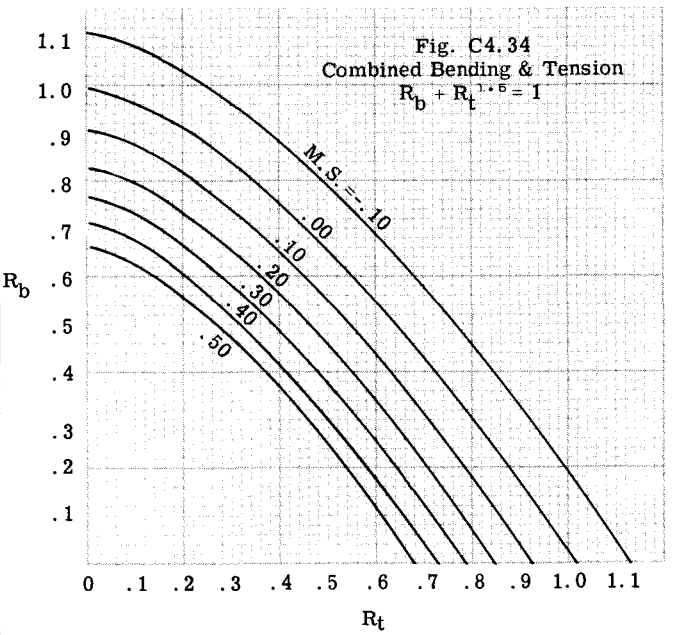

C4.24 Combined Bending and Torsion.

The interaction equation for combined bending and torsion from (Ref. 1) is,

$R_b^2 + R_{st}^2 = 1 \qquad$ - - - - - - - - - - - - - -(C4.16)

This equation is plotted in Fig. C4.35 for M.S. = 0. Curves showing various M.S. values

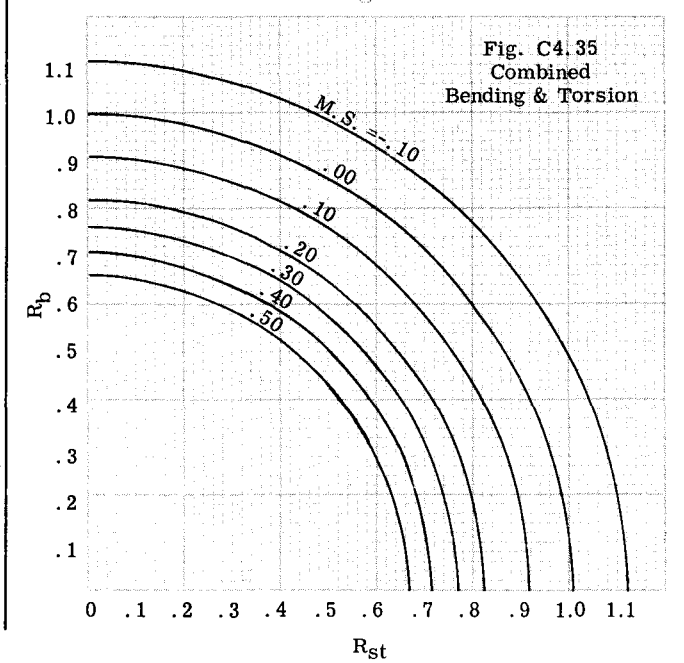

for various values of R_b and R_{st} are also shown on the figure.

The expression for Margin of Safety is,

$$M.S. = \frac{1}{\sqrt{R_b^2 + R_{st}^2}} - 1 \quad \text{- - - - - - - - - (C4.17)}$$

ILLUSTRATIVE PROBLEM 1

A 1-1/2 -..058 round steel tube (F_{tu} = 125000) is 30 inches long. It is subjected to an ultimate design bending moment of 10,000 in. lbs. and a torsional moment of 6000 in. lbs. Find the Margin of Safety.

Solution: D/t = 25.85, I/y = .0912, L/D = 20

To find F_b, we refer to Fig. C4.11 where for D/t = 25.85 and F_{tu} = 125000 we read F_b = 148000. Then $M_a = F_b I/y$ = 148000 x .0912 = 13500 in. lb.

$$\text{Then } R_b = \frac{M}{M_a} = \frac{10000}{13500} = .74$$

To find F_{st}, we refer to Fig. C4.18 where for D/t = 25.85 and L/D = 20 we read $F_{st}/1000$ to be 61, whence F_{st} = 61000.

$$R_{st} = \frac{T}{T_a} = \frac{6000}{11120} = .54$$

$$M.S. = \frac{1}{\sqrt{R_b^2 + R_{st}^2}} - 1$$

$$= \frac{1}{\sqrt{.74^2 + .54^2}} - 1 = \frac{1}{.917} - 1 = .09$$

thus the ultimate strength of the tube has 9 percent Margin of Safety under the combined loading.

In a design problem which involves a trial and error procedure, using an equivalent torsional moment T_e which will produce the same torsional stress as produced by the combined bending and torsional loads is quite useful in shortening the trial and error procedure.

Let $f_{s(max)} = T_e r/2I$ - - - - - - - - (C3.18)

$f_{s(max)}$ also equals $\sqrt{f_s^2 + (f_b/2)^2}$ - - - (C4.19)

Also $f_s = Tr/2I$, and $f_b = Mr/I$

Substituting these values in C4.18,

$$f_{s(max)} = \frac{r}{2I}\left[M\sqrt{1 + (T/M)^2}\right] \quad \text{- - - - - - - (C4.20)}$$

Equating C4.20 and C4.18 and solving for T_e,

$$T_e = M\sqrt{1 + (T/M)^2} \quad \text{- - - - - - - - - - - (C4.21)}$$

Having the value of T_e, select tube sizes that will develop this torsional moment T_e as was done in Problem 2 of Art. C4.21. These sizes are then checked for combined bending and torsion as illustrated above in the example problem.

C4.24a Ultimate Strength in Combined Compression, Bending and Torsion.

The interaction equation for combined compression, bending and torsion from (Ref. 1) is,

$$R_{b'}^2 + R_{st}^2 = (1 - R_c)^2 \quad \text{- - - - - - - - - - (C4.22)}$$

Figs. C4.36 and 37 show a plot of this equation. The expression for the Margin of Safety is,

$$M.S. = \frac{1}{R_c + \sqrt{R_{b'}^2 + R_{st}^2}} - 1 \quad \text{- - - - - (C4.23)}$$

To illustrate the use of the interaction curves, let us assume the following values for the three stress ratios: -

$$R_c = .333, \quad R_b' = .20, \quad R_{st} = .20$$

Then R_{st}/R_c = .20/.333 = .60.

In Fig. C4.36 locate point (a) at the Intersection of R_c = .333 and R_b' = .20. Since the intersection point (a) lies inside the R_{st}/R_c = .60 curve, we know that a positive margin of safety exists. A line is now drawn through (o) and (a) and extended to an intersection with the R_{st}/R_c = .60 curve at point (b). Projecting vertically downward to R_c scale, we read R_c = .538. Then M.S. = (.538/.333) - 1 = .62.

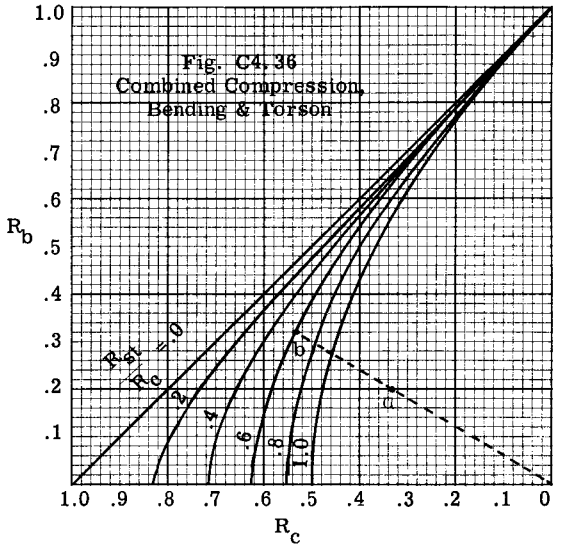

Projecting horizontally from point (b) to R_b scale, we read $R_b = .323$. Then M.S. = (.323/.200) - 1 = .62, which checks value previously found. If the ratio of R_{st}/R_c is greater than one, we use the curves in Fig. C4.37 and use the ratio R_c/R_{st}.

Substituting in equation C4.23,

$$\text{M.S.} = \frac{1}{.333 + \sqrt{.20^2 + .20^2}} - 1 = .62,$$ as given from use of curves.

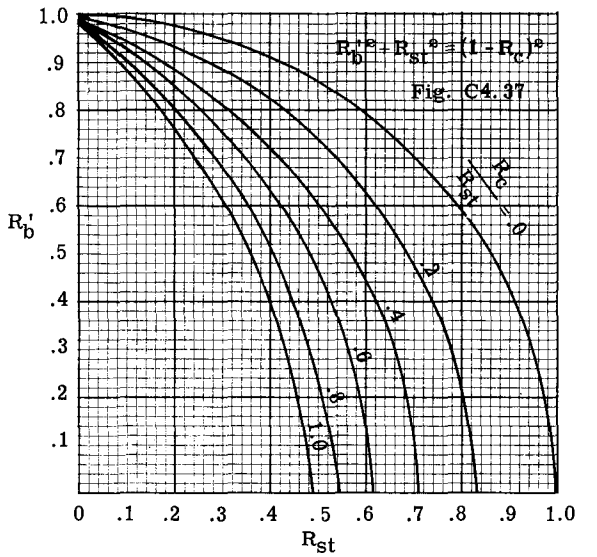

ILLUSTRATIVE PROBLEM

A 1-1/8 - .049 round tube made from 2024-T3 aluminum alloy carries the ultimate design loads as shown in Fig. C4.38. Find the margin of safety under the combined loading.

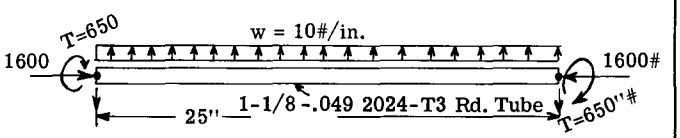

Fig. C4.38

Solution:

The maximum bending moment due to symmetry will occur at midpoint of tube. For a beam column carrying a uniform side load with no end moments, the maximum moment is given by the following expression. (See Chapter A5, Table A5.1).

$$M_{max.} = wj^2 \left(1 - \sec \frac{L}{2j}\right)$$

$$j = \sqrt{\frac{EI}{P}} = \sqrt{\frac{10{,}300{,}000 \times .0240}{1600}} = \sqrt{154.7} = 12.43$$

$$\frac{L}{2j} = \frac{25}{2 \times 12.43} = \frac{25}{24.86} = 1.005$$

$$\sec \frac{L}{2j} = \frac{1}{\cos L/2j} = \frac{1}{.5361} = 1.87$$ (See Table A5.2)

hence,

$$M_{max.} = 10 \times 154.7 \ (1 - 1.87) = -1347 \text{ in. lb.}$$

The column strength for a 25 inch length and end fixity c = 1 can be read from Fig. C4.6 and equals 3700 lb. Then $R_c = P/P_a = 1600/3700 = \underline{.432}$.

To find the ultimate bending strength, we refer to Fig. C4.12, where for D/t = 1.125/.049 = 22.95, we read $F_b/F_{tu} = 1.04$. Then $F_b = 1.04 \times 62000 = 64500$. Thus $M_a = F_b I/y = 64500 \times .0427 = 2760$ in. lb.

Therefore $R_b' = \frac{1347}{2760} = \underline{.487}$.

To find the ultimate torsional strength we refer to Fig. C4.26 where for D/t = 22.95 and estimating location of L/D = 25/1.125 = 22.2 line, we read $F_{st} = 27500$.

Then $T_a = F_{st} J/r = 27500 \times .0427 \times 2 = 2350$

Whence $R_{st} = \frac{T}{T_a} = \frac{650}{2350} = \underline{.276}$

$$\text{M.S.} = \frac{1}{R_c + \sqrt{R_b'^2 + R_{st}^2}} - 1$$

$$= \frac{1}{.432 + \sqrt{.487^2 + .276^2}} - 1 = \frac{1}{.992} - 1 = .01$$

C4.25 Ultimate Strength in Combined Bending and Flexural Shear.

The interaction curve from this type of combined loading from (Ref. 2) is,

$$R_b^2 + R_s^2 = 1 \quad \text{- - - - - - - - - - - - - (C4.24)}$$

$$\text{M.S.} = \frac{1}{\sqrt{R_b^2 + R_s^2}} - 1 \quad \text{- - - - - - - - - (C4.25)}$$

The allowable flexural or transverse shear stress is taken as 1.2 times the allowable torsional stress of the tube (F_{st}).

ILLUSTRATIVE PROBLEM

A 1-1/4 - .058 round aluminum alloy 2024-T3 tube is used as a simple beam and carries an ultimate design load of 600 lb. as shown in Fig. C4.39.

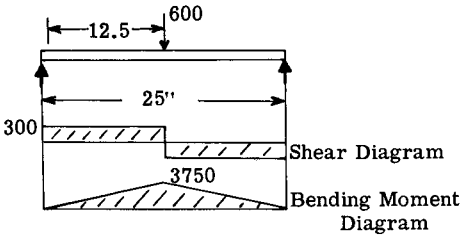

Fig. C4. 39

The critical section is adjacent to the midpoint of beam where shear and bending forces are largest.

The ultimate bending strength can be found from Fig. C4.26 where for D/t = 21.60 we read F_b/F_{tu} = 1.07. Then F_b = 62000 x 1.07 = 66300 and therefore $M_a = F_b I/y$ = 66300 x .06187 = 4100. Then $R_b = M/M_a$ = 3750/4100 = .915.

The allowable shear stress F_s can be taken as 1.2 F_{st} (Ref. 2).

To find F_{st}, we refer to Fig. C4.26 where for D/t = 21.6 and L/D = 20, we read F_{st} = 28400. Then F_s = 1.2 x 28400 = 34000.

The maximum shear stress in a round tube which occurs at the centerline axis is given by the equation,

$$f_s = \frac{4}{3}\frac{V}{A}\left(1 + \frac{dD}{d^2 + D^2}\right)$$

where V = vertical beam shear load
A = tube area
D = outside diameter
d = inside diameter

An approximate formula is

$$f_s = 2\frac{V}{A}, \text{ for } D/t > 10 \text{ error less than 1\%.}$$

Using the approximate equation,

$$f_s = \frac{2 \times 300}{.2172} = 2760 \text{ psi.}$$

$$R_s = \frac{f_s}{F_s} = \frac{2760}{34000} = .081$$

$$M.S. = \frac{1}{\sqrt{R_b^2 + R_s^2}} - 1 = \frac{1}{\sqrt{.915^2 + .081^2}} - 1$$

$$= .09$$

The effect of the shear stress is less than 1 percent. In using F_s = 1.2 F_{st}, if the result is greater than F_{su} for the material, use F_{su} for F_s.

C4. 26 Ultimate Strength in Combined Compression, Bending, Flexural Shear and Torsion.

The interaction equation for this combined loading as presented in Ref. 2 is,

$$R_c + R_{st} + \sqrt{R_b^2 + R_s^2} = 1 \quad \text{- - - - - - (C4.26)}$$

Interaction curves for this equation are given in Fig. C4.40, where R_s the stress ratio for flexural shear can be found as explained in the previous article.

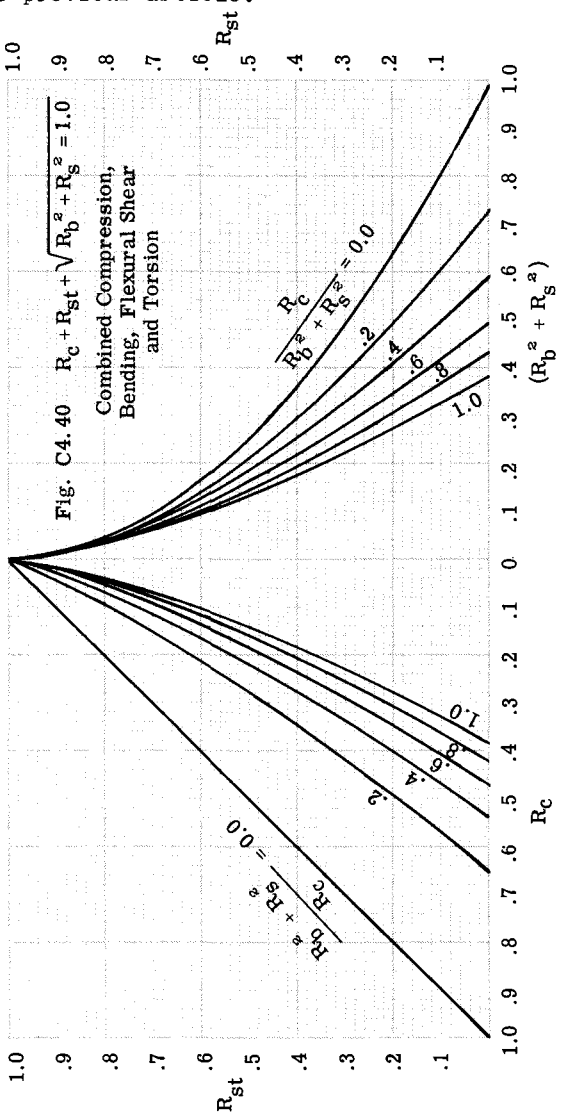

C4. 27 Ultimate Strength in Combined Tension and Torsion.

The interaction equation for this type of loading as presented in Ref. 3 is,

$$R_t^2 + R_{st}^2 = 1 \quad \text{- - - - - - - - - - - - - - (C4.27)}$$

Where $R_t = f_t/F_{tu}$

$$M.S. = \frac{1}{\sqrt{R_t^2 + R_{st}^2}} - 1 \quad \text{- - - - - - - - - (C4.28)}$$

C4. 28 Ultimate Strength in Combined Tension, Torsion and Internal Pressure p in psi.

Ref. 3 gives the following interaction equation,

$$R_t^2 + R_{st}^2 + R_p^2 = 1 \quad \text{- - - - - - - - - - - (C4.29)}$$

Where $R_p = p/p_{max}$, where $p_{max} = \frac{2tF_{tu}}{d}$

where t = wall thickness and d = tube diameter.

The expression for Margin of Safety is,

$$M.S. = \frac{1}{\sqrt{F_t^2 + F_{st}^2 + R_p^2}} - 1 \quad \text{- - - - - - - (C4.30)}$$

PROBLEMS

(1) Fig. 1 shows a portion of a steel tubular fuselage of a small airplane. The critical tension and compression load is shown adjacent to each truss member. Assuming and end fixity coefficient c = 2 for all members, select tube sizes for all members of the truss. The minimum size to be used is 3/4 - .035. The top and bottom longerons should be spliced at least once using telescoping sizes. The material is alloy steel F_{tu} = 95000 and truss is welded.

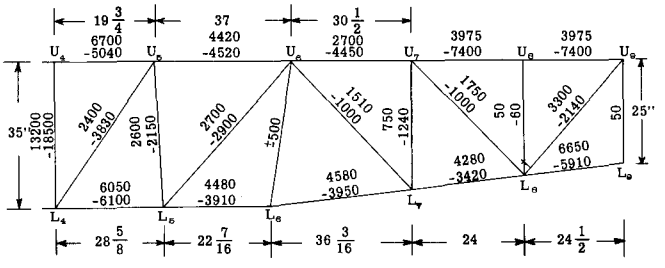

Fig. 1

(2) For the cantilever welded steel tubular truss of Fig. 2, select the lightest members for the truss loading as shown.

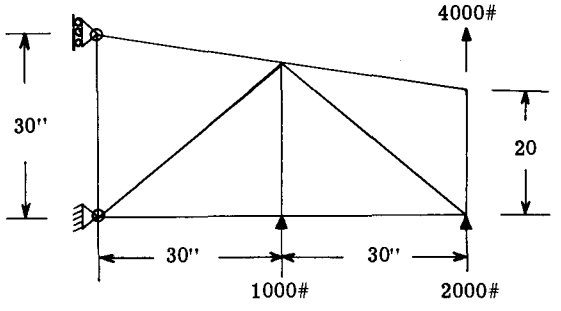

Fig. 2

The top and bottom longerons should be continuous members. Minimum size 3/4 - .035. Use C = 2 for web members and C = 1.5 for longerons. Material (chrome-moly steel F_{tu} = 95000 psi).

(3) If the truss of Fig. 2 is heat treated to 180000 psi after welding, how much weight could be saved over the results obtained in problem (2).

(4) Same as problem (2) but change material to 2024-T3 aluminum alloy round tubes. Members to be fastened together by rivets and gusset plates. For design of tension members assume that rivet or bolt holes cutout 10% of tube area.

(5) Fig. 3 shows a typical tubular engine mount structure. The engine is supported at points A and B. For design purposes assume that engine torque is reacted 60% at A and 40% at B. Tube material is steel F_{tu} = 95000 psi. Use C = 1 for all members. Determine tube sizes for the following design conditions:

Condition I Vertical Load factor = 10 (down)
Thrust Load factor = 2 (forward)
Engine Torque Load factor = 2

Condition II (Same as I except vertical load factor is 5 up.

General Data: Weight of power plant installation = 440 lb.

Maximum engine thrust = 400 lb. Engine H.P. = 120 at 2000 R.P.M.

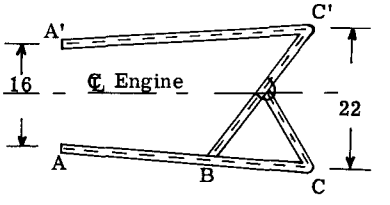

Fig. 3

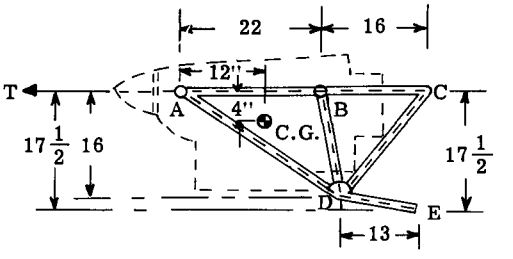

(6) The loads shown in Fig. 4 are to be transmitted to the support at the left, or in other words, a cantilever structure.

The problem is to design the lightest truss configuration using round tubes of alloy steel F_{tu} = 95000 and welded together at the truss joints. Use C = 1.5 for end fixity of all members. There are

no restrictions on type of truss or arrangement of members, however, the goal is the lightest truss. Omit consideration of weight of any gusset plates at truss joints.

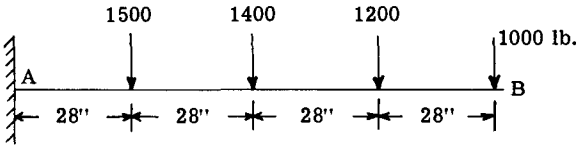

Fig. 4

(7) Same as problem (6), but instead of a cantilever truss use a simply supported truss with supports at points (A) and (B).

(8) Fig. 5 shows a front beam and front lift strut in an externally braced monoplane. The wing beam and lift strut are in the same vertical plane. The ultimate design loads on the beam for the critical conditions are w = 50 lb./in. and w = -30 lbs. per inch. Minus means load is acting down.
   (a) Design a streamline tube to act as the lift strut. Material is 2024-T3 aluminum alloy.
   (b) Same as (a) but made from alloy steel F_{ty} = 75000. Compare the weights of the two designs.

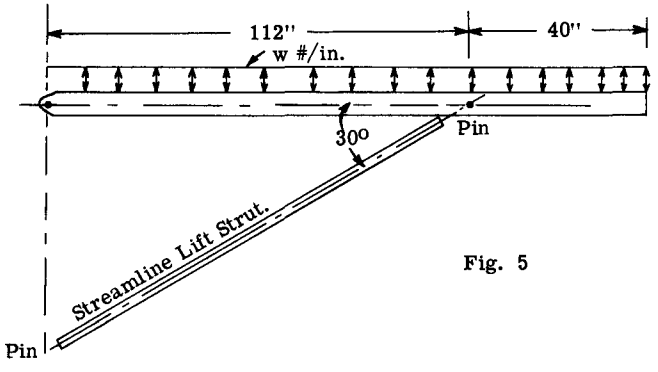

Fig. 5

(9) Fig. 6 illustrates the strut and wire bracing for attaching float to fuselage of a seaplane. Determine the necessary sizes for the streamline struts AC and BD for the following load conditions.

Condition 1. V = -32000 lbs.,
H = - 8000 lbs.
Condition 2. V = - 8000 lbs.,
H = -28000 lbs.
Material 2024-T3 aluminum alloy. Use C=1.

(10) Tube size 2 - .065 round. L = 44 in., C = 1.5. Material alloy steel F_{tu} = 95000, welded at ends. Design ultimate loads equal 22000 lb. compression and 28000 lbs. tension. Find margin of safety.

(11) Same as Problem 10 but heat treated to F_{tu} = 150000 after welding.

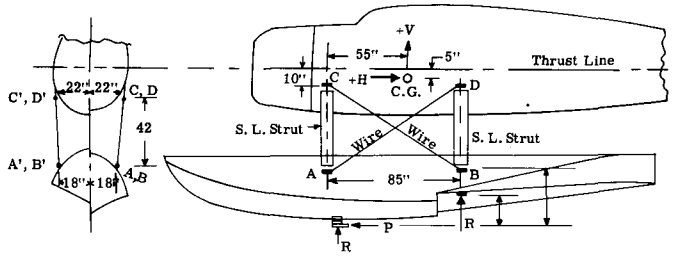

Fig. 6

(12) The ultimate design load if 20,000 lbs. compression. L = 30 in. Use C = 1. Design the lightest round tube from the following materials and compare their weights.
   (a) Aluminum alloy 2024-T3
   (b) Alloy steel F_{tu} = 180,000
   (c) Magnesium alloy F_{cy} = 10,000

(13) Same design load as in problem (10) but design the lightest streamline tube from 2024-T3 aluminum alloy material.

(14) A round tube is to carry an ultimate pure bending moment of 14000 in. lbs. Select the lightest tube size from the following materials and compare their weights.
   (a) Alloy steel F_{tu} = 240,000, (b) 2024-T3 aluminum alloy, (c) Magnesium alloy F_{cy} = 30000, (d) Titanium 6AL-4V alloy.

(15) A round tube 20 inches long is to carry an ultimate torsional moment of 15000 in. lb. Select the lightest tube size from the following materials and compare their weights.
   (a) Alloy steel F_{tu} = 180,000, (b) Aluminum alloy 2024-T3, (c) Magnesium alloy F_{tu} = 36000.

(16) Determine the lightest 2024-T3 aluminum alloy round tube 10 inches long to carry a combined bending and torsional design load of 4500 and 3000 in.lbs. respectively.

(17) Same as Problem 16, but change material to alloy steel F_{tu} = 95000.

(18) A 1-1/2 - .065 2024-T3 round tube 50 inches long is used as a beam-column. The distributed load on beam is 12 lb. per inch and the axial load is 700 lbs. What is the M.S. under these loads.

(19) If the tube in problem (19) was also subjected to a torsional moment of 1400 in.lb., what would be the M.S.

References

(1) Military Handbook. MIL-HDBK-5. March, 1961.
(2) Lockheed Report 2072.
(3) M. A. Sadowsky, "A Principle of Maximum Plastic Resistance," Journal of Applied Mechanics, June, 1943.

CHAPTER C5
BUCKLING STRENGTH OF FLAT SHEET IN COMPRESSION, SHEAR, BENDING AND UNDER COMBINED STRESS SYSTEMS

C5.1 Introduction.

Chapter A18, Part 2, introduced the student to the theoretical approach to the problem of determining the buckling equation for flat sheet in compression with various edge or boundary conditions. A similar theoretical approach has been made for other load systems, such as shear and bending, thus the buckling equations for flat sheet have been available for many years. This chapter will summarize these equations and provide design charts for practical use in designing sheet and plate structures. Most of the material in this chapter is taken from (Ref. 1), NACA Technical Note 3781-Part I, "Buckling of Flat Plates" by Gerard and Becker. This report is a comprehensive study and summary of practically all important theoretical and experimental work published before 1957. The report is especially useful to structural design engineers.

C5.2 Equation for Elastic Buckling Strength of Flat Sheet in Compression.

From Chapter A18, the equation for the elastic instability of flat sheet in compression is,

$$\sigma_{cr} = \frac{\pi^2 k_c E}{12\,(1-\nu_e^2)} \left(\frac{t}{b}\right)^2 \qquad \text{- - - - - - (C5.1)}$$

Where k_c = buckling coefficient which depends on edge boundary conditions and sheet aspect ratio (a/b)

E = modulus of elasticity

ν_e = elastic Poisson's ratio

b = short dimension of plate or loaded edge

t = sheet thickness

C5.3 Buckling Coefficient k_c

Fig. C5.1 shows the change in buckled shape as the boundary conditions are changed on the unloaded edges from free to restrained.

In Fig. (a) the sides are free, thus sheet acts as a column. In Fig. (b) one side is restrained and the other side free, and such a restrained sheet is referred to as a flange. In Fig. (c) both sides are restrained and this restrained element is referred to as a plate.

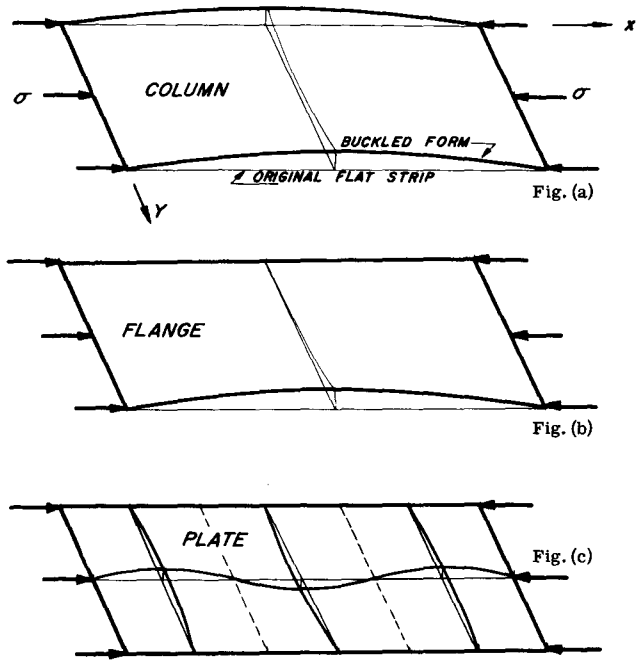

Fig. C5.1 (Ref. 1) Transition from column to plate as supports are added along unloaded edges. Note changes in buckle configurations.

Fig. C5.2 gives curves for finding the buckling coefficient k_c for various boundary or edge conditions and a/b ratio of the sheet.

The letter C on edge means clamped or fixed against rotation. The letter F means a free edge and SS means simply supported or hinged. Fig. C5.3 shows curves for k_c for various degrees of restraint (ε) along the sides of the sheet panel, where ε is the ratio of rotational rigidity of the plate edge stiffener to the rotational rigidity of the plate.

Fig. C5.4 shows curves for k_c for a flange that has one edge free and the other with various degrees of edge restraint. Fig. C5.5 illustrates where the compressive stress varies linearly over the length of the sheet, a typical case being the sheet panels on the upper side of a cantilever wing under normal flight condition.

Fig. C5.6 gives the k_c factor for a long sheet panel with two extremes of edge stiffener, namely a zee stiffener which is a torsionally weak stiffener and a hat section

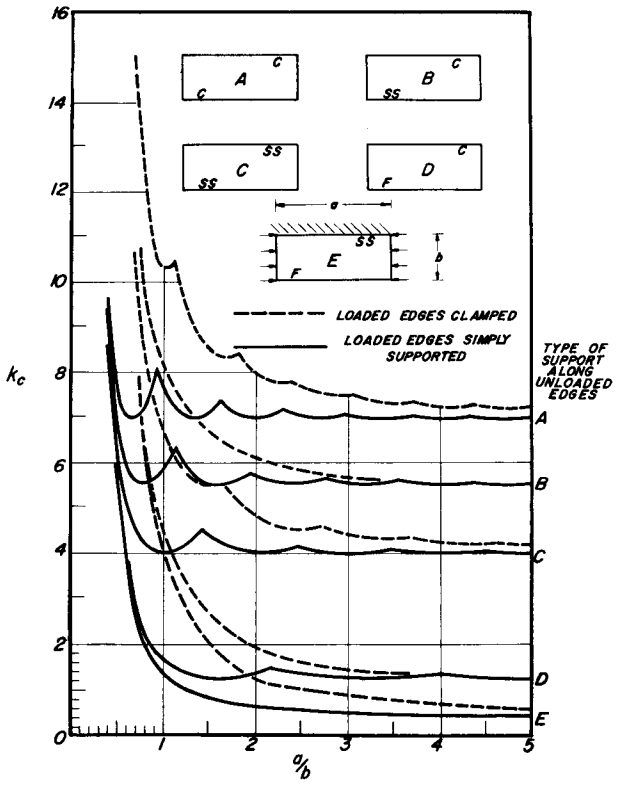

Fig. C5.2 (Ref. 1) Compressive-buckling coefficients for flat rectangular plates.

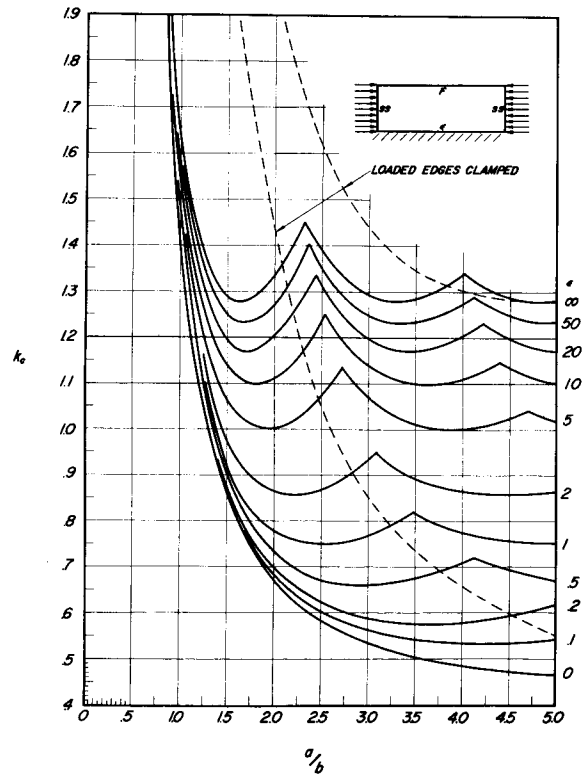

Fig. C5.4 (Ref. 1) Compressive-buckling-stress coefficient of flanges as a function of a/b for various amounts of edge rotational restraint.

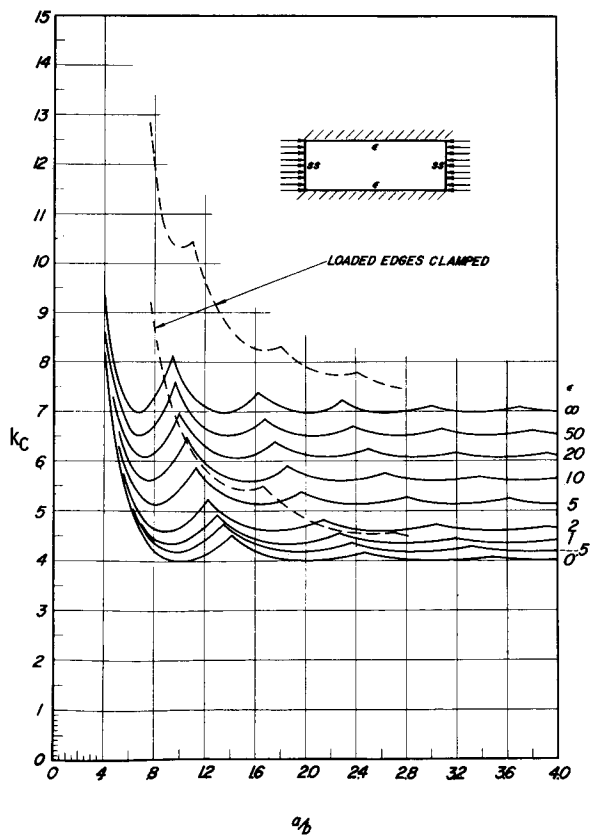

Fig. C5.3 (Ref. 1) Compressive-buckling-stress coefficient of plates as a function of a/b for various amounts of edge rotational restraint.

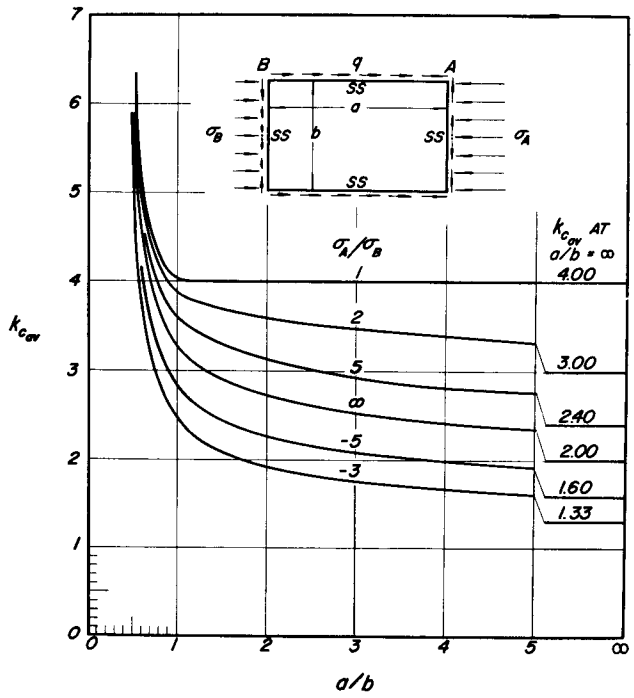

Fig. C5.5 (Ref. 1) Average compressive-buckling-stress coefficient for rectangular flat plate of constant thickness with linearly varying axial load. $\sigma_{av} = \frac{k_{c_{av}} \pi^2 E}{12(1-\nu_e^2)} \left(\frac{t}{b}\right)^2$.

which is a closed section and, therefore, a relatively torsionally strong stiffener. Fig. C5.6a gives the compression buckling coefficients k_c for isosceles triangular plates.

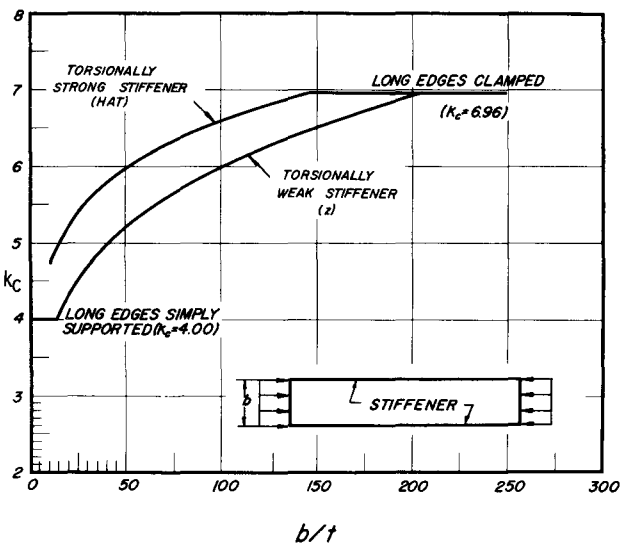

Fig. C5.6 (Ref. 1) Compressive-buckling coefficient for long rectangular stiffened panels as a function of b/t and stiffener torsional rigidity.

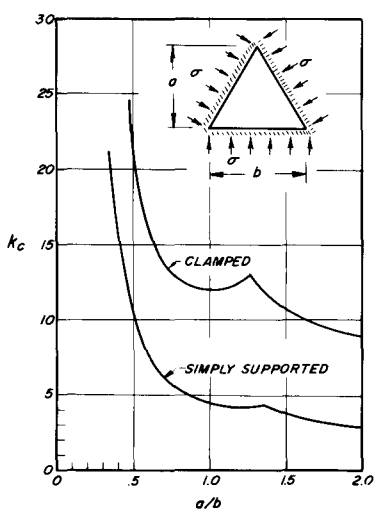

Fig. C5.6a (Ref. 1) Uniform Compression.

Illustrative Problem. Find the compressive buckling stress for a sheet panel with (a) = 10 and b = 5 inches, thickness t = .04 and all edges are simply supported. Material is 2024-T3 aluminum alloy.

Solution: E = 10,700,000. ν_e = 0.3, a/b = 10/5 = 2. The boundary or edge condition corresponds to Case (c) in Fig. C5.2. Thus using curve (c) for a/b = 2, we read k_c = 4.0.

Substituting in Eq. C5.1,

$$\sigma_{cr} = \frac{\pi^2 \times 4.0 \times 10{,}700{,}000}{12\,(1 - .3^2)} \left(\frac{.04}{5}\right)^2 = 2480 \text{ psi.}$$

This stress is below the proportional limit stress for the material, thus equation C5.1 applies and needs no plasticity correction.

C5.4 Equation for Inelastic Buckling Strength of Flat Sheet in Compression.

If the buckling or instability occurs at a stress in the inelastic or plastic stress range, then E and ν are not the same as for elastic buckling, thus a plasticity correction factor is required and equation C5.1 is written,

$$\sigma_{cr} = \frac{\eta\, \pi^2\, k_c\, E}{12(1 - \nu_e^2)} \left(\frac{t}{b}\right)^2 \quad \text{- - - - - - - - - - (C5.2)}$$

Where η is the plasticity reduction factor and equals σ_{cr} plastic/σ_{cr} elastic.

The values of k_c and ν_e are always the elastic values since the coefficient η contains all changes in those terms resulting from inelastic behavior.

A tremendous amount of theoretical and experimental work has been done relative to the value of the so-called plasticity correction factor. Possibly the first values used by design engineers were $\eta = E_t/E$ or $\eta = E_{sec}/E$. Whatever the expression for η it must involve a measure of the stiffness of the material in the inelastic stress range and since the stress-strain relation in the plastic range is non-linear, a resort must be made to the stress-strain curve to obtain a plasticity correction factor. This complication is greatly simplified by using the Ramberg and Osgood equations for the stress-strain curve which involves 3 simple parameters. (The reader should refer to Chapter B1 for information on the Ramberg-Osgood equations.) Thus using the Ramber-Osgood parameters (Ref.1) presents Figs. C5.7 and C5.8 for finding the compressive buckling stress for flat sheet panels with various boundary conditions for both elastic and inelastic buckling or instability.

C5.5 Simple Problems to Illustrate Use of Curves in Figs. C5.7 and C5.8.

The sketch shows a 3 x 9 inch sheet panel. The sides are simply supported. The material is aluminum alloy 2024-T3. The thickness is .094". E = 10,700,000.

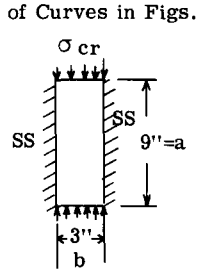

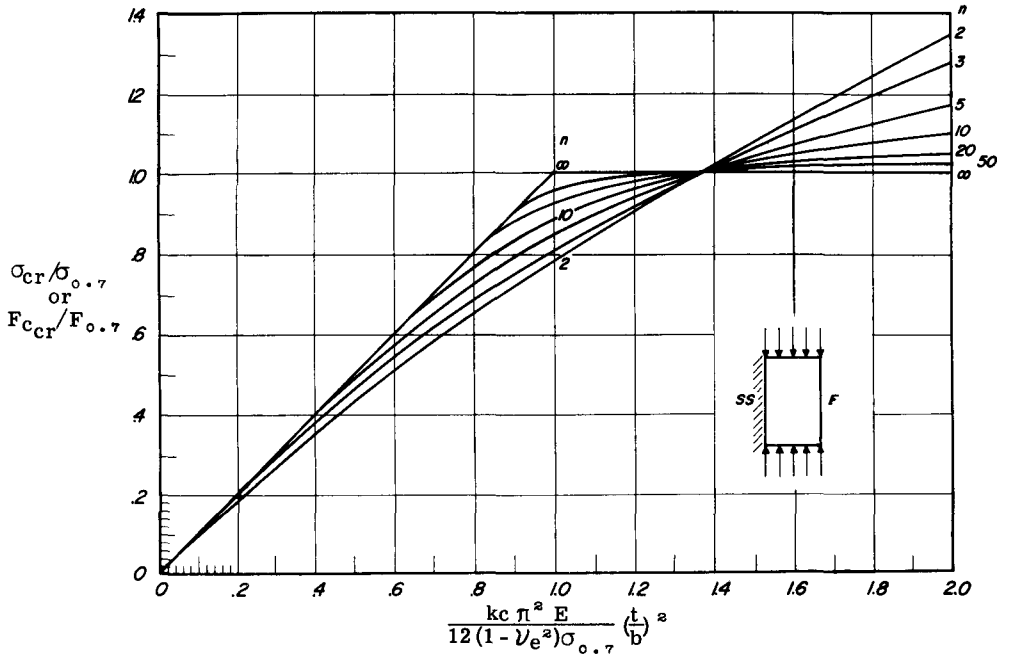

Fig. C5.7 Chart of Nondimensional Compressive Buckling Stress for Long Hinged Flanges. $\eta = (E_s/E)(1 - \nu_e^2)/(1 - \nu^2)$.

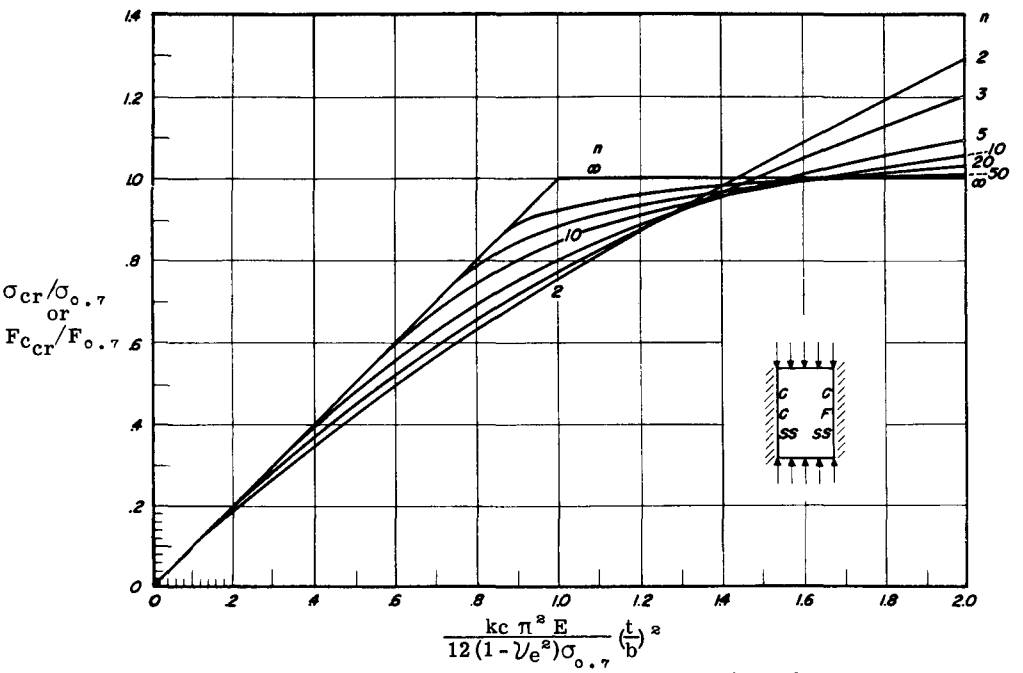

Fig. C5.8 Chart of Nondimensional Compressive Buckling Stress for Long Clamped Flanges and for Supported Plates with Edge Rotational Restraint.

$$\eta = (E_s/2E)\left\{1 + 0.5\left[1 + (3Et/E_s)\right]^{1/2}\right\}(1 - \nu_e^2)/(1 - \nu^2).$$

$\nu_e = 0.3$. Find the buckling stress σ_{cr}.

Solution: We use Fig. C5.8 since it covers the boundary conditions of our problem. The parameter for bottom scale is,

$$\frac{k_c \pi^2 E}{12 (1-\nu_e^2) \sigma_{o.7}} (\frac{t}{b})^2 \quad - - - - - - - - - - - - \quad (A)$$

For a/b = 9/3 = 3, we find k_c from curve (c) of Fig. C5.2 equals 4.0.

The use of Fig. C5.8 involves the use of $\sigma_{o.7}$ and n the Ramberg-Osgood parameters. Referring to Table B1.1 of Chapter B1, we find for 2024-T3 aluminum alloy that $\sigma_{o.7} = 39000$ and the shape factor n = 11.5.

Substituting in (A):-

$$\frac{4.0 \pi^2 \times 10{,}700{,}000}{12 (1 - .3^2) 39{,}000} (\frac{.094}{3})^2 = .98$$

From Fig. C5.8 using .98 on bottom scale and n = 11.5 curve, we read on left hand scale that $\sigma_{cr}/\sigma_{o.7} = .84$.

Then $\sigma_{cr} = 39000 \times .84 = \underline{32800}$ psi.

If we neglected any plasticity effect, then we would use equation C5.2 with $\eta = 1.0$, or,

$$\sigma_{cr} = \frac{\pi^2 \times 4.0 \times 10{,}700{,}000}{12 (1 - .3^2)} (\frac{.094}{3})^2 = \underline{38400} \text{ psi}$$

Whereas the actual buckling stress was 32800, or in this case the plasticity correction factor is 328/384 = .854.

The sheet thickness used in this example of .094 is relatively large. If we change the sheet thickness to .051 inches the results would be practically no correction within the accuracy of reading the curves, and the buckling stress σ_{cr} would calculate to be 11200 psi, which is below the proportional limit stress and thus no plasticity correction.

C5.6 Cladding Reduction Factors.

Aluminum alloy sheet is available with a thin covering of practically pure aluminum and is widely used in aircraft structures. Such material is referred to as alclad or clad aluminum alloy. The mechanical strength properties of this clad material is considerably lower than the core material. Since the clad is located at the extreme fibers of the alclad sheet, it is located where the strains attain their highest value when buckling takes place. Fig. C5.9 shows make up of an alclad sheet and Fig. C5.10 shows the stress-strain curves for cladding, core and alclad combinations.

Thus a further correction must be made for alclad sheets because of the lower strength clad covering material. Thus the buckling stress for alclad sheets can be written:

$$\bar{\sigma}_{cr} = \bar{\eta}\, \sigma_{cr} \quad - - - - - - - - - - - - - - \quad (C5.3)$$

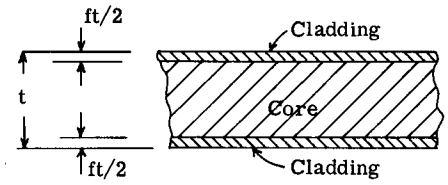

Fig. C5.9

Reference 1 gives simplified cladding reduction factors as summarized in Table C5.1. Thus the buckling stress for alclad sheets is determined for the primary strength properties as normally listed for such materials as illustrated in the two previous example problems. The resulting σ_{cr} is then reduced by use of equation C5.3, using values of $\bar{\eta}$ from Table C5.1.

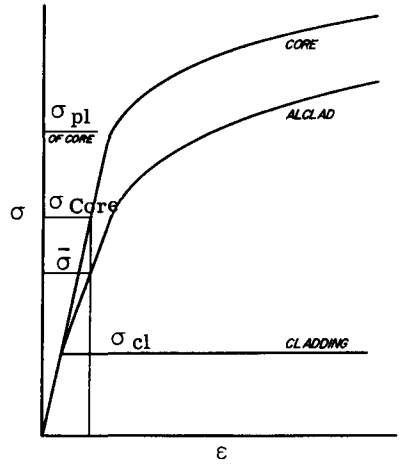

Fig. C5.10 (Ref. 1) Stress-strain Curves for Cladding, Core, and Alclad Combinations. $\bar{\sigma}/\sigma_{core} = 1 - f + \beta f$; $\beta = \sigma_{cl}/\sigma_{core}$.

Table C5.1 (Ref. 1) Summary of Simplified Cladding Reduction Factors

Loading	$\sigma_{cl} < \bar{\sigma}_{cr} < \sigma_{pl}$	$\bar{\sigma}_{cr} > \sigma_{pl}$
Short plate columns	$\frac{1 + (3\beta f/4)}{1 + 3f}$	$\frac{1}{1 + 3f}$
Long plate columns	$\frac{1}{1 + 3f}$	$\frac{1}{1 + 3f}$
Compression and shear panels	$\frac{1 + 3\beta f}{1 + 3f}$	$\frac{1}{1 + 3f}$

BUCKLING UNDER SHEAR LOADS

C5.7 Buckling of Flat Rectangular Plates Under Shear Loads.

The critical elastic shear buckling stress for flat plates with various boundary conditions is given by the following equation:

$$\tau_{cr} = \frac{\pi^2 k_s E}{12 (1 - \nu_e^2)} \left(\frac{t}{b}\right)^2 \quad \text{- - - - - - - - (C5.4)}$$

Where (b) is always the shorter dimension of the plate as all edges carry shear. k_s is the shear buckling coefficient and is plotted as a function of the plate aspect ratio a/b in Fig. C5.11 for simply supported edges and clamped edges.

If buckling occurs at a stress above the proportional limit stress, a plasticity correction must be included and equation C5.4 becomes

$$\tau_{cr} = \frac{\eta_s \pi^2 k_s E}{12 (1 - \nu_e^2)} \left(\frac{t}{b}\right)^2 \quad \text{- - - - - - - - (C5.5)}$$

Test results compare favorably with the results of equation C5.5 if $\eta_s = G_s/G$ where G is the shear modulus and G_s the shear secant modulus as obtained from a shear stress-strain diagram for the material.

A long rectangular plate subjected to pure shear produces internal compressive stresses on planes at 45 degrees with the plate edges and thus these compressive stresses cause the long panel to buckle in patterns at an angle to the plate edges as illustrated in Fig. C5.12, and the buckle patterns have a half wave length of 1.25b.

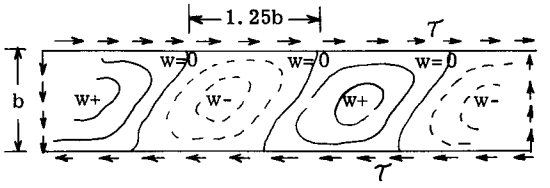

Fig. C5.12 (Ref. 7)

Fig. C5.13 is a chart of non-dimensional shear buckling stress for panels with various edge rotational restraint. This chart is similar to the chart in Figs. C5.7 and C5.8 in that the values $\sigma_{0.7}$ and n must be known for the material before the chart can be used to find the shear buckling stress.

BUCKLING UNDER BENDING LOADS

C5.8 Buckling of Flat Plates Under Bending Loads.

The equation for bending instability of flat plates in bending is the same as for compression and shear except the buckling coefficient k_b is different from k_c or k_s. When a plate in bending buckles, it involves relatively short wave length buckles equal to 2/3 b for long plates with simply supported edges (see Fig. C5.14). Thus the smaller buckle patterns cause the buckling coefficient k_b to be larger than k_c or k_s.

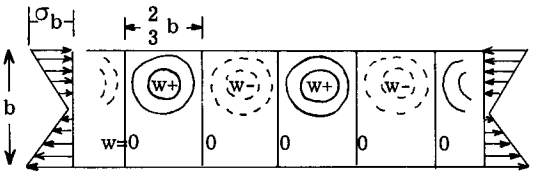

Fig. C5.14 (Ref. 7) Bending Buckle Patterns

For bending elastic buckling the equation is,

$$\sigma_{cr} = \frac{\pi^2 k_b E}{12 (1 - \nu_e^2)} \left(\frac{t}{b}\right)^2 \quad \text{- - - - - - - - (C5.6)}$$

For bending inelastic buckling,

$$\sigma_{cr} = \frac{\eta_b \pi^2 k_b E}{12 (1 - \nu_e^2)} \left(\frac{t}{b}\right)^2 \quad \text{- - - - - - - - (C5.7)}$$

Where k_b is the buckling coefficient and is obtained from Fig. C5.15 for various a/b ratios and edge restraint ε against rotation. In the a/b ratio the loaded edge is (b).

The plasticity reduction factor can be obtained from Fig. C5.8 using simply supported edges.

BUCKLING OF FLAT SHEETS UNDER COMBINED LOADS

The practical design case involving the use of thin sheets usually involves a combined load system, thus the calculation of the buckling strength of flat sheets under combined stress systems is necessary. The approach used involves the use of inter-action equations or curves (see Chapter C1, Art. C1.15 for explanation of inter-action equations).

C5.9 Combined Bending and Longitudinal Compression.

The interaction equation that has been widely used for combined bending and longi-

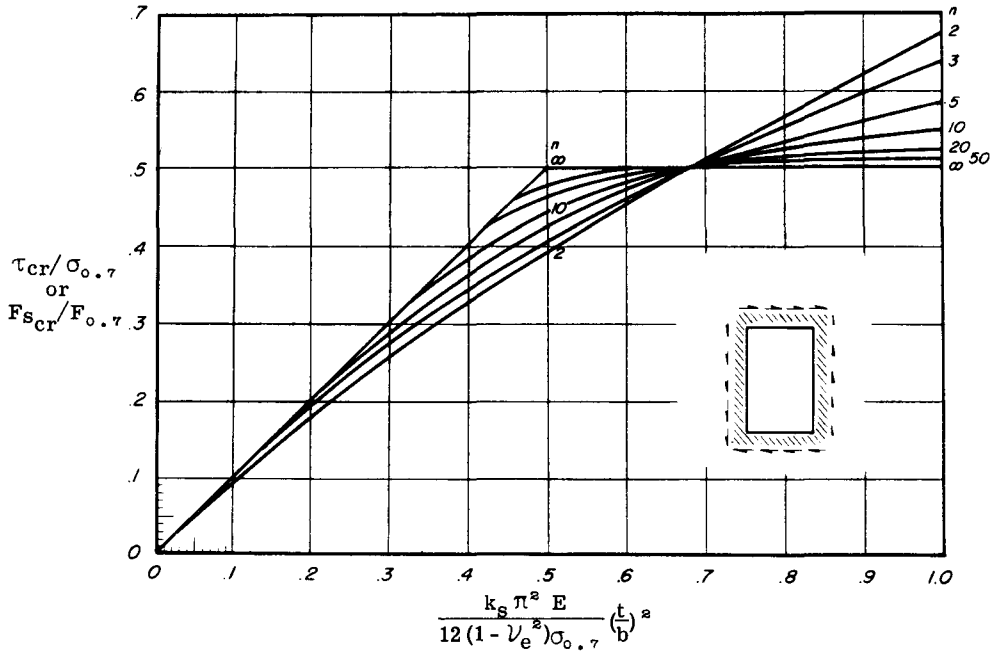

Fig. C5.13 (Ref. 1) Chart of Nondimensional Shear Buckling Stress for Panels With Edge-Rotational Restraint. $\eta = (E_s/E)(1-\nu_e^2)/(1-\nu^2)$.

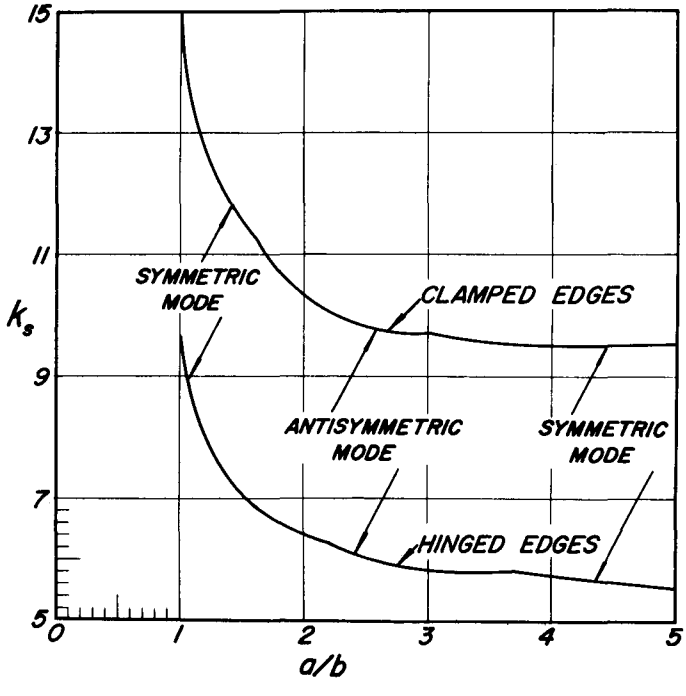

Fig. C5.11 (Ref. 1) Shear-Buckling-Stress Coefficient of Plates as a Function of a/b for Clamped and Hinged Edges.

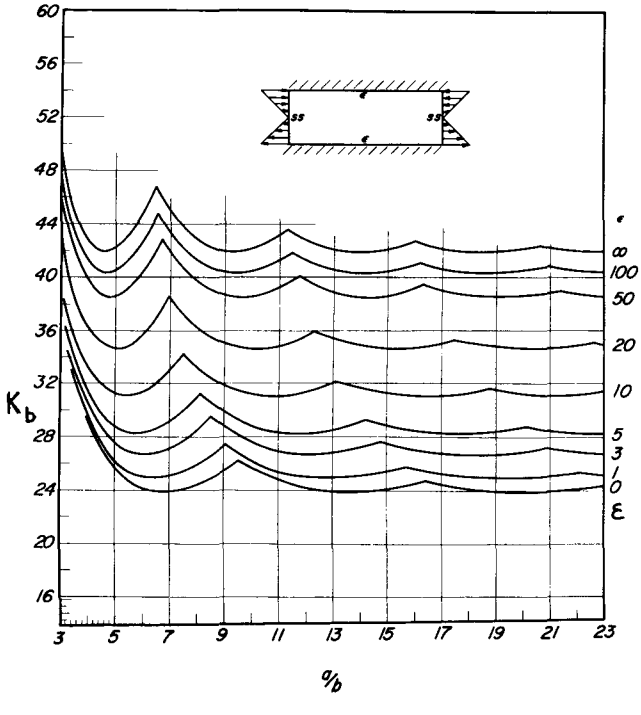

Fig. C5.15 Bending-Buckling Coefficient of Plates as a Function of a/b for Various Amounts of Edge Rotational Restraint.

tudinal compression is,

$$R_b^{1.75} + R_c = 1.0 \quad \text{- - - - - - - - - - - (C5.8)}$$

This equation was originally presented in Ref. 2 and the interaction curve from plotting this equation is found in many of the structures manuals of aerospace companies.

Fig. C5.15 is a plot of eq. C5.8. It also shows curves for various margin of safety values.

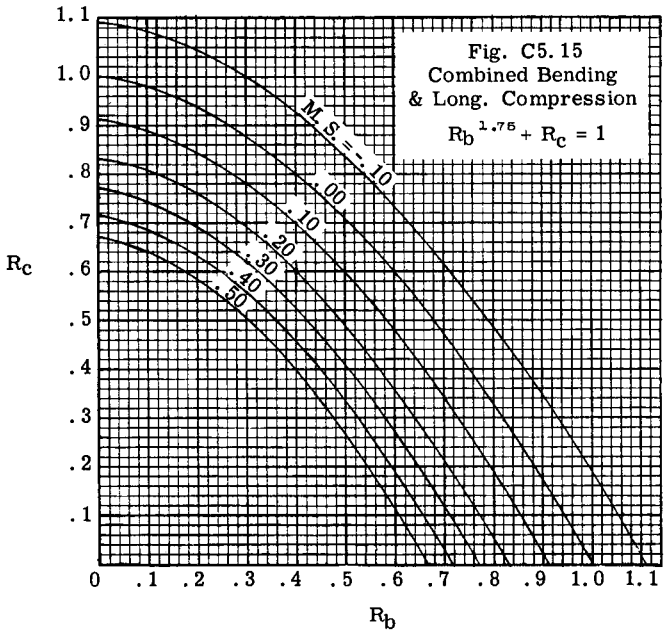

C5.10 Combined Bending & Shear.

The interaction equation for this combined loading (Ref. 1 & 2) is,

$$R_b^2 + R_s^2 = 1 \quad \text{- - - - - - - - - - - - - - (C5.9)}$$

The expression for margin of safety is,

$$M.S. = \frac{1}{\sqrt{R_b^2 + R_s^2}} - 1 \quad \text{- - - - - - - - - (C5.10)}$$

Fig. C5.16 is a plot of equation C5.9. Curves showing various M.S. values are also shown. R_s is the stress ratio due to torsional shear stress and R_{st} is the stress ratio for transverse or flexural shear stress.

C5.11 Combined Shear and Longitudinal Direct Stress. (Tension or Compression.)

The interaction equation is (Ref. 3,4)

$$R_L + R_s^2 = 1.0 \quad \text{- - - - - - - - - - - - - (C5.11)}$$

$$M.S. = \frac{2}{(R_L + \sqrt{R_L^2 + 4R_s^2})} - 1 \quad \text{- - - - (C5.12)}$$

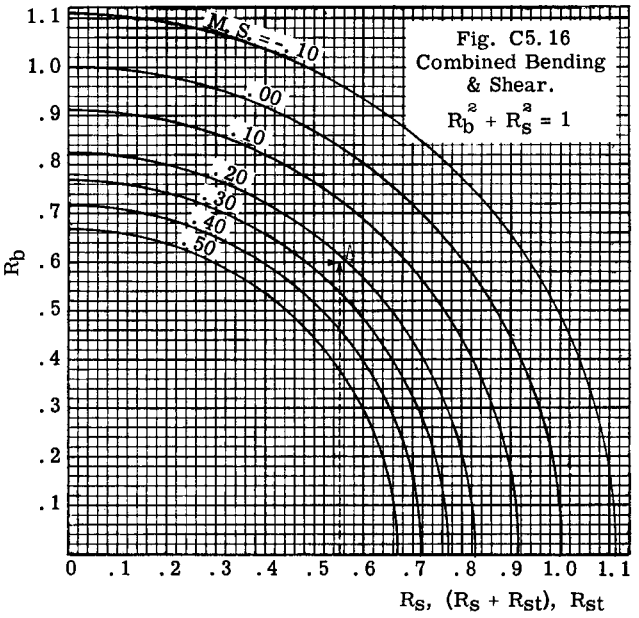

Fig. C5.17 is a plot of equation C5.11. If the direct stress is tension, it is included on the figure as negative compression using the compression allowable.

C5.12 Combined Compression, Bending & Shear.

From Ref. 5, the conditions for buckling are represented by the interaction curves of Fig. C5.18. This figure tells whether the sheet will buckle or not but will not give the margin of safety. Given the ratios R_c, R_s and R_b:- if the value of the R_c curve defined by the given value of R_b and R_s is greater numerically than the given value of R_c, then the panel will buckle.

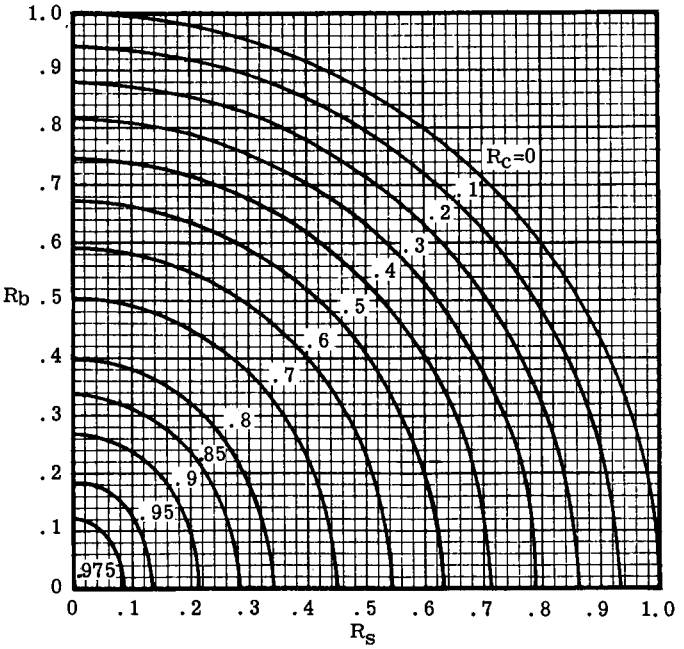

Fig. C5.18 (Ref. 5)

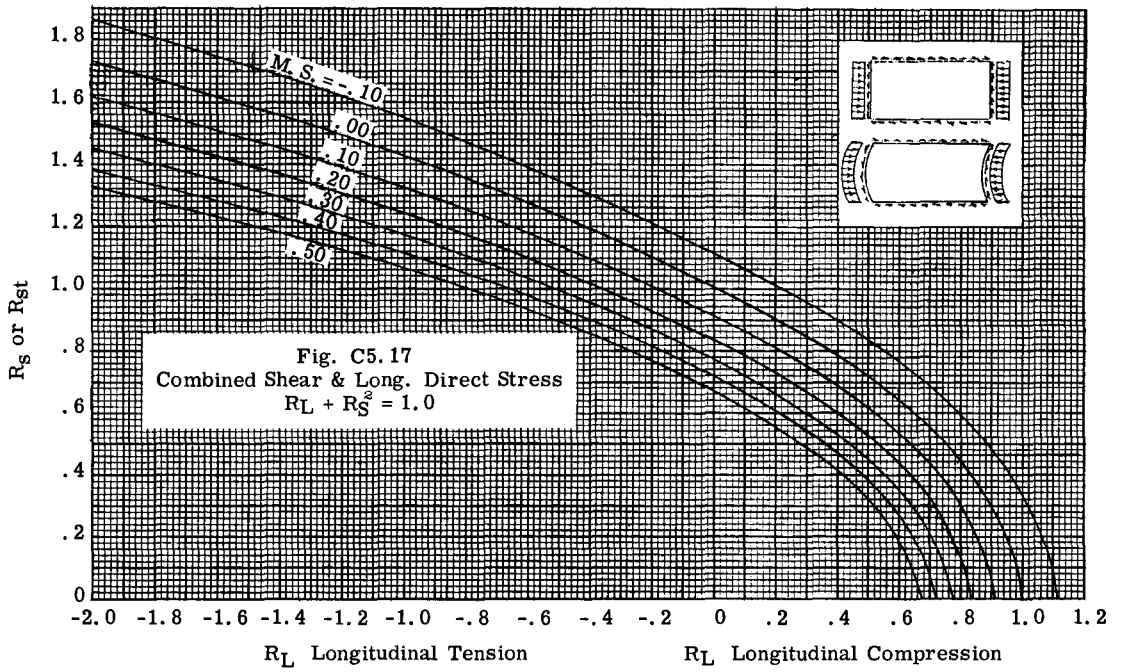

Fig. C5.17
Combined Shear & Long. Direct Stress
$R_L + R_S^2 = 1.0$

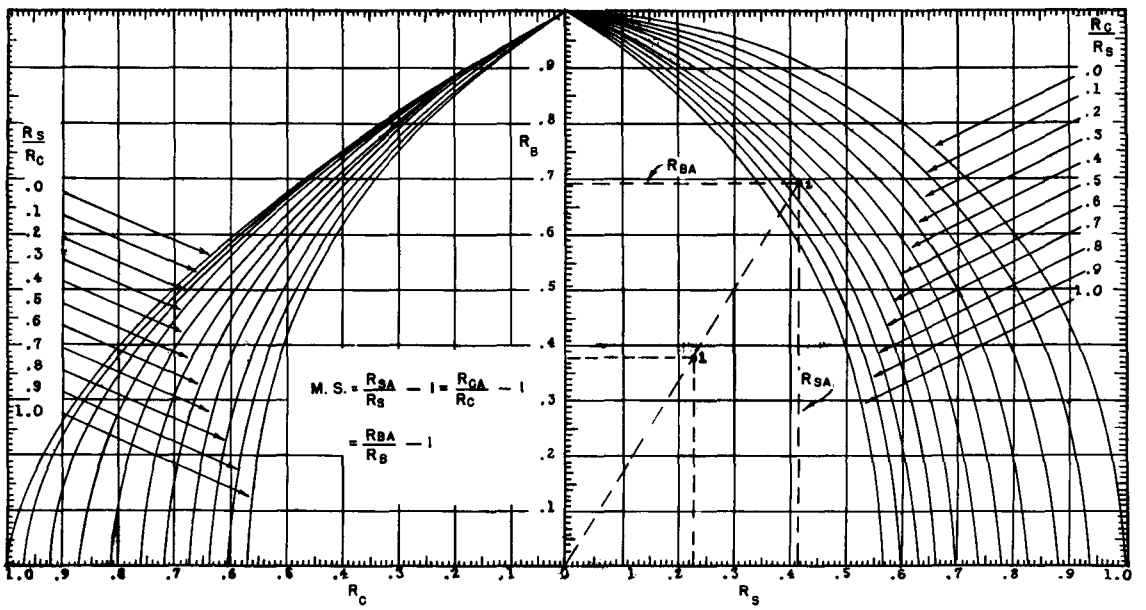

Fig. C5.19 (Ref. 5) Combined Compression, Bending and Shear.

The margin of safety of elastically buckled flat panels may be determined from Fig. C5.19. The dashed lines indicate a typical application where R_c = .161, R_s = .23, and R_b = .38. Point 1 is first determined for the specific value of R_s and R_b. The dashed diagonal line from the origin 0 through point 1, intersecting the related R_c/R_s curve at point 2, yields the allowable shear and bending stresses for the desired margin of safety calculations. (Note when R_c is less than R_s use the right half of the figure; in other cases use the left half).

C5.13 Illustrative Problems.

In general a structural component composed of stiffened sheet panels will not fail when buckling of the sheet panels occurs since the stiffening units can usually continue to carry more loading before they fail. However, there are many design situations which require that initial buckling of sheet panels satisfy certain design specifications. For example, the top skin on a low wing passenger airplane should not buckle under accelerations due to air gusts which occur in normal every day flying thus preventing passengers from observing wing skin buckling in normal flying conditions. Another example would be that no buckling of fuselage skin panels should occur while airplane is on ground with full load aboard in order to prevent public from observing buckling of fuselage skin. In many airplanes, fuel tanks are built integral with the wing or fuselage, thus to eliminate the chances of leakage developing, it is best to design that no buckling of sheet panels that bound the fuel tanks occur in flying and landing conditions. In some cases aerodynamic or rigidity requirements may dictate no buckling of sheet panels. To insure that buckling will not occur under certain load requirements, it is good practice to be conservative in selecting or calculating the boundary restraints of the sheet panels.

Problem 1.

Fig. C5.20 shows a portion of a cantilever wing composed of sheet, stiffeners and ribs. The problem is to determine whether skin panels marked (A), (B) and (C) will buckle under the various given load cases. The sheet material is aluminum alloy 2024-T3.

Load Case 1.

P_1 = 700 lb., P_2 = 0, P_3 = 0

With only loads P_1 acting, the one cell stiffened cantilever beam is subjected to a compressive axial load of 2 x 700 = 1400 lb. Since the P_1 loads are not acting through the centroid of the cross-section, a bending moment is produced about the x-x axis equal to 1400 x 3.7 = 5170 in. lb. = M_X, where 3.7 is distance from load P_1 to x-x axis.

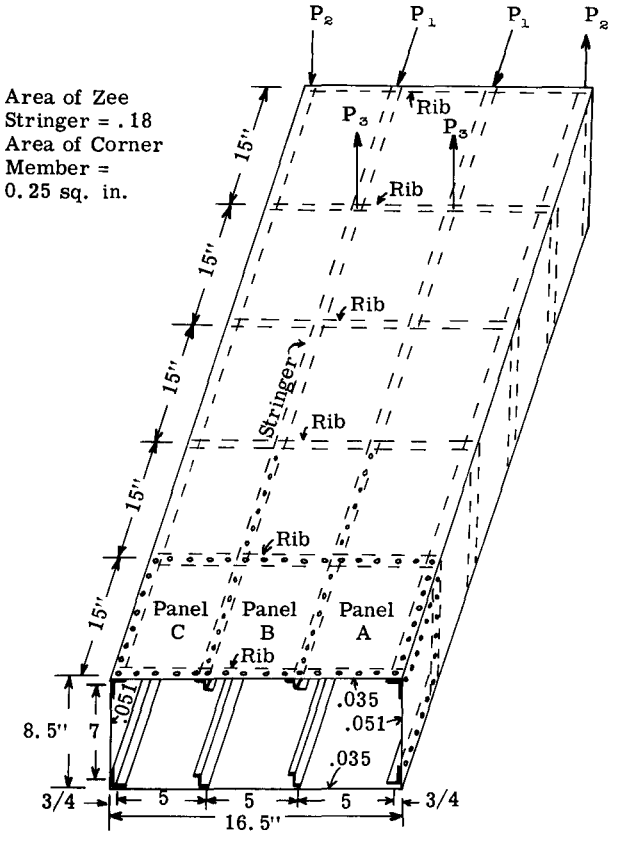

Fig. C5.20

The sheet thicknesses, stiffener areas and all necessary dimensions are shown on Fig. C5.20. The total cross-sectional area of beam section including all skin and stringers is 3.73 sq. in. The moment of inertia about x-x centroidal axis calculates to be 49.30 $in.^4$.

Since the beam section is symmetrical, the top panels A, B and C are subjected to the same stress under the P_1 load system.

Compressive stress due to transferring loads P_1 to centroid of beam cross-section is,

$f_c = 2P_1/\text{area} = 1400/3.73 = 375$ psi

Compressive stress due to constant bending moment of 5170 in. lbs. is,

$f_c = M_X Z/I_X = 5170 \times 4.233/49.30 = 444$ psi

Total f_c = 375 + 444 = 819 psi.

The skin panels are subjected to compression as shown in Fig. a. The boundary edge conditions given by the longitudinal stiffeners

and the rib flanges will be conservatively assumed as simply supported. ($F_{c_{cr}}$ is same as σ_{cr})

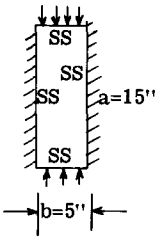

Fig. (a)

$$F_{c_{cr}} = \frac{\pi^2 k_c E}{12 (1-\nu_e^2)} \left(\frac{t}{b}\right)^2$$

(See Eq. C5.1)

a/b of skin panel = 15/5 = 3

From Fig. C5.2 for Case C, we read $k_c = 4.0$

$$F_{c_{cr}} = \frac{\pi^2 \times 4.0 \times 10{,}700{,}000}{12 (1 - 0.3^2)} \left(\frac{.035}{5}\right)^2 = 1900 \text{ psi}$$

Since $F_{c_{cr}}$ the buckling stress is greater than the applied stress f_c, the panels will not buckle.

M.S. = $(F_{c_{cr}}/f_c) - 1 = (1900/819) - 1 = 1.32$

Load Case 2.

$P_1 = 700$ lb., $P_2 = 500$, $P_3 = 0$

The two loads P_2 acting in opposite directions produce a couple or a torsional moment of 500 x 16.5 = 8250 in. lb. on the beam structure, which means we have added a pure shear stress system to the compressive stress system of Case 1 loading.

The shear stress in the top panels A, B and C is,

$f_s = T/2At = 8250/2 \times 138 \times .035 = 854$ psi.

(Where A is the cell inclosed area)

The shear buckling stress is

$$F_{s_{cr}} = \frac{\pi^2 k_s E}{12 (1 - \nu_e^2)} \left(\frac{t}{b}\right)^2 \quad - - - - \text{(See Eq. C5.4)}$$

a/b = 15/5 = 3. From Fig. C5.11, for hinged or simply supported edges, we read $k_s = 5.8$.

$$F_{s_{cr}} = \frac{\pi^2 \times 5.8 \times 10{,}700{,}000}{12 (1 - .3^2)} \left(\frac{.035}{5}\right)^2 = 2760 \text{ psi.}$$

The sheet panels are now loaded in combined compression and shear so the interaction equation must be used. From Art. C5.12 the interaction equation is $R_c + R_s^2 = 1$.

$R_c = f_c/F_{c_{cr}} = 819/1900 = .431$

$R_s = f_s/F_{s_{cr}} = 854/2760 = .309$

The $R_c + R_s^2 = .431 + .309^2 = .526$. Since the result is less than 1.0, no buckling occurs.

$$\text{The M.S.} = \frac{2}{R_c + \sqrt{R_c^2 + 4R_s^2}} - 1$$

$$= \frac{2}{.431 + \sqrt{.431^2 + 4 \times .309^2}} - 1 = .69$$

Load Case 3.

$P_1 = 700$, $P_2 = 500$, $P_3 = 100$ lb.

The two loads P_3 produce bending and flexural shear on the beam. The bending moment produces a different end compressive stress on the three sheet panels since the bending moment is not constant over the panel moment. To simplify we will take average bending moment on the panel.

$M_{x(av)} = 200 \times 52.5 = 10500$ in. lb.

f_c due to this bending = $M_x Z/I_x = 10500 \times 4.233/49.3 = 903$ psi.

Total $f_c = 903 + 819 = 1722$ psi.

$R_c = f_c/F_{c_{cr}} = 1722/1900 = .906$

The two loads P_3 produce a traverse shear load V = 200 lb. The flexural shear stress must be added to the torsional shear stress as found in Case 2 loading.

Due to symmetry of beam section and P_3 loading the shear flow q at midpoint of sheet panel (B) is zero. We will thus start at this point and go clockwise around cell. The shear flow equation (see Chapter A15) is,

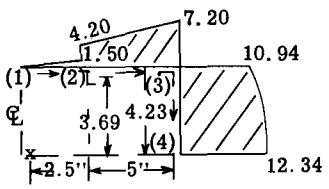

Fig. (b)

$$q = \frac{V}{I_x} \Sigma ZA$$

$$q = -\frac{200}{49.3} = 4.05 \Sigma ZA$$

$q_1 = 0$ (Refer to Fig. b)

$q_{21} = -4.05 \times 2.5 \times .035 \times 4.23 = -1.50$

$q_{23} = -1.50 - 4.05 \times .18 \times 3.69 = -4.20$

$q_{32} = -4.20 - 4.05 \times 5 \times .035 \times 4.23 = -7.20$

$q_{34} = -7.20 - 4.05 \times .25 \times 3.69 = -10.94$

$q_{43} = -10.94 - 4.05 \times .051 \times 3.69 \times 3.69/2 = -12.34$

(See Fig. b for plot of shear flow)

The shear flow q on panel (A) varies from 4.20 to 7.20 or the average q = (4.2 + 7.2)/2 = 5.7. Thus the average shear stress is 5.7/.035 = 163 psi. It is in the same direction as the torsional shear flow and thus is additive.

Total f_s = 163 + 854 = 917 psi

$$R_S = f_s/F_{s_{cr}} = 917/2760 = .332 \quad .$$

$R_c + R_s^2 = 1$, Subt.:- $.906 + .332^2 = 1.016$, since the result is greater than 1.0, initial buckling has started. The margin of safety is slightly negative and equals,

$$M.S. = \frac{2}{.905 + \sqrt{.905^2 + 4 \times .332^2}} - 1 = -.01$$

In this example problem, the panels were assumed simply supported, which is conservative. Reference to Fig. C5.6 shows that k_c could be assumed higher as the panel is riveted to a zee shaped stringer which has some torsional resistance and thus panel is not free to rotate at its boundaries.

Panel (C) is less critical because the flexural shear is acting opposite to the torsional shear stress, thus f_s total = 845 - 163 = 682 psi. The R_s = 682/2760 = .246.

$R_c + R_s^2 = .905 + .246^2 = .966$. Since the result is less than 1.0, panel will not buckle.

Panel (B) carries a small shear flow, being zero at center of panel and increasing uniformly to 1.5 lb. per inch at the edges, and flowing in opposite directions from the centerline. Thus transverse shear will have negligible effect. Thus R_s = 854/2760 = .309.

$R_c + R_s^2 = .905 + .309^2 = 1.00$, or panel (B) is on the verge of buckling under the assumptions made in the solution.

C5.14 Problems.

(1) A sheet panel is 3" x 9" x .051" in size. Consider all sides as simply supported. Determine the buckling load if the compressive load is applied normal to the 3" sides. Do so for 3 different materials, (1) aluminum alloy 7075-T6, (2) magnesium HK31A, (3) Titanium Ti-8Mn.

(2) In Problem (1) if all edges were clamped, what would be the buckling load.

(3) In Problem (1) if the 9" sides were clamped or fixed and the 3" sides simply supported, what would be the buckling load.

(4) A sheet panel 5" x 12.5" x .051 has all edges simply supported. The panel is subjected to combined compression and shear loads which produce the following stresses:-

f_c = 2400 psi, applied normal to 5" side.

f_s = 2800 psi. Will the sheet buckle under the given load system if made of aluminum alloy 2024-T3 material. What is the margin of safety.

(5) If the material in problem (4) is changed to alloy steel F_{tu} = 95000 psi, what would be the margin of safety. If sheet was heat treated to F_{tu} = 180,000, what would be the M.S.

(6) A 3" x 12" x .040" sheet panel is subjected to the following combined stresses. f_c = 3000, f_b = 10000, f_s = 8000. The f_c and f_b stresses are normal to the 3" side. If sides are simply supported, will panel buckle if made of 7075-T6 aluminum alloy. What is M.S.

What will be the M.S. if material is changed to Titanium Ti-8Mn.

References:-

(1) NACA Tech. Note 3781, 1957.

(2) ANC-5 Amendment 2. Aug. 1946.

(3) NACA ARR.No. L6A05

(4) NACA ARR.No. 3K13

(5) ANC-5 Revision of 1942

General References on Theory

(6) NACA Tech. Note 3781.

(7) "Introduction to Structural Stability Theory". By Gerard. Book published by McGraw-Hill.

(8) "Theory of Elastic Stability", by Timoshenko, McGraw-Hill Co.

(9) "A Unified Theory of Plastic Buckling of Columns and Plates", NACA Report 898. By Stowell.

(10) "Plastic Buckling of Simply Supported Compressed Plates", NACA T.N. 1817. By Pride & Heimerl.

(11) "Buckling of Metal Structures" by Bleigh. McGraw-Hill Co.

CHAPTER C6
LOCAL BUCKLING STRESS FOR COMPOSITE SHAPES

C6.1 Introduction.

Thin flat sheet is inefficient for carrying compressive loads because the buckling stresses are relatively low. However, this weakness or fault can be greatly improved by forming the flat sheet into composite shapes such as angles, channels, zees, etc. Most of the many composite shapes can also be made by the extruding process. Formed or extruded members are widely used in Flight Vehicle Structures, thus methods of calculating the compressive strength of such members is necessary.

C6.2 Compressive Buckling Stress for Equal Flanged Elements.

The simplest equal flanged member that can be formed is the angle shape. Other shapes with equal flanges are the T section and the cruciform section as shown in Fig. C6.1.

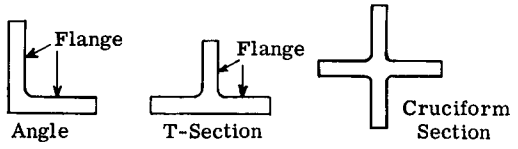

Fig. C6.1

These sections can be considered as a group of long flanges, as illustrated, for the angle section in Fig. C6.2. Since the flanges which make up the section are equal in size, each flange will buckle at the same stress. Therefore each flange cannot restrain the other and thus it can be assumed that each flange is simply supported along the flange junction as illustrated in Fig. C6.2.

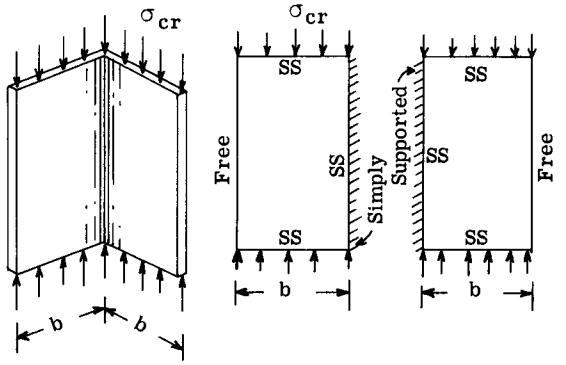

Fig. C6.2

From Equation C5.1 of Chapter C5, the buckling compressive stress for a long flange is,

$$\sigma_{cr} = \frac{\pi^2 k_c E}{12(1-\nu_e^2)} \left(\frac{t}{b}\right)^2$$

From Fig. C5.2 of Chapter C5, $k_c = .43$, then

$$\sigma_{cr} = \frac{0.43\,\pi^2 E}{12(1-0.3^2)} \left(\frac{t}{b}\right)^2 = 0.388\,E\left(\frac{t}{b}\right)^2 \quad - - - \text{C6.1}$$

If the buckling stresses are above the proportional limit stress, use Fig. C5.7 in Chapter C5 to take care of the plasticity effect.

For formed angles, the flange width b extends to centerline of adjacent leg, but for extruded angles, the width b extends to inside edge of the adjacent flange or leg.

C6.3 Compressive Buckling Stress for Simple Flange-Web Elements.

The most common flange-web structural shapes are channels, zees, and hat sections. A flange has one unloaded edge free, whereas a web has no free unloaded edge and thus has an unknown restraint on the boundary between the web and the flange. Fig. C6.3 shows the break down of a Z section into two flange and one web plate elements.

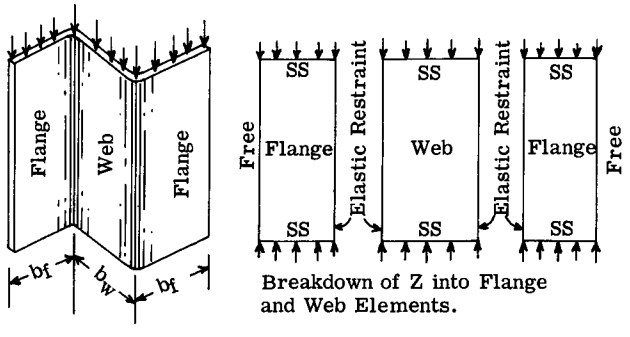

Breakdown of Z into Flange and Web Elements.

Fig. C6.3

The buckling strength of the web and flange elements depends on the boundary restraint between the two elements. If this restraint which is unknown could be found in terms of a known rotational restraint ε as presented in Chapter C5, the buckling coefficients could be found from charts in Chapter C5. Having the

buckling stress for each element, the critical buckling stress will be the smaller of the two. The buckling load based on the buckling stress is not the failing load as more load can be taken by the material in the corner regions before local failure or crippling takes place. The subject of local crippling of formed and extruded shapes is covered in Chapter C7.

Using the moment distribution method or a step by step analysis procedure, several research studies have determined the restraint factors between web and flange elements for simple shapes like channels, Z, H, square tubes and formulated design charts for such shapes. (Refs. 1 to 5 inclusive.)

C6.4 Design Charts for Local Buckling Stresses of Some Composite Web-Flange Shapes.

Figs. C6.4 to C6.7 inclusive give charts for determining the local buckling stress of channel, Z, H, square tube and hat shaped sections. For formed sections, the width b extends to centerline of adjacent element and for extruded sections the width b extends to inside edge of adjacent element.

C6.5 Problems Illustrating Use of Charts.

PROBLEM 1.

The Z section in Fig. (a) is formed from aluminum alloy 2024-T3 sheet. What compressive stress will start local buckling of an element of the member.

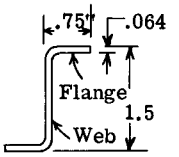

Fig. (a)

Solution:-

$b_w = 1.5 - .064 = 1.436$

$b_f = 0.75 - .032 = 0.718$

$b_f/b_w = 0.718/1.436 = .50$

$t_w/t_f = .064/.064 = 1.0$

From Fig. C6.4, we read $k_w = 2.9$

$$\sigma_{cr} = \frac{k_w \pi^2 E}{12(1-\nu_e^2)} \left(\frac{t_w}{b_w}\right)^2 \quad \text{- - - - - - - - - - (A)}$$

$$\sigma_{cr} = \frac{2.9\ \pi^2 \times 10{,}700{,}000}{12(1-.3^2)} \left(\frac{.064}{1.436}\right)^2 = 56100 \text{ psi}$$

This stress is above the proportional limit stress of the material, thus a plasticity correction must be made. The buckling occurs on the flange.

From Table B1.1 of Chapter B1, we obtain for 2024-T3 aluminum alloy:- $\sigma_{o.7} = 39000$ and $n = 11.5$.

For the plasticity correction of shapes covered in Fig. C6.4 (Ref. 4), the plasticity correction for a flange free on one edge can be used with accuracy. Thus we can use chart in Fig. C5.7 of Chapter C5.to correct for plasticity effects.

The parameter for bottom scale of Fig. C5.7 is equation (A) divided by $\sigma_{o.7}$, or 56100/39000 = 1.44. Using this value and the n = 11.5 curve, we read from Fig. C5.7 that $\sigma_{cr}/\sigma_{o.7} = 1.02$.

Therefore the local buckling stress is

$\sigma_{cr} = 39000 \times 1.02 = \underline{39800}$ psi.

PROBLEM 2.

If the member in Problem 1 is subjected to a 300°F temperature for 2 hours duration, what would be the local buckling stress.

From Table B1.1 for this temperature condition,

$\sigma_{o.7} = 35700$, $E_c = 10{,}300{,}000$, $n = 15$

$$\frac{k_w \pi^2 E}{12(1-\nu_e^2)(\sigma_{o.7})} \left(\frac{t_w}{b_w}\right)^2 = \frac{2.9\ \pi^2 \times 10{,}300{,}000}{12(1-.3^2)\ (35700)}$$

$$\left(\frac{.064}{1.436}\right)^2 = 1.51.$$

Using this value on bottom scale of Fig. C5.7 and n curve = 15, we read $\sigma_{cr}/\sigma_{o.7} = 1.03$. Thus $\sigma_{cr} = 1.03 \times 35700 = \underline{36800}$ psi.

PROBLEM 3.

Same as Problem 1, but change material to Titanium Ti-8Mn Sheet.

From Table B1.1 we obtain for this material:- $E_c = 15{,}500{,}000$, $\sigma_{o.7} = 119500$, $n = 13.7$.

$$\sigma_{cr} = \frac{2.9\ \pi^2 \times 15{,}500{,}000}{12(1-.3^2)} \left(\frac{.064}{1.436}\right)^2 = \underline{81200} \text{ psi.}$$

This stress is near the proportional limit stress so plasticity correction should be small if any.

$\sigma_{cr}/\sigma_{o.7} = 81200/119500 = .68$

From Fig. C5.7, using n = 13.7 curve, we read $\sigma_{cr}/\sigma_{o.7} = .68$. Then $\sigma_{cr} = 119500 \times 0.68 = 81300$, thus no plasticity correction.

PROBLEM 4.

The rectangular tube has the dimensions as shown in Fig. (b). It is extruded from aluminum alloy 2014-T6. Determine the local compressive buckling stress.

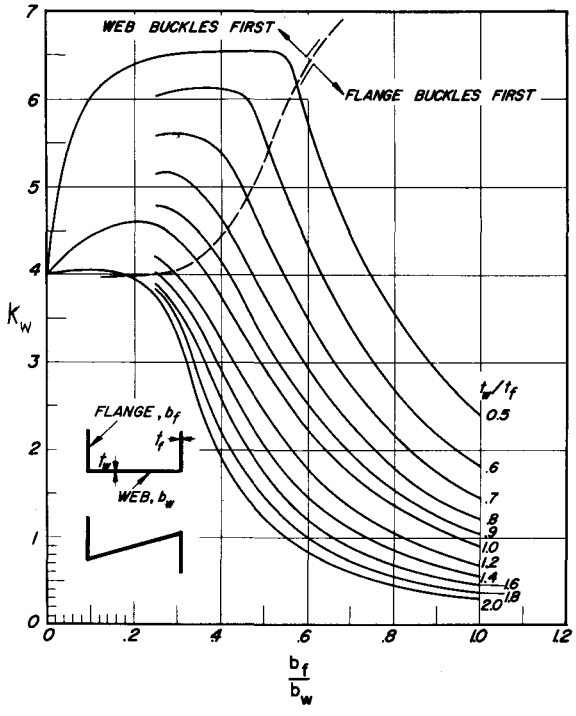

Fig. C6.4 (Ref. 2) Channel- and Z-section stiffeners.

$$\sigma_{cr} = \frac{k_w \pi^2 E}{12\,(1 - \nu_e^2)} \frac{t_w^2}{b_w^2}$$

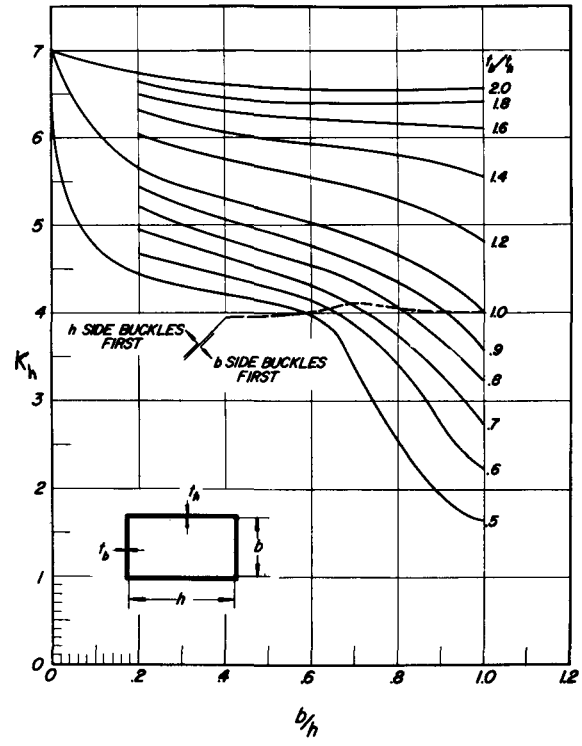

Fig. C6.6 (Ref. 2) Rectangular-tube-section stiffeners.

$$\sigma_{cr} = \frac{k_h \pi^2 E}{12\,(1 - \nu_e^2)} \left(\frac{t_h}{h}\right)^2$$

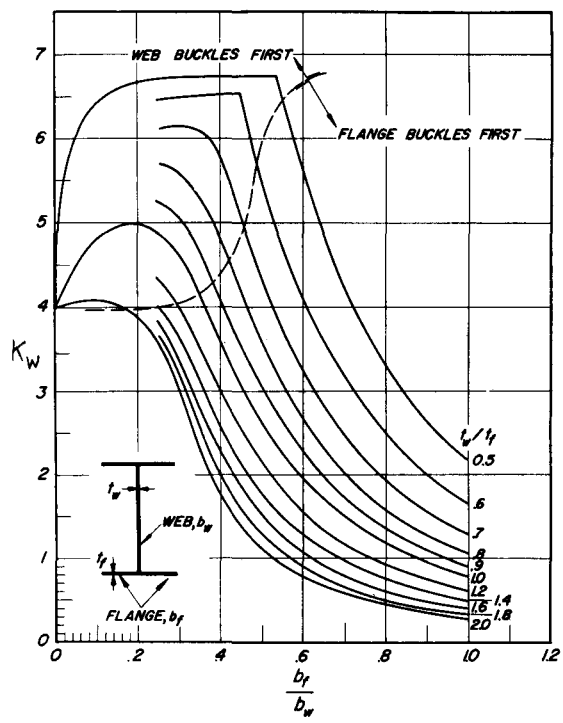

Fig. C6.5 (Ref. 2) H-section stiffeners.

$$\sigma_{cr} = \frac{k_w \pi^2 E}{12\,(1 - \nu_e^2)} \frac{t_w^2}{b_w^2}$$

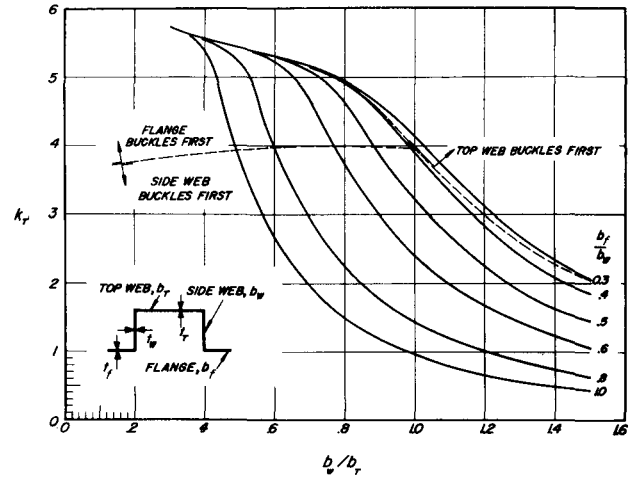

Fig. C6.7 (Ref. 5) Buckling stress for hat-section stiffeners.

$t = t_f = t_w = t_T$; $\sigma_{cr} = \dfrac{k_T \pi^2 E}{12\,(1 - \nu_e^2)} \dfrac{t^2}{b_T^2}$. (Data of Ref. 12.)

Solution:-

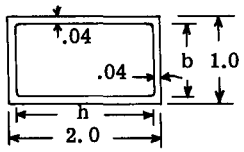

Fig. (b)

b = 1 - .08 = .92

h = 2 - .08 = 1.92

b/h = .92/1.92 = .479

t_b/t_h = 1.0

From Fig. C1.6, we read k_h = 5.2.

$$\sigma_{cr} = \frac{5.2\ \pi^2 \times 10{,}700{,}000}{12(1-.3^2)} \left(\frac{.04}{1.92}\right)^2 = 21900 \text{ psi.}$$

As shown in Fig. C6.6, buckling occurs on the h side of the tube. The computed buckling stress is below the proportional limit stress, thus no plasticity correction.

PROBLEM 5.

Same as Problem 4 but change the thickness of the h side to .072, but leave the b side .04 in thickness.

Solution:-

b = 1 - .144 = .856

h = 2 - .08 = 1.92

b/h = .856/1.92 = .446

t_b/t_h = .04/.072 = .555

From Fig. C6.6, k_h = 4.3

$$\sigma_{cr} = \frac{4.3\ \pi^2 \times 10{,}700{,}000}{12(1-.3^2)} \left(\frac{.072}{1.92}\right)^2 = 58600 \text{ psi.}$$

This stress is above the proportional limit stress thus a plasticity correction is necessary. (Ref. 4) gives no value for a plasticity correction but recommends the correction for a clamped long flange which is a slightly conservative correction. This plasticity correction should also be used for the hat shape as shown in Fig. C6.7.

Thus Fig. C5.8 of Chapter C5 can be used to correct for effect of plasticity.

From Table B1.1, for our material $\sigma_{o.7}$ = 53000 and n = 18.5.

The value of the parameter for bottom scale of Fig. C5.8 is $\sigma_{cr}/\sigma_{o.7}$ = 58600/53000 = 1.10.

From Fig. C5.8, using n = 18.5 curve, we read $\sigma_{cr}/\sigma_{o.7}$ = .91. Therefore σ_{cr} = 53000 x .91 = 48100.

Thus by changing the long side of tube from .04 to .072, the buckling stress was increased from 21900 to 48100 psi.

In the design of rectangular tubes, the designer should select the tube thicknesses for both long and short sides so that buckling occurs on both sides, thus giving the lightest section for buckling strength.

As pointed out previously in this chapter, the load on the member which causes local buckling is not the failing or maximum load for a short length of the member. This local failing or crippling stress is treated in the next chapter. Since the buckling stress may fall in the inelastic stress range, the buckles will not entirely disappear when load is removed. Since limit or applied loads must be carried without permanent distortion, it is thus important to know when local buckling starts. For those missile and space vehicles that carry no humans, the factor of safety on limit loads is considerably less than for aircraft, thus the spread between local buckling and local failing strength becomes important in design.

C6.6 Buckling of Stiffened Flat Sheets Under Longitudinal Compression.

In supersonic aircraft, it is important that the surface skin, particularly that on the wing, not buckle under flight conditions since a buckled surface could effect the aerodynamic characteristics of the airflow around the wing, thus it is important to know when the skin or its stiffening units initially buckle in order to design so that such buckling will not occur under flight conditions.

Gallaher and Boughan (Ref. 6) and Boughan and Baab (Ref. 7) determined the local buckling coefficients for idealized web, Z and T stiffened plates. The results of their studies are shown in Figures C6.8 to C6.12 and were taken from (Ref. 4). The initial local buckling stress for plate or stiffener is given by the equation:-

$$\sigma_{cr} = \frac{k_s\ \pi^2\ E}{12(1-\nu_e^2)} \left(\frac{t_s}{b_s}\right)^2 \quad \text{- - - - - - - - - - - (B)}$$

If the buckling stress is above the proportional limit stress of the material, correct for plasticity effect by using Fig. C5.8 of Chapter C5.

Problem Illustrating Use of Charts.

Fig. C shows a plate with idealized Z section stiffeners. The material is 2024-T3

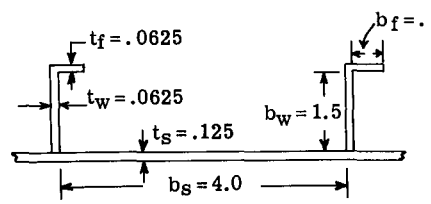

Fig. (c)

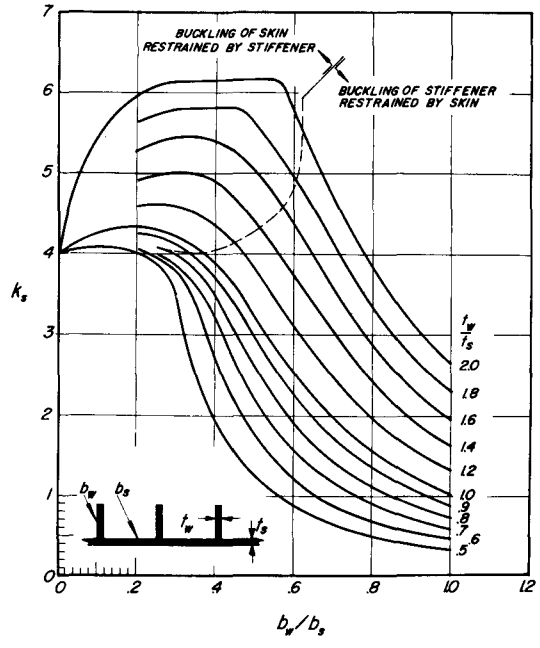

Web stiffeners. $0.5 < t_w/t_s < 2.0$

Fig. C6.8 (Ref. 7) Compressive-local-buckling coefficients for infinitely wide idealized stiffened flat plates.

$$\sigma_{cr} = \frac{k_s \pi^2 E}{12\,(1 \times \nu_e^2)} \left(\frac{t_s}{b_s}\right)^2$$

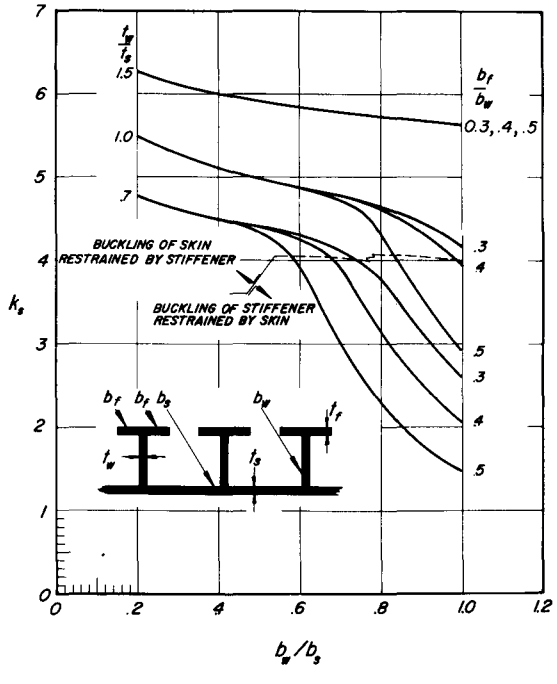

Fig. C6.11 (Ref. 7) T-section stiffeners.
$t_w/t_f = 1.0$; $\frac{b_f}{t_f} > 10$; $\frac{b_w}{b_s} > 0.25$.

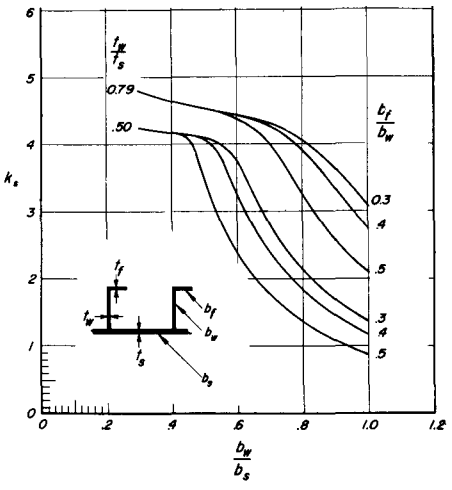

Fig. C6.9 (Ref. 6) Z-section stiffeners.
$t_w/t_s = 0.50$ and 0.79.

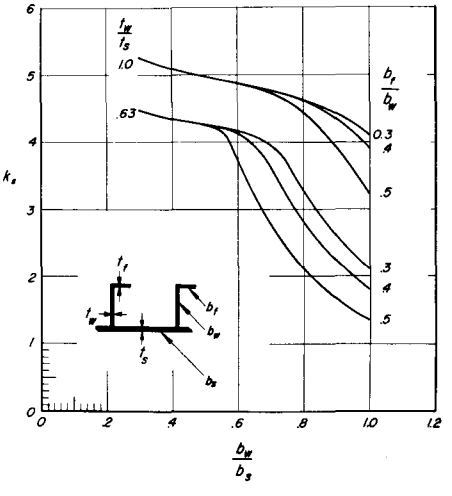

Fig. C6.10 (Ref. 6) Z-section stiffeners.
$t_w/t_s = 0.63$ and 1.0.

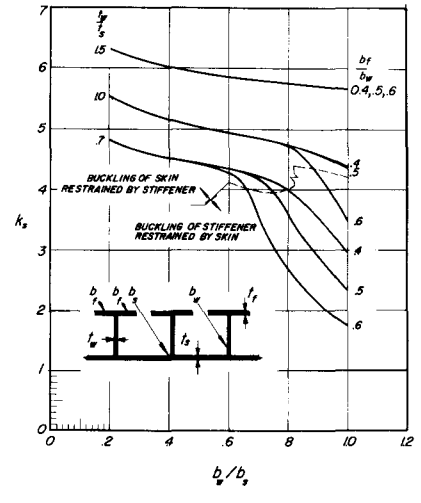

Fig. C6.12 (Ref. 7) T-section stiffeners.
$t_w/t_f = 0.7$; $b_f/t_f > 10$; $b_w/b_s > 0.25$.

aluminum alloy. Determine the initial buckling stress under longitudinal compression.

$$\frac{b_f}{b_w} = \frac{0.5}{1.5} = 0.333, \quad \frac{b_w}{b_s} = \frac{1.5}{4.0} = .375,$$

$$\frac{t_w}{t_s} = \frac{.0625}{0.125} = .50$$

Using the above three values and referring to Fig. C6.9, we read the buckling coefficient k_s to be 4.2. Substituting in equation (B)

$$\sigma_{cr} = \frac{4.2\ \pi^2 \times 10{,}700{,}000}{12(1-.3^2)} \left(\frac{.125}{4.0}\right)^2 = 39800 \text{ psi.}$$

This stress is no doubt above the proportional limit stress so a check for plasticity effect will be made. For this effect we use Fig. C5.8 of Chapter C5.

For our 2024-T3 material, we find from Table B1.1 of Chapter B1, that $\sigma_{0.7} = 39000$ and the shape parameter n = 11.5.

The bottom scale parameter on Fig. C5.8 is equation (B) divided by $\sigma_{0.7}$, thus it equals 39800/39000 = 1.02. Using this value and the n = 11.5 curve on Fig. C5.8, we read on left side scale that $\sigma_{cr}/\sigma_{0.7} = .86$. Therefore the buckling stress $\sigma_{cr} = .86 \times 39000 = \underline{33600}$ psi.

References

(1) Lundquist, Stowell and Schuette: Principles of Moment Distribution Applied to Stability of Structures Composed of Bars and Plates. NACA WRL-326, 1943.

(2) Kroll, Fisher and Heimerl: Charts for Calculation of the Critical Stress for Local Instability of Columns with I, Z, channel and Rectangular Tube Sections. NACA WRL-429, 1943.

(3) Kroll: Tables of Stiffness and Carry-over Factor for Flat Rectangular Plates Under Compression: NACA WRL-398, 1943.

(4) Becker: Handbook of Structural Stability. Part II. Buckling of Composite Elements. NACA TN.3782, July 1957.

(5) Van Der Maas: Charts for the Calculation of the Critical Compressive Stress for Local Instability of Columns with Hat Sections. Jour. Aero. Sci. Vol. 21, June 1954.

(6) Gallaher and Boughan: A Method for Calculating the Compressive Strength of Z Stiffened Panels that Develop Local Instability. NACA TN.1482, 1947.

(7) Boughan and Baab: Charts for Calculating the Critical Compressive Stress for Local Instability of Idealized T Stiffened Panels. NACA WRL-204, 1944.

CHAPTER C7

CRIPPLING STRENGTH OF COMPOSITE SHAPES AND SHEET-STIFFENER PANELS IN COMPRESSION

SHEET EFFECTIVE WIDTHS. COLUMN STRENGTH.

C7.1 Introduction.

Chapter C6 was concerned with the local buckling stress of composite sections when loaded in compression. Tests of short lengths of sections composed of flange-plate elements often show that after the section has buckled locally, the unit still has the ability to carry a greater load before failure occurs. In other words, the local buckling and local failure loads are not the same. For cases where local buckling occurs at low stress, the crippling or failing stress will be higher. When local buckling occurs at high stress such as .7 to .8 F_{cy}, buckling and crippling stress are practically the same. Fig. C7.1 illustrates the stress distribution on the cross-section after local buckling has occurred but prior to local crippling or failure.

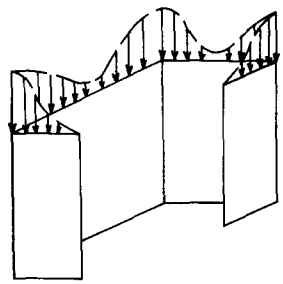

Fig. C7.1

As the load on the section is increased, the buckles on the flat portions get larger but most of the increasing load is transferred to the much stiffer corner regions until the stress intensity reaches a high enough value to cause sufficient deformation to cause failure.

A theoretical solution for the local crippling stress for all types of shapes has not been developed as the boundary restraint between flange and plate elements is unknown and also the manner in which the stress builds up in the corner regions is not well understood. Consequently, the methods of solution are semi-empirical in character, and the results of such methods have been sufficiently proven by tests. Two methods of calculating crippling stresses will be presented in this chapter.

C7.2 METHOD 1. THE ANGLE METHOD, or the Needham Method.

This method which will be referred to as the angle method or the Needham method was presented in (Ref. 1). In this method the member section is divided into equal or unequal angles as illustrated in Fig. C7.2. The strength of these angle elements can be established by theory or tests. The ultimate strength or failing strength can then be found by adding up the strengths of the angle elements that make up the composite section.

Needham made a large number of tests on angle and channel sections. From a study of these test results as well as other published test data on channels, square and rectangular tubes, etc., he arrived at the following equation for the crippling or failing stress of angle sections.

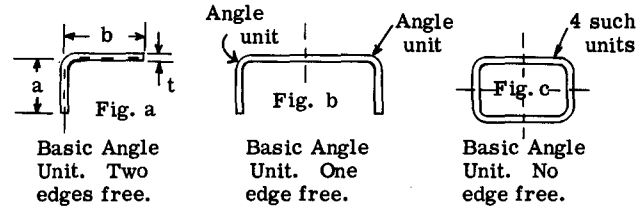

Fig. C7.2

$$F_{cs}/(F_{cy}E)^{1/2} = C_e/(\frac{b'}{t})^{0.75} \text{ - - - - (C7.1)}$$

where,

F_{cs} = crippling stress (psi)
F_{cy} = compression yield stress (psi)
E = Young's modulus of elasticity in compression (psi)
b'/t = equivalent b/t of section = $(a + b)/2t$
C_e = coefficient that depends on the degree of edge support along the edges of contiguous angle units. Specifically they are:-
$C_e = 0.316$ (two edges free)
$C_e = 0.342$ (one edge free)
$C_e = 0.366$ (no edge free)

The crippling stress for angles, channels, zees and rectangular tubes can be determined directly from use of equation C7.1. The crippling load on an angle unit is then,

$$P_{cs} = F_{cs}A \text{ - - - - - - - - - - - - (C7.2)}$$

where A is the area of the angle.

The crippling stress of other formed

structural shapes can be determined by dividing the shape into a series of angle units and computing the crippling loads for these individual angle units by use of equations C7.1 and C7.2. The weighted crippling stress for the entire section is obtained from the following equation:-

$$F_{cs} = \frac{\Sigma \text{ (crippling loads of angles)}}{\Sigma \text{ (area of angles)}} \quad \text{(C7.3)}$$

C7.3 Design Curves.

Fig. C7.3 gives curves for determining the crippling stress of angle units as per equation C7.1, and Fig. C7.4 gives curves for determining the crippling loads for angle units. Using these curves and equation C7.3, the crippling stress of composite shapes other than angles, channels, zees and rectangular tubes can readily be calculated.

Illustrative problems, using this method, will be given later and the results compared with method 2. Crippling stresses for composite sections should be limited to the values given in Table C7.1 unless substantiated by test results.

C7.4 METHOD 2. For Crippling Stress Calculation. (The Gerard Method).

Introduction: References 2 and 3 give the results of a very comprehensive study by Gerard on the subject of crippling stresses. From a thorough study of published theoretical studies and most available test or experimental results, Gerard has developed and presented a more generalized or broader semi-empirical method of determining crippling stresses. In one sense it is generalization or broader application of the Needham method which was presented as method 1. The student and practicing structures engineer should refer to the above references for a complete discussion of how the resulting crippling stress equations were obtained and how these check the extensive test results. In this short chapter we can only present the resulting equations, design curves for same and example problems in the use of the information, in the determination of crippling stresses.

C7.5 Stresses and Displacements of Flat Plates After Buckling Under Conditions of Uniform End Shortening.

Fig. C7.5 shows a picture of the resulting stress distribution on flat plates after buckling under conditions of uniform end shortening as determined by Coan in (Ref. 4). The Gerard method recognizes the effect of distortion of the free unloaded edges upon the failing strength of the member section.

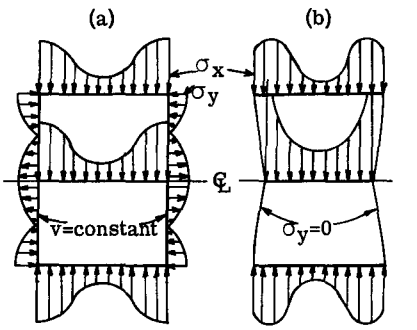

Fig. C7.5 Stresses and displacements of flat plates after buckling under conditions of uniform end shortening (reference 4). (a) Straight unloaded edges, (b) stress free unloaded edges free to warp in the plane of the plate.

C7.6 The Gerard Equations for Crippling Stress.

The following equations are taken from (Ref. 3).

For sections with distorted unloaded edges as angles, tubes, V groove plates, multi-corner sections and stiffened panels, the following crippling stress equation applies within ± 10 percent limits:-

$$F_{cs}/F_{cy} = 0.56 \left[(gt^2/A)(E/F_{cy})^{1/2}\right]^{0.85} \quad \text{(C7.4)}$$

For sections with straight unloaded edges such as plates, tee, cruciform and H sections, the following equation for crippling stress applies within ± 5 percent limits.

$$F_{cs}/F_{cy} = 0.67 \left[(gt^2/A)(E/F_{cy})^{1/2}\right]^{0.40} \quad \text{(C7.5)}$$

For 2 corner sections, Z, J, and channel sections, the following equation applies within ±10 percent limits.

$$F_{cs}/F_{cy} = 3.2 \left[(t^2/A)(E/F_{cy})^{1/2}\right]^{0.75} \quad \text{(C7.6)}$$

F_{cs} = crippling stress for section (psi)
F_{cy} = compressive yield stress (psi)
t = element thickness (inches)
A = section area (in.^{2})
E = Young's modulus of elasticity
g = number of flanges which compose the composite section, plus the number of cuts necessary to divide the section into a series of flanges. See Fig. C7.6 for method of cutting composite sections to determine value of g.

The cut-off or maximum crippling stress F_{cs} for a composite section should be limited to the

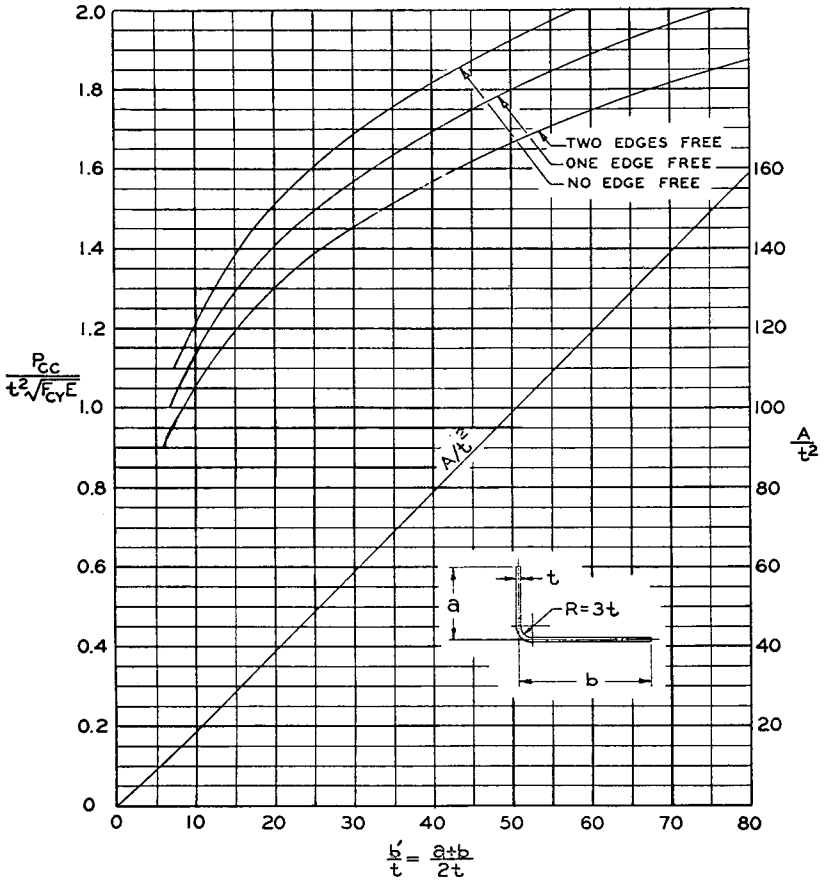

(Note: P_{cc} same as P_{cs})

Fig. C7.4 Dimensionless Crippling Load vs. b'/t (Ref. 1)

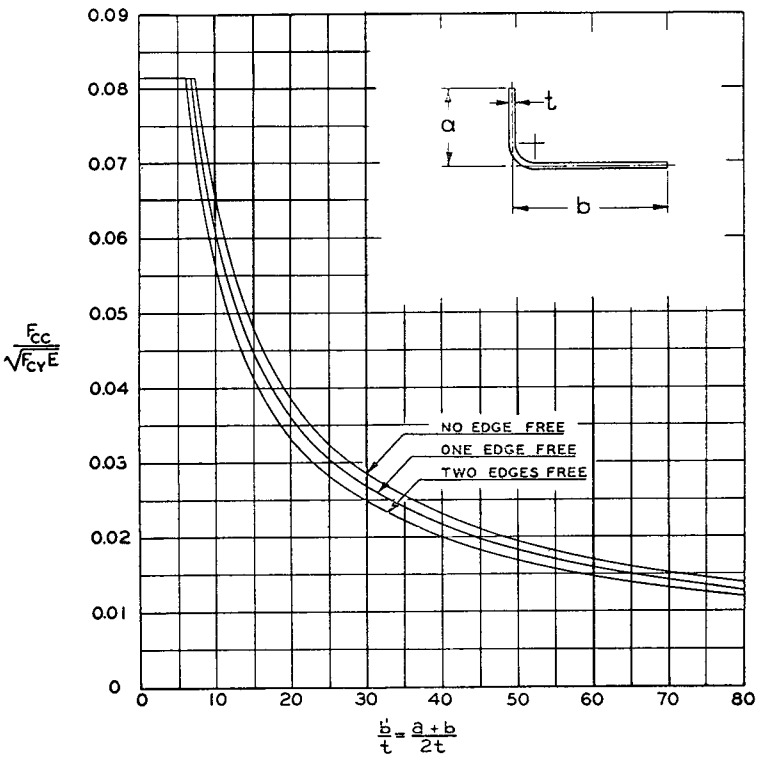

(Note: F_{cc} same as F_{cs})

Fig. C7.3 Dimensionless Crippling Stress vs. b'/t (Ref. 1)

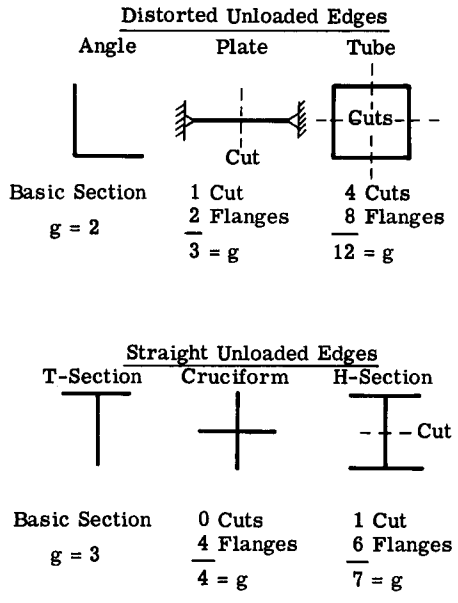

Fig. C7.6 Method of cutting simple elements to determine g.

values in Table C7.1 unless higher values can be substantiated by test results. The cut-off values given in Table C7.1 are no doubt slightly conservative. Design curves for equation C7.4, 5 and 6 are given in Figs. C7.7, C7.8 and C7.9.

C7.7 Correction for Cladding.

Since many formed sections are made from alclad sheets, the clad covering acts to reduce the value of buckling stress and thus a correction factor $\bar{\eta}$ must be used to take care of this reduction in strength. This correction from (Ref. 3) is,

$$\bar{\eta} = \left[1 + 3\,(\sigma_{cl}/\sigma_{cr})f\right]/(1 + 3f) \quad - - - \quad (C7.7)$$

where,

σ_{cl} = cladding yield stress
σ_{cr} = buckling stress
f = ratio of total cladding thickness to total thickness. f = 0.10 for alclad 2024-T3 and .08 for alclad 7075-T3.

C7.8 Maximum Values for Crippling Stresses.

The cut-off or maximum crippling stress for a composite section should be limited to the values in Table C7.1 unless test results are obtained to substantiate the use of higher crippling stresses.

Table C7.1

Type of Section	Max. F_{cs}
Angles	.7 F_{cy}
V Groove Plates	F_{cy}
Multi-Corner Sections, Including Tubes	.8 F_{cy}
Stiffened Panels	F_{cy}
Tee, Cruciform and H Sections	.8 F_{cy}
2 Corner Sections. Zee, J, Channels	.9 F_{cy}

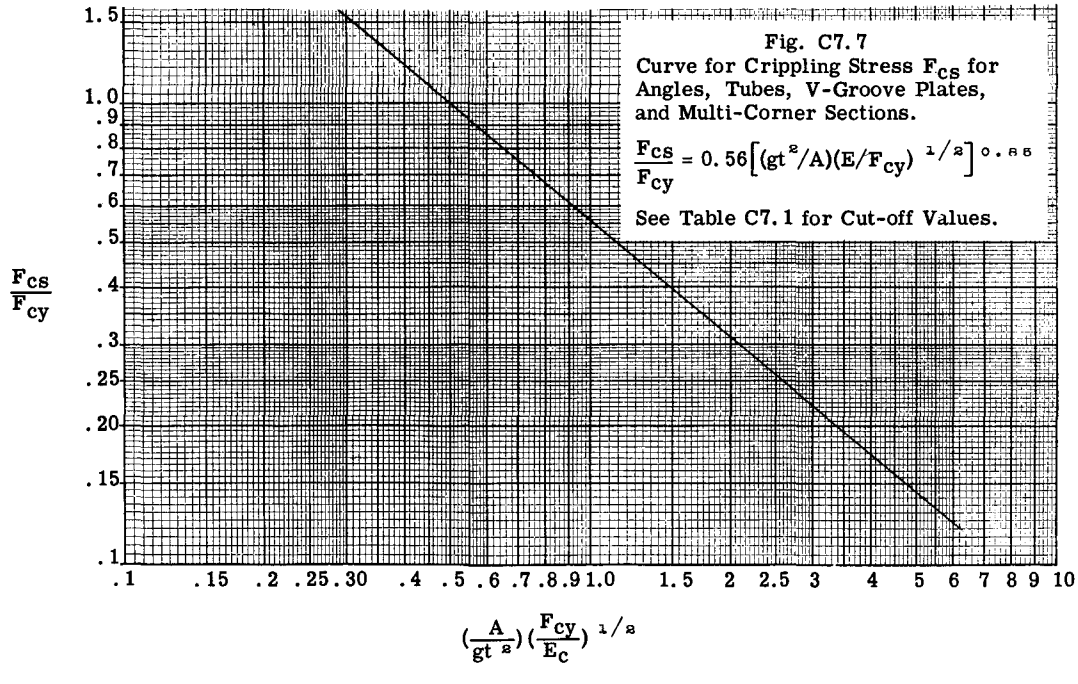

Fig. C7.7
Curve for Crippling Stress F_{cs} for Angles, Tubes, V-Groove Plates, and Multi-Corner Sections.

$$\frac{F_{cs}}{F_{cy}} = 0.56\left[(gt^2/A)(E/F_{cy})^{1/2}\right]^{0.85}$$

See Table C7.1 for Cut-off Values.

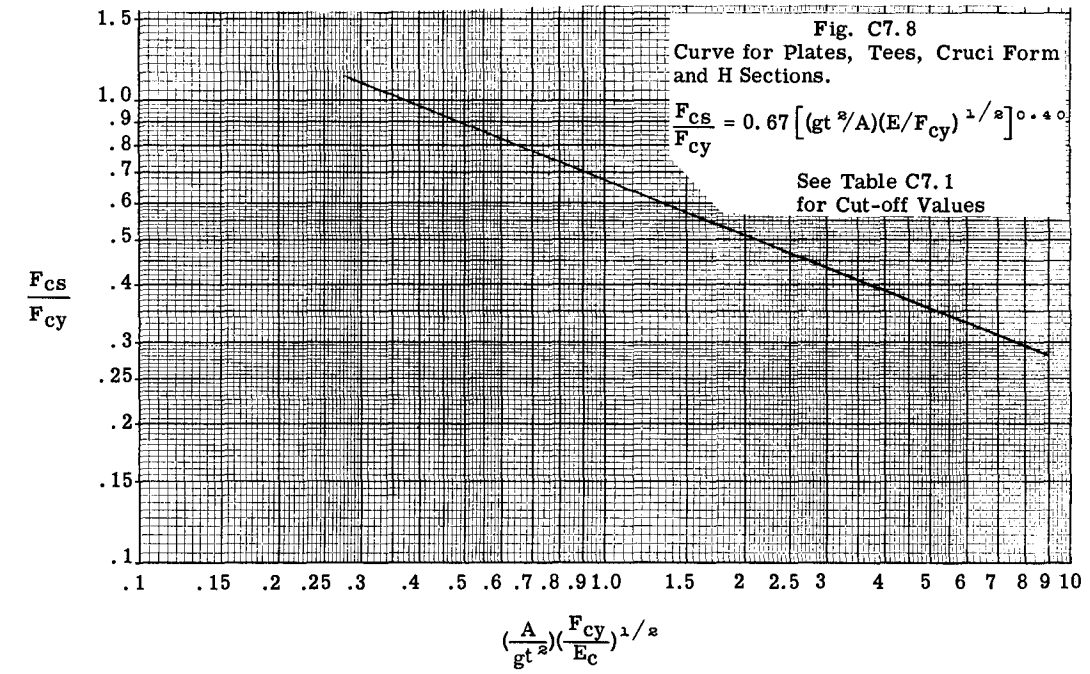
Fig. C7.8
Curve for Plates, Tees, Cruci Form and H Sections.
$\frac{F_{cs}}{F_{cy}} = 0.67\left[(gt^2/A)(E/F_{cy})^{1/2}\right]^{0.40}$
See Table C7.1 for Cut-off Values
$\frac{F_{cs}}{F_{cy}}$
1.5
1.0
.9
.8
.7
.6
.5
.4
.3
.25
.2
.15
.1
.1 .15 .2 .25 .3 .4 .5 .6 .7 .8 .9 1.0 1.5 2 2.5 3 4 5 6 7 8 9 10
$(\frac{A}{gt^2})(\frac{F_{cy}}{E_c})^{1/2}$

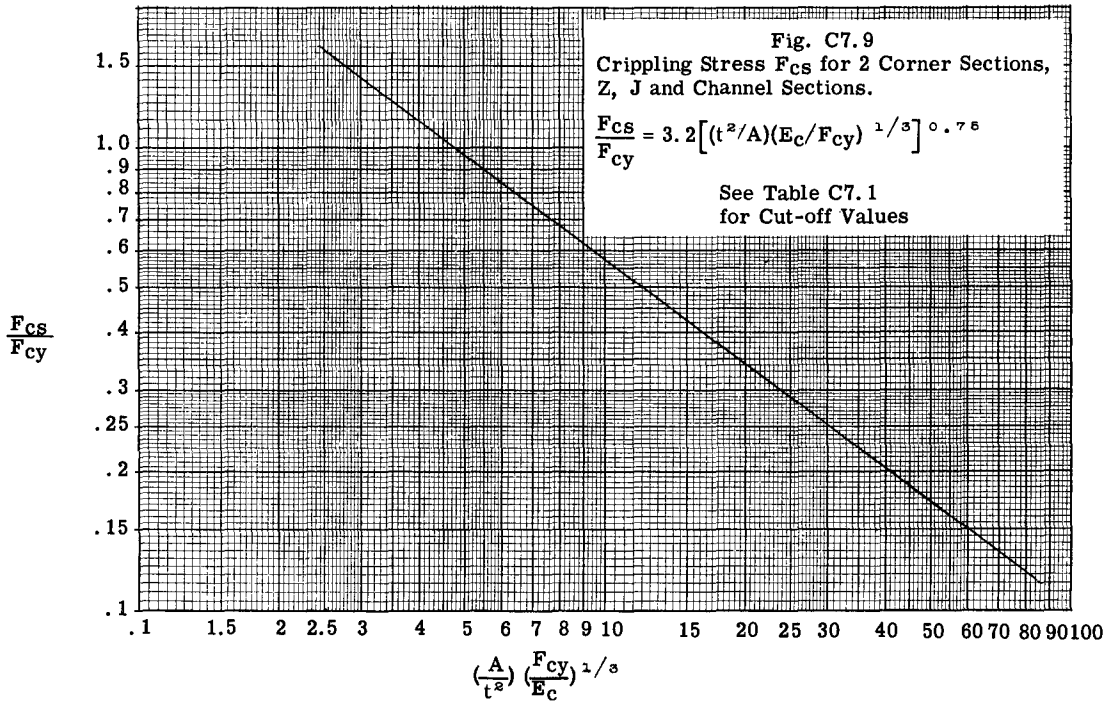
Fig. C7.9
Crippling Stress F_{cs} for 2 Corner Sections, Z, J and Channel Sections.
$\frac{F_{cs}}{F_{cy}} = 3.2\left[(t^2/A)(E_c/F_{cy})^{1/3}\right]^{0.75}$
See Table C7.1 for Cut-off Values
$\frac{F_{cs}}{F_{cy}}$
1.5
1.0
.9
.8
.7
.6
.5
.4
.3
.25
.2
.15
.1
.1 1.5 2 2.5 3 4 5 6 7 8 9 10 15 20 25 30 40 50 60 70 80 90 100
$(\frac{A}{t^2})(\frac{F_{cy}}{E_c})^{1/3}$

C7.9 Restraint Produced by Lips and Bulbs.

Quite often in formed sections, the flange element which has a free edge is rather small in width as illustrated in Fig. a. Also for extruded sections, a bulb is often used as illustrated in Figs. b. The question then arises, is the lip or bulb sufficiently large enough to provide a simple support to the adjacent plate element. Since the compressive buckling coefficient for a plate element is

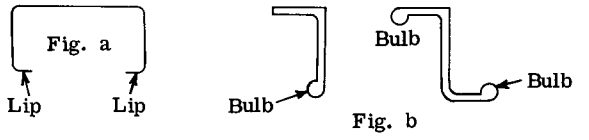

Fig. b

4.0 and 0.43 for a flange element, the use of a small lip or bulb can increase the value of the coefficient considerably above 0.43 and thus produce a more efficient load carrying element. The problem of determining the dimensions of a lip or bulb to give at least a simply supported edge condition to the adjacent plate element has been investigated theoretically by Windenburg (Ref. 5). The results of his studies gives the following design criterion.

$$2.73\frac{I_L}{b_f t^3} - \frac{A_L}{b_f t} \geqq 5 \qquad \text{- - - - - - - - (C7.8)}$$

Where I_L and A_L are the moment of inertia and area of the lip or bulb respectively. (See Fig. C7.10).

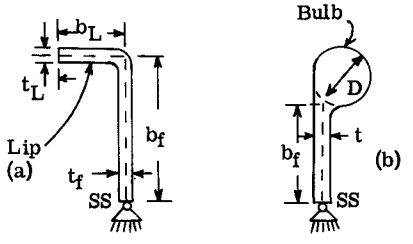

Fig. C7.10

From Fig. C7.10a for the lip, $A_L = b_L t$, and $I_L = t b_L^3/3$.

In substituting these values in equation (C7.8), the dimensions of the lip are expressed as

$$0.910\left(\frac{b_L}{t}\right)^3 - \frac{b_L}{t} = 5\frac{b_f}{t} \qquad \text{- - - - - (C7.9)}$$

To determine b_L and t, an additional requirement is specified, namely, that the buckling stress of the lip must be greater or equal to the buckling stress of the adjacent plate element.

From Chapter C5, the compressive buckling coefficient using $\nu_e = .3$ is 0.388 for a flange element and 3.617 for a plate element. Therefore,

$$0.388\ E\left(\frac{t_L}{b_L}\right)^2 \geqq 3.617\ E\left(\frac{t_f}{b_f}\right)^2 \qquad \text{- - - (C7.10)}$$

From equations C7.9 and C7.10, the following relationship is obtained,

$$\frac{b_L}{t_L} \leqq 0.328\frac{b_f}{t_f} \qquad \text{- - - - - - - - - - (C7.11)}$$

Fig. C7.11 shows the results as a curve.

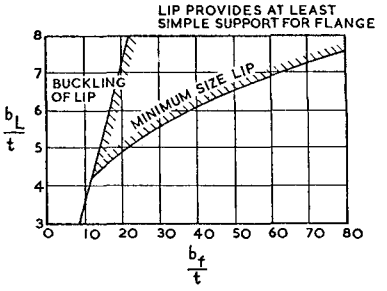

Fig. C7.11 Minimum lip dimensions required for flange to buckle as simply supported plate (Ref. 5).

In extruded sections, a circular bulb is often used to stiffen a free edge as illustrated. in Fig. C7.10b. The moment of inertia of the bulb area about the centerline of the plate element is,

$$I = \frac{\pi D^4}{64} + \frac{\pi D^2}{4}\left(\frac{D-t}{2}\right)^2$$

As for the case of the lip, the buckling stress of the bulb must be greater or equal to the buckling stress of the adjacent plate element, which gives,

$$\left(\frac{D}{t}\right)^4 - 1.6\left(\frac{D}{t}\right)^3 - 0.374\left(\frac{D}{t}\right)^2 = 7.44\ b_f/t \qquad \text{- (C7.12)}$$

Fig. C7.12 shows design curve representing the above equation.

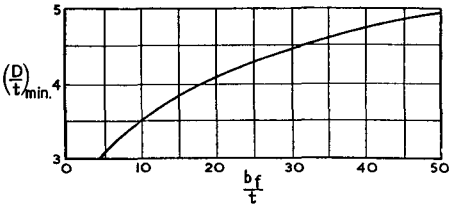

Fig. C7.12 Minimum bulb dimensions required for buckle as simply supported plate (Ref. 5).

C7.10 Illustrative Problems in Calculating Crippling Stresses.

Problem 1. Find the crippling stress for the equal leg angle shown in Fig. a. The material is aluminum alloy 2024-T3.

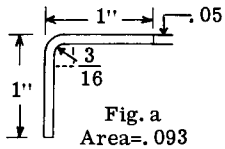

Fig. a

Solution by Method 1.

Material properties are:-

F_{cy} = 40000, E_c = 10,700,000

For this method, we use Fig. C7.3. The parameter for bottom scale of Fig. C7.3 is (a + b)/2t, where (a) and (b) are leg lengths measured to centerline of adjacent leg of angle. For our case a = b = 1 - .025 = 0.975. Thus (a + b)2t = 1.95/0.1 = 19.5.

From Fig. C7.3 using 19.5 on lower scale, and the curve for two edges free, we read on the left hand scale that $F_{cc}/\sqrt{F_{cy}E}$ = .0330. Since we have only one angle, the crippling stress $F_{cs} = F_{cc} = .0330 \times \sqrt{40{,}000 \times 10{,}700{,}000}$ = 21600 psi.

Solution by Method 2 (Gerard Method)

For angle sections we use equation C7.4. A plot of this equation is given in Fig. C7.7. The parameter for lower scale is, $(\frac{A}{gt^2})(\frac{F_{cy}}{E})^{1/2}$, where A = section area and g equals the number of flanges plus cuts, or g = 2 for an angle section. Substituting,

$$(\frac{.093}{2 \times .05^2})(\frac{40{,}000}{10{,}700{,}000})^{1/2} = 1.138$$

Using this value in Fig. C7.7, we read F_{cs}/F_{cy} = 0.50. Therefore F_{cs} = 0.50 x 40,000 = 20,000 psi.

Problem 2. Same as Problem 1, but change material to aluminum alloy 7075-T6.

F_{cy} = 67,000, E_c = 10,500,000

Solution Method 1.

$F_{cs} = F_{cc} = .0330\sqrt{67000 \times 10{,}500{,}000}$ = 28,000 psi

Solution by Method 2.

$$(\frac{.093}{2 \times .05^2})(\frac{67{,}000}{10{,}500{,}000})^{1/2} = 1.485$$

From Fig. C7.7, F_{cs}/F_{cy} = 0.40, whence F_{cs} = .40 x 67,000 = 26800 psi.

Problem 3. Same as Problem 1 but change material to Titanium Ti-8Mn. F_{cy} = 110,000, E_c = 15,500,000.

Solution Method 1.

$F_{cs} = F_{cc} = .0330\sqrt{110{,}000 \times 15{,}500{,}000}$ = 43000 psi

Solution Method 2.

$$(\frac{.093}{2 \times .05^2})(\frac{110{,}000}{15{,}500{,}000})^{1/2} = 1.565$$

From Fig. C7.7, F_{cs}/F_{cy} = 0.38, whence F_{cs} = 0.38 x 110,000 = 41,800.

Problem 4.

Find the crippling stress for the channel section shown in Fig. b if the material is aluminum alloy 2024-T3. F_{cy} = 40,000, E_c = 10,700,000.

Solution Method 1.

As shown in Fig. c, the channel is composed of 2 equal angle units (1) and (2). Since they are the same size, we need only calculate the failing stress for one angle.

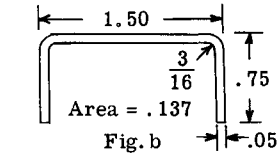

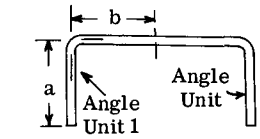

Fig. c

$$\frac{a+b}{2t} = \frac{.725 + .725}{0.1} = 14.5$$

From Fig. C7.3 for b'/t = 14.5, we read $F_{cc}/\sqrt{F_{cy}E}$ = .045 (for one edge free)

Then $F_{cs} = F_{cc} = .045 \times \sqrt{40{,}000 \times 10{,}700{,}000}$ = 29400 psi

Solution Method 2.

For a channel section we use equation C7.6 which is plotted on Fig. C7.9. The parameter for bottom scale of Fig. C7.9 is,

$$\frac{A}{t^2}(\frac{F_{cy}}{E})^{1/3} = (\frac{.137}{.05^2})(\frac{40{,}000}{10{,}700{,}000})^{1/3} = 8.50$$

From Fig. C7.9 F_{cs}/F_{cy} = .65, whence, F_{cs} = .65 x 40,000 = 26,000 psi.

Problem 5. Same as Problem 4 but change material to aluminum alloy 7075-T6. F_{cy} = 67,000, E_c = 10,500,000.

Solution by Method 1.

$F_{cs} = .045 \times \sqrt{67{,}000 \times 10{,}500{,}000}$ = 38200 psi

Solution by Method 2.

$$(\frac{.137}{.05^2})(\frac{67{,}000}{10{,}500{,}000})^{1/3} = 10.17$$

From Fig. C7.9, F_{cs}/F_{cy} = .57, whence F_{cs} = .57 x 67,000 = 38,200

Problem 6.

Find the crippling stress for the square tube as shown in Fig. d. Material is 2024-T3 aluminum alloy. F_{cy} = 40,000, E_c = 10,700,000.

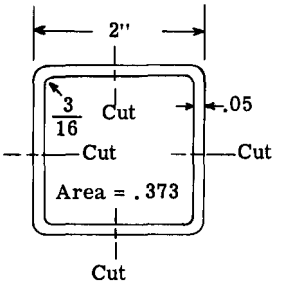

Fig. d

Solution by Method 1.

The square tube is considered as made up of 4 equal angles with no edge free.

$b'/t = (a+b)/2t = 1.95/0.1 = 19.5$

From Fig. C7.3, using upper curve, we obtain $F_{cc}/\sqrt{F_{cy}E}$ = .0392. Whence,

$F_{cs} = F_{cc} = .0392 \times \sqrt{40,000 \times 10,700,000}$ = 25,600 psi

Solution by Method 2.

Area A = .373. g = number of cuts plus flanges or 4 + 8 = 12.

For rectangular tubes we use equation C7.4 or Fig. C7.7.

$$\frac{A}{gt^2}\left(\frac{F_{cy}}{E}\right)^{1/2} = \left(\frac{.373}{12 \times .05^2}\right)\left(\frac{40,000}{10,700,000}\right)^{1/2} = 0.758$$

From Fig. C7.7, F_{cs}/F_{cy} = .70

Therefore F_{cs} = 40,000 x .70 = 28,000 psi

Problem 7. Same as Problem 6, but change material to magnesium HK31A-O Sheet, subjected to a temperature of 300°F for 1/2 hour.

Solution by Method 1.

From Table B1.1 of Chapter B1, F_{cy} = 11,100, E_c = 6,160,000.

$F_{cs} = .0392\sqrt{11,100 \times 6,160,000}$ = 10,250 psi

Solution by Method 2.

$$\frac{A}{gt^2}\left(\frac{F_{cy}}{E}\right)^{1/2} = \left(\frac{.373}{12 \times .05^2}\right)\left(\frac{11,100}{6,160,000}\right)^{1/2} = .528$$

From Fig. C7.7, F_{cs}/F_{cy} = .96

F_{cs} = .96 x 11,100 = 10,600 psi

From Table C7.1, the cut-off or maximum crippling for rectangular tubes is .8 F_{cy} or .8 x 11,100 = 8900 psi. Thus unless tests substantiate higher values, the crippling stress should be taken as 8900 psi.

Problem 8. Same as Problem 6, but change material to stainless steel 17-7PH(TH1050), F_{cy} = 162,000, E_c = 29,000,000

Method 1.

$F_{cs} = .0392\sqrt{162,000 \times 29,000,000}$ = 85,000 psi

Method 2.

$$\left(\frac{.373}{12 \times .05^2}\right)\left(\frac{162,000}{29,000,000}\right)^{1/2} = .93$$

From Fig. C7.7, F_{cs}/F_{cy} = .595. F_{cs} = 162,000 x .595 = 96,200 psi.

Problem 9.

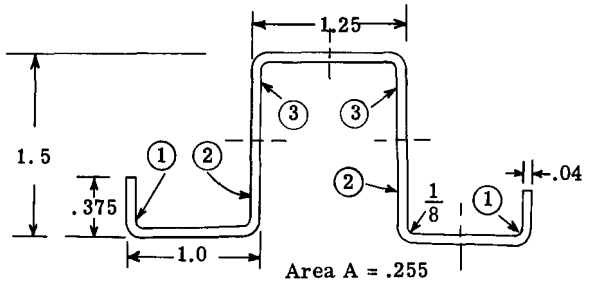

Fig. e

Determine the crippling stress for the formed section shown in Fig. e if material is aluminum alloy 2024-T3. F_{cy} = 40,000, E_c = 10,700,000.

Solution by Method 1 (Needham)

The section is divided into 6 angle units by the dashed lines in Fig. e. They are numbered (1) to (3) since we have symmetry.

The procedure will be to find the failing load for each angle and add up the total for the 6 angle units. The crippling stress will then equal this total load divided by the section area.

Angle unit (1) (One edge free)

$b'/t = (a+b)/2t = \left[(.375 - .02) + (.5 - .02)\right]/.08$ = 10.44

From Fig. C7.3, $F_{cc}/\sqrt{F_{cy}E}$ = .06

Whence, $F_{cc} = .06 \times \sqrt{40,000 \times 10,700,000}$ = 39,300 psi

Area of angle (1) = .0309 = A

P_{cc} = .0309 x 39,300 = 1215 lb.

Angle unit (2) Area = .0459 (no edge free)

b'/t = (a + b)/2t = (.48 + .73)/.08 = 15.1

From Fig. C7.3 $F_{cc}/\sqrt{F_{cy}E}$ = .0475

$F_{cc} = \sqrt{40,000 \times 10,700,000} \times .0475$ = 31,100 psi

P_{cc} = 31,100 x .0459 = 1428 lb.

Angle unit (3) Area = .0509 (no edge free)

b'/t = (.73 + .605)/.08 = 16.7

From Fig. C7.3, $F_{cc}/\sqrt{F_{cy}E}$ = .046

$F_{cc} = .046 \times \sqrt{40,000 \times 10,700,000}$ = 30,200 psi

P_{cc} = .0509 x 30,200 = 1540 lb.

$F_{cs} = \Sigma P_{cc}$/area

= (2 x 1215 + 2 x 1428 + 2 x 1540)/0.255 = 32,800 psi

Solution by Method 2 (Gerard)

$$\frac{A}{gt^2}\left(\frac{F_{cy}}{E_c}\right)^{1/2}$$

g = number of flanges plus number of cuts = 12 + 5 = 17.

Substituting in the above term,

$$\left(\frac{.255}{17 \times .04^2}\right)\left(\frac{40,000}{10,700,000}\right)^{1/2} = .573$$

From Fig. C7.7, F_{cs}/F_{cy} = .895, whence F_{cs} = 40,000 x .895 = 35,600 psi.

From Table C7.1, it is recommended for multi-corner sections that F_{cs} maximum be limited to .8 F_{cy} unless tests can prove higher values.

$F_{cs_{max.}}$ = .8 x 40,000 = 32,000 psi. Since this is less than the above calculated values, it should be used.

Problem 10. Find the crippling stress for the extruded bulb angle shown in Fig. f if material is 2014-T6 extruded aluminum alloy.

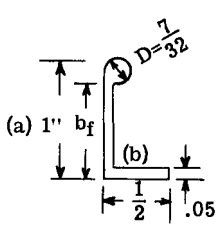

Fig. f

This particular bulb section is taken from Table A3.16 of Chapter A3 as Section No. 2. The area from that table is 0.113 sq. in.

Solution by Method 2 (Gerard)

For this material F_{cy} = 53,000, E_c = 10,700,000.

The first question that arises is the bulb size sufficient to give an end stiffness to the (a) leg so that the bulb may be equivalent to the normal corner.

In Fig. f, b_f = 0.78, hence b_f/t = 15

Referring to Fig. C7.12, we observe that for a b_f/t value of 15 we need a D/t ratio of at least 3.8. The D/t value for our bulb angle is (7/32)/.05 = 4.4, thus bulb has sufficient stiffness to develop a corner. The next question that arises should the bulb angle still be classed as an angle section for which equation C7.4 applies or be classed as a channel or 2 corner section with the bulb acting as a short thick leg of the channel. For this case, equation C7.6 would apply.

The crippling stress will be calculated by both equations.

By equation C7.4 or Fig. C7.7:-

If bulb is considered as a full corner then g = 4 flanges plus 1 cut = 5.

$$\frac{A}{gt^2}\left(\frac{F_{cy}}{E_c}\right)^{1/2} = \left(\frac{.113}{5 \times .05^2}\right)\left(\frac{53,000}{10,700,000}\right)^{1/2} = .636$$

From Fig. C7.7,

F_{cs}/F_{cy} = .82, hence F_{cs} = .82 x 53000 = 43500

By equation C7.6 or Fig. C7.9,

$$\frac{A}{t^2}\left(\frac{F_{cy}}{E_c}\right)^{1/2} = \left(\frac{.113}{.05^2}\right)\left(\frac{53,000}{10,700,000}\right)^{1/2} = 7.70$$

From Fig. C7.9, F_{cs}/F_{cy} = .7, hence F_{cs} = .7 x 53,000 = 37,100.

Possibly the best estimate of the crippling stress would be the average of the two above results or 40,300 psi.

In Table C7.1, the so-called cut-off stress for angles is .7 F_{cy} and channels .9 F_{cy}. If we use the average value or .8 F_{cy}, it gives F_{cs} = .8 x 53,000 = 42,400 as maximum permissible because of limited test results on bulb angles.

For the case where the bulb or lip does not develop the stiffness necessary to assume a full corner, then the bulb is only

considered as an additional flange and the g count would be four instead of 5, thus reducing the crippling stress.

EFFECTIVE SHEET WIDTHS

C7.11 Introduction.

The previous discussion in this chapter has dealt with the crippling stress of formed or extruded sections when acting alone, that is not fastened to any other structure along its length. However, the major structure of aerospace vehicles, such as the wing or body, involves a sheet covering which is strengthened by attached or integral fabricated stiffeners such as angles, zees, tees, etc. Since the sheet and stiffeners must deform together, the sheet will therefore carry compressive load and to neglect this load carrying capacity of the sheet would be too conservative in aerospace structural design where weight saving is very important.

C7.12 Sheet Effective Widths.

Fig. C7.13a illustrates a continuous flat thin plate fastened to stiffener and the entire unit is subjected to a uniform compressive load. Up to the buckling strength of the sheet the compressive stress distribution is uniform over both stiffeners and sheet as in (Fig. b) assuming same material for sheet and stiffeners. As the load is increased the sheet buckles between the stiffeners and does not carry a greater stress than the buckling stress. However as the stiffeners are approached, the skin being stabilized by the stiffeners to which it is attached can take a higher stress and immediately over the stiffeners the sheet can take the same stress as the ultimate strength of the stiffener, assuming that the sheet has a continuous connection to the stiffener. Fig. c shows the general stress distribution after the sheet has buckled. This distribution depends on the degree of restraint provided by the stiffeners and the panel dimension.

Various theoretical studies (Ref. 6) have been made to determine this stress distribution after buckling. In general they lead to long and complicated equations. To provide a simple basis for design purposes, an attempt has been made to find an effective width of sheet w which would be considered as taking a uniform stress (Fig. d) which would give the same total sheet strength as the sheet under the true non-uniform stress distribution of Fig. c.

The question of sheet effective sheet has been considered by many individuals. The names of VonKarman, Sechler, Timoshenko, Newell, Frankland, Margurre, Fischel, Gerard, and many more are closely associated with the present knowledge on effective sheet width.

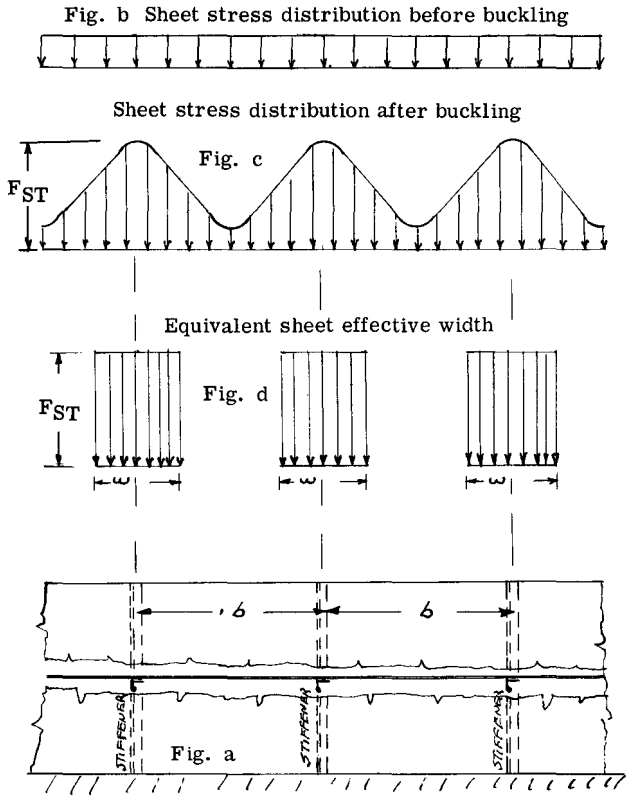

Fig. C7.13

From Chapter C5, the buckling compressive stress of a sheet panel is,

$$F_{cr} = \frac{k_c \pi^2 E}{12\,(1-\nu_e^2)} \left(\frac{t}{b}\right)^2 \quad \text{- - - - - - - - -} \quad (C7.13)$$

If we assume that the stiffener to which the sheet is attached provides a boundary restraint equal to a simple support, then $k_c = 4.0$, and if Poisson's ratio ν_e is taken as 0.3, then equation C7.13 reduces to,

$$F_{cr} = 3.60E(t/b)^2 \quad \text{- - - - - - - - - - -} \quad (C7.14)$$

The Von-Karman-Sechler method as first proposed consisted of solving equation C7.14 for a width (w) in place of (b), when F_{cr} was equal to the yield stress of the material since experiments had shown that the ultimate strength of a sheet simply supported at the edges was independent of the width of the sheet. Thus equation C7.14 changes to,

$F_{cy} = 3.60E(t/w)^2$, whence,

$$w = 1.90t\sqrt{E/F_{cy}} \quad \text{- - - - - - - - - - - -} \quad (C7.15)$$

Since the crippling or local failing stress of a stiffener can exceed the yield strength of the material, equation C7.15 was later changed by replacing F_{cy} by the stress in the stringer F_{ST}, thus giving,

$$w = 1.90t\sqrt{E/F_{ST}} \qquad \text{- - - - - - - - - - - (C7.16)}$$

Some early experiments by Newell indicated the constant 1.90 was too high and for light stringers a value of 1.7 was more realistic, thus 1.7 has been widely used in industry.

If we assume the stiffness of the stiffener and its attachment to the sheet as developing a fixed or clamped edge condition for the sheet, then

$$F_{cr} = 6.35E(t/b)^2 \text{ or } w = 2.52t\sqrt{E/F_{ST}}$$

For general design purposes, it is felt that 1.9 or equation C7.15 is appropriate for determining the effective width w. If stiffener is relatively light, use 1.7. Fig. C7.14 illustrates the effective width for sheet-stiffener units which are fastened together by a single attachment line for each flange of the stiffener.

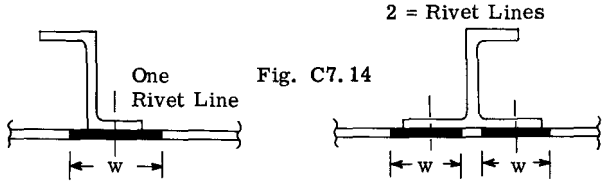

Fig. C7.14

The crippling stress is determined for the stiffener alone. This stress is then used in equation C7.15 to determine the effective widths w. The total area then equals the stiffener area plus the area of the effective sheet width w. The radius of gyration should include the effect of the effective skin area.

Fig. C7.15 illustrates the case where stiffeners are fastened to sheet by two rows of rivets on each stiffener flange. In this case, the rivet lines are so close together that the effective width w for each rivet line would overlap considerably. A common practice in industry for such cases is to use the effective width for one rivet line attachment as per equation C7.16 to represent sheet width to go with each stiffener flange. However, in calculating the crippling stress of the stiffener alone, the stiffener flange which is attached to sheet is considered as having a thickness equal to 3/4 the sum of the flange thickness plus the sheet thickness.

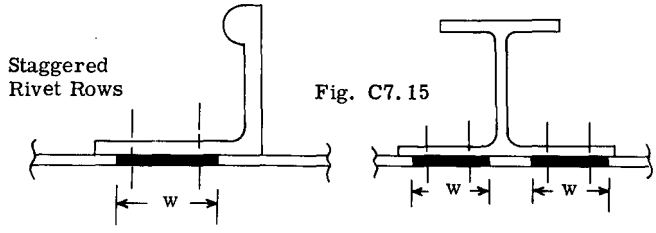

Fig. C7.15

The effective sheet width as calculated by equation C7.16 assumes that no inter-rivet buckling of the sheet occurs or, in other words, the rivet or spot welds are close enough together to prevent local buckling of the sheet between rivets when the sheet is carrying the stiffener crippling stress. The subject of inter-rivet sheet buckling is discussed later in this chapter.

Fig. C7.16 illustrates a procedure to follow for determining the effective width w when sheet and stiffener are integral in manufacture.

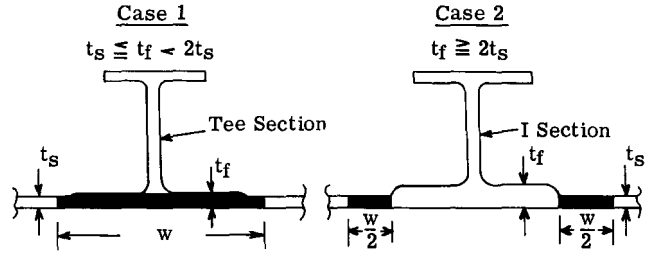

Fig. C7.16

For Case 1, find the crippling stress for the tee section alone, assuming the vertical stem of the tee has both ends simply supported. For value of t in equation C7.15, use $(t_s + t_f)/2$. The effective stiffener area equals the area of the tee plus the area of the sheet of width w.

For Case 2, determine the crippling stress for the I section acting alone. Calculate w/2 from equation C7.15 to include as effective sheet area. The column properties should include I section plus effective sheet.

C7.12 Effective Width W_1 for Sheet with One Edge Free.

In normal sheet-stiffener construction, the sheet usually ends on a stiffener and thus we have a free edge condition for the sheet as illustrated in Fig. C7.16a. The sheet ends at

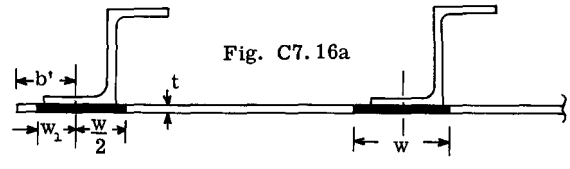

Fig. C7.16a

a distance b' from the rivet line. For a sheet free on one edge, the buckling coefficient in equation C7.13 is 0.43, thus equation C7.13 reduces to,

$F_{cr} = .387E(t/b')^2$, and replacing b' by w , we obtain,

$$w_1 = .62t\sqrt{E/F_{ST}} \qquad \text{- - - - - - - - - - - (C7.17)}$$

Then the total effective sheet width for this end stiffener would thus equal $w_1 + w/2$.

C7.13 Effective Width When Sheet and Stiffener Have Different Material Properties.

In practical sheet-stiffener construction it is common to use extruded stiffeners which have different material strength properties in the inelastic stress range as compared to the sheet to which the stiffener is attached. For example, in Fig. C7.17 the stiffener material could have the stress-strain curve represented by curve (1) and the sheet to which it is attached by the curve (2). Now when the stiffener is stressed to point (B), the sheet directly adjacent to the stiffener attachment line must undergo the same strain as the stiffener and thus the stress in the sheet will be that given at point (A) in Fig. C7.17. This difference in stress will influence the effective width w. Correction for this condition can be made in equation C7.17 by multiplying it by F_{SH}/F_{ST}, which gives

$$w = 1.90t(F_{SH}/F_{ST})\left(\sqrt{\frac{E}{F_{ST}}}\right) \text{ - - - - - - (C7.18)}$$

Where f_{ST} is the stiffener stress and f_{SH} is the sheet stress existing at the same strain as existing for the stiffener and obtained from a stress-strain curve of the sheet material.

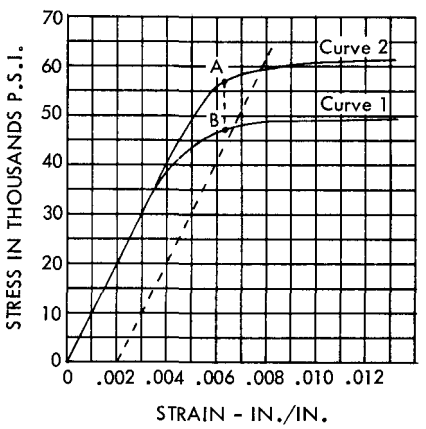

Fig. C7.17

For a rather complete study and comparison of the various effective widths theories as compared, see article by Gerard (Ref. 7). Equation C7.15 is in general conservative for higher b/t ratios.

C7.14 Inter-Rivet Buckling Stress.

The effective sheet area is considered to act monolithically with the stiffener. However, if the rivets or spot welds that fasten the sheet to the stiffener are spaced too far apart, the sheet will buckle between the rivets before the crippling stress of the stiffener is reached, which means the sheet is less effective in helping the stiffener carry a subjected compressive load. Thus, in general, to save structural weight, structural designers select rivet spacings that will prevent inter-rivet buckling of the sheet. In general, the rivet spacing along the stiffeners in the upper surface of the wing will be closer together than on the bottom surface of the wing since the design compressive loads on the top surface are considerably larger than those on the bottom surface.

The following method is widely used by engineers concerned with aerospace structures relative to calculating inter-rivet buckling stresses. It is assumed that the sheet between adjacent rivets acts as a column with fixed ends.

The general column equation from Chapter C2 for stable cross-sections is,

$$F_c = C\pi^2 E_t/(L/\rho)^2 \text{ - - - - - - - - - - - (C7.19)}$$

Where C is the end fixity coefficient and varies from a value of 1 for a pin end support to 4 for a fixed end support.

The effective column length $L' = L/\sqrt{C}$, thus equation C7.19 can be written

$$F_c = \pi^2 E_t/(L'/\rho)^2 \text{ - - - - - - - - - - - (C7.20)}$$

Let p the rivet spacing be considered the column length L. Assume a unit of sheet 1 inch wide and t its thickness. Then moment of inertia of cross section = $1 \times t^3/12$, and area $A = 1 \times t = t$. Then radius of gyration $\rho = 0.29t$. Then substituting in equation C7.20 to obtain the inter-rivet buckling stress F_{ir},

$$F_{ir} = \frac{\pi^2 E t}{\left(\frac{p}{\sqrt{C}}/0.29t\right)^2} \text{ - - - - - - - - - - - (C7.21)}$$

For clamped ends C = 4, thus

$$F_{ir} = \frac{\pi^2 E t}{(p/0.58t)^2} \text{ - - - - - - - - - - - (C7.22)}$$

To plot this equation, the tangent modulus E_t for the material must be known. However, we can use the various column curves in Chapter C2 which show a plot of F_c versus L'/ρ and in equation C7.22 the term $p/0.58t$ corresponds to L'/ρ.

The fixity coefficient C = 4 can be used for flat head rivets. For spot welds it should be decreased to 3.5. For the Brazier rivet type use C = 3 and for counter-sunk or dimpled rivets use C = 1.

Figs. C7.18 and C7.19 show a plot of equation C7.22 for aluminum alloy materials.

If the inter-rivet buckling stress calculates to be more than the crippling stress of the stiffener, then the effective sheet area can be added to the stiffener area to obtain the total effective area. This total effective area times the stiffener crippling stress will give the crippling load for the total sheet-stiffener unit.

When the sheet between rivets buckles before the crippling stress of the stiffener is reached, the sheet in the buckled state has the ability to approximately hold this stress as the stiffener continues to take load until it reaches the stiffener crippling stress. This buckling sheet strength can be taken advantage of by reducing the effective sheet area. Thus effective sheet width equals,

$$W_{corrected} = W(F_{ir}/F_{cs}) \quad \text{- - - - - - - -} \quad (C7.23)$$

The area of the corrected effective sheet is then added to the area of the stiffener. The crippling load then equals the crippling stress of the stiffener times the total area.

The use of sheet effective widths in finding the moment of inertia of a wing or fuselage cross-section is a widely used procedure in the analysis for bending stresses in conventional wing and fuselage construction. Reference should be made to article A19.13 of Chapter A19 and article A20.3 of Chapter A20 for practical illustrations in the use of effective widths.

C7.15 Illustrative Problem Involving Effective Sheet.

Conventional airplane wing construction is illustrated in Fig. C7.20. The wing is covered with sheet, generally referred to as skin, and this skin is stiffened by attaching formed or extruded shapes referred to as skin stiffeners or skin stringers. A typical wing section involves one or several interior straight webs and to tie these webs to the skin, a stringer often referred to as the web flange member, is required to facilitate this connection. Fig. C7.21 is a detail of the flange member and the connection at point (1) in Fig. C7.20.

The stiffener or flange member is an extrusion of 7075-T6 aluminum alloy. The skin and web sheets are 7075-T6 aluminum alloy. The skin is fastened to stiffener by two rows of 1/8 inch diameter rivets of the Brazier head type, spaced 7/8 inch apart. The web is attached to stiffener by one row of 3/16 diameter rivets spaced 1 inch apart. The

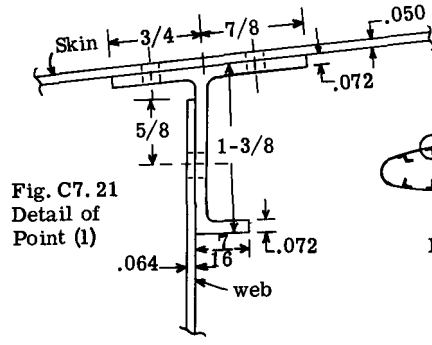

Fig. C7.21 Detail of Point (1)

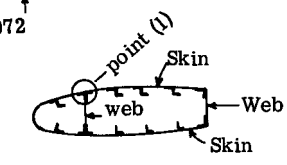

Fig. C7.20

problem is to determine the crippling stress of the stiffener, the effective skin area and the total compressive load that the unit can carry at the failure point. Since the stiffener is braced laterally by the web and the skin, column bending action is prevented and thus the crippling strength is the true resulting strength of this corner member under longitudinal compression. (Additional stresses are produced on these corner members if web buckles under shear stresses and web diagonal tension forces are acting. This subject is treated in the chapter on semi-tension field beams.)

Solution:

Area of stiffener = 0.24 sq. in.
For 7075-T6 extrusion, F_{cy} = 70,000, E_c = 10,500,000.

The Gerard method will be used in calculating the crippling stress. Equation C7.4, or the design curve of Fig. C7.7, applies to this multi-corner shape. The lower scale parameter for Fig. C7.7 is,

$$\frac{A}{gt^2}\left(\frac{F_{cy}}{E_c}\right)^{1/2} = \frac{0.24}{6 \times .072^2}\left(\frac{70{,}000}{10{,}500{,}000}\right)^{1/2} = 0.63$$

Using this value, we read from Fig. C7.7 that F_{cs}/F_{cy} = 0.82. Thus F_{cs} = .82 x 70,000 = 57,400 psi. The g value of 6 was determined as shown in Fig. (a).

Effective Sheet Widths:

Equation C7.16 will be used to determine the sheet effective widths.

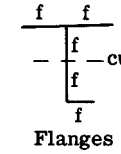

Flanges (f) = 5
No. of cuts = 1
g = 6

Fig. a

For the skin t = .05. Material is 7075-T6 aluminum alloy. E_c = 10,500,000.

$$W = 1.9t\sqrt{E/F_{cs}} = 1.9 \times .05\sqrt{10{,}500{,}000/57{,}400}$$

$$= 1.28 \text{ in.}$$

Thus a piece of sheet 1.28/2 = .64 wide acts to each side of the rivet centerline. Observation

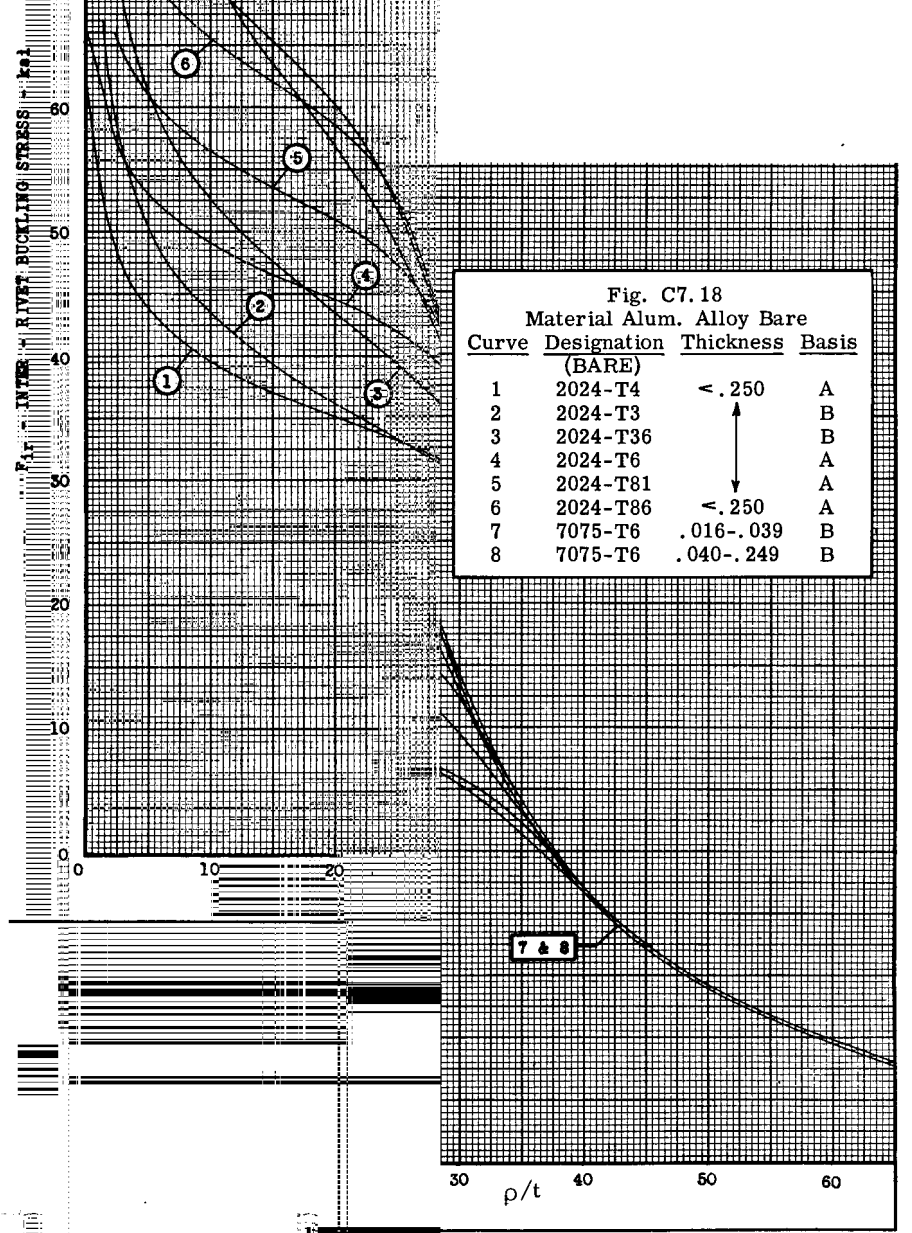

Fig. C7.18
Material Alum. Alloy Bare

Curve	Designation (BARE)	Thickness	Basis
1	2024-T4	≤.250	A
2	2024-T3	↕	B
3	2024-T36	↕	B
4	2024-T6	↕	A
5	2024-T81	↕	A
6	2024-T86	≤.250	A
7	7075-T6	.016-.039	B
8	7075-T6	.040-.249	B

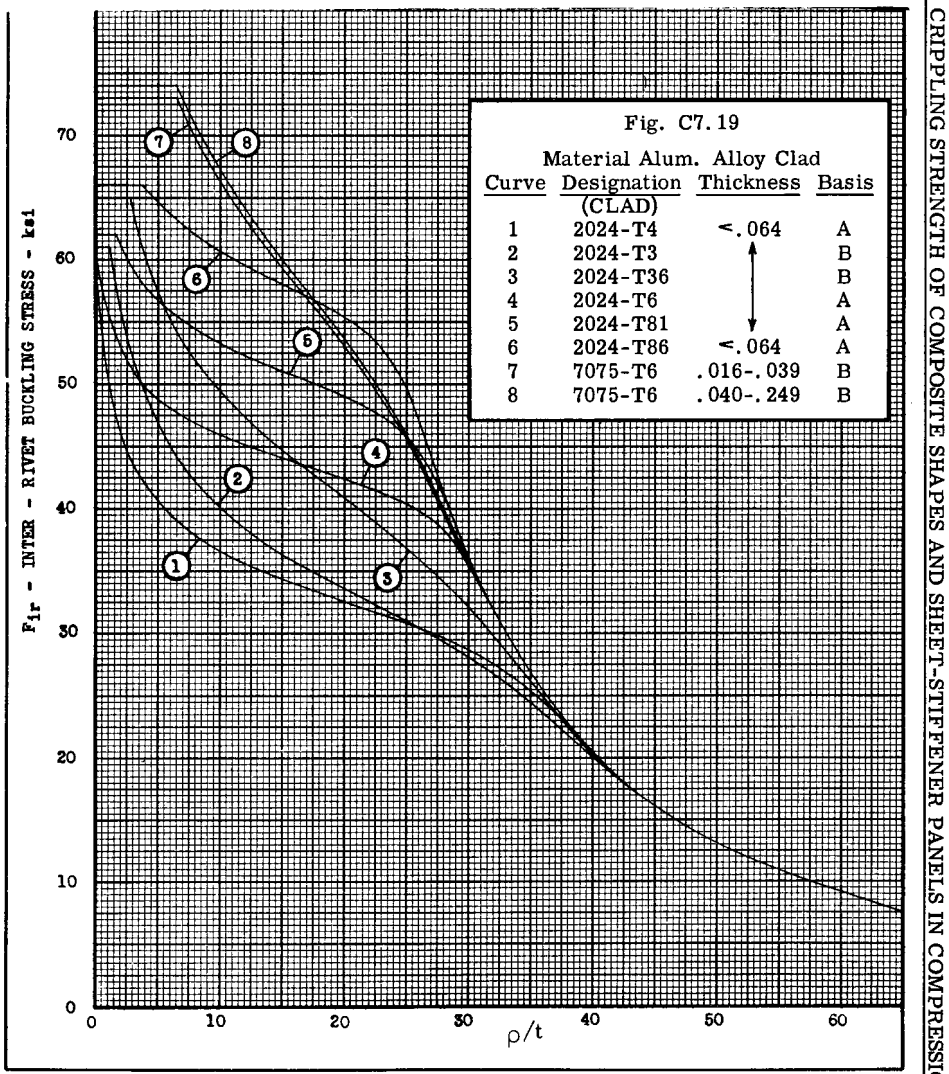

Fig. C7.19
Material Alum. Alloy Clad

Curve	Designation (CLAD)	Thickness	Basis
1	2024-T4	≤.064	A
2	2024-T3	↕	B
3	2024-T36	↕	B
4	2024-T6	↕	A
5	2024-T81	↕	A
6	2024-T86	≤.064	A
7	7075-T6	.016-.039	B
8	7075-T6	.040-.249	B

of the dimensions in Fig. C7.21 shows the effective width with each skin rivet line would overlap slightly thus we use only the width between rivet line (see Fig. b).

For the web t = .064. Since the web has a free edge, the effective width calculation will be in two steps.

$$\frac{W}{2} = \frac{1.9}{2} \times .064 \sqrt{10{,}500{,}000/57{,}400} = 0.82$$

W_1 from equation C7.18 = $.62t \sqrt{E/F_{cs}}$ = .62 x .064 $\sqrt{10{,}500{,}000/57{,}400}$ = 0.55 inch.

Fig. (b) shows the effective sheet width as calculated. Total effective sheet area = 1.28 x .05 + .875 x .05 + (0.55 + 0.82) .064 = .195. Total area = .195 + 0.24 = .435.

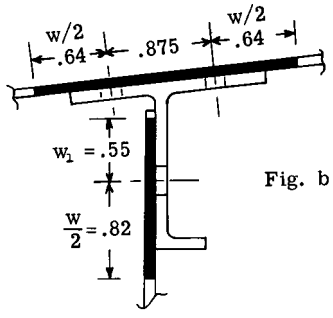

Fig. b

The total compressive load that entire unit can carry before failure is then equal to AF_{cs} = .435 x 57,400 = 25,000 lbs.

This result assumes that no inter-rivet buckling occurs under the stress of 57,400 psi in the sheet between rivets.

The skin rivets are Brazier head type spaced 7/8 inch apart or p = 7/8.

As discussed under inter-rivet buckling, the end coefficient c for this type of rivet should be less than 4 or assumed as 3.

Fig. C7.18 gives the inter-rivet buckling stress versus the p/t ratio. This chart is based on a clamped end condition or C = 4. Since C = 3 will be used for the Brazier type rivet, we correct the p/t ratio by the ratio $\sqrt{4} / \sqrt{3}$ = 1.16.

The corrected p/t = 1.16 x .875/.05 = 20.3

From Fig. C7.18 using curve (8) which is our material, we read F_{ir} = 60,000 psi, thus skin will not buckle between rivets as crippling stress is 57,400 psi.

The web rivets are of the flat head type and C = 4 can be used. Spacing is 1 inch. Hence p/t = 1/.064 = 15.6 and from Fig. C7.18, curve 8, we read F_{ir} = 64,600, which is considerably more than the unit crippling stress.

In wing construction, the skin rivets are usually of the flush surface type, either countersunk or dimpled. If we make the skin rivets of the countersunk type, the end fixity coefficient must be reduced to 1 to be safe. Then the corrected p/t ratio to use with Fig. C7.18 would be $(\sqrt{4} / \sqrt{1})$p/t = 2 x .875/.05 = 35. From Fig. C7.18 and curve 8, F_{ir} = 29,000 which is far below the calculated crippling stress, thus the rivet spacing would have to be reduced. Use 9/16 inch spacing corrected p/t = 2 x .5625/.05 = 22. From Fig. C7.18, F_{ir} = 57,400 psi, which happens to be the crippling stress and therefore satisfactory.

C7.16 Failing Strength of Short Sheet-Stiffener Panels in Compression.

Gerard (Refs. 2, 3) from a comprehensive study of test results on short sheet-stiffener panels in compression, has shown that his equation C7.4, or Fig. C7.7, can be used to give the local monolithic crippling stress for sheet panels stiffened by Z, Y and H at shaped stiffeners. The method of calculating the value of the g factor is illustrated in Fig. C7.22. Fig. C7.23 is a photograph showing the crippling type of failure for a short panel involving the Z shape stiffener.

C7.17 Failure by Inter-Rivet Buckling.

Howland (Ref. 8) assumed that the sheet acts as a wide column which is clamped at its ends and whose length is equal to the rivet spacing. The inter-rivet buckling stress equation is then,

$$F_{ir} = \frac{c\pi^2 \eta \bar{\eta}}{12\,(1 - \nu_e^2)} \left(\frac{t_s}{p}\right)^2 \quad \text{- - - - - - - - -} \quad (C7.24)$$

The end fixity coefficient C is taken as 4 for flat head rivets and reduced for other types as previously explained for equation C7.21.

η is the plasticity correction factor

$\bar{\eta}$ is the clad correction factor

ν_e is Poisson's ratio (use 0.30)

t_s = sheet thickness, inches.

p = rivet spacing or pitch in inches.

For non-clad materials the curves of Fig. C7.24 can be used. This figure is the same as Fig. C5.8 of Chapter C5. For the clad correction see Table C5.1 of Chapter C5.

C7.18 Failure of Short Panels by Sheet Wrinkling.

In a riveted sheet-stiffener panel, if the rivet spacing is relatively large, the sheet will buckle between rivets, such as illustrated in the photograph of Fig. C7.25. This inter-rivet buckling stress was discussed in the previous

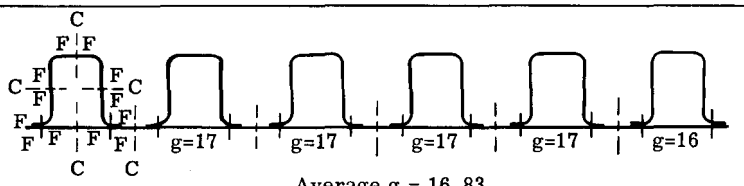

5 Cuts
12 Flanges
17 = g

Average g = 16.83

(c) Hat-stiffened panel.

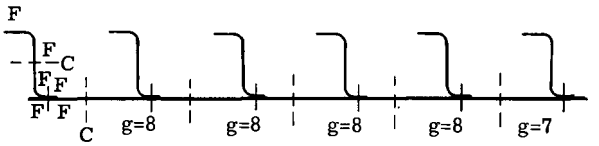

2 Cuts
6 Flanges
8 = g

Average g = 7.83

(b) Z-stiffened panel.

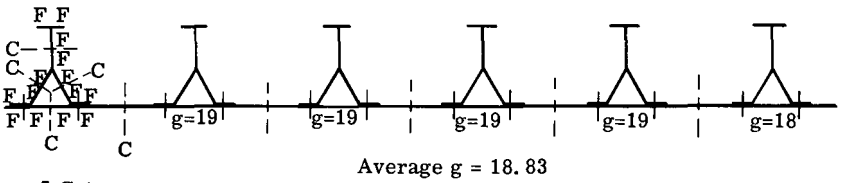

5 Cuts
14 Flanges
19 = g

Average g = 18.83

(a) Y-stiffened panel.

Fig. C7.22 Method of cutting stiffened panels to determine g.

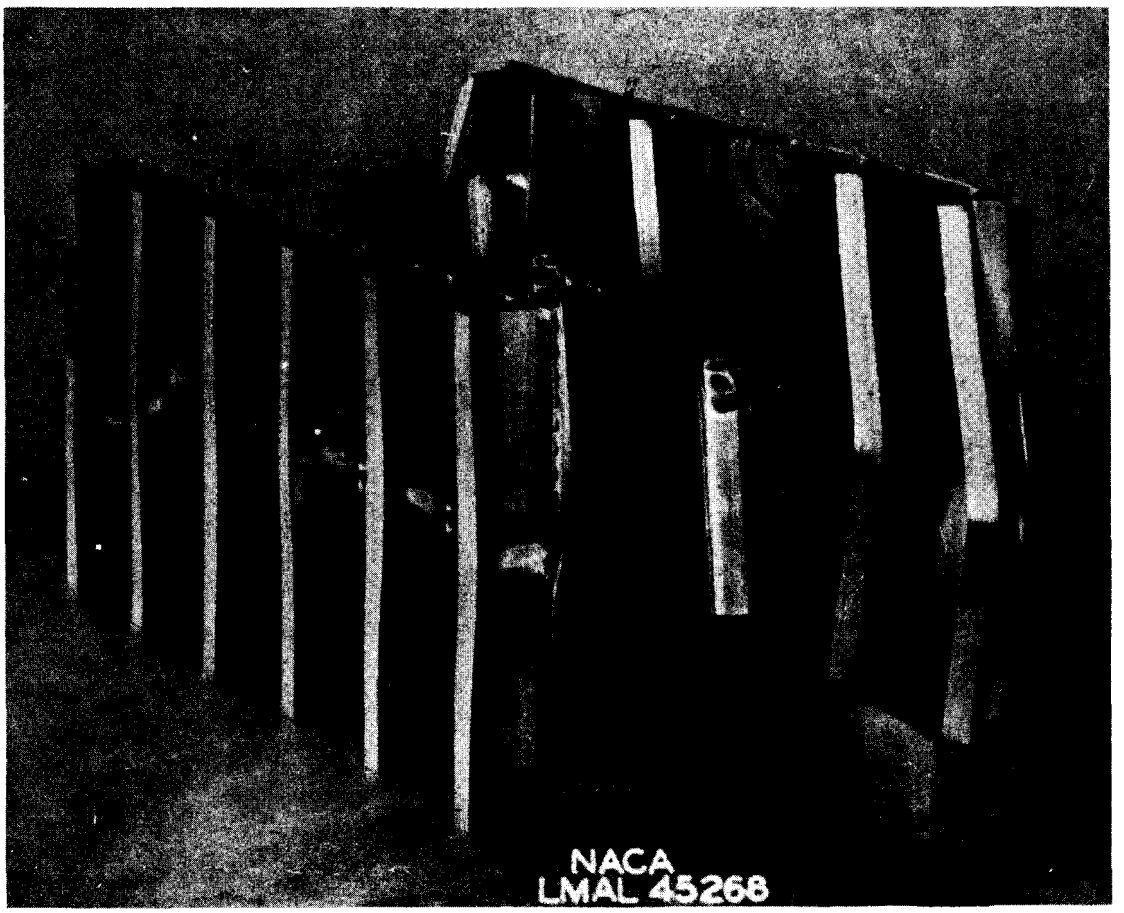

Fig. C7.23 A 24S-T aluminum-alloy Y-stiffened panel (on the left) and its 75S-T counterpart after failure.

article. This sheet buckling does not deform the flange of the stiffener to which the sheet is attached. However, if the rivet or spot weld spacing is such as to prevent inter-rivet buckling of the sheet, then failure often occurs by a larger wrinkling of the sheet as illustrated in Fig. C7.26. The larger wrinkle shape subjects the flange of the stiffner to which the sheet is attached to lateral forces and thus the stiffener flange often deforms with the sheet wrinkle shape. This deforming of the stiffener flange produces stresses on the stiffener web, thus wrinkling failure is a combination of sheet and stiffener failure. The action of the wrinkling sheet to deform the stiffener flange places tension loads on the rivets, thus rivet design enters into the failing strength of sheet-stiffener panels under compression.

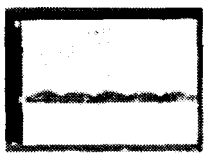

Fig. C7.25
Inter-Rivet Buckling



Fig. C7.26
Wrinkling Failure

Several persons have studied this wrinkling or forced crippling of riveted panels (Refs. 9 and 10). A rather recent study was carried out by Semonian and Peterson (Ref. 11), which is reviewed and simplified somewhat by Gerard in (Ref. 2). The results as given in (Refs. 11 and 2) are used to calculate the wrinkling stress.

C7.19 Equation for Wrinkling Failing Stress F_w.

From Ref. 2 we obtain,

$$F_w = \frac{k_w \pi^2 \eta \bar{\eta} E}{12 (1-\nu_e^2)} \left(\frac{t_s}{b_s}\right)^2 \quad \text{- - - - - - - - - (C7.25)}$$

k_w, the wrinkling coefficient is obtained from Fig. C7.27. This coefficient is a function of the effective rivet offset f which is obtained from Fig. C7.28. Having determined k_w from Fig. C7.27, equation C7.25 can be solved by use of Fig. C7.24.

C7.20 Rivet Criterion for Wrinkling Failure.

A criterion for the rivet pitch found from test data which results in a wrinkling mode failure is,

$$p/b_s \leq 1.27/k_w^{1/2} \quad \text{- - - - - - - - - - (C7.26)}$$

The lateral force required to make the stringer attachment flange conform to the wrinkled sheet, loads the rivet in tension. An approximate criterion for rivet strength from Ref. 2 is,

$$S_r > \frac{0.7}{E_{st}} \frac{b_s}{d} \frac{p}{d} (F_w)^2 \quad \text{- - - - - - - - - - (C7.27)}$$

The tensile strength of the rivet S_r is defined in terms of the shank area and it may be associated with either shank failure or pulling of the countersunk head of the rivet through the sheet.

For aluminum alloy 2117-T4 rivets whose tensile strength is s = 57 ksi, the criteria are:-

$$\left.\begin{aligned} &s = 57 \text{ ksi.}, \; d_e/t_{av} \leq 1.67 \\ &s = \frac{190}{d_e/t_{av}} - \frac{160}{(d_e/t_{av})^2}, \; d_e/t_{av} > 1.67 \end{aligned}\right\} \quad \text{(C7.28)}$$

where t_{av} is the average of sheet and stiffener thickness in inches. The effective diameter d_e is the diameter for a rivet made from 2117-T4 material.

The effective diameter of a rivet of another material is,

$$d_e/d = (S_r/S)^{1/2} \quad \text{- - - - - - - - - - - - (C7.29)}$$

where S_r is the tensile strength of a rivet defined as maximum tensile load divided by shank area in ksi units.

C7.21 Problem 1. Illustrating Calculation of Short Panel Failing Strength.

Fig. C7.29 shows a sheet-stiffener panel composed of formed Z stiffeners. The material is aluminum alloy 2024-T3. F_{cy} = 40,000. $F_{0.7}$ = 39,000, n = 11.5, E_c = 10,700,000. The problem is to determine the compressive failing. strength of a short length of this panel unit.

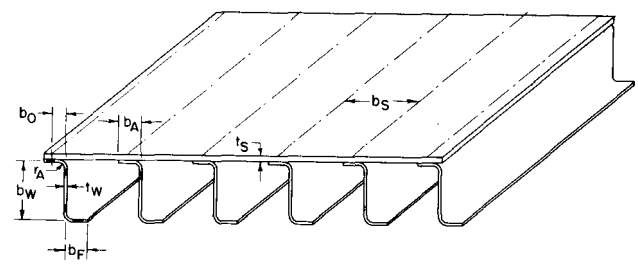

Fig. C7.29

General Panel Data:

t_w = .064	b_w = 2.437	b_A = 0.593
t_s = .064	b_f = 0.905	b_o = 0.343
b_s = 2.00		

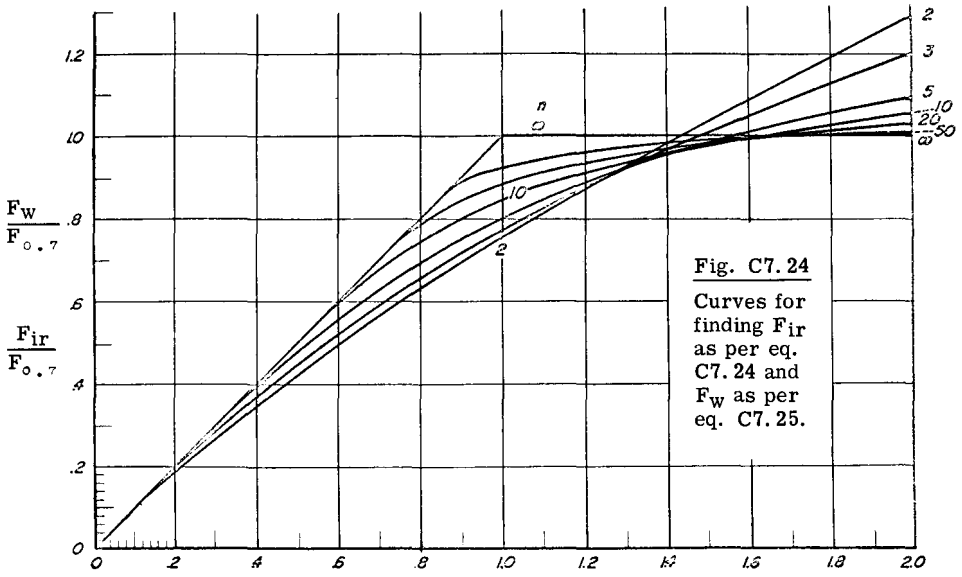

Fig. C7.24
Curves for finding F_{ir} as per eq. C7.24 and F_w as per eq. C7.25.

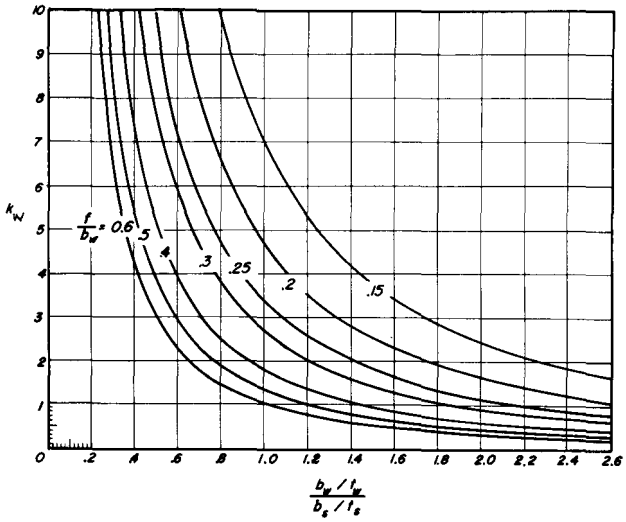

Fig. C7.27 Experimentally determined coefficients for failure in wrinkling mode. (Ref. 2)

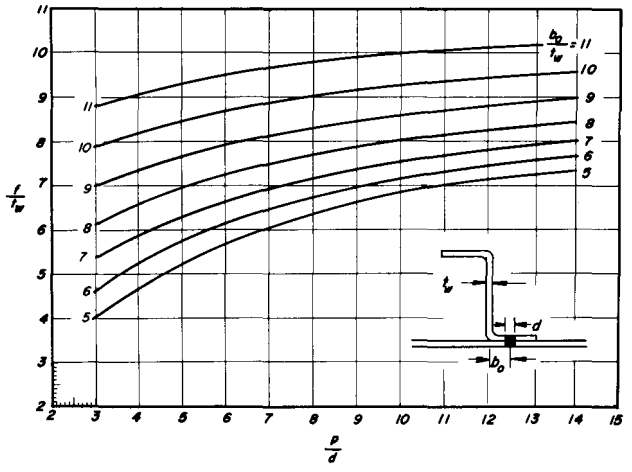

Fig. C7.28 (Ref. 2) Experimentally determined values of effective rivet offset.

whence, $b_W/t_W = 38$, $b_F/b_W = 0.372$

$b_A/t_W = 9.27$, $b_o/t_W = 5.36$

The rivets are 3/32 diameter Brazier head type AN456, 2117-T3 material spaced at 0.75 inches.

Area of Z stiffener = 0.252 in.^{2}
Area of skin for b_s = 2 inches = 2 x .064 = 0.128
Total area of sheet and stiffener = 0.380 in.^{2}

Crippling Stress of Stiffener Acting Alone. $F_{cs(ST)}$.

Since we have a Z type of stiffener, equation C7.6 and Fig. C7.9 applies. The lower scale parameter in Fig. C7.9 is,

$$(\frac{A}{t^2})(\frac{F_{cy}}{E_c})^{1/3} = (\frac{0.252}{.064^2})(\frac{40,000}{10,700,000})^{1/3} = 9.56$$

From Fig. C7.9, $F_{cs}/F_{cy} = 0.6$. Hence, F_{cs} = .6 x 40,000 = 24,000 psi = $F_{cs(ST)}$.

Crippling Stress of Panel Considered as a Monolithic Limit. $F_{cs(M)}$.

Equation C7.4 or Fig. C7.7 applies for monolithic failure of sheet-stiffener panels.

The lower scale parameter on Fig. C7.7 is,

$$(\frac{A}{gt^2})(\frac{F_{cy}}{E_c})^{1/2} = (\frac{0.380}{7.83 \times .064^2})(\frac{40,000}{10,700,000})^{1/2} = 0.73$$

g = 7.83 (see Fig. C7.22b)

From Fig. C7.7, we read F_{cs}/F_{cy} = .725, hence F_{cs} = 40,000 x .725 = 29,000 psi = $F_{cs(M)}$.

Inter-Rivet Buckling Stress (F_{ir})

The rivet type is Brazier head and the spacing p is 3/4 inch.

Equation C7.24 applies and Fig. C7.24 is used to solve the equation. The lower scale parameter in Fig. C7.24 is,

$$\frac{C \pi^2 E}{12 (1 - \nu_e^2) F_{o.7}} (\frac{t_s}{p})^2$$

For Brazier head rivet C = 3. ν = .3. Substituting:-

$$\frac{3\pi^2 \times 10,700,000}{12 (1 - .3^2)(39,000)} (\frac{.064}{.75})^2 = 5.45$$

The shape parameter n for our material is 11.5. Reference to Fig. C7.24 for a value of 5.45 on bottom scale which is off the scale, we estimate the $F_{ir}/F_{o.7}$ as above 1.1. Thus F_{ir} = 39,000 x 1.1 = 43,000. This value is far above the stiffener or panel crippling stress as previously calculated so inter-rivet buckling is not at all critical.

Failure by Sheet or Face Wrinkling. (F_W)

The wrinkling failure stress by equation C7.25 is,

$$F_W = \frac{k_W \pi^2 \eta E}{12(1 - \nu_e^2)} (\frac{t_s}{b_s})^2$$

To determine value of k_W, we use curves in Figs. C7.28 and C7.27.

$p/d = .75/.0937 = 8$, $b_o/t_W = 5.36$

From Fig. C7.28, we read f/t_W = 6.5, whence
$f = .064 \times 6.5 = 0.416$
$f/b_W = .416/2.437 = .17$
$(b_W/t_W)/b_S/t_S = 38/(2.0/.064) = 1.21$

From Fig. C7.27, we read k_W = 4.4.

To solve equation for F_W we use Fig. C7.24. The lower scale parameter is,

$$\frac{k_W \pi^2 E}{12 (1 - \nu_e^2)(F_{o.7})} (\frac{t_s}{b_s})^2 =$$

$$\frac{4.4 \pi^2 \times 10,700,000}{12 (1 - .3^2)(39,000)} (\frac{.064}{2.0})^2 = 1.15$$

For n = 11.5, we read from Fig. C7.24 that $F_W/F_{o.7}$ = .9, whence F_W = .9 x 39,000 = 35,100 psi. Thus wrinkling failure is not critical as F_W is larger than $F_{cs(M)}$ and $F_{cs(ST)}$.

The results show that the crippling stress for the stiffener alone of 24,000 psi is the smallest value, or the stiffener is unstable as it fails first. The entire panel unit will not reach its failing strength when stiffener stress is 24,000 because the skin wrinkling stress f_W is higher. An approximation suggested in (Ref. 2) is to assume stiffeners carry the same stress as the skin up to $F_{cs(ST)}$ and beyond this the stiffener carries no additional load. Thus the panel failing stress $F_{(F)}$ can be calculated from the following equation.

$$F_F = \frac{F_W b_s t_s + F_{cs(ST)} A_{ST}}{b_s t_s + A_{ST}}$$

$$= \frac{35,100 \times 2 \times .064 + 24,000 \times 0.252}{2 \times .064 + 0.252} = 27,800 \text{ psi}$$

The total load carried by each stiffener plus its sheet is 27,800 x .380 = 10,600 lbs.

The failing strength of the riveted panel cannot exceed the monolithic panel failing stress $F_{cs(M)}$, which was 29,000 psi for our panel or

greater than the calculated failing stress of 27,800 psi.

Check of Rivet Strength.

From expression C7.26

$$p/b_s < 1.27/k_w^{1/2}$$

$$\frac{0.75}{2.0} = .375 < 1.27/(4.4)^{1/2} = .603 \text{(satisfactory)}$$

The criterion for required rivet strength to make the stiffener flange follow the wrinkled sheet is from C7.27

$$S_r > \frac{0.7}{E_{ST}} \frac{b_s}{d} \frac{p}{d} (F_w)^2$$

$$S_r > \left(\frac{0.7}{10{,}700{,}000}\right)\left(\frac{2}{3/32}\right)\left(\frac{0.75}{3/32}\right)(35{,}100)^2$$

$S_r > 13.7$ psi.

From expression C7.28

$S = 57$ ksi for $d_e/t_{av.} \leq 1.67$

For given panel $d_e/t_{av.} = 3/32/.064 = 1.46$, thus rivets have plenty of tensile strength to produce a wrinkling failure.

C7.22 General Design Limitations to Prevent Secondary Failure in Sheet-Stiffener Panels.

Sheet stiffener units can be designed as columns if the secondary forms of failure such as inter-rivet buckling and face wrinkling are avoided. The following design rules referring to Fig. (A) will usually avoid these secondary weaknesses.

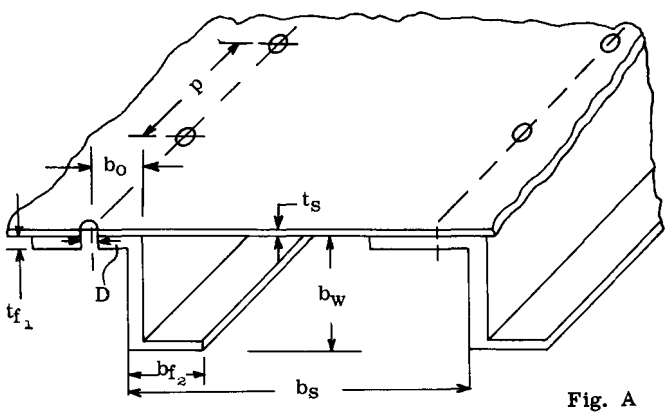

Fig. A

(1) $t_{f_1}/t_s \geq 0.5$ - - Promotes overall crippling

(2) $0.4 < b_{f_2}/b_w < 0.5$ -- Rolling versus local buckling

(3) Make b_o as small as possible -- Face wrinkling

(4) $p/b_s < 0.5$ - - - - - - Inter-rivet buckling

(5) $p/D \leq 8$ - - - - - - - - - - Face wrinkling

(6) Tensile strength of rivet or spot weld attachment per inch should be $\geq 0.05 F_{cy} t_s$ in order to prevent failure in wrinkling.

(7) As a rough guide do not use bent up stringers if $b_s/t_s < 30$ in order to prevent face wrinkling weakness.

C7.23 Y Stiffened Sheet Panels.

A Y shape cannot be formed from sheet, thus it must be extruded. To make the Y shape efficient, the various parts usually have a different thickness. Furthermore, the extruded material has different mechanical properties in the inelastic stress range as compared to rolled sheet that is used for the panel, thus these effects must be considered in calculating the crippling stress of the stiffener and the complete panel unit.

The effective thickness $\bar{t}_w$ of the stiffener is determined by the following equation (Ref. 3):

$$\bar{t}_w = \Sigma\, b_i t_i / \Sigma\, b_i \quad - - - - - - - - - - - - \text{(C7.29)}$$

where b_i and t_i refer to the length and thickness, respectively, of the cross-section elements.

When the yield stress F_{cy} of stiffener and sheet are different and effective $\bar{F}_{cy}$ can be estimated as follows (Ref. 3):

$$\bar{F}_{cy} = \left\{ F_{cy(SH)} + F_{cy(ST)} \left[(\bar{t}_w/t_s) - 1 \right] \right\} / \bar{t}_w/t_s \quad - - - - - - - - - - - - \text{(C7.30)}$$

The monolithic crippling stress for the sheet stiffener panel can be calculated from equation C7.4 or by the curve in Fig. C7.7. Equation C7.4 is

$$F_{cs(M)}/F_{cy} = 0.56 \left[(gt^2/A)(E/F_{cy})^{1/2} \right]^{0.85}$$

The constant 0.56 in this equation applies for Y and hat-stiffened panels when the ratio $t_w/t_s = 1.0$. For other ratios the correction of this constant which is referred to as βg in Gerard's basic equation can be obtained from curve in Fig. C7.30.

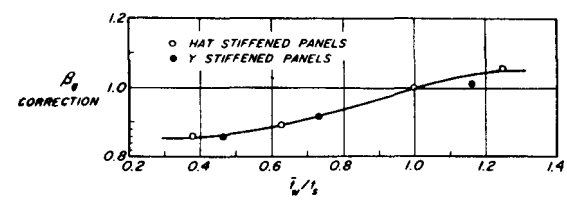

Fig. C7.30 β_g correction for $\bar{t}_w/t_s$ effect on Y- or hat-stiffened panels.

C7.24 Example Problem Y Stiffened Panel.

The compressive monolithic failing stress of a Y stiffened panel, as illustrated in Fig. C7.22a, will be calculated by the Gerard method. Fig. C7.31 shows details of the panel unit. The stiffener is extruded from 2014-T6 aluminum alloy for which F_{cy} = 53000 and E_c = 10,700,000. The skin or panel sheet is aluminum alloy 7075-T6 for which F_{cy} = 67,000 and E_c = 10,500,000.

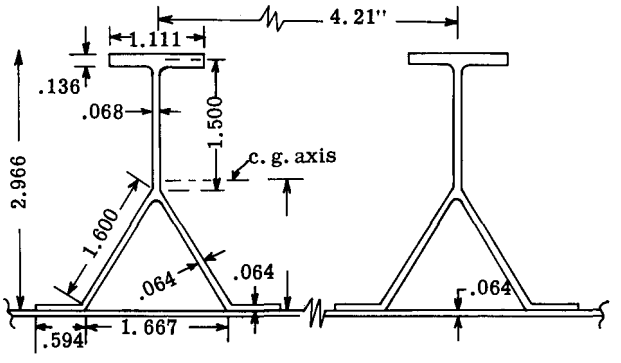

Fig. C7.31

Stiffener area = 0.538 in.^{2}
Sheet area = 4.21 x .064 = .270 in.^{2}
Total area (A) per stiffener unit = 0.808 in.^{2}
Radius of gyration of stiffener alone = 1.123 in.

Solution:-

Since the elements of the Y stiffener have different thicknesses, the effective t_w by equation C7.29 is needed.

$$\bar{t}_w = \frac{\Sigma\, b_1 t_1}{\Sigma b_1} =$$

$$\frac{1.111 \times .136 + 1.432 \times .068 + 3.2 \times .064 + 1.188 \times .064}{1.111 + 1.432 + 3.2 + 1.188}$$

or $\bar{t}_w$ = .0763 inches

Since stiffener and sheet have different material properties, an effective F_{cy} from equation C7.30 will be calculated.

$$\bar{F}_{cy} = \left\{67{,}000 + 53000\left[\left(\frac{.0763}{.064}\right)-1\right]\right\} / \frac{.0763}{.064} = 64700$$

The curve in Fig. C7.7 will be used to solve the equation for $F_{cs(M)}$. The lower scale parameter for Fig. C7.7 modified by $\bar{t}_w$ and $\bar{F}_{cy}$ is,

$$\frac{A}{g\, \bar{t}\, t_s}\left(\frac{\bar{F}_{cy}}{E_c}\right)^{1/2}$$

The value of g from Fig. C7.22a is 18.83 as the average value for a 6 stiffener panel unit. E_c will be taken as 10,600,000 which is the average E for stiffener and sheet. Substituting in the above parameter:-

$$\left(\frac{.808}{18.83 \times .0763 \times .064}\right)\left(\frac{64{,}700}{10{,}600{,}000}\right)^{1/2} = .686$$

From Fig. C7.7 we read

$$F_{cs}/\bar{F}_{cy} = .76$$

Thus the monolithic crippling a failing stress $F_{cs_M} = \bar{F}_{cy} \times .76 = 64{,}700 \times .76 =$ 48,200 psi.

The curve as plotted in Fig. C7.7 is for a $\bar{t}/t_s$ ratio of 1.0. The ratio for our panel is .0763/.064 = 1.19. The correction factor from Fig. C7.30 is 1.03. Therefore $F_{cs(M)}$ = 1.03 x 48200 = 49,600 psi.

Load carried by one stiffener-sheet unit = 0.808 x 49600 = 40100 lb.

COLUMN STRENGTH

C7.25 Column Curve for Members With Unstable Cross-Sections.

Chapter C2 dealt with the column strength of members with stable cross-sections. For example, if we took a round tube with relatively heavy wall thickness and tested various lengths in compression to obtain the failing stress and then plotted these stress values F_c against the slenderness ratio L'/ρ of the member, the test results would closely follow the curves ABFC in Fig. C7.32. The type of failure would be elastic overall bending instability at stresses between points B-C and inelastic bending instability at stresses for most of the range BA. Euler's equation as shown in Fig. C7.32 can be used to determine the failing stress for both elastic and inelastic bending instability with the tangent modulus E_t being used in the inelastic stress range.

Now suppose we test various lengths of a member composed of the same material as used for obtaining curve ABC, but use a member with an open cross-section, such as a channel, hat section, etc., with relatively small material thickness. The test results for such members would often follow a curve similar to DEFC in Fig. C7.32. Thus it is obvious that Euler's equation cannot be used in the range DEF, as the true failing stresses are far less than that given by the Euler column equation. A short length of the member with L'/ρ less than 20 will fail at practically the same stress, thus the failing stress for lengths up to L'/ρ = 20 will be practically the same and this stress has been given the name of crippling stress (F_{cs}) and the previous portion of this chapter has been con-

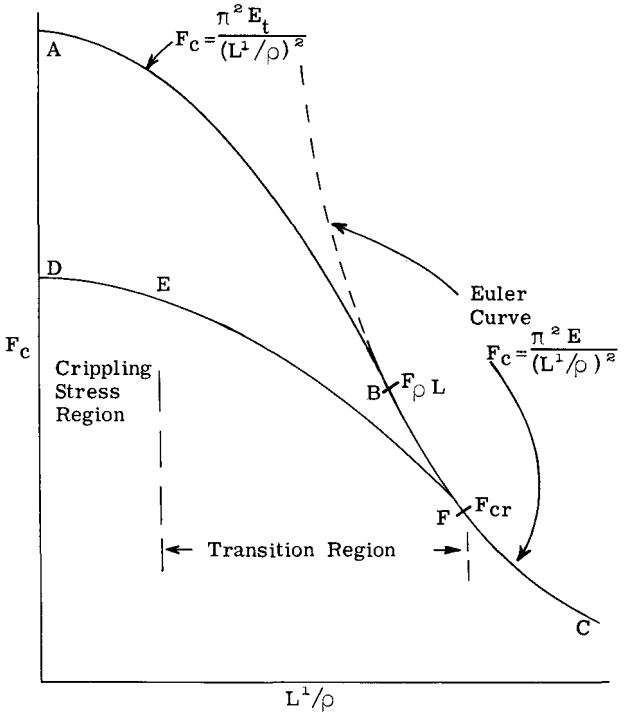

Fig. C7.32

cerned with methods of calculating this local crippling or failing stress. At point (F) the elastic buckling of some part of the cross-section begins. Between stress points F to E the action for the member involves both overall elastic bending instability plus local buckling which becomes more extensive as the stress increases. The portion EF of the column strength curve is often referred to as the transition range. At present no reliable theoretical theory has been developed for determining the failing stresses in this transition range, thus resort is made to semi-empirical methods which have been checked against test results and found to give reasonably close results.

C7.26 Methods Used for Determining the Column Failing Stress in the Transition Region.

METHOD 1. JOHNSON-EULER EQUATION.

Possibly the first method used in calculating the column failing stress F_c in the transition range EF in Fig. C7.32 was the well known Johnson-Euler equation which involves the crippling stress. The equation is,

$$F_c = F_{cs} - \frac{F_{cs}^2}{4\pi^2 E}(L'/\rho)^2 \quad \text{- - - - - - - - (C7.31)}$$

where, F_c = column failing stress (psi)
F_{cs} = crippling stress, assumed to occur at $L'/\rho = 0$, where $L' = L/\sqrt{c}$.

The equation gives a parabolic curve starting from the crippling stress at $L'/\rho = 0$, and becomes tangent to the Euler curve at a stress value equal to one half the crippling stress. Fig. C7.33 shows a plot of equation C7.31 for aluminum alloy material for various values of the crippling stress which is the F_c stress at $L'/\rho = 0$.

This method is quite simple to use as the only additional calculation required is the crippling stress of the column section which is obtained by methods previously explained in this chapter. The other methods usually involve the buckling stress as well as the crippling stress. Since the crippling stress is normally constant below $L'/\rho = 20$, the assumption that F_{cs} is zero at $L'/\rho = 0$ is slightly conservative.

METHOD 2.

The following method or slight variations of it appears in the structural design manuals of a number of aerospace companies. The method or procedure for determining the column failing stresses in the so-called transition range involves the use of the basic column curve for stable cross-sections. The procedure can best be explained by reference to Fig. C7.34.

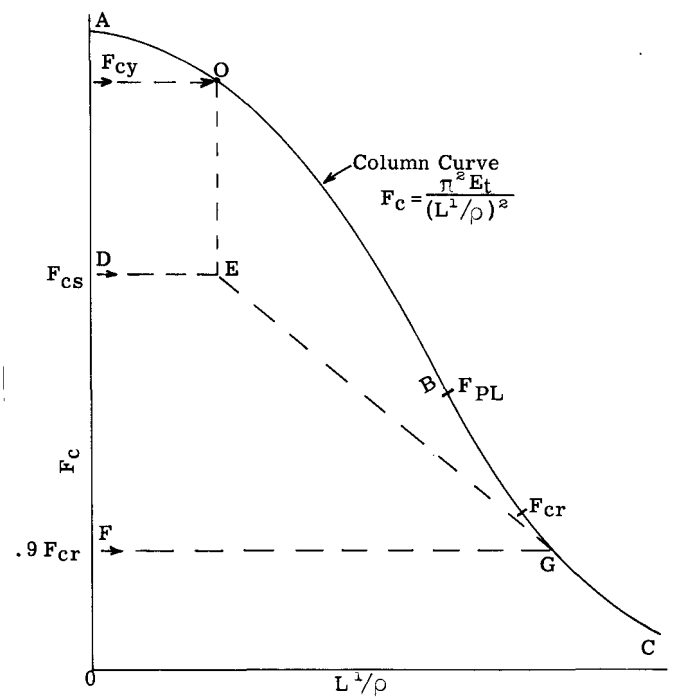

Fig. C7.34

The curve ABC is the Euler column curve for a column with a stable cross-section and for a given material. It involves using the tangent modulus E_t in the inelastic stress range. The following steps are taken to determine the column curve for the so-called transition range:-

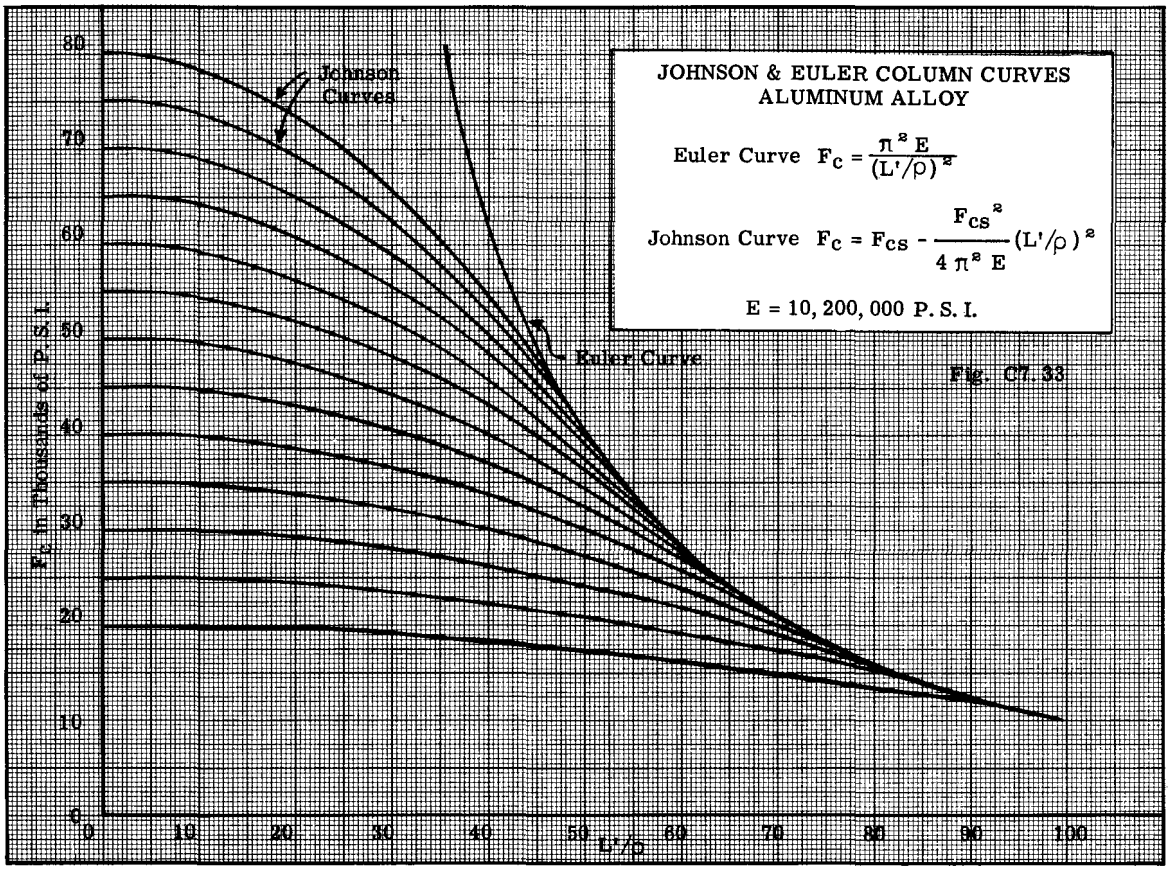

(1) Locate point (O) on the basic column curve by drawing a horizontal line through an F_c value equal to F_{cy}, the yield stress of the particular material being used.

(2) Draw a horizontal line starting at point D. Point D is at an F_c value equal to the (F_{cs}) crippling stress for the column section being considered. Point (E) on this line is determined by projecting vertically downward from point (O).

(3) Locate point (F) at a value of $F_c = .9\ F_{cr}$ where F_{cr} is the buckling stress for the cross-section. Draw a horizontal line through point (F) to intersect the column curve at point (G).

(4) Connect points E and G with a straight line. The line EG then represents the column failing stress F_c for values of L'/ρ between points E and G.

This method requires the use of the column curve for stable sections and the determination of the buckling stress and thus requires more calculations than Method 1. It also requires a graphical construction.

METHOD 3.

Another method that is widely used also uses a parabolic curve to represent the column strength in the transition range (see Ref. 12)

The parabolic approximation has the following form:-

$$\frac{F_c}{F_{cs}} = 1 - (1 - \frac{F_{cr}}{F_{cs}})(\frac{F_{cr}}{F_E}) \qquad \text{- - - - - - - - (C7.32)}$$

where

F_c is the column failing stress.
F_{cs} is the crippling stress.
F_{cr} is buckling stress for the column cross-section.
F_E is the Euler column stress for the particular column being considered as found from equation $F_E = \pi^2 E/(L'/\rho)^2$

The equation applies for $F_c > F_{cr}$. For cases where $F_{cr} > F_{\rho L}$ where $F_{\rho L}$ is the proportional limit stress for the material use $F_{\rho L}$ instead of F_{cr} in equation C7.32.

C7.27 Example Problems Involving the Finding of the Column Strength of Columns With Unstable Cross-Sections.

PROBLEM 1.

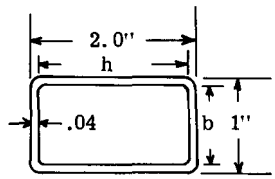

Fig. a

A rectangular tube 21 inches long has the cross-section as shown in Fig. (a). The material is aluminum alloy sheet 7075-T6, with F_{cy} = 67,000 and E_c = 10,500,000. If the member has a pinned end condition, what is the column failing stress.

Solution. The area of cross-section = .234 in.^{2} The least radius of gyration is 0.42 inches.

Before the column failing stress F_c for the 21 inch length can be found, the crippling stress F_{cs} and the buckling stress F_{cr} must be determined.

The crippling stress will be calculated by the Gerard Method. The parameter for use with Fig. C7.7 is,

$$\frac{A}{gt^2}\left(\frac{F_{cy}}{E_c}\right)^{1/2} = \frac{.234}{12 \times .04^2}\left(\frac{67{,}000}{10{,}500{,}000}\right)^{1/2} = 0.976$$

From Fig. C7.7, F_{cs}/F_{cy} = .57, hence F_{cs} = .57 x 67,000 = 38,200 psi.

The initial buckling stress F_{cr} will be determined by the theory of Chapter C6.

b = 1 - .08 = .92, h = 2 - .08 = 1.96

b/h = .92/1.96 = .479, t_b/t_h = 1.0

From Fig. C6.6 of Chapter C6, K_h = 5.2

$$F_{cr} = \frac{K_h \pi^2 E_c}{12(1-\nu_e^2)}\left(\frac{b}{h}\right)^2$$

$$F_{cr} = \frac{5.2\pi^2 \times 10{,}500{,}000}{12(1-.3^2)}\left(\frac{.04}{1.92}\right)^2 = 21{,}500 \text{ psi.}$$

Column Strength by Method 1 (Johnson-Euler eq.)

L = 21 inches $L' = L/\sqrt{c} = 21/\sqrt{1} = 21$

$L'/\rho = 21/.42 = 50$

The Johnson-Euler equation is,

$$F_c = F_{cs} - \frac{F_{cs}^2}{4\pi^2 E}(L'/\rho)^2 \text{ , substituting,}$$

$$F_c = 38{,}200 - \frac{38{,}200^2}{4\pi^2\ 10{,}500{,}000}(50)^2 = 29{,}400 \text{ psi}$$

This value could be read directly from Fig. C7.33 for a value of L'/ρ = 50 and a value of $F_c = F_{cs}$ = 38,200 at L'/ρ = 0.

Column Strength by Method 2

This method requires a graphical construction which involves the column curve for the given material and for a stable cross-section.

Fig. C7.35 shows the column curve for our material for a column with stable cross-section. It is identical to Fig. C2.10 of Chapter C2 for the room temperature condition, except the curve in Fig. C7.35 has been drawn to a smaller vertical scale.

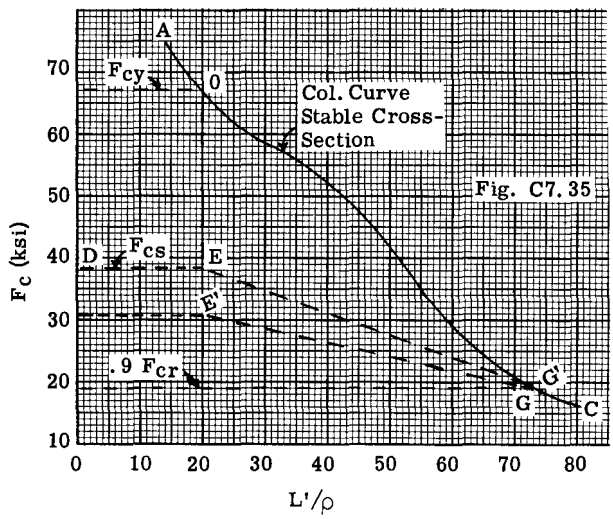

Fig. C7.35

The graphical construction to obtain the column curve in the region between the crippling stress and the buckling stress is as follows:

At a column stress $F_c = F_{cy}$ = 67,000, draw a horizontal line to intersect the basic column curve at point (O). Draw a horizontal line from point (D) which equals the crippling stress of 38,200 psi. Locate point (E) by projecting vertically downward from point (O). Locate point (G) at an F_c stress equal to .9 F_{cr} = .9 x 21,500 = 19,350 psi. Connect points (E) and (G) by a straight line. This line represents the column failing curve for the member of our problem for L'/ρ values between points (E) and (G). Taking L'/ρ = 50, we project upward to EG line and then horizontally to scale at left to read F_c = 27,700 psi.

Column Strength by Method 3

In this method equation C7.32 is used.

$$\frac{F_c}{F_{cs}} = 1 - (1 - F_{cr}/F_{cs})(F_{cr}/F_E) \quad \text{------ (A)}$$

F_{cr} = 21,500, F_{cs} = 38,200

F_E is the Euler column stress for column with a stable cross-section. To find F_E, we project upward from $L'/\rho = 50$ to the curve AOC in Fig. C7.35 and then horizontally to read $F_c = F_E = 41{,}700$ psi.

Substituting in eq. (A),

$$\frac{F_c}{38{,}200} = 1 - (1 - 21{,}500/38{,}200)(21{,}500/41{,}700)$$

$$F_c = 38{,}200\ (1 - 0.225) = \underline{29{,}600}\ \text{psi}$$

Example Problem 2.

A formed Z section as shown in Fig. (b) is used as a column. The length L = 30". The member is braced in the x-x direction thus column bending failure must occur about x-x axis. Material is aluminum alloy, $F_{cy} = 67{,}000$, $E_c = 10{,}500{,}000$. Assume the end fixity coefficient c = 1.5.

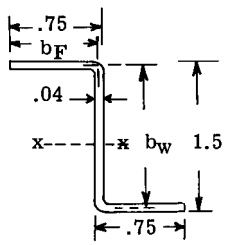

Fig. b

Find the column failing stress.

Solution:

Area of Section = 0.117 in.^{2}
$\rho_x = .535$ in.

The initial buckling stress is needed in finding the column strength.

$b_W = 1.5 - .04 = 1.46$, $b_f = 0.75 - .02 = 0.73$

$b_F/b_W = .73/1.46 = 0.5$, $t_W/t_F = 1.0$

From Fig. C6.4 of Chapter C6, we read $K_W = 2.9$.

$$F_{cr} = \frac{2.9\ \pi^2 \times 10{,}500{,}000}{12\ (1 - .3^2)} \left(\frac{.04}{1.46}\right)^2 = 20{,}900\ \text{psi}$$

The crippling stress will be calculated by the Gerard Method using Fig. C7.9, which applies for Z shapes. The lower scale parameter is,

$$\frac{A}{t^2}\left(\frac{F_{cy}}{E_c}\right)^{1/3} = \left(\frac{.117}{.04^2}\right)\left(\frac{67{,}000}{10{,}500{,}000}\right)^{1/3} = 13.6$$

From Fig. C7.9, we read, $F_{cs}/F_{cy} = .455$, hence, $F_{cs} = 67{,}000 \times .455 = \underline{30{,}600}$ psi.

Column Strength by Method 1

$$L' = L/\sqrt{c} = 30\ \sqrt{1.5} = 24.5$$

$$L'/\rho = 24.5/.535 = 45.8$$

Substituting in Johnson-Euler equation,

$$F_c = 30{,}600 - \frac{30{,}600^2}{4\ \pi^2 \times 10{,}500{,}000}(45.8)^2 = \underline{25{,}860}\ \text{psi}$$

Column Strength by Method 2

On Fig. C7.35 point E' is located at $F_c = F_{cs} = 30{,}600$. Point G' is located at .9 x 20,900 = 18,800 psi. The line E'G' is the column curve. For $L'/\rho = 45.8$, we project upward to line E'G' and then horizontally to left scale to read $F_c = \underline{25{,}000}$ psi.

Column Strength by Method 3

To find F_E, use Fig. C7.35 with $L'/\rho = 45.8$ and basic Euler curve, gives a value of $F_E = 47{,}000$ psi.

Substituting in equation (A):-

$$\frac{F_c}{30{,}600} = 1 - (1 - 20{,}900/30{,}600)(20{,}900/47{,}000)$$

$$F_c = 30{,}600\ (1 - .141) = \underline{26{,}300}\ \text{psi}$$

C7.28 Column Strength of Stiffener With Effective Sheet.

Column members are often attached to thin sheet by rivets or spot welding. If the rivet spacing is such as to prevent inter-rivet buckling, then the sheet will assist the stiffener to carry a compressive load and to neglect the sheet would be too conservative.

If the attached sheet is relatively thin, that is, less than the stiffener thickness, the method of using the effective sheet width as a part of the column area is widely used by structural designers and will be used in this example solution.

Example Problems.

For an example problem, we will assume that the Z stiffener in Problem 2 is one of several stiffeners riveted to a sheet of .025 thickness and of the same material as the stiffener.

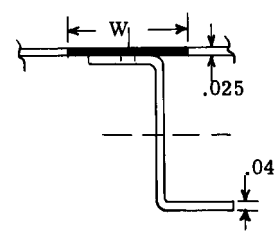

Fig. c

Solution.

The rivet or spot weld spacing is made such as to prevent inter-rivet buckling. Thus the column area will be as shown in Fig. c, namely, the stiffener area plus the area of the sheet for the effective width w. Since the effective sheet width w is a function of the stiffener stress and since the stiffener

stress is a function of the radius of gyration, the design procedure is of the trial and error category.

First Trial.

Assume the effective sheet width is based on column strength of Z stiffener acting alone. The average column failing stress by the 3 methods in the Problem 2 solution was (25,860 + 25,000 + 26,300)/3 = 25,700 psi.

The effective width equation to be used is,

$w = 1.9\ t\sqrt{E/F_{ST}}$

$= 1.9 \times .025 \times \sqrt{10{,}500{,}000/25{,}700} = .965$ in.

Effective sheet area = $0.965 \times .025 = .0242$

Area of stiffener = $A_o = .117$

Total area = .1412

Adding the effective sheet to the stiffener will change the radius of gyration. Mr. R. J. White (Ref. 13) has developed equation C7.33 which gives the variation in the radius of gyration in terms of known variables for any stiffener cross-section. Since the failing stress of a column is directly proportional to the radius of gyration squared, equation C7.33 can be equated to the ratio of the column stresses.

$$\left(\frac{\rho}{\rho_o}\right)^2 = \frac{F_c}{F_{ST}} = \frac{1+\left[1+\left(\frac{S}{\rho_o}\right)^2\right]\frac{wt}{A_o}}{1+\left(\frac{wt}{A_o}\right)^2} \quad \text{- - - - (C7.33)}$$

where, ρ_o = radius of gyration of stiffener alone.

ρ = radius of gyration of sheet and stiffener.

S = distance from centerline of sheet to neutral axis of stiffener.

t = sheet thickness. w = sheet effective width.

Equation C7.33 has been put in curve form as shown in Fig. C7.36, which will now be used to compute the radius of gyration ρ_o for the stiffener plus effective sheet.

S = .75 + .0125 = .7625

ρ_o for stiffener alone = .535

$S/\rho_o = .7625/.535 = 1.425$

w = .965

$wt/A_o = .965 \times .025/.117 = .2063$

From Fig. C7.36 for the above values of S/ρ_o and wt/A_o, we obtain

$(\rho/\rho_o)^2 = 1.05$, whence $\rho^2 = .535^2 \times 1.05$, which gives $\rho = .548$ in.

Then $L'/\rho = 24.5/.548 = 44.8$.

Use Method 1 for column strength:-

$$F_c = 30{,}600 - \frac{30{,}600^2}{4\ \pi^2 \times 10{,}500{,}000}\ 44.8^2 = \underline{26{,}050}\ \text{psi}$$

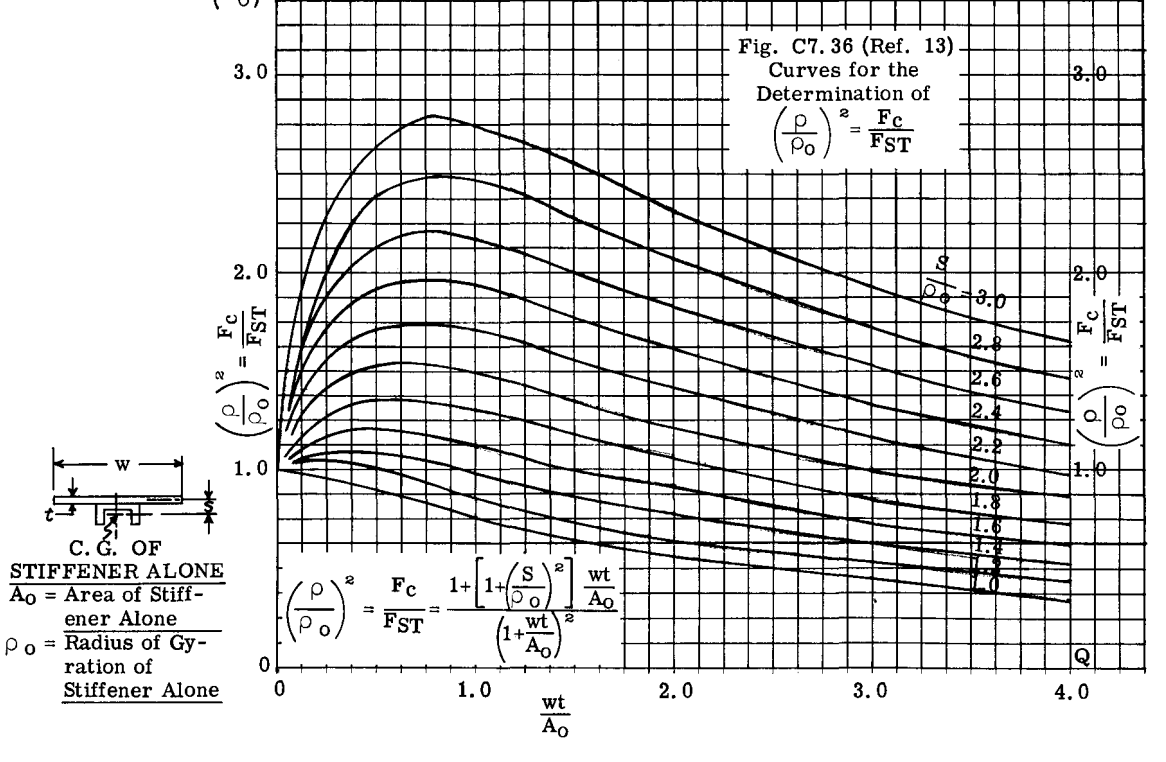

The revised effective width based on this stiffener stress is,

$w = 1.9 \times .025 \sqrt{10,500,000/26,050} = .99$ in.

This value is only .03 inch more than the value of .96 previously, thus the effect on the radius of gyration ρ will be negligible. The column failing stress for the sheet stiffener combination is therefore 26,050 psi, and the compressive failing load would be 26,050 x .1412 = 3675 lbs.

C7.29 Sheet-Stiffener Panels With Relatively Heavy Sheet Thickness.

For Z, Y and hat shaped stiffener-sheet panels as previously discussed relative to local failing stress, use entire sheet and stiffener area in computing radius of gyration or, in other words, due not use effective sheet widths but use entire sheet as effective.

PROBLEMS

(1) Find the crippling stress for the angle sections of Figs. (a) and (b) when formed from the following materials. Use both Needham and Gerard Methods. (1) 2024-T3 aluminum alloy. (2) 7075-T6 aluminum alloy. (3) 17-7PH(TH1050) stainless steel. (4) Same as (3) but subjected to an elevated temperature of 700°F for 1/2 hour duration.

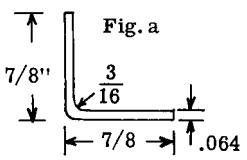

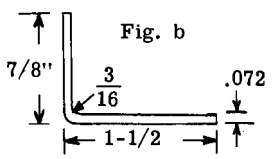

(2) Find the crippling stress for the two channel shapes of Figs. c and d when formed of following materials. (1) AISI 4130 steel, heat-treated to F_{tu} = 180,000. (2) Same as (1) but subjected to an elevated temperature of 500°F for 1/2 duration. (3) Ti-8Mn Titanium. (4) 7075-T6 aluminum alloy.

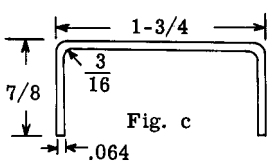

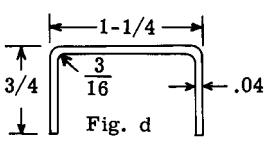

(3) Find the crippling stress of the rectangular tubes in Figs. e and f when formed from following materials. (1) 2024-T3 aluminum alloy. (2) HK31A-0 magnesium. (3) Ti-8Mn Titansium.

(4) Same as (2) but subjected to 300°F for 1/2 hour duration.

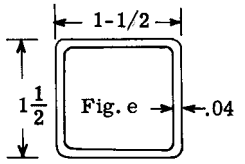

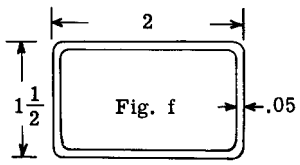

(4) Find the crippling stress for sections of Figs. g and h when formed from 2024-T3 and 7075-T6 aluminum alloy material.

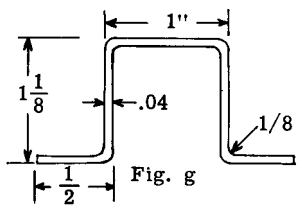

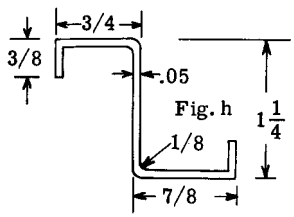

(5) Find the crippling stress for the extruded sections numbers 4, 8, 16, 22, 28 and 34 as given in Table A3.16 of Chapter A3. Material 2014-T3 aluminum alloy.

(6) Fig. i shows a corner member, in a stiffened wing section. The skin is fastened to the stiffener by one row of 1/8 diameter rivets at 3/4 inch spacing. The web is fastened to stiffener by 2 staggered rows of rivets, with rivet spacing in each of 1-1/8 inch, and rivets are of the flat head type. Material is 2024-T3 aluminum alloy. Also use 7075-T6 aluminum material.

Find crippling stress for stiffener. Will inter-rivet buckling occur. Find effective sheet widths and total failing load unit will carry.

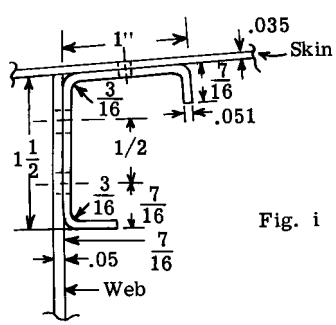

(7) Determine the compressive failing strength of a short Z stiffened sheet panel unit such as that illustrated in Fig. C7.29. The various dimensions are as follows. Refer to Fig. C7.29 for meaning of symbols.

$t_W = .072$ $b_F = 1.0$ $b_S = 2.50$
$t_S = .072$ $b_A = 0.625$
$b_W = 2.50$ $b_O = 0.375$

Stiffener and sheet material is 2024-T3 aluminum alloy. Rivets are 1/8 diameter Brazier Head type 2117-T3 material and spaced 7/8 inch.

(8) Same as (7) but change material to 7075-T6 aluminum alloy.

(9) Same as (7) but change material to Ti-8Mn Titanium.

(10) In the Example Problem on a Y stiffened panel as given in Art. C7.25, change sheet thickness from .064 to .081 and calculate the resulting panel strength.

(11) The hat stiffener in Fig. g of Problem (4) is one of several stiffeners riveted to skin of thickness .032 and of the same material as the stiffener. If the length of the panel is 20 inches, what will be the column failing stress if end fixity c = 1.5. Also for c = 2.0. Use method involving effective sheet widths.

(12) Same as Problem 11 but use Z stiffener of Fig. h of Problem 4.

References

(1) Needham, R. A.:- The Ultimate Strength of Aluminum Alloy Formed Structural Shapes in Compression. Jour. Aero. Sci. Vol. 21 April, 1954.

(2) Gerard, G.:- Handbook of Structural Stability. Part IV. Failure of Plates and Composite Elements. NACA TN 3784. August, 1957.

(3) Gerard, G.:- The Crippling Strength of Compression Elements. Jour. Aero. Sci., Vol. 25, Jan. 1958.

(4) Coan, J. M.:- Large Deflection Theory for Plates with Small Initial Curvature Loaded in Compression. Jr. Applied Mech., Vol. 18, June 1951.

(5) Windenberg, D. F.:- Proc. 5th International Congress for Applied Mechanics. pp. 54-61, 1939.

(6) Experimental Study of Deformation and Effective Widths in Axially Loaded Sheet Stringer Panels. NACA TN 684, 1939.

(7) Gerard, F.:- Effective Width of Elastically Supported Flat Plates. Jour. Aero. Sci., Vol. 13, Oct. 1946.

(8) Howland, W.L.:- Effect of Rivet Spacing on Stiffened Thin Sheet in Compression. Jour. Aero. Sci., Vol. 3, Oct. 1936.

(9) Argyris, J. H. and Dunne, P.C.:- Structural Principles and Data. Handbook of Aero., 4th Edition, 1952.

(10) Bizlaard, P. D. and Johnston, G. S.:- Compression Buckling of Plates Due to Forced Crippling of Stiffeners. Preprint No. 408. S.M.F. Fund Paper. Inst. of Aero Sci. Jan. 1953.

(11) Semonian, J. W. and Peterson, J. P.:- An Analysis of the Stability and Ultimate Compressive Strength of Short Sheet-Stringer Panels with Special Reference to the Influence of Riveted Connection Between Sheet and Stringer. NACA TN 3431, March, 1955.

(12) Gerard, G.:- Handbook of Structural Stability, Part V. Compressive Strength of Flat Stiffened Panels. NACA TN 3785. Aug. 1957.

(13) Thesis by R. J. White:- The Ultimate Compressive Strength of Thin Sheet Metal Panels. Appendix A. C.I.T. 1935.

CHAPTER C8
BUCKLING STRENGTH OF MONOCOQUE CYLINDERS

This chapter presents information on the buckling strength of circular cylinders under compressive, bending and torsional loads acting separately and in combination, without and with internal pressure. Some information on the buckling strength of conical cylinders is presented.

C8.1 Introduction.

Before the advent of the high speed aircraft and particularly the missile and space vehicle, the use of the unstiffened cylinder or monocoque type of structure was quite limited. However, the arrival of the space age has caused the thin walled cylinder to become important in the design of missiles and space structures.

The classical small deflection theory which has proved adequate for determining the buckling strength of flat sheet structures as covered in Chapter A18, has not proved adequate for determining the buckling strength of thin walled cylinders or curved sheet panels since the theory gives results much too high when compared with the experimental or test results.

A more recent large deflection theory has shown closer agreement with experimental results, however, the theory requires a prior knowledge of cylinder imperfections. As a result of the theoretical limitations to date, the strength design of such structures is based primarily on best fit curves for experimental or test results, using theoretical parameters and curves when they appear applicable.

A missile structure in handling operations and flight maneuvers is subjected to tensile, compressive, bending and torsional load systems. The cylinders may be pressurized or unpressurized. The structural design of such structures thus requires a knowledge of the buckling strength under the various load systems, acting separately and in combination. This chapter will be confined to giving test data and design curves for the buckling strength of cylinders under the various types of stress systems.

C8.2 Buckling of Monocoque Circular Cylinders Under Axial Compression.

The term monocoque cylinder means a thin walled cylinder without longitudinal skin stiffeners or transverse intermediate frames attached to cylinder skin.

Investigation by the author of the procedure used by a number of aerospace companies for the strength design of monocoque structures indicated that the design curves given in (Ref. 1) were widely used. It thus seems appropriate to give some design material from (Ref. 1).

Cylinders are usually given four classifications relative to length:-

(1) Short Cylinders. Short cylinders tend to behave as flat plate columns (cylinders with infinite radius). They develop buckles in a sinusiodal wave form similar to flat plate buckling. The end fixity has considerable influence.

(2) Intermediate or Transition Length of Cylinders. Buckling involves a mixed pattern combining sinusiodal and diamond shapes. The effect of end fixity and cylinder length are only of nominal importance.

(3) Long Cylinders. Such cylinders buckle in a diamond shaped pattern, and the length and end conditions are not of much importance.

(4) Very Long Cylinders. Such cylinders buckle by over-all column instability or act as a Euler type column.

Fig. C8.1 shows a photograph of the buckle failure of an intermediate length cylinder under axial compression.

The name of Donnell is prominent in the development of a theory for the buckling strength of cylinders. From (Ref. 2), Donnell's eight-order differential equation can be used to provide a small-deflection theoretical solution to the behavior of cylinders in the short to long length range. A solution of Donnell's equation by Batdorf (Ref. 3) gives the critical stress in terms of the buckling coefficient K_c, which for simply supported cylinder ends is defined by the equation:-

$$K_c = \left[(m^2+\beta^2)^2/m^2\right] + \left[12Z^2m^2/\pi^4(m^2+\beta^2)\right] \qquad \text{- - - - - - C8.1}$$

where,

m = number of half waves in longitudinal direction

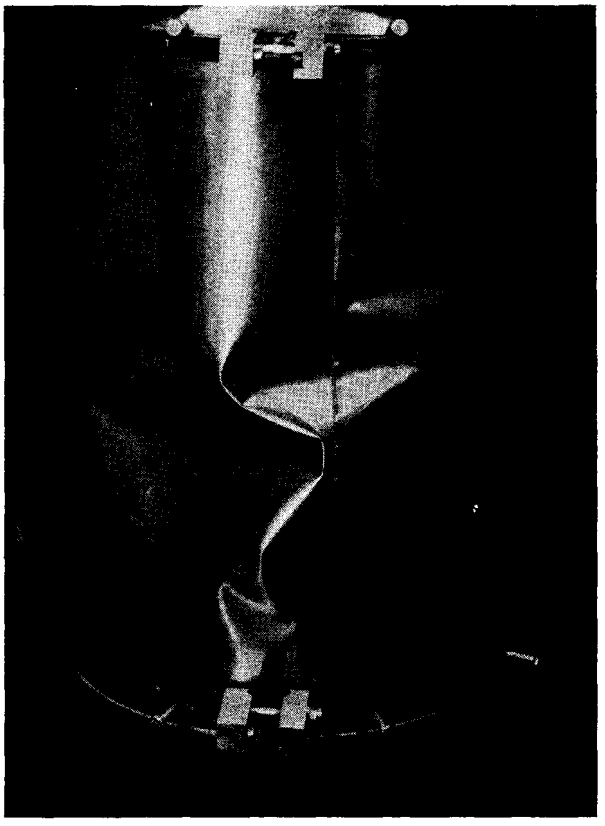

Fig. C8.1 Type of Failure Axial Compression and No Internal Pressure. (Ref. 1.)

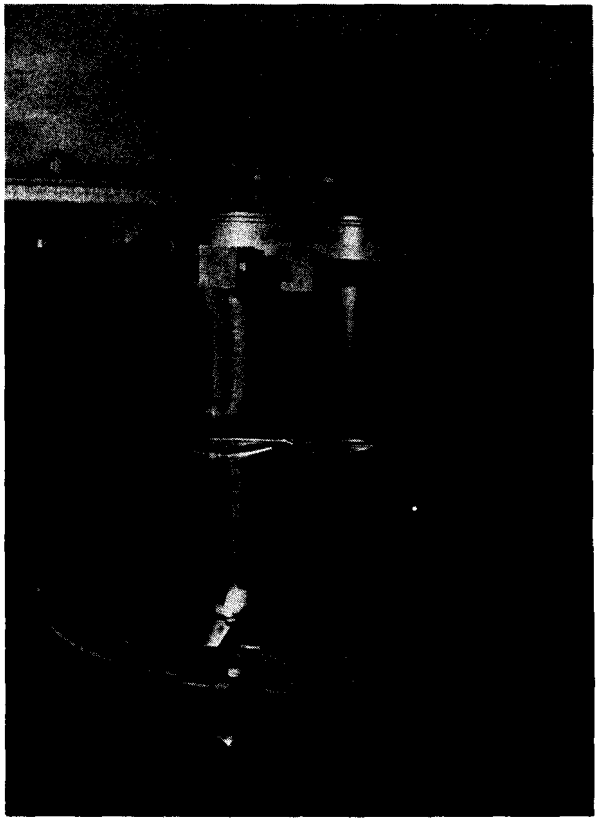

Fig. C8.1a Type of Failure Under Axial Load With Internal Pressure. (Ref. 1.)

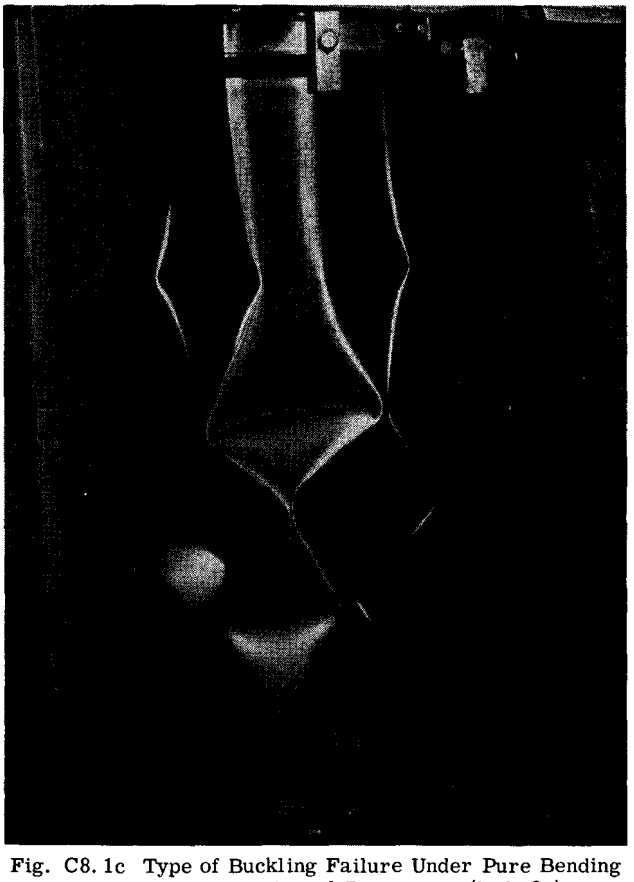

Fig. C8.1c Type of Buckling Failure Under Pure Bending Load. No Internal Pressure. (Ref. 9.)

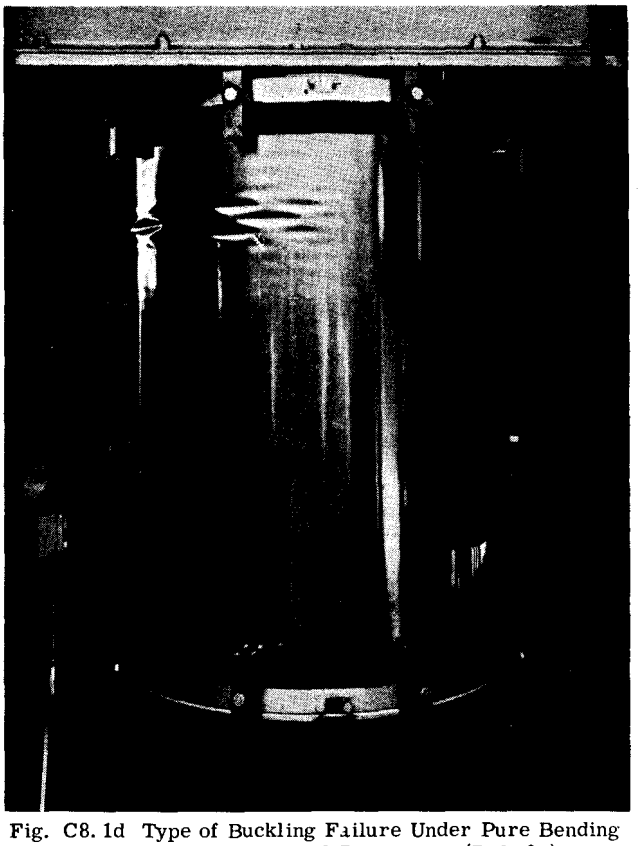

Fig. C8.1d Type of Buckling Failure Under Pure Bending With High Internal Pressure. (Ref. 9.).

$\beta = L/\lambda$

λ = half wave length of buckles in circumferential direction.

The compressive buckling stress is given by,

$$F_{cr}/\eta = \frac{K_c \pi^2 E}{12(1-\nu^2)} \left(\frac{t}{L}\right)^2 \quad \text{- - - - - - - - - - C8.2}$$

where, t = wall thickness, L is the cylinder length and ν is Poisson's ratio. The term η is the plasticity correction factor and equals 1.0 for elastic buckling.

Minimization of Eq. C8.1 with respect to the parameter $(m^2 + \beta^2)^2/m^2$, gives the critical buckling coefficient for long cylinders in the following form:-

$$K_c = (4\sqrt{3}/\pi^2)Z = 0.702Z \quad \text{- - - - - - - - - C8.3}$$

$$\text{where } Z = (L^2/rt)\sqrt{1-\nu^2} \quad \text{- - - - - - - - - C8.4}$$

Substitution of Eq. C8.3 into Eq. C8.2 reduces to the well known classical equation

$$F_{cr} = CE(t/r) \quad \text{- - - - - - - - - - - - - - - C8.5}$$

where, $C = 1/\sqrt{3(1-.3^2)} = 0.605$ for $\nu = .30$

The buckling coefficient for simply supported end conditions in the transition range can be determined by substituting the limiting values of $\beta = 0$ and m = 1 in Eq. C8.1. A similar solution for cylinders with fixed edges deviates from the solution for simply supported cylinders only in the flat plate and transition ranges.

Figs. C8.2 to C8.5 inclusive taken from Reference 1, show the theoretical curve which shows the buckling coefficient as a function of the geometrical parameter Z. Theoretically, the short cylinder range would occur at Z = 0. The values of K_c of 1.12 and 4.12 for Z = 1 correspond quite closely to the buckling coefficients of simply supported and fixed ended plate columns. The long cylinder behavior is represented by a 45 degree sloping straight line portion of the curve. The curve connecting the short and long cylinder ranges is referred to as the transition range.

Figs. C8.2 to C8.5 show the plot of extensive test data and a 90 per cent probability curve derived by the author of (Ref. 1) by a statistical approach. Fig. C8.6 from (Ref. 1) shows a plot of much test data on a logarithmic chart of r/t versus K_c for Z = 10,000. A best fit curve and 90 and 99 percent probability derived curves are also seen as well as the theoretical curve for C = .605. Observation shows that the theoretical results are far above the test values. Fig. C8.7 (from Ref. 1) is a set of design curves of K_c versus Z for various r/t values and for 90 percent probability.

C8.3 Additional Convenient Design Charts for Determining Compressive Buckling Stress.

Figs. C8.8a and C8.8b are more convenient design charts as the buckling stress $F_{c_{cr}}$ can be read from the chart, thus avoiding the calculations involved in using curves in Fig. C8.7. Fig. C8.8a is for 99 percent probability and 95 percent confidence level and Fig. C8.8b for 90 percent probability and 95 percent confidence level. The curves are based on tests of steel and aluminum alloy cylinders only. The accuracy of these curves when used for other materials has not been substantiated by tests. The 99 percent probability curves are recommended as design allowables for structures whose failure would be highly critical. The 90 percent curves can be used for less critical structures.

C8.4 Plasticity Correction.

The plasticity correction for cylinders in the long range ($L^2/rt > 100$) is given by the curves in Fig. C8.9 taken from (Ref. 4). In general most practical cylinders in aerospace structures will fall in the long cylinder range.

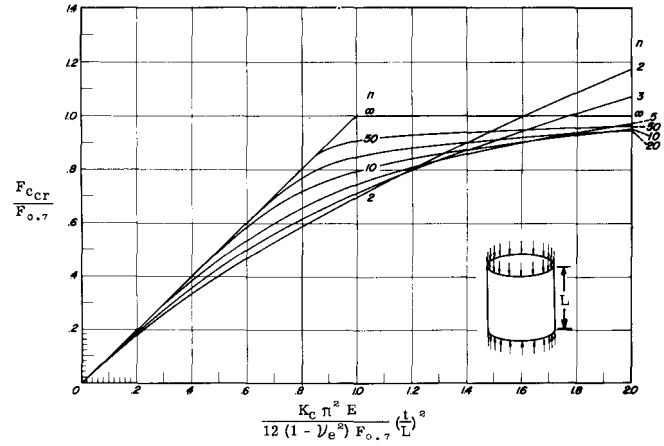

Fig. C8.9 (Ref. 4) Nondimensional Buckling Chart for Axially Compressed Long Circular Cylinders. $\eta = (E_s/E)\left[(E_t/E)(1-\nu_e^2)/(1-\nu^2)\right]^{1/2}$. Applicable When $L^2/rt > 100$.

C8.5 Buckling of Monocoque Circular Cylinders Under Axial Load and Internal Pressure.

Experiments conducted many years ago definitely showed that the compressive buckling strength of monocoque cylinders was increased if internal pressure was added to the closed cylinder. Since weight saving is very important in missile design, the use of pressurized

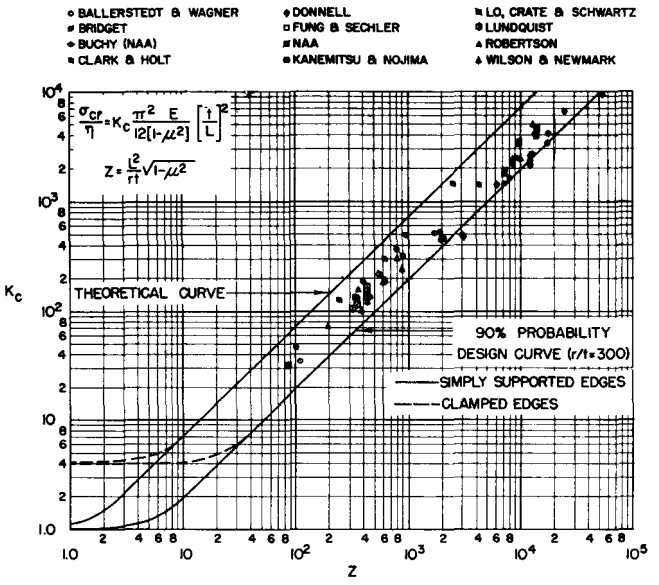

Fig. C8.2 r/t = 100 to 500.

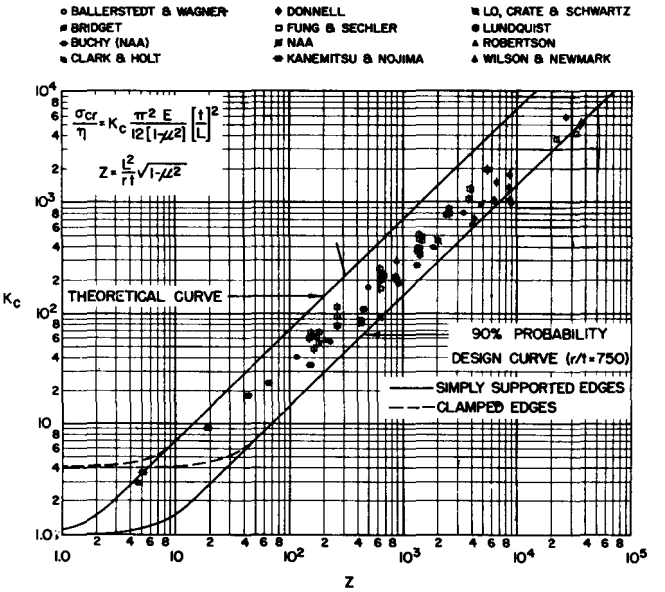

Fig. C8.3 r/t = 500 to 1,000.

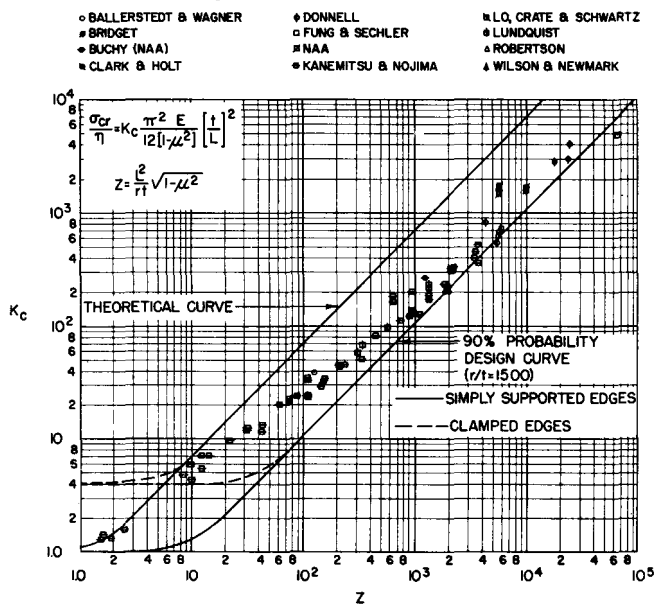

Fig. C8.4 r/t = 1,000 to 2,000.

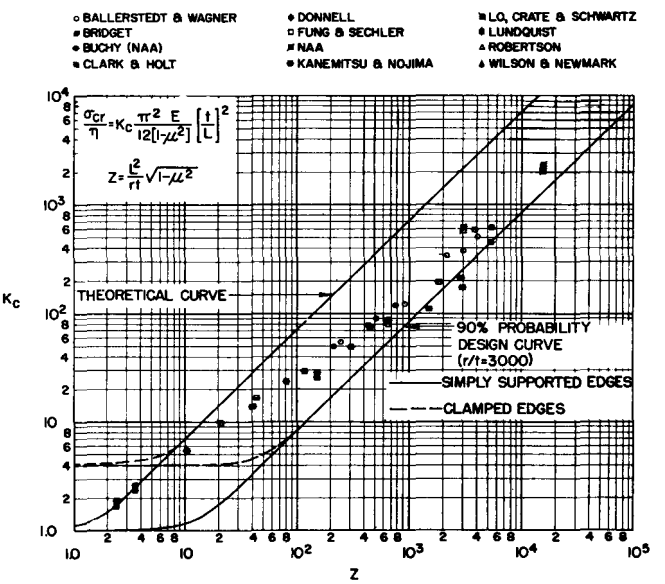

Fig. C8.5 r/t over 2,000.

Fig. C8.2-C8.5 (Ref. 1) Compressive Buckling Coefficients for Unpressurized Circular Cylinders.

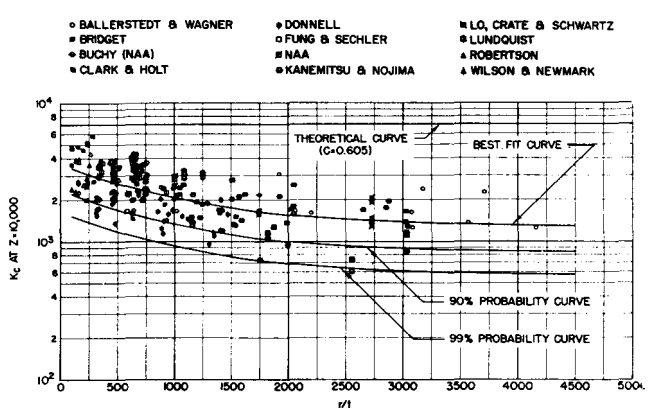

Fig. C8.6 (Ref. 1) Compressive Buckling Coefficients as a Function of r/t.

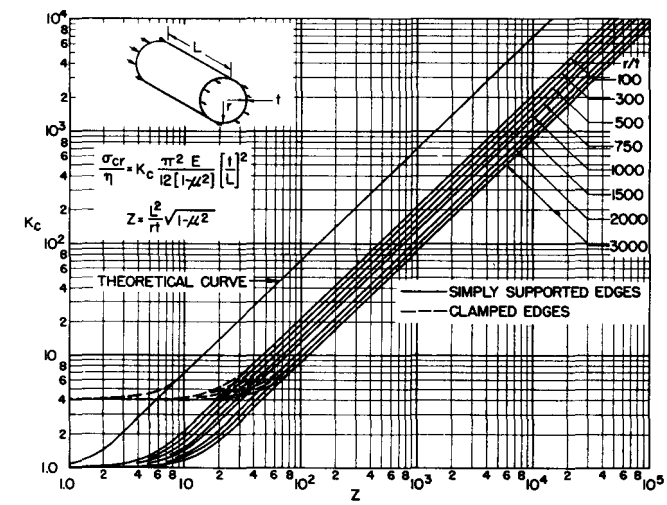

Fig. C8.7 (Ref. 1) Compressive Buckling Stress Coefficients for Unpressurized Circular Cylinders. (90 Percent Probability)

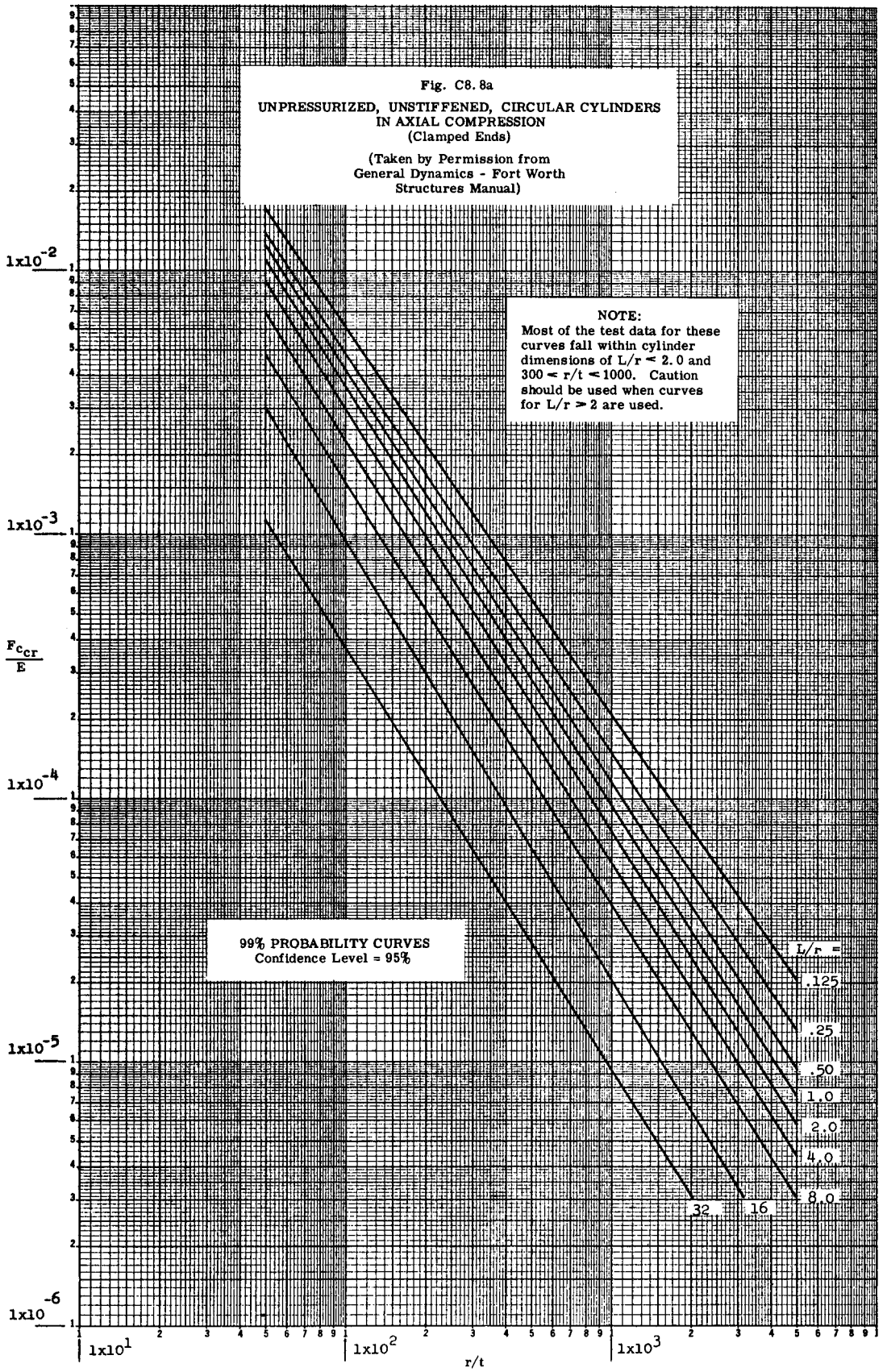
Fig. C8.8a
UNPRESSURIZED, UNSTIFFENED, CIRCULAR CYLINDERS
IN AXIAL COMPRESSION
(Clamped Ends)
(Taken by Permission from
General Dynamics - Fort Worth
Structures Manual)
NOTE:
Most of the test data for these curves fall within cylinder dimensions of L/r < 2.0 and 300 < r/t < 1000. Caution should be used when curves for L/r > 2 are used.
99% PROBABILITY CURVES
Confidence Level = 95%
Fccr/E
1x10-2
1x10-3
1x10-4
1x10-5
1x10-6
1x101
1x102
1x103
r/t
L/r =
.125
.25
.50
1.0
2.0
4.0
8.0
16
32

Fig. C8.8a

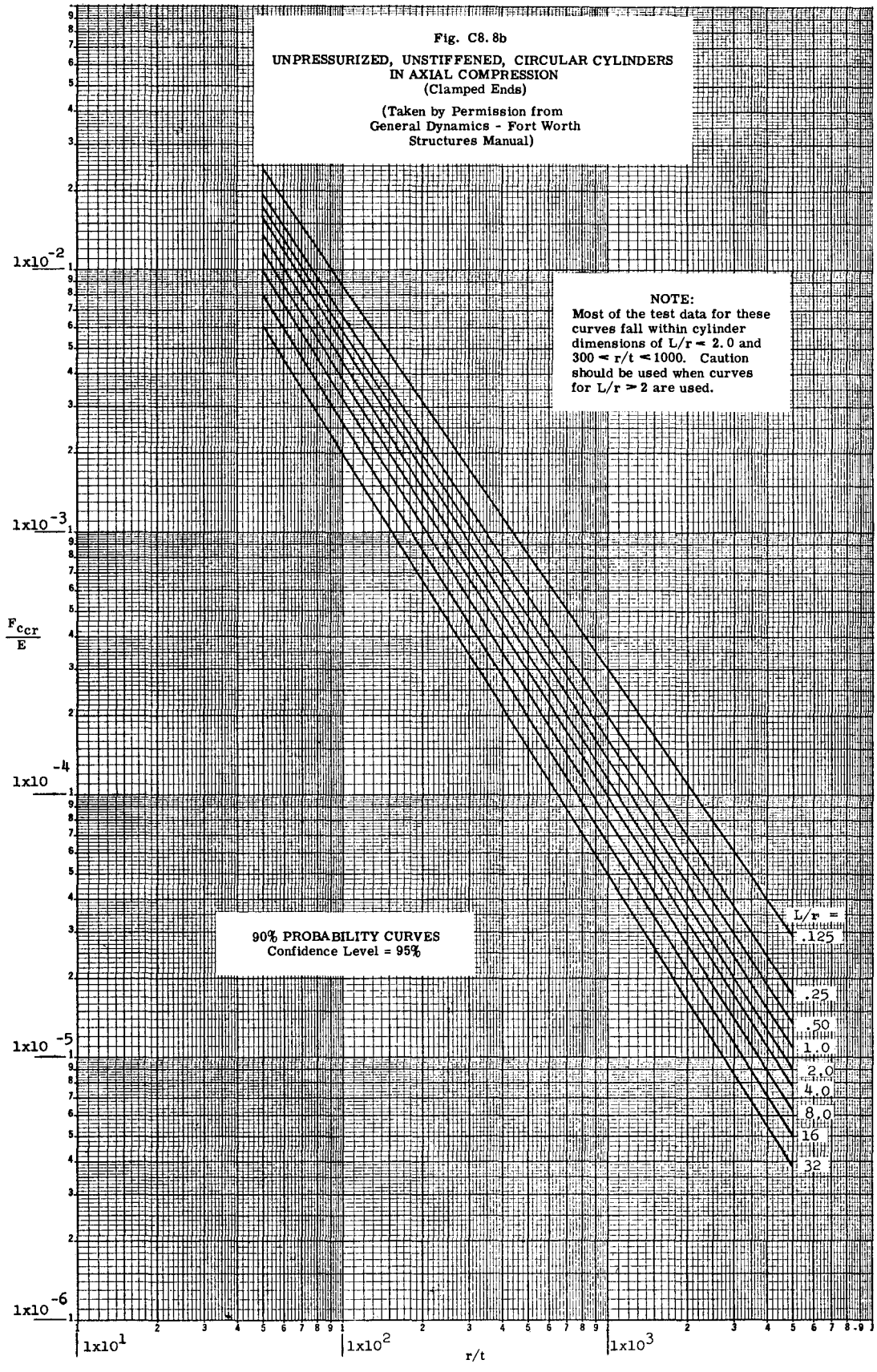
Fig. C8.8b
UNPRESSURIZED, UNSTIFFENED, CIRCULAR CYLINDERS
IN AXIAL COMPRESSION
(Clamped Ends)
(Taken by Permission from
General Dynamics - Fort Worth
Structures Manual)
NOTE:
Most of the test data for these curves fall within cylinder dimensions of L/r ≤ 2.0 and 300 ≤ r/t ≤ 1000. Caution should be used when curves for L/r ≥ 2 are used.
90% PROBABILITY CURVES
Confidence Level = 95%
L/r =
.125
.25
.50
1.0
2.0
4.0
8.0
16
32
Fccr / E
1x10-2
1x10-3
1x10-4
1x10-5
1x10-6
1x10^1
1x10^2
1x10^3
r/t

Fig. C8.8b

cylinders in missile structures ha[illegible] become a common type of missile structural design. The famous Atlas missile was one of the first to use a pressurized monocoque type of structure.

The major reason for the large discrepancy between the actual test strength and the theoretical strength by the linear small deflection theory that is generally accepted is that the discrepancy is due to geometrical imperfections and the associated stress concentrations. Now large internal pressures should smooth out such imperfections and approach a perfect cylinder and thus the resulting buckling strength should approach that given by the linear small deflection theory. However, much of the available test data for pressurized cylinders gives values below that given by the linear small deflection theory. (See Fig. C8.1a for buckling action of pressurized cylinder.)

One of the first experimental and theoretical investigations of the effect of internal pressure upon the buckling compressive stress of monocoque cylinders was by Lo, Crate and Schwartz (Ref. 5). They analyzed the problem of long pressurized cylinders using an extension of the large deflection theory of Von Karman and Tsien (Ref. 6). Plotting their results in terms of the non-dimensional parameters $(p/E)(r/t)^2$ and $(F_{cr}/E)(r/t)$, they found that the buckling coefficient C increased from the Tsien value (Ref. 7) of 0.375 at zero internal pressure to the maximum classical value of 0.605 at $(p/E)(r/t)^2 = 0.169$. Fig. C8.10 taken from (Ref. 1) shows the large deflection theoretical curve. Also shown are the experimental values obtained in (Ref. 5) as well as those obtained by the investigators in (Ref. 1) and by other investigators in (Ref. 8). From Fig. C8.10 it is apparent that large discrepancies exist between the theoretical predicted values and the experimental values. Lo, Crate and Schwartz suggested that better correlation with test results could be obtained if the increment in the buckling stress parameter $(\Delta F_{cr}/E)(r/t)$ were plotted as a function of the pressure parameter as shown in Fig. C8.11. The increase in the critical stress ΔF_{cr} due to the internal pressure directly represents the beneficial effect of the internal pressure. The total critical stress is thus obtained by adding the critical stress for the unpressurized cylinder to the increase in the critical stress due to the internal pressure. In order to plot the test points in Fig. C8.11, it was necessary to determine the unpressurized critical buckling stress for each test. The 90 percent probability values from Fig. C8.7 were used. As shown in Fig. C8.11, the general trend of the test data agrees fairly well with the theoretical curve. The investigations in Ref. 1 have shown a best fit curve and a 90 percent probability curve obtained by a statistical approach and this 90 percent curve in Fig. C8.11 is recommended as a design curve for taking into account the effect of internal pressure.

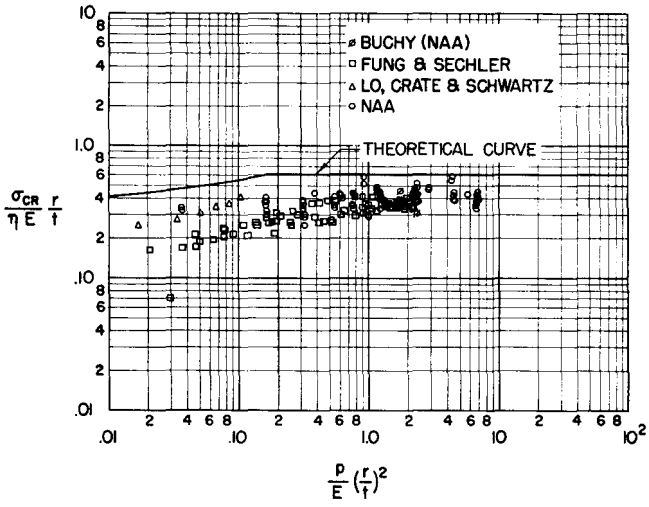

Fig. C8.10 Compressive Buckling Stress for Pressurized Circular Cylinders. (Ref. 1)

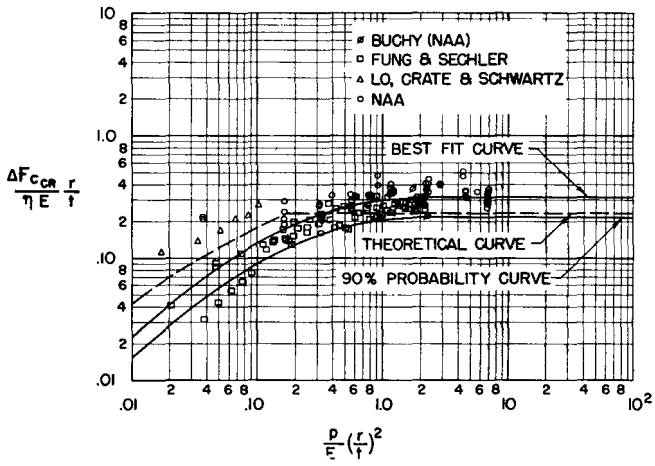

Fig. C8.11 Increase in Compressive Buckling Stress Due to Internal Pressure.

BUCKLING OF MONOCOQUE CIRCULAR CYLINDERS UNDER PURE BENDING

C8.6 Introduction.

Flight vehicles are subjected to forces in flight and in ground operations that cause bending action on the structure, thus it is necessary to know the bending strength of cylinders. Two rather extremes have been used in past design practice. One design assumption takes the value of the bending buckling stress as 1.3 times the buckling stress under axial compression. The other assumption is to assume the bending buckling

stress is equal to the axial compressive buckling stress. The first assumption is considered by some designers as somewhat unconservative while the second assumption is no doubt somewhat conservative.

It is relatively recent (Ref. 10) that a small deflection approach has been completely solved for a cylinder in bending. Tests of cylinders in bending show that the theoretical result is lower than the test results but higher than the buckling stress in axial compression. No large deflection analysis which involves a consideration of initial imperfections of the cylinder has been formulated to date for the buckling strength in bending. Since the stress in bending varies from zero at the neutral axis to a maximum at the most remote element, the lower probability of imperfections occurring within the smaller highest stressed region would lead one to conclude that higher buckling stresses in bending, as compared to the buckling stress in axial compression, should be expected.

C8.7 Available Design Curves for Bending Based on Experimental Results.

The same investigators (Suer, Harris, Skene and Benjamin) that carried out tests on cylinder in axial compression (Ref. 1), have also carried on an extensive investigation of the buckling strength of monocoque cylindrical cylinders in pure bending (see Ref. 9).

As originally developed by Flugge (Ref.11) for long cylinders, the buckling stress in bending is expressed as:-

$$F_{b_{cr}} = C_b E(t/r) \quad \text{- - - - - - - - - - - - - - - C8.6}$$

The theoretical vlue of the bending buckling coefficient as found by Flugge was about 30 percent higher than the corresponding classical buckling coefficient of 0.605 in axial compression.

Fig. C8.12 (from Ref. 9) gives a plot of considerable test data and a plot of C_b versus (r/t). A best fit curve, a 90 percent probability curve and a 99 percent probability curve, are shown. The dashed curve is a plot of the 90 percent probability curve as previously given in Fig. C8.6 for buckling in axial compression, thus giving a comparison between bending and compressive buckling strengths. As indicated by the plotted test points, the test data above an r/t value of 1500 is quite limited, thus the accuracy of the curves is somewhat unknown.

Figs. C8.13 and C8.13a give convenient design curves for finding the bending buckling stress based on 99 percent probability and 90

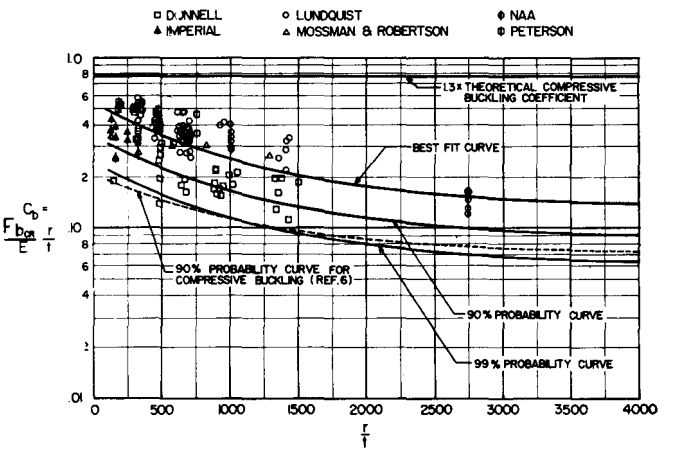

Fig. C8.12 Unpressurized Bending Buckling Stress Coefficients as a Function of r/t.

percent probability and confidence level of 95 percent. These curves are from the structures manual of the General Dynamics Corp. (Fort Worth.) Their manual states that most of the test data upon which the curves are based fall within the range of cylinder dimensions $.25 < L/r < 5$, and $300 < r/t < 1500$, and the curves are based on tests of steel, aluminum and brass cylinders only.

C8.8 Buckling Strength of Circular Cylinders in Bending with Internal Pressure.

The published information on the buckling strength of circular cylinders in bending with internal pressure is very limited and the status of theoretical studies to date leave much unknown regarding this subject.

Reference 9 gives the results of a series of tests of circular cylinders in bending with internal pressure. Fig. C8.14 is taken from that published report. In Fig. C8.14 the experimental data are plotted in terms of the increment ΔC_{bp} to the buckling coefficient C_b. The increase in the buckling stress coefficient ΔC_{bp} represents the beneficial effect of internal pressure. The total value of the buckling coefficient is obtained by adding the buckling coefficient for unpressurized cylinders to the increase in the buckling coefficient due to the internal pressure. In order to plot the data, it was first necessary to determine the unpressurized buckling coefficient for each specimen. The 90 percent probability design curve of Fig. C8.12 was used for this purpose. The direct benefit of lateral internal pressure to the stability of cylinders in bending is indicated by those specimens with no net axial stress (the balanced specimens) represented by the circular symbols. At large values of the pressure parameter, the additional benefit of the axial pretention is clearly demonstrated by the large increase in ΔC_{bp} of the pretensioned

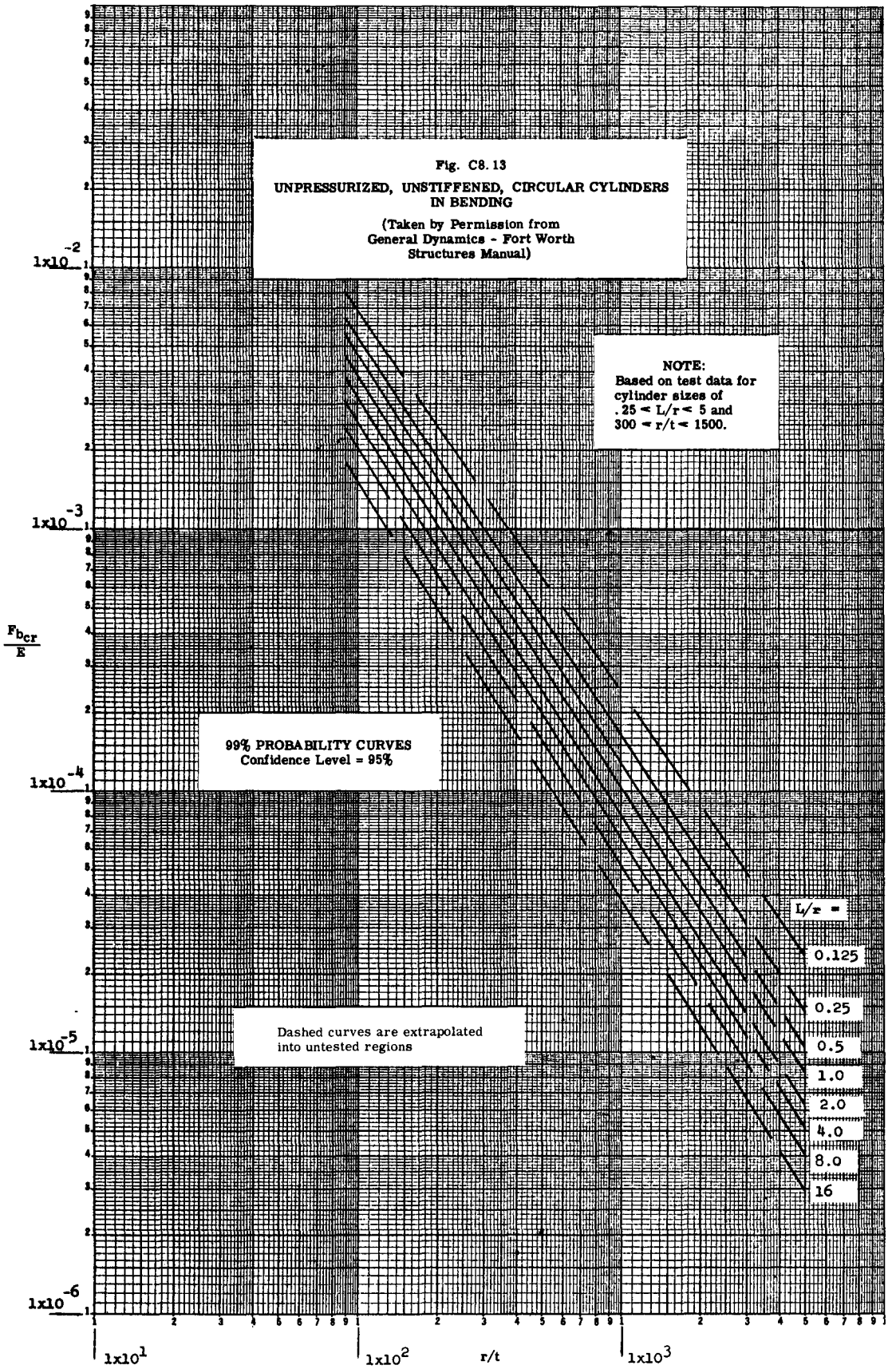
Fig. C8.13
UNPRESSURIZED, UNSTIFFENED, CIRCULAR CYLINDERS IN BENDING
(Taken by Permission from General Dynamics - Fort Worth Structures Manual)
NOTE:
Based on test data for cylinder sizes of
.25 ≤ L/r ≤ 5 and
300 ≤ r/t ≤ 1500.
99% PROBABILITY CURVES
Confidence Level = 95%
Dashed curves are extrapolated into untested regions
L/r =
0.125
0.25
0.5
1.0
2.0
4.0
8.0
16
$\frac{F_{b_{cr}}}{E}$
1x10^-2
1x10^-3
1x10^-4
1x10^-5
1x10^-6
1x10^1
1x10^2
1x10^3
r/t

Fig. C813

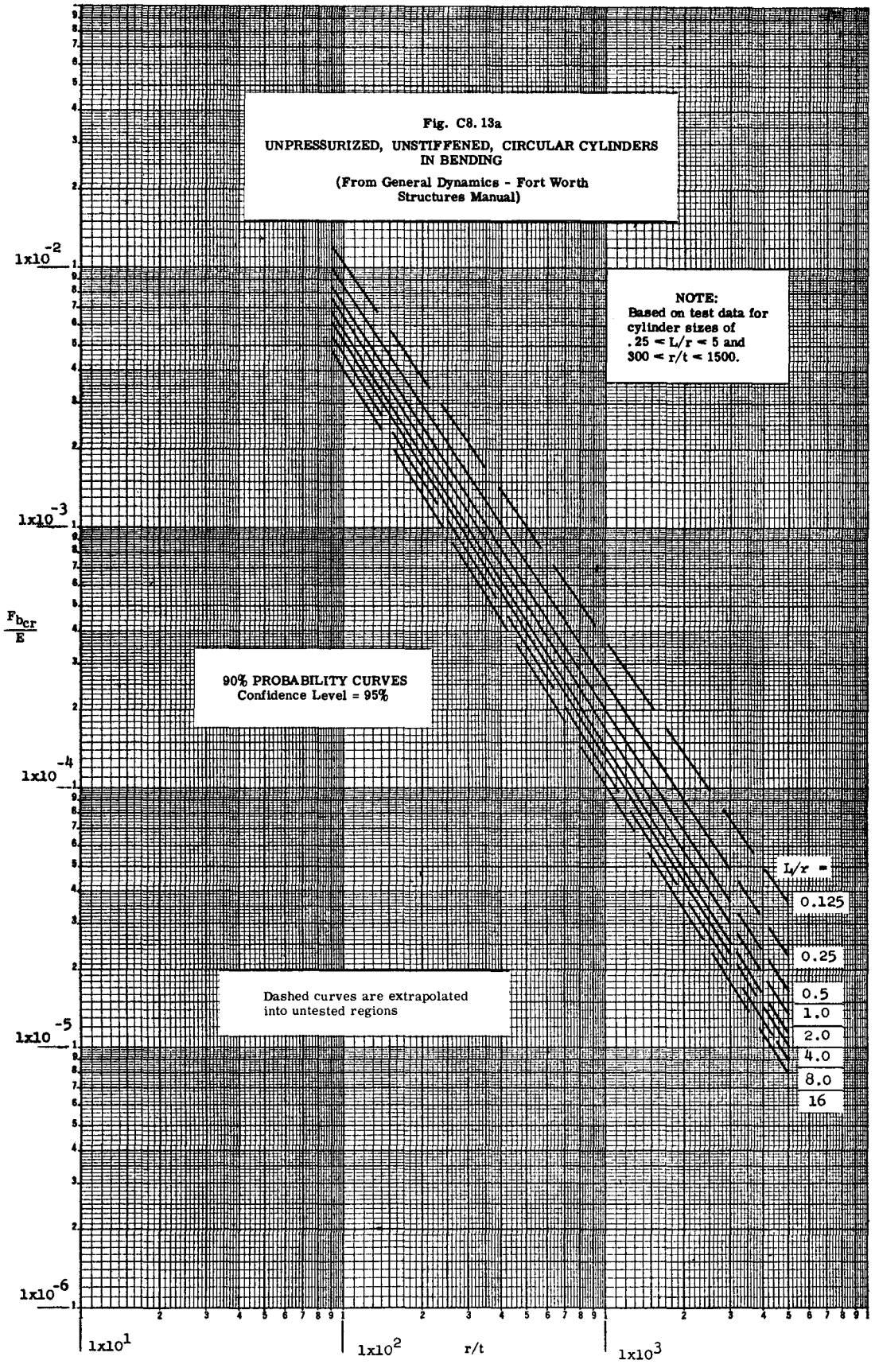
Fig. C8.13a
UNPRESSURIZED, UNSTIFFENED, CIRCULAR CYLINDERS IN BENDING
(From General Dynamics - Fort Worth Structures Manual)
NOTE:
Based on test data for cylinder sizes of
.25 ≤ L/r ≤ 5 and
300 ≤ r/t ≤ 1500.
90% PROBABILITY CURVES
Confidence Level = 95%
Dashed curves are extrapolated into untested regions
L/r =
0.125
0.25
0.5
1.0
2.0
4.0
8.0
16
$\frac{F_{b_{cr}}}{E}$
1x10^-2
1x10^-3
1x10^-4
1x10^-5
1x10^-6
1x10^1
1x10^2
1x10^3
r/t

Fig. C8.13a

specimens, represented by the triangular symbols, over that for balanced specimens. The limiting value of the increase in the buckling stress coefficient for pretensioned pressurized cylinders at very high values of the pressure parameter is given by the line $\sigma_{cr} = pr/2t$.

The analysis of the pressurized cylinder data was achieved by selecting a best fit curve for those specimens in which the axial pretension was balanced. This curve (shown in Fig. C8.14) was selected by the investigators as best indicating the general trend of the experimental data. At large values of the pressure parameter, the curve is drawn to approach an asymptote agreement between the best fit curve and experimental data is apparent in Fig. C8.14. A statistical analysis of the test data was performed for the specimens with no axial pretension to establish the 90 percent probability design curve shown in Fig. C8.14. Because data were available only from the tests made by the investigators, they indicate the sample may not be representative and a lower probability curve should perhaps be used for design purposes. The data was not considered sufficient to permit a statistical analysis of the pretensioned test data, and therefore they suggest a lower bound curve be used in the design of pretensioned cylinder. Additional tests are needed too for unpressurized cylinders with r/t ratios greater than 1500 to verify the shape of the design curve.

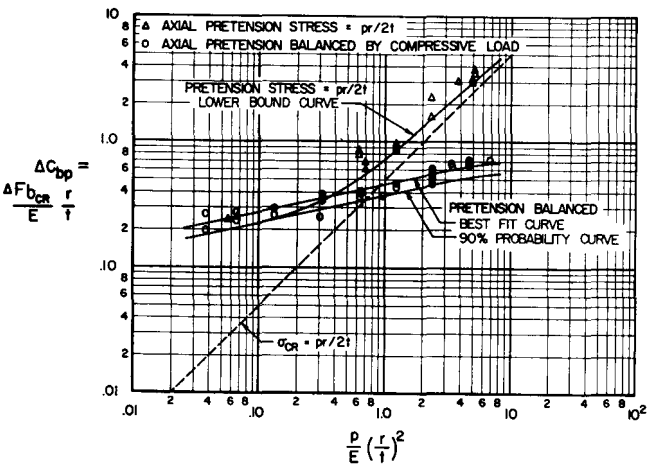

Fig. C8.14 Increase in Bending Buckling Stress Coefficients Due to Internal Pressure.

BUCKLING OF MONOCOQUE CIRCULAR CYLINDERS UNDER EXTERNAL PRESSURE

C8.9 External Hydrostatic Pressure.

Under this type of loading, the cylinder shell is placed in circumferential compressive stress equal to twice the longitudinal compressive stress.

The buckling compressive stress for this type of loading is given by the following equation (Ref. 12):-

$$F_{c_{cr}} = \frac{k_p \pi^2 E}{12 (1 - \nu_e^2)} \left(\frac{t}{L}\right)^2 \quad \text{- - - - - - - - - - C8.7}$$

Values of the buckling coefficient k_p are given in Fig. C8.15. Equation C8.7 is for buckling stresses below the proportional limit stress of the material.

C8.10 External Radial Pressure.

Under an inward acting radial pressure only the circumferential compressive stress produced is $f_c = pr/t$ where p is the pressure.

The buckling stress under this type of loading from (Ref. 12) is,

$$F_{c_{cr}} = \frac{k_y \pi^2 E}{12 (1 - \nu_e^2)} \left(\frac{t}{L}\right)^2 \quad \text{- - - - - - - - - - C8.8}$$

Values of the buckling coefficient k_y are given in Fig. C8.16. Equation C8.8 is for buckling stresses within the proportional limit stress of the material.

C8.11 Buckling of Monocoque Circular Cylinders Under Pure Torsion.

Fig. C8.17 (from Ref. 12) shows the results of tests of thin walled circular cylinders under pure torsion. The theoretical curve in Fig. C8.17 is due to the work of Batdorf, Stein and Schildcrout (Ref. 15). Their theoretical investigation utilized a modified form of the single equilibrium form of Donnell (Ref. 2) and by use of Galerkins Method obtained the curve shown in Fig. C8.17. This theoretical curve falls above the test results and thus for safety a lowered curve should be used for design purposes. Fig. C8.18 shows a design curve which appears in the structural design manuals of a number of aerospace companies.

The torsional buckling stress is given by the equation:-

$$F_{s_{cr}} = \frac{k_t \pi^2 E}{12 (1 - \nu_e^2)} \left(\frac{t}{L^2}\right) \quad \text{- - - - - - - - - - C8.9}$$

Fig. C8.18 gives the value of the torsion buckling coefficient k_t and applies for buckling below the proportional limit stress.

To correct for plasticity effect when buckling stress is above the proportional limit stress, the non-dimensional chart of Fig. C8.19 can be used. Figs. C8.20 and C8.21 give other convenient design curves involving buckling stresses for 90 and 99 percent probability.

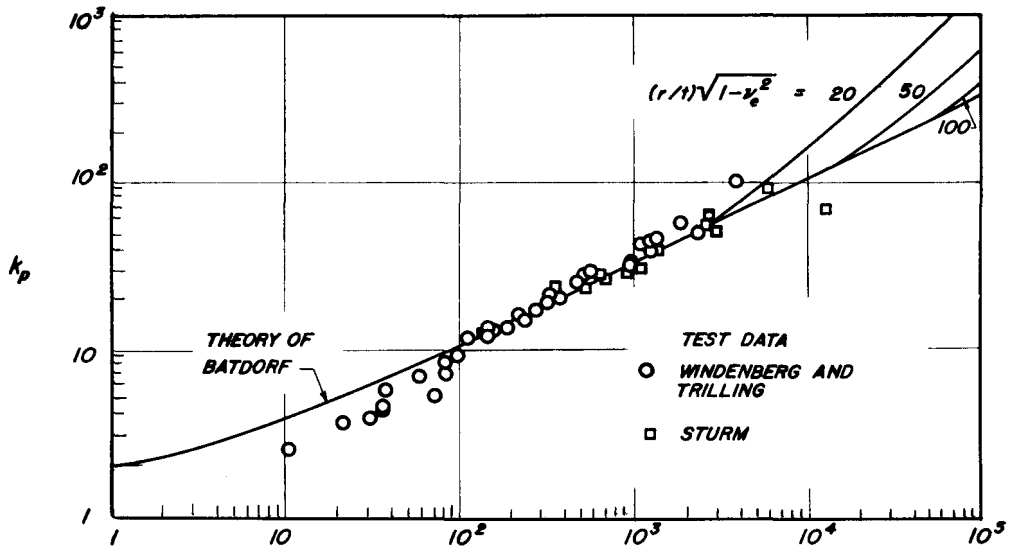

$$Z_L = \frac{L^2}{rt}\sqrt{1 - \nu_e^2}$$

Fig. C8.15 Buckling Under External Hydrostatic Pressure. $F_{c_{cr}} = \frac{k_p \pi^2 E}{12\,(1 - \nu_e^2)}\left(\frac{t}{L}\right)^2$.

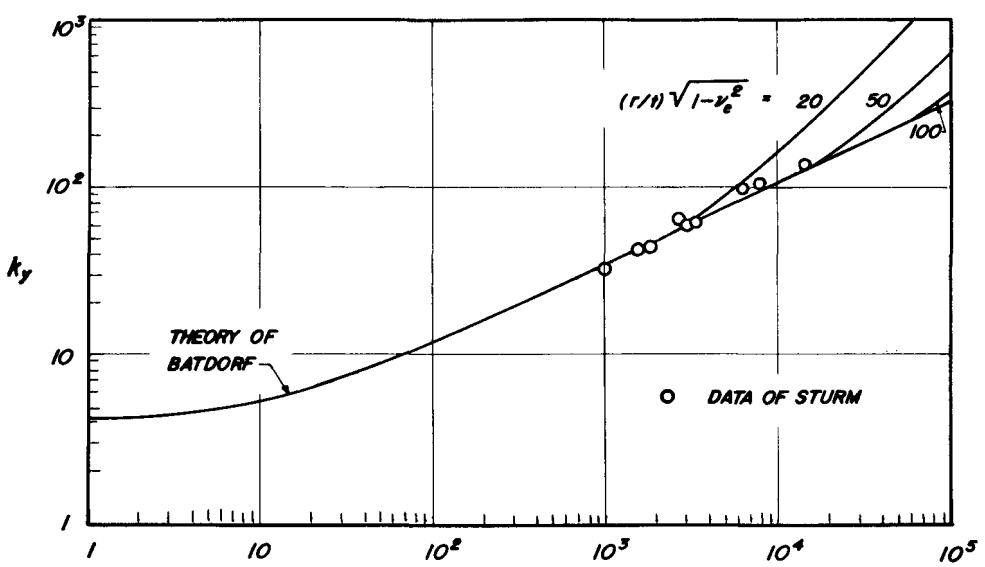

$$Z_L = \frac{L^2}{rt}\sqrt{1 - \nu_e^2}$$

Fig. C8.16 Buckling Under External Radial Pressure. $F_{c_{cr}} = \frac{k_y \pi^2 E}{12\,(1 - \nu_e^2)}\left(\frac{t}{L}\right)^2$.

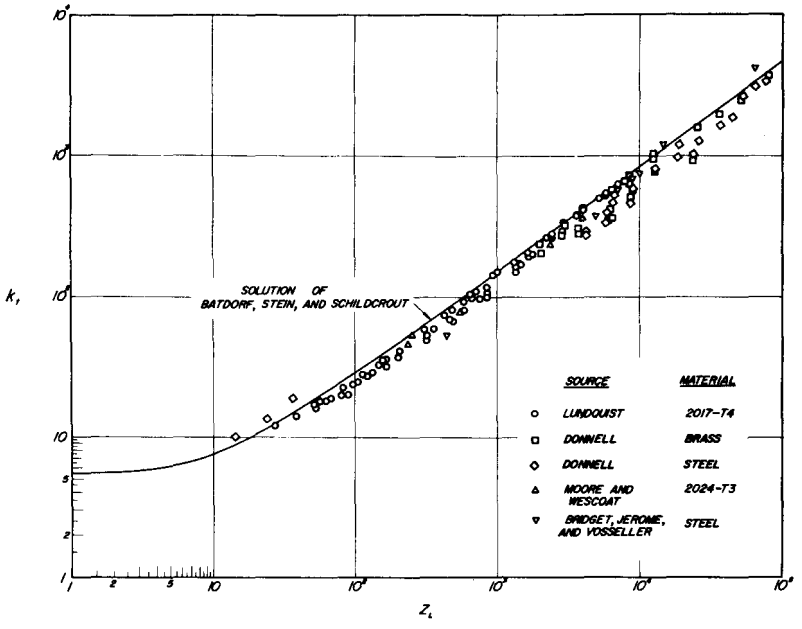

Fig. C8.17 Comparison of Test Data and Theory for Simply Supported Circular Cylinders in Torsion.

$$F_{s_{cr}} = \frac{k_t \pi^2 E}{12\,(1 - \nu_e^2)} \left(\frac{t}{L}\right)^2 ; \quad Z_L = \frac{L^2}{rt}(1 - \nu_e^2)^{1/2}.$$

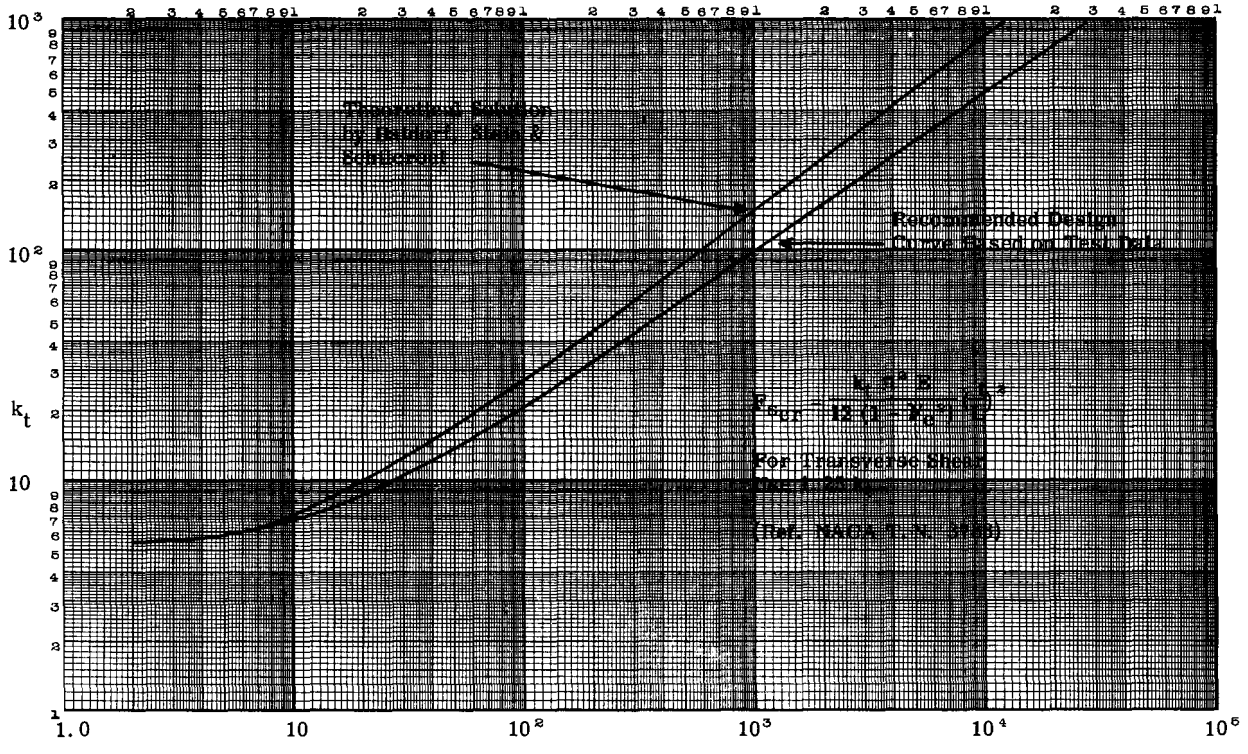

$$Z_L = \frac{L^2}{rt}\sqrt{1 - \nu_e^2}$$

Fig. C8.18 Buckling of Simply Supported Circular Cylinders in Torsion or Transverse Shear

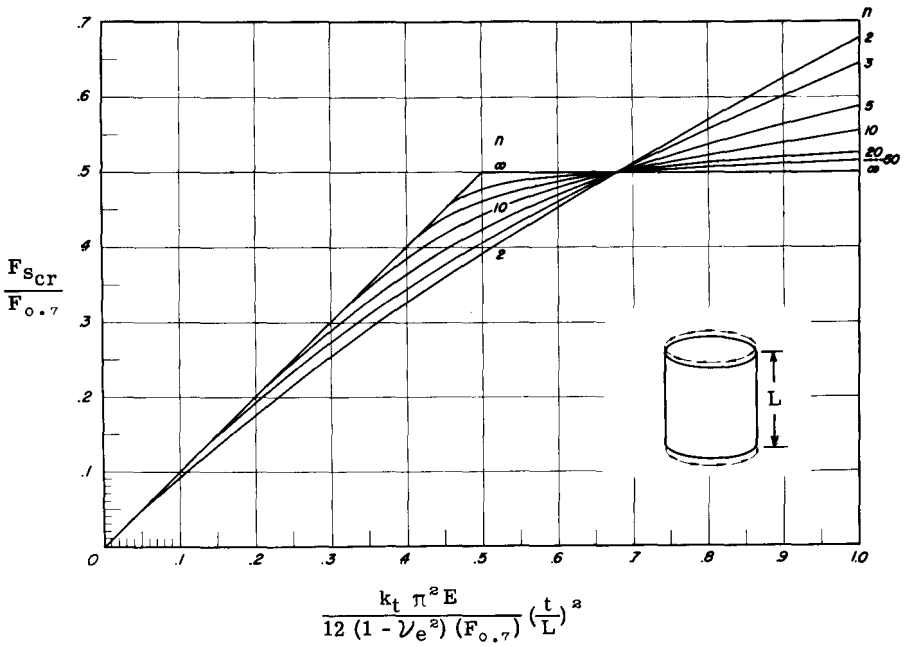

Fig. C8.19 Nondimensional-Buckling-Stress Curves for Long Cylinders in Torsion.

$$\eta = (E_s/E)\left[(1-\nu_e^2)/(1-\nu^2)\right]^{3/4}.$$

C8.12 Buckling Under Transverse Shear.

Shear stresses are also produced under bending due to transverse loads. These shear stresses are maximum at the neutral axis and zero at the most remote portion of the cylinder wall, whereas the torsional shear stress is uniform over the entire cylinder wall. Limited tests indicate a higher buckling shear stress under a transverse shear loading as compared to the torsional buckling stress. A general procedure in industry is to increase the shear buckling stress under torsion by using 1.25 times k_t. Thus in Fig. C8.18 find k_t for buckling under torsion and then multiply it by 1.25 in using Equation C8.9 to find buckling stress under transverse shear.

C8.13 Buckling of Circular Cylinders Under Pure Torsion With Internal Pressure.

Internal pressure places the cylinder walls in tension, thus the torsional buckling stress is increased as torsional buckling is due to the compressive stresses that are produced under shear forces.

Hopkins and Brown (Ref. 13), using Donnell's equation, calculated the effect of internal pressure on the buckling stress of circular cylinders in torsion and the results were in fair agreement with test results.

Crate, Batdorf and Baab (Ref. 14), utilized an empirical interaction equation to fit test data. The derived interaction equation was:-

$$R_{st}^2 + R_p = 1 \quad \text{- - - - - - - - - - - - - - - C8.10}$$

where,

R_{st} = ratio of $\dfrac{\text{applied torsion shear stress}}{\text{allowable torsion shear stress}}$

R_p=ratio of $\dfrac{\text{applied internal pressure}}{\text{external hydrostatic buckling pressure}}$

Note that R_p has a negative sign. The value of the external hydrostatic buckling pressure can be determined by use of Fig. C8.15. Fig. C8.22 shows a plot from Equation C8.10 and its comparison with test data.

C8.14 Buckling of Circular Cylinders Under Transverse Shear and Internal Pressure.

For this load system, the derived interaction equation is similar to Eq. C8.10.

$$R_s + R_p = 1 \quad \text{- - - - - - - - - - - - - - - C8.11}$$

where,

$R_s = \dfrac{\text{applied transverse shear stress}}{\text{allowable transverse shear stress}}$

R_p is same as explained in Article C8.13.

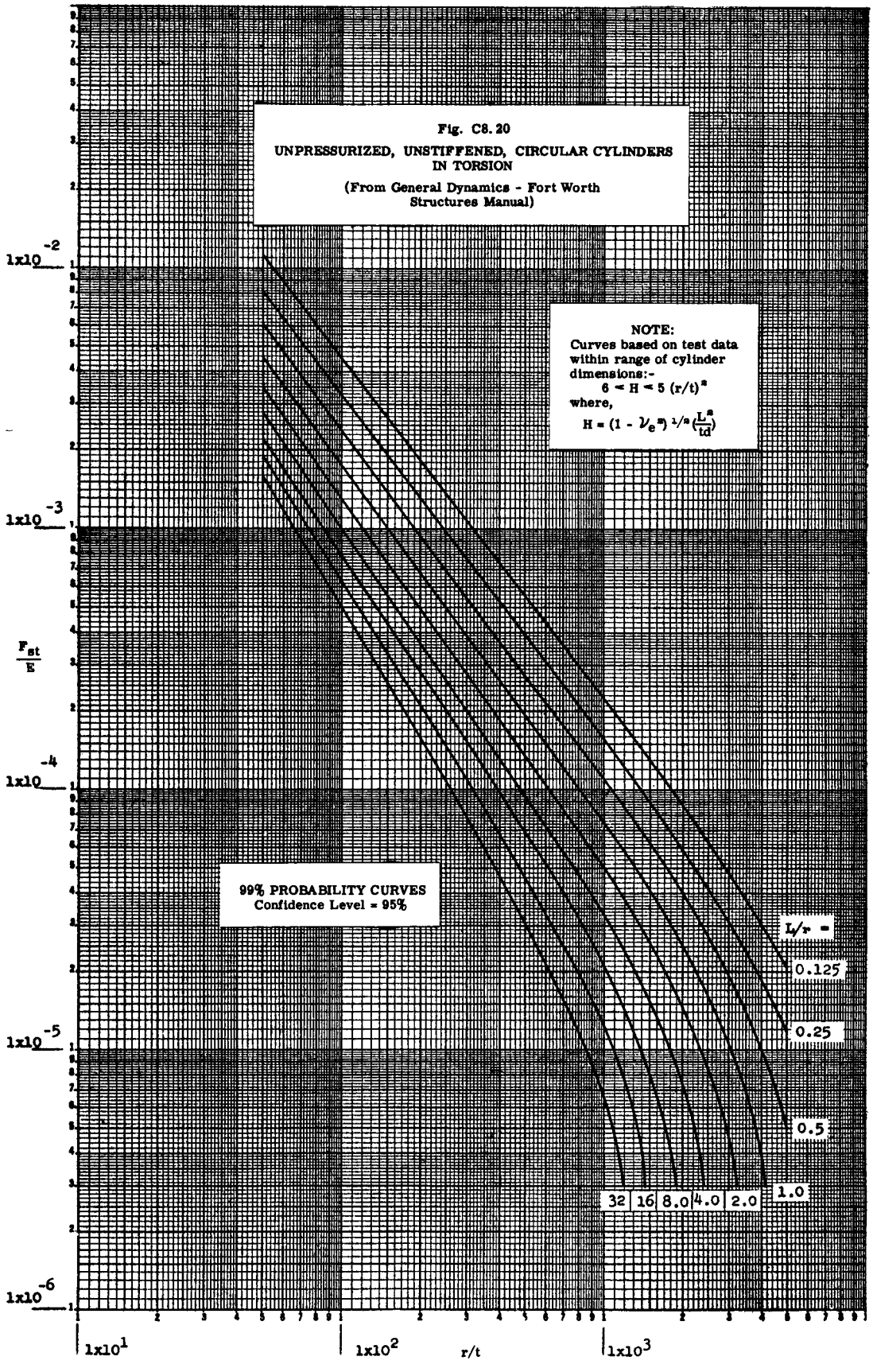
Fig. C8.20
UNPRESSURIZED, UNSTIFFENED, CIRCULAR CYLINDERS IN TORSION
(From General Dynamics - Fort Worth Structures Manual)
NOTE:
Curves based on test data within range of cylinder dimensions:-
$6 \leq H \leq 5\,(r/t)^2$
where,
$H = (1 - \nu_e^2)^{1/2}(\frac{L^2}{rt})$
99% PROBABILITY CURVES
Confidence Level = 95%
F_{st}/E
$1x10^{-2}$
$1x10^{-3}$
$1x10^{-4}$
$1x10^{-5}$
$1x10^{-6}$
$1x10^{1}$
$1x10^{2}$
$1x10^{3}$
r/t
L/r =
0.125
0.25
0.5
1.0
32
16
8.0
4.0
2.0

Fig. C8.20

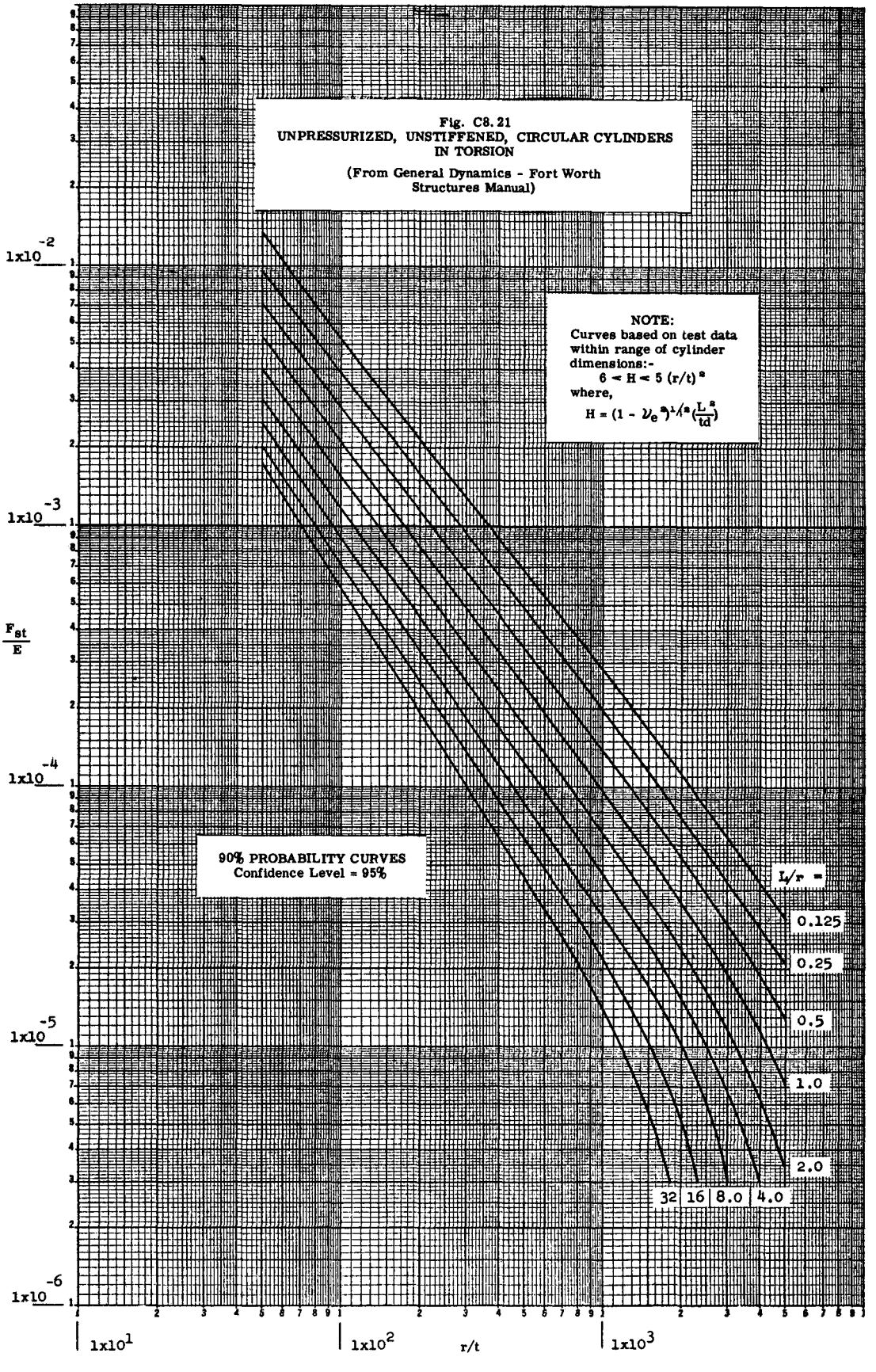
Fig. C8.21
UNPRESSURIZED, UNSTIFFENED, CIRCULAR CYLINDERS IN TORSION
(From General Dynamics - Fort Worth Structures Manual)
NOTE:
Curves based on test data within range of cylinder dimensions:-
$6 \leq H \leq 5\,(r/t)^2$
where,
$H = (1 - \nu_e^2)^{1/2}(\frac{L^2}{td})$
90% PROBABILITY CURVES
Confidence Level = 95%
$\frac{F_{st}}{E}$
$1x10^{-2}$
$1x10^{-3}$
$1x10^{-4}$
$1x10^{-5}$
$1x10^{-6}$
$1x10^{1}$
$1x10^{2}$
$1x10^{3}$
r/t
L/r =
0.125
0.25
0.5
1.0
2.0
32
16
8.0
4.0

Fig. C8.21

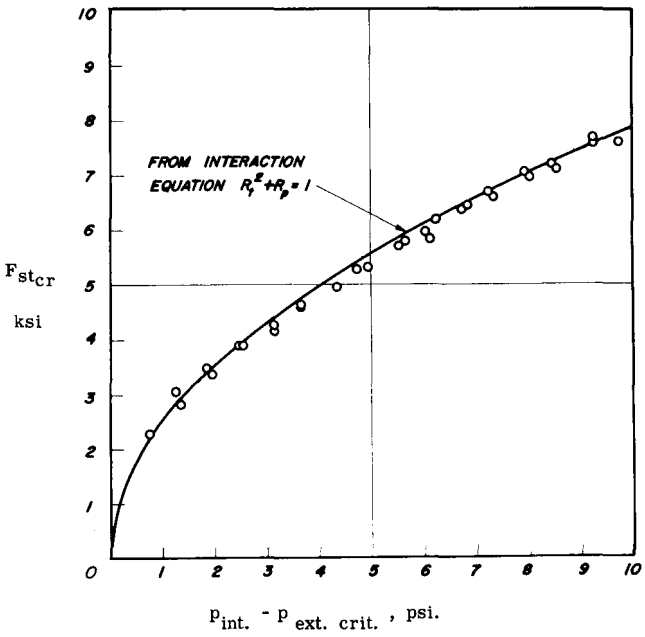

Fig. C8.22 Effect of Internal Pressure on Torsional-Buckling Stress of Long Cylinders. Test Results are from Ref. (14).

C8.15 Buckling of Circular Cylinders Under Combined Load Systems.

It is very seldom that a circular cylinder used in an aerospace structure such as a missile is subjected to a load system causing only one internal stress system such as axial stress, bending stress, and shearing stress. Therefore it is necessary to be able to safely determine the buckling strength under the practical cases of combined stress systems. This problem is handled by the use of interaction equations.

Table C8.1 summarizes the interaction equations that appear in the structures design manuals of several aerospace companies. These equations no doubt have been proven reliable by checking against test data. Fig. C8.23 gives a plot of three interaction curves. These curves are useful in quickly observing whether cylinder is weak and to determine margins of safety.

C8.16 Illustrative Problems for Finding the Buckling Strength of Circular Monocoque Cylinders.

Problem 1. Axial Compressive Strength.

A circular cylinder has a radius r = 50 inches, a length L = 75 inches, and a wall thickness t of .05 inches. The material is aluminum alloy 2024-T3, for which E_c 10,700,000 psi. What compressive load will it

Table C8.1

Summary of Interaction Equations for Buckling of Pressurized and Unpressurized Circular Cylinders

Combined Loading Condition	Interaction Equation	Equation For Margin of Safety
Longitudinal Compression and Pure Bending	$R_c + R_b = 1$	M.S. $= \frac{1}{R_c + R_b} - 1$
Longitudinal Compression and Torsion	$R_c + R_{st}^2 = 1$ (See Fig. C8.23)	M.S. $= \frac{2}{R_c + \sqrt{R_c^2 + 4R_{st}^2}} - 1$
Longitudinal Tension and Torsion	$R_{st}^3 - (R_t) = 1$ (See Note 1)	
Pure Bending and Torsion	$R_b^{1.5} + R_{st}^2 = 1$ (See Fig. C8.20)	
Pure Bending and Transverse Shear	$R_b^3 + R_s^3 = 1$ (See Fig. C8.23)	
Longitudinal Compression, Pure Bending and Transverse Shear	$R_c + \sqrt[3]{R_s^3 + R_b^3} = 1$	
Longitudinal Compression, Pure Bending and Torsion	$R_c + R_b + R_{st}^2 = 1$	M.S. $= \frac{2}{R_c + R_b + \sqrt{(R_c + R_b)^2 + 4R_{st}^2}} - 1$
Longitudinal Compression, Pure Bending, Transverse Shear and Torsion	$R_c + R_{st}^2 + \sqrt[3]{R_s^3 + R_b^3} = 1$	

NOTE 1. $R_t = \frac{\text{applied tensile stress}}{\text{compression buckling allowable}}$

$R_t < 0.8$

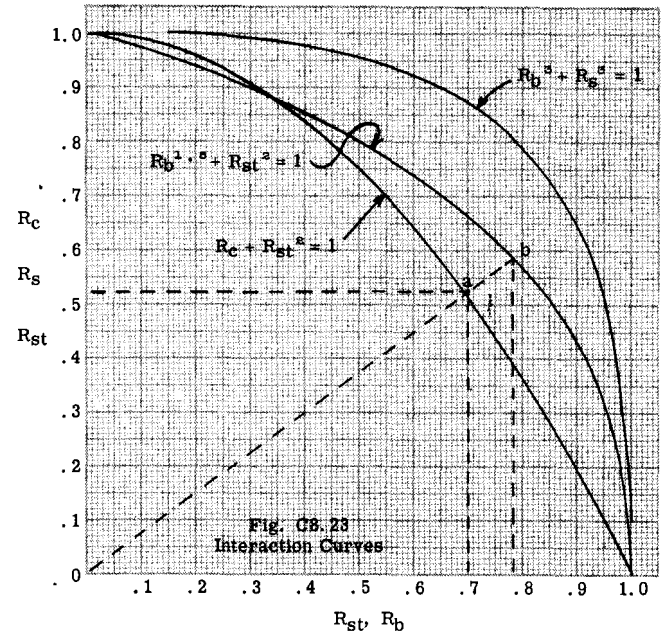

Fig. C8.23 Interaction Curves

C.8.23

carry using design curves based on 90 percent probability.

Solution:

$r/t = 50/.05 = 1000$, $L/r = 75/50 = 1.5$

$$F_{cr} = \frac{k_c \pi^2 E}{12 (1 - \nu_e^2)} \left(\frac{t}{L}\right)^2 \quad \text{(See Eq. C8.2)}$$

To find the buckling coefficient k_c, we use Fig. C8.7.

$$Z = \frac{L^2}{rt} \sqrt{1 - \nu_e^2}$$

$$Z = \frac{75^2}{50 \times .05} \sqrt{1 - .3^2} = 2140$$

From Fig. C8.7 using $Z = 2140$ and $r/t = 1000$, we read $k_c = 280$, then

$$F_{cr} = \frac{280 \pi^2 \times 10{,}700{,}000}{12 (1 - .3^2)} \left(\frac{.05}{75}\right)^2 = \underline{1210} \text{ psi}$$

The buckling axial compressive load $P = 2\pi rt\, F_{cr} = 2\pi \times 50 \times .05 \times 1205 = \underline{18950}$ lb.

If we use the design curves of Fig. C8.8b based on 90 percent probability and 95 percent confidence, we read for $r/t = 1000$ and $L/r = 1.5$, that $F_{c_{cr}}/E = .000121$. Thus $F_{c_{cr}} = 10{,}700{,}000 \times .000121 = 1295$ psi. If we multiply this value by the .95 confidence value, we obtain 1230 psi which is practically the same as obtained above using Fig. C8.7.

$P_a = 1295 \times 2\pi \times .05 \times 50 = \underline{20350}$ lbs.

If we require 99 percent probability and 95 percent confidence, we use Fig. C8.8a. For $r/t = 1000$ and $L/r = 1.5$, we read $F_{s_{cr}}/E = .000082$ or $F_{s_{cr}} = 10{,}700{,}000 \times .000082 = 877$ psi, which would give an axial buckling load of $\underline{13{,}700}$ lbs. Thus requiring a 99 percent probability decreases the buckling load considerably.

Problem 2. Bending Strength

The same cylinder as used in Problem 1 will be used in this example problem. What bending moment will buckle this cylinder under 90 percent probability.

Solution. The curve in Fig. C8.12 will be used. For $r/t = 1000$ and $L/r = 1.5$, we read from Fig. C8.12 that the bending buckling coefficient $C_b = .16$.

$$F_{b_{cr}} = C_b E t/r \quad \text{(See Eq. C8.5)}$$

$$= .16 \times 10{,}700{,}000 \times .05/50 = \underline{1710} \text{ psi}$$

The bending moment developed at this buckling stress is,

$$M = F_{b_{cr}} I/r = F_{b_{cr}} \pi r^2 t$$

$$= 1710 \pi \times 50^2 \times .05 = \underline{670{,}000} \text{ in. lb.}$$

If we use Fig. C8.13a based on 90 percent probability and 95 percent confidence, we read for $r/t = 1000$ and $L/r = 1.5$ that $F_{b_{cr}}/E$ is .000160. Thus $F_{b_{cr}} = 10{,}700{,}000 \times .000160 = 1710$ psi. Since it is difficult to read Fig. C8.12, it is recommended that Fig. C8.13a be used in design.

If we require 99 percent probability, we use Fig. C8.13 and obtain $F_{b_{cr}}/E = .000092$, which gives $F_{b_{cr}} = 10{,}700{,}000 \times .000092 = 985$ psi as against 1710 for 90 percent probability.

Problem 3. Torsional Strength.

Same cylinder as in Problem 1. What torsional moment will this cylinder develop.

Solution. Using design curve in Fig. C8.18

$$Z = \frac{L^2}{rt} \sqrt{1 - \nu_e^2} = \frac{75^2}{50 \times .05} \sqrt{1 - .3^2} = 2140$$

For this value of Z, we read the torsional buckling coefficient k_t from Fig. C8.18 to be 170.

$$F_{st_{cr}} = \frac{k_t \pi^2 E}{12 (1 - \nu_e^2)} \left(\frac{t}{L}\right)^2 \quad \text{(See Eq. C8.9)}$$

$$F_{st_{cr}} = \frac{170 \pi^2 \times 10{,}700{,}000}{12 (1 - .3^2)} \left(\frac{.05}{75}\right)^2 = \underline{735} \text{ psi}$$

The torsional moment developed by this buckling stress is,

$$T = F_{st_{cr}} J/r. \quad J/r = 2\pi r^3 t/r = 2\pi r^2 t$$

whence,

$$T = F_{st_{cr}} 2\pi r^2 t$$

$$T = 735 \times 2\pi \times 50^2 \times .05 = \underline{578000} \text{ in.lbs.}$$

The result will also be calculated using Figs. C8.20 and C8.21 based on 99 percent and 90 percent probability respectively and 95 percent confidence. Using Fig. C8.21:-

For $r/t = 1000$ and $L/r = 1.5$, we read $F_{st}/E = 000082$. Then $F_{st} = .000082 \times 10{,}700{,}000 = 876$ psi. $T = 876 \times 2\pi \times 50^2 \times .05$

$$= \underline{688000} \text{ in.lbs.}$$

Using Fig. C8.20 which is for 99 percent proba-

bility, we read $F_{st}/E = .000060$ which gives $F_{st} = 642$ psi which, in turn, gives allowable torque T = 504000 in. lbs.

Problem 4. Combined Compression and Bending.

The cylinder of Problem 1 is subjected to an axial compressive load P of 10,700 lbs. and a bending moment M of 282,000 in. lbs. What is the margin of safety under this combined loading for 90 percent probability and 95 percent confidence.

Solution. The interaction equation for this type of combined loading from Table C8.1 is,

$R_c + R_b = 1$

$R_c = P/P_a$. (P_a from Problem 1 solution is 20350 lb.)

$R_c = 10700/20350 = .527$

$R_b = M/M_a$ (From Problem 2 results:- M_a = 670,000 in.lbs.)

$R_b = 282,000/670,000 = .421$

$R_c + R_b = .527 + .421 = .948$. Since the result is less than 1.0, we have a small margin of safety.

$$M.S. = \frac{1}{R_c + R_b} - 1 = \frac{1}{.948} - 1 = .055$$

Problem 5. Combined Compression, Bending and Torsion.

Same cylinder as in Problem 1. The loading is the same as Problem 4 plus a torsional moment T of 89300 in. lb. Fing the M.S. under this combined loading for 90% probability.

Solution.

The interaction equation for this combined load system from Table C8.1 is,

$$R_c + R_b + R_{st}^2 = 1 \quad - - - - - - - - - - - - (A)$$

From Problem 4, $R_c = .527$, $R_b = .421$, $R_{st} = T/T_a$. (From Problem 3 results: T_a is 688,000 in. lb.)

$R_{st} = 89300/688,000 = .13$

Subt. in Eq. (A):-

$.527 + .421 + .13^2 = .965$, (since this result is less than 1.0, we have a small margin of safety. From Table C8.1,

$$M.S. = \frac{2}{R_c + R_b + \sqrt{(R_c + R_b)^2 + 4R_{st}^2}} - 1$$

$$= \frac{2}{.527+.421+\sqrt{(.527+.421)^2+4x.13^2}} - 1 = .035$$

Problem 6. Combined Compression, Bending, Torsion and Transverse Shear.

The same cylinder as in Problem 1 is subjected to the following loads:-

P = 10700 lbs. compression, M = 282,000 in.lbs., T = 715000 in.lb., V = 1790 lb., (transverse external shear). Will the cylinder carry this combined loading under 90 percent probability.

Solution:

From Table C8.1 the interaction equation for this combined loading is,

$$R_c + R_{st}^2 + \sqrt[3]{R_s^3 + R_b^3} = 1 \quad - - - - - - - - (B)$$

$R_c = 10700/20350 = .527$

$R_b = 282000/670000 = .421$

$R_{st} = 71500/688000 = .104$

The equation for shear stress due to transverse shear load V is,

$$f_s = \frac{V}{I} \int ydA$$

I for cylinder section = $\pi r^3 t$

$\int ydA = \pi rt \times .6366r = 2 r^2 t$

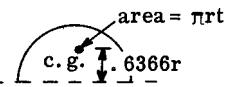

$$f_s = \frac{V}{\pi r^3 t}(2 r^2 t) = \frac{V}{\pi rt}$$

$f_s = 1790/\pi \times 50 \times .05 = 228$ psi.

From Article C8.12 we use buckling coefficient for transverse shear to be 1.25 times that for torsional buckling.

From Problem 3 the torsional buckling stress calculated to be $F_{st} = 876$ psi. Therefore the transferse shear buckling stress is 1.25 x 876 = 1095 psi, = F_s

$R_s = f_s/F_s = 228/1095 = .208$

Substituting in Equation (B),

$.527 + .104^2 + \sqrt[3]{.208^3 + .421^3} = .975$. This result is less than 1.0 so a small margin of safety exists.

Problem 7. Combined Compression, Bending and Transverse Shear.

Same cylinder and loads as in Problem 6, but without the torsional moment load.

Solution: The interaction equation is,

$R_c + \sqrt[3]{R_s^3 + R_b^3} = 1$ - - - - - - - - - - - (C)

$R_c = .527$, $R_b = .421$ and $R_s = .208$ (from Problem 6)

Subt. in Equation (C),

$.527 + \sqrt[3]{.208^3 + .421^3} = .964$ (less than 1.0 thus cylinder will not buckle.)

Problem 8. Combined Bending and Torsion.

Using the same cylinder as in previous problems, the combined loading is:-

M = 478,000 in.lbs., T = 358,000 in. lb.

Will the cylinder buckle under this loading.

Solution:

$R_b = 470{,}000/670{,}000 = .701$

$R_{st} = 358{,}000/688{,}000 = .520$

The interaction equation from Table C8.1 is,

$R_b^{1.5} + R_{st}^2 = 1$

$.701^{1.5} + .520^2 = .88$ less than 1.0, therefore cylinder will not buckle.

The margin of safety can be determined graphically by using Fig. C8.21 as follows:-

Find point (a) as indicated on Fig. C8.21 using $R_b = .701$ and $R_{st} = .520$. Draw line from origin o through point (a) and extend it to intersect interaction curve at point (b). Projecting downward and horizontally from point (b), we read $R_b = .78$ and $R_{st} = .58$.

The factor of utilization U = .70/.78 = .52/.58 = .895. Therefore Margin of Safety = (1/U) - 1 = (1/.895) - 1 = .12.

Problem 9. Combined Compression and Torsion.

Same cylinder as in previous problems. The loads are P = 12900 lbs. T = 358000 in.lbs. What is M.S.

Solution: The interaction equation from Table C8.1 is, $R_c + R_{st}^2 = 1$

$R_c = 12900/20350 = .634$

$R_{st} = 358000/688000 = .520$

$.634 + .520^2 = .904$ (less than 1.0, therefore no buckling.)

$$M.S. = \frac{2}{.634 + (.634^2 + 4 \times .520^2)^{1/2}} - 1 = .08$$

C8.17 Problems Involving Internal Pressure with External Loadings.

The same cylinder and material as was used in Problems 1 to 9 will be used in the following example problems, namely, r = 50, t = .05, L = 75, E = 10.7×10^6.

Problem 10. Axial Compression with Internal Pressure.

The cylinder is subjected to an axial compressive load of 50000 lbs. and an internal pressure of 5 lbs. per sq. in. What is the margin of safety under this combined load system with 90 percent probability.

Solution. From Problem 1, the buckling compressive stress $F_{c_{cr}}$ with no internal pressure was 1295 psi. To obtain the increase in the compressive buckling due to the internal pressure, we use Fig. C8.11. The horizontal scale parameter is,

$$\frac{p}{E}\left(\frac{r}{t}\right)^2 = \frac{5}{10{,}700{,}000}\left(\frac{50}{.05}\right)^2 = .467$$

From Fig. C8.11, we read on vertical scale,

$$\frac{\Delta F_{c_{cr}}}{\eta}\left(\frac{r}{Et}\right) = .19, \text{ whence}$$

$\Delta F_{c_{cr}} = (\eta \times .19 \times 10{,}700{,}000 \times .05)/50 = 2035\eta$ psi

Since the stress is below the proportional limit stress the plasticity correction is zero or $\eta = 1.0$. Thus $\Delta F_{c_{cr}} = \underline{2035}$ psi.

Then the total buckling stress with the internal pressure is 1295 + 2035 = 3330 psi.

Now the internal pressure produces a longitudinal tensile stress in the cylinder wall. This tensile stress is,

$F_t = pr/2t = 5 \times 50/2 \times .05 = 2500$ psi

This tensile stress must be cancelled before walls can be subjected to a compressive stress due to an external compressive axial load. The allowable failing load P_a thus equals,

$P_a = 2\pi rt\,(F_{c_{cr}} + \Delta F_{c_{cr}} + F_t)$

$= 2\pi \times 50 \times .05\,(3330 + 2500) = \underline{91500}$ lb.

$M.S. = (P_a/P) - 1 = (91500/50000) - 1 = .83.$

This result shows the tremendous effect of internal pressure in increasing the compressive strength of a thin walled unstiffened circular cylinder. With no internal pressure, the failing compressive load as calculated in

Problem 1 was only 20350 lbs. as compared to 95000 lbs. with 5 psi internal pressure.

Problem 11. Bending with Internal Pressure.

If the same cylinder as used in the preceding example problems is subjected to a bending moment of 3,000,000 in. lbs. when internal pressure is 5 psi, what is the M.S. use 90 percent probability.

Solution. For bending without internal pressure, the bending buckling stress $F_{b_{cr}}$ was found in Problem 2 to be 1710 psi. The increase in this bending buckling stress due to internal pressure is obtained from the curves in Fig. C8.14. The horizontal scale parameter is,

$$\frac{p}{E}\left(\frac{r}{t}\right)^2 = \frac{5}{10{,}700{,}000}\left(\frac{50}{.05}\right)^2 = 4.67$$

From Fig. C8.14, we read

$$\frac{\Delta F_{b_{cr}}}{E}\left(\frac{r}{t}\right) = .51 \text{ for 90 percent probability.}$$

whence, $\Delta F_{b_{cr}} = (.51 \times 10{,}700{,}000 \times .05)/50 = 5350$ psi.

As calculated in Problem 11, the internal pressure of 5 psi produces a longitudinal tensile stress in the cylinder wall equal to $F_t = 2500$ psi. The allowable bending moment that cylinder can develop is,

$$M_a = F_{b(total)} I/r = F_{b_{total}} \times \pi r^2 t$$

$$F_{b(total)} = F_{b_c} + \Delta F_{b_c} + F_t =$$

$$= 1710 + 5350 + 2500 = 9560 \text{ psi.}$$

$$M_a = 9560 \times \pi \times 50^2 \times .05 = 3760000 \text{ in. lbs.}$$

$$M.S. = (M_a/M) - 1 = (3760000/3000000) - 1 = .25$$

Again note the tremendous effect of internal pressure on the bending strength. With no internal pressure, the failing bending moment was 670000 as compared to 3760000 with 5 psi internal pressure.

Problem 12. Combined Compression, Bending and Internal Pressure.

The same cylinder will be subjected to an axial load P = 51000 lbs., a bending moment M = 1475000 in. lbs., and an internal pressure of 5 psi. Use 90 percent probability. What is the margin of safety under these load conditions.

Solution:

Interaction equation is, $R_c + R_b = 1$

From Problem 10, the allowable load P_a for compression plus 5 psi, internal pressure is 95000 lbs.

$$R_c = P/P_a = 51000/95000 = .536$$

From Problem 11, the allowable bending moment M_a with an internal pressure is 3,760,000 in. lbs.

$$R_b = M/M_a = 1475000/3760000 = .392$$

$R_c + R_b = .536 + .392 = .928$ (less than 1, thus will not buckle)

$$M.S. = (1/.928) - 1 = .08$$

Problem 13. Torsion with Internal Pressure

If the same cylinder is subjected to an internal pressure of 5 psi, what pure torsional moment T_a will it carry without buckling.

Solution:

With no internal pressure, the torsional shearing buckling stress as calculated in Problem 3 was 876 psi. for 90 percent probability.

The increase in shear buckling stress due to the internal pressure will be determined by use of interaction curve in Fig. C8.22. To use this curve, the external hydrostatic pressure ($p_{ext.}$) to cause buckling of the cylinder must be determined. This buckling stress $F_{c_{cr}}$ is determined by equation C8.7, which is,

$$F_{c_{cr}} = \frac{k_p \pi^2 e}{12(1 - \nu_e^2)}\left(\frac{t}{L}\right)^2$$

The buckling coefficient k_p is found by use of Fig. C8.15.

$$Z = \frac{L^2}{rt}(1 - \nu_e^2)^{1/2} = 2140 \text{ (See Problem 1)}$$

From Fig. C8.15, we read $k_p = 60$

$$F_{c_{cr}} = \frac{60\pi^2 \times 10{,}700{,}000}{12(1 - .3^2)}\left(\frac{.05}{75}\right)^2 = 258 \text{ psi}$$

The external pressure to produce this circumferential stress in the cylinder wall would be

$$p_{ext.} = F_{c_{cr}} t/r = 258 \times .05/50 = .258 \text{ psi}$$

Fig. C8.22 is now used to find the increase in the torsional shear buckling stress due to

the internal pressure of 5 psi. The lower scale parameter is,

$p_{int} - p_{ext} = 5 - .258 = 4.74$

Using this value we read from C8.22 that $F_{st_{cr}} = 5280$ psi. This buckling stress will develop a torsional moment of

$T_a = F_{st_{cr}} (2\pi r^2 t)$

$= 5280 (2\pi \times 50^2 \times .05 = \underline{4,150,000}$ in. lb.

Reference to the interaction curve in Fig. C8.22 shows most of the test data falling below the curve. A 90 or 99 percent probability would give a curve considerably below the curve shown. A correction factor of around .8 would seem to be in order or .8 x 5280 = 4220 psi.

The buckling stress can be calculated by use of the interaction equation:

$R_{st}^2 + R_p = 1$, $R_{st} = f_{st}/F_{st_{cr}}$

$R_p = 5.0/.258 = 19.4$ (use minus sign)

$\frac{f_{st}^2}{876^2} = 1 + 19.4$, or $f_{st} = 3940$ psi.

Thus to cause torsional buckling with 5 psi internal pressure requires a torsional shear stress of 3940 psi.

Then the torsional moment developed = 3940 $(2\pi \times 50^2 \times .05) = \underline{3,100,000}$ in.lb.

Problem 14. Combined Compression, Bending, Torsion and Internal Pressure.

The same cylinder is subjected to a combined loading of P = 40750, M = 1,670,000, T = 700,000 and internal pressure of 5 psi. Will cylinder buckle.

From Problem 10, $P_a = 95,000$

From Problem 11, $M_a = 3,760,000$

From Problem 13, $T_a = 3,100,000$

The stress ratios then are: -

$R_c = 40,750/95,000 = .431$

$R_b = 1,670,000/3,760,000 = .444$

$R_{st} = 700,000/3,100,000 = .226$

The interaction equation is $R_c + R_b + R_{st}^2 = 1$.

$.431 + .444 + .226^2 = .926.$

This is less than 1.0, thus cylinder will not buckle under the given combined loading.

C8.17 Buckling Strength of Thin-Walled (Monocoque) Conical Shells.

In a multi-stage missile, the upper stages normally have smaller diameters than the lower stages, thus a conical shell provides a type of structure to permit changing the missile diameter between the various stages.

As for the case of the cylindrical monocoque shell, the theoretical analysis for the buckling strength of conical shells by either the small or large deflection theories gives results considerably above those given by tests, thus design of conical shells at present is based primarily on results obtained by tests. The material presented in this chapter will thus be limited to presenting a few design buckling curves.

C8.18 Allowable Compressive Buckling Stress for Thin-Walled Conical Shells.

Fig. C8.24 shows design curves for the compressive buckling stress of a conical shell as derived from a statistical study of test data by Hausrath and Dittoe (Ref. 16). The expression for the buckling compressive stress along a generator at mid-height of cone is,

$$F_{c_{cr}} = \frac{P_{cr}}{2 \pi \bar{\rho} t \cos^2 \alpha}$$

where, P_{cr} is the buckling axial compressive load on cone.

$\bar{\rho}$ = radius of curvature of cone at mid-height.

t = cone wall thickness.

α = semi-vertex angle of cone.

Data from 170 tests by various investigators were statistically evaluated for expected men, 90 percent and 99 percent probability strength levels. Dispersion of data was found to be slightly less than that of monocoque cylinders. Non-linear effects of radius to thickness ratio or strength deterioration with length to radius ratio were not discernible.

The "A" level curve in Fig. C8.24 is that level which would be exceeded by at least 99 percent of the entire test population with 95 percent confidence; that is, the confidence is 95 percent that at least 99 percent of the compressive strengths of all cones can be expected to exceed the "A" level curve. The "B" level curve is for 90 percent probability and 95 percent confidence.

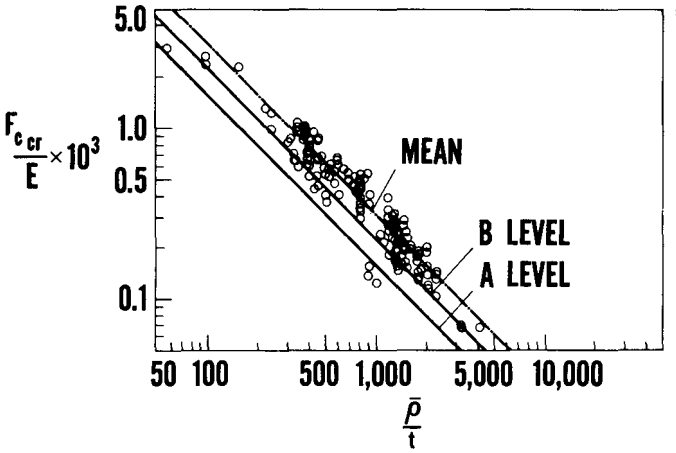

Fig. C8.24 (Ref. 16)

The "A" and "B" curves are recommended for practical design. The "A" level curve is recommended for use for those structures where a single failure would result in catastrophic loss or injury to personnel. The stress level at the small end of the cone should be checked to preclude the possibility of an early failure precipitated by inelastic stresses.

C8.19 Additional Design Buckling Curves for Thin-Walled Conical Shells.

Figs. C8.25, 26, 27 gives curves for determining the allowable buckling stress for thin-walled conical shells in compression, bending and torsion respectively. These curves are reproduced by permission of the Boeing Company from their report D2-3617. Fig. C8.28 gives a design curve for the allowable external buckling pressure for thin-walled conical shells, also from same Boeing Report. These curves were used for minuteman interstage and skirt design and the conical shells had ring stiffeners designed by method given in (Ref. 17).

DEFINITION OF TERMS:-

F_c = allowable compressive buckling stress (psi)
F_b = allowable bending buckling stress (psi)
F_{st} = allowable torsional buckling stress (psi)
f_c = compressive stress
f_b = bending stress
f_v = transverse shear stress
L = slant height of conical shell
t = wall thickness
α = one half cone apex angle
ν_e = Poisson's ratio
ρ = minimum radius of curvature
ρ_{avg} = average radius of curvature
q = external pressure (psi)
q_{cr} = allowable external pressure

Buckling Under Combined Loading

From Boeing Report (D2-3617) the effects of simultaneous compression, bending, shear and overpressure can be considered using the interaction equation:-

$$(R_c + R_b + R_v)^{1.2} + R_q^{1.2} = 1$$

where, $R_c = f_c/F_c$, $R_b = f_b/F_b$, $R_v = \frac{f_v}{1.4\ F_{st}}$

$R_q = q/q_{cr}$

C8.20 Example Problem.

A conical shell with wall thickness t = .05 and other dimensions shown in Fig. (a) is fabricated from aluminum alloy (E = 10,700,000). Determine the following values:-

(1) Allowable compressive load P_c.

(2) Allowable bending moment M_{cr}.

(3) Allowable torsional moment T_{cr}.

(4) External buckling pressure q_{cr}.

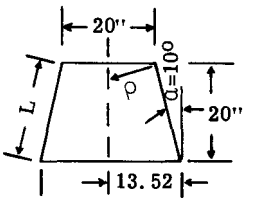

Fig. a

Solution:

ρ = 10/cos 10° = 10.16 in.
ρ/t = 10.16/.05 = 203
L = 20/cos 10° = 20.32 in.
L/ρ = 20.32/10.16 = 2.0

To find P_c:-

From Fig. C8.25 with ρ/t = 203 and L/ρ = 2.0, we read $F_c \times 10^3/E$ equals 1.20. Whence F_c = 1.20 x 10,700,000/1000 = 12,820 psi. Then
$P_c = F_c\ 2\ \pi\ rt$
= 12820 x 2π x 10 x .05 = 40,300 lbs.

To find M_{cr}:-

From Fig. C8.26 with ρ/t = 203 and L/ρ = 2.0, we read $F_b \times 10^3/E$ = 1.48. Whence F_b = 1.48 x 10,700,000/1000 = 15820 psi. Then
$M_{cr} = F_b\ \pi\ r^2 t$
= 15820 π x 10^2 x .05 = 248,500 in. lb.

To find T_{cr}:-

From Fig. C8.27, with ρ/t = 203 and L/ρ = 2.0, we read $F_{st} \times 10^3/E$ = .61. Whence, F_{st} = .61 x 10,700,000/1000 = 6520 psi. Then
$T_{cr} = F_{st}\ 2\ \pi\ r^2 t$
= 6520 x 2π x 10^2 x .05 = 205,000 in. lb.

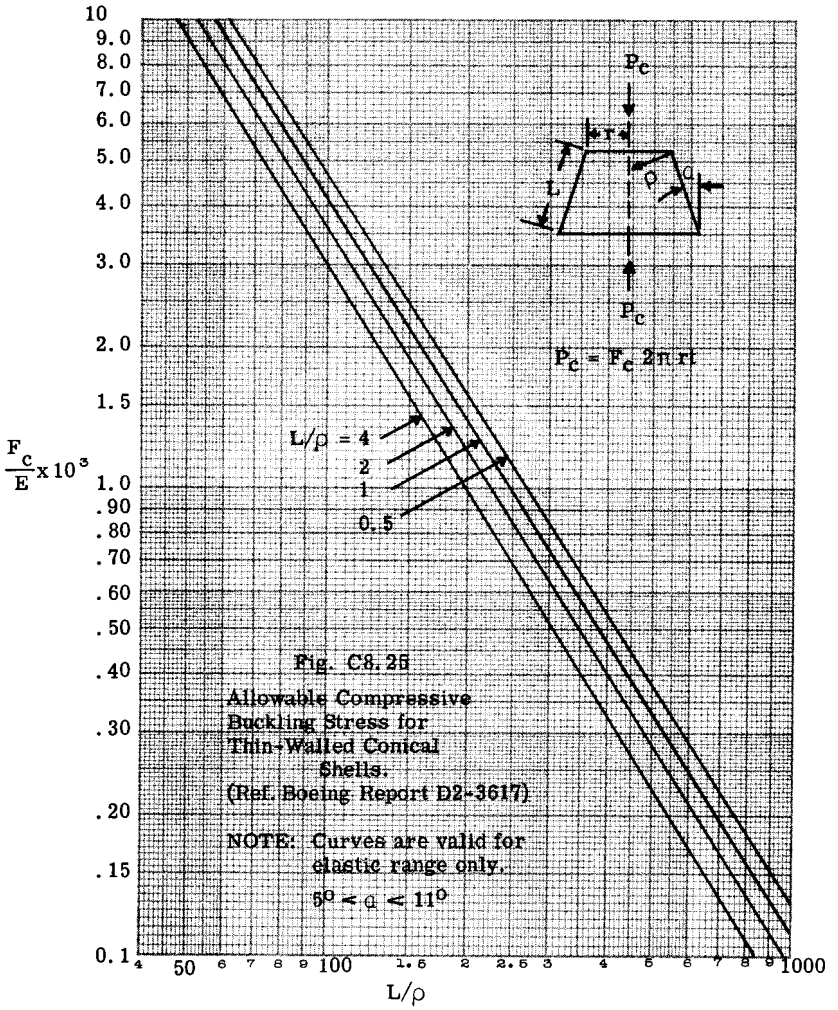

Fig. C8.25
Allowable Compressive Buckling Stress for Thin-Walled Conical Shells.
(Ref. Boeing Report D2-3617)

NOTE: Curves are valid for elastic range only.
$5^o < \alpha < 11^o$

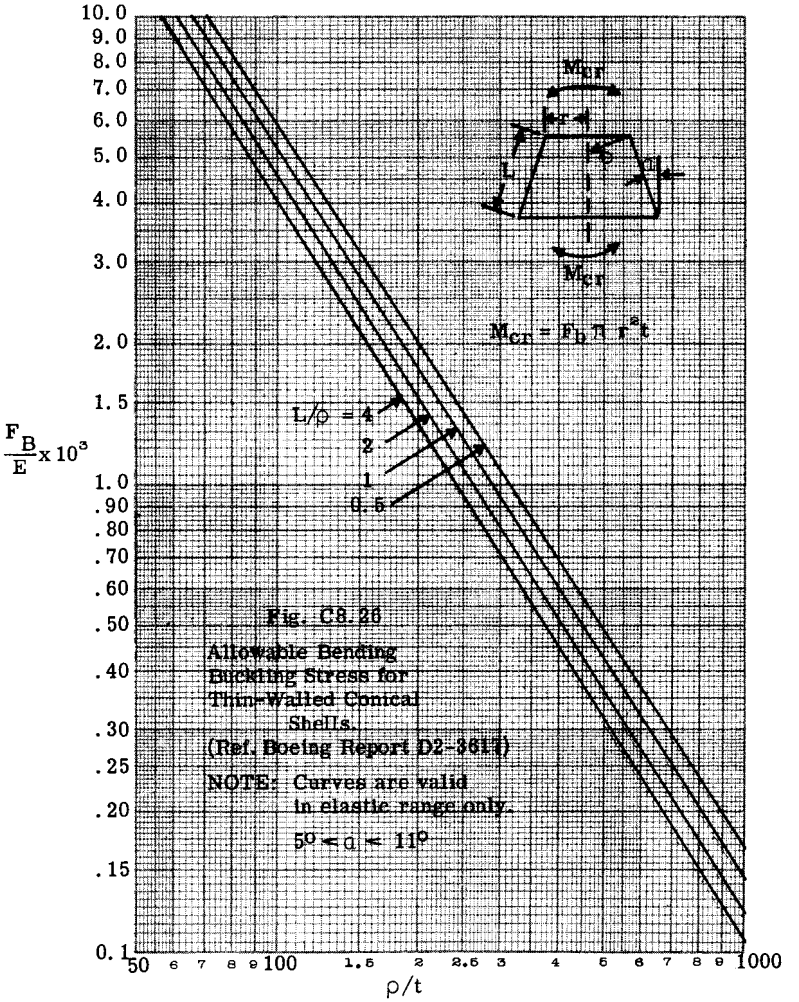

Fig. C8.26
Allowable Bending Buckling Stress for Thin-Walled Conical Shells.
(Ref. Boeing Report D2-3617)

NOTE: Curves are valid in elastic range only.
$5^o < \alpha < 11^o$

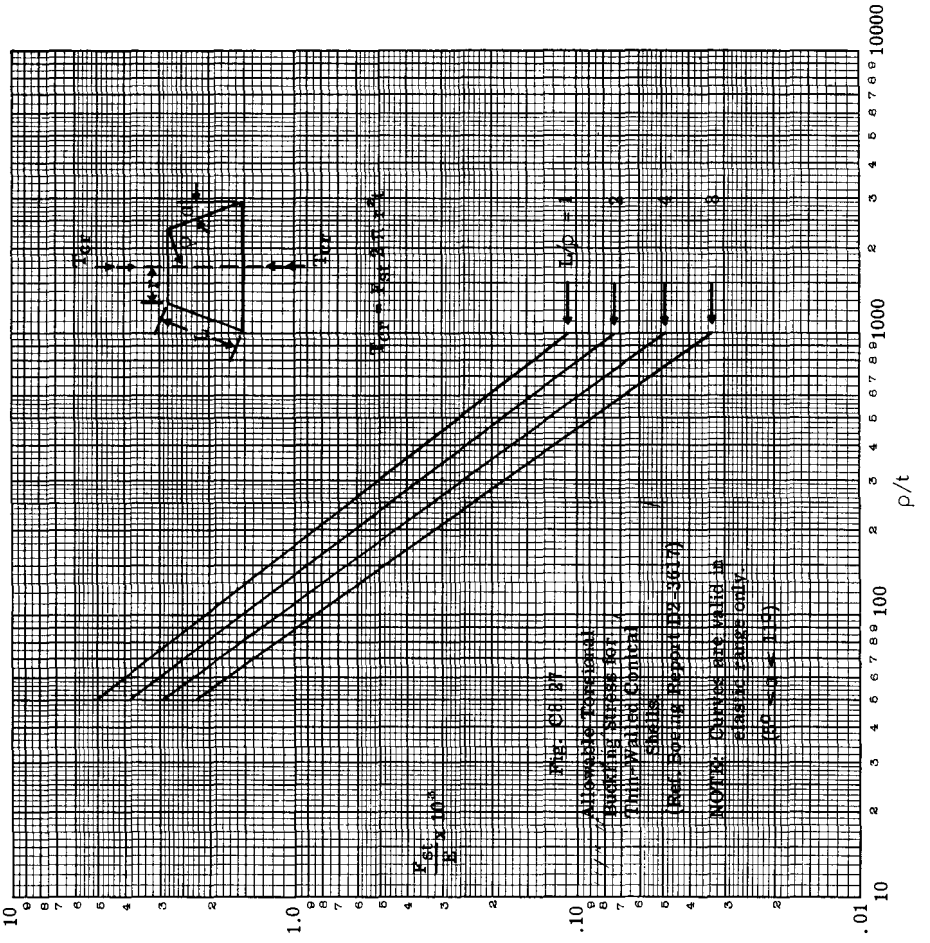

Fig. C8.27

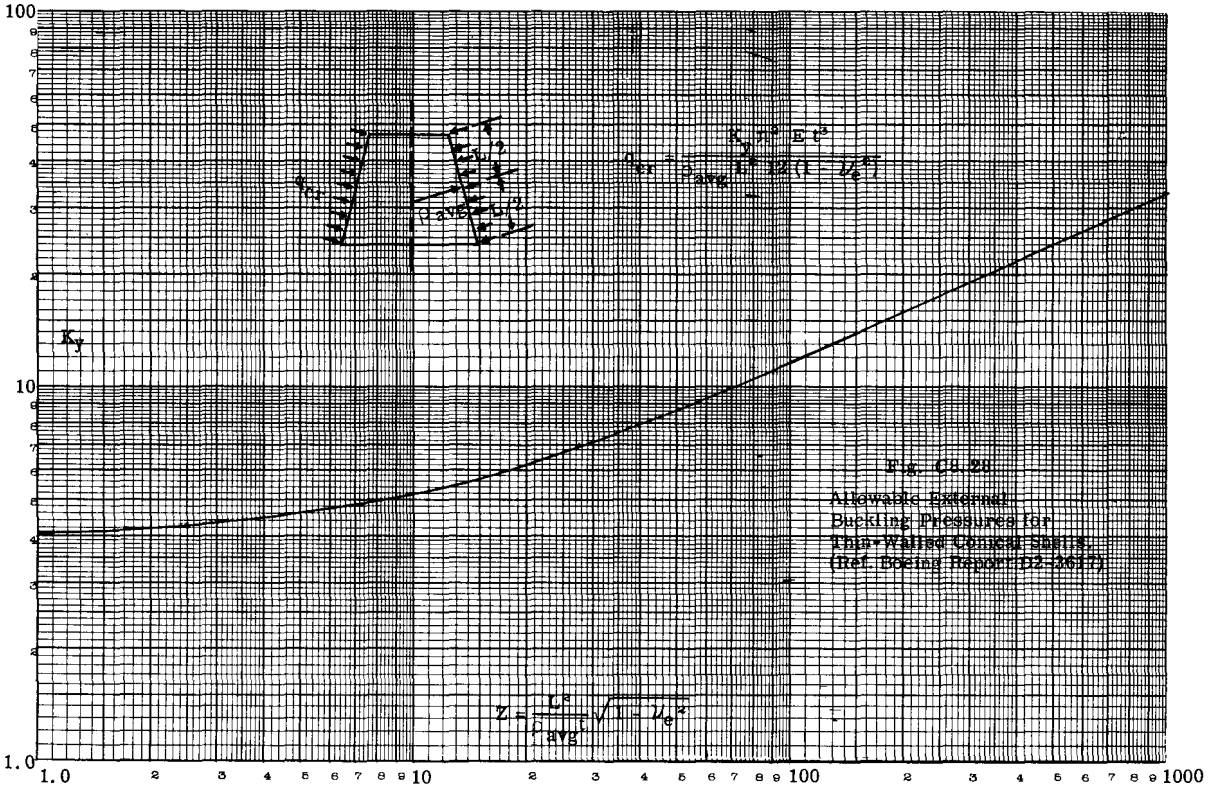

Fig. C8.28

Allowable External Buckling Pressures for Thin-Walled Conical Shells. (Ref. Boeing Report D2-3617)

To find external buckling pressure q_{cr}:-

Use is made of Fig. C8.28.

$$\rho_{avg} = \frac{10 + 13.52}{2 \cos 10^\circ} = 11.92 \text{ in.}$$

$$\rho_{avg}/t = 11.92/.05 = 238$$

The lower scale parameter of Fig. C8.28 is,

$$Z = \frac{L^2}{\rho_{avg} t} \sqrt{1 - \nu_e^2}$$

$$Z = \frac{20.32^2}{11.92 \times .05} \sqrt{1 - .3^2} = 660$$

From Fig. C8.28 for Z = 660, we read $K_y = 27.5$. The equation for buckling pressure from Fig. C8.28 is,

$$q_{cr} = \frac{K_y E t^3 \pi^2}{\rho_{avg} L^2 12 (1 - \nu_e^2)}$$

$$= \frac{27.5 \times 10{,}700{,}000 \times .05^3 \times \pi^2}{11.92 \times 20.32 \times 12 (1 - .3^2)} = \underline{5.37} \text{ psi}$$

PROBLEMS

(1) A monocoque circular cylinder is fabricated from aluminum alloy for which E is 10,500,000. Wall thickness is .064. Cylinder diameter is 80 inches. Length is 60 inches. Using a probability factor of 90 percent, determine the following values:-

(a) Buckling compressive load for cylinder.
(b) Buckling bending moment for cylinder.
(c) Buckling torsional moment for cylinder.

(2) The cylinder in Problem (1) is subjected to the following design loads. Will the cylinder fail under these various design conditions:-

Condition 1
P = 30000 lbs. compression
M = 50000 in. lbs.

Condition 2
P = 25000 lbs. compression
M = 45000 in. lbs.
T = 50000 in. lbs.

(3) If the cylinder in Problem 1 is pressurized to 6 psi, what ultimate compressive load will it carry. What ultimate bending moment will it carry. What ultimate torsional moment will it carry.

(4) A conical shell has a small end diameter of 30 inches, a length of 30 inches, a semi-vertex angle of 8 degrees and a wall thickness of .057. Material is aluminum alloy with E = 10,500,000. Determine the ultimate compressive load, the ultimate bending moment, and the ultimate torsional moment the cone will sustain when each load is acting separately.

Determine the external pressure that will buckle the cone.

REFERENCES

(1) Harris, Seurer, Skeene and Benjamin. The Stability of Thin-Walled Unstiffened Circular Cylinders Under Axial Compression. Jour. Aero. Sciences. Vol. 24, August, 1957.
(2) Donnell, L. H. Stability of Thin-Walled Tubes Under Torsion. NACA Report 479.
(3) Batdorf, S. B. A Simplified Method of Elastic Stability Analysis for Thin Cylindrical Shells. NACA Report 874 (1947).
(4) Weingarten, Morgan and Siede. Final Report of Design Criteria for Elastic Stability of Thin Shell Structures. Contract AFO4(647)619 Air Force Ballistic Missile Division). Space Tech. Labs. Dec., 1960.
(5) Lo, Crate and Schwartz. Buckling of Thin Walled Cylinders Under Axial Compression and Internal Pressure. NACA T. N. 2021, Jan. 1950.
(6) VonKarman and Tsien. The Buckling of Thin Cylindrical Shells Under Axial Compression. Jour. of Aero. Sciences. Vol. 8, June 1941.
(7) Tsein. A Theory for Buckling of Thin Shells. Jour. of Aero. Sciences. Vol. 9, August 1942.
(8) Fung and Sechler. Buckling of Thin Walled Circular Cylinders Under Axial Compression and Internal Pressure. Jour. of Aero. Sciences. Vol. 24, May 1957.
(9) Harris, Seurer, Skeene and Benjamin. The Bending Stability of Thin Walled Unstiffened Circular Cylinders Including Effects of Internal Pressure. Jour. of Aero. Sciences, Vol. 25, May 1958.
(10) Siede and Weingarten. On the Bending of Circular Cylindrical Shells Under Pure Bending. Jour. of Applied Mechanics. Vol. 28, March 1961.
(11) Flugge. Die Slabititat der Kruszylinderschole. Ingenieur Archiv. Vol. 3, 1932.
(12) Gerard & Becker. Handbook of Structural Stability. Part III. Buckling of Curved Plates and Shells. NACA T. N. 3783, Aug. 1957.
(13) Hopkins and Brown. The Effect of Internal Pressure on the Initial Buckling of Thin Walled Circular Cylinders Under Torsion. R & M. No. 2423. British A. R. C. 1946.
(14) Crate, Batdorf and Baab. The Effect of Internal Pressure on the Buckling Stress of Thin Walled Circular Cylinders Under Torsion. NACA WRL-67, 1940.
(15) Batdorf, Stein and Schildcrout. Critical Stress of Thin Walled Cylinders in Torsion. NACA T. N. 1344 (1947).
(16) Hausrath & Dittoe. Development of Design Strength Levels for the Elastic Stability of Monocoque Cones Under Axial Compression. NASA T. N. D-1510 (1962).
(17) Hess and Garber. Stability of Ring Stiffened Conical Shells Under Simultaneous Lateral Pressure and Axial Compression. General Electric Report No. R58SD226. April 1958.

CHAPTER C9

BUCKLING STRENGTH OF CURVED SHEET PANELS. ULTIMATE STRENGTH OF STIFFENED CURVED SHEET STRUCTURES.

PART 1. BUCKLING STRENGTH OF CURVED SHEET PANELS

C9.1 Introduction.

Curved sheet panels represent a common external part of flight vehicle structures. Examples are the skin of the fuselage and the missile. If the curved sheet has no longitudinal stiffeners, failure will occur when buckling occurs. If the curved sheet has stiffening elements attached then the composite unit will not fail on the development of sheet buckling, that is, the composite unit has an ultimate strength much greater than the load which caused initial buckling of the curved sheet panels between the stiffening units commonly referred to as sheet stiffeners. In some flight vehicle designs it may be specified that under a certain percentage of the limit loads that no buckling of the curved sheet panels shall occur. Thus it is necessary to be able to determine what stresses will cause curved sheet panels to buckle and also to determine what external loads will cause a stiffened sheet panel to fail.

C9.2 State of the Theory.

In Chapter A18, the small deflection linear theory was used to determine the compressive buckling stress of flat sheet panels. The theoretical results compare favorably with experimental test results. However, when the same theory is applied to unstiffened curved sheet panels or thin-walled cylinders, the theoretical results are considerably above the test results on such units. A large deflection theory gives closer comparison to test results, but this theory involves a consideration of initial imperfections in the sheet and thus an unknown quantity. For the application of both small and large deflection theories to the buckling of curved sheet and cylinders, the reader is referred to the references listed at the end of Chapter C8, particularly those reports which give the results of such investigators as Donnell, Batdorf and Gerard.

C9.3 Compressive Buckling Stress of Curved Sheet Panels.

The expression for the buckling stress under axial compression is of the same form as for flat sheets, the value of the buckling coefficient K_c having a higher value.

$$F_{c_{cr}} = \frac{K_c \pi^2 E}{12 (1 - \nu_e^2)} \left(\frac{t}{b}\right)^2 \qquad \text{C9.1}$$

Fig. C9.1 gives curves for determining the buckling coefficient K_c. The theoretical derived curve is shown along with the recommended design curves which were dictated by test results. These curves apply for buckling stresses in the elastic range.

C9.4 Shear Buckling Stress of Curved Sheet Panels.

The equation for the buckling shear stress is,

$$F_{s_{cr}} = \frac{K_s \pi^2 E}{12 (1 - \nu_e^2)} \left(\frac{t}{b}\right)^2 \qquad \text{C9.2}$$

Figs. C9.2 to C9.5 gives curves for finding the buckling stress coefficient K_s to use in Equation C9.2. These curves apply when buckling stresses are in the elastic range.

C9.5 Buckling Strength of Curved Sheet Panels Under Combined Axial Compression and Shear.

The studies by Schildcrout and Stein (Ref. 1) gave the following interaction equation for combined longitudinal compression and shear on curved sheet panels:-

$$R_S^2 + R_L = 1 \qquad \text{C9.3}$$

where, $R_S = \frac{f_s}{F_{s_{cr}}}$, $R_L = \frac{f_c}{F_{c_{cr}}}$

If the longitudinal stress is tension instead of compression, then R_L is considered as a negative compression using the compression allowable. The equation for margin of safety is:-

$$M.S. = \frac{2}{R_L + \sqrt{R_L^2 + 4 R_S^2}} - 1 \qquad \text{C9.4}$$

C9.6 Compressive Buckling Stress of Curved Panels with Internal Pressure.

As for the case of monocoque cylinders, internal outward pressure increases the axial buckling compressive stress of the curved sheet panel. Rafel and Sandlin (Ref. 3) and Rafel (Ref. 4) performed tests on curved panels under axial compression and internal outward pressure. The results correlate with the interaction equation:-

$$R_c^2 + R_p = 1 \qquad \text{C9.5}$$

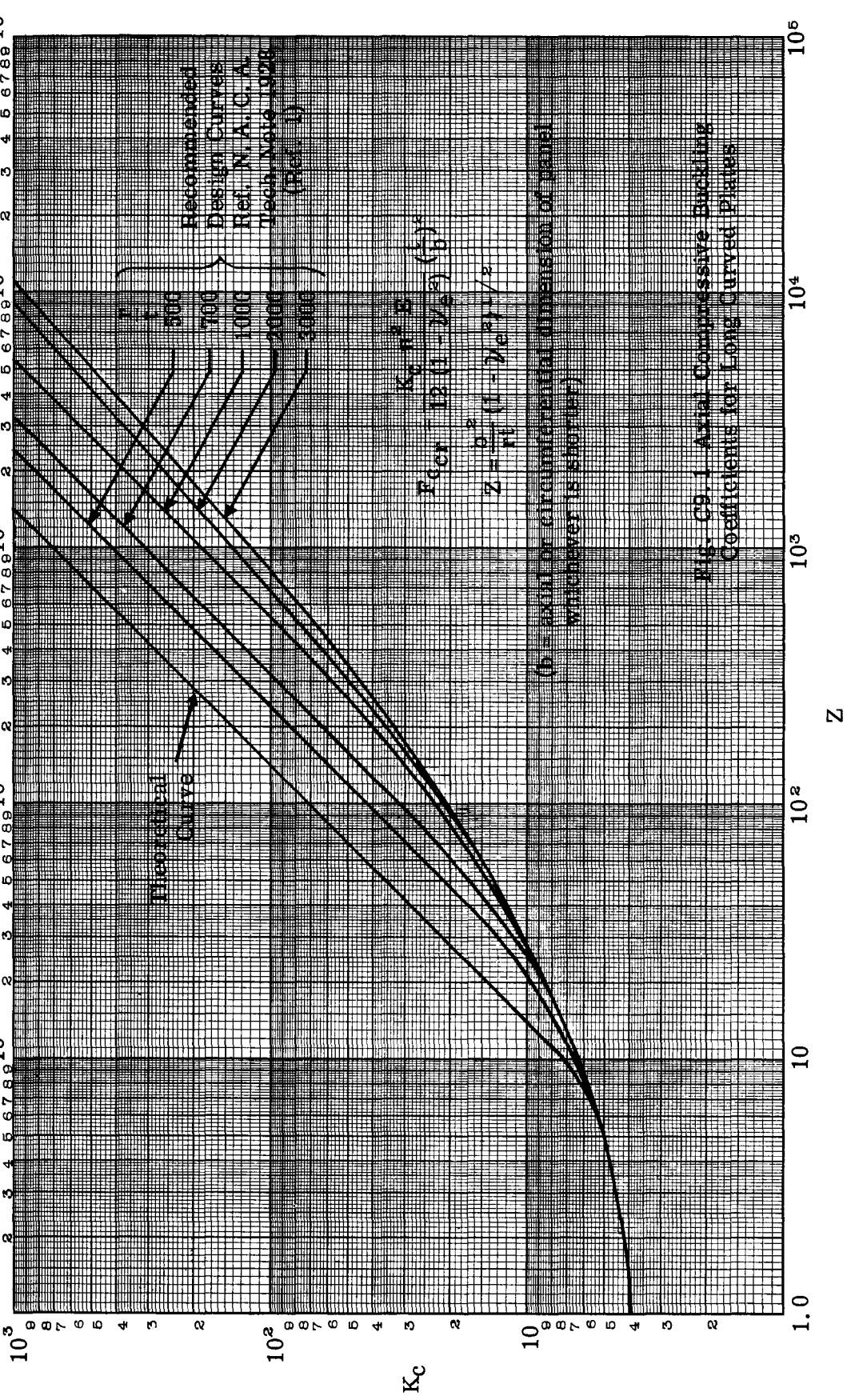
Recommended Design Curves Ref. N.A.C.A. Tech. Note 1028 (Ref. 1)
R/t = 500
700
1000
2000
3000
Theoretical Curve
$K_c = \sigma_{cr} \frac{b^2}{\pi^2 E} \left(\frac{t}{b}\right)^2$
$\sigma_{cr} = \frac{\pi^2 E}{12(1-\nu^2)} \left(\frac{t}{b}\right)^2$
$Z = \frac{b^2}{Rt}\sqrt{1-\nu^2}$
(b = actual or circumferential dimension of panel whichever is shorter)
Fig. C9.1 Axial Compressive Buckling Coefficients for Long Curved Plates
K_c
Z

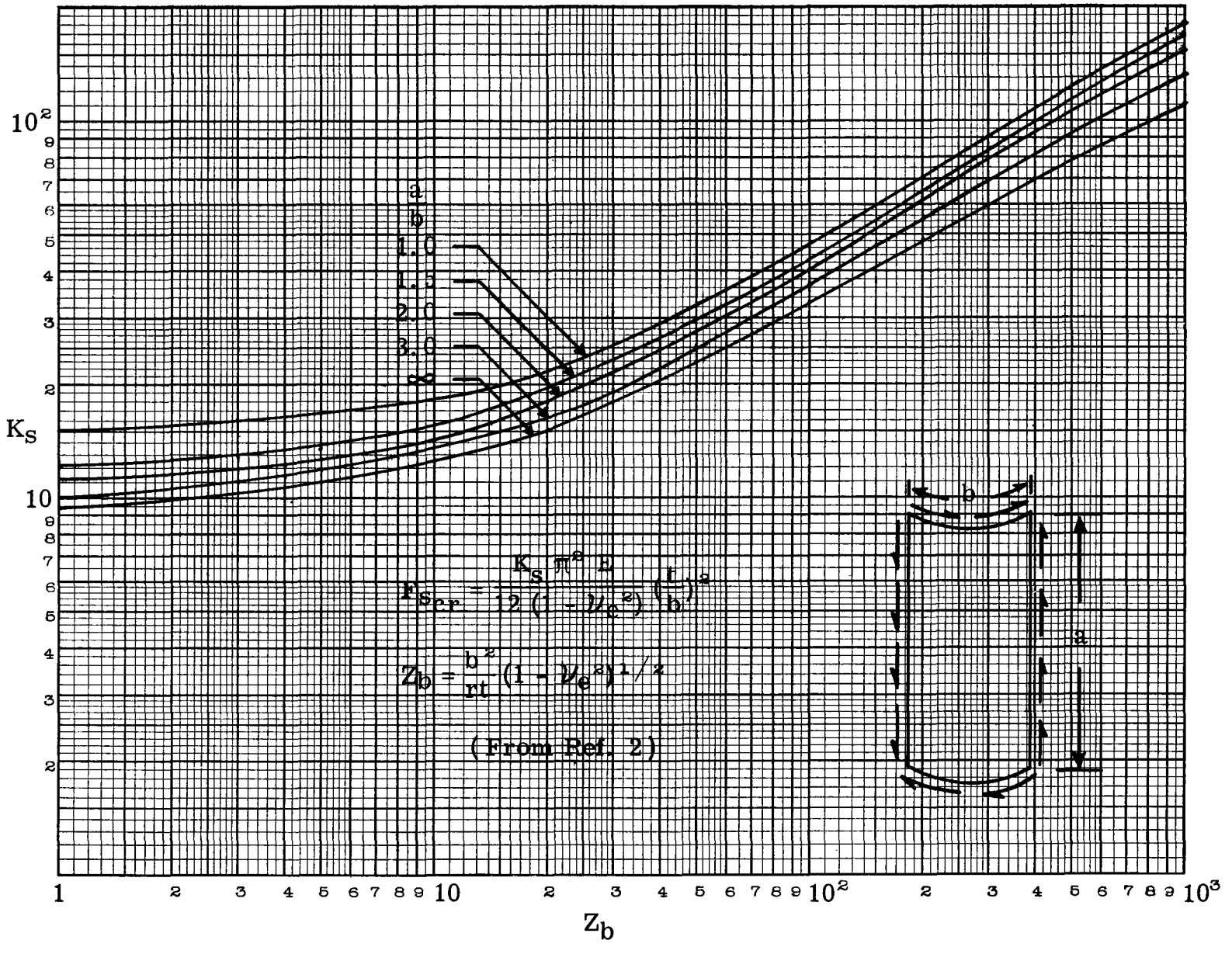

Fig. C9.2 Shear Buckling Coefficients for Long Clamped Curved Plates

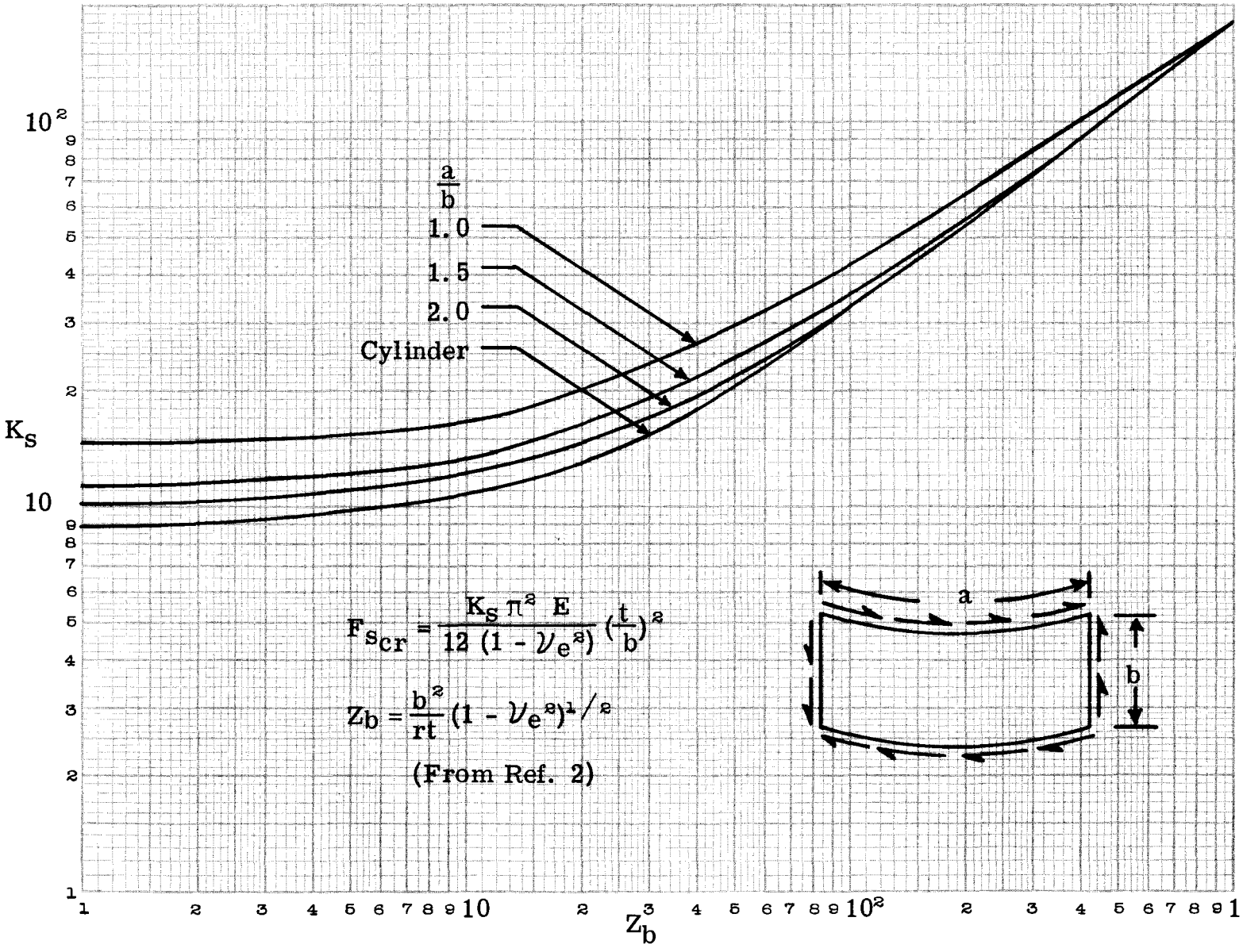

Fig. C9.3 Shear Buckling Coefficients for Wide Clamped Curved Plates.

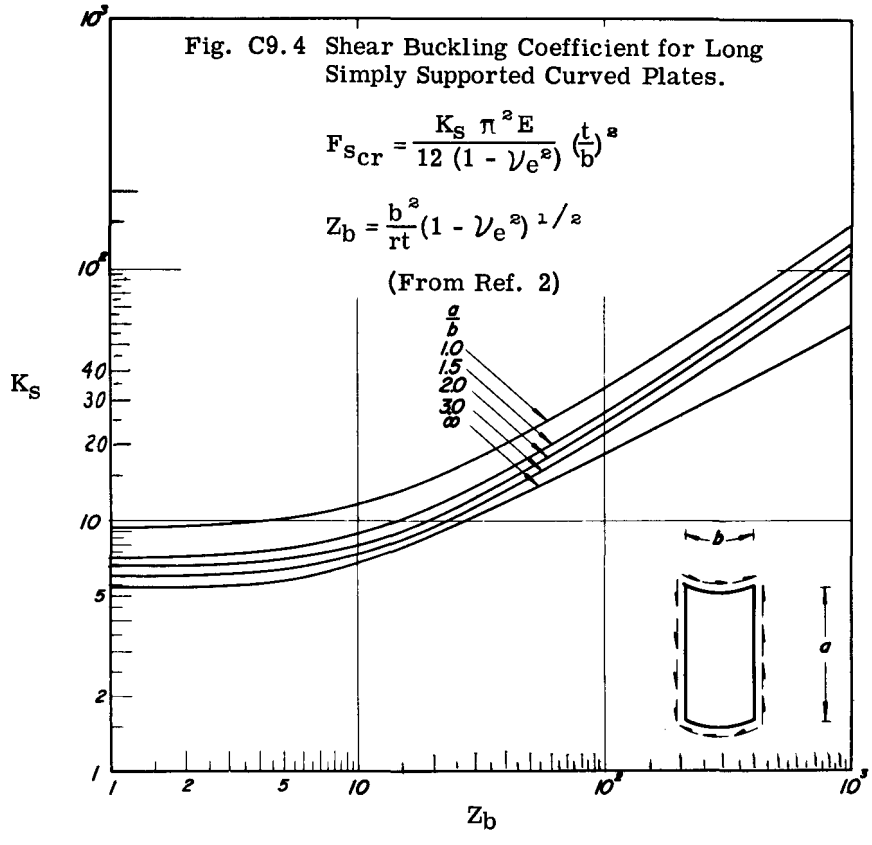

Fig. C9.4 Shear Buckling Coefficient for Long Simply Supported Curved Plates.

$$F_{s_{cr}} = \frac{K_s \pi^2 E}{12 (1 - \nu_e^2)} \left(\frac{t}{b}\right)^2$$

$$Z_b = \frac{b^2}{rt}(1 - \nu_e^2)^{1/2}$$

(From Ref. 2)

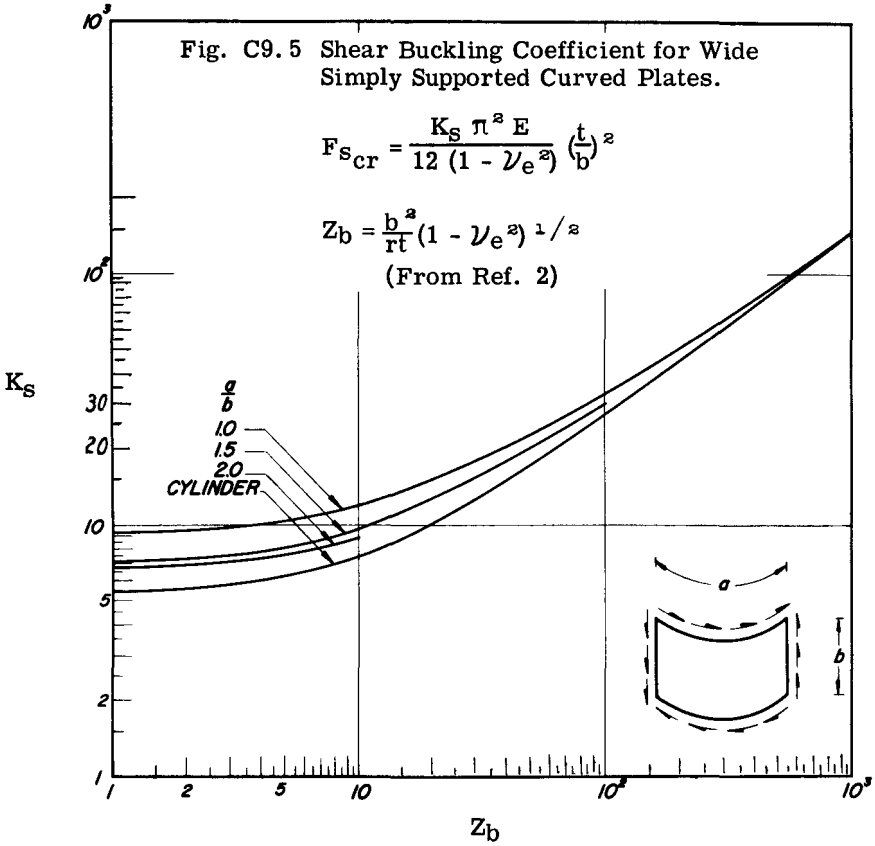

Fig. C9.5 Shear Buckling Coefficient for Wide Simply Supported Curved Plates.

$$F_{s_{cr}} = \frac{K_s \pi^2 E}{12 (1 - \nu_e^2)} \left(\frac{t}{b}\right)^2$$

$$Z_b = \frac{b^2}{rt}(1 - \nu_e^2)^{1/2}$$

(From Ref. 2)

where $R_c = f_c/F_{c_{cr}}$

R_p = ratio of [applied internal pressure / external inward pressure that would buckle the cylinder of which the curved panel is a section. Found by use of Fig. C8.16 in Chapter C8.]

In using Equation C9.5, the value of R_p is negative as inward pressure is opposite to the inward acting outward pressure.

C9.7 Shear Buckling Stress of Curved Sheet Panels with Internal Pressure.

As in the case of monocoque cylinders, internal pressure increases the shear buckling stress of the curved sheet panel. Brown and Hopkins (Ref. 5) solved the classical equilibrium equations to determine the effect of radially outward pressure upon the shear buckling stress of curved panels and obtained fair agreement with test data by Rafel and Sandlin (Ref. 3). The test data also correlates with the interaction curve used for the effect of internal pressure upon cylinders in torsion (see Chapter C8). The interaction equation is:

$$R_s^2 + R_p = 1 \qquad \text{- - - - - - - - - - - - - - - C9.6}$$

where $R_s = f_s/F_{s_{cr}}$

R_p = ratio of [applied internal pressure / external inward pressure that would buckle the cylinder of which the curved sheet panel is a section. Found by use of Fig. C8.16 of Chapter C8.]

In using Equation C9.6, R_p is given a minus sign.

C9.8 Example Problems.

PROBLEM 1.

Fig. C9.6 illustrates a circular fuselage section with longitudinal stringers represented by the small circles. The area of each stringer is .15 sq. in. The skin thickness is .04 inches. All material is aluminum alloy with E_c = 10,700,000. The fuselage frame spacing (a) is 15.75 inches. The fuselage section is subjected to the following load system:-

M_y = 600,000 in.lb. (causing compression on top half)
V_z = 5175 lbs. (acting up)
T = Torsional moment = 210,000 in.lbs. (acting counterclockwise)

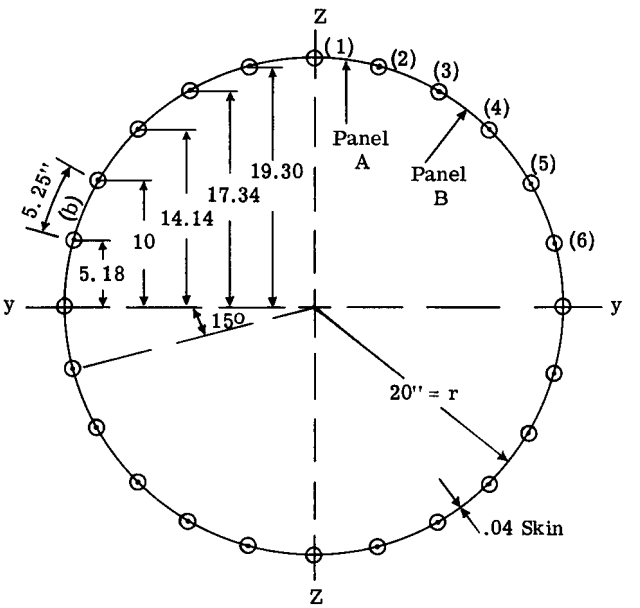

Fig. C9.6

The problem is to determine whether skin panels (A) and (B) will buckle under the given combined loading on the fuselage section.

Solution.

To find the bending stresses, the moment of inertia of the cross section about axis y-y is necessary, which axis is also the neutral axis since all material is effective. The moment of inertia will equal 4 times that due to material in one quadrant.

I_y due to stringers is,

$$I_y = 4\left[.075 \times 20^2 + .15\,(19.30^2 + 17.34^2 + 14.14^2 + 10^2 + 5.18^2)\right] = 720 \text{ in.}^4$$

Due to skin:-

$$I_y = \pi r^3 t = \pi \times 20^3 \times .04 = 1005 \text{ in.}^4.$$

$$\text{Total } I_y = 720 + 1005 = 1725 \text{ in.}^4.$$

Consider Skin Panel (A):

$r/t = 20/.04 = 500$, $a/b = 15.75/5.25 = 3.0$

To determine the compressive buckling stress, use will be made of Fig. C9.1.to find the buckling coefficient K_c.

$$Z = \frac{b^2}{rt}(1 - \nu_e^2)^{1/2}$$

$$= \frac{5.25^2}{20 \times .04}(1 - .3^2)^{1/2} = 32.9$$

From Fig. C9.1, K_c = 14

$$F_{c_{cr}} = \frac{K_c \pi^2 E}{12 (1 - \nu_e^2)} \left(\frac{t}{b}\right)^2$$

$$= \frac{14 \pi^2 \times 10{,}700{,}000}{12 (1 - .3^2)} \left(\frac{.04}{5.25}\right)^2 = \underline{7850} \text{ psi}$$

To find the shear buckling stress, we use Fig. C9.2. Z is the same as calculated above or 32.9. Thus from Fig. C9.2 we read for a/b = 3, that $K_s = 20$.

$$F_{s_{cr}} = \frac{20 \pi^2 \times 10{,}700{,}000}{12 (1 - .3^2)} \left(\frac{.04}{5.25}\right)^2 = \underline{11{,}200} \text{ psi}$$

The bending stress at midpoint of Panel (A) will be calculated:

$f_c = MZ/I_y = (600{,}000 \times 19.7)/1725 = 6850$ psi

Thus stress ratio $R_c = f_c/F_{c_{cr}} = 6850/7850$

$= .874$

Shear stress on Panel (A) due to torsion is,

$f_s = T/2At$, where A is inclosed area of fuselage cell.

$f_s = 210{,}000/2 \times \pi \times 20^2 \times .04 = \underline{2090}$ psi.

The panel is also subjected to shear stress due to transverse shear of $V_z = 5175$ lbs.

The shear flow equation is,

$$q = -\frac{V_z}{I_y} \Sigma ZA = -\frac{5175}{1725} \Sigma ZA = -3 \Sigma ZA.$$

The shear flow will be zero on Z axis. The shear flow at top edge of Panel (A) will be due to effect of one-half the area of stringer (1).

$q_{1-2} = -3 \times .075 \times 20 = -4.5$ lb./in.

Area of skin between stringers (1) and (2) is $5.25 \times .04 = .21 = \bar{A}$.

Distance from centroid of Panel (A) from neutral axis is $Z = r \sin \alpha/\alpha$. $\alpha = 15^\circ$. which gives Z = 19.8 in.

Thus $q_{2-1} = -4.5 - 3 \times .21 \times 19.8 = -17$ lb./in

Then average shear flow on panel is $(17 + 4.5)/2 = 10.75$.

Then shear stress = $q/t = 10.75/.04 = 269$ psi.

This shear stress has the same sense or direction as the torsional shear stress so we add the two to obtain the true shear or:

$f_{s(total)} = 269 + 2090 = 2359$ psi.

Then shear stress ratio $R_s = f_s/F_{s_{cr}} = 2359/11200 = .21$.

The interaction equation for combined compression and shear is,

$R_c + R_s^2 = 1$

$.874 + .21^2 = .918$. This is less than 1.0 so panel will not buckle.

$$M.S. = \frac{2}{.874 + \sqrt{.874^2 + 4 \times .21^2}} - 1 = .09$$

Consider Skin Panel (B).

Arm Z to midpoint of panel = 15.88 in.

$f_c = Mz/I = 600{,}000 \times 15.88/1725 = \underline{5520}$ psi

$R_c = 5520/7850 = .704$

The torsional shear stress is the same on all panels or $f_s = 2090$ psi as previously calculated.

Shear flow q due to transverse shear load:

$q = \frac{V}{I} \Sigma ZA = 3 \Sigma ZA.$

Calculation of ΣZA at upper edge of panel:

For stringers = $.075 \times 20 + .15 (19.3 + 17.34)$

$= 7.0$

For skin: Area = $2 \times 5.25 \times .04 = .42$.

Vertical distance $\bar{Z}$ to centroid of skin portion = $r \sin \alpha/\alpha$. $\alpha = 30^\circ$. The result is $\bar{Z} = 19.1$ in. The $\bar{Z}A = 19.1 \times .42 = 8.03$. Total $\Sigma ZA = 8.03 + 7.0 = 15.03$. Then $q = 3 \Sigma ZA = 3 \times 15.03 = 45.09$ lb./in.

A similar calculation for shear flow at lower edge of Panel (B) would give q equal 55.0. Thus average shear flow on panel is $(55 + 45.09)/2 = 50.04$. Then $f_s = q/t = 50.14/.04 = 1251$ psi. The total shear stress f_s on panel then equals $1251 + 2090 = 3341$ psi.

$R_s = f_s/F_{s_{cr}} = 3341/11200 = .299$

Substituting in interaction equation $R_c + R_s^2 = .704 + .299^2 = .793$. The result is less than 1.0, thus panel will not buckle.

The student should check other panels for buckling and compare their margins of safety.

General Comment:-

In general the compressive stress is the dominant factor in causing the panel buckling. Thus to increase the buckling stress of the panels and also to give a more effective stringer arrangement to carry the bending moment, the stringers should be spaced closer in the top and bottom regions of the cross-section and with increased spacing as the neutral axis is approached.

PROBLEM 2.

The fuselage section in Problem 1 is subjected to an internal outward pressure of 5 psi. What would be the compressive buckling stress of a panel and also the shear buckling stress with this internal pressure existing.

Solution.

From Art. C9.6, the interaction equation is,

$$R_c^2 + R_p = 1, \quad R_c = \frac{f_c}{F_{c_{cr}}}$$

From Problem 1, the compressive buckling stress $F_{c_{cr}} = 7850$ psi.

To evaluate R_p, the external inward radial acting pressure that would cause buckling of a circular cylinder having a radius equal to that of the curved sheet panel must be determined. Use is made of Fig. C8.16 of Chapter C8 to determine the backing stress under such a loading. The lower scale parameter for Fig. C8.16 is,

$$Z_L = \frac{L^2}{rt}\sqrt{1 - \nu_e^2}$$

$$= \frac{15.75^2}{20 \times .04}\sqrt{1 - .3^2} = 296$$

From Fig. C8.16, we read $K_y = 19$

$$F_{c_{cr}} = \frac{K_y \pi^2 E}{12 (1 - \nu_e^2)} \left(\frac{t}{L}\right)^2$$

$$= \frac{19 \pi^2 \times 10{,}700{,}000}{12 (1 - .3^2)} \left(\frac{.04}{15.75}\right)^2 = 1215 \text{ psi}$$

The external radial pressure to produce this buckling stress is,

$$p = F_{c_{cr}} t/r = 1215 \times .04/20 = 2.43 \text{ psi}$$

$$R_p = \frac{5.0}{2.43} = 2.06$$

Subt. in interaction equation with a minus sign for R_p,

$$\frac{f_c^2}{F_{c_{cr}}^2} - R_p = 1$$

$$\frac{f_c^2}{7850^2} - 2.06 = 1, \text{ or } f_c = 13750 \text{ psi}$$

Thus the internal outward pressure of 5 psi increases the axial compressive buckling stress from 7850 to 13750 psi.

Shear Buckling Stress Under 5 psi Internal Radial Pressure.

From Art. C9.7, the interaction equation is,

$$R_s^2 + R_p = 1$$

From Problem 1, $F_{s_{cr}}$ or our panel was 11200 psi. The value of R_p is determined as above or $R_p = 2.06$. Subt. in interaction equation:

$$\frac{f_s^2}{F_{s_{cr}}^2} - 2.06 = 1$$

$$f_s^2 = 11200^2\ (3.06), \text{ or } f_s = \underline{19500} \text{ psi.}$$

The internal pressure of 5 psi thus increases the shear buckling stress from 11200 to 19500 psi.

PART 2. ULTIMATE STRENGTH OF STIFFENED CYLINDRICAL STRUCTURES.

C9.9 Introduction.

A cylindrical structure composed of a thin skin covering and stiffened by longitudinal stringers and transverse frames or rings is a common type of structure for airplane fuselages, missiles and various types of space vehicles, and such structures are often referred to as the semi-monocoque type of structure. The design of a semi-monocoque structure involves the solution of two major problems, namely, the stress distribution in the structure under various external loadings and the check of the structure to see if these stresses can be safely and efficiently carried by individual components of the structure as well as the structure acting as a whole.

C9.10 Types of Instability Failure of Semi-Monocoque Structures.

(1) Skin Instability.

In general, thin curved sheet panels buckle under relatively low compressive stress and thus if design requirements specified no buckling of the sheet under limit or design loads, the sheet would have to be relatively thick or the stringers placed very close together and the fuselage or body structure would be unsatisfactory from a strength weight standpoint. In missile structures, internal pressurization increases the buckling stress greatly, thus the buckling weakness of thin sheet is improved, but keeping a structure pressurized under all operating conditions has its difficulties.

In a semi-monocoque body, the longitudinal stringers provide efficient resistance to compressive stresses and buckled sheet panels can transfer shear loads by diagonal tension field action, thus the buckling of the sheet panels is not an important factor in limiting the ultimate strength of the over-all structural unit. When buckling of the skin panels takes place, a stress redistribution over the entire structure takes place, thus it is important to know when skin buckling begins. Furthermore, design requirements may often specify that no skin buckling should take place under a certain percent of the limit or design loads. The equations and design curves in Part 1 of this chapter can be used to determine the buckling stress of curved sheet panels under various stress systems.

(2) Panel Instability.

The internal rings or frames in a semi-monocoque structure such as a fuselage divide the longitudinal stringers and their attached skin into lengths called panels. If these frames are sufficiently rigid, a semi-monocoque structure if subjected to bending will fail on the compression side as illustrated in Fig. C9.7a. The stringers act as columns with an effective length equal to the panel length which is the ring spacing. Initial failure thus occurs in a single panel and thus is referred to as a panel instability failure. In general, this type of failure occurs in most practical aircraft and aerospace semi-monocoque structures because the rings are sufficiently stiff to promote this type of failure. Since the inside of a fuselage carries various loads, such as passengers, cargo, etc., the rings must act as structural units to transfer such loads to the shell skin, thus requiring rings of considerable strength and stiffness. Even lightly loaded frames must be several inches deep to provide conduits required in various installations to pass through the web of the ring cross-section, thus providing a relatively stiff ring for supporting the stiffeners in their column action. When the skin buckles under shear and compressive stresses, the skin panels transfer further shear forces by semi-diagonal tension field action which produces additional axial loads in stringers and also bending which must be considered in arriving at the panel failing strength. This subject is treated in detail in Part 2 of Chapter C11.

(3) General Instability.

In general instability, failure is not confined to the region between two adjacent frames or rings but may extend over a distance of several frame spacings as illustrated in Fig. C9.7b for a stiffened cylindrical shell in bending. In panel instability, the transverse stiffeners provided by the frames on rings is sufficient to enforce nodes in the stringers at the frame support points as illustrated in Fig. C9.7a. Any additional stiffeners in excess of this amount does not contribute to additional buckling strength. General instability may thus occur when the stiffeners of the supporting frames is less than this minimum value.

C9.11 The Determination of the Stresses in a Stiffened Cylindrical Structure Under External Loads.

The stresses in a stiffened cylindrical structure such as used in typical fuselage or missile design can be fairly accurately determined by the modified beam theory as presented in Chapter A20. A more rigorous approach is given in Chapter A8 involving matrix formulation but this approach requires the use of a large electronic computor to handle the required calculations. For details of applying the modified beam theory, the reader should refer to Articles A20.3 and A20.4 of Chapter A20. In the example problem solution as given in Article A20.4, the effective area to use for the curved sheet was based on the ratio of the buckling stress of the curved panel to the bending compressive stress on the panel due to bending of the entire effective cross-section of the fuselage under the design loads. In the example problem as given in Table A20.2, a conservative buckling compressive stress equal to .3 Et/r was used for the curved panel and no consideration of the effect of shear stress on the compressive buckling stress was considered.

A more accurate procedure would be to calculate the effective area of the curved panels taking into account the influence of combined compression and shear on the buckling strength of the panel. Thus in Table A20.2 on page A20.5 of Chapter A20, the shear stress on each curved panel should also be calculated and then the buckling stress of the panel under the combined compression and shear calculated.

The buckling stress under pure compression

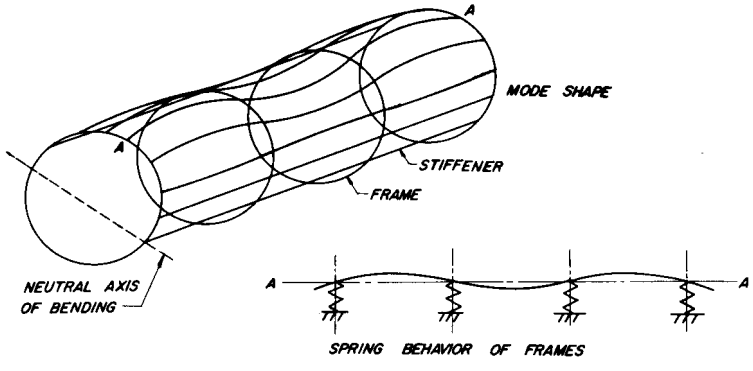

(a) Panel instability.

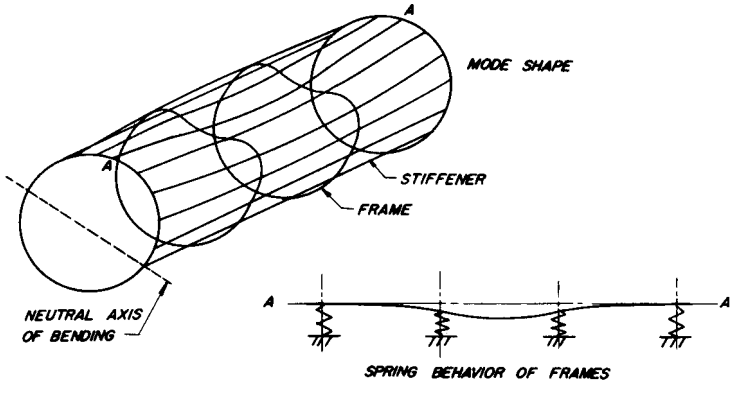

(b) General instability.

Fig. C9.7 Mode Shapes for Panel and General Instability of Stiffened Cylinders in Bending. (From Ref. 7.)

and shear should be calculated using Equations C9.1 and C9.2. The buckling stress under combined compression and shear is given by the interaction equation:-

$R_c + R_s^2 = 1$, where $R_c = f_c/F_{c_{cr}}$, $R_s = f_s/F_{s_{cr}}$.

The expression for margin of safety is,

$$M.S. = \frac{2}{R_c + \sqrt{R_c^2 + 4R_s^2}} - 1$$

Let $\bar{f}_c$ be the compressive stress that will buckle the curved sheet panel when subjected to combined compression and shear when the ratio of the applied compressive and shear stresses in a constant. Then,

$$\bar{f}_c = f_c \left(\frac{2}{R_c + \sqrt{R_c^2 + 4R_s^2}}\right) \quad - - - - - - - - \text{C9.6}$$

These $\bar{f}_c$ values should then replace the values in column 5 of Table A20.2.

The author has noted that one aerospace company in their missile design uses only 90 percent of the theoretical buckling stress in computing the effective area of the buckled curved panels. This correction assumes that the curved sheet fails to hold the buckling stress as the fuselage section as a whole is further loaded and the curved sheet suffers more buckling distortion.

C9.12 Panel Instability Strength.

Panel instability means failure of the stringer and its effective skin between two adjacent frames. The bending of the stiffened shell as a whole produces a compressive load or stress on the stringer. The semi-tension field action of the skin after buckling produces an additional compressive load on the stringer and also a bending moment.

The compressive stress due to bending of the stiffened shell as a whole is found by the methods discussed in Article C9.11. The additional stringer loads due to semi-tension field action are determined by the theory and procedure given in Part 2 of Chapter C11.

These calculated stringer loads are then compared to the stringer strength to determine whether a positive margin of safety exists. The local crippling and column strength of a stringer plus its effective skin can be found by the theory and analysis methods given in Chapter C7. The bending strength of the stringer cross-section can be found by the theory and analysis method given in Chapter C3. The strength of the stringer in combined compression and bending is found by use of the proper interaction equation.

C9.13 Calculation of General Instability.

A great deal of theoretical and experimental work has been done on the subject of general instability of stiffened shells. The general goal in the design of such structures is to insure the frames have sufficient stiffness so as to prevent the type of failure illustrated in Fig. C9.7b or, in other words, to insure the type of failure illustrated in Fig. C9.7a which is panel instability.

Shanley (Ref. 6) has derived an expression for the required frame stiffness to prevent general instability failure of a stiffened shell in pure bending.

$(EI)_f = C_f MD^2/L$

In a study of available test data, C_f was found to be 1/16000. Thus,

$(EI)_f = MD^2/16000L \quad - - - - - - - - - - - - \text{C9.7}$

where, E = modulus of elasticity

I = moment of inertia of frame section

D = diameter of stiffened shell

L = frame spacing

M = bending moment on shell

Becker (Ref. 7) in a comprehensive study of most published theoretical and experimental material relative to the general instability of stiffened shells, summarizes the results of his studies as given in Table C9.1.

Bending.

For the case of bending, the constant of 4.80 in the equation given in Table C9.1 is for the condition where the frames are attached to the skin between the stringers. For frames not attached to the skin between stringers, the constant should be 3.25.

The effective sheet width for use with the stringers may be found from the equation,

$$\frac{W_e}{b} = 0.5\,(F_{c_{cr}}/F_c)^{1/2} \quad - - - - - - - - - - - \text{C9.8}$$

where, W_e = effective width of skin per side of stringer (in.)

b = stringer spacing (in.)

$F_{c_{cr}}$ = compressive buckling stress for curved skin panel

F_c = compressive stress at bending general instability (psi)

Table C9.1
(Ref. 7)

THEORETICAL GENERAL INSTABILITY STRESSES OF ORTHOTROPIC CIRCULAR CYLINDERS

(Results are based on the assumption that spacings of longitudinal stiffeners and circumferential frames are uniform and small enough to permit assumption that cylinder acts as orthotropic shell)

Loading	Moderate-length cylinders	Long cylinders
Bending	$F_c = gE\,(I_f t)^{1/2}/Rt_s$ $g = 4.80\left[(b/d)(\rho_s/\rho_f)(t_s/t_f)^2(\rho_s/b)^2\right]^{1/4}$	
External radial or hydrostatic pressure	$F_y = 5.51E\,(\frac{t_s}{t_f})^{1/4}\,(\frac{\rho_f}{R})^{1/2}(\frac{R}{L})$	$F_y = 3E\,(\rho_f/R)^2$
Torsion	$F_{sT} = 3.46\,(\frac{t_s}{t})^{3/8}\,(\frac{I_f}{R^2t})^{5/8}\,(\frac{R}{L})^{1/2}$	$F_{sT} = 1.754\,(\frac{t_s}{t})^{1/4}(\frac{I_f}{R^2t})^{3/4}$

F_c = Compressive stress at bending general instability (psi)

F_y = Circumferential normal stress under external pressure at general instability (psi)

F_{sT} = Shearing stress at torsional general instability (psi)

b = Stringer spacing (in.)

d = Frame spacing (in.)

R = Cylinder radius (in.)

t = Skin thickness (in.)

A_s = Stringer area (in.^{2})

A_f = Frame section area (in.^{2})

t_s = Distributed stringer area = A_s/b

t_f = Distributed frame area = A_f/d

$\bar{I}_f$ = Bending moment of inertia of frame section (in.^{4})

I_f = Distributed bending moment of inertia of frame = $\bar{I}_f/d$

ρ_s = Stringer section radius of gyration (in.)

ρ_f = Frame section radius of gyration (in.)

L = Length of cylinder (in.)

E = Modulus of Elasticity.

For the frames the effective skin width should be taken as the total frame spacing (d). For inelastic stresses, the use of the secant modules appears to be applicable on the basis of limited test data.

External Radial or Hydrostatic Pressure.

The effective skin width to be used in computing the stringer and frame section properties may be determined from the following equation.

$$\frac{W_{e_s}}{b} = \frac{W_{e_f}}{d} = 0.5\,(F_{c_{cr}}/F_c)^{1/2} \quad \text{- - - - - - - -} \quad C9.9$$

The subscript s refers to stringer and f refers to frame. The term d is the frame spacing.

Torsion.

The effective skin to be used can be determined from the following equation:-

$$\frac{W_{e_s}}{b} = \frac{W_{e_f}}{d} = 0.5\,(F_{s_{cr}}/F_{st})^{1/2} \quad \text{- - - - -} \quad C9.10$$

where $F_{s_{cr}}$ is the shear buckling stress for the curved skin panel. F_{st}, the torsional shear stress at torsional general instability (psi).

The equations for torsion as given in Table C9.1 would not apply to shells in which there is a strong tension field that could introduce appreciable secondary stresses in the frame. The reader should refer to Part 2 of Chapter C11 for a treatment of this subject involving the effect of semi-tension field action in the skin panels.

Transverse Shear General Instability.

From Ref. 7, it is stated that a conservative shear general instability shearing stress may be made by utilizing the relation.

$$F_s = 0.85\,F_{st} \quad \text{- - - - - - - - - - - - -} \quad C9.11$$

where F_s is the transverse shear stress under transverse shear general instability.

General Instability in Combined Torsion and Bending.

From (Ref. 7) the following interaction relation may be used to compute the permissible combinations of applied torsion and bending moments to a stiffened cylinder.

$$M/M_o + (T/T_o)^2 = 1 \quad \text{- - - - - - - - - - -} \quad C9.12$$

where M = applied moment

M_o = moment causing bending general instability acting alone

T = applied torsional moment

T_o = torsional moment causing torsional general instability acting alone

General Instability in Combined Transverse Shear and Bending.

(Ref. 7) concludes there is no interaction for this combination of transverse shear and bending loads. General instability occurs only for either type of loading acting alone and thus both loadings may be examined separately.

C9.14 Buckling of Spherical Plates Under Uniform External Pressure.

Classical Theory using 0.3 for Poisson's ratio gives the following buckling stress for a perfect spherical shell subjected to a uniform external pressure:-

$$F_{cr} = 0.606\,Et/r \quad \text{- - - - - - - - - - - - -} \quad C9.13$$

Available test data on practical shells show this theoretical buckling stress to be much too high. Thus to satisfy experimental results, reduced values must be used. The buckling equation which is similar to that for curved plates, under external pressure (from Ref. 2) is,

$$F_{cr} = \frac{K_p\,\pi^2\,E}{12\,(1-\nu_e^2)}\left(\frac{t}{d}\right)^2 \quad \text{- - - - - - - - - -} \quad C9.14$$

Fig. C9.8 shows curves for determining the buckling coefficient K_p and shows how test data falls considerably below the theoretical buckling curve. Equation C9.14 is for buckling stresses below proportional limit stress of material.

Report AS-D-568 of the Astronautics Division of General Dynamics Corp. from a statistical study of test data gives the following equations for the buckling stress of spherical shells under uniform external pressure for use in preliminary design.

For Mean expected value:-

$$F_{cr} = \frac{0.1561\,Et}{r(\sin\alpha)^{1/3}} \quad \text{- - - - - - - - - - -} \quad C9.15$$

For probability = 90 percent and .95 confidence factor:

$$F_{cr} = \frac{0.1138\,Et}{r(\sin\alpha)^{1/3}} \quad \text{- - - - - - - - - - -} \quad C9.16$$

For 99 percent probability and .95 confidence factor:

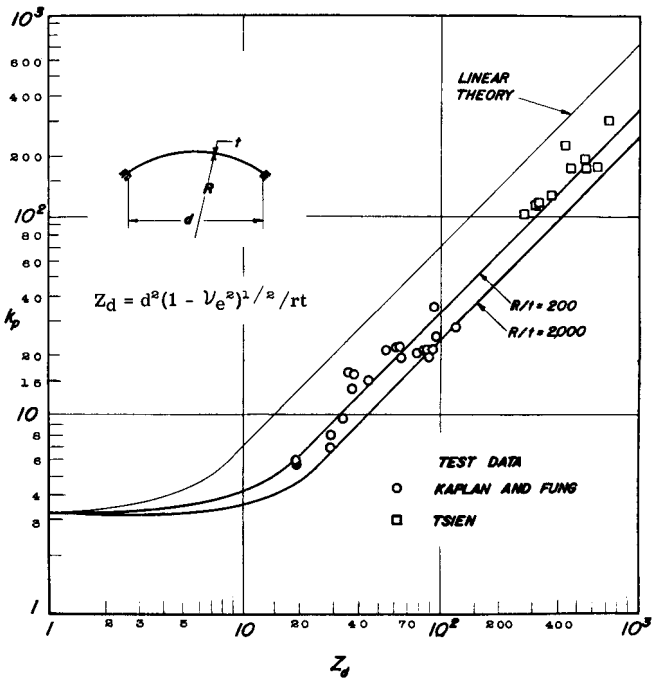

Fig. C9.8 (Ref. 2) Test Data for Spherical Plates under External Pressure Compared with Empirical Theory.

$$F_{cr} = \frac{k_p \pi^2 E}{12(1 - \nu_e^2)} \left(\frac{t}{d}\right)^2$$

$$F_{cr} = \frac{0.0908\ Et}{r(\sin \alpha)^{1/3}} \qquad \text{C9.17}$$

For explanation of angle α see Fig. A.

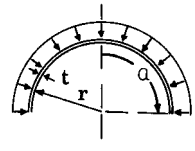

Fig. A

When $\alpha = 90$ or a hemisphere $(\sin \alpha)^{1/3}$ is one.

The test range covered was

$70 \leq \alpha \leq 90^0$

$175 \leq r/t \leq 2000$

The equations are for buckling stresses below the proportional limit stress of the material.

PROBLEMS

(1) The fuselage cross-section as given in Fig. C9.6 of example problem 1 is changed by increasing the skin thickness to .05 inches. The design loads are increased to the following values:

$M_y = 700{,}000$ in. lb., $V_z = 6040$ lbs.

$T = 245{,}000$ in. lb.

Will any of the skin panels buckle under this combined loading.

(2) The fuselage section as given in problem 1 above is subjected to an internal outward pressure of 6 psi. What would be the compressive and shear buckling stress for the skin panels under this internal pressure.

REFERENCES

(1) Schildcrout & Stein. Critical Combinations of Shear and Direct Axial Stress for Curved Rectangular Panels. NACA T.N. 1928.

(2) Gerard & Becker. Handbook of Structural Stability. Part III. Buckling of Curved Plates and Shells. NACA T.N. 3883.

(3) Rafel & Sandlin. Effect of Normal Pressure on the Critical Compression and Shear Stress of Curved Sheet. NACA WRL-57.

(4) Rafel. Effect of Normal Pressure on the Critical Compressive Stress of Curved Sheet. NACA WRL-258.

(5) Brown & Hopkins. The Initial Buckling of a Long and Slightly Curved Panel under Combined Shear and Normal Pressure. R&M No. 2766, BRITISH ARC (1949).

(6) Shanley F.R. Simplified Analysis of General Instability of Stiffened Shells in Pure Bending. Jour. of Aero. Sciences, Vol. 16, Oct. 1949.

(7) Becker H. Handbook of Structural Stability. Part VI. Strength of Stiffened Curved Plates and Shells. NACA T.N. 3786.

CHAPTER C10

DESIGN OF METAL BEAMS. WEB SHEAR RESISTANT (NON-BUCKLING) TYPE.

PART 1. FLAT SHEET WEB WITH VERTICAL STIFFENERS.

C10.1 Introduction.

The analysis and design of a metal beam composed of flange members riveted or spot-welded to web members is a frequent problem in airplane structural design. In this chapter, the general theory for beams with non-buckling webs is considered. In Chapter C11, the more common case where the beam web wrinkles and goes over into a semi-tension field condition is considered. The advantages and disadvantages of the non-buckling and the buckling or semi-tension field web are discussed in Chapter C11. The general beam theory as given in this chapter is basic to that given in Chapter C11, thus the student should study this chapter before C11.

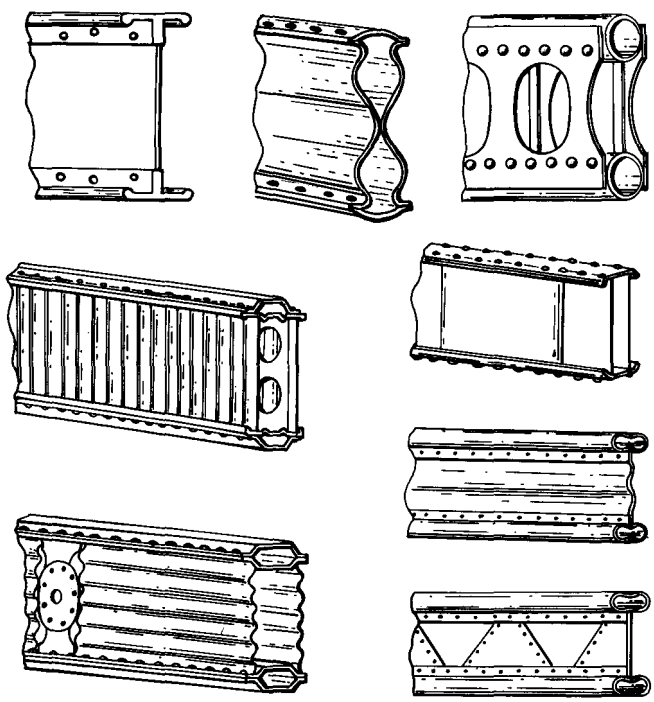

Fig. C10.1 (From ACI Circular No. 622)

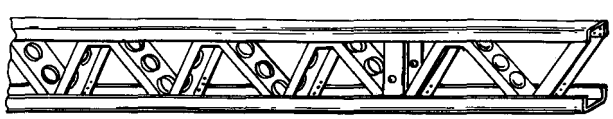

Fig. e Truss type of beam with channel section flange member.

C10.2 Flange Design.

For strength/weight efficiency, the beam flange should be designed to make the radius of gyration of the beam section as large as possible, and at the same time maintain a flange section which will have a high local crippling or crushing stress. Furthermore, the flange sections for large cantilever beams which are frequently used in wing design should be of such shape as to permit efficient tapering or reducing of the section as the beam extends outboard. This tapering of section should also be considered from a fabrication or machining standpoint. The most efficient flange from a strength/weight standpoint might be very costly or entirely impractical from a fabrication and assembly standpoint.

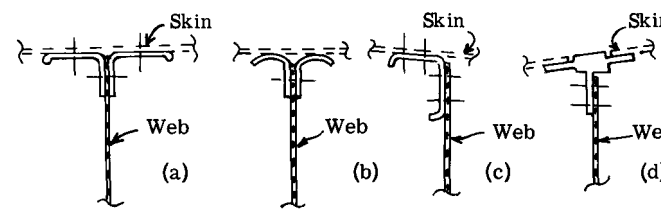

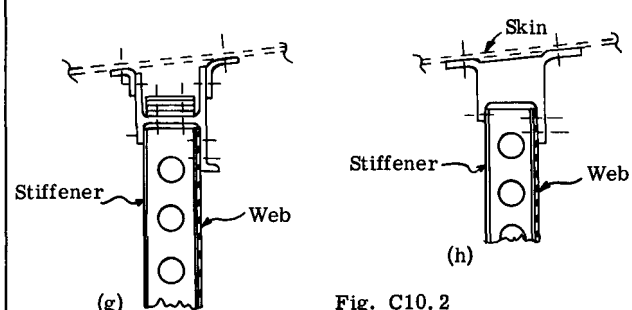

Fig. C10.2

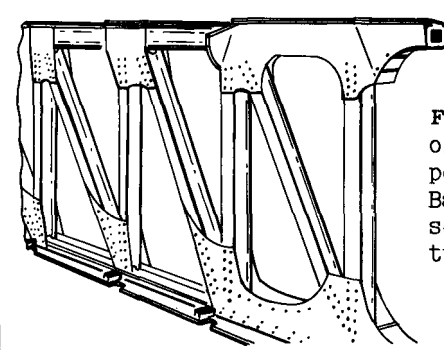

Fig. f Wing beam of Boeing "Clipper" flying boat. Basic flange section is square tube.

Fig. C10.1 shows a few typical metal beam sections for externally braced wings. Such beams must carry large axial compressive loads as well as bending loads. Fig. C10.2 shows typical beam flange sections for cantilever

metal covered wing construction. Sections (a), (b), (c) and (d) are typical beam flange sections for wide box beams where additional stringers or skin stiffeners are also used to provide bending resistance. These flange sections are generally of the extruded type although such sections as (b) and (c) are frequently made from sheet stock. These flange sections are almost always used with a beam web composed of flat sheet, which is stiffened by vertical stiffeners riveted or spot-welded to the web or stiffened by beads or flanged lightening holes.

Figs. (e) and (f) illustrate two types of flange sections used in truss beams which land themselves readily to connection with truss web members. Beam flange sections (g) and (h) are typical sections for wing construction in which no additional spanwise stringers are used. In section (g) tapering of sectional area is provided by first omitting the reinforcing plates, and then gradually decreasing the extruded shape by machining until only a small angle remains. In section (h) a gradual decrease in section area is produced by milling out the center portion to form an H section and then cutting this section down finally to a simple angle.

C10.3 Allowable Flange Design Stresses

The calculating of the stresses in the beam flanges is in general not a difficult procedure if the usual assumptions are made in the flexure theory. The question as to what flange stresses will cause failure is the difficult one from a theoretical standpoint. The only sure way to determine the design allowable is to make sufficient static tests of specially designed test beams.

For beam sections as illustrated in Fig. C10.1, the following tests are usually necessary for forming the basis of design allowable stresses.

(1) A test subjecting the beam to pure bending.

(2) A test of a short length of beam in bending so that failure will occur in web instead of flange.

(3) A test of a short length of beam in pure compression to obtain local crippling strength.

(4) Several tests of beams in combined bending and compression, using different ratios of bending to compressive loads.

Enough data from the above tests can usually be obtained to give rather complete allowable stress curves for the design of the beam. For the approximate design of beam flanges, the method given in this chapter can be used.

The beam flange sections (a), (b), (c) and (d) of Fig. C10.2 are stabilized by the sheet covering and also by the beam web; thus compressive tests of short lengths to obtain crippling stress, and a test of a length equal to the wing rib spacing should give sufficient information on which to base design allowables. Several lengths of the flange section for the truss type of beam should be tested in compression to obtain the column curve since the distance between panel points of the truss will vary.

Before designing any test beams, the structural designer would like to know approximately what his proposed beam flange sections will carry from a stress standpoint, since it is desirable to make test specimens closely approximate to the sections to be finally used in the completed structure. For most of the sections of Fig. C10.2, the ultimate stresses can be calculated approximately by the methods of Chapter C7. For heavy sections similar to (g) and (h) of Fig. C10.2, where the ultimate stresses fall far above the yield strength of the material, and where some parts of the section buckle before other parts, and also where two different kinds of material are used in the same flange section, a logical procedure in trying to calculate ultimate strength of the section would be to make use of the stress-strain diagrams of the materials.

C10.4 Use of Stress-Strain Diagrams in Computing Beam Flange Bending Allowable Design Stresses.

In the beam type of wing construction, where the flange material is concentrated over the web members instead of distributed over the surface in the form of stringers, the allowable ultimate compressive stress which can be developed is considerably above the yield strength of the material since the flange is composed of a section with thick elements which promotes a high crippling stress and since the beam flange is stabilized in both vertical and horizontal directions by the web and skin covering respectively, the influence of column action is negligible. Fig. (a) illustrates this type of beam. The general flexure formula assumes that stress is proportional to strain which is correct for stresses below the proportional limit of the beam material, but the ultimate resisting stresses for the flange of a beam such as in Fig. (a) is far above the proportional limit, thus the actual stress distribution is more like the dashed line in Fig. (b) instead of the triangular distribution as assumed in the common beam theory. Thus to obtain beam fiber stresses above the proportional limit, it is necessary to consider strain and the stress which accompanies such a strain, which relation-

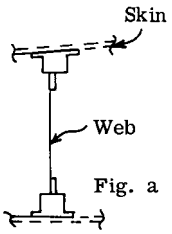

Fig. a

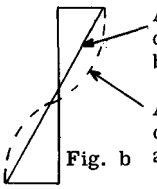

Fig. b

ship can be obtained from the stress-strain diagram of the material. A straight line distribution for strain, that is, plane sections remains plane after bending is a reasonable one, and verified by tests.

In a beam in bending, one side is in tension and the other in compression. The tensile and compressive stress-strain diagrams for materials like aluminum alloy are different above the proportional limit, and the same unit strain will cause different stresses on the two sides of the beam. In frequent cases of large beam design, the beam flange may be composed of two kinds of material and certain portions for attaching to skin or web may buckle before the ultimate strength of the section as a whole is obtained. The solution for the ultimate internal resisting moment for such a beam requires that consideration be given to the stress-strain diagram of the various materials and units making up the beam section. This general method of approach in studying the ultimate internal resisting moment of a beam section can best be explained by an example problem.

Example Problem

Fig. C10.3 shows the cross-section of a beam in a metal covered wing. The main flange members are composed of heavy 24ST extruded shapes. The extrusions are reinforced by 24SRT sheet strips. The beam web is made from 24ST alclad material. The problem is to calculate the ultimate internal resisting moment for this beam section.

Fig. C10.4 shows the stress-strain diagram for these various materials. The 1/8 inch thick outstanding legs of the extrusions act as a plate stiffened on three sides and free on the fourth. These legs will buckle at a stress of 35,000 psi in compression as determined by the methods given in Chapter C7. The stress-strain diagram of the two outstanding legs will be horizontal at 35,000 psi as shown in Fig. C10.4. Although the legs buckle, they will tend to hold the buckling stress under farther flange strain. In Fig. C10.5, each beam section has been broken down into narrow horizontal strips designated from (a) to (w). Only that portion of the web in way of flange has been considered in this example. Fig. C10.5a shows the strain distribution assumed for the trial solution. A heavy aluminum alloy section in compression will usually fail at a strain between .008 to .01 inch per inch if column failure is prevented. In Fig. C10.5a, the compressive unit strain at the upper beam fiber has been taken as .008"/". The neutral axis of the section has been assumed at 1.25" above center line of beam. Taking zero strain at this point the beam section strain diagram is as shown in Fig. C10.5a.

For equilibrium the total compressive bending stresses above the neutral axis must equal the total tensile bending stresses below the neutral axis.

Tables C10.1 and C10.2 give the detail calculations for calculating the resisting moment. The bending unit stress in column (5) is obtained from Fig. C10.4 using the unit strain in column (4). If the summation of column (6) in each Table is the same, the assumed location of the neutral axis is correct. The total ultimate resisting moment for this section equals 1032000 + 1360110 = 2393000 in. lb. Using the ordinary beam formula with properties about the geometric neutral axis as given in Fig. C10.3 and taking extreme fiber stresses of 46000 and 52000 psi which correspond to stresses as per strain diagram of Fig. C10.5a, the internal resisting moment would equal, M = f I/c = 46000 x 436/969 = 2070000 in. lb. as compared to 2392000 in. lb. by the more logical solution, which is a difference of 16 percent. The discrepancy would still be larger if the outstanding leg (a) did not buckle, since the more exact solution only allowed 35000 psi on this element whereas the general beam formula stresses it to 46000 psi.

Trial and Error Approach

The location of the neutral axis is unknown, thus the calculations in Tables C10.1 and 2 are for the final assumption which is the true location of the neutral axis. The general procedure would be as follows: Assume neutral axis as center line axis of beam, and find total axial load on each side of axis. The results will usually show excess load on one flange. For the next trial move neutral axis so as to give excess load on other flange. Plot the results as indicated in Fig. C10.5b to obtain true location of neutral axis and then make final calculations as illustrated in Tables C10.1 and 2.

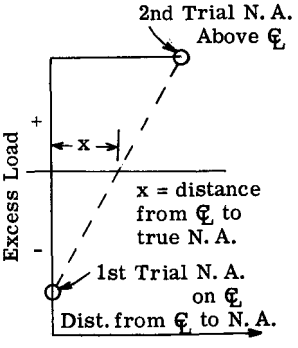

Fig. C10.5b

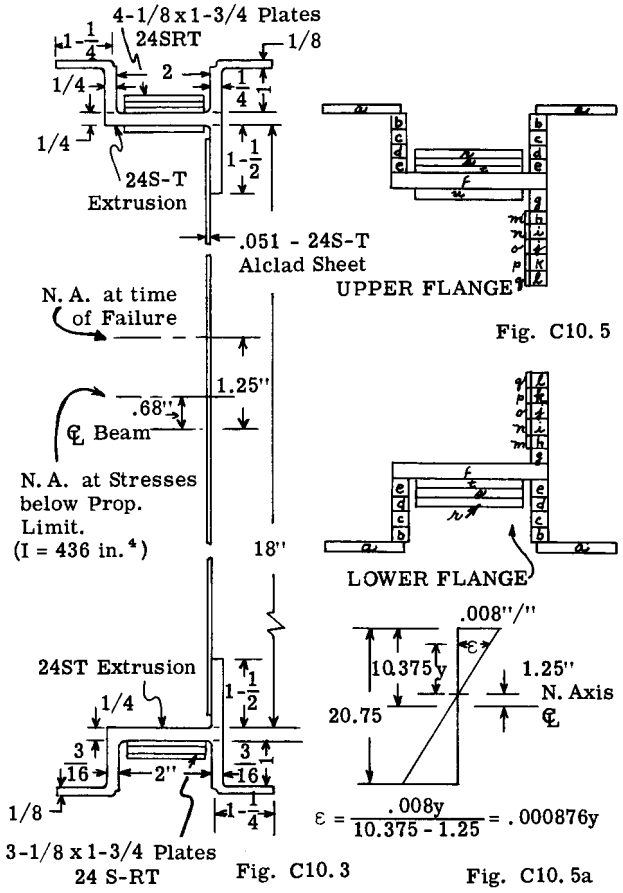

Fig. C10.3 Fig. C10.5a

Fig. C10.5

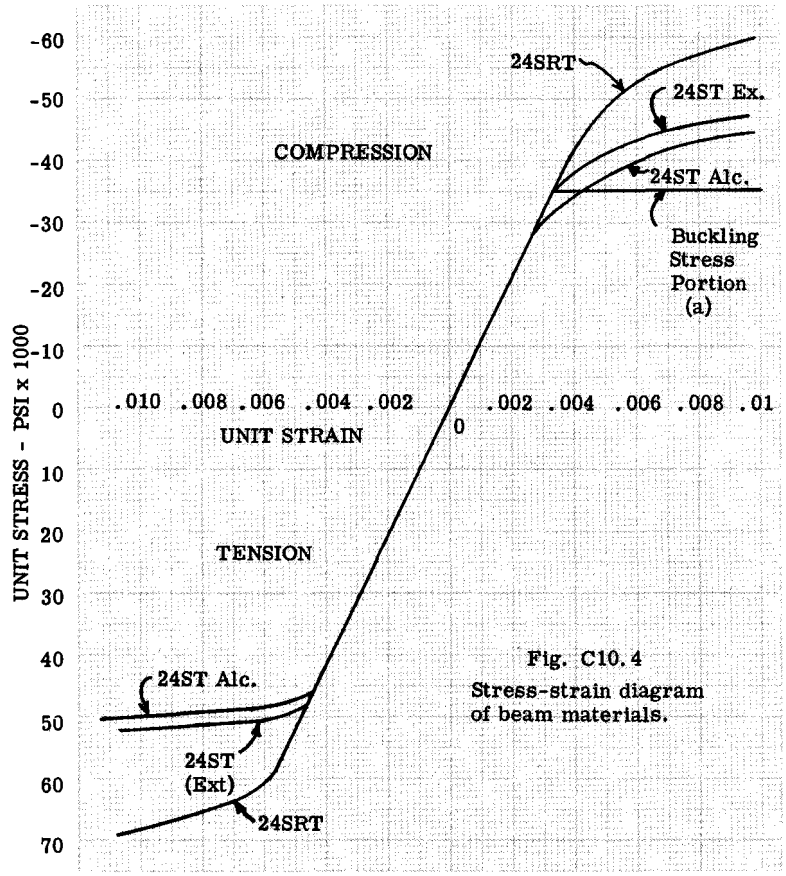

Fig. C10.4
Stress-strain diagram of beam materials.

Table C10.1

Resisting Moment of Comp. Bending Stresses about Neutral Axis							
Strip Port.		A = area of strip	y = area to strip from N.A.	Unit strain ξ = .00876y	f_c=unit stress	Load on Strip = f_c A	Mom. about N.A. = f_c A y
24ST Extru.	a	.3125	9.0625	.00795	-35000*	10940	99200
	b	.1250	8.875	.00778	-45800	5725	50800
	c	.1250	8.625	.00756	-45400	5660	48900
	d	.1250	8.375	.00734	-45150	5640	47200
	e	.1250	8.125	.00712	-45000	5620	45700
	f	.6250	7.875	.00691	-44700	27900	220000
	g	.0625	7.625	.00668	-44300	2770	21150
	h	.0625	7.375	.00646	-44000	2750	20300
	i	.0625	7.125	.00625	-43300	2710	19300
	j	.0625	6.875	.00603	-43100	2695	18610
	k	.0625	6.625	.00581	-42700	2670	17700
	l	.0625	6.375	.00559	-42000	2625	16720
24ST Alc	m	.01275	7.375	.00646	-40700	519	3830
	n	.01275	7.125	.00625	-40100	511	3640
	o	.01275	6.875	.00603	-39700	506	3480
	p	.01275	6.625	.00581	-39000	497	3290
	q	.01275	6.375	.00559	-38600	492	3130
24S-RT	r	.21875	8.3125	.00728	-55500	12230	101800
	s	.21875	8.1875	.00718	-55200	12080	98700
	t	.21875	8.0625	.00706	-55100	12050	97100
	u	.21875	7.6875	.00674	-54400	11900	91450
TOTALS						128490	1032000

*Buckling stress

Table C10.2

Resisting Moment of Tensile Bend. Stresses about Neutral Axis							
Strip Port.		A = area of strip	y = arm to strip	Unit strain ξ = .000876y	f_t=unit stress	Load on Strip = f_t A	Mom. about N.A. = f_t A y
24ST Extru.	a	.31250	11.5625	.01014	52050	16280	188000
	b	.09375	11.375	.00997	52000	4870	55450
	c	.09375	11.125	.00976	51950	4865	54100
	d	.09375	10.875	.00954	51900	4860	52900
	e	.09375	10.625	.00931	51800	4855	51600
	f	.59375	10.375	.00910	51750	30700	318000
	g	.0469	10.125	.00887	51700	2425	24550
	h	.0469	9.875	.00866	51600	2420	23900
	i	.0469	9.625	.00844	51500	2415	23250
	j	.0469	9.375	.00822	51400	2410	22600
	k	.0469	9.125	.00800	51300	2405	21950
	l	.0469	8.875	.00778	51200	2400	21300
24ST Alc	m	.01275	9.875	.00866	49600	633	6250
	n	.01275	9.625	.00844	49400	629	6050
	o	.01275	9.375	.00822	49300	628	5890
	p	.01275	9.125	.00800	49200	627	5720
	q	.01275	8.875	.00778	49100	625	5500
24 SRT	r	.21875	10.8125	.00948	67500	14770	159600
	s	.21875	10.6875	.00936	67300	14720	157200
	t	.21875	10.5625	.00926	67100	14700	156300
TOTALS						128237	1360110

C10.5 Flange Strength (Crippling).

In many cases of beam design, the flange is braced laterally because it is part of a cell construction and the sheet covering which is fastened to the beam flange provides a continuous lateral bracing to the flange or prevents lateral bending-column action for the beam flange. The beam web prevents column bending of the flange in the web direction, thus the flange fails by local crippling action and the crippling stress is determined by the methods of Chapter C7. In many cases the beam loads are relatively small and thus the area required for the flange may be relatively small, which means a flange shape with elements of small thickness, thus the failing local strength may be in the elastic stress range or relatively low.

In many cases, such as a frame in a fuselage, the inner flange of the frame cross-section is free from a lateral brace, thus provisions must be taken to brace the flange laterally or the flange must be designed for lateral column action. This subject is discussed further in Chapter D3.

C10.6 Web Strength. Stable Webs.

A stable web beam is one that carries its design load without buckling of the web, or in other words it remains in its initially flat condition. The design shear stress is not greater than the buckling shear stress for the individual web panels and the web stiffeners have sufficient stiffness to keep the web from buckling as a whole.

In general, a thin web beam with web stiffeners designed for non-buckling is not used widely in flight vehicle structures as its strength/weight ratio is relatively poor. In built-in or integral fuel tanks, it is often desirable to have the beam webs and the skin undergo no buckling or wrinkling under the design loads in order to give better insurance against leaking along riveted web panel boundaries.

The student should realize that the buckling web stress is not a failing stress as the web will take more before collapse of the web takes place, thus in general the web is not loaded to its full capacity for taking load and the web stiffeners are only designed for sufficient stiffness to prevent web buckling and not for the full failing strength of the web.

Equation for Web Buckling Shear Stress

Equation C5.5 of Chapter C5 gives the buckling stress of a flat sheet panel under shear loads. The equation is

$$F_{s_{cr}} = \frac{\eta_s \pi^2 k_s E}{12(1-\nu_e^2)} \left(\frac{t}{b}\right)^2 \quad \text{- - - - - - - - (C10.1)}$$

The curves of Fig. C5.13 and C5.11 of Chapter C5 are used to solve this equation and the reader should refer to Art. C5.8 of Chapter C5 for a review of sheet buckling under shear loads.

Equation for Web Buckling Bending Stress

If the web does not buckle it will be subjected to longitudinal bending stresses of compression and tension with zero stress at the beam neutral axis. Thus in general, the beam is subjected to a combined shear and bending stress system.

Equation C5.7 of Chapter C5 gives the bending buckling stress. It is,

$$F_{b_{cr}} = \frac{\eta_b \pi^2 k_b E}{12(1-\nu_e^2)} \left(\frac{t}{b}\right)^2 \quad \text{- - - - - - - - (C10.2)}$$

In solving this equation, Figs. C5.15 and C5.8 of Chapter C5 are used.

Buckling of Web Panels Under Combined Shear and Bending

From Art. C5.11 of Chapter C5, the interaction equation for a flat sheet panel under combined bending and shear is,

$$R_b^2 + R_s^2 = 1 \quad \text{- - - - - - - - - - - - - (C10.3)}$$

The expression for margin of safety is,

$$M.S. = \frac{1}{\sqrt{R_b^2 + R_s^2}} - 1 \quad \text{- - - - - - - - (C10.4)}$$

C10.7 Web Bending and Shear Stresses.

Since the web is designed not to buckle under the design loads, the web will be effective in taking bending stresses and the following well known equation applies.

$$f_b = My/I_x \quad \text{- - - - - - - - - - - - - - - (C10.5)}$$

where I_x is the moment of inertia of the beam section and the web is included.

In Art. A14.3 of Chapter A14, the well known flexural shear stress equation was derived, namely,

$$f_s = \frac{V}{Ib} \int ydA \quad \text{- - - - - - - - - - - - - (C10.5)}$$

Since the term $\int ydA$ is maximum for a section at the neutral axis, the shearing stress in a beam will be maximum at the neutral axis. In general, the webs of aircraft beams are relatively thin; thus the term $\int ydA$ for the web is quite small so that the shearing stress intensity over the web is approximately uniform. Thus a simple formula $f_s = V/hb$ has been widely used for calculating the maximum web shearing stress. In this equation h is a distance which will make the shear stress f_s check the maximum value of the shear stress as given by equation C10.5.

A simple consideration of the internal stresses on a small element cut from a beam in bending and shear will indicate what value of h to use in the simplified shear equation $f_s = V/hb$.

Fig. C10.6a shows a beam element of length dx cut from a beam which is subjected to a

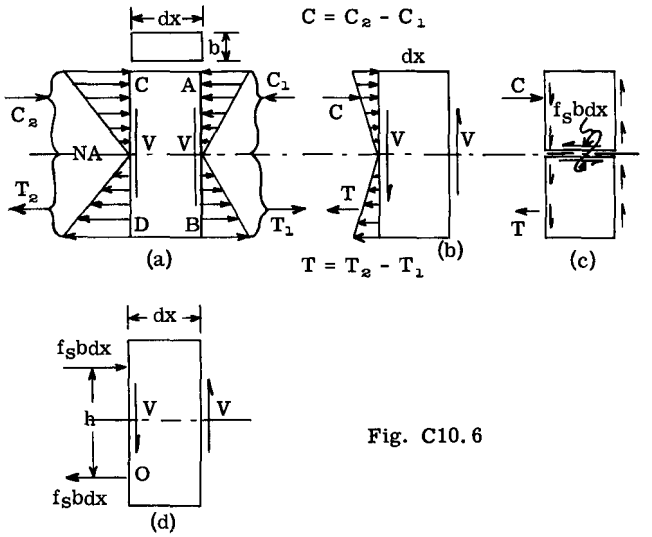

Fig. C10.6

bending moment which produces compression on the upper portion. The bending moment on section (AB) is M and on section (CD) M + ΔM, thus the vectors representing the stress on face (CD) are drawn longer than on face (AB). The beam element is also subjected to a total shear force V on each face. C_2 and C_1 represent the resultant of the total compressive forces on each face and T_2 and T_1 the resultant of the tensile stresses. Fig. (b) shows the same free body but with the tensile and compressive stresses on each face replaced by a simple force C and T which tends to move the block with the same results as the system of Fig. (a). In Fig. (c) the beam element of Fig. (b) has been cut along the neutral axis, and a force applied to the cut faces equal to f_s bdx, where f_s equals the horizontal shear stress intensity.

Writing the equilibrium equation, that the sum of the horizontal forces on the upper portion must equal zero, we obtain

$$C - f_s\, bdx = 0, \text{ hence } C = f_s\, bdx$$

and likewise for the lower - $T + f_s\, bdx = 0$, hence $T = f_s\, bdx$.

Fig. (d) shows the free body of Fig. (b), but with C and T replaced by their above equivalent values.

Taking moments about point (O)

$$M_O = f_s\, bdx \cdot h - Vdx = 0, \text{ hence}$$

$$f_s = \frac{V}{bh} \qquad \text{(C10.6)}$$

Thus to obtain a value f_s equal to the maximum value given by equation (a) use an effective arm (h) equal to the distance between the bending stress centroids. For a rectangular section the effective arm is obviously equal to 2/3 the beam height, but for the common beam sections as illustrated in Figs. C10.11 or C10.12, the distance between bending stress centroids is not so obvious particularly if the web is considered effective in bending. A close approximation of the effective arm (h) and a procedure which is common practice is to assume (h) equal to the distance between the centroids of the web-flange rivets. The student should take several example beam sections and check this assumption for (h) using Eq. (C10.6) against the exact values by Eq. (C10.5).

Some structural designers make assumptions as to the proportion of the total vertical beam shear which is carried by the beam web. For example, it is sometimes assumed that the web takes the entire beam shear, or it may take only 90 percent. The percentage of the shear load carried by the web depends of course upon the size of the flange sections and the form of the web section. For example, in Fig. C10.7, the same flange is connected by a web which is attached to the flanges in two ways as illustrated in Figs. (a) and (b). In Fig. (a), the shear flow on portions (AB) and (CD) help resist the external shear, whereas the shear flow on these portions in Fig. (b) act in the same direction as the external shear load; thus causing the shear load on the web to be greater than the external shear load. (See Chapter A14 and A15 for general discussion of shear flow in open and closed sections).

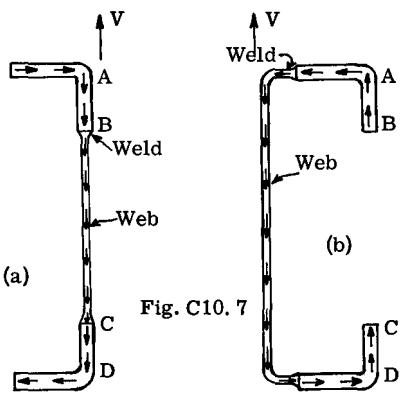

Fig. C10.7

C10.8 Shear Resistance Provided by Sloping Flanges.

A large majority of the beams in airplane wing and tail surfaces have sloping flanges because of the taper of the structure in both planform and thickness. This sloping of the beam flanges relieves the beam web of considering shear load and should not be neglected. Fig. C10.8 shows a beam (abcd) carrying a load system P_1, P_2, etc. The top flange is sloping as shown. If both flanges were extended, they would intersect at point (O).

Let M = bending moment at section (ac)

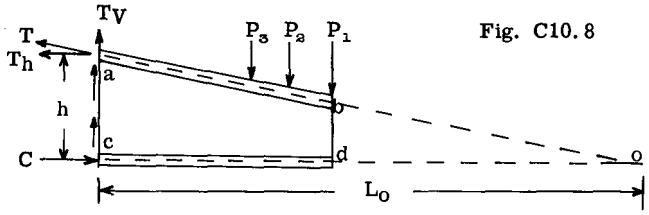

Fig. C10.8

Then $C = T_h = M/h$ (h = distance between flange stress centroids)

The vertical component T_V of the load T in the upper flange equals $T_h\ h/L_O$, but $T_h = M/h$, hence

$$T_V = \frac{M}{h}\frac{h}{L_O} = \frac{M}{L_O}$$

Let V_F = shear load carried by beam flanges

Then $V_F = M/L_O$ - - - - - - - - - - - - - - (C10.7)

Thus the shear component carried by the axial loads in the sloping flange members equals the bending moment at the section being considered divided by the distance from the section to the point of intersection (O) of the flanges.

The above derivation was based on the assumption that the entire resisting moment M was developed by the flanges. With the web effective in bending, the moment developed by the web should be subtracted from the total bending moment M.

Let $I = I_{Fl.} + I_{Web}$

The moment developed by web = $M\frac{I_{Web}}{I}$,

where

M = total bending moment on section

In airplane construction the centilever beam with sloping flange members is the common case, and the shear resistance by the flange axial loads is an important factor which should not be neglected if an efficient structure is desired from a strength-weight standpoint.

C10.9 Effect of Variable Moment of Inertia on Flexural Shear Stress Distribution.

The fundamental shear stress equation C10.5 as derived in Chapter A14 applies strictly to beams of constant moment of inertia. For airplane beams the common case is one with variable moment of inertia; thus the stresses obtained by equation C10.5 are incorrect, although the discrepancy in most cases is not large. The student should realize this fact in studying the shear flow picture in tapered wing structures. See Art. A15.15 of Chapter A15.

C10.9a Flange Discontinuities.

From a weight saving standpoint, it is necessary to taper flange sections in order to approach a beam of constant strength relative to the applied loads.

Fig. a illustrates how such tapering of the flange section may produce local eccentric flange loads. Between sections (1) and (2) the upper flange tapers in side view as shown which

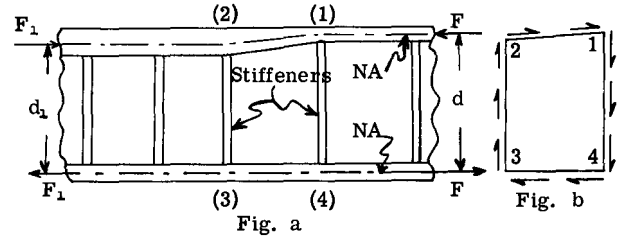

Fig. a Fig. b

displaces the flange neutral axis as shown. Assuming there is no change in bending moment over the beam portion as shown, the force F must be greater than F since resisting arm d is less than d. For equilibrium this moment due to F_1 and F not being colinear must be balanced in some manner. If the flanges are rigidly connected to web and stiffeners, this moment can be balanced by an additional shear stress on the web panel between points (1, 2, 3 and 4) as illustrated in Fig. b. Thus in cases of rather abrupt changes in flange sections which produce the eccentricity as illustrated the web and stiffeners should be checked for the additional shear flow load on the web. If such displacements in the flange neutral axis occur in the plan view, the skin covering should be investigated for the additional shearing stresses.

C10.10 Stiffener Size to Use with Non-Buckling Web.

A web stiffener is used to decrease the size of web panel; thus when buckling of the web starts, the stiffener tends to keep buckles from extending across the stiffener or causes the sheet to buckle in two panels instead of one. Mr. H. Wagner in a paper presented before a meeting of the A.S.M.E. in 1930 offered the following expression as the required moment of inertia of a stiffener to be used with a shear resistant web.

$$I_V = \frac{2.29d}{t}\frac{V\,h_W^{4/3}}{33\,E} \qquad \text{- - - - - - - - - - (C10.8)}$$

where

I_V = moment of inertia of stiffener

d = center line distance between stiffeners

h_W = depth of web plate

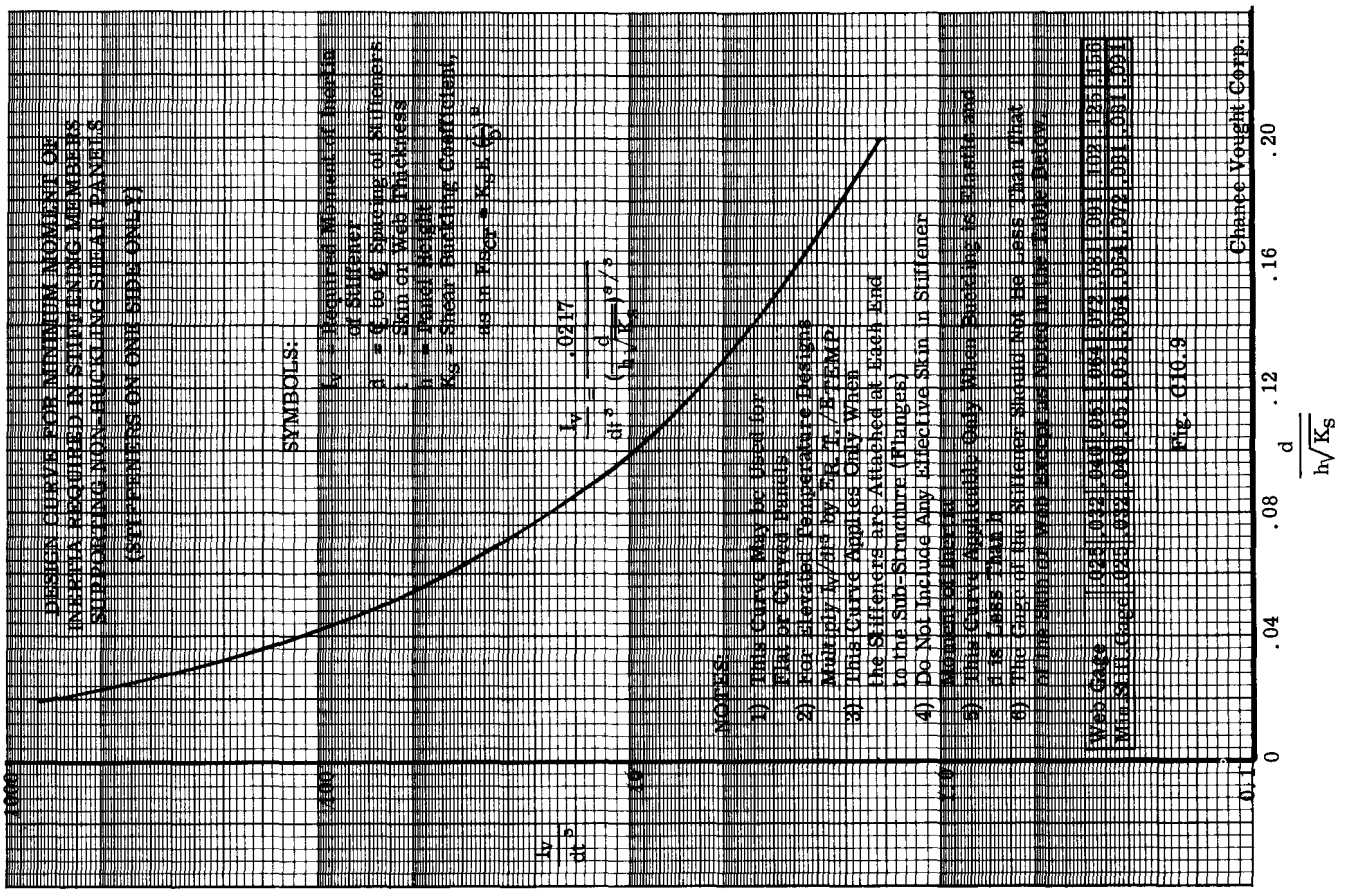

V = vertical shear at section

t = web thickness

E = modulus of elasticity

A more recent criteria for stiffener stiffness (I_V) for both flat and curved webs is given by the curve in Fig. C10.9. When the stiffener is used purely as such and not as a means to transfer a concentrated external load to the beam web, the question arises as to what is the minimum number of fasteners required in attaching the stiffener to the web. For non-buckling webs, two criteria are suggested:-

(1) The stiffener should be attached to the flange at each end.

(2) The rivet pitch (spacing) should according to (Ref. 1) be at the most equal to 1/4 times the stiffener spacing, or 1/4 the web height if this is smaller, in order to justify the assumption of simple support at the edges of the web panel. Normal practice uses more rivets.

C10.11 Notes on Beam Rivet Design.

Except for very small beam sections which may be extruded as one piece, the usual beam consists of separate web and flange members, fastened together by rivets, bolts, spot welding or continuous welding. In the design of such beams it is thus necessary to know what loads the rivets, bolts, etc., are subjected to in order to provide the proper connective strength. It is quite easy to substitute in simple formulas to find the loads on beam flange rivets, however, the student should be sure that he understands the fundamental beam action behind these formulas.

Fig. C10.10 illustrates a beam portion equal in length to the flange rivet pitch p. The beam section at (AA') is subjected to a bending moment M and M + ΔM at section (CC'). The bending stress distribution on the beam faces is indicated by the stress triangles. In this example section it will be assumed that the web takes no bending stresses.

Let P_F equal the total pull on the flange angles due to bending stresses at section AB due to bending moment M. Then total pull on flange angles at section CD due to a moment M + ΔM on beam section CC' equals $P_F + \Delta P_F$.

Under the action of these two forces the flange angles would move to the left, but this movement is prevented by the rivet which ties

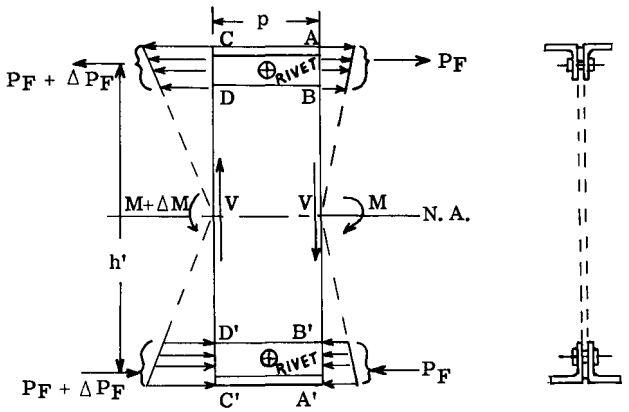

Fig. C10.10

the flange angles to the web. Thus load on rivet equals ΔP_F. The same reasoning applies to the rivet holding the bottom flange angles to the web.

The beam portion of Fig. C10.10 as a whole is in equilibrium under the bending stresses and the shear load V on each face.

Taking moments about the intersection of the lower flange bending load and the beam face CC',

$$\left[P_F - (P_F + \Delta P_F)\right] h' + Vp = 0 \quad ---- \quad (C10.9)$$

hence,

$$\Delta P_F = \frac{Vp}{h'} \quad ---------- \quad (C10.10)$$

Equation C10.10 says that the change in flange axial load in a distance p equals the vertical shear on beam times rivet pitch p divided by the distance between flange bending stress centroids. ΔP_F is also the horizontal shear flow produced by flange angles over a length of p. The horizontal shear (q) per inch due to flange would be

$$q = V/h' \quad ---------- \quad (C10.11)$$

The general expression for shear flow (see chapter A14) is,

$$q = \frac{V}{I} \int ydA \quad ---------- \quad (C10.12)$$

Eq. (C10.11) is easier to use since the terms I and $\int ydA$ of Eq. (C10.12) are not required, and the distance h can be estimated closely without calculation, and will be greater than the distance between the centroids of the flange areas.

Equation (C10.11) was derived on the assumption that the beam web took no bending stresses. In general this is not true or only partially true. With the web taking bending, equation (C10.9) would be wrong because the moment of the bending stresses on the web about our moment center is not included. Thus to make the simplified equation (C10.11), check the exact result as given by equation (C10.12), the distance (h) would have to be greater than the distance between the flange stress centroids. In fact, taking (h) equal to beam depth would not be far off from the results of equation (C10.12).

C10.12 Loads on Rivets Attaching Reinforcing Plates to Flange Member.

The beam flange is commonly composed of a main unit plus several reinforcing plates or parts which are held to the main unit by rivets or spot welds. Fig. C10.11 illustrates typical beam flanges. The basic section of the upper flange is reinforced by the plates (a) and (b), and the lower flange by the plates (c) and (d). The purpose of the rivets is to keep the reinforcing plates from sliding along the flange tee section due to the bending of the beam; thus making the plates effective in bending. This horizontal force tending to slide reinforcing plates and which is prevented by the rivets in shear is given by the fundamental shear flow equation (C10.12), namely

$$q = \frac{V}{I} \int ydA, \text{ which}$$

equals the horizontal shear per inch along the beam. To find the load or rivet section 1-1 of the upper flange of Fig. C10.11, the term $\int ydA$ equals the area of the plate (a) times the distance from its centroid to the neutral axis. For shear load on rivet at section (2-2), the term $\int ydA$ equals the area of plate (b) times distance to neutral axis. On the lower flange rivet section (3-3) is critical since both reinforcing plates are on same side, and the entire shear flow produced by plates (c) and (d) must be resisted by rivet section (3-3). The term $\int ydA$ would thus equal area of both plates times the distance to the neutral axis of the beam.

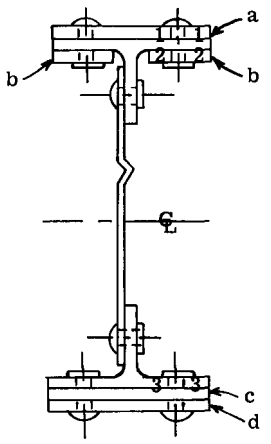

Fig. C10.11

A simplified method which yields good results is based on the relative areas of the units of the total flange. To design connection of flange to beam web, the total horizontal shear q produced by entire flange is always necessary and involves the use of the entire flange area in the shear flow calculation

$$q = \frac{V}{I} \int ydA.$$

The shear flow produced by a reinforcing plate is then taken as proportional to the area of the plate over the total flange area times the total flange shear flow. Using simplified equation (C10.11), we can write

$$q = \frac{V}{h'}\frac{a_p}{A_F} \quad \text{- - - - - - - - - - - - - - - - (C10.13)}$$

where

a_p = area of plates under consideration

A_F = total area of flange

q = load per inch on rivet

V and h' same as explained before

For rivet loads in beams with sloping flanges the shear V is the net shear as explained before in discussing web shear stresses.

C10.13 Web Splices.

Usually in designing a sheet girder beam, it is necessary from a weight saving standpoint to use several web sheet thicknesses, which means web splices. Fig. C10.12 illustrates typical web splices. Fig. (a) is typical for a

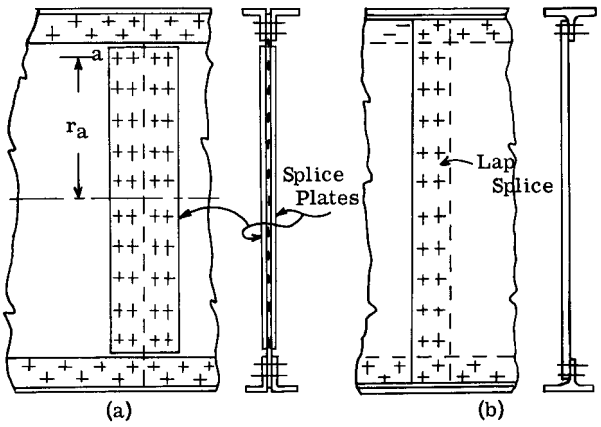

Fig. C10.12

comparatively heavy web which prevents joggling of web as in the case of Fig. (b). In the case of Fig. (b), the lap is usually made under a web stiffener which provides a support for the web in driving the rivets through the thin web sheets.

Loads on Web Splice Rivets

The web is subjected to shear loads and for stable webs, the web undergoes bending stresses.

For rivet design it is usually assumed that the web shear stress is constant over the depth. Thus the vertical component of load on each web splice rivet is the same or

$$R_V = \frac{V}{n} \quad \text{- - - - - - - - - - - - - - - - (C10.14)}$$

where

V = net web shear

n = number of rivets in splice. If butt splice, n, equals the number of rivets on one side of splice.

In bending the splice rivets must transfer the bending moment due to the bending moment M developed by the web. The largest rivet load on a rivet due to bending will be on the most remote rivet, e.g., rivet (a) at distance r_a from center of rotation of the rivet group. Then load on this rivet due to web moment equals

$$R_{m_a} = \frac{M_W r_a}{\Sigma r^2} \quad \text{- - - - - - - - - - - - - - - - (C10.15)}$$

where

Σr^2 = moment of rivet group which equals the sum of the squares of the distances of the rivets from the center of rotation of bolt group.

The resultant load on the critical rivet will equal the vector sum of the values of equations (C10.14) and (15).

Since in most cases only two rows of rivets are used in a web splice, a close approximation for the moment load on critical rivet can be written by using the vertical distances (y) to the rivets instead of the radial distances (r), the resulting force acting in the horizontal direction. Hence

$$R_{m_a} = \frac{M_W y_a}{\Sigma y^2} \quad \text{- - - - - - - - - - - - - - - - (C10.16)}$$

The resultant combined load on critical rivet is

$$R = \sqrt{R_{V_a}^2 + R_{m_a}^2} \quad \text{- - - - - - - - - - - (C10.17)}$$

The student should review Chapter D1 for more detailed information on rivet loads due to moment loads on riveted connections.

When the web of one beam is joined to that of another beam using shear "clips," a special problem may sometimes arise regarding the adequacy of the clips. This design problem is discussed in Chapter D3.

C10.14 Example Rivet Problem.

Fig. C10.13 shows the cross-section of a riveted beam. If the design vertical shear on the section is 3000 lb., check the strength of the riveted connection.

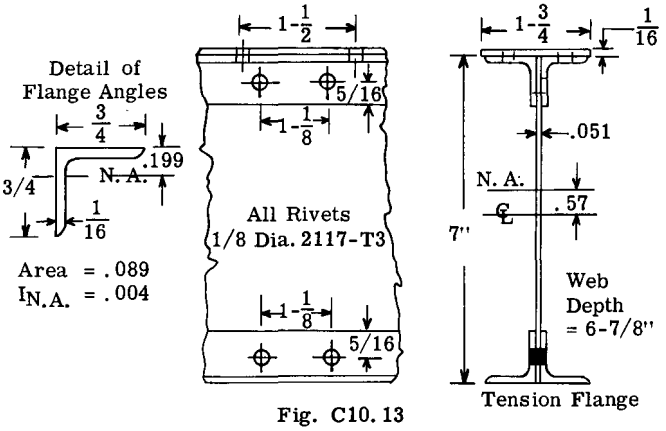

Fig. C10.13

Solution:

The loads on the rivets will be calculated by the "exact" and also by the simplified approximate equations.

The exact shear flow equation is

$$q = \frac{V}{I} \int ydA$$

The first step will be the calculation of the moment of inertia of the beam section about the neutral axis. The bending loads are such as to put the upper flange in compression.

The moment of inertia will be calculated about the centerline axis of the beam section and then transferred to the neutral axis. Table C10.3 gives the detailed calculations.

Table C10.3

Part	Area (A)	y	Ay	Ay^2	I_o*	$I = Ay^2 + I_o$
Upper angles	.1780	3.301	.588	1.94	.008	1.948
Upper reinforcing plate	.1093	3.531	.386	1.36	negl.	1.360
Web	.3510	0	0	0	1/12 x .051 x 6.875^3 = 1.38	1.380
Lower angles	.1780	-3.301	-.588	1.94	.008	1.948
Rivet hole lower flange	-.022	-3.062	.067	- .206	-	-0.206
SUM =	.7943		.453			6.43

$\bar{y} = \frac{\Sigma Ay}{\Sigma A} = \frac{.453}{.7943} = .57"$

$I_{N.A.} = 6.43 - .7943 \times .57^2 = 6.17$ in.^{4}

* I_o = moment of inertia about its own centroidal axis.

Rivet load on upper flange rivets which attach angles to web:

Rivet pitch = 1-1/8 inch

Horizontal shear load per 1-1/8 inch distance equals

$$q = 1.125 \frac{V}{I} \int ydA \text{ - - - - - - - - - - - - - - - (A)}$$

$\int ydA$ = first moment of flange area about N.A.

= angles = 2 x .089 x 2.731 = .486

Reinforcing plate = 1.75 x .0625 x 2.961 = .324

Total = .810

Substituting in equation (A)

$$q = 1.125 \times \frac{3000}{6.17} \times .810 = 443 \text{ lb.}$$

Shear flow by simplified equation $q = \frac{V}{h'}$

h' = beam depth = 7.062" (see Art. C10.10)

hence

$$q = 1.125 \times \frac{3000}{7.062} = 478 \text{ lb.}$$ which is conservative compared to 443 by exact expression.

The web is attached to angles by 1/8 diameter 2117-T3 aluminum alloy rivets and are acting in double shear.

From Chapter D1:

Double shear strength of 1/8 - 2117-T3 rivet = 2 x 388 x .870 = 675 lb.

Bearing strength on 2024-T3 - .051 web plate = 655 x 1.24 = 813 lb., thus shear is critical and

Margin of safety = $\frac{675}{443} - 1 = .52$ and with the approximate method the margin of safety would equal (675/478) - .1 = .41.

Check of Cover Plate Rivets:-

Rivet spacing = 1.5" with two rows of rivets.

By exact equation, load on two rivets

$$q = 1.5 \frac{V}{I} \int ydA$$

$$= 1.5 \times \frac{3000}{6.17} \times .1093 \times 2.961 = 236 \text{ lb.}$$

Load per unit = 236/2 = 118 lb.

By simplified formula:

$$q = \left(\frac{V}{h'} \frac{a_{plate}}{a_{flange}}\right) 1.5 = \left(\frac{3000}{7.062} \times \frac{.1093}{.2873}\right) 1.5$$

= 243 lb. = 122 lb./rivet.

The rivets are in single shear which is critical and equals 388 lb. as given above.

Hence margin of safety = $\frac{388}{118} - 1 = 2.28$

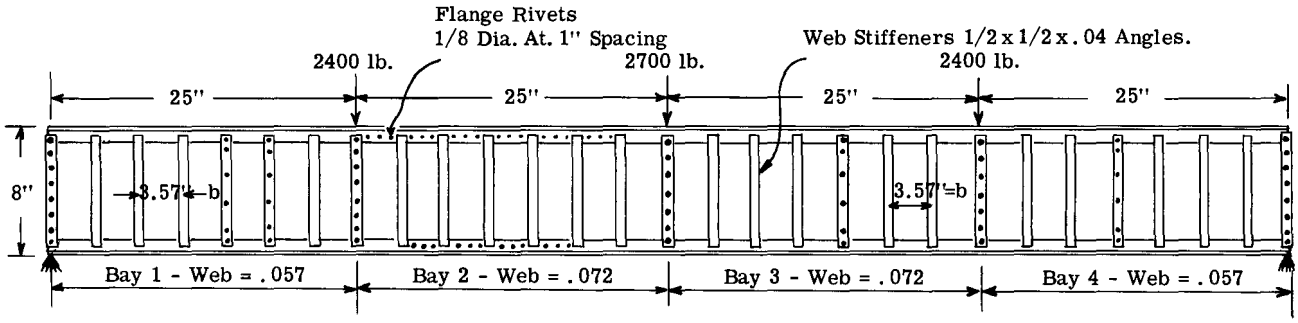

Fig. C10.14. Sketch of Beam (See Fig. C10.15 for Cross-section of Beam)

C10.15 Example Problem. Strength Check of Beam.

Fig. C10.14 shows a built up (I) section beam, simply supported and carrying its three concentrated loads as shown as the design load for the beam.

Check on Bending Strength of Beam

Since the beam cross-section is constant, the critical section is at the midpoint of the beam where the bending moment is:

$$M_{max} = 3750 \times 50 - 2400 \times 25 = 127500 \text{ in.lb.}$$

As indicated in Fig. C10.14, the beam is riveted to the sheet covering. On the upper flange which is in compression under the given loading, a certain effective sheet width will act with the beam flange. This effective sheet width depends upon the beam flange stress which is unknown as yet. As a preliminary value, the assumption that a width of skin sheet equal to 30 t as acting with each rivet line is a reasonable one. On the tension or bottom side, the entire skin sheet is effective or 2 inches to each side of the beam which is the distance half way to the first skin stiffener on each side.

Fig. C10.15 shows the details of the effective cross-section at midspan of the beam. Three rivet holes are assumed in the tension flange. Table C10.4 shows the calculations for the section properties, first about centerline reference axis, then transferred to the neutral axis.

Bending stress at midpoint of horizontal leg of upper angles:- $I_{N.A.} = 10.44$.

$f_b = My/I = 127500 \times 3.614/10.44 = 44200$ psi

The assumption of 30t = 0.75 inch as the skin effective width w will be checked. From Chapter C7,

$$w = 1.9t \sqrt{E/F_{ST}}$$

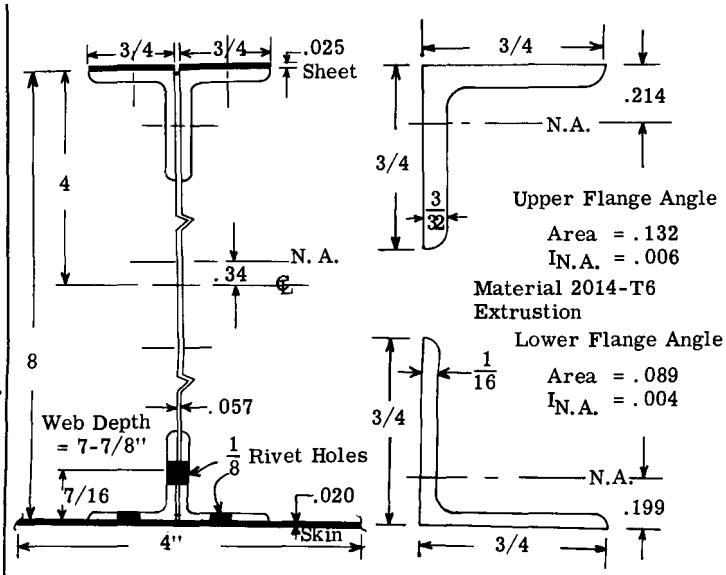

Fig. C10.15

Table C10.4

Part	Area A	y	Ay^2	Ay	I_o	$I_o + Ay^2$
Upper angles	.264	3.786	1.000	3.786	.012	3.798
Upper skin	.0375	4.012	0.1504	0.604	-	0.604
Web	.4490	0	0		1/12 x .072 x 7.875 = 2.31	2.310
Lower angles	.1780	-3.801	-0.676	2.570	.008	2.578
Lower skin	.080	-4.01	-0.321	1.290	-	1.290
Skin rivet holes	-.0206	-3.959	0.082	-0.323	-	-0.323
Web flange rivet holes	-.0227	-3.562	0.081	-0.288	-	-0.288
SUM	.9249		0.316			9.980
$\bar{y} = .316/.9249 = .34$						
$I_{N.A.} = 9.98 - .925 \times .34^2 = 9.87$ in.^{4}						
Section with .072 web:- $I_{N.A.} = 10,44$ (N. A. Location Same.)						

F_{ST} = flange compressive stress which 44200 psi. Then,

$$w = 1.90 \times .025 \sqrt{10{,}700{,}000/44200} = .74 \text{ in.}$$

Since 30t or 0.75 inches was assumed for w, the error is quite small and no revision is necessary.

Calculation of Allowable Failing Compressive Stress for Flange.

Since the flange is braced in two directions at right angles to each other by the skin and the web, column action is prevented and the allowable stress will be the crippling stress of the flange unit.

Chapter C7 gives methods of calculating the crippling stress. In this example problem the Needham method will be used and the crippling stress for a single angle will be calculated.

$$\frac{b'}{t} = (.75 - 3/64)/3/32 = 7.55$$

From Fig. C7.5 of Chapter C7, we obtain

$$F_{cs}/\sqrt{F_{cy}E_c} = .068$$

For 2014-T6 Ext., F_{cy} = 57000, E_c = 10,700,000.

Whence $F_{cs} = .068 \times \sqrt{57000 \times 10{,}700{,}000}$ = 53,000 psi

Since the angle legs which attach to web are riveted together, the crippling stress for these legs would be higher than for the angle legs connecting to the skin, thus the value of 53,000 is somewhat conservative.

The margin of safety for the upper flange is (53,000/44,200) - 1 = .20.

Check of Bottom Flange Tensile Strength:-

$$f_b = My/I = 127{,}500 \times 4.35/10.44 = 53{,}000 \text{ psi}$$

The material for lower skin = 2024-T3 sluminum alloy, which has an ultimate tensile strength of F_{tu} = 65,000 psi; and the extruded angles have a F_{tu} = 60,000. Thus M.S. (60000/53000) - 1 = .13.

As a practice problem for the student, the ultimate bending resisting moment should be calculated by the method of Article C10.4 and compared with the above margins of safety. The result would show a greater margin of safety.

Check of Web Buckling Stress

The maximum shearing stress occurs at the support point and equals 3750 lbs. The web thickness at this point is .057 and the web stiffener spacing is 3.57 inches. The maximum shearing stress on the web by the simplified equation is,

$f_s = V/ht = 3750/7.125 \times .057 = 9230$ psi

By the more exact equation,

$$f_s = \frac{V}{It}\int ydA = \frac{3750}{9.87 \times .057}(.264 \times 3.446 + .0375 \times 3.673 + .057 \times 3.6 \times 1.8) = 9450 \text{ psi}$$

Since the bending moment in the first web panel adjacent to beam end support is practically zero, the web can be considered as subjected to shear stress only.

The buckling stress is given by equation C10.1.

$$F_{s_{cr}} = \frac{\eta_s \pi^2 k_s E}{12(1 - e^2)}\left(\frac{t}{b}\right)^2$$

b = 3.57 inches

a = distance between rivet lines = 7.125

a/b = 7.125/3.57 = 2.0. Assuming simply supported edge conditions, we obtain k_s = 6.4 from Fig. C5.11 of Chapter C5.

$$F_{s_{cr}} = \frac{\pi^2 \times 6.4 \times 10{,}700{,}000}{12(1 - .3^2)}\left(\frac{.057}{3.57}\right)^2 = 15{,}800 \text{ psi}$$

This stress is below the proportional limit stress of the material so no plasticity correction is necessary or η_s = 1.0.

The margin of safety against buckling is therefore (15,800/9450) - 1 = .67. This value is somewhat conservative as boundary condition for web panel is no doubt larger than for simply supported, which condition was assumed.

Check of .057 Web at End of Bay 1.

The web will be more critical at this point because the beam is still subjected to an external shear load of 3750 lbs., plus a bending moment of 3750 x 23.22 = 87000 in.lb. at the midpoint of the end panel.

Since the web is clamped between the flange angles, buckling of the web will occur adjacent to the lower end of the upper flange angles or at a distance of 2.91 inches from neutral axis.

$f_b = My/I = 87000 \times 2.91/9.87 = 25600$

The bending buckling equation is,

$$F_{b_{cr}} = \frac{\pi^2 k_b E}{12 (1 - \nu_e^2)} \left(\frac{t}{b}\right)^2$$

b = 6.5 in. taken as distance between edges of flange angles since web is clamped in between flange angles. a = stiffener spacing = 3.57. The a/b = .55. From Fig. C5.15 of Chapter C5:-

k_b for simply supported edges = 36

k_b for clamped edges = 50

We will assume an average value of k_b = 43.

$$F_{b_{cr}} = \frac{\pi^2 \times 43 \times 10{,}700{,}000}{12 (1 - .3^2)} \left(\frac{.057}{6.5}\right)^2 = \underline{32200} \text{ psi}$$

The shear stress at this section will be same as at support since the external shear load is the same. Thus f_s = 9450 and $F_{s_{cr}}$ = 15800.

The interaction equation for combined bending and shear is,

$$R_b^2 + R_s^2 = 1$$

$$R_b = f_b/F_{b_{cr}} = 25600/32200 = .795$$

$$R_s = f_s/F_{s_{cr}} = 9450/15800 = .598$$

$$\text{M.S.} = \frac{1}{\sqrt{R_b^2 + R_s^2}} - 1 = \frac{1}{\sqrt{.795^2 + .598^2}} - 1$$

M.S. = .01

Check of .072 Web at Centerline of Beam

The bending moment at the midpoint of the web panel adjacent to the beam centerline is 123,200 in. lb. The shear load on the panel is 1350 lb.

$f_b = My/I = 123200 \times 2.91/10.44 = 34200$ psi

$$F_{b_{cr}} = \frac{\pi^2 \times 43 \times 10{,}700{,}000}{12 (1 - .3^2)} \left(\frac{.072}{6.5}\right)^2 = 51500 \text{ psi}$$

This value is in the inelastic stress range so correction must be made for plasticity. The curves of Fig. C5.8 of Chapter C5 will be used. For 2024-T3 sheet, $F_{o.7}$ = 39000 and n = 11.5.

The value of the lower scale parameter in Fig. C5.8 will be $F_{b_{cr}}/F_{o.7}$ = 51,500/39000 = 1.32. From Fig. C5.8 for n = 11.5 we read $F_{b_c}/F_{o.7}$ = .93. Therefore, $F_{b_{cr}}$ = 39000 x .93 = <u>36300</u> psi.

The shear stress is,

$$f_s = \frac{V}{It} \int ydA = \frac{1350}{10.44 \times .072}(1.51) = \underline{2710} \text{ psi}$$

$$F_{s_{cr}} = \frac{\pi^2 \times 6.4 \times 10{,}700{,}000}{12 (1 - .3^2)} \left(\frac{.072}{3.57}\right)^2 = 25300 \text{ psi}$$

R_s = 2710/25300 = .107

R_b = 34200/36300 = .94

$$\text{M.S.} = \frac{1}{\sqrt{.107^2 + .94^2}} - 1 = .01$$

Check of Stiffness of the Web Stiffeners.

The web is stiffened by 1/2 x 1/2 x .04 angles on one side of the web. From Equation (C10.8), the moment of inertia required of web stiffener to prevent web buckling is,

$$I_{ST} = \frac{2.29d}{t} \left(\frac{V h_w}{33 E}\right)^{4/3}$$

$$= \frac{2.29 \times 3.57}{.057} \left(\frac{3750 \times 7.875}{33 \times 10{,}700{,}000}\right)^{4/3}$$

$$= .00050$$

The moment of inertia of stiffener cross-section is .00094, thus stiffness is satisfactory.

The required moment of inertia will also be checked using curves in Fig. C10.9. The lower scale parameter in Fig. C10.9 is $d/h \sqrt{k_s}$ where k_s as used in buckling equation must be multiplied by $\pi^2/1 - .3^2 = .905$. Thus,

$d/h \sqrt{k_s} = 3.57/7.125 \sqrt{6.4 \times .905} = .208$

From Fig. C10.9 we read 1.1 for I_V/dt^3. Whence $I_V = 1.1 \times 3.57 \times .057^3 = .000735$. (Stiffener O.K.).

Check of Rivets Attaching Web to Flange Angles.

End Bay. V = 3750 lb., t = .057

The horizontal shear load q per inch by approximate formula C10.11 is

$q = V/h' = 3750/8 = 468$ lb. per inch

By the most exact C10.12 equation,

$$q = \frac{V}{I} \int ydA = \frac{3750}{9.87} (.264 \times 3.446 + .0375 \times 3.673)$$

q = 398

The single shear strength of 1/8 diameter rivets made from 2117-T3 aluminum alloy is 388 lbs. Since rivets are in double shear and 1 inch spacing, rivet shear strength is 2 x 388 = 776 lbs. versus the design load of 398 lbs.

The bearing strength of a 1/8 diameter rivet on .057 web is 790 lbs. as against load

of 398 lb. Thus rivets could be spaced further apart as margin of safety is rather large.

The rivets attaching the skin to the upper flange should be spaced to prevent inter-rivet buckling of the skin, since the skin was assumed effective in computing the beam moment of inertia. The rivets attaching the lower skin to the lower angles would be checked for the shear flow load and not for inter-rivet buckling since skin is in tension. The general subject of rivet design for structures is treated in Chapter D1.

The web stiffeners at the external load points and at the beam support points must be designed to transfer the concentrated load to the beam web. Refer to Chapter A21, which treats of loads in such stiffeners.

General Comments

The reader should understand that the margin of safety for the beam web in the preceding beam check was based on the design requirement of no initial buckling under the design load. The buckling stress as calculated is not the stress that would cause web to fail or collapse, as the web could take considerably more load in the buckled state. The subject of beam design with buckling webs is treated in Chapter C11.

In general, this type of beam web design is not widely used in flight vehicle structures because it is heavy construction since the web thickness must be relatively large to prevent buckling and the cost of fabrication and assembly is relatively high because of many parts and much riveting. The aerospace structures engineer decreases these disadvantages by using a web sheet with closely spaced beads or a series of flanged lightening holes which stabilize web against buckling and provide low fabrication and assembly cost. This type of web design is treated in Part 2 of this chapter.

C10. 15a Use of Longitudinal Stiffener to Increase Bending Buckling Stress of Web Sheet.

The strength check of the beam in the example problem showed that the compressive stress on the web due to beam bending was the factor that had great effect in producing the web buckling. This web weakness can be improved by adding a single longitudinal stiffener on the compression side as illustrated in Fig. C10.16. Theoretical and experimental information on the effect of such a stiffener is quite limited (see Ref. 3). Such a stiffener can raise the buckling coefficient k_b to around 100 or more, thus the web can be made somewhat thinner if bending stresses are critical. Adding this longitudinal stiffener means another structural part and more assembly cost and therefore such construction is not widely used although it is a structural arrangement that will save structural weight under certain conditions of beam depth, span and external loading.

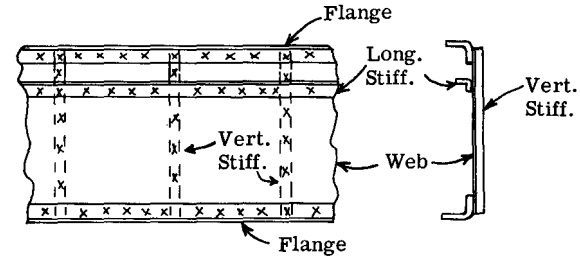

Fig. C10. 16

PART 2. OTHER TYPES OF NON-BUCKLING BEAM WEBS.

(BY W. F. McCOMBS)

C10.16 Other Types of Web Design.

At this point it should be noted that the web design discussed in Part 1 required a large number of parts (the stiffeners) to achieve lightness. To keep manufacturing costs down, the number of parts must be kept to a minimum. A balance, or economic compromise must be found between manufacturing expense and weight penalty. This can be arrived at since in every airplane design some "dollar" penalty can be assigned to every extra pound of weight. The exact figure will depend upon the type of airplane being designed. Thus, eliminating parts may incur some weight penalty but if the savings in manufacturing cost is greater, then the reduction in parts is economical.

Three types of shear resistant, non-buckling webs are frequently used in aircraft design to save the expense of stiffeners. Actually, the web in most cases is as light, or lighter, than a web with separate stiffeners. There is a general limitation, however, in that a stiffener must be provided wherever a significant load is introduced into the beam. The web types are:

a) web with formed vertical beads at a minimum spacing.

b) web with round lightening holes having 45° formed flanges at various spacing.

c) web with round lightening holes having formed beaded flanges and vertical formed beads between holes.

The webs with holes, (b) and (c), also provide lots of built-in access space for the many hydraulic and electrical lines and control linkages in airplanes.

C10.17 Beaded Webs.

Figure C10.17 shows a web having "male" beads formed into it at the minimum spacing forming will allow. The cross-section of the bead is described in Table C10.5.

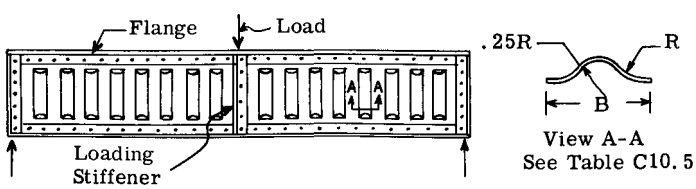

Fig. C10.17

Table C10.5

t	B	R
.020	.95	.32
.025	1.05	.40
.032	1.16	.52
.040	1.27	.64
.051	1.42	.81
.064	1.55	1.02
.072	1.65	1.15
.081	1.73	1.30
.091	1.81	1.45
.102	1.92	1.63
.125	2.12	2.00

The allowable shear flow, q in pounds per inch at collapse, is given in Fig. C10.18, by the solid lines. The dotted lines indicate initial buckling setting in but this is not failure (which is given by the solid lines). This is the strongest of the web systems not having separate stiffeners. Failure occurs

Fig. C10.18

BEADED SHEAR PANELS

DESIGN CURVES FOR CLAD 2024-T4 AND 7075-T6 SHEAR PANELS STIFFENED BY MALE BEADS AT MINIMUM SPACING

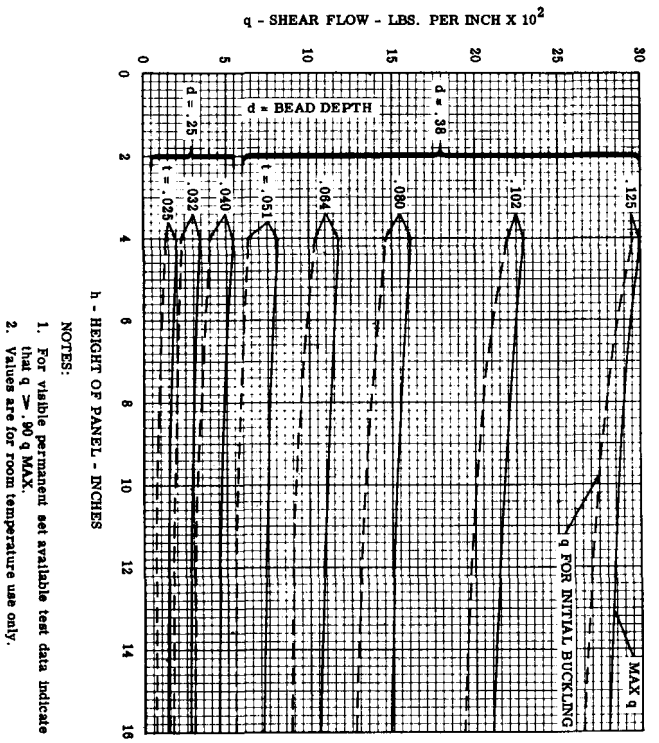

REFERENCE: STRUCTURAL DESIGN MANUAL SECTION 4.230

when the beads collapse. An example will follow later in C10.19. A suitable stiffener must be used (replacing a bead) wherever a load is introduced to prevent earlier collapse of the bead. The allowables are for pure shear only, no normal loads (see Art. D3.7).

C10.18 Webs With Round Lightening Holes Having Formed 45° Flanges.

This is a simple easily formed web. Fig. C10.19 shows such a beam with a cross-section through the web at the holes. The geometry of the hole and its flanges is given in Table C10.6 for typical forming.

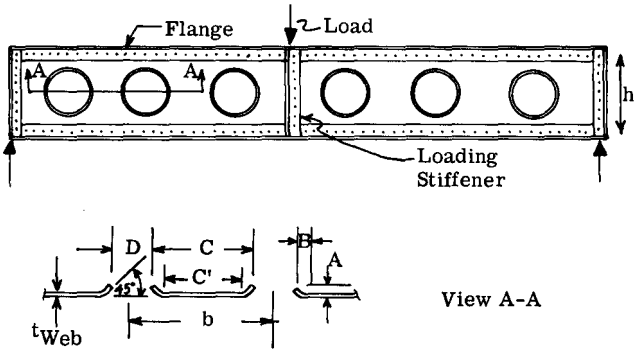

Fig. C10.19

The N.A.C.A. has developed, from an extensive test program, an empirical formula that gives the allowable shear flow (collapse) for webs having this type of hole. Referring to Fig. C10.19, the allowable shear flow is, from Ref. (2).

$$q_{ALL.} = k\,t\left[f_{s_h}\left(1 - \left(\frac{D}{h}\right)^2\right) + f_{s_c}\sqrt{\frac{D}{h}}\right]\frac{C'}{b} \qquad ----(C10.18)$$

where

$k = .85 - .0006\,\frac{h}{t}$

f_{s_h} = Collapsing shear stress of a long plate of width h and thickness t; obtained from Fig. C10.20.

f_{s_c} = Collapsing shear stress of a long plate of width c and thickness t, obtained from Fig. C10.20.

b = hole centerline spacing.

h = height of web, between flange to web rivets.

C' = C-2B where B is given in Table C10.6 for a typical hole.

C = b - D

For this type of web design, in general, those webs designed to take ultimate load will probably not show any permanent set at yield

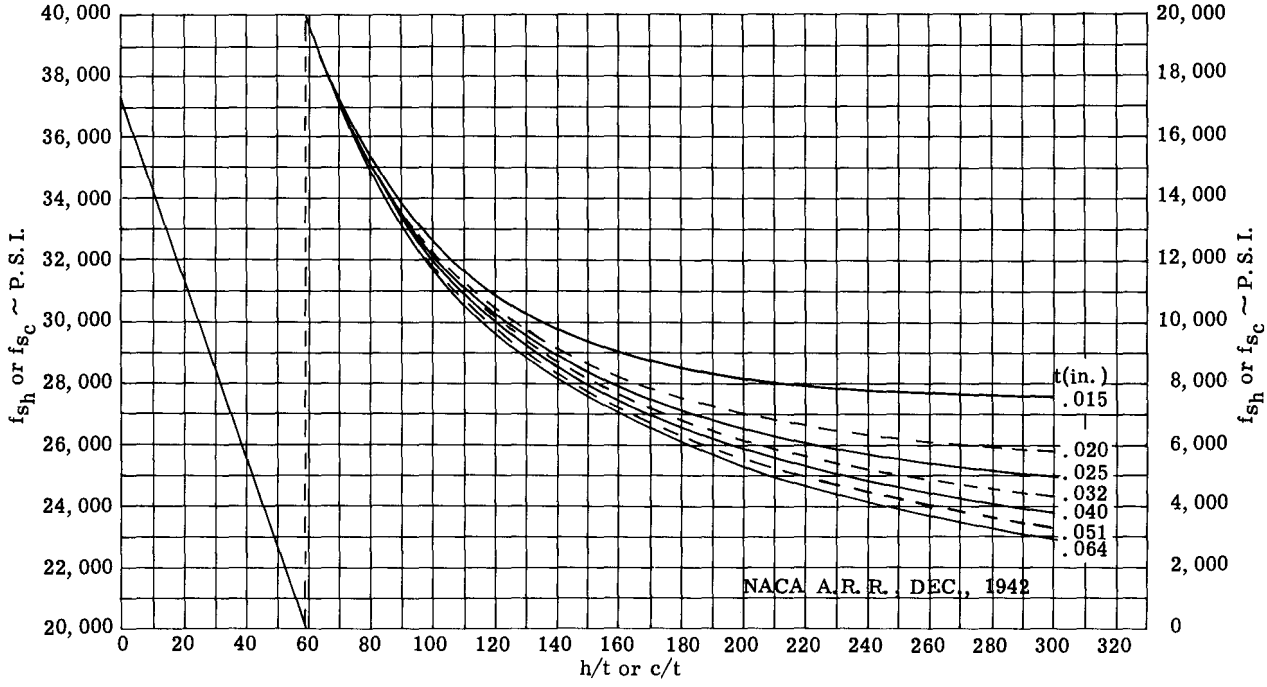

COLLAPSING SHEAR STRESSES, f_{s_h} OR f_{s_c}, FOR SOLID WEBS OF 24S-T ALUM. ALLOY

Fig. C10.20

Table C10.6

D	B	A	D	B	A	D	B	A
1.31	.13	.13	3.61	.19	.19	6.16	.25	.25
1.56	.13	.13	3.86	.19	.19	6.66	.25	.25
1.81	.13	.13	4.11	.19	.19	7.16	.25	.25
2.08	.16	.16	4.36	.19	.19	7.71	.32	.25
2.33	.16	.16	4.61	.19	.19	8.21	.32	.25
2.58	.16	.16	4.86	.19	.19	8.71	.32	.25
2.83	.16	.16	5.11	.19	.19	9.27	.37	.25
3.08	.16	.19	5.36	.19	.19	9.77	.37	.25
3.36	.19	.19	5.61	.19	.19	10.27	.37	.25

load if the shear stress at the yield load over the net sections, C' x t and $\frac{h}{h-D}$ x t, is about equal to the yield stress of the web material, F_{s_y}.

In general, it will be found, from formula (18), that the larger holes (about D ≈ .8h) with wider spacings, b, will give the lightest web in designing for a given shear flow q, but the stiffness will be less, of course.

Again, the allowables per formula (18) are for pure shear only, no normal loads on the web. Thus a stiffener must be provided wherever a load is introduced into the beam and also in areas where the beam may have significant curvature as in round and elliptical bulkheads, see Chapter D3.8. An example is given in Art. C10.19.

In addition to the above (collapse), the web should be checked for net shear stresses through the holes to be sure that $f_{s_{NET}} < F_{su}$ at ultimate load, q x h.

For a more complete discussion of this type of web design and the test data, the reader should review Refs. (2) and (1). Design charts can be prepared from formula (18), Fig. C10.18, and Table C10.6 for use in designing without having to resort to formula (18). Figure C10.21 shows such a chart taken from Ref. (2) for the cases of D/h = .80 and D/h = .50.

C10.19 Webs With Round Beaded Flange Lightening Holes and Intermediate Vertical Male Beads.

A third type of web has round holes with beaded flanges and vertical "male" beads between the holes. Such a beam is shown in Fig. C10.22. The vertical bead is as described in Table C10.5. The beaded flange shown is described in Table C10.7. For the particular case where $\frac{O.D.}{h} \approx .6$ and the hole spacing is equal to h, the allowable shear flows shown in Fig. C10.23 apply.

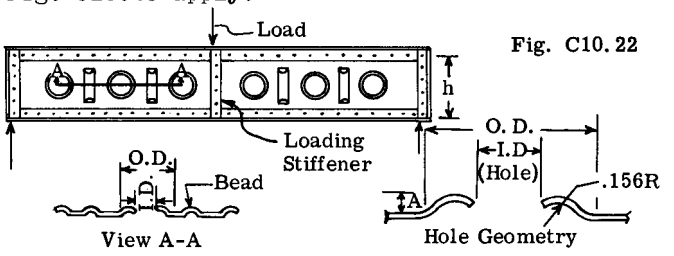

Fig. C10.22

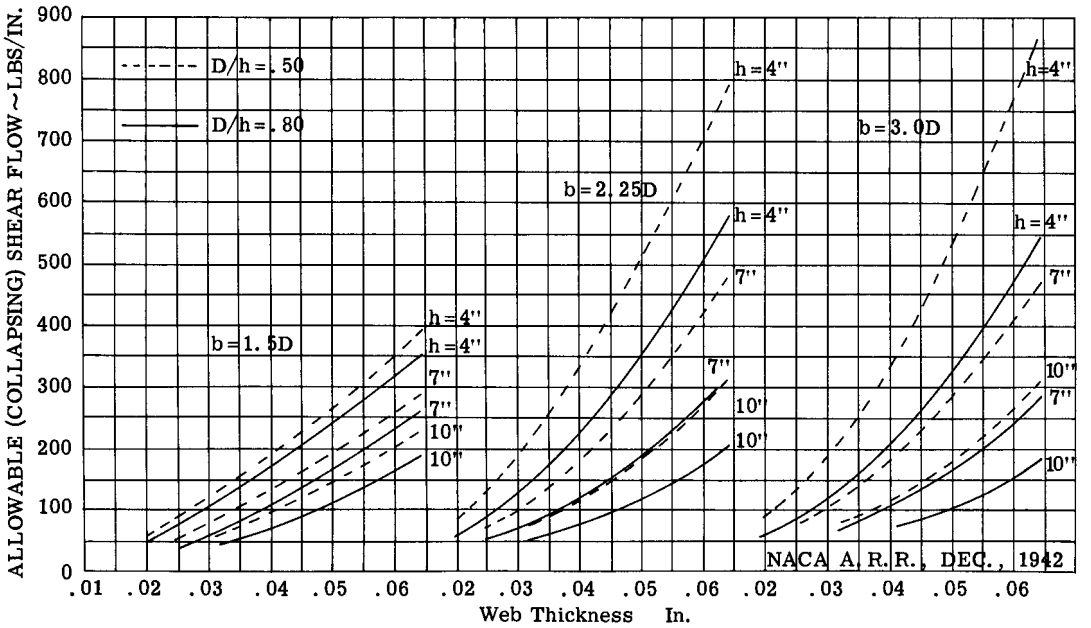

ALLOWABLE (COLLAPSING) SHEAR FLOWS FOR 24S-T WEBS WITH ROUND LIGHTENING HOLES HAVING FORMED 45° FLANGES

Fig. C10.21

Table C10.7

O.D.	I.D.	A
1.69	.81	.19
1.81	.94	.19
1.94	1.06	.19
2.06	1.19	.19
2.19	1.31	.19
2.31	1.44	.19
2.63	1.69	.25
2.75	1.81	.25
2.88	1.94	.25
3.00	2.06	.25
3.13	2.19	.25
3.38	2.44	.25
3.63	2.69	.25

O.D.	I.D.	A
3.88	2.94	.25
4.43	3.31	.38
4.94	3.81	.38
5.43	4.31	.38
5.94	4.81	.38
6.44	5.31	.38
6.94	5.81	.38
7.44	6.31	.38
7.94	6.81	.38
8.44	7.31	.38
8.94	7.81	.38
9.45	8.31	.38

The solid lines of Fig. C10.23 give the ultimate strength, q, of the web as a function of web height, h. This represents the total collapsing strength of the web. The dotted lines indicate the shear flow, q, at which initial buckling begins. If the O.D. is greater than .6 x h, or if the spacing of holes is reduced, the allowables will be reduced but no data is included for other geometries. As in other cases, Arts. C10.16 and C10.17, the data is for pure shear only, no normal loads. Hence loading stiffeners must be used (replacing the vertical bead locally) and Article D3.8 should be reviewed.

Fig. C10.23

CHANCE VOUGHT AIRCRAFT, INCORPORATED

REFERENCE: STRUCTURAL DESIGN MANUAL SECTION 4.230

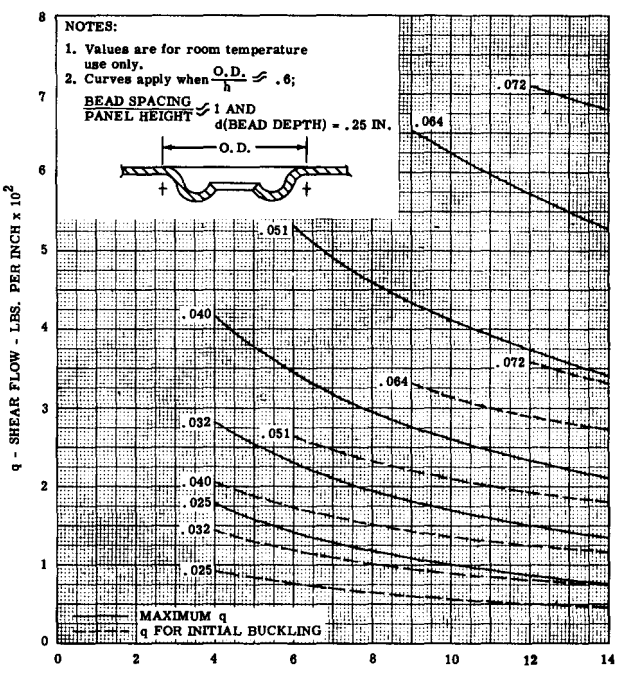

DESIGN CURVES FOR CLAD 2024-T4 AND 7075-T6 SHEAR PANELS WITH CVC-3030 LIGHTENING HOLES AND STIFFENED BY MALE BEADS

BEADED SHEAR PANELS WITH LIGHTENING HOLES

Of course, in all three types of formed webs, a small amount of normal loading can be tolerated, but no limit is defined. Typical cases are wing ribs and fuselage frames where only relatively light normal airloads are distributed by the rib without loading stiffeners. In such cases some extra margin of safety above the shear load is usually used, depending upon the designers judgment and/or substantiating element tests. Where large distributed loads are involved, as in a beam supporting a fuel cell, or where the beam curvature is significant (See D3.7), stiffeners should be used for the lightest design.

As a final note, whenever using webs with formed beads as in C10.17 and C10.19, it is important that the beads be formed with a length long enough to extend as close to the beam flanges as assembly will allow. Short beads, ending well away from the flanges, will not develop the strength indicated by the allowables given in the figures. Rivets attaching the web to the flange above a hole also need be more closely spaced to take the higher "net" shear locally.

C10.20 Example Problems.

For the beam shown in Fig. C10.24, determine the web gages required for

a) a beaded web, as in C10.17.

b) a 45° flanged hole web as in C10.18.

c) a beaded flange hole web with intermediate beads as in C10.19.

The beam shown in Fig. C10.24 has the same external dimensions and design load system as the beam shown in Fig. C10.14 and used for the example problem in Part 1 of this chapter. In these example problems, we are replacing the web design by the three variations (a), (b) and (c). Since the webs cannot be considered fully

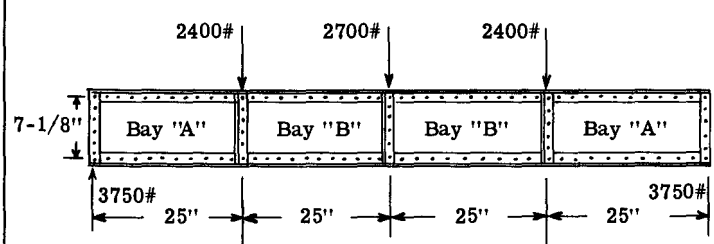

Fig. C10.24

effective in resisting beam bending stresses, the flanges would be stressed slightly higher than found in the example problem of Part 1. Using the same beam dimensions and beam design loading will provide a comparison of the web weights for the various web designs.

Using the simplified formula, the shear flows in bays A and B are

$$q_A = \frac{V}{h} = \frac{3750}{7.125} = 526 \text{ lb./in.}$$

$$q_B = \frac{3750 - 2400}{7.125} = 189 \text{ lb./in.}$$

Thus, for lightest weight, 2 web gages should be used, the lighter one for bays "B", and these could be spliced at the loading stiffeners introducing the 2400 lb. loads.

a) Beaded Web Gage Requirements.

Entering Fig. C10.18 with q = 526 lb./in. and h = 7.125" we find that the minimum acceptable gage is .051". Thus the web of Bay A should be .051", giving $q_{allow.}$ = 770 lb./in., from Fig. C10.18.

$$\text{M.S.} = \frac{770}{526} - 1 = \underline{\underline{.46}}$$

Repeating for the web of Bay B, enter with q = 189 lb./in. and h = 7.125" and find the minimum acceptable gage is .032, which has q_{ALL} = 310 lb./in. Thus for Bay B,

$$\text{M.S.} = \frac{310}{189} - 1 = \underline{\underline{.64}}$$

b) A 45° Flange Round Lightening Hole.

Since the larger diameter (and more widely spaced) holes are more efficient weightwise, try a hole having D ≈ .8h or D = 5.61" from Table C10.6. Spacing two holes in the 25" bays would indicate a spacing b = 12.5". Then, from C10.19

$$C = b - D = 12.5 - 5.6 = 6.9$$

$$B = .19, \text{ from Table C10.6}$$

$$C' = C - 2B = 6.9 - 2\,(.19) = 6.52$$

Now determine the allowable value of q for, say, t = .081" for Bay A.

$$\frac{h}{t} = \frac{7.125}{.081} = 88$$

$$k = .85 - .0006\,(88) = .80$$

From Fig. C10.20, for $\frac{h}{t} = 88$ and $\frac{c}{t} = 85$

$$f_{s_n} = 13{,}200$$

$$f_{s_c} = 13{,}800$$

Substituting values in equation (13)

$$q_{ALL.} = .79(.081)\left[\left[13{,}800\left[1 - \left(\frac{5.61}{7.125}\right)^2\right] + 13{,}800\sqrt{\frac{5.61}{7.125}}\right]\right]\frac{6.52}{12.5}$$

$$= .064\left[13{,}200\,(.38) + 13{,}800\,(.887)\right](.521)$$

$$= \underline{\underline{573}} \text{ lb./in.}$$

Also, the net shear stresses on any section through the holes must be less than F_{su}. Checking a vertical section through the hole we get

$$f_{s_{NET}} = \frac{V}{(h-D)t} = \frac{526(7.125)}{(7.125-5.61)(.081)} = \frac{3750}{.123} = 30{,}500$$

$$\text{Thus, M.S.}_{COLL.} = \frac{573}{526} - 1 = \underline{\underline{.09}}$$

$$\text{M.S.}_{NET} = \frac{F_{su}}{f_{s_{NET}}} = \frac{37{,}000}{30{,}500} - 1 = \underline{\underline{.21}}$$

Repeating with the above geometry and using t = .051 for Bay "B" where q = 189 lb./in., we get

$$q_{ALL.} = .77(.051)\left[\left[7900(.38) + 8300(.887)\right]\right](.521)$$

$$= .0393\,\left[10{,}630\right](.521) = \underline{\underline{217}} \text{ lb./in.}$$

$$\text{M.S.}_{COLL.} = \frac{217}{189} - 1 = \underline{\underline{.15}}$$

and

$$\text{M.S.}_{NET} = \frac{37{,}000}{17{,}400} - 1 = \underline{\underline{1.12}}$$

The reader can repeat the above for smaller sizes of holes and thickness to see if a lighter arrangement (NET web weight) can be obtained. It can be seen that the example gages are confirmed by the data of Fig. C10.21 extrapolating in the case of the .081 web.

c) A Beaded Flange Hole with Intermediate Vertical Beads.

The geometry for this is as previously discussed (O.D. ≈ .6h and b ≈ h).

First determine gage for Bay A. Entering Fig. C10.23 with h = 7.125" and q = 526 lb./in., the closest acceptable gage is t = .064 (solid line), giving

$q_{ALL.}$ = 700 lb./in.

M.S. $= \frac{700}{526} - 1 = \underline{\underline{.33}}$

Repeating for Bay B with q = 189 and h = 7.125" the closest acceptable gage is t = .032.

$q_{ALL.}$ = 208 lb./in.

M.S. $= \frac{208}{189} - 1 = \underline{\underline{.10}}$

Actually, a hole with O.D. = 4.43 (from Table C10.7) could be used even though $\frac{O.D.}{h} = \frac{4.43}{7.125} = .62$ is a little larger than .6, since the M.S. above is well above zero.

A comparison of the total weights of each of the 3 types of webs is given in Table C10.8, using a hole diameter of 5.61" for webs (b) and 3.31" (from Table C10.7) for webs (c) and a density of .10 lb./in. for aluminum.

Table C10.8

Type of Web	Weight in Pounds		
	Bays "A" (2)	Bays "B" (2)	Total Web Wt.
(a)	1.82	1.14	2.96
(b)	2.06	1.30	3.36
(c)	2.06	1.03	3.09
Web of Fig. C10.14 (with extra Stiffeners)			5.82

Thus for a "non-distributed" load, web (a), a beaded web, is lightest for Bays "A" and (c) is lightest for Bays "B". If "access" for lines is required then a web of type (c) or (b) should be used for Bays "A".

The weight of the web and vertical stiffeners designed for no initial buckling under combined bending and shear gave a value of 5.82 lbs., or much heavier than the other designs.

PROBLEMS

(1) Fig. C10.25 shows the cross-section of a wing beam. Calculate the ultimate resisting moment for the beam section using the stress-strain curve for the extruded 24ST material given in Fig. C10.4. Use .008 unit strain at the extreme fiber of the upper flange. Compare the results with the resisting moment given by the general beam formula $M = f_b I/y$.

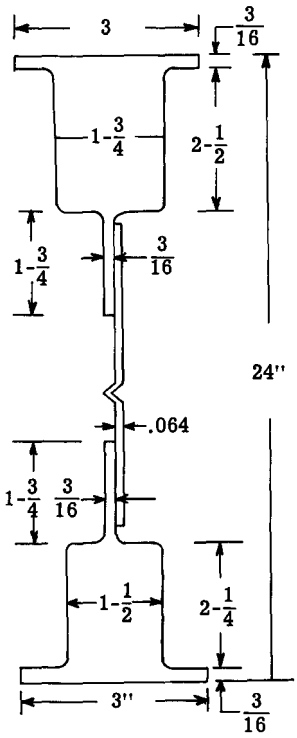

Fig. C10.25

(2) Design a butt web splice for the beam section of C10.13 for a design shear load V = 3000 lb. and a bending moment of 50,000 in. lbs.

(3) Fig. C10.26 shows a simply supported beam carrying a 2000 lb. design load located as shown. The cross-section of the beam is shown in Fig. C10.27. The design requirement for the web is no initial buckling under the design external load. Check the given design for strength and modify if too weak or too strong, or in other words, improve the design. Assume beam flanges are braced against lateral column failure.

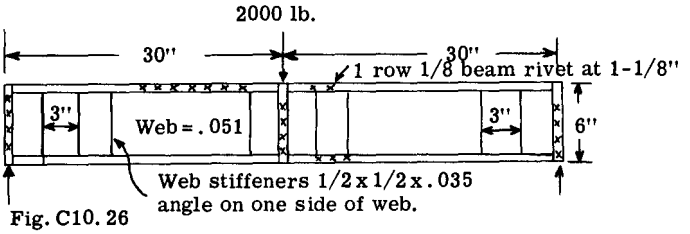

Fig. C10.26

(4) Re-design the beam of Problem (3) to use the 3 types of stiffened web as presented in Part 2 of this chapter. Compare the web weights with the web weight required in Problem 3.

(5) Fig. C10.28 shows the external dimensions of a tapered cantilever beam carrying the distributed design load as shown. The web is not to buckle under the design load.

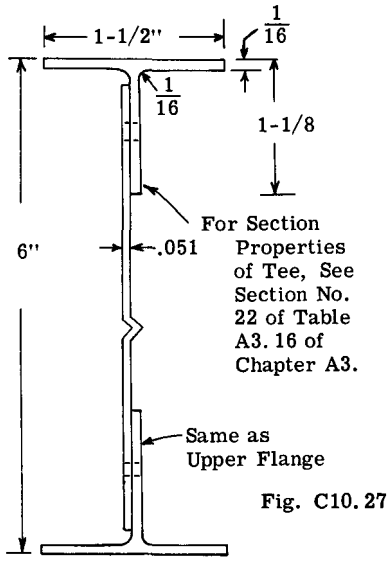

Fig. C10.27

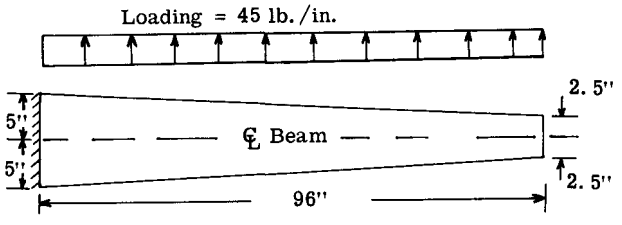

Fig. C10.28

Make a complete structural design of beam showing size of all parts. For flange use 7075-T6 extrusion material and 7075-T6 clad material for web and web stiffeners. Show rivet design.

(5) Same as Problem (4) but use web with vertical beads.

REFERENCES

(1) Kuhn, Paul:- The Strength and Stiffness of Shear Webs With and Without Lightening Holes. NACA. ARR. June 1942.

(2) Kuhn, Paul:- The Strength and Stiffness of Shear Webs with Round Lightening Holes Having 45° Flanges. NACA. ARR. L-323 Dec. 1942.

(3) Bleich, F.:- Buckling Strength of Metal Structures - Book - Publisher, McGraw-Hill pp. 418-24.

CHAPTER C11

DIAGONAL SEMI-TENSION FIELD DESIGN

PART 1. BEAMS WITH FLAT WEBS. PART 2. CURVED WEB SYSTEMS.

PART 1

C11.1 Introduction.

The aerospace structures engineer is constantly searching for types of structures and methods of structural analysis and design which will save structural weight and still provide a structure which is satisfactory from a fabrication and economic standpoint. The development of a structure in which buckling of the webs is permitted with the shear loads being carried by diagonal tension stresses in the web is a striking example of the departure of the design of aerospace structures from the standard structural design methods in other fields of structures, such as beam design for bridges and buildings. The first study and research on this new type of structural design involving diagonal semi-tension field action in beam webs was by Wagner (Ref. 1), and because of this fact, this type of beam design is often referred to as a Wagner beam.

In Chapter C10, Part 1, the subject of beam design with shear resistant (non-buckling) flat webs was covered. This type of web design leads to a comparatively heavy weight, which fact prevents its wide use in aerospace structures. Part 2 of Chapter C10 dealt with webs stiffened by closely spaced beads, flanged lightening holes, etc., a design which shows an improvement relative to web weight over the flat sheet web with vertical stiffeners. However, a large proportion of sheet panels used in aerospace structures is part of the external surface and holes and deep beads in the surface skin cannot be permitted, thus continuous sheet is required and to save structural weight, semi-tension field action in the webs and surface sheet panels must be permitted, which means a wrinkling type of structure.

Since the original work by Wagner, much further study and testing of structures involving semi-tension field design has been carried out by both industry and government agencies, hence a fairly accurate procedure for the design of such structures has been developed and this chapter is concerned with a limited presentation of the principles involved and the design procedures that have been developed.

C11.2 Elementary Approximate Explanation of Tension-Field Beam Action.

Fig. C11.1 shows a single bay truss with double diagonal members (A) and (B) and carrying an external load P. The load P will cause a compressive load in member (A) and a tensile load in member (B). If member (A) is quite flexible it will buckle as a long column as shown in Fig. C11.1b, when load P is relatively small, however, panel will not collapse. As the load P is increased, the member (A) cannot take any more load but it will practically hold its column buckling load as the bending deflection or bowing gets larger. However, member (B) being in tension can take further load until it reaches its ultimate tensile strength. Thus any increase of the shear in the panel due to an increase of load P after diagonal (A) has buckled can be carried by a further increase of tension load in member (B).

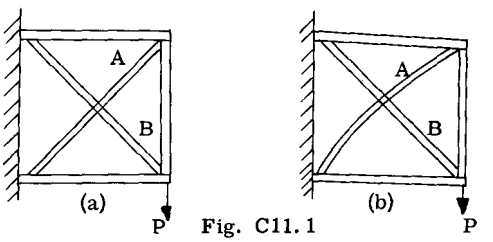

Fig. C11.1

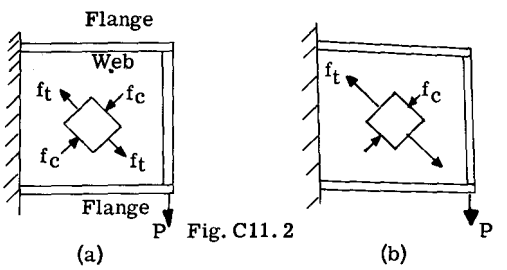

Fig. C11.2

Fig. C11.2 shows the same panel but with the two diagonals replaced by a flat sheet web. Under a small load (P), the web will not buckle and the stress picture on a small web element is shown in Fig. C11.2a, and $f_c = f_t = f_s$ where f_s is the shear stress in the web at this particular point on the web. Now thin flat sheet is relatively weak under compression, thus when panel load P is increased, the compressive stress f_c reaches the buckling stress of the panel in the diagonal direction and the web buckles, however, the panel does not collapse as further increase in load P can be handled by

further increase in f_t or diagonal tension in the web sheet. The web has an ability to hold the f_c stress that caused buckling but cannot increase it. Fig. C11.2b shows the web stress picture after the load P has been increased considerably, thus increasing the diagonal web tensile stress as shown by the length of the vector for f_t. Since the shear load on the panel is transferred by diagonal tension in the web and since flat sheet is efficient in tension, this method of carrying the shear load permits the use of relatively thin webs because of the high allowable design stresses in tension. Fig. C11.3 shows a photograph of a thin web beam under load. Since the diagonal wrinkling appears severe, the external load being carried is no doubt approaching the failing point of the web. The student should realize that such a degree of web wrinkling does not occur under normal flying accelerations since the loads carried in normal flying conditions are only a fraction of the design loads, and thus the buckling and wrinkling is barely noticeable under accelerations of 1/2 gravity, which may be encountered often in flying in gusty weather conditions.

C11.3 Elementary Derivation of Approximate Tension-Field Beam Formulas.

In order to give the student a general picture of the influence of web tension field action upon the beam component parts, an elementary approximation of the beam equations will be given.

Fig. C11.4 shows a cantilever beam with parallel chords and vertical stiffeners subjected to a single shear load V at the free end. The dashed diagonal lines indicate the direction of the wrinkles as the thin sheet buckles under the load V.

Assuming that the flange angles develop all the bending resistance, the vertical and horizontal shearing stress is constant over the web and equals

$$f_s = \frac{V}{ht} \qquad \text{- - - - - - - - - - - - - - - - (1)}$$

where

t is web thickness
h is taken as the distance between centroids of flange rivets.
V = vertical shear load.

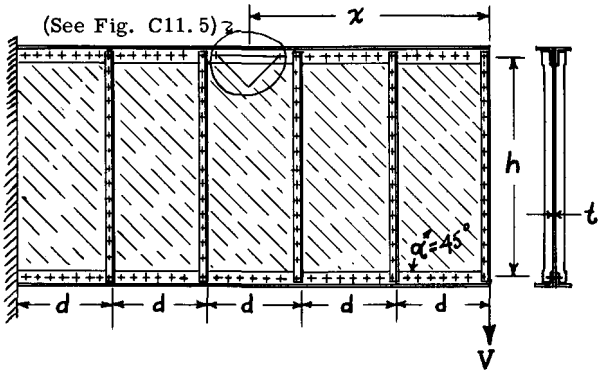

Fig. C11.4

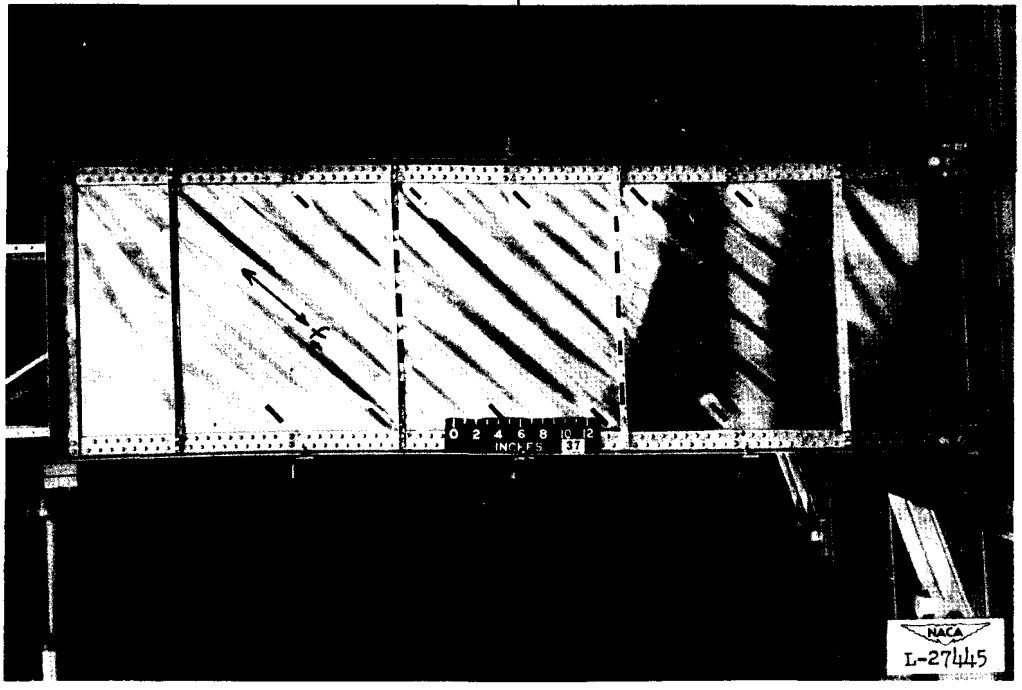

Fig. C11.3 Loaded Cantilever Beam Showing Severe Diagonal Web Wrinkling (Ref. 3)

Fig. C11.5 shows the free body diagram of a small triangular segment of the web cut from the upper portion of the beam.

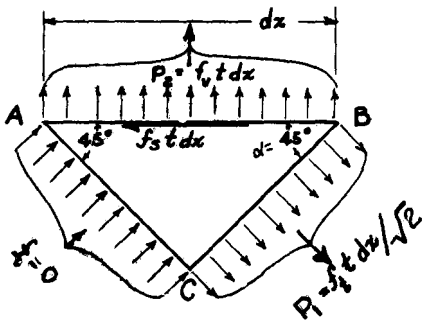

Fig. C11.5

From elementary mechanics the horizontal and vertical shearing stresses produce compressive and tensile stresses on planes at 45° with the shearing planes.

The web, being very thin, can carry very little compression stress on the surface (AC) of Fig. C11.5 before buckling; thus this small stress which produces buckling on AC will be neglected or $f_c = 0$. The edge BC is subjected to tensile stresses which the sheet can carry effectively. The forces acting on the sheet element are shown in Fig. C11.5.

For equilibrium of the element:

$$\Sigma F_x = 0 \text{ or } -f_s\, tdx + f_t \frac{tdx}{\sqrt{2}} \cdot \frac{1}{\sqrt{2}} = 0$$

whence

$$f_t = 2\, f_s \qquad \text{- - - - - - - - - - - - - - - (2)}$$

or the web tensile stress equals twice the web shearing stress:

From (1) $f_s = V/ht$

whence

$$f_t = 2V/ht \qquad \text{- - - - - - - - - - - - - - - (3)}$$

Likewise for equilibrium:

$$\Sigma F_y = 0 \text{ or } f_v\, tdx - f_t \frac{tdx}{\sqrt{2}} \cdot \frac{1}{\sqrt{2}} = 0$$

whence

$$f_t = 2\, f_v \qquad \text{- - - - - - - - - - - - - - - (4)}$$

hence

$$f_v = f_s \qquad \text{- - - - - - - - - - - - - - - (5)}$$

Rivet Loads

The sheet element is held to the flange angles by the rivets along line (AB). The rivets are subjected to two loads, one parallel to AB and one normal to AB; and each force equals $f_s\, tdx$. The resultant rivet load therefore equals $\sqrt{2}\, f_s\, tdx$; and if dx is taken as one inch, the resultant load will be $\sqrt{2}\, f_s\, t$.

But $f_s = V/ht$, hence

Rivet load/inch = 1.41 V/h - - - - - - (6)

Web Stiffener Load

The tendency of the web in Fig. C11.4 which has broken down into the tension bands, is to pull the flanges together; this action is prevented by the vertical stiffeners which keep the flanges apart. Thus if a pure tension field is assumed, the axial compressive load P_s in the stiffeners from Fig. C11.6 equals the vertical component of the web tensile stresses over a distance (d), the stiffener spacing.

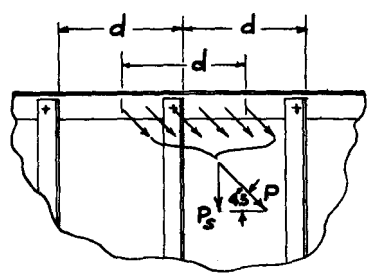

Fig. C11.6

whence

$$P_s = P \sin \theta$$

But

$$P = f_t\, dt\, 1/\sqrt{2}$$

hence

$$P_s = \frac{1}{\sqrt{2}} \cdot \frac{1}{\sqrt{2}} f_t\, dt = f_t\, dt/2$$

but

$$f_t = 2\, f_s \text{ and } f_s = V/ht$$

whence

Stiffener load $P_s = Vd/h$ (compression)
- - - (7)

Flange Axial Loads

Fig. C11.7 shows a free body of the portions of the beam to the right of a section a distance x from the end of the beam.

Let M_x = external bending moment at Section AB. For equilibrium the internal resisting moment on Section AB must equal external bending moment M_x.

Taking moments about point B:

$$\Sigma M_B = M_x - F_t\, h' - f_t \cos 45^\circ h'\, t \cdot \cos 45^\circ \frac{h'}{2} = 0$$

- - - - - - (8)

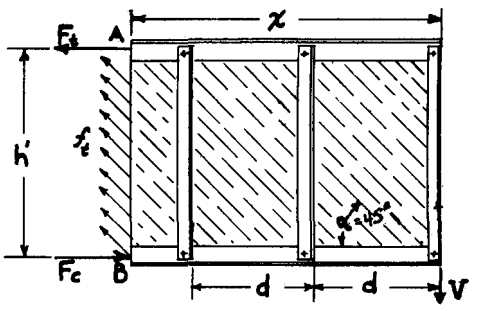

Fig. C11.7

where

h' = distance between flange centroids.

But

$f_t = 2\ f_s$ and $f_s = F/h't$, hence $f_t = \frac{2\ V}{h't}$

Substituting this value of f_t in Eq. (8)

$$M_x - F_t\ h' - \frac{Vh'}{2} = 0$$

whence

$$F_t = \frac{M_x}{h'} - \frac{V}{2} \quad \text{- - - - - - - - - - - - - - -(8a)}$$

Then to make $\Sigma H = 0$ on Section AB:

$$F_c = \frac{M_x}{h'} - \frac{V}{2} \quad \text{- - - - - - - - - - - - - - (9)}$$

Thus the compressive flange axial load due to bending is increased by a value equal to V/2 lbs. and the tension flange load due to bending is decreased by V/2 due to the horizontal components of the web tension field.

C11.4 General Wagner Equations for Tension Field Beams.

The approximate elementary derivation given in the previous article was for the purpose of giving the student a general idea of the influence of a complete tension field beam on the various beam stresses. The angle α is in general not 45° but depends on flange areas, beam height, stiffener spacing, etc.

The general equations derived by Wagner (Ref. 1) are as follows:

For beams with infinitely rigid and parallel flanges with vertical web stiffeners:

Diagonal tensile stress in web:

$$f_t = \frac{2V}{ht} \cdot \frac{1}{\sin 2\ \alpha} \quad \text{- - - - - - - - - -(10)}$$

Axial load in tension flange:

$$F_t = \frac{M}{h'} - \frac{V}{2} \cot \alpha \quad \text{- - - - - - - - - - (11)}$$

Axial load in the compression flange:

$$F_c = \frac{M}{h'} - \frac{V}{2} \cot \alpha \quad \text{- - - - - - - - - - (12)}$$

Axial force in stiffeners:

$$F_{Stiff.} = - V \frac{d}{h} \tan \alpha \quad \text{- - - - - - - - - (13)}$$

In the above equations:

V = applied shear load
h = distance between centroids of flange-web rivets
h' = distance between centroids of flange sections
t = web thickness
d = vertical web stiffener spacing
α = angle of web buckle (see Fig. C11.7)

In deriving equations (10) to (13) Wagner assumed that the beam flanges were infinitely stiff in bending. Actually the flanges due to the lateral pull of the web tension field will act somewhat as a continuous beam over the web stiffeners as supports, as illustrated in Fig. C11.8a. The deflections of the beam flanges relieves the web stress in the midportion of the panels and concentrates the web stress near the stiffeners where deflection of the flange is prevented (see Fig. C11.8b).

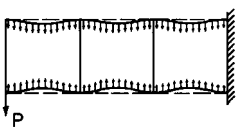

Fig. C11.8a

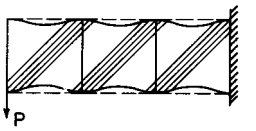

Fig. C11.8b

Wagner (Ref. 2, Part III) has developed a correction factor R to take care of this web stress concentration due to flange deflection. This stress ratio factor is obtained from Fig. C11.9 and the following equations:

$$wd = 1.25\ d \sin \alpha \sqrt[4]{\frac{t}{(I_u + I_L)h}} \quad \text{- - - (14)}$$

d = stiffener spacing

I_u and I_L = moment of inertia of upper and lower beam flanges about their own neutral axis.

Wagner also has derived the following equations for determining the web buckle angle α as follows:

$$\sin^2 \alpha = \sqrt{a^2 + a} - a \quad \text{- - - - - - - - - (15)}$$

$$a = \frac{1 + \frac{ht}{A_u + A_L}}{\frac{dt}{A_s} - \frac{ht}{A_u + A_L}} \quad \text{- - - - - - - - - - - (16)}$$

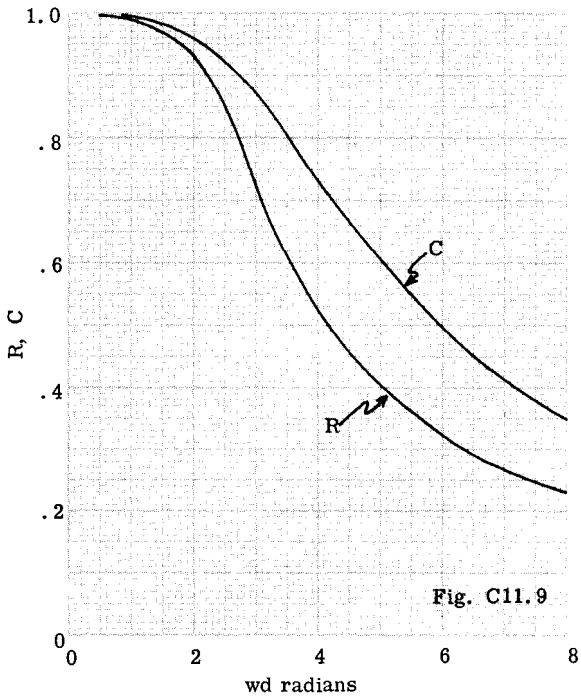

Fig. C11.9

A_U and A_L = area of upper and lower flanges including reinforcing plates but neglecting web material.

A_S = area of stiffener

METHOD 1

C11.5 Modified Wagner Equations for Use in Design.

The Wagner equations are too conservative for design, particularly in the web stresses and the loads in the vertical stiffeners. The shear stress carried by the web before it buckles is in many cases an appreciable part of the total resistance, as the buckled sheet normal to the diagonal compressive stresses has the ability to hold this buckling shear load after wrinkling. The load in the vertical stiffener is too conservative, since the stiffener is riveted to the web and the web is riveted to the flange; thus the web acts as a large gusset plate instead of a pin end condition as assumed in the Wagner equation.

The following general method of analysis of Wagner beams has been used by many airplane companies. Instead of assuming that the entire beam shear is taken by the web in diagonal tension, the following assumptions are made relative to the resistance for carrying the beam vertical shear.

(1) The shear strength of the beam flanges is not neglected.

(2) The shear carried by the web before it buckles, that is, as a shear resistant member is considered as an effective resistance and not neglected.

(3) The remainder of the beam shear after subtracting that carried by (1) and (2) is considered carried by the web in a buckled state in the form of a diagonal tension field.

The above assumptions apply to beams with parallel flange members. If the beam has sloping flanges, part of the beam shear will be carried by the shear component of the flange axial loads, and thus the assumptions should be applied to the net beam shear.

C11.6 Shear Carried by the Beam Flanges.

The general flexural shear flow equation is

$$q = \frac{V \int ydA}{I} = \frac{VQ}{I} \quad (\text{if } \int ydA \text{ is given symbol } Q)$$

For beam flange and web arrangements commonly used in aircraft structures the shear stresses are approximately constant over the web, that is, between the centroids of the flange-web rivets. Using this assumption, the value Q in the above equation equals the static moment of the flange area about the neutral axis of the beam, and I equals the moment of inertia of the flange area about neutral axis. (web area is neglected).

The shear load resisted by the web alone therefore equals

$$V_W = \frac{VQh}{I} = \frac{V}{I/Qh} \quad - - - - - - - - - - - - \quad (17)$$

where

h = effective web depth = distance between centroids of flange-web connection rivets.

The total beam shear V which equals the resistance of both web and flange, equals

$$V = \frac{V_W \, I}{Qh} \quad - - - - - - - - - - - - - - - \quad (18)$$

The difference between (17) and (18) gives the shear carried by flanges.

C11.7 Shear Load Carried by Web.

Up to the buckling stress of the web plate, the shear flow is assumed to be of constant intensity over the effective web depth. When the web buckles, it is assumed that the web maintains the diagonal critical compressive stress that produced the buckling of the plate. For further increase of shear load on the web, the entire resistance is provided by the increase in diagonal tensile stresses with no increase in the diagonal compressive stresses. In other words, for loads above the web buckling point, the web acts as a pure tension field beam. Fig. C11.10 illustrates these assumptions.

Shear Load Carried by Web at Web Buckling Stress

Fig. (C11.10a) shows the shear resistance

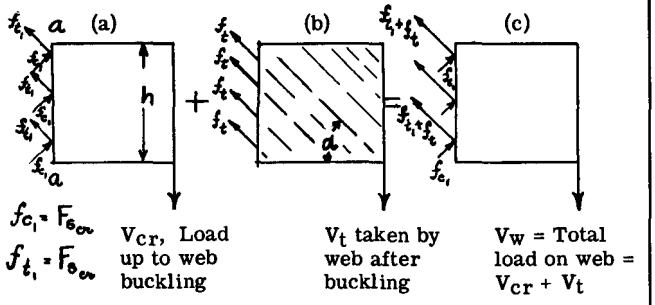

Fig. C11.10

on the web face (aa) when the web is shear resistant. The vertical shear stresses on (aa) have been replaced by the diagonal compressive and tensile stresses. The intensity of these diagonal stresses equals the intensity of the critical shearing stress $F_{s_{cr}}$.

Hence the shear load carried by the web at the web buckling stress equals

$$V_{cr} = F_{s_{cr}} h t \quad - - - - - - - - - - - - - (19)$$

The critical shear buckling stress is given by the following equation from C5.4 of Chapter C5.

$$F_{s_{cr}} = \frac{\pi^2 k_s E}{12 (1 - \nu^2)} \left(\frac{t}{b}\right)^2 \quad - - - - - - - - (20)$$

where k_s is a function of the aspect ratio a/b of the shear panel and of the edge conditions. Fig. C5.11 of Chapter C5 gives the value of k_s for edges simply restrained. Taking a value of k_s for this edge condition is no doubt slightly conservative.

Shear Load Carried by Web after Buckling

Fig. C11.10b shows the web stress distribution that is assumed to be subjected to the web when the web shear load is increased above that which caused the web to break down into a tension field. The diagonal tensile stress f_t tends to pull the beam flanges together, and thus to bend the flanges. The diagonal tensile stress f_t for the shear resistant web does not produce such action. To obtain the maximum combined tensile stress in the web, the stress f_t must be multiplied by a concentration factor 1/R from Fig. C11.9.

Hence

$$f_{t_{(max.)}} = \left(\frac{f_t}{R} + F_{s_{cr}}\right) \quad - - - - - - - (21)$$

Solving for f_t

$$f_t = (f_{t_{(max.)}} - F_{s_{cr}}) R \quad - - - - - - (22)$$

If the web is riveted to the flanges and web stiffeners, part of the web material is cut away due to the rivet holes thus the tensile stress of equation (21) must be multiplied by a rivet correction factor $1/K_r$ to obtain the true $f_{t_{max.}}$.

Hence for riveted connections:

$$f_{t_{(max.)}} = \left(\frac{f_t}{R} + F_{s_{cr}}\right) \frac{1}{K_r} \quad - - - - - - (23)$$

whence

$$f_t = \left(f_{t_{(max.)}} - \frac{F_{s_{cr}}}{K_r}\right) K_r R \quad - - - - - (24)$$

where

$$K_r = \frac{\text{rivet spacing - rivet diameter}}{\text{rivet spacing}}$$

Equation (22) would apply for webs spot welded to flange members.

The vertical components of the total f_t stresses on the web effective depth (h) would thus equal the shear load V_t developed by the web after buckling.

For spot welded flange, web and stiffeners connections:

$$V_t = (f_{t_{max.}} - F_{s_{cr}}) \, Rht \sin\alpha \cos\alpha \quad - (25)$$

For riveted connections:

$$V_t = \left(f_{t_{max.}} - \frac{F_{s_{cr}}}{K_r}\right) K_r \, Rht \, \sin\alpha \cos\alpha \quad - - (26)$$

If $f_{t_{max.}}$ is taken as the tensile yield point stress F_{ty} or the ultimate tensile stress F_{tu} equations (25) and (26) will give the shear load carried by the web above the buckling load when the web is stressed to the yield and ultimate tensile strengths respectively.

Thus for yield strength:

$$V_{ty} = \left(F_{ty} - \frac{F_{s_{cr}}}{K_r}\right) K_r \, Rht \, \sin\alpha \cos\alpha \quad \text{(riveted connect.)} \quad - (27)$$

$$V_{ty} = (F_{ty} - F_{s_{cr}}) \, Rht \, \sin\alpha \cos\alpha \quad - - (28) \quad \text{(Spot welded connect.)}$$

For ultimate strength:

$$V_{tu} = \left(F_{tu} - \frac{F_{s_{cr}}}{K_r}\right) K_r \, Rht \, \sin\alpha \cos\alpha \quad \text{(riveted connect.)} \quad - (29)$$

$$V_{tu} = (F_{tu} - F_{s_{cr}}) \, Rht \, \sin\alpha \cos\alpha \quad - - (30) \quad \text{(spot welded connect.)}$$

The total yield shear resistance of the web equals

$$V_{w_{ty}} = (V_{cr} + V_{ty}) \quad \text{- - - - - - - - - - (31)}$$

Total ultimate web shear resistance:

$$V_{w_{tu}} = (V_{cr} + V_{tu}) \quad \text{- - - - - - - - - - (32)}$$

Total beam shear resistance equals equations (31) or (32) multiplied by $\frac{1}{Qh}$ (Ref. Equation 18)

Hence

$$V_{yield} = \frac{1}{Qh}(V_{cr} + V_{ty}) \quad \text{- - - - - - (33)}$$

$$V_{ult.} = \frac{1}{Qh}(V_{cr} + V_{tu}) \quad \text{- - - - - - (34)}$$

Substituting values from equations (27 to 30) for V_{ty} and V_{tu},

For spot welded connections:

$$V_{yield} = \frac{It}{Q}\left[F_{s_{cr}} + (F_{ty} - F_{s_{cr}})\, R \sin\alpha \cos\alpha\right] \quad \text{- - - - (35)}$$

$$V_{ult.} = \frac{It}{Q}\left[F_{s_{cr}} + (F_{tu} - F_{s_{cr}})\, R \sin\alpha \cos\alpha\right] \quad \text{- - - - (36)}$$

For riveted connections:

$$V_{yield} = \frac{It}{Q}\left[F_{s_{cr}} + (F_{ty} - \frac{F_{s_{cr}}}{K_r})\, K_r R \sin\alpha \cos\alpha\right] \quad \text{- - - - (37)}$$

$$V_{ult.} = \frac{It}{Q}\left[F_{s_{cr}} + (F_{tu} - \frac{F_{s_{cr}}}{K_r})\, K_r R \sin\alpha \cos\alpha\right] \quad \text{- - - - (38)}$$

C11.8 Beams with Parallel Flanges but with Oblique Web Stiffeners.

Wagner has developed equations for the condition where stiffeners are placed at an angle with the parallel flange members, (Fig.A). In this case equations (27) to (30) should be multiplied by a correction factor equal to $(1 - \tan\alpha \cot\beta)$ where β is the upright angle. For oblique stiffeners the wrinkle field angle α is equal to $\beta/2$ and the concentration factor R can be taken as unity. Hence the equations for V_{ty} and V_{tu} become as follows:

$$V_{ty} = 1/2\,(F_{ty} - \frac{F_{s_{cr}}}{K_r})\, K_r\, h\, t\, \frac{1-\cos\beta}{\sin\beta} \quad \text{- -(38a)}$$

$$V_{tu} = 1/2\,(F_{tu} - \frac{F_{s_{cr}}}{K_r})\, K_r\, h\, t\, \frac{1-\cos\beta}{\sin\beta} \quad \text{- -(38b)}$$

(For spot welded joints, omit term K_r)

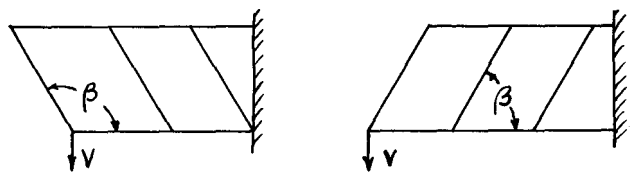

Fig. A

C11.9 Rivet Loads.

The loads on the rivets connecting the flanges to the web consists of two parts, (1) that due to the web acting as a shear resistant member subjected to stresses which cause web buckling, and (2) that due to the web tension field for web stresses above the web buckling stress.

Rivet Load at Web Buckling Stress

$$P_{x_{cr}} = \frac{V_{cr}\, I_F}{h\, I} \quad \text{- - - - - - - - - - - - (39)}$$

where

- $P_{x_{cr}}$ = load on rivet parallel to flange in lb./in.
- I_F = moment of inertia of flanges about beam neutral axis
- I = moment of inertia of total beam section
- h = distance between flange rivet centroids
- V_{cr} = buckling shear strength of web, lbs.

Rivet Loads for Tension Field Action

In Fig. C11.11 the web element (abc) is attached to the flange along line (ab). A vertical depth (bc) of 1 inch has been taken. The shearing stress on this length due to V_{tu} equals V_{tu}/h. This load represents the vertical component of the tension field, hence

$$P_t = \frac{V_{tu}}{h \sin\alpha} \quad \text{- - - - - - - - - - - - - (40)}$$

Resolving the tension load P_t into x and y components on rivet line (ab) and dividing by the length ab to get rivet loads per inch, we obtain

$$P_y = \frac{V_{tu} \sin\alpha \sin\alpha}{h \sin\alpha \cos\alpha} = \frac{V_{tu}}{h} \tan\alpha \quad \text{- - (41)}$$

$$P_x = \frac{V_{tu} \cos\alpha \sin\alpha}{h \sin\alpha \cos\alpha} = \frac{V_{tu}}{h} \quad \text{- - - - - (42)}$$

Combining the three component rivet forces as given in equations 39, 42 and 41 to obtain resultant load R on rivet:-

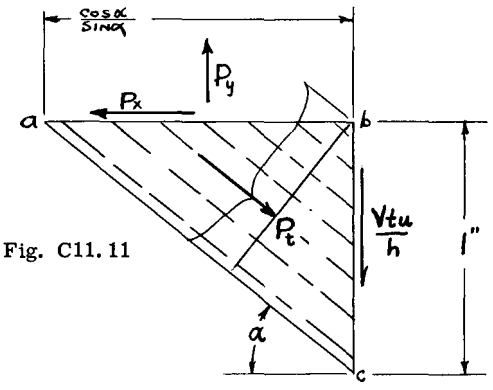

Fig. C11.11

$$P_r = \left[\left(\frac{V_{cr}\, I_F}{h\, I} + \frac{V_{tu}}{h} \right)^2 + \left(\frac{V_{tu}}{h} \tan \alpha \right)^2 \right]^{1/2} \quad ---- \quad (43)$$

C11.10 Flange Loads.

The axial flange loads are due to two primary causes, namely

(1) Stresses due to primary bending of the beam by the usual flexural theory.

(2) Additional stresses produced by the web tension field.

In addition to these two primary effects, secondary bending stresses due to the bending of the flange because of the tension field are produced as illustrated in Fig. C11.8.

Stresses for Primary Bending:

$$f_b = \pm \frac{M_{cr}\, y}{I} \pm \frac{(M - M_{cr})y}{I_F} \quad ------ \quad (44)$$

where

I = moment of inertia of total section including web about neutral axis

I_F = moment of inertia of section without web about neutral axis

M_{cr} = bending moment for load which causes web buckling

M = total bending moment on section

The first term in the above equation gives the bending stresses at the point where the web breaks down into a tension field. The web is thus effective in computing the moment of inertia I. The second term in the equation gives the bending stresses when the beam web acts as a tension field web, or in other words the buckled web is assumed ineffective in bending.

To be slightly conservative the bending stresses can be computed by the following equation which neglects the resistance of the web in bending before buckling.

$$f_b = \pm \frac{My}{I_F} \quad ---------- \quad (45)$$

The total flange loads can be calculated by equating the internal resisting couple to the external resisting couple to the external bending moment, or

$$F_c = F_t \pm \frac{M}{h'} \quad ---------- \quad (46)$$

where

F_c and F_t = total compressive and tensile flange load respectively

h' = distance between flange centroids

Equation (46) neglects the resistance of the web in bending.

Flange Axial Stresses Due to Web Tension Field

Due to the horizontal components of the diagonal tension field each flange is subjected to a compressive load equal to

$$F_c = F_t = -\frac{V_t}{2} \cot \alpha \quad --------- \quad (47)$$

(Reference see Equation (12) and general derivation when $\alpha = 45^0$ see Equation (8) and (9).

In Equation (47) V_t = shear load carried by tension field action.

Secondary Bending Stresses

For estimating the secondary bending moments on flanges due to lateral pull of web tension field, the flange can be treated as a continuous beam with spans equal to the stiffener spacing.

The component of the web diagonal tensile stresses normal to flange.

$$w_v = \frac{V_t}{h} \tan \alpha \text{ (pounds per inch)} \quad --- \quad (48)$$

where

V_t = shear carried by web in diagonal tension

For a continuous beam of equal spans, the moment over the supports = $1/12\ w_v\ d^2$, where d equals the stiffener spacing. The deflection of the flanges tends to relieve the pull in the center portion between stiffeners which then decreases the continuity moment over the support. Wagner (Ref. 1) gives a relieving factor C (See

Fig. C11.9) for use with the bending moment expression.

Therefore, the secondary bending moment on flanges is

$$M_{sec} = 1/12\ C \frac{V_t}{h} d^2 \tan \alpha \quad - - - - - - - \quad (49)$$

C11.11 Loads in Web Vertical Stiffeners.

The following method of checking the strength of vertical web stiffeners was originally proposed by Wagner (Refs. 1, 2) and can be considered conservative.

The axial column load in the web stiffener equals

$$F_{stiff.} = - V_t \frac{d}{h} \tan \alpha \quad - - - - - - - - \quad (50)$$

This is the same as equation (13) except V is replaced by V_t, the shear carried by the web in diagonal tension field action. Under this load Wagner considers the stiffeners as columns with elastic supports as the web tension restrains the struts from buckling out of the plane of the web. Wagner's calculations yield a reduction factor C_2 which the actual length of the stiffener is multiplied by to obtain a reduced length L', or

$$L' = C_2 L \quad - - - - - - - - - - - - - - - - - (50a)$$

With this reduced length L', and the actual cross section of the strut, the column strength can be calculated by the methods of Chapters C2 and C7. Fig. C11.12 by Wagner shows a plot of the reduction factor C which is a function of the parameter as shown.

Since the work of Wagner, the NACA has conducted an extensive research program on the strength and design of semi-tension field beams and the strength design of the web stiffeners has been based on a more rational basis. The NACA method is given later in this chapter and it is recommended that for final check of web

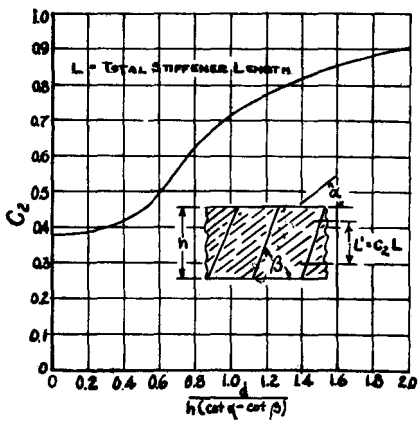

Fig. C11.12

stiffener design, the NACA method be used. The method above, proposed originally by Wagner, can be used for quick preliminary design of the web stiffener.

C11.12 Beams with Non-Parallel Flanges.

In many aircraft beams the flanges are not parallel but have a slight taper. For this case equations (46) and (47) give only the horizontal components of the flange loads. The total flange forces and their vertical components can be computed from the horizontal components and the slope of the flanges. Thus from Fig. C11.12a subtracting the vertical components of the flange forces we obtain the net web shear load V_{w_n}.

$$V_{w_n} = V_w - (F_t \tan \theta_t + F_c \tan \theta_c) \quad - (51)$$

where

V_{w_n} = net web shear for beam with non-parallel flanges

V_w = web shear for parallel flanges

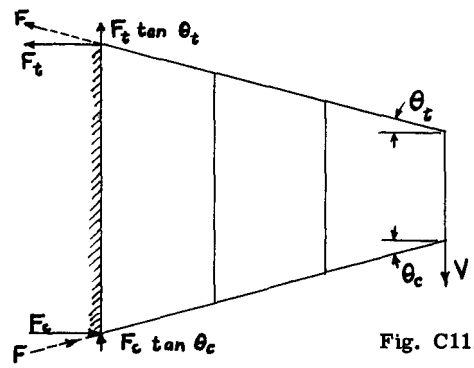

Fig. C11.12a

C11.13 Example Problem Using Method 1.

Fig. C11.13 shows a cantilever beam of constant cross-section carrying a 13500 lb. load at the free end. The beam will be strength checked for the given load. The material properties are:

Web: 2024-T3 alum. sheet. F_{tu} = 64000, F_{ty} = 42000, E = 10,500,000.

Flanges: 7075-T6 alum. alloy extruded. F_{tu} = 78000, F_{ty} = 70000, E = 10,300,000.

Investigation of Web Strength

Web panel size between web stiffeners and centroid of flange rivets = 10 by 28.56.

Aspect ratio of panel = a/b = 28.56/10 = 2.856.

The critical buckling shear stress is given by Eq. C5.4 from Chapter C5:-

$$F_{s_{cr}} = \frac{\pi^2 k_s E}{12 (1 - \nu_e^2)} \left(\frac{t}{b}\right)^2 \quad - - - - - - - (A)$$

The buckling coefficient k_s for an a/b ratio of 2.856 and simply supported edges is obtained from Fig. C5.11 of Chapter C5 which gives $k_s = 5.8$. Substituting in (A),

$$F_{s_{cr}} = \frac{\pi^2 \times 5.8 \times 10{,}500{,}000}{12 (1 - .3^2)} \left(\frac{.025}{10}\right)^2 = 342 \text{ psi}$$

Therefore shear load resistance developed by web up to buckling stress equals

$$V_{cr} = F_{s_{cr}} h t = 342 \times 28.56 \times .025 = 244 \text{ lb.}$$

The shear strength of the web acting as a tension field after buckling is given by the following equations, when stressed to the yield point in tension

$$V_{ty} = \left(F_{ty} - \frac{F_{s_{cr}}}{K_r}\right) K_r \, R h t \sin\alpha \cos\alpha$$

(See Eq. 27)

when stressed to ultimate stress in tension

$$V_{tu} = \left(F_{tu} - \frac{F_{s_{cr}}}{K_r}\right) K_r \, R h t \sin\alpha \cos\alpha$$

(See Eq. 29)

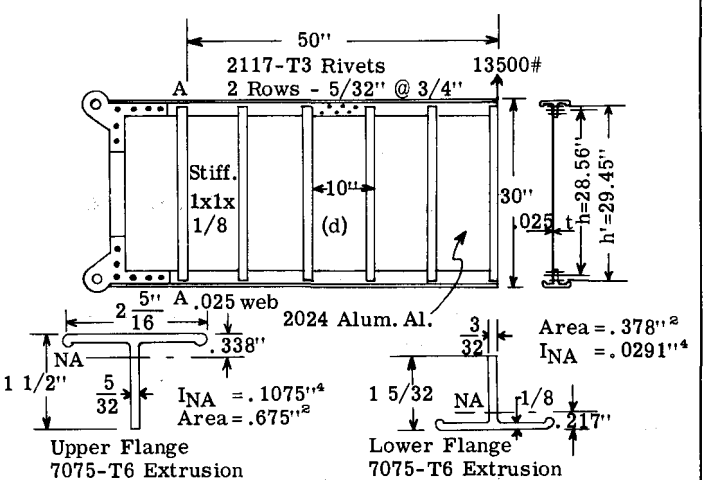

Fig. C11.13

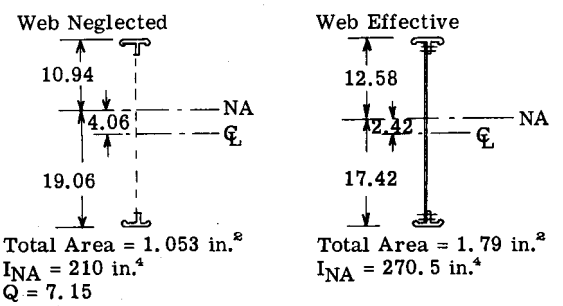

Before solving these equations, the terms α, R, and K_r must be determined:

The angle of the diagonal tension field with horizontal is

$$\sin^2\alpha = \sqrt{a^2 + a} - a \qquad \text{(see Eq. 15)}$$

where

$$a = \frac{1 + \dfrac{ht}{A_u + A_L}}{\dfrac{dt}{As} - \dfrac{ht}{A_u + A_L}} \qquad \text{(see Eq. 16)}$$

Substituting

$$a = \frac{1 + \dfrac{28.56 \times .025}{.675 + .378}}{\dfrac{10 \times .025}{.23} - \dfrac{28.56 \times .025}{.675 + .378}} = 4.05$$

hence

$$\sin^2\alpha = \sqrt{4.05^2 + 4.05} - 4.05 = .47$$

$$\sin\alpha = .685, \quad \alpha = 43^\circ, \quad \cos\alpha = .73$$

To determine the web stress concentration factor R, we solve for term wd and use curve of Fig. C11.9.

$$wd = 1.25 \, d \sin\alpha \sqrt[4]{\frac{t}{(I_u + I_L)h}} \quad \text{(Ref.Eq.14)}$$

$$wd = 1.25 \times 10 \times .685 \sqrt[4]{\frac{.025}{(.1075 + .0291)\, 28.56}}$$

$$= 2.43$$

From curve Fig. C11.9, R = .86

Since the web is riveted to the flange, correction must also be made for net area of web.

$$K_r = \frac{\text{rivet spacing - rivet diameter}}{\text{rivet spacing}} = \frac{.75 - .156}{.75}$$

$$= .79$$

For 2024-T3 material, $F_{ty} = 42000$ and $F_{tu} = 64000$ psi.

$$V_{ty} = \left(42000 - \frac{342}{.79}\right) .79 \times .86 \times 28.56 \times .025$$

$$\times .685 \times .73$$

$$V_{ty} = (41565)\ .242 = 10100 \text{ lb.}$$

$$V_{tu} = \left(64000 - \frac{342}{.79}\right) .242 = 15400 \text{ lb.}$$

The total shear load including strength of flanges is given by equations (33) and (34), namely

$$V_{yield} = \frac{1}{Qh} (V_{cr} + V_{ty})$$

$$V_{ult.} = \frac{1}{Qh}(V_{cr} + V_{tu})$$

From Fig. C11.13

$I_{N.A.}$ of section without web = 210 in.^{4}

Q of flange about N.A. = 7.15

$$V_{yield} = \frac{210}{7.15 \times 28.56}(244 + 10{,}100) = 10{,}670 \text{ lb.}$$

$$V_{ult.} = \frac{210}{7.16 \times 28.56}(244 + 15{,}400) = 16{,}070 \text{ lb.}$$

The design ultimate shear load = 13,500 lb. hence

M.S. = (16,070/13,500) - 1 = .19

The applied shear load using a factor of safety of 1.5 is 13,500/1.5 = 9000 lb.

The yield strength is 10,670 lb. Thus for margin of safety of yield strength over applied load, we have (10,670/9000) - 1 = .18.

The results show that the beam shear resistance is proportioned as follows for a total ultimate strength of 16,070 lb., (244/16,070 x 100 = 1.5% carried by web in pure shear, and 15,400/16,070) 100 = 96.0% carried by web as a diagonal tension field.

The remainder or 2.5% is carried by the shear strength of the flanges. This value is relatively low for this particular beam, as in general the flange may provide considerably more of the resistance. Due to the thin web thickness and the large web panels, the web buckles at a relatively low stress, thus the percent of the external shear load carried by the web at the buckling stress is quite small.

Check of Rivet Attachment - Web to Flange

The .025 web is attached to the flange member by 2 rows of 5/32 diameter 2117-T3 rivets at 3/4 inch spacing.

The resultant load on the rivets per inch of flange is given by equation (43), namely

$$P_r = \left[\left(\frac{V_{cr}\, I_F}{h\, I} + \frac{V_{tu}}{h}\right)^2 + \left(\frac{V_{tu}}{h}\tan\alpha\right)^2\right]^{1/2} \quad --(B)$$

The web is not stressed to its ultimate tensile stress since we have 4% margin of safety. We will therefore solve equation (A) for V_{tu} using the given external shear load V = 13,500 lb., and call this value V_t, the shear load carried by the tensile field under the given shear load of 13,500 lb.

$$13500 = \frac{210}{7.15 \times 28.56}(244 + V_t)$$

$$13500 = 1.03\,(244 + V_t)$$

whence

V_t = 12,850 lb., which represents V_{tu} in equation (B) for P_r

Substitute in Equation (B)

$$P_r = \left[\left(\frac{244}{28.56}\,\frac{210}{270.5} + \frac{12850}{28.56}\right)^2 + \frac{12850}{28.56} \times .933^2\right]^{1/2}$$

$$P_r = \left[(6 + 450)^2 + 420^2\right]^{1/2} = 624 \text{ lb./per inch.}$$

Load per rivet pitch of .75 inch = .75 x 624 = 468 lb.

Single shear strength of 5/32 - 2117-T3 rivet = 596 x .86 = 512 lb. (See Chapter D1).

Bearing strength on 2024-T3 sheet = 1.24 x 392 = 486 lb. (See Chapter D1).

Bearing is critical and the rivet strength per rivet pitch is 2 x 486 = 972 lb. (2 rows of rivets).

Margin of Safety = (972/468) - 1 = 1.08

Due to large M.S., the rivet diameter could be made 1/8 inch, or 5/32 rivets could be spaced farther apart.

CHECK OF FLANGE STRENGTH

The end bay of the cantilever beam involves special design considerations such as the two beam fittings and the special end stiffener. Therefore, the basic flange areas will be checked at Section A-A, which is 50 inches from the load point, which is where the end fitting would possibly begin to take load out of the flange members.

Design bending moment at beam Section A-A is,

50 x 13,500 = 675,000 in. lb.

Since V_{cr} = 244 lb., which is the shear load the web carries without buckling, the bending moment due to a shear of 244 lb. will be resisted by the entire cross-section including the web. Above this value the remaining moment is resisted by the section with the web neglected in computing the moment of inertia.

Thus bending moment at web buckling load = 244 x 50 = 12200 in. lb.

Bending moment for tension field beam = 675,000 - 12200 = 662800 in. lb.

Bending Stresses

Upper Flange Bending Stresses:

$$f_b = -\frac{12200 \times 12.58}{270.5} - \frac{662,800 \times 10.94}{210}$$

(See Eq. 44)

$$= -567 - 34600 = -35167 \text{ psi.}$$

If the entire bending moment were assumed resisted by the flanges alone, then,

$$f_b = \frac{675000 \times 10.94}{210} = -35200 \text{ psi.}$$

Lower Flange Bending Stresses

$$f_b = \frac{-12200 \times -17.42}{270.5} + \frac{-662800 \times 19.06}{210}$$

$$= 783 + 60200 = 60980 \text{ psi.}$$

(Note: Section properties were computed without taking out one 5/32 rivet hole in vertical leg of flange tee, thus stresses are slightly unconservative. To be on the safe side, the net section properties should be used in figuring stresses).

Average Axial Flange Loads Due to Bending

Total Flange Load = $\frac{M}{h'} = \frac{675000}{29.45} = 22900$ lb.

Upper Flange $f_{c(aver.)} = -22900/.675 = -33900$ psi.

Lower Flange $f_{t(aver.)} = 22900/.378 = 60500$ psi.

Flange Axial Loads Due to Tension Field Action

The axial load in each flange due to diagonal tension in web equals

$$F_t = F_c = -.5\, V_t \cot \alpha \quad \text{(See Eq. 47)}$$

$$= -.5 \times 12850 \times 1.07 = -6860$$

Average stress on upper flange

$f_c = -6860/.675 = -10,170$ psi.

Lower flange, $f_t = -6860/.378 = -18180$ psi.

Combined Flange Axial Stresses

Upper Flange - Extreme Fiber

$f_c = -35167 - 10770 = -45337$ psi.

Average stress:-

$f_{c(av.)} = -33900 - 10170 = -44070$ psi.

Lower Flange - Extreme Fiber

$f_t = 60980 - 18180 = 42800$ psi.

Average $f_t = 60500 - 18180 = 42320$ psi.

Since the tension field action tends to decrease the tension load in the lower flange, it is good practice not to include the entire relieving effect as tension field action is not an exact theory.

Flange Secondary Bending Stresses

Since the web is in a diagonal tension condition, it pulls on the flange members, or in other words, each flange acts as a continuous beam with the web stiffeners as the support points and the transverse load on the flange is equal to the vertical component of the web diagonal tensile stresses. This secondary bending moment is approximated by equation (49).

$$M_{sec.} = 1/12\ C \frac{V_t}{h} d^2 \tan \alpha$$

From Fig. C11.9, C = .925 when wd = 2.43

whence

$$M_{sec.} = 1/12 \times .925 \times \frac{12850}{28.56} \times 10^2 \times .933 = 3230 \text{ in.lb.}$$

Secondary Bending Stresses on Upper Flange

$I_{N.A.}$ upper flange = .1075 (See Fig. C11.13)

I/y lower fiber = .1075/1.16 = .0925
I/y upper fiber = .1075/.338 = .318

$f_{b(lower\ fiber)} = 3230/.0925 = 34900$ psi Compression as flange bends over the support.

$f_{b(upper\ fiber)} = 3230/.318 = 10140$ psi. (tension)

The combined stress on the lower fiber then would be -34900 - 44070 = -78970 psi.

The combined stress on the upper fiber would be 10140 - 45337 = - 35197 psi.

Secondary Bending Stresses on Lower Flange

$I/y_{lower\ fiber} = .0291/.217 = .134$ (from Fig. C11.13) $I/y_{upper\ fiber} = .0291/.939 = .031$

$f_{b(upper\ fiber)} = 3230/.031 = 104000$ psi (Compression)

$f_{b(lower\ fiber)} = 3230/.134 = 24100$ psi tension

The combined stresses on lower flange are:-

$f_{(\text{upper fiber})} = 42320 - 104000 = \underline{-61880}$ psi

$f_{(\text{lower fiber})} = 42800 + 24100 = \underline{66900}$ psi

Calculation of Failing Compressive Stress for Upper Flange.

It will be assumed that lateral column action is prevented by lateral bracing from adjacent structure, thus failure of flange will be by local crippling.

The crippling stress for the flange as a whole will be calculated by the Gerard method as given in Chapter C7. The bulbs on the Tee Section (see Fig. C11.13) will be assumed as only partially effective in producing a simple support to the adjacent plate. The g number for the Tee Section will be taken as 4 which is no doubt slightly conservative. The design curve of Fig. C7.7 of Chapter C7 will be used.

$$\frac{A}{gt^2}\left(\frac{F_{cy}}{E_c}\right)^{1/2} = \frac{0.675}{4 \times .1562^2}\left(\frac{70{,}000}{10{,}300{,}000}\right)^{1/2} = .572$$

From Fig. C7.7 we read $F_{cs}/F_{cy} = .90$, hence $F_{cs} = .9 \times 70000 = \underline{63000}$ psi. compression.

Without the effect of secondary bending of flanges, the average axial stress on upper flange was previously calculated to be -44070 psi. Thus margin of safety would be (63000/44070) - 1 = .43. However, the upper flange must also carry the stresses due to the flange acting as a continuous beam with the web vertical stiffeners as the support points. This bending moment over the support points was previously calculated to be 3230 inch lbs. The bending moment midway between the support points would be about 50 percent of this value since lateral deflection of flange produces a relieving effect. The previous calculations gave the combined stress on upper fiber as -35197 psi, and on the lower fiber as -78970 psi. This compressive stress is above the F_{cy} value of 70000 for 7075-T6 material and thus the vertical leg of the Tee is obviously weak. The permissible average stress on the vertical leg can be calculated by considering it part of an equal angle section and computing the crippling stress by the Needham method of Chapter C7. The result would be -51500 psi, thus with a stress of -78970 existing weakness is indicated and re-design is necessary.

The question now arises, what changes can be made without adding any weight to the present flange. Two obvious faults exist in the flange design. (1) For a beam 30 inches deep, increasing the depth of the flange by a small amount such as 0.5 inch would not effect appreciably the over-all beam bending strength, however, the 0.5 inch increase in depth of the Tee would raise the moment of inertia of the Tee considerably. (2) The strength of the vertical leg of the Tee can be improved by adding a lip. This addition will likewise increase the flange moment of inertia, which is needed to decrease the stresses due to the secondary bending action.

Fig. (A) shows a re-design of the flange section with the same area as before, thus no weight is added. The Tee has been made 0.5 inch more in height and an 0.5 inch wide lip has been added to bottom of Tee. The thickness and bulb size has been reduced to cancel the area added. The new section properties are given in Fig. A.

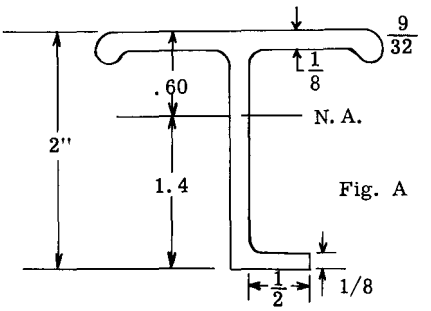

Fig. A

Area = .675
I_{NA} = 0.35
I/y upper fiber = .584
I/y lower fiber = .25

The secondary bending stresses will now be recalculated.

$$f_{b(\text{upper})} = \frac{3230}{.25} = -12900$$

$$f_{b(\text{lower})} = \frac{3230}{.584} = 5530$$

The combined stress on the lower fiber is -44070 - 12900 = -56970 psi as against the previous value of -78970 before Tee was modified. Adding the lip on the bottom of the Tee would raise the allowable stress above the -51500 previously calculated, thus stress of -56970 can now be carried.

This example problem has brought out the fact that the secondary bending stresses can be a major stress factor unless proper attention is given to designing the flange to reduce the secondary bending stresses.

Another approach to calculating or checking the strength of the flange would be to use the inter-action equation,

$$R_c + R_b = 1$$

where R_c is equal to the flange load due to beam

bending and web diagonal tension effect, divided by the crippling stress F_{cs} of the flange section.

R_b is the ultimate bending moment that the flange can develop as per the method presented in Chapter C3, divided by the design secondary bending moment.

Strength Check Lower Flange (Tension Flange)

As previously calculated, the stress on bottom fiber was 66900 psi tension and -61880 psi compression on the upper fiber of the lower flange. The tension is O.K. since the F_{tu} of the material is 78000 psi which should give enough margin of safety to take care of rivet holes. However, the compressive stress of -61880 is too high and re-design is necessary. The difficulty is due to the large stress from secondary bending. Thus making similar changes for the lower flange Tee as was done for upper flange Tee would solve the problem without adding appreciable weight.

Check of Web Vertical Stiffener Strength.

Column load in web stiffener is given in Eq. (50).

$$F_{stiff.} = -V_t \frac{d}{h} \tan \alpha$$

$$= -12850 \frac{10}{28.56} \times .933 = -4200 \text{ lb.}$$

The reduced column length factor C of the web stiffener is obtained from Fig. C11.12 for a parameter of

$$\frac{d}{h\ (\cot \alpha \cot \beta)} = \frac{10}{28.56\ (\cot 40^0)} = .304$$

and gives $C_e = .38$

hence

$$L' = .38 \times 28.56 = 10.8"$$

Assuming an effective width of web sheet equal to 30 t as acting with the 1 x 1 x 1/8 angle stiffener the radius of gyration equals .267 and the area equals .253,

hence

$$L'/\rho = 10.8/.267 = 40.5$$

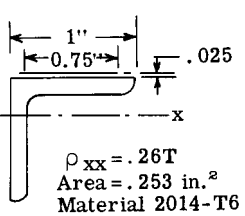

The crippling stress will be calculated by Needham method of Chapter C7.

$$b'/t = .9375/.125 = 7.5$$

From Fig. C7.3 of Chapter C7, $F_{cs}/\sqrt{F_{cy}E} = .07$. $F_{cs} = .07\sqrt{53000 \times 10{,}700{,}000} = 52500$ psi.

Using Johnson-Euler equation of Chapter C7,

$$F_c = F_{cs} - \frac{F_{cs}^2}{4\pi^2 E} (L'/\rho)^2$$

$$F_c = 52500 - \frac{52{,}500}{4\pi^2\ 10{,}700{,}000} (40.5)^2 = 41800 \text{ psi.}$$

Stiffener strength = $P = F_c A = 41800 \times .253 = -10600$ lb.

The load being only 4200 lb., the stiffener is far overstrength and should be re-designed to save structural weight.

METHOD 2

C11.14 NACA Method of Strength Analysis for Semi-Tension Field Beams with Flat Webs.

Method 1, or the modified Wagner equations and procedure used in example problem, are somewhat conservative relative to web and web stiffener design. To eliminate this conservatism and place the web and stiffener design on a more rational or truer basis, the NACA carried on a comprehensive study and testing program to develop a better understanding of semi-tension field beam action and to present a design procedure for use by the aeronautical structures engineer. The results of this program are summarized in (Refs. 3 and 4). The material which follows is taken from those reports.

NACA SYMBOLS

The list of symbols which follows is the same as used in Refs. 3 and 4 except σ, τ and σ_o have been replaced by f_n, f_s and F_u respectively, in order to be consistent with the symbols used in the first part of this chapter.

A cross-sectional area, square inches.
E Young's modulus, KSI.
G shear modulus, KSI.
P force in KIPS.
Q static moment about neutral axis of parts of cross-section as specified by subscripts. in.
R coefficient of edge restraint.
S transverse shear force, kips.
d spacing of uprights, inches.
e distance from median plane of web to centroid of (single) upright, inches.
h depth of beam, inches.
k diagonal-tension factor.

t thickness, inches (used without subscript) signifies thickness of web).
α angle between neutral axis of beam and direction of diagonal tension, degrees.
ρ centroidal radius of gyration of cross-section of upright about axis parallel to web, inches (no sheet should be included).
f_n normal stress ksi.
f_s shear stress ksi.

Subscripts

DT diagonal tension
F flange
S shear
u upright
W web
cr critical
ult ultimate
e effective

Special Combinations

P_u internal force in upright, kips.
R" shear force on rivets per inch run kips. per inch.
R_{tot} total shear strength (in single shear) of all rivets in one upright, kips.
d_c upright spacing measured as shown in Fig. C11.16a.
h_c depth of web as measured as shown in Fig. C11.16a.
h_e depth of beam measured between centroids of flanges, inches.
h_r depth of beam measured between centroids of web to flange rivet patterns, inches.
h_u length of upright measured between centroids of upright to flange rivet patterns, inches.
k_{ss} theoretical buckling coefficient for plates with simply supported edges.
F_u "basic" allowable stress for forced crippling of uprights.
wd flange flexibility factor $(.7d\sqrt[4]{\frac{t}{(I_C+I_T)}}h_e$ where I_C and I_T are moments of inertia of compression and tension flanges respectively.

C11.15 Engineering Theory of Incomplete Diagonal Tension.

In a beam with a thin flat sheet as a web, if the external shear load is less than the buckling load for the web, then the web is in a state of pure shear at the neutral axis as indicated in Fig. C11.14 (Fig. a). If we neglect the normal stresses due to bending over the depth of the web, this shear stress arrangement can be assumed constant over the full depth of the web.

If a web is thin, it will buckle under a certain critical load and if the load is increasing beyond this critical buckling value, the buckle pattern will approach a pure tension field as indicated in (b) of Fig. C11.14b.

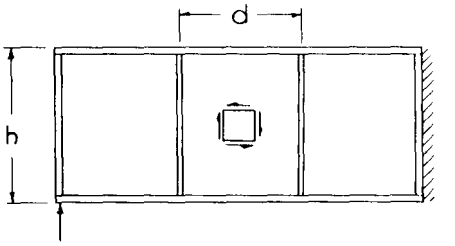

(a) Nonbuckled ("shear-resistant") web.

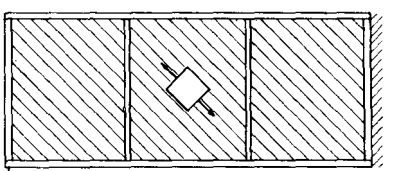

(b) Pure diagonal-tension web.

Fig. C11.14 - State of Stress in a Beam Web.

In the usual practical thin web beam in aircraft construction, the state of stress in the web is intermediate between pure shear and pure diagonal tension. The engineering theory as developed by the NACA considers that this intermediate state of incomplete diagonal tension may be based on the assumption that the total shear force in the web can be divided into two parts, a part S_S carried by pure shear and a part S_{DT} carried by pure diagonal tension.

Thus under this assumption one can write,

$S = S_S + S_{DT}$, which can be written in the form

$$S_{DT} = kS$$

$$S_S = (1-k)S \quad - - - - - - - - - - - - - - (52)$$

where k is the "diagonal-tension factor" which expresses the degree to which the diagonal tension is developed by a given load. Thus the state of pure shear is measured by $k = 0$ and the state of pure diagonal tension by $k = 1$. Fig. C11.15 illustrates the stress condition for the limiting cases of $k = 0$ and $k = 1$ and for the intermediate case. The letters PS, DT and PDT as labeled on Fig. C11.15 mean pure shear, diagonal tension and pure diagonal tension respectively relative to web stress conditions.

C11.16 Formulas for Stress Analysis.

Limitations of Formulas:

The NACA believes the formulas which follow will give reasonable strength predictions if

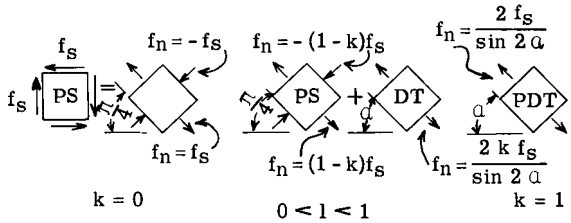

Fig. C11.15 Resolution of Web Stresses at Different Stages of Diagonal Tension.

normal design practices are used. The following limitations should be observed.

(1) Uprights on web stiffeners should not be too thin. $\frac{t_u}{t} > 0.6$

(2) The upright or web stiffener spacing should not be too much outside the range $0.2 < \frac{d}{h} < 1.0$

(3) The tests by NACA did not cover beams with very thin or very thick webs, hence some possibility of inconservative predictions may exist if $\frac{h}{t} >$ 1500 or less than 200.

C11.17 Critical Shear Stress.

In the elastic range, the critical shear stress between two web uprights is calculated by the formula:-

$$F_{s_{cr}} = k_{ss} E \left(\frac{t}{d_c}\right)^2 \left[R_h + \frac{1}{2}(R_d - R_h)\left(\frac{d_c}{h_c}\right)^3\right] \quad (53)$$

where,

k_{ss} = theoretical buckling coefficient (given in Fig. C11.16a for panel length of h_c and width d_c with simply supported edges.

d_c = width of sheet between uprights measured as shown in Fig. C11.16a.

h_c = depth of web measured as shown in Fig. C11.16a.

R_h = restraint coefficient for edges of sheet along upright (See Fig. C11.16b).

R_d = restraint coefficient for edges of sheet along flanges. (See Fig. C11.16b).

(If $d_c > h_c$, substitute h_c for d_c; d_c for h_c; R_d for R_h; and R_h for R_d).

Curves of the critical shear stresses for plates of 2024 aluminum alloy with simply supported edges are given in Fig. C11.17. To the right of the dashed line the curves in Fig. C11.17 are plots of the theoretical equation,

$$F_{s_{cr}} = k_{ss} E \left(\frac{t}{d_c}\right)^2 \quad \text{- - - - - - - - - - (54)}$$

and may be used for most aluminum alloys. To the left of the dashed line, the curves represent straight line tangents to the theoretical curves in a nonlogarithmic plot and are valid only for 2024 aluminum alloy.

If the critical shear buckling stress is above the proportional limit stress for the material, a plasticity correction must be made. Fig. C11.18 presents curves for correcting the calculated elastic values for this plasticity effect. The plasticity correction for other materials can be obtained as explained in Art. C5.8 and Fig. C5.13 of Chapter C5.

C11.18 Loading Ratio.

The loading ratio is the ratio $f_s/F_{s_{cr}}$ where f_s is the depth-wise average or nominal shear stress.

When the depth of the flanges is small compared with the depth of the beam and the flanges are angle sections, the stress f_s may be computed by the formula

$$f_s = \frac{S_w}{h_e t} \quad \text{- - - - - - - - - - - - - - - (55)}$$

In beams with other cross-sections, the average nominal shear stress should be computed by the formula

$$f_s = \frac{S_w Q_F}{It}\left(1 + \frac{2 Q_w}{3 Q_F}\right) \quad \text{- - - - - - - - - (56)}$$

Where Q_F is the static moment about the neutral axis of the flange material and Q_W is the static moment about the neutral axis of the effective web material above the neutral axis. For the computation of I and Q, the effectiveness of the web must be estimated in the first approximation. As second and final approximation, the effectiveness of the web may be taken as equal to (1 - k), where k is the diagonal-tension factor determined in the next step. Thus in computing I and Q the effective web thickness is (1 - k) t.

C11.19 Diagonal-Tension Factor k.

Having determined the loading ratio $f_s/F_{s_{cr}}$, the diagonal tension factor k can be read from Fig. C11.19.

C11.20 Average and Maximum Stress in Upright or Web Stiffener.

The average stress over the length of the upright for a double upright (stiffener on each side of web) can be calculated by the formula,

$$f_u = \frac{k\, f_s \tan \alpha}{\frac{A_u}{dt} + .05\,(1 - k)} \quad \text{- - - - - - - - - (57)}$$

This equation can be evaluated with the use of Fig. C11.20. The stress f_u is uniformly distributed over the cross-section of the upright until buckling of the upright begins.

Eq. 57 assumes the values f_s, k, and α to be the same in the panels on each side of the stiffener. If they are not, then average values should be used, or a conservative check should be made using the largest shear value.

Single Upright (or Web Stiffener on one side of Web)

The stress f_u for a single upright is obtained in the same manner, except that the ratio A_u/dt is replaced by A_{u_e}/dt, where

$$A_{u_e} = \frac{A_u}{1 + (\frac{e}{\rho})^2} \quad \text{- - - - - - - - - - - - (58)}$$

For the single upright f_u is still an average over the length of the upright, but it applies only to the median plane of the web along the line of rivets connecting the upright to the web. In any given cross-section of the upright, the compressive stress decreases with increasing distance from the web, because the upright is a column loaded eccentrically by the web tension. Thus formulas for local crippling based on uniform distribution of stress over the cross-sections do not apply.

Maximum Stress in Upright

The stress f_u in the upright varies from a maximum at (or near) the neutral axis of the beam to a minimum at the ends of the upright ("gusset effect"). The maximum value is given by the following equation:-

$$f_{u_{max.}} = f_u\, (\frac{f_{u_{max.}}}{f_u}) \quad \text{- - - - - - - - - (59)}$$

where, $(f_{u_{max.}}/f_u)$ is the value of the ratio when the web has just buckled, Fig. C11.21 gives the value of this ratio.

C11.21 Angle of Diagonal Tension.

Having determined k and f_u/f_s, the angle α between the direction of the diagonal tension and the axis of the beam can be determined by the use of Fig. C11.22.

C11.22 Allowable Stresses in Uprights.

Four types of failure are conceivable.

(1) Column Failure.
(2) Forced Crippling Failure.
(3) Natural Crippling Failure.
(4) General elastic instability failure of web and stiffeners.

Column Failure

Column failures in the usual meaning of the word (failure due to instability, without previous bowing) are possible only in double uprights. When column bowing begins, the uprights will force the web out of its original plane. The web tensile forces will then develop components normal to the plane of the web which tend to force the uprights back. This bracing action is taken into account by using a reduced "effective" column length L_e of the upright, which is given by the following empirical formula,

$$L_e = \frac{h_u}{\sqrt{1 + k^2\,(3 - 2\,\frac{d}{h})}} \quad \text{- - - - - - - (60)}$$

The stress f_u at which column failure takes place can be found using the standard column curve with the slenderness ratio L_e/ρ as shown.

The problem of "column" failures in a single upright has not been investigated to any extent and test results are greatly at variance with theoretical results. Two criterions are suggested for strength design, namely:-

(a) The stresses f_u should be no greater than the column yield stress for the upright material. This accounts for the upright acting as an eccentrically loaded compression member.

(b) The stress at the centroid of the upright (which is the average stress over the cross-section) should be no greater than the allowable column stress for the slenderness ratio $h_u/2\rho$. This is an attempt to take in account a two-wave type of buckling failure that has been observed in very slender uprights.

Forced Crippling Failure

The shear buckles in the web will force buckling of the upright in a leg attached to the web, particularly if the upright leg is thinner than the web. These buckles give a lever arm to the compressive force acting in the leg and therefore produce a severe stress condition. The buckles in the attached leg will in turn induce buckling of the outstanding legs.

In single uprights the outstanding legs are relieved to a considerable extent by virtue of the fact that the compressive stress decreases with distance from the web; the allowable stresses for single uprights are therefore somewhat higher than those for double uprights. Because the forced crippling is of local nature, it is assumed to depend on the peak value $f_{u_{max.}}$ of the upright stress rather than on the average value.

The upright stress at which final collapse occurs is obtained by the following empirical method:-

(1) Compute the allowable value of $F_{u_{max.}}$ for a perfectly, elastic upright material by the formula:-

For 2024-T3 Aluminum Alloy:-

$F_u=21000k^{2/3}(t_u/t)^{1/3}$ (For double uprights)-(61a)

$F_u=26000k^{2/3}(t_u/t)^{1/3}$ (For single uprights)-(61b)

For 7075-T6 Aluminum Alloy:-

$F_u=26000k^{2/3}(t_u/t)^{1/3}$ (For double uprights)-(61c)

$F_u=32500k^{2/3}(t_u/t)^{1/3}$ (For single uprights)-(61d)

(2) If F_u exceeds the proportional limit for the upright material, use as allowable value the stress corresponding to the compressive strain F_u/E.

F_u can also be obtained for various materials from Fig. C11.38.

Natural Crippling Failure

The term "natural crippling failure" is used to denote a crippling failure resulting from a compressive stress uniformly distributed over the cross-section of the upright. By this definition it can occur only in double uprights. To avoid natural crippling failure, the peak stress in the upright $F_{u_{max.}}$ in the upright should be less than the crippling stress of the section for $L/\rho \rightarrow 0$. It appears that crippling failure does not appear to be a controlling factor in actual designs.

General Elastic Instability of Web and Uprights

Test experience so far has not indicated that general elastic instability need be considered in design. Apparently the web system is safe against general elastic instability if the uprights are designed to fail by column action or by forced crippling at a shear load not much less than the shear strength of the web.

C11.23 Web Design.

For design purposes, the peak value of the nominal web shear stress within a bay is taken as,

$$f_{s_{max.}} = f_s\,(1+kC_1)(1+kC_2) \quad ----(62)$$

Refer to Figs. C11.23 and C11.24 to determine values of factors C_1 and C_2. The C_1 term constitutes a correction factor to allow for the angle α of the diagonal tension field differing from 45 degrees. C_2 makes allowance for the stress concentration due to the flexibility of the beam flanges.

Allowable Shear Stress F_s.

The allowable shear stress F_s is determined by tests and depends on the value of the diagonal-tension factor k as well as on the details of the web to flange and web to upright fastenings. Fig. C11.25 gives empirical allowable curves for two aluminum alloys. It should be noted that these curves contain an allowance for the rivet factor; inclusion of this factor in these curves is possible because tests have shown that the ultimate shear stress based on the gross section (that is, without reduction of rivet holes) is almost constant within the normal range of rivet factor ($C_R > 0.6$).

For the allowable stress for other materials refer to Fig. C11.42.

Permanent Buckling of Web.

A check for the development of permanent shear buckles can be made using Fig. C11.46. In this figure $F_{s_{P.B.}}$ is the allowable web gross shear stress for no permanent buckles. The Air Force usually specifies no permanent buckles at limit load.

C11.24 Rivet Design.

Web to Flange Rivets

The load per inch run acting on web to flange rivets is taken as,

$$R'' = \frac{S_W}{h_R}(1 + 0.414\,k) \quad --------(63)$$

With double uprights the web to upright rivets must provide sufficient longitudinal shear strength to make the two uprights act as an integral unit until column failure occurs. The total shear strength (single shear strength of all rivets) required in an upright is

$$R_{total} = \frac{2\,F_{co}\,Q\,h_u}{b\quad L_e} \quad --------(64)$$

where

F_{co} = column yield strength of upright material. (If F_{co} is expressed in ksi, R_{total} will be in kips.)

Q = static moment of cross-section of one upright about an axis in the median plane of the web in.^{3}

b = width of outstanding leg of upright.

h_u/L_e = ratio obtainable from formula (60).

The rivets must also have sufficient tensile strength to prevent the buckled sheet from lifting off the stiffener. The necessary strength is given by the criterion.

Tensile strength per inch of rivets > $0.15 \times t F_{tu}$ - - - - - - - - - - - - - (65)

where F_{tu} is the tensile strength of the web.

For Web to Upright Rivets on Single Uprights.

The required tensile strength is given by the tentative criterion,

Tensile strength per inch of rivets > $.22 \times t F_{tu}$ - - - - - - - - - - - - - (66)

(The tensile strength of a rivet is defined as the tensile load that causes any failure; if the sheet is thin failure will consist in the pulling of the rivet through the sheet.)

No criterion for shear strength of the rivets on single uprights has been established; the criterion for tensile strength is probably adequate to insure a satisfactory design.

The pitch of the rivets on single uprights should be small enough to prevent inter-rivet buckling of the web (or the upright leg if thinner than the web), at a compressive stress equal to $f_{u_{max}}$. The pitch should also be less than d/4 in order to justify the assumption on edge support used in the determination of $F_{s_{cr}}$.

Upright to Flange Rivets

These rivets must carry the load existing between upright and beam flange. These loads are,

$P_u = f_u A_u$ (for double uprights) - - (67)

$P_u = f_u A_{u_e}$ (for single uprights) - - (68)

These formulas neglect the gusset effect (decrease of f_u towards the ends of the upright) in order to be conservative. Two fasteners should be used to attach the upright to the flange, especially when the upright is joggled. (See Chapter D3.)

C11.25 Secondary Bending Moments in Flanges.

The secondary moment in a flange, caused by the vertical component of the diagonal tension may be taken as,

$$M = \frac{1}{12} k f_s t d^2 C_3 \text{ - - - - - - - - - - (69)}$$

where C_3 is a factor given in Fig. C11.24. The moment given by this formula is the maximum moment and exists at the ends of the bay over the uprights. If C_3 and k are near unity, the moment in the middle of the bay is half as large as that given by formula (69) and of opposite sign.

C11.26 Shear Stiffness of Web.

The theoretical effective shear modulus of a web G_e in partial diagonal tension is given in Figs. C11.26a and C11.26b. In Fig. C11.26a, G_{IDT} is valid only in the elastic range. The correction factor for plasticity is given for 2024-T3 aluminum alloy in Fig. C11.26b.

The effective modulus should be used in deflection calculations.

$$G_e = \frac{G_{IDT}}{G} \times \frac{G_e}{G_{IDT}} \text{ - - - - - - - - - - (70)}$$

G_e, for example, should be used in place of G in the flexibility coefficients for shear panels in Art. A7.10 of Chapter A7, if buckling skins or webs are present.

C11.27 Example Problem. Using NACA Method. (Method 2).

The beam used in example problem of Art. C11.13 will be checked by the NACA Method.

First check to see if given beam falls within the limitations of the NACA formulas.

From Art. C11.16:-

$\frac{t_u}{t}$ should be greater than 0.6

For our beam t_u the leg thickness of the upright is .125" and the web thickness is .025", hence .125/.025 = 5, which is greater than .6.

Also from Art. C11.16, the d/h value for the beam should fall between .2 and 1.0.

The d/h value for our beam is 10/30 = .333 which falls within the given range.

Calculation of the Critical Shear Stress ($F_{s_{cr}}$)

Use will be made of Fig. C11.17,

$\frac{d_c}{t} = \frac{10}{.025} = 400 = \frac{\text{Stiffener spacing}}{\text{Web thickness}}$ (See Fig. C11.16)

$\frac{h_c}{d_c} = \frac{27.94}{10} = 2.79$, See Fig. C11.16 for h_c.

Using the above values, we find from Fig. C11.17 that

$F_{s_{cr}} = 370$ psi.

Calculation of the Loading Ratio $f_s/F_{s_{cr}}$

From equation 55

$$f_s = \frac{S_w}{h_e t} = \frac{13500}{29.45 \times .025} = 18350 \text{ psi.}$$

where, S_w = external shear load on web.
h_e = distance between flange centroids.

Equation 55 was used because the flanges will take very little of the shear load.

Therefore the loading ratio,

$$\frac{f_s}{F_{s_{cr}}} = \frac{18350}{370} = 49.6$$

Calculation of Diagonal-Tension Factor k

With $f_s/F_{s_{cr}} = 49.6$, we use Fig. C11.19 to find value of k = .69, for zero curve since sheet is flat or R = 0.

Calculation of Average Stress in Upright

Upright consists of one 1 x 1 x 1/8, 2024 extruded angle section.

To obtain effective area, we use eq. 58

$$A_{u_e} = \frac{A_u}{1 + (\frac{e}{\rho})^2} = \frac{.234}{1 + (\frac{.3025}{.29})^2} = .112$$

where,

A_u = area of web upright or stiffener
e = distance from median plane of web to centroid of single upright.
ρ = centroidal radius of gyration of cross section of upright about axis parallel to web.

Using Fig. C11.20, with $A_{u_e}/dt = \frac{.112}{10 \times .025}$ = .45 and k = .69, we obtain value of f_u/f_s = .92.

Hence, f_u = 18350 x .92 = 16900 psi, which represents the average stress over the length of the upright but applies only along the median plane of the web or along the line of rivets connecting upright to web.

Calculation of Maximum Stress Upright

Value of $\frac{d}{h_u} = \frac{10}{28.50} = .352$

where, d = upright spacing
h_u = distance between centroids of upright-flange rivet connections.

Using .352 as value of d/h_u and k = .69, we find from Fig. C11.21 that $f_{u_{max}}/f_u = 1.17$. Hence,

$f_{u_{max.}} = -16900 \times 1.17 = -19800$ psi.

Calculation of Diagonal Tension Angle α

From Fig. C11.22 for values of k = .69 and $f_u/f_s = 16900/18350 = .92$, we obtain tan α = .815.

Calculation of Allowable Stresses for Upright

Check allowable stress for failure as a column:-

Since the design is of the single upright type, we check the following two criteria:-

(1) Stress f_u should be no greater than the column yield stress for the upright material.

In the previous solution of this beam by Method 1, the crippling stress of the web upright was calculated to be -52500 psi., which corresponds to the column yield stress F_{co}. Since f_u (average) was -16900 psi., the upright is far overstrength for this particular strength check.

(2) The stress at the centroid of the upright should be no greater than the allowable column stress for a slenderness ratio of $h_u/2\rho = 28.50/2 \times .29 = 49$

The Johnson-Euler column equation is,

$$F_c = F_{cs} - \frac{F_{cs}^2}{4\pi^2 E}(L'/\rho)^2$$

$$F_c = 52500 - \frac{52500^2}{4\pi^2 \times 10{,}700{,}000}(49)^2 = -38000 \text{ psi}$$

M.S. = (38000/16900) - 1 = 1.14.

Allowable Stress for Upright for Forced Crippling

For a single member upright equation (61b) applied.

$$F_u = 26000\ k^{2/3}\ (t_u/t)^{1/3}$$

$$F_u = 26000 \times .69^{2/3}\ (.125/.025)^{1/3} = 34600 \text{ psi}$$

The F_{cy} for 2014-T6 Ext. = 53000

Correcting from F_{cy} = 42000 for 2024 material by directly as the $\sqrt{\ }$ of the yield stresses, which is approximately true, we obtain,

$$F_u = \frac{(57000)^{1/2}}{(42000)^{1/2}} \times 34600 = 38800 \text{ psi}$$

M.S. = (38800/19800) - 1 = 0.96

The stress is below the proportional limit stress of the material so no correction is necessary.

The stress F_u could also be found by use of curves in Fig. C11.38.

The web stiffener or upright is too much overstrength and should be re-designed.

Check Web Design

The peak value of the nominal web shear stress within a beam bay is taken as,

$$f_{s_{max.}} = f_s\ (1 + k\ C_1)\ (1 + k\ C_2)$$

From Fig. C11.23 using tan α = .815, we find C_1 = .022.

Using Fig. C11.24, we must find value of term

$$wd = 0.7\ d \sqrt[4]{\frac{t}{(I_C + I_T)\ h_e}}$$ before the value of C_2 can be found.

$$wd = 0.7 \times 10 \sqrt[4]{\frac{.025}{(.1075 + .0291)\ 29.45}} = 1.96$$

hence from Fig. C11.24, C_2 = .075

Substituting:-

$$f_{s_{max.}} = 18350\ (1 + .69 \times .022)(1 + .69 \times .075)$$

$$= 19600 \text{ psi.}$$

Allowable Web Shear Stress

From Fig. C11.25a for k = .69, the allowable $F_{s_{all.}}$ for 24ST (F_{tu} = 62000 psi.) equals 21000 psi for web without rivet washer and 23700 psi for web with rivet washer. The margin of safety for web with rivets without washer is (21000/19600) - 1 = .07. For rivets with washer the margin of safety would be (23700/19600) - 1 = .21.

Check of Rivets

Loads per inch of run web to flange rivets is given by the following equation.

$$R'' = \frac{S_w}{h_r}\ (1 + 0.414\ k)$$

$$= \frac{13500}{28.50}\ (1 + 0.414 \times .69) = 610 \text{ lb.}$$

Load per rivet pitch of 3/4 inch = .75 x 610 = 456 lb.

These values are practically the same as by the first method of solution in Art. C11.13.

Single shear strength of 5/32 2117-T3 rivet = 512 lb. Bearing strength on .025 web = 486 lb. (critical).

Strength per rivet pitch = 2 x 486 = 972 lb.
M.S. = (972/456) - 1 = 1.12

Web to Upright Rivets

The required tensile strength is given by the criterion, that the tensile strength of rivets per inch of stiffener should be greater than 0.22 to F_{tu} which equals 0.22 x .025 x 62000 = 340 lb./inch.

In our rivet problems we have specified no web-stiffener rivets. Thus rivets should be specified that will develop 340 lb. tension strength per inch of stiffener. See Fig. C11.37a for tension strength for some fastener-skin combinations. Refer to further discussion in latter part of Art. C11.32.

Upright to Flange Rivets

The web uprights are fastened to the flange both upper and lower by 1/4 dia. AN steel bolt.

The load on the upright at its ends is, $P_u = f_u\ A_{u_e}$ = 16900 x .112 = -1895 lb.

Shear strength of 1/4 bolt = 3681.

Bearing on vertical 3/32 leg of lower flange = 1.25 x 2340 = 2930 lb. (critical).

M.S. = (2930/1895) - 1 = .54

Since a 1/4" dia. rivet A17ST, F_{su} = 38 ksi has a shear strength of 1970 lb. it could be used instead of the 1/4" bolt and the M.S. would be .04.

Check of Flange Strength

Section 50" from end. Design external

bending moment = 50 x 13500 = 675000" lb.
Diagonal tension factor = .69
Thus bending moment developed as a shear resistant beam = (1 - .69) 675000 = 209000" lb.

The remainder of the bending moment is developed as a pure tension field beam, or a moment of 466000" lb.

Bending Stresses

Upper flange bending stresses, (extreme fiber) $f_b = -\frac{209000 \times 12.58}{270.5} - \frac{466000 \times 10.94}{210}$

$= -9700 - 24300 = -34000$ psi.

Lower Flange Bending Stresses (extreme fiber)

$$f_b = -\frac{209000 \times -17.42}{270.5} + \frac{-466000 \times -19.06}{210}$$

$= 13450 + 42400 = 55850$ psi.

Average Axial Flange Loads Due to Bending

As a shear resistant beam average axial flange load equals

$$\left(\frac{I - I_W}{I}\right)\left(\frac{M\,(1-k)}{h_e}\right)$$

where M (1 - k) = 675000 (1 - .69) = 209000" lb. at time of web buckling.

h_e = distance between flange centroids
I = moment of inertia of entire beam section about neutral axis
I_W = moment of inertia of web about beam N.A.

Substituting

$$\text{Flange load} = \frac{209000}{29.45}\left(\frac{270.5-60.5}{270.5}\right) = \pm 5510 \text{ lb.}$$

Average axial flange load due to bending with beam in diagonal tension state,

$$= \frac{466000}{29.45} = \pm 15840 \text{ lb.}$$

Total Flange Average Axial Loads Due to Bending:

Upper flange $F_c = -15840 - 5510 = -21350$ lb.
Lower flange $F_t = F_c = 21350$ lb.

Flange Axial Loads Due to Tension Field Action

$$F_F = -\frac{S_{DT}}{2}\cot\alpha$$

S_{DT} = shear load carried by diagonal tension field action = ks, where k = .69

Hence $F_F = -\frac{.69 \times 13500}{2} \times 1.228 = -5710$ lb.

Total Flange Average Axial Loads

Upper flange $F_c = -21350 - 5710 = -27060$ lb.
Lower flange $F_t = 21350 - 5710 = 15640$ lb.

Average stress upper flange $= \frac{-27060}{.675} =$ -40000 psi.

Average stress lower flange $= \frac{15640}{.378} =$ 40300 psi.

Comparing these values with the values obtained by the first method of solution we find -44000 and 42450 respectively. Thus the NACA method decreases the load on the flanges.

Check of Flange Stresses Due to Secondary Flange Bending Moments

From Formula 65

$$M = \frac{1}{12} k f_s t d^2 C_s$$

From Fig. C11.24, $C_s = .97$ when wd = 1.96

Hence,

$$M = \frac{1}{12} \times .69 \times 18350 \times .025 \times 10^2 \times .97 =$$ 2560 in.lb.

This compares with 3210 in.lb. by the first method of solution. The flange stresses could be found as in solution method 1.

C11.28 General Conclusion.

In general the NACA method gives higher margins of safety. The NACA method is recommended for actual design of semi-tension field beams. The NACA method has been extended to cover curved webs and this subject is presented in Part 2 of this chapter.

In the example problem the web was relatively thin and the diagonal tension factor k of .69 means that wrinkling is quite severe as 69 percent of the shear load is carried by diagonal tension. In heavily loaded and rather shallow depth beams, such as wing spars or wing bulkheads subjected to large external loads, the webs are much thicker and the k factor much less.

The great saving in web weight over that required for a non-buckling web design easily exceeds the weight increase in the flanges and the web uprights that diagonal tension field action produces. The rivet design in semi-tension field design presents more detailed design problems since the rivet loads are larger

and more complex than for a beam with non-buckling web.

C11.29 End Bay Effects.

The previous discussion has been concerned with the "interior" bays of a beam. The vertical stiffeners in these areas are subject, primarily, to only axial compression loads, as discussed. The outer or "end bay" is a special case. Since the diagonal tension effect results in an inward pull on the end stiffener, it produces bending in it, as well as the usual compression axial load. This action can be clearly seen in Fig. C11.27. Obviously, the end stiffener must be considerably heavier than the others, or at least supported by additional members to reduce the stresses due to bending.

Actually an end bay effect exists wherever a buckled panel ends and structural members along the edge of the panel must carry the bending due to the diagonal tension loads.

Typical examples, in addition to the end stiffener discussed, would be the edge members bordering a cut-out or a non-structural door in a flat beam, or a curved fuselage or wing panel. Illustrations are shown in Fig. C11.27.

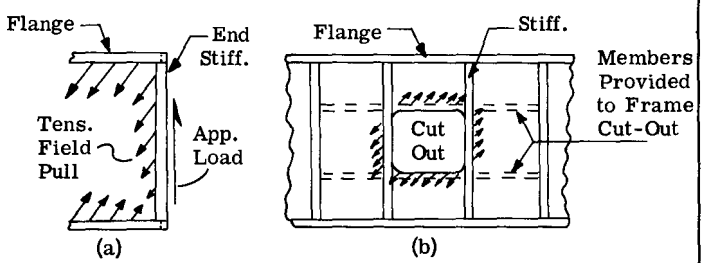

Fig. C11.27

The component of the running load per inch that produces bending in such edge members is given by the formulas

$$w = k\, q \tan \alpha$$

for edge members parallel to the neutral axis (stringers) and

$$w = k\, q \cot \alpha$$

for members normal to the neutral axis (stiffeners or rings). The longer the unsupported length of the edge member subjected to w, the greater will be the bending moment it must carry.

For example, consider the end stiffener of the beam of Fig. C11.13 in Art. C11.13. Using the data from Art. C11.27,

$$w = k\, q \cot \alpha$$

$$= .69\ (18{,}350 \times .025) \times 1.228 = \underline{388\ \text{lb./in.}}$$

This is a severe loading for the end stiffener to carry in bending in addition to its other loads. A heavy member would be required.

There are in general 3 ways of dealing with the edge member subjected to bending, the object being to keep the weight down.

(1) Simply "beef-up" or strengthen the edge member so it can carry all of its loads (this is inefficient for long unsupported lengths).

(2) Increase the thickness of the end bay panel to either make it non-buckling or to reduce k and thereby the running load producing bending in the edge member (this is usually inefficient for large panels).

(3) Provide additional member (stiffeners) to support the edge member and thereby reduce its bending moment due to w. (this requires additional parts).

Actually a combination of these methods might be best.

Consider method (3) above. This will sometimes increase the local shear in the bay and should be considered. Assume that 3 additional stiffeners are added (equally spaced in this case) to support the end stiffener against bending and analyze the end bay internal loads resulting for the beam of Fig. C11.13 and the analysis used for it in Art, C11.27 (NACA Method).

Fig. C11.28a shows the end bay and the loads applied to it.

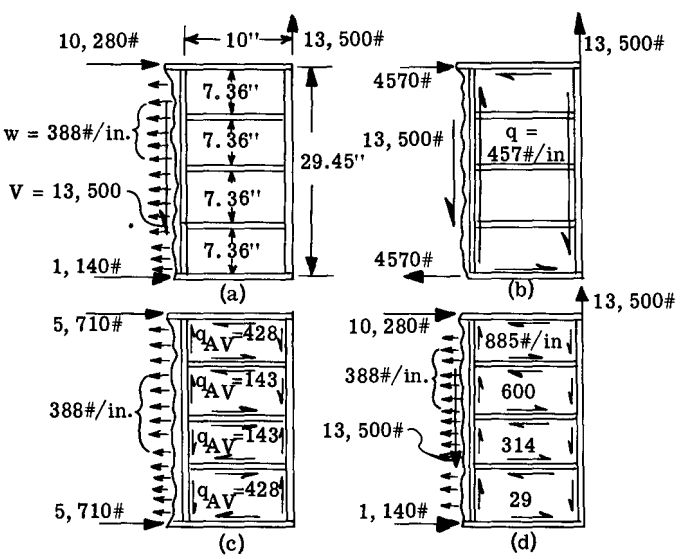

Fig. C11.28

Note that in Fig. (a) there are two sets of applied loads. One is the basic applied shear load of 13,500 lb. and the other is the component of the tension field load, w, calculated as 388 lb./in. earlier in this article.

Fig. (b) shows the shear flows in the end bay panels, taken as constant in all the panels, due to the 13,500 lb. load applied. The shear flows are shown as they act on the edge members.

Fig. (c) shows the shear flows in the panels due to the applied load w. Average shear flows (in the center of each panel) are shown. Actually the shear flow in the end bay will vary from a maximum of $q = 388 \times \frac{29.45}{2 \times 10} = 571$ lb./in. to 0 lb./in. at the center. The values of this variation at the center of each bay are shown for analysis purposes.

In Fig. (d) the load systems of (b) and (c) are added to obtain the final (preliminary) loads. It can be seen here that the shear flow in the upper two panels of the end bay is significantly increased over the nominal value of $q = \frac{13,500}{29.45} = 457$ lb./in. existing in the other bays of the beam. This means that the diagonal tension effects in this area will be greater (for the same web thickness) and must be considered locally here in checking the upper flange, the end stiffener, the added support stiffeners, the rivets, the web, etc.

Having determined the basic internal loads, the members involving the end bay can be checked for strength using the methods and data of Art. C11.14 to C11.26. When, as in the case of the upper added support stiffener, the shear flows are different in the adjacent bays, average values of q and k should be used in checking the stiffener for strength. Formula 57 assumes equal shears in adjacent bays.

In general, there is no simple analytical way of calculating exact tension field load variations when shear flows vary from panel to panel in a structural network. The procedure outlined above is but an elementary "approximation" that can be used for design purposes. If all margins are near zero, substantiating element tests are in order.

Fig. C11.16 Graphs for Calculating Buckling Stress of Webs.

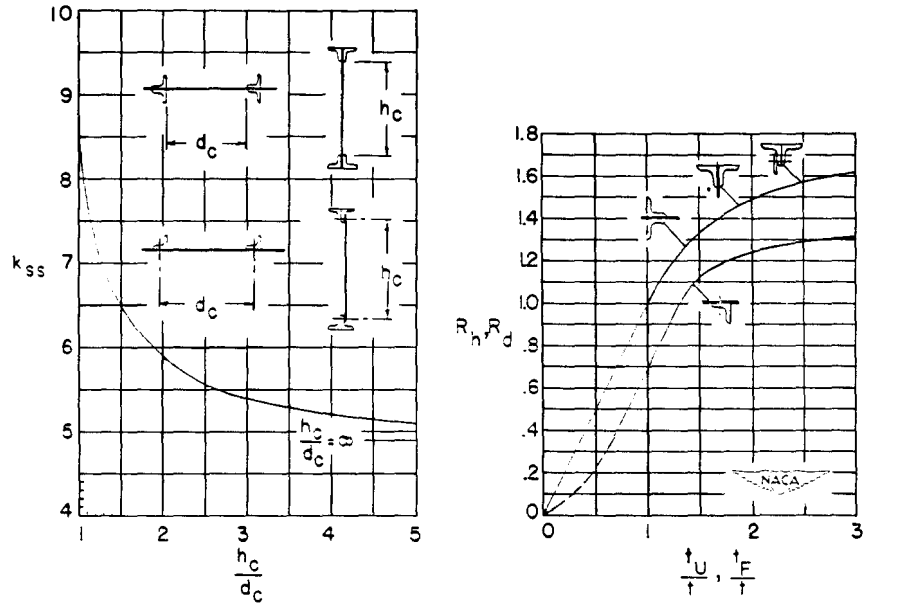

(a) Theoretical coefficients for plates with simply supported edges. (b) Empirical restraint coefficients.

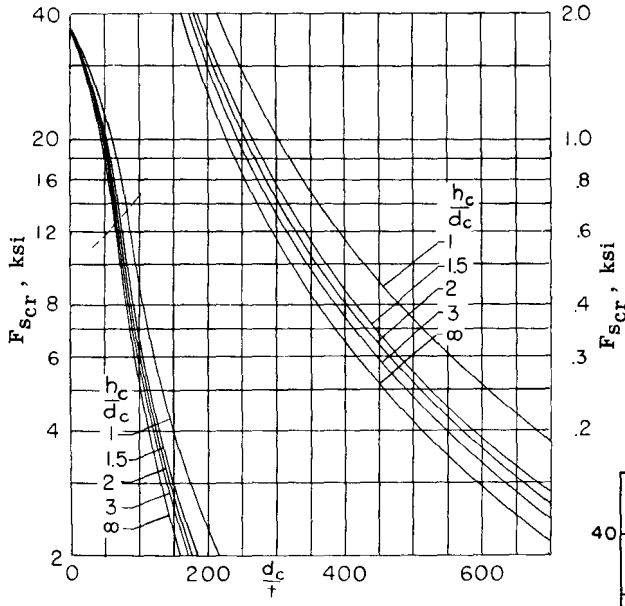

Fig. C11.17 Buckling Stresses $F_{s_{cr}}$ for Plates with Simply Supported Edges. E = 10, 600 ksi. (To left of dashed line, curves apply only to 24ST aluminum alloy.)

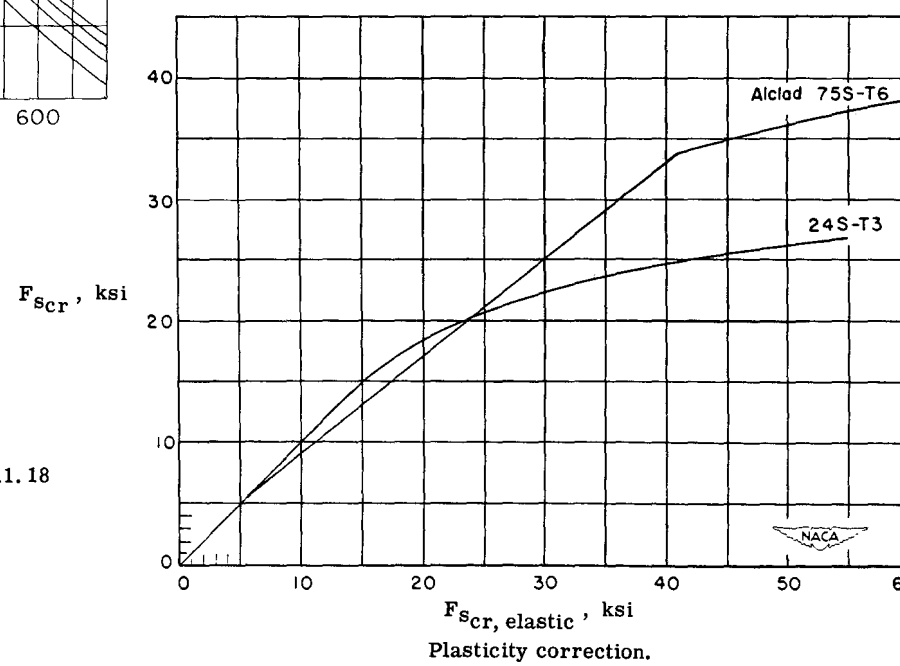

Fig. C11.18 Plasticity correction.

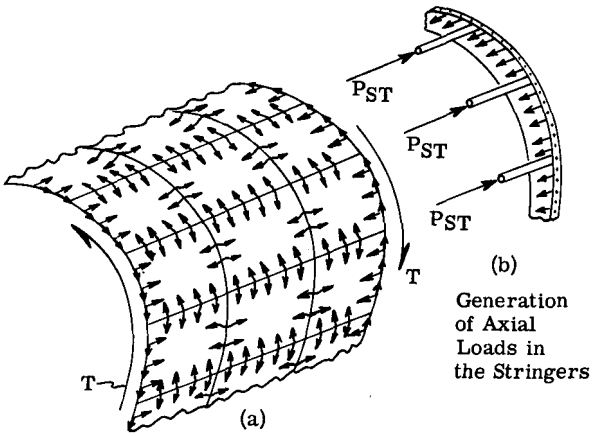

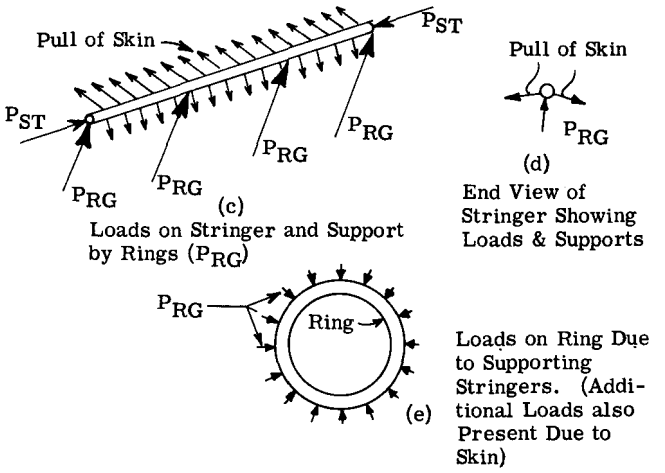

Fig. C11.30

stringers, coming entirely from (3) above, and is thus concentrated at points. This concentration produces not only compression but also internal bending moments in the floating rings. This is shown in Fig. C11.30e.

5. Any fasteners splicing skins together or fastening the skins to the end rings feel not only a shear panel type of loading but also a normal loading, as in the case of a plane web beam. Also, the "folds" in the skin due to the diagonal buckles pry on the rivets as they "attempt" to extend across the rivet lines at the stringers and rings.

The important thing to realize here is that, although only a pure torsion has been applied, considerable axial loads have been generated in the stringers and rings. And even some bending moments have been induced in the stringers and in the rings of the "floating" type.

Now, assume that at the same time the torsion load is being applied an increasing compressive axial load, P, is being applied, simultaneously, as shown in Fig. C11.31.

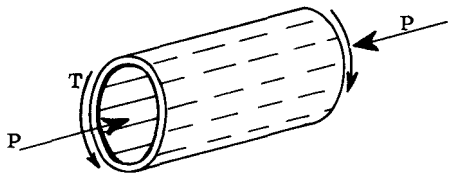

Fig. C11.31

The following will now happen due to the presence of P.

1. The stringers will, of course, have to carry the compressive load, P, which will be divided among them. There will be some "effective" skin to help.

2. Less obvious, but very important, is the fact that the diagonal tension loads due to the torsion, T, will be considerably affected by the presence of the axial load, P. The larger P is, with respect to T, the greater will be its effect upon the diagonal tension effects. This is as follows.

   a) The skin panels will now buckle at a lower amount of applied torsion since they are now also strained axially in compression. Actually there is a "combined" buckling consisting of compression and shear buckling. This can be obtained from an interaction equation, discussed later.

   b) Since the critical shear buckling stress is now lower the diagonal tension factor, k, is larger.

   c) All of the diagonal tension effects dependent upon k are increased. These include the axial loads induced in the stringers., the normal loads bending the stringers inward, the loads induced in the rings and the loads felt by the fasteners.

   d) The angle of diagonal tension will be larger, closer to 45°.

Thus we see that the effect of compression is to increase the loads due to diagonal tension.

Now assume that instead of being compression, the axial load, P, is tension. In this case, the effects of diagonal tension, due to T, are reduced.

1. The stringers and skin feel tension due to P, which opposes compression due to diagonal tension.

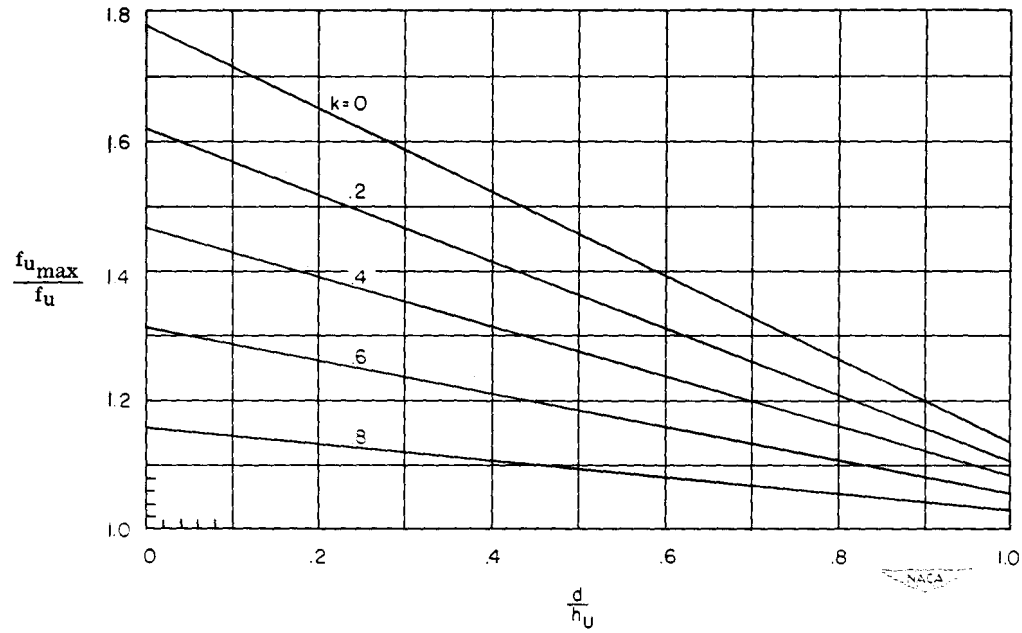

Fig. C11.21 Ratio of Maximum Stress to Average Stress in Web Stiffener.

NOTE for use on curved webs:
For rings, read abscissa as $\frac{d}{h}$; for stringers, read abscissa as $\frac{h}{d}$.

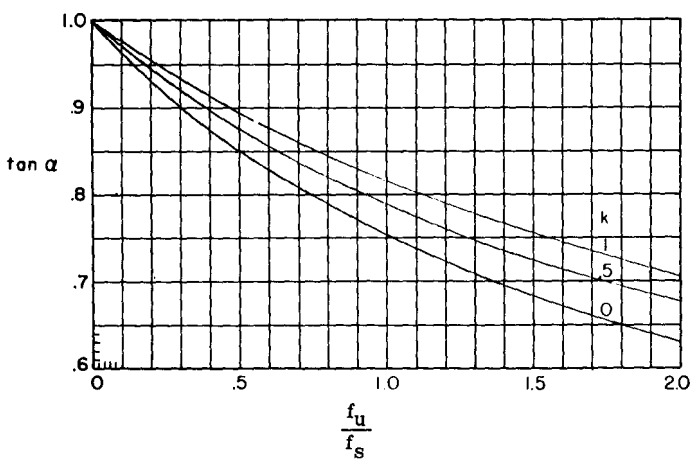

Fig. C11.22 Incomplete Diagonal Tension.

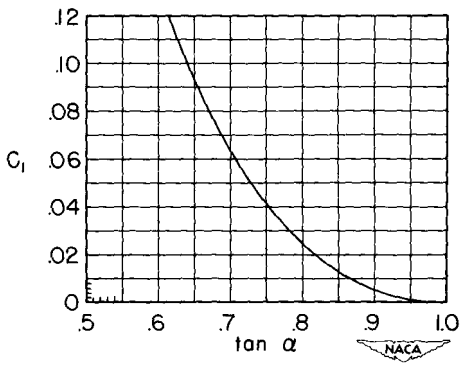

Fig. C11.23 Angle Factor C_1.

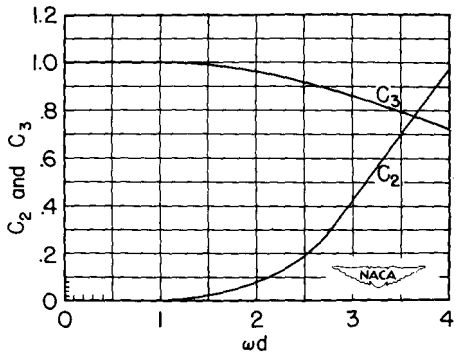

Fig. C11.24 Stress-Concentration Factors C_2 and C_3.
$\left(\omega d = 0.7d \sqrt[4]{\frac{t}{(I_c + I_T)h_e}}\right)$

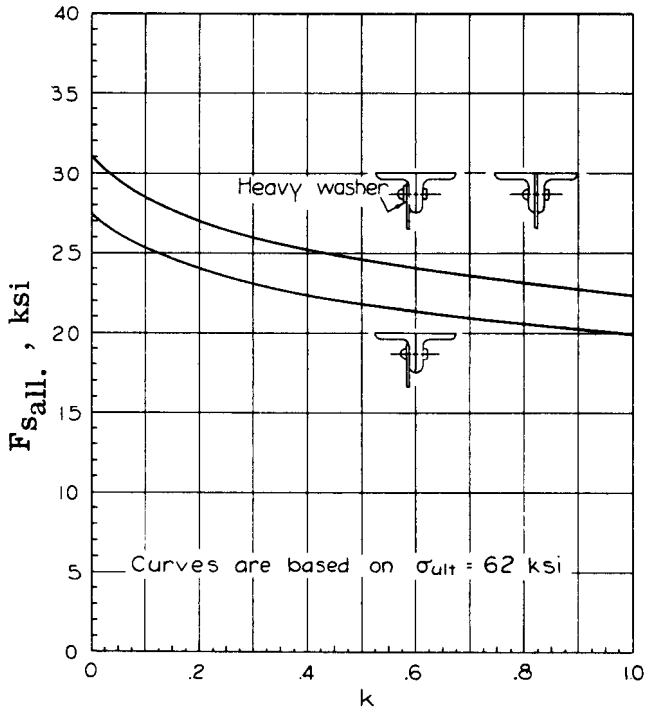

(a) 2024 Aluminum Alloy.

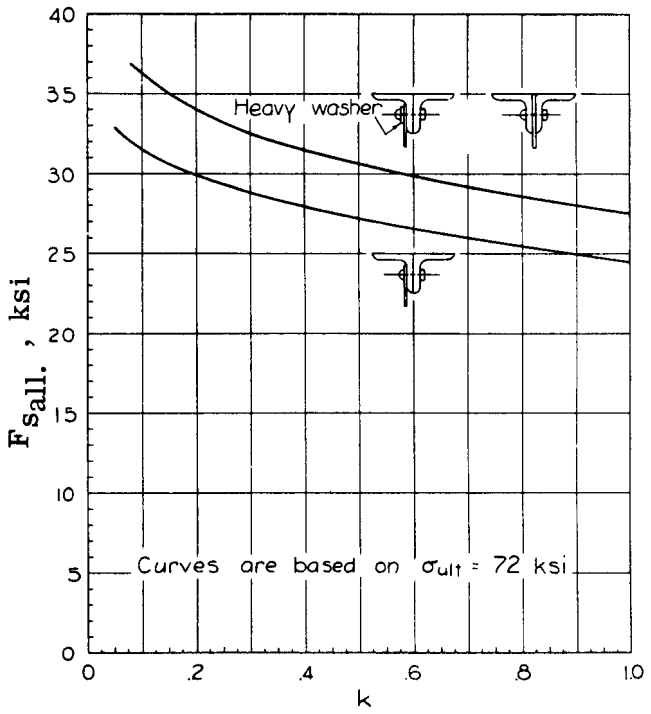

(b) Alclad 7075 Aluminum Alloy.

Fig. C11.25 Allowable Values of Nominal Web Shear Stress.

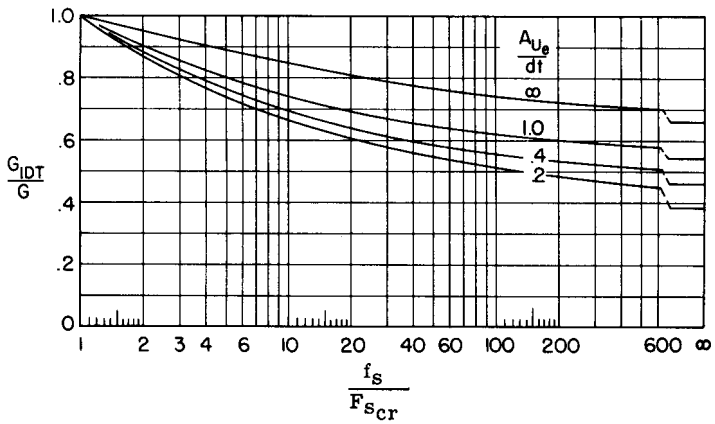

(a) Modulus Ratio for Elastic Web.

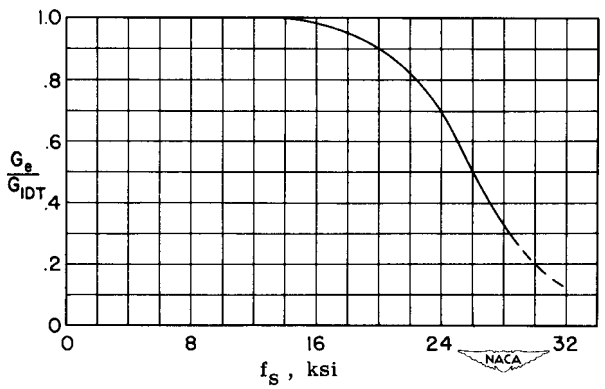

(b) Plasticity Correction for 24S-T3 Aluminum Alloy.

Fig. C11.26 Effective Shear Modulus of Diagonal-Tension Webs.

PART 2. CURVED WEB SYSTEMS.

(BY W. F. McCOMBS)

C11.30 Diagonal Tension in Curved Web Systems - Introduction.

This type of structure has an important place in the design of light metal structures. The structural designer should have as good an understanding of it as he must have for the somewhat simpler plane web system. Actually, most airframe shear web systems are curved rather than flat, the fuselage of a modern aircraft being the oustanding example. To make a fuselage skin entirely non-buckling would require a very thick skin and/or a closely spaced substructure supporting it. This would involve a considerable weight penalty compared to the buckling skin arrangement. The typical metal skin in a modern fighter or transport airplane thus carries its limit and ultimate loads with a considerable degree of skin buckling. In view of this, the need for an understanding of diagonal tension effects in curved web systems is obvious.

C11.31 General Discussion.

Before getting into the details of design, a general discussion of what happens in a curved web system as the web buckles is helpful. Consider a semi-monocoque structure with a circular (or elliptical) cross-sectional shape as shown in Fig. C11.29.

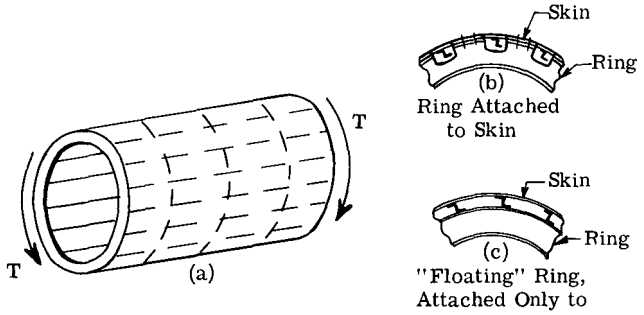

Fig. C11.29

The structure consists of a number of axial members (called "stringers" if they are numerous and "longerons" if they are few in number, say 3 to 8) which are supported by frames or rings and covered with a skin. The rings may be attached to the skin and "notched" to let the stringers pass through, as in Fig. (b), or they may be located entirely under the stringers and not, therefore, attached to the skin. In this latter case they are called "floating" rings, as in Fig. (c). Sometimes both types of rings are present. Comparing this structure to a plane web beam, the stringers correspond to the flanges, the rings correspond to the uprights and the skin corresponds to the web. Thus, the stringers carry (or resist) axial loads. The rings support the stringers and, if not of the "floating" type, also divide the skin panels into shorter lengths. The skin carries (or resists) shear loads.

Now, assume the structure to be subjected to a pure torsion, T, as shown in Fig. C11.29. Before the skin buckles, this torsion produces a shear in the skin panels given by the well-known formula

$$q = \frac{T}{2A}$$

Only the skin is loaded. As in the case of the uprights of a plane web beam, the rings are not loaded. There is no load in the stringers.

As the torsion is increased, however, the skin shear stress eventually becomes larger than the critical buckling stress and the panels buckle. Any further increase in torsion must now be carried as diagonal tension. Five main things then occur as the torsion is increased above the buckling value, as illustrated in Fig. C11.30.

1. The skin panels buckle and flatten out between rings fastened to the skin, from their original curved shape. This gives a polygonal cross-section (away from a ring). The angle of diagonal tension is less than that for a plane web beam, however, in the range of 20° - 30°.

2. The stringers now feel an axial load, due to the pulling on the ends, (C11.30b), of the structure by the buckled skin, just as in the case of the plane web beam.

3. The stringers also feel a normal loading that tends to bend, or "bow", them inward between supporting rings, as shown in Fig. C11.30c.

4. The supporting rings feel an inward loading which puts them in "hoop" compression. For rings attached to the skin this loading is applied by the stringers and the skin, and is thus "spread out". For floating rings this loading is applied only by the

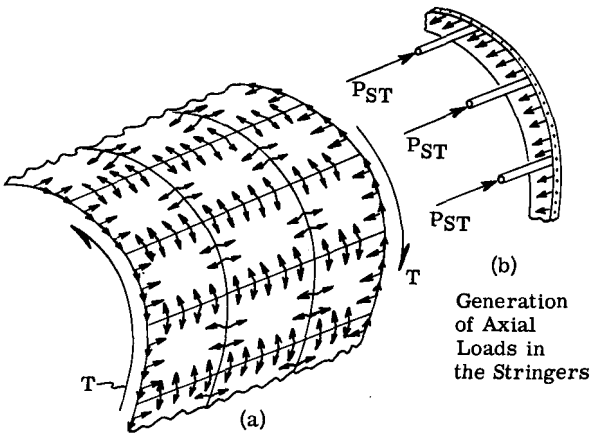

Net Loads Applied by the Skin to the Sub-Structure (Stringers and Rings)

Generation of Axial Loads in the Stringers

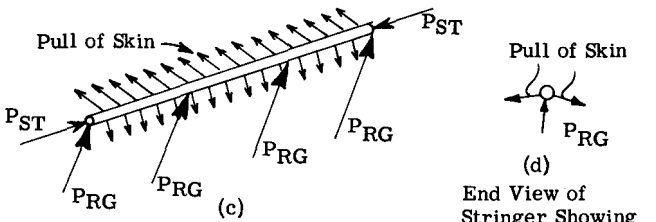

Loads on Stringer and Support by Rings (P_{RG})

End View of Stringer Showing Loads & Supports

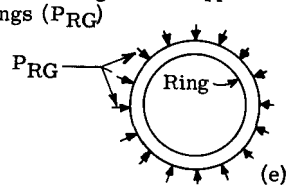

Loads on Ring Due to Supporting Stringers. (Additional Loads also Present Due to Skin)

Fig. C11.30

stringers, coming entirely from (3) above, and is thus concentrated at points. This concentration produces not only compression but also internal bending moments in the floating rings. This is shown in Fig. C11.30e.

5. Any fasteners splicing skins together or fastening the skins to the end rings feel not only a shear panel type of loading but also a normal loading, as in the case of a plane web beam. Also, the "folds" in the skin due to the diagonal buckles pry on the rivets as they "attempt" to extend across the rivet lines at the stringers and rings.

The important thing to realize here is that, although only a pure torsion has been applied, considerable axial loads have been generated in the stringers and rings. And even some bending moments have been induced in the stringers and in the rings of the "floating" type.

Now, assume that at the same time the torsion load is being applied an increasing compressive axial load, P, is being applied, simultaneously, as shown in Fig. C11.31.

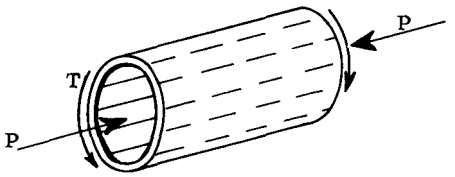

Fig. C11.31

The following will now happen due to the presence of P.

1. The stringers will, of course, have to carry the compressive load, P, which will be divided among them. There will be some "effective" skin to help.

2. Less obvious, but very important, is the fact that the diagonal tension loads due to the torsion, T, will be considerably affected by the presence of the axial load, P. The larger P is, with respect to T, the greater will be its effect upon the diagonal tension effects. This is as follows.

   a) The skin panels will now buckle at a lower amount of applied torsion since they are now also strained axially in compression. Actually there is a "combined" buckling consisting of compression and shear buckling. This can be obtained from an interaction equation, discussed later.

   b) Since the critical shear buckling stress is now lower the diagonal tension factor, k, is larger.

   c) All of the diagonal tension effects dependent upon k are increased. These include the axial loads induced in the stringers., the normal loads bending the stringers inward, the loads induced in the rings and the loads felt by the fasteners.

   d) The angle of diagonal tension will be larger, closer to 45°.

Thus we see that the effect of compression is to increase the loads due to diagonal tension.

Now assume that instead of being compression, the axial load, P, is tension. In this case, the effects of diagonal tension, due to T, are reduced.

1. The stringers and skin feel tension due to P, which opposes compression due to diagonal tension.

2. The skin panels can carry a larger shear stress before buckling in shear. In fact, a relatively small amount of axial tension can prevent them from buckling at all, as will be discussed later.

3. The diagonal tension factor, k, will be smaller (or zero if no buckling occurs).

4. All diagonal tension effects dependent upon k are reduced and the diagonal tension angle is smaller.

Finally, suppose that instead of an axial load, P, a bending moment is being applied simultaneously with the torsion, T, as in Fig. C11.32.

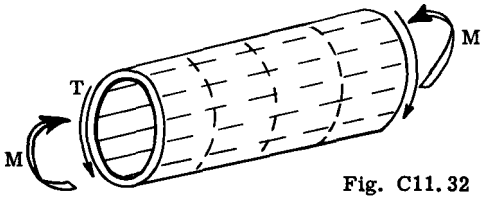

Fig. C11.32

In this case, also, as the torsion is being increased from a small mount, M is also being increased, (the ratio of M to T being constant, as was the case for axial load, P). Then, from the usual bending theory, $f = \frac{Mz}{I}$, the following will occur.

1. The stringers (and skin) above the neutral axis will feel compression loads, the further away the greater the load. The upper skin panels will thus buckle earlier in combined compression and shear and produce the largest diagonal tension loads on the stringers and rings.

2. The skins below the neutral axis will buckle later (or not at all) due to the tension strain produced by M. Thus the diagonal tension effects will be smaller (or non-existant) in the rings and stringers in this region.

3. The skins near the neutral axis will feel little or no strains due to bending and will buckle about as in the case for the pure torsion, T, producing equivalent effects.

In an actual airplane structure, a fuselage for example, the applied loading is more complex. Instead of simply an applied torsion, there is also, usually, a vertical and perhaps a sideward set of loads which produce shears that vary from panel to panel. And there may be not only a bending moment, which changes, along the fuselage, but also axial loads due to landings, catapulting requirements, etc. Obviously all of this complicates the calculations,and experience and judgment are of great help; but the method of going about it is fundamental and will now be discussed.

The N.A.C.A. has conducted an extensive program over the years with the object of determining a system for the design of structures having curved webs in diagonal tension. The theory for this system, as in the case for the plane web beam, was given by Wagner and others and modified as necessary from the results of many tests. The design method is fully discussed in Ref. (3) and the substantiating test program in Ref. (4). The reader is encouraged to consult these references for a fuller presentation of the theoretical development and test results.

As mentioned earlier, curved web systems are of two general types. One of these has an arrangement which results in the web, or skin, panels being longer in the axial direction, d, than in the circumferential direction, h. This is typical of the stringer system in a fuselage, as shown in Fig. C11.33.

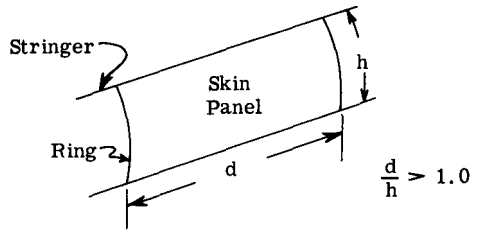

Fig. C11.33

That is, the geometry of the stringer spacing, h, and the ring spacing, d, is such that

$$\frac{d}{h} > 1$$

"Floating" rings, not being attached to the skin, do not determine the spacing, d.

A second type of curved web structure may be referred to as the longeron system. Its main characteristic is that the skin panels are long in the circumferential direction. This type of structure would, typically, in a fuselage, consist of a few axial members (a minimum of 3 but more usually 4 to 8 for a "fail safe" design) and a large number of closely spaced frames. The frames would, in this system, be at about a 4" to 6" spacing as compared to a 15"-20" spacing for a stringer system. This gives

$$\frac{d}{h} < 1$$

as indicated in Fig. C11.34

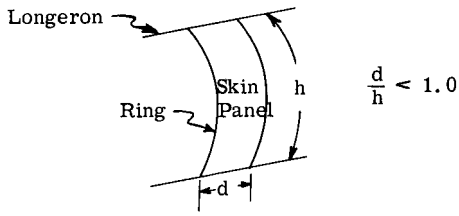

Fig. C11.34

In the longeron system the frames are attached to the skin and longerons; there are no "floating" rings.

Most of the NACA data and design method is for the stringer system. The design method for the longeron system, also presented herein, has evolved from Ref. (3) and also from the results of an investigation and test program at Chance-Vought Aircraft Corp. These latter checks are in some places different from the ones in the stringer system. The main problem is the determination of the angle of diagonal tension, for either system. Once this is known all of the diagonal tension stresses are known.

The stringer system will be discussed first and the longeron system will be discussed secondly. The basic approach is similar to that for plane web beams.

C11.32 Analysis of Stringer Systems in Diagonal Tension.

Before the diagonal tension effects can be calculated, the primary internal loads in the structure, due to the applied loads, must be determined. This can be done as discussed in Chapter A20. The engineers theory of bending can usually be used to determine the axial loads in the stringers, as in Art. A20.2-A20.5. The shear flows in the various skin panels can be determined as in A20.6-A20.8. In the case of stringer construction a more accurate determination of the skin shear flows may, if desired, be obtained if the skin panels are considered flat, rather than curved, between stringers. This is because the panels, after buckling, actually flatten out, giving a polygonal cross-sectional shape, except immediately adjacent to non-floating rings, as shown in Fig. C11.30a.

The diagonal tension effects can now be evaluated.

1. DETERMINATION OF CRITICAL BUCKLING STRESS OF SKIN PANELS.

The buckling strength of curved panels under pure shear and compressive stresses is covered in Chapter C9. The equation for buckling shear stress $F_{s_{cr}}$ is,

$$F_{s_{cr}} = \frac{\pi^2 \eta\, k_s\, E}{12\,(1-\nu_e^2)}\left(\frac{t}{b}\right)^2$$

where simple support is usually conservatively assumed in determining k_s.

When axial loads (and strains) are present, as in practical structures subjected to bending as well as shear, the situation is more complicated. As discussed in Chapter C9, the presence of compressive stresses together with shear stresses causes the panel to buckle at a lower value of shear than if no compression were present. The presence of tension stresses, along with shear stresses, enables the panel to stand larger shear stresses before buckling occurs. In fact, a relatively small amount of tension stress may prevent the panel from ever buckling in shear.

It is important to determine the actual shear buckling stress when axial stresses, particularly compression, are present. The reason is that this affects the diagonal tension factor, k, and all of the ensuing stresses affected by k.

First consider a shear panel subjected to a shear stress f_s and a compression stress f_c. It has been demonstrated experimentally at the NACA, Ref. (5) that a curved panel, thusly loaded, buckles according to the interaction formula

$$\frac{f_c}{F_{c_{cr}}} + \left(\frac{f_s}{F_{s_{cr}}}\right)^2 = 1.0 \qquad \text{- - - - - - - (71)}$$

where $F_{c_{cr}}$ and $F_{s_{cr}}$ are the critical panel buckling stresses for pure compression and pure shear respectively. From Chapter C9, the buckling stress for a curved sheet panel, in end compression is given by the equation,

$$F_{c_{cr}} = \frac{\pi^2 \eta\, k_c\, E}{12\,(1-\nu_e^2)}\left(\frac{t}{b}\right)^2$$

Now for any particular panel,

$$\frac{F_{c_{cr}}}{F_{s_{cr}}} = A \text{ , (a constant)} \qquad \text{- - - - - - - (72)}$$

and

$$F_{c_{cr}} = A\, F_{s_{cr}}$$

Now, also for any given applied loading condition being checked we can calculate f_c $(= \frac{Mz}{I})$ at the center of the panel (before buckling) and also f_s (previously done). These stresses will bear a constant ratio to each other until buckling occurs, after which the

compression stress no longer increases. Thus we can write

$$\frac{f_c}{f_s} = B \quad \text{- - - - - - - - - - - - - - - - - (73)}$$

or $f_c = B\, f_s$

Substituting these formulas for $F_{c_{cr}}$ and f_c back into the interaction formula (71) we obtain,

$$\frac{B\, f_s}{A\, F_{s_{cr}}} + \left(\frac{f_s}{F_{s_{cr}}}\right)^2 = 1.0$$

Solving this quadratic for f_s we get

$$f_s = F_{s_{cr}} \left[\frac{-\frac{B}{A} + \sqrt{\left(\frac{B}{A}\right)^2 + 4}}{2} \right] \quad \text{- - - - (74)}$$

where f_s is the actual shear stress at which the panel buckles due to the presence of compression stresses. Calling this stress $f_{s_{cr}}$ and calling the expression in the brackets R_c

$$f_{s_{cr}} = F_{s_{cr}} R_c \quad \text{- - - - - - - - - - - - (75)}$$

where R_c is always less than 1.0 when compression stresses are present.

Next, consider a shear panel subjected to a shear stress, f_s, and a tension stress, f_t. For this case it has been experimentally demonstrated, Ref. (6), that the interaction relationship defining buckling is

$$\frac{f_s}{F_{s_{cr}}} - \frac{1}{2}\frac{f_t}{F_{c_{cr}}} = 1.0 \quad \text{- - - - - - - - - - (76)}$$

where $F_{s_{cr}}$ and $F_{c_{cr}}$ are as previously discussed.

The shear stress, f_s, at which the panel will buckle when the tension stress present is f_t can be solved for directly from equation (76),

$$\frac{f_{s_{cr}}}{F_{s_{cr}}} = 1.0 + \frac{f_t}{2F_{c_{cr}}} \quad \text{- - - - - - - - - - (77)}$$

or,

$$f_{s_{cr}} = \left(1.0 + \frac{f_t}{2F_{c_{cr}}}\right) F_{s_{cr}} \quad \text{- - - - - - (78)}$$

Calling the expression in parenthesis in (78) R_T we get,

$$f_{s_{cr}} = F_{s_{cr}} R_T \quad \text{- - - - - - - - - - - - (79)}$$

Since R_T is always greater than 1.0 when tension stresses are present, the actual shear buckling stress will always be greater than $F_{s_{cr}}$, the buckling stress for pure shear loads only. Inspection of the term in parenthesis in (78) making up R_T shows that as the tension stress becomes several times larger than $F_{c_{cr}}$ the value of $f_{s_{cr}}$ will become several times larger than $F_{s_{cr}}$. Thus, if f_t is large enough no buckling will occur even when large shear stresses are present.

2. DIAGONAL TENSION FACTOR, k.

The next step is the determination of the diagonal tension factor, k. This is a function of $\frac{f_s}{f_{s_{cr}}}$ where, as discussed above,

$$f_{s_{cr}} = F_{s_{cr}} R_c \quad \text{or} \quad f_{s_{cr}} = F_{s_{cr}} R_T$$

depending upon whether compression or tension stresses are present.

For a curved panel the formula for k, as determined from much test data, Ref. (3) is the empirical relationship,

$$k = \tanh \left[\left(.5 + 300 \frac{td}{Rh}\right) \log_{10} \frac{f_s}{f_{s_{cr}}} \right] \quad \text{- (80)}$$

R = radius of curvature

with the auxiliary rules that

a) if $\frac{d}{h} > 2$ use only 2

b) if $h > d$ replace $\frac{d}{h}$ by $\frac{h}{d}$ ("longeron" system) and, in this case, if $\frac{h}{d} > 2$ use only 2.

Rather than calculate k from the formula, it can more easily be obtained from Fig. C11.19.

3. STRINGER LOADS, STRESSES, AND STRAINS

As in the case of the plane web system, the total stringer load will consist of the primary axial loads, P_P , due to applied bending moments and/or axial loads, plus the diagonal tension induced loads, $P_{D.T.}$

$$P_{STR} = P_P + P_{D.T.} \quad \text{- - - - - - - - - - - (81)}$$

P_P is determined as in Chapter A20.2-A20.5. $P_{D.T.}$ is determined, similarly to the case for the flanges of a plane web beam, from the "pulling" of the buckled skin on the end frames.

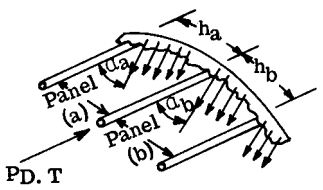

Fig. C11.35

As shown in Fig. C11.35, $P_{D.T.}$ is the diagonal tension load in a stringer bounded by panel "a" on one side and panel "b" on the other. Let the width of panel (a) be h_a and the width of panel (b) be h_b. (For equally spaced stringers, of course, $h_a = h_b$). Let the shear flow in panel (a) be q_a and that in panel (b) be q_b. Then we can write

$$P_{D.T.} = \frac{k_a\, q_a\, h_a\, \cot \alpha_a}{2} + \frac{k_b\, q_b\, h_b\, \cot \alpha_b}{.2} \quad \text{------ (82)}$$

To keep the calculations simpler (as will be appreciated later) we can accept some inaccuracy and use average values for the respective terms ($\frac{h_a + h_b}{2}$, $\frac{q_a + q_b}{2}$, etc.) and get

$$P_{D.T.} = k\, q\, h \cot \alpha \quad \text{--------- (83)}$$

remembering that this is an "average" load, which, for closely spaced stringers, is sufficient, especially for preliminary design. The total stringer load is then, from 80 and 82

$$P_{STR} = P_P + k\, q\, h \cot \alpha$$

where all terms are known except α.

The stringer stress is obtained by dividing the terms on the right side by their respective effective areas

$$f_{STR.} = \frac{P_{STR}}{A} = \frac{P_P}{A_{e_p}} + \frac{k\, q\, h \cot \alpha}{A_{e_{D.T.}}}$$

a) A_{e_p} is the total effective area, stringer and skin, used in determining the primary loads as in Chapter A20. If P_P is tension the area is equal to ht, panel is fully effective.

b) $A_{e_{D.T.}} = A_{STR} + .5\ ht\ (1-k)\ R_{c,T}$ see Ref. (3) ---------- (84)

Ref. (3) suggests a more accurate calculation.

$R_{c,T}$ depending upon whether axial compression or tension is present. Again, k and R_c or R_T are also average values for the panels on each side of the stringer. Thus we can write

$$f_{STR} = \frac{P_P}{A_{STR} + A_{e_{SKIN}}} + \frac{k\, q\, h \cot \alpha}{A_{STR} + .5ht\ (1-k)R_{c,T}}$$

or

$$f_{STR} = \frac{P_P}{A_{STR} + A_{e_{SKIN}}} + \frac{k\, f_s \cot \alpha}{\frac{A_{STR}}{ht} + .5(1-k)R_{c,T}} \quad \text{------ (85)}$$

where all terms are known on the right hand side of the equation except α.

The total stringer strain is then

$$\varepsilon_{STR} = \frac{f_{STR}}{E} \quad \text{---------- (86)}$$

If f_{STR} is larger than the proportional limit stress, or in the neighborhood of the yield stress, E is not a constant and a stress strain diagram should be used to read ε directly, using f_{STR}. Again, $f_{STR.}$ and hence $\varepsilon_{STR.}$ cannot be determined until α is known (later).

There is also a secondary loading on the stringer which tends to bend or "bow" it inward. This is caused by the fact that the taut skins are pulled flat on each side of the stringer. Thus as in Fig. C11.30 there is an inward component of the skin diagonal tension loading that pulls the stringer inward. This loading is not a simply distributed one; it is largest in the middle of the stringer and becomes smaller at the supports. Ref. (3) recommends that the effect of this loading be considered as producing secondary bending moments in the stringer, taken as

$$M_{STR} = \frac{f_s\, ht\, d^2\, k \tan \alpha}{24R} \quad \text{------ (87)}$$

R = radius of curv.

This represents a "peak" moment at the middle and at the ring supports. It will produce tension on the inside of the stringer at the middle and compression on the inside of the stringer at the supports. The recommended value of M_{STR} is the result of many test measurements, therefore it is of a semi-empirical nature.

4. STRESSES AND STRAINS IN RINGS

There are two types of rings, those attached to the skin and those not attached to the skin, called "floating rings," which support, and are therefore loaded only by, the stringers.

Rings attached to the skin are usually "notched" to let the stringers pass through.

The stringers are attached to these rings locally by some shear clip arrangement. The rings feel an inward acting loading which puts them in "hoop compression". These loads come from the stringers and from the skin. The stringer being pulled inward by the skin, as described above and in Fig. C11.30, in turn pushes inward on the supporting rings. The skin, not being flat at the ring, also pulls inward on the ring. The result of all of this is, essentially, according to Ref. (3) a hoop compression stress in the ring for the case of a cylinder under pure torsion. This is because the loading is approximately equivalent to an evenly distributed inward acting radial loading. For this case the radial loading can be taken as, per inch along the ring,

$$p_{RG} = \frac{f_s \, dt \, k \tan \alpha}{R_{RING}}$$

The axial (hoop) compression load in the ring will then be

$$P_{RG} = pR = f_s \, dt \, k \tan \alpha \quad \text{- - - - - - - (88)}$$

The axial compression stress in the ring will be

$$f_{RG} = \frac{P_{RG}}{A_{e_{RG+SKIN}}} = \frac{k \, f_s \tan \alpha}{\frac{A_{RG}}{dt} + .5 \, (1-k)} \quad \text{- - (89)}$$

where all terms on the right are known except α.

The axial strain in the ring will be

$$\varepsilon_{RG} = \frac{f_{RG}}{E} \quad \text{- - - - - - - - - - - - - - (90)}$$

where f_{RG} and hence ε_{RG} are unknown until α is determined.

When loads other than pure torsion are applied f_s and k will vary from panel to panel and the hoop compression stress will not be constant around the ring. There will also be some varying secondary shear stresses in the panel due to unequal "pulls" on each side of the panel, at the stringer, by the buckled skin.

When "floating" rings are used concentrated inward acting radial loads are applied by the stringers. This produces hoop compression and, since all the loads are concentrated, also some bending moments. There is, of course, no effective skin acting with these rings. The axial compression load is

$$P_{D.T.} = f_s \, dt \, k \tan \alpha$$

The axial compression stress is then,

$$f_{RG} = \frac{k \, f_s \tan \alpha}{\frac{A_{RG}}{dt}} \quad \text{- - - - - - - - - - (91)}$$

where all terms on the right hand side are known except α.

The axial strain is given by

$$\varepsilon_{RG} = \frac{f_{RG}}{E} \quad \text{- - - - - - - - - - - - - - - (92)}$$

or can, of course, be gotten from a stress strain diagram for the material.

The maximum bending moment present in a floating ring is given by

$$M_{RG} = \frac{k \, f_s \, t \, h^2 \, d \tan \alpha}{12R} \quad \text{- - - - - - - - (93)}$$

R = radius of curv.

This occurs at the junction with the stringer. There is a secondary moment, half as large, midway between stringers in the ring.

5. STRAINS IN THE SKIN PANELS

The strain in the skin panels is given in Ref. (3) as

$$\varepsilon = \frac{f_s}{E}\left[\frac{2k}{\sin 2\alpha} + \sin 2\alpha \, (1-k)(1+u)\right] \quad \text{- - - - - - - (94)}$$

where u = Poisson's Ratio = .32 for aluminum, every term on the right hand side of the equation is known except α. Fig. C11.36 is of help in calculating ε, giving the value of the bracketed term.

6. DETERMINATION OF α*

For the stringer system (d > h) Ref. (3) shows that α is related to the stringer strain, the ring strain and the web, or skin panel, strain by the formula

$$\tan^2 \alpha = \frac{\varepsilon - \varepsilon_{ST}}{\varepsilon - \varepsilon_{RG} + \frac{1}{24}\left(\frac{h}{R}\right)^2} \quad \text{- - - - - (95)}$$

R = radius of curv.

where ε is a tension strain (+) and ε_{RG} and ε_{STR} are entered as negative members for compression, thus adding to ε.

α is determined by successive approximation using the three prior formulas for ε, ε_{ST} and ε_{RG} and then checking with the formula (95) above. That is,

* For a faster estimate or for preliminary design, step 6 can be skipped for panels in compression and shear and α simply assumed to be 45^0.

1) Assume a value for α.

2) Determine ε, ε_{RG} and ε_{STR} using this assumed value of α.

3) Substitute ε, ε_{RG} and ε_{STR} into the formula for $\tan^2 \alpha$ and get a "new" value for α.

4) Repeat steps (1) to (3) as many times (say 3) as necessary to get α to a "converged" value.

If rings attached to the skin are being used then ε_{RG} in step (2) above is obtained from (90), using (89) for f_{RG}. If "floating" rings are used then ε_{RG} is obtained from (92), using (91) for f_{RG}.

Once α is determined, the stringer stresses and ring stresses are known, having been used in getting the strains ε_{STR} and ε_{RG} for the final check of α in (95). The bending moments in the stringers can then be calculated from (87) and the bending moments in floating rings, if used, from (93).

7. LOADS ON THE RIVETS

The only remaining internal loads to be calculated are those acting on the rivets. These are of two types.

a) There are the primary loads, in the plane of the skins which try to cause shear or bearing failures at the riveted joints, as in any spliced skin.

b) There are also, "prying" forces on the rivets which try to "pop off" the rivet heads or to pull the skin up and around the rivet heads. This latter may occur, particularly, when countersunk or dimpled skins and flush head rivets are used and the rivet diameter is too small or the rivet spacing is too large. These are "secondary" loads.

The primary rivet loads occur whenever the skin is spliced, which is usually, but not necessarily, along a stringer or along a ring. These loads would also be present if the skin panel ended at stringer or ring, as at an opening or "cut-out" and the panel had not been re-enforced by a doubler to prevent buckling.

At a splice parallel to a stringer the load per inch along the rivet line is due to the same effects as discussed for the plane web beam. It is

$$\text{Load/inch} = f_{st}\, t \left[1 + k\left(\frac{1}{\cos \alpha} - 1\right)\right] \quad - - \quad (96)$$

At a splice (or opening) along a ring (a vertical splice) the loading is

$$\text{Load/inch} = f_s\, t \left[1 + k\left(\frac{1}{\sin \alpha} - 1\right)\right] \quad - - \quad (97)$$

Note that in either case, if the panels involved are made non-buckling (on <u>each</u> side of the splice) $k = 0$ and the load per inch is the same as for a non-buckled web. It is only around a "cut-out" or opening that the panels are made either non-buckling or made to buckle to a lesser extent, and this is done to "relieve" the loading on the edge member rather than on the rivets (see Art. C11.29).

The second type of rivet loads, the prying loads, are not determinable by any formula. Ref. (3) recommends that an arbitrary criteria be used as follows. The tensile strength of the rivet-skin combination, P_T, should be such that it is as large as the number given by

$$P_T \text{ per inch} = .22\, t\, F_{TU} \quad - - - - - - - \quad (98)$$

where F_{TU} is the ultimate tensile strength of the skin or web material being used.

P_T is usually most critical for flush attachments. As an aid in getting this, Figs. C11.37a and C11.37b give information on the tensile strength of various rivet types and sizes.

C11.33 Allowable Stresses (and Interactions).

1. STRINGERS

Just as there are two types of basic loads (and stresses) in the stringers and rings (the primary ones and the ones due to diagonal tension effects) there are also two types of allowable stresses for <u>local failure</u>. An interaction formula is thus used to predict adequate strength. This is, for the stringer

$$\frac{f_p}{F_{cc}} + \frac{f_{ST_{MAX}}}{F_{ST}} \leq 1.0 \quad - - - - - - - - - - \quad (99)$$

where

f_p = stringer stress due to the applied loads, this is the <u>first term</u> on the <u>right</u> hand side of equation (85).

*F_{cc} = the allowable crippling stress for the stringer, obtained as in Chapter C7.

$$f_{ST_{MAX}} = f_{ST} \times \frac{f_{ST_{MAX}}}{f_{ST}}$$

f_{ST} is the <u>second term</u> on the <u>right hand side</u> of equation (85).

* F_{cc} is same as F_{cs} in Chapter C7.

1) Assume a value for α.

2) Determine ε, ε_{RG} and ε_{STR} using this assumed value of α.

3) Substitute ε, ε_{RG} and ε_{STR} into the formula for $\tan^2 \alpha$ and get a "new" value for α.

4) Repeat steps (1) to (3) as many times (say 3) as necessary to get α to a "converged" value.

If rings attached to the skin are being used then ε_{RG} in step (2) above is obtained from (90), using (89) for f_{RG}. If "floating" rings are used then ε_{RG} is obtained from (92), using (91) for f_{RG}.

Once α is determined, the stringer stresses and ring stresses are known, having been used in getting the strains ε_{STR} and ε_{RG} for the final check of α in (95). The bending moments in the stringers can then be calculated from (87) and the bending moments in floating rings, if used, from (93).

7. LOADS ON THE RIVETS

The only remaining internal loads to be calculated are those acting on the rivets. These are of two types.

a) There are the primary loads, in the plane of the skins which try to cause shear or bearing failures at the riveted joints, as in any spliced skin.

b) There are also, "prying" forces on the rivets which try to "pop off" the rivet heads or to pull the skin up and around the rivet heads. This latter may occur, particularly, when countersunk or dimpled skins and flush head rivets are used and the rivet diameter is too small or the rivet spacing is too large. These are "secondary" loads.

The primary rivet loads occur whenever the skin is spliced, which is usually, but not necessarily, along a stringer or along a ring. These loads would also be present if the skin panel ended at stringer or ring, as at an opening or "cut-out" and the panel had not been re-enforced by a doubler to prevent buckling.

At a splice parallel to a stringer the load per inch along the rivet line is due to the same effects as discussed for the plane web beam. It is

$$\text{Load/inch} = f_{st}\, t \left[1 + k \left(\frac{1}{\cos \alpha} - 1\right)\right] \quad - - \quad (96)$$

At a splice (or opening) along a ring (a vertical splice) the loading is

$$\text{Load/inch} = f_s\, t \left[1 + k \left(\frac{1}{\sin \alpha} - 1\right)\right] \quad - - \quad (97)$$

Note that in either case, if the panels involved are made non-buckling (on each side of the splice) $k = 0$ and the load per inch is the same as for a non-buckled web. It is only around a "cut-out" or opening that the panels are made either non-buckling or made to buckle to a lesser extent, and this is done to "relieve" the loading on the edge member rather than on the rivets (see Art. C11.29).

The second type of rivet loads, the prying loads, are not determinable by any formula. Ref. (3) recommends that an arbitrary criteria be used as follows. The tensile strength of the rivet-skin combination, P_T, should be such that it is as large as the number given by

$$P_T \text{ per inch} = .22\, t\, F_{TU} \quad - - - - - - \quad (98)$$

where F_{TU} is the ultimate tensile strength of the skin or web material being used.

P_T is usually most critical for flush attachments. As an aid in getting this, Figs. C11.37a and C11.37b give information on the tensile strength of various rivet types and sizes.

C11.33 Allowable Stresses (and Interactions).

1. STRINGERS

Just as there are two types of basic loads (and stresses) in the stringers and rings (the primary ones and the ones due to diagonal tension effects) there are also two types of allowable stresses for local failure. An interaction formula is thus used to predict adequate strength. This is, for the stringer

$$\frac{f_p}{F_{cc}} + \frac{f_{ST_{MAX}}}{F_{ST}} \leqq 1.0 \quad - - - - - - - - - \quad (99)$$

where

f_p = stringer stress due to the applied loads, this is the first term on the right hand side of equation (85).

*F_{cc} = the allowable crippling stress for the stringer, obtained as in Chapter C7.

$$f_{ST_{MAX}} = f_{ST} \times \frac{f_{ST_{MAX}}}{f_{ST}}$$

f_{ST} is the second term on the right hand side of equation (85).

* F_{cc} is same as F_{cs} in Chapter C7.

$\frac{f_{ST_{MAX}}}{f_{ST}}$ is a ratio obtained from Fig. C11.21. It is explained in the plane web beam discussion.

F_{ST}= the "forced crippling" (diagonal tension effect) allowable stress for the stringer is obtained from Fig. C11.38, as in the case for the uprights in the plane web beam, or calculated from the formulas (also for F_{RG} and t_{RG}).

$F_{ST} = 26{,}000\ k^{2/3}\ (\frac{t_{STR}}{t_{WEB}})^{1/3}$ for 24ST material.

$F_{ST} = 32{,}500\ k^{2/3}\ (\frac{t_{STR}}{t_{WEB}})^{1/3}$ for 75ST material with the same restrictions noted in C11.22. (The total axial stringer stress is $f_p + f_{ST}$ at the area near the supporting rings, and $f_p + f_{ST_{MAX}}$ in the middle between supports.)

The stress in the stringer due to the bending moment, M_{STR}, of equation (87) can be calculated and added to f_p in the proper manner.

Ref. (3) also suggests the stringer be checked as a column, fully fixed at the supporting rings and carrying the stress f_{STR}. Some allowance should be made for beam column action, due to the bending moment present in the middle of the stringer. This can be done using some effective loading producing the moments discussed or by carrying some extra margin of safety over and above the column buckling stress.

2. RINGS

The rings have allowable stresses similar in nature to the stringers. The interaction equation is,

$$\frac{f_p}{F_{cc}} + \frac{f_{RG_{MAX}}}{F_{RG}} \leqq 1.0 \quad \text{- - - - - - - - -} \quad (100)$$

for the case of rings attached to the skin.

f_p is the stress due to the ring carrying loads other than the tension field ones (as a bulkhead analysis would show). F_{RG} is the allowable forced crippling stress for the ring, obtained in the same manner as that for the stiffener, (Fig. C11.38),

$f_{RG_{MAX}} = f_{RG} \times \frac{f_{RG_{MAX}}}{f_{RG}}$, obtained in the same manner as discussed for the stiffener. It occurs in the ring midway between stiffeners. F_{cc} is the "normal" allowable crippling stress for the ring. If $F_{RG} > F_{cc}$ then use F_{cc} for F_{RG}.

Floating rings, not being subject to forced crippling by the skin, are checked in the usual manner for the stresses due to hoop compression loads and the accompanying bending moment, equations (91) and (93). The interaction equation is,

$$\frac{f_{RG} + f_M}{F_{cc}} - 1 \leqq 0 \quad \text{- - - - - - - - - - -} \quad (101)$$

f_{RG} is a constant stress between stringer junctions; it does not have a maximum peak as do the rings attached to skin.

3. GENERAL INSTABILITY

A general instability check for the stringers and skin can be made from the empirical criteria presented in Fig. C11.39. This is obtained from test data and recommendations of Ref. (7) and Ref. (3). The allowables are based upon pure torsion tests. The adequacy of the structure is checked by

$$\frac{f_s}{F_{s_{INST}}} - 1 \leqq 0 \quad \text{- - - - - - - - - - -} \quad (102)$$

It is suggested that a respectable margin of safety be held (M.S. $\geqq$ .15). The radii of gyration in Fig. C11.39 should be made assuming the full width of sheet to act with the stringer or ring respectively and that the sheet is flat because the criterion was obtained under these assumptions.

4. ALLOWABLE STRESSES IN THE SKIN (OR WEB)

Ref. (3) recommends that the allowable stress in a web or skin be taken as, for non-flush attachments,

$$f_{s_{ALL.}} = f^*_{s_{ALL.}}\ (.65 + \Delta) \quad \text{- - - - -} \quad (103)$$

where $\Delta = .3 \tanh \frac{A_{RG}}{dt} + .1 \tanh \frac{A_{ST}}{ht}$; Δ can, more easily, be read from Fig. C11.40. $f^*_{s_{ALL}}$ is obtained from Fig. C11.41b or C11.41c after obtaining α_{PDT} from Fig. C11.41a. Data from tests by the Chance-Vought Aircraft Corp. indicate that the allowable web stress can simply be read from Fig. C11.42. In either case, the allowables apply to f_s, the gross stress in the panel. The net shear stress between rivet holes can be carried up to the ultimate shear stress F_{su} of the material.

C11.34 Example Problem.

The foregoing explanation can be better explained or clarified through the presentation of an example problem.

Assume that we have a fuselage with a structural arrangement as in the example problem of A20.5 and Fig. A20.3 and A20.4 of Chapter A20. Also, assume the moment of inertia and neutral axis for a linear bending stress distribution to apply. These values are given on page A20.8*. Also let it be assumed that the supporting rings are attached to the skin and spaced at 15". The rings are 1" x 3" x 1" 24ST Z sections, .040" in thickness (see Fig.C11.43).

An analysis will be made of stringer #3, skin panels 2-3 and 3-4, and the ring. It is assumed also that an axial skin splice occurs along stringer #3 and a vertical splice along the ring to show a check of the fasteners.

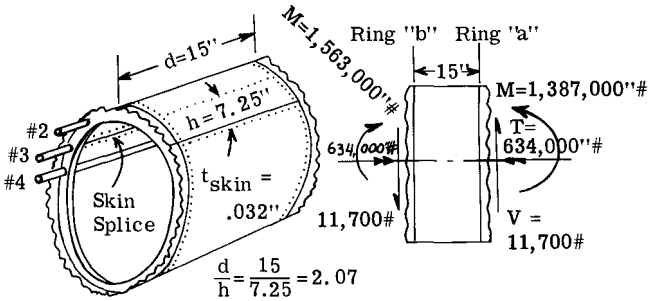

Fig. C11.43

First the internal loads in the stringer and skin panels are determined. The "average" loads at the middle of the bay will be used in this example to get the diagonal tension effects.

At the center of the bay,

M = 1,475,000 in. lb.
T = 634,000 in. lb.
V = 11,700 lb.

Max. stringer stress occurs at Ring b:-

$$f_{p_{MAX}} = \frac{MZ}{I} = \frac{1,563,000\ (32.9)}{2382} = 21,600 \text{ psi.}$$

$$f_{p_{AV.}} = \frac{1,475,000\ (32.9)}{2382} = 20,400 \text{ psi.}$$

Shear flows in skin panels:-

$$q_{2-3} = \frac{VQ}{I} + \frac{T}{2A}\text{, where A consists of area of 26 triangles}$$

$$= \frac{11,700\left[.167(38.3) + .169(36.4)\right]}{2382} +$$

$$\frac{634,000}{2\left[26 \times \frac{29.8}{2} \times 7.25\right]}$$

$$= 61.6 + 113 = 175 \text{ lb./in.}$$

$$q_{3-4} = \frac{11,700\left[.167(38.3) + .169(36.4) + .216(32.9)\right]}{2382}$$

$$+ 113 = 96 + 113 = 209 \text{ lb./in.}$$

The diagonal tension effects will now be calculated assuming average q's, bending stresses, etc., for the panels 2-3 and 3-4.

$$q_{AV_{2-4}} = \frac{175 + 209}{2} = 192 \text{ lb./in.}$$

$$f_{s_{AV_{2-4}}} = \frac{192}{t} = \frac{192}{.032} = \underline{6000} \text{ psi.}$$

The average critical shear buckling stress will now be calculated using equation (75).

First, if no skin buckling occurred the average compression stress in the two panels would be, approximately, the stress in the stringer between them, thus

$$f_{c_{panels}} = f_{p_{AV.}} = 20,400 \text{ psi.}$$

then the constant, B, would be

$$B = \frac{f_c}{f_s} = \frac{20,400}{6,000} = 3.40$$

The critical pure shear buckling stress equation from Chapter C9 is,

$$F_{s_{cr}} = \frac{\pi^2\ k_s\ E}{12\ (1 - \nu_e^2)} \left(\frac{t}{b}\right)^2 .$$ From Chapter C9, $k_s = 16.8$.

$$F_{s_{cr}} = \frac{\pi^2 \times 16.8 \times 10,600,000}{12\ (1 - .3^2)} \left(\frac{.032}{7.25}\right)^2 =$$

$$\underline{3140} \text{ psi.}$$

For pure compression the critical buckling stress equation from Chapter C9 is,

$$F_{c_{cr}} = \frac{\pi^2\ k_c\ E}{12\ (1 - \nu_e^2)} \left(\frac{t}{b}\right)^2 .$$ $k_c = 15.9$ (from Chapter C9).

$$F_{c_{cr}} = \frac{\pi^2 \times 15.9 \times 10,600,000}{12\ (1 - .3^2)} \left(\frac{.032}{7.25}\right)^2 = \underline{2980} \text{ psi}$$

Thus, $A = F_{c_{cr}}/F_{s_{cr}} = 2980/3140 = .950.$

Since buckling stresses are below the proportional limit stress of the material, no plasticity correction was necessary as is usually the case in thin walled structures. Thus stress ratio (A) could be obtained directly as k_c/k_s.

* A non-linear bending stress distribution can be used, but it also is affected by the diagonal tension compressive stresses and involves considerable iteration. Linear ones are often used.

Next: -

$$R_c = \frac{-\frac{B}{A} + \sqrt{(\frac{B}{A})^2 + 4}}{2} =$$

$$\frac{-\frac{3.40}{.950} + \sqrt{(\frac{3.40}{.950})^2 + 4}}{2} = .26$$

and, from equation (75)

$$f_{s_{cr_{2-4}}} = F_{s_{cr}} \times R_c = 3140\ (.26) = 815 \text{ psi}$$

which is quite small, due to the presence of compression.

Next,

$$\frac{f_{s_{AV}}}{f_{s_{cr_{2-4}}}} = \frac{6000}{815} = 7.36$$

now k can be determined:

$$300\,\frac{td}{Rh} = \frac{300\ (.032)}{30}\ (2.0)^* = .64$$

From Fig. C11.19, k = .75

The expressions for stringer and ring stresses can now be written in terms of α: Substituting into equation (85) and using $f_{p_{AV}}$ for the first term on the right side,

$$f_{STR.} = 20{,}400 + \frac{.75\ (6000)\ \cot\alpha}{\frac{.180}{(7.25)(.032)} + .5(1-.75)(.26)}$$

$$= 20{,}400 + 5570 \cot\alpha$$

this is the "average" stress in the stringer.

Substituting into equation (89) for rings, and using A_{RG} = (1" + 3" + 1")(.040") = .20 in.²,

$$f_{RG} = \frac{.75\ (6000)\ \tan\alpha}{\frac{.20}{(15)(.032)} + .5\ (1 - .75)}$$

$$= 8{,}300 \tan\alpha$$

α will now be determined, by successive approximation using equations (94), (86), (90) and the above expressions for stresses in them, and also Fig. C11.36 for equation (94). Since there is so much compression involved, assume α = 45°, to start with. From Fig. C11.36

$$\frac{\varepsilon E}{f_s} = 1.83 \qquad \varepsilon = \frac{1.83\ (6000)}{10.6 \times 10^6} = 1036 \times 10^{-6}$$

$$\varepsilon_{STR} = \frac{20{,}400 + 5570\ (1.0)}{10.6 \times 10^6} = 2450 \times 10^{-6}$$

$$\varepsilon_{RG} = \frac{8{,}300\ (1.0)}{10.6 \times 10^6} = 782 \times 10^{-6}$$

Now solve for "new" α using equation (95)

$$\tan^2\alpha = \frac{(1036 + 2450)10^{-6}}{(1036 + 782)10^{-6} + \frac{1}{24}(\frac{7.25}{30})^2} = 0.822$$

$$\tan\alpha = .907$$

$$\alpha = 42.2^\circ, \text{ which is less than the assumed } 45^\circ.$$

As a second trial assume α = 42.4°.

$$\frac{\varepsilon E}{f_s} = 1.84 \text{ (from Fig. C11.36)}$$

$$\varepsilon = 1.84 \times 6000/10.6 \times 10^6 = 1041 \times 10^{-6}$$

$$\varepsilon_{STR} = 20400 + 5570\ (\cot\alpha)/10.6 \times 10^6 = 2505 \times 10^{-6}$$

$$\varepsilon_{RG} = 8{,}300 \times \tan\alpha/10.6 \times 10^6 = 752 \times 10^{-6}$$

$$\tan^2\alpha = \frac{(1041 + 2505)10^{-6}}{(1041 + 752)10^{-6} + .00243} = .84$$

whence α = 42.6° as against 42.4° assumed. The accuracy of the theory does not warrant a closer check, thus α will be taken as 42.4°.

The corresponding stringer and ring stresses are as follows:

$$f_{STR} = 20{,}400 + 5570\ (1.092)$$

$$= 20{,}400 + 6090$$

These are not added for local strength checks. They are added for a column stability check. The term on the right is the average stress, forced crippling, due to the diagonal tension effects.

$$f_{RG} = 8{,}300\ (.917) = 7{,}610 \text{ psi.}$$

Also, from equation (87),

$$M_{STR} = \frac{6000(7.25)(.032)(15)^2(.75)(.917)}{24\ (30)} =$$

299 lb./in.

and

$$f_b = \frac{M_{STR}\ c}{I_{STR}} = \frac{299\ (.562)}{.0418} = 4020 \text{ psi.}$$

The rivet load/in. along the axial splice is, from eq. (96),

$$\text{Load/in.} = 6000(.032)\left[1 + .75(\frac{1}{.74}) - 1)\right] =$$

243 lb./in.

* Since $\frac{d}{h} > 2.0$, use 2.0 (See page C11.33)

and, along the circumferential splice, from (97)

$$\text{Load/in.} = 6000(.032)\left[1 + .75\left(\frac{1}{.675}\right) - 1\right] = 262 \text{ lb./in.}$$

From the above stresses, f_{MAX}/f ratios, and the allowables, checks for adequate strength can be made as follows:-

STRINGERS:-

At the junction with ring (b),

$$f_{STR} = (21{,}600 + f_b) + 6090 \text{ psi.}$$

For adequate local strength,

$$\frac{f_c + f_b}{F_{cc}} + \frac{f_{ST}}{F_{ST}} \leq 1.0$$

$$F_{ST} = 26{,}000k^{2/3}\left(\frac{t_{ST}}{t}\right)^{1/3}$$

$$= 26{,}000(.75)^{2/3}\left(\frac{.05}{.032}\right)^{1/3} = 24{,}900 \text{ psi}$$

(Also determinable from Fig. C11.38).

Thus,*

$$\frac{21{,}600 + 4020}{27{,}000} + \frac{6090}{26{,}500} = 1.19 \text{ (stringer is inadequate)}$$

At the center of the stringer,

$$f_{ST_{MAX}} = f_{ST}\left(\frac{f_{ST_{MAX}}}{f_{ST}}\right)$$

from Fig. C11.21 $\dfrac{f_{ST_{MAX}}}{f_{ST}} \approx 1.02$.

Therefore,

$$f_{ST_{MAX}} = 6090\ (1.02) = 6210 \text{ psi.}$$

then we get, using the interaction formula,

$$\frac{20{,}400 + 4020}{27{,}000} + \frac{6210}{26{,}500} = 1.14 \text{ (stringer is inadequate)}$$

Checking as a fixed end column,

$$\rho = \sqrt{\frac{I}{A}} = \sqrt{\frac{.0418}{.18}} = .482$$

$$L/2\rho = \frac{15}{2(.482)} = 15.6$$

$$F_{COL.} \approx 26{,}500 \text{ (See Fig. C7.33)}$$

thus

$$\frac{20{,}400 + 6090}{26{,}500} = 1.00 \text{ (should be a little less than 1.00, say 0.85, to allow for beam-column action)}$$

RINGS

The rings attached to the skin are subject only to the forced crippling stresses, f_{RG}.

Midway between stringer junctions this action is a maximum and for adequate local strength,

$$\frac{f_{RG_{MAX}}}{F_{RG}} \leq 1.0$$

Using the data in Fig. C11.21,

$$f_{RG_{MAX}} = f_{RG} \times \frac{f_{RG_{MAX}}}{f_{RG}}$$

$$= 7{,}610 \times 1.0 = 7{,}610 \text{ psi.}$$

and thus

$$\frac{f_{RG_{MAX}}}{F_{RG}} = \frac{7{,}610}{23{,}100} = .33 \text{ (sufficient)}$$

The same compression stress (and load, $P = f_{RG} \times A_{RG}$) exists at the stringer junction. If the ring is notched to let the stringer pass through, as is usually done, the net section at the ring must be made capable of carrying this load, which is located at the centroid of the un-notched ring cross-section. Usually this means some "beef-up", locally, around the notched section; sometimes incorporated into the clip attaching the stringer to the ring.

Actually the rings, like the stringers, are subject to the average of the shear stresses in the panels fore and aft of them. These have been assumed equal in this example.

SKIN

The allowable shear stress taken from Fig. C11.42 is

$$F_s = 21{,}800$$

Using the method of Ref. (3)

$$F_{s_{ALL}}^{*} = 20{,}800 \text{ (from Fig. C11.41a and b)}$$

$$\Delta = .38 \text{ (from Fig. C11.40)}$$

Thus

$$F_s = 20{,}800\ (.65 + .38) = 21{,}400 \text{ psi.}$$

* $F_{cc} = 27{,}000$ (calculation not shown)

Either case shows there to be a large margin of safety for the actual shear stress of f_s = 6000 psi, (average value shown).

(Panels nearer the neutral axis will, of course, feel a larger shear stress.)

FASTENERS

Any fasteners used in this area must, of course, be able to transfer the load/inch at the splices as previously calculated. This criterion might not design the spacing however. They must also have a tension allowable, when installed in .032 skin, of, equation (98),

$$\text{Tens.All.Load/Inch} = .22\ (.032)(62{,}000)$$
$$= 435 \text{ lb.}$$

From Fig. C11.37 it can be seen that 1/8" flush head aluminum rivets in a dimpled .032 skin at .50" spacing should be adequate, or 1/8" brazier head rivets at a spacing of .65" if a "flush" joint is not required. The tension requirement is most severe in this case.

GENERAL INSTABILITY

A check against overall instability of the "network" of rings and stringers can be made using Fig. C11.39. This is analagous to the column stability check for the uprights of a plane web beam. In the case of curved webs, however, no "help" is given by the taut skin in preventing instability.

For this example problem the values used in calculating the shear stress in the skin at which "collapse" due to instability would occur are:

ρ_{ST} = .414 (Stringer S_a of Fig. A20.4 in Chapter A20)

ρ_{RG} = .819

(Both of these radii of gyration are gotten by including a full width of skin acting with the stringer, $w_e = h$, and with the ring, $w_e = d$, per Ref. (3).

Then

$$\frac{(\rho_{ST}\,\rho_{RG})^{7/8} \times 10^4}{(dh)^{1/2}\,R^{3/4}} = \frac{(.414 \times .819)^{7/8} \times 10^4}{(15 \times 7.25)^{1/2}\,(30)^{3/4}}$$

$$= \frac{.386 \times 10^4}{133} = 29$$

From Fig. C11.39

$\frac{F_{s_{INST}}}{E_c} > 3.0$; hence $F_{s_{INST}} > 3 \times 10.3 \times 10^6 >$ 30,900 psi

and the margin of safety against collapse is,

$$\text{M.S.} = \frac{F_{s_{INST}}}{f_s} - 1 = \frac{30{,}900}{6{,}000} = \underline{\text{large}}$$

Other panels, of course, might have a larger shear stress and a smaller allowable $F_{s_{INST}}$ and thus be more critical, but there is too much stiffness available, as seen, to expect any instability troubles.

LONGERON TYPE SYSTEM

C11.35

The longeron type of structural system is somewhat simpler from a total analysis standpoint. This is, of course, primarily because there are fewer members carrying the axial loads and not as many shear panels with varying shear loads. This type of structure may, or may not, be the most optimum arrangement from a weight and manufacturing cost consideration for a particular airplane. But this is not the subject of this discussion since it depends upon an optimization study. The methods of analysis presented here would, however, have a place in the calculations behind such a study.

Some typical types of longeron structural systems cross-sections for a fuselage are shown in Fig. C11.44.

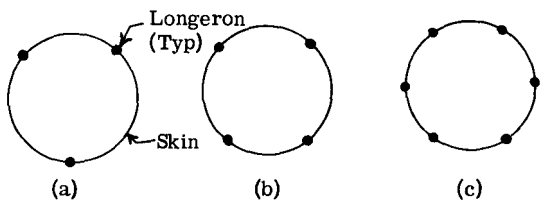

Fig. C11.44

Fig. (a) shows the minimum arrangement, as to number of longerons, since at least 3 axial load carrying members are necessary for equilibrium when bending moments in more than one plane are involved. This arrangement, however, has a disadvantage in that it is not a "fail safe" design. This means that the failure of any one member will not leave a structure capable of still carrying some arbitrary percentage (usually 50% to 67%) of the design ultimate loads.

The system shown in Fig. C11.44b is capable of doing this and is, therefore, the minimum type acceptable from the "fail safe" standpoint (4 longerons). More longerons may be used, as in Fig. (c), occasionally, depending upon other factors of design and manufacturing.

The longeron system, however, requires more closely spaced rings than does the stringer

system for strength-weight efficiency, as mentioned before. The optimum spacing of the supporting rings, or frames, is determined after many trial calculations have been made involving different gauges and sizes and spacings of rings and thicknesses of skins.

As in the previous discussion of stringer construction, the rings support the skin, dividing it into smaller panels, lengthwise. They also support the longerons, similarly to the uprights (stiffeners) in a plane web beam, against bending due to unequal tension field "pulls" by the skin on each side of the longeron. There are no "floating" rings in a longeron structural system.

After buckling, the skin in this system has tension diagonals which, rather than being "flat" between closely spaced stringers, instead lie on a hyperboloid of revolution. That is, they flatten diagonally between the closely spaced rings. This action is discussed in Ref. (8) and the reader should consult it for the basic theory as presented by Wagner originally. In this system the ring spacing "d" is such that d < h; see Fig. C11.34.

C11.36

The engineering procedure for calculating stresses and allowables for the longeron system is somewhat similar to that used for the stringer system. The reader will note the differences.

1. First, at any bay being checked, determine the primary internal load distributions in the longerons and shear panels due to the applied loads. This can be done as in Art. C11.34 using the engineers theory of bending in most cases. In other cases where judgment and experience and the nature of the structure indicate it, the method of Chapter A8 may be used in determining the primary load distribution due to the applied loads.

2. Next determine the critical shear buckling stresses in the skin panels. Since compression stresses are nearly always also present in practical situations, pure shear buckling does not occur. Thus, as discussed in the case for stringer design, some rational interaction must be used to obtain a "reduced" shear buckling stress. This can be done, for example, by using some "average" compression stress in the panel, weighted toward the high side for conservatism. Thereby the interaction method of Article C11.32 can be used where

$$R_C = \frac{-\frac{B}{A} + \sqrt{\left(\frac{B}{A}\right)^2 + 4}}{2}, \text{ as in (74)}$$

and (A) is determined for a curved panel of length "d" between rings and height (h) between longerons measured along the circumference as in Fig. C11.34. (B) is the ratio of the compression stress to the shear stress, (f_c/f_s), for the particular loading condition being investigated. The compression stress should be calculated as if the panel being calculated had not yet buckled. Then, as in equation (75)

$$f_{s_{cr}} = R_C \, F_{s_{cr}}$$

gives the reduced shear buckling stress, $f_{s_{cr}}$.

When tension strains, rather than compressive ones, are present with the shear we have, as in equation (77)

$$R_T = 1.0 + \frac{f_t}{2F_{c_{cr}}}$$

and then

$$f_{s_{cr}} = R_T \, F_{s_{cr}} \text{ as in equation (79).}$$

3. Next, the loading ratio, $f_s/f_{s_{cr}}$ can be calculated using $f_{s_{cr}}$ as determined in (2) above.

4. Following this, the diagonal tension factor, k, can be obtained from Fig. C11.19.

5. The total axial stress in the longeron can now be written as

$$f_L = f_p + f_{D.T.}$$

$$= f_p - \frac{k_1 f_{s_1} \cot \alpha_1}{\frac{2A_L}{h_1 t_1} + .25\,(1-k_1)R_C} - \frac{k_2 f_{s_2} \cot \alpha_2}{\frac{2A_L}{h_2 t_2} + .25\,(1-k_2)R_C} \quad - - - \quad (104)$$

where

f_p = primary longeron stress from Step (1) (+) if tension and (-) if compression

A_L = Longeron Area

and

k, f_s, cot α, R_C (or R_T), h, and t are as previously defined. One set, subscript (1), is for the panels above the longeron and the other, (2) for the panel below the longeron.

6. The average stress in the supporting ring (or frame) due to diagonal tension effects is given by the following formula (and note that this is different from the stringer case)

$$f_{RG} = \frac{k\, f_s \tan \alpha}{\frac{A_{RG_e}}{dt} + .5\,(1-k)} \quad \text{- - - - - - - (105)}$$

where, as in equation (58),

$$A_{RG_e} = \frac{A_{RG}}{1 + (\frac{e}{\rho})^2}$$

This formula is similar to the one for the "effective" area of a single upright in a plane web beam system, (Art. C11.20), where

e = distance from c.g. of ring to the skin

ρ = radius of gyration of the ring (cross-section) about an axis parallel to the skin.

Equation (105) assumes that k, f_s, d, t, etc., are the same for the panels on each side of the ring. If not, then some average value should be used, or else f_{RG} must be written as the sum of 2 diagonal tension effects (for each side panel) as was done for the longeron in (5) above.

The "maximum" stress, $f_{RG_{MAX}}$, in the ring will be, as before, eq. (59)

$$f_{RG_{MAX}} = f_{RG}\,(\frac{f_{RG_{MAX}}}{f_{RG}})$$

where

$\frac{f_{RG_{MAX}}}{f_{RG}}$ is obtained from Fig. C11.21.

7. The next problem is the determination of the angle of diagonal tension, α. There are several ways in which α can be evaluated. Four are as follows:-

a) When there is a significant amount of compressive strain, simply assume $\alpha = 45^0$.

b) When there is no, or very little, axial strain present (only shear) use Fig. C11.45 to obtain α.

c) If sufficient tension stress (or strain) is present to prevent buckling, from eq. (78), then, of course, $\alpha = 0^0$.

d) Calculate α by the method of successive approximation as follows. This is the most tedious method and (a) and (b) above will suffice in most cases, especially for preliminary design.

The angle, α, must satisfy the equation, from Ref. (3), and this is different from the case for stringers,

$$\tan^2 \alpha = \frac{\varepsilon - \varepsilon_L}{\varepsilon - \varepsilon_{RG} + \frac{1}{8}(\frac{d}{R})^2 \tan^2 \alpha} \quad \text{- - (106)}$$

where, as before, from equation (94)

$$\varepsilon = \frac{f_s}{E}\left[\frac{2k}{\sin 2\alpha} + \sin 2\alpha\,(1-k)(1+\nu)\right]$$

or use Fig. C11.36 for bracketed expression.

$$\varepsilon_L = \frac{f_L}{E} \quad (f_L \text{ from equation (104)})$$

$$\varepsilon_{RG} = \frac{f_{RG}}{E} \quad (f_{RG} \text{ from equation (105)})$$

Equation (106) must be solved by successive approximation as was done in the stringer system discussion.

8. Strength checks can then be made as follows, using stress ratios.

a) Longerons:

$$\frac{f_p}{F_{cc}} + \frac{f_{D.T.}}{F_L} \leqq 1.0$$

where F_{cc} is the "natural" crippling strength and F_L is obtained from Fig. C11.38.

Frequently, in the case of thicker longerons, the following is used as a strength check:

$$\frac{f_p + f_{D.T.}}{F_{cc}} \leqq 1.0$$

That is, the primary and diagonal tension effects are simply added and checked against F_{cc}.

b) Rings:

$$\frac{f_{RG}}{F_{RG}} \leqq 1.0$$

If the rings have stresses in them due to loads other than diagonal tension (i.e. bulkhead type loads, see Chapter A21), then an interaction equation is used.

$$\frac{f_p}{F_{cc}} + \frac{f_{RG}}{F_{RG}} \leqq 1.0$$

where f_p is the stress due to loads other than diagonal tension effects.

c) Skins:

Strength check:

$$\frac{f_s}{F_s} \leqq 1.0$$

where F_s is obtained from Fig. C11.42.

Permanent Buckling:

Usually no perm. buckling is allowed at limit load.

$$\frac{f_{s_{LIMIT}}}{F_{s\ p.b.}} \leqq 1.0$$

where $F_{s_{p.b.}}$ is obtained from Fig. C11.46.

d) General Instability:

$$\frac{f_s}{F_{s_{INST.}}} \leqq 1.0$$

where $F_{s_{INST}}$ is obtained from Fig. C11.39. It is recommended that a margin of safety of .15 to .20 be maintained here. Note in Fig. C11.39 that no effective skin is used and that ρ_{LONG} is at most .34.

e) The loads on rivets at splices, etc. are the same as for the stringer system, eq. (96) and (97).

The procedure outlined in (1) to (8) above can best be illustrated through the use of an example problem.

Fig. C11.37 Example Problem.

Consider a longeron type fuselage structure having a cross-section as shown in Fig. C11.47. The details and section properties of the longerons and rings are included in the figure.

The properties of the structural cross-section are given in Fig. C11.48. The properties shown are for the case where the bending moment causes the upper skin to be in compression and the lower in tension. The upper skin thus buckles out early, as indicated.

For this example problem assume that the applied loads are,

M = 2,135,000 in.lb. (compression in upper skin)

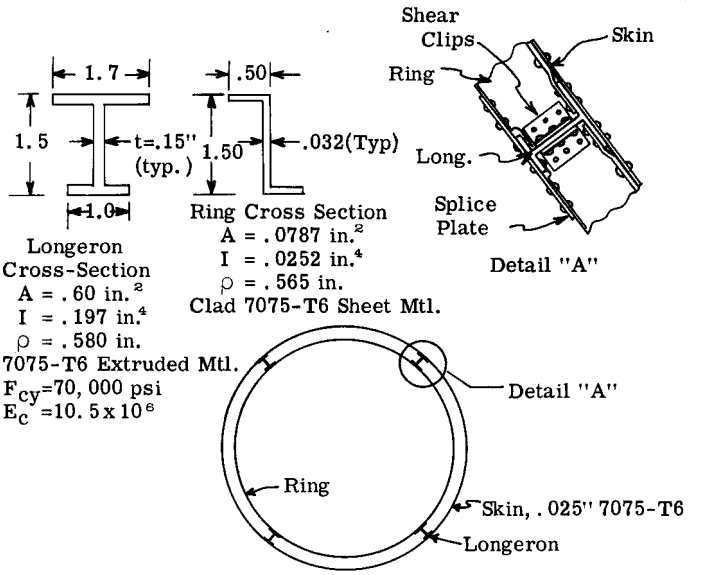

Cross-Section and Details of Members

Fig. C11.47

T = 600,000 in. lb. (reversible)
V = 18,000 lb. (produces comp. in upper skin)

These are the loads at the middle of the bay being checked.

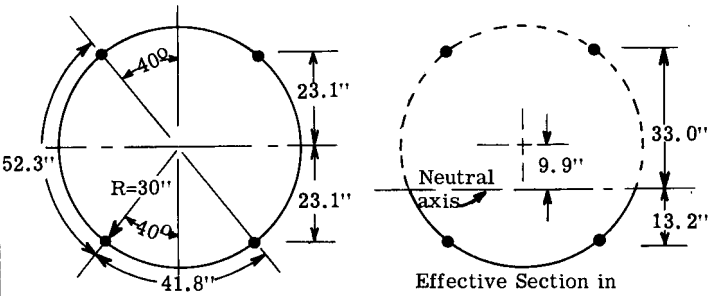

Fig. C11.48

1. Using the geometry and properties of Fig. C11.48 and the engineering theory of bending, we find the primary internal stresses to be,

$$f_{upper\ long.} = \frac{MZ}{I} = \frac{-2,135,000(33)}{1895} =$$

-37,200 psi (comp.)

$$f_{s_{top\ skin}} = \frac{T}{2At} = \frac{600,000}{2(2830)(.025)} = 4240 \text{ psi}$$

$$f_{s_{side\ skins}} = \pm \frac{T}{2At} + \frac{VQ}{2It} = 4240 +$$

$$\frac{18,000(2 \times .60 \times 33)}{2\ (1895)(.025)} = 11,780 \text{ psi}$$

$$f_{lower\ long.} = \frac{MZ}{I} = \frac{-2,135,000(-13.2)}{1895} =$$

+14,800 (tens.)

2a. Check top skin panel for $f_{s_{cr}}$ and k.

Use properties of Fig. C11.47 and the applied loads to get R_c, eq. (74). The skin compression stresses will be "fictitious" since the skin buckles out early, but will give the proper constant, B, for interaction. Assume $f_{c_{skin}}$ at a point 2/3 up from upper longeron to top surface as governing compressive buckling.

$$f_{c_{skin}} = \frac{MZ}{I} = \frac{-2,135,000(27.7)}{1895} = -31,200 \text{ psi (comp.)}$$

$$f_s = \frac{T}{2At} = \frac{600,000}{2(2830)(.025)} = 4240 \text{ psi}$$

Then, from eq. (73),

$$B = \frac{f_c}{f_s} = \frac{31,200}{4240} = 7.35$$

For this upper panel, 5" long (d), 41.8" wide (h) and R = 30", the critical pure shear and compression buckling stresses can be found from buckling equations in Chapter C8.

From Chapter C8, for our panel dimensions, $k_c = 10$ and $k_s = 12.83$, thus

$$F_{c_{cr}} = \frac{\pi^2 \times 10 \times 10,300,000}{12\,(1 - .3^2)} \left(\frac{.025}{5}\right)^2 = \underline{2310} \text{ psi}$$

$$F_{s_{cr}} = \frac{\pi^2 \times 12.83 \times 10,300,000}{12\,(1 - .3^2)} \left(\frac{.025}{5}\right)^2 = \underline{2980} \text{ psi}$$

hence, from eq. (72)

$$A = \frac{F_{c_{cr}}}{F_{s_{cr}}} = \frac{2310}{2980} = .774$$

Then, from eq. (74)

$$R_c = \frac{-\frac{B}{A} + \sqrt{\left(\frac{B}{A}\right)^2 + 4}}{2} = \frac{-\frac{7.35}{.774} + \sqrt{\left(\frac{7.35}{.774}\right)^2 + 4}}{2} = .105$$

and

$$f_{s_{cr}} = R_c F_{s_{cr}} = .105\ (2980) = 313 \text{ psi}$$

3a. The loading ratio, $\frac{f_s}{f_{s_{cr}}}$, is

$$\frac{f_s}{f_{s_{cr}}} = \frac{4240}{313} = 13.54$$

4a. k is then, from (3a) and Fig. C11.19, for

$$\frac{300\ t\ h}{R\ d} = \frac{300\ (.025)}{30}\ (2)^* = .5$$

$$k = .81$$

Next, repeat steps 2a-4a for the side panels. This involves an arbitrary interaction to serve as a criterion for buckling under combined shear and compression.

2b. The stresses at the top (upper longeron) and bottom (lower longeron) of the side panels are -37,200 (comp.) and 14,800 (tension) respectively. This gives an average "fictitious" stress of -11,200 axial and ± 26,000 psi bending stress (equivalent). The actual reduced buckling stress for the side panels could be obtained from an interaction for these axial and bending stresses.

Another way is to use an axial stress only, "weighted" on the high side of the average, arbitrarily, to account for the effect of the bending stress. For this problem a compression stress value half-way between the average, -11,200, and the maximum, -37,200, is used.

Thus $f_c = \frac{-11,200 - 37,200}{2} = -24,200$ psi

then, since $f_s = 11,780$,

$$B = \frac{f_c}{f_s} = \frac{24,200}{11,780} = 2.05$$

and, as before,

$$A = .774\ \left(= \frac{F_{c_{cr}}}{F_{s_{cr}}}\right)$$

Hence

$$R_c = \frac{-\frac{2.05}{.774} + \sqrt{\left(\frac{2.05}{.774}\right)^2 + 4}}{2} = .335$$

and

$$f_{s_{cr}} = R_c F_{s_{cr}} = .335\ (2980) = 998 \text{ psi}$$

3b. The loading ratio is then

$$\frac{f_s}{f_{s_{cr}}} = \frac{11,780}{998} = 11.8$$

4b. From Fig. C11.19, using 11.8 from (3b)

$$k = .79$$

5. The upper longeron stress can then be gotten from eq. (104);

---

* Since $\frac{h}{d} > 2.0$ use 2.0 (See page C11.33).

$$f_L = f_p - \frac{k_1 f_{s_1} \cot \alpha_1}{\frac{2 A_L}{h_1 t_1} + .5 (1-k_1) R_C} - \frac{k_2 f_{s_2} \cot \alpha_2}{\frac{2 A_L}{h_2 t_2} + .5 (1-k_2) R_C}$$

$$= -37{,}200 - \frac{.81 (4240) \cot \alpha_1}{\frac{2 (.6)}{(41.8)(.025)} + .5 (1-.81)(.105)}$$

$$- \frac{.79 (11{,}780) \cot \alpha_2}{\frac{2(.6)}{52.4 (.025)} + .5 (1-.79)(.335)}$$

$$= -37{,}200 - 2970 \cot \alpha_1 - 9810 \cot \alpha_2$$

6a. The stress in the rings supporting the upper skin is obtained from eq. (105).

First,

$$A_{RG_e} = \frac{A_{RG}}{1 + (\frac{e}{\rho})^2} = \frac{.0787}{1 + (\frac{.75}{.58})^2} = .0285$$

Then,

$$f_{RG} = \frac{.81 (4240) \tan \alpha_1}{\frac{.0285}{5(.025)} + .5 (1 - .81)} = 10{,}600 \tan \alpha$$

As discussed earlier, this assumes the upper panels on each side of the frame to have the same shear stress.

6b. The stress in the rings supporting the side panels is, similarly,

$$f_{RG} = \frac{.79(11780) \tan \alpha_2}{\frac{.0285}{5(.025)} + .5 (1 - .79)} = 27{,}900 \tan \alpha_2$$

α_1 and α_2 in the above equations refer to the upper panels and side panels respectively.

7. Angle of diagonal tension.

The compression in the upper panel is so large that α_1 can be reasonably taken as 45^0.

For the side panel the same is probably true, in the upper portion, but this will be checked using the method of successive approximation and equations (106), (105), (104) and (94).

Assume $\alpha = 44^0$ (and $\alpha = 45^0$). From Fig. C11.36 and equations above,

$$\varepsilon = 1.88 (\frac{f_s}{E}) = 1.88 (\frac{11{,}780}{10.3 \times 10^6}) = .00215$$

$$\varepsilon_L = \frac{f_L}{E} = -.00361 - .00028(1.19) - .00095 (1.19) = -.00507$$

$$\varepsilon_{RG} = \frac{f_{RG}}{E} = \frac{-27{,}900 (.967)}{10.3 \times 10^6} = -.00262$$

then,

$$\tan^2 \alpha_2 = \frac{\varepsilon_1 - \varepsilon_L}{\varepsilon_1 - \varepsilon_{RG} + \frac{1}{8} (\frac{d}{R})^2 \tan^2 \alpha}$$

$$= \frac{.00215 - (-.00507)}{.00215 - (-.00262) + \frac{1}{8} (\frac{5}{30})^2 (.705)} = 1.00$$

Thus, $\alpha_2 = 45^0$ which is close to the 44^0 assumed. Let $\alpha_2 = 45^0$. This bears out the statement that any significant compression stress (or strain) forces α towards 45^0.

Had there been no significant average axial strain (or stress) present α could be gotten from Fig. C11.45 which is based on pure shear (no axial loads present). Using this for the above side panels, for example, we would proceed as follows:

$$\frac{E}{f_s} (\frac{d}{R})^2 = \frac{10.3 \times 10^6}{11{,}780} (\frac{5}{30})^2 = 23.5$$

$$\frac{A_{RG_e}}{dt} = .228 \; ; \frac{A_L}{ht} = \frac{.6}{52.3 (.025)} = .459$$

Then from Fig. C11.45, using the above parameters,

$\alpha = 36^0$ (for no compression)

Thus the effect of compression, as previously calculated, is significant in forcing α towards 45^0, as frequently assumed for simplicity.

8. Now that α has been established as 45^0 for the upper skin panels and for the upper portion of the side skin panels, the stresses are available (from (5) and (6)) and strength checks can be made.

a. Longerons:

$f_p = -37{,}200$; $f_{D.T.} = -2970(1.0) - 9810(1.0) = -12{,}780$

$F_{cc} = 65{,}000$

Using Fig. C11.38, and the formula for "C" in the figure,

$F_L = N \times C = 27{,}700 (1.28) = 35{,}400$

then using the interaction equation suggested,

$$\frac{37{,}200}{65{,}000} + \frac{12{,}780}{35{,}400} = .935 < 1.0 \text{ (adequate)}$$

b. Rings:

The ring under the side panel skin will be most critical (f_s is larger):

$f_{RG} = 27,900\ (1.0) = 27,900$

$f_{RG_{MAX}} = 27,900\ (1.15) = 30,500$ (Using Fig. C11.21)

$k^{2/3}\ (\frac{t_r}{t})^{1/3} = .79^{2/3}\ (\frac{.032}{.025})^{1/3} = .927$

Then, using Fig. C11.38,

For R = 30"

N = 19,200

$F_{RG} = N \times C = 19,200 \times 1.187 = 22,800$

$M.S. = \frac{F_{RG}}{f_{RG}} - 1 = \frac{22,800}{30,500} - 1 = -.25$

Thus the ring is not adequate. Either more area (thickness) is required or a closer ring spacing (or both) are needed to lower f_{RG}.

c. Skins:

The side panel has the highest stress and will be, therefore, more critical from an ultimate shear strength than the top panel.

$f_s = 11,780$ psi

From Fig. C11.42, for k = .79 and F_{TU} = 72,000, $F_{s_{ALL.}} = 25,000$ psi. M.S. = (25,000/11,780) - 1 = 1.13.

d. Check for Permanent Buckling

Usually there is the requirement that no permanent skin buckles shall occur at limit load. This is checked as follows:

$f_{s_{limit}} = \frac{f_s}{1.5} = \frac{11,780}{1.5} = 7,840$ psi

Using Fig. C11.46

$\frac{4\ F_{s_{cr}} \times 10^6}{E_c \times F_{cy}} = \frac{4\ (2,980) \times 10^6}{10.3 \times 10^6 \times 62,000} = 1.87$

$\frac{F_{s_{P.B}}}{F_{s_{cr}}} = 2.8,\ F_{s_{P.B}} = 2.8(2980) = 8,340$ psi

$M.S._{P.B.} = \frac{F_{s_{P.B}}}{f_{s_{limit}}} - 1 = \frac{8,340}{7,840} - 1 = .065$

e. General Instability

Using Fig. C11.39, with

$\rho_{LONG} = .554$ and $\rho_{RG} = .565$

(Using no effective skin, per the figure)

$\frac{.39\ (\rho_{RG})^{7/8}}{(dh)^{1/2}\ R^{3/4}} \times 10^4 = \frac{.39(.565)^{7/8}}{(5 \times 52.3)^{1/2}\ (30)^{3/4}}$

$\times 10^4 = 11.35$

From Fig. C11.39

$F_{s_{INST.}} = 3.0 \times E \times 10^{-3} = 30,900$ psi

Thus

$M.S. = \frac{F_{s_{INST}}}{f_s} - 1 = \frac{30,900}{11,780} - 1 = 1.62$ (large)

f. Rivets

The rivet requirements can be checked in the same manner as was done for the stringer type structure along any skin splices and for the tension field "prying" forces.

The load transferred between the longeron and the ring can be calculated as

$P_{RG} = f_{RG} \times A_{RG_e}$, from (8b) and (6a)

$= 27,900 \times .0285$

$= 795$ lb.

This load is actually carried by the rivets attaching the outer ring flange to the longeron flange (next to the skin) and also by the gusset action of the skin at the ring-longeron junction. Two fasteners, staggered if necessary, should be used to attach the outer ring flange to the longeron flange. (See discussion of joggles in Chapter D3).

C11.38 Summary.

From these examples involving both stringer and longeron type construction it can be seen that the effect of axial compression stresses (or strains) along with the shear stresses in the panels is two-fold:

a) It brings about, through interaction, earlier buckling of the panels than would result from shear stresses alone. The result is, of course, a higher value of k and, hence, of all the ensuing loads and stresses that are a function of k.

b) The angle of diagonal tension is forced to approach 45°, more than would result from shear stresses only.

The effect of tension stresses is just the opposite and can thus be conservatively* ignored, or evaluated if desired.

From a time-saving standpoint, in preliminary design, an arbitrarily large value of k and an angle of diagonal tension of 45° can be assumed where significant axial compression strains are present.

The exact magnitude of the various diagonal tension effects throughout a network of skin panels defies simple evaluation from an analytical standpoint. This is particularly true when both shear stresses and axial stresses change from panel to panel as in most practical structures and loadings. No simple analytic expressions are available. But some rational approach is necessary to complete the design, or specimens for test programs, and the approaches given in this chapter represent one such procedure. If margins are extremely small, element tests for substantion are in order. The reader is encouraged to consult the references for a more thorough understanding of the basic theory and its limitations, particularly with regards to areas where substantiating test data is relatively meager.

The stringer system is usually found, for example, in fuselage structures where there are relatively few large "cut-outs" to disrupt the stringer continuity. This is more typical of transport, bomber and other cargo carrying aircraft. The longeron type structure is more efficient and suitable where a large number "quick-access" panels and doors and other "cut-outs" are necessary to service various systems rapidly. These would "chop-up" a stringer system rather severely, making it quite expensive from both a weight and manufacturing standpoint. Therefore, longeron systems are more usually found in fighter and attack type aircraft, and in others with unusual features. There are also, of course, other factors influencing the choice of structural arrangement.

Some further notes concerning this general subject are included in Chapter D3. This includes "beef-up" of panels and axial members bordering cut-outs or non-structural doors, which is also related to "end-bay" effects discussed in C11.29.

* It is not conservative to ignore the reducing effect of tension stresses on k if the compression stresses due to diagonal tension are being relied upon to reduce any primary load tension stresses in stringers or longerons.

C11.39 Problems for Part 2.

1. In the example problem of Art. C11.34, what M.S. would exist if the ring were made of .032 2024 (instead of .040). (Assume $\alpha = 45^\circ$).

2. In the example problem of Art. C11.34, how wide could the ring spacing, d, be made and still show a positive M.S. for the ring. (Assume $\alpha = 45^\circ$.)

3. In the example problem of Art. C11.34, how much additional torsion, T, could be applied before the ring would show a M.S. = 0. (Assume $\alpha = 45^\circ$.)

4. Repeat example problem Art. C11.34 using applied loads

   M = 2,600,000 in./lb.
   T = 0
   V = 40,000 lb.

   Assume the general section properties (I and neutral axis location) remain the same as in C11.34.

5. In the example problem of Art. C11.37

   a) What (standard) gauge of 7075-T6 sheet aluminum would the ring have to be to show a minimum positive M.S.

   b) What ring spacing, d, would be required for the .032" ring to show a minimum positive M.S. (M.S. $\approx$ 0)

6. Repeat the example problem of Art. C11.37 using as applied loads.

   M = 2,400,000 in./lb.
   T = 0
   V = 28,000 lb.

   (Assume section properties are not changed.)

7. What is required to eliminate any negative margins of safety in Problem (6).

C11.40 Problems for Part 1.

(1) The beam as shown in Fig. (A) is subjected to a shear load of 8000 lb. as shown. Determine the margin of safety for the given loading for the following units: (1) web, (2) web flange rivets, (3) web stiffeners. Use NACA method.

(2) Same as problem (1) but with web upright spacing = 4".

(3) Design a semi-tension field beam for the beams and loading of Fig. (B). Take web as 2024-T3 with minimum thickness being .020.

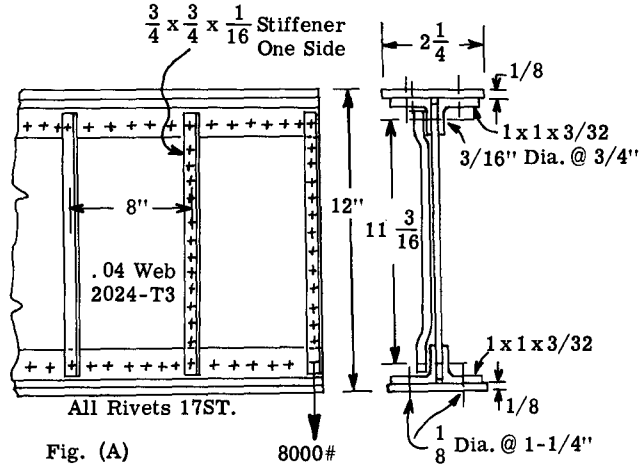

Fig. (A)

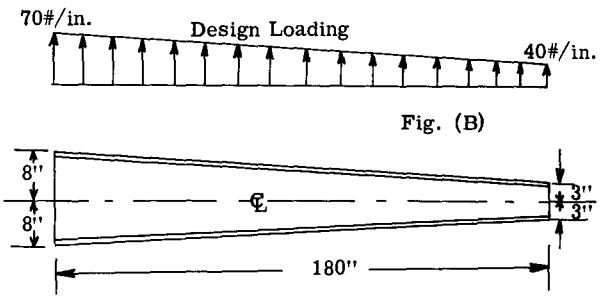

Fig. (B)

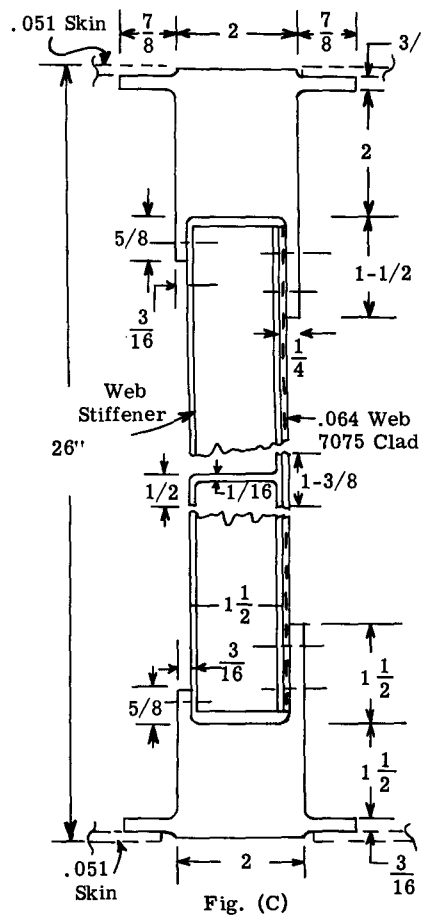

Fig. (C)

Web uprights and flange members to be 2014-T6 extrusions. Rivets to be 2117-T3. Show calculations for at least four sections along beam length. Assume the beam braced laterally by .025 skin on top and bottom.

(4) Fig. (C) shows the cross-section of a single spar wing beam. Strength check the following units of the beam section. (1) web, (2) web uprights. The upright spacing is 8 inches and the design shear load on section is 35000 lb. web material is 7075 alclad.

REFERENCES

(1) H. Wagner, "Structures of Thin Sheet Metal, Their Design and Construction", N.A.C.A. Memo. 490.

(2) H. Wagner, "Flat Sheet Girder With Thin Metal Web."
Part I - N.A.C.A. Technical Memo. 604
Part II - N.A.C.A. Technical Memo. 605
Part III - N.A.C.A. Technical Memo. 606

(3) Kuhn, Peterson, Levin:- A Summary of Diagonal Tension. Part 1. Methods of Analysis. N.A.C.A. T.N. 2661.

(4) Kuhn, Peterson, Levin:- A Summary of Diagonal Tension. Part 2. Experimental Evidence. N.A.C.A. T.N. 2662.

(5) N.A.C.A. T.N. 1347.

(6) Ebner, H., The Strength of Shell Bodies. N.A.C.A. T.N. 838.

(7) N.A.C.A. T.N. 1197.

(8) N.A.C.A. T.N. 774.

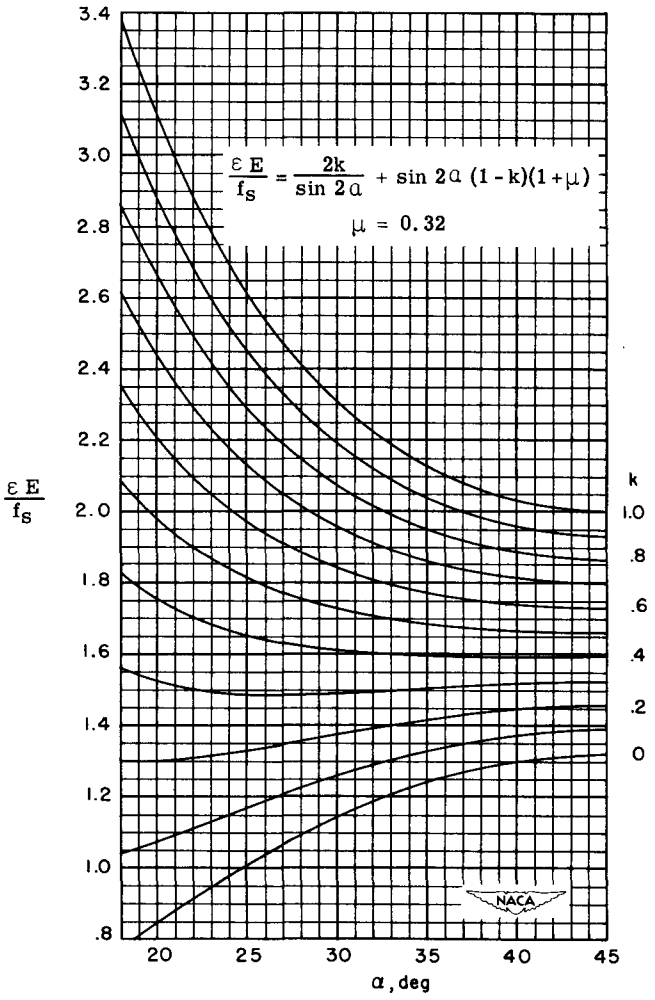

Fig. C11.36 Graph for Calculating Web Strain (Ref. 3)

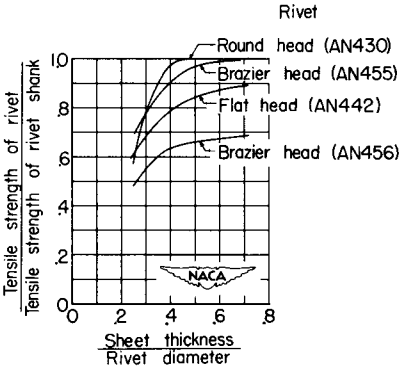

Fig. C11.37a Tensile Strength of Four Types of A17S-T3 Aluminum-Alloy Rivet in 24S-T3 Aluminum-Alloy Sheet. (Ref. 3)

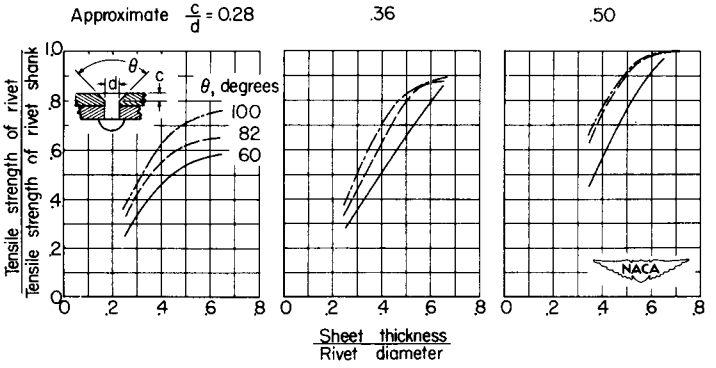

Fig. C11.37b Tensile Strength of NACA Machine-Countersunk Flush Rivets of A17S-T3 Aluminum-Alloy in 24S-T3 Aluminum Alloy Sheet. (Ref. 3).

FORCED CRIPPLING ALLOWABLES FOR STRINGERS (F_{ST}), UPRIGHTS (F_U), RING STIFFENERS (F_{RG}) AND LONGERONS (F_{ST})

Some Typical "C" Values

Matl	Thickness Range	"C"
Clad 2024-T3	.010-.063	.852
	.064-.249	.867
Clad 2024-T4	≤ .064	.803
	.064-.249	1.000
Clad 2024-T6	≤ .064	1.027
	.064-.249	1.107
Clad 2024-T81	≤ .064	1.133
	.064-.249	1.187
Clad 7075-T6	.016-.039	1.209
	.040-.249	.541
AZ31A-H24	.020-.250	1.963
AMS4909	All	1.474
AMS4901	All	1.646
18-8 — 1/4 H	All	

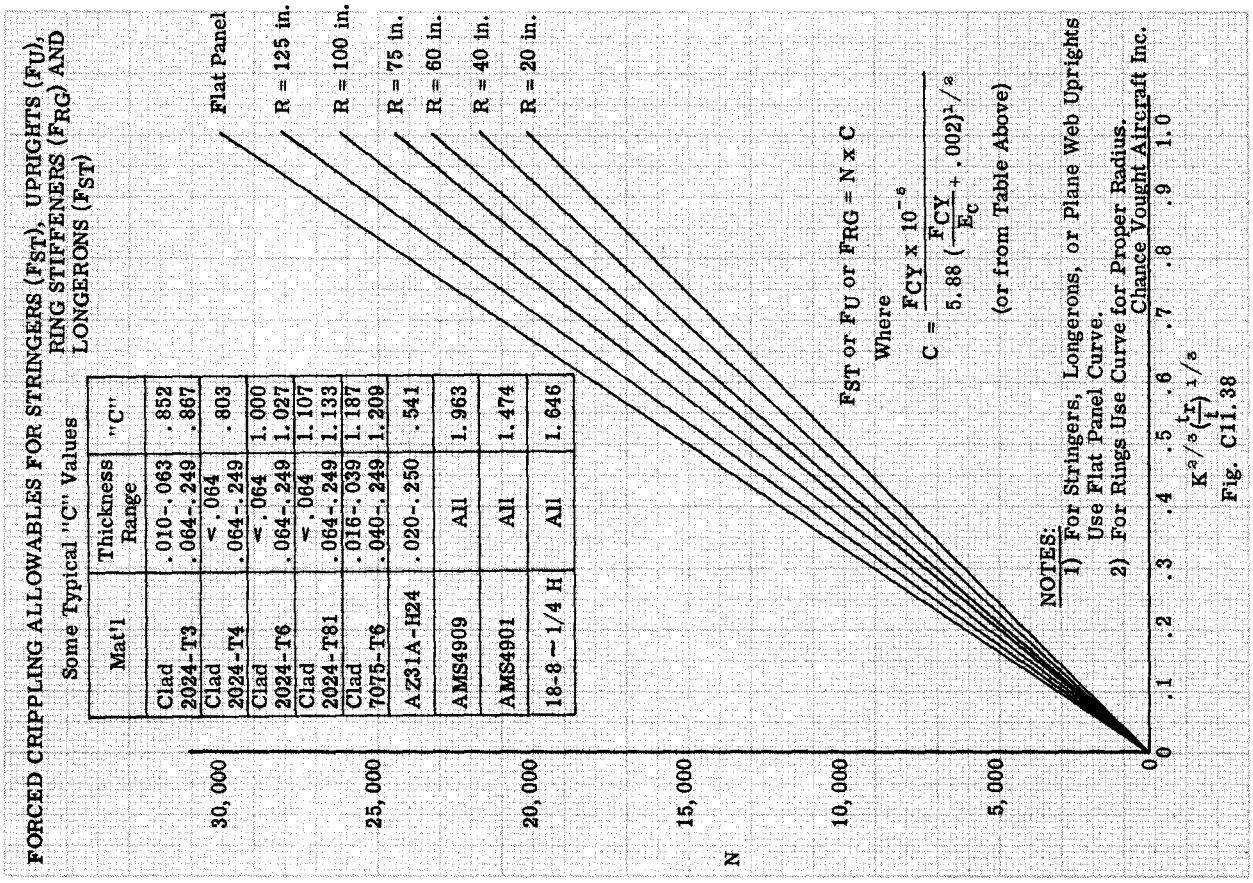

Fig. C11.38

GENERAL INSTABILITY CRITERIA FOR CURVED SHEAR PANELS

(N. A. C. A. T. N. 1197)

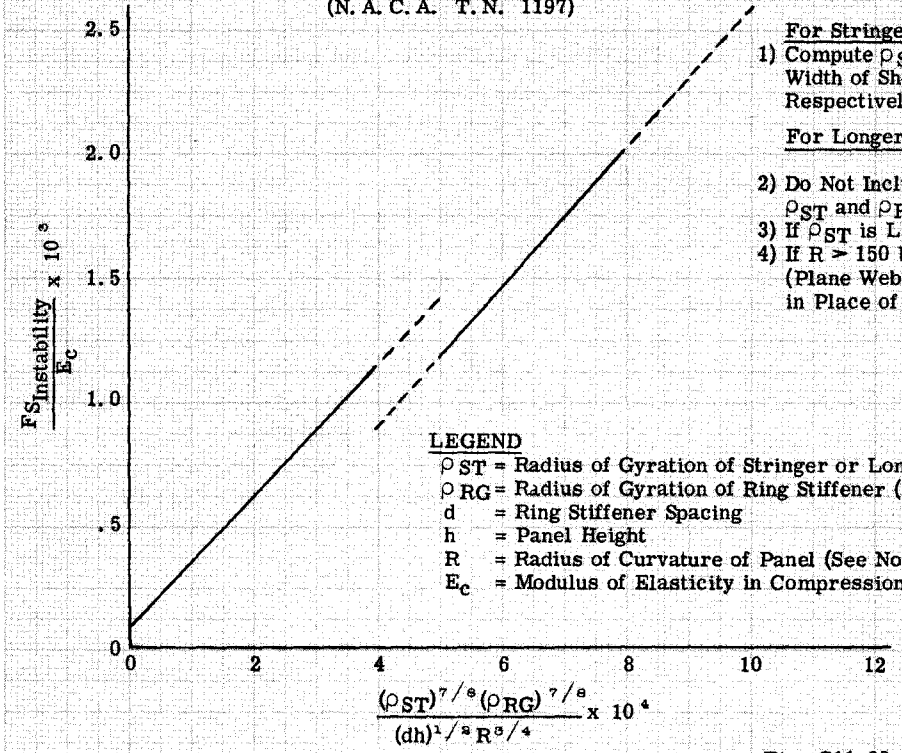

NOTES

For Stringer System (Ref. 3)

1) Compute ρ_{ST} and ρ_{RG} Assuming Full Width of Sheet Acts With Stringer or Ring Respectively and that Sheet is Flat.

For Longeron System (Chance Vought Aircraft, Inc.)

2) Do Not Include Effective Skin in Computing ρ_{ST} and ρ_{RG}.
3) If ρ_{ST} is Larger than 0.34, Use $\rho_{ST} = 0.34$
4) If R ≥ 150 Use Column Analysis for Flat (Plane Web) Tension Field Beam Stiffeners in Place of this Curve.

LEGEND

ρ_{ST} = Radius of Gyration of Stringer or Longeron (See Notes 1, 2 & 3 above)
ρ_{RG} = Radius of Gyration of Ring Stiffener (See Notes 1 & 2 above)
d = Ring Stiffener Spacing
h = Panel Height
R = Radius of Curvature of Panel (See Note 4 above)
E_c = Modulus of Elasticity in Compression

Fig. C11.39

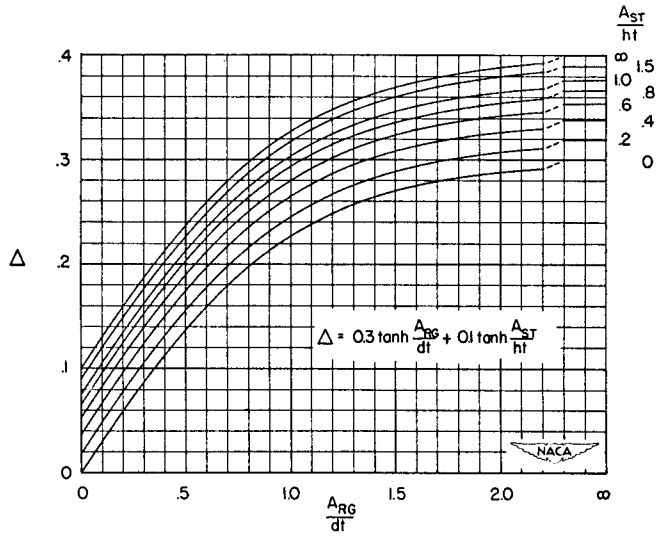

Fig. C11.40 Correction for Allowable Ultimate Shear Stress in Curved Webs.

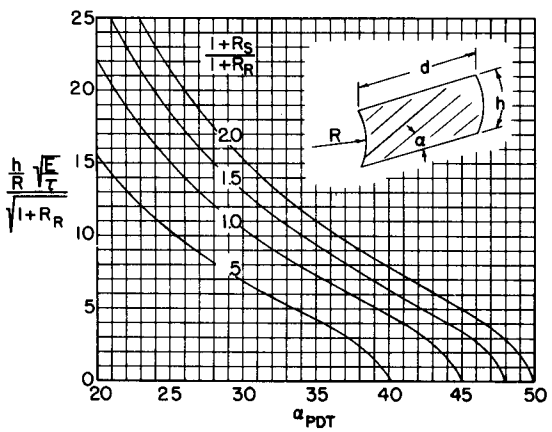

$$R_R = \frac{dt}{A_{RG}} \; ; \; R_S = \frac{ht}{A_{ST}}$$

Fig. C11.41a

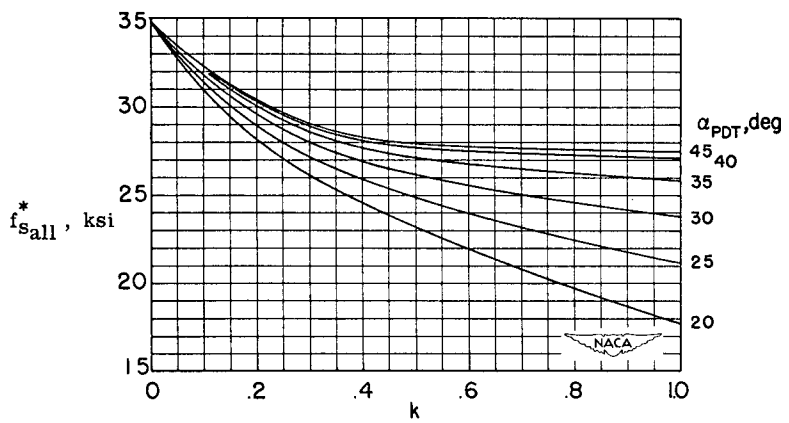

Fig. C11.41c Alclad 7075-T6 Aluminum Alloy. σ_{ult} = 72 ksi

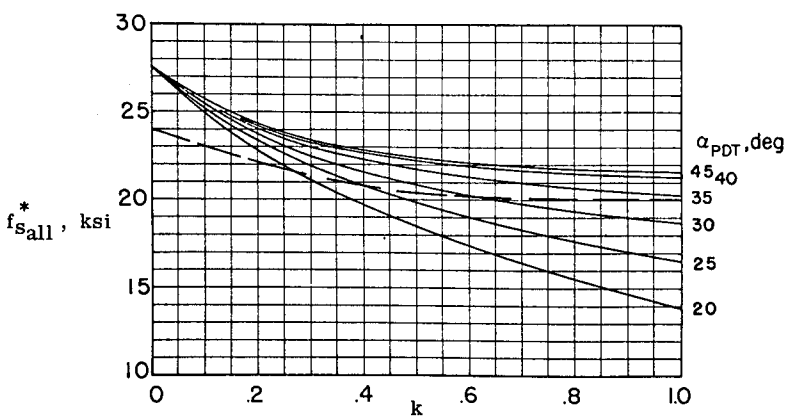

Fig. C11.41b 2024-T3 Aluminum Alloy. σ_{ult} = 62 ksi. Dashed Line is Allowable Yield Stress.

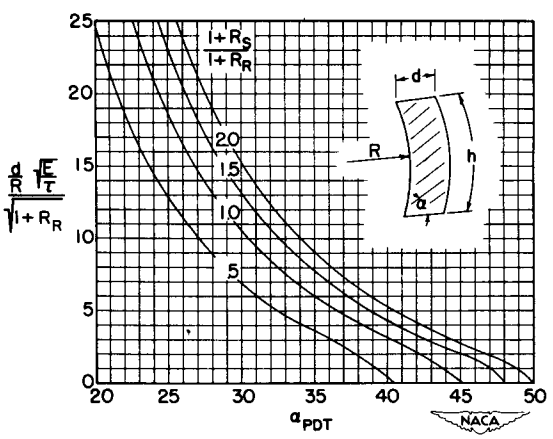

Fig. C11.41d Angle of Pure Diagonal Tension.

$$R_R = \frac{dt}{A_{RG}} \; ; \; R_S = \frac{ht}{A_{ST}}$$

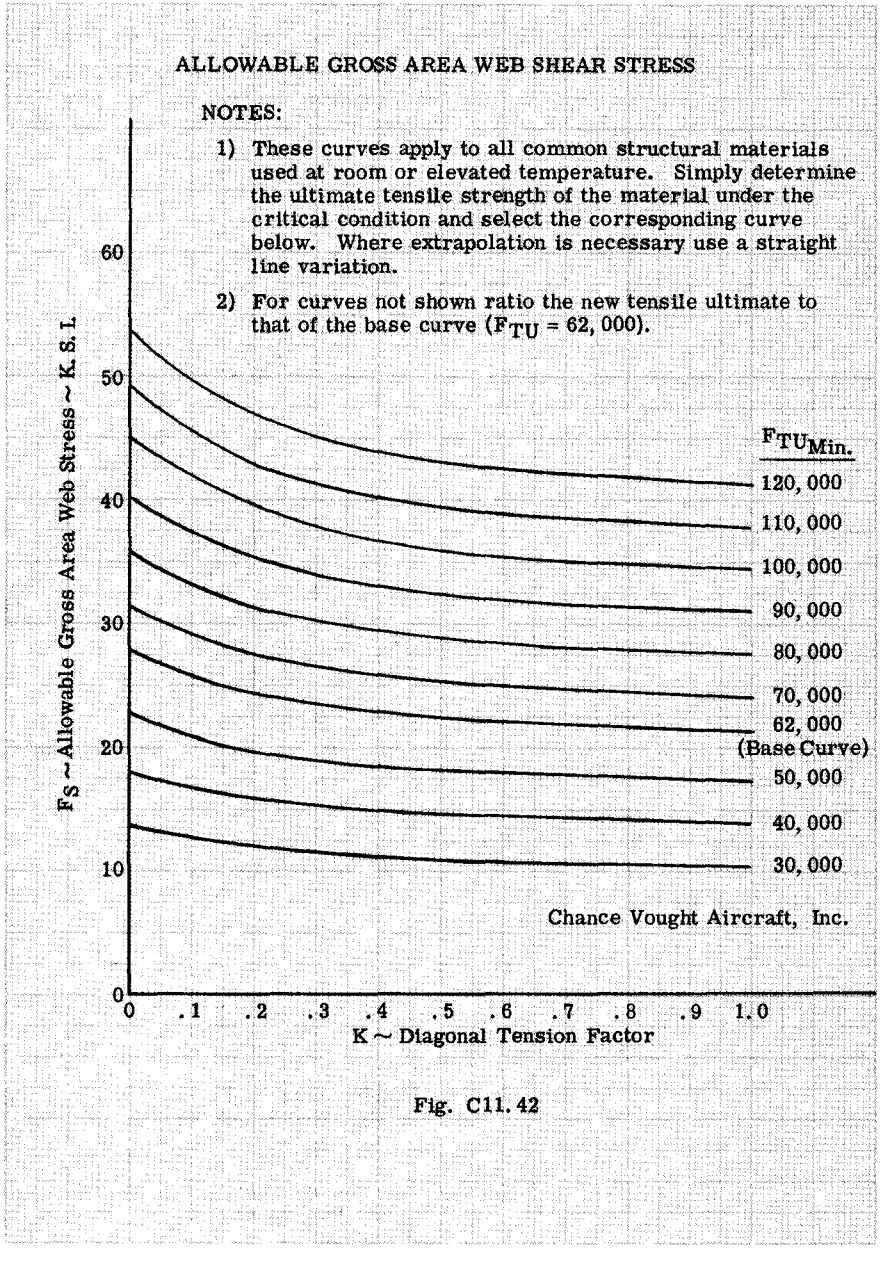
ALLOWABLE GROSS AREA WEB SHEAR STRESS
NOTES:
1) These curves apply to all common structural materials used at room or elevated temperature. Simply determine the ultimate tensile strength of the material under the critical condition and select the corresponding curve below. Where extrapolation is necessary use a straight line variation.
2) For curves not shown ratio the new tensile ultimate to that of the base curve (F_{TU} = 62, 000).
F_S ~ Allowable Gross Area Web Stress ~ K. S. I.
0
10
20
30
40
50
60
$F_{TU_{Min.}}$
120, 000
110, 000
100, 000
90, 000
80, 000
70, 000
62, 000
(Base Curve)
50, 000
40, 000
30, 000
Chance Vought Aircraft, Inc.
0
.1
.2
.3
.4
.5
.6
.7
.8
.9
1.0
K ~ Diagonal Tension Factor

Fig. C11. 42

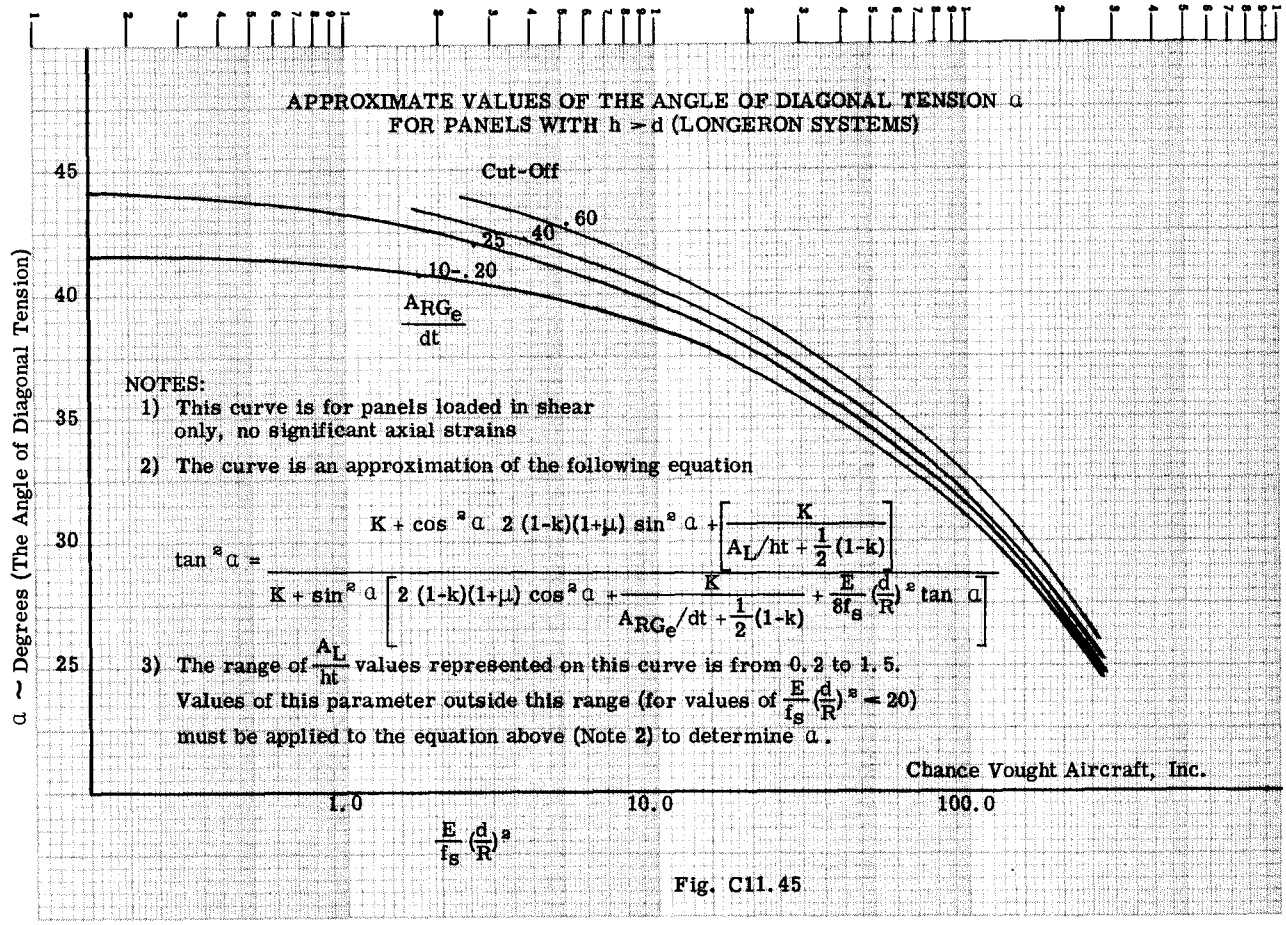

Fig. C11.45

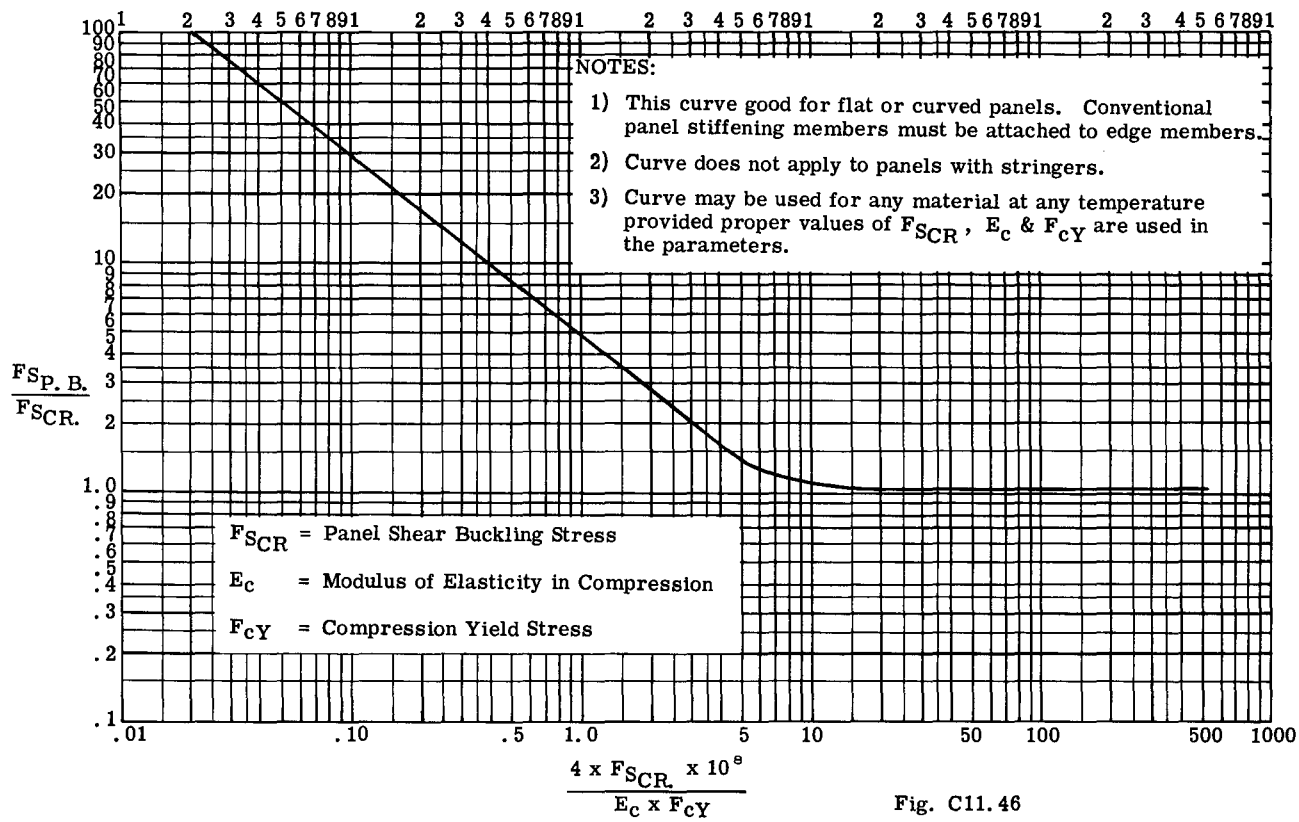

Fig. C11.46

CHAPTER C12
SANDWICH CONSTRUCTION AND DESIGN

BY

LLOYD E. HACKMAN - SR. TECHNICAL SPECIALIST, N. AMERICAN AVIATION, COLUMBUS, OHIO

C12.1 Introduction.

In the past decade sandwich construction has been developed until it is now a widely accepted type of construction in the aircraft industry. This acceptance is due to the continuous development of the sandwich components, sandwich design and fabrication, and the confidence gained through the years in which the sandwich concept has been applied.

The components of sandwich construction are facings, cores and core-to-facing bonding materials. A sandwich panel is analogous to an I-beam with the facings and core corresponding to the flanges and web, respectively. The facings carry axial tensile and compressive stresses and the core sustains shear and compressive stresses normal to the panel and prevents wrinkling or buckling of the facings under axial compressive loading. The continuous support of the facings provided by the core material is also important to aerodynamic performance in aircraft applications. The core-to-facing bond must be adequate to transfer the stresses from facings to core so that the full properties of the core and facings may be realized.

Materials commonly used as facings include metal sheet such as aluminum, titanium, stainless steel, or reinforced plastic laminate. Adhesives used for core-to-facing bonding are normally of the liquid and supported film types. Reinforced plastic laminate facings may be attached to certain cores by a "wet layup" technique which is accomplished by allowing the uncured impregnating resin to act as the bonding agent. This method generally provides bonds of lower strength than when an adhesive is used.

Although a discussion of sandwich adhesive development is not a part of this section, it is to be noted that the core-to-facing bonding materials are extremely important. Like a chain, a sandwich is no better than its weakest link - the facing, core, or core-to-facing bond.

Core materials for sandwich construction may be divided into two classes - metallic and non-metallic. The metallic cores include aluminum, titanium and stainless steel honeycomb and are employed where high shear strength, shear modulus and, in the case of stainless steel, where high temperature resistance is required. In the lower temperature ranges, aluminum honeycomb is generally preferred because of its relatively low cost. Stainless steel honeycomb may be adhesive-bonded or brazed to facings. The brazing technique is relatively expensive and difficult, and is used only when necessary, which is in the temperature range from about 500 degrees F upward, where adhesive-bonded sandwich is not, at present, adequate for extended periods of time.

Foams, balsa, and reinforced plastic honeycombs comprise the non-metallic core materials. The foams possess a wide range of properties but it may be generally said that they have relatively low strength in comparison with the other core materials. However, the thermal insulation properties of the foams, and the ability of certain foams to be "foamed in place", thus conforming to any contour, make them an attractive core material in certain applications. The high strength properties of honeycomb and thermal insulation of low density foams can be advantageously combined to provide a high-strength insulating core material.

Within the family of metallic cores of which there are many different core types, honeycomb has emerged as the best known. However, the corrugated or truss core sandwich is of equal importance in the design of high performance aircraft. The corrugated core sandwich construction will be discussed in section C12.9 in greater detail.

The design procedures of this section are based principally on analyses and tests performed by the U. S. Forest Products Laboratory under the sponsorship of the Composite Construction Subcommittee (formerly ANC-23 Panel) of the Federal Aircraft Design Criteria Committee.

C12.2 Basic Design Principles.

Structural sandwich is a layered construction formed by bonding two thin facings to a thick core. It is a type of stressed-skin construction in which the facings resist all, or nearly all, of the applied edgewise loads and flatwise bending moments. The thin spaced facings provide all, or nearly all, of the bending rigidity to the construction. The core spaces the facings and transmits shear between them so that they are effective about a common neutral axis. The core also provides most of the shear rigidity of the sandwich construction. By proper choice of materials for facings and core,

constructions with high ratios of stiffness to weight can be achieved.

A basic design concept is to space strong, thin facings far enough apart to achieve a high ratio of stiffness to weight; the lightweight core that does this must provide the required resistance to shear and be strong enough to stabilize the facings to their desired configuration through a bonding medium such as an adhesive layer, braze, or weld.

In order that sandwich cores be lightweight, they are usually made of a low-density material, of some type of cellular construction (honeycomb-like core formed of thin sheet material), or of corrugated sheet material. As a consequence of employing a lightweight core, design methods must account for core shear deformation because of the low effective shear modulus of the core. The main difference in design procedures for sandwich structural elements as compared to design procedures for homogeneous material is the inclusion of the effects of core shear properties on deflection, buckling, and stress.

Because thin facings can be used to carry loads in sandwich, consideration must be given to the prevention of local failure under edgewise direct or flatwise bending loads just as local crippling of stringers must be considered in the design of sheet-stringer construction. Modes of failure that may occur in sandwich under edge load are shown in Fig. C12.2.1.

Shear crimpling failure (Fig. C12.2.1B) appears to be a local mode of failure, but is often a form of general overall buckling (Fig. C12.2.1A) in which the wavelength of the buckles becomes very small because of low core shear modulus. The crimping of the sandwich occurs very suddenly and usually causes the core to fail in shear at the crimp; it may also cause shear failure in the bond between the facing and core. Crimping may also occur in conjunction with overall buckling of the sandwich. In such cases, the overall buckle begins to appear and the crimp occurs suddenly because of severe local shear stresses at the ends of the overall buckle. As soon as the crimp appears, the overall buckle may disappear.

Therefore, although examination of the failed sandwich indicates crimping or shear instability, failure may have begun by overall buckling that finally caused crimping.

If the core is of cellular (honeycomb) or corrugated material, it is possible for the facings to buckle or dimple into the spaces between core walls or corrugations as shown in Fig.C12.2.1C. This dimpling of the facings may not lead to failure unless the amplitude of the dimples is large enough to cause the dimples to

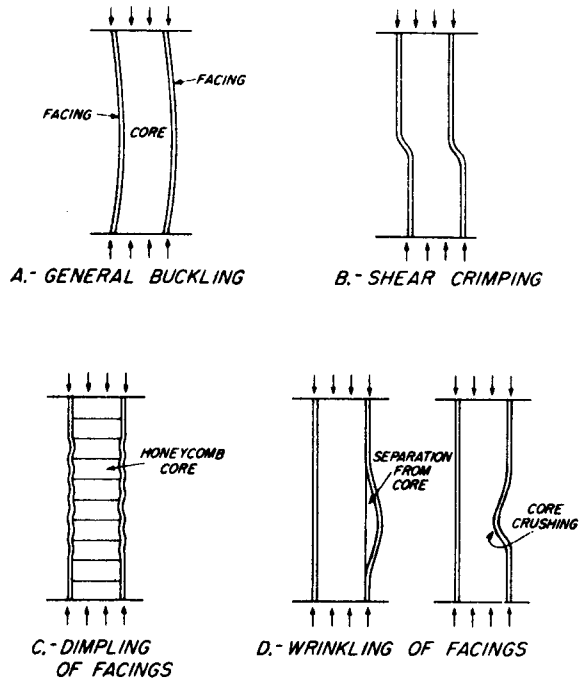

Fig. C12.2.1 Possible modes of failure of sandwich construction under edgewise loads: General buckling, shear crimping, dimpling of facings, and wrinkling of facings either away from or into the core.

grow across the core cell walls and result in a wrinkling of the facings. Dimpling that does not cause total structural failure may, of course, be severe enough so that permanent dimples remain after removal of load.

Wrinkling, as shown in Fig. C12.2.1D, may occur if a sandwich facing subjected to edgewise compression buckles as a plate on an elastic foundation. The facing may buckle inward or outward, depending on the flatwise compressive strength of the core relative to the flatwise tensile strength of the bond between the facing and core. If the bond between facing and core is strong, facings can wrinkle and cause tension failure in the core. Thus, the wrinkling load depends upon the elasticity and strength of the foundation system; namely, the core and the bond between facing and core. Since the facing is never perfectly flat, the wrinkling load will also depend upon the initial facing eccentricity or original waviness.

The local modes of failure may occur in sandwich panels under edgewise loads and/or under normal loads. In addition to overall buckling and local modes of failure, sandwich shall be designed so that facings do not fail in tension, compression, shear, or combined stresses due to edgewise loads and/or normal loads, and cores do not fail in shear or flatwise compression due to normal loads.

The basic design principles can be summarized into four required conditions as follows:

1. Sandwich facings shall be at least thick enough to withstand chosen design stresses under design[1] loads.

2. The core shall be thick enough and have sufficient shear rigidity and strength so that overall sandwich buckling, excessive deflection, or shear failure will not occur under design[1] loads.

3. The core shall have high enough moduli of elasticity, and the sandwich shall have great enough flatwise tensile and compressive strength so that wrinkling of either facing will not occur under design[1] loads.

4. If the core is cellular (honeycomb) or of corrugated material and dimpling of the facing is not permissible, the cell size or corrugation spacing shall be small enough so that dimpling of either facing into the core spaces will not occur under design[1] loads.

In the choice of materials and methods of sandwich assembly, consideration must be given to the environment in which the sandwich is to perform, and material properties used for design should be compatible with the expected environment. Included as environment are effects of heat, cold, water or moisture, corrosive atmosphere or fluids, fatigue, creep, or any other conditions that may affect material properties. Design details should be such as to prevent difficulties insofar as possible in regard to proper performance.

Certain nonstructural characteristics, such as thermal conductivity, resistance to surface abrasion, dimensional stability, permeability, and electrical properties of the sandwich materials should be considered in arriving at a thoroughly efficient design for the intended purpose.

Detailed procedures giving formulas and graphs for use in structural design are given in the following sections of C12. The formulas and graphs can be used to determine dimensions of facings and core as well as necessary core properties for sandwich components under various types of loading. Graphs and formulas are presented in terms of general parameters, and are not for specific materials. Design criteria involving buckling are based on theoretical buckling coefficients. These coefficients have been in fair agreement with average test results, but allowance can be made in the final design to account for the scatter characteristic of buckling test results, perhaps by choosing a slightly thicker core, so that buckling of the sandwich component does not occur at design[1] load.

[1] Design load shall be not less than "design ultimate load" when composite structures are to be designed for use in military aircraft where the requirements of military specifications series MIL-A-8860 (ASG) through MIL-A-8870 (ASG) must be met.

C12.3 Nomenclature.

The following nomenclature is used in this chapter. Each section devoted to a particular sandwich component will define the symbols used the first time in that section. Sketches in Fig. C12.3.1 show nomenclature for cores and sandwich construction.

1	- Subscript denoting facing 1 of a sandwich
2	- Subscript denoting facing 2 of a sandwich
a,b	- Length of panel edge, b parallel to compressive load
c	- Subscript denoting "core" or "compression", core depth
cr	- Subscript denoting "critical"
D	- Bending stiffness or twisting stiffness depending on subscripts
d	- Total sandwich depth or thickness
E	- Young's modulus of elasticity
E'	- Effective modulus of elasticity
F	- Allowable stress; subscript denotes facing
f	- Calculated stress
G	- Modulus of rigidity
G'	- Effective modulus of rigidity
H	- Extensional stiffness
h	- Distance between facing centroids
K	- A constant
L	- Length
M	- Bending moment
m	- Number of half waves
N	- Load per unit length of edge
n	- Number of half waves
P	- Load
p	- Intensity of distributed load
r	- Radius; subscript denoting "reduced"
R	- Ratio
S	- Shear load normal to surface of panel
s	- Core cell size; subscript denoting "shear" when applied to stress and "secant" when applied to moduli
T	- Torque
t	- Thickness; with subscript denotes type of thickness; subscripts denoting "tangent" when applied to moduli
U	- Transverse shear stiffness
u	- Subscript to stress denoting "ultimate"
V	- Parameter relating shear and bending stiffness
w	- Density; subscript denoting "wrinkling"
x	- Axis; subscript denoting "parallel to x-axis"
y	- Axis perpendicular to x-axis; subscript denoting "parallel to y-axis;" or denoting "yield" when applied to stress
z	- Axis normal to surface of sandwich; subscript denoting "parallel to z-axis"

γ - Shear strain
δ - Deflection
ε - Compression or extension strain
η - Plasticity coefficient
λ - One minus the product of two Poisson's ratios
μ - Poisson's ratio
ρ - Radius of gyration

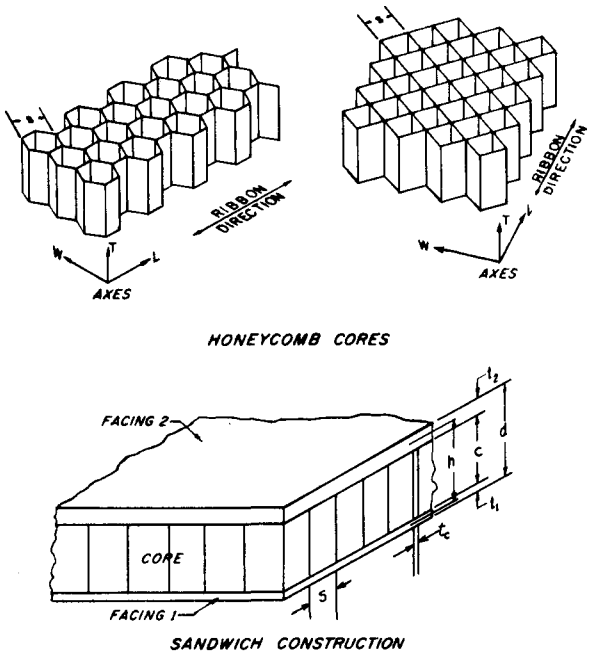

Fig. C12.3.1 Sketches showing nomenclature used for cores and sandwich construction.

C12.4 Basic Sandwich Structural Properties.

C12.4.1 Sandwich Bending Stiffness.

A sandwich that has thin facings on a core of negligible bending stiffness has a transverse stiffness per unit width given by the formula

$$D = \frac{E'_1 t_1 E'_2 t_2 h^2}{(E'_1 t_1 + E'_2 t_2)\lambda} \text{ (for unequal facings)} \quad - - - - - - \text{(C12.4.1)}$$

$$D = \frac{E' t h^2}{2\lambda} \text{ (for equal facings)} \quad - - - - \text{(C12.4.1a)}$$

where E' is the effective modulus of elasticity of facing, $\lambda = 1 - \mu^2$; μ is Poisson's ratio of facings (in formula it is assumed that $\mu = \mu_1 = \mu_2$); t_F is facing thickness and h is distance between facing centroids.

If the facings are thick, the sandwich stiffness is given by the formula

$$D = \frac{E'_1 t_1 E'_2 t_2 h^2}{(E'_1 t_1 + E'_2 t_2)\lambda} + \frac{1}{12\lambda}(E'_1 t_1^3 + E'_2 t_2^3) \quad - - - - - - \text{(C12.4.2)}$$

$$D = \frac{E' t h^2}{2\lambda} + \frac{E' t^3}{6\lambda} \quad - - - - - - - - - - \text{(C12.4.2a)}$$

C12.4.2 Sandwich Shear Stiffness

A sandwich that has fairly thin facings on a thick core has a transverse shear stiffness per unit width given approximately by the formula

$$U = \frac{h^2}{c} G'_c \approx h G'_c \quad - - - - - - - - - - \text{(C12.4.3)}$$

where c is the core thickness and G'_c is the effective core shear modulus.

C12.4.3 Core Properties

The mechanical properties of isotropic square celled honeycomb core and orthotropic hexagonal cell core are presented in this section. The values shown are based on the theory that square celled core has equal properties in the longitudinal (parallel to foil ribbon) and transverse (perpendicular to foil ribbon) directions. Where values are orthotropic, both longitudinal and transverse values will be given.

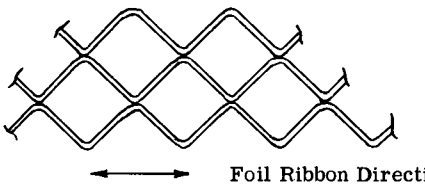

Plan View - Square Cell Core

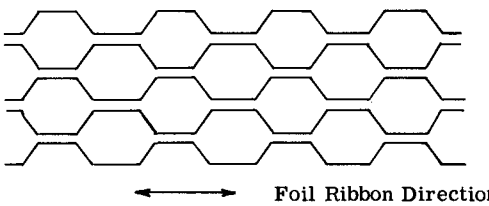

Plan View - Hexagonal Cell Core

The core properties obtained from brazed or adhesive bonded honeycomb sandwich tests are for complete braze node flow or bonded joint. The charts presented in this section are based on formulas derived from empirical data.

C12.4.4 Core Density

The theoretical square cell core density (ρ'_c) can be expressed in terms of cell size (s),

foil gage (t_c) and material density (ρ_c) as:

$$\rho'_c = \frac{2t_c}{s}\ \rho_c \quad - - - - - - - - - - - - - \text{(C12.4.4)}$$

The theoretical hexagonal cell core density (ρ'_c) can be expressed in terms of cell size (s), foil gage (t_c) and material density (ρ_c) as:

$$\rho'_c = \frac{3t_c}{s}\ \rho_c \quad - - - - - - - - - - - - - \text{(C12.4.5)}$$

C12.4.5 Core Shear Properties

BRAZED SQUARE CELL

The core shear strength varies principally as a function of core density. Other factors which affect core shear strength are:

a. Core depth: Core shear strength decreases as the core depth is increased.

b. Braze node flow: Restricted or no node flow conditions reduce the core shear strength.

c. Ribbon direction: Use 80% of longitudinal ribbon direction strength for the transverse ribbon direction.

d. Braze alloy: Braze (core-to-face bond) strength can be expressed by the following equation:

$$F'_s = 1.25\ (\frac{w}{s})\ F_{s_{br}} \quad - - - - \text{(C12.4.6)}$$

Where: w = fillet width
s = cell size
$F_{s_{br}}$ = braze lap shear strength

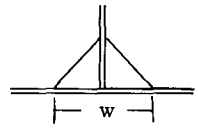

e. Temperature: Elevated temperatures reduce both the core shear strength and the braze strength. It should be noted that elevated temperature reduction for braze strength is greater than that for core shear strength. Therefore, it is possible for a configuration to be critical for core shear strength at room temperature and braze strength at elevated temperature.

The design core shear strength can be expressed by the empirical formula:

$\rho'_c < 18.0$ lbs/ft^3

$$F'_s = 1.307(\frac{\rho'_c}{\rho_c})^{1.64}\ \frac{F_{su}}{c^{0.44}} \quad - - - - \text{(C12.4.7)}$$

$\rho'_c > 18.0$ lbs/ft^3

$$F'_s = 0.427\ (\frac{\rho'_c}{\rho_c})\ \frac{F_{su}}{c^{0.44}} \quad - - - - - \text{(C12.4.8)}$$

The core shear modulus varies principally as a function of core density. Other factors which affect the core shear modulus are:

a. Ribbon direction: Use 70% of longitudinal ribbon direction value for transverse ribbon direction.

b. Temperature: Temperature reduction is proportional to the reduction of the shear modulus of the core material.

Node flow condition, core depth and cell size do not directly affect the modulus.

The design curve for the core shear modulus can be expressed by the empirical formulae:

$\rho'_c < 16.7$ pcf

$$G'_c = 2.43\ (\frac{\rho'_c}{\rho_c})^{1.64}\ G_c \quad - - - - - \text{(C12.4.9)}$$

$\rho'_c \geq 16.7$ pcf

$$G'_c = .4\ (\frac{\rho'_c}{\rho_c})\ G_c \quad - - - - - - - - \text{(C12.4.10)}$$

Most of the test data fall between the design curve and a curve which is about 240% of the design curve. The average (median) value is about 128% of the design curve. Half of the test points are above this average and half of them are below. The theoretical modulus can be expressed by the formula:

$$G'_c = .5\ (\frac{\rho'_c}{\rho_c})\ G_c \quad - - - - - - - - - - - \text{(C12.4.11)}$$

The theoretical equation above assumes that the cell walls are not buckled during the initial portion of the stress-strain diagram. In actual practice, however, the cell walls buckle at very low load levels or even have built-in buckles from fabrication. This would partially account for the stress-strain diagram with initial slopes generally less than theoretical.

BONDED HEXAGONAL CELL CORE

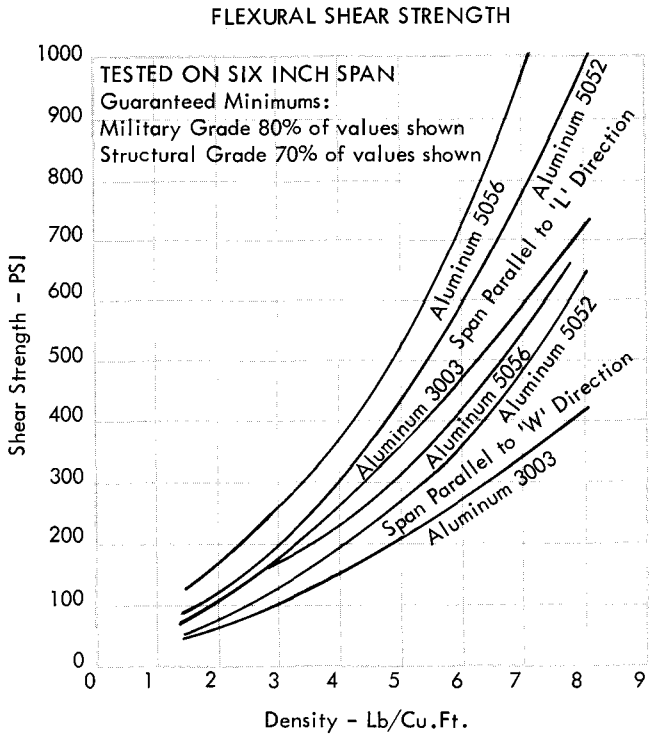

Fig. C12.4.1

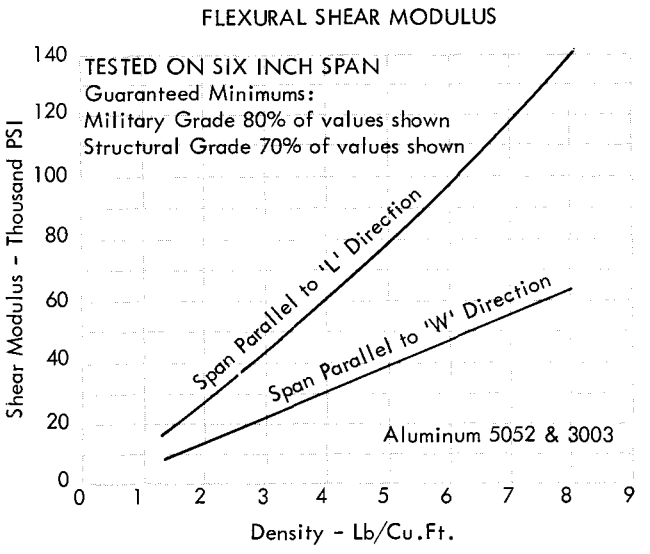

Fig. C12.4.2

C12.4.6 Core Flatwise Compression Properties

BRAZED SQUARE CELL

The core flatwise compression strength varies principally as a function of core density. Other factors which affect the core flatwise compression strength are:

a. Core depth: Strength decreases as the core depth is increased.

b. Braze node flow: Restricted or no node flow conditions reduce the strength.

c. Temperature: The temperature reduction factor is empirical and indicates that at elevated temperatures F'_c ceases to be proportional to F_{cy}.

Cell size and braze alloy do not directly affect the strength.

The design core flatwise compression strength can be expressed by the empirical formula:

$$F'_c = 2.31 \left(\frac{\rho'_c}{\rho_c}\right)^{1.464} \frac{F_{cy}}{c^{.16}} \quad \text{------(C12.4.12)}$$

F_{cy} = compression yield stress

The average (median) is about 115% of the design core strength.

The flatwise compression modulus is a function of core density. Node flow, core depth and cell size do not directly affect the modulus. Elevated temperature values show a reduction from room temperature values. The temperature reduction factor presented is empirical and indicates that with elevated temperatures E'_c ceases to be proportional to E_c.

The design curve for the core compression modulus can be expressed by the empirical formula:

$$E'_c = 2.13 \left(\frac{\rho'_c}{\rho_c}\right)^{1.415} E_c \quad \text{------(C12.4.13)}$$

Most of the test data fall between the design curve and a curve which is about 250% of the design curve. The average (median) value is about 157% of the design curve. Half of the test points are above this average and half are below.

The theoretical core flatwise compression modulus can be expressed by the formula:

$$E'_c = \left(\frac{\rho'_c}{\rho_c}\right) E_c \quad \text{----------(C12.4.14)}$$

This formula assumes that the total cross-section of the cell walls deflects uniformly due to axial stress. In actual practice, however, the cell walls between nodes buckle at a relatively low stress level and the nodes are then required to operate at a higher stress level than indicated by a uniform stress distribution. Therefore, core compression modulus values indicated by tests are considerably lower than the theoretical values.

BONDED HEXAGONAL CELL CORE

In the case of Young's Modulus, the theoretical equation remains the same in the case of hexagonal cell core. Therefore it is suggested that equation C12.4.12 and C12.4.13 be used to represent the design curves.

C12.4.7 Core Flatwise Tension Properties.

BRAZED SQUARE CELL CORE

The core flatwise tension strength varies principally as a function of core density. Other factors which affect the core flatwise tension strength are:

a. Node flow: Restricted or no node flow condition reduce core flatwise tension strength.

b. Braze alloy: Braze (core-to-face bond) strength can be expressed by the following equation:

$$F'_t = 1.41 \left(\frac{W}{s}\right) F_{s_{br}} \quad \text{- - - - -(C12.4.15)}$$

$F_{s_{br}}$ = Braze lap shear strength

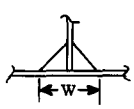

c. Temperature: Elevated temperatures reduce both the core flatwise tension strength and the braze strength. It should be noted that elevated temperature reduction for braze strength is greater than that for core flatwise tension strength. Therefore, it is possible for a configuration to be critical for core flatwise tension strength at room temperature and braze strength at elevated temperature.

Core depth does not directly affect the strength.

The design core flatwise tension strength can be expressed by the empirical formula:

$$F'_t = .5 \left(\frac{\rho'_c}{\rho_c}\right) F_{tu} \quad \text{- - - - - - - - - - -(C12.4.16)}$$

Most of the test data fall between the design curve and a curve which is 160% of the design curve. The average (median) is about 130% of the design curve. Half of the test points are above this average and half are below.

BONDED HEXAGONAL CELL CORE

The following equation can be used for bonded honeycomb panels to compute the flatwise tension strength as affected by the adhesive bond.

$$F'_t = \frac{bt_{AD}}{s} F_{s_{AD}} \quad \text{- - - - - - - - - - -(C12.4.17)}$$

t_{AD} = Adhesive thickness

$F_{s_{AD}}$ = Adhesive lap shear strength

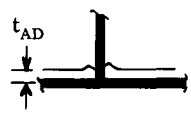

The design core flatwise tension strength remains the same as equation C12.4.16.

C12.4.8 Combined Load Strength.

The design curve for combined load strength can be expressed by the equation:

$$R_a^2 + R_s = 1 \quad \text{- - - - - - - -(C12.4.18)}$$

Where: $R_a = \dfrac{\text{Applied core normal stress}}{\text{Allowable core normal stress}} = \dfrac{f'_c}{F'_c}$ or $\dfrac{f'_t}{F'_t}$

$$R_s = \frac{\text{Applied core shear stress}}{\text{Allowable core shear stress}} = \frac{f'_s}{F'_s}$$

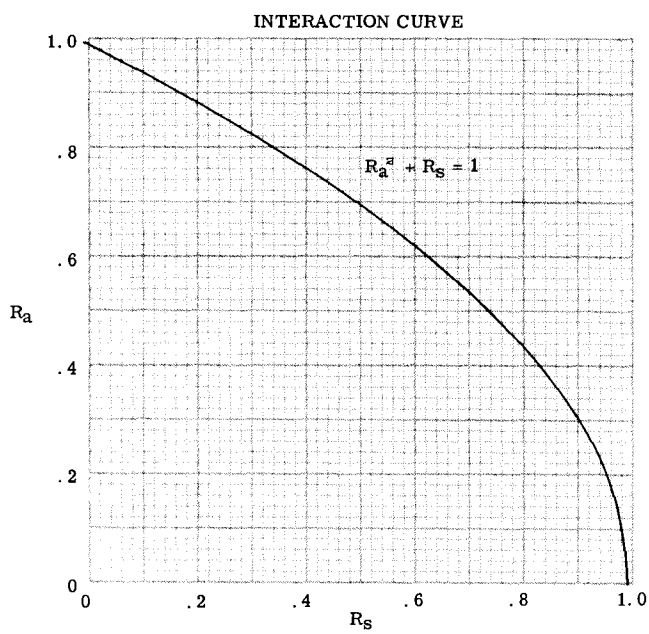

Fig. C12.4.3

C12.4.9 Other Isotropic Cores

Although honeycomb cores find the greatest use in the aircraft industry along with the corrugated core concept, other core materials find many uses. The more important materials used as cores are thoughs of Balsa wood and foamed plastics. Core properties such as density, tension, compression, and shear allowables, compression and shear moduluses, can be found in producers handbooks. These core materials can be handled much the same as honeycomb but in general with less efficiency and less cost.

C12.5 Honeycomb Flat Panel Failure Modes.

C12.5.1 General.

Honeycomb sandwich is subject to three forms of local instability. They are (1) intracell buckling, (2) face sheet wrinkling and (3) shear crimping. (Ref. Section C12.2)

In general, intracell buckling will be critical for elements with thin face sheets; wrinkling will be critical for light density cores; and shear crimping will be critical for light density cores in combination with high K_t, (t_F/c), values.

C12.5.2 Intracell Buckling.

C12.5.2.1 Compression (Ref. 1, 2).

Intracell buckling is a local instability failure of the faces. If the face thickness is reduced while the cell size and material are held constant, a certain thickness will be reached at which the face will fail between the cell walls. A typical intracell buckling failure is shown on Fig. C12.5.1.

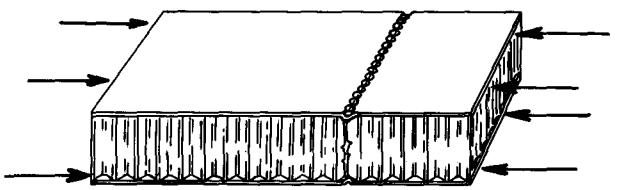

Fig. C12.5.1

The empirical intracell buckling equations in the following sections were developed from tests. Although the probability of meeting or exceeding these allowables is not known, the chosen allowables will be met by almost all future sandwich tests.

The intracell buckling stress varies principally as a function of face thickness and cell size. Core density, core depth and node flow condition do not directly affect the intracell buckling stress. The effect of transverse ribbon direction is negligible.

The design curve for intracell buckling failure under a uniaxial compression load in the direction of the ribbon can be expressed by the equation:

$$\frac{F_{ci}}{\eta} = .75\, E_f \left(\frac{t_F}{s}\right)^{3/2} \qquad \text{(C12.5.1)}$$

Where: $\eta = \dfrac{2E_T}{E_f + E_T}$ for F_{ci} (C12.5.2)

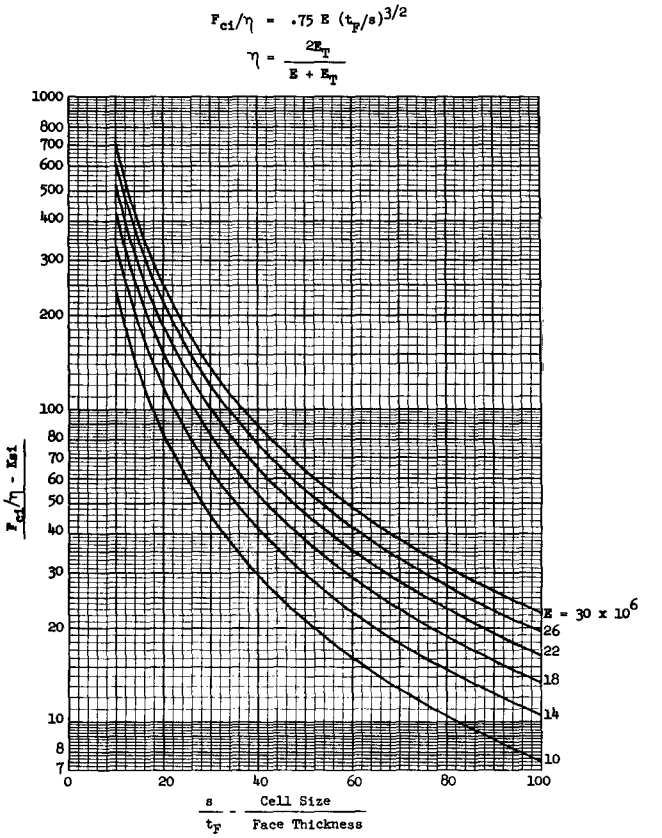

Fig. C12.5.2a

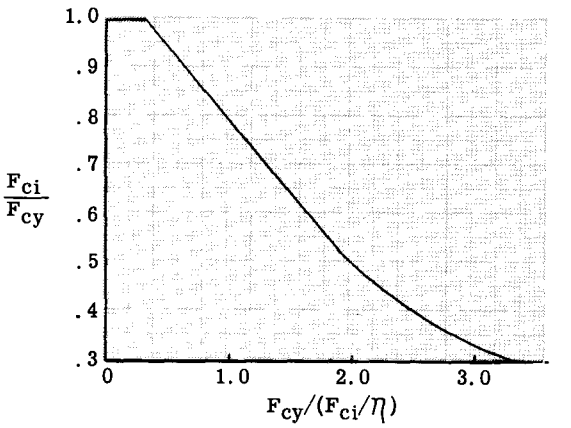

Fig. C12.5.2b

The average (median) can be represented by the equation:

$$\frac{F_{c1}}{\eta} = .9\ E_f\ (\frac{t_F}{s})^{3/2}$$

The procedure to analyze an element for an intracell buckling failure is as follows:

1. Orient the loads so that the loads are perpendicular and parallel to the ribbon direction (Ref. Fig. C12.5.3a and C12.5.3b).

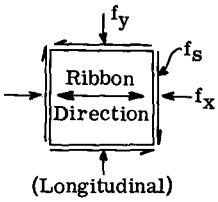

Fig. C12.5.3a

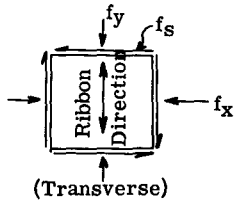

Fig. C12.5.3b

Note: a. $f_x > f_y$

b. f_x is compression

c. f_y may be either compression or tension

This is normally the manner in which loads are presented.

The following example illustrates the method to analyze an element:

Given: 1. Material: PH15-7Mo (RH1050) at R.T.

2. Property: $E_f = 30 \times 10^6$ psi
$F_{cy} = 190{,}000$ psi

3. Geometry: $s = 3/16$ in.
$t_F = .006$ in.

4. Loads: $f_x = 110{,}000$ psi

$\frac{F_{c1}}{\eta} = 129{,}000$ psi (Ref. Fig. C12.5.2a or Eq. C12.5.1)

$\gamma_1 = 1.0$ (See page C12.52)

$F_{c1} = 190{,}000 \times .65$

$F_{c1} = 124{,}000$ psi (Ref. Fig. C12.5.2b)

$M.S. = \frac{F_{c1}}{f_x} - 1 = .13$

INTRACELL BUCKLING

C12.5.2.2 Shear.

The design curve for intracell buckling failure under a shear load (Ref. Fig. C12.5.4) can be expressed by the equation:

$$\frac{F_{si}}{\eta} = .6\ E_f\ (\frac{t_F}{s})^{3/2} \quad \text{- - - - - - - - - (C12.5.3)}$$

Where: $\eta = \frac{2E_T}{E_f + E_T}$ for $F_i = \sqrt{3}\ F_{si}$

- - - - - (C12.5.4)

$\therefore \gamma_1$ (Stress Intensity Ratio) $= \sqrt{3}$

(See page C12.52)



Fig. C12.5.4

The following example illustrates the method to analyze an element:

Given: 1. Material: PH15-7Mo (RH1050) at R.T.

2. Property: $E_f = 30 \times 10^6$ psi
$F_{cy} = 190{,}000$ psi

3. Geometry: $s = 3/16$ in.
$t_F = .006$ in.

4. Loads: $f_s = 80{,}000$ psi

$F_{c1}/\eta = 129000$ psi (Ref. Fig. C12.5.2a)

$F_{si}/\eta = .8 \times F_{c1}/\eta = .8 \times 129000 = 103200$ psi

NOTE: The factor .8 is always applicable $= \frac{.6}{.75}$

$\gamma_1 = \sqrt{3}$ (See page C12.52)

$\frac{F_i}{\eta} = 103200 \times \sqrt{3} = 178000$ psi

$F_i = 145000$ psi (Ref.Fig.C12.5.2b)

F_i = stress intensity -VonMises' Yield Criteria

$F_{si} = \frac{145000}{\sqrt{3}} = 84000$ psi

$$M.S. = \frac{F_{si}}{f_s} - 1 = .05$$

C12.5.2.3 Biaxial Loading

The design curve for intracell buckling failure for biaxial loading in the direction or transverse to the direction of the ribbon can be expressed by the equations:

1. f_y is compression

$$R_x^n + R_y^n = 1 \quad \text{- - - - - - -} \quad (C12.5.5)$$

or $$F_{ci_x} = \frac{F_{ci}}{\sqrt[n]{1+\gamma^n}} \quad \text{- - - - - - -} \quad (C12.5.6)$$

a. $s/t_F \geq 15.63$

$n = 3$

b. $s/t_F < 15.63$

$$n = 2 + \left(\frac{15.63}{s/t_F}\right)^2$$

Where: $R_x = f_x/F_{ci}$

$R_y = f_y/F_{ci}$

$\gamma = f_y/f_x$

F_{ci} = Uniaxial intracell allowable (Ref. Sec. 3.11)

s = Cell size

t_F = Face thickness

2. f_y is tension

$$R_x^2 + R_y = 1 \quad \text{- - - - - - -} \quad (C12.5.7)$$

Where: $R_y = \frac{f_y}{F_{tu}}$

$R_x = \frac{f_x}{F_{ci}}$

C12.5.2.4 Biaxial and Shear Loading.

The design curve for intracell buckling failure of an element under biaxial and shear loading (Ref. Fig. C12.5.5a or C12.5.5b) can be expressed by the equation:

$$R_a + R_s^2 = 1 \quad \text{- - - - - - - - - - - - -} \quad (C12.5.8)$$

and $$M.S. = \frac{2}{R_a + (R_a^2 + 4R_s^2)^{1/2}} - 1 \quad - \quad (C12.5.9)$$

where: $R_a = \frac{f_x}{F_{ci_x}}$

$R_s = \frac{f_s}{F_{si}}$

F_{ci_x} = Allowable load in x-direction with biaxial loading only (Ref. Sec. C12.5.2.1)

F_{si} = Allowable load in element with shear loads only (Ref. Sec. C12.5.2.2)

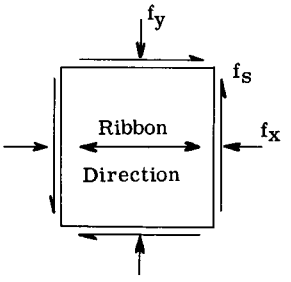

(Longitudinal)

Fig. C12.5.5a

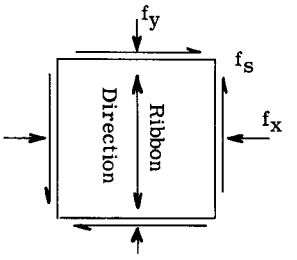

(Transverse)

Fig. C12.5.5b

Note: a. $f_x > f_y$

b. f_x is compression

c. f_y may be either compression or tension

The following example illustrates the method to analyze an element:

Given: 1. Material: PH15-7Mo (RH1050) at R.T.

2. Property: $E_f = 30 \times 10^6$ psi

$F_{cy} = 190000$ psi

3. Geometry: $s = 3/16$ in.

$t_F = .006$ in.

4. Loads: $f_x = 100000$ psi

$f_y = 50000$ psi

$f_s = 20000$ psi

Procedure:

Method A - Specific Solution

1. $F_{ci_x} = 124000$ psi (Ref. Sec. C12.5.2.1)

2. $F_{si} = 84000$ psi (Ref. Sec. C12.5.2.2)

3. $$R_a = \frac{f_x}{F_{ci_x}} = \frac{100000}{124000} = .806$$

$$R_s = \frac{f_s}{F_{si}} = \frac{20000}{84000} = .238$$

$$M.S. = \frac{2}{R_a + (R_a^2 + 4R_s^2)^{1/2}} - 1 = .15$$

C12.5.3 Wrinkling.

The wrinkling phenomenon of the faces of honeycomb sandwich is a stability problem of thin sheets on an elastic foundation. Two distinct failure modes are possible, symmetrical (Fig. C12.5.6a) and antisymmetrical (Fig. C12.5.6b). For large values of K_t, (t_F/c), the wrinkle will be antisymmetrical, while for small values of K_t the wrinkle will be symmetrical.

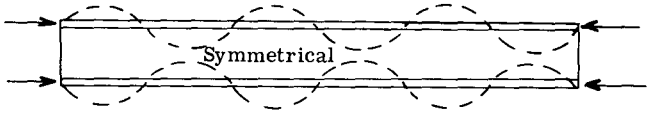

Fig. C12.5.6a

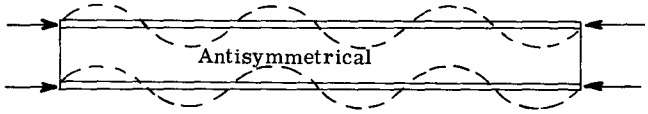

Fig. C12.5.6b

The empirical wrinkling equations in sections C12.5.3.1 through C12.5.3.4 were developed from tests and are applicable to both types of failure. Although the probability of meeting or exceeding these allowables are not known, the chosen allowables will be met by almost all future sandwich tests.

The wrinkling allowable varies principally as a function of core density. Transverse ribbon values show a reduction (.95) from longitudinal values. Node flow, core depth, face thickness and cell size do not directly affect the allowable.

C12.5.3.1 Compression.

The design curve for wrinkling failure under a uniaxial compression load in the direction of the ribbon can be expressed by the equation:

$$\frac{F_{cw}}{\eta_e} = .43\sqrt[3]{E_f\ E'_c\ G'_c} \quad - - - -(C12.5.10)$$

Where: $\eta_e = \sqrt[3]{\frac{3E_T + E_s}{4E_f}}$ for F_{cw} - -(C12.5.11)

The average (median) value is approximately 120% of the design value.

The following example illustrates the method to analyze an element for uniaxial compression.

Given: 1. Material: PH15-7Mo (RH1050) at R.T.

2. Property: $E = 30 \times 10^6$ psi

$F_{cy} = 190000$ psi

3. Geometry: $s \times t_c = 3/16 \times .001$ in.

$\rho'_c = 5.4$ pcf longitudinal ribbon direction

4. Load: $f_x = 120000$ psi

$s/t_c = 187.5$

$\frac{F_{cw}}{\eta_e} = 182000$ psi (Ref.Eq.C12.5.10 or Fig. C12.5.7a)

$\gamma_1 = 1.0$ (uniaxial compression)

$F_{cw} = 158000$ psi (Ref.Eq.C12.5.11 or Fig. C12.5.7b)

$$M.S. = \frac{F_{cw}}{f_x} - 1 = .32$$

WRINKLING PARAMETER

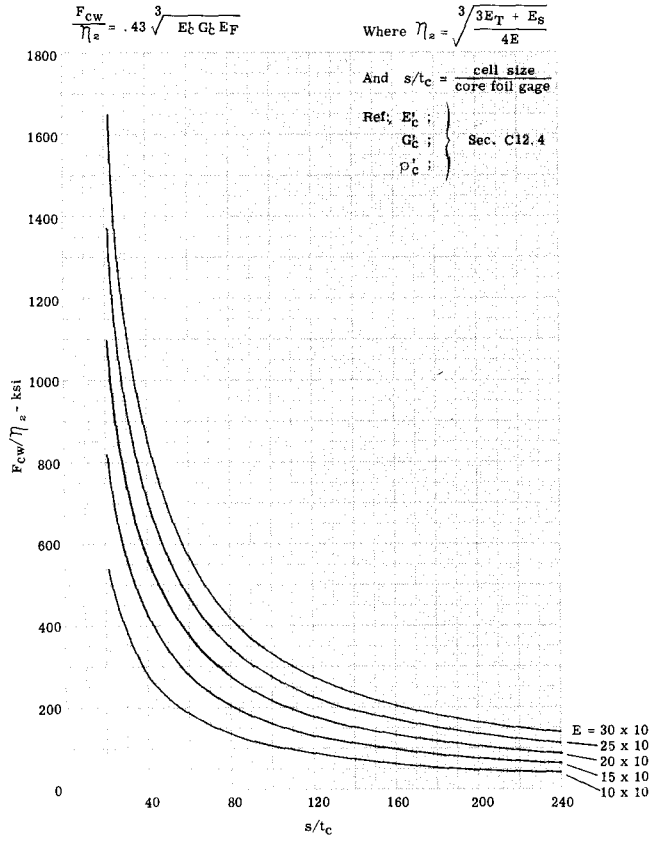

Fig. C12.5.7a

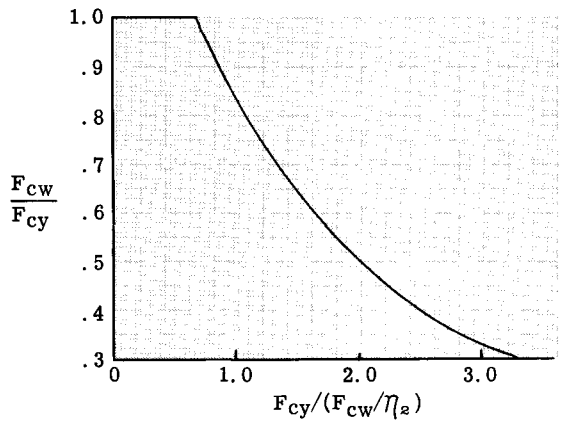

Fig. C12.5.7b

C12.5.3.2 In-Plane Shear

The design curves for a wrinkling failure of a honeycomb sandwich element under shear load may be expressed by the following equation:

$$\frac{F_{sw}}{\eta_e} = .43\sqrt[3]{E_f\, E'_c\, G'_c} \quad \text{- - - - - - - -(C12.5.12)}$$

Where: $\eta_e = \sqrt[3]{\frac{3E_T + E_S}{4E}}$ for $F_i = \sqrt{3}\ F_{sw}$

$$\therefore \gamma_i = \sqrt{3}$$ (See page C12.52)

The following example illustrates the method used to analyze an element.

Given: 1. Material: PH15-7Mo Steel (RH1050) at R.T.

2. Property: $E = 30 \times 10^6$ psi

$F_{cy} = 190000$ psi

3. Geometry: $s \times t_c = 3/16 \times .001$ in.

$\rho'_c = 5.4$ lb/ft.^{3}

4. Load: $f_s = 100{,}000$ psi

$s/t_c = 187.5$

$\frac{F_{sw}}{\eta_e} = 182000$ psi (Ref.Fig.C12.5.7a)

Note: $\frac{F_{sw}}{\eta_e} = \frac{F_{cw}}{\eta_e}$

$\gamma_i = \sqrt{3}$ (See page C12.52)

$F_i/\eta = 182000 \times \sqrt{3} = 314000$

$F_i = 190000$ psi (Ref.Fig.C12.5.7b)

$$F_{sw} = \frac{190000}{\sqrt{3}} = 110500 \text{ psi}$$

$$M.S. = \frac{F_{sw}}{f_s} - 1 = .10$$

C12.5.3.3 Biaxial Loading.

The design curve for wrinkling failure of an element under biaxial loading with the primary load in the direction of the ribbon (longitudinal) can be expressed by the equation:

1. f_y is compression

$$\frac{F_{cw_x}}{\eta_e} = \frac{.43\sqrt[3]{E_f\, E'_c\, G'_c}}{\sqrt[3]{1 + \gamma^3}} \quad \text{- - -(C12.5.13)}$$

2. f_y is tension

$$\frac{F_{cw_x}}{\eta_e} = .43\sqrt[3]{E_f\, E'_c\, G'_c} \quad \text{- - -(C12.5.14)}$$

Where: $\eta_e = \sqrt[3]{\frac{3E_T + E_S}{4E_f}}$ for $F_i = \gamma_i\, F_{cw_x}$

$\gamma = f_y/f_x$

$\gamma_i = \sqrt{1 - \gamma + \gamma^2}$ - - - - -(C12.5.15)

(See page C12.52)

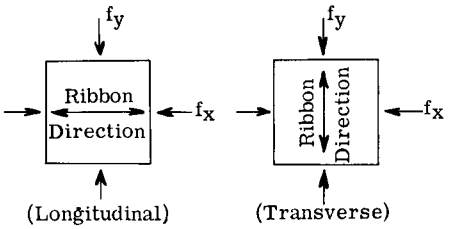

Fig. C12.5.8a Fig. C12.5.8b

The following examples illustrate the method to analyze an element:

Example 1

Given: 1. Material: PH15-7Mo (RH1050) at R.T.

2. Property: $E = 30 \times 10^6$ psi

$F_{cy} = 190000$ psi

3. Geometry: $s \times t_c = 3/16 \times .001$ in.

$\rho'_c = 5.4$ pcf longitudinal ribbon direction

4. Loads: $f_x = 120000$ psi (Comp.)

$f_y = 60000$ psi (Comp.)

$\gamma = f_y/f_x = .5$

$$\frac{s}{t_c} = \frac{3/16}{.001} = 187.5$$

$$\frac{F_{cw}}{\eta_2} = 182000 \text{ psi (Fig. C12.5.7a)}$$

$$\gamma_1 = \sqrt{1 - \gamma + \gamma^2} = .866$$

$$\frac{F_{cw_x}}{\eta_2} = \frac{F_{cw}/\eta_2}{\sqrt[3]{1 + \gamma^3}} = \frac{182000}{1.040} = 175000 \text{ psi}$$

$$F_1/\eta = 175000 \times .866 = 152000 \text{ psi}$$

$$F_{1_x} = 142000 \text{ psi (Ref.Fig.C12.5.7b)}$$

$$F_{cw_x} = \frac{142000}{.866} = 164000 \text{ psi}$$

$$\text{M.S.} = \frac{F_{cw_x}}{f_x} - 1 = .37$$

Example 2

Given: Same geometry as in example 1
Transverse ribbon direction

Loads: $f_x = 120000$ psi (Comp.)

$f_y = -30000$ psi (Tens.)

$\gamma = -.25$

$$\frac{s}{t_c} = \frac{3/16}{.001} = 187.5$$

$$\frac{F_{cw}}{\eta_2} = 182000 \text{ psi (Ref.Fig.C12.5.7a)}$$

$$\gamma_1 = \sqrt{1 - \gamma + \gamma^2} = 1.147$$

$F_{cw_x} = 150000$ psi (Ref.Fig.C12.5.7b)
for transverse ribbon

$F_{cw_x} = .95 \times 150000 = 143000$ psi

$$\text{M.S.} = \frac{F_{cw_x}}{f_x} - 1 = .19$$

C12.5.3.4 Biaxial and Shear Loading.

The design curve for wrinkling failure of an element under biaxial and shear loading (Ref. Fig. C12.5.9a or C12.5.9b) can be expressed by the equation:

$$R_a + R_s^2 = 1 \quad \text{----------(C12.5.16)}$$

$$\text{and M.S.} = \frac{2}{R_a + \sqrt{R_a^2 + 4R_s^2}} - 1 \quad \text{--(C12.5.17)}$$

Where: $R_a = \dfrac{f_x}{F_{cw_x}}$

$R_s = \dfrac{f_s}{F_{sw}}$

F_{cw_x} = allowable load in x-direction with biaxial loading only (Ref. Sec. C12.5.3.3).

F_{sw} = allowable load in element with shear loading only (Ref. Sec. C12.5.3.2).

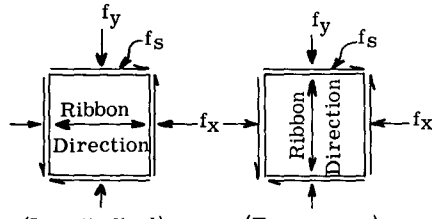

Fig. C12.5.9a

Fig. C12.5.9b

Note: a. $f_x > f_y$

b. f_x is compression

c. f_y may be either compression or tension.

The following example illustrates the method to analyze an element:

Given: 1. Material: PH15-7Mo (RH1050) at R.T.

2. Property: $E = 30 \times 10^6$ psi
$F_{cy} = 190000$ psi

3. Geometry: $s \times t_c = 3/16 \times .001$ in.
$\rho'_c = 5.4$ pcf
longitudinal ribbon direction

4. Loads: $f_x = 120000$ psi (Comp.)
$f_y = 60000$ psi (Comp.)
$f_s = 60000$ psi

$F_{cw_x} = 164000$ psi (Ref. Example 1, Sec. C12.5.3.3)

$F_{sw} = 110500$ psi (Ref. Example Sec. C12.5.3.2)

$$R_a = \frac{f_x}{F_{cw_x}} = \frac{120000}{164000} = .73$$

$$R_s = \frac{f_s}{F_{sw}} = \frac{60000}{110500} = .54$$

$$\text{M.S.} = \frac{2}{R_a + (R_a^2 + 4R_s^2)} - 1 = -.18$$

C12.5.4 Shear Crimping.

Shear crimping failure is a form of general instability failure where the wave length of the buckle becomes very small due to low core shear modulus. This failure occurs suddenly and causes the core to fail in shear at the crimp.

The following equation is used to calculate the critical shear crimping stress:

$$F_{cs_{max}} = \frac{U}{2t_F} = \frac{G'_c\ (c + 2t_F)}{2t_F} \quad - - - -(C12.5.18)$$

Where: $F_{cs_{max}}$ = maximum allowable shear crimping stress in the direction of the maximum principle stress

The following example illustrates the method to analyze an element:

Given: 1. Material: PH15-7Mo (RH1050) at R.T.

2. Geometry: t_F = .050 in.
c = .55 in.
$s \times t_c$ = 3/16 x .001 in.
$\therefore \rho'_c$ = 5.4 pcf
G'_c = 27600 psi

3. Loads: f_x = 150000 psi (Comp.)
f_y = -10000 psi (Tens.)
f_s = 68000 psi
$\therefore f_{max}$ = 175000 psi (form Moore's Circle)

Procedure:

$$F_{cs_{max}} = \frac{G'_c\ (c + 2t_F)}{2t_F} = \frac{27600 \times .65}{.10}$$

$$= 179500 \text{ psi}$$

$$M.S. = \frac{F_{cs_{max}}}{f_{max}} - 1 = .03$$

C12.5.5 General Instability - Uniaxial Compression.

General Buckling Allowables - This section presents the general compression buckling allowables. They are general in that they are not restricted to any particular material.

The compression buckling equation is:

$$\frac{F_{c_{cr}}}{\eta} = \frac{K_c}{J} \times \frac{U}{2t_F} \quad - - - - - - - - - -(C12.5.19)$$

where: $\eta = \frac{2E_T}{E + E_T}$ for panels and $\frac{E_T}{E}$ for columns

for $F_i = F_{c_{cr}} \therefore \gamma_i = 1.0$

$$J = \frac{b^2 U}{\pi^2 D}$$

$K_c = K_m + K_F$

K_m can be obtained from the graphs of Figs. C12.5.10 thru C12.5.14.

K_F is generally negligible. If you desire to calculate it, it is equal to

$$K_{m\infty} \times \frac{K_t^2}{3(1 + K_t)^2}$$

$K_{m\infty} = K_m$ for $J = \infty$

The following example illustrates the method to find the compression buckling allowable.

Given: 1. Material: PH15-7Mo (RH1050) at R.T.

2. Properties: $E = 30 \times 10^6$ psi
G'_c = 38000 psi (s = 3/16 in. and t = .001 in.)
F_{cy} = 190000 psi

3. Geometry: c = .50 in.
t_F = .010 in.
a = 40 in.
b = 20 in.

4. Edges are simply supported

Calculate:

1. a/b = 2 b/c = 40 K_t = .02

2. U = $G'_c\ (c + 2t_F)$ = 19800 lb./in.
D = $\frac{Et_F(c + t_F)^2}{2\ (1 - \mu^2)}$ = 42900

3. J = $\frac{b^2 U}{\pi^2 D} = \frac{400 \times 19800}{\pi^2\ \ 42900}$ = 18.7

4. K_c = K_m (K_F is negligible) = 3.60 (Ref. Fig. C12.5.10)

5. $\frac{F_{c_{cr}}}{\eta} = \frac{K_c}{J} \times \frac{U}{2t_F}$ = 190000 psi

γ_i = 1.0

6. $F_{c_{cr}}$ = 152000 psi (Ref.Fig.C12.5.2b)

C12.5.6 General Shear Buckling Allowables.

This section presents the general shear buckling allowable curves. These curves are general in the sense that they are not restricted to any particular material.

The shear buckling equation is:

$$\frac{F_s}{\eta} = \frac{K_s}{J} \cdot \frac{U}{2t_F} \qquad \text{----------(C12.5.20)}$$

$$\eta = \frac{2E_T}{E + E_T} \quad \text{for } F_i = \sqrt{3}\ F_{scr} \quad \therefore \gamma_i = \sqrt{3}$$

$$J = \frac{b^2 U}{\pi^2 D}$$

Given the geometry, material properties, and edge fixity for a particular panel, the shear buckling allowable can be found from the above equations and the curves given in this section. The K_s values for clamped, and simply supported edges are given on Figs. C12.5.15 and C12.5.16, respectively. The simple support allowables are based on equations given in Ref. 4, and the clamped edge allowables are taken from Ref. 5.

The following example illustrates the method for finding the shear allowable:

Given: 1. Material: PH15-7Mo (RH1050) Steel at R.T.

2. Properties: $E = 30. \times 10^6$ psi

$G'_c = 38000$ psi (for s = 3/16 and t_c = .001 in.)

$F_{cy} = 190000$ psi

$\mu = 0.3$

3. Geometry: $c = .25$ in.

$t_F = .0075$ in.

$a = 40$ in.

$b = 20$ in.

$s \times t_c = 3/16 \times .001$ in.

Procedure:

1. Calculate $a/b = 2$, $b/c = 80$, $K_t = .03$

2. Calculate $U = G'_c\,(c + 2t_F) = 10{,}075$ lb./in.

$$D = \frac{ET_F\,(c + t_F)^2}{2\,(1 - \mu^2)} = 8230$$

3. $$J = \frac{b^2 U}{\pi^2 D} = \frac{400 \times 10075}{\pi^2 \times 8230} = 49.8$$

4. Obtain K_s from Figs. C12.5.15 and C12.5.16.

K_s (Simply supported edges) = 6.05

K_s (Clamped edges) = 8.80

5. Calculate allowable buckling stress for simply supported edges.

$$\frac{F_s}{\eta} = \frac{6.05}{53} \cdot \frac{10075}{.015} = 86800 \text{ psi}$$

$\gamma_i = \sqrt{3}$

$F_s = 78800$ psi (Ref. Fig. C12.5.2b)

6. Calculate allowable buckling stress for clamped edges.

$$\frac{F_s}{\eta} = \frac{8.80}{49.8} \cdot \frac{10075}{.015} = 118{,}700 \text{ psi}$$

$\gamma_i = \sqrt{3}$

$F_s = 88000$ psi (Ref. Fig. C12.5.2b)

COMPRESSION BUCKLING CURVES FOR SIMPLY SUPPORTED HONEYCOMB PANELS

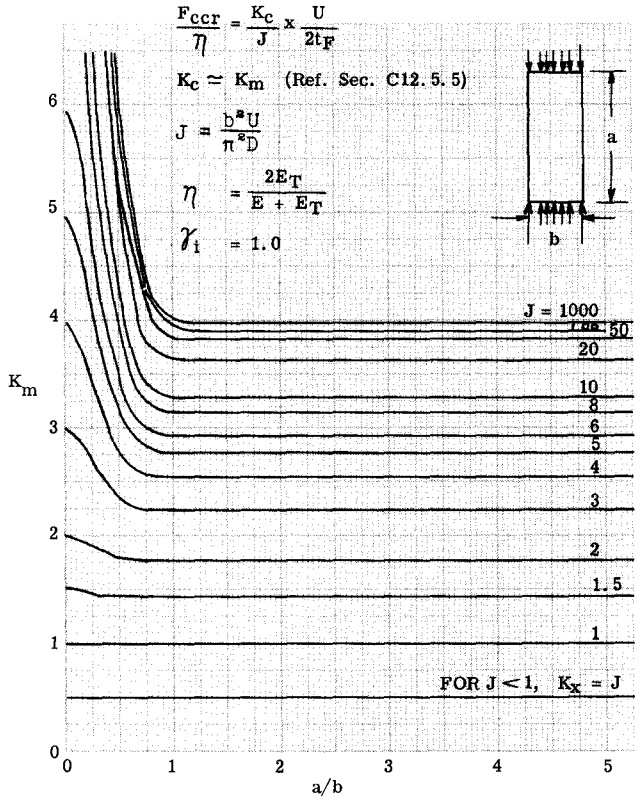

Fig. C12.5.10

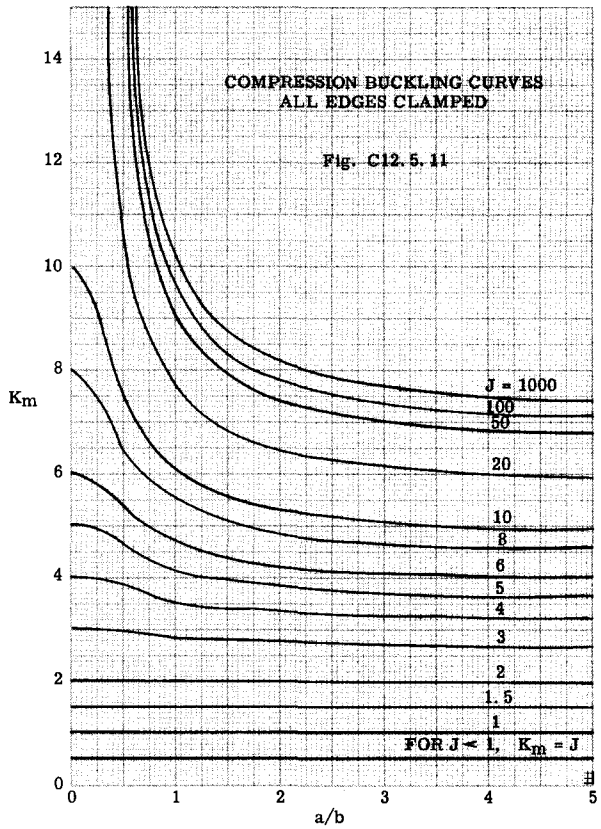
COMPRESSION BUCKLING CURVES
ALL EDGES CLAMPED
Fig. C12.5.11
J = 1000
100
50
20
10
8
6
5
4
3
2
1.5
1
FOR J < 1, Km = J
Km
a/b

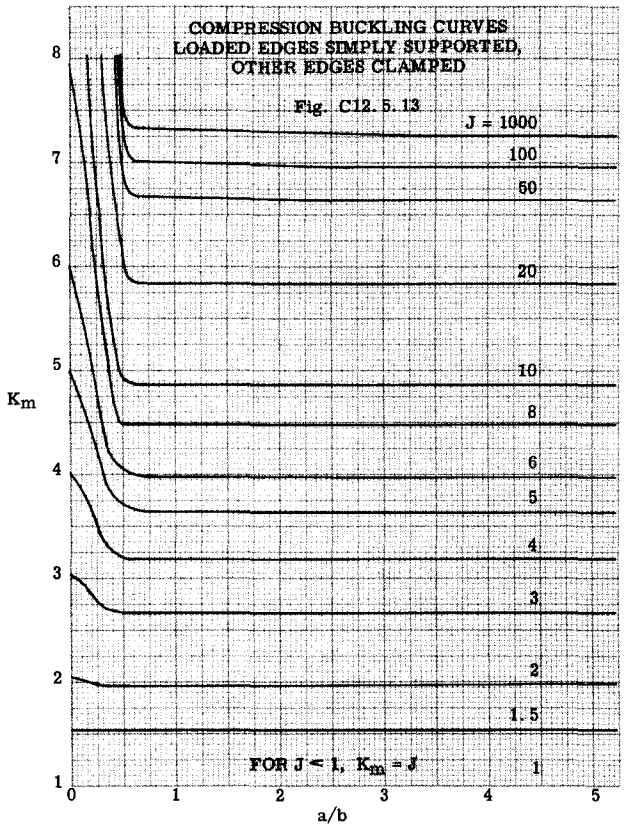
COMPRESSION BUCKLING CURVES
LOADED EDGES SIMPLY SUPPORTED,
OTHER EDGES CLAMPED
Fig. C12.5.13
J = 1000
100
50
20
10
8
6
5
4
3
2
1.5
1
FOR J < 1, Km = J
Km
a/b

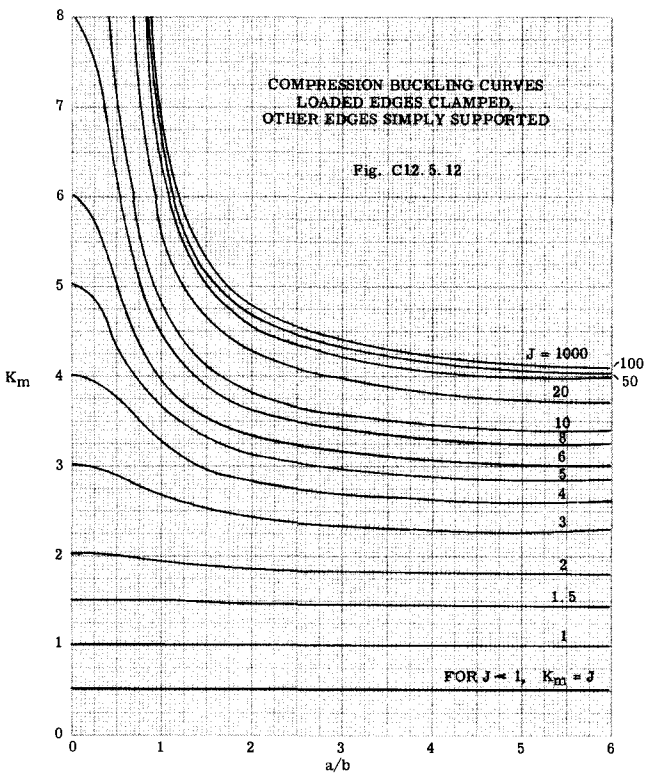
COMPRESSION BUCKLING CURVES
LOADED EDGES CLAMPED,
OTHER EDGES SIMPLY SUPPORTED
Fig. C12.5.12
J = 1000
100
50
20
10
8
6
5
4
3
2
1.5
1
FOR J < 1, Km = J
Km
a/b

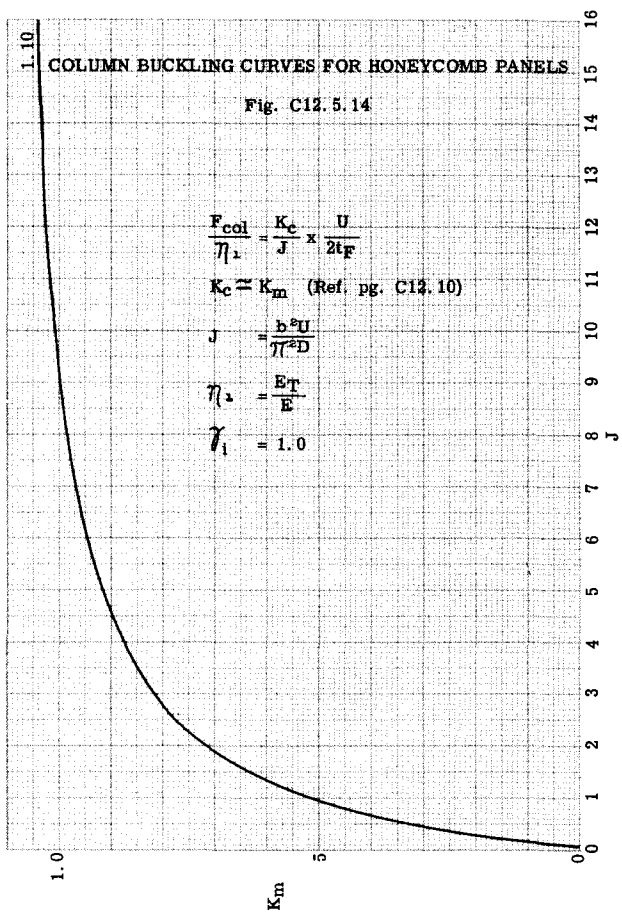
COLUMN BUCKLING CURVES FOR HONEYCOMB PANELS
Fig. C12.5.14
Fcol/η2 = Kc/J x U/2tF
Kc ≃ Km (Ref. pg. C12.10)
J = b²U/π²D
η2 = ET/E
γ1 = 1.0
1.10
1.0
Km
J

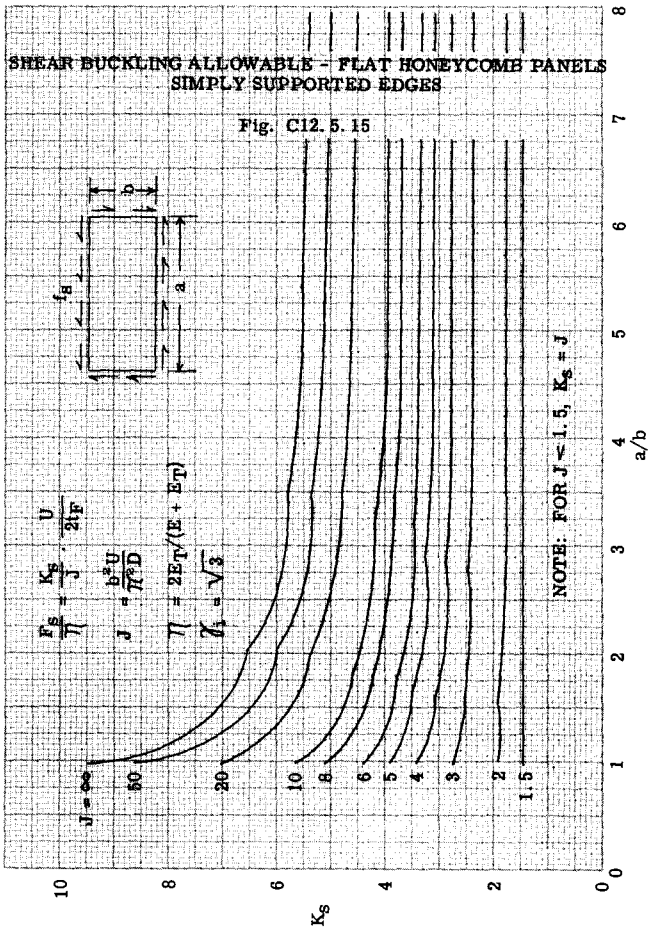

SHEAR BUCKLING ALLOWABLE - FLAT HONEYCOMB PANELS
CLAMPED EDGES

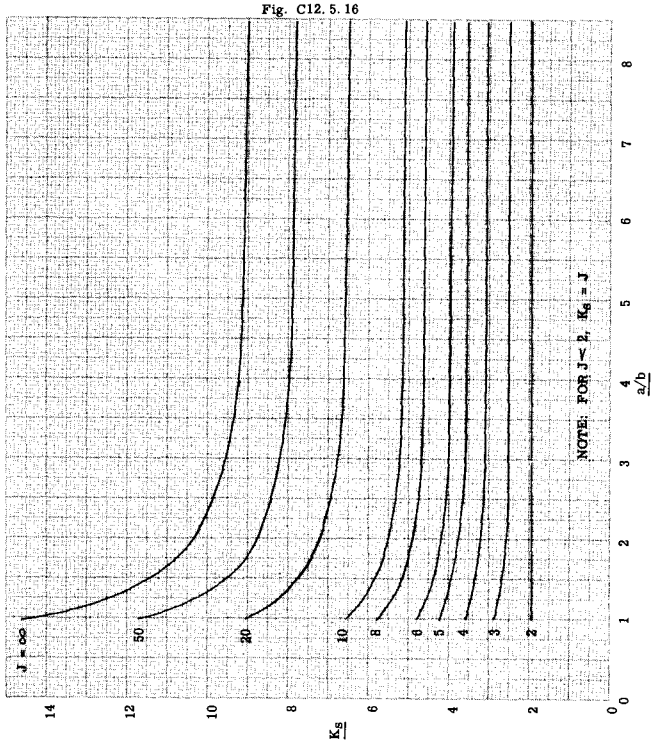

C12.5.7 Biaxial Compression.

General Buckling Allowables - This section presents the general biaxial compression buckling allowables. They are general in that they are not restricted to any particular material. The biaxial compression buckling equation is:

$$\frac{F_{x_{cr}}}{\eta} = \frac{K_x}{J} \cdot \frac{U}{2t_F} \text{ or } \frac{F_{y_{cr}}}{\eta} = \frac{K_y}{J} \cdot \frac{U}{2t_F} \quad \text{-(C12.5.21)}$$

$$\eta = \frac{2E_T}{E + E_T} \text{ for } F_1 = F_{x_{cr}} \sqrt{1 - \gamma + \gamma^2}$$

$$\gamma = \frac{f_y}{f_x} \quad \therefore \gamma_1 = \sqrt{1 - \gamma + \gamma^2}$$

$$J = \frac{b^2 U}{\pi^2 D}$$

The following example illustrates the method to find the biaxial compression buckling allowables.

Given: 1. Material: PH15-7Mo (RH1050) at R.T.

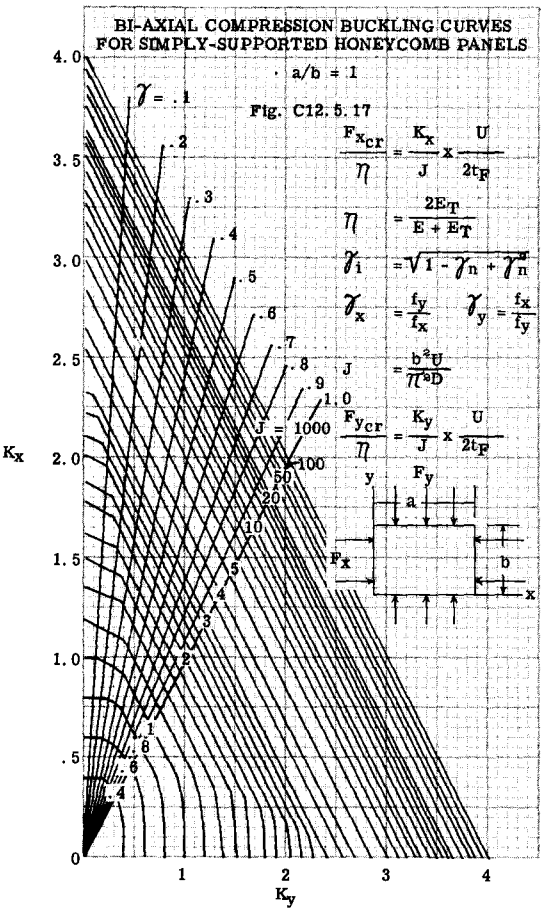

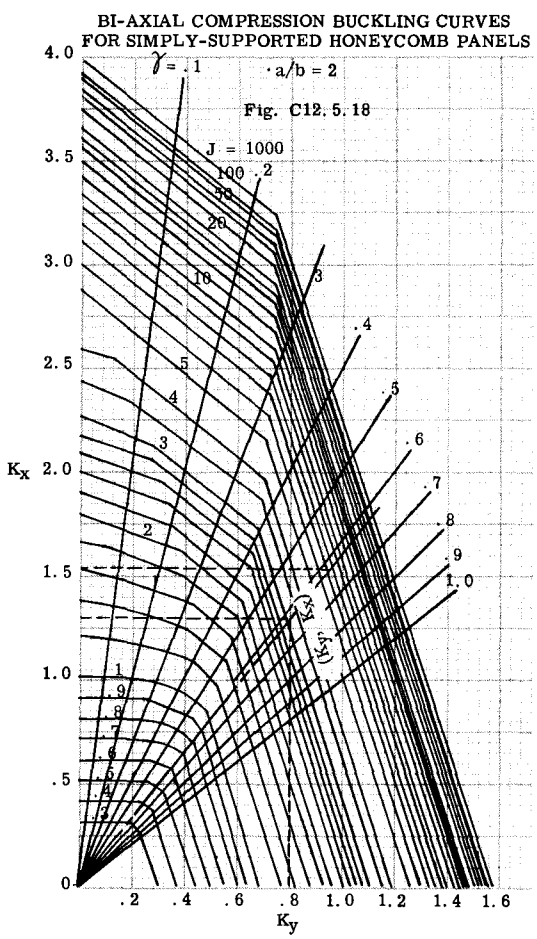

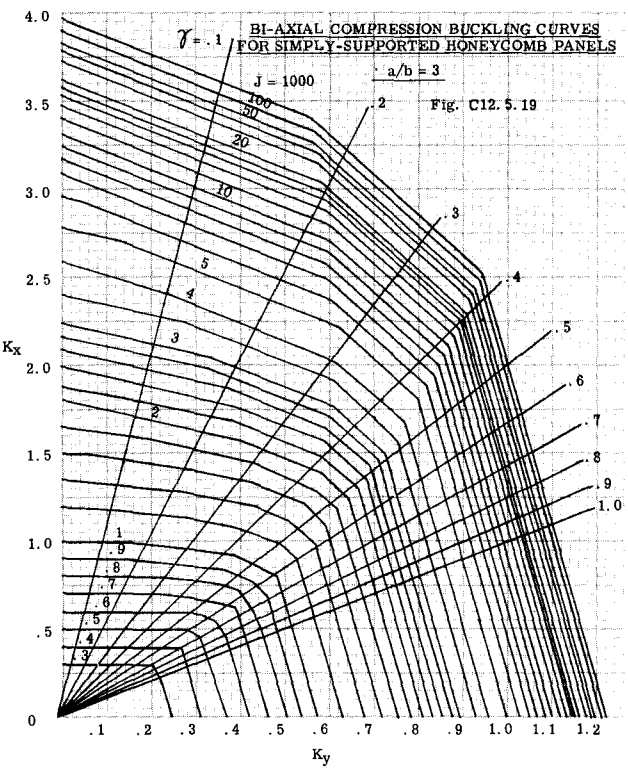

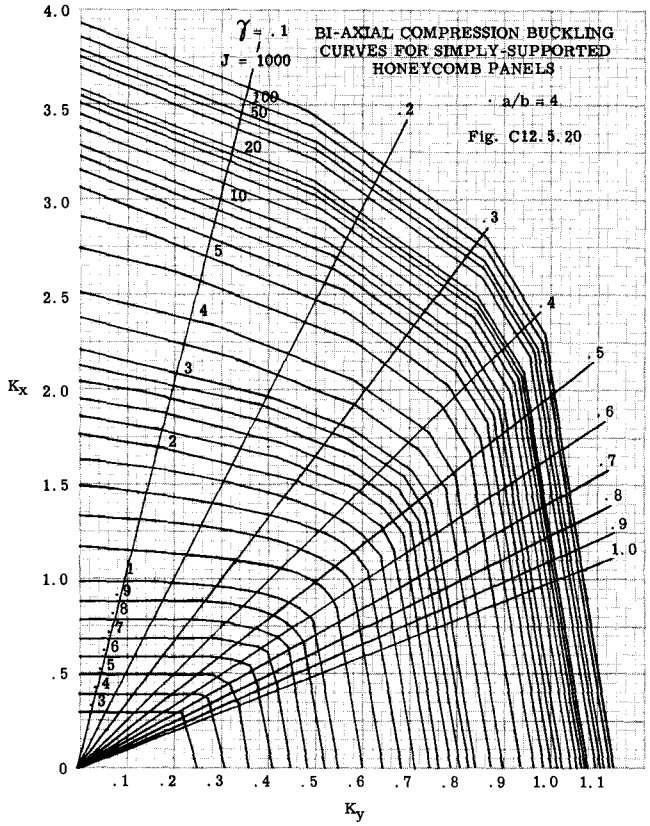

2. Properties: $E = 30 \times 10^6$ psi

$G'_c = 38000$ psi (s = 3/16 in., $t_c = .001$ in.

$F_{cy} = 190000$ psi

3. Geometry: c = .50 in.

$t_F = .010$ in.

a = 40 in.

b = 20 in.

4. Edges are simply supported

5. Loads: $f_x = 100000$ psi

$f_y = 50000$ psi

$\therefore \gamma = .5$

Calculate:

1. a/b = 2, b/c = 40, $K_t = .02$

2. $U = G'_c (c + 2t_F) = 19800$ lb./in.

$$D = \frac{Et_F (c + t_F)^2}{2 (1 - \mu^2)} = 42900$$

BUCKLING OF SIMPLY-SUPPORTED SANDWICH CYLINDER UNDER TORSION LOADS

Fig. C12.5.21

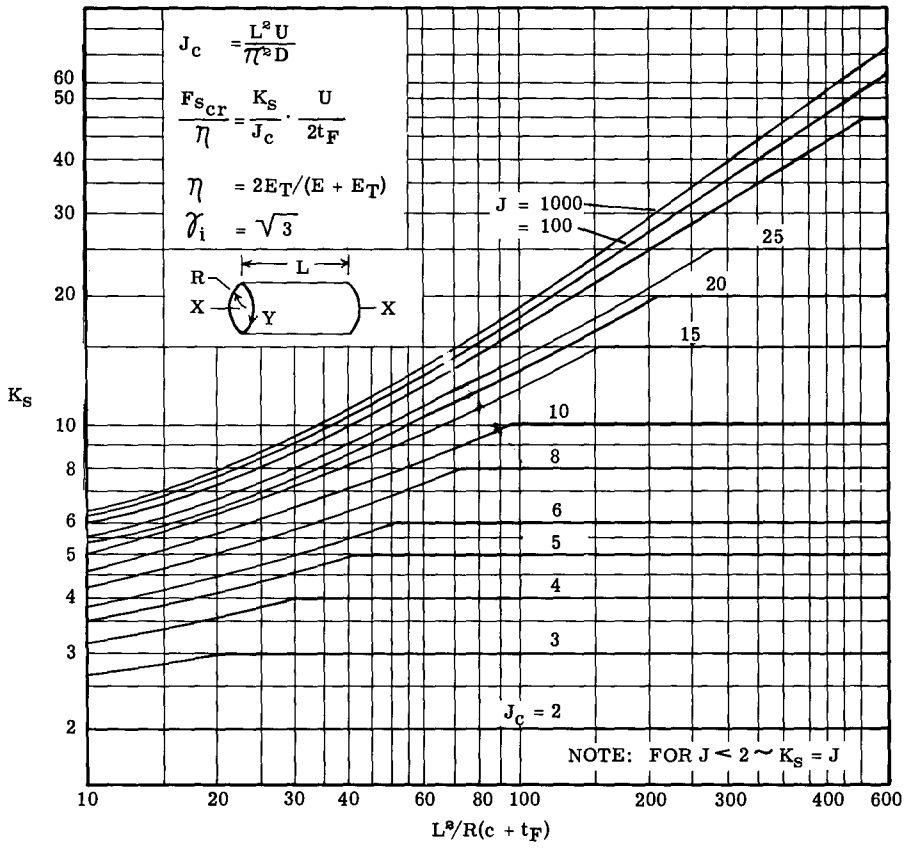

3. $J = \frac{b^2 U}{\pi^2 D} = 20.3$

4. Kx = 1.95 (Ref. Fig. C12.5.18)

5. $\frac{K_{X_{cr}}}{\eta} = \frac{K_X}{J} \cdot \frac{U}{2t_F} = \frac{1.95 \times 19800}{18.4 \times .020} =$

105000 psi

6. $\gamma_i = .866$

7. $F_{X_{cr}}$ = 105000 psi (Ref.Fig.C12.5.26)

8. M.S. $= \frac{F_{X_{cr}}}{f_x} - 1 = \underline{.05}$

C12.5.8 Biaxial Compression and Shear.

The stress ratio concept can be used to analyze flat honeycomb sandwich panels with biaxial compression and shear loading. Curves in Ref. 4 are used to derive the approximate interaction equation:

$$R_c + R_s^2 = 1 \quad \text{- - - - - - -(C12.5.22)}$$

where: $R_c = \frac{F_{x_{max}}}{F_x}$ or $\frac{F_{y_{max}}}{F_y}$

$$R_s = \frac{F_{s_{max}}}{F_s}$$

$$\frac{F_x}{\eta}, \frac{F_y}{\eta} \& \frac{F_s}{\eta} = \frac{(K_x, K_y \& K_s)}{J} \cdot \frac{U}{2t_F}$$

Respectively

$$\eta = \frac{2E_T}{E+E_T} \quad \begin{matrix} \gamma_i = (1 - \gamma + \gamma^2 + 3\lambda^2)^{1/2} & \text{for } F_x \\ \gamma_i = [\lambda_i^2 (1 - \gamma + \gamma^2) + 3]^{1/2} & \text{for } F_s \end{matrix} \quad \text{(C12.5.23)}$$

(See page C12.52)

$$\gamma = f_y/f_x$$

$$\lambda = \frac{1}{\lambda_1} = \frac{f_s}{f_x}$$

$F_{x_{max}}$ and $F_{y_{max}}$ are allowable compression stresses in the x and y directions respectively, if γ and λ remain constant.

$F_{s_{max}}$ is the allowable shear stress if γ and λ remain constant.

then:

$$\frac{F_{x_{max}}}{\eta} = \frac{K_X K_\lambda}{J} \cdot \frac{U}{2t_F} \quad \text{----------(C12.5.24)}$$

or:

$$\frac{F_{s_{max}}}{\eta} = \frac{K_S K_{\lambda_1}}{J} \cdot \frac{U}{2t_F} \quad \text{---------(C12.5.25)}$$

where:

$$K_\lambda = \frac{1}{2\lambda^2 (K_X/K_S)^2} \left\{ -1 + \left[1 + (2\lambda \frac{K_X}{K_S})^2 \right]^{1/2} \right\} \quad \text{(C12.5.26)}$$

$$K_{\lambda_1} = \frac{(K_S/K_X)\lambda_1}{2} \left\{ -1 + \left[1 + (\frac{2}{\lambda_1} \frac{K_X}{K_S})^2 \right]^{1/2} \right\} \quad \text{(C12.5.27)}$$

Procedure:

1. Given: a,b,c,t_F,s and t_c,f_x,f_y,f_s and material.

2. From appropriate page (C12.15 and C12.16) find K_x and K_y.

3. From page C12.17 find K_s

4a. If f_s/f_x (λ) $\leq$ 1
Calculate K_λ from Eq. C12.5.26.

5a. Calculate γ_1 from Eq. C12.5.23.

6a. $\frac{F_{x_{max}}}{\eta} = \frac{K_X K_\lambda}{J} \cdot \frac{U}{2t_F}$

η for $f_i = \gamma \pm \cdot F_{x_{max}}$

4b. If f_x/f_s (λ_1) < 1
Find K_λ from Eq. C12.5.27.

5b. Find γ_1 from Eq. C12.5.23.

6b. $\frac{F_{s_{max}}}{\eta} = \frac{K_S K_{\lambda_1}}{J} \cdot \frac{U}{2t_F}$

η for $F_i = \gamma_1 F_{s_{max}}$

7. Find $F_{x_{max}}$ or $F_{s_{max}}$ from Fig.C12.5.2b.

8. M.S. = $\frac{F_{x_{max}}}{f_x} - 1$ or $\frac{F_{s_{max}}}{f_s} - 1$

C12.6 Failure Modes in Curved Honeycomb Panels.

C12.6.1 General.

Curved panels constructed of honeycomb sandwich can fail either by general instability of the total panel or by local instability of the face sheets. This section considers the former failure while the local instability failure considered for flat panels can be used for curved panels. Loads that affect the general instability of a panel are axial compression in either direction (N_x or N_y), in-plane shear (q_s) and in-plane bending moments (M_{bx} and M_{by}).

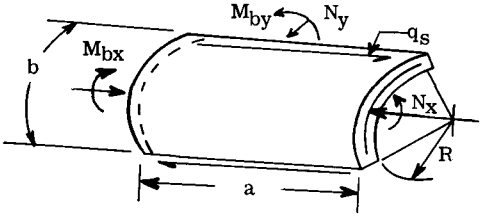

C12.6.2 Uniaxial Compression - Curved Panel (Ref. 6)

The uniaxial compression allowable is presented as a general buckling equation.

The curves can be developed from the following equations:

$$K_X = \frac{\left[1 + (\frac{n}{m})^2 (\frac{a}{b})^2 \right]^2}{\frac{1}{m^2}(\frac{a}{b})^2 + \frac{1}{J}\left[1 + (\frac{n}{m})^2 (\frac{a}{b})^2 \right]} + \frac{\frac{Z^2 (\frac{a}{b})^2}{\pi^4 m^2}}{\left[1 + (\frac{n}{m})^2 (\frac{a}{b})^2 \right]^2}$$

---------(C12.6.1)

$$J = \frac{b^2 U}{\pi^2 D}$$

$$Z = \frac{2 b^2 \sqrt{1 - \mu^2}}{R (c + t_F)} \quad \text{----------(C12.6.2)}$$

$$\frac{F_x}{\eta} = \frac{K_X}{J} \cdot \frac{U}{2t_F} \quad \text{-------------(C12.6.3)}$$

$$\eta = \frac{2E_T}{E + E_T} \text{ for } F_i = F_X$$

$\therefore \gamma_1 = 1.0$

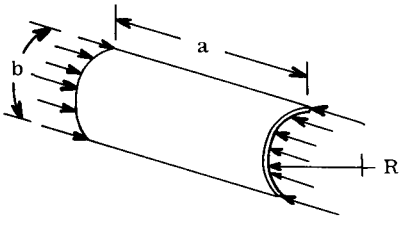

The following example illustrates the application of these equations.

Given: 1. Material: PH15-7Mo (RH1050) at R. T.

2. Properties: $E = 30 \times 10^6$ psi

$G'_c = 38000$ (sxtc = 3/16 x .001 in.)

$F_{cy} = 19000$ psi

$\mu = .30$

3. Geometry: $t_F = .005$ in.

$c = .5$ in.

$b = 25$ in. (Circumferential width)

$R = 50$ in. (Radius of Curvature)

4. Edges are simply supported.

Calculate:

1. $D = \dfrac{Et_F\,(c + t_F)^2}{2\,(1 - \mu^2)} = 21000$

2. $U = G'_c\,(c + 2t_F) = 38000 \times .51 =$ 19400 lb/in.

3. $J = \dfrac{b^2 U}{\pi^2 D} = 59$

4. $Z = \dfrac{2b^2\sqrt{1 - \mu^2}}{R\,(c + t_F)} = 47.0$

$K_X = 9.2$ (min.)(Ref. Eq. C12.6.1)

6. $\dfrac{F_X}{\eta} = \dfrac{9.2 \cdot 19400}{59 \cdot .010} = 303000$ psi

7. $\gamma_i = 1.0$

8. $F_X = 170000$ psi (Ref.Fig.C12.5.2b)

GENERAL INSTABILITY - CYLINDER

C12.6.3 Uniaxial Compression.

The uniaxial compression allowable for a cylinder is presented as a general buckling equation.

A curve can be developed from the following equation:

$$K_X = \frac{(m^2 + n^2\beta_1^2)^2}{m^2\left[1 + \dfrac{m^2 + n^2\beta_1^2}{J_c}\right]} + \frac{.0374\,m^2\left[\dfrac{L^2}{R(c + t_F)}\right]^2}{(m^2 + n^2\beta_1^2)^2} \qquad \text{- - - - - - (C12.6.4)}$$

$$J_c = \frac{L^2 U}{\pi^2 D}$$

$$\beta_1 = L/2\,\pi\,R$$

$$\frac{F_{X_{cr}}}{\eta} = \left(\frac{K_X}{J_c}\right) - \frac{U}{2t_F} \qquad \text{- - - - (C12.6.5)}$$

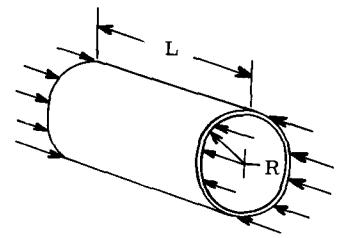

$$\eta = \frac{2E_T}{E + E_t} \text{ for } F_i = F_X$$

$\therefore \gamma_i = 1.0$

The following example illustrates the application of the buckling coefficient equation for cylinders.

Example: Find the buckling stress of a honeycomb cylinder with the edges simply-supported.

Given: 1. Material: PH15-7Mo (RH1050) Steel

2. Properties: $E = 30 \times 10^6$ psi

$G'_c = 38000$ psi (for s = 3/16 and $t_c = .001$)

$F_{cy} = 190000$ psi

3. Geometry: $c = .5$ in.

$t_F = .020$ in.

$L = 50$ in.

$R = 50$ in.

Calculate:

1. $D = \dfrac{Et_F\,(c + t_F)^2}{2(1 - \mu^2)} = 9000$

2. $U = G'_c\,(c + 2t_F) = 20500$ lb/in.

3. $J_c = \dfrac{b^2 U}{\pi^2 D} = 58.3$

Steps:

1. Compute $K_X = 30.8$ From Eq. C12.6.4

2. Compute $\dfrac{F_{X_{cr}}}{\eta} = \dfrac{30.8 \times 20500}{.040 \times 58.3} = 270000$ psi

3. $\gamma_i = 1.0$

4. To find the actual buckling stress, refer to the plasticity correction curve on Fig. C12.5.2b and read $F_{X_{cr}} = 166000$ psi.

C12.6.4 Torsion (Ref. D12).

The torsion buckling allowable equations are presented for the general buckling allowable and are applicable to any material.

The equations give the allowable as a shear stress. The following relationships should be remembered:

$$q_s = \frac{T}{2\pi R^2} \quad \text{- - - - - - - - - (C12.6.6)}$$

$$f_s = \frac{q_s}{2t_F} = \frac{T}{4\pi R^2 t_F} \quad \text{- - - - - - (C12.6.7)}$$

$$\frac{F_{s_{cr}}}{\eta} = \frac{K_S}{J_c} \frac{U}{2t_F} \quad \text{- - - - - - - - (C12.6.8)}$$

where: T is torsion in in.lb.

The curves presented in this section are general for any material and any given cylinder geometry. The curves are in the form of shear buckling coefficients vs defined parameters.

The critical buckling stresses must be corrected for platicity effect if they exceed the proportional limit of the material.

To illustrate the use of these curves the following example is presented.

Given: 1. Material: PH15-7Mo (RH1050) Steel

2. Properties: $E = 30 \times 10^6$ psi
$G'_c = 38000$ psi (for s = 3/16 and $t_c = .001$)
$F_{cy} = 190000$ psi

3. Geometry: $t_F = .05$ in.
$c = .5$ in.
$L = 40$ in.
$R = 25$ in.

Steps: 1. Compute:

$$J_c = \frac{b^2 U}{\pi^2 D} = 14.95$$

$$\frac{L^2}{R\,(c + t_F)} = 116$$

2. From curve on Fig. C12.5.21 $K_S = 13.0$

3. $U = 38000\ (.60) = 22800$

4. $$\frac{F_{s_{cr}}}{\eta} = \frac{13 \times 22800}{14.95 \times .10} = 198000 \text{ psi}$$

5. Using Fig. C12.5.2b for $\gamma_1 = \sqrt{3}$

$F_{s_{cr}} = 102000$ psi

C12.6.5 Uniform External Lateral Pressure (Ref. 7).

The following section presents equations to determine allowable buckling stresses for simply supported honeycomb cylinders.

The allowables are developed from the following equation:

$$K_y = \frac{(1 + n^2 \beta_1^2)^2}{n^2 \beta_1^2 \left[1 + \frac{1 + n^2 \beta_1^2}{J_c}\right]} + \frac{.0374 \left[\frac{L^2}{R\,(c + t_F)}\right]^2}{n^2 \beta_1^2 (1 + n^2 \beta_1^2)^2}$$

$$\text{- - - - - - (C12.6.9)}$$

$$J_c = \frac{L^2 U}{\pi^2 D}$$

$$\beta_1 = \frac{L}{2\pi R}$$

$$\frac{F_{y_{cr}}}{\eta} = \frac{K_y}{J_c} \times \frac{U}{2t_F} \quad \text{- - - - - - - - - - (C12.6.10)}$$

$$F_{y_{cr}} = \frac{pR}{2t_F} \qquad p = \frac{2F_{y_{cr}} t_F}{R} \quad \text{- - - - - (C12.6.11)}$$

p = Uniform external lateral pressure (psi)

The following example illustrates the application of the lateral buckling coefficient equation for cylinders.

Example: Find the buckling stress of a honeycomb cylinder with the edges simply supported and subjected to lateral pressure only.

Given: 1. Material: PH15-7Mo (RH1050) Steel

2. Properties: $E = 30 \times 10^6$ psi
$G'_c = 38000$ psi (for s = 3/16 and $t_c = .001$)
$F_{cy} = 190000$ psi

3. Geometry: $c = 1$ in.
$t_F = .1$ in.
$L = 50$ in.
$R = 30$ in.

Calculate:

1. $$D = \frac{E t_F (c + t_F)^2}{2 (1 - \mu^2)} = 1990000$$

2. $U = G'_c (c + 2t_F) = 45600$ lb./in.

3. $J_c = \frac{L^2 U}{\pi^2 D} = 5.8$

Steps: 1. From Eq. C12.6.9, $K_y = 4.30$

2. $F_{y_{cr}}/\eta = (4.30/5.8) \times (45600/.2) =$ 168000 psi $\quad \gamma_1 = 1.$

3. $F_{y_{cr}} = 141000$ psi (Ref.C12.5.2b)

4. $p_{cr} = \frac{F_{y_{cr}} \times 2t_F}{R} = \frac{141000 \times .2}{30} =$ 940 psi

C12.6.6 Bending Moment.

The allowable buckling stress for a simply supported cylinder with a bending moment is the same as the allowable stress for a cylinder loaded in uniaxial compression. The bending stress f_{bx} can be calculated from the equation

$$f_{bx} = \frac{M}{2 \pi R^2 t_F} \text{ - - - - - - - - - - - -(C12.6.12)}$$

This stress can now be compared with the allowable stress calculated in section C12.6.3. If axial compression load (f_x) is also present, f_{bx} can be directly added to f_x and the summation ($f_{x\Sigma}$) can be handled as a revised or modified uniaxial compression load. This load can also be used with torsion and/or lateral pressure.

The following examples illustrate the method:

Example 1

Given: 1. Material: PH15-7Mo (RH1050) Steel

2. Properties: $E = 30 \times 10^6$ psi

$G'_c = 38000$ psi ($s \times t_c$ = 3/16 x .001 in.)

3. Geometry: $c = .5$ in.

$t_F = .020$ in.

$L = 50$ in.

$R = 50$ in.

4. Loads: $M = 51 \times 10^6$ in.lb.

Procedure:

$$f_{bx} = \frac{M}{2\pi R^2 t_F} = \frac{51 \times 10^6}{2\pi \cdot 50^2 \cdot .020} = 162000 \text{ psi}$$

$F_{x_{cr}} = 170000$ psi (Ref. Sec. C12.6.3)

$$M.S. = \frac{170000}{162000} - 1 = .05$$

Example II

Given: 1. Material: PH15-7Mo (RH1050) Steel

2. Property: $E = 30 \times 10^6$ psi

$G'_c = 38000$ psi ($s \times t_c$ = 3/16 x .001 in.)

$F_{cy} = 190000$ psi

3. Geometry: $c = .80$ in.

$t_F = .080$ in.

$L = 50$ in.

$R = 50$ in.

4. Loads: $F_x = 50000$ psi

$M = 88 \times 10^6$ in. lb.

$f_y = 60000$ psi

$f_s = 24000$ psi

Procedure:

$$f_{bx} = \frac{M}{2\pi R^2 t_F} = \frac{88 \times 10^6}{2\pi 50^2 \times .080} = 70000 \text{ psi}$$

$f_{x\Sigma} = f_x + f_{bx} = 50000 + 70000 =$ 120000 psi

$$\gamma = \frac{f_y}{f_{x\Sigma}} = \frac{60000}{120000} = .5$$

$$\lambda = \frac{f_s}{f_{x\Sigma}} = \frac{24000}{120000} = .2$$

$F_x = 150000$ psi (Ref. Sec. C12.6.8)

$$M.S. = \frac{F_x}{f_{x\Sigma}} - 1 = \frac{150000}{120000} - 1 = .25$$

C12.6.7 Lateral Load and Axial Compression.

The following section presents equations to determine allowable buckling stresses for simply supported honeycomb cylinders under external uniform lateral pressure and axial compression.

$$K_X = \frac{(m^2 + n^2 \beta_1^2)^2}{(m^2 + n^2 \beta_1^2)\left[\frac{1 + m^2 + n^2 \beta_1^2}{J_c}\right]} + \frac{.0374\, m^4 \left[R \frac{L^2}{(c + t_F)}\right]^2}{(m^2 + n^2 \beta_1^2)(m^2 + n^2 \beta_1^2)^2} \text{ - -(C12.6.13)}$$

$$J_c = \frac{L^2 U}{\pi^2 D}$$

$$\beta_1 = \frac{L}{2\pi R}$$

$$\frac{F_{x_{cr}}}{\eta} = \frac{K_x}{J_c} \times \frac{U}{2t_F} \quad \text{----------(C12.6.14)}$$

$$\gamma = \frac{N_y}{N_x} = \frac{1}{\gamma'}$$

$$N_y = pR$$

The following example illustrates the application of the buckling coefficient equations for cylinders.

Example: Find the buckling stress of a simply supported sandwich cylinder subjected to combined lateral and axial loads.

Given: 1. Material: PH15-7Mo (RH1050) Steel

2. Properties: $E = 30 \times 10^6$ psi

$G'_c = 38000$ (For s = 3/16 and $t_c = .001$) psi

$F_{cy} = 190000$ psi

3. Geometry: $c = 1$ in.

$t_F = .1$ in.

$L = 50$ in.

$R = 50$ in.

4. Load Ratio: $\gamma = \frac{N_y}{N_x} = \frac{pR}{N_x} = 1/2$

Calculate:

1. $D = \frac{Et_F (c + t_F)^2}{2(1 - \mu^2)} = 1990000$

2. $U = G'_c (c + 2t_F) = 45600$ lb./in.

3. $J_c = \frac{b^2 U}{\pi^2 D} = 5.80$

Steps:

1. Refer to the Eq. C12.6.13, $\gamma = 1/2$, and compute $K_x = 5.5$

2. $\frac{F_x}{\eta} = \frac{5.5}{5.83} \times \frac{45600}{.2} = 215000$ psi

3. Using $\gamma_1 = \sqrt{1 - 1 \times .5 + .5^2} = .866$

From Fig. C12.5.2b, $F_x = 172000$ psi

4. $P_{cr} = \frac{172000 \times .5 \times .2}{50} = 345$ psi

C12.6.8 Axial Compression, Lateral Load and Torsion.

The following section presents curves to determine the allowable buckling stresses for a simply supported honeycomb sandwich cylinder under axial compression, lateral loads and torsion. The curves were derived from the equations presented in Ref. 7.

The following example illustrates the application of the equations.

Example: Find the buckling stress for a simply supported honeycomb sandwich cylinder under the following loads.

Given: 1. Material: PH15-7Mo (RH1050) Steel at R.T.

2. Properties: $E = 30 \times 10^6$ psi

$G'_c = 38000$ psi (For s = 3/16 and $t_c = .001$ in.)

$F_{cy} = 190000$ psi

3. Geometry: $c = .80$ in.

$t_F = .080$ in.

$L = 50$ in.

$R = 50$ in.

4. Load Ratio: $\gamma = \frac{N_y}{N_x} = \frac{pR}{N_x} = 1/2 \quad \frac{f_s}{f_x} = .2$

Calculate:

1. $D = \frac{Et_F (c + t_F)^2}{2(1 - \mu^2)} = 1025000$

2. $U = G'_c (c + 2t_F) = 36400$ lb./in.

3. $J_c = \frac{7150 \times 38000}{30 \times 10^6} = 9.05$

4. From Eq. C12.5.21, $K_X = 7.1$

5. From Fig. C12.5.21, $K_S = 7.6$

6. Since $\frac{R_x}{R_s} = \frac{f_x}{f_s} \times \frac{K_s}{K_x} = \frac{7.6}{.2 \times 7.1} = 5.36$

7. $R_x + R_s^2 = 1 \quad \therefore R_x = .96$

8. $K'_x = R_x K_x = .96 \times 7.1 = 6.8$

9. $\frac{F_x}{\eta} = \frac{K'_x}{J_c} \times \frac{U}{2t_F} = \frac{6.8}{9.05} \times \frac{36400}{.16} = 171000$ psi

10. $\gamma_1 = \sqrt{\frac{f_x^2 - f_x f_y + f_y^2 + 3f_s^2}{f_x}} = \sqrt{1 - \gamma + \gamma^2 + 3\left(\frac{f_s}{f_x}\right)^2} = .933$

11. From Fig. C12.5.2b, $F_x = 150000$ psi.

12. $F_y = .5\ F_x = 75000$ psi or

$$P_{cr} = \frac{F_y \times 2t_F}{R} = 240 \text{ psi}$$

13. $F_s = .2F_x = 30800$ psi

C12.7 Buckling of Flat Panels with Dissimilar Faces.

C12.7.1 General.

The capability to handle the buckling of panels with unequal facings or facings of dissimilar materials is particularly important in a refined aircraft design. The need for such a method is made necessary quite often by the requirements of minimum external gauges to prevent damage during ground servicing and handling. In recent years with the advent of thermal stresses, the requirement for design with different gauge faces or even different facing materials has become important. Even though a design at room temperature may be considered as similar facing materials, because of the material property effects at temperature, the facings must be considered dissimilar for a more exact analysis.

The buckling of a sandwich panel with facings of unequal thickness or dissimilar materials was treated in Ref. 8. The equations presented in this section will deal only with dissimilar isotropic facings. The referenced report deals further with dissimilar orthotropic facings and similar isotropic facings, all with unequal gauges. All the equations consider orthotropic core material.

C12.7.2 Uniaxial Compression.

The design of a honeycomb panel with unequal or dissimilar faces must still consider the local failure modes discussed in sections C12.5.2, C12.5.3, and C12.5.4. The general buckling allowable equation presented here is in terms of load. The equation is a function of two unequal isotropic facing thicknesses with different material properties, core depth, core density, edge fixity, and panel size. This equation can be written as follows:

$$N = \frac{P_M A h^2}{a^2} \qquad a = \text{Loaded edge} \qquad \text{(C12.7.1)}$$

$$A = \frac{\pi^2 t_1 t_2 E_1 E_2}{(1-\mu^2)(t_1 E_1 + t_2 E_2)} \equiv \frac{\pi^2 Y}{(1-\mu^2)} \qquad \text{(C12.7.2)}$$

$$h = \left(c + \frac{t_1 + t_2}{2}\right) \equiv c + x \qquad \text{(C12.7.3)}$$

$$P_M = \frac{K + \left[\left(\frac{V_x}{c_4} + V_y\right)\right] F}{1 + L + \left(\frac{V_x V_y}{c_4}\right) F} \qquad \text{(C12.7.4)}$$

$$K = c_1 + 2c_2 + c_3$$

$$F = c_1 c_3 - c_2^2 + \frac{1-\mu}{2} c_2 K$$

$$L = \left(c_1 + \frac{1-\mu}{2} c_2\right) \frac{V_x}{c_4} + \left(c_3 + \frac{1-\mu}{2} c_2\right) V_y$$

The core shear parameters are:

$$V_y = \frac{K_1 Y C}{G'_{cy}} \qquad V_x = \frac{K_1 Y C}{G'_{cx}}$$

Where

$$K_1 = \frac{\pi^2}{a^2 (1-\mu^2)} \qquad Y = \frac{t_1 t_2 E_1 E_2}{(t_1 E_1 + t_2 E_2)}$$

$G'_{cx} = G'_{cy}/2$ for hexacell core

$G'_{cx} = G'_{cy}$ for square cell core

The edge fixity constants, c_1, c_2, c_3, and c_4 are listed as follows with their respective edge fixity conditions:

All Edges Simply Supported

$$c_1 = \frac{b^2}{n^2 a^2}, \quad c_2 = 1, \quad c_3 = \frac{n^2 a^2}{b^2}, \quad c_4 = c_1$$

Loaded Edges Simply Supported and the Remaining Edges Clamped

$$c_1 = \frac{16 b^2}{3 n^2 a^2}, \quad c_2 = \frac{4}{3}, \quad c_3 = \frac{n^2 a^2}{b^2}, \quad c_4 = \frac{c_1}{4}$$

Loaded Edges Clamped and the Remaining Edges Simply Supported

$$c_1 = \frac{3b^2}{4a^2} \text{ if } n = 1, \quad c_1 = \frac{b^2}{(n^2+1)a^2} \text{ if } n \geq 2$$

$$c_2 = 1, \quad c_3 = \frac{a^2 (n^4 + 6n^2 + 1)}{b^2 (n^2 + 1)}$$

$$c_4 = \frac{3b^2}{na^2} \text{ if } n = 1, \quad c_4 = \frac{b^2}{(n^2+1)a^2} \text{ if } n \geq 2$$

All Edges Clamped

$$c_1 = \frac{4b^2}{a^2} \text{ if } n = 1, \quad c_1 = \frac{16b^2}{3\,(n^2+1)a^2} \text{ if } n \geq 2$$

$$c_2 = \frac{4}{3}, \quad c_3 = \frac{a^2\,(n^4 + 6n^2 + 1)}{b^2\,(n^2+1)}$$

$$c_4 = \frac{b^2}{a^2} \text{ if } n = 1, \quad c_4 = \frac{4b^2}{3\,(n^2+1)a^2} \text{ if } n \geq 2$$

The following example illustrates the application of the buckling equation in finding the allowable elastic load for a honeycomb panel.

Given: Material: PH15-7Mo (RH1050) Steel

$E_1 = 30 \times 10^6$ psi

$E_2 = 25 \times 10^6$ psi

$G_{cx} = G_{cy} = 40000$ psi

Geometry: $\mu = .3$

$c = .1$ in.

$t_1 = .01$ in.

$t_2 = .02$ in.

$a = 10$ in.

$b = 10$ in.

Simply supported panel, $n = 1$

Calculate:

$c_1 = 1, \; c_2 = 1, \; c_3 = 1, \; c_4 = 1$

$$K_1 = \frac{\pi^2}{100\,(1 - .09)} = .1083$$

$$Y = \frac{.01 \times .02 \times 30 \times 10^6 \times 25 \times 10^6}{.01 \times .30 \times 10^6 + .02 \times 25 \times 10^6} = .188 \times 10$$

$$V_x = V_y = \frac{.1083 \times .188 \times 10^6 \times .1}{40000} = .0511$$

$$L = \left(1 + \frac{.7}{2} \times 1\right) \frac{.0511}{1} + \left(1 + \frac{.7}{2} \times 1\right) .0511 = .138$$

$$K = 1 + 2 \times 1 + 1 = 4$$

$$F = 1 \times 1 - 1 + \frac{.7}{2} \times 1 \times 4 = 1.4$$

$$P_M = \frac{4 + \left[\left(\frac{.0511}{1} + .0511\right)\right] 1.4}{1 + .138 + \left(\frac{.0511 \times .0511}{1}\right) 1.4} = 2.17$$

$$h = \left(.1 + \frac{.01 + .02}{2}\right) = .115$$

$$A = \frac{\pi^2 \times .188 \times 10^6}{.91} = 2.04 \times 10^6$$

The allowable load N from Eq. C12.7.1 is:

$$N = \frac{2.17 \times 2.04 \times 10^6 \times (.115)^2}{100} = 584 \text{ lb/in.}$$

C12.8 Core Shear Induced by Loads Applied at an Insert.

C12.8.1 General.

In the use of structural sandwich construction, particularly for aircraft structures, it is often necessary to carry loads into the sandwich through fittings that allow loads to be applied in a direction normal or inclined to the plane of the sandwich. The fittings are usually fastened to the sandwich by attachment to a small insert that locally replaces the sandwich core. This insert may be of metal or of denser core, and it is bonded between the facings at the time the sandwich is manufactured.

The theoretical and experimental work performed in Ref. 9 was conducted on relatively large circular sandwich panels that had a small, circular insert at their center. Loads were applied at the insert in a direction normal to the sandwich panel. In order to measure core strains the work was limited to continuous core materials, one of end grain balsa wood representing a core of moderate shear modulus and one of cork board representing a core of low shear modulus.

Since the results of this work was limited to an insert in the center of a panel and to isotropic core materials, in the final design case, corrections to this data must be made to account for orthotropic cores and non-centrally located inserts. The correction in the case of orthotropic cores can be made in proportion to the directional shear modulus G_x and G_y. The correction for the case of non-centrally located inserts can be made on the basis of beam shears to their end supports, or inversely proportional to the distance of the load from the supports.

C12.8.2 Shear Stress Distribution.

The shear stresses are a maximum at or near the edge of the insert and are given for a plate with clamped outer rim and clamped insert. The radial distribution of the stress is expressed by the following equation:

$$f_s(r) = \frac{PI_m K}{\pi 2h I} \qquad \text{(C12.8.1)}$$

$$I_m = \frac{t_F h^2}{2} \qquad I = I_m + I_f \qquad I_f = \frac{t^3}{6}$$

$$K = \frac{1}{r}\left[1 - \sqrt{r}\,\frac{\sqrt{r_I}\,\sinh \alpha(r-r_I) + \sqrt{r_p}\,\sinh \alpha(r_p-r)}{\sqrt{r_p r_I}\,\sinh \alpha\,(r_p-r_I)}\right] \qquad \text{(C12.8.2)}$$

$$\alpha = \sqrt{\frac{2\,G'_c\,I}{c\,t_F\,E\,I_f}} \qquad \text{(C12.8.3)}$$

r_I = radius of Insert, r_p = radius of Panel

The facing stresses are a maximum at the edge of the insert and are given by the following equation:

$$f = \frac{P(h+t)}{2\pi t h^2}\left[1 + \frac{2h}{(h+t)\,\alpha\,r_I} - \frac{2r_p^2}{r_p^2 - r_I^2}\,\mathrm{Log}\,\frac{r_p}{r_I} - \frac{3h^2}{(h+t)\,t\,\alpha\,r_I}\right] \qquad \text{(C12.8.4)}$$

The following calculated shear stress distributions, Fig. C12.8.1, in the core demonstrate the variation with α and r.

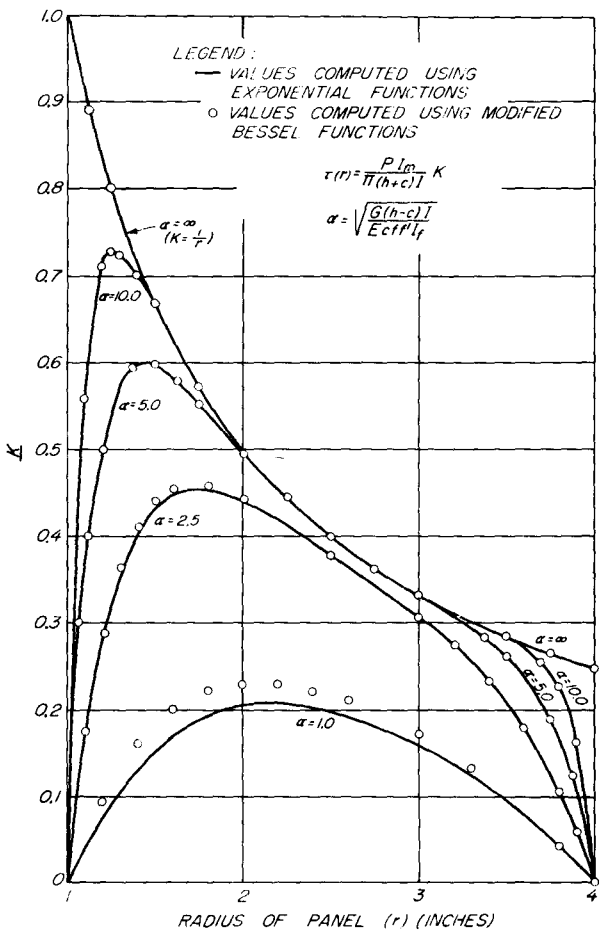

Fig. C12.81. Radial variation in shear stress in the core of a sandwich panel 8 inches in diameter with a central insert 2 inches in diameter.

The calculated shear stresses must be compared with the allowable core shear stresses of section C12.4.5.

C12.9 Corrugated Core Sandwich Failure Modes - Ref. 10.

C12.9.1 General.

Of the wide variety of sandwich constructions available, two important types are those with isotropic cores and those with corrugated cores. Basic theories for the stability analysis of sandwich plates with isotropic facing sheets have been published in the technical literature. Extensive application of these theories has been given to isotropic or nearly isotropic core sandwich under combined in-plane loads. Of the highly orthotropic cores, the corrugated core has important practical use and is the type considered in the paper of Ref. 10 and presented in this section.

Whereas the treatment of isotropic panels under various edgewise loads has been extensive, a similar treatment for corrugated core sandwich has been somewhat limited. This section presents solutions to these cases of corrugated core sandwich subjected to in-plane, combined longitudinal compression and bending, transverse compression and bending, and shear using a variation of the theory formalized in Ref. 11.

The basic element of the idealized corrugated core sandwich panel (shown in Fig. C12.9.1) considered in this paper, consists of relatively thin isotropic facings, which have negligible flexural rigidities about their own centroidal axes, and a highly orthotropic core for which shear distortions are assumed to be admissible only in the plane perpendicular to the corrugations. Furthermore, the bending rigidity of the core is assumed to be negligible in the transverse direction. In general, for the corrugated core, the core shear modulus is many times greater in the plane along the corrugations (longitudinal) than it is perpendicular to the corrugations (transverse) and the above assumption regarding the shear distortions appears to be realistic for many such configurations. Both the facings and the core are assumed to be elastic.

Beside the general buckling allowables developed in this section for the corrugated sandwich panel, local instability must also be considered. The local buckling of the corrugated sandwich panel elements can be handled through the use of standard isotropic panel buckling equation $F_{cR} = KE\,(\frac{t}{b})^2$ using K for the respective type element and element loading.

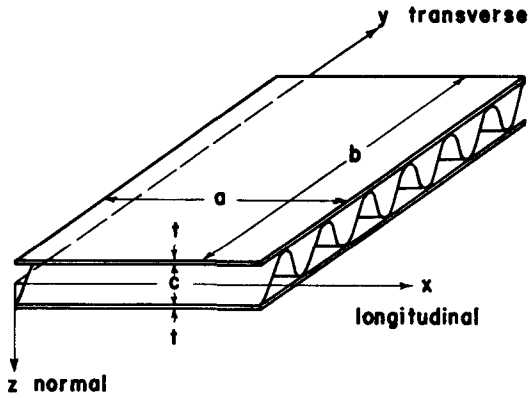

Fig. C12.9.1 Corrugated Core Sandwich

NOMENCLATURE

a	length of panel in x direction
b	length of panel in y direction
c	core depth
D	bending rigidity of facing sheets about sandwich centroidal axis
D_c	core flexural rigidity in direction of corrugations
U	core shear stiffness in plane perpendicular to corrugations $U = G'_y C$
E	Young's modulus of facings
G'_y	core shear modulus in plane perpendicular to corrugations
J	sandwich stiffness parameter
K	buckling coefficient
N_{ox}, N_{oy}	maximum compressive loads per unit length
N_x, N_y	$N_{ox}(1 - \alpha_x y/b)$, $N_{oy}(1 - \alpha_y x/a)$, respectively
N_{xy}	shear load per unit length of edge
t	thickness of each facing
x,y,z	cartesian coordinates
μ	Poisson's ratio of the facings

C12.9.2 Corrugated Sandwich Panel General Buckling Coefficients.

The Rayleigh-Ritz energy method was used to formulate the stability criterion. The buckled shape is assumed in the form of a double sine series which is substituted into energy equation. Minimization of the resulting expression with respect to the coefficients of the assumed series and the ratio of the bending and twisting deflection to the total deflection yields a system of linear homogeneous equations from which the buckling coefficients are evaluated by a matrix iteration procedure.

Curves of the buckling coefficients are plotted in Figs. C12.9.2 through C12.9.10. The validity of the present results is restricted to those cases for which the bending rigidities of the facings about their individual axes is negligible. In general, the bending rigidity of the individual facings becomes increasingly important as the parameter G_{cb} becomes smaller. The accuracy of the results also decreases as J decreases.

All of the curves presented are for values of $D_c/D = 0$ and for $\mu = 0.3$. An indication of the effect of variations in the D_c/D ratio from 0 to 0.4 is shown in Fig. C12.9.11 for the cases of axial compression and shear. Many practical sandwich constructions fall in this range of D_c/D, for which the effect on the buckling coefficient appears small over the wide range of the J parameter.

The effect of variations in Poisson's ratio, μ, on compression and shear buckling coefficients was investigated for values of J of 5.0 and 0.5. The effect decreases for increasing values of J and the buckling coefficients corresponding to a J of infinity are independent of Poisson's ratio.

The effect of the core direction on the buckling coefficient was investigated for compression and shear. For compression, the buckling coefficient is greater if the corrugations are parallel to the applied load. In addition, the core area reduces the applied compressive stress for a given load per inch if the corrugations are parallel to the applied load. For shear, the buckling coefficient is greater if the corrugations are oriented in the short direction. These conclusions are consistent with the behavior of stiffened plate.

Seide (Ref. 12) has presented curves for the buckling coefficients of simply supported, corrugated core sandwich under longitudinal compression with the core longitudinal. A comparison which was made between the results presented graphically by Seide and those presented in this section showed good agreement exists between the results obtained by the two analyses.

Buckling coefficient curves are presented for a number of important loading conditions. For many practical sandwich configurations, the effect on the buckling coefficients of Poisson's ratio and of the core longitudinal bending rigidity appears to be relatively small compared to the effect of the core shear rigidity.

In addition to overall instability, sandwich plates must be analyzed for local modes of failure which have not been considered in the presented curves.

Axial Compression

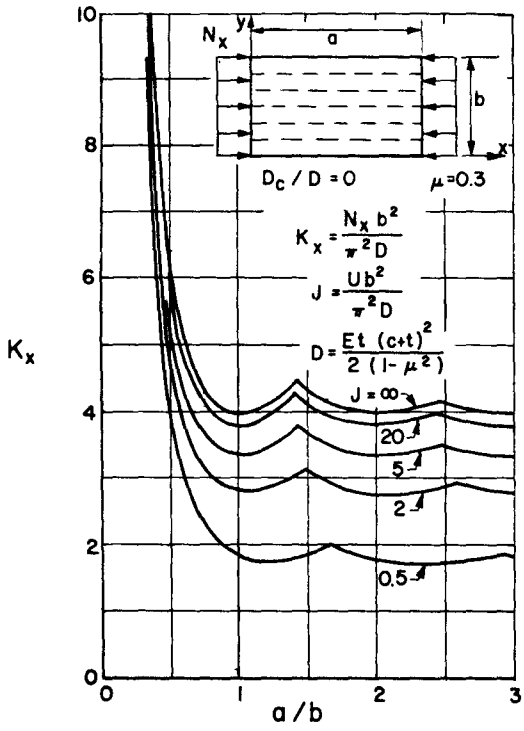

Fig. C12.9.2 Buckling Coefficients for Longitudinal Compression with Longitudinal Core

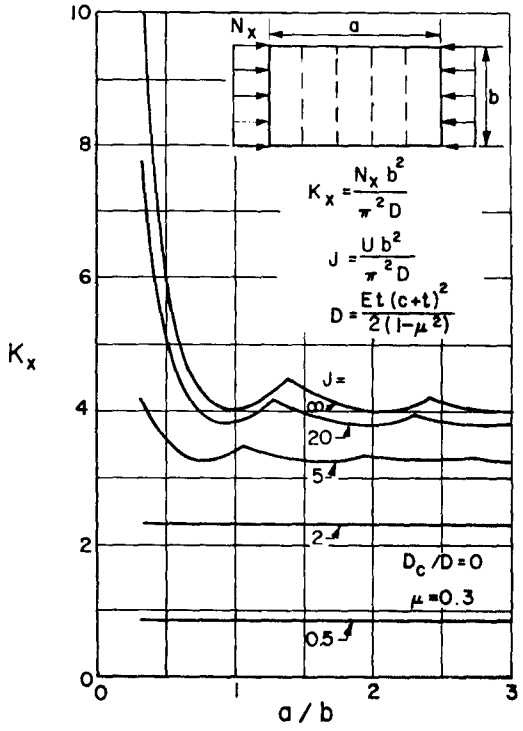

Fig. C12.9.3 Buckling Coefficients for Longitudinal Compression with Transverse Core

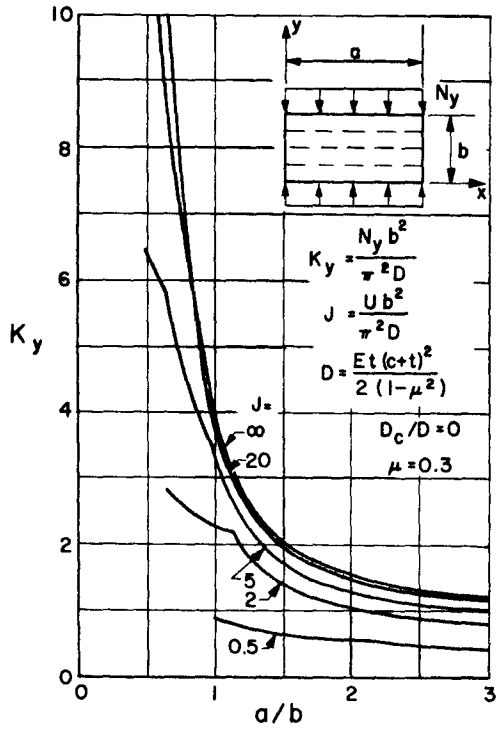

Fig. C12.9.4 Buckling Coefficients for Transverse Compression with Longitudinal Core

Biaxial Compression

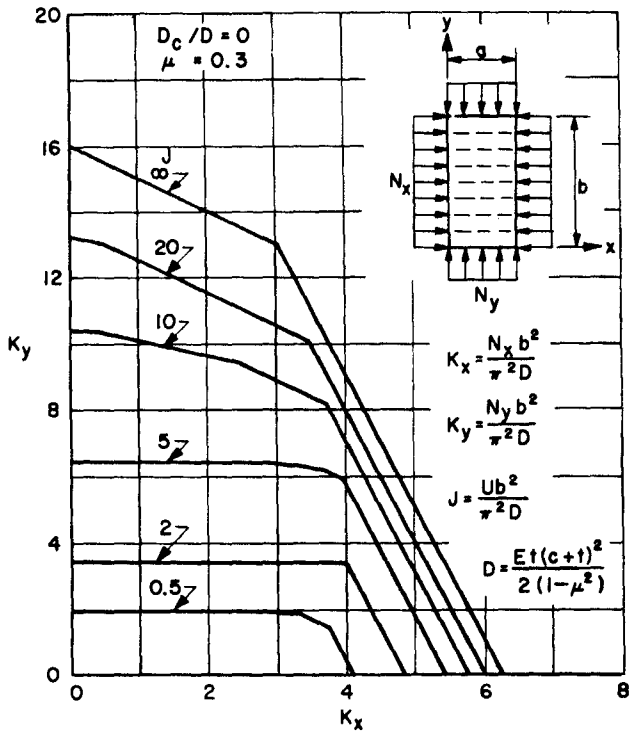

Fig. C12.9.5a Buckling Coefficients for Biaxial Compression; a/b = 1/2

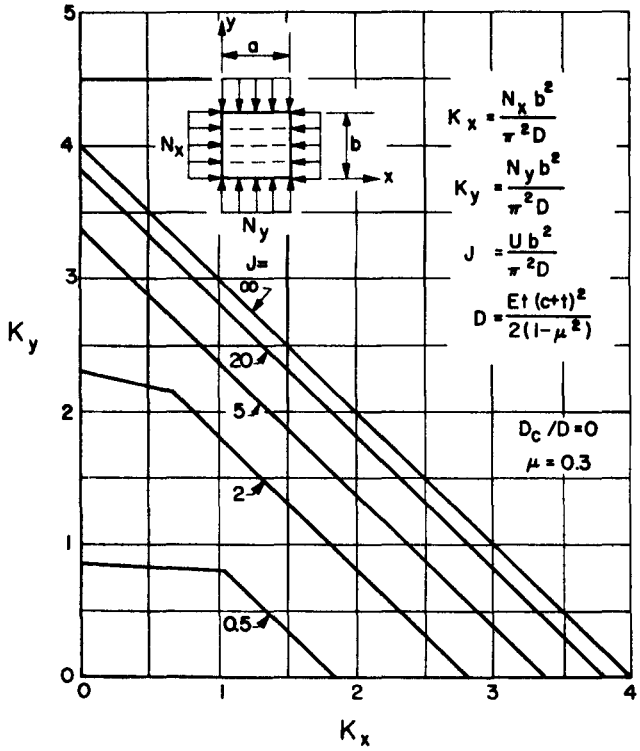

Fig. C12.9.5b Buckling Coefficients for Biaxial Compression, a/b = 1.

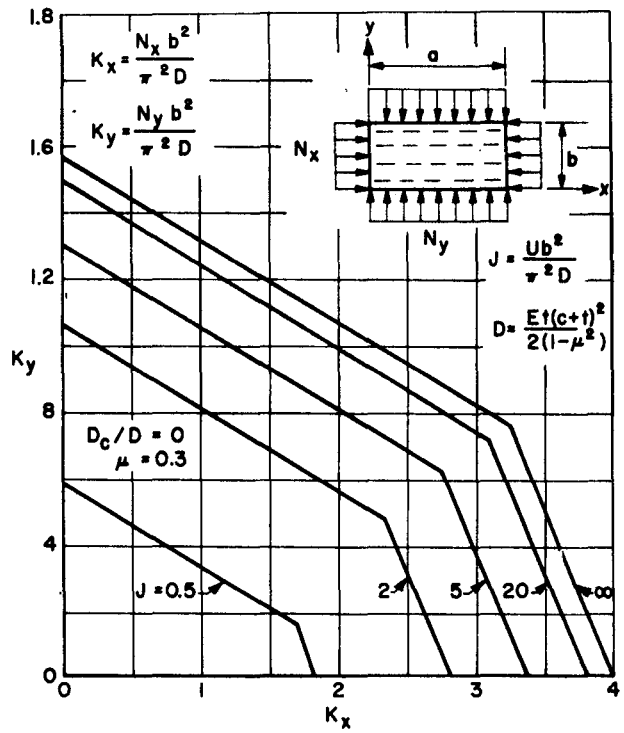

Fig. C12.9.5c Buckling Coefficients for Biaxial Compression, a/b = 2.

Shear

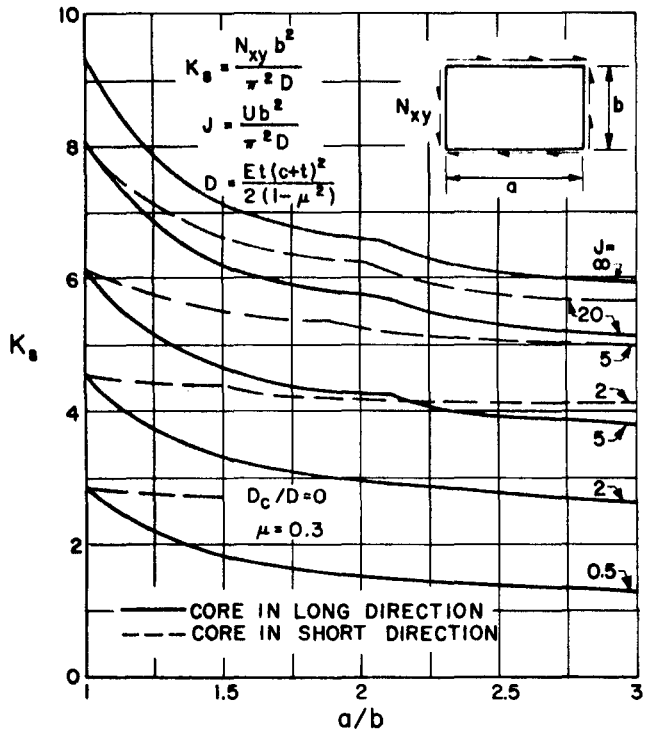

Fig. C12.9.6 Buckling Coefficients for Shear with Longitudinal and Transverse Core

Axial Compression and Shear

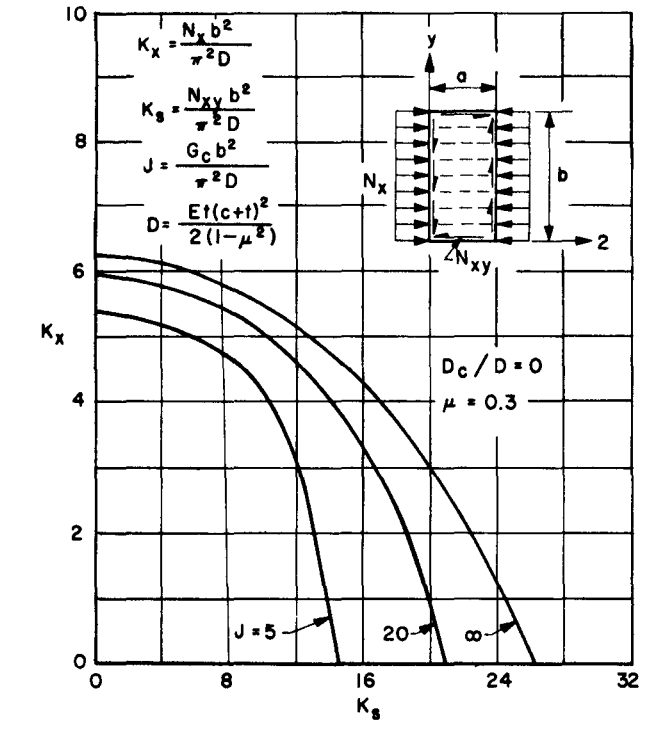

Fig. C12.9.7a Buckling Coefficients for Combined Longitudinal Compression and Shear with Longitudinal Core, a/b = 1/2

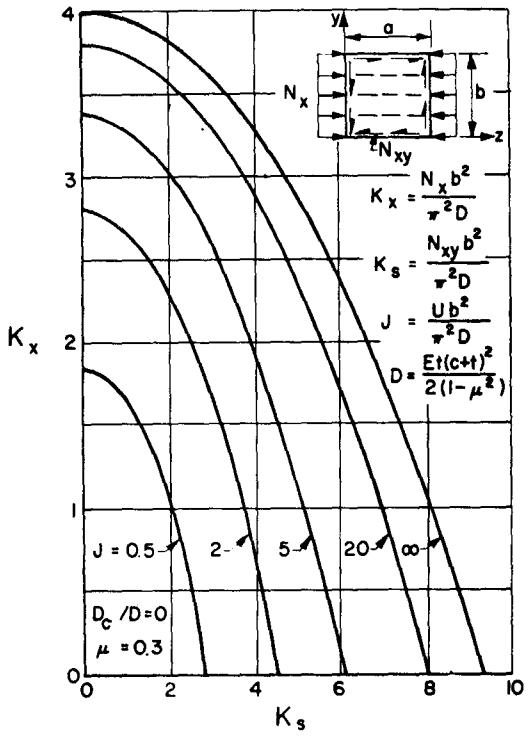

Fig. C12.9.7b Buckling Coefficients for Combined Longitudinal Compression and Shear with Longitudinal Core, a/b = 1.

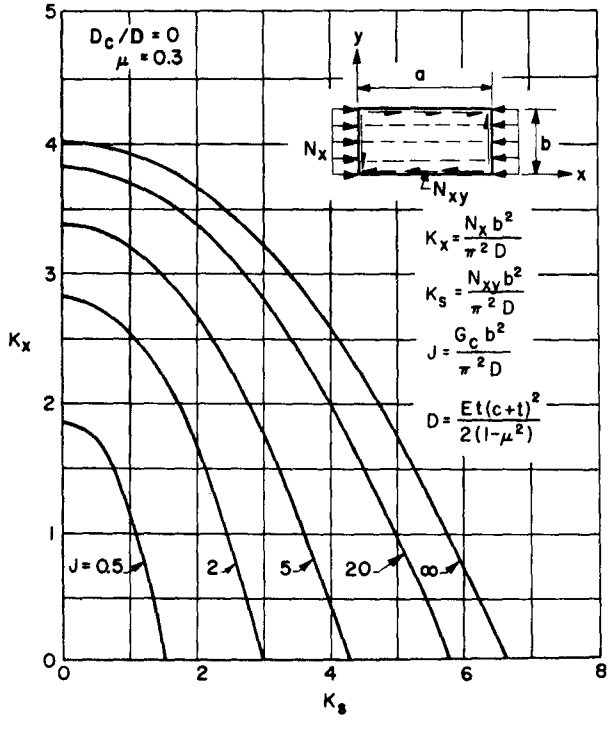

Fig. C12.9.7c Buckling Coefficients for Combined Longitudinal Compression and Shear with Longitudinal Core, a/b = 2

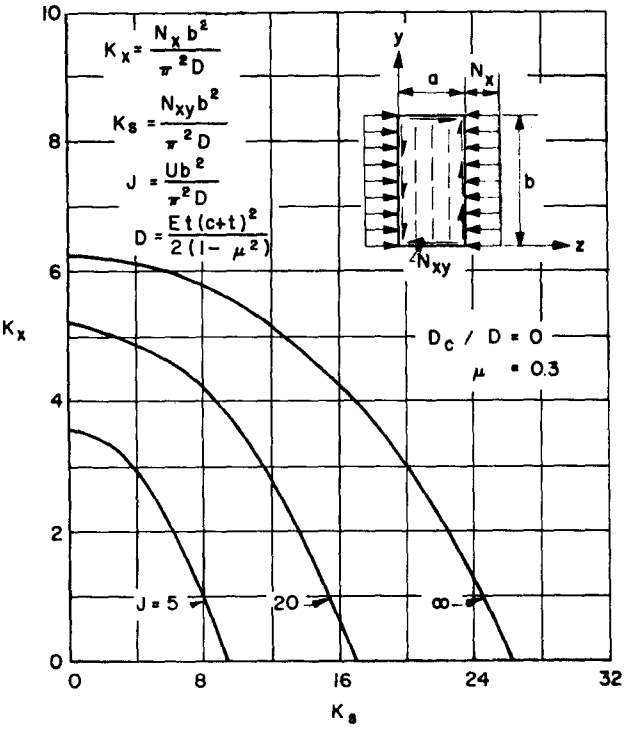

Fig. C12.9.8a Buckling Coefficients for Combined Longitudinal Compression and Shear with Transverse Core, a/b = 1/2

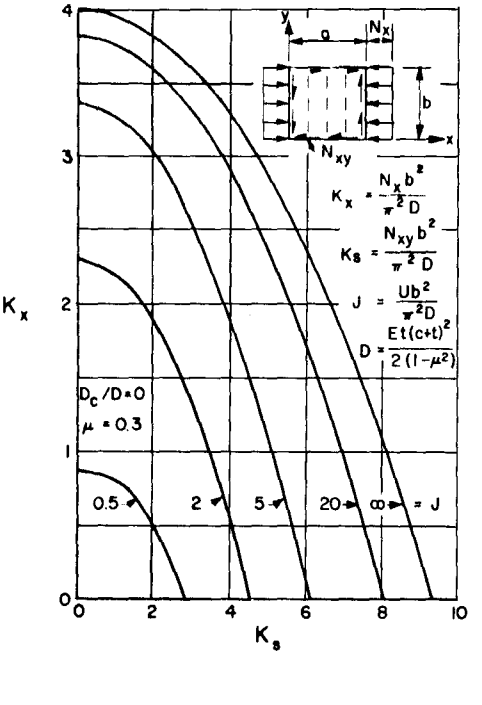

Fig. C12.9.8b Buckling Coefficients for Combined Longitudinal Compression and Shear with Transverse Core, a/b = 1

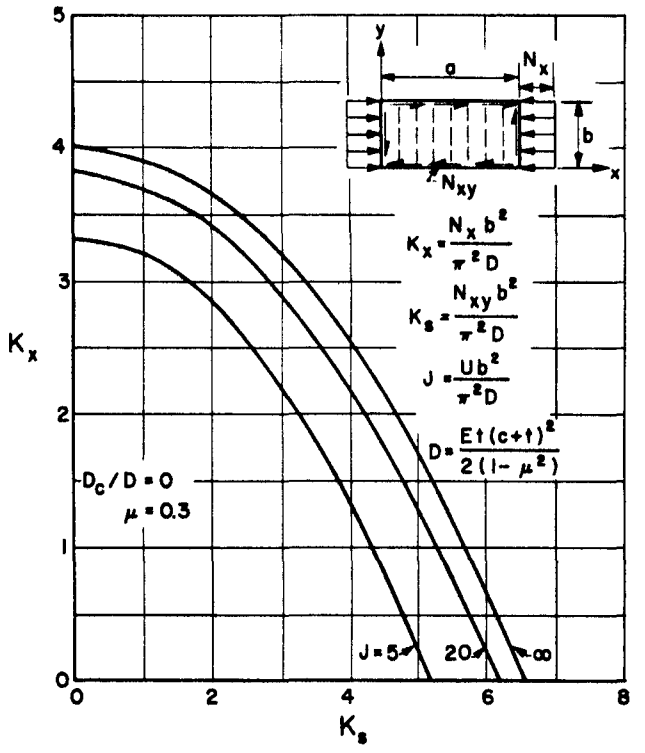

Fig. C12.9.8c Buckling Coefficients for Combined Longitudinal Compression and Shear with Transverse Core, a/b = 2

Biaxial Compression and Shear

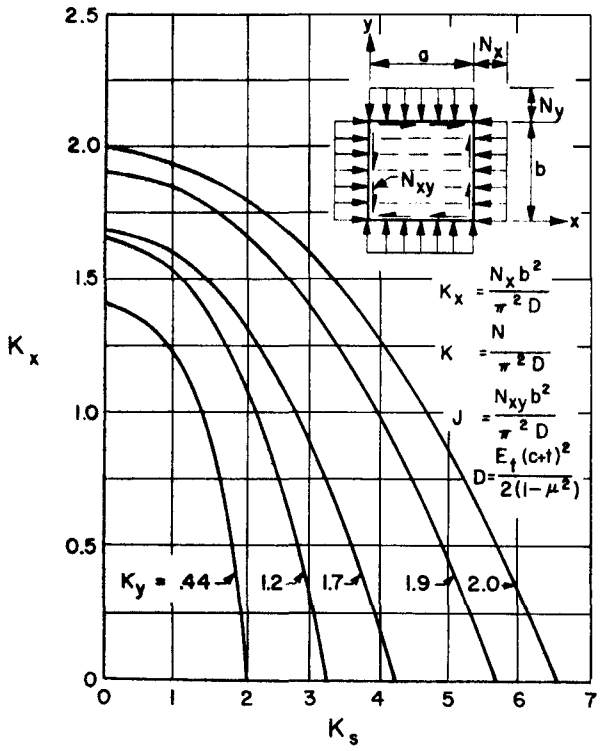

Fig. C12.9.9 Buckling Coefficients for Combined Longitudinal Compression, Transverse Compression, and Shear with Longitudinal Core.

Bending

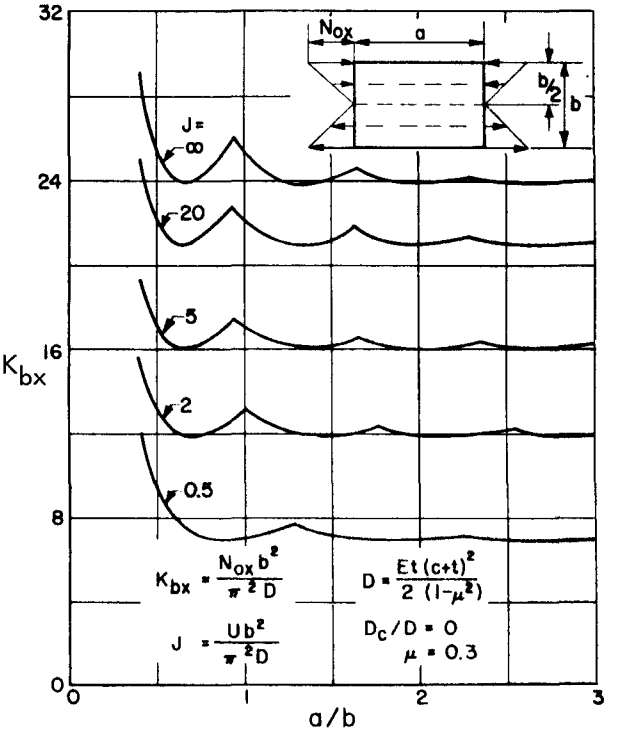

Fig. C12.9.10 Buckling Coefficients for Longitudinal Pure Bending ($\alpha_x = 2$) with Longitudinal Core

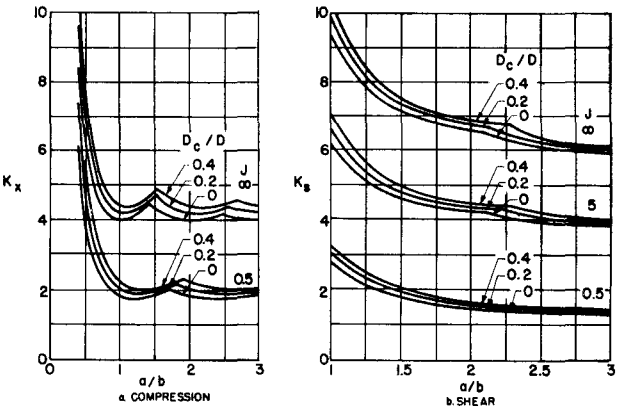

Fig. C12.9.11 Effect of D_c/D Ratio on Buckling Coefficients for Compression and Shear with Longitudinal Core

The following example illustrates the application of the buckling coefficient curves in finding the allowable elastic load for a corrugated sandwich panel.

Given: Material: 2024-T4 Aluminum

$E = 10 \times 10$ psi

$G'_y = 50{,}000$ psi

$F_{cy} = 40{,}000$ psi

Geometry: $c = .5$ in.

$t = .05$ in.

$b = 20$ in.

$a = 20$ in.

Compute allowable load for longitudinal axial compression,

$$U = G'_y c = 50000 \times .5 = 25000 \quad \text{REF(10)}$$

$$D = \frac{10 \times 10^6 \times .05\ (.5 + .05)^2}{2\ (1 - .09)} = 83000$$

$$J = \frac{25000\ (20)^2}{\pi^2\ 83000} = 12.1$$

$K_x = 3.6$ Ref. Fig. C12.9.2.

$$\text{Allowable } N_x = \frac{K_x \pi^2 D}{b^2} = \frac{3.6 \times \pi^2 \times 83000}{(20)^2} =$$

7370 lb./in.

Compute allowable load for biaxial compression,

Ultimate N_x applied = 5000 lb./in.

$U = 25000$

$J = 12.1$

$D = 83000$

$$K_x = \frac{5000\ (20)^2}{\pi^2\ 83000} = 2.45$$

$K_y = 1.35$ Ref. Fig. C12.9.5b.

$$\text{Allowable } N_y = \frac{K_y \pi^2 D}{b^2} = \frac{1.35 \times \pi^2 \times 83000}{(20)^2} =$$

2840 lb./in.

C12.10 Design of Sandwich Structures.

C12.10.1 General.

With increased performance requirements in present day aircraft minimum weight design is being stressed more and more. The present state-of-the-art dictates the use of honeycomb type structure in many areas to achieve a minimum weight design. Great care must be used in the design of a honeycomb panel to take advantage of the possible efficiencies. The magnitude of this problem exceeds acceptable design time if the designer is required to start each panel design from allowable equations. With as many as five (5) parameters (t_{F_1}, t_{F_2}, h, $t_{c/s}$, S) to describe the cross-section of a honeycomb panel, two (2) parameters (b, a/b) to describe the panel configuration, and six (6) parameters, (P_x, P_y, Q, V, M_x, M_y) to describe the panel loading, it can be seen that the problem of honeycomb design optimization can become laborious.

This section will demonstrate the use of the allowable equations presented in Section C12.4 through C12.9 for the design of sandwich structures. With reference to Section C12.2 and Fig. C12.2.1, each of the allowable equations for the primary failure modes must be considered for the simplest honeycomb panel design. For efficient design of sandwich structures, a general rule can be established that the critical stress for each failure mode should be equal to the ultimate applied stress. Compliance with this rule alone, however, does not insure the most efficient sandwich structure. In many structures the higher the allowable stress level the more efficient the structure. This is not necessarily true for a sandwich structure. It must be remembered that for the higher stress level in the sandwich facings the more core material that is required. If a true optimization is performed it can show that the optimum stress level is a function of the applied load level. In this section, data is also presented which will eliminate requirements for the designer to manipulate the large number of parameters through the many possible allowable equations. The data indicates to the designer the most efficient panel for the given conditions. The method used to arrive at such general data, is to write a weight equation in terms of the respective allowables. This weight equation is then minimized by one of several methods to produce a minimum weight as a function of the variable parameters. The digital computer must be used to compute the optimum panel configurations from the derived minimum weight equations in most cases. The data produced with this iterative process presents the data in a form from which an optimum design may be selected directly.

C12.10.2 Dimpling of Sandwich Facings.

If the core of a sandwich construction is of cellular (honeycomb) or corrugated material, it is possible for the facings to buckle or dimple into the spaces between core walls. Dimpling of the facings may not lead to failure unless the amplitude of the dimples becomes large and causes the dimples or buckles to grow across core cell walls and result in wrinkling of the facings. Dimpling that does not cause total structural failure may, of course, be

severe enough so that permanent dimples remain after removal of load.

If dimpling of the facings is not permissible, the core cell size shall be small enough so that dimpling will not occur under design loads. The design procedures assume that a facing thickness (t) is known (facing thickness having been determined by consideration of design loads and chosen design compressive facing stresses), that facing compressive stress F_c and effective compressive modulus of elasticity E'_F are known, and that the core cell size is to be determined. The facing properties shall be values at the condition of use; that is, if application is at elevated temperature, then facing properties at elevated temperature shall be used in design. The facing modulus of elasticity is the effective value at the facing stress. If this stress is beyond the proportional limit value, an appropriate tangent, reduced, or modified compression modulus of elasticity shall be used.

Sandwich with Cellular (Honeycomb) Core

This section gives the procedure for determining the core cell size such that a sandwich facing will not dimple.

The facing stress at which dimpling of the sandwich facing will occur is given by the empirical formula C12.5.1.

$$F_c = 0.75\, E'_F\, (t_F/s)^{3/2}$$

where E'_F is effective compressive modulus of elasticity of the facing $E_F\eta$ at stress F_c; t_F is facing thickness, and s is core cell size (diameter of inscribed circle). Solving formula C12.5.1 for s results in

$$s = 0.825\, t_F\, (F_c/E'_F)^{-2/3} \quad \text{------(C12.10.1)}$$

Maximum core cell size can be determined from formula C12.10.1. If the core cell size is smaller than available, it is necessary to use a thicker facing and a lower stress in order that dimpling will occur at the same edge load. The equation C12.10.1 can also be used to find facing thicknesses and stresses for dimpling of sandwich facings on cores of a particular cell size.

A similar derivation can be made for face dimpling for the panel in shear. The following equation results:

$$s = .71\, t_F\, (F_s/E'_F)^{-2/3} \quad \text{------(C12.10.2)}$$

Sandwich Having Corrugated Core

This section gives the procedure for determining the spacing between core corrugations such that sandwich facing or core elements will not buckle (Ref. 13). For edge compression load in a direction parallel to the core axis, the design procedure is based on the buckling load of the unsupported facing or core element, whichever is the lower, although it may be possible to utilize a sandwich in which the core elements are buckled. For edge compression load in a direction perpendicular to the core axis, the design procedure is based on the buckling load of the unsupported facing element and the core is assumed to be rigid enough to cause rotational restraint at the ends of the facing element. If the core is double corrugated, it may not have sufficient strength to cause the facing elements to buckle as assumed.

The facing stress at which buckling of the facing element or core element will occur is given by the formula

$$F_c = K\, E'\, \left(\frac{t_F}{b_c}\right)^2 \quad \text{----------(C12.10.3)}$$

where E' is the effective compressive modulus of elasticity of the facing $E\eta$ at stress F_c; t_F is facing thickness; b_c is unsupported width of facing element; and K is a coefficient dependent upon the ratio (t_c/t_F) of the corrugation thickness (t_c) to the facing thickness (t_F), the angle (θ) between the corrugation element and the facing, and the type of applied load.

Solving formula (C12.10.3) for b_c results in

$$b_c = \sqrt{K}\; t_F\, \left(\frac{F_c}{E'}\right)^{-1/2} \quad \text{-------(C12.10.4)}$$

C12.10.3 Wrinkling of Sandwich Facings.

The face wrinkling mode of failure described in Section C12.2 cannot be allowed to occur to any extent in a sandwich panel. Thus the design procedure presented here will preclude any such failure at the design load. The design procedures assume that the facing compressive stress F_c and the effective compressive modulus E'_F are known, and that the core density parameter t_c/s is to be determined. The facing properties shall be values at the condition used.

This section gives the procedure for determining the core density parameter t_c/s such that the sandwich facing will not wrinkle (or separate away from the core). The facing stress at which wrinkling of the sandwich facing will occur is given by the empirical equation C12.5.10

$$F_c = .43 \sqrt[3]{E'_F\, E'_c\, G'_c}$$

Where E'_F is the effective compressive modulus of elasticity of the facing $E_F \eta_z^3$ at stress F_c; E'_c is effective core compressive modulus of elasticity as given by equation C12.4.13; G'_c is effective core shear modulus as expressed by equation C12.4.9 or C12.4.10. Substituting the expressions for E'_c and G'_c in to equation C12.5.10, the following equation results:

$$F_c = .43 \sqrt[3]{E_F \eta_z^3 \; 2.13 \left(\frac{2t_c}{s}\right)^{1.415} E_c \times 2.43 \left(\frac{2t_c}{s}\right)^{1.64} G_c}$$

where $\left(\frac{\rho'}{\rho}\right) = \frac{2t_c}{s}$ For Square Cell Core

$$F_c = .43 \sqrt[3]{E_F \eta_z^3 \; E_c G_c \; 5.1 \left(\frac{2t_c}{s}\right)^{2.065}} \quad - - -(C12.10.5)$$

Solving this equation for t_c/s, the following equation resulst:

$$\frac{t_c}{s} = .5 \left[\frac{1.35 \, F_c}{(E_F \eta_z^3 \; E_c G_c)^{1/3}}\right]^{1.015} \quad - - - - -(C12.10.6)$$

The minimum core density can be determined from equation C12.10.6. If the core density required is lower than that available, a lower density can be used or the facing stress increased. If the core density is greater than can be obtained, the facing stress should be reduced. This same equation holds for design for in-plane shear loads.

C12.10.4 Shear Crimping of Sandwich Panels.

The shear crimping mode of failure described in Section C12.2 is not considered one of the primary failure modes but must be checked for any sandwich design. The shear crimping allowable equation can be used primarily to determine the core depth c when the core density t_c/s is known. The equation can also be used to determine t_c/s when the core depth c is known. It is assumed in both cases that the facing thickness t_F and facing stress F_c are known.

This section gives the procedure for determining the core depth and density parameter t_c/s such that the sandwich panel will not fail in shear crimping. The facing stress at which shear crimping of the sandwich panel will occur is given by equation C12.5.18.

$$F_c = \frac{G'_c \; (c + 2t_F)}{2t_F}$$

$$F_c = \frac{1.21 \left(\frac{2t_c}{s}\right)^{1.64} G_c \; (c + 2t_F)}{t_F}$$

Solving this equation for c results in:

$$c = \frac{F_c \; t_F}{1.21 \left(\frac{2t_c}{s}\right)^{1.64} G_c} - 2t_F \quad - - - -(C12.10.7)$$

Solving this equation for t_c/s results in:

$$\frac{t_c}{s} = .5 \left[\frac{F_c \; t_F}{1.21 \, G_c \; (c + 2t_F)}\right]^{.65} \quad - - -(C12.10.8)$$

The core depth thus derived must be compared with that depth derived from the general buckling equation in Section C12.10.5 as the core density t_c/s must be compared with that derived in Section C12.10.3. The maximum values must be used unless the stress or other parameters are adjusted.

C12.10.5 General Buckling of Sandwich Panels.

The general buckling mode of failure described in Section C12.2 must not occur with the application of the ultimate design load. The design procedures assume that the facing compressive stress F_c and the effective compressive modulus E'_F are known, the facing thickness t_F and core density parameter t_c/s and panel size (a, b) are known, and the core depth c is to be determined. The material properties shall be values at the condition used.

This section presents a procedure for determining the core depth such that the sandwich panel will not fail in general instability buckling. The facing stress at which general buckling of the sandwich panel will occur is given by the equation C12.5.19.

$$F_c = \frac{K_c \; U \eta}{J \; 2t_F}$$

$$U = G'_c \; (c + 2t_F)$$

$$J = \frac{b^2 U}{\pi^2 D}$$

$$D = \frac{E t_F \; (c + t_F)^2}{2(1 - \mu^2)}$$

$$F_c = \frac{\pi^2 \; K_c \; \eta E_F \; (c + t_F)^2}{4b^2 \; (1 - \mu^2)} \quad - - - - - -(C12.10.9)$$

Solving this equation for c results in:

$$c = \left[\frac{4F_c \; b^2 \; (1 - \mu^2)}{\pi^2 \; K_c \; \eta E_F}\right]^{1/2} - t_F \quad - - - \; (C12.10.10)$$

For the case when all the panel parameters are known with the exception of panel size b, the following equation can be used to determine b:

$$b = \left[\frac{\pi^2 \; K_c \; \eta E_F \; (c + t_F)^2}{4 \; F_c \; (1 - \mu^2)}\right]^{1/2} \quad - - - \; (C12.10.11)$$

If the core depth should be greater than is practical or greater than volume requirements will allow, the stress level F_c or the panel size b must be changed. For a case where the structural sandwich panels are being used as insulation of fuel cells or equipment bays, if the core depth c can be made greater the panel size b should be increased to reduce the back up structure required.

A similar derivation can be made for other loading cases and results only in the change of K_c to that for the respective load condition.

C12.10.5 Design of Flat Sandwich Panels.

Assuming that a design begins with a given load to transmit and chosen design stresses, a flat rectangular panel of sandwich construction under edgewise compression load shall be designed to comply with the following four conditions:

(1) The facings shall be at least thick enough to withstand the chosen design compressive stresses.

(2) The core shall be thick enough and have a shear modulus high enough so that overall buckling of the sandwich panel will not occur under the design compression load.

(3) The core shall have high enough moduli of elasticity, and the sandwich shall have great enough flatwise tensile and compressive strength, so that wrinkling of either facing will not occur. (Design procedure given in Section C12.10.3.)

(4) If the core is of honeycomb type and dimpling of the facing is not permissible, the cell size shall be small enough so that dimpling of either facing into the core cells will not occur. (Design procedure given in Section C12.10.2.)

These four conditions must be met. Overall buckling of the sandwich or dimpling or wrinkling of the facings cannot occur without possible total collapse of the panel. Detailed procedures giving theoretical formulas are presented in this section.

C12.10.5.1 Determining Facing Thicknesses and Panel Parameters.

For honeycomb panels in compression:

$$t_{F_1} F_{c_1} + t_{F_2} F_{c_2} = N \text{ (for unequal facings)} \quad ---- \text{(C12.10.12)}$$

$$t_F = \frac{N}{2F_c} \text{ (for equal facings)} \quad --- \text{(C12.10.13)}$$

where t_F is facing thickness; F_c is chosen design facing compressive stress; N is design compression load per inch of panel edge; and 1, 2 are subscripts denoting facings 1 and 2.

In determining thicknesses of facings for sandwich with facings of different materials, equation C12.10.12 must be satisfied, but also the stresses F_{c_1} and F_{c_2} must be chosen so that $F_{c_1}/E_{s_1} = F_{c_2}/E_{s_2}$ (where E_s is facing secant modulus of elasticity), thus avoiding overstressing of either facing. For example, if facing 1 is a material such that the ratio $F_{cy_1}/E_{s_1} = 0.005$ and facing 2 is a material such that the ratio $F_{cy_2}/E_{s_2} = 0.002$, the design must be based on a strain of 0.002, otherwise facing 2 will be overstressed. In order to accomplish this, the chosen design stress for facing 1 must be lowered.

This section also gives procedures for determining core thickness and core shear modulus so that overall buckling of the sandwich panel will not occur. The facing stress at which buckling of a sandwich panel with isotropic facings will occur is given by the theoretical formula C12.5.19 from which the primary relation for core depth c was derived as equation C12.10.10.

$$c = \left[\frac{4F_c b^2 (1 - \mu^2)}{\pi^2 K_c \eta E_F}\right]^{1/2} - t_F$$

The core density relation (or shear modulus) was derived from the face wrinkling stress equation C12.5.10 and resulted in equation C12.10.6:

$$\frac{t_c}{s} = .5 \left[\frac{1.35 F_c}{(E_F \eta_2^3 E_c G_c)^{1/3}}\right]^{1.016}$$

C12.10.5.2 Determining Facing Thickness and Panel Parameters for Honeycomb Panels in Shear.

$$t_{F_1} F_{s_1} + t_{F_2} F_{s_2} = N_{xy} \text{ (unequal facings)} \quad ---- \text{(C12.10.14)}$$

$$t_F = \frac{N_{xy}}{2F_s} \text{ (equal facings)} \quad ---- \text{(C12.10.15)}$$

where t_F is facing thickness; F_s is chosen design facing shear stress; N_{xy} is design shear load per inch of panel edge; and 1, 2, are subscripts denoting facings 1 and 2.

In determining the thickness of facings for sandwich with facings of different materials, equation C12.10.14 must be satisfied, but also the stresses F_{s_1} and F_{s_2} must be chosen so that $F_{s_1}/G_{s_1} = F_{s_2}/G_{s_2}$ (where G_s is facing shear modulus).

The core shear modulus can be determined by the local failure criteria discussed in

Section C12.10.3 by deriving the relationship of core density t_c/s similar to that given by equation C12.10.6 with the exception that equation C12.5.12 must be used in place of C12.5.10 which differ as in the derivation of $F_{s_{cr}}/\eta_2$.

$$\frac{t_c}{s} = .5 \left[\frac{1.35\ F_s}{(E_F \eta_2^3\ E_c G_c)^{1/3}}\right]^{1.016}$$

The core depth or thickness c must be derived from the buckling stress equation C12.5.20 similar to the derivation of equation C12.10.10

$$c = \left[\frac{4F_s b^2\ (1 - \mu^2)}{\pi^2\ K_s\ \eta E_F}\right]^{1/2} - t_F$$

C12.10.5.3 Determining Facing Thickness and Panel Parameters for Corrugated Panels in Compression

$$t_{F_1} F_{c_1} + t_{F_2} F_{c_2} + \frac{t_c\ F_{cc}}{\cos\theta} = N_x \quad \text{(unequal facings and core thickness)} \quad \text{- - - - - (C12.10.16)}$$

$$t_F = \frac{N_x}{(2 + \frac{1}{\cos\theta})F_c} \quad \text{(equal facings and core thickness)} \quad \text{- - (C12.10.17)}$$

where t_F is facing thickness; t_c is corrugation thickness; F_c is chosen design compression stress; N_x is design compression load per inch of panel edge; θ angle between corrugation element and facing; and 1, 2, c are subscripts denoting facings 1 and 2 and corrugation.

In determining the thickness of facings for sandwich with facings and corrugation of different materials, equation C12.10.16 must be satisfied, but also stresses F_{c_1}, F_{c_2} and F_{cc} must be chosen so that $F_{c_1}/E_{s_1} = F_{c_2}/E_{s_2} = F_{cc}/E_{sc}$ (where E_s is the secant modulus of the respective sandwich element).

The core depth or thickness c must be derived from the buckling stress equation

$$N_x = \frac{K_x \pi^2 D}{b^2} \quad \text{of}$$

$$D = \frac{E_F t_F\ (c + t_F)^2}{2\ (1 - \mu^2)}$$

$$N_x = \frac{K_x \pi^2\ E_F t_F\ (c + t_F)^2}{2\ b^2\ (1 - \mu^2)}$$

$$c = \left[\frac{2N_x\ b^2\ (1 - \mu^2)}{\pi^2\ E_F t_F\ K_x}\right]^{1/2} - t_F \quad \text{- - (C12.10.18)}$$

The corrugation spacing is given by equation C12.10.4.

C12.10.5.4 Determining Facing Thickness and Panel Parameters for Corrugated Panels in Shear.

$$t_{F_1} F_{s_1} + t_{F_2} F_{s_2} + t_c F_{sc} = N_{xy} \quad \text{(unequal facings and core thickness)} \quad \text{- - - - - (C12.10.19)}$$

$$t_F = \frac{N_{xy}}{2F_{sF} + F_{sc}} \quad \text{(equal facings and core thickness)} \quad \text{- - - - - (C12.10.20)}$$

Where t_F is facing thickness; t_c is corrugation thickness; F_s is chosen design shear stress (note when facing and corrugation thickness are equal, F_{s_c} is equal to $F_{sF} \cos\theta$, due to equal shear strain requirement and longer corrugation element); N_{xy} is design shear load per inch of panel edge; θ angle between corrugation element and facing; and 1, 2, c are subscripts denoting facing 1 and 2 and corrugation.

The core depth or thickness c must be derived from the buckling equation $N_{xy} = \frac{K_s \pi^2 D}{b^2}$ of Section C12.9.

$$c = \left[\frac{2N_{xy}\ b^2\ (1 - \mu^2)}{\pi^2\ E_F t_F\ K_s}\right]^{1/2} - t_F$$

The corrugation spacing b_c is given by equation C12.10.4.

C12.10.6 Design of Sandwich Cylinders.

Assuming that a design begins with a given load to transmit and chosen design stresses, a cylinder with walls of sandwich construction under axial compression load shall be designed to comply with the following five conditions:

(1) The facings shall be at least thick enough to withstand the chosen design compressive stresses.

(2) The core shall be thick enough and have a shear modulus high enough so that buckling of the sandwich cylinder walls will not occur under the design compression load.

(3) The core shall have high enough moduli of elasticity, and the sandwich shall have great enough flatwise tensile and compressive strength so that wrinkling of either facing will not occur. (Design procedure given in Section C12.10.3.)

(4) If the core is of honeycomb type and dimpling of the facing is not permissible, the cell size shall be small enough so that dimpling of either facing into the core cells will not occur. (Design procedure given in Section C12.10.2.)

(5) The entire cylinder shall have sufficient bending stiffness so that buckling as a long column will not occur.

These five conditions must be met. Buckling of the cylinder or the sandwich walls, or dimpling or wrinkling of the facings, cannot occur without possible total collapse of the cylinder. Detailed procedures giving theoretical formulas and graphs for determining dimensions of the facings and core, as well as necessary core properties, are given in the following paragraphs. Double formulas are given, one formula for sandwich with facings of different materials and thicknesses and another formula for sandwich with each facing of the same material and thickness. Facing modulus of elasticity, E'_F, and stress values, F_c, shall be compression values at the condition of use, that is, if application is at elevated temperature; then facing properties at elevated temperature shall be used in design. The facing modulus of elasticity is the effective value at the facing stress. If this stress is beyond the proportional limit value, an appropriate tangent, reduced, or modified compression modulus of elasticity shall be used.

C12.10.6.1 Determining Facing Thicknesses and Panel Parameters for Cylinder in Axial Compression.

$$t_{F_1}F_{c_1} + t_{F_2}F_{c_2} = N \text{ (for unequal facings)} \quad - - - - - \text{(C12.10.21)}$$

$$t_F = \frac{N}{2F_c} \text{ (for equal facings)} \quad - - - \text{(C12.10.22)}$$

where t_F is facing thickness; F_c is chosen design facing compressive stress; N is design compression load per inch of cylinder circumference; and $_1$, $_2$, are subscripts denoting facings 1 and 2.

In determining thicknesses of facings of different materials, equation C12.10.21 must be satisfied, but also the stresses F_{c_1} and F_{c_2} must be chosen so that $F_{c_1}/E_{s_1} = F_{c_2}/E_{s_2}$ (where E_s is facing secant modulus of elasticity), thus avoiding overstressing of either facing. For example, if facing 1 is a material such that the ratio $F_{c_1}/E_{s_1} = 0.005$ and facing 2 is a material such that the ratio $F_{c_2}/E_{s_2} = 0.002$, the design must be based on a ratio of 0.002, otherwise facing 2 will be overstressed. In order to accomplish this, the chosen design stress for facing 1 must be lowered.

If the cylinder is long and slender and the radius is limited, the facing thicknesses may have to be increased in order to prevent column buckling.

This section also gives procedures for determining core thickness and core shear modulus so that overall buckling of the sandwich walls of the cylinder will not occur. The procedures are applicable to cylinders longer than the length of one ideal buckle such as would form in the wall of a long cylinder. Generally, the ideal buckle length is about equal to the radius of the cylinder if the core shear modulus is high. It becomes shorter than the radius as the core shear modulus decreases. For cylinders shorter than the ideal buckle length the load at which buckling of the wall occurs will be higher than given here.

The facing stress at which buckling of the sandwich wall will occur is given by the theoretical formula C12.6.5.

The core shear modulus can be determined by the local failure criteria discussed in Section C12.10.3 by deriving the relationship of core density t_c/s given by equation C12.10.6.

$$\frac{t_c}{s} = .5\left[\frac{1.35\,F_c}{(E_F\eta_2^3\,E_cG_c)^{1/3}}\right]^{1.015}$$

The core depth or thickness c must be derived from the buckling stress equation C12.6.5 as follows:

$$\frac{F_{x_{cr}}}{\eta} = \frac{K_x}{J_c}\frac{U}{2t_F}$$

$$K_x = \frac{(m^2 + n^2\beta_1^2)^2}{m^2\left[1 + \frac{m^2 + n^2\beta_1^2}{J_c}\right]} + \frac{.0374m^2\left[\frac{L^2}{R\,(c + t_F)}\right]^2}{(m^2 + n^2\,\beta_1^2)^2}$$

$$J_c = \frac{L^2U}{\pi^2 D} \qquad U = G'_c\,(c + 2t_F)$$

$$D = \frac{E_Ft_F\,(c + t_F)^2}{2\,(1 - \mu^2)} \qquad \beta_1 = L/2\pi R$$

$$\frac{F_{x_{cr}}}{\eta} = \left[\frac{(m^2 + n^2\,\beta_1^2)^2}{m^2\left[1 + \frac{m^2 + n^2\beta_1^2}{J_c}\right]} + \frac{.0374m^2\left[\frac{L^2}{R(c + t_F)}\right]^2}{(m^2 + n^2\,\beta_1^2)^2}\right] \frac{\pi^2\,E_F\,(c + t_F)^2}{L^2\,4(1 - \mu^2)}$$

$$\frac{F_{x_{cr}}}{\eta} = \left[\frac{(m^2 + n^2\beta_1^2)^2}{m^2\left[1 + \frac{\pi^2E_Ft_F(c + t_F)^2(m^2 + n^2\beta_1^2)}{2L^2\,G'_c\,(c + 2t_F)\,(1 - \mu^2)}\right]} + \frac{.0374\,L^4\,m^2}{R^2(c + t_F)^2(m^2 + n^2\beta_1^2)^2}\right] \times \frac{\pi^2\,E_F\,(c + t_F)^2}{4L^2\,(1 - \mu^2)}$$

$$m^2 + n^2\beta_1^2 = M$$

$$\frac{F_{x_{cr}}}{\eta} = \left[\frac{M^2}{m^2\left[\frac{1}{(c+t_F)^2} + \frac{\pi^2 E_F t_F M}{2L^2 G'_c (c+2t_F)(1-\mu^2)}\right] + \frac{.0374\, L^4 m^2}{R^2 M^2}}\right] \frac{\pi^2 E_F}{4L^2(1-\mu^2)}$$

$$m^2\left[\frac{F_{x_{cr}}}{\eta} - \frac{.00935\, L^2 \pi^2 m^2 E_F}{R^2 M^2 (1-\mu^2)}\right] = \frac{M^2}{\left[\frac{4L^2(1-\mu^2)}{\pi^2 E_F (c+t_F)^2} + \frac{2t_F M}{G'_c (c+2t_F)}\right]}$$

$$\text{if} \quad \frac{4L^2(1-\mu^2)}{\pi^2 E_F} = \left[\ \right], \quad \frac{2t_F M}{G'_c} = \left\{\ \right\}$$

and

$$m^2\left[\frac{F_{x_{cr}}}{\eta} - \frac{.00935\, L^2 m^2 \pi^2 E_F}{R^2 M^2 (1-\mu^2)}\right] = \frac{M^2}{(\ )}$$

$$c^3(\ ) + c^2\left[4t_F(\ ) - \left\{\ \right\}\right] + c\left[5t_F^2(\ ) - 2t_F\left\{\ \right\} - \left[\ \right]\right] + \left[2t_F^3(\ ) - t_F^2\left\{\ \right\} - 2t_F\left[\ \right]\right] = 0 \quad \text{- - - - - - - - - - - - - (C12.10.16)}$$

C12.10.6.2 Determining Facing Thickness and Panel Parameters for Cylinders in Torsion.

$$(t_{F_1}F_{S_1} + t_{F_2}F_{S_2}) = \frac{T}{2A} \quad \text{(unequal facings, approx. for large R/c)} \quad \text{- - - - - (C12.10.23)}$$

$$t_F = \frac{T}{4A\,F_S} \quad \text{(equal facings)} \quad \text{- - - - (C12.10.24)}$$

$$(t_{F_1}F_{S_1}R_1^2 + t_{F_2}F_{S_2}R_2^2) = \frac{T}{2\pi} \quad \text{(unequal facings, for low R/c ratio)} \quad \text{- - - - - (C12.10.25)}$$

where t_F is facing thickness; F_S is chosen design facing shear stress; T is design torsional load on cylinder; 1, 2, are subscripts denoting facing 1 and 2; A is inclosed area of cylinder; and R is radius of cylinder.

In determining thickness of facings of different materials, equation C12.10.23 and C12.10.25 must be satisfied, but also the stresses F_{S_1} and F_{S_2} must be chosen so that $F_{S_1}/G_{S_1}R_1 = F_{S_2}/G_{S_2}R_2$ (where G_S is the facing shear modulus).

The core shear modulus can be determined by the local failure criteria discussed in Section C12.10.3 by deriving the relationship of core density t_c/s as in Section C12.10.5.2.

$$\frac{t_c}{s} = .5\left[\frac{1.35\, F_S}{(E_F \eta_2^3 E_c G_c)^{1/3}}\right]^{1.015}$$

The core depth or thickness c must be derived from the buckling stress equation C12.6.8 similar to the derivation of equation C12.10.10.

$$c = \left[\frac{4\, F_S L^2 (1-\mu^2)}{\pi^2 K_S \eta E_F}\right]^{1/2} - t_F \quad \text{- - (C12.10.26)}$$

C12.10.6.3 Determining Facing Thickness and Panel Parameters for Cylinders Under Lateral Pressure.

$f_X = \frac{PR}{4t_F}$ longitudinal stress

$f_y = \frac{PR}{2t_F}$ circumferential stress

$$t_F = \frac{PR}{2F_y} \quad \text{(equal facings)} \quad \text{- - - - (C12.10.27)}$$

$$t_{F_1}F_{y_1} + t_{F_2}F_{y_2} = \frac{PR}{2} \quad \text{(unequal facings)} \quad \text{- - - - (C12.10.28)}$$

where t_F is facing thickness; F_y is chosen design facing circumferential compression stress compatible with F_X equal .5 F_y; P external lateral positive pressure; R external radius of cylinder; and 1, 2, are subscripts denoting facings 1 and 2.

In determining thickness of facings of different materials equation C12.10.28 must be satisfied, but also the stresses F_{y_1} and F_{y_2} must be chosen so that $F_{y_1}/E_{S_1} = F_{y_2}/E_{S_2}$ (where E_S is the secant modulus of elasticity).

The core shear modulus can be determined by the local failure criteria discussed in Section C12.10.3 by deriving the relationship of core density t_c/s similar to that given by equation C12.10.6 with the exception that equation C12.5.13 must be used in place of C12.5.10.

$$\frac{t_c}{s} = .5\left[\frac{1.35\, F_y (1+\gamma^3)^{1/3}}{(E_F \eta_2^3 E_c G_c)^{1/3}}\right]^{1.015}$$

where γ in this case $= \frac{f_y}{f_X} = 2$

$$\frac{t_c}{s} = .5\left[\frac{2.81\, F_y}{(E_F \eta_2^3 E_c G_c)^{1/3}}\right]^{1.015}$$

The core depth of thickness c must be derived from the buckling stress equation C12.6.10 similar to the derivation of equation C12.10.16.

$$c^3 ( ) + c^2 \left[4t_F ( ) - \{ \} \right] + c \left[5t_F^2 ( ) - 2t_F \{ \} - [ ] \right] + \left[2t_F^3 ( ) - t_F^2 \{ \} - 2t_F [ ] \right] = 0$$

where,

$$[ ] = \frac{4L^2 (1 - \mu^2)}{\pi^2 E_F} \quad , \quad \{ \} = \frac{2t_F M}{G'_c}$$

$$( ) = \frac{M^2}{n^2 \beta_1^2 \left[\frac{F_y}{\eta} - \frac{.00935 L^2 \pi^2 E_F}{n^2 {}^2R^2M^2 (1 - \mu^2)} \right]}$$

$$M = 1 + n^2 \beta_1^2$$

C12.11.1 Example Problem.

The following example problem illustrates the method of computing the honeycomb panel design parameters when loaded in uniaxial compression.

Given:

1. Materials: PH15-7Mo (RH 1050) at R.T.

2. Properties: $E_F = 30 \times 10^6$ psi
   $E_c = 30 \times 10^6$ psi
   $G_c = 10 \times 10^6$ psi
   $F_{cy} = 190{,}000$ psi
   $\mu = .3$

3. Geometry and Load:
   a = 20 in.
   b = 20 in.
   N = 6000 lb/in.
   F_c = 190,000 psi
   Equal facings
   Simply Supported Panel

Calculate:

1. $t_F = \frac{N}{2F_c} = \frac{6000}{2 \times 190{,}000} = .016$ in.

2. $\eta = .32$ Ref. Fig. C12.5.2b

3. $\eta_s = .7$ Ref. Fig. C12.5.7b

4. $\frac{t_c}{s} = .5 \left[\frac{1.35 F_c}{(E_F \eta_s^3 E_c G_c)^{1/3}} \right]^{1.015}$ Ref. Eq. C12.10.6

$$\frac{t_c}{s} = .5 \left[\frac{1.35 \times 190000}{(30 \times 10^6 \times .343 \times 30 \times 10^6 \times 10 \times 10^6)^{1/3}} \right]^{1.015}$$

$$\frac{t_c}{s} = .0083$$

5. $G'_c = 2.43 \left(\frac{2t_c}{s}\right)^{1.54} G_c$ Ref. Equations C12.4.9 and C12.4.4

$G'_c = 2.43 (.0166)^{1.54} \times 10 \times 10^6 = 43800$ psi

6. Assume J = 10

   $K_c = 3.3$ Ref. Fig. C12.5.10

7. $c = \left[\frac{4 F_c b^2 (1 - \mu^2)}{\pi^2 K_c \eta E_F} \right]^{1/2} - t_F$ Ref. Eq. C12.10.10

$$c = \left[\frac{4 \times 190000 \times 400 \times .91}{\pi^2 \times 3.3 \times .32 \times 30 \times 10^6} \right]^{1/2} - .016$$

$c = .924$ in.

8. $J = \frac{b^2 G'_c (c + 2t_F) 2(1 - \mu^2)}{\pi^2 E_F t_F (c + t_F)^2}$

$$J = \frac{400 \times 43800 (.924 + .032) 2(.91)}{\pi^2 \times 30 \times 10^6 \times .016 (.924 + .016)^2}$$

$J = 7.28$

$K_c = 3.05$ Ref. Fig. C12.5.10

9. Recalculate c
   $c = .964$ in.

10. Recalculate J
    $J = 7.33$
    $K_c = 3.05$

11. Recalculate c
    $c = .964$ in.

12. Plot J assumed vs. J calculated

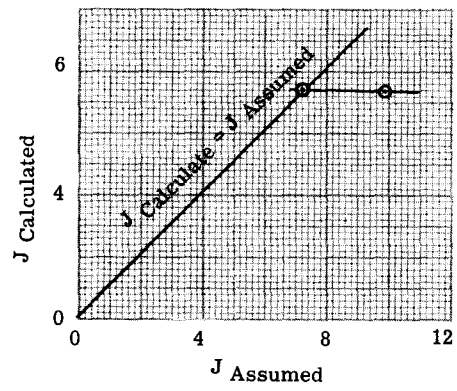

Pick J = 7.33 from plot intersection

$K_c = 3.05$

14. Recalculate c

c = .964 in.

15. c is now sufficiently converged to use c = .964 as final answer.

16. Check panel for shear crimping

$$F_{cs} = \frac{G'_c\ (c + 2t_F)}{2t_F}$$ Ref. Eq. C12.5.18

$$F_{cs} = \frac{43{,}800\ (.964 + .032)}{.032} = 1{,}365{,}000 \text{ psi}$$

Shear crimping will not occur.

17. Compute maximum core cell size and foil thickness.

$$s = .825\ t_F\ (F_c/E_F\eta)^{-2/3}$$ Ref. Eq. C12.10.1

$$s = .825 \times .016\ (\frac{30 \times 10^6 \times .32}{190000})^{2/3} = .181 \text{ in.}$$

$$t_c = .0083 \times .181 = .0015 \text{ in.}$$

These values must be adjusted for practical design to meet available material sizes.

C12.11.2 Example Problem.

The following example problem illustrates the method of computing the honeycomb panel design parameters when loaded in biaxial compression and shear.

Given:

1. Material: PH15-7Mo (RH1050) at R.T.

2. Properties: $E_F = 30 \times 10^6$ psi
   $E_c = 30 \times 10^6$ psi
   $G_c = 10 \times 10^6$ psi
   $F_{cy} = 190000$ psi
   $\mu = .3$

3. Geometry and Load
   a = 20 in.
   b = 10 in.
   $N_x = 5000$ lb./in.
   $N_y = 2000$ lb./in.
   $N_{xy} = 2000$ lb./in.
   $F_{c_{max}} = 120000$ psi

Equal Facings

Panel edges simply supported

Calculate:

1. $$N_n = \frac{N_x + N_y}{2} \pm \sqrt{(\frac{N_x - N_y}{2})^2 + N_{xy}^2}$$ Ref. Eq. 10, Sec. C1.6

$$N_n = \frac{5000 + 2000}{2} \pm \sqrt{(\frac{5000 - 2000}{2})^2 + (2000)^2}$$

$N_n = 6000$ lb./in.

2. $$t_F = \frac{N_n}{2F_{c_{max}}} = \frac{6000}{2 \times 120000} = .025 \text{ in.}$$

3. $\frac{F_{c_{max}}}{F_{cy}} = .631$ $\eta_s = .985$ Ref. Fig. C12.5.7b

4. $$\frac{t_c}{s} = .5 \left[\frac{1.35\ F_{c_{max}}}{(E_F \eta_s^3 E_c G_c)^{1/3}}\right]^{1.015}$$ Ref. Eq. C12.10.6

$$\frac{t_c}{s} = .5\left[\frac{1.35 \times 120000}{(30 \times 10^6 \times .956 \times 30 \times 10^6 \times 10 \times 10^6)^{1/3}}\right]^{1.015}$$

$$\frac{t_c}{s} = .00368$$

5. Check face wrinkling allowable Ref. Section C12.5.3.4.

$$f_x = \frac{N_x}{2t_f} = \frac{5000}{2 \times .025} = 100000 \text{ psi}$$

$$f_{xy} = f_y = \frac{2000}{2 \times .025} = 40000 \text{ psi}$$

$$\frac{s}{t_c} = 272$$

$$\frac{F_{cw}}{\eta_s} = \frac{F_{sw}}{\eta_s} = 123000$$ Ref. Fig. C12.5.7a or Eq. C12.5.10

$$\gamma = \frac{f_y}{f_x} = \frac{40000}{100000} = .4$$

$$\gamma_1 = \sqrt{1 - \gamma + \gamma^2} = .872$$ (See page C12.52)

$$\frac{F_{cw_x}}{\eta_s} = \frac{F_{cw}}{\eta_s \sqrt[3]{1 + \gamma^3}} = 120500 \text{ psi}$$

$F_{cw_x} = 118500$ psi Ref. Fig. C12.5.7b

$\gamma_1 = \sqrt{3}$ for $\frac{F_{sw}}{\eta_s}$

$F_{sw} = 97200$ psi Ref. Fig. C12.5.7b
Ref. Example Prob. C12.5.3.2

$$M.S. = \frac{2}{R_a + \sqrt{R_a^2 + 4R_s^2}} - 1$$

$$R_a = \frac{f_x}{F_{cw_x}} = \frac{100000}{118500} = .84$$

$$R_s = \frac{f_s}{F_{sw}} = \frac{40000}{97200} = .41$$

$$M.S. = \frac{2}{.84 + \sqrt{.84^2 + 4 \times .41^2}} - 1 = \underline{-.004}$$

The M.S. is sufficiently close to zero to use $t_c/s = .00368$. Had the M.S. been too large or more negative, a change in .00368 would be required as follows.

$$\left(\frac{t_c}{s}\right)_{new} = \left(\frac{t_c}{s}\right)_{old} \left(\frac{1}{M.S. + 1}\right)$$

6. $G'_c = 2.43 \left(\frac{2t_c}{s}\right)^{1.64} G_c$ Ref. Eq.C12.4.9 & & C12.4.4

$G'_c = 2.43(.00736)^{1.64}\ 10 \times 10^6 = 12600$ psi

7. Assume $J = 1.0$, $K_x = 1.0$ Ref. Fig. C12.5.18

$K_s = 1.0$ Ref. Fig. C12.5.15

8. $\lambda = \frac{f_s}{f_x} = .4$

$$K_\lambda = \frac{1}{2\lambda^2 (K_x/K_s)^2} \left\{ -1 + \left[1 + (2\lambda \frac{K_x}{K_s})^2 \right]^{1/2} \right\}$$

Ref. Eq. C12.5.26

$$K_\lambda = \frac{1}{2 \times .16 \left(\frac{1.0}{1.0}\right)^2} \left\{ -1 + \left[1 + \left(\frac{2 \times .4 \times 1.0}{1.0}\right)^2 \right]^{1/2} \right\} = .878$$

9. $\gamma_1 = (1 - .4 + .16 + 3 \times .16)^{1/2} = 1.114$

Ref. Fig. C12.5.23

$$\gamma_1 F_{x_{max}} = \frac{1.114 \times 5000}{2 \times .025} = 111400 \text{ psi}$$

$$\frac{F_x \gamma_1}{F_{cy}} = .587$$

$$\frac{F_{cy}\, \eta}{\gamma_1 F_{x_{max}}} = 1.68 \quad \text{Ref. Fig. C12.5.2b}$$

$$\frac{F_{x_{max}}}{\eta} = \frac{F_{cy}}{1.68 \gamma_1} = 101500 \text{ psi}$$

10. $$c = \left[\frac{4\, F_{x_{max}} b^2 (1 - \mu^2)}{\pi^2 K_x K_\lambda \eta E_F} \right]^{1/2} - t_F$$

Ref. Eq. C12.10.10

$$c = \left[\frac{4 \times 101500 \times 1.00 \times .91}{\pi^2\ 1.0 \times .878 \times 30 \times 10^6} \right]^{1/2} - .025$$

$c = .347$ in.

11. $$J = \frac{b^2 G'_c\ (c + 2t_F)\ 2\ (1 - \mu^2)}{\pi^2\ E_F t_F\ (c + t_F)^2}$$

$$J = \frac{100 \times 12600 \times (.347 + .050)\ 2\ (.91)}{\pi^2\ 30 \times 10^6 \times .025\ (.347 + .025)^2}$$

$J = .89$

$K_x = .85$ $K_s = .89$

12. $K_\lambda = .88$

$c = .377$ in.

$J = .82$

From a plot of J assumed vs. J calculated, choose $J = .72$ as next value.

$c = .417$ in.

$J = .74$

The value of J has converged sufficiently close to $J_{assume} = J_{cal.}$ to use $c = .41$.

13. Check shear crimping

$$F_{cs} = \frac{G'_c\ (c + 2t_F)}{2t_F} \quad \text{Ref. Eq. C12.5.18}$$

$$F_{cs} = \frac{12600\ (.41 + .050)}{.050} = 116000 \text{ psi}$$

Shear crimping is critical and t_c/s or c must be adjusted to prevent this failure mode.

14. Adjust $\frac{t_c}{s}$

$$\frac{t_c}{s} = .5 \left[\frac{F_{c_{max}} t_F}{1.21\ G_c\ (c + 2t_F)} \right]^{.65} \quad \text{Ref. Eq. C12.10.8}$$

$$\frac{t_c}{s} = .5 \left[\frac{120000 \times .025}{1.21 \times 10 \times 10^6\ (.41 + .050)} \right]^{.65}$$

$$\frac{t_c}{s} = .00375$$

15. Or adjust c

$$c = \frac{F_{c_{max}} t_F}{1.21 \left(\frac{2t_c}{s}\right)^{1.64} G_c} - 2t_F \quad \text{Ref. Eq. C12.10.7}$$

$$c = \frac{120000 \times .025}{1.21 \times .000531 \times 10 \times 10^6} - .050$$

$c = .416$ in.

16. The equation expressing the effective cross-sectional area of the panel is:

$$\text{Area/in.} = 2t_F + \frac{2t_c}{s} c$$

Since the increase in weight thus reflected by adjusting t_c/s or c is the least for an adjustment of c, the final configuration will be used as:

$t_F = .025$ in.

$\frac{t_c}{s} = .00368$

$c = .416$ in.

17. Compute maximum cell size s

$$\gamma = \frac{f_y}{f_x} = .4$$

$$F_{ci_x} = \frac{F_{ci}}{\sqrt[n]{1+\gamma^n}} \qquad n = 3 \qquad \text{Ref. Eq. C12.5.6}$$

$$\frac{F_{ci_x}}{\eta} = 1.02 \times .75 E_F \left(\frac{t_F}{s}\right)^{3/2}$$

$$\frac{F_{si}}{\eta} = .6 E_F \left(\frac{t_F}{s}\right)^{3/2}$$

$$\frac{F_{ci_x}}{.765} = \frac{F_{si}}{.6}$$

$$F_{ci_x} = F_{si}\ 1.275$$

$$\frac{f_x}{F_{ci_x}} + \left(\frac{f_s}{F_{si}}\right)^2 = 1 \qquad f_x = \frac{f_s}{.4}$$

$$\frac{f_s}{F_{si}\ .51} + \left(\frac{f_s}{F_{si}}\right)^2 = 1$$

$$1.96 \frac{f_s}{F_{si}} + \left(\frac{f_s}{F_{si}}\right)^2 = 1$$

$$\frac{f_s}{F_{si}} = \frac{-1.96 \pm \sqrt{(1.96)^2 + 4}}{2} = .42$$

$f_s = 40000$ psi $\therefore F_{si} = 95000$ psi

$\gamma_1 = \sqrt{3}$ (See page C12.52)

$$\frac{F_{cy}\eta}{\gamma_1 F_{si}} = .74 \qquad \text{Ref. Fig. C12.5.2b; Ref. Sample Prob. C12.5.2.2}$$

$$\frac{F_{si}}{\eta} = \frac{190000}{1.73 \times .74} = 148000 \text{ psi}$$

$$S_{max} = .71 t_F (F_{si}/\eta E_f)^{-2/3} \qquad \text{Ref. Eq. C12.10.2}$$

$$S_{max} = .71 \times .025 \left(\frac{30 \times 10^6}{148000}\right)^{2/3}$$

$S_{max} = .61$ in.

A standard cell size of .50 in. would be used.

18. Core foil thickness t_c would be:

$t_c = .50 \times .00368 = .00184$ in.

If this foil thickness had been below the standard minimum of .001 in. a new $t_{c/s}$ and c would be calculated as follows:

$$\therefore \frac{t_c}{s} = \frac{.001}{.50} = .002$$

19. $$c = \frac{F_c\ t_F}{1.21 \left(\frac{2t_c}{s}\right)^{1.64} G_c} - 2t_F$$

This c must then be compared with c calculated from the buckling equation to insure a satisfactory configuration. The final configuration for this design problem is:

$t_F = .025$

$t_c = .00184$

$s = .50$

$c = .416$

C12.11.3 Example Problem.

The following example problem illustrates the method of computing the honeycomb panel design parameters when loaded in bending by a loaded insert at the center of the panel.

Given:

1. Material: PH15-7Mo (RH1050) at R.T.

2. Properties: $E_F = 30 \times 10^6$ psi
   $E_c = 30 \times 10^6$ psi
   $G_c = 10 \times 10^6$ psi
   $F_{cy} = 190000$ psi
   $F_{su} = 110000$ psi
   $\mu = .3$

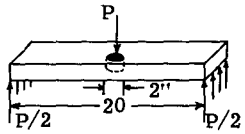

3. Geometry and Load:
   Panel beam span L = 20 in.
   Beam width b = 5 in.
   Load on insert = 10,000 lb.
   Insert size = 2 in. dia.
   Allowable bending deflection at center δ = 1.0 in.

$F_{c_{max}} = 150000$ psi

Simply supported beam

Calculate:

1. Deflection at center of panel is expressed by the following equation:

$$\delta = \frac{PL^3}{48E_S I} = 1.0 \text{ in.}$$

$$E_S = E_{secant} = \frac{E}{1 + \frac{3}{7}\left(\frac{F_c}{F_{cy}}\right)^8} \text{ (Ref.1, Sec.C.2) (Ref. Sec. C2.4)}$$

2. Maximum bending stress is expressed by:

$$f_b = \frac{M}{I}\left(\frac{c + t_F}{2}\right) = 150000 \text{ psi}$$

$$M = \frac{P}{2} \times \frac{L}{2} = \frac{10000 \times 20}{4} = 50000 \text{ in. lb.}$$

$$I = 2t_F b\left(\frac{c + t_F}{2}\right)^2$$

3. Combine equations for δ and f_b and solve for t_F

$$\delta = \frac{PL^3}{24E_S t_F (c + t_F)^2 b} = 1.0 \text{ in.}$$

$$f_b = \frac{M}{t_F b(c + t_F)} = 150000 \text{ psi}$$

$$c = \left[\frac{PL^3}{\delta 24 E_S t_F b}\right]^{1/2} - t_F, \quad c = \frac{M}{150000 t_F b} - t_F$$

$$\left[\frac{PL^3}{\delta 24 E_S t_F b}\right]^{1/2} = \frac{M}{150000\, t_F b}$$

$$t_F = \left[\frac{M}{150000}\right]^2 \frac{24E_S\delta}{PL^3 b}$$

$$E_S = \frac{30 \times 10^6}{1 + \frac{3}{7}\left(\frac{150000}{190000}\right)^8} = 28.5 \times 10^6 \text{ psi}$$

$$t_F = \left(\frac{50000}{150000}\right)^2 \frac{24 \times 28.5 \times 10^6}{10000 \times 8000 \times 6} = .105 \text{ in.}$$

$$c = \frac{M}{150000 t_F} - t_F = \frac{50000}{150000 \times .105 \times 5} - .105 = .527 \text{ in.}$$

4. Compute core shear at end of beam.

$$f_{sc} = \frac{P}{2cb} = \frac{5000}{.527 \times 5} = 1900 \text{ psi}$$

5. Compute core requirements.

$$F'_s = 1.307\left(\frac{2t_c}{s}\right)^{1.34} \frac{F_{su}}{c^{.44}} \quad \text{Ref. Eq. C12.4.7 \& C12.4.4}$$

$$\frac{t_c}{s} = \left[\frac{F'_s\, c^{.44}}{1.307\, F_{su}}\right]^{.747} \times .5$$

$$\frac{t_c}{s} = \left[\frac{.1900 \times .75}{1.307 \times 110000}\right]^{.747} \times .5 = .016$$

From braze shear strength compute cell size s.

$F_{s_{br}} = 26000$ psi

$$F'_s = 1.25\left(\frac{w}{s}\right) F_{s_{br}}$$

Fillet width w = .016

$$s = \frac{1.25\, w\, F_{s_{br}}}{F'_s}$$

$$s = \frac{1.25 \times .016 \times 26000}{1900} = .285 \text{ in.}$$

6. Compute core shear at insert.

$$f_{sc} = \frac{P\, I_m\, K}{\pi\, 2(c + t_F) I} \quad \text{Ref. Eq. C12.8.1}$$

$$I_m = \frac{t_F\,(c + t_F)^2}{2} \qquad I = I_m + \frac{t_F^3}{6}$$

Assume $a = \infty$ $K = 1.0$ Fig. C12.81

$$f_{sc} = \frac{P\,(c + t_F)\,K}{\pi\, 4\left[\frac{(c + t_F)^2}{2} + \frac{t_F^2}{6}\right]}$$

$$f_{sc} = \frac{10000 \times .632 \times 1.0}{\pi \times 4\left[.20 + .00184\right]} = 2490 \text{ psi}$$

Since the panel in this case is not supported on all sides, an adjustment must be made to the calculated stress. It will be assumed that shear is taken out over only 2/3 the circumference of the insert. The shear stress then becomes:

$$f_{s_c} = \frac{2490}{.667} = 3740 \text{ psi}$$

In this case then an increased core density is required locally around the insert and can be determined as above.

$t_c/s = .0317$

7. Check facing for face wrinkling.

$$\frac{F_{cw}}{\eta_s} = .43\sqrt[3]{E_F E_c G_c\, 5.1\left(\frac{2t_c}{s}\right)^{2.955}} \quad \text{Ref. Eq. C12.10.5}$$

$$\frac{F_{cw}}{\eta_e} = .43 \times \left[30 \times 10^6 \times 30 \times 10^6 \times 10 \times 10^6 \times 5.1 \times .000035\right]^{1/3}$$

$$\frac{F_{cw}}{\eta_e} = 502000 \text{ psi}$$

F_{cw} = 190000 psi Ref. Fig. C12.5.7b

$$M.S. = \frac{190000}{150000} - 1 = \underline{\underline{.26}}$$

8. Check facing for intercell buckling or dimpling.

$$\frac{F_{ci}}{\eta} = .75\, E_F\, (t_F/s)^{3/2} \quad \text{Ref.Eq.C12.5.1}$$

$$\frac{F_{ci}}{\eta} = .75 \times 30 \times 10^6 \left(\frac{.105}{.285}\right)^{3/2} = 5020000 \text{ psi}$$

F_{ci} = 190000 psi Ref. Fig. C12.5.2b

$$M.S. = \frac{190000}{150000} - 1 = \underline{\underline{.26}}$$

C12.11.4 Example Problem.

The following example problem illustrates the method of computing the corrugated panel design parameters when loaded in axial compression.

Given:

1. Materials: 7075-T6 Aluminum
2. Properties: $E = 10 \times 10^6$ psi
   $G_c = 4 \times 10^6$ psi
   $F_{cy} = 70000$ psi
   $\mu = .3$
   $G'_{cy} = 55000$ psi
3. Geometry and Load:
   $a = 20$ in.
   $b = 20$ in.
   $N = 4000$ lb./in.
   $F_{c_{max}} = 60000$ psi

   For axial compression loads, the thickness of the facings will be equal to the thickness of the corrugations. The optimum angle of the corrugation will be $\theta = 60^0$.

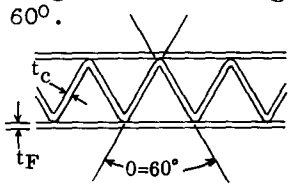

The panel is simply supported.

Calculate:

1. $$f_c = \frac{N}{2t_F + \frac{t_F}{\cos 60^0}}$$

$$t_F = \frac{N}{F_c \left(2 + \frac{1}{\cos 60^0}\right)}$$

$$t_F = \frac{4000}{60000 \times 4} = .0167 \text{ in.}$$

2. Compute the corrugation depth c

$$c = \left[\frac{2N_x\, b^2\, (1 - \mu^2)}{K_x\, \pi^2\, E_F\, t_F}\right]^{1/2} - t_F \quad \text{Ref. Eq. C12.10.18}$$

Assume $J = 5$, $K_x = 3.3$ Ref.Fig.C12.9.2

$$c = \left[\frac{2 \times 4000 \times 400\ (.91)}{3.3 \times \pi^2 \times 10 \times 10^6 \times .0167}\right]^{1/2} - .0167$$

$c = .720$ in.

$$J = \frac{b^2\, G'_{cy} c\, (1 - \mu^2)\, 2}{\pi^2\, E_F t_F\, (c + t_F)^2}$$

$$J = \frac{400 \times 55000 \times .720 \times .91 \times 2}{\pi^2\, 10 \times 10^6 \times .0167 \times .542} = 32.2$$

$K_x = 3.9$ Ref. Fig. C12.9.2

$c = .659$ in., $J = 34.8$

$K_x = 3.90$ Ref. Fig. C12.9.2

$c = .659$ in.

c has been sufficiently converged to use the value of c = .659 in.

The panel configuration is then:

$t_F = .0167$ in., $c = .659$ in.

$a = b = 20$ in., $\theta = 60^0$

3. Check for buckling of the facings between corrugations.

$$F_{cr} = K_c E_F \left(\frac{t_F}{b}\right)^2$$

$$K_c = 4 \qquad b = \frac{c}{\sin 60^0} = .76 \text{ in.}$$

$$F_{cr} = 4 \times 10 \times 10^6 \left(\frac{.0167}{.76}\right)^2 = 17100 \text{ psi}$$

$$M.S. = \frac{17100}{60000} - 1 = \underline{\underline{-.715}}$$

The inter-corrugation buckling is unsatisfactory. The facing thickness and core depth must be changed.

$$F_{cr} = F_c = \frac{N_x}{2t_F + \frac{t_F}{\cos 60^\circ}} = K_c E_F \left(\frac{t_F \sin 60^\circ}{c}\right)^2$$

$$c = \left[\frac{K_c E_F \left(2t_F + \frac{t_F}{\cos 60^\circ}\right)}{N_x}\right]^{1/2} t_F \sin 60^\circ$$

Set this c equal to c derived from the buckling equation C12.10.18.

$$\left[\frac{K_c E_F (2t_F + \frac{t_F}{\cos 60^\circ})}{N_x}\right]^{1/2} t_F \sin 60^\circ = \left[\frac{2N_x b^2 (1 - \mu^2)}{K_x \pi^2 E_F t_F}\right]^{1/2} - t_F$$

$$t_F^{1.5} \left[\frac{K_c E_F \left(2 + \frac{1}{\cos 60^\circ}\right)}{N_x}\right]^{1/2} \sin 60^\circ + t_F - \frac{1}{t_F^{.5}} \left[\frac{2 N_x b^2 (1 - \mu^2)}{K_x \pi^2 E_F}\right]^{1/2} = 0$$

$$170\, t_F^{1.5} + t_F - .0619 \frac{1}{t_F^{.5}} = 0$$

$$170\, t_F^2 + t_F^{1.5} = .0619$$

$$t_F^{1.5} (170\, t_F^{.5} + 1) = .0619$$

Plot this equation to solve for t_F.

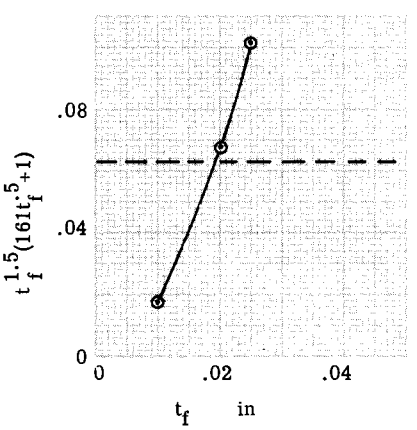

t_F = .0190 in.

$$c = \left[\frac{K_c E_F t_F \left(2 + \frac{1}{\cos 60^\circ}\right)}{N_x}\right]^{1/2} t_F \sin 60^\circ$$

$$c = \left[\frac{4 \times 10 \times 10 \times .0190 \times 4}{4000}\right]^{1/2} .0195 \times .867$$

c = .46 in.

C12.11.5 Example Problem.

The following example problem illustrates the method of computing the corrugated panel design parameters when loaded in axial compression and shear.

Given:

1. Material: PH15-7Mo (RH1050) at R.T.
2. Properties: $E_F = 30 \times 10^6$ psi
   $G_c = 10 \times 10^6$ psi
   $F_{cy} = 190000$ psi
   $\mu = .3$
   $G'_{cy} = 150000$ psi
3. Geometry and Load:
   $b = 20$ in.
   $a = 40$ in.
   $\theta = 60^\circ$
   $N_x = 5000$ lb./in.
   $N_{xy} = 2000$ lb./in.
   $F_{c_{max}} = 160000$ psi

Assume facing thickness and corrugation thickness equal and the panels are simply supported.

Compute:

1. $f_c = \frac{N_x}{2t_F + \frac{t_F}{\cos 60^\circ}}$ Ref. Eq. C12.10.17

$$f_s = \frac{N_{xy}}{2t_F + t_F \cos \theta}$$ Ref. Eq. C12.10.20

It must be noted that only half the thickness of the corrugation is used to compute the shear stress. This accounts for an equal shear deformation in the facings and corrugations and the reduced effectiveness of the corrugation material because of its extra length.

$$f_{c_{max}} = \frac{f_c}{2} + \sqrt{\left(\frac{f_c}{2}\right)^2 + f_s^2}$$

$$f_{c_{max}} = \frac{N_x}{2t_F + \frac{t_F}{.5}} + \sqrt{\left(\frac{N_x}{2t_F + \frac{t_F}{.5}}\right)^2 + \left(\frac{N_{xy}}{2t_F + .5t_F}\right)^2}$$

$$f_{c_{max}} = \frac{N_x}{4t_F} + \sqrt{\frac{N_x^2}{16t_F^2} + \frac{N_{xy}^2}{6.25t_F^2}}$$

$$t_F = \frac{N_x}{4f_{c_{max}}} + \frac{1}{f_{c_{max}}}\sqrt{\frac{N_x^2}{16} + \frac{N_{xy}^2}{6.25}}$$

$$t_F = \frac{5000}{4 \times 160000} + \frac{1}{160000}\sqrt{\frac{25 \times 10^6}{16} + \frac{4 \times 10^6}{6.25}}$$

$t_F = .0171$ in.

2. Compute the corrugation depth c

$$N_x = \frac{K_x \pi^2 D}{b^2} \qquad N_{xy} = \frac{K_s \pi^2 D}{b^2}$$

$$\frac{N_x}{N_{xy}} = \frac{K_x}{K_s} = \frac{5000}{2000} = 2.5$$

Assume J = 20

$K_x = 3.6$ $K_s = 1.44$ Ref. Fig. C12.9.7c

$$c = \left[\frac{2N_x b^2 (1 - \mu^2)}{K_x \pi^2 E_F t_F}\right]^{1/2} - t_F \qquad \text{Ref. Eq. C12.10.18}$$

$$c = \left[\frac{2 \times 5000 \times 400 \ (.91)}{3.6 \times \pi^2 \times 30 \times 10^6 \times .0171}\right]^{1/2} - .0171$$

$= 1.398$ in.

$$J = \frac{b^2 G'_{cy} \ c \ (1 - \mu^2) 2}{\pi^2 E_F t_F (c + t_F)^2}$$

$$J = \frac{400 \times 150000 \times 1.398 \times .91 \times 2}{\pi^2 \times 30 \times 10^6 \times .0171 \times (1.398 + .0171)^2}$$

$J = 15.1$ $K_x = 3.5$ $K_s = 1.40$

$c = 1.413$ in. $J = 14.95$

$K_x = 3.5$

$c = 1.413$ in.

c is sufficiently converged to use c = 1.413 in.

3. Check for buckling of the facing between corrugations.

$$F_{cr} = K_c E_F \left(\frac{t_F}{b}\right)^2$$

$K_c = 4$ $\qquad b = \frac{c}{\sin 60^\circ} = 1.64$ in.

$$F_{cr} = 4 \times 30 \times 10^6 \left(\frac{.0171}{1.64}\right)^2 = 13100 \text{ psi}$$

$$F_{s_{cr}} = K_s E_F \left(\frac{t_F}{b}\right)^2$$

However, it is obvious that the panel will not meet the requirement of inter-corrugation buckling.

4. The combined stress equation is:

$$R_c + R_s^2 = 1$$

$$\frac{f_c}{F_{cr}} + \left(\frac{f_s}{F_{s_{cr}}}\right)^2 = 1$$

Solve for c:

$$\frac{N_x}{4t_F K_c E_F}\left(\frac{c}{t_F \sin 60^\circ}\right)^2 + \left[\frac{N_{xy}}{2.5t_F K_s E_F}\left(\frac{c}{t_F \sin 60^\circ}\right)^2\right]^2 = 1$$

$$c^4\left[\frac{N_{xy}}{2.5 \ t_F K_s E_F}\left(\frac{1}{t_F \sin 60^\circ}\right)^2\right]^2 + c^2\left[\frac{N_x}{4 \ t_F K_c E_F}\left(\frac{1}{t_F \sin 60^\circ}\right)^2\right] - 1 = 0$$

$$c^2 = -\frac{\left[\frac{N_x}{4 \ t_F K_c E_F}\left(\frac{1}{t_F \sin 60^\circ}\right)^2\right]}{2\left[\frac{N_{xy}}{2.5 \ t_F K_s E_F}\left(\frac{1}{t_F \sin 60^\circ}\right)^2\right]^2} \pm \frac{\sqrt{\left[\frac{N_x}{4t_F K_c E_F}\left(\frac{1}{t_F \sin 60^\circ}\right)^2\right]^2 + 4\left[\frac{N_{xy}}{2.5t_F K_s E_F}\left(\frac{1}{\sin 60^\circ}\right)^2\right]^2}}{2\left[\frac{N_{xy}}{2.5t_F K_s E_F}\left(\frac{1}{t_F \sin 60^\circ}\right)^2\right]^2}$$

$$c^2 = -\frac{\frac{N_x t_F E_F}{8K_c} + t_F E_F \sqrt{\left[\frac{N_x}{4K_c}\right]^2 + 4\left[\frac{N_{xy}}{2.5K_s}\right]^2}}{\left[\frac{N_{xy}}{2.5 \ K_s \ t_F \sin 60^\circ}\right]^2}$$

c from buckling eq. is: Ref. Eq.C12.10.18

$$c = \left[\frac{2 \ N_x b^2 (1 - \mu^2)}{K_x \pi^2 E_F \ t_F}\right]^{1/2} - t_F$$

5. Combine these equations and solve for t_F.

$$\left[\frac{2N_x b^2 (1 - \mu^2)}{K_x \pi^2 E_F \ t_F}\right]^{1/2} - t_F = \frac{\left[-\frac{N_x t_F E_F}{8K_c} + t_F E_F\left(\left[\frac{N_x}{4K_c}\right]^2 + 4\left[\frac{N_{xy}}{2.5 \ K_s}\right]^2\right)^{1/2}\right]^{1/2}}{\left[\frac{N_{xy}}{2.5 \ K_s \ t_F \sin 60^\circ}\right]}$$

$$\left[\frac{2\,N_x\,b^2\,(1-\mu^2)}{K_x\,\pi^2\,E_F\,t_F^3}\right]^{1/2} - \frac{4.66\,K_s^2}{N_{xy}^2}$$

$$\left[\frac{-\,N_x\,t_F\,E_F}{8\,K_c} + t_F\,E_F\left(\left[\frac{N_x}{4\,K_c}\right]^2 + 4\left[\frac{N_{xy}}{2.5\,K_s}\right]^2\right)^{1/2}\right]^{1/2} = 1 \quad \text{Eq. C12.11.1}$$

$K_x = 3.65 \qquad K_c = 4 \qquad K_s = 5.4$

Plot Equation C12.11.1 vs. t_F

$$\frac{.0581}{t_F^{1.5}} - 27.8\,t_F^{1/2} = 1$$

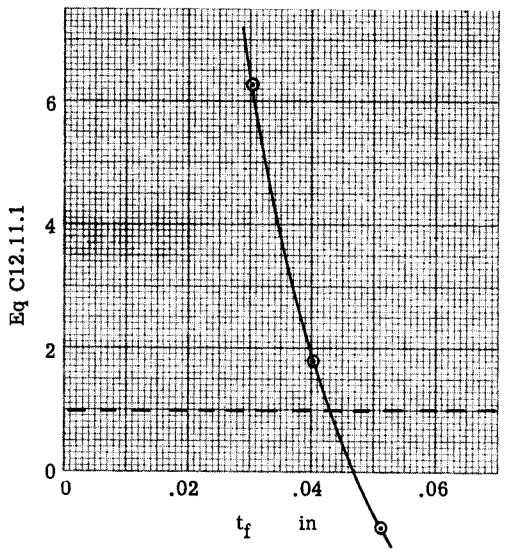

Select $t_F = .0425$ from intersertion of Equation C12.11.1 with 1.0

$$C = \left[\frac{2\,N_x\,b^2\,(1-\mu^2)}{K_x\,\pi^2\,E_F t_F}\right]^{1/2} - t_F$$

$$C = \left[\frac{2 \times 5000 \times 400 \times .91}{3.65 \times \pi^2 \times 30 \times 10^6 \times .0425}\right]^{1/2} - .0425$$

$C = .848$ in.

C12.11.6 Example Problem.

The following example problem illustrates the method of computing the honeycomb cylinder design parameters when loaded with an external lateral pressure.

Given:

1. Material: 2024-T4 Aluminum
   5052 Honeycomb core

2. Properties: $E_F = 10 \times 10^6$ psi
   $G_c = 4 \times 10^6$ psi
   $F_{cy} = 40000$ psi
   $\mu = .3$

3. Geometry and Load:
   $R = 25$ in.
   $L = 100$ in.
   $P = 20$ psi
   $F_y = 10000$ psi

Compute:

1. $t_F = \dfrac{PR}{2F_y}$ Ref. Eq. C12.10.27

$$t_F = \frac{20 \times 25}{2 \times 10000} = .025 \text{ in.}$$

2. Compute t_c/s Eq. from Section C12.10.6.3

$$\gamma = \frac{f_y}{f_x} = 2 \qquad \eta_2 = 1.0$$

$$\frac{t_c}{s} = .5\left[\frac{2.81\,F_y}{(E_F\,\eta_2^3\,E_c G_c)^{1/3}}\right]^{1.015}$$

$$\frac{t_c}{s} = .5\left[\frac{2.81 \times 10000}{(10 \times 10^6 \times 1.0 \times 10 \times 10^6 \times 4 \times 10^6)^{1/3}}\right]^{1.015}$$

$$\frac{t_c}{s} = .00131$$

3. Compute G_c' from Fig. C12.4.1.

$\rho_c' = 3\,\dfrac{t_c}{s}\,\rho_c$ Ref. Eq. C12.4.5

$\rho_c = .1$ lb./in.^{3}

$\rho_c' = 3 \times .00131 \times .1 \times 1728$

$\rho_c' = .679$ lb./ft.^{3}

Density too low use $\rho_c' = 2$ lb./ft.^{3}

$G_c' = 23000$ psi

4. Compute core depth c from equation of Section C12.10.6.3 when n = 6

$$M = 1 + n^2\,(\frac{L}{2\pi R})^2 = 1 + (\frac{2}{\pi})^2\,36 = 15.6$$

$$[\,] = \frac{4L^2\,(1-\mu^2)}{\pi^2 E_F} = \frac{4 \times 10000\,(.91)}{\pi^2 \times 10 \times 10^6}$$

$= .00368$

$$\left\{\ \right\} = \frac{2t_F M}{G'_c} = \frac{2 \times .05 \times 15.6}{23000} = 6.8 \times 10^{-5}$$

$$( ) = \frac{M^2}{n^2\beta^2\left[\frac{F_y}{\eta} - \frac{.00935\ L^2\ \pi^2\ E_F}{n^2\beta^2 R^2 M^2\ (1-\mu^2)}\right]}$$

$$( ) = \frac{243.5}{14.6\left[\frac{10000}{1} - \frac{.00935 \times 10000\ \pi^2 \times 10 \times 10^6}{14.6 \times 625 \times 243.5 \times .91}\right]}$$

$$( ) = .00306$$

Eq. C12.10.16

$$.00306\ c^3 + c^2\left[.01224\ t_F - 6.8 \times 10^{-5}\right] + c\left[.01530\ t_F^2 - 13.6 \times 10^{-5} t_F - .00368\right] + \left[.00612\ t_F^3 - t_F^2\ 6.8 \times 10^{-5} - .00736\ t_F\right] = 0$$

$$.00306\ c^3 + .000238\ c^2 - .00368\ c - .000184 = 0 \qquad \text{Eq. C12.11.2}$$

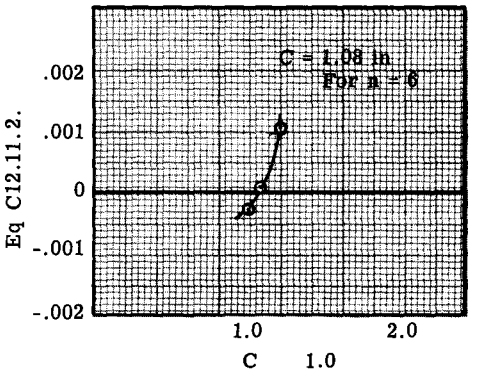

Different values of n must be investigated to obtain the largest value of c required. Only even values of n are applicable.

When n = 8 c = 1.09 in.

When n = 10 c = .92 in.

c = 1.09 in. must be used.

5. Compute the maximum cell size S using Equation C12.10.1.

$$S = .825\ t_F \left(\frac{F_c}{E\eta}\right)^{-2/3}$$

$$F_c = \gamma F_y = 2.0 \times 10000 = 20000 \text{ psi}$$

$$S = .825 \times .25 \left(\frac{20000}{10 \times 10^6 \times 1}\right)^{-2/3}$$

$$S = 1.25 \text{ in.}$$

Final configuration:

t_F = .025 in.

C = .92 in.

t_c/s = .00386

S_{max} = 1.25 in.

C12.11.7 Example Problem.

The example problems demonstrated to this point have designed the sandwich panel for a specific stress which the designer must select. In the case of many structural elements, the designer can select the design stress for an efficiently designed structure. However, in the case of sandwich type structures, the stress for the best efficiency cannot be chosen so easily. It can be demonstrated that the optimum stress level is a function of the applied load level. The following example problem will demonstrate a method of optimization and the direct determination of the optimum stress level. The method will be demonstrated on the design of a honeycomb column element.

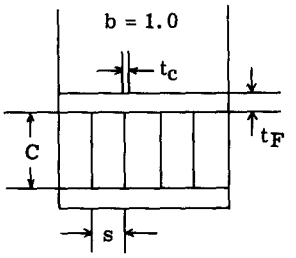

The weight or cross-sectional area equation for square cell honeycomb can be written as:

$$A = 2t_F + 2\frac{t_c}{s}\,c$$

The allowable stress equations used are:

$$F_{cw} = .43(E_F E_c G_c\ 5.1(\frac{2t_c}{s})^{2.955})^{1/3} \qquad \text{Ref. Eq. C12.10.5}$$

$$F_{cc} = \frac{\pi^2 E}{(L/\rho)^2} \qquad \rho^2 = \frac{I}{A}$$

L = Column length

$$I = 2t_F\ (\frac{c + t_F}{2})^2 = \frac{t_F}{2}\,(c^2 + 2ct_F + t_F^2)$$

$$\rho = \frac{(c^2 + 2ct_F + t_F^2)}{4}$$

$$f_{applied} = \frac{N}{2t_F}$$

$$F_{cw} = F_{applied} = \frac{N}{2t_F} = .43\ (E_F E_c G_c 5.1 \left(\frac{2t_c}{s}\right)^{2.955})^{1/3}$$

$$\frac{2t_c}{s} = \left[\frac{N}{.86\ t_F\ (E_F E_c G_c\ 5.1)^{1/3}}\right]^{1.015}$$

$$\frac{2t_c}{s} = \left[\frac{N}{t_F\ K_1}\right]^{1.015}$$

$$A = 2t_F + \left[\frac{N}{t_F\ K_1}\right]^{1.015} c$$

$$F_{cc} = f_{applied} = \frac{N}{2t_F} = \frac{\pi^2 E(c^2 + 2ct_F + t_F^2)}{4L^2}$$

$$c^2 + 2ct_F + t_F^2 = \frac{2\ NL^2}{\pi^2\ t_F\ E} = 0$$

$$c = -\ t_F + \frac{L}{\pi}\left(\frac{2N}{t_F\ E}\right)^{1/2}$$

$$A = 2t_F + \left[\frac{N}{t_F K_1}\right]^{1.015}\left[\frac{L}{\pi}\left(\frac{2N}{t_F E}\right)^{1/2} - t_F\right]$$

$$A = 2t_F + \frac{L}{\pi}\left(\frac{2}{E}\right)^{1/2} \frac{N^{1.515}}{t_F^{1.515} K_1^{1.015}} - \left(\frac{N}{K_1}\right)^{1.015} \frac{1}{t_F^{.015}}$$

The weight equation now in terms of a single variable can be differentiated to solve for minimum Area A.

$$\frac{dA}{dt_F} = 2 - \frac{L}{\pi}\left(\frac{2}{E}\right)^{1/2} \frac{N^{1.515}}{t_F^{2.515} K_1^{1.015}} + \left(\frac{N}{K_1 t_F}\right)^{1.015}$$

$$\frac{dA}{dt_F} = 2t_F^{2.515} - K_2 + K_3 t_F^{1.5} = 0$$

Solving this equation for t_F will give the t_F and stress level for minimum column weight or area.

The results of this equation for various load levels and column lengths are shown in Figure C12.11.1.

It can clearly be seen from Fig. C12.11.1 that for the lower load levels and for the 7075-T6 aluminum, the yield stress F_{cy} is not optimum. The curve also shows the effect of column length on the optimum stress level.

The optimization problem demonstrated here is a relatively simple problem. In this case the area equation was written explicitly in terms of the facing thickness t_F. For the case

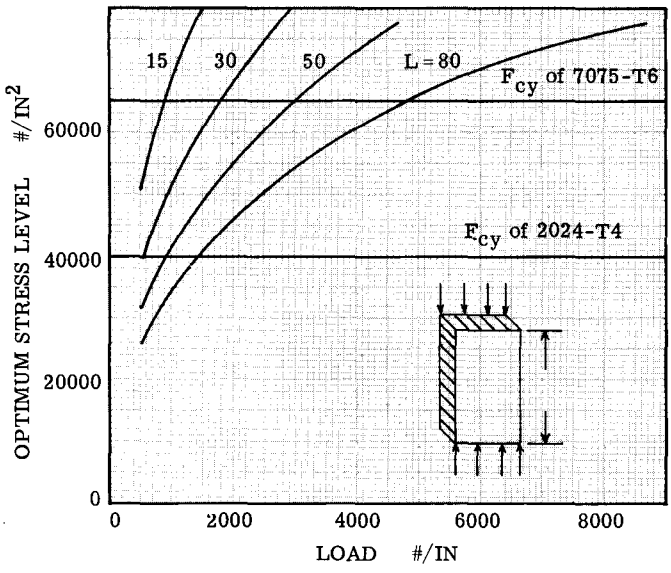

Fig. C12.11.1

of a more complex problem involving more variables, this is not always the case. However, the weight equation can be expressed in terms of the variables and step by step optimization performed through partial differentiation. This method was demonstrated in a paper by the author entitled "Design Optimization of Aircraft Structures with Thermal Gradients", Reference (14).

REFERENCES

1. Forest Products Laboratory Report No. 1817, "Short Column Compressive Strength of Sandwich Construction", C. B. Norris and W. J. Kommers, August 1950.

2. NA59-1597 Structural Development of Brazed Honeycomb Sandwich Construction for the Model F-108 Air Vehicle (North American Aviation, Inc.)

3. "Buckling of Sandwich-type Panels", N. J. Hoff and S. E. Mautner - Journal of the Aeronautical Sciences, July 1945.

4. NAA-STR65 R.R. Anelmann and L. A. Harris (North American Aviation, Inc.).

5. ANC-23 Sandwich Construction for Aircraft.

6. NASA TN2601 "Compressive Buckling of Simply Supported Curved Plates and Cylinders of Sandwich Construction", M. Stein and J. Meyers, January 1952.

7. NA60-1270 "Stability of Honeycomb Sandwich Cylinders", M. O. Kiciman and D. Y. Konish.

8. Forest Products Laboratory Report No. 1583-B, "Compressive Buckling of Sandwich Panels

Having Dissimilar Facings of Unequal Thickness", W. S. Erickson and H. W. March, November 1958.

9. Forest Products Laboratory Report No. 1845, "Stress Induced in a Sandwich Panel by Load Applied at an Insert", W. G. Youngquist and E. W. Kuenzi, March, 1955.

10. "Stability of Flat, Simply Supported Corrugated Core Sandwich Plates", IAS Paper No. 59-87, L. A. Harris and R. R. Anelmann.

11. "A Small-Deflection Theory for Flat Sandwich Plates, NACA Report No. 898, 1948, C. Libove and S. B. Batdorf.

12. "The Stability Under Longitudinal Compression of Flat Symmetric Corrugated-Core Sandwich Plates", NACA TN2279, April 1952, P. Seide.

13. Anderson, Melvin S. "Local Sustability of the Elements of a Truss-Core Sandwich Plate," NASA Techn. Report TR-R-30. 1959.

14. "Design Optimization of Aircraft Structures with Thermal Gradients", AIAA, J. Aircraft January 1964, Lloyd E. Hackman and James E. Richardson.

TYPICAL JOINTS, EDGINGS AND INSERTS IN SANDWICH STRUCTURE

JOINTS

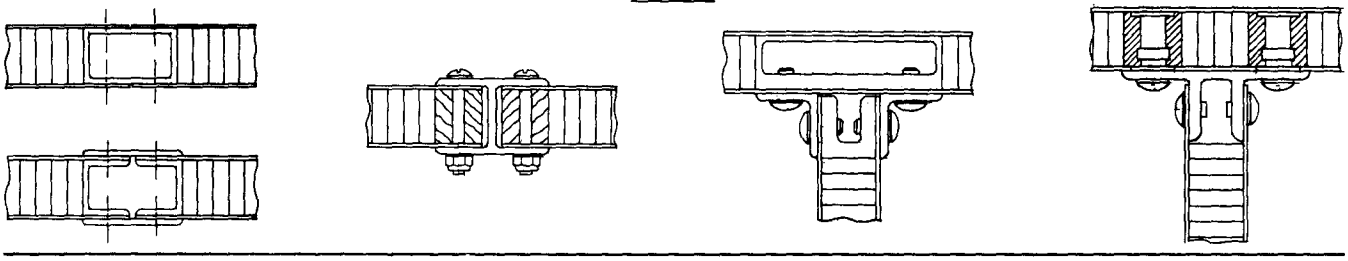

EDGINGS

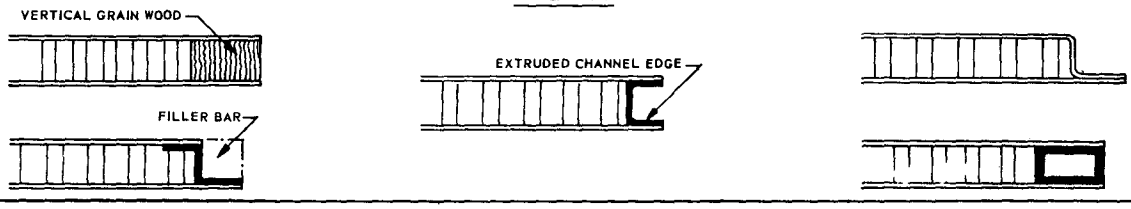

INSERTS

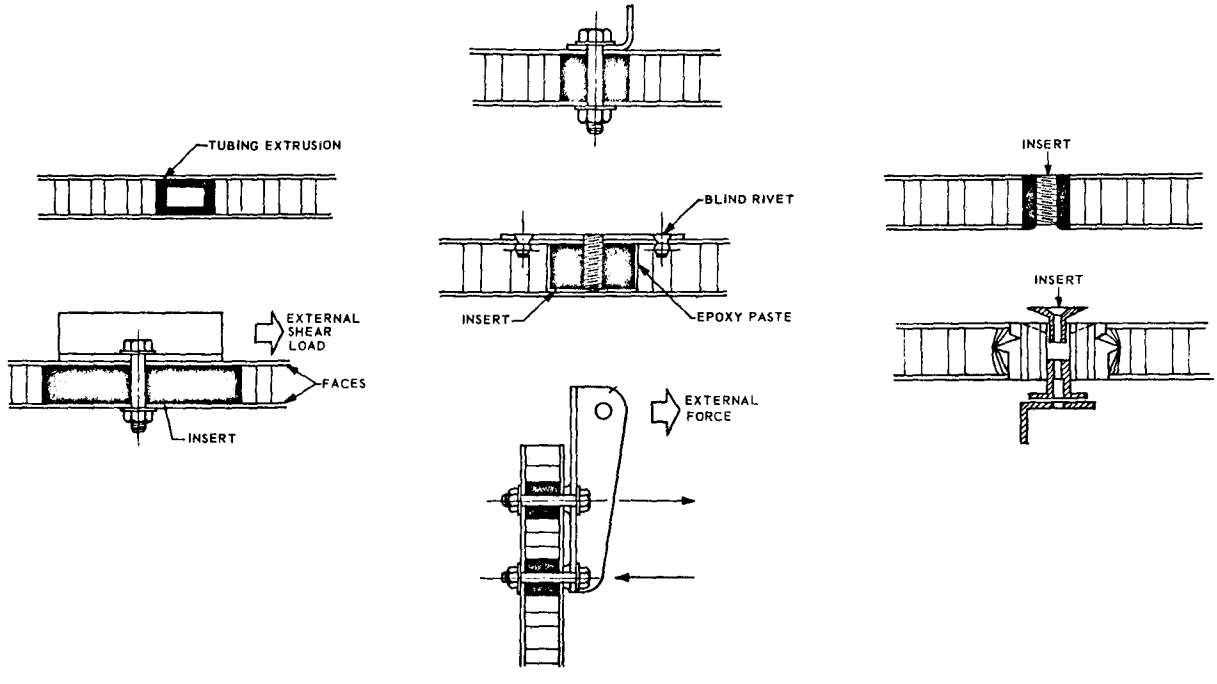

TYPICAL SANDWICH PARTS USED IN AIRCRAFT CONSTRUCTION

Boeing 727 - Thrust Reverser Door
PH15-7 Stainless Steel

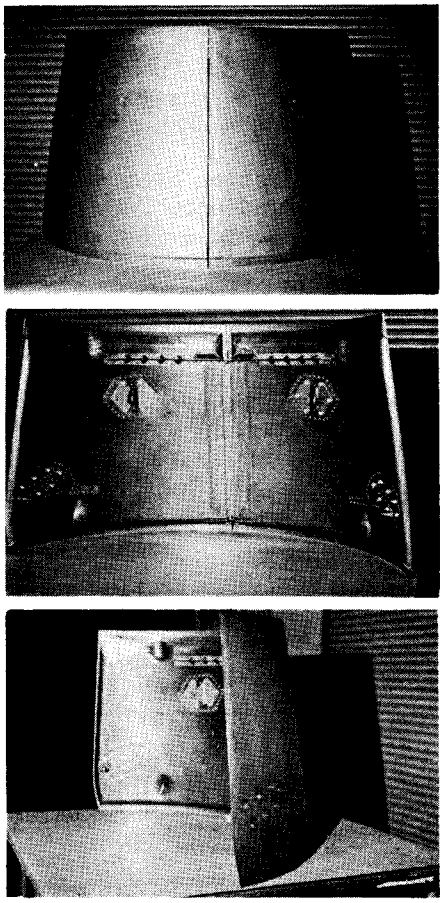

Made by John J. Foster Mfg. Co., of "Stresskin", An All Welded Honeycomb Construction

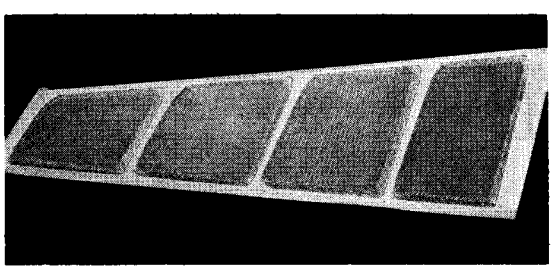

A5A Fixed Trialing Edge - Aluminum Honeycomb

XB-70 Fuselage Panels - Stainless Steel

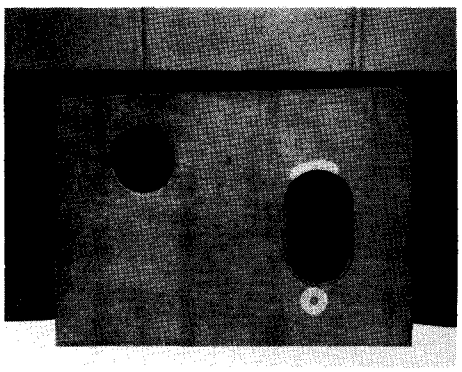

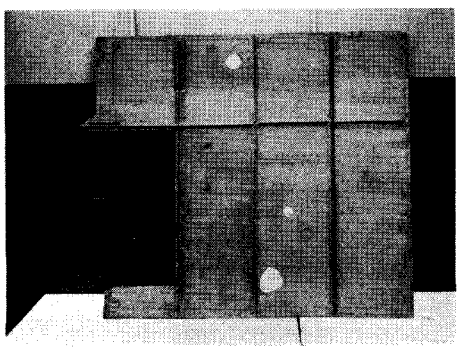

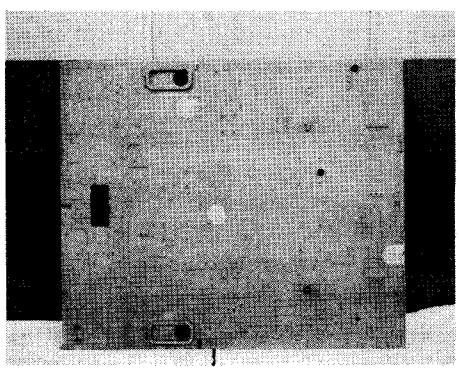

Von Mises Yield Criteria

The deviation of γ_1 from the Von Mises Yield Criteria provides a relation from which an effective stress can be derived for comparison with compression yield of the material. The Von Mises Yield Criteria is one of several forms for expressing material failure criterion. Another name for the same criterion is distortion energy criterion. The criterion relates the onset of gross plastic deformation or yielding under various stress conditions. In the case of compression or tension the yield stress is well defined by simple tests, however data is not normally available for yield stress levels under combined stress conditions. Thus there is a requirement for such a yield relation as used in this chapter to relate the compression yield stress to an effective yield stress under combined or non-compressive stresses.

Values for γ_1 under combined stress conditions are as follows:

Compression: $\gamma_1 = 1.0$

Shear: $\gamma_1 = \sqrt{3}$

Biaxial Loading: $\gamma_1 = \sqrt{1 - \gamma + \gamma^2}$

where $\gamma = f_y / f_x$

Biaxial Compression and Shear:

$$\gamma_1 = \sqrt{1 - \gamma + \gamma^2 + 3\gamma^2}$$

$$\lambda = \frac{f_s}{f_x} \qquad \lambda \leq 1$$

$$\gamma_1 = \sqrt{\lambda_1^2 + (\gamma \lambda_1)^2 - \gamma\lambda_1^2 + 3}$$

$$\lambda_1 = \frac{f_x}{f_s} \qquad \lambda_1 \leq 1$$

CHAPTER C13

F A T I G U E

By Clarence R. Smith

C13.1 INTRODUCTION

The fatigue problem relating to metals has been investigated experimentally for more than a century. In 1849, Jones and Galton investigated cast iron bars in bending. They found that failure occurred in fewer than 100,000 cycles if loaded to more than one-third of ultimate bending strength. Similar work on wrought iron built-up girders by Fairborn (1860-1861) showed comparable results. Wohler's work for the Prussian State Railways goes back to the 1850's when he made an extensive series of tests of various grades of iron and steel subjected to repeated direct tensile and compressive loads, to repeated bending loads, and to repeated torsional loads.

Airplanes in the past were not subjected to loads experienced by present day high speed aircraft. Also, they were built of materials whose tensile strengths were so low that in order to satisfy static strength requirements, stresses for service loading would automatically fall within ranges that would provide an adequate fatigue life.

The fatigue problem has risen at an alarming rate with present day airplanes in that they are built of materials which are stronger, yet have no better (and in some cases, poorer) fatigue properties than those used formerly. The result has been an accumulation of service failures, some with fatalities involved. Such situations have involved the designer in unfamiliar areas. Besides, more accurate methods of stress analysis enable us to design structures with greater efficiency and precision. This causes working stresses to more nearly approach what heretofore had been designated as limit values. In fact, specifications for fighter aircraft require fatigue cycling as high as 1.25 times the design limit loading, while transports are tested to 1.05 times limit loading.

Those of us who have experienced a broken automobile axle while driving along a perfectly smooth highway, realize that fatigue failure is not necessarily caused by a sudden overload or even a load slightly higher than average. Subsequent examination of the broken part revealed the tell-tale striations or "beach marks" that accompany fatigue failures. This is not to say that fatigue is always accompanied by such markings; however, it is usually the case. A typical fatigue failure of an airplane rim is shown in Figure C13.1. Note that the striations started in the highest stressed area of the radius and progressed outward until final static failure as evidenced by the outstanding lip.

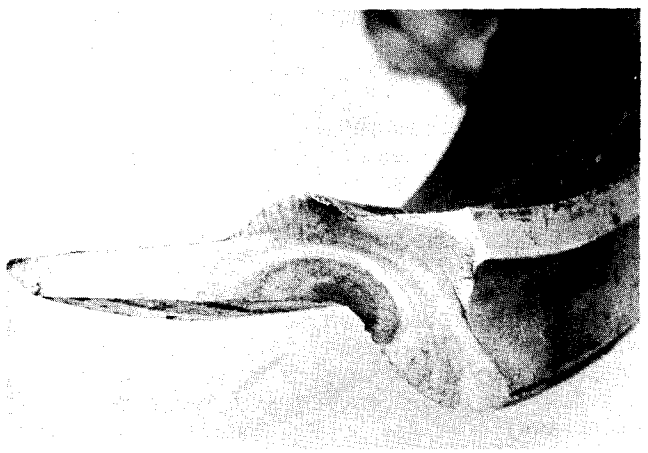

Fig. C13.1 Airplane wheel rim showing striations at fatigue fracture.

Fatigue failures can also be identified by the plain visibility of crystals at the fracture. This largely accounts for the old belief that the metal had become crystallized. This appearance, however, is because fatigue fractures directly through the crystal "transcrystalline failure" as opposed to tearing apart at the grain boundaries or "intracrystalline failure" of static rupture. Both types of failure involve metallic crystals and neither is necessarily more crystalline than the other, notwithstanding the fact that the crystals in fatigue failure are better defined and more visible.

Fatigue failures originate at some discontinuity as a focal point of crack initiation. These are called stress concentrations. Prior to cracking, however, mismatched atoms called "dislocations" tend to pile up along grain boundaries and finally penetrate to cause a fatigue crack. This happens at a very early stage; however, the visible "engineering" type crack usually does not occur until more than 50 % of life to rupture is consumed.

Cracks, however, will always initate at the surface unless special surface preparation or residual compressive stresses are introduced

along the surface. This stems from the fact that interior atoms are shielded on all sides by other atoms, while those on the surface have one side unprotected. Shanley attributes this to surface unbonding.[1] Whatever it is, special surface preparation will help to reduce fatigue failures. More on this later.

C13.2 STRESS CONCENTRATIONS

Were it not for stress concentrations, there would be no need to write the present chapter. This is because the principles used in static designs would be sufficient to compensate for the stresses imposed by service loading. Unfortunately, we do have stress concentrations so that a discussion of this subject is needed before tackling fatigue.

A stress concentration factor may be defined as a coefficient by which the nominal stress away from the interruption of stress is multiplied to reveal actual stress. Handbook values may vary in that some values are based on nominal gross area stresses while others are based on net areas through the least section. Thus we can have a 1-inch wide tensile coupon having a centrally drilled hole of 1/4-inch diameter whose concentration factor turns out to be 3.2 when based on stress through the section away from the hole. However, if based on net area through the hole, the concentration turns out to be 2.4.

Some handbook values for stress concentrations may vary for the same configuration and loading condition. This might be because some may have been derived mathematically, while others experimentally through the use of photoelasticity or other experimental stress analysis techniques. A common value assessed for the concentration at the edge of a hole in a wide sheet is 3. Obviously, as the hole increases in size in comparison to sheet width, the concentration based on gross area stress becomes larger. The stress concentration for a pin loaded hole can vary from infinity for a very small pin in a wide sheet to about 4.5 where the sheet is 2.5 times the hole diameter and then up to higher values where the hole diameter is very nearly the width of the sheet. This is illustrated in Fig. C13.2 where stress concentrations for pin loaded holes and unloaded holes are presented for a sheet loaded in tension. Here we see that the concentration for a lug in terms of gross area stress away from the hole is least at a/b ratios of about 0.4 (2.5 hole diameters), where a is the hole diameter and b is lug width. Since a mechanically fastened joint is essentially a number of lugs side by side, it follows that the optimum fastener spacing would be about 2.5 diameters. Such a joint would have an efficiency $(\frac{\text{net area}}{\text{gross area}})$ of 0.6. This is not in keeping with static designs where joint efficiencies of at least 0.75 are required.

Obviously, for designing lugs, the use of stress concentrations in terms of gross area is inapplicable since many lugs, such as rod ends, have two critical areas--through the shoulder and through the major diameter. Accordingly, we usually work with net stress and use concentration factors as given in Fig. C13.3.

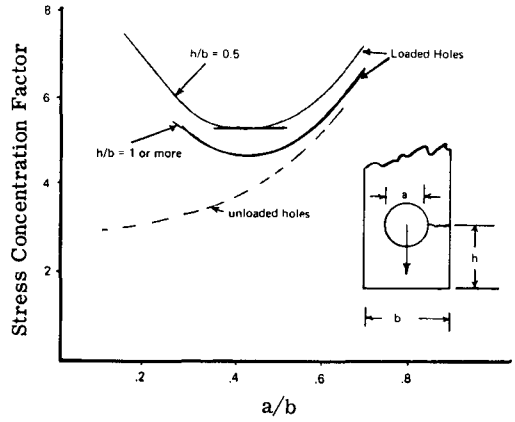

Fig. C13.2 -- Stress concentration factors for loaded and unloaded holes in sheet stressed in tension. Adapted to gross area stress from works of Frocht & Hill.[2]

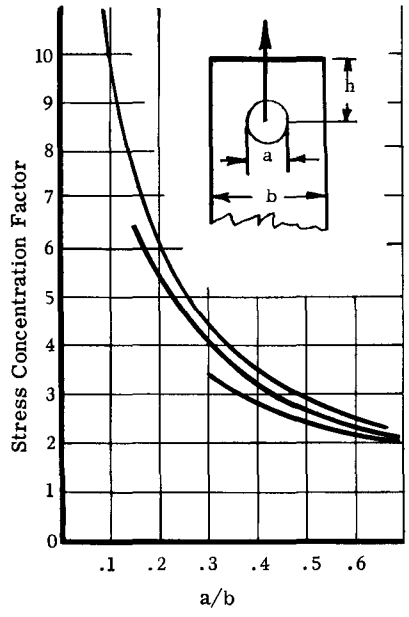

Fig. C13.3 -- Concentration factors for lugs in terms of net area stress.[2]

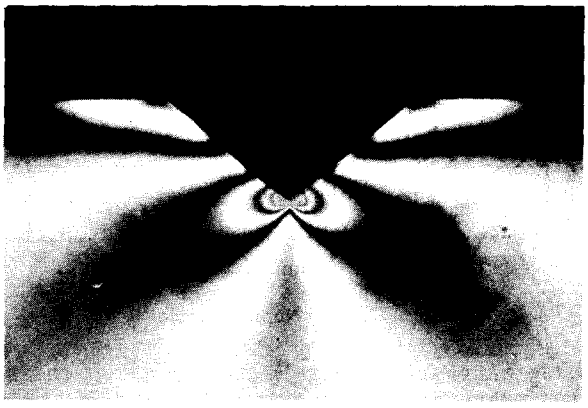

Fig. C13.4 - Photoelastic pattern of sharp edge notch.

In practically every case involving a stress concentration, the stress gradient is very steep as shown in Fig. C13.4 by the photoelastic pattern caused by a sharp edge-notch in a wide sheet loaded in tension. Here the number of dark lines (fringes) are directly proportional to stress. This is further illustrated in Fig. C13.5 where the stress gradient from the edge of a hole in a wide sheet loaded in tension is given in terms of radii from edge of hole.

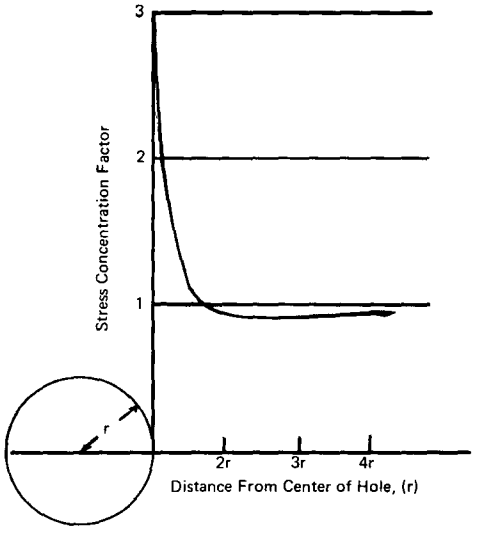

Fig. C13.5 - Stress distribution at edge of hole in wide sheet. (3)

The steep gradient at the concentration has particular significance in that stresses at concentrations can be manipulated at the expense of stresses a short distance away from the concentration. Thus we have such practices as shot peening, surface nitriding, and others which shift the stress at the concentration to more favorable locations.

Other geometrical stress concentrations are given in Figs. C13.6, 13.7, and 13.8. The term "geometrical stress concentration" is used here to distinguish it from the term "fatigue stress concentration factor" which is more or less a ficticious value derived from the ratio of stress for a given life of an unnotched specimen divided by the stress of a notched specimen at the same life and loading condition. This will be discussed in detail later.

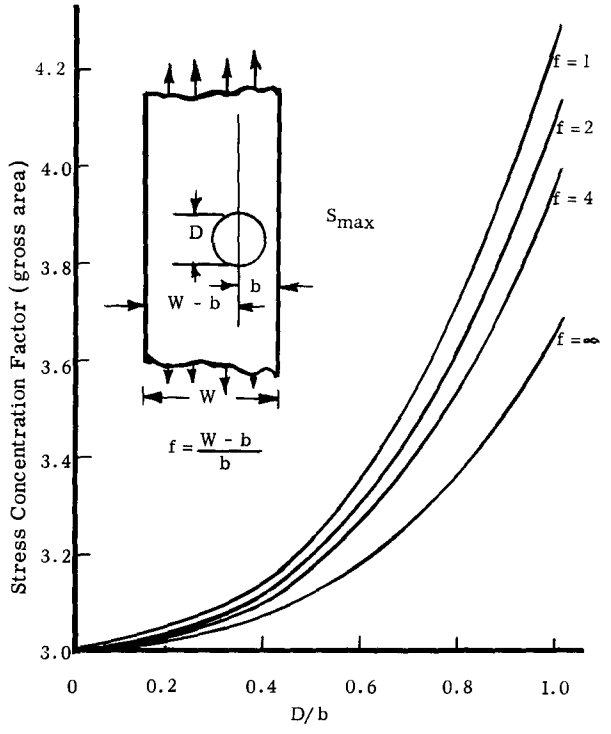

Fig. C13.6 - Semi-infinite plate with hole near edge. (4)

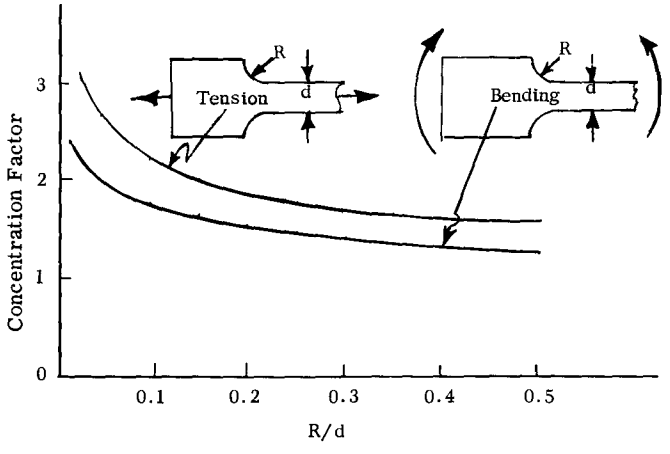

Fig. C13.7 - Rectangular plate with fillets. (5)

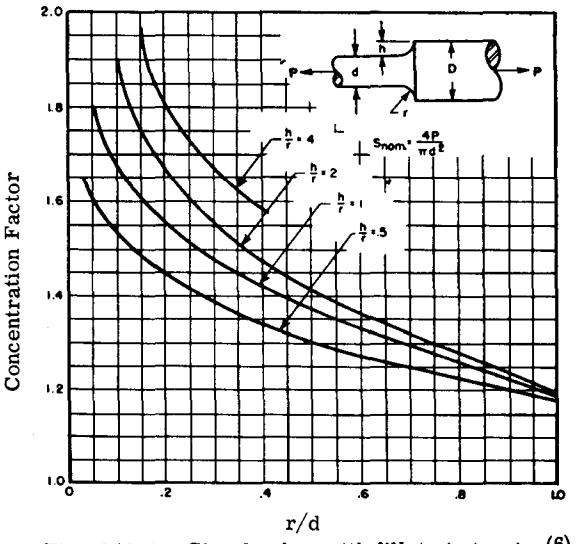

Fig. C13.8 - Circular bar with fillets in tension(6)

C13.3 FATIGUE DATA

C13.3.1 Unnotched Data

Unnotched data in fatigue are comparable to static properties as determined by the standard tensile coupon. As the static stress-strain curves describe static properties, the S-N curves describe basic fatigue properties. The term "basic" is used here to designate a fundamental property of a given material. This is not in agreement with S-N data for notched specimens where residual machining stresses can influence results by more than 10 times, thereby eliminating them from the realm of basic material properties. While it might be argued that ε-N curves would be even more basic, we will use S-N data because of being more available in handbooks.

Whereas static properties are presented in terms of tension and/or compressive yield and ultimate strengths, fatigue data are presented for many intermediate values and manners of loading. To facilitate description, the term Stress Ratio (R) is used, the definition being $R = S_{min}/S_{max}$. Accordingly, for loading from 0 to maximum stress, the stress ratio, R, is $0/S_{max} = 0$. For reversed loading, S_{min} is equal and of opposite sign to S_{max} in which case, R = -1. The nomenclature for conventional laboratory fatigue testing is presented in Fig. C13.9. A Family of S-N curves for 7075-T6 aluminum alloy is given in Figure C13.10. Here, the solid lines represent average (log mean) values for axially loaded 0.1-inch thick sheet material. Dashed lines are interpolations to aid estimating intermediate values.

Frequently fatigue data are presented in terms of constant mean stress or constant ratio of alternating stress to mean stress. The use

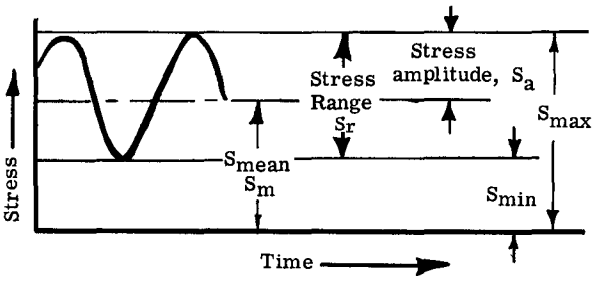

Fig. C13.9 - Nomenclature

of such curves are largely dependent on individual preference; however, for convenience, the data are generally presented in constant life or modified Goodman diagrams as shown in Fig. C13.11.(8) Here, life for any given stress ratio can be found by the intercept of appropriate life with the diagonal lines. It is usually necessary to interpolate between life lines for actual values. As seen in Fig. C13.11, lives are given for even exponents with intermediate values of 4 x the previous increment.

EXAMPLE 1) Find the life for cycling at R = 0 and a maximum stress of 50 KSI (Ref. Fig. C13.11)

Reading from the maximum stress scale at 50 KSI, we see that the life is about midway between 4 x 10^4 and 10^5 cycles. Considering that life is presented on the basis of logarithmic values, we find that life should be slightly over 60,000 cycles.

2) Find the life for cycling ± 20 KSI over a mean stress of 30 KSI.

Along the line for 30 KSI mean stress, we see the intercept for alternating stress to be at 10^5 cycles. Note that this same intercept gives a maximum stress of 50 KSI at R = +0.2. The value of A = 0.67 is simply the ratio of 20 KSI/30 KSI.

While the presentation of data as shown in Figure C13.11 has become more common in recent years, it is usually easier to interpolate life for a given stress when plotted as in Fig. C13.10. In addition, the curves shown in Fig. C13.10 lend themselves for visually demonstrating possible corrections for fatigue critical situations. This will be discussed in detail later.

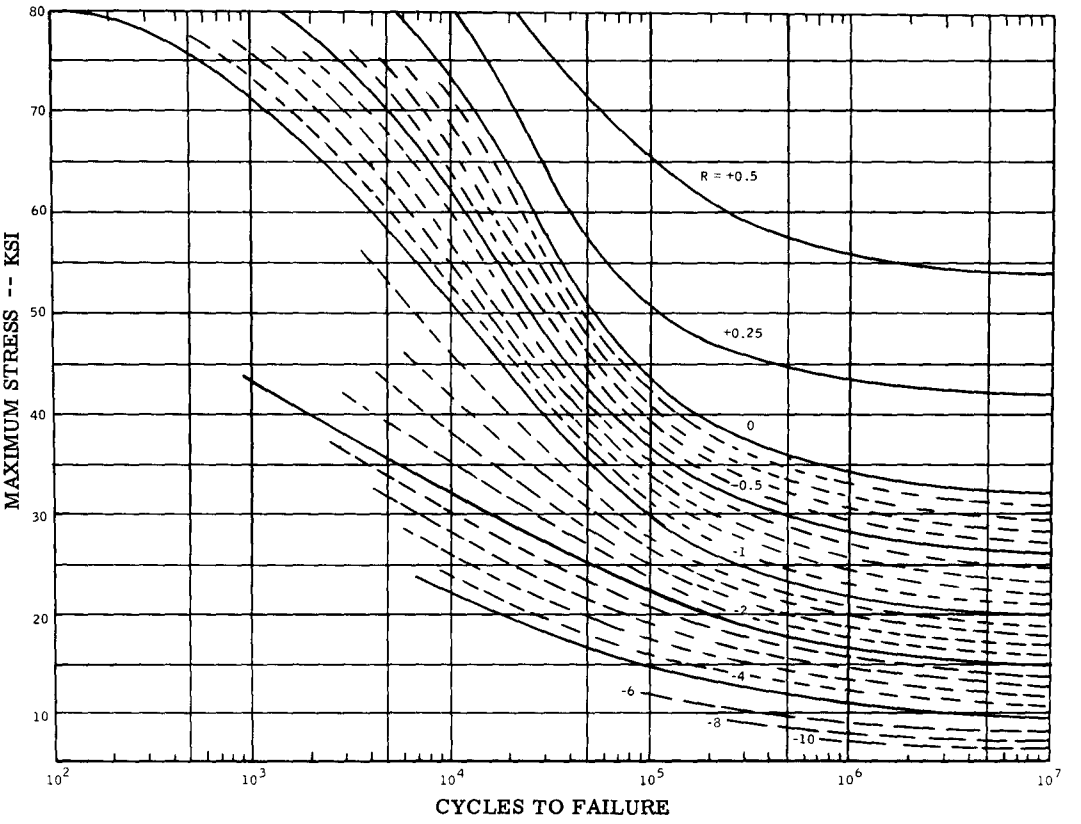

Fig. C13.10
S-N Curves for Unnotched 7075-T6 Aluminum Alloy(7)

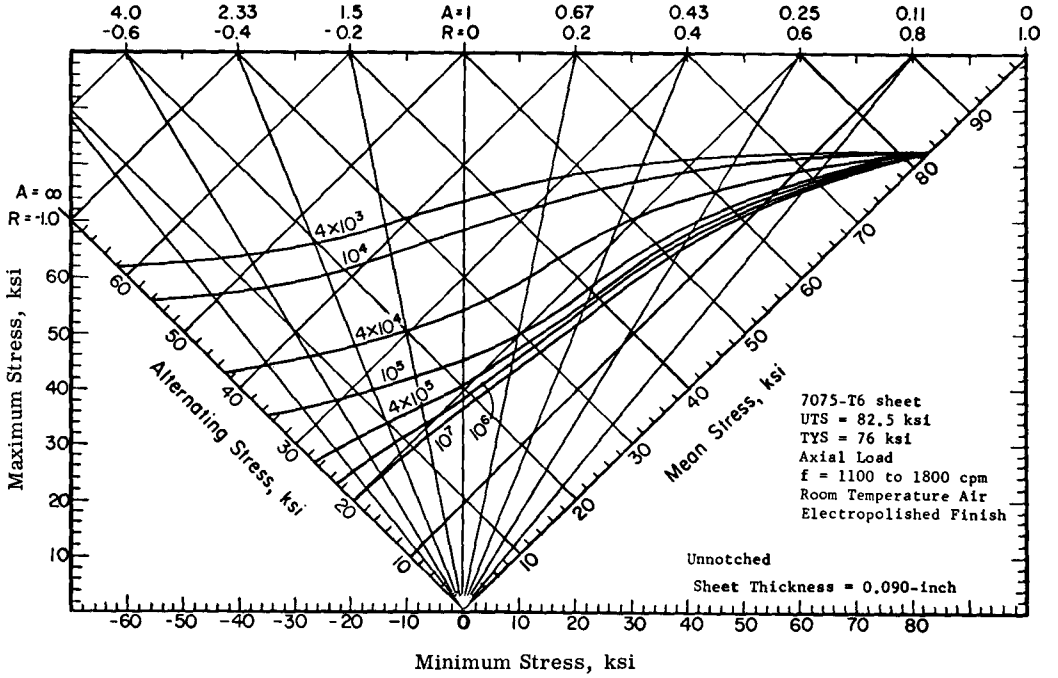

Fig. C13.11
Typical Constant-life diagram for unnotched fatigue behavior of 7075-T6 aluminum alloy.

C13.3.2 Notched Data

Notched data are used to demonstrate fatigue properties of a material in the presence of stress concentrations. This provides a comparison for use with built-up structures having an equivalent concentration. For service life predictions, which will be discussed in detail later, it is common practice to design a structure to some known stress concentration factor and assume that it would behave as a specimen having an equivalent stress concentration. While it is usually too expensive to develop an S-N curve for a full-scale structural component during early stages of design, it is common practice to make spot checks at one or two points to determine the validity of the stress concentration assumed for design. This assures the airplane's ability to pass the fatigue tests required of the complete airframe before certification is granted - at least on the particular component involved.

S-N curves for axially loaded specimens of 7075-T6 having theoretical concentration factors (K_t) of 1 (unnotched), 2.6 (center hole notched), and 3.6 (small lugs) are given in Figure C13.12. K_t values are given in terms of net area. A fourth curve (Theoretical for K_t = 2.6) is shown for comparison with the curve generated by testing. Here it is seen that the theoretical curve (S-N curve for K_t = 1 divided by 2.6) falls short of the experimental curve except at about 10^7 cycles. It is generally conceded that the reason for experimental values being higher is because of beneficial residual stresses acquired by plastic deformation at the notch in the short life ranges.

Were we to divide the stress for a given life as shown by the curve for unnotched specimens (K_t = 1) by the stress exhibited by the notched specimens at the same life, we would end up with a factor which is commonly called a "fatigue notch factor". The fatigue notch factor, (defined as $K_f = \frac{\text{nominal maximum stress, unnotched specimen}}{\text{nominal maximum stress, notched specimen, same life}}$) is usually lower than K_t. An exception exists, however, where fretting is involved. Accordingly, we see that at long life, the K for small lugs is about 5.5 instead of the theoretical 3.6 as derived from the geometric configuration. Fretting is a term used for damage caused by rubbing of solid surfaces in contact under pressure.

The above comparisons point to a very important factor in that there is a difference in the effects of stress concentration, depending on whether or not rubbing surfaces are involved. Virtually all mechanically fastened joints fall into the "closed notch or fretting sensitive region" and therefore need to be treated differently from the simple notch or "open concentration". Commercial airliners are particularly sensitive to fretting because of their long-life expectancy.

While all stress concentrations found by ratioing unnotched to notched fatigue data are fatigue stress concentrations, the validity of many notched data can usually be determined by comparing with the theoretical value at about 10^7 cycles. The fatigue notch factor and theoretical stress concentration should be equal at this point. If not, the fault may lie in residual stresses set up by machining the notches. A dull drill will usually introduce a residual compressive stress which causes the specimen to last longer than it should. Such data would be unconservative for design purposes.

An exception to the above is the very sharp notch. Neuber has shown that the notch effect is less if very sharp in that the notch cannot be smaller than a grain of the material involved.(10)

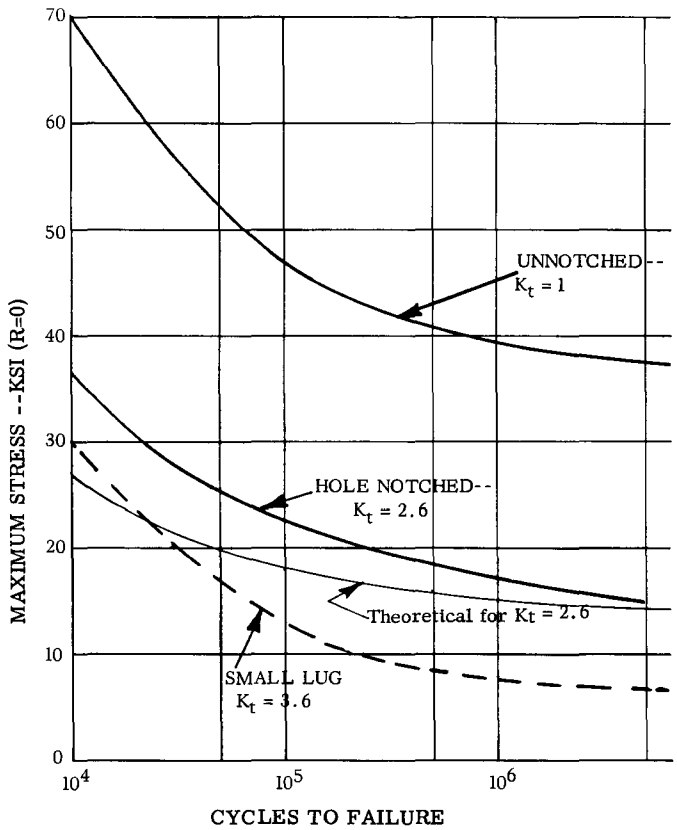

Fig. C13.12
S-N curves for notched and unnotched 7075-T6 sheet.

C13.3.3 Endurance Limit

Endurance limit is defined as the maximum stress below which a material can presumably endure an infinite number of stress cycles. While many materials, including steels, exhibit a definite stress below which fatigue failure will not occur, aluminum and many other alloys have no specific endurance limit. Accordingly, a fatigue limit for those metals is defined as that stress corresponding to a life of 200,000,000 cycles.

C13.3.4 Fatigue Testing Machines

The above data were acquired by fatigue testing axially loaded specimens at frequencies varying from about 1200 cpm to about 1800 cpm. Practically all commercially available axial loading fatigue machines are of the constant-load type - that is, special provision is made for maintaining proper loading even though the specimen may experience creep. An automatic shut-off and cycle count is provided to record cycles at specimen failure.

Another type of data not heretofore mentioned is that of reversed bending and/or torsion. Most early data on steels were acquired by rotary beam tests which flex the specimen in reverse bending. This supposedly simulated fatigue failures of railroad car axles whose service loading was in reverse bending. Unfortunately, the rotary beam tests do not lend themselves to testing at stress ratios other than at R = -1.

J. Goodman(10) used a special technique for converting reverse bending data to stress ratios other than R = -1. Fig. C13.13 shows a Goodman Diagram for the 7075-T6 aluminum alloy specimens which were used to develop the data for Fig. C13.10. In this diagram the maximum, mean, and minimum stresses are ordinates to the curves and the abscissas are any convenient scale. The ultimate tensile strength is first plotted and the straight line of mean stress drawn to it at zero abscissa. Stresses for cycling at R = -1 are then plotted along the ordinate axis for appropriate lives - in this case 10^6, 10^5, and 10^4 cycles. Connecting lines are then drawn to the point representing the ultimate tensile strength of the material at one abscissa.

EXAMPLE 1) The stress for 10^6 cycles at R = -1 is ± 30 KSI. Find Stress for R = 0.

Note that the intercept for 10^6 cycles and zero stress is at abscissa 0.27. Note maximum stress to be 44 KSI for 10^6 cycles at abscissa 0.27. Note that this is in aggrement with the stress shown on the S-N curve for R = 0 in Fig. C13.10.

2) The stress for 10^4 cycles at R = -1 is ± 51 KSI. Find Stress for R = 0.

Note that the intercept for 10^4 cycles and zero stress is at abscissa 0.39. Maximum stress is found to be 63 KSI at the same abscissa. This does not agree with the S-N curve for R = 0 and 10^4 cycles in Fig. C13.10 where the maximum stress is shown to be 73 KSI.

Values for stress ratios other than zero are estimated by scaling between appropriate life lines, moving right or left until finding the desired stress ratio. A good pair of dividers helps. However, a better way is to replot data on a modified Goodman diagram (Ref. Fig. C13.11). Using the mean stress line as independent coordinate, plot maximum stresses wherever they happen to fall and draw constant life curves. Note that the curves will be straight lines, whereas those shown in Fig. C13.11 are curved. Fig. C13.11 was plotted from actual data for a number of stress ratios. Lack of agreement between the two is an indication of the reliability of the Goodman diagram.

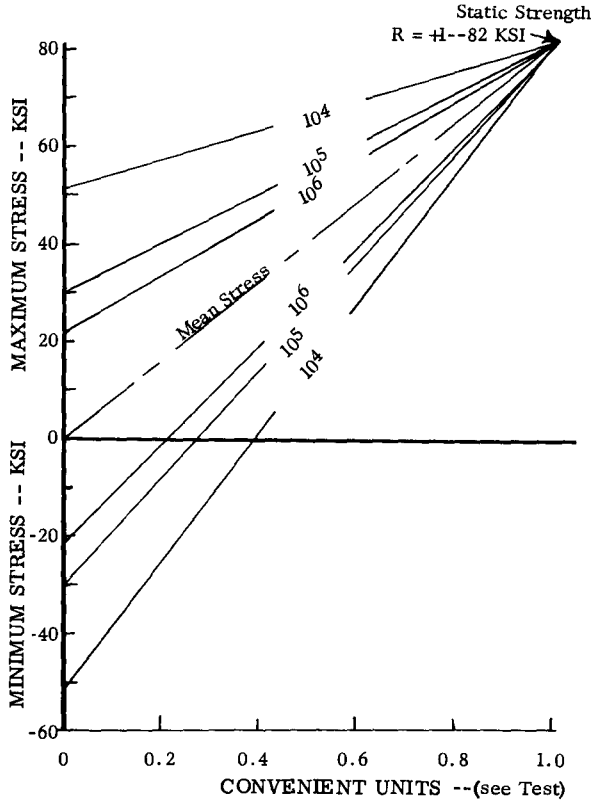

Fig. C13.13 - Goodman Diagram for 7075-T6

Inasmuch as the fatigue data furnished on new alloys by steel companies are usually from rotary beam tests (perhaps because of speed and cost), the Goodman diagram definitely has a

place. However, a certain amount of caution is needed as can be seen by comparing data shown in the appendix of this chapter.

Although many axially loading machines have adapters for torsion tests, few data are available. Accordingly, a logical procedure is to prorate axial or bending properties to torsion. Table I shows experimental data for evaluating ratio of torsion to bending-fatigue strength for various materials.(11) Theoretical development for converting bending to torsion

TABLE 1
RATIO OF TORSION TO BENDING-FATIGUE STRENGTH FOR VARIOUS MATERIALS

Material	Fatigue life, cycles			Reference
	10^5	10^6	10^7	
0.1 C steel (solid specimen)	0.57	0.56	0.57	13
3.5 Ni steel (solid specimen)	.65	.68	.67	13
0.1 C steel (hollow specimen)	.53	.53	.53	13
3.5 Ni steel (hollow specimen)	.62	.67	.64	13
Silal cast iron	.83	.82	.86	13
0.25 C, 3.09 Cr, 0.51 Mo steel	.59	.60	.60	14
0.24 C steel	.....	.....	.55	15
0.38 C steel; oil quenched, 1,550°F.; tempered, 800° F	.....	.....	.61	15
0.38 C steel; oil quenched, 1,550°F.; tempered, 1,250°F	.....	.....	.64	15
0.81 C steel; annealed	.....	.....	.60	15
0.31 C, 3.35 Ni steel; oil quenched, 1,475°F.; tempered, 900°F	.....	.....	.642	15
76S-T61 aluminum	.63	.65	.63	12

fatigue properties are given in references 12 and 13. For design purposes, however, it would seem safe to use 0.5 of tensile values.

C13.3.5 Test Scatter

Test scatter is a problem that has plagued fatigue specialists for years. One of the reasons is that it is virtually impossible to have identical specimens. Another is that all fatigue testing machines do not have the same responses, although their indicated loads may be the same. Accordingly, it is common practice to design to the lower part of a scatter band as shown in Fig. C13.14(16) or use a median value for calculation purposes and then use a scatter factor for final design. A scatter factor of 4 is the criteria by which most airplane structures are contractually obliged to demonstrate by test--that is, the test structure has to withstand 4 lifetimes of simulated service loading. Accordingly, a 4000-hour fighter airplane has to withstand an equivalent of 16,000 hours of service. While there are cases where a scatter factor of 2 is used, the severity of loading is usually increased to compensate for scatter factor.

Practically all of the fatigue data presented in handbooks are log-median or log-mean

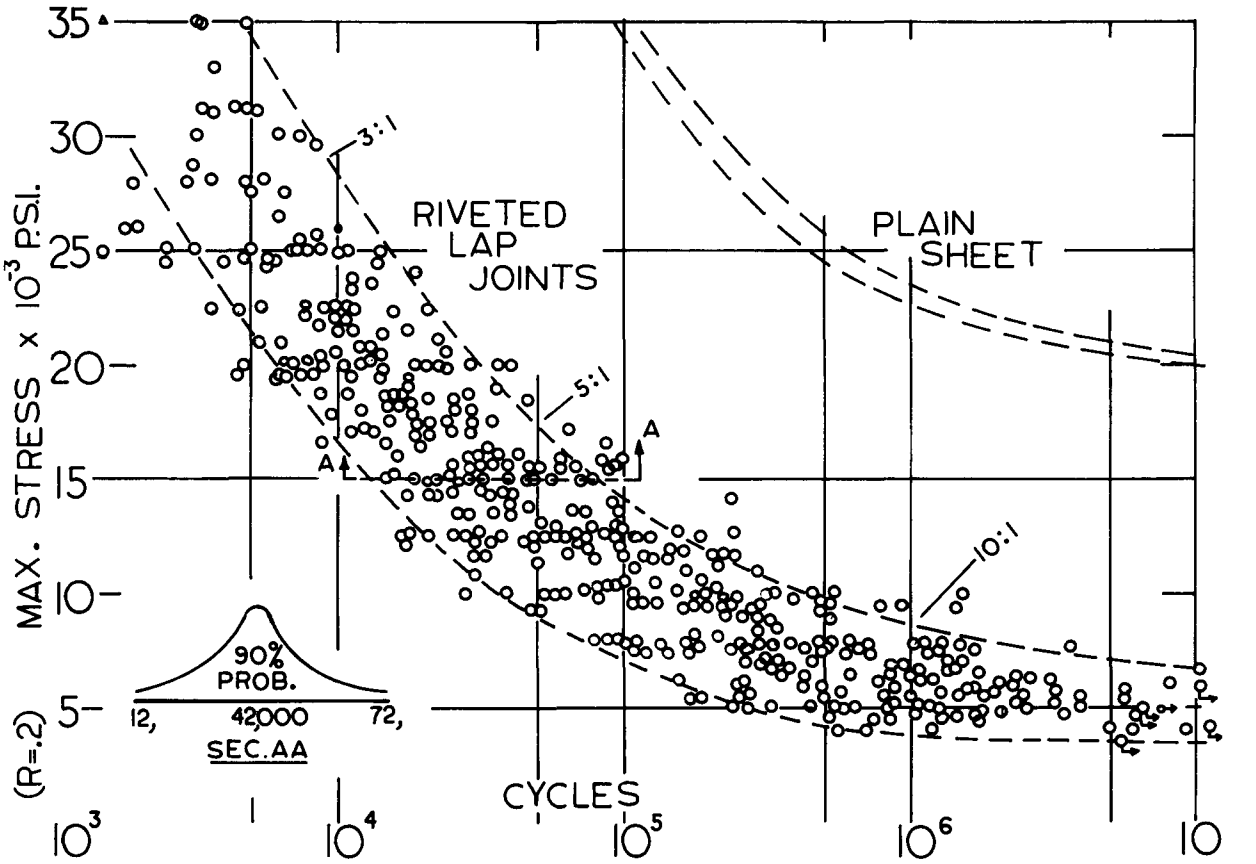

Fig. C13.14

values. Usually there is but little difference between the two. The designer, accordingly, has to use discretion in allowing for test scatter when using handbook data. Statisticians use a factor called standard deviation,(17), usually identified by the Greek letter σ, or Sigma, which relates scatter data to reliability.

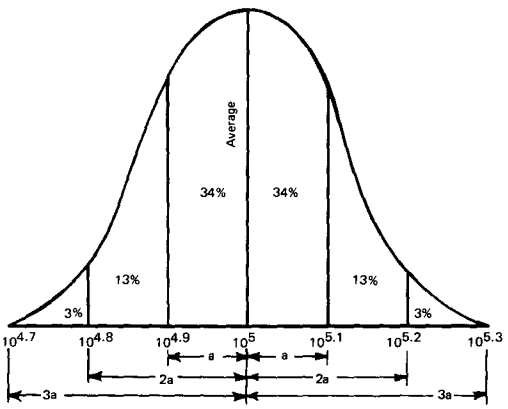

Fig. C13.15 - Bell curve indicates probabilities of fatigue failure based on standard deviations from average life of 10^5 cycles. Standard deviation is assumed to be 0.1 based on log-normal distribution.

Standard deviation takes into account the number of specimens and data spread. In terms of percentages, 99.9% of a group of specimens are expected to have lives in excess of 3σ below the average. For example, if the average life of a group of specimens is 100,000 cycles (10^5), and the standard deviation is 0.1 based on log-normal distribution, then the so-called guaranteed life would be $_{10}(5 - 0.3) = 10^{4.7}$ whose antilog is about 51,000 cycles. A diagram of assumed test lives in terms of standard deviations is presented in Fig. C13.15.

The standard deviation, Sigma, is 0.1 in this example since it happens to be a good value for a life of about 10^6 cycles. Further, averages for full-scale tests on airplanes at the Naval Air Engineering Center, Philadelphia(18) and the Aeronautical Research Laboratories, Melbourne, Australia(19) indicate that 0.1 is a good average value for Sigma on full-scale structures.

Standard deviation, or Sigma, is very important in comparing the relative merits of fastened assemblies where cycles to failure are in the neighborhood of 100,000 cycles. For example, assume that specimens joined with Fastener A average 100,000 cycles to failure for a given loading while specimens with Fastener B average 200,000 cycles. Sigma is 0.1 for specimens with Fastener A. However, there is more scatter in data for specimens with Fastener B so the standard deviation is 0.2 based on the logarithm of average life.

For a guaranteed minimum life of 3σ below the respective average lives, it was found that specimens with Fastener A can be expected to last a minimum of 50,000 cycles. In the case of Fastener B, where average life is 200,000 cycles, but with a standard deviation of 0.2, the logarithm of 200,000 is 5.3010. From this value, 3 x 0.20 (3σ) is subtracted to obtain 4.7010, whose antilogarithm shows the life to be 50,000 cycles. This is no better than specimens fastened with Fastener A with its 100,000 cycle average life.

The value of Sigma, however, is highly dependent on actual life, especially for small unnotched specimens. Where lives exceed one million cycles, Sigma may exceed one or more. At this point, the significance of a standard deviation based on life disappears and other statistical methods must be employed. ASTM's Special Technical Publication No. STP-91A is a good source of information for use of statistics for fatigue.

C13.3.6 Load-N Curves

Load-N curves are frequently used where stress is unknown. Usually plotted in percentage of breaking strength, they are valuable in that structures are designed in terms of limit or ultimate loads. Fig. C13.16 presents data comparing lives of airplane structures in terms of ultimate failing loads.(18) All of the structures shown are of World War II vintage where design for fatigue resistance was not a requirement. None would pass present day fatigue requirements. The author has demonstrated that such structures would have to last for 30,000 or more cycles at limit loading (66.7% of ultimate) in order to pass tests required of an airplane designed for 4000 hours of service. Note that the P51 wing would sustain only 40% of ultimate for a life of 30,000 cycles.

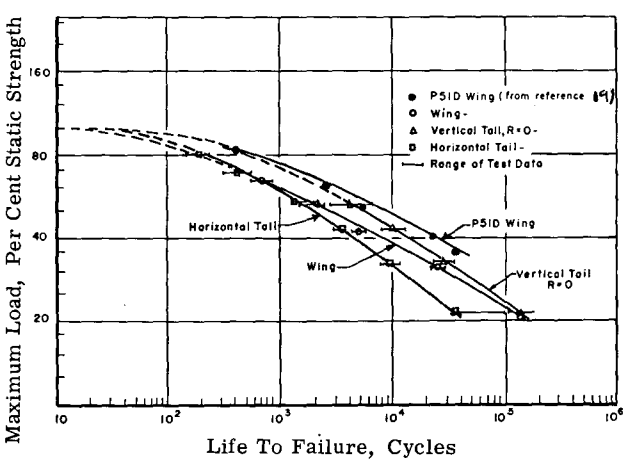

Fig. 2 - Medium Life to Failure, R ≅ O

Fig. C13.16 - Load-N Curves for Full-Scale Structures.

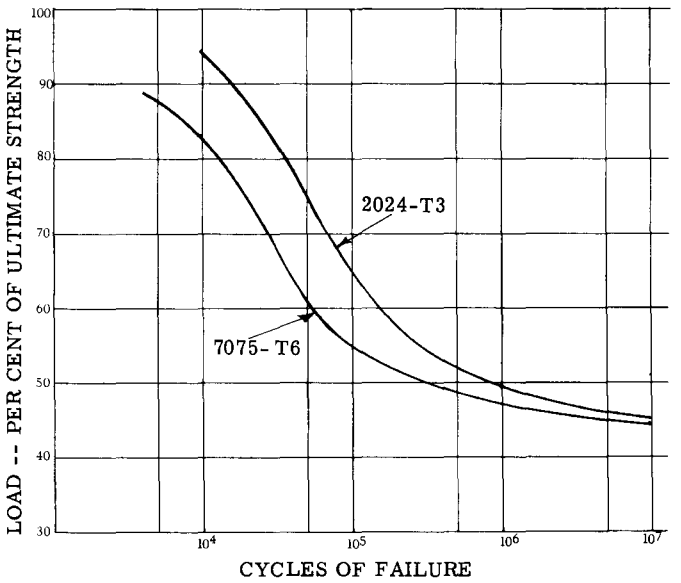

Fig. C13.17
Load-N Curves Comparing Fatigue Strengths of Unnotched 2024-T3 and 7075-T6 Aluminum Alloys

Fig. C13.16 are Load-N curves which compare strengths of unnotched specimens of 2024-T3 and 7075-T6 aluminum alloys. Here we see that for a 30,000 cycle life that 2024-T3 (lower strength alloy) will sustain 82 percent of its ultimate strength whereas 7075-T6 (higher strength alloy) will sustain but 68 percent of its ultimate strength. The 30,000 cycle life, as in the previous paragraph, is used as a fatigue strength index for comparative purposes on a 4000-hour airplane. Comparisons for a 50,000-hour airplane should probably be made at a different life. Irrespective of which particular life is chosen, the graphs do show why fatigue problems have become more prevalent and illustrate why special emphasis on fatigue is important when designing with higher strength alloys.

What has been said of aluminum alloys is also true of steels. Steels, however, especially of 200 ksi and higher strengths, are vulnerable to flaws which reduce fatigue life.

Tests reported by Cummings, Stulen, and Schulte on SAE 4340 steel having inclusions ranging between 0.001 and 0.003-inch diameter, showed that material heat treated between 200 and 250 ksi lasted only 1/4 as long as the same steel heat treated between 100 and 150 ksi. This steel heat treated between 250 and 300 ksi had even shorter life. Where inclusions were smaller than 0.00025-in. diameter, however, fatigue strengths were more or less proportional to their ultimate strengths.

C13.3.7 Elevated Temperature

While fatigue properties of metals at elevated temperatures is a study within itself and is beyond the scope of the present chapter, a few salient facts concerning elevated temperature properties are in order:

1. It is not only the temperature, but the time at temperature that influences life. Referring to the curves on 6Al-4V titanium alloy shown in the appendix, we see that tests were made at 1850 cpm. Accordingly, the data are correct for the duration of the tests. Allowance should be made for periods of longer duration.

2. In general, static properties are reduced as much or more than fatigue properties at elevated temperatures. While this does not nullify the need for fatigue analysis, static considerations may make fatigue problems less acute.

3. Stresses due to thermal expansion or contraction need to be considered. These may or may not be additive to flight loads.

4. The effects of superposition of creep plus fatigue are not well defined at present. Due to the time required for creep testing, but meager data are available. These were more or less acquired on accelerated tests.

C13.5 INCREASING FATIGUE RESISTANCE

C13.5.1 Introduction

The need for increasing fatigue resistance should be obvious by now. As probably anticipated from the stress concentrations shown in Figs. C13.2 through C13.8, most structural failures due to fatigue are likely to occur at holes--particularly those having fasteners loaded in shear. Accordingly, each structural splice would behave more or less as a series of pin-loaded lugs where concentration is higher than for simple unloaded holes or even fillet radii. This is not to say that fillet radii may not also be critical, the point here is simply that the first place to look for trouble would be in mechanically fastened joints.

Although most fatigue failures of airplane structures have been at fastener holes, notches and fillets have also taken their tolls. In looking at handbook values for stress concentrations in fillets of all kinds, it would appear that it would be impossible to have a fillet so poor that failure would not occur first at fastener holes.

Using the lug analogy for shear-loaded fasteners, one explanation for almost as many

failures at fillets could be that stresses at loaded fasteners cannot be reversed even though load is completely reversed, whereas a reversal of load would reverse stress at an open hole or fillet radius. This is shown in Fig. C13.18 where a sponge rubber lug loaded in tension (A) and compression (B) show the deformations at the edge of the lug to be in tension for either load direction.

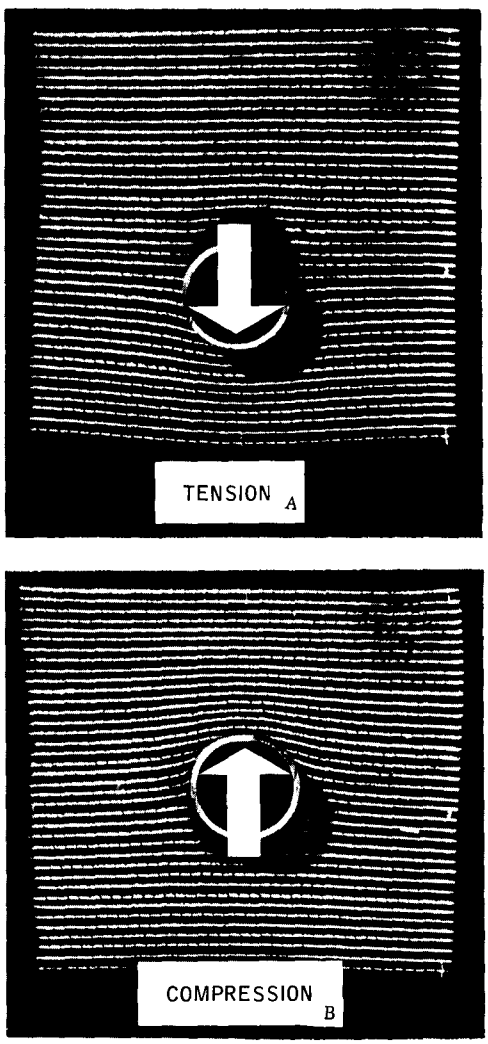

Fig. C13.18 - Sponge rubber model of lug ruled with white lines is loaded in Tension (A) and in compression (B). Stress at concentration causes tension stress for both.

The model is ruled with white lines which are about 0.10-inch apart when unloaded. Since the tensile stresses for compressive loading result from shear transfer from compressively loaded material away from the hole, the tensile stresses due to compressive loading cannot be as high as when loaded directly in tension. Nevertheless, a complete reversal of load results in two tensile stresses of unequal magnitude. Since the location of peak tensile stresses due to compressive and tensile loading are slightly removed from one another, and the stress due to tensile loading is the highest, it follows that failure should always occur at the high stress point for tensile loading. Accordingly, tensile stresses due to compressive loading could be ignored insofar as fatigue life calculations are concerned for reversed loading; however, they must be considered where loading is primarily in compression. This is clearly shown in Table II where test data are presented to compare lives of small lugs subjected to tension-tension and reversed loading. There is no indication that reversed loading is more harmful than tension-tension loading.

The behavior of metals under static and cyclic loading conditions now will be considered to provide an understanding of what can be done to improve fatigue life of structures. Beginning with static stress-strain properties of simple

TABLE II

Maximum Gross Stress (psi)	Fatigue Life: Reversed Loading (Cycles)	Fatigue Life: 0 to Maximum Loading (Cycles)
	7,000	9,000
	9,000	10,000
30,000	10,000	10,000
	12,000	13,000
	37,000	23,000
20,000	37,000	28,000
	42,000	29,000
	63,000	30,000

Results of fatigue tests with small aluminum alloy lugs which were subjected to reversed loading and tension-tension loading are shown here. There is no indication that reversed loading is more harmful than tension-tension loading.

specimens and continuing with S-N data for unnotched specimens, the behavior of stresses at a notch will be likened to stresses in unnotched static and fatigue specimens to see what happens in a structure.

Although most design analyses are made in terms of stress, it is very important to consider strain where deformations exceed the elastic limit of a given material.

Normally, the specified limit loading condition assumes no plastic deformation. However, in view of stresses that may be encountered at stress concentrations, it is unlikely that a structure can be designed where absolutely no local plastic deformation will occur during the lifetime of the structure.

Limit load, at least for airplane structures, is defined as a working load which can be withstood without any permanent deformation

that will impair the performance of the vehicle. Ultimate load usually is defined as 1.5 times the limit load. However, this safety factor may vary depending on the particular circumstances in each case.

The material used in the illustrative examples throughout the remainder of this chapter will be 7075-T6 aluminum alloy because of its almost universal use in airplane structures. Although the principles involved here will apply to other alloys and structures, airplane structures will be considered primarily because of their fatigue sensitivity and the number of mechanical fasteners used.

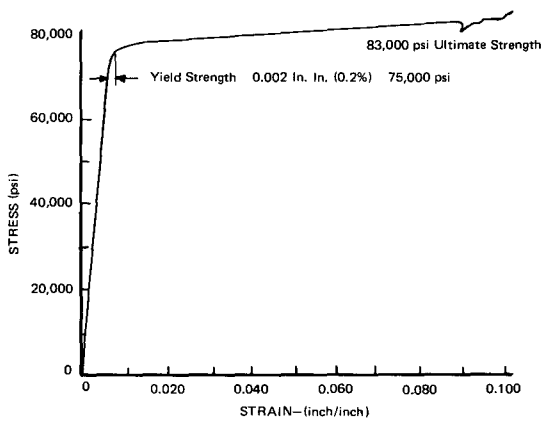

Fig. C13.19
Stress-strain Curve for 7075-T6 Aluminum Alloy

C13.5.2 Stress, Strain & Plastic Deformation

A stress-strain curve for 7075-T6 aluminum alloy is shown in Fig. C13.19. Here it is seen that the yield strength is about 75 ksi with ultimate breaking strength of 83 ksi. Although the rated modulus of elasticity, E, is 10,500,000 psi, for this and subsequent discussions involving aluminum alloys, we will use 10 million psi as a good round number.

Supposedly, the behavior of this material at a stress concentration would be very much as shown in Fig. C13.19 only with this difference: the stress is not based on the entire cross sectional area, but on a very small area at the point of highest stress. When localized yielding occurs, the small increment of area at the stress concentration will refuse to carry additional load (even though the load actually is increased) and the material adjacent to the stress concentration will be forced to carry a larger share of the load.

This ability of material to shed load by yielding at a concentration, along with the residual stresses which result from yielding, has more importance in fatigue strength characteristics of a structure than any other single item.

To further explain this behavior of materials, consider a structure which has a stress concentration of 4 and stress at limit load of 25 ksi based on an average cross-sectional area. If this structure were made of a brittle material with an ultimate strength of 83 ksi (for comparison with 7075-T6), the structure would fail because 4 x 25 ksi = 100 ksi.

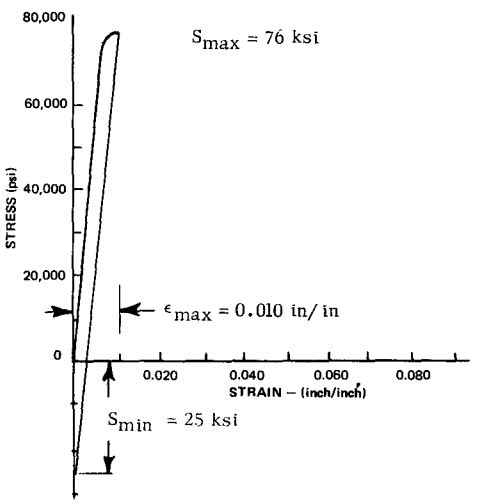

Fig. C13.20
Stress as a function of strain at point of stress concentration--Residual compressive stress in unloaded position.

However, if the structure were 7075-T6 having stress-strain properties as shown in Fig. C13.19, the material would yield locally, transferring the excess load to the yet unyielded adjacent material.

Obviously, the 25 ksi average stress would not fail the structure so that the local yielding would have to stop when the load carrying ability of the yielded plus unyielded material averaged 25 ksi. Exactly when this occurs is not known, however, a good guess can be made by considering the stress concentration to be a strain concentration. That is, the strain corresponding to 25 ksi nominal stress multiplied by 4 to get the maximum strain at the concentration and the maximum stress is found from the stress-strain curve. Assuming E = 10 million psi, we find

$$\epsilon_{nom.} = \frac{25{,}000}{10{,}000{,}000} = 0.0025 \text{ in/in}$$

and $\epsilon_{max} = 4 \times 0.0025 = 0.010$ in/in

From Fig. C13.19, $s_{max} = 76$ ksi*

* Units such as ksi and psi are intermingled here for semantics. While most S-N data are given in ksi, we say E = 10 million psi rather than 10 thousand ksi.

Having yielded locally, the local material now is longer than the remainder so that when the structure is unloaded, this permanently elongated material is forced into compression by the relatively larger bulk of material trying to return to its original point of zero strain. An analogy to this condition is something like trying to fit an old cork back into a bottle. If the area of the yielded material were very small compared to the area of the remaining material, there would be no apparent permanent set; however, a residual stress of 25 ksi would result as graphically illustrated in Fig. C13.20.

Increasing tensile deformation would cause greater amounts of permanent set with correspondingly greater values of residual stress. However, it would be inconceivable that a residual stress greater than the compressive yield for the material could be introduced, no matter how high the preceding tensile load. Even if it were possible to introduce a greater amount, given time, the residual stress would relax to a value below the compressive yield. Actual retainable values are not known; however, experience in the shot-peening industry indicates that up to two-thirds of the compressive yield strength can be retained indefinitely at ambient temperature.

Measurements of strains at a hole in a wide sheet show rate of strain to increase after reaching the plastic state.(21) This would imply an even larger amount of residual stress than assumed; however, since greater strain would increase the ratio of $\frac{\text{plastic}}{\text{elastic}}$ areas, the strain would not return to zero on unloading. Thus, the linear assumption incorporates 2 errors that more or less cancel each other when used for estimating residual stress.(22)

The accuracy of the linear strain concept is not in contention at this point, however, it does illustrate the presence of some residual compressive stress at a concentration after a high preload. Conversely, one would expect a residual tensile stress to exist after yielding in compression. It also explains why some fatigue failures occur in structures which are subjected to NOTHING BUT COMPRESSIVE LOADS. More on this later.

C13.5.3 Effect of Residual Stress on Fatigue

The locked-in residual stress at a point of stress concentration causes a preloaded structure to behave in a manner different from a structure which has never been loaded to the point of local yielding.

For example, if the loading were such as to cause stressing at the concentration to be from 0 to 60 ksi, one would expect that where preloading caused a residual compressive stress of -30 ksi, the loading which previously caused 0 to 60 ksi in the virgin structure would result in ± 30 ksi in the preloaded structure. While the original life of such a structure would be 25,000 cycles (see Fig. C13.10, S_{max} = 60 ksi, R = 0) the preloaded structure would last for 100,000 cycles (see Fig. C13.10, S_{max} = 30 ksi, R = -1).

Similarly, if preloading were such as to leave a residual stress of -40 ksi, the life for cycling at R = 0 would be found to be

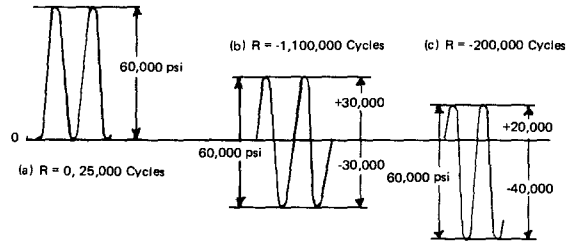

Fig. C13.21 - Examples show changes in fatigue life with addition of residual stress at concentration. All test samples are cycled at the same load which produces a stress range of 60,000 psi.

200,000 cycles (see Fig. C13.10, S_{max} = -2). Since the definition of R is S_{min}/S_{max}, being of minus sign, the -40 ksi stress is lower than +20 ksi, even though numerically larger. Thus, we can have stress ratios of -10 or even minus infinity. The above calculations are presented graphically in Fig. C13.21.

C13.5.4 Mechanically Introduced Residual Stresses

In the above discussion, the compressive residual stress was introduced by overloading so as to cause local yielding. There are, however, many other methods of acquiring favorable residual stresses, perhaps the best known is shot peening. As the name implies, peening is accomplished by small round shot under air pressure which blast the surface concerned. The part to be peened is placed in an enclosure that traps the used shot and returns them to a reservoir. Special mechanical arms or rubber arm protectors permit handling parts being peened.

Shot sizes range from 0.007 to 0.175-inch diameter. Large shot sizes are used to produce deep layers of compressive stress; small shot sizes are used to reach into small radii. Velocities range from 100 to 200 ft/sec.

Since the object of shot peening is to obtain a layer of compressive material on the surface, completeness may be checked visually

by coverage of shot impressions. However, peening works even when the shot is no harder than the surfact to be peened, in which case it may not leave a visible dimple. To overcome these difficulties, the Almen(23) gage is used. The Almen gage is nothing more than a strip of steel (Hardness 47 R_C) which when shot peened on one side causes the metal to hump on the peened side. The Almen intensity is simply the arc height of the strip as measured with dial indicator. Thus, an intensity of 12-14 Almen A means that the arc height of an A strip (0.051-inch thick) is 0.012 to 0.014-in.

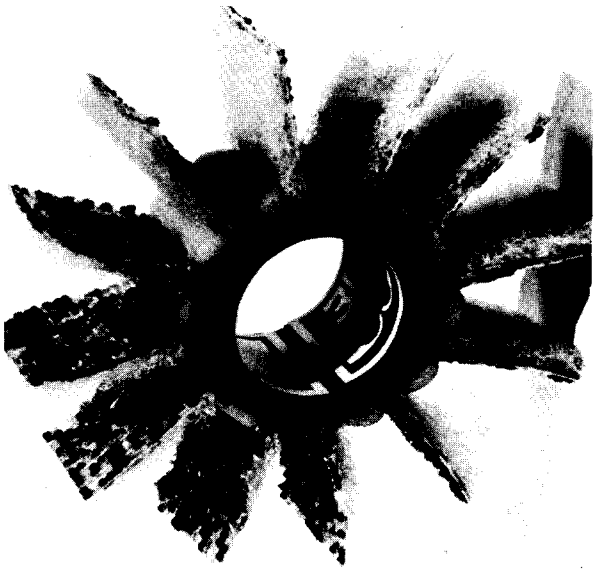

Fig. C13.22 - Shot Peening Wheel -- Cast Steel Shot is Randomly Bonded to Flaps with Resilient Adhesive.

While conventional shot peening works well for removable parts, problems frequently arise in structures already built. Special hammer peening has been used for accessible fillet radii and holes(24). A more recent development in the way of portable peening tools is that of the shot peening wheel called Roto Peen.* Comprised of two or more polymeric flaps (See Fig. C13.22) which extend from a steel mandrel and to which cast steel shot particles are bonded, rotational speeds of from 2000 to 8000 rpm cause the flaps to slap the surface to be peened.

Fig. C13.23 compares residual stresses obtained by two methods of peening. Although two distinct curves are shown, the data are too meager to statistically determine that an actual difference exists. It is known throughout the shot peening industry that incomplete coverage with more severe blast will produce the same intensity as greater coverage at lower intensity. Visual inspection of the two peened surfaces in this instance, however, indicated complete coverage in both cases.

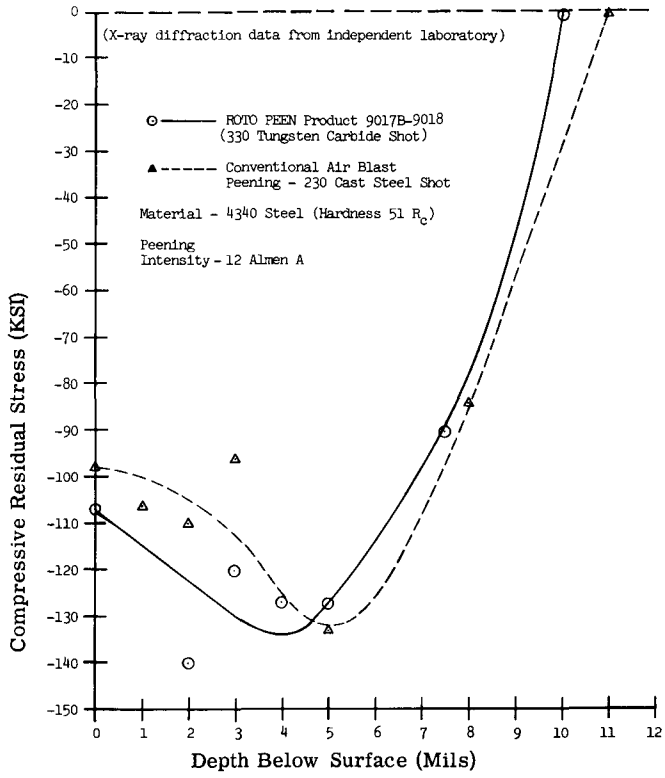

Fig. C13.23 - Comparison of Residual Stresses Produced by Two Methods of Peening.

Although shot peening is probably the most popular method for acquiring a beneficial residual compressive stress, other methods of providing a residual stress include "bearingizing," "coining", and cold rolling. Bearingizing is a trade name used by the Cogsdill Tool Products, Inc. This method consists of inserting a shaft with tight fitting surface rollers into the holes to be treated. This produces a burnishing effect on the sides of the holes.

Coining(26) consists of pressing a concentric groove around the hole or opening to be protected. This squeezes the material adjacent to the hole inward such that the hole diameter is decreased and the amount of compressive residual stress is dependent on the depth of the coin. Generally, the bigger the radius, the greater the residual stress.

Cold rolling is a common practice in preparing bolt threads and under-head radii. An example of the benefits gained in this manner is shown in Fig. C13.24.

* Trade name for peening system by 3M Co., St. Paul, Minnesota.

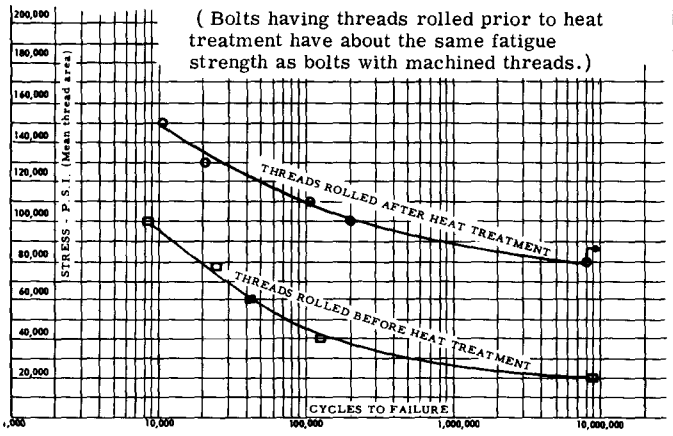

Fig. C13.24 - Thread Rolling

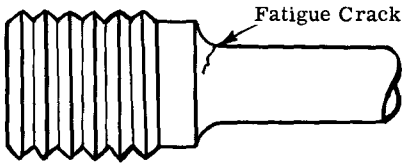

Fig. C13.25 - Fatigue failure at fillet

EXAMPLE PROBLEM (1)

Fig. C13.25 represents a part of a turnbuckle assembly which failed after 50,000 cycles during test. A life of 500,000 cycles is desired. Assume that the part lends itself to shot peening and that the S-N curves of Fig. C13.10 would apply, what residual stress is required to provide the required life? Loading is at R = 0.

Step 1. S_{max} for R = 0 at 50,000 cycles is 51 ksi. This also happens to be the stress range, Ref. Figs. C13.10 and C13.9.

Step 2. $S_{max} - S_{min}$ = 51 ksi stress range (minus a minus = +)

Step 3. We have two unknowns and one equation; however, we can assign a value for S_{max} at some negative R (negative because shot peening introduces compressive stresses) and determine the corresponding minimum stress. Remember, fatigue is not an exact science. Should $S_{max} - S_{min}$ turn out to be greater than 51 ksi, the life mould be more than the needed for 500,000 cycles which is fine, provided that the residual stress is within a range where relaxation is not a problem.

Step 4. Let's assume R = -1. We find S_{max} at 500,000 cycles to be 23 ksi. By definition, S_{min} = -23 ksi which would give a range of 46 ksi which is short of the desired amount.

Step 5. Assume again that R = -2, where S_{max} for 500,000 cycles turns out to be 18 ksi. By definition, S_{min} = -2 x 18 = -36 ksi. The corresponding stress range is 18 - (-36) = 54 ksi which is more than needed. This would indicate a life greater than 500,000 cycles where the stress range is actually 51 ksi and a residual stress of -36 ksi exists -- S_{max} would be 15 ksi.

Although the shot peening industry claims residual stresses as high as two thirds of the yield strength of the material can be retained, a value of one-half would be more conservative. The -36 ksi in the above would be well within reason. Using the 51 ksi stress range, actual life should be slightly more than 2 million cycles (see at R = -2.4).

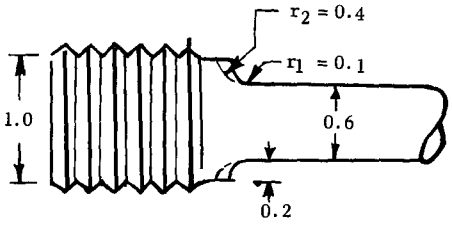

Fig. C13.26 - Fillet Revision

EXAMPLE PROBLEM (2)

Fig. C13.26 shows the same part as used in the previous example; however, appropriate dimensions are added. Suppose that the original part lasted but 10,000 cycles and a life of 500,000 cycles is needed. How do we go about acquiring the needed life?

Step 1. Using the same procedure as in the previous problem, we see that the maximum stress must have been about 74 ksi (Fig. C14.10, R = 0, N = 10^4).

Step 2. Obviously, more residual stress is needed than in the previous problem, so we go directly to R = -4 where S_{max} is found to be 12 ksi at 500,000 cycles. S_{min} would be -4 x 12 = -48 ksi, and the stress range turns out to be 60 ksi which is short of the 74 ksi needed.

Even if we went to R = -8 (S_{max} = 8 ksi, S_{min} = -64 ksi), the 64 ksi residual stress would be more than we could hold because of relaxation.

Step 3. What now? Suppose we try reducing the the stress concentration by providing a more generous radius as indicated by r_2 in the figure. Referring to Fig. C13.8, we see that the original K_t = 1.86 as found along the curve for h/r = 2, $(\frac{0.2}{0.1} = 2)$.

Step 4. For the proposed configuration
h/r = 0.2/0.4 = 0.5
and r/d = 0.4/0.6 = 0.67
from which K_t = 1.26 found along the curve for h/r = 0.5 and r/d = 0.67

Step 5. The new stress range is 74 ksi x 1.26/1.86 = 50 ksi

Step 6. Now that we have a reasonable stress range to work with, we treat the problem exactly as in the previous example.

C13.5.5 Residual Stresses by Diffusion Hardening

While the fatigue resistance of aluminum alloy structures are not affected by residual stresses introduced by diffusion hardening, practically all steels can benefit or suffer from such processing.

Surface nitriding always produces a residual surface compressive stress, provided that the material is sufficiently thick to prevent excessive stretching of the core. While expecially adaptable for medium carbon steels, a special alloy "Nitralloy" provides excellent fatigue properties when surface nitrided, see Fig. C13.27. Nitriding also provides an excellent

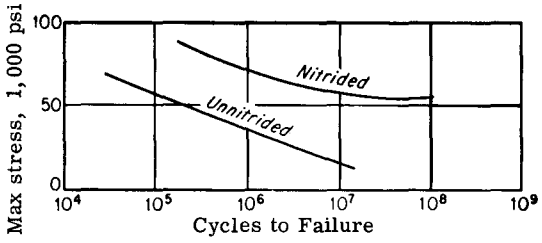

Fig. C13.27 - Effect of nitriding Nitralloy on the corrosion fatigue strength; rotating beam(26).

wear surface. For that reason, its use in aircraft would be in the nature of roller surfaces, such as on flap tracks.

Carburizing or "case hardening", while producing excellent wear surface on steels, may introduce either compression or tensile residual stresses. Accordingly, its presence as a fatigue deterrent is questionable.

Chrome Plating is nearly always damaging; however, parts can be restored to original fatigue strength by shot peening prior to plating, as shown in Fig. C13.28.(27) While chrome plating is used extensively for wear and corrosion resistance, caution should be taken where plating covers fatigue critical radii, etc. In such cases, the shot peening might be required to bring the part up to fatigue requirements even without the chrome. Thus, to bring the strength back to original properties is not enough and other corrosion inhibitors plus shot peening is needed. A mixture of cadmium plate in fatigue critical areas (plus shot peening) with chromium only at wear surfaces might be the answer. Some aircraft companies make it a point to prohibit chromeplate within 1/8-inch of the point of tangency of a fillet.

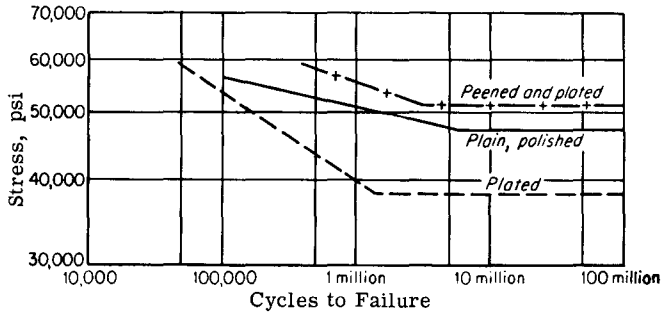

Fig. C13.28 - Rotating beam fatigue test results showing effect of chromium plating with and without shot peening.

Chrome-ite* is a trade name for a high dense chromium plating which has a thickness of under 0.0002-inch. Contrary to the damaging effect of normal chrome plating, fatigue life is increased. Fig. C13.29 shows comparative lives of 0.050-inch thick axially loaded specimens of 4130 steel heat treated to 160 - 180 ksi range. Since the specimens were but 0.050-inch thick, it is doubtful that the core thickness was sufficient to impose enough residual compressive stress on the surface to increase life in the amounts shown.

Tests on aluminum alloys showed similar improvements(28); however, prestressing above 50 ksi caused all benefits to be lost. The one preloaded specimen shown in Fig. C13.29 did not indicate a damaging effect due to preloading for steels.

While Chrome-ite apparently has little to do with residual compressive stresses, it was included at this point so as to be adjacent to the discussion on chrome plating where a residual compressive stress is a must. Why there should be an increase in fatigue life is a matter of conjecture at this point; however,

* Trade name of the Chrome-ite Co., Gardena, California.

similar improvements have been achieved by coating specimens with kerosene or other oleophobic films.(29)

Discussion of Benefits Due to Compressive Residual Stresses

In Example Problem (1) we assumed that the maximum stress at the concentration was 51 ksi because that happened to have been the maximum stress corresponding to a life of 50,000 cycles at R = 0. This would be true only if no residule stresses were present at the time of testing. Had there been residual compressive stresses due to machining or other, an increase in compressive stress by peening would probably be of little benefit. On the other hand, had there been a residual tensile stress, peening would not only remove the tensile stress, but introduce favorable compressive stresses which would increase life even more than estimated in Problem (1).

Whereas we cannot always tell whether residual stresses are present in a structure, should a part fail at fewer than 10,000 cycles for tension-tension loading, we can feel sure that some plastic deformation exists. In such a case any residual tensile stress would have been wiped out because of local yielding and local yielding would have introduced some residual compressive stresses in any event. This would limit the value of introducing additional residual compressive stress by peening or other methods.

For example, let us assume that the original part failed after 2500 cycles and that there was no way to reduce the stress concentration as in example (2). In viewing the stress-strain curve shown in Figure C13.19, we see that the yield strength of 7075-T6 was 75 ksi. Also we see that a substantial amount of strain could be tolerated without an appreciable increase in stress.

Let us assume that the maximum stress at concentration (corresponding to a 2500 cycle life) was 76 ksi, the reason being that very little more stress would cause the entire cross sectional area to yield. At this point, however, it is not too important whether the actual stress is 76, 77, or 80 ksi, the argument being that whatever the maximum stress, the minimum stress could not be zero, but some negative value. This would be true even if the entire cross section yielded, as the elastic return would cause compression at the concentration.

Continuing with our assumption that the maximum stress was 76 ksi, we find that the life of 2500 cycles intercepts the S-N curve for

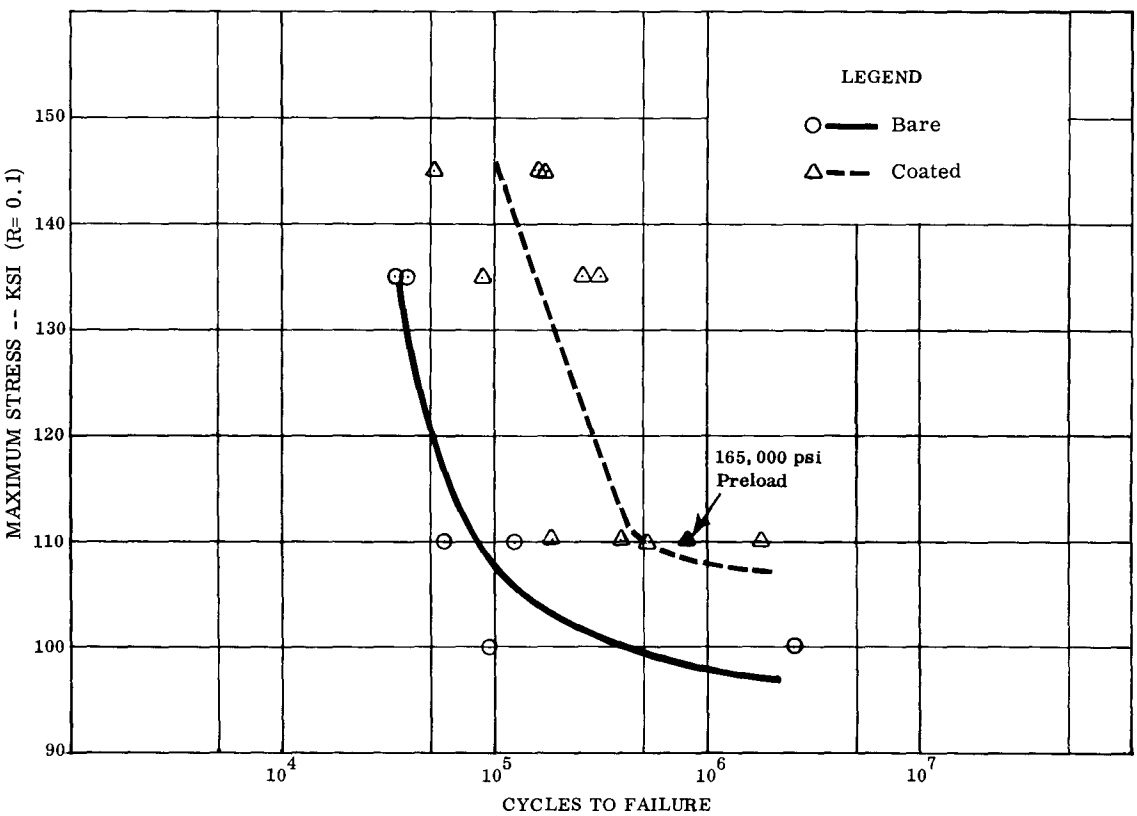

Fig. C13.29 - Effect of Chrome-ite Coating on Unnotched Specimens of 4130 Steel -- H.T.

R = -0.5 at 76 ksi (Ref. Fig. C13.10). This would indicate that the minimum stress, by definition, would be -0.5 x 76 ksi = -38 ksi. Let us further assume that a compressive stress of -50 ksi could be achieved by shot peening. Since the total stress range is 76 ksi - (-38 ksi) = 114 ksi, the maximum stress of the peened structure would be 114 - 50 ksi = 64 ksi for the same loading. The corresponding stress ratio would be -50/64 = -0.78 where life is found in Fig. C13.10 to be about 4000 cycles or less than double the original life.

The above points to the fact that a certain amount of caution is needed in determining whether or not a problem can be solved by introducing residual compressive surfaces stresses. In Problem (1), we found that it would take a residual stress of but -36 ksi to increase life by more than a factor of ten. Accordingly, if the life increase needed is ten times or more, compressive surface stresses would help only if maximum stresses in service did not cause localized yielding. This would be true whether or not loading is of a constant-amplitude or variable-amplitude nature.

Although cold working as in the above in itself might be considered as an improvement in material properties, tests on aluminum alloys have not born this out. Unnotched specimens of 7075-T6 can be stretched 4% prior to fatigue testing with no change in fatigue life. Accordingly, it can be assumed, at least for heat treatable aluminum alloys, that any benefits achieved by cold working are due to beneficial residual stresses.

C13.5.6 Increasing Rigidity

The following discussion has to do with increase of fatigue life by reducing stress amplitude through change of spring constant of a structure. Again referring to the S-N curves in Fig. C13.10, the curve for R = +0.5 is of special interest. Here it can be seen that a structure which lasts 50,000 cycles when loaded at R = 0 could be made to last almost indefinitely if the stress could be made to cycle at R = +0.5. In other words, a substantial increase in fatigue life will result if the minimum stress can be "propped up" even though the maximum stress remains unchanged or even slightly higher.

Torquing a bolt is a good example of how this "propping" effect can be achieved. However, general consensus is that a bolt torqued to a stress higher than the working stress remains static. What really happens is that the torqued bolt makes use of the extra rigidity of the abutting material to reduce stress amplitude.

This is more easily understood by visualizing a bolt which cycles as shown in Fig. C13.30. The cyclic amplitude shown here is exaggerated for easy visualization.

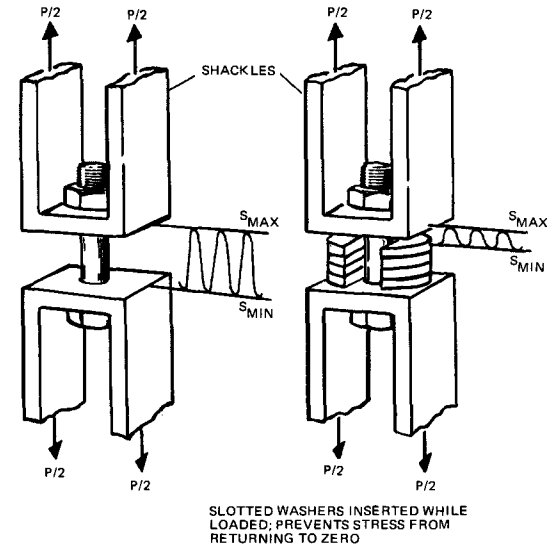

Fig. C13.30
Analogy of Stress for Loose and Pretorqued Bolts

Now suppose with the load fully applied, slotted washers are inserted in the gap as shown in Fig. C13.30 (right). The washers prevent the stress from returning to zero; however, they do not influence the maximum stress as shown by the clearance between washers and shackle. What this means is that the washers have added to the stiffness of the bolt so that the stress amplitude shown in Fig. C13.30 (right) is exactly the same as though the area of the bolt were increased by the cross-sectional areas of the washers.

Since the bolt experiences tensile stresses while resting on the washers in the unloaded position, the same effect can be achieved by torquing the bolt to the same tightness as when unloaded and resting on the washers.

Torquing to higher tensile stress will not change the stress amplitude as the amplitude is determined by the combined factors of bolt stiffness and abutment material (shackles in this case). However, maximum stress is increased and, therefore, a reduction in fatigue life will follow as compared with the fatigue life when exactly the right amount of torque is applied.

Accordingly, there is no point in using exceedingly high torque values unless loading is exceptionally high. This means that there is only one torque value that is optimum for a given loading condition. In the example given in Fig. C13.30, the torque value would permit

the shackle to float clear when fully loaded. Thus, the torque does not increase the stress due to loading.

This principle of increased rigidity for added fatigue life applies to interference-type fasteners. Interference fit introduces residual tensile stresses around the periphery of a hole which are not beneficial per se; however, they do permit structures to gain extra stiffness afforded by the fastener. The interference fastener serves as a seat on which the stressed material rests when unloaded, very much like the stack of washers in the bolt example.

A graph of taper pin interference versus fatigue life of lugs tested at 12 ksi (gross area stress, R = 0.1) is shown in Fig. C13.31. Note that a drop in fatigue life is experienced after 0.0035-inch interference. This agrees with the previous statement regarding one torque value being optimum for a given loading. The lugs were 0.1-in. thick 7075-T6, 1.31-inches wide and were loaded through 3/8-inch diameter taper pins.

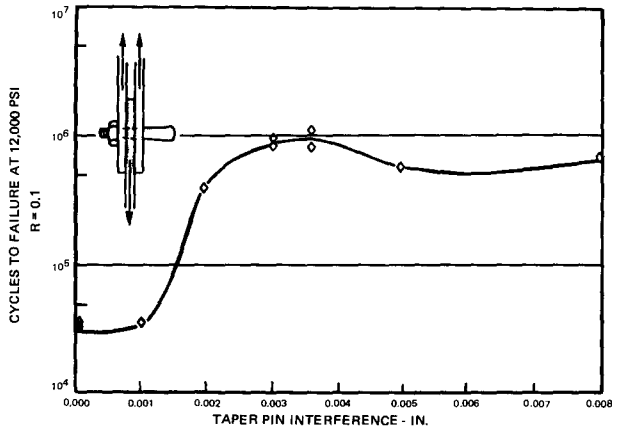

Fig. C13.31 - Effect of taper pin interference on fatigue life of small lugs. (from Ref. 21)

Schematic diagrams of stress cycling which correspond to interferences of zero, 0.002, 0.0035, and 0.008-inch are shown in Fig. C13.32. The amplitude for 0.008-inch interference is the same as for the 0.0035-inch interference; however, maximum stress is increased by too much interference.

Although 0.008-inch interference produced a shorter life than where 0.0035-inch interference was used, fatigue life was still greater than where no interference was used, indicating a wide tolerance of interference fits for fatigue life improvements. Too much interference, however, will invite stress corrosion when fasteners are installed in an adverse grain direction.

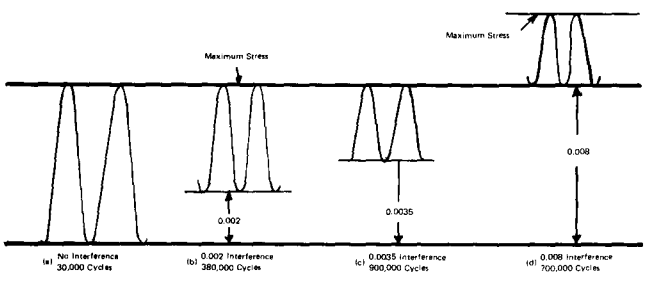

Fig. C13.32 - Schematic diagrams of stress cycle for lugs loaded with 3/8-inch diameter taper pins show how fatigue life is affected by interference type fasteners. It is assumed that no increase in maximum stress results from interferences below 0.0035-inch. The amplitude for 0.008-inch interference is the same as for 0.0035-inch interference, however, the maximum stress is raised which accounts for shorter life.

The previous discussion is further confirmed by tests on 3.75-inch wide lugs where interferences as high as 0.010 (0.008-in./in.) were used. The hole diameter was 1.25 inches, giving a theoretical stress concentration of 3.5. Bushings of hardened steel having wall thickness of 1/4 and 1/8 inch were pressed in at varying amounts of interference from zero to 0.010 in. Bushings were chamfered 10 degrees to enable pressing in without extruding material from the lugs. Chamfered ends were ground off after pressing (see Fig. C13.33)

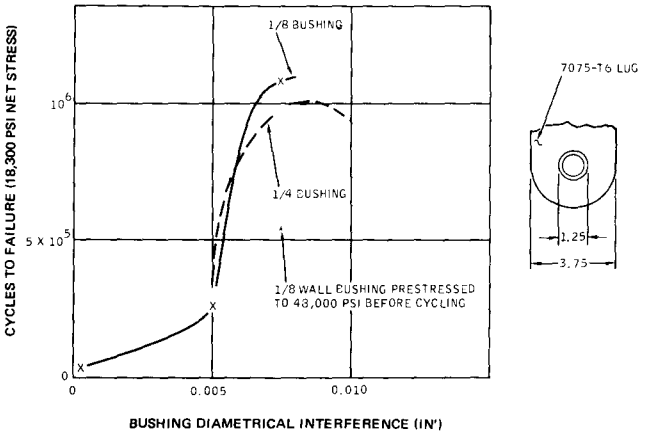

Fig. C13.33 - Effect of Interference-fit bushings on fatigue life of lugs (30).

The points plotted represent an average of 4 tests each. Of special interest is the case where the lugs were prestressed 48 ksi prior to testing. Having a stress concentration of 3.6, the 48 ksi nominal net stress caused local yielding which relieved some of the interference. At the same time; however, beneficial compressive residual stresses were being accumulated -- that is, they would be compressive if it were not for the bushings.

Fig. C13.34 compares lives of small lugs for cycling at 20 ksi gross area stress after various preloads. These specimens were the same as used for Fig. C13.31, except tapered bolts were used to transmit the load instead of tapered pins. Here it is seen that life was increased from about 30,000 cycles to 500,000 cycles where no preloads were present (20 ksi prestress is same as cycling stress). With 30 ksi prestress (10 ksi above cycling stress) no apparent change existed with those specimens having 0.003-inch interference; however, the non-interference lugs experienced a slight gain. By the time preloading was up to 40 ksi, there was practically no difference between specimens with and without interference. In other words, the gain in residual compressive stresses offset the advantages of interference. This holds true up to prestresses of 50 ksi. Gross area stresses are used here to simulate structural joints where net areas are hard to determine.

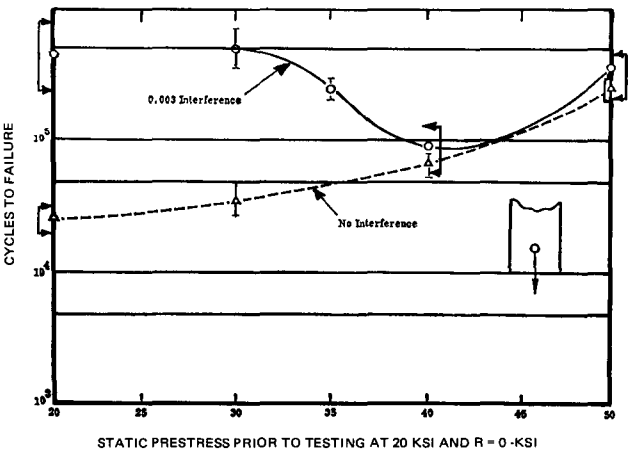

Fig. C13.34 - Effect of static prestress upon subsequent fatigue life of 7075-T6 lugs cycled at 20 ksi gross stress, R = 0[31]

On a percentage basis, because of increased lives of specimens without interference, it appears that the greatest percentage loss on beneficial effect of tapered bolts occurs at prestresses between 30 and 35 ksi (see Fig. C13.35).

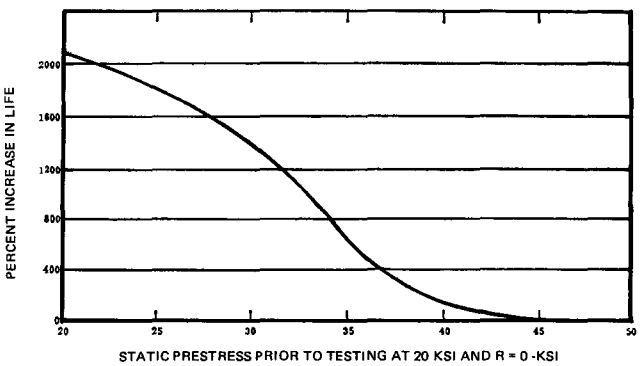

Fig. C13.35 - Effect of static prestress upon percentage life increase produced by using tapered bolts.

C13.5.7 Combined Rigidity and Residual Stress

The object of presenting the effects of preloading on the life of specimens with interference fasteners is to acquaint the reader with what might be expected when high loads in service do essentially the same thing. This would infer that, if indeed such stresses were experienced in service, the main advantage of using interference fasteners would be for that percentage of life consumed prior to encountering the high load. In fact, some airplanes may never experience a load sufficiently high to relieve the prestress provided by interference fasteners. However, most designs have to be made on the assumption that a high load will occur fairly early in life; in fact, the test airplane will undergo such loading, even if the service airplanes do not. Accordingly, the designer is contractually obligated to design the airplane to a specific set of test loads which include loads high enough to cause local yielding unless special precautions are followed.

A solution to the problem of interference relief due to high loading can be visualized by a recap of approximately what happens. Fig. C13.36 shows schematic stress cycling at 20 ksi after preloading as in Fig. C13.34. Here, the stress cycling for specimens with 0 interference is determined by using the unnotched S-N curves of Fig. C13.10, using a stress range (58 ksi in this case) and appropriate stress ratio to agree with life after preloading. The 58 ksi stress range was found from the original life for cycling at R = 0, assuming that no residual stresses were present in the virgin specimens. A try and fit procedure is then used as for Steps 4 and 5 of Example Problem (1).

Stresses for specimens with 0.003 interference are found by using S_{max} for the non-interference specimens and determining stress ratio from the intercept or S-N curve and appropriate life. It is necessary to interpolate between curves to agree with test life. The assumption that S_{max} is the same for specimens with and without interference could be in error if the interference alone caused a higher stress than that caused by loading. However, such an error would not affect the purpose of the illustrations.

The schematics in Fig. C13.36 show a gradual increase in residual compressive stress with preload increase. This produces an increase in life for those specimens having 0 interference and a decrease in life for those with 0.003 interference until a low of 86,000 cycles is reached after a 40 ksi preload. The trend is then reversed where both types experience gains in life. Presumably, the benefits

interference should have disappeared with the 50 ksi preload; however, some benefit might be due to the lateral constraint afforded by the interference fit. In any event, the difference in life is sufficiently small to discount any improvement due to interference.

Considering now the residual stress of -36 ksi in Fig. C13.36 (d), the 50 ksi preload could probably be reapplied without a change in residual stress. Also, it would appear that the -36 ksi could have been introduced by coining or other methods prior to installation of the interference fit fastener. This would mean that a structure fabricated in such a manner could withstand high loads encountered in service without experiencing a lowering of subsequent life.

Not only would the pre-coined interference fastener type construction provide relief from the damage done by overstressing, but the actual life would be increased. Using the S-N curves of Fig. C13.10, consider a case where a structure fails after 11,000 cycles when loaded at R = 0. From the S-N curves, it appears as though the actual stress at the concentration must have been about 70 ksi (see 11,000 cycles and R = 0). Were it possible to use an interference type fastener at the location of failure such that the actual stress cycle was at R = +0.5, the life would be increased to 60,000 cycles.

Instead of using an interference fastener, suppose that the part were coined to produce a residual compressive stress of -35 ksi. The stress for the same load condition then would be ± 35 ksi (still a range of 70 ksi) which would result in a life of 55,000 cycles, which is no improvement over just using an interference fastener.

However, if the part were coined in addition to using an interference fastener, the life would be about 700,000 cycles as found in Fig. C13.10 for stressing at 35 ksi and R = 0. In this case, the -35 ksi due to coining is

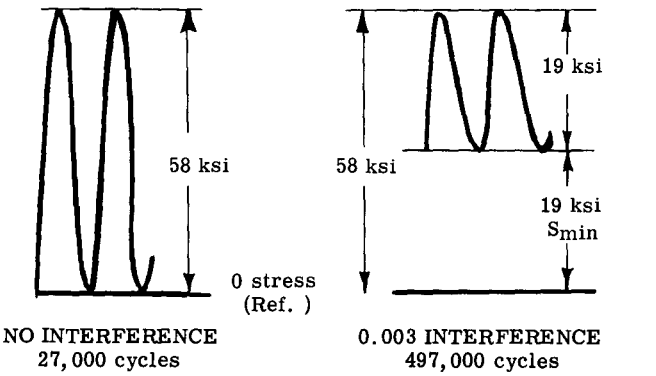

(a) Stress cycle before preload

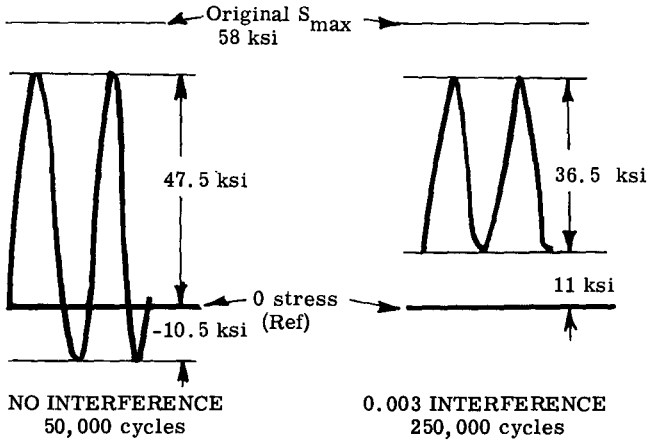

(b) Stress cycle after 35 ksi preload

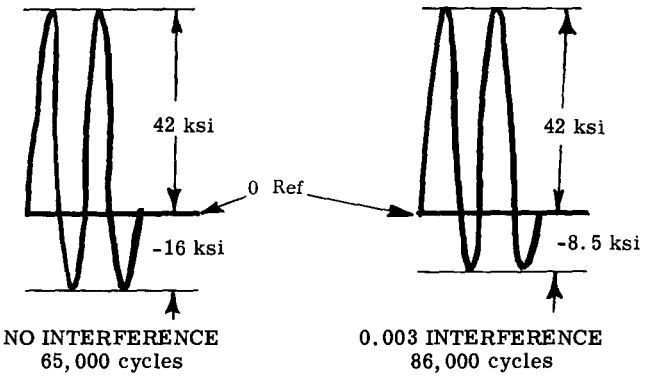

(c) Stress cycle after 40 ksi preload

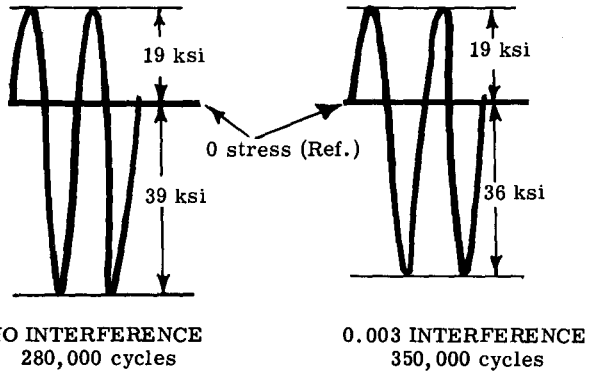

(d) Stress cycle after 50 ksi preload

Fig. C13.36 - Effect of preloads on subsequent cycling of lugs having interference and non-interference-fit loading pins.

taken up by the interference fastener so that the stress range becomes 35 ksi. These are schematically shown in Fig. C13.37.

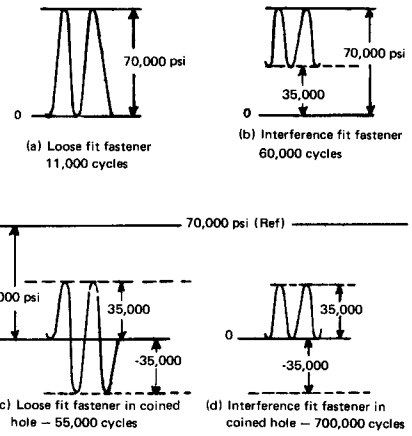

Fig. C13.37 - Diagrams show comparison and improvement in fatigue life obtained with interference fasteners, coining, and combined coining and interference.

Static and fatigue properties were discussed above to illustrate the effect of residual compressive stresses, added rigidity, and combinations of residual stress and rigidity. The discussion on rigidity covered the effects of torqued bolts and interference fasteners.

In the case of torqued bolts it was shown that pre-stress introduced by torquing enables bolts to employ the extra stiffness or rigidity afforded by abutting material. Although interference creates peripheral tensile stresses at the edge of a hole, it is beneficial because the extra stiffness afforded by the fastener reduces stress amplitude.

Coining was described as a method of introducing favorable residual stresses. While coining is usually thought of as a sort of ring staking, other methods such as burnishing inside of holes by mandrel operation, would not apply to tapered holes -- at least at the present state-of-the-art. To achieve the benefits anticipated by the foregoing, a method for achieving interference with straight fasteners or a method of coining tapered holes is needed.

One method for coining a tapered hole would be to over-drive a tapered mandrel to achieve given amounts of permanent set prior to installation in a normal manner. At present, this is not a common practice.

Until recently there has been no fastener specifically designed to introduce residual compressive stresses. A cross section of a newly developed fastener is shown in Fig. C13.38.(32) The fastener is squeezed or bucked more or less like a conventional rivet; however, the head is embedded flush with the surface. The special feature is a lip around the periphery of the head, which coins the hole as the fastener is embedded into the material, displaced material flows into the annular groove under the head and along the reduced section of the shank, thus making the fastener head and material being fastened an integral part of the structure. This reduces hole deformation more or less as though a staple were driven across the hole (more on this later). Corresponding stress reduction is not known at the present time; however, fatigue data indicate that the combination of coining, load transfer, and interference fit contribute substantially to fatigue life increase. Interference is attained by fastener swelling and by flow of metal toward the shank as a result of coining.

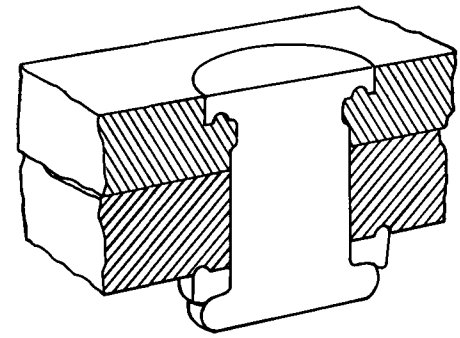

Fig. C13.38 - Newly developed fastener that coins

S-N data comparing fatigue strengths of one-and-one-half dogbone specimens fastened with aluminum rivets, tapered bolts, and Stress Pins* are shown in Fig. C13.39. Here we see that a substantial increase in life is shown by using Stress Pins except for the extreme higher load levels. It is of interest to note that the curves for specimens with tapered bolts and those with aluminum rivets appear to converge at the lower load levels. The reason for this is that the interference used for specimens with

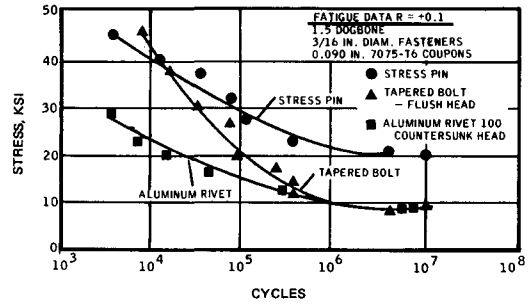

Fig. C13.39 - S-N curves showing fatigue strengths of specimens fastened with countersunk aluminum alloy rivets, tapered bolts, and Stress Pins.

---

* Trade name for fastener developed by Standard Pressed Steel Co., Jenkintown, Pa.

tapered bolts actually raised the stress at low load levels; however, it will be shown later that proportion of damage in this area is small as compared to that experienced at higher load levels (see Sec. C13.6). A lower interference would raise the life at low loads and reduce life at high loads with the net result of reducing service life--service life being a function of all load types. Had the interference been lower, the curve for specimens with tapered bolts would probably fall about midway between the curves for specimens with rivets and with Stress Pins.

A word about the one-and-one-half dogbone specimen shown in Fig. C13.40. The object of the particular configuration was to simulate the spar-to-skin attachment of an airplane wing wherein about 50% of the axial stress in the skin is due to the load transferred from the web through the fasteners. Strain gage measurements, however, revealed that but 40% of the load was transferred from the half dogbone (representing the web) to the full dogbone in the case of specimens with tapered bolts and those with Stress Pins. Transfer for specimens with aluminum alloy rivets was 26%. The special advantage of using such a specimen is that but one fastener is needed per specimen. A complete description of the specimen is given in Ref. 32.

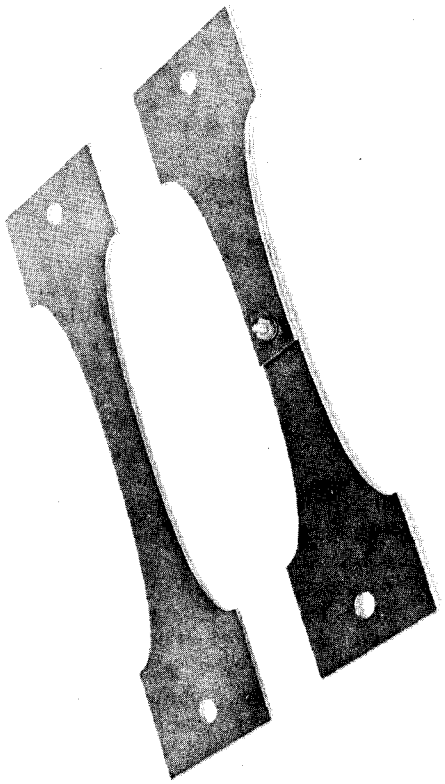

Fig. C13.40 - One-and-one-half dogbone test specimen simulates spar-to-web attachment.

C13.5.8 Load Relief at Fasteners

So far, we have discussed methods of "living with" the stress at a concentration. A better way is to reduce the stress if it can be done without increasing weight. Following are methods which have been proven and add little if any weight--sometimes weight is reduced.

Redistribution of Load

In most mechanically fastened joints, stress concentrations fall somewhere between those for open holes and those for pin-loaded holes. This stems from the fact that these joints (except for lugs) usually incorporate more than one fastener. In these cases, the load is not equally divided between fasteners

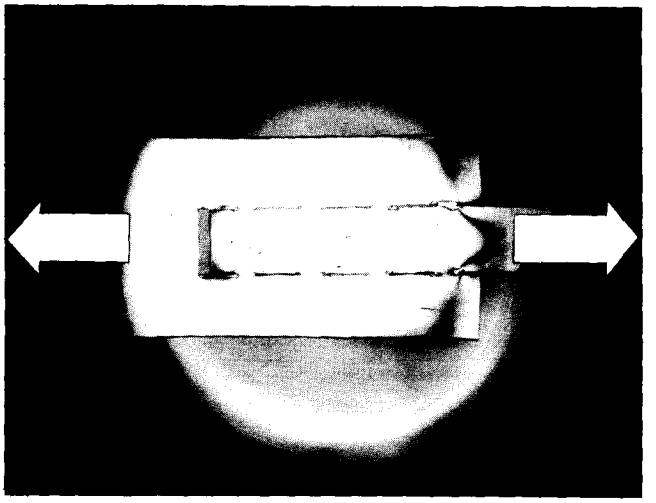

Fig. C13.41 - Photoelastic model showing load distribution between fasteners in a clevis joint.

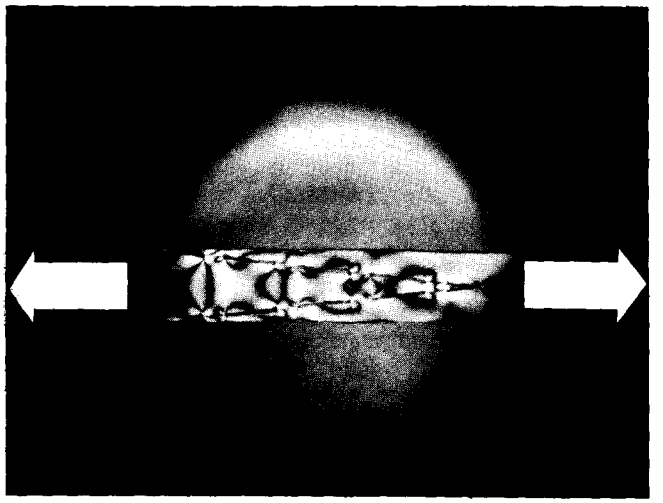

Fig. C13.42 - Improved load distribution is had by scarfing.

and the fastener nearest source of load introduces stresses more like those in the pin-loaded hole as shown in Fig. C13.3. Fig. C13.41 shows the load distribution in a four-fastener clevis joint.(33) Here the amount of stress is demonstrated by the number of photoelastic fringes at each of the fasteners. Scarfing the joint reduces the stress at the first fastener as shown in Fig. C13.42. However, scarfing is not very practical from a fabrication point. A similar effect can be had by using an auxiliary thin doubler(34) that picks up one fastener nearest source of load. The thin doubler is incapable of carrying more than its share of load. Adjustments would have to be made for static strength because of bearing strength in the thin doubler; however, an easy method is simply to assume that the fastener through the thin doubler carries no load. A comparison of the fatigue lives of conventional joints and joints with auxiliary thin doublers is shown in Fig. C13.43.

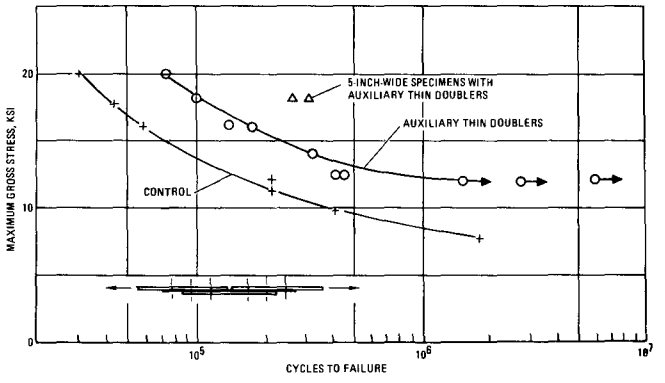

Fig. C13.43 - Effect of auxiliary thin doubler on fatigue strength of 2024-T3 aluminum alloy single-shear butt joints.

Separate Axial from Bending Stresses

Since airplane structures employ single-shear joints because of aerodynamic smoothness, bending stresses are added to the stresses due to load transfer in the joint. This is illustrated in the single-shear butt joint shown in Fig. C13.44 where a rivet driven through the edge of the doubler causes it to last 5 times as long. Here, the edge-driven rivet is incapable of carrying other than a clamping force, leaving the loaded rivets free of bending stresses.(34) The nested angle specimens were designed to eliminate as much bending as possible without the aid of edge-driven rivets. The effect of bending is even more pronounced in lap joints. Because of this, lap joints should be avoided wherever possible except where stresses are extremely low.

Sculptured Skins

With the advent of profile milling, it has become common practice to machine material away from low-stressed areas to reduce weight, leaving full-thickness material at splices. Thus entire airplane wing skins might be machined except for the raised lands in splices and other critical areas.

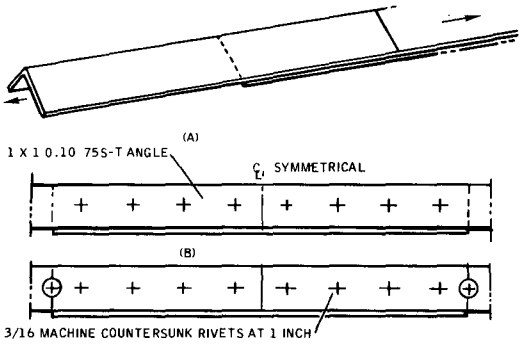

Fig. C13.44 - Edge driven rivet improves fatigue strength of single-shear butt joints.

While it is never possible to achieve a situation where the structure away from the splice is completely free of concentrations, the thickened lands in the splice area permit working the remaining areas to higher stresses than would be possible by other means.

Since the raised lands involve fillets at the juncture of machined skin and parent material, there could be a situation wherein the stress at the fillet is worse than at the fastener holes being protected. This comes about by virtue of the single-shear attachment of a flush joint, introducing bending stresses that are exaggerated by the increase in moment arm separating the centroids of skin and doubler when the land thickness is increased. Furthermore, as load is increased, a certain amount of alignment takes place so that the ratio of bending to axial stress is not proportional to load. Accordingly, the effect of stress concentration at fillets is load related and has to be considered in the design of the structure.

A typical example is a single-shear butt joint having equal thickness skin and doubler. Here, the bending stress alone turns out to be 3 P/A at the time P = 0. When the load is increased, the skin and doubler tend to align themselves so that eventually an increase in load does not increase stress due to bending. Certainly, by the time the entire cross-sectional area has yielded, the stress can be assumed to be P/A even though a substantial difference exists in strains due to bending. Fig. C13.45 presents stress-corrected concentration factors for a 7075-T6 aluminum alloy joint having equal land and doubler thickness.(36) These curves were obtained by multiplying the ratio of calculated bending stress/axial stress times the

concentration factors shown in Fig. C13.46. Calculations were checked experimentally with electrical resistance strain gages.

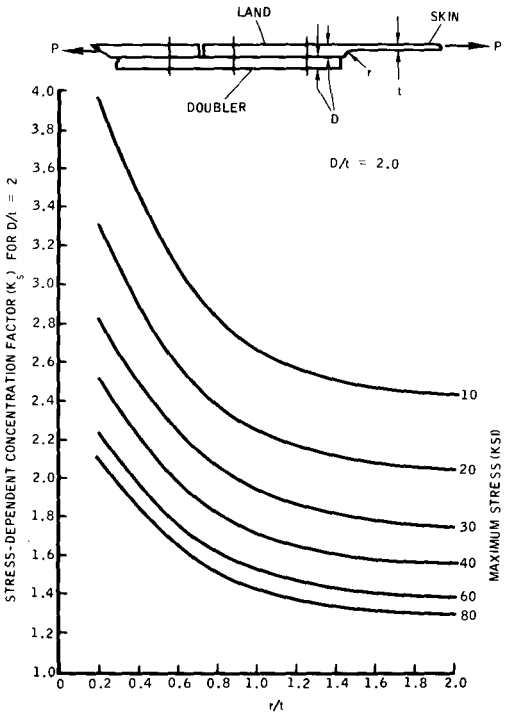

Fig. C13.45 - Stress-dependent concentration factors for fillets in landed structures having equal land and doubler thicknesses.

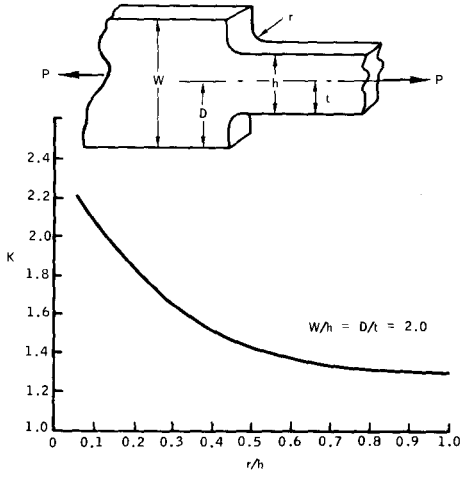

Fig. C13.46 - Stress Concentration for Bar with Fillets Loaded in Tension--D/t = 2 --(Taken from Ref. 6)

From the foregoing, an even larger radius would further reduce the stress. However, there are times when there is no room to permit using a radius sufficiently large to reduce the stress the required amount. In such cases, a variable radius that is generated by intersections of straight lines as shown in Fig. C13.47 will lower the stress.(37) However, if space permits, an even greater reduction in stress can be had by using unequally spaced divisions on the vertical and horizontal axes as shown in Fig. C13.48.

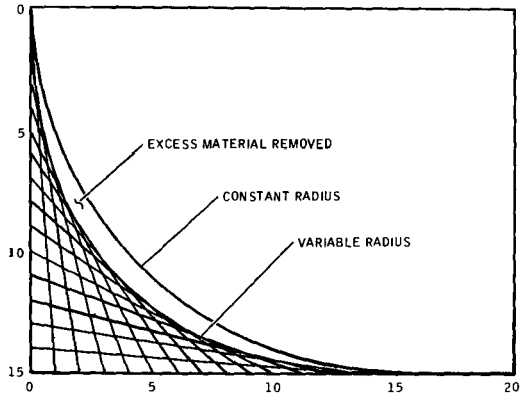

Fig. C13.47 - Variable-radius fillet generated by intersections of straight lines removes material while reducing stress.

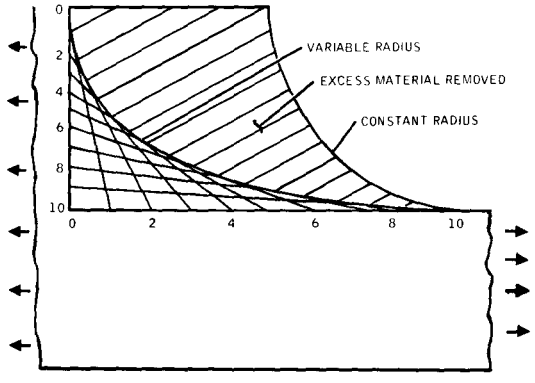

Fig. C13.48 - Approximate streamline fillet

From the above, it would appear that even with lands, the effect of stress concentrations cannot be entirely eliminated. This is particularly true for spanwise lands where the stress is directly proportional to the wing depth and radius of curvature of the deflected wing. Unless local reinforcing reduces the curvature, the bending stress will not be reduced. This usually is the case because local increase in thickness over spar attachemnts adds little to total wing moment of inertia.

This concept is more easily understood by visualizing the stresses in a bar like that shown in Fig. C13.49a. With the bar stressed in tension, the strain is defined as elongation divided by original length: $\varepsilon = \frac{\Delta \ell}{\ell}$, However, when the bar is bent 180° as shown in Fig.

C13.49b, the bend angle cancels out in the computation as follows: $\ell = \pi R$ (assuming length does not change at neutral axis) and

$$\Delta \ell = \pi (R + \frac{h}{2}) - \pi R = \pi \frac{h}{2}$$

(difference between length at neutral axis and periphery)

$$\varepsilon = \frac{\Delta \ell}{\ell} = \frac{\pi (h/2)}{\pi R} = \frac{h}{2R}$$

(or difference in strain at periphery and at neutral axis).

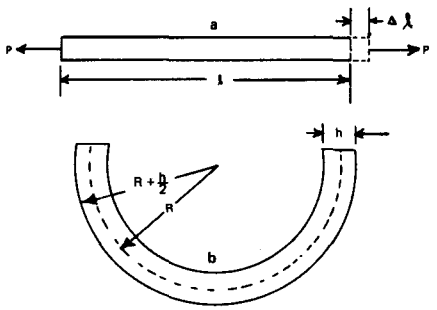

Fig. C13.49 - Strain in bar at (a) which is loaded in tension is found by dividing elongation by original length. When the bar is bent as shown at (b) strain equals h/2R.

Thus, we have the case of the skin having the same stretch whether or not spanwise lands are added. In such cases, the stress at fastener holes cannot be cut in half by doubling skin thickness with lands as one might first suspect. However, lands do provide extra bearing area which permit using countersunk fasteners that might otherwise leave sharp edges instead of bearing surfaces. Unless material is removed from the lands between holes, the axial component of stress will be exactly the same. In other words, we have to force the material in areas away from the concentration to deform more in order to reduce deformation at holes.

The above illustrates a basic principle that should be followed in all designs--STRESS AT A CONCENTRATION CAN BE REDUCED BY REMOVING MATERIAL AWAY FROM THE CONCENTRATION. Thus in the case of the auxiliary doubler (Ref. Fig. C13.43), the same effect could have been attained by removing material from the doubler between the first and second rows of fasteners. In the case of the improved fillets (Ref. Fig. C13.47) we see that material can be removed to reduce the stress.

C13.6 CUMULATIVE FATIGUE DAMAGE

C13.6.1 Introduction

We have seen that the life of a structure or a specimen can be represented by S-N or Load-N curves when cycling at constant amplitude. However, in service, a random mixture of loads occur at each flight with no one flight being exactly like another.

Not only does each flight vary, but aerospace structures have different required lives in terms of usage over a time interval. Examples of what flight vehicles are expected to endure are given in Table III[38]. Here it is seen that lives can vary from 20 years to but a minute or so, the twenty-year life for commercial aircraft being interpreted as 50,000 hours of flight. This means the manufacturer has to demonstrate by design and test that the structure will withstand loads whose cumulative effects are equivalent to 50,000 hours of flight. Military airplanes have expected lives of from 3000 hours for a fighter to 30,000 hours for a trainer.

C13.6.2 Loads

Flight data are usually obtained by means of counting accelerometers located near the G.G. of the airplane and such information is then plotted in the form of ogive curves as shown for gust loading in Fig. C13.50[39]. In addition, maneuver, ground-air-ground (G.A.G.), landing, and taxi loads are added to

TABLE III

FATIGUE REGIMES RELATED TO FLIGHT VEHICLE STRUCTURES

Structure	Target Life	Magnitude of Repeated Loads	Frequency of Occurrence of Repeated Loads	Operational Experience	Effect of Natural Environment in Reducing Vehicle Fatigue Strength
Commercial Aircraft	Approx. 20 yr.	Medium	High	High	Low to medium
Military Aircraft	4-8 yr.	High	Medium	Medium to high	Medium to high
* Launch	min.	High to very high	High	Low	Low to medium
Spacecraft	1-10 yr.	Low to medium	Low	Nil	Low to unknown

* Reusable boosters not considered

make the complete load spectrum.

Actual loads for design purposes, being related to speed, aerodynamic, rigidity, and various other properties of a given airplane, are usually specified by agreement with the contacting agency. Since loads for a particular airplane are largely due to the type of operation and flight paths contemplated, it is usually common to use a set of conditions which will involve the more critical of a fleet of airplanes. Despite this, one airlines operator may experience fatigue proglems while another, using the same make of airplane, may experience no difficulties whatsoever. In any event, the designer has to design a structure which will pass a simulated service loads test for a required number of equivalent hours.

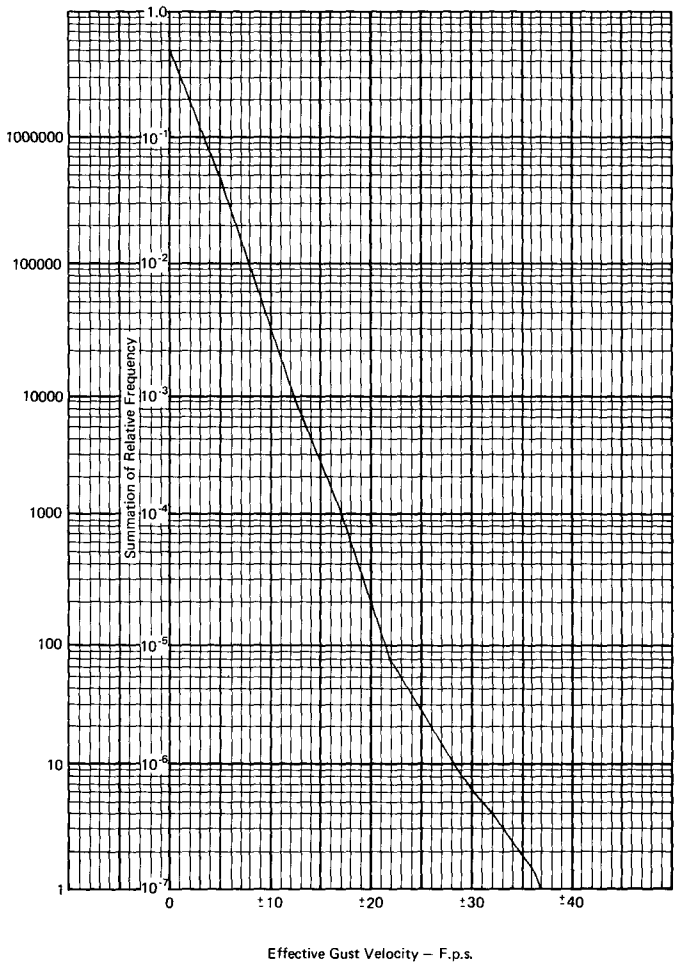

Fig. C13.50 Ogive curve from Ref. 39

The loads used for design and test may not reflect actual loads in service in that compromises are usually made such that the most critical of one flight condition is blended with other critical conditions to end up with a composite of all conditions.

In general, fighter airplanes are more critical in maneuver and landing conditions than for gust. Transport airplanes, on the other hand, are more critical for gust loading. Table IV(40) shows maneuver load spectrums for various military airplane where Fighters, Patrol, Utility, and Transport airplanes fall into classes A, B, C, and D, respectively.

TABLE IV

FREQUENCY OF MANEUVER LOADS

Number of times per thousand hours that load factor is experienced				
Percent of maximum (positive) symmetrical limit load factor	Flight maneuver load spectrum A	B	C	D
35	17,000	25,000		
45	9,500	10,000	10,000	
55	6,500	3,500	3,000	1,000
65	4,500	1,000	1,000	150
75	2,500	500	300	20
85	1,500	200	200	3
95	300	75	30	0.5
105	150	25	10	0.05
115	40	10	3	
125	16	3	2	

TABLE IV (cont'd)

Percent of minimum (negative) symmetrical limit load factor)	Flight maneuver load spectrum A	B	C	D
0	500	5	0.7	
10	200	2	0.5	
20	100	1	0.25	
30	60	0.25		
40	35			
50	30			
60	25			
70	20			
80	15			
90	10			
100	5			
110	3			

NOTE: Above load factors are considered to vary from unity to each specified maneuver load factor to unity again for each occurrence.

While the above loads to not include gust, landing, nor taxiing loads, they will serve for the illustrative problems to follow. It should be noted that effects of gusts are largely dependent on individual characteristics of a given airplane. A conversion of gust velocities (Ref. Fig. C13.50) to load factors, while suitable for the individual airplane concerned, might be misleading for other airplanes.

The loads in Table IV, while seemingly severe, justify themselves in that airplanes which successfully passed fatigue tests using such spectra have given but few fatigue problems, while those using less severe loading have given numerous problems, notwithstanding the fact that all airplanes met the same static requirements.

One problem lies in when the highest load in the spectrum occurs. Early applications of

high loads may either increase life or lower it. This will be discussed in C13.6.4.

C13.6.3 Predicting Life

Cumulative fatigue damage may be defined as a degradation due to repeated stressing which is additive with each cycle. If an airplane were critical only at but one point, and no residual stress or fastener loosening due to high loading influenced subsequent life, then, supposedly if 50% of life were spent at one load level, there should be 50% of life remaining which could be spent at any load or mixture of loads before failure occurs.

First proposed by Palmgren in 1923[41], a method for adding fractional damages had not come into general usage until a paper by Milton Miner[42] presented considerable data that substantiated the method.

In general, the method proposes that if a structure were to fail after N_1 cycles for loading at a stress S_1, N_2 cycles at a stress of S_2 and N_n cycles at a stress corresponding to S_n, then that structure would fail when $\Sigma\, n/N = 1$, where n_1, n_1, and n_n are partial lives spend at their respective stress levels.

Since the method is still being used throughout industry and various services, examples of how to use the method will be presented here. However, the reader must bear in mind that, while being a method still accepted, that consideration needs to be made regarding the type of structure involved. While the method is usually conservative for cases involving open notches (open holes, fillet radii, etc.), structures having rivet filled holes or employing interference-fit fasteners have to be critically examined to determine whether the highest load in the spectrum enhances or is detrimental to subsequent performance at lower stresses. As shown by effects or preloading on lugs (Ref. Fig. C13.34), more than half the anticipated life can be lost when preloading is such as to loosen the fastener.

Consider a 4000-hour fighter airplane whose limit stress is 30 ksi based on gross area. From Table IV, we first compute the stresses corresponding to the specified loads. For simplification, let us consider that loading is with respect to zero instead of 1G and omit the negative loads on the assumption that the extension of each load cycle to zero will produce damage equivalent to the loads omitted.

Assume further that the equivalent stress concentration factor for the structure is 3.1 based on gross area. This enables us to use an S-N curve for hole-notched speciments for loading at R = 0 (Ref. Fig. C13.51). Now we simply

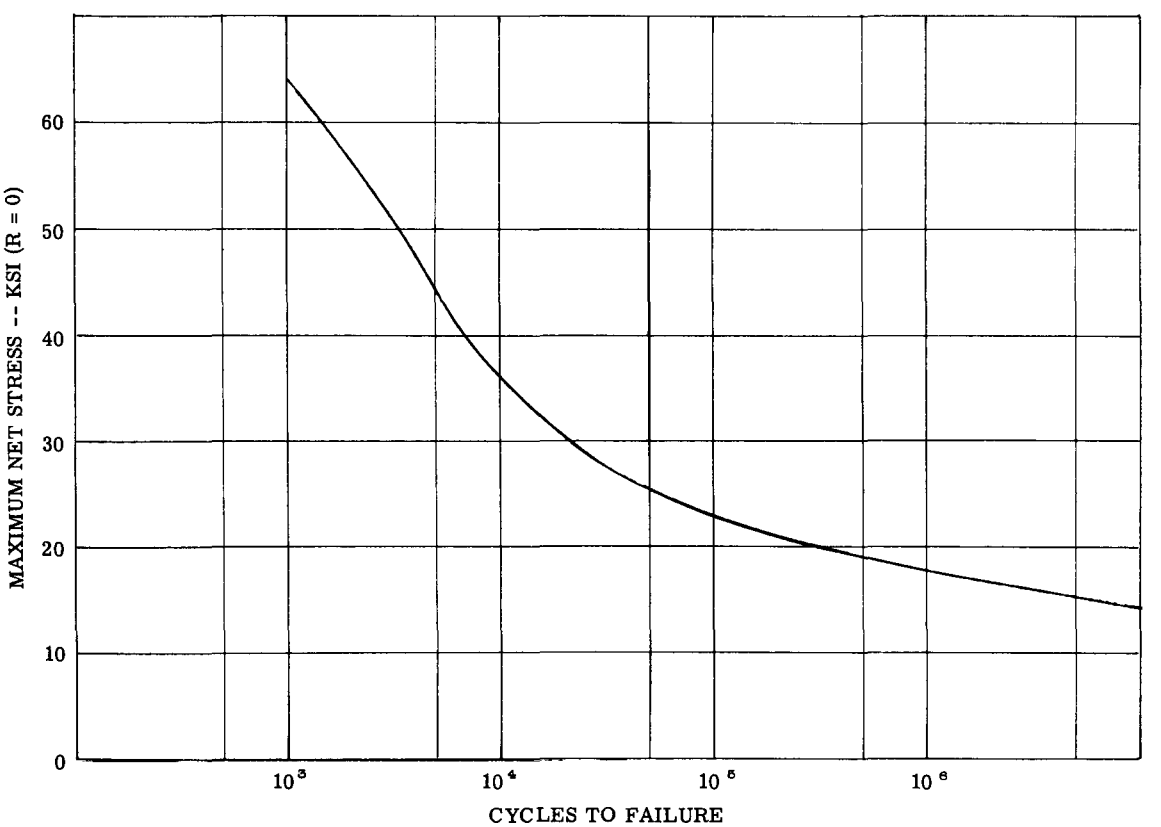

Fig. C13.51 S-N Curve for 7075-T6 Aluminum Alloy -- K_t = 3.1 (gross area)

record the lives for each stress level (N) and compute the ratio of n/N as shown in Table V. The sum of the incremental damages add up to 0.107 so that the life is found to be 1/0.107 = 8,876 hours, say 8,900 hours because of significant figures.

TABLE V

CALCULATIONS FOR FATIGUE LIFE OF 4000-HOUR AIRPLANE (Ref. Table IV)

Load % Limit	n (per 1000 hr.)	Stress (ksi)	N	n/N
35	17,000	10.5		0
45	9,500	13.5	10^7 +	0.00095
55	6,500	16.5	1,700,000	0.00382
65	4,500	19.5	350,000	0.01286
75	2,500	22.5	100,000	0.04000
85	1,500	25.5	50,000	0.03000
95	300	28.5	27,000	0.01110
Limit (Ref)		30.0		
105	150	31.5	17,000	0.00882
115	40	34.5	12,000	0.00333
125	16	37.5	9,000	0.00178

$$\Sigma n/N = 0.11266$$

$$\text{Life} = \frac{1}{0.11266} = 8,876 \text{ hours}$$

To allow for a scatter factor of 4, the calculated life should be 16,000 hours. Accordingly, our assumption of a 30 ksi limit stress was too high, assuming that the stress cannot be reduced by reducing the stress concentration. The problem now is to "guess" the stress reduction needed. For the time being, let us assume that the reduction in stress at limit load would be proportional to lives of notched specimens for a stress at a lifetime which is 16,000/8,876 greater than the life corresponding to the limit stress of 30 ksi, 20,000 cycles in this case. Accordingly, we have 1.802 x 20,000 = 36,040 cycles whose corresponding maximum stress turns out to be 27.0 ksi. Using the same procedure as shown in Table V, we determine the life to be about 21,000 hours. Successive calculations for limit stresses of 28 ksi and 29 ksi yielded lives of 17,000 and 13,000 hours. Plotting limit stresses vs. calculated hours of flight, we have a straight line as shown in Fig. C13.52. From this we interpolate the allowable stress at limit load to be 28.3 ksi.

While the above computations imply a greater accuracy than is justified by the source of data, we have to work to something and that is the reason for the scatter factor requirement in design. Depending on the contracting agency, the airplane when finally built will have to undergo simulated service loading for an equivalent of 4 lifetimes. While it can hardly be expected that the test will be completed without some failures, minor though they may be, the designer should be cognizant of what the penalties might be should an early failure occur. Penalties as used here refers to costs of rectifying deficiencies and loss of time. Accordingly, it behooves the designer to be more conservative in the design of a wing spar than for replaceable parts, such as hinge brackets.

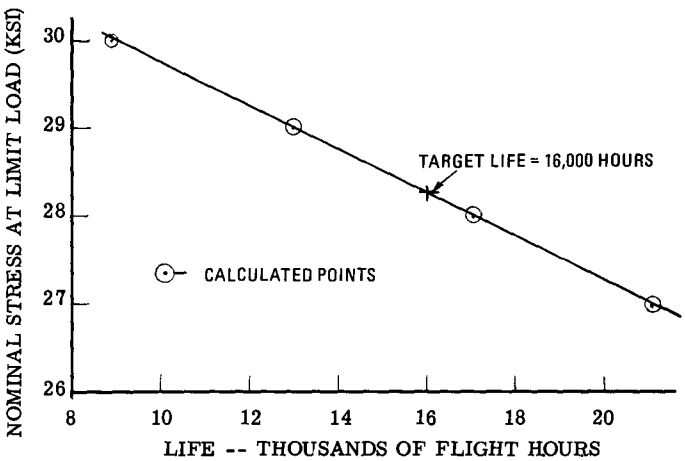

Fig. C13.52 Stress at limit load vs. valculated hours of flight (Ref. Table IV, Spectrum A, positive loads only)

In the above, we assumed $K_t = 3.1$ because of available test data. However, many airplane parts have concentrations far in excess of 3.1 while some may be lower. Having plotted limit stress vs. life as in the above, we are now in a position to estimate life for any stress concentration. For example, had the stress concentration been 4.0 instead of 3.1, we would simply lower the design stress by the ratio of 4.0/3.1.

Whether or not the design stresses, as plotted above, fall on a straight line depends largely on the load spectrum. However, whatever the spectrum, plotting computed lives as shown will enable the designer to visualize the steps needed to bring the structure up to fatigue requirements.

PROBLEM -- Find allowable limit stress for an airplane loaded according to Spectrum D of Table IV if required life is 50,000 hours. Actual life should be 200,000 hours to allow for scatter factor -- use $K_t = 3.1$, R = 0 -- positive loading only.

C13.6.4 Stress Interaction

Fig. C13.53 shows how simply deleting the two highest loads in a spectrum can greaty influence spectrum life, particularly for specimens using tapered bolts. Here it is seen that deleting the two highest loads increased life of specimens with tapered bolts by more than 4 times, while the same deletion reduced life of specimens with conventional fasteners. Specimens

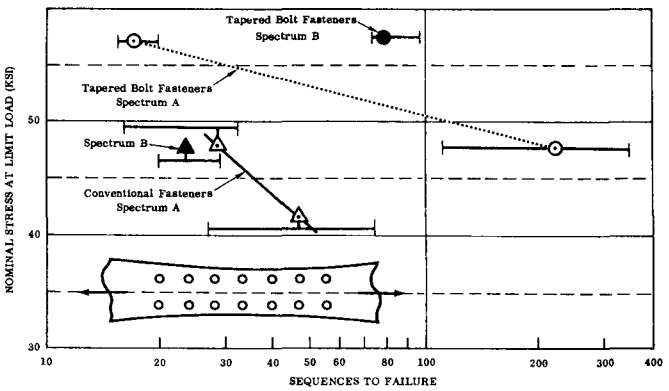

Fig. C13.53 Effect of varying the limit stress level in a spectrum on the fatigue life of specimens with unloaded fasteners (Ref. 31)

TABLE VI

LOAD SPECTRA FOR FIGURE C13.53

Per Cent Limit Load Factor		Cycles Per 100-Hour Sequence	
Maximum Load	Minimum Load	A	B
35	15.4	1200	1200
45	15.4	910	910
55	15.4	550	550
65	15.4	315	315
75	15.4	137	137
85	15.4	67	67
95	15.4	16	16
103.3	15.4	4	4
110.7	15.4	1	...
118.4	15.4	1 every 5 sequences	...

were 0.625-inch thick 7075-T651 rolled plate having multiple 1/4-inch diameter holes filled with unloaded tapered bolts or conventional fasteners. Test spectra given in Table VI, are roughly the same as for Spectrum A in Table IV.

The loading in the above is less conservative than used in Table V in that loads were not complete removed. However, for comparative purposes they are adequate. Referring to the total damage of 0.11266 given in Table V, we see that the two highest loads contributed but 4.5% of the total damage. Yet removal of equivalent loads in the above resulted in a loss of life for those specimens having conventional fasteners. Intuitively, we should think that removal of any load whatsoever would increase life. However, referring to residual stresses gained by overloading (Ref. Fig. C13.20), the above results are not surprising. However, this does point to the extreme care needed in anticipating the effects of high loading on a structure before attempting to predict fatigue life.

While it is not so easy to anticipate effects of high loads on structures using interference fasteners, if we consider a driven rivet as an interference fit fastener, we see in Fig. C13.54 that preloading can have the effect of both, reducing fatigue life, and again increasing life. Here riveted joints

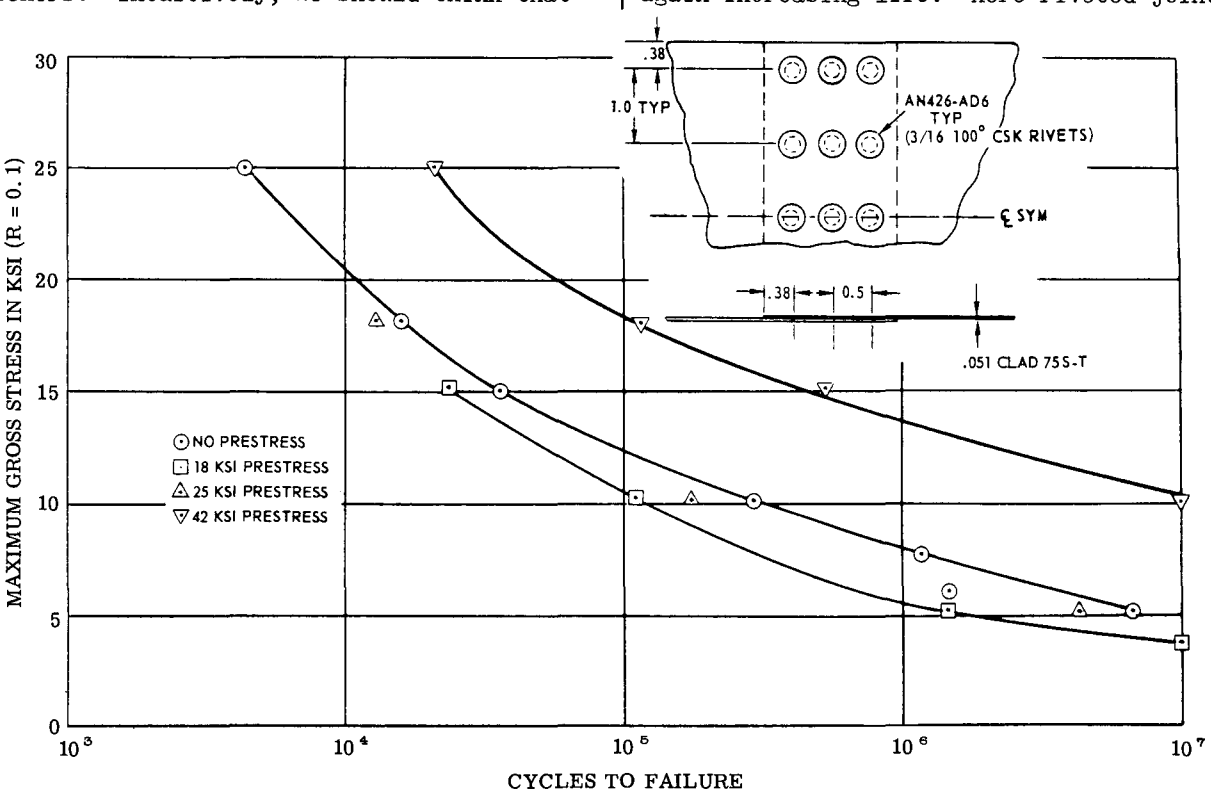

Fig. C13.54 Effect of prestress on fatigue life of riveted joints

were tested after varying preload conditions.[43] The center graph is the case where no preload is imposed and is the S-N curve normally used for estimating fatigue cumulative damage. The lower curve, the one we should be concerned with, represents specimens which were preloaded 18 ksi prior to testing. The average life is reduced to about 1/4 of the original. However, referring to Table V, we see that most of the damage is done in the 50,000 - 350,000 cycle life range (see lives for 65, 75, and 85 percent loading) where the average life (for riveted joints shown in Fig. C13.54) is reduced to about one-third of the original.

Had we used the middle curve for our previous calculations and then subjected the structure to a spectrum load test wherein 18 ksi was the highest load in the spectrum, we should have fell short of the design life by a factor of 3. On the other hand, had the highest load been 25 ksi (shown by triangles in the graph), the test life would have fell short by not more than 25%. Had the highest load been 42 ksi, the life would have exceeded calculated values by more than ten times.

In view of the wide discrepancies in fatigue life caused by stress interaction, we have now reached a point where an S-N curve for a complete structure or structural component appears only remotely related to its spectrum life. While most of the discrepancies can be definitely related to gains in residual stresses or loosening of fasteners, other factors such as fretting and corrosion have not been taken into account.

C13.6.5 Fatigue Strength Index -- An Easy Out

In the days of static designs, the limit load was supposed to be one which would never be exceeded during the lifetime of an airplane. Accordingly, some of the earliest fatigue tests were made using repeated limit loads wherein it was believed that 3000 - 4000 cycles were ample for any fatigue requirement. Referring to Figs. C13.52 and again to Fig. C13.51, we see that the calculated design limit stress of 28.3 ksi corresponds to a life of between 25,000 and 30,000 cycles. Accordingly, were we to design to this particular spectrum, why not simply design to a life of 30,000 cycles and not bother with trying to estimate cumulative damage?

While such a design is no guarantee that the structure will pass a spectrum load test, unless it could withstand 30,000 cycles of limit load, its chances of passing a spectrum test would be remote. This applies to the one particular spectrum; however, there should be some life (fatigue strength index) at limit loading which corresponds to an appropriate life for any given spectrum.

The choice of limit stress is used here because it is convenient in that it is a reference for static designs. Moreover, the stress should be high enough to impose whatever gains in residual stress or loosening of fasteners that might occur in service.

In 1963 (Ref. 7) the author introduced a method for predicting fatigue life of structures for service loading. It incorporated effects of residual stress resulting from the highest load in the spectrum. Prorating the stress ranges (including residual stress) due to limit loading with other loads in the spectrum, a good correlation between life at limit load and spectrum life was established for full-scale structures; however, the method was slightly unconservative for small specimens. Notwithstanding the discrepancies, a number of tests on small specimens did confirm the relation between constant-amplitude life at limit loading and spectrum life -- at least where conventional fasteners were used.

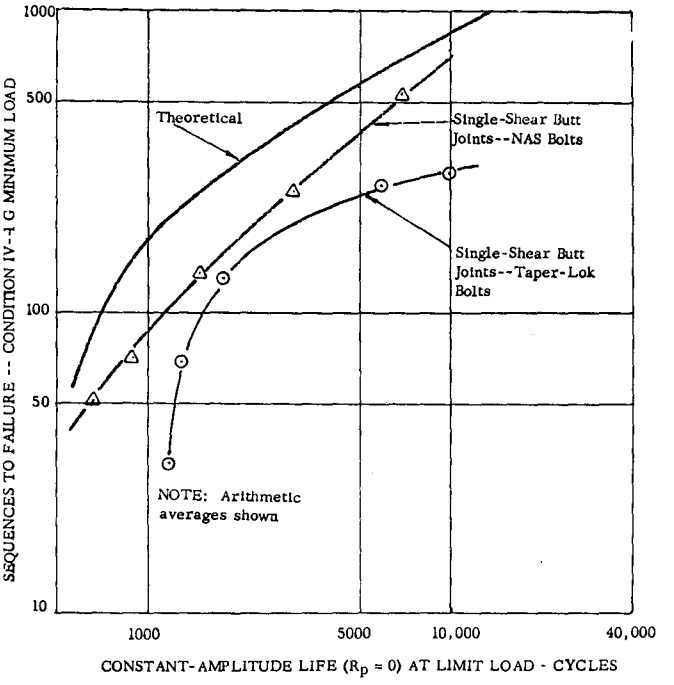

Fig. C13.55 Constant-Amplitude Life at 100 Percent Limit Loading (R = 0) versus Sequences to Failure (1 G Minimum Load)

Test results are shown in Fig. C13.55. Here we see that the theoretical curve and graph for single-shear butt joints would intersect at a constant-amplitude life of 30,000 cycles, in which case the design and actual life would concur. The curve for specimens with tapered bolts does not behave in a like manner, however. As might be expected from their behavior in Fig. C13.53, they are very sensitive to high loads in a spectrum. Also, their lower position with respect to spectrum

life is not because their spectrum life was lower, but that spectrum life in relation to their own constant-amplitude lives was lower. Note that the graphs are constant-amplitude life vs. spectrum life.

Constant-amplitude life vs. spectrum life for full-scale structures is presented in Fig. C13.56. Here we have excellent agreement between calculated and test lives. The calculations in this particular case involved using the life of the structure for limit loading in conjunction with a stress-strain curve for the material and S-N curves from Fig. C13.10 which are replotted in Fig. C13.57 to include a maximum stress cutoff line.

Here, it is assumed that the maximum stress at a concentration involves plastic deformation if life is fewer than 10,000 cycles. The slope of the cutoff line is determined by a point representing 3% strain at R = 0.9* and the yield strength of the material at R = 0.5

* R = 0.9 was chosen as a limiting value for residual compressive stress because of Bauschinger effects, which lowers compressive yield after once yielding in tension. The 3% strain conforms with a stress concentration of 4 times 0.75 (strain at 0.2% offset). Higher straining would supposedly yield the entire cross sectional area.

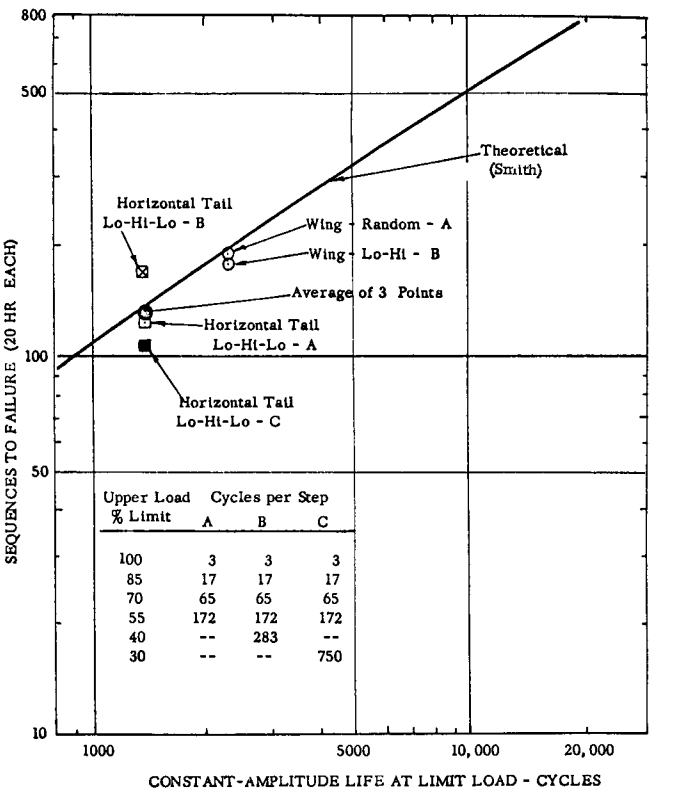

Fig. C13.56 Comparison of Predicted and Test lives of Full-Scale Structures - Minimum Load = 1 G = 13.3 Percent

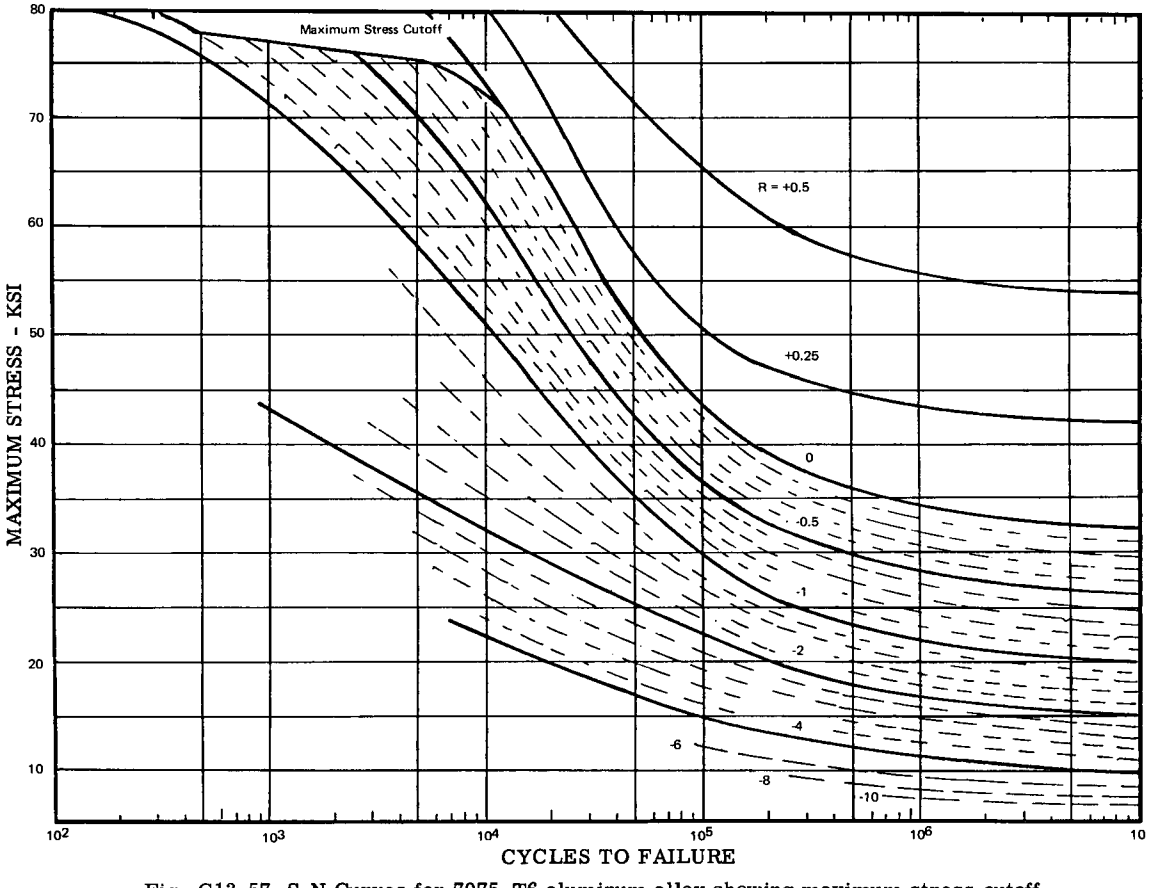

Fig. C13.57 S-N Curves for 7075-T6 aluminum alloy showing maximum stress cutoff for stressing at a concentration

and being faired in to intercept the curve for R = 0 at 72 ksi (proportional limit). In essence, it is a mirror image of the stress-strain curve.

Accordingly, if an airplane or component fails after fewer than 10,000 cycles when subjected to tension-tension constant-amplitude loading, the maximum stress at the point of failure is found at the intercept of life with the cutoff line. The minimum stress, by definition, is the maximum stress times whatever R curve exists at the intercept.

Knowing the maximum stress and minimum stress, we have the total stress range which can be prorated for any other load in a spectrum. Note that we do not even have to know the nominal stress nor stress concentration.

NUMERICAL EXAMPLE

Consider a structure which is cycled at R = 0 and which fails after 1000 cycles of limit load. How long will a similar structure last when loaded according to the following spectrum?

Load - % Limit	n per sequence
100	3
85	17
70	65
55	172
40	283

Referring to Fig. C13.57, we find that the maximum stress at the cutoff line corresponding with a life of 1000 cycles is 77 ksi and that the intercept is at R = 0.76 (using interpolated values). See sketch below.

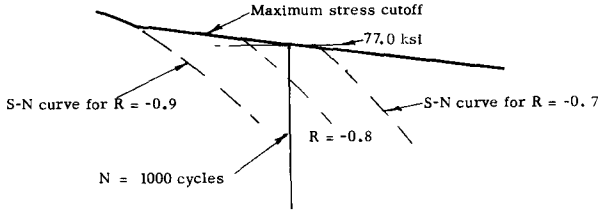

The minimum stress (by definition of R) = 77 x = 0.76 = 58.5 ksi and the stress range = 1.76 x 77.0 = 135.5 ksi.

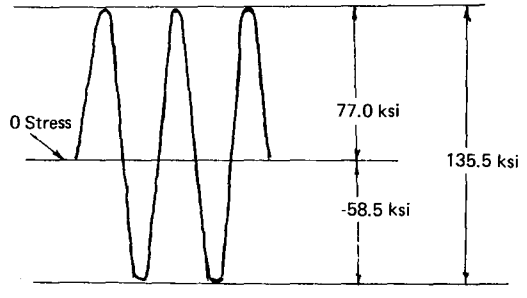

Using the stress range of 135 ksi, we can now compute the stress range for other loads in the spectrum.

Load - % Limit	Stress Range
100	135.5
85	115.2
70	94.8
55	74.5
40	54.2

Since the order of loading shows that 3 cycles of 100 percent were applied first, the residual stress of 58.5 ksi will remain throughout remaining load steps. The residual stress is then to be subtracted from the stress range to find maximum stresses at other loads.

Load - % Limit	Stress Range	Minimum Stress	Maximum Stress
100	135.5	-58.5	77.0
85	115.2	↑	56.7
70	94.8	↓	36.3
55	74.5	-58.5	16.0

We now have the maximum and minimum stress for each load step. By dividing the minimum stress by the maximum stress, we obtain the stress ratio (R) and find corresponding lives (N) from the S-N curves in Fig. C13.57. Knowing the number of cycles per step (n) in each sequence, the proportion of damage is found by dividing n by N. The structure will fail (according to the Miner rule) when Σ n/N = 1. The work is simplified by arranging all steps as in the following table:

Load - % Limit	n	Stress Range	S_{min}	S_{max}	R	N	n/N
100	3	135.5	-58.5	77.0	-0.76	1,000	0.00300
85	17	115.2	↑	56.7	-1.04	5,500	0.00315
70	65	94.8	↓	36.3	-1.60	12,500	0.00520
55	172	74.5		16.0	-3.65	100,000	0.00172
40	283	54.2	-58.5	-4.3	+13.6	∞	0

Σ n/N = 0.01307

Life = 1/0.01307 = 76.5 sequences

While the Smith method is used in some aircraft companies and by the Navy, unless computer programmed, the calculations are tedious and probably not necessary. The purpose of showing roughly how the Smith method works is to acquaint the reader with how the relation between constant-amplitude life at limit load and spectrum life came about (Ref. Fig. C13.56), in fact, that there is a relation at all. While someone in an organization will need to compute the appropriate constant-amplitude life for an individual aircraft, the designer need not go through the computations each time, but simply use the

the life at limit loading for assurance that the structure will have a good chance of passing the spectrum test.

As previously indicated, life predictions can be so spadmodic that the effort is seldom really necessary. As an example of predictions and test results on full-scale airplane structures, Table VII(44) shows predictions and test results where predictions, except one, were made by the linear or Miner rule. The one exception (2nd item from top) was predicted by the Smith method.

C13.6.6 Summary on Life Production

In view of the discrepancies shown in Table VII between predicted and test lives, we have reached a point where any prediction seems futile. Perhaps we have overlooked the need for designing a structure that will not fail, rather than trying to predict how long it will last. As shown in C13.5, there are means of increasing life to where an estimate of fatigue life becomes unnecessary inasmuch as static strength will design the part.

However, since a fatigue analysis is frequently a part of a contractual obligation, and the Miner method is an accepted way, the simple integration of lives from S-N curves (Ref. C13.6.3) supposedly having the same stress concentration factor as the structure will fill contractual obligations. However, a full-scale test is also a contractual obligation, so that whatever analysis is made, the final proof will lie in withstanding the required simulated service tests.

If there is doubt whether the structure will meet the required tests, and the stress concentration is known, one can simply multiply the nominal stress at limit load times the stress concentration to obtain stress range. Having the stress range, if more than 70 ksi, the residual stress may be found from Fig. C13.58. The difference between residual stress and stress range is the maximum stress. Stress ratio, R, is obtained by dividing residual stress by maximum stress and appropriate lives can be found from the S-N curves shown in Fig. C13.57, using the same procedure as outlined in the numerical example to estimate cumulative damage.

Since it would be impossible to introduce a greater residual stress than the compressive yield strength of the material (71 ksi for 7075-T6), an arbitrary cutoff of about 69 ksi is shown in Fig. C13.58. This is more of academic interest than of practical value, since a structure having a service load that introduces more than 69 ksi residual stress is unlikely to be satisfactory in any event.

TABLE VII

FATIGUE LIFE SUMMARY

Structural Elements	Max. Spectrum Net Stress (PSI)	Stress Conc. Factor (K_T)	Predicted Life (hours)	Full-Scale Test Life(1) (hours)	Serv. Life(1) (hours)
Skin fillet, wing sta 33.875 wing outer panel, upper skin ("Thunderbird" fillet)	23,000	4.7	12,670	4,491	2,300
Skin fillet, wing sta 33.875 wing outer panel, lower skin ("Thunderbird" fillet)	23,000	4.7	4,460 (3)	5,508	2,530
Wing outer panel lower skin 51% spar bolt hole, wing canted sta 102	34,300	2.5 (2)	1,120	4,870	2,140
Wing center section lower skin	39,000	2.5	2,600	6,192	2,890 (T-Bird)
Wing center section to wing outer panel lower skin splice	25,000	3.4	30,000	9,116	No failures reported
Fuselage upper longeron, fus sta 305	25,500	3.2 (2)	91,000	12,224	2,580
Fuselage fitting, fus sta 222.5, wing-to-fuselage forward attach			No prediction made	13,227	No failures reported
Fuselage upper longeron, field break splice, fus sta 389			No prediction made	14,587	No failures reported

NOTE: 1. Where more than one failure occurred in service or in test, the life quoted is average.
2. Without consideration for fastener bearing.
3. C.R. Smith Method.

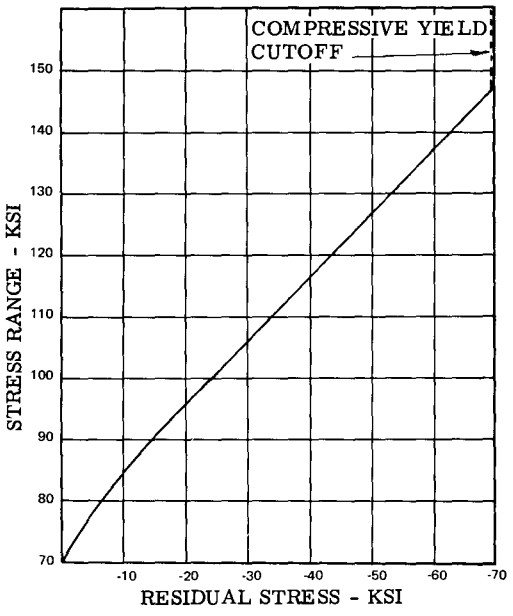

Fig. C13.58 Computed stress range vs. residual stress for cycling at R = 0

Finally, there is no positive way of predicting service life; however, the use of unnotched specimen data with appropriate stress concentrations will come closer than any method so far devised. The reason for this is that much of the published notched data include hidden residual stresses due to specimen fabrication which lead to unconservative estimates (see C13.3.2).

The above applies to 7075-T6 only. For estimating life of other materials, use the unnotched data shown in the appendix. Such data should be plotted as in Fig. C13.58, using a stress-strain curve for the material to establish the cutoff line.

C13.7 SAFE LIFE, FAIL SLOW, AND FAIL SAFE

C13.7.1 Safe Life and Crack Propagation

So far we have discussed methods of increasing life and of estimating life. A structure whose only claim to reliability is through analysis and simulated service fatigue tests is called "safe life". Such a structure is definitely limited to the flying hours to which the airplane was certified.

The single spar Viscount is an example of a safe life airplane. Needless to say, careful analysis and thorough testing is needed in such cases. However, even with single spar construction, inspection procedures are usually such that a fatigue crack can be detected long before it becomes critical. Crack growth at critical sections is measured during the fatigue test so that airplanes in service having similar cracks usually have ample warning before anything like catastrophic failures occur. Recent studies in fracture mechanics have disclosed methods of estimating crack tolerance for many situations.

Generally, thin skins are less susceptible to catastrophic failures due to fatigue cracks than thick-skins. Accordingly, commercial airlines have standard policies for thin skins as to length of crack permissible before repairs are needed. The usual procedure for such repairs is to stop-drill (drill a hole at the end of a crack) the crack and patch the skin with a patch of equal thickness material. Unfortunately, such repairs are of short duration in that the crack eventually progresses through the crack-stop hole and out from under the patch. It is commonly believed that this is because the crack-stop hole did not actually encompass the end of the crack.

Grover(45) considers crack growth to be in four stages. The first is simply initiation, second is the first stage of growth, third is a steady growth stage (the one usually measured in propagation studies), and finally a stage of rapid propagation. The total time between stages depends on stress; however, the ratios between the stages is about the same for all stress levels where loading is constant-amplitude. A high load in a spectrum will cause local yielding and result in a retardation for a short period at subsequent lower loads.

Fig. C13.59 (graph a) shows a typical crack growth graph for an 8-inch wide sheet of 7075-T6 aluminum alloy in which cracks were aided in starting by drilling a small hole in the center and notching edges of the hole with a jeweler's saw. Measurements were made after the crack had been allowed to grow to 0.037-inch. Cycled at 20 ksi gross stress, R = 0.1, final failure did not occur until after 41,000 cycles. This represents 3/4 of the total life; however, it must be remembered that the crack generated in the first 10,000 cycles was aided by the superimposed stress concentrations. Had the specimen simply been hole-notched (Ref. Fig. C13.12), the first crack should not have appeared until more than 100,000 cycles had been sustained. Accordingly, had this been representative of a structure, roughly 25% of life was spent in propagation of the crack.

To determine the effectiveness of stop-crack holes, a second experiment was made wherein 3/16-inch diameter holes were drilled at the ends of the crack. The specimen lasted for 51,000 cycles (see Fig. C13.59, graph b) or an extension of 20% in total life. Two additional experiments were made wherein a Stress Pin (Ref. Fig. C13.38) was driven in the crack-stop hole, and a second wherein the crack was permitted to grow 3/8-inch after which a Stress Pin was inserted in such a manner that 1/16-inch of crack

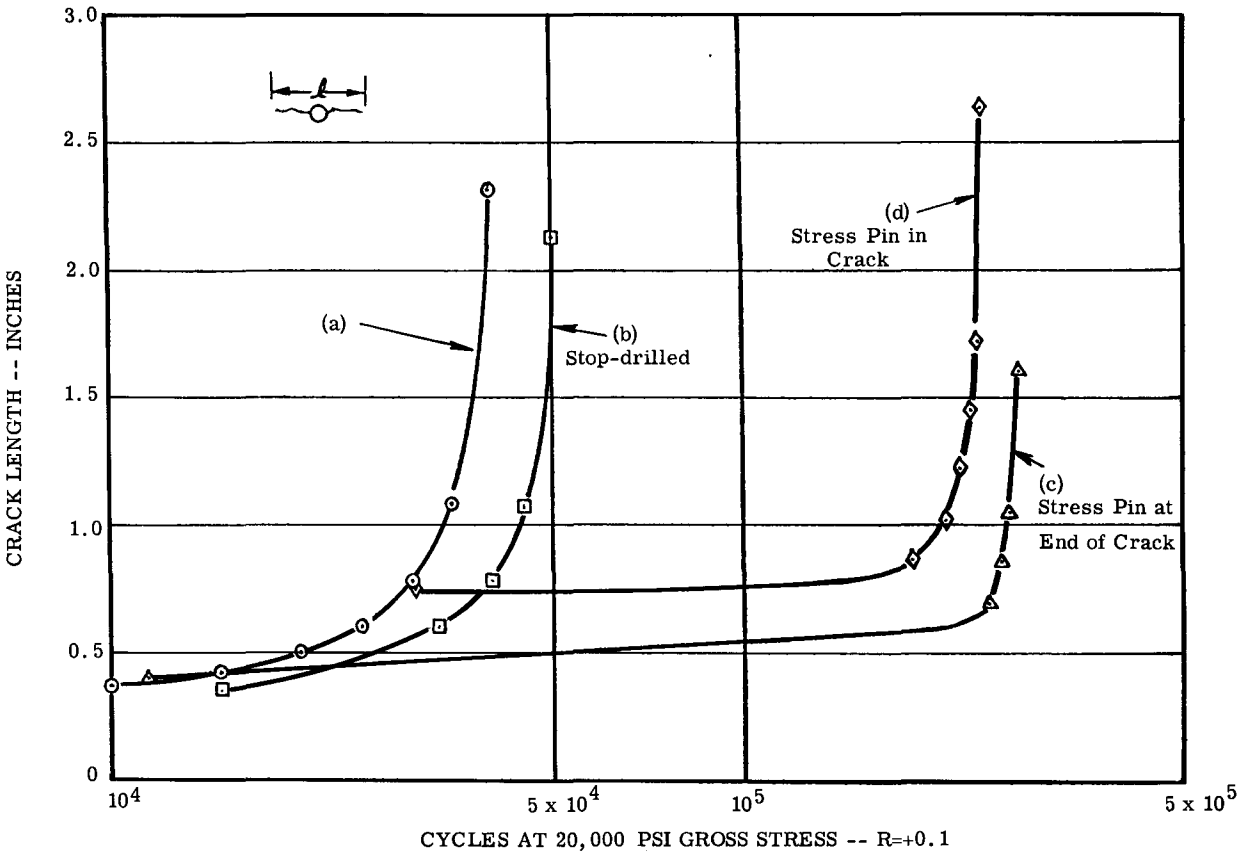

Fig. C13.59 Results of crack propagation tests

extended beyond the fastener head to simulate the case where the crack-stop hole missed the end of the crack. These are shown in graphs (c) and (d) of Fig. C13.59. Here it is seen that an increase in life of more than 5 times is achieved by using the fastener in the crack-stop hole. The reason for this is that the outstanding flanges of the fastener act as a bridge for load to be carried across the crack, more or less as though a staple were driven across the crack.

C13.7.2 Fail Safe

Having no positive way of guaranteeing that a structure might not fail before its so-called guaranteed lifetime, it is now common practice to provide multiple load paths so that should any one of a number of load carrying members fail, the airplane is still able to carry a guaranteed percentage of the design limit load without failure. Thus, a wing having five spars could lose one spar entirely and still carry 80% of the original design load. This is figuratively speaking, since, depending on which of the 5 spars failed, the torsional resistance could not be proportional to the number of spars.

A system of having fail-safe lugs is to have them laminated so that one of the laminates can fail without effecting the strength of the remainder. This is somewhat different from the fail-slow idea of allowing a crack to progress a given depth, say the thickness of one laminate, where fracture toughness would be the governing feature. In other words, the strength of the remaining area in a cracked lug is only a fraction of its rated P/A value. This is also true of cracked skins, however, the thin skin has a greater fracture toughness than thick plates. Wilhelm(46) shows skins having thickness of less than 0.15-inch to be 2.4 times as tough as when thickness is more than 0.80-inch.

The use of stiffener and skin combinations adds to an airplane's fail-safe integrity. Not only does it provide multiple load paths, but the stringers act as crack arrestors. That is, a crack will progress to a stringer and cease to propagate for a period before continuing to the next stringer. This is fail-slow rather than fail-safe. In any event, it permits time to make repairs before the crack becomes dangerous.

Integral fuel tanks are, in a way, fail safe features. This stems from the fact that fuel leaks will reveal cracks long before being detected by conventional inspection processes.

Although the slow propagation of cracks constitutes a fail-safe measure in a way, no airlines operator can afford to spend much time in repairing cracks. This is not only because of repair costs in themselves, but down time for the airplane. The daily interest on a 7-million dollar airplane not being used, assuming 6% rate, is $1,150 per day. Thus we see that prevention of cracks is most important, even if no fail-safe feature were involved.

C13.8 FREQUENTLY OVERLOOKED PROBLEM AREAS

C13.8.1 Fatigue Failures of Compressive Surfaces

While an airplane structure has to be designed to both fatigue and static requirements, the usual practice is to design to static strength and then do whatever is needed to bring the structure up to fatigue strength. Because of fatigue problems, however, the recent trend is to use a lower strength material (2024-T3) for wing lower surfaces, tail surfaces, and fuselage structures. 2024-T3 (or T851) has a slower crack propagation rate than 7075 alloys--also higher brittle fracture toughness.

Upper surfaces, and other members loaded primarily in compression are usually designed of 7075-T6 or 2014-T6 material because of their high compressive yield strengths. However, because loading is primarily in compression does not exempt a structure from fatigue problems. A fatigue crack in a wing upper surface may come as a surprise because tension stresses due to negative maneuvers, gust, or landing conditions are usually much less than corresponding stresses in the lower surface. What happens is that a high positive load can yield the material at a concentration in compression so as to introduce a residual tension stress (just the reverse of examples shown in tension) so that the stress at the concentration suffers a tensile stress every time the structure is unloaded.

Eventually, a fatigue crack develops and progresses until the area of the crack is sufficient to carry the compressive load without further yielding. From then on, only the negative loads will increase crack length; however, because of brittle fracture characteristics, such a structure becomes dangerous for negative loading, however small such loads might be. Thus, a fatigue test having only positive loads may not reveal the fault, nor will the analysis unless consideration is given to residual stresses.

Failures in compressive surfaces usually occur at fillets, fastener holes, or at corners of access doors. A correction is to use generous fillets (see Figs. C13.46 - 48) or to have fastener holes completely filled. While an interference fit is best we presently have no interference-fit fasteners which are satisfactory for removable panels. In thick skins, it is possible to use countersunk fasteners with a steep bevel (60° instead of 100°) so that when installed the fastener head can carry the compressive load required without permitting plastic flow at the hole.

Where skin is too thin to permit a 60° countersink and it is not possible to use an interference fit fastener, the following should be used as a guideline for maximum allowable clearance. Since it takes but 0.006 in. in strain (proportional limit) to cause plastic deformation in 7075 or 2014 alloys, and the concentration factor for a hole in a wide sheet is 3, it follows that the maximum clearance for a 1-inch diameter bolt would be 0.006/3 = 0.002-inch before risking compressive plastic flow at the hole. By the same token, a 1/4-inch diameter bolt could have no more than 0.0005-inch clearance. Should lower strength alloys be used in compressive surfaces, the tolerance would have to be reduced in proportion to differences in proportional limits.

C13.8.2 Heavy Forging Attachments on Stressed Parts

While forgings in themselves are sometimes fatigue prone in that they are sometimes loaded in an adverse grain direction, they are frequently attached to highly stressed parts, and, although supposedly having nothing to do with the stress pattern in the stressed member, are catalysts for early fatigue failure. An example of this is a heavy support bracket attached through a stressed spar web to a wing bulkhead (see Fig. C13.60). Here, a fatigue crack was started at a fastener used to attach the forging to a wing bulkhead; however, it did not permit the spar web to deform properly with results as shown.

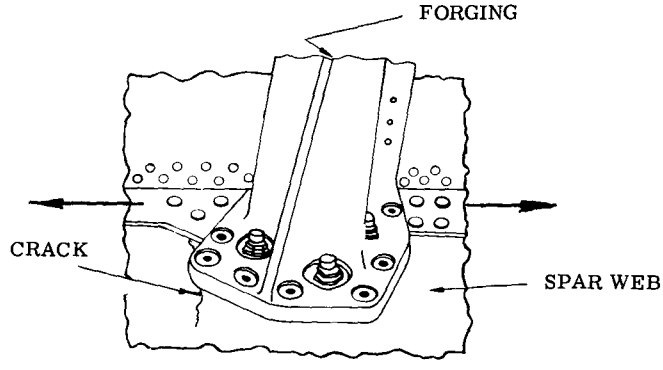

Fig. C13.60 - Heavy forging prevents underlying spar web from deforming properly--causes crack at fastener hole.

Wherever situations like this arise, a solution is to feed out the stress through successive layers of thinner material or to provide gradual taper to the first point of attachment.

If this is not possible, perhaps the heavy piece could be split normal to the direction of stress in the spar to permit "breathing room". To lower the stress fluctuation resulting from the hole itself, tapered bolts at points of attachment will help. However, because of stress corrosion susceptibility of forgings in the transverse grain direction, the interference should be in the spar web and not in the forging.

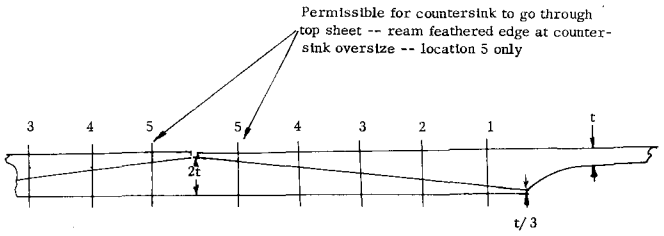

Fig. C13.61 - Flush joint designed for fatigue resistance.

C13.8.3 Single Shear Flush Joints

A common fault in designing mechanically fastened flush type joints is that of using splice plates which are too thick. This is a result of designing for static strength where it is considered a good practice to have fastener shear, sheet tensile strength, bearing and tear out all equal. A splice plate which is equal to or heavier than the material being spliced overloads the first fastener nearest load source (See Fig. C13.41) so as to cause fatigue cracks at the first fastener.

In designing for fatigue, the first fastener nearest load should be incapable of carrying a load which will cause the material being spliced to fail in fatigue. A smaller diameter fastener is simply to invite trouble with the fastener itself. A better way is to thicken the ends of the material being spliced (sculptured skins) as shown in Fig. C13.61, using a scarf to afford better load distribution.

Critical areas are in the skin at Fastener No. 1 and in the splice plate at Fastener No. 5. Accordingly, anything we can do to relieve stress in these locations is beneficial. In the case of Fastener No. 5, we have permitted the countersink going all the way through the outer sheet. While this should never be permitted ordinarily, it is one way of assuring that the splice plate will not fail at this location. This is particularly important in that this is the location of maximum bending in the splice plate and is hidden from view where fatigue cracks would be hard to detect.

A similar situation exists at Fastener No. 1 where special precaution should be taken to assure that the shearing strength of the fasteners exceed bearing strength in the splice plate. Accordingly, overloading will not loosen the fastener in the material we are trying to protect. Permanent bearing deformation in the doubler, if it occurs, is not critical since it merely relieves loads that cause fatigue. Fasteners at locations 2, 3, and 4 should be capable of carrying very nearly the full static requirement.

C13.8.4 Fastener Sizes

A common fault is to use fasteners which are too small. Remember that the stress concentration for a hole is about the same, whatever the hole size. The larger fastener provides more bearing area, doesn't bend so much, and has greater installation tolerance (see Fig. C13.62). Furthermore, the material stack-up ratio (ratio of fastener diameter/material thickness) is better when using larger fasteners. Fatigue tests have shown that specimens having 3-diameter stackup ratios lasted from 1/10 to 1/5 as long as those having ratios of 1 or 2 diameters.

One reason for the trend towards small fasteners is because of having higher strength fasteners available. This has resulted in some weight saving, however, there are probably better ways of reducing weight than by using undersize fasteners.

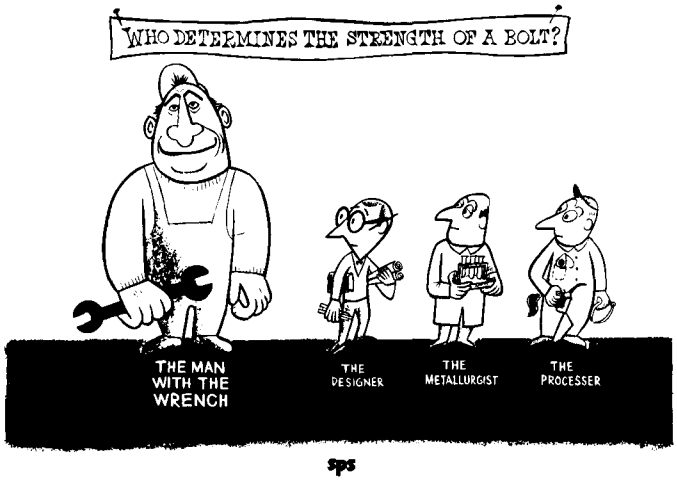

Fig. C13.62 - Manufacturing Tolerances--Courtesy of SPS Co.

C13.8.5 Acoustic Fatigue

While acoustic fatigue is a study all within itself and therefore beyond the scope of the present section, certain precautions can be

taken where exposure to sonic vibration induced by jet noises or propeller blasts invite fatigue problems which are somewhat different from those caused by aerodynamic loading.

The most common fault in design is that of using unsymmetrical rib structures where rolling causes cracks to form through the line of rivets or over the rib web as shown in Fig. C13.63(a). A correction for this can be made by adding an angle to make the section more symmetrical as shown in Fig. C13.63(b); however, an even better solution is to use extruded T or H sections having rounded flange edges. The rounded flanges help to prevent cracking the skin over the edges as in Fig. C13.63(a).

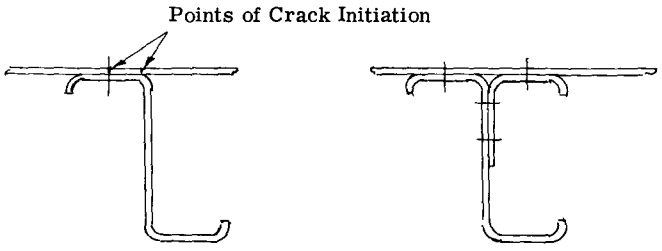

Fig. C13.63 - Fatigue critical areas in acoustical environment

A layer of viscoelastic material between skin and stringers or ribs helps. There have been cases where known critical areas were helped by painting inside of skin with fuel sealing compounds.

Offhand, it would appear that the best design against accoustical fatigue is to design parts of such mass and rigidity that they will be above resonance frequencies of the system. However, this is virtually impossible as the whole spectrum of frequencies is experienced during engine runup and takeoff. Fortunately, the duration at each frequency is very short. However, stresses can be reduced by using appropriate damping materials.

C13.9 Check List

1. Has proper surface finish been specified? 125 r.m.s. or better in general with 60 or smoother at concentrations.

2. Have machined mismatches been avoided? Specify hand finishing if needed to blend machined surfaces at changes of section.

3. Has shot peening in critical areas been specified? Consult design manuals or get help regarding appropriate processes to use.

4. Have high stresses in transverse grain direction been avoided?

5. Have generous radii been used throughout?

6. How about spotfacing? Have spotface tools been modified to provide suitable corner radii?

7. Are changes in cross section as gradual as possible? Use streamline fillets where helpful.

8. How about open holes? It is useless to use tapered bolts for fatigue enhancement and leave an open hole in the area for other purposes. See that appropriate measures are taken to either plug the hole or use an interference fit bushing. If this is not possible material at hole area has to be thickened.

9. Are joints, parts, fittings, etc., eccentric -- if so, is it possible to design them otherwise?

10. Have all sharp edges been broken? Have holes been deburred?

11. Where hard plating has been used, has shot peening been specified to compensate for loss in fatigue strength?

12. How about anodic coating? Hard coatings (sulphuric acid) are vulnerable to fatigue cracking--use chromic acid or soft anodize.

13. Stress corrosion? Have suitable precautions been taken to prevent sustained stresses in short transverse grain direction?

14. Has each joint been examined to make sure that the first fastener nearest load carries less load than remaining fasteners? Splicing material at first fastener should be thin enough to assure bearing failure before fastener shears (see Fig. C13.8.3).

15. Has access been provided for inspection of fatigue critical areas?

C13.10 Concluding Remarks

While it was impossible to cover more than the most rudimentary facets of fatigue in the foregoing, it is hoped that the reader will use the material in the references to further his ability to foresee and correct fatigue problem areas.

While fatigue has not, as of this writing, moved to a position where structures are designed for fatigue resistance rather than for static

strength, it would appear futile to design to the last ounce of weight for static considerations and not consider fatigue. This is why we have experienced so many fatigue problems to date. It is not that we are designing to excessive stresses so much as we are not taking pains to see that the stress has proper distribution.

We have tried to consider many of the possibilities which confront the designer; however, these were confined to those normally found in airplane structures. Some of the points not covered are: low cycle fatigue, strain cycling, wear, corrosion, thermal cycling, fractography, adhesive bonding, sandwich structures and many others. Some of these are included in the references, however, it should be remembered that the references are but a partial list of presently available literature.

Finally, one cannot stress the point too strongly that, as of the present writing, a design for fatigue resistance does not necessarily cost weight. An example of this is a case where 300 military airplanes were modified to bring them up to desired fatigue life. It cost 3200 man hours per airplane which amounted to $11,000,000 for the job, including materials (from Ref. 33). The final airplane was no heavier than the original. It might be argued that the original weight was not based on optimum design and that even the modified airplanes might not meet fatigue standards set in the future. Be that as it may, while we can expect more efficient designs which will reduce weight for static considerations, we can also expect design innovations that will increase fatigue resistance.

REFERENCES

1. Shanley, F.R., "Fatigue Analysis of Aircraft Structures," RAND Report No. 1127, July 1953.
2. Frocht, Max M. & Hill, Stress-Concentration Factors Around a Central Circular Hole in a Plate Loaded Through a Pin in the Hole," Journal of Applied Mechanics, March, 1940.
3. Frocht, Max M., Photoelasticity, Vol. 1, John Wiley & Sons, Inc., 1941.
4. Sjostrom, S., "Stress Concentration Factor at the Edge of an Eccentrically Located Circular Hole in a Sheet in Tension.", Swedish Aeronautical Institute Report No. 36.
5. Timoshenko, S., Theory of Elasticity, McGraw-Hill Book Co., Inc., New York 1934.
6. Lipson, Noll, & Clock, Stress and Strength of Manufactured Parts, McGraw-Hill, New York 1950.
7. Smith, Clarence R., "A Method for Estimating the Fatigue Life of 7075-T6 Aluminum Alloy Aircraft Structures," U.S. Naval Air Engineering Center Report No. NAEC-ASL 1096, December 1965.
8. Metallic Materials and Elements for Aerospace Vehicle Structures, MIL Handbook 5, Department of Defense, Washington 25 DC.
9. Neuber, H. & Bertele, L., "Stress Concentration with Fatigue Loading", Air Force Materials Laboratory Report AFML-TR-70-45, February 1970.
10. Goodman, J., Mechanics Applied to Engineering, Longmans, Green & Co., London 1899.
11. Grover, H.J., Gordon, S.A., and Jackson, L.R., Fatigue of Metals and Structures, U.S. Govt. Printing Office, 1954.
12. Findley, W.N., "Fatigue of 76S-T61 Aluminum Alloy under Bending & Torsion", ASTM Proceedings, 1952.
13. Gough, H.J. and Pollard, H.V., "The Strength of Metals under Combined Alternating Stresses", Institution of Mechanical Engineers, Vol. 131 1935; The effect of Specimen Form on the Resistance of Metals to Combined Alternating Stresses", Vol. 132, 1936.
14. Fritte, P.H., "Fatigue Tests on Crankshaft Steels," Journal of the Iron and Steel Institute, Vol. 159, 1948.
15. McAdam, D.J. Jr., "Endurance Properties of Steel: Their Relation to Other Physical Properties and to Chemical Composition, ASTM Proc. Vol. 23, 1923.
16. Christensen, R.H., "The Fatigue of Materials and Structures", Collection of Notes for In-Plant Course on Fatigue at Douglas Aircraft Co., Inc., Santa Monica, Calif. 1954.
17. Moroney, N.J., Facts from Figures, Penguin Books, Baltimore 1954.
18. Rosenfeld, M.S., "Navy Research on Structural Fatigue", ASTM Special Technical Publication No. 338, 1962.
19. Payne, A.O., Ford, D.G., et al, "Fatigue Characteristics of Riveted 24S-T Aluminum Alloy Wing, Part V: Discussion of Results and Conclusions", Aeronautical Research Laboratories Report SM 268, Melbourne 1959.
20. Cummings, H.N., Stulen, F.B., & Schulte, W.C. "investigation of Materials Fatigue Problems Applicable to Propellor Design", WADC-TR 54-531, May 1954.
21. Smith, Clarence R., "Preventing Fatigue Failures", Assembly Engineering, April 1968.
22. Griffith, George E., "Experimental Investigation of the Effects of Plastic Flow in Tension Panel with a Circular Hole," NACA T.N. 1705, Langley Field, Va.
23. Almen, J.O., "Shot Blasting to Increase Fatigue Resistance", SAE Journal (Transactions), Vol. 51, No. 7.
24. Fuchs, Henry O., "Techniques of Surface Stressing to Avoid Fatigue", Published in Metal Fatigue, Edited by George Sines & J.L. Waisman, McGraw Hill Book Co., Inc., N.Y. 1959.
25. Whaley, Richard E., "Improvement in 7075-T6 Aluminum Alloy Fatigue Life by Coining", ASTM Proceedings, Vol. 63, 1963.
26. Inglis, I.N., "Nitriding Offsets Notch Weakness", Abstract, Iron Age, Vol. 147, No. 1.
27. Almen, J.O., "Fatigue Loss and Gain by Electro-plating", Product Engineering, Vol. 22, No. 6, June 1951.
28. Smith, Clarence R., "Evaluation of Fatigue Life of Chrome-ite Plated Specimens", AFFDL-TR-65-166, Wright-Patterson AFB, Ohio, December 1965.

29. Holshouser, W.L. & Utech, H.P., "Effect of Oleophobic Films on Fatigue Crack Propagation", paper presented at the 64th annual meeting of ASTM, June 1961.

30. Smith, C.R., "Design Applications for Improving Fatigue Resistance of Airplane Structures," Proc. ASTM, Vol. 60, 1960.

31. Smith, Clarence R., "The Effect of Tapered Bolts on Structural Integrity," Assembly Engineering, July 1967.

32. Smith, Clarence R., "Ftontiers in Fastener Design", Assembly Engineering, Jan. 1969.

33. Smith, Clarence R., "Tips on Fatigue, NAVWEPS 00-25-559, U.S. Govt. Printing Office, Washington DC, 1963, Price 70¢.

34. Smith, C.R., "Thin Doublers for Fatigue-Resistant Aluminum Alloy Structures", Aero/Space Engineering, Feb. 1959.

35. Smith, C.R., and Zandman, F., "Photostress Plastic for Measuring Stress Distribution Around Rivets", SESA Proceedings, Vol. XVII, No. 1, 1958.

36. Smith, Clarence R., "Effective Stress Concentrations for Fillets in Landed Structures", Experimental Mechanics, April 1971.

37. Peterson, R.E., Stress Concentration Design Factors, John Wiley & Sons, Inc., New York 1953.

38. Christensen, R.H., & Bellinfonte, R.J., "Some Considerations in the Fatigue Design of Launch and Spacecraft Structures", NASA - CR-242, June 1965.

39. Rhode, Richard V., and Donely, Phillip, "Frequency of Occurrence of Atmospheric Gusts and Related Loads on Airplane Structures", NACA ARR No. L4121.

40. "Airplane Strength and Rigidity, Reliability Requirements, Repeated Loads, and Fatigue", MIL-A-8866 (ASG), 1960.

41. Palmgren, A., "Die Lebensdauer von Kugellagern", Z. Ver. Deut. Ing., Vol. 68, 1924.

42. Miner, M.A., "Cumulative Damage in Fatigue", J. Appl. Mech., Vol. 12, 1945.

43. Smith, C.R., and Lindeneau, G.D., "Riveted Joints -- Fatigue Strength", ASTM Special Publication STP 203, 1957.

44. Fitch, G.E., Jr., Jackman, R.E., and Horsfall, W.P., "The F-100 Structural Integrity Program (ASIP)", Proceedings of the Air Force Conference on Fatigue and Fracture of Aircraft Structures and Materials", Air Force Flight Dynamics Laboratory Report No. AFFDL TR 70-144, 1970.

45. Grover, Horace J., Fatigue of Aircraft Structures, NAVAIR 01-1A-13, U.S. Govt. Printing Office, Washington DC, 20402, 1966 (Price $1.25)

46. Wilhelm, D.P., "Fracture Mechanics Guidelines for Aircraft Structural Applications", AFFDL-TR 69-111, 1969.

BIBLIOGRAPHY

A.S.T.M. Special Publications, Published by the American Society for Testing and Materials, 1916 Race St., Philadelphia, Pa. 19103:

STP 9, References on Fatigue

STP 91, Manual on Fatigue Testing

STP 203, Fatigue of Aircraft Structures, 1957

STP 237, Symposium on Basic Mechanism of Fatigue, 1959

STP 274, Symposium on Fatigue of Aircraft Structures, 1960

STP 284, Symposium on Acoustical Fatigue, 1961

STP 338, Symposium on Fatigue Tests of Aircraft Structures: Low-cycle Full-Scale, and Helicopters,

STP 378, Internal Friction, Damping, and Cyclic Plasticity, 1965

STP 467, Achievement of High Fatigue Resistance in Metals and Alloys.

American Society for Mechanical Engineers. Conference (International) on Fatigue of Metals -- Proceedings, 29 West 39th St., New York 1956.

American Society for Metals. Metals Handbook, Vol. 1, 8th Edition, Metals Park, Novelty, Ohio, 1961.

Baldi, Robert W., "The Smith Hypothesis on Metal Fatigue", Master's Thesis, San Diego State College, Dept. of Mechanical Engineering, January 1971.

Baum, C.P., "Reliability of Airframe Structures -- General Aspects of the Problem and Outline of Methods for Attaining," SAE-ASME-AIAA, Reliability and Maintainability Conference, 1964.

Bennett, J.A., "The Distinction between Initiation and Propagation of a Fatigue Crack," International Conference on Fatigue of Metals (London and New York), 1956.

Carter, T.L., Zaretsky, E.V., and Anderson, W.J., "Effect of Hardness and Other Mechanical Properties on Rolling-Contact Fatigue of Four High-Temperature Bearing Steels," NASA-TN-D270, 1960.

Cazaud, Roger, Fatigue of Metals, Champion & Hall, London 1953.

Corten, H.T., and Dolan, T.J., "Cumulative Fatigue Damage." IME-ASME International Conference on Fatigue, 1956.

Critchlow, W., "The Ultimate Strength of Damaged Structure", Symposium on Full-Scale Fatigue Testing of Aircraft Structures, Pergamon Press, N.Y., 1961.

Dixon, J.R., "The Effect of Local Plastic Deformation on the Stress Distribution around a Crack, National Engineering Laboratory Report No. 71, 1962.

Douglas Aircraft Co., "Investigation of Thermal Effects on Fatigue," WADD TN-50-410, Part I, 1960, Part II, 1961.

Durelli, A.J., "Elastoplastic Stress and Strain Distribution in a Finite Plate with a Circular Hole Subjected to Unidimensional Load," Journal of Applied Mech. (ASME), Vol. 30, March 1963.

Forrest, P.G., Fatigue of Metals, Pergamon Press, N.Y. 1962.

Forsythe, P.J.E., "Fatigue Damage and Crack Growth in Aluminum Alloys," Acta Metallurgica, vol. II, 1963.

Freudenthal, A.M., (Editor). Fatigue in Aircraft Structure (Proceedings of the International Conference Held at Columbia University), January 30, 31, and February 1, 1956.

Freudenthal, A.M., and Heller, R.A., "On Stress Interaction in Fatigue and a Cumulative Damage Rule," Journal of Aero-Space Science, Vol. 26, No. 7, 1959.

Gurney, T.R., "Influence of Artificially Induced Residual Stresses on Fatigue Strength of Load-Carrying Fillet Welded Joints in Mild Steel," Welding Research Council Bulletin, Vol. 8, 1962.

Halford, G.R., and Morrow, J., "Low Cycle Fatigue in Torsion," University of Illinois TAM Report No. 203, 1961.

Harris, W.J., Metallic Fatigue with Particular Reference to Significance of Certain Standard Aircraft Fabrication and Finishing Process, Pergamon Press, N.Y. 1961.

Heywood, R.B., Designing by Photoelasticity, Academic Press Inc., Publishers, N.Y. 1952.

Heywood, R.B., Designing Against Fatigue of Metals, Reinhold Publishing Co., N.Y. 1962.

Hardrath, H.F., and Ohman, L., "A Study of Elastic and Plastic Stress Concentration Factors Due to Notches and Fillets in Flat Plates," NACA Report 1117, 1953.

Illg. W., "Fatigue Tests on Notched and Unnotched Sheet Specimens of 2024-T3 and 7075-T6 Aluminum Alloys and of SAE 4130 Steel with Special Consideration of Life Range from 2 to 10,000 Cycles," NACA TN 3866, Dec. 1956.

Kuhn, P., and Figge, I., "Unified Notch Strength Analysis for Wrought Aluminum Alloys," NASA - TN-D-1259, 1962.

Manson, S.S., Thermal Stress and Low-Cycle Fatigue, McGraw-Hill, N.Y. 1966.

Marin, J., Mechanical Behavior of Engineering Materials, Prentice-Hall, N.Y. 1962.

Melcon, M.A. and McCullogh, A.J., "Simulation of Random Aircraft Service Loading in Fatigue Tests," Third AGARD - ICAF Symposium on Aeronautical Fatigue, 1963.

Paris, P.C. "The Fracture Mechanics Approach to Fatigue," Proc. 10th Sagamore Army Materials Research Conference, Syracuse University Press, Syracuse, N.Y. 1964.

Plantema, F.J. & Schijve, (Editors), Full-Scale Fatigue Testing of Aircraft Structures, Pergamon Press, N.Y. 1961.

Plunkett, R. and Lee, C.T., "Optimum Configurations for Damping by Constrained Viscoelastic Layers," AFML-TR-68-376, Air Force Materials Lab., Wright Patterson AFB, Ohio 1969.

Schive, J., "Endurance Under Program Fatigue Testing" Amsterdam Symposium on Full-Scale Fatigue Testing of Aircraft Structures, Pergamon Press, N.Y. 1961.

Stowell, E.Z., "Stress and Strain Concentration at a Circular Hole in an Infinite Plate," NACA TN2073, April 1950.

Teed, P.L. "Fretting," Metallurgical Review, Vol. 5, 1960.

Wang, D.Y., "The Effect of Stress Distribution on the Fatigue Behavior of Adhesive Bonded Joints," ASD-TDR-63-93, 1963.

Weibull, W., Fatigue Testing and Analysis of Results, Pergamon Press, N.Y. 1961.

APPENDIX A--FATIGUE DATA

This appendix includes fatigue properties of some aircraft materials taken from Ref. 40. While fatigue properties of metals are being developed daily, it is impossible to include all that might be available. Accordingly, one should refer to original sources for additions. Balfour Engineering Co., Suttons Bay, Mich. is continuing to collect fatigue data and is a likely source of new data. Another data source, not necessarily for aircraft materials, is given in Cazaud's Fatigue of Metals (see bibliography).

Some caution should be used in applying these data in that the values presented are for averages and are not guaranteed minimums. Also, it would appear that much of the notched data were acquired on specimens having notches small enough to experience the "Neuber" effect which relates severity of a notch to grain size. Accordingly, it follows that the concentration might be more severe for the same geometrical configuration on a larger piece of structure. Since K_t is approximately equal to K_f at about 10^7 cycles (see C13.2), one can judge the severity of the notches used in these data and make appropriate corrections if needed.

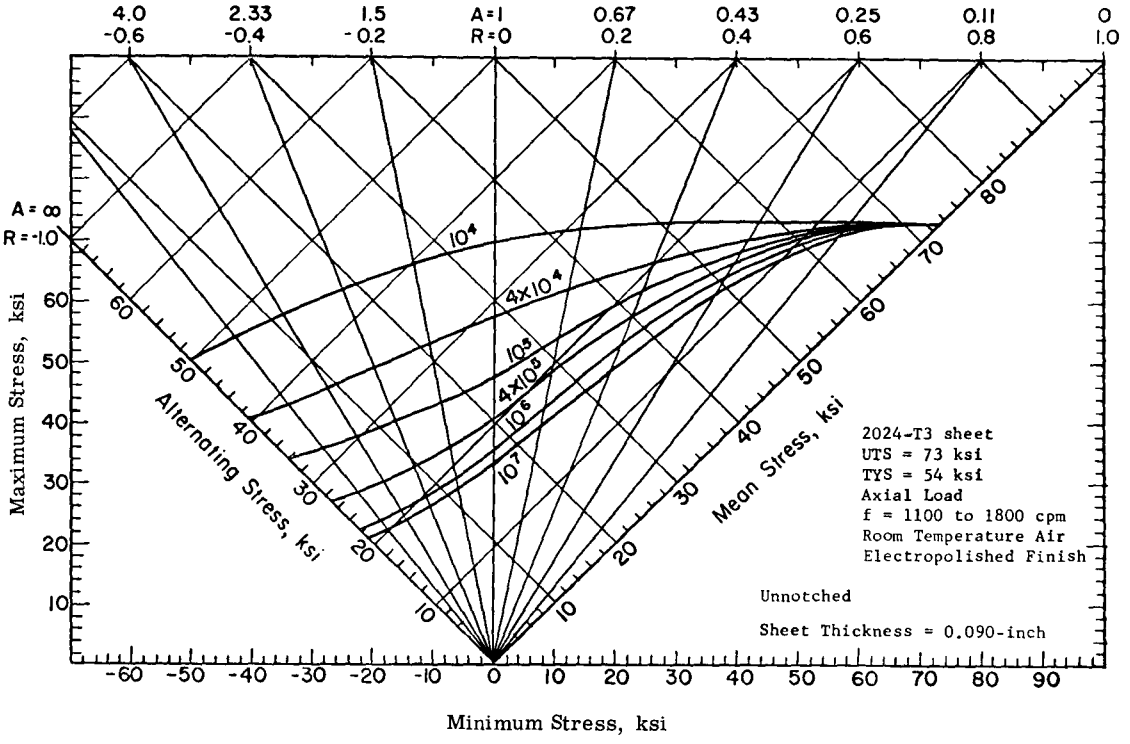

Fig. C13.A1 - Typical Constant-life diagram for unnotched fatigue behavior of 2024-T3 aluminum alloy.

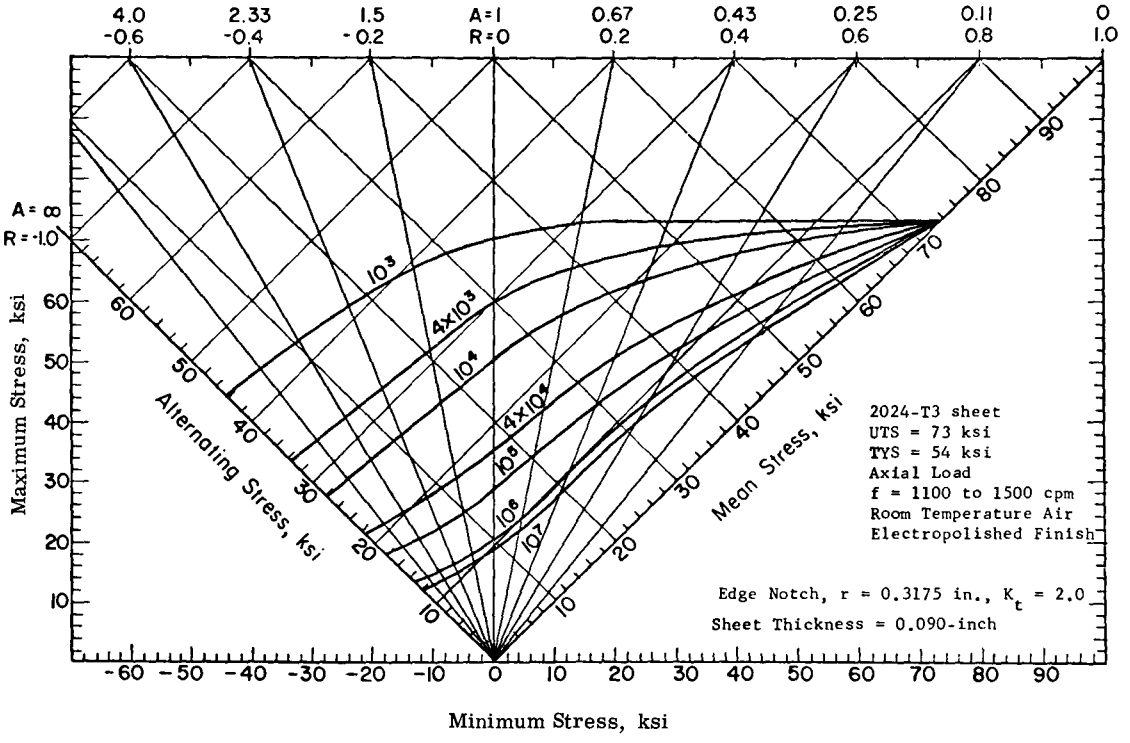

Fig. C13.A2 - Typical Constant-life diagram for notched fatigue behavior of 2024-T3 aluminum alloy.

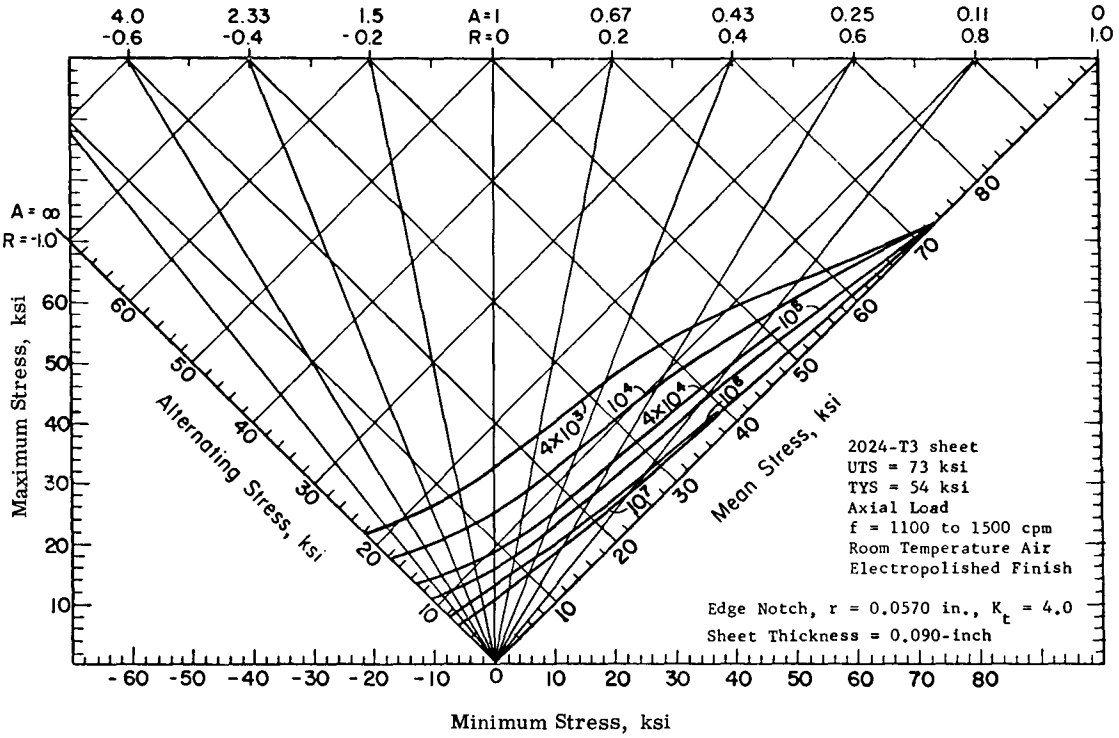

Fig. C13.A3 - Typical Constant-life diagram for notched fatigue behavior of 2024-T3 aluminum alloy.

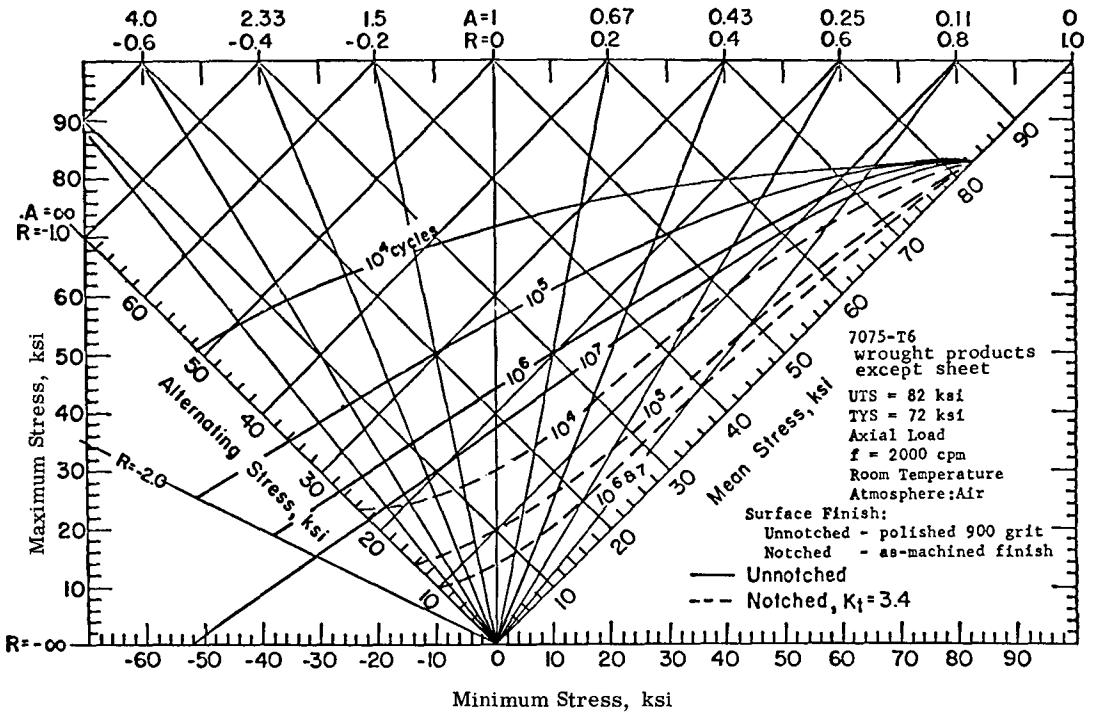

Fig. C13.A4 - Typical constant-life diagram for fatigue behavior of various wrought products of 7075-T6 aluminum alloy.

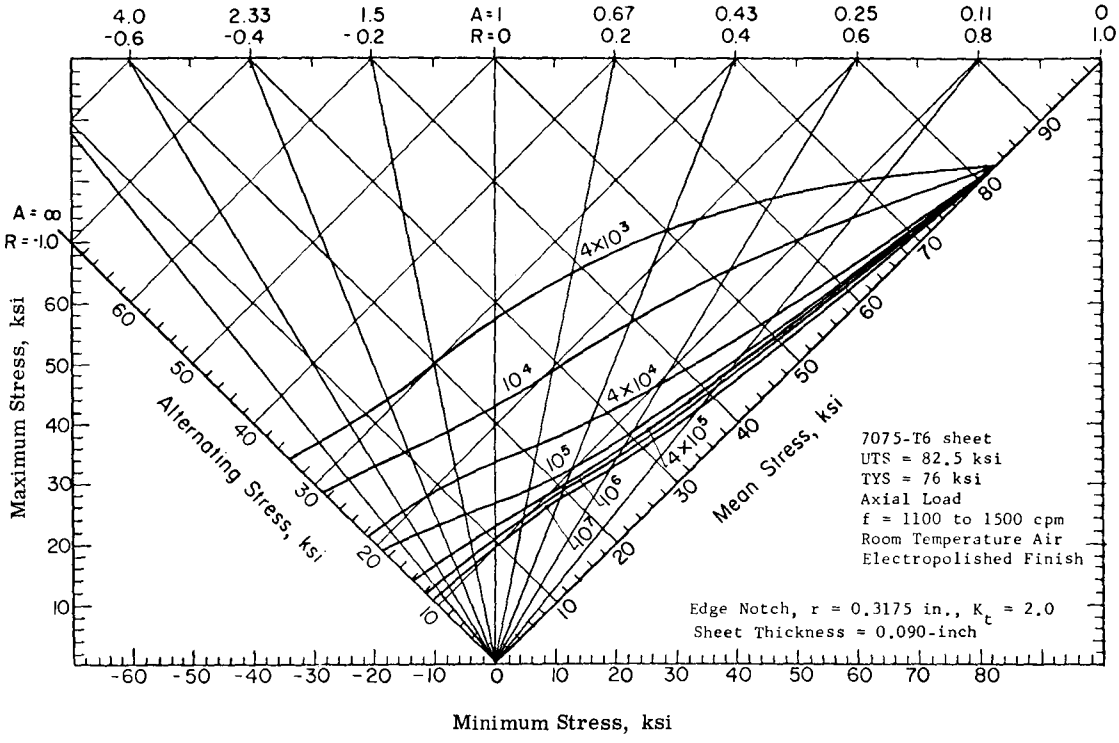

Fig. C13.A5 - Typical Constant-life diagram for notched fatigue behavior of 7075-T6 aluminum alloy.

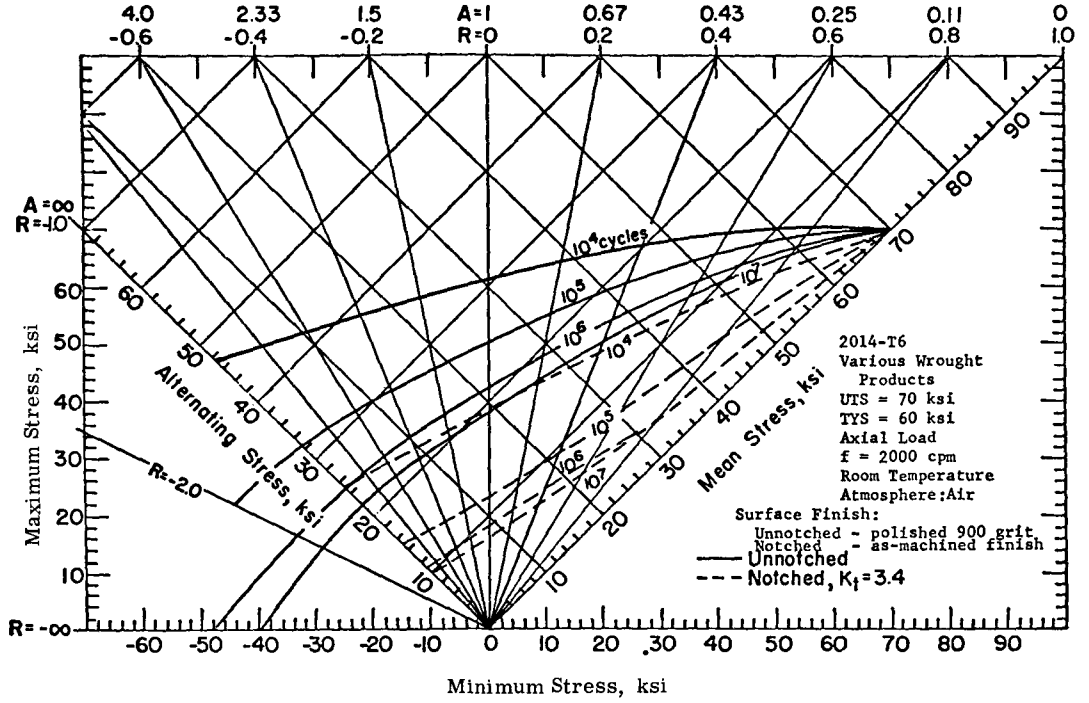

Fig. C13.A6 - Typical constant-life diagram for fatigue behavior of various wrought products of 2014-T6 aluminum alloy.

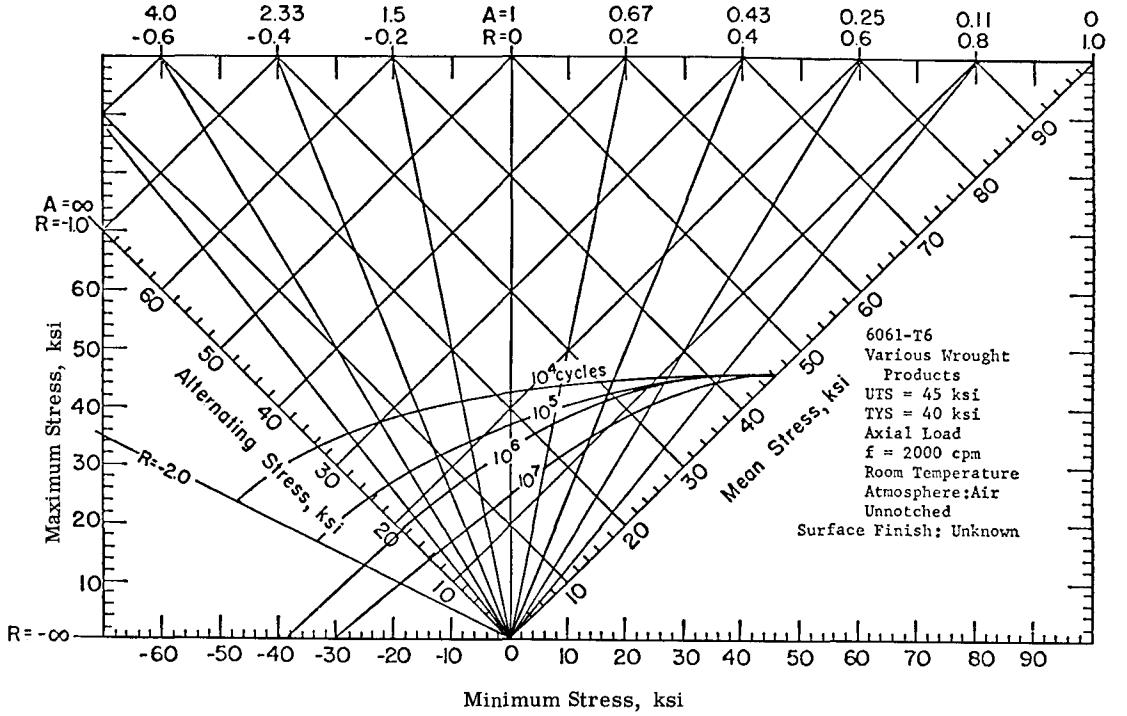

Fig. C13.A7 - Typical constant-life diagram for fatigue behavior of various wrought products of 6061-T6 aluminum alloy.

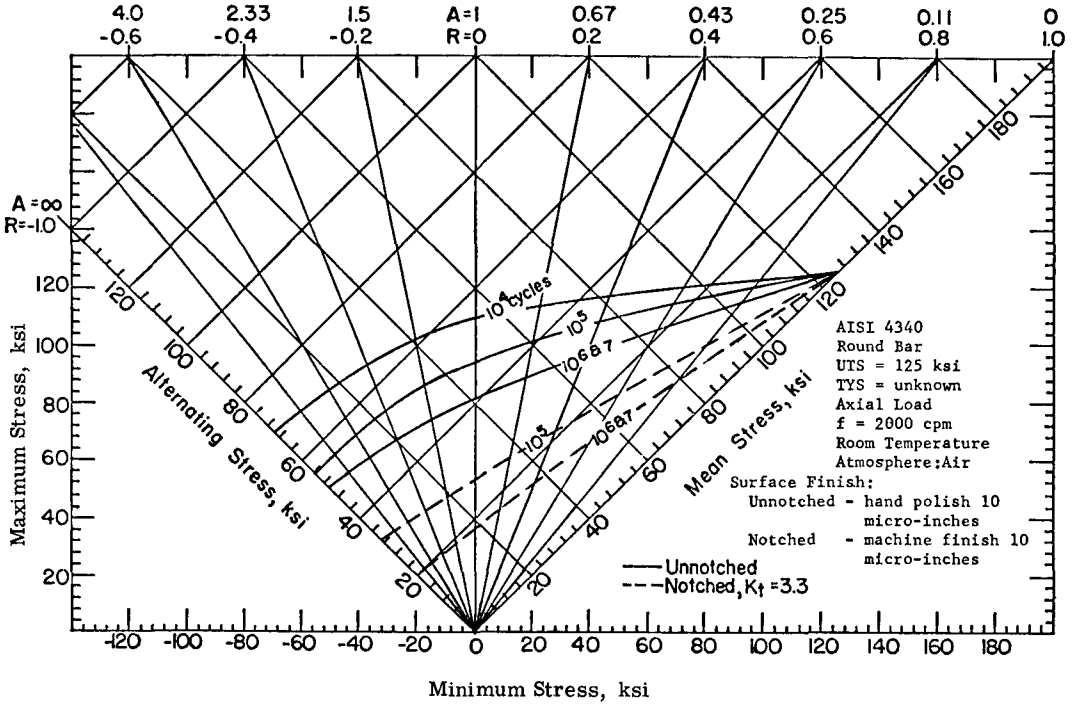

Fig. C13.A8 - Typical constant-life fatigue diagram for heat-treated AISI 4340 alloy steel (bar), F_{tu} = 125 ksi.

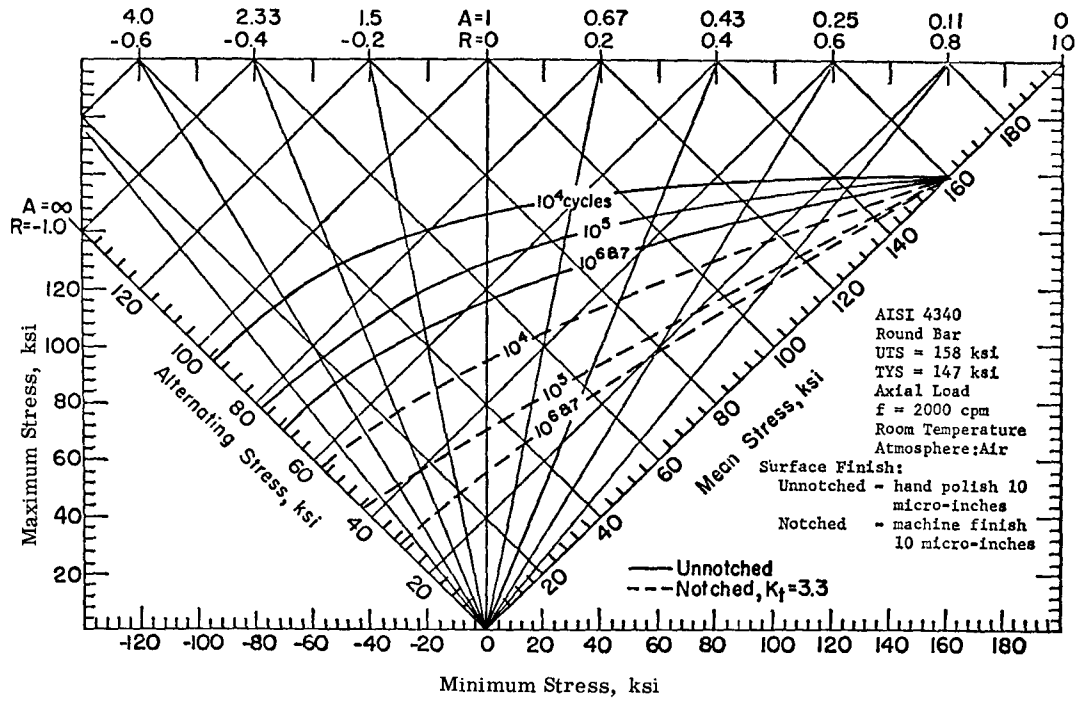

Fig. C13.A9 - Typical constant-life fatigue diagram for heat-treated AISI 4340 alloy steel (bar), F_{tu} = 150 ksi.

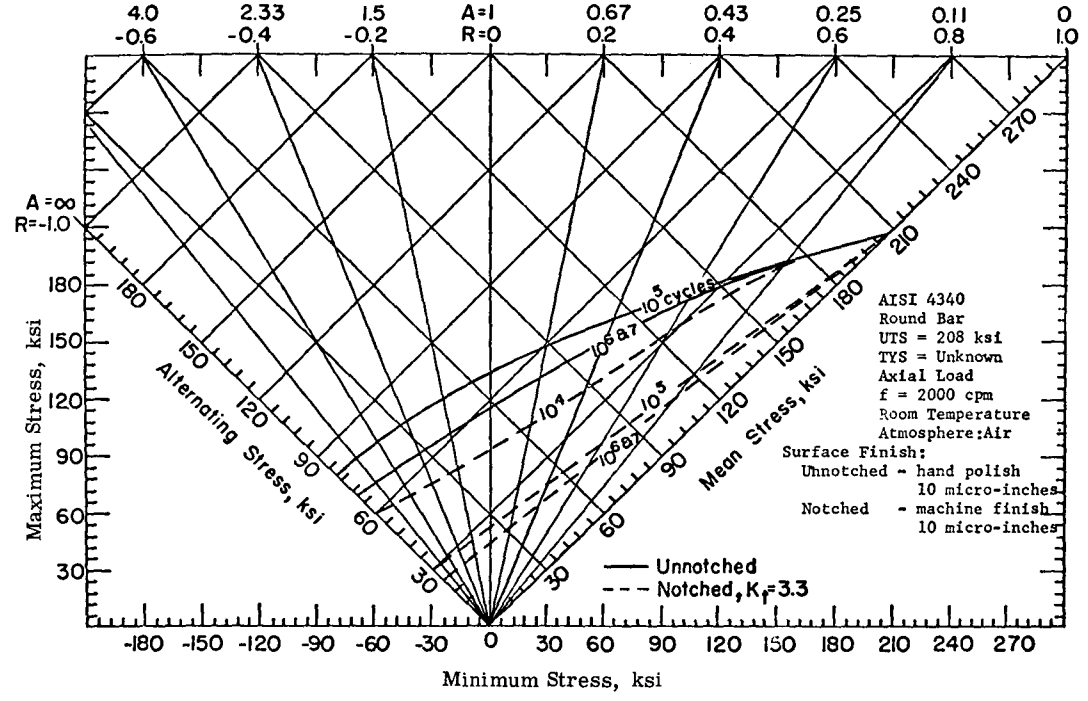

Fig. C13.A10 - Typical constant-life fatigue diagram for heat-treated AISI 4340 alloy steel (bar), F_{tu} = 200 ksi.

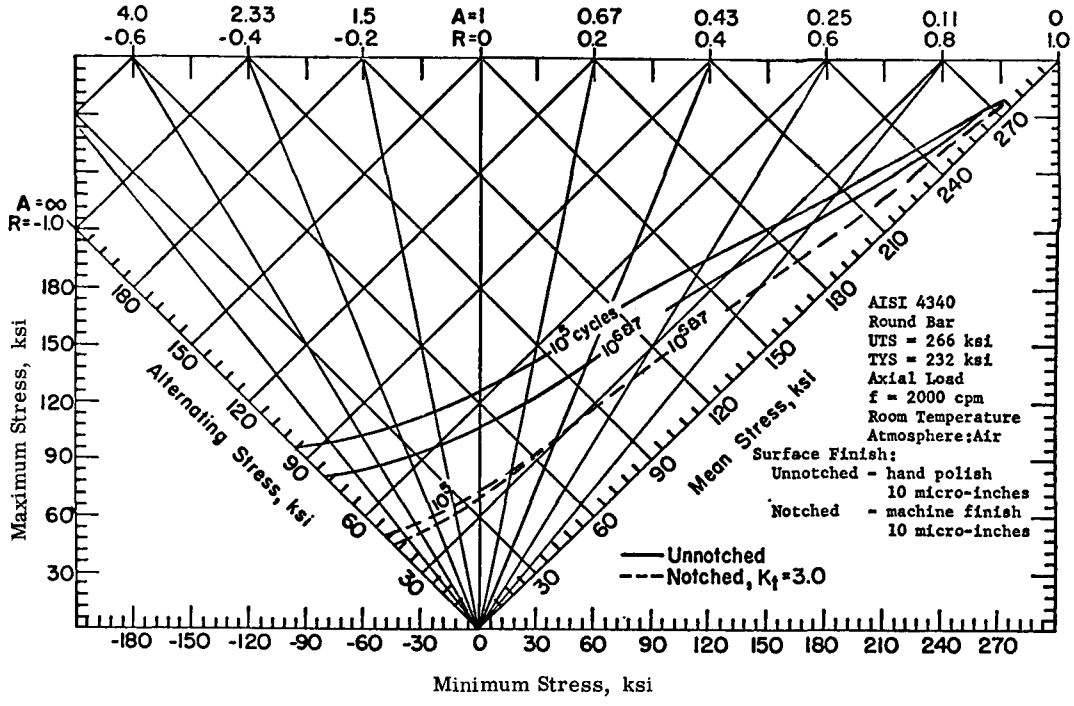

Fig. C13.A11 - Typical constant-life fatigue diagram for heat-treated AISI 4340 alloy steel (bar), F_{tu} = 260 ksi.

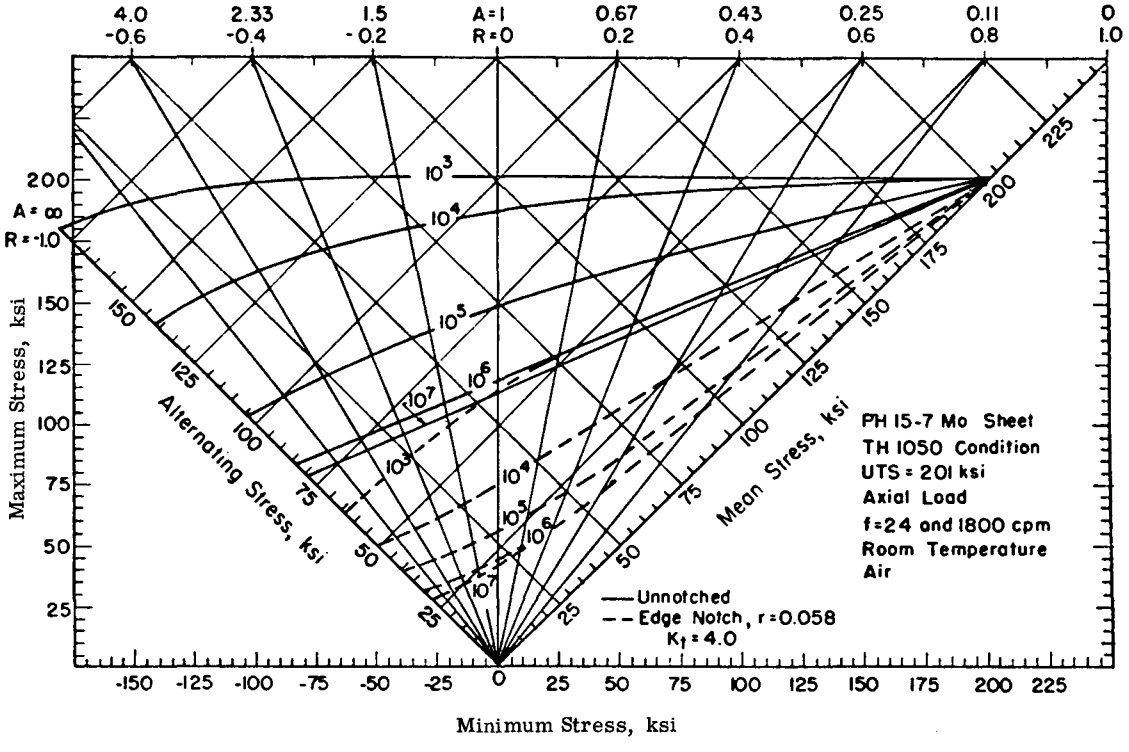

Fig. C13.A12 - Typical constant-life fatigue diagram for PH 15-7 Mo (TH 1050) at room temperature.

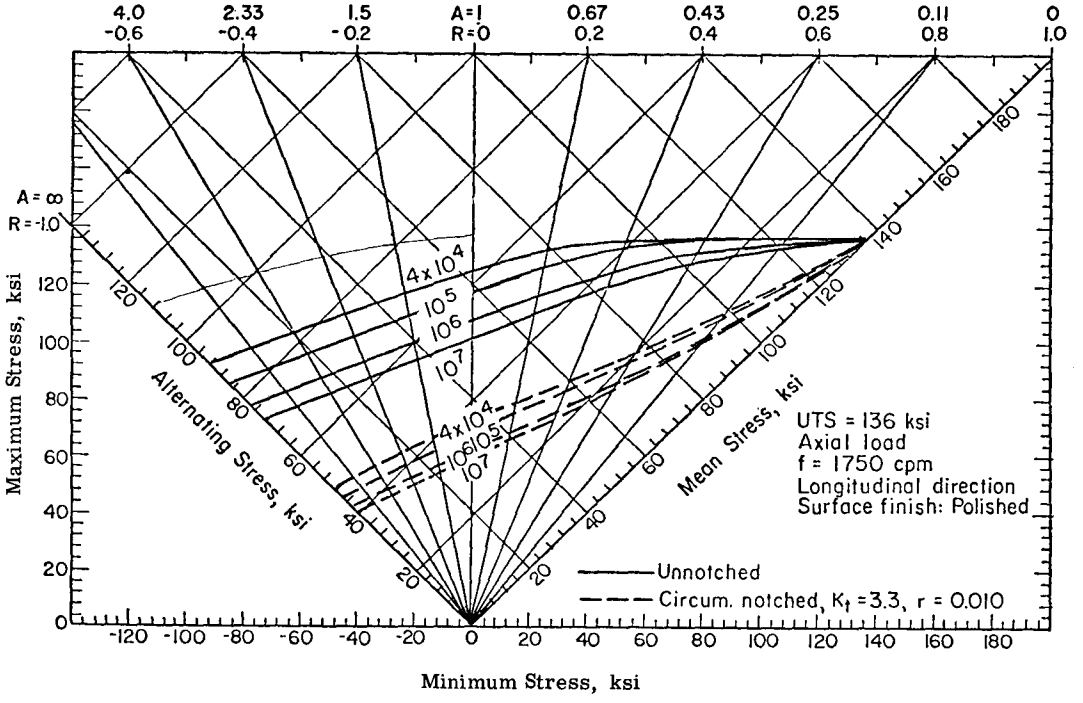

Fig. C13.A13 - Typical constant-life fatigue diagram for annealed Ti-6Al-4V alloy (bar) at room temperature.

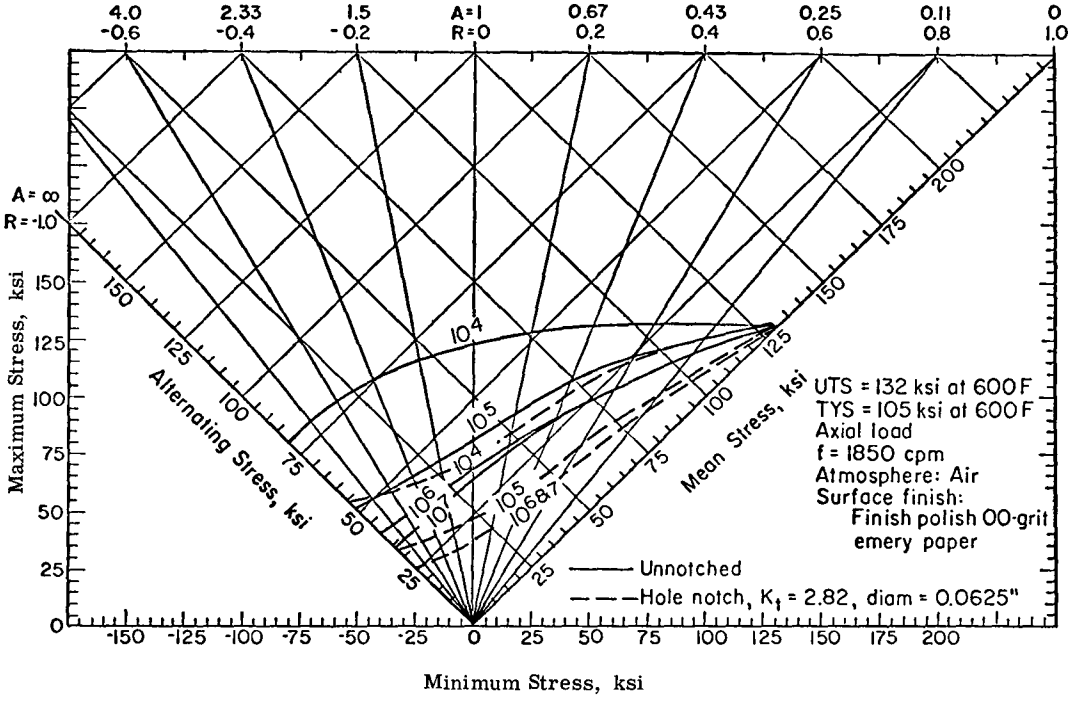

Fig. C13.A14 - Typical constant-life fatigue diagram for solution-treated and aged Ti-6Al-4V alloy (sheet) at 600 F.

CHAPTER D1
FITTINGS AND CONNECTIONS. BOLTED AND RIVETED.

D1.1 Introduction.

The ideal flight vehicle structure would be the single complete unit of the same material involving one manufacturing operation. Unfortunately the present day types of materials and their method of working dictates a composite structure. Furthermore general requirements of repair, maintenance and stowage dictate a structure of several main units held to other units by main or primary fittings or connections, with each unit incorporating many primary and secondary connections involving fittings, bolts, rivets, welding, etc. No doubt main or primary fittings involve more weight and cost per unit volume than any other part of the aerospace structure, and therefore fitting and joint design plays an important part in aerospace structural design.

D1.2 Economy in Fitting Design.

For structural economy the structural designer in the initial layout of the flight vehicle should strive to use a minimum number of fittings particularly those fittings connecting units which carry large loads. Thus in a wing structure splicing the main beam flanges or introducing fittings near the centerline of the airplane are far more costly than splices or fittings placed farther outboard where member sizes and loads are considerably smaller. Avoid changes in direction of heavy members such as wing beams and fuselage longerons as these involve heavy fittings. If joints are necessary in continuous beams place them near points of inflection in order that the bending moments to be transferred through the joint be kept of small magnitude. In column design with end fittings avoid introducing eccentricities on the beam and on the other hand make use of the fitting to increase column end fixity thus compensating some of the weight increase due to fitting weight by saving in the weight of the beam.

For economy of fabrication, the structural designer should have a good knowledge of shop processes and operations. The cost of fitting fabrication and assembly varies greatly with the type of fitting, shape and the required tolerances. Poor layout of major fitting arrangement may require very expensive tools and jigs for shop fabrication and assembly.

Fittings likewise add considerably to the cost of inspection and rejections of costly fittings because of faulty workmanship or materials are quite frequent, thus adding greatly to the unit cost.

D1.3 Fitting Design Loads. Minimum Margins of Safety.

As discussed in other chapters, limit loads are the maximum loads, which a flight vehicle may be subjected to during its lifetime, when carrying out the required ground and flight operations. The limit loads must be carried by the structure without exceeding the yield stress of the material used in the structure. The ultimate or design loads are the limit loads multiplied by a factor of safety, usually 1.5 for aircraft and less for missiles. The structure must have sufficient strength to carry the ultimate or design loads without failure.

The normal flight vehicle structure involves many parts which are joined together by various types of connections. In general, an additional blanket factor of safety is required for design of these connections. This blanket factor of safety is normally 1.15 to 1.20. The stress analysis of most connections or fittings is more complicated than for the primary structural members due to such factors as combined stresses, stress concentration, bolt-hole tightness, etc., thus an additional factor of safety is necessary to give a similar degree of strength reliability for connections as provided in the strength design of the members being connected.

D1.4 Special or Higher Factors of Safety.

A blanket factor of safety for all types of fittings or load conditions is not logical. The manner in which a load is applied to a joint often involves a dynamic or shock load, as for example joints or fittings in landing gear. Single pin connections often undergo rotation or movement between adjacent parts, thus producing faster wearing away of material in operation. Repeated loads often present a fatigue problem. In an airplane or missile there are certain main fittings which, if they failed, would definitely cause the loss of the vehicle. Thus the design fitting requirements of the military and civil aviation agencies involve many special or higher factors of safety. This is so particularly in design involving castings.

D1.5 Aircraft Bolts.

The aircraft bolt is used primarily to transfer relatively large shear or tension loads from one structural member to another. Fig. D1.1 shows three standard aircraft bolts in common use. There are other types but they will not be presented in this limited chapter on connections.

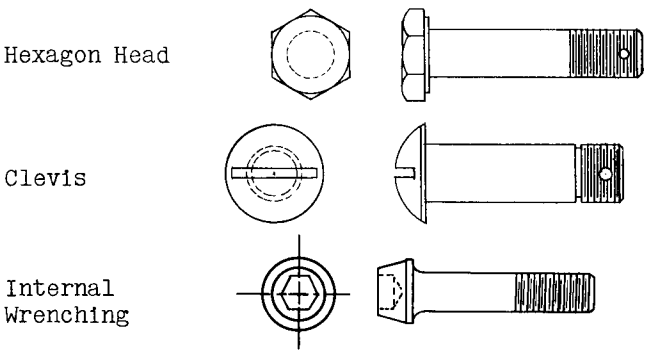

Fig. D1.1

The hexagon head bolt is an Army-Navy standard bolt made from SAE 2330-3.5 percent nickel steel, heat treated to an ultimate tensile strength of 125,000 psi. The bolt head is of sufficient size as to develop the full tensile strength of the bolt.

The internal-wrenching bolt is a high strength steel bolt usually heat treated from 160,000 to 180,000 psi. It is especially suitable for main splice fittings because of its high strength and the relatively small space required for the bolt head.

The clevis bolt is referred to as a shear bolt because its head is not designed to develop the full tensile strength of the bolt. The clevis bolt is usually used when a group or cluster of bolts is required to transfer a load by shear loads on the bolts. The smaller bolt heads thus save weight and also provide greater bolt head clearances. The clevis bolt will develop about one half the tensile strength of the standard AN hexagon head bolt.

The three bolts are also made from aluminum alloy for diameters over 1/4 inch. In many fitting designs weight can be saved by using aluminum alloy bolts.

General Rules in Using Bolts.

Bolt threads should not be placed in bearing or shear. The length of the bolt shank should be such that not more than one thread extends below fitting surface, which can be done by the use of washers.

Bolts less than 3/8 diameter should not be used in major fittings. For steel bolts, 3/16 inch diameter should be the smallest size to be used in any fitting.

Bolts connecting parts having relative motion or stress reversal should have close tolerances to decrease shock loads.

For bolts connecting members having relative motion a lubricator should be incorporated in the surrounding parts of the fitting; the fitting should not be drilled to provide lubrication.

Bolts should be used in double or multiple shear if possible in order to increase strength efficiency in bolt shear and to decrease bending tendency on bolt.

D1.6 Aircraft Nuts.

Fig. D1.2 illustrates four standard steel aircraft nuts. Nut material is more ductile than bolt material, thus when the nut is tightened the threads will deflect to seat on the bolt threads.

The Castle nut is probably the most common aircraft nut. It develops the full rated strength of the bolts. The nut has slots milled in it so that nuts can be prevented from turning.

The Shear nut is only one half as thick as the Castle nut, and thus has only threads enough to develop one half of bolt tensile strength. It is used with a clevis bolt which has a screw driver slot to limit the torsion in tightening the nut. The nut is also castellated for cotter pin lock.

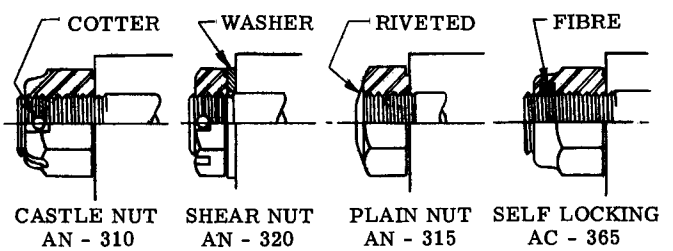

Fig. D1.2

The Plain nut which is very seldom used in present design is used for permanent locations and is locked by "peening" or riveting the end of the bolt over the nut, an operation which destroys the bolt protective coating or finish.

Aluminum Alloy Nuts. Aluminum alloy nuts are not used on bolts designed for tension. Sometimes aluminum alloy nuts are used on steel bolts on land planes to save weight provided the bolts are cadmium plated. If the bolt is used in places where the nut is repeatedly removed, neither bolt or nut should be aluminum alloy because of the danger of injuring the relatively soft threads.

Self Locking Nuts. Self locking nuts are widely used in aircraft industry and there are a number of types on the market. Fig. D1.2 shows one type of self locking nut involving a fiber insert. When the bolt reaches the fiber collar it tends to push the fiber up because the hole in the collar is smaller than the bolt, and is not threaded. The fiber ring thus sets up a heavy downward pressure on the bolt automatically throwing the load carrying sides of the nut and bolt threads into positive contact. Thus all play in the threads is eliminated and a friction is set up between every bolt and nut thread in constant. This constant pressure which is maintained on threads, provides the friction which prevents nut from moving under vibration. The use of the self locking nut reduces the assembly costs as it eliminates the bothersome cotter pin which takes extra operations of the mechanic and is very difficult to install on the nut in the many joints and corners of an airplane. In another type of self locking nut, the locking force is provided by the spring action of the upper part of a specially designed nut.

D1.7 Bolt Shear, Tension & Bending Strengths.

Table D1.1 gives the section properties and the ultimate shear, tension and bending strengths for AN Standard Steel bolts at room temperature. Fig. D1.3 shows the correction to be applied to the strength values in Table D1.1 when bolts are subjected to elevated temperatures. Table D1.2 gives the tensile and double shear strengths of Steel Internal Wrenching bolts. Table D1.2a gives ultimate shear, tension and bending strengths for aluminum alloy bolts. The value of F_b, the modulus of rupture, was determined by the method given in Chapter C3.

Table D1.1

Ultimate Shear, Tensile & Bending Strengths of AN Steel Bolts (F_{tu} = 125,000, F_{su} = 75,000, F_b = 180,000)

Size of pin or bolt	Area of solid section, in.^{2}	Moment of inertia of solid, in.^{4}	Ultimate single shear strength at full diameter, lb.	Ultimate tensile strength (in thread), lb.	Ultimate Bending Moment in. lbs.
0.190	.02835	.0000640	2,126	2,210	121
1/4	.04908	.0001918	3,680	4,080	276
5/16	.07669	.0004682	5,750	6,500	539
3/8	.1105	.0009710	8,280	10,100	932
7/16	.1503	.001797	11,250	13,600	1,480
1/2	.1963	.003069	14,700	18,500	2,210
9/16	.2485	.004914	18,700	23,600	3,140
5/8	.3068	.007492	23,000	30,100	4,320
3/4	.4418	.01553	33,150	44,000	7,450
7/8	.6013	.02878	45,050	60,000	11,850
1	.7854	.04908	58,900	80,700	17,670

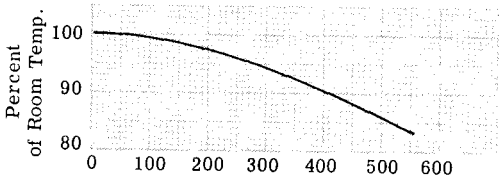

Table D1.2

Ultimate Shear and Tensile Strengths of Steel Internal Wrenching Bolts (F_{tu} = 160,000)

Size Dia.	Ult. Tensile Strength lbs.	Double Shear Strength lbs.	Size Dia.	Ult. Tensile Strength lbs.	Double Shear Strength lbs.
1/4	6,190	9,300	5/8	43,600	58,300
5/16	9,820	14,600	3/4	63,200	83,900
3/8	15,200	21,000	7/8	86,100	114,200
7/16	20,600	28,600	1.0	114,000	149,200
1/2	27,400	37,300	1-1/8	144,000	188,900
9/16	34,800	47,200	1-1/4	180,000	233,200

Table D1.2a

Ultimate Shear, Tensile and Bending Strengths of 2024 Aluminum Alloy Bolts

Dia.	SHEAR F_{su}-35,000	TENSION F_{tu}-62,000	BENDING F_b-72,000
3/16	992	1,059	46
1/4	1,717	1,975	110
5/16	2,684	3,189	216
3/8	3,868	4,937	373
7/16	5,261	6,663	592
1/2	6,871	9.104	884
9/16	8,697	11,563	1,260
5/8	10,738	14,719	1,730
3/4	15,463	21,573	2,980
7/8	21,046	29,520	4,740
1.0	27,489	39,759	7,070

D1.8 Bolts in Combined Shear and Tension.

When bolts are subjected to both shear and tension loads, the resulting strength is given by the following interaction equation:- (Ref. 1, 2)

$$\frac{x^3}{a^3} + \frac{y^2}{b^2} = 1 \quad \text{- - - - - - - - - - - - - - - - (D1.1)}$$

where,

x = shear load
y = tension load
a = shear allowable load from Table D1.1
b = tension allowable load from Table D1.1

Figs. D1.4 and D1.5 is a plot of equation for the various AN steel bolt sizes. The curves are not applicable where shear nuts are used. The curves are based on the results of combined load tests with nuts fingertight.

D1.8a Bushings.

It is customary to provide bushings in the lugs of single bolt or pin fittings subjected to reversal of stress or to slight rotation. Thus if wear and tear takes place a new bushing can be inserted in the lug fitting. Steel bushings are commonly used in aluminum alloy

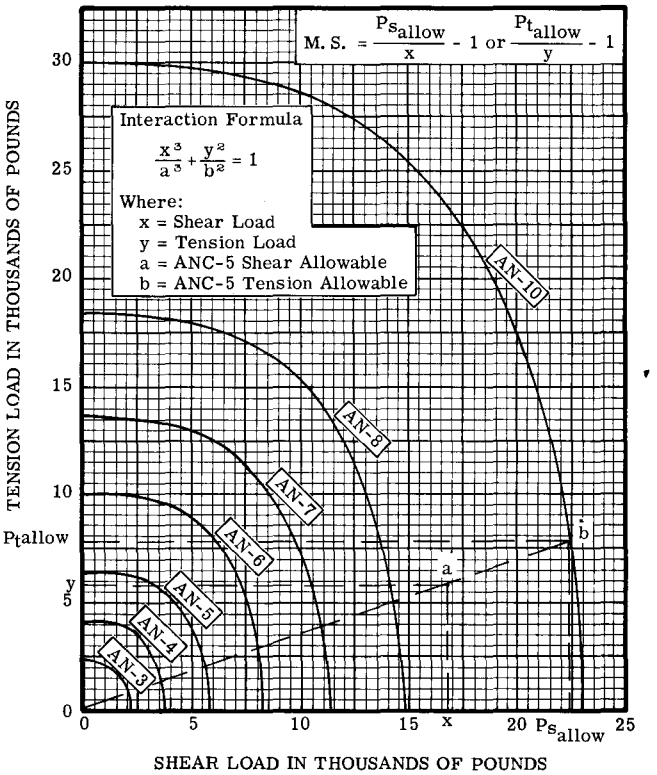

Fig. D1.4 Combined Shear and Tension on AN Steel Bolts (F_{tu} = 125,000, F_{su} = 75,000)

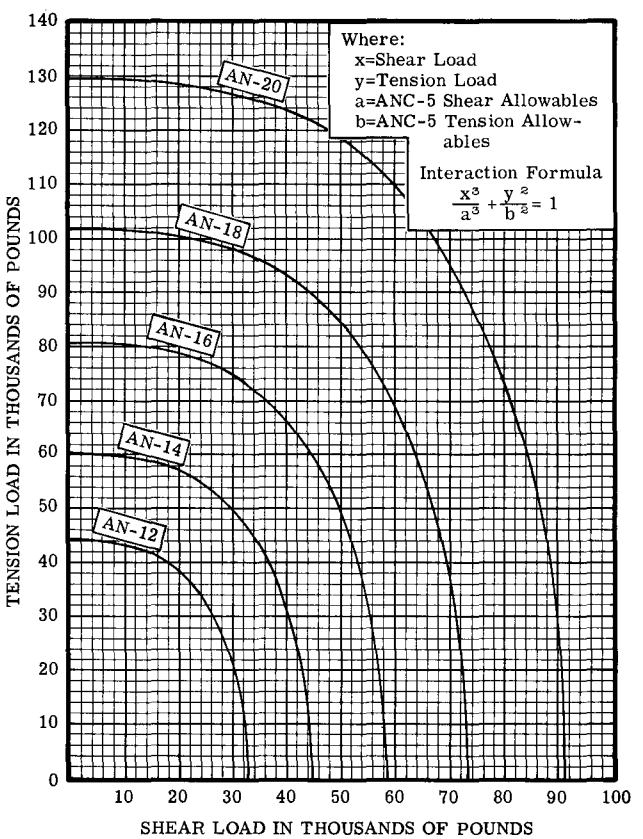

Fig. D1.5 Combined Shear and Tension on AN Steel Bolts

single bolt fitting lugs to increase the allowable bearing stress on the lug since the bushing increases the bearing diameter 1/8 inch since bushings are usually 1/16 inch in wall thickness. If bushings are not used on single bolt connections sufficient edge distance should be provided to ream hole for next size bolt in case of excessive wear of the unbushed hole. If considerable rotation occurs a lubricator should be provided for a plain bushing or an oil-impregnated bushing should be used.

D1.9 Single Bolt Fitting.

Possibly the simplest method of joining two members together is the use of a single bolt or pin connection. Such a joint can transmit relatively large loads and yet the joint is easily and quickly disconnected.

Fig. D1.6 illustrates the four general methods of connecting two members by a single bolt. First the connection is made symmetrical about the centerline of the load on the joint. Thus is Fig. D1.6a the load P on the male part of the fitting divides equally and symmetrically to the two female plates or units which make up part of the fitting unit. If the male and female parts of the connection are to be tied together by a single bolt it is evident that the connecting plates will be weakened due to the bolt hole unless extra material is added at the bolt hole section.

Fig. D1.6a shows a fitting consisting of three rectangular plates of uniform section throughout fastened together by a single bolt. Obviously the weak section for the plates in tension would be a section through the centerline of the hole. If this section is strong enough to carry the given loads, then the remaining part of the fitting members are considerably over strength. To avoid this over-strength which means extra weight of fitting units, a single bolt fitting unit is often made like one of the examples indicated in Fig. b, c and d of Fig. D1.6.

In Fig. b, the plates are made constant thickness but increased in width in the vicinity of the hole section. In Fig. c, the width of the plates is kept constant but the thickness of the plates are increased in the vicinity of the hole section, and in Fig. d, both width and thickness of plates are changed.

D1.10 Methods of Failure of Single Bolt Fitting and the Allowable Failing Loads.

As the load on a fitting is transferred from one side of the fitting to the other, internal stresses are produced which tend to cause the fitting to fail in several different ways.

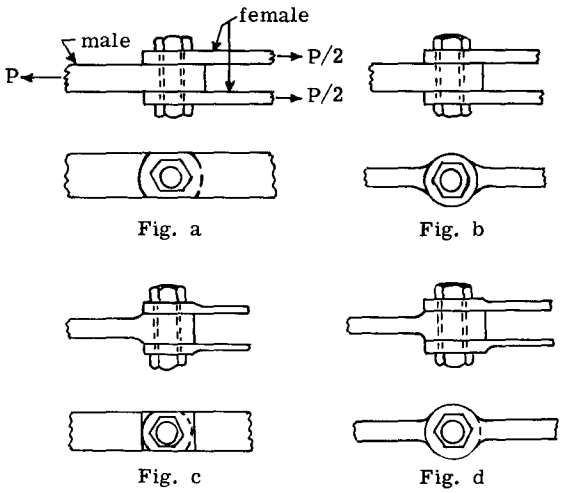

Fig. a Fig. b

Fig. c Fig. d

Fig. D1.6

Failure by Bolt Shear.

In Fig. D1.7 the bushing is not continuous between the plates, but each of the three plates have separate bushings. As the pull P is placed on the fitting it tends to shear the bolt at sections (1-1) and (2-2), (Fig. D1.7a). Fig. D1.7b illustrates the forces or pressures on the bolt and the failure which can take place if the stresses are sufficient.

Let P_u represent the maximum or ultimate load on the fitting. This force P_u must be resisted by the shear strength of the bolt at the two sections (1-1) and (2-2). Hence,

$$P_{u(\text{bolt shear})} = F_{su} \cdot A \cdot 2 \quad \text{- - - - - - - - - - (1)}$$

where F_{su} = ultimate shearing stress for bolt material.
A = cross-sectional area of bolt.

Failure by Bolt Bending.

The main concern regarding bolt bending is that under the limit loads any bending deflection of the bolt be not permanent as such deformation would make removal of the bolt difficult. The subject of bolt bending stresses is discussed in a later article.

Failure of Lug Portion of Fitting.

The lug portion of the fitting refers to that portion of the fitting that involves the hole for the single bolt that connects the male and female parts of the fitting unit. The simplified assumptions regarding failing action and the resulting equations which follow have been widely used for quick approximate check of the lug strength. The procedure which follows will be referred to as Method 1.

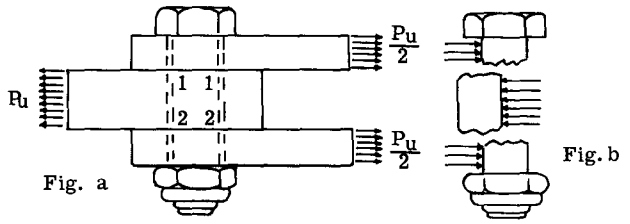

Fig. a Fig. b

Fig. D1.7

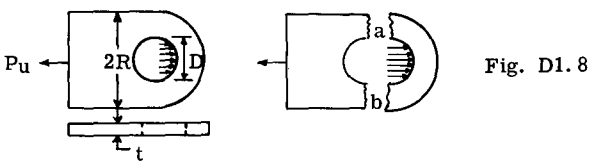

Fig. D1.8

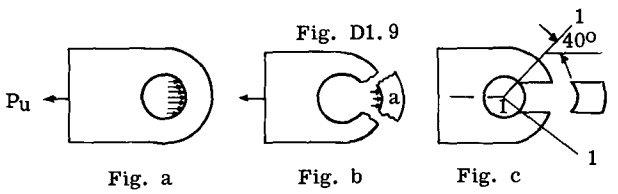

Fig. D1.9

Fig. a Fig. b Fig. c

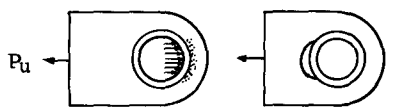

Fig. a Fig. b

Fig. D1.10

METHOD 1 OF BOLT & LUG STRENGTH ANALYSIS

Failure in Tension.

Fig. D1.8 indicates how a fitting plate can pull apart due to tension stresses on a section through the centerline of the bolt hole. Both the male and female parts of the fitting must transfer the load past the centerline of the hole, thus both parts must be considered in the design of a fitting. Equating the allowable load P_u to the ultimate resisting tensile stresses at points (a) and (b) Fig. D1.8, we obtain,

$$P_{u(\text{tension})} = F_{tu}\,(2R - D)t \quad \text{- - - - - - - - - (2)}$$

where F_{tu} = ultimate tensile strength of plate material.

Equation (2) assumes that the tensile stress on the cross-section is uniform. This is not true as the flow of stress around the hole causes a stress concentration. To take care of this stress concentration requires a margin of safety of 25 percent.

Failure by Shear Tear Out.

Fig. D1.4 illustrates the manner in which failure can occur by the shearing tear out of a plate sector in front of the bolt. In Fig. a,

the load P causes the bolt (not shown) to press on the plate around the bolt hole edge. Stresses are produced which tend to cause the portion (a) in Fig. (b) to tear out as shown. Equating the load P_u to the ultimate shear resistance of the material times the area of the two shear out areas, we can write,

$$P_{u(\text{shear out})} = F_{su} A_s \quad \text{- - - - - - - - - - - (3)}$$

where F_{su} = ultimate shearing strength of the plate material.
A_s = shear out area.

It is very common practice to take the shear out area A_s equal to the edge distance at the centerline of the hole times the thickness t of the plate times two since there are two shear areas. This is slightly conservative because the actual shear area is larger. Ref. 1 permits one to use the area along line 1-1 which is limited by the 40 degree line as shown in Fig. D1.9c.

Failure by Bearing of Bushing on Plate.

In Fig. D1.10a, the pull P causes the bolt (not shown) to press against bushing wall which in turn presses against the plate wall. If the pressure is high enough the plate material adjacent to the hole will start to crush and flow thus allowing the bolt and bushing to move which results in the elongated hole as illustrated in Fig. b. Equating the load P_u to the ultimate bearing strength on the bearing surfaces we can write,

$$P_u = F_{br} D t \quad \text{- - - - - - - - - - - - - - - - (4)}$$

where F_{br} = allowable bearing stress
D = diameter of bushing
t = plate thickness

It is good practice to require a margin of safety of 50 percent.

Failure by Bearing of Bolt Bushing.

A bushing is pressed into the plate hole and thus it is considered as a tight fit. A fitting bolt is usually considered as removable therefore a certain tolerance between the bolt and bushing inside diameters is necessary in order to insert and remove bolt. If fitting is subjected to reversible loads the small slop in the fitting tends to cause shock on the fitting. Also the fitting may be such that slight rotation takes place on the bolt, which tends to cause wear between bolt and bushing. It is therefore customary to check the bearing pressure between the bolt and the bushing since failure of the bushing could take place in a manner explained in the previous article dealing with bearing of bushing on plate. Then as before,

$$P_u = F_{br} D t \quad \text{- - - - - - - - - - - - - - - - (5)}$$

where D = bolt diameter

A margin of safety of 50 percent should be maintained. If the fitting is subjected to infrequent rotation under load but with load involving no shock or vibration, require a margin of safety of 100 percent. If shock or vibration with infrequent rotation is present, require a margin of safety of 150 percent. Shock is considered to occur in such structures as landing gears, gun mounts, hoisting, mooring and towing connections.

General Comment on Margins of Safety for Lugs.

In general it is good design practice to design lugs conservatively as the weight of lugs is small relative to their importance in insuring the safety of the flight vehicle. Inaccuracies in manufacture are difficult to control. It is good design practice to provide sufficient material to permit drilling for a bushing if bushing is not used in original design. If castings are used as fittings, much higher factors of safety on the limit loads are specified because of the low ductibility of the material in castings.

D1.11 Method 2. Lug Strength Analysis Under Axial Loading.

Due to a comprehensive study and test program by Cozzone, Melcon and Hobbit (Refs. 3 and 4), the procedure as given in Method 1 is somewhat modified. The important difference is that curves derived from test results give the stress concentration factor to use for tension on the net section and the shear out failure as assumed in Method 1 has been replaced by a combined shear-out bearing failure. Fig. D1.11 shows the lug-pin combinations and types of failure as taken from Ref. 3.

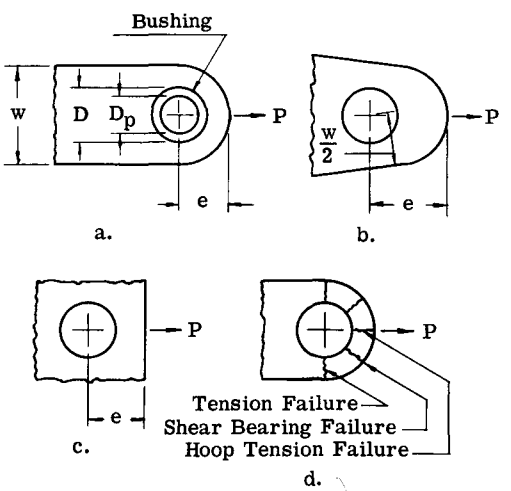

Fig. D1.11

The methods of failure and the methods of lug strength analysis are as follows:

Tension Across the Net Section.

Because of stress concentration, the stress on the net cross-section cannot be taken as uniform. The ultimate allowable tension load P_u for lug equals,

$$P_u = K_t F_{tu} A_t \quad - - - - - - - - - - - - - - - - (6)$$

where K_t is the stress concentration factor as found from Fig. D1.12 and Table D1.3. F_{tu} = ultimate tensile strength of the material and A_t = net tension area.

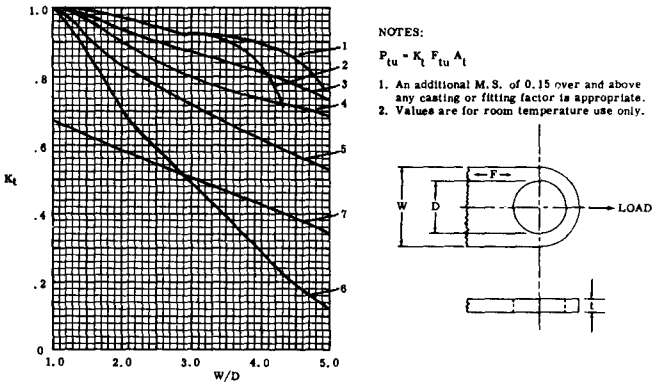

Fig. D1.12 Lug Design Data
Tension Efficiency Factors for
Axially Loaded Lugs (Ref. 3, 4)

Table D1.3

Curve Nomenclature for Axial Loading for Fig. D1.12

L, LT and ST Indicate Grain in Direction F in Sketch
L - Longitudinal
LT - Long Transverse
ST - Short Transverse (Normal)

MATERIALS

Curve 1 - 2014-T6 and 7075-T6 Die Forging (L)
4130 and 8630 Steel
2014-T6 and 7075-T6 Plate ≤ 0.5 (L, LT)
7075-T6 Bar and Extrusion (L)
2014-T6 Hand Forged Billet ≤ 144 in.^{2} (L)

Curve 2 - 2014-T6 and 7075-T6 Plate > 0.5 in. ≤ 1.0 in. (L, LT)
7075-T6 Extrusion (LT, ST)
2014-T6 Hand Forged Billet > 144 in.^{2} (L)
2014-T6 Hand Forged Billet ≤ 36 in.^{2} (LT)
2014-T6 and 7075-T6 Die Forgings (LT)

Curve 3 - 2024-T4, 2024-T2 Extrusion (L, LT, ST)

Curve 4 - 2014-T6 and 7075-T6 Plate > 1 in. (L, LT)
2024-T4 Bar (L, LT)
2024-T3, 2024-T4 Plate (L, LT)

Curve 5 - 2014-T6 Hand Forged Billet > 36 in.^{2} (LT)

Curve 6 - Aluminum Alloy Plate, Bar, Hand Forged Billet and Die Forging (ST). NOTE: For Die Forgings ST Direction Exists Only at Parting Plane.
7075-T6 Bar (T)

Curve 7 - AZ91C-T6 Mag. Alloy Sand Casting
356-T6 Aluminum Alloy Casting

Shear Out-Bearing Strength.

Failure due to shear out and bearing are closely related and are covered by a single calculation based on empirical curves. The ultimate or failing load in this shear-bearing type of failure is:-

$$P_{bru} = K_{bru} F_{tu} A_{br} \quad - - - - - - - - - - - - - - (7)$$

The values of K_{bru}, the shear-bearing efficiency factor, is given by curves in Fig. D1.13.

For shear-bearing yield strength the equation is,

$$P_{bry} = K_{bry} F_{tu} A_{br} \quad - - - - - - - - - - - - - - (8)$$

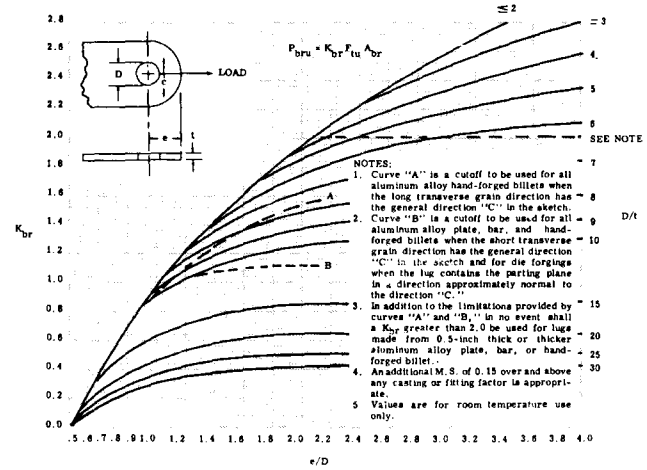

Fig. D1.13 Lug Design Data
Shear-Bearing Efficiency Factors for
Axially Loaded Lugs (Ref. 3, 4)

Fig. D1.14 gives curves for finding K_{bry}.

Bushing Yield.

Take A_{br} as the smaller of the bearing areas of bushing on pin or bushing on lug. (The latter may be smaller as a result of external chamfer of the bushing, oil grooves, etc.) The allowable yield bearing load on bushing is then,

$$P_{bry} = 1.85 F_{cy} A_{br} \quad - - - - - - - - - - - - - - (9)$$

where F_{cy} is compressive yield strength of bushing material.

Bolt or Pin Shear Strength.

The bolt shear strength is calculated in the same manner as given in Method 1.

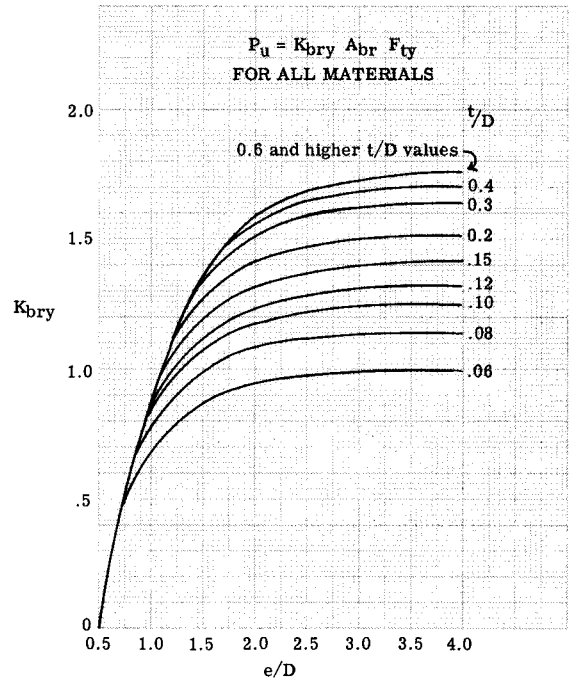

Fig. D1.14 (Ref. 5)
Values of Shear-Bearing Factors of Lugs

Bolt or Pin Bending.

The subject of bolt bending strength is treated in Art. D1.14.

D1.12 Lug Strength Analysis Under Transverse Loading.

Cases arise where the lug of a fitting unit is subjected to only a transverse load. Melcon and Hobbit in (Ref. 4) express the ultimate transverse or failing load by a single equation:-

$$P_{tu} = K_{tu} A_{br} F_{tu} \quad \text{- - - - - - - - - - - - -(10)}$$

Similarly the yield strength of lug is,

$$P_{ty} = K_{ty} A_{br} F_{ty} \quad \text{- - - - - - - - - - - - -(11)}$$

The efficiency failing and yield coefficients K_{tu} and K_{ty} are given by the curves in Fig. D1.15. The curve nomenclature for the curves in Fig. D1.15 is given in Table D1.4. In using Fig. D1.15, a value called A_{av} is needed, the value of which is shown in the equation shown on Fig. D1.15

D1.13 Lug Strength Analysis Under Oblique Loads.

Fitting lugs are often subjected to oblique loads. Ref. 4 gives the following approach to this loading case.

Resolve the applied load into axial and transverse components. Then use the following interaction equation;-

$$R_a^{1.6} + R_{tr}^{1.6} = 1 \quad \text{- - - - - - - - - - - - -(12)}$$

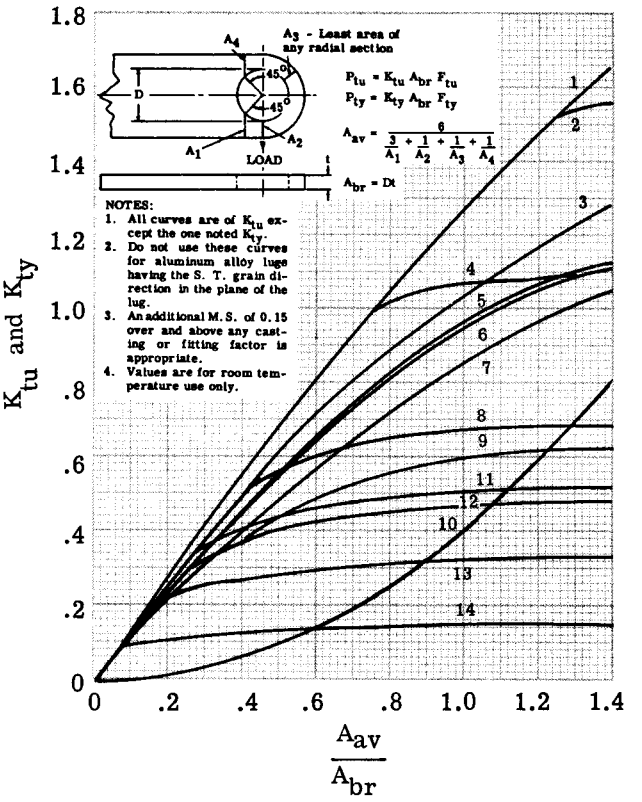

Fig. D1.15 Lug Design Data
Tension Efficiency Factors for Transversely Loaded Lugs (Ref. 3, 4)
(See Table D1.4 for Curve Nomenclature)

Table D1.4
(To be Used with Fig. D1.15)
Curve Nomenclature for Transverse Loading

Curve 1 - 4130 and 8630 Steel thru 125 KSI H. T.
Curve 2 - 4130 and 8630 Steel 150 KSI H. T.
Curve 3 - K_{ty} for All Aluminum and Steel Alloys
Curve 4 - 4130 and 8630 Steel 180 KSI H. T.
Curve 5 - 356-T6 and AZ91C-T6 Sand Castings
Curve 6 - 2024-T3 and 2024-T4 Plate ≤ 0.5 in.
Curve 7 - 220-T4 Sand Casting
Curve 8 - 2014-T6 and 7075-T6 Plate ≤ 0.5 in.
Curve 9 - 2024-T3 and 2024-T4 Plate > 0.5 in. also 2024-T4 Bar
Curve 10 - Approximate Cantilever Strength for All Aluminum and Steel Alloys. If K_{tu} is Below this Curve a Separate Calculation as a Cantilever Beam is Warranted.
Curve 11 - 2014-T6 and 7075-T6 Plate > 0.5 in. ≤ 1.0 in.
7075-T6 Extrusions
2014-T6 Hand Forged Billet ≤ 36 in.[2]
2014-T6 and 7075-T6 Die Forgings
Curve 12 - 2024-T6 Plate, 2024-T4 & 2024-T42 Extrusions
Curve 13 - 2014-T6 and 7075-T6 Plate > 1 in.
Curve 14 - 2014-T6 Hand Forged Billet > 36 in.[2]

or margin of safety is,

$$M.S. = \frac{1}{(R_a^{1.6} + R_{tr}^{1.6})^{0.625}} - 1 \quad \text{- - - -(13)}$$

where, R_a = axial component of applied ultimate load divided by the smaller of the

values obtained for equations (6) or (7).

R_{tr} = transverse component of applied ultimate load divided by the values of P_{tu} in equation (10).

D1.14 Bolt Bending Strength.

In general static tests of single bolt fittings will not show a failure due to bolt bending failure. However, it is important that sufficient bending strength be provided to prevent permanent bending deformation of the fitting bolt under the limit loads so that bolts can be readily removed in maintenance operations. Furthermore, bolt bending weakness can cause peaking up a non-uniform bearing pressure on the fitting lugs thus influencing the lug tension and shear strength. The unknown factor in bolt bending is the true value of the bending moment on the bolt because the moment arm to the resultant bearing forces is unknown. An approximate method (Ref. 4) for determining the arm (b) to use in calculating the bending moment on bolt is given in Fig. D1.16, which gives $b = .5t_1 + .25t_2 + g$ where g is clearance or gap between lugs. The resulting bending moment is considered to be conservative. (See Ref. 4 for other refinements relative to determining moment arm b.)

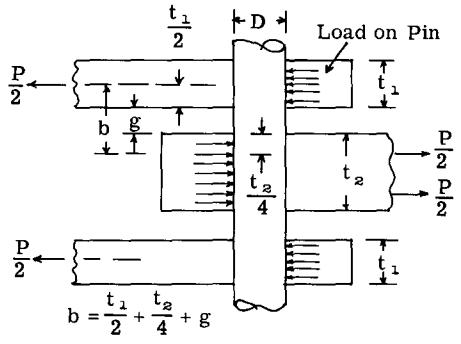

Fig. D1.16

D1.15 Illustrative Problems.

PROBLEM 1. An engine mount fitting is attached to the nacelle fitting by a 5/8 diameter AN steel bolt. The ultimate or design loads on the bolt are tension = 5800 lbs. and shear = 16700 lbs. Due to vibration a 25 percent margin of safety will be required.

Solution:- This is a problem of combined tension and shear on a bolt. Use is made of curves in Fig. D1.4 which are interaction curves for combined tension and shear. On Fig. D1.4 at a value on lower scale equal to the shear load of 16700 lb., labeled point (x) on the figure, we erect a vertical dashed line as shown. On the vertical scale we locate point (y) at tension load of 5800 lbs., and draw horizontal dashed line to give point (a). A straight line through points (o) and (a) is drawn and extended to intersect the curve for a 5/8 AN bolt at point (b). Projecting downward from point (b) to lower scale, we obtain $P_{s(allow)}$ = 22400 lb. and projecting horizontally we obtain $P_{t(allow)}$ = 7700 lb.

Then M.S. = $(P_{s(allow)}/x) - 1$ = (22400/16700) - 1 = .34 or M.S. = $(P_{t(allow)}/y) - 1$ = (7700/5800) - 1 = .34.

The specified required M.S. was .25, thus bolt strength is satisfactory.

PROBLEM 2.

Fig. D1.17 shows a single pin fitting. The lug material is AISI Steel, heat treated to F_{tu} = 125000 psi. The bolt is AN steel, F_{tu} = 125000. The bushing is steel with F_{tu} = 125000. The fitting is subjected to an ultimate tension load of 15650 lb. The fitting will be strength checked for the design load. The check will be made by both Methods 1 and 2.

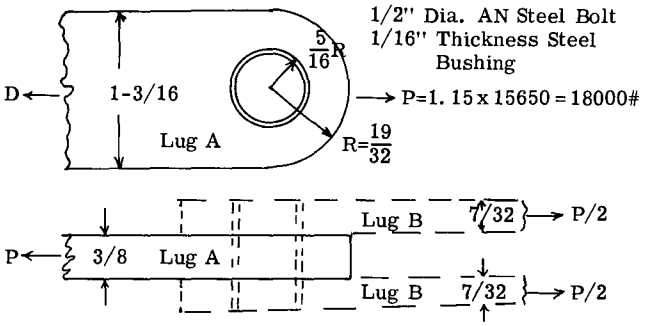

Fig. D1.17

SOLUTION BY METHOD 1.

A fitting factor of safety of 1.15 will be used which is standard practice for military airplanes.

Design Fitting Load = 1.15 x 15650 = 18000 lb.

Check of Bolt Shear Strength.

Bolt is in double shear. From Table D1.1, single shear strength of 1/2 inch diameter AN steel bolt is 14700 lb.

Whence P_u = 2 x 14700 = 29400 lb.

M.S. = (29400/18000) - 1 = .62

Check Bending of Bolt.

Referring to Fig. D1.16, the moment arm for calculating bending moment on bolt is,

$b = 0.5t_1 + 0.25t_2 + g$ (take g as 1/64 inch)
$b = 0.5\ (.218) + 0.25\ (.375) + .0156 = .218$ inches
Bending moment on bolt = $.5Pb = .5 \times 18000 \times .218$
= 1965 in.lb.
$f_b = Mr/I = (1965 \times .25)/.003069 = 160000$ psi.
(See Table D1.1 for bolt moment of inertia)

From Table D1.1, F_b for AN Steel bolts is 180,000.

Therefore M.S. = (180000/160000) - 1 = .12

Check of Lug A.

This lug is more critical than lug B since thickness of lug B is more than one-half of lug A.

Check of Tension Through Bolt Hole.

$P_u = F_{tu} A_t$

$P_u = 125000 \times (1.1875 - .625)\ .375 = 26400$ lb.

M.S. = (26400/18000) - 1 = .46

To take care of stress concentration, Method 1 says maintain a M.S. of .25, thus lug tensile strength is O.K.

Check of Shear Out Strength of Lug.

$P_u = F_{su} A_s$, $F_{su} = 82000$

$P_u = 82000 \times (.5937 - .3125)2 \times .375 = \underline{17300}$ lb.

This value is under the design fitting load of 18000 lb. It is permissible to take a slightly greater shear out distance than the edge distance as used (see Fig. D1.9c). The additional distance to the 40 degree line would add enough shear out area to give a positive margin of safety. This method of calculating shear out strength is conservative as will be brought out by the result in Method 2 solution.

Bearing Strength.

The bushing and lug have the same ultimate strength (F_{tu}), thus bearing will be critical for bolt on bushing since bearing area is less.

$P_u = F_{br} A_{br}$

An extra 50 percent margin of safety is required or the allowable bearing stress F_{br} should be divided by 1.5.

$P_u = (194000/1.50).50 \times .375 = \underline{24300}$ lb.

M.S. = (24300/18000) - 1 = .35

SOLUTION BY METHOD 2.

Bolt Shear Strength and Bolt Bending Strength are calculated in the same manner as in Method 1 and thus the calculations will not be repeated.

Tension Net Section

$P_u = K_t F_{tu} A_t$

K_t is the tension efficiency factor to take care of stress concentration due to the hole and is determined from Fig. D1.12. Table D1.3 says to use curve number 1 for all steels. To use Fig. D1.12 requires the ratio W/D = (1.1875/.625) = 1.9. Then from Fig. D1.12 we read $K_t = .98$, whence,

$P_u = .98 \times 125000 \times (1.1875 - .625).375 =$
$\underline{25800}$ lb.

M.S. = (25800/18000) - 1 = .43.

Fig. D1.12 says that a M.S. of .15 is appropriate over that of all required fitting factors of safety, thus our M.S. of .43 provides more than this additional M.S. of .15.

Shear Bearing Strength.

$P_{bru} = K_{bru} F_{tu} A_{br}$

K_{bru} is the shear-bearing efficiency factor and is obtained from Fig. D1.13.

D/t = .625/.375 = 1.65
e/D = .5937/.625 = .95

From Fig. D1.13, we read $K_{bru} = .80$

$P_{bru} = .80 \times 125000 \times .625 \times .375 = 23400$ lb.

M.S. = (23400/18000) - 1 = .30

The reader should note shear out strength by Method 2 is considerably larger than by Method 1. Fig. D1.13 says a .15 M.S. is appropriate, thus our 0.30 is satisfactory.

Bushing Yield.

$P_{bry} = 1.85 F_{cy} A_{br}$, F_{cy} = 113000 for steel with F_{tu} = 125000.

$P_{bry} = 1.85 \times 113000 \times .500 \times .375 = \underline{39000}$ lb.

M.S. = (39000/18000) - 1 = 1.17

General Conclusion.

Since all margins of safety are positive, the strength of fitting unit is satisfactory. It could be redesigned to save weight. Moving

the hole slightly back of the center of the lug radius would help shear out strength. This change would permit decreasing the thickness of lug slightly. Decreasing the lug thickness would decrease the bolt bending moment and possibly permit use of 7/16 diameter bolt. The student should redesign the lug.

PROBLEM 3.

A lug identical to lug A in Problem 2 is subjected to a transverse load, P_{tu}, which is the failing load. Find the load P_{tu}.

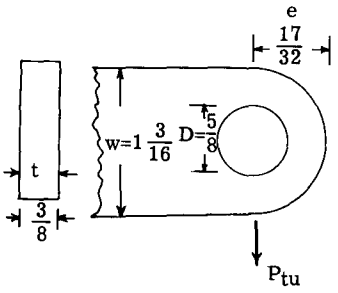

SOLUTION: From equation (10) the failing load is,

$$P_{tu} = K_{tu}\, A_{br}\, F_{tu}$$

The failing coefficient K_{tu} is determined by use of curves in Fig. D1.15. The lower scale parameter for Fig. D1.15 is A_{av}/A_{br}, where

$$A_{av} = \frac{6}{\frac{3}{A_1} + \frac{1}{A_2} + \frac{1}{A_3} + \frac{1}{A_4}}$$

For the meaning of these (A) areas, refer to sketch of lug in Fig. D1.15. Simple calculations give the following values for these areas.

$A_1 = A_4 = .14$, $A_2 = A_3 = .105$

whence, $A_{av} = \dfrac{6}{\frac{3}{.14} + \frac{1}{.105} + \frac{1}{.105} + \frac{1}{.14}} = .126$

$A_{br} = .375 \times .625 = .234$, $A_{ar}/A_{br} = .126/.234 = .54$

Table D1.4 indicates curve 1 is used for steel material with F_{tu} up to 125000 psi. Then from Fig. D1.15, we read $K_{tu} = .74$.

Then, $P_{tu} = .74 \times .234 \times 125000 = \underline{21600}$ lb.

PROBLEM 4.

Fig. D1.18 shows a steel forked fitting bolted to a double channel section made from 7075-T6 aluminum alloy. The hinge pin is 5/8 diameter AISI Steel, heat treated to F_{tu} = 150000. Steel fitting is also 150000 steel. A strength check of the fitting will be carried out.

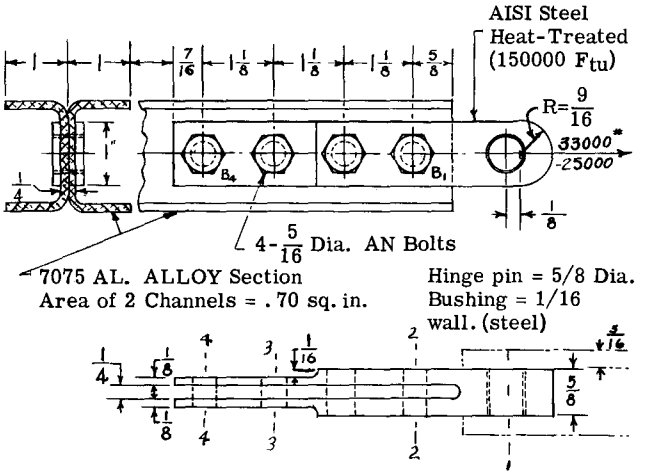

Fig. D1.18

SOLUTION:

Design fitting load = + 33000 tension and -25000 lbs. compression. These loads include the fitting factor of safety of 1.15.

Let P_u equal ultimate strength of the fitting unit in the various failing modes.

Check Shear Strength of Hinge Pin.

The hinge pin diameter is 5/8 and material is AISI Steel, heat treated to F_{tu} = 150000. F_{su} = 95000. Pin is in double shear.

$P_u = F_{su}\, A_s = 95000 \times .3068 \times 2 = 58300$ lb.

M.S. = (58300/33000) - 1 = .77.

Check Bending Strength of Hinge Pin.

The bending moment arm (b) on pin from Fig. D1.16 is

$b = .5t_1 + .25t_2 + g$. The clearance g will be taken as 1/64 inch.

$b = .5 \times .3125 + .25 \times .625 + 1/64 = .328$ in.

Pin bending moment $M = .5Pb = .5 \times 33000 \times .328 = 5410$ in.lb.

$f_b = Mr/I = 5410 \times .3125/.00749 = 226000$ psi.

The modulus of rupture in bending F_b will be calculated by the method of Chapter C3.

$F_b = F_{tu} + f_o\,(k - 1)$

From Table C3.2 for steel with F_{tu} = 150000, we find f_o = 146000.

For a solid round bar K = 1.7 (see Fig. C3.7 of Chapter C3).

F_b = 150000 + 146000 (1.7 - 1) = 258000 psi

M.S. = (258000/226000) - 1 = .14

Check Shear-Bearing Tear Out of Lug.

$P_{bru} = K_{bru} F_{tu} A_{br}$

D/t = .75/.625 = 1.2, e/D = .6875/.75 = .92

From Fig. D1.13, K_{bru} = .72

P_{bru} = .72 x 150000 x .75 x .625 = 51500 lb.

M.S. = (51500/33000)-1 = .56 (margin desirable at least 0.15).

Check Tensile Strength of Lug Section Through Pin Hole.

$P_u = K_t F_{tu} A_t$

K_t obtained from Fig. D1.12 using curve 1.

W/D = 1.125/.75 = 1.5

From Fig. D1.12, K_t = .99

P_u = .99 x 150000 x (1.125 - .75).625 = 34800

M.S. = (34800/33000) - 1 = .06.

It would be desirable to have a M.S. of .15.

Check Tensile Strength of Section 2-2 of Steel Fitting.

From Fig. D1.18, four 5/16 diameter AN Steel bolts are used to attach fitting to channel members. Since bolts are the same size, it will be assumed that each of the 4 bolts transfers 1/4 of the total fitting load. Fig. D1.19 shows the load in the steel fitting and the channel members. The total load passes by section 2-2.

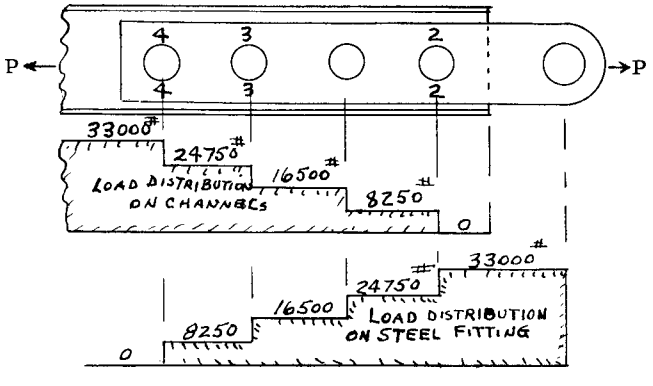

Fig. D1.19

Net tension area = (1.125 - .3125).375 = .305.

A stress concentration factor K_t from Fig. D1.12 will be used to be conservative. W/D = (1.125/.3125) = 3.6. Fig. D1.12 gives K_t = .91.

P_u = .91 x 150000 x .305 = 41700 lb.

M.S. = (41700/33000) - 1 = .26.

Check Section of Steel Fitting at Section 3-3.

Load from Fig. D1.19 = 16500 lb. Net Section = (1.125 - .3125).25 = .204 sq. in. Use same K_t as before.

P_u = .91 x 150000 x .204 = 27900 lb.

M.S. = (27900/16500) - 1 = .69

Check Shear Strength of 4 - 5/16 Dia. Bolts.

Bolts in double shear.

P_u = 4 x 2 x 5750 = 46000 lb.

M.S. = (46000/33000) - 1 = .39.

Check Bearing of Bolts on Steel Fitting.

Section 3-3 or 4-4 is critical as bearing area is less.

Allowable bearing stress for 150000 steel is 218000.

$P_u = F_{br} A_{br}$ = 218000 x .3125 x .25 = 17000 lb.

M.S. = (17000/8250) - 1 = 1.06.

Bearing of Bolts on 7075-T6 Channels.

F_{br} for 7075 aluminum alloy = 106000.

P_u = 106000 x .3125 x .25 = 8300.

M.S. = (8300/8250) - 1 = .01.

Check Tensile Strength of Channels at Section 4-4.

Load on Section = 33000.

Net area = .70 - .25 x .3125 = .622.

Ftu for 7075 material = 78000

P_u = 78000 x .622 = 48500.

M.S. = (48500/33000)-1 = .47 (which will take care of any stress concentration.

Check Shear Out of Channels Behind Bolt B_1.

Shear out distance = .625 - .156 = .469.

Shear out area = 2 x .469 x .25 = .234.

$P_u = F_{su} A_s = 43000 \times .234 = 10100$ lb.

M.S. = (10100/8250) - 1 = .23 (figured conservatively by Method 1)

Shear Out of Steel Fitting Behind Bolt B_4.

$F_{su} = 95000$

Shear out area $A_s = (.4375 - .1565)2 \times .25 = .141$

$P_u = .141 \times 95000 = 13400.$

M.S. = (13400/8250) - 1 = .62.

Bushing Yield Strength.

$P_{bry} = 1.85 F_{cy} A_{br}$. $F_{cy} = 113000$ for 125000 steel.

$P_{bry} = 1.85 \times 113000 \times .625 \times .625 = 81700$ lb. Load = 33000, not critical.

D1.16 Bolt Loads for Multiple Bolt Fitting. Bolts Sizes Different. Concentric Loading.

In designing or strength checking a multiple bolt fitting, the question arises as to what proportion of the total fitting load does each bolt transfer. This distribution could be affected by many things such as bolt fit or bolt tightness in the hole; bearing deformation or elongation of the bolt hole; shear deformation of the bolt or pin; tension or compressive axial deformation of the fitting members and the member being connected, and a number of other minor influences.

Since aircraft materials have a considerable degree of ductility, if the fitting is properly designed, the loads on the bolts when the loads on the fitting approach their maximum value, will tend to be in proportion to the shear strength of the bolt. That is, if the combined shear strength of the bolts is the critical strength, the yielding of the fitting material in bearing, shear and tension will tend to equalize the load on the bolts in proportion to their shear strengths. For stresses below the elastic limit of the fitting plates the bolt load distribution no doubt is more closely proportional to the bearing area of each bolt. Since the primary interest is failing strength, the bolt load distribution in proportion to the bolt shear strengths is usually assumed.

Let:-

P = design load on fitting.
P_s = allowable shear strength of any bolt.
P_n = load on bolt n.
P_{sn} = allowable shear strength of bolt n.

Therefore we can write,

$$P_n = P \left(\frac{P_{sn}}{\Sigma P_s}\right) \quad \text{- - - - - - - - - - - - - - - - (A)}$$

Example Problem of Bolt Load Distribution.

Fig. C1.20 shows a multiple bolt fitting unit subjected to a concentric load of 100000 lbs. Determine the load transferred by each bolt.

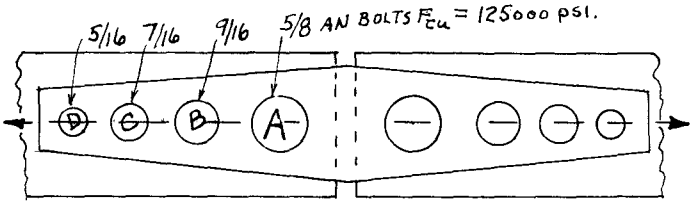

Fig. D1.20

Bolt Sym.	Bolt Dia.	Double Shear Strength = P_s
A	5/8	23010 x 2 = 46020
B	9/16	18637 x 2 = 37274
C	7/16	11272 x 2 = 22544
D	5/16	5751 x 2 = 11502
		ΣP_s = 117340

Distribution of loads to each bolt:-

$$P_a = P \left(\frac{P_{sa}}{\Sigma P_s}\right) = 100000 \times \frac{46020}{117340} = 39200 \text{ lb.}$$

$P_b = 100{,}000 \times 37274/117340 = 31800$ lb.

$P_c = 100{,}000 \times 22544/117340 = 19200$ lb.

$P_d = 100{,}000 \times 11502/117340 = 9800$ lb.

Total load on the four bolts adds up to 100,000 lb.

D1.17 Multiple Riveted or Bolted Joints Subjected to Eccentric Loads.

Fig. D1.21 shows a plate fitting attached to another member by means of four bolts or rivets. (The circles represent the bolts). The fitting plate is subjected to the loads P_H and P_V acting as shown. Let it be required to find the resultant loads on the bolt group due to the given loads.

The centroid of resistance for the bolt group will then correspond to the centroid of the bolt areas. Fig. D1.22 shows the fitting unit with the force P_H and P_V replaced by an equivalent force system at the bolt group centroid point (O). This equivalent force system will be:-

$P_V = -200$ lb., $P_H = 1000$ lb.

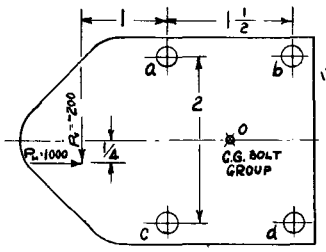

Fig. D1.21

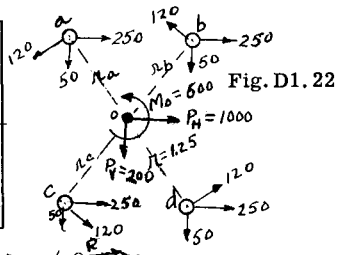

Fig. D1.22

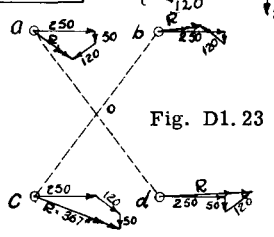

Fig. D1.23

and M_O = -200 x 1.75 - 1000 x .25 = -600 in.lb.

Since P_V and P_H act through the bolt centroid they will be reacted equally by each bolt, hence V load on each bolt due to P_V = -200/4 = -50 lb.; H load on each bolt due to P_H = 1000/4 = 250 lb.

The load produced on each bolt due to the moment load M_O = -600 in.lb. will vary directly as the distance of the bolt from the center of resistance which coincides with the bolt group centroid.

Let r_a equal the distance from the bolt group centroid to bolt (a). Then the resisting moment developed by bolt (a) equals $F_a r_a$, where F_a equals the load on bolt (a). Since the bolt loads are proportional to their distance from O, the resisting moment M_b developed by bolt (b) will equal

$(F_a \frac{r_b}{r_a}) r_b$ or $F_a \frac{r_b^2}{r_a}$, and similarly for bolt (c)

$M_c = F_a \frac{r_c^2}{r_a}$ and for bolt d = $F_a \frac{r_d^2}{r_a}$.

The total moment resistance of the bolt group therefore equals,

$$M = \frac{F_a r_a^2 + F_a r_b^2 + F_a r_c^2 + F_a r_d^2}{r_a} \quad ----(14)$$

hence,

$$F_a = \frac{Mr_a}{r_a^2 + r_b^2 + r_c^2 + r_d^2} = \frac{Mr_a}{I} \quad ----(15)$$

where $I = \Sigma r^2$ of bolt group.

Therefore for the loads on the other bolts,

$$F_b = \frac{Mr_b}{I}; \quad F_c = \frac{Mr_c}{I}; \quad F_d = \frac{Mr_d}{I}$$

For the bolt group of Fig. D1.22 $r_a = r_b = r_c = r_d$ = 1.25".

Hence, $I = \Sigma r^2 = 4 \times 1.25^2 = 6.25$ in.

Therefore the moment load F_m on each bolt will equal

$$F_m = \frac{Mr}{I} = \frac{-600 \times 1.25}{6.25} = 120 \text{ lb.}$$

Fig. C4.31 shows the resulting H, V and moment loads applied to each bolt. The resultant load can be found graphically by drawing the force polygons as shown in Fig. C1.23. The resultant bolt loads can likewise be determined analytically. For example consider bolt (c)

$$\Sigma H = 250 + 120 \times \frac{1}{1.25} + 0 = 346 \text{ lb.}$$

$$\Sigma V = -50 - 120 \times \frac{.75}{1.25} + 0 = -122 \text{ lb.}$$

Hence $R = \sqrt{\Sigma H^2 + \Sigma V^2} = \sqrt{346^2 + 122^2} = 367$ lb.

Case Where Bolts or Rivets are of Different Diameters.

When the joint bolts or rivets are not all the same size, the moment load on each bolt is proportional to the bolt area times its distance to the bolt group centroid. Thus the bolt areas must enter equation (15).

hence,

$$F_a = \frac{MA_a r_a}{n_a A_a r_a^2 + n_b A_b r_b^2 + n_c A_c r_c^2 + n_d A_d r_d^2} \quad -------(16)$$

n = number of bolts of each size.

Since theory of loads on a multiple bolt group is only approximate, reasonable margins of safety should be maintained.

RIVETED CONNECTIONS

D1.18 Types of Rivets.

From an aerospace structural standpoint rivets may be placed into two general classifications, namely:-

(1) The Protruding Head type of rivet.

(2) The Flush type rivet.

Fig. D1.24 illustrates the protruding head type of rivet. Fig. D1.25 illustrates a number of modifications of the protruding head type of rivet that have been used in the past.



Fig. D1.24

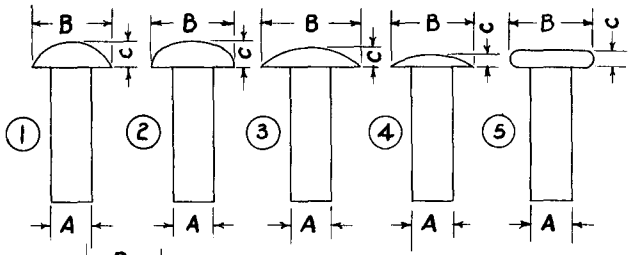

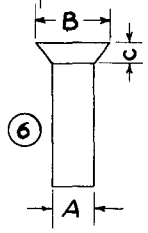

Fig. D1.25

No.	Rivet Types	B	C
1	Round Head	2A	.75A
2	Mushroom Head	2A	.625A
3	Brazier	2.5A	.50A
4	Modified Brazier	2A	.25 to .33A
5	Flat Head	2A	.4A
6	Ctsk. Head	1.81A	.5A

For many years the round head rivet was used for all interior work and before the era of high speeds it was used as a surface rivet as well. When wind tunnel experiments showed that such rivets gave appreciable drag, designers turned to rivets with less head protrusion, thus the development of the Brazier and modified Brazier type of rivet head. Then as the age of relatively high airplane speeds arrived a flush surface was needed, particularly on certain sensitive portions of the airplane surface, thus various modifications of the countersunk head involving press and machine countersinking of the sheets were developed.

Fig. D1.26 illustrates the flush type of rivet. As illustrated in Fig. D1.26, this flush type rivet can be used in several different ways, thus the method shown in Fig. D1.26a is referred to as the machine countersunk type; that in Fig. D1.26b as the press countersunk double dimpled type; and that in Fig. D1.26c as the combined press and machine countersunk type or the dimpled machine countersunk type.



Machine Countersunk Type

Fig. a

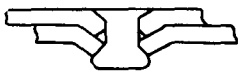

Press Countersunk - Double Dimpled Type.

Fig. b



Combined Press and Machine Countersunk; or Dimpled Machine Countersunk Type.

Fig. c

Fig. D1.26

Fig. D1.27 illustrates the approximate sheet thickness limitations for the three methods of flush riveting.

Approx. Sheet Limitations For Machine Countersunk Rivets (AN-426)

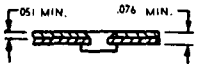

1/8 Dia. Rivet.

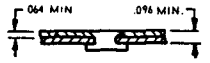

5/32 Dia. Rivet

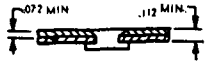

3/16 Dia. Rivet.

Approx. Limitations For Press Countersunk or Double Dimpled Rivets (AN-426)



1/8 Dia. Rivet.



5/32 Dia. Rivet



3/16 Dia. Rivet

Approx. Limitations For Press-Machine Countersunk Rivets (AN-426)

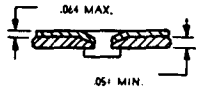

1/8 Dia. Rivet

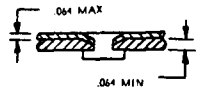

5/32 Dia. Rivet

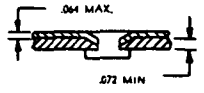

3/16 Dia. Rivet

Fig. D1.27

D1.19 Rivet Material.

Since aluminum alloy is by far the most widely used material in the aircraft industry, it follows that aluminum alloy is the material most widely used for rivets. Table D1.5 (column 1) lists the 5 aluminum alloys used for rivets and the ultimate shearing stress F_{su} for each material. Rivets made from 2017-T3 (F_{su} = 34000) and 2024-T31 (F_{su} = 41000) are rivets that must be driven soon after heat treatment or before age hardening takes place. The aging or hardening is slowed by keeping rivets in refrigeration after heat treatment. The other rivet material is less hard or less brittle in the aged state and thus can be stored in air and driven anytime. These so-called softer rivets have less shear strength, but since a great deal of aircraft construction involves thin sheet, bearing is often critical and thus rivet shear is not critical. Most surface or skin riveting involves the softer rivet, usually 2117-T3 (F_{su} = 30,000).

D1.20 Strength of Rivets. Protruding Head Type.

Rivets are widely used in airplane structures to fasten or tie together two or more structural units. Standard methods of stress analyses of riveted joints consider two primary types of failure, namely, the shear of the shank of the rivet and the bearing or compressive failure of the metal at the point where the rivet bears against the connecting sheet or plate.

Fig. D1.28 illustrates the main forces on a rivet in transferring a load from one plate to another. The load is transferred to the rivet from the plate by bearing of the plate on the rivet. The load is then transferred along the rivet and resisted by bearing action on the other plate. Since the plate bearing forces on the rivet are not in the same line, the forces tend to shear and bend the rivet. Bending of the rivet is usually neglected if there are no intermediate filler plates. In Fig. (a) of D1.28, the rivet is in single shear, whereas in Fig. (b) the rivet is in double shear.

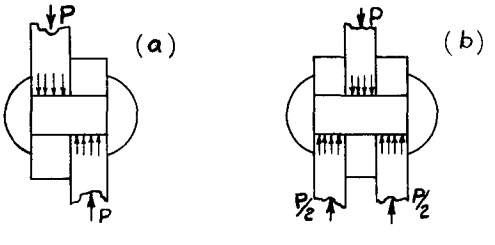

Fig. D1.28

The ultimate shear strength of a rivet is given by the following equation:-

$$P_a = F_{su} A n \quad \text{----------(17)}$$

where, P_a = ultimate shear strength of rivets (lbs.)
F_{su} = ultimate allowable shear stress for rivet (psi)
A = area of rivet cross-section = $\pi D^2/4$, where D equals the nominal rivet hole diameter.
n = number of shear areas per rivet.

Reference (17) shows that the shear strength of protruding head aluminum alloy rivets is affected by increasing D/t (Diameter of rivet over sheet thickness) ratios. The conclusions in Reference (17) are as follows:-

Rivets in Single Shear:-

For values of D/t up to 3:-
Single shear strength = basic allowable single shear strength.

For values of D/t greater than 3:-
Single shear strength = basic allowable single shear strength times $\left[1 - 0.04\ (D/t - 3)\right]$

For Rivets in Double Shear:-

For values of D/t up to 1.5:-
Double shear strength = basic allowable double shear strength.

For values of D/t greater than 1.5:-
Double shear strength = basic allowable double shear strength times $\left[1 - 0.13\ (D/t - 1.5)\right]$

Table D1.5 (from Ref. 2) gives the shear strength of protruding and flush head aluminum alloy rivets and the corrections to take care of the D/t influence on the rivet shear strength. Table D1.8 gives the allowable bearing strengths between the protruding head rivet and the various aluminum alloy sheet and plate material. The bearing values are given for two e/D ratios, namely 1.5 and 2.0, where e is the edge distance measured from the center of the hole to the edge of the plate. Any reduction in edge distance may cause bulging of the edge of the sheet due to driving energy. Edge distance should not be less than e/D = 1.5.

D1.21 Strength of Rivets. Flush Type.

Since flush rivets have no protruding head on the flush end of the rivet and also since flush riveting involves machine countersinking or press countersinking or both, the strength of the flush type rivet is different than the common protruding head type.

Fig. D1.29 illustrates a machine countersunk rivet. Due to the pull P on the two sheets which are held together by the rivet and induced force P_1 is produced on the sloping side of the head of the rivet. This induced force tends to shear and bend the portion 1-1 of the rivet head. The sharp edge of the countersunk sheet at point (a) tends to cut into the rivet. These combined influences tend to cause excessive deflections and finally failure as roughly illustrated in Fig. D1.30.

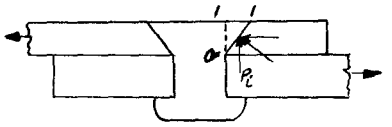

Fig. D1.29

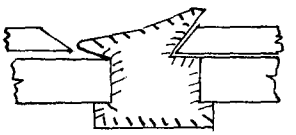

Fig. D1.30

In the press countersunk or dimpled type of flush rivet connection, see Fig. D1.26b and c, because of the interlocking of the sheets due to the dimple, the joint could transmit a load without a rivet if the sheets were held together. Since there is no clearly defined bearing or shear surface in this type of joint, the manner in which the loads are transferred is quite complex. As a result resort must be made to tests to establish design allowables. Tables D1.7, D1.11 and D1.12 give the ultimate and yield strength of flush type rivets (Ref. 2).

D1.22 Blind Rivets.

The name "Blind" rivet is given to that type of rivet which can be completely installed from one side of the joint, and is therefore almost exclusively used where it is impossible or impractical to drive the normal rivet, which requires access to both sides of the joint. There are two general types of blind rivets, namely where the inside or blind head is formed mechanically or where it is formed by an explosive force.

Fig. D1.31 illustrates the Dupont explosive type and Figs. 32 to 34a inclusive illustrate the mechanically formed head type.

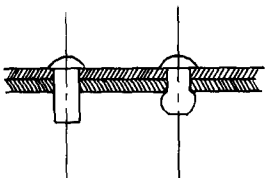

Fig. D1.31 Dupont Explosive

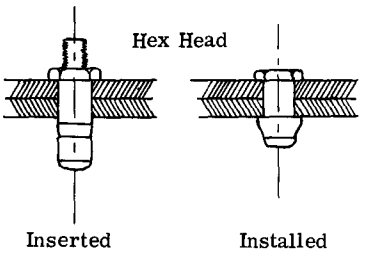

Fig. D1.32 Jo Bolt

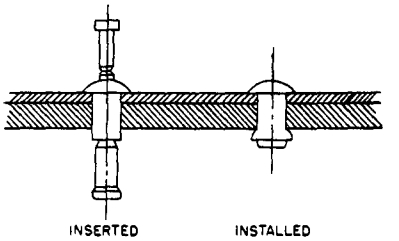

Fig. D1.33 Cherry Type

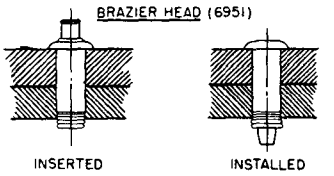

Fig. D1.34 Deutch Type

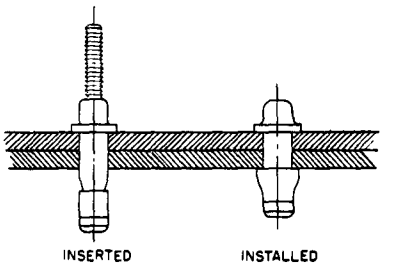

Fig. D1.34a Huck Lock Bolt

D1.23 Riveted Sheet Splice Information.

In splicing or connecting two sheets together by means of rivets or bolts, the joint or connection may fail in the various ways as explained in detail for single and multiple bolt fitting units. Thus one must check the shear strength of the rivets; bearing of rivets on the sheets; tear out of the sheet edges and tension on sections through the rivet holes.

Types of Sheet Splices or Connections.

Fig. D1.35 illustrates the various types of sheet splices. In the offset lap splice between two sheets of different gauges, the offset should be in the heavier material. For a single shear butt splice, the butt splice plate should be equal to the thinnest of the two sheets being spliced and likewise in the

double shear butt splice the splice plates should be of the same thickness and should be equal to the thinnest plate being spliced.

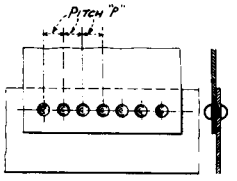

Lap Splice

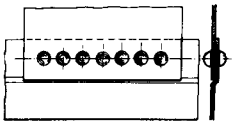

Offset Lap Splice

Fig. D1.35

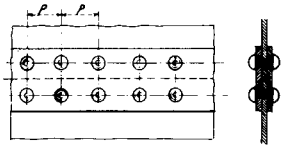

Butt-Double Strap Splice

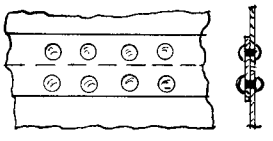

Butt-Single Strap Splice

Proper Rivet Size to Use.

No exact rules can be given relative to the optimum rivet for a given splice, because a number of practical considerations usually enter into the design of a sheet splice. Small rivets, namely 1/16 and 3/32 diameters are hard to handle and are seldom used as structural rivets. The common size of rivets are 1/8, 5/32, 3/16 and 1/4 inch diameters. The larger sizes should not be used in sheet splices unless there is a backing up structure as the sheet may buckle under the driving of the large rivets. From a structural design standpoint, the optimum joint is one in which the allowable rivet shear strength and bearing strength of the given sheets are practically the same for the largest practical size rivet.

Rivet Spacing. Sheet Edge Distance.

The allowable rivet-sheet bearing loads as given in (Ref. 1) are based on an edge distance of two diameters. Therefore in general no edge distance in a joint should be less than 2 rivet diameters for protruding head rivets, and 2-1/2 diameters for press and machine countersunk flush rivets.

The minimum pitch (distance between centerline of rivets in the same row) for a given size rivet should not be less than that given in Tables A and B.

Table A

PROTRUDING HEAD RIVET NORMAL MINIMUM SPACING				
Rivet Diameter	1/8	5/32	3/16	1/4
Normal Minimum Spacing	1/2	9/16	11/16	7/8

Table B

NORMAL MINIMUM SPACING PRESS AND MACHINE COUNTERSUNK FLUSH RIVETS				
Rivet Diameter	1/8	5/32	3/16	1/4
Normal Minimum Spacing	11/16	27/32	1-1/32	1-1/4

In general the minimum rivet row spacing should be such as to make the distance between any two rivets in the two rows not less than the minimum rivet spacing for the rivet size being used.

Splice Sheet Tension Efficiency.

When a sheet is spliced by means of rivets or bolts it means the sheet is weakened since the rivet holes cut away a part of the sheet material. The ratio of the tension strength of the spliced sheet to the unspliced sheet is called the sheet tension efficiency of the joint. If the minimum rivet spacing is used and only one row of rivets the sheet efficiency will be around 70 to 75 percent. The designer should strive for a higher efficiency.

D1.24 Illustrative Problems Involving Use of Rivets.

PROBLEM 1. Horn Connection to Torque Tube.

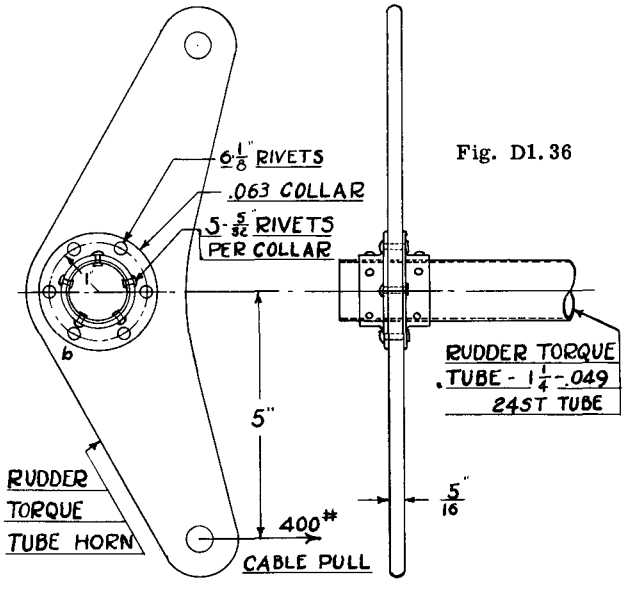

Fig. D1.36

Fig. D1.36 illustrates a rudder horn attachment to the lower end of a rudder torque tube for a small airplane. The horn is fastened to the tube by two collars riveted to the horn and likewise to the tube. The design load cable pull is 400 lb. which includes a fitting factor of safety of 1.15. The rivet material is 2117-T3 aluminum alloy. The horn and tube is 2024-T3 aluminum alloy. The margin of safety for the riveted connection will be calculated.

Solution:-

The horizontal cable pull of 400 lb. can be replaced by an equivalent force system at the centerline of the tube, consisting of a torsional moment of 400 x 5 = 2000 in.lb., and a horizontal 400 lb. force.

Consider attachment of collars to horn:-

6 - 1/8 diameter rivets are used in double shear.

Load per rivet due to torque = 2000/6 x 1 = 334 lb. (Rivet arm is 1 inch).

Load per rivet due to horizontal force = 400/6 = 67 lb.

Resultant load on most critical rivet is 334 + 67 = 401 lb.

From Table D1.5 the single shear strength of a 1/8 diameter rivet of 2117-T3 material is 388 lb. Since the rivets are in double shear the shear strength of one rivet would be 2 x 388 = 776 lb. Referring to the table at the bottom of Table D1.5, we find a rivet factor of .935 to apply for a 1/8 rivet on .063 sheet thickness. Therefore rivet strength is .935 x 766 = 718 lb.

M.S. in rivet shear = (718/401) - 1 = .79

Each rivet bears on two collars each of which is .063 in thickness. The bearing strength of a 1/8 rivet on .063 2024-T3 aluminum alloy material is obtained from Tables D1.9 and D1.8.

From Table D1.9, bearing strength of 1/8 diameter rivet on .063 sheet based on an allowable bearing stress F_{br} = 100,000 is 810 lb. Then referring to Table D1.8 for 2024-T3 material and e/D of 1.5, we find a correction factor of .98. Thus bearing strength is .98 x 810 = 794 lb. Since each rivet bears on two collars, the bearing strength for one rivet = 2 x 794 = 1588 lb.

M.S. = 1588/401 = 2.96

Consider attachment of collars to horn.

10 - 5/32 diameter rivets are used.

Load on each rivet due to torque = 2000/10 x .6 = 334 lb. The horizontal force of 400 lb. can be taken by direct bearing between collars and tube.

The rivets are in single shear. The single shear strength of a 5/32 rivet from Table D1.5 = 596 x .996 = 594 lb. (The value of .996 is the correction from middle table of Table D1.5.

M.S. = (594/334) - 1 = .78

Bearing strength on .049 tube wall from Table D1.9 for .050 thickness and F_{br} = 100,000 is 795 lb. correcting to .049 = (.049/.050) 795 = 780. For 2024-T3 tube material and e/D = 2.0 we obtain a material factor of 1.24. Therefore bearing strength of one rivet on tube wall is 1.24 x 780 = 967 lb.

M.S. = (967/334) - 1 = 1.9

PROBLEM 2.

Fig. D1.37 shows a plate fitting attached to a double channel section by 6 - 1/4 diameter rivets. The design fitting loads are shown in the figure. The riveted connection will be checked for strength under the given design fitting loads.

Solution:-

The given force system will be replaced by an equivalent force system acting at the center of gravity of the rivet group. This force system will consist of:

$H_{c.g.}$ = 8000 lb., $V_{c.g.}$ = 3000 lb.

$M_{c.g.}$ = 8000 x 0 + 3000 x 3 = 9000 in. lb.

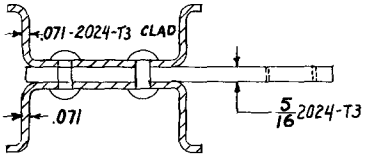

Fig. D1.37

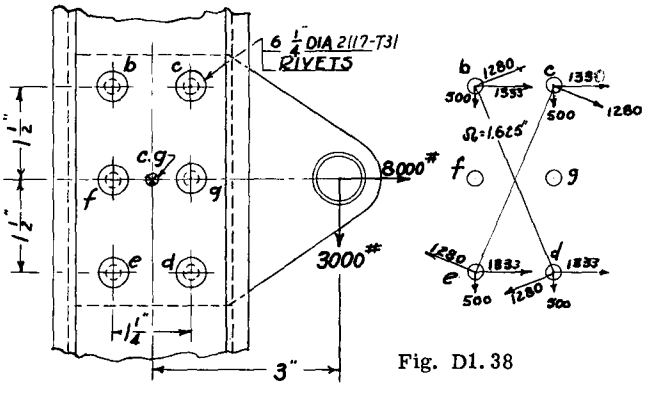

Fig. D1.38

Table D1.5 Shear Strengths of Protruding and Flush-Head Aluminum-Alloy Rivets

Diameter of rivet, in	1/16	3/32	1/8	5/32	3/16	1/4	5/16	3/8
Shear strength, lb:								
5056, $F_{su}=28$ *ksi*	99	203	363	556	802	1,450	2,290	3,280
2117-T3, $F_{su}=30$ *ksi*	106	217	388	596	862	1,550	2,460	3,510
2017-T31[a], $F_{su}=34$ *ksi*	120	247	442	675	977	1,760	2,790	3,970
2017-T3, $F_{su}=38$ *ksi*	135	275	494	755	1,090	1,970	3,110	4,450
2024-T31[a], $F_{su}=41$ *ksi*	145	296	531	815	1,180	2,120	3,360	4,800

Single-shear rivet strength factors

Sheet thickness, in.:								
0.016	0.964							
0.018	.984							
0.020	.996							
0.025	1.000	0.972						
0.032		1.000	0.964					
0.036			.980					
0.040			.996	0.964				
0.045			1.000	.980				
0.050				.996	0.972			
0.063				1.000	1.000	0.964		
0.071						.980	0.964	
0.080						.996	.974	
0.090						1.000	.984	
0.100							.996	0.972
0.125							1.000	1.000
0.160								
0.190								
0.250								

Double-shear rivet strength factors

Sheet thickness, in.:								
0.016	0.688							
0.018	.753							
0.020	.792							
0.025	.870	0.714						
0.032	.935	.818	0.688					
0.036	.974	.857	.740					
0.040	.987	.896	.792	0.688				
0.045	1.000	.922	.831	.740				
0.050		.961	.870	.792	0.714			
0.063		1.000	.935	.883	.818	0.688		
0.071			.974	.919	.857	.740		
0.080			1.000	.948	.896	.792	0.688	
0.090				.974	.922	.831	.753	
0.100				1.000	.961	.870	.792	0.714
0.125					1.000	.935	.883	.818
0.160						.987	.935	.883
0.190						1.000	.974	.935
0.250							1.000	1.000

NOTE: Values of shear strength should be multiplied by the factors given herein whenever the D/t ratio is large enough to require such a correction.

Shear values are based on areas corresponding to the nominal hole diameters specified in table 8.1.1.1.1(*d*), note *e*.

Shear stresses in table 8.1.1.1.1(*d*) corresponding to 90 percent probability data are used wherever available.

Sheet thickness is that of the thinnest sheet in single-shear joints and the middle sheet in double-shear joints.

[a] The -T31 designation refers to rivets that have been heat-treated and then maintained in the heat-treated condition until driving.

Table D1.6 Standard Rivet-Hole Drill Sizes and Nominal Hole Diameters

Rivet size, in.	1/16	3/32	1/8	5/32	3/16	1/4	5/16	3/8
Drill No.	51	41	30	21	11	F	P	W
Nominal hole diameter, (in.)	0.067	0.096	0.1285	0.159	0.191	0.257	0.323	0.386

Table D1.7 Ultimate and Yield Strengths of Solid 100° Machine-Countersunk Rivets

	Strength, lb								
Rivet material	2117-T3				2017-T3			2024-T31	
Clad sheet material	2024-T3, 2024-T4, 2024-T6, 2024-T81, 2024-T86, and 7075-T6								
Rivet diameter, in	3/32	1/8	5/32	3/16	5/32	3/16	1/4	3/16	1/4
	Ultimate strength								
Sheet thickness, in.: [a] [b]									
0.020	132	163	.....	.....	.....	.....	.....	.....	.....
0.025	156	221	[c]250	.....	.....	.....	.....	.....	.....
0.032	178	272	[c]348	.....	.....	.....	.....	[c]324	.....
0.040	193	309	[c]418	[c]525	[c]476	.....	.....	[c]555	.....
0.050	206	340	[c]479	[c]628	[c]580	[c]726	.....	758	[c]975
0.063	216	363	523	705	[c]657	[c]859	[c]1,200	886	[c]1,290
0.071	.....	373	542	739	690	[c]917	[c]1,338	942	[c]1,424
0.080	.....	.....	560	769	720	[c]969	[c]1,452	992	[c]1,543
0.090	.....	.....	575	795	746	1,015	[c]1,552	1,035	[c]1,647
0.100	.....	.....	.....	818	.....	1,054	[c]1,640	1,073	[c]1,738
0.125	.....	.....	.....	853	.....	1,090	1,773	1,131	1,877
0.160	.....	.....	.....	.....	.....	.....	1,891	.....	2,000
0.190	.....	.....	.....	.....	.....	.....	1,970	.....	2,084
Shear	217	388	596	862	755	1,090	1,970	1,180	2,120
	Yield strength								
0.020	91	98	.....	.....	.....	.....	.....	.....	.....
0.025	113	150	110	.....	.....	.....	.....	.....	.....
0.032	132	198	200	.....	.....	.....	.....	204	.....
0.040	153	231	265	273	270	.....	.....	362	.....
0.050	188	261	321	389	345	419	.....	538	594
0.063	213	321	402	471	401	515	610	614	811
0.071	.....	348	453	538	481	557	706	669	902
0.080	.....	.....	498	616	562	623	788	761	982
0.090	.....	.....	537	685	633	746	861	842	1,053
0.100	.....	.....	.....	745	.....	854	1,017	913	1,115
0.125	.....	.....	.....	836	.....	1,018	1,313	1,021	1,357
0.160	.....	.....	.....	.....	.....	.....	1,574	.....	1,694
0.190	.....	.....	.....	.....	.....	.....	1,753	.....	1,925

NOTE: The values in this table are based on "good" manufacturing practice, and any deviation from this will produce significantly reduced values.

a Sheet gage is that of the countersunk sheet. In cases where the lower sheet is thinner than the upper, the shear-bearing allowable for the lower sheet-rivet combination should be computed.

b Increased attention should be paid to detail design in cases where $D/t > 4.0$ because of possibly greater incidence of difficulty in service.

c Yield values of the sheet-rivet combinations are less than 2/3 of the indicated ultimate values.

Table D1.8 Aluminum-Alloy Sheet and Plate Bearing Factors[a]
(K = ratio of actual bearing strength to 100 ksi)

Material	Thickness, in.	A values				B values			
		K (Ultimate)		K (Yield)		K (Ultimate)		K (Yield)	
		$e/D=2.0$	$e/D=1.5$	$e/D=2.0$	$e/D=1.5$	$e/D=2.0$	$e/D=1.5$	$e/D=2.0$	$e/D=1.5$
2024-T42 (heat treated by user)	<0.250	1.18	0.93	0.64	0.56	.....	.....	.....	.....
	0.250–0.500	1.22	.96	.61	.53	.....	.....	.....	.....
	.501–1.000	1.18	.93	.61	.53	.....	.....	.....	.....
2024-T3	<.250	1.24	.98	.79	.69	1.29	1.02	0.82	0.71
2024-T4	.250– .500	1.24	.98	.74	.64	1.27	1.01	.78	.69
	.501–1.000	1.20	.95	.70	.62	1.29	1.02	.77	.67
2024-T36	≤.500	1.33	1.05	.96	.84	1.37	1.08	1.00	.88
2024-T4 (coiled)	≤0.063	1.18	.93	.64	.56	1.26	.99	.66	.57
Clad 2024-T42 (heat treated by user)	<.063	1.06	.84	.54	.48	1.10	.87	.56	.49
	.063– .249	1.12	.89	.58	.50	1.16	.92	.61	.53
	.250– .499	1.18	.93	.61	.53	.....	.....	.....	.....
	.500–1.000	1.14	.90	.58	.50	.....	.....	.....	.....
Clad 2024-T3	.010– .062	1.14	.90	.73	.64	1.18	.93	.76	.67
	.063– .249	1.20	.95	.74	.64	1.24	.98	.78	.69
Clad 2024-T4	.250– .499	1.20	.95	.74	.64	1.24	.98	.78	.69
	.500–1.000	1.16	.92	.67	.59	1.24	.98	.74	.64
Clad 2024-T36	.019– .062	1.20	.95	.88	.77	1.25	.99	.93	.81
	.063– .500	1.27	1.01	.93	.81	1.31	1.04	.96	.84
Clad 2024-T4 (coiled)	.012– .062	1.10	.87	.59	.52	1.16	.92	.61	.53
	.063	1.16	.92	.61	.53	1.20	.95	.64	.56
Clad 2024-T6	<.063	1.14	.90	.75	.66	.....	.....	.....	.....
	≥.063	1.18	.93	.78	.69	.....	.....	.....	.....
Clad 2024-T81	<.063	1.22	.96	.90	.78	.....	.....	.....	.....
	≥.063	1.27	1.00	.94	.83	.....	.....	.....	.....
Clad 2024-T86	<.063	1.33	1.05	1.04	.91	.....	.....	.....	.....
	≥.063	1.35	1.06	1.09	.95	.....	.....	.....	.....
7075-T6	.016– .039	1.44	1.14	1.06	.92	1.48	1.17	1.10	.97
	.040– .249	1.49	1.16	1.07	.94	1.50	1.19	1.12	.98
	.063– .488	1.39	1.08	1.00	.87	1.42	1.10	1.04	.90
	.500–1.000	1.42	1.10	1.04	.90	1.47	1.15	1.08	.94
Clad 7075-T6	.015– .039	1.33	1.05	.98	.85	1.39	1.10	1.02	.90
	.040– .062	1.37	1.08	1.01	.88	1.41	1.11	1.04	.91
	.063– .187	1.39	1.10	1.02	.90	1.42	1.12	1.06	.92
	.188– .249	1.42	1.12	1.04	.91	1.46	1.16	1.07	.94
	.250– .499	1.35	1.05	.98	.84	1.39	1.08	1.00	.87
	.500–1.000	1.39	1.08	.99	.86	1.42	1.11	1.02	.88
7178-T6	.015– .044	1.58	1.24	1.17	1.02	1.61	1.27	1.20	1.05
	.045– .249	1.60	1.26	1.18	1.04	1.63	1.29	1.22	1.06
	.250– .499	1.51	1.18	1.11	.96	1.55	1.20	1.14	.99
	.500–1.000	1.51	1.18	1.12	.97	1.55	1.20	1.15	1.00
Clad 7178-T6	.015– .044	1.44	1.14	1.07	.94	1.48	1.17	1.10	.96
	.045– .249	1.48	1.17	1.10	.96	1.52	1.20	1.14	.99
	.250– .499	1.40	1.09	1.04	.90	1.44	1.12	1.06	.92
	.500–1.000	1.40	1.09	1.05	.91	1.44	1.12	1.08	.93
Clad 2014-T6	≤.039	1.22	.96	.90	.78	1.22	.96	.90	.78
	.040–1.000	1.24	.98	.93	.81	1.27	1.01	.96	.84
2014-T6	.040–1.000	1.29	1.02	.96	.84	1.33	1.05	.99	.87
5052-H32 (¼H)	.....	.65	.50	.34	.29	.....	.....	.....	.....
5052-H34 (½H)	.....	.71	.54	.38	.34	.....	.....	.....	.....
5052-H36 (¾H)	.....	.78	.59	.46	.41	.....	.....	.....	.....
5052-H38 (H)	.....	.82	.62	.53	.46	.....	.....	.....	.....
6061-T4	.....	.63	.48	.26	.22	.....	.....	.....	.....
6061-T6	.....	.88	.67	.58	.50	.....	.....	.....	.....

[a] For e/D values between 1.5 and 2.0 bearing factors may be obtained by linear interpolation. (e=edge distance, D=hole diameter.)

Table D1.9 Unit Bearing Strength of Sheet on Rivets, F_{br} = 100 ksi

Sheet thickness in.	Unit bearing strength for rivet diameter indicated, lb[a]							
	1/16 in.	3/32 in.	1/8 in.	5/32 in.	3/16 in.	1/4 in.	5/16 in.	3/8 in.
0.012	80	.....	.....	.....	.....	.....	.....	.....
0.016	107	.....	.....	.....	.....	.....	.....	.....
0.018	121	173	.....	.....	.....	.....	.....	.....
0.020	134	192	.....	.....	.....	.....	.....	.....
0.025	168	240	321	.....	.....	.....	.....	.....
0.032	214	307	411	509	.....	.....	.....	.....
0.036	241	346	463	572	688	.....	.....	.....
0.040	268	384	514	636	764	.....	.....	.....
0.045	302	432	578	716	860	.....	.....	.....
0.050	335	480	643	795	955	1285	.....	.....
0.063	422	605	810	1002	1203	1619	2035	.....
0.071	476	682	912	1129	1356	1825	2293	2741
0.080	536	768	1028	1272	1528	2056	2584	3088
0.090	603	864	1157	1431	1719	2313	2907	3474
0.100	670	960	1285	1590	1910	2570	3230	3860
0.125	838	1200	1606	1988	2388	3213	4038	4825
0.160	1072	1536	2056	2544	3056	4112	5168	6176
0.200	1340	1920	2570	3180	3820	5140	6460	7720
0.250	1670	2400	3210	3970	4770	6420	8070	.....

[a] Bearing values are based on areas computed using the nominal hole diameters specified in table 8.1.1.1.1(d).

Table D1.10 Unit Bearing Strengths for Pin Size Indicated; lb.[a]

Sheet thickness, in.	Bearing strength of sheet for rivet size indicated, lb												
	1/16 in.	3/32 in.	1/8 in.	5/32 in.	3/16 in.	1/4 in.	5/16 in.	3/8 in.	1/2 in.	5/8 in.	3/4 in.	7/8 in.	1 in.
0.025	156	234	313	.....	.....	.....	.....	.....	.....	.....	.....	.....	.....
0.032	200	300	400	500	.....	.....	.....	.....	.....	.....	.....	.....	.....
0.036	225	338	450	563	675	.....	.....	.....	.....	.....	.....	.....	.....
0.040	250	375	500	625	750	.....	.....	.....	.....	.....	.....	.....	.....
0.045	281	422	563	704	845	.....	.....	.....	.....	.....	.....	.....	.....
0.050	313	469	625	781	940	1, 250	.....	.....	.....	.....	.....	.....	.....
0.063	394	590	788	985	1, 180	1, 575	1, 969	.....	.....	.....	.....	.....	.....
0.071	444	665	888	1, 110	1, 330	1, 775	2, 219	2, 663	.....	.....	.....	.....	.....
0.080	500	750	1, 000	1, 250	1, 500	2, 000	2, 500	3, 000	.....	.....	.....	.....	.....
0.090	563	845	1, 125	1, 407	1, 690	2, 250	2, 813	3, 375	4, 500	.....	.....	.....	.....
0.100	625	938	1, 250	1, 562	1, 875	2, 500	3, 125	3, 750	5, 000	.....	.....	.....	.....
0.125	781	1, 170	1, 563	1, 953	2, 340	3, 125	3, 906	4, 688	6, 250	7, 812	.....	.....	.....
0.160	1, 000	1, 500	2, 000	2, 500	3, 000	4, 000	5, 000	6, 000	8, 000	10, 000	12, 000	.....	.....
0.200	1, 250	1, 875	2, 500	3, 125	3, 750	5, 000	6, 250	7, 500	10, 000	12, 500	15, 000	17, 500	20, 000
0.250	1, 563	2, 344	3, 125	3, 916	4, 688	6, 250	7, 813	9, 375	12, 500	15, 625	18, 750	21, 875	25, 000

[a] Bearing values are based on areas computed using the nominal pin diameters indicated.

Since rivets are same size, all rivets are assumed to share equally in resisting H and V loads.

Load on each rivet due to $H_{c.g.}$ = 8000/6 = 1333 acting in H direction and to the right. Load on each rivet due to $V_{c.g.}$ = 3000/6 = 500 lb. acting down.

From equation (15), the load on a rivet due to $M_{c.g.}$ on rivet group equals F = Mr/I.

$$I = \Sigma r^2 = 1.625^2 \times 4 + 0.625^2 \times 2 = 11.4$$

Consider rivet marked c;

r = 1.625 = arm to c.g. of bolt group.

$$F_c = Mr/I = (9000 \times 1.625)11.4 = 1280 \text{ lb.}$$

Since rivets b, d and e are the same distance as rivet c from the c.g., the moment load on these bolts will also equal 1280. Fig. D1.38 shows the H, V, and M loads on the rivets b, c, d and e. Since the arm r to the rivets f and g is only 0.625, the load due to moment will be considerably smaller and thus these rivets will not be critical. Observation of Fig. D1.38 shows rivet c is the rivet with the largest resultant load.

$$R_c = \sqrt{\Sigma F_H^2 + \Sigma F_V^2}$$

$$\Sigma F_H = 1333 + 1280 \times 1.5/1.625 = 2513 \text{ lb.}$$

$$\Sigma F_V = -500 - 1280 \times 0.625/1.625 = -992$$

Hence, $R = \sqrt{2513^2 + 992^2} = 2700$ lb.

The rivets are in double shear. Rivet material is 2117-T31.

From Table D1.5, single shear value = 1760 lb. or double shear strength = 3520 lb.

Bearing strength of 1/4 rivet on the.071 2024-T3 clad channel section from Tables D1.9 and D1.8 is 1825 x 1.20 = 2190. Since rivet bears on two channels, bearing strength of one rivet = 2 x 2190 = 4380 lb. Rivet shear is critical.

$$M.S. = (3520/2700) - 1 = .30$$

As a problem for the reader, change rivets f and g to 3/16 diameter and determine whether rivet attachment still shows a positive margin of safety (use equation 16).

PROBLEM 3.

Fig. D1.39 shows a lap joint involving two rows of rivets as shown. Sheet material is 2024-T3 clad, and rivets are 5/32 diameter and 2117-T3 material and of the protruding head type.

The ultimate design tension load in the sheet including a 1.15 fitting factor of safety is 1000 lb./inch. The limit fitting load is 2/3 x 1000 = 667 lb./in.

The margin of safety of the sheet splice will be determined.

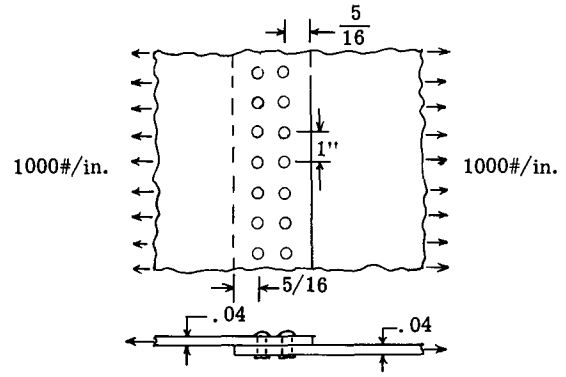

Fig. D1.39

Solution:-

As an analysis unit, a width of sheet equal to the rivet pitch of 1 inch will be used. Thus load on 1 inch unit = 1000 lb.

Check Tension in Sheet at Section Through Holes.

$$P_{t(allow)} = A F_{tu}$$

A = net area = (1 - .159).04 = .0336

(.159 = drill diameter for 5/32 rivet, Table D1.6)

F_{tu} for 2024-T3 clad = 60,000 psi.

$$P_{t(allow)} = .0336 \times 60000 = 2016 \text{ lb.}$$

$$M.S. = (2016/1000) - 1 = 1.01$$

Check Shear of Rivets.

Rivets are in single shear and two rivets act in the 1 inch unit which was assumed. From Table D1.5, single shear strength for 5/32, 2117-T3 rivet is 596 lb. The strength factor middle table of Table D1.5 for .04 sheet thickness is .964. Thus for two rivets the shear strength is 2 x .964 x 596 = 1150 lb.

$$M.S. = (1150/1000) - 1 = .15$$

Check Bearing of Rivets on .04 Sheet.

From Table D1.9, the ultimate bearing strength based on F_{br} of 100,000 psi for 5/32 rivet on .04 sheet = 636 lb. Then referring to

Table D1.8 for 2024-T3 clad material and an e/D ratio of 2.0, we find correction factor K = 1.14. Therefore rivet bearing strength is 1.14 x 636 x 2 = 1450 lb.

M.S. = (1450/1000) - 1 = .45

Check Rivet Shear Out.

Since edge distance is 5/16 in. or e/D = 2.0, shear out strength is satisfactory.

PROBLEM 4.

Assume rivets are changed to the solid 100° dimpled type. What would be the M.S. for the rivets. Referring to Fig. D1.27, we find the sheet thicknesses are such as to prevent double dimpling. From Table D1.11 and D1.12, we obtain the ultimate and yield strength of a 5/32 rivet on .04 sheet as 635 and 506 lbs. respectively.

Whence, Ultimate M.S. = (2 x 635/1000) - 1 = .27

Yield M.S. = (2 x 506/667) - 1 = .49

NOTE: In checking tensile strength of sheet through hole section, the drill size for dimpled rivets is slightly larger than for protruding head type.

PROBLEM 5.

This is a typical problem involving the rivet loads in a sheet-stringer type of construction as illustrated in Fig. D1.40. Before the rivet size and spacing at the points (1) to (10) can be determined, the rivet loads at these points must be known. The shear flow in direction and magnitude on the webs and skin are shown on the figure and are in lbs. per inch. These values represent the results in one of the flight conditions. The structural designer must look at all the shear flows in the various flight and landing conditions in order to obtain the critical rivet loads. It is assumed the shear flows as shown include any diagonal tension effect in the various sheet panels.

The rivet loads in lbs./in. at rivet lines 1 to 10 will be as follows:-

Rivet line (1). Since .05 vertical web ends at point (1), the shear flow of 1075 lbs./in. in the vertical web must obviously be reacted by the rivets in rivet line (1), thus load on rivet line (1) is 1075 lbs./in.

Rivet line (2). By the same reasoning since skin ends at point (2), the load on rivet line (2) equals shear flow in panel 2-3 or 575 lbs./in.

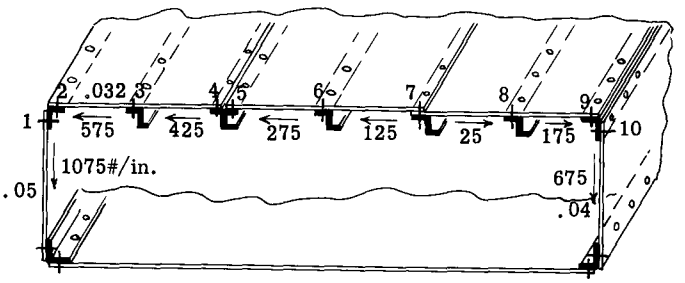

Fig. D1.40

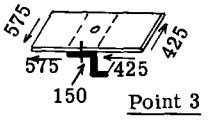

Sketch a

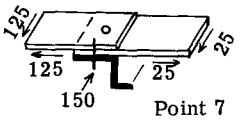

Sketch b

Rivet line (3). The skin is continuous over stringer at point (3). Sketch (a) shows a free body of the skin and stringer at point (3). Since the summation of the forces parallel to the stringer must equal zero, it is observed that the load transferred to the stringer is 150 lbs./in.

Rivet lines (4) and (5). Since the sheets end over the stringer, the load in rivet lines (4) and (5) are 425 and 275 lbs./in. respectively.

Rivet line (6). Rivet load = 275 - 125 = 150 lbs./in.

Rivet line (7). The skin is lap spliced over the stringer at point 7. Sketch (b) shows a free body. The load produced on the stringer is 150 from equilibrium. Thus the worst shear load on the rivet is 150 lbs./in. which is greater than the shear on another cross-section of the rivet which equals 125 lbs./in. as the shear flow in panel 6-7.

Rivet Load at (8) = 175 - 25 = 150 lbs./in.
Rivet Load at (9) = 175 lbs./in.
Rivet Load at (10) = 675 lbs./in.

D1.25 Rivets in Tension.

Great judgment should be used in using rivets in tension. There is a general saying, "Never use a rivet in tension." If this requirement was strictly followed, it would be difficult to design a conventional airplane. For example, the skin on the upper surface of the wing, due to the upward suction air forces places the rivets that hold the skin to the stringers and ribs in tension, however these tension loads in most cases are relatively small.

The following general criteria apply relative to rivets in tension.

Table D1.11 Ultimate Strength of Solid 100° Dimpled Rivets

	Ultimate strength, lb															
Rivet material	2117-T3							2017-T3						2024-T31			
Clad sheet material	2024-T3, 2024-T4, 2024-T6, and 2024-T81		2024-T86	2024-T3, and 2024-T4		2024-T6, 2024-T81, 2024-T86, 7075-T6		2024-T3, 2024-T4, 2024-T6, and 2024-T81		2024-T86 and 7075-T6		2024-T3 and 2024-T4	2024-T6, 2024-T81, 2024-T86, and 7075-T6	2024-T3, and 2024-T4		2024-T6, 2024-T81, 2024-T86, and 7075-T6	
Rivet diameter (in.)	3/32	1/8	1/8	5/32	3/16	5/32	3/16	5/32	3/16	5/32	3/16	1/4	1/4	3/16	1/4	3/16	1/4
Sheet thickness, in.:[a]																	
0.016	177	.....	.....	.....	.....	.....	.....	.....	.....	.....	.....	.....	.....	.....	.....	.....	.....
0.020	209	299	302	.....	.....	.....	.....	.....	.....	.....	.....	.....	.....	.....	.....	.....	.....
0.025	235	360	383	474	.....	462	.....	419	.....	530	.....	.....	.....	.....	.....	.....	.....
0.032	257	413	454	568	722	599	725	600	681	672	822	.....	.....	744	.....	786	.....
0.040	273	451	505	635	839	695	891	728	905	775	1,000	845	1,108	941	879	982	1,300
0.050	.....	484	548	693	940	778	1,036	840	1,097	864	1,153	1,332	1,508	1,110	1,359	1,152	1,705
0.063	.....	.....	.....	736	1,012	840	1,142	922	1,240	930	1,267	1,695	1,803	1,236	1,727	1,277	2,010
0.071	.....	.....	.....	755	1,045	867	1,190	958	1,301	957	1,315	1,853	1,930	1,291	1,883	1,332	2,150
0.081	.....	.....	.....	.....	1,074	.....	1,230	.....	1,357	.....	1,358	1,995	2,044	1,340	2,025	1,380	2,260
0.090	.....	.....	.....	.....	1,098	.....	1,267	.....	1,405	.....	1,398	2,115	2,145	1,382	2,150	1,424	2,365
0.100	.....	.....	.....	.....	.....	.....	.....	.....	.....	.....	.....	2,220	2,232	.....	2,255	.....	2,455

NOTE: The values in this table are based on "good" manufacturing practice and any deviation from this will produce significantly reduced values.

a These allowables apply to double dimpled sheets and to the upper sheet dimpled into a machine-countersunk lower sheet. Sheet gage is that of the thinnest sheet for double dimpled joints and of the upper dimple sheet for dimpled, machine-countersunk joints. The thickness of the machine-countersunk sheet must be at least 1 tabulated gage thicker than the upper sheet. In no case shall allowables be obtained by extrapolation for skin gages other than those shown.

Table D1. 12 Yield Strength of Solid 100° Dimpled Rivets

Rivet material	Yield strength, lb																	
	2117–T3						2017–T3						2024–T31					
Clad sheet material	2024–T3, 2024–T4, 2024–T6, and 2024–T81	2024–T3, 2024–T4, 2024–T6, 2024–T81, and 2024–T86	2024–T3, 2024–T4, 2024–T6, and 2024–T81		2024–T86 and 7075–T6		2024–T3, 2024–T4, 2024–T6, and 2024–T81			2024–T86 and 7075–T6			2024–T3, and 2024–T4		2024–T6 and 2024–T81		2024–T86 and 7075–T6	
Rivet diameter (in.)	3/32	1/8	5/32	3/16	5/32	3/16	5/32	3/16	1/4	5/32	3/16	1/4	3/16	1/4	3/16	1/4	3/16	1/4
Sheet thickness, in.:[a]																		
0.016	154	.....	.....	.....	.....	.....	.....	.....	.....	.....	.....	.....	.....	.....	.....	.....	.....	.....
0.020	184	257	.....	.....	.....	.....	.....	.....	.....	.....	.....	.....	.....	.....	.....	.....	.....	.....
0.025	209	315	324	.....	410	.....	336	.....	.....	450	.....	.....	.....	.....	.....	.....	.....	.....
0.032	231	367	430	512	525	640	483	546	.....	581	705	.....	582	.....	649	.....	786	.....
0.040	246	404	506	644	606	782	589	730	845	675	867	978	666	879	816	962	982	978
0.050	.....	436	571	757	677	905	681	888	1,187	756	1,007	1,508	738	1,308	961	1,308	1,152	1,543
0.063	.....	.....	619	841	729	995	748	1,006	1,415	816	1,111	1,803	925	1,564	1,068	1,564	1,277	1,958
0.071	.....	.....	641	878	752	1,034	778	1,056	1,656	842	1,156	1,930	1,045	1,711	1,115	1,711	1,332	2,140
0.080	.....	.....	.....	910	....	1,070	....	1,102	1,870	....	1,196	2,044	1,152	1,928	1,177	1,928	1,380	2,260
0.090	.....	.....	.....	939	....	1,100	....	1,142	2,057	....	1,231	2,145	1,246	2,121	1,324	2,121	1,424	2,365
0.100	.....	.....	.....	.....	.....	.....	.....	.....	2,220	.....	.....	2,232	.....	2,255	.....	2,268	.....	2,455

Note: The values in this table are based on "good" manufacturing practice and any deviation from this will produce significantly reduced values.

[a] These allowables apply to double dimpled sheets and to the upper sheet dimpled into a machine-countersunk lower sheet. Sheet gage is that of the thinnest sheet for double dimpled joints and of the upper dimple sheet for dimpled, machine-countersunk joints. The thickness of the machine-countersunk sheet must be at least 1 tabulated gage thicker than the upper sheet. In no case shall allowables be obtained by extrapolation for skin gages other than those shown.

(1) Tension on rivets shall be restricted to conditions in which tension load is incidental to the major shear carrying purpose of the rivet. When it is difficult to determine if the tension component is incidental or major, a bolt shall be used.

(2) The following are examples of joints where rivets are considered to be satisfactory tension carrying mediums.

(a) Skin attachment to ribs and frames

(b) Attachment of sheet panels to beam flanges and stringers, where inter-rivet buckling or diagonal sheet wrinkling produce tension loads on rivets.

(c) Skin attachment on a pressurized nacelle or body.

(3) Do not use rivets to fasten control brackets to a supporting structure.

(4) If there is no load reversal on the assembly, the tension allowables given in the following tables can be used.

(5) If there is load reversal on the assembly, the tension load on the rivet should not exceed 25 percent of the values in the table.

(6) Rivets loaded in both shear and tension should be checked for combined stresses, using the interaction equation,

$$R_t^2 + R_s^2 = 1$$

(7) A sufficient number of rivets shall be used to insure that failure of any one rivet due to improper installation, cracked head, etc., shall not result in the failure of the structure that is being held together by the rivets.

D1.26 Rivet Tension Strengths.

Reference to the structures design manuals of various aircraft companies shows that rivet tensile strengths are not the same or, in other words, not standardized as in the case of shear and bearing. Tables A, B & C have been taken from the (Ref. 5). The values given are conservative relative to values found in other company manuals.

Table A
PROTRUDING HEAD RIVETS (AN470, AN442)
ULTIMATE TENSILE STRENGTH



Use this table for 24ST Alclad sheet and harder

Sheet Gauge	Allowable Rivet Load, Lbs. Per Rivet						
	3/32	1/8	5/32	3/16	1/4	5/16	3/8
.016	89						
.020	120	142					
.025	159	197	223				
.032	214	269	311	354			
.040	277	353	420	474	568		
.051	277	471	561	649	799	929	
.064		495	736	854	1077	1262	
.072		495	758	981	1245	1482	1669
.081			758	1094	1440	1721	1952
.091				1094	1651	1982	2265
.102					1882	2274	2622
.125					1982	2890	3353
.156					1982	3130	4336
.188						3130	4470
.250							4470

Table B
100° FLUSH HEAD RIVET (AN426) MACHINE COUNTERSUNK
JOINT ULTIMATE TENSILE STRENGTH

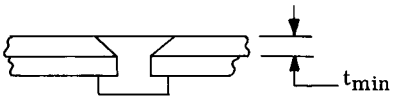

Use this table for 24ST Alclad sheet and harder

Sheet Gauge	Allowable Rivet Load, Lbs. Per Rivet						
	3/32	1/8	5/32	3/16	1/4	5/16	3/8
.040	191						
.051	249	319					
.064	249	438	501				
.072		446	592	653			
.081		446	683	773			
.091			683	912			
.102				985	1275		
.125				985	1698	1941	
.156					1783	2660	2950
.188					1783	2817	3827
.250						2817	4023
t_{min}	.040	.051	.064	.072	.102	.125	.156

Table C
100° FLUSH HEAD RIVET (AN426) DOUBLE DIMPLE
ULTIMATE TENSILE STRENGTH

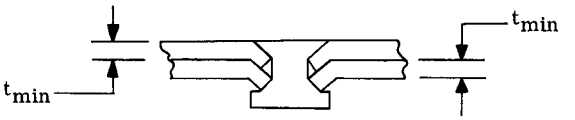

Use this table for 24ST Alclad sheet and harder

Sheet Gauge	Allowable Rivet Load, Lbs. Per Rivet				
	3/32	1/8	5/32	3/16	1/4
.020	103				
.025	137	168			
.032	185	233	271		
.040	241	305	362	409	
.051		408	485	562	694
.064		446	635	737	931
.072				850	1077
.081				970	1242
t_{min}	.020	.025	.032	.040	.051

PROBLEMS

(1) The single bolt fitting unit as shown in Fig. 1 is subjected to a design fitting load of 12000 lbs. in axial tension. The pin is an AN Steel bolt 3/8 inch diameter. Bushing is 1/16 wall and steel F_{tu} = 125000. Lug material is 2014-T6 bar, F_{tu} = 68000. The fitting is not subjected to shock or vibration. Strength check the bolt and lug (A) and give all margins of safety.

(2) Same fitting as in Problem 1 but design fitting load is a transverse load of 10,000 lb. Strength check and give all margins of safety.

(3) Same fitting as in Problem 1 but lug (A) is subjected to a design fitting load acting at 45° with a value of 11000 lb. Strength check for this loading.

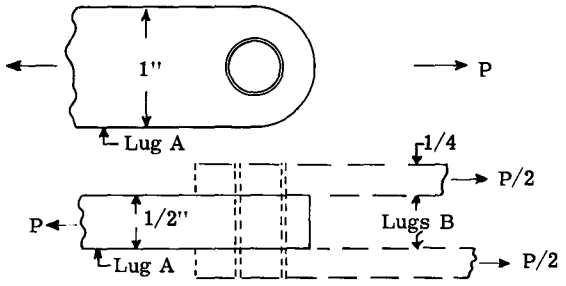

Fig. 1

(4) A 1/2 inch diameter AN steel bolt is subjected to a combined shear and tension load. The shear load on the bolt is 10,000 lbs. and the tension load is 12,000 lbs. Find margin of safety under this combined loading.

(5) Design a hinge pin using a standard AN steel bolt and a male lug to carrying an axial tensile load of 25,000 lbs. Use fitting factor of 1.15. Use steel bushing. No shock or vibration. Assume lugs of female part of fitting 1/2 as thick as male lug. Design the male lug from two materials. (1) 2024-T4 aluminum alloy and (2) AISI steel, F_{tu} = 180000.

(6) Fig. 2 illustrates an end fitting for a streamline strut. The tube is flattened slightly at the end to fit a simple block fitting. Loads shown are design strut loads. Using a fitting factor of 1.20, check the strength of the entire fitting unit. Assume no shock or vibration.

(7) Fig. 3 illustrates a fitting unit on the end of an extruded (I) section. The web on the (I) section extends out to form

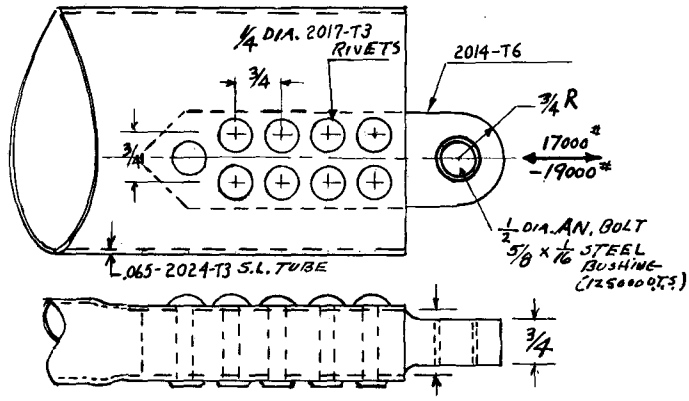

Fig. 2

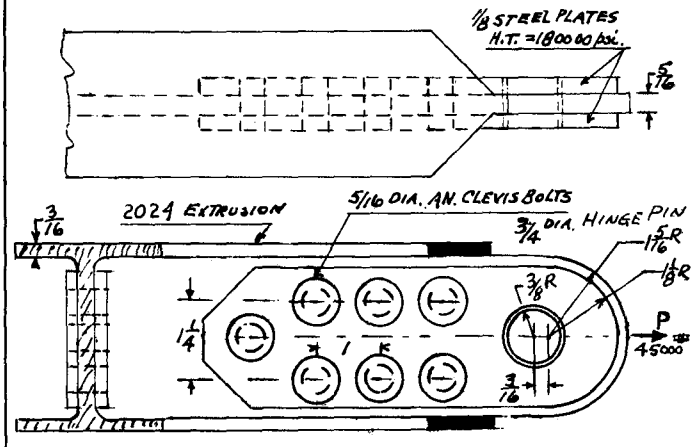

Fig. 3

part of the fitting lug, which is reinforced by steel fitting plates. Strength check the fitting for a design load of 45000 lb. Use fitting factor of 1.15.

(8) Fig. 4 shows a typical beam end-single pin fitting unit. The fitting plate is attached to beam section by the rivet pattern as shown. The loads shown on figure are applied loads. Using a factor of safety on applied loads of 1.5 and a fitting factor of 1.2, determine the margin of safety of the rivet attachment of fitting plate to beam section.

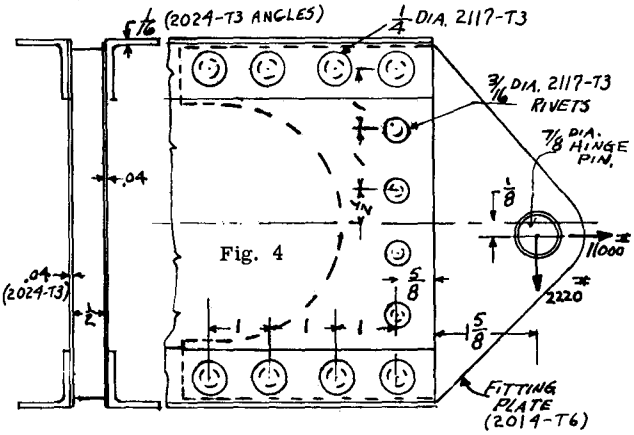

Fig. 4

(9) Fig. 5 shows a flap hinge fitting attached to supporting structure by 4 - 1/4" dia. AN steel bolts. The bolts are in double shear. Check the most critical bolt in shear and bearing for load of 3500 lbs. acting as shown. Fitting material is 2014-T3.

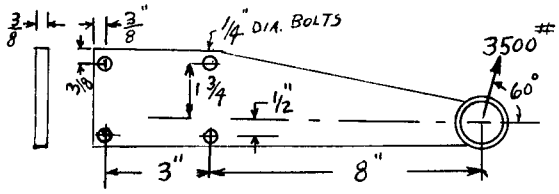

Fig. 5

(10) In the eccentrically loaded multiple bolt fitting of Fig. 6, determine the resultant load on each of the five AN steel bolts in resisting the 24000 lbs. load acting as shown.

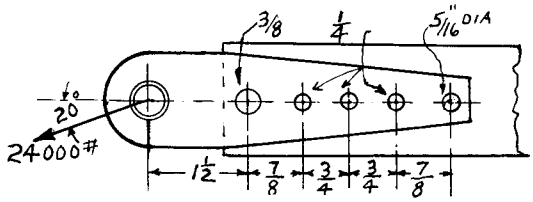

Fig. 6

(11) In Fig. 7 the fitting is attached to a fuselage frame by four 1/4 dia. AN steel bolts. The design fitting loads are as shown. Determine the margin of safety on the most critical bolt. Use Fig. D1.4 to obtain equation for combined tension and shear stresses.

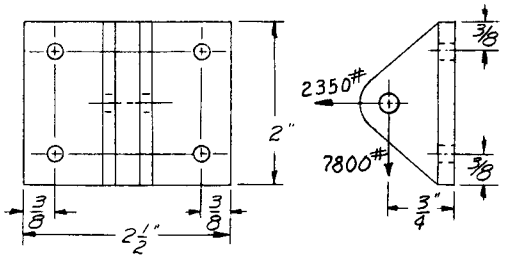

Fig. 7

(12) In Fig. 8 find the size of 2017-T3 rivets necessary to carry the ultimate fitting design load of 3000 lbs. as shown. The fitting plate is steel 1/8 thick, F_{tu} = 95000, and the 2024-T3 channel frame is .081 inch thick.

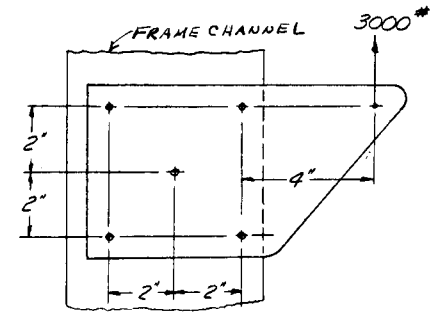

Fig. 8

(13) Design the lightest overlap sheet splice for .051 clad 2024-T6 and protruding head type rivet. Design tension load on sheet = 2350 lb./in. Give all details of joint.

(14) Rework design in Problem 13 to use double dimpled rivets.

REFERENCES

(1) ANC-5. Strength of Metal Aircraft Elements. March, 1955.

(2) Military Handbook MIL-HDBK-5. August, 1962. Metallic Materials and Elements for Flight Vehicle Structures.

(3) Cozzone, Melcon, and Hoblit: Analysis of Lugs and Shear Pins Made of Aluminum and Steel Alloys. Product Engineering Vol. 21, May, 1950.

(4) Melcon and Hoblit: "Developments in the Analyses of Lugs and Pins." Product Engineering. June, 1953.

(5) Martin Co. Structures Manual.

(6) Various Structural Manuals of Various Aircraft Companies.

CHAPTER D2
WELDED CONNECTIONS

D2.1 Introduction.

Since the overall structure of an airplane, missile or space vehicle cannot be fabricated as a single continuous unit, such structures involve many structural parts which must be fastened together. For certain materials and types of structural units, welding plays an important role in joining or connecting structural units. Research is constantly going on to develop better welding machines and welding techniques and also to develop new materials that can be welded without producing a detrimental strength influence on the base or unwelded material. A fair size book could be written on the subject of welding and design for welding. This brief chapter can only be a brief introduction to the subject.

D2.2 Gas Welding.

There are two types of gas welding, namely, oxyacetylene and oxyhydrogen. Practically all gas welding in aircraft work is oxyacetylene. Some welders prefer the oxydrogen flame in welding aluminum alloys because the flame is not so hot. The major aircraft structural units in which gas welding plays an important part are welded steel tubular fuselages, engine mounts, and landing gears and the attachment of plate and machined fittings to such structure.

D2.3 General Notes on the Practical Design of Welded Joints.

The designer of welded structures in steel can greatly help the welder obtain good joints or connections by adherring to the following general rules.

(1) It is much easier to obtain a good weld when the parts being welded together are of equal thickness. It is general design practice to try and keep thickness ratio between the two welded parts less than 3 to 1. Some designers try to keep within a 2 to 1 ratio in order to eliminate possibilities of welders burning the thinner sheet.

(2) Designers usually consider .035 as the minimum thickness to be welded in general practical structural joints as there is considerable danger that the average welder might burn a thinner gauge.

(3) In general avoid welds in tension since they produce a weakening effect. In some connections it is difficult to avoid all tension loads on welds, thus weld stresses should be kept low and if possible incorporate a fishmouth joint or finger patch to put part of weld in shear.

(4) A weld should not encircle a tube in a plane perpendicular to the tube length. Standard splices or joints for overlapping tubes, and end socket fittings in tubes have been developed, which require no strength check. These are the diagonal weld and the fishmouth welds as illustrated in Fig. D2.1.

(5) Tapered gusset plates should be incorporated in all important welded joints to insure gradual change in stress intensity in members. These gussets lessen the danger of fatigue failure by reducing stress intensity.

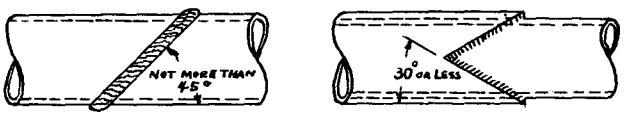

BUTT WELD FISHMOUTH WELD

Fig. D2.1

(6) A weld over a weld should not be made.

(7) To prevent burning of sheet welds should not be made on both sides of a thin sheet.

(8) If two welds are placed close together lack of shrinkage space may cause cracking.

(9) Cracks usually develop if welding is done on bends.

(10) When tubes are spliced by welding locate splice near one end of the tube, to avoid effecting column properties. In general it is not good practice to weld brackets to the middle of column members. Clamps are preferable.

(11) In welding members together local internal stresses are set up. On most weld assemblies it is therefore customary to "normalize" the assemblies after welding. This heating permits the equalization of the internal localized stresses thus preventing cracking in service.

(12) Standard aircraft bolts should not be welded in place since they are made of nickel steel and therefore cannot be satisfactorily welded. Since standard aircraft nuts are made of 1025 steel they can be welded in place if desired.

D2.4 General Types of Welded Steel Fitting Units.

Fig. D2.2 taken from aircraft tubing handbook of the Summerill Tubing Company summarizes the common types of tube terminals and discusses their structural merit. Fig. D2.3 illustrates the conventional concentric butt welded fuselage joint which tests show is satisfactory where vibration is not present. Tests have shown that the fatigue strength of a welded joint as illustrated in Fig. D2.3 when the members are subjected to reverse bending is reduced considerably, thus it is common practice to add additional joint reinforcement such as finger plates or insert gussets as illustrated in Figs. D2.4 and D2.5 to joints subjected to vibration.

Figs. D2.6 to D2.8 illustrate methods of splicing a longeron at a truss joint. The vertical and diagonal members strengthen the butt weld on the spliced member.

Figs. D2.9 and D2.10 illustrate fitting plate attachments to tubes. Except for light fitting loads, the fitting plate should extend through to both sides of tube or to the adjoining members. The fitting type illustrated in Fig. D2.11 is only used for secondary conditions where loads or plate are relatively light.

Since eccentricity of member forces on a joint produce bending in the connecting members which may lower the fatigue strength of the joint, such cases of joint eccentricity as illustrated in Figs. D2.12 to D2.14 should be eliminated in joint design.

D2.5 Electric Arc Welding.

This method of welding is based upon the heat generated in an electric arc. Arc welding to a limited extent has been used for many years in aircraft fabrication. No doubt the flexibility and general all around good results obtained with gas welding retarded its extensive use, however in recent years its use is increasing rapidly as its economies and advantages become apparent to the designer. In arc welding the applied heat is more concentrated and quicker welding results with less expansion and warming as compared to gas welding. In the design of tubular joints, care should be taken to make all welds as accessible as possible. To secure proper stress distribution in arc welded joints the designer should follow the recommendations as illustrated in Figs. D2.15 to D2.18.

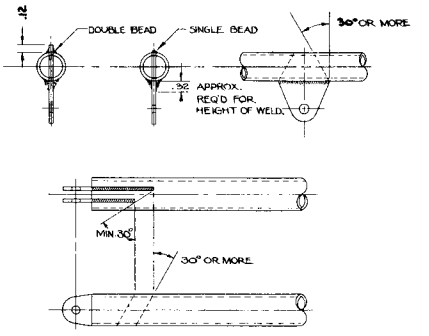

Fig. D2.15

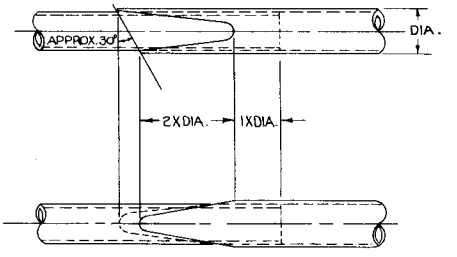

Fig. D2.16

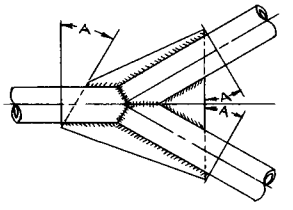

Angle "A" to be not less than 30°

Fig. D2.17

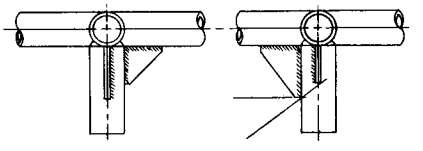

30° or more

Fig. D2.18

The fact that less expansion and warping takes place since the heat is concentrated makes it possible to hold to closer tolerances on parts requiring machining after welding an allowance of 1/16 inch is generall sufficient on most assemblies. Electric welding permits welding of thin sheets as low as .016 inch thickness.

D2.6 Effect of Welding on Base Metal.

Tests show that plain carbon and chrome-molybdenum steels suffer very little in loss of tensile strength due to welding. For cold rolled sheet or tubing the refinement in grain

Fig. D2. 2

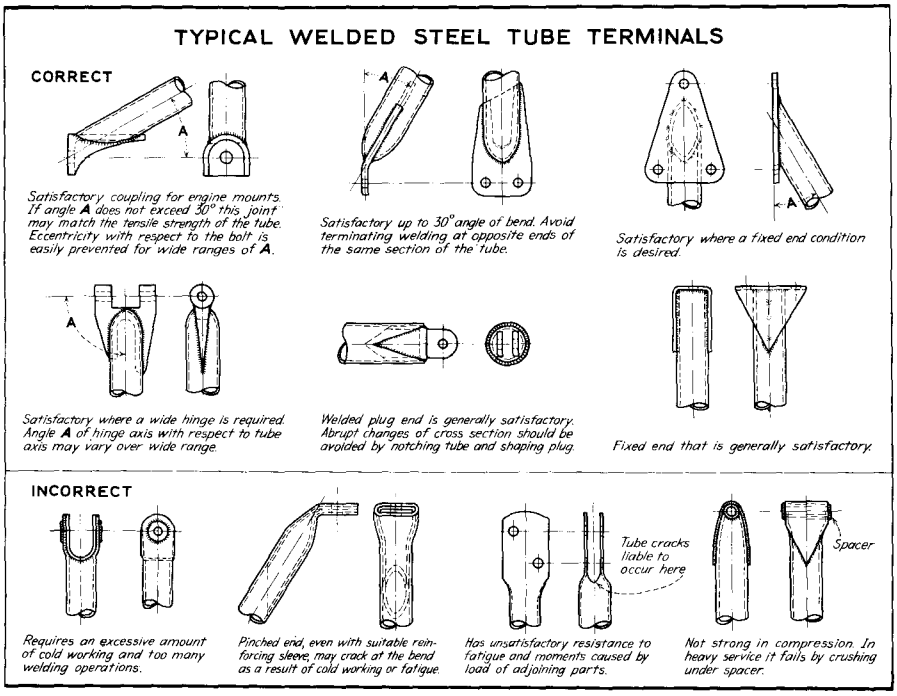

Reproduced by permission from Summerill "Aircraft Tubing Data"

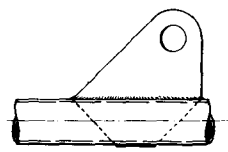

Fig. D2. 9

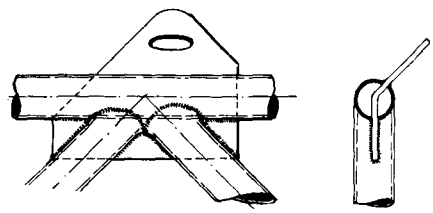

Fig. D2. 10

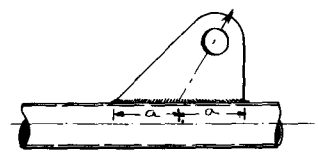

Fig. D2. 11

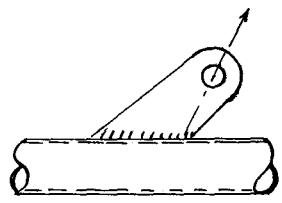

Fig. D2. 12

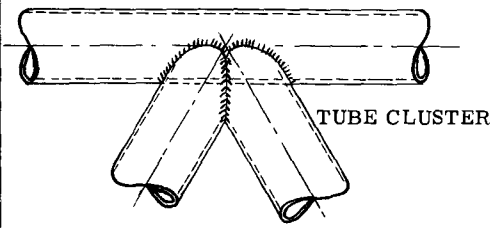

Fig. D2. 3

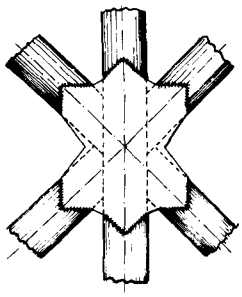

Fig. D2. 4

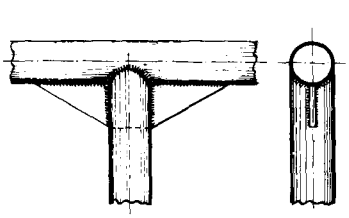

Fig. D2. 5

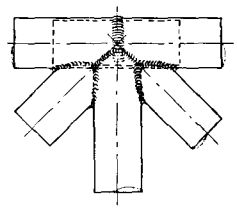

Fig. D2. 6

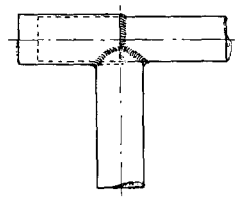

Fig. D2. 7

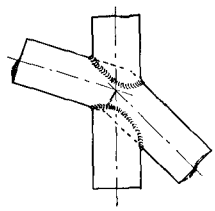

Fig. D2. 8

Bending on tube tends to out lower weld in tension

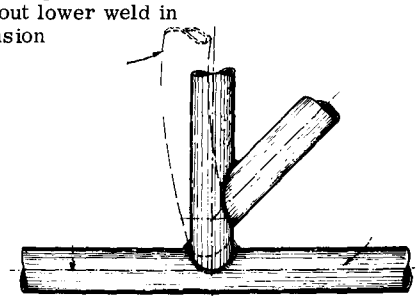

Fig. D2. 13

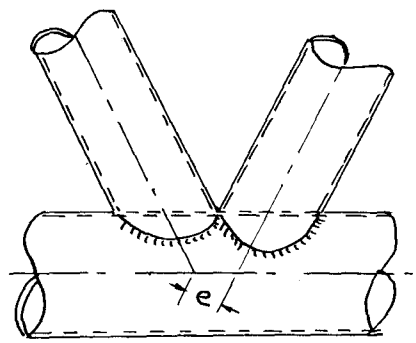

Fig. D2. 14

due to cold working is lost in the material adjacent to the weld which lowers strength to a small degree. Welding, however, does produce a more brittle material which has lower resistance to shock, vibration and reversal of stress, thus it is customary to assume an efficiency of weld joints less than 100 percent.

Table D2.1 gives the allowable ultimate tensile stress for alloy steels for material adjacent to weld when structure is welded after heat treatment.

Table D2.1 (Ref. 1)
Allowable Ultimate Tensile Stresses Near Fusion Welds in 4130, 4140, 4340, or 8630 Steels[a]

(Section thickness 1/4 inch or less)	
Type of joint	Ultimate tensile stress, ksi
Tapered joints of 30° or less[b]	90
All others	80

[a] Welded after heat treatment or normalized after weld.
[b] Gussets or plate inserts considered 0° taper with center line.

For welding members subjected to bending, the allowable modulus of rupture for alloy steels when welded after heat-treatment should not exceed the following as specified in (Ref. 1).

For tapered joints of 30° or less, use modulus of rupture F_b equivalent to that for steel having F_{tu} = 90000 psi.

For all other types of welds, use F_b equal to .9 of that for steel having F_{tu} = 90000 psi. Chapter C4 gives chart for determining the modulus of rupture F_b for alloy steel tubes and Chapter C3 gives a procedure of determining F_b for other shapes subjected to bending.

Strength of Base Material When Structure is Heat-Treated After Welding.

Reference (1) says that for materials heat-treated after welding, the allowable stresses in the parent material near a welded joint may equal the allowable stress for the heat-treated material, in other words, no reduction for welding. However, it is good design practice to be conservative on welded joints, thus a reduction of 10 to 20 percent of the heat-treated properties is often used in calculating the tensile or bending strength in the member adjacent to the weld.

D2.6 Weld-Metal Allowable Stress.

Table D2.2 (from Ref. 1) gives the allowable weld-metal strengths for the various steels. These design allowable stresses for the weld material are based on 85 percent of the respective minimum tensile ultimate test values.

Table D2.2 (Ref. 1) Strength of Welded Joints

Material	Heat treatment subsequent to welding	F_{su}, ksi	F_{tu}, ksi
Carbon and alloy steels .	None	32 32	51 51
Alloy steels	None	43	72
Alloy steels	Stress relieved . . .	50	85
Alloy steels	Stress relieved . . .	60	100
Steels	Quench and temper .		
4130.	125 ksi	63	105
4140.	150 ksi	75	125
4340.	180 ksi	90	150

D2.7 Allowable Load for Welded Seams.

The allowable load on a welded seam can be calculated by the following equation:-

$$P_a = F_{su} \text{ or } F_{ST} \, (Lt) \quad \text{- - - - - - - - - - - - D2.1}$$

where,

P_a = allowable load in lbs.
F_{su} and F_{ST} from Table D2.2
L = length of welded seams in inches
t = thickness of thinnest material joined by the weld in the case of lap welds between two steel plates or between plates and tubes. (inches)
t = average thickness in inches of the weld metal in the case of tube assemblies, but not to be greater than 1.25 times the thickness of the welded stock.

D2.8 Brazing.

Brazing as applied to aircraft work is a process of uniting steel parts by means of a copper-zinc mixture, which is applied by melting with an air-gas flame or by dipping into the molten mixture. The strength of the joint depends on the surface areas of contact and the clearance between the parts to be joined.

Although the brazing mixture may develop a shearing strength of 40000 psi, a general allowable value of 10000 psi is used in aircraft work because many factors, particularly the skill of the workman, effects the strength of a brazed joint.

The requirements of the procuring or government agencies should be noted before using brazing in aircraft work.

D2.9 Welding of Aluminum Alloys.

The heat-treatable alloys, commonly referred to as the strength alloys, such as 2014, 2024, 7075, cannot be welded with the oxyacetylene torch without destroying their mechanical properties, which are not restored even if heat-treated after welding. These alloys are generally classed as unweldable. Constant research is going on to develop aluminum alloys that have relatively high strength which can be welded without appreciable decrease of the strength properties. A recent development by the Aluminum Company of America is a new alloy designated X7005, which develops high strength after welding.

The strain-hardened alloys, namely, 1100 and 3003, are readily joined by gas welding. Either aa oxyacetylene, or an oxyhydrogen flame is used and sheet thicknesses as low as .020 are successfully welded. It is common practice to use these materials in welded fuel or oil tank for aircraft.

D2.10 Illustrative Problems Involving Welding.

PROBLEM 1. Fig. D2.19 shows two plates welded together to form a lap joint. The material is alloy steel F_{tu} = 95000 psi. Find the margin of safety of the welded seams under the load of 5200 lbs. acting as shown.

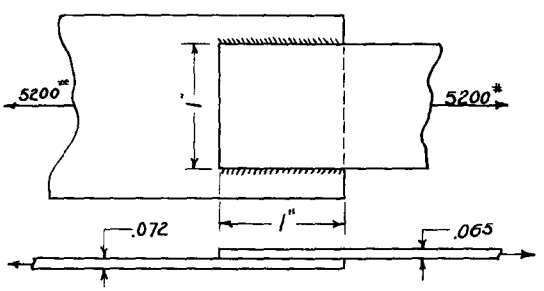

Fig. D2.19

From equation D2.1,

$P_a = F_{su}\, Lt$

F_{su} from Table D2.2 = 43000

L = total weld seam length = 2 x 1 = 2 in.

t = .065

P_a = 43000 x 2 x .065 = 5580

M.S. = (5850/5000) - 1 = .11

Tensile strength of .065 plate using a reduced allowable stress due to welding of 80000 as per Table D2.1, gives

P_a = 1 x .065 x 80000 = 5200 lb.

This is conservative since weld does not extend across the plate, thus any decrease of tensile strength properties should be less than that assumed above.

PROBLEM 2.

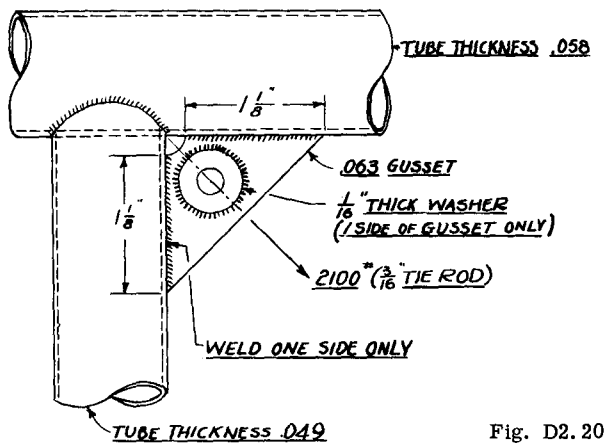

Fig. D2.20

Fig. D2.20 shows a gusset plate inserted between the ends of two tubes of a truss. The gusset is used as a fitting to take the pull from a 3/16 diameter steel tie rod. Determine the margin of safety of connection of gusset to tubes. All material steel, F_{tu} = 95000.

Resolving the wire pull into components parallel to the tubes, we obtain P = 2100 x sin 45^0 = 1480 x 1.2 (fitting factor) = 1780 lb. The allowable weld load is governed by thinnest material or .049 of the vertical tube.

$P_a = F_{su}\, Lt$

= 43000 x 1.125 x .049 = 2370 lb.

M.S. = (2370/1780) - 1 = .33

PROBLEM 3.

In general welded fittings involving plates and tubes present conditions for which it is difficult to determine the actual stress flow through the joint, thus the general procedure is to make conservative assumptions regarding the stress flow distribution and check the fitting units for these conservative assumptions. The following example illustrates this approximate procedure of strength checking a welded fitting joint.

In Fig. D2.21 the fitting plate which is welded to the three steel tubes is subjected to a tension load of 14000 lb. as shown. The fitting will be investigated for possible weakness.

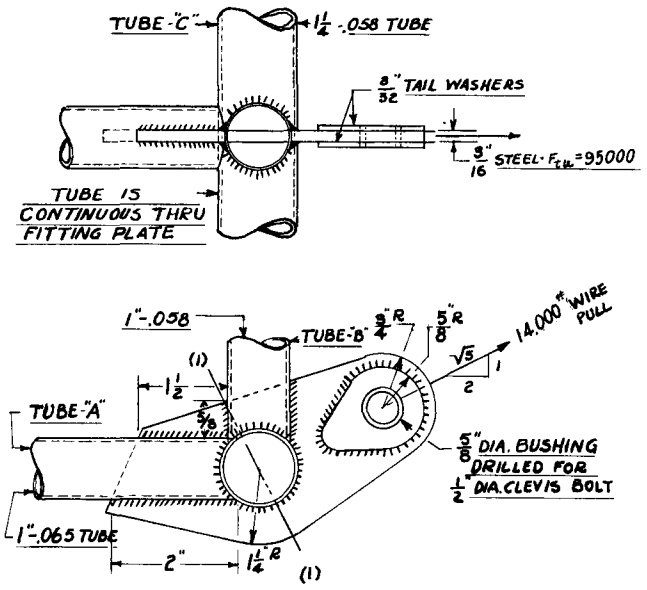

Fig. D2.21

Solution

Shear Strength of Clevis Pin:

Load on pin = 14000 lb.

Double shear strength of 1/2 diameter AN clevis bolt = 2 x 14722 = 29444. M.S.=(294444/14000) - 1 = 1.1

Bearing of Clevis Bolt on Bushing:

Bearing stress $f_b = \frac{14000}{.5 \times .375} = 59500$ psi

Ultimate bearing stress = 175000 psi. Thus a large margin of safety is available to take care of wear due to slight rotation or shock.

Bearing Stress Bushing on Lug:

$f_b = \frac{14000}{.625 \times .375} = 59500$ psi

Allowable bearing stress F_{br} = 140,000 psi (See Chapter B2).

The result shows that bearing on lug is not at all critical.

Shear Out Strength of Fitting Plate:

Shear area main plate = (.75 - .3125) .1875 x 2 = .164
Washers = (.625 - .3125) .1875 x 2 = .118
Total shear out area = .282 sq.in.

f_s = 14000/0.282 = 49700 psi

F_{su} for steel when F_{tu} = 95000 is 55000. See Chapter B2.

This value will be decreased to 50000 because of welding effect on material properties.

M.S. = (50000/49700) - 1 = .01

This margin of safety is conservative since shear out area is conservative.

Tension Stress on Section Through Bolt Hole:

Area of Section Through Hole:

Main plate = (1.5 - .625) .1875 = .164
Washers = (1.25 - .675) .1875 = .118
Total net area = .282 sq.in.

f_t = 14000/.282 = 49700 psi.

F_{tu} from Table D2.1, allowing full correction for welding effect, equals 80000 psi.

M.S. = (80000/49700) - 1 = .61

Tension stress on fitting plate at Section 1-1 (See Fig. D2.21).

Net area = (2.5 - 1.25) .1875 = .235 sq.in.

The entire load of 14000 will be assumed to pass this section, which is no doubt conservative.

f_t = 14000/.235 = 59500, F_t = 80000 psi. o.k.

Check of Connection Between Fitting Plate and Tubes.

It will be assumed that the horizontal component of the wire pull will be transferred to tube (A) by the weld between the tube and the fitting place. This is a conservative assumption.

Horizontal load component = 14000 x $2/\sqrt{5}$ = 12500 lb.

The weld length between tube (A) and the fitting plate is 1.5 inches on the upper tube surface and 2 inches on the lower surface. To be conservative, a total weld length of 2 x 1.5 = 3 inches will be assumed acting.

The fitting plate is welded to the tube on both sides and since twice .065, the tube thickness is less than the plate thickness, a total weld length based on tube strength is 2 x 3 = 6 inches.

$P_a = F_{su} Lt$ = 50000 x 6 x .065 = 19500 lb.

M.S. = (19500/12500) - 1 = .56

It will be assumed that the vertical component of the wire pull will be taken into tube (B) by the weld along each side of the tube.

Load = 14000 x $1/\sqrt{5}$ = 6250 lb.

The weld length on one side of tube is 0.625 inches long and 1 inch on the other. A total weld length of only 2 x 0.625 = 1.25 inches will be assumed which is conservative.

P_a = 50000 x 1.25 x 2 x .058 = 7250.

Thus even under the assumed conservative assumption, the weld attachment for transferring vertical component to tube (B) is more than adequate.

SPOT WELDING

D2.11 Spot Welding.

After many years of research and testing, spot welding of aluminum alloys, magnesium alloys and corrosion resistant steels has become a reliable established practice of joining many parts or units of flight vehicle structures.

The spot welding process is accomplished by clamping two or more sheets of metal between copper or copper alloy electrodes, under comparatively high pressure and causing an electric current of low voltage to flow between the electrodes for a predetermined interval. The current creates an intense heat at point "A" (See Fig. a) which melts the metal locally due to the resistance set up by the sheets. As soon as the metal is molten to the extent shown at "B", the predetermined time of current flow is completed and the sheets are forged together by the pressure on the electrodes "P". This pressure depends on the thickness of the sheet.

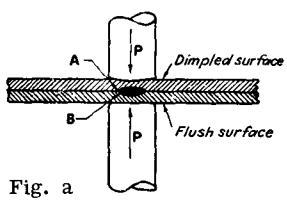

Fig. a

D2.12 Spot Welding of Aluminum Alloys.

In general, aluminum alloy spot welded joints should not be used in primary or critical structures without the specific approval of the military or civil aeronautic authorities. The following are a few types of structural connections in aerospace structures where spot welding should not be used.

(1) Attachment of flanges to shear webs in stiffened cellular construction in wings.

(2) Attachment of shear web flanges to wing sheet covering.

(3) Attachment of wing ribs to beam shear webs.

(4) Attachment of hinges, brackets and fittings to supporting structure.

(5) At joints in trussed structures.

(6) At juncture points of stringers with ribs unless a stop rivet is used.

(7) At ends of stiffeners or stringers unless a stop rivet is used.

(8) On each side of a joggle, or wherever there is a possibility of tension load component, unless stop rivets are used.

(9) In general most aluminum and aluminum alloy material combinations can be spot welded. Table D2.3 gives information on this subject.

Table D2.3 Acceptable Material Combinations for Spot Welding

Material	5052	5052	6061	3003	Clad 2024	1100	1100	Clad 7075[c]	Bare 7075[b]	Bare 2024[b]	Clad 2014	Bare 2014[b]
5052	...	...	...	...	...	...	...	...	...	...	...	...
5052	...	...	...	...	...	...	...	...	...	...	...	...
6061	...	...	...	...	...	...	...	...	...	...	...	...
3003	...	...	...	...	...	...	...	...	...	...	...	...
Clad 2024	...	...	...	...	...	...	...	...	...	...	...	...
1100	...	...	...	...	...	...	...	...	...	...	...	...
1100	...	...	...	...	...	...	...	...	...	...	...	...
Clad 7075[c]	...	...	...	...	...	...	...	...	...	...	...	...
Bare 7075[b]	...	...	...	...	...	...	...	...	(*)	(*)	(*)	(*)
Bare 2024[b]	...	...	...	...	...	...	...	...	(*)	(*)	(*)	(*)
Clad 2014	...	...	...	...	...	...	...	...	(*)	(*)	...	(*)
Bare 2014[b]	...	...	...	...	...	...	...	...	(*)	(*)	(*)	(*)

[a] The various aluminum and aluminum-alloy materials referred to in this table may be spot welded in any combinations except the combinations indicated by the asterisk (*) in the table. The combinations indicated by the asterisk (*) may be spot welded only with the specific approval of the procuring or certificating agency.

[b] This table applies to construction of land- and carrier-based aircraft only. The welding of bare, high-strength alloys in construction of seaplanes and amphibians is prohibited unless specifically authorized by the procuring or certificating agency.

[c] Clad heat-treated and aged 7075 material in thicknesses less than 0.020 inch shall not be welded without specific approval of the procuring or certificating agency.

D2.13 Spot Strengths.

Design shear strength allowables for spot welds in aluminum alloys are given in Table

D2.4, for magnesium alloys in Table D2.5, and for steels in Table D2.6. The minimum edge distances from spot welds is also given in the tables.

Fig. D2.22 gives the maximum static strength of spot welded joints having the same pitch in all rows in aluminum alloys together with the maximum pitches with which these values can be obtained. For joints having larger pitches, use Table D2.4.

Fig. D2.23 gives the tensile strength single spot welds in 7075-T6 clad material.

D2.14 Reduction of Tensile Strength of Parent Metal Due to Spot Welding.

Spot welding decreases the ultimate tensile strength of the sheet material being spot welded. Fig. D2.24 gives the efficiency in tension for spot welding of aluminum alloy sheets.

Table D2.4 (Ref. 1)

Shear Strengths and Minimum Edge Distances for Bare and Clad Aluminum Alloys

Nominal Thickness of Thinner Sheet, Inches	Materials & Tensile Strength, ksi				Minimum Edge Distance, inches
	Above 56	28 to 56	20 to 27.5	19.5 and below	
	Shear Strength of Sheet, Pounds				
0.012	60	52	24	16	3/16
0.016	86	78	56	40	3/16
0.020	112	106	80	62	3/16
0.025	148	140	116	88	7/32
0.032	208	188	168	132	1/4
0.040	276	248	240	180	9/32
0.051	384	354	329	240	5/16
0.064	552	500	451	320	11/32
0.072	678	589	524	364	3/8
0.081	842	691	620	424	13/32
0.091	1020	810	703	484	7/16
0.102	1230	960	760	548	7/16
0.114	1465	1085	803	591	7/16
0.125	1698	1300	840	629	9/16
0.156	2400				5/8

Table D2.5 (Ref. 1) Shear Strengths for Magnesium Alloys

Nominal Thickness of Thinner Sheet, Inches	Magnesium Alloy		Minimum Edge Distance, Inches
	QQ-M-54	QQ-M-44	
	Shear Strength of Sheet, Lbs.		
0.020	51	69	3/16
0.025	71	97	7/32
0.032	102	139	1/4
0.040	137	185	9/32
0.051	186	251	5/16
0.064	242	328	11/32
0.072	279	378	3/8
0.081	320	434	13/32
0.091	368	498	7/16
0.102	433	586	7/16
0.114	488	658	7/16
0.125	544	735	9/16

Table D2.6 Spot-Weld Maximum Design Shear Strengths for Uncoated Steels[a] and Nickel Alloys (Ref. 1)

Nominal Thickness of Thinner sheet, in.	Material Ultimate Tensile Strength, lb.		
	150 ksi and above	90 ksi to 150 ksi	Below 90 ksi
0.006	70	57	.....
0.008	120	85	70
0.010	165	127	92
0.012	220	155	120
0.014	270	198	142
0.016	320	235	170
0.018	390	270	198
0.020	425	310	225
0.025	580	425	320
0.030	750	565	403
0.032	835	623	453
0.040	1,168	850	650
0.042	1,275	920	712
0.050	1,700	1,205	955
0.056	2,039	1,358	1,166
0.060	2,265	1,558	1,310
0.063	2,479	1,685	1,405
0.071	3,012	2,024	1,656
0.080	3,540	2,405	1,960
0.090	4,100	2,810	2,290
0.095	4,336	3,012	2,476
0.100	4,575	3,200	2,645
0.112	5,088	3,633	3,026
0.125	5,665	4,052	3,440

[a] Refers to plain carbon steels containing not more than 0.20 percent carbon and to austenitic steels. The reduction in strength of spotwelds due to the cumulative effects of time-temperature-stress factors is not greater than the reduction in strength of the parent metal.

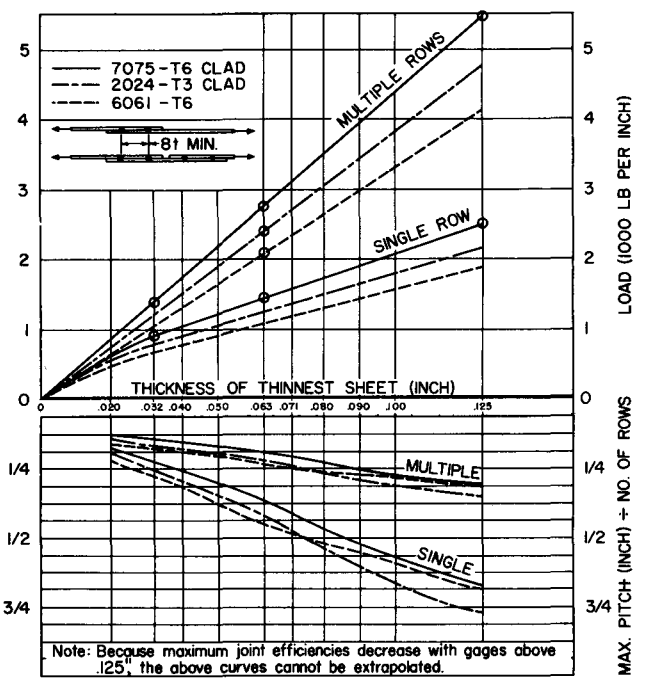

Fig. D2.22 (Ref. 1) Maximum Static Strength of Spot Welded Joints in Aluminum Alloys and Corresponding Maximum Spot Weld Pitch

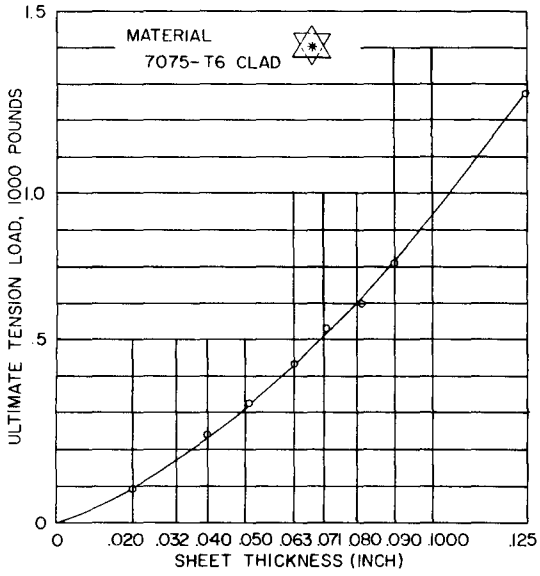

Fig. D2.23 (Ref. 1) Static Strength of Typical Single Spot Welds In Tension Using Star Coupons

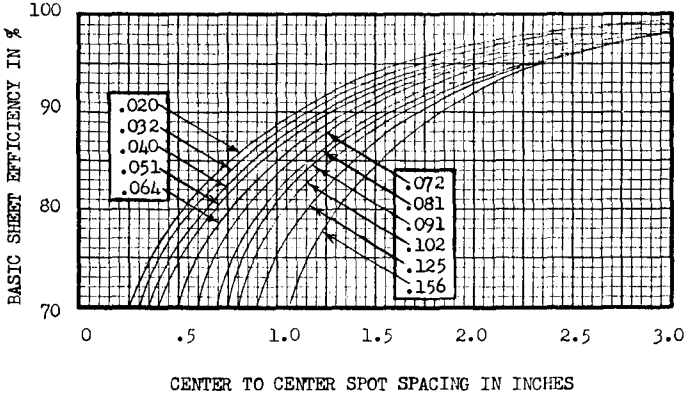

Fig. D2.24 (Ref. 1) Efficiency in Tension for Spot Welding Aluminum Alloys

PROBLEMS

(1) Fig. (A) illustrates a welded plate fitting unit fastened to a round steel tube. Both fitting plate and tube are steel F_{tu} = 95000. What is the maximum design load P which the fitting can be subjected to if a fitting factor of 1.2 is used. Fitting is not subjected to vibration or rotation on hinge pin.

(2) Same as Problem 1 but tube and fitting is heat-treated after welding to F_{tu} = 150,000.

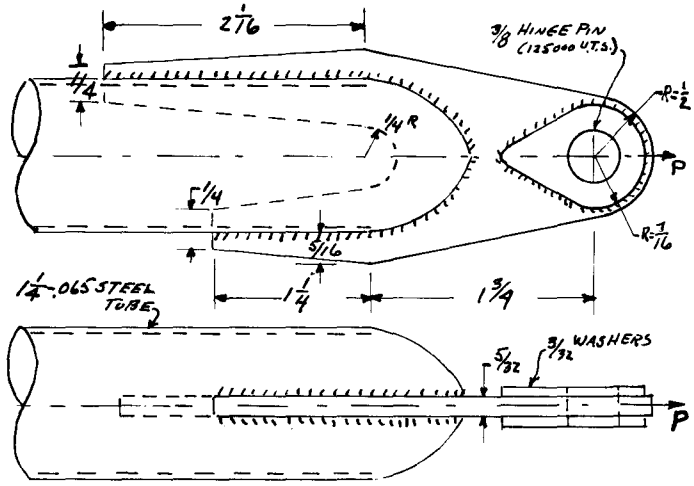

Fig. A

(3) A -.051, 2024-T3 aluminum sheet carries an ultimate tension load of 700 lbs. per inch. It is spliced by a lap joint involving one row of spot welds spaced at 0.5 inch. Is the spot weld strength satisfactory.

(4) A 7075-T6 aluminum sheet carries an ultimate tensile stress of 30000 psi. The sheet is to be spliced. Design a spot welded joint for a lap joint.

(5) In a wing section involving skin and stringers, the shear flow in adjacent panels to a particular stringer is 400 and 600 lbs. per inch, and acting in the same direction. Assuming no diagonal tension action due to skin wrinkling, what spot spacing is required to fasten the stringer to the skin if the skin is .04 thick and 2024-T6 aluminum alloy material.

REFERENCES

(1) Military Handbook - MIL-HDBK-5, August, 1962.

(2) ANC-5, March, 1955.

CHAPTER D3
SOME IMPORTANT DETAILS IN STRUCTURAL DESIGN

BY
WILLIAM F. McCOMBS
(DESIGN SPECIALIST - CHANCE VOUGHT CORP.)

D3.1 Introduction.

In the design and fabrication of an airplane the major components receive a thorough review and evaluation. Many of the smaller parts, however, are designed at the last minute and, not receiving so much attention, sometimes have faulty details. It is these which frequently lead to trouble in service and in tests. This chapter represents an attempt to point out some of the more common details that seem, somehow, to be overlooked from time to time. This should be of help to those involved in designing or dealing in other ways with the structural components of airplanes or of similar types of structures. With regard to specific details, many aircraft companies have standard methods of design. The reader should always consult his company's data on these, if available. In the event such are not available, the following suggested practices should be of practical help.

D3.2 Shear Clips.

There are hundreds of these in a typical military airplane. They are used in joining together both primary structural components and secondary structural parts such as equipment mounting brackets, etc. The function of the shear clip is to transfer a shear load from one part to another. It is not intended to transfer axial load or bending moment or twist, only shear.

A typical example is shown in Fig. D3.1. Here bracket, or beam, (a) is supported by beams (b) and (c). The load P is thus "beamed out" to (b) and (c), passing as a shear load through the clips into the webs of (b) and (c) as illustrated.

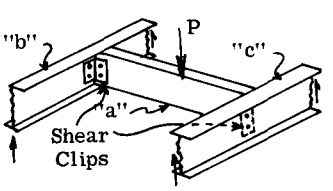

Fig. D3.1

When a significant axial load or bending moment must also be transferred, additional members must be provided or the shear clip must be replaced by a heavier fitting. This is illustrated in Fig. D3.2. Here a beam, (a),

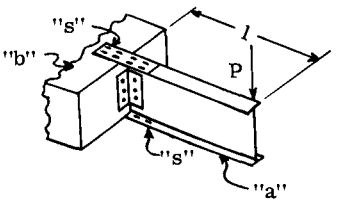

Fig. D3.2

is cantilevered off of a heavy piece of structure, (b). The load, P, passes through the shear clip as a shear load from web (a) to (b). There is also the bending moment, P x l, to be transferred. Additional splice plates, "S", are provided for this purpose. They transfer the moment in the form of axial loads from the flanges of beam (a) to member (b).

Shear clips are usually seen in two forms:

(a) bent up sheet metal or extruded angles (the angle being anywhere from 0° to 180° between the legs).

(b) extruded "tees".

These shear clips are shown in their "minimum acceptable" form in Fig. D3.3. The

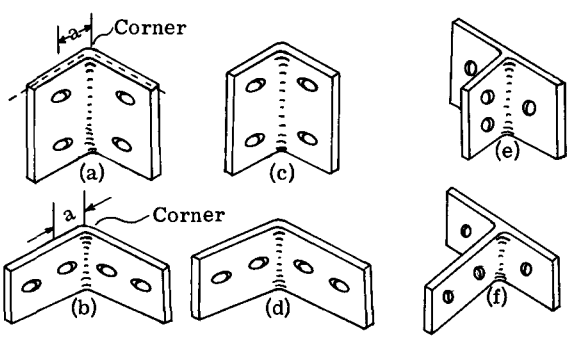

"Minimum" Type Shear Clips

Fig. D3.3

minimum requirement is that each leg of an angle type clip must have at least 2 fasteners through it. The "top" of the tee type clip and its leg must also have at least 2 fasteners each, as shown in (e) and (f).

The load "balance" of an angle type shear clip is illustrated in Fig. D3.4. The corner edge of the clip should be assumed to carry

only the shear being transferred, taken as 1000 lb. in this figure. The net loads on the fasteners are then as illustrated. Once the loads are known, the clip and fasteners can be checked for strength using standard methods.

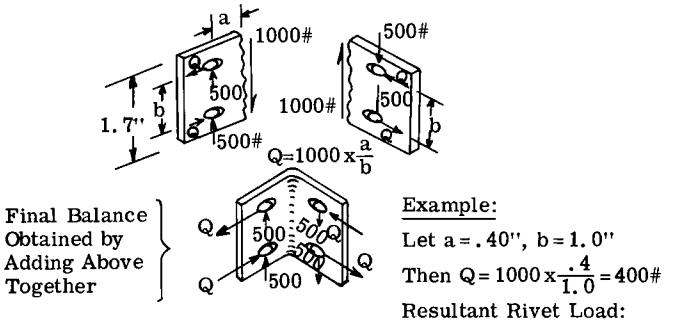

Fig. D3.4

Fig. D3.5 illustrates what will happen if only one fastener is provided in a leg of an angle clip. The single fastener cannot (ignoring friction) balance any shear at the corner. In other words, it can receive only a shear from the web to which it is fastened. This, in turn, puts a twist, P x a, into the other leg of the clip and, hence, into the other web. This is unacceptable, of course, since a much thicker leg would be needed to carry the torsion, and an undue twist would be present in the other web being joined. Of course, several fasteners, rather than just two, may be used when space allows.

Clips of type (a), (c) and (e) in Fig. D3.3 are more efficient than are types (b), (d) and (f). The latter are used when this is all that space limitations will allow. In all cases the dimension "a" should be kept as small as practical installation will allow.

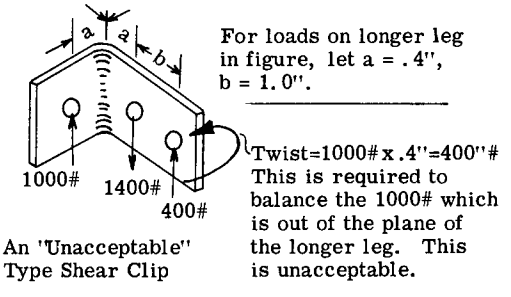

Fig. D3.5

Another type of deficiency sometimes arises when a minimum type shear clip is being used. This is illustrated in Fig. D3.6 where it has been necessary to "joggle" one leg of the angle clip, say to fit over some locally thicker part of the member being attached. If the joggle is a significant one, say to the

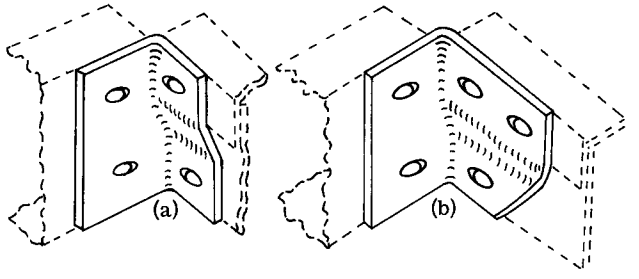

Fig. D3.6

order of the clip's thickness or greater, it can considerably reduce the clip's rigidity and cause it to function as 2 "one rivet clips" with the adverse twist effects mentioned previously. In this case at least 2 fasteners should be provided on one side of the joggle in the joggled leg, as illustrated in Fig. D3.6(b), to maintain rigidity and proper functioning. The load should be assumed to be carried by the 2 fasteners above the joggle, similar to case (b) or (d) in Fig. D3.3. Joggles are discussed further in Art. D3.4.

D3.3 Tension Clips

These are also quite numerous in military airplanes, being used to splice relatively light tension loads from one member to another. The tension clip is a very inefficient type of splice. It has a relatively poor fatigue life, particularly, and should be used only when the load is small and other design factors prevent the use of the more efficient lap shear splice.

It is usually resorted to when some structural member such as a bulkhead web or flange or fitting cannot be efficiently "opened up" to let an axially loaded member pass through. It is also frequently used to attach cantilevered brackets to bulkheads or ribs or other structure.

Consider Fig. D3.7. Member (a) is, say, on one side of a bulkhead and is to be spliced to member (b) on the other side. There is an axial tension load to be transferred and since the bulkhead cannot be cut, a tension clip arrangement must be used as shown. Angle clips in this case are illustrated.

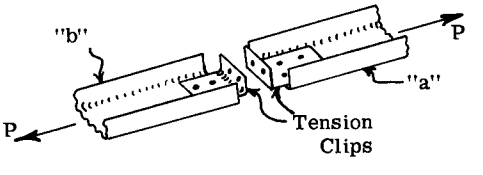

Fig. D3.7

Simple tension clips are used for relatively light loads, large loads requiring a machined fitting of a "bathtub" type. These clips are usually seen in 3 forms.

(a) single angles - either bent up sheet metal or extrusions.

(b) double angles (back to back)

(c) clips cut from extruded tee sections

Type (c) is the strongest and stiffest for a given thickness.

To obtain maximum strength and stiffness, bolts should be used for attachment purposes. Allowable load data is given in Fig. D3.8 for the single angle clip arrangement illustrated. The method of obtaining the allowable load is also illustrated by the dashed lines in the figure.

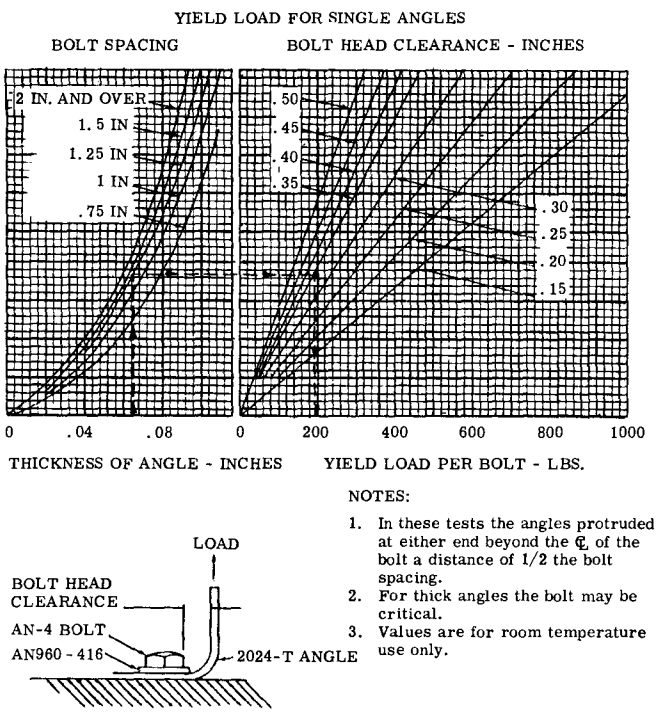

NOTES:

1. In these tests the angles protruded at either end beyond the ℄ of the bolt a distance of 1/2 the bolt spacing.
2. For thick angles the bolt may be critical.
3. Values are for room temperature use only.

Fig. D3.8
(Ref. Vought Structures Manual)

It is noted that for larger clip thicknesses the bolt may become critical and begin to yield (the same would apply to smaller bolts than those specified for the thicknesses shown). This is because of the prying action on the bolt. Because of the prying action, the load in the bolt is always greater than the applied load. Consider Fig. D3.9(a) illustrating an angle type clip arrangement. As the applied loads, P, begin to "open-up" the clips the bolt feels an increasing tension load, Q, and the "toes" of the clip bear down

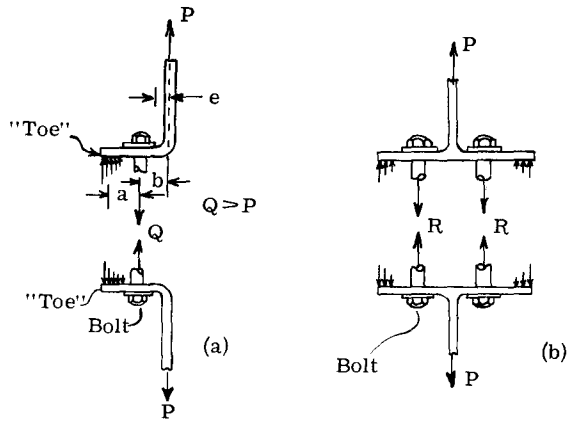

Fig. D3.9

more on each other. From statics, taking moments about the center of pressure on the toes, $Q = P \times (\frac{a+b}{a})$. Thus Q is greater than P. Obviously a small enough bolt will yield or fail in tension before a thick clip will yield or fail in bending near the washer ($M_{clip} = P \times e$). There is also a prying action in the tee type clip, as illustrated.

This prying action is the reason why the designer should be cautious in using rivets even for light tension loads, as is sometimes done. When rivets are used, as in mounting equipment brackets, it is best to use steel types and carefully check the prying load maintaining an ample margin of safety. In any event, riveted clips are inferior and no design data for them is given here.

Another point in using tension clips is frequently overlooked. The structure to which the clip is attached must be capable of taking the loads applied to it. These loads consist of the tension load from the bolt and the load from the toe action. Several examples are shown in Fig. D3.10. In these examples the term "unacceptable" means that the allowable loads of Fig. D3.8 are not applicable.

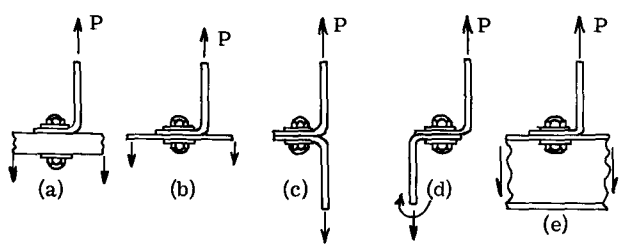

Fig. D3.10

Cases (b), (d) and (e) require a rearrangement of, or additional structure in, the back-up

structure which is receiving the load from the clips in order to achieve the full allowables of Fig. D3.8. The resultant load on the back-up structure is, of course, the applied vector, P.

Tension clips, aside from having a low static strength and stiffness, also exhibit a relatively poor fatigue life. If the load is of such a nature as to occur many times, say due to symmetrical flight conditions such as pull-ups and gusts, there should be a large margin of safety at limit load levels in the neighborhood of 200% or more. If the load is due only to some non-recurring type of loading, such as a crash condition or "jammed" system load, the large margin of safety would not be necessary.

Other suggested practices involving tension clips are:

1. Keep the bolt head as close to the bend radius or fillet radius as is possible.

2. Avoid their usage, if possible, when repeated loadings are dominant.

3. If part of the structure is continuous across a joint and part is interrupted, do not use tension clips to join the interrupted structure - instead a heavier, stiffer, machined fitting is required.

D3.4 Joggled Members.

A "joggle" is an offset formed in a member. It usually involves one or more flanges of a member of the "open" cross-section type. Joggles are quite common in typical metal airplane structures. They are used most often when it is desired to fasten together two intersecting members without using an extra part at the joint. The joggle is a compromise. It saves an extra part but the price paid is a loss in strength and stiffness of the joggled member. If the load in the member at the joint is small enough, the saving is justified. If not, an extra part, instead of or in addition to the joggle, must be used. A typical joggled installation is shown in Fig. D3.11 where one leg of an angle member has been joggled over and fastened to another member lying in the same plane.

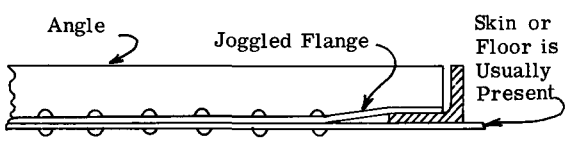

Fig. D3.11

Some aircraft companies have specific strength data and practices for the design of joggled members. This should, of course, be consulted by the designer, if available. Some companies use a 6:1 joggle length to depth ratio, others use a 3:1 ratio, or both may be used. Strength or stiffness data for one ratio should not be used blindly for another. Some of this data indicates that when, in the case of angle members, the depth of the joggle is to the order of the thickness of the joggled leg or more, the loss in strength is about equivalent to the loss of the leg outboard of the bend radius. A "rule-of-thumb" design practice is therefore suggested as follows. Assume that the net effect of the joggle, from a strength and stiffness standpoint, is equivalent to a slot cut into the joggled leg that extends inward to the bend radius tangent point. This is illustrated in Fig. D3.12.

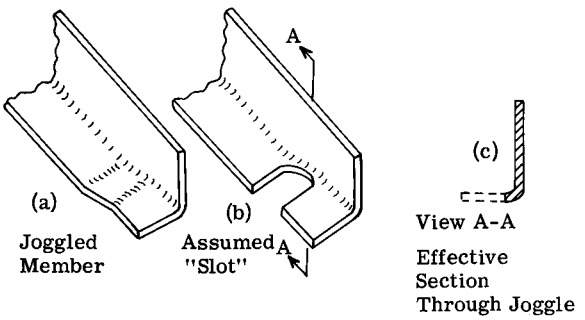

Fig. D3.12

With this assumption, the flat portion of the joggled leg will carry no axial load across the joggled area but will provide support for the curved element. The effective net section, Fig. D3.12(c), can then be checked using standard methods of analysis for whatever forces are acting on it. It is obvious that the net section shown will have little strength for carrying bending moment normal to the remaining leg. Thus, care should be taken to insure that any axial loads are introduced as near the corner as possible - which in turn means that at least two fasteners should be used on each side of the joggle.

The above approach, considering the joggle equivalent to a slot, will give the designer a much better "feel" of what he is really doing when he specifies a joggled member. The basic reason for the loss of strength and stiffness can be seen in Fig. D3.13.

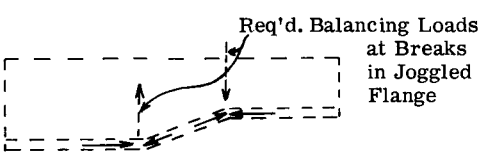

Fig. D3.13

The axial loads in the joggled leg being inclined to each other require a balancing load. Such a balancing load is not available except as shear in the thin leg and this results in the loss of stiffness and strength. If the symmetrical leg of a tee member were joggled there would be more stiffness than in the case of an angle, but the same approach, though more conservative, is recommended in the absence of test data.

As an example of the foregoing discussion assume that an angle member is supporting another member locally which is loaded by the forces Q as shown in Fig. D3.14. If a skin is present, as shown, part of the load can be carried across the joggle by the gusset effect of the skin. This can be approximated by using the methods of calculating inter-rivet buckling of skins discussed in another chapter. The rest of the load must be carried across by the net effective section of the angle in the joggled area.

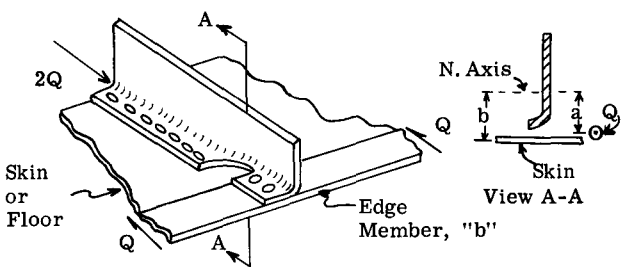

Fig. D3.14

Thus if the total load at the joint were 2Q and the load carrying ability of the skin were R, then the net section of the angle would be subjected to a load P = 2Q - R and a bending moment M = 2Q x a - R x b. The stress at the lower curved edge would be the sum of the compressive stresses,

$$f_c = \frac{MC}{I}_{\text{Net Section}} + \frac{P}{A}_{\text{Net Section}}$$

For ultimate strength, f_c could be carried up to F_{cy}, conservatively, in the typical case.

In order to realize the maximum strength and stiffness, the load in the net section must be applied in the "corner". This is to prevent stresses due to bending out of the plane of the remaining leg. This requires that a minimum of 2 fasteners be provided to receive the load at the joint. The reasoning here is the same as discussed in Art. D3.2 concerning minimum type shear clips, and the fastener loads can be calculated in the same manner as discussed there.

If the load is too large for the net section to carry, then an additional member should be provided locally. Two ways of doing this are shown in Fig. D3.15

Sometimes local requirements are such as to necessitate both legs of an angle member being joggled. In such cases it should be assumed that the angle has no significant load carrying ability at the joggle. Thus, the existence of any significant load at the joint would require an additional member and the angle should be ended just short of the joint rather than joggled up onto it.

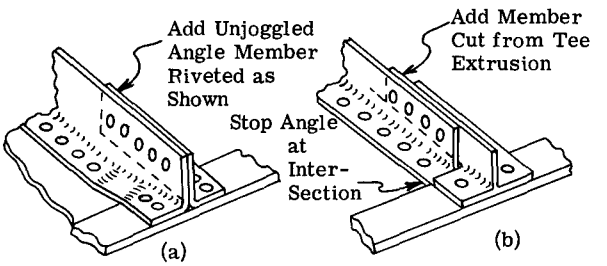

Fig. D3.15

The suggested effective net sections of members having other types of cross-sections are shown in Fig. D3.16 where the legs indicated by dotted lines are joggled. In general if the joggle is slight, considerably less than the thickness of the joggled leg, its effect can be ignored, but proper fasteners should still be provided as discussed. The smaller the length to depth ratio used for joggling, the greater the effect of the joggle. Joggled members lose stiffness and strength when subjected to tension loads as well as when under compression (but any skin present is, of course, much more effective as a gusset than when in compression).

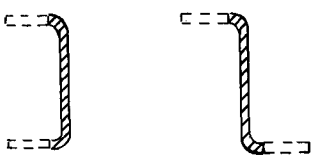

Fig. D3.16

D3.5 Fillers.

As the name implies, fillers are used to fill up a void. It is when they become a part of the structural load path that they need particular attention. Fillers also represent an item that is quite common in typical large or complicated metal airplane structures.

As an example consider Fig. D3.17. Here two tees, "a" and "b" carrying an axial load, P, are seen to be spliced together by a pair of angles "c". Since the lower leg of "b" is thicker than that of "a", a filler is needed. This filler is part of the structural load

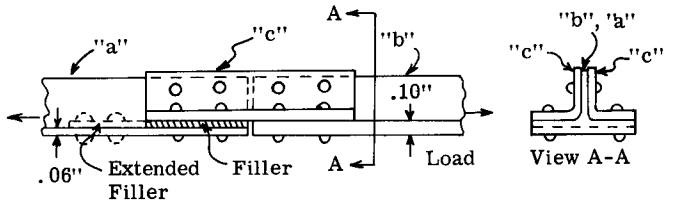

Fig. D3.17

path, from "c" to "a". In this case, to realize full strength of the fasteners, the filler must be "extended" and additional fasteners provided to tie the extended portion into member "a". If this is not done, it is said to be a "floating" filler. As explained later, a floating filler, if thick enough, will cause a loss in fastener strength.

In the above example let the total load P be 8000 lbs. and assume that 2000 lbs. of this must be transferred from "c" to "a" by the two fasteners in the filler area. The part of the load put into the filler by bearing pressure can be taken as

$$P_{Filler} = P_{Fasteners} \times \frac{t_{Filler}}{t_{Filler} + t_a}$$

$$= 2000 \times \frac{.04}{.04 + .06} = 800 \text{ lb.}$$

Sufficient fasteners should be put in the extended part of the filler to transfer this 800 lbs. into member "a".

Thus, whenever a thick filler is inserted between two members being spliced together in shear, the filler should be assumed to be a part of one of them. The part of the total splice load it will carry can be calculated as illustrated above. The fasteners can then be considered as being in two sets. One set must have the strength to splice the total shear load from the single member to the combination "filler plus member". The other set of fasteners must have the strength (meaning in shear and in bearing) to transfer the calculated filler load to the member it is assumed to be a part of. Another example uses Fig. D3.18.

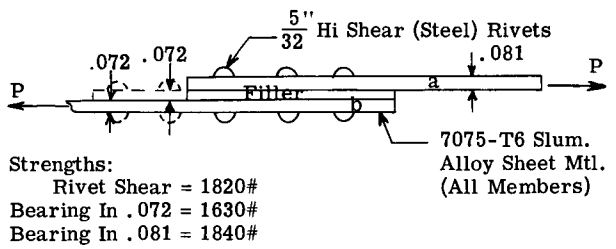

Fig. D3.18

Assume filler to be integral with the lower member, "b".

Case I.

P = 3000 lbs.

1. Rivets required to splice 3000 lbs. from "a" to combination of "b" plus filler:

   No. Rivets = $\frac{3000}{1820}$ = 1.65, or $\underline{2}$

2. Load carried by filler (to be spliced to "b"):

   $P_{Filler} = 3000 \times \frac{t_F}{t_F + t_b} = \frac{3000(.072)}{.072 + .072} =$

   1500 lbs.

3. Fasteners required to transfer P_F to "b"

   No. Fasteners = $\frac{1500}{1630}$ = .92 or $\underline{1}$

   Total Fasteners required = 2 + 1 = 3.

Splice is adequate since 3 rivets are present. Had no filler been present, 2 fasteners would have sufficed.

Case II.

P = 5000 lbs.

Repeating the same steps as in Case I:

1. No. Rivets required = $\frac{5000}{1820}$ = 2.75 or $\underline{3}$

2. Load in Filler = $5000 \times \frac{.072}{.072 + .072} =$

   2500 lbs.

3. No. Rivets required = $\frac{2500}{1630}$ = 1.54 or $\underline{2}$

Thus the 3 rivets are required to transfer load, P, from "a" and 2 additional rivets are needed to unload the filler into member "b". The filler should be extended over "b" and 2 additional fasteners added as shown by the dotted lines in Fig. D3.18.

Admittedly, the above procedure is approximate, but it provides a quick way of evaluating the effect of the filler. When the filler thickness is less than about 15% of the fastener diameter, its presence can be ignored.

The effect of the filler is to reduce the allowable strength of the fastener. The reason for this can be seen from Fig. D3.19 where the presence of the filler causes greater prying loads and hence more tension in the fastener, along with the shear load.

Any filler in the structural load path should, of course, be made from a material compatible in stiffness with that of the

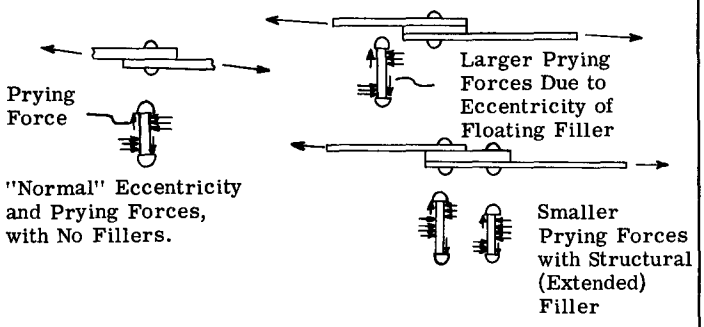

Fig. D3.19

structure around it. That is, one should not use a soft aluminum filler between high heat-treated steel parts or a phenolic or fiberglas filler between aluminum parts. The need for fillers arises not only from design considerations but frequently from manufacturing problems. In these latter cases "mis-match" between parts sometimes occurs in assembly. To prevent expensive re-work, structural fillers must be used to make the spliced area adequate. In these cases detailed attention is necessary. In the occasional instances when floating fillers cannot be avoided, the fasteners should have quoted allowables well in excess of the shear being transferred locally, if the filler is of significant thickness. It is common practice also to use a bonding agent (glue) in addition to the fasteners in installing fillers.

D3.6 Cut-outs in Webs or Skin Panels.

The aircraft structure is continually faced with requirements for opening up webs and panels to provide access or to let other members such as control rods, hydraulic lines, electrical wire bundles, etc., pass through. The designer or liaison engineer should be familiar with some of the various methods of providing structurally sound cut-outs.

There are several ways of providing cut-outs. Three will be mentioned here. These are:

(a) Providing suitable framing members around the cut-out.

(b) Providing a doubler or "bent" where framing as in (a) cannot be done.

(c) Providing standard round flanged holes which have published allowables as discussed in chapter on beam design.

(a) Framing Cut-Outs in Webs

As an example assume that a beam web requires a cut-out as shown in Fig. C3.20.

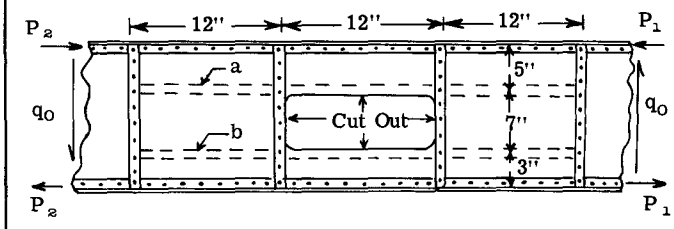

Fig. D3.20

Before the cut-out was made the members shown by solid lines (flanges, stiffeners, webs) are present. The members "a" and "b" are added to frame the cut-out, as shown by the broken lines.

There are 2 ways to determine the loads in the area framed around the cut-out. The first is to assume a shear flow equal and opposite to that present with no cut-out (q_o in the figure above) and determine the corresponding balancing loads in the framed area. Adding this load system to the original one will give the final loads and, of course, q = 0 in the cut-out panel. The other method is to use standard procedures assuming the shear to be carried in reasonable proportions on each side of the cut-out. The first method will be illustrated here.

All shear flows are shown as they act on the edge members (on the flanges and stiffeners) in this discussion.

If there were no cut-out there would be a constant shear flow, q_o, in all of the panels, as shown in Fig. D3.21a. Next a shear flow equal and opposite to that in the center panel of Fig. (a) is applied to the center panel of

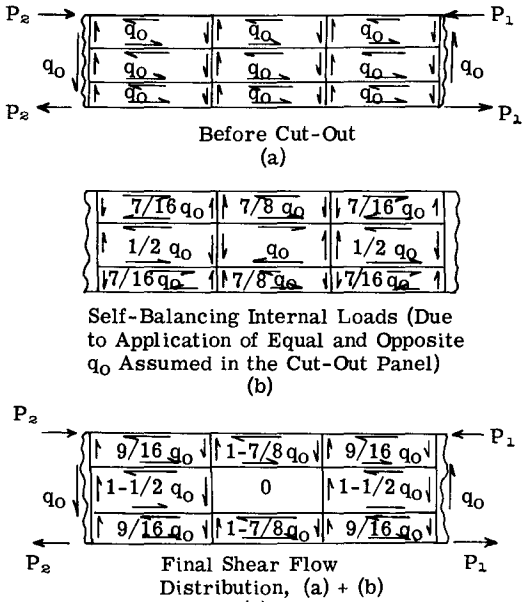

Fig. D3.21

Fig. (b). Since this represents a self-balancing load system, no external reactions outside of the framing areas are required. This is an important concept and the reader should think about it. The loads in the framed areas due to q_o in (b) are next determined. To eliminate redundancies, it is usually assumed that the same shear flow exists in the panels above and below the cut-out. It is also assumed that shear flows are the same in the panels to the left and right of the cut-out.

a) the shear flow in the panels above and below the center panel must statically balance the force due to q_o, or

$$\text{Since } \Sigma F_t = 0,\ q_o \times 7 = q \times (5+3)$$

$$q = 7/8\ q_o$$

b) the shear flows in the panels to the left and right of the center panel must also statically balance the force due to q_o.

$$\text{Since } \Sigma F_y = 0,\ q_o \times 12 = q \times (12+12)$$

$$q = 1/2\ q_o$$

c) the shear flows in the corner panels must also balance the force due to the shear flow in the (any) panel between them. Considering the panels in the right hand bay

$$\Sigma F_z = 0;\ 1/2\ q_o \times 7 = q \times (5+3)$$

$$q = \frac{\frac{1}{2} q_o \times 7}{8} = \frac{7}{16} q_o$$

d) the final shear flows are gotten by adding the values in (a) and (b) together, algebraically. Note that:

1. the shear flow in the center panel (the cut-out) is $q = q_o - q_o = 0$, as it should be.

2. the shear flows above and below and to the left and right of the cut-out add, giving a number greater than the original q_o.

3. the shear flows in the corner panels are smaller than the original value of q_o.

This is the way the changes always occur in the area framed about a cut-out.

e) Finally, and importantly, there are axial loads developed in all of the framing members due to the cut-out. These will add or subtract, depending upon their directions, to any loads present before the cut-out was made (as in the case of the beam flanges). The axial loads due to the cut-out can be gotten from Fig. (b). Or the total axial loads in all of the members can be gotten from (c). These are illustrated in Fig. D3.22.

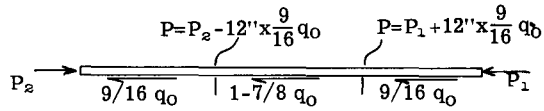

Axial Load Distribution in Upper Flange from Fig. D3.21c
(a)

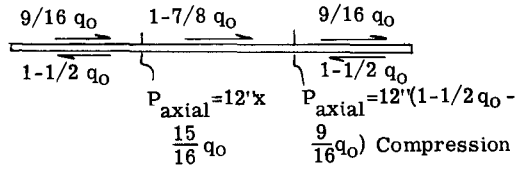

Axial Load Distribution in Framing Member Above Cut-Out Obtained from D3.21c (Same Result Could be Gotten from Fig. D3.21b).
(b)

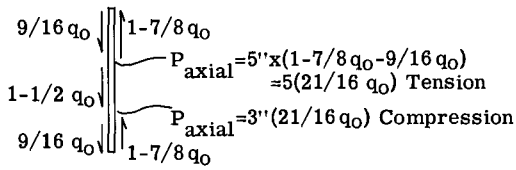

Axial Load Distribution in Stiffener Bordering Cut-Out on Left Side, from Fig. D3.21c (Same Result Obtained from D3.21b)

Fig. D3.22

Once the internal loads are known, the members can be checked for strength using standard methods of stress analysis.

The cut-out could have been framed without extending the framing members into the bay on the right of the cut-out. This case is illustrated in Fig. D3.23.

Had the 7" deep cut-out been required at the bottom of bay, the framing could have been done with only one member (as could the preceding cases also) as illustrated in Fig. D3.24. This represents the minimum of adequate framing for any cut-out. That is, there must be a minimum of one redistribution bay on one side of the cut-out and at least two redistribution bays on the other side, and there must be the framing members defining the bays. These framing members will always be loaded axially.

Note that in the previous examples in Case (b) the sum of the loads on all edge members (framing members) is zero. No external loads are needed for equilibrium. This is

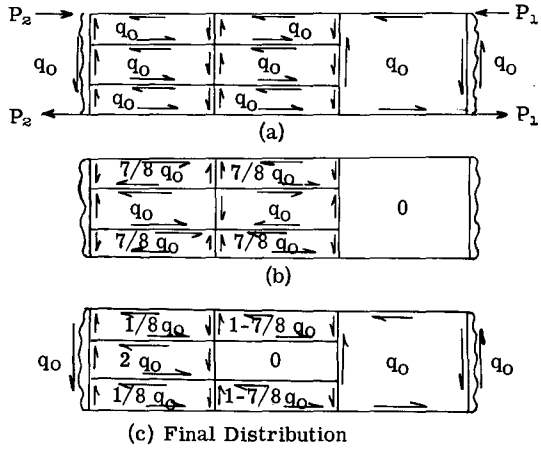

Fig. D3.23

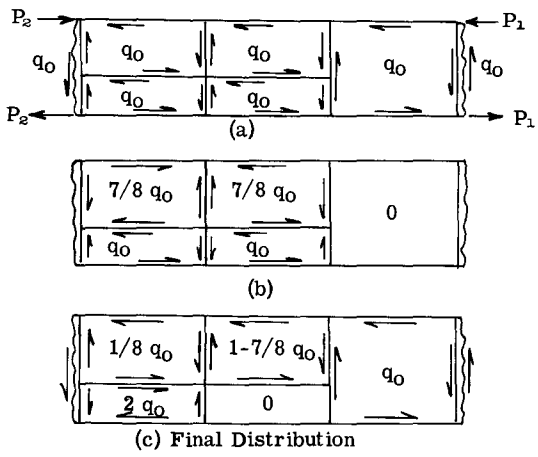

Fig. D3.24

always the case when a set of self-balancing shear flows are applied to a flat panel structure or to a 3 dimensional box structure with a cut-out on any side. The reader should study the examples closely. Although the method is shown only for a flat beam it is also applicable to any structure with a cut-out, such as the box beam of Article A21.8. This has actually been illustrated in Solution No. 2 of that article and the reader should review it at this time.

Sometimes framing members for a cut-out are not conveniently available as were the stiffeners and flanges of the beam used in the previous examples. In such cases they must, of course, be provided.

(b) Framing Cut-Outs With Doublers or Bents

Frequently a cut-out in the web of a beam must be so deep that it removes nearly all of the web. In this case the method previously described cannot be used. Instead the "brute-force" approach is necessary and a heavy doubler, or bent, is provided around the cut-out to carry the shear. This is illustrated in Fig. D3.25.

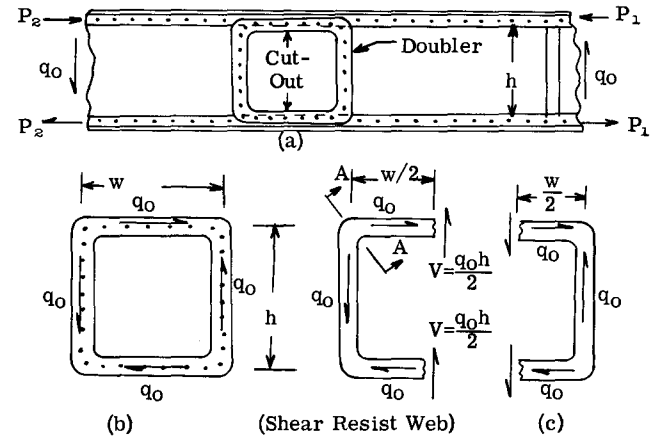

Fig. D3.25

As shown in (a) the doubler whose thickness is yet to be determined is made to fit around the cut-out as shown. Reasonable internal radii are in the cut web and doubler at the corners to keep stresses due to curved beam bending reasonable (see Chapter C11). Attachments are provided as shown to pick up the basic shear flow in the web.

The loading imposed on the doubler is shown in (b), namely the shear flow q_o. Strictly speaking, the doubler should be analyzed as a frame. With reasonable symmetry the loading in (c) can be assumed at the center of the frame. That is, one half of the total shear, $q_o \times h/2$ is resisted in the top of the frame, one half in the bottom and a pin joint (no bending moment) exists at the cut. The bending moment axial loads and shears at any section of the frame follow as a matter of statics. For example,

At A-A,

$$M = V \times \frac{w}{2} = \frac{q_o\, h\, W}{4}$$

(there may also be a little relieving moment due to q_o)

$$F_Z = V = \frac{q_o h}{2}$$

$$F_y = q_o \times \frac{W}{2}$$

The thickness of doubler required to take the loads can thus be determined using standard methods of stress analysis. The doubler should have sufficient out of plane stiffness, also, to provide simple support for the beam web, as discussed in Chapter C10. This will normally be provided by the thickness required for strength purposes.

Sometimes the nature of the cut-out is such that the frame (doubler) can be deeper at the top (or bottom). In such a case, the

deeper part can be assumed to carry a greater portion of the total shear, V, and the lower part a smaller portion. This is illustrated in Fig. D3.26 where the cut-out does not extend as high as in Fig. D3.25 and the upper part is assumed to carry 4/5 of the total shear and the lower part only 1/5.

The cases illustrated are for shear resistant webs. If a tension field is present the doubler must also be designed for the end-bay effects discussed in Chapter C11.

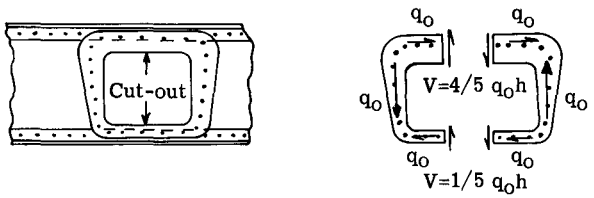

Fig. D3.26

(c) Providing Access With Standard Round Flanged Holes or "Donut Doublers"

Frequently a cut-out size requirement is such that a standard round flanged hole will provide the needed open space and strength. In such cases either of the following can be done when the beam is of the shear resistant type:

1) replace the web, locally, with a panel having a standard round hole that has a 45° flange, as discussed in Chapter C10.

2) Cut the required diameter hole into the web and attach a "donut" doubler (ring) that has the same (or greater) stiffness in a direction normal to the web as does the flange of (1) above.

In either case the allowable shear can be calculated as discussed in Chapter C10. Th se allowables apply only to round holes, not to elliptical or rectangular holes with flanged edges, which are weaker.

Item (2) above is illustrated in Fig. D3.27. Note that the hole spacing "b" of Chapter C10 will be quite large if only one hole is present and is not near the end of the beam. The hole spacing "b" is, of course, used in determining the allowable shear if no stiffeners are present.

If a beaded web is cut, a panel can be inserted locally, containing a hole with a beaded flange, as discussed in Chapter C10 and these allowables used conservatively.

If the beam is of the tension field type, method (c) does not apply. In such cases, a heavier frame, as in method (b), that can take the tension field effects should be used.

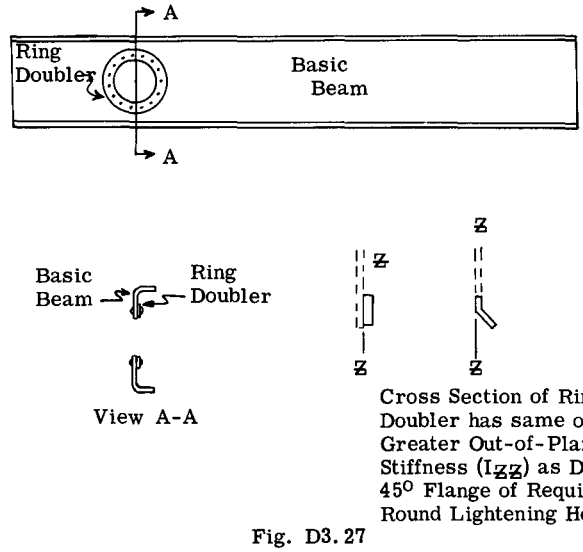

Fig. D3.27

D3.7 Special Cases of Beam Design.

There are several cases involving beam design not discussed in Chapters C10 and C11, since these chapters are intended primarily to present fundamental design principles. The designer will encounter in practice, however, the following situations which include ordinary straight beams and beams in the form of bulkheads or frames:

a) Curved beams

b) Flanges with local changes in direction ("bent" flanges)

c) Flanges subject to "normal" loads which tend to bend them.

d) Flanges requiring "stabilization" against buckling out of the plane of the web.

(a) Curved Beams

Consider a portion of a curved beam as shown in Fig. D3.28. The curvature is taken as constant, as is the bending moment, for purposes of illustration.

When the outer (upper flange in (a)) is in tension and the inner flange in compression there will be a collapsing (compression) loading on the web as shown in (b). This is because a "hoop" loading is required to keep the flanges from moving inward, towards each other. For a constant load, P, in the flange and from simple statics.

$$2P = 2wR$$

$$w = \frac{P}{R}$$

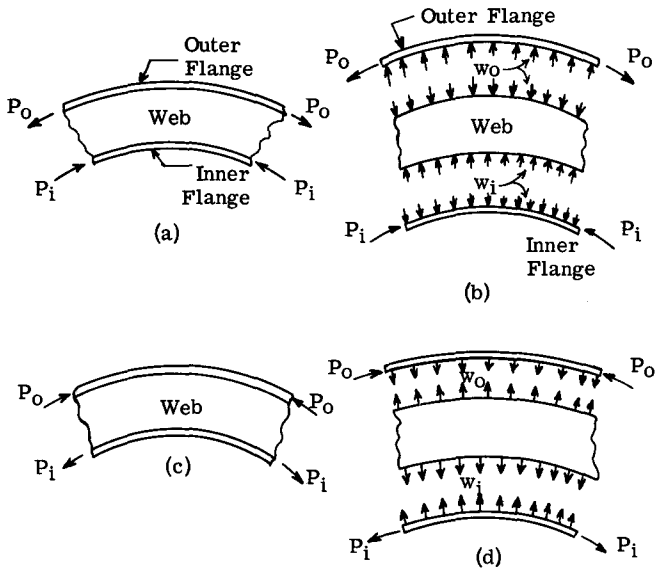

Fig. D3.28

w is, of course, larger at the inner flange, since R is smaller, than at the outer flange.

This compressive loading tends to collapse the web. If the web is also carrying shear, as is the usual case in practice, an interaction formula which includes compression and shear stresses should be used to predict buckling. This is the reason that the allowable stresses quoted for beaded panels and panels with flanged holes in Chapter C10 do not apply. These allowables were for straight webs with no normal loads, as are present in curved beams.

If the curvature is enough to cause significant compression in the web, stiffeners should be provided to take this load. This can be done as shown in Fig. D3.29.

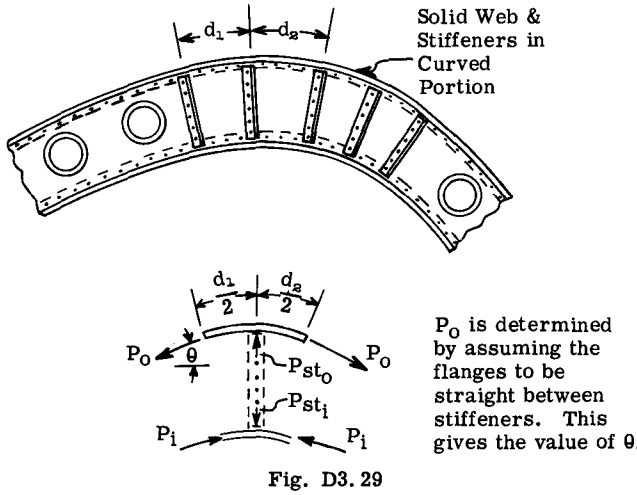

P_o is determined by assuming the flanges to be straight between stiffeners. This gives the value of θ.

Fig. D3.29

P_o and P_i can be taken as the calculated flange loads at the stiffener junction as determined from statics, or from a bulkhead internal load analysis. Then the stiffener loads will be,

$$P_{st_o} = 2P_o \tan \theta$$

$$P_{st_i} = 2P_i \tan \theta$$

Any difference in stiffener end loads will be sheared into the web through the attaching fasteners.

The flanges should be designed for the axial loads, P, in them. Some allowance for bending moment, M, (Fig. D3.30) can be made by taking M as P x e x 1/2 at the center and - P x e x 1/2 at the stiffener junctions. These secondary effects are sometimes ignored when obviously small, in practice.

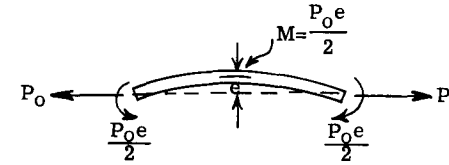

Fig. D3.30

"e" is the eccentricity between stiffener junctions due to the flanges being curved rather than straight. The same applies to the inner flange, except that it is in compression in this discussion.

When the outer flange is in compression and the inner one in tension, all of the loadings are reversed, as in Fig. D3.28(c) and (d). The web is then subjected to tension loads and there is no collapsing problem. No stiffeners are required, other than for the "normal" reasons. However, in practice, most loadings are reversible to some degree, and some compression on the webs will then, of course, be present.

(b) Flanges With Local Changes in Direction (Bent Flanges).

This is a special case of (a) above. Instead of a general curvature the flange has a local change in direction as in Fig. D3.31.

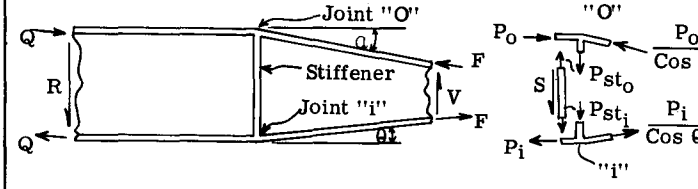

Fig. D3.31

The outstanding legs of the flanges will move upwards unless a stiffener provides the load required to hold them down. This can be calculated from statics at the joint. The

load in the stiffener is then sheared into the web. If the stiffener is not provided, some strength will be present unless the kick load puts the web in compression, in which case it will buckle if thin. If the beam is machined from bar stock the stiffener can be machined in place. If the beam is "built up" from separate flanges and web parts a stiffener can be made up from a tee member attached to the flange and an angle member attached to the web and to the tee. This is illustrated in Fig. D3.32. The kick load path is from the flange to the tee to the angle to the web.

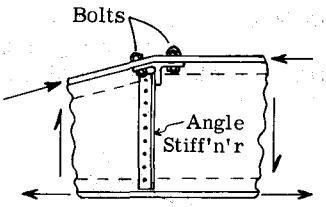

Fig. D3.32

The loading shown will produce an up load on the bolts, putting tension into the leg of the tee and the stiffener angle. A reversed loading would push down on the tee producing compression. The above tee and angle combination could, of course, be replaced by a single machined fitting. The important thing is that an adequate stiffener, attached to the outstanding legs, be present if all of the outstanding leg is to function effectively.

(c) Flanges Subjected to Normal Loads Tending to Bend Them.

Frequently the flanges of a beam are subjected to loads which pull outward or push inward. It is important in each case that the flange be "backed up" by a stiffener. The effect is the same as in the case just discussed, (b), involving kick loads due to bent flanges. A similar stiffener arrangement can be used.

(d) Flanges Requiring Stabilization Against Out-of-Plane Buckling.

In the cases of flange design discussed in Chapters C10 and C11, it was assumed that any flange in compression was stabilized, or prevented from buckling as a column, by some supporting member. This member was usually shown there as a floor or a skin to which the flange was attached. Thus the flange could not buckle since it was restrained in one plane by the beam web and in a plane normal to this by some skin.

Occasionally, however, this out-of-plane (normal to the web) supporting member is not inherently present and must be provided. A typical example is the inner flange of a fuselage bulkhead or frame (the outer flange is stabilized, usually, by the outer skin). The inner flange will usually be subject to a compression load over much of its length for some design condition. Since the flange will have little stiffness of its own, its L/ρ will be small and it will buckle at very low compressive stress levels as a long column. It is then necessary to provide supporting members, as shown in Fig. D3.33, to reduce the unsupported length and bring the buckling stress up to an efficiently high level, nearer to the local crippling strength of the flange.

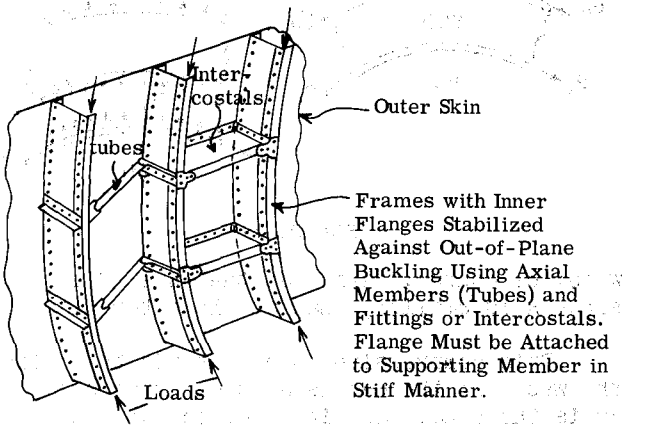

Fig. D3.33

The supporting member will not be subject to any appreciable load but it must have sufficient stiffness to prevent column buckling. The required stiffness criteria will not be discussed here but the reader should consult Ref. (1) or similar textbooks to obtain such criteria. Since the supporting members are sized by stiffness rather than strength requirements they can usually consist of light tubes or intercostals. Their weight is usually less than would result from beefing-up the bulkhead flange for out-of-plane strength. The stiffness of the supporting member must, of course, include the end fitting attaching it to the flange.

D3.8 Structural Skin Panel Details.

The general principles involving the design of structural skin or floor panels are covered in Chapters C10 and C11. Chapter C11 concerning buckling panels, in particular, should be thoroughly understood by the designer. In addition to this information, several details of design are presented below.

a) Rectangular holes

b) Recessed panels

c) Installation of long axial members on panels

d) Spot welding sheet metal doublers

e) Tension skin splices

(a) Rectangular Holes.

It is frequently necessary to cut rectangular holes into load carrying panels to provide doors or to mount equipment. These holes must, of course, be framed as discussed in Art. D3.6. Equally important from a fatigue standpoint is that the internal corner radii not be too small or cracks will eventually start there. As an arbitrary design requirement it is suggested that the corner radii be maintained at R = .35 inches or larger with the normally obtained finish. In those cases where a smaller radius is absolutely necessary, it is suggested that the lower limit of R = .10 be maintained, and that an f-40 finish be specified around the edge of the panel at the corner.

(b) Recessed Panels.

It is sometimes necessary to recess a structural panel locally in order to mount equipment, as shown in Fig. D3.34.

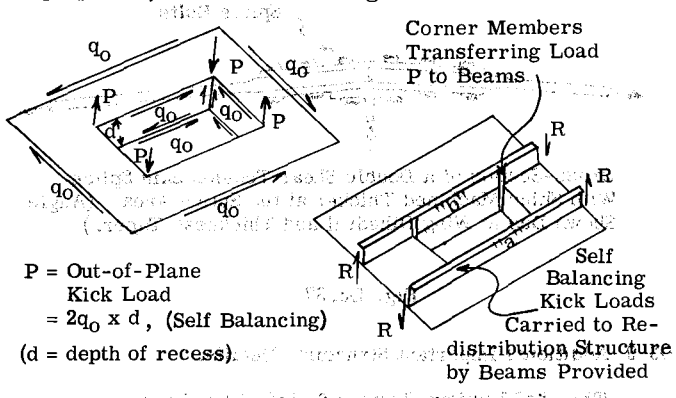

Fig. D3.34

The recessed panel can continue to carry its shear load but there will be out-of-plane "kick" loads. These are resisted by the framing members "a" and "b" as shown in the figure and carried over to some beam or frame that can redistribute them into the main side panels. If the recess must be very deep and its size is not too large, it may be better to omit the panel and simply frame the resulting hole. This is more likely to be the case if highly buckling skins are involved. The recessed panel cannot, of course, carry tension stresses, only shear. The hole in the basic skin at the recess must not have sharp corners, as discussed in (a) above.

(c) Installation of Axial Members on Skin Panels.

Whenever a local axial member, meaning one lying in the direction of the main bending stresses of the overall structure (i.e. fore-and-aft in a fuselage), is installed, care should be observed. This member will tend to become "effective". That is, it will develope axial stresses as it strains along with the skin, particularly in tension. Most of the load picked up will enter through the fasteners near the ends of the members. The member tends to strain the same amount as the panel it is attached to though it never is as much due to the flexibility of the fasteners. Thus the total load will be $P = f_{skin} \times A_{member}$ as an upper limit, but only 60% to 80% of the skin axial stress is normally developed in the member. The larger the member and the greater its length the more axial load it will develope. Most of this load can be considered to enter through the outer (end) 20% of the fasteners at each end. High loads and relatively large bearing stresses will thus be present here. When these are present in the skin panel along with high skin tension stresses, the fatigue life of the skin panel will suffer. Therefore to keep these induced fastener loads lower, axial members (other than primary structure) should be kept as short as is practical. If their area is large then their ends should be tapered. There are methods for evaluating these effects more specifically, but they are beyond the scope of this article. The possible deleterious effect should be anticipated as it can sometimes cause cracks in panels.

Whenever a member is installed on a buckling (diagonal tension) shear panel it must be strong enough to prevent the possibility of "forced crippling" failure due to the action of the buckling skin. The reader should consult Chapter C11 in this respect for design criteria.

(d) Spot Welded Doublers.

Frequently some bay or area of a skin or floor panel must be made thicker than other bays because of higher local shear flows. For example, a skin of .040 thickness might have to be made .064 in a bay because of higher loads as shown in Fig. D3.35.

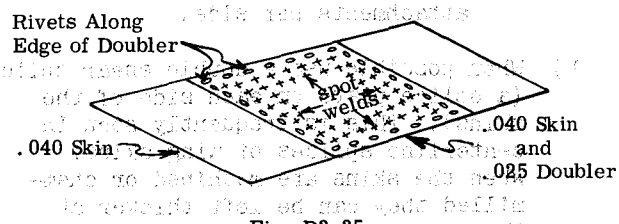

Fig. D3.35

One common way of achieving this, for large panels, is to spot weld (or sometimes to bond) an .025 doubler to the .040 skin. The spot welds should be put in at a close spacing to make the combination act as unit rather than as two separate skins, which would

be weaker. It is considered good practice to use rivets along the edge of the doubler, particularly if the panel is of a tension field design with its accompanying buckles.

(e) Tension Skin Splices.

Skin splices should be kept to a minimum number, but they are common in aircraft structures. The splices of major structural skins should be given due consideration since they always contain stress concentrations and limit the fatigue life.

There are two factors present in tension splices which reduce the fatigue life:

a) There is the basic tension stress in the skin being spliced and the stress concentration due to the holes.

b) There is also the bearing stress in the holes, due to the fastener splice loads, which worsens the situation. That is, the combination of tension and high bearing stresses in the skins is worse than tension stresses only.

To keep the fatigue life as large as possible, the following practices should be observed:

a) When more than one row of fasteners per side is required, as is the usual case:

   1. Do not "stagger" the fastener pattern but keep the holes in line, as shown in Fig. D3.36. This gives a lower stress concentration than staggered holes. It is an interesting fact that two or more holes in line in the direction of the load gives a lower stress concentration factor than does a single hole.

   2. Avoid using more than 3 rows of attachments per side.

b) When possible use a double shear splice (a splice plate on each side of the skins). This is frequently seen in centerline splices of wing skins. When the skins are machined or chem-milled they can be left thicker at the splice to reduce the tension and bearing stresses locally, as shown in Fig. D3.37.

c) Maintain a fastener spacing in each row and between rows of approximately four times the fastener diameter (the rows should be kept as close together as is practicable).

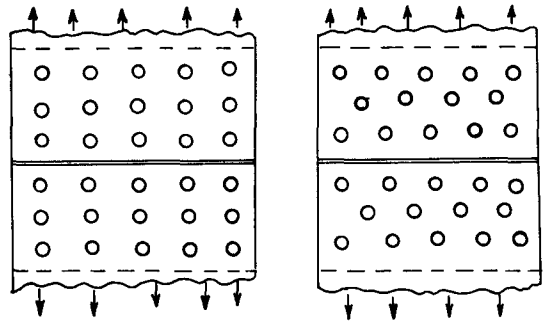

Fig. D3.36

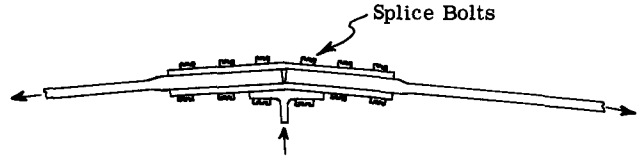

Cross-Section of a Double Shear Tension Skin Splice With Skins Machined Thicker at the Splice Area. (Angle Shown Due to Wing Dihedral and Thickness Taper.)

Fig. D3.37

D3.9 Additional Important Structural Details.

The following list of details is presented with a minimum amount of comment as representative of "good practice". In addition to the following list, the details listed in Chapter B25 "Fatigue Analysis and Fail Safe Design" should be observed.

1. Avoid mixing hole-filling and non-hole-filling fasteners in the same pattern (i.e. aluminum and hi-shear type rivets or steel bolts). When this cannot be avoided, ream the holes for the non-hole-filling fasteners to insure their picking up load better than a plain drilled hole, with its "slop", would produce.

2. When using less than four non-hole-filling fasteners in a pattern, use reamed holes to insure a better distribution of load among the fasteners.

3. When using fasteners in thin sheets where the value of D/t (fastener diameter to sheet thickness is greater than 5.5) determine allowables from tests or use

conservative extrapolations. The thin sheet tends to "buckle" around the hole at relatively low bearing stresses.

4. Do not use hi-shear type fasteners in joints where the bottom skin is dimpled.

5. Maintain an arbitrary margin of safety of .15 in shear joints for fastener patterns to allow for uneven distribution of loads.

6. Do not use spot welds to attach buckling skins to their supporting frames unless a "one-shot" structure, such as a missile, is involved. Even in these cases do not use spot welds on either side at the joggled area of a joggled member; use rivets at the joggle.

7. Do not use a "long string" of fasteners in a splice. In such cases the end fasteners will load up first and yield early. Three, or at most 4, fasteners per side is the upper limit unless a carefully tapered, thoroughly analyzed splice is used. Such a design can be fashioned but is beyond the scope of this article.

8. Carefully insure against feather edges in all fitting design. Re-entrant surface intersections must have their edges rounded or else fatigue cracks will inevitably begin in such places. Any angle between surfaces less than 70° can be considered a feather-edge. These commonly occur in design if not watched, in drilling and other machining operation call-outs.

9. The permanent buckling data presented in Chapter C11 applies to structures similar to fuselages where the sub-structure rings are closely spaced as compared to the radius of curvature of the skin. That is, the ratio of skin support spacing to radius of curvature is small, considerably less than one. When the spacing of the sub-structure becomes larger, permanent buckling should be considered to occur at approximately the same shear stress that produces initial buckling; that is when the above ratio approaches unity.

10. Avoid the use of "open section" members when torsion is present. Open section members are extremely flexible compared to closed sections as can be seen from Chapter A6. For a given torsional stiffness, an open section member will be far heavier than a closed one. In the example below, member "b" is 65 times as stiff as member "a" for pure torsion applied at each end (see also the example in Chapter

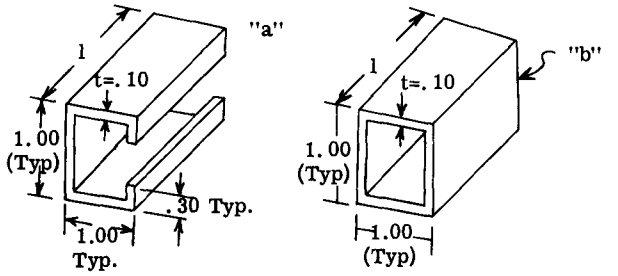

Fig. D3.38

A6). For even a closed section to operate efficiently the torsion should be capable of being distributed into all sides of the closed section. This may require a "bulkhead" type end fitting, or a much thicker section locally where the torsion is put in. The action is similar to a fuselage bulkhead distributing a twist loading into the skins of the fuselage or a wing rib distributing an applied twist into the skins and spar webs.

11. Compressive buckling does not necessarily mean failure. It means failure only if there is no other member to keep taking additional load. Shear buckling simply indicates that additional load must be carried as diagonal tension as discussed in Chapter C11. Of course, the members supporting the web must be able to withstand the ensuing so-called "secondary" effects.

When the compression skins of a fuselage or wing buckle they will carry no additional compression load but the stringers and flanges are still capable of this, as discussed in Chapter A19. The buckled skins can, however, carry additional shear load through tension field action. Thus to achieve a light efficient design the designer should have a thorough understanding of the factors involved after members have buckled as covered in other chapters of this book.

12. Probably the most single important item regarding detail structural design is the matter of equilibrium. If the designer will show the load equilibrium for every part of his assembly, most errors will be prevented. The majority of all structural strength problems occur simply because the laws of statics have not been observed, and it is usually in the smaller detail parts that the time is not taken to do this. It takes a considerable amount of experience to safely substitute the "eyeball" for the slide rule and data book. The beginning detail designer and many others who have been at it for a while simply do not have this experience

in all areas of structural design. The only safe course in such circumstances is always to show the member loads in static balance. for every part of a structural assembly. When this is done it will also give the designer a better feel as to how the structure is actually deflecting under load. This can be of significant help in anticipating problems where members are joined together and therefore must push, pull or pry on each other when loaded.

REFERENCES:

1. "Theory of Elastic Stability", Timoshenko.
"Buckling of Metal Structures", Bleich, F.

APPENDIX A

I - Elementary Arithmetical Rules of Matrices.

Definition of a Matrix - $\left[A_{ij}\right]$

A matrix is a group of numbers and/or symbols arranged in an array so as to take advantage of certain arbitrarily defined rules and operations. Those rules which have proven to be the most convenient are now commonly accepted: some of these are set forth here.

Matrix Forms

A matrix may be formed of numbers and/or symbols arranged in various ways. Some of these, along with examples, are:

NAME	SYMBOL	EXAMPLE
Column Matrix	$\left\{\ \right\}$	$\begin{Bmatrix} 3 \\ -1 \\ 8 \end{Bmatrix}$
Row Matrix	$\lfloor\ \rfloor$	$\begin{bmatrix} 4 & 6 & -6 & 3 \end{bmatrix}$
Rectangular Matrix	$\left[\ \right]$	$\begin{bmatrix} a & b & c \\ d & e & f \end{bmatrix}$
Square Matrix* (special case of a rectangular matrix)	$\left[\ \right]$	$\begin{bmatrix} b_{11} & b_{12} \\ b_{21} & b_{22} \end{bmatrix}$
Diagonal Matrix (special case of a square matrix: elements on "main diagonal" only)	$\not\left[\ \right]\not$	$\begin{bmatrix} 1 & 0 & 0 \\ 0 & -7 & 0 \\ 0 & 0 & 6 \end{bmatrix}$
Unit Matrix (a diagonal matrix with only "ones" on the main diagonal)	$\left[\ I\ \right]$	$\begin{bmatrix} 1 & 0 & 0 & 0 \\ 0 & 1 & 0 & 0 \\ 0 & 0 & 1 & 0 \\ 0 & 0 & 0 & 1 \end{bmatrix}$

Subscript Notation

In the notation $\left[A_{ij}\right]$, indicating a rectangular matrix, the i are the indices of the rows while the j are the indices of the columns. Thus, the element A_{34} is in the third row, fourth column (counting from the upper left).

Matrix Equality $\left[A_{ij}\right] = \left[B_{ij}\right]$

Two matrices are said to be equal when (and only when) each term in one is equal to its corresponding term in the other. Thus the equality indicated above means that

$$A_{11} = B_{11}$$
$$A_{12} = B_{12}$$
$$\cdots\cdots$$
$$\cdots\cdots$$
$$A_{21} = B_{21}$$
$$A_{22} = B_{22}$$
$$\cdots\cdots$$
$$\text{etc.}$$

It follows that, for this definition to make sense, the two matrices involved must be of equal size. The equality $\begin{bmatrix} a \\ b \end{bmatrix} = \begin{bmatrix} c & d & e \end{bmatrix}$ makes no sense.

Matrix Addition $\left[A_{ij}\right] + \left[B_{ij}\right] = \left[C_{ij}\right]$

Two matrices are added together by adding corresponding terms. Thus, in the above, $A_{11} + B_{11} = C_{11}$, $A_{12} + B_{12} = C_{12}$, etc. For example,

$$\begin{bmatrix} 4 & 2 & -1 \\ 6 & 0 & -1 \end{bmatrix} + \begin{bmatrix} -3 & 7 & 0 \\ 0 & 4 & 2 \end{bmatrix} = \begin{bmatrix} 1 & 9 & -1 \\ 6 & 4 & 1 \end{bmatrix}$$

Here too, the operation only has meaning for matrices of equal size.

Matrix Subtraction $\left[A_{ij}\right] - \left[B_{ij}\right] = \left[C_{ij}\right]$

The same rules apply as for addition but with a change in sign. For example,

$$\begin{bmatrix} 6 & -5 \\ 3 & 2 \\ 7 & -8 \end{bmatrix} - \begin{bmatrix} 6 & 2 \\ 0 & 2 \\ 9 & 0 \end{bmatrix} = \begin{bmatrix} 0 & -7 \\ 3 & 0 \\ -2 & -8 \end{bmatrix}$$

---

* A square matrix should be carefully distinguished from a determinant, which it resembles superficially. A determinant has a numerical value obtained by certain rules of operation. A matrix, by itself, has no value.

Matrix Multiplication $[A_{ij}][B_{jk}] = [C_{ik}]$

MULTIPLICATION BY A SCALAR

A scalar quantity multiplied into a matrix multiplies every element in the matrix. Thus,

$$6\begin{bmatrix} 2 & 2 & 3 \\ -4 & 0 & 7 \\ 1 & 0 & 1 \end{bmatrix} = \begin{bmatrix} 12 & 12 & 18 \\ -24 & 0 & 42 \\ 6 & 0 & 6 \end{bmatrix}$$

(Note how this rule differs from that applied to a determinant multiplied by a scalar).

MULTIPLICATION OF A COLUMN MATRIX BY A ROW MATRIX

The product of a column matrix by a row matrix forms the basis for all matrix multiplications. The product is a scalar quantity (a single number) formed by the following rule:

$$\begin{bmatrix} a_1 & a_2 & a_3 & \cdots & a_n \end{bmatrix}\begin{Bmatrix} b_1 \\ b_2 \\ b_3 \\ \vdots \\ b_n \end{Bmatrix} = a_1b_1 + a_2b_2 + a_3b_3 + \cdots + a_nb_n$$

More concisely,

$$\begin{bmatrix} a_i \end{bmatrix}\begin{Bmatrix} b_i \end{Bmatrix} = \sum_i a_ib_i$$

Example:

$$\begin{bmatrix} 3 & -2 & 17 \end{bmatrix}\begin{Bmatrix} 4 \\ 6 \\ 2 \end{Bmatrix} = 12 - 12 + 34 = 34$$

Obviously there must be an equal number of elements in each matrix.

MULTIPLICATION OF A COLUMN MATRIX BY A RECTANGULAR MATRIX

If the premultiplier (matrix in front) has several rows of numbers, the matrix multiplication between each row of the premultiplier and the postmultiplier column matrix is carried out as above. Each row is treated separately and there are as many independent results as there are rows in the premultiplier. These results are arranged in a column.

Example: (2 rows in the premultiplier)

$$\begin{bmatrix} 4 & -1 & 2 \\ 6 & 1 & 0 \end{bmatrix}\begin{Bmatrix} 3 \\ 2 \\ 9 \end{Bmatrix} = \begin{Bmatrix} 28 \\ 20 \end{Bmatrix}$$

Example: (4 rows in the premultiplier)

$$\begin{bmatrix} 7 & 6 \\ -1 & 0 \\ 2 & 4 \\ 4 & -3 \end{bmatrix}\begin{Bmatrix} 1 \\ 2 \end{Bmatrix} = \begin{Bmatrix} 19 \\ -1 \\ 10 \\ -2 \end{Bmatrix}$$

MULTIPLICATION OF A RECTANGULAR MATRIX BY A ROW MATRIX

If the postmultiplier matrix has several columns, the premultiplier row matrix is multiplied onto each column independently of the other columns. As many separate results are obtained as there are columns in the postmultiplier. These results form a row.

Example: (3 columns in postmultiplier)

$$\begin{bmatrix} 3 & -2 & 1 \end{bmatrix}\begin{bmatrix} 7 & 1 & 6 \\ 4 & 0 & -3 \\ 4 & -2 & 1 \end{bmatrix} = \begin{bmatrix} 17 & 1 & 25 \end{bmatrix}$$

PRODUCT OF TWO RECTANGULAR MATRICES

The operation in this case is a combination of the two previous cases. One proceeds by taking row one of the premultiplier and multiplying successively with each column of the postmultiplier. The set of independent results thus obtained forms the first row of the matrix. The second row of the premultiplier matrix is then employed in like fashion to obtain the second row of the result matrix, and so forth.

Example:

$$\begin{bmatrix} 6 & -4 & 3 \\ 2 & 2 & -1 \end{bmatrix}\begin{bmatrix} -2 & 7 & 0 & 4 \\ 3 & 3 & 1 & -1 \\ -4 & 6 & 9 & 12 \end{bmatrix} = \begin{bmatrix} -36 & 48 & 23 & 64 \\ 6 & 14 & -7 & -6 \end{bmatrix}$$

Note that the product of the first row of the premultiplier by the first column of the postmultiplier gave the element in first row first column position of the result. In general the rth row by the sth column gives the element in the rth row, sth column position.

Obviously, the number of columns of the premultiplier must equal the number of rows in the postmultiplier.

The process of matrix multiplication is not commutative. That is, the order of multiplication must be preserved. In general,

$$[A][B] \neq [B][A].$$

Matrix Transposition - $[A']$

The transpose of a matrix is obtained by interchanging rows and columns. Thus if

$$[A] = \begin{bmatrix} 6 & 2 \\ -1 & 4 \\ 0 & -4 \end{bmatrix} .$$

Then its transpose, denoted by $[A']$, is

$$[A'] = \begin{bmatrix} 6 & -1 & 0 \\ 2 & 4 & -4 \end{bmatrix}$$

When the subscript notation is used (see below), transposition is indicated by interchanging subscripts. Thus, the transpose of $[A_{ij}]$ is shown as $[A_{ji}]$. This notation is followed in the text.

Matrix Inversion - $[A^{-1}]$

The process of matrix inversion may be likened to division in elementary arithmetic. The inverse of the matrix $[A]$ is denoted by $[A^{-1}]$ and is computed such that

$[A][A^{-1}] = [I]$ where $[I]$ is the unit matrix.

Unlike most matrix products, the order of multiplication is immaterial in this case:

$$[A][A^{-1}] = [A^{-1}][A] = [I]$$

i. Only square matrices have inverses.

ii. An inverse cannot be found for a matrix, the determinant of whose coefficients is zero. Such a matrix is called singular. This rule will appear obvious in light of the method given below for finding an inverse.

One method of finding the inverse of a given matrix is as follows:

1. Form the matrix of cofactors. The cofactor of the element in the mth row and n^{th} column is found by computing the value of the determinant remaining after the mth row and n^{th} column are struck from the matrix; this value is then multiplied by $(-1)^{m+n}$

Thus, in the matrix

$$\begin{bmatrix} 3 & 7 & -4 \\ 2 & 0 & 2 \\ -1 & 3 & 2 \end{bmatrix} ,$$

the cofactor of the element in the first row, first column is

$$(-1)^{(1+1)} \begin{vmatrix} 0 & 2 \\ 3 & 2 \end{vmatrix} = (1)(0 - 6) = -6 .$$

The cofactor of the element in the first row, second column is

$$(-1)^{(1+2)} \begin{vmatrix} 2 & 2 \\ -1 & 2 \end{vmatrix} = (-1)(4 + 2) = -6$$

2. Transpose the matrix of cofactors.

3. Divide by the value of the determinant of the original matrix (conveniently and quickly found as the sum of products of corresponding terms in the first column of the original matrix and the first column of the matrix of cofactors).

Example: Find the inverse of

$$[A] = \begin{bmatrix} 3 & 7 & -4 \\ 2 & 0 & 2 \\ -1 & 3 & 2 \end{bmatrix}$$

1. Find the matrix of cofactors

$$\begin{bmatrix} -6 & -6 & 6 \\ -26 & 2 & -16 \\ 14 & -14 & -14 \end{bmatrix}$$

2. Transpose

$$\begin{bmatrix} -6 & -26 & 14 \\ -6 & 2 & -14 \\ 6 & -16 & -14 \end{bmatrix}$$

3. Find the determinant of $[A]$

$$|A| = 3(-6) + 2(-26) - 1(14) = -84$$

and, Divide (2) by $|A|$, giving

$$[A^{-1}] = -\frac{1}{84} \begin{bmatrix} -6 & -26 & 14 \\ -6 & 2 & -14 \\ 6 & -16 & -14 \end{bmatrix} =$$

$$= \begin{bmatrix} .0714 & .3095 & -.1667 \\ .0714 & -.0238 & .1667 \\ -.0714 & .1905 & .1667 \end{bmatrix}$$

4. Check

$$\begin{bmatrix} 3 & 7 & -4 \\ 2 & 0 & 2 \\ -1 & 3 & 2 \end{bmatrix}\begin{bmatrix} .0714 & .3095 & -.1667 \\ .0714 & -.0238 & .1667 \\ -.0714 & .1905 & .1667 \end{bmatrix} =$$

$$= \begin{bmatrix} 1.00 & 0 & 0 \\ 0 & 1.00 & 0 \\ 0 & 0 & 1.00 \end{bmatrix}$$

The above method of matrix inversion is only practical for small size matrices (2x2 or 3x3). It is presented here primarily to demonstrate the impossibility of inverting a singular matrix. This impossibility should be clear in view of step (3), above.

Methods satisfactory for hand inversion of matrices of moderate size may be found in references (1), (2) and (3). In general, hand computation of large matrix inversions is to be avoided.

Useful Rules for Dealing With Inverses

While the structural engineer will (it is to be hoped) be able to delegate the main task of forming inverses to automatic machine computation, the following rules and techniques will prove useful for dealing with inverses in structural problems.

INTERCHANGE OF ROWS (OR COLUMNS)

If two rows of a matrix are interchanged the corresponding two columns of the inverse are interchanged. If two columns of a matrix are interchanged the corresponding two rows of the inverse are interchanged.

SCALING OF A ROW OR COLUMN

If a row (column) of a matrix is multiplied by a constant, the corresponding column (row) of the inverse is divided by this constant.

EXTRACTING INVERSES OF REDUCED MATRICES

If one has a large matrix out of which a smaller (reduced) matrix is to be employed, the inverse of the reduced matrix often may be found from the inverse of the original, large matrix (assuming this had already been computed). Thus, if

$$\left[\begin{array}{c|c|c} A & B & C \\ \hline D & E & F \\ \hline G & H & J \end{array}\right] \leftarrow k^{th} \text{ row}$$

$\uparrow$ k^{th} column

has a known inverse

$$\left[\begin{array}{c|c|c} a & b & c \\ \hline d & e & f \\ \hline g & h & j \end{array}\right] \leftarrow k^{th} \text{ row}$$

$\uparrow$ k^{th} column ,

then the inverse of the reduced matrix $\left[\begin{array}{c|c} A & C \\ \hline G & J \end{array}\right]$, obtained by dropping out the kth row and k^{th} column, is:

$$\left[\begin{array}{c|c} A & C \\ \hline G & J \end{array}\right]^{-1} = \left[\begin{array}{c|c} a & c \\ \hline g & j \end{array}\right] - \frac{1}{e}\left\{\begin{array}{c} b \\ \hline h \end{array}\right\}\left[\begin{array}{c|c} d & f \end{array}\right]$$

INVERSE OF A MODIFIED MATRIX

Given a matrix

$$\left[A_o\right] = \left[\begin{array}{c|c} B & C \\ \hline D & E \end{array}\right]$$

and its inverse

$$\left[A_o^{-1}\right] = \left[\begin{array}{c|c} K & L \\ \hline M & N \end{array}\right]$$

If now a portion of $\left[A_o\right]$ is to be modified to give a matrix

$$\left[A_1\right] = \left[\begin{array}{c|c} B_1 & C \\ \hline D & E \end{array}\right] \text{ , where } \left[B_1\right] = \left[B\right] + \left[b\right],$$

then the inverse of the modified matrix may be found as

$$\left[A_1{}^{-1}\right] = \left[A_o^{-1}\right] - \left[\begin{array}{c} K \\ \hline M \end{array}\right]\left[q^{-1}\right]\left[b\right]\left[\begin{array}{c|c} K & L \end{array}\right]$$

where

$$\left[q\right] = \left[I\right] + \left[b\right]\left[K\right]$$

Partitioning of Matrices

Matrices are sometimes "partitioned" into smaller submatrices for convenience. When performing matrix multiplications with partitioned matrices these submatrices may be handled as though they were simply matrix elements. For example, we multiply two partitioned matrices:

$$\left[\begin{array}{c|c} A & B \\ \hline C & D \end{array}\right]\left\{\begin{array}{c} E \\ \hline F \end{array}\right\} = \left\{\begin{array}{c} [A][E] + [B][F] \\ \hline [C][E] + [D][F] \end{array}\right\} .$$

Of course, the requirements as to sizes of matrices to be multiplied, will have to be observed in performing the partitioning.

An example with numbers:

$$\left[\begin{array}{cc|c} 4 & 7 & 3 \\ -1 & 3 & -3 \\ \hline 1 & 6 & 0 \\ -5 & 8 & 4 \end{array}\right]\left[\begin{array}{cc} 6 & -1 \\ -4 & 0 \\ \hline 9 & 2 \end{array}\right] = \left[\begin{array}{c} \left[\begin{array}{cc} 4 & 7 \\ -1 & 3 \end{array}\right]\left[\begin{array}{cc} 6 & -1 \\ -4 & 0 \end{array}\right] + \left\{\begin{array}{c} 3 \\ -3 \end{array}\right\}\left[\begin{array}{cc} 9 & 2 \end{array}\right] \\ \hline \left[\begin{array}{cc} 1 & 6 \\ -5 & 8 \end{array}\right]\left[\begin{array}{cc} 6 & -1 \\ -4 & 0 \end{array}\right] + \left\{\begin{array}{c} 0 \\ 4 \end{array}\right\}\left[\begin{array}{cc} 9 & 2 \end{array}\right] \end{array}\right]$$

$$= \left[\begin{array}{c} \left[\begin{array}{cc} -4 & -4 \\ -18 & 1 \end{array}\right] + \left[\begin{array}{cc} 27 & 6 \\ -27 & -6 \end{array}\right] \\ \hline \left[\begin{array}{cc} -18 & -1 \\ -62 & 5 \end{array}\right] + \left[\begin{array}{cc} 0 & 0 \\ 36 & 8 \end{array}\right] \end{array}\right] = \left[\begin{array}{cc} 23 & 2 \\ -45 & -5 \\ -18 & -1 \\ -26 & 13 \end{array}\right]$$

II - Applications of Matrix Notation.

It is true that the applications of matrix notation here and elsewhere in the text are no more than rearrangements of arithmetic operations into a more concise and compact form; no important new concepts or methods are introduced thereby. Superficially, these same criticisms may be levelled at most mathematical tools. Only with continued use and increased familiarity with the tool, do new concepts and improved methods suggest themselves to the analyst.

Sum as a Product

The sum, $\sum_{i=1}^{3} a_i b_i$, may be written as either the matrix product

$$\left\lfloor a_1\ a_2\ a_3 \right\rfloor \left\{\begin{array}{c} b_1 \\ b_2 \\ b_3 \end{array}\right\}$$

or

$$\left\lfloor b_1\ b_2\ b_3 \right\rfloor \left\{\begin{array}{c} a_1 \\ a_2 \\ a_3 \end{array}\right\} .$$

In a more concise notation

$$\sum_{i=1}^{n} a_i b_i = \left\lfloor a_i \right\rfloor \left\{ b_i \right\} \quad i=1,2,\ldots.n$$

Sum of a Multiple Product

The sum $\sum_{i=1}^{3} a_i b_i c_i$ is written in matrix form as

$$\left\lfloor a_1\ a_2\ a_3 \right\rfloor \left[\begin{array}{ccc} b_1 & 0 & 0 \\ 0 & b_2 & 0 \\ 0 & 0 & b_3 \end{array}\right] \left\{\begin{array}{c} c_1 \\ c_2 \\ c_3 \end{array}\right\} .$$

In a more concise notation

$$\sum_{i=1}^{n} a_i b_i c_i = \left\lfloor a_i \right\rfloor \left[b_i \right] \left\{ c_i \right\} \quad i=1,2,\ldots.n$$

Since the product $a_i b_i c_i$ is commutable, the matrix form above may be written equally well as

$$\left\lfloor b_i \right\rfloor \left[a_i \right] \left\{ c_i \right\} \text{ or } \left\lfloor c_i \right\rfloor \left[a_i \right] \left\{ b_i \right\} , \text{ etc.}$$

Double Sum ("Bilinear Form")

The double sum $S = \sum_{i}^{m} \sum_{j}^{n} x_i a_{ij} y_j$ writes out as

$$\begin{aligned} S = {} & a_{11} x_1 y_1 + a_{12} x_1 y_2 + \ldots + a_{1n} x_1 y_n \\ & + a_{21} x_2 y_1 + a_{22} x_2 y_2 + \ldots + a_{2n} x_2 y_n \\ & + a_{31} x_3 y_1 + \ldots \qquad\qquad \vdots \\ & \vdots \qquad\qquad\qquad\qquad\quad \vdots \\ & + a_{m_1} x_m y_1 + \ldots\ldots\ldots + a_{mn} x_m y_n . \end{aligned}$$

In matrix form one has,

$$S = \left\lfloor x_1\ x_2\ \ldots x_m \right\rfloor \left[\begin{array}{ccc} a_{11} & a_{12} \ldots & a_{1n} \\ a_{21} & a_{22} \ldots & \cdot \\ \cdot & & \cdot \\ \cdot & & \cdot \\ \cdot & & \cdot \\ a_{m_1} & \ldots\ldots & a_{mn} \end{array}\right] \left\{\begin{array}{c} y_1 \\ y_2 \\ \cdot \\ \cdot \\ \cdot \\ y_n \end{array}\right\} .$$

More concisely,

$$S = \left\lfloor x_i \right\rfloor \left[a_{ij} \right] \left\{ y_j \right\} \quad \begin{array}{l} i=1,2,\ldots m \\ j=1,2,\ldots n \end{array}$$

Simultaneous Equations

The equations

$$\begin{aligned} a_{11} x_1 + a_{12} x_2 + a_{13} x_3 &= k_1 \\ a_{21} x_1 + a_{22} x_2 + a_{23} x_3 &= k_2 \\ a_{31} x_1 + a_{32} x_2 + a_{33} x_3 &= k_3 \end{aligned}$$

are written in matrix form as

$$\begin{bmatrix} a_{11} & a_{12} & a_{13} \\ a_{21} & a_{22} & a_{23} \\ a_{31} & a_{32} & a_{33} \end{bmatrix} \begin{Bmatrix} x_1 \\ x_2 \\ x_3 \end{Bmatrix} = \begin{Bmatrix} k_1 \\ k_2 \\ k_3 \end{Bmatrix}$$

In a more concise form:

$$\left[a_{ij}\right]\left\{x_j\right\} = \left\{k_i\right\} \quad i,j = 1,2,3 \ .$$

The solution of a set of simultaneous equations may be either indicated (for symbolic purposes) or actually obtained, by the use of the inverse matrix definition. Thus, the equations

$$\left[a_{ij}\right]\left\{x_j\right\} = \left\{k_i\right\}$$

may be solved for the x_j if one first computes the inverse of the coefficient matrix $\left[a_{ij}\right]$,

and then multiplies through by it.

$$\left[a^{-1}_{ij}\right]\left[a_{ij}\right]\left\{x_j\right\} = \left[a^{-1}_{ij}\right]\left\{k_i\right\}$$

$$\left\{x_j\right\} = \left[a^{-1}_{ij}\right]\left\{k_i\right\}$$

(Solution)

For example, if one has the equations

$$\begin{bmatrix} 3 & 7 & -4 \\ 2 & 0 & 2 \\ -1 & 3 & 2 \end{bmatrix} \begin{Bmatrix} x_1 \\ x_2 \\ x_3 \end{Bmatrix} = \begin{Bmatrix} 4.02 \\ 9.90 \\ -.635 \end{Bmatrix},$$

the solution is (the inverse of this matrix of coefficients was found in an example above).

$$\begin{Bmatrix} x_1 \\ x_2 \\ x_3 \end{Bmatrix} = \begin{bmatrix} .0714 & .3095 & -.1667 \\ .0714 & -.0238 & .1667 \\ -.0714 & .1905 & .1667 \end{bmatrix} \begin{Bmatrix} 4.02 \\ 9.90 \\ -.635 \end{Bmatrix}$$

$$= \begin{Bmatrix} 3.46 \\ -.0544 \\ 1.49 \end{Bmatrix} \quad \text{(Solution)}$$

Matrix Transformations

Linear transformations play an important role in the matrix methods of structural analysis. The principle ones are indicated here.

A linear relationship between two sets of variables, such as

$$\left\{f_j\right\} = \left[a_{ij}\right]\left\{x_j\right\} \text{ - - - - - - - - - - - - - - - } (1)$$

may be transformed, if a new set of variables $\left\{y_k\right\}$ are related linearly to the $\left\{x_j\right\}$ by equations such as

$$\left\{x_j\right\} = \left[T_{jk}\right]\left\{y_k\right\} \text{ - - - - - - - - - - - - - - - } (2)$$

A direct substitution of (2) into (1) gives the new relationship:

$$\left\{f_i\right\} = \left[a_{ij}\right]\left[T_{jk}\right]\left\{y_k\right\}$$

$$= \left[b_{ik}\right]\left\{y_k\right\} \text{ - - - - - - - - - - - - - - - - } (3)$$

where

$$\left[b_{ik}\right] \equiv \left[a_{ij}\right]\left[T_{jk}\right]$$

Equation (3) now gives the f_i as functions of the new variables y_k.

For example, if the deflections of a structure are related to the internal forces q_i by

$$\begin{Bmatrix} \delta_1 \\ \delta_2 \end{Bmatrix} = \frac{L}{6EI} \begin{bmatrix} 1 & 2 \\ 0 & 1 \end{bmatrix} \begin{Bmatrix} q_1 \\ q_2 \end{Bmatrix}$$

and the q_i are in turn related to the external loads on the structure by

$$\begin{Bmatrix} q_1 \\ q_2 \end{Bmatrix} = \begin{bmatrix} .8 & 0 \\ 1.6 & .8 \end{bmatrix} \begin{Bmatrix} P_1 \\ P_2 \end{Bmatrix}$$

then

$$\begin{Bmatrix} \delta_1 \\ \delta_2 \end{Bmatrix} = \frac{L}{6EI} \begin{bmatrix} 1 & 2 \\ 0 & 1 \end{bmatrix} \begin{bmatrix} .8 & 0 \\ 1.6 & .8 \end{bmatrix} \begin{Bmatrix} P_1 \\ P_2 \end{Bmatrix}$$

$$= \frac{L}{6EI} \begin{bmatrix} 4.0 & 1.6 \\ 1.6 & 0.8 \end{bmatrix} \begin{Bmatrix} P_1 \\ P_2 \end{Bmatrix}$$

This last expression relates the deflections directly to the external loads.

In the case of a bilinear form,

$$S = \left[x_i\right]\left[a_{ij}\right]\left\{y_j\right\} \text{ - - - - - - - - - - - - - - } (4)$$

where the sum is a function of two sets of independent variables, x_i and y_j, transformations of either or both variables may be made. Thus if two new sets of variables σ_k and τ_l are introduced by the linear equations

$$\left\{x_i\right\} = \left[T_{ik}\right]\left\{\sigma_k\right\} \quad \text{- - - - - - - - - - - - - - -} \quad (5)$$

$$\left\{y_j\right\} = \left[U_{jl}\right]\left\{\tau_l\right\}, \quad \text{- - - - - - - - - - - - - - -} \quad (6)$$

a direct substitution may be made (note that equation 5 will have to be transposed to get the x_i in row-matrix form).

$$S = \left\lfloor\sigma_k\right\rfloor\left[T_{ki}\right]\left[a_{ij}\right]\left[U_{jl}\right]\left\{\tau_l\right\}$$

$$= \left\lfloor\sigma_k\right\rfloor\left[b_{kl}\right]\left\{\tau_l\right\} \quad \text{- - - - - - - - - - - - - - -} \quad (7)$$

where

$$\left[b_{kl}\right] \equiv \left[T_{ki}\right]\left[a_{ij}\right]\left[U_{jl}\right] \quad \text{- - - - - - - - - -} \quad (8)$$

and $\left[T_{ki}\right]$ is the transpose of $\left[T_{ik}\right]$ (transposition denoted by interchange of subscripts).

Remarks on Subscript Notation

A useful check procedure may be formulated by the observation that if one "cancels" alike adjacent subscripts in a matrix multiplication, the remaining subscripts should agree on each side of the equality. Thus, in equation (7) above, all subscripts "cancel" on the right hand side, which is as it should be, since S is a scalar quantity. The same procedure checks the arrangement of equation (8), above.

In checking subscripts by this scheme the order of the subscripts must be (mentally) interchanged in the case of an inverse. For example,

$$\left[A_{mn}\right] = \left[a_{mn}\right] - \left[a_{ms}\right]\left[a_{rs}^{-1}\right]\left[a_{rn}\right]$$

and

$$\left\{q_j\right\} = \left[A_{ij}^{-1}\right]\left[A_{im}\right]\left\{P_m\right\}$$

Some caution must be exercised in applying the simple rule given with this scheme of notation. It is necessary that the subscripts follow this rule but not sufficient. Thus, the scheme cannot by itself distinguish between

$$\left\{q_\rho\right\} = \left[B_{\rho r}\right]\left\{q_r\right\}$$

or

$$\left\{q_\rho\right\} = \left[B_{r\rho}^{-1}\right]\left\{q_r\right\}$$

Either of these sets of equations could be correct: one would have to work carefully from the equation originally defining the $B_{\rho r}$ transformation, in order to choose between the above relations. Hence, while the rule can serve as a check, it should be used as a guide only with caution.

Check Rows and Check Columns in Matrix Multiplication

The greatest source of errors in the handling of numerical computations by matrix methods lies in the forming of matrix products. Whether the matrix product is formed automatically or manually it is advisable to carry along check rows and check columns as shown in the following.

Before forming the matrix product

$$\left[A\right]\left[B\right] = \left[C\right] ,$$

form an extra row under $\left[A\right]$, called a check row. Each element in this check row is the sum of elements in the column immediately above it. Next, form an extra column after $\left[B\right]$, called a check column. Each of its elements is the sum of elements in the adjacent horizontal row.

Thus,

$\left[A\right]\left[B\right]\square$ ← check column.

check row ↑

Now multiply out, treating the new row and new column as though they were regular parts of the $\left[A\right]$ and $\left[B\right]$ matrices. The product matrix which results will have an extra row and an extra column.

$$\left[A\right]\left[B\right]\square = \left[C\right]\square$$

If there are no errors, the sums of the elements in the rows and columns of $\left[C\right]$ should check against the corresponding elements in the extra row and column.

Example:

$$\begin{bmatrix} 6 & -4 & 3 \\ 2 & 2 & -1 \\ \hline 8 & -2 & 2 \end{bmatrix}\begin{bmatrix} -2 & 7 & 0 & 4 \\ 3 & 3 & 1 & -1 \\ -4 & 6 & 9 & 12 \end{bmatrix}\begin{bmatrix} 9 \\ 6 \\ 23 \end{bmatrix} = \begin{bmatrix} -36 & 48 & 23 & 64 \\ 6 & 14 & -7 & -6 \\ \hline -30 & 62 & 16 & 58 \end{bmatrix}\begin{bmatrix} 99 \\ 7 \end{bmatrix}$$

References

(1) Frazer, R., Duncan, W. and Collar, A. "Elementary Matrices", Cambridge Univ. Press, England, 1952.

(2) Crout, P. A Short Method of Evaluating Determinants and Solving Systems of Linear Equations with Real or Complex Coefficients, Transactions A.I.E.E., vol. 60, 1941.

(3) "Simultaneous Linear Equations and the Determination of Eigenvalues", National Bureau of Standards, Applied Mathematics Series, vol. 29, 1953.